18.9.87

AJR

Cuk-
Cuk-H03515-5 Pg2 (15)
Pg24440

American
Journal of
Roentgenology





October 1986

Procedure trays to control costs ...new from E-Z-EM

The objective:
Respond to the demand for a set of disposable trays to help hospitals and private practices control biopsy costs on a per-procedure basis.

The result:
E-Z-EM's new PercuSet line of disposable biopsy trays creating a system of procedure trays—a system of trays which offers the doctor progressive degrees of procedure capability.

The PercuSet Skin Prep Tray includes every implement and agent needed to cleanse, aseptisize, and anesthetize the procedure area—for biopsy, or for any percutaneous procedure.

The PercuSet Basic Biopsy Tray includes all the elements of the Prep Tray, *plus* a needle stop, and a ruler/protractor, *and* the option of an E-Z-EM biopsy needle.

The PercuSet Expanded Biopsy Tray adds a specimen-handling section, for complete biopsy procedure capability, also with the option of an E-Z-EM biopsy needle.

PercuSet Biopsy Trays assure absolute sterility, minimize component handling, eliminate cross-contamination, and are laid out in a logical procedural sequence.

They provide effective cost control, and reduce inventory management of components.

For additional information and a color brochure that details the PercuSet System, contact your local representative, or call E-Z-EM toll-free at 800-645-3052. In New York call 516-333-8230.

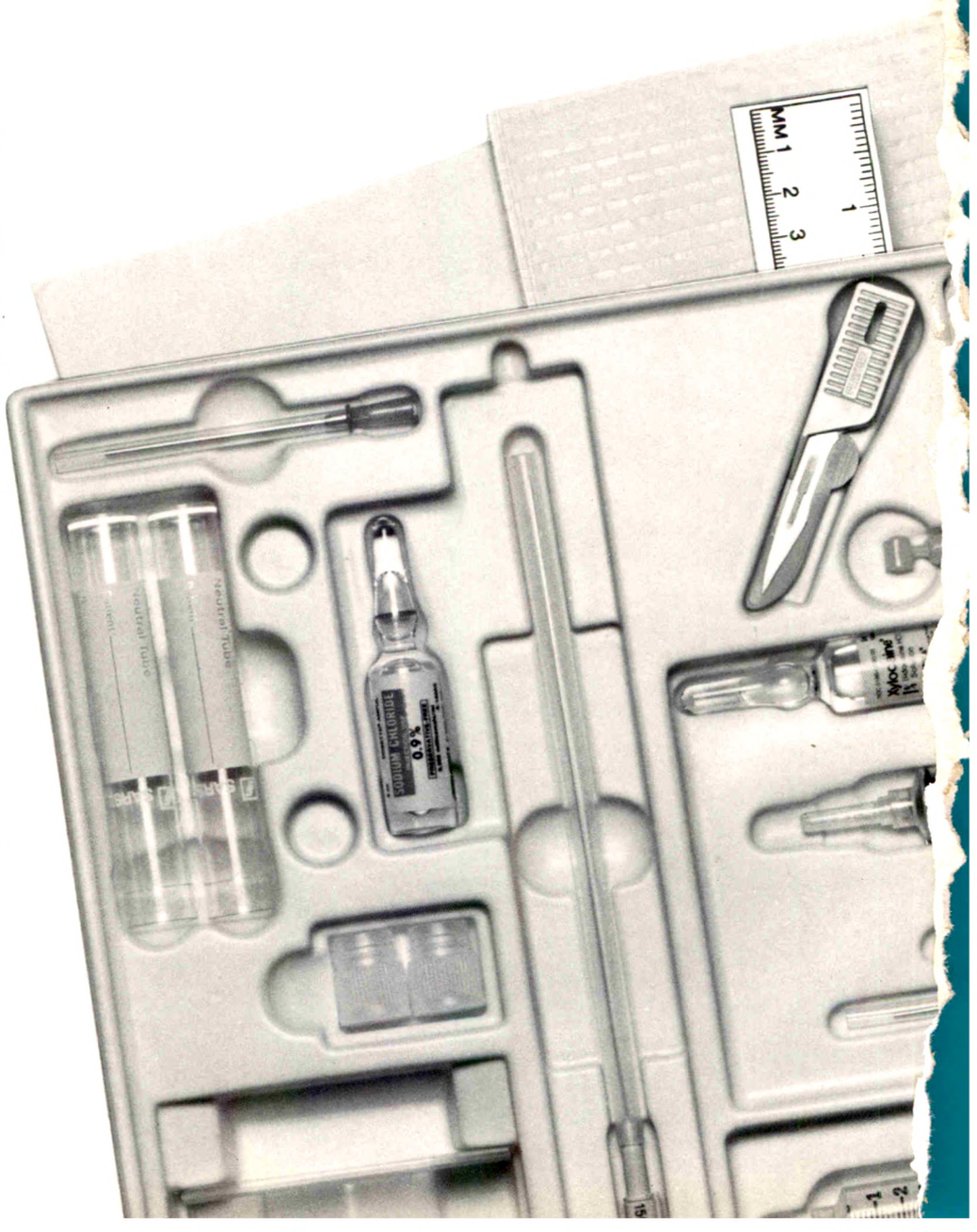
E-Z-EM

More than barium—
much more

E-Z-EM®
E-Z-EM, Inc.
7 Portland Avenue
Westbury, N.Y. 11590

© 1986 E-Z-EM, Inc.

PercuSet™



Official Journal of the American Roentgen Ray Society

AJR

American Journal of Roentgenology
Diagnostic Imaging and Related Sciences

P24,440

Editor-In-Chief Robert N. Berk, *San Diego, California*

Editor Emeritus Melvin M. Figley, *Seattle, Washington*

Associate Editors Alan J. Davidson, *Washington, District of Columbia*
Saskia von Waldenburg Hilton, *San Diego, California*
Juan M. Taveras, *Boston, Massachusetts*

Assistant Editors William L. Ashburn, *San Diego, California*
Charles C. Berry, *San Diego, California*
William G. Bradley Jr., *Pasadena, California*
Edward Buonocore, *Knoxville, Tennessee*
Peter L. Cooperberg, *Vancouver, British Columbia*
Peter Doubilet, *Boston, Massachusetts*
N. Reed Dunnick, *Durham, North Carolina*
Ronald G. Evens, *St. Louis, Missouri*
Henry I. Goldberg, *San Francisco, California*
William R. Hendee, *Chicago, Illinois*
John R. Hesselink, *San Diego, California*
Charles B. Higgins, *San Francisco, California*
Helen C. Redman, *Dallas, Texas*
Donald L. Resnick, *San Diego, California*
Stewart R. Reuter, *San Antonio, Texas*
Stuart S. Sagel, *St. Louis, Missouri*
Edward A. Sickles, *San Francisco, California*
Michel M. Ter-Pogossian, *St. Louis, Missouri*
Eric vanSonnenberg, *San Diego, California*

Editorial Staff: Gita S. Braude, *managing editor*; Elizabeth A. Whalen, Barbara Rose, and Linda Wood, *manuscript editors*; Nancy Rydbeck, *administrative assistant*; Sandra Wood, *administrative secretary*; Fay Lau, *secretary*.

All business correspondence, including display (not classified) advertising, subscriptions, address changes, reprints, and permission requests should be addressed to Williams & Wilkins, 428 East Preston Street, Baltimore, MD 21202. Correspondence regarding editorial matters and classified advertising should be addressed to the editorial office, AJR, 2223 Avenida de la Playa, Suite 200, La Jolla, CA 92037. For manuscript submission, see Guidelines for Authors, next page. Undelivered or damaged copies replaced within 60 days of publication; 90 days for foreign subscribers. Allow 90 days for address changes.
AJR AMERICAN JOURNAL OF ROENTGENOLOGY (ISSN 0361 803X) is published monthly by American Roentgen Ray Society, 428 E. Preston Street, Baltimore, MD 21202. Annual dues include $50 for journal subscription. Second class postage paid at Baltimore, MD and at additional mailing offices. Postmaster send address changes (Form 3579) to Williams & Wilkins, 428 East Preston St., Baltimore, MD 21202. Subscription rates $75 ($100 foreign); institutions $95 ($120 foreign); in training $25; single copy $14 ($17). Japanese Yen price is available from our sole agent USACO Corporation, 13-12, Shimbashi 1-Chome, Minato-Ku, Tokyo 105, Japan, telephone 03-502-6471. Airmail rates furnished on request. Indexed by *Current Contents* and *Index Medicus*.
Copyright © 1986 by American Roentgen Ray Society.
0361-803X/86$2.00

AJR Guidelines for Authors

Address new and revised manuscripts, correspondence, and classified ads to:

AJR Editorial Office
2223 Avenida de la Playa, Suite 200
La Jolla, CA 92037
telephone: (619) 459-2229

Make inquiries regarding subscriptions, display advertising, reprints, or permission to republish *AJR* material to the publisher:

The Williams & Wilkins Co.
428 E. Preston St.
Baltimore, MD 21202
telephone: (301) 528-4133

Publication Policy

The *AJR* publishes original and timely contributions to the advancement of medical diagnosis and treatment with radiologic methods. Although content is predominantly clinical, laboratory investigations are accepted when their relevance to clinical practice is demonstrable. In prospective clinical investigations, authors should document that informed consent was obtained from patients. The material submitted **must** not have been previously published nor be currently submitted for publication elsewhere (prior publication of simple abstracts without illustrations or tables will not prejudice publication of the complete study). Papers dealing with **neuroradiology** should be addressed to: Editorial Office, American Journal of Neuroradiology, Dept. of Radiology, Massachusetts General Hospital, Boston, MA 02114; telephone: (617) 726–8342. At the discretion of the Editor of *AJR*, *AJNR* articles may be republished in *AJR*.

Decisions on manuscripts are based on peer review. Reviewers receive manuscripts without title pages to protect the identity of authors and to ensure an unbiased review; names of reviewers, in turn, are not revealed to the authors. Accepted manuscripts are subject to editing. Statements within an article, including changes made by the Editor or copy editor, are the responsibility of the author and not *AJR* or its publisher. Authors will receive the edited manuscript, galley proof, and proofs of illustrations usually 6–8 weeks after acceptance. If the corresponding author will not be available, arrangements should be made for a coauthor or colleague to read and return the proof.

Copyright Information

In accordance with *AJR* implementation of the U.S. Copyright Law, authors must release first and subsidiary rights to their manuscript at submission (unless the study was performed as part of their duties as an employee of a U.S. government agency). A dated letter with the signatures of all authors should state: "We, the authors, assign first and subsidiary rights to the American Roentgen Ray Society in the event that our manuscript [insert title] is published by *AJR*. We guarantee that this manuscript contains no matter libelous or otherwise unlawful or which invades individual privacy or which infringes any proprietary right. *AJR*, in turn, grants us the right of republication, subject only to crediting the original source of publication and receiving written permission from the publisher. We understand we will receive no royalty or other compensation from *AJR*. We guarantee that this article and illustrations have not been previously published elsewhere or, if previously published in part or in whole, that permission has been obtained for republication. Copies of these permissions are included and previously published text or illustrations have been identified in the manuscript." (Delete the last sentence if it does not apply.) The covering letter also should state that the manuscript has been seen and approved by all the authors.

Manuscript Form

AJR complies with the Uniform Requirements for Manuscripts Submitted to Biomedical Journals (*Ann Intern Med* 1979;90:95–99). Manuscripts must be ***typed double-space throughout***, including references, tables, and figure legends. Each table, the footnotes, and the figure legend section should begin on separate sheets; a separate title page should be provided. Send the original typescript, one copy, and two sets of illustrations (not photocopies). Authors' names should be on the title page **only** so that author anonymity can be maintained during the review process. Permission to reprint previously published material should accompany the manuscript.

Organization of Major Articles

Title Page

Titles should be brief yet precise, accurately conveying the content of the paper. Limit authors to those who made substantial contributions to the work. Include an address for *each* author, and ZIP or postal code; acknowledgment of grant or other financial support when appropriate; name of meeting, location, and date if the paper was presented; a running head (shortened title); and the name, address, and telephone number of the author to whom correspondence and requests for reprints should be addressed.

Abstract

A description of the purpose, methods, results, and conclusions of the study is required. The factual highlights of each section should be recapitulated.

Introduction

Clearly state the purpose of the investigation, including necessary background facts that indicate its current relevance.

Materials [or Subjects] and Methods

Describe the research plan, the materials or subjects, and the methods, in that order. Proof of disease and control of subjectivity in observations should be detailed. Metric measurements should be used throughout. Put measurements in the International System of Units (SI) in parentheses when appropriate; for example, 400 rad (4 Gy).

Results

Present results in logical sequence. If tables are used, do not duplicate tabular data but do describe important points and trends.

Case Reports

Individual cases can be described if there are only a few; one or more cases from a large series can be described individually as Representative Case Reports. Each report should concentrate on the radiologic information and its usefulness.

Discussion

Offer appropriate limitations about the research plan, materials or subjects, and methods to give perspective to their adequacy for the purpose of the study. Interpret the results to lend meaning and importance to the observations. Hypotheses and speculation based

on the results are encouraged. When results differ from those of previous investigations, an attempt should be made to explain the discrepancy. Conclude with a brief statement regarding clinical significance.

Acknowledgments

Acknowledge only persons who have made *substantive* contributions to the study. Mention grant support on the title page.

References

References should be offered to document major assertions of fact and any opposing evidence and concepts. Discretion in number is requested. References should be cited in the text by number (e.g., [3, 4]). The reference list should be arranged in the numeric order that references are cited in the text and ***typed double-spaced throughout***. References cited *first* or *only* in tables or figure legends should be numbered by the sequence in which the table or figure is first identified in the text. Data for each reference should be arranged according to the style adopted by the U.S. National Library of Medicine and used in *Index Medicus*. ***Accuracy of reference data is the responsibility of the author.*** Provide all authors' (or editors') names when fewer than seven; when seven or more, list the first three and add et al. Provide inclusive page numbers; if an article is only one page, please indicate. Abbreviations for titles of medical periodicals should conform to those published in *Index Medicus*. Articles that appear in both *AJR* and *AJNR* should be a single reference that cites both journals (example 3). Examples:

1. Kirks DR, Fram EK, Vock P, Effmann EL. Tracheal compression by mediastinal masses in children: CT evaluation. AJR 1983;141:647–651
2. Khansur T, Yam LT, Tavassoli M. Serum monitors of bone metastasis. In: Stoll BA, Parbhoo S, eds. Bone metastases: monitoring and treatment. New York: Raven, 1983:165–180
3. Sage MR. Review. Kinetics of water-soluble contrast media in the central nervous system. AJNR 1983;4:897–906, AJR 1983; 141:815–824

Unpublished data and personal communications should not be numbered references but should be put in parentheses in the text (e.g., Smith JD, personal communication).

Tables

Tables should be concise and organized to show trends, not merely compilations of raw data. (The Editor may request that tables of backup data too extensive to be published be deposited with the National Auxiliary Publications Service or made available by the author.) Include only data pertinent to the subject. Long itemized case histories are better presented in the text as case reports or summaries. Do not repeat in tabular form material presented in the text. Tables should have titles and headings, but no vertical or horizontal rules.

Illustrations

Figures should be submitted as 13 × 18 cm (5 × 7 inch) glossy, black-and-white prints, ***untrimmed and unmounted***. Labels and arrows must be of professional quality and removable. Number each figure to correspond with the figure legends and indicate the top. Avoid writing directly on the back of the print. Special permission for publication of facial photographs of patients or for previously published pictures is required. Line illustrations or graphs must be professionally drawn in black ink on white background; please send photographic prints (not photocopies), not originals, to avoid damage in handling. Color illustrations will be used at the discretion of the Editor; send color prints. Firm estimates of cost will be sent to the author(s) for approval before publication. Identical anatomic structures in color prints should be the same size to facilitate reproduction and reduce cost.

Legends

Figure legends should carry a title identifying the message of the illustration and the case number if individual cases are described in the text. Legends should be as brief as possible for the informed reader to understand the figure. Detailed clinical data should be avoided. Legends for previously published illustrations should cite the reference number of the source (e.g., Reprinted from [8]).

Organization of Case Reports

Concise case reports will be considered for publication if they present unusual experiences that are medically important and instructive. Clarity and brevity are essential. After preliminary screening by an editor to determine whether the requirement of medical significance has been met, qualifying papers will undergo the same peer review as major papers. To facilitate planning the order and layout of each issue, case reports are limited in length to two journal pages. The introduction should be one short paragraph that gives some general background of the disorder and the specific interest and message of the case presented. Only one case should be described in detail. The case report should concentrate on the radiologic information and its usefulness. The discussion should focus on the specific message of this report and the relevance of radiology in this instance. If the author has encountered other cases, they may be briefly mentioned, and possibly illustrated, but not described in detail. There should be no more than eight references. The figures should be limited to the minimum required to document the case findings, probably not more than four pictures, each a column wide (or the equivalent). Excess illustrations would require severely shortening the text. Figure legends should be as short as possible and should not repeat the text. There can be no tables and no acknowledgments. See previous sections for detailed instructions regarding references and illustrations.

Other Contributions

Technical Notes

Brief descriptions of new techniques or significant modifications of older ones that are directly applicable to the clinical practice will be accepted if review is favorable. Technical notes do not carry abstracts or acknowledgments.

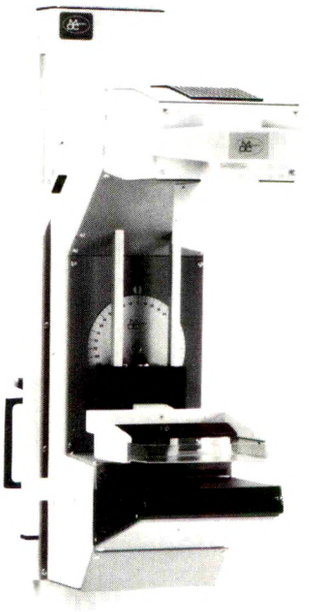
Letters to the Editor

Letters are subject to editing and condensation. Criticism of published articles should be objective and constructive. Letters also may discuss matters of general interest to radiologists.

Tecnomed USA

Mamex DC

MAMMOGRAPHIC SYSTEM





Original MAMEX DC

In the beginning...
The original MAMEX DC

The Mamex DC is a complete mammographic system, consisting of a modern, efficient DC generator which virtually eliminates "ripple" and gives a higher resolution image with consistently higher subject contrast; a molybdenum anode x-ray tube; and a motorized compression system with floor remote control.

Standard features:

- ★ Compact DC generator with automatic exposure control.
  Exposures can be made once every 30 seconds.
- ★ Stand designed for x-ray examination of the breast.
- ★ Hardened glass screen protects technician during exposure.
- ★ Floor remote compression control.
- ★ Phototiming detector position selector.
- ★ Field light.
- ★ Breast compression plate;
  Biopsy compression plate;
  Spot cone compression plate.
- ★ 18x24cm Kodak Min-R cassette with screen.
- ★ Film identification markers.
- ★ Automatic line voltage compensation.
- ★ .6x.6 stationary anode molybdenum x-ray tube with beryllium window.

Options:

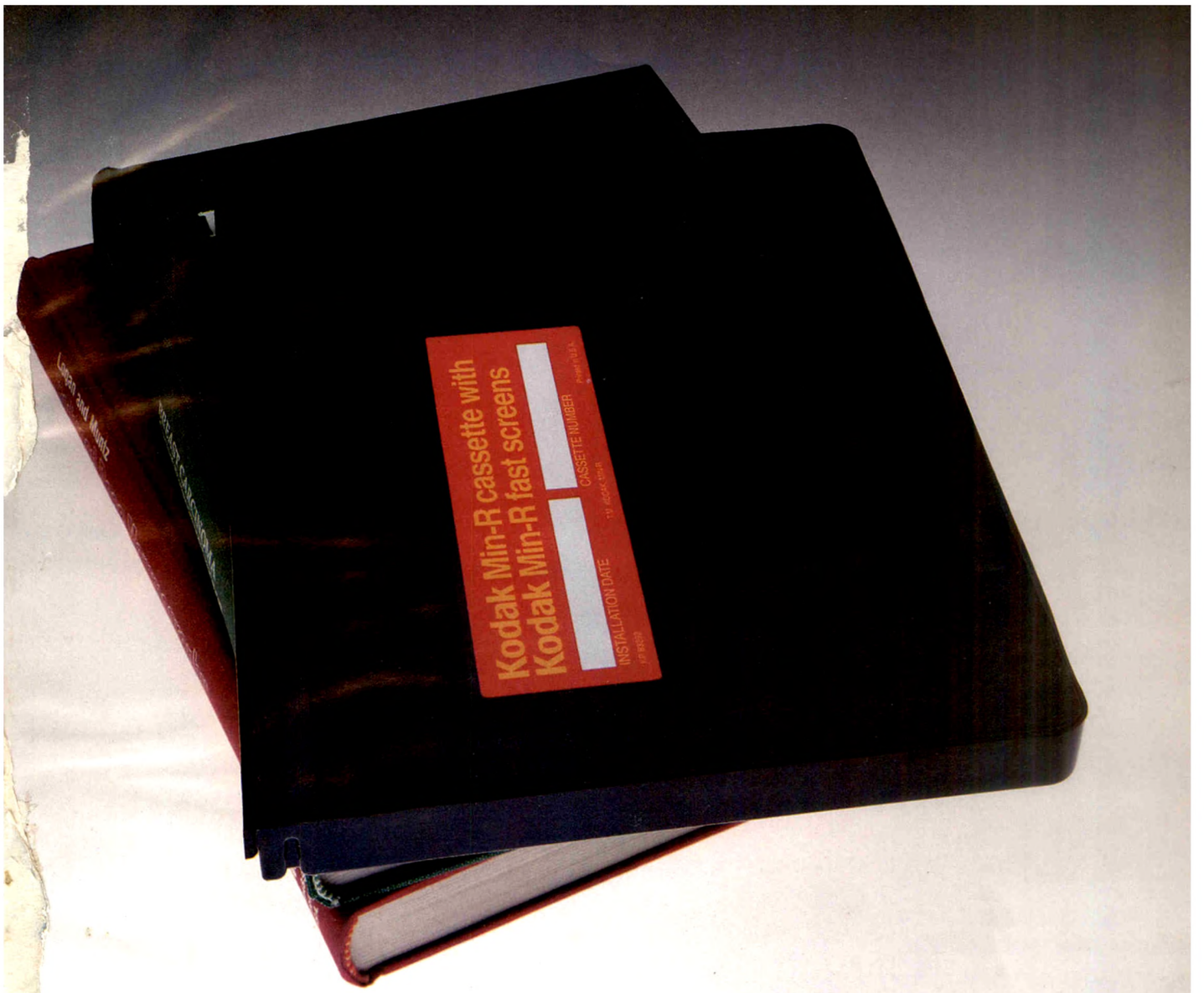
- ★ 200L 3.5:1 grid.
- ★ Carbon fiber cassette tunnel with grid pocket.
- ★ In-hospital wheel assembly (shown).
- ★ Van wheel assembly.

Mamex DC . . .

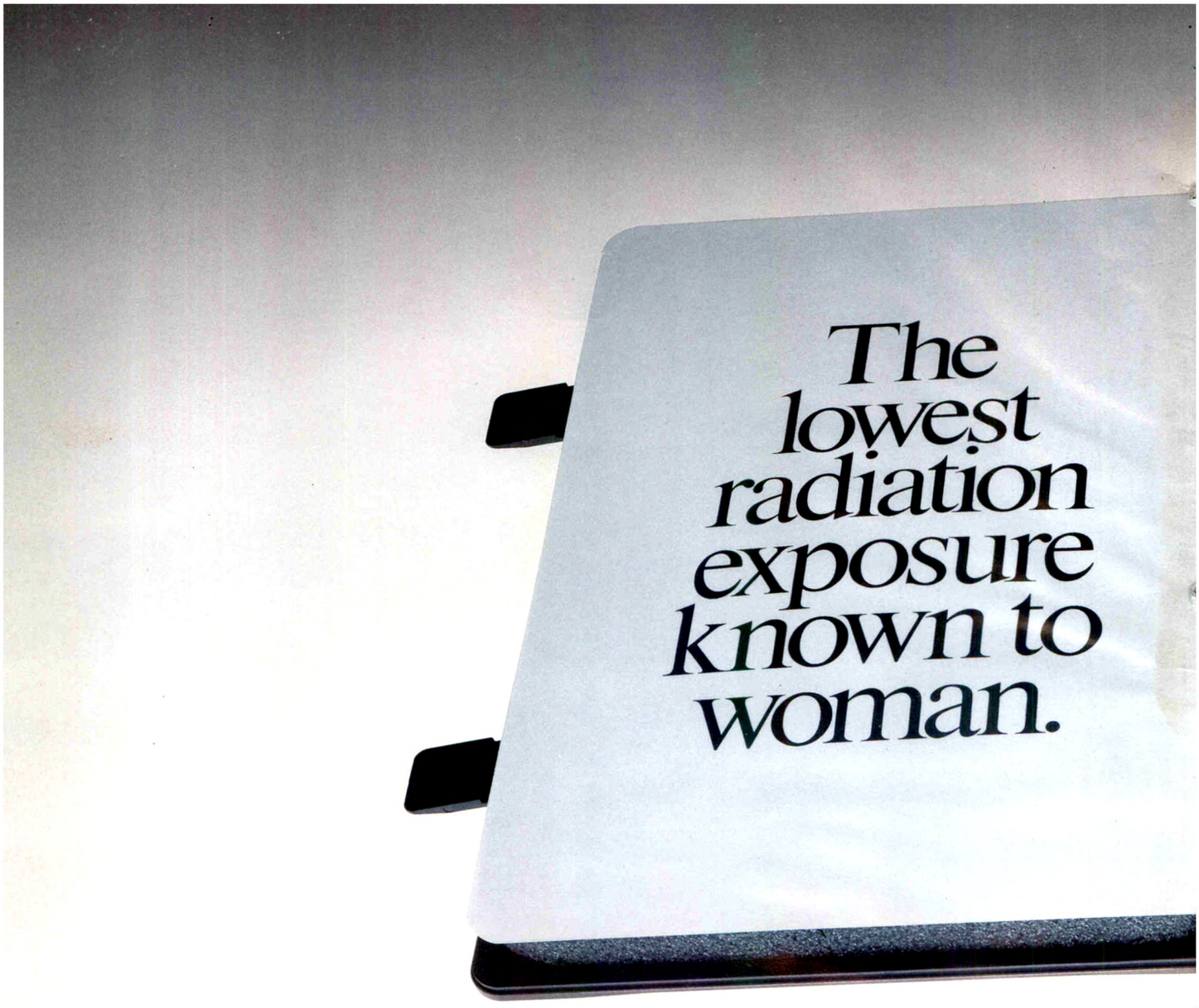
- ★ Five-year proven track record of performance and reliability;
- ★ Hundreds of satisfied physicians, clinics, and hospitals throughout the United States and internationally;
- ★ Full 12-month non-prorated warranty on the x-ray tube;
- ★ Average midbreast dosages, on a 2-film exam of a 6cm compressed breast, of .07R or less (as documented by the University of Michigan Breast Cancer Detection Center - Ingvar Andersson, M.D.)

. . . offers your facility the very best in diagnostic equipment available in today's marketplace.

Tecnomed USA 235 South Fehr Way, Bay Shore, New York 11706 • 516/586-1991-Telex II 510-227-9837



Kodak opens a new chapter in screen-film mammography.



New two-screen, double-emulsion film combination.

Introducing KODAK MIN-R Fast Screens and KODAK T-MAT M Film

For years, Kodak has been writing the book on mammographic imaging. Now a new chapter unfolds.

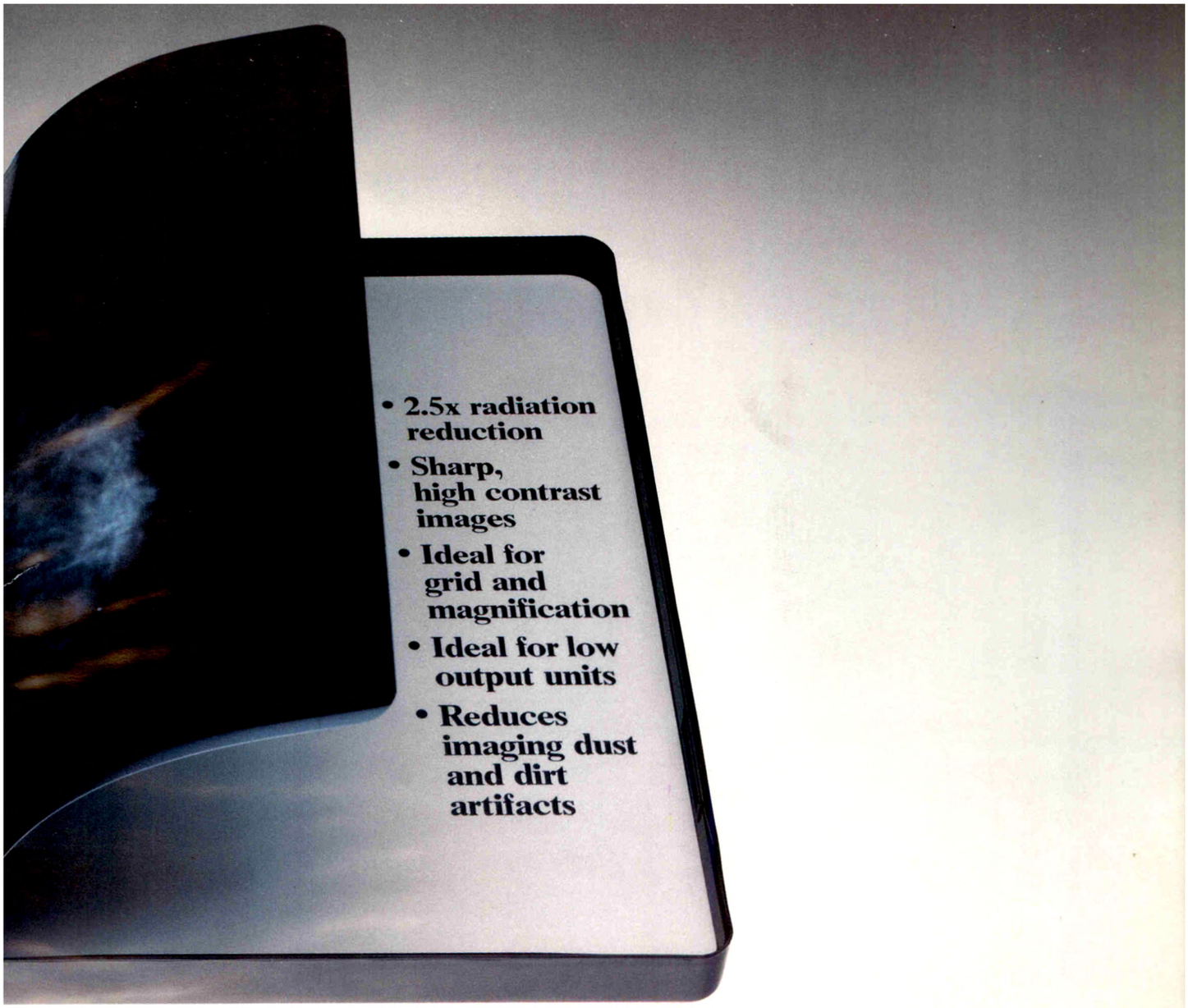
For the first time, you can use a two-screen, double-emulsion film combination for mammography. A combination that Kodak has created specifically for mammographic applications.

It's the new KODAK MIN-R Fast Screens and KODAK T-MAT M Film combination. And it's the fastest, high-quality, low-radiation-exposure mammographic imaging system in existence. It's so efficient, it reduces radiation exposure by 2.5x.

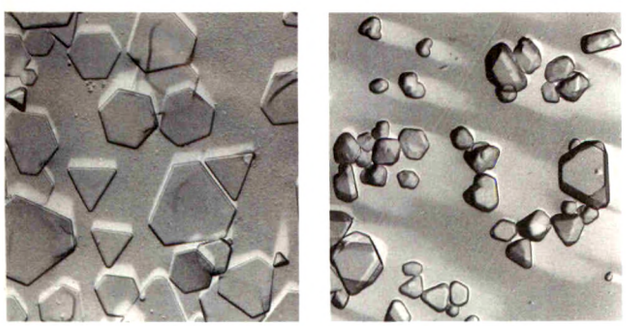
This technological breakthrough is the result of new screen-coating capabilities combined with Kodak's innovative T-Grain emulsion technology.

The proprietary new screens comprise a thin front screen and a conventional thickness mammographic back screen. These new screens are important elements that make possible the use of a double-emulsion film for mammography.

© Eastman Kodak Company, 1986



T-Grain emulsions are perhaps the biggest advance in silver halide imaging in 50 years. The new tablet-shaped silver halide grains used in KODAK T-MAT M Film capture more light, afford increased speed, and don't compromise image quality.



T-Grain emulsion technology is the basis for the new KODAK T-MAT M Film. The emulsions employ flat, tabular grains of silver halide (left) rather than the conventional pebble-shaped grains.

In addition, the T-MAT M Film has a magenta dye adsorbed onto the T-Grain crystals to absorb the green light emitted by the rare earth intensifying screens, reducing crossover without sacrificing system speed.

The double MIN-R Fast Screens and the T-MAT M Film are provided in low-absorbing KODAK MIN-R Cassettes or mounted in folders for use in vacuum devices. The result is a state-of-the-art system customized for mammography. A system that eliminates imaging dust and dirt artifacts, and provides an intimate screen-film contact to further maintain image sharpness. A system that can be used with grids to deliver the high-contrast image you need, while reducing radiation dose.

To open a new chapter in mammography for you and your patients, contact your Kodak technical sales representative.

New KODAK MIN-R Fast Screens and KODAK T-MAT M Film, the combination with a 2.5x radiation dose reduction.

Relative contrasts, speeds, and average glandular dose comparisons of Kodak films used with Kodak screens for mammography

Film	Contrast[1]	Relative Speed[2]	Average Glandular Dose[3] (Rads)
KODAK Ortho M Film KODAK MIN-R Screen	2.85	100	0.05
KODAK T-MAT M Film KODAK MIN-R Fast Screens	3.05	250	0.02

Development—KODAK *RP* X-OMAT Processors using seasoned KODAK *RP* X-OMAT Chemicals or equivalent at recommended temperatures.

Contrast[1]—Measured as the average gradient between densities 0.25 and 2.00 above gross fog.

Relative Speed[2]—Determined from matched density radiographs. KODAK Ortho M Film arbitrarily assigned a relative speed of 100.

Technique[3]—Based on average size breast, craniocaudal view, molybdenum target tube, 0.03 mm molybdenum filter, 28 kVp setting.

New KODAK MIN-R Fast Screens

The KODAK MIN-R Fast Screens incorporate phosphors which contain metals from the lanthanide series of "rare earth" elements. Using a molybdenum target x-ray tube with a beryllium window, 30 microns molybdenum filtration, and a 4 cm clear plastic breast test object, energy absorption by the screens is approximately 90 percent. The MIN-R Fast Screens are to be used in a KODAK MIN-R Cassette or suitable vacuum holder, with KODAK T-MAT M Film.

New KODAK T-MAT M Film

The new double-coated KODAK T-MAT M Film is a high-speed, high-contrast orthochromatic x-ray film specially designed for mammographic imaging. It incorporates light-sensitive dyes to absorb green light emitted by the intensifying screens and reduce image blur.

It is ideal for applications where high film speed is desired to reduce exposure times and radiation dose —for example, with the use of grids, small focal spots, and magnification techniques.

The KODAK MIN-R Cassette

The KODAK MIN-R Cassette provides fast, easy loading of films for the mammographic procedure. The all-plastic molded cassette provides intimate screen-film contact and low absorption. The tube-side panel of the cassette is thin, injection-molded polycarbonate, with low x-ray absorption. Combined with appropriate compression, the design of the MIN-R Cassette permits good visualization of soft-tissue information near the chest wall of the patient. MIN-R Cassettes can be supported with a holding device available on most dedicated mammography x-ray units.

Availability

KODAK T-MAT M Film

24 x 30 cm . . . . . CAT No. 810 9456
18 x 24 cm . . . . . CAT No. 809 6091
8 x 10 in. . . . . CAT No. 847 4975

KODAK MIN-R Fast Screens (in KODAK MIN-R Cassettes)

24 x 30 cm . . . . . CAT No. 813 3332
18 x 24 cm . . . . . CAT No. 810 1412

(in folder for vacuum devices)

8 x 10 in. . . . . CAT No. 847 6673

Kodak, X-Omat, Min-R, T-Grain, and T-Mat are trademarks.

M3-299

Printed in U.S.A.

7/86

The LORAD M-II™ Dedicated Mammography System...ideal for both Low Cost Screening and Sophisticated Diagnosis

✓	HIGH THRUPUT OF PATIENTS
✓	EASY, QUICK CASSETTE AND GRID CHANGES
✓	FAST ACCESS TO MAGNIFICATION AND BIOPSY MODES
✓	SUPERB RESOLUTION AND CONTRAST
✓	LOW DOSAGE



LOrad M-II meets the increasing demand for cost-effective mammographic screening systems. When operating in a screening mode, outstanding thruput results from LOrad M-II's compression and positioning controls, quick change cassette holders, continuously adjustable collimator, and automatic exposure. Easily mobile on large wheels, it plugs into any standard 115 volt power source, yet automatically delivers clean power at constant potential. And when a suspicious reading makes sophisticated diagnostic procedures advisable, LOrad's magnification and biopsy modes are easily attached.

Standard equipment includes:

Contact Film-screen Mode, with specially-designed breast compression devices and matching cassette holders.

Magnification Mode, including complete assembly which quickly attaches as a unit. It works with the new microfocus x-ray tube with rotating molybdenum target and alternative microfocal spot of .1 mm to give sharp, clearly-resolved magnified images. The special built-in LOrad 5-plate collimator with a light field indicator makes it easy to confine the beam precisely to the area of concern.

Biopsy localization mode. Its special compression device is perforated for a biopsy needle. The side-loading cassette allows the technologist to maintain positioning during film changes.

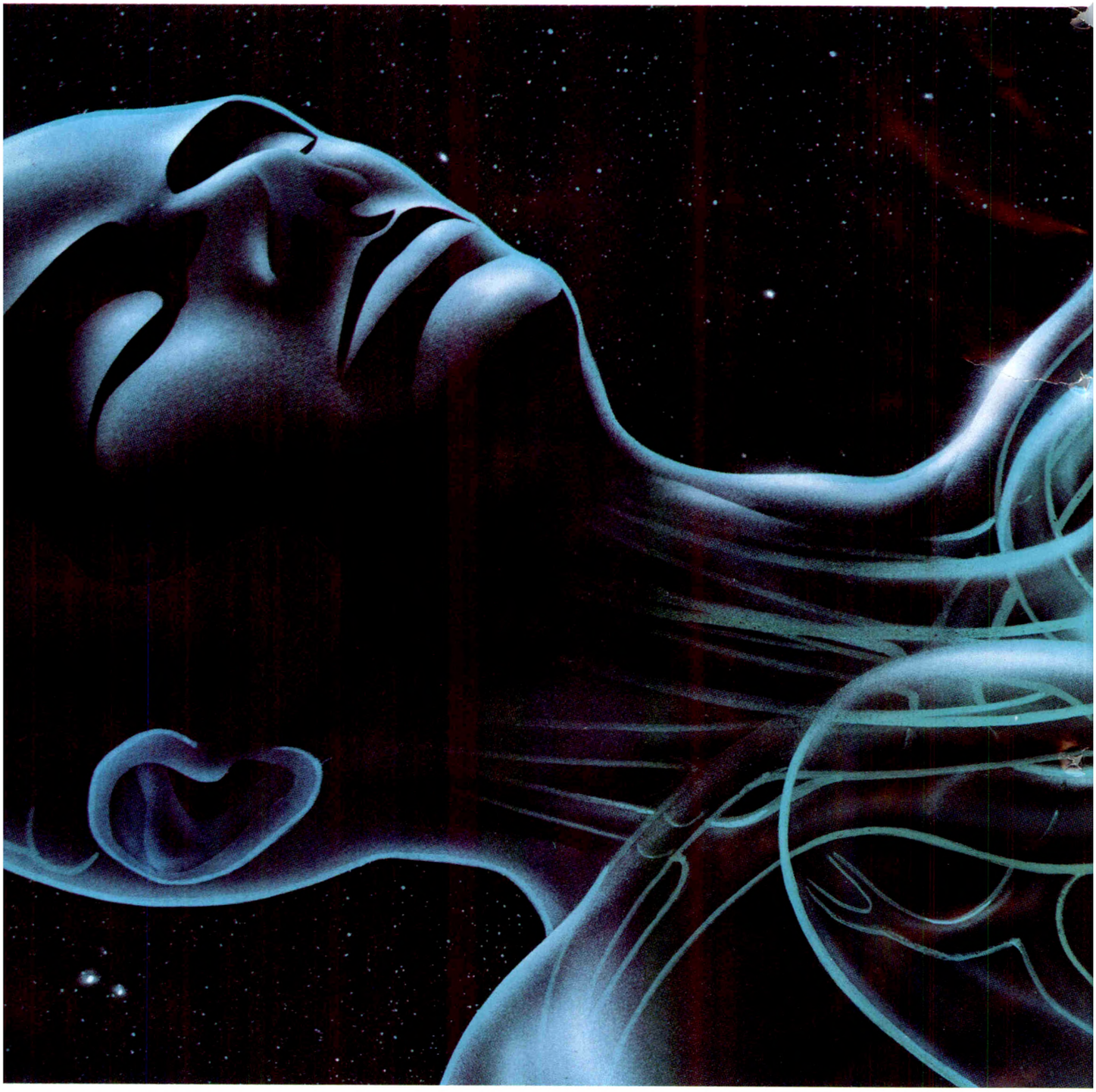
Grid Systems available.
The money-saving, time-saving new LOrad Permagrid™ has a stationary grid built into a specially engineered LOrad cassette holder. This slips easily onto the image receptor and accepts standard cassettes, and may be loaded and unloaded from either side. For those who prefer them, a Bucky moving grid or separate stationary grids are available.



LEASING PLANS AVAILABLE THROUGH YOUR DEALER. For his name, phone:

LOrad Medical Systems, Inc.
Eagle Road
Danbury, CT 06810
(203) 798-1127

Toshiba's TCT-900S...



)ne giant leap for CT!



CT beyond the fourth generation.

Toshiba's TCT-900S scanner is indisputably unique to the CT imaging industry. In fact, Toshiba's leading edge technology actually takes CT beyond the fourth generation into another dimension with these technological features found in no other comparable system:

1. Consistently superior image quality: just what you expect from Toshiba.
2. Nutate/Rotate geometry with continuous scan: thirty scans in thirty seconds.
3. True dynamic scan: no inter-scan delay.
4. Sub-second scanning: quality images in 0.6 seconds.

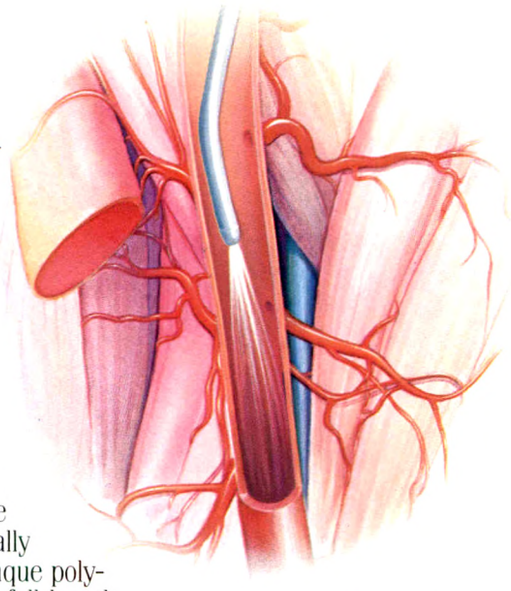
Let the competition tell you that CT technology can go no further. But you owe it to yourself to see just how far Toshiba can really go . . .

Call or write: Toshiba Medical Systems, 2441 Michelle Drive, Tustin, CA 92680. In California, call (714) 669-5419. Outside California, call toll-free (800) 421-1968. In Canada, call (416) 298-6100.

In Touch with Tomorrow

TOSHIBA

GLOBAL IMAGING SPECIALISTS



THE MOST SIGNIFICANT IMPROVEMENT IN DIAGNOSTIC RADIOLOGY CATHETERS IN RECENT YEARS.

Shiley SOFTIP® Standard and High Flow diagnostic radiology catheters.* Now they provide increased safety for patients. And better torqueability for you.

SOFTIP's improved patient safety comes from a unique, patented catheter tip which deforms on contact with vessel walls. Catheter forces previously directed against the intima are now absorbed by the catheter tip itself. As a result, the risks of intimal/subintimal lesions, intramural dissection, perforation and related vessel thrombosis and clot or plaque embolism may be reduced.

STUDIES CONFIRM SOFTIP PATIENT SAFETY.

In-vivo and in-vitro studies compared SOFTIP with two other conventional catheters. Both studies suggest that SOFTIP reduces the likelihood of angiography complications.

In the first study, light-micrograph cross sections of canine aortic tissue (Fig. 1A & 1B) demonstrated a reduction of intimal abrasions with SOFTIP.

The second study measured catheter tip indentation depths. Here SOFTIP showed 43% to 56% less indentation than other catheters tested (Fig. 2).

TORQUE SUPERIORITY YOU CAN FEEL.

A 16-strand stainless steel wire braid within specially formulated radiopaque polyurethane runs the full length of the catheter body. In the 5 and 6 French catheter, braiding extends to the deformable tip. In all cases, the result is a precise one-to-one torque ratio for optimum control, plus added memory. Yet longitudinal flexibility is never compromised.

The same special polyurethane also results in a superior curve memory. Consequently, positioning is easier while recoil and whipping may be minimized.

SOFTIP provides outstanding visualization, too.

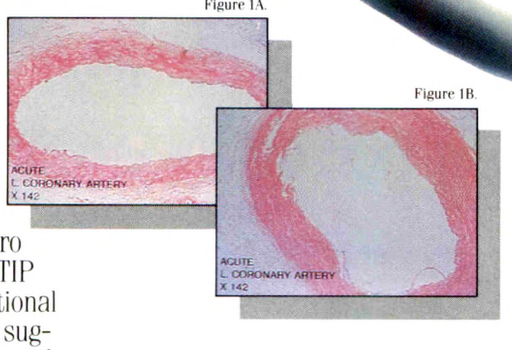


Fig. 1A *Canine histology studies demonstrated a reduction of intimal abrasions with the SOFTIP catheter's patient-safe deformable tip.*

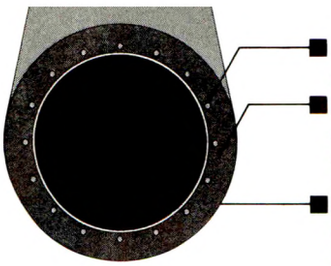
Fig. 1B *In contrast, conventional catheters showed significant endothelial disruption.*



Hard Facts

Shiley Incorporated, 17600 Gillette Avenue, Irvine, CA 92714-5751 USA, (714) 250-0500 (800) 854-3683, Cable: SHILEYINC IRIN, Telex: 68-5585.
Shiley-Europe, Staines House, 158-162 High Street, Staines, TW184AZ, England, Tel: (44) 784-61533, Telex: 919851 PFHPGS-G.
Shiley Canada, 251 Bartley Drive, Toronto Ontario, M4A-2N7, Canada, Tel: (416) 752-9990, Telex: 389-06963811.

For detailed information describing intended use, warnings, precautions and contraindications, refer to the instructions provided with each device or contact the Shiley Corporate Office.



- ***16-Strand Wire Braiding*** *helps produce one-to-one torque control.*
- ***Angithane,™****** *a specially formulated radiopaque polyurethane, improves handling, shape retention and visualization.*
- ***CELGARD™****** *silicone coating demonstrates superior catheter thromboresistance and increased lubricity.*

And its walls withstand high-pressure injections without compromising expected flow rates.

HIGH FLOW AND MORE.

In addition to Standard Flow catheters, SOFTIP offers a range of High Flow French sizes. High Flow catheter lumens have been enlarged without increasing outside catheter diameters. The benefits include improved flow capacity, greater media concentrations and better visualization, all without increasing French sizes.

Winged SOFTIP hubs are clearly marked with catheter length and French size for easy identification. A secure grip facilitates more efficient on-off connections. And a tapered hub lumen promotes smooth injections.

The exterior of each SOFTIP catheter is coated with silicone CELGARD™** for improved thromboresistance and lubricity. Studies demonstrated that silicone coated SOFTIP catheters yielded the lowest thrombogenicity index of any catheters tested.[1]

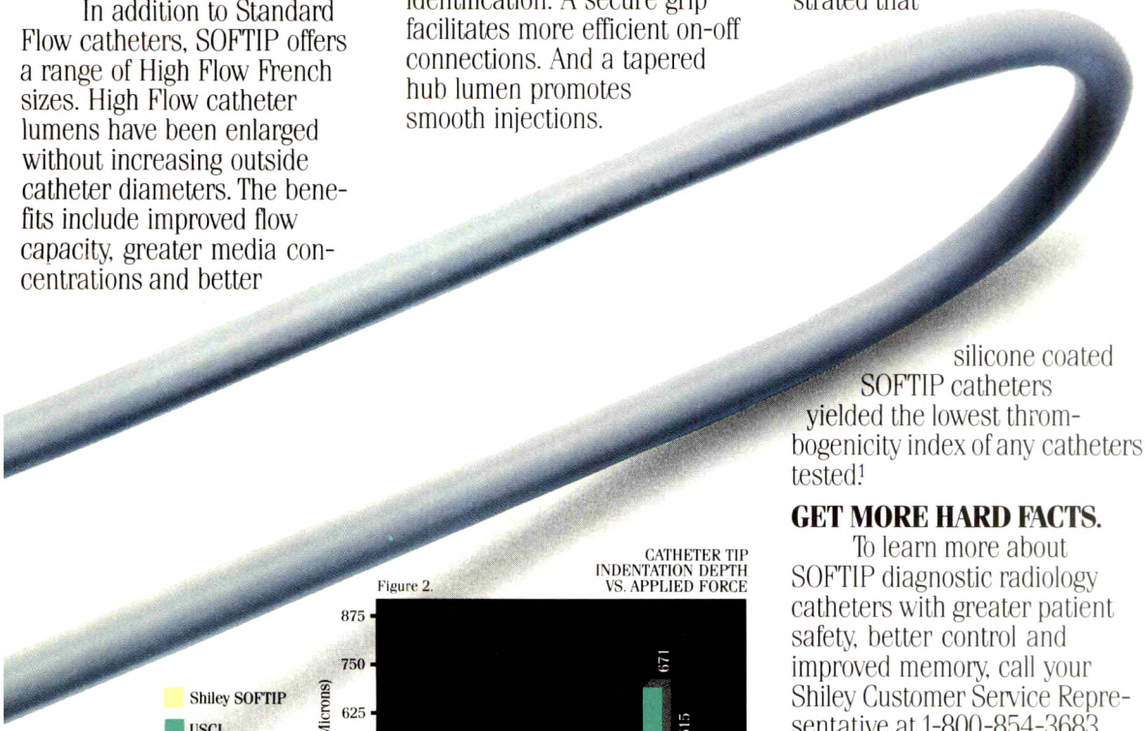
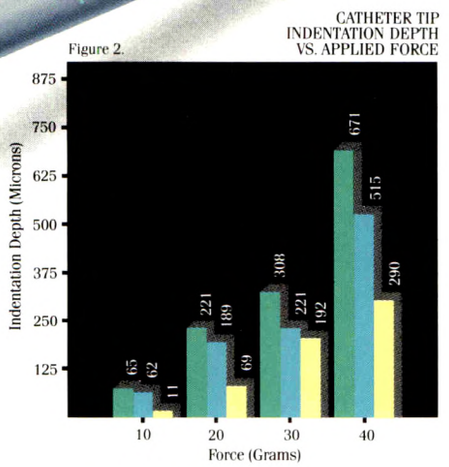


Figure 2.



Indentation depths in a semi-soft wax medium simulating vascular tissue were reduced 43% to 56% with SOFTIP angiography catheters when measured against conventional catheter tips.

Shiley SOFTIP = 140 ±13 μ's
USCI = 246 ±15μ's
Cordis = 318 ±20μ's

GET MORE HARD FACTS.

To learn more about SOFTIP diagnostic radiology catheters with greater patient safety, better control and improved memory, call your Shiley Customer Service Representative at 1-800-854-3683. In Alaska, call 714-250-0500 collect. In Europe, contact your Schneider-SOFTIP representative.

[1]*"Acute Canine Intra-Arterial Implantation Screening for Thrombogenicity," Utah Biomaterials Test Lab.*

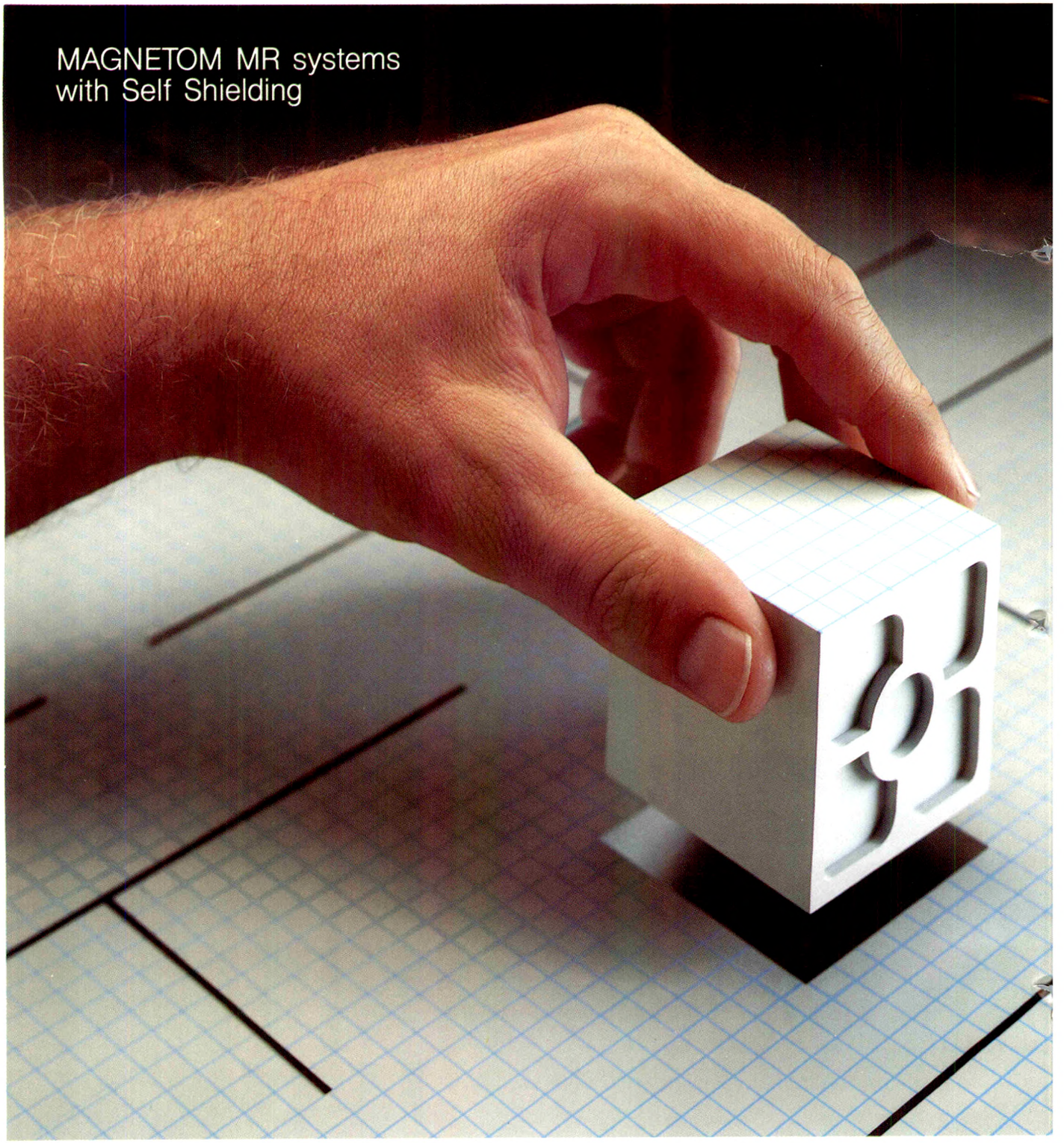
About SOFTIP®

Standards of excellence... beyond excellent standards.

Shiley
A Pfizer Company ®

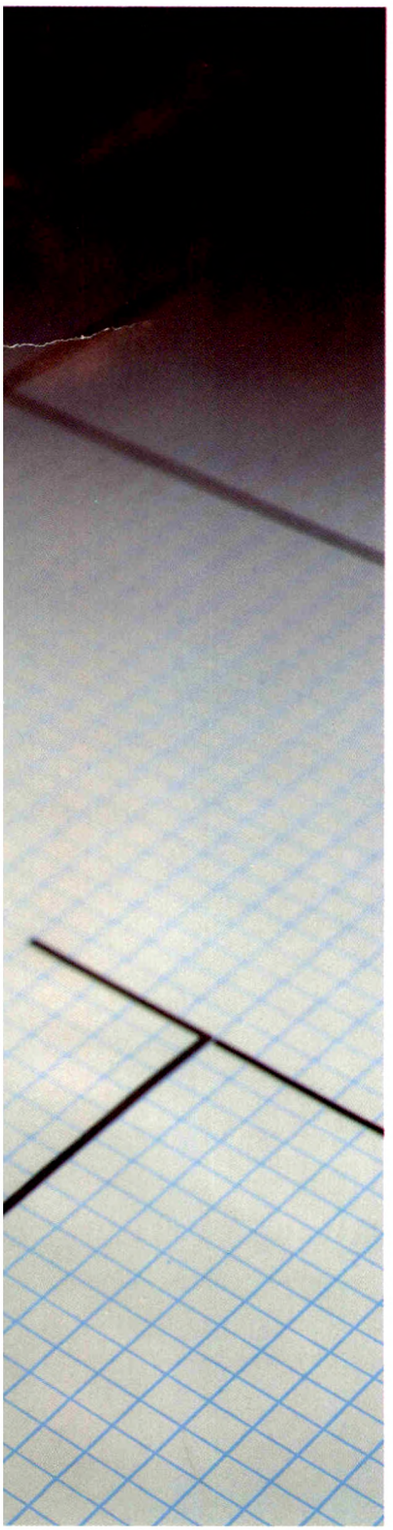
©Shiley Incorporated. All rights reserved. 086SP184 (5/86).
SOFTIP® is a registered trademark of Angiomedics Incorporated.
**CELGARD and Angithane are trademarks of Angiomedics Incorporated.
*U.S. Patent Numbers 4,551,292; 4,531,943.

SIEMENS



It's a fact that superconducting m
superior image quality and less ris
But site selection can be a proble
limitations lead to expensive room
Or worse, compromising your MR

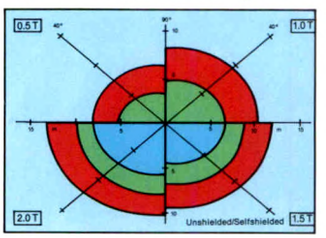
But you can have both the quality
system and an economical site la
Self Shielding comes in. Tucked n
MAGNETOM's covers, it shrinks t
directions.



More than better
A better fit.

Installation space is cut

How much space can you save? C
m
lir
m
W
sp
ab
na
Sh
ac
sp
0.



The diagram above shows the 0.5 mT line for (clockwise from upper left) a 0.5 T, 1.0 T, 1.5 T, and 2.0 T MAGNETOM. The 0.5 mT is shown for the unshielded (red), Type 1 Self Shielded (green) and Type 1 Self Shielded (Blue).

N
in

With its symmetrical design, Self S
harm the homogeneity of the imag
homogeneity is often *better* than u
in typical sites because asymmetr
has less interaction with the magn



Self Shielding's symmetry means no sacrifice in magnet homogeneity.

N
Be
fit
ar
ex
pl
bu
af
tic

No intimidating structures

Self Shielding fits inside the MAGN
it's invisible to staff and patients. T
architecture is needed. And patien
comfort—key to high throughput—

Siemens Medical Systems, Inc.
186 Wood Avenue South
Iselin, NJ 08830

In
Sie
11
Mi

**The Siemens MAGNETOM has received FDA p certain configurations and applications, includ Configurations and applications that are curre available for investigational use in the US.*

Siemens...
technology with int

"THERE'S NO DIFFERENCE BETWEEN PHASED ANNULAR ARRAYS AND COMPUTED SONOGRAPHY.

acuson
COMPUTED SONOGRAPHY

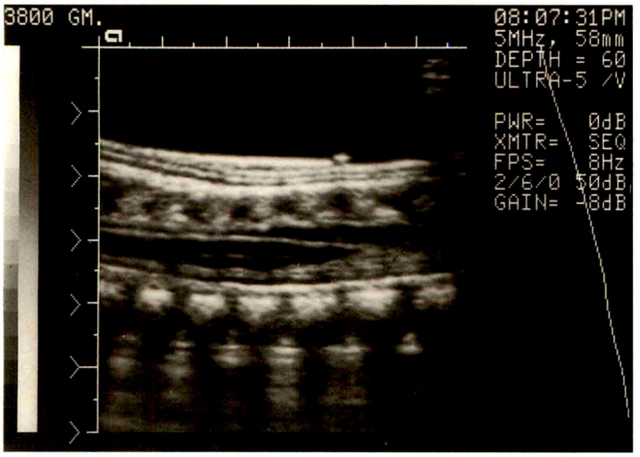
THE GOLD STANDARD IN ULTRASOUND



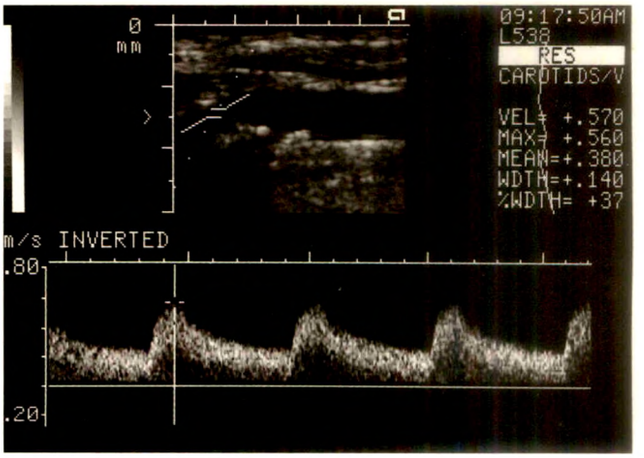
Contrast Resolution: Enlarged spleen, normal left kidney
Arkansas Children's Hospital, Little Rock, AK.



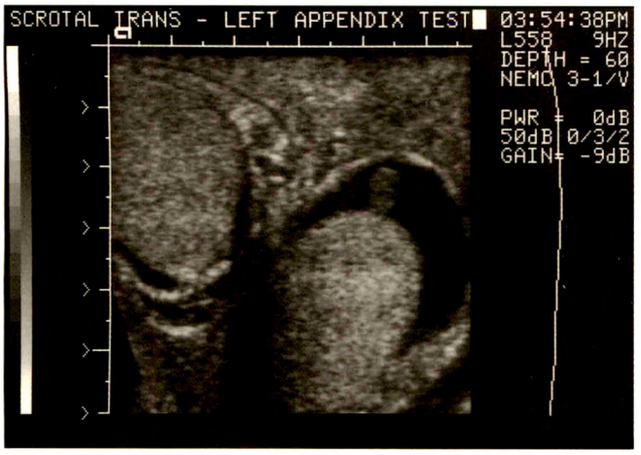
Penetration: Diffuse liver disease, small pleural effusion



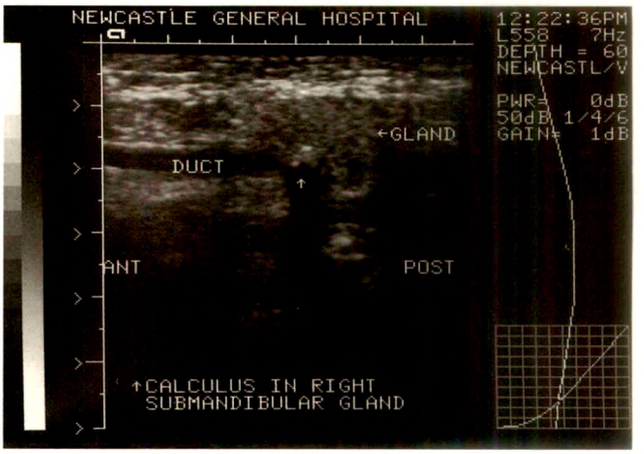
Detail and Contrast Resolution: Pediatric spine
Wylers Children's Hospital, University of Chicago, Chicago, IL.



Imaging and Doppler: 15-49% ICA Stenosis



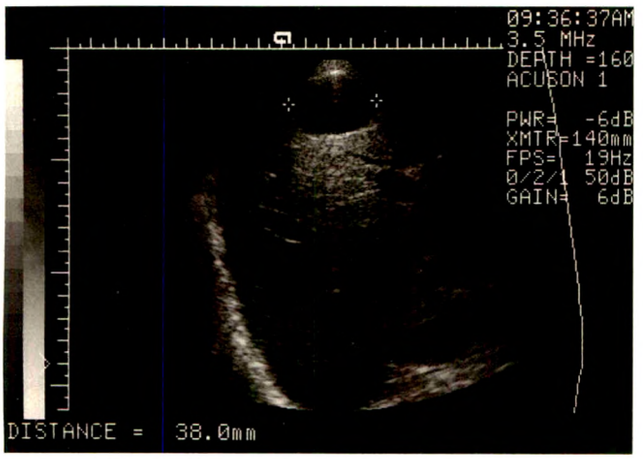
Tissue Differentiation: Bilateral testes, epididymis
Tufts New England Medical Center, Boston, MA.



Clinical Versatility: Submandibular gland
Newcastle General Hospital, Newcastle, U.K.



THE GOLD STANDARD IN ULTRASOUND



Near-Field Resolution: Liver Mass
University of Alabama, Birmingham, AL.

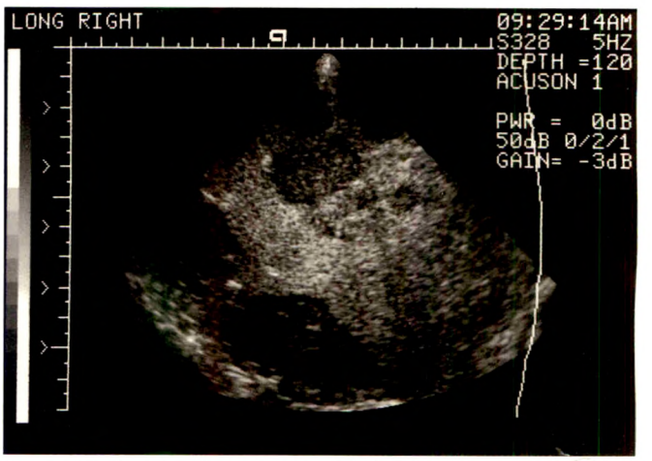
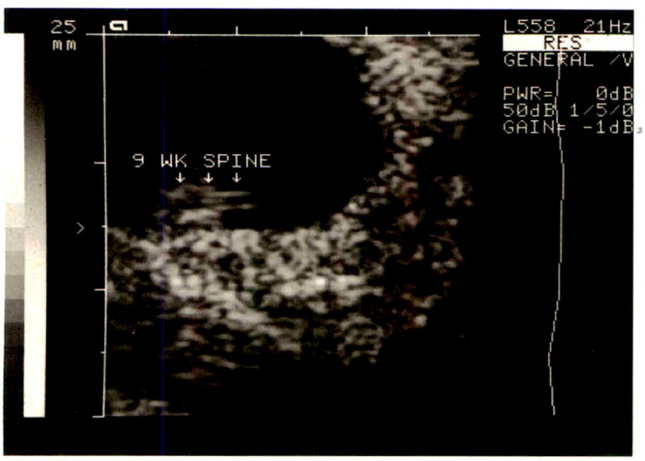
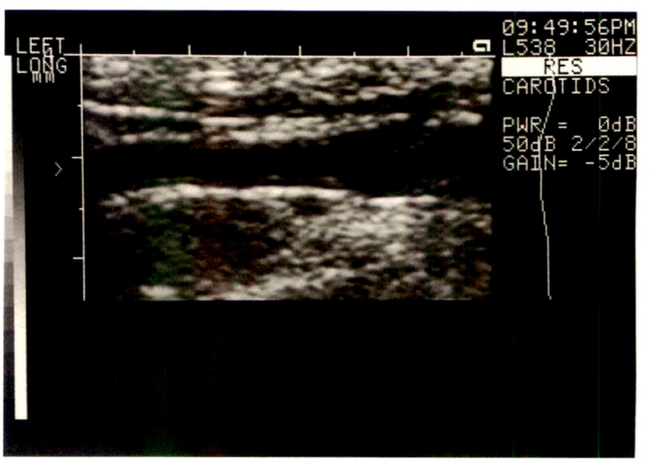


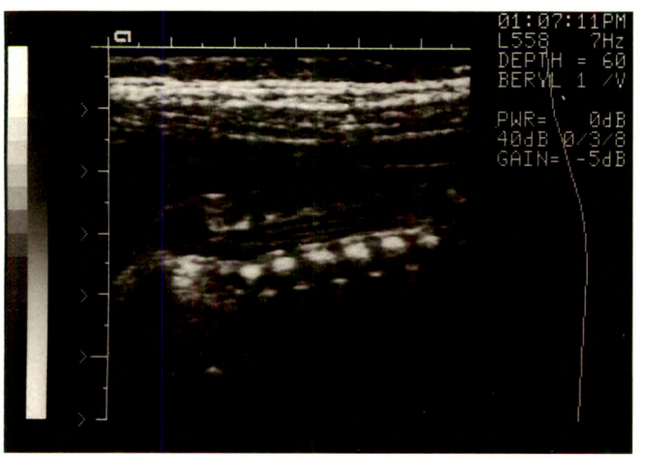
Image Uniformity: Near and far-field liver lesions
University of Alabama, Birmingham, AL.



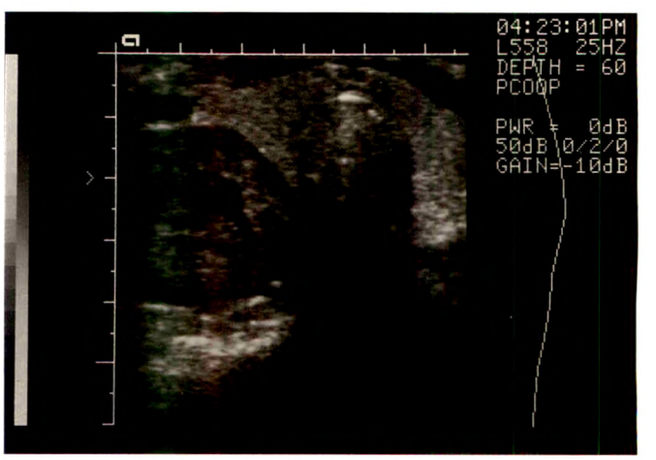
Early Diagnosis: Nine-week fetal spine
Frauenklinik, Salzburg, Austria



PV Scan Format: ICA, intimal defect, soft plaque
Huntington Memorial Hospital, Pasadena, CA.



Diagnostic Confidence: 2nd Trimester spinal defect
Diagnostic Ultrasound Association, Boston, MA.



Contrast Resolution: Differentiated neurogenic tumor, normal thyroid.
Vancouver General Hospital, Vancouver, B.C.

acuson
COMPUTED SONOGRAPHY

L O O K A T T H E F A C T S

Comparing phased annular arrays and Computed Sonography™ is like comparing a calculator to a computer. Phased annular arrays are conventional ultrasound technology—they are still mechanical scanners with all their inherent problems. Computed Sonography is new technology—the image is formed under total software control by our proprietary ultrasound computer. Look at the technologies. Then look at the images. There really is no comparison.

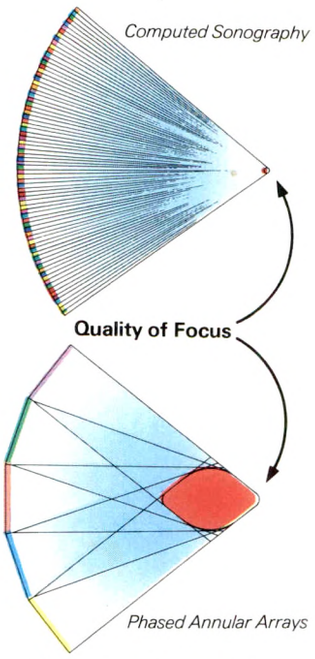
COMPARE THE TECHNOLOGIES

Image Quality

- Phased annular arrays have typically 5 information channels—not enough to maintain the uniform quality of focus necessary for the best detail and contrast resolution.
- Computed Sonography has 128 independent image resolution channels—producing images recognized as the Gold Standard in Ultrasound.

Reliability

- Phased annular arrays are mechanical, fluid-filled sector scanners with a known history of reliability problems.



Only Computed Sonography has enough channels to maintain excellent focal quality throughout the field of view.

- Computed Sonography delivers documented 99.9% up-time.

Linear Format

- Now recognized as the best format for Small Parts, Peripheral Vascular and Obstetric applications.
- Computed Sonography provides both linear and sector formats—phased annular arrays are sector only.

Simultaneous Imaging

- Only Computed Sonography provides simultaneous real-time imaging and Doppler or M-Mode—and from the same transducer.
- Simultaneous real-time imaging makes Doppler faster to learn and easier to perform.

EVALUATE THE TECHNOLOGIES AND THE IMAGES: THERE IS NO COMPARISON.

- Call 1-800-4-ACUSON.
  Or in California 1-800-5-ACUSON.
  We'll make a believer out of you.

BELIEVE YOUR EYES!



American Roentgen Ray Society
Officers, Committees, and Meeting Informatio

Officers

President: Jerome F. Wiot
President- elect: Raymond A. Gagliardi
1st Vice-president: Lee F. Rogers
2nd Vice-president: Gerald D. Dodd
Secretary: Glen W. Hartman
Treasurer: Ronald G. Evens

Executive Council: E. Gedgaudas, J. F. Wiot, L. F. Rogers, R. A. Gagliardi, R. G. Evens, R. N. Berk, F. L. Angell, J. E. Madewell, M. P. Capp, G. W. Hartman, B. G. Brogdon, G. A. Kling, H. C. Carlson, A. K. Poznanski, A. E. James, Jr., J. A. Kirkpatrick, Jr., G. R. Leopold, G. D. Dodd, J. T. Ferrucci, Jr., R. H. Troupin, chairman

Committees 1986–1987

Editorial Policy: S. S. Sagel, W. J. Casarella, J. T. Ferrucci, Jr., N. C. Whitley, S. Hilton, A. J. Davidson, J. M. Taveras, R. N. Berk, M. P. Capp, chairman

Education and Research: C. E. Putman, A. R. Margulis, J. R. Thornbury, R. A. McLeod, J. T. Ferrucci, Jr., ex officio, B. G. Brogdon, chairman

Finance and Budget: B. P. Wood, L. R. James, J. A. Kirkpatrick, Jr., A. E. James, F. L. Angell, chairman

Instruction Courses: R. A. McLeod, associate chairman, J. T. Ferrucci, Jr., chairman

Program: J. Wiot, G. W. Hartman, J. A. Kirkpatrick, Jr., R. H. Troupin, M. P. Capp, J. E. Madewell, B. G. Brogdon, J. T. Ferrucci, Jr., G. A. Kling, G. G. Ghahremani, M. Viamonte, R. A. Gagliardi, chairman

Publications: W. J. Casarella, J. T. Ferrucci, Jr., S. S. Sagel, N. C. Whitley, M. P. Capp, chairman

Scientific Exhibits: S. G. Kirchner, A. V. Proto, S. M. Goldman, J. E. Madewell, chairman

Nominating: W. J. Casarella, H. C. Carlson, A. E. James, chairman.

Representatives to Other Organizations

American Board of Radiology: E. C. Klatte, R. W. McConnell, L. I Rogers

American College of Radiology: J. L. Gwinn, G. A. Kling, G. V Hartman, J. M. Dennis, E. J. Ferris, J. E. Madewell

American Medical Association House of Delegates: S. F. Ochsne K. C. Krabbenhoft, alternate

American National Standards Institute: M. Haskin

National Council on Radiation Protection and Measurement E. L. Saenger, H. L. Friedell

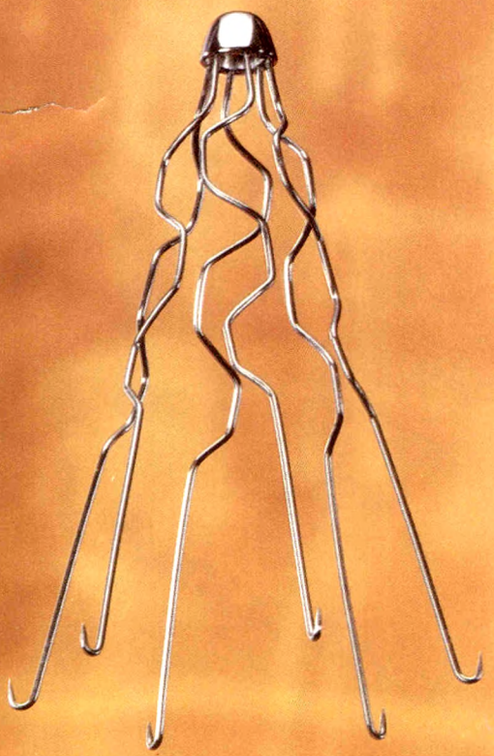
Meetings, Membership, Business Information

Annual Meetings: April 26–May 1, 1987, Fontainebleau Hilton, Miami Beach; May 1–6, 1988, Westin Bonaventur Los Angeles; May 7–13, 1989, Hilton, New Orleans.

Director Annual Meeting: George A. Kling, Harper Hospita Detroit, MI 48201

ARRS Membership: Rosalind H. Troupin, Dept. of Radiology, Hospit of University of Pennsylvania, 3400 Spruce St., Philadelphia, P 19104. The ARRS has two membership categories: active and i training. For active membership, applicants must practice radiolo in the U.S. or Canada. Each must have graduated in good standir from an approved medical school or hold an advanced degree in physical, chemical, or biological science and be certified by th American Board of Radiology, the Royal College of Physicians ar Surgeons of Canada, or otherwise adequately document training ar credentials. A member-in-training must be in a radiology residency, postresidency fellowship program, or a postgraduate student in a allied science. Status must be verified by the program director. Fo consideration during the 1987 ARRS meeting, completed applicatior must be received by Dr. Troupin no later than Feb. 1, 1987.

Business Office: Paul Fullagar, executive director, George J. O'Ho controller, American Roentgen Ray Society, 1891 Preston White Dr Reston, VA 22091.



The Case For Quality.

Patient: 39-year-old male. Five days post excisio of meningioma.

Diagnosis: Deep vein thrombosis with evidence of major vein involvement.

Considerations: Patient cannot be treated with anticoag-ulants due to recent intracranial surgery Patient is at risk of pulmonary embolism

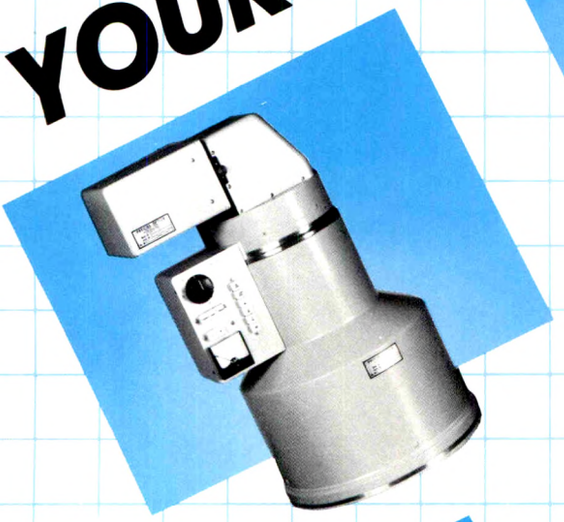
Treatment Selected: Percutaneous transvenous placement of Greenfield® Vena Cava Filter under loc anesthesia. This unique Medi-tech produ affords definitive and permanent protec tion against pulmonary embolism, whil avoiding the risks associated with alter-native treatments. It combines advanced technology with strict clinical standards of quality and reliability.

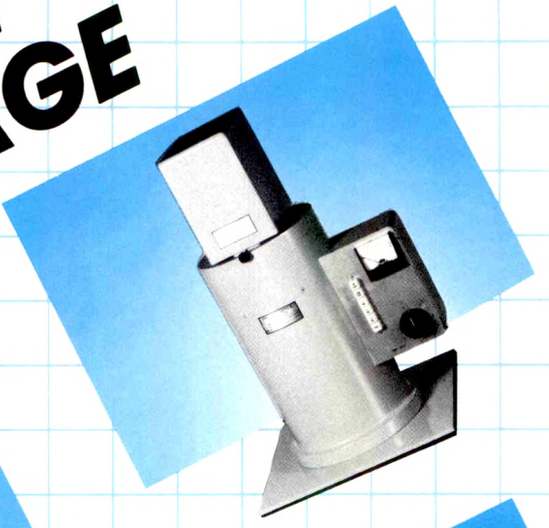
Medi-tech®

Medi-tech, Incorporated
480 Pleasant Street
P.O. Box 7407
Watertown, Massachusetts 02272
(617) 923-1720 Telex 922-453

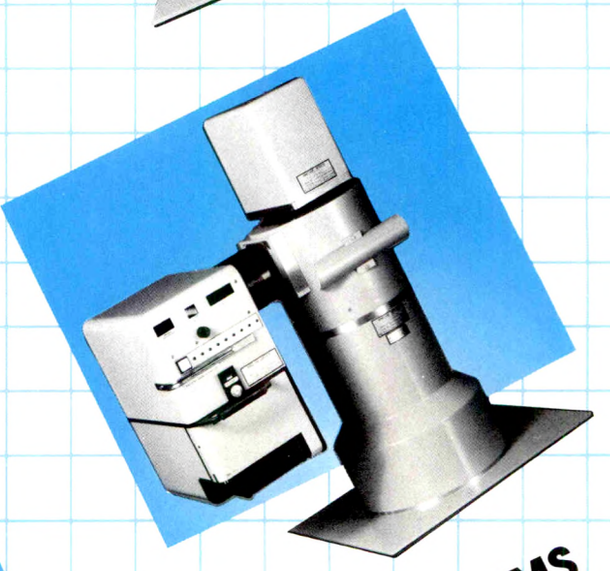
Ordering Information (800) 225-3238

IMPROVE YOUR IMAGE







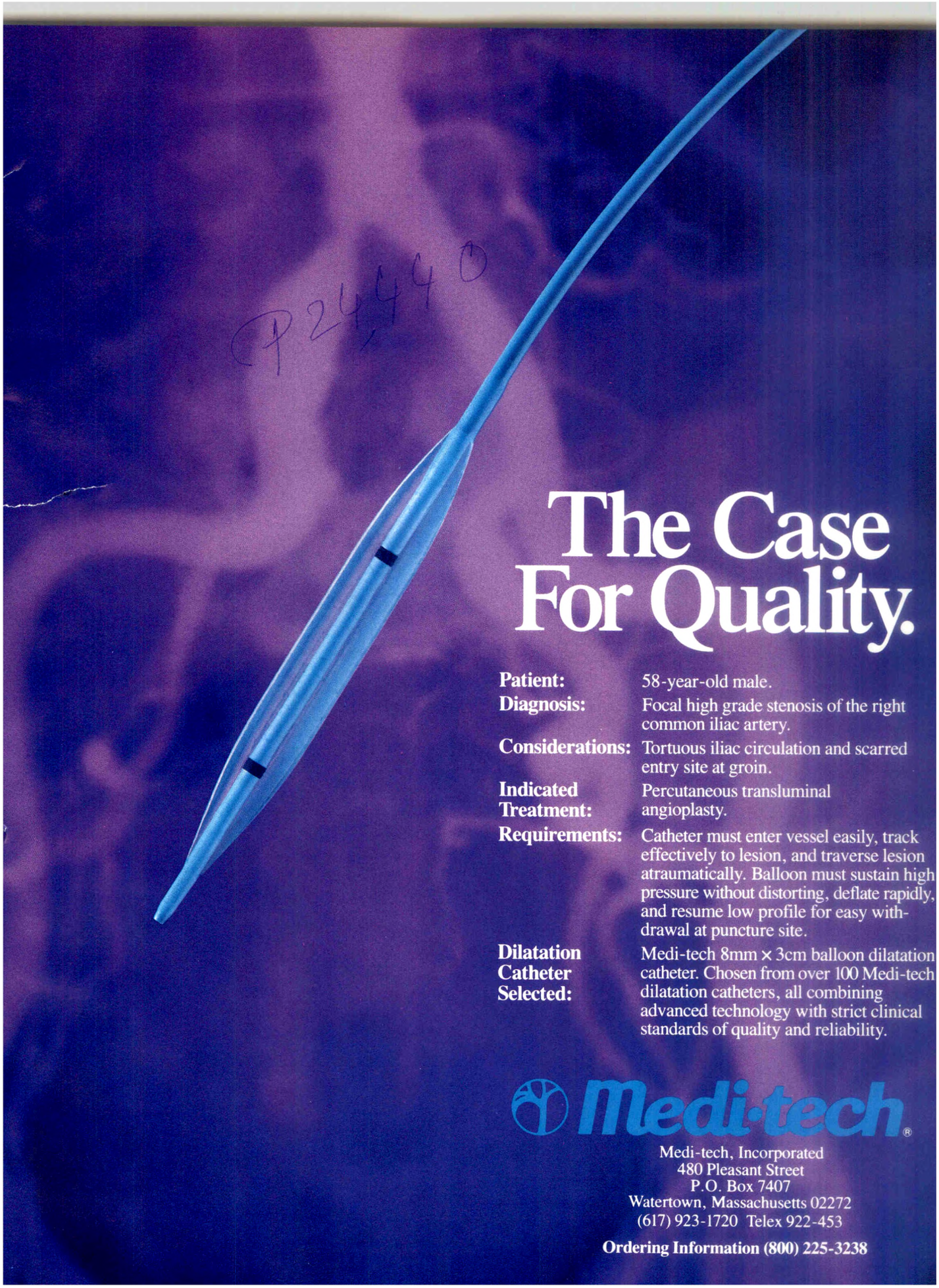


WITH PRECISE OPTICS IMAGE INTENSIFIER SYSTEMS

- The world's largest independent manufacturer of Image Intensifier Systems and components
- Over 30 years of experience in design and manufacture
- 6,9,12, and 16-Inch latest series image tubes for optimum performance
- 525/875/1023 line CCTV's, 6fps 100mm/105mm cameras
- Cost effective, versatile, reliable
- Compatible with new or existing x-ray equipment
- Extend the life of existing apparatus
- Worldwide dealer network

Precise® Optics
PHOTO MEDIC EQUIPMENT, INC.

239 South Fehr Way
Bay Shore, New York 11706
Tel.: 516 242-6600
TWX: 510-227-9837



The Case For Quality.

Patient:	58-year-old male.
Diagnosis:	Focal high grade stenosis of the right common iliac artery.
Considerations:	Tortuous iliac circulation and scarred entry site at groin.
Indicated Treatment:	Percutaneous transluminal angioplasty.
Requirements:	Catheter must enter vessel easily, track effectively to lesion, and traverse lesion atraumatically. Balloon must sustain high pressure without distorting, deflate rapidly, and resume low profile for easy withdrawal at puncture site.
Dilatation Catheter Selected:	Medi-tech 8mm × 3cm balloon dilatation catheter. Chosen from over 100 Medi-tech dilatation catheters, all combining advanced technology with strict clinical standards of quality and reliability.

Medi-tech®

Medi-tech, Incorporated
480 Pleasant Street
P.O. Box 7407
Watertown, Massachusetts 02272
(617) 923-1720 Telex 922-453

Ordering Information (800) 225-3238

The NEW Ackrad H/S Catheter Set for Hysterosalpingography

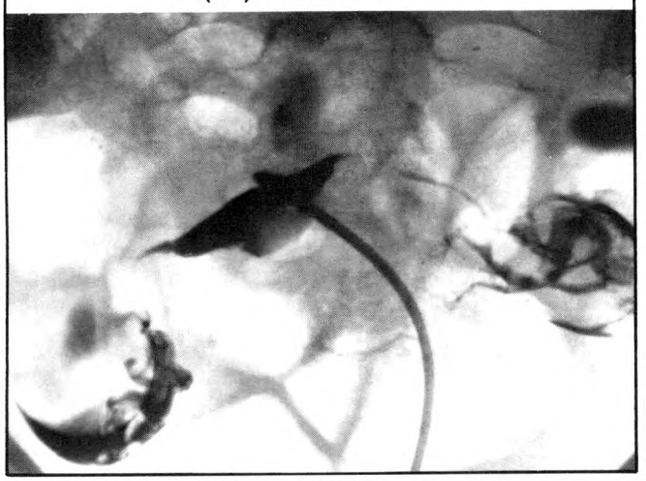


Now: Easier on the Patient . . .
Better for the Physician

The unique small sizes (5 and 7F) of the flexible balloon-bearing catheter provide previously unavailable freedom from trauma for the patient. A placement sheath and inflation syringe are included in the set for a rapid and efficient procedure.

Sample furnished on request.

ACKRAD LABORATORIES, Inc.
70 Jackson Drive, P.O. Box 1085, Cranford, NJ 07016
(201) 276-6390



Help us to serve you better.....



USE YOUR ZIP CODE

Remember, your zip code provides faster, more direct delivery of your journals. Use it on all correspondence, too.

Two step film control

Minimize X-ray exposure. Optimize image quality. Stabilize film processor performance, film speed and contrast. Quickly. Easily.

1. The Tobias Model RF Wejex Sensitometer

Produces a precise 11-step wedge exposure on *your* X-ray film. Exposure made just before processing eliminates latent image fade problem.* Features: Precise shutter exposure control. Variable lamp intensity. Provisions for 2″×2″ ANSI blue, green or other filters, double sided exposures, 8″×10″ and 35mm test film alignment. And more.

*Lawrence, D.J.: **A Simple Method of Processor Control,** Med. Rad. and Photog. 49, 2-6, 28, 1973 (Reprints available on request)

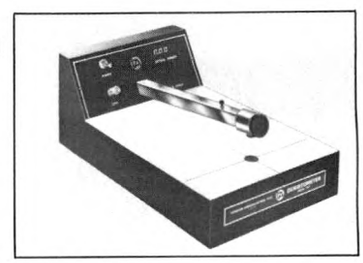


Wejex Universal Model RF
Also available: Wejex Standard Model R

For a demonstration, call your Tobias dealer.
Or write for our brochure. Ask about our 30 day free trial.

2. The Tobias Model TBX Digital Densitometer

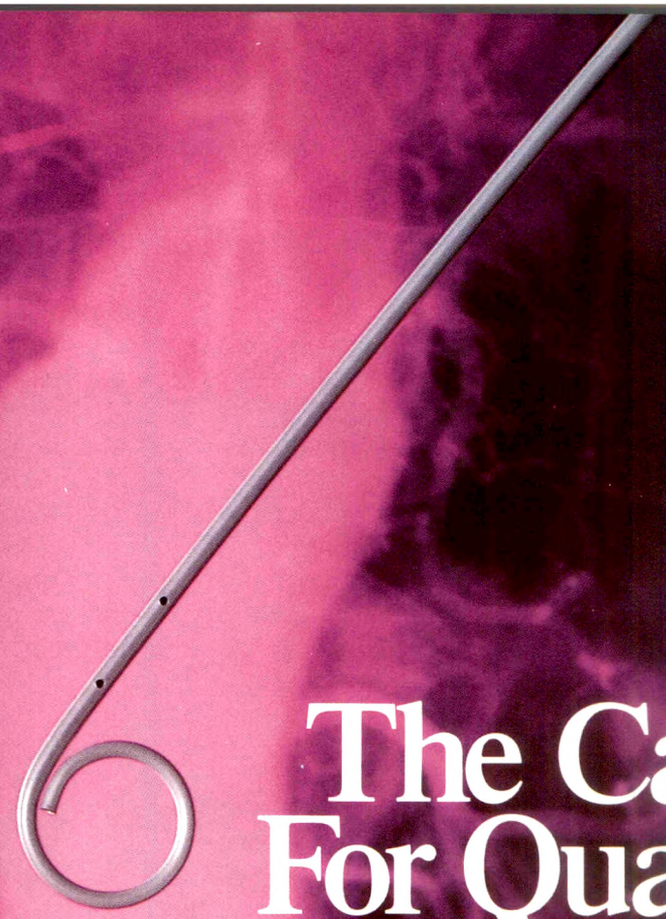
Measures optical transmission density of the Wejex-exposed step wedge over a density range of 0 to 4.50. Accuracy ±0.02. Repeatability ±0.01. State-of-the-art electronics. Lighted digital display. 5 second warm up. Easily portable. Virtually no zero drift.



TOBIAS ASSOCIATES, INC.
50 Industrial Drive, P.O. Box 2699, Ivyland, PA 18974, (215) 322-1500

☐ Send literature on the Wejex Sensitometer and TBX Densitometer.
☐ Please send me a copy of D.J. Lawrence's "A Simple Method of Processor Control."
☐ Tell me more about your 30 day free trial policy.

Name _____
Title/Organization _____
_____
Address _____
City _____ State _____
Zip _____ Tel. _____



The Case For Quality.

Patient: 60-year-old male with palpable abdominal mass.

Diagnosis: Abdominal aortic aneurysm.

Treatment: Surgical aorto-bifemoral bypass.

Considerations: Abdominal aortogram requires high contrast flow for maximum filling and superior visualization of the aorta. Pig-tail catheter must retain shape during injection for safe delivery of large contrast bolus.

Catheter Selected: 5 French Medi-tech High Flow pigtail, 65 cm. One of the complete line of High Flow Angiographic Catheters for flush and selective studies, combining advanced technology with strict clinical standards of quality and reliability.

Medi-tech®

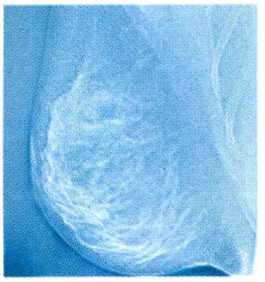
Medi-tech, Incorporated
480 Pleasant Street
P.O. Box 7407
Watertown, Massachusetts 02272
(617) 923-1720 Telex 922-453

Ordering Information (800) 225-3238

© 1986 Medi-tech, Inc.

Radiograph courtesy of Michael E. Jay, M.D., Harvard Medical School

Compare the two images below. Both are the same breast tissue specimen. One is a film screen image, the other, a Xeroradiograph. As you can clearly see, Xeroradiography shows calcifications easier.



Small wonder that Xeroradiography is the most widely used method for mammography.

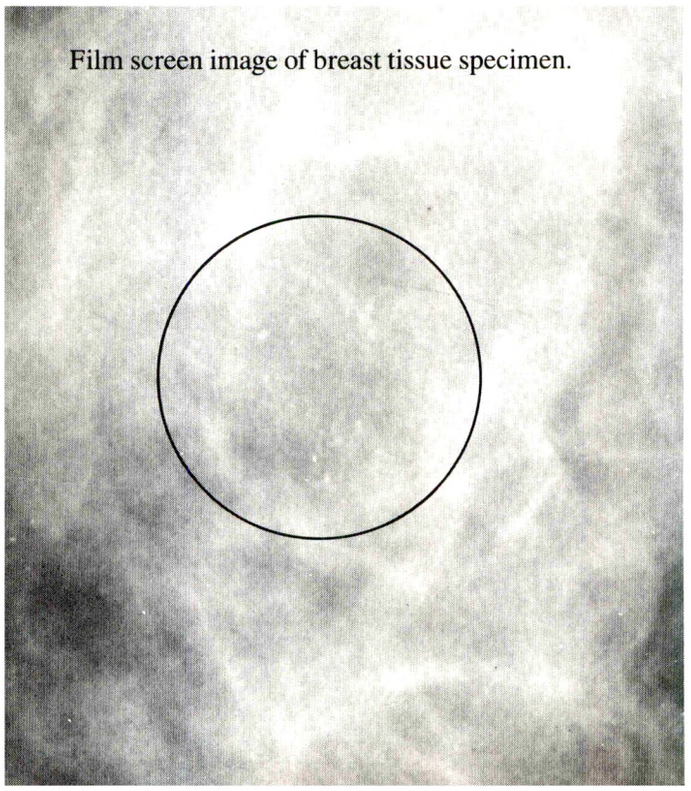
Its wide recording latitude shows you the nipple to the chest wall on one image. This, together with the clarity provided by superior resolution and edge enhancement allows calcifications to be seen anywhere i the breast.

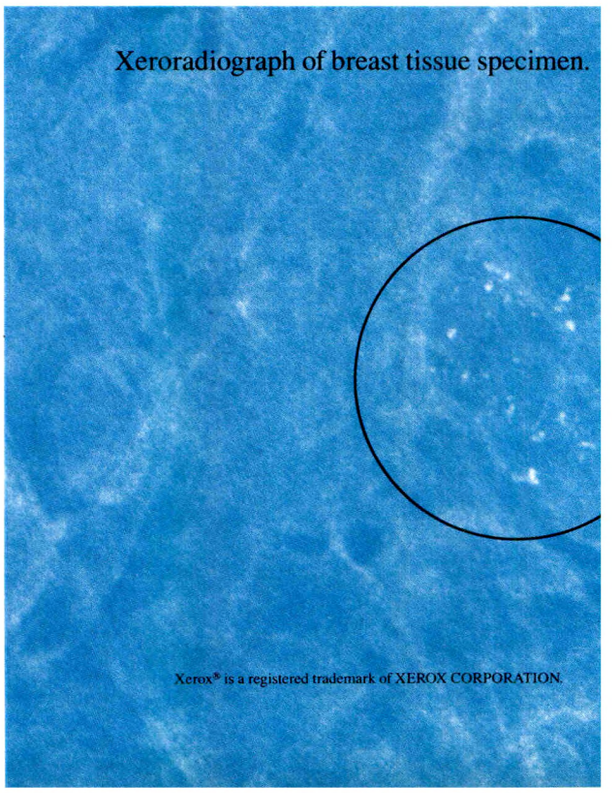
For more information, call or write Xerox Medical Systems, P.O. Box 5786, Pasadena, CA 91107, (818) 356-1221.

Team Xerox

Xeroradiography. It's easy to see. And that's why radiologists have made it the image of choice.

It's easy to see why our image is #1

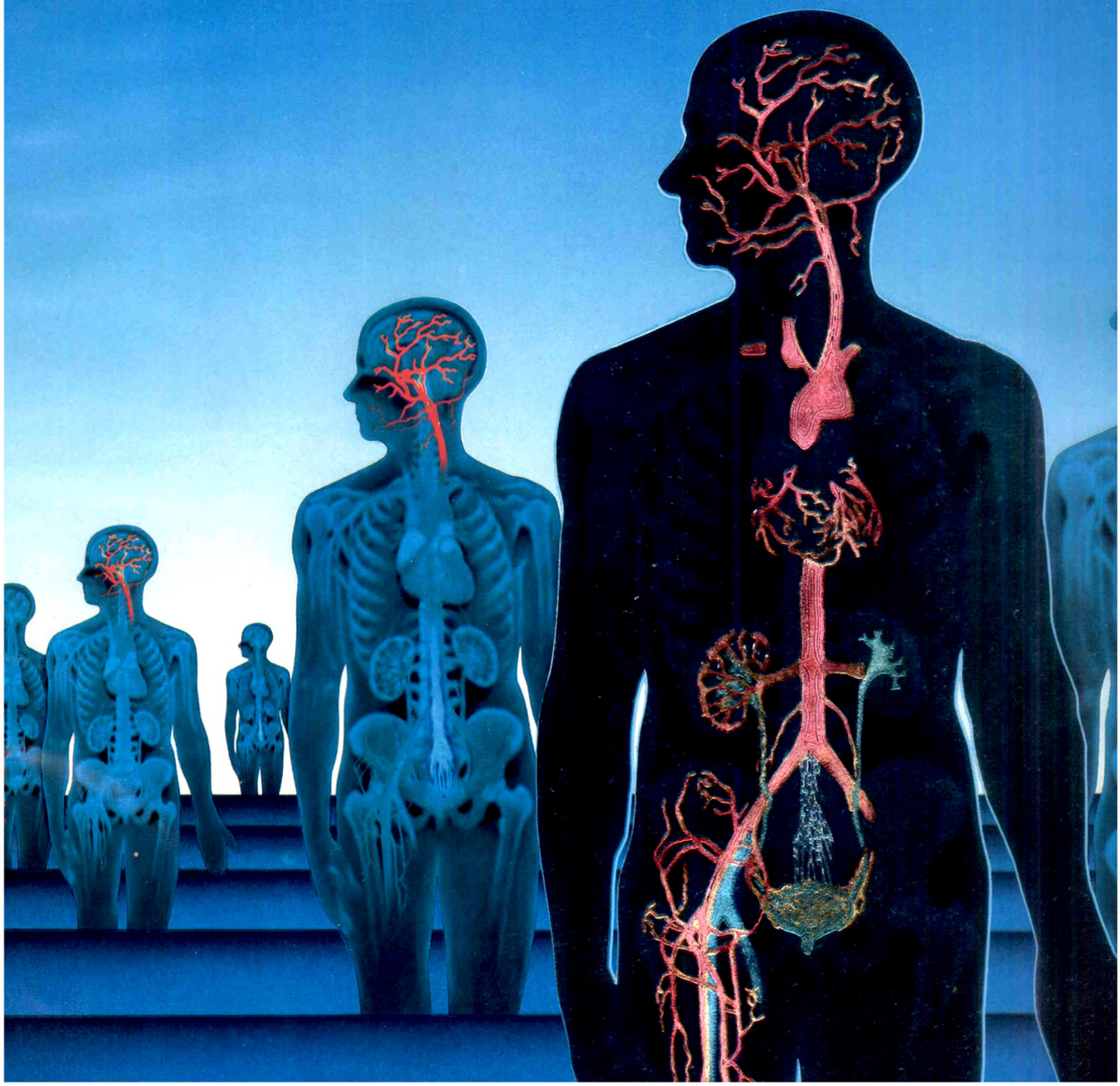




Xerox® is a registered trademark of XEROX CORPORATION.

FROM
Winthrop-Breon
LEADER IN THE DEVELOPMENT OF NONIONIC CONTRAST MEDIA

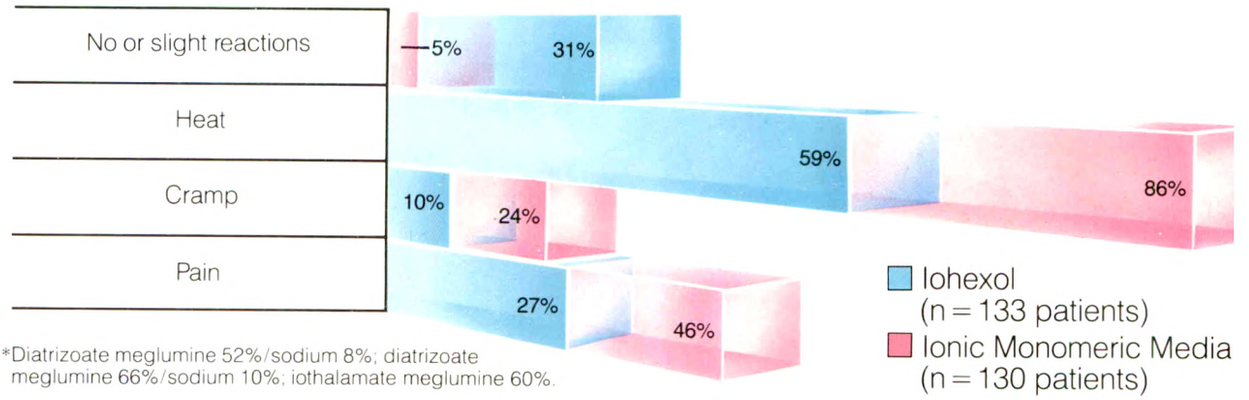
Improving the safety profile in a broad spectrum of applications.



Excellent vascular tolerance: low incidence of postphlebographic thrombosis.[1]

Significant improvement in comfort reduces patient motion[4,5]: Less need for repeat examinations.

Subjective Sensations in Peripheral Arteriography



*Diatrizoate meglumine 52%/sodium 8%; diatrizoate meglumine 66%/sodium 10%; iothalamate meglumine 60%.

Improved hemodynamic profile over conventional ionic media. Systolic and diastolic pressures are maintained near baseline levels.[6,7]

Improving the nephrotoxicity profile: Minimal effect on glomerular filtration rate, permeability, or albumin excretion.[8,9]

Not recommended for patients with anuria. Since adverse reactions can occur with nonionic media, similar preparations to those recommended for ionic media should be planned to handle severe or potentially fatal reactions.

Wider margin of safety even at higher iodine concentrations.[1-3] Less potential for renal damage compared to conventional ionic media. Minimal effect on creatinine levels and renal enzymes.[10]

Significant improvement in patient comfort in cerebral arteriography.

Significant improvement over conventional ionic contrast media: Fewer and milder pain and warmth sensations.[11-15] Excellent neurotoxicity profile.†

Excellent cardiovascular safety profile: Fewer injections accompanied by major changes in heart rate.[6,14,15]

For peripheral arteriography: Recommended concentrations—OMNIPAQUE 300 (300 mgI/mL) or OMNIPAQUE 350 (350 mgI/mL).
For cerebral arteriography: Recommended concentration—

Adapted from Wolf[4]; data on file, Winthrop-Breon Laboratories.[5]
Comparable concentration and volume per injection.

Excellent diagnostic quality in intravenous digital subtraction angiography.

Greater patient comfort, better tolerance: Most subjective side effects are mild.[6,16-18]

Excellent diagnostic images: Significantly less image degradation secondary to swallowing, motion, coughing.[16]

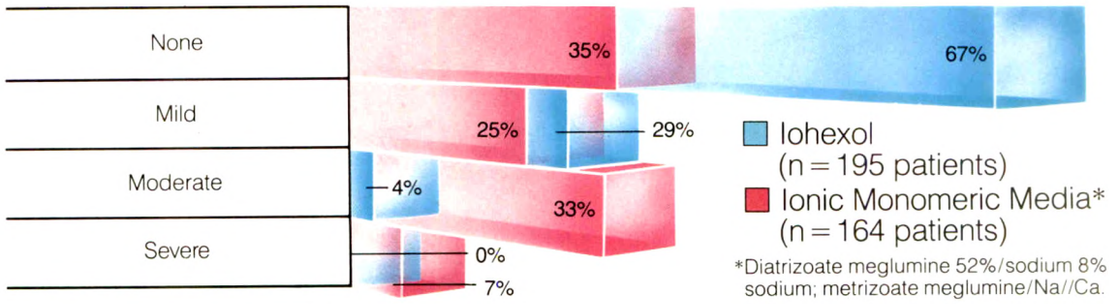
Good to excellent radiographic quality achieved in 94% of patients studied (n = 81).[6,16-18] 94% of carotid DSA studies conducted with no or only slight artifacts.[17]

Excellent patient tolerance in excretory urography.

Less nausea, vomiting, and heat sensation compared to conventional ionic contrast media.

In 96% of patients, discomfort was absent or mild.[6]

Discomfort in Urography



*Diatrizoate meglumine 52%/sodium 8%; iothalamate sodium; metrizoate meglumine/Na//Ca.

Data on file, Winthrop-Breon Laboratories.[6]

NONIONIC

OMNIPAQUE®

(IOHEXOL)

†See following pages for important product information concerning contraindications, warnings, adverse reactions, patient selection, and precautionary recommendations.

Improving the safety profile in a broad spectrum of applications.

Less chemotoxicity than ionic contrast media.[19]

Lower osmolality than conventional ionic media.[19]

Minimal effect on key physiologic parameters[19]**:** Well tolerated by most patients.

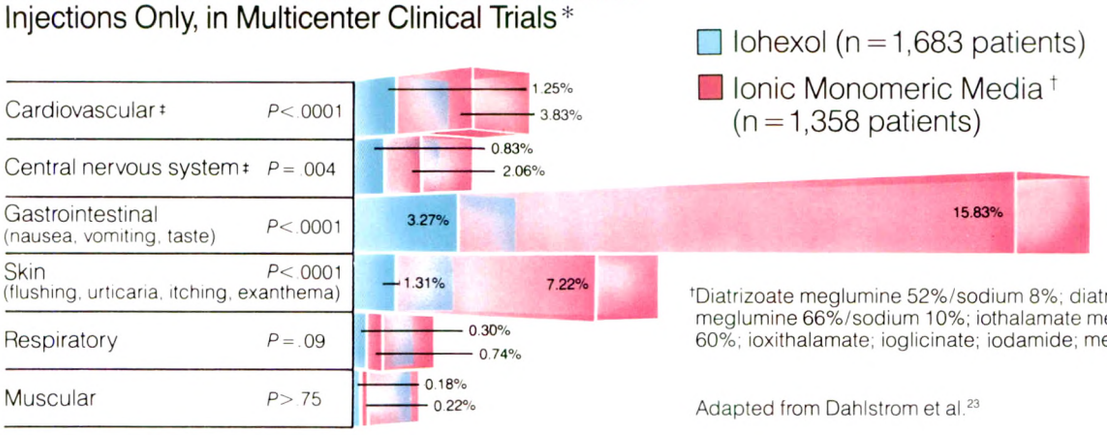
Less neurotoxic than conventional ionic media.

Few direct or indirect cardiovascular effects.[20,21]

Improved patient comfort: Fewer artifacts due to motion and swallowing.[16-18]

Less potential for allergic reactions.[22] Since adverse reactions can occur with nonionic media, similar preparations to those recommended for ionic media should be planned to handle severe or potentially fatal reactions.

Incidence of Adverse Reactions After Intravenous Injections Only, in Multicenter Clinical Trials *



†Diatrizoate meglumine 52%/sodium 8%; diatrizoate meglumine 66%/sodium 10%; iothalamate meglumine 60%; ioxithalamate; ioglicinate; iodamide; metrizoate.

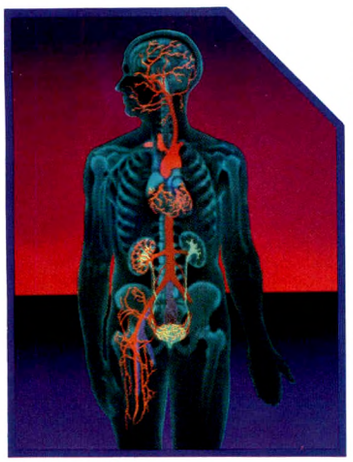
Adapted from Dahlstrom et al.[23]

Supplied in ready-to-use vials and bottles. No dilution or reconstitution necessary.

Product	Size (mL/unit)	Use
OMNIPAQUE® 180 (180 mgI/mL)	10 mL, 20 mL vials, Myelo-Kit™	Lumbar, Thoracic, and CT Myelography
OMNIPAQUE® 240 (240 mgI/mL)	10 mL, 100 mL vials, 200 mL bottle, Myelo-Kit	Lumbar and Thoracic Myelography, Peripheral Venography
OMNIPAQUE® 300 (300 mgI/mL)	10 mL, 30 mL, 50 mL, 100 mL vials	Urography, Cerebral Arteriography, Peripheral Arteriography, Peripheral Venography
OMNIPAQUE® 350 (350 mgI/mL)	50 mL, 100 mL vials, 200 mL bottle	Angiocardiography, Urography, Peripheral Arteriography, I.V. Digital Subtraction Angiography

*See following pages for important product information concerning contraindications, warnings, adverse reactions, patient selection, and precautionary recommendations.

‡In general, adverse reactions to the intravascular use of OMNIPAQUE have been mild and of short duration. The general incidence of these occurrences following total intravascular use is slightly higher, as shown in the product information on the last page.



OMNIPAQUE®
INJECTION (IOHEXOL)

180

240

300

350

PLEASE CONSULT FULL PRODUCT INFORMATION BEFORE USING.
A SUMMARY FOLLOWS:
OMNIPAQUE is a nonionic, water-soluble; radiographic contrast medium.
INDICATIONS AND USAGE: OMNIPAQUE is indicated in adults for angiocardiography (ventriculography, selective coronary arteriography); aortography, including studies of the aortic root, aortic arch, ascending aorta, abdominal aorta, and its branches; cerebral arteriography; digital subtraction angiography; peripheral angiography including arteriography and venography (phlebography); excretory urography; and lumbar and thoracic myelography, by conventional technique and in computerized tomography.

Administration of contrast media should be performed by qualified personnel familiar with the procedure and an appropriate technique should be utilized.
CONTRAINDICATIONS: OMNIPAQUE should not be administered to patients with a known hypersensitivity to iohexol.

Lumbar puncture ordinarily should not be performed in the presence of local or systemic infection where bacteremia is likely.

Intrathecal administration of corticosteroids with OMNIPAQUE is contraindicated.

Because of the possibility of overdosage, immediate repeat myelography in the event of technical failure is contraindicated (see DOSAGE AND ADMINISTRATION).
WARNINGS—General: OMNIPAQUE should be used with extreme care in patients with severe functional disturbances of the liver and kidneys, severe thyrotoxicosis, or myelomatosis. Diabetics with a serum creatinine level above 3 mg/dL should not be examined unless the possible benefits of the examination clearly outweigh the additional risk. OMNIPAQUE is not recommended for use in patients with anuria.

Radiopaque contrast agents are potentially hazardous in patients with multiple myeloma or other paraproteinemia, particularly in those with therapeutically resistant anuria. Although neither the contrast agent nor dehydration has separately proven to be the cause of anuria in myeloma, it has been speculated that the combination of both may be causative factors. The risk in myelomatous patients is not a contraindication; however, special precautions are necessary. Partial dehydration in the preparation of these patients prior to injection is not recommended since this may predispose the patient to precipitation of the myeloma protein in the renal tubules. No form of therapy, including dialysis, has been successful in reversing the effect. Myeloma, which occurs most commonly in persons over age 40, should be considered before instituting intravascular administration of contrast agents.

Ionic contrast media, when injected intravenously or intraarterially, may promote sickling in individuals who are homozygous for sickle cell disease.

Administration of radiopaque materials to patients known or suspected of having pheochromocytoma should be performed with extreme caution. If, in the opinion of the physician, the possible benefits of such procedures outweigh the considered risks, the procedures may be performed; however, the amount of radiopaque medium injected should be kept to an absolute minimum. The patient's blood pressure should be assessed throughout the procedure and measures for the treatment of hypertensive crisis should be readily available.

Reports of thyroid storm following the use of iodinated, ionic radiopaque contrast media in patients with hyperthyroidism or with autonomously functioning thyroid nodule suggest that this additional risk be evaluated in such patients before use of any contrast medium.

Urography should be performed with caution in patients with severely impaired renal function and patients with combined renal and hepatic disease.

Caution is advised in patients with a history of epilepsy, severe cardiovascular disease, chronic alcoholism, or multiple sclerosis.

Elderly patients may present a greater risk following myelography. The need for the procedure in these patients should be evaluated carefully. Special attention must be paid to dose and concentration of the medium, hydration, and technique used.

Patients who are receiving anticonvulsants should be maintained on this therapy. Should a seizure occur, intravenous diazepam or phenobarbital sodium is recommended. In patients with a history of seizure activity who are not on anticonvulsant therapy, premedication with barbiturates should be considered.

Prophylactic anticonvulsant treatment with barbiturates should be considered in patients with evidence of inadvertent intracranial entry of a large or concentrated bolus of the contrast medium since there may be an increased risk of seizure in such cases.

Drugs which lower the seizure threshold, especially phenothiazine derivatives, including those used for their antihistamine properties, should not be used with OMNIPAQUE. Others include MAO inhibitors, tricyclic antidepressants, CNS stimulants, and psychoactive drugs described as analeptics, major tranquilizers, or antipsychotic drugs. Such medication should be discontinued at least 48 hours before myelography, should not be used for the control of nausea and vomiting, and should not be resumed for at least 24 hours postprocedure.

Care is required in patient management to prevent inadvertent intracranial entry of a large dose or concentrated bolus of the medium. Also, effort should be directed to avoid rapid dispersion of the medium causing inadvertent rise to intracranial levels (eg, by active patient movement). Direct intracisternal or ventricular administration for standard radiography (not CT) is not recommended.

In most reported cases of major motor seizures with other nonionic myelographic media, one or more of the following factors were present. Therefore avoid:
- Deviations from recommended procedure or in myelographic management.
- Use in patients with a history of epilepsy.
- Overdosage.
- Intracranial entry of a bolus or premature diffusion of a high concentration of the medium.
- Medication with neuroleptic drugs or phenothiazine antinauseants.
- Failure to maintain elevation of the head during the procedure, on the stretcher, or in bed.
- Excessive and particularly active patient movement or straining.

If grossly bloody CSF is encountered, the possible benefits of a myelographic procedure should be considered in terms of the risk to the patient.

PRECAUTIONS—General: Diagnostic procedures which involve the use of radiopaque diagnostic agents should be carried out under the direction of personnel with the prerequisite training and with a thorough knowledge of the particular procedure to be performed. Appropriate facilities should be available for coping with any complication of the procedure, as well as for emergency treatment of severe reactions to the contrast agent itself. After parenteral administration of a radiopaque agent, competent personnel and emergency facilities should be available for at least 30 to 60 minutes since severe delayed reactions have occurred (see ADVERSE REACTIONS).

Preparatory dehydration is dangerous and may contribute to acute renal failure in patients with advanced vascular disease, diabetic patients, and in susceptible nondiabetic patients (often elderly with preexisting renal disease). Dehydration in these patients seems to be enhanced by the osmotic diuretic action of urographic agents. It is believed that overnight fluid restriction prior to excretory urography generally does not provide better visualization in normal patients. *Patients should be well hydrated prior to and following iohexol administration.*

In patients with severe renal insufficiency or failure, compensatory biliary excretion of the drug is anticipated to occur, with a slow clearance into the bile. Patients with hepatorenal insufficiency should not be examined unless the possibility of benefit clearly outweighs the additional risk.

Acute renal failure has been reported in diabetic patients with diabetic nephropathy and in susceptible nondiabetic patients (often elderly with preexisting renal disease) following excretory urography. Therefore, careful consideration of the potential risks should be given before performing this radiographic procedure in these patients.

Immediately following surgery, excretory urography should be used with caution in renal transplant recipients.

The possibility of a reaction, including serious, life-threatening, fatal, anaphylactoid, or cardiovascular reactions should always be considered (see ADVERSE REACTIONS). It is of utmost importance that a course of action be carefully planned in advance for immediate treatment of serious reactions, and that adequate and appropriate personnel be readily available in case a severe reaction should occur.

The possibility of an idiosyncratic reaction in susceptible patients should always be considered (see ADVERSE REACTIONS). The susceptible population includes patients with a previous reaction to contrast media, patients with a known sensitivity to iodine per se, and patients with a known clinical hypersensitivity: bronchial asthma, hay fever, and food allergies.

The occurrence of severe idiosyncratic reactions has prompted the use of several pretesting methods. However, pretesting cannot be relied upon to predict severe reactions and may itself be hazardous for the patient. It is suggested that a thorough medical history with emphasis on allergy and hypersensitivity, prior to the injection of any contrast media, may be more accurate than pretesting in predicting potential adverse reactions.

A positive history of allergies or hypersensitivity does not arbitrarily contraindicate the use of a contrast agent where a diagnostic procedure is thought essential, but caution should be exercised (see ADVERSE REACTIONS). Premedication with antihistamines or corticosteroids to avoid or minimize possible allergic reactions in such patients should be considered. Recent reports indicate that such pretreatment does not prevent serious life-threatening reactions, but may reduce both their incidence and severity.

Even though the osmolality of OMNIPAQUE is low compared to diatrizoate- or iothalamate-based ionic agents of comparable iodine concentration, the potential transitory increase in the circulatory osmotic load in patients with congestive heart failure requires caution during injection. These patients should be observed for several hours following the procedure to detect delayed hemodynamic disturbances.

General anesthesia may be indicated in the performance of some procedures in selected adult patients; however, a higher incidence of adverse reactions has been reported in these patients, and may be attributable to the inability of the patient to identify untoward symptoms, or to the hypotensive effect of anesthesia which can reduce cardiac output and increase the duration of exposure to the contrast agent.

Angiography should be avoided whenever possible in patients with homocystinuria, because of the risk of inducing thrombosis and embolism.

In angiographic procedures, the possibility of dislodging plaques or damaging or perforating the vessel wall should be borne in mind during the catheter manipulations and contrast medium injection. Test injections to ensure proper catheter placement are recommended.

Selective coronary arteriography should be performed only in those patients in whom the expected benefits outweigh the potential risk. The inherent risks of angiocardiography in patients with chronic pulmonary emphysema must be weighed against the necessity for performing this procedure.

Administration of contrast media should be performed by qualified personnel familiar with the procedure and appropriate patient management. Sterile technique must be used with any spinal puncture.

When OMNIPAQUE is to be injected using plastic disposable syringes, the contrast medium should be drawn into the syringe and used immediately.

If nondisposable equipment is used, scrupulous care should be taken to

prevent residual contamination with traces of cleansing agents.

Parenteral products should be inspected visually for particulate matter and discoloration prior to administration. If particulate matter or discoloration is present, do not use.

Repeat Procedures: If, in the clinical judgment of the physician, sequential or repeat subarachnoid examinations are required, a suitable interval of time between administrations should be observed to allow for normal clearance of the drug from the body.

Information for Patients: Patients receiving injectable radiopaque diagnostic agents should be instructed to:

1. Inform your physician if you are pregnant.
2. Inform your physician if you are diabetic or if you have multiple myeloma, pheochromocytoma, homozygous sickle cell disease or known thyroid disorder (see WARNINGS).
3. Inform your physician if you are allergic to any drugs, food, or if you had any reactions to previous injections of dyes used for x-ray procedures.
4. Inform your physician about any other medications you are currently taking, including nonprescription drugs, before you are administered this drug.

Drug/Laboratory Test Interaction: If iodine containing isotopes are to be administered for the diagnosis of thyroid disease, the iodine-binding capacity of thyroid tissue may be reduced for up to two weeks after contrast medium administration. Thyroid function tests which do not depend on iodine estimation, eg, T_3 resin uptake or direct thyroxin assays, are not affected.

Drug Interactions: Drugs which lower the seizure threshold—especially phenothiazine derivatives including those used for their antihistaminic or antinauseant properties—should not be used with OMNIPAQUE. Others include monoamine oxidase (MAO) inhibitors, tricyclic antidepressants, CNS stimulants, and psychoactive drugs described as analeptics, major tranquilizers, or antipsychotic drugs. Such medications should be discontinued at least 48 hours before myelography, should not be used for the control of nausea or vomiting during or after myelography, and should not be resumed for at least 24 hours postprocedure. In nonelective procedures in patients on these drugs, consider prophylactic use of anticonvulsants.

Carcinogenesis, Mutagenesis, Impairment of Fertility: No long-term animal studies have been performed to evaluate the potential of iohexol in these areas.

Pregnancy Category B: Reproduction studies have been performed in rats and rabbits with up to 100 times the recommended human dose. No evidence has been established of impaired fertility or harm to the fetus due to OMNIPAQUE; there are, however, no studies in pregnant women. Because animal reproduction studies are not always predictive of human response, this drug should be used during pregnancy only if clearly indicated.

Nursing Mothers: Caution should be exercised when OMNIPAQUE is administered to a nursing woman; it is not known to what extent iohexol is excreted in human milk.

Pediatric Use: Safety and effectiveness in children have not been established.

ADVERSE REACTIONS:

Intrathecal: Adverse reactions to the intrathecal use of OMNIPAQUE in general have been mild to moderate in degree, and of short duration. The incidence of these occurrences, based on clinical trials of 584 patients, is as follows:

Headaches: The most frequently occurring adverse reaction following myelography with OMNIPAQUE has been headache, with an incidence of less than 20%. Headache may be caused either as a direct effect of the contrast medium or by CSF leakage at the dural puncture site. However, in managing the patient, it is considered more important to minimize intracranial entry of contrast medium by postural management than to attempt to control possible CSF leakage.

Pain: Mild pain including backache, stiffness, and neuralgia occurred following injection with an incidence of about 8%.

Nausea and Vomiting: Nausea was reported, with an incidence of about 6%, and vomiting of about 3% (based on clinical trials of 584 patients—see PATIENT MANAGEMENT). Maintaining normal hydration is very important. The use of phenothiazine antinauseants is contraindicated. Reassuring the patient that the nausea will clear is usually all that is required.

Dizziness: Transient dizziness was reported in about 2% of the patients.

Other Reactions: Other reactions, occurring with an individual incidence of less than 0.1%, included feeling of heaviness, hypotension, hypertonia, sensation of heat, sweating, vertigo, and loss of appetite. All were transient and mild, with no clinical sequelae.

General Adverse Reactions to Contrast Media: Physicians should remain alert for the occurrence of adverse effects in addition to those discussed above, particularly those already reported in the literature for other nonionic, water-soluble myelographic contrast media. These have included but are not limited to aseptic and bacterial meningitis, and CNS and other neurologic disturbances.

Intravascular: Adverse reactions to the intravascular use of OMNIPAQUE have usually been of mild to moderate severity. However, serious, life-threatening and fatal reactions, mostly of cardiovascular origin, have been associated with the administration of iodine-containing contrast media, including OMNIPAQUE. The injection of contrast media is frequently associated with the sensation of warmth and pain, especially in peripheral angiography; pain and warmth are less frequent and less severe with OMNIPAQUE than with many ionic media, but lower osmolality media are similar in this respect. The incidence of these occurrences in clinical trials is as follows:

Cardiovascular System: Arrhythmias including PVCs and PACs (3%), angina/chest pain (2%), and hypotension (1%). Others including cardiac failure, asystole, bradycardia, tachycardia, and vasovagal reaction were reported with an individual incidence of less than 0.8%. In controlled clinical studies involving 900 patients, one fatality occurred. In widespread clinical use, the incidence of fatality is estimated at 0.0003%.

Nervous System: Pain (6%), photomas (3%), headache (2%), and metallic taste (0.8%). Others including anxiety, blurred vision, dizziness, fever, motor and speech dysfunction, convulsion, light-headedness, paresthesia, somnolence, vertigo, stiff neck, hemiparesis, and nystagmus were reported, with an individual incidence of less than 0.3%.

Respiratory System: Dyspnea, laryngitis, and throat irritation, with an individual incidence of 0.1%.

Gastrointestinal System: Nausea (2%) and vomiting (0.5%). Others including diarrhea, dyspepsia, and dry mouth were reported, with an individual incidence of 0.1%.

© 1986 WINTHROP-BREON LABORATORIES 41368/3737

OMNIPAQUE® (iohexol)

Skin and Appendages: Urticaria (0.3%) and purpura (0.1%).

Individual adverse reactions which occurred to a significantly greater extent for a specific procedure are listed under that indication.

General Adverse Reactions to Contrast Media: Physicians should remain alert for the occurrence of adverse effects in addition to those discussed above. The following reactions have been reported after administration of other intravascular iodinated contrast media. *Reactions due to technique:* hematomas and ecchymoses. *Hemodynamic reactions:* vein cramp and thrombophlebitis following intravenous injection. *Cardiovascular reactions:* rare cases of cardiac arrhythmias, reflex tachycardia, chest pain, cyanosis, hypertension, hypotension, peripheral vasodilatation, shock, and cardiac arrest. *Renal reactions:* occasionally, transient proteinuria, and rarely, oliguria or anuria. *Allergic reactions:* Asthmatic attacks, nasal and conjunctival symptoms, dermal reactions such as urticaria with or without pruritus, as well as pleomorphic rashes, sneezing and lacrimation and, rarely, anaphylactic reactions. Rare fatalities have occurred, due to this or unknown causes. *Signs and symptoms related to the respiratory system:* pulmonary or laryngeal edema, bronchospasm, dyspnea; *or to the nervous system:* restlessness, tremors, convulsions. *Other reactions:* flushing, pain, warmth, metallic taste, nausea, vomiting, anxiety, headache, confusion, pallor, weakness, sweating, localized areas of edema, especially facial cramps, neutropenia, and dizziness. Rarely, immediate or delayed rigors can occur, sometimes accompanied by hyperpyrexia. Infrequently, "iodism" (salivary gland swelling) from organic iodinated compounds appears two days after exposure and subsides by the sixth day.

CONSULT PACKAGE INSERT FOR A MORE DETAILED DISCUSSION OF ADVERSE REACTIONS to both intrathecal and intravascular use of OMNIPAQUE.

DOSAGE AND ADMINISTRATION: CONSULT FULL PACKAGE INSERT BEFORE USE. Details on dose, concentration, and administration are provided for each of the indicated procedures.

HOW SUPPLIED: OMNIPAQUE is available in the following packaging and concentrations, *requiring no dilutions or reconstitution:*

Vials of 10 mL, 180 mgI/mL, boxes of 10 (NDC 0024-1411-10)
Vials of 20 mL, 180 mgI/mL, boxes of 10 (NDC 0024-1411-20)
Vials of 10 mL, 240 mgI/mL, boxes of 10 (NDC 0024-1412-10)
Vials of 100 mL, 240 mgI/mL, boxes of 5 (NDC 0024-1412-15)
Bottles of 200 mL, 240 mgI/mL, boxes of 5 (NDC 0024-1412-25)
Vials of 10 mL, 300 mgI/mL, boxes of 10 (NDC 0024-1413-10)
Vials of 30 mL, 300 mgI/mL, boxes of 10 (NDC 0024-1413-30)
Vials of 50 mL, 300 mgI/mL, boxes of 10 (NDC 0024-1413-50)
Vials of 100 mL, 300 mgI/mL, boxes of 5 (NDC 0024-1413-15)
Vials of 50 mL, 350 mgI/mL, boxes of 10 (NDC 0024-1414-50)
Vials of 100 mL, 350 mgI/mL, boxes of 5 (NDC 0024-1414-15)
Bottles of 200 mL, 350 mgI/mL, boxes of 5 (NDC 0024-1414-25)
MYELO-KIT™ containing: One vial of 10 mL, 180 mgI/mL, and one sterile myelogram tray, boxes of 5 (NDC 0024-1411-05)
MYELO-KIT™ containing: One vial of 20 mL, 180 mgI/mL, and one sterile myelogram tray, boxes of 5 (NDC 0024-1411-51)
MYELO-KIT™ containing: One vial of 10 mL, 240 mgI/mL, and one sterile myelogram tray, boxes of 5 (NDC 0024-1412-05)

References: 1. Enge I: Phlebography: Survey and present state. *Acta Radiol* 1983; suppl 366, pp 50-53. **2.** Gjølberg T, Andrew E, Enge I: Iohexol in phlebography of the leg: A comparative investigation with meglumine metrizoate. *Acta Radiol* 1983; suppl 366, pp 65-69. **3.** Albrechtsson U, Fagher B, Lagerstedt C, et al: Double blind comparison between iohexol and metrizoate in phlebography of the lower limb. *Acta Radiol* 1983; suppl 366, pp 58-64. **4.** Wolf GL: Adult peripheral angiography: Results from four North American randomized clinical trials of ionic media versus iohexol. *Acta Radiol* 1983; suppl 366, pp 166-170. **5.** Gordon IJ, Skoblar RS, Chicatelli PD, et al: A comparison of iohexol and Conray-60 in peripheral angiography. *AJR* 1984; 142:563-565. **6.** Data on file, Winthrop-Breon Laboratories. **7.** Egsgaard H, Hørup A, Praestholm J: A controlled clinical trial of iohexol and diatrizoate in aortofemoral angiography. *Eur J Radiol* 1983; 3:14-17. **8.** Kolbenstvedt A: Iohexol in lower extremity, renal and visceral angiography: Survey and present state.*Acta Radiol* 1983; suppl 366, pp 153-157. **9.** Törnquist C, Holtås S: Renal angiography with iohexol and metrizoate. *Radiology* 1984; 150:331-334. **10.** Albrechtsson U, Hultberg B, Lárusdóttir H, et al: Nephrotoxicity of ionic and non-ionic contrast media in aorto-femoral angiography. *Acta Radiol* 1985; 5:615-618. **11.** Cronqvist S: Iohexol in cerebral angiography: Survey and present state. *Acta Radiol* 1983; suppl 366, pp 135-139. **12.** Åhlgren P: Iohexol compared to urografin meglumine in cerebral angiography: A randomized, double-blind cross-over study. *Neuroradiology* 1982; 23:195-198. **13.** Nakstad P, Sortland O, Aaserud O: Iohexol compared to meglumine-Ca-metrizoate in common carotid angiography: A randomized double-blind cross-over study in man. *Neuroradiology* 1983; 23:33-36. **14.** Kido DK, Morris TW, Ekholm S, et al: Comparison of iohexol and meglumine-Na diatrizoate in cerebral angiography. *Acta Radiol* 1983; suppl 366, pp 142-146. **15.** Amundsen P, Dugstad G, Presthus J, et al: Cerebral angiography with iohexol: A multicentre clinical trial. *Acta Radiol* 1982; 23:529-534. **16.** Cacayorin ED, Bernstein AD, Fruehan CT, et al: Intravenous digital subtraction angiography with iohexol. *AJNR* 4:329-332. **17.** Nakstad P: Digital subtraction angiography of the carotid arteries: A comparison of iohexol and metrizoate. *Acta Radiol* 1983; suppl 366, pp 89-93. **18.** Sackett JF, Bergsjordet B, Seeger JF, et al: Digital subtraction angiography: Comparison of meglumine-Na diatrizoate with iohexol. *Acta Radiol* 1983; suppl 366, pp 81-84. **19.** Dawson P: Some aspects of contrast medium toxicity. *Acta Radiol* 1983; suppl 366, pp 174-179. **20.** Bryan RN, Miller SL, Roehm JOF Jr, et al: Neuroangiography with iohexol. *AJNR* 1983; 4:344-346. **21.** Higgins CB, Mancini GBJ, Bloomquist JN, et al: Cardioangiography in man using iohexol and meglumine-Na diatrizoate: A comparison of hemodynamic and electrocardiographic effects. *Acta Radiol* 1983; suppl 366, pp 111-114. **22.** Holtås S: Iohexol in patients with previous adverse reactions to contrast media. *Invest Radiol* 1984; 19:563-565. **23.** Dahlstrom K, Shaw DD, Clauss W, et al: Summary of U.S. and European intravascular experience with iohexol based on the clinical program. *Invest Radiol* 1985; 20(suppl 1), pp 117-121.

Winthrop-Breon

Winthrop-Breon Laboratories
Division of Sterling Drug Inc.
New York, NY 10016

illumination

EXCELLENCE

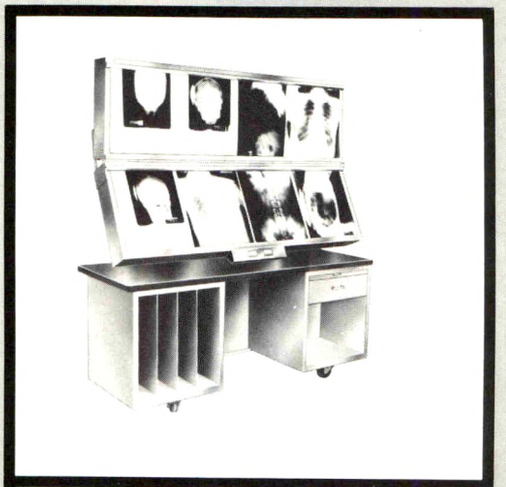
S&S X-Ray medical film reading illumination excellence has provided radiologists with unequalled quality and reliability for over 30 years.

The S&S commitment to quality and R&D has earned the reputation for excellence we enjoy, and has made S&S the world's largest manufacturer of Motorized Viewers.

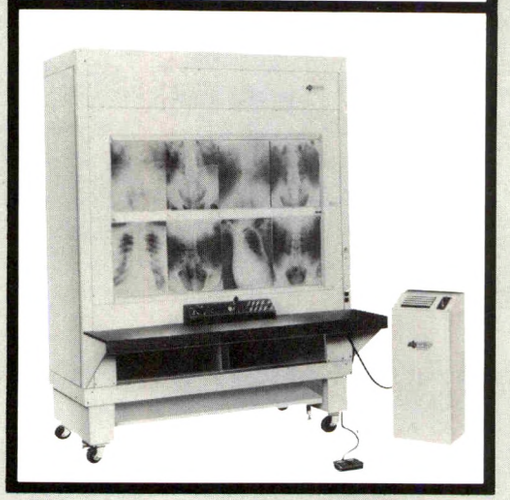
Models' film capacity range from 48 14″x17″ radiographs to 400 (4 over 4).

Whether stationary or motorized, S&S viewers together with our complete line of x-ray accessories are designed and engineered to fit every need, every budget.

Catalog available upon request.



Modular Mobile Illuminator



Model MV200A with optional MV 200C and MV200T

Engineered and produced by the world's leading manufacturer of X-Ray Accessories

S&S X-RAY PRODUCTS, INC.

87-93 Jay Street, Brooklyn, NY 11201
Telex: 219262 TLX UR
Tel: In NY State: (718) 852-6900
Toll Free: (800) 221-6634

Efficient bowel evacuants for diagnostic procedures

Take one

X-Prep®

for a cleaner, clearer film

Excellent visualization...fewer retakes

■ 95% efficacy proven with X-PREP® Liquid in 749 patients prepared for diagnostic procedures such as barium enemas and IVPs*

■ Effective for colonoscopy and sigmoidoscopy*

X-PREP® Liquid
2½ fl. oz. (74 ml) (standardized extract of senna fruit)

*Data on file, Medical Department, The Purdue Frederick Company.

Gray Pharmaceutical Co., Affiliate
The Purdue Frederick Company
Norwalk, CT 06856

X-PREP® Bowel Evacuant Kit-1
Contains two SENOKOT-S® Tablets (standardized senna concentrate and docusate sodium), one bottle of X-PREP Liquid 2½ fl. oz. (74 ml), one RECTOLAX® Suppository (bisacodyl 10 mg), plus easy-to-follow instructions.

X-PREP® Bowel Evacuant Kit-2
Contains one pack CITRALAX® Granules 1.06 oz. (effervescent citrate/sulfate of magnesia), one bottle of X-PREP Liquid 2½ fl. oz. (74 ml), one RECTOLAX Suppository, plus easy-to-follow instructions.



© 1984, Gray Pharmaceutical Co. PFR-081/84

Special Article

Vascular Complications After Liver Transplantation: A 5-Year Experience

Paul Wozney[1]
Albert B. Zajko[1]
Klaus M. Bron[1]
Stuart Point[1]
Thomas E. Starzl[2]

During the past 5 years, 104 angiographic studies were performed in 87 patients (45 children and 42 adults) with 92 transplanted livers for evaluation of possible vascular complications. Seventy percent of the studies were abnormal. Hepatic artery thrombosis was the most common complication (seen in 42% of children studied, compared with only 12% of adults) and was a major complication that frequently resulted in graft failure, usually necessitating retransplantation. In six children, reconstitution of the intrahepatic arteries by collaterals was seen. Three survived without retransplant. Arterial stenosis at the anastomosis or in the donor hepatic artery was observed in 11% of patients. Portal vein thrombosis or stenosis occurred in 13% of patients. Two children and one adult with portal vein thrombosis demonstrated hepatopetal collaterals that reconstituted the intrahepatic portal vessels. Uncommon complications included anastomotic and donor hepatic artery pseudoaneurysms, a hepatic artery–dissecting aneurysm, pancreaticoduodenal mycotic aneurysms, hepatic artery–portal vein fistula, biliary–portal vein fistula, hepatic vein occlusion, and inferior vena cava thrombosis.

Liver transplantation, once an experimental procedure, has become an accepted therapy for end-stage liver disease in both adults and children. With the advent of cyclosporine, 1-year survival rates have steadily risen from 50% in 1980 to 80% in 1984 [1]. Most mortality occurs in the first 6 months after transplant. Four-year survival is 75% in children (≤ 18 years old) and 50% in adult patients, reflecting the poorer first-year statistics of 4 years ago [1]. Most patients enjoy a satisfactory quality of life after transplantation [1–4].

The number of centers performing liver transplants has increased to 11 in the United States and nine in Europe, with a combined total of 992 recipients by June 1984 [1]. Two key ingredients to widespread liver transplantation, immunosuppression with cyclosporine and training of multiple-organ harvest and implantation teams, are quite recent (since 1980 and 1982, respectively). As surgical skill advances and diffuses throughout the medical world, liver transplants will become increasingly common [2, 4–6]. During 1985, 250 liver transplants were performed at our institution.

A vascular complication is a primary diagnostic consideration in the liver-transplant patient with fulminant hepatic failure, bile leak, relapsing bacteremia, gastrointestinal or abdominal bleeding, or hemobilia. Angiography is the test of choice in the evaluation of possible vascular complications. We report our 5-year experience with the angiographic diagnosis and the clinical outcome of patients with vascular complications after liver transplantation.

Materials and Methods

During the 5-year period ending December 1985, 477 patients received 625 liver transplants at the University of Pittsburgh Health Center (Table 1). The four leading indications were cirrhosis, biliary atresia, primary biliary cirrhosis, and inborn metabolic errors. Few transplants were for primary liver tumors [1]. The principle indications for retransplantation were rejection,

Received April 25, 1986; accepted after revision May 29, 1986.

Presented at the annual meeting of the American Roentgen Ray Society, Washington, DC, April 1986.

[1] Department of Radiology, Presbyterian-University Hospital, DeSoto at O'Hara Sts., Pittsburgh, PA 15213. Address reprint requests to A. B. Zajko.

[2] Department of Surgery, University of Pittsburgh Health Center, 1084 Scaife Hall, Pittsburgh, PA 15261.

AJR 147:657–663, October 1986
0361–803X/86/1474–0657
© American Roentgen Ray Society

TABLE 1: **Liver Transplants and Posttransplant Angiography Performed During the 5-Year Period**[a]

	Liver Transplants	Posttransplant Angiography (%)[b]
Total patients	477	87 (18)
Children (≤18 years old)	204	45 (22)
Adults (>18 years old)	273	42 (15)
Retransplants	148	12 (8)
Children	70	9 (13)
Adults	78	3 (4)
Total transplanted livers	625	92 (15)
Female: male	1:0.8	1:0.85

[a] Ending December 1985.
[b] Expressed as a total number and as a percentage of the number of liver transplants for each category.

technical failures, and primary graft nonfunction [5].

All posthepatic transplant angiograms performed at our institution during the past 5 years were analyzed retrospectively. Adults (> 18 years old) and children were grouped separately because complications and prognoses for the two groups are different; children commonly fare better [1]. One hundred four angiographic studies were performed in 87 patients (42 adults and 45 children) with 92 homograft livers; five children studied had two different transplants. The group included 40 males and 47 females, ranging in age from 4 months to 62 years old. Fifteen patients were studied twice, and one patient was studied three times. In 12 patients, the liver represented a retransplant. In one of the 12, the liver was a third transplant. Studies were performed from 2 days to more than 11 years after transplant. Seventy-seven studies (74%) were performed within the first 2 months after transplant.

All studies were performed by conventional angiographic techniques. Adult patients were only lightly sedated. Patients under 12 years old were evaluated under general anesthesia. All angiograms were performed from the femoral artery, except that the left axillary artery was used in one patient with bilateral external iliac artery occlusion. An aortogram was performed in 30 cases. Selective catheterization for evaluation of the hepatic artery or portal vein was performed in 82 cases. In general, angiography was performed on a semiemergent basis, within 4 to 24 hr of the clinical request. Performing the study on an emergent basis (within 2 hr) was rarely necessary.

In all but one patient, liver transplantation was orthotopic (i.e., the donor liver anatomically replaced the recipient's organ). In the single heterotopic transplant, an auxiliary liver was placed in the right lower abdomen in a patient with situs inversus and polysplenia.

In most patients, hepatic artery revascularization consisted of an end-to-end anastomosis between the donor celiac and recipient common hepatic artery. With anomalies of hepatic arterial supply, techniques were employed to create a single hepatic arterial pedicle [1, 7, 8]. Use of the donor's aorta or iliac artery for an arterial graft was more commonly necessary in children than in adults [8]. The donor and recipient extrahepatic portal veins were usually anastomosed end-to-end, except in a few patients with an abnormally small or occluded portal vein, for whom revascularization was performed with a venous homograft from the donor's vena cava, iliac vein, or pulmonary vein [9]. For the inferior vena cava, the infra- and suprahepatic vena cava segments of the donor were anastomosed end-to-end to the respective vessels of the recipient.

Results

All patients in this study were arbitrarily numbered from 1 through 47 with letters to designate separate livers where applicable. Throughout the Results and Discussion sections these numbers are used for easy reference to Figures 1, 5, and 6. Sixty-four (70%) of the 92 homografts studied were abnormal (Table 2).

TABLE 2: **Vascular Complications After Liver Transplantation in 87 Patients with 92 Allografts**

	Children	Adults
Normal	12	16
Hepatic artery		
Complete occlusion	21	5
Branch artery occlusion	1	1
Stenosis	3	7
Portal vein		
Occlusion	3	2
Stenosis	5	1
Miscellaneous findings	6	3
Pseudoaneurysm	1	1
Dissecting aneurysm	1	0
Mycotic aneurysms	0	1
Inferior vena cava occlusion	1	0
Hepatic vein occlusion	1	0
Hepatic artery–portal vein fistula	0	1
External iliac artery occlusion	1	0
Biliary–portal vein fistula	1	0
Possible rejection	7	11

Hepatic Artery Complications

The most frequently encountered complication was hepatic artery thrombosis, which occurred in 21 (42%) of 50 pediatric grafts (Fig. 1A), compared with only 5 (12%) of 42 adult grafts (Fig. 1B). Hepatic artery thrombosis was diagnosed from 5 days to 3 months after transplantation. All adults with complete hepatic arterial occlusion required immediate retransplantation, within days (Fig. 1B). However, five (24%) children (cases 2, 4a, 5, 6, 7) survived without retransplant, with follow-up from 3 to 42 months. In three of the five, hepatopetal arterial collaterals were demonstrated (Fig. 2). An additional three organs (cases 8, 9a, 12b) were retransplanted 2 to 5 months after hepatic artery thrombosis. Most children, however, required immediate retransplant. Intraarterial thrombolytic therapy with streptokinase was employed in one patient (case 32), without success.

In one child (case 12b) with hepatic artery occlusion, an intrahepatic biloma developed and was treated by percutaneous drainage. This revealed a biliary–portal vein fistula (Fig. 3). Conservative treatment resulted in fistula resolution, allowing retransplant 1 month later when a suitable donor became available.

Isolated occlusion of the right hepatic artery was seen in two patients (cases 11 and 33). Both showed intrahepatic collaterals (Fig. 4A) and had a benign clinical course. One of these, the child with the auxiliary graft (case 11), required retransplant 6 months later for chronic rejection. The other patient (case 33) demonstrated a right lobe infarct on CT (Fig. 4B). Treatment was conservative, and the patient was asymptomatic 6 weeks later.

Arterial stenosis occurred in 10 patients (Figs. 1A and 1B). In three children and four adults the stenosis was at the

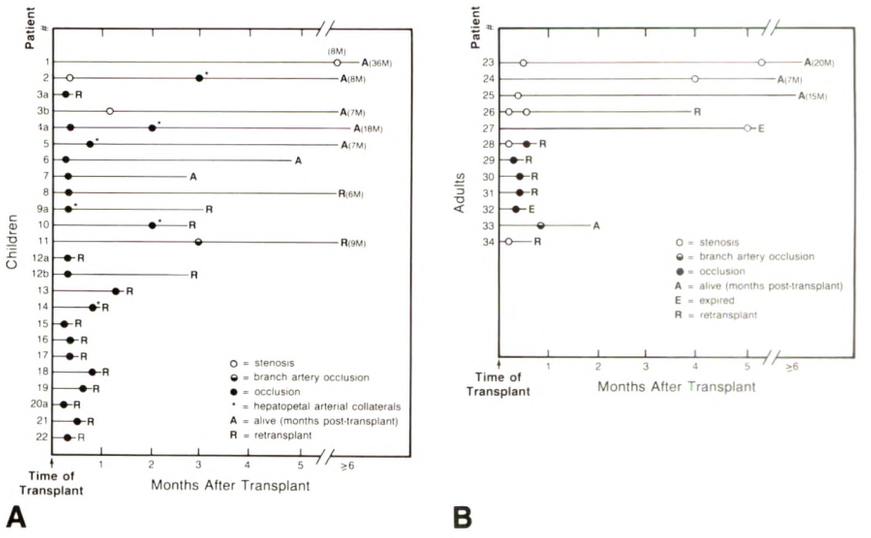


Fig. 1.—Hepatic artery complications in liver transplants. **A**, Children. **B**, Adults. Placement of circles indicates time of angiographic study after transplant. Patients are numbered consecutively, with letters indicating separate transplanted livers. Numbers refer to case numbers in Results and Discussion sections. Numbers followed by M are number of months (e.g., 8M = 8 months).

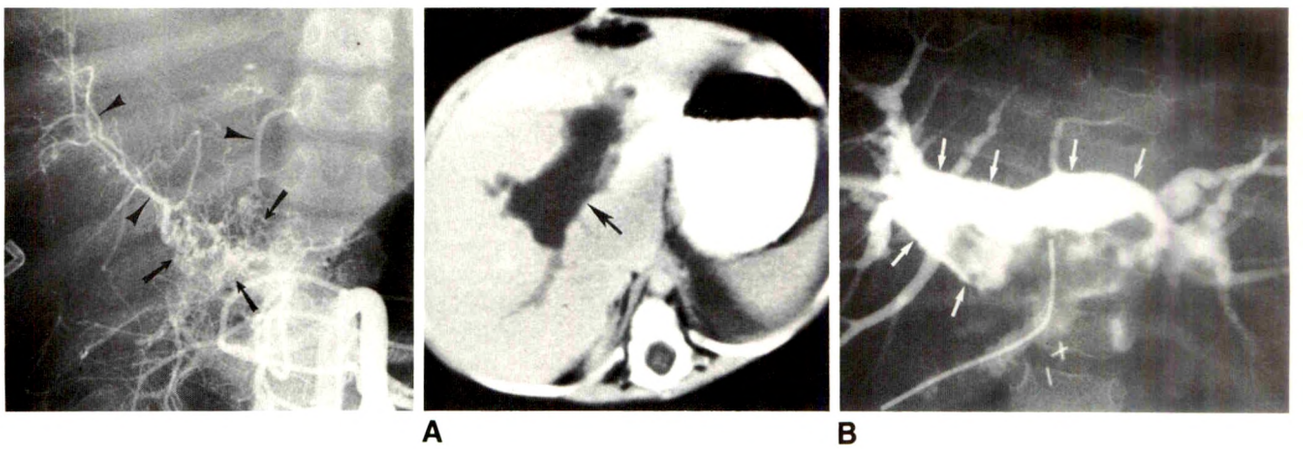


Fig. 2.—Collateral circulation after hepatic artery thrombosis. Extensive arterial collaterals (*arrows*), which reconstitute intrahepatic arteries (*arrowheads*), are demonstrated on selective superior mesenteric arteriogram 2 months after transplant.

Fig. 3.—Biliary–portal vein fistula in a 1-year-old girl with hepatic artery thrombosis and recurrent intermittent sepsis. **A**, Large intrahepatic fluid collection (*arrow*) is seen on CT 2 months after transplant. **B**, A biloma (*arrows*) communicating with intrahepatic portal veins is demonstrated after percutaneous drainage.

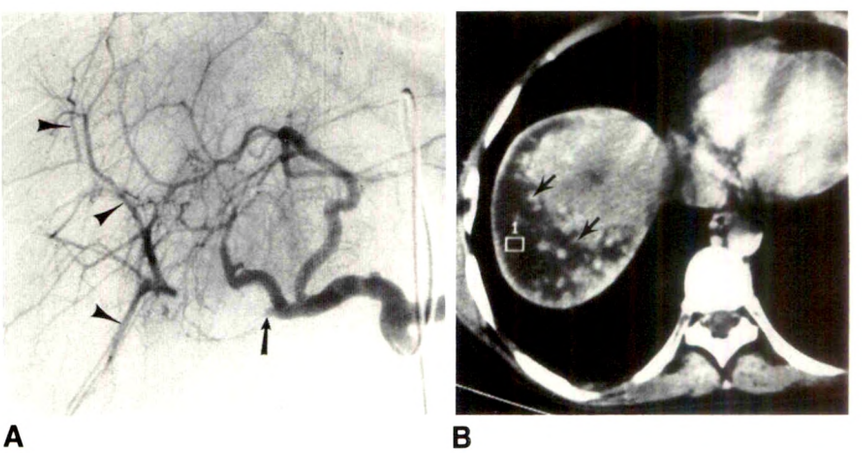
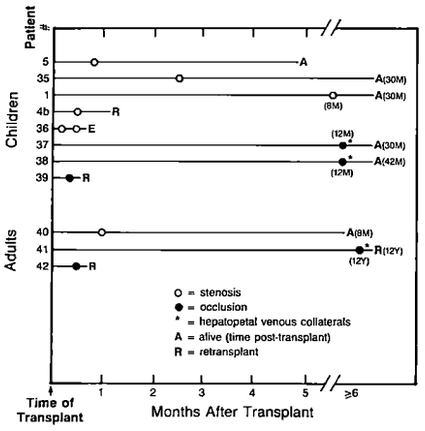
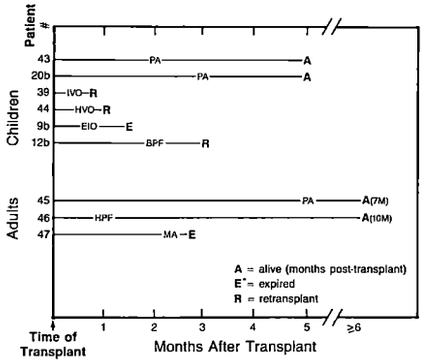


Fig. 4.—Branch hepatic artery occlusion. **A**, Occlusion of proximal right hepatic artery (*arrow*) is seen on celiac arteriogram 3 weeks after transplant. The peripheral branches (*arrowheads*) are reconstituted by intrahepatic collaterals. **B**, Probable right hepatic lobe infarct (*arrows*) seen on abdominal CT performed the same day.



5



6

Fig. 5.—Portal vein complications in liver transplants. Placement of circles indicates time of angiographic study after transplant. Numbers followed by M or Y are number of months or years (e.g., 30M = 30 months).

Fig. 6.—Miscellaneous vascular complications in liver transplants. PA = pseudoaneurysm, IVO = inferior vena cava occlusion, HVO = hepatic vein occlusion, EIO = external iliac artery occlusion, BPF = biliary–portal vein fistula, HPF = hepatic artery—portal vein fistula, MA = mycotic aneurysms. Numbers followed by M are number of months (e.g., 7M = 7 months).

anastomosis. One child with arterial stenosis (case 2) later demonstrated thrombosis. All three children survived without retransplant. In one adult with an anastomotic stenosis (case 23), a follow-up angiogram 5 months later showed almost complete resolution. A second adult patient (case 26) underwent balloon angioplasty but required retransplant for chronic rejection 4 months later. At surgery the hepatic artery was patent. A third adult with a severe anastomotic stenosis (case 27) developed a hepatic abscess and died during retransplant. Presumably the stenosis had progressed to occlusion. In the fourth adult (case 28), an anastomotic stenosis progressed to occlusion after 14 days, and retransplantation was required.

Stenosis within the donor right hepatic artery was seen in two adults. In one (case 24) the stenosis was an incidental finding. The second patient (case 34) required retransplant 3 days later for acute rejection. In one adult (case 25) a kink was seen in the hepatic artery near the anastomosis. At surgery for revision of the biliary anastomosis the next day, the hepatic arterial pulse was strong. The vessel was straightened but the kink was not thought to be hemodynamically significant. The patient was asymptomatic 1 year later.

Portal Vein Complications

Portal vein thrombosis developed in three children and two adults (Fig. 5). All demonstrated evidence of portal hypertension with massive gastroesophageal varices. Retransplantation was required in one child (case 39). In the other two children (cases 37 and 38), portal vein occlusion was diagnosed 1 year after transplantation. Massive hepatopetal venous collaterals had reconstituted the intrahepatic portal veins. Both patients were treated with endoscopic esophageal sclerotherapy although one eventually required a distal splenorenal shunt for control of portal hypertension. One adult also developed hepatopetal collaterals (case 41), and retransplantation was required for chronic rejection.

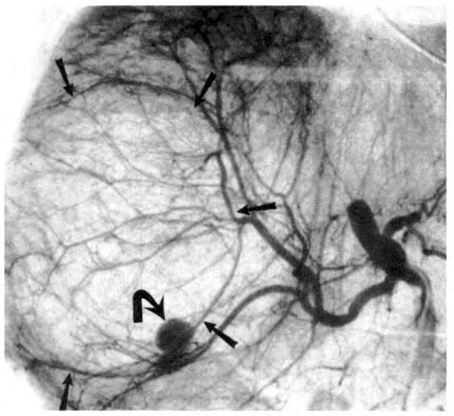
Portal vein stenosis at the anastomosis was observed in five children and one adult from 4 days to 8 months after transplantation (Fig. 5). Four presented with upper gastrointestinal tract bleeding from gastroesophageal varices. In the other two (cases 5 and 35), portal vein stenosis was an incidental finding. Varices were not present.

Miscellaneous Vascular Complications

Pseudoaneurysms occurred in two patients (Figs. 6 and 7), and a dissecting aneurysm occurred in one (Fig. 8). In one adult (case 45), abdominal CT for back pain demonstrated an aneurysm adjacent to the abdominal aorta. At angiography, this proved to be an anastomotic pseudoaneurysm. The patient underwent successful revision of the anastomosis. In one child (case 43) angiography was performed for possible hepatic artery thrombosis. A pseudoaneurysm of a branch of the right hepatic artery and a large intrahepatic hematoma were demonstrated (Fig. 7). A hemorrhagic right-lobe infarct was found at surgery. A right hepatic lobectomy was performed. In another child (case 20b), sonography and CT revealed a possible infarct in the posterior right lobe of the liver, indicating possible hepatic artery thrombosis. Angiography revealed a large aneurysm (Fig. 8), which in retrospect was evident on the CT study. At surgery a 4-cm dissecting aneurysm of an aortic graft was resected and a new arterial graft was placed.

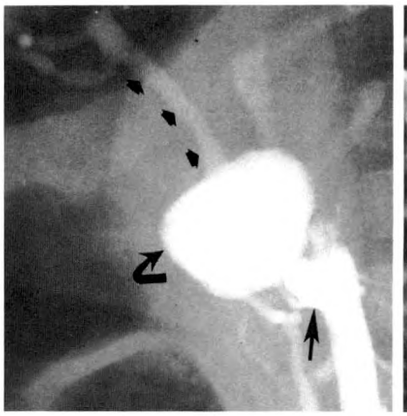
In one patient, abdominal CT was obtained because of an acute decrease in hematocrit. CT demonstrated evidence of intraabdominal hemorrhage that appeared to arise from the proximal anastomosis of an aortic graft (Fig. 9). Angiography was performed to evaluate for a pseudoaneurysm, but the study was normal. Hemorrhage that originated from the anastomosis was found at surgery.

Unusual complications (Fig. 6) included an adult (case 47) with aneurysms in pancreaticoduodenal arterial collaterals that at laparotomy proved to be mycotic in origin. Progressive hemorrhage resulted in death within 6 days. Another adult (case 46) developed a hepatic artery–portal vein fistula, probably secondary to needle biopsy. This was an incidental finding, with no clinical sequelae. One child (case 9b) developed bilateral external iliac thrombosis, which was initially thought to be secondary to thrombosis of an aortic graft with embolization to the iliac arteries. Angiography confirmed oc-



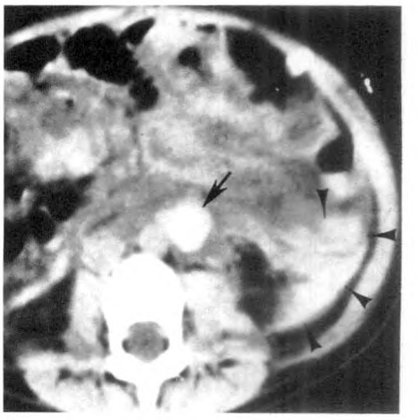
7

Fig. 7.—Pseudoaneurysm (*curved arrow*) with large right-hepatic-lobe hematoma (*straight arrows*) seen on hepatic arteriogram 7 weeks after transplant.



8

Fig. 8.—Large aneurysm (*curved arrow*) just beyond proximal anastomosis (*straight arrow*) of aortic graft with preservation of distal arterial flow (*small arrows*) demonstrated on angiogram 3 months after transplant. Surgery showed this to be a dissecting aneurysm starting at proximal anastomosis of graft.



9

Fig. 9.—Paraaortic (*arrow*) and retroperitoneal (*arrowheads*) hematoma originating from proximal anastomosis of aortic graft seen on nonenhanced abdominal CT scan 1 week after transplant. Angiography was normal.

clusion of the iliac arteries but the graft was patent. The iliac occlusion was attributed to previous indwelling femoral catheters. A second child (case 39) developed inferior vena cava thrombosis and portal vein occlusion, and retransplantation was done the next day. In a third child (case 44), attenuation of the intrahepatic arteries and late portal venous filling were seen on hepatic angiography. The angiographic impression was rejection and hepatic venous occlusion. At retransplant the next day, the large hepatic veins were patent. However, histologic evaluation showed central venous endophlebitis with necrosis and occlusion. Indications of rejection were also present.

In 18 studies, intrahepatic arterial attenuation and narrowing or decreased flow was seen, suggesting rejection. Because the diagnosis of rejection is complex [10, 11], these studies are being analyzed separately and are excluded from the present discussion.

Discussion

By far the most common and most significant complication diagnosed at angiography was hepatic artery thrombosis. It was seen in 42% of pediatric and 12% of adult angiographic studies. The overall prevalence in all liver transplants at our center was 3% of adults and 12% of children between March 1980 and June 1984 [12, 13]. Only 25% were diagnosed by angiography. The remainder were diagnosed during retransplant, exploratory laparotomy, or autopsy. With retransplant the mortality was 27%, while without retransplant the mortality was 73% [13]. Only pediatric patients have survived without retransplantation.

The pathophysiology is often difficult to deduce, because biopsy is not available in all patients. Hepatectomy specimens (at retransplant) frequently are not intact, while autopsy specimens are complicated by supervening factors, such as sepsis, extensive hemorrhage, and hypotension. A clear cause was identified in only three (14%) of 22 cases recently reviewed at our institution [13]. Certain risk factors are, however, clear. Patients at increased risk include children and those requiring complex vascular reconstruction, either because of multiple arterial supply to the liver or because of the small size of donor and recipient vessels [3, 13].

Rejection probably plays a role in hepatic artery thrombosis in some cases. Liver biopsies or pathologic material obtained within 1 week of the angiogram were only available in 10 of the 26 cases of hepatic artery thrombosis. One sample showed no rejection, four showed mild rejection, while marked rejection was seen in five. Arterial lesions of rejection are said to be more evident in medium-sized hepatic vessels [10]. In chronic rejection, there is deposition of subintimal foam cells, myointimal hyperplasia, and intimal sclerosis [10]. The end result is progressive arterial narrowing and slow flow, with subsequent thrombosis.

Other potential causes for hepatic artery occlusion are speculative. Thrombosis may be related to turbulent flow at difficult anastomoses. In three cases infection may have been the cause. In two other patients (cases 2 and 28) stenosis progressed to occlusion. Stenosis probably resulted in slow flow with subsequent thrombosis.

Clinically, hepatic artery thrombosis presents in three forms with equal frequency [12, 13]. Massive hepatic necrosis is a dramatic clinical emergency, requiring rapid retransplantation for survival. A second presentation is delayed biliary leak seen in 7 (32%) of 22 patients with thrombosis [13]. After transplantation, the donor bile duct is entirely dependent on hepatic arterial blood supply, usually the right. Occlusion may result in bile-duct ischemia and necrosis. In our series, five children (cases 6, 8, 9a, 10, 12b) with hepatic artery thrombosis had

intrahepatic bilomas (Fig. 3), presumably due to bile-duct necrosis. All but one required retransplantation. A third presentation is intermittent episodes of sepsis without an evident source, probably caused by focal abscesses within infarcted areas of the liver. In these patients, evaluation with CT or sonography may demonstrate bilomas, infarcts, or abscesses, suggesting arterial occlusion [14]. Eighty-six percent of transplant patients with hepatic abscesses or infarcts seen with CT or sonography had hepatic artery thrombosis [15].

Although graft function is usually poor enough to warrant retransplant, the prognosis is not inevitably grim. The patient's clinical condition dictates management, and if liver function is stable, retransplant is postponed. As Figure 1A illustrates, 24% of children with hepatic artery thrombosis survived without retransplantation. This probably is a manifestation of the ability of the liver to recruit collateral arterial supply (Fig. 2). Collaterals were demonstrated in three cases within 2 weeks of transplant, and, if we judge by patient survival, an additional three patients probably also developed collaterals within 2 weeks of transplant. Three other patients developed collaterals within 3 months of transplant, making a total of nine (43%) of 21 pediatric arterial occlusions.

Collateral development is clearly a characteristic of the immediate posttransplant period. The source of these collaterals was from the superior mesenteric artery (two cases) (Fig. 2), superior mesenteric and splenic arteries (one case), and right inferior phrenic artery (one case). Surgery has shown that collaterals supply the liver from adhesions to the diaphragm, omentum, and bowel [5].

The presence of collaterals has significant implications for survival and for surgical blood loss. Half of the patients with collaterals ultimately did not require retransplant, and in an additional patient who did require retransplant for a hilar abscess, the liver was considered viable at surgery. All adult patients with complete arterial thrombosis ultimately required retransplant, and in none of them were collaterals observed. Surgical blood loss during retransplantation is usually half that of the first transplant, but with collaterals, blood loss typically exceeds the first transplant by a factor of three or more. Thus the actual blood loss at retransplantation may be sixfold or higher, information of significant interest to the surgical team as well as to the blood bank [5]. Actuarial survival after retransplant is lower than for primary transplants. Four-year survival is 60% in children and 40% in adults [5]. Our study population was similar. Eight (57%) of 14 children and one (25%) of four adults survived after retransplantation.

Extrahepatic portal vein complications were unusual, constituting six cases of stenosis and five of thrombosis over the past 5 years (Fig. 5). Potential causes include surgical technique, misalignment or excessive vessel length, hypercoagulable states, thrombus formation from the portal venous bypass cannula used at transplantation, and previous portal vein surgery (R. D. Gordon, unpublished data). Although occasionally diagnosed incidentally, most portal vein complications were accompanied by symptoms of portal hypertension (i.e., varices and upper gastrointestinal hemorrhage). Presentation of these symptoms warrants angiography to evaluate the portal venous system. Other clinical presentations include hepatic failure, intestinal swelling, and massive ascites (R. D. Gordon, unpublished data). In most of our patients, treatment consisted of endoscopic sclerotherapy for esophageal varices, although one eventually required a splenorenal shunt and one patient required retransplantation.

Three of the five cases of portal vein thrombosis demonstrated massive hepatopetal venous collaterals that reconstituted the intrahepatic portal veins. Angiographically, the appearance was similar to cavernous transformation of the portal vein [16]. The mechanism by which these collaterals develop a communication with the intrahepatic vessels is unknown. However, they must arise de novo, since all potential collateral communications are severed at transplantation.

Occlusion of the inferior vena cava or hepatic veins was rare. This contrasts with a recent series of 18 posttransplant studies in which thrombosis was as common in the vena cava as in the hepatic artery [11]. In the same series, arteriovenous fistulae after biopsy were demonstrated twice and thought to compromise the graft. Despite frequent percutaneous transhepatic intervention [17], including cholangiography, biliary drainage, and biopsy during the past 5 years, we have seen only two procedure-related vascular complications. One case (case 46) was an incidental finding of a hepatic artery–portal vein fistula. The other case (case 43) was an intrahepatic pseudoaneurysm with an infarct (Fig. 7). Both were secondary to biopsy.

During the past 5 years, angiography has been the principle technique for the evaluation of possible vascular complications after liver transplantation. CT (even with bolus technique), radionuclide scanning, and real-time sonography have all been disappointing in patency evaluation. CT and sonography, however, are valuable in identifying abscesses, bilomas, and hematomas that may result from vascular complications. CT has been the most useful study for evaluation of possible hepatic infarction after transplant [14]. The identification of pseudoaneurysms may be difficult. CT and sonography both have definite roles in addition to angiography (Fig. 9).

Since 1984, we have increasingly employed duplex sonography (combined real-time and pulsed Doppler) for evaluation of suspected hepatic arterial thrombosis after transplant. In 29 cases, duplex sonography correctly diagnosed thrombosis in eight and patency in 21 [15]. These encouraging results have led the transplant team to commonly request duplex sonography to screen for hepatic artery thrombosis. This has resulted in some decrease in angiography.

The practical treatment of end-stage liver disease with homograft liver transplant is quite new, dating from the availability of cyclosporine in 1980 [1–4, 6]. Surgical technique and intra- and postoperative management of transplant patients are still evolving [1, 4]. Our results cover the first 5 years of the cyclosporine era. As surgical and medical management evolves, the vascular complications observed as well as the clinical outcome may change.

ACKNOWLEDGMENT

We thank Donna Scahill for manuscript preparation.

REFERENCES

1. Starzl TE, Iwatsuki S, Shaw BW Jr, Gordon RD. Orthotopic liver transplantation in 1984. *Transplant Proc* **1985**;17:250–258
2. Iwatsuki S, Shaw BW Jr, Starzl TE. Five-year survival after liver transplantation. *Transplant Proc* **1985**;17:259–263
3. Iwatsuki S, Shaw BW Jr, Starzl TE. Current status of hepatic transplantation. *Semin Liver Dis* **1983**;3:173–180
4. Starzl TE, Iwatsuki S, Shaw BW Jr, et al. Analysis of liver transplantation. *Hepatology* **1984**;4:47S–49S
5. Shaw BW Jr, Gordon RD, Iwatsuki S, Starzl TE. Hepatic retransplantation. *Transplant Proc* **1985**;17:264–271
6. Starzl TE, Iwatsuki S, Van Thiel DH, et al. Report of Colorado-Pittsburgh liver transplantation studies. *Transplant Proc* **1983**; 15:2582–2585
7. Gordon RD, Shaw BW Jr, Iwatsuki S, Todo S, Starzl TE. A simplified technique for revascularization of homografts of the liver with a variant right hepatic artery from the superior mesenteric artery. *Surg Gynecol Obstet* **1985**;160:474–476
8. Zajko AB, Bron KM, Starzl TE, et al. Angiography of liver transplantation patients. *Radiology* **1985**;157:305–311
9. Shaw BW Jr, Iwatsuki S, Bron K, Starzl TE. Portal vein grafts in hepatic transplantation. *Surg Gynecol Obstet* **1985**;161:66–68
10. Demetris AJ, Lasky S, Van Thiel DH, Starzl TE, Dekker A. Pathology of hepatic transplantation. A review of 62 adult allograft recipients immunosuppressed with a cyclosporine/steroid regimen. *Am J Pathol* **1985**;118:151–161
11. Cardella JF, Castaneda-Zuniga WR, Hunter D, Young A, Amplatz K. Angiographic and interventional radiologic considerations in liver transplantation. *AJR* **1986**;146:143–153
12. Tzakis AG. The dearterialized liver graft. *Semin Liver Dis* **1985**; 5:375–376
13. Tzakis AG, Gordon RD, Shaw BW Jr, Iwatsuki S, Starzl TE. Clinical presentation of hepatic artery thrombosis after liver transplantation in the cyclosporine era. *Transplantation* **1985**;40:667–671
14. Penkrot RJ. Noninvasive evaluation of complications of orthotopic liver transplantation. *Semin Intervent Radiol* **1986**;3:120–122
15. Segel MC, Zajko AB, Bowen A, et al. Hepatic artery thrombosis after liver transplantation: radiologic evaluation. *AJR* **1986**; 146:137–141
16. Zajko AB, Bron KM. Hepatopetal collaterals after portal vein thrombosis following liver transplantation. *Cardiovasc Intervent Radiol* **1986**;9:46–48
17. Zajko AB, Campbell WL, Bron KM, et al. Cholangiography and interventional biliary radiology in adult liver transplantation. *AJR* **1985**;144:127–133

American Roentgen Ray Society 87th Annual Meeting April 26–May 1, 1987, Miami Beach, FL Fontainebleau-Hilton Hotel

Registration and Hotel Reservations

Forms for advance registration and hotel reservations will be in the January and February 1987 issues of the *AJR*.

Refresher Course Program

A summary of the refresher courses will appear in the *AJR* in January along with advance registration forms. Early registration is an advantage in assuring preferred courses in this popular program. Dr. J. T. Ferruci, Jr. is program director.

Local Program

A program of sightseeing, shopping, and entertainment will be developed by the Local Arrangements Chairman. Information and advance registration forms will be in the January and February issues of the *AJR*.

President's Award Papers

The society offers several cash awards for the best scientific papers prepared by residents in radiology. The President's Award has a $1000 prize. There are two Executive Council awards of $500 each. All are presented at the annual meeting. Papers should be submitted by Jan. 31 for consideration in this competition. Send entries to:

B. G. Brogdon, M.D.
Dept. of Radiology
University of South Alabama Medical Center
2451 Fillingim Street
Mobile, AL 36617

ARRS Membership Requirements

The American Roentgen Ray Society (ARRS) has two membership categories: active and in-training. For active membership, applicants must practice radiology in the U.S. or Canada. Each must have graduated in good standing from an approved medical school or hold an advanced degree in physical, chemical, or biological science and be certified by the American Board of Radiology, the Royal College of Physicians and Surgeons of Canada, or otherwise adequately document training and credentials.

A member-in-training must be in a radiology residency or postresidency fellowship program or be a postgraduate student in an allied science. Status must be verified by the program director.

For consideration during the 1987 ARRS meeting, completed applications must be received no later than Feb. 1. Obtain forms and details from:

Rosalind H. Troupin, M.D.
Department of Radiology
Hospital of University of Pennsylvania
3400 Spruce St.
Philadelphia, PA 19104

Associated Society Meetings

Society for Pediatric Radiology and European Society of Pediatric Radiology

The inaugural conjoint International Pediatric Radiology '87 meeting will meet May 30–June 4, 1987 at the Westin Hotel, Toronto, Ontario, Canada. Deadline for receipt of abstracts is February 1, 1987. For details contact: Donald R. Kirks, M.D., Secretary, Society for Pediatric Radiology, c/o Dept. of Radiology, Childrens Hospital Medical Center, Elland and Bethesda Aves., Cincinnati, OH 45229, (513) 559-4880

Deadlines

President's Award papers: January 31
Membership applications February 1

Society of Gastrointestinal Radiologists Roscoe E. Miller Award

Monitoring Hepatic Cryosurgery with Sonography

Gary Onik[1,2]
Robert Kane[1]
Glen Steele[3]
William McDermott[3]
Urmila Khettry[4]
Blake Cady[3]
Roger Jenkins[3]
Judith Katz[1]
Melvin Clouse[1]
Boris Rubinsky[5]
Brenda Chase[1]

The intraoperative sonographic appearance of frozen hepatic tumors and frozen normal liver was correlated with the histologic appearance of pathologic specimens from six patients. Frozen tissue was visualized as a hyperechoic rim with posterior acoustic shadowing. Normal liver that was frozen and then thawed appeared hypoechoic when compared with normal unfrozen liver. These findings allowed visualization of the extent of freezing in relation to tumor margins. Pathologically, frozen tumors showed definite evidence of necrosis. Normal liver tissue was extremely sensitive to cold and was completely necrotic after freezing. The sonographic appearance of frozen and thawed liver correlated precisely with the gross morphologic and histologic changes seen in the cryolesion. It appears that intraoperative sonography allows accurate monitoring of hepatic cryosurgery.

Cryosurgery, the in situ destruction of tissue by means of subzero temperatures, has been suggested for the treatment of hepatic malignancies that are unresectable by traditional surgery [1]. Because the tumor is not resected, larger amounts of normal liver surrounding the malignancy can be saved, and therefore more than one hepatic segment can be treated. Although techniques for hepatic freezing have been investigated in animals, a major drawback to its use in patients has been the inability to monitor the freezing process.

Previous in vitro studies have shown that the freezing process can be visualized by sonography [2]. Animal work has shown that a cryolesion produced in normal liver has a characteristic appearance after thawing: it is hypoechoic in comparison to the adjacent unfrozen liver [3]. It was suggested that this characteristic of the cryolesion would make hepatic cryosurgery feasible by permitting visualization of the cryosurgical margin.

We studied the sonographic appearance of frozen and thawed hepatic metastases to evaluate the technical feasibility of using intraoperative sonography to monitor hepatic cryosurgery.

Subjects and Methods

With the permission of the New England Deaconess Hospital Human Experimentation Committee, six patients (five with metastatic colon carcinoma of the liver and one with multiple hepatic lesions of unknown cause) had lesions frozen. All lesions were then resected in the usual manner. Each patient had a preoperative CT, sonogram, and hepatic angiogram, and each was determined to have resectable disease by the usual criteria [4].

A laparotomy was performed on each patient. If the hepatic lesions were deemed resectable and no extrahepatic metastatic disease was found, the entire liver was surveyed for occult lesions by using the Technicare OR330 Intraoperative Ultrasound Unit (Codman Co., Randolph, MA) with a 7.5-MHz linear-array T or I configuration transducer (Fig. 1). Subsequently, one of the lesions to be resected was localized sonographically, and a sharp, trocar cryoprobe (8 mm in diameter) was placed into the tumor nodule via sonographic guidance. The cryoprobe

Received March 6, 1986; accepted after revision May 28, 1986.

Recipient of the Roscoe E. Miller Award of the Society of Gastrointestinal Radiologists. Presented at the annual meetings of the Society of Gastrointestinal Radiologists, Acapulco, January 1986, and the American Roentgen Ray Society, Washington, DC, April 1986.

[1] Department of Radiology, New England Deaconess Hospital, Boston, MA 02215.

[2] Present address: Allegheny General Hospital, 320 E. North Ave., Pittsburgh, PA 15212. Address reprint requests to G. Onik.

[3] Department of Surgery, New England Deaconess Hospital, Boston, MA 02215.

[4] Department of Pathology, New England Deaconess Hospital, Boston, MA 02215.

[5] Department of Mechanical Engineering, University of California at Berkeley, Berkeley, CA 94720.

AJR 147:665–669, October 1986
0361–803X/86/1474–0665
© American Roentgen Ray Society

was driven by a Frigitronics, Inc. (Shelton, CT) CE4 cryosurgical system, which circulated liquid nitrogen at −196°C through the cryoprobe (Fig. 2). When the position of the probe was deemed adequate by sonography, freezing was begun by circulating liquid nitrogen through the probe. It was continued for 8 min while the freezing front was continuously monitored by sonography. The frozen tissues were then allowed to thaw and were rescanned. The lesion was then resected and correlation was made with the gross and microscopic pathologic changes. In three of the six patients, tumor only was frozen. The other three patients had a portion of tumor and a portion of the normal adjacent liver included in the cryolesion.

Results

Freezing was carried out in all six patients without complications. The freezing process was visualized in all cases as a hyperechoic rim with posterior acoustic shadowing. The high-frequency sound waves were completely reflected at the interface between the nonfrozen tissue and the ice ball. For complete visualization of the frozen tissue, it was necessary to scan the liver in several different areas while the nonfrozen liver tissue was used as an acoustic window to the cryolesion. The largest volume of frozen liver that could be generated by using our 8-mm cryoprobe was approximately 3 cm in diameter. Thawing of the frozen region took approximately 15 min, and the hyperechoic rim, representing the freezing front, could be monitored as it receded during the thawing process.

In all six patients the tumor or the part of the tumor that was frozen and subsequently thawed did not change significantly in echogenicity. However, in the three patients in whom a portion of normal liver was frozen in addition to tumor, the normal liver showed a marked decrease in echogenicity after thawing when compared with unfrozen liver. After thawing there was no acoustic shadowing, and the altered echogenicity of the thawed liver made it possible to determine that the freezing had extended beyond the tumor margin into adjacent liver (Fig. 3). Visual correlation between the sonographic

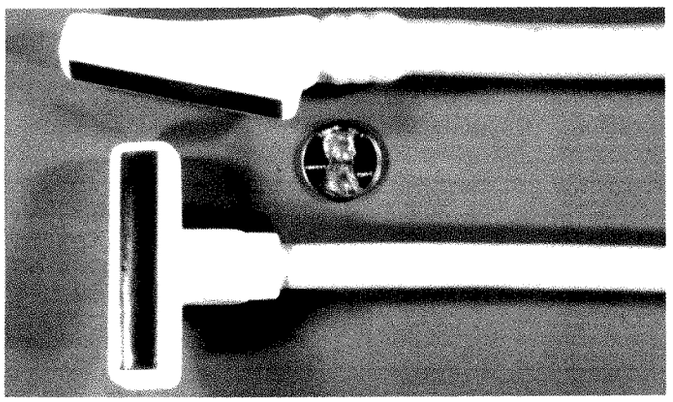


Fig. 1.—Two 7.5-MHz linear-array transducers specifically designed for intraoperative hepatic sonography. The sound beam emanates from the transducer perpendicular to the cable, allowing the transducer to be cradled between the fingers and to scan flat on the liver surface.



Fig. 2.—Cryoprobe freezing hepatic lesion. The cryoprobe (*small arrow*) is seen piercing the liver. The white area around the probe on the surface of the liver represents frozen tissue. The transducer (*larger arrow*) monitoring the freezing is seen beneath the liver.

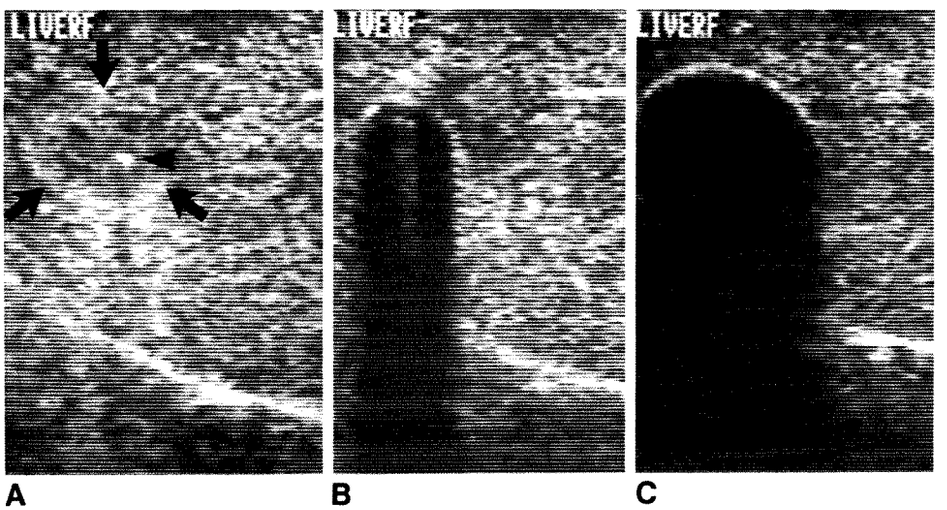


Fig. 3.—Sonograms demonstrating the freeze-thaw cycle of a hepatic lesion. **A**, Lesion (*arrows*) has a slightly hyperechoic rim surrounding a more hypoechoic center. Cryoprobe tip (*arrowhead*) appears as a tiny echogenic focus with slight posterior acoustic shadowing. **B**, Partial freezing. Ice ball appears as a hemispherical, hyperechoic rim with posterior acoustic shadowing. A reverberation artifact is seen centrally within the acoustic shadow, emanating from the tip of the cryoprobe. **C**, Fully developed cryolesion. At 8 min the frozen zone is much larger, as indicated by the increased radius of the echogenic rim and larger area of acoustic shadowing.

images and the gross pathologic changes seen in the resected specimens was excellent (Figs. 4 and 5).

Pathologically, the cryolesions produced in normal liver and tumor had a distinctive morphology. Grossly, the normal liver could be separated into frozen and nonfrozen zones by a sharp line of demarcation. The frozen normal liver was darker (somewhat red-brown) and softer than the nonfrozen normal liver. The capsular surface had tiny red petechiae. The line of demarcation was sharp on the capsular surface as well. The tumor, however, could not be separated into frozen or nonfrozen areas as readily and showed little if any gross morphologic change in the previously frozen areas. Microscopically, however, both the tumor and normal liver could be easily separated into frozen and nonfrozen zones. The zone of separation in each case was again sharp and abrupt. The frozen liver (Fig. 6) showed coagulative necrosis of individual hepatocytes with small, shrunken, pyknotic nuclei. All of the nuclear details were lost. The cytoplasm was fuzzy and granular with indistinct cell borders. The sinusoids were moderately congested, a finding that could be seen clearly under low power alone. Tumor tissue similarly underwent coagulative necrosis with loss of nuclear detail and cytoplasmic shrinkage in the frozen area (Fig. 7). Histologic changes after freezing were much more striking in the tumor tissue than in the normal liver, with definite cytologic changes consistent with necrosis even after only one freeze-thaw cycle.

In one patient whose preoperative workup indicated metastatic colon carcinoma limited to the left lobe, intraoperative sonographic survey of the liver showed several tiny echogenic nodules ranging in size from 2 to 5 mm in the right lobe. Again, no lesions could be seen on follow-up CT scan 10 weeks after surgery, but a scan at 6 months showed several lesions within the same area of the right lobe. Subsequently, pathologic examination proved that the nodules were metastatic.

Discussion

Several investigators [5, 6] have proposed cryosurgery as a treatment for unresectable hepatic tumors. In a study of 20

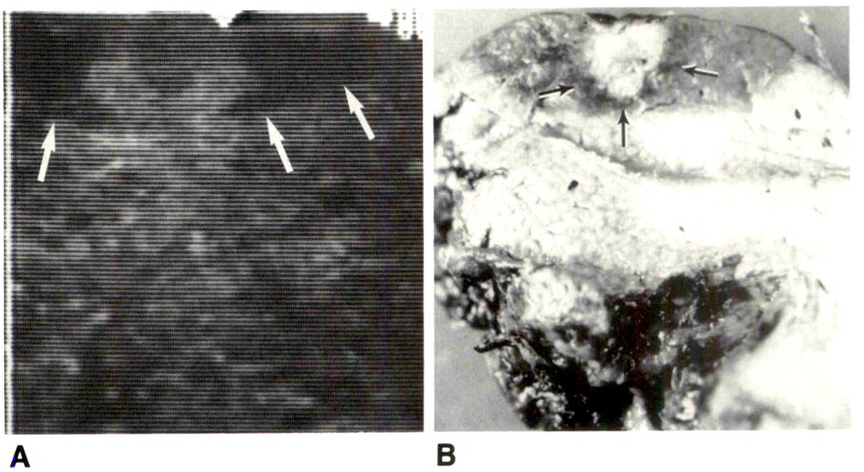


Fig. 4.—Cryolesion after thawing. **A.** Intraoperative scan through lesion shown in Fig. 3, with transducer repositioned on surface of tumor nodule. Tumor nodule is unchanged in appearance with an echogenic rim and hypoechoic center. Adjacent frozen and thawed liver (*arrows*) is hypoechoic compared with the unfrozen liver, making the lesion more obvious. **B**, Pathologic specimen shows hepatic cryolesion is dark and hemorrhagic compared with adjacent unfrozen liver. Tumor nodule (an unsuspected and largely fibrosed hemangioma) reaches just to edge of cryolesion, as depicted on sonogram. Edges of hemangioma are slightly darker (*arrows*); the central lighter area has undergone fibrosis.

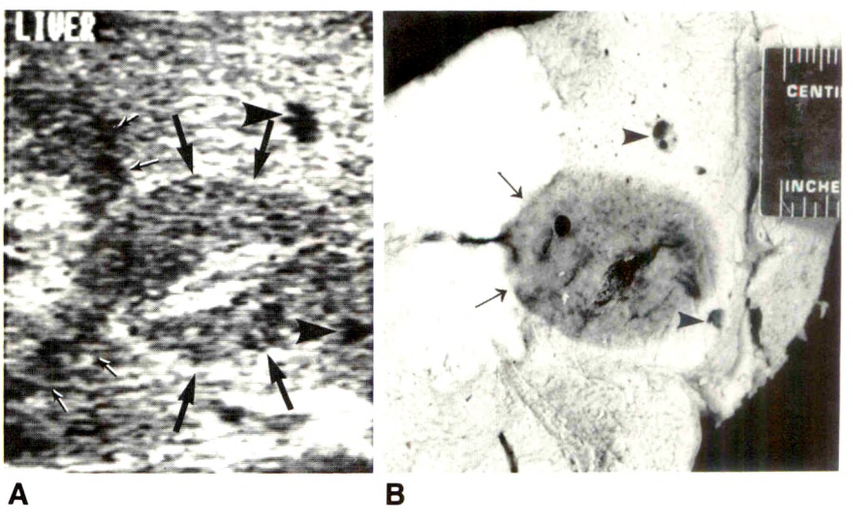
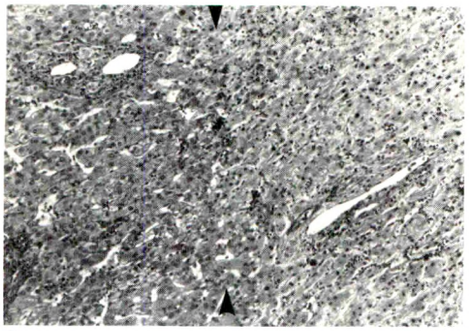
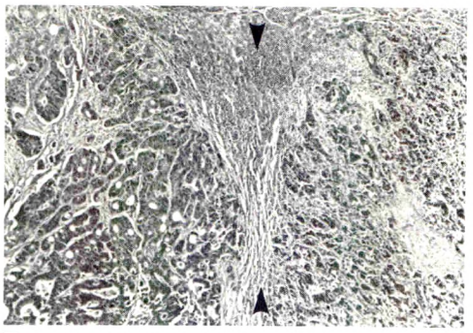


Fig. 5.—**A**, Sonogram shows thawed cryolesion (*large arrows*) largely within normal liver, with one margin extending into a colon metastasis (*small arrows*). Linear hyperechoic area, centrally within the cryolesion, represents the laceration caused by cryoprobe. *Arrowheads* indicate hepatic vessels to be used as landmarks for comparison with pathologic specimen. **B**, Pathologic specimen through approximate plane of sonogram shown in Fig. 5A. Cryolesion appears dark compared with adjacent unfrozen liver. Note margin of contact of cryolesion with tumor nodule (*arrows*) and correlation of vessels shown in pathologic specimen (*arrowheads*) with those in sonogram.



6



7

Fig. 6.—Normal unfrozen liver (left) containing a portal tract is separated from frozen and thawed liver (right) by a sharp line of demarcation (*arrowheads*) running through center of photomicrograph. Hepatocytes in affected area show coagulative necrosis. Sinusoids are moderately congested. (H and E, ×10)

Fig. 7.—Tumor separated into unfrozen (left) and frozen and thawed (right) areas by a sharp line of demarcation (*arrowheads*). The difference in histology is more striking here than in the normal liver. (H and E, ×10)

dogs, Dutta et al. [6] showed the feasibility of freezing large volumes of hepatic tissue with no sequelae. Hepatic cryolesions underwent total necrosis, which was followed by inflammatory cell migration in the margins of the lesions. At 6 to 8 weeks after the initial freezing, only fibrotic scars remained. No hepatic abscesses were formed. Gage [5] showed that larger arteries and veins tolerated freezing extremely well without rupture or occlusion, as long as the vessels were not ligated before the freezing. Gage et al. [7] postulated that this would allow freezing of tumors in technically difficult locations, such as those near the confluence of hepatic veins.

Jacob et al. [1] studied the cryodestruction of Walker carcinomas implanted in rat liver and showed significantly increased survival in those rats undergoing cryodestruction of the tumors rather than surgical resection or tumor infarction. Zhou et al. [8] reported the freezing of hepatocellular carcinomas in 35 patients who had tumors that were unresectable by traditional surgical means. Cryosurgery was monitored via thermocouple needles blindly placed into the margins of the tumor, and the freezing was monitored visually from the hepatic surface. There was no surgical mortality and no complications such as bleeding, tumor rupture, bile leakage, or infection. Survival rates were 55.5% for 1 year, 24.3% for 2 years, and 10% for 3 years. By comparison, patients with a similar stage of disease who received chemotherapy had survival rates of 13% for 1 year and 0% for 2 years [8].

There are several problems with monitoring cryosurgery of the liver either visually or via thermocouple needles [9]. Visual monitoring is only possible for surface lesions, and even in that situation the depth of the cryolesion can only be estimated by extrapolating the radius of the ice ball as seen on the surface of the liver. Thermocouples allow accurate assessment of temperature at specific points within the liver, but only a limited number of points can be monitored. Placement of the thermocouples is largely guided by palpation, which can be difficult when lesions have irregular contours and heterogeneous consistency. The deep margins of palpable lesions are often difficult to assess by palpation, and therefore inaccurate placement of the thermocouple probes may be greater for these lesions. Additionally, lesions that are not visible or palpable cannot be monitored or treated by using visual guidance or thermocouple monitoring. Sheu et al. [10] reported on the contribution of intraoperative sonography in 47 operations for hepatocellular carcinoma. In their patients 45% of the tumors smaller than 3 cm and 14.2% of tumors between 3 and 6 cm were not palpable and were identified only at the time of surgery through the use of intraoperative sonography. For these reasons, visual monitoring of hepatic cryosurgery, with or without thermocouple monitoring, is inadequate.

Intraoperative sonography, however, allows excellent visualization of even extremely small lesions deep within the hepatic parenchyma and can be used to guide the cryoprobe to the correct position within the lesion. The freezing can then be monitored as it extends out from the cryoprobe as a hyperechoic rim with posterior acoustic shadowing. The hyperechoic rim can be observed as it extends beyond the tumor margin into normal liver tissue. After thawing, a decrease in echogenicity of the previously frozen normal liver indicates the adequacy of the cryosurgical margin. The cryosurgical margin is particularly easy to discern because the tumor, which does not change in echogenicity after freezing, stands out against the low-echogenicity background of the frozen normal liver. Cryosurgical protocols suggest three freeze-thaw cycles to ensure tumor destruction [11]. In our study, because of time considerations, only one freeze-thaw cycle was completed. There may be changes in tumor echogenicity after more freeze-thaw cycles.

A tissue temperature of at least −50°C is necessary for adequate cryosurgical treatment of malignant disease as measured by needle-mounted thermocouples at the tumor margins [5]. It was thought that temperatures warmer than −50°C would be inadequate for complete tumor destruction. Although the histologic appearance of cryosurgically treated tumors in our series showed definite evidence of necrosis, we cannot conclude that all of the frozen portions of the tumors were totally destroyed because the lesions were resected immediately after freezing. Gage et al. [12] have shown that normal liver is very sensitive to thermal destruction, and our pathologic examinations showed changes consistent with coagulative necrosis of the previously normal liver tissue. Therefore, by freezing both the tumor and a surrounding margin of normal liver, one may attack the neoplastic lesion both directly by freezing and indirectly by depriving the

tumor tissue of its vascular supply from the surrounding frozen liver tissue.

There are several technical difficulties in the performance of hepatic cryosurgery. With a standard right subcostal incision, access to the dome of the liver and extreme lateral aspect of the right lobe is limited. For treatment of lesions in these areas, the liver must be well mobilized, either by taking down the hepatic ligaments (as is done in hepatic transplantation procedures) or by extending the surgical incision into the right side of the chest and incising the right hemidiaphragm, thereby allowing access to the high lateral right lobe and dome. This better exposure of the right lobe allows for greater accuracy in placement of the cryoprobe as well as better sonographic monitoring of the freezing process.

Placement of the cryoprobe in lesions deep within the liver is difficult and requires several manipulations to finally position the cryoprobe correctly. If we consider the size of the cryoprobes, the associated trauma to the liver requires that a better stereotactic technique be developed for probe placement. A biopsy guide, developed for the linear-array transducer, may solve this problem. In addition, visualizing deeper lesions can sometimes be difficult because the 7.5-MHz transducer does not penetrate very deeply. Deep penetration requires that a 5-MHz transducer be used, although it has slightly decreased resolution. Lastly, the greatest limitation is the small freezing volume associated with the cryoprobes presently available. If a larger cryoprobe is used, a greater freezing volume is obtainable. However, with large cryoprobes, the trauma associated with placement becomes unacceptable. The 8-mm cryprobe that we used can freeze a volume of only 3 cm. Therefore, creating larger cryolesions is impossible without several probe placements, which then significantly prolongs the procedure.

In summary, it appears that intraoperative hepatic sonography can provide a satisfactory method for guiding the placement of cryoprobes, monitoring the freezing process itself, and assessing the adequacy of the margins of the cryolesion around the tumor nodule. This may permit more widespread application of cryotherapy in the treatment of selected patients with hepatic neoplastic disease.

REFERENCES

1. Jacob G, Li A, Hobbs K. A comparison of cryodestruction with excision or infarction of an implanted tumor in rat liver. *Cryobiology* **1984**;21:148–156
2. Onik G, Cooper C, Goldberg H, Moss A, Rubinsky B, Christianson N. Ultrasonic characteristics of frozen liver. *Cryobiology* **1984**;21:321–328
3. Onik G, Gilbert J, Hoddick W, et al. Sonographic monitoring of hepatic cryosurgery in an experimental model. *AJR* **1985**; 144:1043–1047
4. Foster JH. Treatment of metastatic cancer to liver. In: DeVita VT Jr, Hellman S, Rosenberg SA, eds. *Cancer: principles and practice of oncology.* Philadelphia: Lippincott, **1982**:1558–1563
5. Gage AA. Current issues in cryosurgery. *Cryobiology* **1982**; 19:219–222
6. Dutta P, Montes M, Gage A. Large volume freezing in experimental hepatic cryosurgery: avoidance of bleeding in hepatic freezing by an improvement in technique. *Cryobiology* **1979**; 16:50–55
7. Gage A, Fazekas G, Riley E. Freezing entry to large blood vessels in dogs. *Surgery* **1967**;615:748–754
8. Zhou X, Tang Z, Yu Y. Cryosurgery for liver cancer: experimental and clinical study. *Chung-Hua Wai Ko Tsa Chih (Chinese J Surg)* **1979**;17:480–483
9. Orpwood J. Biophysical and engineering aspects of cryosurgery. *Phys Med Biol* **1981**;26:555–595
10. Sheu J, Lee C, Sung J, Chen D, Yang P, Lin T. Intraoperative sonography: an indispensable procedure in resection of small hepatocellular carcinomas. *Surgery* **1985**;97:97–103
11. Neel HB III, Ketcham AS, Hammond WG. Cryonecrosis of normal and tumor-bearing rat liver potentiated by inflow occlusion. *Cancer* **1971**;28:1211–1218
12. Gage AM, Montes M, Gage AA. Destruction of hepatic and splenic tissue by freezing and heating. *Cryobiology* **1982**; 19:172–179

Case Report

Mosaic Oligemia Simulating Pulmonary Infiltrates on CT

Kenneth W. Martin,[1] Stuart S. Sagel, and Barry A. Siegel

CT examination of the pulmonary parenchyma is a useful and sensitive diagnostic technique because of its tomographic format and high contrast-sensitivity; the latter is especially important for evaluation of the lung. Blood vessels are a major contributor to lung density, and CT is capable of demonstrating both physiologic and pathologic changes in these structures. Regional alterations in pulmonary blood flow and the accompanying changes in pulmonary blood volume may result in remarkable differences in lung density when the organ is examined on lung window settings. Adjacent areas of hyperperfused and hypoperfused lung may have density differences so great that the former resemble pulmonary infiltrates.

Case Reports

Case 1

A 20-year-old woman with pulmonary hypertension and right ventricular failure due to chronic recurrent pulmonary embolism was admitted for consideration of possible pulmonary embolectomy.

A chest radiograph on admission showed moderate cardiomegaly with enlargement of the right side of the heart and huge central pulmonary arteries. A faint right-middle-lobe opacification was present (Fig. 1).

Pulmonary ventilation scintigraphy with Xe-133 was normal. Perfusion scintigraphy with Tc-99m macroaggregated albumin showed no perfusion of the left lung and right lower lobe and diminished perfusion of the right upper lobe (Fig. 2).

Magnetic resonance imaging (MRI) was performed in an attempt to determine the size and location of thromboemboli before embolectomy. Large thrombi in the central pulmonary arteries were observed (Fig. 3). However, unsuspected hilar lymph node enlargement was queried on the MRI. To resolve this problem, a CT examination was performed. No lymphadenopathy was seen, but there appeared to be scattered pulmonary infiltrates in both lungs (Fig. 4). These apparent infiltrates were of homogeneous density and had sharply

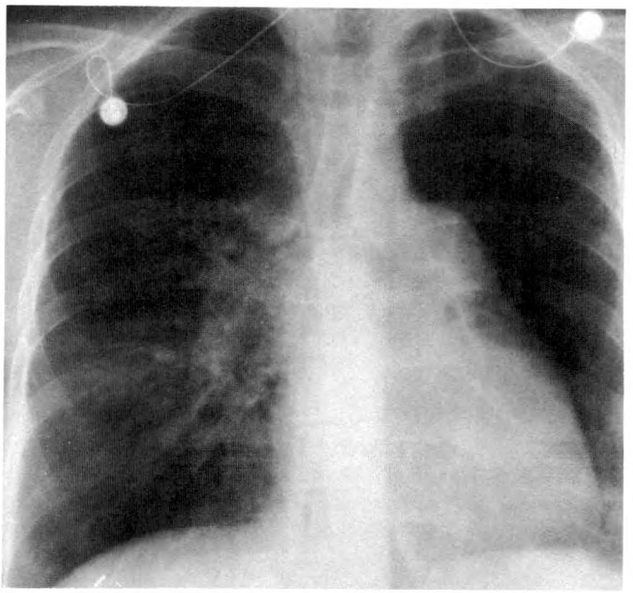


Fig. 1.—Case 1. Posteroanterior chest radiograph shows enlarged central pulmonary arteries and cardiomegaly with slightly increased density inferior to minor fissure.

Received March 3, 1986; accepted after revision May 2, 1986.

[1] All authors: Edward Mallinckrodt Institute of Radiology, Washington University School of Medicine, 510 S. Kingshighway Blvd., St. Louis, MO 63110. Address reprint requests to S. S. Sagel.

AJR **147:670–673, October 1986** 0361–803X/86/1474–0673 © American Roentgen Ray Society

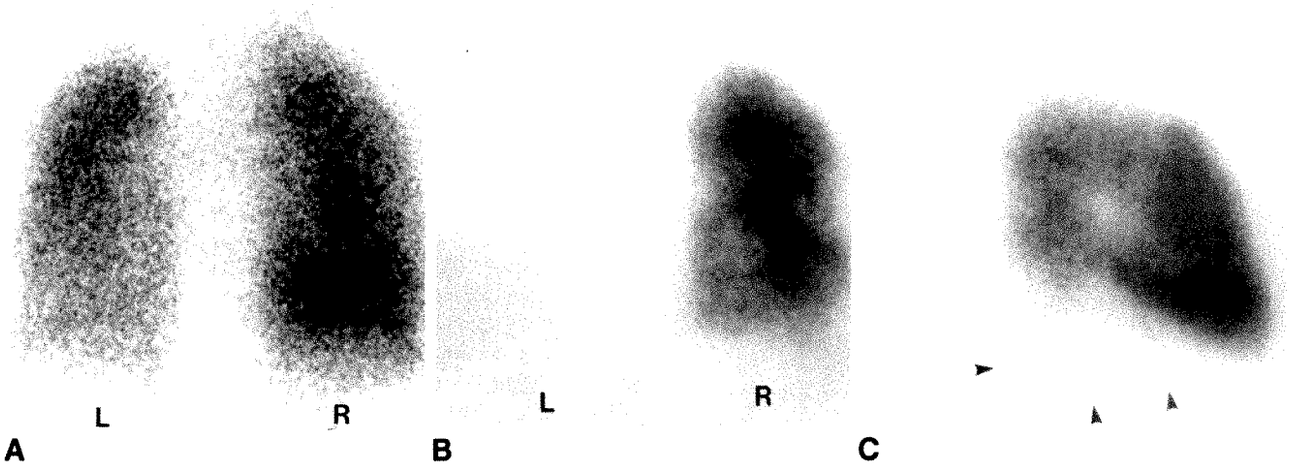


Fig. 2.—Case 1. Ventilation-perfusion lung scintigraphy. **A**, Posterior view of equilibrium phase of Xe-133 ventilation study shows normal ventilation.
B, Posterior view of Tc-99m macroaggregated-albumin perfusion image shows absent perfusion to left lung.
C, Lateral view of right lung shows absent perfusion of right lower lobe (*arrowheads*) and diminished perfusion of right upper lobe.

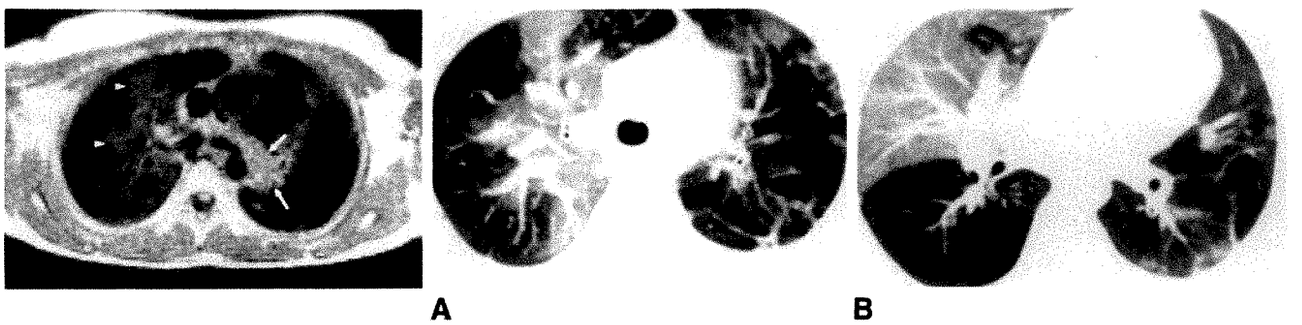


Fig. 3.—Case 1. MRI showed bilateral central pulmonary emboli. T1-weighted SE 500/30 image shows a large thrombus in left pulmonary artery (*arrows*) and a faint increase in signal anteriorly in right upper lobe (*arrowheads*).

Fig. 4.—Case 1. **A**, CT scan with lung window settings shows apparent infiltration of right upper lobe. Diameter of vessels in lucent lung is substantially less than in more opaque areas.
B, A similar "infiltrate" is seen in right middle lobe. Comparison with other studies (Figs. 1–3) shows, however, that it actually represents the only remaining perfused lung and that more lucent zones are oligemic or nonperfused.

defined boundaries with the more lucent adjacent lung. Careful comparison with the perfusion scintigrams showed that these areas of pulmonary infiltration actually represented the only remaining areas of perfused lung.

A pulmonary angiogram, performed via the digital subtraction technique to minimize the dose of contrast medium, corroborated the CT and scintigraphic findings. Pulmonary arterial pressure before administration of contrast medium was 100/45 mm Hg. Enlarged bronchial arterial collaterals supplying the left lung and right lower lobe were seen.

The patient died during embolectomy; the surgical and postmortem findings confirmed the clinical and radiologic diagnosis of massive, chronic pulmonary thromboembolism.

Case 2

A 38-year-old man was admitted for evaluation of atypical chest pain. Eight months before admission tuberculosis had been diagnosed and the patient had been started on antituberculous therapy.

The admission chest radiograph showed biapical linear densities and apical lucency suggestive of bullous disease (Fig. 5). Chest CT examination was performed for evaluation of a possible dissection of the aorta as the cause of the chest pain. The aorta was normal, but the apical and anterior portions of both upper lobes of the lung were relatively lucent, whereas the surrounding pulmonary parenchyma appeared diffusely increased in density (Fig. 6). There was a sharp distinction between dense and lucent lung.

Ventilation-perfusion scintigraphy showed no evidence of obstructive-airways disease or bullous disease on Xe-133 ventilation images. Perfusion to the lung apices was diminished in a nonsegmental pattern that matched the lucency seen on the lung window settings of the CT scans (Fig. 7). No wedge-shaped mismatched defects were present to suggest the diagnosis of pulmonary embolism.

Discussion

Areas of increased pulmonary parenchymal density resulting from hyperperfusion may be misinterpreted as pulmonary

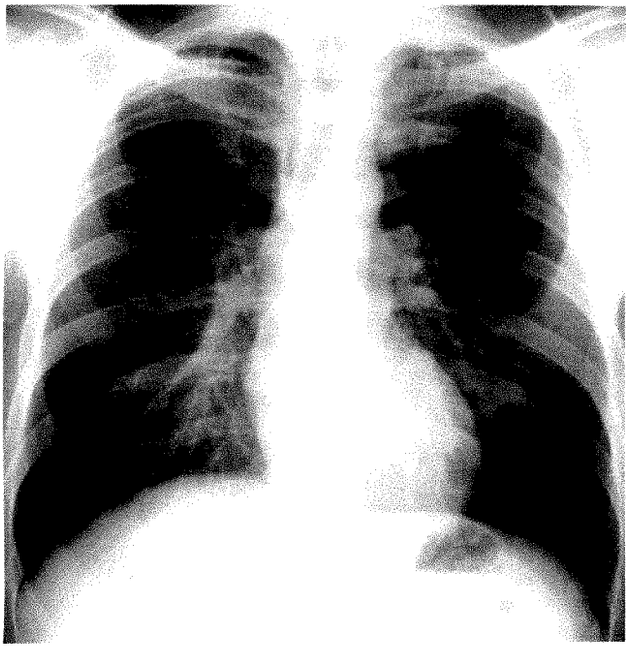


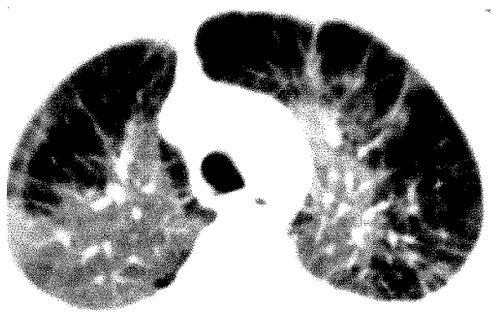
Fig. 5.—Case 2. Posteroanterior chest radiograph shows linear streaks in lung apices with biapical pleural-based thickening and probable apical bullae.

infiltrates on CT. First, there may be no visual standard for "normal" lung density. Ordinarily, the patient's own lung serves as a control. Areas of increased density are usually called infiltrates, whereas the more lucent areas are considered normal except in the presence of obvious bullous or centrilobular emphysema. In the cases presented the relatively lucent lung was the abnormal tissue and initially was used as an inappropriate baseline for comparison. Second, in patients studied with CT parenchymal abnormalities are usually smaller than the remaining normal lung. In Case 1 the entire left lung, right lower lobe, and most of the right upper lobe were diminished in density. Given the increased attenuation values in the relatively confined right middle lobe, the abnormality was mistakenly localized to the smaller area and ascribed to pulmonary infiltration. In fact, the density difference was secondary to altered blood flow and blood volume in both regions, with increased and decreased density caused by hyperperfusion and hypoperfusion, respectively, a phenomenon to which the term *mosaic oligemia* has been applied [1, 2].

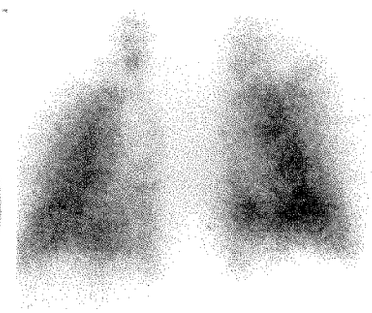
The physiology of mosaic oligemia is relatively simple. When large areas of the pulmonary vascular bed are occluded, there must be a reciprocal increase in blood flow to the remaining patent areas to maintain the cardiac output. Blood in the lung is a major contributor to lung density, and most is in the capillary bed. Alterations in regional blood flow affect lung density by increasing or decreasing blood volume in the capillary bed. Physiologic changes in blood flow secondary to gravitational effects have been well described [3]. In the supine patient the anterior-to-posterior gradient difference may be greater than 200 H. It is reasonable to assume that similar, if not greater, differences would be apparent in cases of mosaic oligemia due to occlusive pulmonary vascular disease.

In Case 1, it is readily apparent after correlating the ventilation-perfusion scintigrams and the pulmonary angiogram with the CT images that the denser areas represent hyperperfused lung. In a recent review of the chest radiographs of 22 patients with chronic pulmonary embolism, mosaic oligemia was found in 68% [2]. The faint right-middle-lobe density seen on the chest radiograph of our patient represents an extreme example of this finding. Pulmonary ischemia without infarction has been studied previously on CT scans of dogs with experimentally induced emboli [4]. On the clinical CT images presented (Fig. 4), oligemia of the left lung, right lower lobe, and right upper lobe is highlighted by the hyperperfused right middle lobe. The absolute density of this oligemic lung may not be as low as in instances of acute vascular occlusion because of the presence of extensive bronchial collaterals, which were demonstrated by pulmonary angiography.

We believe Case 2 represents an example of vasculitis associated with tuberculosis [5, 6]. The chest radiograph may return to normal in treated tuberculosis in spite of severe regional vascular disease. Associated occlusive vascular disease may be demonstrated by both perfusion scintigraphy and pulmonary angiography. Vasoconstriction may be important because, in some instances, pulmonary arteries not perfused in the body are shown to be patent in the resected lungs of patients with tuberculosis. Thus, in a manner similar to that due to embolism, other types of regional occlusive



6



7

Fig. 6.—Case 2. CT scan with lung window settings shows regional areas of increased and decreased density. Lucent areas are shown in Fig. 7 to correspond to nonperfused lung on pulmonary scintigraphy, indicating oligemia as cause for density difference.

Fig. 7.—Case 2. Pulmonary scintigraphy. Xe-133 ventilation images were normal. Tc-99m macroaggregated-albumin perfusion study shows diminished or absent perfusion laterally in both lung apices corresponding to areas of lucency seen on the CT scan (Fig. 6).

vascular disease can cause mosaic oligemia. CT examination of the patient in Case 2 showed regional areas of increased density surrounded by relatively lucent lung. The scintigraphic study revealed no evidence of ventilatory abnormality to explain the lucency on the CT scans. Bullous disease or focal emphysema is therefore unlikely. There was, however, a significant perfusion deficit in a distribution matching the CT abnormality. Oligemia of the lung apices secondary to pulmonary arteritis induced by tuberculosis with reciprocal hyperperfusion undoubtedly accounts for the CT appearance.

REFERENCES

1. Genereux GP. CT of acute and chronic distal air space (alveolar) disease. *Semin Roentgenol* **1984**;19:211–221
2. Woodruff WW III, Hoeck BE, Chitwood WR, Lyerly HK, Sabiston DC Jr, Chen JTT. Radiographic findings in pulmonary hypertension from unresolved embolism. *AJR* **1985**;144:681–686
3. Rosenblum LJ, Mauceri RA, Wellenstein DE, et al. Density patterns in the normal lung as determined by computed tomography. *Radiology* **1980**;137:409–416
4. Ovenfors C-O, Godwin JD, Brito AC. Diagnosis of peripheral pulmonary emboli by computed tomography in the living dog. *Radiology* **1981**;141:519–523
5. Thomas HM III. The effect of tuberculosis on the distribution of pulmonary blood flow and ventilation. *Clin Nucl Med* **1978**; 3:243–244
6. Ramos M, Baumann HR, Muhlberger F. Perfusion and ventilation imaging in pulmonary tuberculosis. *Clin Nucl Med* **1978**;3:233–242

Pictorial Essay

Thoracic Venous Anatomy

J. David Godwin[1, 2] and James T. T. Chen[1]

Chest radiography is essential to evaluate the placement of IV pressure-monitoring catheters or pacing wires, because none of the indirect techniques (such as measuring the pressure, observing pulsation, or obtaining the return of blood in the catheter) is accurate.

Usually, the desired position of the catheter tip is the subclavian vein, the brachiocephalic vein, or the superior vena cava [1, 2]. Malposition occurs in about one-third of insertions. It is essential to determine, that the catheter is actually in a vein (rather than in an artery or free in the mediastinum or pleural space); that it is in a vein with sufficient flow to tolerate infusion; and, if the catheter is for central venous pressure measurements, that it is proximal to any competent valve. In assessing the position of a pacing wire intended for the right ventricle, it is important to determine that the electrode is in the ventricular apex rather than in a cardiac vein or the pericardial space.

A knowledge of normal and anomalous venous anatomy is required to identify the locations of venous catheters on chest radiographs. This paper reviews the anatomy of the thoracic veins as determined by catheter positions on radiographs.

Normal Veins

Subclavian, Jugular, and Vertebral Veins

The subclavian vein (Figs. 1 and 2) is the continuation of the axillary vein and arises at the outer margin of the first rib [3]. It passes along the inner surface of the clavicle and drains the arms, shoulders, and part of the anterior thoracic wall to the brachiocephalic vein. The most proximal valve is near the venous angle, where the subclavian and jugular veins join to form the brachiocephalic vein.

The internal jugular vein (Fig. 3) drains the brain and parts of the face and neck. A pair of valves is located about 2.5 cm above the termination of the vessel. Despite these valves, the jugular vein is the most common location of a malpositioned catheter entering from the subclavian vein [2]. The jugular is not an appropriate vein for infusion because of the risks of thrombosis, erosion of the vessel because of torque on the catheter, and pooling of infused solutions near the brain in a supine patient [1].

The vertebral vein (Fig. 4) drains the upper cervical spine and neck and descends in the transverse foramina of the cervical vertebrae to the dorsal aspect of the origin of the brachiocephalic vein. A pair of valves is located near its opening. Because of the small size of the vertebral vein, catheters rarely extend into it.

Brachiocephalic (Innominate) Vein and Superior Vena Cava

The brachiocephalic vein (Fig. 5) is formed by the junction of the internal jugular and subclavian veins behind the sternoclavicular joint. The left brachiocephalic vein passes obliquely downward, and the right passes steeply downward behind the manubrium. They join to form the superior vena cava. The left vein is longer than the right; neither has a valve.

On lateral view, the proximal parts of the subclavian vein and the distal parts of the brachiocephalic vein contribute to the retromanubrial opacity that has been termed the anterior

Received December 20, 1985; accepted after revision April 17, 1986.
[1] Department of Radiology, Duke University Medical Center, Durham, NC 27710.
[2] Present address: Department of Radiology, SB-05, University of Washington, Seattle, WA 98195. Address reprint requests to J. D. Godwin.

AJR 147:674–684, October 1986 0361–803X/86/1474–0674 © American Roentgen Ray Society

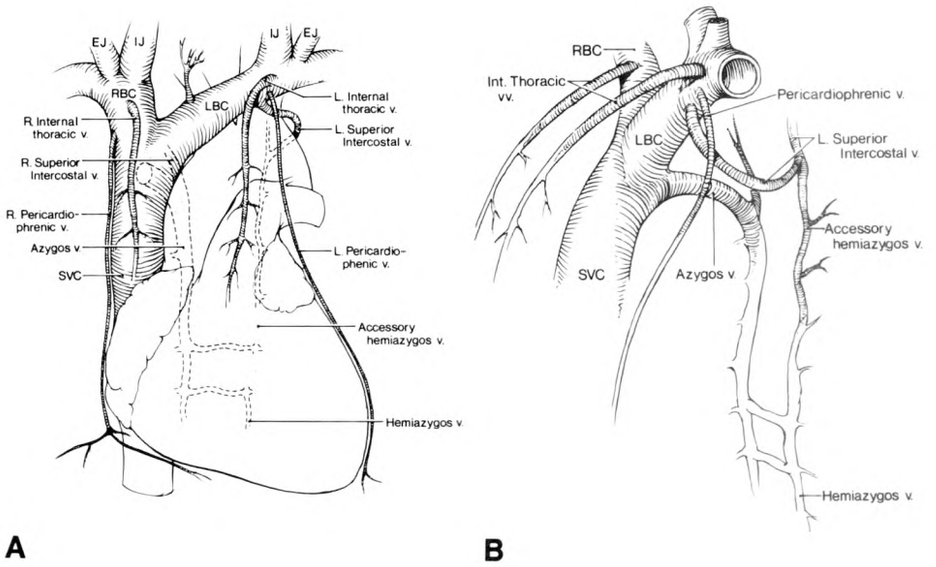


Fig. 1.—Thoracic veins. **A**, Frontal view. **B**, Left lateral view. Right internal thoracic vein terminates more proximally on its bachiocephalic vein than does the left. Left pericardiophrenic vein terminates on left brachiocephalic vein; it may also terminate on internal thoracic or superior intercostal vein. SVC = superior vena cava; RBC = right brachiocephalic vein; LBC = left brachiocephalic vein; EJ = external jugular vein; IJ = internal jugular vein.

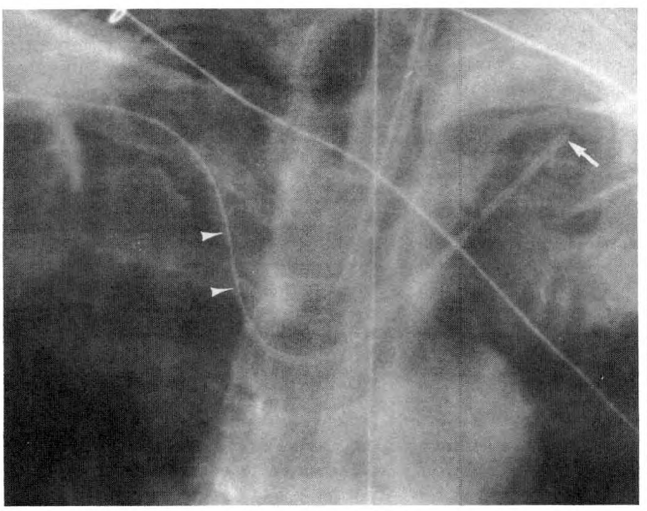


Fig. 2.—Subclavian and brachiocephalic veins. Catheter inserted in right arm vein dips across midline and crosses from right brachiocephalic vein into left brachiocephalic vein. Tip (*arrow*) is distal to sternoclavicular joint and is therefore in left subclavian vein. Because of steeper downward slope of right brachiocephalic vein (*arrowheads*) compared with the left, a catheter inserted on the right is more likely to continue down superior vena cava and not cross into the opposite brachiocephalic vein than is one inserted on the left.

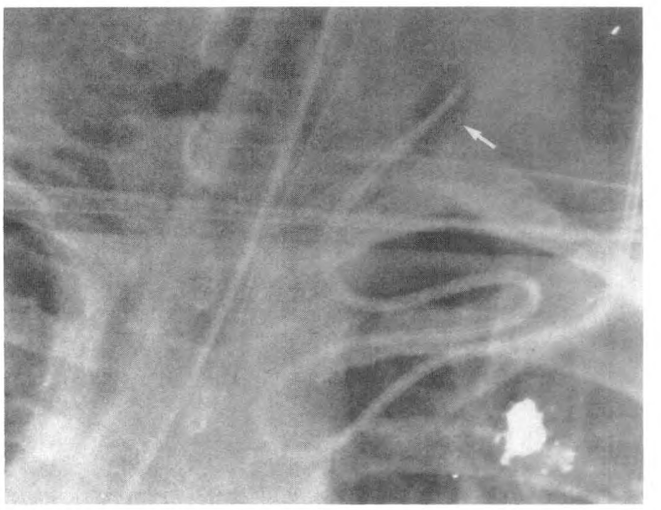


Fig. 3.—Left internal jugular vein. Swan-Ganz catheter inserted into left subclavian vein extends into left jugular vein. Note inflated balloon (*arrow*) at catheter tip. Bullet fragment in left thoracic apex.

extrapleural line [4]. Since the posterior margin of this opacity is defined by lung, the opacity must arise to the right or left of the midline. CT often shows a corresponding indentation of both the right and left lungs by the subclavian and brachiocephalic veins near their junction. However, CT also shows that the main sweep of left brachiocephalic vein, where it arcs anteriorly and downward across the mediastinum, does not contribute to the posteriorly marginated retrosternal opacity because, where it crosses the mediastinum, the brachiocephalic vein has no lung behind it that could create a visible margin.

On lateral view of the chest, the anterior arc of a catheter in the left brachiocephalic vein is often below the anterior extrapleural line. A catheter in the right brachiocephalic vein, however, descends obliquely but straight downward without an anterior arc (see Fig. 15). Lack of an arc on a catheter inserted on the left suggests that the catheter is extravascular [5].

Rather than descend into the superior vena cava, a catheter may cross the midline from one brachiocephalic vein into the other, typically with a dip at the junction of the two veins. This occurrence is less likely when the catheter is inserted on

the right because the steep descent of the right brachiocephalic vein aligns the catheter to pass directly into the vena cava.

The superior vena cava drains blood from the upper half of the body. It is formed by the junction of the brachiocephalic veins behind the first intercostal space just to the right of midline behind the sternum, and it receives the azygos vein. Its lower half is within the fibrous pericardium. It has no valves.

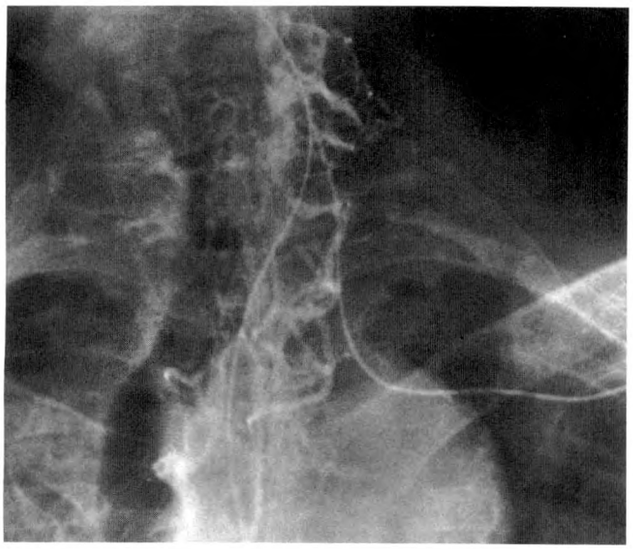


Fig. 4.—Vertebral vein and vertebral venous plexus. Injection of catheter inserted via left subclavian vein opacifies the external and internal vertebral plexus via the vertebral vein.

Internal Thoracic Vein

The internal thoracic (mammary) vein (Figs. 6 and 7) receives the anterior intercostal veins and some abdominal branches (including the inferior epigastric vein) and travels along the border of the sternum just medial to the internal thoracic artery to drain into the brachiocephalic vein. The insertion of the right internal thoracic vein is often more proximal on the brachiocephalic vein than is the insertion of the left on its brachiocephalic vein. The vein has multiple valves.

Because the orifice of the right internal thoracic vein is often close to the origin of the superior vena cava, it can be entered by a catheter coming from either brachiocephalic vein. Conversely, because the orifice of the left thoracic vein is more remote from the right-sided veins, it can be entered only by a catheter coming from the left brachiocephalic vein.

Pericardiophrenic Vein

The pericardiophrenic (pericardiacophrenic, lateral mediastinal-phrenic) vein (Fig. 8) drains the pericardium, pleura, and diaphragm. Small and either single or multiple, it ascends along the phrenic nerve between the mediastinal pleura and the pericardium to drain either into the internal thoracic vein or the left superior intercostal vein, or directly into the left brachiocephalic vein opposite the orifice of the left jugular vein [3, 6]. Its diaphragmatic branches anastomose with those

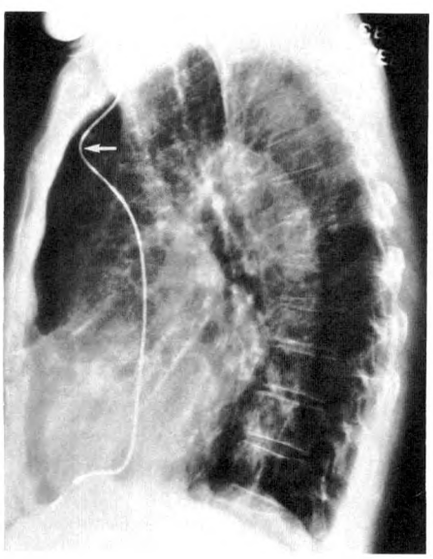
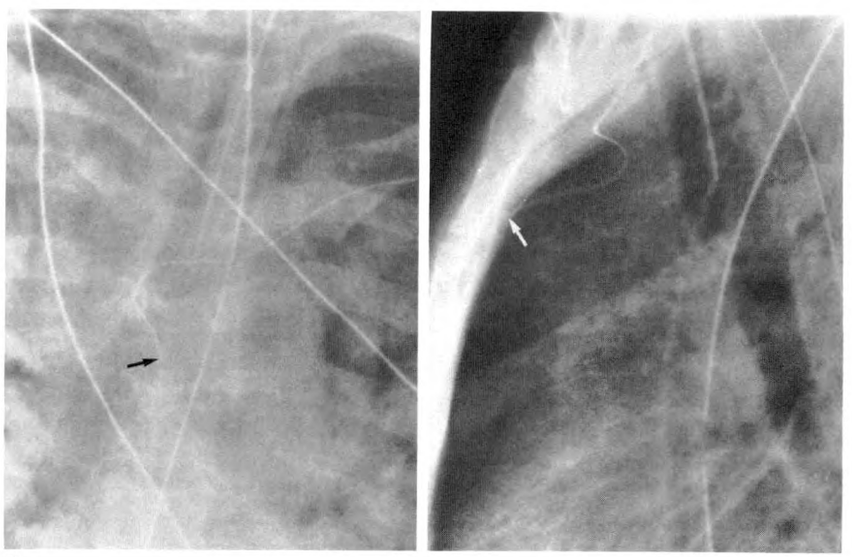


Fig. 5.—Left brachiocephalic vein. Lateral radiograph shows typical anterior bend (*arrow*) of wire where left brachiocephalic vein crosses mediastinum from left to right.



A B

Fig. 6.—Right internal thoracic vein. Catheter inserted in left subclavian vein enters right internal thoracic vein. Tip (*arrow*) is medial to superior vena cava on frontal view (**A**) and anterior to it on lateral view (**B**). A catheter in thymic vein could have same course.

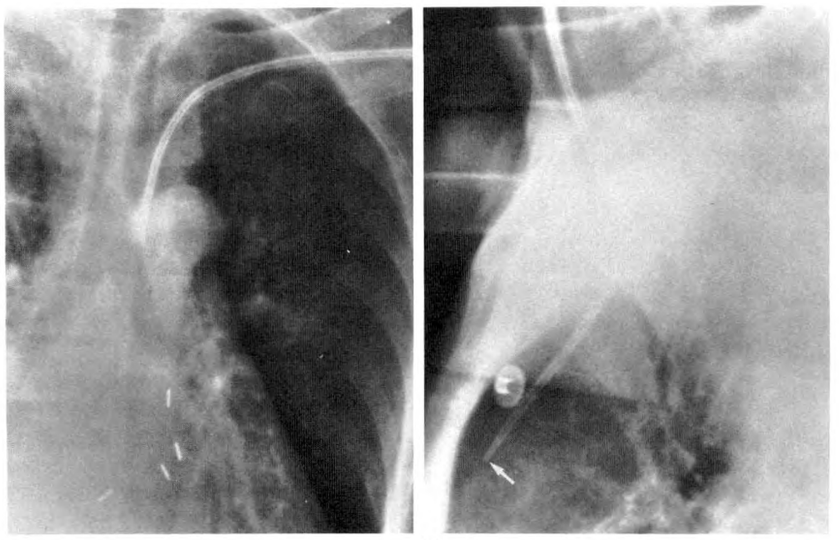


Fig. 7.—Left internal thoracic vein. Anteroposterior (**A**) and lateral (**B**) radiographs. Catheter tip (*arrow*) is more medial and anterior than if it were in superior vena cava, or pericardiophrenic vein, or left superior vena cava. Thymic vein could also account for this catheter position.

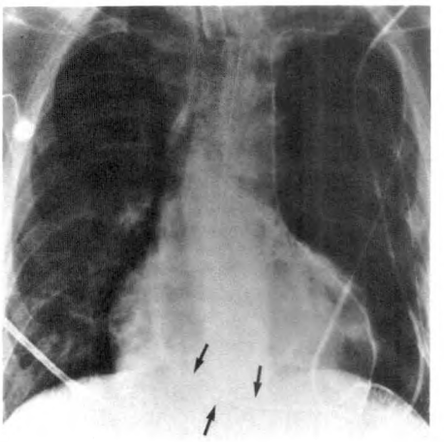


Fig. 8.—Left pericardiophrenic vein. Catheter inserted into left subclavian vein follows left superior mediastinal border then curves laterally along left heart border. Injection of contrast material opacifies distal part of vein and its connections to inferior phrenic vein (retouched) under hemidiaphragm. The lateral swing of catheter along heart border distinguishes pericardiophrenic vein from left superior vena cava, which curves medially near left atrium. A catheter in internal thoracic vein has a straighter downward course and does not swing laterally near heart border. On lateral view (not shown), a catheter in internal thoracic vein is more anterior than one in pericardiophrenic vein, and a catheter in a persistent left superior vena cava is more posterior.

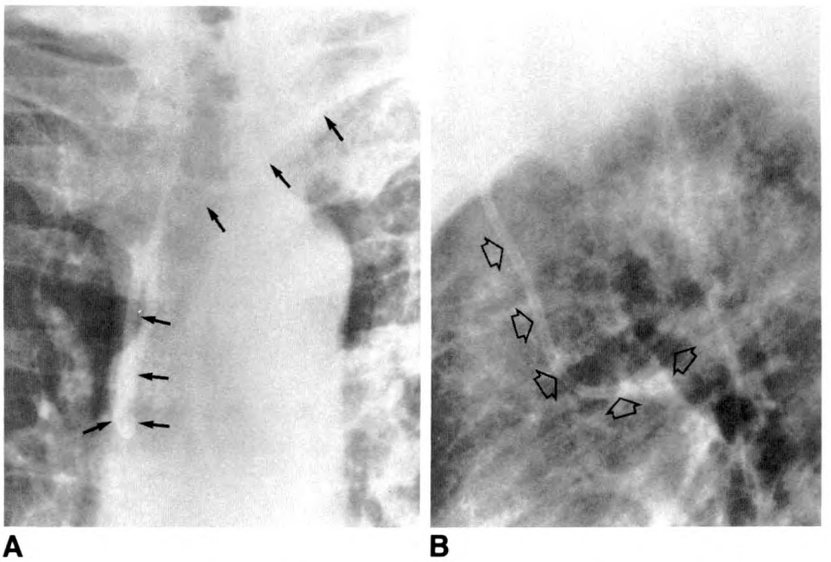


Fig. 9.—Azygos vein. On frontal view (**A**), a catheter (*arrows*) entering azygos arch is often projected over superior vena cava. Catheter may arc upward and slightly laterally before turning downward and medially [14]. On lateral view (**B**), catheter (*arrows*) extends posteriorly from superior vena cava with an upward convexity, then parallels spine downward toward diaphragm.

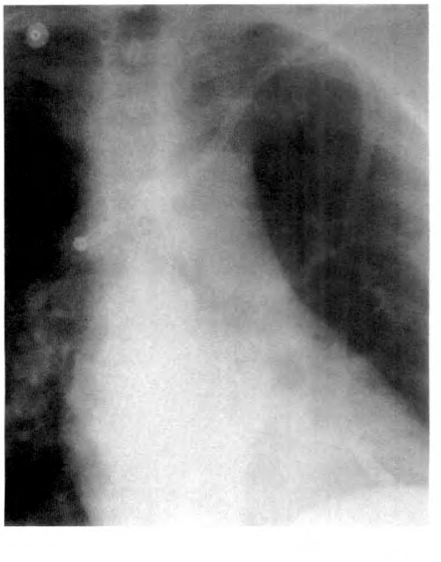


Fig. 10.—Azygos vein. Anteroposterior view. Double lumen catheter entering azygos vein is projected end-on in azygos arch.

of the inferior phrenic vein, which drains to the inferior vena cava or left renal vein. It may serve as a collateral pathway in superior vena caval obstruction [7]. Inadvertent catheterization of the left pericardiophrenic vein is rare [7–10] and usually occurs when the catheter has been inserted into the jugular vein. The pericardiophrenic vein is not a suitable location for a catheter because the vein is small and moves with transmitted cardiac motion. Thrombosis, erosion, and perforation are all risks. Larsen and Rieke [10] suggest that hemopericardium could result from perforation, but that would require rupturing a branch within the fibrous pericardium.

Azygos Vein

The azygos vein (Figs. 9 and 10) is the continuation of the right ascending lumbar vein. It enters the thorax either through the aortic hiatus or behind or through the right crus of the diaphragm. Passing along the right anterior surface of the spine, it receives the lower right posterior intercostal veins, the hemiazygos vein at the level of the eighth thoracic vertebra, and the accessory hemiazygos vein at the seventh thoracic vertebra. About the fourth vertebra, it arcs anteriorly and to the right, passing over the right upper lobe bronchus and truncus anterior of the right pulmonary artery to drain into the posterior surface of the superior vena cava just above the cava's entry into the pericardium [11–13]. The posterior part of the arch receives the right superior intercostal vein, which is a common trunk draining the right second, third, and fourth posterior intercostal veins. There are usually one to four incomplete valves in the azygos arch [12]. Because the azygos vein, along with the ascending lumbar veins and their tributaries, connects the superior and inferior vena cava, the azygos vein functions as an important collateral pathway in cases of superior or inferior vena caval obstruction. The azygos vein is also the route for venous return from the lower half of the body in cases of congenital interruption of the inferior vena cava (azygos continuation). Depending on the site of caval obstruction, blood flow in the azygos vein can be craniad or caudad.

Left Superior Intercostal, Hemiazygos, and Accessory Hemiazygos Veins

The left superior intercostal vein (Figs. 11 and 12) forms an arch on the left side of the mediastinum that is analogous to the azygos arch on the right. This vein drains the second, third, and fourth posterior intercostal veins, then passes forward and upward along the aortic arch to drain into the left brachiocephalic vein near the venous angle. About 75% of the time the vein connects to the accessory hemiazygos vein [15, 16].

On a frontal radiograph, the left superior intercostal vein is

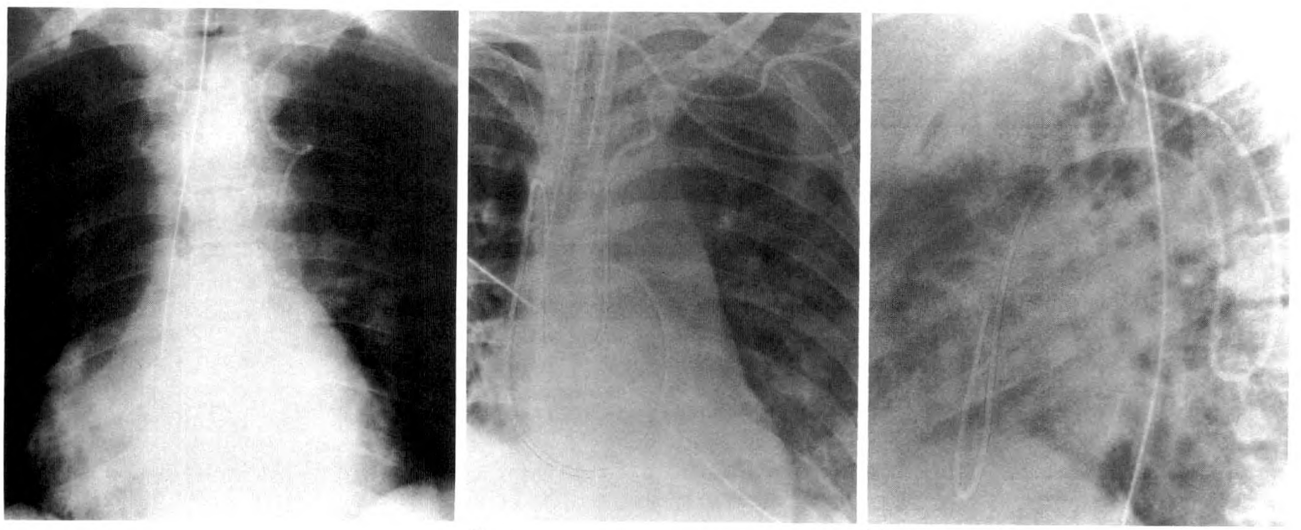


Fig. 11.—Left superior intercostal vein. Catheter inserted in left subclavian vein arcs laterally along aortic arch in superior intercostal vein. A short downward course is consistent with location in posterior part of vein, but longer downward course here indicates entry into accessory hemiazygos vein. The course of a catheter in superior intercostal vein is distinguishable from that of a catheter in a persistent left superior vena cava or in a pericardiophrenic vein because the latter two descend along left side of mediastinum without arcing laterally along aortic arch.

Fig. 12.—Left superior intercostal, accessory hemiazygos, azygos veins, and superior vena cava. **A**, Posteroanterior radiograph. **B**, Lateral radiograph. Catheter (retouched) inserted into left subclavian vein has shallow lateral and posterior curve in superior intercostal vein just above aortic arch, then descends medially in accessory hemiazygos vein, crosses posterior mediastinum behind descending aorta to ascend in azygos vein, and arches forward to superior vena cava, in which it descends to right atrium. Tip is in pulmonary artery on posteroanterior view and in right ventricle on lateral view. (courtesy of M. M. Figley)

sometimes visible as a discrete bulge, called the aortic nipple [17, 18], along the aortic arch. Most often the nipple projects laterally off the aortic arch, but it may be located just above the arch or just below it.

The hemiazygos vein (Fig. 1) is the continuation of the left ascending lumbar vein and usually connects to the left renal vein as well [13]. It enters the thorax through the left crus or the aortic hiatus, just posterior to and to the left of the descending aorta. It receives the lower left posterior intercostal veins and ascends on the left anterior surface of the spine to the eighth or ninth thoracic vertebra, where it crosses to the right behind the aorta to drain into the azygos vein. It often connects with the accessory hemiazygos vein above.

The accessory hemiazygos vein (Figs. 11 and 12) drains the fifth through eighth left posterior intercostal veins. It usually crosses to the right over the seventh thoracic vertebra to drain into the azygos vein, or it may drain to the hemiazygos vein or to both.

Cardiac Veins

The cardiac veins can be entered intentionally (for investigation of an arrhythmia or for atrial pacing via the coronary sinus) or inadvertently with a catheter or pacing wire intended for the right ventricular apex [19]. The coronary sinus drains most of the cardiac veins. Located in the posterior part of the atrioventricular groove [3], it is 2–3 cm long and terminates in the right atrium near the inferior vena cava.

The continuation of the coronary sinus in the posterior atrioventricular groove is the great cardiac vein (Figs. 13 and 14), which originates alongside the left anterior descending coronary artery in the anterior interventricular groove. The small cardiac vein runs in the anterior atrioventricular groove, and the middle cardiac vein (Fig. 15) runs in the posterior interventricular groove from the apex to join the coronary sinus. The oblique vein (of Marshall) of the left atrium descends on the back of the left atrium and is part of the drainage of a persistent left superior vena cava. The coronary sinus and all the cardiac veins have valves at their orifices.

Because the middle cardiac vein travels on the surface of the heart, a catheter in it may be confused for one that has perforated the heart and entered the pericardial space. Fluoroscopy may be required with special attention to the motion of the pacer tip and to the relationship of the cable to the pericardium and subepicardial fat [19].

A catheter or pacing wire entering a persistent left superior vena cava enters the oblique vein and coronary sinus in almost all cases.

Other Veins

Occasionally an IV catheter lodges in a right superior intercostal vein [20], a thymic vein arising from the left brachiocephalic vein [6], or an inferior thyroid vein arising from the right or left brachiocephalic vein [20]. A catheter may pass through the right atrium from above to enter the inferior vena cava or a hepatic vein.

Anomalous Veins

Persistent Left Superior Vena Cava

Persistent left superior vena cava (Figs. 13, 16–18) is the most common variant of systemic venous drainage. It occurs

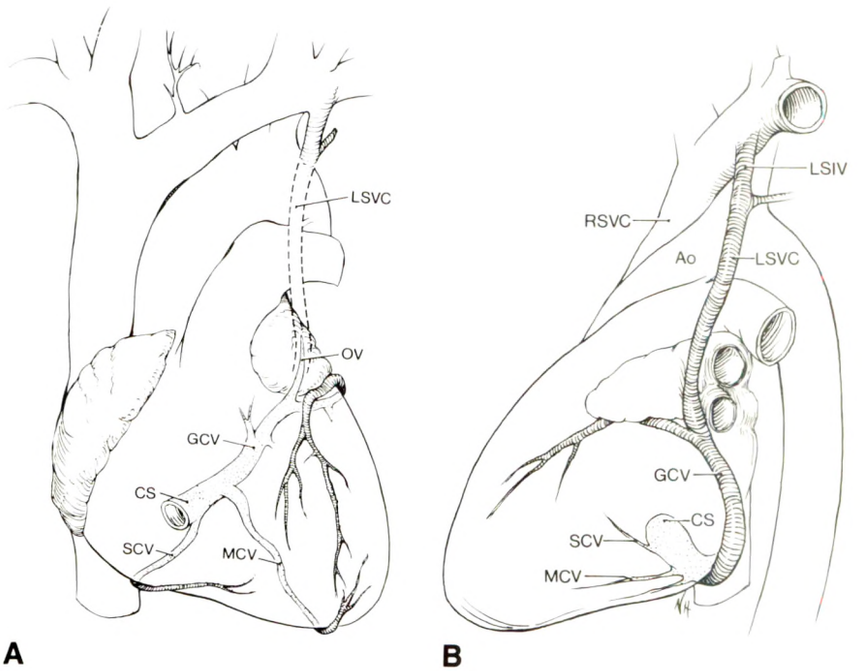


Fig. 13.—Cardiac veins and left superior vena cava. Course of anomalous persistent left superior vena cava (LSVC) and relationship to the oblique vein of left atrium (OV) are indicated by dashed lines in frontal view (**A**) and by solid lines in lateral view (**B**). CS = coronary sinus; GCV = great cardiac vein; SCV = small cardiac vein; MCV = middle cardiac vein; Ao = aorta; RSVC = right superior vena cava; LSIV = left superior intercostal vein.

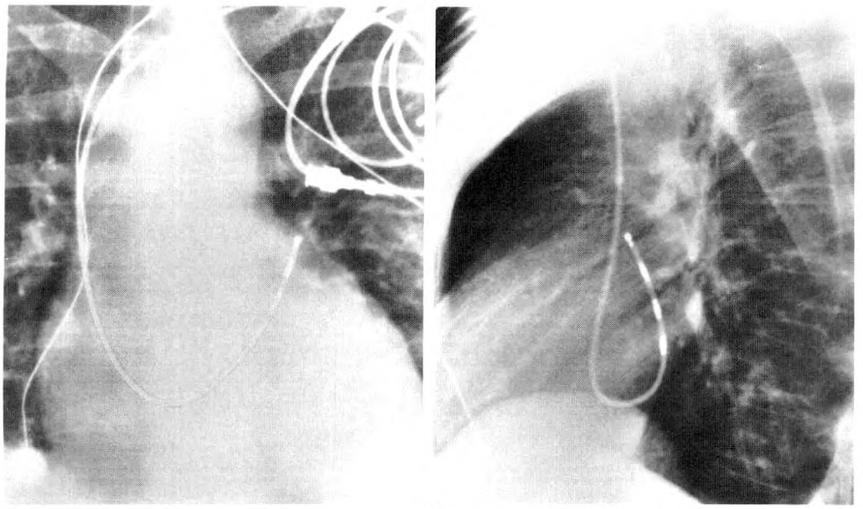


Fig. 14.—Coronary sinus and great cardiac vein pacing wire. **A**, Frontal radiograph shows pacing wire (retouched) arcing upward. Its course could be mistaken for location in right ventricle and pulmonary artery. **B**, Lateral radiograph shows posterior position of wire, following posterior atrioventricular groove, excluding location in right ventricle and pulmonary artery. Occasionally, a wire extends into a branch of great cardiac vein.

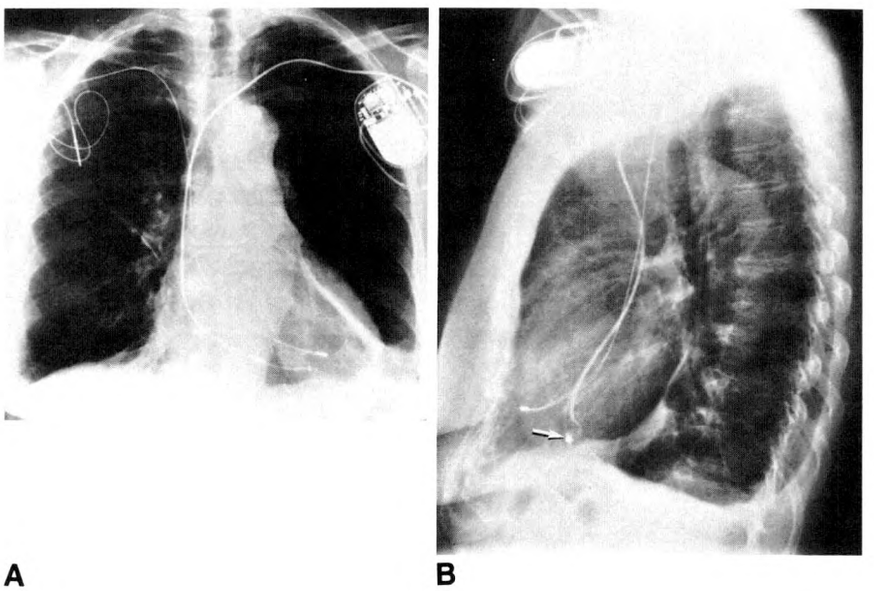


Fig. 15.—Middle cardiac vein. **A**, Posteroanterior radiograph. **B**, Lateral radiograph. Pacing wire entering middle cardiac vein resembles one in right ventricle, but its curve is slightly lower and its tip may extend more distally toward cardiac apex. On lateral view, it has a farther posterior location of electrode (*arrow*), projecting roughly over middle of heart. Note anterior arc of pacing cable in left brachiocephalic vein vs straight course of wire in right brachiocephalic vein high in mediastinum in **B**. (Compare with Fig. 3.)

in 0.3% of persons with otherwise normal hearts and in 4.3% of patients with congenital heart disease [21]. It results from failure of parts of the left anterior and common cardinal veins to regress. The vein drains the left subclavian and jugular veins to the coronary sinus via the oblique vein of the left atrium. The left superior intercostal vein becomes a tributary of the left superior vena cava, analogous to the azygos arch on the right. When the drainage is to the coronary sinus (as it is in almost all cases), there are no important hemodynamic effects. However, there may be an increased risk of arrhythmia during cardiac catheterization via the anomalous vein [22]. Further, cardiopulmonary bypass for open-heart surgery may have to be modified.

In all but about 18% of cases, a right superior vena cava is also present, although it may be smaller than usual. When it is not present, the incidence of congenital heart disease increases; atrial septal defect is most common [21]. Rarely, the drainage of the left superior vena cava is not into the coronary sinus, but instead into the left atrium. In these cases as well, the incidence of congenital disease increases [21].

In about 40% of cases, the left brachiocephalic vein connecting the two vena cavae is absent [23]. When present, this vein may be smaller than usual and its course may be more horizontal. In most cases, the left superior vena is visible as a vertical contour along the upper left mediastinal border [22, 23].

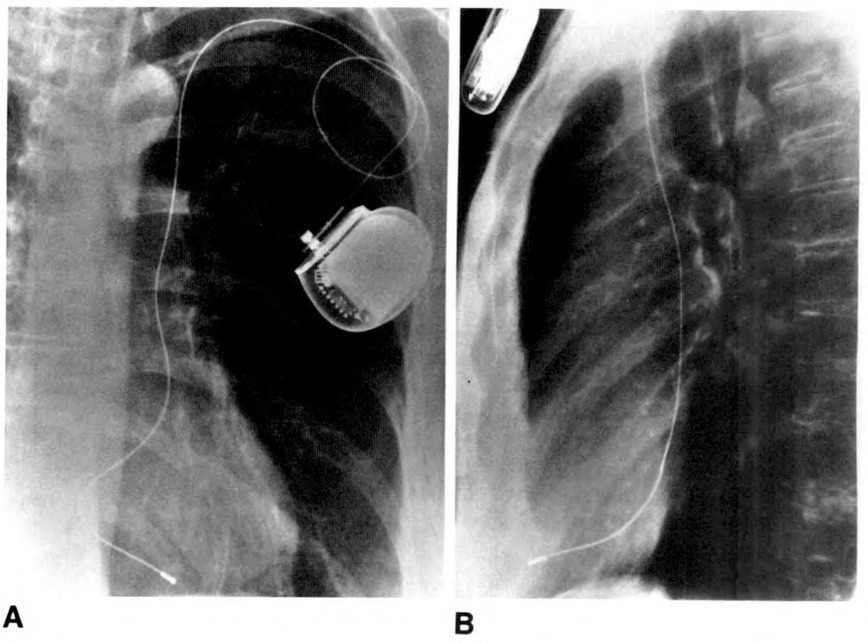


Fig. 16.—Persistent left superior vena cava. Posteroanterior (**A**) and lateral (**B**) radiographs show pacing wire inserted in left subclavian vein entering persistent left superior vena cava and descending along left border of superior mediastinum. Catheterization of vein is more likely if catheter is inserted on the left. Catheter delineates vein as it descends lateral to arch and in front of pulmonary hilum toward posterior surface of heart, where it enters coronary sinus via oblique vein of left atrium and arcs anteriorly to enter right atrium near insertion of inferior vena cava. Electrode is in right ventricular apex. Faint shadow of left superior vena cava is visible lateral to aortic arch in (**A**). Posterior swing of wire on lateral view distinguishes course of left superior vena cava from that of the right.

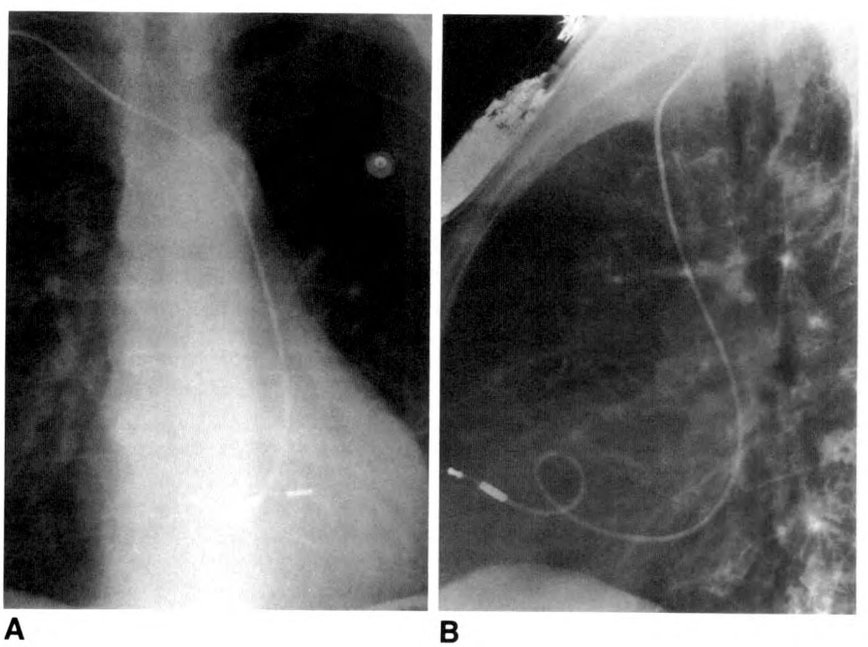


Fig. 17.—Persistent left superior vena cava with absence of right superior vena cava. Posteroanterior (**A**) and lateral (**B**) radiographs. Pacing wire crosses mediastinum in right brachiocephalic vein (note anterior arc in superior mediastinum in **B**) and then descends to posterior surface of heart in left superior vena cava draining via oblique vein to coronary sinus. Electrode is in right ventricular apex. CT scan (not shown) confirmed absence of right superior vena cava.

Partial Anomalous Pulmonary Venous Connection

Although total anomalous pulmonary venous connection is such a severe derangement that it is diagnosed in infancy, partial anomalous pulmonary venous connection (Figs. 19 and 20) may be undetected until the patient is an adult. Usually 50% or more of the lung must be drained anomalously for the patient to be symptomatic [24]. The lesion causes a left-to-right shunt. Atrial septal defect is frequently present, especially when the anomalous drainage is from the right upper lobe to the superior vena cava [25].

The embryology is complex. Briefly, anomalous drainage arises from failure of the developing pulmonary veins to establish normal connections with the heart and subsequent persistence of primitive splanchnic venous connections of the lung [24].

The right lung is involved twice as often as the left, and upper lobes are involved more frequently than lower. The

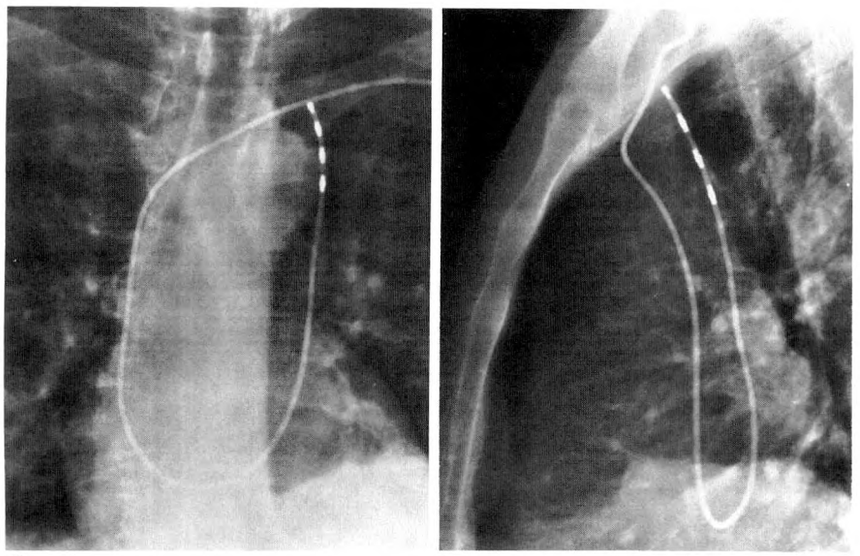


Fig. 18.—Persistent left superior vena cava. Posteroanterior (**A**) and lateral (**B**) radiographs. Pacing wire intended for coronary sinus crosses mediastinum in left brachiocephalic vein to right superior vena cava then enters coronary sinus and extends upward to left brachiocephalic vein via persistent left superior vena cava. Lateral view (**B**) shows posterior position of left superior vena cava compared with the right. Reproduced by permission of Hewitt et al. [19].

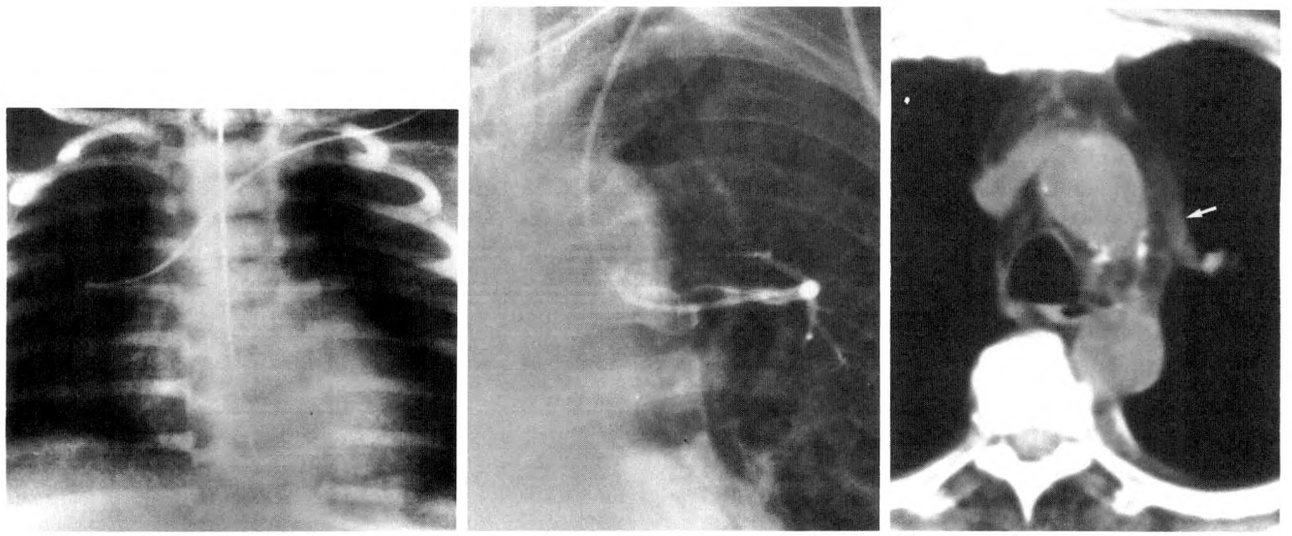


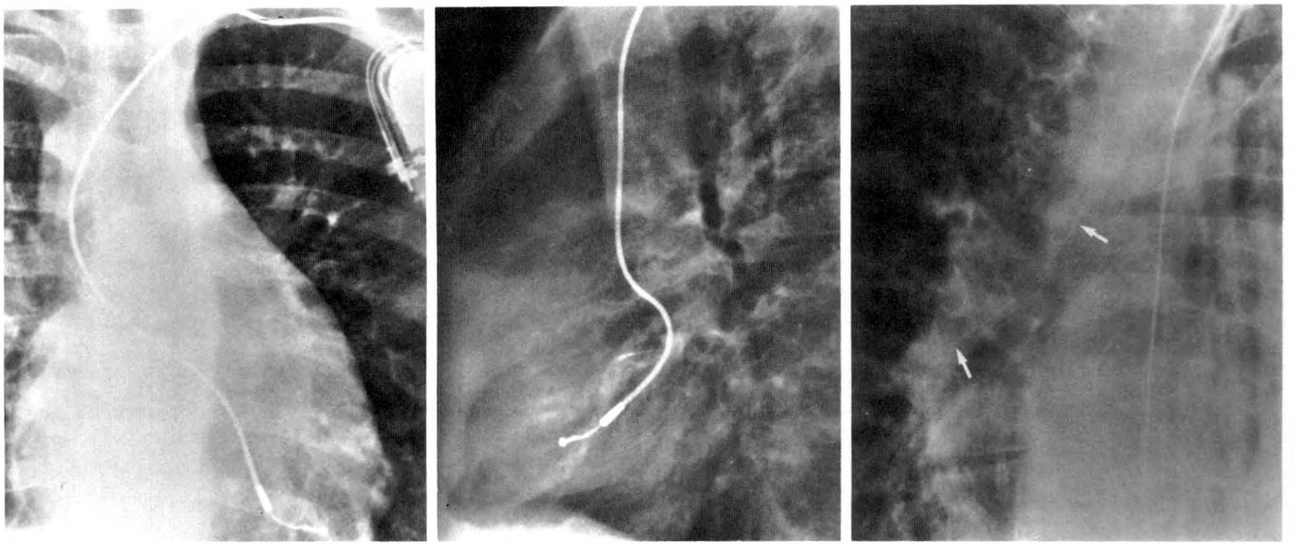
Fig. 19.—Partial anomalous pulmonary venous connection from right upper lobe. Anteroposterior radiograph. Catheter enters anomalous pulmonary vein draining into superior vena cava.

Fig. 20.—Partial anomalous pulmonary venous connection. **A**, Anteroposterior radiograph. Catheter extends via vertical vein along left mediastinal border into anomalously draining left pulmonary vein, into which contrast media has been injected. A CT scan (**B**) confirmed left vertical vein (*arrow*) draining to left brachiocephalic vein.

usual sites of termination of the anomalous vein are, in decreasing frequency, the superior vena cava, right atrium, left brachiocephalic vein (via a vertical vein), coronary sinus, and the azygos vein. Less common are the portal vein, ductus venosus, inferior vena cava, and left subclavian vein [24]. The left vertical vein is a remnant of the anterior cardinal vein. It drains to the left brachiocephalic vein as does the left superior intercostal vein, which is in roughly the same location.

Radiographic findings of partial anomalous pulmonary venous connection are (1) increased pulmonary blood flow caused by the left-to-right shunt and resembling atrial septal defect, and (2) the anomalous course of the pulmonary vein within the lung [26].

A catheter entering an anomalous pulmonary vein may appear to be extravascular and to have perforated the lung. False diagnosis of anomalous pulmonary venous connection



A B

Fig. 21.—Mustard procedure [27] for treatment of complete transposition of the great arteries. Pericardial baffle installed in atrium so that systemic venous blood is directed into left ventricle. Posteroanterior (**A**) and lateral (**B**) radiographs. Pacing wire descends from superior vena cava across right atrium into left ventricle via surgically created baffle.

Fig. 22.—Glenn procedure [28] for treatment of severe right ventricular outflow obstruction. Superior vena cava is separated from right atrium and anastomosed to right pulmonary artery. IV catheter (*arrows*) descends from superior vena cava into interlobar right pulmonary artery along bronchus intermedius.

can occur when a catheter crosses an atrial septal defect or patent foramen ovale from the right atrium into the left atrium and then extends into a normal pulmonary vein.

Surgically-Altered Veins

Figures 21 and 22 illustrate two surgical procedures (Mustard [27] and Glenn [28], respectively) that alter venous anatomy.

REFERENCES

1. Langston CS. The aberrant central venous catheter and its complications. *Radiology* **1971**;100:55–59
2. Gilday DL. The value of chest radiography in the localization of central venous pressure catheters. *Can Med Assoc J* **1969**;101:363–364
3. Warwick R, Williams PL. *Gray's anatomy*, 35th Br. ed. Philadelphia: Saunders, **1973**:700–704
4. Whalen JP, Oliphant M, Evans JA. Anterior extrapleural line: superior extension. *Radiology* **1975**;115:525–531
5. Proto AV, Speckman JM. The left lateral radiograph of the chest. *Med Radiogr Photog* **1979**;55:30–74
6. Yune HY, Klatte EC. Mediastinal venography. *Radiology* **1972**;105:285–291
7. Ovenfors C-O, Ounjian ZJ. Aberrant position of central venous catheter introduced via internal jugular vein. *AJR* **1977**;128:483–484
8. Jantsch H, Lechner G, Mauritz W, Waneck R. Fehllagen und Komplikationen des oberen Cavakatheters. *Radiologe* **1981**;21:463–469
9. Belda FJ, Frasquet FJ, Maruenda A, et al. Malposicion de los cateteres venosos centrales con el abordaje de la vena jugular interna. *Rev Esp Anestesiol Reanim* **1981**;28:306–310
10. Larsen R, Rieke H. Ungewohnliche Fehllage eines V. jugularis interna-Katheters. *Anaesthesist* **1981**;30:95–97
11. Heitzman ER, Scrivani JV, Martino J, Moro J. The azygos vein and its pleural reflections. *Radiology* **1971**;101:249–258
12. Tori G, Garusi GF. The azygos vein arch and its valvular apparatus. *AJR* **1962**;87:235–247
13. Abrams HL. The vertebral and azygos venous systems, and some variations in systemic venous return. *Radiology* **1957**;69:508–526
14. Stauffer HM, LaBree J, Adams FH. The normally situated arch of the azygos vein: its roentgenologic identification and catheterization. *AJR* **1951**;66:353–360
15. Pagniez B, Denies JL, Dupuis C, Remy J. La veine intercostale superieure gauche. *J Radiol Electrol* **1975**;56:285–298
16. Ball JB Jr, Proto AV. The variable appearance of the left superior intercostal vein. *Radiology* **1982**;144:445–452
17. McDonald CJ, Castellino RA, Blank N. The aortic "nipple." *Radiology* **1970**;96:533–536
18. Friedman AC, Chambers E, Sprayregen S. The normal and abnormal left superior intercostal vein. *AJR* **1978**;131:599–602
19. Hewitt MJ, Chen JTT, Ravin CE, Gallagher JJ. Coronary sinus atrial pacing: radiographic considerations. *AJR* **1981**;136:323–328
20. Wechsler RJ, Byrne KJ, Steiner RM. The misplaced thoracic venous catheter: detailed anatomical consideration. *CRC Crit Rev Diagn Imaging* **1984**;21:289–305
21. Cha EM, Khoury GH. Persistent left superior vena cava. *Radiology* **1972**;103:375–381
22. Fraser RS, Dvorkin J, Rossall RE, Eidem R. Left superior vena

cava. *Am J Med* **1961**;31:711–716
23. Winter FS. Persistent left superior vena cava. *Angiology* **1954**;5:90–132
24. Edwards JE. Pathologic and developmental considerations in anomalous pulmonary venous connection. *Proc Staff Meet Mayo Clin* **1953**;28:441–452
25. Shumacker HB, Judd D. Partial anomalous pulmonary venous return with reference to drainage into the inferior vena cava and to an intact atrial septum. *J Cardiovasc Surg* **1964**;5:271–278
26. Chen JTT. Radiologic demonstration of anomalous pulmonary venous connection and its clinical significance. *CRC Crit Rev Diagn Imaging* **1979**;11:383–422
27. Mustard WT. Successful two-stage correction of transposition of the great vessels. *Surgery* **1964**;55:469–472
28. Glenn WWL. Circulatory bypass of the right side of the heart. *N Engl J Med* **1958**;259:117–120

Digital Subtraction Venography in Central Venous Obstruction

James F. Benenati[1]
Gary J. Becker
John T. Mail
Robert W. Holden

Thirty-five patients had central venous digital subtraction venography (DSV) to assess its value in detecting central line/shunt patency (13 patients) and central venous obstruction (22 patients). All examinations were easily performed and provided diagnostic images without conventional venographic supplementation. The disadvantages of DSV are outweighed by the advantages, which include saving time and money, superior contrast resolution, flexibility of image display, and reduced dosage of contrast agent.

One source of difficulty in the evaluation of obstruction of the superior vena cava (SVC) or subclavian vein is the superimposition of soft tissue and osseous structures, including the mediastinum, ribs, clavicles, sternum, and thoracic spine. These structures often produce obstacles to conventional venography because they increase radiodensity in the precise area of interest. While photographic film subtraction has been helpful in alleviating this problem, it is both expensive and time consuming. Oblique and lateral positioning are potentially beneficial, but infrequently employed. We undertook the present study in order to (1) assess the feasibility of routine use of digital subtraction venography (DSV) instead of conventional superior vena cavography and subclavian venography for suspected obstruction, (2) perfect the technique, and (3) determine the advantages, disadvantages, and approximate cost savings of the digital method for a series of patients.

Subjects and Methods

Thirty-five patients suspected of having obstruction of the SVC, *subclavian vein*, or central venous line on the basis of clinical, CT, or radionuclide-flow study findings were referred to the radiology department for venography. All underwent DSV of one or both subclavian veins and/or the SVC. In cases involving a question of catheter patency, injections were also made directly into the catheters. All exams were performed on a Diasonics DF-100 (Milpitas,CA), Philips DVI II (Philips Medical Systems, Shelton, CT) or ADAC DPS-1000 (ADAC Laboratories, Sunnyvale, CA). Our preferred study method evolved into the one described in the following paragraphs.

At the beginning of each procedure, patients are instructed about holding their breath. With the arms abducted and elevated approximately 30°, an antecubital venous injection of 40 ml of meglumine iothalamate 43% (Conray-43, Mallinckrodt, Inc., St. Louis, MO) is made unilaterally for suspected SCV obstruction or bilaterally (80 ml total) for suspected SVC obstruction using 18-gauge butterfly needles. Centering depends on the area of interest. The field size most commonly used is 12 in. (30 cm). For assessments of central venous catheter patency, contrast material is injected directly into the catheter. In all instances, contrast material is manually injected as rapidly as possible. The framing sequence is 1 frame/sec. Durations of injection and acquisition are determined by real-time monitoring of the study with special attention to the acquisition of late mask frames. Postprocessing primarily includes remasking, reregistration, and changes in window and level.

Studies were quantitatively assessed for contrast resolution in structures frequently obscured within the mediastinal shadows on conventional venography (SVC brachiocephalic

Received December 17, 1985; accepted after revision May 5, 1986.

[1] All authors: Department of Radiology, Indiana University School of Medicine, 926 W. Michigan St., Indianapolis, IN 46223. Address reprint requests to J. F. Benenati.

AJR 147:685–688, October 1986
0361–803X/86/1474–0685
© American Roentgen Ray Society

TABLE 1: **Digital Subtraction Venogram Findings in Obstruction of the Superior Vena Cava or Subclavian Vein**

Cause	Frequency (%)	No. of Film Sequences	Finding	
			Obstruction	Collaterals
Carcinoma	18 (82)	1	15	13
Fractured clavicle	1 (5)	1	1	1
Thoracic inlet syndrome	1 (5)	1	1	1
Unknown	2 (9)	1	0	0

TABLE 2: **Digital Subtraction Venogram Findings in Evaluation of Catheter or Shunt Patency**

Catheter type	Frequency (%)	No. of Film Sequences	Findings
Central line	8 (62)	1	6 fibrin sheath surrounding catheter 2 normal
	3	2	2 thrombus in SVC; fibrin sheath surrounding catheter 1 catheter in small tributary of SCV
LaVeen shunt	1 (8)	2	1 fibrin sheath; thrombus in SVC
Denver shunt	1 (8)	2	1 extensive fibrin sheath; patent SVC and SCV

Note.—SVC = superior vena cava; SCV = subclavian vein.

TABLE 3: **Cost Comparison of Digital Subtraction[a] and Conventional Venography[b] for Typical Superior Vena Cava Study**

Costs	Conventional	Digital
Film	$12.88	$ 0.76
Contrast material	13.88	10.90
Technologist	6.42	4.30
Total	33.18	15.96

[a] Includes only one sequence.
[b] Includes only one sequence and no photographic subtraction.

veins, medial one-third of the subclavian veins, and central venous catheters).

An average cost saving on film was computed by using (1) the number of films usually employed at our institution for a conventional subclavian venogram or superior venacavogram and (2) the average number of films used for DSV studies in this group of 35 patients. Other cost considerations studied in our limited analysis include contrast media and technologist time.

Results

DSV was diagnostic in all 35 patients. The results are provided in Tables 1 and 2. In no instance was conventional venography necessary to supplement the diagnostic impression. No complications were encountered.

Our average number of 14 × 14 in. (36 × 36 cm) films per sequence in conventional venography of the subclavian vein and SVC is eight. Our average for the digital method is four frames on one 8 × 10 in. (20 × 25 cm) film per sequence. Since the cost of 14 × 14 in. film is $1.61 per sheet (TMG-1, Eastman Kodak Company, Rochester, NY) and the cost of 8 × 10 in. film is $0.76 per sheet (NMC-1, Eastman Kodak Company), the minimum savings in film cost per sequence is $12.12. In conventional cases requiring photographic subtraction, there is obviously additional procedure time and expense; each sheet of X-Omat subtraction film (Eastman Kodak) is $2.24. In the majority of our DSV cases, only one sequence was necessary to obtain diagnostic information.

Meglumine iothalamate 60% (Conray-60, Mallinckrodt, Inc.) is used for our conventional upper-extremity venograms at a cost of $6.94 per 50-ml vial. Meglumine iothalamate 43% (Conray-43, Mallinckrodt, Inc., St. Louis, MO) is used for our DSV studies at a cost of $5.45 per 50-ml vial.

Our average cost for technologist time including salary plus fringe benefits is $12.84/hr, and a DSV study takes approximately 20 minutes or two-thirds the time of a conventional upper-extremity venogram.

Table 3 summarizes the differences in cost between the two types of exams in the case of a study for SVC obstruction. Figures 1–4 are representative DSVs from our series.

Discussion

It is often necessary to study the SVC and subclavian vein for clinically suspected obstruction (e.g., upper extremity edema, cyanosis, superficial collaterals) [1] or evaluation of the patency of central venous lines. In our experience, malfunction of central lines is most commonly due to thrombosis or sheathing of the catheter with a layer of fibrin. Less commonly, the catheter tip may be found positioned within a small tributary to the brachiocephalic or subclavian vein or in an extravascular position.

Venography has been considered the diagnostic method of choice in SVC obstruction [2]. However, the density of the mediastinum presents an inherent problem in the evaluation of thoracic venous structures. Because of this problem, photographic subtraction is often a necessary supplement to conventional venography of the SVC and subclavian vein. This increases the cost and time of the examination. Film costs for such procedures, even without subtraction, are considerably higher than for most DSVs.

With the method we have described for DSV, the examination is easily tailored to the specific needs of the patient. The amount of contrast material used is variable. Because meglumine iothalamate 43% (202 mg I/ml) is employed, repeat sequences are possible even when bilateral antecubital injections are made.

Instructions for holding of breath deserve special emphasis when the digital method is used. Patients who cannot cooperate with holding their breath are poor candidates for this technique. Practicing holding breath before the actual acquisition sequence provides a good measure of the patient's ability to cooperate. Late mask frames often prove useful for

Fig. 1.—Patient with poor venous return through Hickman catheter; digital subtraction venography done to rule out obstruction shows Hickman catheter in patent subclavian vein with no fibrin sheathing.

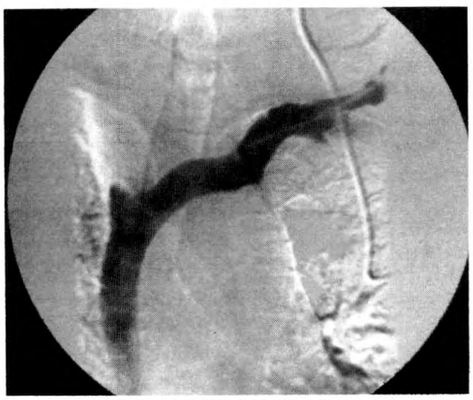
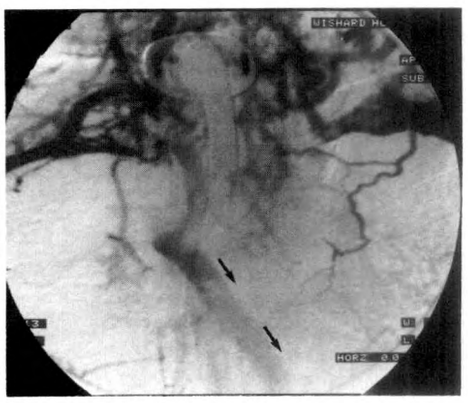


Fig. 2.—72-year-old woman with small-cell undifferentiated carcinoma of lung. Digital subtraction venogram reveals infraazygos superior vena cava obstruction and multiple collateral channels. *Arrows* indicate retrograde direction of blood flow in azygos vein.



1 2

Fig. 3.—83-year-old man with squamous-cell carcinoma of lung. Digital subtraction venogram reveals supraazygos obstruction of superior vena cava (SVC) with complete occlusion of right brachiocephalic vein and narrowing of left brachiocephalic vein. Note multiple collateral channels. Antegrade flow from left brachiocephalic vein to SVC is shown. *Arrows* indicate antegrade direction of blood flow in azygos vein.

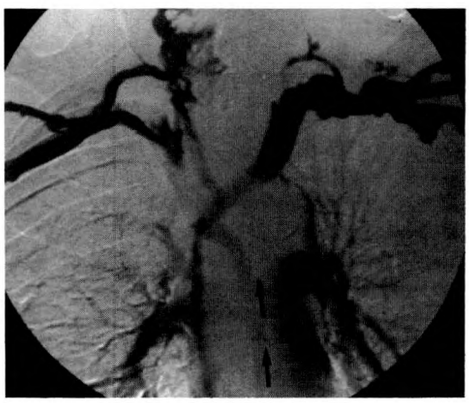


Fig. 4.—52-year-old man with LaVeen shunt in left subclavian vein (SCV). Digital subtraction venogram with antecubital venous injection demonstrates extensive thrombus in SCV with collateral flow.



3 4

remasking studies in which the patient has moved or breathed. Misregistration remains a significant limitation of the digital method in uncooperative patients. Arm elevation should precede acquisition to assure filling of the subclavian vein and SVC without misregistration. While ECG gating could potentially alleviate misregistration due to cardiac motion, the latter has not proved a significant limitation in our studies.

The digital venography method has several real and potential advantages. Real-time subtraction (instead of photographic film subtraction), decreased film cost, improved flexibility of display and archival, and time efficiency are a few of the real advantages. High-quality images result from injection of a relatively low concentration of contrast medium, which is important in patients who have renal insufficiency or who require more than one contrast injection. In addition, a theoretical advantage is that meglumine iothalamate 43% is less likely to induce venous endothelial injury than other more highly concentrated media [3, 4], and this is important in patients with venous obstruction and stasis. Although the spatial resolution of DSV is less than that of the conventional method, this limitation has never hindered the diagnostic accuracy of any of our studies.

Other techniques used to image central venous obstruction are CT and MRI. CT is excellent at showing masses in the mediastinum and the numerous collaterals that occur in venous obstruction but is limited to axial scanning. Frontal projection radiography and coronal MR imaging are better for imaging vascular structures in continuity. MR imaging may prove the technique of choice, but its wide application is presently hampered by expense, acquisition time, and lack of availability. In addition, not all patients are suitable candidates for MR imaging.

Our cost comparison does not include differences in room-utilization time and certain other operating costs, but it does provide a fair representation of the differences in film cost, contrast material cost, and technologist time. On the basis of this limited analysis, we believe that DSV is more cost efficient than conventional upper-extremity venography.

In summary, digital subtraction venography of the SVC and subclavian vein is a time-efficient, cost-efficient, and useful method of examination. It is easily performed and is readily adaptable to the clinical situation. DSV offers several real and theoretical advantages over conventional venography and is recommended as the diagnostic procedure of choice in all cases of suspected occlusion of the SVC, subclavian vein, and central venous catheters.

REFERENCES

1. Hudson GW. Venography in superior vena cava obstruction. *Radiology* **1963**;68:499–505
2. Shim DS, Logue GL, Rigsby LC. Evaluating the superior vena cava syndrome. *JAMA* **1981**;245:951–953
3. Bettman MA, Paulin S. Leg phlebography: the incidence, nature and modification of undesirable side effects. *Radiology* **1977**;122:101–104
4. Laerum F. Acute damage to human endothelial cells by brief exposure to contrast media in vitro. *Radiology* **1983**;147:681–684

Screening Mammography: Referral Practices of Los Angeles Physicians

Lawrence W. Bassett[1]
Daniel H. Bunnell[1]
Julie A. Cerny[2]
Richard H. Gold[1]

The American Cancer Society (ACS) recommends annual screening mammography for asymptomatic women over 50 years old. In a survey of attitudes and referral practices toward screening mammography, one-fifth (886) of the 4200 physicians queried returned a postage-paid questionnaire. Only 11% of respondents followed the ACS guidelines. Physicians under 40 years old, in group practice, or in surgical specialties were more apt to refer their patients for screening. The major deterrent to referral was the perceived high cost and low yield of screening. However, 80% of the physicians indicated they would refer patients over 50 who requested annual screening. Annual mammography screening is underused; greater efforts must be directed toward educating physicians and patients regarding its value and toward lowering its cost.

Breast cancer is the most common cancer in American women; one in 11 will develop breast cancer at some time in her life [1]. The results of the Breast Cancer Detection Demonstration Project and other ongoing screening investigations indicate that mammography is the most sensitive and accurate method for the early detection of breast cancer [2–9]. For these reasons, the American Cancer Society (ACS) now recommends guidelines that include a baseline mammogram for asymptomatic women aged 35 to 40, mammograms at 1–2 year intervals for women aged 40 to 50, and annual examinations thereafter [10]. We surveyed physicians in our community to assess their attitudes and practices with regard to mammography screening in asymptomatic women over 50 years old.

Subjects and Methods

In September 1984, we sent questionnaires (return postage paid) to 4200 physicians in the Los Angeles area. This group included all members of the Los Angeles County Medical Association listed as actively practicing internal medicine, surgery, family practice, general practice, or obstetrics and gynecology. The survey postcard sought general demographic information and responses to specific questions about using mammography in asymptomatic women over age 50 (Table 1). We felt the ACS guidelines for screening this group would be the most familiar to physicians.

Results

Of the 4200 physicians surveyed, 886 (21%) returned the questionnaire. A comparison of the demographics of the respondents with the whole survey population yielded no major differences (Table 2). Sixty-four percent of the responding physicians were in solo practice, and 33% in group practice.

Only 11% (95) of the respondents followed the ACS guidelines with regard to screening asymptomatic women over 50 years old. Although compliance with the ACS guidelines was poor in all medical specialties queried, variations in referral practices occurred (Table 3). In addition, there was a significant difference ($p <$

Received March 11, 1986; accepted after revision May 15, 1986.

[1] Department of Radiological Sciences, UCLA School of Medicine, Los Angeles, CA 90024. Address reprint requests to L. W. Bassett.

[2] The American Cancer Society, Los Angeles Coastal Cities Unit 2, Los Angeles, CA 90230.

AJR 147:689–692, October 1986
0361–803X/86/1474–0689
© American Roentgen Ray Society

TABLE 1: **Mammography Questionnaire**

(Check Box)

1. How frequently do you refer *asymptomatic* women *over 50* for mammography?
   [ ] Never
   [ ] On a regular basis (every 1–3 years) when there is a family pesonal history of breast cancer.
   [ ] Every year regardless of patient history or symptoms.
   [ ] Every 2–3 years regardless of patient history or symptoms.
   [ ] Every 4–5 years regardless of patient history or symptoms.
   [ ] Other _____
2. If you selected the first or second choice in Question #1, please indicate why you do not refer all asymptomatic women for screening mammograms:
   [ ] High cost/low yield
   [ ] Risk of radiation exposure
   [ ] Other screening methods are adequate
   [ ] Other reasons: _____
3. Would you refer a woman over 50 for mammograms every year if she requested annual screening regardless of risk factors or symptoms?
   [ ] Yes [ ] No
4. Your Speciality:
   [ ] General practice
   [ ] Family practice
   [ ] Internal medicine
   [ ] OB/Gyn
   [ ] Surgery
5. Type of Practice (Majority of Time)
   [ ] Solo private
   [ ] Group private
   [ ] Private hospital based
   [ ] County hospital based
   [ ] HMO
   [ ] University based
6. Your Sex:
   [ ] Male [ ] Female
7. Your age:
8. If you would like the results of this survey, please provide your name, address and zip code:

TABLE 2: **Characteristics of Survey Respondents Compared to All Physicians Surveyed**

	Respondents	Active members LACMA[a] (n = 5363)
Age (mean)	55	53
Sex (%)		
Male	95	93
Female	5	7
Specialty (%)		
General practice	16 (n = 143)	17 (n = 887)
Family practice	17 (n = 154)	15 (n = 821)
Internal medicine	35 (n = 314)	38 (n = 2060)
OB/Gyn	15 (n = 129)	12 (n = 653)
Surgery	17 (n = 146)	18 (n = 942)

[a] Demographics provided by Los Angeles County Medical Association (LACMA). (4200 members were surveyed.)

0.01) in compliance with the ACS guidelines between physicians younger than 40 years old and those older than 40; the younger physicians were more apt to refer their asymptomatic patients for screening mammography. Although physicians practicing in a group had a slightly greater tendency to refer their patients for screening mammography, they usually did not do so annually. There was no significant difference in referral practices between male and female physicians. Of those physicians who did not refer all asymptomatic women for annual screening, 55% gave high cost and low yield as the major reasons for not screening, 17% were concerned about high cost, low yield, and radiation risk, 7% listed radiation risk as their only concern, and 7% thought that other screening methods were adequate. While most physicians did not refer women for regular screening mammograms, 81% indicated that they would refer women over 50 regardless of risk factors or symptoms if the patients requested annual screening.

Discussion

Clinical trials in North America and Europe have shown that mammography is the most effective method for detection of early breast cancer [2, 3, 7] and that screening with mammography decreases mortality from the disease [3, 7–9]. Although the ACS and other professional medical societies recommend regular mammographic screening, mammography is not widely used in the United States as a screening examination [11–13].

In a 1982 mail survey of 509 family physicians in New York State, Cummings et al. [11] found that, although family physicians recognized that mammography could detect breast cancer in its early stages, most of these physicians did not recommend routine mammograms for their patients. In that study, the reason most commonly given for not recommending mammography was the possibility of radiation risk. Other reasons included concerns over the reliability of the procedure, the low probability of cancer detection, poor patient acceptance, and high cost. Our survey found a similar noncompliance with the ACS guidelines, with high cost being the most common reason given.

In 1984, the Ohio Division of the ACS conducted a telephone survey of 1035 primary-care physicians to ascertain their detection practices for all types of cancers [12]. The part of the study concerned with breast cancer detection yielded results similar to our investigation: (1) 11% of the Ohio physicians followed the ACS guidelines; (2) the high cost of mammography was the primary deterrent to compliance with ACS guidelines; and (3) there were differences in mammography-screening practices among the various specialties, with obstetricians/gynecologists being more apt to follow the ACS guidelines than general practitioners/family physicians or internists.

A computer-assisted assessment [13] of 306 family physicians' knowledge of ACS screening guidelines indicated that only 55% of the participants were aware of the newest

TABLE 3: **Percentages of Physicians Referring Asymptomatic Women Over 50 for Mammography**

Frequency of Referral	General Practice (n = 143)	Family Practice (n = 154)	Internal Medicine (n = 314)	OB/Gyn (n = 129)	Surgery (n = 146)	All Respondents (n = 887)
Never	40	24	23	13	14	23
High-risk patients only (family or personal history of breast cancer)	34	38	34	33	35	36
All patients						
Annual	4	11	12	11	15	11
Every 2–3 years	18	20	19	31	24	22
Every 4–5 years	4	4	10	9	9	7
Other	1	4	3	3	3	3

guidelines for baseline mammography at 35–40 years and regular screening after 40. In our survey, we chose to query screening practices for woman over 50 because some physicians might have been unaware of the more recent recommendations for screening younger women.

Our survey disclosed that physicians in all specialties were most likely to recommend regular screening mammograms for women with a family or personal history of breast cancer. Although this approach is rational in a cost-benefit analysis, 75% of women with breast cancer have no known risk factors [14]. Furthermore, in a survey of 257 women undergoing mammography, Fox et al. [15] found that only 9% were asymptomatic; 46% had breast symptoms and were seeking mammographic confirmation of clinical findings. Fox et al. further noted that many women did not know why they were having mammograms. She concluded that women would more willingly participate if they were informed about the value of screening mammography, and that its underuse might be more the result of a lack of acceptance by physicians than resistance by patients. Although our survey showed that most physician respondents do not follow the ACS guidelines for mammographic screening, 80% answered that they would refer patients that requested annual mammographic screening.

In summary, our survey revealed that only a small fraction of Los Angeles physicians currently follow the ACS guidelines for mammographic screening in women over 50. Nevertheless, even though the demographic characteristics of the responding and nonresponding physicians were similar, our finding that about 10% of physicians follow the ACS guidelines may be an overestimate for the whole population. The physicians who returned the questionnaire may have been more convinced of the value of mammography than those who did not. They may have been more likely to refer patients for mammography and more likely to reply to our questionnaire than nonreferring physicians.

The major reason given for not screening was the perception of the examination as being high in cost and low in yield. In our study, these two issues (cost and yield) were combined to provide an index of the perceived cost effectiveness of mammographic screening. Fear of radiation-induced cancer was less important in preventing screening. It is encouraging that most of the physicians would not resist annual screening if requested by their patients and that younger and more recently trained physicians are more aware of the importance of screening mammography. Radiologists should accept the challenge of providing lower cost and high-quality screening mammographic examinations, as well as contributing to the education of both the public and referring physicians.

Physicians, women's advocacy groups, the mass media, and professional organizations can aid in the dissemination of information about the importance of screening mammography. Several successful pilot projects of low-cost mammography, supported by the ACS and the mass media, have recently been completed. Further projects are in the planning stages and will aid in introducing women to the concept of breast-cancer screening.

REFERENCES

1. Silverberg E. Cancer statistics, 1985. *CA* **1985**;35(1):19–35
2. National Task Force on Breast Cancer Control. Mammography 1982: a statement of the American Cancer Society. *CA* **1982**;32(4):226–230
3. Baker LH. Breast cancer detection demonstration project: five-year summary report. *CA* **1982**;32(4):194–225
4. Tabar L, Gad A. Screening for breast cancer: the Swedish trial. *Radiology* **1981**;138:219–222
5. Miller AB, Howe GR, Wall C. The national study of breast cancer screening. Protocol for a Canadian randomized controlled trial of screening for breast cancer in women. *Clin Invest Med* **1981**;4:227–258
6. Doll R, Atkinson AB, Chamberlain J, et al. Trial of early detection of breast cancer: description of method. UK trial of early detection of breast cancer group. *Br J Cancer* **1981**;44:618–627
7. Collette AJ, Day NE, Rombach JJ, DeWard F. Evaluation of screening for breast cancer in a non-randomized study (The DOM Project) by means of a case-control study. *Lancet* **1984**;1(8388):1224–1226
8. Verbeck ALM, Holland R, Sturmans F, Hendriks JHCL, Mravunac M, Day NE. Reduction of breast cancer mortality through mass screening with modern mammography. First results of the Nijmegen project, 1975–1981. *Lancet* **1984**;1(8388):1222–1224
9. Tabar L, Gad A, Holmberg LM, et al. Reduction in mortality from breast cancer after mass screening with mammography. Randomized trial from the Breast Cancer Screening Working Group

of the Swedish National Board of Health and Welfare. *Lancet* **1985**;1(8433):829–832
10. American Cancer Society. Mammography guidelines 1983: background statement and update of cancer-related checkup guidelines for breast cancer detection in asymptomatic women age 40 to 49. *CA* **1983**;33(5):255
11. Cummings KM, Funch DP, Mettlin C, Jennings E. Family physicians' beliefs about breast cancer screening by mammography. *J Fam Pract* **1983**;17(6):1029–1034
12. Survey of physicians' attitudes and practices in early cancer detection. *CA* **1985**;35(3):197–213
13. Groveman HD, Ganiats TG, Klauber MR, Holden MG. Computer-assisted assessment of family physicians' knowledge about cancer screening guidelines (health care delivery). *West J Med* **1985**;143:541–544
14. Seidman H, Stellman SD, Mushinski MH. A different perspective on breast cancer risk factors: some implications of the nonattributable risk. *CA* **1982**;32(4):301–313
15. Fox S, Baum JK, Klos DS, Tsou CV. Breast cancer screening: the underuse of mammography. *Radiology* **1985**;156:607–611

Radiologic and Manometric Correlation in "Nutcracker Esophagus"

David J. Ott[1]
Joel E. Richter[2]
Wallace C. Wu[2]
Yu Men Chen[1]
David W. Gelfand[1]
Donald O. Castell[2]

"Nutcracker esophagus" is a newly described esophageal motor disorder seen in some patients with chest pain and/or dysphagia and characterized manometrically by normal primary peristalsis with distal contractions of high amplitude. The radiographic and manometric examinations in 20 patients with nutcracker esophagus were correlated. Normal primary peristalsis was observed radiographically in 16 patients, and a nonspecific motor disorder was diagnosed in the remaining four patients. Mild-to-severe nonspecific tertiary activity was seen in about half of the patients, esophageal wall thickness was normal. It is concluded that nutcracker esophagus is primarily a manometric diagnosis made in the appropriate clinical setting, and that the radiographic findings are normal or nonspecific.

Esophageal motor disorders have long been recognized as a cause of chest pain or dysphagia. Disruption of primary esophageal peristalsis, spontaneous and repetitive contractions, and dysfunction of the lower esophageal sphincter are the major radiographic and manometric findings used to characterize many of these motor disorders. Radiographic evaluation of the esophagus is often diagnostic of the more specific types of primary esophageal motor disorders, such as achalasia. Additionally, it may suggest other primary or secondary motility disorders, such as diffuse esophageal spasm or scleroderma.

In recent years, low-compliance infusion systems for esophageal manometry have been introduced. The improved fidelity of these systems for recording esophageal body pressure has permitted more accurate assessment of peristaltic amplitude and duration [1, 2]. This has led to the identification of a group of patients presenting with chest pain and/or dysphagia having normal peristaltic contractions with distal amplitudes exceeding the normal range [3–6]. This entity has been called "high-amplitude peristaltic esophageal contractions" or, more simply, "nutcracker esophagus." We present 20 patients with nutcracker esophagus having manometric and radiographic correlation.

Materials and Methods

Over a period of 22 months, a diagnosis of nutcracker esophagus was made in our esophageal manometry laboratory in 20 patients, who also had a radiographic examination of the esophagus done within 1 week of their manometric examination. The group consisted of seven women and 13 men with a mean age of 50 years (range, 24–71 years). Eleven patients presented with both chest pain and dysphagia, eight patients had only chest pain, and one patient had only dysphagia.

Esophageal manometry was performed using a round 8-lumen polyvinyl catheter with four distal openings 1 cm apart at 90° angles, and four more proximal openings 5 cm apart. Each lumen was continuously infused using a low-compliance pneumohydraulic capillary infusion system (Arndorfer Specialities, Greensdale, WI). The individual catheters were connected to external transducers with output directed to a Beckman physiograph recorder (model R-612, Norcross, GA). The catheter was positioned in the esophageal body at 3, 8, 13, and 18 cm

Received April 15, 1986; accepted after revision May 30, 1986.

[1] Department of Radiology, Bowman Gray School of Medicine, Winston-Salem, NC 27103. Address reprint requests to D. J. Ott.

[2] Department of Medicine, Bowman Gray School of Medicine, Wake Forest University, Winston-Salem, NC 27103.

AJR 147:692–695, October 1986
0361–803X/86/1474–0692
© American Roentgen Ray Society

above the lower esophageal sphincter. Esophageal contractions were recorded in response to 10 wet swallows (5 ml H_2O) at 30-sec intervals. Based on 95 healthy controls, normal mean distal amplitude in our laboratory is 100 ± 80 mm Hg (mean ± 2 SD). The nutcracker esophagus therefore was defined by the presence of distal peristaltic contractions with a mean amplitude greater than 180 mm Hg.

Radiographic examination of the esophagus was performed using remote-control machinery. A multiphasic examination of the esophagus was done on all patients and consisted of double-contrast, mucosal-relief, and full-column techniques [7]. Esophageal motility was assessed with the patient in the prone oblique position by observing several single swallows of barium traversing the length of the esophagus. The presence of tertiary activity and its severity were noted. A nonspecific esophageal motor disorder was defined radiographically if primary esophageal peristalsis was disturbed, but no specific motor disorder could be diagnosed. Esophageal wall thickness was also measured in 18 of the 20 patients with nutcracker esophagus, and was compared with 20 patients (seven women; 13 men; mean age, 49 years) having both normal radiographic and manometric examinations of the esophagus.

Results

All patients were classified manometrically as nutcracker esophagus (i.e., normal primary peristalsis with high-amplitude distal contractions). The mean distal esophageal amplitude was 237 ± 49 mm Hg (mean ± 1 SD) with a range of 185–359 mm Hg. Lower esophageal sphincter function was normal in 19 patients, and showed incomplete relaxation in the remaining patient. The Bernstein test for evaluating acid sensitivity of the lower esophagus was performed on 16 patients, but was positive in only four. The edrophonium test [8] to provoke chest pain was used in 14 patients, but was positive in only two.

Radiographic examination showed normal esophageal peristalsis in 16 patients, with eight patients also demonstrating mild-to-severe tertiary activity of the esophageal body (Fig. 1A). A nonspecific esophageal motor disorder was diagnosed in the remaining four patients on the basis of disruption of primary peristalsis, with tertiary activity demonstrated in three (Fig. 1B). The tertiary activity most often occurred spontaneously. The mean esophageal wall thickness in those with nutcracker esophagus was 2.64 mm (range, 1.5–4.0 mm), compared with 2.55 mm (range, 2.0–3.5 mm) in the manometrically and radiographically normal patients ($p > 0.05$). Other radiographic diagnoses included hiatal hernia in 14, reflux esophagitis in three, and esophageal diverticula in three.

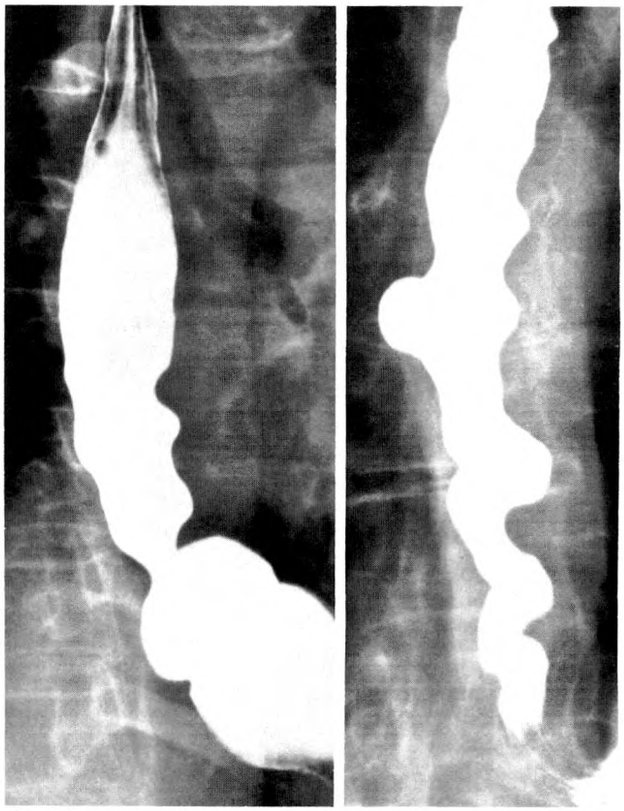


Fig. 1.—**A**, 66-year-old woman with chest pain. Primary peristalsis was normal radiographically, but moderate tertiary activity and hiatal hernia were present. Mean esophageal body pressure was 256 mm Hg (normal mean, 100 mm Hg). **B**, 70-year-old man with dysphagia diagnosed as a nonspecific motor disorder with severe tertiary activity radiographically. Esophageal manometry showed normal primary peristalsis and a mean body pressure of 287 mm Hg (normal mean, 100 mm Hg).

Discussion

The nutcracker esophagus, one of the more recently described esophageal motility disorders, is characterized by normal progressive peristalsis with distal contractions of high amplitude and long duration. The recent description of this manometric entity reflects the development of new technology and improvements in the equipment used in performing esophageal manometry. Nutcracker esophagus probably represents a common motility disorder in patients presenting with chest pain and dysphagia, particularly if structural abnormalities of the esophagus and cardiac disease have been excluded. Currently, however, the prevalence of this esophageal motor abnormality and its significance in relationship to symptoms have not been fully determined [4–6].

The nutcracker esophagus is primarily a manometric diagnosis made in the appropriate clinical setting. Our findings confirm previous reports that the radiographic examination of the esophagus in this disorder is usually normal or shows only nonspecific findings, such as tertiary contractions [3–5]. This would be expected since primary esophageal peristalsis progresses normally in nutcracker esophagus. Four patients in our series, however, were diagnosed radiographically as nonspecific esophageal motor disorders on the basis of intermittent disruption of primary peristalsis and the presence of tertiary activity. Because primary peristalsis was intact manometrically in these four patients, the radiographic interpretations most likely represented false-positive errors. Perhaps, the presence of tertiary activity in three of these patients made radiographic evaluation of primary peristalsis more difficult. Another possibility, since our examinations were not performed simultaneously, is that intermittent motor disturbances may affect some patients with nutcracker esophagus.

Interestingly, mild-to-severe tertiary activity was demonstrated radiographically in approximately half of our patients. On manometric examination, however, spontaneous contractions were noted in only one of the patients with nutcracker esophagus. The significance of tertiary activity in our patients with nutcracker esophagus and the reason for its discrepant manometric and radiographic demonstration are uncertain. Spontaneous contractions may be seen less often manometrically because the 30-sec swallowing interval inhibits spontaneous activity, or because low-amplitude pressure waves are generally ignored owing to confusion with respiratory artifacts. In addition, nonocclusive esophageal contractions, which are easily visualized radiographically, may not alter the intraluminal pressure and will not be detected manometrically.

Also, the natural history of nutrcracker esophagus is not completely known, and such considerations as transformation of nutcracker esophagus to other primary motor disorders (e.g., diffuse esophageal spasm) or the presence of intermittent motor abnormalities (e.g., spontaneous contractions) in these patients remain possibilities. We have seen one patient in whom nutcracker esophagus progressed to diffuse esophageal spasm, but have rarely observed manometric features of both diffuse esophageal spasm and nutcracker esophagus in the same individual. Similarly, Narducci et al. [9] have also reported a case of transition from nutcracker esophagus to diffuse spasm. These observations support the concept that intermediate types of motility disorders exist and possibly represent transitional forms within a spectrum of related motor disorders [10]. Prolonged manometric monitoring and simultaneous radiographic-manometric studies in patients with nutcracker esophagus, along with long-term evaluation, will be needed to study these questions.

The presence of tertiary activity radiographically is often a nonspecific finding that may relate to the patient's age or to the presence of an inflammatory, neoplastic, or motor disorder of the esophagus. In particular, the observation of spontaneous esophageal contractions is important in the diagnosis of diffuse esophageal spasm, which may mimic the clinical and radiographic findings seen in some patients with nutcracker esophagus. The major manometric criterion for diagnosing diffuse esophageal spasm is intermittent normal peristalsis with simultaneous contractions, which are often repetitive and spontaneous in nature [10, 11]. Radiographic findings in diffuse esophageal spasm are usually nonspecific, but may suggest a diagnosis that will require manometric confirmation [12]. Thickening of the esophageal wall is frequently present in patients with diffuse esophageal spasm and was not found in our patients with nutcracker esophagus [12].

In conclusion, nutcracker esophagus appears to be a common esophageal motor disorder in patients with otherwise unexplained chest pain and dysphagia. These patients are being increasingly diagnosed and are often referred for radiographic evaluation of the esophagus. The radiologist must be aware that there are no specific findings to make this diagnosis radiographically. Although tertiary activity may be seen in nutcracker esophagus, its significance is not known at the present time. Nutcracker esophagus, therefore, remains a clinical consideration in the patient who has chest pain or dysphagia but who has a normal radiologic evaluation of the esophagus. The radiographic examination remains useful, however, in evaluating structural or other functional disturbances of the esophagus in patients with chest pain or dysphagia.

REFERENCES

1. Dodds WJ. Instrumentation and methods for intraluminal esophageal manometry. *Arch Intern Med* **1976**;136:515–523
2. Arndorfer RC, Stef JJ, Dodds WJ, Linehan JH, Hogan HJ. Improved infusion system for intraluminal esophageal manometry. *Gastroenterology* **1977**;73:23–27
3. Benjamin SB, Gerhardt DC, Castell DO. High amplitude, peristaltic esophageal contractions associated with chest pain and/or dysphagia. *Gastroenterology* **1979**;77:478–483
4. Traube M, Albibi R, McCallum RW. High-amplitude peristaltic esophageal contractions associated with chest pain. *JAMA* **1983**;250:2655–2659
5. Herrington JP, Burns TW, Balart LA. Chest pain and dysphagia in patients with prolonged peristaltic contractile duration of the esophagus. *Dig Dis Sci* **1984**;29:134–140
6. Richter JE, Obrecht WF, Bradley LA, Young LD, Anderson KO. Psychological comparison of patients with nutcracker esophagus and irritable bowel syndrome. *Dig Dis Sci* **1986**;31:131–138
7. Ott DJ. Radiologic evaluation of the esophagus. In: Castell DO, Johnson LF, eds. *Esophageal function in health and disease.* New York: Elsevier, **1983**:211–235
8. Richter JE, Hackshaw BT, Wu WC, Castell DO. Edrophonium: a useful provocative test for esophageal chest pain. *Ann Intern Med* **1985**;103:14–21
9. Narducci F, Bassotti G, Gaburri M, Morelli A. Transition from nutcracker esophagus to diffuse esophageal spasm. *Am J Gastroenterol* **1985**;80:242–244
10. Vantrappen G, Janssens J, Hellemans J, Coremans G. Achalasia, diffuse esophageal spasm, and related motility disorders. *Gastroenterology* **1979**;76:450–457
11. Blackwell JN, Castell DO. Motility disorders of the lower esophagus. *Surv Dig Dis* **1983**;1:157–168
12. Stewart ET. Radiographic evaluation of the esophagus and its motor disorders. *Med Clin North Am* **1981**;65:1173–1194

Book Reviews

Radiology of Adverse Reactions to Drugs and Toxic Hazards. By George Ansell. Rockville: Aspen, 357 pp., 1985. $40

This book underlines the importance of the ever-increasing number of morbid reactions to drugs, toxins, and professional hazards, and it stresses the role of radiology in diagnosing and evaluating these entities. It represents the revised second edition of a similar book published in 1974 by a British radiologist, Dr. Ansell, who for many years manifested interest and acquired great expertise in this important facet of radiology. The book is divided into five chapters according to the organ or system involved. The effects of different toxic substances are described whenever feasible under specific subheadings, such as allergic reactions, coagulopathies, and ulcerations. A great variety of drugs and toxic agents from common to esoteric, including their source of origin, pathophysiology, and the expected radiographic abnormalities are concisely discussed. A comprehensive index is available and an impressive list of references is provided at the end of each chapter to satisfy the need for a more exigent investigator. Examples of some radiographic abnormalities are found in the 154 illustrations, most of which are plain films or old conventional contrast examinations. Unfortunately, many of the reproductions are poor or of limited quality and the few CT images shown are probably done on primitive early-generation scanners.

Despite these deficiencies, this is a well-written, useful summary that permits easy access in a single comprehensive volume to information difficult to obtain otherwise. It should be helpful not only to radiologists but to clinicians and investigators concerned with adverse reactions to drugs, poisons, and industrial hazards in humans.

Emil J. Balthazar
NYU Medical Center
New York, NY 10016

Radiology of Lymphomas. Edited by J.-N. Bruneton and M. Schneider. Berlin: Springer-Verlag, 115 pp., 1986. $56.50

This small text was a pleasure to review. Its 115 pages are extremely well-referenced (681 references, but 1984 the most recent). The book must have been completed in 1984 because there are few MR images and the extensive references are complete through 1983 with only a few from 1984.

After an introductory section on the classification of the lymphomas, the text is organized along anatomic lines, which I found to be logical and easy to follow. The first chapter includes an understandable overview of the numerous classifications of the lymphomas, including the newer *Working Formulation for Clinical Usage*.

Differential considerations are included in each of the anatomic chapters with tables to show clinical and radiologic issues that affect the diagnosis. Most of the discussions assume that the patient is seen on initial disease presentation, with only a brief overview of the imaging challenges on follow-up, subsequent to treatment. In the pulmonary section, there is a brief and incomplete discussion on radiation changes. The reproductions throughout the book are of excellent quality (with only one reversal error).

As with any new text, there are a few errors, but none that detracts from the readability of the book, which can serve either as a primary review of this group of diseases or as a reference. I would have included a more complete discussion of the implications of the low- and high-grade non-Hodgkin's lymphomas because I believe they have a major impact on the understanding of the behavior of the non-Hodgkin's lymphomas. Greater emphasis on the challenge of disease recurrence would have been helpful, as would more discussion of the role that CT and, now, MR can play in making this differential diagnostic challenge more specific. Inclusion of some interventional procedures, including a discussion of the difficulties of percutaneous biopsy on initial diagnosis, also would have been useful. Finally, an inclusion of the primary forms of non-Hodgkin's lymphoma and how they differ from disseminated lymphoma would help in understanding the presenting features of primary non-Hodgkin's lymphoma and the implications for treatment in both the localized forms of disease and the high- vs low-grade settings of non-Hodgkin's lymphoma.

Despite these deficiencies, I recommend *Radiology of Lymphomas* as a concise, well-referenced, well-illustrated, and nicely organized review of the radiologic implications of this fascinating group of diseases.

David G. Bragg
University of Utah School of Medicine
Salt Lake City, UT 84132

Radiographic Efficacy in Gastric Ulcer: Comparison of Single-Contrast and Multiphasic Examinations

David J. Ott[1]
Yu Men Chen[1]
David W. Gelfand[1]
Wallace C. Wu[2]

The efficacies of single-contrast and multiphasic examinations of the stomach for gastric ulcer detection were compared in 90 patients with 102 gastric ulcers, and in a control group of 382 patients without gastric ulcer. Single-contrast and multiphasic sensitivities were 62% and 64%, respectively. Radiographic detection depended significantly on ulcer size: Only 24% of ulcers under 5 mm were detected, compared with 89% of ulcers 5 mm or larger. Radiographic specificities and positive predictive values were similar for both types of examination. Moderate variation of the sensitivities and specificities of the three radiologists was observed, with ranges of 53–69% and 90–98%, respectively. Results indicated that gastric ulcer detection is more related to ulcer size and to individual interpretive variations than to the type of examination.

In a previous study we noted that no significant difference may exist between the sensitivities of single- and double-contrast upper gastrointestinal examinations for detection of gastric ulcer, and that the size of an ulcer strongly affected its likelihood of detection [1]. However, the double-contrast method used for that study did not routinely include compression or mucosal relief films of the stomach, and we proposed multiphasic examination of the stomach as a more effective method for detecting gastric inflammatory lesions. For the present study, we compared the efficacies of single-contrast and multiphasic examinations of the stomach in the diagnosis of gastric ulcer. Gastric-ulcer size and examiner variability were also investigated as determinants of successful radiologic detection.

Materials and Methods

We reviewed all the endoscopic and radiographic records at our institution from July 1980 to June 1985; we consecutively selected the patients who had both radiographic and endoscopic examination of the stomach done within 1 week of each other, and who had an endoscopic diagnosis of gastric ulcer or normal stomach. The patients were divided into two groups: (1) the gastric ulcer (GU) group consisted of 90 patients (47 women, 43 men) with a mean age of 57 years (range 17–82) and with 102 gastric ulcers diagnosed endoscopically, and (2) the normal (NL) group consisted of 382 patients (214 women, 168 men) with a mean age of 52 years (range 17–88) and with a normal stomach diagnosed endoscopically.

In the GU group, single-contrast upper gastrointestinal examinations were done in 41 patients and multiphasic examinations were performed in 49 patients. In the NL group, 206 patients were examined by the single-contrast method and 176 patients by the multiphasic technique. Patients were selected for single-contrast examination if they were scheduled for a small-bowel study afterward or if they were debilitated or uncooperative. In the GU group, 14 (34%) of 41 patients having a single-contrast examination had a concomitant small-bowel series, suggesting that many of these patients were debilitated and more difficult to examine than those who had multiphasic examinations.

Endoscopy was performed with Olympus instruments (Olympus Corp., Lake Success, NY) by faculty gastroenterologists or by directly supervised fellows. An endoscopic diagnosis of gastric ulcer was made when a surface excavation was felt to have sufficient depth to indicate penetration beyond the muscularis mucosae. Gastric ulcers were routinely biopsied and their

Received April 14, 1986; accepted after revision May 30, 1986.

[1] Department of Radiology, Bowman Gray School of Medicine, Wake Forest University, Winston-Salem, NC 27103. Address reprint requests to D. J. Ott.

[2] Department of Medicine, Bowman Gray School of Medicine, Wake Forest University, Winston-Salem, NC 27103.

AJR 147:697–700, October 1986
0361–803X/86/1474–0697
© American Roentgen Ray Society

size noted, as determined by comparison with the known diameter of the endoscopic biopsy forceps.

Radiology was performed by gastrointestinal radiologists or by residents supervised by faculty during fluoroscopy and film interpretation. Single-contrast examinations included compression and mucosal relief films of the stomach using a small amount of barium suspension of moderate density (Liquid Sol-o-pake, E-Z EM Co., Westbury, NY). After further barium filling of the stomach, prone, right anterior oblique, right lateral, supine, and left posterior oblique films were obtained, the latter depicting variable portions of the gastric antrum in double-contrast relief. Multiphasic examinations included initial compression and mucosal relief films of the stomach using a small amount of a high-density barium suspension (E-Z-HD, E-Z EM Co.). Double-contrast views (obtained after ingestion of gas-producing granules, 10 ml water, and additional high-density barium) consisted of supine, left posterior oblique, right lateral, right anterior oblique, and prone films. Further visualization of portions of the gastric antrum in double-contrast relief were obtained during filming of the duodenum.

Final assessment of gastric-ulcer size was based on direct measurement of the ulcers when they were visible radiographically, or on endoscopic estimation when they were not. Ulcers were categorized by size as under 5 mm, 5–10 mm, and over 10 mm. All radiographic examinations were reviewed to determine the type of study performed, the radiologist interpreting the examination, and the confidence level for the diagnosis of gastric ucler by each of three faculty radiologists. A radiographic confidence level of 1–3 (low to high) was assigned retrospectively to each ulcer diagnosed, using previously defined criteria [2].

Radiologic sensitivity and specificity were determined using the original radiologic reports. The results of endoscopy were accepted as the final criterion in assessing radiographic efficacy. Chi-square statistics were calculated to test for equality of frequency distributions of ulcers by size, assuming that multiple ulcers in the same person were independent observations. We also assumed that patients examined by each radiologist were a random sampling from the consecutive series.

Results

A total of 102 gastric ulcers were found endoscopically in the GU group. The overall radiographic sensitivity was 63%, with only 24% of ulcers under 5 mm detected, compared with 89% (54/61) of ulcers that were 5 mm or larger (Table 1). The overall sensitivity of single-contrast radiography was 62%, with 32% detection of ulcers less than 5 mm and 82% (23/28) detection of larger ulcers (Table 2). The sensitivity of the multiphasic examination was 64%, with 18% detection of ulcers less than 5 mm and 94% (31/33) sensitivity for ulcers 5 mm or larger (Table 2). Statistical analysis showed a significant relationship ($p < 0.01$) between ulcer size and radiographic detection, regardless of the technique used. No significant difference in sensitivity was noted between the two types of examinations.

In the NL group, 358 patients had normal radiographic examinations, and 24 had false-positive ulcer diagnoses, for an overall specificity of 94%. The specificities for the single-contrast and multiphasic examinations were 96% and 92%, respectively. In addition, seven false-positive diagnoses were made in patients with gastric ulcers. Based on a total of 31 false-positive diagnoses, the overall positive predictive value for all gastric-ulcer diagnoses was 67% (64/95) in a population with an ulcer prevalence of 19%. The positive predictive values and ulcer prevalences were not significantly different between the two types of radiographic examinations.

Comparison of the sensitivities and specificities of the three faculty radiologists showed ranges of 53–69% and 90–98%, respectively (Table 3). The true-positive and false-positive fractions were inversely related, the opposite of what we would expect if we were operating on the same receiving-operator-characteristic curve [3]. The positive predictive values, using the total number of false-positive diagnoses for each radiologist, varied from 53% to 84% (Table 3). Individual positive predictive values correlated directly with the average confidence level for each examiner, suggesting that a more confident diagnosis of gastric ulcer was associated with a better predictive value.

TABLE 1: **Radiographic Sensitivity for Gastric Ulcers by Size**

Ulcer Size (mm)	No. Seen Endoscopically	No. Detected Radiographically	Radiographic Sensitivity (%)
<5	41	10	24
5–10	29	25	86
>10	32	29	91
Total	102	64	63

TABLE 2: **Gastric-Ulcer Sensitivities for the Single-Contrast and Multiphasic Examinations**

Ulcer Size (mm)	Single-Contrast		Multiphasic	
	No.[a]	No. Dectected[b] (%)	No.[a]	No. Dectected[b] (%)
<5	19	6 (32)	22	4 (18)
5–10	15	12 (80)	14	13 (93)
>10	13	11 (85)	19	18 (95)
Total	47	29 (62)	55	35 (64)

Note.—Single-contrast examinations were done in 41 patients; multiphasic examinations were done in 49 patients.
[a] No. = Number of ulcers determined by endoscopy.
[b] No. detected = Number of ulcers detected radiographically.

TABLE 3: **Statistical Parameters and Average Confidence Level of Three Radiologists**

Parameter	Radiologist		
	A	B	C
Sensitivity (%)	9/17 (53)	24/40 (60)	31/45 (69)
Specificity (%)	56/62 (90)	146/160 (91)	156/160 (98)
Positive PV[a] (%)	9/17 (53)	24/41 (59)	31/37 (84)
Average confidence level (range 1–3)	2.56	2.71	2.87

[a] Predictive value (includes false-positive diagnoses in both normal and gastric-ulcer groups).

Discussion

The results of this study confirm our previous investigations that radiographic detection of peptic ulcer depends largely on ulcer size [1, 2, 4]. In this investigation, only 24% of gastric ulcers under 5 mm were detected, compared with 89% of larger ulcers. Previous results were 48% for the minute ulcers and 81% for larger ulcers. The reason for poorer sensitivity in the current study for ulcers under 5 mm is unclear. Radiographic techniques were similar except for the incorporation of compression and mucosal relief filming into the double-contrast examination. Possibly the endoscopic criteria for inclusion of minute ulcers (vs gastric erosions) may have varied between investigations, or the attitudes of the radiologists interpreting the examinations may have changed, with less attention paid to the diagnosis of minute ulcers.

Comparison of gastric-ulcer detection by the single-contrast and multiphasic examinations showed sensitivities of 62% and 64%, respectively. Both examinations poorly detected gastric ulcers less than 5 mm, with detection rates depending significantly on the size of the ulcer rather than on the type of examination. The multiphasic examination showed a slightly better sensitivity (94% vs 82%) for detection of ulcers 5 mm or larger, while the single-contrast study detected more minute ulcers (32% vs 18%). Our previously reported gastric-ulcer detection rate for the double-contrast examination was 62%, almost identical to the 64% sensitivity of the multiphasic examination achieved in the present investigation.

Thus, the multiphasic examination used in this study, incorporating early compression and mucosal relief filming along with standard double-contrast views, did not significantly improve detection of gastric ulcer in comparison with single-contrast radiography or a simple double-contrast method. One potential criticism of our multiphasic technique is the use of a high-density barium suspension for compression filming. This suspension may have made the compression technique less effective than that performed with a less dense barium.

The finding that many minute gastric ulcers were not detected radiographically, regardless of the technique used, is not surprising. As a comparison, radiographic sensitivities in patients with erosive gastritis have also been shown to be poor, with reported detection rates ranging from 0–57% [5]. We would expect small and relatively shallow gastric ulcers to be similarly difficult to demonstrate radiographically. Endoscopy depends on a difference in color, as well.

The specificities and predictive values were similar for both types of examinations. The overall specificity of the radiographic examination was 94%, reflecting a relatively low false-positive fraction. However, the positive predictive value was only 67%, indicating that about one-third of the gastric ulcer diagnoses were false-positive errors. This proportion is not unexpected in view of the low prevalence (19%) of gastric ulcer in this series [6]. Therefore, our overall results suggest that approximately one-third of gastric ulcers, mostly those under 5 mm in size, will not be detected radiographically, and that about one-third of ulcer diagnoses will be incorrect in a population with a low gastric-ulcer prevalence.

The radiologists interpreting the examinations in this study showed moderate variability in their sensitivities and specificities. The false-positive fraction for each radiologist showed an inverse relationship to his sensitivity, suggesting that the receiving-operator-characteristic curves were different for each radiologist if we assume that the populations were similar. However, a direct correlation was demonstrated between the positive predictive values of each radiologist and his average confidence level for gastric-ulcer diagnosis. We have previously shown a similar relationship in the diagnosis of duodenal ulcer [2, 4].

The results of this investigation and our previous studies on gastric and duodenal ulcer suggest that the radiologic detection of peptic ulcer is primarily related to ulcer size, and secondarily to variations among the radiologists performing and interpreting the examinations. The specific type of radiographic examination had no significant relationship to the detection of gastric ulcer. Furthermore, the multiphasic examination of the stomach, contrary to expectation, did not improve our detection of minute ulcers.

Our results suggest that in the upper gastrointestinal tract a threshold exists for the accurate radiographic demonstration of small mucosal excavations, and that tiny peptic lesions are poorly detected with current radiologic methods. Minute gastric ulcers and isolated erosions, which are easily discernible endoscopically, will not be demonstrated radiographically in many patients with these lesions. As a result, the added time and expense of a thorough multiphasic examination of the stomach may not be justified if the goal is detection of subtle mucosal inflammations.

A matter that warrants comment, however, is the necessity for detecting all minute mucosal lesions of the stomach before treatment is started. Most patients with dyspepsia have benign, often minor, inflammatory disease of the upper gastrointestinal tract, with a risk of malignancy estimated to be less than 1% [7]. Because of cost, routine initial diagnostic evaluation of dyspepsia has been discouraged [7–9]. The general strategy of reserving radiographic or endoscopic examination for those with persistent symptoms after a course of therapy is increasingly recommended [7–9]. Because upper gastrointestinal radiology is currently less expensive and safer than endoscopy, the radiographic examination, if desired, remains a reasonable approach to exclude potentially serious disease before starting therapy [9–12].

REFERENCES

1. Ott DJ, Gelfand DW, Wu WC. Detection of gastric ulcer: comparison of single- and double-contrast examination. *AJR* **1982**;139:93–97
2. Ott DJ, Chen YM, Gelfand DW, et al. Positive predictive value and examiner variability in diagnosing duodenal ulcer. *AJR* **1985**;145:1207–1210
3. Metz CE. Basic principles of ROC analysis. *Semin Nucl Med* **1978**;8:283–298
4. Gelfand DW, Dale WJ, Ott DJ, Wu WC, Meschan I. The radiologic detection of the duodenal ulcers: effects of examiner variability, ulcer size and location, and technique. *AJR* **1985**;145:551–553

5. Ott DJ, Gelfand DW, Wu WC, Kerr RM. Sensitivity of single- vs double-contrast radiology in erosive gastritis. *AJR* **1982**; 138:263–266
6. Kundel HL. Disease prevalence and radiological decision makings. *Invest Radiol* **1982**;17:107–109
7. Endoscopy in the evaluation of dyspepsia: position paper by the Health and Public Policy Committee, American College of Physicians. *Ann Int Med* **1985**;102:266–269
8. Marton KI, Sox HC Jr, Wasson J, Duisenberg CE. The clinical value of the upper gastrointestinal tract roentgenogram series. *Arch Intern Med* **1980**;140:191–195
9. Read L, Pass TM, Komaroff AL. Diagnosis and treatment of dyspepsia. A cost-effectiveness analysis. *Med Decis Making* **1982**;2:415–438
10. Overholt BF. Gastrointestinal endoscopy in the 1980s: cost, challenge, and change. *Gastrointest Endosc* **1984**;30:325–328
11. Armington WG, Mann FA, Nelson JA. Cost-effective means of diagnosing and following benign and malignant gastric ulcers. *Invest Radiol* **1985**;20:171–176
12. Munitz HA, Gelfand DW, Ott DJ. Upper gastrointestinal series: patient management and a study of 199 cases. *Gastrointest Radiol* **1985**;10:277–281

Radiologic Findings of Linear Gastric Erosions

Suketaka Momoshima[1]
Yutaka Imai
Yoshinori Sugino
Yoshiyuki Sekine
Kenji Kumakura

Long, linear, shallow barium collections were observed on the surface of the gastric rugae on barium studies of the upper gastrointestinal tract in 12 patients. These abnormalities have been confirmed endoscopically to represent long, continuous linear erosions of the gastric mucosa due to erosive gastritis.

Using the double-contrast technique, we have noted long, linear barium collections on the surface of the gastric rugae in patients with abdominal symptoms. Although little has been reported about such radiologic abnormalities, linear lesions on the gastric rugae have been recognized by endoscopists as a finding of erosive gastritis [1, 2].

Subjects and Methods

Twelve patients, whose upper gastrointestinal (UGI) series demonstrated linear niches on the surface of gastric mucosal folds and whose endoscopy showed linear redness, were analyzed. There were three men and nine women ranging in age from 18 to 60 years. All were symptomatic, the major symptoms being upper abdominal pain and discomfort. The radiologic and endoscopic findings were compared.

The UGI study was performed with 200 ml of barium suspension. An intramuscular anticholinergic agent was administered before the examination. The posterior and the anterior walls of the stomach were individually studied by the double-contrast technique [3]. Endoscopy was performed within 3 weeks before or after the radiologic study.

Results

The shallow, linear niches were seen most frequently in the distal portion of the body of the stomach and antrum. No linear niches were demonstrated in the fornix. Associated lesions such as varioliform erosions or gastric ulcer scars occurred in all but one of the cases. The linear lesions were not demonstrated on single-contrast studies, except for one case in which the lesions were shown with compression. Radiographs of a representative case are shown in Figure 1.

The shape, number, and location of the lesions detected on radiographs correlated well with the abnormality seen on endoscopy in all 12 cases. In one case, the UGI series showed linear erosions only in the antrum, while endoscopy revealed linear lesions in the body of the stomach as well. Linear lesions with pooling of indigo carmine instilled into the stomach through the endoscope were noted endoscopically in the lesions (Fig. 2). The lesions in the body were not accompanied by dye pooling, showing only linear redness.

Discussion

The usefulness of the double-contrast technique for delineating minute gastric

Received December 13, 1985; accepted after revision April 16, 1986.

[1] All authors: Department of Diagnostic Radiology, Keio University, School of Medicine, 35 Shinanomachi, Shinjuku-ku, Tokyo 160, Japan. Address reprint requests to S. Momoshima.

AJR 147:701–703, October 1986
0361–803X/86/1474–0701
© American Roentgen Ray Society

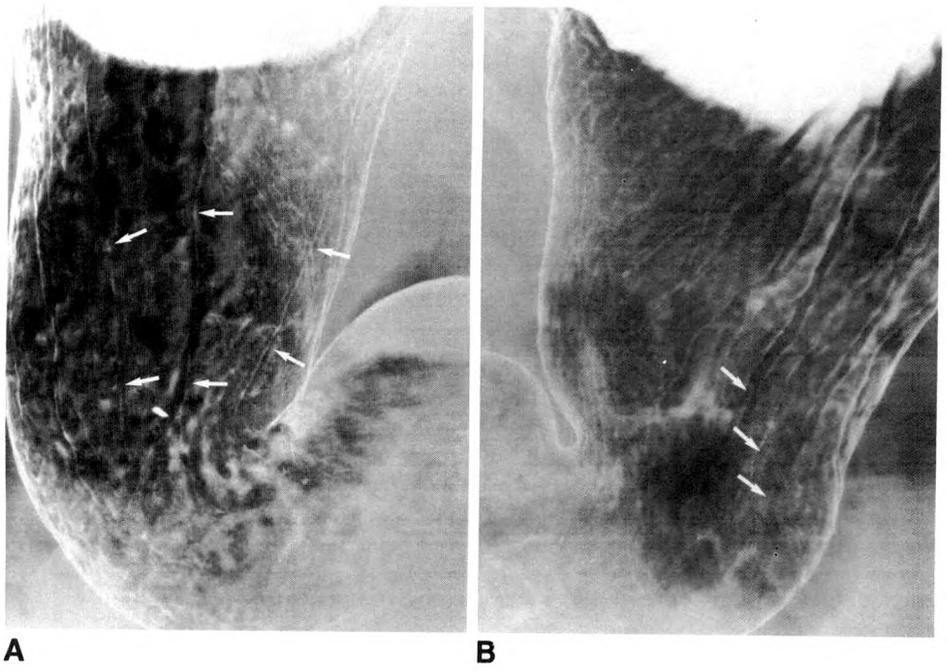


Fig. 1.—Double-contrast upper gastrointestinal examination of stomach. **A**, Prone projection shows several long linear niches on gastric rugae of anterior wall (*arrows*). **B**, Supine projection shows long linear niches on posterior wall (*arrows*).

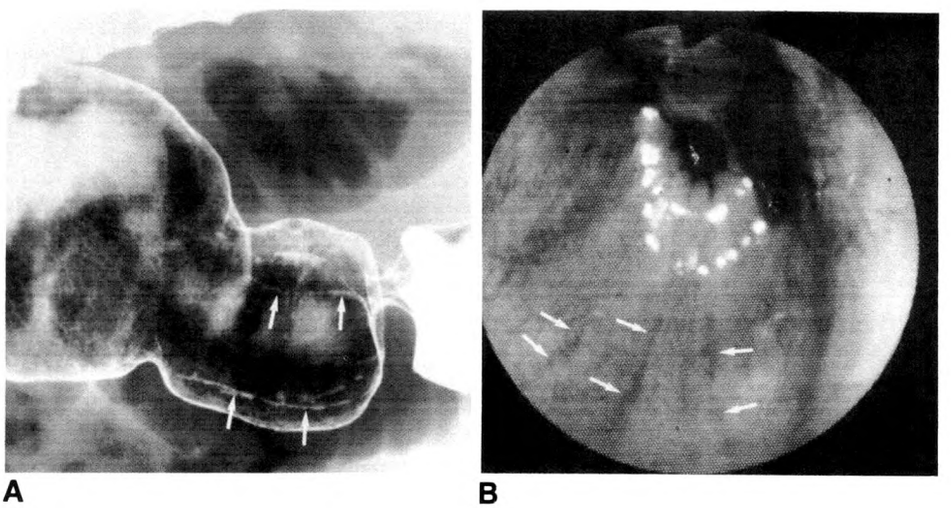


Fig. 2.—**A**, Prone projection of stomach demonstrates prominent linear shadows in anterior wall of antrum (*arrows*). Varioliform erosions are also noted. **B**, Endoscopy of corresponding region reveals linear areas on which instilled dye (indigo carmine) is pooled (*arrows*).

lesions has been well established [3–7]. We have frequently encountered a long linear niche situated on the ridges of the gastric rugae using this technique. Although little has been published about such radiologic findings, similar linear lesions have been recognized by endoscopists as a sign of erosive gastritis since their first description by Henning in 1956 [8]. The morphologic similarities have led us to assume that the linear collections on UGI studies are radiologic equivalents of the endoscopic linear erosion.

In our series of 12 cases, shallow, linear, depressed lesions accompanied by redness were confirmed endoscopically in the regions where a linear niche on the mucosal ridges had been radiologically demonstrated. The radiologic findings almost certainly represent barium pooled in the linear depressions located on the rugal ridges. This presumption is confirmed in the case mentioned earlier in which there was no radiologic evidence of linear lesions in the region where no depression was noted endoscopically, but where there was linear redness.

It has been previously reported that varioliform erosions are inclined to align along the gastric rugae [9], and short linear shadows also have been found as a result of erosive gastritis [6, 10, 11]. However, the linear barium collections in our series are longer and more continuous, and correspond

in location to the top of the gastric rugae. Three cases with similar findings were reported by Nanaumi [12], who called them "comb niches."

We have seen a number of cases in which endoscopy performed more than a month after the barium study failed to demonstrate linear lesions corresponding to the radiologic linear shadows. This is due to the rapid resolution of erosive gastritis with or without treatment, which is well documented [13, 14].

The pathologic significance of these long linear lesions is uncertain, but they most likely constitute a part of the acute gastric mucosal lesion described by Katz and Siegel [15] and Katoh et al. [16]. No characteristic clinical symptom or sign is associated with these lesions, and there is no therapeutic significance in differentiating long linear erosions from short linear or varioliform erosions. With improvement of the double-contrast technique, it has become increasingly common to note these long linear shadows on the gastric rugae on UGI studies. It is clinically useful to recognize them considering that most patients with linear lesions have erosive gastritis and are symptomatic. However, because of the relatively low sensitivity of the radiologic study [5, 7], the endoscopic examination should remain the primary method of examining patients with suspected erosive gastritis.

REFERENCES

1. Demling L, Elster K, Koch H, Rosch W. *Endoscopy of esophagus, stomach, and duodenum.* Philadelphia: Saunders, **1982**:110
2. Kasugai T. Endoscopy of the stomach. In: Kasugai T, ed. *Endoscopic diagnosis in gastroenterology.* Tokyo: Igaku Shoin, **1982**:60
3. Sugino Y, Imai Y, Kaneda S, Sekine Y, Kumakura K. Kinsetsu X-sen TV souchi ni yoru fukuga-i niju-zouei-hou no kokoromi. (Double contrast study of anterior wall of the stomach in prone position with conventional X-ray TV.) *Nippon Shokakibyo Gakkai Zasshi* **1983**;80:2165
4. Kumakura K. *Zufu ni yoru i X-sen shindangaku (X-ray diagnosis of gastric diseases).* Tokyo: Kanehara Shuppan, **1968**:223–251
5. Ott DJ, Gelfand DW, Wu WC, Kerr RM. Sensitivity of single- vs. double-contrast radiology in erosive gastritis. *AJR* **1982**; 138:263–266
6. Catalano D, Pagliari U. Gastroduodenal erosions: radiological findings. *Gastrointest Radiol* **1982**;7:235–240
7. Thoeni RF, Goldberg HI, Ominsky S, Cello JP. Detection of gastritis by single- and double-contrast radiography. *Radiology* **1983**;148:621–626
8. Henning N. *Lehrbuch der Verdauungskrankheiten.* Stuttgart: Georg-Thieme, **1956**:118
9. Green PHR, Gold RP, Marboe CC, Weinberg LM, Goldfarb JP, Brasitus TA. Chronic erosive gastritis: clinical, diagnostic, and pathological features in nine patients. *Am J Gastroenterol* **1982**;77:543–547
10. McLean AM, Paul RE Jr, Philipps E, et al. Chronic erosive gastritis—clinical and radiological features. *J Can Assoc Radiol* **1982**;33:158–162
11. Laufer I, Hamilton J, Mullens JE. Demonstration of superficial gastric erosions by double contrast radiography. *Gastroenterology* **1975**;68:387–391
12. Nanaumi K. X-ray appearance of comb erosion. *Rinsho Hoshasen* **1980**;25:1223–1225
13. Tragardh B, Wehlin L, Ohashi K. Radiologic appearance of complete gastric erosions. *Acta Radiol [Diagn]* (Stockh) **1978**;19:634–642
14. Kawai K, Masaki F, Murakami K, Masuda K. The evolution of the erosion. *Gastroenterol Jpn* **1968**;1:377–380
15. Katz D, Siegel HI. Erosive gastritis and acute gastrointestinal mucosal lesions. In: Glass GBJ, ed. *Progress in gastroenterology*, vol. 1. New York: Grune & Stratton, **1968**:67–96
16. Katoh Y, Kuga H, Harada T. A clinical study of longitudinal linear redness on the gastric mucosa. *Gastroenterol Endoscopy* **1985**;27:362–369

Forthcoming Articles

SPECIAL ARTICLES

Caldwell lecture. Armchair research and the practicing radiologist. *Felson B*

ARRS Executive Council Award paper. MR imaging of the lumbar spine: anatomic correlations and the effects of technical variations. *Reicher MA, Gold RH, Halbach VV, Rauschning W, Wilson GH, Lufkin R*

Pictorial essay. The retroperitoneal spaces revisited. *Dodds WJ, Darweesh RMA, Lawson TL, et al.*

THORACIC RADIOLOGY

Radiographic manifestations of bronchiolitis obliterans with organizing pneumonia vs usual interstitial pneumonia. *Chandler PW, Shin MS, Friedman SE, Myers JL, Katzenstein A*

CT of esophageal-pleural fistulae. *Wechsler RJ*

Postoperative recurrence of lung cancer: detection by whole-body gallium scintigraphy. *Hatfield MK, MacMahon H, Ryan JW, et al.*

GASTROINTESTINAL RADIOLOGY

The diagnosis of acute acalculous cholecystitis: a comparison of sonography, scintigraphy, and CT. *Mirvis SE, Vainright JR, Nelson AW, et al.*

Morphine-augmented cholescintigraphy in the diagnosis of acute cholecystitis. *Kim EE, Pjura G, Lowry P, Nguyen M, Pollack M*

Pseudotumor of the quadrate lobe in hepatic sonography: a sign of generalized fatty infiltration. *Sauerbrei EE, Lopez M*

Anomalous hepatic duct inserting into the cystic duct: a report of three cases. *Reid SH, Cho S-R, Shaw C-I, Turner MA*

Benign pancreatic insulinoma: preoperative and intraoperative sonographic localization. *Gorman B, Charboneau JW, James EM, et al.*

Case report. Spontaneous rupture of a pancreatic pseudocyst into the portal venous system. *Takayama T, Kato K, Sano H, Katada N, Takeichi M*

Retractile mesenteritis involving the colon: barium enema, sonography, and CT findings. *Perez-Fontan FJ, Soler R, Sanchez J, Iglesias P, Sanjurjo P, Ruiz J*

Case report. CT diagnosis of primary small bowel volvulus. *Jaramillo D, Raval B*

SKELETAL RADIOLOGY

Gaucher's disease type 1: assessment of bone involvement by CT and scintigraphy. *Hermann G, Goldblatt J, Levy RN, Goldsmith SJ, Desnick RJ, Grabowski GA*

GENITOURINARY RADIOLOGY

MR imaging of renal transplants. *Baumgartner BR, Nelson RC, Ball TI, et al.*

Commentary. The differential diagnosis of renal transplant rejection: is MR imaging the answer? *Halasz NA*

The role of excretory urography in patients with prostatism. *Bundrick TJ, Katz PG*

Case report. Congenital urethral polyp. *Caro PA, Rosenberg HK, Snyder HM III*

NEURORADIOLOGY

CT changes in dementing diseases: a review. *LeMay M*

Neuroradiologic findings in AIDS; a review of 200 cases. *Levy RM, Rosenbloom S, Perrett LV*

MR and CT of occult vascular malformations of the brain. *New PFJ, Ojemann RG, Davis KR, et al.*

Penetrating vascular injuries of the face and neck: clinical and angiographic correlation. *North CM, Ahmadi J, Segall HD, Zee C-S*

Editorial. Angiography in penetrating neck injuries. *Quencer RM*

INTERVENTIONAL RADIOLOGY

Interventional radiology rounds. Interventional radiologic management of sclerosing cholangitis. *Kerlan RK, LaBerge JM, Goldberg HI, Pogany AC, Ring EJ*

Percutaneous aspiration and drainage of pancreatic pseudocysts. *Torres WE, Evert MB, Baumgartner BR, Bernardino ME*

Technical note. Basket extraction of esophageal foreign bodies. *Shaffer HA Jr, Alford BA, de Lange EE, Meyer GA, McIlhenny J*

Technical note. Effect of suction on biopsy sample size. *Hueftle MG, Haaga JR*

Technical note. A method for retrieval of retained subcutaneous catheter fragments. *Sibbitt RR, Palmaz JC, Garcia F*

Case report. Small bowel obstruction due to an intestinal balloon: treatment by percutaneous needle puncture. *Sato Y, Frey E, Foderaro A, Pringle KC*

ANGIOGRAPHY

A comparison of techniques for improved visualization of the arteries of the distal lower extremity. *Cohen MI, Vogelzang RL*

Technical note. Lower extremity venography: value of femoral vein compression. *Smith TP, Cardella JF, Darcy MD, Hunter DW, Castaneda-Zuniga WR, Amplatz K*

PEDIATRIC RADIOLOGY

MR evaluation of the portal vein in pediatric liver transplant candidates. *Day DL, Letourneau JG, Allan BT, Ascher NL, Lund G*

Imaging of acute renal infection in children. *Sty JR, Wells RG, Starshak RJ, Schroeder BA*

Pediatric hypertrophic gastropathy. *Marks MP, Lanza MV, Kahlstrom EJ, Mikity V, Marks SC, Kvalstad RP*

MAGNETIC RESONANCE

Technical note. A technique for image salvage in MR imaging. *Lund G, Morin R*

OBSTETRIC AND FETAL SONOGRAPHY

Sonographic findings in abdominal pregnancy. *Stanley JH, Horger EO III, Fagan CJ, Andriole JG, Fleischer AC*

Fetal omphalocele and gastroschisis: a review of 24 cases. *Bair JH, Russ PD, Pretorius DH, Manchester D, Manco-Johnson ML*

RADIOLOGIC LITERATURE

The scientific literature in diagnostic radiology for American readers: a survey and analysis of journals, papers, and authors. *Chew FS*

MISCELLANEOUS

The fibromatoses: CT-pathologic correlation. *Francis IR, Dorovini-Zis K, Glazer GM, Lloyd RV, Amendola MA, Martel W*

CT of fibrous tissues and fibrous tumors with sonographic correlation. *Rubenstein WA, Gray G, Aun YH, et al.*

COMPUTER PAGE

Computer page. Some applications for a personal computer database system in radiology. *Sommer G*

CT of Appendicitis

Emil J. Balthazar[1]
Alec J. Megibow
Donald Hulnick
Richard B. Gordon
David P. Naidich
Elliot R. Beranbaum

The CT findings of 38 consecutive patients with acute appendicitis are analyzed, described, and illustrated. CT showed intraabdominal disease in 92% of patients and made a specific diagnosis of appendicitis in 79% of cases. The most common CT findings were pericecal inflammation (68%), abscess (55%), calcified appendicolith (23%), and an abnormal appendix (18%). CT had a sensitivity similar to that of contrast enema examinations, but it correlated much better with the surgical findings in detecting the precise nature, extent, and location of the disease process. Normal CT does not exclude appendicitis, since mild forms without periappendiceal disease may escape detection.

The diagnosis of appendicitis is usually made on the basis of clinical and laboratory findings. In clinical practice, however, many patients with atypical presentations require radiographic examinations for diagnosis or confirmation. While the usefulness and shortcomings of plain abdominal films and barium enema examinations are well established [1–13], the sensitivity and potential role of CT in the diagnosis of appendicitis have not yet been adequately analyzed and reported in the literature [14–16]. Recently, the high-resolution images obtained with the new-generation CT scanners have permitted a more comprehensive evaluation of other primary inflammatory intestinal lesions, such as Crohn's disease and diverticulitis [17–22]. These findings prompted us to review the cases of 38 consecutive patients with proven appendicitis who were examined at our institution during the past 4 years. This report attempts to assess the role played by CT in the diagnosis and evaluation of patients with acute appendicitis. We will (1) describe and illustrate the specific and suggestive CT findings, (2) analyze the sensitivity and pitfalls of CT diagnosis, and (3) compare and correlate CT features with those seen on plain films and barium enema examinations.

Normal Appendix

During routine CT abdominal examinations the appendix is seldom visualized. Visualization depends in great measure on the amount of intraperitoneal fat, the adequate demonstration of terminal ileal loops and cecum, the type and quality of CT examination, and the diligence of the examiner. Depending on its orientation, the normal appendix appears as a small tubular or ringlike density in the right lower abdomen (Fig. 1). It can be fluid- or air-filled and has a thin wall and sharp outer contour. It is enveloped by the homogeneous fat density of the normal mesenteric structures and may be located in the pelvis or posterior to the right colon in a retrocecal position. Appendicoliths may be seen in asymptomatic individuals presenting as ringlike or homogeneous calcific densities associated with a normal-looking appendix. Without the expected inflammatory changes indicative of appendicitis, the presence of air, fecal matter, or calcifications in the appendix has no immediate clinical implications.

Received March 6, 1986; accepted after revision May 6, 1986.

[1] All authors: Department of Radiology, NYU Medical Center, 550 1st Ave., New York, NY 10016. Address reprint requests to E. J. Balthazar, Dept. of Radiology, Bellevue Hospital, 1st Ave. and 27th St., New York, NY 10016.

AJR 147:705–710, October 1986
0361–803X/86/1474–0705
© American Roentgen Ray Society

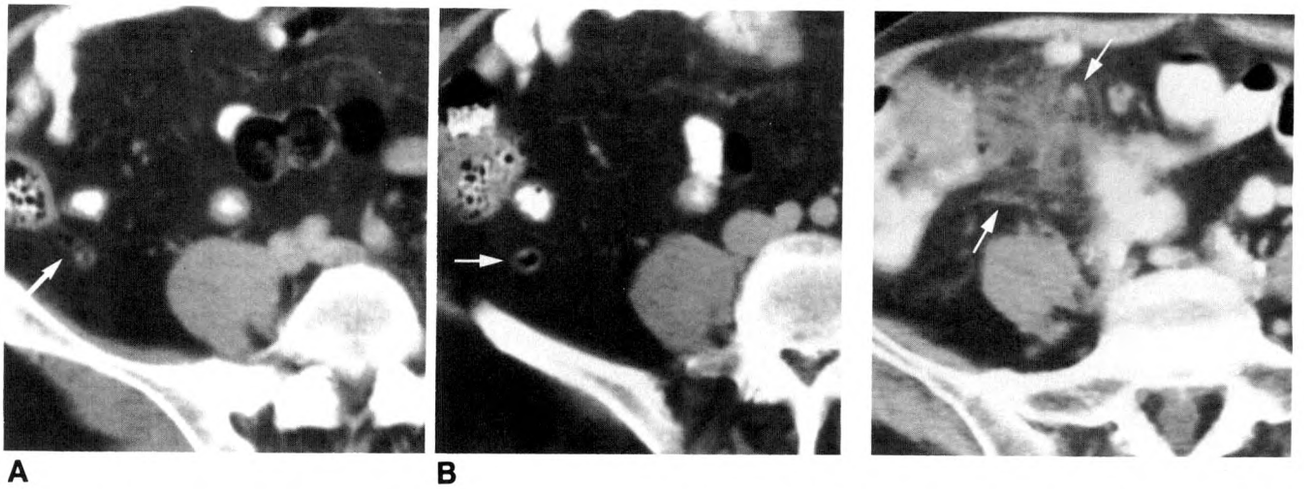


Fig. 1.—Normal appendix. **A**, Small, thin-walled tubular structure is seen arising from a partially distended, fecal-filled cecum (*arrow*). Terminal ileum is filled with barium. **B**, Adjacent section shows appendix as a small, air-filled ringlike structure with a sharp inner and outer contour (*arrow*).

Fig. 2.—Acute appendicitis with severe pericecal inflammation. Hazy, ill-defined, linear, and streaky densities are seen in right lower quadrant (*arrows*). Process is focal and is located inferior and medial to the cecum and adjacent to terminal ileal loops.

Materials and Methods

This series included 38 patients with acute appendicitis, all proven by surgery and pathologic examination. There were 27 men and 11 women with an age range of 16 to 80 years and a mean age of 43.3 years. The clinical presentation was generally suggestive of an intraabdominal septic process, but many patients had atypical features such as pyuria, hematuria, normal white blood count, pain without localized tenderness, small-bowel obstruction, and normal temperature. For this reason radiographic examinations, including CT, were requested and performed to assess the presence, origin, and extent of the suspected intraabdominal disease. All patients had plain abdominal radiographs and CT examinations done within 48 hr of admission, and in 19 patients, contrast enemas (barium or water soluble contrast material) were also performed. In most patients CT was performed initially, and in all cases the CT findings were interpreted without the knowledge of the barium enema results. CT examinations were done on 8800 and 9800 GE units using standard techniques. Unless contraindicated, patients received an IV infusion of contrast material, and 36 patients were given 750–800 ml of diluted barium solution 40 to 45 min before scanning. Transaxial images 10 × 10 mm (21 patients) and 10 × 15 mm (17 patients) were obtained initially. In addition, in five patients 5 × 5 mm sections over the region of interest were repeated.

Results

On the basis of the original CT interpretation, a diagnosis of acute appendicitis was made in 30 patients (79%) but was missed in eight patients (21%). In this latter group, CT was reported as normal in three patients (8%), but showed intraabdominal disease interpreted to be of a different origin in five patients.

Pericecal inflammation appearing as a hazy, ill-defined, increased density of the pericolic fat was the most common finding (26 patients, 68%) (Fig. 2). The process was either localized, usually adjacent and medial to the cecum, or more diffuse involving a larger portion of the mesentery. It was seen alone or associated with other findings; it commonly contained linear and streaky densities and occasionally acted as a phlegmonous mesenteric mass displacing adjacent ileal loops (Fig. 2).

Abscesses were the second most common abnormalities and were seen in 21 patients (55%). They appeared as extraluminal, low-attenuated fluid collections that were either ill defined or partially encapsulated (15 patients) (Fig. 3) or as mixed soft-tissue and fluid densities accompanied by blurring and thickening of the surrounding fascial planes (6 patients) (Fig. 4). Abscesses varied in size from 2 to 10 cm and were located (in order of frequency) (1) in the right lower quadrant medial to cecum, (2) in the pelvis, (3) posterior to the ascending colon, or (4) within the right paracolic gutter. In this series, three abscesses had air-fluid levels.

Appendicoliths were seen in nine patients (24%), appearing either as a ringlike (Fig. 3) or as a homogeneous round calcific density. They were located in the right lower abdomen in the vicinity of the cecum and were always accompanied by a focal inflammatory reaction or an adjacent abscess (Fig. 3). Solitary appendicoliths were seen in eight patients, and two small appendicoliths were present in one patient.

An abnormal appendix was identified in seven patients (18%). The appendix was located in the right pelvis, inferior to the cecum and adjacent to barium-filled intestinal loops (Figs. 5 and 6). On cross section it appeared as a ringlike structure having a symmetrically and circumferentially thickened wall and an associated periappendiceal inflammatory reaction. The lumen was either slightly distended and fluid-filled (Fig. 5) or almost totally collapsed (Fig. 6).

Small regional mesenteric nodes were seen in two patients (5%). Three patients (8%) had evidence of mechanical small-bowel obstruction presenting with markedly distended, fluid-filled intestinal loops and a collapsed colon. Circumferential thickening of the wall of the cecum and terminal ileum and regional mesenteric inflammation were identified in two pa-

Fig. 3.—Appendiceal abscess. Extraluminal, ill-defined fluid collection is present in right lower quadrant (*arrows*). Ringlike calcification (*arrowhead*) represents an appendicolith.

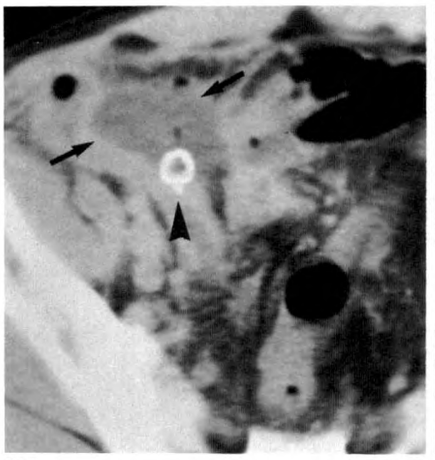
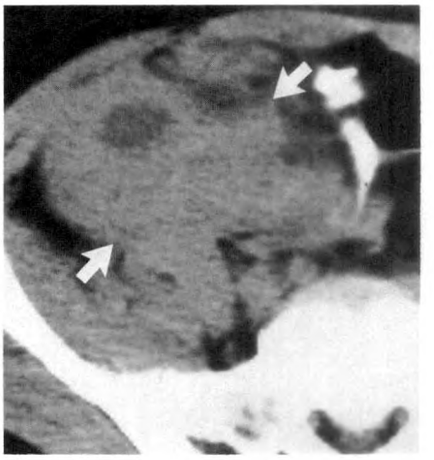
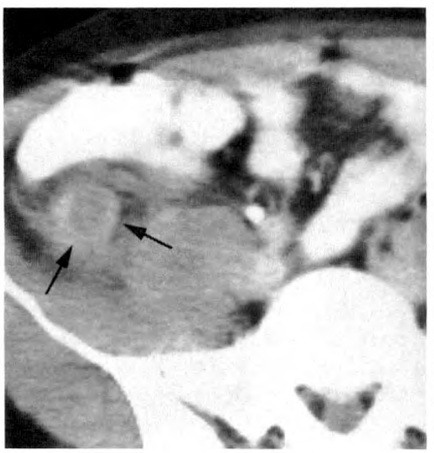
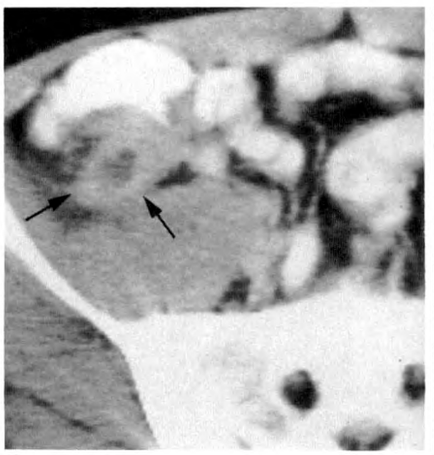


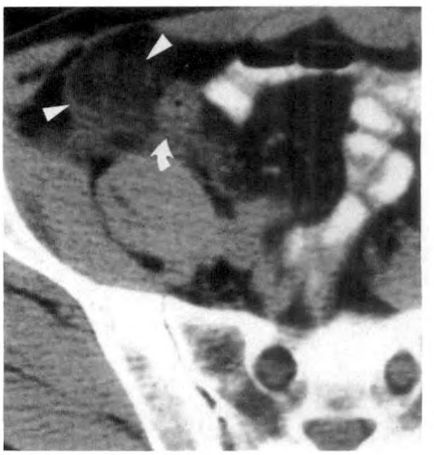
Fig. 4.—Appendiceal abscess presenting as a large soft-tissue density with areas of decreased attenuation (*arrows*) displacing adjacent small-bowel loops.



3 4







A B

Fig. 5.—Acute appendicitis with demonstration of an abnormal appendix. Cross section (**A**) and a slightly oblique section (**B**) demonstrate fluid-filled thick-walled appendix (*arrows*) and periappendiceal inflammatory changes. Surgery revealed a markedly distended and inflamed appendix measuring 8.5 × 1.3 cm.

Fig. 6.—Appendicitis causing symmetric thickening of appendix (*arrow*) and evidence of inflammation in adjacent fat (*arrowheads*).

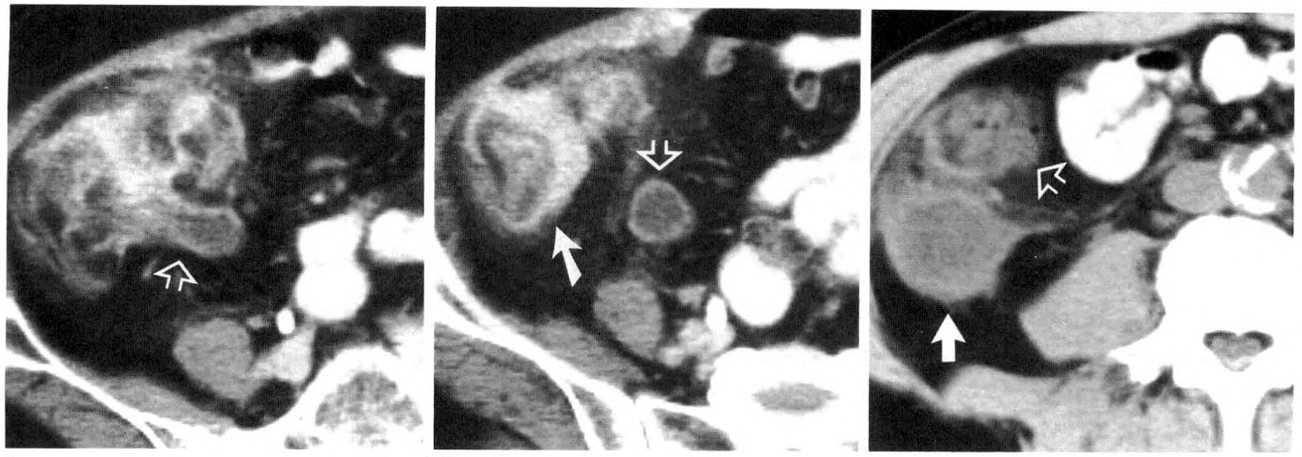
tients (5%). The bowel wall was dense, probably secondary to contrast enhancement, and the appearance was similar to other inflammatory processes, particularly Crohn's disease (Fig. 7).

CT Contrast Enema Correlation

In five cases (13%), calcified appendicoliths were recognized on plain abdominal films. In addition to the CT studies, contrast enema examinations were performed in 19 patients. In this group, 18 had abnormal CT examinations (sensitivity 94%) and 17 had abnormal contrast studies consistent with appendicitis (sensitivity 89%). There were two cases with abnormal CT and normal contrast enema examinations (Fig. 8) and one case with normal CT but positive contrast enema. Contrast enema studies missed retrocolic abscesses in two patients with retrocecal appendices, and CT failed to visualize a pericecal abscess in a patient with distended, fluid-filled small-bowel loops. Calcified appendicoliths were visualized almost twice as often on CT (24%) as on conventional studies (13%); however, the sensitivity of CT and contrast studies to diagnose appendicitis was approximately equal in this series.

Discussion

Although some of the CT findings of appendicitis have been described [14–16], the role of CT in the diagnosis and evaluation of patients with acute appendicitis has not been previously evaluated. CT has been shown to be a valuable adjunct to conventional contrast enema and to be particularly useful in diagnosing severe forms of appendicitis associated with phlegmons or periappendiceal abscesses. Like other



A B

Fig. 7.—Pericecal phlegmon secondary to perforated appendicitis. **A**, At level of ileocecal junction, CT reveals pericecal inflammation and enhancement of wall of terminal ileum (*open arrow*). **B**, Adjacent section shows markedly thickened cecal wall (*solid arrow*) and slight wall thickening of terminal ileum (*open arrow*). CT and surgical findings were consistent with Crohn's disease. Pathologic specimen revealed indurated and chronically inflamed terminal ileum and cecum secondary to perforated appendix.

Fig. 8.—Retrocecal appendicitis. CT examination reveals an encapsulated fluid collection representing an abscess (*solid arrow*) located posterior to ascending colon (*open arrow*). Barium enema showed no abnormalities.

radiographic methods, CT is performed mainly in patients presenting with atypical clinical and laboratory findings when the diagnosis is unknown or when an intraperitoneal inflammatory process is suspected, but the therapeutic approach is based mainly on the radiographic confirmation. This is the case for the use of CT in this series of cases. These patients are not representative of all patients with appendicitis since they had atypical clinical features, a greater mean age, and were selected by clinicians for radiographic examinations. Depending on the severity of the disease and the time of the examination, the CT findings should be expected to vary in different series.

In this series of patients with proven appendicitis, the CT examination established the presence of intraabdominal disease in 35 cases (92%), while making a specific diagnosis in 30 cases (79%). A retrospective analysis of the CT studies indicates that various radiographic features have different diagnostic significance. They can be divided into primary and secondary signs: (1) Primary signs are represented by the demonstration of a diseased appendix and/or appendicolith with associated inflammatory response in the pericecal fat. These findings can be considered pathognomonic. They were present in 13 patients (34%) in our series. (2) Secondary signs such as pericecal inflammation and/or pericecal, retrocecal, and right paracolic abscesses are highly suggestive and were seen in 15 cases (39%) in our series. Mesenteric or pelvic phlegmons or abscesses far away from the cecal caput, particularly in the pelvis (Fig. 9), are additional secondary signs compatible with but not diagnostic of appendiceal disease. They were present in 10 patients (26%) in our series. Because of the mobility of the right colon as well as variations in the size and position of the appendix, abscesses of appendiceal origin often have an unexpected intraperitoneal or retroperitoneal location. They may be located in the left pelvis, subhepatic space, or in the mesentery between loops of small bowel, making their origins difficult to identify (Figs. 9 and 10).

Among the eight cases in which the diagnosis of appendicitis was missed, three were interpreted as normal and five were incorrectly diagnosed. In the former group two patients had proven appendicitis with small appendices and without periappendiceal disease and one had an appendiceal abscess. A second abscess was missed on CT in a patient with small-bowel obstruction. In both cases the abnormal fluid collections were interpreted as loops of bowel not opacified with barium at the time of the examination. A complete opacification of the distal ileal loops and cecum is essential in the CT diagnosis of an appendiceal abscess. Terminal ileal loops and cecum should be clearly identified either with positive contrast or by repetition of the examination after air insufflation of the colon. A fluid-filled cecum that can be seen occasionally, even when the ascending colon is filled with barium, may be misinterpreted as an abscess and lead to a diagnostic error. Although calcified appendicoliths may occasionally be missed when the distal bowel is opacified, we consider it more important to be able to identify small interloop abscesses in this group of patients (Fig. 10). In addition, we think that most appendicoliths can still be visualized despite the presence of barium in the bowel (Fig. 3).

Among the five patients with misdiagnosed abnormal CT scans, two were considered to have diverticulitis, one pelvic inflammatory disease, one Crohn's disease, and one simple small-bowel obstruction. Because of the nature of our study, false-positive examinations were not surveyed. In the same period of time, however, we have seen a few patients with pericecal fluid collections or abnormal fat in whom an erroneous initial CT diagnosis of appendicitis was made. In the absence of primary CT signs, the diagnosis of appendicitis should be made with caution and should include a careful

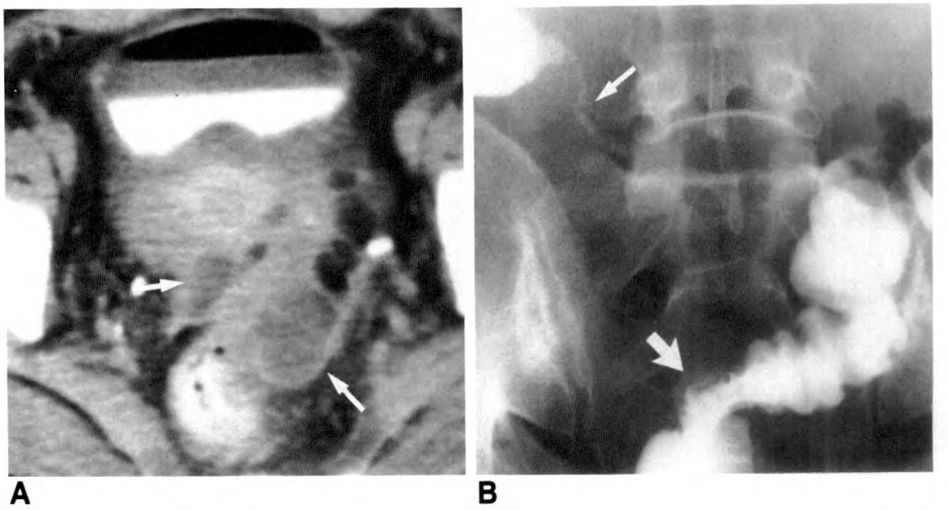


Fig. 9.—Appendiceal perforation presenting as a pelvic abscess in a 54-year-old woman. **A**, CT shows fluid collections in pelvis adjacent to sigmoid colon (*arrows*). CT findings can be misinterpreted as sigmoid diverticulitis. Air in bladder is secondary to a Foley catheter. **B**, Barium enema visualizes partially filled appendix (*small arrow*) and narrowed and slightly spiculated sigmoid colon (*large arrow*).

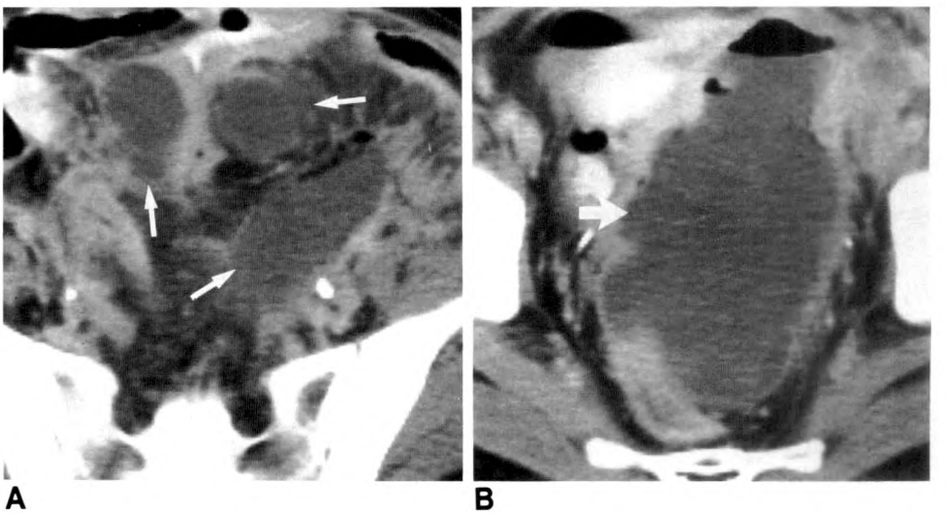


Fig. 10.—Perforated appendicitis with peritonitis in 28-year-old man. **A**, Multiple ill-defined mesenteric abscesses are visualized in lower abdomen (*arrows*). **B**, Large abscess containing an air-fluid level is seen in pelvis (*arrow*).

clinical evaluation and a contrast enema study when indicated.

Other entities can present with pericolic or pelvic phlegmons or abscesses and thus mimic appendicitis. Conditions such as cecal diverticulitis, typhlitis, foreign-body perforations, pelvic inflammatory disease, Crohn's disease, and, in older individuals, perforated cecal carcinoma should be considered in the differential diagnosis. Occasionally patients with pancreatitis, trauma, or loculated ascetic fluid may show suspicious ill-defined pericecal fluid collections. In most cases, the demonstration of an intraabdominal abscess requires surgical drainage independent of the cause of the abscess. A careful history and clinical evaluation in addition to a thorough CT evaluation of the entire abdomen can establish the correct preoperative diagnosis in most patients. When the diagnosis is in doubt, contrast enema studies should be performed.

CT examinations, like contrast enema studies, can miss appendicitis, particularly when the inflammation is mild and the appendix is not visualized. Compared with contrast enema, CT correlates far better with the surgical and pathologic findings, distinguishes phlegmons from abscesses, shows disease directly rather than inferentially, and provides a more exact evaluation of the extent and location of intraabdominal disease. In addition, CT can detect disease in the solid organs or peritoneal cavity, such as abscesses or metastatic disease, that are clinically unsuspected. The CT demonstration of a normal appendix excludes appendicitis; however, the appendix is seldom seen during routine examinations. Contrast enema, on the other hand, can exclude appendicitis by demonstrating a contrast-filled appendix.

In our experience, CT has been a sensitive and noninvasive method of diagnosing appendicitis in patients presenting with atypical clinical features and suspected of harboring intraabdominal sepsis. In our group of patients with acute appendicitis, CT demonstrated intraabdominal disease in 92% while

making a specific diagnosis in 79% of cases. A normal CT examination does not exclude appendicitis, because mild forms without periappendiceal disease may escape detection and abscesses can be missed if terminal ileal loops and cecum are not adequately visualized. CT and contrast enema studies should be considered complementary examinations. At this time, we advocate the primary use of CT imaging in these patients for the following reasons: (1) CT has a high sensitivity in diagnosing acute appendicitis similar to that of barium enema; (2) It provides a more precise evaluation of the nature, extent, and location of the pathologic process; and (3) It can detect intraabdominal disease unrelated to appendicitis that explains the patient's clinical presentation. When the diagnosis is in doubt, contrast enema examinations are very helpful in establishing or excluding acute appendicitis.

ACKNOWLEDGMENT

The authors wish to thank Jane Crafts for manuscript preparation.

REFERENCES

1. Steinert R, Hareide I, Christiansen T. Roentgenologic examination of acute appendicitis. *Acta Radiol* (Stockh) **1943**;24:13–37
2. Brooks DW, Killen DA. Roentgenographic findings in acute appendicitis. *Surgery* **1965**;57:377–384
3. Rulfs DM, Fisher RG. Radiographic findings in acute appendicitis. *Tex Med* **1971**;67:89–93
4. Smith DE, Kirchmer NA, Stewart DR. Use of the barium enema in the diagnosis of acute appendicitis and its complications. *AJR* **1979**;138:829–834
5. Shimkin PM. Radiology of acute appendicitis. *AJR* **1978**; 130:1001–1004
6. Graham AD, Johnson HF. The incidence of radiographic findings in acute appendicitis compared to 200 normal abdomens. *Milit Med* **1966**;131:272–276
7. Fagenberg D. Fecaliths of the appendix: incidence and significance. *AJR* **1963**;89:752–759
8. Beneventano TC, Schein CJ, Jacobson HG. The roentgen aspects of some appendiceal abnormalities. *AJR* **1966**;96:344–360
9. Vaudagna JS, McCort JJ. Plain film diagnosis of retrocecal appendicitis. *Radiology* **1975**;117:533–536
10. Fedyshin P, Kelvin FM, Rice RP. Nonspecificity of barium enema in acute appendicitis. *AJR* **1984**;143:99–102
11. Halls JM, Meyers HI. Acute appendicitis with abscess simulating carcinoma of the sigmoid. *AJR* **1977**;129:1057–1059
12. Harned RK. Retrocecal appendicitis presenting with air in the subhepatic space. *AJR* **1976**;126:416–418
13. Meyers MA, Oliphant M. Ascending retrocecal appendicitis. *Radiology* **1974**;110:295–299
14. Fish B, Smulewicz JJ, Barek L. Role of computed tomography in diagnosis of appendiceal disorders. *NY State J Med* **1981**;81:900–904
15. Jones B, Fishman EK, Siegelman SS. Computed tomography and appendiceal abscess: special applicability in the elderly. *J Comput Assist Tomogr* **1983**;7:434–438
16. Gale ME, Birnbaum S, Gerzof SG, Sloan G, Johnson WC, Robbins AH. CT appearance of appendicitis and its local complications. *J Comput Assist Tomogr* **1985**;9:34–37
17. Berliner L, Redmond P, Purow E, Megna D, Sottile V. Computed tomography in Crohn's disease. *Am J Gastroenterol* **1982**; 77:548–553
18. Goldberg HJ, Gore RM, Margulis AR, Moss AA, Baker EL. Computed tomography in the evaluation of Crohn disease. *AJR* **1983**;140:277–282
19. Frager DH, Goldman M, Beneventano TC. Computed tomography in Crohn disease. *J Comput Assist Tomogr* **1983**;7:819–824
20. Kerber GW, Greenberg M, Rubin JM. Computed tomography evaluation of local and extraintestinal complications of Crohn's disease. *Gastrointest Radiol* **1984**;9:43–48
21. Hulnick MA, Megibow AJ, Balthazar EJ, Naidich DP, Bosniak MA. Computed tomography in the evaluation of diverticulitis. *Radiology* **1984**;152:491–495
22. Lieberman JM, Haaga Jr. Computed tomography of diverticulitis. *J Comput Assist Tomogr* **1983**;7:431–433

Hepatic Hemangioma: Dynamic Bolus CT

Patrick C. Freeny[1]
William M. Marks

Forty-seven patients with 58 hepatic hemangiomas were studied prospectively with a dynamic bolus CT protocol (single-level or incremental scans) that included precontrast scans, rapid-sequence scanning during the IV bolus injection of 150 ml of 60% contrast agent, and delayed scans taken as long as 60 min after contrast. Three CT criteria are believed to be necessary to make a specific diagnosis of hemangioma: (1) lesion with diminished attenuation on precontrast scan; (2) peripheral contrast enhancement during the dynamic bolus phase of scanning; and (3) complete isodense fill-in on delayed scans obtained up to 60 min after contrast. These CT criteria were seen in only 32 (55%) of 58 hemangiomas, making CT a relatively poor imaging technique for diagnosis.

Hemangioma is the most common benign hepatic neoplasm and has a frequency on autopsy of about 4% [1]. As hemangiomas are usually asymptomatic, most frequently they are discovered incidentally by abdominal imaging studies, such as sonography, CT, or radionuclide hepatic scintigraphy [2–4]. Once a hepatic lesion is detected, however, a specific diagnosis should be made to exclude a primary or metastatic malignant lesion, especially in an oncology patient.

Previous reports [3, 5–9] have suggested that CT is an accurate and efficient method for diagnosing hepatic hemangioma. However, a review of these reports reveals that a variety of techniques were used for CT evaluation of the liver and that the hemangiomas manifested a broad spectrum of morphologic patterns, thus raising questions about the specificity of the CT diagnosis.

We therefore designed a prospective CT protocol for evaluation of focal liver lesions suspected of being hemangiomas. This report describes the results of this protocol and presents our current approach to the evaluation of patients with incidentally detected hepatic lesions.

Subjects and Methods

Forty-seven patients with 58 hemangiomas were studied with single-level or incremental bolus dynamic CT and delayed scanning. In this group were 32 women and 15 men; their average age was 54 years (range, 30 to 72 years). Single lesions were present in 38 patients, two lesions in seven patients, and three lesions in two patients.

Techniques of Computed Tomography

CT scans were obtained using a General Electric CT/T 8800 scanner (scan speed, 4.5 sec for single-level bolus dynamic scans and 9.6 sec for precontrast and delayed scans) or 9800 scanner (scan speed, 2 sec for all scans).

Single-level bolus dynamic scans.—Single-level bolus dynamic scans were obtained in 44 patients with known hepatic lesions. Non–contrast-enhanced scans were obtained of the entire liver at 10-mm intervals to localize the lesions. Single-level bolus dynamic CT scans were then obtained at the level that contained either the largest lesion or the greatest number of lesions. Using a scan speed of 4.5 sec (8800 scanner) or 2 sec (9800 scanner), four groups

Received February 28, 1986; accepted after revision May 5, 1986.

Presented at the annual meeting of the American Roentgen Ray Society, Washington, DC, April 1986.

[1] Both authors: Department of Radiology, The Mason Clinic, P.O. Box 900, 1100 9th Ave., Seattle, WA 98111. Address reprint requests to P. C. Freeny.

AJR 147:711–719, October 1986
0361–803X/86/1474–0711
© American Roentgen Ray Society

of four 10-mm collimated scans were obtained with a 2.5-sec interscan delay and a 10-sec intergroup delay (to allow for patient breathing). Scanning was begun simultaneously with the IV bolus injection of 150 ml of a 60% iodinated contrast agent (42 g of iodine). The contrast agent was injected by hand over 1.5–2 min using a butterfly needle placed in a peripheral vein. This technique proved to be simple to perform, and few if any patients experienced difficulty with breath-holding.

With the 4.5-sec scan speed, 16 single-level bolus dynamic images were obtained in 132 sec (average of one scan per 8.25 sec). Thus, the last five scans were collected during a range of 2 to 37.5 sec after the completion of injection of a 90-sec contrast bolus, or the last two scans were collected during a range of 0.5 to 7.5 sec after the completion of injection of a 120-sec contrast bolus. With the 2-sec scan speed, 16 single-level bolus dynamic images were obtained in 92 sec (average of one scan per 5.75 sec). Thus, essentially all of the scan images were obtained during the 90–120-sec bolus injection of contrast agent.

Delayed scans were obtained at 5, 10, 15, 20, 30, 45, and 60 min, unless the lesion became isodense, at which time the delayed-scan sequence was stopped in most cases. One patient with a giant hemangioma was rescanned at 90 min.

Incremental-bolus dynamic scans.—Incremental-bolus dynamic scans were obtained in three patients. Noncontrast scans were not obtained in these patients. The cranial and caudal limits of the hepatic scans were determined from a digitalized scout radiograph. Scans were obtained using automatic table incrementation, contiguous 10-mm collimated scans, and a scan speed of 2 sec. Groups of three scans were obtained with a 3.5-sec interscan delay and a 10-sec intergroup delay. The first scan was obtained after the initial 50 ml of the 150-ml bolus of 60% iodinated contrast agent had been injected (about 40 sec after the start of the bolus injection). The total bolus was delivered by hand over 1.5–2 min using a butterfly needle placed in a peripheral vein. Thus, the first 12 scans were collected during the 120-sec bolus injection, and the last six scans were collected at a range of 10 to 34 sec after the bolus was injected. Delayed scans were obtained at the level or levels of the lesions at 5, 10, 15, 20, 30, and 45 min after contrast injection. The delayed sequence was stopped if the lesion became isodense.

Initial Studies

Single-level bolus dynamic CT was performed after identification of the hepatic lesion by sonography in 29 patients, by radionuclide ^{99m}Tc-sulfur colloid liver scans in two patients, and after a routine incremental-bolus dynamic CT scan (without delayed images) in 13 patients. In the remaining three patients, the lesions were identified during incremental bolus dynamic scans, and delayed images were obtained.

Indications for the initial studies were right upper abdominal pain or discomfort (suspected gallbladder disease) in 10 patients; nonspecific epigastric or diffuse, nonlocalized abdominal pain or discomfort in 14 patients; evaluation of suspected renal abnormality in five patients; survey study for metastatic disease in 10 oncology patients; evaluation of the biliary tract for jaundice in one patient; and miscellaneous reasons in eight patients.

Liver function tests (bilirubin, serum glutamic oxaloacetic transaminase, and alkaline phosphatase) were normal in 44 patients and abnormal in two patients (one patient with jaundice and one with Gaucher's disease). Test results were not available in one patient.

Associated Diseases

Twenty-three patients had associated medical diseases. Thirteen patients had benign conditions. These included cholelithiasis in four patients; benign lung nodules in two patients; and one case each of cardiomyopathy, renal disease, immune complex syndrome, adrenal adenoma, Gaucher's disease, hepatic focal nodular hyperplasia, and pancreatic insulinoma. Ten patients had malignant tumors. Breast, cervical, and colon carcinomas were present or had been resected previously in two patients each, and one patient each had lung carcinoma, carcinoma of the ampulla, melanoma of the eye, and leukemia.

Final Diagnosis of Hemangioma

A diagnosis of hepatic hemangioma was made in 28 patients by selective hepatic angiography (10 patients), ^{99m}Tc red blood cell (RBC) radionuclide scan (six patients), surgical biopsy (11 patients), percutaneous biopsy (two patients), and autopsy (one patient). Several patients had more than one confirming study.

A presumed diagnosis of hepatic hemangioma was made in 19 patients: on the basis of clinical follow-up only (24 months or longer) in two patients; clinical follow-up plus no change on repeat sonography (6 months to 2 years) in 13 patients; and clinical follow-up plus repeat CT (6 months to 2 years) in four patients. In each case in which sonography or CT was performed, the lesions showed no change in size or morphology (with the exception of one patient with a surgically proved giant hemangioma, which became smaller after radiation therapy). All 19 patients are alive and well.

Results

Non–Contrast-Enhanced Scans

Fifty-five of 58 hemangiomas were identified initially on non–contrast-enhanced scans before single-level bolus dynamic scans were performed. Fifty-three of the 55 hemangiomas were of diminished attenuation relative to the surrounding hepatic parenchyma. One patient with diffuse fatty infiltration of the liver had two hemangiomas that were hyperdense before contrast injection.

Three patients with single hemangiomas had only incremental bolus dynamic scans, and initial non–contrast-enhanced scans were not obtained. However, in all three cases, the central portions of the lesions were hypodense relative to the surrounding hepatic parenchyma during the dynamic scan, and the lesions showed peripheral contrast enhancement; none arose in livers with CT evidence of fatty infiltration. We believe that, in these three cases, all three lesions would have been hypodense relative to the normal liver if non–contrast-enhanced scans had been obtained.

Dynamic Contrast-Enhancement Patterns

The patterns of dynamic contrast enhancement in the 58 scans were categorized as peripheral in 74% (43 hemangiomas) (Fig. 1); central (focal zone of contrast enhancement within the center of the lesion) in 12% (seven hemangiomas) (Fig. 2); diffuse (complete, homogeneous contrast enhancement of the entire lesion) in 2% (one hemangioma); mixed (central and peripheral) in 9% (five hemangiomas) (Fig. 3); and absent in 3% (two hemangiomas).

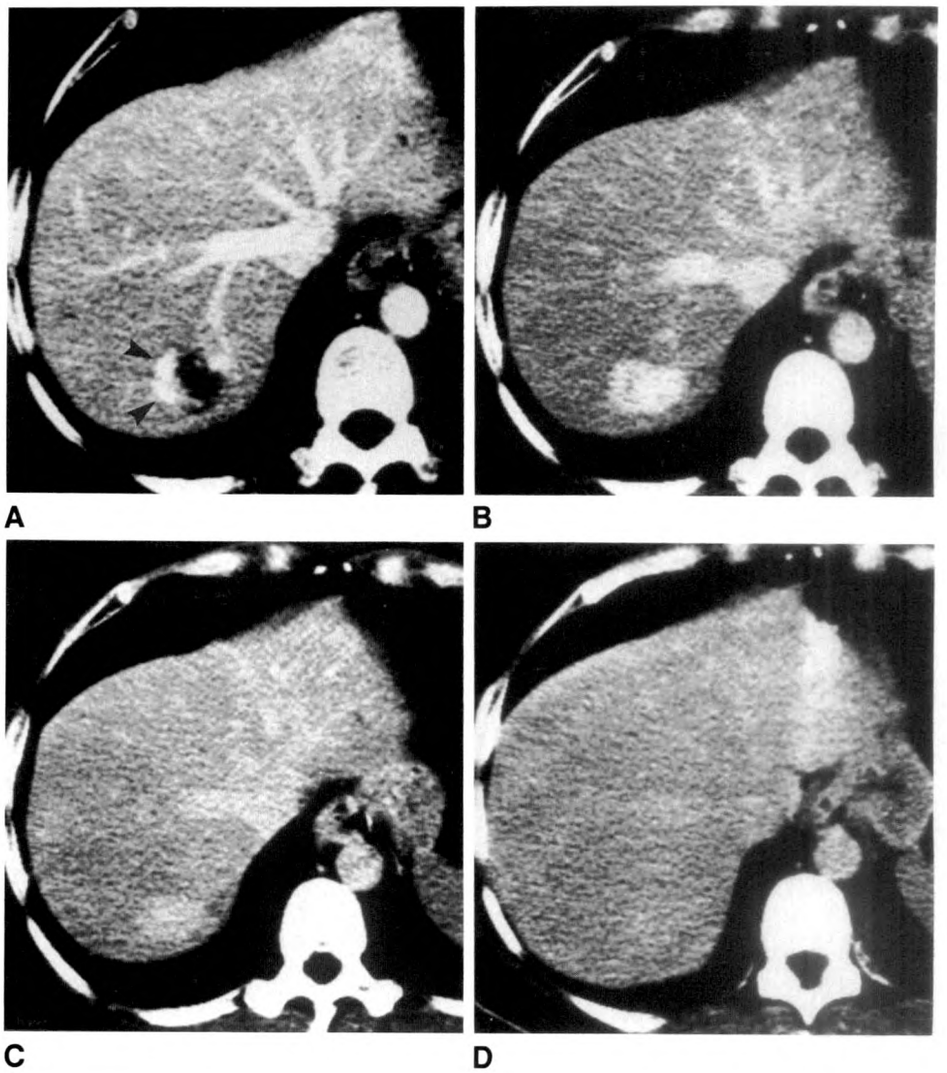


Fig. 1.—Typical hemangioma: single-level bolus dynamic scan.

A, Dynamic scan at 87 sec shows intense peripheral contrast enhancement of right-lobe lesion (*arrowheads*).

B, Delayed scan at 5 min shows diffuse contrast enhancement of lesion.

C, Delayed scan at 20 min shows persistent diffuse contrast enhancement.

D, Delayed scan at 30 min shows isodense lesion.

Delayed Patterns of Fill-in

The degree of isodense fill-in was categorized as complete in 72% (42 hemangiomas) (Figs. 1–3), partial (a remaining zone of diminished attenuation within the lesion) in 21% (12 hemangiomas) (Fig. 4), and none (no fill-in or decrease in lesion size) 7% (four hemangiomas). Included in the last group were two hemangiomas in the same patient that arose in a diffusely fatty liver. The lesions remained hyperdense on delayed scans and therefore were categorized as having no fill-in.

The time required to reach complete isodense fill-in was determined for each hemangioma (Fig. 5). There was no direct relationship to size and time required to reach isodense fill-in, although the largest lesion (12 cm) required the longest time (90 min). Only two of the 42 hemangiomas required more than 30 min to reach fill-in (45 and 90 min, respectively).

During the delayed scan sequences, 13 lesions remained diffusely hyperdense for 5–15 min before becoming isodense (Fig. 1). All lesions that were diffusely hyperdense became isodense. In five cases, delayed scans were obtained after isodense fill-in had occurred. These scans showed that the lesions subsequently returned to their precontrast appearance (hypodense relative to the surrounding hepatic parenchyma).

Discussion

The experience of several investigators has led to the suggestion that most hepatic hemangiomas can be diagnosed specifically by CT if certain characteristic patterns or appearances are recognized [3, 5–9]. However, for CT evaluation to be translated into a clinically useful method, the techniques of the CT examination and contrast administration must be similar, the characteristic morphologic patterns of the hemangiomas must be easily recognized and reproducible, and the patterns must be present in most cases to obviate additional diagnostic procedures, such as angiography or biopsy.

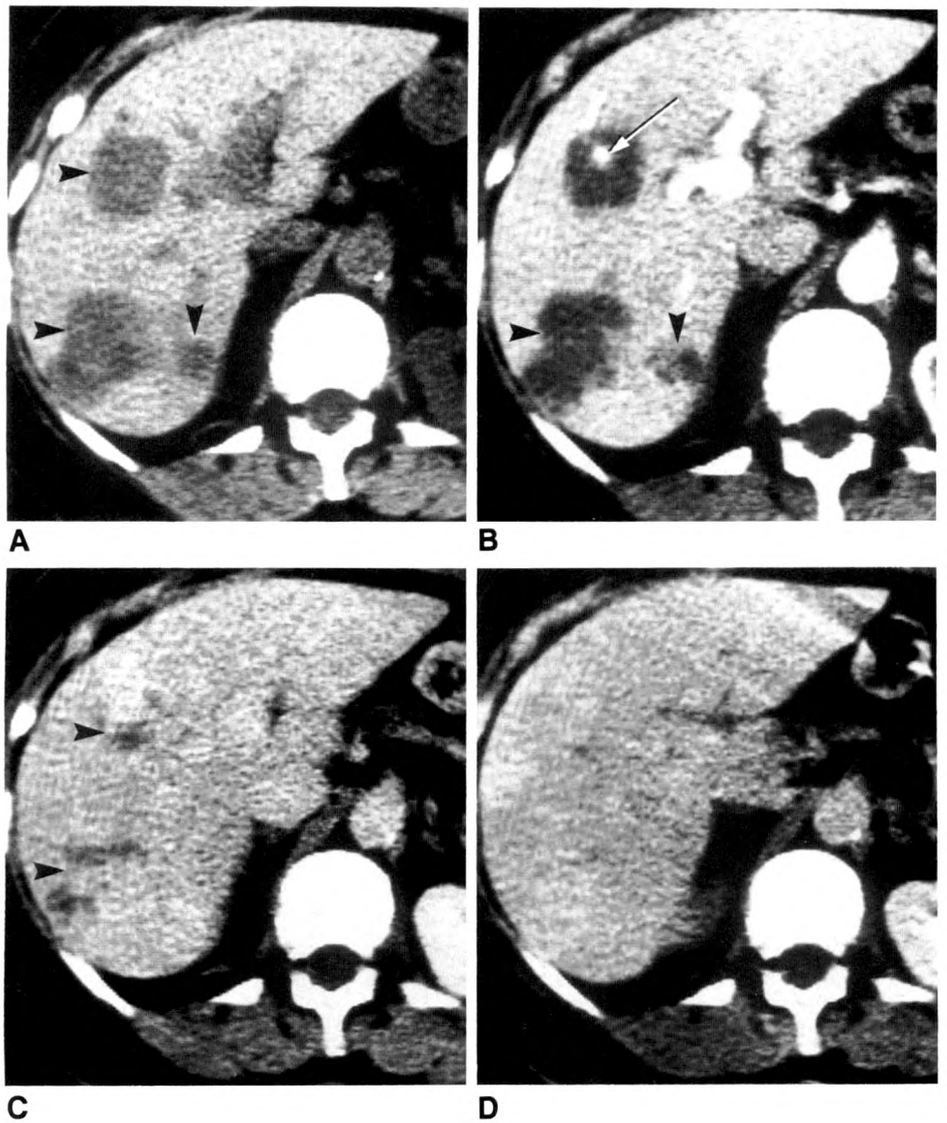


Fig. 2.—Atypical hemangioma: single-level bolus dynamic scan.

A, Scan without contrast shows three low-attenuation lesions in right lobe (*arrowheads*).

B, Dynamic scan at 106 sec shows central contrast enhancement of one lesion (*arrow*) and minimal peripheral enhancement of the other two lesions (*arrowheads*).

C, Delayed scan at 10 min shows incomplete fill-in of two lesions (*arrowheads*) and a complete isodense fill-in of third lesion.

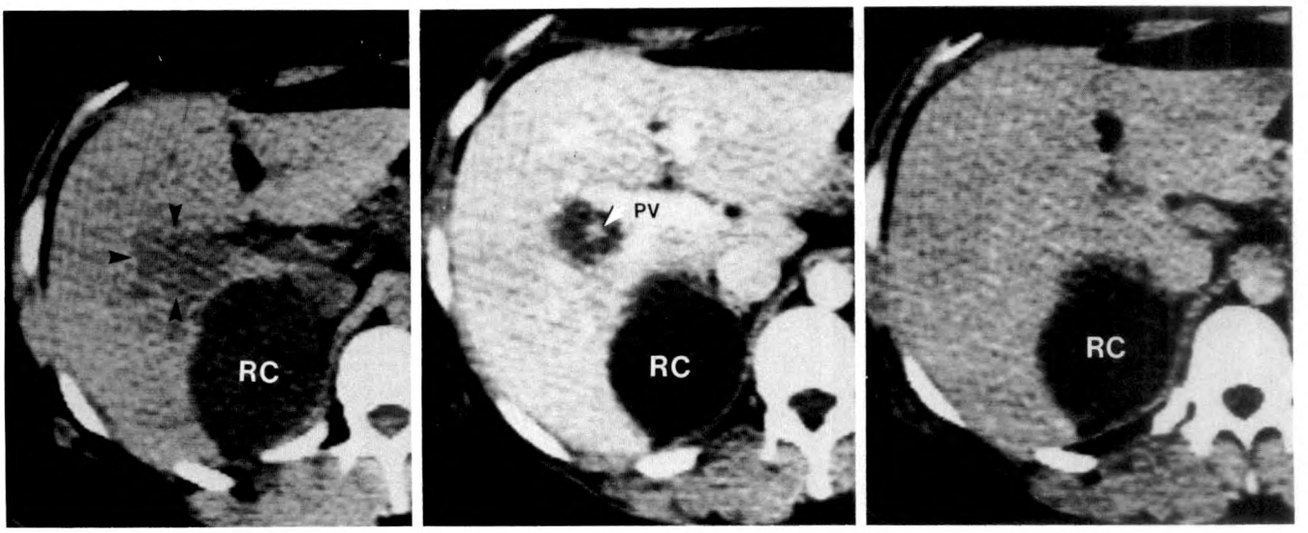
D, Delayed scan at 15 min shows complete isodense fill-in of all three lesions.

Four groups of investigators have published six reports describing the CT appearance of hepatic hemangiomas [3, 5–9]. Unfortunately, the techniques of the CT examinations and the methods of contrast enhancement varied, not only from report to report but also within the same series. The scan speed ranged from 9.6 to 18 sec (speed was not given in one report). Some examinations were performed using contiguous 10-mm collimated scans, whereas others used 13-, 15-, or 20-mm collimation. Each investigator obtained initial non–contrast-enhanced scans.

Techniques of contrast administration varied from drip infusion to bolus injection; iodine concentrations ranged from 30% to 66.8% (concentration was not stated in one series); and volumes varied from 40 to 300 ml. In some series, both drip infusion and bolus injections were used, whereas in others different volumes were used in the same series (40–60 ml in one series, 50–100 ml in another). The contrast-enhanced scans were begun simultaneously with contrast injection in one series, whereas in other series either there was a delay or scanning was begun at the conclusion of the contrast injection. The speed of contrast administration was stated in only one report (10–20 sec). Single-level bolus dynamic scan technique was used in two series, and the scanning technique was not specified in the others.

In four series, the investigators obtained delayed scans, whereas in one series only the first contrast-enhanced scans were used for evaluation. Delayed scans were obtained only at 2 min after contrast in one series, at variable times from 3 to 37 min in two series, and every 5 min for up to 20 min in one series.

The five series [3, 5–9] describing the CT appearance of hemangiomas included 87 lesions. One group reported two series, one in 1980 and one in 1983 [5, 6]; for purposes of evaluation, only the larger (1983) series was evaluated [5].



A B C

Fig. 3.—Atypical hemangioma: single-level bolus dynamic scan. PV = portal vein; RC = renal cyst.

A, Scan without contrast shows low-attenuation lesion in right lobe (*arrowheads*).

B, Dynamic scan at 132 sec shows small area of central contrast (*arrowhead*) and peripheral contrast enhancement.

C, Delayed scan at 15 min shows isodense lesion.

CT Appearance of Hepatic Hemangioma (Series Review)

Non-contrast-enhanced scans.—Scans were obtained before IV contrast administration for all 87 lesions. The hemangiomas were of diminished attenuation relative to the surrounding liver in 86 (99%) of 87 cases. In one lesion, a central area of increased attenuation was noted.

Contrast-enhanced scans.—Scans were obtained during or after contrast administration in 70 (80%) of 87 cases. As noted earlier, the method, rate, volume, and concentration of contrast administration varied from series to series and within series. The patterns of contrast enhancement were described as peripheral (or edge enhancement) in 64 (91%) of 70 cases, central in 3 (4%) of 70 cases, and diffuse (enhancement of the entire lesion) in 3 (4%) of 70 cases. Because there was such a wide variation in technique of contrast administration, particularly in the time between the delivery of the contrast agent and the collection of the scans, these data are impossible to evaluate more specifically.

Delayed scans.—Scans were obtained after administration of contrast agent in 64 (91%) of 70 cases. The timing of the delayed scans was different for each series, as noted earlier. Most importantly, delayed scans were obtained for no more than 15 min in 41 cases, at variable times for no more than 37 min in six cases, and for no more than 20 min in 13 cases [3, 5, 9].

Hemangiomas were reported as hyperdense relative to the surrounding liver in four cases in one series (scans at 2 min after contrast) and in two cases in another series in which scans were obtained for as long as 20 min after contrast. Hemangiomas became isodense with the liver in 23 cases (variable lengths of delay) and showed incomplete isodense fill-in (remaining central areas of diminished attenuation or "central clefts") in 30 cases (also with variable delay times).

Each group concluded that CT was an accurate technique for diagnosis of hemangioma if specific criteria were observed. These included the following: (1) rapid, prolonged, high contrast enhancement of tumor [7]; (2) low attenuation of tumor on precontrast scan, same tumor size on postcontrast scan, and peripheral tumor enhancement with an inner corrugated appearance [8]; (3) dense accumulation of contrast material in tumor that progressively spreads in all directions in sequential scans over minutes or diffuse tumor density higher than that of normal hepatic parenchyma lasting 2 min or more [5, 6]; (4) early peripheral tumor enhancement, low-attenuation center, and variable degree of central fill-in on delayed scans [9]; and (5) precontrast low-attenuation tumor, peripheral contrast enhancement, and either complete or partial isodense fill-in or hyperdense appearance of tumor on delayed scans [3].

CT Appearance of Hemangiomas (Current Series)

The current series used single-level bolus dynamic scanning in 44 patients with 55 hemangiomas and incremental bolus dynamic technique in three patients with one hemangioma each. The technique, volume, concentration, and speed of contrast injection were identical in both groups. Only the exact timing of the scans collected during the bolus dynamic phase of the scan sequences varied (single-level scans at 4.5 or 2 sec/scan and incremental scans at 2 sec/scan). However, analysis of the 55 lesions studied with the single-level technique did not show any lesions that changed their pattern of enhancement during the bolus dynamic phase (i.e., lesions with peripheral, central, or mixed enhancement patterns main-

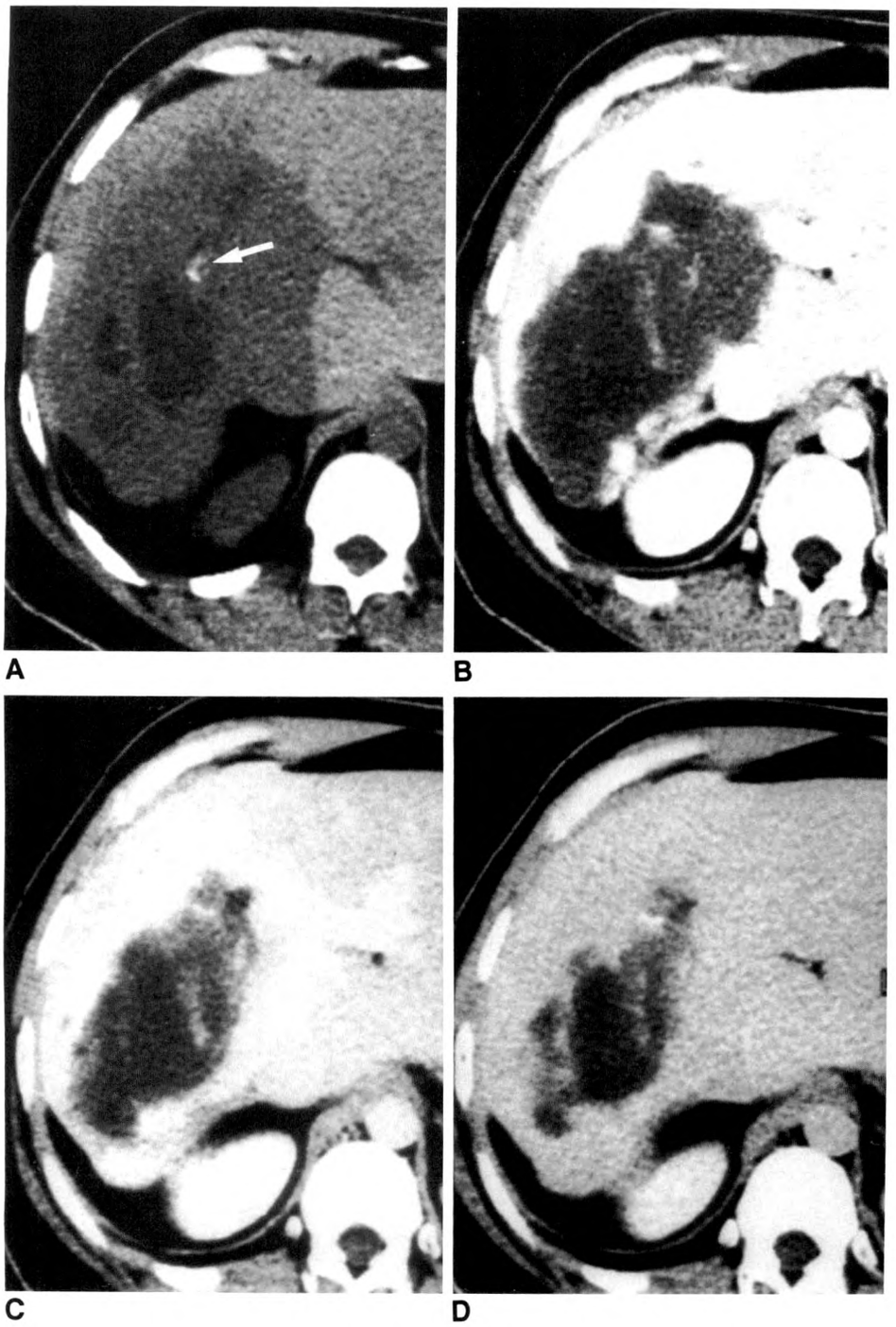


Fig. 4.—Atypical hemangioma: single-level bolus dynamic scan.

A, Scan without contrast shows large low-attenuation lesion in right lobe. Center is of lesser attenuation than periphery. Small central calcification is present (*arrow*).

B, Dynamic scan at 76 sec shows intense peripheral contrast enhancement.

C, Dynamic scan at 92 sec shows some fill-in of peripheral portion of lesion.

D, Delayed scan at 45 min shows isodense fill-in of periphery but persistent central area of decreased attenuation.

tained these patterns throughout the bolus dynamic phase).

Analysis of our data and those from the series reported [3, 5–9], plus our experience with contrast-enhancement patterns of malignant tumors [10], indicates that the following pattern is the most frequent and "typical" of hepatic hemangioma: (1) low-attenuation lesion before IV contrast administration; (2) peripheral contrast enhancement during the rapid IV-bolus dynamic phase of contrast administration; and (3) complete isodense fill-in of the lesion on delayed scans extended to at least 30 min (Fig. 1).

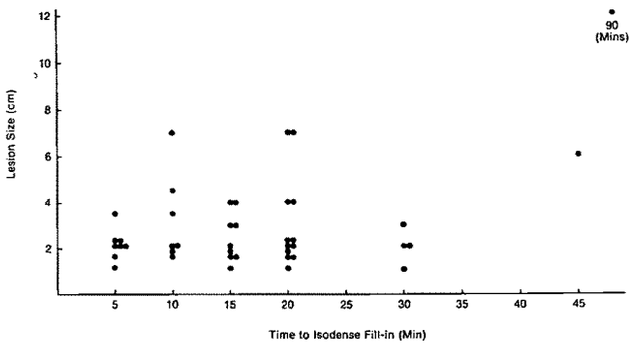


Fig. 5.—Isodense fill-in: time (min) vs lesion diameter (cm).

Several important technical and morphologic features should be emphasized. First, hemangiomas should be of diminished attenuation on non–contrast-enhanced scans. In our series, one patient with diffuse fatty infiltration of the liver had two hemangiomas that were hyperdense before contrast administration. No cases of fatty infiltration were reported in the previous series [3, 5–9]. Because it is not possible to evaluate precisely the pattern of contrast enhancement or delayed fill-in of lesions within fatty livers, we believe that lesions arising in livers with fatty infiltration should be excluded from CT evaluation for suspected hemangiomas.

Second, scans must be obtained during the dynamic phase of bolus contrast injection. If more delayed scans are obtained, the pattern of enhancement may change from peripheral to diffuse enhancement or to a mixed or heterogeneous pattern (Fig. 1).

Third, assessment of the delayed fill-in pattern is essential for accurate CT evaluation of lesions suspected of being hemangiomas. Complete isodense fill-in was present in 23 (36%) of 64 hemangiomas in the previously reported series and in 42 (72%) of 58 cases in the current series. The increased frequency of isodense fill-in in the current series occurred because many of the lesions did not become isodense until 20–30 min after contrast injection (Fig. 1). In the previously reported series, only 19 lesions were followed for 20 min or longer (longest delay was 37 min, number of lesions not stated) [3, 9].

Fourth, peripheral contrast enhancement or isodense fill-in alone is not diagnostic of hemangioma, as both of these can be seen in other benign liver tumors as well as in hepatic metastases (Fig. 6) [10–12].

The three "typical" hemangioma criteria described earlier were present in only 32 (55%) of the 58 hemangiomas in our series. If less rigid criteria had been accepted as typical, such as central contrast enhancement or incomplete isodense fill-in, 56 (97%) of the 58 hemangiomas would have been classified as typical. However, the use of less rigid criteria would result in many other benign and malignant lesions being diagnosed incorrectly as hemangiomas (Fig. 6) [5, 7]. In our previous report of contrast-enhancement patterns of malignant hepatic tumors, 77% of patients manifested one or more of the atypical hemangioma criteria, but only one showed typical criteria [10].

Current Approach to Imaging of Suspected Hemangioma

In our current approach to evaluation of suspected hemangiomas, patients are divided into two groups on the basis of the imaging technique used for initial lesion detection: group 1, sonography or radionuclide hepatic scintigraphy (^{99m}Tc-sulfur colloid); and group 2, CT.

Group 1

Patients who have (1) discrete, hyperechoic liver lesions detected incidentally by sonography, (2) normal liver function tests, (3) no clinical symptoms referable to the liver, and (4) no known primary tumor are followed up only with clinical and laboratory evaluation and repeat sonography in 3–6 months [3].

Lesions detected by hepatic scintigraphy are evaluated with sonography to define their echographic morphology. Patients with discrete, hyperechoic lesions who also fulfill the clinical and laboratory criteria for group 1 patients also are followed up as outlined previously.

Patients who have (1) lesions with atypical sonographic patterns, (2) abnormal clinical or laboratory findings, or (3) a known primary tumor require additional imaging studies. The choices include CT, MRI, angiography, and hepatic scintigraphy using ^{99m}Tc-labeled RBC [13–20].

The current procedure of choice at our institution is ^{99m}Tc-labeled RBC scintigraphy [19]. Combining our current series of 40 cases with that of Brunetti et al. [18] (36 cases) (using single-photon emission CT imaging for small lesions less than 3 cm in diameter), the accuracy of the examination is 95% (72/76) [18–19]. The finding of persistent, increased blood-pool activity is characteristic of hemangioma (Fig. 7) [15–17].

Group 2

Patients in whom focal hepatic lesions with peripheral contrast enhancement are detected during routine dynamic bolus CT should have delayed images obtained up to 30 min after contrast injection. Patients with diffuse fatty infiltration of the liver should be excluded from CT evaluation for suspected hemangioma. If the CT appearance is typical, and if the patient is asymptomatic, has normal liver function tests, and has no known primary tumor, no further evaluation is necessary.

If the CT appearance is atypical, or if any of the clinical and laboratory studies are abnormal, ^{99m}Tc-labeled RBC scintigraphy should be performed. Angiography should be performed if the RBC scintigram is negative or if the clinical or laboratory findings indicate that surgical exploration is necessary (Fig. 6).

Percutaneous fine-needle aspiration biopsy can be performed if atypical lesions are identified in group 1 or group 2 patients. Although risk of bleeding has been a relative contraindication to percutaneous biopsy of suspected hemangioma, the technique has been found to be safe if a segment

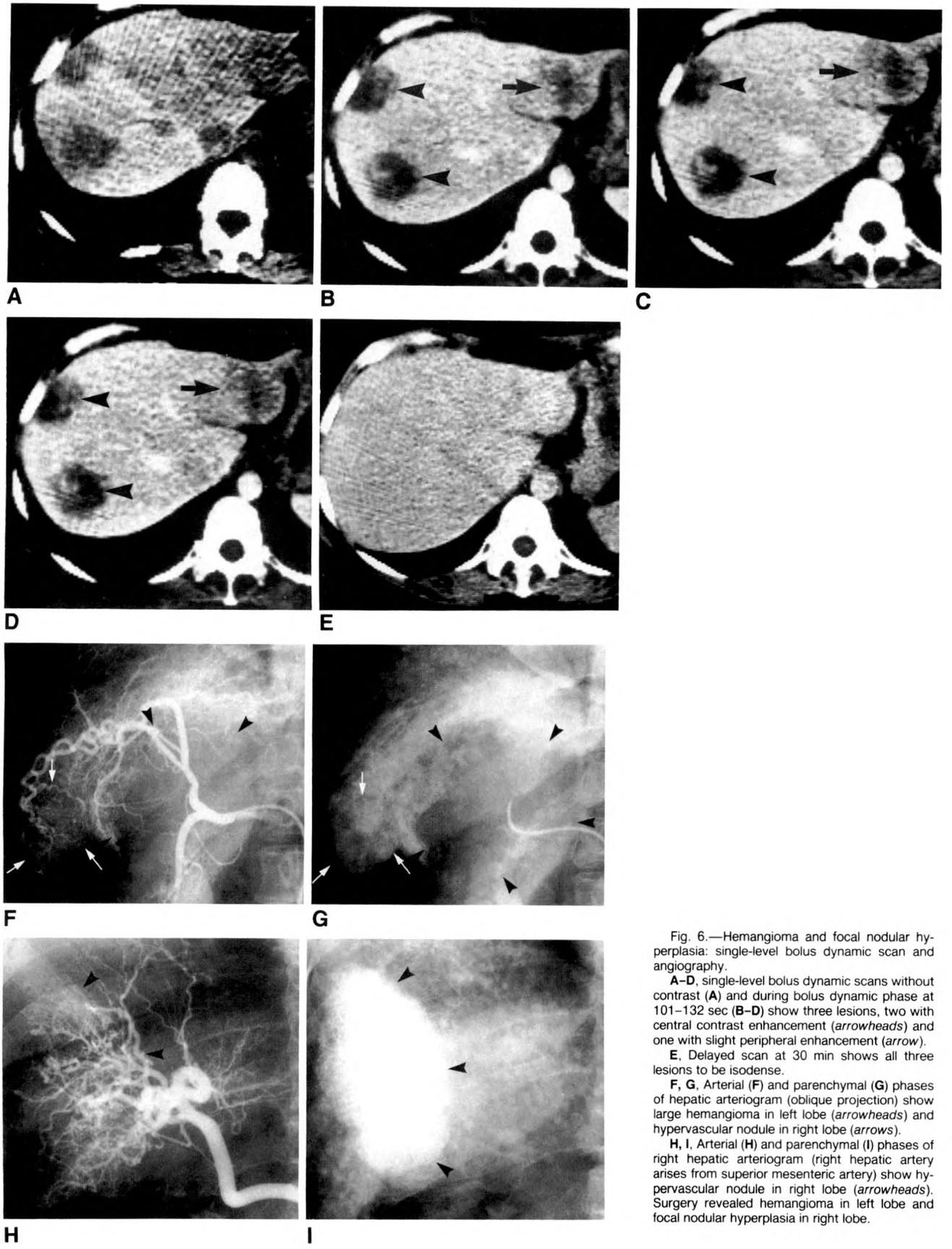


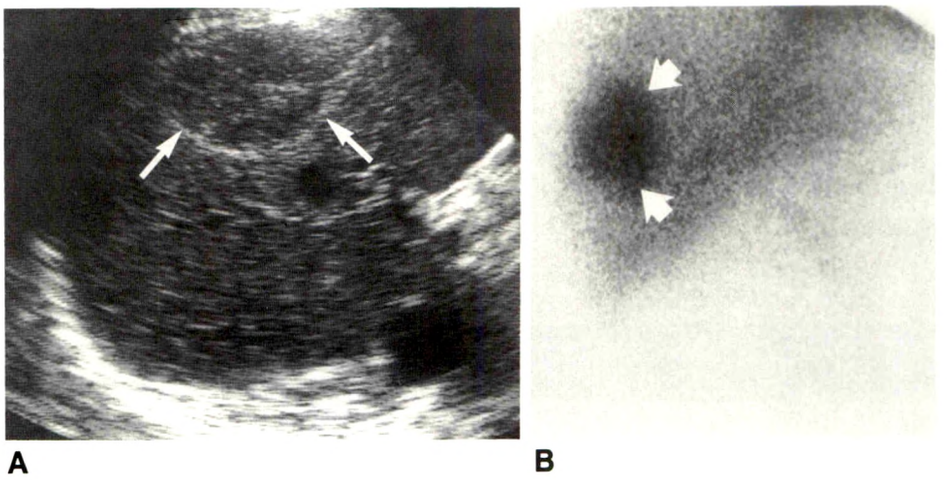
Fig. 6.—Hemangioma and focal nodular hyperplasia: single-level bolus dynamic scan and angiography.

A–D, single-level bolus dynamic scans without contrast (**A**) and during bolus dynamic phase at 101–132 sec (**B–D**) show three lesions, two with central contrast enhancement (*arrowheads*) and one with slight peripheral enhancement (*arrow*).

E, Delayed scan at 30 min shows all three lesions to be isodense.

F, G, Arterial (**F**) and parenchymal (**G**) phases of hepatic arteriogram (oblique projection) show large hemangioma in left lobe (*arrowheads*) and hypervascular nodule in right lobe (*arrows*).

H, I, Arterial (**H**) and parenchymal (**I**) phases of right hepatic arteriogram (right hepatic artery arises from superior mesenteric artery) show hypervascular nodule in right lobe (*arrowheads*). Surgery revealed hemangioma in left lobe and focal nodular hyperplasia in right lobe.



A B

Fig. 7.—Sonographically atypical hemangioma.

A, Real-time sector scan of liver shows hypoechoic lesion in right lobe (*arrows*).

B, ^{99m}Tc-labeled RBC scintigram (planar gamma camera image) shows focal area of increased blood-pool activity (*arrows*), typical of hemangioma.

of normal hepatic parenchyma is interposed between the entrance of the needle on the surface of the liver and the lesion [3, 4]. Some controversy still exists over whether a specific cytologic diagnosis of hemangioma can be made if only blood or normal endothelial cells are obtained. At our institution, biopsies of focal hepatic lesions are used only to confirm, not to exclude, malignancy. Thus, normal or "benign" findings on biopsy in an oncology patient are not considered final proof of either the presence of hemangioma or the absence of malignancy.

REFERENCES

1. Edmondson HA. Tumors of the liver and intrahepatic bile ducts. In: *Atlas of tumor pathology*, sect. VII, fasc. 25. Washington, DC: Armed Forces Institute of Pathology, **1958**:113
2. Freeny PC, Vimont TR, Barnett DC. Cavernous hemangioma of the liver: ultrasonography, arteriography, and computed tomography. *Radiology* **1979**;132:143–148
3. Bree RL, Schwab RE, Neiman HL. Solitary echogenic spot in the liver: is it diagnostic of a hemangioma? *AJR* **1983**;140:41–45
4. Solbiati L, Livraghi T, De Pra L, Lerace T, Masciadri N, Ravetto C. Fine-needle biopsy of hepatic hemangioma with sonographic guidance. *AJR* **1985**;144:471–474
5. Itai Y, Ohtomo K, Araki T, Furui S, Iio M, Atomi Y. Computed tomography and sonography of cavernous hemangioma of the liver. *AJR* **1983**;141:315–320
6. Itai Y, Furui S, Araki T, Yashiro N, Tasaka A. Computed tomography of cavernous hemangioma of the liver. *Radiology* **1980**;137:149–155
7. Araki T, Itai Y, Furui S, Tasaka A. Dynamic CT densitometry of hepatic tumors. *AJR* **1980**;135:1037–1043
8. Johnson MC, Sheedy PF II, Stanson AW, Stephens DH, Hattery RR, Adson MA. Computed tomography and angiography of cavernous hemangiomas of the liver. *Radiology* **1981**;138:115–121
9. Barnett PH, Zerhouni EA, White RI Jr, Siegelman SS. Computed tomography in the diagnosis of cavernous hemangioma of the liver. *AJR* **1980**;134:439–447
10. Freeny PC, Marks WM. Patterns of contrast enhancement of benign and malignant hepatic neoplasms during bolus dynamic CT scanning. *Radiology*, In press
11. Rogers JV, Mack LA, Freeny PC, Johnson ML, Sones PJ. Hepatic focal nodular hyperplasia: angiography, CT, sonography, and scintigraphy. *AJR* **1981**;137:983–990
12. Welch TJ, Sheedy PF II, Johnson CM, et al. Focal nodular hyperplasia and hepatic adenoma: comparison of angiography, CT, US, and scintigraphy. *Radiology* **1985**;156:593–595
13. Freeny PC. Angiography of hepatic neoplasms. *Semin Roentgenol* **1983**;18:114–122
14. Stark DD, Felder RC, Wittenberg J, et al. Magnetic resonance imaging of cavernous hemangioma of the liver: tissue-specific characterization. *AJR* **1985**;145:213–222
15. Front D, Royal HD, Israel O, Parker JA, Kolodny GM. Scintigraphy of hepatic hemangiomas: the value of Tc-99m-labeled red blood cells. Concise communication. *J Nucl Med* **1981**;22:684–687
16. Engle MA, Marks DS, Sandler MA, Shetty P. Differentiation of focal intrahepatic lesions with 99mTc-red blood cell imaging. *Radiology* **1983**;146:777–782
17. Lubin E, Lewitus Z. Blood pool scanning in investigating hepatic mass lesions. *Semin Nucl Med* **1972**;2:128–132
18. Brunetti JC, Van Heertum RL, Yudd AP. SPECT in the diagnosis of hepatic hemangioma (abstr). *J Nucl Med* **1985**;26:8
19. Hanelin LG, Lee ME. The evaluation of hepatic hemangiomas: contribution of SPECT imaging (abstr). *Clin Nucl Med* **1985**;10:25
20. Itai Y, Ohtomo K, Furui S, Yamauchi T, Minami M, Yashiro N. Noninvasive diagnosis of small cavernous hemangioma of the liver: advantage of MRI. *AJR* **1985**;145:1195–1199

Book Review

Single Photon Emission Computed Tomography. By Barbara Y. Croft. Chicago: Yearbook Medical Publ., 306 pp., 1986. $29.50; paper $18.00

The book, *Single Photon Emission Computed Tomography* (SPECT), is an excellent introduction to SPECT imaging and should be read by anyone interested in SPECT imaging.

The book is divided into four sections. First, the author reviews the historical and scientific principles that form the bases of SPECT imaging. The second section of the book is devoted to the instrumentation that is required for imaging and data processing in SPECT imaging. This is followed by a section concerning the technical aspects of SPECT imaging, and finally the book ends with a section on the clinical applications of SPECT imaging.

The book begins with a brief history of emission-CT and is followed by an explanation of the tomographic process and how the images are reconstructed. The author uses a descriptive fashion first and then a slightly more rigorous mathematical, but still largely descriptive, manner.

In the next section, the author reviews the different instrumentation requirements for SPECT. This section begins with an in-depth discussion of the important features in a SPECT camera and then discusses the instruments, both gamma camera and other, that are available for SPECT imaging. A review of many SPECT cameras is included. The section ends with a description of the computing needs for SPECT.

These introductory chapters are followed by a discussion of the actual production of SPECT images. First, a description of the data acquisition and processing is considered. Such topics as uniformity, linearity, center of rotation, pixel size, and collimator selection are considered. A rather detailed chapter on the importance of quality assurance and acceptance testing for SPECT units is included.

Finally, the application of SPECT in various clinical situations is considered. Naturally, SPECT of the head is predominant, but other types, such as SPECT of lung, heart, liver, and bone, are considered.

This is the best available introductory book on SPECT imaging. It is written from a single perspective and, therefore, shows a unity of purpose and style that is frequently lacking in multiauthor books. The book is well written at an introductory level so that newcomers to SPECT can read the book with ease, but an extensive bibliography is included so that people who seek more detailed information can find it. The references in the clinical section are relatively complete through 1984 with some additional references from 1985. The well-done illustrations and images add to the book's value.

I recommend this book strongly to anyone who is interested in beginning or has recently started a SPECT-imaging program. It covers everything from filter kernels to air-conditioning in the computer room in a manner that is clear, concise, and pleasant to read.

G. Donald Frey
Medical University of South Carolina
Charleston, SC 29425-0744

Chronic Acalculous Gallbladder Disease:

Multiimaging Evaluation with Clinical-Pathologic Correlation

Vassilios Raptopoulos[1]
Carolyn C. Compton[2, 3]
Paul Doherty[4]
Edward H. Smith[1]
Carl J. D'Orsi[1]
Nilima A. Patwardhan[5]
Robert Goldberg[6]

Despite the recent advances in hepatobiliary imaging, the diagnosis of chronic acalculous gallbladder disease remains difficult. A retrospective study was undertaken to assess the value of a multiimaging approach in detecting chronic acalculous gallbladder disease and in predicting which patients would obtain symptomatic relief after cholecystectomy. Of 199 patients with chronic cholecystitis, 26 (13%) had no gallstones. Of these 26, only 17 (65%) had symptoms related to chronic cholecystitis; in the remainder, the histologic diagnosis was made incidentally. After cholecystectomy, 13 (76%) of the 17 symptomatic patients obtained long-term symptomatic relief, while in four, the symptoms recurred. Among patients with histologic changes of chronic cholecystitis, biliary scintigraphy was the most sensitive technique (sensitivity, 89%). The sensitivity of sonography and oral cholecystography was 61.5% and 66%, respectively. However, for identifying symptomatic patients who may obtain long-term symptomatic relief after cholecystectomy, the accuracy of sonography, oral cholecystography, and biliary scintigraphy was 82%, 86%, and 38%, respectively. When two tests were in agreement the accuracy was 88%. For chronic acalculous cholecystitis, more than one study must be performed in order to make the correct diagnosis and to predict good results from cholecystectomy.

Detection of gallstones is the only objective evidence of chronic cholecystitis, and cholecystectomy is the only definitive treatment [1–3]. However, for the diagnosis of chronic acalculous gallbladder disease there is no such single criterion. The value of an oral fatty meal in conjunction with oral cholecystography or cholecystosonography is not considered reliable, and there is confusion as to both the optimal technique and the proper interpretation of biliary scintigraphy and the use of cholecystokinin [1–7].

We have reviewed the studies performed in 26 patients with a pathologic diagnosis of chronic acalculous gallbladder disease in an attempt to determine which radiologic features and techniques are the most sensitive and to identify the value of these tests to predict which patients would obtain long-term symptomatic relief after cholecystectomy.

Materials and Methods

Over a period of 3½ years, 26 patients were identified as having a histologic diagnosis of chronic acalculous cholecystitis. These patients were drawn from a larger pool of 199 consecutive patients who had a histologic diagnosis of chronic cholecystitis and who had undergone sonographic evaluation of the upper abdomen within 2 months of cholecystectomy (179 patients) or autopsy (20 patients). Gallstones were found in 173 patients who were exluded from this study. In the remaining 26 (13%), no gallstones were identified within the gallbladder or the bile ducts. All 26 patients had a minimum of two sonographic examinations of the gallbladder performed at least 1 week apart; oral cholecystography was performed in 15 patients and biliary scintigraphy in nine within 1 week of sonography.

Sonography was done using commercially available static and dynamic (real-time) scanners. The results were considered abnormal when there was persistent (1) diffuse thickness of the

Received December 9, 1985; accepted after revision May 28, 1986.

Presented at the 16th International Congress of Radiology, Honolulu, July 1985.

[1] Department of Radiology, University of Massachusetts Medical Center, 55 Lake Ave. N., Worcester, MA 01605. Address reprint requests to V. Raptopoulos.

[2] Department of Pathology, University of Massachusetts Medical Center, Worcester, MA 01605.

[3] Present address: Department of Pathology, Massachusetts General Hospital, Boston, MA 02114.

[4] Department of Nuclear Medicine, University of Massachusetts Medical Center, Worcester, MA 01605.

[5] Department of Surgery, University of Massachusetts Medical Center, Worcester, MA 01605.

[6] Department of Medicine, University of Massachusetts Medical Center, Worcester, MA 01605.

AJR 147:721–724, October 1986
0361–803X/86/1474–0721
© American Roentgen Ray Society

TABLE 1: **Findings in 26 Patients with Chronic Acalculous Gallbladder Disease**

Case No.	Histology	Age	Gender	Clinical Group[a]	Sonogram	Oral Cholecystogram	Cholescintigraphy	Preoperative Diagnosis/ Duration of Symptoms	Postoperative Diagnosis	Follow-up/ Duration
1	Chronic cholecystitis and marked adenomyomatosis	57	F	S	Thick wall (localized)	RA[b] sinuses	Not performed	Adenomyomatosis/3 mo	Adenomyomatosis	Asymptomatic/1 yr
2		50	M	S	Thick wall, RA sinuses	Thick wall, RA sinuses	Not performed	Adenomyomatosis/2 mo	Adenomyomatosis	Asymptomatic/2 yr
3		35	M	S	Thick wall, septum	Hourglass	Not performed	Adenomyomatosis/6 mo	Adenomyomatosis	Asymptomatic/1 yr
4	Chronic cholecystitis and minimal adenomyomatosis	44	M	S	Thick wall (localized)	Nonvisualized	Not performed	Chronic cholecystitis/3 mo	Chronic cholecystitis	Asymptomatic/ 1½ yr
5		31	F	S	Thick wall (localized)	Thick wall (localized)	Not performed	Chronic cholecystitis/6 mo	Chronic cholecystitis	Asymptomatic/3 yr
6		67	M	S	Thick wall	Nonvisualized	Not performed	Chronic cholecystitis/2 mo	Chronic cholecystitis	Asymptomatic/3 yr
7		64	F	S	Thick wall	Not performed	Not performed	Chronic cholecystitis/2 mo	Chronic cholecystitis	Asymptomatic/1 yr
8		19	M	S	Thick wall	Not performed	No contraction (CCK)[c]	Chronic cholecystitis/1 yr	Chronic cholecystitis	Asymptomatic/2 yr
9		31	F	S	Normal	Normal	No contraction (CCK)	Chronic cholecystitis/1 yr	Chronic cholecystitis	Asymptomatic/1 yr
10		37	F	S	Normal	Normal	No contraction (CCK)	Chronic cholecystitis/3 yr	Chronic cholecystitis	Symptoms recurred within 4 mo/3 yr
11		67	F	S	Normal	Normal	No contraction (CCK)	Chronic cholecystitis/1 yr	Chronic cholecystitis	Symptoms recurred within 4 mo/2 yr
12		26	M	S	Normal (thick bile in only 1 of 2 exams)	Normal	No contraction (CCK)	Chronic cholecystitis/1 yr	Chronic cholecystitis	Symptoms recurred within 3 mo/hepatocellular carcinoma diagnosed 5 mo later
13	Chronic cholecystitis and cholesterolosis	37	F	S	Normal	Nonvisualized	No contraction (CCK)	Chronic cholecystitis/1 yr	Chronic cholecystitis	Asymtomatic/3 yr
14		74	M	I	Thick bile	Not performed	Not performed	Pancreatic carcinoma/3 mo	Pancreatic carcinoma	Died
15		57	M	I	Normal	Not performed	Not performed	Cholangiocarcinoma/4 mo	Cholangiocarcinoma	Died
16		76	M	I	Thick bile	Not performed	Not performed	No GI symptoms[d]	No surgery	Died
17	Chronic cholecystitis	42	M	S	Normal	Normal	Normal	Pancreatic carcinoma (tail)/3 mo	Chronic cholecystitis	Asymptomatic/2 yr
18		33	F	S	Normal	Not performed	No contraction (CCK)	Chronic cholecystitis/6 mo	Chronic cholecystitis	Symptoms recurred within 1 mo/2 yr
19		52	M	I	Normal	Not performed	Not performed	Ischemic colon	Ischemic colon	No data
20		52	M	I	Thick wall	Not performed	Not performed	Sclerosing cholangitis/6 mo	Sclerosing cholangitis	No data
21	Chronic and subacute cholecystitis	59	M	S	Indistinct wall	Nonvisualized	Not performed	Chronic cholecystitis/1 yr	Chronic cholecystitis	Asymptomatic/1 yr
22		70	M	S	Thick bile	Nonvisualized	Not performed	Adhesions/1 yr	Chronic cholecystitis	Asymptomatic/1 yr
23		60	M	I	Indistinct wall	Nonvisualized	Not performed	Perforated ulcer	Perforated ulcer	Died
24		57	F	I	Normal	Not performed	Not performed	Sclerosing cholangitis/6 mo	Sclerosing cholangitis	Died
25		57	M	I	Small gallbladder	Not performed	Not performed	No surgery	No GI symptoms	Died
26		68	F	I	Thick bile	Not performed	Delayed visualization	No surgery	No GI symptoms	Died

[a] S = symptomatic group; I = incidental.
[b] Rokitansky-Aschoff sinuses.
[c] Sincalide, which is the carboxy terminal octapeptide of cholecystokinin. See text for details.
[d] GI-gastrointestinal.

TABLE 2: **Correlation Between Outcome After Cholecystectomy and Results of Preoperative Imaging Tests**

Symptoms After Cholecystectomy	Sonogram[a]		Oral Cholecystogram[b]		Biliary Scintigraphy[c]	
	Abnormal	Normal	Abnormal	Normal	Abnormal	Normal
Asymptomatic[d]	10	3	9	2	3	1
Symptomatic[e]	0	4	0	4	4	0

Note.—All patients had symptoms preoperatively and were found to have chronic acalculous cholecystitis at surgery.
[a] No. of patients = 17.
[b] No. of patients = 15.
[c] No. of patients = 8.
[d] Patients were followed for 1–3 years.
[e] Symptoms recurred 1–3 months after cholecystectomy.

gallbladder wall greater than 3 mm, with or without visual impression of contracted gallbladder and/or (2) medium- to high-level nonshadowing echoes filling more than half of the gallbladder lumen, provided the patients were eating before the overnight fast required for the test [8, 9].

In oral cholecystography, overhead and upright spot films were obtained after ingestion of 3 g of iopanoic acid (Telepaque, Sterling-Winthrop, NY) the afternoon before the examination and after overnight fast. When the gallbladder was not opacified, the study was repeated the following day after ingestion of an additional 3 g of Telepaque. This examination was considered abnormal when there was no opacification after the second day of Telepaque ingestion or when there were thick septations or intramural outpouching of contrast (Rokitansky-Aschoff sinuses) either before or after a fatty-meal ingestion [10, 11].

Biliary scintigraphy was also performed after an overnight fast. Five to 10 mCi (370 MBq) of Tc-99m diisopropyl-phenylcarbamoylmethyl iminodiacetic acid (Hepatolite, New England Nuclear, Boston) was injected intravenously. A series of images was obtained over 1 hr. If the gallbladder was not visualized, delayed images were obtained for up to 4 hr. When the isotope had sufficiently filled the gallbladder, sincalide (Kinevac, Squibb, Princeton, NJ), the carboxy terminal octapeptide of cholecystokinin, was infused over 2 min in three divided doses of 10–30 ng/kg separated by 15 min. A continuous series of images was collected on a computer, and time-activity curves were generated over the gallbladder region. An ejection fraction was then calculated. Biliary scintigraphy was considered abnormal when it showed delayed visualization or when, after injection of sincalide, the gallbladder showed no evidence of active emptying on the time-activity curve and the serial images. A total ejection fraction between 40 and 60% was considered the normal response to IV sincalide stimulation [5, 12–14].

All pathologic specimens were reviewed. The diagnosis of chronic cholecystitis was made according to well-accepted histologic criteria, and the cases were divided into five histologic groups [15–19] (Table 1). Patients with a "minimal" degree of chronic inflammation were not included in the study because it is difficult to differentiate normal from "minimal" chronic inflammation. In part, this is due to the difficulty of preventing some degree of autolysis of the mucosa after removal of the gallbladder, especially in the postmortem specimen. Furthermore, the question of whether histologic evidence of "minimal" chronic inflammation is in fact within the range of "normal" gallbladder has not been resolved. For these reasons, only patients with a "mild" or "marked" degree of chronic cholecystitis were studied.

Clinically, the patients were divided into two groups: symptomatic (17) and incidental (nine) (Table 1). Patients in the incidental group did not have any symptoms attributable to chronic cholecystitis, and the gallbladder was either examined at autopsy or excised incidentally during the course of a surgical intervention performed for another reason. In the symptomatic group, all 17 patients had a primary postoperative diagnosis of chronic acalculous cholecystitis. Preoperatively, 15 suffered repeated attacks of typical gallbladder symptoms for 2 to 36 months. These included fatty-food intolerance, heartburn, flatulence, epigastric fullness, upper abdominal discomfort or pain, colic, and occasional vomiting. In addition, two patients who did not have typical gallbladder symptoms were also included in this group because, although the preoperative diagnosis was not substantiated at surgery, they obtained long-term relief of their symptoms after cholecystectomy.

Results

The results of the imaging procedures performed on 26 patients with a histologic diagnosis of chronic acalculous cholecystitis are summarized in Table 1. Sonography showed abnormal findings in 16 (62%) patients. Oral cholecystography was abnormal in 10 (67%) of 15 and biliary scintigraphy in eight (89%) of nine patients on whom they were performed. Overall, 22 patients (85%) had at least one abnormal study.

With the exception of marked adenomyomatosis, no direct correlation between the histologic groups and the imaging findings could be made. There was also no objective correlation between the histologic degree of chronic cholecystitis (mild or marked) and the degree, duration, or type of clinical symptoms. Reviewing the hospital records, however, one could have the impression that in general patients with superimposed subacute cholecystitis had more severe symptoms than the rest.

The 17 patients who had symptoms preoperatively and who had a primary postoperative diagnosis of chronic cholecystitis were followed for 1–3 years. Thirteen (76%) remained asymptomatic, while in four the symptoms recurred 1–3 months after cholecystectomy (Table 2). In this group, sonography accurately identified the patients who did or did not benefit from cholecystectomy in 14 (82%) of 17, oral cholecystography in 13 (86%) of 15, and biliary scintigraphy in three (38%) of eight cases. Sixteen patients of the 17 had more than one test. When the results of at least two techniques were in agreement, the accuracy of this combination to predict benefit from cholecystectomy rose to 88%. This also increased our subjective confidence for the correct clinical diagnosis.

These findings must nonetheless be interpreted with appropriate reservation, given the small sample size of patients studied. In addition, while no conscious effort was made by the physicians involved in this study to selectively perform the various diagnostic procedures used, it is possible that aside from those measured, additional clinical characteristics of the patients studied may have contributed to the differential accuracy of the results obtained.

Discussion

Acalculous cholecystitis is not uncommon. In a recent report, no calculi were found in 20% of cases of both acute and chronic cholecystitis [7]. In our series, 13% of 199 patients with histologically proven chronic cholecystitis had the acalculous variety.

In contrast to cholelithiasis and acute cholecystitis, there are no specific imaging criteria defined for the diagnosis of chronic acalculous cholecystitis. The numerous conditions associated with thick gallbladder wall, contracted gallbladder, and intraluminal nonshadowing echoes on sonography have been well described [8, 20–23]. Similarly, there are many causes of nonopacification of the gallbladder on a 2-day repeated-dose oral cholecystography [10, 11]. Finally, in patients with acalculous cholecystitis (acute and chronic combined), the sensitivity of biliary scintigraphy has been reported to be as high as 93.3% and as low as 68 to 76%, and reports are conflicting as to the value of cholecystokinin cholecystoscintigraphy [2, 6, 7, 13, 24, 25].

To complicate matters even more, not all patients with chronic cholecystitis are symptomatic, and even with the presence of symptoms and chronic cholecystitis and cholelithiasis, only 45 to 70% of patients may benefit from cholecystectomy [1–3]. In our series of a highly selected group, only 65% of the patients had symptoms that may have been related to chronic gallbladder disease, and 24% did not benefit from cholecystectomy. Therefore, surgeons are justified in being reluctant to operate in the absence of gallstones, especially because the available diagnostic techniques offer indirect evidence of disease or nonspecific images.

Our data indicate that among patients with histologic changes of chronic cholecystitis, biliary scintigraphy may be the most sensitive technique. In patients with repeated gallbladder-type symptoms, an abnormal sonogram or oral cholecystogram accurately predicts benefit from cholecystectomy, provided the other causes of the abnormal findings can be excluded. In the same type of patients, however, normal sonography or oral cholecystography findings do not exclude symptomatic relief of symptoms after cholecystectomy. Although the value of biliary scintigraphy alone as an indicator for cholecystectomy was not substantiated in our material, this may be due to the relatively small number of patients examined with this technique.

None of the different tests reviewed provide any specific sign for chronic cholecystitis. In general, however, in the various techniques used, these nonspecific findings depend on different underlying factors. Thus, for chronic acalculous cholecystitis, more than one study must be performed in order to make the correct diagnosis and predict good results from cholecystectomy.

ACKNOWLEDGMENTS

The authors are grateful to Elizabeth Shultis for editorial assistance, Elizabeth Bohanan for secretarial assistance, and Ellen Hubbell for administrative support.

REFERENCES

1. Berk RN. Oral cholecystography. In: Berk RN, Clemett AR, eds. *Radiology of the gallbladder and bile ducts.* Philadelphia: Saunders, **1977**:101–199
2. Berk RN, Ferrucci JT Jr, Fordtran JS, Cooperberg PL, Weissmann HS. The radiologic diagnosis of gallbladder disease: an imaging symposium. *Radiology* **1981**;141:49–56
3. Douglas-Wilson I. When do gallstones matter? (editorial). *Lancet* **1976**;1:1061
4. Goldberg HI. Cholecystokinin cholecystography. *Semin Roentgenol* **1976**;11:175–179
5. Griffen WO Jr, Bivins BA, Rogers EL, Shearer GR, Liebschutz D, Lieber A. Cholecystokinin cholecystography in the diagnosis of gallbladder disease. *Ann Surg* **1980**;191:636–640
6. Davis GB, Berk RN, Scheible FW, et al. Cholecystokinin cholecystography, sonography, and scintigraphy: detection of chronic acalculous cholecystitis. *AJR* **1982**;139:1117–1121
7. Shuman WP, Rogers JV, Rudd TG, Mack LA, Plumley T, Larson EB. Low sensitivity of sonography and cholescintigraphy in acalculous cholecystitis. *AJR* **1984**;142:531–534
8. Yeh H-C. Update on the gallbladder. In: Saunders RC, ed. *Ultrasound annual, 1982.* New York: Raven, **1982**:135–172
9. Durrell CA III, Vincent LM, Mittelstaedt CA. Gallbladder ultrasonography in clinical context. *Semin Ultrasound CT MR* **1984**; 5:315–332
10. Mujahed Z, Evans JA, Whalen JP. The nonopacified gallbladder on oral cholecystography. *Radiology* **1974**;112:1–3
11. Palayew MJ. Chronic cholecystitis and cholelithiasis. *Semin Roentgenol* **1976**;11:107–115
12. Krishnamurthy GT, Bobba VR, McConnel D, Turner F, Mesgarzadeh M, Kingston E. Quantitative biliary dynamics: introduction of a new noninvasive scintigraphic technique. *J Nucl Med* **1983**;24:217–223
13. Freeman LM, Sugarman LA, Weissmann HS. Role of cholecystokinetic agents in ^{99m}Tc-IDA cholecystography. *Semin Nucl Med* **1981**;11:186–193
14. Hopman WPM, Rosenbusch G, Jansen JBMJ, deJong AJL, Camers CBHW. Gallbladder contraction: effects of fatty meals and cholecystokinin. *Radiology* **1985**;157:37–39
15. Beilby JO. Diverticulosis of the gallbladder: the fundal adenoma. *Br J Exp Pathol* **1967**;48:455–461
16. Elfving G, Silvonen E, Tier H. Mucosal hyperplasia of the gallbladder in cases of cholecystolithiasis. *Acta Chir Scand* **1969**;135:519–522
17. Jutras JA, Levesque HP. Adenomyoma and adenomyomatosis of gallbladder: radiologic and pathologic correlations. *Radiol Clin North Am* **1966**;4:483–500
18. King ESJ. Cholecystitis glandularis and diverticula of the gallbladder. *Br J Surg* **1953**;41:156–161
19. Weismann RE, MacDonald JR. Cholecystitis. *Arch Pathol* **1948**;45:639–657
20. Finberg HJ, Birnholz JC. Ultrasound evaluation of the gallbladder wall. *Radiology* **1979**;133:693–698
21. Engel JM, Deitch EA, Sikkema W. Gallbladder wall thickness: sonographic accuracy and relation to disease. *AJR* **1980**; 134:907–909
22. Shlaer WJ, Leopold GR, Scheible FW. Sonography of the thickened gallbladder wall: a nonspecific finding. *AJR* **1981**;136:337–339
23. Cooperberg P, Golding RH. Advances in ultrasonography of the gallbladder and biliary tract. *Radiol Clin North Am* **1982**;20:611–633
24. Shuman WP, Gibbs P, Rudd TG, Mack LA. PIPIDA scintigraphy for cholecystitis: false positive in alcoholism and total parenteral nutrition. *AJR* **1982**;138:1–5
25. Kalff V, Froelich JW, Lloyd R, Thrall JH. Predictive value of an abnormal hepatobiliary scan in patients with severe intercurrent illness. *Radiology* **1983**;146:191–194

Sonography in the Diagnosis of Hepatic Artery Aneurysms

Patricia A. Athey[1]
Steven L. Sax[1]
Neela Lamki[2]
Gilberto Cadavid[2]

In five cases of hepatic artery aneurysms, the findings on sonography suggested the diagnosis or indicated the need for angiography. The intrahepatic aneurysms (four cases) were anechoic, well-circumscribed masses with good through transmission of sound. None were pulsatile, but flow within the mass was observed in one case. An intrahepatic mass adjacent to the aneurysm was identified in every case, representing hematoma in three and postoperative abscess in one. The sonogram in a patient with a common hepatic artery aneurysm (one case) showed a lobulated, pulsatile, anechoic mass within a pancreatic head pseudocyst. Sonography offers a noninvasive means of screening for this abnormality.

Hepatic artery aneurysms are uncommon lesions that are rarely diagnosed preoperatively. Clinical presentation is frequently nonspecific, and diagnosis is often delayed, leading to high morbidity and mortality if rupture occurs.

Before the advent of angiography, radiographic imaging had little to offer. However, angiography is an invasive technique and is not likely to be employed without a high index of suspicion.

Five cases of hepatic artery aneurysms are presented in which the findings on sonography either suggested the correct diagnosis or indicated the need for angiography.

Materials and Methods

The hospital records and sonograms of five patients with hepatic artery aneurysms were reviewed. Four patients were scanned using both a contact B-scanner (3.5 MHz) and a real-time sector scanner (3.5 MHz). One patient had only static scans.

The sonographic features that were assessed included location, size, and shape of the aneurysm, detection of pulsations or any motion within the aneurysm, and presence of associated intrahepatic mass. Findings were correlated with angiography and/or surgery.

Results

Four of five patients were men. The patients ranged in age from 15 to 64 years. The cause of the aneurysm was blunt trauma in two, penetrating trauma in one, chronic pancreatitis in one, and previous biliary tract surgery in one. Three patients experienced right upper quadrant pain and one had sharp periumbilical pain. Hematemesis or hematochezia was noted in three patients, and a fourth patient had bright red blood per nasogastric tube. Three patients had some abnormality of liver enzymes or bilirubin. Only one had a palpable mass. One experienced fever secondary to postoperative liver abscess.

Two aneurysms arose from the right hepatic artery, two from the left hepatic artery, and one from the common hepatic artery. Sonographically the intrahepatic aneurysms were well-circumscribed anechoic masses with good through transmis-

Received September 18, 1985; accepted after revision May 22, 1986.

[1] Department of Radiology, Baylor College of Medicine, and Ben Taub General Hospital, 1 Baylor Plaza, Houston, TX 77030. Address reprint requests to P. A. Athey, Baylor College of Medicine, 1 Baylor Plaza, Houston, TX 77030.

[2] Department of Radiology, Baylor College of Medicine, and Veterans Administration Medical Center, 2002 Holcomb Blvd., Houston, TX 77030.

AJR 147:725–727, October 1986
0361–803X/86/1474–0725
© American Roentgen Ray Society

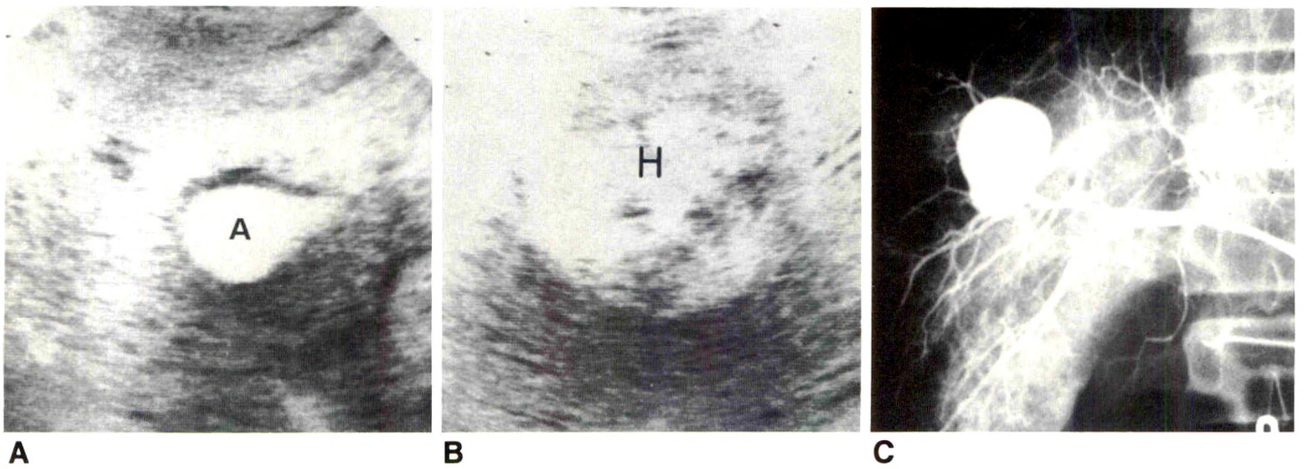


Fig. 1.—16-year-old boy with aneurysm of right hepatic artery caused by blunt trauma. **A**, Sagittal sonogram of aneurysm (A), which is anechoic and well circumscribed with good sound transmission. **B**, Transverse scan of right lobe of liver demonstrating hematoma (H) as a hypoechoic mass with good through transmission. **C**, Angiographic confirmation of aneurysm arising from right hepatic artery.

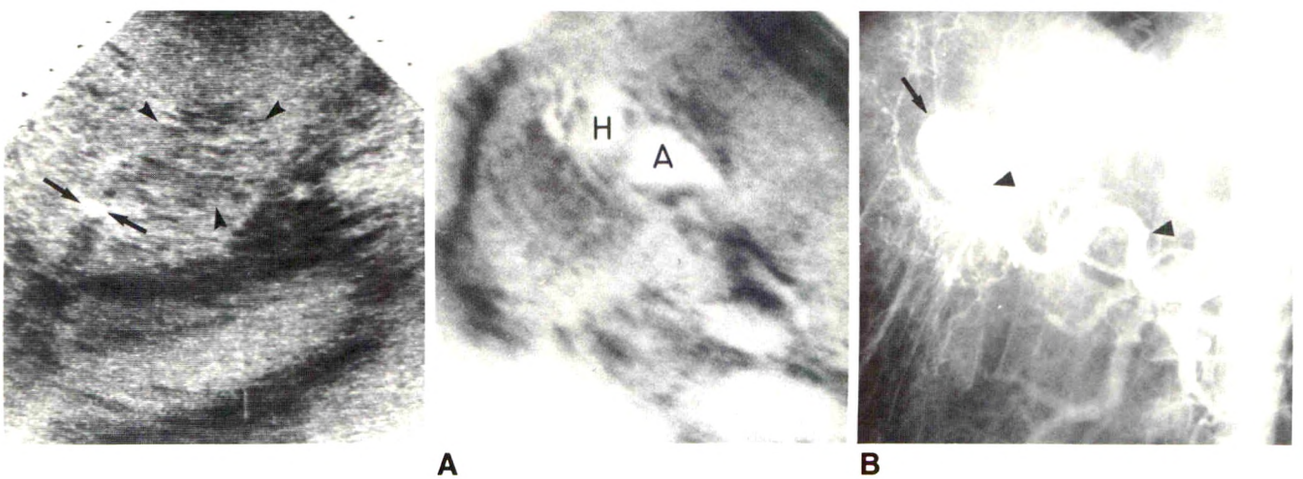


Fig. 2.—56-year-old man with aneurysm of left hepatic artery caused by blunt trauma. Sagittal sonogram of left lobe of liver demonstrates irregular echogenic hematoma (*large arrowheads*) superior to a small anechoic mass (*arrows*) with good through transmission corresponding to location of aneurysm.

Fig. 3.—64-year-old woman with aneurysm of left hepatic artery resulting from previous biliary tract surgery. **A**, Oblique sonogram of right lobe of liver demonstrates aneurysm (A) as well-circumscribed anechoic mass adjacent to an ill-defined, relatively anechoic area corresponding to hematoma (H). **B**, Celiac angiography demonstrates moderate-size aneurysm (*arrow*) arising from medial aspect of left hepatic artery. Two smaller aneurysms (*arrowheads*) are also seen. (Angiogram courtesy of Richard G. Fisher.)

sion of sound (Figs. 1A, 2, and 3A). None were pulsatile, but swirling of echoes arising from a point source was seen in one aneurysm (Fig. 4). Deep Doppler was not available in these cases. All of the intrahepatic aneurysms were closely associated with another intrahepatic mass, less well defined than the aneurysm and ranging from entirely echogenic (Fig. 2) to hypoechoic (Fig. 1B).

The common hepatic artery aneurysm was a lobulated, pulsatile, anechoic mass within a larger mass of mixed echogenicity located in the pancreatic head region (Fig. 5A). The latter proved to be a pseudocyst that had eroded into the common hepatic artery.

Discussion

Hepatic artery aneurysms make up one-fifth of all visceral aneurysms [1]. In the 1966 review of 170 cases by Guida and Moore [2], systemic infection and arteriosclerosis were the most common causes. The number of traumatic aneurysms is currently rising owing to an increase in blunt trauma secondary to motor vehicle accidents and to increasing iatrogenic forms of trauma such as biliary tract surgery or instrumentation, percutaneous interventional radiologic procedures, and hepatic biopsy [3].

Clinical presentation is variable and nonspecific. The most

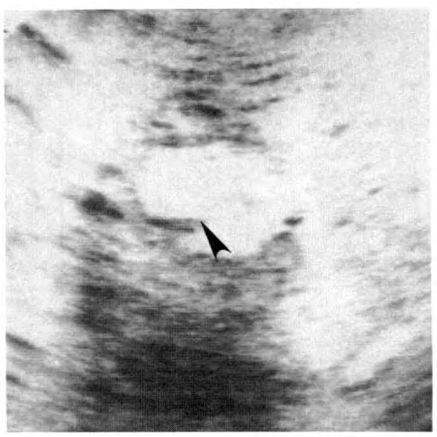
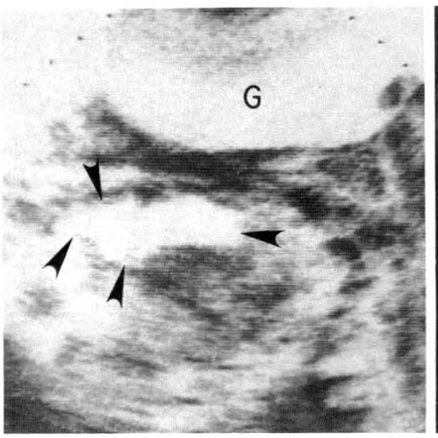
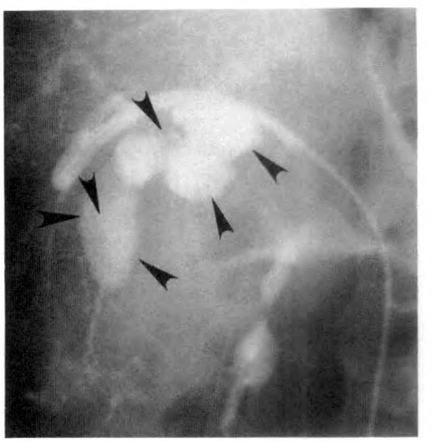


Fig. 4.—15-year-old boy with aneurysm of right hepatic artery caused by penetrating trauma. Sagittal sonogram of right lobe of liver demonstrates anechoic mass. On real-time, bursts of echoes were seen to arise from echogenic focus (*arrowhead*) and swirl around within mass.





A B

Fig. 5.—51-year-old man with aneurysm of common hepatic artery resulting from erosion by a pancreatic pseudocyst. **A**, Sagittal sonogram with patient in left decubitus position demonstrates gallbladder (G) anterior to a large pancreatic head pseudocyst filled with clot. In anterosuperior aspect of mass there is an ill-defined lobulated anechoic area (*arrowheads*) from which strong pulsations arose during real-time scanning, corresponding to a pseudoaneurysm on angiography. **B**, Right hepatic angiogram demonstrates marked displacement of right hepatic artery by mass in head of pancreas (pseudocyst) as well as a large lobulated pseudoaneurysm (*arrowheads*).

frequent complaint is epigastric or right upper quadrant pain followed in frequency by gastrointestinal hemorrhage and jaundice [2]. The aneurysm is seldom detected on physical examination, and conventional radiographic imaging has little to offer diagnostically. Angiography is currently the definitive diagnostic technique for this abnormality.

There have been sporadic case reports of the sonographic visualization of hepatic artery aneurysms [1, 4–11]. Of nine cases reported, six arose from the common hepatic artery, two from the right hepatic artery, and one from the left hepatic artery. Sonographically the aneurysms were anechoic (three cases), hypoechoic (one case), or of mixed echogenicity (five cases). In five patients, aneurysm was suspected on the basis of the following sonographic findings: pulsation was observed (one case); Doppler sonography demonstrated turbulent arterial flow (two cases); a channel was seen within a fusiform mass suggesting vascular origin (one case); and a tubular structure was seen in continuity with the mass (two cases). Five of six common hepatic artery aneurysms, in addition to one arising from a replaced right hepatic artery, presented as pancreatic head masses that were thought to represent neoplasm or pseudocyst.

Our series of five cases yielded a higher percentage of aneurysms of the right and left hepatic arteries. The only aneurysm to exhibit pulsation was one arising from the common hepatic artery. In one case a burst of echoes was seen arising from a projection from the wall of the aneurysm, which suggested active bleeding. This phenomenon was reported by Savage et al. [12] in a case of massive abdominal-wall hemorrhage with turbulence from a point source, but has not been described in aneurysm detection. Intrahepatic hematoma (three cases) and abscess (one case) in close proximity to the aneurysm were also demonstrated sonographically.

Sonography, already the primary screening technique for right upper quadrant pain or jaundice, offers a noninvasive means of screening for hepatic artery aneurysms. If blood flow within the mass can be documented by real-time or Doppler sonography, the diagnosis is secure and angiography is necessary only for surgical planning or for embolization.

REFERENCES

1. Countryman D, Norwood S, Register D, Torma M, Andrassy R. Hepatic artery aneurysm: report of an unusual case and review of the literature. *Am Surg* **1983**;49:51–54
2. Guida PM, Moore SW. Aneurysm of the hepatic artery. Report of five cases with a brief review of the previously reported cases. *Surgery* **1966**;60:299–310
3. Sandblom P. Hemobilia. *Surg Clin North Am* **1973**;53:1191–1201
4. Greenberg M, Rubin JM, Crass JR. The ultrasound appearance of an arterio-biliary fistula. *J Clin Ultrasound* **1983**;11:323–325
5. Gavin PM, Matalon TAS, Petasnick JP, Roseman DL. Congenital hepatic artery aneurysm simulating pancreatic carcinoma. *Radiology* **1984**;152:607–608
6. Shultz S, Druy EM, Friedman AC. Common hepatic artery aneurysm: pseudocyst of the pancreas. *AJR* **1985**;144:1287–1288
7. Stokland E, Wihed A, Ceder S, Lukes P, Hasselgren PO, Seeman T. Ultrasonic diagnosis of an aneurysm of the common hepatic artery. *J Clin Ultrasound* **1985**;13:369–370
8. Paolella LP, Scola FH, Cronan JJ. Hepatic artery aneurysm: an ultrasound diagnosis. *J Clin Ultrasound* **1985**;13:360–362
9. Kibbler CC, Cohen DL, Cruicshank JK, Kushwaha SS, Morgan MY, Dick RD. Use of CAT scanning in the diagnosis and management of hepatic artery aneurysm. *Gut* **1985**;26:752–756
10. Wolinski AP, Gall WJ, Dubbins PA. Hepatic artery aneurysm following pancreatitis diagnosed by ultrasound. *Br J Radiol* **1985**;58:768–770
11. Falkoff GE, Taylor KJW, Morse S. Hepatic artery pseudoaneurysm: diagnosis with real-time and pulsed Dopper ultrasound. *Radiology* **1986**;158:55–56
12. Savage PE, Joseph AEA, Adam EJ. Massive abdominal wall hematoma: real-time ultrasound localization of bleeding. *J Ultrasound Med* **1985**;4:157–158

Book Reviews

Nuclear Pharmacy. An Introduction to the Clinical Application of Radiopharmaceuticals. By Henry M. Chilton and Richard L. Witcofski. Philadelphia: Lea & Febiger, 190 pp., 1986.

This slim text is a superficial introduction to radiopharmacy. In addition to describing the principal applications of the major radiopharmaceuticals, it covers the nature, production, and detection of radioactivity, dosimetry, health physics, elementary radiopharmaceutical compounding and quality control, and regulatory affairs. Rigorous coverage in all of these areas is neither intended nor achieved.

Anyone setting out to provide brevity to the uninitiated has a responsibility for accuracy and relevance. Unfortunately, this is not always the case in this text. For example, one wonders about the chapter on the physics of "PETT (Positron Emission Transmission Tomography)." A table of conceptus-absorbed dose estimates is a fine idea, but one-third of the entries are for I-131-rose bengal, Se-75-selenomethionine, and Fe-59 citrate—not exactly the mainstays of today's radiopharmaceutical offerings. A table containing thyroid-dose estimates for I-123 states that the most important radiocontaminants are I-125 and I-131. The authors do not even mention I-124. The section on disofenin imaging is misleading. The authors state that "Patients should fast for at least four hours prior to injection since false positive studies may result if the gallbladder has been emptied by the ingestion of food." The converse has more truth to it, and they do not even mention the use of cholecystokinin to empty a full gallbladder. In their discussion of radiopharmaceuticals for spleen imaging, the authors compare Tc-99m and Cr-51–labeled heat-damaged red cells. They do not mention that it is probably more common to perform a liver-spleen scan with Tc-99m-sulfur colloid followed 2 days later by an early Tc-99m-disofenin image of the liver and to discern the spleen by mental-image subtraction. In the section on gallium imaging, the authors state "There are no known contraindications to the use of Ga-67 citrate." There should be a caveat about lactation. The section on ferrokinetics could probably be omitted. The discussion of the use of lasix in renal scanning is simplistic enough to be misleading. If long-standing obstruction has led to parenchymal damage, the kidney will not produce a bolus of urine in response to lasix, and a flat response renogram gives no information about functional vs anatomic obstruction. This is a common situation, and the user of this test should be warned before he makes a diagnostic error.

The organization of the book is logical and the style is straightforward. Many vague statements could have been more specific (and much more useful) without taking up any more space. Many of the conclusions have no preceding rationale so that the reader may memorize effectively but often not understand very well. The illustrations are good and the subject matter is well indexed. The section on regulatory affairs is necessarily brief but helpful. This is not generally offered in a text and I was very pleased to see it included.

This book would probably be useful to diagnostic radiology residents rotating through nuclear medicine, but the clinical portions would have to be supplemented with other textbooks. It might also be handy for Boards review. Undergraduate pharmacists taking a radiopharmacy elective as well as radiopharmacy and nuclear medicine technologists may also find this book helpful.

Carol S. Marcus
Harbor-UCLA Medical Center
Torrance, CA 90509

Guide Pratique D'Echographie Scrotale. A Guide to Scrotal Ultrasonography. By Kathlyn Marsot-Dupuch and Brigitte Martin. Paris: Masson, 134 pp., 1986.

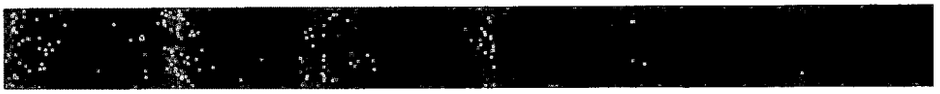
Written in French, this book covers all topics relevant to sonography of the scrotum. It consists of 11 chapters and begins with two chapters on embryology and anatomy. It continues with well-balanced discussions on inflammations, tumors, torsion, trauma, and varicocele. Chapters nine and 10 discuss the postoperative scrotum and pitfalls in scrotal sonography. The last chapter is dedicated to case discussions.

The book is well organized. The text is lucid, concise, and offers an adequate amount of detail. It is surprising that almost all the illustrations were obtained with articulated arm scanners; however, they are judicially chosen, are of good quality, and have clear labeling.

This book is an atlas on scrotal sonography. Through it, the authors have reached their goal to provide a guide to residents and practitioners.

Joseph Fakhry
New York Medical College
Valhalla, NY 10595

Bile-Duct Dilatation After Laparotomy: A Potential Effect of Intestinal Hypomotility



Vassilios Raptopoulos[1]
Edward H. Smith[1]
Thomas Cummings[1,2]
Wayne Silva[3]
Andrew Karellas[1]

Dilatation of unobstructed extrahepatic bile ducts was observed in patients with conditions associated with intestinal hypomotility. For further investigation of this association, a prospective study was undertaken in which the common hepatic duct was measured in 15 patients before and 1 day after laparotomy, when all patients had postoperative paralytic ileus. A statistically significant ($p < 0.01$) increase in the mean diameter of the hepatic duct was observed postoperatively. When compared with the preoperative measurement, the mean diameter of the duct almost doubled, from 3.3 to 5.9 mm. This phenomenon may be due to persistent contraction of the sphincter of Oddi that occurs when intestinal hypomotility eliminates the stimuli for cholecystokinin release.

Diagnostic sonography, which can accurately assess the caliber of the common hepatic duct (CHD), is widely accepted as the screening method of choice for the detection of biliary obstruction [1–3]. Although some controversy exists about the normal range of the internal diameter of the CHD, most investigators consider a measurement of 6 mm or smaller normal, and that of 7 mm or larger abnormal [3]. However, this distinction does not always correlate with biliary obstruction. Extrahepatic bile-duct obstruction may be present before the development of, or without, biliary dilatation [4, 5]. Conversely, patients without obstruction may show dilatation [3, 4, 6–8]. In some of these patients, previous obstruction, aging, and inflammation have adversely affected the elastic recoil and contractility of the extrahepatic duct wall [4, 8–10]. In others, no cause can be identified; often an incidental sonographic finding of extrahepatic biliary dilatation may start a battery of biochemical and imaging tests and, ultimately, surgical exploration. The fatty-meal stimulation test in such patients significantly improves diagnostic accuracy [8]. However, in some patients, administration of a fatty meal may be contraindicated, while in others the test provides inconclusive results.

In our practice, we identified 33 patients with unexplained CHD dilatation, up to 15 mm. None of the causes of biliary dilatation mentioned earlier were present. The only common denominator we could identify was an association with a variety of conditions of intestinal hypomotility, including paralytic ileus resulting from miscellaneous abdominal and thoracic inflammatory processes or trauma. Several patients were receiving parenteral hyperalimentation or narcotics, or they had undergone previous vagotomy. In 21 patients, bile-duct obstruction was excluded by direct opacification, surgery, or autopsy. In the remaining 12, there was strong clinical and biochemical evidence to exclude obstruction. Follow-up sonograms showed nondilated CHD.

These observations suggested association of intestinal hypomotility with extrahepatic bile-duct dilatation. To study the problem more systematically, we studied prospectively 15 patients scheduled for elective major abdominal surgery to evaluate CHD diameter changes during physiologic postoperative ileus.

Received March 13, 1986; accepted after revision May 28, 1986.

[1] Department of Radiology, University of Massachusetts Medical Center, 55 Lake Ave. N., Worcester, MA 01605. Address reprint requests to V. Raptopoulos.

[2] Present address: Department of Radiology, Health Sciences Center, St. John's, Newfoundland, Canada A1B 326.

[3] Department of Surgery, University of Massachusetts Medical Center, 55 Lake Ave. N., Worcester, MA 01605.

AJR 147:729–731, October 1986
0361–803X/86/1474–0729
© American Roentgen Ray Society

TABLE 1: **Common Hepatic Duct Diameters Measured Pre- and Postlaparotomy**

Patients		Age (yr)	Operation	Common Hepatic Duct Diameter		
No.	Gender			Preop. (mm)	Postop. (mm)	Difference (mm)
1	M	50	Colectomy	2.0	2.3	+0.3
2	F	45	Hysterectomy	2.3	2.7	+0.3
3	F	42	Hysterectomy	2.7	5.0	+2.3
4	M	61	AAA repair	2.7	5.7	+3.0
5	M	59	Colectomy	2.7	6.0	+3.3
6	F	49	Hysterectomy	2.7	6.3	+3.6
7	M	53	Nephrectomy	3.0	5.7	+2.7
8	M	67	AAA repair	3.0	6.0	+3.0
9	F	61	Colectomy	3.3	5.3	+2.0
10	M	74	Colectomy	3.3	6.3	+3.0
11	M	63	AAA repair	4.0	4.7	+0.7
12	F	56	Hysterectomy	4.0	6.7	+2.7
13	F	71	AAA repair	4.3	7.3	+3.0
14	M	57	Colectomy	4.7	8.3	+3.7
15	F	62	Colectomy	5.3	9.7	+4.4
M = 58 (SD = 9)				M = 3.3	M = 5.9	M = 2.6

Note.—The common hepatic duct diameter is the mean of three measurements. Preop. measurement was taken on the evening before operation. Postop. measurement was taken on second postoperative day. AAA = abdominal aortic aneurysm. M = mean; SD = standard deviation.

Subjects and Methods

Biliary sonography was performed prospectively in 15 patients scheduled for elective major abdominal surgery. The CHD was measured the day before and again the day after laparotomy. An informed consent, approved by the Human Subjects Committee, was obtained from all patients.

The following criteria were followed for inclusion of patients in this study. The patients were in good general condition, with normal liver-function tests; the operative procedures and the postoperative course were uneventful; the indications for operation did not include cholecystectomy, other hepatobiliary, pancreatic, or gastric surgery; they did not have inflammatory bowel disease or abdominal abscess. Patients with cholelithiasis or previous cholecystectomy were not studied, although it has been shown that the latter condition does not affect the caliber of the CHD [4, 11, 12]. The surgical procedures included right or left hemicolectomy for carcinoma of the colon, total abdominal hysterectomy and bilateral oophorectomy for uterine or ovarian carcinoma, abdominal aortic aneurysm repair, and nephrectomy with anterior abdominal approach for renal cell carcinoma (Table 1).

All sonograms were performed at the bedside with a commercially available dynamic (real-time) scanner, utilizing a 3-MHz or 5-MHz transducer. The patients were examined in the right anterior oblique position, and sagittal images of the extrahepatic bile duct just anterior to the portal vein were obtained. The anteroposterior internal diameter of the CHD was measured at the level of the hepatic artery with electronic calipers [3].

The CHD diameters were obtained by one examiner and represent the mean of three measurements. Because of the small number of subjects and because the observations were made on the same patients on two separate occasions (pre- and postlaparotomy), the significance in the change of the mean CHD diameter was calculated with the t-test applied to a paired comparison [13].

Results

Postoperatively, the 15 patients' general condition was satisfactory and their liver-function tests remained normal. None had eaten, had a bowel movement, or passed gas per rectum before the second examination.

The preoperative CHD diameters ranged from 2.0 to 5.3 mm (mean = 3.3, SD = 1.0) (see Table 1). On the second postoperative day, during physiologic postoperative ileus, the mean CHD diameter almost doubled. The measurements ranged from 2.3 to 9.7 mm (mean = 5.9, SD = 1.9). The 2.6-mm change in the mean CHD diameter was statistically significant ($p < 0.01$).

Discussion

The use of CHD size alone for screening biliary obstruction is valuable but does not always correspond with obstruction. Patients with early obstruction or conditions affecting the bile-duct wall may have a CHD caliber of less than 6 mm, while measurements larger than 7 mm have been observed in unobstructed biliary systems [3–8]. Aging and previous inflammation and obstruction have been shown to affect the elastic recoil of the duct wall, resulting in CHD dilatation without obstruction [4, 8–10].

Our data indirectly support the role that the sphincter of Oddi plays in affecting the diameter of the CHD. The wall of the extrahepatic bile duct consists mainly of fibroelastic tissue, with very little smooth muscle [9]. Considerable and rapid changes in the caliber of the extrahepatic ducts related to intermittent distal obstruction and bile flow have been observed, and in experimental animals, the CHD caliber doubles 24 hr after distal obstruction [3, 4, 14].

Failure of relaxation of the sphincter of Oddi may act in a manner similar to distal biliary obstruction. A fatty-meal stimulus that indirectly results in relaxation of the sphincter of Oddi may produce a decrease in CHD diameter [8]. This sphincter exhibits both tonic and phasic contractions. In humans, the mean pressure in the sphincter is 4–5 mm Hg higher than in the bile ducts, but the peak pressures during the phasic contractions are 10 times greater (15, 16). The phasic contractions can be abolished by a 20 ng/kg IV bolus of cholecystokinin octapeptide. At the same time, the pressure in the sphincter falls by nearly 50% [17]. During fasting, electrical spike bursts recorded from the sphincter of Oddi correlate with the migrating myoelectrical complex in the upper small intestine, while feeding abolishes this cycle [18]. Thus, a prolonged period of decreased upper-intestinal muscular activity would produce a prolonged contraction of the sphincter of Oddi, resulting in a dynamic distal common-bile-duct obstruction. This hypothesis is supported by our clinical observations in patients with intestinal hypomotility, as well as by the increase in the CHD diameter noted in our patients with physiologic postoperative ileus.

Parenteral hyperalimentation and prolonged fasting result in failure of relaxation of the sphincter of Oddi from lack of stimulus to release endogenous cholecystokinin. Sponta-

neous resolution of hyperalimentation-induced biliary dilatation has been described [19]. Morphine and other narcotics result in decreased intestinal activity. Narcotics, however, also have a direct effect on the sphincter of Oddi, increasing its contractility and preventing its relaxation [20]. Vagus-nerve stimulation increases upper-intestinal motility and relaxes the sphincter of Oddi. This effect is reversed after vagotomy [17, 21]. Progesterone appears to have a direct effect on the sphincter of Oddi, preventing its relaxation. Increased bile-duct caliber has been noted in pregnant women and in those who take oral contraceptives, while it returns to normal postpartum or after administration of estrogens [17, 21].

In patients with nonobstructive bile-duct dilatation, a fatty meal, known to release endogenous cholecystokinin, relaxes the sphincter of Oddi and results in reduction of the CHD caliber [8]. However, some patients with CHD dilatation do not respond to a fatty meal [8, 22]. In these patients, other conditions may be responsible for spasm of the sphincter, such as narcotics, increased serum progesterone levels, or vagotomy, which act irrespective of cholecystokinin levels. It must be emphasized, however, that the proposed mechanisms involved in the CHD dilatation are speculative: The status of sphincter pressure and contractions has not been studied in our patients.

Our data support the clinical observation of extrahepatic bile-duct dilatation in response to factors inhibiting the relaxation or prolonging the contraction of the sphincter of Oddi. Most of these factors are associated with decreased or absent intestinal motility. This phenomenon should be kept in mind to avoid misdiagnosing biliary obstruction under these circumstances. Furthermore, incidentally observed biliary dilatation in the early postoperative period should be viewed as a physiologic response to the surgical trauma.

ACKNOWLEDGMENT

The authors are grateful to Ellen Hubbell for administrative assistance.

REFERENCES

1. Cooperberg PL, Li D, Wong P, Cohen MM, Burhenne HJ. Accuracy of common hepatic duct size in the evaluation of extrahepatic biliary obstruction. *Radiology* **1980**;135:141–144
2. Baron RL, Stanley RJ, Lee JKT, et al. A prospective comparison of the evaluation of biliary obstruction using computed tomography and ultrasonography. *Radiology* **1982**;145:91–98
3. Mueller PR, Simeone JF. New concepts in biliary ultrasound. *Semin Ultrasound* **1984**;5:333–348
4. Raptopoulos V, Fabian TM, Silva W, et al. The effect of time and cholecystectomy on experimental biliary tree dilatation. A multi-imaging evaluation. *Invest Radiol* **1985**;20:276–286
5. Muhletaler CA, Gerlock AJ Jr, Fleischer AC, James AE Jr. Diagnosis of obstructive jaundice with nondilated bile ducts. *AJR* **1980**;134:1149–1152
6. Zeman R, Taylor KJW, Burrell MI, Gold J. Ultrasound demonstration of anicteric dilatation of the biliary tree. *Radiology* **1980**;134:689–692
7. Weinstein BJ, Weinstein DP. Biliary tract dilatation in the nonjaundiced patient. *AJR* **1980**;134:899–906
8. Simeone JF, Butch RJ, Mueller PR, et al. The bile ducts after a fatty meal: further sonographic observations. *Radiology* **1985**;154:763–768
9. Mahour GH, Wakim KG, Soule EH, et al. Structure of the common bile duct in man. *Ann Surg* **1967**;166:91–94
10. Wu CC, Ho YH, Chen CY. Effect of aging on common bile duct diameter: a real time ultrasonographic study. *J Clin Ultrasound* **1984**;12:473–478
11. Graham MF, Cooperberg PL, Cohen MM, et al. The size of the normal common hepatic duct following cholecystectomy: an ultrasonographic study. *Radiology* **1980**;135:137–139
12. Mueller PR, Ferrucci JT Jr, Simeone JF, et al. Postcholecystectomy bile duct dilatation: myth or reality? *AJR* **1981**;136:355–358
13. Hill AB. *Principles of medical statistics*, 9th ed. London: Lancet, **1971**
14. Scheske GA, Cooperberg PL, Cohen MM, Burhenne HJ. Dynamic changes in the caliber of the major bile ducts, related to obstruction. *Radiology* **1980**;135:215–216
15. Geenan JE, Hogan WJ, Dodd WJ, Stewart ET, Arndorfer RC. Intraluminal pressure recording from the human sphincter of Oddi. *Gastroenterology* **1980**;78:317–324
16. Csendes A, Kruse A, Funch-Jensen P, Oster MJ, Arnshold J, Amdrup E. Pressure measurements in the biliary and pancreatic duct systems in controls and in patients with gallstones, previous cholecystectomy or common bile duct stones. *Gastroenterology* **1979**;77:1203–1210
17. Brooks FP. Movements and muscular activity in the gastrointestinal system. In: West JB, ed. *Best and Taylor's physiological basis of medical practice*, 11th ed. Baltimore: Williams & Wilkins, **1985**:642–679
18. Toouli J, Honda R, Doods WJ, et al. Manometric and electromyographic features of the opossum sphincter of Oddi (abstr). *Gastroenterology* **1980**;78:1279
19. Oppenheimer DA, Carroll BA. Spontaneous resolution of hyperalimentation-induced biliary dilatation: ultrasound description. *J Ultrasound Med* **1982**;1:213–214
20. Jaffe JH, Martin WR. Opioid analgesics and antagonists. In: Gilman AG, Goodman LS, Gilman A, eds. *Goodman and Gilman's the pharmacological basis of therapeutics*, 6th ed. New York: Macmillan, **1980**:494–534
21. Schwartz SL. Gallbladder and extrahepatic biliary system. In: Schwartz SL, ed. *Principles of surgery*, 3rd ed. New York: McGraw-Hill, **1979**;1317–1352
22. Willson SA, Gosink BB, vanSonnenberg E. Unchanged size of a dilated common duct after fatty meal: results and significance (abstr). *Radiology* **1985**;157(p):242

Review Article

MRI of the Bladder and Prostate

Joseph K. T. Lee[1] and Kenneth S. Rholl

Since the advent of MRI of the body, several reports have attested to its utility for the evaluation of the bladder and prostate [1–7]. Respiratory motion, which often degrades the quality of upper abdominal and thoracic MR images, is virtually absent in the pelvis. The ability of MR to produce images in multiple planes is often helpful with complex pelvic anatomy. Finally, MR has superior contrast sensitivity and causes no known biologic effects. In this article, the value of MRI in the evaluation of the bladder and prostate will be reviewed and illustrated.

Imaging Techniques

Patients scheduled for MR examination of the pelvis require no special preparation. They are usually examined supine during shallow respiration, with the urinary bladder at least half full before the study is begun. A full bladder displaces the small bowel out of the true pelvis, thereby allowing better delineation of the seminal vesicles in males. Likewise, the wall of the urinary bladder can be better assessed.

Both T1-weighted (TR 300–500 msec, TE 15–35 msec) and T2-weighted (TR 1500–2100 msec, TE 90–120 msec) spin-echo sequences are necessary for complete examination of the pelvis. While the T1-weighted images are best for detecting lymphadenopathy and extension of bladder or prostatic carcinoma into adjacent fat, T2-weighted images provide a clear separation of urine from the bladder wall.

One-centimeter slices are usually obtained with 0- to 1-cm center-slice gap. Depending on the TR and TE intervals used, 5–21 slices are produced during a single imaging sequence. Transaxial images are obtained in every case, but additional imaging in coronal or sagittal planes may be performed if needed. Coronal images are useful for evaluating seminal vesicles and bladder neoplasms that involve the lateral wall. Sagittal views are necessary if the bladder neoplasm is located along the anterior or posterior wall.

A 59-cm cylindrical body coil is used routinely. Data are acquired using a 256 × 256 matrix. The matrix size is 2 × 2 mm for the body coil.

Normal MR Appearance

Urinary Bladder

The urinary bladder appears as a low-intensity structure on T1-weighted images because urine has an extremely long T1 (Fig. 1). The bladder wall cannot be differentiated from urine with this sequence [1, 3]. The signal intensity of urine compared with adjacent perivesical structures increases with prolongation of TR and TE. On a T2-weighted spin-echo sequence, urine can be distinguished from the bladder wall because of the high signal intensity of urine and the low intensity of the bladder wall (Fig. 1). However, the low-intensity bladder wall may be obscured by the chemical-shift artifact that results from the difference in resonance frequency between fat and water protons. The chemical-shift artifact occurs at the water/fat interface (bladder/perivesical fat) in the direction of the readout gradient, which is different for different imaging planes (i.e., for transaxial views, chemical-shift artifact would affect lateral walls; for sagittal sections, it would affect the superior and inferior bladder wall). The chemical-shift artifact can be recognized on a transverse image as a dark band along the lateral wall on one side and a bright band along the lateral wall on the opposite side. Becoming

Received February 26, 1986; accepted after revision May 21, 1986.

[1] Both authors: Mallinckrodt Institute of Radiology, Washington University School of Medicine, 510 S. Kingshighway, St. Louis, MO 63110. Address reprint requests to J. K. T. Lee.

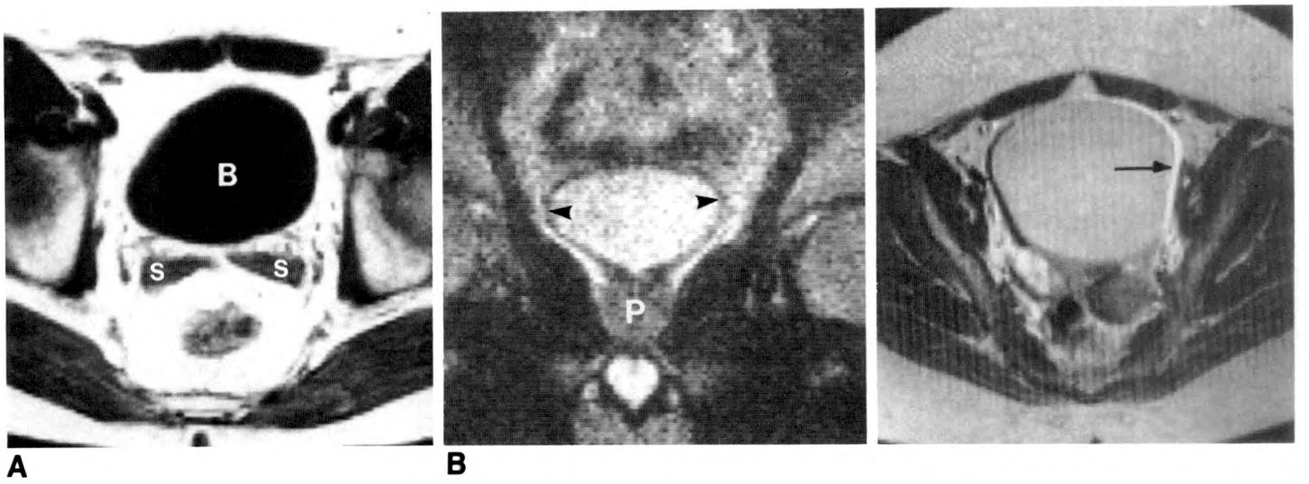
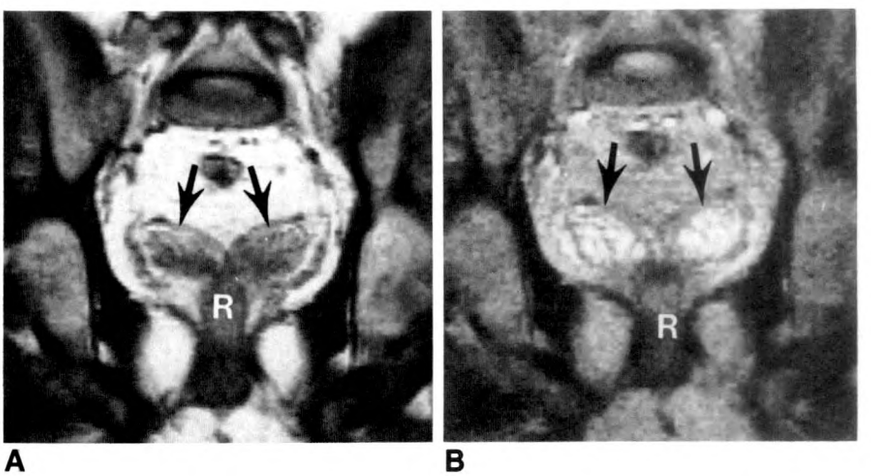


Fig. 1.—Normal urinary bladder. **A**, Axial view (TR 500 msec/TE 30 msec). The urinary bladder (B) has low signal intensity. Bladder wall cannot be distiguished from urine. s = seminal vesicle. **B**, Coronal view (TR 2100 msec/TE 90 msec). Bladder wall (*arrowheads*) has a low signal intensity and can be distinguished from high-intensity urine. P = prostate.

Fig. 2.—Chemical-shift artifact at water-fat interface. Axial view (TR 2100 msec/TE 90 msec) of pelvis obtained on 1.5-T-unit demonstrates black line on right of bladder-perivesical fat interface and white line (*arrow*) on opposite side. This artifact may lead to erroneous interpretation of bladder-wall invasion by neoplasm.

Fig. 3.—Normal seminal vesicles. **A**, Coronal view (TR 2100 msec/TE 30 msec). Seminal vesicles (*arrows*) have medium signal intensity. **B**, Coronal view (TR 2100 msec/TE 90 msec). Signal intensity of seminal vesicles (*arrows*) is higher than that of subcutaneous fat. Multiseptated appearance is demonstrated. R = rectum.



more pronounced with increasing field strength, in an extreme case the chemical-shift artifact may appear as thickening of the bladder wall on one side and absence of the bladder wall on the other (Fig. 2).

Prostate

With present equipment, the prostate gland has a homogeneous MR appearance [1, 4–7]. On T1-weighted images, the signal intensity is similar to that of skeletal muscle; on T2-weighted images, it is slightly less than that of fat [1, 4–7] (Fig. 1B). One group of investigators reported that the central and peripheral zones can be distinguished because the peripheral zone has a high signal intensity on T2-weighted images [8]. The low signal intensity of the central zone has been partly attributed to striated muscle within the prostatic sphincters.

Although the prostatic capsule is not usually visible, the prostate gland can be distinguished from adjacent structures because of interposed fatty tissue. The Denonville's fascia is infrequently seen on MR but may appear as a low-intensity band separating the rectum from the prostate gland.

Seminal Vesicles

The seminal vesicles are well visualized on MR images. With T1-weighted spin-echo sequence, they have a medium-to-low signal intensity. On T2-weighted images, they appear brighter than fat because of their high water content (Fig. 3).

Pathology

Urinary Bladder

Bladder wall hypertrophy secondary to bladder outlet obstruction can be identified with a signal intensity similar to that of the normal wall [3]. Both mucosal edema and inflammation of the bladder wall have a high signal intensity on T2-weighted images, thereby allowing easy differentiation from the low-intensity normal or hypertrophied bladder wall. However, the signal intensity of inflammation or edema of the bladder wall overlaps that of bladder neoplasms [9].

Tumors of the bladder, whether infiltrative, sessile, or pedunculated, can be detected if they exceed 1–2 cm [9]. The signal intensity of a bladder neoplasm is higher than urine but lower than fat on both T1-weighted and balanced images (long TR, short TE); the signal intensity of a bladder neoplasm is similar or slightly lower than that of urine on T2-weighted images. Thus, a bladder neoplasm can be best seen on a spin-echo sequence with a short TE (Fig. 4).

Therapy for carcinoma of the bladder depends on the clinical stage of disease at the time of initial examination. Patients with carcinoma in situ and T1 lesions (mucosal and submucosal involvement) can be treated adequately with fulguration or transurethral resection; patients with T2 lesions (involvement of superficial muscle layer) are often treated with segmental cystectomy. Radical cystectomy is the procedure of choice for patients with T3 lesions (T3A—deep muscle invasion; T3B—perivesical fat involvement). Palliative radiation therapy with an ileal loop is a common form of management for stage T4 lesions (involvement of perivesical organs and rectum) [10].

At present, MR cannot differentiate T1 and T2 stage tumors [9, 11]. However, MR can identify deep muscular invasion (stage T3A) on a T2-weighted sequence. Gross tumor involvement of deep muscular layer often leads to disruption of the low-intensity line. Of eight patients with proven deep-muscle invasion evaluated at our institute, the low-intensity bladder wall was definitely disrupted on MR in five and was equivocal in three [12]. In nine patients with superficial or no muscle invasion, eight had an intact bladder wall on MR. Therefore, the finding of a disrupted bladder wall on MR signifies an advanced stage lesion (T3 or above), while an intact bladder wall usually implies a more localized lesion. Because bladder neoplasms and bladder wall have a similar CT attenuation value, deep muscular invasion cannot be determined on a CT study.

Tumor extension into the perivesical fat (stage T3B) also can be detected and is best appreciated on T1-weighted images because of sharp contrast between fat and tumor (Fig. 5A). Tumor invasion into adjacent organs, such as the seminal vesicles and the rectum, can similarly be detected (Fig. 5B). Lymph node metastases can be seen if the involved nodes are enlarged. Lymphadenopathy is best appreciated on T1-weighted images. MR is superior to CT in distinguishing an enlarged lymph node from a small blood vessel [13]. Unfortunately, tissue characterization based on MR signals is not yet reliable. Lymphadenopathy from benign causes cannot be distinguished from malignant disease. Likewise, a normal-sized lymph node replaced with tumor cannot be recognized as abnormal by MR [13, 14].

As yet, no large prospective studies have compared the accuracy of MR and CT for staging bladder neoplasms. However, preliminary data show MR at least as accurate as CT [9, 11, 12]. In one study, MR staging was correct in 12 of 14 patients [9]. MR failed to detect one case of carcinoma in situ and understaged a T4 tumor as a T3A because peritoneal metastases were not detected [9].

Prostate

There have been conflicting reports on the ability of MR to differentiate prostatic carcinoma from benign hyperplasia.

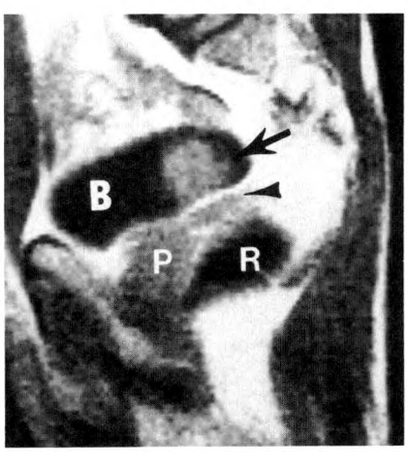


Fig. 4.—Transitional cell carcinoma of urinary bladder. Sagittal view (TR 500 msec/TE 30 msec). Polypoid tumor (*arrow*) has medium signal intensity and can easily be distinguished from surrounding low-intensity urine (B = bladder). P = prostate; R = rectum; seminal vesicles (*arrowhead*).

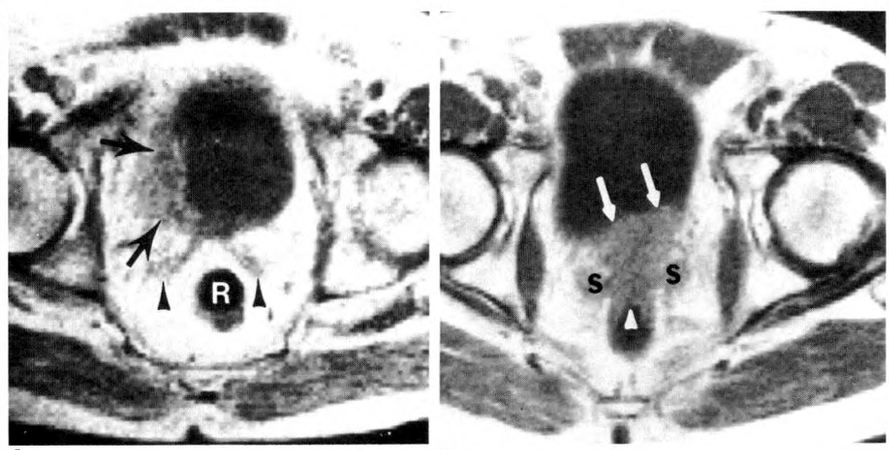


Fig. 5.—**A**, Transitional cell carcinoma of urinary bladder with extension into right perivesical fat (*arrows*). Axial view (TR 500 msec/TE 30 msec). Seminal vesicles (*arrowheads*); R = rectum. **B**, Transitional cell carcinoma (*arrows*) of urinary bladder invading anterior wall of rectum (*arrowhead*). Axial view (TR 500 msec/TE 30 msec). s = seminal vesicles.

Steyn and Smith [15, 16] found that T1 of carcinoma was longer than that of benign hyperplasia when they used a 0.04-T resistive imager but the same when measured on a 0.08-T resistive unit. When imaged with either unit, benign hyperplasia had a regular outline and a homogeneous texture, while carcinoma had an irregular outline and nonhomogeneous texture [15, 16]. More recently, Larkin et al. [7], using a 0.15-T resistive imager, showed that heterogeneous signal texture was a nonspecific finding and could be seen in both carcinoma and hyperplasia, but a focal nodule with prolonged T1 and T2 was specific for carcinoma. The results based on medium-field (0.3–0.6 T) superconducting imagers have been less encouraging. With the exception of one early report [2], most investigators found it difficult to distinguish carcinoma from benign hyperplasia [5, 6, 17]. While prostatic carcinoma often creates an area of high signal intensity on T2-weighted images (Fig. 6), this appearance is by no means specific for carcinoma. Benign prostatic hyperplasia may also appear as hyperintense nodules [6]. Benign hyperplasia has a variable appearance (high or low signal intensity), a reflection of its heterogeneous composition. Some nodules are cellular, while others are fibrous. Other benign conditions, such as acute and chronic prostatitis, are also heterogeneous on MR, with areas of high signal intensity indistinguishable from carcinoma [4].

Although differentiation between benign prostatic hyperplasia and carcinoma is not possible, MR has value because of its promise for staging prostatic carcinoma [7, 17, 18]. Because the prostatic capsule is not reliably visualized, the periprostatic venous plexus, which appears as a high signal-intensity rim on a second-echo image, may be a useful landmark for detecting extracapsular invasion [5]. Tumor extension into periprostatic fat is best detected on T1-weighted images; involvement of seminal vesicles is best seen on T2-weighted images, on the basis of recognition of alteration in size or signal intensity. Normal seminal vesicles have a high signal intensity on T2-weighted images; invasion of the seminal vesicles by carcinomas may lead to a lower signal intensity. Recognition of changes in the signal intensity of seminal vesicles may sometimes be a more sensitive indicator of tumor invasion than changes in size (Fig. 7). However, we do not know whether other conditions, such as inflammation or atrophy and fibrosis, may cause a similar decrease in signal intensity.

Extension of prostatic carcinoma into adjacent pelvic organs can be detected by MRI. Because of Denonville's fascia, the tumor often grows around the rectum to occupy the presacral space rather than invading the rectum directly (Fig. 8). Metastases to lymph nodes can be seen on MR if the involved nodes are enlarged. Because lymph nodes have a longer T1 than fat, lymphadenopathy can best be appreciated on a T1-weighted pulse sequence. Using a spin-echo technique with a TR of 500 msec and a TE of 30–35 msec, lymph nodes, which appear as medium-intensity structures, can be easily separated from high-intensity fat. Likewise, lymph nodes can be readily distinguished from the surrounding blood vessels, which can either appear black because of "flow void" phenomenon or bright because of "even echo rephasing" phenomenon [19]. In our experience, MR is superior to CT in differentiating small pelvic vessels from lymphadenopathy (Fig. 9). Unfortunately, tissue characterization based on MR signals is not yet possible. As stated previously, lymphadenopathy secondary to metastatic disease cannot be distinguished from lymphadenopathy due to other causes [13, 14].

Conclusions

MR is a promising technique for the evaluation of the urinary bladder and prostate and, although clinical experience is still

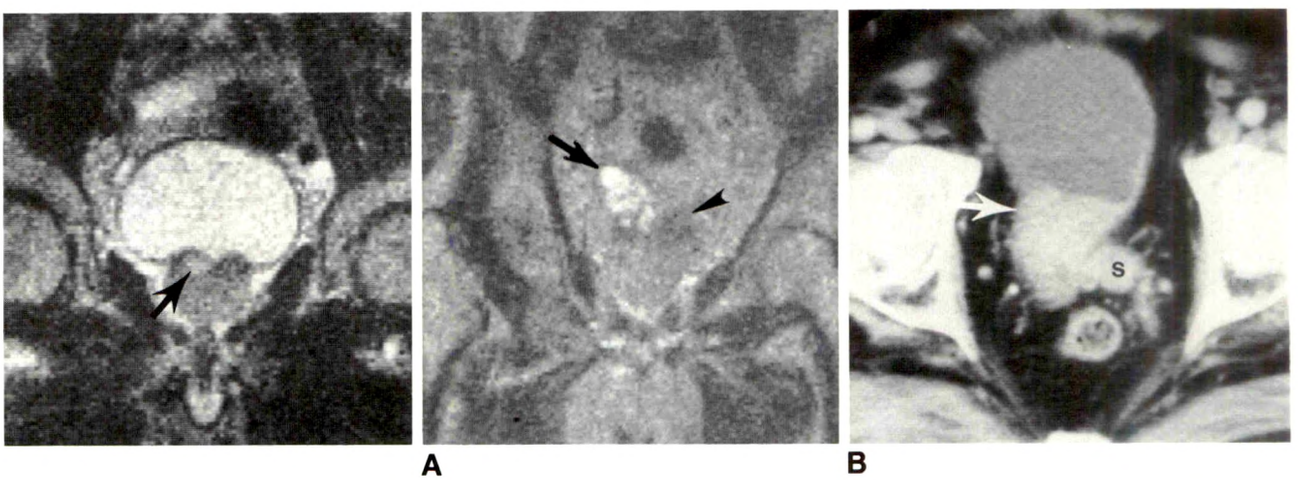


Fig. 6.—Adenocarcinoma of prostate. Coronal view (TR 2100 msec/TE 90 msec). High-intensity lesion (*arrow*) located in right lobe of prostate corresponding to a palpable nodule.

Fig. 7.—Prostatic carcinoma involving left seminal vesicle. **A**, Coronal image (TR 2100 msec/TE 90 msec). Right seminal vesicle (*arrow*) large but has normal signal intensity. Left seminal vesicle (*arrowhead*) smaller but has abnormally low signal intensity. Pathologic examination of resected specimen showed total replacement of left seminal vesicle by prostate carcinoma. Right seminal vesicle was normal. **B**, CT scan shows enlargement of right seminal vesicle with obliteration of right seminal vesicular angle (*arrow*); changes suggest seminal vesicular invasion. s = left seminal vesicle.

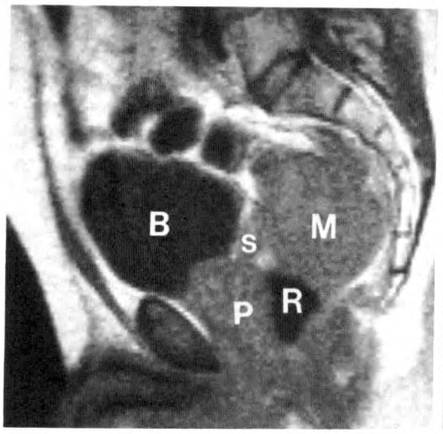


Fig. 8.—Advanced prostatic carcinoma. Sagittal view (TR 500 msec/TE 30 msec). Large mass (M) representing contiguous spread of prostatic carcinoma lies posterior to rectum (R). s = seminal vesicles; B = bladder; p = prostate.

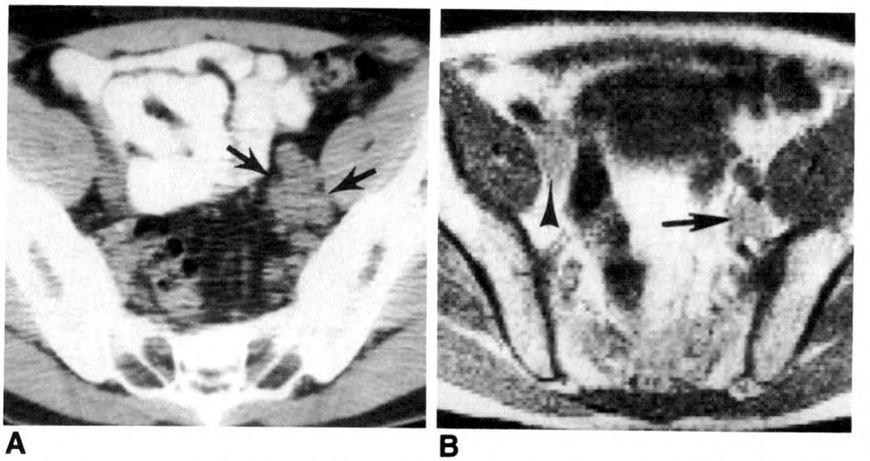


Fig. 9.—Pelvic lymphadenopathy secondary to prostatic carcinoma. **A**, Noncontrast CT scan demonstrates increased soft-tissue densities around left iliac vessels (*arrows*) indicating possible lymphadenopathy. **B**, Axial MR image (TR 900 msec/TE 30 msec) confirms presence of enlarged left external iliac node (*arrow*). Enlarged right iliac lymph node (*arrowhead*), not suspected on previous CT study, also evident. Lymphadenopathy easily distinguished from adjacent low-intensity iliac vessels.

limited, initial results suggest that MR may be useful for staging carcinoma of these organs, as well. In contrast to CT, in which the diagnosis of tumor invasion is based on size or morphologic changes alone, MR has the added advantage of being able to detect changes in signal intensity. Determination of the accuracy of MR for staging pelvic neoplasms awaits large, prospective studies.

REFERENCES

1. Bryan PJ, Butler HE, LiPuma JP, et al. NMR Scanning of the pelvis: initial experience with a 0.3 T system. *AJR* **1983**; 141:1111–1118
2. Hricak H, Williams RD, Spring DB, et al. Anatomy and pathology of the male pelvis by magnetic resonance imaging. *AJR* **1983**; 141:1101–1110
3. Fisher MR, Hricak H, Crooks LE. Urinary bladder MR imaging. Part I. Normal and benign conditions. *Radiology* **1985**;157:467–470
4. Buonocore E, Hesemann C, Pavlicek W, Montie JE. Clinical and in vitro magnetic resonance imaging of prostate carcinoma. *AJR* **1984**;143:1267–1272
5. Poon PY, McCallum RW, Henkelman MM, et al. Magnetic resonance imaging of the prostate. *Radiology* **1985**;154:143–149
6. Ling D, Lee JKT, Heiken JP, Balfe DM, Glazer HS, McClennan BI. Prostatic carcinoma and benign prostatic hyperplasia: inability of MR imaging to distinguish between the two diseases. *Radiology* **1986**;158:103–107
7. Larkin BT, Berquist TH, Utz DC. Evaluation of the prostate by magnetic resonance imaging. *Magnetic Resonance Imaging* **1986**;4:53–58
8. Hricak H. Pelvis. In: Margulis AR, Higgins CB, Kaufman L, Crooks LE, eds. *Clinical magnetic resonance imaging*. San Francisco: Radiology Research and Education Foundation, **1983**:229–250
9. Fisher MR, Hricak H, Tanagho EA. Urinary bladder MR imaging. Part II. Neoplasm. *Radiology* **1985**;157:471–477
10. Droller MJ. Transitional cell cancer: upper tracts and bladder. In: Walsh PC, Gittes RF, Perlmutter AD, Stamey TA, eds. *Campbell's urology*. Philadelphia: Saunders, **1986**:1343–1440
11. Bryan PJ, Butler HE, LiPuma JP. Magnetic resonance imaging of the pelvis. *Radiol Clin North Am* **1984**;22:897–915
12. Lee JKT, Rholl KS, Heiken JP, et al. Staging of bladder neoplasms by MRI. Presented at the scientific assembly and annual meeting of the Radiological Society of North America, Chicago, November **1985**.
13. Lee JKT, Heiken JP, Ling D, et al. Magnetic resonance imaging of abdominal and pelvic lymphadenopathy. *Radiology* **1984**; 153:181–188
14. Dooms GC, Hricak H, Moseley ME, Bottles K, Fisher M, Higgins CB. Characterization of lymphadenopathy by magnetic resonance imaging and tissue characterization. *Radiology* **1985**; 155:691–697
15. Steyn JH, Smith FW. Nuclear magnetic resonance imaging of the prostate. *Br J Urol* **1982**;54:726–728
16. Steyn JH, Smith FW. Nuclear magnetic resonance (NMR) imaging of the prostate. *Br J Urol* **1984**;56:679–681
17. Bryan PJ, Butler HE, Nelson AD, et al. Magnetic resonance imaging of the prostate. *AJR* **1986**;146:543–548
18. Hricak H, Dooms GC, Jeffrey RB, Fisher MR, Tanagho E, Higgins CB. MR imaging and CT in the evaluation of carcinoma of the prostate. Presented at the scientific assembly and annual meeting of the Radiological Society of North America, Chicago, November **1985**
19. Bradley WG, Waluch V. Blood flow: magnetic resonance imaging. *Radiology* **1985**;154:443–450

Case Report

Reversible Renal Fibromuscular Dysplasia

Albert A. Nemcek, Sr.,[1] and Charles E. Holmburg[2]

Because fibromuscular dysplasia of the renal artery is considered a progressive disease, most authorities agree that patients with renovascular hypertension caused by the disease should be treated either surgically or by percutaneous transluminal angioplasty of the renal artery [1–4].

We have observed a patient with hyperreninemic hypertension and fibromuscular dysplasia of the right renal artery who refused surgical correction 11 years ago. Her hypertension was satisfactorily treated medically during this period. A second renal arteriogram performed recently showed complete reversal of the fibromuscular dysplasia.

Case Report

A 41-year-old woman, known to be normotensive when seen in 1969 (at age 25 years) for pregnancy, was found to be hypertensive in 1970. A rapid-sequence urogram was normal and she was treated with Hygroton (chlorthalidone). Hypertension persisted through 1974 despite treatment with Butizide (hydrochlorothiazide and butabarbital) and Aldactone (spironolactone). At this time a second rapid-sequence urogram revealed a small right kidney. In a random sample taken from a peripheral vein with the patient in an upright position, renin was 3000 ng/100 dl. The left and right renal-vein renins were 1530 and 1740 ng/100 dl, respectively. A flush aortogram revealed decreased visualization of the right kidney. Renal arteriography showed dysplasia of the right renal artery (Fig. 1).

The patient refused surgery and was placed on medical therapy consisting of Aldomet (methyldopa), Inderal (propranolol hydrochloride), hydrochlorothiazide and Lasix (furosemide). Her blood pressure, which previously ranged from 180/120 to 134/84, with most readings in the higher ranges, became normal.

Eleven years later, in 1985, while still normotensive, the patient was reevalulated for renovascular disease. Left and right renal-vein renins were 81 and 72 ng/dl/hr, respectively, and the aortic renin was 56 ng/dl/hr, all normal values.

Right renal arteriography revealed a completely normal right renal artery with a mild stenosis of the origin of the right inferior polar artery (Fig. 2). Kidney size was normal.

Discussion

The cause of fibromuscular dysplasia is unknown, but the disease is considered to be progressive. The only previously reported case we are aware of that documents improvement, but not a reversal to normal, was an 8-year-old girl described by Siegler et al. [5]. This hypertensive patient was treated medically after fibromuscular dysplasia developed in two left renal arteries following failed right renal artery bypass for histologically proven fibromuscular disease.

Current theories of renin release suggest that renin secretion is stimulated by baroreceptor cells in the juxtaglomerular apparatus when there is a gradient between intraluminal arterial pressure and renal interstitial pressure. In fibromuscular dysplasia, renal arterial pressure in the affected kidney is reduced because of mechanical obstruction, and renin is stimulated. If the mechanical obstruction is hereditary, it should be unresponsive to pharmacologic intervention.

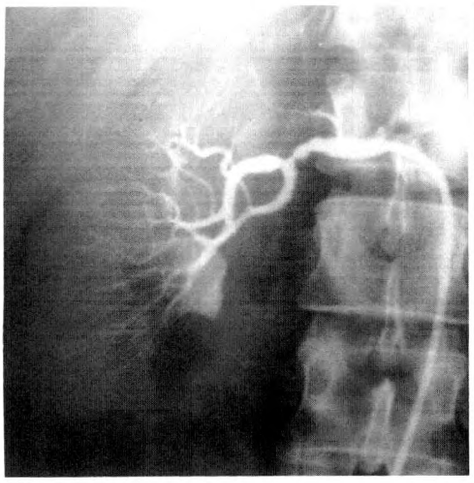
The possibility that pharmacologic therapy reversed a mechanical obstruction suggests that the dysplasia is under metabolic control. Since the agents that were used suppress renin secretion, it is possible that Angiotensin II, the vasoactive end point of renin metabolism, may perpetuate and mediate fibromuscular dysplasia. If so, drugs such as captopril, by blocking metabolic conversion of renin to Angiotensin II, would also be able to reduce renin output. Conversely, patients with the highest renin output might have the highest risk of progression of fibromuscular dysplasia if nothing is done to alter the renin-angiotensin cycle. Such pharmacologic effects may be slowly mediated, and observation over a

Received February 10, 1986; accepted after revision April 22, 1986.

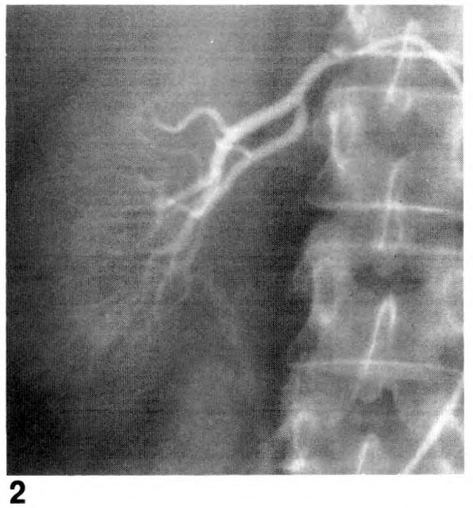
[1] Department of Radiology, Medical College of Wisconsin, Milwaukee, WI 53226, and Community Memorial Hospital, Menomonee Falls, WI 53051. Address reprint requests to A. A. Nemcek, Dept. of Radiology, Community Medical Hospital, W 180 N8085 Town Hall Rd., Menomonee Falls, WI 53051.

[2] Department of Medicine, Medical College of Wisconsin, Milwaukee, WI 53226, and Medical Associates Health Center, Menomonee Falls, WI 53051.

AJR 147:737–738, October 1986 0361–803X/86/1474–0737 © American Roentgen Ray Society



1



2

Fig. 1.—Selective right renal arteriogram done in 1974 shows fibromuscular dysplasia.

Fig. 2.—Selective right arteriogram 11 years later shows normal renal artery. There is mild stenosis of right inferior polar artery.

period of years may be needed to establish that fibromuscular dysplasia is indeed a disease under metabolic control susceptible to pharmacologic intervention.

If renovascular hypertension and abnormal anatomy can be reversed with medical treatment, perhaps surgical and/or angiographic intervention need not be the procedure of choice. Further study of successful cases of medically treated patients may demonstrate normal vasculature.

REFERENCES

1. Goncharenko V, Gerlock AJ Jr, Shaff MI, et al. Progression of renal artery fibromuscular dysplasia in 42 patients as seen on angiography. *Radiology* **1981**;139(1):45–51.
2. Tegtmeyer CJ, Elson J, Glass TA, et al. Percutaneous transluminal angioplasty: the treatment of choice for renovascular hypertension due to fibromuscular dysplasia. *Radiology* **1982**;143(3):631–637
3. Martin EC, Diamond NG, Casarella WJ. Percutaneous transluminal angioplasty in nonatherosclerotic disease. *Radiology* **1980**;135(1):27–33
4. Martin EC, Mattern RF, Baer L, et al. Renal angioplasty for hypertension: predictive factors for long term success. *AJR* **1981**;137(5):975–982
5. Siegler RL, Miller FJ, Mineau DE, et al. Spontaneous reversal of hypertension caused by fibromuscular dysplasia. *J Pediatr* **1982**;100(1):83–85

Case Report

Intraosseous Glomus Tumor: Report of a Case and Review of the Literature

Ann G. Bjorkengren,[1] Donald Resnick, Parviz Haghighi, and David J. Sartoris

The glomus tumor has, despite its rarity, received attention in the clinical literature because of its characteristic symptoms and its typical location at the fingertips. Radiographic examination is negative in most cases, but a small scalloped bony defect in a terminal phalanx has been described in 9–60% of cases [1, 2]. Primary intraosseous location of a glomus tumor, of which nine cases have been previously described [3–9], all in the nonradiologic literature, has a place in the differential diagnosis of lytic lesions of the phalanges. Previously described cases have all been located in the distal phalanx. We describe a case of primary intraosseous glomus tumor, not in the phalangeal tuft, but in the base of a middle phalanx, mimicking an enchondroma.

Case Report

A 68-year-old man was evaluated for pain that worsened at night and that had been present in the fifth finger of his right hand for approximately 5 years. Physical examination demonstrated a tender prominence just distal to the proximal interphalangeal joint. Radiographic examination demonstrated a well-circumscribed radiolucent lesion that involved the proximal aspect of the middle phalanx of the fifth finger and that produced endosteal erosion of the adjacent cortex (Fig. 1). An enchondroma was considered the most likely diagnosis. The lesion was subsequently curretted, and the residual osseous defect was filled with cancellous bone graft. The specimen consisted of multiple fragments of tan and white tissue, the largest of which measured 4 × 3 × 1 mm. Microscopic examination demonstrated prominent vascular structures with perivascular nests of glomus cells, diagnostic of a glomus tumor of the glomangioma type (Fig. 2). Two months after surgery, the clinical manifestations had completely disappeared, and repeat radiographs documented successful incorporation of the bone graft material into the adjacent bone.

Discussion

The cutaneous neuromyoarterial glomus is a structure located in the skin whose function in temperature regulation is related to arteriovenous shunting of blood. The normal glomus, Latin for "ball" or "spherical mass," was first described by Hoyer in 1877 [13]; it consists of a specialized vascular anastomotic complex surrounded by nerve elements. Glomus structures are present diffusely in the skin layer, are more common in the palmar and plantar regions, and are particularly frequent in the fingertips, especially the region of the nailbeds.

A glomus tumor is an uncommon neoplasm characterized by excessive proliferation of vascular structures with distinctive large cells, the glomus cells, associated with the smooth muscle layer of arteriolar walls and with thickened endothelium [10]. If the lesion mainly consists of prominent vessels, it is called a glomangioma. Masson provided the first accurate pathologic description of the glomus tumor in 1924 [13]. In 1958, Jaffe [11] proposed that the lesion arose in a normal glomus organelle, which occasionally can be located in the medullary cavity of a bone. Pericytes within the walls of intraosseous blood vessels have also been suggested as potential cells of origin [4].

The characteristic clinical presentation of a glomus tumor was first described in 1812 by Wood [13]. The lesion most

Received February 21, 1986; accepted after revision May 9, 1986

[1] All authors: Department of Radiology, Veterans Administration Medical Center and University of California Medical Center, San Diego, CA. Address reprint requests to D. Resnick, Department of Radiology, Veterans Administration Medical Center, 3350 La Jolla Village Dr., San Diego, CA 92161.

AJR 147:739–741, October 1986 0361–803X/86/1474–0739 © American Roentgen Ray Society

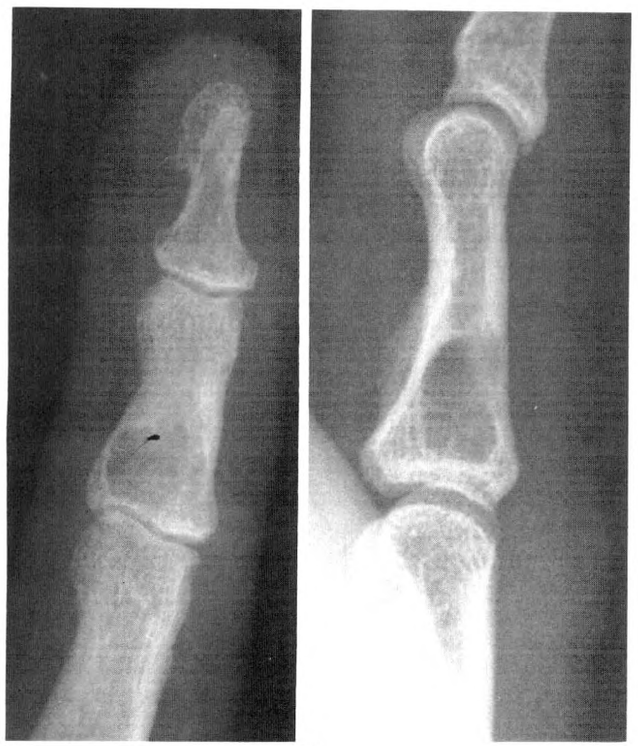


Fig. 1.—Posteroanterior (**A**) and lateral (**B**) views of fifth finger demonstrate a lytic lesion involving base of middle phalanx. No soft-tissue mass demonstrated, no evidence of matrix calcification or ossification. Cortex is attenuated but not interrupted. Lesion is well demarcated and extends to subchondral cortex of proximal interphalangeal joint.

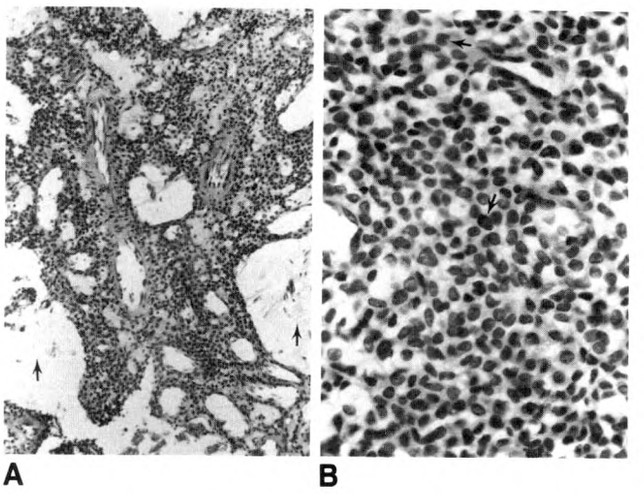


Fig. 2.—**A**, Microscopic section showing many variously sized vascular channels with variable medial thickness. Pericytes are seen between vessels. Perivascular edema noted (*arrows*). (H and E, ×40)

B, Higher magnification (×160) demonstrates pericytes with ill-defined cytoplasmic membranes and uniform round-to-oval nuclei, some of which have nuclear grooves (*arrows*), and evenly distributed chromatin.

commonly involves the soft tissue, and it frequently is not palpable or visible on physical examination because of its small size. A small pink or bluish nodule may be observed, typically beneath the nail. Characteristic symptoms are usually present, including aching pain, exquisite point tenderness, and temperature sensitivity. Exposure to cold or minimal trauma may trigger severe paroxysmal attacks of pain. This combination of findings has been considered specific enough for an accurate clinical diagnosis of a glomus tumor in most patients. Almost all glomus tumors are benign and do not metastasize; exceptionally rarely, a glomangiosarcoma may occur [12]. Adequate treatment consists of excision, usually by currettage in the setting of an intraosseous localization. Incomplete removal of the tumor may result in local recurrence, usually within a few months of surgery.

Glomus tumors are most commonly soft-tissue lesions that do not involve bone. However, in various series, osseous abnormalities have been observed in 9% of 23 cases [1], 14% of 28 cases [13], 15% of 20 cases [14], and 60% of 15 cases [2]. These abnormalities consist of shallow, well-corticated osseous defects, generally involving the tufts of the distal phalanges adjacent to the tumor, and they are believed to result from pressure on the cortex induced by vascular pulsations from the lesion. An entirely intraosseous localization of a glomus tumor was first reported by Iglesias de la Torre and collaborators in 1939 [3]. Subsequently, eight additional cases have been documented [4–9]. In all nine previously described cases, the intraosseous glomus tumor has been located in the medullary space of a terminal phalanx and encased by cortical bone. The radiographic appearance in all instances resembled that of an enchondroma, epithelial inclusion cyst, or simple bone cyst, and the correct diagnosis was usually made only after excision and pathologic examination of the specimen.

In our patient, the radiographic abnormalities were interpreted as most compatible with an enchondroma. The clinical history, suggesting the correct diagnosis and consisting of several years of point tenderness and localized pain, at times awakening the patient at night, had not, however, been made available to the radiologist at the time of interpretation of the radiographs. This information would have rendered the diagnosis of enchondroma less likely, even in the setting of pathologic fracture. Other less common diagnostic considerations would have included epithelial inclusion cyst, simple bone cyst, aneurysmal bone cyst, metastasis (particularly from bronchogenic carcinoma), sarcoidosis, tuberous sclerosis, and xanthoma.

REFERENCES

1. Raisman V, Mayer L. Tumor of the neuromyoarterial glomus. Report of cases. *Arch Surg* **1935**;30:911–929
2. Mathis W Jr, Schulz M. Roentgen diagnosis of glomus tumors. *Radiology* **1948**;51:71–76
3. Inglesias de la Torre L, Gomez Camejo M, Palacios G. Consideraciones clínicas, anatómicas, radiológicas y quirúgical del glomus tumoral de Masson. *Cirurgía Ortopédica y Traumatol (Habana)* **1939**;7:11–17
4. Lattes R, Bull D. A case of glomus tumor with primary involve-

ment of bone. *Ann Surg* **1948**;127:187–191
5. Lehman W, Kraissl C. Glomus tumor within bone. *Surgery* **1949**;25:118–121
6. Mackenzie DH. Intraosseous glomus tumours. *J Bone Joint Surg [Br]* **1962**;44:648–651
7. Siegel MW. Intraosseous glomus tumor. *Am J Orthoped* **1967**;9:68–69
8. Ishii S, Minami M, Asai M, Usui M, Itagaki T, Kobayashi S. Glomus tumor of the hand. *Hok J Orthoped Traum Surg* **1973**;18:52–55
9. Sugiura I. Intra-osseous glomus tumour. *J Bone Joint Surg [Br]* **1976**;58:245–247
10. Wilner D. Glomus tumor of bone. In: *Radiology of bone tumors and allied disorders*, 1st ed. Philadelphia: Saunders, **1982**:766–776
11. Jaffe H. Glomus tumor of bone. In: *Tumors and tumorous conditions of bones and joints*. Philadelphia: Lea & Febiger, **1958**:254–255
12. Enzinger F, Weiss S. Glomus tumor. In: *Soft tissue tumors*. St. Louis: Mosby, **1983**:450–462
13. Carroll R, Berman A. Glomus tumors of the hand. *J Bone Joint Surg [Am]* **1972**;54:691–703
14. Riveros M, Pack GT. The glomus tumor. *Ann Surg* **1951**; 133:394–398

Case Report

Calcific Tendinitis of the Longus Coli: Diagnosis by CT

Ferris M. Hall,[1] William P. Docken,[2] and Hayes W. Curtis[1]

We describe a case of calcific tendinitis of the longus coli muscle in which plain radiographs could not definitively demonstrate calcific deposits in the prevertebral soft tissues of the neck. The diagnosis was made by CT.

Case Report

A 50-year-old black woman was admitted to the hospital with severe neck discomfort. Symptoms had progressed over the period of 1 month to the point of disabling pain for the 5 days before admission. There was moderate dysphagia. Oral temperature ranged from 99–101°F for the 2 days before admission. There was no pertinent past medical history.

The physical examination was normal except for excruciating pain on any movement of the neck. The sedimentation rate was 58. Multiple other laboratory examinations were normal including CSF. Extensive evaluation, including lumbar puncture, was unrevealing. Admission plain neck radiographs showed only prominence of the prevertebral soft tissues. The diagnosis of calcific tendinitis of the longus coli was entertained but characteristically located soft-tissue calcifications could not be definitively identified despite repeat neck radiographs with multiple views including flexion and extension (Fig. 1). However, these were clearly demonstrated on subsequent CT (Fig. 2).

The patient was treated with high-dose indomethacin, analgesics, and a cervical collar. Her symptoms gradually subsided over 2 weeks. Follow-up imaging studies were not obtained.

Discussion

Calcific tendinitis of the longus coli is associated with and presumably caused by hydroxyapatite crystals in musculotendinous tissues. It is one of the crystalline deposition diseases that characteristically occurs near periarticular tendinous insertions. The diagnosis is most commonly made in the shoulder where the calcifications usually lie in the supraspinatus tendon of the rotator cuff or the adjacent subacromial bursa. However, calcific tendinitis is a well-known cause of acute pain about the wrist (flexor carpi ulnaris), hip (gluteus maximus), and ankle (peroneus longus), as well as the neck (longus coli).

Acute calcific tendinitis of the shoulder is occasionally seen without radiographically demonstrable soft-tissue calcifications, and typical calcifications are sometimes seen without acute symptoms. The lack of demonstrable soft-tissue calcifications should not detract from this diagnosis. Knowledgeable orthopedists and rheumatologists will often treat patients with a classic history by using anesthetic/steroid injections or antiinflammatory agents, without obtaining radiologic confirmation. However, in the less common cases of presumed calcific tendinitis, occurring at sites other than the shoulder, the lack of demonstrable calcifications often prompts consideration of other diagnoses.

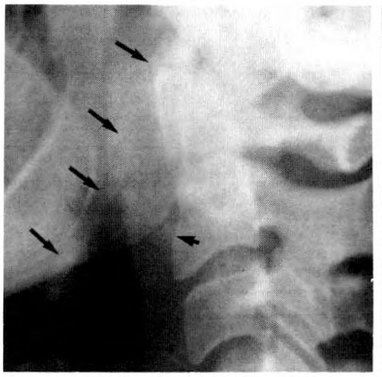
Calcific tendinitis of the longus coli was first described in 1964 [1]. A 1984 report and literature review found 34 reported cases [2]. Relatively few of these cases have appeared in the radiologic literature [3–7]. The radiologist needs to be familiar with this disease because the symptoms are in the purview of a variety of medical specialists, many of whom may be unfamiliar with its existence. The typical history is that of a middle-aged man or woman with acute or subacute posterior neck pain. The pain is often severe and may be

Received March 24, 1986; accepted after revision April 28, 1986.

[1] Department of Radiology, Beth Israel Hospital and Harvard Medical School, Boston, MA 02215. Address reprint requests to F. M. Hall, Dept. of Radiology, Beth Israel Hospital, 330 Brookline Ave., Boston, MA 02215.

[2] Department of Rheumatology, Beth Israel Hospital and Harvard Medical School, Boston, MA 02215.

AJR 147:742–743, October 1986 0361–803X/86/1474–0742 © American Roentgen Ray Society



1



2

Fig. 1.—Admission lateral neck film shows prevertebral soft-tissue swelling. There are equivocal amorphous calcifications anterior to C2 (*short arrow*) but none appreciated anterior to C1. Calcified styloid-hyoid ligaments (*arrows*) overlie the soft tissues anterior to C1.

Fig. 2.—CT scan at level of C1 shows swollen and calcified right longus coli muscle and/or its tendinous insertions (*arrow*). There is calcification of both styloid-hyoid ligaments, greater on the right, seen anterior to the lateral masses of C2. Scan at level of C2 (not shown) showed similar calcifications as suggested on plain radiograph (Fig. 1).

accompanied by dysphagia. Range of motion about the cervical spine is limited. There may be a mild fever, leukocytosis, and an elevation of the erythrocyte sedimentation rate, raising the suspicion of retropharyngeal infection. Radiographs demonstrate prevertebral soft-tissue swelling and focal amorphous calcifications anterior to the first and second cervical vertebrae.

We could find no published examples of a CT diagnosis of calcific tendinitis of the longus coli muscle, although a number of authors have described the typical calcifications on conventional tomography. In our case, despite clinical suspicion, the characteristically located calcifications could not be definitively identified despite multiple radiographs specifically looking for them. CT, because of its enhanced contrast resolution and axial anatomic display, frequently demonstrates faint calcifications not seen on plain radiographs or even on conventional tomograms. We are aware of one case in which faint rotator cuff calcifications, not visualized on plain radiographs, were demonstrated on CT of the shoulder because of the greater contrast resolution (Newberg A, unpublished data).

To our knowledge the definitive diagnosis of calcific tendinitis of the longus coli is always based on the radiologic findings of characteristic amorphous calcifications in the prevertebral soft tissues. As awareness of this entity increases, the diagnosis will be considered in earlier and more subtle cases. We recommend that CT be performed if clinical suspicion is high, and if plain films fail to demonstrate calcification.

REFERENCES

1. Hartley J. Acute cervical pain associated with retropharyngeal calcium deposit: a case report. *J Bone Joint Surg* [Am] **1964**;46:1753–1754
2. Kaplan MJ, Eavey R. Calcific tendinitis of the longus coli muscle. *Ann Otol Rhinol Laryngol* **1984**;93:215–219
3. Haun CL. Retropharyngeal tendinitis. *AJR* **1978**;130:1137–1140
4. Newmark H, Forrester DM, Brown JC, Robinson A, Oiken SM, Bledsoe R. Calcific tendinitis in the neck. *Radiology* **1978**; 128:355–358
5. Karasick D, Karasick S. Calcific retropharyngeal tendinitis. *Skeletal Radiol* **1981**;7:203–205
6. Newmark H, Zee CS, Frankl P, Robinson A, Blau L, Gans DC. Chronic calcific tendinitis of the neck. *Skeletal Radiol* **1981**;7:207–208
7. Wallington G, Palmer MK. Retropharyngeal tendinitis. *Br J Radiol* **1983**;36:52–54

Case Report

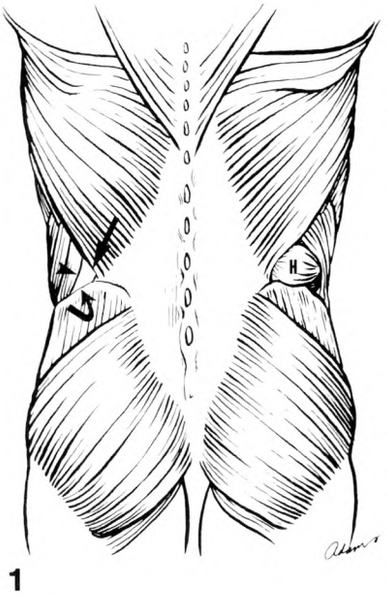
Inferior Lumbar (Petit's) Hernia

Richard B. Lawdahl,[1] C. Neil Moss, and Jerrold A. Van Dyke

The inferior lumbar triangle is a normal area of weakness in the posterior abdominal wall. It is bounded by the free border of the latissimus dorsi posteromedially, the external oblique anterolaterally, and the iliac crest inferiorly (Fig. 1) [1]. Herniation through this triangle is rare and is known as Petit's hernia or inferior lumbar hernia [2]. The cause may be congenital, spontaneous, postinflammatory, traumatic, or surgical [3].

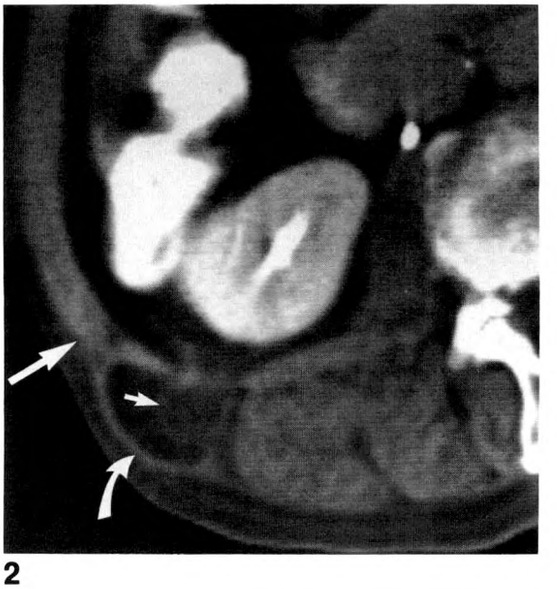
Case Report

A 78-year-old man was admitted to University of Alabama Hospital for treatment of congestive heart failure. He had had an asymptomatic mass in his right flank for several years. There was no history of surgery. Physical examination revealed a 4 × 6 cm soft right-flank mass that increased when the patient coughed or during the Valsalva maneuver. No bowel sounds were heard over the mass. An abdominal CT was performed to exclude malignancy. CT showed herniation of



1

Fig. 1.—Posterior view of back demonstrates external oblique (*arrowhead*), latissimus dorsi (*arrow*), and iliac crest (*curved arrow*), which form the borders of the inferior lumbar triangle. A Petit's hernia (H) is shown on right.



2

Fig. 2.—CT scan shows Petit's hernia, which contains retroperitoneal fat as well as a portion of Gerota's fascia (*short arrow*). Without other structures in the hernia, the presence of Gerota's fascia differentiates it from a lipoma. At this level, hernia is bounded by attenuated inferior margin of latissimus dorsi (*curved arrow*) and external oblique (*long arrow*).

Received February 29, 1986; accepted April 27, 1986

[1] All authors: Department of Radiology, University of Alabama at Birmingham, School of Medicine, 619 S. 19th St., Birmingham, AL 35233. Address reprint requests to R. B. Lawdahl.

AJR **147:744–745, October 1986** 0361–803X/86/1474–0745 © American Roentgen Ray Society

right retroperitoneal fat and Gerota's fascia through the inferior lumbar triangle (Fig. 2). No other abnormalities were found. The patient received no treatment for the hernia and was discharged after treatment of his congestive heart failure.

Discussion

In 1738 Petit described a case of strangulated lumbar hernia through the triangle that now bears his name [3]. Lumbar hernias are often asymptomatic, but may produce low-back pain, colic, or a pulling sensation that may resolve with reduction of the hernia. Diagnosis is usually established by the presence of a reducible soft-tissue mass above the iliac crest, which enlarges with the Valsalva maneuver or coughing. Bowel sounds may be heard over the area of the hernia.

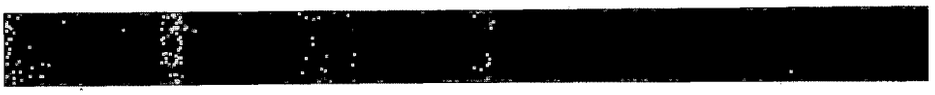
Lumbar hernias may contain peritoneum and intraperitoneal organs, or may be entirely extraperitoneal. Contents, in order of frequency, include bowel, retroperitoneal fat, and kidney. Less frequently, the hernia contains omentum, stomach, ovary, spleen, or appendix [4]. Once formed, these hernias gradually enlarge. Because the neck of the hernia is usually wide, strangulation is uncommon, occurring in about 10% of cases [2, 3]. Treatment may require surgical reduction and closure, or simply the use of a belt or truss.

Lumbar hernias are difficult to diagnose by physical examination when they are small, occur in obese individuals, or contain only fat. CT is valuable and may be useful to define the muscular walls and contents of the hernia, such as bowel, kidney, or Gerota's fascia, before surgery. It is important that this abnormality be differentiated from a retroperitoneal tumor or abdominal-wall lipoma.

REFERENCES

1. Goss CM, ed. *Gray's anatomy*, 29th ed. Philadelphia: Lea & Febiger, **1973**:448
2. Nyhus LM, Bombeck CT. Hernias. In: Sabiston DC, ed. *Textbook of surgery*, 12th ed. Philadelphia: Saunders, **1981**:1348–1349
3. Wakeley C. Rare types of external abdominal hernias. In: Maingot R, ed. *Abdominal operations*, 5th ed. East Norwalk, CT: Appleton-Century-Crofts, **1969**:1282–1283
4. Swartz WT. Lumbar hernias. In: Nyhus LM, Harkins HN, eds. *Hernia*. Philadelphia: Lippincott, **1964**:361–379

Primary Central Nervous System Lymphoma: CT and Pathologic Correlation



Ya-Yen Lee[1]
Janet M. Bruner[2]
Pamela Van Tassel[1]
Herman I. Libshitz[1]

CT findings of 15 patients with histologically proven primary central nervous system (CNS) lymphoma were reviewed with pathologic correlation in order to evaluate variable CT patterns. There were a total of 32 lesions. Of the 15 patients studied, seven had acquired immunodeficiency syndrome (AIDS), all diagnosed within the past 3 years. The CT observations of eight non-AIDS patients were consistent with findings reported previously. Most of the lymphomatous lesions were either hyper- or isodense, round or oval masses with homogeneous contrast enhancement and variable surrounding edema. Pathologic examination showed tightly packed preserved lymphoma cells without necrosis. in AIDS patients, rim or ring enhancement of lymphoma, indistinguishable from brain abscess, was frequently seen. Histologic examination consistently showed extensive tumor necrosis with preservation of viable tumor cells at the periphery. A third and infrequent CT pattern was multiple infiltrative nonnodular solid enhancement with extensive edema. Pathologic correlation showed infiltrating viable tumor cells without necrosis. The rim- or ring-enhancing brain lesion seen in AIDS patients can either be an abscess or a primary lymphoma; proper tissue collection is essential for correct diagnosis and appropriate treatment.

Primary CNS lymphoma is still a relatively rare primary brain tumor, even with the recent increase in AIDS patients. The classic CT observations of primary CNS lymphoma have been described as solid, well-circumscribed hyperdense mass(es) with homogeneous contrast enhancement and predilection for the basal ganglia, corpus callosum, periventricular white matter, and cerebellar vermis. Other CT observations, however, such as rim- or ringlike and gyrallike patterns, have not been previously emphasized, and to our knowledge there has been no report describing the pathologic correlation. In this paper we will describe the spectrum of CT findings on primary CNS lymphoma in 15 patients and correlate these findings with tissue specimens obtained before initiation of treatment.

This article appears in the July/August 1986 issue of *AJNR* and the October 1986 issue of *AJR*.

Received July 18, 1985; accepted after revision October 29, 1985.

[1] Division of Diagnostic Imaging, The University of Texas M. D. Anderson Hospital and Tumor Institute at Houston, 6723 Bertner Ave., Houston, TX 77030. Address reprint requests to Y.-Y. Lee.

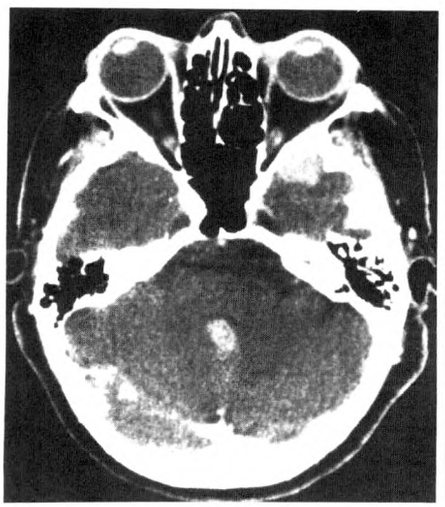
[2] Department of Pathology, The University of Texas M. D. Anderson Hospital and Tumor Institute at Houston, Houston, TX 77030.

***AJR* 147:747–752, October 1986**
0361–803X/86/1474–0747
© American Roentgen Ray Society

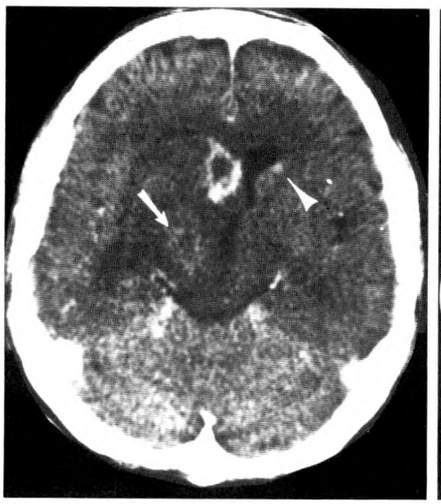
Materials and Methods

From June 1977 to June 1985, 15 patients with biopsy-proven primary CNS lymphoma were seen at The University of Texas M. D. Anderson Hospital and Tumor Institute in Houston. Ten of the patients were men and five were women. They ranged in age from 12 to 65 years (mean age, 38.4 years).

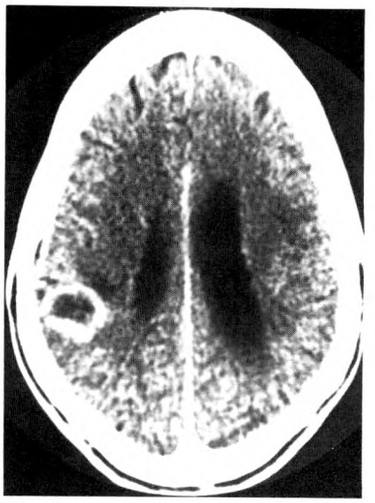
All CT scans were done before needle or open biopsy and were obtained before and after intravenous administration of 300 ml of 30% contrast medium (42 g iodine). The scans were performed on different scanners, including GE-8800 (Milwaukee, WI), GE-9800, EMI-1010 (Hayes, Middlesex, England), Siemens Somatom 2, and Siemens DR-3 (Iselin, NJ). Thirty-two lesions in our 15 patients were evaluated with CT. All biopsy or resected specimens (n = 15) were reviewed by one of the authors (JMB) and the results were correlated with the CT findings.



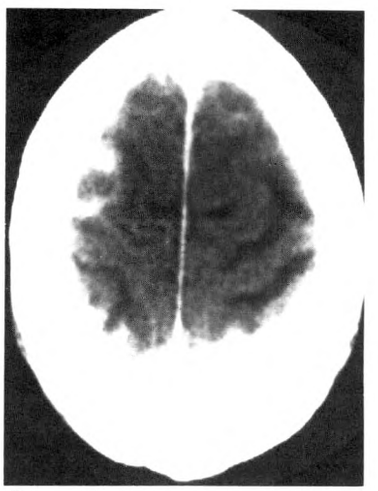
1



2



3



4

Fig. 1.—Two solid nodular-enhancing lesions in previously healthy 66-year-old woman. Diagnosis of primary CNS lymphoma was made on surgical specimen of left temporal lesion.

Fig. 2.—Multiple-enhancing lesions in 32-year-old male AIDS patient. Irregular rim-enhancing lesion is seen in head of right caudate nucleus, in addition to poorly defined rim-enhancing lesion in right thalamus and posterior limb of internal capsule (*arrow*) and solid nodular-enhancing lesion in head of left caudate nucleus (*arrowhead*). Needle biopsy of right caudate lesion revealed lymphoma. Patient received whole brain irradiation of 5200 rad (52 Gy). Autopsy 3½ months after initial diagnosis revealed extensive necrotic lymphoma involvement in both basal ganglia and in right thalamus. There was no evidence of intracranial infection and no dissemination of lymphoma beyond CNS.

Fig. 3.—Well-defined right parietal thick ring-enhancing lesion in 24-year-old male AIDS patient proved to be lymphoma with extensive necrosis in an open biopsy specimen. Autopsy 2 months after initial diagnosis confirmed diagnosis of primary CNS lymphoma without intracranial infection.

Fig. 4.—"Gyral"-enhancing lesion in right high-convexiety parietal lobe of 35-year-old male AIDS patient. Open biopsy revealed lymphoma. Autopsy 1 month later confirmed diagnosis without evidence of CNS infection or extraneural lymphomatous involvement.

Results

CT Evaluations

Thirty-two lesions were identified on CT in 15 patients (eight non-AIDS and seven AIDS). Fifteen (47%) of the lesions were predominantly in the cortex; of these, three showed extensive infiltration into the periventricular white matter. The cortico-medullary junction was primarily involved in only three (9%) of the 32 lesions. Of the remaining 17 lesions, 15 (47%) were periventricular and the other two (6%) were in the lateral basal ganglia. Vermis and basal ganglia were the favorite sites in the non-AIDS patients, and frontal lobe was the most common location in the AIDS patients. Edema surrounded 26 (81%) of the lesions; the edema/tumor ratio was greater or equal to one in 20 lesions.

A summary of the CT observations is given in Table 1. The contrast-enhancing pattern was the only significantly different CT feature between non-AIDS and AIDS patients. In the non-AIDS patients, the solid nodular pattern (Fig. 1) was the predominant pattern and was observed in 12 (75%) of the lesions. Only two (13%) of the lesions had a rimlike pattern (Figs. 2 and 3). In the AIDS patients, the rimlike pattern was observed in seven (44%) of 16 lesions and the solid nodular pattern was seen in six (38%). The gyrallike pattern (Fig. 4) was observed infrequently (it occurred in two (13%) of 16 lesions in each group).

Pathologic Correlation

In all 15 patients the tissue diagnosis was diffuse large-cell lymphoma, which was in accordance with the working formulation for classification of non-Hodgkin's lymphoma [1]. None of the 15 lesions examined had an associated infectious process microscopically. The microbiologic cultures in seven AIDS patients were negative for bacteria, viruses, and protozoa. Of the 15 lesions biopsied or resected, the enhancing CT patterns were solid nodular in six, rim or ringlike in seven, and gyrallike in two.

TABLE 1: **CT Characteristics of Primary CNS Lymphoma**

	Non-AIDS (n = 8)	AIDS (n = 7)
Number of Lesions	16	16
Multiplicity	3	4
Location		
Frontal lobe	2	8
Parietal lobe	1	3
Temporal lobe	2	0
Occipital lobe	1	1
Basal ganglia	4	2
Thalamus	0	1
Vermis	6	1
Size (cm)		
<2	9	6
2–5	6	7
>5	1	3
Shape		
Round	8	7
Oval	5	4
Multilobular	1	3
Infiltrative	2	2
Precontrast CT Density		
Hyperdense	6	3
Isodense	10	9
Hypodense	0	3
Mixed	0	1
Degree of Contrast Enhancement		
Marked	14	13
Moderate	2	3
Contrast-Enhancing Pattern		
Solid nodular	12	6
Rim or ringlike	2	7
Gyrallike	2	2
Mixed (nodular + rim)	0	1

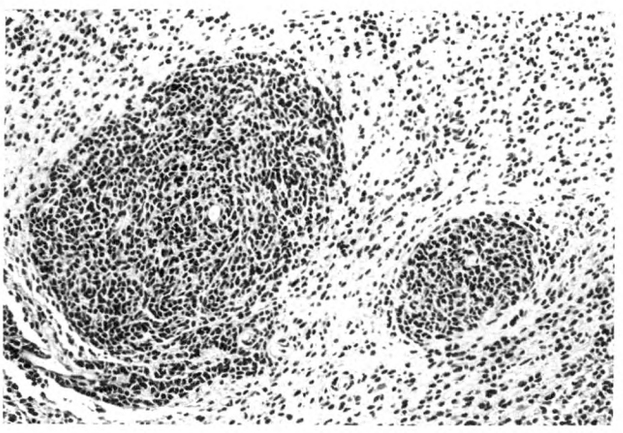


Fig. 5.—Extensive lymphomatous infiltration (same patient as in Fig. 1) with characteristic dense concentric perivascular cuffing. No necrosis is present. ×525.

The solid nodular patterns (six patients) all showed tightly packed and preserved lymphoma cells without necrosis (Fig. 5). Only one of these patients was immunosuppressed.

The rim- or ringlike patterns (seven patients) all demonstrated extensive necrosis with preservation of tumor cells at the periphery (Fig. 6). Five of these seven patients had AIDS.

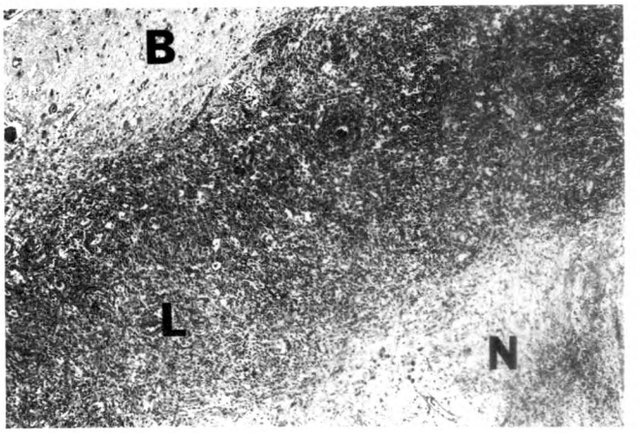


Fig. 6.—Extensive central necrosis (N) surrounded by rim of viable lymphoma (L). Normal brain tissue is identified outside lymphoma (B). ×200 (same patient as in Fig. 3).

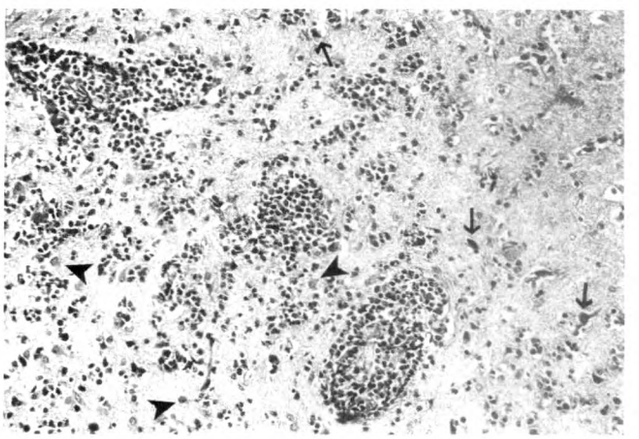


Fig. 7.—Loosely clustered perivascular cuffings of viable lymphoma cells, with minimal infiltration into intervening brain tissue where residual neurons (*arrows*) and reactive astrocytes (*arrowheads*) can be identified. No necrosis is present. ×525 (same patient as in Fig. 4).

The gyrallike patterns (two patients) were seen in the cortical region. Microscopically, the tumor cells were loosely clustered, forming perivascular cuffs with infiltration into the interlacing reactive brain tissue (Fig. 7). One lesion was observed in an AIDS patient and the other in an immunecompetent 12-year-old patient.

Discussion

Primary CNS lymphoma is a relatively rare primary brain tumor and there is controversy regarding its cell of origin. "Perithelial sarcoma" [2], primary reticulum cell sarcoma of brain [3, 4], and microgliomatosis [5], with its possible perivascular or microglial origin, have been used to describe the same primary neoplastic lymphoproliferative process in the CNS. The term "primary malignant lymphomas of CNS" has generally been accepted in recent years because these lym-

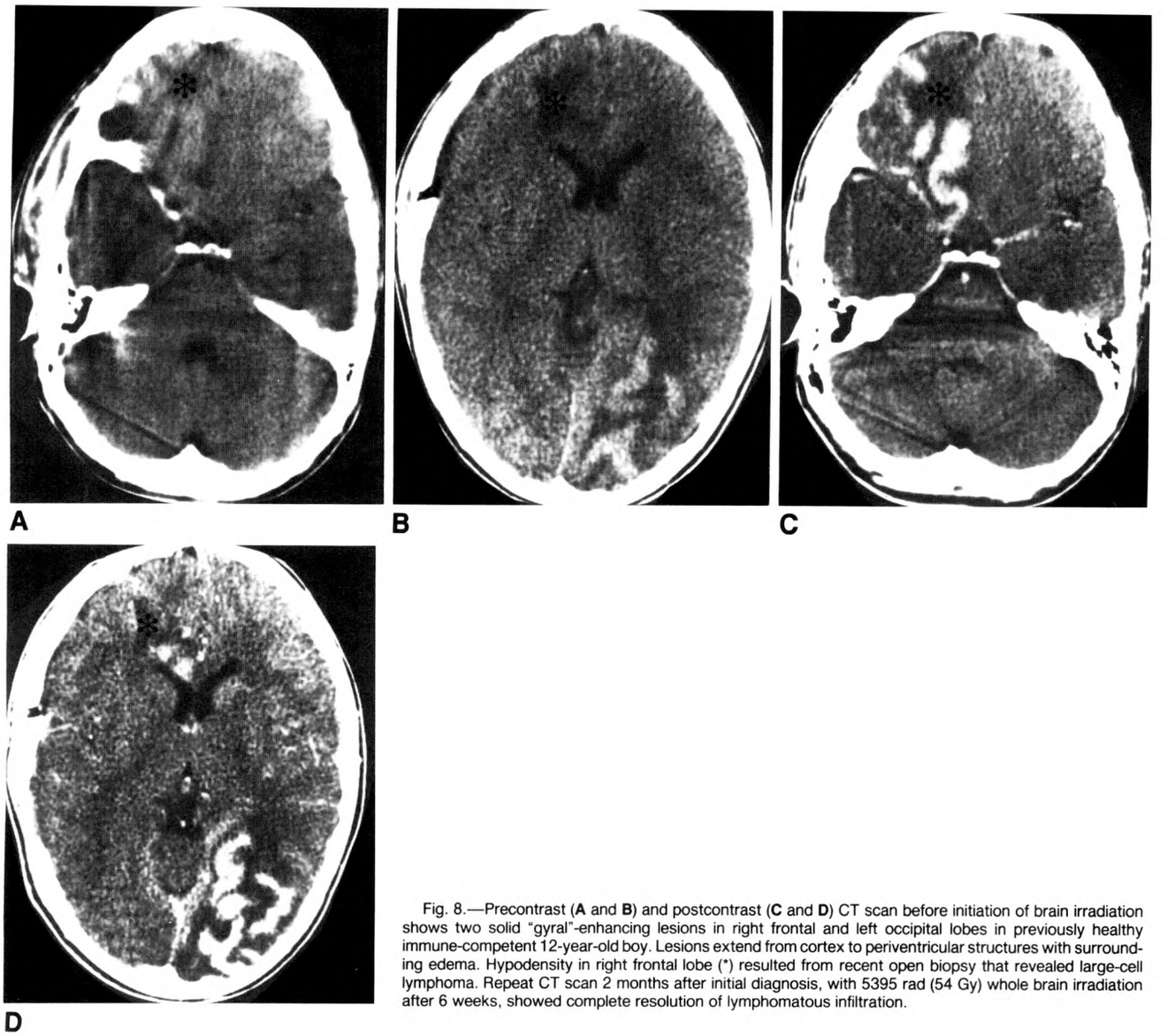


Fig. 8.—Precontrast (**A** and **B**) and postcontrast (**C** and **D**) CT scan before initiation of brain irradiation shows two solid "gyral"-enhancing lesions in right frontal and left occipital lobes in previously healthy immune-competent 12-year-old boy. Lesions extend from cortex to periventricular structures with surrounding edema. Hypodensity in right frontal lobe (*) resulted from recent open biopsy that revealed large-cell lymphoma. Repeat CT scan 2 months after initial diagnosis, with 5395 rad (54 Gy) whole brain irradiation after 6 weeks, showed complete resolution of lymphomatous infiltration.

phomas are similar to a wide range of extraneural malignant lymphomas [6–11]. It is postulated that these lymphomas might be the neoplastic counterparts of the normal process of lymphocyte transformation [12, 13]. There is evidence of an increasing incidence in recent years, particularly among allograft transplant recipients [14–16] and AIDS patients [17–19]. The AIDS epidemic, however, has contributed most significantly to this increase. Of the 15 patients in this series, five diagnoses were made between 1977 and 1982 and none was related to AIDS. Of the remaining 10 patients, all seen within the past 3 years, seven had AIDS.

The classic CT appearance of primary CNS lymphoma has been well described [20–25]. In general, these lymphomas present as relatively large, sharply demarcated, hyper- or isodense, round or oval mass lesions located in the basal ganglia, corpus callosum, periventricular white matter, and cerebellar vermis. Moderate-to-marked homogeneous contrast enhancement is usually observed without central hypodensity. Multiple lesions are frequently present.

CT observations of 16 lesions in our eight non-AIDS patients agree with previous reports [20–25]. The tumor masses are pathologically composed of densely packed neoplastic cells of lymphoreticular origin with a characteristic pattern of dense perivascular concentric cuffing. Hypercellularity, not hypervascularity, without necrosis may be responsible for the hyper- or isodensity of the tumor mass on the noncontrast CT and for the homogeneous enhancement on the postcontrast CT. The pathologic examination of our tissue specimens with the solid nodular CT pattern supports this postulation.

The CT and pathologic findings in the AIDS patients, however, are frequently different from the classic pattern. Nearly half the lesions have an abscesslike appearance, with rim or

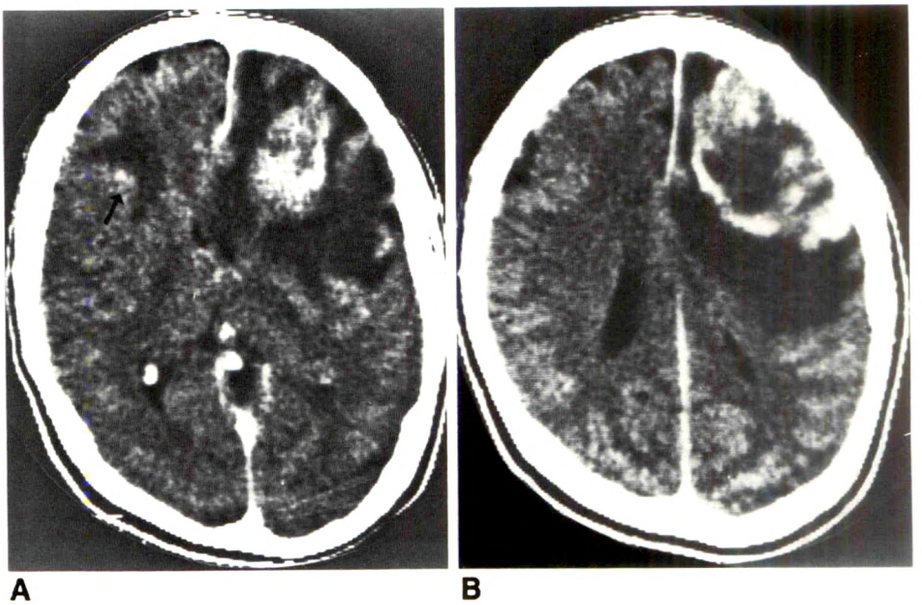


Fig. 9.—**A** and **B**, Left frontal irregular rim-enhancing lesion with partial solid nodular mass in 35-year-old male AIDS patient. This pathologically proven necrotic lymphomatous lesion cannot be differentiated from glioblastoma multiforme. A small additional solid-enhancing lesion is seen in right frontal corticomedullary junction (*arrow* in **A**).

ring enhancement and central hypodensity. This observation is less common in non-AIDS patients. Pathologic examination consistently showed extensive necrosis of the tumor mass with preservation of viable tumor cells at the periphery. Central necrosis had also been reported as a common finding of CNS or extraneural lymphomas in the organ transplant recipients who, like AIDS patients, are immunocompromised [26, 27]. We have no explanation for this central necrosis. Extensive immunomorphologic examinations of these cases should provide further understanding.

An unusual gyrallike, solid-enhancing pattern, which to our knowledge has not been previously described, occurred in three patients. One child with normal immune status had extensive gyrallike lesions interlacing with edematous but tumor-free brain tissue in two different locations (Fig. 8). The lesions extended from the cortex into the periventricular white matter. The tissue specimen revealed viable tumor cells clustered together without necrosis. The lesions responded to cranial irradiation and disappeared completely (by CT) immediately following the completion of treatment. The second patient, who had AIDS, had more subtle gyrallike enhancement in the parietal cortex (Fig. 4). The biopsy specimen showed loose clusters of viable cells without necrosis. The patient died of cytomegaloviral pulmonary infection and sepsis 3 weeks later. Autopsy results showed extensive necrosis of lymphoma, probably resulting from radiation therapy. There was a small number of viable neoplastic cells within the meninges and around the large vessels bordering the necrosis. No evidence of infection was found in the brain. The biopsy specimens in these two patients were unfortunately too small and fragmented for a more detailed CT-pathologic correlation. The third patient, also an AIDS patient, had associated solid-nodular and ring-enhancing lesions. Biopsy of the gyrallike lesion was not done.

Differential diagnosis of primary CNS lymphoma includes meningioma, metastasis, brain abscess, enhancing infarction, and primary glial tumor. Solitary hyperdense-enhancing lymphoma, when situated near the surfaces of the brain, should be differentiated from meningioma; angiography may be necessary to confirm or exclude the latter. Metastatic lesions, either solitary or multiple, are more difficult to differentiate. Classic CT findings of hyper- or isodensity, homogeneous enhancement, and periventricular location might be helpful to make primary CNS lymphoma the more likely diagnosis. Nevertheless, tissue proof is mandatory, particularly when no primary malignancy is known. The solid-enhancing pattern and the favored locations can distinguish lymphoma from brain abscess without difficulty, although the early cerebritis stage of an abscess might be confusing.

It is impossible to differentiate ring- or rim-enhancing CNS lymphoma from brain abscess, particularly when the patient is immunosuppressed. Opportunistic CNS infections in immunocompromised patients are common [19, 28, 29]. Toxoplasmosis is the most frequent CNS parenchymal infection in AIDS patients [28, 29]. Common findings of extensive necrosis in malignant lymphoma and toxoplasmosis in immunocompromised patients often cause a diagnostic dilemma and delay the proper management. Cases of lymphoma misdiagnosed as toxoplasmosis at biopsy have been reported in AIDS patients [19, 28]. An example of how this might occur was seen in a patient with AIDS in our series. On two occasions, needle biopsy of a ring-enhancing lesion revealed only necrotic tissue without viable cells. The third tissue collection, open biopsy, finally revealed a small portion of viable lymphoma cells at the periphery of extensive necrotic tissue. A large necrotic-enhancing lymphomatous mass may occasionally mimic a malignant glial tumor (Fig. 9). The rare gyrallike lymphomatous involvement can sometimes be confused with an enhancing-resolving infarction.

In conclusion, adequate tissue specimens are essential for

correct diagnosis and initiation of appropriate treatment of primary CNS lymphoma, since lymphomas may mimic brain abscesses on CT, particularly in immunosuppressed patients. Multiple samples or a carefully directed biopsy with immediate frozen section confirmation of the adequacy of viable tissue is mandatory.

REFERENCES

1. National Cancer Institute sponsored study of classifications of non-Hodgkin's lymphomas. Summary and description of a working formulation for clinical usage. *Cancer* **1982**;49:2112–2135
2. Bailey P. Intracranial sarcomatous tumors of leptomeningeal origin. *Arch Surg* **1929**;18:1359–1402
3. Yuile CL. Case of primary reticulum cell sarcoma of the brain. *Arch Pathol* **1938**;26:1036–1044
4. Kinney TD, Adams RD. Reticulum cell sarcoma of the brain. *Arch Neurol Psychiatr* **1943**;50:552–564
5. Russell DS, Marshall AHE, Smith FB. Microgliomatosis. *Brain* **1948**;71:1–15
6. Henry JM, Heffner RR, Dillard SH, Earle KM, Davis RL. Primary malignant lymphomas of the central nervous system. *Cancer* **1974**;34:1293–1302
7. Jellinger K, Radaskiewicz T, Slowik F. Primary malignant lymphomas of the central nervous system in man. *Acta Neuropathol [Suppl]* (Berl) **1975**;6:95–102
8. Houthoff HJ, Poppema S, Ebels EJ, Elema JD. Intracranial malignant lymphomas: a morphologic and immunocytologic study of twenty cases. *Acta Neuropathol* **1978**;46:203–210
9. Letendre L, Banks PM, Reese DF, Miller RH, Scanlon PW, Kiely JM. Primary lymphoma of the central nervous system. *Cancer* **1982**;49:939–943
10. Mendenhall NP, Thar TL, Agee OF, et al. Primary lymphoma of the central nervous system. *Cancer* **1983**;52:1993–2000
11. Helle TL, Britt RH, Colby TV. Primary lymphoma of the central nervous system. *J Neurosurg* **1984**;60:94–103
12. Lukes RJ, Collins RD. Immunological characterization of human malignant lymphomas. *Cancer* **1974**;34:1488–1503
13. Lukes RJ, Parker JW, Taylor CR, et al. Immunologic approach to non-Hodgkin's lymphomas and related leukemias: analysis of the results of multiparameter studies of 425 cases. *Semin Hematol* **1979**;15:322–351
14. Penn I. Development of cancer as a complication of clinical transplantation. *Transplant Proc* **1977**;9:1121–1127
15. Hoover R, Fraumeni JF. Risk of cancer in renal-transplant recipients. *Lancet* **1973**;2:55–57
16. Sloan GM, Cole P, Wilson RE. Risk indicators of de novo malignancy in renal transplant recipients. *Transplant Proc* **1977**;9:1129–1132
17. Gapen P. Neurologic complications now characterizing many AIDS victims. *JAMA* **1982**;248:2941–2942
18. Snider WD, Simpson DM, Aronyk KE, Nielsen SL. Primary lymphoma of the nervous system associated with acquired immune-deficiency syndrome. *N Engl J Med* **1983**;308:45
19. Kelly WM, Brant-Zawadzki M. Acquired immunodeficiency syndrome: neuroradiologic findings. *Radiology* **1983**;149:485–491
20. Tadmor R, Davis KR, Roberson GH, Kleinman GM. Computed tomography in primary malignant lymphoma of the brain. *J Comput Assist Tomogr* **1978**;2:135–140
21. Enzmann DR, Krikorian J, Norman D, et al. Computed tomography in primary reticulum cell sarcoma of the brain. *Radiology* **1979**;130:165–170
22. Lukin R, Tomick TA, Chambers AA. Lymphoma and leukemia of the central nervous system. *Semin Roentgenol* **1980**;15:246–250
23. Spillane J, Kendall B, Moseley IS. Cerebral lymphoma: clinical radiological correlation. *J Neurol Neurosurg Psychiatry* **1982**; 45:199–208
24. Holtas S, Nyman U, Cronqvist S. Computed tomography of malignant lymphoma of the brain. *Neuroradiology* **1984**;26:33–38
25. Whelan MA, Kricheff II. Intracranial lymphoma. *Semin Roentgenol* **1984**;19:91–99
26. Frizzera G, Hanto DW, Gail-Peczalaska KJ, et al. Polymorphic diffuse B-cell hyperplasia and lymphomas in renal transplant recipients. *Cancer Res* **1981**;41:4262–4279
27. Tubman DE, Frick MP, Hanto DW. Lymphoma after organ transplantation: radiologic manifestations in the central nervous system, thorax, and abdomen. *Radiology* **1983**;149:625–631
28. Whelan MA, Kricheff II, Handler M, et al. Acquired immunodeficiency syndrome; cerebral computed tomographic manifestations. *Radiology* **1983**;149:477–484
29. Bursztyn EM, Lee BCP, Bauman J. CT of acquired immunodeficiency syndrome. *AJNR* **1984**;5:711–714

Minimal Asymmetry of the Brain: A Normal Variant

Robert Shapiro[1]
Shelby J. Galloway[2,3]
Marc D. Shapiro[3]

Normal cerebral asymmetry, well-known to neuroradiologists, is not widely recognized by radiologists in general. In our review of CT brain scans, 31 of 300 patients with a negative neurologic examination and no history of birth injury, head trauma, or seizure had recognizable asymmetry of the frontal horns of the lateral ventricles. The right frontal horn and the right cerebral hemispheres were larger than the left twice as often as left were larger than right. The right frontal lobe was wider than the left in 44% of patients and extended as far anteriorly or more anteriorly than the left in 22% of patients. The right central hemispheric mass tended to be wider than the left, resulting in slight displacement of the pineal gland to the left, in approximately 45% of cases. The posterior end of the left Sylvian fissure projected farther posteriorly in 10% of the patients. Occipital petalia and a more posterior position of the calcified glomus of the choroid plexus of the lateral ventricle were both common on the left side of 56%. Earlier studies of the brain by other methods have also shown asymmetry. An awareness of these anatomic asymmetries in normal individuals should preclude the erroneous diagnosis of an atropic or mass lesion.

In the era of pneumoencephalography, a dilated lateral ventricle with a shift of the septum pellicidum indicated an atrophic lesion on the side of the shift, unilateral obstruction of the foramen of Monro, or a mass on the side opposite to the shift. Symmetry of the ventricular system, and parenthetically, of the cerebral hemispheres, was the sine qua non of a normal study, except for asymmetry of the occipital horns without displacement or deformity, which was empirically accepted as a normal variant. Despite these criteria, normal cerebral asymmetry has been recognized by anatomists, anthropologists, and neurologists for some time [1–11]. Although neuroradiologists [12–19] are familiar with normal cerebral asymmetry, there is insufficient recognition of this entity among radiologists in general. The purpose of this paper is to familiarize radiologists with normal ventricular asymmetry on the CT scan as an expression of asymmetric brain development.

Materials and Methods

We reviewed 300 well-positioned, axial transverse CT scans of the brain carried out on patients who presented one of the following: nonspecific headache, dizziness with normal hearing and no cerebellar signs; or depressive disorder. None of the patients had a history of previous birth injury, head trauma, or seizure. All of the patients had had a negative neurologic examination. The age of the patients was 15–62 years (mean: 36.2). There were 159 men and 141 women. Unfortunately, information regarding right- or left-handedness was unavailable because of the retrospective nature of the study.

Scans were performed on a GE 8800 or 9800 high-resolution CT scanner with the scanning angle 20° craniocaudad to the orbitomeatal line. Ten-millimeter contiguous sections were obtained before and after IV contrast enhancement. Soft-tissue and bone-window radiographs of the monitor images were used for measurement. All scans were reviewed and measurements made independently by two observers on two separate occasions. The observers recorded the presence of asymmetry of the frontal, temporal, and occipital horns of the lateral

Received May 13, 1985; accepted after revision April 10, 1986.

[1] Department of Radiology R-130, University of Miami School of Medicine, P. O. Box 016960, Miami, FL 33101. Address reprint requests to R. Shapiro.

[2] Department of Radiology, Hospital of Saint Rapheal, 1450 Chapel St., New Haven, CT 06511.

[3] Department of Medical Imaging, Yale New Haven Medical Center, New Haven, CT 06510.

AJR 147:753–756, October 1986
0361–803X/86/1474–0753
© American Roentgen Ray Society

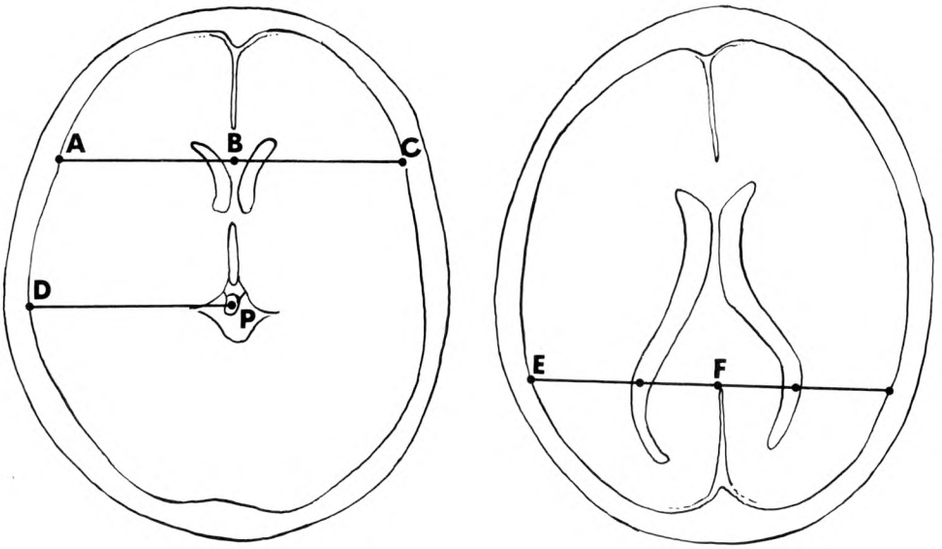


Fig. 1.—**A**, Diagram of axial CT scan though frontal horns. AB = width of right frontal lobe; BC = width of left frontal lobe; P = pineal; DP = distance from center of pineal to right inner skull table. **B**, Diagram of axial CT scan through trigones and occipital horns of lateral ventricles. EF = width of right occipital lobe.

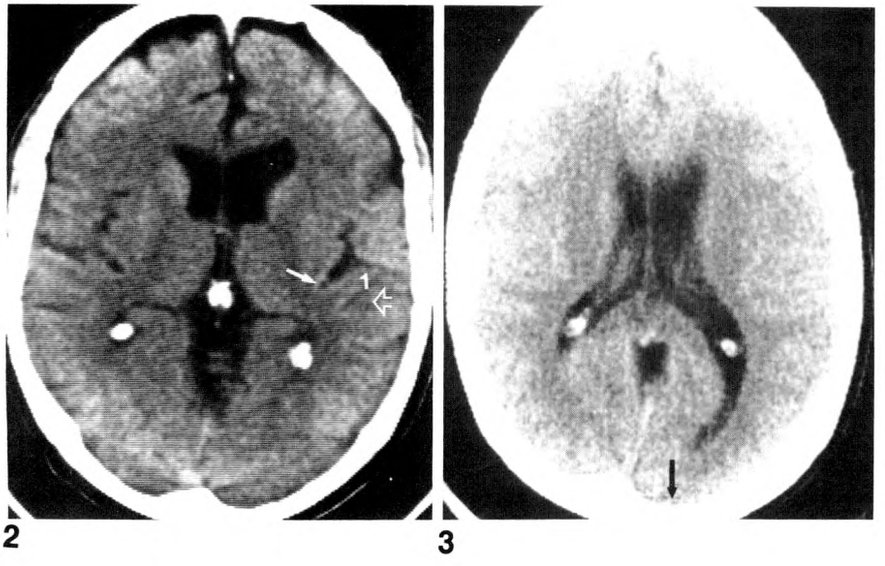


Fig. 2.—Sixty-year-old woman with mild generalized atrophy and asymmetry of Sylvian fissures. Note displacement of septum to right. Did patient have asymmetric normal ventricles before onset of atrophy? Posterior end of Sylvian fissure (*arrow*); planum temporale (*arrowhead*); 1 = anterior tranverse temporal gyrus (Heschl).

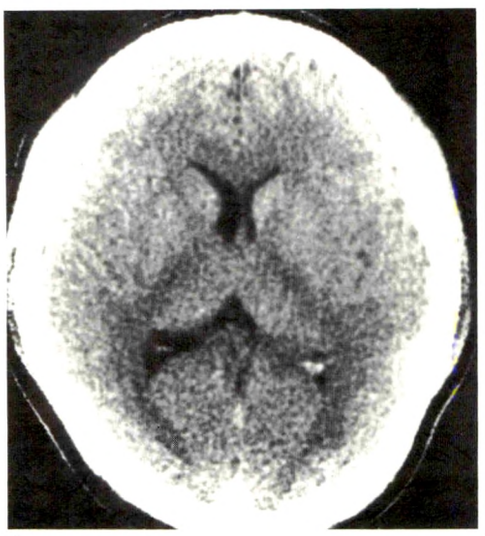
Fig. 3.—Prominent left occipital petalia (*arrow*) with more posterior location of left glomus.

ventricles and of the corresponding lobes. The position of the septum pellucidum and the widths of the frontal lobes from the inner table of the skull to the septum were measured on scans made through the frontal horns (Fig. 1A). The position and relative size of the occipital horns and the measurement of the widths of the occipital lobes were determined from scans made through the trigones or occipital horns of the lateral ventricles (Fig. 1B). The widths of the occipital lobes were measured from the inner table of the occipital bone to the interhemispheric fissure.

Asymmetry of the temporal lobes was judged by differences in the anteroposterior length and width of the Sylvian fissure. However, no actual measurements of the distance between the frontal and temporal opercula were made. The posterior limit of the Sylvian fissure was determined from the scan demonstrating the third ventricle, the atria, and the insular region (Fig. 2). Whenever the pineal gland was calcified, the distance from the inner table of the skull to the center of the calcified gland was measured to determine the width of the midportion of the hemispheres. The presence or absence of frontal or occipital petalia (i.e., anterior or posterior extension of one hemisphere beyond the other) was also noted [20] (Fig. 3). Similar observations were made with respect to the calcified glomera of the choroid plexi of the lateral ventricles. The mean was calculated from each observer's measurements. Intra- and interobserver agreement were 89.5% and 92.8%, respectively.

Results

Thirty-one (10.3%) of the 300 patients had recognizable asymmetry of the frontal horns of the lateral ventricles. In 21 patients, the right frontal horn was larger than the left with a slight shift (1–2 mm) of the septum pellucidum to the left (Fig.



4

Fig. 4.—Slight dilatation of right frontal horn with shift of septum pellucidum to left indicating relative increase in width of right frontal lobe. Note mild left occipital petalia associated with slightly more posterior location of left glomus (normal variant).



5

Fig. 5.—Dilated left frontal horn and localized porencephaly without shift of septum in 6-year-old boy with left cerebral atrophy and history of right hemiplegia since birth.



6

Fig. 6.—Asymmetry of frontal horns with smaller right lateral ventricle and shift of septum to left. Note obliteration of right sulci by subdural hematoma.

4). In 10 patients, the left frontal horn was larger than the right with a similar septal shift to the right. In 269 patients, the frontal horns were equal in size.

The right frontal lobe was wider than the left in 132 cases (44%), the left frontal lobe wider than the right in 59 patients (20%), and both frontal lobes equal in 109 patients (36%).

There was equal anterior extension of both frontal lobes in 60% of the patients, right anterior extension (right frontal petalia) [21] in 22%, and left anterior extension (left frontal petalia) in 18%.

Sixty-two percent of the patients had calcified pineal glands. The pineal was situated to the right of the midline by 0.5 mm or more in 2% of the cases, indicating a wider left central hemispheric mass. Similar displacement of the calcified pineal gland to the left by a wider right central hemispheric mass was found in 45%. Using this criterion, the central hemispheric masses were equally wide in 53% of the cases.

In 20% of the patients, the right parietooccipital areas was wider than the left; the left parietooccipital area was wider than the right in 49%; both areas were equal in 31% of cases.

There was equal posterior extension of the occipital lobes in 86 patients (29%), right occipital posterior extension (right occipital petalia) in 46 patients (15%), and left occipital posterior extension (left occipital petalia) in 168 cases (56%).

There were 126 patients (42%) with bilateral calcification of the glomus of the choroid plexus of the lateral ventricles. In this group, the calcifications were symmetrically aligned in the anteroposterior axis in 42 patients. There was a more posterior position of the right glomus in 17 patients and of the left glomus in 67 patients. The posterior end of the left Sylvian fissure was situated more posteriorly than the right in 70% of the patients. There was no apparent correlation between normal cerebral asymmetry and the gender of the patient.

Discussion

"Normal" asymmetry of the cerebral hemispheres has been reported at necropsy [22, 23] and on various imaging studies such as cerebral pneumoencephalography [15, 18], cerebral angiography [13, 14], CT [12, 17, 19, 24, 25] and sonography [26, 27]. This asymmetry bears no relationship to the gross asymmetry secondary to early unilateral ischemia or hypoplasia, which are frequently associated with corresponding abnormalities in the calvarium. The right cerebral hemisphere is heavier than the left [22], associated with enlargement of the right lateral ventricle. As LeMay and Kido [17] noted, and as we found, also, the central portion of the right cerebral hemisphere is commonly wider than the left, regardless of cerebral dominance, probably an explanation for the location of calcified pineal gland slightly to the left of the midline (1–2 mm) in many normal patients. Indeed, a minimal shift of the pineal gland to the right may be a subtle sign of a space-occupying lesion in the left cerebral hemisphere. Hadžiselimović and Cus [20] noted asymmetry of the occipital pole in 56% of 250 skulls. In their series, the left occipital pole was wider and extended more posteriorly (occipital petalia) in 37%. Enlargement of the left occipital pole was often accompanied by right frontal and temporoparietal enlargement [17, 28].

Asymmetry may affect an entire hemisphere, one or more lobes, or a specific gyral area. The area most frequently involved is the retroinsular cortex, that is, the posterior speech area [5, 6]. In a large adult series published in 1980, Eberstaller [23] noted that the posterior horizontal ramus of the left Sylvian fissure was longer than the right in 63% of brains. Cunningham [3] reported the left Sylvian fissure to have a more shallow upward slope than the right. Similarly, Wada et al. [9] found that the newborn child commonly had a larger

left planum temporale, the triangular area caudal to the transverse gyrus of Herschl on the dorsal surface of the temporal lobe. This finding was confirmed by Chi and his coworkers [29], who demonstrated asymmetry of the temporal lobes, including the Sylvian fissure, in a study of fetal brain development. Further confirmation was provided by Rubens et al. [30], who compared Sylvian fissures in a series of 36 adult brains and noted a characteristic pattern of emergence of the posterior portion of the fissure in approximately 70%. After an initial similar course on both sides, the right fissure angled sharply upward into the inferior parietal area, while the left continued posteriorly. Consequently, the right hemicerebrum had a smaller parietal operculum and planum temporale, a high Sylvian point, and enlargement of the inferior parietal area posterior to the Sylvian fissure. These reports agree with the angiographic findings of LeMay and Culebras [14] that normal enlargement of one cerebral hemisphere is commonly associated with a wider postcentral gyrus, a longer Sylvian fissure, and a lower Sylvian point in the ipsilateral hemisphere.

A number of investigators have correlated anatomic findings with functional dominance [5, 6, 28]. Because the anatomic differences between the two hemispheres are present at birth [26, 27, 31], a genetic basis for the functional asymmetries has been suggested [5, 6, 22, 28]. The widened left Sylvian fissure is a reflection of the larger left temporal lobe. Along these lines, Gerschwind and Levitsky [6] found that the left planum temporale, part of Wernicke's speech area, was significantly larger than the right in 65 of 100 adult brains (mean difference 0.9 cm). This observation lends further support to the hypothesis of functional anatomic correlation on a genetic basis.

The normal variant can be differentiated from minimal atrophy by a shift of the septum pellicidum away from the dilated ventricle, absence of dilated sulci, and a normal calvarial thickness on the side of the dilated ventricle (see Fig. 4). The atrophic hemicerebrum is characterized by a shift of the septum pellicidum toward the ipsilateral hemisphere, dilated sulci, and, at times, thickening of the corresponding calvarium (Fig. 5). A frontal-space–occupying lesion is characterized by some compression of the corresponding ventricle as well as displacement of the septum to the opposite side (Fig. 6).

REFERENCES

1. Bailey P. Variations in the shape of the lateral ventricles due to difference in the shape of the head (abstr). *Arch Neurol Psychiatry* **1936**;35:932
2. Connolly CJ. *External morphology of the primate brain.* Springfield, IL: Thomas, **1950**
3. Cunningham DJ. *Contribution to the surface anatomy of cerebral hemispheres.* Dublin: Royal Irish Academy, **1893**:131–136
4. Forty H. Eine neue theorie über die materielle grundlageder funktionallen Superioretat der linken Hemisphare. *Dtsch Med Wochenschr* **1922**;48:312–313
5. Galaburda AM, LeMay M, Kemper TL, Geschwind N. Right-left asymmetries in the brain. *Science* **1978**;199:852–856
6. Geschwind N, Levitsky W. Human brain: left-right asymmetries in temporal speech region. *Science* **1968**;161:186–187
7. Iglessis M. Eineges über Seitenventrikel und Hirnschwellung. *Arch Psychiatry* **1919**;74:159–168
8. Iglessis M. Untersuchungen über Symmetrie und Asymmetrie der menschlichen Grosshirnhemispharen. *Z ges Neurol Psychiatr* **1925**;95/96:464–475
9. Wada JA, Clarke R, Hamm A. Cerebral hemispheric asymmetry in humans. *Arch Neurol* **1975**;32:239–246
10. Weil A. Measurements of cerebral and cerebellar surfaces, comparative studies of the surfaces of endocranial casts of man, prehistoric man and anthropoid apes. *Am J Phys Anthropol* **1929**;13:69–90
11. Von Bonin G. Anatomical asymmetries of the cerebral hemispheres. In: Mountcastle VB, ed. *Interhemispheric relations and cerebral dominance.* Baltimore: Johns Hopkins Press, **1962**:1–6
12. Habib M, Renicci RL, Vanier M, et al. CT assessment of right-left asymmetries in the human cerebral cortex. *J Comput Assist Tomogr* **1984**;8:922–927
13. Hochberg FH, LeMay M. Arteriographic correlates of handedness. *Neurology* **1975**;25:218–222
14. LeMay M, Culebras A. Human brain: morphologic differences in the hemispheres demonstrable by carotid arteriography. *N Engl J Med* **1972**;287:168–180
15. LeMay M. Morphological cerebral asymmetries of modern man, fossil man and non-human primates. *Ann NY Acad Sci* **1976**;280:349–366
16. LeMay M. Asymmetries of the skull and handedness; phrenology revisited. *J Neurol Sci* **1977**;32:243–253
17. LeMay M, Kido DK. Asymmetries of the cerebral hemispheres on computed tomograms. *J Comput Assist Tomogr* **1978**;2:471–476
18. McRae DL, Branch DL, Milner B. The occipital horns and cerebral dominance. *Neurology* **1968**;18:95–98
19. Strauss E, Fitz C. Occipital horn asymmetry in children. *Ann Neurol* **1980**;8:437–439
20. Hadžiselimovič H, Cus M. The appearance of the internal structures of the brain in relation to the configuration of the human skull. *Acta Anat (Basel)* **1966**;63:289–399
21. Chang Chui H, Domasio AR. Human cerebral asymmetries evaluated by computed tomography. *J Neurol Neurosurg Psychiatry* **1980**;43:873–878
22. Weinberger DR, Luchins DJ, Morbisa J, Syatt RJ. Asymmetrical volumes of the right and left frontal and occipital regions of the human brain. *Ann Neurol* **1982**;11:97–100
23. Eberstaller O. *Das Stirnhirn.* Vienna: Urban & Schwarzenberg, **1980**
24. Deuel RK, Moran CC. Cerebral dominance and cerebral asymmetries on computed tomograms in childhood. *Neurology* **1980**;30:934–938
25. Seidenwurm D, Bird CR, Enzmann DR, Marshall WH. Left-right temporal region asymmetry in infants and children. *AJNR* **1985**;6:777–779
26. Hobar JD, Leahy KA, Lucey JF. Ultrasound identification of lateral ventricular asymmetry in the human neonate. *J Clin Ultrasound* **1983**;11:67–69
27. Winchester P, Brill PW, Cooper R, Krauss AN, deC Peterson H. Prevalence of compressed lateral ventricle in healthy full-term neonates: sonographic study. *AJNR* **1986**;7:149–153
28. Geschwind N. The anatomical basis of hemispheric differentiation. In: Diamond SG, Beaumont JG, eds. *Hemispheric function in the human brain.* London: Eleh Science, **1974**
29. Chi JG, Dooling EC, Gilles FH. Gyral development of the human brain. *Ann Neurol* **1977**;1:86–93
30. Rubens AB, Mahowald MW, Hutton JT. Asymmetry of the lateral (Sylvian) fissures in man. *Neurology* **1976**;26:620–624
31. Kleinman PK, Zito JL, Davidson RI, Raptopoulos V. The subarachnoid spaces in children: normal variations in size. *Radiology* **1983**;147:455–457

Lumbar Herniated Disk Disease and Canal Stenosis: Prospective Evaluation by Surface Coil MR, CT, and Myelography

Michael T. Modic[1]
Thomas Masaryk[2]
Francis Boumphrey[3]
Marlene Goormastic[4]
Gordon Bell[3]

Sixty patients with suspected lumbar herniated disk and/or canal stenosis were studied prospectively with surface coil MRI, CT, and/or myelography, and the results were compared with the surgically confirmed abnormality. Forty-eight patients had lumbar surgery at 62 levels. There were no negative explorations. Thirty-nine patients had a myelogram and CT. Thirty of the CTs were performed following the injection of metrizamide for myelography. Nine patients had a CT without intrathecal contrast material 1 to several days before the myelogram. Six patients had myelography only, and three patients had CT only. All studies were evaluated for the location and type of disease in a forced choice fashion. Independent of the surgically correlated levels, there was 86.8% agreement between the MR and CT studies in all patients at 151 levels and 87.2% agreement between MR and myelography at 218 levels. At the operative levels, there was 82.6% agreement between MR and surgical findings for both type and location of disease; 83% agreement between CT and surgical findings; and 71.8% agreement between myelography and surgical findings. There was 92.5% agreement when MR and CT were used jointly, and 89.4% agreement when CT and myelography were used jointly. The results of this study indicate that a technically adequate MR examination was equivalent to CT and myelography in the diagnosis of lumbar canal stenosis and herniated disk disease. CT and MR can be complementary studies, and surface coil MR can be viewed as an alternative to myelography.

Previous experience has indicated that MR can identify lumbar canal stenosis and herniated nucleus pulposus. However, current experience shows that with conventional body coil imaging, MR cannot be considered equivalent to CT and/or myelography for the evaluation of small or lateral disk herniations, neural foraminal disease, and canal stenosis. The reasons most often cited for this are the slice thickness and spatial resolution of MR and its inability to discriminate cortical bone from soft tissue [1–6]. It has been suggested by us and others that the introduction of surface coil imaging, which provides an improved signal-to-noise ratio over a limited distance, might obviate these disadvantages by trading off the increased signal-to-noise for thinner slices and thus a smaller voxel element with a concomitant improvement in spatial resolution. This could then provide an MR examination that would be equivalent to CT or myelography [4, 7, 8].

To test this hypothesis we undertook a prospective study on a group of patients who were presumed to have herniated disk, lumbar canal stenosis, or both. We compared the results of surface coil MR with CT and/or myelography without reference to either the clinical information or other imaging observations. These findings were then compared with the surgically confirmed pathology for an objective measure of accuracy.

Materials and Methods

Sixty patients were admitted to this study between September 1984 and February 1985. The patients were referred for enrollment in the study on the basis of their clinical history and

This article appears in the July/August 1986 issue of *AJNR* and the October 1986 issue of *AJR*.

Received August 6, 1985; accepted after revision November 7, 1985.

[1] Department of Radiology, University Hospitals/Case Western Reserve University, 2074 Abington Rd., Cleveland, OH 44106. Address reprint requests to M. T. Modic.

[2] Division of Radiology, Cleveland Clinic Foundation, Cleveland, OH 44106.

[3] Department of Orthopedic Surgery, Cleveland Clinic Foundation, Cleveland, OH 44106.

[4] Department of Biostatistics, Cleveland Clinic Foundation, Cleveland, OH 44106.

***AJR* 147:757–765, October 1986**
0361–803X/86/1474–0757
© American Roentgen Ray Society

a physical exam that indicated a strong probability of herniated disk or lumbar canal stenosis, with the likelihood they would require surgery. Patients with a known diagnosis and/or a prior imaging study—for example, CT and/or myelography—were excluded. All patients who entered the study were scheduled for an MR and either a CT, myelogram, or both. Although most patients had a myelogram followed by high-resolution CT, in some, the number and sequence of examinations were determined by patients' convenience, clinical preference, and financial considerations. All exams were completed within 1 week. In most cases, MR was the first examination, followed by myelography and then CT. Forty-eight patients aged 19–73 years (mean, 46) had lumbar surgery at 62 levels. There were no negative explorations.

In the operated group, all 48 patients had an MR and at least one other study (CT and/or myelography). Thirty-nine patients had a myelogram and CT. Thirty of the CTs were performed after the patient was injected with metrizamide for myelography at delays of 2 to 6 hr. Nine patients had CT 1 to several days before the myelogram, without an injection of intrathecal contrast. Six patients had myelography only, and three patients had CT only.

CT was performed on either a Delta 2060 or Pickerview 1200 synerview unit with a 120–130 kV and 400–800 mAs. Lateral scout images were obtained in all patients for alignment of the sections. Sections of 5 mm were obtained through at least the L5 and L4 levels, and the L3 level if indicated.

Myelography was performed after the installation of 8–14 ml of 190 mg/dl metrizamide in the lumbar subarachnoid space. Routine anteroposterior, lateral, and oblique films were obtained with the side of interest in the dependent position.

The MR examinations were performed on a 0.6 T superconductive unit (Teslacon-Technicare, Solon, OH) using a prototype surface coil. The surface coil was circular, 12 cm in diameter, and composed of ⅝-in. copper tubing. It served as a receiver only; a 50-cm body coil served as the radiofrequency transmitter.

The MR study involved four separate acquisitions. First, patient position and coil placement were determined with a single coronal image with the X-gradient turned off for orientation. The remaining acquisitions were obtained with a 4-mm slice thickness, 1-mm gap, and four averages. The first of these was a 32-msec echo time (TE)/0.5 sec repetition time (TR) sagittal study consisting of 10 sections obtained in 4.4 min. The second was a 90-msec TE/2-sec TR sagittal study with 12 sections obtained in 18 min. The last was a transverse 32-msec TE/2-sec TR study with 12 sections obtained in 18 min through the suspected level(s) of abnormality, with the angle of acquisition adjusted, if necessary, for true transverse images through the disk space. The matrix size for all studies was 128 × 256.

When the study was complete, copies of the examination were collected for subsequent, independent interpretation with only the hospital number for identification. The MR, CT, and myelographic examinations were interpreted by three of us, without access to the patients' names, clinical information, or results of other imaging studies. All studies were evaluated via a forced-choice method for the location and type of disease(s) and for compression of the spinal nerve(s) or thecal sac. An attempt was made to determine if the abnormality was caused by a herniated disk or by canal stenosis from bony or soft-tissue compression. The two major types of stenosis, central and lateral, including both foraminal and lateral recess stenosis, were grouped under the broad heading of spinal stenosis. The abnormalities in the last category were grouped under the broad heading of spinal stenosis.

Other observations noted were the presence or absence of arachnoiditis, signal changes within the vertebral body, and whether the herniated disk appeared to be protruding or whether it seemed to be a free fragment.

The three separate MR acquisitions were interpreted in the following manner. First, the sagittal T1-weighted short TE/TR images were evaluated for disk-space height; canal compression; presence and configuration of epidural fat and nerve root in the neural foramina in the parasagittal plane; disk position and configuration; vertebral body signal; and upper lumbar neural canal, including the conus (Figs. 1A and 1B). The signal intensity of the disk and adjacent vertebral endplates were evaluated on the T2-weighted sagittal image (long TE/TR) (Fig. 1C). In addition, the CSF–extradural interface was examined for the presence or absence of herniated disk and canal stenosis. The axial images, which produced the highest signal intensity, were evaluated for the disk, thecal sac, and canal contour as well as for the nerve roots within the epidural fat (Fig. 1D).

The MR and CT criteria for herniation were similar. Briefly stated, they involved identifying a focal extention of the disk margin beyond the vertebral margin, with resulting epidural-fat, nerve-root, or thecal-sac displacement. On myelography, the changes sought were a sharp wedge- or tent-shaped indentation of the anterior or lateral aspect of the thecal sac and/or nerve root sleeve.

Criteria for lumbar stenosis on MR or CT were (1) a distortion or paucity of epidural fat either in the neural foramina, lateral recess, or posteriorly between the ligamentum flavum, and (2) a diminution in the overall size of the neural foramina, neural canal, and /or thecal sac. An attempt was made to determine the contribution of hypertrophied facet joints and bony overgrowth as well as hypertrophy of the ligamentum flavum.

The surgical operative findings were then reviewed and included on a general demographic form with the patient's name, age, gender, and clinical data. Subsequently, a computer match was made with the imaging studies at the operative levels.

Results

Tables 1 and 2 list the agreement and disagreement, respectively, among MR, CT, and myelography with the surgical findings. A match was also made with the combined results of MR and CT, and of CT and myelography. In this last grouping, if one of the diagnostic tests was confirmed at surgery, it was rated as an agreement.

Independent of the surgically correlated levels, there was an 86.8% agreement between the MR and CT findings in all patients (operated or not) at 151 levels. The agreement with myelography at 218 levels was 87.2%. The difference in the number of levels reflects the visualization of the L1 through L3 levels by MR and myelography, areas not routinely examined by CT.

At the operative levels, there was an 82.3% agreement between MR and surgical findings for both type and location of disease; an 83% agreement between CT and surgical findings, and a 71.4% agreement between myelography and surgical findings. When the operated levels were broken down into those studied with plain CT and those studied with metrizamide CT, the agreement with surgical findings was 91% (11 of 12) and 81% (33 of 41), respectively. There was a 92.5% agreement when MR and CT were used jointly, and an 89.4% agreement when CT and myelography were used jointly. All disks shown to be normal by MR were also shown to be normal on both CT and myelography.

For the 11 cases in which there was disagreement between the MR and surgical findings, the breakdown was as follows. In four patients the MR diagnosis was that of a herniated disk

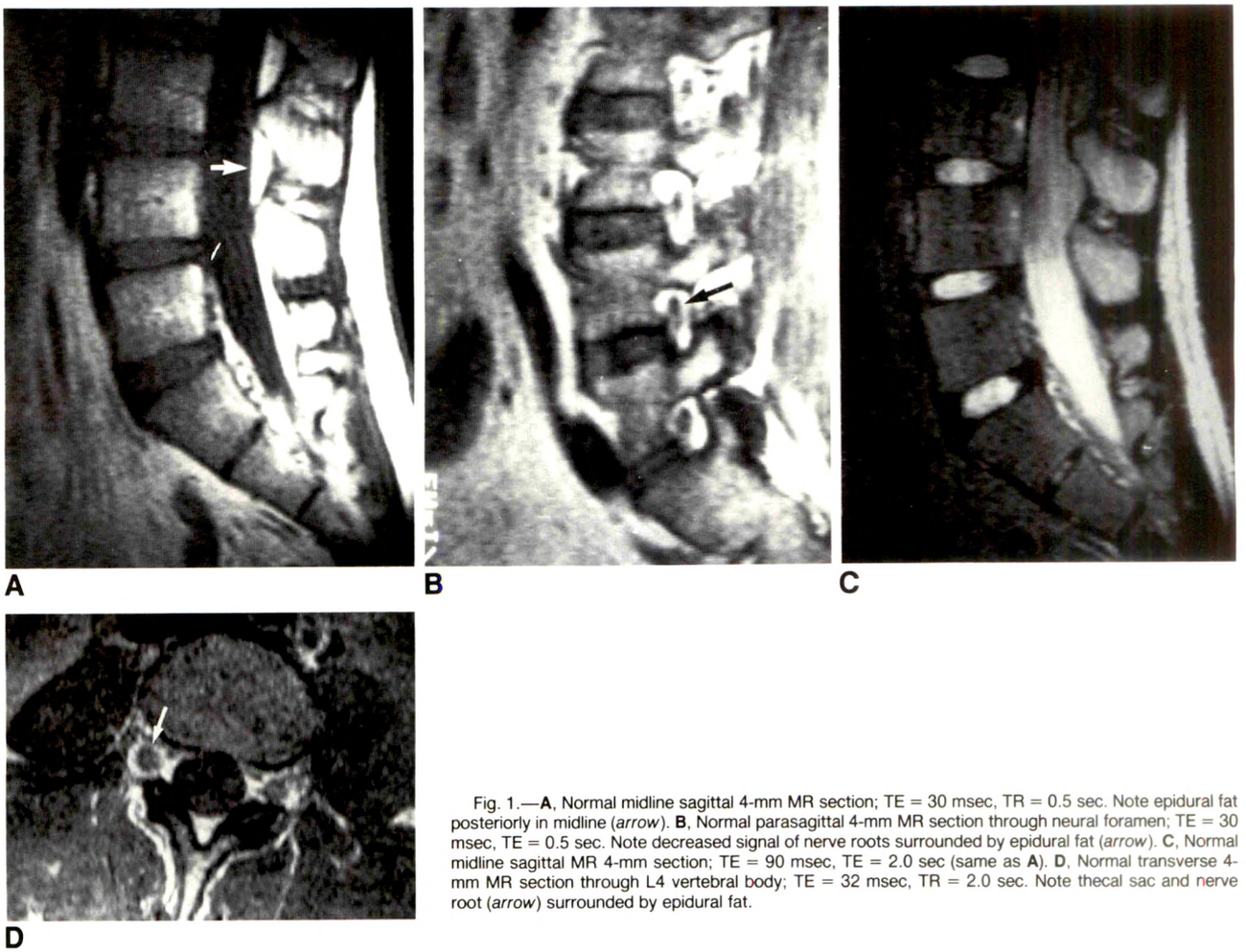


Fig. 1.—**A**, Normal midline sagittal 4-mm MR section; TE = 30 msec, TR = 0.5 sec. Note epidural fat posteriorly in midline (*arrow*). **B**, Normal parasagittal 4-mm MR section through neural foramen; TE = 30 msec, TE = 0.5 sec. Note decreased signal of nerve roots surrounded by epidural fat (*arrow*). **C**, Normal midline sagittal MR 4-mm section; TE = 90 msec, TE = 2.0 sec (same as **A**). **D**, Normal transverse 4-mm MR section through L4 vertebral body; TE = 32 msec, TR = 2.0 sec. Note thecal sac and nerve root (*arrow*) surrounded by epidural fat.

TABLE 1: **Lumbar Surgical Findings and Imaging Results: Agreement by Location and Disease Type**

	Surgical Findings/MR	Surgical Findings/CT	Surgical Findings/ Myelography	Surgical Findings/MR & CT	Surgical Findings/CT & Myelography
No. of levels	62/62	53/53	56/56	53/53	47/47
Herniation	32/28	29/25	32/27	29/26	28/26
Stenosis	30/23	24/19	24/13	24/23	19/16
% Agreement	82	83	71	92	89

TABLE 2: **Lumbar Surgical Findings and Imaging Results: Disagreement by Location and Disease Type**

Imaging/Surgical Findings	MR	CT	Myelography
Herniation/Stenosis	4	2	3
Stenosis/Herniation	1	3	3
No disease/Stenosis	3	3	8
No disease/Herniation	0	1	2
Herniation and stenosis/Herniation only	3	0	0
Total	11	9	16

and the surgical findings were those of canal stenosis. In one case, MR diagnosed stenosis of the neural foramina, but surgery demonstrated a lateral disk. In three cases, there was narrowing of the lateral recesses noted at surgery, while the MR was interpreted as normal at these levels. In three cases, MR was read as disk herniation with stenosis posteriorly, while surgery demonstrated only a herniated disk.

Of the total of 28 surgically confirmed herniated disks, MR predicted a free fragment in six. This was surgically confirmed in four patients.

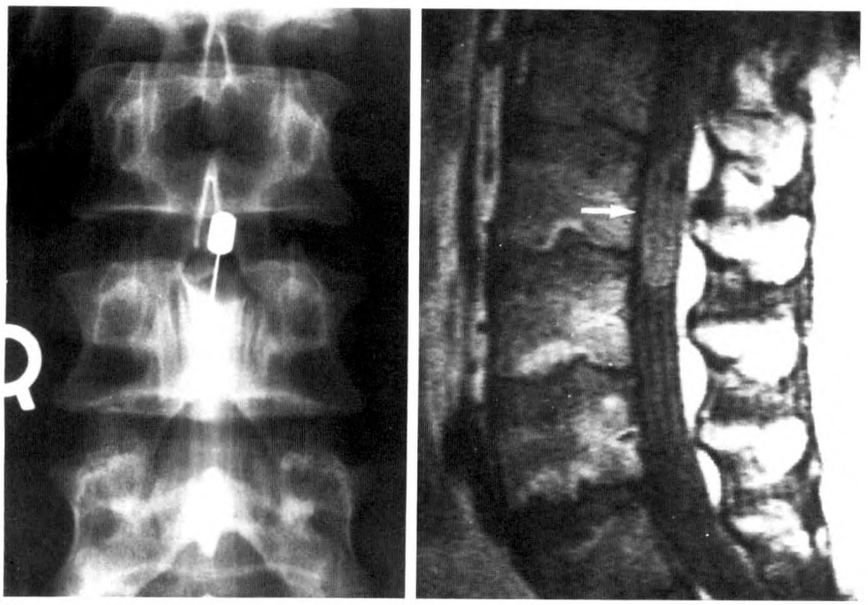


Fig. 2.—32-year-old man with L5 radiculopathy. **A**, Anteroposterior radiograph of lumbar spine at L3 level after installation of metrizamide into thecal sac. Note intradural filling defect at level of needle. CT without metrizamide performed before this study was normal to level of L3 pedicles. **B**, Sagittal 4-mm MR section (TE = 30 msec, TR = 0.5 sec) showed intradural mass of intermediate signal intensity at L2 and L2–L3 levels (*arrow*). An ependymoma was identified at surgery.

Disagreements between the CT and surgical findings were similar to those found between MR and surgery. Exceptions were that CT misdiagnosed two cases of lateral stenosis and one herniated disk, which were accurately identified by MR. Three cases identified by MR as herniation and stenosis were accurately diagnosed by CT as herniation only.

The disagreements between myelographic and surgical findings occurred at 16 levels; eight of these were at the L5–S1 levels. The remaining eight cases were those in which myelography failed to show lateral stenosis, which was identified at the time of surgery.

In the 12 patients studied but not operated on, one had metastatic disease identified by MR where there was diminished signal intensity on the T1-weighted images of the involved vertebral bodies. Bony changes were not noted on either CT or myelography. One patient had an ependymoma at the L2–L3 level identified by both MR and myelography but not by CT, because it was above the level of the study (the patient had an L5 radiculopathy clinically) (Fig. 2). Two patients had arachnoiditis identified by myelography but not by MR. Two patients had lumbar canal stenosis, and one had a disk herniation identified by MR and/or CT and myelography, but all three chose conservative management. Five patients had normal MRs and normal CTs and/or myelographic studies.

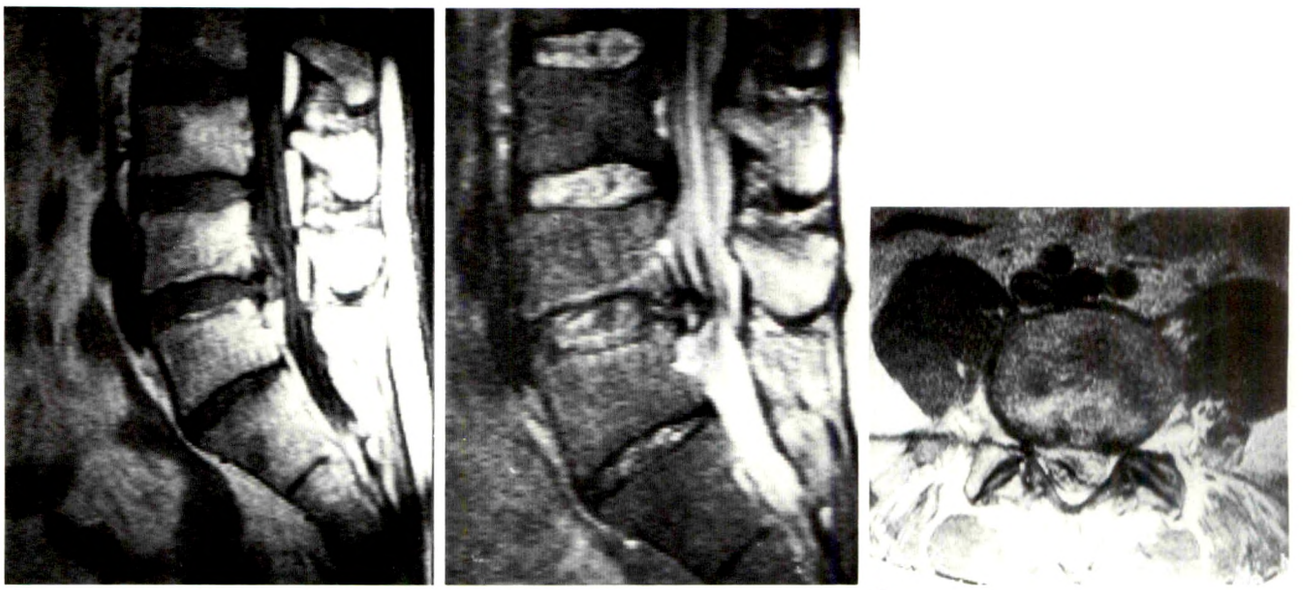
Discussion

In this study, surface coil MR was as accurate as CT and slightly more accurate than myelography in evaluating lumbar disk disease and canal stenosis. The combined results of MR and CT were as accurate as those of CT and myelography.

The accuracy of MR in this study can be ascribed to the use of a surface coil, which produces an improved signal-to-noise ratio and allows the use of a smaller imaging voxel element. The coil itself is not responsible for the thinner sections that are usually achieved with a stronger imaging gradient. Rather, the surface coil allows the signal-to-noise in the smaller voxel elements to remain adequate for imaging. In addition, it serves to reduce the patient-generated noise and is not as affected by artifacts from respiratory motion and blood flow.

The contour of herniation of the intervertebral disk was characteristic in the majority of cases. An angular protrusion of the disk with sharp (rather than rounded) margins was the rule in most cases on both the transverse and sagittal images (Fig. 3). Lateral herniations of the intervertebral disks could be identified by distortion of this epidural fat on parasagittal images (Fig. 4) but were better seen on transverse images. On the more T2-weighted sagittal images (90-msec TE/2-sec TR) there is a relative increase in the signal of the central portion of the normal disk. In cases of disk degeneration this central region demonstrates a decreased signal intensity. Thus, suspected levels of abnormality related to disk degeneration could be identified on the sagittal images and were helpful in directing the transverse examination. All levels of herniation identified were associated with a decreased signal intensity of the disk on the sagittal 90-msec TE/2-sec TR images relative to normal disks and adjacent CSF.

The transverse 30-msec TE/2-sec TR images produced the highest signal of the three techniques, and the long TR allowed a sufficient number of slices at 4 mm to cover three



A B C

Fig. 3.—28-year-old woman with left L4 radiculopathy. **A** and **B**, Sagittal midline 4-mm MR sections; TE = 30 msec, TR = 0.5 sec, and TE = 90 msec, TR = 2.0 sec. There is a "pinched off" herniated appearance of L4 disk with an increased signal intensity of herniated segment when compared with remainder of intervertebral disk. **C**, Transverse 4-mm MR section (TE = 32 msec, TR = 2.0 sec) through L4 disk. There is a large disk herniation, with herniated fragment showing slightly higher signal than remaining disk. At surgery, a large free fragment was identified.

disk spaces. There was excellent demonstration of the epidural fat and nerve roots in the neural foramina laterally, and the overall dimensions of the lateral recesses and neural foramina could be consistently and accurately assessed. The posterior and lateral configurations of the disk (Fig. 5) were seen best with this pulse sequence and it was the most accurate for demonstrating lateral disk herniation and imaging of the neural foramina (Fig. 6).

There were five cases in which the signal intensity of the herniated disk segment remained higher than the CSF on the axial images (30-msec TE/2-sec TR). In two of these, free fragments were identified at surgery (Fig. 3).

These three pulse sequences were also complementary in the evaluation of canal stenosis (Fig. 7). The T1-weighted image was useful in evaluating the size and contour of the neural canal, foramen, and thecal sac as well as the location of the conus medullaris, which can be obscured by the relatively increased signal intensity of the CSF on longer TE and TR images. However, cortical bone and surrounding fibrous or ligamentous structures are manifested by a decreased signal intensity on this pulse sequence, and may be difficult to separate.

The more T2-weighted sagittal images allowed an accurate assessment of the extradural–CSF interface and overall canal dimensions, and were particularly accurate for identifying anterior and/or posterior extradural defects in cases of canal stenosis.

The techniques in this study were kept constant to reduce variability from patient to patient; and although this approach provided satisfactory results, there is certainly room for further study of various pulse sequences and other technical factors. For instance, in work done subsequent to this study it has become apparent that certain modifications of the exam technique can produce equivalent, and in some cases improved, accuracy. This would include a multislice-multiecho technique in the sagittal plane that allows a 30- and 90-msec TE to be acquired simultaneously with a 2-sec TR. This produces a high-signal sagittal image as well as a heavily T2-weighted image without increasing the exam time. Experience at 1T suggests the transverse images can be acquired with a shorter TR (e.g., 0.5 sec), which produces an adequate signal for anatomic evaluation in much less time. This allows multiple separate acquisitions with the appropriate angle for the various disk levels without increasing the overall exam time. With this pulse sequence technique the lumbar nerve roots can be identified within the thecal sac on the transverse images by the higher signal intensity from the surrounding CSF.

In comparing the results of surface coil MR with high-resolution CT and water-soluble myelography, certain recognizable advantages and disadvantages of the various studies became apparent. Despite the accuracy of high-resolution CT and plain-film myelography [with studies showing from 72–97% agreement with surgical findings (9–15)], recognizable problems exist, and in many clinical situations these modalities are used together.

Myelography still involves considerable radiation and the need for intrathecal contrast medium, and, despite reasonably acceptable side effects with nonionic agents, is still an invasive procedure and in most situations is performed only on hospitalized patients. The diagnostic accuracy of myelography is questionable in cases of far lateral disease and at the L5–S1 level, where the epidural space may be large. MR, on

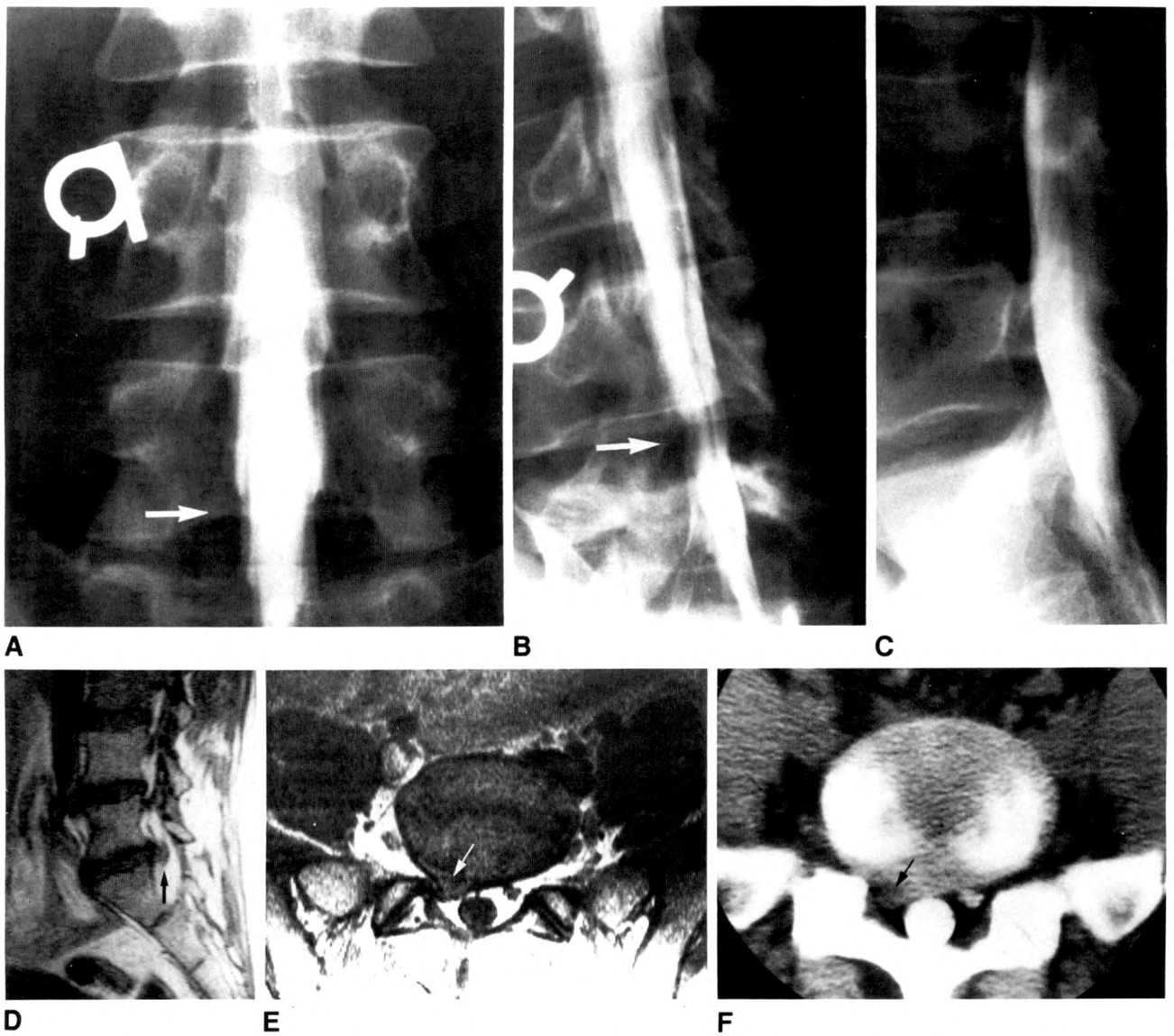


Fig. 4.—40-year-old woman with right S1 radiculopathy. **A, B,** and **C,** Anteroposterior lateral and oblique radiographs of lumbar spine from metrizamide myelogram. There is a subtle extradural defect involving right S1 nerve root on anteroposterior and oblique radiographs (*arrows*) and a mildly increased anterior extradural space at L5–S1 level on lateral radiograph. **D,** Parasagittal 4-mm MR section (TE = 30 msec, TR = 0.5 sec) 1 cm off midline. There is posterior lateral herniation of L5 disk indenting the epidural fat (*arrow*). **E,** Transverse 4-mm MR section (TE = 30 msec, TR = 2.0 sec) angled to L5 disk. Note right posterior lateral herniation of L5 disk (*arrow*). **F,** Transverse 5-mm high-resolution CT section through L5 disk showing right posterior lateral herniation of L5 disk similar to MR study (*arrow*).

the other hand, requries no intrathecal contrast agent or ionizing radiation, and, in this study, was as accurate or more so than myelography for lateral disease and at the L5–S1 level. However, at present, myelography still has some advantages in certain situations. In this study there were two cases in which myelography was more sensitive to changes of arachnoiditis than was either MR or CT. And while surface coil MR can examine the entire lumbar canal, the potential exists for the entire spinal axis to be studied in a shorter period of time with myelography.

At our institution, CT is usually performed only to the L3 level. Moreover, owing to time and radiation considerations, it may be impractical to examine the entire lumbar canal with an appropriate slice thickness and spatial resolution. Transverse imaging is the rule; reformatting and secondary reconstruction, while sometimes helpful, result in a corresponding loss of spatial and contrast resolution. Appropriate scan angles are needed for the intervertebral disks and this may be difficult at the L5–S1 level because of limitation in gantry angulation. With MR, the entire lumbar canal, including the

Fig. 5.—**A** and **B**, Sagittal midline 4-mm MR section (TE = 30 msec, TR = 0.5 sec, and TE = 90 msec, TR = 2.0 sec) through lumbar spine. There is a decrease signal of L3 and L4 disks and, to a lesser extent, of L5 disk on TE = 90 msec, TR = 2.0 sec image. There is mild posterior protrusion of disk at L3 and L4 levels. **C**, High-resolution CT and **D**, transverse 4-mm MR section (TE = 32 msec, TR = 2.0 sec) through the L4 disk. On high-resolution CT image, there is a smooth central protrusion of L4 disk (*arrow*). On MR image, there is protrusion of L4 disk with sharp margins suggestive of herniation (*arrow*). Herniation was confirmed at surgery. Similar angulations of disk margin were also noted at L3, but surgery was performed only at L4 level.

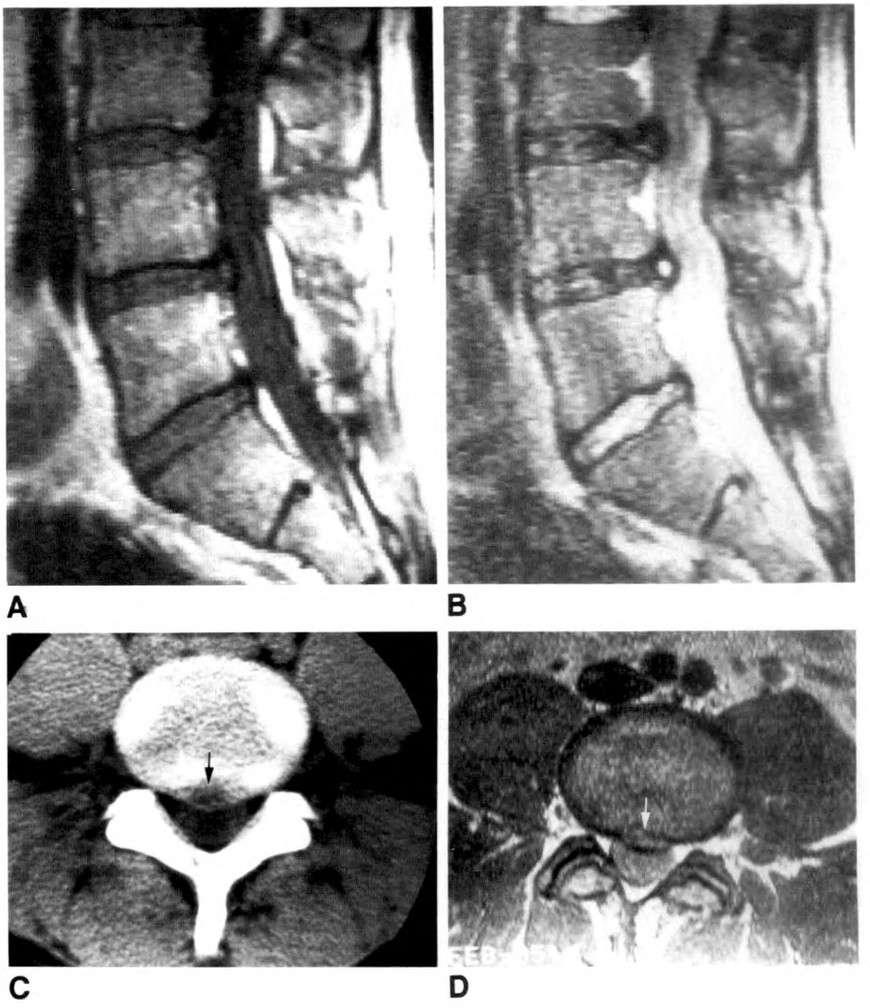
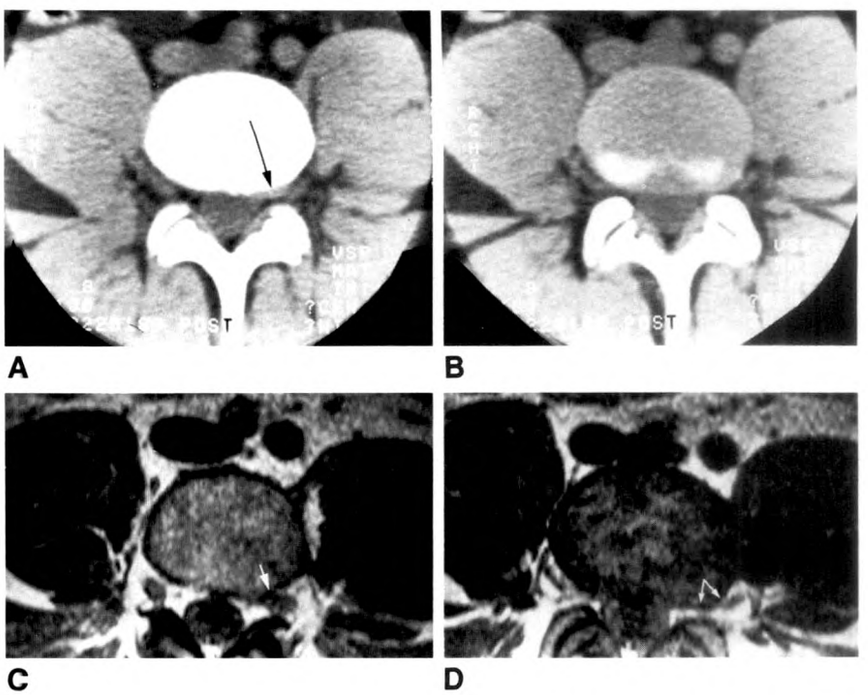


Fig. 6.—**A** and **B**, Contiguous 5-mm transverse high-resolution CT images through lower L4 vertebral body and disk level. There is paucity of epidural fat laterally on left as well as mild prominence of L4 disk on left (*arrow*). **C** and **D**, Contiguous transverse MR images (TE = 30 msec, TR = 2.0 sec) through same levels as **A** and **B.** Note reduction of epidural fat and narrowing of neural foramina surrounding L4 nerve root (*arrow*). There is acute angulation of margins of L4 disk laterally on left (*arrows*) that was found to represent a lateral disk herniation at surgery. Note decreased signal of disk in **D** when compared with **C**, which is partially through vertebral body.



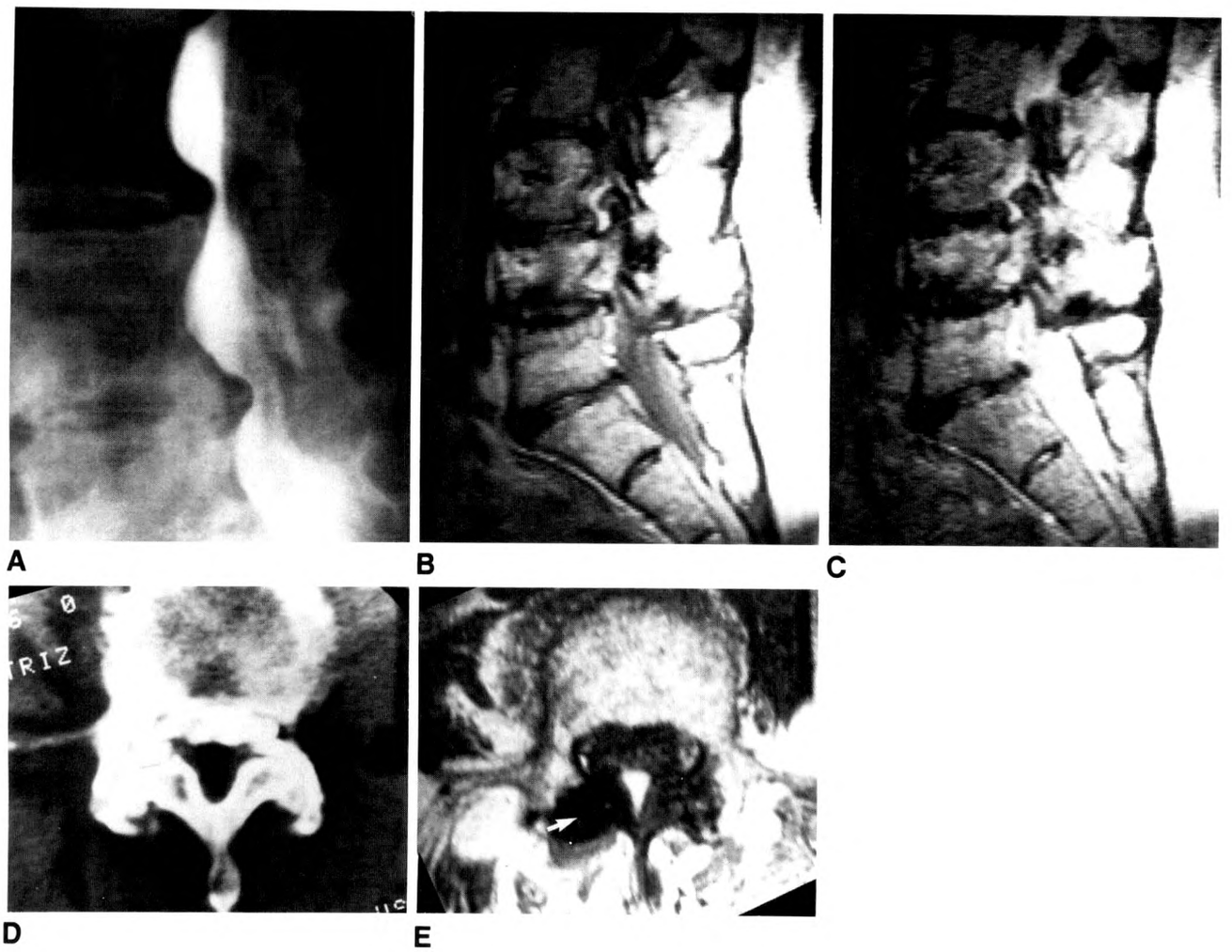


Fig. 7.—62-year-old man with pseudoclaudication consistent with lumbar canal stenosis. **A**, Lateral view on metrizamide myelogram. Anterior extradural defects are noted at L3, L4, and L5 levels. **B**, Sagittal midline 4-mm MR section (TE = 32 msec, TR = 0.5 sec) showing marked canal stenosis from both anterior and posterior extradural elements. There is minimal scoliosis at L3 and L4. **C**, Sagittal midline 4-mm MR section (TE = 90 msec, TE = 2.0 sec) again showing marked canal stenosis, further emphasizing major contribution from posterior elements, proven at surgery. All visible disk levels show a decreased signal, presumably secondary to degeneration. **D**, High-resolution CT after metrizamide myelogram at L4 level. There is marked compression of thecal sac from hypertrophic bony changes involving facet joints and posterior elements. **E**, Transverse MR image (TE = 30 msec, TR = 2.0 sec) through same level as **C**. Compression of thecal sac is similar to that in high-resolution CT. Epidural fat is well seen, but signal from ligamentum flavum and posterior bony elements is confluent. Note decreased signal intensity within bony changes in right facet joint, which is seen in certain cases of degenerative disease (*arrow*).

region of the conus, may be examined in the sagittal plane without prolonging the exam time. Images can be obtained in any plane and at any angle off the primary orthogonal planes. On the other hand, unlike CT, the angle of acquisition of MR is set for an entire acquisition and is not as flexible in terms of changing disk levels.

Although every effort was made to eliminate bias in this study, certain potential flaws became apparent. First, although herniated disks were treated in a precise fashion, the treatment of spinal stenosis as a broad category was advantageous to MR. In order to facilitate statistical analysis we chose to treat stenosis in a more global manner. We felt this was appropriate because of the diffuse and multilevel nature of the process and because the surgical approach in the lumbar region is usually more encompassing, entailing a bilateral laminectomy at more than one level.

Second, while the surgical appraisal of herniation was precise, that of stenosis was often more general in the operative description; yet it must be assumed to be correct because it cannot be tested. This can produce problems in the analysis, and it must be assumed that at least one false surgical diagnosis was probably made. This is illustrated by one of the 11 patients for whom there was disagreement between the operative findings and those of MR, CT, and myelography. The surgical diagnosis was that of bony facet overgrowth. Postoperatively, there was no improvement in this patient, and a subsequent MR study again identified what appeared to be a herniated L5 disk with the surgical changes

predominately at the L4 level. Another problem, noted by Haughton et al. [11], is that a nuclear fragment lodged behind the posterior longitudinal ligament, which may be diagnosed correctly as a herniated disk by CT and MR, may appear as a bulging anulus (which would be assumed to be secondary to a spondylitic process in conjunction with other spondylitic changes) and thus might be categorized as stenosis at the time of surgery.

A final criticism would be our grouping of all CTs together, those performed with metrizamide (30 of 42) and those performed without it (12 of 42). We chose to do this to simplify the analysis. It has been suggested by some that metrizamide CT is superior to plain CT [10, 16]; but similar accuracy, especially with herniated disk disease, has been reported with plain CT [11, 17]. In this study the results showed a slightly greater agreement of surgery with plain CT, but the numbers are too small to draw any meaningful conclusion. It is further understood that metrizamide CT, while an invasive test, can potentially provide a more accurate delineation of the thecal sac and the evaluation of intradural and intramedullary lesions.

Despite these limitations, the results of this study indicate that a technically adequate MR examination was equivalent to CT and myelography in diagnosing lumbar canal stenosis and herniated disk disease. In this study, there was still significant disagreement, ranging from 17–29%, with the surgical findings when any of the three techniques was used alone. This disagreement was most apparent in cases of lumbar stenosis. Thus, in both herniated disk disease and lumbar canal stenosis, a combination of studies may be indicated for preoperative evaluation. In such cases, CT and MR can be complementary studies and MR can be viewed as an alternative to myelography.

REFERENCES

1. Chafetz NI, Genant HK, Moon KL, Helms CA, Morris JM. Recognition of lumbar disk herniation with NMR. *AJNR* **1984**;5:23–26, *AJR* **1983**;141:1153–1156
2. Han JS, Kaufman B, El Yousef SJ, et al. NMR imaging of the spine. *AJNR* **1983**;4:1151–1159, *AJR* **1983**;141:1137–1145
3. Modic MT, Pavlicek W, Weinstein MA, et al. Nuclear magnetic resonance imaging of the spine. *Radiology* **1983**;148:757–762
4. Modic MT, Pavlicek W, Weinstein MA, et al. Magnetic resonance imaging of intervertebral disk disease. *Radiology* **1984**;152:103–111
5. Moon KL, Genant HK, Helms CA, Chafetz NI, Crooks LE, Kaufman L. Musculoskeletal applications of nuclear magnetic resonance. *Radiology* **1983**;147:161–171
6. Maravilla KR, Lesh P, Weinreb JC, Selby DK, Mooney V. Magnetic resonance imaging of the lumbar spine with CT correlation. *AJNR* **1985**;6:237–245
7. Schenck JF, Foster TH, Henkes JL, et al. High-field surface-coil MR imaging of localized anatomy. *AJNR* **1985**;6:181–186
8. Edelman RR, Shoukimas GM, Stark DD, et al. High-resolution surface-coil imaging of lumbar disk disease. *AJNR* **1985**;6:479–485, *AJR* **1985**;144:1123–1129
9. Bell GR, Rothman RH, Booth RE, et al. A study of computer assisted tomography. II. Comparison of metrizamide myelography and computed tomography in the diagnosis of herniated lumbar disc and spinal stenosis. *Spine* **1984**;9(6):552–556
10. Dublin AB, McGahan JP, Reid MH. The value of computed tomographic metrizamide myelography in the neuroradiological evaluation of the spine. *Radiology* **1983**;146:79–86
11. Haughton VM, Eldevik OP, Magnaes B, Amundsen P. A prospective comparison of computed tomography and myelography in the diagnosis of herniated lumbar discs. *Radiology* **1982**;142:103–110
12. Landman JA, Hoffman JC, Braun IF, Barrow DL. Value of computed tomographic myelography in the recognition of cervical herniated disc. *AJNR* **1984**;5:391–394
13. Moufarrij NA, Hardy RW, Weinstein MA. Computed tomographic, myelographic, and operative findings in patients with suspected herniated lumbar discs. *Neurosurgery* **1983**;12(2):184–188
14. Sobel DF, Barkovich AJ, Munderloh SH. Metrizamide myelography and postmyelographic computed tomography: Comparative adequacy in the cervical spine. *AJNR* **1984**;5:385–390
15. Williams AL, Haughton VM, Syvertsen A. Computed tomography in the diagnosis of herniated nucleus pulposus. *Radiology* **1980**;135:95–99
16. Anano AK, Lee BCP. Plain and metrizamide CT of lumbar disc disease: comparison with myelography. *AJNR* **1982**;3:567–571
17. Firooznia H, Benjamin V, Kricheff II, Rafi M, Golimbu C. CT of lumbar spine disk herniation: correlation with surgical findings. *AJNR* **1984**;5:91–96, *AJR* **1984**;147:587–592

Book Review

Diagnostic Imaging of the Acutely Injured Patient. Edited by Thomas H. Berquist. Baltimore: Urban & Schwarzenberg, 250 pp., 1985, $47.50

The purpose of this book as stated in the introduction is to serve as a basic reference guide to aid in selection of various imaging techniques for evaluation of the acutely injured patient. It comprises 12 chapters. Eight chapters are written by the editor and the remaining chapters by four contributing authors.

The first chapter is a review of the traumatologist's approach to the acute trauma patient, with a nice overview of the clinical assessment and the use of a trauma score system to judge the severity of injury. The chapter contains several tables, including imaging studies most frequently used and indications for arteriography in the acute trauma setting. The 11 remaining chapters are divided by anatomic regions of interest. In each anatomic area the discussion includes imaging studies that are applicable to the particular situation. Use of tables and algorithms is extensive. Although not referenced in the text, a short list of references follows each chapter. There is no index; in order to find a specific topic, the text concerning appropriate anatomic area must be perused. Most of the radiographs are of excellent quality, although several are reversed or printed upside down. Also, it would be desirable to print all lateral views of the spine oriented in the same direction throughout (either right or left) for consistency. The two CT head scans in the section on skull trauma are vintage 1979 and 1982, and are not cropped well; most of the remaining CT scans are of appropriate quality.

The main problem with the book, which limits its appeal to radiologists, is the superficial coverage of the use of imaging studies and the inclusion of some basic normal radiographic anatomy, all of which will be familiar to practicing radiologists and most traumatologists. In addition, the normal anatomic examples are all radiographs, not special imaging studies, and usually appear in the text after illustrations of pathologic conditions. The limited scope of the discussion excludes, for example, the typical osteochondral fractures of the patella or femoral condyle associated with patellar dislocation. Injuries to the immature skeleton are not discussed as a separate section, and receive scant coverage throughout the text. Plastic deformity is excluded. Most of the issues in the selection of proper imaging studies are not discussed in enough detail to make the text a useful guide to the radiologist. Although MR is included in the introduction as an imaging technique to be discussed, its limited mention in the text presumably reflects the shortcomings of MR in the acute trauma setting.

Although not stated in the introduction, the book's primary audience may be the trauma physician, medical student, and emergency medical technologist. It does not fill a needed gap in reference material for the practicing radiologist.

Thomas G. Goergen
UCSD Medical Center
San Diego, CA 92103

Cystic Necrosis of the Spinal Cord in Compressive Cervical Myelopathy:

Demonstration by Iopamidol CT-Myelography

John R. Jinkins[1]
Rifaat Bashir[2]
Ossama Al-Mefty[3]
M. Zuheir Al-Kawi[2]
John L. Fox[3,4]

Seven consecutive patients with compressive cervical myelopathy were studied with standard water-soluble contrast myelography and immediate CT followed by delayed CT of the spinal canal at 10 to 12 hr. Every case demonstrated findings suggestive of necrosis and/or cavitation of the central portions of the spinal cord on the delayed CT study. Two types of abnormalities were visualized in the form of delayed collections of contrast media inside the cord: (1) bilateral enhancement, a double-barreled "snake-eyes" appearance at or near the level of compression (consistent with central gray matter necrosis and/or cavitation—local syringomyelia ex-vacuo); and (2) longitudinally oriented, "pencil-shaped" central enhancement of variable length distant from the level of compression (consistent either with an enlarged central canal—hydromyelia ex-vacuo—or with necrosis and/or cavitation extending craniad and caudad from the area of maximal compression and located in or near the anterior portion of the dorsal columns—distant syringomyelia ex-vacuo). These findings, supported by previous reports of autopsy specimens, may explain in part: (1) the frequent discrepancy between the levels of maximal cervical compression and the variable neurologic signs; and (2) the frequent lack of improvement in clinical signs after surgical decompression of the spinal cord at this late stage of the illness. We believe similar intramedullary lesions may be present in other cases of chronic compression of varying etiology at any location within the spinal cord.

Compressive lesions of the cervical spinal canal commonly present in three ways: incidental radiographic findings; signs of cervical nerve root compression; and/or signs of cervical spondylotic myelopathy (CSM). This paper deals with the latter phenomenon, which has created much consternation as a result of the following clinical inconsistencies [1–15]. Frequently, the neurologic findings do not correlate with the level of maximal compression as seen on myelography. Often there are variable sensory and motor findings suggestive of a transverse spinal lesion, amyotrophic lateral sclerosis, central cord syndrome, Brown-Sequard syndrome, or syringomyelia syndrome. Atrophy of the hand muscles (whose motor cells are at the C8 and T1 spinal cord levels) is often seen in association with lesions present at higher cervical levels. At surgery, the cord may appear not to be compressed. Surgical decompression often does not improve the clinical signs and occasionally may worsen the neurologic condition. After surgery the myelopathy may continue to progress. Wilson et al. [15] concluded, "Mounting evidence now implicates etiologic factor(s) in addition to, or instead of, compression of neural structures because: (a) levels of dysfunction often do not correspond to the location of vertebral osteophytes; (b) evidence of spinal cord compression by ventral osteophytes is often slight or absent at laminectomy; and (c) myelographic findings do not always correlate with neurologic involvement."

In 1958, Brain and Wilkinson [4] found radiographic signs of cervical spondylosis in 24 out of 52 cases of syringomyelia. They hypothesized that the process of cervical bony joint degeneration was intensified in patients with syringomyelia. A 1981 publication by Lucci et al. [16] suggests, at first glance, a similar phenomenon.

This article appears in the July/August 1986 issue of *AJNR* and the October 1986 issue of *AJR*.

Received May 20, 1985; accepted after revision December 10, 1985.

Presented at the annual meeting of the Research Society of Neurological Surgeons. Chapel Hill, NC, April 1985.

[1] Division of Neuroradiology, King Faisal Specialist Hospital and Research Centre; P.O. Box 3354, Riyadh 11211, Saudi Arabia. Address reprint requests to J. R. Jinkins.

[2] Division of Neurology, King Faisal Specialist Hospital and Research Centre, Riyadh 11211, Saudi Arabia.

[3] Division of Neurosurgery, King Faisal Specialist Hospital and Research Centre, Riyadh 11211, Saudi Arabia.

[4] Present address: Department of Neurosurgery, Georgetown University Hospital, Washington, DC 20007.

***AJR* 147:767–775, October 1986**
0361–803X/86/1474–0767
© American Roentgen Ray Society

However, they postulate that two of their cases of CSM had syringes secondary to the cervical spondylosis. Although no CT photographs of these cases were shown, they stated that the nonenchanced CT scans revealed cervical intramedullary cavities. In 1982, Tsuji [17] mentioned a case of cervical canal stenosis and syringomyelia, but gave no details. Another single case was reported in 1983 by Mossman and Jestico [18]. They performed an immediate and a delayed (6 hr) CT scan of the cervical spine after intrathecal injection of metrizamide in a patient who already had a laminectomy for CSM. The delayed scan revealed a large-enhancing cavity or syrinx in the center of the spinal cord.

Despite the recent suggestion that the various forms of secondary syringohydromyelia are exceptionally rare [19], we elected to follow the advice of Quencer et al. [20]: "This case [of spinal cord glioma] points out the need to perform delayed metrizamide CT even in the face of normal myelography when there is a strong clinical indication of spinal cord abnormality." We wished to investigate the possibility that the aforementioned inconsistencies found with CSM may, in fact, be explained by radiographically demonstrable intramedullary lesions (i.e., syringomyelia ex-vacuo) secondary to various causes of cervical cord compression.

Materials and Methods

From July 1984 through January 1985, we investigated seven consecutive patients admitted with symptoms arising from severely stenotic spinal canals of developmental and acquired origin. In each case, the patient presented with a long (months or years) history of progressive myelopathy and with clinical finidngs of sensory, motor and reflex deficits consistent with a cervical myelopathic process.

All the patients in this study had low lumbar punctures with instillation of 10 ml of iopamidol (Niopam 300). The contrast material was then manipulated into the cervical region, and routine filming was done. Subsequently, an immediate CT was performed followed by a delayed CT 10–12 hr later. Earlier (6–8 hr) and later (24 hr) scanning done in these cases showed inadequate contrast-medium penetration at 6–8 hr and poor cord/cavity differentiation (i.e., nearly isodense) at 24 hr. The CT examination was performed both at the level of maximal spinal stenosis as well as above and below the stenotic canal, with the exam extending into the upper cervical and lower thoracic regions, respectively. Narrow window level and width CT filming was performed on the delayed study to electronically enhance the accumulation of contrast medium within the spinal cord at these various levels. In examinations where the sections were contiguous, reformatting was performed in both the sagittal and coronal planes to further elucidate the nature and extent of the lesion.

All of the myelographic procedures were performed on a standard radiographic tilt table under fluoroscopic control. The CT examination was carried out on a General Electric 9800 scanner (Milwaukee, WI). Slice thicknesses of 3, 5, and 10 mm were obtained depending on the level examined. Our control group of patients included a total of eight individuals examined for reasons other than myelopathy. They had the identical myelographic procedure (the same amount and concentration of contrast medium was administered) and the same type of subsequent CT evaluation. None of these controls demonstrated any evidence of abnormality on the immediate CT examination, nor was there an abnormal accumulation of contrast medium within the spinal cord on delayed evaluation. No patient in either the control group or the tested group had any adverse reaction or clinical deterioration during or after the intrathecal iopamidol injection.

Case Reports

Case 1

This 58-year-old woman was first seen because she had been unable to walk for 1 year on account of weakness. On examination, there was mild touch and pinprick sensory deficit in the C8 and T1 distribution bilaterally and severe hypesthesia (all sensory modalities) below the knees in both legs. The ankle jerks were absent, but knee jerks and upper limb deep tendon reflexes were 3+. Bilateral Hoffmann's reflexes were present. Plantar stimulation caused down-going toe reflexes. There was a positive Romberg test. The upper limbs were moderately weak and spastic throughout. The lower limbs were moderately weak throughout, but the patient could not walk, mainly because of severe sensory ataxia.

The myelogram showed a nearly complete block at the C6–C7 interspace due to developmental stenosis coupled with acquired spondylotic changes as well as severe lumbar stenosis. Immediate CT evaluation at this same cervical level revealed a remarkably atrophied spinal cord surrounded by a moderate-sized subarachnoid space and sagittal narrowing of the spinal canal (Fig. 1A). A repeat CT exam 10 hr later at the C6–C7 level indicated that contrast medium had collected inside the cord and concentrated in areas corresponding to the right and left gray-matter zones (Fig. 1B). This "snake-eyes" appearance was seen only at and near the level of the spondylotic bar. However, extending above (Fig. 1C) and below (Figs. 1D and 1E) this level was a separate, longitudinally oriented, "pencil-shaped" zone of intramedullary contrast collection. This central, longitudinal lesion was well seen only when the window setting of the CT computer console was sufficiently narrow to enhance the accumulated contrast (Figs. 1D and 1E).

The patient underwent a lumbar laminectomy for decompression of the cauda equina. There has been gradual improvement in her lower-limb function. To date, a cervical decompression has not been done.

Case 2

This 40-year-old man was seen in May 1984. He had a 3-year history of electriclike sensations radiating into his back, left thumb, and left leg when he flexed his neck. He also complained of general body weakness. On examination, he was found to have a positive Lhermitte's sign. There was touch and pinprick sensory deficit over the left C8 and T1 zones. His strength was good, but the deep tendon reflexes were 3+ to 4+ throughout and there was a left ankle clonus.

Radiographs of the cervical spine revealed developmental spinal stenosis. A subsequent myelogram demonstrated interruption of contrast medium by a C6–C7 spondylotic process. An immediate CT study at the same level confirmed the narrowed sagittal diameter of the spinal canal, the posterolateral osteophyte, and the associated spinal cord atrophy (Fig. 2A). On delayed CT examination 10 hr later, an intramedullary lesion appearing as a pencil-shaped contrast density was found extending longitudinally below the point of compression and into the thoracic spinal cord (Fig. 2B). The "snake-eyes" lesions were not identified in this patient.

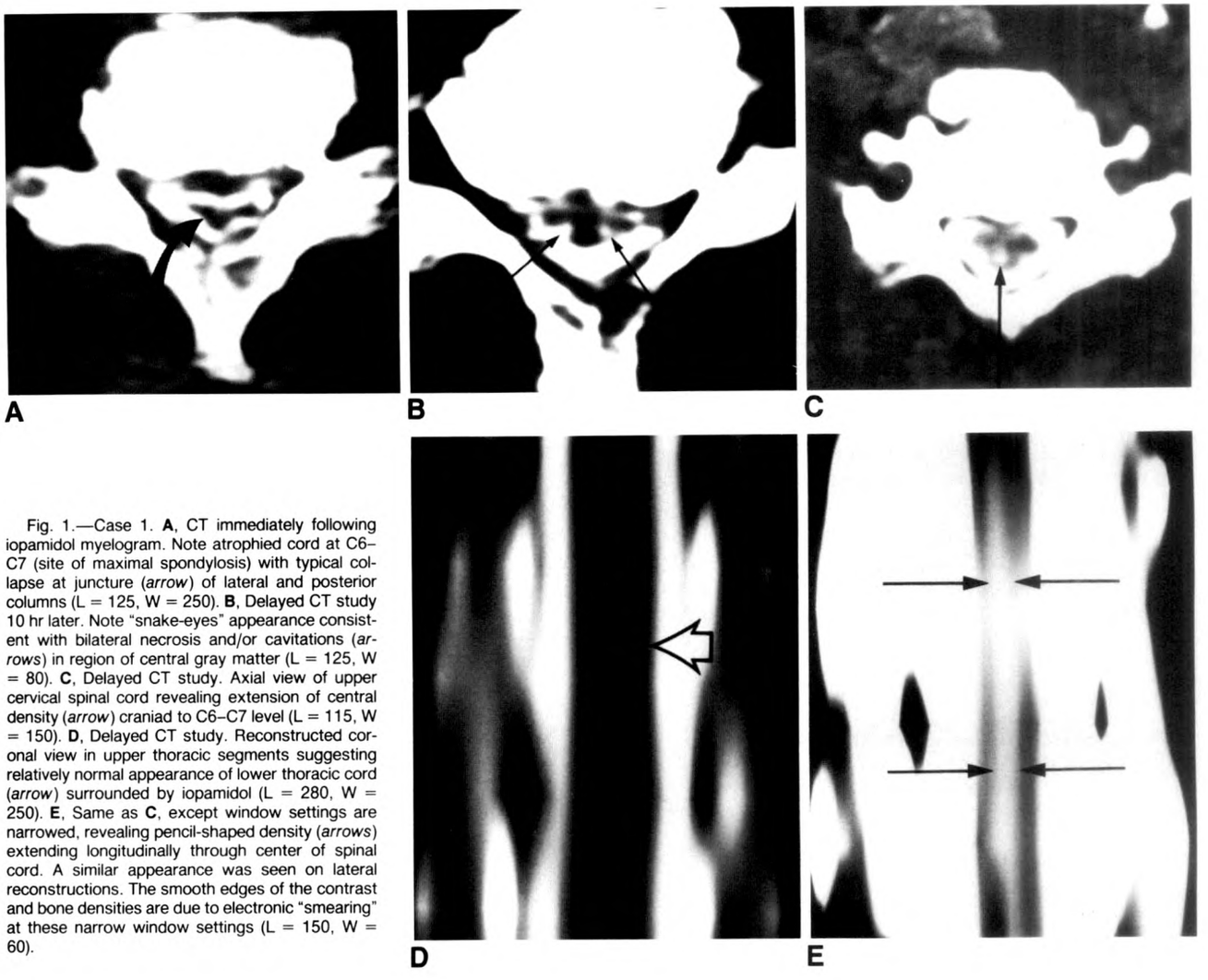


Fig. 1.—Case 1. **A**, CT immediately following iopamidol myelogram. Note atrophied cord at C6–C7 (site of maximal spondylosis) with typical collapse at juncture (*arrow*) of lateral and posterior columns (L = 125, W = 250). **B**, Delayed CT study 10 hr later. Note "snake-eyes" appearance consistent with bilateral necrosis and/or cavitations (*arrows*) in region of central gray matter (L = 125, W = 80). **C**, Delayed CT study. Axial view of upper cervical spinal cord revealing extension of central density (*arrow*) craniad to C6–C7 level (L = 115, W = 150). **D**, Delayed CT study. Reconstructed coronal view in upper thoracic segments suggesting relatively normal appearance of lower thoracic cord (*arrow*) surrounded by iopamidol (L = 280, W = 250). **E**, Same as **C**, except window settings are narrowed, revealing pencil-shaped density (*arrows*) extending longitudinally through center of spinal cord. A similar appearance was seen on lateral reconstructions. The smooth edges of the contrast and bone densities are due to electronic "smearing" at these narrow window settings (L = 150, W = 60).

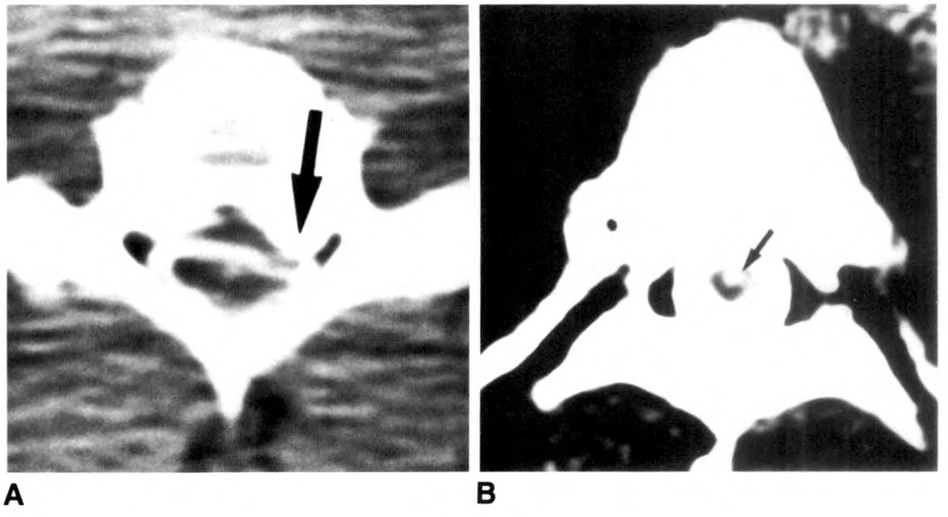


Fig. 2.—Case 2. **A**, Immediate postmyelographic CT study demonstrating C6–C7 osteophyte formation (*arrow*) and cord atrophy with flattening (L = 75, W = 350). **B**, Mid-thoracic cord axial CT examination 10 hr later. The centrally enhancing lesion (*arrow*) is seen when narrow window settings are used (L = 85, W = 60).

The patient underwent a cervical laminectomy. Postoperatively, his neurologic exam has been unchanged, but the electric shocks he experienced during neck flexion have disappeared.

Case 3

This 64-year-old man had a 2-year history of stiffness and weakness in both legs, with his legs often giving way while he was walking. On examination, he had good extremity strength and sensation, but his tone was moderately spastic in all four limbs. Deep tendon reflexes were 4+ in his arms and legs. He had positive Babinski and Hoffmann signs. He walked slowly with a spastic gait. The Romberg test was normal.

The conventional radiographs and myelogram revealed developmental stenosis and a prominent spondylotic bar at C3–C4. Bar and cord atrophy were confirmed on an immediate CT study (Fig. 3A). The typical "Napoleonic hat" appearance (upside down in the CT view) of the spinal cord in cross section was seen. Immediate CT examinations above and below the primary, compressive lesion showed moderate but less severe atrophy. At the C3–C4 level a 10-hr delayed CT scan (Fig. 3B) demonstrated the "snake-eyes" appearance resulting from an apparent intramedullary collection of contrast medium in the right and left central gray matter. Above (Figs. 3C and 3D) and below the C3–C4 spondylosis, proper settings of window levels allowed presentation of centrally located intramedullary contrast enhancement, the contrast medium that was presumably lying in central zones of necrosis and/or cavitation.

The patient underwent a decompressive cervical laminectomy. To date, his neurologic examination remains as it was before surgery.

Case 4

This 57-year-old man had had a ventriculoperitoneal shunt inserted 4 years earlier for normal pressure hydrocephalus, which was diagnosed as a cause of his gait disturbance. In the same year, a metrizamide myelogram was attempted by a C1–C2 level puncture, but without success. The patient's gait disturbance accelerated into a progressive quadriparesis and spasticity of unclear origin (i.e., from normal pressure hydrocephalus, cord injury during attempted myelography, or cervical spondylosis). A zone of suspended, painful dysesthesia from C4 to T4 levels evolved. On examination, there was mild loss of temperature and pinprick sensation bilaterally

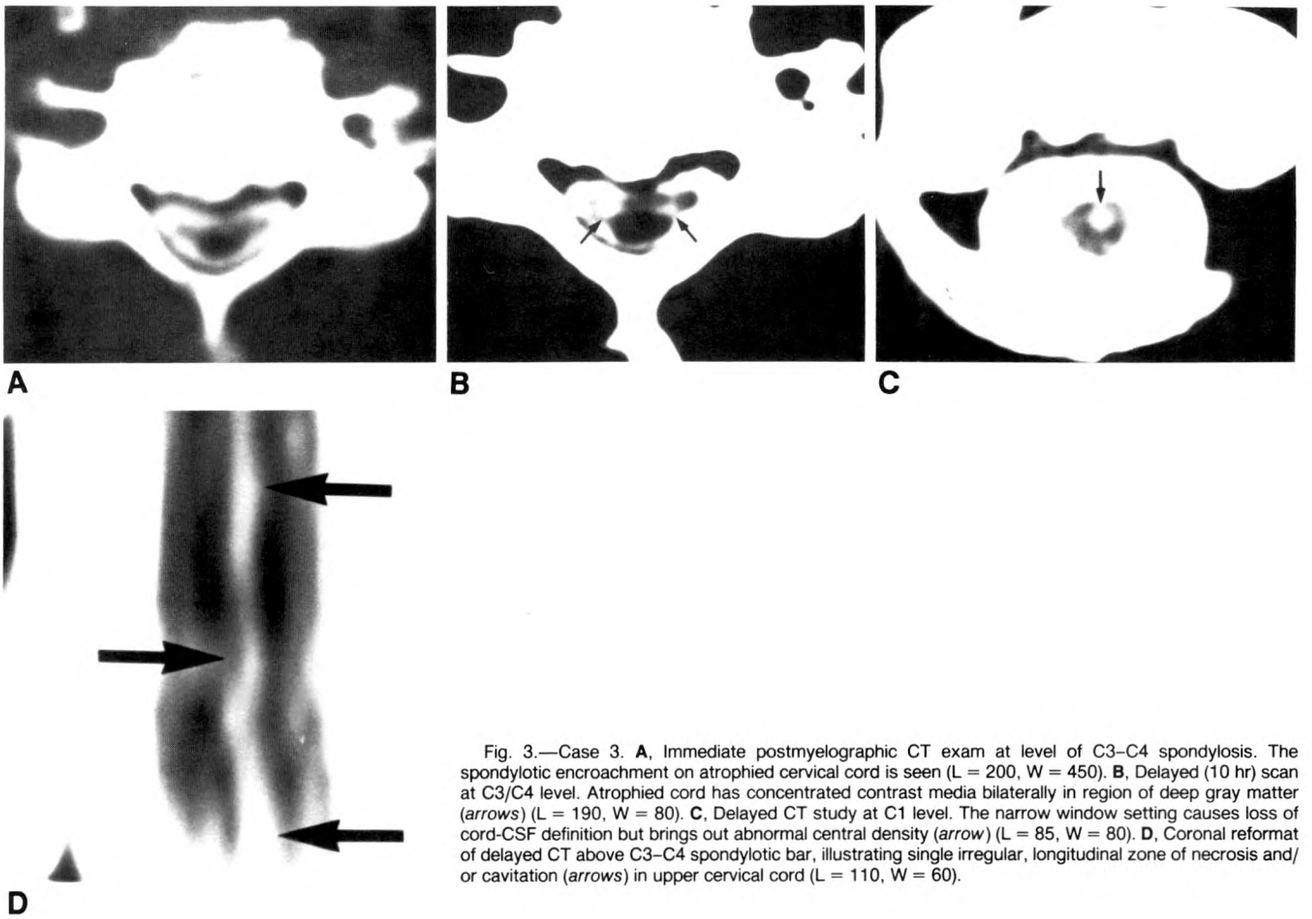


Fig. 3.—Case 3. **A**, Immediate postmyelographic CT exam at level of C3–C4 spondylosis. The spondylotic encroachment on atrophied cervical cord is seen (L = 200, W = 450). **B**, Delayed (10 hr) scan at C3/C4 level. Atrophied cord has concentrated contrast media bilaterally in region of deep gray matter (*arrows*) (L = 190, W = 80). **C**, Delayed CT study at C1 level. The narrow window setting causes loss of cord-CSF definition but brings out abnormal central density (*arrow*) (L = 85, W = 80). **D**, Coronal reformat of delayed CT above C3–C4 spondylotic bar, illustrating single irregular, longitudinal zone of necrosis and/or cavitation (*arrows*) in upper cervical cord (L = 110, W = 60).

from C4 to T4, inclusively. He had a mild spasticity of all limbs, but his strength was good. There were bilateral, positive Hoffmann's reflexes and a normal response to plantar stimulation. Deep tendon reflexes were 3+ throughout.

The myelogram revealed a developmentally narrow canal with spondylotic bars at C4–C5 and C5–C6. A CT scan done immediately thereafter demonstrated a severely atrophied cord surrounded by a moderate-sized subarachnoid space. The delayed study failed to suggest any pencil-shaped central cavitation, but the classical double-barreled "snake-eyes" abnormality was seen at the level of the spondylosis (Figs. 4A and 4B). These intramedullary lesions appeared to lie within the central gray matter.

The patient has been followed in the neurology clinic. No cervical decompression has been performed, and his neurologic status remains unchanged.

Case 5

This 48-year-old man was seen for a prolactinoma that was well controlled by bromocriptine. His chief complaint was difficulty in walking and occasionally falling during the past year. On examination, there was slight, bilateral optic atrophy and reduced visual acuity. His strength was good, but severe spasticity was present in all four limbs. Deep tendon reflexes were 4+ throughout, and Hoffmann and Babinski signs were positive bilaterally. The sensory examination was within normal limits.

The axial CT and sagittal reformat showed ossification of the posterior longitudinal ligament at C5 and C6 levels (Fig. 5A). Marked focal cord atrophy was present at these same levels. A delayed (10 hr) CT exam at the level of cord compression again illustrated the abnormal bilateral contrast collections in the central gray-matter zones (Fig. 5B). Above and

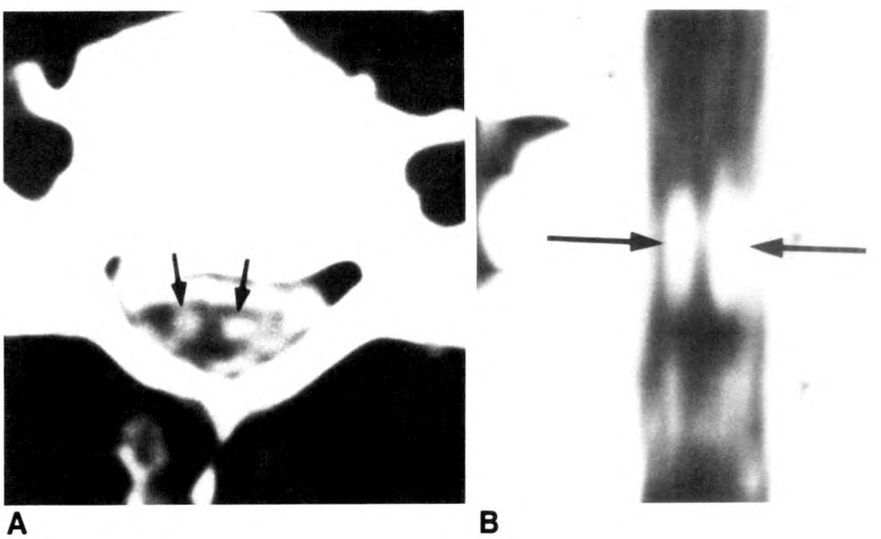


Fig. 4.—Case 4. **A**, This delayed postmyelographic CT scan (10 hr) at C5 illustrates bilateral collection of contrast media in central gray zones (*arrows*) giving typical "snake-eyes" appearance at level of spondylosis (L = 120, W = 150). **B**, The double-barreled, 1-cm-long lesion (*arrows*) is well seen on coronal reformat (L = 120, W = 150).

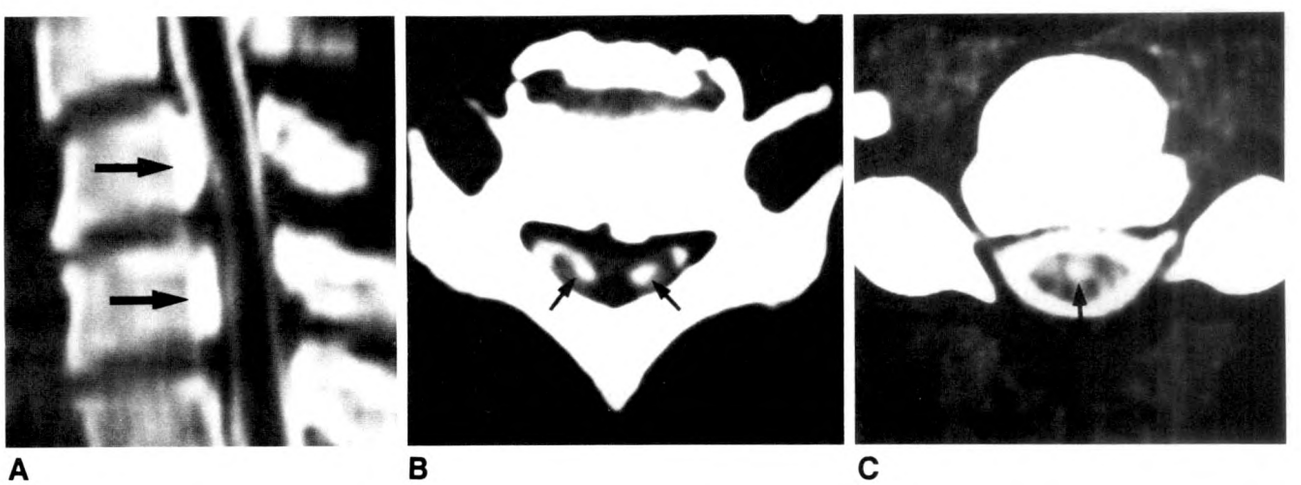


Fig. 5.—Case 5. **A**, Lateral reformat of immediate CT myelogram at midcervical level. Ossification at the posterior longitudinal ligament at C5 and C6 is seen (*arrows*) and adjacent cord is atrophied (L = 330, W = 850). **B**, Delayed (10 hr) CT scan at C5 level. Window levels set to show bilateral, intramedullary collection of contrast media (*arrows*) (L = 160, W = 150). **C**, Delayed CT scan at C3 with narrow window settings revealing abnormal central intramedullary enhancement (*arrow*) (L = 100, W = 100).

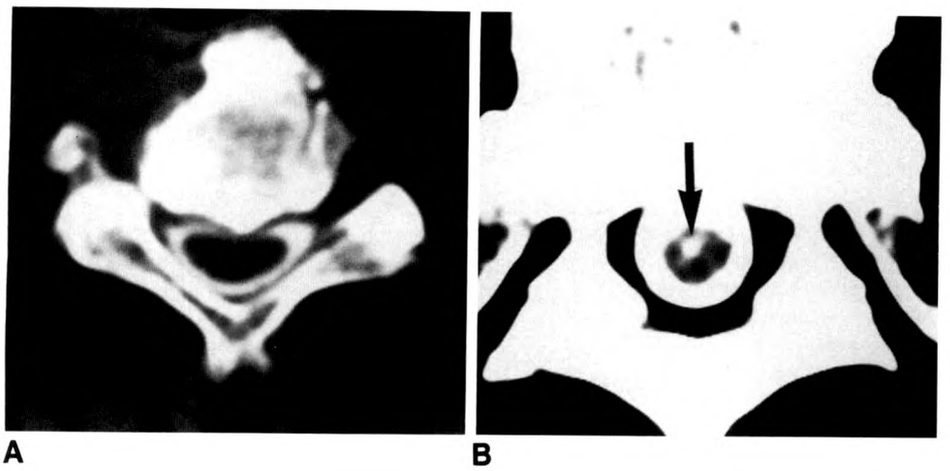


Fig. 6.—Case 6. **A**, Initial CT section at level of cervical spondylosis immediately after iopamidol myelogram. Note moderate flattening of spinal cord (L = 70, W = 650). **B**, Delayed (12 hr) CT scan in lower thoracic region. Iopamidol concentrated (*arrow*) within spinal cord is noted at narrow window settings (L = 75, W = 60).

below the levels of ossification of the posterior longitudinal ligament, the spinal cord appeared relatively normal at wide window settings. However, at narrower window levels (Fig. 5C), these same sites now were seen to have centrally located, abnormal contrast collections within the spinal cord.

A decompressive cervical laminectomy was done. Postoperatively, there has been minimal improvement in the patient's gait and spasticity.

Case 6

This 65-year-old man had a history of cervical injury. He complained chiefly of pain in the left thumb and index finger that had been present for several months. He had a 3-month history of electriclike sensations radiating into both arms and legs during neck flexion. On examination, his reflexes, strength, and tone were normal. Touch and pinprick sensations in the thumb and index finger were reduced bilaterally. A positive Lhermitte's sign was present.

Conventional spine films revealed mid- and lower-cervical developmental spinal stenosis, Forestier's disease (idiopathic skeletal hyperostosis) of the cervical spine, and an old fracture of the hyperostotic mass at C6. Myelography with CT demonstrated moderate cord atrophy (Fig. 6A). A delayed CT scan failed to show any necrosis/cavitation in the cervical region, but an intramedullary density coursed through the thoracic spinal cord (Fig. 6B).

This patient's signs and symptoms have remained unchanged without surgical intervention.

Case 7

This 63-year-old man complained of neck pain, loss of strength in all limbs, and difficulty urinating for 8 months. On examination, he had a wide-based, spastic gait. There was marked spasticity and mild weakness in all four limbs. Sensation was intact. Deep tendon reflexes were 4+ throughout. There was ankle clonus on the right, and bilaterally positive Babinski and Hoffmann reflexes.

The iopamidol myelogram demonstrated a prominent C4–C5 spondylotic bar with partial obstruction to contrast flow in cervical extension. The subsequent CT demonstrated a markedly atrophic cervical spinal cord (Fig. 7A). "Double-barrel" necrosis/cavitation was seen in the mid-cervical region at 10 hr, and contrast material had collected centrally within the thoracic cord (Fig. 7B), but no abnormal accumulation could be identified craniad to C4–C5.

A C4–C5 diskectomy by the anterior approach was carried out. Since then, there has been little improvement in the patient's clinical symptoms and signs, although his clinical course seems to have stabilized.

Discussion

It appears that special techniques of CT examination of the spinal cord 10–12 hr after water-soluble contrast (iopamidol) myelography permit demonstration of intramedullary lesions at and distant from levels of known spinal cord compression. These studies, while placing additional demands on time and scheduling, provide rather solid evidence, not heretofore demonstrated in a consecutive series of patients, that spinal cord compression can and does create both local and remote intramedullary spinal cord zones of destruction and apparent cavitation. The occurrence of such remote, pencil-shaped lesions (whether they are necroses, cavitations, or hydromyelia ex-vacuo) are frequently seen in severe cases and clearly explains some of the puzzling clinical aspects of compressive cervical myelopathy and the surgical results mentioned in the introduction. Certainly a patient with mid-cervical spondylosis and secondary necrosis and/or cavitation (syrinx) extending up into the upper cervical spinal cord and down into the thoracic spinal cord can be expected to show signs of muscle atrophy of the hands; electromyographic signs of fasciculations in the arms and legs [8, 21–23]; and misinterpreted signs of motor neuron degeneration, demyelinating disease, amyotrophic lateral sclerosis, or primary syringomyelia [2, 5, 8, 22].

Secondary, usually noncommunicating syringomyelia has

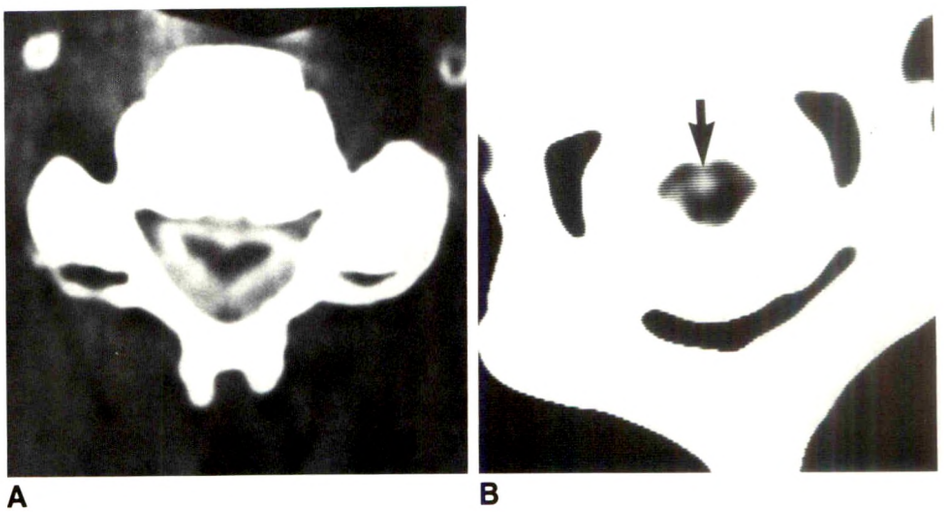


Fig. 7.—Case 7. **A**, Initial CT section near level of cervical spondylosis immediately after iopamidol myelogram. Note severe flattening and atrophy of spinal cord (L = 65, W = 200). **B**, Delayed (10 hr) CT scan in lower thoracic region. Iopamidol concentrated (*arrow*) within spinal cord is noted at narrow window settings (L = 150, W = 60).

been reported in association with spinal cord neoplasms, Pott's disease (tuberculosis) of the spine, spinal trauma, foramen magnum tumors, arachnoiditis (from infection, hemorrhage, trauma, or other inflammatory causes), vascular disorders and infarcts, intramedullary hematomas, malformations of the central nervous system, extramedullary tumors, vertebral body tumors, myelitis, and spondylotic compression of the spinal cord [16, 18, 20, 24–33]. Brain and Wilkinson [4] in 1958, McRae and Standen [28] in 1966, and Smith [12] in 1968 suggested the possible coexistence of syringomyelia and cervical spondylosis. As previously noted, Lucci et al. [16] in 1981 and Mossman and Jestico [18] in 1983 related instances of CSM in which CT had shown signs of intramedullary cavitation.

Sotaniemi et al. [34] observed, "When an intramedullary cavitation filled with contrast medium is demonstrated, the diagnosis of syringomyelia seems clear." However, at this point we cannot confirm whether the abnormal intramedullary collections of contrast material demonstrated in our cases of CSM represent actual cavities (syringomyelia) or whether they are necrotic tissue retaining contrast medium. Stevens et al. [32] found that 15% of their operated cases of posttraumatic syringes diagnosed by delayed CT examinations after myelography did not have intramedullary cavities. Instead, necrotic zones appeared to be present. Certainly, liquifaction necrosis often precedes cavitation.

The use of delayed CT examinations after subarachnoid injection of water-soluble contrast material has been in common use for demonstrating posttraumatic syringes [31, 34], classical syringomyelia or hydromyelia [19, 35–39], syrinx secondary to arachnoiditis [27], and an occasional cystic spinal cord glioma [20]. Many of the cerebrospinal fluid (CSF)-enhanced CT studies nicely showed the syringes after a delay of only 4–8 hr. The fact that our lesions were seen best with iopamidol at 8–12 hr suggests one or more of the following: (1) there may be differences between the transparenchymal spinal cord diffusion rates of metrizamide (used mostly by others) and iopamidol (used in our cases); (2) the cavities in our cases are much smaller, requiring a longer diffusion and collection time; and (3) some or all of the lesions in our cases represent a form of central cord necrosis (without cavitation), which more slowly concentrates the inwardly diffusing contrast media.

We expect that in the future MR studies will reveal these lesions as spinal MR technology improves. The MR studies of cervical spondylosis to date have been somewhat useful for evaluating spinal stenosis and spondylosis [40, 41], but spinal cord anatomic details have been limited. Such imaging has been much more useful for classical syringomyelia [19, 38, 40–42].

Up to now, most CT examinations of cases of CSM have been performed either without contrast enhancement or with CSF-contrast enhancement studied without delay [16, 43, 44]. The same is true for cases of ossification of the posterior longitudinal ligament [45] and the developmentally narrowed cervical canal [46]. Whereas Lucci et al. [16] apparently were the first to relate syringomyelia causally to cervical spondylotic cord pressure, Mossman and Jestico [18] in 1983 were the first to report delayed CT scanning after intrathecal injection of contrast medium in one postoperative case of CSM and thus demonstrate the presence of a large syrinx. While one possibly may assume that these were incidentally coexisting lesions in their three cases, our findings confirm a significant relationship between the chronic spinal cord pressure and intramedullary spinal cord cavitations.

CSF-enhanced contrast medium may enter a classical (Arnold-Chiari type) hydromyelic cavity by one of two postulated routes: downward reflux via the fourth ventricle or transmyelon migration [37]. In our cases, we believe that the iopamidol crossed the pia and passed through the parenchymal, extracellular spaces of the white matter and then into the lesions. This is consistent with the theories and observations of other investigators regarding metrizamide: water-soluble contrast material in the CSF penetrates the brain and spinal cord through extracellular spaces communicating directly with the CSF [47–49]. Isherwood et al. [48] noted it took 3–6 hr for intrathecally administered metrizamide to achieve an equilibrium between the spinal cord parenchyma and the surround-

ing CSF of patients. It is possible that iopamidol has a different equilibrium time than does metrizamide, one factor that may account for the longer (10–12 hr) delay to reach optimum visualization of the lesions in our cases. As a control, we have studied eight cases without evidence of spinal cord compression. The focal intramedullary contrast collections were not seen at 10 or 12 hr.

We cannot give precise measurements of the lesion demonstrated on our delayed CT scans. Observed absolute and relative sizes of the imaged lesion, spinal cord, and surrounding CSF vary depending on the operator-selected window-density settings of the CT console [50]. We can state that: (1) the lesions shown are smaller than most previously demonstrated syringomyelic cavities; (2) no communication with the fourth ventricle has been proven; and (3) two separate types of lesions have been demonstrated. On the basis of our radiologic studies, we cannot confirm the histologic classification of the two types of lesions. We can postulate that the focal "snake-eyes" lesions at the cervical site of compression represent zones of repeated traumatic and/or ischemic damage leading to necrosis with almost certain subsequent deep gray-matter cavitation, or local syringomyelia ex-vacuo [11, 51–54]. The somewhat smaller, pencil-shaped lesions extending caudal and/or cranial to the primary compressive site may represent similar liquifaction necrosis and cavitation near the anterior part of the dorsal columns [3, 11, 14, 51, 55–57] or distant syringomyelia ex-vacuo. Alternatively, this may represent a dilated central canal, or hydromyelia ex-vacuo, secondary to severe atrophy of ascending and descending spinal cord pathways. This combination of changes explains why, outwardly, the spinal cord exhibits the markedly severe focal atrophy at the site of maximal cervical compression while the remainder of the cord only shows moderate, diffuse shrinkage. At the same time, it may well be the key to understanding and interpreting the medical and surgical dilemma of patients manifesting compressive myelopathy.

ACKNOWLEDGMENT

We thank Ms. Virginia D. Lacson for the invaluable assistance she provided in the preparation of this manuscript.

REFERENCES

1. Adams CBT, Logue V. Studies in cervical spondylotic myelopathy. III. Some functional effects of operations for cervical spondylotic myelopathy. *Brain* **1971**;94:587–594
2. Bradshaw P. Some aspects of cervical spondylosis. *Quart J Med* **1957**;26:177–208
3. Brain WR, Northfield D, Wilkinson M. The neurological manifestations of cervical spondylosis. *Brain* **1952**;75:187–225
4. Brain WR, Wilkinson M. Cervical arthropathy in syringomyelia, tabes dorsalis and diabetes. *Brain* **1958**;81:275–289
5. Bucy PC, Heimburger RF, Oberhill HR. Compression of the cervical spinal cord by herniated discs. *J Neurosurg* **1948**;5:471–492
6. Crandall PH, Batzdorf U. Cervical spondylotic myelopathy. *J Neurosurg* **1966**;25:57–66
7. Good DC, Couch JR, Wacaser L. "Numb clumsy hands" and high cervical spondylosis. *Surg Neurol* **1984**;22:285–291
8. Liversedge LA, Hutchinson EC, Lyons JB. Cervical spondylosis simulating motor-neurone disease. *Lancet* **1953**;2:652–655
9. Nugent GR. Clinicopathologic correlations in cervical spondylosis. *Neurology* **1959**;9:273–281
10. Nurick S. The natural history and the results of surgical treatment of the spinal cord disorder associated with cervical spondylosis. *Brain* **1972**;95:101–108
11. Ogino H, Tada K, Okada K, et al. Canal diameter, anteroposterior compression ratio, and spondylotic myelopathy of the cervical spine. *Spine* **1983**;8:1–15
12. Smith BH. *Cervical spondylosis and its neurological complications.* Springfield, Ill: Charles C. Thomas, **1968**
13. Stern WE, Rand RW. Spinal cord dysfunction from cervical intervertebral disk disease. *Neurology* **1954**;4:883–893
14. Wilkinson M. The morbid anatomy of cervical spondylosis and myelopathy. *Brain* **1960**;83:589–617
15. Wilson CB, Bertan V, Norrell HA Jr, Hukuda S. Experimental cervical myelopathy. II. Acute ischemic myelopathy. *Arch Neurol* **1969**;21:571–589
16. Lucci B, Reverberi S, Greco G. Syringomyelia and syringomielic syndrome by cervical spondylosis. Report on three cases presenting with neurogenic osteoarthropathies. *J Neurosurg Sci* **1981**;25:169–172
17. Tsuji H. Laminoplasty for patients with compressive myelopathy due to so-called spinal canal stenosis in cervical and thoracic regions. *Spine* **1982**;7:28–34
18. Mossman SS, Jestico JV. Central cord lesions in cervical spondylotic myelopathy. *J Neurol* **1983**;230:227–230
19. Batnitzky S, Price HI, Gaughan MJ, Hall PV, Rosenthal SJ. The radiology of syringohydromyelia. *RadioGraphics* **1983**;3:585–611
20. Quencer RM, Montalvo BM, Green BA, Eismont FJ. Intraoperative spinal sonography of soft-tissue masses of the spinal cord and spinal canal. *AJNR* **1984**;5:507–515
21. Kasdon DL. Cervical spondylotic myelopathy with reversible fasciculations in the lower extremities. *Arch Neurol* **1977**; 34:774–776
22. King RB, Stoops WL. Cervical myelopathy with fasciculations in the lower extremities. *J Neurosurg* **1963**;20:948–952
23. Stark RJ, Kennard C, Swash M. Hand wasting in spondylotic high cord compression: an electromyographic study. *Ann Neurol* **1981**;9:58–62
24. Appleby A, Bradley WG, Foster JB, Hankinson J, Hudgson P. Syringomyelia due to chronic arachnoiditis at the foramen magnum. *J Neurol Sci* **1969**;8:451–464
25. Blaylock RL. Hydrosyringomyelia of the conus medullaris associated with a thoracic meningioma. Case report. *J Neurosurg* **1981**;54:833–835
26. Poser CM. *The relationship between syringomyelia and neoplasms.* Springfield, Ill: Charles C. Thomas, **1956**
27. Simmons JD, Norman O, Newton TH. Preoperative demonstration of postinflammatory syringomyelia. *AJNR* **1983**;4:625–628
28. McRae DL, Standen J. Roentgenologic findings in syringomyelia and hydromyelia. *AJR* **1966**;98:695–703
29. Barnett HJM, Jousse AT. Posttraumatic syringomyelia (cystic myelopathy). In: Vinken PJ, Bruyn GW, eds. *Handbook of neurology*, vol 26. *Injuries of the spine and spinal cord*. Amsterdam: **1976**:113–157
30. Nurick S, Russell JA, Deck MDF. Cystic degeneration of the spinal cord following spinal cord injury. *Brain* **1970**;93:211–222
31. Quencer RM, Green BA, Eismont FJ. Posttraumatic spinal cord cysts: clinical features and characterization with metrizamide computed tomography. *Radiology* **1983**;146:415–423
32. Stevens JM, Olney JS, Kendall BE. Posttraumatic cystic and non-cystic myelopathy. *Neuroradiology* **1985**;27:48–56

33. Williams B, Terry AF, Jones HWF, McSweeney T. Syringomyelia as a sequel to traumatic paraplegia. *Paraplegia* **1981**;19:67–80
34. Sotaniemi KA, Pyhtinen J, Myllylä VV. Computed tomography in the diagnosis of syringomyelia. *Acta Neurol Scand* **1983**;68:121–127
35. Bradley WG Jr, Waluch V, Yadley RA, Wycoff RR. Comparison of CT and MR in 400 patients with suspected disease of the brain and cervical spinal cord. *Radiology* **1984**;152:695–702
36. Rossier AB, Foo D, Naheedy MH, Wang A-M, Rumbaugh CL, Levine H. Radiography of posttraumatic syringomyelia. *AJNR* **1983**;4:637–640
37. Aubin ML, Vignaud J, Jardin C, Bar D. Computed tomography in 75 clinical cases of syringomyelia. *AJNR* **1981**;2:199–204
38. Barbaro NM, Wilson CB, Gutin PH, Edwards MSB. Surgical treatment of syringomyelia. Favorable results with syringoperitoneal shunting. *J Neurosurg* **1984**;61:531–538
39. Di Chiro G, Axelbaum SP, Schellinger D, Twigg HL, Ledley RS. Computerized axial tomography in syringomyelia. *New Engl J Med* **1975**;292:13–16
40. Han JS, Kaufman B, El Yousef SJ, et al. NMR imaging of the spine. *AJNR* **1983**;4:1151–1159; *AJR* **1983**;141:1137–1145
41. Modic MT, Weinstein MA, Pavlicek W, et al. Nuclear magnetic resonance imaging of the spine. *Radiology* **1983**;148:757–762
42. Yeates A, Brant-Zawadzki M, Norman D, Kaufman L, Crooks LE, Newton TH. Nuclear magnetic resonance imaging of syringomyelia. *AJNR* **1983**;4:234–237
43. Badami JP, Norman D, Barbaro NM, Cann CE, Weinstein PR, Sobel DF. Metrizamide CT myelography in cervical myelopathy and radiculopathy: correlation with conventional myelography and surgical findings. *AJNR* **1985**;6:59–64
44. Miyasaka K, Isu T, Iwasaki Y, Abe S, Takei H, Tsuru M. High resolution computed tomography in the diagnosis of cervical disc disease. *Neuroradiology* **1983**;24:253–257
45. Yamamoto I, Kageyama N, Nakamura K, Takahashi T. Computed tomography in ossification of the posterior longitudinal ligament in the cervical spine. *Surg Neurol* **1979**;12:414–418
46. Thijssen HOM, Keyser A, Horstink MWM, Meijer E. Morphology of the cervical spinal cord on computed myelography. *Neuroradiology* **1979**;18:57–62
47. Dubois PJ, Drayer BP, Sage M, Osborne D, Heinz MR. Intramedullary penetrance of metrizamide in the dog spinal cord. *AJNR* **1981**;2:313–317
48. Isherwood I, Fawcitt RA, Forbes WS, Nettle JRL, Pullan BR. Computer tomography of the spinal canal using metrizamide. *Acta Radiol [Suppl]* (Stockh) **1977**;355:299–305
49. Winkler SS, Sackett JF. Explanation of metrizamide brain penetration: a review. *J Comput Assist Tomogr* **1980**;4:191–193
50. Seibert CE, Barnes JE, Dreisbach JN, Swanson WB, Heck RJ. Accurate CT measurement of the spinal cord using metrizamide: physical factors. *AJNR* **1981**;2:75–78; *AJR* **1981**;136:777–780
51. Ono K, Ota H, Tada K, Yamamoto T. Cervical myelopathy secondary to multiple spondylotic protrusions. A clinicopathologic study. *Spine* **1977**;2:109–125
52. Inoue K, Mannen T, Nakanishi T, Toyokura Y, Nagashima K. An autopsy case of ossification of the posterior longitudinal ligament of the cervical spine. *Adv Neurol Sci (Tokyo)* **1967**;20:425–433
53. Hashizume Y, Iijima S, Kishimoto H, Yanagi T. Pathology of spinal cord lesions caused by ossification of the posterior longitudinal ligament. *Acta Neuropathol (Berl)* **1984**;63:123–130
54. Hoff J, Nishimura M, Pitts L, Vilnis V, Tuerk K, Lagger R. The role of ischemia in the pathogenesis of cervical spondylotic myelopathy. A review and new microangiographic evidence. *Spine* **1977**;2:100–108
55. Hughes JT. *Pathology of the spinal cord.* London: Lloyd-Luke, **1966**
56. Greenfield JG. Lesions of the nervous system associated with diseases or malformations of the cranium and spinal cord. In: Greenfield JG, Blackwood W, McMenemy WH, Meyer A, Norman RM, eds. *Neuropathology.* London: Edward Arnold, **1958**:616–630
57. Mair WGP, Druckman R. The pathology of spinal cord lesions and their relation to the clinical features in protrusion of cervical intervertebral discs. A report of four cases. *Brain* **1953**;76:70–91

Book Reviews

Lymphatic Imaging: Lymphography, Computed Tomography and Scintigraphy, 2nd ed. Edited by Melvin E. Clouse and Sidney Wallace. Baltimore: Williams & Wilkins, 526 pp., 1985. $87.50

This definitive, comprehensive text deals with the anatomy, physiology, pathology, and imaging of the lymphatic system. It opens with a historical review dating back to the Alexandrian School in ancient times and closes with chapters on CT imaging and percutaneous biopsy of the lymph nodes. In between are dispersed chapters on all of the advances that have occurred in the diagnosis of lymphatic system abnormalities.

Anatomy of the lymph system is described through the use of multiple correlative illustrations of line drawing, lymphograms, CT scans, and histologic specimens. Many of these are presented in "eye strain reduction" full-page figures for easy study of their minute detail. This is one of the many features that has made *The Golden's Diagnostic Radiology Series*, of which this volume is part, so popular throughout the years. The normal anatomy section completely covers the pelvic, abdominal, and thoracic nodal groups. Completing the basic science portion of this text is an excellent chapter on lymphatic physiology by Adair and Guyton.

Another feature that grants this text its well-deserved adjective "definitive" is its broad scope. Represented are the peripheral lymphatic abnormalities, mesenteric lymphatic malformations, and benign lymph-node diseases. Jing and Wallace expound generously upon their M. D. Anderson Hospital experience in an excellent chapter on lymphatic imaging of solid tumors. They begin by placing in perspective the most commonly employed techniques for imaging lymph-node involvement by tumors. Included are lymphangiography, CT, and sonography. The mechanisms and nodes of metastasis are described comprehensively for tumors of the female genital organs, the genitourinary tract, the large intestine, the breast, malignant tumors of the skin, sarcomas of the soft tissue, and malignant tumors of bone. Countless images of nodal abnormalities and tables defining the accuracy of the various imaging techniques are given throughout this superbly illustrated chapter. There is no doubt that the way to learn about disease, staging, and diagnosis of solid tumor metastasis is to read this chapter.

Separate chapters are dedicated to the lymph-node imaging of the thorax and cervical region. Again, the text and illustrations in these are excellent.

This book represents a rare collection of masterpieces put together by those at the pinnacle of their professions. Who should read it? All of us who are faced with the daily dilemma of diagnosing lymph-node disease.

Amil J. Gerlock, Jr.
Louisiana State University Medical Center
Shreveport, LA 71130-3932

Clinical Radiology of the Spine and Spinal Cord. By Mohamed Barna. Rockville, MD: Aspen, 449 pp., 1985. $78

This book was intended to be a comprehensive work covering all types of disease affecting the spine. Indeed, practically everything is mentioned, but the discussions are uneven and at times the written text is awkward.

The book is beautifully illustrated with superb radiographs and many excellent line drawings to enhance interpretation. In many cases the routine radiographs are supplemented with CT. The author's choice of emphasis is difficult to understand. Some rare entities are discussed in detail while some common and important subjects are dismissed with a paragraph. In the references, there are too many anecdotal case reports. There is an MRI illustration on the cover of the book, but this is misleading. The chapter on MRI is only a 23-page afterthought in which a typical discussion of an entire major subject consists of two sentences.

Most sophisticated *AJR* readers would find this book disappointing, but it would be useful and satisfactory as a first text dealing with the spine or a supplementary reference.

Adele K. Friedman
Hospital of the University of Pennsylvania
Philadelphia, PA 19104

Cognitive and Affective Changes After Myelography: A Comparison of Metrizamide and Iohexol

Graham Ratcliff[1]
Susan Sandler[2]
Richard Latchaw[2]

A battery of brief cognitive tests and a mood scale were administered to 42 patients before and after cervical myelography with either metrizamide (20 patients) or iohexol (22 patients). The patients receiving metrizamide experienced a deterioration in mood after myelography and a relatively greater decline in cognitive test performance than did those receiving iohexol. These two side effects tended to occur together in the metrizamide group, suggesting a common underlying cause; but there was no correlation between changes in mood and cognitive function after myelography with iohexol. These results suggest that metrizamide has a greater neurotoxic effect than iohexol.

It has been known for several years that the use of metrizamide (Amipaque) for myelography can be associated with undesirable side effects, including nausea, headache, back and leg pain, and florid neuropsychiatric symptoms [1–6]. However, the more recent literature suggests that adverse reactions are not limited to spontaneously reported or obviously observable physiological reactions but may include subclinical disturbances of mood and cognitive function that can only be reliably detected by close questioning of the patient and formal psychometric testing [6–10]. Further, there is increasing evidence that the use of other, newer, nonionic contrast media may lead to a reduction in the incidence of these complications [9–14], and an active search for a less toxic alternative to metrizamide has been recommended [15].

Accordingly, we report the results of a study in which alterations in affect and cognitive test performance from a premyelogram baseline were assessed in patients undergoing myelography with either metrizamide or iohexol (Omnipaque), a relatively new nonionic contrast medium.

Subjects and Methods

Subjects were 42 patients in the Presbyterian University Hospital in Pittsburgh who had agreed to participate in another, larger, randomized double-blind trial of the two contrast media for cervical myelography, the results of which have been reported elsewhere [16]. Twenty patients (12 men and 8 women; mean age 43.6 years) were subsequently found to have received metrizamide, and 22 (14 men and 8 women; mean age 49.7 years) to have received iohexol. All patients were tested on two occasions—between 14 and 18 hr before myelography and between 6 and 10 hr after myelography.

Myelograms were accomplished via C1–C2 puncture using 300 mg I/ml concentration for both contrast agents, and all patients were premedicated with 10 mg of Valium. All patients were encouraged to drink liberally before myelography and to consume at least 2 liters of fluid over 8 hr after myelography. Patients were maintained in a head-up position for at least 3 min following myelography, and all received post myelographic CT scans.

Each evaluation took about 1 hr and involved administration of a standard questionnaire about the patient's mood followed by a series of brief cognitive tests. The test battery was designed to be brief yet reasonably comprehensive in terms of the cognitive functions sampled so as to minimize the burden to the patient while maximizing the probability of detecting any

This article appears in the July/August 1986 issue of *AJNR* and the October 1986 issue of *AJR*.

Received June 11, 1985; accepted after revision December 4, 1985.

Presented in part at the annual meeting of the American Society of Neuroradiology, Boston, June 1984.

[1] Harmarville Rehabilitation Center, Inc., P.O. Box 11460, Guys Run Rd., Pittsburgh, PA 15238. Address reprint requests to G. Ratcliff.

[2] Department of Radiology, University of Pittsburgh, Scaife Hall, DeSoto and Terrace St., Pittsburgh, PA 15261.

***AJR* 147:777–781, October 1986**
0361–803X/86/1474–0777
© American Roentgen Ray Society

deficits that might have occurred. It included measures sensitive to verbal and nonverbal memory impairment, disturbances of attention and concentration, perceptual and scanning disorders, constructional apraxia, difficulty with calculation, and some conventional neuropsychological measures of cerebral dysfunction. The group of tests chosen, which should be regarded as a screening battery rather than a full neuropsychological evaluation, yielded a total of 28 scores. The individual tests are described briefly below; a fuller discussion of most of these measures is provided by Lezak [17].

Profile of Mood States (POMS) [18]: A 65-item questionnaire on which the subject rates on a 5-point scale (not at all, a little, moderately, quite a bit, extremely) the extent to which he feels "tense," "miserable," "angry," "lively," "bushed," "muddled," and so on.

Wechsler Memory Scale [17, 19]: A memory scale in standard clinical use that includes measures of general information, orientation, mental control (e.g., counting backward), memory for prose passages, digit span, paired associate word learning, and memory for designs. The visual reproduction subtest was not administered in this study, and since no subject's performance on the information or orientation subtests deteriorated following myelography, they were excluded from the analysis. Different forms were used at the two evaluations to reduce the effect of learning, and 11 scores were derived reflecting immediate and delayed recall of prose and paired associate words, digit span forward and backward, and the three items from the mental control subtest.

Mooney's Visual Closure Test [20, 21]: A measure of visual perception involving recognition of camouflaged faces. The score is the number of correctly identified faces. Even-numbered items were used at the first evaluation and odd-numbered items at the second evaluation.

Repetitive Psychometric Measures [22, 23]: These tests are designed for use in drug studies and involve rapid processing of relatively simple information; subtests include perceptual speed, number facility, visualization, and speed of closure. Parallel forms were used at the two evaluations and, while the subtests used in this study variously demand visual scanning, rapid addition, oculomotor control, and word recognition, all require good concentration. Five scores were derived reflecting the number of items correctly completed within the time limit on each subtest plus the number of errors of addition on the number-facility subtest.

Grooved Peg Board [17]: A manual dexterity test. The two scores are the time taken to insert ridged pegs into 25 keyhole-shaped slots with either hand.

Stroop Color/Word Test [17, 24]: The test involves reading color names, naming colors, and naming the color of the ink in which inappropriately colored color names are printed (e.g., the word "red" printed in green). Scores are the time taken to complete each part of the test.

Trail Making Test [17, 25]: A standard neuropsychological test in which the subject draws lines to connect numbered circles in the appropriate order (part A) or alternates between numerical and alphabetical series (part B). Scores are the time it takes to complete each part.

Rey and Taylor Figures [17]: Parallel forms of a difficult constructional and nonverbal memory task in which the subject must copy a complex geometrical figure and then redraw it from memory after a delay. The scores are the number of elements accurately drawn on each occasion.

Results

Two patients who had been examined prior to myelography declined the postmyelogram evaluation. Two additional patients elected to discontinue the postmyelogram evaluation at an early stage when less than half the tests had been attempted. All four of these patients were subsequently found to have received metrizamide and they were discarded from the analysis. The data reported below, therefore, came from 38 patients, 22 of whom received iohexol and 16 metrizamide.

Changes in expressed mood following myelography as measured by the POMS are shown in Figure 1. Patients receiving metrizamide rated themselves as more anxious, more depressed, more angry, less vigorous, more fatigued, and more confused 6–10 hr after myelography than they had before the investigation. Conversely, patients receiving iohexol reported slightly less anxiety and confusion following myelography (possibly because of relief from worry about the impending investigation) and exhibited virtually no change on

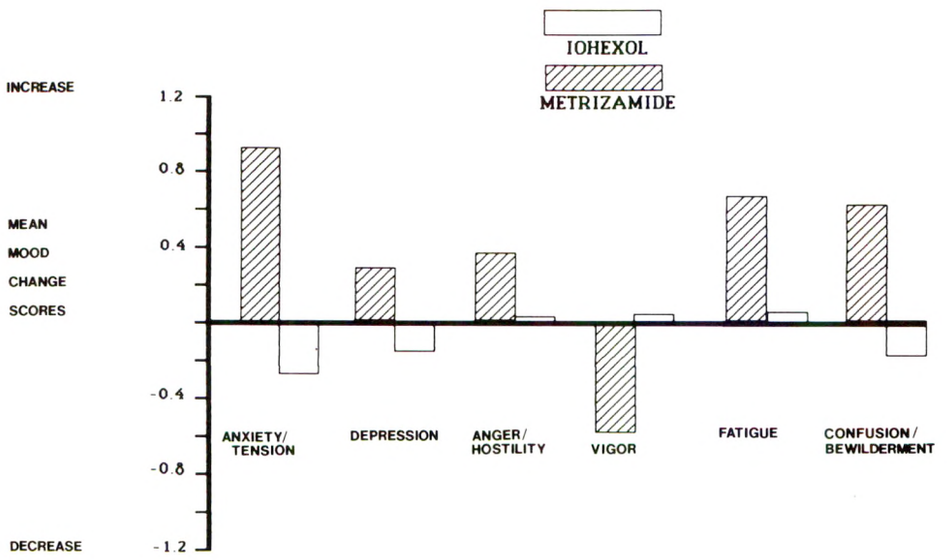


Fig. 1.—Changes in mood following myelography. Mean change from premyelogram baseline on each Profile of Mood States scale is shown for both groups.

the other scales. An overall mood-change score was calculated for each group by subtracting the overall POMS mood-disturbance score obtained at the postmyelogram evaluation from that recorded before myelography. The difference in mood change between the groups was significant at the 0.01 level ($t = 2.99$).

The cognitive test results are not subject to such simple analysis because parallel forms were not available for all the measures used and because the extent of any practice effects attributable to the repetition of the same or similar tests within 24 hr is not known with certainty. Therefore, a simple comparison of pre- and postmyelogram scores on cognitive tests would not necessarily be a valid measure of absolute cognitive change—if normal subjects improved on retesting because of increased familiarity with the task, no change in performance would actually imply a deterioration in level of functioning. However, *relative* change following myelography (i.e., a difference between groups in the *amount* of improvement or decline in test performance from the premyelogram baseline) can be calculated and is a valid basis on which to decide whether one of the contrast media employed has *more* effect on cognitive function than the other. As it is unlikely that the intrathecal injection of either contrast medium would improve cognitive function, it can be assumed that the group that exhibits the greater deterioration after myelography has been more adversely affected by the contrast medium involved.

Bearing this in mind, the difference between pre- and postmyelogram performance was calculated for each subject on each test and the raw difference scores transformed into z scores (i.e., standard deviation units) to allow comparison and summation across tests. An overall cognitive-change score was calculated for each subject by computing the mean of the transformed difference scores for each test. The change scores allow each subject to serve as his or her own control, and the distribution of scores for each group is shown in Figure 2. A t-test applied to the group mean indicates that metrizamide had significantly more adverse effect on cognitive test performance than did iohexol ($t = 3.09$; $p < 0.005$).

Considering the tests individually and excluding the two on which no subject showed any change, the metrizamide group performed less well than the iohexol group on 21 of the 26 measures, a result that departs from chance at the 0.01 level (Fisher exact probability). The between-group difference reached conventional levels of significance on five individual measures (rapid simple addition, immediate recall of a short story, paired associate-word learning, counting by threes and fours, and rapid color naming), all of them favoring the iohexol group.

These two sets of changes, decline in cognitive test performance and deterioration in mood, were correlated in the metrizamide group (rho = 0.489; $p < 0.01$), raising the possibility that a third variable (e.g., fatigue, pain, or nausea) underlies both phenomena. No such relationship was found in the iohexol group (rho = 0.045). Not surprisingly, subjects in either group who spontaneously reported adverse reactions such as nausea, headache, and back pain (five in the iohexol group and 12 in the metrizamide group) tended to experience a deterioration in mood. But there was also a suggestion that

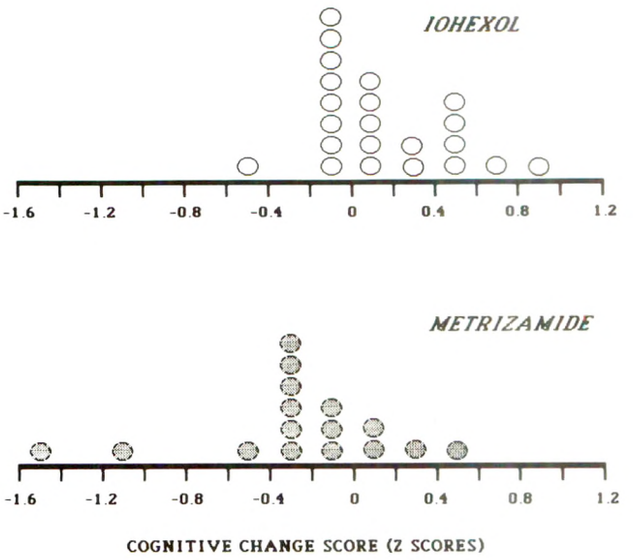


Fig. 2.—Changes in cognitive test performance following myelography. Changes in cognitive test score, averaged across tests and transformed to Z scores, are shown for each subject. Negative numbers indicate relatively poorer performance after myelography.

adverse reactions were associated with greater cognitive impairment in the metrizamide group whereas the cognitive functioning of the few subjects who reported adverse reactions to iohexol did not differ from that of the remainder of the group. Thus, the evidence tends to suggest that such adverse reactions are not by themselves sufficient to account for poor cognitive test performance. However, because of the small numbers and the imbalance in the frequency of adverse reactions between the two groups, no attempt was made to examine this phenomenon statistically, and the conclusion must remain tentative.

Finally, there was no clear relationship between age and either affective or cognitive change following myelography. It is in any case unlikely that our results could be explained on the basis of greater sensitivity of the elderly to the effects of metrizamide [5], as the patients receiving metrizamide in this study were, on average, slightly younger than the iohexol group.

Discussion

Psychometric retesting was performed 6–10 hr after myelography, because it is well known clinically that symptoms are maximal during this period, although they may persist for at least 24 hr [8, 10]. Our results indicate that metrizamide used as a contrast medium in cervical myelography leads to a deterioration in affective state shortly after myelography but that iohexol employed in a similar role does not. Metrizamide also affects cognitive function more than iohexol, but our data do not allow us to conclude with certainty that iohexol has no adverse effects on cognitive test performance.

Although the cognitive test scores of the great majority of

our iohexol subjects remained unchanged or improved after myelography, it is possible that this is attributable to a practice effect—that is, the possibility that subjects who take similar tests twice do better on the second occasion because of their increased familiarity with the material. Further, it is conceivable that unoperated control subjects would have improved to an even greater extent. If this were the case, it would imply that iohexol or the fact of myelography itself had limited the ability of the subjects receiving it to benefit from prior exposure to the test battery. The only way to determine whether the performance of our iohexol subjects was entirely unaffected by the use of this contrast medium would, therefore, be to compare them either with a sham-operated control group or with a group receiving a contrast medium that is *known* to have no adverse effect. The former would clearly be unethical and the latter is not currently possible. Therefore, we conclude only that iohexol has a less adverse effect on cognitive function than does metrizamide, and note that Cronqvist et al. [8] recently reported subtle psychic changes after iohexol myelography though they agree that these are less frequent and much less pronounced than those associated with metrizamide.

Our finding that there was a correlation between the severity of the cognitive deficits and the extent of the deterioration in mood after myelography with metrizamide but not with iohexol, together with the suggestion of a stronger association between these changes and other side effects in the former group, also strengthens the case for a direct neurotoxic effect of metrizamide. It suggests that all these effects have a common cause or may be manifestations of a single underlying disorder, and that the more commonly reported side effects of nausea, headache, back and leg pain, and overt psychic disturbances are only the more obvious manifestations of a more diffuse toxic abnormality.

Galle et al. [9] were able to show that the slowing of mental function 6 hr after metrizamide myelography was directly related to the intracranial concentration of contrast medium at that time but that there was no relationship between mental function and concentration of contrast medium in the subarachnoid space after myelography with iopamidol. Both our results and their findings would be compatible with a direct toxic effect of metrizamide but allow the possibility that some of the milder effects seen after myelography with iopamidol and iohexol are not directly attributable to the contrast medium used. Little or no correlation between mood and level of cognitive function would be expected in patients in whom mood but not cognition had been affected, and postmyelogram changes in mood need not be directly related to myelography. One patient in our iohexol group who became quite depressed after the myelogram had been told that the results, by exclusion, suggested a diagnosis of multiple sclerosis, and it is possible that the diagnosis rather than the myelogram *per se* was the cause of his depression. This may be an extreme case, but anxiety about diagnosis, lack of sleep prior to myelography, and other nonspecific factors can be expected to affect patients' moods.

While the adverse effects of metrizamide myelography reported here are comparatively mild, and there is good reason to suppose that they are transient [9], they are nevertheless definite. The between-group difference in our study accounted for over 20% of the total variance in both cognitive and affective change, and it is possible that this is an underestimate—the four subjects, all from the metrizamide group, who declined to complete the postmyelogram evaluation may well have been more adversely affected by their experience than the remaining subjects; and, had their data been available, the between-group differences may have been greater.

Although the number of subjects included in this study was small, the results suggest that in the absence of any indication to the contrary, and given that the radiographic quality of the two contrast media is equivalent, iohexol may be preferable to metrizamide for cervical myelography because its effects on mental function, if any, are less severe than those of metrizamide.

REFERENCES

1. Skalpe IO. Adverse effects of water-soluble contrast media in myelography, cisternography and ventriculography. *Acta Radiol [Suppl]* (Stockh) **1977**;355:409–416
2. Sackett JF, Strother CM, Quaglieri CE, Manucher JJ, Levin AB, Duff TA. Metrizamide. Analysis of clinical application in 215 patients. *Radiology* **1977**;123:779–782
3. Baker RA, Hillman BJ, MacLennan JE, Strand RD, Kaufman SM. Sequelae of metrizamide myelography in 200 examinations. *AJR* **1978**;130:499–502
4. Gelmers HJ. Adverse side effects of metrizamide myelography. *Neuroradiology* **1979**;18:119–124
5. Schmidt RC. Mental disorders after myelography with metrizamide and other water-soluble contrast media. *Neuroradiology* **1980**;19:153–157
6. Richert S, Sartor K, Holl B. Subclinical organic psychosyndromes on intrathecal injection of metrizamide for lumbar myelography. *Neuroradiology* **1979**;18:177–184
7. Hauge O, Falkenberg H. Neuropsychologic reactions and other side effects after metrizamide myelography. *AJNR* **1982**;3:229–232, *AJR* **1982**;139:357–360
8. Cronqvist SE, Holtas SL, Laike T, Ozolins A. Psychologic tests in the evaluation of psychic changes after myelography with metrizamide. *Acta Radiol [Diagn]* (Stockh) **1984**;25:257–260
9. Galle G, Huk W, Arnold K. Psychopathometric demonstration and quantification of mental disturbances following myelography with metrizamide and iopamidol. *Neuroradiology* **1984**;26:229–233
10. Hammeke TA, Grogan JP, Haughton VM, Pfeiffer MM, Harrington GJ, Sudilovsky A. Evaluation of myelographic contrast-medium tolerance with psychometric testing. *AJNR* **1985**;6:343–348
11. Trevisan C, Malaguti C, Manfredini M, Tampieri D. Iopamidol vs. metrizamide myelography: clinical comparison of side effects. *AJNR* **1983**;4:306–308
12. Turski PA, Sackett JF, Gentry LR, Strother CM, Matozzi F. Clinical comparison of metrizamide and iopamidol for myelography. *AJNR* **1983**;4:309–311
13. Bannon KR, Braun IF, Pinto RS, Manuell M, Sudilovsky A, Kricheff II. Comparison of radiographic quality and adverse reactions in myelography with iopamidol and metrizamide. *AJNR* **1983**;4:312–313
14. Witwer G, Cacayorin ED, Bernstein AD, Huballah MY, Yuan HA, Keiffer SA. Iopamidol and metrizamide for myelography: pro-

spective double-blind clinical trial. *AJNR* **1984**;5:403–407
15. Bockenheimer SAM, Hillesheimer W. Clinical experience with iopamidol for myelography. *AJNR* **1983**;4:314–316
16. Latchaw RE, Hirsch WL, Horton JA, Bissonette D, Shaw WW. Iohexol vs. metrizamide: a study of efficacy and morbidity in cervical myelography. *AJNR* **1985**;6:931–933
17. Lezak M. *Neuropsychological assessment*. New York: Oxford University Press, **1983**
18. McNair DM, Lorr M, Droppleman LF. *Profile of mood states*. San Diego: Educational and Industrial Testing Service, **1971**
19. Wechsler D. A standardized memory scale for clinical use. *J Psychol* **1945**;19:87–95
20. Mooney CM. Recognition of ambiguous and unambiguous visual configurations with short and long exposures. *Br J Psychol* **1960**;51:119–125
21. Newcombe F, Russell WR. Dissociated visual perceptual and spatial deficits in focal lesions of the right hemisphere. *J Neurol Neurosurg Psychiatry* **1969**;32:73–81
22. Moran LJ, Mefford RB. Repetitive psychometric measures. *Psychol Rep* **1959**;5:269–275
23. Moran LJ, Kimble JP, Mefford RB. Repetitive psychometric measures; equating alternate forms. *Psychol Rep* **1964**;14:335–338
24. Golden C. *The Stroop color/word test*. Chicago: Stoelting, **1978**
25. Reitan RM. Validity of the Trail Making Test as an indicator of organic brain damage. *Percept Mot Skills* **1958**;8:271–276

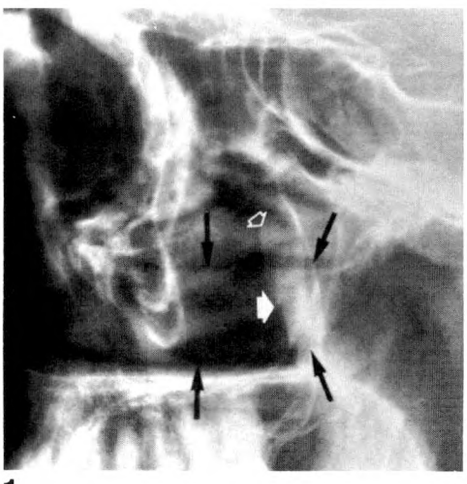
Technical Note

The Anatomic Basis of the Pseudotumor of the Nasal Cavity

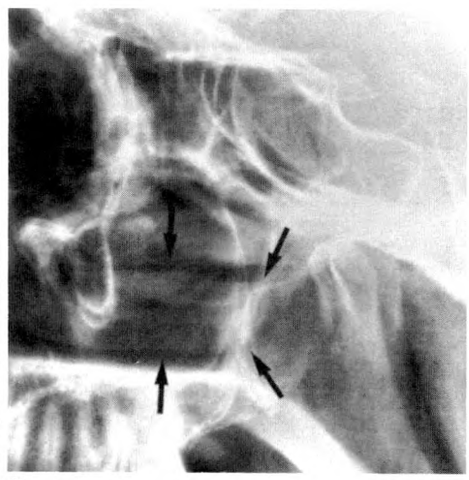
Christopher L. Sistrom,[1] Theodore E. Keats,[1] and Charles M. Johnson III[2]

On lateral radiographs of the skull or sinuses, an ovoid density is sometimes seen overlying the posterior and inferior nasal cavity. This finding does not signify disease and, indeed, is considered to be a normal variant, often termed the "pseudotumor of the nasal cavity" [1]. It has been suggested that in patients with prominent inferior turbinates, the posterior aspect of the turbinates and the coronoid process of the mandible are superimposed creating a discrete ovoid density. An alternative explanation is that the torus tubarius is responsible for the density in question. We endeavored to determine what anatomic structures are responsible for the pseudotumor.

A plain lateral radiograph of the skull of a normal volunteer, made with the mouth closed, shows the rounded density in the nasal cavity (Fig. 1). A second radiograph was obtained with the subject's mouth open as wide as possible, an action that results in downward displacement of the coronoid process. Figure 2 shows the subsequent change in contour of the



1



2

Fig. 1.—Lateral radiograph of a normal volunteer. Inferior turbinates (*black arrows*), anterior margin of pseudotumor (*white arrow*), mandibular coronoid processes (*open arrow*).

Fig. 2.—Same subject as in Fig. 1 with mouth wide open. Inferior turbinates (*black arrows*). Coronoid processes are displaced inferiorly and density and extent of pseudotumor are decreased.

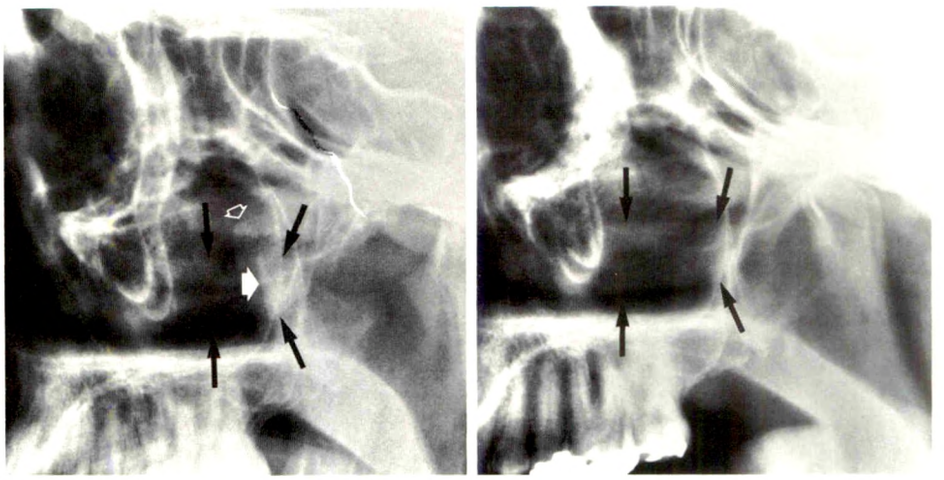
Received March 17, 1986; accepted after revision May 29, 1986.

[1] Department of Radiology, University of Virginia Medical Center, Charlottesville, VA 22908. Address reprint requests to C. L. Sistrom, Box 170.
[2] Department of Otolaryngology–Head and Neck Surgery, University of Virginia Medical Center, Charlottesville, VA 22908.

AJR **147:782–783, October 1986** 0361–803X/86/1474–0782 © American Roentgen Ray Society

Fig. 3.—Lateral radiograph of same volunteer with mouth closed after ephedrine shrinkage of turbinates. Inferior turbinates (*black arrows*), anterior extent of the pseudotumor (*open white arrow*), mandibular coronoid processes (*white arrow*). Note shrinkage of turbinates and concomitant change in contour of pseudotumor.

Fig. 4.—Lateral radiograph of same volunteer with mouth open after shrinkage of turbinates. Inferior turbinates (*black arrows*). Pseudotumor is no longer evident.



3 4

anterior aspect of the density. To determine the role of the turbinates in the pseudotumor, we repeated the radiographs in the volunteer after shrinking the turbinates. This was achieved by first spraying the nasal cavity with nebulized 3% ephedrine solution bilaterally and then applying cotton pledgets soaked with 3% ephedrine solution directly to the turbinates for 5 min. Upon removal of the pledgets, about 50% reduction in size of the turbinates was noted by direct visualization. Repeat radiographs were immediately obtained with the mouth closed and fully opened (Figs. 3 and 4). These films clearly show that the turbinates as well as the pseudotumor are smaller. With shrunken turbinates and an open jaw the pseudotumor is virtually invisible (Fig. 4).

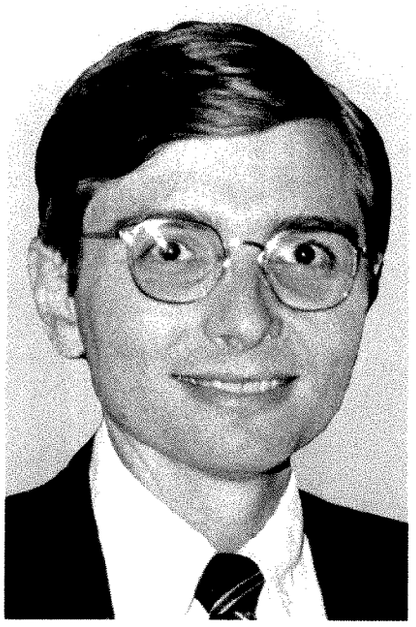
We conclude that the anatomic basis for the nasal cavity pseudotumor seen on lateral radiographs of the skull is a combination of the posterior aspect of the inferior turbinates and the mandibular coronoid processes.

REFERENCE

1. Keats TE. *Atlas of normal roentgen variants that may simulate disease*. Chicago: Year Book Medical Publishers, **1984**

Memorial

Daniel R. Biello, 1947–1986



Dr. Daniel R. Biello died June 4, 1986, after a 12-year struggle with Hodgkin's disease. Dr. Biello was born February 26, 1947, in Cleveland, OH. After graduating from Ohio Wesleyan University cum laude in 1969 and from Case-Western Reserve School of Medicine with honors in 1973, he came to the Mallinckrodt Institute of Radiology at Washington University School of Medicine where he completed his internship and residency training in diagnostic radiology and a fellowship in nuclear medicine. During his fourth year of training, he served as the Chief Resident in diagnostic radiology at the Institute. In 1978, he joined the faculty of the Institute's Division of Nuclear Medicine as Assistant Professor of Radiology, and the medical staffs of Barnes Hospital and St. Louis Children's Hospital. At the time of his death, Dr. Biello was Professor of Radiology and Associate Director of the Division of Nuclear Medicine.

During his all too brief academic career, Dr. Biello was highly productive as a scientist, having over 50 journal articles and chapters to his credit. He delighted in the search for new knowledge and new approaches to common clinical problems, and was particularly interested in cardiovascular nuclear medicine and in pulmonary embolism. Through a series of studies, performed in collaboration with investigators at several different institutions, he developed new criteria for the interpretation of ventilation-perfusion scintigrams (the "Biello criteria," as they are now usually labeled in the literature). His approach has been adopted into general use by the nuclear medicine community.

Dr. Biello was a master diagnostic radiologist and nuclear physician, who found great satisfaction in solving complex clinical problems. He was never satisfied with doing an adequate job, but always sought to do the best he could for every patient. His empathy and compassion for patients were unparalleled. He loved teaching, and scores of residents benefited from his wisdom and learned the art of nuclear medicine from his example.

Dan was a gentle, unpretentious human being. Virtually everyone who knew him considered him a friend. No matter how busy or preoccupied with his own problems, he always found time to help others deal with their problems. His sound advice and calming influence will be particularly missed. The optimism and courage with which he faced his long illness inspired his friends and coworkers, and the physicians who cared for him. In his honor, the Mallinckrodt Institute of Radiology has established the Daniel R. Biello Memorial Lectureship to serve as a lasting testimonial of our love and respect for this unique man.

He is survived by his wife, Elizabeth, his sons, David and Timothy, his parents, Dante and Jeane Biello, and his sister, Nancy Biello.

Barry A. Siegel
Mallinckrodt Institute of Radiology
Washington University Medical Center
St. Louis, MO 63110

Imaging the Pediatric Liver: MRI and CT

Jeffrey C. Weinreb[1]
Jesse M. Cohen[1]
Edward Armstrong[2]
Thomas Smith[2]

The livers of 27 children, 2 weeks to 16 years old, were examined with MRI and CT. Fourteen children had normal livers, 9 had focal liver disease, and 4 had diffuse liver disease. Normal intrahepatic venous anatomy was visualized more frequently with MRI than with CT, regardless of presence of disease, type of disease, or age. Focal hepatic lesions were either iso- or hypointense on relatively T1-weighted images and were hyperintense on T2-weighted images regardless of the pathology. In three cases, lesions seen with MRI were not detected with CT. In two other cases, CT was interpreted as equivocal or abnormal, but the liver was normal on MRI. MRI was superior to CT for evaluation of patency of the intrahepatic portion of the inferior vena cava. Other than in cases of fatty infiltration, CT provided no information additional to MRI. MRI has the potential to replace CT as a technique for imaging the pediatric liver in many cases, especially for infants and young children.

Several reports have described early experience with MRI of the liver, and some investigators have shown that it offers advantages compared to CT for detection and assessment of hepatic disease [1–9]. At the same time, many investigators acknowledge that image degradation from respiration and other sources of motion often results in poor image quality [5, 7, 10]. In this study, we reviewed MR and CT studies in 27 patients to compare the merits of the two procedures in evaluating the liver of infants and children.

Materials and Methods

We examined MRI and CT studies of the livers of 27 children, 2 weeks to 16 years old (mean 6 years, median 4 years). In 24 of the children, liver disease was suspected. Three children with no evidence of hepatic disease had abdominal CT and MRI for other reasons. The absence or presence of liver disease had been documented by surgical exploration in 19 and by tissue biopsy in six. The other two children proved to have normal livers by clinical, laboratory, and radiologic follow-up.

The MR imager used was a Diasonics 0.35-T cryogenic system. The minimum study consisted of multislice transaxial spin-echo images through the entire liver with relatively T1-weighted (TR = 500 or 1000) and T2-weighted (TR = 1500 or 2000) pulse sequences. Echo delay times (TE) were 28 (or 30) and 56 (or 60) msec for each section, except in some cases where only the first echo (TE = 30 msec) was used with TR = 500 msec. These images were sometimes supplemented with coronal and sagittal scans, especially if we were uncertain about the hepatic origin or extension of a mass on transaxial images alone. In-plane spatial resolution was 1.7 mm. For 20 studies, section thickness was 7 mm with an intervening 3-mm gap. In the seven most recent cases, sections were 10 mm thick with 1-mm gaps or continuous 5-mm slices. Neither respiratory nor ECG gating was employed. Two or four excitations were used for data acquisition.

Small children (14 patients) were studied in a head coil with a useful aperture of 30 cm, while larger children (13 patients) were studied in an elliptical neck coil (30 × 50 cm). In general, oral sedation consisting of 40–70 mg/kg chloral hydrate was administered to children under 6 years old. An accompanying adult visually monitored each child's respiration [11].

Received January 13, 1986; accepted after revision May 22, 1986.

[1] Department of Radiology, University of Texas, Health Science Center at Dallas, 5323 Harry Hines Blvd., Dallas, TX 75235. Address reprint requests to J. C. Weinreb, NMR Imaging Center, 1311 Record Crossing, Dallas, TX 75235.

[2] Department of Radiology, Children's Medical Center of Dallas, 1934 Amelia St., Dallas, TX 75235.

AJR 147:785–790, October 1986
0361–803X/86/1474–0785
© American Roentgen Ray Society

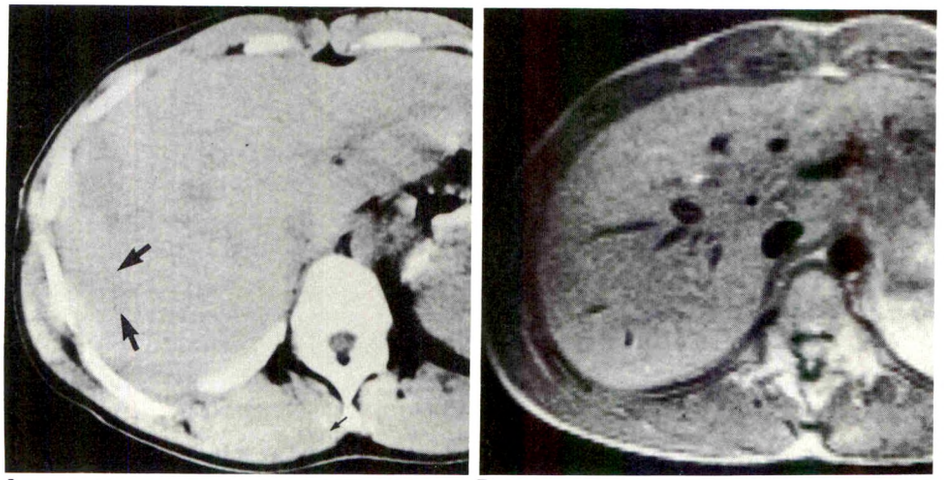


Fig. 1.—15-year-old boy who underwent leg amputation for osteogenic sarcoma presented 1 year later with chest mass. Tc^{99m} sulfur-colloid liver scintigram showed probable mass in right hepatic lobe. **A**, Contrast-enhanced CT. Low-attenuation region in periphery of right lobe (*arrows*) corresponded to abnormality on scintigram and was thought to confirm liver metastases. Note that hepatic vasculature is not visualized in right lobe. **B**, Transaxial MRI, SE 2000/28. No masses; normal hepatic vasculature. Absence of liver disease was confirmed with sonography and clinical and MRI follow-up at 1 year.

Children over 6 were usually able to cooperate for the 30–90 min required for the exam.

CT scans were obtained in 25 children within 2 weeks (mean 3 days) of the MR study. In one patient, the CT was obtained 5 months before MRI, and in another case, 3 months before MRI. The studies were performed with a variety of CT scanners (GE 8800, GE 9800, or Picker 1200); the technique varied. Scans were obtained at 1-cm intervals using 1-cm collimation (20 patients), or at 5-mm intervals with 5-mm collimation (7 patients). In three subjects, CT scans were performed without IV contrast because of poor renal function (1 patient) or difficulty finding a suitable vein (1 patient), or because the study was a follow-up (1 patient) in which the findings were visible on a previous noncontrast CT. Fifteen scans were obtained after a bolus injection, seven had a bolus followed by a rapid infusion of contrast material, and two had a rapid infusion only. Oral contrast agents were used for all CT studies.

MRI and CT scans were retrospectively and independently evaluated by two radiologists. When there was disagreement in interpretation, a consensus was always reached. The quality of the transaxial MR scans was subjectively rated as excellent, adequate, or poor, depending on whether the margins of the abdominal organs and vascular structures were sharp, slightly blurred, or grossly distorted. An effort was made to identify specific normal anatomic structures on the MRI and CT scans: the inferior vena cava; the main, right, and left portal veins and their segmental branches; the hepatic veins; the common hepatic artery and its branches; the intersegmental fissure/falciform ligament; and the bile ducts. In the nine cases with focal liver disease, the scans were scrutinized for (1) number of lesions, (2) appearance in relation to surrounding liver, (3) homogeneity of lesions, (4) presence of calcifications, and (5) lesion margins (clear or poorly defined). In the four cases with diffuse hepatic disease, the homogeneity of the liver was evaluated, and the size of the liver was subjectively rated as large, normal, or small.

Results

Quality of MR Scans

Twenty-two of 27 (81%) transaxial MR scans of the liver were rated as excellent, five (19%) as adequate, and none as poor. Four of the "adequate" scans were in children who were studied in the larger neck coil without sedation. Only one of these children was less than 8 years old. Thirteen of 14 (93%) studies performed in the head coil, whether with or without sedation, were rated as excellent.

Normal Anatomy

Normal extrahepatic vascular anatomy was visualized more frequently with MRI than with CT in both normal and diseased livers and regardless of age. This difference was most pronounced in the 0- to 5-year age group. The common hepatic artery was seen at the origin from the celiac axis in 74% of the cases with MRI and in only 15% with CT. Except in one case where the right hepatic artery was visible with MRI, branches of the common hepatic artery were not detected with either MRI or CT.

The left intersegmental fissure/falciform ligament was usually not visible with either MRI or CT in the patients younger than 10 years but was visible with CT more frequently in the older children. Normal intrahepatic bile ducts were not identified with either MRI or CT.

MRI consistently demonstrated intrahepatic venous structures better than CT in the 14 normal livers. Four of these children were studied for hepatic disease suspected on the basis of earlier imaging studies or biochemical data and were later proved to have disease-free livers. In two of these cases, a hepatic abnormality was suggested by the CT study, but MR images were unremarkable (Fig. 1). In the other two, the livers were depicted as normal by both MRI and CT.

Extrahepatic Masses

Seven children had extrahepatic masses that appeared on CT to originate in or invade the liver (5 with right Wilms' tumors, 1 right adrenal neuroblastoma, 1 yolk sac tumor) because either their epicenters appeared to be within the liver, the liver/lesion interface was poorly defined, or normal hepatic vessels in the region of the mass were not visualized. In one case, transaxial MRI indicated no liver invasion because of a sharp liver/lesion interface and the presence of normal (displaced but not amputated) hepatic vessels in the region of the mass. In six cases, hepatic origin or invasion by the mass could not be determined on transaxial MR images. In two of these cases, coronal and sagittal images correctly

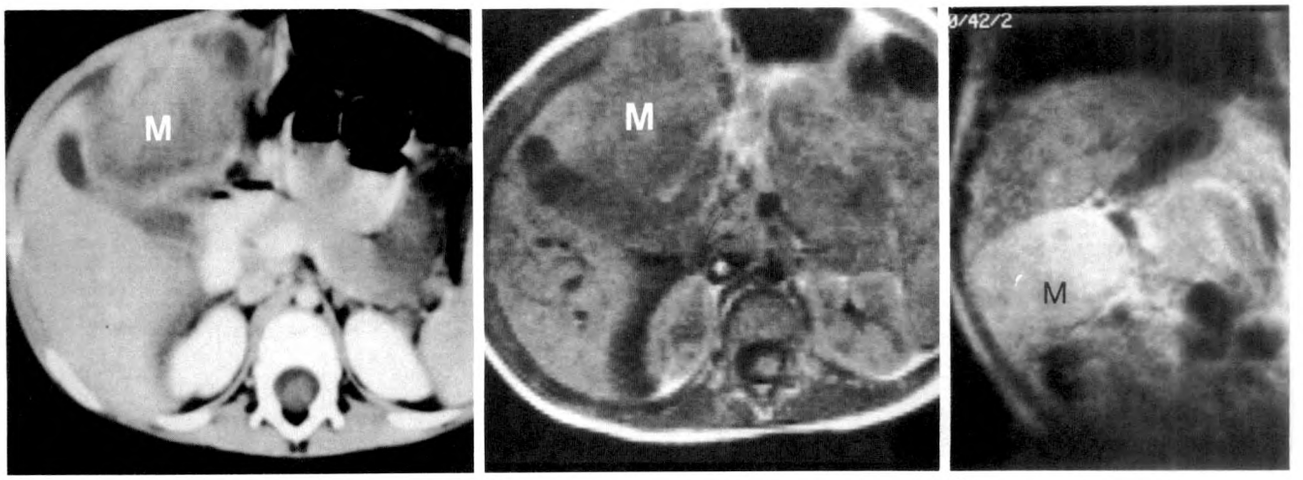


Fig. 2.—2-year-old girl with right upper quadrant mass. Surgery demonstrated yolk sac tumor that invaded anterior abdominal wall but not liver. **A**, Contrast-enhanced CT. Mass (M) appears to originate in or invade left lobe of liver. **B**, Transaxial MRI, SE 500/28. As with CT, mass (M) appears to be within liver. **C**, Coronal MRI, 1500/56. Epicenter of mass (M) is outside liver, suggesting its extrahepatic origin. Clear, sharp interface between mass and liver indicates probable absence of hepatic extension.

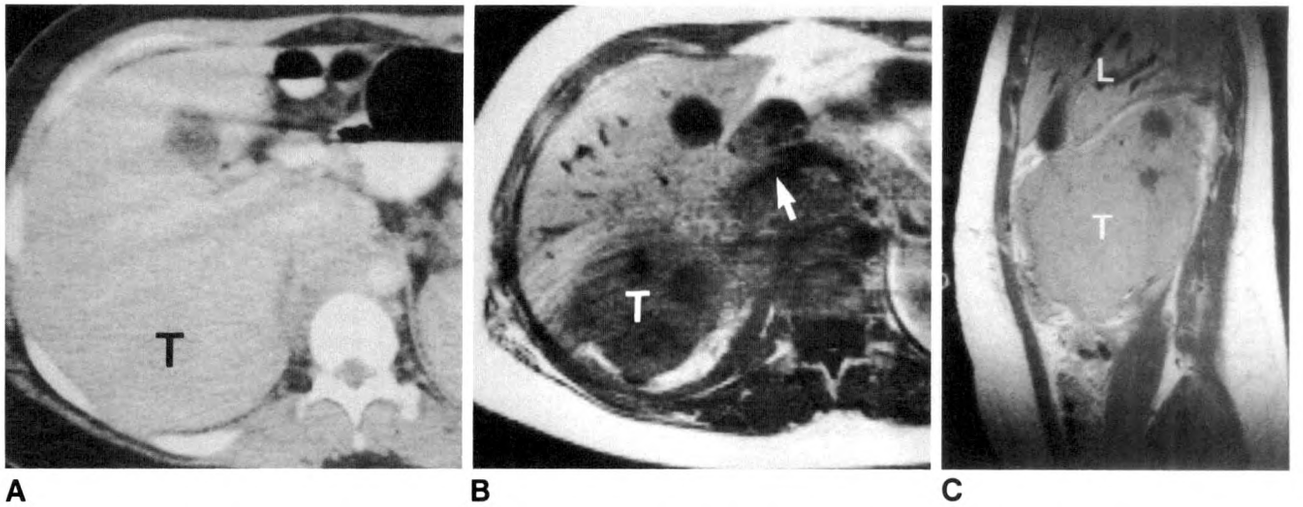


Fig. 3.—14-year-old girl with Wilms' tumor. Patent inferior vena cava was not seen with sonography. **A**, Contrast-enhanced CT. Renal mass/liver interface unclear and hepatic involvement cannot be excluded. Patent inferior vena cava not depicted. Non-contrast-enhanced CT and different window settings were not helpful. Note retrocrural adenopathy. T = tumor. **B**, Transaxial MRI, SE 500/30. Mass/liver interface not clear. Anteriorly displaced but patent inferior vena cava (*arrow*) was confirmed with sagittal MRI (not shown). Retrocrural adenopathy is present. T = tumor. **C**, Sagittal MRI, SE 1000/60. Tumor (T) indents liver (L) but clear plane between mass and liver indicates no invasion. Confirmed at surgery.

depicted extrahepatic epicenters and liver indentation without invasion (Figs. 2 and 3). In the other four, clear margins between mass and liver could not be defined in any imaged plane, and thus liver invasion could not be excluded on the basis of either MR or CT. All of the masses were hyperintense compared with liver parenchyma on relatively T2-weighted images, and iso- or hypointense with T1 weighting. In each instance, the liver was ultimately proved free of disease.

Focal Disease

Nine patients had lesions that originated in the liver. Of these patients, three had solitary masses (2 hepatoblastomas and 1 hemangioendothelioma), and six had multiple masses (metastatic neuroblastoma, metastatic islet cell tumor, nodular Hodgkin's lymphoma, caseating granulomas, hemangioendotheliomatosis, and cystic hamartomas). All were hyperintense on relatively T2-weighted images and hypo- or isointense on relatively T1-weighted images, compared with surrounding liver parenchyma. Lesions were always more conspicuous on the T2-weighted images.

MRI and CT always agreed about the homogeneity of these lesions, but the lesion margins were clearer and better defined with MR in three cases. No calcifications were seen with either MRI or CT.

Of the children with solitary hepatic masses, segmental or

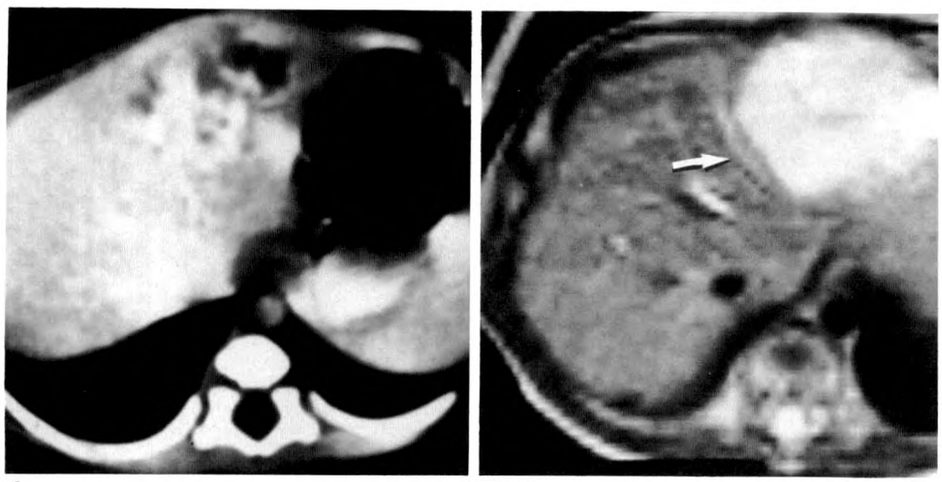


Fig. 4.—14-day-old boy presented with a right upper quadrant mass. At surgery, hemangioendothelioma was confined to lateral segment of left lobe about 1 cm from falciform ligament. Curative left lateral segmentectomy was performed. **A**, Contrast-enhanced CT. Lesion margins are poorly defined and hepatic vessels cannot be distinguished in region of mass. On the basis of this appearance, mass was thought to involve both segments of left lobe. **B**, Transaxial MRI, SE 1500/56. Lesion/liver interface sharp and left hepatic vein (*arrow*) laterally displaced but patent. This appearance indicated that mass was confined to lateral segment of left lobe.

lobar localization of masses was equally accomplished with MRI and CT in two. However, in one patient, the mass was more accurately localized with MRI (Fig. 4).

In a case of metastatic neuroblastoma, several 3- to 10-mm lesions seen with MRI were not detected on contrast-enhanced CT, sonography, or Tc^{99m} sulfur-colloid liver spleen scan. In a child with caseating granulomas, MRI unequivocally demonstrated more hepatic masses than CT. One child had nodular lymphomatous infiltrates of the liver that were clearly depicted on MRI but that were not visible or that mimicked beam-hardening artifacts on CT (Fig. 5).

Diffuse Disease

Four patients had diffuse liver disease (fatty metamorphosis and fibrosis of unknown cause, schistosomiasis with periportal fibrosis, liver transplant rejection, and cystic fibrosis with cirrhosis). Liver size was subjectively equivalent with both CT and MRI. In the patient with fatty metamorphosis, fatty infiltration of the liver was apparent on CT but was not detected on MRI. The parenchyma of all other diffusely diseased livers appeared normal on MRI and CT.

Other Observations

With MRI, the intrahepatic inferior vena cava was visibly patent in every instance. With CT, it was identifiable in only 60% of children, and in less than half of those below the age of 6. Furthermore, even when it was visible on CT, its patency was occasionally equivocal. In two cases the inferior vena cava appeared occluded on contrast-enhanced CT but was later proved patent (Fig. 6).

Discussion

CT of the pediatric liver has not achieved complete acceptance because of shortcomings such as radiation exposure, cost, motion, and the necessity for sedation [12]. Enhancement with IV contrast media is important, but it may be difficult both to establish a suitable route of injection in small children and to inject and scan in the appropriate time interval. Even with optimal CT technique, the absence of well-visualized fat planes and the presence of technical artifacts, such as streaking from air/contrast interfaces and beam hardening from adjacent ribs, may render examinations difficult to interpret. Furthermore, because CT is limited to the transverse plane, it may be impossible to differentiate between invasion and simple indentation of the liver by an extrahepatic mass or to differentiate between an extrahepatic and intrahepatic tumor. Finally, the diagnostic specificity of hepatic CT is limited [13].

Many investigators [2–9, 14, 15] have reported their early experience with MRI of the liver and have generally concluded that MRI has the ability to depict hepatic disease with an accuracy approaching or surpassing CT. The most obvious advantages of MRI are the superior contrast sensitivity and the depiction of major blood vessels without IV contrast medium. At the same time, many of these authors have indicated that the utility of MRI in the liver is often limited by image degradation that results from breathing and technical artifacts [5, 7, 10]. In one study with 54 MRI hepatic examinations [5], 19 (35%) were rated as poor or fair, and only 35 (65%) were rated as good. Some authors [10] have suggested that respiratory gating may be required to improve image quality. Others have advocated the use of respiratory-ordered phase-encoding techniques [16]; short TR, short TE spin-echo pulse sequences [17]; and short TI inversion recovery sequences [18] to diminish respiratory artifacts. However, we have been continually impressed by the quality of the upper-abdomen MR images in children obtained with standard, widely available MR pulse sequences without respiratory gating.

All but one of the children that could be imaged in the 30-cm head coil had studies rated excellent, probably because of: (1) the small size of the RF coil resulting in a better filling factor, higher signal-to-noise ratios, and less RF inhomogeneity; (2) more frequent sedation with younger patients; (3) smaller and more frequent respiratory excursions in smaller

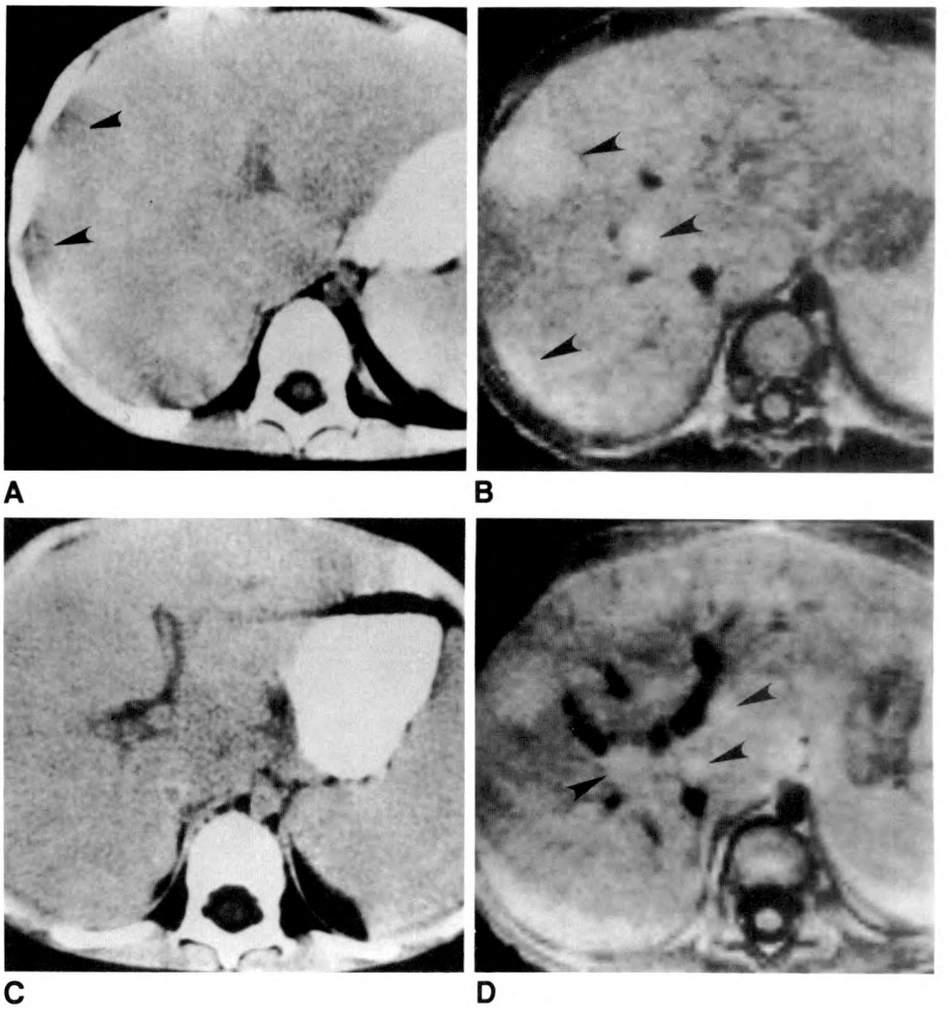


Fig. 5.—5-year-old boy with nodular sclerosing Hodgkin's disease. **A**, Contrast-enhanced CT. No masses detected prospectively. Low-density areas in periphery (*arrowheads*) were interpreted as "beam hardening" artifacts from ribs. (Compare to Fig. 1A). **B**, Transaxial MRI, SE 2000/50. Three hepatic masses (*arrowheads*), two of which correspond to supposed artifacts on CT. Masses later confirmed with sonography; one proven by laparoscopic biopsy to represent lymphomatous infiltrate. **C**, Contrast-enhanced CT. There appears to be a filling defect in inferior vena cava. **D**, Transaxial MRI, SE 2000/28. Inferior vena cava is patent. Note multiple masses (*arrowheads*) not visible on corresponding CT.

children; and (4) less body fat, resulting in less conspicuous respiratory "ghosts." These results suggest that respiratory gating should not be necessary for most pediatric liver examinations with MRI, and that appropriate body coils should be developed for children of different sizes [19].

Previous reports [20] have demonstrated the ability of MRI to depict the hepatic vasculature and surgical anatomy in adults. This capability is particularly important in children because limited, potentially curative, surgical resection of hepatic masses is guided by preoperative knowledge of their precise segmental distribution, hepatic arterial supply, and evidence of vascular invasion [21]. The results of this study suggest that MRI can depict venous anatomy in the pediatric liver better than CT, regardless of presence of disease, type of disease, or age. Even when the vascular anatomy was visible with CT, it was almost always depicted more clearly with transaxial MRI, and vessel patency could be assessed with a much higher degree of confidence.

With MRI, the common hepatic artery was visible in 74% of cases at its origin from the celiac axis. Replaced hepatic arteries and intrahepatic arteries were not detected. Unquestionably, the 3-mm gap between contiguous sections in many of our studies contributed to this result, but even with thinner contiguous sections this limitation may still be significant for MRI (as well as CT); preoperative angiography may be required to define hepatic arterial anatomy.

The normal biliary system was never apparent. The ability to visualize normal and mildly or moderately dilated biliary ducts has not yet been convincingly demonstrated with MRI and may represent another potential limitation. The left intersegmental fissure/falciform ligament was not usually visible in young children with either MRI or CT. A previous report [21] stated that the intersegmental fissure was visible in 13 of 15 consecutive unselected patients with CT (ages not stated). This apparent discrepancy with our results may arise from the different age distribution and, possibly, the relative paucity of perivisceral fat in sick children. Because the fissure may not be visible in children, identification of the left hepatic vein for locating the boundary between the medial and lateral segments of the left hepatic lobe is critical.

In general, we found hepatic masses most conspicuous on relatively T2-weighted spin-echo images, in agreement with

previous reports [2, 5, 8, 9]. However, others have suggested the inversion recovery [18], chemical shift [6], or short TR/TE spin-echo pulse sequences [17] are the most sensitive for liver lesion detection. Although we are unable to draw any definite conclusions about the sensitivity of MRI compared to CT for detection of hepatic masses, three cases had lesions seen with MRI and not on CT. In three cases, the borders of liver masses were more sharply defined with MRI than with CT, an important finding for localization and surgical resection.

Two pitfalls in interpreting MR images of liver lesions are well-established [5]. Dilated bile ducts may simulate focal masses, and calcifications may make it difficult to detect masses on T2-weighted images. None of our patients had dilated bile ducts, nor did we enounter any calcified lesions, and we suspect that this pitfall may be less critical in the pediatric patient.

The inability to detect fatty infiltration of the liver with MRI using spin-echo technique is a shortcoming of the procedure that may be avoided with the chemical-shift technique [4].

Our results indicate that detection and localization of hepatic lesions and the definition of hepatic vascular anatomy in children may be successfully accomplished with MRI more frequently than with CT. However, a prospective, double-blind study with a larger number of patients and state-of-the-art CT and MRI is required before the relative roles of each technique can be firmly established. Nevertheless, MRI has the potential to replace CT as an imaging technique in the pediatric liver in many cases, especially for infants and young children.

REFERENCES

1. Smith FW, Mallard JR. NMR imaging in liver disease. *Br Med Bull* **1984**;20(2):194–196
2. Moss AA, Goldberg HI, Stark DB, et al. Hepatic tumors: magnetic resonance and CT appearance. *Radiology* **1984**;150:141–147
3. Weinreb JC, Brateman L, Maravilla KR. Magnetic resonance imaging of hepatic lymphoma. *AJR* **1984**;143:1211–1214
4. Lee JKT, Dixon WT, Ling D, Levitt RG, Murphy WA Jr. Fatty infiltration of the liver: demonstration by proton spectroscopic imaging. *Radiology* **1984**;153:195–201
5. Heiken JP, Lee JKT, Glazer HS, Ling D. Hepatic metastases studied with MR and CT. *Radiology* **1985**;156:423–427
6. Lee JKT, Heiken JP, Dixon WT. Detection of hepatic metastases by proton spectroscopic imaging. *Radiology* **1985**;156:429–433
7. Vermess M, Leung AW-L, Bydder GM, Steiner RE, Blumgart LH, Young IR. MR imaging of the liver in primary hepatocellular carcinoma. *J Comput Assist Tomogr* **1985**;9(4):749–754
8. Glazer GM, Aisen AM, Francis IR, Gyves JW, Lande I, Adler DD. Hepatic cavernous hemangioma: magnetic resonance imaging. *Radiology* **1985**;155:417–420
9. Stark DD, Felder RC, Wittenberg J, et al. Magnetic resonance imaging of cavernous hemangioma of the liver: tissue-specific characterization. *AJR* **1985**;145:213–222
10. Ehman RL, McNamara MT, Pollack M, Hricak H, Higgins CB. Magnetic resonance imaging and respiratory gating: techniques and advantages. *AJR* **1984**;143:1175–1182
11. Weinreb JC, Maravilla KR, Peshock R, Payne J. Magnetic resonance imaging: improving patient tolerance and safety. *AJR* **1984**;143:1285–1287
12. Fletcher BD. CT in pediatric patients. *Computed tomography of the whole body*. St. Louis, MO: Mosby, **1983**:953–964
13. Burgener FA, Hamlin DJ. Contrast enhancement of focal hepatic lesions in CT: effect of size and histology. *AJR* **1983**;140:297–301
14. Brasch RC, Wesbey GE, Gooding CA, Koerper MA. Magnetic resonance imaging of transfusional hemosiderosis complicating thalassemia major. *Radiology* **1984**;150:767–771
15. Stark DD, Moseley ME, Bacon BR, et al. Magnetic resonance imaging and spectroscopy of hepatic iron overload. *Radiology* **1985**;154:137–142
16. Bailes DR, Gilderdale DJ, Bydder GM, Collins AG, Firmin DN. Respiratory ordered phase encoding (ROPE): a method of reducing respiratory motion artifacts in MR imaging. *J Comput Assist Tomogr* **1985**;9(4):835–838
17. Stark DD, Wittenberg J, Edelman RR, et al. Detection of hepatic metastases: analysis of pulse sequence performance in MR imaging. *Radiology* **1986**;159:365–370
18. Bydder GM, Steiner RE, Blumgart LH, Khenia S, Young IR. MR imaging of the liver using short TI inversion recovery sequences. *J Comput Assist Tomogr* **1985**;9(6):1084–1089
19. Pennock JM, Dubowitz LMS, Payne JA, Young IR. Recent technical developments leading to improvements in image quality in magnetic resonance during infancy (abstr). Annual meeting of Society of Magnetic Resonance in Medicine, London, August **1985**:733–734
20. Fisher MR, Wall SD, Hricak H, McCarthy S, Kerlan RK. Hepatic vascular anatomy on magnetic resonance imaging. *AJR* **1985**;144:739–745
21. Korobkin M, Kirks DR, Sullivan DC, Mills SR, Bowie JD. Computed tomography of primary liver tumors in children. *Radiology* **1981**;139:431–435

Interventional Genitourinary Radiology in Children: A Review of 61 Procedures

William S. Ball, Jr.[1,2]
Richard Towbin[3]
Janet L. Strife[3]
Roberto Spencer[1]

Forty-nine children underwent 61 interventional uroradiologic procedures. These included percutaneous nephrostomy, internal ureteral stenting, ureteral stricture dilatation, perirenal abscess drainage, and percutaneous removal of renal calculi. Of the 61 procedures, 60 (98%) were technically successful. Of the 60 successful procedures, 24 (40%) were considered "definitive," 33 (55%) favorably "altered the course," and 3 (5%) "failed" to have any beneficial effect. Technical success at minimal risk can be achieved in even the smallest patients by modifying equipment and by attending to the special needs of the pediatric patient.

The applications, efficacy, and technical modifications of interventional procedures of the genitourinary tract in adults have been well described [1–6]. Despite recent publications on the use of similar procedures in children [7–12], these techniques have not been used as widely in children. Radiologists may not be aware of how they can safely and effectively intervene in the management of disease processes that affect the genitourinary system in children. An additional problem is the vast array of equipment designed for adults that is cumbersome, occasionally damaging, and, at times, ineffective in the younger and smaller patient. This paper describes the necessary indications and technical modifications that permit successful and safe performance of interventional genitourinary radiology in children.

Materials and Methods

From January 1980 until February 1985, 49 patients underwent 61 interventional procedures of the genitourinary tract either at Children's Hospital Medical Center at the University of Cincinnati College of Medicine or at the University of New Mexico Medical Center. Included in this group were 34 percutaneous nephrostomies in 28 patients, placement of seven internal ureteral stents in five patients, dilatation of eight ureteral strictures in six patients, six perirenal drainages in five patients, four percutaneous removals of renal stones in three patients, and placement of two circle tubes in two patients. Ages of the patients ranged from 1 day to 22 years, with a mean age of 10 years (Table 1). All procedures were performed in fluoroscopic/radiographic rooms; a 1000-mA generator was used to allow for fast exposure times. The focal spot ranged from 0.3 to 1.0 for greater resolution. Radiant warmers or increased room temperatures were used to prevent heat loss in newborns. Informed consent was obtained from the parents before each procedure. A registered pediatric nurse familiar with pediatric drug dosages was present to monitor each patient. In most cases, the procedures were performed after consultation with the pediatric surgical service.

The results of the procedures were divided into three groups: (I) definitive, (II) altered the course of therapy, or (III) failed to modify therapy. A procedure was considered definitive if, as a result of the procedure, the patient's problem was resolved and no further intervention or surgery was required. A procedure altered the course of therapy if the patient benefited from it but required further intervention or surgery and failed if there was no measurable benefit to the patient. Complications were considered major if there was loss of a kidney, significant morbidity requiring additional hospitalization, or mortality from the procedure.

Received February 10, 1986; accepted after revision May 9, 1986.

Presented at the annual meeting of the Society of Pediatric Radiology, Boston, April 1985.

[1] Department of Radiology, University of New Mexico Medical Center, Albuquerque, NM 87131.

[2] Present address: Department of Radiology and Pediatrics, Children's Hospital Medical Center, University of Cincinnati College of Medicine, Cincinnati, OH 45229. Address reprint requests to W. S. Ball, Jr.

[3] Department of Radiology and Pediatrics, Children's Hospital Medical Center, University of Cincinnati College of Medicine, Cincinnati, OH 45229.

AJR **147:791–796, October 1986**
0361–803X/86:1474–0791
© American Roentgen Ray Society

Local anesthesia consisted of infiltration with 1% mepivacaine hydrochloride (Carbocaine). Chloral hydrate at a dose of 50–75 mg/kg was used to orally sedate children less than 1 year old. Sodium pentobarbital (Nembutal) at 2–6 mg/kg and fentanyl at 1–4 μg/kg were used separately or in combination for IV sedation in children more than 1 year old. Temperature, heart rate, and respiration were monitored for all patients.

To assure technical success, modifications were required for initial percutaneous access, catheter selection, dilatation of the tract, and securing of the catheter.

Access for Percutaneous Nephrostomy

Percutaneous nephrostomy has been greatly facilitated by the use of introducer sets (Cook Co., Bloomington, IN) that require only a single puncture [3]. These sets consist of a thin walled 22-gauge needle that is used to gain access to the kidney and through which a 0.018-in. (0.046-cm) stainless steel guidewire is passed into the pelvis. Over the stainless steel wire, a tapered dilator with a proximal side hole is placed into the renal pelvis. A 0.038-in. (0.097-cm) guidewire is then passed through the dilator, out the side hole, and into the pelvis. A nephrostomy catheter or progressive dilator or both can then be passed over the guidewire.

This system can be used in older children with minimal problems [13, 14], but it has additional shortcomings in the younger child or infant. The side-hole dilator frequently will not enter far enough into a small renal pelvis so that the proximal side hole still lies within the pelvis. If the side-hold dilator is coiled in a small renal pelvis, the angle created at the side hole will not allow passage of the larger guidewire. The larger guidewire may injure the parenchyma or perforate the infant pelvis and will not accommodate the smaller drainage catheter. We have found that a smaller drainage catheter such as a 5-French pigtail catheter can be advanced into the renal pelvis directly over the stainless steel guidewire. This may be facilitated by strengthening the catheter with the metal obturator provided with the introducer set, as long as the obturator is advanced under fluoroscopic control through the renal parenchyma only to just inside the collecting system. By using the metal obturator, we avoided both kinking of the catheter in the subcutaneous tissues and the necessity of using a larger 0.038-in. guidewire for delivery of the catheter. A 7.5-cm, 22-gauge Chiba needle (Cook) may replace the longer, thin-walled needle in the introducer set for better control. If a larger guide is necessary, in place of the side-hole dilator we use a standard 5-French fascial dilator (Cook) mounted on the metal obturator to enter the collecting system. Once the end hole is within the collecting system, a standard 0.035-in. (0.089-cm) guidewire may be passed through the straight dilator into the pelvis.

Catheter Selection

Proper catheter selection is crucial for successful percutaneous drainage, especially in the young infant. Newer flexible drainage catheters from 6.0- to 10.0-French (Medi-tech, Watertown, MA), which offer both patient mobility and comfort, are too large for the neonate or small infant but do work well in the older infant or child who weighs more than 10 kg. For the smaller neonate and infant, we have successfully used a modified 5-French polyethylene catheter mounted on a 15-cm metal obturator (Towbin Cath, Cook) (Figs. 1A and 1B). The catheter and obturator can be passed over either the stainless steel wire or a standard 0.018-in. guidewire.

Nephrostomy Tract Dilatation

Percutaneous nephrolithotomy, placement of internal stents, and ureteral stricture dilatation all require establishing wide tracts, even in small children. We have used the Amplatz dilator set (Cook) with success but have found that the standard set is limited since the smallest sheath provided is 24-French. Sheaths for the Amplatz set may be ordered in 12-, 14-, 16-, and 18-French, which allow adequate and safe access into the kidney for instrumentation even in the small child (Fig. 2). Shortening of these sheaths may be required to accommodate the shorter pediatric nephroscope and to permit easier maneuverability. Except in patients with a sensory deficit, all large-tract dilatations were performed under general anesthesia to maximize patient cooperation. Tracts up to 10-French diameter were made by using standard fascial dilators.

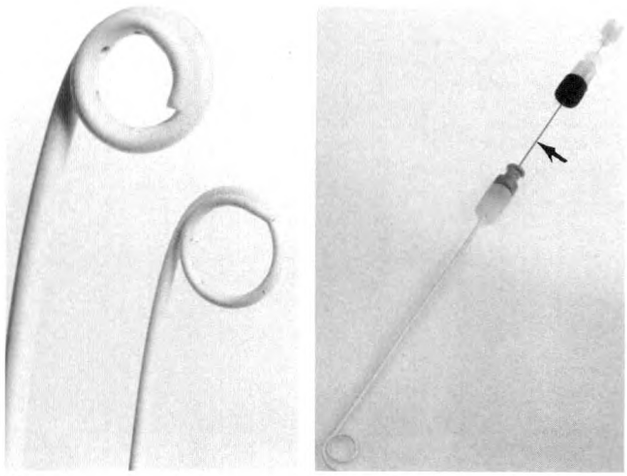


Fig. 1.—**A**, Modified 5-French polyethylene nephrostomy tube compared to standard 8-French nephrostomy drain. **B**, The 5-French nephrostomy catheter is strengthened by a thin-walled metal obturator (*arrow*), which locks to the hub of the catheter to prevent separation during advancement.

Securing the Catheter

Numerous methods have been devised for securing the catheter to the patient. Internal methods such as pigtail or "loop" catheters are of limited help in the active child. External fixation by using mylar discs or suturing the catheter will not adequately secure smaller size catheters. We have found that constructing a tape bridge (Fig. 3), frequently used to secure umbilical artery catheters, is a good first step in securing the system. Benzoin is used on both the skin and the catheter to enhance adhesiveness and to protect the skin. With the catheter supported by gauze to prevent kinking, the site is covered by a breathable dressing (Tegoderm, 3M, Roseville, MN) to keep the area dry and intact. Finally, if all else fails in long-term drainage of the active child, the single nephrostomy tube can be percutaneously converted to a silastic "circle tube" (Heyer Shulte, Goleta, CA) which cannot be dislodged by pulling [15].

Results

Forty-nine patients underwent a total of 61 interventional procedures during the review period (Table 1). Eight patients were less than 1 month old; their interventions were percutaneous nephrostomies only. Three patients were 1 to 12 months old, fourteen were 1 to 10 years old, and 24 were 10 to 22 years old (mean age 14 years).

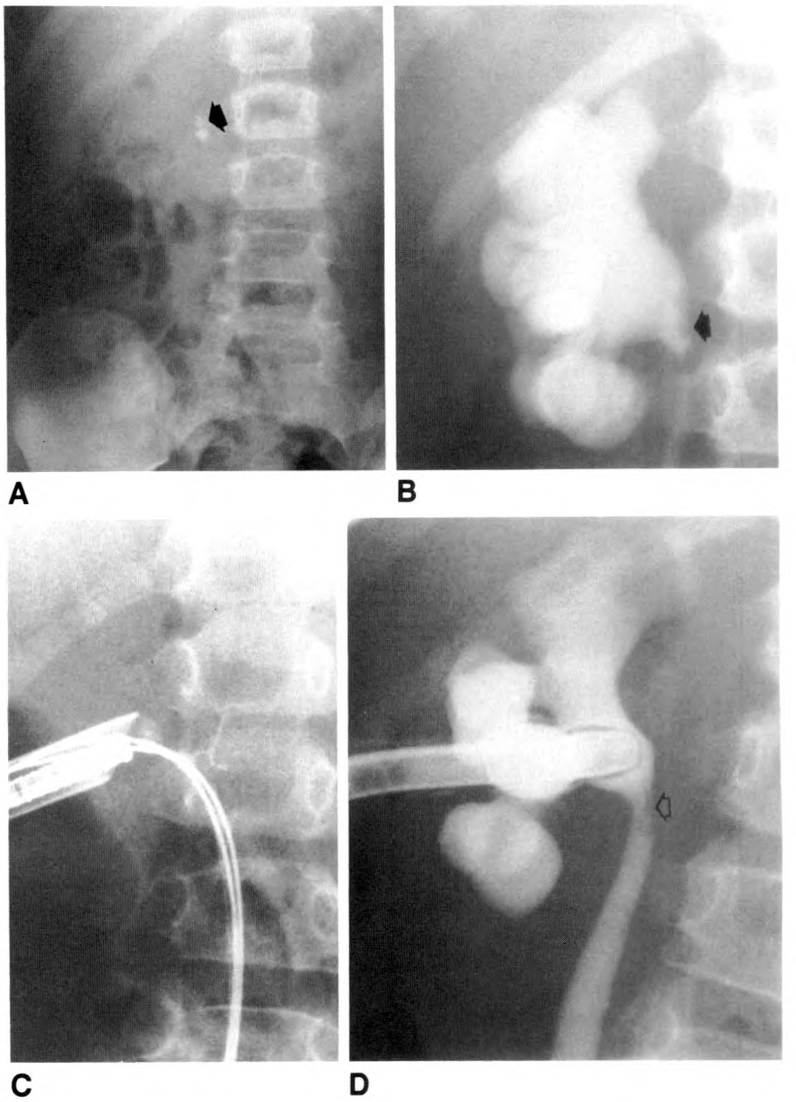


Fig. 2.—Percutaneous retrieval of renal calculus in a 7-year-old. **A**, Radiodense calculus on right (*arrow*). **B**, Excretory urography confirms calculus (*arrow*) obstructing ureteropelvic junction. **C**, Flexible nephroscope passed readily through 18-French Amplatz sheath. **D**, Minimal edema of ureteropelvic junction (*open arrow*) after procedure.

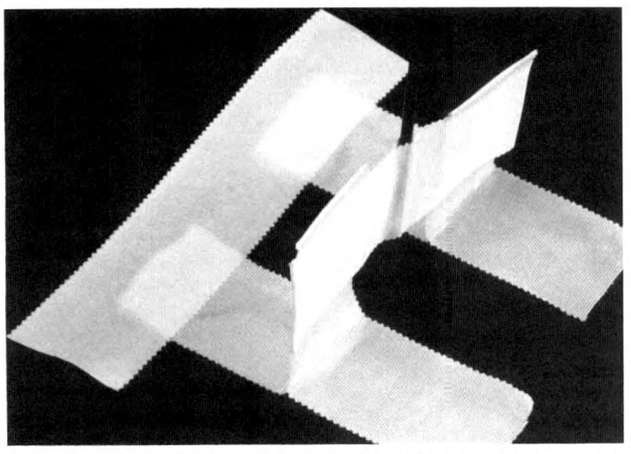


Fig. 3.—Simple bridge constructed from adhesive tape. Benzoin applied directly to the catheter enhances adhesiveness with the tape.

Of the 61 procedures, 60 (98%) were technically successful. In only one patient (2%) was there a technical failure. This occurred early in the study and was caused by the inability to pass an internal ureteral stent through a ureterovesical junction obstruction in an 18-year-old boy with recurrent stricture following reimplantation. Of the 60 procedures considered technically successful, 24 (40%) were considered definitive and required no further surgery or intervention. In an additional 33 (55%), the intervention altered the course and therefore favorably benefited the patient. In only 3 (5%), did the patient fail to benefit as a result of the intervention. All three failed cases were ureteral strictures that did not remain patent for more than a week after an initially successful balloon dilatation. Complications occurred in five patients in the percutaneous nephrostomy group. One patient developed Gram-negative sepsis 6 hours after tube placement. In two patients, intrarenal hemorrhage was brisk enough to fill the pelvis with clot. Only one patient required transfusion, and in both pa-

TABLE 1: **Summary of 61 Interventional Procedures in 49 Patients**

Age	Type of Procedure[a]	No. of Patients	No. of Procedures (Successful)	Results[b] I	II	III	Indications (No. of Patients)
<1 month	PN	8	11 (11)	4	7		Obstruction (6) Pyonephrosis (2)
1–12 months	PN	2	3 (3)	1	2		Pyonephrosis (1) Postoperative complication (1)
	UD	1	1 (1)	1			Postoperative stricture (1)
13 months to 10 years	PN	7	7 (7)	2	5		Trauma (1) Obstruction (4) Stones/obstruction (2)
	PSR	2	2 (2)	2			
	UD	1	1 (1)	1			Postoperative stricture (1)
	US	1	1 (1)	1			Functional obstruction in transplanted ureter (1)
	PD	2	2 (2)	1	1		Urinoma (2)
	CT	1	1 (1)		1		Postoperative atresia, ureteropelvic junction (1)
>10 years	PN	11	13 (13)	3	10		Obstruction (9) Pyonephrosis (1) Stones (1)
	PSR	1	2 (2)	1	1		
	UD	4	6 (6)	2	1	3	Postoperative stricture (4)
	US	4	6 (5)	2	3		Obstruction tumor (1) Multiple strictures (3)
	PD	3	4 (4)	3	1		Abscess (2) Urinoma (1)
	CT	1	1 (1)		1		Ureteropelvic obstruction in poor surgical risk (1)
Totals		49	61 (60)	24	33	3	

[a] PN = percutaneous nephrostomy, UD = ureteral dilatation, PSR = percutaneous stone removal, US = ureteral stent, PD = perirenal drainage, CT = circle tube.
[b] I = definitive—no further intervention required, II = altered the course—beneficial but further intervention or surgery required, III = failed—no measurable benefit.

tients the pelvic clot completely resolved in 48 hr. Urinomas developed in two patients after percutaneous puncture. One was less than 1 month old, and the second had thin renal parenchyma because of chronic reflux in a transplanted kidney. One urinoma, which became infected, required drainage.

Local anesthesia alone was required in seven patients (14%), a combination of local anesthesia and sedation in 24 (49%), and general anesthesia in 15 (31%). No anesthesia was required in an additional three patients (6%) in whom sensory deficits allowed performance of the procedure without patient discomfort. There were no complications as a result of anesthesia or sedation.

Discussion

Babcock et al. [7] described the successful use of a percutaneous nephrostomy in a pediatric patient in 1979. Winfield et al. [8] later described the successful use of percutaneous nephrostomy in 10 patients, including four neonates. Other reports have also described the use of this procedure in children [9, 10, 12]. Despite these important contributions, not much emphasis has been placed on the safety, effectiveness, and technical modifications necessary to perform these procedures in even the smallest of neonates. Little attention has been focused on the broad variety of procedures, frequently performed in adults, that can be successfully and beneficially performed in children.

Congenital stenotic obstructions of the genitourinary system in children are presently amenable only to surgical repair. Percutaneous nephrostomy may be beneficial in temporizing before definitive surgical repair by allowing drainage of the infected system, in assessment of the degree of return of function to the nonfunctioning kidney, and in stabilization of the patient in acute renal failure. There is likely little or no place for presurgical drainage for obstructions that are uncomplicated or asymptomatic. Percutaneous nephrostomy may be all that is necessary to treat certain types of obstruction such as "fungus balls" in the newborn (Fig. 4), obstruction from postoperative ureteral edema, or temporary obstructions of the upper collecting system and ureter due to extrinsic ureteral compression. Obstruction due to renal calculi may also be resolved successfully through a percutaneous approach. Through the use of smaller diameter sheaths, calculi may be retrieved easily without having to establish a larger (≥24-French) tract (Fig. 2).

We and others have been successful in performing ureteral dilatation in the patient with a postoperative stricture [16]. In four (67%) of six patients percutaneous dilatation was the only procedure needed. This preliminary experience suggests that percutaneous dilatation of the postsurgical stricture should be attempted before subjecting the patient to further surgery.

Most equipment now available for genitourinary intervention was designed primarily for use in the adult. These same

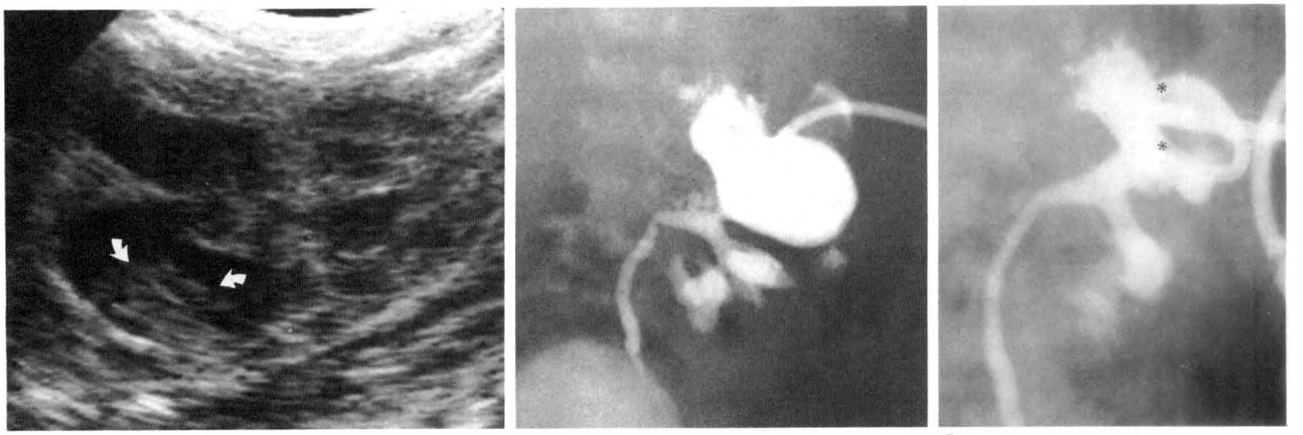


Fig. 4.—"Fungus ball" obstruction in a neonate with known *Candida* sepsis. **A**, Sonogram shows hydronephrotic upper-pole moiety left kidney and fungus ball in dilated upper-pole calyx (*arrows*). **B**, Percutaneous drainage of upper-pole collecting system shows high-grade partial obstruction due to the fungus ball. **C**, Nephrostogram performed within 2 weeks shows resolution of obstruction after therapeutic infusion of amphotericin through indwelling 5-French nephrostomy catheter (*asterisks*).

systems can be used, as designed, in the older child at or approaching adult proportions. Unfortunately, this same equipment not only may be ineffective but also may be dangerous if used in the small infant or neonate. These systems are quite adaptable via substitutions of equipment that may be available in most radiology departments or that can be ordered from the manufacturers without modifications. Performing interventional procedures in children without a thorough familiarity of what modifications are necessary and without adequate availability of the appropriate equipment may result in technical failure. We had no technically unsuccessful procedures in patients less than 10 years old when we used this approach. The only unsuccessful procedure was in an older child in whom we were unable to pass a stent beyond the ureterovesical junction into the bladder even though a guidewire had crossed the stricture. We have subsequently encountered this same problem but have succeeded by retrieving the wire through a cystoscope and fixing it at both ends. Graded dilators or a balloon catheter can then be used to dilate the stricture to facilitate passage of a more flexible stent.

Continuous monitoring of heart rate, respirations, and body temperature is important, especially in the infant or newborn. In addition to radiant warmers, control of room temperature is critical. Draping of the sterile field often is not enough to keep the infant warm, especially if the drapes are wet. We have found that using a sterile plastic underdrape not only keeps the infant dry but also prevents significant heat loss.

As in the adult, general anesthesia is not required except in those procedures that are prolonged or that result in significant patient discomfort. In only one patient less than 12 months old was general anesthesia required for placement of a nephrostomy tube. General anesthesia was not necessary for nephrostomy tube placement in children more than 10 years old. Using the described regimen, we encountered no technical failures as a result of inadequate sedation. Eleven patients had general anesthesia for procedures such as stone removal, internal stenting, and stricture dilatation. Adequate sedation is most difficult for this group because the young child cannot be expected to provide maximal cooperation, especially if the procedure is prolonged or produces significant discomfort.

Regardless of the safety and capability of performing any interventional procedure, a critical look at the effectiveness of such procedures is necessary. In only 24 (40%) of the 60 procedures, could we consider the intervention definitive. In 33 (55%) of the 60 procedures, the procedure, although not definitive, did alter the course and have some beneficial effect. Most often, this beneficial effect was an improvement in renal function or a control of infection in an obstructed system. In only three (5%) of 60 procedures, did we fail to see any beneficial effect. At surgery, periureteral scar tissue was found at the site of two of the three failed strictures, in addition to inflammation and edema of the ureter itself. These failures were likely a result either of dilating ureteral strictures in the face of a coexistent chronic infection or of attempting to dilate a narrowing of the ureter caused by extrinsic compression.

As a result of our experience, we believe that interventional uroradiologic procedures are both safe and effective in children. Technical success at minimal risk can be achieved by modifying equipment and by attending to the special needs of the pediatric patient.

ACKNOWLEDGMENT

The authors wish to thank Juanita Hunter for manuscript preparation and administrative support.

REFERENCES

1. McLean GK, Gorden RD, Ring EJ. Interventional uroradiology. In: Ring EJ, McLean GK, eds. *Interventional radiology: principles and techniques*. Boston: Little, Brown, **1984**:379–410

2. Castaneda-Zuniga WR, Clayman RV. Interventional uroradiology. *Semin Interventional Radiol* **1984**;1(1):1–123
3. Cope C. Single stick percutaneous nephrostomy. *Semin Interventional Radiol* **1984**;1:1–4
4. Leroy AJ, May GR, Bender CE, et al. Percutaneous nephrostomy for stone removal. *Radiology* **1984**;151:607–612
5. Barbaric ZL. Percutaneous nephrostomy for urinary tract obstruction. *AJR* **1984**;143:803–809
6. Lang EK, Lanasa JA, Garrett J, et al. The management of urinary fistulas and strictures with percutaneous ureteral stent catheters. *J Urol* **1979**;122:736–740
7. Babcock JR, Shkolnic A, Cook WA. Ultrasound guided percutaneous nephrostomy in the pediatric patient. *J Urol* **1979**;121:327–329
8. Winfield AC, Kirchner SG, Brun ME, et al. Percutaneous nephrostomy in neonates, infants and children. *Radiology* **1984**; 151:617–619
9. Alyaderani MK, Kalinowski D, Gabrielle OF. Percutaneous nephrostomy by pigtail catheter in children. *South Med J* **1981**;74:421–423
10. Diament MJ, Boechat MI, Kangarlso H. Interventional radiology in infants and children: clinical and techical aspects. *Radiology* **1985**;154:359–361
11. Woodside J, Stevens GF, Stask GL, Borden TA, Ball WS. Percutaneous stone removal in pediatric patients. *J Urol* **1985**;134:1166–1167
12. Stanley P, Bear JW, Reid BS. Percutaneous nephrostomy in infants and children. *AJR* **1983**;141:473–477
13. Chuang VP, Alspaugh JP, Harris SA, et al. A modified application of the Cope introduction set. *AJR* **1985**;145:1073–1074
14. Greenwood LH, Yrizarry JM, Brown SB. Observations on the use of the Cope introduction set. *AJR* **1985**;144:257–258
15. Raddy P, Smith AD. Circle tube nephrostomy and nephroureterostomy. *Urol Clin North Am* **1982**;9(1):69–73
16. Banner MP, Pollack HM, Ring EJ, et al. Catheter dilatation of benign ureteral strictures. *Radiology* **1983**;147:427–433

Fetal Omphalocele and Gastroschisis: Pitfalls in Sonographic Diagnosis

Karen K. Lindfors[1]
John P. McGahan[1]
John P. Walter[1]

The prenatal sonographic findings in 10 infants with omphalocele or gastroschisis diagnosed either by sonogram or by physical examination at birth are reviewed. There were six true-positive diagnoses, as well as two false-positive and two false-negative diagnoses by sonography. The false-positive cases resulted from confusion of umbilical cord with extruded bowel (1 case) and oligohydramnios coupled with improper scanning technique (1 case). The false-negative cases resulted from poor documentation of fetal anatomy (1 case) and confusion of extruded bowel with umbilical cord (1 case). These pitfalls may be avoided by using optimal scanning technique with documentation of fetal anatomy and pulsed Doppler sonography.

Developmental defects in the fetal anterior abdominal wall with resultant omphalocele or gastroschisis are rare anomalies having a frequency of approximately 1 in 2500 births [1, 2]. Omphalocele, which is a herniation of abdominal contents into the base of the umbilical cord, is the more common and carries an increased risk for concomitant abnormalities [1, 3]. Gastroschisis occurs when there is evisceration of abdominal contents through a paraumbilical defect in the abdominal wall and is less commonly associated with other abnormalities.

Prenatal diagnosis of omphalocele and gastroschisis is important for appropriate obstetric and perinatal management. Termination of the pregnancy can be considered if severe abnormalities are diagnosed early. If the pregnancy is continued, knowledge of an anterior abdominal defect can aid in planning optimal route of delivery [4]. Forewarning of the birth of an infant with one of these anomalies allows time to alert pediatricians and surgeons so that resuscitation and corrective surgery can be accomplished without delay.

Sonography offers a means for accurate diagnosis of omphalocele and gastroschisis in the fetus. However, the recognition of these abnormalities can be difficult. We reviewed a series of patients with omphalocele or gastroschisis diagnosed at birth or by prenatal sonography and found several pitfalls in these sonographic evaluations.

Materials and Methods

During the period from January 1, 1980, through September 30, 1985, approximately 7500 fetal sonographic examinations were performed at the University of California, Davis, Medical Center. We reviewed all examinations in which prenatal diagnosis of either gastroschisis or omphalocele was made, and we compared them with the findings on physical examination of each child at birth.

To discover any false-negative or additional outside examinations, we reviewed the medical records of all children admitted with the diagnosis of gastroschisis or omphalocele during the same period to see whether a prenatal sonogram had been performed. We compared the sonograms for these patients with the findings on physical examination as recorded in their medical records. In cases of outside prenatal sonograms, we included only those in which the actual study could be obtained for review.

Received January 23, 1986; accepted after revision April 19, 1986.

[1] All authors: Department of Radiology, University of California, Davis, School of Medicine, 4301 X St., Room 109R, Sacramento, CA 95817. Address reprint requests to K. K. Lindfors.

AJR 147:797–800, October 1986
0361–803X/86/1474–0797
© American Roentgen Ray Society

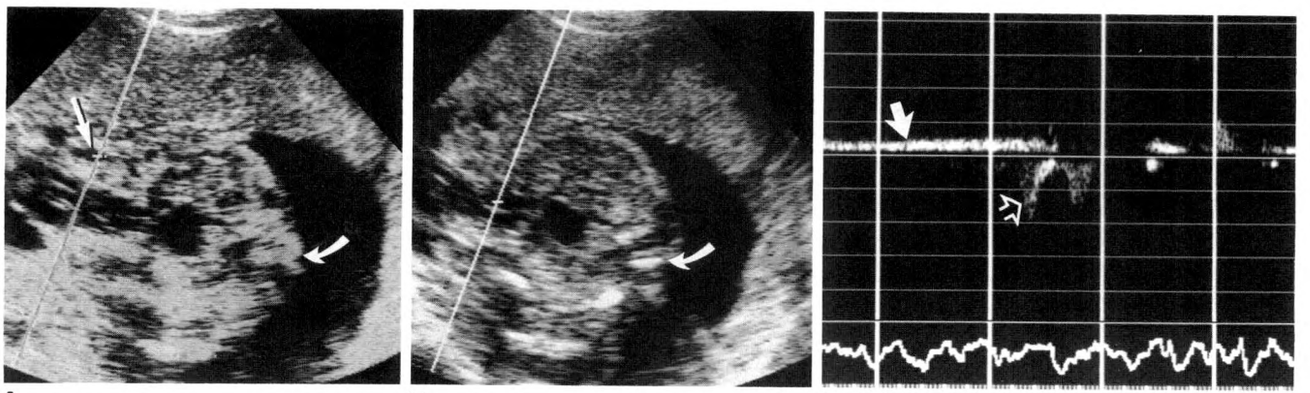


Fig. 1.—Gastroschisis. **A**, Sonogram of fetal abdomen at 25 weeks menstrual age demonstrates a complex mass containing cystic areas anterior to abdominal wall with Doppler cursor (*straight arrow*) on one cystic structure. Spectral analysis at this level showed no evidence of blood flow through area (*curved arrow* shows fetal spine). **B, C,** Transverse real-time examination (**B**) with Doppler cursor over umbilical vessels located at left of mass; spectral analysis (**C**) at this level shows both arterial (*open arrow*) and venous (*closed arrow*) flow (*curved arrow* shows fetal spine).

The sonograms were performed with a variety of both static and linear array real-time sonographic systems using 3- or 5-MHz transducer frequencies. Pulsed Doppler sonography using an ATL 600 instrument (Advanced Technology Laboratories, Bothell, WA) operating at 3 MHz was used whenever appropriate during the past 2 years.

Results

We include in this report 10 cases of infants diagnosed as having abdominal-wall defects by prenatal sonography or physical examination at birth. Three cases of gastroschisis and three cases of omphalocele were correctly diagnosed by prenatal sonography. Two cases of gastroschisis were missed by sonography; one false-positive sonographic diagnosis of omphalocele and one false-positive diagnosis of gastroschisis were made by sonography.

The menstrual ages of the fetuses at sonography ranged from 22 weeks to 35 weeks (mean = 29.2 weeks). The indications for sonography included confirmation of probable abnormalities seen on outside studies (4 cases), preterm labor (2 cases), premature rupture of membranes (2 cases), fetal age determination (1 case), and maternal abdominal pain (1 case).

In all three correctly diagnosed cases of gastroschisis, complex masses could be seen anterior to a defect in the fetal abdominal wall on the prenatal sonogram. In two of these cases there was total evisceration of abdominal contents through large defects in the abdominal wall (i.e., body-stalk anomaly) at birth. The course of the umbilical vessels was impossible to define sonographically in these two cases, but no membranous covering of the herniated viscera was seen. Associated orthopedic abnormalities were seen sonographically in one case. Both infants died shortly after birth. A Doppler instrument was used in the sonogram of the third correctly diagnosed case of gastroschisis (Fig. 1). Arterial and venous flow were demonstrable in the umbilical vessels that inserted normally into the abdomen, but no evidence of flow was demonstrable within any of the cystic or tubular structures composing the viscera that had herniated through a right abdominal-wall defect. This infant underwent primary surgical closure of the gastroschisis shortly after birth.

Sonograms for the three correctly diagnosed cases of omphalocele all demonstrated midline defects with herniation of intraabdominal contents into the base of the umbilicus. Membranous coverings of the herniated viscera were visible in all three cases. In all cases the transverse diameter of the abdominal-wall defect was smaller than the transverse diameter of the hernia sac, and the edge of the hernia sac formed an acute angle with the fetal abdominal wall (Fig. 2). Additional prenatal sonographic findings in these cases included polyhydramnios (1 case) and a probable endocardial cushion defect (1 case). All three infants underwent primary surgical closure of the omphalocele shortly after birth. Complex congenital heart disease was confirmed at birth in one case, and one infant was found to have Beckwith-Weidemann syndrome.

There were two false-negative sonograms for fetuses found at birth to have gastroschisis. In one case, the sonogram, done at another institution, was a limited study at 29 weeks for determination of fetal age and growth. Biparietal diameter, femur length, and abdominal diameter were measured, but no other documentation of fetal anatomy was made.

In the second false-negative sonogram, multiple tubular and cystic structures appeared anterior to the fetal abdominal wall (Fig. 3). Gastroschisis was considered by the sonographer, but dismissed because the structures appeared pulsatile and because no definite defect in the anterior abdominal wall could be visualized. A Doppler instrument was not available at the time of this study. It was concluded that the structures visualized anterior to the abdominal wall represented an edematous umbilical cord. At birth, the infant had a gastroschisis with protrusion of small bowel and colon through the defect.

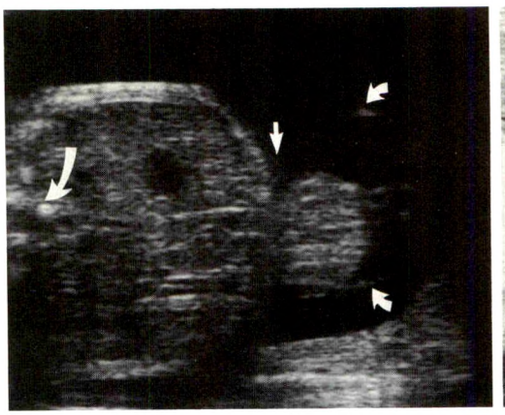


Fig. 2.—Omphalocele. Transverse sonogram of fetal abdomen at 32 weeks menstrual age demonstrating midline defect in abdominal wall with herniation of both solid and cystic structures into base of umbilicus. Membranous covering of herniated viscera was seen (*short curved arrows*). Note acute angle formed by hernia sac and fetal abdominal wall (*straight arrow*). Mild polyhydramnios was also noted (*long curved arrow* shows fetal spine).

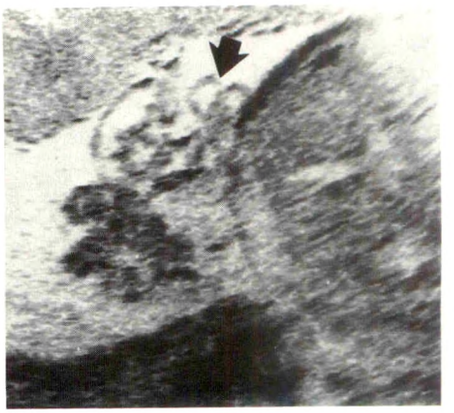


Fig. 3.—False negative diagnosis of gastroschisis. Transverse view of fetal abdomen at 35 weeks demonstrates multiple tubular structures in mass anterior to abdominal wall (*arrow*). Structures appeared pulsatile and were later interpreted as edematous umbilical cord. Doppler examination was not available. Infant had a gastroschisis at birth.

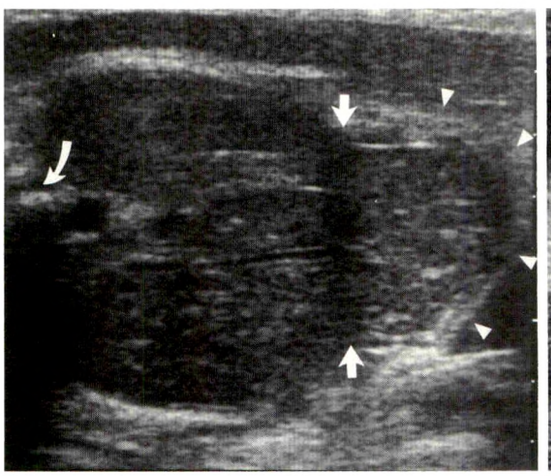


Fig. 4.—False-positive diagnosis of omphalocele. Oblique scan through fetal abdomen at 32 weeks menstrual age after premature rupture of the membranes simulates large defect in anterior wall (*arrows*) and possible omphalocele (*arrowheads*). Note smooth continuous border formed by apparent hernia sac and fetal abdominal wall. Infant was normal at birth (*curved arrow* shows fetal spine).

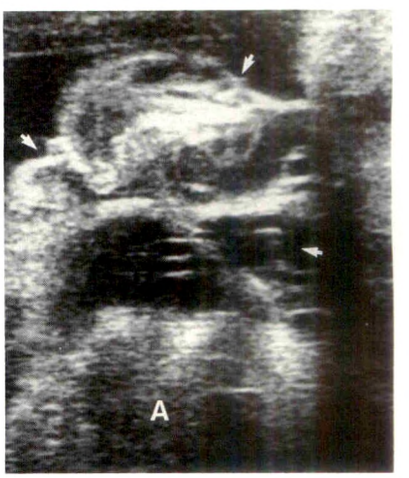


Fig. 5.—False-positive diagnosis of gastroschisis. Transverse sonogram of complex mass simulating gastroschisis anterior to fetal abdomen (A) at 35 weeks menstrual age. At cesarean section the infant was normal; tangled umbilical cord encased by blood clot (*arrows*) corresponded to sonographic abnormality.

One infant who was normal at birth had a prenatal sonogram that was falsely positive for an omphalocele. The mother had premature rupture of membranes with consequent oligohydramnios. On the sonogram, there appeared to be an anterior abdominal wall defect with protrusion of the liver into a hernia sac covered by a membrane (Fig. 4). This appearance might have resulted from compression of the fetal abdomen, secondary to oligohydramnios.

The second false-positive sonogram demonstrated multiple fluid-filled tubular- and cystic-appearing areas in a mass anterior to the fetal abdominal wall that did not appear surrounded by a membrane (Fig. 5). Despite a Doppler examination that demonstrated flow through some of the tubular structures, the mass was reported to be a gastroschisis. At cesarean section 2 days after the sonogram, a complete abruption of the placenta was found. The placenta and umbilical cord were matted together, and blood clot was wrapped around the cord. The infant's abdominal wall was intact.

Discussion

The sonographic appearances of fetal gastroschisis and omphalocele have been discussed in numerous reports in the literature [5–9], and the utility of sonograms in diagnosing such conditions is well known. In gastroschisis, the abdominal-wall defect usually lies to the right, with herniation of abdominal contents into the amniotic cavity. No membranous covering of the herniated viscera is seen in gastroschisis.

One of the reported hallmarks in diagnosis of gastroschisis is the normal insertion of umbilical vessels into the fetal abdomen. However, identification of the position of these vessels can be difficult, particularly when the cord is absent or rudimentary as in body-stalk anomaly, which is the most severe form of gastroschisis [10]. In body-stalk anomalies, a profound error in embryologic development has resulted in failure of formation of the body stalk. The viscera lie outside the abdomen in contact with the placenta. Body-stalk anom-

alies are frequently associated with skeletal abnormalities and other severe congenital anomalies, such a structural malformations in the heart, lungs, and liver. This form of gastroschisis is uniformly fatal [10] and was present in two cases in this series.

Omphalocele, which was correctly diagnosed in three cases in this series, appears as a midline defect in the anterior abdominal wall with herniation of echogenic or cystic-appearing fetal abdominal contents into the base of the umbilicus. The hernia sac is covered by a membrane, which is usually visible sonographically unless in utero rupture has occurred [9].

If it is possible early in pregnancy, the distinction between omphalocele and gastroschisis is important because of the association of omphalocele with chromosomal abnormalities. Identification of a fetus with such an abnormality early in pregnancy suggests the need for amniocentesis. Since both omphalocele and gastroschisis can be associated with other congenital anomalies, a detailed sonographic examination of the remainder of the fetus is imperative in all cases so that optimal management decisions can be made.

Although some patients will be referred for sonography because of an elevated maternal serum alpha fetoprotein, most anterior abdominal-wall defects will be discovered serendipitously while scanning is performed for another indication [11]. In this series, none of the first scans demonstrating anterior abdominal-wall defects were done in response to an elevated maternal serum alpha fetoprotein. This emphasizes the need for complete evaluation and careful documentation of the fetal anatomy in all prenatal sonograms, no matter what the indications for scanning [12]. In one case included in this review, a gastroschisis was probably missed by sonography because a thorough survey with documentation of the fetal anatomy was not undertaken.

The technical quality of a sonographic examination is also important. The position of the fetus and oligohydramnios may make scanning difficult. One case of a false-negative examination of a fetus with omphalocele in the presence of oligohydramnios has been reported in the literature [13]. The oligohydramnios made recognition of the detail of the fetal outline difficult because the omphalocele was in direct contact with the uterine wall. In the one false-positive diagnosis of omphalocele in the presence of oligohydramnios we encountered, some compression and distortion of the abdominal wall resulted from the lack of amniotic fluid. Additionally, the angle of interrogation of the sonogram was, in retrospect, not transverse, but rather oblique through the fetal abdomen. Examination of the spine and umbilical vein or left portal vein can reveal an oblique angle [14]. The appearance of an apparently large defect in the abdominal wall and a hernia sac that forms a smooth continuous border with the abdominal wall (Fig. 4), rather than a smaller defect with the hernia sac forming a more acute angle with the abdominal wall, also suggests a false-positive examination.

In the other two errors of diagnosis in this series, there was confusion in distinguishing anterior abdominal-wall defects from umbilical cord. We report one case of a correctly diagnosed gastroschisis with Doppler examination of the extruded abdominal viscera. As seen in this case, no flow was demonstrable through the herniated bowel, and both arterial and venous flow were detectable by Doppler examination in the umbilical vessels, which were clearly separable from the herniated viscera. Doppler examination of a mass with cystic components located anterior to the fetal abdominal wall can yield valuable information about these structures and help to increase accuracy in diagnosis of anterior abdominal-wall defects.

In summary, a thorough, well-documented fetal sonographic examination, combined with Doppler examination in equivocal cases, can increase the accuracy of in utero diagnoses of omphalocele and gastroschisis. The diagnosis of such anomalies is important in assuring appropriate obstetric and perinatal management. If the pregnancy is maintained with a known diagnosis of omphalocele or gastroschisis, the obstetrician can minimize injury to the bowel at the time of delivery. Fluid loss and incidence of peritonitis can be reduced if surgical closure is performed within 6–8 hr of birth [15]. All of these measures can increase the survival of infants with omphalocele or gastroschisis.

REFERENCES

1. Mann L, Ferguson-Smith MA. Prenatal assessment of anterior abdominal wall defects and their prognosis. *Prenat Diagn* **1984**;4:427–435
2. Ravitch MM, Barton BA. The need for pediatric surgeons as determined by the volume of work and the mode of delivery of surgical care. *Surgery* **1974**;76:754–763
3. Mahour GH, Weitzman JJ, Rosenkrantz JG. Omphalocele and gastroschisis. *Ann Surg* **1983**;177:478–482
4. Davidson JM, Johnson TRB, Rigdon DT, Thompson BH. Gastroschisis and omphalocele: prenatal diagnosis and perinatal management. *Prenat Diagn* **1984**;4:355–363
5. Youngblood JP, Franklin DW, Stein RT. Omphalocele: early prenatal diagnosis. *JCU* **1983**;11:339–341
6. Nelson PA, Bowie J, Filston HC, Crane LM. Sonographic diagnosis of omphalocele in utero. *AJR* **1982**;138:1178–1180
7. Roberts C. Intrauterine diagnosis of omphalocele. *Radiology* **1978**;127:762
8. Giulian BB, Alvear DT. Prenatal ultrasound diagnosis of fetal gastroschisis. *Radiology* **1978**;129:473–475
9. Schaffer RM, Barone C, Friedman AP. The ultrasonographic spectrum of fetal omphalocele. *J Ultrasound Med* **1983**;2:219–222
10. Potter EL, Craig JM. *Pathology of the fetus and infant.* Chicago: Year Book Medical Publishers **1975**:388–392
11. Canty TG, Leopold GR, Wolf DA. Maternal ultrasonography for the antenatal diagnosis of surgically significant neonatal anomalies. *Ann SUrg* **1981**;194:353–365
12. Leopold GR. Controversies in ultrasound: should the obstetrical ultrasound examination be standardized? *Clin Diagn Ultrasound*, in press
13. Verco PW. Omphalocele, hernia of the umbilical cord and gastroschisis. *Australas Radiol* **1983**;27:274–282
14. Chinn DH, Filly RA, Callen DW. Ultrasonic evaluation of fetal umbilical and hepatic vascular anatomy. *Radiology* **1982**; 144:153–157
15. Jassani MN, Gauderer WL, Fanaroff AA, Fletcher B, Merkatz IR. A perinatal approach to the diagnosis and management of gastrointestinal malformations. *Obstet Gynecol* **1982**;59:33–39

Neonatal Renal Candidiasis:
Sonographic Diagnosis



C. Kintanar[1]
B. C. Cramer[2]
W. D. Reid[1]
W. L. Andrews[1]

With improved survival of very-low-birth-weight infants, the incidence of neonatal renal candidiasis is increasing. The clinical and sonographic features of four premature infants with renal candidiasis are presented. Both parenchymal and intrapelvic renal lesions, with or without hydronephrosis, were detected. Abdominal sonography is a useful noninvasive technique for the diagnosis and follow-up management of renal candidiasis. Early diagnosis allows prompt intervention with antifungal therapy and should increase survival.

The occurrence of fungal balls in the renal pelvis, secondary to *Candida albicans* and resulting in hydronephrosis, is well known in adults and children, particularly in those with immune suppression or with diabetes mellitus [1–3]. More recently, there have been several reports of hydronephrosis and renal bezoars secondary to systemic candidiasis [4–7] in low-birth-weight premature neonates. Several authors originally detected hydronephrosis and *Candida* fungal balls by IV urography, voiding cystogram, or retrograde ureterography [2, 6] and, more recently, by sonography [6–8] but none report the associated parenchymal lesions or the small pelvic bezoars in the absence of significant hydronephrosis.

We recently diagnosed renal candidiasis in four premature infants whose sonograms presented various appearances, from small parenchymal lesions to gross hydronephrosis and large fungal bezoars. (Table 1 summarizes clinical data for these patients.)

Subjects and Methods

Sonograms were performed with a 7.5-MHz transducer and a real-time (Advanced Technology Laboratories, Inc., Bothell, WA, Model Mark 600) machine; the images were printed on strip recorder paper except for patient 3, who was recorded on tape.

Case Reports

Patient 1

At 30 days of age, this premature infant developed anuria. Renal sonograms showed marked bilateral hydronephrosis with echodense material forming a cast of the dilated collecting system on the left (Fig. 1A) and, to a lesser extent, on the right (Fig. 1B). Bilateral nephrostomies were performed; the large fungal "casts" of the pelvicalyceal systems were removed and confirmed as *Candida albicans* concretions. The infant was treated with amphotericin B and 5-fluorocytosine for 6 weeks, but she later died from overwhelming staphylococcal septicemia. Autopsy showed bilateral moderate hydronephrosis with multiple cortical abscesses that were positive for *Candida albicans* (Fig. 1C).

Patient 2

At 33 days, the second patient developed necrotic skin lesions; scrapings revealed *Candida*. Antifungal therapy was started and continued for 6 weeks. The patient is now well. The initial

Received February 20, 1986; accepted after revision May 15, 1986.

[1] Department of Pediatrics, The Dr. Charles A. Janeway Child Health Centre, St. John's, Newfoundland A1A 1R8, Canada. Address reprint requests to W. D. Reid.

[2] Department of Radiology, The Dr. Charles A. Janeway Child Health Centre, St. John's, Newfoundland A1A 1R8, Canada.

AJR 147:801–805, October 1986
0361–803X/86/1474–0801
© American Roentgen Ray Society

TABLE 1: **Clinical Data for Four Premature Infants**

Clinical Finding	Case No.			
	1	2	3	4
Gestational age (wk)	25	26	26	24
Birth weight (g)	820	950	620	510
RDS/BPD[a]	Yes/Yes	Yes/Yes	Yes/No	Yes/Yes
Patent ductus arteriosis	Yes	Yes	No	Yes
IVH (S)[b]	Gr 11	Gr 11	Gr IV	Gr 11
Recognition of symptoms of candidiasis (age at onset, days)	30	33	10	34
Broad-spectrum antibiotics	Yes	Yes	Yes	Yes
Central venous catheters	Yes	Yes	No	Yes
Theophylline	Yes	Yes	No	Yes
Abdominal distention	Yes	Yes	Yes	Yes
Intractable hyponatremia	Yes	Yes	Yes	Yes
Candiduria	Yes	Yes	Yes	Yes
Candidemia	Yes	Yes	Yes	Yes
Carbohydrate intolerance	No	Yes	Yes	No
Outcome	Died from staphylococcal septicemia	Well	Died from staphylococcal septicemia	Died from severe necrotizing enterocolitis and septicemia

[a] RDS = respiratory distress syndrome; BPD = bronchopulmonary dysplasia.
[b] IVH = intraventricular hemorrhage; S = sonographic diagnosis.

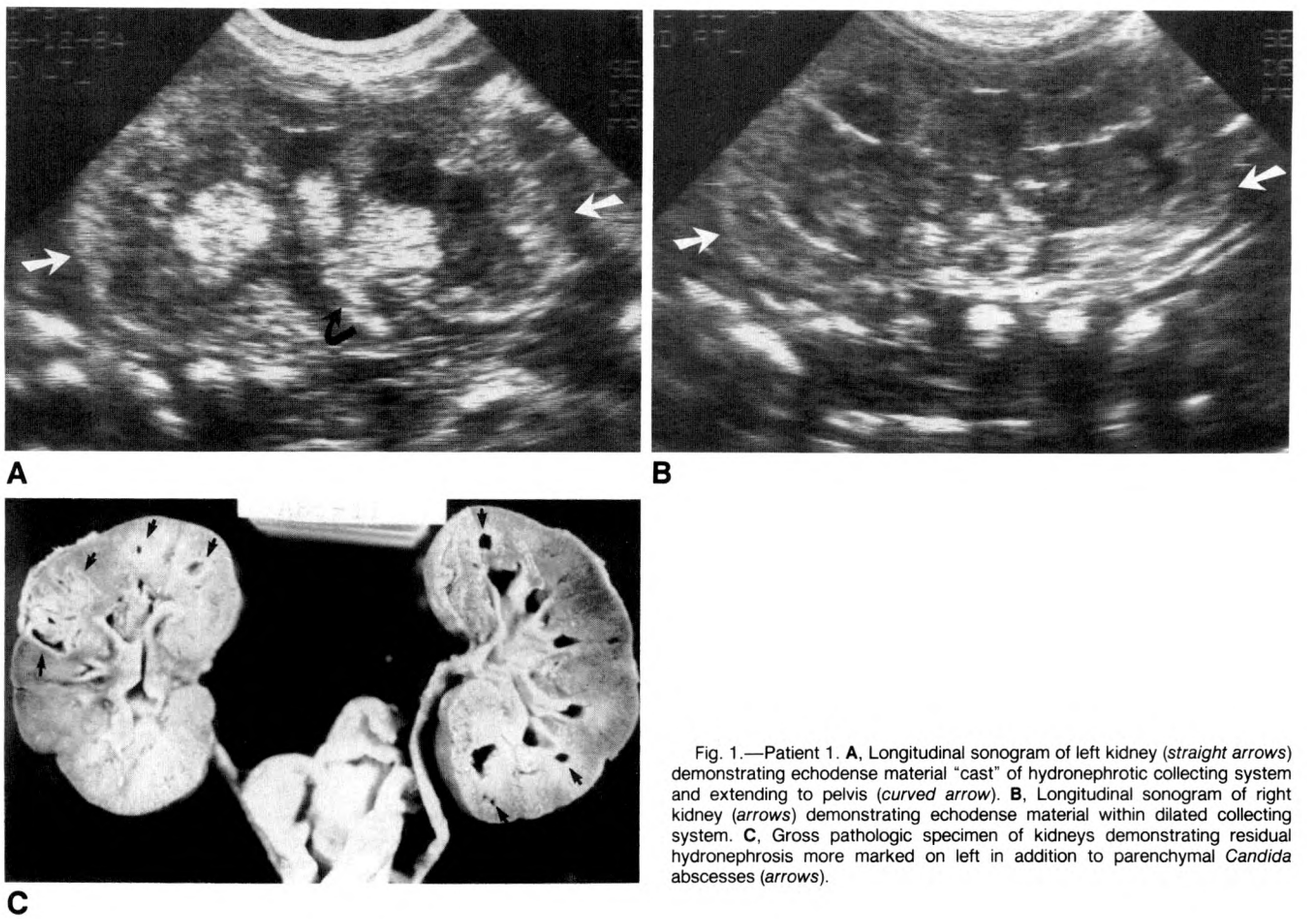


Fig. 1.—Patient 1. **A**, Longitudinal sonogram of left kidney (*straight arrows*) demonstrating echodense material "cast" of hydronephrotic collecting system and extending to pelvis (*curved arrow*). **B**, Longitudinal sonogram of right kidney (*arrows*) demonstrating echodense material within dilated collecting system. **C**, Gross pathologic specimen of kidneys demonstrating residual hydronephrosis more marked on left in addition to parenchymal *Candida* abscesses (*arrows*).

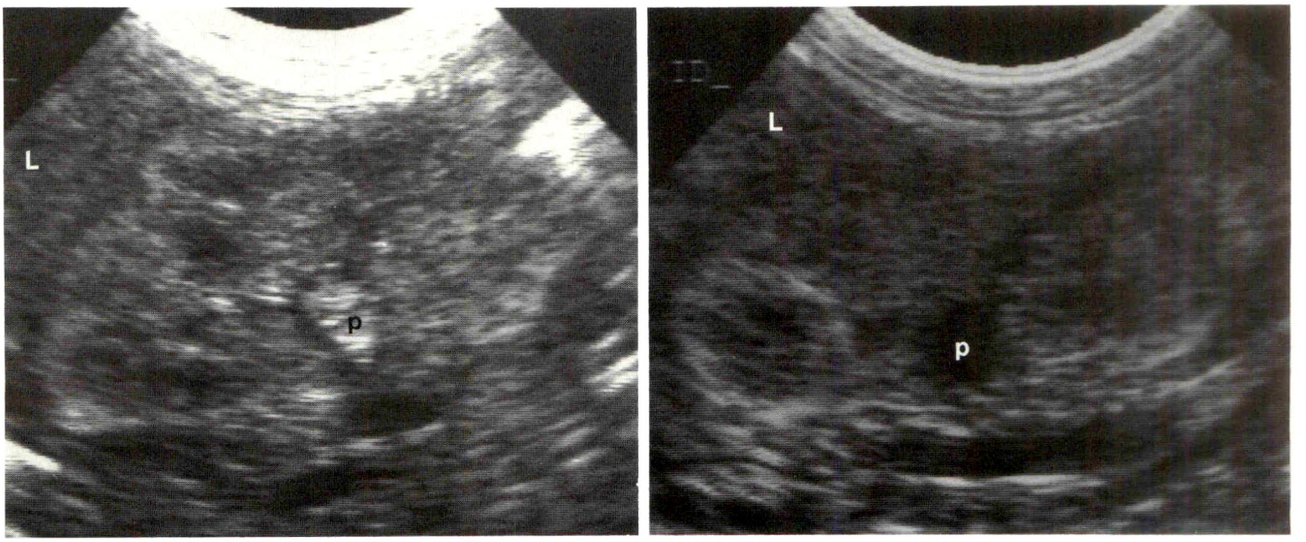
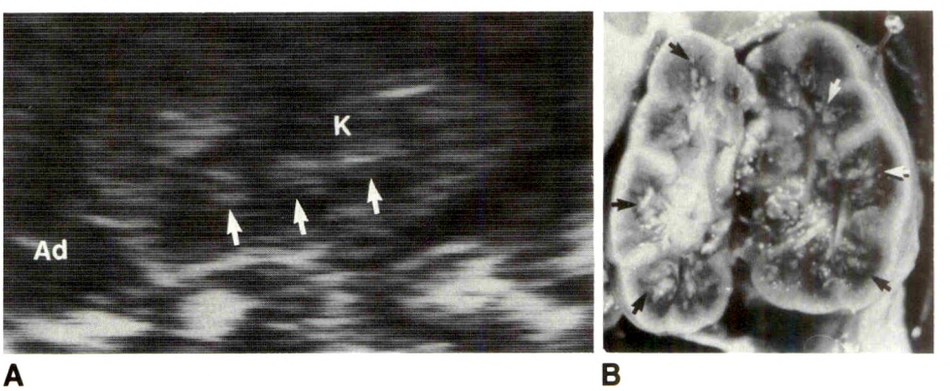


Fig. 2.—Patient 2. **A**, Longitudinal sonogram of right kidney showing a wedge-shaped density within renal pelvis (p). L = liver. **B**, Longitudinal sonogram of right kidney 1 week later showing resolution of lesion in renal pelvis (p). L = liver.

Fig. 3.—Patient 3. **A**, Longitudinal sonogram of right kidney showing focal densities in region of papillae (*arrows*). K = kidney; Ad = adrenal. **B**, Gross pathologic specimen demonstrating widespread papillary abnormalities (*arrows*) secondary to *Candida*.



sonogram showed on the right a wedge-shaped echodense plug in the pelvis, but no hydronephrosis (Fig. 2A). The plug disappeared after antifungal therapy (Fig. 2B), and a focal parenchymal echodensity in the left upper pole gradually disappeared.

Patient 3

The third patient had severely macerated skin at birth and presented with hyponatremia and carbohydrate intolerance. Sonography demonstrated focal densities near the tips of the papillae (Fig. 3A) and, although this finding is not specific for candidiasis, in the presence of candidemia it was considered secondary to the disease. After sonography, candidemia was confirmed by a blood culture. The patient died from overwhelming staphylococcal sepsis. Focal papillary necrosis resulting from *Candida* was confirmed at autopsy (Fig. 3B).

Patient 4

Echodense material was identified in the left renal pelvis and lower major calyx in this patient, without significant hydronephrosis. However, multiple parenchymal lesions were identified in both kidneys (Fig. 4). Follow-up showed marked hydronephrosis on the right and large fungal balls within the dilated collecting system (Fig. 5). This patient's renal candidiasis was detected early and was treated with antifungal agents. However, in spite of therapy, the disease progressed and surgical nephrostomy for decompression of the right hydronephrosis and removal of *Candida* concretions was required. Unfortunately, in spite of treatment this patient also died with severe necrotizing enterocolitis and septicemia. Autopsy was refused.

Discussion

The survival of low-birth-weight infants has improved considerably [9], but their decreased cellular immunity and re-

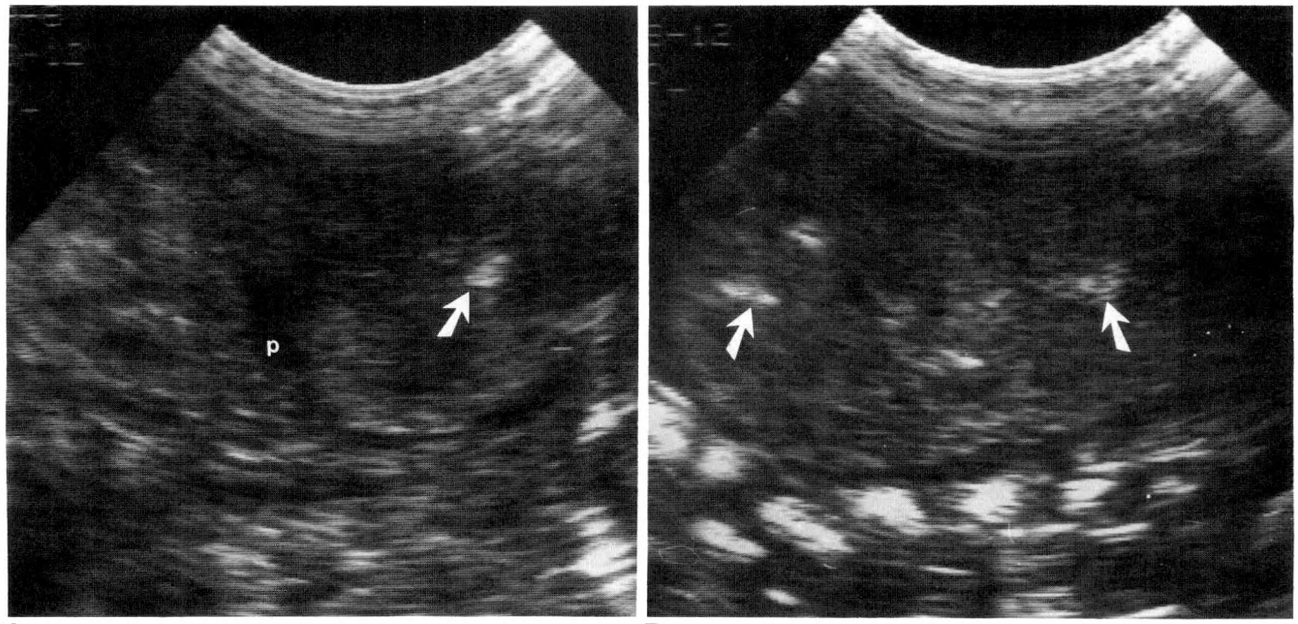


Fig. 4.—Patient 4. Initial longitudinal sonograms medially (**A**) and laterally (**B**) of right kidney. Renal pelvis is normal (p); several focal echodense lesions seen in both views (*arrows*).

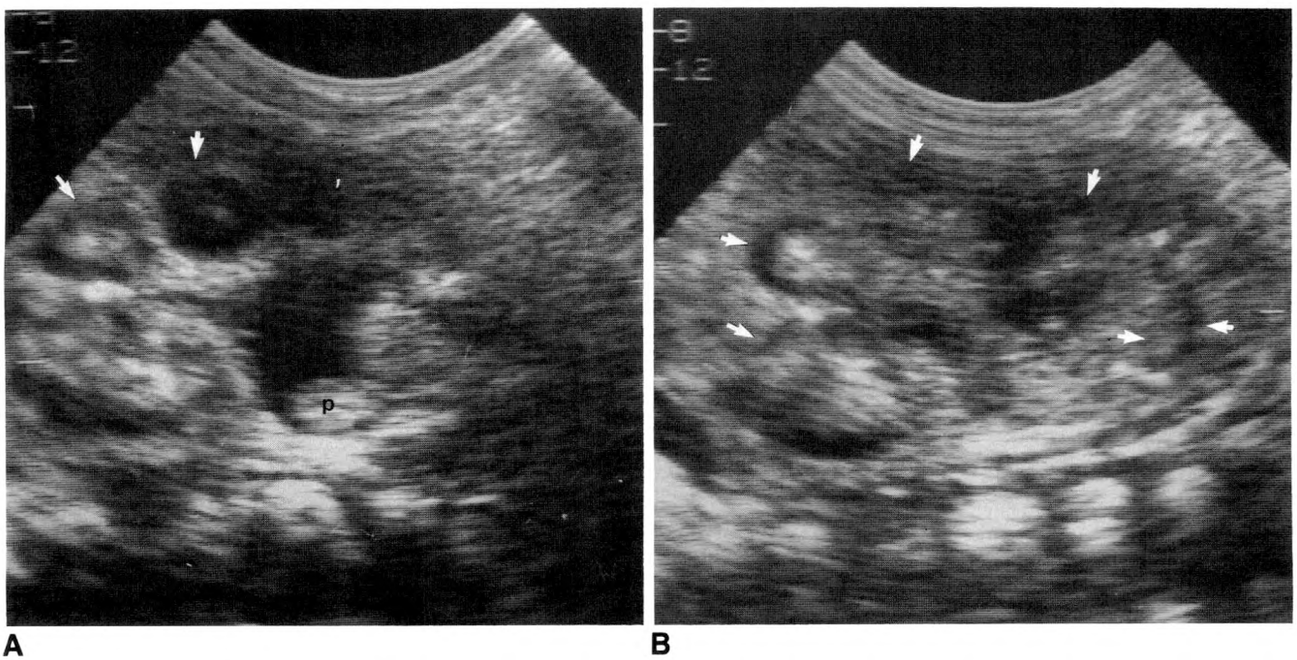


Fig. 5.—Patient 4. Similar views 1 week later show fungus ball (p) within previously normal pelvis (**A**) and echodense filling of dilated collecting system (**B**).

peated courses of broad-spectrum antibiotics predisposes them to systemic candidiasis [10]. In these premature infants, renal candidiasis can be fulminant with rapid development of hydronephrosis and destruction of renal parenchyma [3–5]. Clinical features for *Candida* sepsis are nonspecific and can be confused with bacterial septicemia, making early diagnosis difficult [10]. The clinical characteristics of these four infants were similar to those in previous reports, but in our group possible risk factors included hyponatremia and carbohydrate intolerance.

In most previously reported cases of neonatal candidiasis, the patients had already developed or presented with marked

hydronephrosis. Initial diagnosis was formerly made by standard renal radiologic examinations [4, 5], but has recently been made by sonography [6–8]. Hurley and Winner [11] showed that hydronephrosis was a relatively late development of the disease in white Swiss mice. After introduction of IV organisms, the initial lesions were cortical abscesses and pyelonephritis, followed by mycelia collections in the tubules and later renal pelvis fungal balls resulting in hydronephrosis. *Candida*-associated renal papillary necrosis has also been documented pathologically in premature infants [12].

In the presence of candidemia and the absence of hematuria or pyuria, the calyces and the nonshadowing echodense material in the renal pelvis suggest renal candidiasis even without hydronephrosis. Parenchymal lesions, whether cortical or papillary, are less specific, but, in the presence of candidemia, suggest candidiasis. If clean-catch urine specimens are positive for *Candida albicans* and lesions appear on sonograms, treatment may be started while confirmation by blood culture or suprapubic aspiration is awaited. Focal echodense areas in the medulla have been described in both acute tubular necrosis [13] and nephrocalcinosis [14, 15], thus requiring clinical correlation for correct diagnoses.

We have found renal sonography useful to identify candiduria at an early stage, thus permitting early therapy and improved chances of survival. Follow-up examinations can document the need for intervention if hydronephrosis develops.

REFERENCES

1. Clarke RE, Minagi H, Palubinskas AJ. Renal candidiasis. *Radiology* **1971**;101:567–572
2. Gerle R. Roentgenographic features of primary renal candidiasis. *AJR* **1973**;119:731–738
3. Fisher J, Mayhall G, Duma R, Shadomy S, Shadomy J, Watlington C. Fungus balls of the urinary tract. *South Med J* **1979**; 72:1281–1287
4. Patriquin H, Lebowitz R, Perreault G, Yousefzadeh D. Neonatal candidiasis: renal and pulmonary manifestations. *AJR* **1980**; 135:1205–1210
5. Heckmatt JZ, Meadow SR, Anderson CK. Anuric renal failure in an infant with systemic candidiasis. *Arch Dis Child* **1979**;54:70–72
6. Noe HN, Tonkin ILD. Renal candidiasis in the neonate. *J Urol* **1981**;127:517–519
7. Pappu LD, Purohit DM, Bradford BF, Turner WR, Levkoff AH. Primary renal candidiasis in two preterm neonates. *Am J Dis Child* **1984**;138:923–926
8. Stuck RJ, Silver TM, Joffe MH, Bowerman RA. Sonography demonstration of renal fungus balls. *Radiology* **1982**;142:473–474
9. Greenough A, Robertson NRC. Morbidity and survival in neonates ventilated for the respiratory distress syndrome. *Br Med J* **1985**;290:598–600
10. Baley JE, Kliegman RM, Fanaroff AA. Disseminated fungal infections in very low birth weight infants: clinical manifestations and epidemiology. *Pediatrics* **1984**;73:144–152
11. Hurley R, Winner HI. Experimental renal moniliasis in the mouse. *J Pathol* **1963**;86:75–82
12. Tomashefski JF, Abramowsky CR. *Candida*-associated renal papillary necrosis. *Am J Clin Pathol* **1981**;75:190–194
13. Avni EF, Brion LE. Ultrasound of the neonatal urinary tract. *Urol Radiol* **1983**;5:177–183
14. Jequier S, Cramer B, Kronick J, Reade T. Renal ultrasound in metabolic bone disease. *Pediatr Radiol* **1986**;16:135–139
15. Alon U, Brewer WH, Chan JC. Nephrocalcinosis: detection by ultrasound. *Pediatrics* **1983**;71:970–973

Case Report

Enterocyst Formation: A Late Complication of Neonatal Necrotizing Enterocolitis

Turner I. Ball[1] and J. Bradley Wyly

Necrotizing enterocolitis is a well-recognized, though not thoroughly understood, inflammatory disease of the bowel seen in newborn and primarily premature infants. The disease is characterized by the clinical findings of gastric retention, bilious vomiting, abdominal distension, bloody stools, diarrhea, and sometimes erythema of the abdominal wall. The well-known radiographic signs of this disease include a nonspecific pattern of bowel distension, pneumatosis of the bowel wall, portal venous gas, pneumoperitoneum, signs of intraperitoneal fluid [1], and the so-called "fixed loop" [2]. As medical and surgical management of these infants has improved, survival has increased dramatically [3]. With this better survival rate, the number of late sequelae of the disease has been encountered with increasing frequency. The reported late complications have included stenoses and acquired atresias in both large and small bowel, enteric fistulae, malabsorption, and the formation of enterocysts [4–9]. Strictures and atresias have been the most commonly reported sequelae [5]. We have recently encountered two infants who had previously experienced necrotizing enterocolitis with the resulting complication of large enterocyst formation presenting as a palpable abdominal mass or as abdominal distension. The case histories and clinical presentations in the two infants are almost identical so only one case history is included. A combination of barium examinations of the gastrointestinal tract and abdominal sonography clearly delineated the anatomy of the obstructed, isolated segments.

Case Report

A 26-week-gestation infant girl with a birth weight of 750 g was initially treated for severe hyaline membrane disease with endotracheal intubation for 39 days. Oral feedings with full-strength Pregestimil (Mead Johnson Nutritional, Evansville, IN) were started after extubation and were tolerated for only 2 days, after which time the patient developed abdominal distension, bloody diarrhea, lethargy, apnea, and acidosis. A radiograph of the abdomen revealed pneumatosis and ascites. After neonatal transport, evaluation demonstrated erythema of the abdominal wall, a decreased platelet count, and extensive pneumatosis on repeat abdominal radiographs. Peritoneocentesis revealed brown cloudy fluid with many neutrophils; no bacteria were identified by gram stain. The patient developed increasing abdominal girth and a "fixed loop" on follow-up radiographic examination, in addition to more extensive pneumatosis. Because of her deteriorating clinical status, surgery was performed and revealed a gangrenous distal ileum, ascending colon, and approximately one-half of the transverse colon. These segments were resected and an ileostomy was created. A mucous fistula from the midtransverse colon was also brought to the abdominal skin surface. At the time of discharge, 8 weeks postoperatively, the patient was tolerating oral feedings and gaining weight. Two months after discharge she was readmitted with a history of vomiting, lethargy, and apparent "abdominal pain" for several days. Physical examination at that time showed what appeared to be a functioning ileostomy, but the mucous fistula had retracted and could not be catheterized. The abdomen was slightly distended and a mass was palpable in the left lower quadrant.

Initially, a barium contrast study of the upper intestinal tract and small bowel was performed and was within normal limits, showing

Received April 22, 1986; accepted after revision May 29, 1986.

[1] Both authors: Department of Radiology, Egleston Hospital for Children, Emory University School of Medicine, 1405 Clifton Rd., N.E., Atlanta, GA 30322. Address reprint requests to T. I. Ball.

AJR 147:806–808, October 1986 0361–803X/86/1474–0806 © American Roentgen Ray Society

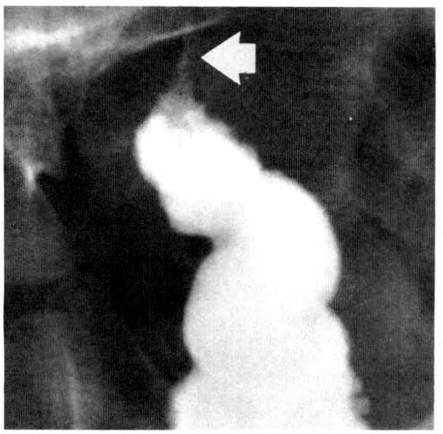


Fig. 1.—Barium enema examination demonstrates filling of rectum only and acquired atresia at rectosigmoid junction (*arrow*).

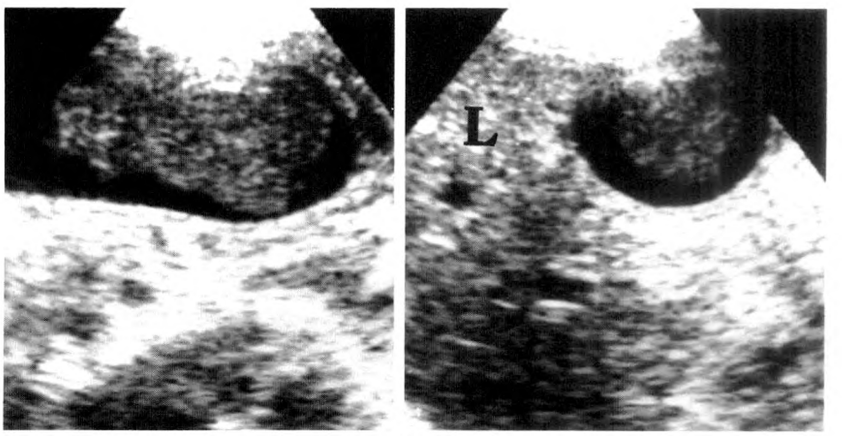


Fig. 2.—**A**, Coronal sonogram of left lateral abdomen shows well-defined enterocyst with intraluminal fluid and solid debris.

B, Longitudinal sonogram of left upper quadrant, 90° angled from view in **A**, shows enterocyst as a mass inferior to left lobe of liver (L).

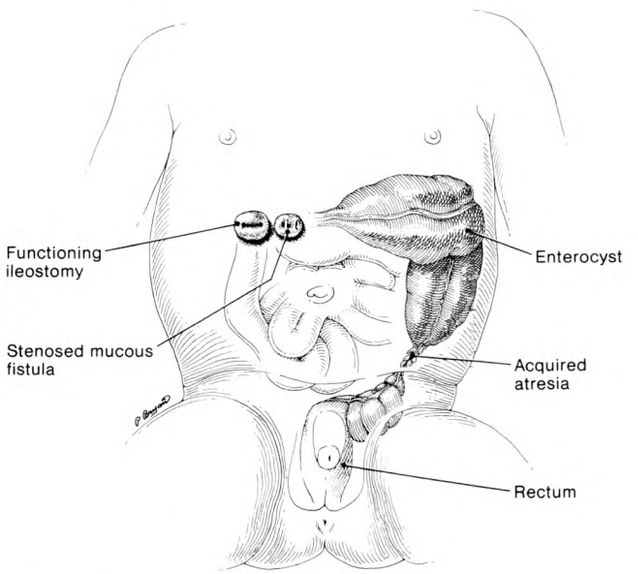


Fig. 3.—Diagram of formed enterocyst with stenosis of proximal mucous fistula and acquired atresia of distal bowel.

no evidence of obstruction or stricture formation in the small bowel. A retrograde barium examination of the colon was then performed and showed filling of the rectum only, without filling of the descending or transverse colon (Fig. 1). Sonography of the abdomen revealed a tubular structure with a well-defined wall across the left upper abdomen and in the left flank that had the course and configuration of the transverse and descending colon (Fig. 2). In view of the retracted mucous fistula and the atretic rectal segment, it was assumed that this tubular structure represented a closed colonic segment filled with secretions. The patient underwent surgery, and an enterocyst involving the distal transverse and descending colon was confirmed. The proximal end of the enterocyst was closed by the retracted and stenosed mucous fistula, and the distal portion was closed by an acquired atresia presumed secondary to ischemia from the patient's previous episode of necrotizing enterocolitis.

Discussion

As both medical and surgical treatment have improved, the survival rate in infants with necrotizing enterocolitis has increased. Virjee et al. [4] reported an overall mortality rate of 17.5% in 1979, whereas a mortality rate of 76% was reported by Touloukian et al. [1] in 1967. As the survival rate has improved, the number of late complications has increased. These late complications include stenoses, acquired atresias, fistulae, enterocyst formation, and malabsorption [4–9]. The first four of these complications can be explained by a common theory of development. Intestinal ischemia is the most important pathologic factor in necrotizing enterocolitis. The degree of damage to the bowel wall will depend on the extent of ischemia to which a segment of bowel is subjected [10]. In milder cases recovery may be complete. In the most severe circumstance full-thickness necrosis results in bowel death and perforation. Cases somewhere between these extremes have varying degrees of healing and therefore present a spectrum from minimal areas of narrowing to total loss of lumen continuity with resulting acquired atresia. Fewer areas of atresia have been reported in those patients who were medically (as oposed to surgically) treated [3]. This is presumably related to milder disease in those medically treated and to more severe disease in patients requiring surgery. In any event the development of strictures in functioning bowel inevitably causes signs and symptoms of clinically evident intestinal obstruction. In defunctionalized bowel, as in our two cases, complete atresia can occur without symptoms. If two areas of atresia occur, a closed loop of bowel results; with accumulation of secretions, enterocyst formation follows (Fig. 3). In such cases, the patient can present with a palpable

abdominal mass and without signs or symptoms of obstruction.

In any infant treated for necrotizing enterocolitis with surgical resection and diversion of the bowel, barium studies to determine patency and possible stenoses are mandatory before reanastomosis. We suggest that sonography be used in any infant with a palpable abdominal mass or in whom the defunctionalized loop cannot be completely filled with barium. If an enterocyst exists, sonography readily demonstrates the presence and the extent of the enterocyst, its mixed fluid and solid debris content, its well-defined wall, and its tubular form.

REFERENCES

1. Touloukian RJ, Berdon WE, Amoury RA, Santulli TV. Surgical experience with necrotizing enterocolitis in the infant. *J Pediatr Surg* **1967**;2(5):389–401
2. Wexler HA. The persistent loop sign in neonatal necrotizing enterocolitis: a new indication for surgical intervention? *Radiology* **1978**;126:201–204
3. Costin BS, Singleton EB. Bowel stenosis as a late complication of acute necrotizing enterocolitis. *Radiology* **1978**; 128:435–438
4. Virjee JP, Gill GJ, Desa D, Somers S, Stevenson GW. Strictures and other late complications of neonatal necrotizing enterocolitis. *Clin Radiol* **1979**;30:25–31
5. Lloyd DA, Cywes S. Intestinal stenosis and enterocyst formation as late complications of neonatal enterocolitis. *J Pediatr Surg* **1973**;8:479–486
6. Beardmore HE, Rodgers BM, Outerbridge E. Necrotizing enterocolitis (ischemic enteropathy) with the sequel of colonic atresia. *Gastroenterology* **1978**; 74:914–917
7. Chiba T, Watanabe I, Kasai M. Colonic atresia following necrotizing enterocolitis. *J Pediatr Surg* **1975**; 10:965–966
8. Krasna IH, Becker JM, Schneider KM, Beck AR. Colonic stenosis following necrotizing enterocolitis of the newborn. *J Pediatr Surg* **1970**; 5:200–206
9. Cockrill H, Oliphant M, Grossman H. Intestinal strictures in the neonate: a complication of ischemic bowel disease. *AJR* **1975**;123:764–769
10. deVilliers DR. Ischaemia of the colon: an experimental study. *Br J Surg* **1966**;53:497–503

Effect of Chronicity of Infection on the Sensitivity of the In-111–Labeled Leukocyte Scan

Frederick L. Datz[1]
David A. Thorne

This study was undertaken to determine the effect of chronicity of infection on the sensitivity of In-111–labeled leukocyte scanning. A total of 332 scans on 290 patients were reviewed retrospectively. The diagnosis of infection was based on culture results and other laboratory data, autopsy findings, radiographic studies, and clinical course. Duration of infection at the time of scanning was determined by the date of onset of fever and symptoms, elevation of white cell count, positive cultures, and abnormal findings on radiographic studies. Sensitivity of leukocyte scanning was 90% for 69 patients who had infections for 0–14 days and 86% for 86 who had infections for 15 days or longer. This difference is not statistically significant.

In-111–labeled leukocyte imaging has been widely used to diagnose intraabdominal abscesses and other sites of infection [1–5]. The overall sensitivity of the leukocyte scan has been excellent, ranging from 85 to 96% [2–7]. Coleman [8], in a summary of the results of three large studies, found the sensitivity to be 90%.

Several investigators [5, 8–10] have speculated that some false-negative findings may be due to factors such as antibiotic or steroid therapy, hyperalimentation, hemodialysis, and hyperglycemia that potentially affect leukocyte chemotaxis and function. Others have wondered if chronic infections are more likely to be missed [5, 8–11]. Sfakianakis et al. [11] compared In-111–labeled leukocytes and uptake of Ga-67 citrate in infected patients and correlated the sensitivity of each with the duration of infection. They found that the sensitivity of the In-111 leukocyte scan fell from 100% for infections less than 2 weeks in duration to 73% for those more than 2 weeks in duration. Using gallium, however, did not result in any false-negative findings in patients whose infections were of more than 2-week duration. On the basis of these data, the authors have recommended that Ga-67 citrate be used in patients with chronic infections that have been present for longer than 2 weeks. However, there are a number of problems with this study; one of the most important is the small number of patients (eight) examined who had chronic infection [12].

To determine the effect of chronicity of infection on the sensitivity of the In-111–labeled leukocyte scan, we undertook a retrospective study of patients with acute (less than 14-day duration) or chronic (15-day or more in duration) infection.

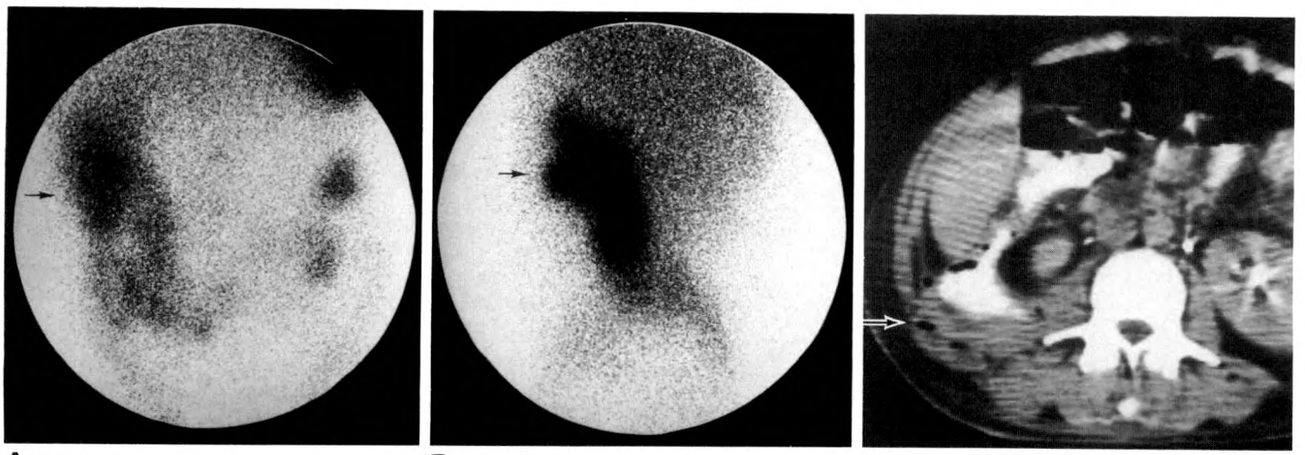
Materials and Methods

A total of 332 consecutive scans on 290 patients (some patients underwent several examinations) were reviewed retrospectively. The scans were classified as positive or negative. The patients' charts were then reviewed to determine if the patients were infected. Classification was based on culture results, white cell counts, other laboratory data, radiographic studies such as CT and sonography, autopsies, and clinical course. In the infected patients, the duration of infection at the time of scanning was determined by the date of onset of fever, onset of other symptoms, elevation of white cell count, abnormal findings on radiographic studies, surgery, and positive cultures.

Received March 5, 1986; accepted after revision May 7, 1986.

[1] Both authors: Department of Radiology, Division of Nuclear Medicine, University of Utah School of Medicine, 50 N. Medical Dr., Salt Lake City, UT 84132. Address reprint requests to F. L. Datz.

AJR 147:809–812, October 1986
0361–803X/86/1474–0809
© American Roentgen Ray Society



A B C

Fig. 1.—38-year-old man with severe thermal burn developed fever, elevated white cell count, and abdominal pain. Abdominal radiograph for Dobhoff placement done 5 days after onset of symptoms showed extraluminal gas in the right upper abdomen. This was missed on the original interpretation.

A, In-111-labeled leukocyte scanning was performed 41 days after the onset of fever, 36 days after abdominal radiograph showing abscess. Anterior view over abdomen shows uptake in right abdomen with linear activity (*arrow*).

B, Right lateral scan shows intense uptake in retroperitoneum with less intense linear activity extending anteriorly (*arrow*).

C, CT scan shows retroperitoneal abscess on right (*arrow*) with a fistula communicating with the bowel. At surgery, a large abscess communicating with the right colon was found.

Patients were divided into two groups: those with infections of 0- to 14-day duration and those with infections of 15-days or longer. The sensitivity of leukocyte scanning was calculated for each group and compared by using the chi-square test.

The leukocyte labeling technique was a modification of that originally described by Thakur et al. [13] and modified by Beightol and Baker [14]. Forty milliliters of venous blood were obtained in a syringe containing 5 ml of acid citrate dextrose solution. The cells were allowed to sediment for 60 min in the inverted syringe. The leukocyte-rich supernatant was then removed from the syringe via a butterfly catheter and placed in a centrifuge tube. To obtain a white-cell button, the supernatant was centrifuged at 300–350 g for 5 min. Leukocyte-poor plasma supernatant was removed and stored in an identical sterile centrifuge tube. The white-cell button was resuspended in 5 ml of sterile saline. One mCi (37 MBq) of In-111 oxine was added to the concentrated cell suspension, and the mixture was incubated for 30–40 min. During the incubation, the suspension was gently agitated every 10 min. Five to 8 ml of leukocyte-poor plasma was added to the suspension of leukocytes, and the mixture was centrifuged for 5 min at 450 g. The supernatant was removed and saved for evaluation of labeling efficiency. Five to 8 ml of the previously obtained leukocyte-poor plasma were gently added to the labeled white-cell button, and the mixture was agitated to resuspend the labeled cells. These cells were assayed in a dose calibrator. The In-111–labeled leukocytes were then drawn into a syringe and reinjected into the patient. The activity in the final product was limited to a maximum of 500 μCi (18.5 MBq). The maximum time from blood drawing to reinjection was approximately 2 hr.

Imaging was done 24 hr after injection by using a large-field-of-view gamma camera equipped with a medium-energy parallel-hole collimator with 20% windows set on the 173- and 247-KeV photopeaks of In-111.

Results

A total of 155 patients had infections; 149 involved soft tissues, and 15 involved bone. Sixty-nine patients had infections with a duration of 0–14 days (range 1–14 days, mean 8.1). Sixty-two were true positives, and seven were false-negatives, for a sensitivity of 90%.

Eighty-six patients had infections with a duration of 15 days or longer (range 15–86 days, mean 29.8). Seventy-four were true positives, and 12 were false-negatives, for a sensitivity of 86%.

The sensitivity of In-111–labeled leukocyte scanning was not significantly different when the two groups were compared ($p > 0.05$). Illustrative cases are shown in Figures 1 and 2.

Discussion

In the other published study of the effect of chronic infection on the sensitivity of the In-111–labeled leukocyte scan [11], the sensitivity was 100% for infections 0–2 weeks in duration but only 73% for infections more than 2 weeks in duration. Consequently, these authors recommended that Ga-67 be used to scan patients with chronic infections that have been present 2 weeks or longer. However, only 19 patients with acute or chronic infections were examined, and of these only 8 had chronic infections. Thus, it is difficult to draw many conclusions from the results.

Data from the same study [11] also indicated problems related to the leukocyte labeling process. Several patients showed leukocyte emboli, a finding that indicates poor labeling technique. In addition, the authors incubated the leukocytes with 600 μCi (22.2 MBq) of In-111 and achieved a labeling efficiency of 80–90%. However, only 150 μCi (5.6 MBq) was available for injection in some patients. This discrepancy seems to indicate a poor labeling efficiency of some patients' leukocytes. Merkel et al. [15] found, in cases of chronic musculoskeletal infection, that low labeling efficiency

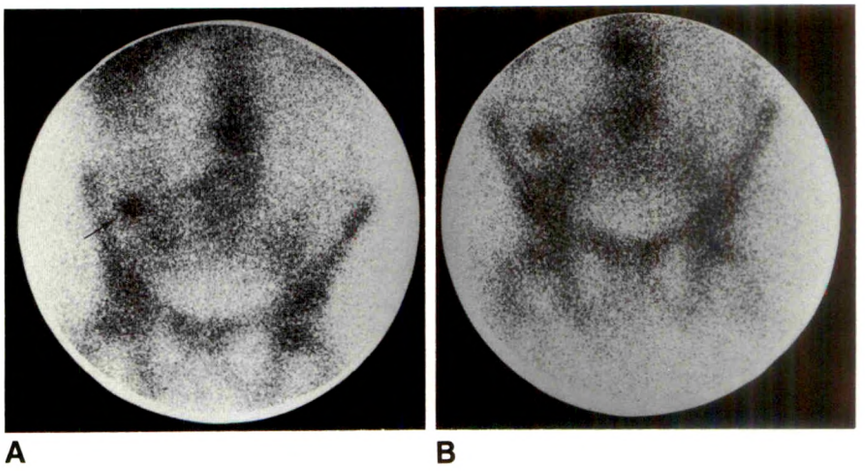


Fig. 2.—60-year-old man who had infected aortofemoral grafts removed became febrile and had an elevated white cell count 1 day after surgery. An In-111-labeled leukocyte scan was performed 7 days later.

A, Anterior scan over pelvis shows small focus of activity (*arrow*). A CT performed because of a suspected abscess was negative.

B, Another leukocyte scan was performed 21 days later because of a continued fever. Anterior pelvis view again shows right lower quadrant focus. Patient was taken to surgery, and a small abscess was drained.

of leukocytes was associated with false-negative results. Thus, a low labeling efficiency in some preparations may have contributed to the false-negative rate in the study of Sfakianakis et al. [11]. Related to this is the more than 400% range of injected activity (150–600 μCi, 5.6–22.2 MBq). Patients receiving the lower dosage may have had such a low photon flux that subtle foci of uptake were missed.

Another problem with the labeling technique was the use of hypotonic hemolysis for 60 sec to remove red cells contaminating the leukocyte fraction. Leukocytes can tolerate only a narrow range of osmolarities [16], and when they are exposed to hypotonic solutions, osmotic damage occurs in less than 30 sec [16]. This has deleterious effects on the function of In-111–labeled leukocytes [12]. Although the results of tests with trypan blue and nitroblue tetrazolium (NBT) were said to be normal, Peters et al. [17] and Eckelman [18] believe that in vitro studies do not necessarily reflect in vivo function. They and others believe that in vivo studies are the ultimate test of leukocyte function [12]. Thus, diminished function secondary to hypotonic hemolysis may have contributed to the decreased sensitivity found by Sfakianakis et al. [11].

Our study involved 155 patients with infection, 89 of whom had chronic infections. Our labeling technique routinely exceeds 90% labeling efficiency [19]. Good in vivo function is confirmed by our overall sensitivity for infection of 95% [6]. We found only a slight decrease in sensitivity in patients with a duration-of-infection of 15 days or more as compared with those with a duration of 0–14 days. This decrease was not statistically significant.

A number of studies have also indirectly supported the high sensitivity of In-111–labeled leukocytes in more chronic infections. Al-Sheikh et al. [20] found no difference in sensitivity between Ga-67 and In-111–labeled leukocyte scans in orthopedic patients with subacute or chronic bone infections (symptoms of 1 to several months). In a prospective study of In-111–labeled leukocyte scans in patients with suspected low-grade or chronic osteomyelitis, Merkel et al. [15] found a sensitivity of 83%. This was significantly higher than the sensitivity for combined technetium and gallium scans. In patients with painful arthroplasties, some of whom were being evaluated for persistent infection 1 year after implantation, the sensitivity of the In-111–labeled leukocyte scan was 86% as compared with 57% for combined technetium and gallium scans. These patients did not have significant systemic signs of infections, and only one had fever. The white cell counts and differentials in these patients were not elevated; white cell counts averaged 7400/μl, and the neutrophil differential was 61%. Other authors [21] have shown similar results with chronically infected arthroplasties. Chronically infected arterial prosthetic grafts also have been successfully diagnosed by means of labeled leukocytes [22–24].

There are several possible explanations for the high sensitivity of In-111–labeled leukocytes in chronic infections. First, chronic inflammation usually results in infiltration by mononuclear cells, principally macrophages, lymphocytes, and plasma cells [25]. However, Robbins and Cotran [25] pointed out that "although polymorphonuclear leukocytes are usually considered the hallmarks of acute infection, many forms of chronic inflammation, lasting for months, continue to show large numbers of neutrophils and to form pus." Second, Merkel et al. [15] speculated that the large number of labeled lymphocytes in leukocyte preparations obtained by gravity sedimentation may account for the high sensitivity of In-111–labeled leukocyte imaging in chronic infections. Milgram and Goodwin [26] have shown uptake of labeled lymphocytes in patients with chronic osteomyelitis and other chronic inflammatory lesions.

REFERENCES

1. McDougall IR, Baumert JR, Lantieri RL. Evaluation of ^{111}In leukocyte whole body scanning. *AJR* **1979**;133:849–854
2. Coleman RE, Welch DM, Baker WJ, Beightol RW. Clinical experience using indium-111-labeled leukocytes. In: Thakur ML, Gottschalk A, eds. *Indium-111 labeled neutrophils, platelets, and lymphocytes*. New York: Trivirum, **1980**:103–118
3. Forstrom LA, Weiblen BJ, Gomez L, et al. Indium-111-oxine-labeled leukocytes in the diagnosis of occult inflammatory disease. In: Thakur ML, Gottschalk, A, eds. *Indium-111 labeled neutrophils, platelets, and lymphocytes*. New York: Trivirum, **1980**:123–130

4. Goodwin DA, Doherty PW, McDougall IR. Clinical use of indium-111-labeled white cells: an analysis of 312 cases. In: Thakur ML, Gottschalk A, eds. *Indium-111 labeled neutrophils, platelets, and lymphocytes.* New York: Trivirum, **1980**:131–150
5. Ascher NL, Forstrom L, Simmons RL. Radiolabeled autologous leukocyte scanning in abscess detection. *World J Surg* **1980**;4:395–402
6. Datz FL, Jacobs J, Baker W, Landrum W, Alazraki N, Taylor A Jr. Decreased sensitivity of early imaging with In-111 oxine-labeled leukocytes in detection of occult infection: concise communication. *J Nucl Med* **1984**;25:303–306
7. Datz FL, Bedone RA, Baker WJ, Alazraki NP, Taylor A Jr. No difference in sensitivity for occult infection between tropolone- and oxine-labeled indium-111 leukocytes. *J Nucl Med* **1985**;26:469–473
8. Coleman RE. Radiolabeled leukocytes. In: Freeman LM, Weissman HS, eds. *Nuclear medicine annual 1982.* New York: Raven, **1982**:119–141
9. Knochel JQ, Koehler PR, Lee TG, Welch DM. Diagnosis of abdominal abscesses with computed tomography, ultrasound, and ^{111}In leukocyte scans. *Radiology* **1980**;137:425–432
10. Kipper MS, Williams RJ. Indium-111 white blood cell imaging. *Clin Nucl Med* **1983**;8:449–455
11. Sfakianakis GN, Al-Sheikh W, Heal A, Rodman G, Zeppa R, Serafini A. Comparisons of scintigraphy with In-111 leukocytes and Ga-67 in the diagnosis of occult sepsis. *J Nucl Med* **1982**;23:618–626
12. Datz FL, Taylor A Jr. Cell labeling: techniques and clinical utility. Section I. Radiolabeled leukocytes. In: Freeman ML, ed. *Freeman and Johnson's clinical radionuclide imaging*, 3rd ed. Orlando, FL: Grune & Stratton, **1986**:1785–1913
13. Thakur ML, Coleman RE, Welch MJ. Indium-111-labeled leukocytes for the localization of abscesses: preparation, analysis, tissue distribution and comparison with gallium-67 citrate in dogs. *J Lab Clin Med* **1977**;89:217–228
14. Beightol RW, Baker WJ. Labeling autologous leukocytes with indium-222 oxine. *Am J Hosp Pharm* **1980**;37:847–850
15. Merkel KD, Brown ML, Dewanjee MK, Fitzgerald RH. Comparison of indium-labeled-leukocyte imaging with sequential technetium-gallium scanning in the diagnosis of low-grade musculoskeletal sepsis. *J Bone Joint Surg [Am]* **1985**;67A:465–476
16. Dooley DC, Takahashi T. The effect of osmotic stress on the function of the human granulocyte. *Exp Hematol* **1981**;9:731–741
17. Peters AM, Saverymuttu SH, Reavy HJ, Danpure HJ, Osman S, Lavender JP. Imaging of inflammation with indium-111 tropolonate labeled leukocytes. *J Nucl Med* **1983**;24:39–44
18. Eckelman WC. Technical considerations of labeling of blood elements. *Semin Nucl Med* **1975**;5:3–10
19. Baker WJ, Datz FL. Preparation and clinical utility of In-111 labeled leukocytes. *J Nucl Med Tech* **1984**;12:131–136
20. Al-Sheikh W, Sfakianakis GN, Mnaymneh W, et al. Subacute and chronic bone infections: diagnosis using In-111, Ga-67 and Tc-99m MDP bone scintigraphy and radiography. *Radiology* **1985**;155:501–506
21. Mulamba L, Ferrant A, Leners N, deNayer P, Rombouts JJ, Vincent A. Indium-111 leucocyte scanning in the evaluation of painful hip arthroplasty. *Orthop Scand* **1983**;54:695–697
22. Stevick CA, Fawcett HD. Aortoiliac-graft infection: detection by leukocyte scan. *Arch Surg* **1981**;116:939–942
23. McKeown PP, Miller DC, Jamieson SW, et al. Diagnosis of arterial prosthetic graft infection by indium-111 oxine white blood cell scans. *Circulation* **1982**;66[Suppl I]:130–134
24. Serota AI, Williams RA, Rose JG, Wilson SE. Uptake of radiolabeled leukocytes in prosthetic graft infection. *Surgery* **1981**; 90:35–40
25. Robbins SL, Cotran RS. *Pathologic basis of disease.* Philadelphia: Saunders, **1979**:82–84
26. Milgram R, Goodwin DA. Human scanning with In-111 oxine labeled autologous lymphocytes. *Clin Nucl Med* **1985**;10:30–34

Case Report

Utility of Indium-111–Labeled Leukocyte Imaging in Acute Acalculous Cholecystitis

Frederick L. Datz[1]

The reported sensitivity of cholescintigraphy in acute acalculous cholecystitis varies from 45 to 100% with an average sensitivity (based on combining the results in the literature) of 75% [1–11]. This figure is significantly lower than the sensitivity reported for acute calculous disease [2, 7, 9]. In addition, acalculous cholecystitis often occurs in patients with severe intercurrent illnesses and those on hyperalimentation, conditions that can cause nonvisualization of the gallbladder on cholescintigraphy in the absence of gallbladder disease [1]. We present two patients with acute acalculous cholecystitis who had indium-111 (In-111) labeled leukocyte uptake in the gallbladder in a doughnut pattern. It appears that the leukocyte scan can detect acalculous cholecystitis. The leukocyte scan may be helpful in diagnosing or excluding acute acalculous cholecystitis in patients in whom the cholescintigram results (either positive or negative) are questioned.

Case Reports

Case 1

A 55-year-old man sustained multiple injuries in an automobile accident. The injuries included multiple rib fractures, crushed T5 and T6 vertebrae, right femoral fracture, liver laceration, left pneumothorax, and a closed head injury that left the patient comatose. Postoperatively, the patient developed fever. A sonogram of the abdomen revealed no evidence of gallstones or an abscess. Since the cause of the fever could not be well localized, an In-111–labeled leukocyte scan was performed (Fig. 1). This showed a doughnut of uptake in the gallbladder fossa. The patient was taken to emergency surgery where a gangrenous gallbladder without stones was removed. The patient went on to regain consciousness and was eventually discharged.

Case 2

A 27-year-old male trauma patient on hyperalimentation developed postoperative fever and vague abdominal pain. An In-111–labeled leukocyte scan showed a doughnut pattern of uptake in the gallbladder fossa (Fig. 2). The patient underwent emergency surgery and acalculous cholecystitis was found.

Discussion

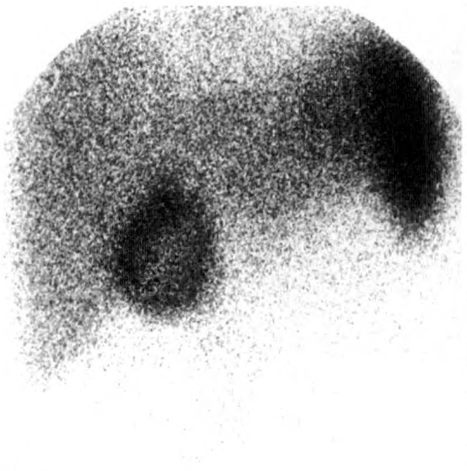
Acalculous cholecystitis is an important cause of cholecystitis. It makes up 5 to 15% of all cases of gallbladder inflammation and is thought to be increasing in prevalence [1]. Twenty-one to 45% of cases of postoperative cholecystitis are acalculous, as are one-third of pediatric cases of cholecystitis [1]. Acute acalculous cholecystitis has a much poorer prognosis than calculous disease. As many as half of all cases progress to serious complications such as gangrene or perforation [1]. Not surprisingly, the rate of mortality is high, ranging from 10 to 50% [3]. Since the disease usually occurs in patients with other severe diseases, the clinical diagnosis is often difficult [1].

Numerous predisposing causes for the development of acalculous cholecystitis have been reported [1, 2, 6–8]. One of the most common is chemical inflammation secondary to hyperconcentrated bile. Prolonged fasting hyperconcentrates the bile as a result of bile stasis and inspissation. Analgesics and increased bile pigments from multiple transfusions lead to a similar result [6].

Another chemical toxin that can acutely inflame the gallbladder is refluxed bile caused by spasm of the sphincter of Oddi [6]. Other etiologic factors include decreased blood flow

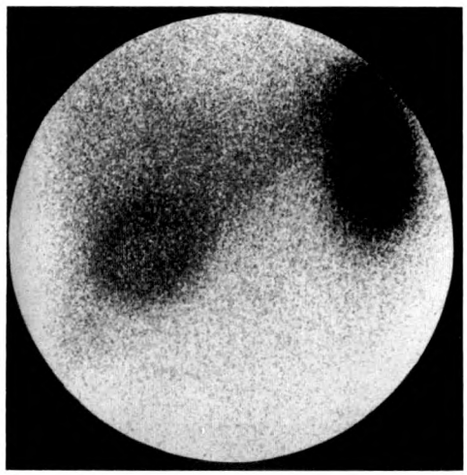
Received April 11, 1986; accepted after revision May 29, 1986.

[1] Division of Nuclear Medicine, Department of Radiology, University of Utah School of Medicine, 50 N. Medical Dr., Salt Lake City, UT 84132. Address reprint requests to F. L. Datz.



1

Fig. 1.—55-year-old male paraplegic after surgery for multiple injuries incurred in an automobile accident developed postoperative fever. Anterior abdominal view of indium-111–labeled leukocyte scan. Doughnut of activity seen in gallbladder fossa. At surgery, acute gangrenous acalculous cholecystitis was found.



2

Fig. 2.—27-year-old male trauma patient on hyperalimentation, with fever and vague abdominal pain. Anterior abdominal view shows doughnut of increased activity in gallbladder region. Acute acalculous cholecystitis was found at surgery.

to the gallbladder wall from episodes of hypotension or mechanical ventilator support [6] and bacterial infection of the gallbladder wall secondary to hematogenous dissemination [2]. The latter appears to be an especially important cause in children [2]. A review of diseases associated with acalculous cholecystitis has been presented by Shuman et al. [1].

The usual radionuclide agents used to diagnose cholecystitis are technetium imino diacetic acids (Tc-IDAs). The sensitivity of IDA scans in acute calculous cholecystitis is excellent [2], with accuracies as high as 98% reported [2, 7, 9]. The diagnosis is based on obstruction of the cystic duct by a stone that prevents flow of the IDA agent into the gallbladder, resulting in nonvisualization of the gallbladder. Because of this, investigators have questioned the sensitivity of the scan in acalculous disease. A number of studies of the sensitivity of cholescintigraphy in acalculous cholecystitis have been reported, but all have involved very small numbers of patients [1–11]. In the reports, the sensitivity has varied from 45 to 100%. By combining the results of these studies, the average sensitivity of the IDA scan is 75–79%, significantly less than the values reported for calculous disease [2, 7, 9].

The cholescintigram can be falsely positive (i.e., nonvisualization of the gallbladder) in patients with severe intercurrent diseases (especially trauma) or those on hyperalimentation [1]. Unfortunately, these are the very patients who are most likely to develop acute acalculous cholecystitis.

Thus, the interpretation of the cholescintigram in patients with suspected acalculous cholecystitis is difficult. False-negative studies are more common than with calculous disease. However, since the false-positive rate is also increased in the patient population that develops acute acalculous cholecystitis, nonvisualization may not be diagnostic in these patients. Clinical correlation to confirm the diagnosis is often difficult because of the underlying multiple diseases present in these patients [1].

We found that the In-111–labeled leukocyte scan showed significant gallbladder uptake in both cases of acalculous cholecystitis. This uptake formed a doughnut of activity in the gallbladder fossa that had a characteristic "gallbladder" appearance. The doughnut of activity is presumably due to uptake of the leukocytes in the gallbladder wall rather than in the lumen.

On the basis of these two cases, the indium-111–labeled leukocyte scan can detect acalculous cholecystitis. It may be helpful in diagnosing or excluding the disease in patients in whom the cholescintigram results (either positive or negative) are questioned. We have not formally studied the sensitivity of the indium-111–labeled leukocyte scan in acalculous cholecystitis. However, on the basis of these two cases, we think it should be helpful in evaluating selected patients who are suspected of having this disease.

REFERENCES

1. Shuman WP, Rogers JV, Rudd TG, Mack LA, Plumley T, Larson EB. Low sensitivity of sonography and cholescintigraphy in acalculous cholecystitis. *AJR* **1984**;142:531–534
2. Fox MS, Wilk PJ, Weissmann HS, Freeman LM, Gliedman ML. Acute acalculous cholecystitis. *Surg Gynecol Obstet* **1984**; 159:13–16
3. Devine RM, Farnell MB, Mucha P Jr. Acute cholecystitis as a complication in surgical patients. *Arch Surg* **1984**;119:1389–1393
4. Lee AW, Proudfoot WH, Griffen WO Jr. Acalculous cholecystitis. *Surg Gynecol Obstet* **1984**;159:33–35
5. Ramanna L, Brachman MB, Tanasescu DE, Berman DS, Waxman AD. Cholescintigraphy in acute acalculous cholecystitis. *Am J Gastroenterol* **1984**;79:650–653
6. Ouriel K, Green RM, Ricotta JJ, DeWeese JA, Adams JT. Acute acalculous cholecystitis complicating abdominal aortic aneurysm resection. *J Vasc Surg* **1984**;1:646–648
7. Mauro MA, McCartney WH, Melmed JR. Hepatobiliary scanning with ^{99m}Tc-PIPIDA in acute cholecystitis. *Radiology* **1982**; 142:193–197
8. Savino JA, Scalea TM, Del Guercio LRM. Factors encouraging laparotomy in acalculous cholecystitis. *Crit Care Med* **1985**; 13:377–380
9. Freitas JE. Cholescintigraphy in acute and chronic cholecystitis. *Semin Nucl Med* **1982**;12:18–26
10. Echevarria RA, Gleason JL. False-negative gallbladder scintigram in acute cholecystitis. *J Nucl Med* **1980**;21:841–843
11. Schneider PB. Acalculous cholecystitis: a case with variable cholescintigram. *J Nucl Med* **1984**;25:64–65

Technetium-99m Pyrophosphate Imaging in Acute Renal Failure Associated with Nontraumatic Rhabdomyolysis

Raman Patel[1]
Fred S. Mishkin[2]

Technetium-99m pyrophosphate (Tc-PYP) imaging was performed in five patients with acute renal failure associated with nontraumatic rhabdomyolysis. Four patients had phencyclidine intoxication and one had viral pneumonia. During the acute phase, marked uptake of pyrophosphate was seen in all patients in several muscle groups, but always in the thigh adductors. The results show that phencyclidine intoxication can result in diffuse muscle uptake of Tc-PYP without overt evidence of muscle injury. Tc-PYP imaging may provide a clue to the cause of acute renal failure in patients with suspected rhabdomyolysis in whom elevations of serum creatine phosphokinase concentrations are equivocal.

Imaging with technetium-99m phosphorus compounds provides a useful and highly sensitive method for the detection of muscle injury in several disease states [1–3]. The mechanisms underlying muscle uptake of these radiopharmaceutical agents are not clear. They are probably similar to the processes that cause labeling of irreversibly damaged myocardium after an acute infarction. The phosphate compounds appear to follow shifts in muscle calcium [4, 5]. We used technetium-99m pyrophosphate (Tc-PYP) imaging in five patients with nontraumatic rhabdomyolysis and acute renal failure to determine the potential usefulness of the procedure in defining the cause of acute renal failure in patients with clinically inapparent muscle injury.

Subjects and Methods

Five men, 20 to 40 years old, were referred because of acute renal failure secondary to nontraumatic rhabdomyolysis. Rhabdomyolysis developed in association with phencyclidine overdose in four patients and in association with viral pneumonia in one. None of the patients had visible evidence of muscle injury, nor were any soft-tissue calcifications apparent on radiographs of the sites shown to be involved by Tc-PYP imaging. The biochemical abnormalities were typical of those commonly seen in rhabdomyolysis-associated acute renal failure [6, 7]. All patients had increased serum levels of creatine phosphokinase (range 3740–350,000 IU/l, mean 154,980), and uric acid (range 9.2–18.6 mg/dl, mean 14.5) and normal serum levels of albumin. Four patients had marked hyperphosphatemia (serum phosphate range 8.1–12.8 mg/dl, mean 10.0) and hypocalcemia (serum calcium range 4.6–6.3 mg/dl, mean 5.6). One patient developed transient hypercalcemia (serum calcium 11.4 mg/dl) during the diuretic phase. Serum creatinine concentration ranged from 4.7 to 18.3 mg/dl (mean 13.1). Four patients required hemodialysis or peritoneal dialysis to control uremia. All recovered with return to normal renal function and electrolyte homeostasis.

For the technetium pyrophosphate scan, each patient was given an IV injection of 20 mCi (740 MBq) of Tc-99m (stannous) pyrophosphate. Three hours later, the body was imaged from head to ankle by means of a commercially available instrument (Siemens Pho-Con [R]), which produces 12 simultaneous coronal plane images from anterior to posterior planes at 2-cm intervals. Detailed views of any area of interest were obtained by using an appropriately collimated large-field-of-view Anger camera. Abnormal muscle uptake of Tc-PYP is not found in acute renal failure due to causes other than rhabdomyolysis ([8] and unpublished observations).

Received February 20, 1986; accepted after revision May 21, 1986.

[1] Department of Medicine, Los Angeles County–King Drew Medical Center and the Charles R. Drew Postgraduate Medical School, 12021 S. Wilmington Ave., Los Angeles, CA 90059. Address reprint requests to R. Patel.

[2] Department of Radiology, Los Angeles County–King Drew Medical Center and the Charles R. Drew Postgraduate Medical School, Los Angeles, CA 90059.

AJR 147:815–817, October 1986
0361–803X/86/1474–0815
© American Roentgen Ray Society



Fig. 1.—Technetium-99m pyrophosphate images in a 21-year-old man with phencyclidine intoxication and rhabdomyoglobinuric acute renal failure. Anterior (**A**) and posterior (**B**) coronal tomographic sections show uptake in the left pectoralis muscle and in right latissimus dorsi. Uptake can also be seen in the musculature of the abdominal wall along the lateral body margin. Localized uptake is marked in the arms, forearms, thighs, and legs.

Results

In all patients, increased uptake of Tc-PYP was seen in several muscle groups (Figs. 1–3) but was always found in the adductor groups of the thighs. In one patient, a repeat scan 8 weeks later showed resolution of the muscle uptake but persisting pulmonary and gastric uptake. The latter are characteristic of secondary hyperparathyroidism that accompanies renal failure [9, 10]. The serum parathyroid hormone level measured as C-terminal fragments at this time was elevated at 2240 pg/ml (normal is 430–1860).

Discussion

Our results confirm the observations of others that diffuse muscle uptake of Tc-99m-labeled phosphate tracers occurs in rhabdomyolysis-associated acute renal failure in the absence of clinically apparent muscle injury [1, 8, 11]. Although the mechanism of localization of these agents in the injured muscle is not certain, experimental and clinical evidence suggests that it may be related to calcium deposition [12, 13].

In rhabdomyolysis-associated renal failure, Tc-99m compounds can be used to visualize the site and extent of localized muscle injury that may or may not be evident clinically [8, 13]. The increased muscle uptake occurs during the oliguric phase and correlates with hypocalcemia [1, 11]. The hypocalcemia may result from the deposition of calcium in muscles [1, 6].

Calcium deposition in damaged muscle may occasionally be visualized by means of radiographs but not in the absence of clinical findings of muscle damage [13, 14]. Tc-99m phosphate compounds, however, may be taken up in muscle for

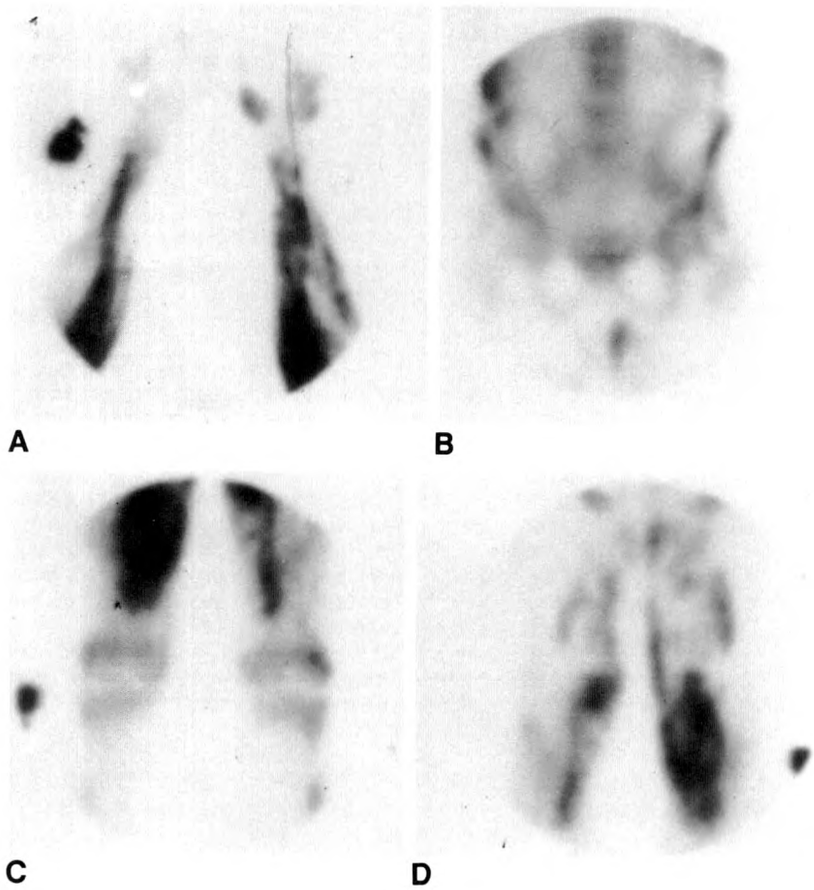
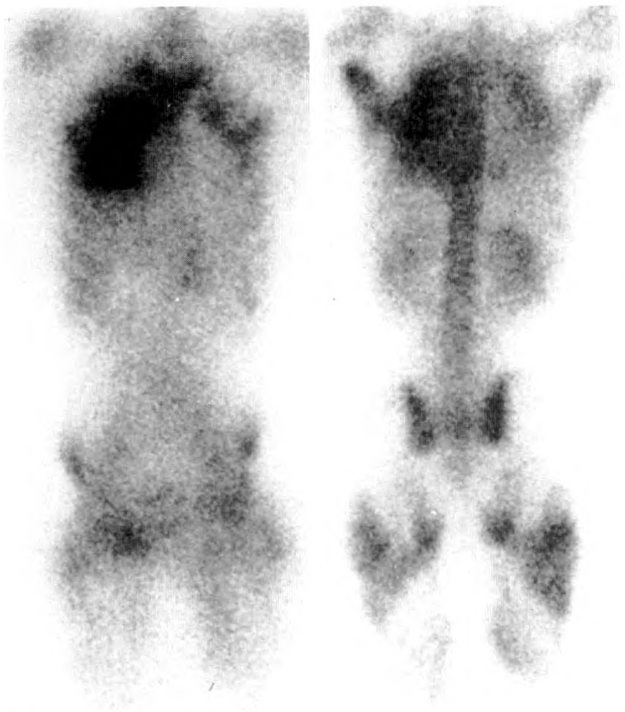


Fig. 2.—Camera images of the forearms (**A**), pelvis (**B**), thighs (**C**), and legs (**D**) of the same patient shown in Fig. 1 delineate involvement of several muscle groups.



A B

Fig. 3.—Technetium-99m pyrophosphate scan in a 20-year-old man who developed rhabdomyolysis and acute renal failure after viral pneumonia. Anterior (**A**) and posterior (**B**) coronal tomograms from an initial study performed 4 days after hospitalization show abnormal isotope concentration in the lungs, particularly the right; the inferior edge of the right latissimus dorsi; and the region of the adductor, gluteal, and biceps femoris muscles in the posterior compartments of the thighs. The diffuse pulmonary uptake is characteristic of hyperparathyroidism due to renal failure. A repeat study performed 8 weeks later showed uptake in the lungs and the stomach but not in the muscles.

which there is no clinical evidence of focal damage. Frymoyer et al. [8] pointed out the usefulness of Tc-99m medronate imaging in defining and localizing occult muscle trauma.

Among hospital-treated phencyclidine users, rhabdomyolysis develops in approximately 2.5% and acute renal failure in 0.5–1.0% [7, 15]. Recent studies suggested that clinical manifestations of phencyclidine intoxication may all be due to a common molecular mechanism, namely blockade of presynaptic potassium ion channels of nerve and muscle [16]. Kuncl and Meltzer [17] indicated that the rhabdomyolysis that develops in rats treated with phencyclidine may be due to the combined influence of phencyclidine and restraint and may be prevented by prior denervation of the muscles involved.

Tc-PYP imaging may have diagnostic value in certain patients with acute renal failure. In five other patients with rhabdomyolysis-associated acute renal failure, we determined by regression analysis that serum levels of creatine phosphokinase would return to normal values in 3–10 days. Therefore, theoretically, some patients with rhabdomyolysis and moderately severe renal failure could have near-normal serum creatine phosphokinase concentrations at the time of hospitalization. In this situation, positive results on Tc-PYP imaging may provide a clue to the cause of acute renal failure.

REFERENCES

1. Blair RJ, Schroeder ET, McAfee JG, et al. Skeletal muscle uptake of bone-seeking agents in both traumatic and non-traumatic rhabdomyolysis with acute renal failure. *J Nucl Med* **1975**; 16:515–516
2. Brown M, Swift TR, Spies SM. Radioisotope scanning in inflammatory muscle disease. *Neurology* **1976**;26:517–520
3. Swift TR, Brown M. Tc-99m pyrophosphate muscle labelling in McArdle syndrome. *J Nucl Med* **1978**;19:295–297
4. Parkey RW, Bonte FJ, Meyer SL, et al. A new method for radionuclide imaging of acute myocardial infarction in humans. *Circulation* **1974**;50:540–546
5. D'Agostino AN, Chiga M. Mitochondrial mineralization in human myocardium. *Am J Clin Pathol* **1970**;53:820–824
6. Koffler A, Fiedler RM, Massry SG. Acute renal failure due to nontraumatic rhabdomyolysis. *Ann Intern Med* **1976**;85:23–28
7. Patel R, Connor G. A review of thirty cases of rhabdomyolysis-associated acute renal failure among phencyclidine users. *J Toxicol Clin Toxicol* **1985**;23:547–556
8. Frymoyer PA, Giammarco R, Farrar FM, Schroeder ET. Technetium 99m medronate bone scanning in rhabdomyolysis. *Arch Intern Med* **1985**;145:1991–1995
9. Rosenthal DI, Chandler HL, Azizi F, et al. Uptake of bone-imaging agents by diffuse pulmonary metastatic calcifications. *AJR* **1977**;129:871–874
10. DeGraaf P, Pauwek EKJ, Schacht M. Scintigraphic detection of gastric calcification in dialysis patients *J Nucl Med* **1980**;21:197
11. Silberstein EB, Bove KE. Visualization of alcohol-induced rhabdomyolysis: a correlative radiotracer, histochemical, and electron microscopic study. *J Nucl Med* **1979**;20:127–129
12. Buja LM, Tofe AJ, Kulkarni PV, et al. Sites and mechanisms of localization of technetium-99m phosphorus radiopharmaceuticals in acute myocardial infarcts and other tissues. *J Clin Invest* **1977**;60:724–736
13. Akmal M, Goldstein DA, Telfer N, Wilkinson E, Massry SG. Resolution of muscle calcification in rhabdomyolysis and acute renal failure. *Ann Intern Med* **1978**;89:928–930
14. Patel R, Ford J. Hypercalcemia in acute renal failure. *NZ Med J* **1976**;84:482–484
15. Akmal M, Valdin JR, McCarron M, Massry SG. Rhabdomyolysis with and without acute renal failure in patients with phencyclidine intoxication. *Am J Nephrol* **1981**;1:91–96
16. Albuquerque EX, Aguayo LG, Warnick JE. Interaction of phencyclidine with ion channels of nerve and muscle: behavioral implications. *Fed Proc* **1983**;42:2584–2589
17. Kuncl RW, Meltzer HY. Pathologic effect of phencyclidine and restraint on rat skeletal muscle structure: prevention by prior denervation. *Exp Neurol* **1974**;45:387–402

Case Report

False-Positive Thallium-201 Parathyroid Scan of the Mediastinum in Hodgkin's Lymphoma

Gary G. Winzelberg,[1] Gary A. Melada,[2] and Jerrold D. Hydovitz[2]

The recent introduction of thallium-201/Tc-99m pertechnetate subtraction scintigraphy for imaging parathyroid adenomas has rekindled interest in parathyroid scintigraphy [1–5]. The sensitivity of this scanning technique has been related to the size and weight of the adenoma, with over 85% of those weighing 500 mg or more being identified [6]. A similar success rate with diffuse parathyroid hyperplasia has not been realized. The factors that control thallium accumulation in the parathyroids are poorly understood. Parathyroid uptake of thallium may be a nonspecific blood-flow–related phenomenon. As our experience with this technique increases, more false-positive studies are being reported. This case report describes a false-positive mediastinal accumulation of thallium in a patient with Hodgkin's lymphoma.

Case Report

A 77-year-old white man was admitted with persistently elevated serum calcium levels from 12.0 to 14.5 mg/dl associated with an elevated intact N-terminal parathyroid hormone (PTH) concentration of 29 pg/ml (normal, 11–24 pg/ml) and C-terminal PTH level of 690 pg/ml (normal, 430–1860). The serum 1,25-dihydroxy-vitamin D_3 concentration was 69 pg/ml (normal, 15–60 pg/ml). The serum phosphorus was 2.2 mg/dl with a serum chloride/phosphate ratio of 46 (normal, < 35). There was a history of recurrent calcium-containing renal stones and increasing azotemia (serum creatinine, 3.7 mg/dl). The patient was also being treated for congestive heart failure, atrial fibrillation, and ventricular arrythmias, but the treatment regimen did not include any preparation that might influence the serum calcium concentration or parathyroid function. Additional laboratory studies demonstrated a modest anemia with a hematocrit of 32%, while the WBC count and serum protein electrophoresis study were normal.

A parathyroid scan was performed after IV injection of 2 mCi (74 MBq) thallium-201 (thallous chloride). The patient's head was immobilized using tape and head restraints. An anterior view of the neck and upper mediastinum was obtained using a regular-field-of-view camera equipped with a pinhole collimator (5-mm insert) placed 6 in. (15.25 cm) from the neck. A 100,000-count image was then stored on the computer. The patient was then injected with 5 mCi (185 MBq) of Tc-99m pertechnetate. Twenty minutes later, a repeat 100,000-count anterior image of the neck was obtained and was stored in the computer. Finally, a direct subtraction view was obtained by subtracting the 100,000-count Tc-99m pertechnetate image from the stored 100,000-count thallium images.

The thallium scan (Fig. 1) demonstrated a large, 3-cm thallium avid collection approximately 4–5 cm inferior to the right lobe of the thyroid in the right superior mediastinum. No other abnormality was seen. A high-resolution sonogram demonstrated no enlarged parathyroids in or around the thyroid. The right mediastinal area could not be visualized because of obscuring lung parenchyma. A CT scan of the chest and mediastinum showed no definite abnormality.

Neck exploration identified three normal parathyroids. One of these (right inferior gland) was located in the thymic remnant. The right superior parathyroid was not identified. Because of the findings on the parathyroid scan, the sternum was split and a mediastinal exploration was performed. Five matted lymph nodes were identified in the right superior mediastinum corresponding to the area where abnormal thallium collection was noted. Their histology demonstrated Hodgkin's lymphoma with histiocytic reaction. No other lymph nodes that

Received March 25, 1986; accepted after revision May 9, 1986.

[1] Department of Diagnostic Imaging, Shadyside Hospital, 5230 Centre Ave., Pittsburgh, PA 15232, and the University of Pittsburgh School of Medicine, Pittsburgh, PA 15213. Address reprint requests to G. G. Winzelberg at Shadyside Hospital.

[2] Department of Endocrinology, Shadyside Hospital, Pittsburgh, PA 15232, and the University of Pittsburgh School of Medicine, Pittsburgh, PA 15213.

AJR 147:819–821, October 1986 0361–803X/86/1474–0819 © American Roentgen Ray Society

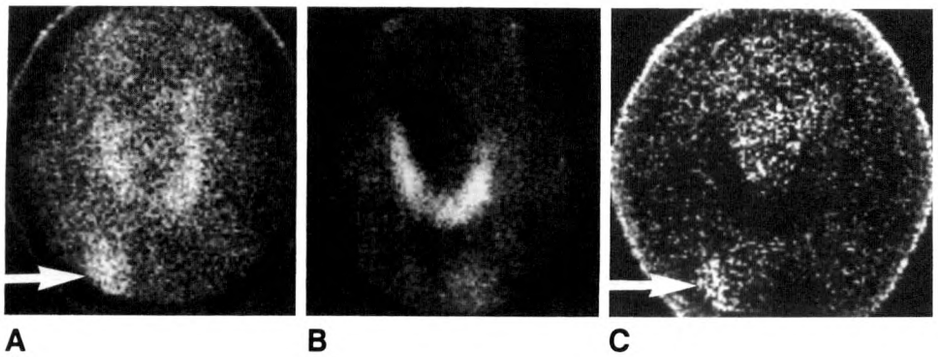


Fig. 1.—Anterior pinhole (**A**) thallium-201 view of neck and mediastinum demonstrating 3-cm collection of thallium in right superior mediastinum (*arrow*). Tc-99m pertechnetate view (**B**) shows normal Tc-99m activity in thyroid. Subtraction view (**C**) again demonstrates abnormal accumulation in right superior mediastinum.

appeared to be abnormal were seen or identified in the neck or mediastinum.

In the postoperative period, the serum calcium ranged from 9.4 to 10.4 mg/dl. The patient was started on chemotherapy but eventually died from recurrent sepsis. A postmortem examination was not obtained, at the family's request.

Discussion

The mechanism for thallium-201 accumulation in enlarged or hyperfunctioning parathyroids is unclear. After IV injection, thallium-201, which is a potassium analog, is distributed to various body organs by blood flow with a short blood-pool half-life [7]. Vascular organs such as the thyroid and parathyroid have increased thallium uptake as compared with surrounding structures. The thallium technetium subtraction technique allows one to identify parathyroid thallium uptake by subtracting out thyroidal activity. Thallium, however, can accumulate in foci of abnormal focal cellular thyroid tissue, as is seen with papillary, follicular, undifferentiated, or mixed thyroid carcinoma [8], adenomatous goiter, chronic thyroiditis, and thyroid adenomas [9]. These areas usually have decreased uptake on routine technetium scanning; thus, thallium technetium subtraction scintigraphy may cause false-positive studies. In the neck, thallium has also been shown to be taken up by lymph nodes involved with sarcoidosis [2], metastatic adenocarcinoma of the ovary [10], and metastatic thyroid cancer [11]. On the basis of several published series [1, 2, 4–6], the overall number of false-positive studies is not large. To date we have studied 115 patients with suspected hyperparathyroidism with thallium-technetium subtraction scintigraphy. Seventy-two patients have been surgically explored. There were four false-positive studies in the neck, two secondary to thyroid adenomas, and two secondary to Hashimoto's thyroiditis. Only one false-positive mediastinal study was noted (current case). The current study demonstrates that Hodgkin's lymphoma of the mediastinum can also accumulate thallium, which could cause false-positive studies in the mediastinum and be misinterpreted as ectopically located parathyroid tissue. Previous work [8, 9] has shown that thallium uptake in malignancy is nonspecific. Thallium accumulation has been documented in lung carcinomas of various cell types, including squamous, undifferentiated, and large cell, and in adenocarcinoma of the lung [12]. Epidermoid carcinomas of the esophagus have also been shown to cause increased uptake. All of these malignancies may therefore cause false-positive studies in the neck or mediastinum. Additionally, any granulomatous process involving lymph nodes may also cause increased uptake, as has been reported with sarcoidosis, and could cause false-positive studies. While careful screening of patients with suspected hypercalcemia should reduce the frequency of false-positive studies, it may not be possible to eliminate them all.

In the current case, the elevated calcium and PTH level strongly suggested the presence of parathyroid disease. The relationship of vitamin D metabolites to the hypercalcemia occasionally noted in association with certain lymphomas [13] is of current interest and is the subject of much investigation [14]. These cellular elements seemingly have the capacity to engage in a variety of extrarenal processes that result in the synthesis of 1,25-dihydroxy-vitamin D_3 (calcitriol) and a number of other vitamin D metabolites. An elevated calcitriol level was demonstrated in the serum of the patient reported here. This hormone does have the capacity to stimulate intestinal calcium absorption and osteoclastic bone resorption, which could result in hypercalcemia. We cannot eliminate other mechanisms (e.g., osteoclastic-activating factor, prostaglandin E) that have been thought to contribute to oncogenic hypercalcemia. Elevated serum levels of calcitriol have been reported in association with primary hyperparathyroidism. If the hypercalcemia in this patient was related to coincidental primary hyperparathyroidism (in the fourth gland, not accounted for at the time of surgery), very high levels of serum-immunoreactive parathyroid hormone should have been recorded with radioimmunoassay that recognizes carboxy-terminal fragments. Such was not the case here.

REFERENCES

1. Ferlin G, Borsato N, Camerani M, Conte N, Zohi D. New perspectives in localizing enlarged parathyroids by technetium-thallium subtraction scan. *J Nucl Med* **1983**;24:438–441
2. Young AE, Gaunt JI, Croft DN, Collins RE, Wells CP, Coakley AJ. Location of parathyroid adenomas by thallium-201 and technetium-99m subtraction scanning. *Br Med J* **1983**;286:1384–1386
3. Winzelberg GG, Hydovitz JD. Radionuclide imaging of parathy-

roid tumors: historical perspectives and newer techniques. *Semin Nucl Med* **1985**;15:161–170
4. Okerlund MD, Sheldon K, Corpuz S, et al. A new method with high sensitivity and specificity for localization of abnormal parathyroid glands. *Ann Surg* **1984**;200:381–388
5. MacFarlane SD, Hanelin LG, Taft DA, Ryan JA, Fredlund PN. Localization of abnormal parathyroid glands using thallium-201. *Am J Surg* **1984**;148:7–13
6. Winzelberg GG, Hydovitz JD, O'Hara KR, et al. Parathyroid adenomas evaluated by Tl-201/Tc-99m pertechnetate subtraction scintigraphy and high resolution ultrasonography. *Radiology* **1985**;155:231–235
7. Strauss HW, Harrison K, Pitt B. Thallium-201: noninvasive determination of the regional distribution of cardiac output. *J Nucl Med* **1977**;18:1167–1170
8. Tonami N, Bunko H, Michigishi T, Kuwajima H, Hisada K. Clinical application of 201-Tl scintigraphy in patients with cold thyroid nodules. *Clin Nucl Med* **1978**;3:217–221
9. Ochi H, Sawa H, Fukuda T, et al. Thallium-201 chloride thyroid scintigraphy to evaluate benign and/or malignant nodules. *Cancer* **1982**;50:236–240
10. Punt CJA, DeHooge P, Hoekstra JBL. False-positive subtraction scintigram of the parathyroid glands due to metastatic tumor. *J Nucl Med* **1985**;26:155–156
11. Fukuchi M, Tachibana K, Kuwata K, et al. Thallium-201 imaging in thyroid carcinoma appearance of a lymph node metastasis. *J Nucl Med* **1978**;19:195–196
12. Tonami N, Hisada K. Clinical experience of tumor imaging with 201 Tl-chloride. *Clin Nucl Med* **1977**;2(3):75–78
13. Breslau NA, McGuire JL, Zerwekh JE, Frenkel EP, Pak CYC. Hypercalcemia associated with increased serum calcitriol levels in three patients with lymphoma. *Ann Int Med* **1984**;100:1–6
14. Avioli LV, Haddad JG. The vitamin D family revisited (editorial). *N Engl J Med* **1984**;311:47

Technical Note

Percutaneous Gastrostomy for Jejunal Feeding: A New Technique

Gregg D. Alzate,[1] Harold G. Coons,[1] James Elliott,[1,2] and Patrick H. Carey[1]

The ability to create a gastrostomy by using percutaneous techniques without general anesthesia has simplified patient care [1–3]. Total parenteral nutrition can frequently be replaced with percutaneous enteral feeding in acute or chronically ill patients in whom the gastrointestinal tract is intact and functioning. A significant reduction in medical cost can be achieved [5–9]. We report our experience with 61 consecutive patients in whom percutaneous gastrostomies were performed by using two systems designed specifically for enteral feeding distal to the ligament of Treitz.

Materials and Methods

Sixty-one consecutive patients, aged 2 to 97 years, underwent percutaneous gastrostomy for enteral feeding between January 1984 and November 1985. These patients were unable to maintain an adequate caloric intake because of carcinoma of the head and neck (one-third), a stroke (one-third), or metastatic carcinoma (one-third). Five children who underwent the procedure carried diagnoses of anoxic encephalopathy (two patients), severe bronchopulmonary dysplasia (two patients), and severe hydrocephalus (one patient). All of these patients had recurrent bouts of aspiration pneumonia. Performing the procedure was complicated by a previous Billroth II anastomosis (one patient), by previous subtotal gastrectomy (one patient), and an unusually high transverse stomach (one patient).

For the percutaneous gastrostomies and enteral-feeding-tube insertions, the patients were given nothing by mouth after midnight the evening before the procedure, and if possible, a soft nasogastric tube was inserted. In cases with esophageal obstruction in which this could not be accomplished, a 90-cm, 5-French catheter was manipulated perorally over a 0.035-in. Bentson guidewire (Cook, Inc., Bloomington; IN) and the tip positioned in the gastric fundus. To avoid puncturing the liver, sonography was used to demarcate the margin of the left lobe of the liver on the anterior abdominal wall. Since the colon can be easily identified at fluoroscopy, opacification of the colon was unnecessary. Approximately 200 cm^3 of room air were injected into the stomach via the nasogastric tube.

An 18-gauge Chiba needle was inserted percutaneously at the junction of the proximal and middle thirds of the stomach under fluoroscopic guidance. A heavy exchange guidewire (0.038 THSF 260 Coons-Cook or 0.035 THSF 260 Cook; Cook, Inc., Bloomington, IN) was advanced through the needle and made to form a fundal loop in the gastric fundus (Fig. 1A). A 90-cm, 5-French Teflon catheter was inserted over the guidewire and manipulated across the pylorus and into the jejunum distal to the ligament of Treitz. The catheter was then removed, leaving the guidewire distal to the ligament of Treitz, and one of two methods was used to achieve proximal jejunal feeding catheter position.

Thirty-six gastrostomies were performed by using a specially designed jejunostomy set (GJS-1020, Cook, Inc.). The tube is 100 cm long and 12 French in diameter. An important feature is the retention device (Friction Lock), which when unexpanded easily slides through a 15-French peelaway sheath (Fig. 2A). When expanded it is greater than 20 French, which hinders dislodgment secondary to peristalsis (Fig. 2B). A suture hub is present on the jejunal feeding catheter approximately 10 cm from the injection port (Figs. 2A and 2B). Also critical to the system is the 15-French peelaway sheath, which when placed into the gastric fundus, effectively eliminates resistance of the anterior abdominal and gastric wall (Fig. 2C). The rigidity of the 15-

Received January 9, 1986; accepted after revision May 5, 1986.
Presented at the annual meeting of the Radiological Society of North America, Chicago, November 1985.
[1] Department of Radiology, Sharp Memorial Hospital, 7901 Frost St., San Diego, CA 92123. Address reprint requests to G. D. Alzate.
[2] Present address: Department of Radiology, Victoria Hospital, London, Ontario, Canada N6A 4G5.

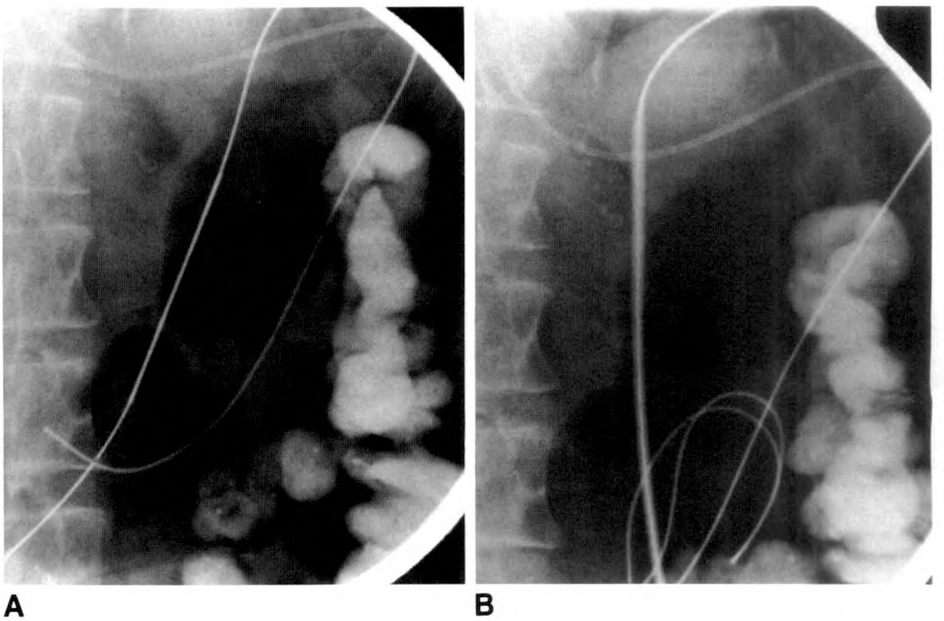


Fig. 1.—**A**, Radiograph of abdomen after puncture of stomach with an 18-gauge Chiba needle under fluoroscopic guidance showing a 260-cm guidewire forming fundal loop with tip placed at pylorus. Needle is then exchanged for a 5-French 90-cm catheter. A nasogastric tube is in place. Barium in colon is unrelated to procedure. **B**, Radiograph of abdomen showing 10-French dilator well into gastric fundus. Guidewire tip is at ligament of Treitz.

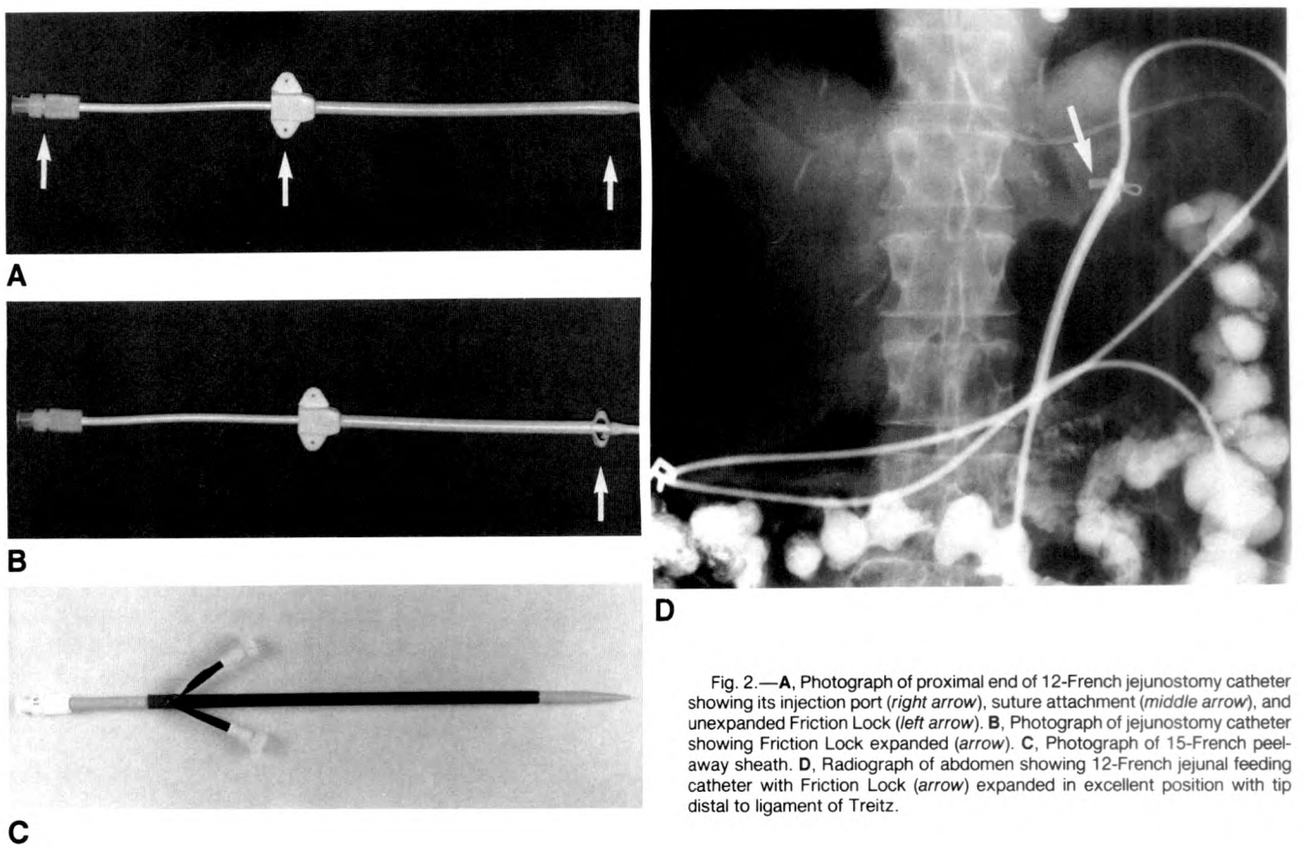
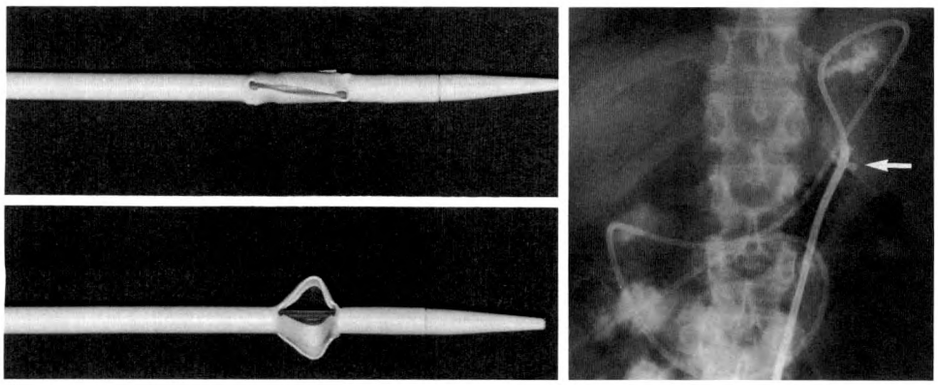


Fig. 2.—**A**, Photograph of proximal end of 12-French jejunostomy catheter showing its injection port (*right arrow*), suture attachment (*middle arrow*), and unexpanded Friction Lock (*left arrow*). **B**, Photograph of jejunostomy catheter showing Friction Lock expanded (*arrow*). **C**, Photograph of 15-French peelaway sheath. **D**, Radiograph of abdomen showing 12-French jejunal feeding catheter with Friction Lock (*arrow*) expanded in excellent position with tip distal to ligament of Treitz.

French peelaway sheath also helps to transmit axial forces more effectively to aid catheter movement. When feeding catheter position is optimal, the peelaway sheath is simply pulled apart leaving the jejunal catheter undisturbed.

This gastrostomy set is used to insert the 12-French jejunal feeding tube. The 5-French catheter used to place the guidewire distal to the ligament of Treitz is removed and exchanged directly for a 10-French dilator (Fig. 1B). This is followed by a 15-French peelaway sheath,



A B

Fig. 3.—**A**, Photograph of Gastrostik and disposable tip. Upper illustration, collapsed retention mechanism. Lower illustration, expanded retention mechanism after central stiffener has been slightly withdrawn. Tip pops off when coaxial 8-French jejunal feeding catheter is advanced over guidewire. **B**, Radiograph of abdomen shows Gastrostik with retention mechanism fully expanded (*arrow*) and coaxial 8-French jejunal feeding catheter in excellent position beyond ligament of Treitz.

which is placed well into the gastric fundus. A 12-French jejunostomy tube, cut to optimal length, is then fed over the guidewire, and its tip is placed just distal to the ligament of Treitz. A jejunal catheter is pushed up to the suture hub and the peelaway sheath is removed. The retention device (Friction Lock) is then expanded and the catheter is sutured into place (Fig. 2D).

In a second group of 24 patients, gastrostomies were performed using the Medi-tech Gastrostik (CGSK-01, Medi-tech, Watertown, MA), which is an 18-cm, 12.3-French gastrostomy sheath catheter with a removable tapered tip (Fig. 3A). An 8-French feeding catheter is pushed coaxially through the Gastrostik sheath pushing the removable tip ahead of it. Once the feeding catheter tip is positioned in the proximal jejunum, the guidewire is removed and the removable tip pops off into the small-bowel lumen and later passes per rectum. A mechanism in the tip of the Gastrostik enhances the retention of the 12.3-French sheath in the gastric lumen (Fig. 3A, lower).

For insertion of the Gastrostik with jejunal feeding catheter, the 5-French catheter used to place the guidewire distal to the ligament of Treitz is removed and then serial dilatations with 10- and 12-French dilators are performed. A 12.3-French Gastrostik sheath is placed over the guidewire. The central stiffener is not removed until the retention mechanism is well into the stomach. If any difficulty is encountered, a 15-French peelaway sheath is placed into the gastric lumen and the Gastrostik is passed coaxially. Thereafter, the stiffener is removed and the 8-French jejunal feeding catheter is pushed coaxially through the Gastrostik, pushing the removable tip ahead of it until the jejunal feeding tube is in place. The guidewire is then removed and contrast material is injected into the jejunal feeding tube to document its position relative to the mucosal surface (Fig. 3B). External tubing is attached to the catheter cuff and a dressing is applied. The removable tip of the Gastrostik will eventually pass per rectum.

After either system is in place, a supine abdominal radiograph is taken to document the final position of the catheter, and the nasogastric tube is attached to suction. The patient is kept in the supine position until the next morning, when feedings through the tube can begin, if the white blood cell count, temperature, and abdominal examination are normal. The enteral tube feedings are given by continuous infusion with the head of the bed elevated. If the feeding is temporarily discontinued, the tube is vigorously flushed with saline [4].

It is mandatory to prevent the patient from pulling on the tube until the tract matures. Because of explicit instruction for care and protection of the tube in the disoriented patient, and close communication with the nursing staff, we have rarely had to attempt to replace an enteral feeding tube in the first 7 postoperative days. If the tube is pulled out after 1 week, the tract can usually be recatheterized with a guidewire and a 5-French catheter. The jejunal feeding catheter can then be easily replaced.

Results

Sixty of 61 initial attempts to insert a jejunal feeding catheter were successful. In the patient in which it failed, a gastrostomy tube was placed. In adults, the procedure was performed under local anesthesia and required less than 45 min. Hepatomegaly did not prevent the procedure.

There were no deaths related to the procedure and no complications that required surgery. Two patients developed signs of peritonitis and fever, but both recovered with antibiotic therapy. Five patients developed minor stomal infections, two of which required antibiotic treatment. Minimal leakage from the stoma occurred in three patients. One had a retrogastric hematoma, and one had diffuse pneumatosis intestinalis, both without sequelae. One patient, who died of an unrelated cause, was found at autopsy to have penetration of the duodenal wall by an occluded catheter without peritonitis. In this case, which was done early in the series, the jejunal feeding tube was a straight 6-French polyethylene catheter, a material that is no longer used. Autopsies in seven patients done up to 2 months after the procedure showed mature tube tracts with minimal adhesions.

Two patients required two percutaneous punctures. One required a second puncture because of intraperitoneal catheter dislodgment, which occurred when a loop of catheter formed outside the stomach secondary to poor guidewire purchase. This complication occurred before an exchange guidewire distal to the ligament of Treitz was placed as the initial step. The second patient pulled his catheter out, and the tract, which was less than 7 days old, could not be reentered.

Discussion

The potential safety of proximal jejunal feeding as compared with nasogastric or nasoduodenal tube feeding has not been emphasized. The ends of nasogastric and nasoenteral tubes are routinely positioned in the stomach or duodenum, and tube feedings carry a risk of pulmonary aspiration as high as 38% [10, 11]. Percutaneous gastrostomy alone will not

reduce this risk. Experimental evidence suggests that nasoduodenal-feeding-tube placement results in gastric reflux of feeding material more than 50% of the time. However, when tube placement is distal to the ligament of Treitz, little gastric reflux occurs [12]. Thus a system of percutaneous catheter placement for jejunal feeding is needed.

Two key technical factors are fundamental to safe and effective percutaneous placement of a catheter for feeding. First, manipulation of the guidewire beyond the ligament of Treitz provides significant purchase to prevent dislodgment of the catheter or looping of the catheter between the stomach and anterior abdominal wall. Second, the secure purchase of the catheter in the jejunum makes the early postoperative period safer than it is with a gastrostomy catheter, because the infusion site is far removed from the gastric puncture site.

The catheters used in this series have several desirable features. We prefer the ease of insertion of the 12-French tube, but consider both systems to be adequate as enteral feeding systems. The 8-French tube/12.3-French gastrostomy sheath is essentially a smaller two-piece version of the 12-French system. A retaining mechanism in each system limits the possibility of accidental or inadvertent dislodgment of the catheter (Figs. 2B and 3A). The jejunal feeding catheters, if dislodged, can be easily remanipulated into the proper position at fluoroscopy. The large bore of the 12-French jejunal feeding tube results in fewer catheter changes and an approximate life of 3–4 months. If occluded, both the 8- and 12-French enteral feeding tubes are easily replaced in 5–10 min at fluoroscopy.

REFERENCES

1. Ho CS, Gray RR, Goldfinger M, Rosen IE, McPherson R. Percutaneous gastrostomy for enteral feeding. *Radiology* **1985**;156:349–351
2. Wills JS, Oglesby JT. Percutaneous gastrostomy: further experience. *Radiology* **1985**;154:71–74
3. Ponsky JL, Gauderer MK, Stellato TA. Percutaneous endoscopic gastrostomy. *Arch Surg* **1983**;118:913–914
4. Rombeau JL, Barot LR. Enteral nutritional therapy. *Surg Clin North Am* **1981**;61(3):605–621
5. Wateska LP, Sattler LL, Steiger E. Cost of home parenteral nutrition program. *JAMA* **1980**;244:2303–2304
6. Howard L, Michalek AV. Home parenteral nutrition (HPN). *Annu Rev Nutr* **1984**;4:69–99
7. Heymsfield SB, Bethel RA, Ansley JD, Nixon DW, Rudman D. Enteral hyperalimentation: an alternative to central venous hyperalimentation. *Ann Intern Med* **1979**;90:63–71
8. Ruppin H, Sailer D. Nasoenteral alimentation: technical procedures and follow-up. *Hepatogastroenterology* **1983**;30:161–165
9. Sheldon GF, Petersen SR, Sanders R. Hepatic dysfunction during hyperalimentation. *Arch Surg* **1978**;113:504–508
10. Miller KS, Tomlinson JR, Sahn SA. Pleuropulmonary complications of enteral tube feedings. Two reports, Review of the literature and recommendations. *Chest* **1985**;88(2):230–233
11. Winterbauer RH, Durning RB, Barran E, McFadden MC. Aspirated nasogastric feeding solution detected by glucose strips. *Ann Intern Med* **1981**;95:67–68
12. Gustke RF, Varma RR, Soergel KH. Gastric reflux during perfusion of the small bowel. *Gastroenterology* **1970**;59:890–895

Case Report

Percutaneous Gastrostomy: Applications in Gastric Carcinoma and Gastroplasty Stoma Dilatation

John S. Wills[1]

Percutaneous gastrostomy is a safe, effective alternative to surgical gastrostomy in patients who are candidates for enteric feeding but in whom transoral or transnasal feeding options are unacceptable [1]. Additional applications of this technique are possible. In a patient with severe vomiting and gastroesophageal reflux secondary to scirrhous carcinoma of the stomach, percutaneous gastrostomy was used to drain secretions. In a second patient with diffuse gastric carcinoma, percutaneous gastrostomy was performed in order to place a catheter in the jejunum for enteric feeding. In another patient with an inappropriately narrow stoma after gastroplasty, gastrostomy was used to supply enteric feeding and as a route for retrograde balloon dilatation of the stoma.

Case Report

A 67-year-old woman was referred for percutaneous gastrostomy to palliate intractable vomiting and gastroesophageal reflux associated with gastric carcinoma of the linitis plastica variety. She had undergone surgical feeding jejunostomy, but a presumed small bowel obstruction had rendered it nonfunctional. Endoscopic percutaneous gastrostomy was attempted but was unsuccessful because of poor gastric transillumination and resistance to passage of the trocar through the gastric wall from within. Several days later, percutaneous gastrostomy was performed in the usual manner. Although the stomach was less distensible than usual, sufficient air insufflation to permit the procedure was possible (Fig. 1). Upon insertion of the 9-cm sheathed trocar, mild resistance was encountered, but the trocar entered the stomach with relative ease. The guidewire, dilators, and 12-French gastrostomy catheter were inserted without incident. Mild transient oozing of blood from the puncture site occurred for several minutes, but ceased spontaneously. No blood was aspirated from the stomach immediately after the procedure nor thereafter, and there was no other evidence of blood loss due to the procedure.

The catheter was used for gastric suction until the patient's death approximately 1 month later. During this time, vomiting ceased promptly with the use of gastric suction.

Discussion

Experience with approximately 70 patients in our institution continues to support the use of percutaneous gastrostomy as a safe, effective alternative to surgical gastrostomy. This procedure has the potential to replace parenteral hyperalimentation in many patients for whom enteric feeding is not contraindicated. Additional applications of the procedure include gastric drainage and dilation of the gastric stoma after surgery for morbid obesity [2–4].

Percutaneous gastrostomy proved to be a satisfactory method to drain the stomach in a patient with vomiting resulting from gastric carcinoma. This patient was not a candidate for surgical gastrostomy, and endoscopic gastrostomy had been unsuccessful. Intractable vomiting represented a serious problem with her management. Difficulties with needle and catheter insertion and with catheter manipulation were expected because of limited distensibility of the stomach caused by the tumor. However, except for a gritty sensation with mild resistance during passage of the catheters, and transient oozing of blood from the puncture site, the

Received December 13, 1985; accepted after revision April 22, 1986.

[1] Department of Radiology, Medical Center of Delaware, Christiana Hospital, P.O. Box 6001, Ogletown-Stanton Rd., Newark, DE 19718. Address reprint requests to J. S. Wills.

AJR 147:826–827, October 1986 0361–803X/86/1474–0826 © American Roentgen Ray Society

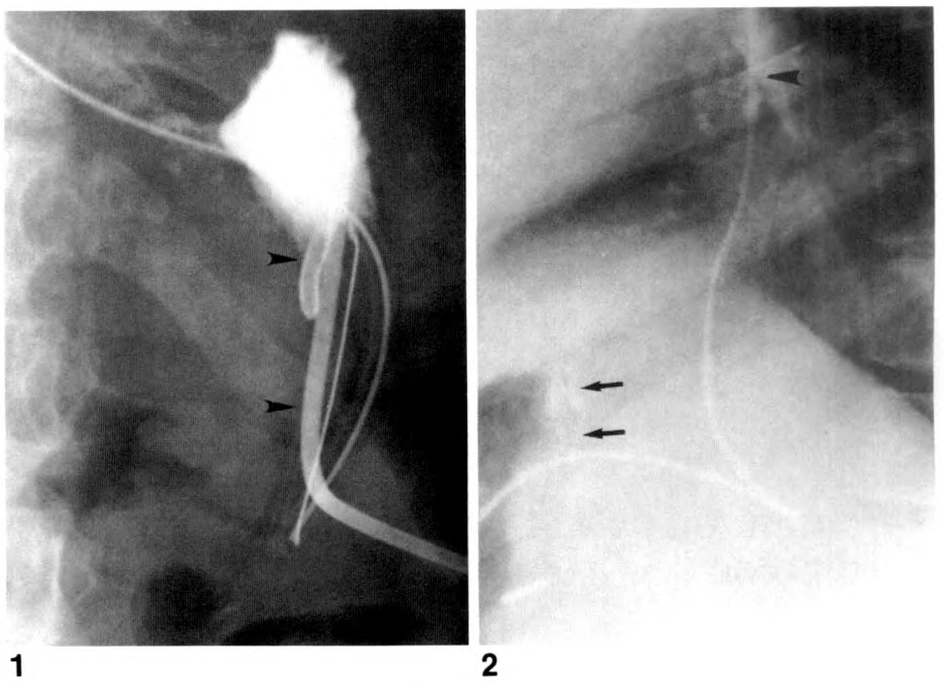


Fig. 1.—Anteroposterior spot film showing a 12-French gastrostomy catheter (*arrowheads*) positioned in proximal stomach. Stomach is markedly contracted by diffuse carcinoma. Nasogastric tube is in place.

Fig. 2.—Lateral radiograph showing Headhunter catheter inserted through gastroplasty stoma (*arrows*) into distal esophagus. A 250-mm exchange guidewire (*arrowhead*) has been introduced through catheter for insertion of balloon dilator.

1 **2**

procedure and the subsequent management of the gastrostomy site and catheter were uncomplicated.

In another patient with diffuse gastric carcinoma, gastrostomy was performed with placement of a catheter in the jejunum for feeding. The procedure was tolerated without incident by the patient, and the catheter continues to function satisfactorily.

After the failure of attempted endoscopic dilatation of a gastroplasty stoma in another patient, fluoroscopically guided antegrade cannulation was attempted. This procedure was unsuccessful despite prolonged effort, largely because of inability to negotiate the stoma. After percutaneous gastrostomy, initially performed to facilitate enteric feeding, retrograde passage through the stoma was accomplished with a 6.5-French Headhunter 1 (Cordis Corp., Miami, FL) catheter. A 250-mm exchange guide was inserted retrograde into the esophagus through the catheter (Fig. 2). Three separate dilations were performed, ultimately using a 20-mm balloon. The patient's tolerance for oral feedings improved, and the gastrostomy catheter was subsequently removed without incident.

Retrograde balloon dilation of a gastric stoma is a logical extension of percutaneous gastrostomy and conventional balloon dilation techniques [5, 6]. Our experience favors the use of multiple dilations, each maintained for 2–10 minutes. Incremental inflation of the same size balloon, using multiple reinflations at the same session, and the use of progressively increasing balloon diameters at separate sessions are suggested [5, 7]. In patients with gastroplasty for obesity, a luminal diameter of 10–12 mm is considered ideal [8]. In one case, Griffin [8] chose a 12-mm balloon for the initial dilation, but because the patient was not a good surgical candidate and because a 12-mm balloon had no effect, then selected larger balloons. The satisfactory results suggested that larger balloons result in dilation of the stoma to the ideal range.

REFERENCES

1. Wills JS, Oglesby JT. Percutaneous gastrostomy: further experience. *Radiology* **1985**;154:71–74
2. Agha FP, Harris HH, Boustany MM. Gastroplasty for morbid obesity: roentgen evaluation and spectrum of complications. *Gastrointest Radiol* **1982**;7:217–223
3. Smith C, Gardiner R, Kubicka RA, Dieschbourg JJ. Radiology of gastric restrictive surgery. *Radiographics* **1985**;5:193–216
4. Wolper JC, Messmer JM, Turner MA, Sugerman HJ. Endoscopic dilatation of late stomal stenosis. *Arch Surg* **1984**;119:836–837
5. Dawson SL, Mueller PR, Ferrucci JT, et al. Severe esophageal strictures: indications for balloon catheter dilatation. *Radiology* **1984**;153:631–635
6. McLean GK, Rosen RJ, Ring ET. Miscellaneous interventional procedures. In: Ring EJ, McLean GK, eds. *Interventional radiology: principles and techniques*. Boston: Little, Brown, **1981**: 441–463
7. Goldthorn JF, Ball WS, Wilkinson LG, Seigel RS, Koslowske AM. Esophageal strictures in children: treatment by serial balloon catheter dilatation. *Radiology* **1984**;153:655–658
8. Griffin WO. Surgical management of morbid obesity. In: Moody FG, Carey LC, Jones RC, et al., eds. *Surgical treatment of digestive disease*. Chicago: Year Book Medical, **1986**:257–263

Technical Note

A Modified Cope Introducer Set for Rapid Insertion of a Safety Wire

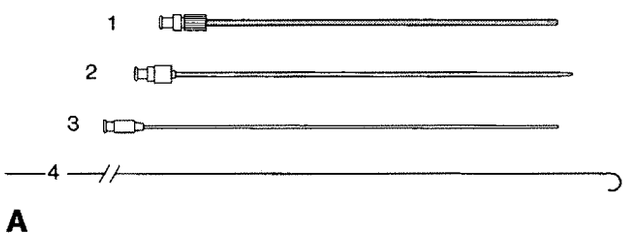
R. Brooke Jeffrey, Jr.[1]

In many interventional procedures it is often desirable to have a second guidewire in place as a safety wire to preserve access [1]. This article describes a modified Cope introducer set [2] consisting of a coaxial sheath and dilator that can be used for rapid insertion of two 0.038-in. guidewires with a 21-gauge needle puncture.

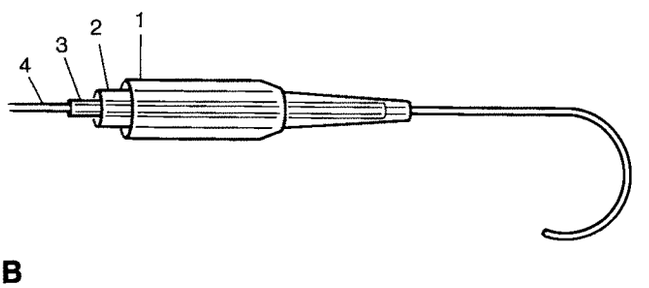
Technique

The modified Cope introducer set (JWGE-10 wire exchange set, Cook, Inc., Bloomington, IN) described in this report includes the following components (Fig. 1): (1) a 21-gauge needle used in the Cope set; (2) a 60-cm, 0.018-in. (0.05 cm) stainless-steel wire with a flexible tip (similar to the 0.018-in. Cope introducer set wire but with a 3-mm closed J configuration); (3) a 19-gauge steel cannula used in the Cope set; (4) 6.3-French tapered to 4-French polyethylene end-hole dilator; and (5) an outer 8-French thin-walled, tapered Teflon sheath that loads coaxially over the inner dilator.

After initial puncture with a 21-gauge needle, the 0.018-in. wire is coiled within the renal collecting system (Fig. 2A, left). The tract is then dilated using the 6.3-French-tapered-to-4-French polyethylene dilator using an inner 19-gauge metal cannula (Fig. 2A, right). The 6.3-French dilator and inner metal cannula are then withdrawn leaving the 0.018-in. guidewire in place. The thin-walled 8-French (0.104-in.) tapered Teflon sheath is then loaded coaxially over the 6.3-French dilator and is inserted as a unit over the 0.018-in. guidewire again with the 19-gauge inner metal cannula in place (Fig. 2B, left). Once the outer 8-French thin-walled sheath has been introduced into the collecting system, both the 19-gauge metal cannula and the inner



A



B

Fig. 1.—**A**, Components of modified Cope introducer set. 1 = 8-French slightly tapered Teflon sheath. 2 = 6.3-French polyethylene dilator tapered to 4 French. 3 = 19-gauge inner metal cannula. 4 = 0.018-in. stainless wire with flexible tip having a 3-mm closed J configuration. **B**, Magnified view of assembled components labeled as in **A**.

Received March 10, 1986; accepted after revision May 5, 1986.

[1] Department of Radiology, University of California and San Francisco General Hospital, San Francisco, CA 94110. Address reprint requests to R. B. Jeffrey, Jr., Dept. of Radiology, San Francisco General Hospital, San Francisco, CA 94110.

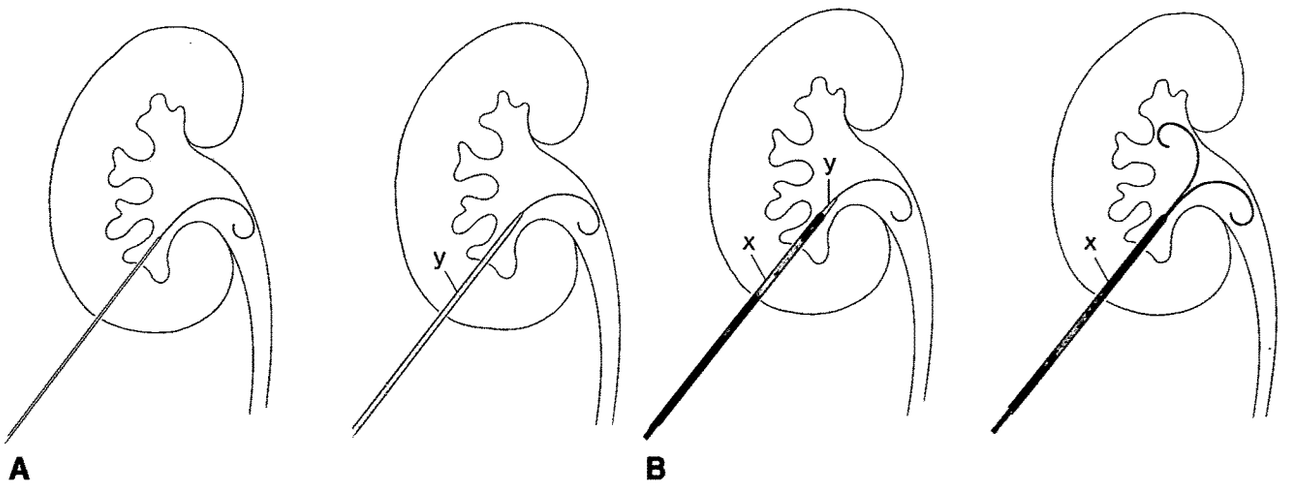


Fig. 2.— **A**, Technique for safety wire insertion using modified Cope introducer set. **A** (left) demonstrates 21-gauge needle puncturing renal collecting system and 0.018-in. wire inserted into renal pelvis. **A** (right) demonstrates first step of tract dilatation with 6.3-French polyethylene dilator tapered to 4 French (y). 19-gauge inner metal cannula has been inserted inside 6.3-French dilator but is not depicted in this drawing. **B** (left) shows second step in tract dilatation using 8-French thin-walled sheath (x) loaded coaxially over 6.3-French dilator (y) and inner metal cannula (metal cannula not shown). **B** (right) shows two 0.038-in. guidewires inserted through 8-French sheath (x). Initial 0.038-in. guidewire is inserted with original 0.018-in. wire in place.

6.3-French dilator are removed, leaving the 0.018-in. guidewire in place. If there is any question about the position of the outer 8-French sheath within the collecting system, contrast material can be injected through a sidearm adapter with the 0.018-in. guidewire in place. A 0.038-in. (0.1 cm) guidewire is then inserted through the sheath and coiled in the collecting system. A second 0.038-in. guidewire may then be introduced through the sheath as a safety wire after removing the first 0.018-in. wire (Fig. 2B, right).

Discussion

This modification of the Cope introducer set using a 21-gauge needle has been used successfully in 25 interventional procedures (18 percutaneous nephrostomies for renal stone extraction, four abscess drainages, and three biliary drainages). In all cases, a second heavy-duty 0.038-inch guidewire was employed as a safety wire. The present coaxial dilator system has several advantages compared with the original Cope introducer system [3]. First, it avoids the difficulty of inserting a 0.038-in. guidewire through the sidehole in an angled dilator [3, 4]. Second, it allows simultaneous introduction of a 0.038-in. guidewire while the 0.018-in. guidewire is still in place. Finally, the 8-French sheath allows for the rapid introduction of a second 0.038-in. guidewire as a safety wire.

We have not used the 21-gauge needle and modified Cope set in cases where extensive perirenal scarring is anticipated, such as in patients with prior renal surgical procedures. However, we have used this system in several obese patients without difficulty. As with the original Cope introducer set, visualization of the 0.018-in. guidewire may be somewhat difficult in obese patients. Visualization can be improved, however, with the use of magnification fluoroscopy. No significant buckling of the 0.018-in. guidewire has been observed during tract dilatation.

REFERENCES

1. Dawson S, Papanicolaou N, Mueller PR. Preserving access during percutaneous catheterization using a double-guidewire technique. *AJR* **1983**;141:407
2. Cope C. Conversion from small (0.018-inch) guidewires in percutaneous drainage procedures. *AJR* **1982**;138:170–171
3. Greenwood LH, Yrizarry JM, Brown SB. Observations on the use of the Cope introduction set. *AJR* **1985**;144:257–258
4. Chuang BP, Alspaugh JP, Harris SA Jr, et al. A modified application of the Cope introduction set. *AJR* **1985**;145:1073–1074

Technical Note

The Universal Stent Introducer: A Simplified Approach to Antegrade Ureteral Stent Insertion

Won J. Lee[1] and Mark Rich[2]

Ureteral stenting is indicated for temporary or permanent urinary diversion for the management of ureteral perforations or fistulae. Also used after dilatation of strictures, after percutaneous surgery (such as endopyelotomy), and for relief of ureteropelvic junction obstruction, stenting may also relieve ureteral obstruction secondary to external compression caused by retroperitoneal fibrosis or treatable neoplasms [1]. As more endourological procedures are performed on the upper urinary tract, the need for ureteral stenting will undoubtedly increase.

Many types of ureteral stents are available, testimony to the fact that no single design is appropriate for all applications and all patients. One of these designs is the universal (Smith) stent, which provides both standard stenting and optional nephrostomy drainage with a single-size tube that is cut to fit the patient [2, 3]. Although there are many advantages to the universal ureteral stent, such as softness, tissue compatibility, ease of exchange, and ready availability of access to the kidney, some reluctance to use this stent has resulted from the difficulties of inserting it percutaneously. We recently solved this problem with a new stent introducer [4], which is described here along with the indications, contraindications, and directions for use of the universal stent.

Materials and Methods

The universal ureteral stent (Heyer-Schulte, Goleta, CA) is 79 cm long and is available in 8-French and 12-French sizes. It is made of radial-compression–resistant silicone rubber with a linear barium strip marker and a 4-cm region of renal pelvic drainage holes marked at both ends with tantalum-impregnated markers. A 40-cm-long segment is distal to this region, and its terminal (15 cm long) also has drainage holes. The beginning of the distal group of holes is also marked with radiopaque material. The distal end is cut by the radiologist to fit the individual patient's needs. The proximal end of the stent, which protrudes from the nephrostomy site, has a Luer-Lock adaptor to facilitate flushing and a silicon rubber cap to occlude the stent if external drainage is not desired. The introducer consists of a 60-cm, 9-French polyethylene catheter that tapers to fit a 0.038-in. (0.1-cm) guidewire and 56-cm, 11-French peel-away Teflon sheath. Peel-away sheath sets (Cook Inc., Bloomington, IN) are now available in 8- to 18-French sizes.

For antegrade insertion of the universal stent, a percutaneous nephrostomy is performed through a posterolateral approach into a calyx (usually posterior-middle calyx) that will make the stent describe a gentle curve into the upper ureter. The tract is dilated to 11-French and the introducer with its peel-away sheath is advanced over the 0.038-in. guidewire through the nephrostomy tract down to the bladder. The 9-French inner polyethylene catheter and the guidewire are removed, and the universal stent, cut to the appropriate length as determined by fluoroscopy and radiographs, is threaded over a well-lubricated 0.038-in. Lunderquist guidewire, leaving only 2 cm of the floppy tip of the guidewire protruding from the stent. The assembly is then passed into the urinary tract and down to the bladder through the lumen of peel-away sheath. The stent is held in position by slight pressure on its proximal portion while the peel-away sheath is progressively withdrawn until it has been totally removed (Fig. 1). The Lunderquist wire is then removed, the proximal portion of the stent

Received February 18, 1986; accepted after revision April 30, 1986.

[1] Department of Radiology, Long Island Jewish Medical Center, New Hyde Park, NY 11042, and State University of New York School of Medicine at Stony Brook, Stony Brook, NY 11797. Address reprint requests to W. J. Lee at Long Island Jewish Medical Center.

[2] Department of Urology, Long Island Jewish Medical Center, New Hyde Park, NY 11042.

AJR 147:830–831, October 1986 0361–803X/86/1474–0830 © American Roentgen Ray Society

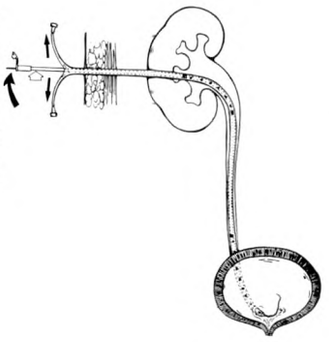
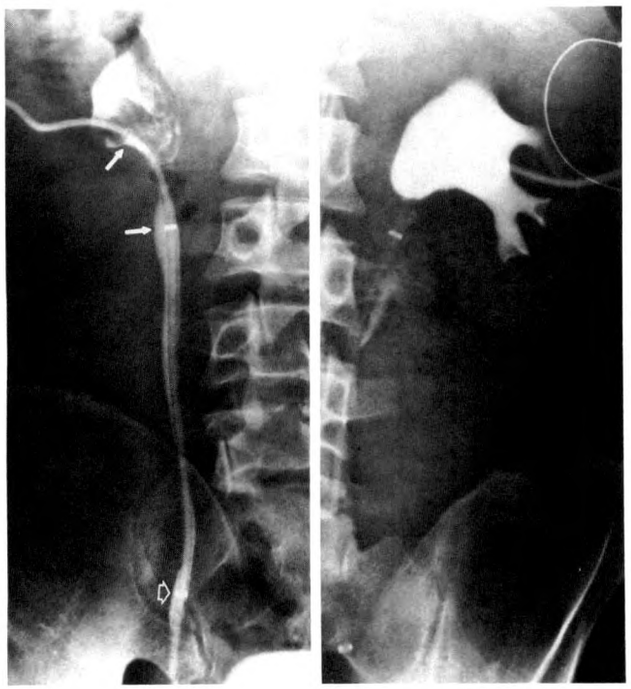


Fig. 1.—11-French peel-away stent introducer (*small straight arrows*) is progressively withdrawn until it is totally removed, while universal stent (*open arrow*) is held in place by either Lunderquist or torque guidewire. Guidewire is then removed and position of stent is checked. Guidewire in catheter is indicated by a *large curved arrow*.



A **B**

Fig. 2.—**A**, Stentogram after percutaneous stone extraction and endopyelotomy shows universal stent in place without obstruction or extravasation. Contrast material within tube indicates patency. Renal pelvic drainage holes marked at both ends are indicated by *arrows*. *Open arrow* indicates beginning of distal group of holes.

B, Occluded stent. Stentogram shows no contrast material within tube, thus indicating occlusion. Irrigation with normal saline and guidewire manipulation were done for cleansing of blood clot or debris in stent. Stent can also be easily replaced with new peel-away stent introducer if other technique fails.

is coiled, and a povidine-iodine dressing is applied to the flank. A few days later, when the urine is clear, the stent is flushed with saline and adjusted if necessary so that one set of drainage holes is in the renal pelvis and the other is in the bladder or lower ureter (Figs. 2A and 2B). This can be checked by injecting contrast medium. The stent is then fixed to the skin with silk sutures and capped if external drainage is not desired. The dressing is changed twice a week. With the peel-away stent introducer system, we have successfully placed the universal stent in 93 of 98 patients with various urological problems and have found them to be effective and easy to use. The patient's tolerance has been excellent and no significant complications have been observed.

Discussion

In patients with malignant obstruction, in whom the ability of the kidney to recover is often in doubt, universal stent is an excellent choice, since it allows one to monitor the urine output of the kidney while relieving the obstruction. Similarly, it is helpful if renal failure may be impending. With an internal stent, it can be difficult to determine whether a patient with anuria has an occluded stent or is truly in renal failure, and cystoscopy and stent replacement are undesirable. If a universal stent is in place, however, it can simply be uncapped. Further, if the stent does prove to be occluded, it can be flushed or exchanged with a new peel-away introducer.

The universal ureteral stent generally is contraindicated when external urinary diversion is not indicated. Some reported problems common to all indwelling stents include encrustation, irritative bladder symptoms, microhematuria, and pyuria. Pyelonephritis and ureteritis cystitica are uncommon and usually secondary to stent occlusion. Urine cultures should be obtained monthly and patients should take appropriate antibiotics. This is particularly important with a silicone elastomer stent, as this material encourages stone formation in the presence of bacteria.

The use of a sheath to introduce a variety of ureteral stents has been previously described [5–7]. The new peel-away system has multiple uses, including antegrade stent introduction, negotiation of tortuous or obstructed ureter, placement of a second guidewire into the ureter during percutaneous stone extraction, stone basketing, and removal of a foreign body such as migrated stent. The thin-wall sheath has a tendency to kink at the ureteropelvic junction and thus to decrease lumen size and usability. However, it can be straightened by gently pulling the sheath.

REFERENCES

1. Coleman CC, Kimura Y, Castaneda-Zuniga WR, et al. Interventional techniques in the ureter. *Semin Intervent Radiol* **1984**; 1:24–37
2. Smith AD. The universal ureteral stent. *Urol Clin North Am* **1982**;9:103–107
3. Smith AD, Lee WJ. Characteristics and uses of the universal (Smith) ureteric stent. *Br J Urol* **1983**;55(Suppl):79–81
4. Smith A, White E, Lee W. The universal stent introducer (abstract). *J Urol* **1984**;131:134A
5. Salazar JE, Johnson JB, Scott R, Pinstein M. A simplified method for placement of internal ureteral stents. *AJR* **1983**;140:611–612
6. Hackethorn JC, Boren SR, Dotter CT, Rösch J. Antegrade internal ureteral stenting: a technical refinement. *Radiology* **1985**;156:827–828
7. Bettman MA, Perlmutt L, Finkelstein J, Meyerovitz MF, Richie JR. Percutaneous placement of soft, indwelling ureteral stent. *Radiology* **1985**;157:817–818

Case Report

Shearing of Percutaneous Nephrostomy Catheter During Indwelling Ureteral Stent Placement

Steven K. Sussman,[1] Edward J. Oke, Louis M. Perlmutt, and N. Reed Dunnick

The use of indwelling ureteral stents for treatment of ureteral obstruction, strictures, or fistulae is a well-established technique that is a viable alternative to either surgery or percutaneous nephrostomy. Complications associated with the use of these stents are problems related to the initial percutaneous nephrostomy (vascular trauma, urinoma, infection), transient ureteral obstruction from mucosal edema, spontaneous breakage of the stent, migration of the stent, and encrustation [1]. We describe a new complication: the shearing off of a portion of a previously established percutaneous nephrostomy catheter during the removal of a nylon safety suture attached to the proximal end of the stent.

Case Report

The patient was a 69-year-old man with peritoneal carcinomatosis and bilateral hydronephrosis secondary to carcinoma of the prostate. A percutaneous nephrostomy catheter had been placed to drain the left kidney. With access through this catheter, a heavy-duty 0.038-in (0.097 cm) guidewire was passed down the ureter into the bladder. A 3-0 nylon safety suture was passed through the end hole and out the proximal side hole of the proximal end of a double pigtail ureteral stent to allow repositioning once the stent was beneath the skin. The ureteral stent was then fed over the guidewire to the level of the skin puncture site. At this point a pusher was used to further advance the stent so that its distal pigtail coiled in the bladder and its proximal pigtail coiled in the region of the renal pelvis. The guidewire was then removed from the stent but not from the collecting system, thus allowing for coiling of the guidewire in the renal pelvis so that an externally draining percutaneous nephrostomy catheter could be placed. A 6-French polyethylene pigtail catheter was passed over the guidewire, and injection of contrast medium verified the intrapelvic position of the proximal stent. The nylon safety suture was then pulled without difficulty. Immediately thereafter it was noticed that the percutaneous nephrostomy catheter was disrupted, with its distal end free in the renal pelvis. A guidewire was placed through the proximal end of the catheter to allow placement of a new percutaneous nephrostomy catheter (Fig. 1). The free distal end was left within the collecting system, as it was decided that removal of this catheter fragment was not essential in this patient.

Discussion

Specific complications associated with the use of indwelling ureteral stents are transient obstruction, encrustation, migration, and spontaneous breakage of the stent. Transient obstruction is a common phenomenon that occurs early and is presumably secondary to edematous changes caused by the pressure effect of the catheter. This usually resolves within 5 to 8 days [2]. Encrustation with phosphate crystals is uncommon and is associated with urinary tract infection and an alkaline urine [1]. Migration can occur both upward into the renal parenchyma [3] and downward into the bladder and may require replacement of the device if the obstruction is no longer stented. Spontaneous breakage is presumably secondary to deterioration of the stent after long-term exposure to the urinary system and to kinking and bending at the time of insertion [1].

The technique for antegrade insertion of indwelling ureteral stents has been described [4]. A commonly used modification is placement of a nylon suture through the proximal end hole and out the most proximal side hole. Once the stent is out of reach within the collecting system, it still can be pulled back-

Received January 29, 1986; accepted after revision April 22, 1986.
[1] All authors: Box 3808, Department of Radiology, Duke University Medical Center, Durham, NC 27710. Address reprint requests to S. K. Sussman.
AJR 147:832–833, October 1986 0361–803X/86/1474–0832 © American Roentgen Ray Society



Fig. 1.—Proximal pigtail of indwelling ureteral stent is well positioned in the renal pelvis. Distal portion of sheared percutaneous nephrostomy catheter has its pigtail within left upper pole collecting system. An intact externally draining percutaneous nephrostomy is also present. Distal end of a right indwelling ureteral stent is seen in bladder.

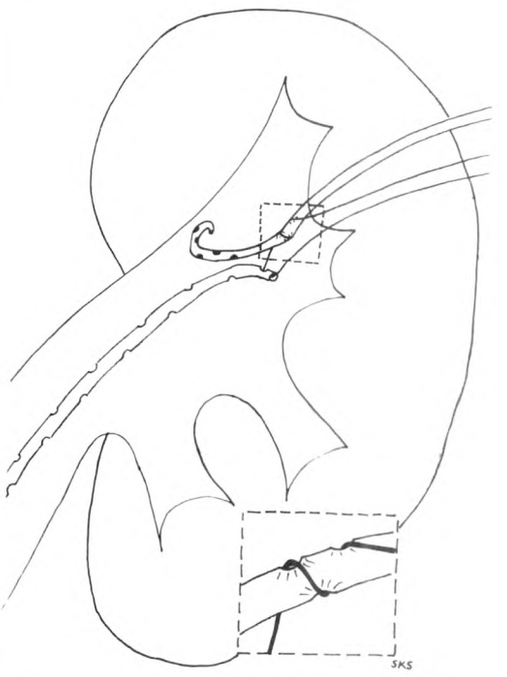


Fig. 2.—Proposed mechanism for shearing of externally draining percutaneous nephrostomy catheter during pulling of nylon safety suture. A loop of nylon safety suture is shown wound around percutaneous nephrostomy catheter. Catheter may be sliced as suture is dragged across it during removal (see insert).

1 2

ward, if necessary, simply by pulling both limbs of the nylon safety suture that are protruding through the skin puncture site. Once the stent is positioned satisfactorily, the suture can be removed by pulling a single limb while maintaining stent position with the pusher.

After placement of an indwelling ureteral stent, an externally draining percutaneous nephrostomy catheter is often left in place for 24 to 72 hr to be certain that the indwelling stent is functioning well [5]. After removal of the pusher the guidewire is removed from the stent but not from the collecting system, thus providing access for final placement of a percutaneous nephrostomy catheter. An alternative method for providing access for the final percutaneous nephrostomy catheter is exchange of the initial catheter for a peel-away sheath through which two guidewires are placed in the renal pelvis. One guidewire is used for stent placement and the other for final placement of the percutaneous nephrostomy catheter. In our case, we wished to verify the position of the proximal pigtail in the renal pelvis by observing the injection of contrast medium; therefore the nylon safety suture was not removed until after placement of the final, externally draining percutaneous nephrostomy catheter. During the pulling of this nylon safety suture the tip of the polyethylene percutaneous nephrostomy catheter was sheared off. A single loop of nylon that may have wound around the catheter during manipulations presumably sliced through it (Fig. 2). Although the indwelling sheared fragment of the percutaneous nephrostomy catheter was not removed in our case, removal of catheter fragments in the renal pelvis can be performed by the radiologist via a percutaneous approach by using forceps, baskets [6], or angiographic guidewire loop-snare devices.

Recently a new method of introducing double-J stent catheters by means of a coaxial sheath system has been described [7]. This may eliminate the problem of shearing of the externally draining percutaneous nephrostomy catheter during the pulling of a safety suture, as the pusher itself functions as the externally draining percutaneous nephrostomy catheter.

To avoid shearing of percutaneous nephrostomy catheters during placement of indwelling ureteral stents, we recommend either careful fluoroscopic monitoring during pulling of the safety suture if another catheter is within the renal pelvis or exchange of the catheter for a guidewire during this manuever, with subsequent replacement of the catheter after the nylon safety suture has been removed.

REFERENCES

1. Elyaderani MK, Kandzari SJ, Castaneda WR, Lange PH. *Invasive uroradiology: A manual of diagnostic and therapeutic techniques*. Lexington, MA: Collamore Press **1984**:55–95
2. Levine RS, Pollack HM, Banner MP. Transient ureteral obstruction after ureteral stenting. *AJR* **1982**;138:323–327
3. Oswalt GC, Bueschen AJ, Lloyd LK. Upward migration of indwelling ureteral stents. *J Urol* **1979**;122:249–250
4. Mazer NJ, LeVeen RF, Call JE, Wolfe G, Baltaxe HA. Permanent percutaneous antegrade ureteral stent placement without transureteral assistance. *Urology* **1979**;14:413–419
5. Elyaderani MK, Gabriele OF, Kandzari SJ, Belis JA. Percutaneous nephrostomy and antegrade ureteral stent insertion. *Urology* **1982**;20:650–656
6. LeRoy AJ, Williams HJ, Segura JW, Patterson DE, Benson RC. Indwelling ureteral stents: percutaneous management of complications. *Radiology* **1986**;158:219–222
7. Mercado S, Hawkins J, Herrera MA, Caridi JG, Hawkins IF. Simplified method of introducing double-J stent catheters using a coaxial sheath system. *AJR* **1985**;145:1271–1273

Case Report

Successful Treatment of Superior Vena Cava Syndrome by Venous Angioplasty

Cynthia S. Sherry,[1] Norman G. Diamond,[1] Thomas P. Meyers,[2] and Russell L. Martin[3]

Obstruction of the superior vena cava is a rare complication of a transvenous cardiac pacemaker [1–3]. Thrombosis and fibrotic stenosis are the usual mechanisms of obstruction [1], and treatment usually involves anticoagulant therapy, thrombolytic agents, or surgical intervention [2, 3]. We report successful balloon dilatation of a superior vena cava stenosis that had developed as a complication of a cardiac pacemaker.

Case Report

An 82-year-old white woman was admitted to Baylor University Medical Center with symptoms of superior vena cava syndrome, including progressive swelling of her face, neck, and arm over a 4-day period. Venous distension and pitting edema of the anterior chest, arm, and neck were noted upon physical examination. A permanent atrioventricular synchronous pacemaker had been inserted from a left subclavian venous approach 2½ years before. Superior vena caval thrombosis was suspected. Findings on a chest radiograph were negative for a mediastinal mass. Venography was performed via simultaneous injection of both upper extremity venous systems. A focal 5-mm stenosis of the superior vena cava was noted at its junction with the right and left innominate veins. Pacemaker leads entered the lumen of the superior vena cava at the point of stenosis. The next day, from a right common femoral venous approach, a 0.035-in. (0.09 cm) J-tipped guidewire was advanced into the superior vena cava and followed by a 5-French straight selective catheter, modified with a gentle distal curve. By means of the J-wire the stenosis was easily traversed, and the 5-French catheter was advanced into the right innominate vein. Systolic pressure above the stenosis was 19 mm Hg. The selective catheter was then exchanged for an 8-French dilatation catheter equipped with a 10-mm balloon. The hourglass deformity was eliminated upon inflation of the balloon. A repeat venacavogram revealed successful dilatation of the stenosis. After dilatation, systolic pressure in the right innominate vein was 12 mm Hg.

The patient was symptom free and remained well until 15 months later, when symptoms recurred. Venography showed recurrence of the stenosis in the same region. Pressure above the lesion, in the right internal jugular vein, was 19/17 mm Hg (mean 18 mm Hg), while that below the lesion, in the superior vena cava was 6/3 mm Hg (mean 4 mm Hg). The stenosis was dilated to 12 mm (2 mm greater than before) by means of a 9-French dilatation catheter with a 12-mm balloon (See Fig. 1).

Pressure readings after dilatation were 19/14 mm Hg (mean 17 mm Hg) and 17/9 mm Hg (mean 13 mm Hg) above and below the level of stenosis. Minimal residual luminal narrowing was evident. Once again the patient was relieved of symptoms. She was discharged the next day on a regimen of 300 mg of aspirin each day.

Discussion

Percutaneous transluminal angioplasty is a well-established treatment for a variety of arterial occlusions and stenoses. Venous angioplasty has been applied primarily to stenoses of saphenous vein bypass grafts [4]. Reports of angioplasty for larger vein stenoses have been limited. Hepatic vein stenosis and inferior vena cava stenosis [5, 6] due to the Budd-Chiari syndrome have been dilated successfully, as has portal vein occlusion secondary to chronic pancreatitis [7]. There is also a report of superior vena cava angioplasty in a 15-month-old

Received April 21, 1986; accepted May 19, 1986.
[1] Department of Radiology, Baylor University Medical Center, 3500 Gaston Ave., Dallas, TX 75246. Address reprint requests to N. G. Diamond.
[2] Department of Surgery, Baylor University Medical Center, 3500 Gaston Ave., Dallas, TX 75246.
[3] Department of Internal Medicine, Baylor University Medical Center, 3500 Gaston Ave., Dallas, TX 75246.

AJR 147:834–835, October 1986 0361–803X/86/1474–0834 © American Roentgen Ray Society

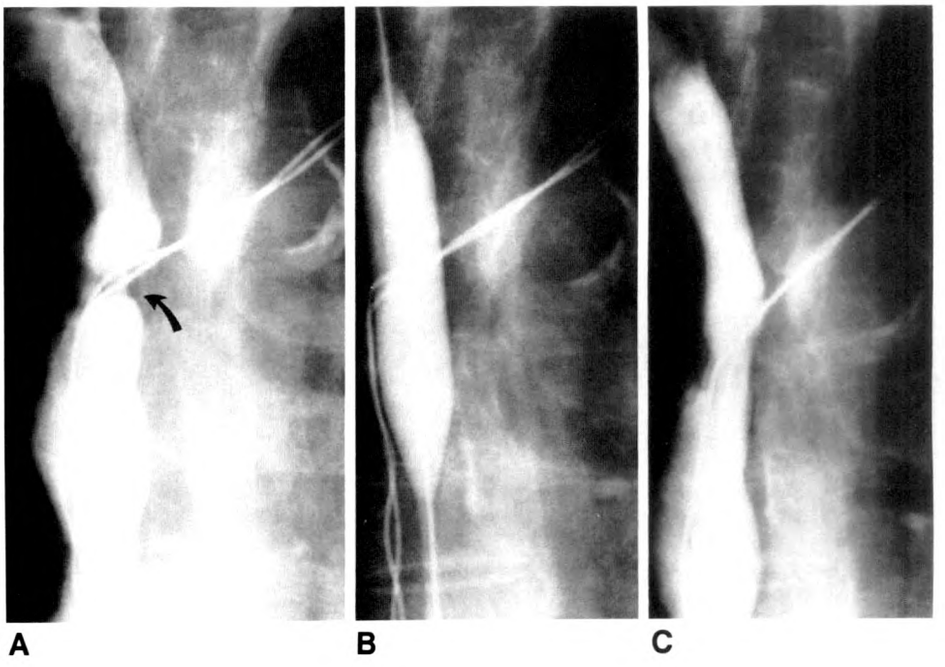


Fig. 1.—**A**, Recurrent superior vena cava stenosis at junction of right and left innominate veins (*curved arrow*).

B, Contrast-inflated 12-mm balloon dilatation catheter.

C, Venacavogram after procedure shows dilatation of the stenosis with minimal residual narrowing.

child in whom the superior vena cava obstruction was a complication of total anomalous pulmonary venous drainage [8].

Stenosis of the superior vena cava is a rare complication of transvenous pacemaker insertion, but it lends itself well to percutaneous angioplasty. Obviously, accurate sizing of the balloon before performing the procedure is desirable to avoid rupture of the superior vena cava. As in arterial angioplasty, a recurrent stenosis can be redilated easily and with good results.

REFERENCES

1. Gunderson T, Abrahamsen AM, Jorgensen I. Superior vena cava obstruction as a complication of transvenous pacemaker treatment. *Acta Med Scand* **1982**;212:85–88
2. Szuman J, Lorkiewicz Z. Superior vena caval stenosis: a rare complication in permanent transvenous cardiac pacing. *J Cardiovasc Surg* **1985**;26(1):79–81
3. Fritz T, Richeson JF, Fitzpatrick P, Wilson G. Venous obstruction: a potential complication of transvenous pacemaker electrodes. *Chest* **1982**;83(3):534–539
4. Alpert JR, Ring EJ, Berkowitz HD, et al. Treatment of vein graft stenosis by balloon catheter dilatation. *JAMA* **1979**;242:2769
5. Uflacker R, Francisconi CF, Rodriguez MP, Amaral NM. Percutaneous transluminal angioplasty of the hepatic veins for treatment of Budd-Chiari syndrome. *Radiology* **1984**;153:641–642
6. Jeans WD, Bourne JT, Read AE. Treatment of hepatic vein and inferior vena caval obstruction by balloon dilatation. *Br J Radiol* **1983**;56(669):687–689
7. Uflacker R, Alves MA, Cantisani GG, Souza HP, Wagner J, Moraes LF. Treatment of portal vein obstruction by percutaneous transhepatic angioplasty. *Gastroenterology* **1985**;88(1 pt. 1):176–180
8. Rocchini AP, Cho KJ, Byrum C, Heidelberger K. Transluminal angioplasty by superior vena cava obstruction in a 15 month-old child. *Chest* **1982**;82(4):506–508

Case Report

Short-Term Prophylaxis of Pulmonary Embolism by Using a Retrievable Vena Cava Filter

Michael D. Darcy,[1] Tony P. Smith, David W. Hunter, Wilfrido Castaneda-Zuniga, Gunnar Lund, and Kurt Amplatz

The most common indications for placement of vena caval filters have been to prevent further pulmonary embolism in patients in whom anticoagulation therapy has failed or who have contraindications to anticoagulants. In Greenfield's series [1], 18% of filters were placed prophylactically in patients who had not had embolic events but were at high risk secondary to having large free-floating iliac or caval thrombus. In that series and in others [2] where filters were used prophylactically, the filters were placed with the intention of leaving them in permanently. Permanent insertion of a Kimray-Greenfield (K-G) filter carries a 3–5% risk of subsequent inferior vena cava thrombosis [3], which may lead to difficulties associated with venous stasis. In addition, clots can embolize through large collateral channels that develop around an obstructed inferior vena cava. We recently reported the development of a caval filter that can be removed percutaneously [4]. The present case report describes the use of the Amplatz Filter for short-term prophylaxis of pulmonary embolism with subsequent percutaneous removal. To our knowledge, this is the first such case reported.

Case Report

A 66-year-old woman with a malignant fibrous histiocytoma involving the right ilium was being treated with a multidrug chemotherapeutic regimen before surgical removal of the tumor. One month after the diagnosis, she developed a fever, and her right leg became warm and swollen. A venogram revealed extensive thrombus in the calf veins and the femoral vein. The common femoral and iliac veins were free of thrombus. Heparin therapy was started. Two days later, a lung perfusion scan was done to evaluate shortness of breath and was normal. Three weeks later, a right hemipelvectomy was planned.

Because of the nature of the surgery, the patient was considered at high risk for pulmonary embolism during the perioperative period. Thus, the day before surgery, an Amplatz retrievable filter was percutaneously inserted through the right internal jugular vein. After doing an inferior vena cavogram, the filter was placed without complications at the L3 level below the renal veins. The patient's post-hemipelvectomy course was complicated by wound hemorrhage, sepsis, and skin-flap necrosis. However, by the 13th postoperative day, the patient was becoming mobile and, no longer confined to bed, was beyond her high-risk period. Therefore, on the 16th postoperative day the filter was percutaneously removed through the left femoral vein.

The retrieval technique used in this case is identical to that described previously [4]. A cavogram, done before removal, showed no thrombus in the inferior vena cava. The caudal hook of the filter was "captured" with a wire snare (Fig. 1). We passed an 8-French Teflon dilator over the snare and used it to secure the snare around the hook. We then passed a 14-French Teflon sheath coaxially over the 8-French dilator with the intent of passing it up over the filter and thus extracting the filter prongs from the caval wall as the filter was collapsed into the sheath. Because we were forced to approach the filter from the left side, the 14-French sheath met the filter at a rather sharp angle (Fig. 2), which prevented the sheath from being gently advanced over the filter as recommended. Instead, the filter was gently pulled into the sheath, without apparent trauma to the inferior vena cava wall (Figs. 3 and 4). The patient tolerated the procedure well, and a cavogram done 3 days after retrieval was normal.

Received February 24, 1986; accepted after revision April 28, 1986.

[1] All authors: Department of Radiology, University of Minnesota Hospital and Clinic, Minneapolis, MN 55455. Address reprint requests to K. Amplatz, Box 701 Mayo Memorial Building, University of Minnesota Hospital, 420 Delaware St. S.E., Minneapolis, MN 55455.

AJR 147:836–838, October 1986 0361–803X/86/1474–0836 © American Roentgen Ray Society

Fig. 1.—Wire snare engages caudal hook of filter.

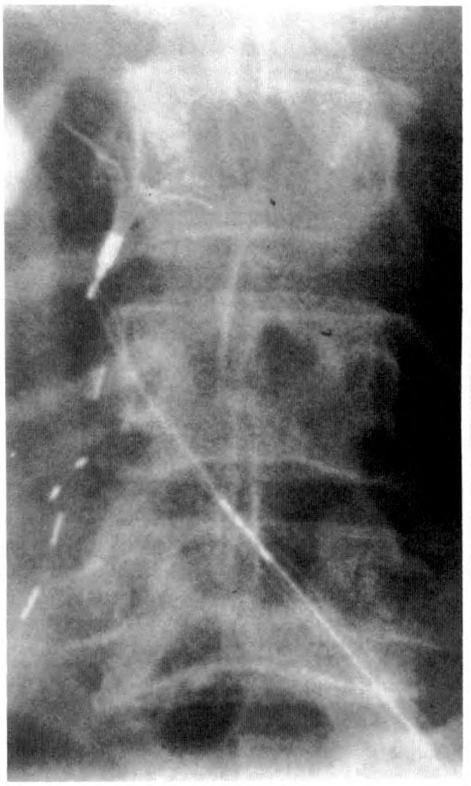
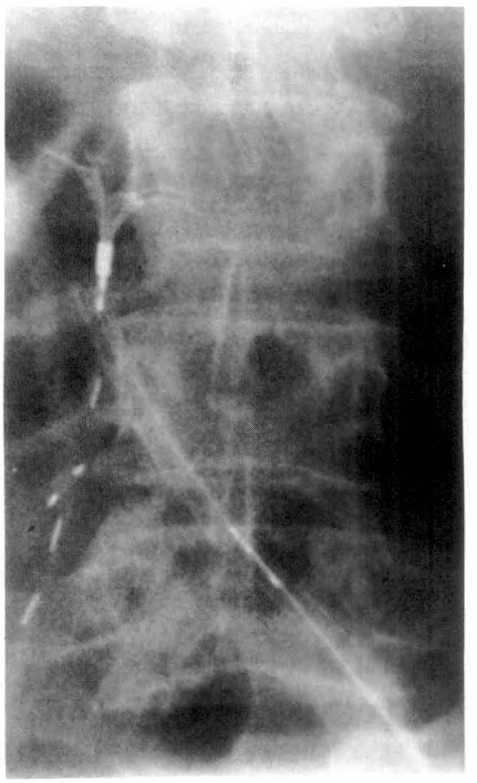


Fig. 2.—14-French Teflon sheath advanced to filter, meeting it at relatively sharp angle.



1 2

Fig. 3.—Filter gently pulled into 14-French sheath.

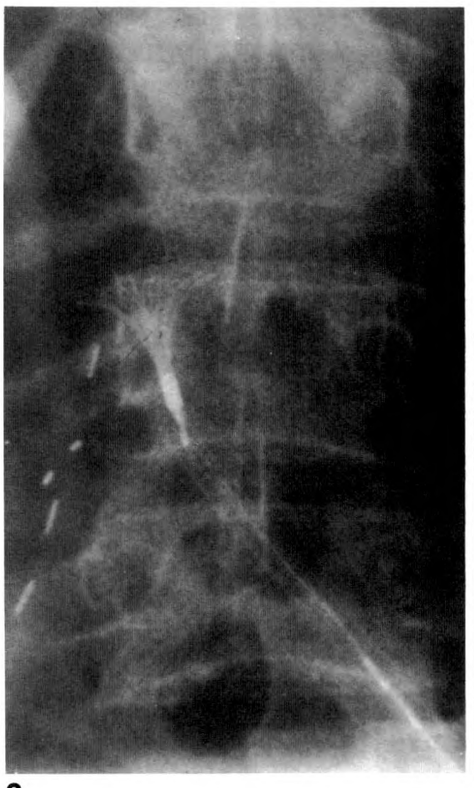
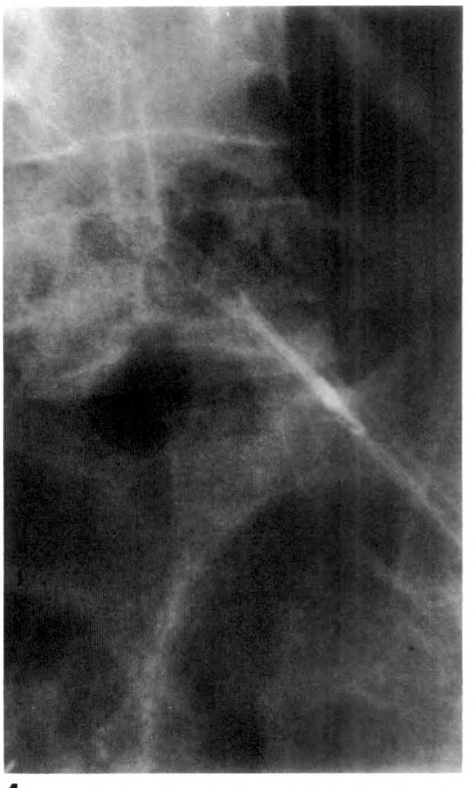


Fig. 4.—Filter completely collapsed and withdrawn into sheath.



3 4

Discussion

The design of the Amplatz retrievable filter [4, 5] allows both placement and retrieval percutaneously, obviating surgical venotomy. Because of the hook's caudal location, retrieval can be performed only by the femoral route. Once the femoral vein is entered, an iliofemoral and caval venogram is done to ensure that no residual thrombi exist that could embolize during filter manipulation. Large iliofemoral or caval thrombus contraindicates a retrieval attempt. The retrieval procedure is technically easy. In this case, the hook was captured after two or three passes of the wire snare. The ease of retrieval was also demonstrated in previous dog experiments, in which almost all attempted retrievals were successful within 2–3 min [6].

The experimental data obtained in dogs have also suggested that percutaneous retrieval of the Amplatz filter remains a safe and easy procedure for up to 2 weeks after insertion. During the third week, the filter can still usually be removed, but there may be slightly more difficulty and potentially more trauma to the inferior vena cava [6]. The removal of the filter in our patient was delayed slightly more than 2 weeks because of postsurgical complications, and yet the retrieval was performed without trauma.

Greenfield and Crute [7] reported a cylinder device for retrieving K-G filters, but it is 11.1 mm (approximately 34 French) in diameter. Not only would this size require a venotomy, but in four of the 15 dogs in whom Greenfield and Crute attempted to use the device, it could not be passed through the jugular veins. In their study, K-G filter retrieval was only possible during the first week after insertion, after which the filters were too securely fixed to the inferior vena cava. This short time during which retrieval can be accomplished limits the usefulness of the K-G filter for short-term prophylaxis because the patient's high-risk period could easily extend beyond 1 week.

In the use of a snare-loop system to retrieve a misplaced K-G filter [8], the filter was repositioned from the renal vein to the inferior vena cava. The snare was used to collapse the filter, but the anchoring hooks were left uncovered. Although the authors stated that complete percutaneous removal could have been performed, it is uncertain how much damage would be done to the veins by the unprotected filter hooks.

The basket filter, also recently described [9], has a caudal hook to allow percutaneous retrieval. Although the authors' pathologic studies suggested that the filter should be retrievable up to 2 weeks after insertion, they had not yet clinically tested this hypothesis. Their one reported retrieval attempt in a dog failed because the filter fractured as a result of a design problem that has since been corrected.

The Amplatz retrievable filter has been shown in our previous work to be at least as efficient as the K-G filter in trapping emboli, especially when the filters are tilted [4]. This advantage, as well as the ease with which the filter can be inserted or retrieved percutaneously, makes it an attractive alternative to the K-G filter. As demonstrated by this case report, the development of the Amplatz retrievable filter has broadened the applications of caval filters by making it practical to use them for short-term prophylaxis of pulmonary embolism. This use will probably be of most benefit in surgical patients at high risk for pulmonary embolism, especially if they cannot be placed on anticoagulants. Although presently limited to use in experimental clinical trials, we anticipate the filter will be commercially available in 1–1½ years (Cook, Bloomington, IN).

REFERENCES

1. Greenfield LJ. Current indications for and results of Greenfield filter placement. *J Vasc Surg* **1984**;1(3):502–504
2. Wingerd M, Bernhard VM, Maddison F, et al. Comparison of caval filters in management of venous thromboembolism. *Arch Surg* **1978**;113:1264–1271
3. Messmer JM, Greenfield LJ. Greenfield caval filters: long term radiographic follow-up study. *Radiology* **1985**;156(2):613–618
4. Lund G, Rysavy JA, Salomonowitz E, et al. A new vena cava filter for percutaneous placement and retrieval: experimental study. *Radiology* **1984**;152(2):369–372
5. Lund G, Rysavy JA, Hunter DW, et al. Retrievable vena caval filter percutaneously introduced. *Radiology* **1985**;155(3):831
6. Hunter DW, Lund G, Rysavy JA, et al. Retrieving the Amplatz retrievable vena caval filter. *Cardiovasc Intervent Radiol*, in press
7. Greenfield LJ, Crute SL. Retrieval of the Greenfield vena caval filter. *Surgery* **1980**;88(5):719–722
8. Schneider PA, Bednarkiewicz M. Percutaneous retrieval of Kimray-Greenfield vena cava filter. *Radiology* **1985**;156(2):547
9. Gunter RW, Schild H, Fries A, Storkel S. Vena caval filter to prevent pulmonary embolism: experimental study. *Radiology* **1985**;156(2):315–320

Renografin-60 for Urography: Effect on Serum Electrolytes and Proteins in Adults

P. Segun Olutola[1]
Linda Hutton[1]
Stephen Karlik[1]
A. R. Henderson[2]

A prospective study was done on 27 adults to assess the changes in serum electrolytes and proteins induced by bolus administration of 100 ml of the ionic contrast medium diatrizoate meglumine and sodium (Renografin-60) for IV urography. Statistically significant changes in serum sodium, chloride, potassium, calcium, bicarbonate, phosphate, total proteins, and albumin were shown at 5 min postinjection. The mean percentage decreases were sodium 2%, chloride 2%, potassium 9%, calcium 13%, bicarbonate 9%, phosphate 10%, and proteins 15%. A mean 3% increase in serum osmolality was observed. By 30 min, sodium and chloride levels had returned to baseline; potassium, calcium, and albumin values were incompletely recovered; bicarbonate was not significantly changed from 5 min; and phosphate values continued to decrease. An in vitro dialysis experiment in which different volumes of Renografin-60 were dialysed against an electrolyte solution (pseudoserum) produced a dilutional factor of 5 to render a given volume of the contrast isoosmotic with plasma. The observed changes from the baseline values of the electrolytes and proteins up to 10% are therefore assumed to be due to hemodilution resulting from movement of fluid from the extravascular to the intravascular compartment. This study confirms alterations in serum levels of several electrolytes after the use of ionic contrast media beyond simple hemodilution. Although these changes appear not to be clinically significant in this investigation, the alterations in potassium and calcium may contribute to arrhythmias, particularly when hypokalemia or hypocalcemia preexists.

Water-soluble iodized ionic contrast media remain the most commonly used intravascular contrast media despite the recent introduction in some countries of nonionic contrast media with less osmolality. Although the frequency of adverse reactions with the administration of contrast media is low, they are no less important; The ideal contrast agent will produce no adverse reactions.

Several alterations in body chemistry after intravascular contrast administration have been documented. These include changes in the electrophoretic mobilities of blood proteins and lipoproteins [1], hematocrit, serum sodium, serum osmolality [2], and acute hypocalcemic effects [3]. Radiographic contrast media also have been shown to cause acute fibrinogenopenia [4] and to produce transient electrocardiographic abnormalities [5, 6]. However, other workers [7] have reported no change in serum sodium, potassium, or creatinine levels.

We have investigated the changes in serum electrolytes and proteins induced by a commonly used ionic urographic contrast medium, diatrizoate meglumine and sodium (Renografin-60, Squibb, Princeton, NJ), during IV urography. Our purpose was to document the electrolyte alterations induced by this contrast medium in our patients, in particular, the changes in serum sodium, calcium, and potassium, and to correlate them with any observed reactions.

Materials and Methods

The subjects were 27 consecutive adult patients who were referred to the Department of

Received October 7, 1985; accepted after revision May 26, 1986.

[1] Department of Diagnostic Radiology, University Hospital, P.O. Box 5339, Station A, London, Ontario, Canada N6A 5A5. Address reprint requests to L. Hutton.

[2] Department of Clinical Biochemistry, University Hospital, London, Ontario, Canada N6A 545.

AJR 147:839–842, October 1986
0361-803X/86/1474–0839
© American Roentgen Ray Society

Diagnostic Radiology for IV urography. The patients were being investigated for genitourinary abnormalities. Those with known electrolyte imbalance, intestinal urinary diversion, chronic renal failure, and renal transplants were excluded. The study protocol was approved by the Health Sciences Standing Committee on Human Research, University of Western Ontario. Written informed consent was obtained from all patients.

Patient preparation for urography consisted of 2 oz (60 ml) of castor oil before 4 p.m. and no solids after 4 on the afternoon before examination, an early low-residue supper, then fasting from 6 a.m. on the day of examination. This regimen was designed to avoid excessive dehydration and promote optimum contrast concentration.

During IV urography, samples of blood were withdrawn before the injection of contrast medium and at 5 and 30 min after injection. The 30-min blood sample could not be obtained from all patients for technical reasons. All the patients received 100 ml of Renografin-60 administered rapidly as a bolus in less than 1 min. Renografin-60 contained diatrizoate meglumine 52%, diatrizoate sodium 8%, 0.32% sodium citrate, and 0.04% disodium edetate; total sodium concentration was 0.1902 molar. The last two samples of blood were withdrawn through the same needle that was used for the first venipuncture after flushing with at least 5 ml of 0.9% saline. The first 2 ml of blood obtained after such flushing were discarded. All patients were observed for contrast reactions, and the presence or absence of subjective changes including warmth, nausea, and itching also were recorded.

The mean values for serum electrolyte and blood proteins were obtained (Table 1) and the analysis of variance was done using a single-factor repeated-measures design. Comparison among the time means, using Tukey's pairwise T-test, was carried out. A p-value of less than 0.05 was considered statistically significant.

To be certain that contrast medium did not interfere with laboratory measurements, five specimens of blood were analyzed with and without the addition of Renografin-60 in a dilution of 1:40 (using a Technicon SMA II Analyzer, Tarrytown, NY and a Beckman Astra 8 Analyzer, Norcross, GA).

An osmolarity dialysis experiment was carried out in vitro to establish the expected ratio for dilution of contrast medium. Different volumes of Renografin-60 were placed into dialysis tubing (Spectapor, Los Angeles, CA, approximately 3500 molecular weight cutoff) and the bags sealed. The tubes were then dialyzed against 4 l of an electrolyte solution (pseudoserum) containing 148 mM Na^+, 4.3 mM K^+, 110 mM Cl^-, 28 mM HCO_3^-, and 10 mM PO_4^{-3} (osmolarity=272 mOsm). After 18 hr the volume and osmolarity of each tube was measured, using a graduated cylinder and a Precision microosmette (Precision Instruments, Sudbury, MA), respectively.

TABLE 1: **Changes in Serum Electrolytes**

	Time (min)	Mean ± SD	Change (%)	No. of Patients	F test p-value
Sodium[a]	0	140 ± 2.2		27	
	5	136 ± 3.3	−2	27	0.001
	30	138 ± 3.4		20	NS
Potassium[a]	0	4.3 ± 0.4		27	
	5	3.9 ± 0.4	−9	27	0.001
	30	4.1 ± 0.4	−6	20	0.008
Chloride[a]	0	105 ± 2.8		27	
	5	103 ± 4.5	−2	27	0.018
	30	106 ± 5.7		20	NS
Calcium[a]	0	2.32 ± 0.11		19	
	5	2.02 ± 0.13	−13	19	0.001
	30	2.07 ± 0.16	−11	13	0.001
Bicarbonate[a]	0	24.0 ± 1.9		26	
	5	21.8 ± 3.2	−9	26	0.001
	30	21.7 ± 2.0	−10	20	0.001
Protein[b]	0	68.3 ± 5.4		19	
	5	58.3 ± 4.7	−15	19	0.001
	30	61.4 ± 5.7	−10	13	0.001
Albumin[b]	0	41.5 ± 3.4		19	
	5	36.5 ± 3.4	−12		0.001
	30	38.6 ± 3.0	−7	13	0.002
Phosphate[a]	0	1.07 ± 0.12		19	
	5	0.95 ± 0.13	−10	19	0.001
	30	0.91 ± 0.13	−15	13	0.001
Osmolality[c]	0	283 ± 3.5		7	
	5	292 ± 5.6	+3	7	0.002

Note.—NS = not significant. $p < 0.05$ was considered significant.
[a] In mmol/l.
[b] In g/l.
[c] In mOsm/kg.

Results

There was a total of 27 patients: 14 women and 13 men. The mean age was 40.6 years with a range of 18–90 years.

Of the first 19 patients, 15 had subjective feelings of increased body warmth; there were nausea in four, itching in one, and sneezing in two patients. The reactions observed were all mild and resolved without treatment.

Table 1 shows the values for sodium, potassium, chloride, calcium, bicarbonate, total proteins, albumin, phosphate, and osmolality at 0, 5, and 30 min after the injection of the contrast medium. There are definite differences in the means at 5 min and/or 30 min compared with the baseline values. Statistically significant decreases occurred at 5 min in the values of sodium, potassium, chloride, bicarbonate, total proteins, albumin, phosphate, and osmolality.

Sodium and chloride values returned to preinjection levels by 30 min postinjection, whereas potassium levels recovered by 40% at 30 min. Smaller changes in serum calcium and protein levels between 5 and 30 min indicate a slower recovery toward baseline. Bicarbonate values showed no significant movement toward baseline by 30 min; phosphate levels continued to decrease.

No significant changes in electrolyte determinations were observed when serum samples were tested before and after the addition of Renografin-60 (1:40 dilution). Therefore, the contrast material does not interfere with established biochemical tests.

The in vitro experiment showed fluid movement into the dialysis bags containing Renografin. Final osmolarity in each bag measured between 279 and 283 mmol/kg. A plot of final volume against initial volume yielded an $r = 0.99$ with a slope of 4.8 (Fig. 1).

Discussion

This study shows that there are alterations in the serum levels of several electrolytes after the use of ionic contrast medium during urography. This is in general agreement with the findings of previous investigators [1, 2, 3, 6], although others have found no changes in serum sodium, potassium,

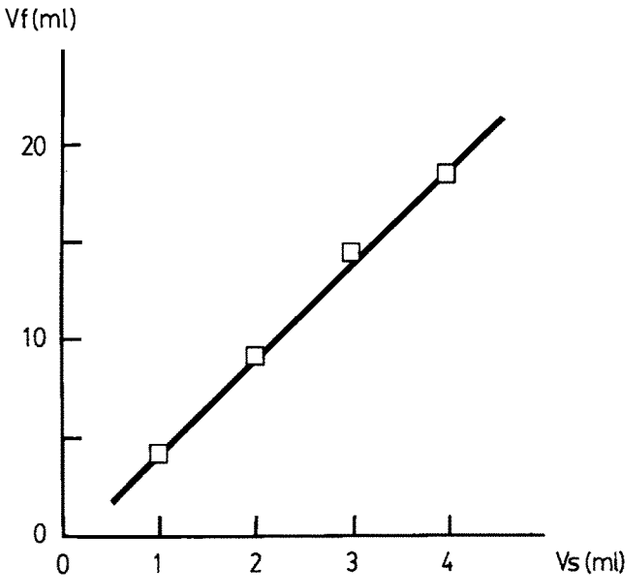


Fig. 1.—Plot of starting volume (Vs) and final volume (Vf) for measured aliquots of Renografin–60 dialyzed for 18 hr (see text).

or creatinine [7]. Statistically significant decreases occur in the serum values of sodium, potassium, calcium, bicarbonate, total proteins, albumin, and phosphate at 5 min after IV injection of Renografin–60. This occurs during the early rapid fall of plasma concentration of contrast medium injected as a bolus [8, 9] and may account for some of the differences from values reported by other workers who took their blood samples at later times. DiSessa et al. [7] using meglumine sodium diatrizoate during angiocardiography in doses of 1–1.5 ml/kg in 30 patients less than 3 years old found that neither serum sodium nor potassium had changed from baseline values at 15 min postinjection. On the basis of our results, this may be too late to detect a significant change in serum sodium, but serum potassium should still be decreased. Using Renografin–76 (diatrizoate meglumine 66% and diatrizoate sodium 10%, Squibb) for angiocardiography in doses of 2 ml/kg in 10 infants less than 2 years old, Baltaxe et al. [6] found an average decrease of 2% in serum sodium and 10% in serum potassium 15 min after injection. These values are similar to the 5-min values in this study.

In another study, Robey et al. [2], using Renografin–60 in doses of 1–3 ml/kg body weight for urography in children up to 10 years old, found mean decreases in serum sodium of 1.8 mEq/l in children less than 5 years and 1.4 mEq/l in those between 5 and 10 years. These investigators, however, got their postinjection samples in 1 hr, by which time serum sodium had returned to baseline values. The reason for this discrepancy is not entirely understood. Berger et al. [3], using Renografin–60 or Renografin–76 in an average dose of 60 ml during angiography in nine adult patients, found a maximum decrease of serum calcium of 0.088 ± 0.038 mM/l at 2–5 min after injection, then a gradual return to baseline values, which was incomplete at 15 min postinjection. This slow recovery was similar to our findings in which calcium had not returned to baseline values by 30 min postinjection.

We think the mechanisms by which the changes occur, although not entirely clear, happen in part because of a rapid shift of fluid from the extravascular compartment to the intravascular compartment as a direct response to the hyperosomotic contrast medium. The in vitro dialysis experiment produced a slope of 4.8 in the graph of initial volume of contrast vs final volume (Fig. 1). This value correlates well with a predicted value of 5 for diluting 1410 mOsm (Renografin–60) to 300 mOsm (blood). A 100-ml dose of contrast material would therefore increase the blood volume a total of 500 ml, including 400 ml of fluid from the extra vascular compartment. The resulting 10% hemodilution could account for a substantial portion of the decrease in potassium, calcium, bicarbonate, and phosphate. The additional decrease in calcium may be attributed to the chelating effect of disodium edetate and citrate contained in Renografin as shown by Berger et al. [3].

The rapid mobilization of extra vascular fluid into the vascular compartment can account for changes in the protein and albumin and protein-bound electrolytes such as calcium in the serum. Bicarbonate, potassium, and phosphate remain low after 5 min, despite the presence of an equilibrium between interstitial and serum fluids. We propose that two mechanisms exist that may account for these reductions in potassium, bicarbonate, and phosphate; both mechanisms may be operative in this instance. The rapid intravascularization of fluid during the first 5 min after injection may occur faster than the processes leading to ionic equilibration. Furthermore, the Gibbs Donnan equilibrium, which establishes the ionic composition and relationship between the serum and the interstitial fluid may be profoundly affected by the sodium and electrolytes in the Renografin–60 as well as its very high osmolarity (1400). These two phenomena, rapid fluid shift and Gibbs Donnan effects of Renografin, may account for the transient reductions in potassium, bicarbonate, and phosphate.

We did not find the serum chemistry changes to be significant clinically. There were three patients in whom serum potassium fell below the normal range. Although an ECG was not performed, no apparent adverse clinical effect was seen during the examination. However, the alteration in potassium and the extended change in serum calcium may contribute to the cardiac arrhythmias previously reported [5], particularly when hypokalemia or hypocalcemia preexists. The movement of large fluid volumes from the extravascular to the intravascular compartment in these patients may contribute significantly to the systemic symptoms such as warmth, headache, and nausea.

In conclusion, we have confirmed that Renografin–60 administered for IV urography decreases the levels of serum electrolytes and proteins. These changes may be important when electrolyte imbalances preexist.

ACKNOWLEDGMENTS

We thank Mercia Mercer for secretarial assistance in preparing this manuscript.

REFERENCES

1. Kutt H, Milhorat TH, McDowell F. The effect of iodinised contrast media upon blood proteins, electrolytes and red cells. *Neurology* **1963**;13:492–499
2. Robey G, Reilly BJ, Carusi PA, Nguyen KB. Pediatric urography. Comparison of metrizamide and methylglucamine diatrizoate. *Radiology* **1984**;150:61–63
3. Berger RE, Gomez LS, Mallette LE. Acute hypocalcemic effects of clinical contrast media injections. *AJR* **1982**;138:283–288
4. Lalli A. *Tailored urologic imaging.* Chicago: Year Book Medical Publ., **1980**:26
5. Pfister RC, Hutter AM, Newhouse JH, Loder ICM, Travers E. Contrast-medium–induced electrocardiographic abnormalities. *AJR* **1983**;140:149–153
6. Baltaxe HA, Mooring P, Krugler J, Pinsky W, Chu W. Comparative hemodynamic effect of Metrizamide and Renografin–76 in infants with congenital heart disease. *AJR* **1983**;140:1097–1101
7. DiSessa TG, Zednikova M, Hiraishi S, Jarmakani JM, Higgins CB, Friedman WF. The cardiovascular effects of Metrizamide in infants. *Radiology* **1983**;148:687–691
8. Newhouse JH. Fluid compartment distribution of intravenous iothalamate in the dog. *Invest Radiol* **1977**;12:364–367
9. Witten DM, Myers GH, Utz DC. *Emmett's urography*, Philadelphia: Saunders, **1977**:17

MRI of the Spleen: Normal Appearance and Findings in Sickle-Cell Anemia

Dorit D. Adler[1]
Gary M. Glazer
Alex M. Aisen

The MRI appearance and characteristics of the normal and diseased spleen were prospectively evaluated using spin-echo imaging with a superconducting magnet operating at 0.35 T. Sixty normal patients and 13 patients with sickle-cell anemia involving the spleen were studied. The normal spleen was isointense or slightly more intense than liver at a repetition time of 0.5 sec. At a longer repetition time (TR 2.0 sec), the normal spleen was usually more intense than liver, becoming markedly hyperintense compared to liver on relatively T2-weighted images (TR 2.0 sec, TE 56 msec). All patients with sickle-cell anemia showed abnormally diminished signal intensity of the spleen.

With increasing use of CT and sonography, there has been renewed interest in radiologic investigation of the spleen [1, 2]. Both these techniques can demonstrate focal lesions larger than 1–2 cm, but are only occasionally useful in evaluation of splenic abnormality due to systemic diseases. In this investigation we evaluated the MRI appearance of the normal spleen and the appearance of the spleen in patients with sickle-cell disease.

Materials and Methods

MR scans of the upper abdomen on 60 patients, ranging in age from 12 to 82 years, without known or suspected splenic disease (nearly all of these patients also had a normal spleen on CT or sonography) were reviewed to establish the normal MR appearance of the spleen. Splenic intensity was visually compared with the intensity of the liver at all pulse sequences. T1, T2, and intensity values of the normal spleen were determined in 20 of these patients. Twelve children and one adult with homozygous sickle-cell disease were also prospectively imaged. These patients ranged in age from 6 to 31 years.

All patients underwent spin-echo MRI using a superconducting magnet (Diasonics) operating at 0.35 T. Imaging was generally performed at repetition times (TR) of 0.5 and 2.0 sec and at echo delay times (TE) of 28 and 56 msec. Two patients were imaged at TR 0.5 and 1.0 sec, one patient was scanned at TR 2.0 sec, and one patient was imaged at TR 0.5 and 1.5 sec. Intensity measurements of the splenic parenchyma and liver were obtained using an electronic cursor to define region of interest. T1 and T2 relaxation times of splenic parenchyma were determined from intensity images as previously described [3].

Results

In 56 of the 60 patients who underwent MR scanning of the abdomen for reasons unrelated to the spleen, the spleen was visually isointense with the liver at TR 0.5 sec and TE 28 msec (Fig. 1A). At TR 0.5 sec, TE 56 msec, the spleen became slightly more intense than liver in 28 of the patients. However, at TR 2.0 sec, TE 28 msec, the spleen was more intense than liver in 55 of the 60 patients (Fig. 1B), and more intense than liver in 57 patients at TR 2.0 sec, TE 56 msec. With the marked increase in splenic intensity on T2-weighted sequences, the spleen often became imperceptible from the surrounding fat.

Received January 17, 1986; accepted after revision April 30, 1986.

Presented in part at the annual meeting of the American Roentgen Ray Society, Washington, DC, April 1986.

[1] All authors: Department of Radiology, University of Michigan Medical Center, Ann Arbor, MI 48109-0010. Address reprint requests to D. D. Adler, Box 013.

AJR 147:843–845, October 1986
0361–803X/86/1474–0843
© American Roentgen Ray Society

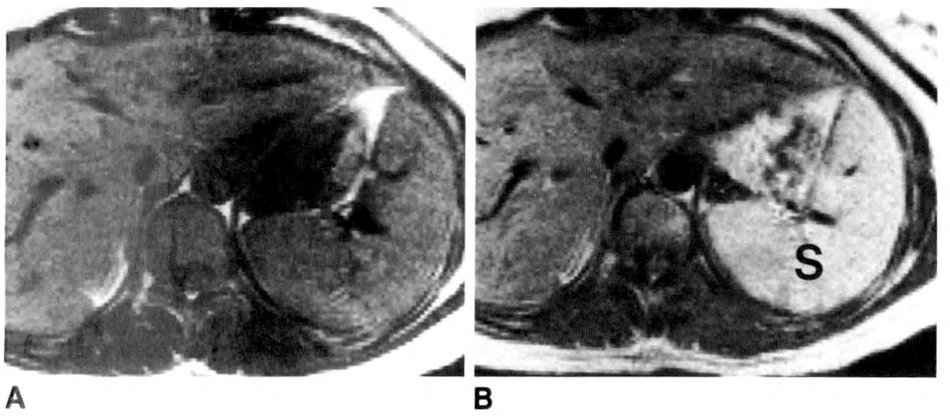


Fig. 1.—**A**, T1-weighted MR image (TR 0.5 sec, TE 28 msec) shows the spleen to be isointense with liver and hyperintense compared with paraspinal musculature. **B**, At TR 2.0 sec, TE 28 msec, normal spleen (S) is markedly hyperintense compared with liver and muscle.

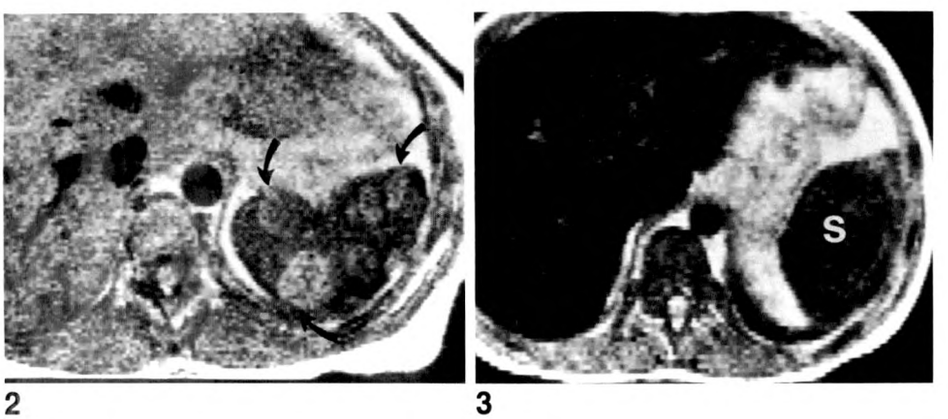


Fig. 2.—Multiple hyperintense splenic lesions (*curved arrows*) seen at TR 2.0 sec, TE 28 msec in a 31-year-old black woman with sickle-cell anemia, consistent with multiple infarcts. Note abnormally diminished intensity of remaining splenic parenchyma relative to surrounding musculature (compare Figs. 1**A** and 1**B**).

Fig. 3.—MR image (TR 2.0 sec, TE 28 msec) in an 11-year-old girl with sickle-cell anemia. Deposition of hemosiderin in liver and spleen has caused these organs to have diminished intensity (hypointense compared with paraspinal musculature).

Quantitative relaxation time measurements of the spleen in 20 patients who were scanned for reasons other than suspected splenic disease were used as normal controls. There was marked variation of these calculated T1 and T2 values with large ranges and standard deviations for the normal splenic parenchyma. Mean T1 was 604 msec (SD = 230) and mean T2 was 61 msec (SD = 19).

Generalized diminished splenic intensity relative to liver and paraspinal musculature was found in the 13 sickle-cell patients, including two who also had focal abnormalities (Figs. 2 and 3). Calculated T1 and T2 relaxation times of the splenic parenchyma in these patients were shorter than values obtained in the normal spleen. Mean T1 was 422 (SD = 112), with a mean T2 of 52 msec (SD = 25). T1 shortening reached statistical significance ($p < 0.01$, unpaired Student's t test), while T2 shortening only showed a trend toward statistical significance ($p = 0.10$).

Since the liver is overloaded with iron in many sickle-cell patients, we also visually compared the intensity of the spleen with that of paraspinal muscle on the same TR 2.0-sec scans. The spleen was less intense than the muscle or equal in intensity to the muscle in all but one of these patients. In normal patients, the spleen was always found to be more intense than muscle at this repetition time.

Discussion

MRI has already proved to be extremely useful in evaluation of the central nervous and cardiovascular systems, and other extracranial applications are rapidly evolving [4–6]. Upper abdominal applications of MR have been slower to develop in part because of image degradation by cardiac, respiratory, and intestinal motion. Despite these difficulties, we have investigated the possible role of MR in splenic imaging. Our data show a consistent appearance of the normal spleen using spin-echo imaging. On T1-weighted images (TR 0.5 sec, TE 28 msec) the spleen is essentially isointense with liver, whereas on T2-weighted images (TR 2.0 sec, TE 56 msec) the normal spleen becomes hyperintense with respect to liver, often becoming inseparable from adjacent abdominal fat. These observations agree with those of Ehman et al. [7]. Any alteration in this relationship suggests the possibility of diffuse splenic disease.

Abnormal splenic intensity was seen in all the patients with sickle-cell disease. In all likelihood, the changes seen in these cases are similar to those previously reported in hemochromatosis [8], in which iron deposition results in marked shortening of T1 and T2 relaxation times and diminished signal intensity using spin-echo imaging. In patients with homozy-

gous sickle-cell anemia, microscopic perivascular and parenchymal calcifications are found in the splenic tissue in addition to iron deposition [9]. These calcifications may also contribute to the diminished splenic intensity.

REFERENCES

1. Piekarski JD, Federle MP, Moss AA, London SS. Computed tomography of spleen. *Radiology* **1980**;135:683–689
2. Mittelstaedt CA. Ultrasound of the spleen. *Semin Ultrasound* **1981**;2:233–240
3. Glazer GM, Aisen AM, Francis IR, Gyves JW, Lande I, Adler DD. Hepatic cavernous hemangioma: magnetic resonance imaging. *Radiology* **1985**;155:417–420
4. Moon KL Jr, Genant HK, Helms CA, Chafetz NI, Crooks LE, Kaufman L. Musculoskeletal applications of nuclear magnetic resonance. *Radiology* **1983**;147:161–171
5. Herfkens RJ, Higgins CB, Hricak H, et al. Nuclear magnetic resonance imaging of the cardiovascular system: normal and pathologic findings. *Radiology* **1983**;147:761–764
6. Brant-Zawadzki M, Badami JP, Mills CM, Norman D, Newton TH. Primary intracranial tumor imaging: a comparison of magnetic resonance and CT. *Radiology* **1984**;150:435–440
7. Ehman RL, Kjos B, Hricak H, Brasch RC, Higgins CB. Relative intensity of abdominal organs in MR images. *J Comput Assist Tomogr* **1985**;9:315–319
8. Runge VM, Clanton JA, Smith FW. Nuclear magnetic resonance of iron and copper disease states. *AJR* **1983**;141:943–948
9. Magid D, Fishman EK, Siegelman SS. Computed tomography of the spleen and liver in sickle cell disease. *AJR* **1984**;143:245–249

Case Report

Extramedullary Hematopoeisis in Acute Lymphocytic Leukemia Masquerading as Hepatic, Renal, and Splenic Microabscesses

Kenyon K. Kopecky,[1] Ann T. Moriarty,[2] Asok C. Antony,[3] and Martin K. Baker[1]

Although extramedullary hematopoeisis (EMH) is known to occur in agnogenic myeloid metaplasia with myelofibrosis, various anemias, and chronic myelogenous leukemia [1], it is rare in acute leukemia. There are no radiographic reports of EMH presenting as multiple focal hepatic lesions, and CT findings in renal EMH have not been described. A 22-year-old man with acute lymphocytic leukemia developed granulocytopenic fever and multiple small hepatic, renal, and splenic lesions on CT. Because of the radiographic appearance and clinical course, these were thought to represent microabscesses. Liver biopsy, however, revealed EMH.

Case Report

A 22-year-old man presented with a 3-week history of malaise, sweats, chills, adenopathy, and weight loss. Physical examination revealed cervical and inguinal lymphadenopathy. Hemoglobin was 8.2 g/dl; leukocyte count was 20,200/mm^3 with 94% lymphoblasts; and platelet count was 16,000/mm^3. Bone-marrow biopsy confirmed the diagnosis of L1 acute lymphocytic leukemia. Treatment was started (day 1) with oncovin, adriamycin, prednisone, and methotrexate in addition to four antibiotics. Amphoterocin was added on day 13. On day 16 an abdominal CT scan was performed because of fever; the scan was normal. On day 27 a repeat bone-marrow biopsy showed acellularity. Because of persistent fever a repeat CT scan (Fig. 1) was done on day 41 that showed many small lesions throughout the liver and kidneys and several very small (5-mm) splenic lesions. At this time the peripheral blood was beginning to recover normally: Hgb 9.3, WBC 13,000 with normal differential, and platelets 77,000. Because microabscesses were suspected, fine-needle aspiration biopsy of the right hepatic lobe was performed under sonographic guidance. Seven aspirations with a 22-gauge needle were obtained for cultures and microscopic examination. Some slides were immediately stained using a rapid Wright-Giemsa method, and others were alcohol-fixed and stained with Papanicolaou stain. Microscopic examination showed scattered reactive hepatocytes and typical EMH. Precursors of all three blood-cell lines were present: normoblasts, myelocytes, and megakaryocytes. Stains and cultures for aerobic and anaerobic bacteria, mycobacteria, and fungi were negative. Owing to persistent culture-negative fevers, all antimicrobial agents were subsequently stopped. Because the fevers subsided, it was concluded that they were probably caused by one or more of the drugs. A third abdominal CT scan (day 75) was normal, showing complete resolution of the hepatic, renal, and splenic lesions. At that time examinations of the peripheral blood and bone marrow were normal, and the patient remains in complete remission at 6 months follow-up.

Discussion

EMH is a compensatory mechanism that occurs when the marrow is unable to maintain sufficient red cell mass. It has been reported in agnogenic myeloid metaplasia with myelofibrosis, anemias, and chronic leukemia [1]. To our knowledge this is the first case reported in a patient with acute leukemia.

Received March 24, 1986; accepted after revision May 5, 1986.
[1] Department of Radiology, University Hospital X-64, Indiana University Medical Center, 926 W. Michigan St., Indianapolis, IN 46223.
[2] Department of Pathology, Indiana University Medical Center, 926 W. Michigan St., Indianapolis, IN 46223.
[3] Department of Medicine, Indiana University Medical Center, 926 W. Michigan St., Indianapolis, IN 46223.

 0361–803X/86/1474–0846 © American Roentgen Ray Society

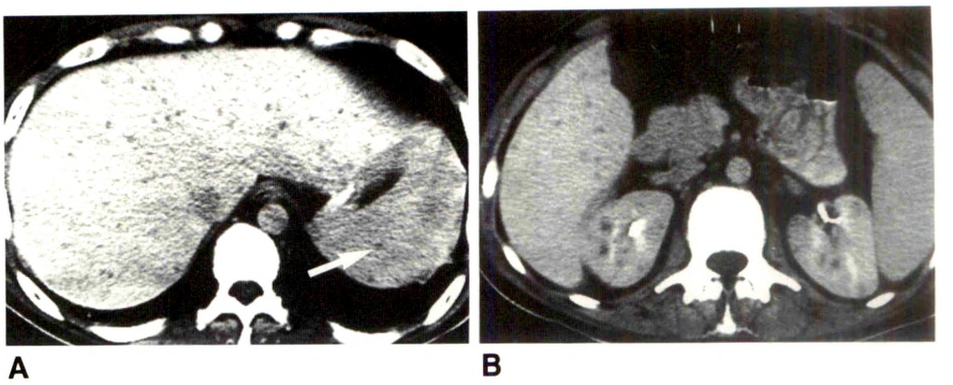


Fig. 1.—CT scan performed 6 weeks after start of chemotherapy, demonstrating **A**, multiple small focal hepatic lesions and a small splenic lesion (*arrow*) and **B**, multiple focal renal lesions.

Histologic examination of the liver in patients with myelofibrosis or chronic myelogenous leukemia commonly reveals EMH [1]. Leigh et al. [2] noted hepatomegaly radiographically on plain films in nine of 14 patients with myelofibrosis. Radiographic findings of focal EMH have not been reported. In our patient the liver was studded with innumerable small (<1 cm) lesions (Fig. 1); the overall liver size was normal.

Renal EMH was detected by Redlin et al. [3] who reported five patients with agnogenic myeloid metaplasia who had abnormal excretory urograms showing renal enlargement and calyceal distortion. Our patient did not have renal enlargement by CT, and the very small size of the lesions (<1 cm) would probably not cause calyceal distortion at excretory urography, had it been performed. Although the kidneys were not biopsied in this case, the evidence for renal EMH is very strong: a baseline CT of the liver and kidneys was normal; 25 days later CT showed many small lesions throughout the liver and kidneys at a time when the hypoplastic marrow was just beginning to recover from chemotherapy (a likely time for EMH to occur); the liver biopsy demonstrated EMH; 34 days later when the marrow and peripheral blood were normal, repeat CT of the liver and kidneys was normal. This resolution of EMH after marrow recovery was not unexpected since the stimulus for EMH (marrow aplasia) was no longer present.

The spleen is the most common site of EMH in patients with myelofibrosis [1]. Although the spleen was not biopsied in this patient, the clinical and radiographic course make splenic EMH likely.

Callen et al. [4] described the CT appearance of hepatic and splenic microabscesses in two patients with acute leukemia. The appearance and clinical setting were strikingly similar to our patient, which led to our biopsy for suspected infection. The therapeutic and prognostic implications of biopsy are great. Callen's patients died with liver microabscesses that grew *Candida albicans*, whereas our patient was taken off antibacterial and antifungal agents and recovered.

Because patients with acute leukemia are immunosuppressed and frequently febrile, abdominal CT scans are commonly requested to exclude abscess. Multiple focal hepatic, renal, or splenic lesions could be due to either abscesses or EMH. The diagnosis can be established by fine-needle aspiration biopsy with cytologic and microbiologic examinations.

REFERENCES

1. Wintrobe MM, Lee GR, Boggs DR, et al. *Clinical hematology*, 8th ed. Philadelphia: Lea & Febiger, **1981**:52,1572,1620
2. Leigh TF, Corley CC, Huguley CM, Rogers JV. Myelofibrosis: the general and radiologic findings in 25 proved cases. *AJR* **1959**;82:183–193
3. Redlin L, Francis RS, Orlando MM. Renal abnormalities in agnogenic myeloid metaplasia. *Radiology* **1976**;121:605–608
4. Callen PW, Filly RA, Marcus FS. Ultrasonography and computed tomography in the evaluation of hepatic microabscesses in the immunosuppressed patient. *AJR* **1980**;136:433–434

Technical Note

The Value of a Worksheet in Reporting Body-CT Examinations

Richard E. Kinard,[1] William W. Orrison,[2] and Byron G. Brogdon[3]

A body-CT worksheet was originally designed to provide consistent reporting of CT examinations, to serve as a preliminary report, and to be used as a computer interface. From this study the worksheet also appears to improve diagnostic accuracy when routinely used in interpreting body-CT scans.

Materials and Methods

During a 6-month period one of the authors reviewed 200 consecutive abdominal or abdominal/pelvic CT examinations using the worksheet shown in Table 1. All examinations had been performed on a GE 8800 CT/T scanner (Milwaukee, WI) with dynamic scanning capabilities. Oral and IV contrast media were administered in most cases. All had previously been interpreted and reported by one of eight other board-certified radiologists. Two of these individuals had had fellowship training in body CT and the other six had had more practical CT experience than the reviewer at the time of the study.

The retrospective reviews were carried out within 2 weeks of the first interpretation and report. The reviewer had access to the same clinical information that the original radiologists had, but he did not have the original reports.

The reviewer meticulously followed the worksheet, checking every item as either normal or abnormal and concisely describing each abnormality. These results then were compared with the original reports. Only positive findings of possible clinical significance in terms of diagnosis, treatment, or follow-up were considered.

Results

In the 200 examinations that were reviewed using the worksheet, 22 additional significant abnormal findings (true positives) were discovered. Those findings did not represent failures to interpret a perceived finding as abnormal; rather, they were errors of oversight (false negatives) on the first interpretations. The errors were distributed evenly among the eight original radiologists. Thus, use of the worksheet increased the number of significant findings in approximately 10% of cases. A list of the overlooked abnormalities and their frequency is presented in Table 2. Adrenal masses and spinal metastases were the lesions most often missed on the interpretations unaided by the worksheet.

Discussion

Although much has been written about observer error and quality control in radiology [1, 2], little attention has been paid to these problems in relation to body CT. Routine abdominal or pelvic CT images display an enormous amount of information regarding abdominal viscera, fascial planes, muscles and bones, and vascular structures in every anatomic section. Although an orderly system for studying each scan is essential for proper interpretation [3, 4], until now, a framework for such a system has not been devised. The body-CT worksheet used in this study (Table 1) was designed to ensure a section-by-section, organ-by-organ, structure-by-structure approach to the evaluation of these complex images. The idea of a worksheet is not new, but to our knowledge no such method has been applied to the area of routine abdominal-pelvic imaging [5, 6]. Improvement in diagnostic performance with use of the body-CT worksheet can be explained in part by

Received January 22, 1986; accepted after revision April 19, 1986.

[1] Department of Radiology, University of Florida College of Medicine, Gainesville, FL 32610. Address reprint requests to R. E. Kinard, Department of Radiology, North Florida Regional Hospital, Box NFR, Gainesville, FL 32608.

[2] University of New Mexico Hospital, Albuquerque, NM 87131.

[3] University of South Alabama Medical Center, Mobile, AL 36617.

 0361–803X/86/1474–0848 © American Roentgen Ray Society

TABLE 1: **Body CT Worksheet**

Patient name _____ Hospital _____
Date _____
Age _____ Sex _____
History _____
Type of Scan
_____ Quality
_____ Extraabdominal—Heart
Lungs
Bones
Soft Tissues
_____ Liver—Parenchyma
Biliary system
Adjacent fluid
_____ Spleen
_____ Pancreas—Size, mass
duct, calcification
_____ Adrenals—Right
Left
_____ Kidneys—Right
Left
Ureters
Pararenal space
_____ Retroperitoneum—Aorta
Inferior vena cava
Nodes
Psoas muscles
_____ GI tract and peritoneal cavity
_____ Pelvis—Male: Bladder
Seminal vesicles
Prostate
Nodes
Inguinal
_____ Female: Bladder
Uterus and adnexa
Nodes
Inguinal
Conclusion

TABLE 2: **Additional Lesions Detected upon Review with the Body-CT Worksheet**

Findings	Number
Adrenal masses	5
Spinal metastases	5
Pelvic masses	2
Fluid collections	2
Low mediastinal node	1
Inguinal hernia	1
Liver hypodense mass	1
Renal calcification	1
Renal cyst	1
Gallstone	2
Biliary duct dilatation	1
Total	22

extrapolation of studies of factors related to perception of pulmonary lesions on chest radiographs. The step-by-step completion of the worksheet forces the observer into a series of directed or focused-search sequences; this system has been shown to have advantages over the free-search method of diagnostic observation [7], although these benefits may be dependent on specific tasks or experimental design [8, 9].

Use of the worksheet helps to safeguard against one of the major hazards of both the free-search and the directed-search when the "direction" is by a specific clinical diagnosis—namely, that a search will be prematurely terminated because a significant signal or finding has been detected. The worksheet requires evaluation of all available imaged information, thereby guarding against defective search patterns due to misinterpretation or distraction.

Hillard et al. [10] suggested that experienced radiologists develop a visual representation ("mind's-eye view") of a prototypical radiograph (a "schema"), which aids them in interpreting chest films. Since it would be considerably more difficult to develop such a schema for a multilevel body-CT examination, use of the worksheet also guards against blind spots in the observer's prototypical memory pattern. Additionally, regular and routine use of the worksheet during training periods and in clinical practice should improve and expedite the observer's acquisition of body-CT schemata.

The body-CT worksheet has other practical applications beyond its principal use as an aid to observer performance. When a copy of the worksheet is attached to the multiviewer or inserted in the film jacket, it provides the clinician with a convenient and helpful means of systematically reviewing the pertinent findings.

Further, the format of the worksheet is such that information can be easily dictated or interfaced with computerized reporting systems [11, 12] and computer-data retrieval systems.

REFERENCES

1. Brogdon BG, Kelsey CA, Moseley RD. Factors affecting perception of pulmonary lesions. *Radiol Clin North Am* **1983**;21:633–654
2. Wheeler PS. Risk prevention, quality assurance, and the missed diagnosis conference. *Radiology* **1982**;145:227–228
3. Balfe DM, Peterson RR, Lee JKT. Normal abdominal anatomy in computed body tomography. In: Lee JKT, Sagel SS, Stanely RL, eds. *Body computed tomography.* New York: Raven Press, **1983**;131
4. Moss AA, Genant HK, Gamsu G. *Computed tomography of the body.* Philadelphia: Saunders, **1983**
5. Glenn WV Jr, Rhodes ML, Altschuler EM, Wiltse LL, Lostanek C, Kuv YM. Multiplanar display computerized tomography applications in the lumbar spine. *Spine* **1979**;4:282
6. Hanafee W, Mancuso A. *Introductory workbook for CT of the head and neck.* Baltimore: Williams & Wilkins, **1984**
7. Parker TW, Kelsey CA, Moseley RD Jr, Mettler FA Jr, Garcia JF, Briscoe DE. Directed versus free search for nodules in chest radiographs. *Invest Radiol* **1982**;17:152–155
8. Swensson RG, Hessel SJ, Herman PG. Radiographic interpretation with and without search: visual search aids the recognition of chest pathology. *Invest Radiol* **1982**;17:145–151
9. Kundel HL. Directed attention and film reader performance (editorial). *Invest Radiol* **1982**;17:117–118
10. Hillard A, Worsley MM, Johnston W, Baxter B. The development of radiologic schemata through training and experience. *Invest Radiol* **1985**;20:422–425
11. Choplin RH, Boehme JM, Cowan RL, et al. A computed assisted radiologic reporting system. *Radiology* **1984**;150:345–348
12. Jost RG, Trachtman MS, Rexford L, Smith BA, Evans RO. A computer system for transcribing radiology reports. *Radiology* **1980**;136:63–66

History of Radiology

Early American Radiology: The Pioneer Years

David J. DiSantis[1]

Very few American radiologists have a more-than-cursory idea of our specialty's beginning in the 19th century. Roentgen's story is widely known, but the Americans who helped lay radiology's foundations in our country remain essentially anonymous, especially to younger members of our profession. This paper chronicles the landmark years of early American radiology.

Can American radiology really have celebrated its 96th anniversary when X-rays are only 90 years old? The saga begins one evening in late February 1890, in a University of Pennsylvania physics laboratory. After an experimental session testing electric sparks as a photographic light source, Professor Arthur Willis Goodspeed began demonstrating the properties of a Crookes cathode-ray tube to William Jennings, a photographer. Next to the tube, Jennings had stacked several unexposed photographic plates, on top of which were two coins, reportedly his fare for the Woodland Avenue trolley [1]. When Jennings later developed the plates, some were mysteriously fogged, and one displayed two peculiar disk-shaped shadows (Fig. 1). Neither man could explain the phenomenon, and so the plates were filed and forgotten for nearly 6 years. Only after Roentgen's discovery did the men recreate the setting of that February night and grasp the magnitude of the observation that they had failed to make. Although he claimed "no credit for the interesting accident," Goodspeed maintained that "without doubt, the first Roentgen picture was produced on February 22, 1890 . . . [at] the University of Pennsylvania" [2].

The scientific furor engendered by Roentgen's announcement can hardly be overestimated. In the ensuing year, 1000 papers dealing with X-rays appeared [1]. America's true introduction to radiography came in early 1896. As is often the case even now, news of a scientific breakthrough arrived first through the lay press (Fig. 2). On January 6, 1896, the Sunday *New York Sun* announced that Professor Routgen [sic] had discovered "the light that never was," which could photograph hidden things including bones within flesh. The "Roentgen fever" in the European scientific community quickly became an American epidemic as well.

Although the race for the first American radiograph had been won inadvertently by Goodspeed even before the starting gun, the contest for the first intentional radiograph was still on. Arthur Wright of the Yale Physics Department won, literally with a photo finish. On January 27, 1896, 80 days after the discovery of X-rays, he placed cardboard-covered photographic paper beneath a cathode-ray tube. On the paper he placed a pencil, a pair of scissors, and a quarter. Using a lengthy exposure time of 15 minutes, he obtained "a very clear representation of the objects employed" [3]. Modern publication delays were not such a problem in 1896: His success was reported in the *Engineering and Mining Journal* dated February 1, only 4 days after the event [2]. Meanwhile, in Boston, John Trowbridge, director of Harvard's Jefferson Physical Laboratory, was working toward the same end. He detailed his success in the *New York Journal* dated February 2, appearing just 1 day after Wright's report.

While Yale and Harvard vied for priority in the laboratory, another Ivy League institution, Dartmouth, was making clinical history. Edwin Brant Frost, a professor of astronomy, was familiar with cathode-ray tubes, and he was asked by his physician brother, G. D. Frost, to radiograph the fractured forearm of one of his patients (Fig. 3). So, on February 3,

Received March 21, 1986; accepted after revision May 22, 1986.

[1] Department of Radiology, DePaul Hospital, Eastern Virginia Medical School, 150 Kingsley Ln., Norfolk, VA 23505. Address reprint requests to D. J. DiSantis.

AJR 147:850–853, October 1986 0361–803X/86/1474–0850 © American Roentgen Ray Society

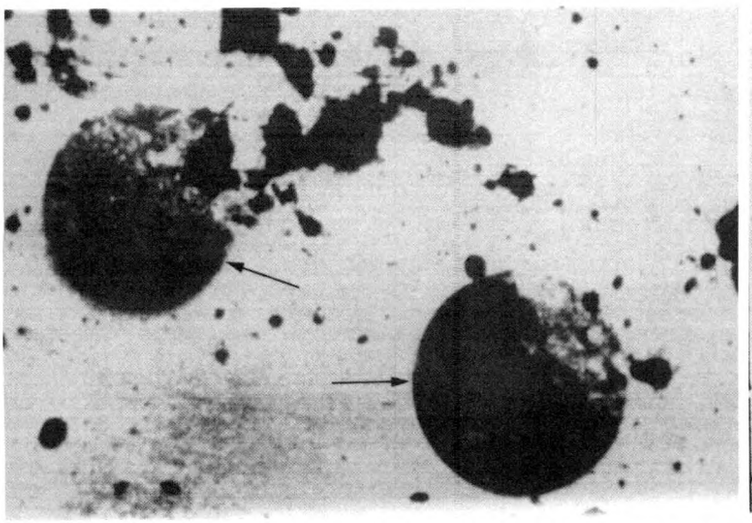
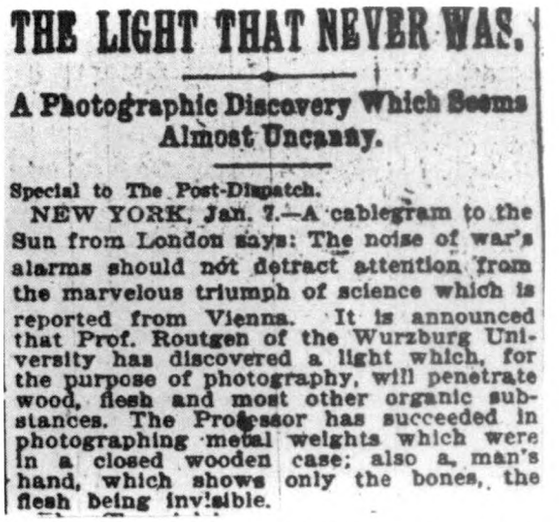


Fig. 1.—Goodspeed-Jennings "trolley fare" radiograph of 1890. *Arrows* point toward presumed coin shadows. (Modified from Grigg [1].)



THE LIGHT THAT NEVER WAS.

A Photographic Discovery Which Seems Almost Uncanny.

Special to The Post-Dispatch.

NEW YORK, Jan. 7.—A cablegram to the Sun from London says: The noise of war's alarms should not detract attention from the marvelous triumph of science which is reported from Vienna. It is announced that Prof. Routgen of the Wurzburg University has discovered a light which, for the purpose of photography, will penetrate wood, flesh and most other organic substances. The Professor has succeeded in photographing metal weights which were in a closed wooden case; also a man's hand, which shows only the bones, the flesh being invisible.

Fig. 2.—America learns of "Routgen's" rays. Reprinted from microfilm record of the *St. Louis Post Dispatch*, January 7, 1896.

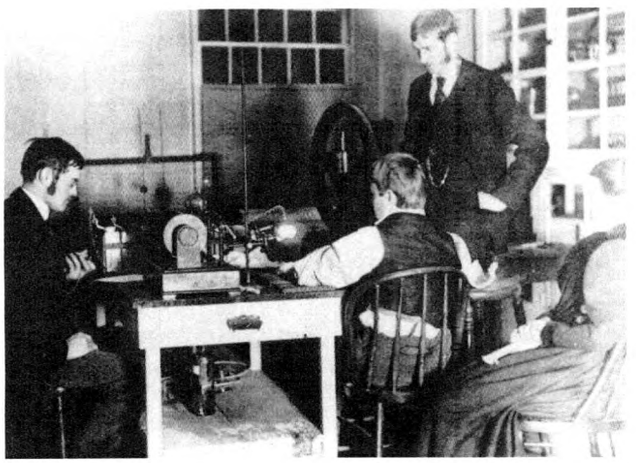


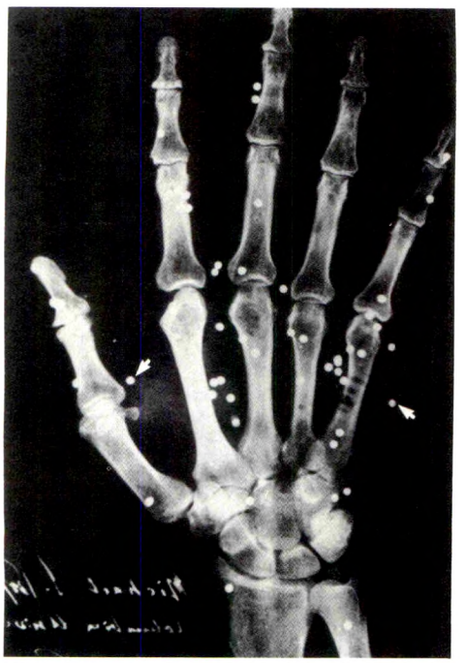
Fig. 3.—First clinical radiograph in America, Dartmouth, 1896. Edwin Brant Frost is on the left (from Brecher and Brecher [2]).

1896, Eddy McCarthy's left forearm was exposed to the tube for 20 min. His Colles' fracture thus became the first clinical radiograph in America [1].

Later that same landmark month, X-ray pioneer Michael Idvorsky Pupin publicized another milestone. A patient named Prescott Butler had been sent to him with painful shot pellets lodged in his hand. Pupin was asked to make an "X-ray photograph" before surgery, which he did on February 18, 1896. However, his method had a key difference. Rather than exposing the plate using the X-rays themselves, he placed a fluorescent screen between subject and plate and used its light to make the exposure. While controversy exists regarding Pupin's claim as discoverer of image intensification [2], the clarity of the radiograph produced only 3 months after Roentgen's discovery is incontrovertible (Fig. 4).

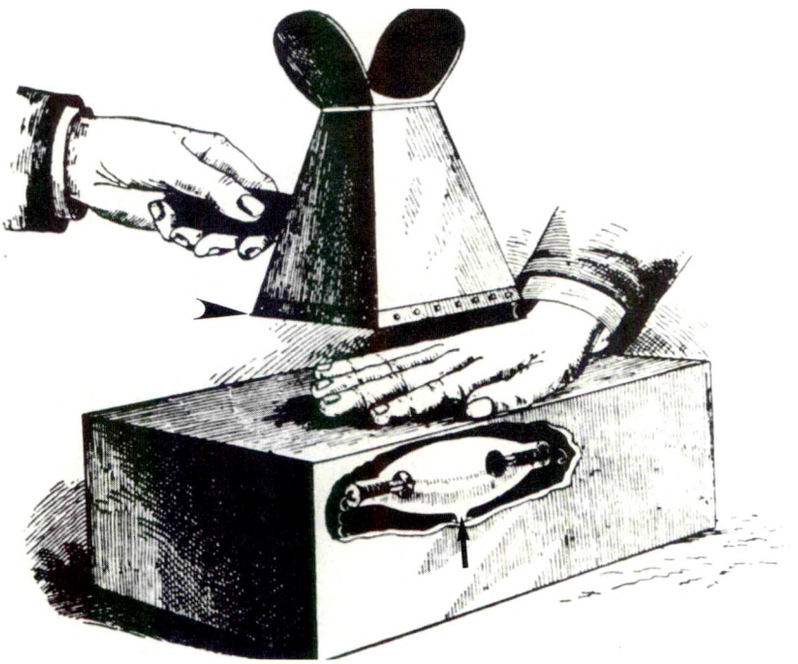
In his 1930 autobiography, Pupin claimed to have received his fluorescent screen from famed inventor Thomas Edison, who had begun investigations with X-rays quite early, in January 1896. His role became much more conspicuous, however, after he received a telegram on February 5, 1896. William Randolph Hearst, publisher of the *New York Journal*, asked Edison if he would . . . as an especial favor to the journal, undertake to make a cathodograph of a human brain" [2]. Edison accepted Hearst's challenge and on February 7, the *New York Times* announced that "tomorrow morning Mr. Edison will attempt further to demonstrate the penetrating powers of the new light by an experiment in photographing a man's brain." Reporters flocked to the West Orange, New Jersey, laboratory. After several delays, the much-touted experiment took place on February 12, 1896. After exposing his assistant's head to the tube for an amazing 1 hr, Edison's result was only a "curvilinear murkiness." The chagrined inventor explained in the February 14th *New York Daily Tribune* that he was skeptical of his brain experiments reaching any results "as the bony structure of the cranium would offer insuperable obstacles" [2]. Even Mr. Edison did not foresee CT.

Despite the theatric air, Edison's laboratory made significant advances. The chief contribution probably was its discovery of an improved fluorescent source to supplant the barium platinocyanide used since Roentgen. After testing up to 8000 substances [1], Edison announced in a cable to Lord Kelvin that calcium tungstate fluoresced most brightly in response to X-rays. This discovery by Edison the scientist sparked Edison the entrepreneur. While fluorescent screens had been described previously, Edison used the brighter calcium tungstate for his screens; he shaped the viewer like the recreational stereoscopes of the day. Thus, in March 1896, the Edison Vitascope was available to the public for home fluoroscopy [2] (Fig. 5). Edison advocated fluoroscopy over photographic plates, presumably in hope of spurring



4

Fig. 4.—Pupin's February 1896, image-intensified radiograph. Note easily visible shot pellets (some highlighted by *arrowheads*) and the excellent bone detail. (Modified from Brecher and Brecher [2].)



5

Fig. 5.—The Edison Vitascope, March 1896. X-ray tube (*arrow*); fluorescent screen (*arrowhead*). (Modified from Brecher and Brecher [2].)

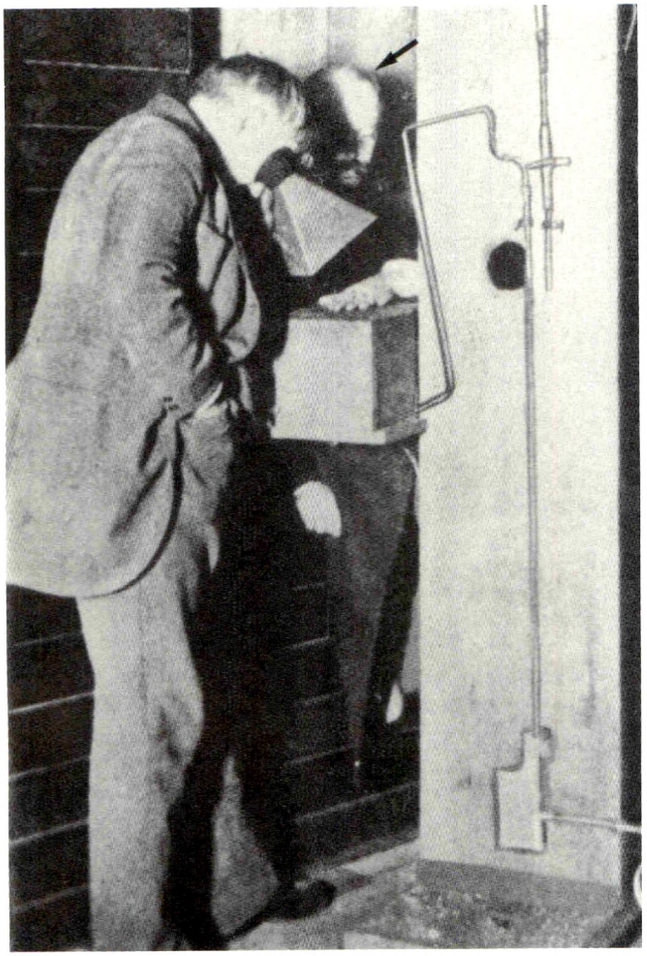
fluoroscope sales [1]. In the same year, the Edison Decorative and Miniature Lamp Department, a division of the General Electric Company, began manufacture of the Edison Roentgen Ray Apparatus, with equipment for both fluoroscopy and photographic plates. General Electric thus has the distinction of being the oldest X-ray manufacturer in the United States.

Unshielded X-ray tubes and unshielded operators were the rule in 1896, with predictable results. Beginning in March, sporadic mention of injury associated with X-rays appeared in the literature. Early reports described a burnlike dermatitis, often with ulceration. Scientific thinking was sharply divided regarding the source of the injurious effects, however. One noteworthy theory was expounded by X-ray tube maker, G. A. Frei, of Boston. In December 1896, he declared that skin damage was "not caused by the action of the X-rays in any way." He ascribed the burns instead to the type of electrical apparatus used to power the tube. In his communication definitively titled "X-Rays harmless with the static machine" [4], Frei proclaimed that " . . . whatever ill effects we get on our skin are caused only when we use induction coils . . . , while no such effects are perceived when we employ the static machine." Interestingly, Frei manufactured static machines. No such potential impediment to objectivity affected famed investigator Nikola Tesla, however, when he, too, asserted in late 1896 that local electrical effects occurring in proximity to a working X-ray tube caused the skin damage. "As to the hurtful actions of the skin . . . ," he stated, "they are not due to the Roentgen rays but merely to the ozone generated in contact with skin" [2].

With such influential voices proclaiming X-rays harmless, the investigators who continued to warn of potential hazard deserve credit. Elihu Thomson of the General Electric Company, in November 1896, detailed an experiment in which he incurred a severe burn after deliberately exposing the little finger of his left hand for ½ hr to an X-ray tube powered by a static machine [5]. Frei's contention that X-rays from such an apparatus were harmless was thus discounted.

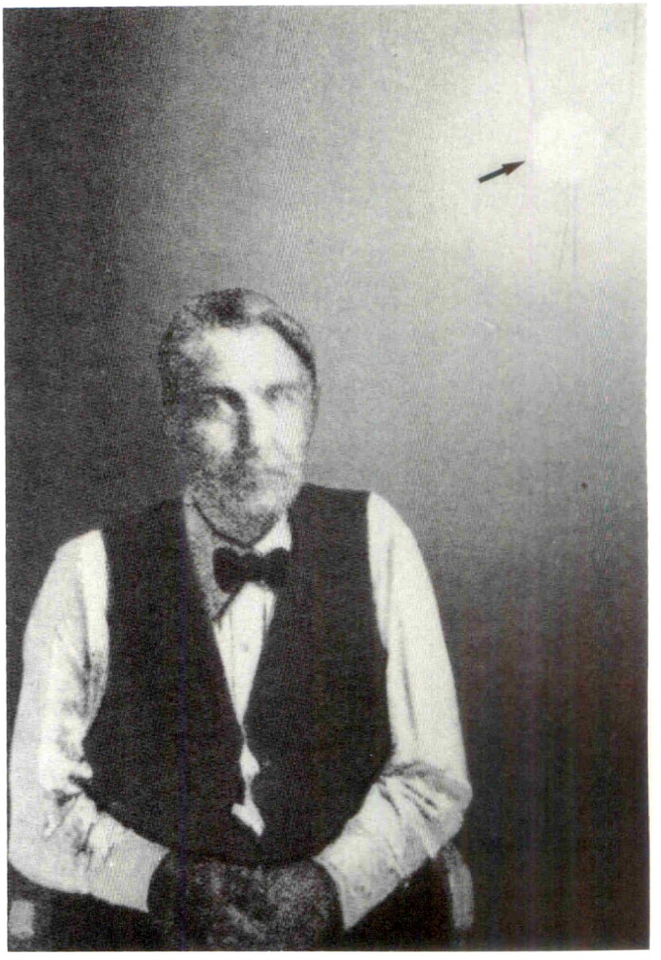
Boston physician and dentist William Herbert Rollins, in the ominously titled work "X-light kills" [6], demonstrated that a guinea pig in a closed, electrically insulated box could be killed by X-rays. This not only cast doubt on Tesla's dictum, but also stressed a previously little-appreciated caveat: Because the guinea pig died with no visible burns, lack of skin damage did not indicate that a given level of X-ray exposure was safe [2]. These conclusions were strongly reinforced on both sides of the Atlantic by a 1916 paper [7] in the Italian literature with the rather melodramatic title of "Autopsy of a radiologist." It detailed the demise of Doctor Emilio Tiraboschi, who had practiced radiology for 14 years without protection. The autopsy showed profound aplastic anemia, and probably equally alarming to the radiologists of the day, both testes were "shrunk to the size of filbert nuts." William Rollins' "X-light axioms" were proving true: The smallest possible beam should strike the patient, and no rays should strike the observer [7].

These revelations came too late, however. The first American casualty was Clarence Madison Dally (Fig. 6), a glasswork artisan employed by Thomas Edison. Edison had de-



6

Fig. 6.—First American X-ray casualty. Clarence Madison Dally (*arrow*) undergoes fluoroscopy by Thomas Edison. (Modified from Brown [8].)



7

Fig. 7.—Thomas Edison photographed with his X-ray tube fluorescent lamp (*arrow*). (Modified from Brown [8].)

vised a project for a new means of illumination, using an X-ray tube coated with fluorescent calcium tungstate (Fig. 7). Dally used his glassblowing skills in forming these tubes, and he performed the preliminary testing in the standard 1896 fashion of placing his hand in the beam. By late that year his hands had been so badly burned that his physician urged him to stop his work. Amazingly, he continued. Speaking of Dally's affliction, Edison commented with pragmatic understatement, " . . . I started to make a number of these lamps, but I soon found that the rays had affected poisonously my assistant, Mr. Dally, so that . . . his flesh commenced to ulcerate. I then concluded that it would not be a very popular kind of light, so I dropped it . . . " [8]. That decision came too late for Dally, however, who died in 1904 of metastatic squamous carcinoma after 144 failed skin grafts and bilateral arm amputations [8]. In addition to Dally, Percy Brown lists 26 Americans who died as a result of their pioneering work with X-rays.

The eclectic group presented here, culled from such diverse fields as photography, physics, and medicine, provides a mere sampling of the people important in our specialty's fledgling years. With the advent of the Coolidge hot cathode-ray tube in 1912, the "gas tube era" came to a close. Taking into account their equipment, which was inefficient, dangerous, and impossible to calibrate, the level of advances achieved by these pioneers remains a tribute to their ingenuity, diligence, and selflessness.

REFERENCES

1. Grigg ERN. *The trail of the invisible light.* Springfield, IL: Thomas, **1965**
2. Brecher R, Brecher E. *The rays. A history of radiology in the United States and Canada*. Baltimore: Williams & Wilkins, **1969**
3. Wright AW. Experiments upon the cathode rays and their effects. *Am J Sci* March **1896**;1(15):235–244
4. Frei GA. X-rays harmless with the static machine. *Elect Engineer* Dec. 23, **1896**;22:651
5. Thomson E. Roentgen rays act strongly on the tissues. *Elect Engineer* Nov. 25, **1896**;22:534
6. Rollins W. X-light kills. *Boston Med Surg J* Feb. 14, **1901**;144:173
7. Bruwer AJ. *Classic descriptions in diagnostic roentgenology*, vol. 1. Springfield, IL: Thomas, **1964**
8. Brown P. *American martyrs to science through the Roentgen rays*. Springfield, IL: Thomas, **1936**

Commentary

Should We X-Ray Halloween Candy?

Jerry Calvanese[1]

Each Halloween, adulterated food is discovered in children's trick-or-treat bags. In order to lessen the risk of such poisoning, schools, neighborhoods, and organizations sponsor Halloween parties as an alternative to trick-or-treating. For the same purpose, the X-raying of Halloween candy has been started in many hospitals in recent years, with the costs of such screening considered justified by the decreased risk of injury to children and the enhanced public image of the participating hospitals. Furthermore, the competitive atmosphere in which many hospitals now operate forces some hospitals to offer the screening program even though their staffs doubt its effectiveness. Because there are no published studies on the costs and effectiveness of X-raying Halloween candy, I gathered such data from three local hospitals in the Reno-Sparks area and 18 outlying hospitals in the referral area of northern Nevada and in the mountain area of northern California for 1985.

The well-intentioned program of X-raying Halloween candy is costly: The annual expenses just to the three local hospitals in the Reno-Sparks area was $1625.62. The price to X-ray each bag (including calculated salary for volunteer time, when applicable) ranged from $2.01 to $5.23 (average, $3.38). The potential annual national costs are staggering; approximately 6900 hospitals nationally are capable of offering this service for an estimated 48 million children below the age of 14 [1, 2]. On the basis of our total regional population statistics, the nation could be spending as much as $0.8–1.4 million to screen Halloween candy [3, 4].

Radiographic screening of Halloween candy is not effective. Of the 394 X-rays taken in the three local hospitals and the 669 taken in the 18 outlying hospitals, no films were positive for hidden radiopaque foreign bodies. Also, no positive findings were found when approximately the same number of X-rays of Halloween candy were done at these same hospitals 1 year earlier. The screening procedures do not ensure that the X-rayed candy is safe to eat. X-raying excludes neither potential toxins nor radiolucent foreign bodies. In fact, radiographs are not reliable in excluding the presence of gastrointestinal foreign bodies. A study by Bender and Anderson [5] revealed radiographic documentation of foreign bodies in only 62% of 125 pediatric cases of foreign-body ingestions. In another study [6] involving 2394 ingested foreign bodies, the radiographic documentation rate was only 14%.

Not only is X-raying of Halloween candy costly and ineffective, it also creates several problems. Children taking their candy to the hospital on Halloween night risk involvement in traffic accidents. The Reno and Sparks police departments reported 13 drunk-driving arrests on Halloween, almost 2½ times the normal number of arrests for driving-under-the-influence. Also, the implication that X-rayed candy is "safe," when toxins or radiolucent foreign bodies may still be present, carries potential liability for the hospital, the X-ray technician, and the physician who interprets the films. Finally, additional drawbacks and risks arise from crowds composed mostly of children in the Radiology Department and Emergency Room and from disruption of vital hospital functions.

The arguments for stopping the X-ray screening of Halloween candy appear overwhelming. The first step is to educate the decision makers in hospitals so they can see that ending the radiographic screening program is a logical, cost-effective move. Then, in order to minimize the public relations damage that might ensue, the staffs of all competing hospitals should

Received March 17, 1986; accepted after revision June 9, 1986.
[1] Department of Emergency Medicine, Washoe Medical Center, 77 Pringle Way, Reno, NV 89502. Address reprint requests to J. Calvanese.

also agree to stop the screening and to use some of the money saved for public education. The public relations departments of these hospitals may start a media campaign that explains the costliness and ineffectiveness of X-ray screening. Such a campaign might emphasize that X-raying candy is no guarantee against contamination and that the "free" X-rays involve health-care costs shared by all.

Most importantly, parents must be informed that their own inspection of Halloween candy is the best guarantee of safety. All four cases of adulterated candy reported in our community over the last 2 years were detected by inspection alone. Parents should be educated to the simple methods of inspection that can decrease the chances of their children eating adulterated candy: (1) Examine candy wrappers carefully; (2) Discard any candy with wrappers that have puncture holes or tears, as well as any candy with signs of being unwrapped, faded wrappers, discoloration, or any other possible signs of tampering; (3) Discard unwrapped candy and candy from unknown manufacturers or sources; (4) Discard home-wrapped "goodie" bags from unknown sources that contain, for example, popcorn, cookies, or cupcakes; (5) Inspect fruits for punctures and discard any from unknown sources, because these can be contaminated with a toxin without visible evidence of tampering; (6) Limit the trick-or-treating area covered, especially in unfamiliar neighborhoods, and encourage, instead, attendance at parties given by friends or organizations.

I hope that hospital administrators and the communities they serve can be convinced that the well-intentioned program of X-raying Halloween candy should be stopped. If the public is properly educated, much money and staff time can be saved without risk to the safety of the children or to the public image of hospitals.

REFERENCES

1. U. S. Census Bureau. *Estimate of population of the United States by age, sex, and race, 1980–84, current population reports* (series P-25, No. 965). Washington, DC: U. S. Government Printing Office, March **1985**
2. *American Hospital Association guide to the health care field.* Chicago: American Hospital Association, **1984**
3. *Population estimates of California cities and counties, January 1, 1984 to January 1, 1985* (report 85 E-1). Sacramento, CA: California Department of Finance, May **1985**
4. *Population of Nevada's counties and incorporated cities, 1980 actual, 1981 through 1985, official state estimates.* Carson City, NV: Nevada State Office of Community Services, January **1985**
5. Bender L, Anderson WA. Pediatric gastrointestinal foreign body ingestions. *Ann Emerg Med* Feb. **1984**;13:112–117
6. Nandi P, Ong GB. Foreign body in the esophagus: review of 2394 cases. *Br J Surg* **1978**;65:5–9

Editorial

The Diffusion of MRI in the United States: What is Fact and What Is Speculation

Ronald G. Evens[1]

The article by Steinberg in the September issue of the *AJR* [1] is the third report in this journal during the last year on the distribution of MRI equipment. In August 1985, Evens et al. [2] reported on data obtained by survey directly from 47 of 72 MRI installations operational in October 1984; Hillman and Schwartz [3] reported in May 1986 on data obtained by telephone directly from 151 MRI installations operational in May 1985; and Steinberg [1] reports data obtained from manufacturers on 371 MRI units assumed to be operational in December 1985.

Each report confirms the results of the others. The number of MRI installations in the United States is growing rapidly, yet the growth curve lags behind that of CT at a comparable time after the introduction of the new technology. Nearly half of the installed MRI units are not in hospitals, "larger" magnets (≥0.5 T) are more popular, and a large portion are owned by physicians. Steinberg [1] reports that the 371 MRI units in the United States are 72% of the estimated 511 worldwide units, and that manufacturers anticipate a continued rapid growth. Steinberg lists 15 manufacturers of MRI equipment, and I know of two additional companies that believe they should be included in the list. The three reports vary with time (installation dates from October 1984 through December 1985) and data-collection method (from the user by written survey, the user by telephone, and manufacturers), yet the data are consistent.

Analysis and discussion resulting from the data are more interesting and controversial. Is the diffusion of MRI in the United States appropriate? While there is no doubt that the installation of MRI units is moving quickly, the determination of "appropriateness" depends on the bias of the evaluator. I suggest that the diffusion curve for MRI is no different from that of any new technology in science, business, or medicine. There is always an "S-shaped" curve with useful technology, and the important questions are the magnitude and time scale of the curve. Similar curves describe the installation and diffusion of CT, image intensifiers, NMR spectrometers, word processors, electronic copiers, and so forth. With any technology, including MRI, the dimensions of the curve depend upon the consumers' analysis of the advantages in the new technology, its cost, and the ability of the suppliers to get the product to market.

Why is the curve for MRI lower than for CT? The analysis of this question in the three *AJR* papers is influenced by the interests of the authors. Hillman and Schwartz [3] and Steinberg [1] emphasize the importance of health-policy issues (e.g., prospective payment, certificate of need, Medicare payment approval), while Evens et al. [2] suggest that the important issues are related to medical and radiologic practice. MRI has important diagnostic utility, but CT is readily available and has excellent diagnostic efficacy in most organ systems, making it difficult for MRI to demonstrate that its diagnostic supremacy is worth a considerable added cost. All authors agree that the current concern about medical costs is a major factor preventing a more rapid diffusion of MRI. If MRI cost half as much to the radiologist and half as much to the patient, if MRI had no installation problems, and if CT weren't available, then the MRI diffusion rate would be spectacular. But wishes are not reality.

What is the future of the MRI diffusion curve? How high will it go and when will it plateau? These questions are important to many, including manufacturers, health-care plan-

[1] Mallinckrodt Institute of Radiology, Washington University School of Medicine, St. Louis, MO 63110. Address reprint requests to R. G. Evens.

AJR 147:856–857, October 1986 0361–803X/86/1474–0856 © American Roentgen Ray Society

ners, and radiologists. The parameters for the dynamics of this curve include many unknowns. Does MR spectroscopy have clinical importance? Can MRI units be installed in hospital and acute-care locations with new technology for shielding? Will the operational and capital costs stay at current levels? Will the current proposed advantages of MRI (e.g., direct sagittal and coronal imaging) be matched by new developments in CT? Are there useful, organ-specific MR contrast agents? Until some of these questions are answered, no one can predict the total number of MRI units or when they will be in operation.

How important is economics to the owner/operator? Freestanding or mobile units account for approximately 50% of all operational units. Economic risk is always accepted by the owner of new technology and traditionally, with radiology equipment, has first been accepted by a hospital or other large medical institutions. A large medical institution has many reasons to accept economic risk with a new technology. In addition to making a profit from the new technology, it can make a profit with increased activity in other cost centers (i.e., a "loss leader") or justify an economic loss for noneconomic reasons (i.e., prestige, research, teaching). The highest priority of the noninstitutional owner/operator will be making a profit, and economic factors should be of great importance. Only one of the papers [2] reports economic data and describes MRI operations in 1984 as a risky business because of low procedure-volume and poor third-party reimbursement. Future studies with economic data will be of interest.

The paper by Steinberg [1] identifies two bits of information worth watching. In 1986, he reports on 15 (or more) manufacturers of MRI equipment, more than double the seven manufacturers identified in 1984. If CT is a model, less than 10 manufacturers will survive, and the battles for market share will be fierce. Steinberg also reports that more than 70% of MRI units now installed are in the United States. The U. S. market is approximately 50% of the world radiology market. Either we are buying fast or the rest of the world is buying slow; I bet on the former.

Technology-watching will be increasingly important because of continued concerns about costs and distribution of expensive resources. Data collection and analyses from careful scientific studies should be subjected to peer and editorial review in the *AJR* and other journals so that we will have a better idea about what is known and what is speculation.

REFERENCES

1. Steinberg EP. The status of MRI in 1986: rates of adoption in the United States and worldwide. *AJR* **1986**;147:453–455
2. Evens RG, Jost RG, Evens RG Jr. Economic and utilization analysis of magnetic resonance imaging units in the United States in 1985. *AJR* **1985**;145:393–398
3. Hillman AL, Schwartz JS. The diffusion of MRI: patterns of siting and ownership in an era of changing incentives. *AJR* **1986**;146:963–969

Letters

Quadriplegia in Diffuse Idiopathic Skeletal Hyperostosis After Minor Trauma

We would like to report two patients with diffuse idiopathic skeletal hyperostosis (DISH), both of whom developed severe neurologic deficits after minor trauma.

The first patient was a 44-year-old man who suffered "backstrain" at work. He subsequently noted pain and decreased sensation in his extremities and difficulty walking. Physical examination disclosed myelopathy with weakness in both upper extremities and diminished sensation in all extremities. Plain-film examination (Fig. 1A) showed thick, rodlike ossification of the posterior longitudinal ligament. Metrizamide CT examination (Fig. 1B) clearly demonstrated the ossified posterior longitudinal ligament, which caused significant narrowing of the vertebral canal and compression of the spinal cord. Lateral view of the thoracic spine showed ossification of the anterior longitudinal ligament and vertebral bridging with normal disc spaces, fulfilling the criteria for DISH [1].

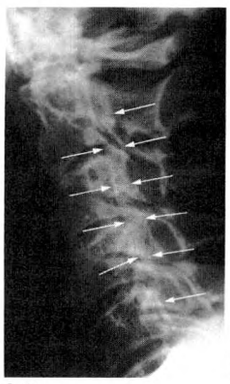
The second patient was a 30-year-old, severely retarded man who fell during a seizure, striking his chin on the floor. Initial examination disclosed weakness of the upper extremities and absence of movement of the lower extremities. The patient became totally quadriplegic over the next 2 days with subsequent respiratory arrest. Plain-film examination of the cervical spine (Fig. 2) showed ossification of the anterior longitudinal ligament from C3 to C6 with a fracture of the ossified ligament at C5–C6 and a fracture through the upper C6 body. The C5–C6 disc space and facet joints were disrupted. An earlier radiograph of the cervical spine showed a dense bony bridge between C5 and C6. On neither cervical spine film were there syndesmophytes to suggest anklyosing spondylitis. The rest of the spine and sacroiliac joints were normal. Postmortem examination of the cervical cord showed contusion and ascending necrosis.

DISH is an ossifying diathesis, characterized by bony proliferation of spinal and extraspinal structures, particularly of the spinous ligaments [1, 2]. Patients with DISH are often asymptomatic [3], but the condition is not innocuous. Thickening and ossification of posterior longitudinal ligament in DISH can narrow the vertebral canal and progressively compress the spinal cord [4]. This was the situation with the first patient, who was in seemingly good health until the time of his back strain. The neurologic deficits after this incident were probably the result of further insult to an already compromised, compressed spinal cord.

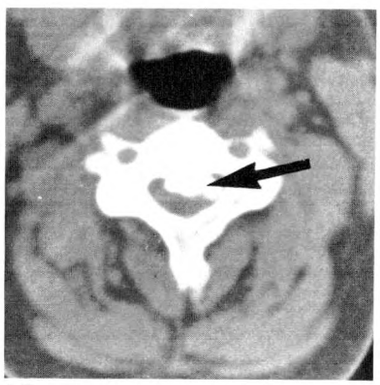
The second patient illustrates another complication of injury in DISH. Ossification of the anterior longitudinal ligament causes rigidity of the spine. The spine is not able to bend in response to a blow to the head or neck, and the blow effectively becomes concentrated at one point, resulting in complete fracture of the spine at that level with potentially catastrophic consequences to the spinal cord. This postulated mechanism of injury in DISH [5] is similar to that in ankylosing spondylitis [6].

Patients with DISH should be particularly careful to avoid situations that may cause back strain or injury.

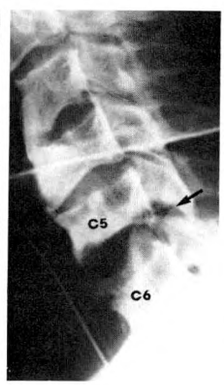
Rauf Yagan
Nathaniel Karlins
Case Western Reserve University
Cleveland Metropolitan General Hospital
Cleveland, OH 44190



1A



1B



2

Fig. 1.—**A**, Lateral view of cervical spine shows rodlike ossification of posterior longitudinal ligament (*arrows*).

B, Metrizamide CT scan of cervical spine shows a thickened, ossified posterior longitudinal ligament (*arrow*). The cord is compressed and displaced to the right.

Fig. 2.—Lateral view of cervical spine shows ossification of anterior longitudinal ligament from C3 to C6, and fracture of ossified anterior longitudinal ligament at C5–C6. Also note fracture of upper C6 vertebral body. There is disruption of C5–C6 facets (*arrow*).

REFERENCES

1. Resnick D, Niwayama G. *Diagnosis of bone and joint disorders*. Philadelphia: Saunders Company, **1981**:1419
2. Resnick D, Niwayama G. Entheses and entheropathy: anatomic, pathologic, and radiologic correlation. *Radiology* **1983**;146:1–9
3. Tsukamoto Y, Onituska H, Lee K. Radiologic aspects of diffuse idiopathic skeletal hyperostosis in the spine. *AJR* **1977**;129:913–918
4. Alenghat JP, Hallet M, Kido DK. Spinal cord compression in diffuse idiopathic skeletal hyperostosis. *Radiology* **1982**; 142:119–120
5. Corke CF. Spinal fracture and paraplegia after minimal trauma in a patient with anklyosing vertebral hyperostosis. *Br Med J* **1981**;282:2035
6. Hunter T, Dubo H. Spinal fractures complicating anklyosing spondylitis. *Ann Intern Med* **1978**;88:546–549

Splenic Hydatid Cyst Opening to:

In the September 1985 issue of the *AJR* Beggs [1] presents an interesting review of the most common locations of echinococcosis. Hydatid disease is endemic in Spain. Its high frequency offers us the opportunity to find hydatid cysts in unusual places with peculiar radiologic manifestations. We recently studied a case of splenic hydatid cyst opening to the colon.

A 65-year-old woman was admitted to our hospital with a 4-day history of fever (39°C), pain in the left hypochondrium, and watery diarrhea. Four years before she had had surgery for a hepatic hydatid cyst. Her physical examination disclosed a tender mass in the left hypochondrium.

The chest radiograph revealed an elevated left hemidiaphragm. On the plain film of the abdomen, extraluminal gas could be seen on the left hypochondrium (Fig. 1). A sonographic examination of the abdomen demonstrated a complex mass underneath the left diaphragm. The upper gastrointestinal series showed a shift of the stomach to the right, without wall lesions. A barium enema revealed the presence of a fistula between the splenic flexure of the colon and a large cavity in the spleen with multiple radiolucent defects (Fig. 2).

The surgical excision revealed a big hydatid cyst in the spleen opening into the colon. The cyst was filled with daughter cysts and feces. Splenectomy and colostomy were performed.

Splenic echinococcosis occurs in about 2 to 3% of hydatid disease [2]. Rupture into the gastrointestinal tract occurs in no more than 0.5% of hydatid cysts of any location [3]. On the plain film of the abdomen a soft-tissue mass displacing adjacent structures may be seen in the left hypochondrium. If the cyst is perforated into the colon, extraluminal gas may be found. This can occur also with abdominal abscesses, making the differential diagnosis difficult. The sonogram performed on our patient showed a tender mass similar to that described for hepatic echinococcus cysts. Initially, a primary tumor of the gastrointestinal tract was suspected. The upper gastrointestinal series demonstrated a normal stomach, and the barium enema revealed contrast material flowing from the splenic colonic flexure into a large cyst filled with multiple daughter cysts with the typical appearance of "a bunch of grapes."

Despite the great number of reports about echinococcosis that have been published in Spain, we have not been able to find a case of splenic hydatid cyst rupture into the colon that had such a radiologic appearance.

P. Caballero
E. Ocon
A. G. Robledo
F. J. Diáz
Universidad Autonoma
Madrid, Spain 28043

REFERENCES

1. Beggs I. The radiology of hydatid disease. *AJR* **1985**;145:639–648
2. Bonakdarpour A. Echinococcus disease: report of 112 cases

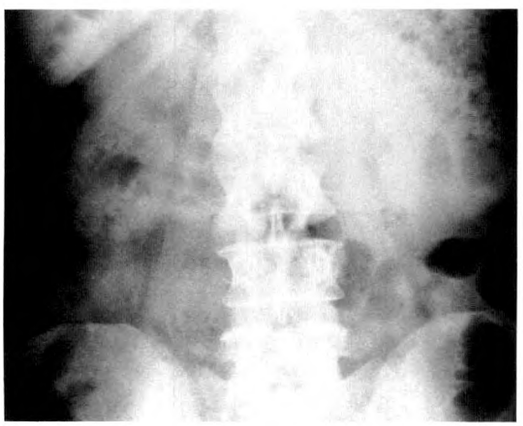


Fig. 1.—Plain film of abdomen shows extraluminal gas on left upper quadrant.



Fig. 2.—Barium enema shows fistula between splenic flexure and a large cavity in spleen. Multiple radiolucent defects are daughter cysts and feces.

from Iran and a review of 611 cases from the United States. *AJR* **1967**;99:660–667
3. Kourias B. Complications principales des kystes hydatiques du foie. Leur thérapeutique actuelle. *J Chir* (*Paris*) **1967**;94:35–52

Reply

Caballero et al. describe an unusual case of hydatid disease. The sonographic examination of their case is not illustrated but is reported to be similar to that of hepatic echinococcosis. The barium enema is typical of a complicated hydatid cyst shown by contrast examination wherever the site (Fig. 1). The daughter cysts appear as multiple round or oval filling defects within the parent cyst on contrast studies and as similarly shaped masses of about water density on CT examination.

The parasite behaves in different ways in different organs but in extraskeletal sites the similarities are striking (Fig. 2) and apparent differences in appearance are often related more to the imaging method required to demonstrate the parasite than to differences in morphology. I should, perhaps, have made this point more clearly in my article and am grateful for the opportunity to do so now.

Ian Beggs
Royal Infirmary
Edinburgh EH3 9YW
United Kingdom

Mammography and Grids

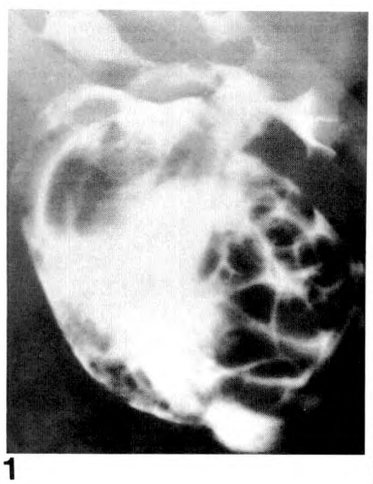
Sickles and Weber [1] found that the use of grids improved the image quality in approximately 60% of film-screen mammograms. However, despite the use of slightly faster film and an increase in kilovoltage, the use of a grid resulted in a 70% increase in radiation from 0.10 to 0.17 rads (cGy) per exposure. In order to maximize information while minimizing radiation, these authors recommend that mammography be performed with "an initial exposure using nongrid rather than grid technique, unless the technologist cannot achieve a compressed breast thickness of 6 cm or less. Then, switch to grid technique only if the initial film shows more than 50% dense fibroglandular tissue."

With the protocol recommended by the authors, 92% of patients would have undergone an initial nongrid mammogram and a total of 37% would have eventually undergone grid mammography. Seventy-eight percent of women selected for grid mammography would have had the image quality of their examination improved by its use. However, 43% of those women not selected for grid mammography also would have had image quality improved by the use of grids. The protocol necessitates keeping track of two different mammographic films.

These recommendations require that in over 90% of patients, first, an initial mammogram be obtained, developed, and evaluated before completing the examination. I estimate that, depending on a number of factors, this would result in a 10–20% increase in examination time. Most mammograms are now performed as screening studies and many low-cost screening centers, charging $25–50 per examination, might not be economically viable with a 10–20% reduction in efficiency. Dr. Sickles, a pioneer in low-cost screening mammography, could speak to this issue better than I. In the case of nonscreening mammography, where there is a positive clinical history or physical examination, I would be reluctant to sacrifice the 43% improved-image quality in those women not selected for use of the grid.

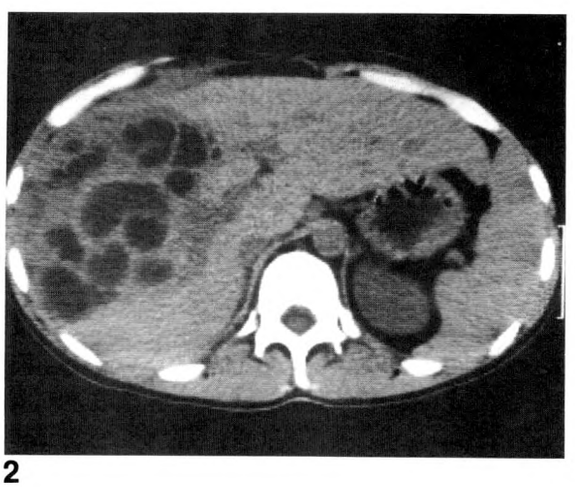
Opinion is nearly unanimous concerning the benefits of screening mammography, which can reduce the mortality from breast cancer by as much as one-third [2]. Because current recommendations make almost one-half of adult women eligible for this examination each year, monetary considerations are often the most important determinant of the success of most large-scale mammographic screening programs. Costs are both direct and indirect in the case of false-negative biopsies [3]. Radiation dangers of screening mammography, while of obvious importance, are in my opinion, dwarfed by economic considerations. Mammographic-screening cancer detection (prevalence of seven and incidence of three) is approximately four breast cancers per year per 1000 women [4] while radiation causes approximately four breast cancers per million women per year per rad [5] with a 10-year latency. Therefore, the cost:benefit (cancers caused:cancers detected) of screening mammography (0.2 rads per breast) is approximately 1:5000, and even with a 70% increase in dose from the use of grids, screening mammography remains a "best buy." Also, the use of a grid would have improved the image quality of almost one-half of women selected in the Sickles and Weber protocol to have nongrid mammography.

I commend the authors for their informative and timely article.



1

Fig. 1.—Multiple daughter cysts in complicated renal hydatid cyst shown by diagnostic cyst puncture. Note similarity to splenic cyst of Caballero et al.



2

Fig. 2.—Unenhanced CT. Large complicated hydatid cyst in right lobe of liver. Daughter cysts appear as well-defined defects of water density.

However, I have some reservations about their recommendations. We hope the recent introduction of faster double-emulsion mammographic films will further reduce radiation dangers and concerns.

Ferris M. Hall
Beth Israel Hospital
Harvard Medical School
Boston, MA 02215

REFERENCES

1. Sickles EA, Weber WN. High-contrast mammography with a moving grid: assessment of clinical utility. *AJR* **1986**;146:1137–1139
2. Tabár L, Fagerberg CJG, Gad A, et al. Reduction in mortality from breast cancer after mass screening with mammography: randomized trial from the Breast Cancer Screening Working Group of the Swedish National Board of Health and Welfare. *Lancet* **1985**;1:829–832
3. Hall FM. Screening mammography–potential problems on the horizon. *N Engl J Med* **1986**;314:53–55
4. Baker LH. Breast cancer detection demonstration project: five year summary report. *CA* **1982**;32:194–230
5. Feig S. Assessment of the hypothetical risk from mammography and evaluation of the potential benefit. *The Radiologic Clinics of North America* **1983**;21:173–191

Reply

We are grateful for the opportunity to clarify a potential source of confusion. Table 1 in our paper catalogs the changes in mammographic image quality seen with grid use, while Table 2 describes the frequency with which these changes actually affect image interpretation. By presenting our data in this fashion, we had hoped to emphasize the *clinical significance* of Table 2. Improved image quality (primarily increased contrast in the case of grids) does not necessarily alter radiologic interpretation, or even the level of confidence with which interpretations are made. The data in Tables 1 and 2 clearly show this to be true. While Dr. Hall's reworking of Table 1 correctly indicates that 43% of women not selected for grid mammography thereby would miss out on improved image quality, Table 2 shows that only 0.6% of these women would really benefit from grid use by virtue of a change in image interpretation. As we stated elsewhere in the paper, "one may readily justify the use of a higher-dose imaging technique if it frequently provides added information that is clinically useful." In our opinion, an increase in clinical utility of only 0.6% is insufficient to justify grid use for women whose breasts are neither thick nor dense.

Dr. Hall's objection to our imaging protocol centers on the practice of developing the first standard mammographic exposure before the other three, and using the information on this film to decide for or against grid use. He suggests that the resultant increase in examination time will drive up the cost of operation. In fact, our protocol does add 2 to 3 min to each examination, but also affords us the opportunity to make adjustments in exposure parameters to optimize technique for the remaining three standard exposures. In many circumstances, this latter advantage alone is sufficient to justify the approach; indeed, we have been recommending it for the past 7 years [1], long before mammography grids were widely available.

Returning to the issue of increased examination time, Dr. Hall is correct to make the distinction between high-volume low-cost screening operations and the remainder of mammography practices, which include individually-directed nonscreening examinations on symptomatic and otherwise complex patients. For the latter, more common type of mammography practice, a difference in examination time of only 2 to 3 min is hardly noticeable; it simply is not practical to shorten the time between patient appointments by such a small interval to actually realize a savings in operating costs. However, the situation is quite different for rapid-throughput screening of asymptomatic patients, because this type of imaging examination can be completed in as little as 5 min. Such a degree of efficiency is achieved only by streamlining imaging procedures, including the batch processing of all films at the end of the work day [2]. Clearly, our protocol for deciding on grid use will not work in this situation. Rather, one must choose either to use grids on every patient or on none at all. In the UCSF low-cost screening program we have based our decision to completely omit grid use on the limited tube output of our X-ray unit, and also on our observation that only 20% of a general patient population will benefit from grid exposures (Table 2). The rate of detecting prevalent cancers in our first round of screening has been even higher than that cited by Dr. Hall, so we are confident that our nongrid technique is clinically successful.

We fully agree that current mammography techniques impart a negligible radiation risk, but wish to emphasize that grid use in a (readily identifiable) majority of women produces a correspondingly negligible benefit. For conventional mammography practices that mix complete cases with screening examinations, we strongly recommend our protocol of limiting grid use to women with thick or dense breasts. For low-cost screening practices, the all-or-none decision on grid mammography is more difficult to make. We share Dr. Hall's hope that the recent introduction of faster mammographic screen-film systems will permit grid use at equal exposure parameters (and dose) to what currently is standard technique. However, we caution

TABLE 1: **Comparative Evaluation of Image Quality of Matched Pairs of Grid and Nongrid Films**

	Total No. of Patients	Grid Inferior	No Difference	Grid Superior
		No. (%)	No. (%)	No. (%)
All patients	1000	69 (7)	363 (36)	568 (57)
Thickness >5 cm	334	16 (5)	111 (33)	207 (62)
Thickness >6 cm	83	8 (10)	10 (12)	65 (78)
>50% dense tissue	308	15 (5)	47 (15)	246 (80)
>75% dense tissue	126	4 (3)	11 (9)	111 (88)
Thickness >5 cm or >50% dense tissue	543	25 (5)	165 (30)	353 (65)
Thickness >5 cm or >75% dense tissue	420	22 (5)	122 (29)	276 (66)
Thickness >6 cm or >50% dense tissue	370	18 (5)	57 (15)	295 (80)
Thickness >6 cm or >75% dense tissue	201	12 (6)	20 (10)	169 (84)

Note.—Breast thickness measured during vigorous compression; percentage of dense tissue (by volume) estimated from combination of craniocaudal and lateral projection nongrid mammograms. Percentage of dense tissue (by area) estimated from a single-projection nongrid mammogram closely parallels the volume estimates used above.

TABLE 2: **Comparative Evaluation of Clinical Utility of Matched Pairs of Grid and Nongrid Images**

	Total No. of Patients	Grid: Less Information	No Difference	Grid: More Information Interpretation Unaided	Grid: More Information Interpretation Aided
All patients	1000	72	359	373	196
Thickness >5 cm or >50% dense tissue	543	28	121	199	195
Thickness >5 cm or >75% dense tissue	420	22	63	142	193
Thickness >6 cm or >50% dense tissue	370	19	53	129	192
Thickness >6 cm or >75% dense tissue	201	15	12	27	147

the reader to await controlled clinical testing of these faster imaging systems, because, as shown in Tables 1 and 2, simple determinations of image quality do not always correlate with clinical results.

Edward A. Sickles
William N. Weber
University of California School of Medicine, San Francisco
San Francisco, CA 94143

REFERENCES

1. Sickles EA. Methods to reduce radiation dose in mammography. In: Margulis AR, Gooding CA, eds. *Diagnostic radiology 1979.* San Francisco: University of California, **1979**:809–823
2. Sickles EA, Weber WN, Galvin HB, Ominsky SH, Sollitto RA. Mammographic screening: how to operate successfully at low cost. *Radiology* **1986**;160:95–97

Ear Acupuncture for Hypotonia in Gastrointestinal Examination

I wish to call your attention to the value of acupuncture to achieve hypotonia of the stomach during radiographic studies of the upper gastrointestinal tract.

Fifty patients (26 men, 24 women) had acupuncture of the ear immediately preceding double-contrast upper gastrointestinal examination. Acupuncture was accomplished in the conventional fashion by inserting 1.5-cm-long steel needles into the tragus of both ears at the "hungry" point. The degree of gastrointestinal hypotonia evident on the radiographs was compared with that of a second group of 44 patients, matched for age and gender, who were given 20 mg of the anticholinergic drug, 654-2, commonly used in China. Barium studies were performed in an identical fashion in both groups with high-density barium suspension and an effervescent agent.

No side effects were noted in the patients having acupuncture; dry mouth, blurred vision, and tachycardia were common in the patients given 654-2.

The average widths of the body and antrum of the stomach, as measured on the radiographs, were the same in the two groups. The films were judged to be excellent, good, or poor in 44, 34, and 22%, respectively, in the acupuncture group, and 14, 50, and 36%, respectively, in the 654-2 group.

The results suggest that acupuncture is as effective as 654-2 in producing hypotonia during radiographic examination of the upper gastrointestinal tract, but does so without causing side effects.

Jing-Huei Jiang
Huai-Hua Railway Hospital
Huai-Hua City, Hunan, China

Abstracts

Heart

Intraoperative evaluation of coronary artery bypass graft anastomoses with high-frequency epicardial echocardiography: experimental validation and initial patient studies. Hiratzka LF, McPherson DD, Lamberth WC Jr, et al. (The University of Iowa Hospitals and Clinics, Iowa City, IA 52242). *Circulation* 73:1199–1205, June 1986

The authors evaluated the use of high-frequency epicardial echocardiography in the intraoperative evaluation of the technical adequacy of coronary artery-bypass-graft anastomoses. Initially, 12 dogs were studied after coronary artery-bypass-grafting with deliberate technical errors created in some grafts. There was good correlation between short-axis (cross-sectional) and longitudinal two-dimensional images of the anastomoses with findings determined histologically. All technical errors were recognized. In 12 patients, 15 coronary artery-bypass-graft anastomoses were examined intraoperatively with high-frequency epicardial echocardiography. The measured maximal luminal diameter of the anastomoses was greater than the maximal luminal diameter of the native artery in all end-to-side anastomoses. The maximum luminal diameter of the side-to-side anastomoses was equal to or slightly greater than that of the native artery. Minor technical errors were noted in two of the 15 grafts. The authors conclude that high-frequency epicardial echocardiography can accurately measure coronary artery-bypass-graft anastomoses and has the potential for intraoperative detection of technical errors and inadequacies.

Richard B. Jaffe

Noninvasive evaluation of aortic regurgitation by continuous-wave Doppler echocardiography. Masuyama T, Kodama K, Kitabatake A, et al. (The First Department of Internal Medicine, Osaka University School of Medicine, 1-1-50 Fukushima, Fukushima-ku, Osaka 553, Japan). *Circulation* 73:460–466, March 1986

The authors examine the feasibility of using continuous-wave Doppler echocardiography to examine the aortic regurgitant-flow-velocity pattern in 32 adults with aortic regurgitation and in 10 patients without aortic regurgitation. The aortic regurgitant-flow-velocity patterns, characterized by a rapid rise in flow velocity immediately after closure of the aortic valve, and high peak-flow velocity and the gradual deceleration until the next aortic valve opening, successfully identified 30 of 32 patients with aortic regurgitation. Generally, as the severity of aortic regurgitation increased, the velocity decline (deceleration) became greater, and the time to decline to half the peak velocity (half-time) shortened. The authors conclude that continuous-wave Doppler echocardiography permits the noninvasive evaluation of aortic regurgitation.

Richard B. Jaffe

Pediatric Radiology

Idiopathic external hydrocephalus: natural history and relationship to benign familial macrocephaly. Alvarez LA, Maytal J, Shinnar S (Division of Pediatric Neurology, VCP-207, Montefiore Medical Center, 111 E. 210th St., Bronx, NY 10467). *Pediatrics* 77:901–907, June 1986

Idiopathic external hydrocephalus was identified in 36 infants. All children were macrocephalic by 1 year of age and maintained head growth at the 95th percentile. Although 89% of the infants were developing normally, 43% of this group had transient developmental delay at 5 to 12 months of age, corresponding to the time of the most rapid head growth. There was a family history of macrocephaly in 88% of cases, and several families had members with external hydrocephalus and benign familial macrocephaly throughout several generations. No children required surgical therapy. The authors suggest that idiopathic external hydrocephalus is a benign self-limiting condition that resolves without therapy and is closely related to benign familial macrocephaly.

Richard Towbin

The chest film in immotile cilia syndrome in children (in French and English). Fauré C, Verderi F, Schmit P, Sirinelli D, Salomon JL, Escalier D (Service de Radiologie, Hôpital Trousseau, 8 av. du Docteur-A.-Netter, F-75571 Paris 12, France). *Ann Radiol* 29:301–311, 1986

In a review of 31 children with immotile cilia syndrome (various ultrastructural anomalies of the cilia), more than half began with lung symptoms in the first year of life. Half of the series showed situs inversus; 13 of the 31 had associated causes of bronchopneumopathy (gastroesophageal reflux or immune compromise). The lung pattern was not specific, but tended to be bilateral, with middle lobes more severely involved and apices spared. Bronchiectasis was present in a majority, most commonly cylindrical. Radiologic progression tended to be slow, but eventual surgical excision of an involved area was necessary in 20% of the patients. Early search for this disease in infants should be beneficial.

Alan E. Oestreich

Stress-related widening of the radial growth plate in adolescents. Fliegel CP (Dept. of Radiology, Basel Children's Hospital, Römergasse 8, CH-4005 Basel, Switzerland). *Ann Radiol* 29:374–376, 1986

Three examples are reported of stress-induced widening of the radial growth plate in young adolescent gymnasts, a condition that may well be more frequent than previously expected (such changes were seen in nearly one-third of 98 adolescent gymnasts reviewed

by Fauré). The radiographic changes include irregular longitudinal widening of the physis soft-tissue zone, irregular metaphyseal border line, flaring of the metaphysis, occasional periosteal new bone, and mildly retarded bone age. Two of these three 13- to 15-year-olds showed bilateral changes. Immobilization of wrist and discontinuation of gymnastics until radiographic repair was successful in 9 to 24 months. Although none of these three children recalled a history of trauma, the pattern is quite similar to the Salter I epiphyseal injury.

Alan E. Oestreich

Hyperimmunoglobulinemia E syndrome: pulmonary imaging considerations. Fitch SJ, Magill HL, Herrod HG, Moinuddin M (Radiology, University of Tennessee Center for the Health Sciences, 848 Adams Ave., Memphis, TN 38103). *Pediatr Radiol* 16:285–288, May 1986

Recurrent sinusitis and pneumonias, as well as chronic dermatitis and elevated serum IgE, are the principal features of the Hyper-IgE (or Job) syndrome. Pneumatoceles are frequently present, often containing air-fluid levels. Pneumatocele rupture may cause intractable pneumothorax, as in one 6-month-old patient. Ventilation and perfusion scanning, as in another patient, gives functional information about the pneumatoceles; CT is valuable in documenting anatomic extent of such disease.

Alan E. Oestreich

CT features of peritoneal and mesenteric involvement in pediatric malignancies. Experience from 13 cases (in French and English). Granier N, Filiatrault D, Garel L, Dubé J, Paillé P (Radiologie, Hôpital des Enfants, 168 cours Argonne, F-33000 Bordeaux, France). *Ann Radiol* 29:275–285, 1986

Although sonography can diagnose mesenteric root and lesser omentum tumor involvement, CT is the best method to image the entire abdomen, including every peritoneal reflection. This seems especially valuable in cases of non-Hodgkin's lymphoma, ovarian immature teratoma or carcinoma, and adrenal neuroblastoma, on the basis of a study of 13 pediatric malignancies. High-quality vascular enhancement is required to recognize involvement of the lesser omentum (6 of the 13 cases), the most frequent site. The greater omentum was always invaded in cases of massive peritoneal seeding. Mesenteric involvement on CT was as discrete masses or stellate infiltration. The transverse mesocolon was shown to be invaded once.

Alan E. Oestreich

Involvement of posterior visual pathways by optic nerve gliomas. Lourie GL, Osborne DR, Kirks DR (Radiology, Children's Hospital, Cincinnati, OH 45229-2899). *Pediatr Radiol* 16:271–274, May 1986

CT in seven children with optic nerve gliomas extending posterior to the chiasm showed involvement of lateral geniculate bodies and adjacent optic radiations in five, each with marked contrast enhancement. These seven patients are 22% of new optic glioma patients in a 4-year period. In one patient, MR image revealed contralateral lateral geniculate and optic radiation involvement not shown on CT. These imaging methods have an increasing role for optic nerve gliomas; the posterior extension aids in diagnosis.

Alan E. Oestreich

Breast Radiology

The significance of calcifications in mammograms in the early detection of breast carcinoma. Rosselli Del Turco M, Ciatto S, Bravetti P, Pacini P (Centro per lo Studio e la Prevenzione Oncologica, Viale A. Volta 171, I-50131 Firenze FI, Italy). *Radiol Med* 72:7–12, 1986

From Nov. 1978 to July 1982, mammography was performed on 47,097 patients; biopsies were recommended for 3126. A carcinoma was found in 1110 specimens and calcifications were seen in 217. In 2016 cases the lesions were of a benign nature and in 111 of 2016 microcalcifications were present. This study reports and discusses (1) distribution of microcalcifications; (2) their various morphologic characteristics; (3) positive predictive value for each radiologic pattern; (4) frequency of microcalcifications in relationship to age group and whether the lesion was benign or malignant; (5) the frequency of calcifications in relation to the histologic type of tumor; and (6) the distribution of the microcalcifications and its relationship to the clinical and pathologic diagnosis and whether the patients were part of a screening program (385) or self-referred (2771). The authors emphasize that the microcalcifications that show a high sensitivity for cancer are also poorly specific, and that those calcifications with a high specificity for cancer show a poor sensitivity. Therefore, since no strict diagnostic criteria can be established, biopsy should always be performed to detect breast cancer early whenever there is any suspicion of malignancy.

A. F. Govoni

Gastrointestinal System

Sonographic and pulsed-Doppler evaluation of the portal venous system (in Italian). Renda F, Di Giandomenico E, Di Giandomenico V, Sanità di Toppi G, Marano P (Istituto di Scienze Radiologiche e Formazione dell'Immagine, Ospedale SS Annunziata, I-66100 Chieti CH, Italy). *Radiol Med* 71:496–505, 1986

To further the diagnostic imaging of the portal venous system, the authors conducted a series of studies in 23 normal subjects and in 13 cirrhotic patients in which sonographic morphologic evaluation of the caliber of the portal vein was associated with a functional study of its pressure and degree of flow by a pulsed-Doppler technique. The studies were conducted before and after a normal meal.

The hemodynamic principles of the portal system and the factors governing the pressure, the flow, and the velocity in blood vessels are reviewed. From a statistical analysis of the data, they conclude that the association of a routine sonographic study of the liver in patients who have a presumed abnormal portal circulation with a pulsed-Doppler evaluation of the portal hemodynamics provides detailed information on the direction, degree of flow, and flow velocity, which results in a comprehensive morphologic and functional study of the portal venous system.

A. F. Govoni

Physics

Xeroangiography: technique and clinical applications (in Italian). Toti A, Mannella P, Benea G, Galeotti R, Borrelli M, Bonari RL (Istituto di Radiologia dell'Università, Corso Giovecca 203, I-44100 Ferrara FE, Italy). *Radiol Med* 71:403–408, 1985

This preliminary report on transarterial (TAXA) and transvenous (TVXA) xeroangiography with a semirapid seriographic unit describes the characteristics of the unit and the techniques used. Conclusions reached from the early results are (1) the poor sensitivity of the plates limits TAXA and TVXA only to segments of the body of limited thickness; (2) the size of the xeroradiographic cassette (24 × 30 cm) is restrictive; and the necessary use of high tensions results in a dosage almost three times that of traditional angiography. The advantages of xeroangiography are (1) the high power of resolution; (2) images with more detailed information; (3) the wide latitude of exposure that permits simultaneous imaging of bones and soft tissues; (4) the lower cost of the equipment; and (5) the reduced incidence of complications.

A. F. Govoni

Society for Pediatric Radiology: Abstracts from 1986 Meeting

The 29th annual meeting of the Society for Pediatric Radiology took place in Washington, DC, on April 10–13, 1986. Donald R. Kirks, M.D., edited the abstracts. They are presented in the order of presentation.

The Renal Cortex & Medulla in the Neonatal Kidney: Sonographic Evaluation of Pathologic States by Thomas L. Slovis, M.D. and Jack O. Haller, M.D.

The neonatal kidney has a unique sonographic appearance. In an attempt to correlate the change of this appearance with specific disease states we evaluated all of the neonatal kidney ultrasound examinations done in the high-risk referral nurseries of 2 institutions (Children's Hospital of Michigan and Downstate Medical Center). From this group of neonates, 5 distinct ultrasonic patterns emerged-1)a normal appearance, 2)increased cortical echogenicity with cortico-medullary differentiation preserved, 3)loss of cortico-medullary differentiation in normal to small kidneys, 4)loss of cortico-medullary differentiation in large kidneys, 5)increased medullary echogenicity. We studied most of the patients during this period with a phased linear array, 5.0MHz transducers on the electronically focused system,[R] and 7.5MHz single frequency, triple loaded mechcanical section sanncer,[R2] All examinations were recorded on video tape and hard copy was made on x-ray film.

A series of diagnoses fell within each of the 5 categories of sonographic appearances:

A. Normal
   1. Normal
   2. Renal artery thrombosis (acute)
   3. Some forms of congenital medical renal disease, i.e., renal tubular acidosis (RTA).

B. Increased Cortical Echogenicity Cortico-Medullary Differentiation Preserved
   1. Prerenal azotemia
   2. Ischemia
   3. Dysplasia
   4. Some forms of congenital medical renal disease, i.e., congenital nephrosis.

C. Loss of Cortico-Medullary Differentiation in normal to small sized kidney
   1. Severe dysplasia
   2. Pyelonephrosis

D. Loss of Cortico-Medullary Differential with Renal Enlargement
   1. Renal vein thrombosis
   2. Fetal renal hamartoma
   3. Recessive polycystic kidney disease
   4. Dominant polycystic kidney disease

E. Increased Medullary Echogenicity
   1. Nephrocalcinosis
   2. Tamm Horsefall protein deposition
   3. Medullary cystic disease

The appropriate work-up based on clinical symptoms and sonographic appearance will be discussed. R = Acuson R2 = ATL

Sonographic Assessment Of The Bladder Wall In The Pediatric Age Group

Jequier S, Rousseau O (The Montreal Children's Hospital, Montreal, PQ H3H 1P3.

Between August 1, 1984 and May 31, 1985, 160 children were thought to have bladder wall thickening by ultrasound. They represent 7% of all abdominal and/or pelvic ultrasounds done. There were 75 boys and 85 girls age one week to 16 years. However, no normal values for bladder wall thickness in different age groups and with different stage of filling of the bladder were known to us. A prospective study was therefore undertaken to evaluate normal wall thickness of empty or full bladders at different ages.

Preliminary results indicate that the normal wall of a moderately filled bladder measures 2mm in most patients and is independant of age. It may vary by 1 to 2mm between empty and full stage. Bladder walls 5mm thick or more when empty and 3mm or more when full are definitely abnormal. There was no bladder wall of 4mm. when empty in the normal control group and this thickness is probably abnormal, although this is still under investigation. Measurements should be taken from the bladder floor or laterally in order not to include the peritoneal reflection of the dome.

Main causes of bladder wall thickening were:
1. Urinary tract infection (44%, 12% in boys, 32% in girls).
2. Neurogenic bladder (12%, 2.5% in boys, 9.5% in girls).
3. Hematuria (7.5%, 6.2% in boys, 1.3% in girls).
4. Enuresis, incontinence (6%, 2.5% in boys, 3.5% in girls).
5. Post chemotherapy (6%, 5% in boys, 1% in girls).
6. Abdominal pain (5.5%, 1% in boys, 4.5% in girls).

The remaining 19% were made out of mostly isolated cases including 17 different entities such as posterior urethral valves, previous surgery, trauma, ect.

Focal bladder wall changes were rare, seen in 12 patients only (post-surgical, benign and malignant tumor, focal inflammation in Crohn's disease, diverticula and ureterocele).

MRI of the Pelvis and Perineum in Children

Dietrich RB, Kangarloo H, Boechat MI (UCLA Medical Center, Los Angeles, CA 90024).

The pelves of 49 children (age 1 to 19 years) were evaluated using 0.3 T spin echo magnetic resonance imaging (MRI). The MR scans of 12 of these patients, who had studies or lesions of structures adjacent to the pelvis, were reviewed to assess the optimal imaging plane (s) for demonstrating specific pelvic structures. Midline structures (urethra, bladder, rectum and sacrum) were best evaluated in the sagittal planes; paired structures (ovaries, pelvic musculature and ectopic gonads) were best evaluated in axial and coronal planes. The remaining 37 patients imaged had pelvic or peritoneal pathology. Results were correlated with the ultrasound (35) and CT (8) scans and surgical and biopsy findings (26). The planes of imaging depended on the suspected pathology; images in two different planes were routinely obtained. T1-weighted sequences (TR 500 msec, TE 28 msec) were obtained in all cases; T2-weighted sequences (TR 1500 or 2000, TE 84 or 112 msec) were also obtained in 20 cases with suspected neoplasms or cystic lesions.

Lesions imaged were divided into three categories: congenital (15), cystic and fluid collections (9), and neoplastic (13). MR demonstrated all lesions well. It gave a better global view of the pelvis than did ultrasonography and was especially useful in evaluating pelvic neoplasms and lesions not directly adjacent to the bladder. It was superior to CT in evaluating the extent of lesions due to its ability to image in any plane and its better tissue differentiation. T1-weighted images gave the best anatomical detail; T2-weighted images were useful in patients with ectopic gonads and pelvic neoplasms. Due to its low cost and availability ultrasonography should remain the modality of choice for screening pelvic pathology in children. MR is, however, a useful adjunct in the evaluation of equivocal cases and in determining the full extent of lesions.

Patterns of Calcium Deposition in the Kidneys of Children: In Vivo Demonstration of the Anderson Carr Progression

Patriquin H, Robitaille P (Hôpital Sainte-Justine, Montréal, Qc, Canada H3T 1C5).

The Anderson Carr theory of renal stone formation, based on cadaver studies, postulates the aggregation of calcium at the

tips and margins of the renal pyramid. Progressive calcium deposition is followed by the formation of calcium plaques, which may perforate into the calyx and provide a nidus for further stone growth. This theory has not been demonstrated in vivo. We studied 50 children with conditions leading to nephrocalcinosis with renal ultrasonography; and 7 of these with high resolution computed tomography. Twenty-four positive ultrasound examinations were used to study patterns of calcium deposition in the kidney. Nephrocalcinosis was confined to the medulla, and was found at the margins of the pyramid, at the fornix or filling the entire pyramid. Five children showed calcium plaques in or near the calyx. The ultrasonographic patterns outlined seem to illustrate, in vivo, the Anderson Carr progression of renal stone formation.

Segmental Function in Duplex Kidneys: Assessment from the Tc-99m DTPA Renogram

Shore RM, Koff SA, Cirulli C, Smith SP, Frye TR, Lloyd TV (Children's Hospital and Ohio State Univ., Columbus, OH 43205).

We have adapted our previously described method of estimating the glomerular filtration rate (GFR) from the Tc-99m DTPA renogram in children to the determination of segmental function in duplex kidneys. This method determines both the total GFR and the relative GFR of each kidney and segment. Segmental GFR was determined 46 times in 25 patients with 30 duplex kidneys. Segmental analysis of diuresis renograms also assessed segmental obstruction. Correlation of scintigraphic images with the excretory renogram was necessary for accurate assignment of regions of interest.

The normal distribution of function was determined by analyzing kidneys without reflux, obstruction, or scarring. For the normal duplex kidney, the upper segment function was: mean = 38%, range = 38-44%, SD = 5%. Where the contralateral kidney was also normal, the relative funtion of the duplex kidney was: mean = 55%, range = 45-60%, SD = 7%.

By comparison to the normal distribution of function, abnormal renal function was evaluated in a wide variety of renal disorders including: segmental reflux nephropathy, reflux and obstruction secondary to ectopic ureteroceles, and segmental analysis of urinary diversions. Segmental function was also followed longitudinally, and sequential changes correlated well with other clinical and surgical findings. Since function was expressed in absolute terms (rather than just relative function), it was possible to distinguish simple functional loss in one kidney or segment from loss in one region with compensatory hypertrophy in another. This feature should make this method valuable not only for clinical use, but also as a tool for clinical investigation in order to determine the conditions under which compensatory hypertrophy might be expected.

The segmental renogram curves were more irregular than curves for the entire kidney, and this appears to be the main limitation of determining segmental urine function by this method. Since individual segment urine collections are seldom available for comparison, it would be desirable to compare this renogram method for evaluating segmental function to that determined by static imaging agents.

The Duplex Collecting System in Female Children with Urinary Tract Infection

Bisset GS III, Strife JL, Dunbar JS (Children's Hospital Medical Center, Cincinnati, OH 45229).

We retrospectively evaluated 40 female children with urinary tract infection who had duplication anomalies documented on excretory urography (EU). The EU's were evaluated for renal scarring, size, and anatomic characteristics of the duplication anomaly. Voiding cystourethrograms (VCUG) were evaluated in each patient for the presence of vesicoureteral reflux (VUR).

The purpose of the study was to evaluate the natural history, the incidence of VUR, and the incidence of parenchymal scarring in children with duplex renal systems. There were 49 duplicated systems in 40 patients (80 kidneys). In the 34 systems with complete duplication, VUR occurred in 23 (68%). VUR occurred into the lower pole in 74%, into the upper pole in 9%, and into both poles of the kidney in 17%. With partial duplication, VUR was noted in 27%. In kidneys with duplication there was associated renal scarring in 7%. This figure is identical to the incidence of parenchymal scarring in a group of 479 females with urinary tract infection and no duplex system. In all but one patient with renal scarring, VUR was present.

In follow-up studies in those patients with duplex systems and VUR, the reflux resolved in 66%. Only one in our series (1 month old) demonstrated late parenchymal scarring. The remaining patients all had scarring at the initial study.

Our conclusions are that in patients with duplication anomalies: (1) there is a high incidence of VUR in complete duplication, (2) the incidence of VUR in partial duplication is identical to the incidence in anatomically normal systems with VUR, (3) a significant percent of the VUR resolved spontaneously, and (4) the incidence and natural history of parenchymal scarring is similar in duplex systems and in normal anatomic kidneys with VUR.

The Pseudohorseshoe Deformity in Children with Congenital Gibbus

Fernbach SK, Davis TM (The Children's Memorial Hospital, Northwestern Univ. Medical School, Chicago, IL 60614)

After noting an abnormal renal axis on excretory urography (EU) in children with myelomeningocele and gibbus deformity, we decided to retrospectively analyze the clinical (operative, autopsy) and radiological (spine films, EU, nuclear scintigrams, ultrasound) data in 96 children with thoracic level myelomeningoceles.

Lack of concurrent spine films and EU caused us to exclude 28 children from the study. Of the remaining 68 children, 21 had both no gibbus deformity and a normal renal axis. Two children (one with gibbus, one without) had unilateral agenesis; two others (one with gibbus, one without) had mild unilateral ectopia.

Gibbus deformity was present in 43 children, two of whom were excluded from our analysis because of scoliosis greater than 35°. In 38 of the remaining 41 children the angle formed by the intersection of the renal axes was abnormal. Regression analysis confirmed that there was 1) a linear relationship between the measured angle of gibbus and the angle of intersection of the renal axes and 2) a high correlation coefficient (r=.62).

Intersection of the renal axes below the renal masses, as in horseshoe kidney, occurred in 19 children. In all of these children correlation was made with other data of renal status: nuclear medicine scintigrams, ultrasound studies, operative reports, and autopsy findings. No instance of parenchymal fusion was detected by these other modalities. We therefore believe that in children with severe gibbus deformity pseudohorseshoe kidney should be considered a diagnostic possibility rather than true horseshoe kidney when there is an abnormality of the renal axes.

Radiologic and Histopathologic Correlates of Posterior Rib Fractures in Abused Infants: An Alternate Mechanism of Injury

Kleinman PK (Univ. of Massachusetts Medical Center, Worcester, MA 01605).

Posterior rib fractures are characteristic findings in abused infants and commonly occur near the costovertebral junctions. These fractures can result from violent shaking and are generally assumed to be due to lateral thoracic compression. An analysis of the plain radiography, computed tomography, and histopathology of posterior rib fractures in fourteen abused infants casts doubt on this traditional view. This study reveals that these fractures often occur at or medial to the costotransverse process articulation. Furthermore, cortical disruption and periosteal reaction occur mainly along the ventral surface of the fracture sites, not dorsally, as would be expected if lateral compression alone induced these fractures. Based upon available data, and assuming that manual thoracic compression during shaking produces the fractures, a plausible mechanism of injury is proposed. As the infant is shaken, the posterior rib is levered over a fulcrum of the costotransverse process articulation. This places maximal stress upon the ventral surface of the posterior aspect of the rib, resulting in the typical patterns of injury defined in this study.

Late Radiological Patterns of the Hip in JRA

Blane CE (Dept. of Radiology), Ragsdale CG (Dept. of Pediatrics and Communicable Diseases), Hensinger RN (Dept. of Surgery). [The University of Michigan, Ann Arbor, MI, 48109-0010.]

The hip is a major weight-bearing joint for walking and sitting in the child. We reviewed the radiographs of 68 children with long-standing juvenile rheumatoid arthritis (JRA) and no significant steroid therapy, and found 36 patients with osseous changes at the hips. Although many changes at the hips in JRA have been described, we report two distinct patterns. One pattern is characterized by progressive primary inflammatory destruction of the hip. Erosive arthritis with progressive joint space narrowing, subchondral cysts and sclerosis, was seen in 7 boys and 1 girl.

The second pattern had the appearance of developmental adaptation in the growing skeleton. Twenty-one girls and 7 boys had a spectrum of changes without erosion or significant joint space narrowing. The hip varied in position from mild valgus, to subluxation, to frank dislocation. The capital femoral epiphyses had various degrees of flattening with medial wedging and lateral squaring. The metaphyses were widened and often a ring of osteophytes, "sagging rope sign," was identified. The changes at the hips are similar to those seen in children with cerebral palsy.

Categorization of the changes at the hip into one of these two patterns has important therapeutic implications. One of the main goals in the child with JRA and hip disease is to maintain function and to prolong mobility. Muscle spasm and reflex guarding, keeping the hip flexed, may be in part responsible for the developmental pattern. Minor surgical procedures and bracing to reposition the femoral head in the acetabulum, used in the child with cerebral palsy, may be of value in these patients. Early recognition of this developmental pattern to identify children who may benefit from aggresive medical management or early orthopedic intervention may improve long-term function and mobility at the hip.

Osteochondrodysplasias: Prenatal Ultrasonographic Diagnosis. Diagnostic's Criteria and Differential Diagnosis

Filiatrault D, Perreault G, Grignon A (Ste-Justine Hospital, Montreal, Qc, Canada H3T 1C5), Paillé N (Toulouse, France).

A retrospective study was performed on 11 patients to determine the prenatal sonographic diagnosis of osteochondrodysplasias. The purpose of this study was mainly to sensitize ultrasonographers to detect these entities by extrapolating the criteria that we, as pediatric radiologists, are used to see on X-Rays in the neonatal period. The ultrasounds were done mainly before or around 20 wks of gestation. All these diagnosis except one were picked up on ultrasounds done routinely as a screening of normal pregnancies. We evaluated the following criteria: 1) limb lenght (femur), 2) bone echogenicity (skull), 3) aspect of the spine, 4) thoracoabdominal disproportion. All the fetuses had postnatal X-Rays and pathological studies to confirm the diagnosis. We have encountered 5 osteogenesis imperfecta (OI) type II, 3 campomelic dwarfism (CD), 1 achondrogenesis type I, 1 thanathophoric dwarfism (TD) and 1 recessive hypophosphatasia. All the fetuses had short to very short femurs and thoracoabdominal disproportions. The 5 cases with OI had moderate to severe lack of mineralisation and multiple fractures. The 3 CD had characteristic bowing of the femurs. The achondrogenic fetus presented a lack of ossification of the lombosacral spine. The TD was characterized by a slight curvature of the short femurs and trigonocephaly. The fetus with hypophosphatasia was the only one where we were oriented for the diagnosis because the mother had already given birth to a child who died shortly after of this entity. There was lack of mineralisation compatible with this diagnosis. Using the four criteria studied we elaborated charts to facilitate a practical differential diagnosis. Even though a precise prenatal diagnosis is not always easy, knowledge of these criteria should assist the clinician in deciding the outcome of the pregnancy and in selecting patients for genetic counselling referral.

ACUTE COMPRESSION INJURIES OF BONE: OR, THE TODDLER'S FRACTURE REVISED

Conway JJ, Poznanski AP (The Children's Memorial Hospital, Chicago, IL, 60614)

The "Toddler's Fracture" is a well-known entity since the report of its significance by Dunbar, et al, in 1964. The tibial fracture may visualize only with fine resolution x-ray techniques, on oblique views or by the delayed appearance of periosteal reaction. With high resolution magnification bone scintigraphy, not only is an earlier diagnosis possible, but of greater importance is the recognition of occult injuries of other bones which clinically simulate "The Toddler's Fracture". This report emphasizes the significance of recognizing occult bone trauma caused by compression.

Compression injuries of bone are more common in children due to the pliable nature of young osseous tissue. Compression causes microtrabecular disruptions which in turn produce a marked vascular and metabolic response of bone. Bone scintigraphy demonstrates this pathophysiologic response by the prominent localization of the radionuclide at the site of injury. Compression injuries produce little, if any, x-ray changes and thus go unrecognized, creating concerns for the parent, pediatrician and radiologist alike.

Compression injuries tend to occur at impact sites much as the metatarsals, sesamoids of the great toe, cuboid, calcaneus and patella. Four cases of "cuboid compression" are presented, three were in toddlers and the other in a young child with a documented hyperflexion injury of the foot. X-rays were normal. Follow-up tomography of the hyperflexion injury demonstrated periarticular sclerosis of the cuboid as evidence of the healing microtrabecular fractures. Multiple other examples of occult compression injuries involving the patella (the Hot Patella sign), calcaneal apophysis (the Hot Heel sign), metatarsals (Stubbed Toe sign) and sesamoid bones of the great toe (the Scintillating Sesamoids sign) are presented.

Compression injuries are a poorly recognized common injury in young children. Bone scintigraphy readily depicts the abnormality. A child who favors an extremity and has normal x-ray findings should be studied with bone scintigraphy.

Changes in Skeletal Scintigraphy Secondary to Bone Aspiration in the Young

Jones BE, Davis RT, Treves ST (The Children's Hospital, Harvard Medical School, Boston, MA 02115)

The dilemma of when to do a skeletal scintigram in relation to bone aspiration in patients suspected of having osteomyelitis, has been a difficult decision. Questions arise: 1. will a bone aspiration cause a change in the scintigram?, 2. if it does, when? This study was designed to answer the above.

Two immature dogs (ages 8 and 10 weeks) weighing 20 Kg each were anesthetized with IV acetoprothezide 1 mg/Kg, followed by IV sodium penthobarbital 20-30 mg/Kg. The animals had a baseline Tc-99m MDP (technetium-99m methylene diphosphonate) scan in order to exclude occult pathology, as well as a control for subsequent scintigrams. Needle aspiration of 8 leg bones were performed under fluoroscopic control. Aspiration of the bone was performed according to the protocol used in the Orthopedic Department at Children's. An 18 gauge needle was placed into/adjacent to the bone, 2-5 ml of sterile, non-bactericidal saline solution was injected to "wash" or irrigate the area and then aspirated. All procedures were done under anesthesia. Tc-99m MDP scans were obtained at 6, 24 and 48 h post aspiration. The images were obtained using a gamma scintillation camera with a high resolution collimator.

There were no detectable differences on the scintigraphic pattern in the baseline and the post-aspiration studies.

This study suggests that needle aspiration of long bones in the young does not cause detectable abnormalities on Tc-99m MDP scintigraphy. Therefore, aspiration of a long bone is not a contraindication to Tc-99m MDP scintigraphy if osteomyelitis is suspected.

Bone Density Changes in Normal Children

Gilsanz V, Senac M, Roe T, Wells T, Landing B (Depts. of Radiology, Pediatrics, and Pathology, Childrens Hospital of Los Angeles), Libaneti C, Schultz E (Loma Linda University School of Medicine), Cann C (University of California, San Francisco).

Since March, 1985, all previously healthy children undergoing CT examinations at Childrens Hospital of Los Angeles because of trauma had their vertebral mineral content measured by computed tomography. Especially designed phantoms scanned with the patients were used to provide corrections for machine drifts. These phantoms, smaller than those commercially available for adults contain exact solutions of dipotassium hydrogen phosphate for calibration. Thus far, 74 children (44 boys, 30 girls) ages 0-18 years have been studied. The bone density in neonates was very high ranging from 310-505 (mean 372) mg/cm^3 K_2HPO_4. Histomorphometric and chemical analysis of three newborn vertebrae obtained at autopsy revealed relative absence of red marrow and closely packed bony spicules. The bone mineral content for children older than one year ranged from 145-240 (mean 183) mg/cm^3 K_2HPO_4. Whereas girls showed no difference in bone density before and after puberty, there was a significant increase in the bone mineral content of boys following puberty. This is consistent with the fact that adult males have higher bone density than adult females. We propose that the relative increase in testosterone levels in post pubertal males account for their higher bone density.

We foresee that quantitative computed tomography will have wider applications than the measurement of bone loss in post menopausal women. The normal values of spinal trabecular bone in children will aid in future studies of pediatric bone diseases.

The Use of CT Scan in Unstable Hip Reconstruction

Mahboubi, S, Horstman H (The Children's Hospital of Philadelphia, Philadelphia, PA 19104).

If the unstable hip (in cerebral palsy) is neglected and allowed to sublux and dislocate, it can become painful. Intervention in this process of subluxation, dislocation, femoral erosion and acetabular dysplasia can allow a more mobile, less painful hip. Surgical intervention is often undertaken with relatively little comprehension of the three dimensional aspects of the femoral-acetabular complex.

Forty infants and children with unstable hips underwent computed tomography of their hip prior to surgery. Computed tomography has shown superiority over conventional radiographic techniques in solving problems relating to the unstable hip in these patients. Computed tomography of the hip allows for information regarding the acetabular arc and containment of the femoral head, acetabular depth or shallowness as contrasted to the femoral head, and shape of the femoral head. We modified measurement of the femoral torsion on CT scans of the hip to allow the more accurate technique for visualization of the femoral torsion. In our modified technique for anteversion study we get a slice through the femoral head and another slice through the femoral neck at the level of the greater trochanter. These slices are superimposed on each other with a double film exposure. A line is drawn from the center of the femoral neck in its most lateral point through the center of the femoral head, and another line through transcondylar axis.

CT scan of the hip is the single most important modality in the assessment and management of the unstable hip as well as postoperative follow-up.

The Position and Mobility of The Normal Ligament of Treitz and Cecum

Katz ME, Siegel MJ, Shackelford GD, McAlister WH (Mallinckrodt Institute of Radiology, St. Louis, MO 63110)

Identification of the fixation points of the small bowel mesentery at the ligament of Treitz and cecum is necessary to assess rotational anomalies of the gut. It is known that the cecum may be mobile and high riding in infants but little is known of the normal range of motion of the ligament of Treitz. We initiated a prospective study to determine the normal position and mobility of the ligament of Treitz and of the cecum.

In a series of over 40 pediatric patients undergoing barium examinations of the gastointestinal tract, we found that the ligament of Treitz could be manually displaced from the left side of the spine to the right side in 60% of infants less than 6 months of age. Lesser mobility was present from 6 months to 3 years (usually to the midline or over the right pedicles of the spine). In all normal patients the distal duodenum sprang back to its original position at the end of manipulation. Very limited or no movement of the fixation point occured in older children. The superior aspect of the ligament of Treitz ranged normally from T11 to the L1-2 disc space, throughout all age groups. Cecal position tended to be at lower vertebral levels as age increased. Cecal mobility was quite variable and did not correlate well with any other parameter.

This study demonstrated that in young patients mobility of the ligament of Treitz does not by itself indicate a rotational abnormality. The immediate return of the distal duodenum to a normal position after manual displacement is a more accurate way to determine if normal mesenteric fixation has occurred.

Contrast Imaging to Improve Specificity in the Diagnosis of Necrotizing Enterocolitis

Uken P, Smith W, Franken E, Jr. (Univ. of Iowa Hospitals, Iowa City, IA 52242), Ellerbroek, C (Iowa Methodist Hospital, Des Moines, IA 50308).

Necrotizing enterocolitis (NEC) is a major source of morbidity and mortality in premature infants. Current standards for diagnosis involve clinical and plain film radiographic criteria, both of which are often vague and imprecise. Many cases of NEC are managed medically and therefore no substantiation of the diagnosis is possible. Treatment for a false positive case of NEC is associated with significant morbidity, mortality, and unnecessary medical expense. A procedure which improves specificity of diagnosis of NEC would be of great value.

Twenty-five infants with suspected NEC were studied using single contrast barium enema. Criteria for entry into the study were either a strong clinical or a strong radiographic suspicion of NEC. Twenty infants had normal single contrast examination of the colon and terminal ileum. All of these infants were fed within 12 hours of the examination and none developed NEC. Five infants had abnormal single contrast examinations. Tissue documentation of the diagnosis of NEC was obtained in 2 of the 5: the other 3 were treated medically and recovered. Although there is a theoretical risk involved in performing contrast studies in patients with severe inflammatory bowel disease no patient suffered a complication owing to the study.

Historical review of the years 1980-1984 documented that approximately 40 cases per year of NEC are diagnosed or cared for at this institution. Thus the 25 cases of this study period represent approximately 40% of the annual census of patients with NEC. Positive contrast imaging can substantially reduce the suspected prevalance of NEC by improving the specificity of the diagnosis by reducing the incidence of false positives.

Massive Esophageal Dilatation in Post Operative Chest Films of Patients with Diaphragmatic Hernia Supported by Extracorporeal Membrane Oxygenation - (ECMO)

Stolar C, Berdon W, Dillon P, Abramson S, Amodio J. (Babies Hospital, New York, NY 10032).

Seven newborn infants supported by extracorporeal membrane oxygenation (ECMO) (after intractable persistent pulmonary hypertension of the newborn, following repair of congenital diaphragmatic hernia) developed post operative masses in the left paravertebral-mediastinal area.

On plain radiographs the masses in four patients appeared solid, in three the masses were air-filled. All patients had portable contrast studies performed that showed the mass to be a markedly ectatic esophagus. Two of the patients later had fluoroscopy that showed both hiatus hernia and gastroesophageal reflux of massive degree, confirmed in 3 of 7 by 24 hour pH analysis. All survivors showed improvement of the megaesophagus over time. Although feeding difficulties were encountered in all, none required anti-reflux surgery.

Recent interest in the association of poor prognosis of diaphragmatic hernia with prenatal detection of polyhydramnios suggests that the finding of the dilated esophagus probably relates to problems of fetal swallowing. It has not been noted in the post operative films of ordinary diaphragmatic hernia patients in any significant number; its finding in all of the ECMO patients is striking.

There are several possible causes of the esophageal dilatation. The first is a partial obstruction due to kinking of the gastroesophageal junction while the stomach was herniated into the chest; the second relates to the effect of transmitted pleural pressures while the lungs are still incompletely expanded, with possible interference to development and tone of the esophagus in utero.

Patterns of Liver Injury in Childhood: CT Analysis

Stalker HP, Kaufman RA and Towbin RB (Children's Hospital Medical Center, Cincinnati, OH 45229).

Blunt abdominal trauma to the liver in childhood commonly causes recognizable patterns of injury which are generally lobar or segmental in distribution and have predictable associated findings, injuries and complications.

We retrospectively reviewed 216 consecutive cases of blunt abdominal trauma studied by computed tomography between 8/81 and 9/85. Among these there were 48 patients with liver injury. We analyzed these cases for location of injury, nature of injury (deep vs superficial, focal vs complex), presence of associated injuries and bleeding, and complications.

The most common patterns of liver injury were posterior segment right lobe and dome of the right lobe. Less common but about equal in occurrence were anterior segment right lobe and left lobe (medial or lateral segment) injuries. Least common were multilobar and isolated caudate injuries.

Focal (simple) injuries outnumbered complex ones by about 3:1, but there was only slight difference between the number of superficial (58%) and deep (42%) injuries. Deep injuries were also often perihilar (17/20).

Right renal and right crus injuries, rib fractures, periadrenal space hematoma, and IVC halo were commonly encountered with posterior right lobe or dome injuries. Twenty-two cases (53%) had associated injuries to the lung base, and in this group there was a 95% likelihood of right lobe liver injury. All 11 pneumothoraces were also associated with right lobe injuries. On the other hand, pancreatic or duodenal injuries (2) occurred only in association with left lobe trauma. Complications such as biloma and hematobilia were uncommon but occurred in a small number of complex, deep, perihilar injuries.

A detailed analysis of these data will be presented.

Doppler Investigation of Children with Portal Hypertension

Patriquin H, Garel L, Weber A, Blanchard H (Hopital Saint-Justine, Montreal, Qc, Canada H3T 1C5).

Pulsed Doppler coupled with real time ultrasound (US) is a rapidly evolving tool for the investigation of abdominal vascular structures. As yet the literature contains few reports of its impact in the investigation of portal hypertension (PHT) in children. Twenty patients aged 6 mo-18 yrs with clinical PHT were examined by duplex US in order to assess the degree of PHT (14), the anatomy of collateral circulation (17), portal and hepatic vein patency (8) and surgical porto-, spleno- or mesenterico-caval shunt patency (6). Three children were studied prior to liver transplantation, and in 4 portal and systemic veins were assessed prior to a shunting procuedure. The results of duplex examinations were confirmed by angiography (4/4), endoscopy (3/3), surgical findings (4/4) and immediate clinical outcome in 4/9.

Doppler correctly defined the presence and direction of flow in the portal vein; intrahepatic portal venous thrombosis; the anatomy of collateral circulation; shunt patency or stenosis in all confirmed studies. In 5 cases of advanced cirrhosis, the small left hepatic lobe limited the examination of the lesser omentum. Portosystemic shunts were performed on Doppler findings alone.

This study suggests that Doppler is a valuable adjunct in the investigation of childhood PHT, replacing angiography in some cases. The hepatofugal flow in the left gastric vein may prove to be a reliable predictor of potential gastro-esophageal hemorrhage.

Cholelithiasis or Sludge In Infancy and in Utero: A Spectrum

Daneman A, Davies C, Roberts E, Stringer DA (The Hospital For Sick Children, Toronto, Canada) and Wilson S (Toronto General Hospital)

The wider use of abdominal sonography has lead to an increased detection of intraluminal echogenic material in the gallbladder in infancy. However to date, no large series has reviewed the clinical and sonographic findings in these infants.

We present 20 infants in whom sonography revealed findings consistent with gallstones as shown by the presence of highly echogenic foci with or without acoustic shadowing. In addition low level intraluminal echoes due to sludge were present in some and were present in previous scans in others. These patients accounted for 15% of all patients with gallstones in our Institution between 1979-1985 inclusive. In 10 the diagnosis was made in the neonatal period and in 3 in utero. In all but 3, gallstones were an incidental finding. Of these 3, 2 had right upper quadrant calcification on plain radiographs and 1 was jaundiced. Follow-up examinations were performed in 13, most within 2 months of initial detection. In 4, follow-up sonography showed disappearance of the stone - 1 within 24 hours. This raises the question of the consistency of the echogenic material. Evidence that these so called "stones" may be a variety of sludge is however lacking.

We therefore reviewed the sonographic appearances of infants who only showed evidence of sludge and who were not included in the above group. Two sonographic appearances were noted: (i) Low level intraluminal echoes usually with layering and (ii) hyperechogenic more globular material which may simulate the appearance of stones. The latter appearance is similar to that which we have observed in 2 infants with cystic fibrosis (proven operatively to be thick inspissated bile in 1) and in older children with metachromatic leukodystrophy (proven to be sulphatide globules).

We therefore believe that there is a spectrum of sonographic appearances of intraluminal material in the gallbladder in infancy reflecting a continuum of sludge→ sludge balls→ stones. We also feel that thick bile secretions may masquerade as stones. The disappearance of "stones" probably reflects dissolution of thick sludge.

Significance of Umbilical Artery Catheter (UAC) Related Aortic Thrombosis (AT) in Neonates

Siebert JJ, Taylor BJ, Williamson SL, Williams BJ, Szabo JS, Corbitt SL (Arkansas Children's Hospital, Little Rock, AR 72202)

The incidence and clinical significance of AT, a well-recognized complication of indwelling UAC's in newborns, is not well defined. Oppenheimer, et al, in 1982, demonstrated how well AT could be detected by abdominal ultrasound. We proposed to follow up their study to determine the incidence of AT formation in asymptomatic and symptomatic children as well as to determine risk factors associated with thrombosis formation to determine which neonates should be routinely studied for catheter complications. We prospectively studied 81 infants (birth weights 680-4650 grams) with UAC's admitted to the NICU at Arkansas Children's Hospital by serial abdominal ultrasound examination to investigate the incidence, risk factors, complications, and natural history of AT. Ultrasound was performed anteriorly through the abdomen and through the flanks, using a small parts transducer routinely when the infant was admitted to the nursery and at least once a week while the catheter was in place and then after catheter removal. Thrombosis was detected in 21/81 (26%) infants. Of these, 6 (28%) were asymptomatic, and 5 (24%) had hematuria only. Major complications occurred in 10 (50%) infants and included leg discoloration, hypertension, poor femoral pulses, necrotizing enterocolitis, renal failure, and cardiovascular collapse. Major AT (>40% aorta occluded and extension into renal and/or iliac arteries) was diagnosed in 4/6 of asymptomatic babies and in 13/15 sympotmatic babies. Risk factors associated with development of AT were presence of Ca++ in the UAC infusate ($p<0.02$) and catheter above renals ($p<0.04$). The primary disease process, quality of femoral pulses, presence of hematuria and/or signs of vascular compromise did not predict AT formation. We conclude that clinical examination does not reliably predict AT and that asymptomatic AT is more frequent than previously recognized. We recommend routine ultrasound screening on babies identified at risk and serial ultrasound in asymptomatic infants with AT to follow for extension and vascular sequelae.

Contribution of MR Imaging to the Anatomical Evaluation of Right AV Valve Atresia

Fletcher BD, Jacobstein MD, Abramowsky CR (University Hospitals of Cleveland, Cleveland, OH 44106), Anderson RH (Brompton Hospital, London, UK)

In the usual form of tricuspid atresia, the muscular floor of the blind-ending right atrium is separated from the right ventricle by the atrioventricular (AV) sulcus. Consequently, epicardial tissue including fat is interposed between the right atrium and the hypoplastic right ventricle. In other rare forms of tricuspid atresia, a valve annulus is present but the potential AV connection is occluded by a complete membrane or by Ebstein's malformation with an imperforate tricuspid valve and there is no intervening epicardial tissue.

In a retrospective review of MR images of seven patients with right AV valve atresia, we observed an increase in signal intensity in the region of the atretic right AV valve on T1-weighted spin echo images made at 0.3 or 1.0T. This finding however, was not apparent in nine patients with hypoplastic right ventricles accompanying other anomalies including Ebstein's malformation, pulmonary atresia, atrioventricular canal and double inlet left ventricle.

Postmortem examination of six other hearts with right AV valve atresia revealed epicardial fat within the AV sulcus between the muscular floor of the right atrium and the right ventricle. In three hearts with Ebstein's anomaly, the sulcus extended only to the level of the tricuspid valve ring.

The characteristic MRI signal of fat adjacent to the muscular floor of the right atrium therefore, serves to identify the AV sulcus and allows differentiation of patients with atresia due to muscular and epicardial separation of the atrium and ventricle from those with a membranous or imperforate valve. MRI is also capable of evaluating atrioventricular relationships and alignment as well as ventricular-arterial relationships and the severity of

right ventricular hypoplasia. These observations have potential relevance to surgical therapy.

Role of CT in the Evaluation of the Pulmonary Arteries in Children with Right Ventricular Outflow Obstructive Lesions

Hernandez RJ, Bank ER, Shaffer EM, Snider AR, Rosenthal A (C.S. Mott Children's Hospital, Univ. of Mich., Ann Arbor, MI 48109).

The distribution and size of the pulmonary arteries are important considerations in determining major surgical options for children with severe right ventricular outflow obstructive lesions. The purpose of this prospective study is to assess the role of CT in the evaluation of pulmonary arteries in such pts.

We prospectively studied by CT 17 children, ages 1-22 (mean 14.4) yrs., with the following diagnoses: pulmonary atresia-6, tetralogy of Fallot-4, pulmonary artery stenosis-2, miscellaneous complex cyanotic cardiac lesions-5. All patients had CT performed with a GE 9800, ultrasound (US) and angiography (AN). AN was performed within 4 mos. of the CT and US in 14 pts. and 1-4 yrs. before the CT in 3 pts. Surgery was performed in 10/17 pts.

The presence of a pulmonary artery was established by surgical inspection and/or visualization at angiography. Visualization of the main (MPA), right (RPA) and left (LPA) pulmonary arteries by the 3 techniques are summarized in the following table.

	MPA			RPA			LPA		
	US	CT	AN	US	CT	AN	US	CT	AN
Visualized	9	15	15	14	15	12	12	16	14
Not Visualizedor/Uncertain	5	2	2	1	2	5	3	1	3
Tech. Failure	3			2			2		

Four of the five pts. who had absent pulmonary arteries (3 RPA/1 LPA) by AN but visualized by CT had the CT findings surgically confirmed. The 5th pt. is scheduled for surgery. The difference between the measurements obtained by CT and US ranged from 0.03 cm to 0.93 cm (mean 0.35 cm) while the difference between CT and AN ranged from 0.02 cm to 1.04 cm (mean of 0.27 cm). Localized narrowing of the RPA was well demonstrated by CT, US and AN. The narrowing was more clearly visualized by CT and US than AN in 1/3 pts. By contrast narrowing of the origin of the LPA seen by AN was not detected by CT and US in 4/4 pts.

We conclude that CT is more sensitive than US and AN in visualization of the presence of branch RPA and LPA. However AN is superior to CT and US in detecting site and severity of narrowing of LPA or peripheral pulmonary stenosis. CT, which is less operator dependent that US, has a complimentary role to angiography.

Evaluation of Chronic Pediatric Airway Obstruction with Cine-CT

Frey E, Smith W, Wagener J, Grandgeorge S, Franken E, McCrae P. (Univ. of Iowa Hospitals, Iowa City, IA 52242)

The radiographic diagnosis of airway lesions, especially laryngomalacia and tracheomalacia is not precise. Endoscopy, which allows detailed examination of the upper airway, is a complex invasive procedure sometimes requiring sedation or anesthesia. A prospective study was undertaken to demonstrate the value of Cine-CT (Imatron) scanning in diagnosing airway lesions in children.

Ten patients, aged 10 days to 4 years and presenting with stridor, were evaluated using both dynamic CT scanning and endoscopy. The results of the scan were then compared to the endoscopic findings. Endoscopy identified 12 diagnostic abnormalities in 10 patients. Eight patients had laryngomalacia or vocal cord paralysis documented by endoscopy. The dynamic CT airway study correctly identified laryngeal lesions in 7 of these 8 patients. The one patient with a false negative laryngeal study had both tracheomalacia and laryngomalacia, with the latter lesion not correctly identified owing to considerable patient motion. Both patients with vocal cord paralysis were correctly identified. One patient had only tracheomalacia and one patient had both laryngeal and tracheomalacia; the tracheomalacia was correctly identified in both of these patients. One patient in the series had a discrete subglottic stenosis which was correctly diagnosed on dynamic airway CT and confirmed by endoscopy. A comparison of the study population to a control group of 10 infants who had Cine CT for other reasons, documented that the dynamic motion of the airway among the affected population was very different from that of their counterparts.

Dynamic CT scanning is a rapid, accurate, and sensitive method for evaluation of patients with chronic stridor. At present it is the most sensitive and specific imaging modality for infants and children with chronic stridor.

The Detection of Sites of Pulmonary Hemorrhage in Patients with Cystic Fibrosis Utilizing Technetium-99m Red Blood Cells

Miller JH, Wong C, Osher A (Childrens Hospital of Los Angeles, Los Angeles, CA 90027).

The occurrence of major pulmonary hemorrhage in patients with cystic fibrosis can be life threatening. Methods previously utilized to identify the site of pulmonary hemorrhage have included bronchography with selective angiography followed by surgical resection. More recently, selective angiography with embolization of bronchial vessels have proved efficacious in the non-surgical treatment of marked pulmonary hemorrhage. Identification of the sites of pulmonary bleeding is difficult. The chest radiograph in patients with cystic fibrosis is very difficult to interpret as is whole lung pulmonary angiography, which carries considerable risk. We utilize the technique of Technetium (Tc)-99m red blood cells (RBC) scintigraphy to identify sites of pulmonary bleeding. Recently, we have added single photon emission computed tomography (SPECT) to this procedure which has further helped localize the sites of pulmonary bleeding. We have evaluated eight patients for pulmonary hemorrhage and successfully identified bleeding points in over one-half of the patients examined. This procedure has virtually no risk. The total body radiation is approximately 300 millirads and once labeled, a patient can be evaluated for a peiod of approximately 24 hours. This procedure provides a method of evaluation of these patients not available by any other imaging method.

Myocardial Scintigraphy in Complete Transposition of the Great Arteries (TGA) After Arterial Switch Repair

Nancarrow P, Hougen T, Potter C, Colan S, Hernanz-Schulman M, Castaneda A, Treves S (The Children's Hospital, Harvard Medical School, Boston, MA 02115).

Thallium-201 (Tl-201) and technetium-99m pyrophosphate (Tc-99m PYR) scintigraphy was used to evaluate the myocardium in children after arterial switch and coronary artery reimplantation for repair of TGA (1/83-11/85). Thirty one patients had Tl-201 scans (Tls) performed 1 wk postop and again 8 mo later in 16. Tc-99m PYR scans (PYRs) were obtained in 27 on the third postop day. The median age at repair was 8 days. Seven patients had TGA-VSD, all repaired without ventriculotomy.

Tl-201 (30 uCi/kg; min 200 uCi) and Tc-99m PYR (600-800 uCi) were used. Magnification scintigraphy in multiple projections was performed. Images were recorded on a 128-128 matrix and smoothed with a median filter.

Tls and PYRs were evaluated independently, and results were correlated with clinical parameters of myocardial ischemia/infarct (ECG, CPK, MB, function by echo). One patient had all clinical and scintigraphic studies positive for ischemia/infarct. Four patients had positive PYRs, negative Tls, but CPK >600 IU and MB >6%. Four patients had Tls positive for ischemia/infarct, negative PYRs, and 1 or less clinical indicators of ischemia. On follow-up, no patients developed positive Tls.

Tls detected physiologically adaptive right ventricular hypertrophy and enlargement in 30 and 26 patients respectively; 25 children had both. Follow-up scans (n=16) showed resolution of hypertrophy in 12 (75%) and return toward normal size in 10 (63%).

Clinical parameters of myocardial ischemia, particularly CPK >600 and MB >6% were found to correlate with PYRs (5/5). However, Tl-201 scintigraphy may represent the most sensitive test for detection of myocardial ischemia.

Normal Ultrasonic Anatomy of the Neonatal Spine

Gusnard DA, Yousefzadeh, DK (University of Chicago Hospitals & Clinics, Chicago, IL 60637), Naidich TP (Children's Memorial Hospital, Chicago, IL 60614)

Closely spaced transverse, sagittal and inclined ultrasonic sections from living human neonates were correlated with axial, sagittal and coronal cryomicrotome sections of frozen human premature and full term cadavers to determine the precise nature of the structures displayed sonographically. Linear array 5.0 MHz Acuson® images readily depict the ossification centers of the lamina and centrum, the cartilaginous neurocentral synchondroses, the unossified cartilage of the spinious process, the intervertebral disk spaces, the neural foramina, the dorsal nutrient foramina,

epidural venous plexus, dura, spinal cord, conus medullaris and some emerging nerve roots. The occipital condyles, roots of clivus, basisphenoid, basiocciput, basisphenoidal-basioccipital synchondrosis and the paraspinal musculature are similarly well displayed. Familiarity with the appearances and relationships of these structures in cadavers permits correct identification of the structures in vivo.

Magnetic Resonance Imaging of the Spinal Neuraxis in Childhood.

Barnes P., Lester P., Galloway D., Prince J., Yamanashi W. (Oklahoma Children's Memorial Hospital and Oklahoma Diagnostic Imaging, Oklahoma City, OK 73126 and City of Faith Hospital, Tulsa, Oklahoma 74137.

Magnetic Resonance Imaging (MRI) has been carried out in 117 pediatric and adolescent patients (age range: 5 days-20 years) for developmental and acquired conditions of the upper and lower spinal neuraxis, including the more recent application of high-field and surface coil imaging techniques (74 patients). MRI was compared with metrizamide myelotomography (MMT) and metrizamide computer tomography (MCT) in 45, ultrasonography (US) in eight, and angiography in two.

Abnormalities were demonstrated in sixty-two patients, including dysraphic myelodysplasias (42), tumors and cysts (17), craniocervical anomalies (13), hydrosyringomyelia (4), and vascular malformations (2). Six MRI studies were nondiagnostic due to motion, sedation, spinal curvature, and patient-compliance factors.

Multisequence, multiplanar, thin-section surface coil MRI provided superior anatomic delineation of the spinal neuraxis and equivalent diagnostic sensitivity as compared with MMT, MCT, or US, such that invasive MMT/MCT was avoided in fifty-one patients. There were two false-positive, and no false-negative MRI results.

At the present time, MRI appears to be a desirable noninvasive method for the initial evaluation of suspected developmental or acquired causes of spinal neurologic disorders in childhood. Although MMT/MCT has usually provided more specific delineation of finer anatomic and pathologic detail, advanced MRI techniques are now affording definitive evaluation of many spinal conditions in childhood.

The Hippocampal Formation

Naidich, TP (The Children's Memorial Hospital, Chicago, IL 60614), Yousefzadeh, DK (University of Chicago Hospitals & Clinics, Chicago, IL 60637), Haughton VM (Medical College of Wisconsin, Milwaukee, WI 53226)

Ultrasound and magnetic resonance images now display some brain structure better than does CT. Correlation of ultrasound and magnetic resonance images of living infants with fresh cadaver specimens, cryomicrotome sections and myelin-stained histologic preparations of human brain documents that both ultrasound and magnetic resonance images routinely display the site and configuration of the amygdaloid nucleus, pes hippocampus, dentate and hippocampal gyri, parahippocampal gyrus, fornix, choroidal and hippocampal fissures and temporal horn. Magnetic resonance images (MRI) also display the alveus and fimbria of the fornx. In nearly all cases, the specific gyri are best appreciated in sagittal sections. The alveus and fimbria of fornix are best appreciated in coronal sections. Those familiar with the anatomic relationships of thesestructures may use ultrasound and MRI to depict the normal anatomy and pathology of the medial temporal lobe and the hippocampal formation.

Magnetic Resonance Imaging of Spinal Dysraphism

Altman NR, Altman DH (Miami Children's Hospital, Miami, FL 33155

Spinal dysraphism includes those anomalies of midline fusion involving bony, mesenchymal and neural elements. A retrospective study of 16 children where this entity was clinically suspected or where plain films revealed errors of ossification of the posterior elements (spina bifida) are reviewed.

The neuroradiological approach should include anteroposterior and lateral roentgenograms of the entire spine. We feel that magnetic resonance imaging should then be the procedure of choice to initially evaluate the cord. If this examination is positive, then myelography with computed tomography may also provide useful information.

Examples of spina bifida cystica, including myelomeningocele and lipomyelomeningocele (lipomyeloschisis) are presented. Occult spinal dysraphism disorders are also presented including dermal sinus, spinal lipoma and the tight filum terminale (thickened filum) syndrome.

NEUROSONOGRAPHIC AND DOPPLER STUDIES IN FULL-TERM ASPHYXIA

Daneman A, Hellmann J, Barks J, Soto G, (The Hospital For Sick Children, Toronto, Canada, M5G 1X8).

The prognostic value of cranial sonography (US) and Doppler findings has not been established in perinatal asphyxia in full-term infants. We correlated the US findings in 43 full-term asphyxiated neonates with the clinical staging of the hypoxic ischemic encephalopathy, CT and short-term outcome. Abnormalities were classified as: (i) Diffuse - increased echogenicity of the brain parenchyma with loss of anatomic land marks, (ii) Focal - increased echogenicity in a specific anatomic location. Increased echogenicity was graded 1 to 4+.

(i) Diffuse hyperechogenicity correlated significantly with clinical severity and neurodevelopmental outcome ($p < .002$). This was seen in 13 infants, 2 of whom also had focal lesions. Of the 13, 5 died and 6 had persistent neurological abnormalities. The other 2 who were developmentally normal, had only mild (1+) increased echogenicity on initial scan.

(ii) Three infants had focal lesions only. Sites included periventricular white matter (normal outcome), temporal cortex and IVH (hemiparesis) and bilateral IVH (died).

Of the 27 patients with no detectable abnormality or slit like ventricles only, 20 were normal, 2 died and 5 were abnormal at discharge. The latter 7 had their only US on days 1 or 2. All US abnormalities diagnosed after day 2 were predictive of outcome. The timing of US is thus critical to its usefulness.

CT was performed in 17 infants and in only 5 did not correlate with US. US failed to detect only 1 lesion of clinical significance.

Doppler studies of intracranial vessels were performed in a further 21 asphyxiated infants. Increased diastolic frequency shift was the usual initial response detectable on day 1 and its degree correlated with clinical severity. In mild asphyxia the abnormal velocity profile returned to normal by day 4 whereas in moderate and severe asphyxia persistence beyond this correlated with neurological outcome.

US with Doppler studies are thus the modalities of choice in this clinical setting, are predictive of outcome and have increased our understanding of the patho—physiologic changes following asphyxia.

Computed Tomography of the Orbital Mass in Children

Ball WS, Towbin RB, Han BK (Children's Hospital Medical Center, Cincinnati, OH 45229).

From 1981 through 1985, 67 children were found to have orbital masses on CT. Age ranged from 1 month to 19 years. The literature has shown that a wide variety of pathologic conditions may present as orbital masses in childhood. We have reviewed our patient population in order to attempt characterization and differentiation of these orbital masses. Of the 67 patients, 16 were intraocular including retinoblastoma (11), with the remainder composed of retinal detachment, drusen body, primary hyperplastic vitreous, and Coats' disease. Fifty-one had extraocular masses which included inflammatory (17), hemangioma (8), dermoid (7), malignancy (6), neurofibroma (3), pseudotumor (3), and miscellaneous (7).

Intraocular masses often have typical features allowing for diagnosis. Description of extraocular pathology has received less attention. Characterization was attempted to differentiate benign from malignant orbital masses. Hemangiomas and dermoids had characteristic CT appearances. Hemangiomas were well defined with homogeneous enhancement (180 to 257 HU) following bolus contrast injection, with prominent associated vascular structures (50%). Bone remodelling without destruction was noted in 29%. Hemangiomas could not be differentiated from malignancy by location or size. Dermoids usually were well defined masses with a sharp, thin, minimally enhancing rim, with a low attenuation center (-8 to -115 HU). Differentiation from malignancy by location or size was not possible.

Although radiologically not distinguishable as a group, malignant masses had ill-defined margins frequently associated with bone

destruction (75%) and with minimal to moderate enhancement. Rapid growth on sequential CT and necrotic areas suggested malignancy. Benign lesions such as ectopic glial tissue, neurofibromas, and pseudotumor did not have characteristic findings allowing for differentiation from malignant processes. Inflammatory masses are generally well localized, exert mass effect, have no gross bone destruction, and are associated with sinus disease.

CT is useful in differentiating certain but not all benign processes and inflammation from malignancy.

COMPUTED EVALUATION OF ORBITAL LESIONS - COMPUTED SONOGRAPHY (CS) AND COMPUTED TOMOGRAPHY (CT)

Thomas L. Slovis, M.D., Frederick B. Watts, Jr., M.D., John Baker, M.D.

Orbital lesions are divided into global and extraglobal. Global lesions are further subdivided into anterior chamber, lens, posterior chamber, and retinal lesions. Extraglobal orbital lesions are divided into those within the muscle cone (intraconal) and those outside the muscle cone (extraconal). When cataracts, hemorrhage or other occular media opacify and obstruct intraocular visualization both CS and CT are of importance in detecting pathology. CS excells in evaluating lesions of the vitreous such as persistent hyperplastic primary vitreous (PHPV) and separating those diseases which compromise the differential diagnosis of leukocoria (PHPV, retinoblastoma, retinal dysplasia, and retrolentofibroplasia). Retinal dysplasia and the extent of retinal detachment are easily detected with CS. Both modalities reveal defects of the posterior globe such as coloboma.

Our current approach to leukocoria is to evaluate first with CT for calcified masses and extent of the lesion when attempting to diagnosis retinoblastoma. When a clear diagnosis of retinoblastoma is not obtained, then further evaluation for the other diagnostic possibilities requires CS.

In the differentiation of extraglobal, intraorbital lesions CT is superior to CS. CS and CT are complimentary in that different anatomical regions are optimally defined by each.

Prevalance of Incidental Sinus Opacification in Children and Adolescents: A Study Based on Computed Tomography

Diament, MJ (Childrens Hospital of Los Angeles, Los Angeles, CA 90027), Senac M, Gilsanz V, Baker S, Gillespie T, Larsson S (Univ. Hospital, Uppsala, Sweden)

A prospective evaluation of the paranasal sinuses was performed on a consecutive series of 137 pediatric patients referred for cranial computed tomography. Approximately one-half of the patients less than 13 years of age had some degree of maxillary or ethmoid sinus opacification. The prevalance and severity of opacification was approximately the same for the maxillary and ethmoid sinuses. Sphenoid sinus abnormality was less common and was usually minimal or mild. No incidental frontal sinus abnormalities were observed.

This study confirms previous reports, based on plain film radiography, of the prevalance of incidental maxillary sinus opacifications in children. However contrary to some prior studies, we did not find a relatively higher rate of opacification in children less than one year of age. This may be due to over-diagnosis of maxillary sinus opacification on plain films, in small children. The diagnosis of sinusitis in childhood must take into account not only the radiographic findings but clinical signs and symptoms. Correlation is needed to avoid over-diagnosis in patients referred for sinus radiography for nonspecific indications or who have incidental opacification noted on radiographic or computed tomographic studies of the skull and brain.

Reliability of Retropharyngeal Soft Tissue Measurements in Infants and Children: New Standards Based on 586 Normals

Rivero HJ, Young LW, Flom L (Children's Hospital of Pittsburgh and the University of Pittsburgh School of Medicine, Pittsburgh, PA 15213)

Previous standards available and advocated for measurement of the normal retropharyngeal soft tissues in infants and children have been widely used, largely because of uncertainty of their validity. We reviewed the various methods and subsequently measured the retropharyngeal soft tissues in 586 children (325 male and 261 female) between the ages of 6 months and 9 years. Several landmarks were used but we finally settled on measurements of the retropharyngeal soft tissues at the anterior margins of the C2-C3 and C5-C6 interspaces.

This simple method of measurement was found to be consistent in each age group. Variable factors such as cervical rotation, flexion, or extension and incomplete distention of the pharynx led to exclusion of roentgenograms showing such findings from the study. Measurements greater than the determined norms were obtained in infants and children who had proven retropharyngeal abscesses. Corroborative findings in this group were obtained with other imaging methods including ultrasound and computed tomography.

These new standards for the measurement of retropharyngeal soft tissues in infants and children are reproducible and reliable. They can be used as a screening mode prior to, or in some cases exclusive of, more complex imaging methods in suspect cases.

Nembutal Sedation for Pediatric CT

Strain JS, Harvey LA, Foley LC and Campbell JB (The Children's Hospital, Denver, Colorado 80218)

A retrospective analysis of 4,910 consecutive patients undergoing CT examination over a three year period was recently completed to evaluate the use of sedation in CT imaging. Although several sedation regimens were initially employed, a marked preference for intravenous Nembutal clearly emerged. In 394 patients sedated with intravenous Nembutal, there have been no sedation related complications and there have been only two sedation failures. Other findings from the study will be briefly presented.

Because of our preference for intravenous Nembutal sedation, a prospective study has been undertaken to further document the safety and efficacy of this method. Patients are being evaluated with pulse oximetry and mechanical blood pressure analysis in addition to our standard monitoring of EKG, pulse and respirations. Sedated patients have shown no significant alteration in blood pressure or oxygen saturation when compared to age matched controls.

We conclude that intravenous Nembutal is a safe, efficient and effective form of sedation and is the sedation of choice for pediatric imaging.

Gastroschisis and Omphalocele: Prenatal Ultrasonographic Diagnosis and Postnatal Evolution

Grignon A, Filiatrault D, Yazbeck S (Ste-Justine Hospital, Montreal, Qc, Canada H3T 1C5).

A retrospective study (1980-85) was done on 47 patients with congenital anomalies of the abdominal wall. The main goals of this study consisted in determining 1) the accuracy of the diagnosis, 2) how to improve it, 3) and to establish an antenatal protocol of follow-up of these patients. The ultrasounds(US) were studied retrospectively and done between 17 and 34 wks of pregnancy. There were 27 omphaloceles (O) and 20 gastroschisis (G). Thirty-seven babies were born in our institution and 12 transferred after birth. The prenatal diagnosis was correct in 35/47 for an overall accuracy of 74%. There were 12 false negative and no false positive. We have found 55% (15/27) of associated malformations in O and/or associated trisomy 18 (3) and 18% (5) with G. Twenty-two (46%) had a therapeutic abortion (O: 17, G: 5) of which 18/22 (80%) had major malformations. The other babies were operated within 24 hours and a surgical correlation established (organs involved at surgery and predicted by US). Three out of 10 O died (2 with cardiac anomalies) and 15/15 (100%) G are alive and well. We have seen 3 pairs of non identical twins both having G! The main causes of error were a non-echogenic patient, lack of amniotic fluid and the position of the fetus. The main points that will improve the accuracy of the diagnosis are: the visualization of the insertion of the ombilical cord, and the presence or not of a membrane. When a diagnosis of G is made, it is important to follow these pregnancies closely as we have picked up in utero 2 well known complications: 1 volvulus and 1 obstruction because of the small size of the defect. These 2 babies were born rapidly by cesarian and operated on immediately with success. In conclusion, it is very important to make the diagnosis of O and G as soon as we can using the criteria included above. We have to look for associated anomalies by US and an amniocentesis. When these 2

entities seem not to be complicated, the pregnancy is allowed to go on and closed follow-up is needed especially in G. Overall in our series, the prognosis of the O is worse than the G as 25% (7/27) of the O are alive and well and 75% (15/20) for the G.

DETECTION OF NEUROBLASTOMA WITH ^{131}I META-IODOBENZYLGUANIDINE

Conway JJ, Weiss S, Cohn S, Karesh S, (Children's Memorial Hospital, Chicago, IL, 60614), Gaynon P, (Wyler Children's Hospital, Chicago, IL, 60637).

^{131}I Meta-iodobenzylguanidine (^{131}I MIBG) is a radiopharmaceutical which localizes in neurosecretory granules of adrenergic tissue. Meta-iodobenzylguanidine is an analog of Norepinephrine. ^{131}I MIBG has been used successfully to localize pheochromocytoma and other paraganglioma tumors. It has recently been shown to also localize in neuroblastoma. Some localization occurs normally in the liver, heart, salivary glands, adrenal glands, kidney and bladder but this can be differentiated from abnormal tumor localization.

We studied 11 children with ^{131}I MIBG scintigraphy between August and November, 1985. All had documented neuroblastoma. Only one patient was studied prior to any therapy and there was an intense localization of the radiopharmaceutical in a mediastinal neuroblastoma. In an infant with Stage IVS neuroblastoma of the liver, increased localization was noted in the liver 11 weeks after receiving 350 rads to the liver in a single administration at two days of age. The liver diminished to normal size following radiotherapy. Another child had residual masses in the adrenal and pelvis areas five years following diagnosis, attempted surgical removal on three occasions, radiotherapy and multiple courses of intensive chemotherapy. There was localization in the pelvis but not the adrenal area. Of interest, previous second-look biopsies of these sites demonstrated maturation of the adrenal mass to elements of ganglioneuroma but persistent neuroblastoma in the pelvis mass.

^{131}I MIBG scintigraphy utilizes a physiologic mechanism for imaging neuroblastoma. Our limited early experience suggests that there is a sensitivity and specificity for neuroblastoma tissues which may allow noninvasive staging of neuroblastoma.

Kevlar® Cassettes: Further Reduction in Radiation Exposure During Routine Pediatric Radiography

Wesenberg RL, Amundson GM, Mueller DL (Alberta Children's Hospital, Calgary, Alberta, CA T2T 5C7).

The Alberta Children's Hospital has replaced all radiographic cassettes in the Department of Radiology with DuPont Kevlar® fiber front cassettes. Kevlar was selected because of its low x-ray absorption characteristics, allowing a 30 to 37.5% reduction in radiation exposure over that commonly utilized with conventional cassettes. Along with the decreased radiation exposure to the patient, there is a subtle improvement in image quality. The cassettes have now been utilized in over 1000 routine pediatric radiographic examinations ranging from chest films to scoliosis series. The Kevlar® cassettes are used in combination with a 700 speed yttrium tantalate rare-earth screen (Quanta Fast Detail) and relatively fast film (Cronex 4L) plus an erbium rare-earth beam filter on the x-ray tube. The addition of the Kevlar® cassettes results in what is effectively, from a radiation exposure standpoint, a 2000 speed system (1/20th the radiation dose of a par speed system). Kevlar cassettes are cost-effective when amortized over a 5 year period. From our experience, it is quite practical to convert an entire pediatric radiology department to high technology Kevlar cassettes.

Digital Teleradiology in a Pediatric Practice

Kuhn JP, Seidel FG (Children's Hospital, Buffalo, NY 14222).

Because of the increasing interest in out-patient imaging, we have performed a study to evaluate the feasibility of providing interpretation of pediatric radiographs by teleradiology at a site remote from a children's hospital.

A commercially available digital teleradiology unit was installed in a radiology office 15 miles from our children's hospital. Digitized images were transmitted over ordinary phone lines to a receiving unit installed in the hospital. A series of 100 test cases was evaluated. Accuracy of greater than 95% was achieved and the unit was then placed into clinical use for transmission of films for which urgent interpretation was requested. All cases were viewed initially and reported on the teleradiology unit. The original radiographs were then reviewed later in the day, normally by the same radiologist. Over 500 cases have been transmitted and interpreted; only very minor discrepancies have been noted between the teleradiology interpretations and the interpretations of the actual films.

Drawbacks of the system include a relative lack of spatial resolution and limitations in contrast range particularly if the original film is overexposed. Image enhancement programs have been developed to compensate for these limitations. We believe the system can be used accurately for remote interpretation of pediatric radiographs. With the availability of a larger storage disc, the system has the potential to serve as a limited PACS system and has promise as a teaching tool.

Magnetic Resonance Appearance of Blood and Blood Products

Cohen MD, Smith JA, Cory DA (Riley Hospital for Children, Indiana Univ. School of Medicine, Indianapolis, IN 46223).

There are conflicting reports of the appearance of blood and blood clot as seen in the human body by magnetic resonance imaging. This study was designed to demonstrate the normal in vitro appearance of human blood and various blood products in the fresh state and to evaluate the changing appearance over a period of two weeks. Old stored plasma and red blood cells were also studied. All the studies were done on a Technicare 0.15 resistive scanner. The blood and blood products are kept at a temperature of 10°C or 37°C. Anticoagulated whole blood, plasma, serum, white cell concentrates, platelet concentrates, lysed red cells, red cell concentrates and blood clot were studied. Serial images of the various blood products in test tubes were obtained for periods up to 14 days. T1 relaxation time measurements were also obtained.

The results indicate a similar T1 relaxation time of plasma and serum; and of lysed and intact erythrocytes. T1 relaxation times of serum and plasma initially rose and then fell. T1 relaxation times of red blood cells, clot and packed red blood cells fell for 48 hours and then remained steady for 10 days. Platelets and white blood cells had little effect on the MR image. Temperature had a significant effect on image intensity, T1 relaxation time and changes in T1 relaxation times during the 14 days of the study.

Urgent and Emergent Embolization of Lesions of the Head and Neck in Children; Indications and Results

Burrows PE (Hospital for Sick Children, Toronto, Canada M5G IX8), Lasjaunias P (Hopital de Bicetre, Universite Paris IX, France), Terbrugge K (Toronto Western Hospital, Toronto, Canada M5T 2S8), Flodmark O (Vancouver Children's Hospital, Vancouver, Canada).

This report describes embolization procedures of the head and neck performed on an urgent or emergent basis in 33 consecutive infants and children up to 15 years of age, since 1980. Indication for emergency embolization included potential loss of vision due to occlusive orbital (palpebral) hemangiomas; respiratory obstruction due to subglottic hemangiomas and vascular malformations (VM); severe hemorrhage related to VM, trauma and coagulopathy; congestive cardiac failure in the presence of cerebral (Galenic) VM and dural AVM; and traumatic aneurysm.

Indications for urgent embolization included moderate bleeding from VM; functionally important masses, usually hemangiomas producing maxillo-mandibular maldevelopment or hypertelorism; and congestive cardiac failure in the presence of dural AVM. The lesions fell into the following etiologic categories: 19 vascular malformations (including 7 predominantly lymphatic VM), 10 hemangiomas, 1 giant carotid artery aneurysm, 1 aneurysmal bone cyst and 2 children with epistaxis and systemic coagulopathy.

Among the 33 patients, embolization was efficacious in 30. Technical failure occurred in one patient with a right aortic arch. Two cervical lymphatic VM's did not respond to embolization; the others decreased in size following embolization of the vascular component. Bleeding and congestive heart failure were satisfactorily controlled in all other patients with VM. Among the hemangiomas, 3 osseous lesions were successfully resected post embolization and the remainder showed satisfactory regression. One complication (necrosis of the anterior 1/3 of the tongue) occurred.

News

Breast Imaging Conference

The sixth Annual Conference in Breast Imaging sponsored by the Medical College of Wisconsin Dept. of Radiology and Continuing Medical Education and Ausonics Corporation of Milwaukee will be held at the Wyndham Hotel Sea World in Orlando, FL, Oct. 5–7. This conference is designed for physicians, nurses, technologists, and other allied health professionals involved in diagnosis, treatment, and management of breast disease. Category 1 credit: 24½ hr. Fee: $350: physicians; $275: nurses, allied health personnel; $500: commercial. Information: program coordinator, Sandra L. Hagen-Ansert, U.C.S.D. Medical Center, San Diego, CA 92103. Registration information: Sixth Annual Breast Imaging Conference; MB Unit 9402, Milwaukee, WI 53268.

Southeast Magnetic Resonance Conference

The 1986 Southeast Magnetic Resonance Conference will be held Oct. 8–10, 1986, in Nashville, TN, hosted by Vanderbilt University. In addition to general plenary sessions, there will be special basic science or clinical tracks, with 44 invited speakers. Category 1 credit available. Fee: $50 for physicians wanting CME credit, $20 for others. Information: Southeast Magnetic Resonance Conference, Division of Continuing Medical Education, Vanderbilt University Medical Center, Nashville, TN 37232; (615) 322–4030.

New Orleans Radiology Conference

The Fall Radiology Conference sponsored by LSU Medical Center will be held at The Royal Orleans Hotel, New Orleans, LA, on Oct. 23–25. The conference will feature sessions on neuroradiology, recent advances in myelography, interventional radiology, MR, and CT. Guest faculty: O. W. Houser, J. Rabinowitz, C. Tegtmeyer, and V. Hegedus. Category 1 credit: 20 hr. Fee: $300: physicians; $200: residents. Information: Office of Continuing Education, LSU School of Medicine, 1542 Tulane Ave., New Orleans, LA 70112; (504) 568-6085.

Radiology Service Development Seminar

The American Hospital Association (AHA) is sponsoring New Opportunities in Imaging Services, Oct. 27–28, 1986, in Philadelphia. There will be sessions on the development and marketing of breast diagnostics, osteoporosis screening, outpatient vascular diagnosis and intervention, and MR. Various models for the organization of outpatient imaging will be presented, as well as strategies to capture a greater share of the HMO market. Selected lecturers: F. D. Rollo, L. Avioli, L. Repa-Eschen, G. Freedman, W. Casarella, R. Evens, E. O. Templeton, and P. Gebhard. Fee: $395 for AHA and ACR members, $450 for nonmembers, $325 for additional attendees from same institution. Information: Mark Goodhart, Division of Clinical Services and Technology, AHA, 840 N. Lake Shore Dr., Chicago, IL 60611; (312) 280-6026.

University of California, San Francisco Courses

The following courses in radiology postgraduate education will be sponsored by UC San Francisco: Diagnostic Radiology Seminars, Nov. 3–7, 1986, Maui Marriott Resort, Maui, Hawaii; Diagnostic Radiology Seminars, Jan. 19–23, 1987, Camino Real, Ixtapa, Mexico; Diagnostic Radiology Seminars, Feb. 1–6, 1987, The Gant, Aspen, CO; Diagnostic Radiology Seminars, Feb. 22–27, 1987, Shadow Ridge, Park City Utah; Diagnostic Imaging: 1987, March 16–21, 1987, Waiohai, Kauai, Hawaii. Information: Radiology Postgraduate Education, Rm. 324, University of California, San Francisco, CA 94143-0628; (415) 476-5731.

Progress in Impotence: Diagnosis and Therapy

The University of California, San Diego, and the Urological Research and Education Fund will present Progress in Impotence: Diagnosis and Therapy at the U. S. Grant Hotel, San Diego, CA, Nov. 13–15, 1986. (Note that this conference date has been changed from Sept. 9–20). This in-depth 2-day interdisciplinary symposium will discuss new concepts regarding the physiology of erection, the causes of impotence, and radiologic imaging procedures in defining causes and therapy of impotence. Radiologic aspects will include angiographic research in an animal model, pharmacoarteriography, pharmacocavernography, pharmacocavernometry, sonography, MR, and possibilities of transluminal angioplasty. Workshops will be offered in angiography, vascular surgery, and other topics. Faculty: I. Goldstein, T. Lue, G. Benson, J. Bookstein, L. Parsons. Credit: 13 hr. Fee: $295. Information: Edith Bookstein, Conference Management Associates, P.O. Box 2586, La Jolla, CA 92038; (619) 343-3212 (Pacific Coast Time)

American Radiological Nurses Association Meeting

The annual meeting of ARNA will be held on Nov. 29–Dec. 3, 1986, in conjunction with the RSNA meeting in Chicago, IL. The theme of

ARNA's educational forum is "The key to quality patient care." Information: Elaine Deutsch, Pres., 502 Forest Ct., Carrboro, NC 27501; (919) 966-1461.

International Continuing Medical Education Series

Boston University School of Medicine will sponsor the following courses. Category 1 credit: 20 hr, (except 24 hr, where noted). Fee: $350, physicians. Maui, Hawaii: Controversies in Medicine & Neurology, Dec. 2–9, 1986; Cancun, Mexico: Advances in Pediatric Clinical Care, Dec. 24, 1986–Jan. 2, 1987; St. Moritz, Switzerland: Controversies in Medicine & Surgery, Jan. 16–24, 1987, Jan. 23–31, 1987 (24 hr); Maui, Hawaii: Clinical Update in Medicine & Surgery, Feb. 10–17, 1987, Feb. 17–24, 1987; Banff, Canada: Topic to be announced, Mar. 14–21, 1987; Japan: Topic to be announced, Apr., 1987 (24 hr); Bermuda: Topic to be announced, May 20–26, 1987; Ireland: Topic to be announced, June, 1987 (24 hr); Pebble Beach, CA: Topic to be announced, July 24–30, 1987; Gstaad, Switzerland: Topic to be announced, Aug., 1987 (24 hr); Banff, Canada: Topic to be announced, Sept. 5–12, 1987. Information: Dept. of CME, Boston University School of Medicine, 80 E. Concord St., Boston, MA 02118; (617) 638-4605.

Los Angeles Radiological Conference

The Continuing Education Committee of The Los Angeles Radiological Society will sponsor its 39th annual midwinter conference for 1987 from Jan. 30–Feb. 1 at the Century Plaza Hotel, Los Angeles, CA. Guest faculty: M. Dalinka, J. Ferruci, J. Lee, T. Naidich, T. Sos, L. Talner, and R. Zimmerman. Category 1 credit: 21 hr. Fee (2-day participation): $200: residents, technologists; $250: LARS members; $300: non-LARS members. Fee (3-day participation): $250: residents, technologists; $300: LARS members; $350: non-LARS members. Their 13th annual postconference seminar will be held Feb. 3–7, 1987, at the Hyatt Regency, Maui, Kaanapali, Maui, Hawaii. Postconference speakers: M. Dalinka, E. R. Heitzman, J. K. T. Lee, and R. A. Zimmerman. Category 1 credit: 18 hr. Fee: $375: physicians; $275: residents. Information: Los Angeles Radiological Society, Attn: Diane L. Johnson, MWR, P.O. Box 91215, Los Angeles, CA 90009-1215; (213) 642-0921.

Big Sky Radiology Conference

The 11th annual Big Sky Radiology Conference, sponsored by the Dept. of Radiology, Columbus Hospital, Great Falls, MT, will be held Feb. 8–13, 1987, at Huntley Lodge, Big Sky, MT. General areas presented will be: pediatrics, sonography, CT, neuroradiology, and emergency room radiology. Category 1 credit: 20 hr. Fee: $300. Information: Audrey Goyette, Educational Services Dept., Columbus Hospital, 500 15th Ave. S., Great Falls, MT 59405; (406) 727-3333, ext. 5592.

Palm Beach Magnetic Resonance Imaging Update

Boston University Medical Center and JFK Memorial Hospital, Lake Worth, FL, will sponsor an MRI update course on Feb. 8–11, 1987, at the Hyatt Palm Beaches, West Palm Beach, FL. Category 1 credit: 18 hr. Fee: $385: physicians; $285: residents, technologists. Course directors: Allan M. Green, Neil Steimetz. Information: Dept. CME, Boston University School of Medicine, 80 E. Concord St., Boston, MA 02118; (617) 638-4605.

Diagnostic Radiology and Nuclear Medicine

The Dept. of Radiology of the Bowman Gray School of Medicine will hold its seventh annual winter continuing education meeting, Feb. 21–28, 1987, at the Frenchman's Reef Beach Resort, St. Thomas, U. S. Virgin Islands. A variety of topics will be covered, and the following Bowman Gray faculty will participate: Drs. Moody (program director), Bechtold, Choplin, Dyer, Formanek, Gelfand, Klein, Maynard, and Watson. Category 1 credit: 23 hr. Fee: $500. Registration is limited to 100 participants. Information: Carolyn Shaver, Dept. of Radiology, Bowman Gray School of Medicine, Winston-Salem, NC 27103; (919) 748-2470.

Society for Magnetic Resonance Imaging

The fifth annual meeting of the SMRI will be held Feb. 28–March 4, 1987, at the Hilton-Palacio del Rio Hotel, San Antonio, TX. The meeting will be divided into two sessions: field strength, joint ventures, and manufacturers' symposium; educational program: clinical techniques and principles of MR, neurologic applications of MR, cardiac and vascular images, clinical studies of musculoskeletal system, pulse sequences and image contrast, equipment choices and magnet selection, costs, economics, site planning, and safety considerations. Faculty: P. A. Bottomley, W. G. Bradley, Jr., B. Flannigan, G. Fullerton, J. G. Gore, C. Higgins, R. Lufkin, K. Maravilla, M. T. Modic, R. Nunnally, V. Runge, F. W. Smith, D. Stark, F. W. Wehrli, J. Weinreb. Information: SMRI Secretariat, 1340 Old Chain Bridge Rd., Ste. 300, McLean, VA 22101; (703) 790-1745.

Meeting and Course Review

For reader convenience, a summary of upcoming meetings and courses is provided. Detailed listings in the *AJR* issues are noted in parentheses.

European Symposium, Oct. 1–4, Vienna (March)
American Board of Radiology Examinations, Oct. 2–3; Oct. 6–7; Oct. 8–9; June 8–12, 1987; May 23–27, 1988.
Courses in Diagnostic Ultrasound, Oct. 6–Nov. 7, Winston-Salem, NC (July)
Angiography and Interventional Radiology, Oct. 6–9, Cambridge, MA (Sept)
AFIP Seminar in Pulmonary and Mediastinal Diagnosis, Oct. 6–9, Bethesda, MD (Sept)
Practical Radiology, Oct. 6–9, Charlottesville, VA (Aug)
University of Texas Continuing Medical Education, Diagnostic Radiology, Oct. 9–11; **Sixth Semi-Annual Fundamentals of MRI**, Nov. 5–8; **Radiation Safety Officer's Course**, Jan. 5–9, 1987, or May 18–22, 1987; **Radiotherapy Treatment Planning Anatomy**, Jan. 26–30, 1987; **Basic Radiological Health**, Feb. 9–13, 1987; **Review of Radiation Calculations**, Feb. 16–18, 1987; **Advanced Radiological Health**, May 11–15, 1987, San Antonio, TX (all in Sept)
Advanced Neuroradiology, Oct. 9–11, Orlando, FL (July)
Sonography and OB/GYN, Oct. 10–11, Sacramento, CA (July)
San Diego Course: Postgraduate Course, Oct. 13–17, San Diego, CA (Sept)
Society for Medical Decision Making, Oct. 19–22, 1986, Chicago, IL (Sept)
Mammography Course, Oct. 20–23, Boston, MA (Feb)
Chest Disease, Postgraduate course, Oct. 20–23, 1986, Boston, MA (Sept)
Diagnostic Radiology of the TMJ, Oct. 23–26, Marco Island, FL (Aug)

Weekend courses. Frontiers in Chest Diagnosis, Bone and Genitourinary Imaging, Nov. 3–7, Marbella, Spain (Feb)
Diagnostic Radiology Seminar, Nov. 3–7, Maui, Hawaii (July)
Interventional Radiology for Practicing Physicians, Nov. 5–7, 1986, Charleston, SC (Sept)
Gastrointestinal Cancers, conference, Nov. 12–14, Houston (May)
Radiology Seminar, Gastrointestinal Diseases, Nov. 14–16, Scottsdale, AZ (Aug)
Brachytherapy of Choroidal Melanoma, Nov. 20–21, New York (Aug)
MRI for Technologists, Dec. 5–6, Houston (June)
Indian Radiation Oncology Congress, Dec. 5–7, Bombay (April)
International Symposium on Breast Cancer, Jan. 1–4, 1987, New Delhi, India (Aug)
International Symposium on MR 1987, Jan. 29–Feb. 1, 1987, Garmisch-Partenkirchen, Bavaria (Aug)
Perspectives on Imaging Modalities, Feb. 2–6, 1987, Cancun, Mexico (Sept)
Gastrointestinal Radiologists Meeting and Course, Feb. 8–13, 1987, Scottsdale, AZ (Aug)
Thoracic Imaging 1987, Feb. 16–19, Orlando, FL (May)
Radiation Research Society Meeting, Feb. 22–26, 1987, Atlanta, GA (July)
Advanced Perinatal Ultrasound Seminar, Feb. 26–28, 1987, Lake Buena Vista, FL (Aug)
Alexandria International Conference on Laryngeal Cancer, April 1–2, 1987, Alexandria, Egypt (Sept)
American Radium Society Meeting, April 6–10, 1987, London (Aug)
Annual Meeting, National Council on Radiation Protection and Measurements, April 8–9, 1987, Bethesda, MD (Sept)
Fleischner Society Annual Symposium, May 21–23, 1987, San Francisco, CA (July)
1987 Radiology Congress, Lisbon, May 31–June 6, 1987 (Aug)
EUROSON '87, June 14–18, 1987, Helsinki, Finland (Sept)
International Conference on Computer Assisted Radiology. July 1–4, 1987, West Berlin (Feb)
Sarcoidosis and Granulomatous Disorders, congress, Sept. 6–11, 1987, Milan (June)
Copenhagen Symposium on Uroradiology, Sept. 7–10, 1987, Copenhagen, Denmark (Sept)

AJR carries announcements of courses, symposia, and meetings of interest to its readers if received a minimum of 4 months before the event. There is no charge; receipt of items by the *AJR* Editorial Office is not acknowledged. Submit items for publication typed double spaced. Provide title, date, location, brief description, sponsor, course directors, fees, category I credit, and address and telephone number for additional information. Faculty from the host institution will not be listed. Guest faculty names will appear **only** if initials are provided. Mail news items to *AJR* Editorial Office, 2223 Avenida de la Playa, Suite 200, La Jolla, CA 92037.

Classified Advertising

Positions Available

NEW YORK CITY SUBURBAN PRACTICE seeks board-certified radiologist. Hands-on ultrasound skills essential. Solid imaging knowledge. Personality counts. High pay with early partnership for special individual. CV to Box 18, Meacham Station, Elmont, NY 11003. 10–11a

BOARD-CERTIFIED RADIOLOGIST–Six man radiology group seeks new associate with fellowship training in CT/ultrasound. The group provides complete radiologic services in fully-equipped 500 bed hospital with two G.E. 9800 CT scanners, and Acuson and Diasonics ultrasound. Private out-patient office also covered by the group. Send CV to Eric R. Rosenberg, M.D., Dept. of Radiology, New Hanover Memorial Hospital, Wilmington, NC 28403. 10–12a

DIAGNOSTIC RADIOLOGY–Immediate opening for well-qualified BC/BE radiologist to join progressive group in 260-bed full-service community hospital in southern Illinois. All modalities are available. Excellent salary leading to early partnership. Please send CV to Richard A. Rudman, M.D., 13 Orchard Drive East, Centralia, IL 62801 or call St. Mary's Hospital (618) 532-6731 ext. 501 or home (618) 533-2066. 10a

STAFF RADIOLOGIST–The University of Virginia, School of Medicine and its affiliated hospitals program are seeking a full-time staff radiologist for its VA Medical Center. Candidates must have an MD degree, be board certified or board eligible in radiology, eligible for licensure in Virginia, and eligible for appointment with the University of Virginia School of Medicine. Candidates must demonstrate experience with general radiology, interventional radiology, CT, ultrasound, and teaching. A clinical research interest is also desirable. Send CV with references to Charles J. Schleupner, M.D., Chairman, Search Committee for Chief, Radiology, Infectious Diseases Section (111L), VA Medical Center, Salem, VA 24153. EEO employer. 10a

CHIEF OF RADIOLOGY–The University of Virginia School of Medicine and its affiliated hospitals program are seeking a full-time Chief of Radiology for its VA Medical Center. Candidates must have an MD degree, be board certified in radiology, eligible for licensure in Virginia, and eligible for appointment with the University of Virginia, School of Medicine. Candidates should be knowledgeable in the broad aspects of radiology, demonstration of prior teaching, administrative experience, and leadership ability is desirable. Send CV with references to Charles J. Schleupner, M.D., Chairman, Search Committee for Chief of Radiology, Infectious Diseases Section (111L), VA Medical Center, Salem, VA 24153. EEO employer. 10a

RADIOLOGY FACULTY POSITIONS. The Dept. of Radiology of the State University of New York, School of Medicine at Stony Brook is currently recruiting two radiologists to keep pace with the rapid growth of its state-of-art division of body CT and ultrasound. Located on the highly desirable North Shore of Long Island, with convenient access to New York City, the Health Sciences Center and 540-bed University Hospital provide the benefits of academic practice in a suburban setting. Requirements include board certification in diagnostic radiology and post-residency training in body CT and ultrasound. Send CV to Roger Baim, M.D., Dept. of Radiology, School of Medicine, Health Sciences Center, Level 4, Room 147, State University of New York at Stony Brook, Stony Brook, NY 11794. 10a

NEURORADIOLOGY/MRI. Private clinic seeks board certified radiologist with MRI experience to oversee and direct diagnostic center. Excellent salary and recreational activities. Reply: P.O. Box 292527, Davie, FL 33324. 6–10ap

RADIOLOGY FACULTY POSITION. The Dept. of Radiology of the State University of New York, School of Medicine at Stony Brook is currently recruiting a skeletal radiologist to keep pace with the rapid growth of its University Hospital and orthopedic service. Located on the highly desirable North Shore of Long Island, with convenient access to New York City, the medical center provides the benefits of academic practice in a suburban setting. Candidates should be board eligible or board certified having completed an accredited training program. Fellowship training or practice experience is desirable. Send resume to Morton A. Meyers, M.D., Professor and Chairman, Dept. of Radiology, School of Medicine, Health Sciences Center, SUNY Stony Brook, Stony Brook, NY 11794. SUNY Stony Brook is an affirmative action/equal opportunity educator and employer. 10a

RADIOLOGY FACULTY POSITION. The Dept. of Radiology of the State University of New York, School of Medicine at Stony Brook is currently recruiting a pediatric radiologist to keep pace with the rapid growth of its University Hospital and pediatric service. Located on the highly desirable North Shore of Long Island, with convenient access to New York City, the medical center provides the benefits of academic practice in a suburban setting. Candidates should be board eligible or board certified having completed an accredited training program. Fellowship training or practice experience is desirable. Send resume to Morton A. Meyers, M.D., Professor and Chairman, Dept. of Radiology, School of Medicine, Health Sciences Center, SUNY Stony Brook, Stony Brook, NY 11794. SUNY Stony Brook is an affirmative action/equal opportunity educator and employer. 10a

CHIEF, BODY CT. The Dept. of Diagnostic Radiology of William Beaumont Hospital, a major tertiary care and academic institution in Michigan, is seeking a candidate to direct the division of body CT and participate in MR. Candidates must be board certified in diagnostic radiology and have significant academic achievements. Income is negotiable and competitive. Send CV to Jalil Farah, M.D., Director, Diagnostic Radiology, William Beaumont Hospital, 3601 West 13 Mile Road, Royal Oak, MI 48072. 10–12a

RADIOLOGY FACULTY–CHIEF POSITION. University and VA Hospital seeking board-certified radiologist for position of Chief of Radiology, commencing Sept. 1, 1986. Cross-appointment with medical school at appropriate rank. Candidates should have extensive clinical radiology experience as well as administrative talents. Position located in San Antonio, one of America's most charming cities. Replies and CVs should be sent to Elliot Weser, M.D., Chief, Medicine Service, AMVAH, 7400 Merton Minter Blvd., San Antonio, TX 78284. 10a

RADIOLOGIST–The Dept. of Radiology of the Brigham and Women's Hospital–Harvard Medical School wishes to recruit a staff for positions in thoracic and skeletal radiology. These positions offer diverse clinical work and opportunities for research and teaching. Rank and salary commensurate with experience. Evidence of interest in academic radiology and certification by the American Board of Radiology are preferred. We are an equal opportunity, affirmative action employer. Please send CV in confidence to B. Leonard Holman, M.D., Acting Chairman, Dept. of Radiology, Brigham and Women's Hospital, 75 Francis St., Boston, MA 02115. 10a

TWO YOUNG RADIOLOGISTS seek a third radiologist in expanding hospital-based practice near Canadian border in northern New York. All modalities available. Write P. Berman, HC 61 Box 454, Massena, NY 13662. 8–7a

DIAGNOSTIC RADIOLOGIST/INTERVENTIONAL RADIOLOGIST. The Dept. of Radiology at the University Hospital of Jacksonville/University of Florida College of Medicine is seeking an additional staff radiologist with special interest, expertise, or training in interventional radiology. Fellowship training is preferable. Salary and fringe benefits are competitive with other similar positions. Academic appointment will be at the assistant professor, associate professor level depending on the qualifications of the applicant. Application recruiting deadline is December 15, 1986 with an anticipated starting date of July 1, 1987. Interested applicants are invited to forward their CV and names and addresses of three references to H. Martin Northup, M.D., Chairman, Search Committee, Dept. of Radiology, University Hospital of Jacksonville, 655 West 8th St., Jacksonville, FL 32209. EEO/AAE. 10a

DIAGNOSTIC RADIOLOGIST/PULMONARY RADIOLOGIST. The Dept. of Radiology at the University Hospital of Jacksonville/University of Florida College of Medicine is seeking an additional staff radiologist with special interest, expertise, or training in pulmonary radiology. Fellowship training is preferable. Salary and fringe benefits are competitive with other similar positions. Academic appointment will be at the assistant professor, associate professor level depending on the qualifications of the applicant. Application recruiting deadline is December 15, 1986 with an anticipated starting date of July 1, 1987. Interested applicants are invited to forward their CV and names and addresses of three references to H. Martin Northup, M.D., Chairman, Search Committee, Dept. of Radiology, University Hospital of Jacksonville, 655 West 8th St., Jacksonville, FL 32209. EEO/AAE. 10a

DIAGNOSTIC RADIOLOGIST/SKELETAL RADIOLOGIST. The Dept. of Radiology at the University Hospital of Jacksonville/University of Florida College of Medicine is seeking an additional staff radiologist with special interest, expertise, or training in skeletal radiology. Fellowship training is preferable. Salary and fringe benefits are competitive with other similar positions. Academic appointment will be at the assistant professor, associate professor level depending on the qualifications of the applicant. Application recruiting deadline is December 15, 1986 with an anticipated starting date of July 1, 1987. Interested applicants are invited to forward their CV and names and addresses of three references to H. Martin Northup, M.D., Chairman, Search Committee, Dept. of Radiology, University Hospital of Jacksonville, 655 West 8th St., Jacksonville, FL 32209. EEO/AAE. 10a

RADIOLOGIST, BOARD ELIGIBLE/BOARD CERTIFIED for 75-physician multispecialty group in Rocky Mountain region. Practice to include hospital and office diagnostic radiology. Special imaging training is necessary. Practice includes angiography, invasive techniques, nuclear medicine, and sonography. Send CV to Box G68, AJR (see address this section). 10a

AGGRESSIVE DIAGNOSTIC RADIOLOGY GROUP in need of new associate. Must be board certified and would prefer multi-talented background including interventional radiology, nuclear medicine, ultrasound, CT, and MRI experience. Our group covers 4 hospitals including regional trauma center and 2 offices. Located in The Sparkling City by the Sea. Kindly send CV to Richard P. Chepey, M.D., 2481 Morgan Ave., P.O. Box 5608, Corpus Christi, TX 78405. 7–10ap

BOARD CERTIFIED diagnostic radiologist. All diagnostic modalities except MR. MR installation planned in 1½ years. Busy in-patient and out-patient practice. Salary negotiable and early partnership available. Send CV to Box C23, AJR (see address this section). 6xa

RADIOLOGIST. Opening for part-time and full-time, board-certified or board-eligible diagnostic radiologists. Large group practice, 2 offices, 3 hospitals, 860 beds. General radiology, CT, ultrasound, nuclear medicine, MRI pending (angio-IV positions filled). Located in Lower Bucks County, PA and Mercer County, NJ, between Philadelphia and Princeton. Prefer postresidency fellowship or practice experience. Available immediately, will consider for July 1987. Send CV to S.L. Meshkov, M.D., 838 W. State St., Trenton, NJ 08618. 10a

FACULTY POSITION AVAILABLE IN DIAGNOSTIC BODY IMAGING. Assistant Professor/Associate Professor of Radiology, University of Colorado School of Medicine. Specialty: ultrasound, body CT, body MRI; Prerequisites: Completion of body-imaging fellowship or ultrasound fellowship; board eligibility or board certified in diagnostic radiology. New diagnostic imaging center now under construction at University Hospital that will house a new high-speed Picker 1200 CT Scanner, over 15 state-of-the-art ultrasound systems, and a new .35 Telsa Diasonic MRI Scanner. Position to share in all clinical, research, and teaching responsibilities with other faculty and two fellows in body imaging. Over 7,000 diagnostic ultrasound procedures are performed annually in all areas of imaging including obstetrical, abdominal, and adult cardiac. Salary and position commensurate with experience. Contact: Michael L. Manco-Johnson, M.D., Professor and Acting Chairman, Director of Body Imaging, Department of Radiology, University of Colorado School of Medicine, 4200 E. 9th Ave., C277, Denver, CO 80262 (303) 394-7719. University of Colorado Health Sciences Center is an affirmative action/equal opportunity employer. 10a

NEURORADIOLOGIST to join 11-member private practice radiology group in southeastern North Carolina. Position available for Director of Neuroimaging including Neuro MRI. Candidate must have at least 2 yr University training in neuroradiology with at least 12 months training/experience in MRI. Neuroradiologist with active clinical expertise in neurology preferred. Please submit CV to Box F46 AJR (see address this section). 9-10a

RADIATION ONCOLOGIST. A 180-member multispecialty group seeks a board certified/board eligible radiation oncologist to expand the service offerings of the Oncology Dept. In addition to the provision of care, the radiation oncologist will have considerable latitude in the design of services including the planning of the proposed radiation therapy plant. Duties will include design of facilities, selection of equipment, and selection and training of personnel. Community has 143,000 population and offers three universities, fine cultural opportunities and four-season recreational activities. Please remit inquiries to Box F48 AJR (see address this section). 9-10a

JR. FACULTY POSITIONS at Wayne State University, Detroit Medical Center in general radiology. Seeking board certified radiologist who will spend 50% of the time in general radiology and the remainder in sub-speciality interests and teaching. Send CV and salary requirements to Dr. Thomas Slovis, Children's Hospital of Michigan, Dept. of Radiology, 3901 Beaubien Blvd., Detroit, MI 48201. Wayne State University is an equal opportunity/affirmative action employer. 8–10a

BOARD CERTIFIED radiologist to do general diagnostic work, including CT, US, biopsies, mammography, and angio. Special training in angio desired. Excellent salary and full partnership 2nd yr. Busy hospital and office practice in suburban Washington, DC area. Send CV to Box F50, AJR (see address this section). 9-11a

THE MEDICAL COLLEGE OF GEORGIA (Augusta, GA) is seeking a Professor and Chairman for the Dept. of Radiology. The department consists of sections of diagnostic radiology (including US, CT, and MRI), nuclear medicine, radiation therapy, and medical physics, and has approved residency programs in diagnostic radiology and radiation therapy. Interested parties please submit CV by Oct. 30, 1986 to Robert R. Nesbit, Jr., M.D., Chairman, Radiology Search Committee, Dept. of Surgery, Medical College of Georgia, Augusta, GA 30912. EOE/AAP 9-10a

RADIOLOGIST TO WORK WEEKENDS only with large group in exciting Las Vegas, NV. Remainder of week free to enjoy Nevada's unlimited recreational activities. University-associated practice. Angio not required. Generous salary and fringe benefits. Contact Richard Ellis, M.D., 828 Vegas Valley Dr., Las Vegas, NV 89109 or call 7am - 4pm PDST (702) 369-7774. 9-10a

GENERAL DIAGNOSTIC RADIOLOGIST, board certified to join hospital-based group. 200-bed hospital equipped with CT, US, nuclear medicine, special procedures, and interventional radiology. 20,000 exams/yr. Located in Alton, IL, 45 min. to downtown St. Louis. Competitive salary leading to early partnership. Contact Sumner Holtz, M.D., 232 So. Woodsmill Rd., Chesterfield, MO 63017 (314) 434-1500, ext. 4250. 9-11a

BOARD CERTIFIED RADIOLOGIST. Six man radiology group seeks new associate with 6–12 mo. fellowship/experience in MRI. New 1.5 T unit to be operational by year-end. The group provides complete radiologic services in fully-equipped 500-bed hospital, and private outpatient office. Send CV to Eric R. Rosenberg, M.D., Dept. of Radiology, New Hanover Memorial Hospital, Wilmington, NC 28403. 8–10ap

ISRAEL, DIAGNOSTIC RADIOLOGY. Opportunities for 3–4 week or longer working vacations in a number of Israeli medical centers, on a volunteer basis. Positions varied, arrangements flexible. For information contact: Jonathan H. Fish, M.D., 1844 San Miguel Dr., #302, Walnut Creek, CA 94596; (415) 947-0560. 8xa

Positions Desired

BOARD-CERTIFIED RADIOLOGIST seeks part-time position in Philadelphia, South Jersey, Wilmington, Delaware area. Experienced in all imaging and invasive modalities except MRI. Reply Box G62, AJR (see address this section). 10–12b

PGY-3 RADIOLOGY RESIDENT seeking PGY-4 position beginning July 1987 at university-based program with MRI. Quality U.S. medical graduate. Dedicated, hard-working, easy-going. Reply Box G64, AJR (see address this section). 10–11b

POST-DOCTORAL RESEARCH ASSOCIATE/FELLOW in diagnostic radiology seeks position. Fully qualified, extensive experience in CT/US, installation to intervention. Over 10,000 CT/US cases, 500 CT/US intervention, biopsies, drainage. Adept also in angiography and general radiology. Write Box G66, AJR (see address this section) or call (914) 591-6234. 10–11b

BOARD-CERTIFIED DIAGNOSTIC RADIOLOGIST with interest in all areas of radiology seeks position beginning July 1987. Will have completed a formal postgraduate fellowship in CT/ultrasound/MRI. Have 1-yr extensive experience in angiography and interventional radiology procedures. Reply 251 Marengo Ave., Apt. 4F, Forest Park, IL 60130, (312) 366-0712. 10–12b

NEURORADIOLOGIST completing 2-yr-UCSD fellowship 6/87 (with 1.5T GE Signa experience throughout) seeks private practice position. P.O. Box 8107, La Jolla, CA 92038. 9-12b

Fellowship and Residencies

POST-DOCTORAL FELLOWSHIP–The Dept. of Medical Physics of Memorial Hospital invites applications for a postdoctoral training fellowship in medical radiological physics of 2-yr duration. The purpose of this program is to provide qualified experimental physicists with "on-the-job" and didactic training—unique to a few hospitals and which cannot be obtained in university courses—in the use of radiation for diagnostic and therapeutic purposes with second year concentration on a significant research project. This will qualify them for professional responsibilities in hospitals and medical research institutions in response to a demonstrated need for medical radiation physicists capable of high standards of performance. To apply send CV and list of publications to Gian D. Ragazzoni, Fellowship Program Coordinator, Dept. of Medical Physics, Memorial Sloan-Kettering Cancer Center, 1275 York Ave., New York, NY 10021. MSKCC is an equal opportunity affirmative action institution. 10c

GASTROINTESTINAL RADIOLOGY–One-year fellowship available at the Hospital of the University of Pennsylvania starting July 1987. Please contact Igor Laufer, M.D., Hospital of the University of Pennsylvania, 3400 Spruce St., Philadelphia, PA 19104 (215) 662-3263. 10c

CARDIOVASCULAR-INTERVENTIONAL RADIOLOGY FELLOWSHIP. Two-year program starting July 1, 1988. Extensive clinical training provided in all types of interventional procedures, diagnostic angiography, coronary angiography and cardiac catheterization, digital imaging, and cardiovascular MRI. Optional time available for laboratory and/or clinical projects. Contact Michael A. Bettman, M.D., Dept. of Radiology, Harvard Medical School-Brigham and Women's Hospital, 75 Francis St., Boston, MA 02115. 9-10c

Tutorials/Courses

CORTINA, ITALY—LONDON, ENGLAND. Winter Congress-Cortina, Jan 31–Feb 7, 1987: Winter Seminar-London, Feb 7–11, 1987. Attend one or both offering CME I accredited and presented by a renowned faculty. Topics in CT, US, MRI with correlation. Fees each meeting: to November 14, US$395, thereafter US$435 (combined fee US$450 and US$495, respectively). Contact Medical Seminars International, 21915 Roscoe Blvd., Ste. 222, Canoga Park, CA 91304 (818) 701-5143. 10–12d

NMR VISITING FELLOWSHIPS in Northern California. Intensive structured 1–6 week courses in clinical magnetic resonance with emphasis on CNS imaging. Integrated live instruction with 20 hr of dual projection slide presentations in week 1, extensive teaching file (600 cases), and updated videotape library. Certificate awarded on completion. References from prior fellows available. For further information contact: Murray A. Solomon, M.D., San Jose MRI Center, 361 S. Monroe St., San Jose, CA 95128. 6–11dp

HAWAII 86–11TH ANNUAL INTERNATIONAL BODY IMAGING CONFERENCE. Oct. 18–26, 1986. Diagnostic medical imaging. CME category I credit. Contact: Body Imaging Conference, Dept. of Radiology, West Park Hospital, 21915 Roscoe Blvd., Ste. #222, Canoga Park, CA 91304; (818) 701-5143. 8–10d

ULTRASOUND AT SEA—Caribbean Cruise. Post RSNA CME 1 presented by Dr. Peter Cooperberg. Registration: $385 before Oct. 1; $425 thereafter. Info: Medical Seminars International, 21915 Roscoe Blvd., Ste. #222, Canoga Park, CA 91304, (818) 701-5143. 7–11d

Other

REALIZE THE VALUE of your practice. A group of successful and well-qualified radiologists is interested in acquiring established radiology practices. Hospital contracts, clinics, and private office settings are desired. Opportunity for radiologists considering retirement or reduction in practice activities to capitalize on the value of the practice they have built up during their careers. Alleviate the problems of professional recruitment or administrative pressures. Practices considered throughout the country. Flexible purchase options with opportunity for continuing relationship arrangements. Write Box C49, AJR, (see address this section). 6–5e

AJR Indexes

AJR CONSOLIDATED INDEXES available in limited quantities. Complete your journal collection. Order by index number. Indexes available, years covered and prices: 2, 1938–1942, $10; 3, 1943–1947, $22.50; 4, 1948–1952, $23.50; 5, 1953–1957, $25; 6, 1958–1962, $23.50; 7, 1963–1967, $30; 8, 1968–1972, $40; 9, 1973–1977, $34. Order from: Subscription Dept. Williams & Wilkins, 428 E. Preston, St. Baltimore, MD 21202; (301) 528-4000.

AJR Classified Advertising Information

Box Responses and Address for Ad Placement

Write Box _____, AJR, Suite 200, 2223 Avenida de la Playa, La Jolla, CA 92037; (619) 459-2229.

How to Place an Ad

AJR accepts classified advertising for Positions Available, Positions Desired, Fellowships and Residencies, and Tutorials/Courses. Ads are accepted by mail or telephone. Institutions should supply purchase orders.

Rates: $6.00/line with a $30 minimum charge. Box service is $10 additional for each month the ad appears. There are discounts for multiple insertions: 10% for 2–3 insertions; 20% for 4 or more. To estimate lines, count all words and divide by 5.5.

Billing: Ads may be prepaid or invoices will be sent after the ad appears.

Deadlines. About 3 weeks before the issue mails. *AJR* issues mail in the middle of the month preceding the cover date (e.g., July mails June 17). For specific deadlines, write or telephone the AJR editorial office.

Estimating Ad Charges

Line charge: divide total words by 5.5 and multiply by $6.00	$ _____
Multiple insertions? If so, multiply by number	× _____
Subtotal	$
Box response requested? If so, multiply number of months by $10.00	+ _____
Subtotal	$
Discount applies to two or more insertions. Subtract 10% if ad appears 2–3 months, 20% if 4 months or more	− _____
Approximate advertising charge	$

Vital new references on 30-day FREE trial

EMERGENCY RADIOLOGY OF THE ACUTELY ILL OR INJURED CHILD
Second Edition

By **Leonard E. Swischuk, MD**

"Only Len Swischuk could produce a book quite like this....The reproductions, particularly of soft tissues, are superb....A true teacher, [Swischuk] stresses the basic facts, the simple, the obvious, the variations, and the pitfalls....This book should be in the library of even the smallest radiology department." — **J Can Assoc Radiol** (of the First Edition)

1986/622 pages/685 illustrations/#8049-0/$75.00

COMPUTED TOMOGRAPHY AND MAGNETIC RESONANCE IMAGING OF THE HEAD AND NECK
Second Edition

By **Anthony A. Mancuso, MD** and **William N. Hanafee, MD**
with a special contribution from ***John A. Kirchner, MD***

The leading guide to head and neck imaging now includes the first comprehensive discussion of otolaryngologic MRI, an extensively revised chapter on temporal bone, extraordinary images generated by state-of-the-art equipment, and more.

1985/504 pages/155 illustrations/#5476-7/$84.75

LYMPHATIC IMAGING
Lymphography, Computed Tomography and Scintigraphy
Second Edition

Edited by **Melvin E. Clouse, MD** and **Sidney Wallace, MD**

For assistance in selecting, performing and interpreting lymphatic images using state-of-the-art equipment and techniques, turn to the new *Second Edition* of the only book-length exploration of lymphatic evaluation.

1985/526 pages/352 illustrations/#1651-2/$87.50

COMPUTED TOMOGRAPHY IN THE EVALUATION OF TRAUMA
Second Edition

Edited by **Michael P. Federle, MD** and **Michael Brant-Zawadzki, MD**

In this new edition you'll find a thorough and up-to-date discussion of the clinical indications for CT scanning in different types of trauma to virtually all areas of the body, keys to techniques of scanning and to accurate interpretation, and comparisons of CT to other radiographic procedures and laboratory tests.

1986/about 300 pages/about 370 illustrations/#3102-3/about $58.95

CLINICAL ARTHROGRAPHY
Second Edition

By **Rolf-D. Arndt, MD, John W. Horns, MD,** and **Richard H. Gold, MD**
with a special contribution by ***Donald D. Blaschke, DDS***

Including inflammatory diseases and other joint abnormalities, the *Second Edition* retains the emphasis on orthopedic disorders as it expands the basic principles of arthrography and adds new, recently published concepts, such as double-contrast CT arthrography.

1985/282 pages/147 illustrations/#0256-2/$62.50

Williams & Wilkins
428 E. Preston Street Baltimore, MD 21202

___ YES! Please rush my copy of _____

_____

_____.

If not completely satisfied, I may return the books within 30 days at no further obligation. (US & Canada only).

PAYMENT OPTIONS
(Enclose payment or charge your order and Williams & Wilkins will pay all postage and handling costs.)

☐ Check enclosed ☐ Bill me
☐ VISA ☐ MasterCard ☐ American Express

card # ☐☐☐☐☐☐☐☐☐☐☐☐☐☐☐☐ exp. ☐☐-☐☐

_____
signature/p.o. #

For fastest service...call 1-800-638-0672 toll free anywhere in the US except AK and HI; MD residents call 528-4221 collect.

Full Name _____

Address _____

City _____ State _____ Zip _____

SWISAD 95401

You learn from your experience with

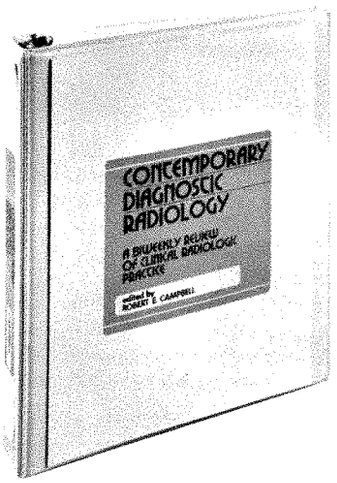
CONTEMPORARY DIAGNOSTIC RADIOLOGY

Editor: **Robert E. Campbell, M.D.**

A Biweekly Review of Clinical Radiologic Practice—26 issues a year!

One of your toughest jobs is keeping up with the many new developments that affect radiology. That's why you want **Contemporary Diagnostic Radiology**... an effective and convenient way to perfect your skills and maintain your professional status.

Contemporary Diagnostic Radiology is designed as a continuing education program that lets you work at your own pace. Every two weeks you'll receive an issue that covers a single topic or procedure in detail. Read the information and study the clearly reproduced radiographs—and then, if you choose, respond to a comprehensive examination in the strictest confidence. You set the pace.
Each biweekly lesson brings you pertinent review of the basics in bone radiology... gastrointestinal radiology... pediatric radiology... genitourinary radiology... MR imaging... and all of the topics you want to know more about.



Contemporary Diagnostic Radiology works *two ways*. You may choose to subscribe to the non-scoring version, receiving every issue as an important element of your professional reading. The scoring version, however, supplements your reading and computer-coded examinations with confidential result responses, making you eligible for Continuing Medical Education credits co-sponsored by the University of Pennsylvania School of Medicine.

"As an organization for continuing medical education, the University of Pennsylvania School of Medicine designates this continuing medical education activity as meeting the criteria for 1 credit hour per bi-weekly issue in Category I for Educational Materials for the Physician's Recognition Award of the American Medical Association provided it has been completed according to instructions."

You can begin this ongoing program **today. Contemporary Diagnostic Radiology** is a year-round program, so you can join at any time. To begin your lessons, just fill out the enclosed card and return it to us. Or call **FREE** 1-800-638-6423 (except from Alaska and Hawaii). In Maryland call **COLLECT** 528-4105. You'll find that **Contemporary Diagnostic Radiology** is the most efficient and inexpensive way to keep up with your dynamic field.

Williams & Wilkins

P.O. Box 23291
Baltimore, Maryland 21203

266 Fulham Road
London SW10 9EL England

clip & mail

CONTEMPORARY DIAGNOSTIC RADIOLOGY

☐ **Yes!** I want to keep pace in my field! Begin my 26-issue subscription:
☐ Send me the scoring version ($220)
☐ Send me the non-scoring version ($180)
☐ Send me the resident non-scoring version ($160)
(add $35 for optional air mail delivery outside the U.S.)
☐ new subscription
☐ renewal

name

address

city/state/zip

payment options
☐ payment enclosed ☐ bill me
☐ American Express ☐ MasterCard ☐ VISA

card # expiration date

signature/P.O. #

Maryland residents add 5% sales tax. Subscriptions outside the U.S. must be prepaid in U.S. dollars only. Rates subject to change without notice. Please allow 8 weeks for delivery of your first issue, up to 16 weeks for surface delivery outside the U.S. Optional airmail rates: add $35 per subscription.

Residents are eligible for the special in-training rate for up to three years. When requesting this rate, please include training status and institution.

Don't forget: you can order with a **FREE** phone call at 1-800-638-6423 (except from Alaska and Hawaii). In Maryland, call collect 528-4105.

Williams & Wilkins

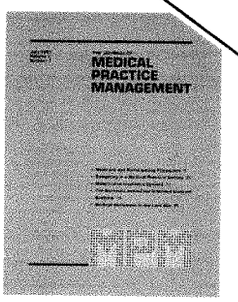
P.O. Box 23291
Baltimore, Maryland 21203

266 Fulham Road
London SW10 9EL England

printed in USA

CDRAD 95191 86

Cont.ol the futu.e of your practice



NEW!

The Journal of MEDICAL PRACTICE MANAGEMENT

Editor: **Marcel Frenkel, MD, MBA**

A new journal gives you the management skills you need to pull ahead

Right now you need information on some important topics that weren't covered in medical school. Topics that are having a profound impact on private practice and hospital-based physicians across the country.

Like competition from HMOs. Industrialization of medicine. The sheer number of physicians competing for your patients. Increasing costs.

You know the issues. What you need to know is the best way to face them so your practice will flourish in years to come.

And that's where **The Journal of Medical Practice Management** comes in.

Keep up with the issues that are changing your way of practice forever

The Journal of Medical Practice Management is a new quarterly publication that covers *your* concerns...issues affecting the way you practice now — and the way you'll practice in the future.

Four times a year, an expert editorial board headed by Dr. Marcel Frenkel brings you concise, readable coverage of today's issues and tomorrow's trends.

You'll find departments covering • office procedures and management • malpractice • marketing • manpower • computers • taxation • legal and legislative affairs • and health policy.

You'll also find pertinent features like the **Washington Report,** telling you what's up in the nation's capital and how it affects you...a **Letter from Abroad,** offering perspectives on how physicians are handling health care issues in other countries...and profiles of profit and not-for-profit health care delivery systems.

A multidisciplinary editorial board

Members of the editorial board for **The Journal of Medical Practice Management** have been carefully chosen for their knowledge of the management aspects of practicing medicine. These experts, many with experience in more than one field, give you the perspectives you need from medicine, law, management, government, and education.

You can control the future of your practice

The issues you can't afford to ignore are in **The Journal of Medical Practice Management.** It's a lot of information for a little money. And that's good business for you.

Reserve your charter subscription today!

Just return the attached coupon, or **call our FREE number,** 800-638-6423, from anywhere in the US except Alaska and Hawaii. In Maryland, call 528-4105 collect. **Quarterly**

Williams & Wilkins

428 East Preston Street
Baltimore, Maryland 21202

266 Fulham Road
London SW10 9EL England

YES, I want to control the future of my practice!

Please enter my subscription to **The Journal of Medical Practice Management** (quarterly)

☐ Individuals and Institutions $40

All subscribers: add $10 outside the U.S.

☐ Check enclosed ☐ Bill me
☐ MasterCard ☐ American Express ☐ VISA

Card # _____ Exp. date _____

Signature _____

Name _____

Address _____

City/State/Zip _____

Maryland residents add 5% sales tax. Subscriptions outside the US must be prepaid. All subscriptions must be paid in US dollars. Rates valid through April 30, 1987.

Please allow 8 weeks for delivery of your first issue, up to 16 weeks for surface delivery outside the US. Airmail rates available on request.

Williams & Wilkins

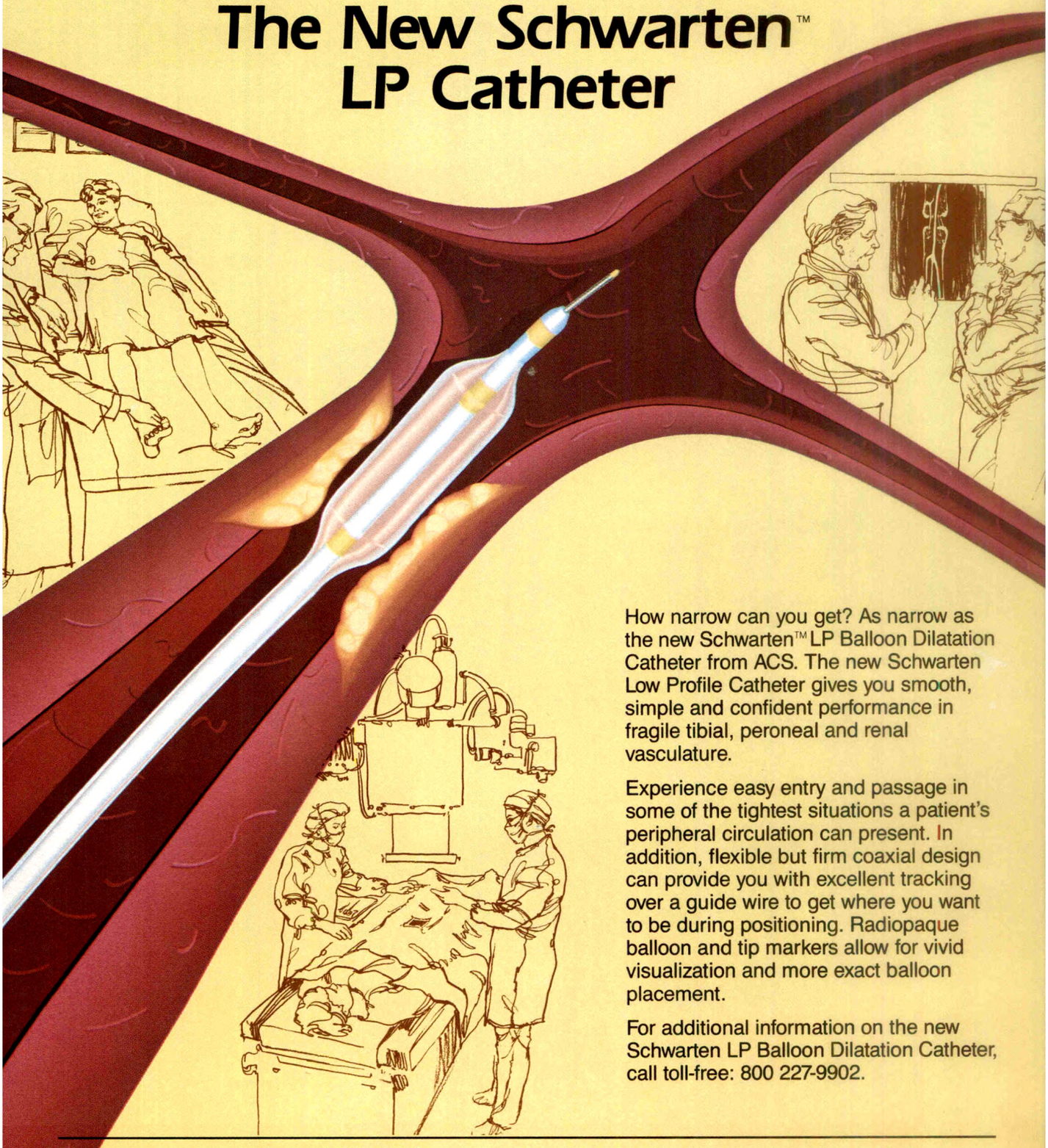
P.O. Box 1496
Baltimore, Maryland 21203

266 Fulham Road
London SW10 9EL England

MPMAD 95048 86

The perfect profile for narrow navigation.

The New Schwarten™ LP Catheter



How narrow can you get? As narrow as the new Schwarten™ LP Balloon Dilatation Catheter from ACS. The new Schwarten Low Profile Catheter gives you smooth, simple and confident performance in fragile tibial, peroneal and renal vasculature.

Experience easy entry and passage in some of the tightest situations a patient's peripheral circulation can present. In addition, flexible but firm coaxial design can provide you with excellent tracking over a guide wire to get where you want to be during positioning. Radiopaque balloon and tip markers allow for vivid visualization and more exact balloon placement.

For additional information on the new Schwarten LP Balloon Dilatation Catheter, call toll-free: 800 227-9902.

ACS®

Where Innovation continues.

Lilly

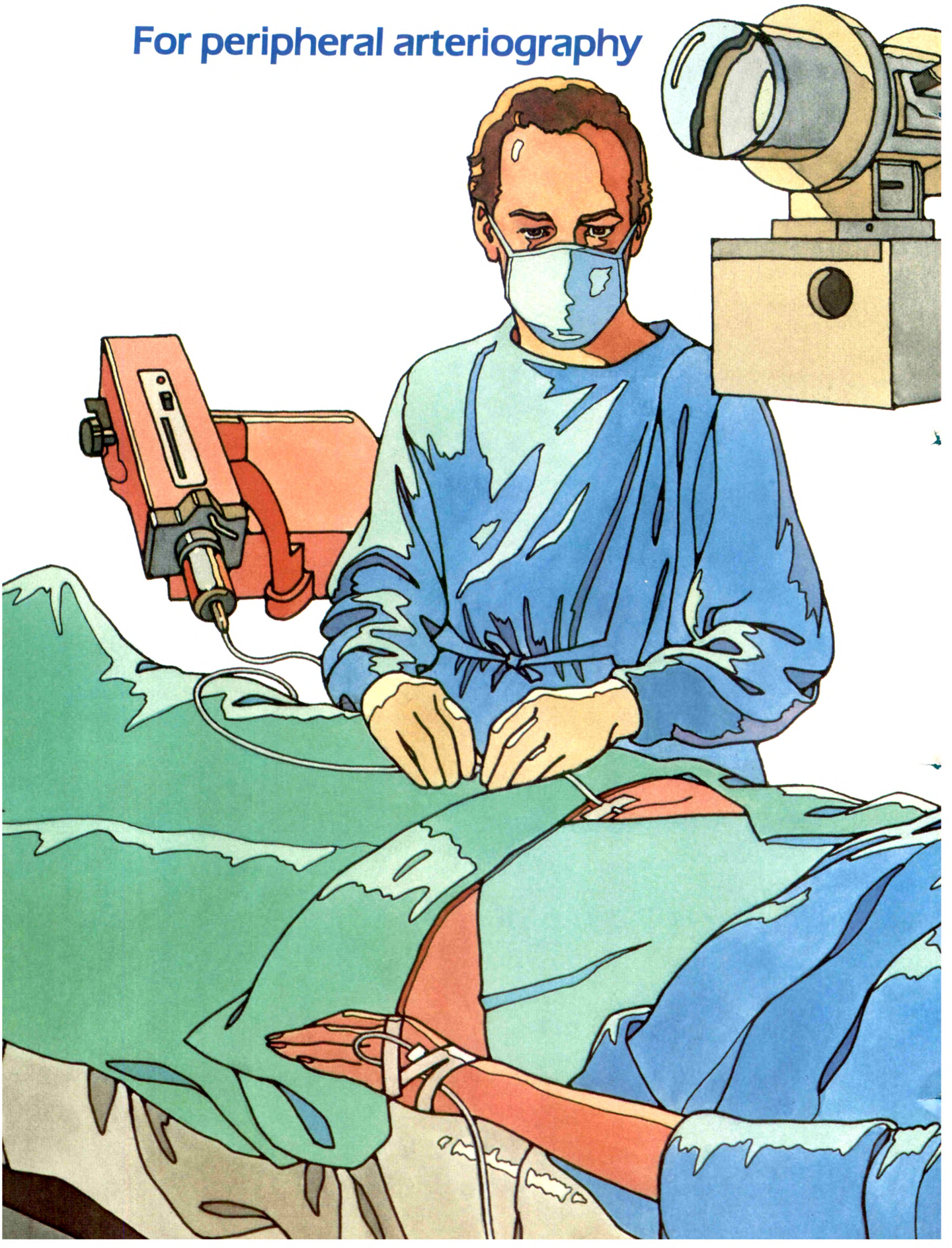
ACS is a wholly owned subsidiary of Eli Lilly and Company.

Advanced Cardiovascular Systems, Inc.

1395 Charleston Road
Mountain View, CA 94039
415 965-7360
Toll free: 800 227-9902
TWX (Telex II) 23-289-720

© 1988 Advanced Cardiovascular Systems, Inc.

For peripheral arteriography





ISOVUE®-300
iopamidol injection 61%

Nonionic contrast media that causes less pain than a leading ionic agent.

With Isovue, patients found procedures less painful; physicians saw fewer signs of distress

Isovue-300 is low in osmolality—616 mOsm/kg water.

Using a visual analog scale, patients undergoing peripheral arteriography ranked their pain from "no pain" to "the worst pain I ever had." On a linear scale from zero to 12.4 cm, the mean pain rating for 99 patients given a total of 155 injections of Isovue-300 was 2.3 cm compared with 6.3 cm for 97 patients given a total of 144 injections of the ionic agent diatrizoate meglumine and diatrizoate sodium 52%/8%.

By observing signs of distress, such as movement and/or vocalization, physicians ranked patient distress as being absent, mild, moderate, or severe. When Isovue was compared with diatrizoate meglumine and diatrizoate sodium 52%/8%, the number of injections judged to cause severe distress was 2/299 (1%) compared with 23/293 (8%); moderate distress, 13/299 (4%) compared with 58/293 (20%); mild distress, 59/299 (20%) compared with 94/293 (32%); and no distress, 225/299 (75%) compared with 108/293 (37%), respectively.

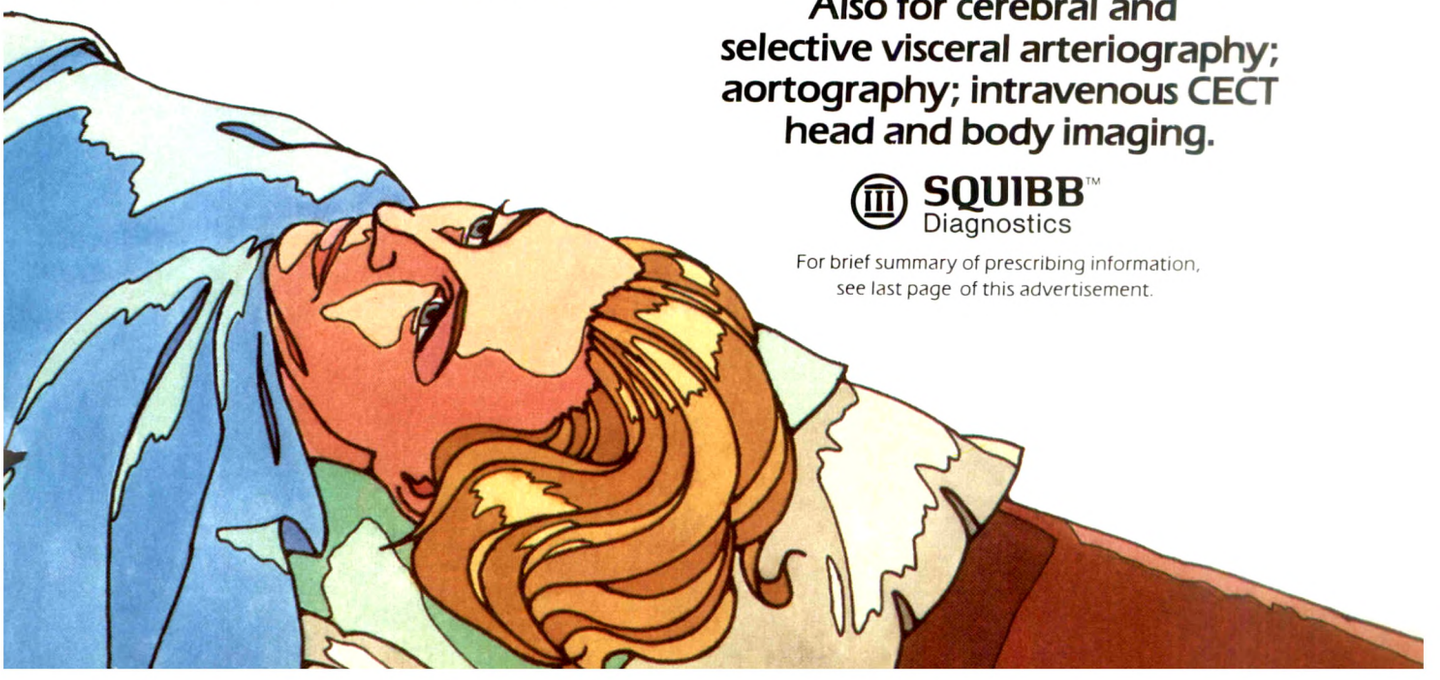
As with all injectable contrast agents, the possibility of severe reactions should be borne in mind. (See brief summary of prescribing information on the last pages of this advertisement for a discussion of CONTRAINDICATIONS, WARNINGS, PRECAUTIONS, and ADVERSE REACTIONS.)

ISOVUE®
iopamidol injection

Nonionic. Low in osmolality. Also for cerebral and selective visceral arteriography; aortography; intravenous CECT head and body imaging.

SQUIBB™
Diagnostics

For brief summary of prescribing information, see last page of this advertisement.



ISOVUE®-300
Iopamidol Injection 61%
ISOVUE®-370
Iopamidol Injection 76%

DESCRIPTION—ISOVUE (iopamidol injection) is a nonionic radiopaque contrast media for diagnostic use. The formulations are stable, aqueous, sterile, and nonpyrogenic solutions for intravascular administration. Each mL of ISOVUE-300 (iopamidol injection 61%) provides 612 mg iopamidol with 1 mg tromethamine and 0.39 mg edetate calcium disodium. The solution contains approximately 0.037 mg (0.002 mEq) sodium and 300 mg organically bound iodine per mL. Each mL of ISOVUE-370 (iopamidol injection 76%) provides 755 mg iopamidol with 1 mg tromethamine and 0.48 mg edetate calcium disodium. The solution contains approximately 0.046 mg (0.002 mEq) sodium and 370 mg organically bound iodine per mL. The pH has been adjusted to 6.5 to 7.5 with hydrochloric acid.

CONTRAINDICATIONS—None.

WARNINGS—Use caution in patients with severely impaired renal function, combined renal and hepatic disease, or anuria, particularly when larger doses are administered. Radiopaque diagnostic contrast agents are potentially hazardous in patients with multiple myeloma or other paraproteinemia, particularly in those with therapeutically resistant anuria. It has been speculated that the combination of the contrast agent and dehydration may be causative of anuria in myelomatous patients. This risk is not a contraindication; however, special precautions are required. Contrast media may promote sickling in individuals who are homozygous for sickle cell disease when injected intravenously or intraarterially. Administration to patients known or suspected of having pheochromocytoma should be performed with extreme caution. If the possible benefits outweigh the considered risks, the procedures may be performed; however, the amount of the medium injected should be kept to an absolute minimum. Assess blood pressure throughout the procedure and have measures for treatment of a hypertensive crisis available. Monitor such patients very closely. Use caution in patients with hyperthyroidism or with an autonomously functioning thyroid nodule because of risk of thyroid storm.

PRECAUTIONS: General—Diagnostic procedures should be carried out under the direction of personnel with the prerequisite training and a thorough knowledge of the particular procedure to be performed. Appropriate facilities should be available for coping with any complication of the procedure, or for emergency treatment of severe reaction to the agent itself. After parenteral administration, competent personnel and emergency facilities should be available for at least 30 to 60 minutes since severe delayed reactions may occur. Preparatory dehydration is dangerous and may contribute to acute renal failure in susceptible patients. *Patients should be well hydrated prior to and following administration.* Reactions to the medium, including serious, life-threatening, fatal, anaphylactoid or cardiovascular reactions, should always be considered (see ADVERSE REACTIONS in the product package insert). Patients at increased risk include those with a history of a previous reaction to a contrast medium, a known sensitivity to iodine per se, and a known clinical hypersensitivity (bronchial asthma, hay fever, and food allergies). Pretesting cannot be relied upon to predict severe reactions and may itself be hazardous for the patient. A thorough medical history with emphasis on allergy and hypersensitivity prior to the injection of any contrast medium may be more predictive and accurate than pretesting. Premedication with antihistamines or corticosteroids to avoid or minimize possible allergic reactions in such patients should be considered. General anesthesia may be indicated in some procedures in selected patients; however, a higher incidence of adverse reactions has been reported in anesthetized patients, which may be attributable to the inability of the patient to identify untoward symptoms, or to the hypotensive effect of anesthesia which can reduce cardiac output and increase the duration of exposure to the agent. Even though the osmolality is low compared to diatrizoate or iothalamate based ionic agents of comparable iodine concentration, the potential transitory increase in the circulatory osmotic load in patients with congestive heart failure requires caution during injection. Observe these patients for several hours following the procedure. In angiographic procedures, be aware of the possibility of dislodging plaques or damaging or perforating the vessel wall during catheter manipulations and contrast medium injection. Test injections to ensure proper catheter placement are suggested.

The inhibitory effects of nonionic contrast media on mechanisms of hemostasis have been shown, in vitro, to be less than ionic contrast media at comparable concentrations. For this reason, standard angiographic procedures should always be followed: angiographic catheters should be flushed frequently, and prolonged contact of blood with contrast in syringes and catheters should be avoided. Perform *selective coronary arteriography* only in those in whom the expected benefits outweigh the procedural risk. The inherent risks of *angiocardiography* in patients with chronic pulmonary emphysema must be weighed against the necessity for performing this procedure. *Angiography* should be avoided whenever possible in patients with homocysfinuria, because of the risk of inducing thrombosis and embolism.

Drug Interactions—Renal toxicity has been reported in a few patients with liver dysfunction who were given oral cholecystographic agents followed by intravascular contrast agents. Administration of intravascular agents should therefore be postponed in any patient with a known or suspected hepatic or biliary disorder who has recently received a cholecystographic contrast agent. Other drugs should not be admixed with iopamidol.

Drug/Laboratory Test Interactions—PBI and radioactive iodine uptake studies will not accurately reflect thyroid function for up to 16 days following administration, however T3 resin uptake and total or free thyroxine (T4) assays are not affected. Any test which might be affected by contrast media should be performed prior to administration of the contrast media.

Carcinogenesis, Mutagenesis, Impairment of Fertility—In animal reproduction studies performed on rats, intravenously administered iopamidol did not induce adverse effects on fertility or general reproductive performance. In studies to determine mutagenic activity, iopamidol did not cause any increase in mutation rates.

Pregnancy Category B—No teratogenic effects attributable to iopamidol have been observed in teratology studies performed in animals. There are, however, no adequate and well controlled studies in pregnant women. It is not known whether iopamidol crosses the placental barrier or reaches fetal tissues. Because animal studies are not always predictive of human response, this drug should be used during pregnancy only if clearly needed. Radiologic procedures involve a certain risk related to the exposure of the fetus to ionizing radiation.

Labor and Delivery—It is not known whether use during labor or delivery has immediate or delayed adverse effects on the labor, the delivery or the newborn.

Nursing Mothers—It is not known whether iopamidol is excreted in human milk. Use caution when contrast media are administered to nursing women because of potential adverse reactions; consideration should be given to temporarily discontinuing nursing.

Pediatric Use—Safety and effectiveness in children have not been established.

ADVERSE REACTIONS—Usually mild to moderate, self-limited and transient. In angiocardiography (597 patients), the adverse reactions with an estimated incidence of one percent or higher are: hot flashes 3.4%; angina pectoris 3.0%; flushing 1.8%; bradycardia 1.3%; hypotension 1.0%; hives 1.0%. Intravascular injection is frequently associated with the sensation of warmth and pain, especially in peripheral arteriography; pain and warmth are less frequent and less severe with ISOVUE (iopamidol injection) than with diatrizoate meglumine and diatrizoate sodium injection. The following table of incidence of reactions is based on clinical studies with ISOVUE in about 1760 patients.

Adverse Reactions
Estimated Overall Incidence

System	>1%	≤1%
Cardiovascular	none	tachycardia hypotension hypertension myocardial ischemia circulatory collapse S-T segment depression bigeminy extrasystoles ventricular fibrillation angina pectoris bradycardia transient ischemic attack thrombophlebitis
Nervous	pain (2.2%) burning sensation (1.4%)	vasovagal reaction tingling in arms grimace faintness
Digestive	nausea (1.2%)	vomiting anorexia
Respiratory	none	throat constriction dyspnea pulmonary edema
Skin and Appendages	none	rash urticaria pruritus flushing
Body as a Whole	hot flashes (1.5%)	headache fever chills excessive sweating back spasm
Special Senses	none	taste alterations warmth in throat/arms/chest nasal congestion visual disturbances
Urogenital	none	urinary retention

Regardless of the agent employed, overall estimated incidence of serious adverse reactions is higher with *coronary arteriography* than with other procedures. Cardiac decompensation, serious arrhythmias, or myocardial ischemia or infarction may occur during *coronary arteriography and left ventriculography.* Following coronary and ventricular injections, certain electrocardiographic changes (increased QTc, increased R-R, T-wave amplitude) and certain hemodynamic changes (decreased systolic pressure) occurred less frequently with ISOVUE (iopamidol injection) than with diatrizoate meglumine and diatrizoate sodium injection; increased LVEDP occurred less frequently after ventricular iopamidol injections. In *aortography,* the risks of procedures also include injury to the aorta and neighboring organs, pleural puncture, renal damage including infarction and acute tubular necrosis with oliguria and anuria, accidental selective filling of the right renal artery during the translumbar procedure in the presence of preexisting renal disease, retroperitoneal hemorrhage from the translumbar approach, and spinal cord injury and pathology associated with the syndrome of transverse myelitis. Adverse effects reported in literature include arrhythmia, arterial spasms, hematuria, periorbital edema, involuntary leg movement, malaise, and triggering of deglutition; some of these may be procedural. Other reactions due to procedural hazards include hemorrhage or pseudoaneurysms at the puncture site, brachial plexus palsy following axillary artery injections, chest pain, myocardial infarction, and transient changes in hepatorenal chemistry tests; and rarely arterial thrombosis, displacement of arterial plaques, venous thrombosis, dissection of the coronary vessels and transient sinus arrest.

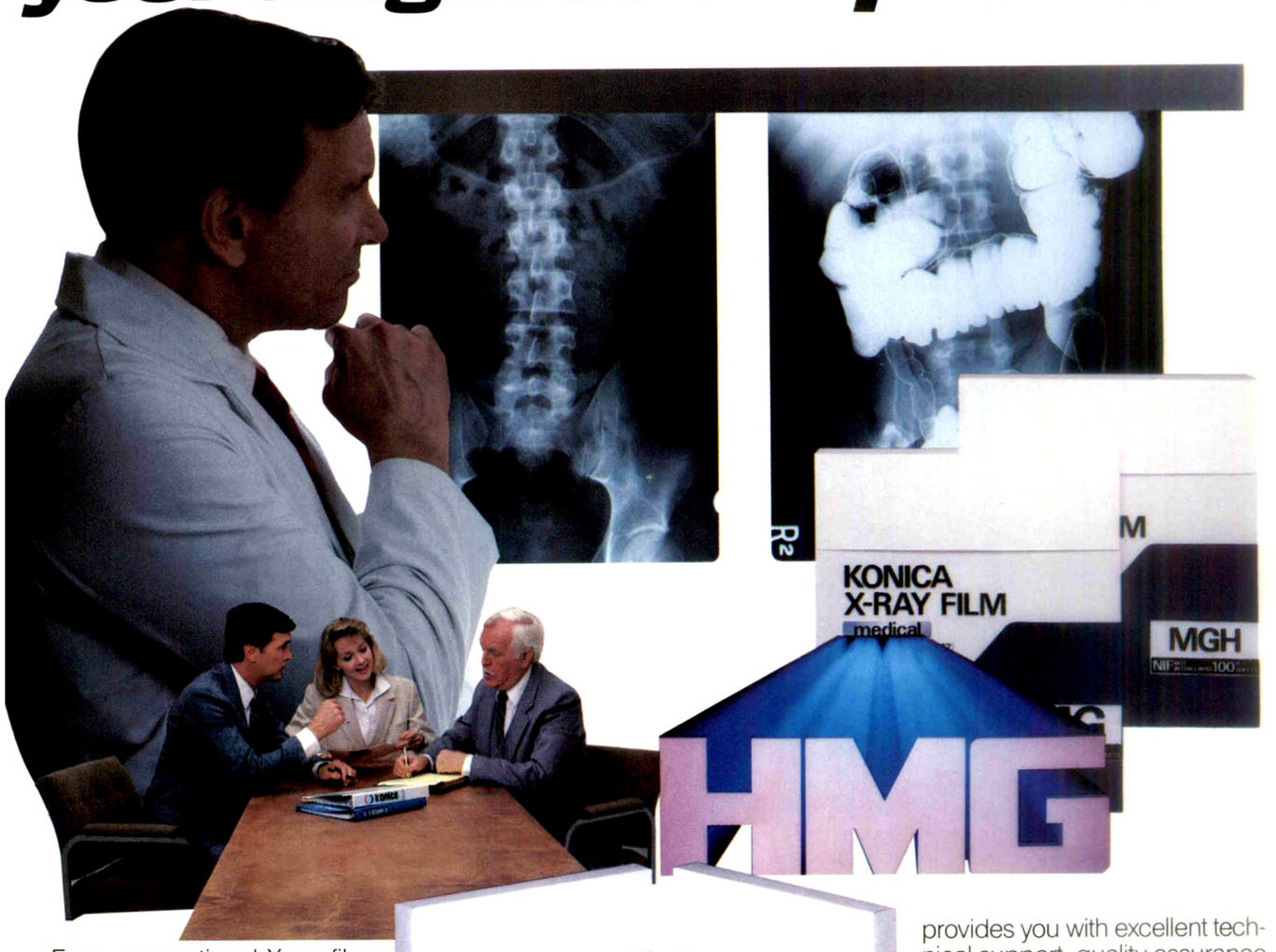
General Adverse Reactions To Contrast Media—Reactions known to occur with parenteral administration of iodinated ionic contrast agents (see the listing below) are possible with any nonionic agent. Life-threatening reactions and fatalities, mostly of cardiovascular origin, have occurred. Reported incidences of death from the administration of other iodinated contrast media range from 6.6 per 1 million (0.00066%) to 1 in 10,000 patients (0.01%). Foreign experience in approx. 2.4 million patients receiving iopamidol suggest a lower risk of mortality. Most deaths occur during injection or 5 to 10 minutes later, the main feature being cardiac arrest with cardiovascular disease as the main aggravating factor. Isolated reports of hypotensive collapse and shock (est. 0.005%) are found in the literature. Experience with iopamidol suggests there is much less discomfort (e.g., pain and/or warmth) with peripheral arteriography. Fewer changes are noted in ventricular function after ventriculography and coronary arteriography. The reported incidence of adverse reactions to contrast media in patients with a history of allergy is twice that for the general population; patients with a history of previous reactions to a contrast medium are three times more susceptible. Most reactions to intravascular contrast agents appear within 1-3 minutes after the start of injection, but delayed reactions may occur (see PRECAUTIONS, General). Adverse reactions reported with other intravascular contrast agents and theoretically possible with iopamidol include: *Cardiovascular:* vasodilation, cerebral hematomas, petechiae; *Nervous:* paresthesia, dizziness, convulsions, paralysis, coma; *Respiratory:* increased cough, asthma, laryngeal edema, pulmonary edema, bronchospasm, rhinitis; *Skin and Appendages:* injection site pain usually due to extravasation and/or erythematous swelling, skin necrosis; *Urogenital:* osmotic nephrosis of proximal tubular cells, renal failure, pain; *Special Senses:* bilateral ocular irritation; lacrimation; conjunctival chemosis, infection, and conjunctivitis; *Other:* neutropenia, thrombophlebitis, flushing, pallor, weakness, severe retching and choking, wheezing, cramps, tremors, and sneezing.

For full prescribing information consult package insert. (J3-652C)

Under license from Bracco Industria Chimica S.p.A. U.S. Patent #4,001,323

© 1986 E.R. Squibb & Sons, Inc., Princeton, NJ 646-503 Issued: Sept. 1986

Konica.... sharpening your diagnostic capabilities.

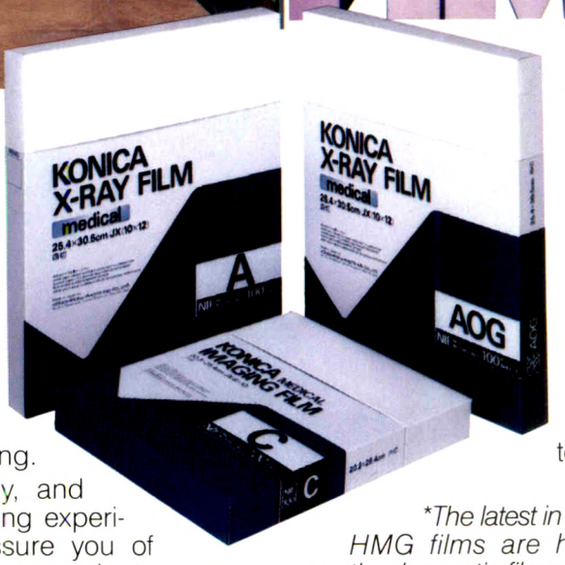


From conventional X-ray films to state-of-the-art HMG* imaging technology, Konica, a world leader in medical imaging films offers a multitude of ways to sharpen your diagnostic capabilities.

Konica offers imaging films for all diagnostic needs, from general radiography through CT, Nuclear Medicine, Ultrasound, Digital Radiology and Magnetic Resonance Imaging.

Our leading-edge technology, and over 112 years of manufacturing experience and quality control assure you of consistently superior imaging products. And to optimize your imaging results, Konica provides you with excellent technical support, quality assurance and educational programs for your staff.

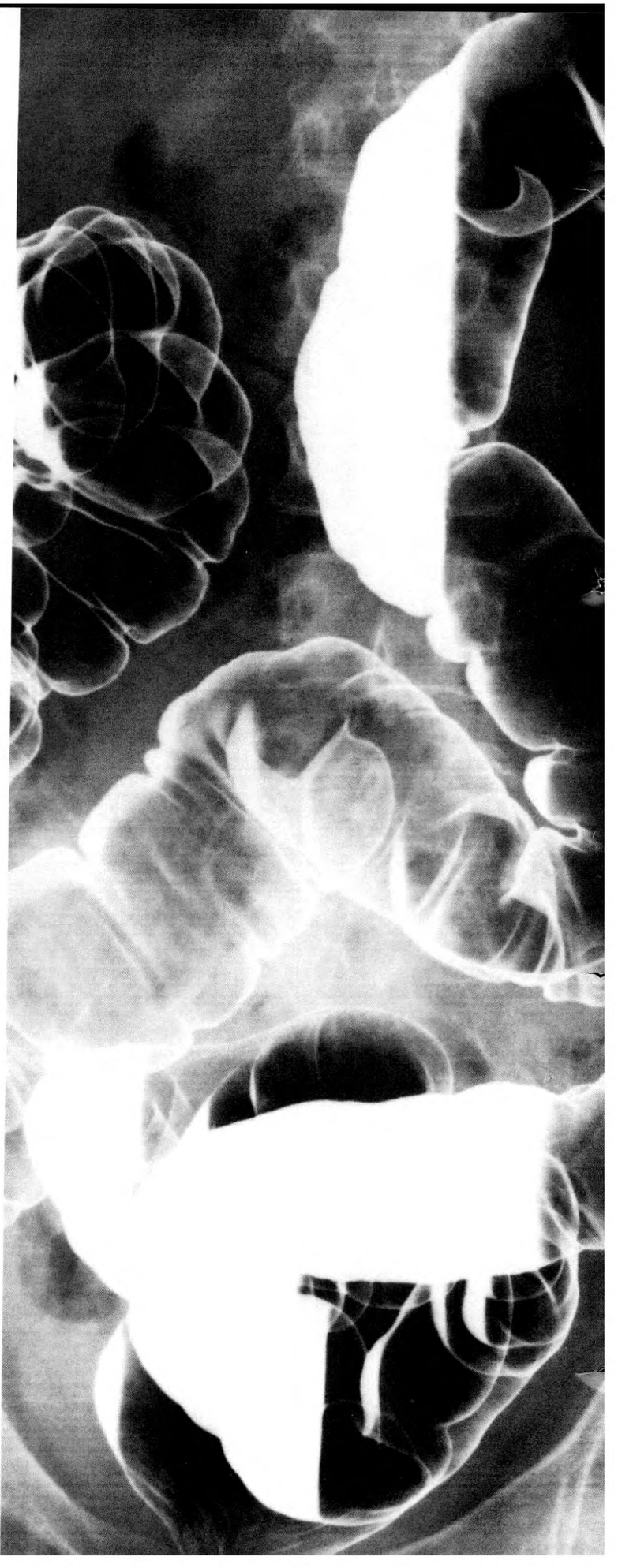
If you'd like to sharpen your diagnostic capabilities, take a good look at Konica. We'll show you how our technology, film products and support services clearly make a difference. Konica-leading medical imaging into the future. Konica Medical Corporation, 411 Newark Pompton Turnpike, Wayne, N.J. 07470



The latest in advanced film technology. Konica HMG films are high-speed, higher resolution, orthochromatic films designed for maximum detail visibility and minimum image graininess.

Konica
The Image of Perfection.

The clear case for the E-Z-EM Prep System.

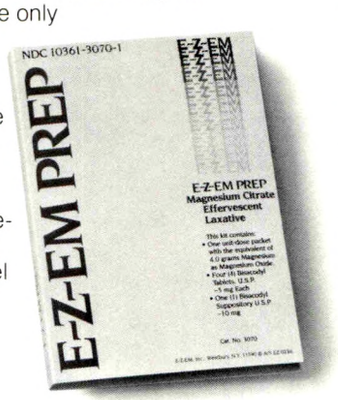


Clear, clean, clinically sound X- ays... the ultimate test of proper bowel preparation.

It's only common sense, then, that the best prepping regimen is the one that consistently yields the most diagnostic X-rays. That's the simple concept behind the design of our E-Z-EM Prep and E-Z-EM Prep II kits.

Not just a prep, but a prepping system.

Proper and thorough bowel cleansing means more than just supplying a series of laxative products. That's why our prep kits are only *part* of a comprehensive system, one specifically aimed at increasing the effectiveness of the entire bowel cleansing program.



enteric coated Bisacodyl tablets and one Bisacodyl suppository. Along with our gentle hydration regimen, these components effectively cleanse the small bowel, colon, and recto-sigmoid.

When a cleansing enema is desired, the E-Z-EM Prep II kit is available. It replaces the suppository with an enema bag.

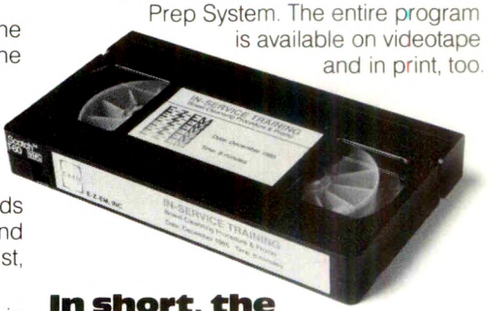
Several schedules, in several languages.

For patient comfort, E-Z-EM recommends using a 24-hour prepping schedule. And each kit comes with a handy check-off list, available in a variety of languages.

When necessary, thorough cleansing is possible using a condensed time schedule with increased hydration.

Complete in-service training.

Our technical representatives are available to train your nursing staff in using the E-Z-EM Prep System. The entire program is available on videotape and in print, too.



In short, the only complete prepping system.

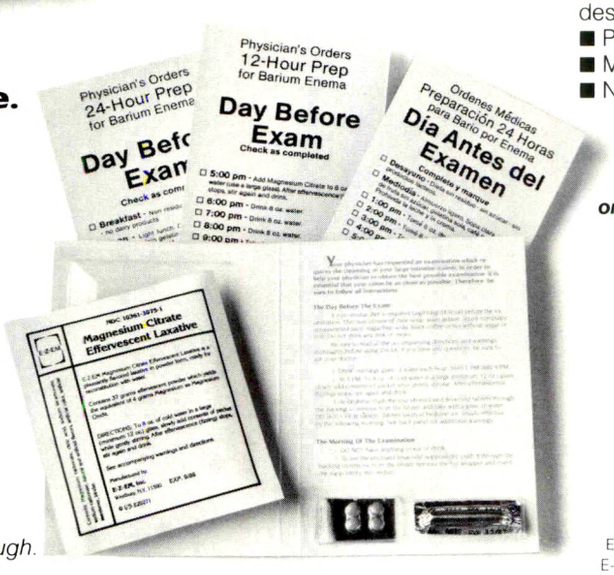
The E-Z-EM Prep System has been designed for: ■ Effective cleansing ■ Patient comfort ■ Ease of use ■ Minimal storage requirements ■ No breakage.

For free samples and additional information, contact your local representative, or call E-Z-EM toll-free at 800-645-3052. In New York call 516-333-8230.

A good-tasting Magnesium Citrate.

E-Z-EM Magnesium Citrate has a pleasant orange flavor, which can significantly improve patient compliance.

E-Z-EM Magnesium Citrate contains no alcohol and is low in sodium. It comes packaged in single dose, foil-wrapped packets which eliminate breakage and greatly reduce storage requirements.



Two complete prep kits.

The E-Z-EM Prep System is *thorough*. In addition to Magnesium Citrate, each E-Z-EM Prep kit includes four

E-Z-EM®
E-Z-EM, Inc.
7 Portland Avenue
Westbury, N.Y. 11590

A complete prepping system for the cost of a prep kit.

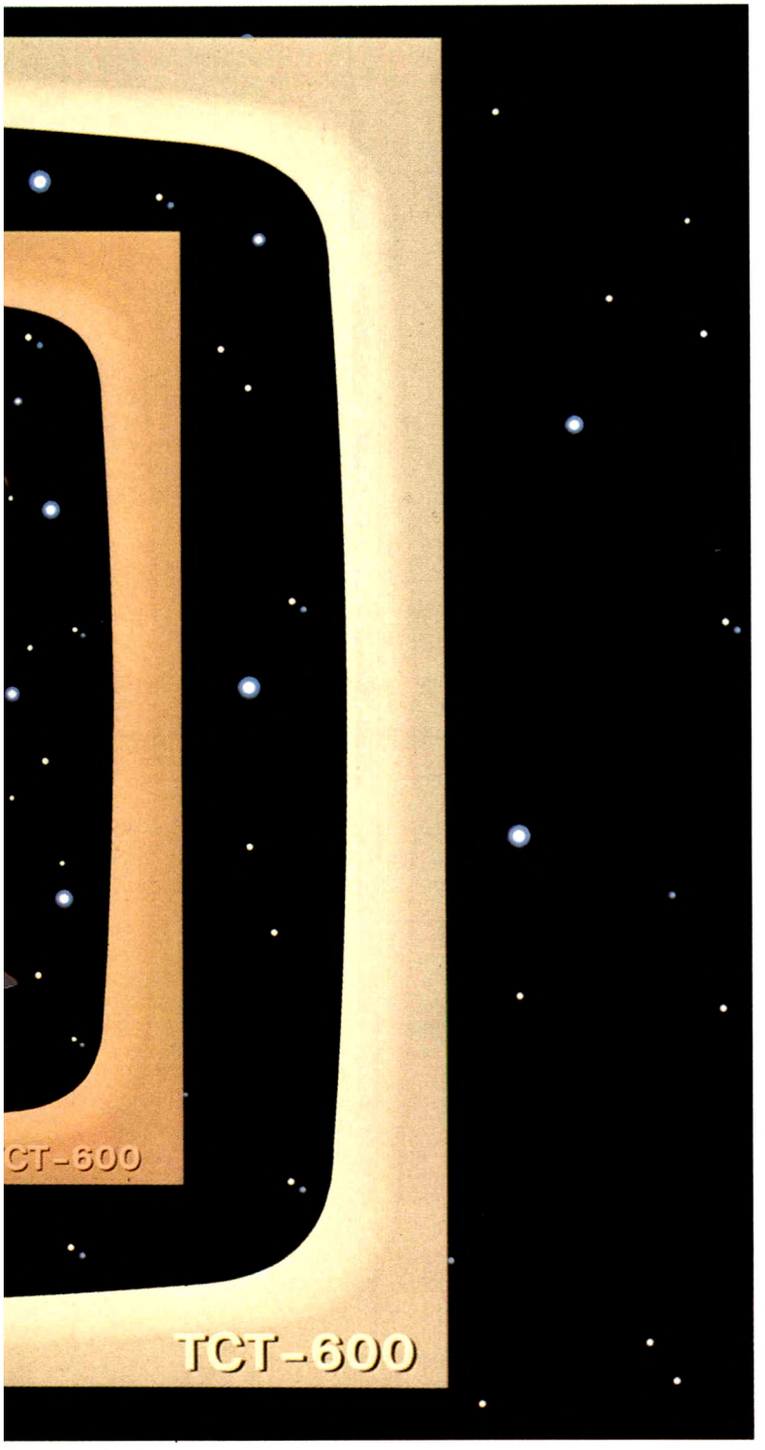
E-Z-EM Prep: Catalog No. 3070 (Packaged 50 kits/carton)
E-Z-EM Prep II: Catalog No. 3072 (Packaged 48 kits/carton)
E-Z-EM Magnesium Citrate: Catalog No. 3075 (Packaged 100 packets/carton)

©E-Z-EM, Inc. 1986

Unparalleled image q



ality. Time after time.



Toshiba's TCT-600 Series

Toshiba's **TCT-600 Series Whole Body CT Scanners** are just what you would expect from a world leader in diagnostic imaging: fast, flexible, and expandable. And that's just what you should ask for. But Toshiba's TCT-600 Series give you even more:

1. Image quality and performance second to none.
2. Reliability, flexibility, and easy "one-touch command" operations for high throughput.
3. System expandability for widening applications.

Ask for more. Ask for the image quality and level of performance you get with Toshiba. Time after time after time.

For more information about the TCT-600 Series Whole Body Scanners, call or write: Toshiba Medical Systems, 2441 Michelle Drive, Tustin, CA 92680. In California, call (714) 669-5419. Outside California, call toll-free **(800) 421-1968.** In Canada, call (416) 298-6100.

In Touch with Tomorrow

TOSHIBA

GLOBAL IMAGING SPECIALISTS

LONG BEACH VETERANS ADMINISTRATION MEDICAL CENTER
UNIVERSITY OF CALIFORNIA, IRVINE

The Long Beach Veterans Administration Medical Center and the University of California, Irvine are seeking a board certified radiologist for a staff position at the Long Beach Veterans Administration Medical Center. A position with an academic rank appropriate to experience is expected in the faculty of the Department of Radiological Sciences at the University of California, Irvine.

The residency program is integrated between the two institutions, and teaching and research programs are closely coordinated. Specific training in ultrasound, body and head CT scanning and in neuro-radiology is necessary. Teaching experience and demonstrated interest in research are desirable. Salary is commensurate with experience.

The University of California, Irvine is an Equal Opportunity and Affirmative Action Employer. Interested candidates should forward their curriculum vitae and appropriate date of availability to:

Richard M. Friedenberg, M.D.
Professor and Chairman
Department of Radiological Sciences
University of California, Irvine Medical Center
101 City Drive, South
Orange, CA 92668

INTERVENTIONAL RADIOLOGIST

Aramco's Dhahran Health Center in Saudi Arabia needs an Interventional Radiologist to join a staff of seven doing general diagnostic radiology, specialty diagnostic procedures including ultrasound nuclear medicine, computed tomography and interventional medicine.

The modern 483-bed hospital has been JCAH accredited since 1956 and has all major specialty services as well as most sub-specialties. The DHC functions as a referral center for a patient population of approximately 200,000. The medical services organization includes four district clinics, one with a new 80-bed hospital.

The position requires American Board certification in Radiology and two years interventional radiology experience.

This overseas position offers an exciting opportunity along with a competitive salary and benefits. For immediate consideration, **call Velma Guy at 1-800-231-7577 or in Texas at (713) 432-8060.** Or send resume to: **Velma Guy, Aramco Services Company, Dept. 06G-007-6, P.O. Box 4530, Houston, Texas 77210-4530.**

ARAMCO
SERVICES COMPANY

RADIOLOGY/NUCLEAR MEDICINE

Excellent opportunity for radiologist with specialty training in nuclear medicine to develop and expand the nuclear medicine department within Kaiser-Permanente. Experience in the area of cardiac nuclear medicine is a plus.

Practice located in midtown location within 10 minutes of downtown Denver. Hospitals within walking distance. Established group practice HMO with excellent benefits including fully paid professional liability insurance.

For additional information, please contact:

Toby P. Cole, M.D., Executive Medical Director, Colorado Permanente Medical Group, P.C., 2045 Franklin Street, 11th Floor, Denver, Colorado 80205 (303) 861-3262. EOE

LONG BEACH VETERANS ADMINISTRATION MEDICAL CENTER
UNIVERSITY OF CALIFORNIA, IRVINE

The Long Beach Veterans Administration Medical Center and the University of California, Irvine are seeking a board certified radiologist for a staff position at the Long Beach Veterans Administration Medical Center. A position with an academic rank appropriate to experience is expected in the faculty of the Department of Radiological Sciences at the University of California, Irvine. The residency program is integrated between the two institutions, and teaching and research programs are closely coordinated.

Fellowship experience in neuro-radiology is necessary. Teaching experience and demonstrated interest in research are desirable. Salary is commensurate with experience.

The University of California, Irvine is an Equal Opportunity and Affirmative Action Employer. Interested candidates should forward their curriculum vitae and approximate date of availability to:

Richard M. Friedenberg, M.D.
Professor and Chairman
Department of Radiological Sciences
University of California, Irvine Medical Center
101 City Drive, South
Orange, CA 92668

How to reduce the costs of bowel preparation before and after the X-ray



Before

Evac-Q-Kwik® helps keep hospital costs down by eliminating the staff time and labor involved in giving enemas. And everything needed for effective bowel evacuation is contained in one cost-effective kit.



Nurses appreciate Evac-Q-Kwik because it can be administered during a single shift and completed during one 6-hour period. Patients prefer the simple, comfortable Evac-Q-Kwik procedure, too. Evac-Q-Kwik contains no sugar, no alcohol, and is low in sodium.

After



Evac-Q-Kwik is the ideal bowel prep for today's cost-conscious climate. It effectively cleans the colon for clear X-rays *the first time*, to reduce the need for expensive, time-consuming retakes that escalate hospital costs.

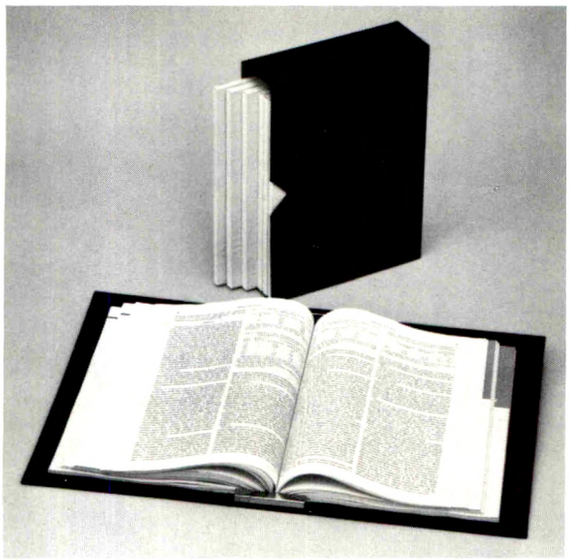
Evac-Q-Kwik®



Adria®

Adria Laboratories
Columbus, OH 43215

078508



Protect your copies of

AJR: AMERICAN JOURNAL OF ROENTGENOLOGY

with Jesse Jones Binders or Files

Keep your journals clean, orderly, and readily accessible with Jesse Jones Binders or Files. Two Binders or two box style Files are all you need to accommodate a full year's worth of issues. Both Binders and Files are handsomely made with rich black leatherette covers and gold leaf embossed lettering.

Jesse Jones Binders open flat for easy reading and reference and are economically priced at only $9.95 each; 3 for $27.95, or 6 for $52.95 postpaid. The rugged, compact box Files are only $7.95 each; 3 for $21.95, or 6 for $39.95. Add $1.00/unit postage and handling. (Outside the U.S. add $2.50/unit.)

For charge orders call toll free 1-800-972-5858. ($15.00 minimum).

Free gold transfer slips included for indexing volume and year.

Please allow four to five weeks for delivery.

TO: Jesse Jones Industries
499 E. Erie Avenue, DEPT. AJR
Philadelphia, PA 19134

I enclose my check or money order for $_____
(PA residents add 6% sales tax)

Send me ____ ☐ Files ☐ Binders for my journals

Name

Address (will not ship to P.O. Box)

City/State/Zip

Satisfaction guaranteed.

INDEX TO ADVERTISERS

Ackrad Laboratories, Inc. A24

Acuson A16, A17, A18, A19

Adria Laboratories A45

Advanced Cardiovascular Systems A35

Aramco Services Company A44

Colorado Permanente Medical Group A44

Eastman Kodak A5, A6, A7, A8

E-Z-EM Company . . . . . Cover 2, A40, A41

Konica Medical Corporation A39

Lorad Medical Systems, Inc. A9

Medi-Tech A21, A23, A25

Precise Optics/PME, Inc. A2

Purdue Frederick Company A34

Pyne Corporation . . . . . Cover 3

Shiley, Inc. A12, A13

Siemens Corporation A14, A15

Squibb A36, A37, A38

S & S X-Ray A33

Tecnomed USA A4

Tobias Associates A24

Toshiba Medical Systems . . A10, A11, A42, A43

University of California-Irvine A44

Winthrop Laboratories . . . A27, A28, A29, A30, A31, A32

Xerox Corporation A26

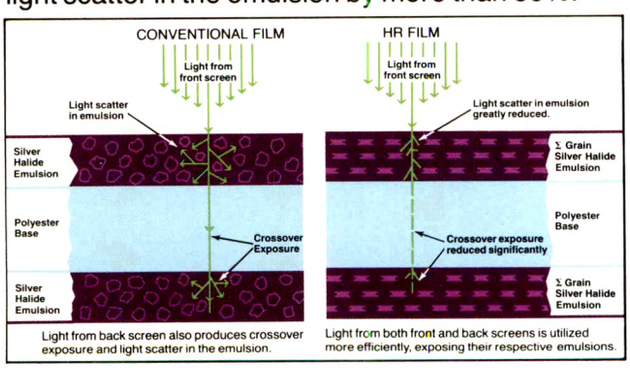
We try to present an accurate index. Occasionally this may not be possible because of a last-minute change or an omission.

THE SHAPE OF SHARPNEΣΣ



Fuji's new HR Series of Orthochromatic Medical X-ray films featuring new Σ (sigma) grain technology

Through the use of new silver halide formation technology and higher optimized amounts of spectral sensitizing dye, Fuji's new Sigma Grain Technology can reduce cross-over exposure and light scatter in the emulsion by more than 50%!



The very small (one micron mean diameter) Σ grains are systematically arranged in the emulsion with their large hexagonal faces oriented toward the intensifying screen for maximum light absorption. The result is increased resolution and extremely fine grain with no loss of film speed.

Prove it to yourself

Simply put, the Fuji HR series of medical x-ray films provide the highest resolution images obtainable today. Call your Pyne representative today toll free 1-800-431-1850 (In NY 914-834-4567)

THE REASON FOR CHANGE

PYNE CORPORATION
20 North Avenue, Larchmont, NY 10538

Volume 147 **American Journal of Roentgenology** October 1986

SPECIAL ARTICLE

657 **Vascular complications after liver transplantation: a 5-year experience.** *Wozney P, Zajko AB, Bron KM, Point S, Starzl TE*

ROSCOE E. MILLER AWARD, SOCIETY OF GASTROINTESTINAL RADIOLOGY

665 **Monitoring hepatic cryosurgery with sonography.** *Onik G, Kane R, Steele G, et al.*

PULMONARY RADIOLOGY

670 **Case report. Mosaic oligemia simulating pulmonary infiltrates on CT.** *Martin KW, Sagel SS, Siegel BA*

674 **Pictorial essay. Thoracic venous anatomy.** *Godwin JD, Chen JTT*

685 **Digital subtraction venography in central venous obstruction.** *Benenati JF, Becker GJ, Mail JT, Holden RW*

BREAST RADIOLOGY

689 **Screening mammography: referral practices of Los Angeles physicians.** *Bassett LW, Bunnell DH, Cerny JA, Gold RH*

GASTROINTESTINAL RADIOLOGY

693 **Radiologic and manometric correlation in "nutcracker esophagus."** *Ott DJ, Richter JE, Wu WC, Chen YM, Gelfand DW, Castell DO*

697 **Radiographic efficacy in gastric ulcer: comparison of single-contrast and multiphasic examinations.** *Ott DJ, Chen YM, Gelfand DW, Wu WC*

701 **Radiologic findings of linear gastric erosions.** *Momoshima S, Imai Y, Sugino Y, Sekine Y, Kumakura K*

705 **CT of appendicitis.** *Balthazar EJ, Megibow AJ, Hulnick D, Gordon RB, Naidich DP, Beranbaum ER*

711 **Hepatic hemangioma: dynamic bolus CT.** *Freeny PC, Marks WM*

721 **Chronic acalculous gallbladder disease: multiimaging evaluation with clinical-pathologic correlation.** *Raptopoulos V, Compton CC, Doherty P, et al.*

725 **Sonography in the diagnosis of hepatic artery aneurysms.** *Athey PA, Sax SL, Lamki N, Cadavid G*

729 **Bile-duct dilatation after laparotomy: a potential effect of intestinal hypomotility.** *Raptopoulos V, Smith EH, Cummings T, Silva W, Karellas A*

GENITOURINARY RADIOLOGY

732 **Review article. MRI of the bladder and prostate.** *Lee JKT, Rholl KS*

737 **Case report. Reversible renal fibromuscular dysplasia.** *Nemcek AA Sr, Holmburg CE*

MUSCULOSKELETAL RADIOLOGY

739 **Case report. Intraosseous glomus tumor: report of a case and review of the literature.** *Bjorkengren AG, Resnick D, Haghighi P, Sartoris DJ*

742 **Case report. Calcific tendinitis of the longus coli: diagnosis by CT.** *Hall FM, Docken WP, Curtis HW*

744 **Case report. Inferior lumbar (Petit's) hernia.** *Lawdahl RB, Moss CN, Van Dyke JA*

NEURORADIOLOGY

747 **Primary central nervous system lymphoma: CT and pathologic correlation.** *Lee Y-Y, Bruner JM, Van Tassel P, Libshitz HI*

753 **Minimal asymmetry of the brain: a normal variant.** *Shapiro R, Galloway SJ, Shapiro MD*

757 **Lumbar herniated disk disease and canal stenosis: prospective evaluation by surface coil MR, CT, and myelography.** *Modic MT, Masaryk T, Boumphrey F, Goormastic M, Bell G*

767 **Cystic necrosis of the spinal cord in compressive cervical myelopathy: demonstration by iopamidol CT-myelography.** *Jinkins JR, Bashir R, Al-Mefty O, Al-Kawi MZ, Fox JL*

777 **Cognitive and affective changes after myelography: a comparison of metrizamide and iohexol.** *Ratcliff G, Sandler S, Latchaw R*

782 **Technical note. The anatomic basis of the pseudotumor of the nasal cavity.** *Sistrom CL, Keats TE, Johnson CM III*

PEDIATRIC RADIOLOGY

785 **Imaging the pediatric liver: MRI and CT.** *Weinreb JC, Cohen JM, Armstrong E, Smith T*

791 **Interventional genitourinary radiology in children: a review of 61 procedures.** *Ball WS Jr, Towbin R, Strife JL, Spencer R*

797 **Fetal omphalocele and gastroschisis: pitfalls in sonographic diagnosis.** *Lindfors KK, McGahan JP, Walter JP*

801 **Neonatal renal candidiasis: sonographic diagnosis.** *Kintanar C, Cramer BC, Reid WD, Andrews WL*

806 **Case report. Enterocyst formation: a late complication of neonatal necrotizing enterocolitis.** *Ball TI, Wyly JB*

NUCLEAR MEDICINE

809 **Effect of chronicity of infection on the sensitivity of the In-III labeled leukocyte scan.** *Datz FL, Thorne DA*

813 **Case report. Utility of In-III labeled leukocyte imaging in acute acalculous cholecystitis.** *Datz FL*

815 **Technetium-99m pyrophosphate imaging in acute renal failure associated with nontraumatic rhabdomyolysis.** *Patel R, Mishkin FS*

819 **Case report. False-positive thallium-201 parathyroid scan of the mediastinum in Hodgkin's lymphoma.** *Winzelberg GG, Melada GA, Hydovitz JD*

INTERVENTIONAL RADIOLOGY

822 **Technical note. Percutaneous gastrostomy for jejunal feeding: a new technique.** *Alzate GD, Coons HG, Elliott J, Carey PH*

826 **Case report. Percutaneous gastrostomy: applications in gastric carcinoma and gastroplasty stoma dilatation.** *Wills JS*

828 **Technical note. A modified Cope introducer set for rapid insertion of a safety wire.** *Jeffrey RB Jr*

830 **Technical note. The universal stent introducer: a simplified approach to antegrade ureteral stent insertion.** *Lee WJ, Rich M*

832 **Case report. Shearing of percutaneous nephrostomy catheter during indwelling ureteral stent placement.** *Sussman SK, Oke EJ, Perlmutt LM, Dunnick NR*

834 **Case report. Successful treatment of superior vena cava syndrome by venous angioplasty.** *Sherry CS, Diamond NG, Meyers TP, Martin RL*

836 **Case report. Short-term prophylaxis of pulmonary embolism by using a retrievable vena cava filter.** *Darcy MD, Smith TP, Hunter DW, Castaneda-Zuniga W, Lund G, Amplatz K*

MISCELLANEOUS

839 **Renografin-60 for urography: effect on serum, electrolytes and proteins in adults.** *Olutola PS, Hutton L, Karlik S, Henderson AR*

843 **MRI of the spleen: normal appearance and findings in sickle-cell anemia.** *Adler DD, Glazer GM, Aisen AM*

846 **Case report. Extramedullary hematopoeisis in acute lymphocytic leukemia masquerading as hepatic, renal, and splenic microabscesses.** *Kopecky KK, Moriarty AT, Antony AC, Baker MK*

848 **Technical note. The value of a worksheet in reporting body-CT examinations.** *Kinard RE, Orrison WW, Brogdon BG*

HISTORY OF RADIOLOGY

850 **Early American radiology: the pioneer years.** *DiSantis DJ*

COMMENTARY

854 **Should we X-ray Halloween candy?** *Calvanese J*

EDITORIAL

856 **The diffusion of MRI in the United States: what is fact and what is speculation.** *Evens RG*

OTHER CONTENT

664 **ARRS 1987 meeting**
704 **Forthcoming articles**
784 **Memorial**
858 **Letters**
863 **Abstracts**
865 **Society for Pediatric Radiology Abstracts**
874 **News**
877 **Classified ads**
Book reviews 696, 720, 728, 766, 776
A2 **Guidelines for authors**
A20 **American Roentgen Ray Society information**

1987 ARRS Meeting: April 26–May 1, Miami Beach, FL

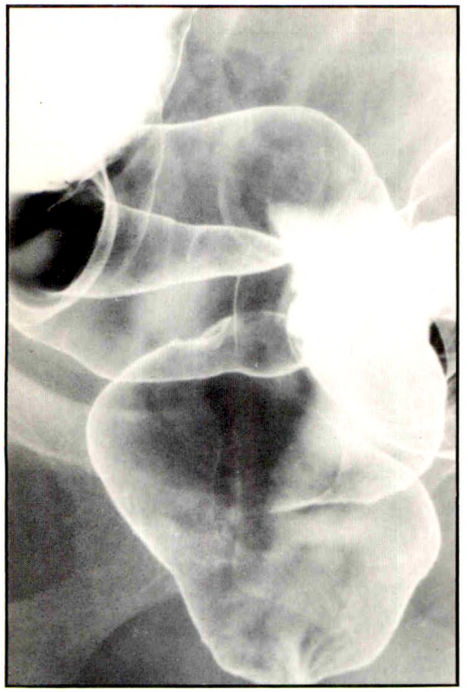
Acc.
18.9.87

AJR

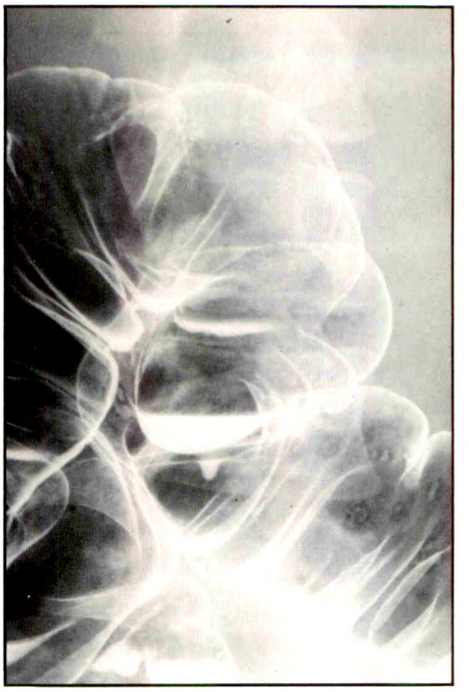
American
Journal of
Roentgenology

M.D. UNIVERSITY OF MEDICINE LIBRARY

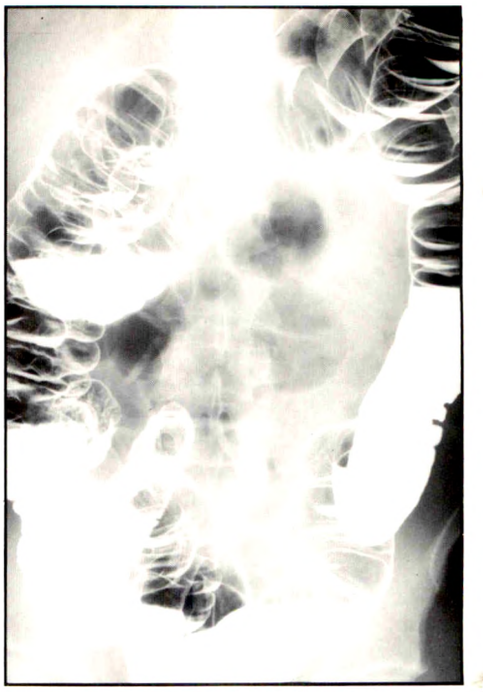
November 1986



LIQUID POLIBAR™
X-Ray courtesy of Dr. Alec J. Megibow
N.Y.U. Medical Center University Hospital
New York, NY 10016



E-Z-AC™
X-Ray courtesy of Dr. Igor Laufer
Hospital of the University of Pennsylvania
Philadelphia, PA 19104



LIQUID POLIBAR™ PLUS
X-Ray courtesy of Dr. David W. Gelfand
Bowman Gray School of Medicine, Wake Forest University
Winston-Salem, NC 27102

Three bariums for superior air-contrast results.

Air Contrast Colon: The procedure of choice with the systems of your choice.

Liquid Polibar™

The original air contrast colon barium with superb coating characteristics. Optimum viscosity assures consistent even coating throughout. Truly the bench mark formulation for air contrast studies.

E-Z-AC™

This fast flowing liquid barium reaches the splenic flexure in only 20 to 30 seconds. Specifically formulated for air contrast procedures where a cleansing enema has not been administered that morning.



Introducing: Liquid Polibar™ Plus

The classic Liquid Polibar formulation modified to achieve a faster flow rate. It has the excellent coating characteristics that you expect from a Polibar formula but is more attuned to the speed necessary in the modern radiology department. Polibar Plus—increased speed and diagnostic consistency.

For samples and additional information, please contact your local E-Z-EM distributor or call E-Z-EM directly.

E-Z-EM®

E-Z-EM, Inc. 7 Portland Avenue, Westbury, NY 11590 516-333-8230 800-645-3052

© E-Z-EM, Inc. 1985

Official Journal of the American Roentgen Ray Society

AJR

American Journal of Roentgenology
Diagnostic Imaging and Related Sciences

Editor-In-Chief Robert N. Berk, *San Diego, California*

Editor Emeritus Melvin M. Figley, *Seattle, Washington*

Associate Editors Alan J. Davidson, *Washington, District of Columbia*
Saskia von Waldenburg Hilton, *San Diego, California*
Juan M. Taveras, *Boston, Massachusetts*

Assistant Editors William L. Ashburn, *San Diego, California*
Charles C. Berry, *San Diego, California*
William G. Bradley Jr., *Pasadena, California*
Edward Buonocore, *Knoxville, Tennessee*
Peter L. Cooperberg, *Vancouver, British Columbia*
Peter Doubilet, *Boston, Massachusetts*
N. Reed Dunnick, *Durham, North Carolina*
Ronald G. Evens, *St. Louis, Missouri*
Henry I. Goldberg, *San Francisco, California*
William R. Hendee, *Chicago, Illinois*
John R. Hesselink, *San Diego, California*
Charles B. Higgins, *San Francisco, California*
Helen C. Redman, *Dallas, Texas*
Donald L. Resnick, *San Diego, California*
Stewart R. Reuter, *San Antonio, Texas*
Stuart S. Sagel, *St. Louis, Missouri*
Edward A. Sickles, *San Francisco, California*
Eric vanSonnenberg, *San Diego, California*

Editorial Staff: Gita S. Braude, *managing editor*; Elizabeth A. Whalen, Barbara Rose, and Linda Wood, *manuscript editors*; Nancy Rydbeck, *administrative assistant*; Sandra Wood, *administrative secretary*; Fay Lau, *secretary*.

All business correspondence, including display (not classified) advertising, subscriptions, address changes, reprints, and permission requests should be addressed to Williams & Wilkins, 428 East Preston Street, Baltimore, MD 21202. Correspondence regarding editorial matters and classified advertising should be addressed to the editorial office, AJR, 2223 Avenida de la Playa, Suite 200, La Jolla, CA 92037. For manuscript submission, see Guidelines for Authors, next page. Undelivered or damaged copies replaced within 60 days of publication; 90 days for foreign subscribers. Allow 90 days for address changes.
AJR AMERICAN JOURNAL OF ROENTGENOLOGY (ISSN 0361 803X) is published monthly by American Roentgen Ray Society, 428 E. Preston Street, Baltimore, MD 21202. Annual dues include $50 for journal subscription. Second class postage paid at Baltimore, MD and at additional mailing offices. Postmaster send address changes (Form 3579) to Williams & Wilkins, 428 East Preston St., Baltimore, MD 21202. Subscription rates $90 ($120 foreign); institutions $100 ($130 foreign); in training $25; single copy $14 ($17). Japanese Yen price is available from our sole agent USACO Corporation, 13-12, Shimbashi 1-Chome, Minato-Ku, Tokyo 105, Japan, telephone 03-502-6471. Airmail rates furnished on request. Indexed by *Current Contents* and *Index Medicus*.
Copyright © 1986 by American Roentgen Ray Society.
0361-803X/86$2.00

AJR Guidelines for Authors

Address new and revised manuscripts, correspondence, and classified ads to:

AJR Editorial Office
2223 Avenida de la Playa, Suite 200
La Jolla, CA 92037
telephone: (619) 459-2229

Make inquiries regarding subscriptions, display advertising, reprints, or permission to republish *AJR* material to the publisher:

The Williams & Wilkins Co.
428 E. Preston St.
Baltimore, MD 21202
telephone: (301) 528-4133

Publication Policy

The *AJR* publishes original and timely contributions to the advancement of medical diagnosis and treatment with radiologic methods. Although content is predominantly clinical, laboratory investigations are accepted when their relevance to clinical practice is demonstrable. In prospective clinical investigations, authors should document that informed consent was obtained from patients. The material submitted **must** not have been previously published nor be currently submitted for publication elsewhere (prior publication of simple abstracts without illustrations or tables will not prejudice publication of the complete study). Papers dealing with **neuroradiology** should be addressed to: Editorial Office, American Journal of Neuroradiology, Dept. of Radiology, Massachusetts General Hospital, Boston, MA 02114; telephone: (617) 726–8342. At the discretion of the Editor of *AJR*, *AJNR* articles may be republished in *AJR*.

Decisions on manuscripts are based on peer review. Reviewers receive manuscripts without title pages to protect the identity of authors and to ensure an unbiased review; names of reviewers, in turn, are not revealed to the authors. Accepted manuscripts are subject to editing. Statements within an article, including changes made by the Editor or copy editor, are the responsibility of the author and not *AJR* or its publisher. Authors will receive the edited manuscript, galley proof, and proofs of illustrations usually 6–8 weeks after acceptance. If the corresponding author will not be available, arrangements should be made for a coauthor or colleague to read and return the proof.

Copyright Information

In accordance with *AJR* implementation of the U.S. Copyright Law, authors must release first and subsidiary rights to their manuscript at submission (unless the study was performed as part of their duties as an employee of a U.S. government agency). A dated letter with the signatures of all authors should state: "We, the authors, assign first and subsidiary rights to the American Roentgen Ray Society in the event that our manuscript [insert title] is published by *AJR*. We guarantee that this manuscript contains no matter libelous or otherwise unlawful or which invades individual privacy or which infringes any proprietary right. *AJR*, in turn, grants us the right of republication, subject only to crediting the original source of publication and receiving written permission from the publisher. We understand we will receive no royalty or other compensation from *AJR*. We guarantee that this article and illustrations have not been previously published elsewhere or, if previously published in part or in whole, that permission has been obtained for republication. Copies of these permissions are included and previously published text or illustrations have been identified in the manuscript." (Delete the last sentence if it does not apply.) The covering letter also should state that the manuscript has been seen and approved by all the authors.

Manuscript Form

AJR complies with the Uniform Requirements for Manuscripts Submitted to Biomedical Journals (*Ann Intern Med* 1979;90:95–99). Manuscripts must be ***typed double-space throughout***, including references, tables, and figure legends. Each table, the footnotes, and the figure legend section should begin on separate sheets; a separate title page should be provided. Send the original typescript, one copy, and two sets of illustrations (not photocopies). Authors' names should be on the title page **only** so that author anonymity can be maintained during the review process. Permission to reprint previously published material should accompany the manuscript.

Organization of Major Articles

Title Page

Titles should be brief yet precise, accurately conveying the content of the paper. Limit authors to those who made substantial contributions to the work. Include an address for *each* author, and ZIP or postal code; acknowledgment of grant or other financial support when appropriate; name of meeting, location, and date if the paper was presented; a running head (shortened title); and the name, address, and telephone number of the author to whom correspondence and requests for reprints should be addressed.

Abstract

A description of the purpose, methods, results, and conclusions of the study is required. The factual highlights of each section should be recapitulated.

Introduction

Clearly state the purpose of the investigation, including necessary background facts that indicate its current relevance.

Materials [or Subjects] and Methods

Describe the research plan, the materials or subjects, and the methods, in that order. Proof of disease and control of subjectivity in observations should be detailed. Metric measurements should be used throughout. Put measurements in the International System of Units (SI) in parentheses when appropriate; for example, 400 rad (4 Gy).

Results

Present results in logical sequence. If tables are used, do not duplicate tabular data but do describe important points and trends.

Case Reports

Individual cases can be described if there are only a few; one or more cases from a large series can be described individually as Representative Case Reports. Each report should concentrate on the radiologic information and its usefulness.

Discussion

Offer appropriate limitations about the research plan, materials or subjects, and methods to give perspective to their adequacy for the purpose of the study. Interpret the results to lend meaning and importance to the observations. Hypotheses and speculation based

on the results are encouraged. When results differ from those of previous investigations, an attempt should be made to explain the discrepancy. Conclude with a brief statement regarding clinical significance.

Acknowledgments

Acknowledge only persons who have made *substantive* contributions to the study. Mention grant support on the title page.

References

References should be offered to document major assertions of fact and any opposing evidence and concepts. Discretion in number is requested. References should be cited in the text by number (e.g., [3, 4]). The reference list should be arranged in the numeric order that references are cited in the text and ***typed double-spaced throughout***. References cited *first* or *only* in tables or figure legends should be numbered by the sequence in which the table or figure is first identified in the text. Data for each reference should be arranged according to the style adopted by the U.S. National Library of Medicine and used in *Index Medicus*. ***Accuracy of reference data is the responsibility of the author.*** Provide all authors' (or editors') names when fewer than seven; when seven or more, list the first three and add et al. Provide inclusive page numbers; if an article is only one page, please indicate. Abbreviations for titles of medical periodicals should conform to those published in *Index Medicus*. Articles that appear in both *AJR* and *AJNR* should be a single reference that cites both journals (example 3). Examples:

1. Kirks DR, Fram EK, Vock P, Effmann EL. Tracheal compression by mediastinal masses in children: CT evaluation. AJR 1983;141:647–651
2. Khansur T, Yam LT, Tavassoli M. Serum monitors of bone metastasis. In: Stoll BA, Parbhoo S, eds. Bone metastases: monitoring and treatment. New York: Raven, 1983:165–180
3. Sage MR. Review. Kinetics of water-soluble contrast media in the central nervous system. AJNR 1983;4:897–906, AJR 1983; 141:815–824

Unpublished data and personal communications should not be numbered references but should be put in parentheses in the text (e.g., Smith JD, personal communication).

Tables

Tables should be concise and organized to show trends, not merely compilations of raw data. (The Editor may request that tables of backup data too extensive to be published be deposited with the National Auxiliary Publications Service or made available by the author.) Include only data pertinent to the subject. Long itemized case histories are better presented in the text as case reports or summaries. Do not repeat in tabular form material presented in the text. Tables should have titles and headings, but no vertical or horizontal rules.

Illustrations

Figures should be submitted as 13 × 18 cm (5 × 7 inch) glossy, black-and-white prints, ***untrimmed and unmounted***. Labels and arrows must be of professional quality and removable. Number each figure to correspond with the figure legends and indicate the top. Avoid writing directly on the back of the print. Special permission for publication of facial photographs of patients or for previously published pictures is required. Line illustrations or graphs must be professionally drawn in black ink on white background; please send photographic prints (not photocopies), not originals, to avoid damage in handling. Color illustrations will be used at the discretion of the Editor; send color prints. Firm estimates of cost will be sent to the author(s) for approval before publication. Identical anatomic structures in color prints should be the same size to facilitate reproduction and reduce cost.

Legends

Figure legends should carry a title identifying the message of the illustration and the case number if individual cases are described in the text. Legends should be as brief as possible for the informed reader to understand the figure. Detailed clinical data should be avoided. Legends for previously published illustrations should cite the reference number of the source (e.g., Reprinted from [8]).

Organization of Case Reports

Concise case reports will be considered for publication if they present unusual experiences that are medically important and instructive. Clarity and brevity are essential. After preliminary screening by an editor to determine whether the requirement of medical significance has been met, qualifying papers will undergo the same peer review as major papers. To facilitate planning the order and layout of each issue, case reports are limited in length to two journal pages. The introduction should be one short paragraph that gives some general background of the disorder and the specific interest and message of the case presented. Only one case should be described in detail. The case report should concentrate on the radiologic information and its usefulness. The discussion should focus on the specific message of this report and the relevance of radiology in this instance. If the author has encountered other cases, they may be briefly mentioned, and possibly illustrated, but not described in detail. There should be no more than eight references. The figures should be limited to the minimum required to document the case findings, probably not more than four pictures, each a column wide (or the equivalent). Excess illustrations would require severely shortening the text. Figure legends should be as short as possible and should not repeat the text. There can be no tables and no acknowledgments. See previous sections for detailed instructions regarding references and illustrations.

Other Contributions

Technical Notes

Brief descriptions of new techniques or significant modifications of older ones that are directly applicable to the clinical practice will be accepted if review is favorable. Technical notes do not carry abstracts or acknowledgments.

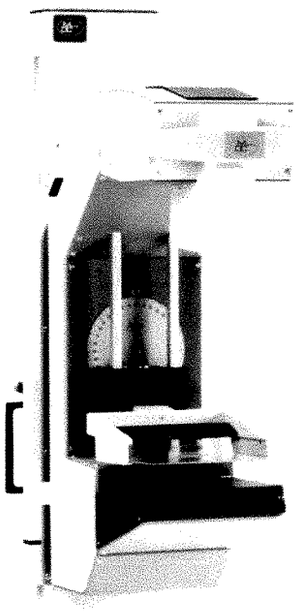
Letters to the Editor

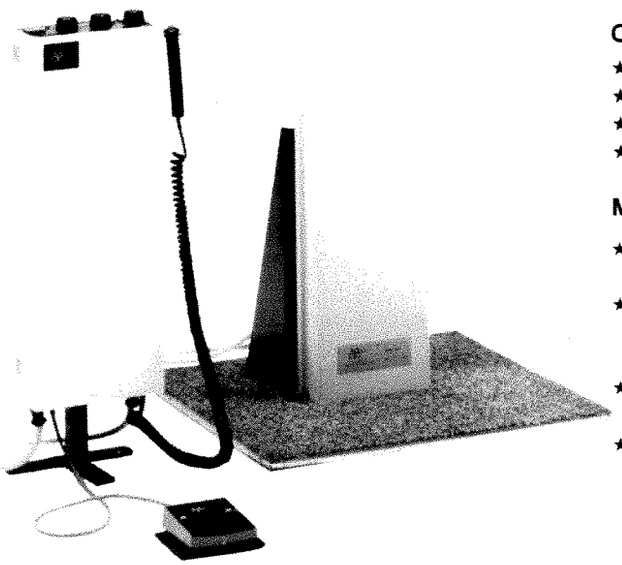
Letters are subject to editing and condensation. Criticism of published articles should be objective and constructive. Letters also may discuss matters of general interest to radiologists.

Tecnomed USA

Mamex DC

MAMMOGRAPHIC SYSTEM





Original MAMEX DC

In the beginning...
The original MAMEX DC

The Mamex DC is a complete mammographic system, consisting of a modern, efficient DC generator which virtually eliminates "ripple" and gives a higher resolution image with consistently higher subject contrast; a molybdenum anode x-ray tube; and a motorized compression system with floor remote control.

Standard features:

- ★ Compact DC generator with automatic exposure control.
  Exposures can be made once every 30 seconds.
- ★ Stand designed for x-ray examination of the breast.
- ★ Hardened glass screen protects technician during exposure.
- ★ Floor remote compression control.
- ★ Phototiming detector position selector.
- ★ Field light.
- ★ Breast compression plate;
  Biopsy compression plate;
  Spot cone compression plate.
- ★ 18x24cm Kodak Min-R cassette with screen.
- ★ Film identification markers.
- ★ Automatic line voltage compensation.
- ★ .6x.6 stationary anode molybdenum x-ray tube with beryllium window.

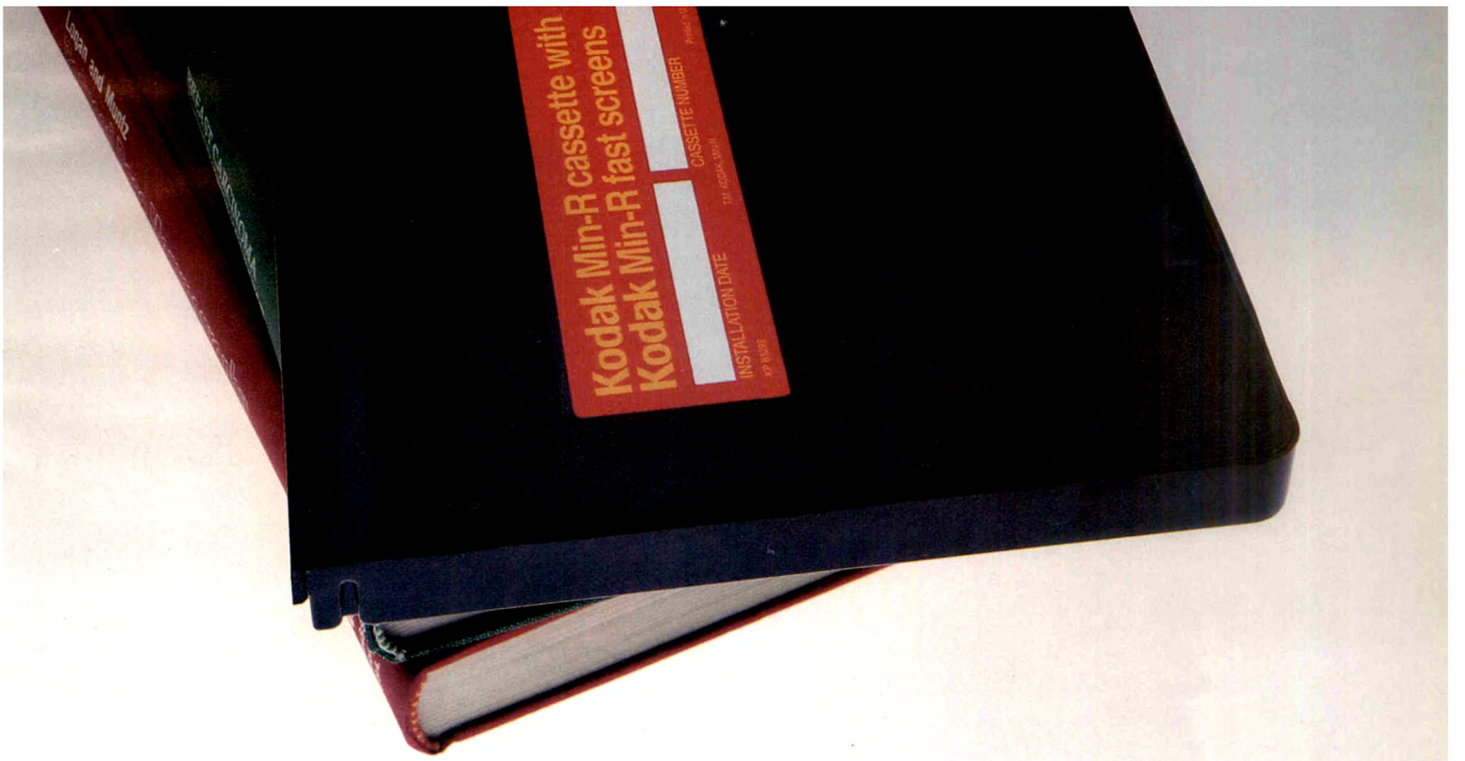
Options:

- ★ 200L 3.5:1 grid.
- ★ Carbon fiber cassette tunnel with grid pocket.
- ★ In-hospital wheel assembly (shown).
- ★ Van wheel assembly.

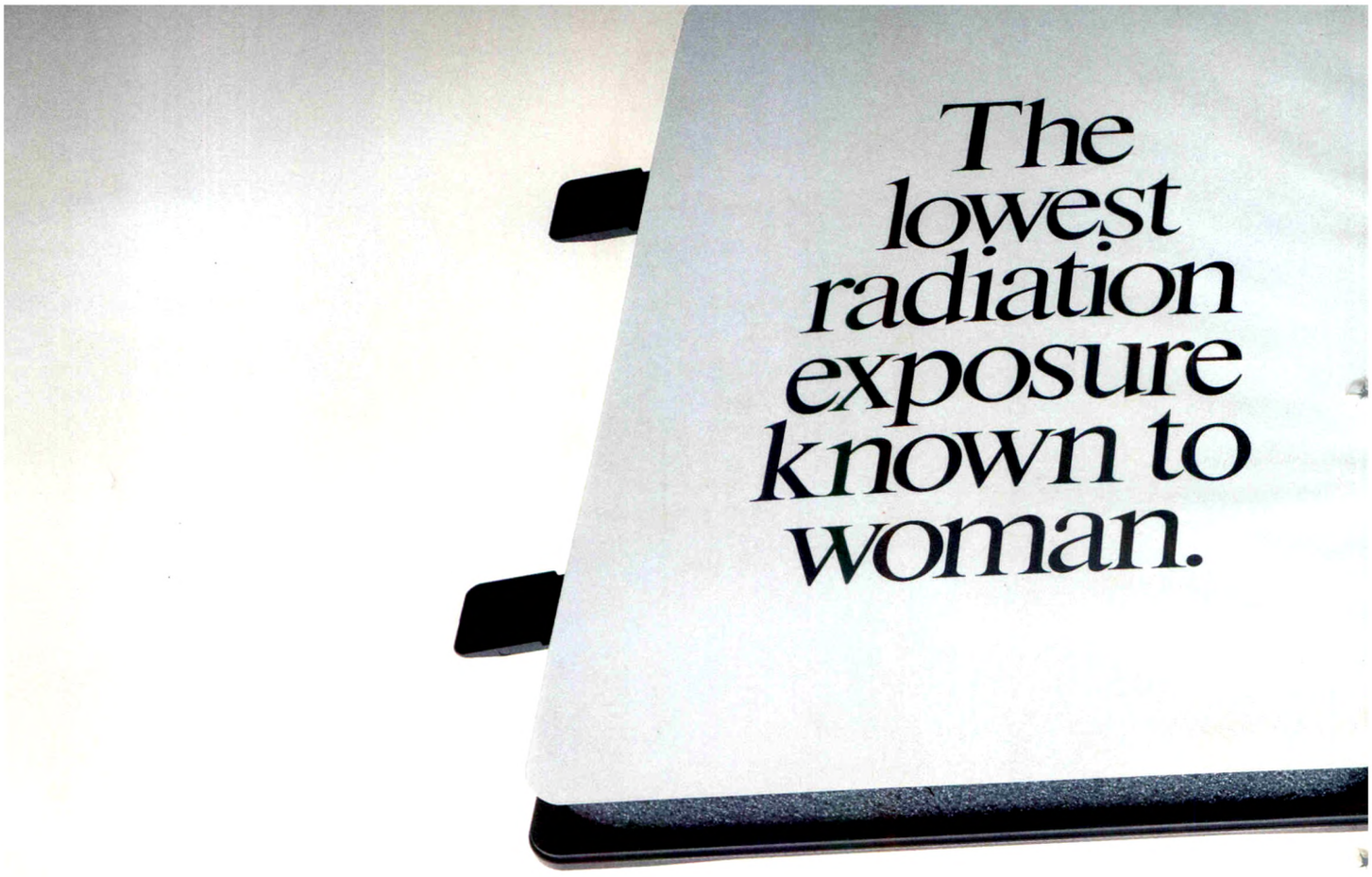
Mamex DC . . .

- ★ Five-year proven track record of performance and reliability;
- ★ Hundreds of satisfied physicians, clinics, and hospitals throughout the United States and internationally;
- ★ Full 12-month non-prorated warranty on the x-ray tube;
- ★ Average midbreast dosages, on a 2-film exam of a 6cm compressed breast, of .07R or less (as documented by the University of Michigan Breast Cancer Detection Center - Ingvar Andersson, M.D.)

. . . offers your facility the very best in diagnostic equipment available in today's marketplace.



Kodak opens a new chapter in screen-film mammography.



New two-screen, double-emulsion film combination.

Introducing
KODAK MIN-R Fast Screens and
KODAK T-MAT M Film

For years, Kodak has been writing the book on mammographic imaging. Now a new chapter unfolds.

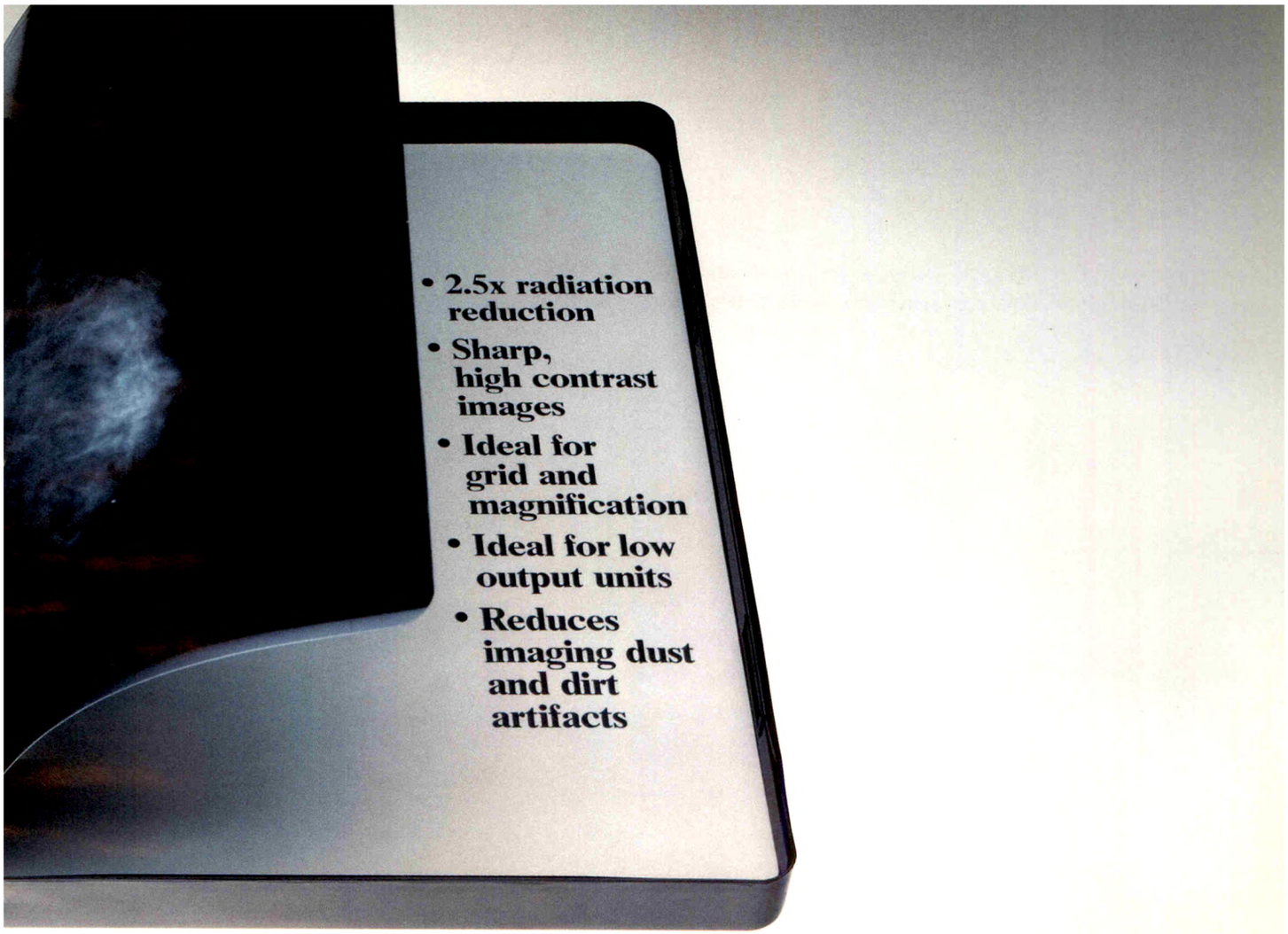
For the first time, you can use a two-screen, double-emulsion film combination for mammography. A combination that Kodak has created specifically for mammographic applications.

It's the new KODAK MIN-R Fast Screens and KODAK T-MAT M Film combination. And it's the fastest, high-quality, low-radiation-exposure mammographic imaging system in existence. It's so efficient, it reduces radiation exposure by 2.5x.

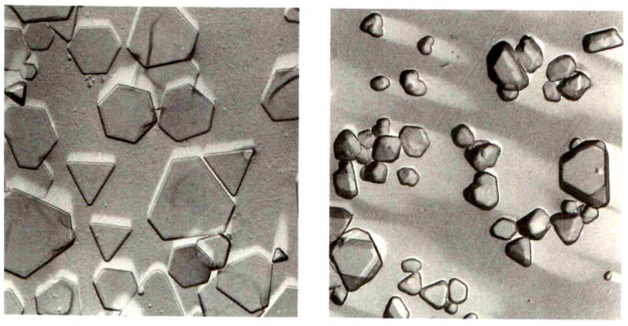
This technological breakthrough is the result of new screen-coating capabilities combined with Kodak's innovative T-Grain emulsion technology.

The proprietary new screens comprise a thin front screen and a conventional thickness mammographic back screen. These new screens are important elements that make possible the use of a double-emulsion film for mammography.

© Eastman Kodak Company, 1986



T-Grain emulsions are perhaps the biggest advance in silver halide imaging in 50 years. The new tablet-shaped silver halide grains used in KODAK T-MAT M Film capture more light, afford increased speed, and don't compromise image quality.



T-Grain emulsion technology is the basis for the new KODAK T-MAT M Film. The emulsions employ flat, tabular grains of silver halide (left) rather than the conventional pebble-shaped grains.

In addition, the T-MAT M Film has a magenta dye adsorbed onto the T-Grain crystals to absorb the green light emitted by the rare earth intensifying screens, reducing crossover without sacrificing system speed.

The double MIN-R Fast Screens and the T-MAT M Film are provided in low-absorbing KODAK MIN-R Cassettes or mounted in folders for use in vacuum devices. The result is a state-of-the-art system customized for mammography. A system that eliminates imaging dust and dirt artifacts, and provides an intimate screen-film contact to further maintain image sharpness. A system that can be used with grids to deliver the high-contrast image you need, while reducing radiation dose.

To open a new chapter in mammography for you and your patients, contact your Kodak technical sales representative.

New KODAK MIN-R Fast Screens and KODAK T-MAT M Film, the combination with a 2.5x radiation dose reduction.

Relative contrasts, speeds, and average glandular dose comparisons of Kodak films used with Kodak screens for mammography

Film	Contrast[1]	Relative Speed[2]	Average Glandular Dose[3] (Rads)
KODAK Ortho M Film KODAK MIN-R Screen	2.85	100	0.05
KODAK T-MAT M Film KODAK MIN-R Fast Screens	3.05	250	0.02

Development—KODAK *RP* X-OMAT Processors using seasoned KODAK *RP* X-OMAT Chemicals or equivalent at recommended temperatures.

Contrast[1]—Measured as the average gradient between densities 0.25 and 2.00 above gross fog.

Relative Speed[2]—Determined from matched density radiographs. KODAK Ortho M Film arbitrarily assigned a relative speed of 100.

Technique[3]—Based on average size breast, craniocaudal view, molybdenum target tube, 0.03 mm molybdenum filter, 28 kVp setting.

New KODAK MIN-R Fast Screens

The KODAK MIN-R Fast Screens incorporate phosphors which contain metals from the lanthanide series of "rare earth" elements. Using a molybdenum target x-ray tube with a beryllium window, 30 microns molybdenum filtration, and a 4 cm clear plastic breast test object, energy absorption by the screens is approximately 90 percent. The MIN-R Fast Screens are to be used in a KODAK MIN-R Cassette or suitable vacuum holder, with KODAK T-MAT M Film.

New KODAK T-MAT M Film

The new double-coated KODAK T-MAT M Film is a high-speed, high-contrast orthochromatic x-ray film specially designed for mammographic imaging. It incorporates light-sensitive dyes to absorb green light emitted by the intensifying screens and reduce image blur.

It is ideal for applications where high film speed is desired to reduce exposure times and radiation dose—for example, with the use of grids, small focal spots, and magnification techniques.

The KODAK MIN-R Cassette

The KODAK MIN-R Cassette provides fast, easy loading of films for the mammographic procedure. The all-plastic molded cassette provides intimate screen-film contact and low absorption. The tube-side panel of the cassette is thin, injection-molded polycarbonate, with low x-ray absorption. Combined with appropriate compression, the design of the MIN-R Cassette permits good visualization of soft-tissue information near the chest wall of the patient. MIN-R Cassettes can be supported with a holding device available on most dedicated mammography x-ray units.

Availability

KODAK T-MAT M Film

24 x 30 cm . . . . . CAT No. 810 9456
18 x 24 cm . . . . . CAT No. 809 6091
8 x 10 in. . . . . CAT No. 847 4975

KODAK MIN-R Fast Screens (in KODAK MIN-R Cassettes)

24 x 30 cm . . . . . CAT No. 813 3332
18 x 24 cm . . . . . CAT No. 810 1412

(in folder for vacuum devices)

8 x 10 in. . . . . CAT No. 847 6673

Kodak, X-Omat, Min-R, T-Grain, and T-Mat are trademarks.

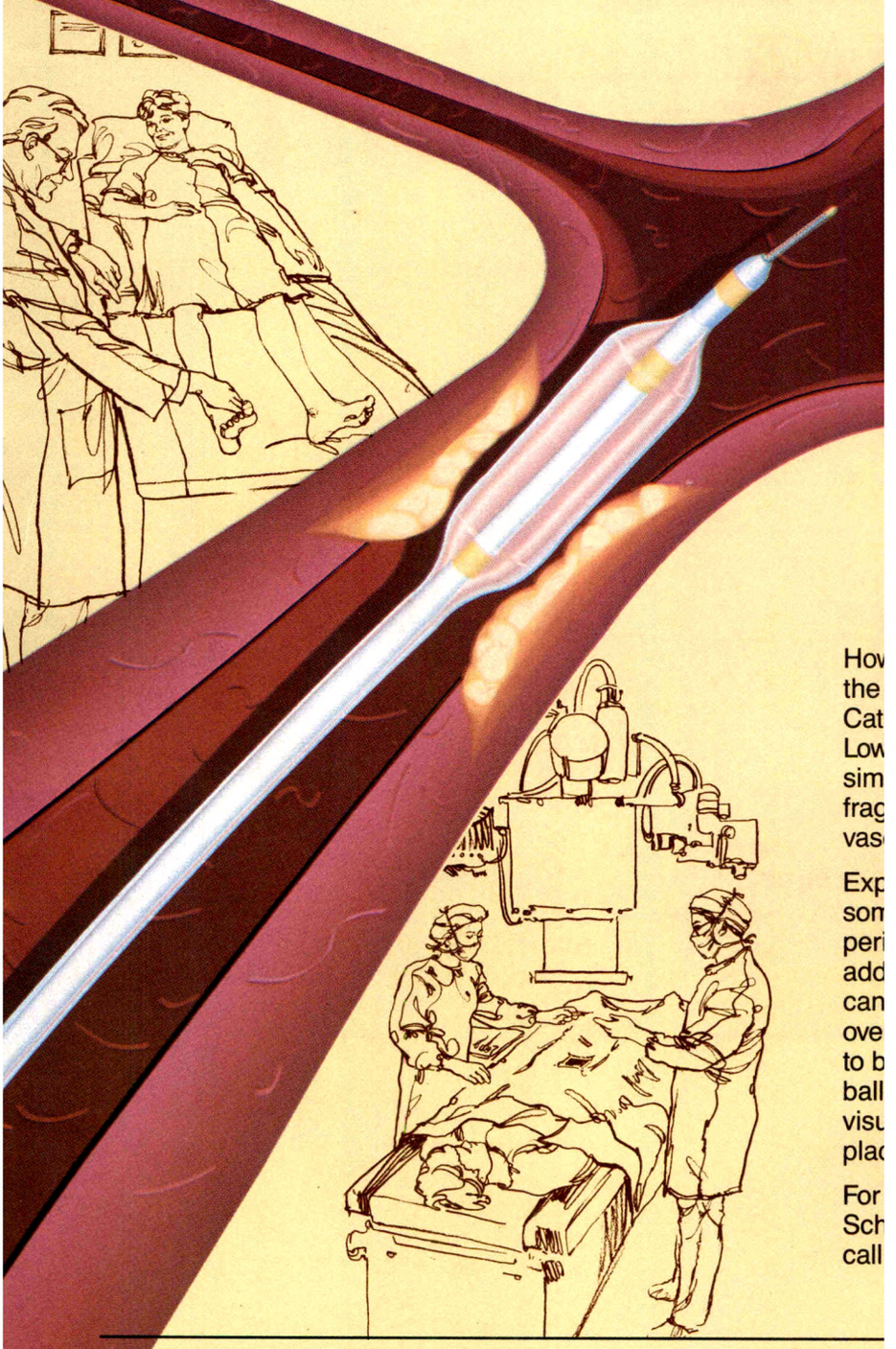
M3-299

Printed in U.S.A.

7/86

The perfect profile for narrow

The New Schwa LP Cathete



How
the
Cat
Low
sim
frag
vas

Exp
som
peri
add
can
ove
to b
ball
visu
plac

For
Sch
call

ACS®

Where Innovation continues.

Lilly

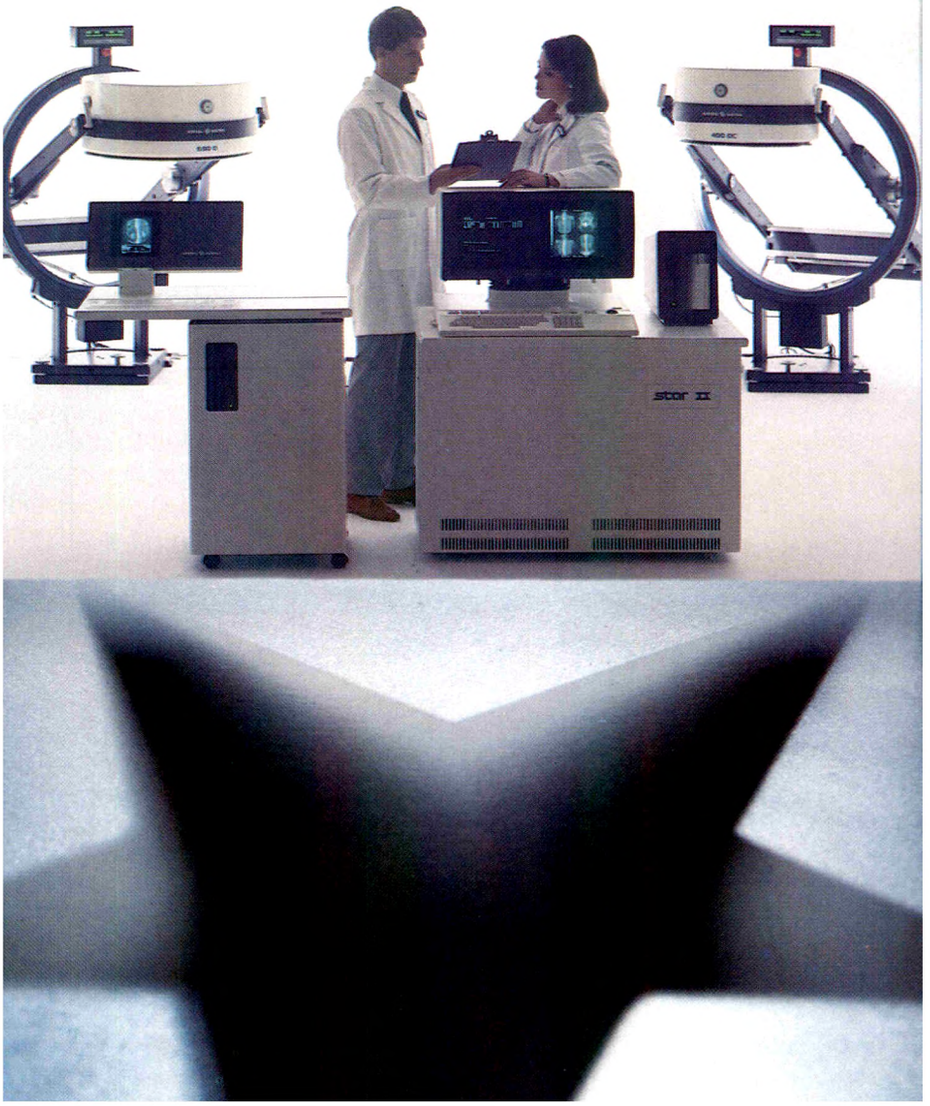
ACS is a wholly owned subsidiary of Eli Lilly and Company.

Advance

1395 Cha
Mountain
415 965-7
Toll free:
TWX (Telex

© 1986 Adva

Star vision



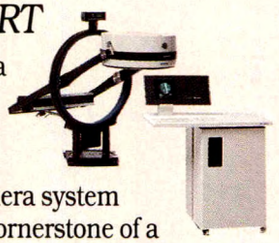
The Star family of nuclear imaging products takes you into the future...no matter where you're growing

The best way to a bright future for your nuclear imaging department is to choose equipment that can grow with you. At your pace. In the direction you choose.

The Star family of nuclear imaging products from General Electric gives you that versatility with advanced technology that easily upgrades as your needs change. These systems not only work with each other to increase your nuclear imaging and processing capabilities, they work with other manufacturers' systems as well.

Meet our family

STARPORT



Ideal for data acquisition and display. This digital gamma camera system can be the cornerstone of a nuclear department because, as requirements grow, the Starport™ system can evolve to meet them.

STARCAM



The best of all worlds: data acquisition, processing and display in an integrated system that performs the most demanding nuclear procedures with ease. With its modular digital design, the Starcam™ system keeps pace with your growth and with emerging technology.

STAR II



Powerful processing in a small system that's compatible with virtually all nuclear imaging equipment. The Star II™ system extends your processing capabilities without making your existing systems obsolete.

STARVIEW



Additional efficiency from a system that combines data processing and display functions. Starview™ saves time for physicians and technologists alike in a busy nuclear department.

STARLINK

The technology that brings the Star family together. With the future Starlink™ network, you will be able to easily access data from any on-line nuclear system, at any station.

STARGATE

Your passport to the multi-modality imaging of the future. Stargate™ will link your nuclear department with other imaging modalities, and bring the complete diagnostic picture to you at a single console.

Look into the future of nuclear imaging . . . discover the Star family of products from GE. And find out about the special financing packages available for a limited time. Call toll free *1-800-433-5566.*

GENERAL ELECTRIC

Expanding your nuclear imaging capabilities? See GE at RSNA!



USCI is Now Bard Interventional Products.

USCI, Products for Radiology, is now Bard Interventional Products. A new group with a strengthened commitment: innovative technologies for the interventional radiologist.

Many of the familiar and fundamental tools of interventional radiology were developed by USCI. New applications for these tools are being defined in the clinical arena, making interventional radiology one of the most dynamic, and demanding, fields in medicine.

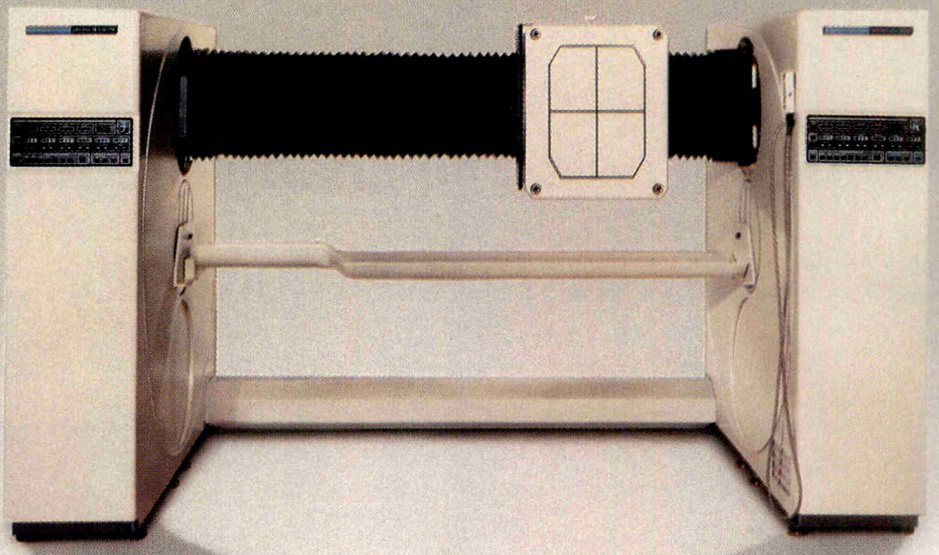
With Bard Interventional Products we are expanding our ability to work with you toward the development of new technologies based on our rigorous standards and applications-oriented know-how.

BARD
Interventional
Products

The Bard Response to the Changes You've Made.

C.R. Bard Inc. 5 Federal Street P.O. Box 5069 Billerica, MA 01822
(617) 663-2244 • (800) 824-8724

A new star



The Star family of nuclear imaging products presents its newest member…Gemini

Meet the Gemini™ system from General Electric—and prepare to meet the future.

Gemini's unique mechanical design helps you perform a comprehensive range of studies, including ECT, planar and whole body imaging. It's the answer for nuclear departments that demand versatility.

Gemini has an extra large rectangular field of view—a logical geometry for simplicity and speed. It delivers high quality whole-body studies while improving throughput by as much as 50%.

Star quality from GE

When combined with the GE Star II™ computer, Gemini delivers the high quality ECT images you've come to expect from GE equipment. And the Star II interface guarantees continuing access to the expanding universe of GE software.

Gemini also allows your department to keep pace with advances in radiopharmaceuticals and optimized high energy collimation. All these features add up to big capability in a compact package.

To find out more about the Gemini system, see your GE Representative today.

GENERAL ELECTRIC

ELE[illegible]-SCHO[illegible]DER

PUCK® Angiographic Filmchanger Systems

THE PUCK ADVANTAGE— durability... reliabilit

- **UNMATCHED HISTORY** of reliability and performance
- **RECOGNIZED DURABILITY** means many years of useful life...lower cost per examination... economy
- **DEDICATED SYSTEMS** for optimized film transport in all positions
- **POSITIVE FILM SEPARATION** through spacers in loading magazine virtually prevents film-sticking and double film-feeding
- **ADEQUATE EXPOSURE TIME** for magnification technique at 4 exp/sec (2 exp/sec in alternate biplane)
- **SYNCHRONIZED BIPLANE OPERATION** for simultaneous or alternate exposures. Two PUCK U4's... or one PUCK UD4 plus one PUCK U4... or two PUCK UD4's.

PUCK UD4...position-independent sheet-fi



PUCK U4...sheet-film changer for a.p. a



solid construction

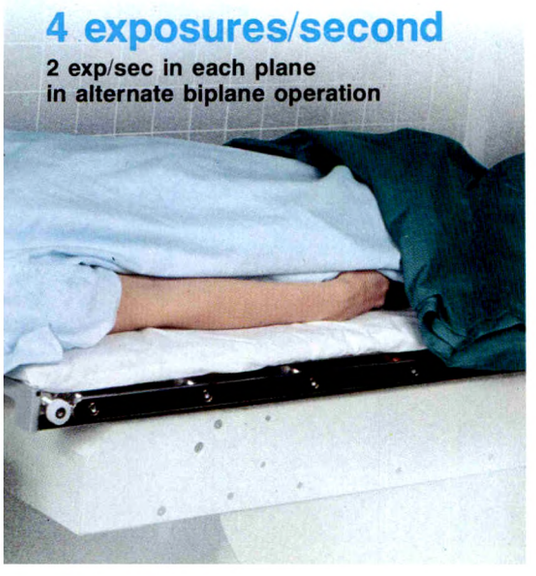


angers



4 exposures/second
2 exp/sec in each plane
in alternate biplane operation

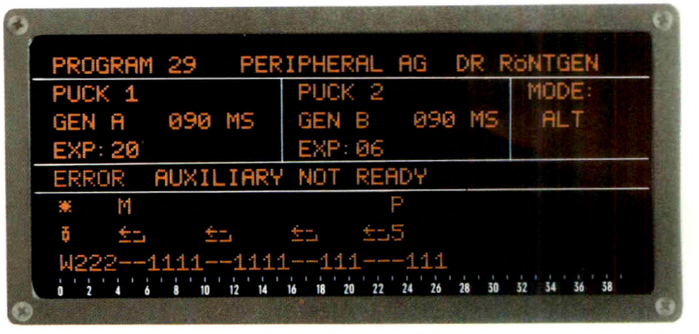
eral projections



4 exposures/second
2 exp/sec in each plane
in alternate biplane operation

SEP U1...computerized program control for PUCK filmchangers

4 exposures/second
2 exp/sec in each plane
in alternate biplane operation



VERSATILE...RESPONSIVE...PROGRAMMABLE

SEP U1 Computerized Program Control allows complex examinations to be conducted conveniently and accurately by utilizing microprocessor technology.

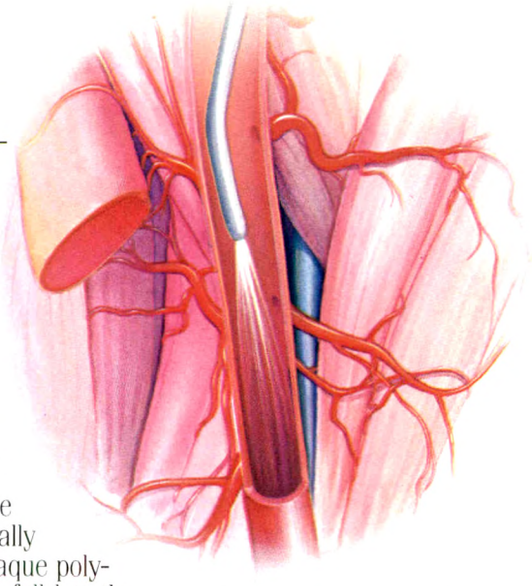
Nineteen user-designed examination programs can be stored in memory and displayed on SEP's screen in real-time, second-by-second. Programs can be temporarily altered, permanently revised, or replaced. Up to 3 PUCKS can be controlled by one SEP U1 in single-plane or biplane operation. Interfaces with other system components, e.g., injector, moving table-top, ECG triggering device.

Model SEP M1 is available for those single-plane applications where film rates greater than 3 exp/sec are not required.

85225

elema-schonander

Elema-Schonander, Inc.
2360 North Palmer Drive
P.O. Box 94517
Schaumburg, IL 60195
Telephone (312) 397-5900



THE MOST SIGNIFICANT IMPROVEMENT IN DIAGNOSTIC RADIOLOGY CATHETERS IN RECENT YEARS.

Shiley SOFTIP® Standard and High Flow diagnostic radiology catheters* Now they provide increased safety for patients. And better torqueability for you.

SOFTIP's improved patient safety comes from a unique, patented catheter tip which deforms on contact with vessel walls. Catheter forces previously directed against the intima are now absorbed by the catheter tip itself. As a result, the risks of intimal/subintimal lesions, intramural dissection, perforation and related vessel thrombosis and clot or plaque embolism may be reduced.

STUDIES CONFIRM SOFTIP PATIENT SAFETY.

In-vivo and in-vitro studies compared SOFTIP with two other conventional catheters. Both studies suggest that SOFTIP reduces the likelihood of angiography complications.

In the first study, light-micrograph cross sections of canine aortic tissue (Fig. 1A & 1B) demonstrated a reduction of intimal abrasions with SOFTIP.

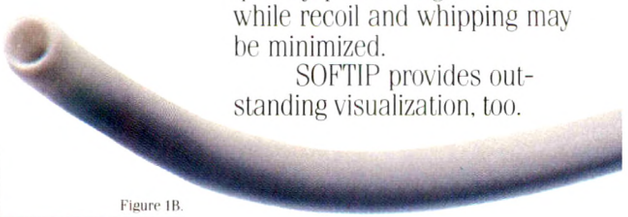
The second study measured catheter tip indentation depths. Here SOFTIP showed 43% to 56% less indentation than other catheters tested (Fig. 2).

TORQUE SUPERIORITY YOU CAN FEEL.

A 16-strand stainless steel wire braid within specially formulated radiopaque polyurethane runs the full length of the catheter body. In the 5 and 6 French catheter, braiding extends to the deformable tip. In all cases, the result is a precise one-to-one torque ratio for optimum control, plus added memory. Yet longitudinal flexibility is never compromised.

The same special polyurethane also results in a superior curve memory. Consequently, positioning is easier while recoil and whipping may be minimized.

SOFTIP provides outstanding visualization, too.



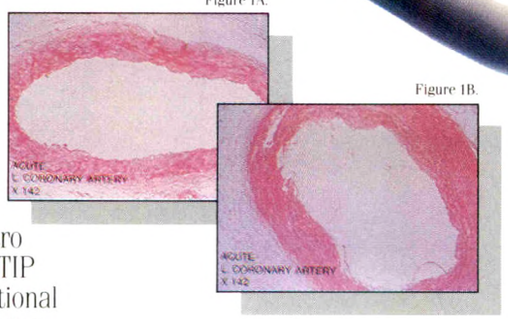


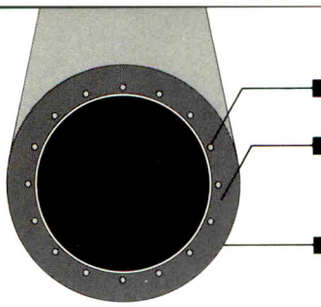
Fig. 1A *Canine histology studies demonstrated a reduction of intimal abrasions with the SOFTIP catheter's patient-safe deformable tip.*

Fig. 1B *In contrast, conventional catheters showed significant endothelial disruption.*



Hard Facts

Shiley Incorporated, 17600 Gillette Avenue, Irvine, CA 92714-5751 USA. (714) 250-0500 (800) 854-3683. Cable: SHILEYINC IRIN. Telex: 68-5585.
Shiley-Europe, Staines House, 158-162 High Street, Staines, TW184AZ, England. Tel: (44) 784-61533. Telex: 919851 PFHPGS-G.
Shiley Canada, 251 Bartley Drive, Toronto Ontario, M4A-2N7, Canada. Tel: (416) 752-9990. Telex: 389-06963811.



- ***16-Strand Wire Braiding*** *helps produce one-to-one torque control.*
- ***Angithane,™***** *a specially formulated radiopaque polyurethane, improves handling, shape retention and visualization.*
- ***CELGARD™***** *silicone coating demonstrates superior catheter thromboresistance and increased lubricity.*

And its walls withstand high-pressure injections without compromising expected flow rates.

HIGH FLOW AND MORE.

In addition to Standard Flow catheters, SOFTIP offers a range of High Flow French sizes. High Flow catheter lumens have been enlarged without increasing outside catheter diameters. The benefits include improved flow capacity, greater media concentrations and better visualization, all without increasing French sizes.

Winged SOFTIP hubs are clearly marked with catheter length and French size for easy identification. A secure grip facilitates more efficient on-off connections. And a tapered hub lumen promotes smooth injections.

The exterior of each SOFTIP catheter is coated with silicone CELGARD™** for improved thromboresistance and lubricity. Studies demonstrated that silicone coated SOFTIP catheters yielded the lowest thrombogenicity index of any catheters tested[1]

GET MORE HARD FACTS.

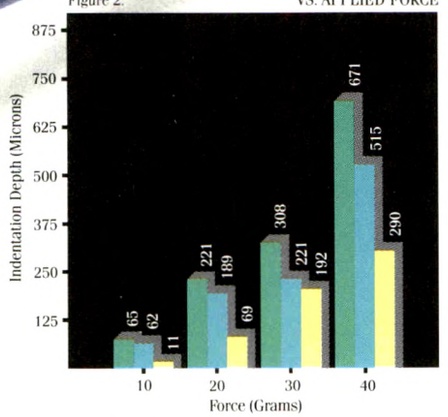
To learn more about SOFTIP diagnostic radiology catheters with greater patient safety, better control and improved memory, call your Shiley Customer Service Representative at 1-800-854-3683. In Alaska, call 714-250-0500 collect. In Europe, contact your Schneider-SOFTIP representative.

[1]*"Acute Canine Intra-Arterial Implantation Screening for Thrombogenicity," Utah Biomaterials Test Lab.*

Indentation depths in a semi-soft wax medium simulating vascular tissue were reduced 43% to 56% with SOFTIP angiography catheters when measured against conventional catheter tips.

Figure 2.

CATHETER TIP INDENTATION DEPTH VS. APPLIED FORCE



Shiley SOFTIP = 140 ±13 μ's
USCI = 246 ±15μ's
Cordis = 318 ±20μ's

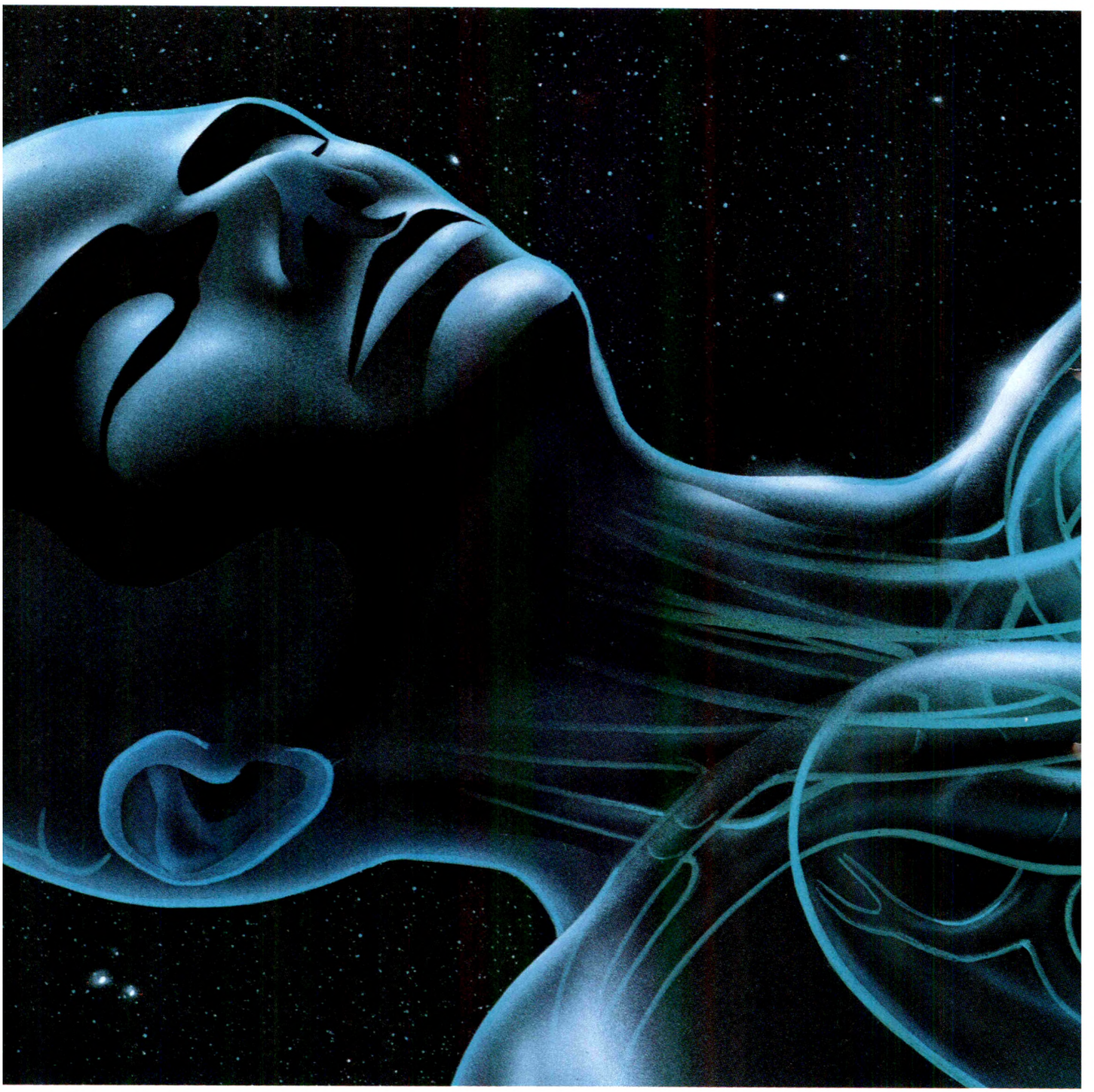
About SOFTIP®

Standards of excellence... beyond excellent standards.

Shiley
A Pfizer Company®

© Shiley Incorporated. All rights reserved. 086SP184 (5/86).
SOFTIP® is a registered trademark of Angiomedics Incorporated.

Toshiba's TCT-900S..



)ne giant leap for CT!



CT beyond the fourth generation.

Toshiba's TCT-900S scanner is indisputably unique to the CT imaging industry. In fact, Toshiba's leading edge technology actually takes CT beyond the fourth generation into another dimension with these technological features found in no other comparable system:

1. Consistently superior image quality: just what you expect from Toshiba.
2. Nutate/Rotate geometry with continuous scan: thirty scans in thirty seconds.
3. True dynamic scan: no inter-scan delay.
4. Sub-second scanning: quality images in 0.6 seconds.

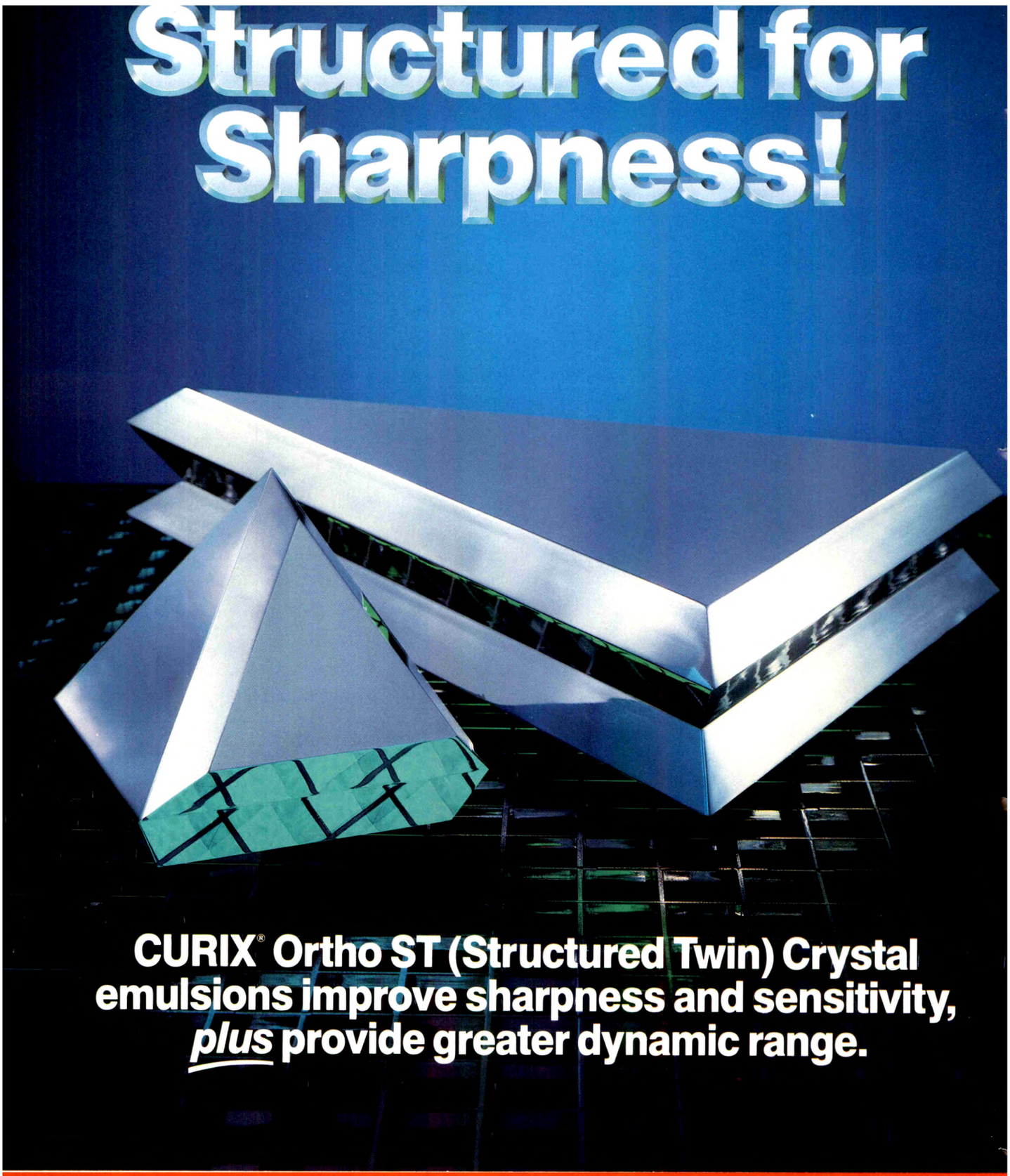
Let the competition tell you that CT technology can go no further. But you owe it to yourself to see just how far Toshiba can really go . . .

Call or write: Toshiba Medical Systems, 2441 Michelle Drive, Tustin, CA 92680. In California, call (714) 669-5419. Outside California, call toll-free (800) 421-1968. In Canada, call (416) 298-6100.

In Touch with Tomorrow

TOSHIBA

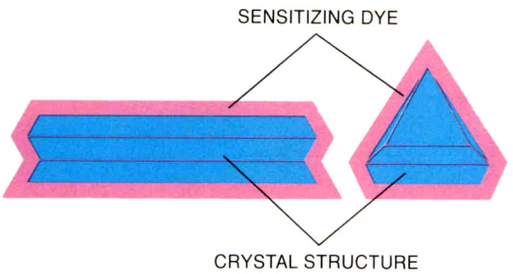
GLOBAL IMAGING SPECIALISTS


Structured for Sharpness!
CURIX® Ortho ST (Structured Twin) Crystal emulsions improve sharpness and sensitivity, plus provide greater dynamic range.

CURIX® Ortho ST Films achieve superior image quality and noise suppression through fundamental innovations in crystal and emulsion technology.

First: AGFA's twin tabular and compact silver halide crystals provide both *increased surface area* for improved sensitivity, and *compact size* for increased sharpness and reduced graininess.

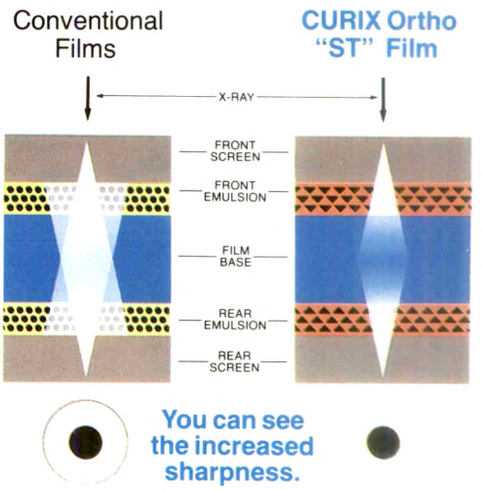
Second: The unique silver bromoiodide crystal structure of CURIX Ortho ST Films enhances image perception and suppresses noise, because of improved adherence of the sensitizing dye upon the crystal surfaces. Thus, the dye is better utilized in image formation than with other tabular grain films, resulting in a cleaner, brighter, sharper image.





CURIX Ortho ST emulsions reduce Crossover Exposure

Screen-emitted light is absorbed in the layers adjacent to the screens, resulting in increased sharpness.



You can see the increased sharpness.

CURIX Ortho ST Films are compatible with standard CURIX Ortho Screens, require no change in technique, and provide the same high speed with greater sharpness and less grain.

AGFA is setting new standards...with innovations in imaging technology, equipment, and service.

CURIX Ortho ST Films provide improvement in sharpness that you can actually see!

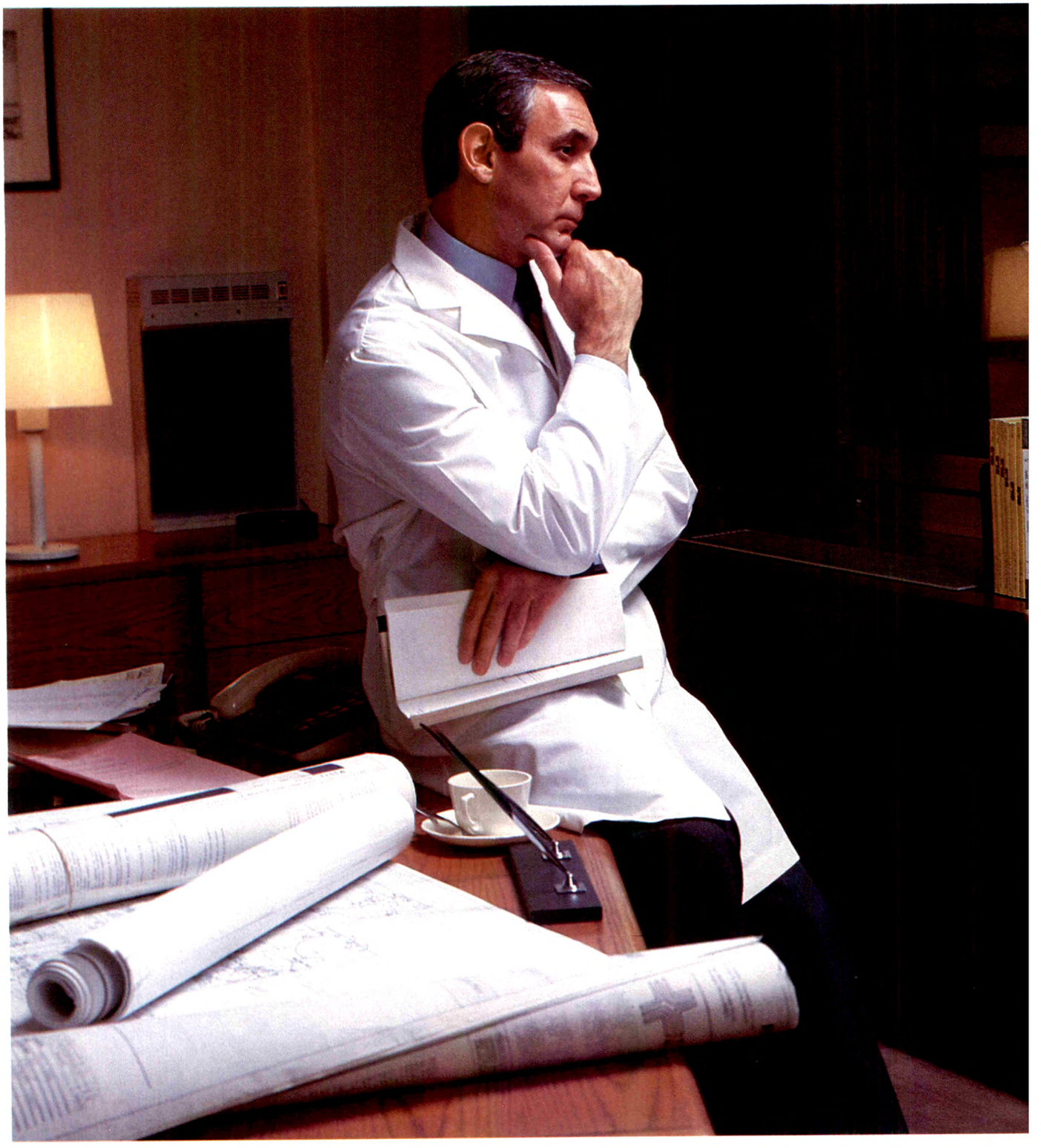
Let us prove it to you. Call 914-682-5650 for a demonstration.

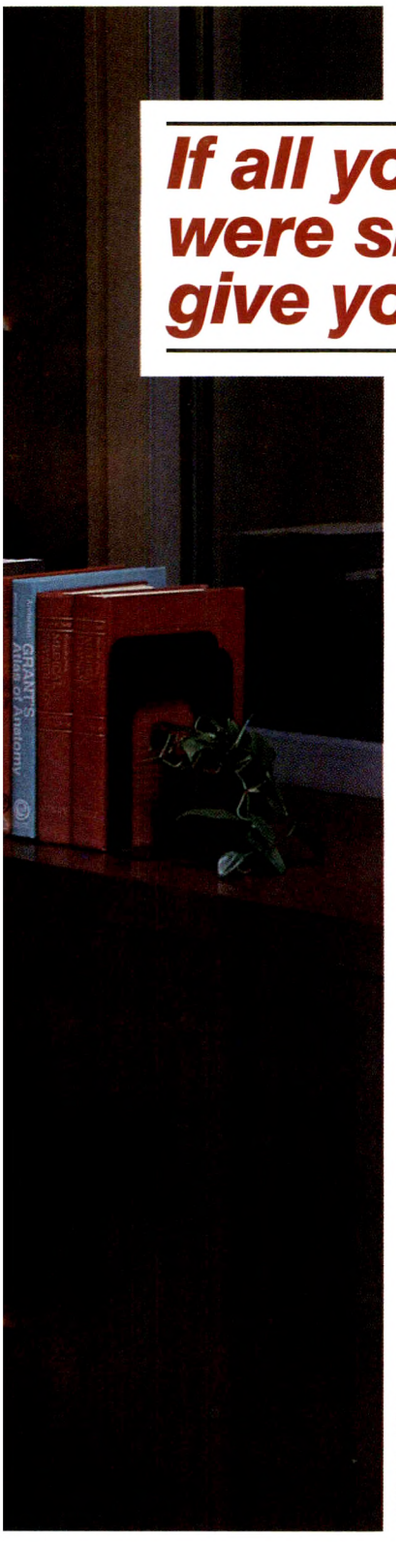
Agfa-Gevaert Rex, Inc.
A Subsidiary of Agfa-Gevaert, Inc.
P.O. Box 190, White Plains, NY 10602
914-682-5650

AGFA

Advancing the Science of Medical Imaging

SIEMENS





If you're in the market for a magnetic resonance scanner, you know how many critical questions must be answered before you choose the right system.

If all your MR questions were simple, anyone cou give you the answers.

That's why it's important to seek sound advice. And when you know MR is right for you, the time is right to talk to Siemens.

Why Siemens? When it comes to magnetic resonance, we have the attributes you'll want in the company you do business with.

A System That's Right For You

Because the needs of clinicians vary, Siemens MAGNETOM MR systems encompass the requirements of a broad range of users. As a full-line supplier, we offer you what limited vendors simply can't: a level-headed, unbiased approach to equipment selection. Our experience is built on thousands of clinical case studies at different field strengths. We can help you choose an MR system that will best do the job at your institution.

Whichever MAGNETOM system you select, you can expect it to fulfill your goals of excellent image quality and high throughput. You'll need this kind of productivity to make your MR investment successful.

Comprehensive Support and Service

Siemens will help you maximize the return on your investment. We offer total, ongoing support. Realistic appraisals of your capital needs and patient volume. Experienced site planning with recommendations on shielding or even complete turnkey installations. Educational programs that begin before your MAGNETOM is delivered and continue with in-depth applications training. And we have the financial services to assist you in acquiring this new technology.

MG/5000-058A WLM 412

A Comp
and Res

The facts
company

already c
MR magı

And as th
equipme
be aroun
in the fut

Talk to u

Contact y
represen
you with
magnetic
custome



Siemens
186 Wooc
Iselin, NJ

In Canada
Siemens E
1180 Court
Mississau

Sieme
techn

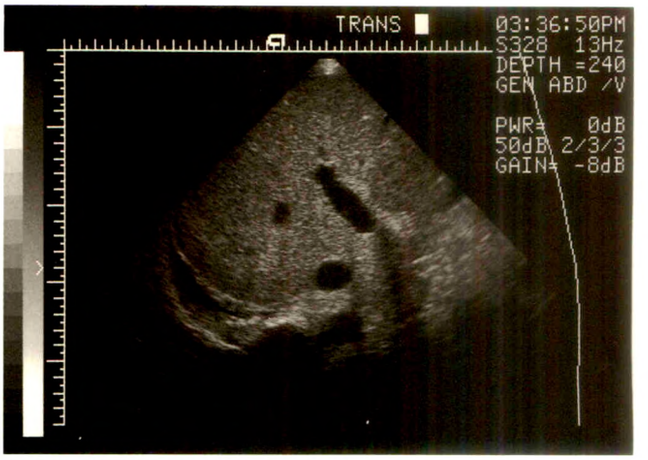
"THERE'S NO DIFFERENCE BETWEEN PHASED ANNULAR ARRAYS AND COMPUTED SONOGRAPHY.

acuson
COMPUTED SONOGRAPHY

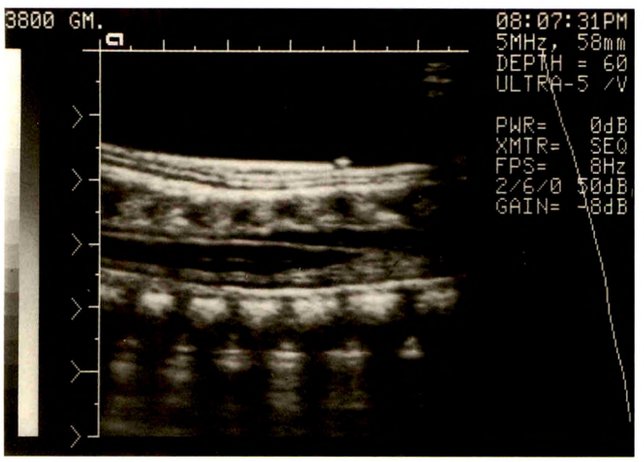
THE GOLD STANDARD IN ULTRASOUND



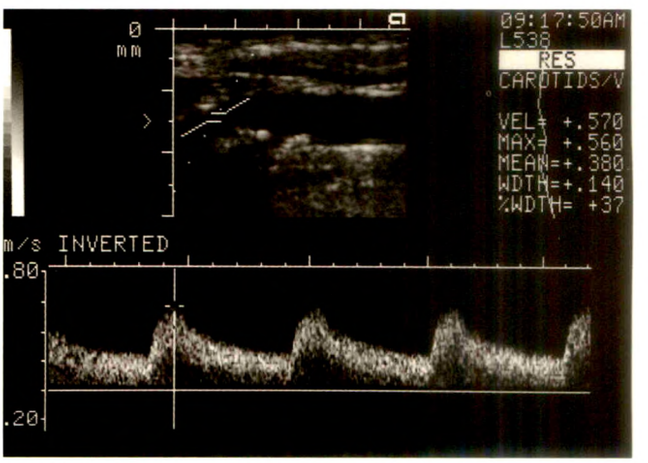
Contrast Resolution: Enlarged spleen, normal left kidney
Arkansas Children's Hospital, Little Rock, AK.



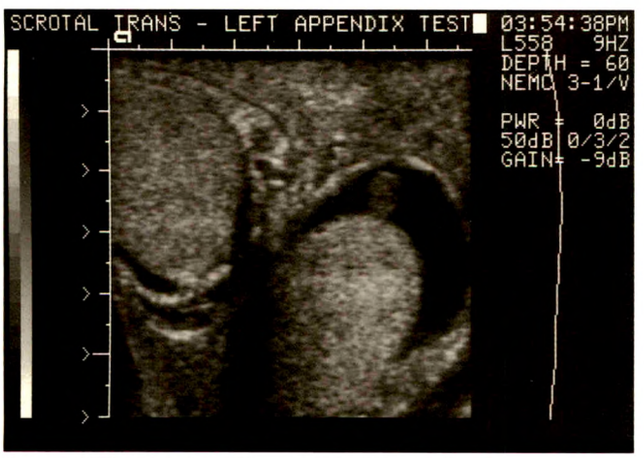
Penetration: Diffuse liver disease, small pleural effusion



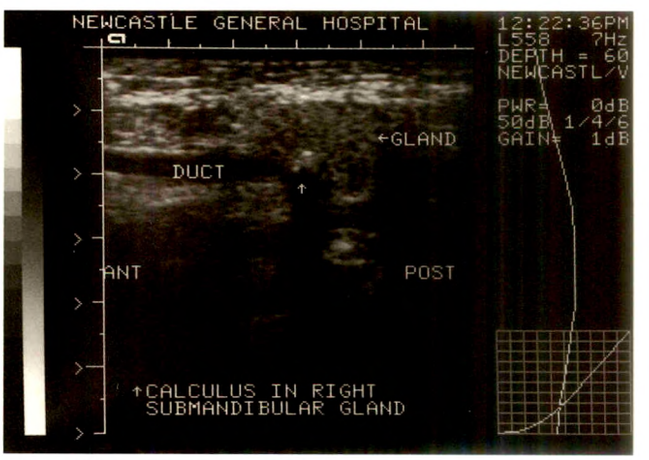
Detail and Contrast Resolution: Pediatric spine
Wylers Children's Hospital, University of Chicago, Chicago, IL.



Imaging and Doppler: 15-49% ICA Stenosis



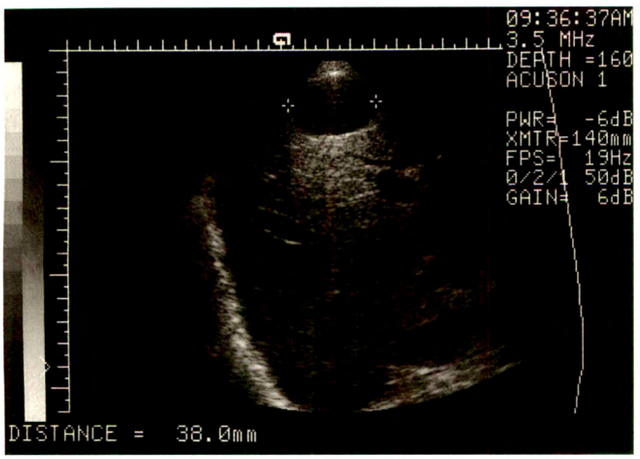
Tissue Differentiation: Bilateral testes, epididymis
Tufts New England Medical Center, Boston, MA.



Clinical Versatility: Submandibular gland
Newcastle General Hospital, Newcastle, U.K.



THE GOLD STANDARD IN ULTRASOUND



Near-Field Resolution: Liver Mass
University of Alabama, Birmingham, AL.

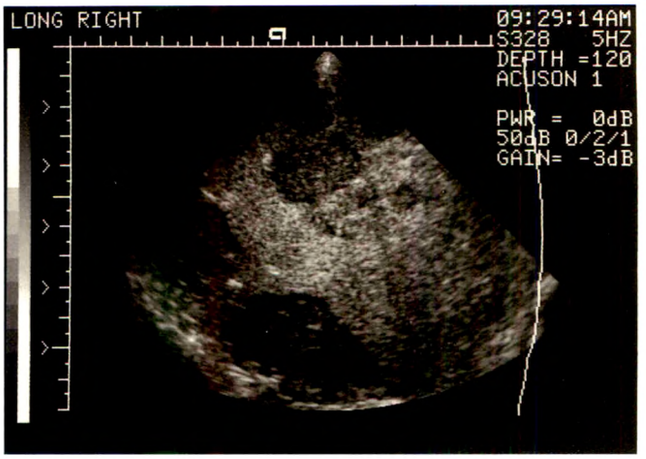
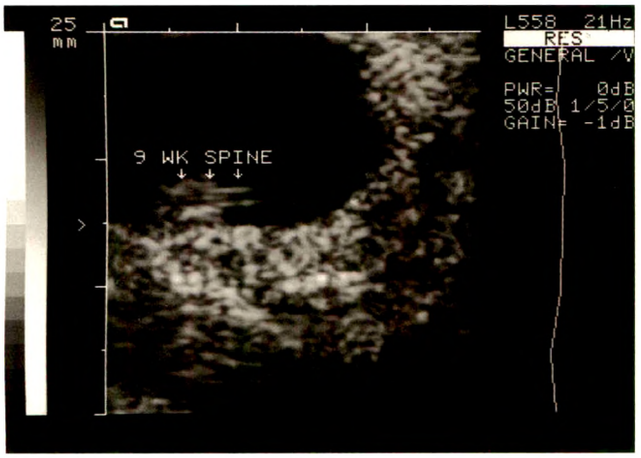
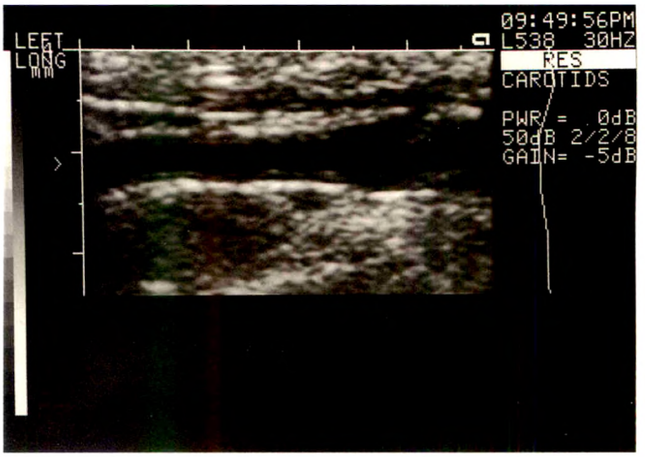


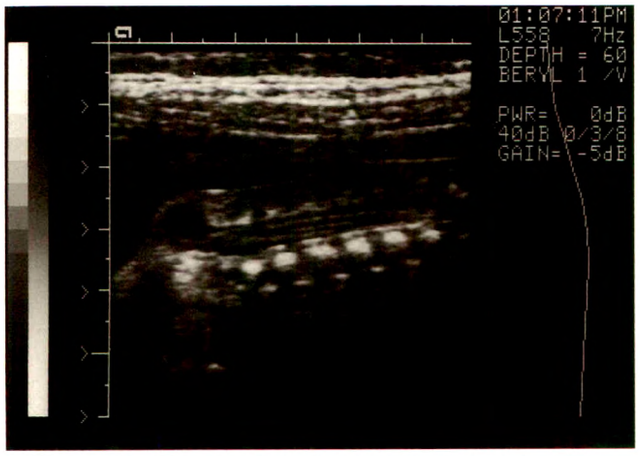
Image Uniformity: Near and far-field liver lesions
University of Alabama, Birmingham, AL.



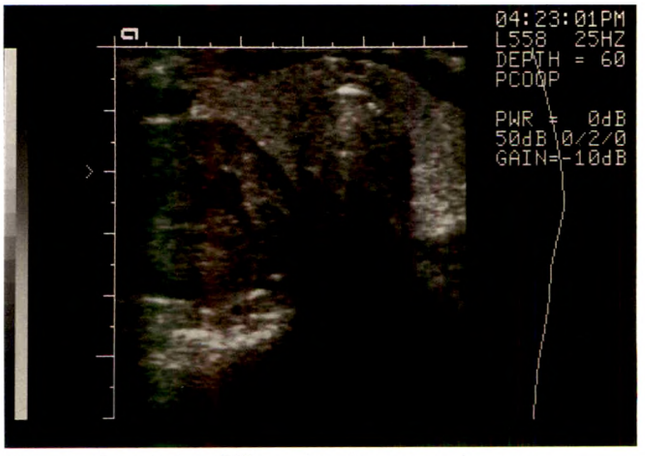
Early Diagnosis: Nine-week fetal spine
Frauenklinik, Salzburg, Austria



PV Scan Format: ICA, intimal defect, soft plaque
Huntington Memorial Hospital, Pasadena, CA.



Diagnostic Confidence: 2nd Trimester spinal defect
Diagnostic Ultrasound Association, Boston, MA.



Contrast Resolution: Differentiated neurogenic tumor, normal thyroid.
Vancouver General Hospital, Vancouver, B.C.

acuson
COMPUTED SONOGRAPHY

L O O K A T T H E F A C T S

Comparing phased annular arrays and Computed Sonography™ is like comparing a calculator to a computer. Phased annular arrays are conventional ultrasound technology—they are still mechanical scanners with all their inherent problems. Computed Sonography is new technology—the image is formed under total software control by our proprietary ultrasound computer. Look at the technologies. Then look at the images. There really is no comparison.

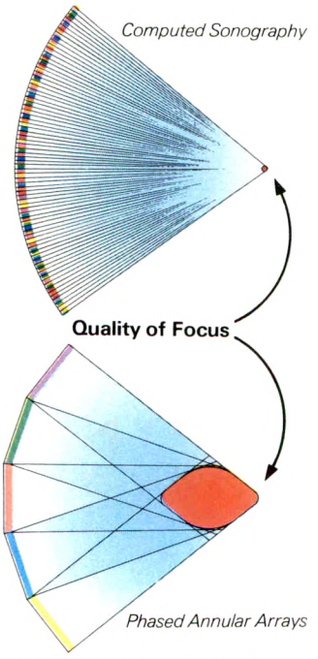
COMPARE THE TECHNOLOGIES

Image Quality

- Phased annular arrays have typically 5 information channels—not enough to maintain the uniform quality of focus necessary for the best detail and contrast resolution.
- Computed Sonography has 128 independent image resolution channels—producing images recognized as the Gold Standard in Ultrasound.

Reliability

- Phased annular arrays are mechanical, fluid-filled sector scanners with a known history of reliability problems.



Only Computed Sonography has enough channels to maintain excellent focal quality throughout the field of view.

- Computed Sonography delivers documented 99.9% up-time.

Linear Format

- Now recognized as the best format for Small Parts, Peripheral Vascular and Obstetric applications.
- Computed Sonography provides both linear and sector formats—phased annular arrays are sector only.

Simultaneous Imaging

- Only Computed Sonography provides simultaneous real-time imaging and Doppler or M-Mode—and from the same transducer.
- Simultaneous real-time imaging makes Doppler faster to learn and easier to perform.

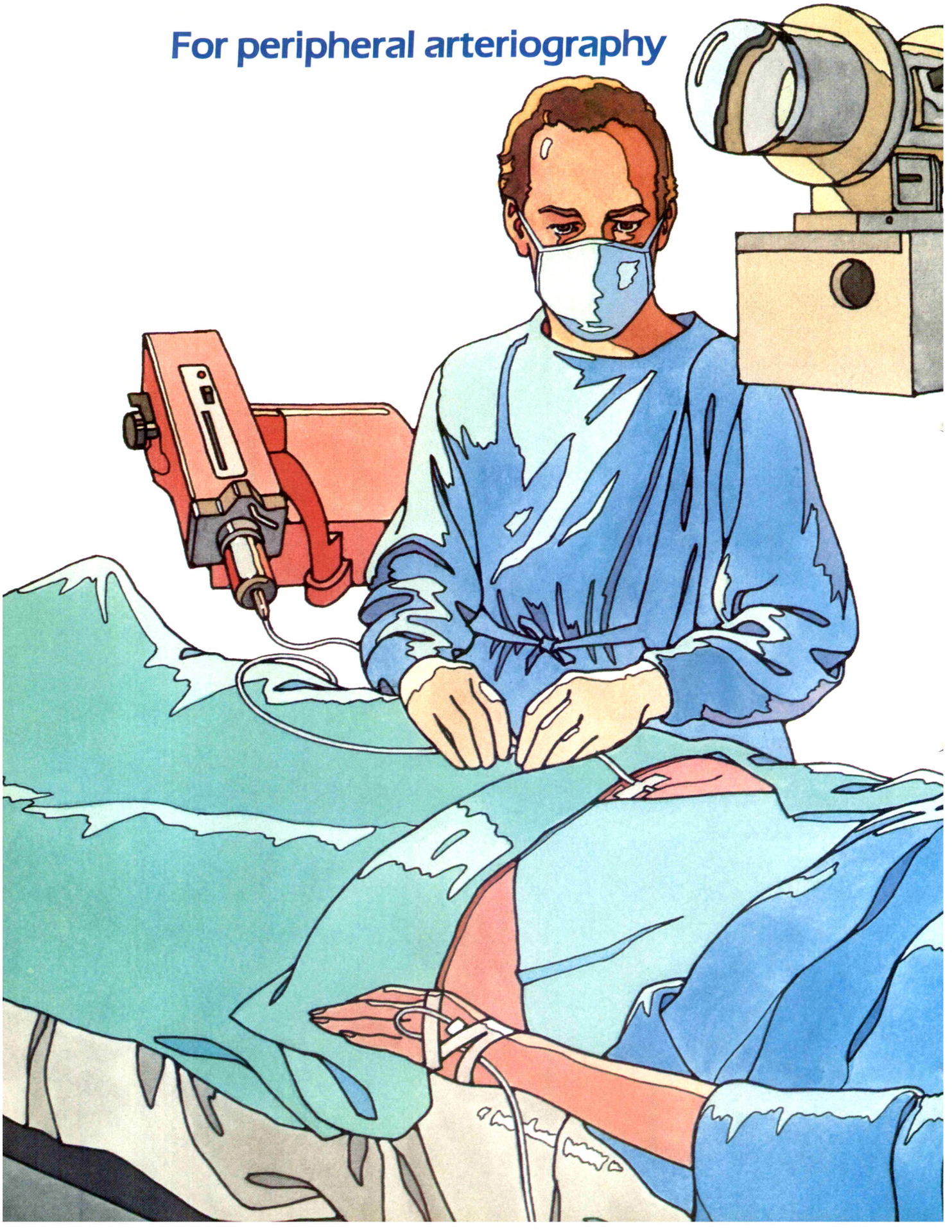
EVALUATE THE TECHNOLOGIES AND THE IMAGES: THERE IS NO COMPARISON.

- Call 1-800-4-ACUSON.
  Or in California 1-800-5-ACUSON.
  We'll make a believer out of you.

BELIEVE YOUR EYES!



For peripheral arteriography





ISOVUE®-300
iopamidol injection 61%

Nonionic contrast media that causes less pain than a leading ionic agent.

With Isovue, patients found procedures less painful; physicians saw fewer signs of distress

Isovue-300 is low in osmolality—616 mOsm/kg water.

Using a visual analog scale, patients undergoing peripheral arteriography ranked their pain from "no pain" to "the worst pain I ever had." On a linear scale from zero to 12.4 cm, the mean pain rating for 99 patients given a total of 155 injections of Isovue-300 was 2.3 cm compared with 6.3 cm for 97 patients given a total of 144 injections of the ionic agent diatrizoate meglumine and diatrizoate sodium 52%/8%.

By observing signs of distress, such as movement and/or vocalization, physicians ranked patient distress as being absent, mild, moderate, or severe. When Isovue was compared with diatrizoate meglumine and diatrizoate sodium 52%/8%, the number of injections judged to cause severe distress was 2/299 (1%) compared with 23/293 (8%); moderate distress, 13/299 (4%) compared with 58/293 (20%); mild distress, 59/299 (20%) compared with 94/293 (32%); and no distress, 225/299 (75%) compared with 108/293 (37%), respectively.

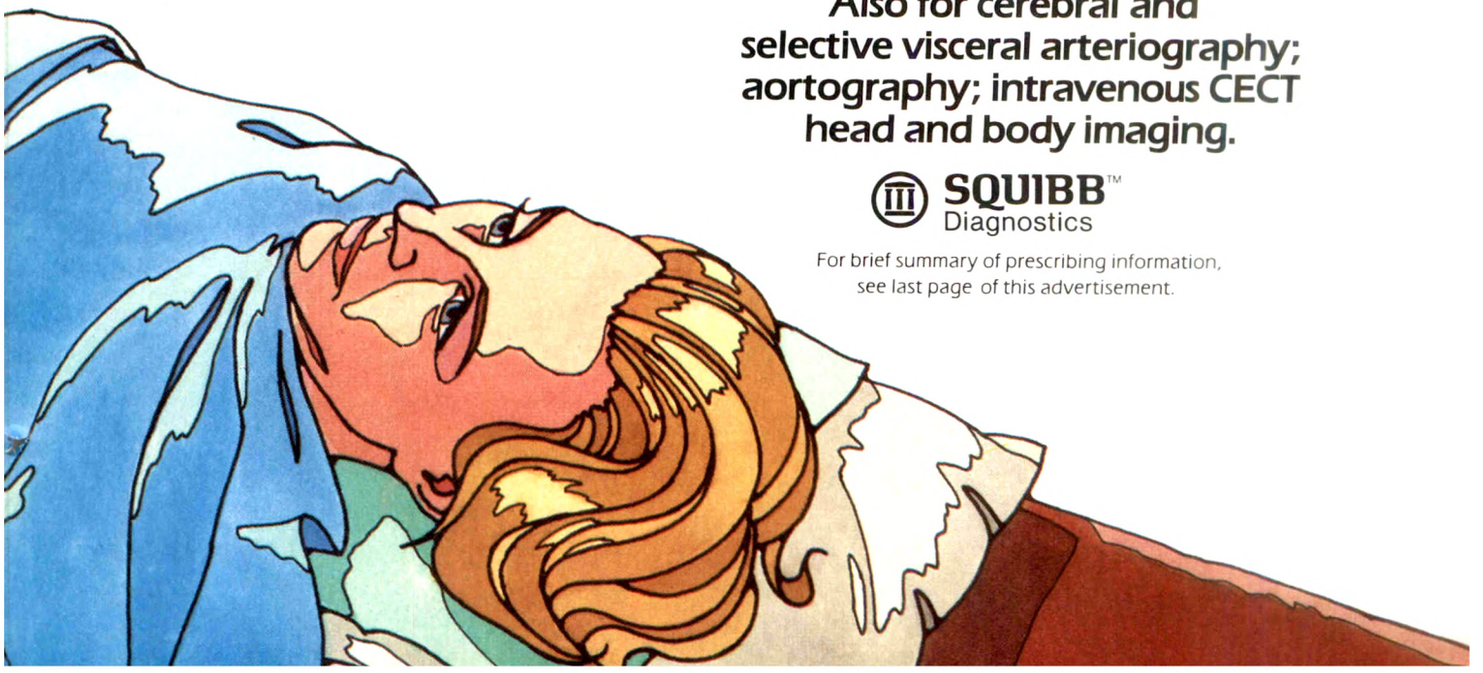
As with all injectable contrast agents, the possibility of severe reactions should be borne in mind. (See brief summary of prescribing information on the last pages of this advertisement for a discussion of CONTRAINDICATIONS, WARNINGS, PRECAUTIONS, and ADVERSE REACTIONS.)

ISOVUE®
iopamidol injection

Nonionic. Low in osmolality. Also for cerebral and selective visceral arteriography; aortography; intravenous CECT head and body imaging.

SQUIBB™
Diagnostics

For brief summary of prescribing information, see last page of this advertisement.



ISOVUE®-300
Iopamidol Injection 61%
ISOVUE®-370
Iopamidol Injection 76%

DESCRIPTION—ISOVUE (iopamidol injection) is a nonionic radiopaque contrast media for diagnostic use. The formulations are stable, aqueous, sterile, and nonpyrogenic solutions for intravascular administration. Each mL of ISOVUE-300 (iopamidol injection 61%) provides 612 mg iopamidol with 1 mg tromethamine and 0.39 mg edetate calcium disodium. The solution contains approximately 0.037 mg (0.002 mEq) sodium and 300 mg organically bound iodine per mL. Each mL of ISOVUE-370 (iopamidol injection 76%) provides 755 mg iopamidol with 1 mg tromethamine and 0.48 mg edetate calcium disodium. The solution contains approximately 0.046 mg (0.002 mEq) sodium and 370 mg organically bound iodine per mL. The pH has been adjusted to 6.5 to 7.5 with hydrochloric acid.

CONTRAINDICATIONS—None.

WARNINGS—Use caution in patients with severely impaired renal function, combined renal and hepatic disease, or anuria, particularly when larger doses are administered. Radiopaque diagnostic contrast agents are potentially hazardous in patients with multiple myeloma or other paraproteinemia, particularly in those with therapeutically resistant anuria. It has been speculated that the combination of the contrast agent and dehydration may be causative of anuria in myelomatous patients. This risk is not a contraindication; however, special precautions are required. Contrast media may promote sickling in individuals who are homozygous for sickle cell disease when injected intravenously or intraarterially. Administration to patients known or suspected of having pheochromocytoma should be performed with extreme caution. If the possible benefits outweigh the considered risks, the procedures may be performed; however, the amount of the medium injected should be kept to an absolute minimum. Assess blood pressure throughout the procedure and have measures for treatment of a hypertensive crisis available. Monitor such patients very closely. Use caution in patients with hyperthyroidism or with an autonomously functioning thyroid nodule because of risk of thyroid storm.

PRECAUTIONS: General—Diagnostic procedures should be carried out under the direction of personnel with the prerequisite training and a thorough knowledge of the particular procedure to be performed. Appropriate facilities should be available for coping with any complication of the procedure, or for emergency treatment of severe reaction to the agent itself. After parenteral administration, competent personnel and emergency facilities should be available for at least 30 to 60 minutes since severe delayed reactions may occur. Preparatory dehydration is dangerous and may contribute to acute renal failure in susceptible patients. *Patients should be well hydrated prior to and following administration.* Reactions to the medium, including serious, life-threatening, fatal, anaphylactoid or cardiovascular reactions, should always be considered (see ADVERSE REACTIONS in the product package insert). Patients at increased risk include those with a history of a previous reaction to a contrast medium, a known sensitivity to iodine per se, and a known clinical hypersensitivity (bronchial asthma, hay fever, and food allergies). Pretesting cannot be relied upon to predict severe reactions and may itself be hazardous for the patient. A thorough medical history with emphasis on allergy and hypersensitivity prior to the injection of any contrast medium may be more predictive and accurate than pretesting. Premedication with antihistamines or corticosteroids to avoid or minimize possible allergic reactions in such patients should be considered. General anesthesia may be indicated in some procedures in selected patients; however, a higher incidence of adverse reactions has been reported in anesthetized patients, which may be attributable to the inability of the patient to identify untoward symptoms, or to the hypotensive effect of anesthesia which can reduce cardiac output and increase the duration of exposure to the agent. Even though the osmolality is low compared to diatrizoate or iothalamate based ionic agents of comparable iodine concentration, the potential transitory increase in the circulatory osmotic load in patients with congestive heart failure requires caution during injection. Observe these patients for several hours following the procedure. In angiographic procedures, be aware of the possibility of dislodging plaques or damaging or perforating the vessel wall during catheter manipulations and contrast medium injection. Test injections to ensure proper catheter placement are suggested.

The inhibitory effects of nonionic contrast media on mechanisms of hemostasis have been shown, in vitro, to be less than ionic contrast media at comparable concentrations. For this reason, standard angiographic procedures should always be followed: angiographic catheters should be flushed frequently, and prolonged contact of blood with contrast in syringes and catheters should be avoided. Perform *selective coronary arteriography* only in those in whom the expected benefits outweigh the procedural risk. The inherent risks of *angiocardiography* in patients with chronic pulmonary emphysema must be weighed against the necessity for performing this procedure. *Angiography* should be avoided whenever possible in patients with homocystinuria, because of the risk of inducing thrombosis and embolism.

Drug Interactions—Renal toxicity has been reported in a few patients with liver dysfunction who were given oral cholecystographic agents followed by intravascular contrast agents. Administration of intravascular agents should therefore be postponed in any patient with a known or suspected hepatic or biliary disorder who has recently received a cholecystographic contrast agent. Other drugs should not be admixed with iopamidol.

Drug/Laboratory Test Interactions—PBI and radioactive iodine uptake studies will not accurately reflect thyroid function for up to 16 days following administration, however T3 resin uptake and total or free thyroxine (T4) assays are not affected. Any test which might be affected by contrast media should be performed prior to administration of the contrast media.

Carcinogenesis, Mutagenesis, Impairment of Fertility—In animal reproduction studies performed on rats, intravenously administered iopamidol did not induce adverse effects on fertility or general reproductive performance. In studies to determine mutagenic activity, iopamidol did not cause any increase in mutation rates.

Pregnancy Category B—No teratogenic effects attributable to iopamidol have been observed in teratology studies performed in animals. There are, however, no adequate and well controlled studies in pregnant women. It is not known whether iopamidol crosses the placental barrier or reaches fetal tissues. Because animal studies are not always predictive of human response, this drug should be used during pregnancy only if clearly needed. Radiologic procedures involve a certain risk related to the exposure of the fetus to ionizing radiation.

Labor and Delivery—It is not known whether use during labor or delivery has immediate or delayed adverse effects on the labor, the delivery or the newborn.

Nursing Mothers—It is not known whether iopamidol is excreted in human milk. Use caution when contrast media are administered to nursing women because of potential adverse reactions; consideration should be given to temporarily discontinuing nursing.

Pediatric Use—Safety and effectiveness in children have not been established.

ADVERSE REACTIONS—Usually mild to moderate, self-limited and transient. In angiocardiography (597 patients), the adverse reactions with an estimated incidence of one percent or higher are: hot flashes 3.4%; angina pectoris 3.0%; flushing 1.8%; bradycardia 1.3%; hypotension 1.0%; hives 1.0%. Intravascular injection is frequently associated with the sensation of warmth and pain, especially in peripheral arteriography; pain and warmth are less frequent and less severe with ISOVUE (iopamidol injection) than with diatrizoate meglumine and diatrizoate sodium injection. The following table of incidence of reactions is based on clinical studies with ISOVUE in about 1760 patients.

Adverse Reactions
Estimated Overall Incidence

System	> 1%	≤ 1%
Cardiovascular	none	tachycardia hypotension hypertension myocardial ischemia circulatory collapse S-T segment depression bigeminy extrasystoles ventricular fibrillation angina pectoris bradycardia transient ischemic attack thrombophlebitis
Nervous	pain (2.2%) burning sensation (1.4%)	vasovagal reaction tingling in arms grimace faintness
Digestive	nausea (1.2%)	vomiting anorexia
Respiratory	none	throat constriction dyspnea pulmonary edema
Skin and Appendages	none	rash urticaria pruritus flushing
Body as a Whole	hot flashes (1.5%)	headache fever chills excessive sweating back spasm
Special Senses	none	taste alterations warmth in throat/arms/chest nasal congestion visual disturbances
Urogenital	none	urinary retention

Regardless of the agent employed, overall estimated incidence of serious adverse reactions is higher with *coronary arteriography* than with other procedures. Cardiac decompensation, serious arrhythmias, or myocardial ischemia or infarction may occur during *coronary arteriography and left ventriculography.* Following coronary and ventricular injections, certain electrocardiographic changes (increased QTc, increased R-R, T-wave amplitude) and certain hemodynamic changes (decreased systolic pressure) occurred less frequently with ISOVUE (iopamidol injection) than with diatrizoate meglumine and diatrizoate sodium injection; increased LVEDP occurred less frequently after ventricular iopamidol injections. In *aortography,* the risks of procedures also include injury to the aorta and neighboring organs, pleural puncture, renal damage including infarction and acute tubular necrosis with oliguria and anuria, accidental selective filling of the right renal artery during the translumbar procedure in the presence of preexisting renal disease, retroperitoneal hemorrhage from the translumbar approach, and spinal cord injury and pathology associated with the syndrome of transverse myelitis. Adverse effects reported in literature include arrhythmia, arterial spasms, hematuria, periorbital edema, involuntary leg movement, malaise, and triggering of deglutition; some of these may be procedural. Other reactions due to procedural hazards include hemorrhage or pseudoaneurysms at the puncture site, brachial plexus palsy following axillary artery injections, chest pain, myocardial infarction, and transient changes in hepatorenal chemistry tests; and rarely arterial thrombosis, displacement of arterial plaques, venous thrombosis, dissection of the coronary vessels and transient sinus arrest.

General Adverse Reactions To Contrast Media—Reactions known to occur with parenteral administration of iodinated ionic contrast agents (see the listing below) are possible with any nonionic agent. Life-threatening reactions and fatalities, mostly of cardiovascular origin, have occurred. Reported incidences of death from the administration of other iodinated contrast media range from 6.6 per 1 million (0.00066%) to 1 in 10,000 patients (0.01%). Foreign experience in approx. 2.4 million patients receiving iopamidol suggest a lower risk of mortality. Most deaths occur during injection or 5 to 10 minutes later, the main feature being cardiac arrest with cardiovascular disease as the main aggravating factor. Isolated reports of hypotensive collapse and shock (est. 0.005%) are found in the literature. Experience with iopamidol suggests there is much less discomfort (e.g., pain and/or warmth) with peripheral arteriography. Fewer changes are noted in ventricular function after ventriculography and coronary arteriography. The reported incidence of adverse reactions to contrast media in patients with a history of allergy is twice that for the general population; patients with a history of previous reactions to a contrast medium are three times more susceptible. Most reactions to intravascular contrast agents appear within 1-3 minutes after the start of injection, but delayed reactions may occur (see PRECAUTIONS, General). Adverse reactions reported with other intravascular contrast agents and theoretically possible with iopamidol include: *Cardiovascular:* vasodilation, cerebral hematomas, petechiae; *Nervous:* paresthesia, dizziness, convulsions, paralysis, coma; *Respiratory:* increased cough, asthma, laryngeal edema, pulmonary edema, bronchospasm, rhinitis; *Skin and Appendages:* injection site pain usually due to extravasation and/or erythematous swelling, skin necrosis; *Urogenital:* osmotic nephrosis of proximal tubular cells, renal failure, pain; *Special Senses:* bilateral ocular irritation; lacrimation; conjunctival chemosis, infection, and conjunctivitis; *Other:* neutropenia, thrombophlebitis, flushing, pallor, weakness, severe retching and choking, wheezing, cramps, tremors, and sneezing.

For full prescribing information consult package insert. (J3-652C)

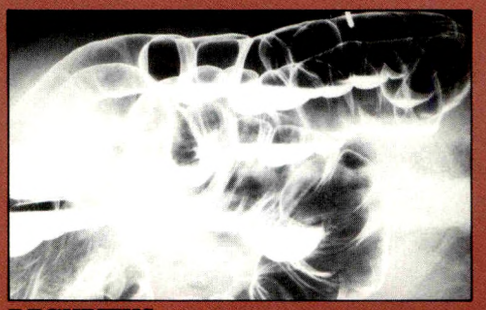
Under license from Bracco Industria Chimica S.p.A. U.S. Patent #4,001,323

© 1986 E.R. Squibb & Sons, Inc., Princeton, NJ 646-503 Issued: Sept. 1986

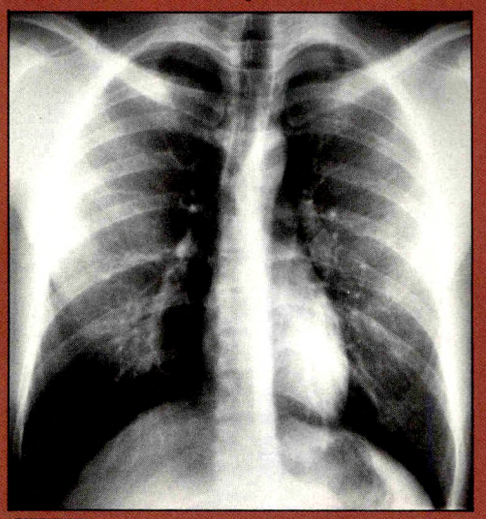
MORE DIAGNOSTIC DETAIL... LESS RADIATION EXPOSURE



FULL-SPINE. Full-spine scoliosis exam using compensation filters (as recommended by the FDA to reduce exposure). Note ideal density throughout the spinal column.



DECUBITUS. Right lateral decubitus radiograph with double contrast (barium and air). CLEAR-Pb Filter ends "image burn-out."

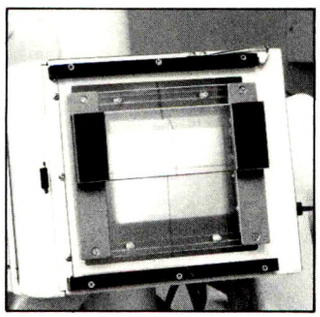


CHEST. Chest radiograph taken with CLEAR-Pb Chest Filter. Reveals all details of lungs and mediastinum.



LONG-LEG. Long-leg radiograph (weight-bearing) obtained with uniform-speed screens and a CLEAR-Pb Long-Leg filter. Note the even film density from hips to ankles.

Radiography Takes a Giant Step Forward with CLEAR-Pb® TRANSPARENT X-RAY COMPENSATION FILTERS



Magnetic mounting system allows instant adjustment of lightweight filter.

- **Improve image quality by providing a more uniform film density.**
- **Reduce patient exposure by selectively attenuating the x-ray beam.**
- **Reduce the need for multiple exposures.**
- **Transparent lead-plastic filters never block the collimator light field.**
- **Easy to use; mount to any collimator.**

For details on our full line of Image Compensators, request Bulletin 361-C.

Finally, there's an easy way to solve your imaging problems. With a CLEAR-Pb Filter you are assured of top-quality images the first time...every time. Over and under-penetration of the patient are eliminated, and important details are improved dramatically.

Try a CLEAR-Pb Filter. You will find one available for most routine exams. There's no easier or better way to obtain superb images...**GUARANTEED!***

* **100% SATISFACTION GUARANTEED!** Buy a CLEAR-Pb Filter and use it for 30 days. If it doesn't meet your expectations, return it for full credit.

® Victoreen, Inc.

NUCLEAR ASSOCIATES

VICTOREEN

A Division of VICTOREEN, INC.
100 VOICE ROAD
CARLE PLACE, NY 11514-1593
(516) 741-6360
A Subsidiary of Sheller-Globe SG

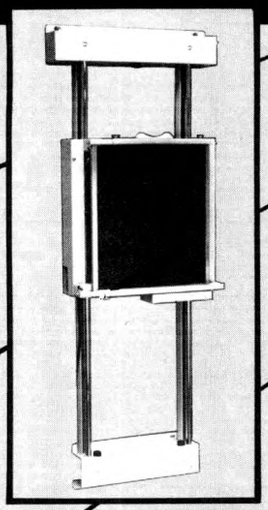
THE BREAKTHROUGH IN IMAGE COMPENSATORS

There are reasons
S.&S. X-RAY ACCESSORIES
are preferred...

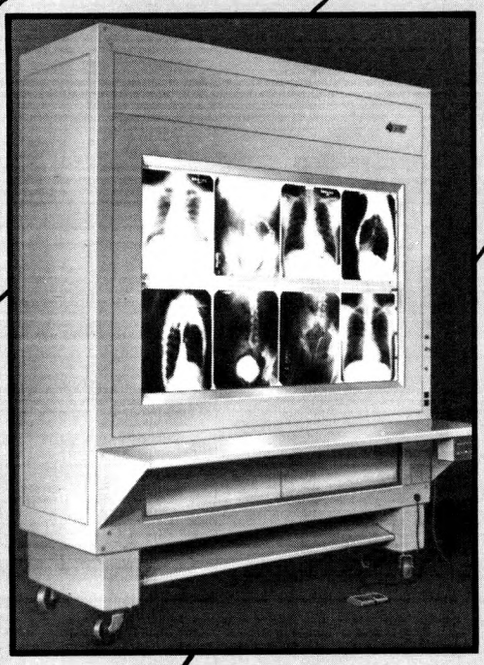
PROVEN the best in X-Ray Departments throughout the world

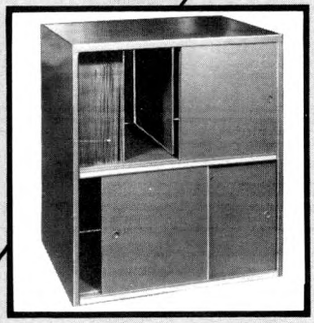
UNEQUALLED in design, construction and—quality

REPUTATION unmatched for RELIABILITY and PERFORMANCE









- Motorized Viewers
- Illuminators
- Transfer Cabinets
- File Cabinets
- Protective Panels
- Protective Aprons
- Wall Cassette Holders
- Dryers
- Safelights
- Dark Room Cabinets
- Storage Chests
- Loading Bins
- X-Ray Accessories

For more than 30 years, S. & S. has been meeting Radiologists' needs with a complete line of illuminators and accessories.

Contact S. & S. or your local x-ray dealer for additional information.

MANUFACTURED BY
S. & S. X-RAY PRODUCTS INC.

The Complete Line of X-Ray Accessories
(800)221-6634

Telephone: (212) 852-6900
87-93 JAY STREET, BROOKLYN, N.Y. 11201

See us at RSNA—Booth #2419

How to reduce the costs of bowel preparation before and after the X-ray



Before

Evac-Q-Kwik® helps keep hospital costs down by eliminating the staff time and labor involved in giving enemas. And everything needed for effective bowel evacuation is contained in one cost-effective kit.



Nurses appreciate Evac-Q-Kwik because it can be administered during a single shift and completed during one 6-hour period. Patients prefer the simple, comfortable Evac-Q-Kwik procedure, too. Evac-Q-Kwik contains no sugar, no alcohol, and is low in sodium.

After



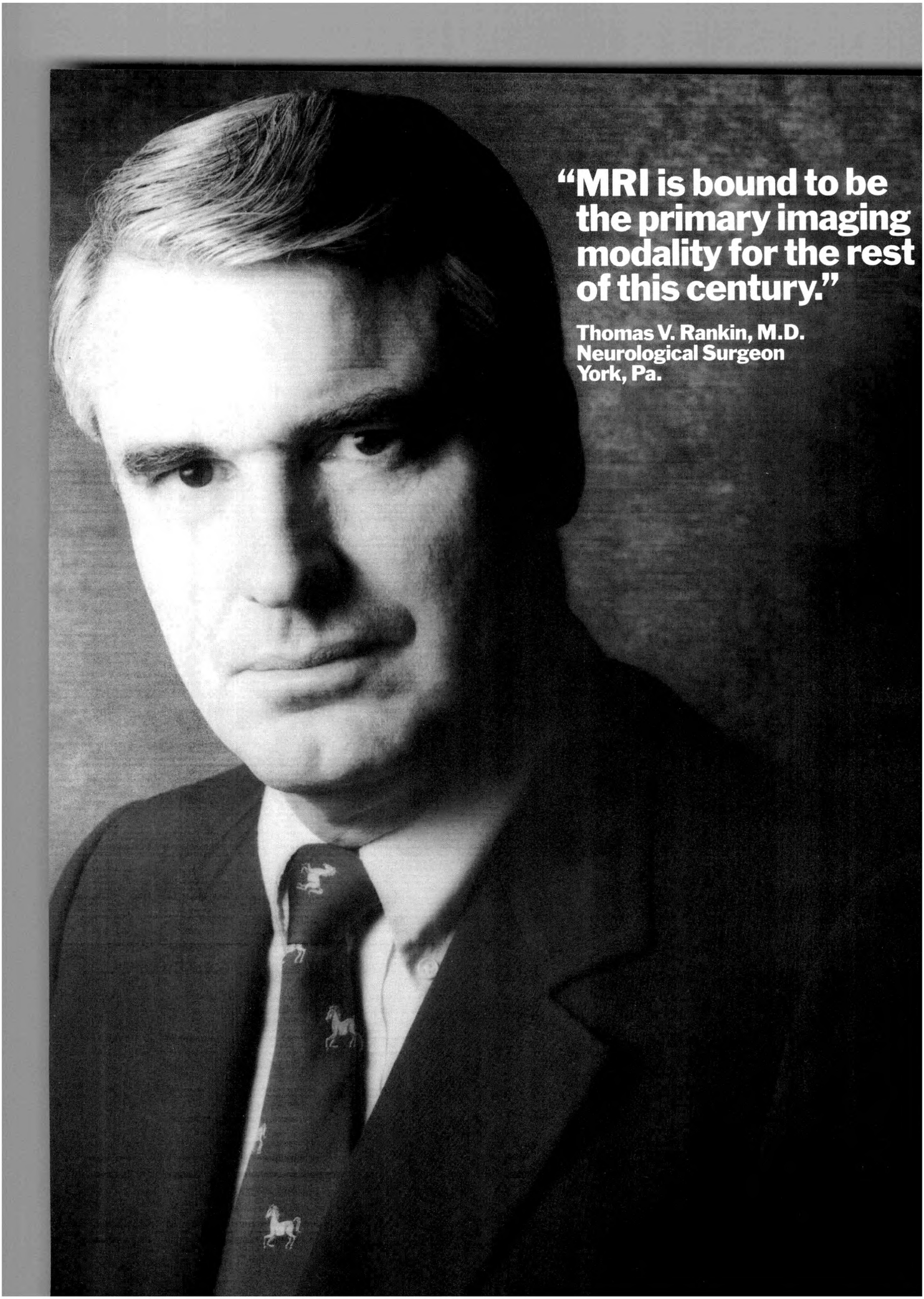
Evac-Q-Kwik is the ideal bowel prep for today's cost-conscious climate. It effectively cleans the colon for clear X-rays *the first time*, to reduce the need for expensive, time-consuming retakes that escalate hospital costs.

Evac-Q-Kwik®



Adria®

Adria Laboratories
Columbus, OH 43215


"MRI is bound to be the primary imaging modality for the rest of this century."
Thomas V. Rankin, M.D.
Neurological Surgeon
York, Pa.

"Magnetic resonance imaging is already becoming standard in the diagnosis of disorders of the central nervous system.

Its noninvasive technology—using low electromagnetic energy instead of conventional x-rays—makes it one of the safest diagnostic tools we have.

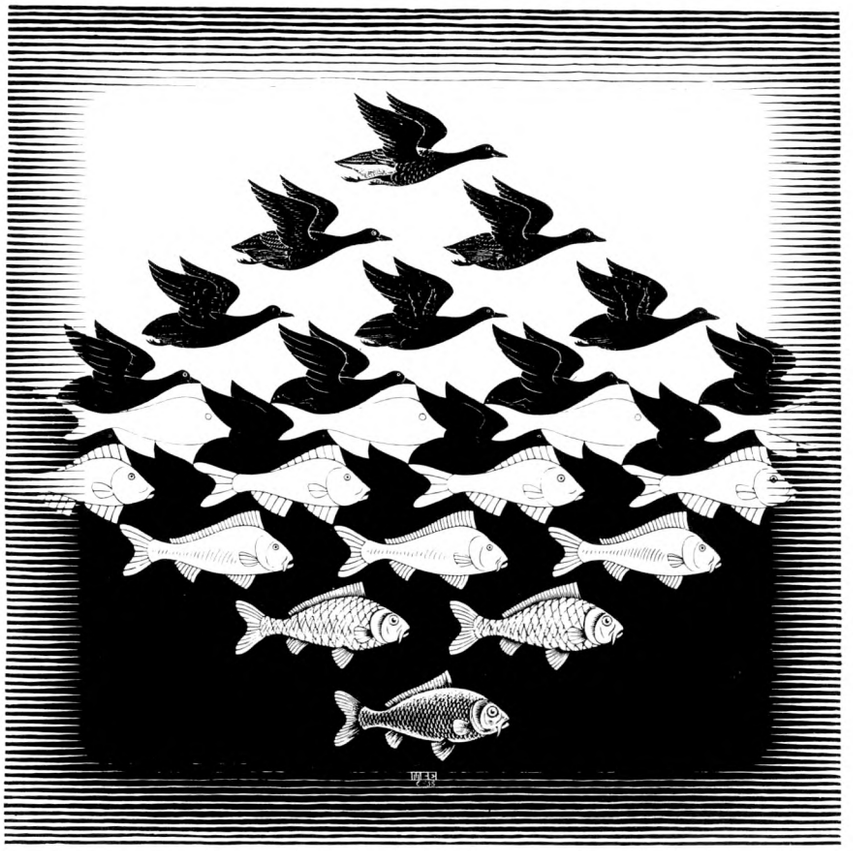
And its ability to observe body chemistry makes it one of the most precise.

The films I see from THOMSON-CGR's Magnascan 5000 are of unprecedented quality. The head images are absolutely the best available.

What we're talking about here is a revolution in medical diagnostics, and a company in the vanguard of that revolution."

For more information call or write THOMSON-CGR, 10150 Old Columbia Road, Columbia, Md. 21046. (301) 964-6600. We're THOMSON-CGR. We want you to know.

THOMSON CGR



© M.C. Escher Heirs c/o Cordon Art-Baarn, Holland

PERCEPTION

No two people see things exactly the same way. Each of us combines what we see with what we know to create our own, unique perceptions.

You've probably used E-Z-EM products for years, and think of us as "the barium company". But we're more than that. Over the years we've expanded to become a full-line supplier of imaging products and services.

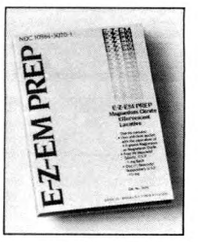
We've grown because we've never stopped looking for new ways to help the radiologist and technologist, or lost our willingness to adapt our products to your personal perception of what you need.

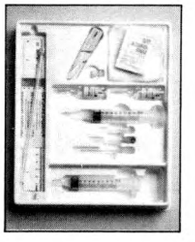
That's why our new PercuSet™ line of disposable procedure trays and our complete line of PercuCut™ biopsy needles can accommodate a wide range of options, and why our Pinnacle™ protective garments can be custom adjusted for your comfort. It's why our E-Z-EM Prep colon prepping systems were developed, and why we've always offered the broadest range of barium sulfate products.

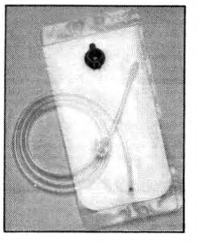
E-Z-EM

More than barium—much more









Protective Products
Colon Prepping Products
Interventional Products
Barium Products

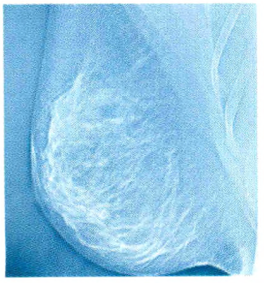
E-Z-EM®

E-Z-EM, Inc., 7 Portland Ave., Westbury, N.Y. 11590, Toll Free 800-645-3052, In New York 516-333-8230

© E-Z-EM, Inc. 1986

XEROX

Compare the two images below. Both are the same breast tissue specimen. One is a film screen image, the other, a Xeroradiograph. As you can clearly see, Xeroradiography shows calcifications easier.



Small wonder that Xeroradiography is the most widely used method for mammography.

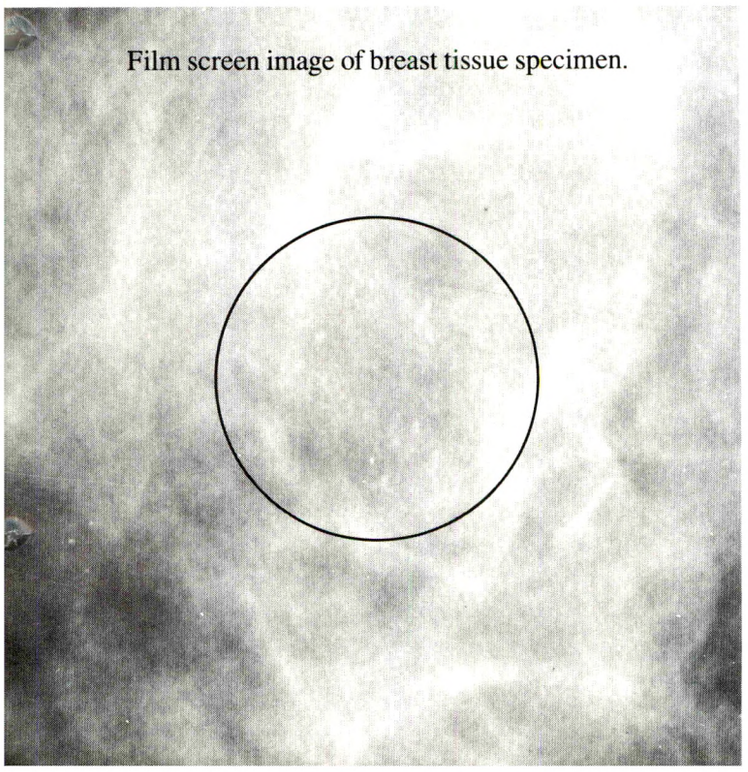
Its wide recording latitude shows you the nipple to the chest wall on one image. This, together with the clarity provided by superior resolution and edge enhancement, allows calcifications to be seen anywhere in the breast.

For more information, call or write Xerox Medical Systems, P.O. Box 5786, Pasadena, CA 91107, (818) 356-1221.

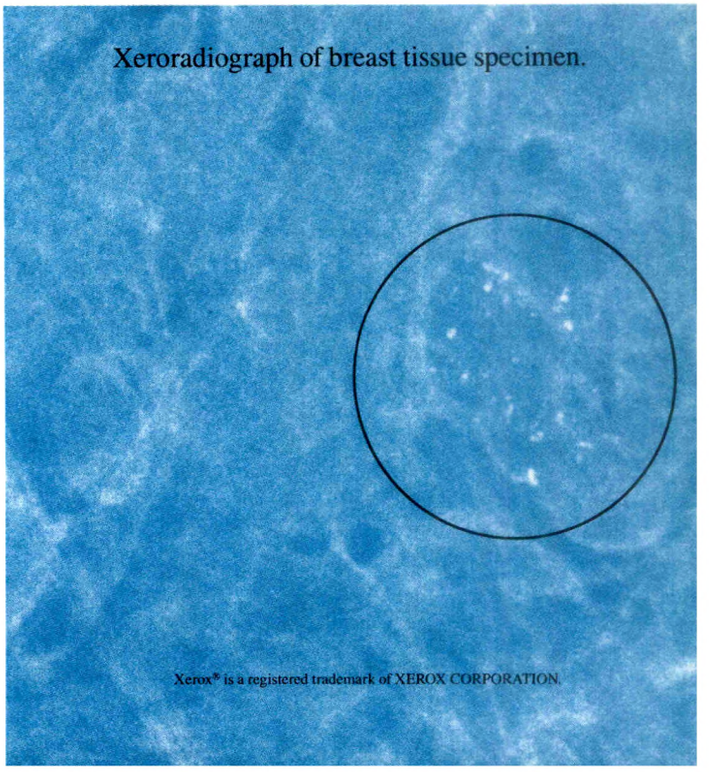
Team Xerox

Xeroradiography. It's easy to see. And that's why radiologists have made it the image of choice.

It's easy to see why our image is #1



Film screen image of breast tissue specimen.



Xeroradiograph of breast tissue specimen.

Xerox® is a registered trademark of XEROX CORPORATION.

Efficient bowel evacuants for diagnostic procedures

Take one

X-Prep®

for a cleaner, clearer film

Excellent visualization...fewer retakes

■ 95% efficacy proven with X-PREP® Liquid in 749 patients prepared for diagnostic procedures such as barium enemas and IVPs*

■ Effective for colonoscopy and sigmoidoscopy*

X-PREP® Liquid
2½ fl. oz. (74 ml) (standardized extract of senna fruit)

*Data on file, Medical Department, The Purdue Frederick Company.

Gray Pharmaceutical Co., Affiliate
The Purdue Frederick Company
Norwalk, CT 06856

X-PREP® Bowel Evacuant Kit-1
Contains two SENOKOT-S® Tablets (standardized senna concentrate and docusate sodium), one bottle of X-PREP Liquid 2½ fl. oz. (74 ml), one RECTOLAX® Suppository (bisacodyl 10 mg), plus easy-to-follow instructions.

X-PREP® Bowel Evacuant Kit-2
Contains one pack CITRALAX® Granules 1.06 oz. (effervescent citrate/sulfate of magnesia), one bottle of X-PREP Liquid 2½ fl. oz. (74 ml), one RECTOLAX Suppository, plus easy-to-follow instructions.



© 1984, Gray Pharmaceutical Co. PFR-081/84

Caldwell Lecture

Armchair Research and the Practicing Radiologist

Benjamin Felson[1]

When he invited me to give the Caldwell Lecture, Jerry Wiot said, "Please make it nonscientific." Perhaps this should have disturbed me, but I knew what he meant. One of the hallmarks of "maturity" is that your assignments become parascientific. To illustrate, I have been relegated recently to making television interviews of *Living Legends in Radiology*, to giving speeches with such titles as *They Still Need the Conventional Radiologist* and *Humor in Medicine*, and to writing about *The Tennis World of the Elderly.* Since Jerry is still my boss, I once more acceded, and I have selected the title *Armchair Research and the Practicing Radiologist.*

First let's define some terms. I said armchair, not wheelchair, indicating that the age of the researcher is not relevant to my thesis. By "armchair research" I mean research that uses instructive case material as a basis for creative thinking. It is also called clinical research, because neither the basic sciences nor animal or laboratory models are emphasized. The project is disease-oriented, and evidence pro and con is collected from information about the patient and from study of the literature.

By "practicing radiologist" I refer to one working in a nonacademic setting. As a group, practicing radiologists are a huge potential source of experience and clinical information. I have heard all the excuses why many practitioners do not write, including the usual too busy, too tired, too many family and social obligations. None of these, in fact, is really valid because many practitioners do contribute to our scientific programs and to our literature. For some radiologists the lure of inquiry and exposition is as compelling in practice as in academics.

Armchair research requires only a few hours each week (but every week, lest you forget where you've left off in your project). It takes self-discipline and a little imagination, but that's about all. University connections, grants, and intellectual brilliance are not necessary. Planning, thinking, and working are all that are required. Remember, virgin wool comes from ugly sheep.

Let me cite some examples. Eugene Caldwell was an engineer, scientist, inventor, physician, and professor, but he later became a practicing radiologist who performed outstanding armchair research.

Albert Einstein was one of the greatest armchair researchers of all time. This photograph (Fig. 1) is not of Albert Einstein, but of his look-alike, my late father-in-law, Jacob Raphaelson, who did some remarkable armchair research in optometry by proving the value of +1 lenses in preserving vision in children.

I have known some splendid armchair researchers. Figure 2 is of Louis Raider, a practicing radiologist in Mobile who called attention to a lucent triangle on the normal lateral chest film where the two lungs come together (Fig. 3). His fine paper was rejected by several well-known radiology journals, but he persisted [1]. This triangle lies along the main vertical thoroughfare through the thorax, and a lesion of the trachea, esophagus, thyroid, lymph nodes, or great vessels, often obscure on conventional posteroanterior and lateral views of the chest, can often be detected by noting opacity in this space (Fig. 4). A glance at Raider's triangle on every lateral chest film is mandatory. This glance has often saved my neck, and more important, the patient's.

Bert Pear (Fig. 5), who practices in Denver, has written some penetrating and scholarly articles. Among other subjects, he has studied amyloidosis and has called attention to

Received May 5, 1986; accepted after revision June 26, 1986.
Caldwell Lecture presented at the American Roentgen Ray Society annual meeting, Washington, DC, April 1986.
[1] Department of Radiology, University of Cincinnati, College of Medicine, Cincinnati, OH 45267-0742. Address reprint requests to B. Felson.

AJR 147:881–890, November 1986 0361–803X/86/1475–0881 © American Roentgen Ray Society

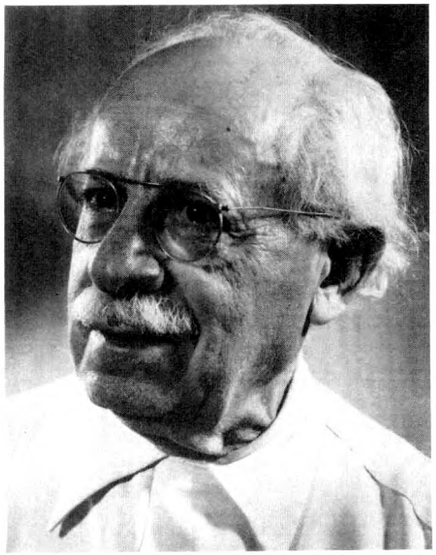


Fig. 1.—Armchair researcher (see text).

calcification in pulmonary amyloid nodules [2, 3]. In fact, this bland form of amyloidosis can sometimes be diagnosed by the presence of multiple large indolent nodules, some calcified, that come in a variety of sizes and shapes (Fig. 6) [4].

Richard Mulvey of Cincinnati (Fig. 7) is another practicing radiologist who does imaginative and innovative armchair research. He was the first to describe the thymic wave sign [5], in which the large normal thymus can be recognized on the frontal chest film by the imprint of the costal cartilages on its lateral borders (Fig. 8). He also extended the concept of inversion of the diaphragm. By the simple expedient of giving a barium swallow to all patients with a large left pleural effusion (Fig. 9), he found that diaphragm inversion is common, and he demonstrated its paradoxical motion with respiration, a cause of life-threatening dyspnea [6]. Inversion of the diaphragm due to pleural effusion is not widely appreciated, even now.

Mulvey called me recently to tell me how to distinguish between pleural fluid and edema in the subpleural or peripheral space of Weibel [7]: simply turn the patient into the lateral decubitus with the involved side up (Fig. 10). CT also shows the fluid in Weibel's space, but it costs a lot more.

University radiologists do a lot of armchair research, too. Our major journals are full of it. I can illustrate this with some of the works of staff members in our department.

Kenneth Kattan is an observant and effective armchairman (Fig. 11). Reading films at our mental hospital one day, he saw a case in which the skull of a youth had thickened considerably over a few years (Fig. 12). Further investigation revealed that the patient was an epileptic. After more sleuthing, Kenneth showed that Dilantin therapy thickens the skull [8]! He also discovered the superior triangle sign of lower-lobe collapse (Fig. 13) [9] and the diaphragmatic tenting sign of upper-lobe collapse (Fig. 14) [10]. Kenneth has the effrontery to discover new signs and refer to illustrations in my book that demonstrate them. The pain is lessened by his use of Fraser and Paré for similar purposes.

Donald Heimbrock (Fig. 15) was the first to observe signs of intramural bleeding in the renal pelvis and ureter from Coumadin (warfarin) overdosage (Fig. 16) [11]. Jerome Wiot (Fig. 17) described the same condition in the duodenum [12]. My own armchair research in regard to the silhouette sign worked out pretty well [13], but I have failed miserably to prove experimentally the physical principle behind it [14].

Apart from advancing medical knowledge, armchair research provides benefits for the researcher. It is a great

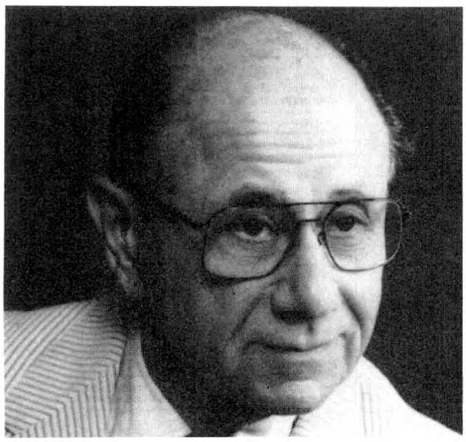


Fig. 2.—Louis Raider, Mobile, AL.

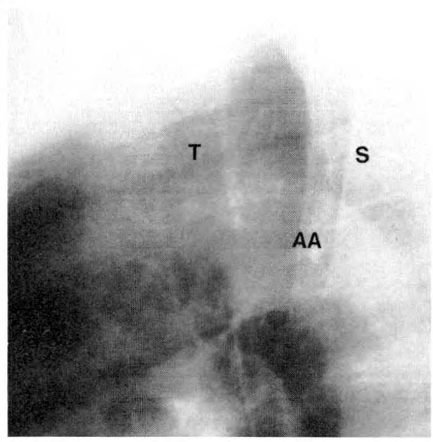


Fig. 3.—Normal lateral view of chest showing Raider's triangle, bounded anteriorly by back of trachea (T), inferiorly by aortic arch (AA), posteriorly by spine (S), and superiorly by thoracic inlet. Scapular margins sometimes project across it.

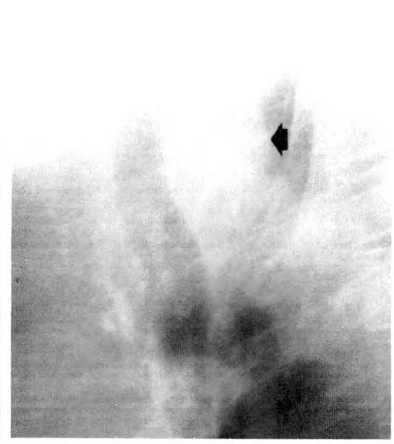


Fig. 4.—Posterior right aortic arch (*arrow*) seen in Raider's triangle.

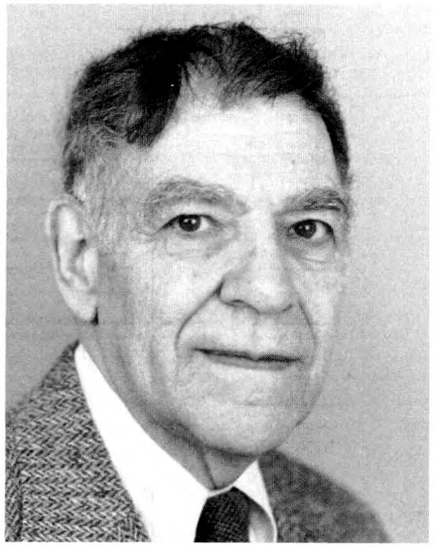
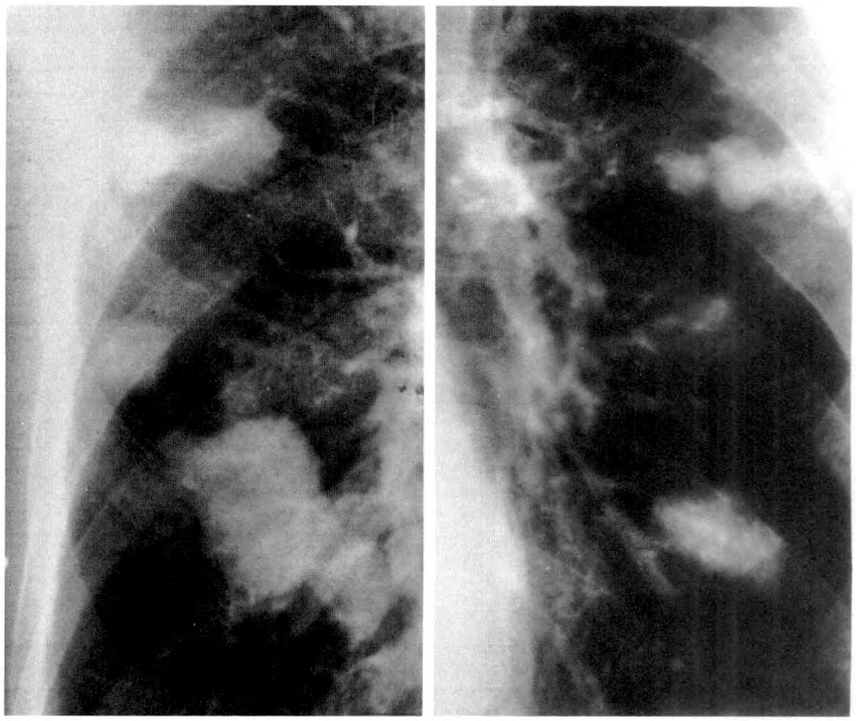


Fig. 5.—Bert Lincoln Pear, Denver, CO.



A B

Fig. 6.—Amyloidosis of the lung. *A*, Right lung. *B*, Left lung. Pulmonary nodules are indolent, sharply outlined, and widely varying in shape and size. Note stippled calcium in lowermost nodule in *B*. This combination of findings is almost diagnostic of nodular pulmonary amyloidosis, a benign disease. (Courtesy of Seminars in Roentgenology [4]).



Fig. 7.—Richard B. Mulvey, Cincinnati, OH.

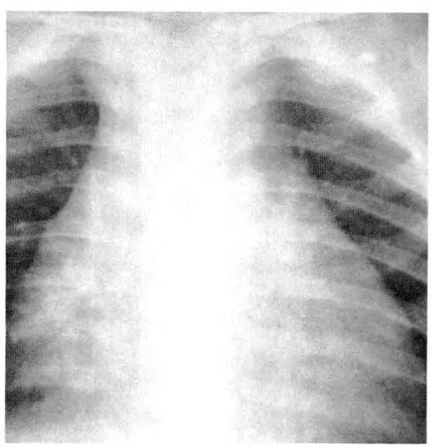


Fig. 8.—Thymic wave sign (on a calm day). Enlargement of right side of mediastinum in this child can be recognized as normal thymus tissue by the wavy indentations produced by third, fourth, and fifth costal cartilages.

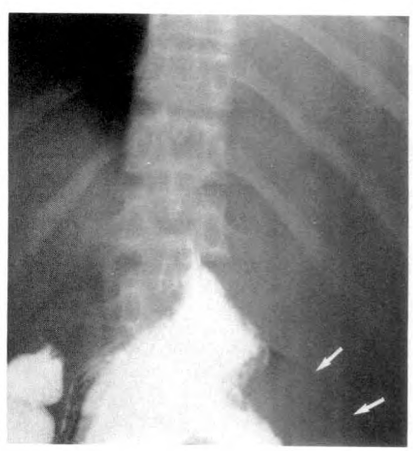
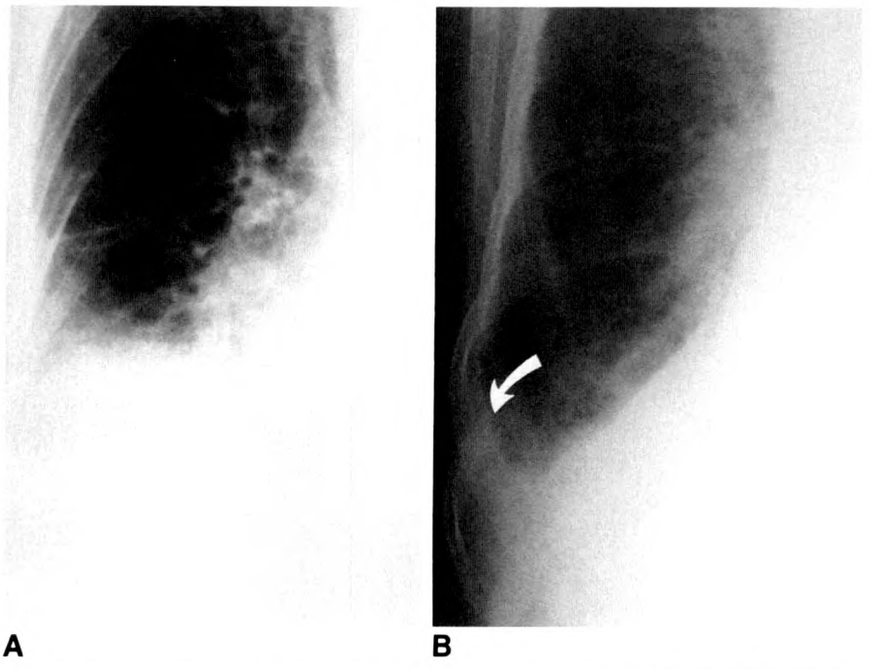


Fig. 9.—Inversion of left hemidiaphragm, indicated by marked downward and medial displacement of fundus of stomach with indentation of left margin. Spleen (*arrows*) is not enlarged. Diaphragm inversion is a common event, generally caused by large left pleural effusion but sometimes by intrathoracic tumor or cyst. Paradoxical motion of the two leaves of diaphragm occurs and may result in severe dyspnea from pendulum breathing.



A B

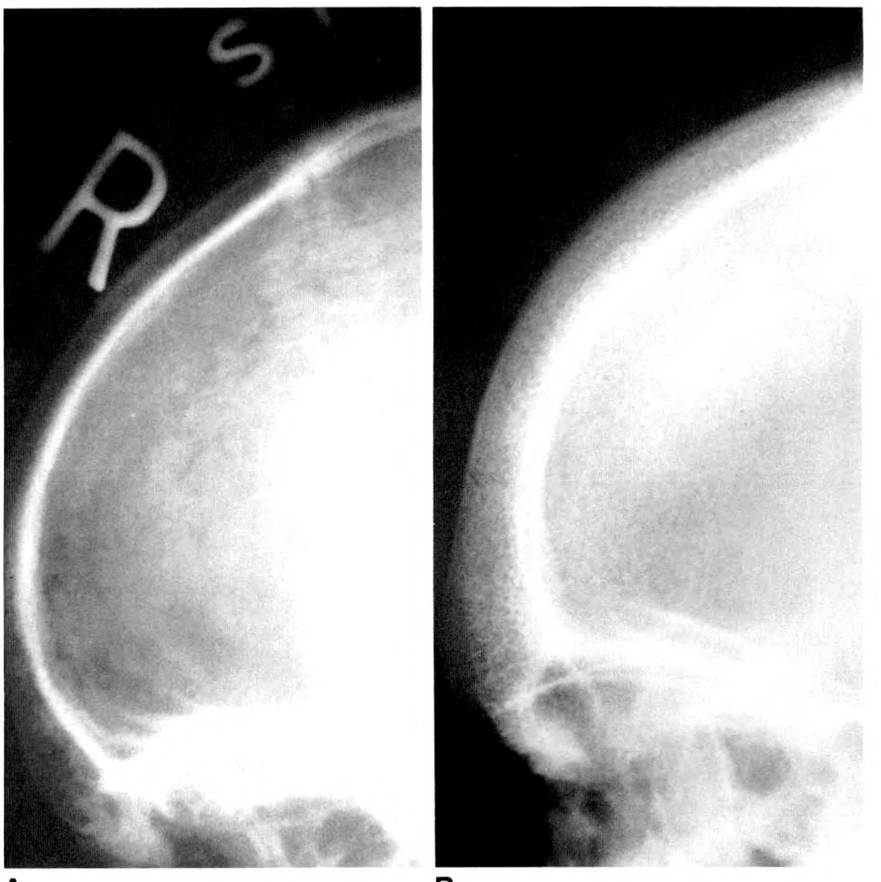
Fig. 10.—Distinction between free pleural fluid and subpleural alveolar edema.

A, Posteroanterior radiograph. Patient is in cardiac failure and there is a moderate-sized right pleural effusion.

B, Left lateral decubitus (film printed upright for comparison). Free pleural fluid has gravitated medially. Remaining density in costophrenic angle (*curved arrow*) is attributable to subpleural alveolar edema, confirmed on CT.



Fig. 11.—Kenneth R. Kattan, Cincinnati, OH.



A B

Fig. 12.—Lateral views of skull in 14-year-old epileptic boy. *A*, Before Dilantin treatment. *B*, After 3 years of Dilantin, 100 mg twice daily. Note marked widening of diploe. (Courtesy of *American Journal of Roentgenology* [8]).

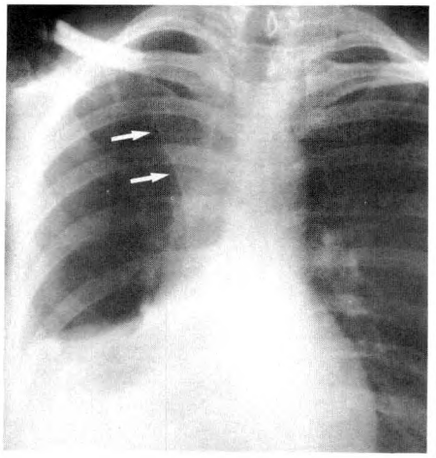


Fig. 13.—Superior triangle sign due to shift of anterior mediastinum (*arrows*), indicating collapse of lower lobe. Middle lobe is also collapsed. Unlike right upper lobe collapse, triangle stops at right clavicle, indicating its anterior location. Lower end of triangle continues downward as anterior junction line. Right hilum is depressed. (Courtesy of *Radiology* [9]).

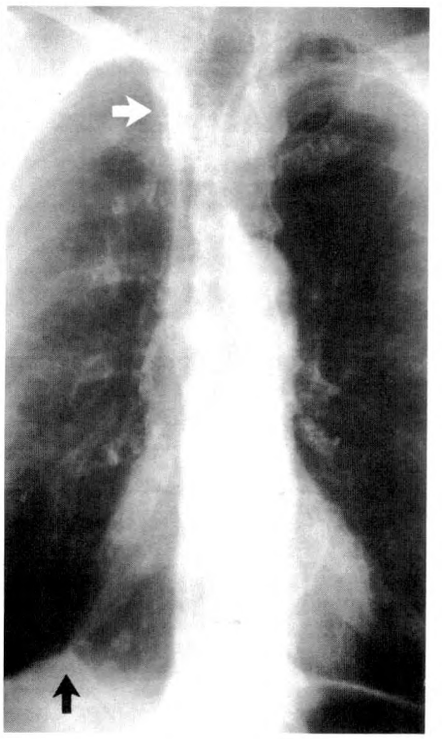


Fig. 14.—Tenting of right hemidiaphragm (*black arrow*) in upper lobe collapse. Note thick strip along right border of trachea (*white arrow*), which represents marked collapse of right upper lobe secondary to tuberculosis. Right hilum is drawn upward and is higher than left. (Courtesy of *Seminars in Roentgenology* [10]).



Fig. 15.—Donald J. Heimbrock, Cincinnati, OH.

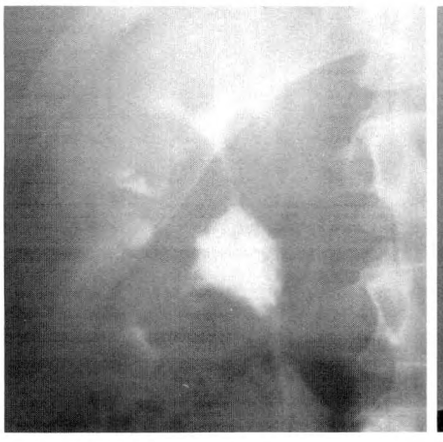


Fig. 16.—Intramural bleeding of renal pelvis and ureter following Coumadin (warfarin) overdosage. Note fine bubbly pattern in pelvis and upper ureter, the "champagne" sign. Subsequent urogram showed normal pelvis and ureter. (Courtesy of *Radiology* [11]).

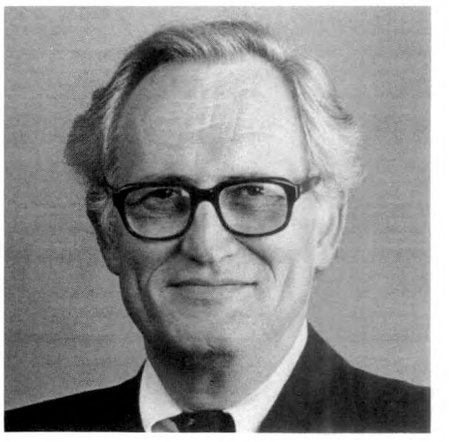


Fig. 17.—Jerome F. Wiot, Cincinnati, OH.

learning device, and the knowledge acquired is never forgotten. To paraphrase Daniel Drake: "Write much, publish little, and learn a lot." Pride and self-respect well up when the author sees his opus in print, and prestige and credibility soon follow. But mostly it's fun—the sheer pleasure of learning and teaching is its own reward.

How to get started? The selection of a topic depends, of course, on one's interest and experience, but the subject

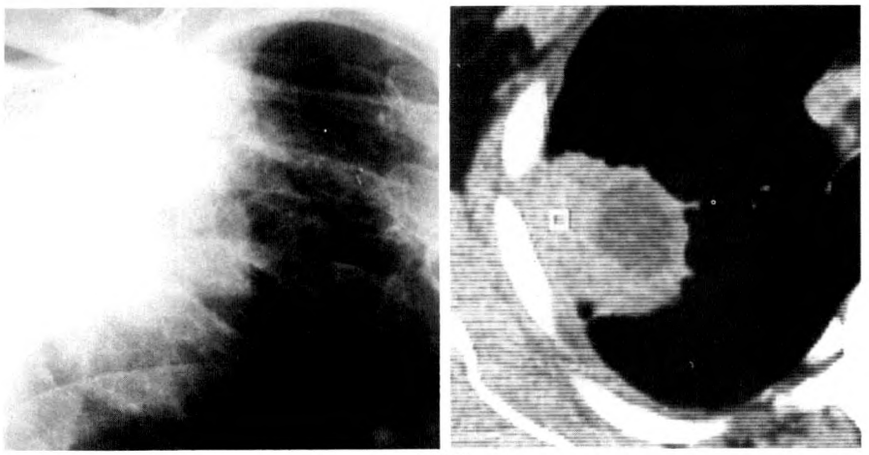


Fig. 18.—Carcinoma of lung complicating lipoid pneumonia.

A, Plain chest film shows large density in right upper lung.

B, CT at mediastinal setting. Note lucency in medial portion of pulmonary lesion. Bronchial brushing of lesion showed oil droplets and intracellular lipid deposits. Patient history indicated that he nightly anointed his throat with vaseline. At surgery 1 month later, right upper lobe was resected, showed squamous carcinoma, grade 1, with cavitation and central necrosis. (Courtesy of John A. Campbell, Los Angeles, and the *American Journal of Roentgenology* [15]).

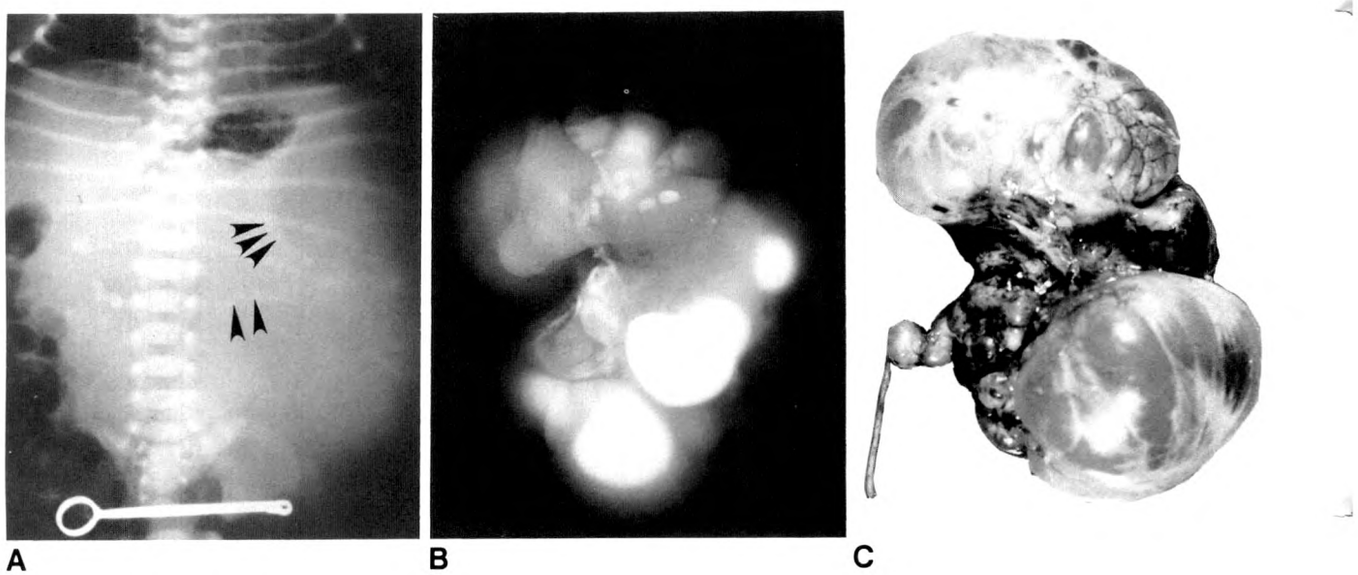


Fig. 19.—Left multicystic kidney.

A, Urogram shows poor renal function and large ringlike shadows (*arrowheads*).

B, Multicystic kidney was resected. Specimen radiograph was obtained after barium suspension was injected into the ureter proximal to atretic segment. All cysts intercommunicated.

C, Surgical specimen of another unilateral multicystic kidney with pelvoinfundibular atresia preventing intercommunication. (Courtesy of *Seminars in Roentgenology* [17, 18].

should not strain credulity. An article on the radiology of heart transplants coming from Minot, ND, would sound as flat as a bugler with a hernia. But many articles on the newer techniques are being written by practicing radiologists who, early on, have acquired the appropriate equipment, often before academic institutions.

Begin with a case report? Fine. I ran across a patient with mineral oil pneumonia who developed bronchogenic carcinoma (Fig. 18), and put it in my "crazy" file. Before I knew it, I had four more cases, some contributed by colleagues [15].

Keep your unique cases at hand. Every 6 months or so, I go through my own file of exceptional cases and reestablish follow-up. This type of file pays dividends. For example, more than 30 years ago, I saw two infants whose urograms showed a very poorly functioning kidney with faint ring shadows (Fig. 19). At surgery, unilateral multicystic kidney with intercommunicating cysts was found in both. I considered this strong evidence that multicystic kidney was really endstage fetal hydronephrosis. But what of the unilateral multicystic kidneys that didn't show communicating cysts? Twenty years later, Thorne Griscom of Boston described a form of multicystic kidney with pelvoinfundibular atresia preventing intercommu-

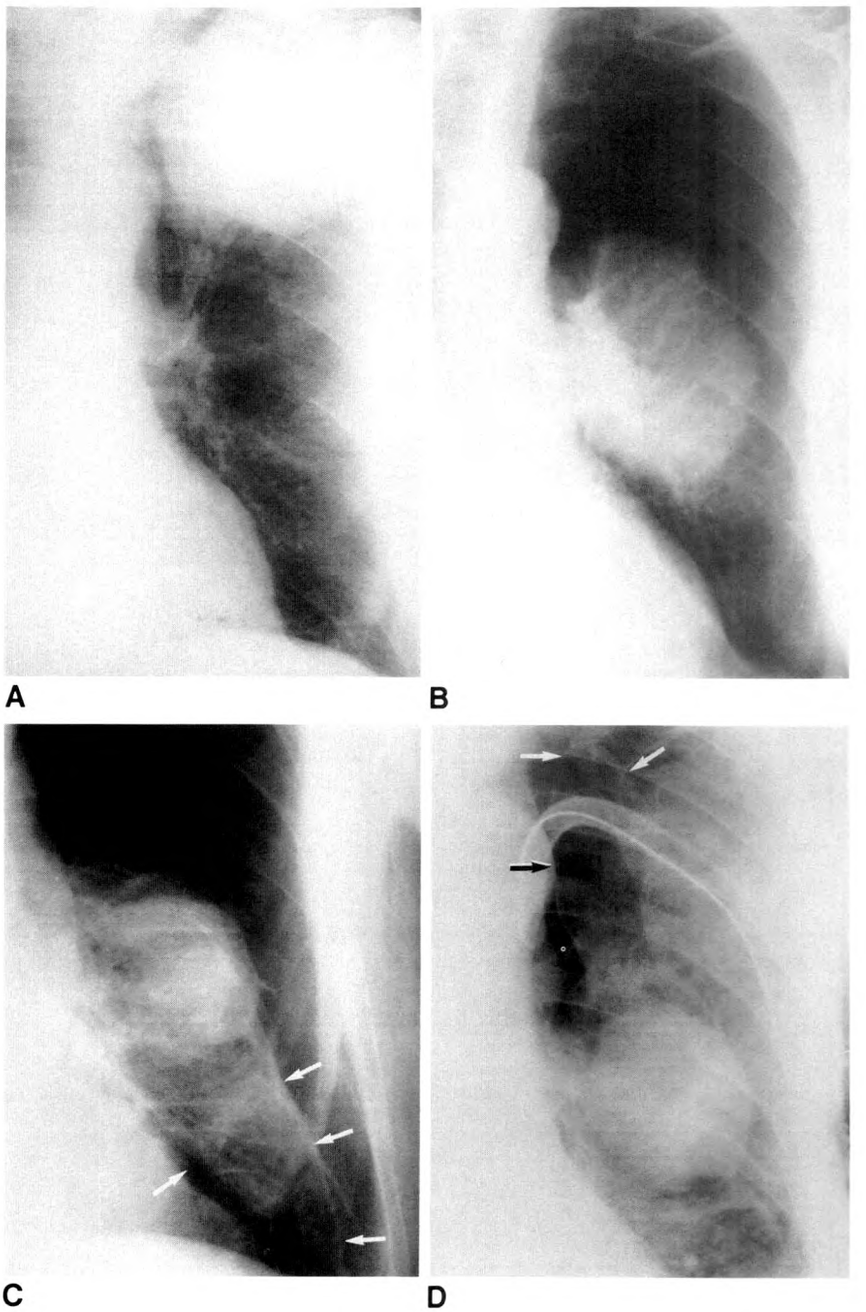


Fig. 20.—Torsion of left upper lobe secondary to a large squamous carcinoma.

***A*, Tumor lies in extreme apex.**

***B*, Tumor has gone "downstairs." Left upper lobe has obviously rotated on its vertical axis. No collapse or air trapping was demonstrated. Mass shifted its position on a number of occasions.**

***C*, *D*, Spontaneous pneumothorax shows mass within upper lobe. Note change in position of lingula (*arrows*).**

nication. This was the missing link that had baffled me. The two observations together, his and mine, have clarified the pathogenesis of unilateral multicystic kidney [16–18].

Someone once showed me a case of torsion or volvulus of the lung. I put it in the crazy file and soon gathered eight more cases of this fascinating condition (Fig. 20). Finding additional cases of an entity is more than coincidence. Awareness of a condition previously overlooked facilitates discovery of more examples.

It is important to wonder and ponder about something you don't understand. Emerson once remarked that there is almost no expense that man will spare to avoid thinking. Let this not apply to you. Some years ago, speculation and observation led me to conclude that there are two types of right aortic arch, an anterior one associated with cyanotic heart disease, and a posterior one without cyanotic heart disease (Fig. 4). A fantastic coincidence occurred in this connection. Showing this material in a conference at Mayo Clinic, I randomly selected a young man in the audience and asked him which patient had cyanotic heart disease. He

responded immediately with the correct answer. How could he have known? Well, he had just completed his graduate treatise on the right aortic arch! At that moment, James Stewart and Ben Felson were probably the only two people in the world aware of the two types of right aortic arch [19, 20].

Collecting and documenting material is much easier today than in the past. Film copiers, indexing methods, home computers, library systems, and copying machines are invaluable to the researcher. Just around the corner is digital videorecording with computer retrieval. One can and should create a personal information system for coding, storing, and retrieving. If I were starting over today, I'd do it with a home computer, but I believe that a computerized videorecorder will be much more effective in the future.

Follow-up of personal cases through the pathology department, medical record room, clinicians, or even direct patient contact is absolutely essential for reliability and validation of conclusions. I like the acronym GOYA, meaning Get Off Your Ass—and check on your patient. Documenting a diagnosis by determining its accuracy has a fascination of its own. Furthermore, I've learned and remembered more medicine through follow-up than any other way.

Literature review must be careful and thorough, lest your accuracy be flawed, your honesty questioned, or your credibility impaired. Our paper on traumatic intramural hematoma had been completed and submitted when I accidentally came upon an article that I had previously read and forgotten on the same subject [21, 22]. Of course, due credit was appended.

Discovery and innovation are not essential for a valuable contribution. Rudolf Hanke and his colleague, Richard Kretschmar, practicing radiologists in Germany who do meticulous armchair research, amassed 90 cases of a little-known condition, rounded atelectasis, recognizing this innocuous lesion by its pathognomonic signs: the comet shadow and the overlying localized peel of pleural thickening (Fig. 21) [23]. I have now seen more than 30 cases personally in less than 10 years [24]. Where were they before?

Writing the paper is an important part of the process, since acceptance for publication often depends on how much editing may be required. It is important to follow the guidelines for authors of each journal. Good grammar and interesting prose are helpful, yet many radiologists are unable to provide them. Elegant phrasing is not needed; simply stated facts and clearly worded conclusions are adequate for most editors. There is no substitute for drudgery here; many drafts are necessary, and review by an experienced writer may be immeasurably helpful. If your message is worthy of publication, invest the effort until the paper conveys it clearly and convincingly. Of course, assistance must be acknowledged. This is not only fair, but will avert ill feelings.

If appropriate, give your discovery a catchy name. It may help it gain attention. I published a sign of traumatic diaphragmatic hernia more than 25 years ago [25]. It has proved infallible in about 100 cases (Figs. 22 and 23), but was generally ignored until about 5 years ago, when I gave it a name, the "lovebird sign." Guess what? It's catching on.

Honesty in fact and in findings is essential. Mistakes can be instructive but it might be prudent to wait for the statute of limitations to expire before airing them, as I did with my report on plaster of Paris GI series [26]. Avoid unverified statements that may be erroneous. It takes only one to make the author appear foolish. In a recent publication, the silhouette sign was attributed to the author of an article published in 1965, some 15 years after it was first reported!

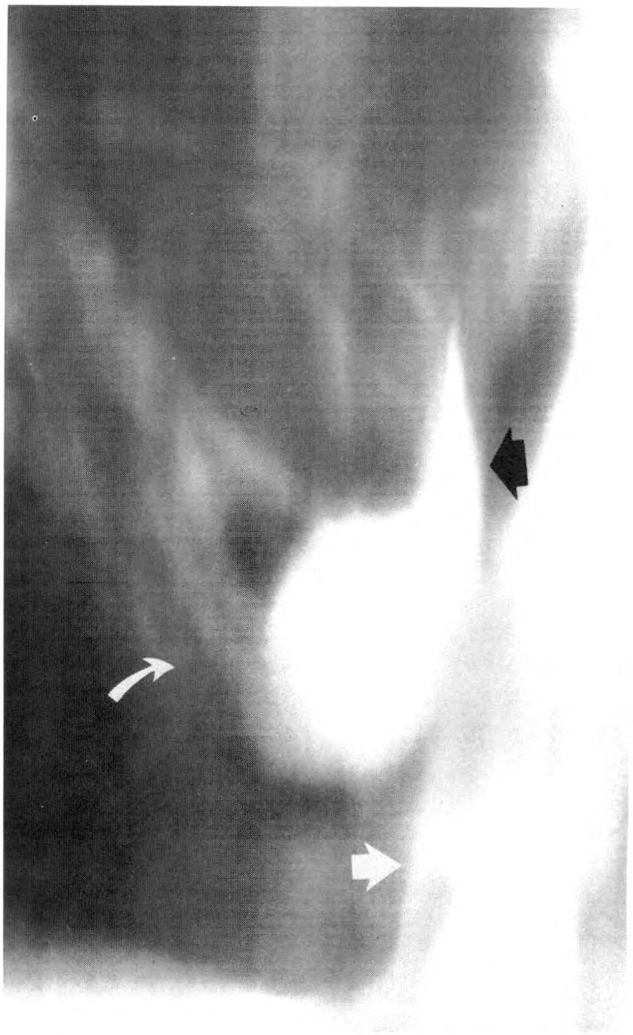


Fig. 21.—Rounded atelectasis. Lateral tomogram shows comet sign, curving tail (*curved white arrow*) extending from lower anterior margin of mass. Thick pleural peel (*straight white arrow*) overlays body of comet. *Black arrow* points to displaced major fissure with opaque pulmonary tissue extending along its margin. On posteroanterior film, right hilum was depressed, indicating partial right lower lobe collapse.

Getting the paper accepted for publication is inordinately difficult and frustrating. The information explosion is as great in radiology as in any other medical field, if not greater, and there is only so much available space, despite the many new journals in our field. Just remember that Saul Bellow, Nobel Prize winner, was an unsuccessful writer until the age of 50. However, many journals now accept nearly 50% of major

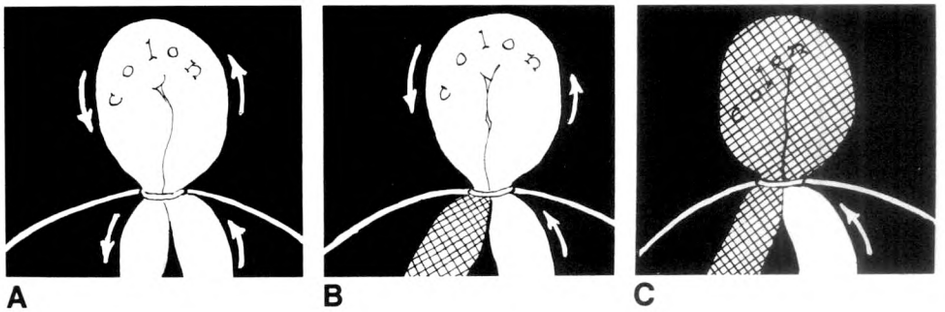


Fig. 22.—Diagram of traumatic hernia of colon through left hemidiaphragm. Barium is indicated in white.

***A*, Note that colon is constricted at four points, causing four beaklike contours, and that points of thoracic entry and exit (*arrows*) lie side by side. "Love-bird sign" is indicated by two beaks on each side of diaphragm, representing two sets of cuddling birds.**

***B*, Colon is obstructed proximally. The cross-hatched transverse colon is distended with gas. Only three beaks are outlined by barium.**

***C*, Distal obstruction. Only one beak is seen, and proximal intrathoracic and abdominal segments of colon (*cross-hatched*) are distended.**

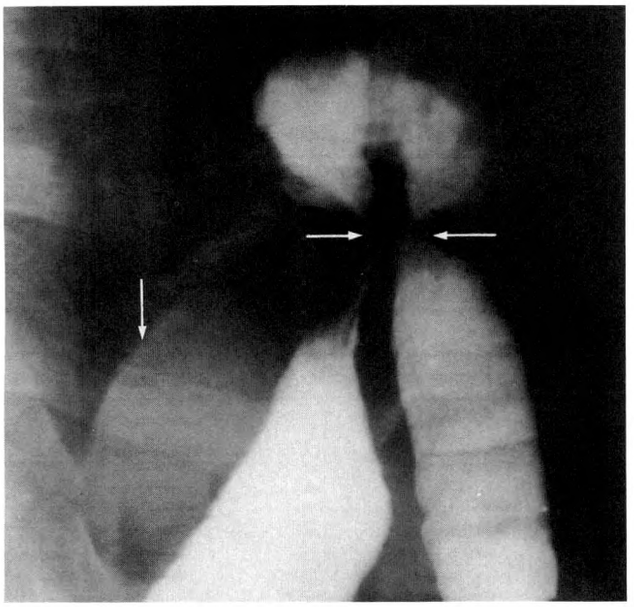


Fig. 23.—Barium study in a nonobstructed traumatic diaphragmatic hernia. Knuckle of colon lies in chest. Note lovebird sign (*transverse arrows*). Intact segment of left hemidiaphragm is visible (*vertical arrow*). (Courtesy of *American Journal of Roentgenology* [25]).

papers (but fewer case reports). A worthwhile paper will generally be accepted by one editor or another. As everyone knows, considerable "junk" does get into print. Why not yours?

Rejection kills initiative, but remember that editors are fallible, human, sometimes inconsistent, and occasionally fickle. What appeals to one may not interest another. Perseverence, rewriting, and resubmission to the same or to a less demanding journal may pay off. In fact, rejection can be constructive and the paper may be improved in the process.

It is an editor and publisher's world, and some make the most of their power. Here is some gratuitous heresy: I believe it is fair to submit a manuscript to several journals simultaneously. Some journals don't even acknowledge receipt of manuscripts for several months, and the publication decision often takes many months more. Why should an author have to go through this process more than once? If concurrent sentences are acceptable in jurisprudence, why not concurrent sentences for editors? Of course, this practice makes for more manuscripts and extra work for editors, so I offer a compromise: If the editorial decision to accept or reject is not received within 3 months, the author can (and should) submit elsewhere. Of course, the contribution should only be published one time, and I suggest first acceptance, first served. In desperation, you might consider publishing and distributing your article yourself. With a book this effort may even prove lucrative. *Gamuts in Radiology* was such a venture [27].

The budding author should take certain precautions. In listing the authors, be the first. Senior authorship is conventionally for the person who did the work. Any other names should only merit coauthorship *if they have contributed.* No gifts! And never be number 4 or higher. Et al. is for drinking, not writing. I don't understand why so many articles have five or more authors. Is the philosophy "I'll scrub your back if you scrub mine," or are the individual authors spreading responsibility for a poor production? I suppose polyauthorship is sometimes appropriate; it is a reality of modern publishing [28].

Stealing and plagiarism are rampant in medicine. The old cliché is, "When you steal from many it is called research, but when you steal from one it is plagiarism." C. P. Li and his colleagues in a small town in Ohio made a magnificent diagnosis of Canada-Cronkhite syndrome in a patient whose colon polyps spontaneously regressed. The patient and his diagnosis were sent to a well-known Ohio institution, from which the case was published without reference to the true heroes. My own black pleural sign [29] suffered a similar fate, but how can I complain when our Gamut book contains so much "borrowed" material?

To sum up, I submit that preparing a publication is a great way to learn and an opportunity to probe deeply into a specific area. An unpublished article becomes a project, and projects are instructive. A published paper is even more; it's a source of pride and can be an exhilarating experience.

I would like to close on a sentimental note. At this moment, I feel a bit like a patriarch surrounded by his extended family. Jerry Wiot is my Number One Son who, like his counterpart, my eldest son Steve, is possessed of many talents, and like my youngest son Ed, looks out for me. My former residents

(my first one, Pat Lynch, deserves special mention) seem like my own children, warm, loyal, and dedicated to me as well as to their profession. The present residents, like my grandchildren, are friendly and respectful but have closer ties elsewhere. Some of my older radiologic colleagues, like my own siblings, have been long-suffering supporters, and several have played a major role in my career. To the rest of you, both academic and practising radiologists, I am indebted for the teaching and learning opportunities you have provided me over these 40 years. For my final acknowledgment there is no counterpart: my wife of 50 years, Virginia, whose warmth, cooperation, and humor have always sustained me. Her approval has been my inspiration and my reward.

REFERENCES

1. Raider L. The retrotracheal triangle. *Chest* **1973**;63:835–838
2. Pear BL. The radiographic manifestations of amyloidosis. *AJR* **1971**;111:821–832
3. Pear BL. Other organs and other amyloids. *Semin Roentgenol* **1986**;21:150–161
4. Gross BH, Felson B, Birnberg FA. The respiratory tract in amyloidosis and the plasma cell dyscrasias. *Semin Roentgenol* **1986**;21:113–127
5. Mulvey RB. The thymic "wave" sign. *Radiology* **1963**;81:834–838
6. Mulvey RB. The effect of pleural fluid on the diaphragm. *Radiology* **1965**;84:1080–1086
7. Weibel ER. *Structure and function in the mammalian respiratory system.* Cambridge, MA: Howard University Press, **1984**:307–310
8. Kattan KR. Calvarial thickening after Dilantin medication. *AJR* **1970**;110:102–105
9. Kattan KR, Felson B, Holder LE, Eyler WR. Superior mediastinal shift in right-lower-lobe collapse: the "upper triangle sign." *Radiology* **1975**;116:305–309
10. Kattan KR, Felson B, Eyler WR. The juxtaphrenic peak in upper lobe collapse. *Semin Roentgenol* **1980**;15:187–193
11. Smith WL, Weinstein AS, Wiot JF. Defects of the renal collecting systems in patients receiving anticoagulants. *Radiology* **1974**; 113:649–651
12. Wiot JF. Intramural small intestinal hemorrhage—a differential diagnosis. *Semin Roentgenol* **1966**;1:219–222
13. Felson B, Felson H. Localization of intrathoracic lesions by means of the postero-anterior roentgenogram: the silhouette sign. *Radiology* **1950**;55:363–374
14. Kattan KR, Felson B, Eyre JT. The silhouette sign revisited experimentally. *Applied Radiology*, May/June **1984**:114–120
15. Felson B, Ralaisomay G. Carcinoma of the lung complicating lipoid pneumonia. *AJR* **1983**;141:901–907
16. Felson B. Letter from the editor. *Semin Roentgenol* **1975**;10:93–94
17. Felson B, Cussen LJ. The hydronephrotic type of unilateral congenital multicystic disease of the kidney. *Semin Roentgenol* **1975**;10:113–123
18. Griscom NT, Vawter GF, Fellers FX. Pelvoinfundibular atresia: the usual form of multicystic kidney: 44 unilateral and two bilateral cases. *Semin Roentgenol* **1975**;10:125–131
19. Felson B, Palayew MJ. The two types of right aortic arch. *Radiology* **1963**;81:745–763
20. Stewart JR, Kincaid OW, Edwards JE. *An atlas of vascular rings and related malformations of the aortic arch system.* Springfield, IL: Thomas, **1964**
21. Felson B, Levin EJ. Intramural hematoma of the duodenum: a diagnostic roentgen sign. *Radiology* **1954**;63:823–831
22. Liverud K. Hematoma of the jejunum with subileus. *Acta Radiol* **1948**;30:163–168
23. Hanke R, Kretzschmar R. Rounded atelectasis. *Semin Roentgenol* **1980**;15:174–182
24. Schneider HJ, Felson B, Gonzalez LL. Rounded atelectasis. *AJR* **1980**;134:225–232
25. Carter BN, Giuseffi J, Felson B. Traumatic diaphragmatic hernia. *AJR* **1951**;65:56–71
26. Felson B. Radiologist on the rocks. *Med Econ* **1959**;36:100–104
27. Reeder MM, Felson B. *Gamuts in radiology. Comprehensive lists of roentgen differential diagnosis.* Cincinnati: Audiovisual Radiology of Cincinnati, **1975**
28. Chew FS. Scientific literature in American radiology. *AJR* **1986**;147:1055–1061
29. Felson B. *Chest roentgenology.* Philadelphia: Saunders, **1973**:479

ARRS Executive Council Award Paper

MR Imaging of the Lumbar Spine: Anatomic Correlations and the Effects of Technical Variations

Murray A. Reicher[1]
Richard H. Gold[1]
Van V. Halbach[1]
Wolfgang Rauschning[1,2]
Gabriel H. Wilson[1]
Robert B. Lufkin[1]

A correlative anatomic study, a retrospective review of MR images performed in 35 patients, and a series of tests of the effectiveness of various MR scanning techniques were performed in order to improve comprehension of lumbar spine anatomy depicted on MR images, and thereby facilitate development of an optimal scanning protocol. Correlation of MR images with cryomicrotomed cadaver specimens enhanced understanding of the MR depiction of the intervertebral disks, ligamentum flavum, nerve roots, epidural fat, and epidural veins. Experiments were performed to assess the efficacy of a surface coil applied to the back, a solenoidal surface coil, a standard body coil, and an abdominal compression device in optimizing image quality. Experiments were also performed to determine the effect of alterations in the pulse sequence and variations of the phase-encoding axis. Based on these results, a protocol is proposed for routine imaging of the lumbar spine that yields high-resolution sagittal and oblique images and that does not require a surface coil. The recommended protocol employs heavily T1-weighted images with phase encoding along the z axis for sagittal images and along the x axis for axial images. This protocol yields multiple sagittal and oblique axial images through each of the lumbar disks, a larger field of view than obtained with surface coils, and a reduction of total imaging time to as little as 10 min.

MR imaging is a valuable tool for the evaluation of disorders of the lumbar spine [1–9]. Although MR evaluation of the lumbar spine was initially limited by low spatial resolution, with continued technologic advances spatial resolution has begun to approach that of CT. MR imaging permits the lumbar spine to be directly imaged in multiple planes and the conus medullaris to be routinely visualized. Furthermore, MR imaging does not require the injection of intrathecal or IV contrast material, is painless, and poses no known biological risk. MR imaging may detect disease of the bone marrow with a high degree of sensitivity, a theoretical advantage in the evaluation of metastatic disease, infarction, and infection. The inherent contrast between the various tissues of the lumbar spine is greater with MR imaging than with CT. For these reasons, MR imaging promises to be a superior technique for evaluating disease of the lumbar spine. Until now, however, two major factors have limited its clinical success: a relatively long examination time and spatial resolution inferior to that obtained with CT or myelography.

We report the results of a correlative anatomic study, a retrospective review of clinical MR images, and a series of tests of the effectiveness of various MR scanning techniques in the evaluation of the lumbar spine. Based on these results, a method is proposed for MR imaging of the lumbar spine that requires as little as 10 min of imaging time, that results in a higher signal-to-noise ratio than has been achieved using conventional methods, and that produces images with a larger effective field of view than those produced using planar surface coils.

Materials and Methods

All scans were performed with 0.3-T imaging systems (Fonar B-3000 permanent magnet

Received February 7, 1986; accepted after revision June 9, 1986.

Presented at the annual meeting of the American Roentgen Ray Society, Washington, DC, April 1986.

[1] Department of Radiological Sciences, 10833 LeConte Ave., UCLA School of Medicine, Los Angeles, CA 90024. Address reprint requests to M. A. Reicher.

[2] Foundation for Advanced Medical Display Technology, Torrance, CA.

AJR 147:891–898, November 1986
0361–803X/86/1475–0891
© American Roentgen Ray Society

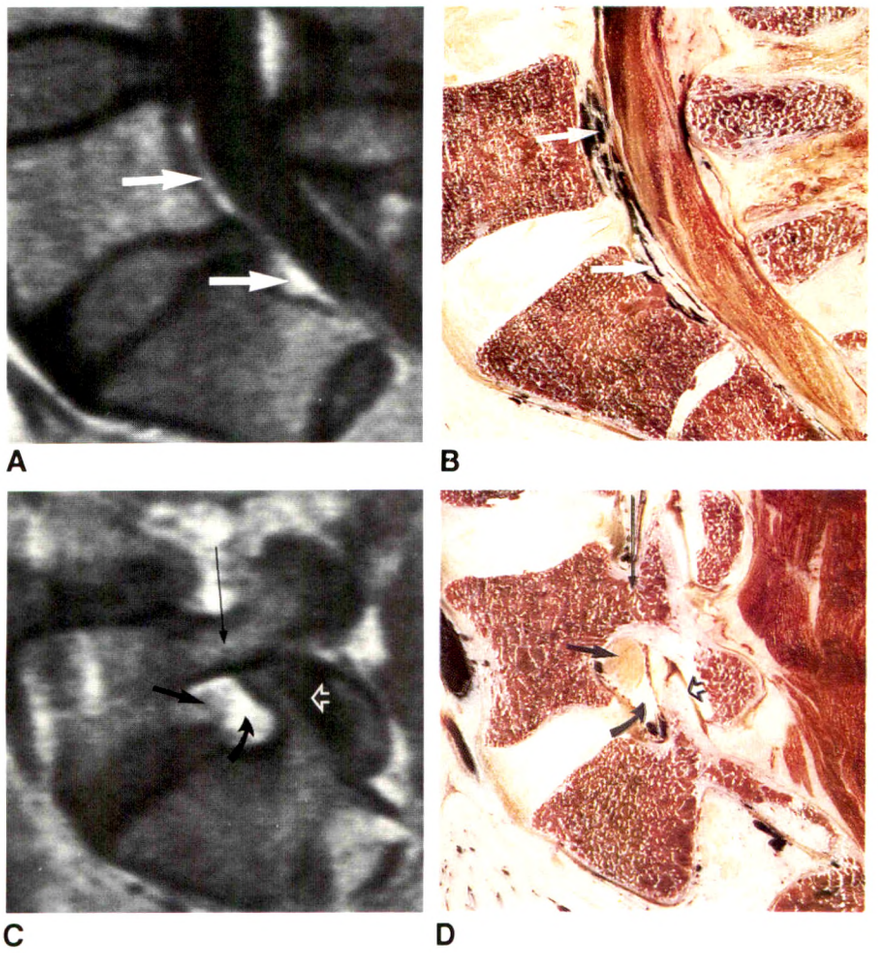


Fig. 1.—Matched sagittal and parasagittal cryomicrotomed specimens and MR images (SE/500/28, four excitations, 5-mm-thick slices, 0.75-mm pixels) of lower lumbar spine.

***A, B,* Midline sagittal section. Region of moderate signal intensity in intervertebral disk represents both nucleus pulposus and surrounding centralmost portion of anulus fibrosus. High-intensity line at region posterior to vertebral bodies (*arrows*) represents epidural fat and veins.**

***C, D,* Parasagittal section. Nerve root is clearly seen as moderate-intensity structure (*shorter black arrow*) surrounded by high-intensity epidural fat (*curved arrow*). Vertical line of moderate intensity within apophyseal joint (*open arrow*) represents hyaline cartilage and synovial fluid. Note direct depiction of medullary bone of pedicle (*long arrow*).**

and B-3000m hybrid permanent/resistive magnet). The anatomy of the lumbar spine as depicted on MR images was analyzed by correlating the scans of nine volunteers with matched color photographs of cryomicrotomed cadaver specimens. The technique of cryomicrotomy has been described and the method of indirect correlation validated in previous studies [10–12]. Three cadaver spines were sectioned in the axial, coronal, and sagittal planes, respectively. Features of normal and pathologic anatomy were also examined by reviewing the scans of 35 patients that were produced with a variety of MR imaging techniques. The volunteers and patients were examined using spin-echo pulse sequences, with TE varying from 14 to 112 msec and TR from 167 to 3450 msec. The scans were performed with a standard body coil, a solenoidal belt coil wrapped circumferentially around the torso, or a surface coil applied to the back. Multislice images were made by employing either a 256 × 256 matrix interpolated to a 512 × 512 matrix or a direct 512 × 512 matrix, employing from two to six acquisitions. Pixels varied from 0.5 to 1.25 mm, and slice thickness varied from 5 mm to 1.25 cm.

A series of tests of the surface coils and of various scanning techniques were also performed, as described below.

Experiment 1

In this experiment, the effects of limiting respiratory motion were studied by obtaining images in the same volunteers both with and without the use of an abdominal compression device. Two volunteers were studied, with both axial and sagittal images obtained by using a standard body coil. For the spin-echo pulse sequence, either TR = 277, TE = 28 (SE/277/28) or TR = 500, TE = 28 (SE/500/28) were used. Phase encoding for this experiment was along the y axis (anterior to posterior). The abdominal compression device consisted of a cloth and plexiglass band ordinarily used for IV urography.

Experiment 2

The effectiveness of various surface coils was studied by examining the same volunteer with a standard body coil, a solenoid surface coil circumferentially wrapped around the torso, and a planar-type surface coil applied to the back. A spin-echo pulse sequence was used (SE/277/28, two excitations, 7-mm slice thickness, 1.0-mm pixels, 256 × 256 matrix).

Experiment 3

The effect of varying the phase-encoding axis was studied by obtaining images in the same subjects with all factors held constant, except that phase encoding was varied from the y axis to the x axis (left to right) for axial images and from the y axis to the z axis (cephalocaudal) for sagittal images. Three volunteers and one patient were studied in this manner, again using T1-weighted spin-echo techniques.

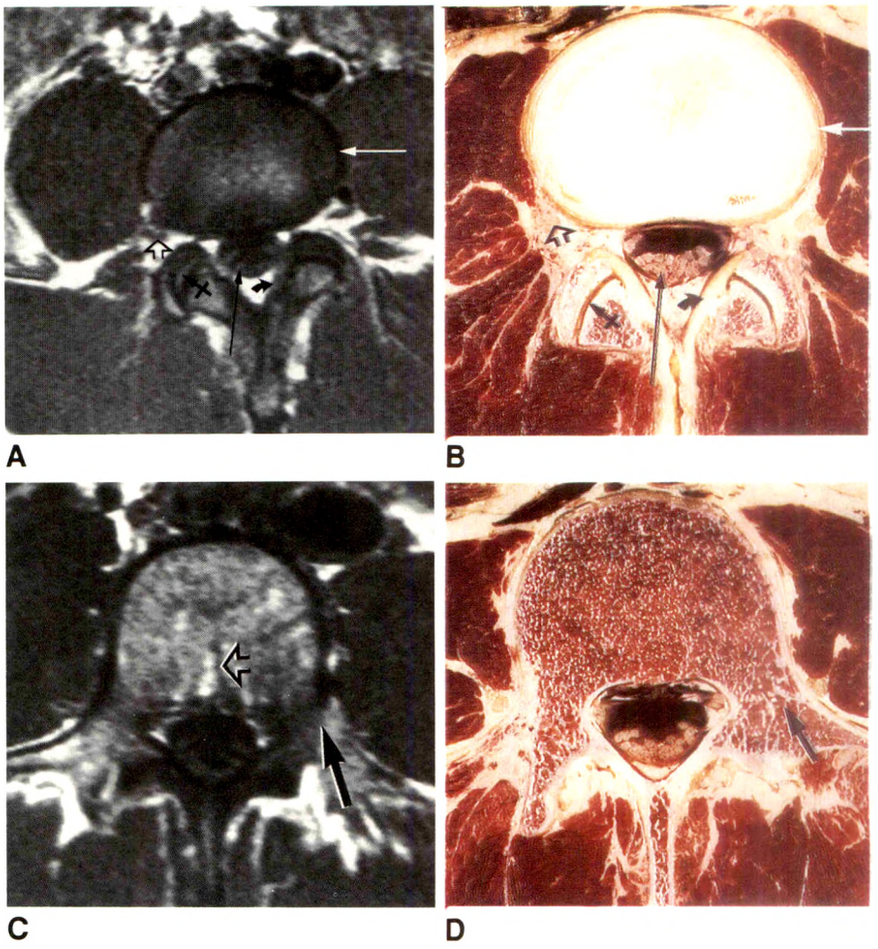


Fig. 2.—Axial cryomicrotomed specimen and matched MR image (SE/500/28, four excitations, 5-mm-thick slices, 0.75-mm pixels).

A, B, L4–L5 disk level. Again note that anulus fibrosus yields moderate signal intensity, blending with nucleus pulposus. Only vertically oriented collagen fibers at periphery of disk (*white arrow*) yield low signal. Individual nerve roots (*long black arrow*) are depicted as moderate-intensity circular structures surrounded by low-intensity CSF. Exiting nerve root is also clearly seen (*open arrow*). Again note moderate-intensity line (*crossed arrow*) within apophyseal joints, representing hyaline cartilage and synovial fluid. Ligamentum flavum (*curved arrow*) yields moderate signal intensity and is distinguishable from both high-intensity epidural fat and adjacent black cortical bone of lamina.

C, D, Section at level of pedicle. Note direct visualization of medullary bone of pedicle (*arrow*) and vertebral body. Intravertebral venous channels (*open arrow*) are also evident on MR image (*C*).

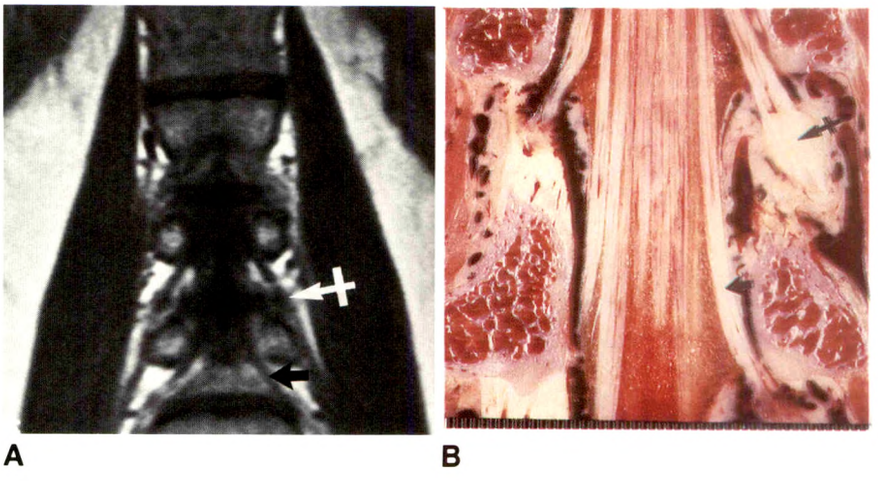


Fig. 3—*A,* Coronal MR image (SE/500/28, four excitations, 5-mm-thick slice, 0.75-mm pixels).

B, More highly magnified cadaver specimen. Exiting nerve roots (*arrows*) are seen coursing under ipsilateral pedicles. Focal nodular enlargement of nerve roots (*crossed arrows*) represents dorsal root ganglion.

Results

Anatomic Correlation

Figures 1–3 illustrate the correlation of the MR images and the matched color photographs of cryomicrotomed cadaver specimens. This technique proved invaluable in the definitive identification of structures seen on the MR images. For example, the ligamentum flavum, thought previously to be a low-intensity structure indistinguishable from the adjacent cortical bone of the lamina, was found instead to yield a

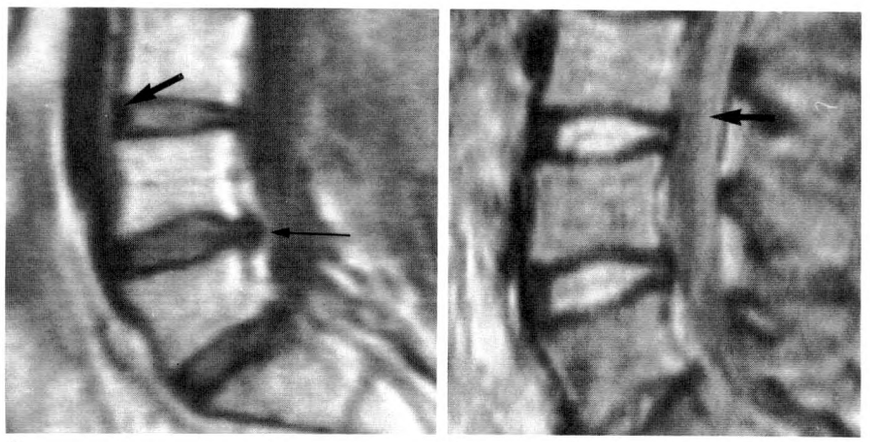


Fig. 4.—Sagittal images of lumbar spine. *A*, SE/500/28. Nucleus pulposus and surrounding centralmost portion of anulus fibrosus are indistinguishable in signal. Only peripheral fibers of anulus fibrosus yield low-intensity signal (*thick arrow*). Note posterior bowing of high-intensity line (*thin arrow*) posterior to bulging L4–L5 disk. This displacement of epidural fat and veins aids in detection of disk bulges on T1-weighted images.

***B*, Same patient imaged using SE/1500/28. With increase in TR, CSF, nerve roots (*arrow*), and normal nucleus increase in signal intensity. Is disk bulge at L4–L5 seen better than in *A*? Acquisition time for scan in *B* was three times that for *A*.**

moderate signal on T1-weighted images (Fig. 2A; also see Fig. 11), and was easily identified as a structure separate from both the cortical bone and thecal sac. A thin line of moderate-to-high signal intensity within the diarthroidal apophyseal joints was found to represent hyaline cartilage and perhaps additionally a thin film of synovial fluid. This correlated well with earlier studies, which revealed that on T1-weighted images hyaline cartilage yielded a relatively high signal intensity [12]. On T1-weighted images (i.e., TE = 28 msec and TR = 500 msec), the nerve roots were easily distinguished within the thecal sac, and the dorsal root ganglia were identified on both coronal and axial images. A thin layer of high signal intensity posterior to the L5 vertebral body and upper sacrum represented epidural fat and epidural veins, and allowed the posterior margin of the L5–S1 disk to be distinguished from the thecal sac even on T1-weighted images (SE/500/28). As other observers have recently reported, the moderately intense signal of the core of the intervertebral disk seen on T1-weighted images was found to represent both the nucleus pulposus and a contiguous portion of the anulus fibrosus, not merely the nucleus pulposus alone, as was initially reported [7]. The medullary bone of the vertebra was visualized, and intravertebral venous channels were identified [13]. Visualization of this detailed anatomy required pixels less than 1.0 mm and slices less than 1.0 cm, both of which were obtainable with the standard body coil or either of the surface coils.

Optimal Scanning Technique

Optimal spatial resolution.—An improvement in anatomic detail compared with that exhibited in previous reports was evident in images with pixels equal to or less than 1.0 mm, a slice thickness equal to or less than 5 mm, and a 256 × 256 matrix. The doubling in image time required to acquire images on a direct 512 × 512 matrix (rather than 256 × 256) resulted in more artifacts due to patient motion, which may contribute to a decrease in resolving power [14]. We empirically observed that when the matrix size was maintained at 256 × 256 (interpolated to 512 × 512 for display) and the pixel size was reduced from 1.25 to 0.75 mm by steepening the coil gradients, the resolution significantly improved.

Optimal pulse sequence.—Since a fundamental advantage of MR imaging over other imaging techniques is excellent inherent soft-tissue contrast, it is imperative to employ pulse sequences that optimize the contrast differences between neighboring tissues. The optimal pulse sequence should allow the discrimination by difference in signal intensity between ligamentum flavum, thecal sac, and intervertebral disks. Retrospective review of the scans performed in 35 patients and nine volunteers disclosed that on conventional T1-weighted images (SE/500/28) the signal intensity of the CSF was homogeneously low, allowing discrimination of the nerve roots and ligamentum flavum from the CSF. However, the peripheral fibers of the anulus fibrosus were also of low signal intensity, resulting in poor discrimination between the posterior margin of the disk and thecal sac. This problem was somewhat alleviated at the L5–S1 level by the high-intensity epidural fat and veins that are interposed between the disk and the thecal sac, providing a consistently visible marker for the posterior margin of the disk when high-resolution scans are performed (pixels ≤0.75 mm) (seen on Fig. 4A; also seen on Figs. 1A, 6, 8, and 12). Even at the L2–L3 and L3–L4 levels, bulging disks were occasionally recognized on T1-weighted images by means of a thin line of moderate signal intensity posterior to the disk, representing displaced epidural veins and/or fat (Fig. 4). This finding has not been previously reported, possibly because of the lower resolution of older images. On T1-weighted images, the nucleus pulposus and the greater part of the anulus were isointense. Only the outer, poorly hydrated fibrocartilaginous elements of the anulus and the vertically oriented collagen fibers at the periphery of the disk were low in signal intensity on T1-weighted images. A progressive increase in TR led to a corresponding increase in the relative signal intensity of the nerve roots, CSF, and normal nucleus pulposus. Neighboring structures could be easily differentiated by differences in signal intensity when a SE/1500/28 pulse sequence was used (Fig. 5). On images produced with this sequence, the nerve roots were higher in signal intensity than the CSF, which in turn was higher in signal intensity than the peripheral fibers of the anulus. With progressive T2 weighting (increase in TE and TR), the signal intensity of the entire thecal sac increased to the point at which nerve roots were no longer visible (Fig. 6). With extreme T2 weighting, the signal intensities of the normal nucleus

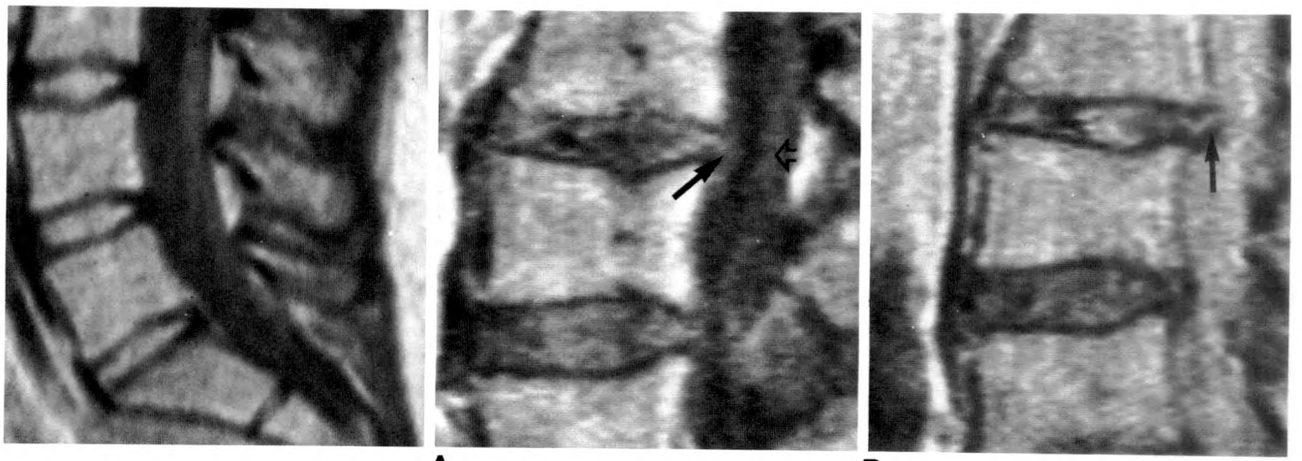


Fig. 5.—Sagittal image of lumbar spine employing SE/1500/28 sequence. Nucleus pulposus and surrounding centralmost portion of anulus fibrosus are isointense, and are easily distinguishable from CSF, nerve roots, and peripheral fibers of anulus fibrosus, each of which yields different signal intensities.

Fig. 6.—Effect of increasing TR. *A* and *B* are sagittal images using SE/500/28 and SE/3500/28, respectively. Bulging disk at L1–L2 is equally well seen in both images (*black arrow*), but relationship of disk to nerve roots (*open arrow*) is better seen with shorter TR.

pulposus and thecal sac became indistinguishable. Within the thecal sac, lesions with a long T2, such as the inflammatory tissue caused by arachnoiditis, could not be distinguished from CSF on heavily T2-weighted images (Fig. 7). Although the resultant "metrizamide effect" on T2-weighted images increased the contrast difference between the anulus and the CSF, this was not significantly greater from a clinical viewpoint than on images produced with an SE/1500/28 sequence. With progressive T2 weighting, the signal intensity of the more central fibers of the anulus fibrosus diminished (Fig. 7). This finding correlated well with the in vitro measurements reported by Modic et al. [6], who found the anulus fibrosus to have significantly shorter T1 and T2 values than the nucleus pulposus. Acquisition time for a pulse sequence with a TR of 3450 msec was, of course, seven times longer than for a TR of 500 msec, resulting in greater motion artifact and a poorer image signal-to-noise ratio. The image signal-to-noise ratio also gradually decreased as the TE was progressively increased.

In an attempt to optimize visualization of T1 differences between the nucleus, anulus, and CSF, a more heavily T1-weighted pulse sequence was employed than has been previously used for spine imaging. On images produced with a SE/266/14 sequence, the anulus fibrosus increased in relative signal, becoming isointense to the nucleus and distinguishable from adjacent low-intensity CSF (Fig. 8). These results correlated well with the single published image of the lumbar spine obtained with a similar sequence [7]. With this sequence, the nerve roots and ligamentum flavum were also readily distinguished from CSF. A very thin low-intensity line continued to be seen at the periphery of the disk, corresponding to the site of vertically oriented collagen fibers anatomically present at the disk margin. This heavily T1-weighted sequence therefore resulted in better contrast resolution of the lumbar spine while requiring only a small fraction of the time necessary to perform T2-weighted images. Furthermore, lesions with a long T2 such as neurofibromata, metastases, and inflammatory tissue, which may not be visible within the thecal sac on heavily T2-weighted images should, in theory, because of T1 differences, be readily differentiated from CSF by using the SE/266/14 sequence. The imaging time was 5 min for a spin-echo pulse sequence with a TR of 300 msec, when four excitations (two averages) and a 256 × 256 matrix were employed.

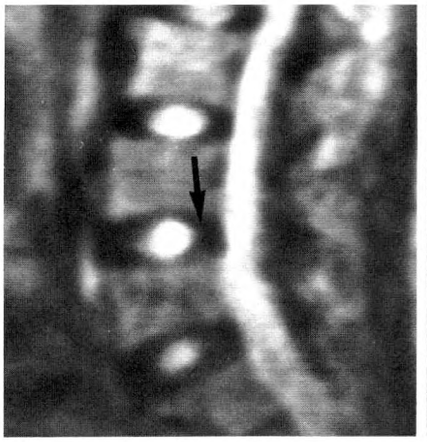
Optimal image signal-to-noise ratio.—Recent reports have advocated the use of surface coils applied to the back for imaging the lumbar spine [1]. Surface coils improve the signal-to-noise ratio within the region adjacent to the coil [1, 15]. The signal-to-noise ratio geometrically decreases proportionally to the increasing distance from the source to the coil when planar-type coils are used [15]. This effectively limits the field of view and, since the spine is a relatively deep structure, may limit visualization of the ventral aspect of the lumbar spine (Fig. 9) or paraspinal structures.

In order to develop a scanning technique that improved the image signal-to-noise ratio without sacrificing the field of view, it was first necessary to determine by experimental means the sources of image noise (see Materials and Methods).

The results of Experiment 1 (Fig. 10) indicated that limitation of abdominal motion improved the depiction of the spine as well as of the abdomen. Degradation of spine images by respiratory, bowel, and vascular motion in the abdomen resulted in errors in phase encoding that degraded sagittal or axial images of the spine when phase encoding was performed along the y axis. The results of Experiment 1 and our empirical experience in patients suggest that these motion-related artifacts may be substantially overcome with the use of abdominal compression and patient instruction.

The results of Experiment 2 indicated that signal-to-noise ratio could be improved with the use of either a solenoid or a planar-type surface coil, but that when either technique was employed, the effective field of view was reduced in compar-





A B

Fig. 7.—Effect of increasing TE and TR. *A* and *B* are sagittal images of same patient obtained using SE/500/28 and SE/2000/112, respectively. With increased TE and TR (*B*), signal intensity from more cental section of anulus fibrosus decreases (*arrow*). This creates impression of "shrinking nucleus" with increased T2-weighting. Although no structural abnormalities are evident in either *A* or *B*, signal intensity of spinal canal is markedly increased in *A*, compared with normals scanned with same T1-weighted sequence. This was due to myelographically proven arachnoiditis, with inflammatory tissue packing the spinal canal, and was not appreciated on T2-weighted image (*B*).

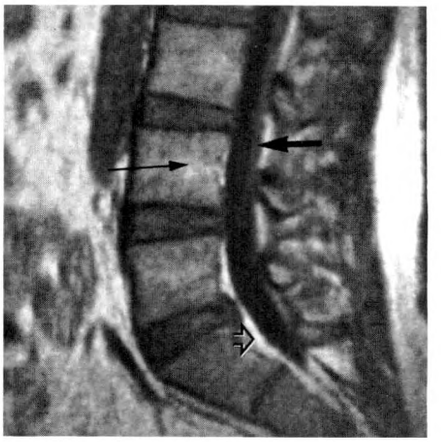
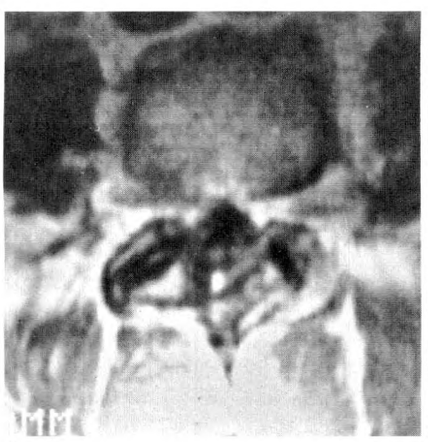
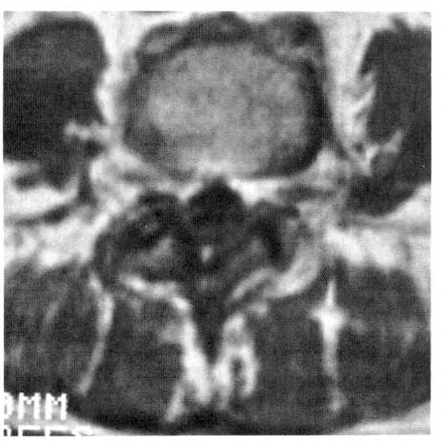


Fig. 8.—Effect of heavy T1 weighting. Sagittal image performed using SE/300/14. Nearly entire anulus fibrosus and nucleus pulposus are isointense, with only vertically oriented collagen fibers at periphery of disk remaining low in signal intensity. Moderate intensity nerve roots (*thick black arrow*) are distinguishable from homogeneously black CSF. Epidural fat (*open arrow*) remains high in signal intensity. Region of bright signal within vertebral bodies (*thin black arrow*) may be related to venous blood flow. Phase encoding was performed along y axis (see text), resulting in poor depiction of abdomen, but excellent depiction of spine. Sequence requires only one-half the time required for similar images with TR = 500.





A B

Fig. 9.—Axial images at L4–L5 level performed with identical technique (SE/500/28, six excitations, 7-mm-thick slice, 1.0-mm pixels, 256 × 256 matrix), except that surface coil was applied to back in *A* and standard body coil was used in *B*. In *A*, although signal intensity is very high adjacent to surface coil, loss of signal in geometric proportion to increasing distance between source and coil results in poor signal-to-noise ratio in more ventral aspect of image. In *B*, using standard body coil, effective field of view is improved without sacrificing signal-to-noise ratio in clinically relevant portion of image.

ison to the standard body coil (Fig. 9). Using a planar coil applied to the back, signal-to-noise decreased geometrically proportionally to increasing distance from the coil [1, 15]. By using a solenoid coil circumferentially applied around the torso, signal-to-noise decreased cephalad and caudal to the coil [15].

The results of Experiment 3 indicated that phase-encoding errors due to abdominal motion could be substantially reduced by altering the phase-encoding axis to the x direction (left to right) for axial images and to the z direction (cephalocaudal) for sagittal images (Figs. 11 and 12). When these techniques were employed, abdominal motion degraded depiction of the abdomen, but not of the lumbar spine.

Multiple-angle, variable-interval, nonorthogonal (MAVIN) imaging.—Oblique imaging parallel to the lumbar disk spaces is a widely accepted method for the CT examination of the lumbar spine. Although oblique images can be obtained with MR imaging, until now the slices produced by a given pulse sequence have been parallel and positioned at a fixed interval. Previously, in order to obtain oblique axial MR images through the L3–L4, L4–L5 and L5–S1 disk spaces, three sets of oblique images would have been required, resulting in a lengthy examination time. Multiple-angle, variable-interval, nonorthogonal (MAVIN) imaging is a recently developed technique that provides an independent choice of obliquity and position for each slice within a multislice pulse sequence (Fig.

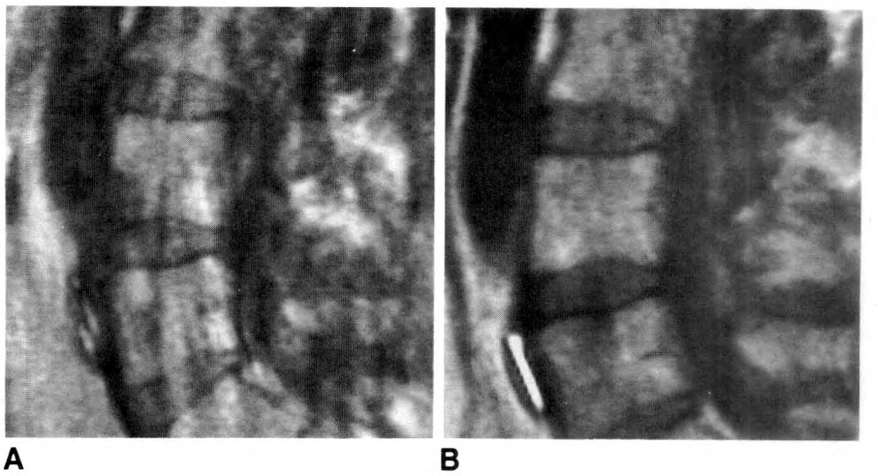


Fig. 10.—Effect of limiting abdominal motion. Sagittal images of volunteer with same technique (SE/277/28, two excitations, 7-mm-thick slice, 1.0-mm pixels, 256 × 256 matrix), except that respiratory motion was unrestricted in *A* and an abdominal compression device was employed in *B*. Phase-encoding artifact in *A* degrades entire image, not simply region of abdomen.

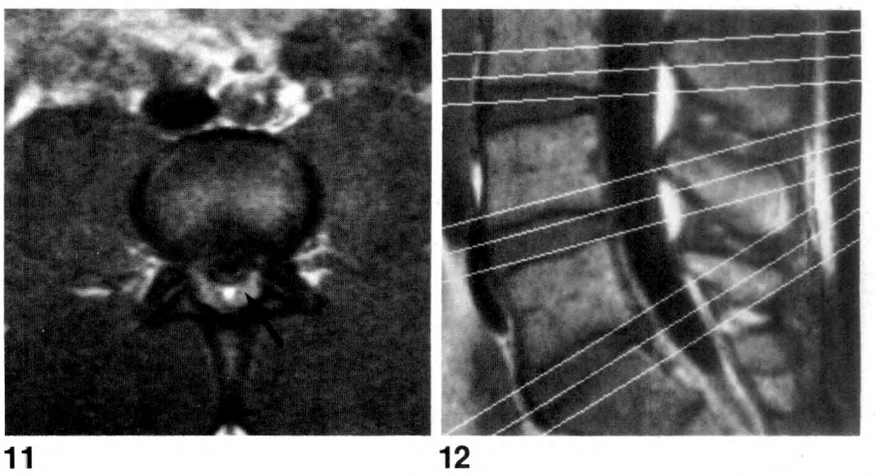


Fig. 11.—Axial image performed by phase encoding along the x axis (see text). Phase-encoding artifact degrades depiction of abdomen, but not spine. Note moderate-to-high-intensity ligamentum flavum (*arrow*) on T1-weighted image (SE/500/28) and stenosis of spinal canal.

Fig. 12.—Multiple-angle, variable-interval, nonorthogonal (MAVIN) imaging sequence. Sagittal scan employed as reference to select oblique axial scans of L3–L4, L4–L5, and L5–S1 disks. Using single pulse sequence (SE/610/28), nine oblique axial images were then obtained through L3–L4, L4–L5, and L5–S1 levels.

13) [16]. The time required for this technique is the same as that for a conventional spin-echo pulse sequence performed with the same TR. When the technique is applied to imaging the lumbar spine, oblique axial images parallel to each of the lumbar disks may be obtained by using a single pulse sequence, resulting in a significant reduction in the time required to perform an optimal examination.

Discussion

The optimal MR examination of the lumbar spine is characterized by the following features: (1) contrast between neighboring structures should be maximized by appropriate selection of the pulse sequence; (2) spatial resolution should be maximized while maintaining an adequate field of view; (3) noise and artifacts should be minimized; (4) oblique imaging, a fundamental advantage of MRI, should be incorporated into the examination where appropriate; and (5) examination time should be held to a minimum. The goal of our research project was to determine rationally an optimal MR scanning protocol for the lumbar spine by analyzing normal and pathologic anatomy and evaluating the efficacy of various scanning techniques. Several conclusions may be drawn from our results.

Correlation of MR images with cryomicrotomed cadaver specimens revealed features of normal anatomy not previously appreciated. The ligamentum flavum was found to be distinguishable from adjacent structures on T1-weighted images. The anulus fibrosus of the disk was found to increase progressively in relative signal intensity with progressive T1 weighting, allowing structural disk abnormalities to be recognized on T1-weighted images. Although a fine line of low intensity remained present at the disk margin when heavily T1-weighted sequences were employed, our initial experience indicated that this line was of a predictively thin dimension. Certainly, by using heavily T1-weighted sequences, most of the anulus fibrosus can be distinguished from the thecal sac. On high-resolution scans, a thin line composed of epidural fat and epidural veins was found posterior to the lumbar disks, further aiding in the detection of disk disease on T1-weighted images. These correlative anatomic findings imply that with high-resolution scanning techniques, disorders of the lumbar spine may be diagnosed with T1-weighted imaging in a fraction of the time necessary to create heavily T2-weighted images. Furthermore, lesions with a relatively long T2, which may not be distinguishable from CSF on T2-weighted images, are occasionally apparent on T1-weighted images.

Retrospective analysis of the efficacy of various pulse

sequences and prospective testing of new heavily T1-weighted pulse sequences also suggested that contrast between neighboring tissues could be maximized with shorter examination times than previously advocated. One proposed disadvantage of T1-weighted imaging of the spine is the inability to discriminate osteophytes from CSF. However, on high-resolution scans, we have never seen a clinically significant osteophyte on a T2-weighted image that was not also apparent on a T1-weighted image. In fact, there are no published examples of osteophytes obscured on T1-weighted images made with high-resolution scanning techniques.

Experiments designed to evaluate sources of noise and to seek methods of maximizing the signal-to-noise ratio also yielded several significant results: Abdominal motion was found to be a major contributor to noise in images of the lumbar spine when phase encoding was performed along the y axis, which until now has been the most widely employed technique. Images of the lumbar spine could be improved by phase encoding along the x axis for axial images, and along the z axis for sagittal images. For systems in which this option is not yet available, the use of abdominal compression and careful patient instruction may lessen artifacts caused by respiratory motion.

We propose that one reason that surface coils applied to the back are effective in improving the signal-to-noise ratio in images of the lumbar spine is their poor detection of noise generated in the relatively distant abdomen. Unfortunately, the loss of signal geometrically proportional to the distance of the source from the coil tends to limit the effective field of view in images produced by using surface coils applied to the back. Even solenoidal-type coils circumferentially applied to the torso tend to limit the field of view. With our imaging system, use of a standard body coil and decrease of noise by appropriate adjustment of the phase-encoding direction produced high-resolution images without limitation of the field of view. As imaging time is progressively reduced, set-up time becomes a more significant component of the total examination time. By avoiding the time usually necessary to apply a surface coil, the total examination time is further reduced.

In order to reduce imaging time and still obtain an optimal examination, a new imaging technique, MAVIN, was developed. This allows oblique axial images to be obtained through each of the lumbar disks by using a single pulse sequence.

While we were unable to unequivocally determine the optimal spatial resolution for depiction of the lumbar spine, evaluation of scans performed by using various pixel sizes led to the following impression: employing 256 phase-encoding levels rather than 512 levels produced clinically superior results, since the use of the 512 × 512 matrix doubled the examination time and tended to result in more motion artifacts. Although there is no mathematical method to quantify human perception, the anatomy apparent on MR scans performed with 0.75-mm pixels and 5-mm-thick slices was thought to be superior to that evident on CT scans. This was due to the superior contrast resolution of the MR images, which allowed nerve roots, medullary bone, CSF, disk material, epidural fat, and the ligamentum flavum to be discriminated without the use of IV or intrathecal contrast material.

On the basis of these observations, we propose the following routine scanning protocol for MR evaluation of the lumbar spine: The examination should begin with a sagittal heavily T1-weighted spin-echo pulse sequence (SE/300/14) with pixels equal to or less than 1.0 mm and slices equal to or less than 5 mm, and phase encoding along the z axis. If four excitations are employed and 256 phase-encoding levels are used, the scan can be completed in 5 min. Multiple oblique axial images may then be performed through each of the lumbar disks using the MAVIN technique, requiring an additional 5 min. This should complete the routine examination, although, as with other diagnostic imaging procedures, the technique may have to be tailored to the clinical indication. We believe that this 10-min examination should suffice for most patients, and we are currently conducting clinical trials to further evaluate its efficacy in a prospective manner.

ACKNOWLEDGMENTS

The authors give special thanks to William Glenn, Jr., and the Foundation for Advanced Display Technology for supporting the cryomicrotomy performed for this publication.

REFERENCES

1. Edelman RR, Shoukimas GM, Stark DD, et al. High-resolution surface coil imaging of lumbar spine disk disease. *AJR* **1985**;144:1123–1129
2. Han JS, Kaufman B, El Yousef SJ, et al. NMR imaging of the spine. *AJR* **1983**;141:1137–1145
3. Norman D, Mills CM, Brant-Zawadski M, Yeates A, Crooks LE, Kaufman L. MRI of the spinal cord and canal: potentials and limitations. *AJR* **1983**;141:1147–1152
4. Chafetz NI, Genant HK, Moon KL, Helms CA, Morris JM. Recognition of lumbar disc herniation with NMR. *AJR* **1983**; 141:1153–1156
5. Modic MT, Weinstein MA, Pavlicek W, et al. NMR imaging of the spine. *Radiology* **1983**;148:757–762
6. Modic MT, Pavlicek W, Weinstein MA, et al. MRI of intervertebral disk disease—clinical and pulse sequence considerations. *Radiology* **1984**;152:103–111
7. Pech P, Haughton VM. Lumbar intervertebral disk: correlative MR and anatomic study. *Radiology* **1985**;156:699–701
8. Aquila LA, Piraino DW, Modic MT, Dudley AW, Duchesneau PM, Weinstein MA. The internuclear cleft of the intervertebral disk: MRI. *Radiology* **1985**;155:155–158
9. Ramsey RG, Zacharias CE. MRI of the spine after radiation therapy—easily recognizable effects. *AJR* **1985**;144:1131–1135
10. Rauschning W. CT and cryomicrotomy of lumbar spine specimens—a new technique for multiplanar anatomic correlation. *Spine* **1983**;8:170–180
11. Bergstrom K, Nyberg G, Pech P, Rauschning W, Utterbergh C. Multiplanar spinal anatomy: comparison of CT and cryomicrotomy in postmortem specimens. *AJNR* **1983**;4:590–592
12. Reicher MA, Rauschning W, Gold RH, Bassett LW, Lufkin RB, Glenn W. High resolution MRI of the knee joint. *AJR* **1985**;145:895–902
13. Sartoris DJ, Resnick D, Guerra J. Vertebral venous channels: CT appearance and differential considerations. *Radiology* **1985**;155:745–749
14. Bradley WG Jr, Kortman KE, Crues JV. Central nervous system high resolution MRI: effect of increasing spatial resolution on resolving power. *Radiology* **1985**;156:93–98
15. Lufkin RB, Vortruba J, Reicher MA, et al. Solenoidal surface coils in MRI. *AJR* **1986**;146:409–412
16. Reicher MA, Lufkin RB, Smith S, et al. Multiple-angle, variable-interval, nonorthogonal MRI. *AJR* **1986**;147:363–366

Radiographic Manifestations of Bronchiolitis Obliterans with Organizing Pneumonia vs Usual Interstitial Pneumonia

Paul W. Chandler[1]
Myung S. Shin[1]
Samuel E. Friedman[1]
Jeffrey L. Myers[2]
Anna-Luise Katzenstein[2]

The radiographic findings in 24 cases of bronchiolitis obliterans with organizing pneumonia and 16 cases of usual interstitial pneumonia were reviewed and compared. Some cases of bronchiolitis obliterans with organizing pneumonia have been mistaken for usual interstitial pneumonia, although the two diseases have distinct pathologic findings. Clinically, the diseases often have different manifestations. Bronchiolitis obliterans with organizing pneumonia has a better prognosis and often responds well to steroids. This study shows that the radiologic findings of bronchiolitis obliterans include alveolar opacities without lung-volume loss. Patients with usual interstitial pneumonia, however, have bilateral diffuse interstitial opacities with occasional honeycomb changes, and there is loss of lung volume in most patients. These findings suggest that the chest radiograph can aid in distinguishing the two diseases.

There has been some confusion in the past concerning the subclassification of lung diseases characterized by pulmonary fibrosis. Various schemata have been proposed depending on certain histologic or etiologic criteria. Some [1, 2] believe that subclassification of pulmonary fibrosis is of clinical and prognostic significance. Bronchiolitis obliterans with organizing pneumonia is a lung disease characterized by fibrosis of the small airways and alveoli. Because pulmonary fibrosis is such a prominent histologic finding in this disease, many cases of bronchiolitis obliterans have been misclassified as idiopathic pulmonary fibrosis or usual interstitial pneumonia (UIP) [2, 3]. UIP is almost always associated with a poor prognosis. Epler et al. [2] studied patients with idiopathic bronchiolitis obliterans with organizing pneumonia, however, and found that patients responded well to steroid therapy. The study concluded that bronchiolitis obliterans with organizing pneumonia is a distinct clinicopathologic entity from UIP [2]. Recently, Katzenstein et al. [4] retrospectively studied bronchiolitis obliterans with organizing pneumonia and UIP and arrived at a similar conclusion. The purpose of this paper is to compare the radiographic findings of bronchiolitis obliterans with organizing pneumonia and UIP to further characterize their distinguishing features because there has been histologic misclassification in the past.

Materials and Methods

We reviewed open-lung biopsies from the pathology files at the University of Alabama Hospitals and found 24 cases of bronchiolitis obliterans with organizing pneumonia and 16 cases of UIP dating from 1972 to 1984. All patients had chest radiographs that were examined by the chest radiologists at University Hospital at the time of diagnosis.

We used the following pathologic criteria to define the two diseases for analysis in this study. Bronchiolitis obliterans with organizing pneumonia was histologically defined as plugs of granulation tissue within bronchioles and extending into the alveoli. The intraalveolar granulation tissue was referred to as organizing pneumonia. There were also varying degrees of interstitial inflammation. In our experience pure bronchiolitis obliterans without organizing pneumonia is rare and was not seen in this series [4]. Histologic criteria for UIP were interstitial

Received March 24, 1986; accepted after revision June 23, 1986.

Presented as scientific paper and exhibit at the annual meeting and scientific exhibit of the American Roentgen Ray Society, April 1986, Washington, DC.

[1] Department of Radiology, University of Alabama School of Medicine, 619 S. 19th, Birmingham, AL 35233. Address reprint requests to M. S. Shin.

[2] Department of Pathology, University of Alabama School of Medicine, 619 S. 19th, Birmingham, AL 35233.

AJR 147:899–906, November 1986
0361–803X/86/1475–0899
© American Roentgen Ray Society

TABLE 1: **Comparison of Clinical Information of 24 Cases of Bronchiolitis Obliterans with Organizing Pneumonia (BOOP) with 16 Cases of Usual Interstitial Pneumonia (UIP)**

Characteristic	BOOP	UIP
Mean age (years)	60	58
Gender (male/female)	11/13	13/3
Common symptoms	Fever, cough, dyspnea	Cough, progressive dyspnea
Mean duration of symptoms	3 months	2–3 years
Number with underlying collagen vascular disease	7 (29)	3 (19)
Number with occupational exposure	0 (0)	5 (31)
Number having steroid therapy	12 (50)	14 (88)
Number surviving	16 (67)	3 (19)
with residual disease	7	3
without residual disease	9	0
Number of deaths[a]	3 (13)	10 (63)

Note.—Numbers in parentheses are percentages.
[a] Does not include deaths due to unrelated causes.

fibrosis with collagen deposition and an interstitial infiltrate of chronic inflammatory cells, particularly lymphocytes and plasma cells.

The radiographs were examined for pulmonary opacities, pleural disease, and lung-volume status. Pulmonary opacities were classified as alveolar if there was consolidation with air bronchograms, patchy consolidation, or air-space nodules. Opacities were also classified as interstitial if they were reticular (fine or coarse), streaky or linear, reticulonodular, or honeycomb. Manifestations were classified according to their distribution as diffuse, lobar, or bibasilar. Lung volume was assessed by counting the number of posterior ribs that could be seen above the diaphragm and the degree of diaphragmatic flattening. Volume was considered reduced if there were less than nine posterior ribs above the diaphragm and the diaphragm was convex. Follow-up radiographs were obtained in 17 of 24 cases of bronchiolitis obliterans with organizing pneumonia and 11 of 16 cases of UIP. These radiographs were assessed in a similar fashion with particular attention to radiographic improvement or worsening. Clinical information was obtained from medical records, private physicians, relatives, and the patients themselves.

TABLE 2: **Comparison of Radiographic Manifestations of 24 Cases of Bronchiolitis Obliterans with Organizing Pneumonia (BOOP) with 16 Cases of Usual Interstitial Pneumonia (UIP)**

Findings	BOOP	UIP
Alveolar opacities	12 (50)	0 (0)
Lobar	11 (46)	0 (0)
Diffuse	0 (0)	0 (0)
Bibasilar	1 (4)	0 (0)
Interstitial opacities	10 (42)	15 (94)
Reticular	10 (42)	10 (63)
Reticulonodular	0 (0)	2 (13)
Honeycomb	0 (0)	3 (19)
Mixed alveolar and interstitial opacities	2 (8)	1 (6)
Lung volume		
Decreased	6 (25)	12 (75)
Normal	18[a] (75)	4 (25)
Pleural thickening	3 (13)	1 (6)
Pleural effusion	2 (8)	1 (6)

Note.—Numbers in parentheses are percentages.
[a] Unilateral hyperinflation was found in one case.

Results

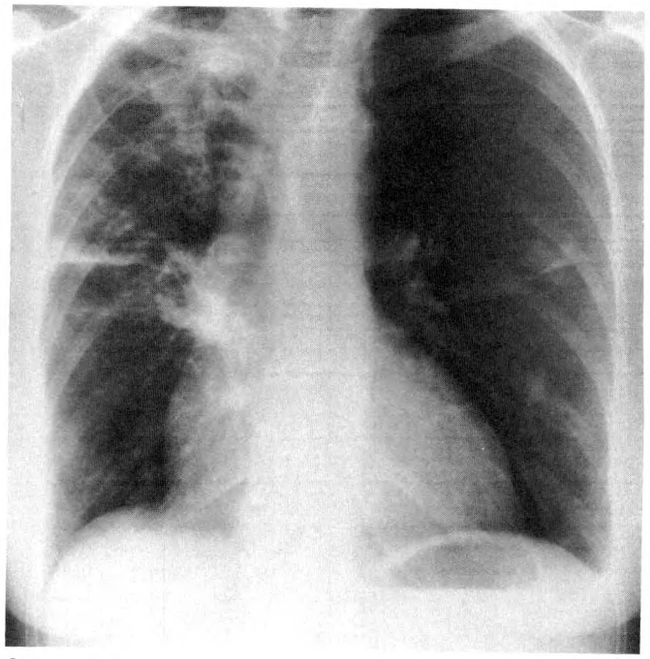
Bronchiolitis Obliterans with Organizing Pneumonia

Clinical information.—The clinical information is summarized in Table 1. The 24 patients, 11 men and 13 women, ranged in age from 28 to 80 years (mean, 60). Most patients presented with symptoms of fever, cough, and dyspnea. The duration of symptoms ranged from 5 days to 6 months (mean, 3 months). Seven patients had underlying connective-tissue diseases, including polymyositis, rheumatoid arthritis, mixed connective-tissue disease, and systemic lupus erythematosus. One patient had arthralgias but a negative antinuclear antibody and rheumatoid factor. Another had a positive antinuclear antibody and Raynaud's phenomenon. Sputum cultures were positive for *Hemophilus influenza*, *Nocardia asteroides*, *Klebsiella*, and *Mycobacterium avium* in one patient each. One patient had bronchial washings that were positive for *H. influenza*. No patient had a history of occupational exposure.

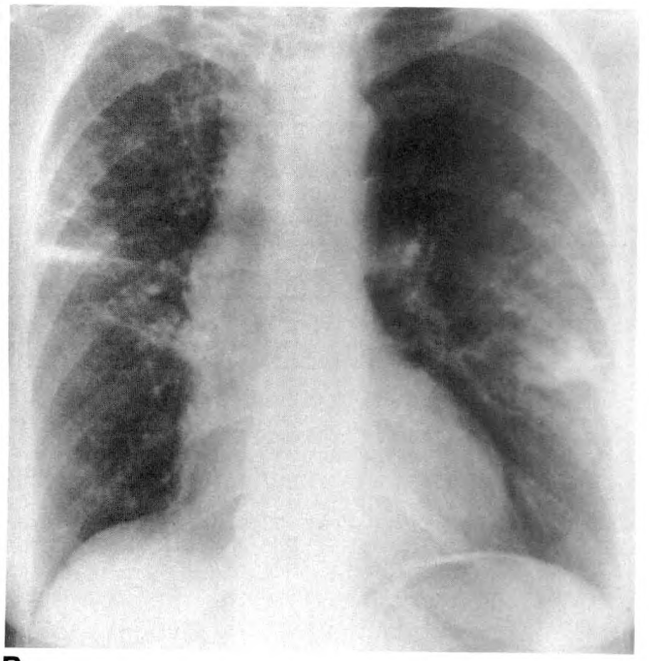
Radiographic findings.—The radiographic findings are summarized in Table 2. Twelve patients manifested alveolar opacities, 11 of which were lobar in distribution (Figs. 1A, 1B, 1D, 2A, and 2C). Six cases involved more than one lobe, whereas five involved only a single lobe. The opacities were bibasilar in one case. Four cases involved the right upper lobe, one the right middle lobe, five the right lower lobe, three the left upper lobe, and four the left lower lobe.

There were 10 patients with coarse reticular interstitial opacities (Figs. 3A and 3C). Three patients had diffuse bilateral involvement. Five cases were lobar in distribution, two of which were multilobar and three unilobar. In two cases the distribution was bibasilar. None had honeycomb changes. Two cases exhibited mixed alveolar and interstitial opacities: one case diffusely involved the upper-lung zones and the other diffusely involved lower-lung zones. Lung volume was decreased in six cases, and these were equally distributed among the patients with alveolar opacities and those with interstitial disease. Lung volume was normal in 17 cases. In one case there was unilateral hyperinflation (Fig. 1A). Pleural thickening was seen in three cases, and pleural effusion was seen in two cases.

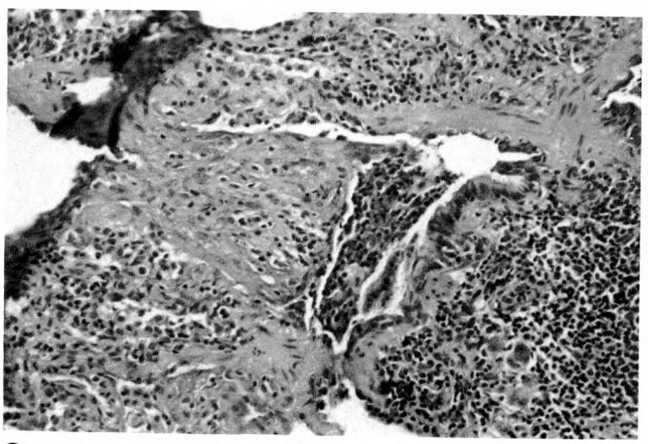
Follow-up radiographs were available in 17 cases. The



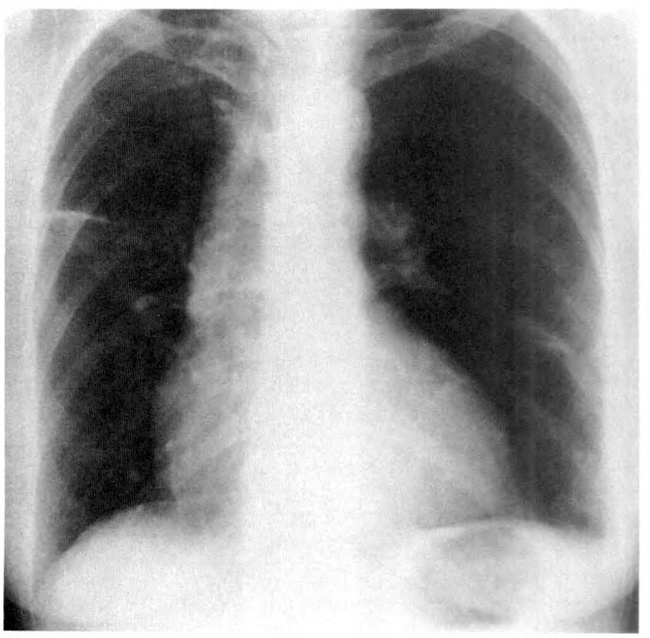
A



B



C



D

Fig. 1.—Case 1, 51-year-old woman with bronchiolitis obliterans with organizing pneumonia.

A, Chest radiograph shows alveolar opacities in right upper lobe and pleural thickening in left base. There are two poorly defined opacities in left midlung zone and hyperinflation of left lung.

B, Chest radiograph 1 month later shows improvement of right upper lobe opacity but new patchy alveolar opacity in lingular segment.

C, Photomicrograph shows proliferating fibroblasts within epithelial-lined bronchiole. Fibroblastic proliferation is associated with inflammatory exudate. Note chronic inflammatory infiltrate in bronchiole wall at upper left. (Original magnification 200×)

D, Follow-up chest radiograph 5 months later shows marked improvement after steroid treatment.

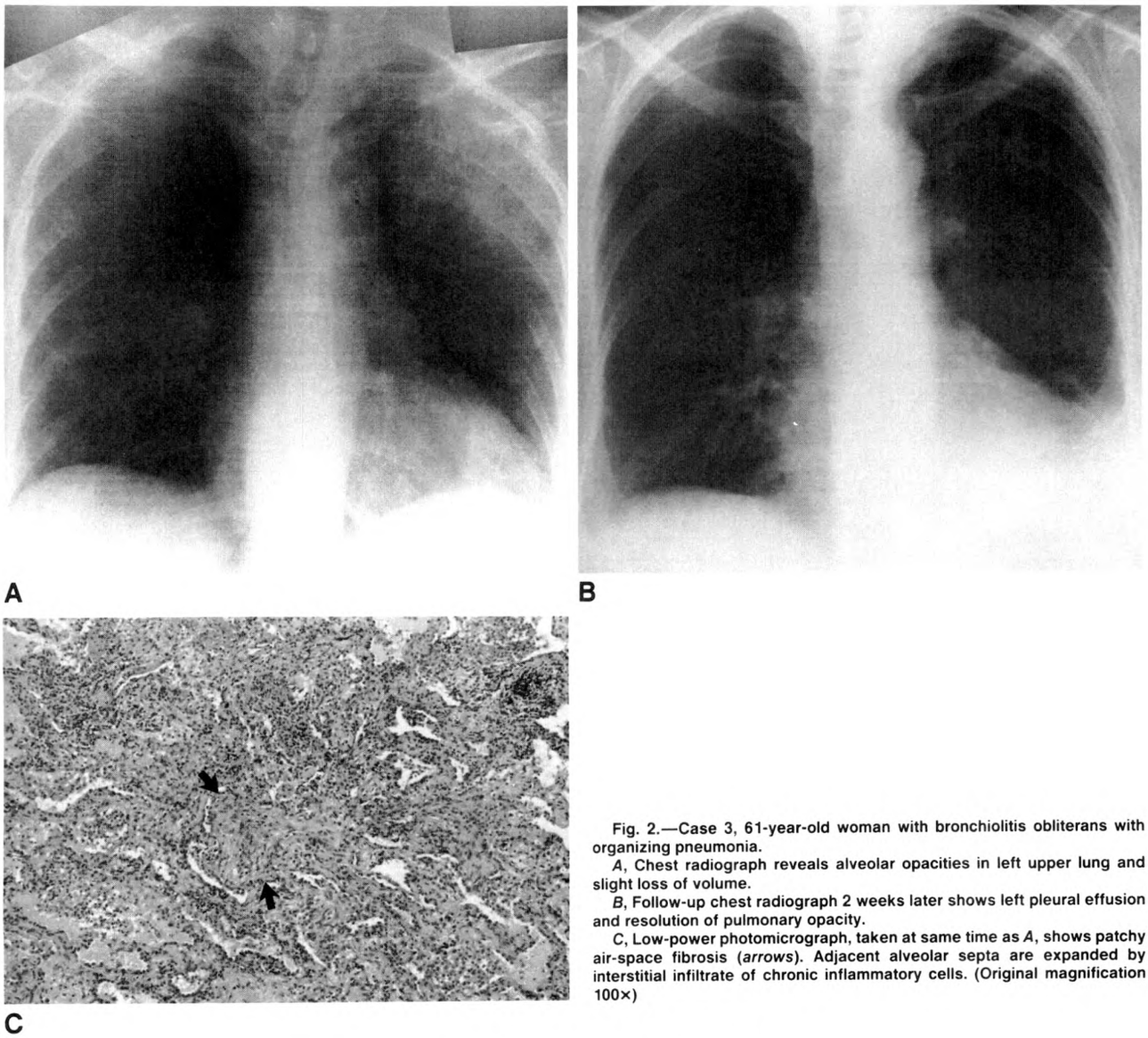


Fig. 2.—Case 3, 61-year-old woman with bronchiolitis obliterans with organizing pneumonia.

A, Chest radiograph reveals alveolar opacities in left upper lung and slight loss of volume.

B, Follow-up chest radiograph 2 weeks later shows left pleural effusion and resolution of pulmonary opacity.

C, Low-power photomicrograph, taken at same time as *A*, shows patchy air-space fibrosis (*arrows*). Adjacent alveolar septa are expanded by interstitial infiltrate of chronic inflammatory cells. (Original magnification 100×)

range of follow-up was 1 week to 48 months (mean, 3 months). Overall, eight patients showed improvement or resolution, six exhibited no change, and three worsened. Of seven patients who presented with alveolar opacities, one showed complete resolution, three improved but had persistent opacities, one demonstrated no change, and two worsened. Of eight cases presenting with interstitial opacities, one resolved completely, two partially improved, four remained unchanged, and one worsened. In the two patients who presented with mixed interstitial and alveolar opacities, one improved and one remained unchanged. Clinical follow-up was available in 23 of 24 patients (Table 1). Range of follow-up was from 2 months to 7¾ years (mean, 3½ years). Twelve (50%) patients were treated with steroids. Nine patients are alive without disease. Seven are alive with residual but stable disease. Three patients died of the disease and four died of other causes.

Usual Interstitial Pneumonia

Clinical information.—The clinical information is summarized in Table 1. The 16 patients, 13 men and 3 women, ranged in age from 29 to 77 years (mean, 58). The mean duration of symptoms was 2 to 3 years, and the most common symptoms were cough and progressive dyspnea. Three patients had evidence of connective-tissue disease. One patient had mixed connective-tissue disease, one had polymyositis, and one had a positive rheumatoid factor. Five patients had a history of occupational exposure. This group consisted of a shipbuilder in World War II, a papermill laborer, a sandblaster, a fiberspinner in a rubber plant, and a foundry laborer.

Radiographic findings.—The radiographic findings are summarized in Table 2. Fifteen patients had interstitial opacities only, and one patient had mixed alveolar and interstitial

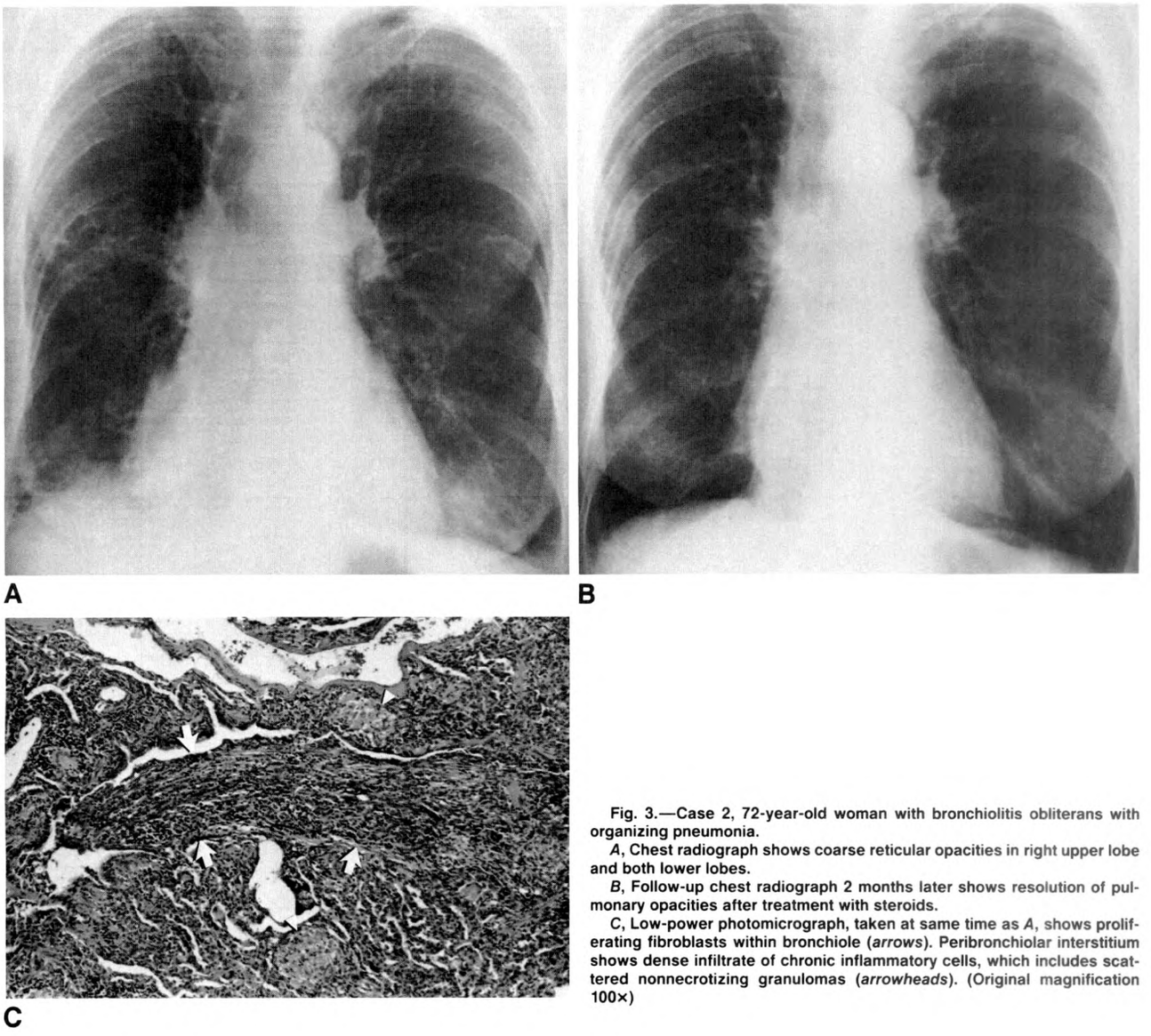


Fig. 3.—Case 2, 72-year-old woman with bronchiolitis obliterans with organizing pneumonia.

***A*, Chest radiograph shows coarse reticular opacities in right upper lobe and both lower lobes.**

***B*, Follow-up chest radiograph 2 months later shows resolution of pulmonary opacities after treatment with steroids.**

***C*, Low-power photomicrograph, taken at same time as *A*, shows proliferating fibroblasts within bronchiole (*arrows*). Peribronchiolar interstitium shows dense infiltrate of chronic inflammatory cells, which includes scattered nonnecrotizing granulomas (*arrowheads*). (Original magnification 100×)**

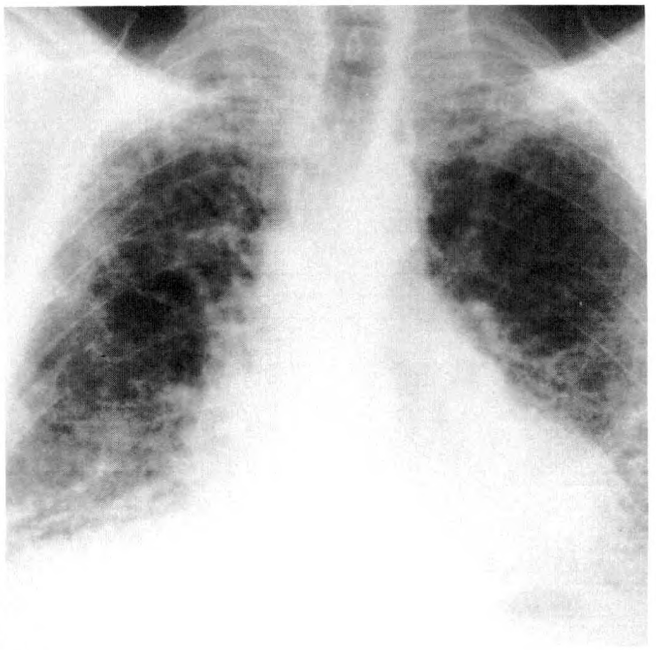
opacities (Figs. 4 and 5). Reticular opacities were seen in 10 patients, a reticulonodular pattern was seen in two patients, and three patients had generalized honeycomb lung. As for the distribution of these opacities, 10 cases were diffuse, four were bibasilar, and one was localized in the left lower lobe. One patient had diffuse, patchy alveolar and reticular opacities. Lung volumes were reduced in most cases. Only one patient had a pleural effusion. One patient had pleural thickening. Follow-up radiographs were obtained in 11 of 16 cases. Range of follow-up was from 1 week to 6½ years (mean, 18 months). Follow-up radiographs after steroid therapy showed partial improvement in five cases, worsening in three, and no change in three. Clinical follow-up was available for all 16 patients (Table 1). Fourteen of 16 were treated with steroids. Ten of the 16 patients died of the disease an average of 15 months after diagnosis whereas three died of other causes. The three who are alive have residual or worsening disease, including one who has been followed for 6½ years. There are no patients without residual disease.

Discussion

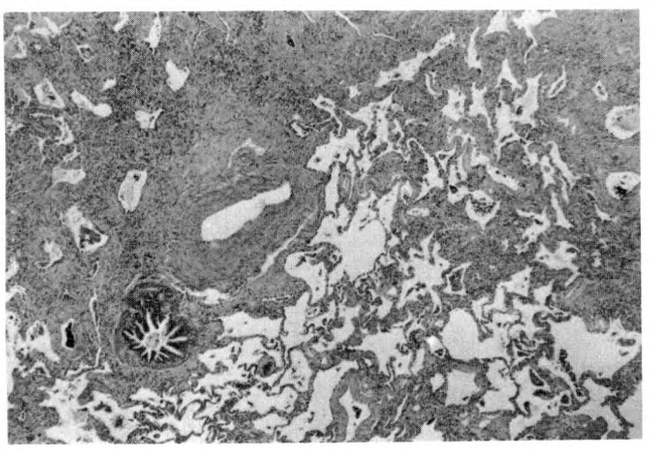
Bronchiolitis obliterans with organizing pneumonia is a disorder that may result from various types of lung injuries. It has been associated with toxic-fume inhalation, connective-tissue disorders, acute and chronic pulmonary infections, various drugs, and heart-lung transplantation [5–10]. It may also be idiopathic [2, 5, 11]. Some [2, 12] believe that prognosis is related to cause and that patients with the postinfectious or idiopathic variety fare better clinically. Histologically, the disease is characterized by plugs of granulation tissue



A



B



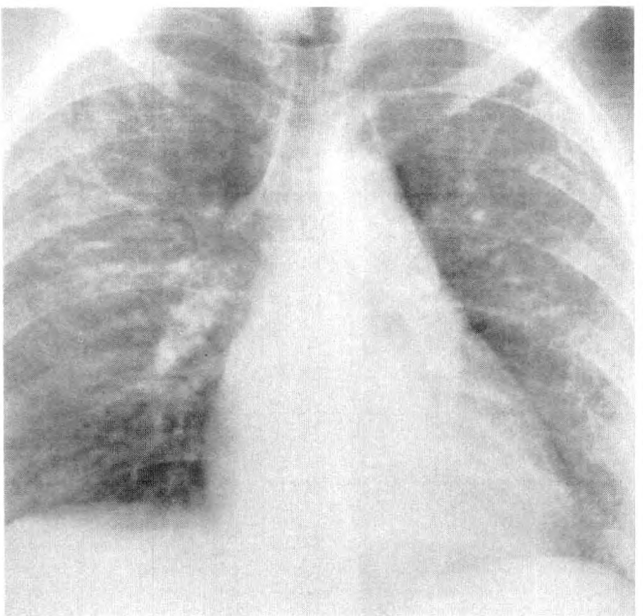
C

Fig. 4.—Case 4, 63-year-old man with usual interstitial pneumonia.
***A*, Chest radiograph shows reticular opacities in left lower lung and diminished lung volume.**
***B*, Follow-up chest radiograph 3 years later shows worsening with honeycomb changes.**
***C*, Low-power photomicrograph, taken at same time as *A*, shows interstitial fibrosis at upper right and left. Interstitial fibrosis is associated with lymphocytic infiltrate. Note relatively uninvolved lung at center. (Original magnification 40×)**

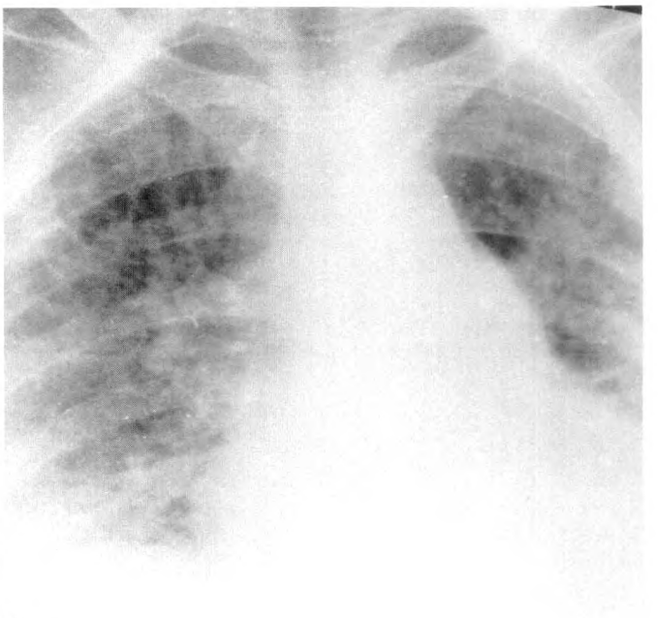
lying within small airways and extending into the alveoli. There is a varying interstitial infiltrate of inflammatory cells.

The term usual interstitial pneumonia (UIP) was first designated by Liebow and Carrington [13]. It is a response of the lung to alveolar damage. It has occurred in association with connective-tissue disease, drugs, or viral penumonia, or as a familial entity [1]. Many cases, however, are idiopathic [1]. UIP carries a poor prognosis, with death usually occurring within a few years after the diagnosis is made. Histologically, the disease is characterized by interstitial fibrosis with collagen deposition and interstitial pneumonia.

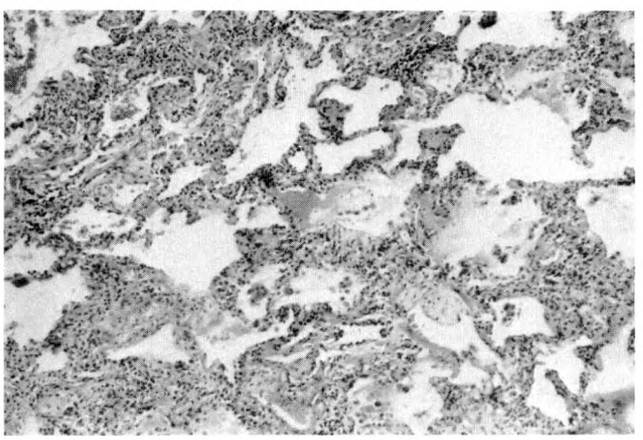
Many different radiographic appearances have been described in bronchiolitis obliterans with organizing pneumonia. Nodular, patchy, linear, lineonodular, alveolar, edemalike, "ground glass," and miliary opacities; lobar consolidation; and occasional hyperinflation have been seen [2, 5–12, 14–16]. In a study of 52 cases, Gosink et al. [5] found 18 cases with nodular densities, 39 with alveolar opacities, and two with hyperinflation. Epler et al. [2] studied 50 patients who had idiopathic bronchiolitis obliterans with organizing pneumonia, 42 of whom had chest radiographs available. These showed patchy densities with a "ground glass" appearance in 81%. This "ground glass" pattern was equated to an alveolar-type opacity [2]. In our study, half of the patients with bronchiolitis obliterans with organizing pneumonia had alveolar opacities, and 42% had an interstitial pattern. Because all cases had an open-lung biopsy it seems likely that we could explain the different radiographic patterns. But, as in the study of Gosink et al. [5], we found no direct correlation between radiographic patterns and histologic findings. A possible reason for this is the restricted sampling of the lung; the biopsy specimen may not contain the area of visualized radiographic abnormality.



A



B



C

Fig. 5.—Case 5, 29-year-old woman with usual interstitial pneumonia.
***A*, Chest radiograph shows diffuse reticulonodular opacities with slightly decreased lung volumes.**
***B*, Follow-up chest radiograph 6½ years later shows worsening of pulmonary disease with diffuse coarse reticular opacities and reduced lung volumes.**
***C*, Low-power photomicrograph, taken at same time as *A*, shows interstitial infiltrate of mononuclear cells. Edema fluid is present in occasional air spaces. (Original magnification 100×)**

We suspect that obstructive pneumonia or extensive intraalveolar organization is responsible for the alveolar opacities and that interstitial opacities were due to interstitial pneumonia. These processes would vary according to the individual patient's response. This response may be related to the cause of the disease, which in our study was usually idiopathic.

In UIP the earliest radiographic manifestations are fine reticular opacities predominantly in the lung bases. As the disease progresses the opacities coarsen and eventually there is honeycomb lung [13, 17]. In a study of 53 patients with UIP, Carrington et al. [1] reported that 40 (75%) had linear or irregular opacities, 26 (49.1%) had alveolar opacities, 26 (49%) had honeycomb changes, and 24 (45%) had diminished lung volume with "small lungs." In our study of 16 cases of UIP there was a marked preponderance of interstitial opacities (94%). Seventy-five percent of the patients had volume loss and in three cases there was honeycomb lung. The pathologic findings in these patients did show some correlation with the radiographs. In all cases there were extensive foci of interstitial fibrosis with collagen deposition and varying degrees of chronic interstitial pneumonia. We believe that this caused the interstitial opacities. Honeycomb changes were seen histologically in all three cases in which there was honeycomb lung radiographically. Perhaps the pathologic correlation in the patients with UIP is better because the radiographic manifestations tended to be more diffuse than in bronchiolitis obliterans with organizing pneumonia, thereby preventing the same degree of sampling error.

Even though the two diseases often have different clinical findings, we think it important to characterize any distinguishing radiographic features because some cases of bronchiolitis obliterans with organizing pneumonia have been confused with UIP histologically. Although there is overlap, our study

revealed that there are often radiographic differences in the two diseases. Half of the patients with bronchiolitis obliterans with organizing pneumonia had alveolar opacities whereas those with UIP displayed a marked tendency for interstitial opacities with volume loss. Honeycomb changes were seen in UIP but not in bronchiolitis obliterans with organizing pneumonia. These findings suggest that the chest radiograph may aid in distinguishing the two diseases.

ACKNOWLEDGMENTS

We would like to thank Cecil Gilman, Harry Germagian, Sam Collins, and Kim Woodward for their assistance in the preparation of the paper and scientific exhibit.

REFERENCES

1. Carrington CB, Gaensler EA, Coutu RE, Fitzgerald MX, Gupta RG. Natural history and course of usual and desquamative interstitial pneumonia. *N Engl J Med* **1978**;298:801–809
2. Epler GR, Colby TV, McLoud TC, Carrington CB, Gaensler EA. Bronchiolitis obliterans organizing pneumonia. *N Engl J Med* **1985**;312:152–158
3. Epler GR, Colby TV. The spectrum of bronchiolitis obliterans. *Chest* **1983**;83:161–162
4. Katzenstein A, Myers JL, Prophet D, Corley LS, Shin MS. Bronchiolitis obliterans and usual interstitial pneumonia: a comparative clinicopathologic study. *Am J Surg Pathol* **1986**;10:373–381
5. Gosink BB, Friedman PJ, Liebow AA. Bronchiolitis obliterans: roentgenologic-pathologic correlation. *AJR* **1973**;117:816–832
6. Williams T, Eidus L, Thomas P. Fibrosing alveolitis, bronchiolitis obliterans and sulfasalazine therapy. *Chest* **1982**;81(6):766–768
7. Murphy KC, Atkins CJ, Ofer RC, Hogg JC, Stein HB. Obliterative bronchiolitis in two rheumatoid arthritis patients treated with penicillamine. *Arthritis Rheum* **1981**;24:557–560
8. Epler GR, Snider GL, Gaensler EA, Cothcart ES, Fitzgerald MX, Carrington CB. Bronchiolitis and bronchitis in connective tissue disease. A possible relationship to the use of penicillamine. *JAMA* **1979**;242:528–532
9. Soto P, Madtes DK, Thorning P, Albert RK. Bronchiolitis obliterans caused by legionella pneumophilia. *Chest* **1985**;87(6):840–841
10. Burke CM, et al. Post transplant obliterative bronchiolitis and other late lung sequelae in human heart lung transplantation. *Chest* **1984**;86(6):824–829
11. Iannuzzi MC, Farhi DC, Bostrom PD, Petty TL, Fisher JH. Fulminant respiratory failure and death in a patient with idiopathic bronchiolitis obliterans. *Arch Intern Med* **1985**;145:733–734
12. McLoud TC, Epler GR, Colby TV, Gaensler EA, Carrington CB. Bronchiolitis obliterans. *Radiology* **1986**;159(1):1–8
13. Liebow AA, Carrington CB. The interstitial pneumonias. In: Simon M, Potchen EJ, LeMay M, eds. *Frontiers of pulmonary radiology*. New York: Grune & Stratton, **1969**:102–141
14. Azizirad H, Polgar G, Borns PF, Chatten J. Bronchiolitis obliterans. *Clin Pediatr (Phila)* **1975**;14(6):572–584
15. Seggev JS, Mason UG III, Worthen S, Stanford RE, Fernandez E. Bronchiolitis obliterans: report of three cases with detailed physiologic studies. *Chest* **1983**;83:169–174
16. Tukiainen P, Poppius H, Taskinen E. Slowly progressive bronchiolitis obliterans: a case report with detailed pulmonary function studies. *Eur J Respir Dis* **1980**;61:77–83
17. Fraser RG, Pare JAP. *Synopsis of diseases of the chest*. Philadelphia: Saunders, **1983**: 651–657

CT of Esophageal-Pleural Fistulae

Richard J. Wechsler[1]

Diagnosis of esophageal-pleural fistulae may be difficult in the absence of mediastinitis. To determine the value of CT in establishing this diagnosis and in detecting mediastinal involvement, CT findings in seven patients with esophageal-pleural fistulae were studied retrospectively. The fistulae were secondary to surgery (five patients), esophageal dilatation (one patient), and esophageal carcinoma (one patient). CT findings included barium, air, and fluid in the pleural space and pneumonia. These abnormalities seemed to distinguish an esophageal fistula from other pathologic processes, such as aspiration pneumonia, lung abscess, spontaneous pneumothorax, pulmonary emboli, and bronchopleural fistulae, and they documented a lack of inflammatory reactions in the mediastinum associated with the fistula. The latter finding is important, because patients with esophageal-pleural fistulae without mediastinitis have a less severe clinical course and respond better to conservative treatment. CT is useful for patients with normal findings on esophagrams when suspicion of esophageal-pleural fistulae remains high and when satisfactory esophagrams cannot be obtained.

Early diagnosis of esophageal-pleural fistula reduces morbidity and mortality but may be difficult to make if mediastinitis is absent [1]. We performed a retrospective study of the CT findings in seven patients with esophageal-pleural fistula to determine the value of this procedure in establishing this diagnosis and in detecting mediastinal involvement.

Subjects and Methods

Between 1982 and 1985, CT scans were obtained on five men and two women 16 to 59 years old who had esophageal-pleural fistulae. The fistulae were secondary to surgery in five patients, to esophageal dilatation in one, and to esophageal carcinoma in one. Four patients had fever, three had dyspnea, and two had lung infections. The length of time between esophageal injury and CT examination ranged from 2 days to 8 years. In five patients other studies established a diagnosis of esophageal perforation before the CT examination was performed; however, the extent of mediastinal involvement was not determined. The fistulae were determined by CT before esophagography in the other two patients. The diagnosis was proven by surgery in four patients and by endoscopy in one. The sixth fistula was diagnosed by esophagography and the seventh by detection of radioactivity in the pleural space after instillation of radionuclide into the esophagus. Five patients had esophagography and all seven had chest radiographs.

Five CT scans were obtained on a Technicare 2020 HR scanner by using a 512 × 512 matrix with a scan time of 2 sec, 120 kV, 100 mA, and a 10-mm collimator. Two studies were obtained on a Pfizer 0200 scanner with a 320 × 320 matrix and a scan time of 28 sec, 140 kV, 35 mA, and a 10-mm collimator. IV contrast enhancement (100 ml of 60% meglumine iothalamate) was used in selected cases. Contrast material was administered orally just before the examination in two patients. Scans were obtained from the apex of the lung through the superior aspect of the liver at 10-mm increments. Additional scans were obtained as necessary.

Received April 15, 1986; accepted after revision June 9, 1986.

[1] Department of Radiology, Thomas Jefferson University Hospital, Philadelphia, PA 19107.

AJR 147:907–909, November 1986
0361–803X/86/1475–0907
© American Roentgen Ray Society

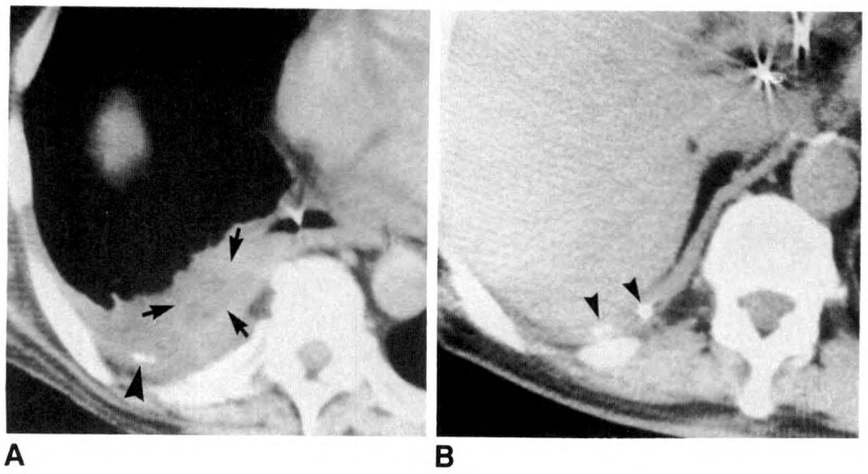


Fig. 1.—68-year-old man with esophageal-pleural fistula after esophagogastrectomy. Esophagography was not done.

A, CT scan made just above diaphragm shows stomach (*arrows*) in right paravertebral region. Adjacent to stomach is pleural reaction containing a small collection of oral barium (*arrowhead*) administered just before scan.

B, CT scan at level of upper abdomen reveals barium (*arrowheads*) in posterior costophrenic angle.

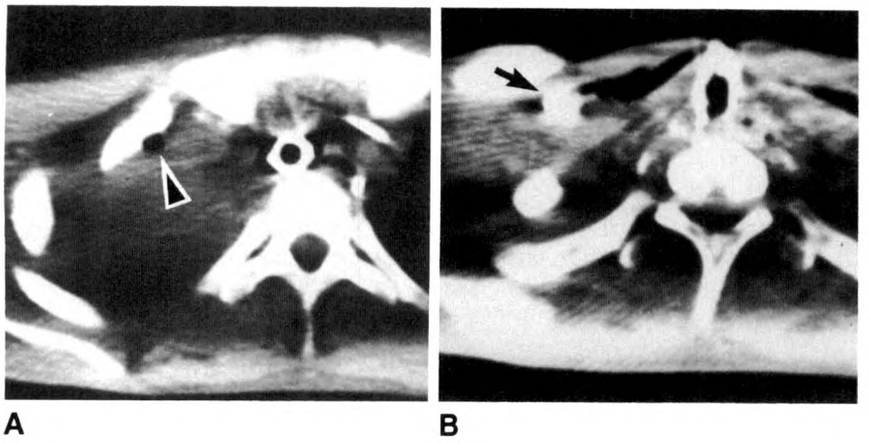


Fig. 2.—*A*, 16-year-old boy with esophageal-pleural fistula after anterior fusion of cervical spine. CT scan shows loculated pleural reaction with small anterior air collections in the pleural space (*arrowhead*). Subsequent esophagram confirmed fistula.

B, Barium (*arrow*) given just before CT scan is noted along with pleural thickening at right apex in scan approximately 2 cm above scan shown in *A*.

Results

CT showed barium from a previous barium swallow in the pleural space in four patients (Fig. 1). Pneumothorax (Fig. 2) was seen in four patients, pleural reaction in six, and pneumonia in five. Mediastinitis was considered present only when CT findings of mediastinal air and soft-tissue reaction were seen remote from the area of previous surgery or esophageal cancer. This was noted in one of two patients who subsequently died.

Discussion

The clinical and radiographic signs and symptoms of esophageal-pleural fistulae are inconstant and nonspecific. Clinical findings include chest pain, fever, dysphagia, and dyspnea. When these symptoms follow esophageal instrumentation or surgery, esophageal trauma must be excluded. The radiologic signs depend on the site, duration, and severity of the perforation. If the pleura remains intact, mediastinal emphysema occurs early and mediastinal widening appears within several hours. Once mediastinitis occurs, rupture of the mediastinal pleura, pneumothorax, or hydrothorax can occur. Radiographic findings may, however, not appear for up to 24 hr [2]. When the pleura is not intact, esophageal-pleural fistulae can occur in the absence of mediastinal involvement because decompression of the esophageal contents into the pleural space spares the mediastinum. In these cases pleural effusion, pneumothorax, and hydropneumothorax may be the only clues to the diagnosis [1]. Other processes that mimic esophageal-pleural fistula are aspiration pneumonia, lung abscess, spontaneous pneumothorax, pulmonary emboli, and bronchopleural fistula.

CT findings of esophageal-pleural fistulae are similar to those seen on chest radiographs. Pleural effusions occur in most cases and are nonspecific. Pneumothorax, however, is seen in the majority of cases and reduces the number of diagnostic considerations. If contrast medium has been given orally, it can be seen in the pleural space. This is pathognomonic of this condition. Although contrast medium was not given orally to some of our patients immediately before the CT scan because of clinician oversight, it is apparent that the routine use of oral contrast medium in these patients is mandatory. Thickening of the esophageal wall at the site of perforation may also be seen. Atelectasis or direct involvement of the lung from the perforated esophagus is a common finding.

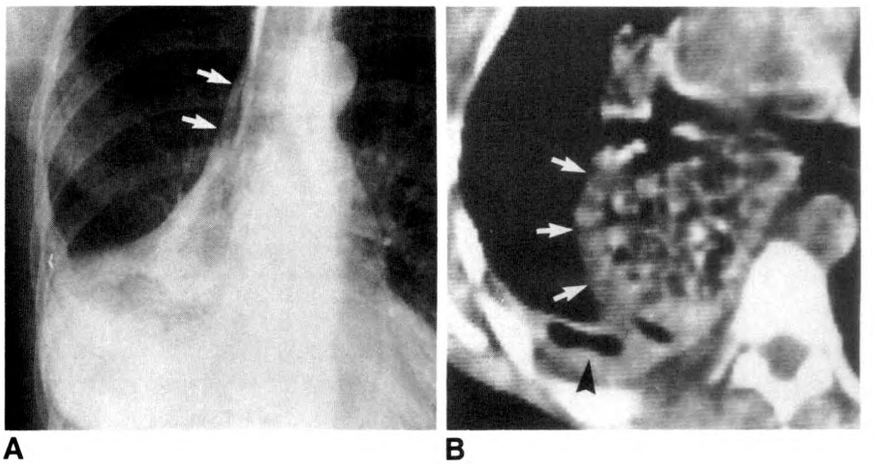


Fig. 3.—48-year-old woman with esophageal-pleural fistula after esophageal dilatation performed 8 years earlier for achalasia. First barium swallow was inadequate because of patient's refusal to cooperate.

***A*, Posteroanterior chest radiograph taken 8 years after dilatation shows dilated esophagus (*arrows*) and right basilar opacification.**

***B*, CT scan made at the same time as *A* shows a dilated esophagus (*arrows*) and pleural air (*arrowhead*) indicating esophageal-pleural fistulae.**

The use of CT to detect esophageal-pleural fistulae offers several advantages. A high-quality esophagram is often difficult to obtain in seriously ill patients. CT is fast, requires little patient cooperation, and is capable of evaluating both the pleura and the mediastinum. Minute amounts of air or oral contrast material in the pleural space can be identified. In a previous report, a patient was described in whom an anastomotic leak was identified on CT after esophagography failed to show it [3]. We made this diagnosis in two patients before using esophagography and showed esophageal-pleural fistulae in another two patients in whom esophagography could not be or was not obtained. CT is more sensitive than plain radiographs and can be used in clinical situations in which findings on esophagography are normal or in those patients for whom a satisfactory esophagram cannot be obtained. In addition, mediastinal, pulmonary, and subphrenic involvement secondary to esophageal trauma can be assessed. In a previous report of seven patients with esophageal-pleural fistulae, two had a concomitant subphrenic abscess and three had associated pneumonia [1].

The major value of CT is to determine the need for surgical intervention. The prognosis of esophageal-pleural fistulae without mediastinal involvement is good, and patients with this condition may respond to percutaneous drainage of the pleural space better than those who have an associated mediastinitis. One patient in this series tolerated an esophageal-pleural fistula for 8 years before her condition was detected by CT (Fig. 3). Two other patients without evidence of mediastinitis were treated medically. Patients with an esophageal-pleural fistula and no mediastinal involvement may respond well to conservative treatment [4, 5, 6]. In addition, CT localization of pleural collections provides useful information for percutaneous drainage.

The use of CT in this setting has several shortcomings. Postoperative changes in the mediastinum may be difficult to distinguish from acute disease, and the exact site of esophageal perforation may not be demonstrated. One patient in this series, despite having positive findings on a water-contrast esophagram, had only a pleural effusion without pneumothorax detected by CT. Barium might have been detectable in the pleural space if it had been administered orally before the CT examination. CT in this patient, however, detected mediastinitis and helped determine the choice of therapy. Other mediastinal collections, such as hematomas or lymphoceles, may be mistaken for anastomotic leaks. However, these are rare surgical complications with a different clinical presentation [7].

In summary, CT can establish the diagnosis of esophageal-pleural fistulae when findings on a barium swallow are negative or when an esophagram cannot be obtained. This occurred in two of seven cases in this series. In addition, CT can detect the presence of mediastinitis. This is important because patients who do not have mediastinal involvement have a less severe clinical course and may respond better to conservative treatment.

ACKNOWLEDGMENTS

I thank Jack Edeiken and Esmond Mapp for their helpful comments and Wendy Bayliss and Ann Prather for assistance in manuscript preparation.

REFERENCES

1. Wechsler RJ, Steiner RM, Goodman LR, Teplick SK, Mapp E, Laufer I. Iatrogenic esophageal-pleural fistula: subtlety of diagnosis in the absence of mediastinitis. *Radiology* **1982**;144:239–243
2. Christoforidis A, Nelson SW. Spontaneous rupture of esophagus with emphasis on the roentgenologic diagnosis. *AJR* **1957**; 78:574–580
3. Heiken JP, Balfe DM, Roper CL. CT evaluation after esophagogastrectomy. *AJR* **1984**;143:555–560
4. Brown RH, Cohen PS. Nonsurgical management of spontaneous esophageal perforation. *JAMA* **1978**;240:140–142
5. Lyons WS, Seremetis MG, deGuzman VC, Peabody JW. Ruptures and perforations of the esophagus: the case for conservative supportive management. *Ann Thorac Surg* **1978**;25:346–350
6. Cameron JL, Kieffer RF, Hendrix TR, Mehigan DG, Baker RR. Selective nonoperative management of contained intrathoracic esophageal disruptions. *Ann Thorac Surg* **1974**;27:404–408
7. Sullivan KL, Wechsler RJ. CT diagnosis of mediastinal lymphocele. *J Comput Assist Tomogr* **1985**;9:1110–1111

American Roentgen Ray Society:
Officers, Committees, and Meeting Information

Officers

President: Jerome F. Wiot
President- elect: Raymond A. Gagliardi
1st Vice-president: Lee F. Rogers
2nd Vice-president: Gerald D. Dodd
Secretary: Glen W. Hartman
Treasurer: Ronald G. Evens

Executive Council: E. Gedgaudas, J. F. Wiot, L. F. Rogers, R. A. Gagliardi, R. G. Evens, R. N. Berk, F. L. Angell, J. E. Madewell, M. P. Capp, G. W. Hartman, B. G. Brogdon, G. A. Kling, H. C. Carlson, A. K. Poznanski, A. E. James, Jr., J. A. Kirkpatrick, Jr., G. R. Leopold, G. D. Dodd, J. T. Ferrucci, Jr., R. H. Troupin, chairman

Committees 1986–1987

Editorial Policy: S. S. Sagel, W. J. Casarella, J. T. Ferrucci, Jr., N. C. Whitley, S. Hilton, A. J. Davidson, J. M. Taveras, R. N. Berk, M. P. Capp, chairman

Education and Research: C. E. Putman, A. R. Margulis, J. R. Thornbury, R. A. McLeod, J. T. Ferrucci, Jr., ex officio, B. G. Brogdon, chairman

Finance and Budget: B. P. Wood, L. R. James, J. A. Kirkpatrick, Jr., A. E. James, F. L. Angell, chairman

Instruction Courses: R. A. McLeod, associate chairman, J. T. Ferrucci, Jr., chairman

Program: J. Wiot, G. W. Hartman, J. A. Kirkpatrick, Jr., R. H. Troupin, M. P. Capp, J. E. Madewell, B. G. Brogdon, J. T. Ferrucci, Jr., G. A. Kling, G. G. Ghahremani, M. Viamonte, R. A. Gagliardi, chairman

Publications: W. J. Casarella, J. T. Ferrucci, Jr., S. S. Sagel, N. C. Whitley, M. P. Capp, chairman

Scientific Exhibits: S. G. Kirchner, A. V. Proto, S. M. Goldman, J. E. Madewell, chairman

Nominating: W. J. Casarella, H. C. Carlson, A. E. James, chairman.

Representatives to Other Organizations

American Board of Radiology: E. C. Klatte, R. W. McConnell, L. F. Rogers

American College of Radiology: J. L. Gwinn, G. A. Kling, G. W. Hartman, J. M. Dennis, E. J. Ferris, J. E. Madewell

American Medical Association House of Delegates: S. F. Ochsner, K. C. Krabbenhoft, alternate

American National Standards Institute: M. Haskin

National Council on Radiation Protection and Measurements: E. L. Saenger, H. L. Friedell

Meetings, Membership, Business Information

Annual Meetings: April 26–May 1, 1987, Fontainebleau-Hilton, Miami Beach; May 1–6, 1988, Westin Bonaventure, Los Angeles; May 7–13, 1989, Hilton, New Orleans.

Director Annual Meeting: George A. Kling, Harper Hospital, Detroit, MI 48201; (313) 494-8405.

ARRS Membership: Rosalind H. Troupin, Dept. of Radiology, Hospital of University of Pennsylvania, 3400 Spruce St., Philadelphia, PA 19104. The ARRS has two membership categories: active and in-training. For active membership, applicants must practice radiology in the U.S. or Canada. Each must have graduated in good standing from an approved medical school or hold an advanced degree in a physical, chemical, or biological science and be certified by the American Board of Radiology, the Royal College of Physicians and Surgeons of Canada, or otherwise adequately document training and credentials. A member-in-training must be in a radiology residency, a postresidency fellowship program, or a postgraduate student in an allied science. Status must be verified by the program director. For consideration during the 1987 ARRS meeting, completed applications must be received by Dr. Troupin no later than Feb. 1, 1987.

Business Office: Paul Fullagar, executive director, George J. O'Hop, controller, American Roentgen Ray Society, 1891 Preston White Dr., Reston, VA 22091; (703) 648-8900.

Postoperative Recurrence of Lung Cancer: Detection by Whole-Body Gallium Scintigraphy

M. K. Hatfield[1]
H. MacMahon[1]
J. W. Ryan[1]
A. G. Little[2]
P. C. Hoffman[3]
M. Ferguson[2]
T. R. DeMeester[4]
H. M. Golomb[3]

The records were reviewed of 111 consecutive patients who had lung cancer resected and who were followed with serial postoperative whole-body gallium scans. Scans were obtained preoperatively at intervals of 3–6 months for about 1 year after surgery and subsequently at yearly intervals. The period of follow-up varied from 1½ to 8 years. Of 55 patients who developed tumor recurrence, a gallium scan was the first indicator of recurrence in 11 (20%) and was judged helpful in confirming or localizing a recurrence in another 14 patients (25%). False-positive rates were determined from 175 postoperative scans in the other 56 patients who did not suffer recurrence. Of these 175 scans, 15 (9%) demonstrated abnormalities that were sufficiently suspicious that an additional diagnostic procedure, other than chest radiography, was performed for clarification. However, in no case did the gallium scan result adversely affect the management of the patient. Our data demonstrate that routine postoperative whole-body gallium scanning can facilitate early detection of recurrence in some cases. Judicious use of gallium scanning in cases with clinically suspected recurrence can enable prompt localization, diagnosis, and treatment of recurrent tumor.

Whole-body gallium scanning has been used successfully for preoperative staging of lung cancer patients, though its utility in that context remains controversial [1, 2]. However, the role of gallium scintigraphy in the postoperative follow-up of these patients has not been defined.

At the University of Chicago Medical Center, gallium scanning has been performed in all patients with lung cancer both before and after surgery at regular intervals. To examine the clinical efficacy of this approach, we analyzed the records of 111 patients who had lung cancer resected and who were evaluated by interview, physical examination, chest radiography, and gallium scintigraphy periodically thereafter. The purpose of this review was to determine how frequently unsuspected recurrences were revealed by gallium scans and to what extent such benefits were offset by false-positive results.

Received February 27, 1986; accepted after revision June 10, 1986.

[1] Department of Radiology, University of Chicago, 5841 S. Maryland Ave., Chicago, IL 60637. Address reprint requests to H. MacMahon.

[2] Department of Surgery, University of Chicago, Chicago, IL 60637.

[3] Department of Medicine, University of Chicago, Chicago, IL 60637.

[4] Department of Surgery, Creighton University, Omaha, NB 68131.

AJR 147:911–916, November 1986
0361–803X/86/1475–0911
© American Roentgen Ray Society

Materials and Methods

The study included all patients resected for cure at this medical center from 1977 through 1983 in whom one or more postoperative gallium scans were obtained. Patients included in the study were followed for a minimum of 18 months and a maximum of 8 years.

Imaging was performed 48–72 hr after IV injection of 10 mCi (370 MBg) of gallium-67 citrate. Whole-body scans were obtained in the longitudinal multiplane tomographic mode with a Pho/Con (Siemens) Tomographic Scanner [1]. Supplemental gamma camera views were obtained when indicated.

All patients had preoperative scans. The first postoperative scan was usually obtained 3–6 months after surgery. A second scan was obtained about 6 months later. Subsequent scans were obtained at 1-year intervals if the patient remained asymptomatic. Patients with suspected or proven recurrence were discussed at a joint multispecialty conference where

TABLE 1: **Proof of Recurrence**

Method	No. of Patients
Tissue diagnosis	27
Progression of lesion on chest radiography	10
Brain CT scan	7
Combination of techniques (plain radiography, bone scanning, CT, sonography)	10
Physical examination (palpable mass)	1
Total	55

TABLE 2: **Role of Gallium Scan in Diagnosis of Recurrence**

Role	No. of Patients (%)
Gallium scan first indicator of recurrence	11 (20)
Suspected recurrence confirmed or localized by gallium scan	14 (25)
Lesion demonstrated by gallium scan, with no influence on clinical decision making	15 (27)
Recurrence detected by other methods and not shown on gallium scan	12 (22)
Recurrence demonstrated by other methods and no gallium scan obtained	3 (5)
Total	55 (100)

scans and other imaging studies were reviewed.

For this investigation, the records of 111 consecutive patients who fulfilled the criteria for the study were reviewed. Clinical records, chest radiographs, and radionuclide scans were analyzed. A judgment as to the usefulness of the gallium scan in the detection of recurrent tumor and in subsequent patient management was made on the basis of the original interpretation of the scan and the recorded consensus of the multispecialty conference group. From these data, each patient was assigned to one of five categories: (1) the gallium scan was the first indicator of recurrence (i.e., there was no prior clinical suspicion of recurrence; (2) the gallium scan confirmed or localized a suspected recurrence and was thus judged helpful in the management of the patient; (3) the gallium scan demonstrated the recurrence but was judged not to have influenced the patient's management; (4) the gallium scan failed to demonstrate the recurrence; or (5) the recurrence was detected by other means and a gallium scan was not obtained at that time. Proof of tumor recurrence was provided by biopsy in 27 cases. The others were deemed to have recurred on the basis of chest radiography, other imaging techniques, or in one instance, by appearance of a palpable, hard, subcutaneous mass (Table 1).

Retrospective review of the relevant scans and radiographs was performed to help identify false-negative or false-positive diagnoses with the benefit of hindsight. "Normal" postsurgical uptake in the chest wall was also recorded during this retrospective review.

TABLE 3: **Sites of Tumor Recurrence**

Site	No. of Patients
Chest (including ribs)	29
Other bones	11
Brain	8
Extrathoracic lymph nodes	6
Liver	1
Total	55

TABLE 4: **Frequency of False-Positive results among Nonrecurrent Postoperative Lung Cancer Patients**

Scan Interpretation	No. of Scans (%)
Probable recurrence	2 (1)
Possible recurrence, additional imaging study recommended	13 (7)
Possible recurrence by gallium scan; considered negative following correlation with chest radiographs	8 (5)
Minor abnormalities described, probably not significant	9 (5)
No evidence of recurrence	143 (82)
Total	175 (100)

Note.—175 scans were done on 56 patients with no evident tumor recurrence.

Results

Of the 111 patients studied, 55 development a recurrence during the period of follow-up. The average interval between resection and recurrence was 12.5 months (range, 2–36 months). The gallium scan was the first indicator of recurrence in 11 patients (20%), and it was judged helpful in confirming or localizing a recurrence in another 14 patients (25%) (Table 2). The chest was the most common site of tumor recurrence followed by extrathoracic skeletal lesions and brain metastases (Table 3). The gallium scan was most frequently helpful in detecting or confirming intrathoracic recurrences. Among the recurrent cases there were 22 examples of squamous cell carcinoma, 19 of adenocarcinoma, and eight of oat cell carcinoma. There were no obvious differences in this series between these cell types in terms of their susceptibility to detection by gallium.

Fifty-six patients showed no evidence of tumor recurrence during the period of follow-up, and a total of 175 gallium scans were obtained on these during the postoperative period. These cases were analyzed for evidence of false-positive scan results. To determine the possible impact of false-positive interpretations on patient management, specific note was made as to how often a false-positive interpretation led to performance of further investigations to exclude recurrence. The rate of false-positive "calls" is listed in Table 4. A question of recurrence was raised in 23 instances. In eight of these, correlation with chest radiographs was adequate to exclude the question. In 15 a further investigation was recommended to exclude recurrence. These additional studies consisted of radiography in six, bone scans in four, and brain CT scans in two cases. One bronchoscopy examination, one

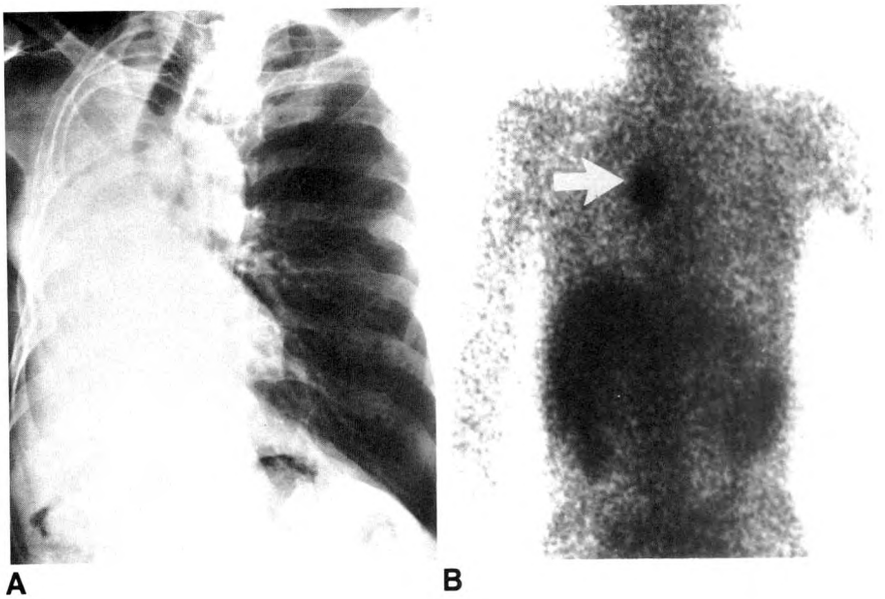


Fig. 1.—Asymptomatic 66-year-old man 4 months after right pneumonectomy for stage III squamous cell carcinoma.

***A*, Chest radiograph shows only normal postoperative findings.**

***B*, Gallium scan reveals focal uptake in right hilum (*arrow*). Bronchoscopy confirmed recurrent tumor at bronchial stump.**

lymph node biopsy, and one repeat gallium scan were also performed to clarify suspicious findings on the initial scan. In no instance was a patient's management otherwise affected by a false-positive reading.

The possible role of postsurgical inflammatory change as a source of false-positive scan interpretation was examined. Among the patients without recurrence, six had scans within 3 months of thoracotomy. In five of these, abnormal accumulation was seen at the surgical site. Of 23 scans obtained 3–6 months after surgery, eight showed uptake attributable to surgical trauma. Intense uptake was seen at the surgical site up to 21 months after surgery and faint uptake occasionally occurred up to 5 years after surgery.

Of the 55 patients whose tumor recurred, there were five whose primary lesion had not shown gallium uptake. The size of these gallium-negative tumors varied from 3.5 to 10.5 cm. However, in two of these five, the recurrent tumor was gallium-positive, with uptake in a supraclavicular node metastasis and iliac bone recurrence, respectively. Thus, absence of uptake in the primary did not preclude identification of metastases by the gallium scan in our series.

Discussion

The most widely recognized role for gallium scintigraphy in lung cancer has been that of a staging technique, though its utility in that context remains controversial [3–9]. In patients with established malignancy, it can be used for periodic reevaluation when the high sensitivity of the technique frequently outweighs the disadvantage of low specificity. Both sensitivity and specificity are improved when previous scans of the same patient are available for comparison. We have found the gallium scan to be particularly helpful in cases in which extensive scarring from previous surgery has rendered radiographs and CT scans difficult to interpret. In this situation, a new focus of gallium accumulation in a patient with no clinical evidence of infection strongly suggests recurrent tumor (Fig. 1). In patients who develop clinical symptoms, the gallium scan can localize a recurrence unsuspected on chest radiography (Figs. 2 and 3).

False-positive results are a potential source of concern with gallium scans in general. In this series, although false positives did occur (Fig. 4), the rate was reasonably low, and the patient's management was not adversely affected in any case. Comparison with previous postoperative scans in most instances undoubtedly increased interpretation accuracy. More importantly, in recognition of the potentially low specificity of the test, the results were generally used as a guide to further, more specific investigations. Therefore, at worst, a false-positive call resulted in additional, otherwise unnecessary, testing.

Administration of chemotherapy less than 24 hr before gallium injection has been reported to impair tracer localization in tumor [10]. Greater temporal separation between chemotherapy and gallium administration can obviate this problem. In this series, 15 of 40 patients with gallium-positive recurrences had received chemotherapy in the weeks or months preceding the scan, and tracer concentration was evidently not impaired.

As treatment for recurrent lung cancer is largely palliative, the cost-effectiveness of routine postoperative testing designed to detect preclinical recurrence may be questioned. However, in an oncology program in which randomized trials for various adjuvant forms of therapy are in progress, it is important to document the "disease-free interval" and to establish the presence of recurrent tumor as early and as accurately as possible. In some instances, detection of preclinical bone metastases can facilitate early radiation therapy, thus preventing pathologic fractures with attendant morbidity. Further, a thorough evaluation that indicates no evidence of

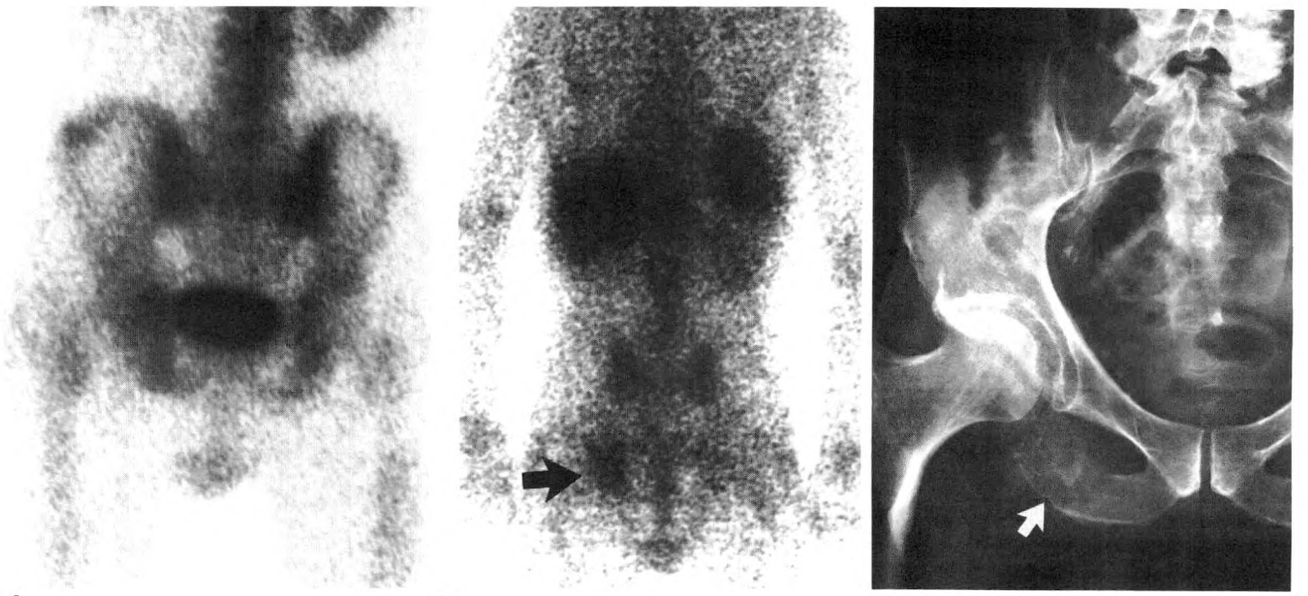


Fig. 2.—63-year-old man with diffuse bone pain 5 months after left pneumonectomy for stage II squamous cell carcinoma.
A, Bone scan was interpreted as normal. In retrospect there is some asymmetry in ischial regions.
B, Gallium scan 3 days later. Uptake in right ischium (*arrow*).
C, Radiograph confirms lytic metastasis (*arrow*).

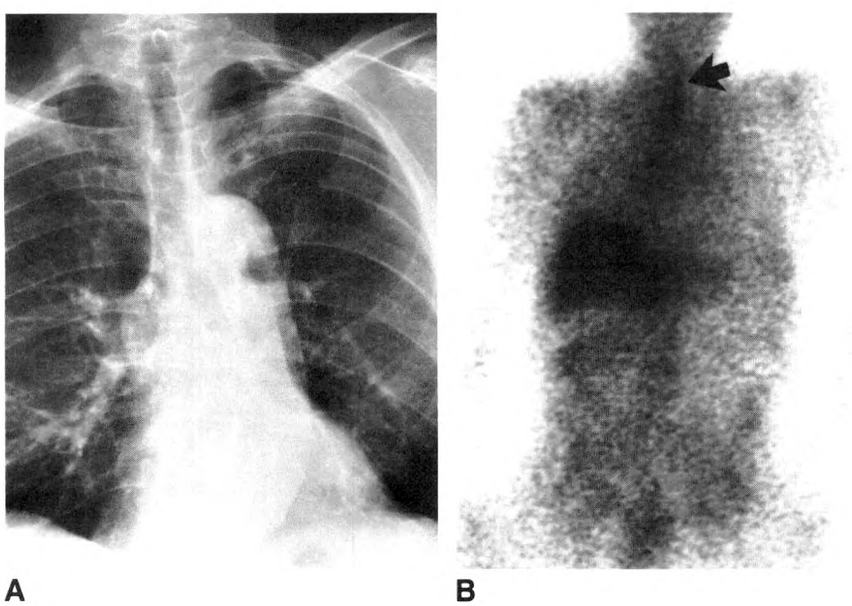


Fig. 3.—75-year-old man with productive cough 9 months after left lower lobectomy for stage I squamous cell carcinoma.
A, Chest radiograph shows postoperative scarring unchanged from previous study.
B, Gallium scan shows focal uptake anteriorly in midsuperior mediastinum (*arrow*). Tracheal metastasis was confirmed by bronchoscopy.

recurrent tumor can provide important reassurance to a concerned patient. In those who develop symptoms such as poorly localized pain, early diagnosis of recurrence by gallium scanning can facilitate timely palliation. Although an abnormal focus of gallium activity is not in itself diagnostic of recurrent tumor, the ability to image the entire body and to localize a potential recurrence is valuable.

Our results demonstrate that use of routine postoperative whole-body gallium scans can facilitate early detection of recurrence in some cases. More importantly, judicious use of

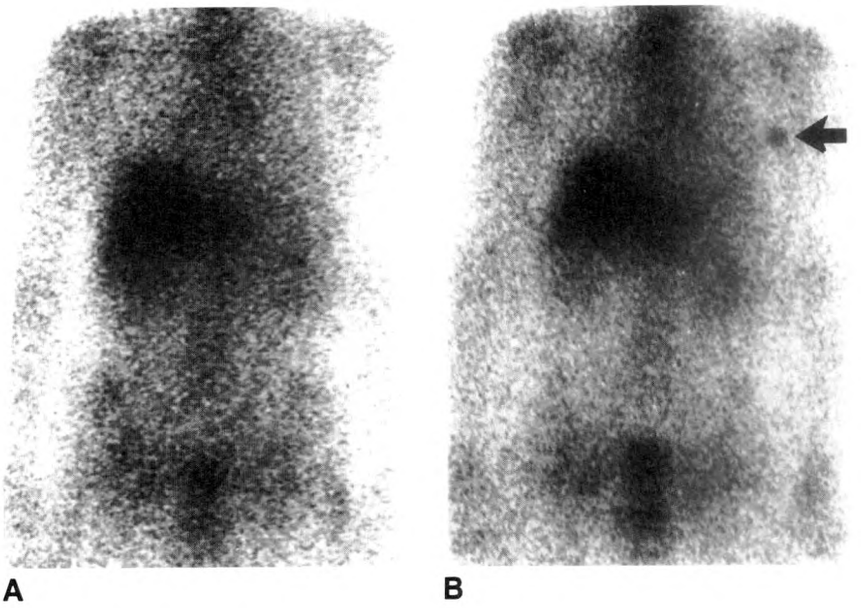


Fig. 4.—Asymptomatic 54-year-old man 5 months after right middle and right lower lobectomy for stage III adenocarcinoma.

***A*, Gallium scan shows no abnormality. Faint hilar uptake of degree observed was not considered significant in these patients.**

***B*, 14 months later. Focal uptake in left axilla (*arrow*) diagnosed as probable lymph node metastasis. Left axillary biopsy showed no evidence of recurrent tumor; follow-up was uneventful.**

gallium scans in patients with clinically suspected recurrence enables prompt localization, diagnosis, and treatment of the recurrent tumor.

REFERENCES

1. DeMeester TR, Golomb HM, Kirchner P, et al., The role of gallium-67 scanning in the clinical staging and preoperative evaluation of patients with carcinoma of the lung. *Ann Thorac Surg* **1979**;28(5):451–464
2. Waxman AD, Julien PJ, Brachman MB, et al. Gallium scintigraphy in bronchogenic carcinoma. The effect of tumor location on sensitivity and specificity. *Chest* **1984**;86(2):178–183
3. McKenna RJ, Haynie TP, Libshitz HI, Mountain CF, McMurtrey MJ. Critical evaluation of the gallium-67 scan for surgical patients with lung cancer. *Chest* **1985**;87(4):428–431
4. Friedman PJ, Feigin DS, Liston SE, et al. Sensitivity of chest radiography, computed tomography, and gallium scanning to metastasis of lung carcinoma. *Cancer* **1984**;54:1300–1306
5. Neumann RD, Sostman MD. Ga-67 scintigraphy of the thorax. *Chest* **1984**;86:253–256
6. Nieweg OE, Beekhuis H, Peirs DA, Sluiter HJ, VanderWal AM, Woldring MG. 57-Co-bleomycin and 67-Ga-citrate in detecting and staging lung cancer. *Thorax* **1983**;38(1):16–21
7. Pannier R, Verlinde I, Puspowidjono I, Willemot JP. Role of gallium-67 thoracic scintigraphy in the diagnosis and staging of patients suspected of bronchial carcinoma. *Thorax* **1982**; 37(4):264–269
8. Higashi T, Nakamura K, Suzuki S, Allison JR, Wakao H. Ga-67 scan as a prognostic indicator in primary lung carcinoma. *Clin Nucl Med* **1982**;7(12):553–557
9. Bitran JD, Bekerman C, Pinsky S. Sequential scintigraphic staging of small cell carcinoma. *Cancer* **1981**;47(8):1971–1975
10. Bekerman C, Pavel DG, Bitran J, Ryo UY, Pinsky S. The effects of inadvertent adminsitration of antineoplastic agents prior to Ga-67 injection: concise communication. *J Nucl Med* **1984**; 25:430–435

Technical Note

Cine-CT Technique for Evaluation of Left Ventricular Function During Supine Exercise

Michael R. Rees,[1,2] Robert M. MacMillan, Barbara Fender,[1] and Donald L. Clark[1]

Rapid-acquisition CT (cine CT) with its 50-msec data acquisition time is a new technique for cardiac imaging that permits the study of left ventricular regional-wall motion [1], left ventricular end-diastolic and end-systolic volumes, and ejection fraction [2]. Wide application of this technique for the detection and evaluation of coronary artery disease requires the combination of exercise with cine/CT scanning. In order to do this, significant technical difficulties must be resolved, including avoidance of motion artifact, angulation of patient, method of exercise, method of bolus delivery, scan timing, and scan levels. This report summarizes our methods for performing an adequate cine-CT exercise study.

Materials and Methods

All scans were performed on the Imatron C-100 scanner, which attains its rapid scan times by elimination of movement of the X-ray tube and gantry. Roentgen rays are produced by a scanning electron beam generated in an electron gun and magnetically focused onto four tungsten targets, producing up to eight near-contiguous 8-mm slices. Total scan time is 58 msec (50-msec scan time, 8-msec interscan delay) [3]. The largest reconstruction-and-scan circle diameter is 47 cm. This permits considerable movement in the positioning of an average-sized patient, which is achieved by table movement of up to 25° leftward and rightward in the horizontal plane and table tilt of up to 25° downward.

The patient is studied in the fasting state. An 18- or 20-gauge cannula is placed in a median antecubital vein. The patient is positioned supine on the scan table with his shoulders in contact with a table-supported shoulder brace. A table-attached bicycle ergometer is adjusted to the patient. The patient is positioned for a long-axis view (Fig. 1) by turning the table 20° leftward and feet-down 5°. The downward table tilt permits greater traction on the ergometer. The long-axis view is preferred over the standard transaxial view because it gives better visibility of the left ventricular apex and allows comparison with cardiac sonography and right anterior oblique left ventriculography (Fig. 2).

The patient is centered in the scan circle, and the anterior chest wall is marked for position. An eight-level localization scan is performed. The levels to be imaged are selected so that slices are obtained through the entire left ventricle, and a two-level flow study is then performed by injecting 5–10 ml Renografin 76 (Squibb, Princeton, NJ) at a rate of 5 ml/sec through the antecubital vein cannula. The vein is checked for patency before injection. Respirations are suspended 5 sec before and during scans. The time to peak appearance of contrast material in the left ventricle is determined along with time-density curves for determination of cardiac output.

Scans for the flow study are triggered to the R wave of the ECG and are acquired 1 scan/cardiac cycle in diastole over 20–40 cardiac cycles, depending on heart rate. From the flow study, six contiguous levels sufficient to slice the entire left ventricle are selected. A six-level scan in the cine or continuous mode is performed at rest by injecting a 33–39 ml bolus of contrast material, depending on heart rate and body size, at a rate of 3 ml/sec (prolonged bolus technique). The scan is started at the previously determined peak-appearance time for the left ventricle. The scan sequence is begun at the peak of the R wave by ECG with successive scans begun consecutively. For a six-level slice acquisition with slow heart rates, the entire cardiac cycle is not covered, since only 13 images/level are permitted by current computer capacity. However, even with this limitation, dias-

Received August 9, 1985; accepted after revision June 2, 1986.
This work was supported by a grant from the W. E. Smith Foundation, Suite 200, 100 Chetwynd Dr., Rosemont, PA 19010.
[1] Department of Cine/CT, Deborah Heart and Lung Center, University of Medicine and Dentistry of New Jersey, Brown Mills, NJ 08015.
[2] Present address: X-ray Department, Killingbeck Hospital, York Rd., Leeds LS14 6UQ, England. Address reprint requests to M. R. Rees.

tole and systole in all patients can be imaged by peak R-wave triggering.

The patient then undergoes graded exercise. The exercise is continued to a predetermined endpoint, for example, angina, target heart rate, dyspnea, fatigue, or drop in blood pressure. Heart rate and blood pressure are monitored during exercise. Immediately before the patient ceases exercise, his chest-wall markings are realigned within the scanner. A prolonged bolus of contrast material is injected (33–39 ml at 3 ml/sec) via the peripheral vein. Exercise is stopped after injection of contrast material is begun, and *respiration* is suspended 5 sec before scanning. Scans are begun 2–4 sec earlier than the peak-appearance time for the left ventricle at rest. The prolonged bolus technique ensures that scanning will take place while the contrast medium is in the left ventricle.

After return of the heart rate to baseline, the patient is repositioned in the short axis [4]. The table is angled rightward 20° and tilted feet-down to a maximum of 25° with the patient's upper body raised from behind with foam wedges, giving a final angulation of the torso of 20–55° with the horizontal (Fig. 3). In some cases a satisfactory

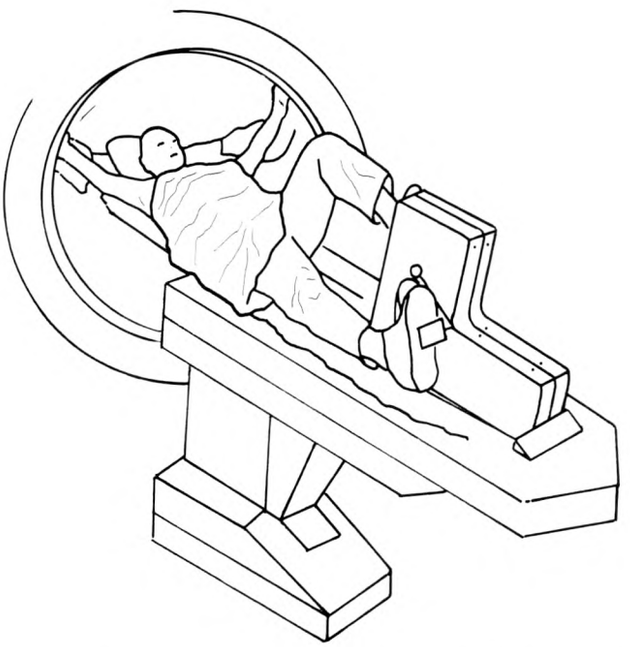


Fig. 1.—Patient positioning for exercise study in long-axis planar view for cine CT.

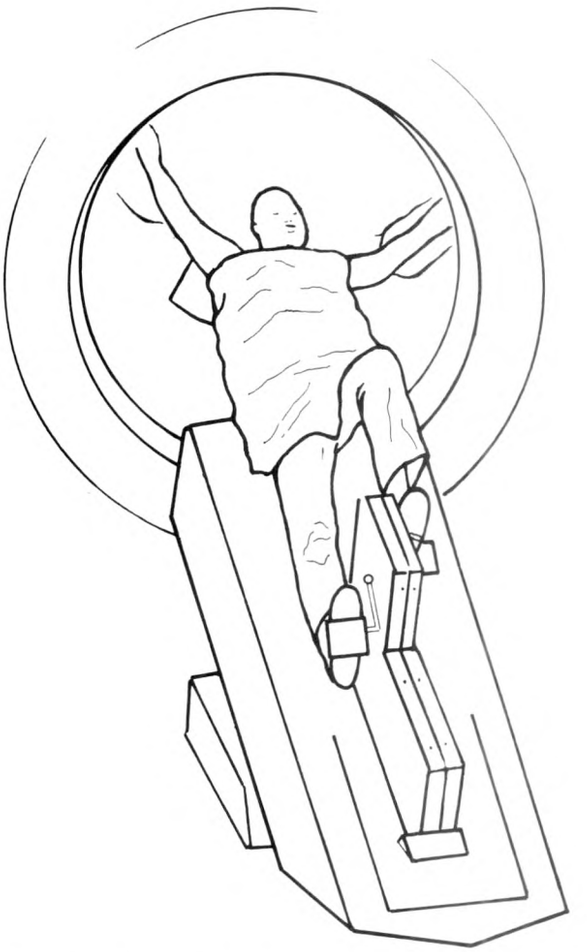


Fig. 3.—Patient positioning for exercise study in short-axis planar view for cine CT.

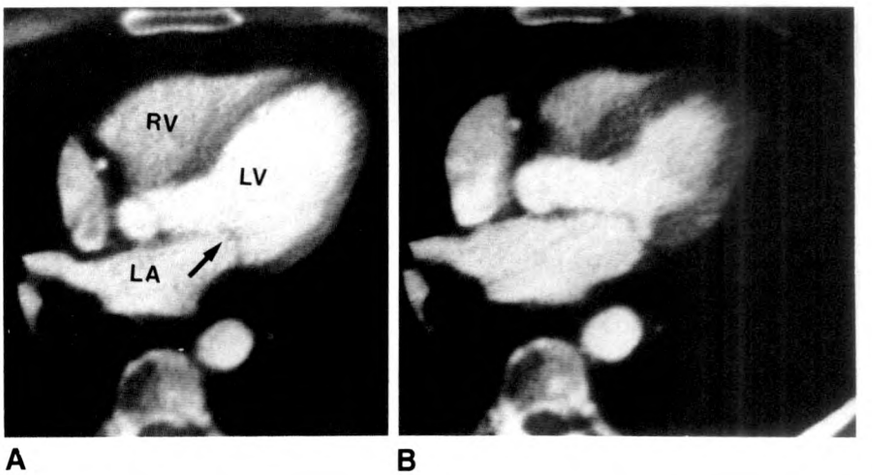


Fig. 2.—Cine-CT images through middle left ventricular slice in long-axis planar view.

***A*, Left ventricle at end-diastole; *arrow* = mitral valve; RV = right ventricle; LV = left ventricle; LA = left atrium.**

***B*, Left ventricle at end-systole.**

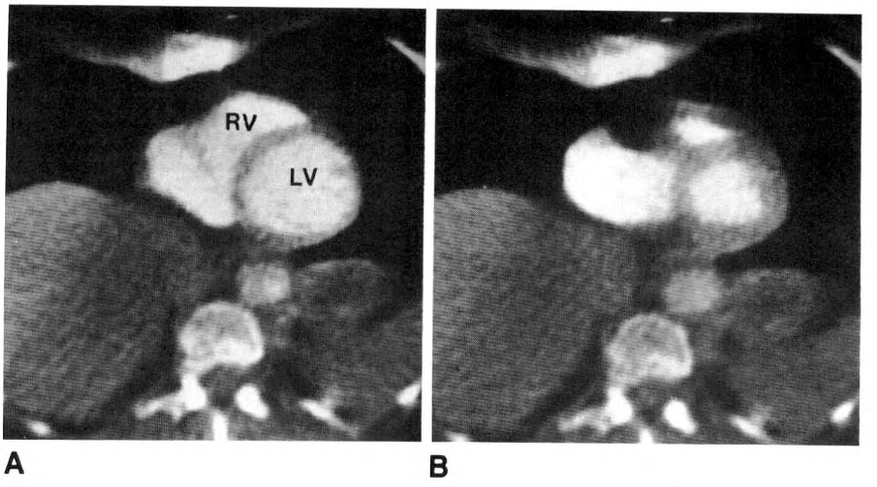


Fig. 4.—Cine-CT images through a middle left ventricular slice in short-axis planar view.
***A*, Left ventricle at end-diastole; LV = left ventricle, RV = right ventricle.**
***B*, Left ventricle at end-systole.**

short-axis position can be achieved with table tilt alone. The short-axis view allows visualization of the entire left ventricular wall and is particularly useful for abnormalities of the anterior and inferior left ventricular wall (Fig. 4).

An eight-level localization is performed to determine that the patient is satisfactorily placed within the reconstruction circle and to determine the levels necessary to scan the left ventricle in the short axis. A six- or eight-level scan in the cine mode triggering at peak R wave is performed by using the prolonged bolus method described above. If the rest study is satisfactory, an exercise study is performed by using the previous exercise protocol and the same scanning protocol. The short-axis view is more sensitive to scan artifacts caused by shifts in body position during exercise, and meticulous care must be taken to reposition the patient before scanning after exercise. Wall-motion abnormalities may be assessed visually either by replaying the scans on the computer in the cine mode in a closed loop or by examining the study frame by frame *with computerized planimetry of the ventricular wall.* End-systolic and end-diastolic frames can be selected either visually or by reference to the patient's ECG, recorded during the study.

Discussion

This method allows performance of a complete study with the patient receiving less than 200 ml of contrast material. By obtaining both long- and short-axis views one can assess all major segments of the left ventricular wall. As wall-motion abnormalities may only be seen during exercise, rest vs exercise segmental wall motion can be compared. Ejection fraction from the long-axis view can be determined for rest vs exercise, and an abnormal response can be detected [5]. Because of current limitations in the size of the reconstruction circle, a true short-axis view may not be possible for large-chested patients; for these patients, we recommend repeat localizations at lesser angulations. If the short axis cannot be scanned, we recommend performing only the long-axis study.

REFERENCES

1. Lipton MJ, Farmer DW, Killebrew EJ, et al. Regional myocardial dysfunction: evaluation of patients with prior myocardial infarction with fast C.T. *Radiology* **1985**;157:735–740
2. MacMillan RM, Rees MR, Maranhao V, Clark D. Comparison of left ventricular ejection fraction by cine computed tomography and single plane right anterior oblique ventriculography. *Angiology*, **1986**;36:299–305
3. Lipton MJ, Higgins CB, Boyd DP. Computed tomography of the heart: evaluation of anatomy and function. *J Am Coll Cardiol* **1985**;5:55S–69S
4. Rees MR, Feiring AJ, Rumberger JA, MacMillan RM, Clark DL. Cine computed tomography of the heart using two new oblique views. *Radiology* **1986**;159:804–806
5. Borer JS, Kent KM, Bachrach SL, et al. Sensitivity, specificity and predictive accuracy of radionuclide cine angiography during exercise in patients with coronary artery disease. Comparison with exercise electrocardiography. *Circulation* **1979**;60:572–580

Pharyngeal Kaposi's Sarcoma in Patients with AIDS

Christine D. Emery[1]
Susan D. Wall[1,2]
Michael P. Federle[1,3]
C. Daniel Sooy[4]

The radiographic appearance of gastrointestinal Kaposi's sarcoma in patients with AIDS has been described previously, but little attention has been paid to pharyngeal involvement. This study compared the radiographic findings of pharyngeal Kaposi's sarcoma in eight patients with AIDS and dysphagia to those of visual inspection by laryngoscopy or bronchoscopy. Barium pharyngography (six patients) demonstrated nodular lesions without ulceration, ranging in extent from a single nodule to extensive confluent disease. CT (two patients) showed nodular or polypoid intraluminal protrusions, distortion of valleculae and pyriform sinuses, infiltration of deep-tissue planes, and adenopathy. A 4-mm nodular lesion was not seen on pharyngography. Radiographic evaluation provided supplemental information in six patients, especially regarding inferior extent of disease in four whose bulky lesions precluded adequate visual assessment. CT aided in defining deep-tissue-plane involvement and extent of nodal disease. It is concluded that barium pharyngography and CT are useful in the diagnostic evaluation of possible Kaposi's sarcoma in patients with AIDS and dysphagia.

Kaposi's sarcoma now occurs in an epidemic form associated with AIDS. The gastrointestinal tract is involved at the time of diagnosis or early thereafter in about 50% of homosexual men with cutaneous disease [1–4]. The radiologic literature contains scattered descriptions of AIDS-related gastrointestinal Kaposi's sarcoma [3–6], but to our knowledge, there are no published radiographs or descriptions of pharyngeal involvement without coexistent opportunistic infection. We compared the radiographic findings of pharyngeal Kaposi's sarcoma in eight patients with AIDS and dysphagia to those of visual inspection by laryngoscopy or bronchoscopy.

Subjects and Methods

Eight patients with AIDS and visually detected oropharyngeal and/or hypopharyngeal Kaposi's sarcoma were studied. The diagnosis of AIDS conformed to the criteria established by the Centers for Disease Control [7]. All patients were homosexual men; their ages ranged from 22 to 44 years. All patients had cutaneous Kaposi's sarcoma, and one also had oral lesions. Presenting symptoms included dysphagia (eight patients), odynophagia (three), dysphonia (two), and hoarseness (one). Time from the diagnosis of AIDS to onset of the above symptoms ranged from 3 to 18 months. Radiographic evaluation was performed from 2 days before to 17 days after visual examination.

In six patients, pharyngograms were performed along with esophagrams in the routine evaluation of dysphagia. In two patients, radiographic findings prompted visual examination. The remaining four patients were evaluated radiographically without knowledge of the details regarding site or extent of disease noted previously by visual inspection. Barium pharyngography was performed by using the air-contrast technique as described by Semenkovich et al. [8]. Briefly, in the erect position, the patient swallows 15–30 ml of a high-density barium suspension and then performs a modified Valsalva maneuver. Exposures are made during maximal pharyngeal distension.

Two patients were studied by CT performed with a GE 9800 CT/T scanner during quiet respiration. Contiguous 0.5-cm-thick images were obtained after a bolus of IV contrast

Received June 16, 1986; accepted after revision July 24, 1986.

Presented at the annual meeting of the American Roentgen Ray Society, Washington DC, April 1986.

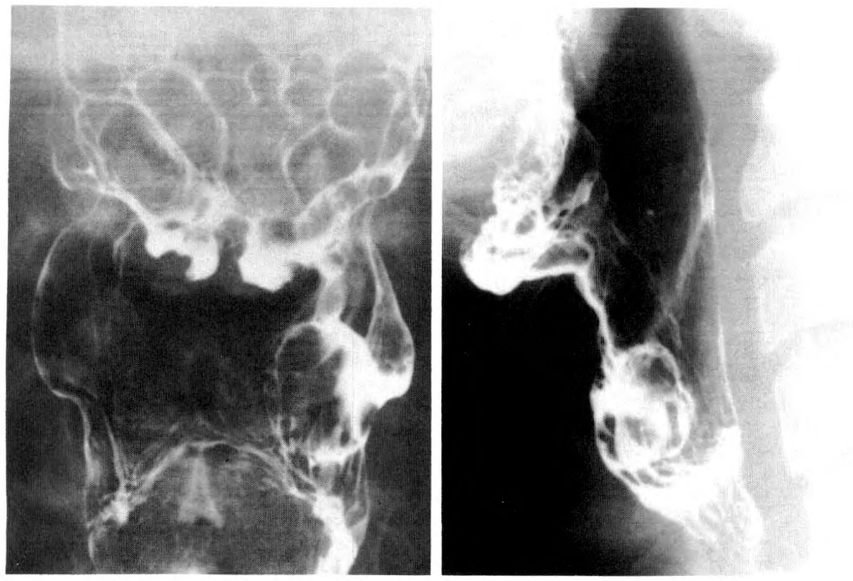
[1] Department of Radiology, University of California, San Francisco, 505 Parnassus Ave., San Francisco, CA 94143.

[2] Veterans Administration Medical Center, 4150 Clement St., San Francisco, CA 94121. Address reprint requests to S. D. Wall at the Veterans Administration Medical Center.

[3] San Francisco General Hospital, San Francisco, CA 94110.

[4] Department of Otolaryngology, University of California, San Francisco, San Francisco, CA 94143.

AJR 147:919–922, November 1986
0361–803X/86/1475–0919
© American Roentgen Ray Society



A B

Fig. 1.—38-year-old homosexual man with dysphagia. Anteroposterior (*A*) and lateral (*B*) views of pharynx show multiple large nodular submucosal lesions involving anterior oropharynx and base of tongue. Valleculae are deformed. There is a lesion measuring 2.5 cm in left pyriform sinus.

material. No patient underwent both pharyngography and CT. Two patients had a follow-up pharyngogram, one after local radiation therapy and one after CO_2 laser therapy.

Visual inspection consisted of indirect laryngoscopy (one patient), indirect laryngoscopy followed by direct laryngoscopy (three), direct laryngoscopy (three), and bronchoscopy (one). Biopsy, performed on six patients, was diagnostic of Kaposi's sarcoma in each. The diagnosis was made in the remaining two patients by the characteristic endoscopic appearance of violaceous nodules or hemorrhagic macules [1]. No patient had concurrent pharyngeal candidiasis. Radiographic and visual findings were compared.

Results

Pharyngography demonstrated one or more nodular lesions of Kaposi's sarcoma in all patients. The extent of disease ranged from a single 1 × 2 cm nodular lesion to innumerable lesions, occasionally as large as 2.5 cm (Fig. 1). Disease was most extensive at the base of the tongue and tonsillar fossae, where confluent nodules were present in four patients. Involvement of the valleculae was noted in four patients, sometimes with prominent effacement (Fig. 2). The posterior hypopharyngeal wall and pyriform sinuses were each involved in three patients. Neither ulceration nor central umbilication was present.

In seven of eight pharyngograms (including two follow-up studies), radiographic findings confirmed or supplemented those of visual examination. The inferior extent of disease was more completely determined in four patients whose bulky lesions precluded adequate visual inspection. Follow-up pharyngography after local radiation therapy in one patient demonstrated marked regression of extensive nodular disease that had involved the base of the tongue, posterior and lateral walls of the oropharynx, valleculae, and the pyriform sinuses (Fig. 1B). However, in one patient, follow-up pharyngography 10 months after CO_2 laser therapy did not demonstrate a single 4-mm lesion at the level of the arytenoids. Pharyngography was used to design the radiation port in three patients.

CT, performed in two patients, demonstrated nodular or polypoid intraluminal protrusion of tumor (Figs. 3 and 4) as had been noted on visual examination. Additional findings on CT included tumor infiltration of the parapharyngeal, paralaryngeal, and preepiglottic spaces, thickening of the posterior pharyngeal wall, distortion of valleculae and pyriform sinuses, tumor extension about the vascular sheath into the sternocleidomastoid muscle, and cervical adenopathy. In one patient, left maxillary sinus opacification was biopsy-positive for Kaposi's sarcoma. This patient later required tracheostomy for acute airway obstruction.

Discussion

In patients with AIDS, Kaposi's sarcoma presents as an aggressive, multicentric neoplasm with early visceral involvement. The gastrointestinal tract is the most common target organ after skin and lymph node disease; gastrointestinal lesions may antedate skin lesions. Radiographically, AIDS-related gastrointestinal Kaposi's sarcoma has been noted to cause intraluminal filling defects of variable size and number. Although central umbilication may be seen, it is not common. Large nodules may protrude into the lumen as polyps or masses. Multiple coalescent lesions may produce an appearance of enlarged nodular gastric rugae or thickened nodular small-bowel folds [3–6]. To our knowledge, there are no reports to date of the radiographic appearance of Kaposi's sarcoma of the pharynx in the absence of concurrent opportunistic infection. Barium pharyngography in our patients demonstrated well-defined nodular lesions without mucosal ulceration. One patient had a single nodular intraluminal protrusion,

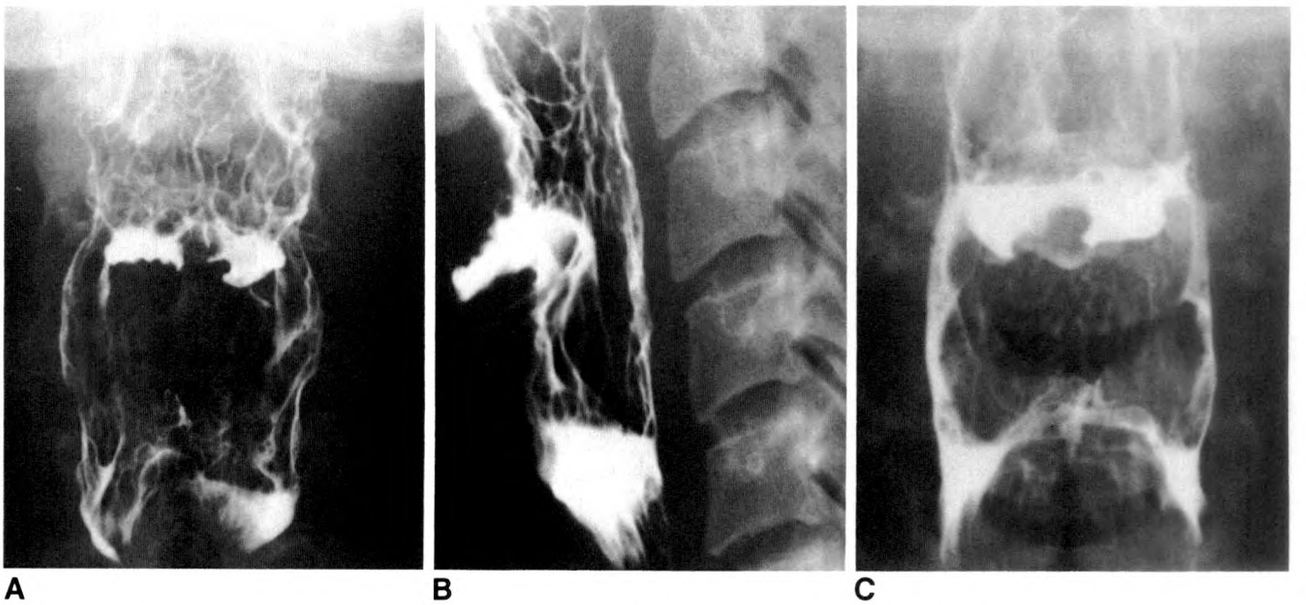


Fig. 2.—30-year-old homosexual man with oral Kaposi's sarcoma and dysphagia. Anteroposterior (*A*) and lateral (*B*) views of pharynx demonstrate extensive coalescent nodules in oropharynx and hypopharynx with deformity of valleculae and pyriform sinuses. *C*, Reevaluation 10 months later, after local radiation treatment, shows fewer lesions and less distortion of valleculae and pyriform sinuses.



Fig. 3.—31-year-old homosexual man. *A*, Left vallecula (*straight arrow*) and orifice of left pyriform sinus (*curved black arrow*) are obliterated. *Curved white arrow* indicates large anterior cervical lymph node.

***B*, At level of hyoid bone, there is thickening of aryepiglottic fold with narrowing of laryngeal vestibule (*arrow*) and infiltration of paralaryngeal spaces bilaterally.**

Fig. 4.—22-year-old homosexual man. Bilateral parapharyngeal space infiltration is seen with extension of tumor on left about carotid sheath into sternocleidomastoid muscle. Ill-defined but enlarged submandibular gland on left was biopsy-positive for Kaposi's sarcoma. *Curved arrow* indicates right submandibular gland; *straight arrow* indicates right carotid artery.

whereas the others had more confluent disease with lesions extending from the base of the tongue to the tonsillar pillars, valleculae, and pyriform sinuses.

The differential diagnosis for this appearance on pharyngography includes coaptation artifact, lymphoma, carcinoma, and candidiasis. Coaptation of one pharyngeal structure against another can simulate a mass, but should be distinguished readily from a true abnormality on repeat swallow. Lymphoma occurs in the submucosal lymphoid tissue of the gastrointestinal tract and commonly involves Waldeyer's ring

in the nasopharynx. At the level of the oropharynx and hypopharynx where there is no submucosal lymphoid tissue, lymphoma involves the lymph nodes. Generally, carcinoma can be distinguished from Kaposi's sarcoma on barium examination by its mucosal location. Moreover, carcinoma tends to occur in patients who are older than the typical AIDS patient. The nodules of Kaposi's sarcoma are notably different from the discrete small mucosal plaques, cobblestoning, and shaggy borders that are typical of candidiasis.

Our findings demonstrate the value of barium pharyngography in patients with AIDS and dysphagia. Barium evaluation detected all lesions of Kaposi sarcoma seen by visual inspection, except a single 4-mm lesion. Moreover, it often supplied additional information regarding inferior extent of disease in those patients whose bulky proximal lesions precluded optimal visual inspection of the hypopharynx, especially the pyriform sinuses. Incomplete indirect laryngoscopy in three patients prompted intraoperative direct laryngoscopy in an attempt to further define the full extent of disease.

Although early Kaposi's sarcoma elsewhere in the gastrointestinal tract is often asymptomatic [1, 2], nodular lesions in the pharynx can produce symptoms because of their location. Radiographic evaluation of possible pharyngeal Kaposi's sarcoma in patients with AIDS may be preferable to laryngoscopy for several reasons. Barium pharyngography can be used to screen symptomatic patients who may benefit from chemotherapy or radiation therapy for palliation and improved quality of life; it also provides a means of defining the radiation port. With barium pharyngography, patients can concurrently undergo evaluation of the remainder of the upper gastrointestinal tract for possible multifocal disease, including other sites of Kaposi's sarcoma, lymphoma, or concurrent opportunistic infection [6]. In addition to detecting the initial lesions, barium pharyngography provides a ready and easy mode of assessing response to treatment. Compared with direct visualization, it is a less invasive and more readily tolerated examination, and it is available at institutions that do not have an experienced otolaryngologist. The cost of pharyngography compares favorably with indirect laryngoscopy and is a small fraction of the total cost of direct laryngoscopy, which requires the operating room and general anesthesia. CT is valuable in determining extent of deep-tissue-plane involvement and nodal disease and may detect clinically unsuspected disease. Finally, both barium pharyngography and CT introduce less risk that the examiner will be exposed to the patient's body fluids. Neither pharyngography nor CT will demonstrate the early macular lesions of Kaposi's sarcoma, but in our experience, these lesions do not cause symptoms.

In summary, our study shows that barium pharyngography can contribute to the evaluation of possible Kaposi's sarcoma in the patient with AIDS and dysphagia. If previous visual inspection is judged to be inadequate, pharyngography may better determine the full extent of disease. CT may be indicated in those patients with palpable adenopathy to assess deep soft-tissue-plane involvement and extent of nodal disease. Both techniques provide data for delineation of radiation ports and a baseline examination for comparison when assessing response to therapy.

ACKNOWLEDGMENTS

Acknowledgment and thanks to Helen Galvin, William Shea, and Bernie Saks for assistance in barium studies.

REFERENCES

1. Friedman SL, Wright TL, Altman DF. Gastrointestinal Kaposi's sarcoma in patients with acquired immunodeficiency syndrome: endoscopic and autopsy findings. *Gastroenterology* **1985**; 89:102–108
2. Gottlieb MS, Groopman JE, Weinstein WM, Fahey JL, Detels R. The acquired immunodeficiency syndrome. *Ann Intern Med* **1983**;99:208–220
3. Rose HS, Balthazar AJ, Megibow EJ, Horowitz L, Laubenstein LJ. Alimentary tract involvement in Kaposi sarcoma: radiographic and endoscopic findings in 25 homosexual men. *AJR* **1982**;139:661–666
4. Wall SD, Friedman SL, Margulis AR. Gastrointestinal Kaposi's sarcoma in AIDS: radiographic manifestations. *J Clin Gastroenterol* **1984**;6:165–171
5. Hill CA, Harle TS, Mansell PWA. The prodrome, Kaposi sarcoma, and infections associated with acquired immunodeficiency syndrome: radiologic findings in 39 patients. *Radiology* **1983**; 149:393–399
6. Wall SD, Ominsky SO, Altman DF, et al. Multifocal abnormalities of the gastrointestinal tract in AIDS. *AJR* **1986**;146:1–5
7. United States Department of Health and Human Services. Update: acquired immunodeficiency syndrome (AIDS)—United States. *MMWR Centers Dis Control* **1982**;31:507–514
8. Semenkovich JW, Balfe DM, Weyman PJ, Heiken JP, Lee JKT. Barium pharyngography: comparison of single and double contrast. *AJR* **1985**;144:715–720

Pseudotumor of the Quadrate Lobe in Hepatic Sonography: A Sign of Generalized Fatty Infiltration

Eric E. Sauerbrei[1]
Michelle Lopez

Sonograms of 43 patients demonstrated a focal area of decreased echogenicity in the medial segment of the left hepatic lobe (quadrate lobe). The shape ranged from ovoid to sheetlike, and the diameter ranged from 0.7 to 8.6 cm. The echogenicity of the right hepatic lobe was abnormally increased in 34 of 37 scans graded. In 20 patients with follow-up sonograms, 11 showed no change, six disappeared and three decreased in size. In 12 patients with unenhanced CT scans, 10 had decreased attenuation of the hepatic parenchyma and normal attenuation in the observed quadrate lobe focus. The hypoechoic focus in the quadrate lobe represents focal sparing in generalized fatty infiltration of the liver. When present, this focus represents a useful qualitative sign of generalized fatty infiltration in the rest of the liver.

Most commonly, fatty infiltration of the liver (FIL) is generalized; both CT scans and sonograms can demonstrate changes related to this condition [1, 2]. Less commonly, FIL is focal, and occasionally it is generalized with focal areas of sparing [3, 4]. Two case reports have demonstrated generalized FIL with apparent focal sparing in the medial segment of the left hepatic lobe (also called the quadrate lobe) [5, 6]. However, the same focal area of decreased echogenicity has been described in 12 patients in whom the presence of FIL could not be confirmed, although the authors state that "it is possible that at least several of the patients had mild fatty infiltration" [7]. We examined records of 43 patients with a hypoechoic focus in the quadrate lobe to establish the clinical significance of this "mass" and to investigate its relationship to FIL.

Materials and Methods

Over a 3-year period, 43 patients demonstrated a hypoechoic area in the medial segment of the left hepatic lobe. There were 24 men and 19 women, ranging in age from 35 to 85 years (mean, 60 years). The reasons for the first sonograms included possible liver metastases from a known primary malignancy (15 patients), upper abdominal pain (13 patients), possible hepatic parenchymal disease (4 patients), and other abdominal symptoms (11 patients).

Follow-up sonograms were obtained in 20 of the 43 patients 1 to 27 months after initial sonograms (mean, 9 months). All scans were performed with real-time sector scanners. CT scans were obtained in 12 patients. The time between the sonogram and CT was 0 days in 6 patients and 1, 2, 3, 6, 12, and 60 days in the others. All CT scans were performed without contrast enhancement. Scan slices were 1 cm thick and 1 cm apart. Where possible, CT attenuation numbers for the right hepatic lobe, the focal "abnormality," and the spleen were obtained. Scans were photographed at the usual window settings (40-H window level and 400-H window width) and also at reduced window widths (160 H). In two patients, a liver biopsy of the right hepatic lobe was performed, and in one patient a fine-needle aspiration of the hypoechoic focus was performed.

Sagittal sonograms of the right hepatic lobe and right kidney allowed scoring of the liver parenchyma according to Scatarige et al. [2]: grade 1, mild FIL (diffuse increase in hepatic echoes with normal visualization of intrahepatic vessels and diaphragm); grade 2, moderate FIL (diffuse increase in hepatic echoes with slightly impaired visualization of intrahepatic

Received April 28, 1986; accepted after revision June 11, 1986.

[1] Both authors: Department of Radiology, Kingston General Hospital, Queen's University, Stuart St., Kingston, Ontario, Canada K7L 2V7. Address reprint requests to E. E. Sauerbrei.

AJR 147:923–927, November 1986
0361–803X/86/1475–0923
© American Roentgen Ray Society

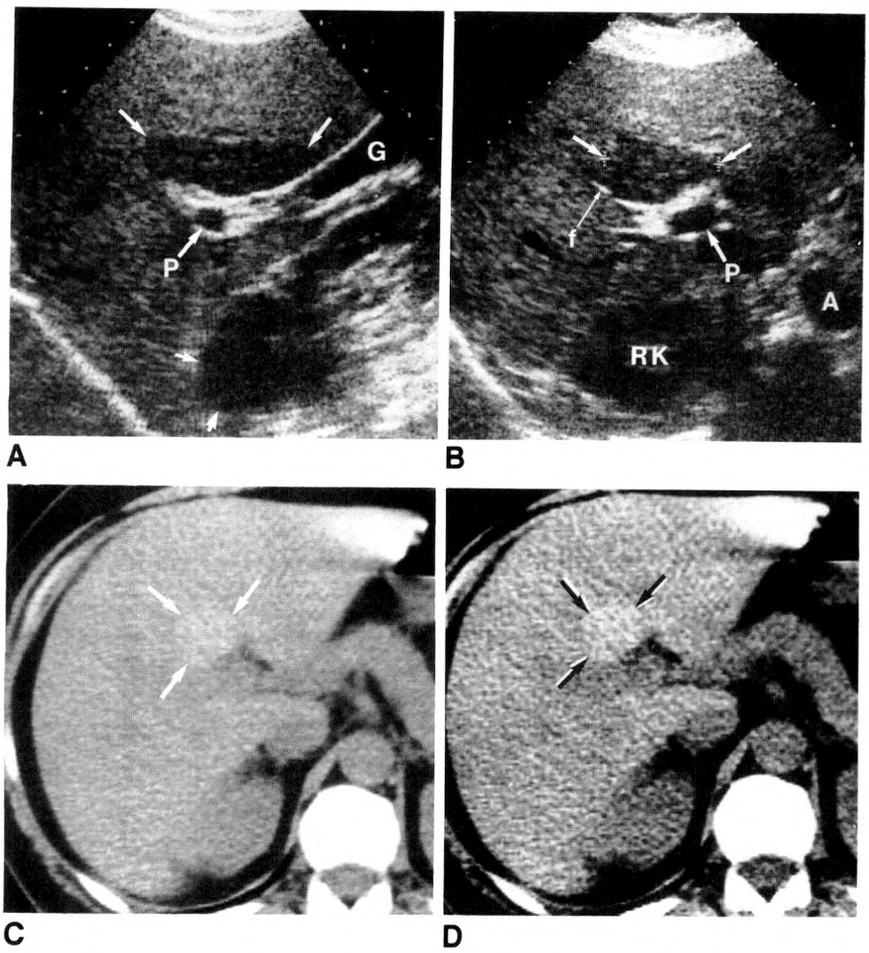


Fig. 1.—*A*, Sagittal sonogram through gallbladder (G) and right kidney (*short arrows* indicate upper pole of right kidney). Note hypoechoic focus (*long arrows*) anterior to right portal vein (P).

***B*, Axial sonogram through same liver as *A* demonstrating hypoechoic focus (*large arrows*) anterior to portal vein bifurcation (P). Focus lies lateral to interlobar fissure (f) that separates right and left lobes of liver. A = aorta; RK = right kidney.**

***C*, Axial CT scan of same patient without IV contrast enhancement, demonstrating hyperdense focus (*arrows*) corresponding in size and location to the hypoechoic focus in sonograms. Scan was photographed at window level 40 H and window width 400 H.**

***D*, Same axial CT scan as *C* with window width narrowed to 160 H. Hyperdense focus (*arrows*) is more easily identified at narrower window width.**

vessels and diaphragm); grade 3, severe FIL (marked increase in hepatic echoes with poor visualization or nonvisualization of vessel borders, diaphragm, and posterior right lobe).

Results

The first sonograms demonstrated the hypoechoic area anterior to the portal vein bifurcation in 38 patients (Fig. 1) and medial to neck of gallbladder, or interlobar fissure in five patients (Fig. 2). In four patients a second hypoechoic area was noted in the caudate lobe (Fig. 3), and in one patient, a second area was noted in the right hepatic lobe. The margins of the focus were fairly well defined but not as sharply as a cyst would be, and the shape varied from a thin sheet of hepatic tissue to a roughly ovoid shape. The mean length of the focus was 3.0 cm (range 1.2–6.0 cm), the mean width 2.6 cm (range 0.9–8.6 cm) and the mean depth 1.5 cm (range 0.7–4.2 cm) (Fig. 4).

The parenchyma of the right hepatic lobe was graded as follows: grade 3, three patients; grade 2, 13 patients; grade 1, 19 patients; normal, three patients; unable to grade, five patients. The parenchymal grade was unobtainable in five patients because a single long-axis view that included the right hepatic lobe and right kidney could not be obtained with the sector scanner.

Follow-up sonograms in 20 patients (1–27 months time lapse) showed no change in the hypoechoic focus in 11, a decrease in size in three, and disappearance in six. In the last six patients, the parenchymal score of the right hepatic lobe changed from 1 (mild FIL) to 0 (normal) in four patients, 2 to 1 in one patient, it remained 0 in one patient.

In 10 of 12 patients, the unenhanced CT scan demonstrated a relatively hyperdense focus corresponding in size and location to the hypoechoic focus in the sonogram. The hyperdense focus was more easily detected with narrow window widths (i.e., 160 H). In fact, the focus was quite subtle in some patients at the usual settings for abdominal CT scan photography (window width, 400 H). In two of 12 patients, the CT scan failed to demonstrate a hyperdense focus while the sonograms demonstrated hypoechoic foci of 3.2 × 2.2 × 2.3 cm and 3.7 × 2.8 × 1.5 cm, respectively. However, the CT scans were available only at 400-H window width, and scan data could not be retrieved for further examination. The time interval between the sonogram and CT for these two patients was 12 days and 2 months, respectively. In follow-up sonograms (at 25 months and 3 months), the foci had

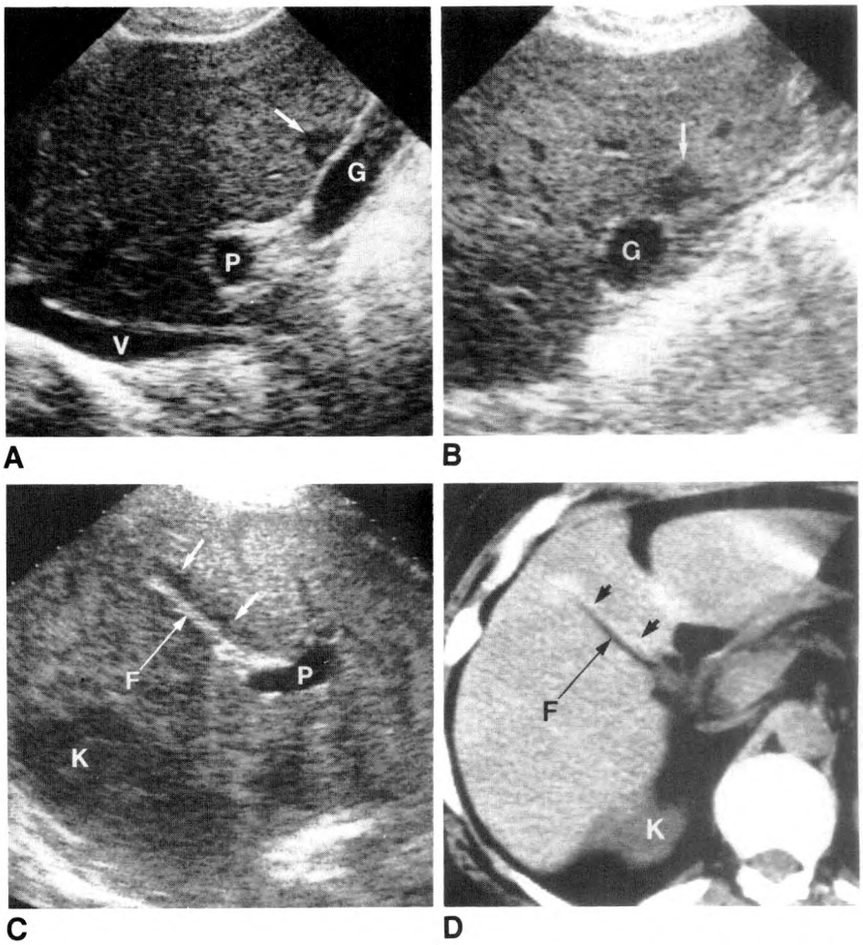


Fig. 2.—*A*, Sagittal sonogram through inferior vena cava (V) and right portal vein (P). Note small hypoechoic focus (*arrow*) anterior to neck of gallbladder (G).

B, Axial sonogram in same patient, demonstrating small hypoechoic focus (*arrow*) medial and anterior to gallbladder neck (G).

C, Axial sonogram through right kidney (K) and portal vein bifurcation (P) in another patient, demonstrating a band of hypoechoic liver tissue (*short arrows*) medial to interlobar fissure (F).

D, Unenhanced axial CT scan in the same patient, demonstrating thin band of hyperdense liver tissue (*short arrows*) medial to interlobar fissure (F). K = upper pole of right kidney.

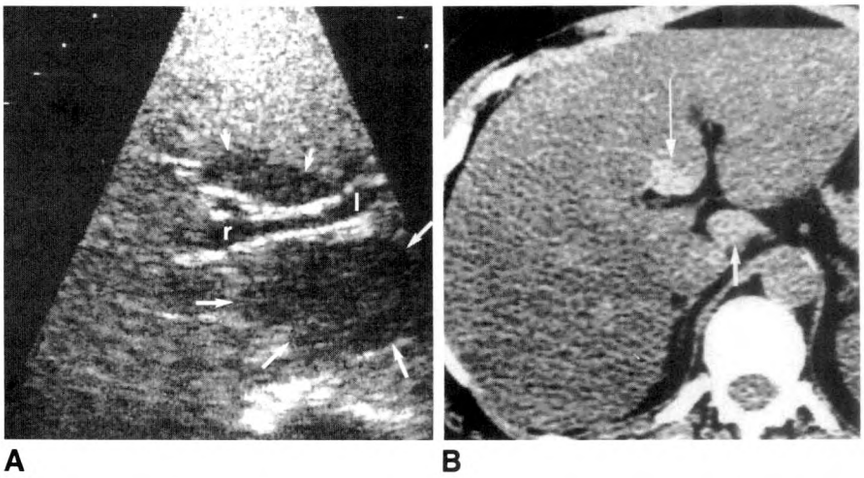


Fig. 3.—*A*, Axial sonogram through right (r) and left (l) portal veins demonstrating hypoechoic focus in medial segment of left hepatic lobe (*short arrows*) and large hypoechoic focus in caudate lobe (*long arrows*).

B, Unenhanced axial CT scan in the same patient, demonstrating hyperdense focus in medial segment of left hepatic lobe (*long arrow*) and another hyperdense focus in caudate lobe (*short arrow*). Right hepatic lobe was less dense than spleen.

disappeared. In one of these two patients, a liver biopsy (right lobe) demonstrated the histology of mild fatty infiltration shortly after the first sonogram. Another patient had a biopsy of the right hepatic lobe that demonstrated moderate fatty infiltration. The previous sonogram demonstrated a hypoechoic focus in the quadrate lobe, and the CT demonstrated a corresponding hyperdense focus. The only other biopsy was a fine-needle aspiration of the hypoechoic focus itself, which demonstrated normal cytology.

In the 10 patients with CT attenuation values determined,

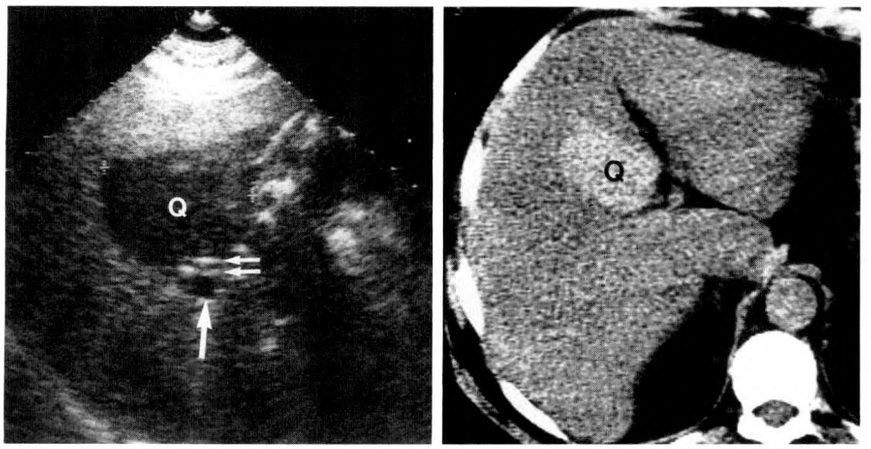


Fig. 4.—*A*, Sagittal sonogram through right portal vein (*large arrow*) and common hepatic duct (*small arrows*) demonstrating large hypoechoic focus (Q) in medial segment of left hepatic lobe.

***B*, Unenhanced CT scan in the same patient, demonstrating hyperdense focus (Q) in same location. Right hepatic lobe was less dense than spleen.**

the attenuation of the right hepatic lobe was less than the quadrate lobe. The mean attenuation of the right lobe was 33 H (range 6–54 H) and the quadrate lobe 53 H (range 36 to 68 H). On average, the attenuation of the right hepatic lobe was 21 H less than the quadrate lobe (range 14–30 H). The mean attenuation of the spleen was 47 H (range 32–56 H). On average, the attenuation of the right hepatic lobe was 14 H less than the spleen (range 0–26 H).

Discussion

The hypoechoic focus described here could be mistaken for a tumor mass except that follow-up sonograms (20 patients) and CT scans (12 patients) demonstrated that these foci were not neoplasms. Although the foci in the medial segment of the left lobe may vary tremendously in shape and size, we now can dismiss the possibility of neoplasm in most patients' first sonogram on the basis of the following observations: (1) The hypoechoic focus had a characteristic location *and* the echogenicity of the right hepatic lobe was increased compared with the cortex of the right kidney; (2) There was no mass effect on surrounding vessels and tissue; (3) There was usually a solitary focus, although the caudate lobe and other areas were sometimes affected. (4) In some cases, a hypoechoic area was more like a sheet of tissue than an ovoid or spherical mass. A straight interface with normal liver tissue would be very unusual for a tumor, and this finding was very suggestive that FIL with focal sparing was present.

In most patients, the echogenicity of the right lobe was clearly increased. This finding represents a reasonably accurate indication of FIL [2]. In 10 of the 12 patients with CT scans, the right hepatic lobe was less dense than normal (mean attenuation of 33 H compared with a normal range of 40–80 H in unenhanced scans) and the right lobe was less dense than the pseudotumor. In addition, the attenuation of the right hepatic lobe was less than the spleen, although the liver is normally denser than the spleen. These findings indicate an increased amount of fat in the right hepatic lobe [1] with relative sparing in a portion of the quadrate lobe, whose mean attenuation was 53 H (normal liver, 40–80 H). As in normal liver tissue, the mean attenuation of the pseudotumor was slightly greater than the spleen (mean of 6.5 H greater).

Some of the pseudotumors were quite subtle on CT, and only scans with narrow window widths clearly demonstrated the area to be relatively hyperdense. The difference between right lobe and spleen density also became clearer with reduced window widths. In two of the 12 patients with CT scans, no focal abnormality was seen, perhaps because CT images with reduced window widths were not available, or because the amount of FIL changed between the first sonogram and subsequent CT scan (time intervals of 12 days and 2 months). It is well known that rapid disappearance of fat (less than 1 week) can occur when the offending agent is removed [8]. Furthermore, a conventional biopsy of the right hepatic lobe in one of these patients revealed mild FIL shortly after the sonograms. We conclude, therefore, that these hypoechoic pseudotumors represent a qualitative sign of fatty infiltration in the rest of the liver, with sparing in the quadrate lobe.

Our clinical practice indicates that the pseudotumor is not present in all cases of FIL, by any means. However, in a patient with increased echogenicity of the right hepatic lobe, rescanning with special attention to the quadrate lobe often allows detection of a small zone of decreased echogenicity, which increases our confidence that FIL is actually present.

The cause of focal sparing in FIL is unclear. A study of 10 liver specimens with focal FIL [9] postulated focal ischemia to explain the fatty deposition. A recent article [10] has demonstrated that in some patients, direct anastomoses between peripheral portal radicles and perforating capsular or accessory cystic veins occur in this area of the liver. These communicating vessels can cause drainage of systemic venous blood into liver sinusoids. The local blood flow may then be dominated by systemic venous blood rather than splanchnic venous blood, and for this reason there may be localized sparing in generalized fatty infiltration of the liver.

ACKNOWLEDGMENTS

The authors would like to thank the ultrasound technologists of the Radiology Department for scanning many of the patients and Yvonne DeRoche for the preparation of the manuscript.

REFERENCES

1. Bydder GM, Kreel L. Accuracy of computed tomography in diagnosis of fatty liver. *Br Med J* **1980**;281:1042–1045
2. Scatarige JC, Scott WW, Donovan PJ, Siegelman SS, Sanders RC. Fatty infiltration of the liver: ultrasonographic and computed tomographic correlation. *J Ultrasound Med* **1984**;3:9–14
3. Scott WW Jr, Sanders RC, Siegelman SS. Irregular fatty infiltration of the liver: diagnostic dilemmas. *AJR* **1980**;135:67–71
4. Halvorsen RA, Korobkin M, Ram PC, Thompson WM. CT appearance of focal fatty infiltration of the liver. *AJR* **1982**;139: 277–281
5. Wilson SR, Rosen IE, Chin-Sang HB, Arenson AM. Fatty infiltration of the liver—an imaging challenge. *J Can Assoc Radiol* **1982**;33:227–232
6. Jennett VM, Keil W, Ludwig J. Echoarme leberpfortennahe pseudolasion bei steatosis hepatis (Non-echo producing pseudolesion near the liver hilus in fatty liver). *Fortschr Rontgenstr* **1983**;138:746–748
7. Berland LL. Focal areas of decreased echogenicity in the liver at the porta hepatis. *J Ultrasound Med* **1986**;5:157–159
8. Bashist B, Hecht HL, Harley WD. Computed tomographic demonstration of rapid changes in fatty infiltration of the liver. *Radiology* **1982**;142:691–692
9. Brawer MK, Austin GE, Lewin KJ. Focal fatty change of the liver: a hitherto poorly recognized entity. *Gastroenterol* **1980**;78: 247–252
10. Marchal G, Tshibwabwa-Tumba E, Verbeken E, et al. "Skip areas" in hepatic steatosis: a sonographic-angiographic study. *Gastrointest Radiol* **1986**;11:151–157

American Roentgen Ray Society 87th Annual Meeting April 26–May 1, 1987, Miami Beach, FL Fontainebleau-Hilton Hotel

Registration and Hotel Reservations

Forms for advance registration and hotel reservations will be in the January and February 1987 issues of the *AJR*.

Refresher Course Program

A summary of the refresher courses will appear in the *AJR* in January along with advance registration forms. Early registration is an advantage in assuring preferred courses in this popular program. Dr. J. T. Ferruci, Jr. is program director.

Local Program

A program of sightseeing, shopping, and entertainment will be developed by the Local Arrangements Chairman. Information and advance registration forms will be in the January and February issues of the *AJR*.

President's Award Papers

The society offers several cash awards for the best scientific papers prepared by residents in radiology. The President's Award has a $1000 prize. There are two Executive Council awards of $500 each. All are presented at the annual meeting. Papers should be submitted by Jan. 31 for consideration in this competition. Send entries to:

B. G. Brogdon, M.D.
Dept. of Radiology
University of South Alabama Medical Center
2451 Fillingim Street
Mobile, AL 36617

ARRS Membership Requirements

The American Roentgen Ray Society (ARRS) has two membership categories: active and in-training. For active membership, applicants must practice radiology in the U.S. or Canada. Each must have graduated in good standing from an approved medical school or hold an advanced degree in physical, chemical, or biological science and be certified by the American Board of Radiology, the Royal College of Physicians and Surgeons of Canada, or otherwise adequately document training and credentials.

A member-in-training must be in a radiology residency or postresidency fellowship program or be a postgraduate student in an allied science. Status must be verified by the program director.

For consideration during the 1987 ARRS meeting, completed applications must be received no later than Feb. 1. Obtain forms and details from:

Rosalind H. Troupin, M.D.
Department of Radiology
Hospital of University of Pennsylvania
3400 Spruce St.
Philadelphia, PA 19104

Associated Society Meetings

Society for Pediatric Radiology and European Society of Pediatric Radiology

The inaugural conjoint International Pediatric Radiology '87 meeting will meet May 30–June 4, 1987 at the Westin Hotel, Toronto, Ontario, Canada. Deadline for receipt of abstracts is February 1, 1987. For details contact: Donald R. Kirks, M.D., Secretary, Society for Pediatric Radiology, c/o Dept. of Radiology, Childrens Hospital Medical Center, Elland and Bethesda Aves., Cincinnati, OH 45229, (513) 559-4880

Deadlines

President's Award papers: January 31

Benign Pancreatic Insulinoma: Preoperative and Intraoperative Sonographic Localization

Brian Gorman[1,2]
J. William Charboneau[1]
E. Meredith James[1]
Carl C. Reading[1]
Angelo K. Galiber[1]
Clive S. Grant[3]
Jon A. van Heerden[3]
Robert L. Telander[4]
F. John Service[5]

Twenty-nine patients with surgically proved benign pancreatic insulinoma were studied by preoperative or intraoperative sonography. Twenty-five patients had solitary pancreatic tumors; four had multiple tumors. Six of the patients with solitary insulinomas and one of the patients with multiple insulinomas had undergone previous unsuccessful exploration. Preoperative sonography was performed in 24 patients with solitary insulinomas, and 15 (63%) were localized. Intraoperative sonography was performed in 22 patients with solitary insulinomas, and 19 (86%) were visualized without having been previously located by palpation. Four of these visible solitary tumors (18%) were not detected by palpation at surgery. All the solitary insulinomas were detected with the combination of palpation and intraoperative sonography. In each of the six patients with solitary insulinoma who had undergone previous surgery, the tumor was visible with intraoperative sonography, which also demonstrated nonpalpable insulinomas in two of the four patients with multiple tumors. Preoperative real-time sonography is a sensitive, noninvasive, inexpensive method for localization of insulinoma. Intraoperative high-frequency sonography is a highly sensitive method for the detection of insulinoma. Intraoperative sonography is also valuable to determine the relationship of the insulinoma to pancreatic and bile ducts and thereby facilitate safe enucleation.

Insulinomas are usually small (<2.0 cm), solitary benign tumors with no predilection for any part of the pancreas [1]. Accurate localization of these tumors facilitates their excision and obviates the poor alternative of "blind" distal pancreatectomy, which is associated with a greater morbidity and mortality [2]. With this goal in mind, many imaging procedures have been used with variable success, including angiography, CT, sonography, pancreatic venous sampling, and more recently, MR imaging.

We have previously described our initial experience with intraoperative sonography in three patients with pancreatic insulinomas [3], and we present here our experience to date with both preoperative and intraoperative sonography in this condition.

Subjects and Methods

During a 4-year period, we studied 29 consecutive patients with benign pancreatic insulinoma: 19 female and 10 male patients, from 12 to 82 years old. All had clinical and biochemical evidence of insulinoma with hypoglycemic symptoms and had documented fasting hypoglycemia with inappropriately elevated levels of serum insulin. Surgical confirmation of a diagnosis of benign pancreatic insulinoma was obtained in all patients. Seven had undergone previous unsuccessful exploration for insulinoma.

Twenty-five of the 29 patients had both preoperative and intraoperative sonography performed. Three had only preoperative sonography, and one had only intraoperative sonography.

The preoperative sonograms were obtained using commercially available real-time scanners equipped with 3.5-MHz or 5-MHz transducers. The intraoperative sonograms were obtained using commercially available real-time scanners. Five patients were examined intraoperatively

Received May 5, 1986; accepted after revision June 9, 1986.

Presented at the annual meeting of the American Roentgen Ray Society, Washington, DC, April 1986.

[1] Department of Diagnostic Radiology, Mayo Clinic and Mayo Foundation, Rochester, MN 55905. Address reprint requests to J. W. Charboneau.

[2] Present address: Department of Radiology, The London Hospital, Whitechapel Rd., London E1 1BB, U.K.

[3] Section of Gastroenterologic and General Surgery, Mayo Clinic and Mayo Foundation, Rochester, MN 55905.

[4] Section of Pediatric Surgery, Mayo Clinic and Mayo Foundation, Rochester, MN 55905.

[5] Division of Endocrinology, Metabolism, and Internal Medicine, Mayo Clinic and Mayo Foundation, Rochester, MN 55905.

AJR 147:929–934, November 1986
0361–803X/86/1475–0929
© American Roentgen Ray Society

with a 5-MHz transducer, and 21 were examined intraoperatively with 7.5-MHz or 10-MHz transducers.

The preoperative examination was conducted systematically as follows: We initiated the examination with the patient supine and obtained both transverse and longitudinal scans of the head, body, and tail of the pancreas. We supplemented supine views with scans of the patient in recumbent oblique positions and then in the semierect position. In the semierect position, each patient drank approximately 700 ml water, and scans were obtained using the fluid-filled stomach as an acoustic window. The tail of the pancreas was often visualized best through the fluid-filled stomach when the patient was in a left posterior oblique position. The tail of the pancreas was also visualized in the coronal plane by using the spleen as an acoustic window. We performed and interpreted the preoperative sonograms without knowing the location of the pancreatic insulinoma, except on one patient who had an insulinoma previously demonstrated angiographically.

For intraoperative sonography, the transducer head was coated with approximately 10 ml acoustic gel and was enclosed in a sterile sheath. The pancreas was mobilized by the surgeon, and the abdominal cavity was filled with warm, sterile saline. The sterile-covered transducer was placed within this "fluid path" approximately 1 cm anterior to the pancreatic surface, and the examination was started in the transverse plane. The confluence of splenic and superior mesenteric veins was identified, as was the superior mesenteric artery, and these large vessels were used as anatomic landmarks for the pancreas, which lay anteriorly. The neck and body of the pancreas were thoroughly imaged in both transverse and longitudinal planes. Attention was then directed to the tail of the pancreas, and the transducer was directed far laterally toward the splenic hilum so that the distal tail could be visualized. Finally, the head of the pancreas was imaged. In most patients, the pancreatic and distal common bile ducts were visible, and the relationship of these structures to the insulinoma was determined. If the tumor was palpable by the surgeon, its location was not revealed to the radiologist who performed the examination.

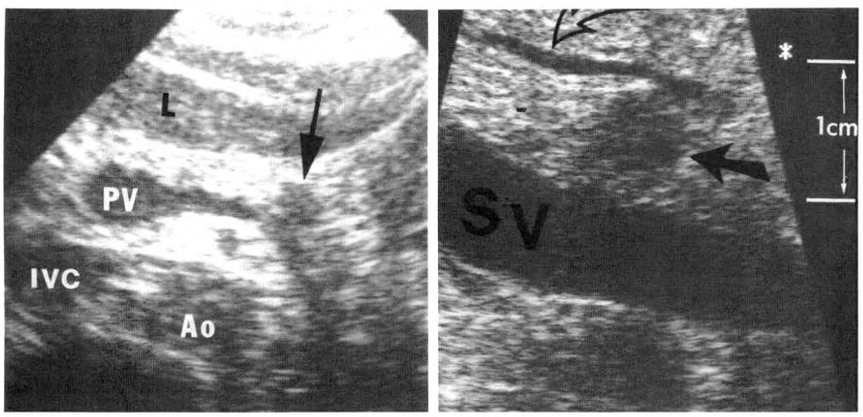


Fig. 1.—*A*, Preoperative transverse sonogram demonstrates typical 1-cm hypoechoic insulinoma (*arrow*) in body of pancreas. L = left lobe of liver; PV = portal vein; IVC = inferior vena cava; Ao = aorta.

***B*, Intraoperative transverse 10-MHz sonogram demonstrates typical 0.8-cm hypoechoic insulinoma (*black arrow*) in body of pancreas. Pancreatic duct (*curved arrow*) lies anterior to tumor. SV = splenic vein.**

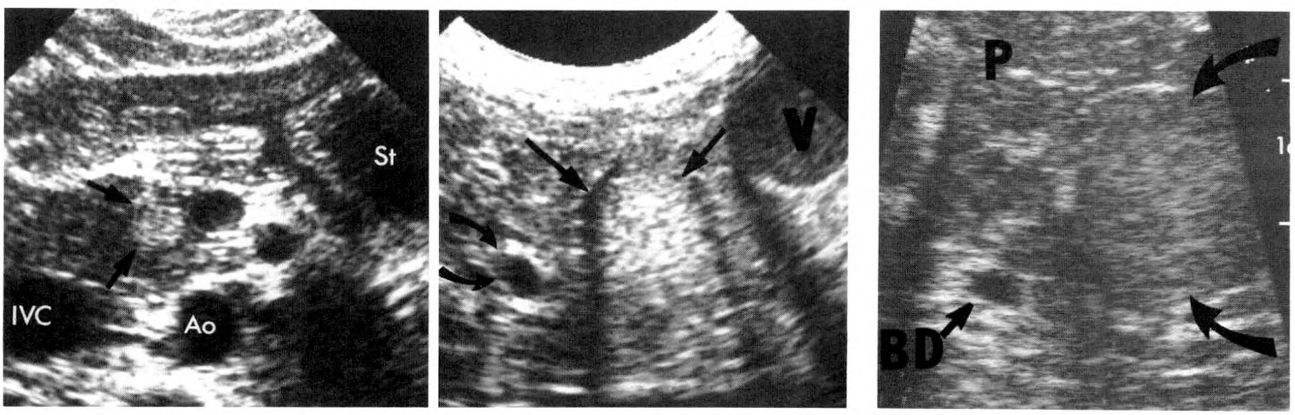


Fig. 2.—*A*, Preoperative transverse sonogram demonstrates 1-cm hyperechoic insulinoma (*arrows*) in pancreatic head. Ao = aorta; IVC = inferior vena cava; St = stomach.

***B*, Intraoperative transverse 7.5-MHz sonogram demonstates 1-cm hyperechoic insulinoma (*straight arrows*) with associated halo and refractive shadow in pancreatic head. Tumor lies 0.3 cm lateral to portal vein (V) and 0.4 cm medial to distal common bile duct (*curved arrows*).**

Fig. 3.—Intraoperative transverse 10-MHz sonogram demonstrates 1.2-cm isoechoic insulinoma with fine internal echoes (*curved arrows*) in pancreatic head of 16-year-old patient. Tumor was not palpable. P = pancreas parenchyma; BD = distal common bile duct.

Results

Of the 29 patients studied, 25 had solitary and four had multiple pancreatic insulinomas excised. Six of the patients with solitary insulinomas had undergone previous unsuccessful exploration; all of these tumors were in the pancreatic head. All four patients with multiple insulinomas had multiple endocrine neoplasia syndrome type 1 (MEN 1). One of these patients had a previous distal pancreatectomy but had two residual insulinomas in the pancreatic head. A total of 48 insulinomas were removed from the 29 patients. The diameters of the tumors ranged from 0.2 to 2.4 cm (mean, 1.1 cm). The diameters of the solitary tumors ranged from 0.5 to 2.0 (mean, 1.3 cm). All patients had surgical cure of hypoglycemia.

Sonographic Appearance

The typical sonographic appearance of a pancreatic insulinoma is a well-circumscribed mass that is hypoechoic in relation to surrounding pancreatic tissue [4] (Fig. 1). Most insulinomas in our series had this sonographic appearance. Two patients had insulinomas that were hyperechoic in relation to pancreatic tissue and were associated with a surrounding hypoechoic halo and refractive shadows (Fig. 2). Two of the 32 tumors seen sonographically were isoechoic in relation to pancreatic tissue and were visualized only because of a subtle echogenic halo around the tumor (Fig. 3). One of the two insulinomas seen at intraoperative sonography with guidance from the surgeon was also isoechoic. One insulinoma contained a central echogenic focus of calcification. The echo texture of insulinomas is often finer than that of the surrounding pancreatic parenchyma. The difference in echo texture is best appreciated by using high-frequency (7.5 to 10 MHz) sonography, which may help to identify the tumors (Fig. 3). A fine echo texture was present in nine of 16 solitary insulinomas detected intraoperatively by high-frequency sonography.

Diagnostic Accuracy

Preoperative sonography.—Of the 28 patients examined preoperatively by sonography, 24 had solitary insulinomas and 4 had multiple insulinomas at surgery. Correct localization was obtained in 15 (63%) of the 24 patients with solitary insulinomas. In three of the nine patients with false-negative findings, the sonographic examination was technically inadequate, because pancreatic tail was not visualized owing to bowel gas. In each of these three patients, a solitary insulinoma was found in the tail of the pancreas at surgery. Excluding these three patients, correct preoperative sonographic localization was obtained in 71% of the patients with solitary insulinomas. Of the 24 solitary insulinomas, 17 were located in the head of pancreas, and 11 of these were visible sonographically. Four of the solitary insulinomas were located in the body of pancreas, and all were visible sonographically. Three of the solitary insulinomas were located in the tail of pancreas; none were visible with preoperative sonography.

In each of the four patients with multiple insulinomas, at least one of the tumors was visible sonographically, but most of the tumors were small (<1-cm diameter) and were not visualized. Of 33 tumors removed from these four patients, 5 (15%) were visualized. The smallest insulinoma seen on preoperative sonography was 0.5 cm.

In the one false-positive preoperative sonogram, an accessory spleen in the patient was misinterpreted as a possible insulinoma in the tail of the pancreas.

Intraoperative sonography.—Of the 26 patients examined intraoperatively by sonography, 22 had solitary insulinomas and 4 had multiple insulinomas at surgery. Intraoperative sonography correctly localized the tumors in 19 (86%) of the 22 patients with solitary insulinomas. Two of the three insulinomas not visualized initially by the radiologist were visible after guidance from the surgeon, who could palpate the tumors. One of these insulinomas was larger than the field of view of the 10-MHz transducer and was isoechoic in relation to the adjacent pancreatic parenchyma; the other insulinoma was small and protruded off the anterior surface of the pancreas into the surrounding fluid path. The third tumor was in the distal pancreatic tail, which had not been mobilized by the surgeon; that region had not been imaged sonographically. Of the 22 solitary insulinomas, 4 (18%) were neither palpable nor grossly visible but were seen by intraoperative sonography. These tumors measured 1.7 cm, 1.5 cm, 1.0 cm, and 0.6 cm in maximum diameter and were all located in the pancreatic head. Two of these four patients were undergoing reoperation. All of the solitary insulinomas were detected with the combination of palpation and intraoperative sonography.

Intraoperative sonography localized more insulinomas than did preoperative sonography in each of the four patients with multiple insulinomas. In the patient with MEN 1, who had a previous distal pancreatectomy but had two residual insulinomas in the pancreatic head, both tumors were visualized intraoperatively, although only one had been seen preoperatively. The second insulinoma, which measured 0.5 cm, was not palpable. Of the 33 insulinomas removed from the four patients with multiple insulinomas, 12 (36%) were visible. Five of the 12 tumors seen by sonography were not palpable. Their diameters ranged from 0.3 cm to 0.7 cm. Intraparenchymal insulinomas surrounded by echogenic pancreas were easier to visualize sonographically than were surface lesions protruding into the anechoic fluid around the pancreas. The smallest insulinoma visible by intraoperative sonography was 0.3 cm [5] (Fig. 4). There were no false-positive intraoperative sonograms.

Value of intraoperative sonography.—The contribution of each intraoperative sonographic examination to surgical management was subjectively assessed by the surgeon. In 15 (58%) of the 26 patients, intraoperative sonography contributed to the surgical management. In four patients with solitary insulinomas, the contribution was vital because the tumors were not palpable, and enucleation was possible only after sonographic localization. In two of the four patients with multiple insulinomas, intraparenchymal tumors that were not palpable were demonstrated sonographically. Visualization of these insulinomas was essential to determine the extent of

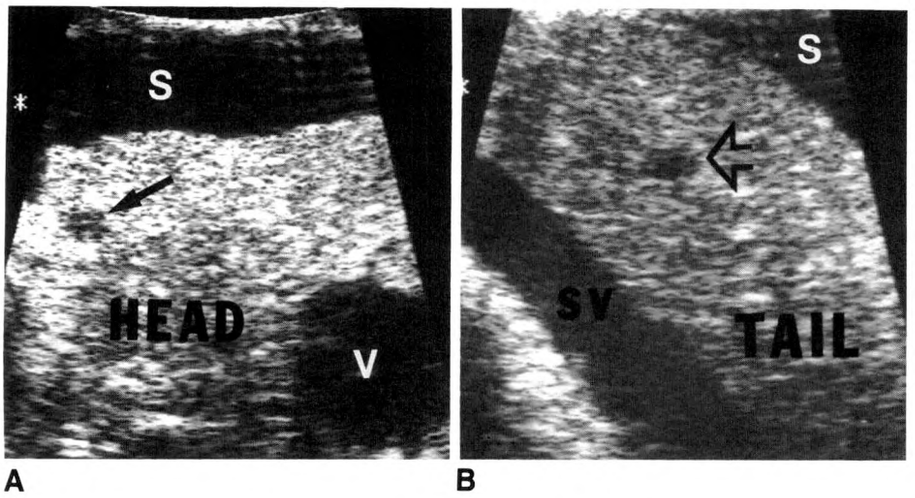


Fig. 4.—Intraoperative sonogram of 12-year-old patient with multiple endocrine neoplasia syndrome type 1.

***A*, Transverse image of head and neck of pancreas demonstrates 0.3-cm hypoechoic insulinoma (*arrow*). S = saline-filled peritoneal cavity; V = superior mesenteric vein.**

***B*, Transverse image of body and tail of pancreas demonstates 0.3-cm hypoechoic insulinoma (*arrow*). SV = splenic vein; S = saline-filled peritoneal cavity. (Figure republished with permission of *Journal of Pediatric Surgery* [5]).**

the pancreatic resection. In the other nine patients, the intraoperative sonographic examination was valuable because it precisely demonstrated the relationship of the insulinoma to the pancreatic and common bile ducts and pancreatic blood vessels (Fig. 1B). This information was useful to determine whether enucleation of the insulinoma was safe or whether pancreatectomy resection was indicated.

Discussion

When the diagnosis of pancreatic insulinoma has been established clinically and biochemically, accurate localization of the tumor is desirable to facilitate surgical resection and to obviate blind partial or subtotal pancreatectomy [6]. Various imaging techniques have been used to achieve this goal. These examinations vary in accuracy, invasiveness, operator dependence, and cost.

The success rate of angiographic localization ranges from 20 to 90% [6]. A high level of accuracy may be achieved by using selective injections and subtraction and magnification techniques [7]. However, angiography is invasive and, although sensitive, may be associated with a significant number of false-positive examinations [8, 9]. Success rates of as high as 97% have been achieved by using pancreatic venous sampling [9], but this procedure is also invasive, technically difficult, uncomfortable for the patient, time consuming, and relatively expensive. The reported success rate of CT for the detection of insulinoma ranges from 50% [10–12] to 80% [13].

The early experience of preoperative localization of insulinomas with sonography by using static scanners was disappointing [14, 15]. However, with the greater versatility and resolution now available with real-time sonography, better results are being reported, with detection rates of 60% [16]. Günther et al. [12] have recommended that sonography be used as the first step in locating islet cell tumors. At our institution, sonography is now the first and frequently the only imaging procedure used in the preoperative localization of insulinomas because it is noninvasive, is relatively inexpensive, and, when adequate visualization of the pancreas is obtained, has a sensitivity of approximately 70% in the detection of solitary insulinomas.

In order to maximize visibility of the pancreas, the examination technique must be meticulous. The patient must be scanned in various posterior oblique and semiupright positions. The left lobe of liver, fluid-filled stomach, gallbladder, and spleen (to visualize the tail) should all be used as acoustic windows to the pancreas.

Most insulinomas are hypoechoic in relation to the surrounding pancreatic parenchyma [17–19]. However, 10% of the insulinomas detected in our series were either isoechoic or hyperechoic relative to pancreatic parenchyma, perhaps because the normal pancreas is less echogenic in younger patients than in older ones [20]. All the patients with either isoechoic or hyperechoic insulinomas were less than 30 years old. Isoechoic insulinomas are difficult to visualize, but the presence of a halo around the tumor allows detection. The two hyperechoic insulinomas in our series were accompanied by refractive shadows that aided their identification. These shadows probably result from differences in acoustic properties between the insulinoma and adjacent pancreatic parenchyma. Awareness of the range of sonographic appearances of insulinomas is important. During the course of learning this range of sonographic appearances, we failed to appreciate one tumor that was isoechoic until it was identified after guidance from the surgeon.

Almost all solitary insulinomas are visible on intraoperative sonography. In our series, 86% were visible without prior knowledge of tumor location by palpation. Of the three tumors that were not visualized initially, two were visible after guidance from the surgeon, who could palpate them, and the other was in the distal tail of the pancreas, which had not

been mobilized and could not be examined. All solitary insulinomas in this series were detected by the combination of palpation and intraoperative sonography. Four of the patients in our series had solitary insulinomas that were not palpable (Fig. 3). Enucleation of the insulinomas in these four patients was possible only with sonographic guidance.

In patients undergoing reoperation for persistent hyperinsulinism, postoperative scarring and fibrosis may make palpation of the insulinoma more difficult. Intraoperative sonography can be especially helpful in this group of patients. In our series, two of six patients with solitary insulinomas and previous surgery had tumors that were not palpable but were visible with intraoperative sonography.

Patients with the MEN 1 present a special clinical problem. These patients have multiple, small insulinomas with diameters usually less than 1 cm; preoperative imaging techniques rarely demonstrate all the tumors. In our experience, intraoperative sonography demonstrated more insulinomas than preoperative sonography and detected small intraparenchymal insulinomas that were not palpable. Some small insulinomas on the surface of the pancreas, which are easily palpable and grossly visible, may not be seen by sonography. The combination of careful surgical palpation and a meticulous intraoperative sonographic examination seems to detect more of the multiple insulinomas than either technique alone. Even with this combination of palpation and intraoperative sonography, some small insulinomas may not be identified. The best treatment of multiple insulinomas is a subtotal pancreatectomy, because enucleation of all of the tiny tumors is not feasible. In two of the four patients with multiple tumors in our series, intraoperative sonography demonstrated nonpalpable tumors in the pancreatic head proximal to the proposed resection line. The demonstration of these additional tumors influenced the extent of the pancreatectomy performed.

The first five patients in our series were examined intraoperatively with a 5-MHz transducer, and 21 others were examined with either a 7.5-MHz or 10-MHz transducer. The superior resolution obtainable with the higher frequency transducers is important, not only in detecting the tiny tumors, but also in displaying with greater clarity the anatomic relationships of the tumor. This unique ability of intraoperative high-frequency sonography to display precisely the relationship of the tumor to the pancreatic and common bile ducts and pancreatic vessels is at least equally important to the surgeon as is its sensitivity of detection. This anatomic information is important in deciding between tumor enucleation or more extensive pancreatectomy. If the tumor lies away from or superficial to the pancreatic or bile duct, a safe enucleation is usually possible. If the tumor lies near or contiguous with the pancreatic or bile duct, this information may influence the method of enucleation or decision to proceed with pancreatectomy. Such precise localization may decrease the incidence of postoperative pancreatic fistulas. If the preoperative localizing studies are positive, we still use intraoperative sonography to display duct and vascular relationships, and to exclude additional occult insulinomas.

Close cooperation between the surgeon and the radiologist, maximizes the potential of intraoperative high-frequency sonography. In our practice, the radiologist "scrubs" for the procedure. The input of the radiologist is crucial because sonographic-imaging experience is necessary to appreciate subtle changes in echo texture, halo, and refractive shadow that may be the only signs of the insulinoma. In addition, familiarity with scanning in multiple planes of section, acquired from daily practice of sonography, is important in displaying the exact relationship of the tumor to ductal and vascular structures.

In conclusion, preoperative real-time sonography of the pancreas can localize 63% of solitary insulinomas. The procedure is noninvasive and relatively inexpensive, and it should be the first imaging technique used in patients with insulinoma. In our study, intraoperative high-frequency sonography detected 86% of solitary insulinomas, including tumors that are not palpable. We believe that almost all solitary insulinomas can be detected by the combined use of careful palpation and carefully performed high-frequency sonography. In addition, high-frequency sonography can precisely demonstrate the relationship of the insulinomas to the pancreatic and bile ducts and can thereby facilitate removal.

REFERENCES

1. Service FJ, Dale AJD, Elveback LR, Jiang N-S. Insulinoma: clinical and diagnostic features of 60 consecutive cases. *Mayo Clin Proc* **1976**;51:417–429
2. Edis AJ, McIlrath DC, van Heerden JA, et al. Insulinoma: current diagnosis and surgical management. *Curr Probl Surg* **1976**;13:1–45
3. Charboneau JW, James EM, van Heerden JA, Grant CS, Sheedy PF II. Intraoperative real-time ultrasonographic localization of pancreatic insulinoma: initial experience. *J Ultrasound Med* **1983**;2:251–254
4. Kuhn F-P, Günther R, Ruckert K, Beyer J. Ultrasonic demonstration of small pancreatic islet cell tumors. *J Clin Ultrasound* **1982**;10:173–175
5. Telander RL, Charboneau JW, Haymond MW. Intraoperative ultrasonography of the pancreas in children. *J Pediatr Surg* **1986**;21(3):262–266
6. Fulton RE, Sheedy PF II, McIlrath DC, Ferris DO. Preoperative angiographic localization of insulin-producing tumors of the pancreas. *AJR* **1975**;123:367–377
7. Stefanini P, Carboni M, Patrassi N, Basoli A. Beta-islet cell tumors of the pancreas: results of a study on 1,067 cases. *Surgery* **1974**;75:597–609
8. Boijsen E, Samuelsson L. Angiographic diagnosis of tumors arising from the pancreatic islets. *Acta Radiol [Diagn]* (Stockh) **1970**;10:161–176
9. Roche A, Raisonnier A, Gillon-Savouret M-C. Pancreatic venous sampling and arteriography in localizing insulinomas and gastrinomas: procedure and results in 55 cases. *Radiology* **1982**;145:621–627
10. Krudy AG, Doppman JL, Jensen RT, et al. Localization of islet cell tumors of dynamic CT: comparison with plain CT, arteriography, sonography, and venous sampling. *AJR* **1984**;143:585–589
11. Stark DD, Moss AA, Goldberg HI, Deveney CW. CT of pancreatic

islet cell tumors. *Radiology* **1984**;150:491–494
12. Günther RW, Klose KJ, Rückert K, et al. Islet-cell tumors: detection of small lesions with computed tomography and ultrasound. *Radiology* **1983**;148:485–488
13. Rossi P, Baert A, Passariello R, Simonetti G, Pavone P, Tempesta P. CT of functioning tumors of the pancreas. *AJR* **1985**;144:57–60
14. Dunnick NR, Long JA, Krudy A, Shawker TH, Doppman JL. Localizing insulinomas with combined radiographic methods. *AJR* **1980**;135:747–752
15. Shawker TH, Doppman JL, Dunnick NR, McCarthy DM. Ultrasonic investigation of pancreatic islet cell tumors. *J Ultrasound Med* **1982**;1:193–200
16. Günther RW, Klose KJ, Rückert K, Beyer J, Kuhn FP, Klotter HJ. Localization of small islet-cell tumors: preoperative and intraoperative ultrasound, computed tomography, arteriography, digital subtraction angiography, and pancreatic venous sampling. *Gastrointest Radiol* **1985**;10:145–152
17. Sigel B, Duarte B, Coelho JCU, Nyhus LM, Baker BJ, Machi J. Localization of insulinomas of the pancreas at operation by real-time ultrasound scanning. *Surg Gynecol Obstet* **1983**;156:145–147
18. Rückert K, Günther R, Klotter HJ, Kümmerle F. Intraoperative sonographische Lokalisation von Insulinomen. *Chirurg* **1983**; 54:589–591
19. Rueckert KF, Klotter HJ, Kümmerle F. Intraoperative ultrasonic localization of endocrine tumors of the pancreas. *Surgery* **1984**;96:1045–1047
20. Worthen NJ, Beabeau D. Normal pancreatic echogenicity: relation to age and body fat. *AJR* **1982**;139:1095–1098

Case Report

Spontaneous Rupture of a Pancreatic Pseudocyst into the Portal Venous System

Tetsuo Takayama,[1] Katsumoto Kato,[2] Hiroshi Sano,[2] Naoyuki Katada,[2] and Masayuki Takeichi[2]

Spontaneous rupture of pancreatic pseudocyst into the portal venous system is a rare but serious complication of chronic pancreatitis [1]. We previously reported one case in which the pancreatic pseudocyst spontaneously ruptured into the splenic vein [2]. In this report we illustrate the radiologic findings of spontaneous rupture of a pseudocyst into the portal venous system in two additional cases.

Case Reports

Case 1

An 82-year-old alcoholic man was admitted with cough and pain of the left hemithorax. Hematologic examination revealed hypochromic and microcytic anemia (RBC: 291 × 10^4/mm^3; hemoglobin: 9.8 g/100 ml). Fecal occult blood was highly positive (guaiac method). Serum amylase, lipase, and trypsin were all elevated: 1780 U/100 ml (normal value 160 U/100 ml), 5.9 U/100 ml (normal 1.5 U/100 ml), and 960 ng/ml (radioimmunoassay, normal 443 ng/ml), respectively. A chest radiograph showed a large left pleural effusion. Thoracocentesis revealed dark brown fluid rich in amylase (10,290 U/100 ml) and protein (3.6 g/100 ml).

A CT scan demonstrated several calcifications in the body of the pancreas and a solitary cyst in the tail. Sonograms showed dilatation of the main pancreatic duct. Celiac angiography revealed extremely dilated and tortuous branches of the hepatic artery, as well as obstruction of the splenic vein with filling of many collateral vessels. An ultrasonically guided percutaneous pancreatic ductogram revealed an irregularly shaped solitary cyst in the tail of the gland (Fig. 1). Contrast medium flowed from the cyst into the main pancreatic duct and splenic vein and into the left pleural cavity. The splenic vein was obstructed proximally and distally. These findings were verified by a CT scan made after the ductogram. The patient died of renal insufficiency 42 days after admission. Autopsy was refused.

Case 2

A 52-year-old alcoholic man was admitted to the hospital with mild epigastric pain and slight tenderness in the region. Hematological examination showed hypochromic and microcytic anemia (RBC: 292 × 10^4/mm^3, Hb: 9.0 g/100 ml). Serum amylase, lipase, and trypsin were all elevated: 972 Caraway U/100 ml with dominant pancreatic type (89%), 36 Cherry-Crandall U/100 ml, and 1217 ng/ml (radioimmunoassay), respectively. The abdominal pain subsided on the day after admission, but serum enzymes were persistently elevated. A guaiac test for occult blood in the stool was highly positive. A CT scan and sonogram revealed ascites and multiple cystic lesions in the pancreatic head.

An ultrasonically guided percutaneous pancreatic ductogram showed the cyst filling (Fig. 2). Percutaneous transhepatic portography showed the filling of the cyst and the portal vein, then the main pancreatic duct, and finally the duodenum. Amylase concentration in the dark brown fluid aspirated from the portal vein was extremely high (33,700 Caraway U/100 ml). On CT of the abdomen made just after this examination, the portal vein, cyst, and main pancreatic duct were all clearly shown. Percutaneous splenoportography demonstrated abrupt obstruction of the splenic vein around the head of the pancreas and dilated tortuous collateral veins running to the distal part of the portal vein.

At surgery, the pancreas was hard and many large collateral veins were present. After a simple drainage of ascites to the exterior, serum amylase gradually returned to normal. The patient was discharged 3 months after his admission, and he has done well.

Received February 11, 1986; accepted after revision June 17, 1986.
[1] Department of Internal Medicine, Sakashita Hospital, Sakashita-cho Ena-gun, Gifu-pref, 509-92 Japan. Address reprint requests to T. Takayama.
[2] Department of Internal Medicine, Kamo Hospital, Toyota, Aichi Japan.

AJR 147:935–936, November 1986 0361–803X/86/1475–0935 © American Roentgen Ray Society

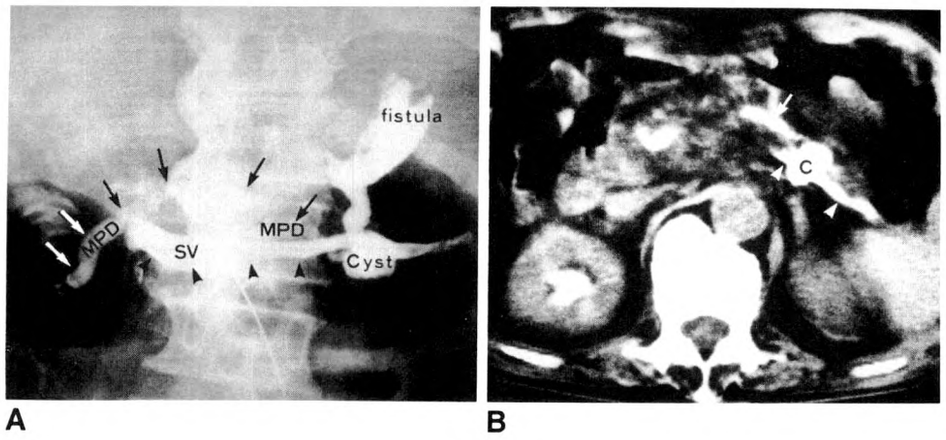


Fig. 1.—Case 1. *A*, Sonographically guided percutaneous pancreatic ductography. Dilated main pancreatic duct (MPD, *arrows*), cyst in tail of pancreas, splenic vein (SV, *arrowheads*), and fistula into pleural cavity, which filled with contrast medium in that order.

***B*, CT scan immediately after *A*. Contrast medium was retained in splenic vein (*arrowheads*), main pancreatic duct (*arrow*), and pancreatic cyst (C).**

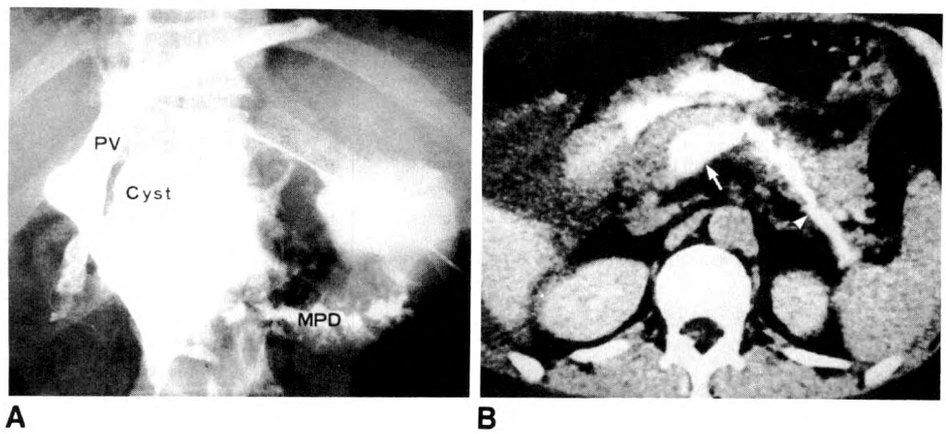


Fig. 2.—Case 2. *A*, Sonographically guided percutaneous transhepatic portogram. Contrast medium drained from portal vein (PV) into duodenum through cyst and main pancreatic duct (MPD).

***B*, CT scan immediately after *A*. Contrast medium was retained in cyst (*arrow*) and main pancreatic duct (*arrowhead*).**

Discussion

Ultrasonically guided percutaneous transhepatic portography, splenoportography, and pancreatic ductography are valuable techniques to detect both communication of the portal venous system with pancreatic cyst and the occluded part of the system. Extremely high amylase level in the dark brown fluid aspirated from the portal venous system can provide further evidence for the rupture of the cyst into it.

Spontaneous rupture of the pancreatic cyst has been reported in about 5% of patients with pancreatic cyst secondary to pancreatitis [3]; once the cyst ruptures into the portal venous system, thrombosis of the veins occurs.

In the present cases and the one reported previously [2], the proximal part of the portal vein was completely obstructed. Both obstruction of the portal vein and communication of the cyst with the splenic vein could be thoroughly demonstrated by sonographically guided examinations, including pancreatic ductography.

ACKNOWLEDGMENT

We wish to thank A. Noda, Department of Internal Medicine, Aichi Medical University, for his critical review and advice.

REFERENCES

1. Zeller M, Hetz HH. Rupture of a pancreatic cyst into the portal vein. *JAMA* **1966**;195:869–871
2. Takayama T, Kato K, Katada N, et al. Radiological demonstration of spontaneous rupture of a pancreatic pseudocyst into the portal system. *Am J Gastroenterol* **1982**;76:55–58
3. Hess W, Rütte B. Die intermittierende und perforierende pancreascyste. *Schweiz Med Wochenschr* **1950**;476–479

Retractile Mesenteritis Involving the Colon: Barium Enema, Sonographic, and CT Findings

F. Javier Pérez-Fontán[1]
Rafaela Soler[2]
Jesús Sanchez[3]
Pilar Iglesias[3]
Pedro Sanjurjo[2]
José Ruiz[2]

Retractile mesenteritis is a rare disorder characterized by either focal or diffuse thickening of the mesentery due to chronic inflammation and fibrosis. Six cases are reported in which stenosis of the colon, an uncommon complication of retractile mesenteritis, was the predominant radiologic finding. Diagnosis was suggested by the tapered, serrated appearance of the stenotic segment on barium enema complemented by the findings on sonography and CT.

Retractile mesenteritis is one of several terms that describe benign, tumorlike mesenteric lesions formed as a result of the chronic inflammation of adipose and fibrous tissue [1]. This disorder mainly affects the small bowel [2–4], with colonic involvement occurring less frequently [5–9]. We present six cases in which involvement of the colon was the major finding.

Materials and Methods

Three men and three women, 29 to 74 years old, were hospitalized with diffuse or localized abdominal pain of variable duration (4 days to 5 months). An abdominal mass was present in two patients. Three others had signs of complete intestinal obstruction. Two of the women had previous abdominal surgery, one for an inflammatory pelvic process of obscure etiology and the other for leiomyomas of the uterus.

All patients had plain abdominal radiographs as well as a barium enema examination, three had sonography, one had excretory urography, one had a small-bowel examination and CT, and one had a colonoscopy.

Results

Plain abdominal radiographs suggested mechanical obstruction of the colon in three patients and were normal in the other three. Barium enema examination showed a concentric stricture with tapered, serrated edges (Figs. 1, 2A, and 3) in all but one patient (Fig. 4). The length of the narrowed segment was 4–18 cm. Double-contrast barium enema examination in two of the cases disclosed a normal mucosa (Fig. 5A). The transverse, descending, and rectosigmoid colon were each affected in two cases. Results of sonography varied from an irregularly shaped hypoechoic area to a hyperechoic mass with central hypoechoic areas (Fig. 2B). Excretory urography performed in one patient revealed a smooth, extrinsic compression of the bladder. A small-bowel examination in another patient showed separation of the intestinal loops with tethered contours (Fig. 5B). CT performed in the same patient showed an epigastric mass, the density of which suggested fat interspersed with streaky soft tissue and some calcification (Figs. 5C and 5D).

All patients underwent surgery. Only one patient was evaluated by colonoscopy before laparotomy. This examination revealed an intact mucosa, which appeared elevated in the area of the obstruction. Four patients had radical resections because

Received September 24, 1985; accepted after revision May 14, 1986.

[1] Departments of Radiology and Surgery, Hospital Montecelo, Pontevedra, Spain. Address reprint requests to F. J. Pérez-Fontán, Dept. of Radiology, Hospital Teresa Herrera, Ciudad Sanitaria Juan Canalejo, La Coruña, Spain.

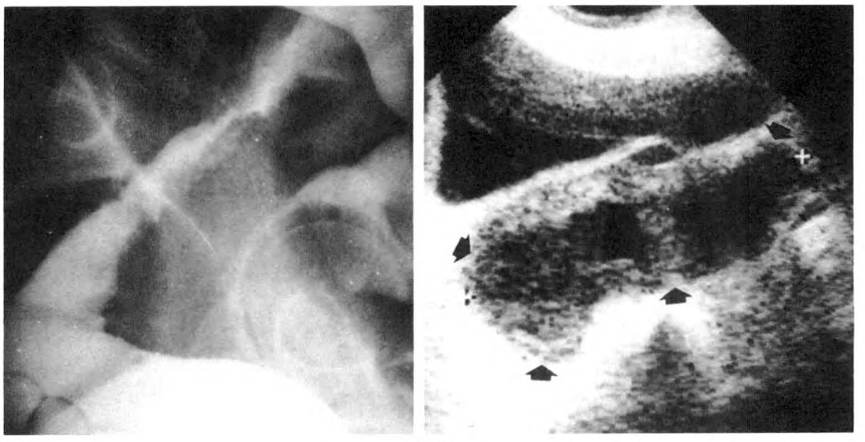
[2] Department of Radiology, Hospital Montecelo, Pontevedra, Spain.

[3] Department of Pathology, Hospital Montecelo, Pontevedra, Spain.

AJR 147:937–940, November 1986
0361–803X/86/1475–0937
© American Roentgen Ray Society

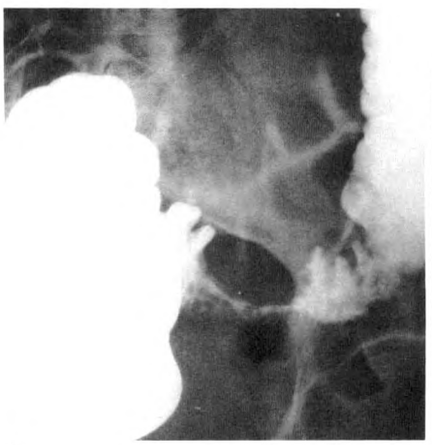


Fig. 1.—74-year-old man complaining of abdominal pain and constipation. Barium enema shows stricture with nonabrupt edges in descending colon.



A B

Fig. 2.—57-year-old woman with low-grade fever and pain in right lower quadrant.
A, Barium enema shows concentric stricture of rectosigmoid colon with tapering edges and serration.
B, Pelvic sonogram shows solid mass (*arrows*) with central hypoechoic areas.



3



4

Fig. 3.—47-year-old woman with constipation and diffuse abdominal pain. Barium enema shows concentric stricture in sigmoid colon with tapered, serrated edges.

Fig. 4.—52-year-old man with high fever and acute abdominal pain in left flank. Barium enema shows narrowing of descending colon. Radiograph was made after glucagon administration.

malignant disease was suspected at laparotomy. Two patients had conservative surgery because retractile mesenteritis was suspected and confirmed by histologic studies.

Discussion

Retractile mesenteritis represents the final stage of a series of inflammatory changes affecting the mesentery. These changes result from a common reparative process arising from various causes [10–12]. The disorder is more common in males and has been described at various ages, but not in children younger than 8 years old.

Histologically, the lesions are composed of fibrous tissue, lipophages, lymphocytes, plasma cells, and eosinophils. These lesions involve the mesenteric and subserosal fat, and often extend into the bowel muscle and submucosa. The mucosa remains intact. Partial or complete obstruction of the small bowel may complicate the course [2–4, 12, 13]. An abdominal mass, suggesting a tumor, is frequently palpable.

Retractile mesenteritis has been described in association with lymphoma [13, 14], Gardner's syndrome [15], and retroperitoneal fibrosis. The simultaneous occurrence of retractile mesenteritis and retroperitoneal fibrosis has led to the hypothesis that these entities are different expressions of the same process [11, 14, 16–18].

Radiologic signs of retractile mesenteritis include separation of the intestinal loops (mass effect); kinking or angulation of the small intestine [2, 3]; and, more rarely, narrowing of the colon [5, 8, 9]. Narrowing of the colon, however, was the predominant finding in our cases. Barium enema showed a concentric stricture with tapered edges in all but one case.

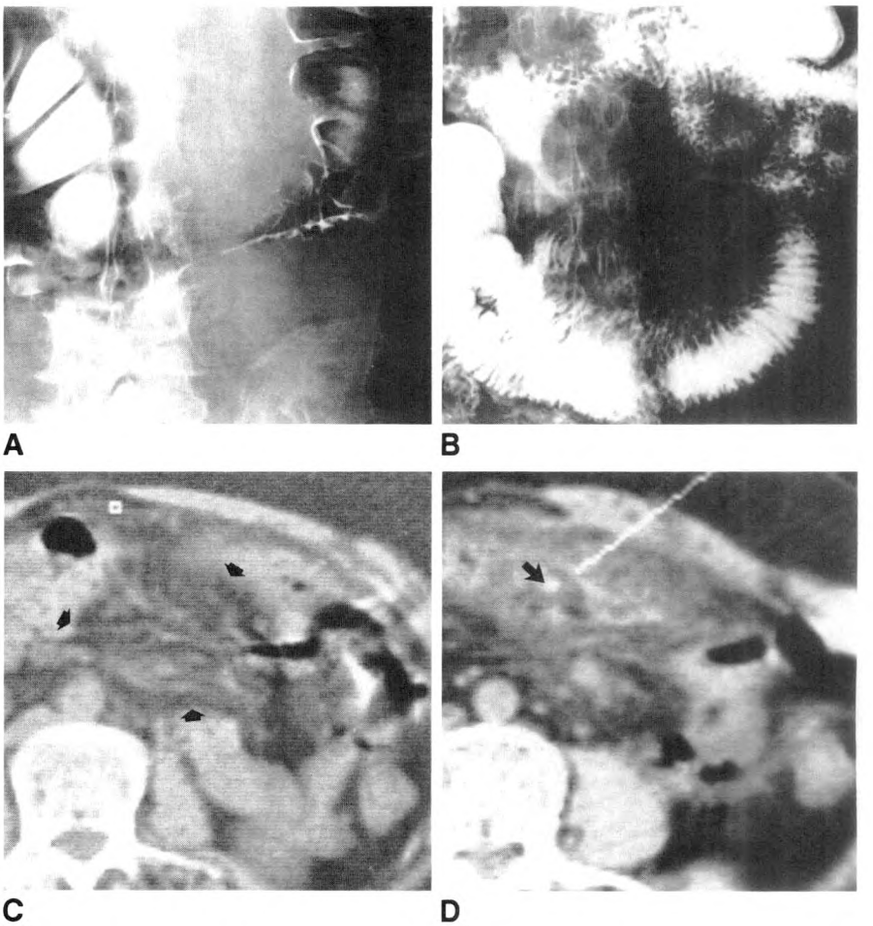


Fig. 5.—37-year-old woman with pain in left upper quadrant.

***A*, Barium enema shows narrowing of transverse colon.**

***B*, Small-bowel examination shows separation of intestinal loops with tethered contours.**

***C*, CT scan of upper abdomen shows heterogeneous mass (*arrows*) with fat density alternating with linear soft-tissue densities.**

***D*, Different CT section shows calcifications within mass (*arrow*).**

The colonic mucosa was unaltered in the patients studied with double contrast. The margin of the colon was serrated, an appearance attributed to the existence of either fibrotic implants on the serosal side of the intestinal wall or venous congestion [8, 9].

Differential diagnosis of narrowing of the colon as seen on barium enema includes inflammatory, neoplastic, and ischemic diseases of the colon. Localized abscesses caused by diverticulitis are leading causes of colonic obstruction in areas where diverticulosis is endemic. The strictures caused by diverticulitis tend to be more eccentric, however, in contrast with the rather concentric strictures seen with retractile mesenteritis. Annular carcinoma of the colon is less likely in the presence of a stricture with tapered edges and normal mucosa. No definitive differences are shown on barium enema between retractile mesenteritis and the rare variant of scirrhous carcinoma and the segmental colonic encasement caused by metastatic involvement. Ischemia of the colon must also be considered in the differential diagnosis, although the patient's age and clinical presentation are usually helpful to establish a distinction.

The sonographic characteristics of retractile mesenteritis have seldom been described [5, 19, 20]. Both our findings and those previously reported suggest that this examination is inconclusive for the diagnosis of retractile mesenteritis, although sonography narrows the possibilities substantially. Sonographic findings similar to those found in our patients can be seen in liposarcoma, leiomyosarcoma, teratoma, abscesses, and hematoma.

CT examination was performed in only one of our patients, revealing a mass of fat density interspersed with soft-tissue density and calcifications. Pathologic examination showed that fibrous tracts were responsible for the soft-tissue density. Because the lesions of retractile mesenteritis contain a variable proportion of fat and fibrous tissue, it is likely that the CT findings vary according to this proportion. A similarly variable appearance can be found in angiomyolipoma, liposarcoma, myelolipoma, and teratoma [21].

Even if sonographic and CT examination are nonspecific for retractile mesenteritis, we believe that both diagnostic procedures are indicated when narrowing of the colon with characteristics similar to those described in our patients is found. Both procedures complement the findings of the barium enema and colonoscopy, corroborate the benign appearance of the lesion, and help to establish its extension and the secondary involvement of adjacent organs. Furthermore, they may serve as a reference to evaluate the response to medical [20, 22] or surgical therapy.

REFERENCES

1. Tedeschi CG, Botta GC. Retractile mesenteritis. *N Engl J Med* **1962**;266:1035–1040
2. Aach RD, Kahn LI, Frech R. Obstruction of the small intestine due to retractile mesenteritis. *Gastroenterology* **1968**;54:594–598
3. Clement AR, Tracht DC. The roentgen diagnosis of retractile mesenteritis. *Radiology* **1969**;107:787–790.
4. Maroy B, Bou G, Duroselle C. Diagnostique radiologique preoperatoire d'une mesenterite retractile. Efficacite prolongee d'une resection localisee. *Ann Radiol (Paris)* **1985**;28:65–67
5. Bendom JA, Poleynard GD, Bordin GM. Fibrosing mesenteritis simulating pelvic carcinomatosis. *Gastrointest Radiol* **1972**; 4:195–197
6. Soumerai S, Kirkland WG, McDonnell WV, Schantz A. Nodular mesenteritis: report of a case simulating carcinoma of the sigmoid colon and analysis of its histologic profile. *Dis Colon Rectum* **1976**;19:448–452
7. Durst AL, Freund H, Rosenmann E, Birnbaum D. Mesenteric panniculitis: review of the literature and presentation of cases. *Surgery* **1977**;81:203–211
8. Williams RG, Nelson JA. Retractile mesenteritis: initial presentation as colonic obstruction. *Radiology* **1978**;126:35–37
9. Thompson GT, Fitzgerald EF, Somers SS. Retractile mesenteritis of the sigmoid colon. *Br J Radiol* **1985**;58:266–267
10. De Castro JA, Calem WS, Papadakis L. Liposclerotic mesenteritis. *Arch Surg* **1967**;94:26–29
11. Handelsman JC, Shelley WM. Mesenteric panniculitis. *Arch Surg* **1965**;91:842–850
12. Reske N, Namiki H. Sclerosing mesenteritis, report of two cases. *Am J Clin Pathol* **1975**;64:661–667
13. Ogden WW, Bradburn DM, Rives JD. Mesenteric panniculitis: review of 27 cases. *Ann Surg* **1965**;161:864–875
14. Kipfer RE, Moertel CG, Dahlin DC. Mesenteric lipodystrophy. *Ann Intern Med* **1974**;80:582–588
15. Richards RC, Rogers SW, Gardner EJ. Spontaneous mesenteric fibromatosis in Gardner's syndrome. *Cancer* **1981**;47:597–601
16. Baum S. Case records of the Massachusetts General Hospital. Case 27. *N Engl J Med* **1972**;287:34–40
17. Harbrecht PJ. Variants of retroperitoneal fibrosis. *Ann Surg* **1966**;165:388–401
18. Rogers CE, Demetrakopoulos NJ, Hyamns V. Isolated lipodystrophy affecting the mesentery, the retroperitoneal area and the small intestine. *Ann Surg* **1961**;153:277–282
19. Gago P, Robles JL, Crespo E. Lipodistrofia del mesenterio. A proposito de una observación. *Rev Esp Enferm Apar Dig* **1978**;54:629–632
20. Tytgat GN, Roozendal K. Winter W, Esseveld MR. Successful treatment of a patient with retractile mesenteritis with prednisone and azothioprine. *Gastroenterology* **1980**;79:352–356
21. Katz ME, Heiken JP, Glazer HS, Lee JKT. Intraabdominal panniculitis: clinical, radiographic and CT features. *AJR* **1985**; 145:293–296
22. Bush RW, Hammar SP, Rudolph RH. Sclerosing mesenteritis: response to cyclophosphamide. *Arch Intern Med* **1986**;146: 503–505

Case Report

CT Diagnosis of Primary Small-Bowel Volvulus

Diego Jaramillo[1] and Bharat Raval

Volvulus of the small bowel can either be primary or secondary to conditions such as malrotation, congenital bands, postoperative adhesions, tumors, intussusception, colostomy, or internal hernias [1]. To the best of our knowledge, the CT appearance of primary small-bowel volvulus has not been reported. In the following case, CT played the major role in preoperative diagnosis. A characteristic CT appearance consists of multiple dilated intestinal loops with edematous mesenteric folds converging radially toward the site of torsion.

Case Report

A 31-year-old black man presented with a 24-hr history of progressive dull epigastric pain, nausea, and vomiting. The past medical history was not significant, and the patient had not undergone any previous surgery.

Physical examination revealed tenderness to deep palpation in the epigastric area and markedly decreased bowel sounds. An abdominal series showed a nonspecific bowel gas pattern without evidence of obstruction or pneumoperitoneum. Because an abdominal sonogram 18 hr after admission suggested enlargement of the pancreatic head, a CT of the abdomen was performed. This study showed no pancreatic abnormalities, but demonstrated multiple distended small-bowel loops anterior to the left lobe of the liver, distributed radially, with marked edema of the mesentery and thickening of the bowel wall (Fig. 1). Intramural gas was present in some of the loops.

Scanning in the left lateral decubitus position confirmed the presence of pneumatosis intestinalis and also demonstrated a fixed, radial arrangement of the involved intestinal loops (Fig. 2). The corresponding portions of the swollen mesentery converged toward a common point (Fig. 3). Ascites was also noted.

An upright radiograph of the abdomen after the CT examination showed a conglomerate of multiple distended, partially fluid-filled small-bowel loops clustered in the upper abdomen. Pneumatosis intestinalis could not be demonstrated.

Twenty-four hours after his admission, the patient developed melena and signs of peritoneal irritation. An exploratory laparotomy revealed a primary volvulus involving 90 cm of small intestine, approximately 60 cm proximal to the ileocecal valve. The rest of the intestine was normal and, except for ascites, no other intraperitoneal abnormalities or anomalies predisposing to small-bowel volvulus were present. The necrotic segment of the intestine was resected, and the uninvolved portions were anastomosed. Microscopic examination of the specimen revealed necrosis of the entire thickness of the wall with hemorrhage and inflammation. The postoperative course was uneventful, and the patient was discharged 1 week later.

Discussion

Primary small-bowel volvulus is a common surgical problem in young males in countries of the Middle East, Asia, and Africa [1]. Dietary habits and abnormalities in the length and height of the mesentery have been implicated in its development. Although there are often few symptoms and signs [1, 2], the development of constant pain suggests infarction. The radiologic findings, and specifically the CT picture, represent a summation of (1) venous and lymphatic obstruction, (2) arterial obstruction and infarction, (3) closed-loop obstruction, (4) abnormal location of intestinal loops, and (5) twisting of the mesenteric root.

Venous and lymphatic obstruction with thickening of the bowel wall, separation of bowel loops, blunting of the valvulae conniventes, and thumbprinting are better demonstrated on CT than on plain films [3]. Furthermore, CT shows the mesenteric edema that is a dominant element of venous occlusion

Received March 18, 1986; accepted April 28, 1986.

[1]Both authors: Department of Radiology, University of Texas Medical School, 6431 Fannin St., Rm. 2. 134, Houston, TX 77030. Address reprint requests to B. Raval.

AJR 147:941–942, November 1986 0361–803X/86/1475–0941 © American Roentgen Ray Society

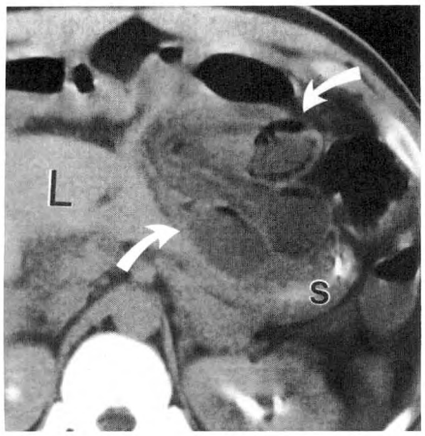


Fig. 1.—CT scan of upper abdomen demonstrates conglomerate of distended small-bowel (*curved arrows*) anterior to left lobe of liver (L) and stomach (S). Pneumatosis intestinalis and thickening of bowel wall also noted.

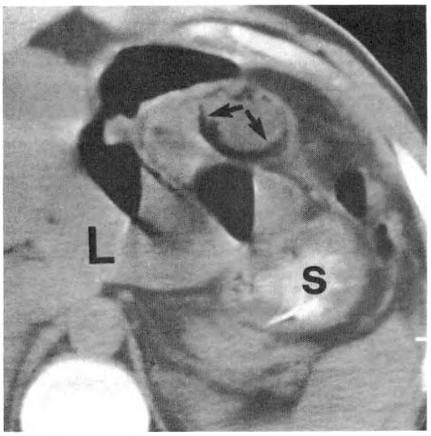


Fig. 2.—CT scan in left lateral decubitus position shows fixed distended bowel loops. Gas in intestinal wall again noted (*arrows*). L = left lobe of liver; S = stomach.



Fig. 3.—CT scan shows edematous mesenteric folds converging toward point of torsion (*arrow*).

[4]. Arterial obstruction and infarction are indicated by thumbprinting, pneumatosis intestinalis, and gas in the portal venous system. Gas in the mesenteric veins in the absence of portal venous gas has also been described with isolated arterial infarction on CT [3].

Closed-loop obstruction can be seen on CT as marked dilation of the involved intestinal segment without significant abnormalities of either the proximal or distal bowel [5]. Fixation of bowel loops, a characteristic finding of closed-loop obstruction, was demonstrated in our case by scanning in the supine and lateral decubitus positions (Fig. 2).

Intestinal loops in an abnormal location are detected after the initial torsion because portions of the uninvolved proximal bowel are trapped under the twisted mesentery, analogous to an internal hernia. In our case, the predominant conglomerate of bowel loops was seen anterior to the liver, where neither normal small intestine nor internal hernias are found.

The rotation of the mesentery, which can be demonstrated with barium [6] and angiography [7], has been described on CT as the "whirl sign" [6, 8]. In the present case, the fixed radial arrangement of dilated bowel loops with their edematous mesenteric folds converging toward the point of torsion strongly suggests volvulus.

REFERENCES

1. Duke JH Jr, Yar MS. Primary small bowel volvulus. *Arch Surg* **1977**;112:685–688
2. Juler GL, Stemmer EA, Connolly JE. Preoperative diagnosis of small bowel volvulus in adults. *Am J Gastroenterol* **1972**;36:235–247
3. Federle MP, Chun G, Jeffrey RB, Raylor R. CT in bowel infarction. *AJR* **1984**;142:91–95
4. Nichols DM. Computed tomography in acute mesenteric vein thrombosis. *J Comput Assist Tomogr* **1984**;8:171–172
5. Balthazar EJ, Bauman JS, Megibow AJ. CT diagnosis of closed loop obstruction. *J Comput Assist Tomogr* **1985**;9:953–955
6. Fisher JK. Computed tomographic diagnosis of volvulus in intestinal malrotation. *Radiology* **1981**;140:145–146
7. Kadir S, Athanasoulis CA, Greenfield AJ. Intestinal volvulus: angiographic findings. *Radiology* **1978**;128:595–599
8. Shaff MI, Himmelfarb E, Sacks GA, Burks DD, Kulkarni MV. The whirl sign: a CT finding in volvulus of the large bowel. *J Comput Assist Tomogr* **1985**;9:410

Gaucher's Disease Type 1: Assessment of Bone Involvement by CT and Scintigraphy

George Hermann[1]
Jack Goldblatt[2]
Roger N. Levy[3]
Stanley J. Goldsmith[4]
Robert J. Desnick[2]
Gregory A. Grabowski[2]

The effectiveness of CT and technetium-99m sulfur colloid (^{99m}Tc SC) bone-marrow scans in determining the extent and severity of skeletal involvement in 23 patients with type 1 Gaucher's disease was compared with the effectiveness of conventional radiographic techniques and technetium-99m methylene diphosphonate (^{99m}Tc MDP) bone scintigrams. Density measurements obtained by CT proved sensitive in differentiating normal marrow (−50 to −120 H). Scintigrams with the sulfur colloid nuclide demonstrated three distinct patterns of uptake: (1) peripheral expansion of normal marrow (profile B), (2) greater marrow expansion with patchy areas lacking uptake (profile C), and (3) greater loss of uptake with retention of the nuclide in other reticuloendothelial organs and circulation (profile D). CT scans provided greater sensitivity in resolving the extent of marrow involvement in affected areas, while the ^{99m}Tc SC scintigrams were more effective in overall assessment of the severity of bone-marrow involvement. Both conventional radiographic techniques and ^{99m}Tc MDP bone scans were useful primarily as screening procedures or for evaluating specific involved areas. ^{99m}Tc MDP scans were useful in evaluating regional defects (i.e., ischemic necrosis) in certain cases, but no consistent patterns were observed. CT and ^{99m}Tc SC scans are useful for determining the extent and severity of Gaucher's disease involvement of bone marrow.

Received November 25, 1985; accepted after revision June 12, 1986.

Parts of this paper were presented as an exhibit at the annual meeting of the Radiological Society of North America, Washington, DC, November 1984.

This work was supported in part by a grant (RR-71) for the General Clinical Research Center by the Division of Research Resources of the National Institutes of Health, a grant (1-857) from the March of Dimes Birth Defects Foundation, and a grant from Florence and Theodore Baumritter to the Mount Sinai Center for Jewish Genetic Diseases. G. A. Grabowski has received a Research Career Development award (1 K04 AM01351) from the National Institutes of Health and a Career Scientist Award from the Irma T. Hirschl Trust.

[1] Department of Radiology, Mount Sinai School of Medicine, City University of New York. The Mount Sinai Hospital, One Gustave L. Levy Pl., New York, NY 10029. Address reprint requests to G. Hermann.

[2] Division of Medical Genetics, Department of Pediatrics, Mount Sinai School of Medicine, City University of New York, New York, NY 10029.

[3] Department of Orthopaedics, Mount Sinai School of Medicine, City University of New York, New York, NY 10029.

[4] Department of Physics–Nuclear Medicine, Mount Sinai School of Medicine, City University of New York, New York, NY 10029.

AJR 147:943–948, November 1986
0361–803X/86/1475–0943
© American Roentgen Ray Society

Type 1 Gaucher's disease, the most prevalent genetic disease among Ashkenazi Jews, is characterized by the deficient activity of the lysosomal hydrolase, acid β-glucosidase [1, 2]. On the basis of gene frequency in this population, it is estimated that about 5000 to 10,000 Jews in the United States are afflicted by this disease [3]. Its clinical manifestations result from abnormal accumulation of the enzyme's major substrate, glucosyl ceramide, primarily in reticuloendothelial cells of the liver, spleen, and bone marrow [3, 4]. The progressive infiltration and replacement of the bone marrow by "Gaucher cells" (lipid-filled macrophages) lead sequentially to diffuse osteoporosis, localized destruction, ischemic necrosis, osteosclerosis, and other bony abnormalities (see Table 1) [3–6].

The marked variability in severity of the disease's manifestations makes it particularly difficult to predict the future course and complications for individual patients. In some, the bony involvement is severely debilitating or crippling [3–6]. Although variability in bone-disease severity has made medical and orthopedic management decisions difficult, no clinical or biochemical predictors have been identified for the rate of progression or future severity of the disease process [7]. Moreover, the extent and severity of the skeletal involvement is often difficult to assess by clinical and radiographic examinations [5–7]. To date, no one has reported using CT for evaluating skeletal involvement; scintigraphic studies have suggested an association between extent of bone-marrow involvement and the severity of radiographically evident bone disease [8].

Because the skeletal manifestations are the most debilitating and disabling complications of Gaucher's disease, we undertook an investigation to determine the value of CT scans and scintigraphy to estimate the extent of bone marrow

TABLE 1: **Radiologic Stages of the Skeletal Lesions in Type 1 Gaucher's Disease**

Stage	Nature of Lesion	Appearance
1	Diffuse osteoporosis	Coarse trabecular pattern of osteoporosis
2	Medullary expansion	Loss of normal concavity above femoral condyles; Erlenmeyer flask deformity
3	Localized destruction (osteolysis)	Small erosions, well defined or moth eaten; cortex rarefied and endosteally notched; ground-glass veiling
4	Ischemic necrosis of long bones; sclerosis; osteitis	Patchy densities and erosions; serpiginous sclerotic streaks; layered periostitis; sequestra
5	Diffuse destruction; epipheseal collapse; osteoarthrosis	Flattening or irregular destruction of femoral heads, with mixed lytic and sclerotic foci; larger "soap bubble" pattern

involvement [9, 10]. We evaluated the results of radionuclide marrow (technetium-99m sulfur colloid [^{99m}Tc SC]) and bone scintigraphy (technetium-99m methylene diphosphonate [^{99m}Tc MDP]) in conjunction with CT scans to assess the extent and severity of the variable bony disease in patients with Gaucher's disease type 1.

Subjects and Methods

Patient Population

Twenty-three patients (5–70 years old; 14 male, nine female) with clinically and biochemically documented Gaucher's disease type 1 were admitted to the General Clinical Research Center for evaluation. Their skeletal disease ranged from minimal to severe. Informed consent for these studies was obtained from all patients or their parents, and assent was obtained from children over the age of 16 years, in accordance with guidelines of our institution and of the U. S. Department of Health and Human Services.

CT Scans

CT scans were performed for 9.6 sec with a GE 8800 scanner. The femora, tibiae, and pelvis were chosen for detailed analyses: 10-mm slices were evaluated from the level of the midpelvis through the hips, and from the upper, middle, and lower thirds of the femurs and tibiae. Density measurements (Hounsfield units) of the long-bone medullary cavities were determined. Because the medullary cavities were heterogenous in cross-sectional density, the largest possible area was used for each measurement, carefully avoiding the cortex. The size of the region of interest varied according to the diameter of the medullary cavity at each level; a slice averaging 0.29 cm^2 was scanned (see Fig. 1 for a typical normal cross-section with negative attenuation coefficient). Each region of interest (Fig. 2A) in the extremities was rated as positive or negative according to the determined mean density.

Scintigraphy

Bone-marrow scintigraphy was performed 20–30 min after IV administration of ^{99m}Tc SC (10 mCi), by using a wide-field-of-view gamma camera and a low-energy, all-purpose, parallel-hole collimator. Images of the lower extremities were acquired for the same time interval as needed to acquire 300,000 counts of the anterior pelvis while excluding the liver and spleen from the field. Similarly, routine skeletal scintigraphy was performed at least 2 hr after IV administration of 20 mCi (740 MBq) of ^{99m}Tc MDP. Skeletal images were obtained during the time required to acquire a 1,600,000-count anterior chest image.



Fig. 1.—Cross section at level of upper thigh. Marrow cavity shows negative attenuation coefficient −29 H. Normal density.

Results

The results of the radiographic studies and CT and ^{99m}Tc SC scans are shown in Table 2. The scoring systems were developed to correlate various images with the radiographic findings. With CT and ^{99m}Tc SC, the degree of involvement of the lower extremities was symmetric; therefore, the CT results in Table 2 are those of the right lower extremity with ^{99m}Tc SC, and the scintigrams from both lower extremities were used in the scoring system. Because the lower extremity was most consistently and severely involved, studies were restricted to this area [11].

Radiographic Studies

The radiographic severity of the lower-extremity bone disease was classified on a scale from 0 to 5, (minimal to most severe, see Tables 1 and 2). The lower-extremity radiographs were normal in four patients.

CT Scans

The results of the CT scans were classified according to the patterns of positive (abnormal) or negative (normal) attenuation coefficients (Table 2). In the femora and tibiae, each of the six scanned areas with a positive attenuation coefficient was assigned a value of 1. The sum of the positive areas provided the numeric score. Compared with the negative

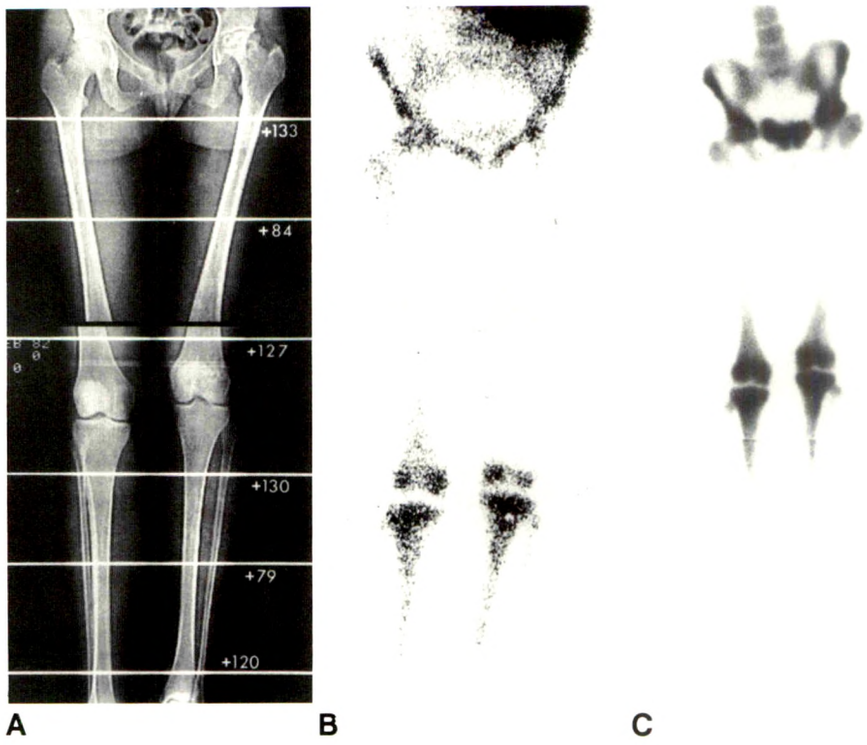


Fig. 2.—*A*, Radiographs and CT density measurements, *B*, ^{99m}Tc sulfur colloid scintigram, and *C*, ^{99m}Tc methylene diphosphonate scintigram from a 32-year-old woman with Gaucher's disease. Horizontal white lines in *A* represent the six levels at which CT density measurements (Hounsfield units) were obtained. ^{99m}Tc sulfur colloid scintigraphy (*B*) was representative of profile C with nonuniform bone marrow expansion. ^{99m}Tc methylene diphosphonate scintigram (*C*) demonstrates nonspecific increased uptake in long bones.

TABLE 2: **Correlation of CT and MS Findings in Various Skeletal Regions in 23 Homozygotes with Gaucher's Disease Type 1**

Case No.	Gender	Age (years)	Radiographic Stage[a]	Overall Score		Proximal Femur		Midfemur		Distal Femur		Proximal Tibia		Midtibia		Distal Tibia	
				MS	CT	CT	MS	CT	MS	CT	MS	CT	MS	CT	MS	CT	MS
1	M	5	4	D	6	+	−	+	−	+	−	+	−	+	−	+	−
2	M	5	2	B	6	+	+	+	+	+	+	+	+	+	+	+	+
3	M	6	0–1	B	4	+	+	+	+	+	+	+	+	−	+	−	−
4	M	15	2	B	4	+	+	+	+	+	+	+	+	−	−	−	−
5	F	19	0	B	0	−	+	−	+	−	+	−	+	−	−	−	−
6	M	23	5	C	6	+	+	+	+	+	+	+	+	+	+	+	+
7	F	25	4–5	B	6	+	+	+	+	+	+	+	+	+	+	+	+
8	M	28	0	B	6	+	+	+	+	+	+	+	+	+	+	+	+
9	M	29	5	D	6	+	−	+	−	+	−	+	−	+	−	+	−
10	F	29	3	D	4	+	−	+	−	+	−	+	−	−	−	−	−
11	F	33	4	C	6	+	+	+	+	+	+	+	+	+	+	+	−
12	F	36	0	C	4	+	+	+	−	+	−	−	+	+	+	−	−
13	F	36	5	C	6	+	+	+	+	+	+	+	+	+	+	+	+
14	F	41	2–3	C	5	+	+	+	−	+	−	+	+	+	−	−	−
15	M	42	4	D	6	+	−	+	−	+	+	+	+	+	+	+	+
16	M	43	4	D	4	+	−	+	−	+	+	+	+	−	−	−	−
17	F	45	3	B	5	+	+	+	+	+	+	+	+	+	+	−	−
18	F	48	4	B	2	+	+	+	+	−	+	−	−	−	−	−	−
19	M	54	3	B	3	+	+	+	+	+	−	−	+	−	+	−	−
20	M	52	0	B	2	+	+	+	+	−	−	−	−	−	−	−	−
21	M	55	5	D	6	+	−	+	−	+	−	+	−	+	−	+	−
22	M	65	3	C	3	+	−	+	+	+	+	−	+	−	+	−	−
23	M	70	4	C	3	+	−	+	−	+	+	−	+	−	−	−	−

Note.—Radiographic stage assessed by criteria in Table 1. MS = ^{99m}Tc sulfur colloid; profile A = normal bone marrow scan (not observed in any Gaucher's disease patient); B = uniform peripheral expansion; C = nonuniform pattern; D = almost total absence of uptake; + = positive finding, − = negative finding (see text for details).

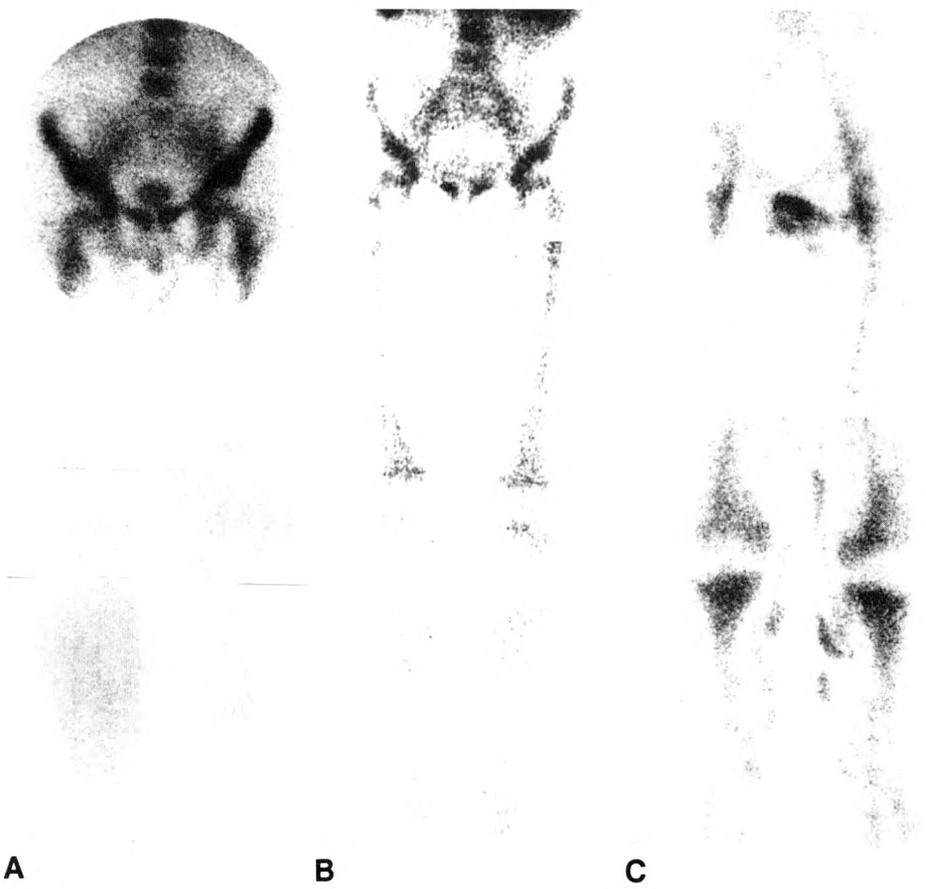


Fig. 3.—^{99m}Tc SC marrow scans from representative normal person (*A*) and Gaucher's disease patients (*B, C*). Profile B has uniform marrow expansion to distal femora (*B*). Profile C has nonuniform marrow expansion (see Fig. 2B). Profile D has total lack of marrow uptake or, as shown in *C*, residual marrow uptake near knees, but lack of pelvic and other lower-extremity marrow uptake, with persistence of ^{99m}Tc sulfur colloid in vessels.

attenuation coefficient of normal bone marrow [9], abnormally high intramedullary attenuation coefficients were observed in the marrow of the Gaucher's patients. For example, in 10 cases, the entire length of femur and tibia had positive attenuation coefficients (score = 6), while four cases had positive values throughout the femur and in only the proximal third of the tibia (score = 4). The density measurements of the marrow in these patients varied in degree and extent, usually ranging from +15 to +80 H. However, in areas of previous infarction, the attenuation coefficients attained values up to +200 H (Fig. 2A).

Three of the four patients (Table 2) with normal radiographs had CT evidence of Gaucher's marrow involvement in the lower extremity. Only one patient (case 5) had normal CT scan and radiographic findings.

^{99m}Tc SC Marrow Scintigraphy

The ^{99m}Tc SC images were obtained to evaluate the distribution of reticuloendothelial cells in the bone marrow. Images were classified as positive or negative, depending on the uptake of sulfur colloid in the region of interest. The normal scan (Fig. 3A), which had uptake only in the proximal femur (profile A), was not observed. The images showed three profiles of increasingly abnormal uptake patterns (Table 2). Profile B (Fig. 3B), observed in 10 patients, was a pattern of bone marrow expansion with a uniformly dense uptake. In some patients, peripheral bone-marrow expansion was extensive and involved the feet. Profile C (Fig. 2B), observed in seven patients, was a pattern of bone-marrow expansion that was mixed in distribution and density; that is, areas of uptake were flanked by regions without uptake. Profile D (Fig. 3C), observed in six patients, showed almost total absence of ^{99m}Tc SC uptake by the marrow, or isolated uptake in the midshaft of the femur or tibia. In four of these patients, the radionuclide was retained primarily in the vascular pool with concomitant extra uptake of marrow-reticuloendothelial cells in lymph nodes, lungs, liver, and spleen (Fig. 3C). Because all patients had normal ECGs, echocardiographs, and ejection fractions, the vascular pattern was attributed to severely compromised marrow-reticuloendothelial function rather than slow circulation times.

Correlation of CT and ^{99m}Tc SC Scans

The results of both the CT and ^{99m}Tc SC scans were required to describe completely the degree of involvement (see Table 2). For example, cases 4, 5, and 18 had extension

of bone-marrow activity throughout the femur (profile B). However, their CT scans indicated normal measurements in case 5, while cases 4 and 18 had abnormal density extending to the midfemur and proximal tibia, respectively, demonstrating that the marrow was more extensively involved although the reticuloendothelial function was still intact.

In addition, CT for cases 1 and 13 showed involvement of the entire lower extremity. Case 1 had no marrow uptake on the ^{99m}Tc SC scans (profile D), while case 13 had nonuniform uptake of the imaging agent throughout the extremity (profile C). Different patterns of bone-marrow uptake activity had been assessed as identical degrees of involvement by CT density measurements.

Correlation of CT and ^{99m}Tc SC Scans with Bone Radiographs

The degree of radiographic abnormality, scored by the criteria in Table 1, was correlated with the severity of bone-marrow disease determined by the CT and ^{99m}Tc SC scans. However, scanning procedures provided greater sensitivity to the extent of bone involvement within and among the different radiographic stages (Table 2). Only in case 18 did the radiographic score contradict the severity assessed by the CT and ^{99m}Tc SC scans. The radiographic abnormalities in this patient were confined to destruction of femoral heads and acetabuli; these abnormalities may have been related to aseptic necrosis induced by high-dose prednisone therapy for thrombocytopenia several years earlier.

^{99m}Tc MDP Bone Scintigraphy

The ^{99m}Tc MDP bone images in the Gaucher's patients were variable, and the pattern of uptake did not indicate the severity of bony involvement assessed by CT and ^{99m}Tc SC scans. Although some scans showed regional defects (e.g., ischemic infarction) in particular patients, we observed no discernible patterns that permitted development of a scoring system for the degree of involvement (Fig. 2C). Fifteen patients had abnormal ^{99m}Tc MDP bone scans, and eight had normal studies. In one patient (case 22), Paget's disease was observed in the right hip. In the 15 abnormal scans, the regional defects also appeared on conventional radiographs.

Discussion

Most patients with type I Gaucher's disease present clinical or radiographic evidence of infiltrative bone disease. To develop more sensitive methods for evaluating presence, extent, and severity of the bony involvement, we compared the ^{99m}Tc MDP, ^{99m}Tc SC, and CT scans, as well as conventional radiographic studies, of 23 patients. We found that the combined CT and ^{99m}Tc SC scans provided more subtle graduations of skeletal involvement and suggested a hypothesis of sequential progression of bone disease in Gaucher's disease.

The classification system was developed independently of the radiographic scheme and provided greater delineation of bone-disease severity within each radiographic group. CT and ^{99m}Tc scans showed that some patients with minimal-to-moderate radiographic evidence of bone disease actually had extensive abnormalities (case 14). Even for patients in radiographic classes 4 and 5, with severe bone disease, the CT and ^{99m}Tc SC scans indicated at least four separate patterns of involvement. Several patients with normal radiographic studies were found to have obvious involvement when evaluated by CT.

Although both CT and ^{99m}Tc SC were required for most effective evaluation of bone involvement, each scan provided specific information. The CT scans were useful in assessing specific skeletal regions, as well as in delineating the extent of the bone-marrow disease. For example, evaluation of nine hips in eight patients before prosthetic hip replacement provided the opportunity to correlate the CT scan results with gross marrow disease. In seven of the femora, the transition from positive to negative attenuation coefficients by CT scan correlated with the juncture between overtly abnormal bone marrow and grossly normal-appearing bone marrow. In the two other patients, entire femoral marrows were involved on CT and by anatomic inspection. This information has proved useful for tailoring prosthetic implants for these patients to enhance the durability of their reconstructed hips. Thus, patients undergoing prosthetic hip replacements should have pelvic and femoral CT scans to determine the extent of involvement in the supraacetabular area and femoral shaft.

The ^{99m}Tc SC scans provided assessments of regional and total bony involvement of the disease process. The extent of marrow involvement correlated directly with the radiographic and clinical severity of the bony disease (i.e., peripheral marrow extension alone was associated with minimal-to-mild radiographic and clinical bone disease, while increasing loss, whether discrete or generalized, of nuclide uptake by peripheral marrow was related directly to more extensive bone disease). The most severely involved patients showed an almost total absence of ^{99m}Tc SC uptake. The CT scan provided further classification of the degree of involvement in these patients. ^{99m}Tc SC scan images may be most useful if baseline data is available, preferably from studies performed early in life, before development of significant bone involvement. Sequential ^{99m}Tc SC images presumably should demonstrate the progressive rate of bone-marrow involvement, particularly in presymptomatic patients, and may provide a basis for estimating the rate of progression. ^{99m}Tc MDP scans provided little additional information about the general extent of bony involvement compared to routine radiographs, except for the investigation of bone pain and possible avascular necrosis.

The exact pathophysiologic events that cause the patterns observed on CT and ^{99m}Tc SC scans have not been explained, but it is tempting to speculate on correlation between the degree of scan abnormalities and the natural history of bone involvement in Gaucher's disease. The progressive infiltration and replacement of normal marrow elements by Gaucher cells result in an increased reticulum (surrounding individual Gaucher cells) that acts as a space-occupying lesion, leading

to vascular compromise and increased intramedullary pressure followed by marrow necrosis and fibrosis [11, 12].

The profiles observed with ^{99m}Tc SC corresponded to increasing levels of disease. Profile A (normal) may represent with an early stage of marrow infiltration by small numbers of Gaucher cells. Profile B suggests an increased Gaucher-cell mass coincident with greater ^{99m}Tc SC uptake in the marrow space. Presumably, the marrow expansion represents a compensatory response to increased marrow infiltration by Gaucher cells or a secondary effect of hypersplenism. Accordingly, profile C may correspond to development of patchy necrotic or fibrotic lesions with insufficient viable Gaucher cells to produce a uniformly dense pattern of ^{99m}Tc SC uptake. Finally, profile D presumably results from pathologic events that preclude uptake of ^{99m}Tc SC in viable marrow-reticuloendothelial cells, such as infarction, necrosis, or decreased blood flow due to increased intramedullary pressure.

This sequence of events is indicated by the increasingly positive CT attenuation coefficients of the medullary space. Because Gaucher cells are glycosphingolipid-laden macrophages, marrow filled with these cells should have the negative attenuation coefficient characteristic of lipid [10, 13]. Their positive coefficients suggested intramedullary fibrotic or calcification processes secondary to destructive events or in reaction to abnormally functioning macrophages (Gaucher cells) [13, 14]. Furthermore, the positive CT attenuation coefficients that appeared after the expansion of marrow observed by ^{99m}Tc SC scan was consistent with the time required for developing secondary pathologic changes.

Although these correlations are speculative, they suggest that the bone involvement occurs in a predictable sequence. Initially, both the marrow expansion and the subsequent loss of ^{99m}Tc SC uptake begin proximally and spread distally, as do the areas with positive CT attenuation coefficients. The oldest affected areas become most severely involved first, a process that may partly explain why the hips are the most common and usually the most severely involved joints. In view of this sequence of progressive disease, it might be anticipated that the severity of the bone disease would be related to age.

However, no strict relationship between age and bone severity (or any other manifestation) has been observed in this series or others [12, 15]. Generally progressive severity of the bone disease was suggested in our patients between the ages of 19 and 43 years old. However, the variability within families (cases 4 and 20, son and father) and among families presumably results from the genetic (allelic) heterogeneity in this disease [16, 17]. Clearly, longitudinal studies (biochemical, clinical, and genetic) in a well-defined population of type 1 Gaucher's disease patients will be required to establish the precise relationship of the scanning abnormalities and the progression of the bony disease. Thus, the use of CT and scintigraphy might provide useful information for monitoring the sequential progression of bone disease and for choosing the most effective orthopedic intervention.

ACKNOWLEDGMENTS

We wish to thank Linda Lugo, Evelyn Pineiro, and Linda Huntley for preparation of this manuscript.

REFERENCES

1. Patrick DA. A deficiency of glucocerebrosidase in Gaucher's disease. *Biochem J* **1965**;97:17C–18C
2. Brady RO, Kanfer JN, Shapiro D. Metabolism of glucocerebrosides II. Evidence of an enzymatic deficiency in Gaucher's disease. *Biochem Biophys Res Commun* **1964**;18:221–225
3. Desnick RJ, Gatt S, Grabowski GA, eds. *Gaucher disease: a century of delineation and research.* New York: Alan R. Liss, **1982**
4. Fredrickson DS, Sloan HR. Glucosyle ceramide lipidoses: Gaucher's disease. In: Stanbury JB, Wyngaarden JB, Frederickson DS, eds. *The metabolic basis of inherited disease.* 3rd ed. New York: McGraw-Hill, **1972**:730–759
5. Siffert RS, Platt A. Gaucher disease: orthopedic considerations. In: Desnick RJ, Gatt S, Grabowski GA, eds. *Gaucher disease: a century of delineation and research.* New York: Alan R. Liss, **1982**:617–624
6. Goldblatt J, Sachs S, Beighton P. The orthopaedic aspects of Gaucher disease. *Clin Orthop* **1978**;137:208–214
7. Desnick RJ. Gaucher disease: A century of delineation and understanding. In: Desnick RJ, Gatt S, Grabowski GA, eds. *Gaucher disease: a century of delineation and research.* New York: Alan R. Liss; **1982**:1–30
8. Chang TH, Holman BL. Radionuclide assessment of Gaucher's disease. *J Nucl Med* **1978**;19:1333–1336
9. Hermann G, Rose JS. Computed tomography in bone and soft tissue pathology of the extremities. *J Comput Assist Tomogr* **1979**;3:58–66
10. Hermann G, Rose JS, Strauss L. Tumor infiltration of the bone marrow. Comparative study using computed tomography. *Skeletal Radiol* **1984**;11:17–21
11. Lee R. Pathology of Gaucher disease. In: Desnick RJ, Gatt S, Grabowski GA, eds. *Gaucher disease: a century of delineation and research.* Alan R. Liss, **1982**:177–217
12. Lee RE, Peters SP, Glew RH. Gauchers's disease: clinical, morphologic and pathologic considerations. In: Sommers SC, ed. *Pathology annual*, vol. 12, part 2. E. Norwalk, CT: Appleton-Century-Crofts **1977**:309
13. Hermann G, Yeh H-C, Schwartz I. Computed tomography of soft tissue lesions of the extremities, pelvic and shoulder girdles: sonographic and pathologic correlations. *Clin Radiol* **1984**;35(3):193–292
14. Gery I, Zigler S Jr, Brady RO, Barranger JA. Selective effects of glucosylceramide (Gaucher's storage material) on macrophage cultures. *J Clin Invest* **1981**;68:1182–1189
15. Noyes FR, Smith WS. Bone crises and chronic osteomyelitis in Gaucher's disease. *Clin Orthop* **1971**;79:132–140
16. Grabowski GA, Goldblatt J, Dinur T, et al. Genetic heterogeneity in Gaucher disease: physicokinetic and immunologic studies of the residual enzyme in cultured fibroblasts from non-neuropathic neuropathic patients. *Am J Med Genet* **1985**;21:529–550
17. Grabowski GA, Dinur T, Osiecki KM, Kruse J, Legler G, Gatt S. Gaucher disease types 1, 2 and 3: differential mutations of the acid B-glucosidase active site identified with conduritol B epoxide derivates and sphingosine. *Am J Hum Genet* **1985**;37:499–510

MR Imaging of Renal Transplants

Bruce R. Baumgartner[1]
Rendon C. Nelson[1]
Turner I. Ball[1]
J. Brad Wyly[1]
Edmund Bourke[2]
Veronica Delaney[2]
Michael E. Bernardino[1]

Fifty-six MR studies were obtained in 32 renal transplant patients, by using T1-weighted, spin-echo, and inversion-recovery pulse sequences. The findings, particularly the loss of corticomedullary differentiation, and the extent of vascular penetration into the renal parenchyma, were compared with the clinical and histologic diagnosis of transplant rejection. Thirteen MR studies on 11 patients with clinically normal renal transplants demonstrated normal corticomedullary differentiation. Renal vessels extended into the parenchyma in all 11 patients and to the cortex in 38%. In 37 MR studies on 22 patients with a clinical or histologic diagnosis of acute and/or chronic transplant rejection, the corticomedullary differentiation was normal in 8%, faint in 24%, and absent in 68%. Renal parenchymal vessels were visualized in 32%, but extended to the level of the cortex in only 8%. In 68% of the studies with transplant rejection, no parenchymal vessels were seen. When the corticomedullary differentiation was either faint or absent, the vascular pattern was normal in 6%; in 68% of cases no parenchymal vessels could be identified. We conclude the corticomedullary differentiation and the renal vascular pattern are useful parameters in the evaluation of renal transplant rejection.

Investigators have emphasized the ability of MR to distinguish the renal cortex from the medulla in normal kidneys [1–8]. This corticomedullary differentiation has been reported absent in several pathophysiologic states, including chronic renal insufficiency, obstructive hydronephrosis, dehydration, and renal transplant rejection. Thus, early studies with MR have suggested its usefulness in the evaluation of renal transplants [2–7]. In addition, the extent of vascular penetration into the renal parenchyma can be determined with MR because of the absence of signal from flowing blood. We attempted to evaluate the MR findings in renal transplant patients and to correlate these findings, especially the loss of corticomedullary differentiation and the penetration of vessels into renal parenchyma, with the clinical and histologic diagnosis of transplant rejection.

Materials and Methods

Fifty-six consecutive MR examinations were obtained in 32 renal transplant patients over a 7-month period. The 18 men and 14 women ranged in age from 3 to 57 years. Twenty-three patients had cadaver transplants; nine had living related donors. All MR studies were performed with a 1.5-T superconductive magnet (Philips Gyroscan) operating at 0.5 T. Thirty examinations used various surface coils placed directly over the transplanted kidney, while 22 examinations were performed with the system body coil. In four, both coils were used. The transplanted kidneys were initially located with a single transverse image by using a spin-echo (SE) pulse sequence with echo time (TE) of 30 msec and repetition time (TR) of 250 msec. Coronal images were then obtained with either SE or combined SE and inversion-recovery (IR) techniques. The SE sequence of TE 30 and TR 500 was used with four measurements, 256 × 256 acquisition, 5- to 10-mm slice thickness, and 2- to 5-mm slice spacing for the surface-coil studies, with either single-slice or three multislice images. When the body coil was used alone, the three multislice images were obtained with the same

Received January 13, 1986; accepted after revision May 30, 1986.

[1]Department of Radiology, Emory University School of Medicine, Atlanta, GA 30322. Address reprint requests to B. R. Baumgartner.

[2]Department of Medicine (Nephrology), Emory University School of Medicine, Atlanta, GA 30322.

AJR 147:949–953, November 1986
0361–803X/86/1475–0949
© American Roentgen Ray Society

parameters, followed by eight multislice coronal or axial images at TE 30 and TR 700, with 10-mm slice thickness and a gap of 2–5 mm between slices. All the studies had SE images; 22 examinations also included the IR technique. The IR pulse sequence of TE 30, TI 400, and TR 1600 was used with both surface and body coils; single or three multislice coronal images were obtained.

All MR images of the renal transplants were examined for kidney appearance with particular attention to corticomedullary differentiation and to the renal vascular pattern. The corticomedullary differentiation was classified as good, faint, or absent. The renal vessels were graded according to visibility within the parenchyma: grade-3 vessels extended to the cortex, grade-2 vessels extended into the renal parenchyma but did not reach the cortex, grade-1 vessels were limited to the renal sinus, and grade-0 vessels could not be identified within either the renal parenchyma or sinus (Fig. 1). The images from each MR examination were evaluated as a group.

Attention was also given to the presence of perinephric fluid collections and hydronephrosis. The findings of the MR examinations were compared with the clinical data, including laboratory tests and radiographic studies (renal sonograms, radionuclide renograms, angiograms, and nephrostograms). Pathologic specimens were available for correlation with 23 (41%) of 56 MR studies, either by kidney biopsy (21) or transplant nephrectomy (2), and provided histologic data for 20 (63%) of 32 patients. Thirteen biopsies were performed within 7 days of the MR imaging, and four were done 8–17 days after the examination. Six patients with normal MR and clinical studies had no biopsy, nor did three others who had ureteral obstruction or renal-artery stenosis. The remaining three patients with clinical evidence of rejection had no biopsy.

Results

Thirteen studies were performed on 11 patients who were determined by clinical and laboratory data to have normally functioning renal transplants. In all 13 studies, the corticomedullary differentiation was normal. Vessels could be identified within the renal parenchyma in all the studies, and in five (38%) the vessels extended to the cortex (Fig. 2). Nine exams (69%) were obtained within 14 days of transplantation. The other four exams ranged from 1 to 11 months after transplantation. Only four of the 11 patients (36%) received kidneys from living related donors. One patient was found to have clinical and laboratory evidence of cyclosporin toxicity; he had normal corticomedullary differentiation and a grade-2 vascular pattern.

Thirty-seven studies were performed on 22 patients with a clinical or histological diagnosis of transplant rejection. Five exams (14%) were obtained within 14 days of surgery, while the remaining 32 studies were performed from 3 weeks to 9 years after transplantation. Three studies (8%) demonstrated normal corticomedullary differentiation. A biopsy was obtained on all three of these patients; however, only one of the biopsies was performed within 7 days of MR imaging. Nine studies (24%) on seven patients demonstrated a poor or faint corticomedullary differentiation (Fig. 3). Twenty-five studies (68%) on 17 patients demonstrated no corticomedullary differentiation.

Only three (8%) of the 37 studies performed on rejected transplants demonstrated grade-3 vessels. Two of the three were histologically confirmed by a biopsy obtained within 7 days of the MR. Nine studies (24%) revealed grade-2 vessels, and in 18 studies (49%), grade-1 vessels could be identified. No vessels (grade 0) could be visualized within either the renal parenchyma or sinus on seven studies (19%) in six patients. Thus, parenchymal vessels were absent in 68% of the rejected kidneys. Of the 22 patients with transplant rejection, 19 (86%) cases were confirmed by biopsy or transplant nephrectomy.

In addition to the evaluation of corticomedullary differentiation and renal vascular pattern on MR scans, other causes of transplant dysfunction were sought, such as hydronephrosis and perinephric fluid collections. Hydronephrosis was noted on 10 MR studies in seven patients. Two of these patients,



Fig. 1.—Grading the vascular pattern in two renal transplants; coronal images SE 30/700.
***A*, Grade 3: vessels extending to cortex. Note normal corticomedullary differentiation.**
***B*, Grade 1: vessels seen only in region of renal hilum. Note absent corticomedullary differentiation.**

Fig. 2.—15-year-old boy several days after transplantation with normally functioning kidney. Surface-coil SE 30/500 coronal image clearly demonstrates normal corticomedullary differentiation and vessels (*arrow*) extending to cortex (grade 3).

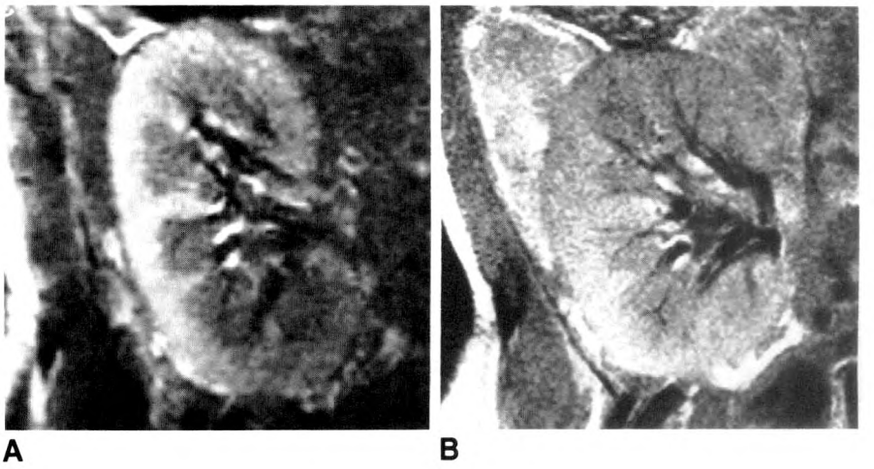


Fig. 3.—*A*, 11-year-old girl 1 day after kidney transplantation. Coronal SE 30/500 surface-coil images show clear corticomedullary differentiation and normal intrarenal vessels.

***B*, Two weeks after transplantation. Coronal SE 30/500 image now reveals enlarged, globular kidney with faint corticomedullary differentiation. Although vessels can be seen through medulla, they appear compressed peripherally when compared with previous study.**

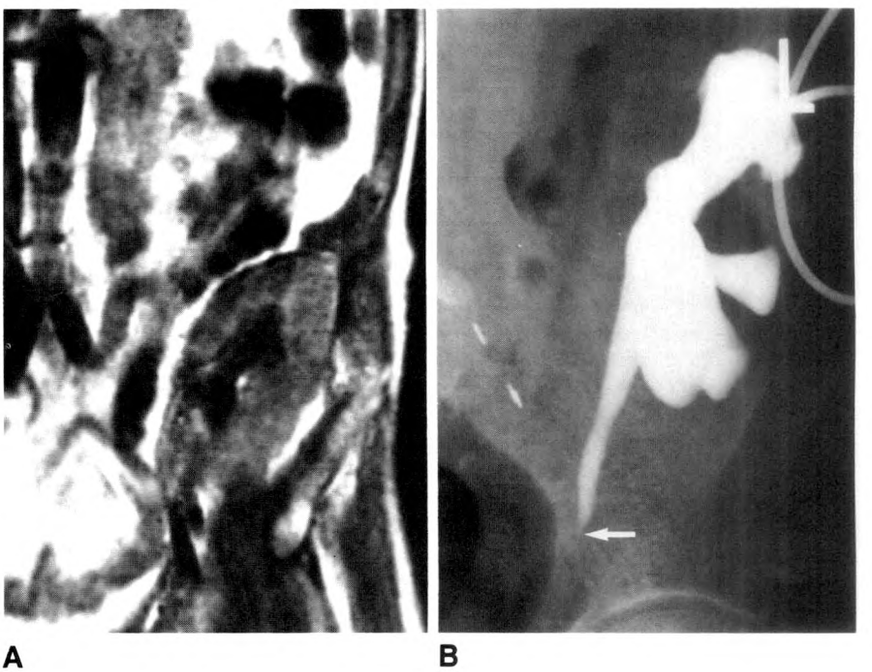


Fig. 4.—*A*, Coronal, body-coil SE 30/700 images demonstrate no corticomedullary differentiation with hydronephrosis in renal transplant.

***B*, After percutaneous nephrostomy 3 days later, contrast study confirms hydronephrosis and reveals obstructed ureter (*arrow*). Continued drainage and subsequent balloon dilation of stricture resulted in return of serum creatinine to normal level.**

each with two MR scans, had ureteral obstruction and subsequent decrease in serum creatinine after percutaneous nephrostomy (Fig. 4). Four patients had biopsy-proven rejection as well as hydronephrosis. The other patient had mild hydronephrosis and renal-artery stenosis with resolution of renal insufficiency after angioplasty. One patient had biopsy-proven acute tubular necrosis without evidence of rejection. In all cases of hydronephrosis, renal-artery stenosis, or acute tubular necrosis, the corticomedullary differentiation was either faint or absent and the renal vessels were negligible. Perinephric fluid collections (Fig. 5), including hematoma, abscess, and lymphocele, were detected on 10 MR scans in five patients.

Discussion

Several authors have reported the value of MR in delineation of renal anatomy as well as of medical and surgical diseases that may affect the kidney [1–3, 8]. Of particular interest has been the role of MR in renal transplants. The ability of MR to distinguish the renal cortex from the medulla in normal kidneys has been emphasized by several investigators [2–7]. The cortex has higher signal intensity than the medulla but lower intensity than the perirenal or renal-sinus fat on T1-weighted images. MR scans with short TE and TR readily delineate corticomedullary differentiation in normal kidneys without iodine or other contrast agents.

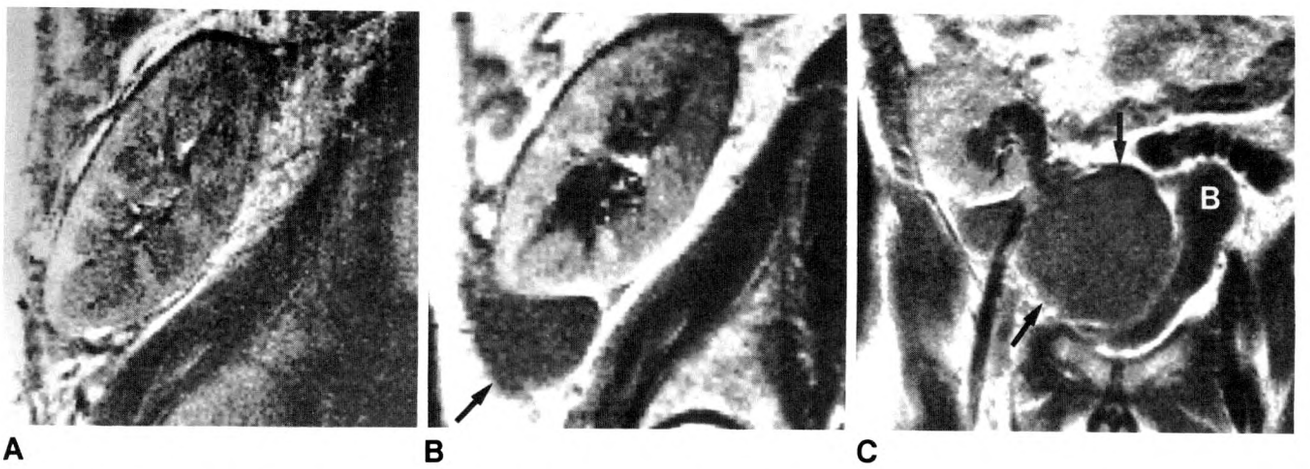


Fig. 5.—*A*, 32-year-old man 1 week after transplantaton. Surface-coil SE 30/500 image of normally functioning kidney shows clear corticomedullary differentiation.

B, Same patient 2 months after transplantation. Body-coil, SE 30/700, long-axis coronal image reveals loss of corticomedullary differentiation, mild hydronephrosis, and a small, low-signal-intensity, perinephric fluid collection (*arrow*) adjacent to lower pole.

C, Straight, coronal, body-coil, SE 30/700 image at same time as *B* shows another, larger perinephric fluid collection (*arrows*) displacing bladder (B) to left.

In the evaluation of renal transplants for corticomedullary differentiation, we noted various patterns in the penetration of vessels into the renal parenchyma. Changes in the vascular pattern could be expected because of vascular compression by renal edema or a distended collecting system. Also, in certain types of rejection, vascular destruction would decrease the number of vessels and their renal penetration.

The MR studies in patients with normally functioning transplants all demonstrated normal corticomedullary differentiation and either grade-2 or grade-3 vessels. None of these patients was biopsied, but the combination of these findings strongly suggests that rejection is not present.

Of the 37 studies in the 22 patients with a clinical or histologic diagnosis of transplant rejection, corticomedullary differentiation was faint or absent in 34 (92%). Of the three patients with normal corticomedullary differentiation, only one demonstrated grade-3 vessels. This patient's biopsy several months before MR was consistent with chronic rejection, and his clinical and laboratory data in the interim supported that diagnosis. Another patient with normal corticomedullary differentiation, grade-1 vessels, and biopsy of rejection had an additional MR scan 5 days later that revealed loss of corticomedullary differentiation. The first study may have been obtained too early to detect the changes of rejection. Thus, there may be a critical threshold of cellular or interstitial changes needed before MR detects corticomedullary differentiation loss—perhaps at 72–96 hr; however, in one patient this loss occurred less than 48 hr after transplantation [9]. The third patient with normal corticomedullary differentiation had grade-0 vessels; biopsy 17 days after MR demonstrated rejection. A repeat MR scan 4 months later showed no corticomedullary differentiation and grade-0 vessels. Two other patients with rejection and grade-3 vessels demonstrated either faint or absent corticomedullary differentiation. In the 34 studies with rejection and faint or absent corticomedullary differentiation, grade-1 or grade-0 vascular pattern was present in 23 (68%). Therefore, combining the findings of both corticomedullary differentiation and the renal vascular pattern should increase the sensitivity of the MR diagnosis of transplant rejection.

Geisinger et al. [4] described variable MR appearance of corticomedullary differentiation in transplants with acute tubular necrosis, while other reports [2, 3] have described preservation of corticomedullary differentiation. In our single patient with biopsy-proven acute tubular necrosis, MR showed poor corticomedullary differentiation and grade-1 vessels. Renal-artery stenosis and ureteral obstruction with hydronephrosis have been associated with absent corticomedullary differentiation [1, 2]. Those cases in our study also had grade-1 or grade-0 vessels.

MR detection of hydronephrosis or perinephric fluid collections was similar to the results of sonography in the same renal transplant patients. If surface coils are used, the study should also include body-coil images for better evaluation of the pelvic region around the kidney transplant and bladder. Confirming these conditions was significant in the overall care of the patients; two patients with poor or no corticomedullary differentiation and hydronephrosis had ureteral obstruction requiring intervention that led to improvement in renal function. Three of the five perinephric fluid collections detected by MR also required percutaneous or surgical drainage as part of the patients' care.

The results of this study indicate an important role for MR in evaluation of renal transplant patients. MR is now being used as an imaging tool for evaluation of transplant rejection by the nephrologists in our hospital. We have found a strong correlation of normal corticomedullary differentiation and grade-2 or grade-3 vascular pattern by MR with the presence of a normal transplant. Faint or absent corticomedullary differentiation and grade-0 and grade-1 vessels are seen more

frequently in transplant rejection. The combination of the latter findings in the absence of hydronephrosis or renal-artery stenosis strongly points to rejection. The value of MR in the differentiation of rejection from acute tubular necrosis and cyclosporin toxicity needs continued investigation.

REFERENCES

1. Hricak H, Crooks L, Sheldon P, Kaufman L. Nuclear magnetic resonance imaging of the kidney. *Radiology* **1983**;146:425–432
2. Leung AW-L, Bydder GM, Steinber RE, Bryant DJ, Young DR. Magnetic resonance imaging of the kidneys. *AJR* **1984**;143:1215–1227
3. Lipuma JP. Magnetic resonance imaging of the kidney. *Radiol Clin North Am* **1984**;22:925–941
4. Geisinger MA, Risius B, Jordan ML, Zelch MG, Novick AC, George CR. Magnetic resonance imaging of renal transplants. *AJR* **1984**;143:1229–1234
5. Lipuma JP, Bryan PJ, Butler HE, D'Andrea DC, Miraldi FD, Hau T. *Renal transplant MRI: a prospective study.* Presented at the scientific assembly and annual meeting of the Radiological Society of North America, Washington, DC, November **1984**
6. Hricak H, Peduska N, Terrier F, Vincenti F. *The potential of MR imaging in post-transplant renal failure.* Presented at the scientific assembly and annual meeting of the Radiological Society of North America, Washington, DC, November **1984**
7. Lipuma JP, Bryan PJ, Cohen AM, et al. *Renal transplant NMR.* Presented at the scientific assembly and annual meeting of the Radiological Society of North America, Chicago, IL, November **1983**
8. Hricak H, Newhouse JH. MR Imaging of the kidney. *Radiol Clin North Am* **1984**;22:287–296
9. Rholl KS, Lee JKT, Ling D, Sicard G, Griffith R. *Differentiation of acute renal rejection and acute tubular necrosis: MR demonstration.* Presented at the scientific assembly and annual meeting of the Radiological Society of North America, Washington, DC, November **1984**

The reader's attention is directed to the Commentary on this article, which appears on the following pages.

Commentary

Differential Diagnosis of Renal Transplant Rejection: Is MR Imaging the Answer?

Nicholas A. Halasz[1]

New immunosuppressive regimens that use cyclosporine and steroids, with or without antilymphocyte globulin preparations, have improved the results of kidney (and other organ) transplants dramatically. However, they have added to the difficulty of monitoring the posttransplantation course of patients. Until the advent of cyclosporine, when a kidney malfunctioned after transplantation, the malfunction could be attributed to two main causes: (1) harvesting or preservational injury (acute tubular necrosis) (ATN) or (2) allograft rejection. Even though vascular or ureteral obstruction occasionally contributed to malfunction, it occurred infrequently and was usually identifiable. Cyclosporine, however, has changed this situation significantly, in two distinct ways. First and most commonly, it depresses established renal function because of its nephrotoxicity. Secondly, if can cause—probably also because of its nephrotoxicity—an occasional ATN-like syndrome that primarily affects marginally preserved organs.

Now the clinical differentiation of the various causes of dysfunction ceases to be easy, and help is needed to resolve the dilemma in differential diagnosis. Invasive though they are, biopsies are now commonly used to differentiate the two most confusing entities, cyclosporine toxicity and graft rejection. When MR imaging was first reported to make this distinction easily, the hopes of many transplant surgeons were raised. It seems to this reader of the accompanying paper by Baumgartner et al. [1], that while MR will help, it will not be THE answer. The authors, themselves, point to 8% false negatives and 24% intermediate results in a study with unblinded observers and with only a loose temporal correlation between the MR studies and biopsies.

Imaging techniques for evaluating renal allografts fall into two major groups: dynamic or static. MR and CT are in the latter category; scintigraphic flow and hippuran studies, on the other hand, are dynamic and potentially quantitative. Sonography overlaps both and can also be quantitative when used to guide duplex scanning. Angiography can similarly be considered both dynamic and static. It has the advantage of having the ability to magnify for a look at fine vessels, but it also has the disadvantage of damaging renal function owing to the amount of contrast material required.

We need a key procedure to follow kidney allografts. Currently, nuclear medicine studies (DTPA and I^{131}-hippuran) seem to retain this role: They are dynamic and functional studies that look at blood flow as well as glomerular and tubular function, give a fair assessment of the patency of the drainage system, and permit monitoring the status of the kidney during acute tubular necrosis, when rejections are most difficult to recognize. The studies are also more accessible and less expensive than MR. Sonography is clearly the ideal technique for recognizing urinary obstruction, but it is closely matched by scintigraphy or MR. A new and potentially exciting application of sonography is evolving. Duplex sonography is being applied to the main renal artery as well as to its intraparenchymal branches, and by analysis of Doppler wave forms can provide semiquantitative information about blood flow and intrarenal impedance. These techniques have

Received June 30, 1986; accepted after revision July 2, 1986.

[1] Director, Transplantation Program, Department of Surgery, University of California, San Diego, School of Medicine, UCSD Medical Center, 225 Dickinson St., San Diego, CA 92103. Address reprint requests to N. A. Halasz.

AJR 147:954–955, November 1986 0361–803X/86/1475–0954 © American Roentgen Ray Society

shown promising correlation with graft rejection in early studies [2, 3]. Sonography also identifies fluid collections and extravasations most economically, another task that MR performs well, but that nuclear medicine studies do poorly.

In addition to the need to distinguish cyclosporine toxicity from rejection, there is an even greater need. Graft rejection is not an all-or-nothing process. Instead it is a crescendo attack by the body, and as such, the earlier it is recognized and treated, the more effectively it can be reversed with the least permanent injury to the kidney. The key to exploiting this situation is early recognition: Graft rejection should be identified early—before it becomes clinically evident or obvious—and at this time we lack imaging, immunologic, or other techniques to accomplish this. MR is not the answer. Better blood-flow measurement techniques, more sophisticated functional studies and quantification of changes by scintigraphy, and recognition of metabolic changes identifiable by spectroscopic MR techniques are a few of the radiologic methods that should be explored to achieve this goal.

REFERENCES

1. Baumgartner BR, Nelson RC, Ball TI, et al. MR imaging of renal transplants. *AJR* **1986**;147:949–953
2. Berland LL, Lawson TL, Adams MB, Melrose BL, Foley WD. Evaluation of renal transplants with pulsed Doppler duplex sonography. *J Ultrasound Med* **1982**;1:215–222
3. Rigsby CM, Taylor KJW, Weltin G, et al. Renal allographs in acute rejection: evaluation using duplex sonography. *Radiology* **1986**;158:375–378

Forthcoming Articles

SPECIAL ARTICLES

Cannon memorial lecture. The impact of radiology on hepatology. *Sherlock S, Dick R*
MR of the liver. *Ferrucci JT*

CARDIOVASCULAR RADIOLOGY

Aortic dissection: a statistical analysis of the usefulness of plain chest radiographic findings. *Jagannath AS, Sos TA, Lockhart SH, Saddekni S, Sniderman KW*
MR of the central pulmonary arterial tree in conotruncal malformation. *Formanek AG, Witcofski RL, D'Souza VJ, Link KM, Karstaedt N*
MR of pulmonary emboli: an experimental study in dogs. *Stein MG, Crues JV III, Bradley WG Jr, et al.*
New cineradiographic methods for assessment of Bjork-Shiley valve integrity. *Cousin AJ, Soto B*

CHEST RADIOLOGY

Rebound thymic hyperplasia after treatment of Cushing's syndrome. *Doppman JL, Oldfield EH, Chrousos GP, et al.*

BREAST RADIOLOGY

Baseline screening mamography: one vs two views per breast. *Sickles EA, Weber WN, Galvin HB, Ominsky SH, Sollitto RA*

ENDOCRINE RADIOLOGY

MR of the thyroid. *Higgins CB, McNamara MT, Fisher MR, Clark OH*

GASTROINTESTINAL RADIOLOGY

Indium-III leukocyte imaging in the diagnosis of acute appendicitis. *Navarro DA, Weber PM, Kang IY, dos Remedios LV, Jasko IA, Sawicki JE*
Hepatic cavernous hemangioma: diagnosis with TC-99m–labeled red cells and SPECT. *Brodsky RI, Friedman AC, Maurer AH, Radecki PD, Caroline DF*
Esophageal intramural pseudodiverticulosis: a reevaluation. *Levine MS, Moolten DN, Herlinger H, Laufer I*
Technical note. Value of flow technique for double-contrast examination of the stomach. *Kikuchi Y, Levine MS, Laufer I, Herlinger H*
Case report. Voice change after barium enema: a sign of extraperitoneal colon perforation. *Rabin DN, Smith C, Witt TR, Holinger LD*
Interventional radiology rounds. Angiographic management of upper gastrointestinal hemorrhage. *Kerlan RK Jr, Pogany AC, Burke DR, Ring EJ*

GENITOURINARY RADIOLOGY

Distal ureteral calculi: diagnosis by transrectal sonography. *Lerner RM, Rubens D*
Simultaneous pancreatic-renal transplant scintigraphy. *Shulkin BL, Dafoe DC, Wahl RL*
Case report. Uterine duplication, unilateral imperforate vagina, and normal kidneys. *Johnson J, Hillman BJ*

PEDIATRIC AND FETAL RADIOLOGY

Patterns of liver injury in childhood: CT analysis. *Stalker HP, Kaufman RA, Towbin R*
Case report. Prenatal sonographic diagnosis of atrial hemangioma. *Leithiser RE Jr, Fyfe D, Weatherby E III, Sade R, Garvin AJ*

NEURORADIOLOGY

Subcortical arteriosclerotic encephalopathy: CT spectrum and pathologic correlation. *Lotz PR, Ballinger WE Jr, Quisling RG*
Head injury: early results of comparing CT and high-field MR. *Zimmerman RA, Bilaniuk LT, Hackney DB, Goldberg HI, Grossman RI*
Gd-DTPA in clinical MR of the brain. 1. Intraaxial lesions. *Brant-Zawadzki M, Berry I, Osaki L, Brasch R, Murovic J, Norman D*
Gd-DTPA in clinical MR of the brain. 2. Extraaxial lesions and normal structures. *Berry I, Brant-Zawadzki M, Osaki L, Brasch R, Murovic J, Newton TH*

INTERVENTIONAL RADIOLOGY

Complications of percutaneous nephrolithotomy. *Lee WJ, Smith AD, Cubelli V, Badlani GH, Lewin B, Vernace F*
Percutaneous drainage of subphrenic abscess: a review of 62 patients. *Mueller PR, Simeone JF, Butch RJ, et al.*
Portable real-time sonography and needle-guidance system in performance of interventional procedures. *McGahan JP, Anderson MW, Walter JP*
Inferior vena caval stent-filter. *Wallace MJ, Ogawa K, Wright K, Carrasco CH, Richli W, Charnsangavej C*
Expandable intrahepatic portocaval shunt stents in dogs with chronic portal hypertension. *Palmaz JC, Garcia F, Sibbitt PR, et al.*

MR

Comparison of the contrast-enhancing properties of albumin-(Gd-DTPA) and Gd-DTPA at 2.0 T. *Schmiedl U, Ogan MD, Moseley ME, Brasch RC*
MR artifacts: a review. *Bellon EM, Haacke EM, Coleman PE, Sacco DC, Steiger DA, Gangarosa RE*
Boundary artifact due to truncation errors in MR. *Lufkin RB, Pusey E, Stark DD, Brown R, Leikind B, Hanafee WN*
Technical note. A new device for exercise MR imaging. *Schaefer S, Peshock RM, Parkey RW, Willerson JT*

MEDICOLEGAL RADIOLOGY

Malpratice and radiologists, update 1986: 11½-year perspective *Berlin L*

MISCELLANEOUS

MR and CT of extrahepatic cavernous hemangiomas. *Levine E, Wetzel LH, Neff JR*
Sonographic localization of hematomas in hemophiliac patients with positive iliopsoas sign. *Graif M, Martinovitz U, Strauss S, Heim M, Itzchak Y*
Case report. Multiple granular cell tumors of the skin and gastrointestinal tract. *Radin DR, Zelner R, Ray MJ, Cohen H, Halls JM*
Tailgut cyst: diagnosis with CT and sonography. *Johnson AR, Ros PR, Hjermstad BM*
Technical note. Double images in plain film radiography: a motion artifact. *Marinelli D, Miller WT*
Communicating the significance of radiologic test results: the concept of likelihood ratio. *Black WC, Armstrong P*

COMPUTER PAGE

Microcomputer-based graphics for radiology. *Taylor GA*

OPINION

Technological volatility and the aging radiologist. *Davidson AJ*

PERSPECTIVES

The American Board of Radiology to consider "Added qualifications." *Rogers LF, Bradd FJ, Kennedy W*
Localized, tissue MR spectroscopy. *Margulis AR, James TL*

Excretory Urography in Patients with Prostatism

Thomas J. Bundrick[1]
P. Gary Katz[2]

The value of performing routine screening excretory urography in patients with prostatism was prospectively evaluated in 180 patients (50 years old or older). All patients had signs and symptoms of prostatism or acute urinary retention, findings of benign prostatic hypertrophy on physical examination, and negative urine cultures. High-risk patients, such as those with hematuria, urinary tract infections, history of bladder tumors, or significant elevation of serum creatinine, were excluded. In four patients (2.2%), findings of excretory urography resulted in an alteration of patient management. Three of these had asymptomatic upper urinary tract malignancies. One had a complicated renal cyst. We conclude that routine screening of patients with prostatism is warranted.

Excretory urography is a common screening procedure in the evaluation of patients with prostatism. Historically, it was used to provide information on bladder disorders, prostate size, renal function, and upper urinary tract disease. Most of this information is now obtained by other techniques. Bladder disorders, prostate size, and degree of obstruction are best evaluated by cystoscopy, cystometry, and measurement of urinary flow rate [1]. Renal function is better evaluated by determining serum creatinine and blood urea nitrogen levels rather than the degree of hydronephrosis [1, 2]. Renal calculi often can be visualized by means of an abdominal radiograph if this information is desired.

On the basis of this background, the appropriateness of screening excretory urography has been challenged [3, 4]. Kumar and Schreiber [3] recommended excretory urography for preprostectomy patients only when there was a history of gross hematuria, urinary calculi, or elevated serum creatinine levels. They suggested that approximately 90% of preprostectomy patients would not need excretory urography if these criteria were used. We performed a prospective study of excretory urography in a group of patients being evaluated for prostatism. Only patients with voiding dysfunction without predetermined clinical and laboratory abnormalities were included. Voiding symptoms included urinary hesitancy, diminished stream, daytime frequency, urgency, and nocturia.

Subjects and Methods

One hundred eighty consecutive patients with the clinical diagnosis of prostatism were prospectively evaluated. Included were all patients 50 years or older (mean age, 65) who had signs and symptoms of prostatism or acute urinary retention, findings of a benign prostate on physical examination, and negative urine cultures. Excluded were patients with history of gross or microscopic (>5 RBC per high-powered field) hematuria, or bladder cancer, clinically significant urethral stricture disease, previous prostate surgery, or serum creatinine concentrations greater than 2 mg/dl.

Patients who fulfilled these criteria underwent excretory urography followed by cystoscopy. Selected patients also underwent cystometry and determination of urinary flow rates. Patients for whom excretory urography revealed an abnormality before cystoscopy or prostate surgery

Received April 3, 1986; accepted after revision June 9, 1986.

[1] Department of Radiology, McGuire Veterans Administration Medical Center, 1201 Broad Rock Blvd., Richmond, VA 23249.

[2] Department of Urology, McGuire Veterans Administration Medical Center, 1201 Broad Rock Blvd., Richmond, VA 23249.

AJR 147:957–959
0361–803X/86/1475–0957
© American Roentgen Ray Society

were included in the study as long as other entry criteria were met.

At the time of the excretory urography, staff radiologists completed data sheets that recorded the excretory urography findings of kidney masses, chronic pyelonephritis, obstruction, congenital defects, ureteral abnormalities, bladder calculi, and renal calculi. Also recorded were significant contrast reactions, including urticaria, angioedema, laryngoedema, bronchospasm, and vascular collapse. A separate data sheet was completed by urology residents and staff. This sheet recorded laboratory and cystoscopy results and whether the excretory urographic resulted in an alteration in clinical management.

Results

Prostatic surgery, usually a transurethral resection of the prostate, was performed on 121 of the 180 patients. The others did not have significant clinical findings warranting surgery, refused surgery, or had findings on excretory urography that required alternative therapy.

Forty-nine (27%) of the 180 patients had upper tract abnormalities incidentally detected by excretory urography (Table 1). Most of the findings were minor and not significant. None of the six cases of hydronephrosis was severe. The renal calculi noted in five patients were small and nonobstructive. In nine patients abnormal findings on the excretory urogram prompted another radiographic examination, which ultimately did not result in an alteration in the patient's management. In three of these nine patients the excretory urogram suggested an abnormality (parapelvic mass, ureteropelvic mass, adrenal mass), but other studies did not confirm the finding. Six of these nine cases were cysts verified by either sonography or CT. One indeterminate mass was not evaluated because the patient died of pulmonary complications before his studies were completed.

The excretory urography findings led to an alteration in management for four patients, including three with malignant tumors and one whose renal cyst was aspirated because it was atypical on both excretory urography and sonography. One patient developed a severe contrast reaction manifested by laryngeal edema, which rapidly responded to subcutaneous epinephrine therapy.

TABLE 1: **Upper Tract Findings in 180 Patients Undergoing Excretory Urography**

Finding	No. of Patients (%)
Congenital abnormalities	
Duplex collecting system	4
Anterior rotation	1
Single kidney	1
Total	6 (3.3)
Miscellaneous	
Chronic pyelonephritis	3
Left renal arterial stenosis	1
Papillary necrosis	1
Total	5 (2.8)
Hydronephrosis	6 (3.3)
Renal calculi	5 (2.8)
False positives	3 (1.7)
Renal mass lesions	
Cysts	20
Hypernephroma	2
Transitional cell cancer	1
Indeterminate mass	1
Total	24 (13.3)

Note.—Numbers in parentheses are percentages of total patient population (180).

Discussion

The entry criteria excluded high-risk patients for whom past studies and experience have proven the value of excretory urography. We evaluated screening excretory urography only in patients who had abnormal voiding patterns. The use of urography in this group of patients has been questioned recently. Most of these studies were retrospective evaluations of patients undergoing prostatectomy, and some patients with prostatism symptoms might have been omitted because their radiographic findings obviated prostatectomy.

Our prospective study included patients with signs and symptoms of prostatism or acute urinary retention. We included patients who had a benign prostate on physical examination, negative urine culture, serum creatinine less than 2 mg/dl, but did not have hematuria, bladder cancer, clinically significant urethral stricture, or history of prostate surgery. The value of screening excretory urography depends on the definition of significance. We chose to describe significant findings as those that could not be obtained by other routine screening tests and that resulted in an alteration of patient management or therapy. On the basis of this definition, only upper urinary tract abnormalities were included because bladder abnormalities are best studied by cystoscopy [2, 5].

Morrison [6], Pinck et al. [7], and Pang et al. [8] favored screening excretory urography. Collectively, they reviewed 841 patients who had undergone prostatectomy. Of these, 16 patients (2%) needed immediate management alterations on the basis of excretory urography findings.

Other authors have not advocated screening excretory urography. In separate retrospective studies of prostatectomy patients, Boerema [9] found, in excretory urography of 125 patients, that none of the results led to alterations in therapy, whereas Christoffersen and Moller [5] found three (2%) of 150 patients with significant findings. In a similar study of 601 postprostectomy patients, Bauer et al. [10] found screening excretory urography unnecessary, but, unfortunately, they did not cite an exact number of significant cases. Ten (1.1%) of 894 patients reviewed by Butler et al. [11] and none of 180 patients reviewed by Marshall et al. [2] had upper urinary tract findings that resulted in alterations of patient management. Both studies were retrospective analyses of patients with acute urinary retention. Abrams [12], in a retrospective review of excretory urography in 201 patients with symptoms of bladder-outflow obstruction, found no abnormalities that led to alterations in therapy. In a prospective study, Andersen et al. [1] found no significant results in their review of 104 patients with a preliminary diagnosis of infravesical obstruction.

Most of our findings did not prompt changes in patient management. The prevalence of renal cysts (11%) is expected

for patients in this age group [13, 14]. In one patient, excretory urography findings suggested renal artery stenosis, but this possibility was not pursued. One patient with an indeterminate mass died of respiratory complications before sonographic findings could be obtained for clarification. The mass was probably a cyst, but the diagnosis remains uncertain. In nine patients, further radiographic studies were necessary to confirm various findings. We do not regard these findings as significant because they did not require an interventional procedure or ultimately lead to changes in patient management.

Despite our attempt to preselect patients without high-risk factors, we uncovered four cases (2.2%) whose management was altered on the basis of excretory urography findings. These included three patients with asymptomatic upper tract malignancies who underwent nephrectomy and one patient with an atypical cyst that required aspiration. Although benign, this cyst was classified as a significant finding because it necessitated an interventional diagnostic procedure. Other findings were potentially valuable, including one patient with a solitary kidney, five with renal calculi, one with papillary necrosis, and three with chronic pyelonephritis. However, none of these findings directly influenced the pre- or postsurgical management of these patients.

Our three asymptomatic cancers (1.7%) are surprising. In a review of the literature, Bauer et al. [10] found six (0.29%) upper urinary tract malignancies on excretory urography among 2024 men with acute urinary retention. They also reported that based on data from Bennington and Beckwith the expected number of upper tract malignancies was 32 (0.03%) per 100,000 70-year-old men. Most of the previous studies of patients with prostatism found a similar prevalence of cancer. However, there was one exception: Pinck et al. [7] found upper urinary tract cancer in eight (1.4%) of 557 patients.

Our higher prevalence of cancer can be partially explained by the prospective nature of our study, which prevented loss of any patients with significant excretory urography findings. Also, unlike some of the retrospective studies, most of our patients did not have acute urinary retention. Previous studies have found fewer abnormalities in this subgroup of patients. Finally, our standard excretory urography routinely included nephrotomography, which permits visualization of more subtle lesions than a conventional examination does. Most of the previous studies did not mention the routine use of nephrotomography.

We conclude that the upper urinary tract should be assessed in patients undergoing prostatism evaluation. Despite excluding potential high-risk patients on the basis of certain clinical and laboratory criteria, we found four patients whose management was directly influenced by the excretory urography findings and other patients with potentially important upper urinary tract abnormalities.

ACKNOWLEDGMENT

We thank Connie Goodyear for assistance in the preparation of this manuscript.

REFERENCES

1. Andersen JT, Jacobsen O, Strandgaard L. The diagnostic value of intravenous pyelography in infravesical obstruction in males. *Scand J Urol Nephrol* **1977**;11:225–230
2. Marshall V, Singh M, Blandy JP. Is urography necessary for patients with acute retention of urine before prostatectomy? *Br J Urol* **1974**;46:73–76
3. Kumar R, Schreiber M. The changing indications for excretory urography. *JAMA* **1985**;254(3):403–405
4. Pollack R, Banner M. Current status of excretory urography: a premature epitaph? *Urol Clin North Am* **1985**;12(4):585–601
5. Christoffersen I, Moller I. Excretory urography: a superfluous routine examination in patients with prostatic hypertrophy? *Eur Urol* **1981**;7:65–67
6. Morrison JD. Help or habit? Excretion urography before prostatectomy. *Br J Clin Pract* **1980**;34:239–241
7. Pinck BD, Corrigan MJ, Jasper P. Pre-prostatectomy excretory urography: does it merit the expense? *J Urol* **1980**;123:390–391
8. Pang SM, Keresteci AG, Rankin JT, Jewett MA. Role of preoperative urography in benign prostatic hyperplasia. *Urology* **1979**;14:292–294
9. Boerema WJ. Intravenous pyelography before prostatectomy: an evaluation of its use. *Aust NZ J Surg* **1972**;42:35–38
10. Bauer DL, Garrison RW, McRoberts JW. The health and cost implications of routine excretory urography before transurethral prostatectomy. *J Urol* **1980**;123:386–389
11. Butler MR, Donnelly B, Komaranchat A. Intravenous urography in evaluation of acute retention. *Urology* **1978**;12:464–466
12. Abrams PH. Use of the intravenous urogram in diagnosis. In: Hinman F, ed. *Benign prostatic hypertrophy*. Berlin: Springer-Verlag, **1983**:605–609
13. Kissane JM. Congenital malformations. In: Heptinstall RH, ed. *Pathology of the kidney*, 2nd ed. Boston: Little, Brown, **1974**:69–119
14. Lang EK. Roentgenologic approach to the diagnosis and management of cystic lesions of the kidney: is cyst exploration mandatory? *Urol Clin North Am* **1980**;7(3):677–688

The reader's attention is directed to the Commentary on this article, which appears on the following pages.

Commentary

Routine Urography in Men with Prostatism

Lee B. Talner[1]

Should all men with symptoms of bladder-outlet obstruction have screening excretory urography? That question is addressed by Bundrick and Katz [1]. The authors found three important surprises, two renal carcinomas and one transitional cell carcinoma, among 180 patients screened, citing this unusually high yield of occult cancers to support their argument in favor of routine urography. With the publication of their relatively small but at least prospective study, we now have a dozen reported series, but rather than allowing a clear-cut conclusion to be drawn, these reports instead underscore the complex and controversial nature of this issue. Formulating policy on the basis of small studies should not be undertaken lightly. We have a responsibility to examine the recommendations of Bundrick and Katz in light of data from larger series, epidemiologic studies, and autopsy surveys.

Previous authors [2–4] generally agree that the decision for prostatectomy should rest on clinical and urodynamic grounds rather than on urographic findings. While the discovery of unsuspected stones, scars, cysts, duplications, mild hydronephrosis, and so forth, is not always trivial, it generally has little or no impact on immediate patient management. Azotemic men with prostatism are best studied by sonography to look for kidney size and hydronephrosis. Only hematuria remains a noncontroversial indication for urography in these men [2]. Therefore, the major, unresolved issue is whether uncovering occult (asymptomatic) upper urinary tract malignancies is worthwhile. The possibility of missing a cancer provokes so much anxiety that the issue cannot be ignored.

To reach a rational decision we need to know the prevalence of renal carcinoma and upper tract transitional cell carcinoma (I will group these together as "renal cancer") in men with prostatism and the risk of renal cancer in these men compared with men of similar age without prostatism.

Of the 12 series reporting the results of urography in men with bladder-outlet obstructive symptoms [3, 5–14], three are from the United States; the remainder are from Europe, Australia, and Canada. The prevalence of upper tract malignancies ranged from 0% to 2%, but as might be expected, the patient populations differed substantially. Some series reviewed results only in men who subsequently underwent prostatectomy, while others included all men with symptoms of prostatism whether or not they eventually had surgery. Still others examined only men who presented with urinary retention. Patients with hematuria were excluded from some series (including that of Bundrick and Katz) but included in others. It is not surprising that the prevalence of renal cancer varied so much.

In all series combined, 15 renal "tumors" were discovered in 3828 patients. Five were specified as renal cancer, two as transitional cell cancer, five as renal "tumors," and three as ureteral "tumors." Assuming that all 15 tumors were malignant, the overall prevalence of "renal cancer" was 0.4%. Bundrick and Katz imply that their figure of 1.7% is nearer the true prevalence of occult cancers in men with prostatism because their study was prospective, while many of the other studies were retrospective and may have omitted patients with renal cancer who never reached prostatectomy. How does their conclusion fit with other data? Data from several sources on the incidence of renal cancer are fairly consistent. From the SEER (surveillance epidemiology and end results) study [15], the age-specific yearly incidence of renal cancer in the United States (including ureteral cancer) per 100,000 men is 17 cases (0.017%) in those aged 50–54 years, 33 cases (0.033%) for ages 60–64, 54 cases (0.054%) for ages 70–74, and 60 cases (0.060%) for ages 80–84. No significant regional differences emerged.

[1] Department of Radiology, University of California, San Diego, Medical Center, 225 Dickinson St., San Diego, CA 92103. Address reprint requests to L. B. Talner.

AJR 147:960–961, November 1986 0361–803X/86/1475–0960 © American Roentgen Ray Society

While autopsy series can provide data on the prevalence of renal cancer, most are not relevant to the present issue of discovering occult cancers. Harvey [16], looking for incidental renal cancers, found eight in 4529 autopsies, for a prevalence of 0.18%. The AFIP series from 1957 [17] cites a 0.3% prevalence of renal cancer among over 200,000 autopsies, including both symptomatic and occult malignancies. Bell [18] found 156 incidental tumors (including adenomas) in 59,000 autopsies, for a prevalence of 0.26%.

What do we learn by comparing the age- and sex-specific population data to the data derived from patients with prostatism? At first inspection it would appear that the prevalence of renal cancer in the prostatism group is as much as five to 10 times the prevalence in men of similar age who were not selected because of prostatism. However, all the reported series suffer from selection bias, which could easily explain the higher prevalence of renal cancer in this group. I suspect that urologists who found one or more occult cancers were more likely to report a series than those who did not. When to begin and end a series is arbitrary and is almost certainly influenced by when cancers are discovered. The inclusion of men with hematuria in some series also raises the chances of finding a cancer. Until larger series of patients are studied prospectively, we will not be sure of the prevalence of renal cancer in prostatism patients without hematuria.

But even if we were to acknowledge a small increased prevalence of renal cancer in men with prostatism, is that sufficient to formulate a policy of routine urography in prostatism patients? Is it worth the cost and risk of doing 1000 excretory urograms to discover three or four malignancies? What will be the stage of these tumors? How many will be curable or cured by prompt treatment? Is longevity affected in this older age group? What about the risks of surgery, contrast media, and the unknown natural history of occult tumors? While the medical profession would like to assume that all tumors removed represent "saves," we don't have enough data to know the ultimate impact of surgery on survival.

None of the published series have reported deaths from urography, but if the policy of routine urography for prostatism is carried out nationwide, and now it probably is close to standard procedure, enough urograms (estimate 200,000) are done yearly to make several deaths per year from contrast media likely. These patients would have been omitted from series that included only men who had survived urography to undergo prostatectomy.

In 1980, the cost of routine preprostatectomy urography was estimated to be near $29 million [3], but that cost did not include the cost of urography performed in prostatectomy candidates who did not undergo surgery. To this must be added the cost of extra time the patient must take from work, extra hospital days, and further workup necessitated by the discovery of space-occupying lesions that are actually cysts. For every renal cancer in this age group, we should find 15–25 renal cysts. Sonography or CT to confirm these as cysts adds substantial time and expense to the already heavy costs. The average cost of IV urography is at least 50% higher now ($200 in San Diego and Imperial Counties in California) than in 1980, and an increasing number of men are presenting with prostatism each year, so it is not unreasonable to project an overall annual expenditure exceeding $100 million nationwide for routine urography.

The two studies with the highest incidence of occult renal cancers were from New Jersey and Virginia. While we should not dismiss lightly the possibility that environmental factors play a role in the genesis of renal cancer, nationwide studies have so far failed to confirm significant regional differences [15]. What we should do is support large, multiinstitutional studies. These are tedious and expensive, but with medical economic pressures likely to escalate, it is the only way to generate data weighty enough to convince both urologists and radiologists. As of now I believe that the balance of evidence is against routine urography in men with prostatism.

REFERENCES

1. Bundrick TJ, Katz PG. Excretory urography in patients with prostatism. *AJR* **1986**;147:957–959
2. Abrams PH. Use of the intravenous urogram in diagnosis. In: Hinman F, ed. *Benign prostatic hypertrophy*. Berlin: Springer-Verlag, **1983**:605–609
3. Bauer DL, Garrison RW, McRoberts JW. The health and cost implications of routine excretory urography before transurethral prostatectomy. *J Urol* **1980**;123:386–389
4. Kumar R, Schreiber M. The changing indications for excretory urography. *JAMA* **1985**;254(3):403–405
5. Abrams PH, Roylance J, Feneley RCL. Excretion urography in the investigation of prostatism. *Br J Urol* **1976**;48:681–684
6. Chant ADB, Sellwood R, Spencer T. The value of intravenous pyelography in the management of patients with acute retention. *J R Coll Surg Edinb* **1974**;19:109
7. Andersen JT, Jacobsen O, Strandgaard L. The diagnostic value of intravenous pyelography in infravesical obstruction in males. *Scand J Urol Nephrol* **1977**;11:225–230
8. Marshall V, Singh M, Blandy JP. Is urography necessary for patients with acute retention of urine before prostatectomy? *Br J Urol* **1974**;47:73–76
9. Christoffersen I, Moller I. Excretory urography: a superfluous routine examination in patients with prostatic hypertrophy? *Eur Urol* **1981**;7:65–67
10. Morrison JD. Help or habit? Excretion urography before prostatectomy. *Br J Clin Pract* **1980**;34:239–241
11. Pinck BD, Corrigan MJ, Jasper P. Pre-prostatectomy excretory urography: does it merit the expense? *J Urol* **1980**;123:390–391
12. Pang SM, Keresteci AG, Rankin JT, Jewett MA. Role of preoperative urography in benign prostatic hyperplasia. *Urol* **1979**; 14:292–294
13. Boerema WJ. Intravenous pyelography before prostatectomy: an evaluation of its use. *Aust NZ J Surg* **1972**;42:35–38
14. Butler MR, Donnelly B, Komaranchat A. Intravenous urography in evaluation of acute retention. *Urology* **1978**;12:464–466
15. Young JL, Percy CL, Asire AJ, et al. Cancer incidence and mortality in the United States. *Natl Cancer Inst Monog* **1981**; 57:1–1082
16. Harvey NA. Kidney tumors. *J Urol* **1947**;57:669–692
17. Lucke B, Schlumberger HG. Tumors of the kidney, renal pelvis and ureter. *Atlas of tumor pathology*, sec. 8, fasc. 30. Washington, DC: Armed Forces Institute of Pathology, **1957**:11–20
18. Bell ET. *Renal diseases*, 2nd ed. Philadelphia: Lea & Febiger, **1950**

Book Review

Radiologic Diagnosis of Renal Transplant Complications. Edited by W. R. Castaneda-Zuniga. Minneapolis: Univ. of Minnesota Press, 298 pp., 1986

Dealing with the great variety of complications that occur in the renal transplant patient can be a perplexing and difficult clinical problem. The authors have nicely compiled a book on diagnosis and uroradiologic management of these situations. The book consists of three major sections: diagnosis of systemic complications, diagnosis of local complications, and therapeutic techniques. The text is written by the editor and 15 contributors, representing six institutions, many of whom are appropriately from the University of Minnesota with its extensive transplant experience.

The first section on systemic complications includes chapters on the chest film; echocardiography; and radiology of pulmonary complications, GI complications, and skeletal and soft-tissue change. Application of these pathologic changes to patients other than transplant patients becomes evident in this section, particularly, pulmonary disease in other immunosuppressed states, complications in patients on chronic steroids, and pathologic changes in patients with chronic renal disease alone. The discussions and extensive, diverse bibliographies are excellent. However, the poorly reproduced images definitely detract from the quality of the chapters, especially the two chapters dealing with chest radiographs. The images are far too small to appropriately illustrate the major points. The illustrations in the skeletal and soft-tissue chapter are of good size and adequate reproduction.

The second section of the book (local complications) has chapters dealing with urologic complications, nuclear medicine, angiography, sonography, and digital subtraction angiography. In the chapter on nuclear medicine, numerous illustrations and examples of scintigraphy and graphs effectively depict the various pathologic changes. In the chapter on angiography, the editor-author's experience is clearly evident; reproduction of the angiograms is adequate. Because of the type of images produced in sonography, the extensively illustrated chapter on that topic is well done and the images are not degraded by reproduction. In this second section of the book, particularly in the chapters on nuclear medicine, angiography, and sonography, the authors make a concerted effort to help the clinician and radiologist differentiate between a rejection reaction and acute tubular necrosis, one of the more difficult clinical dilemmas in the transplant patient. That coordinated effort makes reading of the chapters definitely worthwhile.

The third section on interventional uroradiology and management of complications is well done, showing the broad, innovative experience of the editor and his associates in dealing with these problems.

For radiologists, urologists and nephrologists involved with renal transplant patients, this book offers an extensive compilation of clinical knowledge and experience in recognizing and dealing with a multitude of problems. In its present form, the book is adequate; it would be an excellent book if reproduction of many of the radiographs were improved.

William H. Bush
The Mason Clinic
Seattle, WA 98111-0900

CT Changes in Dementing Diseases: A Review

Marjorie LeMay[1,2]

The present review describes the primary CT features of a variety of dementing disorders. An understanding of the differential neuropathologic and CT changes occurring in dementing illnesses can greatly increase the diagnostic utility of CT. CT is valuable not only in diagnosing space-occupying lesions but also in recognizing numerous degenerative brain diseases.

There are a number of diseases that can cause dementia. Some of these include presenile and senile illnesses of the Alzheimer's type, Pick's disease, Creutzfeldt-Jakob disease, multiple infarcts, dementia pugilistica, normal pressure hydrocephalus, and a variety of metabolic encephalopathies. While numerous studies have attempted to differentiate the CT scans of dementia patients from those of age-matched controls, few have compared and contrasted the CT scans of patients with a variety of dementing syndromes [1–4]. The present review summarizes CT features that typify a number of commonly encountered dementing disorders.

Dementing Disorders

Alzheimer's Type Dementia

Alzheimer's type dementia (ATD) is a primary degenerative brain disease usually occurring in middle and late life that is diagnosed by clincopathologic findings. Microscopic examination of the aging brain shows a decreased number of neurons, amyloid accumulation, senile plaques, neurofibrillary tangles, and granulovacuolar degeneration. These changes are greatly exaggerated in number and extent of distribution in patients with ATD [5–8]. Neuropathologic changes in patients with dementia are marked in the region of the angular gyrus and the inferior and middle temporal gyri; they are particularly striking in the amygdala, hippocampus, and the parahippocampal gyri, which lie in the medial temporal region [9–11] (Fig. 1).

Previously, patients who developed Alzheimer's type dementia at age 65 and older were designated as having "senile dementia" and, then, "senile dementia of the Alzheimer's type." Those who developed symptoms earlier were said to have "Alzheimer's disease." At present, the illness in both age groups is often referred to as Alzheimer's disease, although some clinical differences have been cited. One report noted that patients with dementia beginning before age 65 have a stronger family history of dementia, a relatively shorter life span, more language difficulties, and more left handedness [12]. Neuropathologic changes have been reported to be more marked in patients with an early onset of dementia [9, 11, 13–16].

A close examination of the CT scans of patients with ATD show that a number of characteristic changes can be seen in the temporal regions that appear to correlate with the above neuropathologic findings. As shown in Figure 2, atrophy is striking in the anterior and medial portions of the temporal lobes. This is reflected by widening of the suprasellar cistern, the cisterns between the midbrain and temporal lobes, and, particularly, the temporal horns of the lateral ventricles. The widening of the temporal horns occurs not only at their tips, which lie between the amygdala and hippocampus, but also extends posteriorly. This latter finding may be due to atrophic changes in the white matter of the temporal lobes as well as to cellular changes in the hippocampus. It seems likely that the widening of the cisterns at

This article appears in the September/October 1986 issue of *AJNR* and the November 1986 issue of *AJR*.

Received August 1, 1985; accepted after revision January 12, 1986.

[1] Present address: Harvard University Health Service, 75 Mt. Auburn St., Cambridge, MA 02138. Address reprint requests to M. LeMay.

[2] Department of Radiology, Brigham & Women's Hospital and Harvard Medical School, Boston, MA 02115.

***AJR* 147:963–975, November 1986**
0361–803X/86/1475–0963
© American Roentgen Ray Society

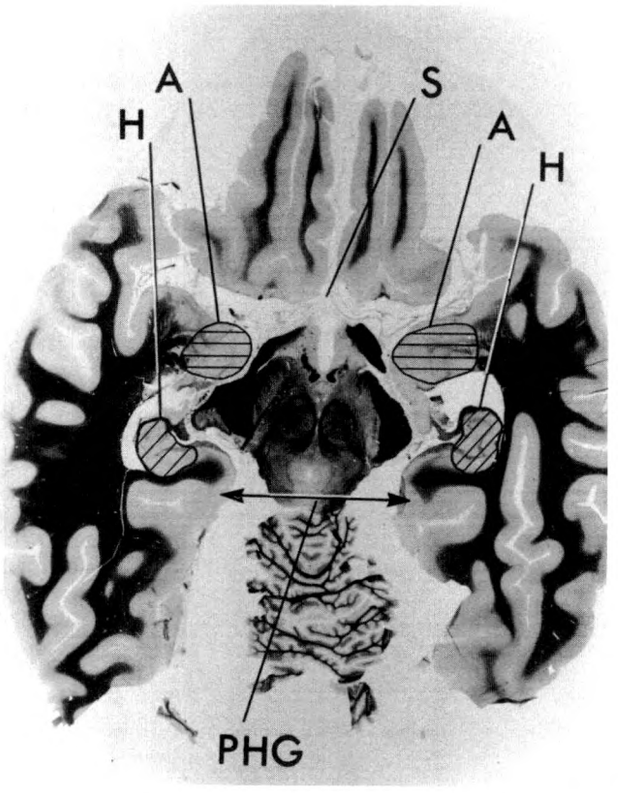


Fig. 1.—Section of brain through temporal lobes showing suprasellar cisterns (S), amygdala (A), and hippocampus (H). Tips of temporal horns of lateral ventricles lie between A and H. *Arrows* overlying midbrain point to parahippocampal gyri (PHG). (From the Yakovlev brain collection, AFIP, Washington, D.C. Courtesy T. Kemper and M. Haleem.)

the lateral margins of the midbrain is largely the result of tissue loss in the adjacent temporal lobes rather than in the midbrain. Most CT scans of patients with ATD, besides showing atrophy in the medial temporal regions, also show increased widening in the anterior portions of the sylvian fissures. Similar changes may be seen in the aging brain, but they are less striking, and the temporal horns are not often appreciably widened in nondemented elderly individuals [17, 18]. Fewer patients with ATD show lesser alterations in the medial temporal lobes but marked atrophy of the gyri in the temporal lobes and along the insula, widening both the sulci and sylvian fissures in these regions (Fig. 3).

The majority of radiographic studies, using both pneumoencephalography (PEG) [19–22] and CT [1, 2, 4, 23–32] have found the third ventricle and bodies of the lateral ventricles, and often the superficial sulci, to be statistically larger in patients with ATD, but there is a great overlap between the studies of patients with dementia and those of mentally normal controls. A progressive widening of the third ventricle is usual with aging [17], but PEG [20] and some CT studies [26, 27, 29] have found widening of the third ventricle to be significantly greater than widening of the bodies of the lateral ventricles in patients with ATD compared to CT studies of age-matched controls. Along with the described changes in the temporal lobes, prominent widening of the third ventricle and global atrophic changes help to strengthen the diagnosis of ATD by CT.

Pick's Disease

Pick's disease is another form of progressive dementia. It is not a common disease but is easily mistaken clinically for ATD. Neuropathologic changes are less generalized, however, and Pick's disease is sometimes called "lobar atrophy" or "progressive circumscribed cerebral atrophy." Microscopically, the brain shows atrophy and sclerosis, especially in the frontal and temporal lobes; however, there is often sparing of the posterior two-thirds of the superior temporal gyrus [33, 34], a gyrus that usually shows atrophy in ATD. Atrophy is often asymmetrically distributed in Pick's disease, and more frequently involves the left hemisphere than the right [34, 35]. There may also be severe atrophy of the basal ganglia [34, 35]. Microscopically, some neurons show local areas of cytoplasmic swelling, which are called Pick's bodies. Clinically, abnormal behavior and difficulty with language are more common in these patients than memory disturbances, which are more likely to be an early manifestation of ATD.

The diagnosis of Pick's disease can be suggested by CT when atrophy is localized and/or asymmetrical in the hemispheres [34, 36]. Figure 4A shows a CT scan through the temporal regions of a 52-year-old man who had presented 1 year earlier with hypomanic and depressive symptoms. At the time of the CT study, he showed a progressive decline in memory and an inability to learn new things. He died 5 years later, and neuropathologic examination showed moderate widening of the third and lateral ventricles. The temporal lobes appeared "shriveled up" bilaterally. The amygdalae could not be identified, but Pick's cells were seen in the hippocampi. No senile plaques or neurofibrillary tangles were seen. Figures 4B and 4C are scans of a 70-year-old woman who presented with paranoid ideation and a 4-year history of progressive dementia. Her EEG showed minor asymmetry in activity organization, with that on the left less well organized than that on the right. Clinically, she was thought to have Pick's disease and she was sent to a nursing home. No autopsy was performed when she died.

Creutzfeldt-Jakob Disease

A more common dementing illness than that described by Pick is Creutzfeldt-Jakob disease, a form of subacute spongiform encephalopathy. It is usually associated with an incubation period of several years and has been attributed to a "slow virus" or what is sometimes referred to as "a slow infectious pathogen, or prion." Patients typically develop the disease between the ages of 40 and 60, but some individuals have developed symptoms in their late teens and early twenties [37, 38]. The average course of the disease after symptoms develop is less than 1 year [38], although some patients have lived longer—one as long as 16 years [39]. Behavioral changes and visual disturbances, such as cortical blindness and hemianopsia, are often early symptoms of the disease. These are usually followed, in weeks or months, by progressive dementia, loss of motor control, and gait disturbances [40]. EEG changes with periodic sharp wave complexes appear during the course of the disease and are said to be characteristic of a viral infection [37, 38, 41, 42]. A familial history of the disease has been reported in at least 15% of the cases of Creutzfeldt-Jakob disease, possibly due to a genetically inherited susceptibility [38]. The disease is not rare. Person-to-person transmission has been reported from neurosurgical operations in which silver electrodes were used that had previously been implanted in a patient with Creutzfeldt-Jakob disease [43] and in patients who were recipients of human pituitary growth hormone [44, 45]. Transmission of the disease via a corneal transplant has also been reported [46], and some scientists speculate that it can be transmitted via absorbable animal-tissue sutures used in head trauma and/or surgery [47].

Histologic changes show widespread loss of neurons and astrogliosis in the cerebral cortex and in the central gray matter and cerebellum. The brainstem also is often affected [38]. The presence of spongiform changes in these areas is thought to suggest active disease, and when present in this distribution is strong evidence of

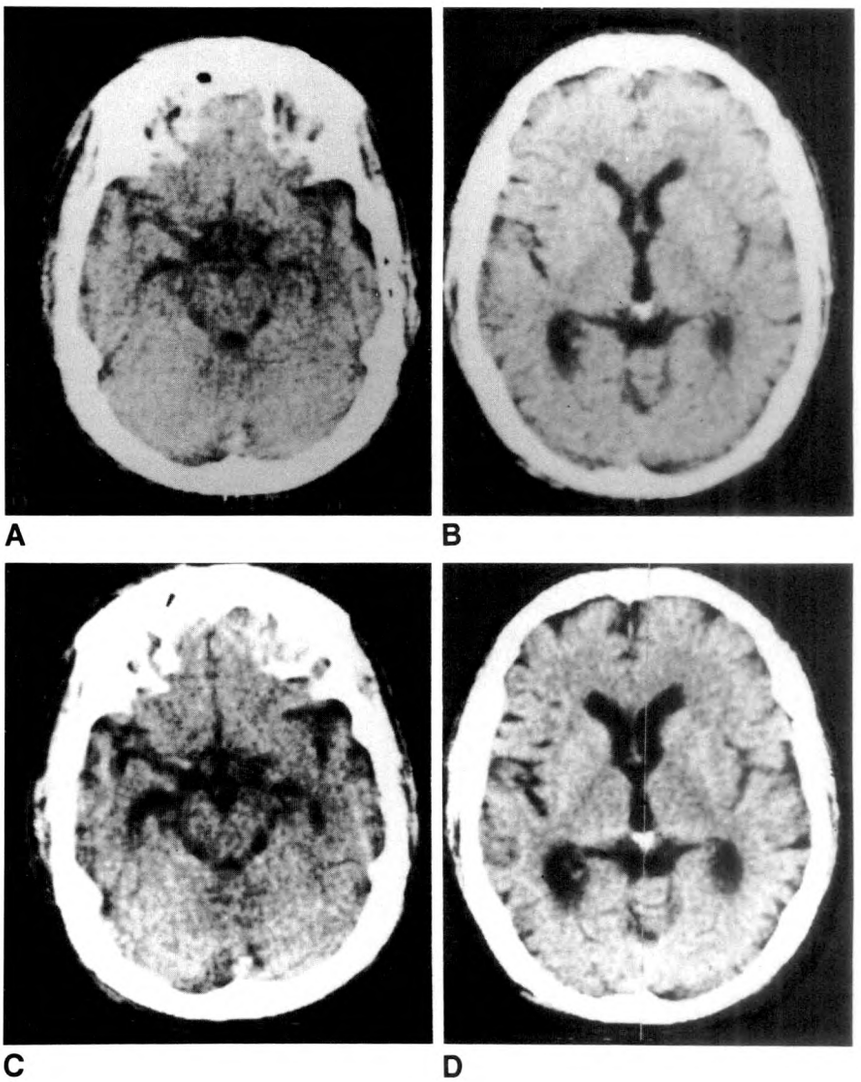


Fig. 2.—Alzheimer's disease. Scans of 58-year-old man who presented with memory deficit, spatial difficulties, and problems with concentration. His mother was said to have had senile dementia. Scans from Feb. 1983 (**A** and **B**) show slight widening of CSF spaces, involving particularly the cisterns above the sella and about the midbrain and slight widening of third ventricle. **A** shows significant widening of temporal horns. Bodies of lateral ventricles showed slight widening on slice above **B**. **C** and **D**, Scans taken 16 months later (June 1984), when symptoms had progressed, also show progression of atrophic changes. The extent of visualization of temporal horns depends particularly on angulation of slice. If scan had been more nearly horizontal, it is probable that one would see widening of temporal horns extending more posteriorly.

Creutzfeldt-Jakob disease [48]. White-matter degeneration is seen in some cases and may be more frequent in those individuals who have a longer course of disease [38, 49]. Extensive white-matter degeneration has been reported in some patients, and this may be caused by a different strain of Creutzfeldt-Jakob virus [50, 51]. Some cases of rapidly progressive Alzheimer's disease develop myoclonus and may be mistaken for Creutzfeldt-Jakob disease. Occasionally, ATD and Creutzfeldt-Jakob disease occur in the same families [38].

The CT findings in Creutzfeldt-Jakob disease vary according to the brain site most affected and to the time at which the scan is performed. Progressively atrophic changes are seen on CT [42, 52–54], with gradual widening of the ventricles and superficial sulci (Fig. 5). The temporal lobes may also be involved but not to the extent that is seen in patients with ATD. If the white matter is involved, this may also show on the CT study [42].

Angiopathic Dementia

Dementia may occur in patients who have suffered multiple cerebral infarcts. These infarcts often follow arteriosclerotic changes in the neck vessels, with ensuing thromboemboli or occlusion [55]. There is usually a neurologic history of focal deficits, and the progressive decline of mental function is usually more punctuated than in individuals with ATD. The presence of dementia depends on the location and the amount of brain loss. The patients are commonly hypertensive and often diabetic. CT studies may show local areas of low density and asymmetry of the lateral ventricles and sylvian fissure enlargement. It is difficult, however, to diagnose multiple infarct dementia radiologically because many patients thought to have multiple infarct dementia by clinical evaluation do not show infarcts by CT or avascular areas by angiography [56]; and many patients with primary degenerative brain disease often show local low-density areas consistent with infarction [56–58].

Subcortical arteriosclerotic encephalopathy is a form of multiple infarct dementia. This condition was described by Binswanger in the late 19th century and is frequently referred to as Binswanger's disease. It is a type of arteriosclerosis that particularly affects the vessels to the white matter about the ventricles and to the basal ganglia. Histologic changes show diffuse and/or localized demyelination in the white matter about the lateral ventricles. Lacunar infarcts

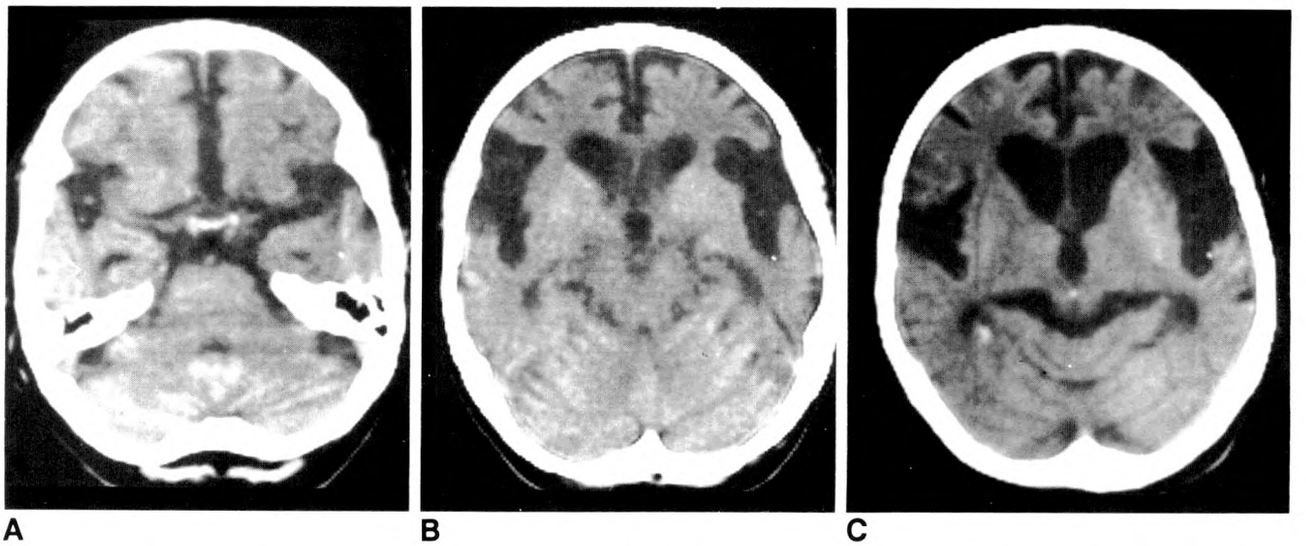


Fig. 3.—Alzheimer's disease. **A**, **B**, and **C**, Scans of 74-year-old woman with 4–5 year history of progressive memory loss that had progressed markedly during past 6–12 months. Four of five siblings also had severe memory loss in their late 60s, which prevented them from functioning normally. A scan was not taken through suprasellar cistern, but scans **A** and **B** do show widening of temporal horns., The most striking atrophic changes are widening of sulci of the temporal opercula and of anterior ends of sylvian fissures.

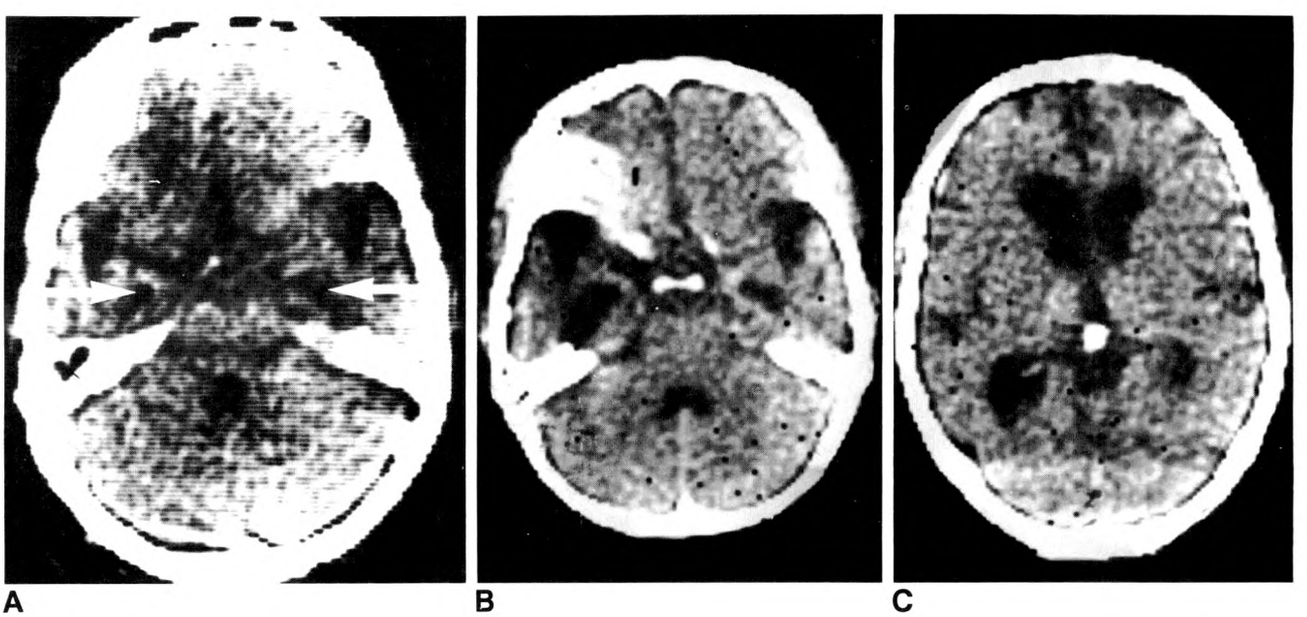


Fig. 4.—Pick's disease. **A**, CT scan of 52-year-old man with progressive memory impairment for 3–4 years that prevented him from functioning normally. He died 5 years later, and neuropathologic changes showed findings of Pick's disease. At time of CT, the bodies of the lateral ventricles were not large but the anterior ends of temporal horns showed asymmetrical widening. (Courtesy of R. K. Rosales, Boston University Medical School and Boston VA Hospital, and E. P. Richardson, Jr., Harvard Medical School and Massachusetts General Hospital.) **B** and **C**, Scans of 70-year-old woman who was thought to have Pick's disease. Scans show asymmetrical ventricular atrophy, particularly striking in temporal region, suggestive of Pick's disease.

may also be seen in the white matter and basal ganglia [59–61]. These patients are frequently hypertensive and commonly develop slowly progressive dementia, pseudobulbar palsy, and signs resembling parkinsonism. CT changes usually show a patchy decrease in density of the white matter about the lateral ventricles and widening of the third and lateral ventricles and superficial sulci [60, 62, 63]. Local small areas of low density suggesting lucunar infarcts may also be seen. Figure 6 shows CT scans consistent with Binswanger's disease, from a study of a hypertensive 71-year-old man with dementia. The patient was in cardiac failure and had diffuse arteriosclerotic

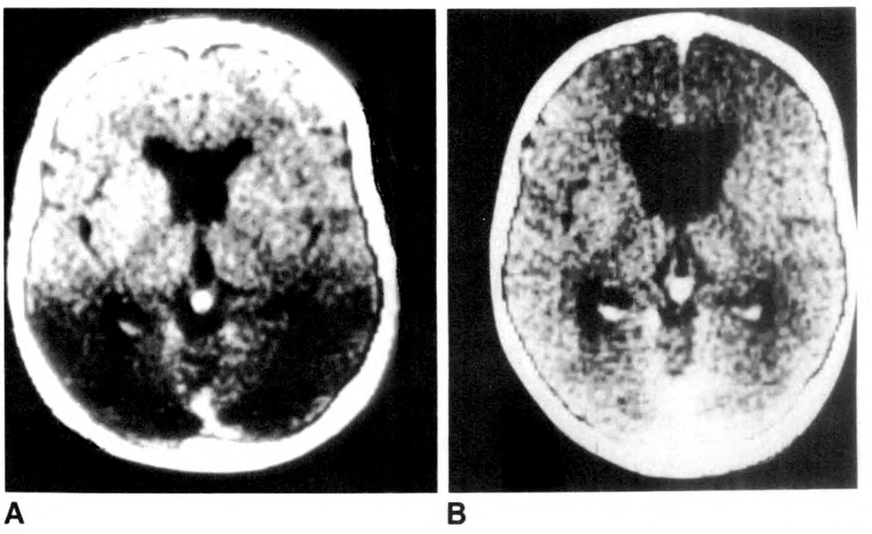


Fig. 5.—Creutzfeldt-Jakob disease. **A**, Scan of 43-year-old man who had a herpes zoster infection on his thorax 1 year previously, which cleared. He developed vertigo 7 months before hospital admission. On admission to hospital, he was dysarthric, showed diplopia and horizontal nystagmus, and had a tremor. He soon became confused and developed jerking movements. **B**, Scan 3 months later. Patient was confused and incontinent. There was progressive widening of third and lateral ventricles compared with the study 3 months earlier. He also had a cyst of the septum pellucidum.

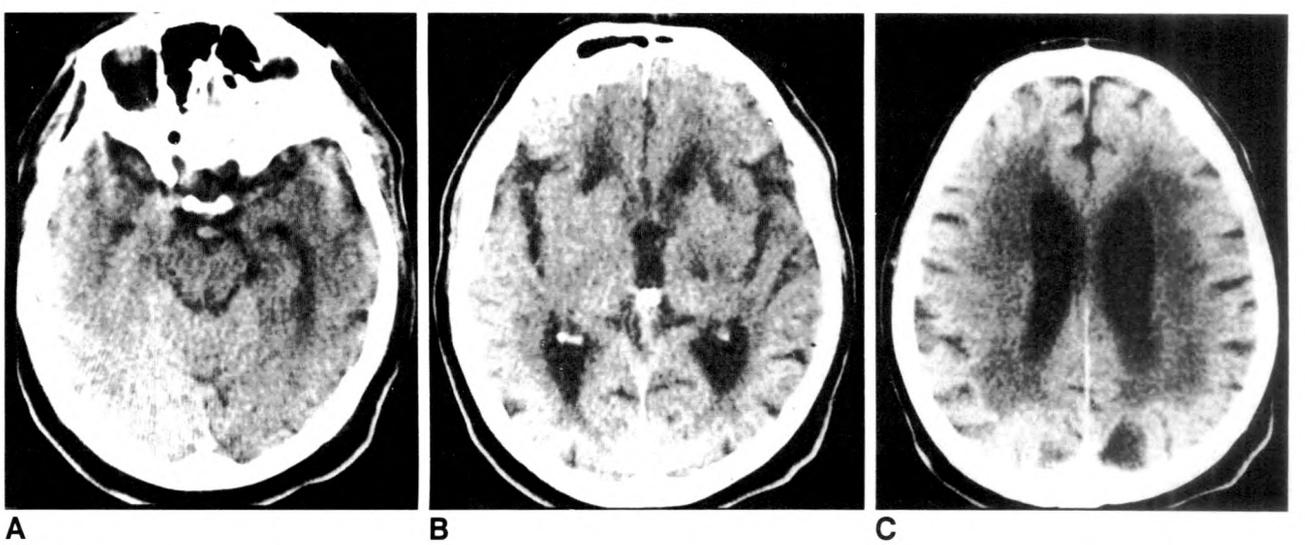


Fig. 6.—Binswanger's disease. **A, B**, and **C**, Scans of 71-year-old man with hypertension and 5-month history of dementia. There is widening of third and lateral ventricles, including some asymmetrical enlargement of temporal horns. There is suggestive evidence of small infarct in left thalamus. Suprasellar cistern was not significantly widened. The most striking changes are in white matter, about the bodies of the lateral ventricles. (Courtesy of M. Savoiardo, Milan.)

disease. Figure 7 shows head scans of a man who died at the age of 67 and whose CT and pathologic findings were consistent with global and Binswanger's type of multiple infarct dementia. There was a history of mild hypertension, multiple episodes of difficulty of speech and gait, and progressive dementia over a period of nearly 20 years. Autopsy showed evidence of large infarcts in both cerebellar hemispheres and the right occipital lobe. Multiple lacunar and microscopic infarcts were present in the basal ganglia bilaterally, both hippocampi, throughout the cortex and both cerebellar hemispheres, and in the brainstem. There was also extensive disease in the white matter, particularly in the periventricular regions, consistent with Binswanger's disease. CT scans were repeated at intervals over a 10-year period; these clearly showed the larger infarcts that occurred in the cerbellar hemispheres and the right occipital lobe and ill-defined densities about the margins of the lateral ventricles. Suggestions of small infarcts were reported in the pons and corona radiata.

Another cause of vascular dementia is congophilic or primary amyloid angiopathy. This is a disease in which amyloid deposits develop in the walls of small vessels and may cause occlusion or necrosis of the vessels, in turn leading to hemorrhage [64–69]. Plaques occur similar to those found in multiple sclerosis (MS) and it has even been suggested that the disease may be a variant of MS [64]. Plaques are common in the periventricular white matter and have also been reported in the optic nerves, brainstem, and spinal cord. Some patients have shown evidence of systemic amyloidosis, and hemorrhage can occur in other organs, such as the gastrointestinal tract [64–65], as well as in the brain. Familial cases of amyloid angiopathy have been reported. Hemorrhages can occur in all the lobes of the brain, most being superficial or subcortical and sometimes extending into the subarachnoid space. These hemorrhages

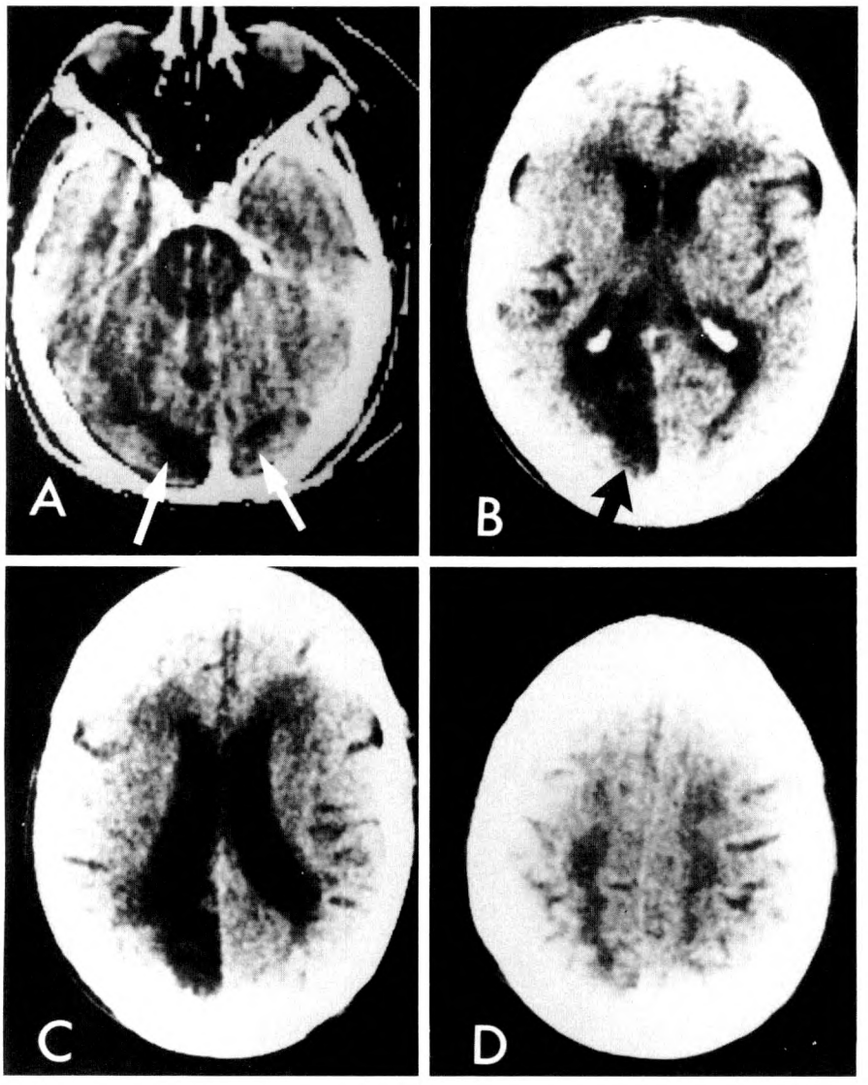


Fig. 7.—Multiple infarct dementia and Binswanger's disease. Scans of 67-year-old man with repeated syncopal episodes and progressive dementia over a 20-year period. Tissue loss due to infarcts is clearly seen in cerebellar hemispheres (**A**) and in right posterior occipital region adjacent to enlarged occipital horn of lateral ventricle (**B**). **C** and **D**, Low densities are present in white matter about and above bodies of lateral ventricles secondary to microangiopathic encephalopathy. Temporal horns were not significantly widened.

differ from those associated with arteriosclerotic hypertensive disease, which more classically involves the basal ganglia, pons, and cerebellum [68]. The patients occasionally present with slowly progressive dementia or, more frequently, with an intracerebral hemorrhage. The changes on CT will of course depend on the form of the disease [70]. Scans taken after a large hemorrhage that invades the ventricles show the hemorrhage to be more often above the basal ganglia and at times to extend over the surface of the brain [68] (Fig. 8). Patients presenting with dementia usually have demonstrated global atrophic changes and show the neuropathologic findings of ATD. If the temporal lobes are involved, the temporal horns are likely to be enlarged. Figure 9 shows CT scans of a 76-year-old man with progressive failure of intellect over a 4-year period. He was thought to have Alzheimer's disease and was placed in a nursing home. When he died, the neuropathologic findings were those of extensive amyloid angiopathy, and there were insufficient neuritic plaques or neurofibrillary tangles to classify the patient as having ATD.

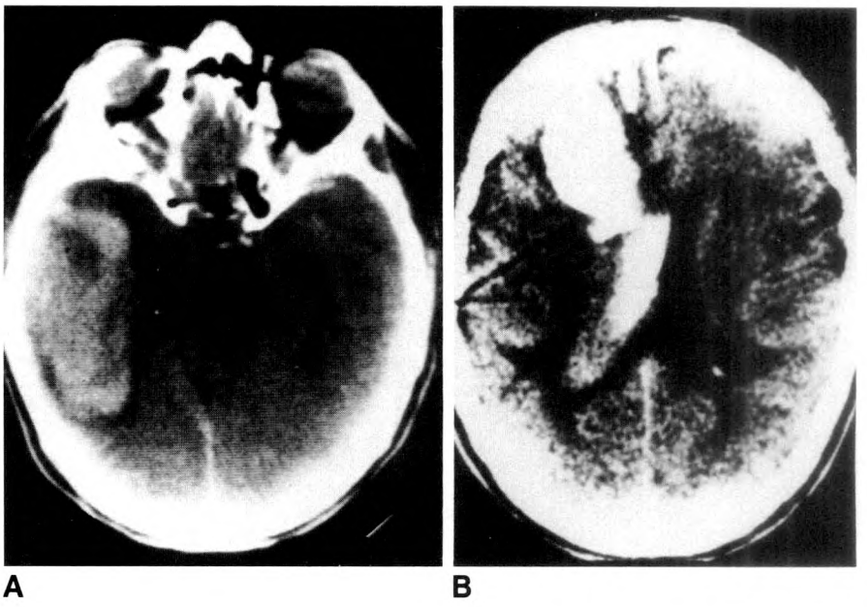
Hydrocephalic Dementia

Hydrostatic hydrocephalus may also be responsible for dementia, and patients' symptoms often clear after ventricular shunting. Spinal cord tumors occasionally prove to be the cause of hydrostatic hydrocephalus and dementia, both of which clear when the tumor is removed [71].

Some patients with hydrocephalus and dementia do not have elevated spinal fluid pressures and are classified as normal pressure hydrocephalus. Many of these treatable patients have obstruction of the CSF pathway outside the ventricles. Normal pressure hydrocephalus may result from many causes, but the most common cause is probably previous hemorrhage or meningeal infection resulting in interference with absorption of the CSF. Normal pressure hydrocephalus may also be caused by long-standing obstructive hydrocephalus, such as that resulting from aqueduct stenosis.

Apart from dementia, the most common symptoms in patients with normal pressure hydrocephalus are gait disturbances and incontinence. Difficulty in walking appears to be particularly frequent, and decreased cognitive functioning may at times be mild [72]. The diagnosis is often difficult to make. Some patients found to have normal pressure hydrocephalus were originally diagnosed as having had lacunar strokes [73] or progressive arthritis and aging because of their increase in walking difficulty and decrease in cognitive function [74]. Normal pressure hydrocephalus has at times been found to be responsible for parkinsonian dementia [75–78].

Fig. 8.—Amyloid angiopathy with hemorrhage. Scans of 62-year-old, nonhypertensive man who had been in good health but suddenly developed a hemorrhage in right temporal lobe (**A**). Angiogram was normal except for showing a mass effect. The clot was evacuated, and patient recovered but developed mild hypertension. One year later a hemorrhage occurred in right frontal lobe, extending into ventricle (**B**). Angiograms were again normal except for a mass effect. The clot was evacuated and a biopsy of adjacent cerebral tissue and leptomeninges showed intramural amyloid deposits consistent wtih amyloid angiopathy. Patient developed a superficial hemorrhage in left frontal lobe 2 weeks later.



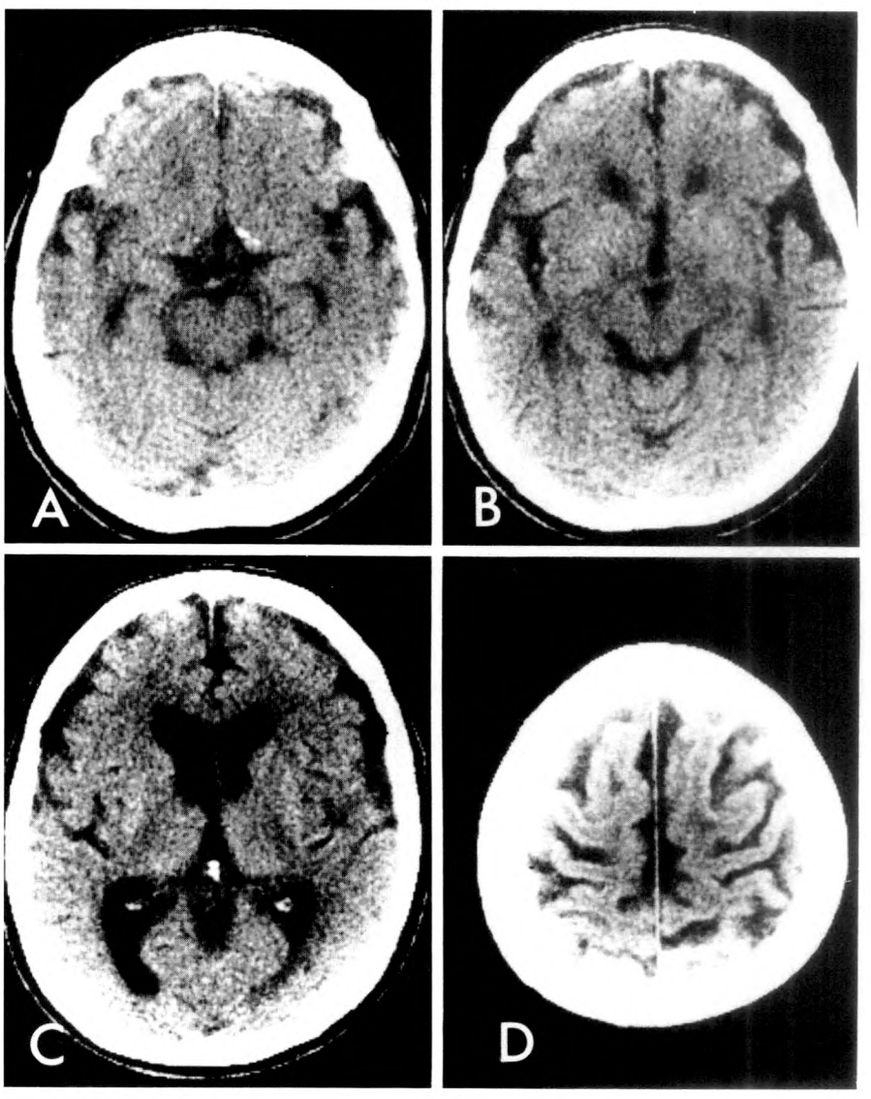


Fig. 9.—Amyloid angiopathy without hemorrhage. **A–D**, Scans of 76-year-old man with progressive dementia over a 4-year period. He was thought to have Alzheimer's disease and placed in a nursing home. He died 3 months after the CT study. Neuropathologic studies showed evidence of extensive amyloid angiopathy, but there were insufficient neuritic plaques or neurofibrillary tangles to make a diagnosis of Alzheimer's disease. (Courtesy of Eric D. Caine, University of Rochester Medical School, Rochester, NY.)

Cisternography shows abnormal CSF flow, but this may also be found in patients with degenerative brain disease [79, 80]. Removal of a small amount of CSF by spinal puncture may improve the symptoms of patients with normal pressure hydrocephalus; when this occurs, it is a good sign that the patient may be helped by shunting fluid from the ventricles [72].

Visualization of the anterior ends of the temporal horn is usually the earliest sign of hydrostatic hydrocephalus, unless it is caused by a centrally located lesion, such as an expanding third ventricle tumor, which may compress the tips of the temporal horns and prevent their enlargement. The temporal horn tips are usually rounder and wider in patients with hydrostatic hydrocephalus than in patients with primary degenerative disease of the brain, but it is sometimes difficult to separate the two disease states by CT. At times, a low density is seen about the margins of the lateral ventricles, particularly the frontal horns, which is thought to be caused mainly by leakage of CSF through the ventricular walls. The third and lateral ventricles are usually larger in patients with normal pressure hydrocephalus than in patients with primary degenerative dementia. On CT studies, the frontal horn ratio (i.e., the width of the frontal horns divided by the internal diameter of the vault at the same level) is often over 0.5 in patients with normal pressure hydrocephalus, which is much less common in patients with ATD [81]. The superficial sulci over the hemispheres and the cisterns about the midbrain and in the suprasellar region tend to be less prominent in patients with normal pressure hydrocephalus than in patients with ATD. Figure 10 is a scan of a patient who presented with difficulty walking and diminished cognitive function who improved with shunting of CSF from the ventricles.

Posttraumatic Dementia

Ventricular enlargement and widening of superficial sulci are often seen by CT after closed head injuries [82–84], but severe reduction of intellectual function is not a common sequel. ATD has been reported after head injuries, usually, but not always, in elderly individuals [84]. Neuropsychiatric symptoms and evidence of cerebral atrophy by CT have been reported in young torture victims [85].

Dementia pugilistica, a dementia occurring in boxers, appears to be related to the length of the boxer's career and to the evidence of brain damage occurring during the fights [86]. Neuropathologic studies usually show some enlargement of the lateral ventricles and fenestration, and sometimes large cysts of the septum pellucidum. There may also be thinning of the corpus callosum and scarring of the lower surface of the cerebellum. Neurofibrillary tangles are often seen in the cerebral cortex and brainstem, but especially in the gray matter of the medial temporal lobes [82, 87]. CT studies [86–88] usually show rather striking ventricular enlargement; large cysts of the septum pellucidum may be apparent, and sometimes expansion of a cavum vergae as well. The temporal horns are often enlarged. A clinical history of repeated head trauma should help to differentiate the changes of dementia pugilistica from those seen in patients with ATD.

Figure 11 shows CT scans of a 77-year-old man who presented with ataxia, memory loss, and diminished cognitive function. When the question of dementia pugilistica was raised by CT, the attending physician at first denied that his patient had any history of boxing. On further questioning, however, the patient admitted that he had boxed in his youth but had quit during his twenties because of head injuries.

Huntington's Chorea

This is a well-known hereditary disease characterized by the development of progressive choreiform movements and dementia. It usually becomes manifest in adult life although it is occasionally seen in young children. The basal ganglia, cerebral cortex, and white matter are involved, but the caudate nuclei, particularly, become shrunken as the disease progresses. CT studies usually show progressive widening of the intercaudate region of the lateral ventricles [89–91]. The extent of the caudate atrophy does not necessarily parallel the apparent clinical stage of the disease, and patients may have gross dementia although their CT scans appear relatively normal. A positive family history is an important aid in the diagnosis of Huntington's chorea, and it is has been reported that Huntington's patients have decreased levels of gamma aminobutyric acid (GABA) in their CSF,

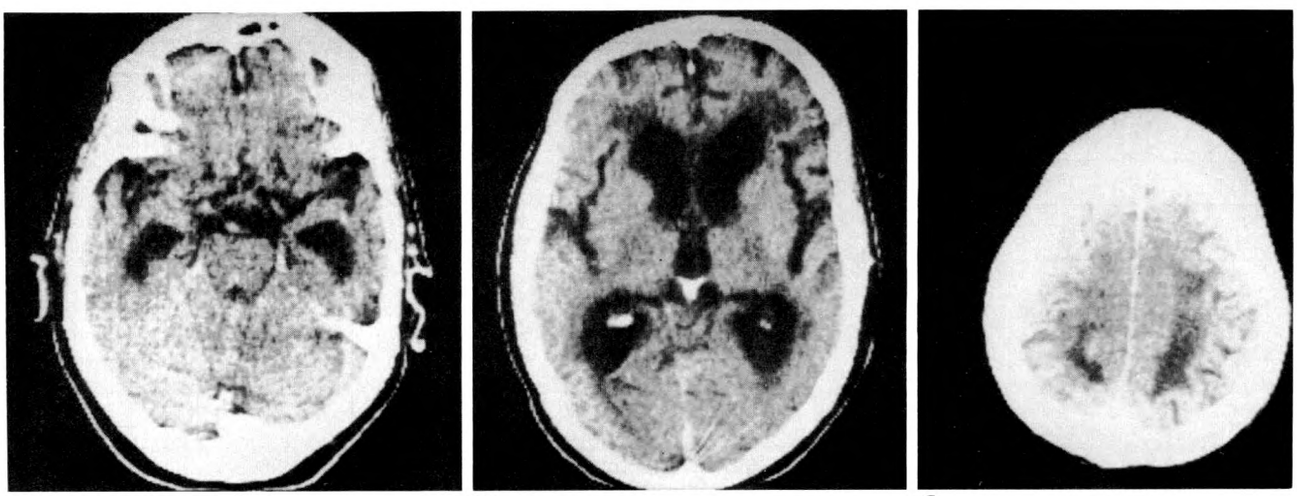


Fig. 10.—Normal pressure hydrocephalus. **A, B,** and **C,** Scans of 87-year-old man with normal pressure hydrocephalus who presented with walking difficulty. Frontal horn ratio was over 0.5. Temporal horn tips are very prominent, and there are areas of low densities about lateral ventricles. Sulci were not prominent over the hemispheres.

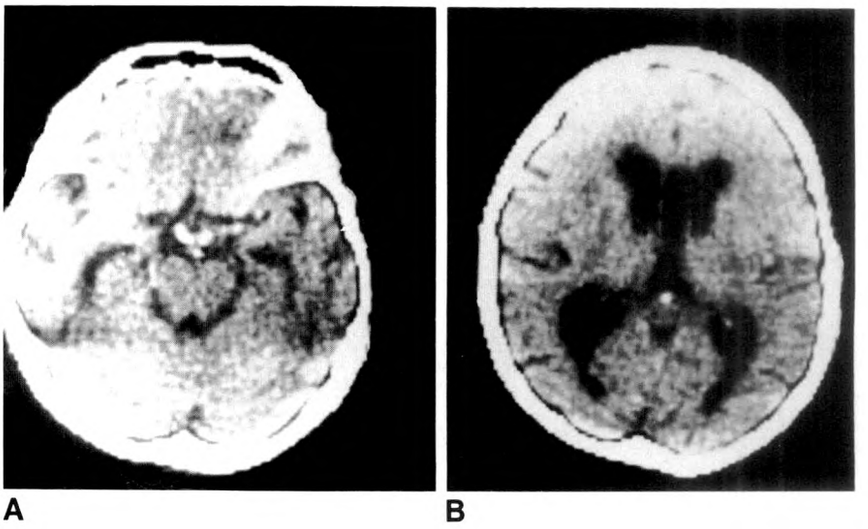


Fig. 11.—Dementia pugilistica. **A** and **B**, Study of a 77-year-old man with ataxia, memory loss, and some decrease in brain function. Patient had been a boxer in his youth. Temporal horns are very prominent and there is a large cyst of the septum pellucidum.

which can help confirm the diagnosis [92]. Huntington's disease has now been found to be linked to a DNA fragment of chromosome 4 [93, 94]. It is probable that soon it will be possible to identify persons who are at high risk for the disease. Chromosomal studies may also lead to effective treatment [95].

Figure 12 is a CT scan of a 37-year-old woman with Huntington's chorea. There was a family history of the disease, she had a severe movement disorder, was demented, and had a decrease of GABA in her CSF.

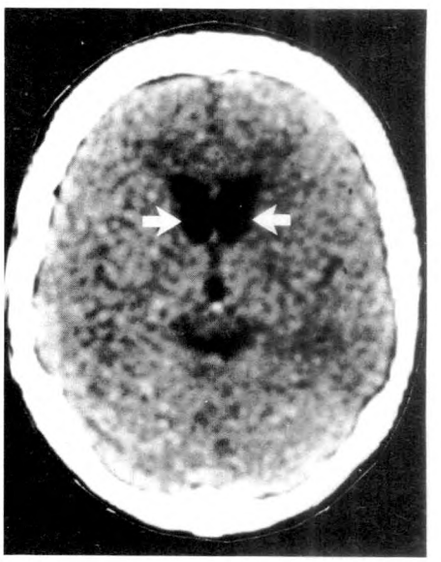


Fig. 12.—Huntington's chorea. Scan of 37-year-old woman with severe movement disorder and decreased mental functioning. There is marked widening of intercaudate distance (*arrows*), which is nearly as wide as frontal horns anterior to caudate nuclei. An earlier scan, taken when her symptoms were developing, showed no obvious widening of intercaudate distance.

Dementia Associated with Metabolic Disorders

Dementia, which is often reversible, may be caused by metabolic disorders of the nervous system [96]. One not uncommon condition is the Wernicke-Korsakoff syndrome, which is associated with alcoholism. These patients often show unsteadiness of gait and a marked memory deficit that is thought to be related primarily to a thiamine deficiency [97]. Histologically, lesions are seen in the thalamus and hypothalamus at the margins of the third ventricle and also in the cerebellum, particularly in the vermis and in the floor of the fourth ventricle. CT studies usually show widening of the CSF spaces, including the temporal horns of the lateral ventricles and vermal sulci of the cerebellum. Although they resemble the changes of ATD in some respects, the temporal lobe alterations are usually not as striking in patients with metabolic disorders. PEG [98, 99] and CT studies of chronic alcoholics have often shown the third ventricle to be strikingly widened. Figure 13 shows CT scans of a 32-year-old chronic alcoholic who entered the hospital mentally confused and with severe difficulty walking. Alcoholics are particularly susceptible to trauma resulting in head injuries, and evidence of asymmetrical tissue loss may be seen on CT scans. The ventricles and sulci of chronic alcoholics can return to normal, or near normal, size if alcohol intake is greatly reduced [100, 101]. Marchiafava-Bignami disease is a rare disorder sometimes seen in chronic alcoholics. It was first reported in Italy and thought to be caused by certain wines. It is associated with loss of tissue in the corpus callosum and usually also some lesions are present in the white matter. Evidence of lesions in the corpus callosum have been reported by CT in two patients who died of the disease [102].

Decreased brain function is sometimes seen in patients with Cushing's disease and other illnesses associated with increased steroid levels in the body [103]. CT changes in these individuals can resemble those seen in patients with ATD; as in alcoholics, however, the brain changes are less striking, and are often reversible when the cause of the metabolic changes is eliminated. Similar CT changes also may occur in individuals who are malnourished or are in renal failure or are receiving chemotherapy for cancer. Figure 14 shows the CT scan of a young man with carcinoid tumor of the ileum and metastasis to the liver. He had increased 5-hydroxyindol acetic acid in the urine resulting from increased serotonin in the body.

Hypoxic encephalopathy is often a more serious form of metabolic disorder of the nervous system and usually causes some permanent

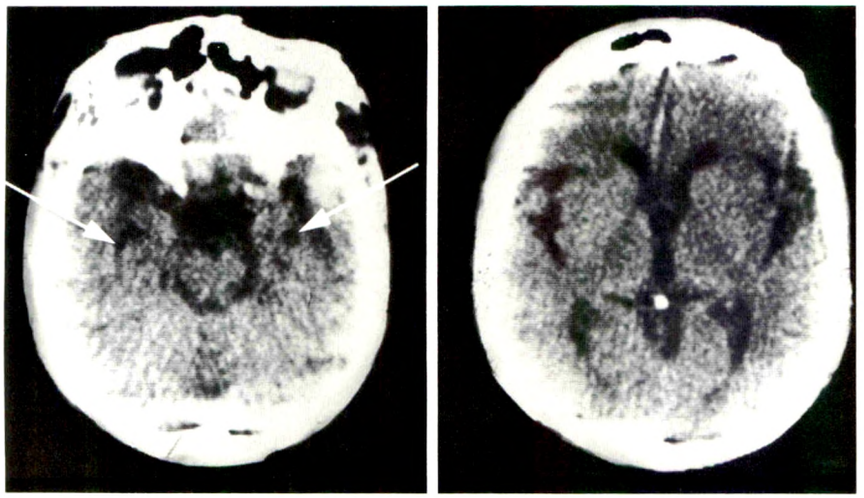


Fig. 13.—Alcoholism. **A** and **B**, Scans of 32-year-old male chronic alcoholic, who entered hospital confused and had marked gait difficulty. Third ventricle, sulci, and fissures are strikingly widened, and there is also some widening of temporal horns of lateral ventricles.

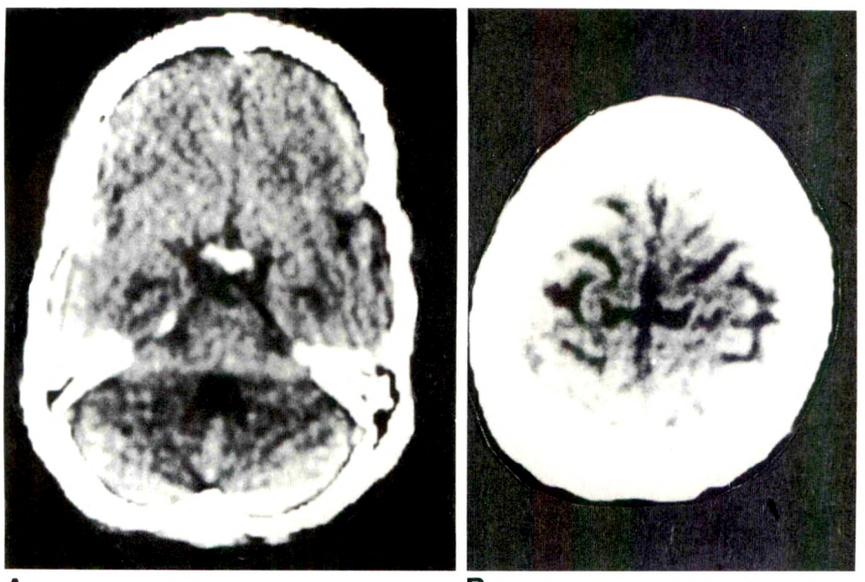


Fig. 14.—Carcinoid tumor. **A** and **B**, Scans show some widening of CSF spaces in 27-year-old man with carcinoid tumor of the ileum and liver metastasis. Patient had periods of flushing of the face and intermittent diarrhea for many months and showed some changes in mental status. Widening of suprasellar cistern and temporal horns are not as striking as is commonly seen in patients with Alzheimer's type dementia.

damage to the brain. It may occur after severe respiratory and heart disease or exposure to chemical poisoning, such as carbon monoxide inhalation, or after the ingestion of methyl alcohol. Neuropathologic studies usually show changes particularly in the globus pallidus, cerebellum, and hippocampus. Clinical symptoms depend on the degree of brain damage; memory loss is frequent. CT studies, besides showing well-defined, low-density lesions in the basal ganglia may also show widening of the temporal horns of the lateral ventricles [104].

Discussion

Less than 15 years ago the diagnosis of mental illnesses depended mainly on clinical criteria, aided by plain x-rays of the skull and PEG. CT has revolutionized the diagnostic capabilities in this area. Positron emission tomography (PET) is another relevant addition to the imaging of mental disease. PET studies [105–107] have shown hypometabolism, especially in the parietal regions, in patients with ATD compared with age-matched controls. The findings cannot be considered entirely diagnostic, since similar changes have been reported with Creutzfeldt-Jakob disease [108]. PET is also able to show, in patients with Huntington's disease, decreased activity in the caudate nuclei. This becomes evident before any changes are seen by CT, and it may help predict the likelihood of young family members developing the disease [105, 107]. In conjunction with CT studies, it is also helpful in the study of patients with strokes [109, 110]. PET is a developing field [111]. MRI is rapidly proving valuable in

the diagnosis of mental illnesses, and many small lesions can be seen with it that are not seen by CT. It will probably be some time, however, before enough data are collected from patients with global degenerative brain disease to utilize MRI to its greatest advantage.

A decrease in mental functioning in adult life may result from innumerable causes such as depression, endocrine disorders, systemic illnesses, drugs, toxins, and space-occupying lesions that may be successfully treated [96]. Alzheimer's disease is presently the most common dementing illness seen. Although global atrophic changes may be observed in brains of Alzheimer patients, the most striking alterations are seen in the temporal lobes. If on CT of a patient suspected of having ATD one does not see enlargement of the temporal horns, a tenacious search should be made for another cause of the dementia. Some scientists have suggested that ATD may be caused by a slow virus, but the difference in CT findings between patients with ATD and those with Creutzfeldt-Jakob disease would suggest they are not caused by similar pathogens. CT, at present, is valuable in diagnosing not only space-occupying treatable lesions, but also in diagnosing primary degenerative brain diseases.

ACKNOWLEDGMENTS

This review was stimulated and encouraged by Marilyn Albert and Juliene Stafford, Departments of Psychiatry and Neurology, Massachusetts General Hospital, Division on Aging; and Tamas Sandor, Department of Radiology, Brigham and Women's Hospital, Harvard Medical School, Boston. Dr. Albert also assisted in the preparation of the manuscript. I also thank T. Kemper and M. Savoiardo for their helpful review of the material.

REFERENCES

1. Huckman MS, Fox J, Topel J. The validity of criteria for the evaluation of cerebral atrophy by computed tomography. *Radiology* **1975**;116:85–92
2. Huckman MS. Computed tomography in the diagnosis of degenerative brain disease. In: Leeds NE, ed. *Symposium on neuroradiology. Radiol Clin North Am* **1982**;20:169–183
3. Bradshaw JR, Thompson JLG, Campbell MJ. Computed tomography in the investigation of dementia. *Br Med J* **1983**;286:277–280
4. Erkinjuntti T, Sipponen JT, Iivanainen M, Ketonen L, Sulkava R, Sepponen RE. Cerebral NMR and CT imaging in dementia. *J Comput Assist Tomogr* **1984**;8:614–618
5. von Braunmühl A. Alterserkrankungen des Zentralnervensystems. In: Lubarsch H, Henke F, Rossle R, eds. *Handbuch der Speziellen Pathologischen Anatomie und Histologie*. Vol. 13. Berlin: Springer-Verlag **1957**:337–539
6. Pantelakis S. Un type particulier de'angiopathie sénile du système nerveux central. L'angiopathie congophile. Topographie et fréquence. *Monatschr Psychiat Neurol* **1954**;128:219–256
7. Surbek B. L'angiopathie dyshorique (Morel) de l-ecore cérébrale. Etude anatomo-clinique et statistique, aspect génétique. *Acta Neuropathol* **1961**;1:168–197
8. Constantinidas J. Is Alzheimer's disease a major form of senile dementia? Clinical, anatomical and genetic data. In: Katzman R, Terry RD, Brick KL, eds. *Aging*. Vol. 7. New York: Raven Press, **1978**:15–25
9. Kemper TL. Neuroanatomical and neuropathological changes in normal aging and in dementia. In: Albert M, ed. *Clinical neurology of aging*. New York: Oxford University Press, **1984**:9–52
10. Kemper TL. Senile dementia: a focal disease in the temporal lobe. In: Nandy K, ed. *Senile dementia: a biomedical approach. Developments in neuroscience*. Vol. 3. New York: Elsevier/North Holland Biomedical Press, **1978**:105–113
11. Kemper TL. Organization of the neuropathology of the amygdala in Alzheimer's disease. Banbury report 15: *Biological aspects of Alzheimer's disease*. Maine: Cold Spring Laboratory, **1983**:31–35
12. Seltzer B, Sherwin I. A comparison of clinical features in early and late-onset primary degenerative dementia. One entity or two? *Arch Neurol* **1983**;40:143–146
13. Shefer VF. Absolute number of neurons and thickness of the cerebral cortex during aging, senile and vascular dementia and Pick's and Alzheimer's disease. *Zh Nevropatol Psikhiatr* **1972**;72:1024–1029
14. Shefer VF. Development of senile plaques in the human brain. *Arkh Anat Gistol Embriol* **1976**;73:97–103
15. Colon EJ. The cerebral cortex in presenile dementia—a quantitative analysis. *Acta Neuropathol* **1973**;23:281–290
16. Simma K. Über Thalamusveränderungen bei seniler Demenz und bei der Alzheimierschen Krankheit. *Monatschr Psychiat Neurol* **1951**;122:156–178
17. LeMay M. Dementia and cerebral atrophy. In: Wolpert SM, ed. *Multiple imaging procedures, central nervous system*. New York: Grune & Stratton, **1979**:109–128
18. LeMay M. Review. Radiologic changes of the aging brain and skull. *AJNR* **1984**;5:269–275
19. Burhenne HJ, Davis H. The ventricular span in cerebral pneumography. *AJR* **1963**;90:1176–1184
20. Engeset A, Sonnun A. Third ventricles of 12 mm width or more. *Acta Radiol* **1958**;50:5–11
21. Gosling RH. The association of dementia with radiographically demonstrated cerebral atrophy. *J Neurol Neurosurg Psychiatry* **1955**;18:129–133
22. Willanger R, Thygesen P, Nielsen R, Peterson O. Intellectual impairment and cerebral atrophy. A psychological, neurological and radiological investigation. *Dan Med Bull* **1968**;15:65–93
23. Earnest MP, Heaton AK, Wilkinson WE, Manke WF. Cortical atrophy, ventricular enlargement and intellectual impairment in the aged. *Neurology* **1979**;29:1138–1143
24. Jacoby RJ, Levy R. Computed tomography in the elderly: II. Senile dementia: diagnosis and functional impairment. *Br J Psychiatry* **1980**;136:256–269
25. Gado M, Patel J, Hughes CP, Danziger W, Berg L. Brain atrophy in dementia judged by CT scan ranking. *AJNR* **1983**;4:499–500
26. Kohlmeyer K, Shamena A. CT assessment of CSF spaces in the brains in demented and non-demented patients over 60 years of age. *AJNR* **1983**;4:706–707
27. Soininen M, Puranen M, Riekkinen PJ. Computed tomography findings in senile dementia and normal aging. *J Neurol Neurosurg Psychiatry* **1982**;45:50–54
28. Roberts MA, Caird FI, Grossart KW, Stevens JL. Computed tomography and intellectual impairment in the elderly. *J Neurol Neurosurg Psychiatry* **1976**;39:986–989
29. deLeon MJ, Ferris SH, George AE, Reisberg B, Kricheff IT, Gershon S. Computed tomography evaluations of brain-behavior relationships in senile dementia of the Alzheimer's type. *Neurobiol Aging* **1980**;1:69–79

30. Ford CV, Winter J. Computerized axial tomograms and dementia in elderly patients. *J Gerontol* **1981**;36:164–169
31. Damasio H, Eslinger P, Damasio AR, Rizzo M, Huang HK, Demeter S. Quantitative computed tomographic analysis in the diagnosis of dementia. *Arch Neurol* **1983**;40:715–719
32. Albert M, Naeser MA, Levine HL, Garvey AJ. Ventricular size in patients with presenile dementia of the Alzheimer's type. *Arch Neurol* **1984**;41:1258–1284
33. Schoene WC. Degenerative diseases of the nervous system. In: Robinson D, Davis R, eds. *Textbook of general neuropathology*. Baltimore: Williams & Wilkins, **1985**:788–823
34. Wechsler AF, Verity A, Rosenschein S, Fried I, Scheibel AB. Pick's disease. A clinical, computed tomographic and histologic study with Golgi impregnation observations. *Arch Neurol* **1982**;39:287–290
35. Cummings JL, Duchen LW. Kluver-Bucy syndrome in Pick's disease: clinical and pathological correlation. *Neurology* **1981**;31:1415–1422
36. Groen JJ, Hekster REM. Computed tomography in Pick's disease: findings in a family affected in three consecutive generations. *J Comput Assist Tomogr* **1982**;6:907–911
37. Monreal J, Collins GH, Masters CL, Fisher CM, Kim RC, Gibbs CJ Jr., Gajdusek DC. Cruetzfeldt-Jakob in an adolescent. *J Neurol Sci* **1981**;52:341–350
38. Masters CL, Gadjdusek DC. The spectrum of Cruetzfeldt-Jakob disease and the virus-induced subacute spongiform encephalopathies. In: Smith WT, Cavanagh JB, eds. *Recent advances in neuropathology*. No. 2. New York: Churchill Livingston, **1982**:139–163
39. Cutler NR, Brown PW, Narayan T, Parisi JE, Janotta F, Baron H. Cruetzfeldt-Jakob disease: a case of 26 years duration. *Ann Neurol* **1984**;15:107–110
40. Bernoulli CC, Masters CL, Gajdusek DC, Gibbs CJ Jr, Harris JO. Early clinical features of Cruetzfeldt-Jakob disease (subacute spongiform encephalopathy). In: *Slow transmissible diseases of the nervous system. Vol. 1. Clinical, epidemiological, genetic, and pathological aspects of the spongiform encephalopathies*. New York: Academic Press, **1979**;229–252
41. Roos R, Gajdusek C, Gibbs CJ Jr. The clinical characteristics of transmissible Cruetzfeldt-Jakob disease. *Brain* **1973**;96:1–20
42. Schneck SA, Hedley-Whyte ET. Case records of the Massachusetts General Hospital: Case 49-1983. *N Engl J Med* **1983**;309:1440–1449
43. Bernoulli C, Siegfried J, Baumgartner G, Regli F, Rabmowicz T, Gajdusek DC, Gibbs CJ. Danger of accidental person-to-person transmission of Cruetzfeldt-Jakob disease by surgery. *Lancet* **1977**;1:478–479
44. Gibbs CJ Jr, Joy A, Heffner R, et al. Clinical and pathological features and laboratory confirmation of Cruetzfeldt-Jakob disease in a recipient of pituitary-derived human growth hormone. *N Engl J Med* **1985**;313:734–738
45. Koch TK, Berg BO, DeArmond SJ, Gravina RF. Cruetzfeldt-Jakob disease in a young adult with idiopathic hypopituitarism. *N Engl J Med* **1985**;313:731–733
46. Duffy P, Wolff J, Collins G, DeVoe AG, Streeten B, Cowen D. Possible person-to-person transmission of Cruetzfeldt-Jakob disease. *N Engl J Med* **1974**;290:692–693
47. Davanipous D, Alter M, Sobel E, Asher D, Gujdusek DC. Cruetzfeldt-Jakob disease: Possible medical risk factors. *Neurology* **1985**;35:1483–1486
48. Masters CL, Richardson EP Jr, Subacute spongiform encephalopathy (Cruetzfeldt-Jakob disease). The nature and progression of spongiform change. *Brain* **1978**;101:333–344
49. Kovanen J, Erkinjuntti T, Iivanainen M, Ketonen L, Haltia M, Sulkava R, Sipponen JT. Cerebral MR and CT imaging in Cruetzfeldt-Jakob disease. *J Comput Assist Tomogr* **1985**;9:125–128
50. Tateishi J, Sato Y, Ohta M. Cruetzfeldt-Jakob disease in humans and laboratory animals. In: Zimmerman HM, ed. *Progress in neuropathology*. No. 5. New York: Raven Press, **1981**:195–221
51. Park TS, Kleinmen GM, Richardson EP Jr. Cruetzfeldt-Jakob disease with extensive degeneration of white matter. *Acta Neuropathol* **1980**;52:239–242
52. Rao CVGK, Brennan TG, Garcia JH. Computed tomography in the diagnosis of Cruetzfeldt-Jakob disease. *J Comput Assist Tomogr* **1977**;1:211–215
53. Brown TR, Richardson EP Jr. Case records of Massachusetts General Hospital, 44-1977. *N Engl J Med* **1977**;297:930–937
54. Wolpow ER, Kleinman GM, Landis DMD, Richardson EP Jr. Case records of Massachusetts General Hospital, 45-1980. *N Engl J Med* **1980**;303:1162–1171
55. Haase GR. Diseases presenting as dementia. In: Wells CE, ed. *Dementia*. 2nd ed. Philadelphia: FA Davis Co., **1977**:27–67
56. Radue EW, duBoulay GH, Harrison MJG. Comparison of angiographic and CT findings between patients with multiple-infarct dementia and those with dementia due to primary neuronal degeneration. *Neuroradiology* **1978**;16:113–115
57. Glatt SL, Lantos P, Danzibea A, Katzman R. Efficacy of CT in the diagnosis of vascular dementia. *AJNR* **1983**;4:703–705
58. Liston EH, LaRue A. Clinical differentiation of primary degenerative and multi-infarct dementia: A critical review of the evidence. Part 1: clinical studies. Part II: Pathological studies. *Biol Psychiatry* **1985**;18:1451–1484
59. Caplan LR, Schoene WC. Clinical features of subcortical arteriosclerotic encephalopathy (Binswanger disease). *Neurology* **1978**;28:1206–1215
60. Zeumer H, Schonsky B, Sturm KW. Predominant white matter involvement in the subcortical arteriosclerotic encephalopathy (Binswanger disease). *J Comput Assist Tomogr* **1980**;4:14–19
61. Kameyama M. Clinicopathologic study of progressive subcortical vascular encephalopathy (Binswanger's type) in the elderly. *J Am Geriatr Soc* **1982**;30:524–529
62. Rosenberg GA, Kornfeld M, Stovering J, Bicknell JM. Subcortical encephalopathy (Binswanger): computerized tomography. *Neurology* **1979**;29:1102–1106
63. Goto K, Ishii N, Fukasawa H. Diffuse white-matter disease in the geriatric population. *Radiology* **1981**;41:687–695
64. Heffner RR, Porro RS, Olson ME, Earle KM. A demyelinating disorder associated with cerebrovascular amyloid angiopathy. *Arch Neurol* **1976**;33:501–506
65. Mandybur TI, Bates SDR, Stephen RD. Fatal massive intracerebral hemorrhage complicating cerebral amyloid angiopathy. *Arch Neurol* **1978**;35:246–248
66. Okazaki H, Reagan TJ, Campbell RJ. Clinopathological studies of primary cerebral amyloid angiopathy. *Mayo Clin Proc* **1979**;54:22–31
67. Adam J, Crow TS, Duchen LW, Scaravilli F, Spokes E. Familial cerebral amyloidosis and spongiform encephalopathy. *J Neurol Neurosurg Psychiatry* **1982**;45:37–45
68. Cosgrove GR, Leblanc R, Meagher-Villemure K, Ethier R. Cerebral amyloid angiopathy. *Neurology* **1985**;35:625–631
69. Ackerman RH, Richardson EP Jr. Case Records of Massachusetts General Hospital: Case 49-1982. *N Engl J Med* **1983**;307:1507–1514
70. Wagle WA, Smith TW, Weiner M. Intracerebral hemorrhage caused by cerebral amyloid angiopathy: radiographic-pathologic

correlation. *AJNR* **1984**;5:171–176
71. Messer HD, Brinker RA. Hydrocephalus and dementia complicating spinal tumor. *J Neurosurg* **1980**;53:544–547
72. Fisher CM. Hydrocephalus as a cause of disturbance of gait in the elderly. *Neurology* **1982**;32:1358–1363
73. Fisher CM. Lacunar strokes and infarcts: a review. *Neurology* **1982**;32:871–876
74. Rasker JJ, Jansen ENH, Haan J, Oostrom J. Normal-pressure hydrocephalus in rheumatic patients: a diagnostic pitfall. *N Engl J Med* **1985**;312:1239–1241
75. Hakim AM, Mathieson G. Dementia in Parkinson disease: a neuropathologic study. *Neurology* **1979**;29:1209–1214
76. Steiner I, Goromi JM, Melamed E. Features of brain atrophy in Parkinson's disease. *Neuroradiology* **1985**;27:158–160
77. Heilig CW, Knopman DS, Mastri AR, Frey W II. Dementia without Alzheimer's pathology. *Neurology* **1985**;35:762–765
78. Syupert GW, Leffman H, Ojemann GA. Occult normal pressure hydrocephalus manifested by Parkinsonism-dementia complex. *Neurology* **1973**;23:234–238
79. Benson DF, LeMay M, Patten DH, Rubens AB. Diagnosis of normal pressure hydrocephalus. *N Engl J Med* **1970**;283:609–617
80. Messart B, Levin AB. Iodinated serum albumin dynamic cerebrospinal fluid flow studies. *Arch Neurol* **1972**;26:49–59
81. LeMay M, Hochberg FH. Ventricular differences between hydrostatic hydrocephalus and hydrocephalus ex-vacuo by computed tomography. *Neuroradiology* **1979**;17:191–195
82. Corsellis JAN, Bruton CJ, Freeman-Browne D. The aftermath of boxing. *Psychol Med* **1973**;3:270–303
83. Levin HS, Meyers CA, Grossman RG, Sarwar M. Ventricular enlargement after closed head injury. *Arch Neurol* **1981**;38:623–629
84. Rudelli R, Strom RI. Post-traumatic premature Alzheimer's disease. Neuropathological findings and pathological considerations. *Arch Neurol* **1982**;39:570–575
85. Jensen TS, Genefke IK, Hyldebrandt N, Pedersen H, Peterson HD, Weile B. Cerebral atrophy in young torture victims. *N Engl J Med* **1982**:307–1341
86. Casson IR, Sham R, Campbell EA, Tarlau M, Didomenico A. Neurological and CT evaluation of knocked-out boxers. *J Neurol Neurosurg Psychiatry* **1982**;45:170–174
87. Lampert PW, Hardmen JM. Morphological changes in brains of boxers. *JAMA* **1984**;251:2676–2679
88. Ross RJ, Cole M, Thompson JS, Kim KH. Boxers—computed tomography, EEG, and neurological evaluation. *JAMA* **1983**;249:211–213
89. Terrence CF, Delaney JF, Alberts MC. Computed tomography for Huntington's disease? *Neuroradiology* **1977**;13:173–175
90. Lang C. Is direct CT caudalometry superior to indirect parameters in confirming Huntington's disease? *Neuroradiology* **1985**;27:161–163
91. Neophytides AN, DiChiro G, Barron SA, Chase TN. Computed axial tomography in Huntington's disease and persons at risk for Huntington's disease. *Adv Neurol* **1979**;23:185–191
92. Manyam NVB, Hare TA, Katz L, Glaeser BS. Huntington's disease. *Arch Neurol* **1979**;35:728–730
93. Gusella JF, Wexler NS, Conneally PM, et al. A polymorphic DNA marker genetically linked to Huntington's disease. *Nature* **1983**;306:234–238
94. Folstein SE, Phillips JA III, Meyers DA, et al. Huntington's disease: two families with differing clinical features show linkage to the G8 probe. *Science* **1985**;229:776–779
95. Ferrante RJ, Kowall NW, Beal MF, Richardson EP Jr, Bird ED, Martin JB. Selective sparing of a class of striatal neurons in Huntington's disease. *Science* **1985**;230:561–563
96. Cummings J, Benson DF, LoVerme S. Reversible dementia: illustrative cases, definition, and review. *JAMA* **1980**;243:2434–2439
97. Adams RD, Victor M. Wernicke-Korsakoff's syndrome. In: *Principles of neurology*. New York: McGraw-Hill, **1981**:704–711
98. Haug JO. Pneumocephalographic evidence of brain damage in chronic alcoholics. *Acta Psychiatr Scand* [*Supp*] **1968**; 203:135–143
99. Lying-Tunell U, Marion SO. A triad of airencephalographic findings in patients with mental impairment: a controlled prospective study. *Neuroradiology* **1975**;9:251–265
100. Cala LA, Burns P, Davis R, Jones B. Alcohol-related brain damage-serial studies after abstinence and recommencement of drinking. *Aust Alcohol/Drug Rev* **1984**;3:127–140
101. Artmann G, Gall MV, Hacker H, Herrlich J. Reversible enlargement of cerebral spinal fluid spaces in chronic alcoholics. *AJNR* **1981**;2:23–27
102. Bourrat C, Tommasi M, Bochu M, Kopp N, Malsch S. Donnécs du scanner X dans la maladie de Marchiafava-Bignami. *Rev Neurol* (Paris) **1984**;140:426–431
103. Bentson J, Reza M, Winter J, Wilson G. Steroids and apparent cerebral atrophy on computed tomography scans. *J Comput Assist Tomogr* **1978**;2:16–23
104. Nardizzi LR. Computerized tomographic correlate of carbon monoxide poisoning. *Arch Neurol* **1979**;36:38–39
105. Phelps ME, Mazziotta JC. Positron emission tomography: human brain function and biochemistry. *Science* **1985**;228:799–809
106. de Leon MJ, George AE, Ferris SH, et al. Regional correlation of PET and CT in senile dementia of the Alzheimer's type. *AJNR* **1983**;4:553–556
107. Kuhl DE. Imaging local brain function with emission computed tomography. *Radiology* **1984**;150:625–631
108. Friedland RP, Prusiner SB, Jagust WJ, Budinger TF, Davis RL. Bitemporal hypometabolism in Creutzfeldt-Jakob disease measured by positron emission tomography with [^{18}F]-2-fluorodeoxhylucose. *J Comput Assist Tomogr* **1984**;8:978–981
109. Ackerman RH, Correia JA, Alpert NM, et al. Positron imaging in ischemic stroke disease using compound labeled with oxygen 15. *Arch Neurol* **1981**;38:537–543
110. Ackerman RH, Alpert NM, Davis SM, et al. The occurrence of hypermetabolisms adjacent to subcortical infarcts and hemorrhages. *Stroke* **1982**:118
111. Powers WJ, Raichle ME. Positron emission tomography and its application to the study of cerebrovascular disease in man. *Stroke* **1985**;16:362–376

Book Review

Clinical Diagnostic Ultrasound, Edited by E. Barnett and P. Morley. Oxford: Blackwell Scientific Publ., 617 pp., 1985. $216

The technology of ultrasound has changed tremendously over the past 5 years, and it is difficult to incorporate all of the latest developments into a timely textbook. This may explain the paucity of books dealing with the entire field.

This book covers the whole of diagnostic ultrasound, including sections on instrumentation; eye and orbit; heart; vascular system; small parts; abdomen, gastrointestinal tract, and peritoneum; liver and pancreas; spleen and lymphatic system; renal tract; obstetrics, gynecology; and pediatrics, with detailed chapters in each section. The writing is clear and well organized. However, as with any multiauthored text, there is a considerable lag-time between writing and publication. Thus, while some chapters are fairly up-to-date, many are less current, with few references beyond 1980. The images are adequate to good: few are state-of-the-art.

The chapter on apparatus and scanning techniques is comprehensive, clearly worded, and easily understood. The second chapter, including volume measurements, needle-puncture techniques, radiotherapy planning, and tissue characterization is an odd combination. Information on volume measurement, which is dependent for the most part on B-scanning, could have been included in the sections on the specific organs measured. An expanded section on percutaneous biopsy and puncture techniques would be useful, since these procedures are so much in demand today.

In the United States, most radiologists do not perform ultrasound examinations of the eye. The four chapters on the subject are interesting and well written, and serve to make the book complete. However, some of the techniques described have been changed because of newer equipment. In this country, CT has supplanted ultrasound in the evaluation of the orbit.

The strongest chapters are those on congenital heart disease; abdomen, gastrointestinal tract, and peritoneum; bladder and prostate; uterus, ovaries; pelvic inflammatory disease; and fetal anomalies. These are well written, clinically useful, and well illustrated. Several chapters suffer from lack of recent information, notably those on early pregnancy; late pregnancy; breast (which is well written, but contains no references beyond 1977, and should include data from some of the more recent screening studies); acute abdomen, especially the section on ectopic pregnancy; pancreas (excellent discussion of anatomy, but not current technique).

Aside from problems regarding out-of-date techniques or data, this reviewer disagreed with the text in few areas. I must take issue with the statement on page 379 that ". . . the ultrasound appearances of the various focal lesions (in the liver) are usually specific." Although ultrasound is certainly a sensitive test in many clinical situations, I would hesitate to call it specific in evaluating liver lesions.

This book is well written with much clinical information. It would be useful in a department or hospital library for general background information from specific chapters. For a personal library, however, one may be better advised to obtain more recent publications, narrower in scope but more suitable for specific needs.

Beverly A. Spirt
SUNY Health Science Center at Syracuse
Syracuse, NY 13210

Neuroradiologic Findings in AIDS: A Review of 200 Cases

Robert M. Levy[1]
Scott Rosenbloom[2,3]
Lance V. Perrett[2,4]

The radiologic studies of 200 consecutive AIDS patients with neurologic symptoms were evaluated to determine their diagnostic specificity and prognostic value. Of 81 patients with initially normal CT scans, four (5%) later developed progressive neurologic illness. Of 75 patients with CT evidence of diffuse cerebral atrophy, 12 (16%) later developed CT abnormalities or had postmortem CNS disease. CT scans showed mass lesions initially in 44 patients and later in an additional seven patients. Although *toxoplasma gondii* infection was the most frequent cause of these lesions, the CT characteristics of cerebral toxoplasmosis are too nonspecific to warrant diagnosis without biopsy. Preliminary evidence suggests that MRI may be more sensitive than CT in detecting intracranial disease in patients with AIDS.

As AIDS has become more widespread, it has become apparent that the neurologic manifestations of this disease are common: 39% of patients with AIDS have neurologic symptoms and 10% have these symptoms as their initial complaint [1–3]. Some of the neuroradiologic findings in AIDS patients have been described in earlier reports [4–7]. With dramatically increased numbers of such patients has come greater experience in neuroradiologic evaluation of AIDS, particularly with respect to the neuropathologic correlates of the radiologic findings. In this report, we describe the neuroradiologic findings in 200 AIDS patients with neurologic symptoms who were evaluated at the San Francisco General Hospital or the University of California Medical Center, San Francisco, from 1983 to 1985. The neuroradiologic studies were evaluated to determine their diagnostic specificity and prognostic value in this patient population.

Materials and Methods

The neuroradiologic studies of 200 consecutive patients with AIDS and neurologic symptoms were reviewed. Histopathologic examination of tissue obtained by biopsy or at autopsy was performed in 40 patients; the remaining 160 patients were followed for up to 2 years. The patients were all homosexual men ranging in age from 23 to 60 years, and the majority (56%) were in the fourth decade of life. The diagnosis of AIDS was made according to the criteria established by the Centers for Disease Control [8].

The CT scans were obtained with a GE 8800 or GE 9800 CT/T scanner using standard techniques; slice thickness was 10 mm. Intravenous contrast material (average dose, 42 g/l) was administered up to 30 min before scanning in all patients; double-dose contrast enhancement was not used. MRI was performed using a spin-echo technique on a Diasonics imager with a 0.35-T superconducting magnet. The T1-weighted scans were obtained with TR = 500 msec and TE = 28 msec; for the T2-weighted images, TR = 2000 msec and TE = 56 msec. A total of 240 CT scans and six MRI scans were obtained.

Results

The neuroradiologic findings defined three groups of patients (Table 1). The first

This article appears in the September/October 1986 issue of *AJNR* and the November 1986 issue of *AJR*.

Received October 2, 1985; accepted after revision February 22, 1986.

Dr. Levy is supported by a fellowship from the Research Foundation of the American Association of Neurological Surgeons.

[1] Department of Neurological Surgery, School of Medicine, University of California, San Francisco, CA 94122. Address reprint requests to R. M. Levy, c/o The Editorial Office, Department of Neurological Surgery, 1360 Ninth Avenue, Suite 210, San Francisco, CA 94122.

[2] Department of Radiology (Neuroradiology), School of Medicine, University of California, San Francisco, CA 94122.

[3] Present address: Staff Neuroradiologist, The Cleveland Clinic Foundation, 9500 Euclid Avenue, Cleveland, OH 44106.

[4] Present address: Staff Neuroradiologist, Royal Adelaide Hospital, South Australia 5000.

***AJR* 147:977–983, November 1986**
0361–803X/86/1475–0977
© American Roentgen Ray Society

TABLE 1: **Initial CT Findings vs Outcome in 200 Patients with AIDS**

Initial CT Findings	No. of Patients	New CT Lesions	CNS Abnormality at Autopsy	Risk of Progression*
Normal	81	2	2	4/81 (5%)
Atrophy	75	5	7	12/75 (16%)
Focal lesion	44	N/A	29	N/A

* Defined as the percentage of patients who later developed focal lesions on CT scans or who had significant neuropathologic findings at autopsy.

TABLE 2: **Histopathologic Diagnoses and CT Findings in 45 Patients with AIDS**

Diagnosis	No. of Patients	CT Findings		
		Normal	Atrophy Only	Focal Lesions
Toxoplasma gondii	22[a]			22
T. gondii + primary CNS lymphoma	5			5
Primary CNS lymphoma	3	1[b]	1	1
Kaposi's sarcoma	2	1[b]		1
Leukoencephalopathy	2			2
Herpes simplex II	2		1	1
Herpes simplex I & cytomegalovirus	1		1	
Cryptococcus neoformans	2		2	
Coccidioides immitis	1		1	
Candida albicans	1			1
Sterile abscess	1			1
Nondiagnostic biopsy (gliosis, inflammation)	3			3
Total	45	2	6	37[c]

[a] Includes five patients with compelling clinical evidence of cerebral toxoplasmosis but without histopathologic confirmation.
[b] CT scans performed several months before autopsy.
[c] Fourteen additional patients had focal lesions on CT, but no biopsy or autopsy was performed.

group consisted of 81 patients (40.5%) whose initial CT scans were normal. In two of these patients, CT scans obtained 6 and 32 days later, respectively, showed multiple bilateral lesions representing cerebral toxoplasmosis. In two additional patients, postmortem examination revealed CNS disease: one was found to have diffuse lymphoma 3 months after a normal CT scan had been obtained; the second, who died several months after his single CT scan showed no abnormalities, had metastatic Kaposi's sarcoma. Thus, 77 of these 81 patients had no progression of their neurologic symptoms and no CT abnormalities during follow-up.

The second group consisted of 75 patients (37.5%) whose initial CT scans showed evidence of diffuse cerebral atrophy only. Five of these patients later developed focal lesions on CT that were shown to be caused by *Toxoplasma gondii* infection. At postmortem examination, seven additional patients were found to have CNS disease, including two cases of cryptococcal meningitis, two cases of herpes simplex encephalitis, and one case each of toxoplasmosis, coccidioidomycosis, and primary CNS lymphoma. Sixty-three of the 75 patients had unchanged repeat CT scans or remained neurologically stable during follow-up.

The third group included 44 patients (22%) who had one or more focal lesions, with or without concomitant atrophy, on initial CT scans. Thus, a total of 51 patients (including seven patients from groups 1 and 2) had focal lesions that were detected on initial or subsequent CT scans. Neuropathologic diagnoses, obtained at autopsy or by biopsy, were available for 29 of these patients; compelling clinical diagnoses were made in five patients. No diagnosis was available for 17 patients who either refused biopsy or autopsy or were lost to further clinical follow-up.

The histopathologic diagnoses and CT findings in 40 patients (20%) who had a biopsy or postmortem examination are listed in Table 2; the five patients with compelling clinical evidence of cerebral toxoplasmosis, including positive serum and CSF titers and an objective clinical response to chemotherapy, but without histopathologic confirmation, are also included in this table. Infection with *T. gondii* was the most frequent histopathologic diagnosis, either alone (17 patients) or in conjunction with primary CNS lymphoma (five patients). There were no demonstrable differences in the CT scans of patients with toxoplasmosis only and those with toxoplasmosis and lymphoma. The most common CT finding associated with toxoplasmosis was a large low-density area that showed ring enhancement upon injection of contrast material (18 of 27 patients, 68%) (Fig. 1). These lesions were multiple in 11 patients and the most common site was within the basal ganglia (20 patients, 75%) (Fig. 2). The mass effect of basal lesions often resulted in compression of the third ventricle, dilatation of the lateral ventricles, and obliteration of the sylvian fissures (Fig. 3). Smaller low-density lesions that showed variable enhancement after injection of contrast material were noted in 16 of these 27 patients (Fig. 4).

In eight patients with toxoplasmosis and focal abnormalities other than ring-enhancing lesions, the CT scans showed single or multiple hypodense areas with less mass effect. These hypodense lesions were usually peripheral rather than central, and in the majority of cases there was slight enhancement adjacent to the lesion, usually around its cortical surface (Fig. 5). In two patients the CT scans showed high-density areas within low-density lesions (Fig. 6) that enhanced homogenously upon injection of contrast medium; these findings were thought to represent hemorrhage into necrotic lesions and were confirmed by histopathologic evaluation in both cases. One additional patient had CT evidence of ventricular dilatation only; postmortem examination 24 hours later revealed diffuse cerebral toxoplasmosis. Most of the patients with toxoplasmosis had CT evidence of atrophy.

Eighteen patients in whom histopathologic data are available did not have toxoplasmosis, either alone or with lymphoma (Table 2). Of three patients with primary CNS lymphoma, one had bilateral, small ring-enhancing lesions in the paraatrial regions (Fig. 7), one had evidence of atrophy, and the third had a normal CT scan 2 months before his autopsy diagnosis. One patient with metastatic Kaposi's sarcoma had a single diffusely enhancing mass lesion in the right frontal lobe; the second patient with Kaposi's sarcoma had a normal

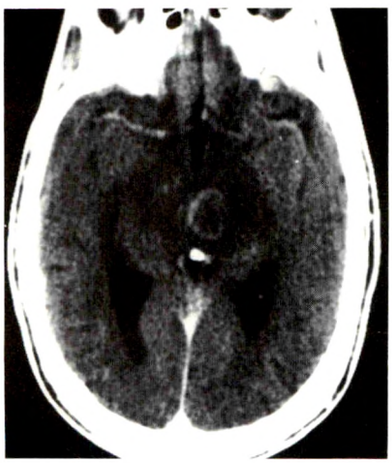


Fig. 1.—Toxoplasmosis abscess. Single ring-enhancing lesion in left thalamus with extension to upper brainstem and into right thalamus as well.

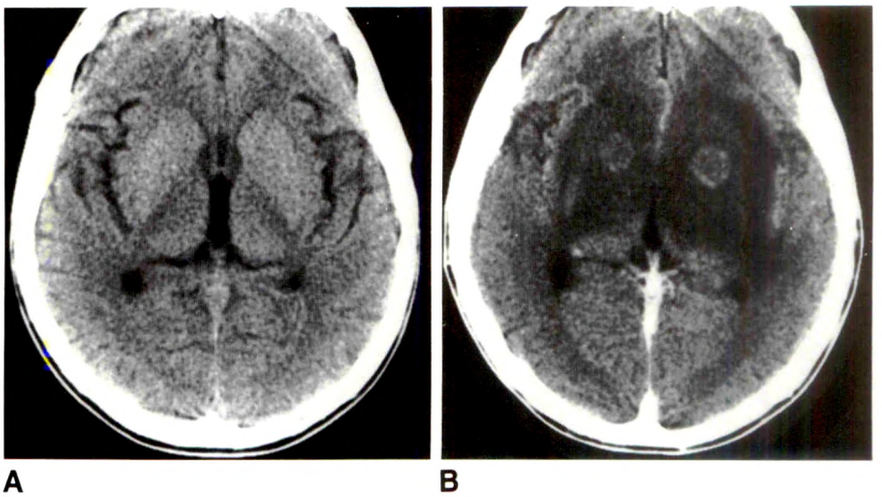


Fig. 2.—Bilateral toxoplasmosis abscesses. **A**, Normal scan. **B**, Bilateral ring-enhancing lesions with surrounding edema 30 days later. Note compression of third ventricle.

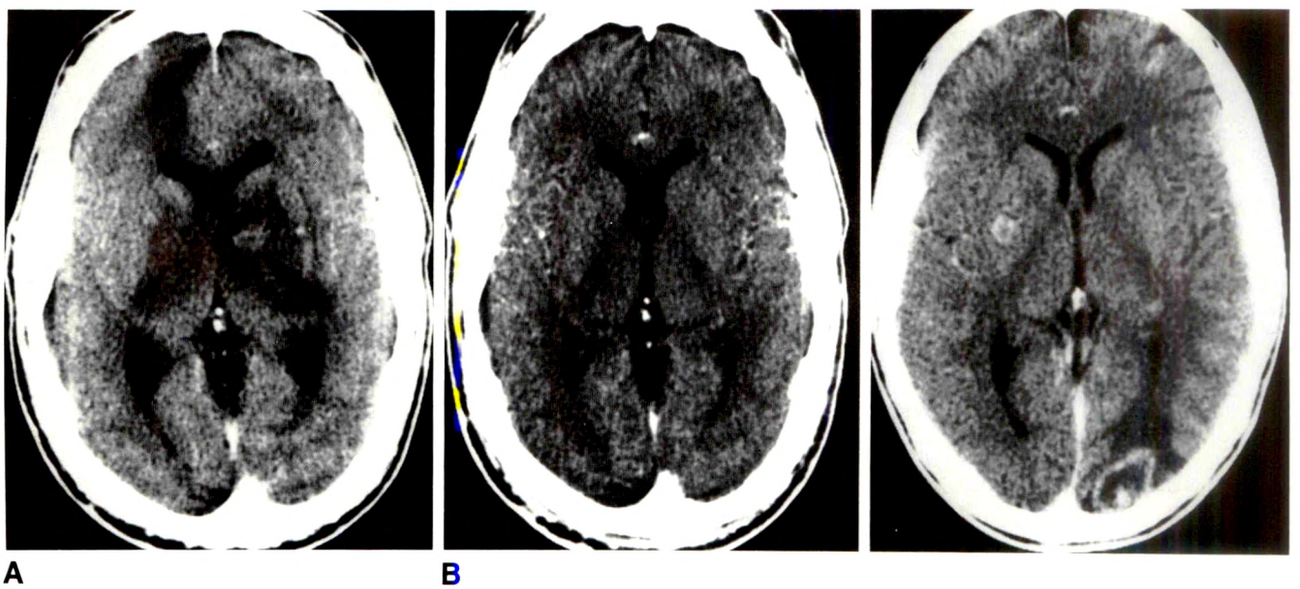


Fig. 3.—Multifocal toxoplasma abscesses. **A**, Right frontal nonenhancing and left basal ganglia ring-enhancing lesions with secondary compression of third ventricle and slight hydrocephalus. **B**, Near-complete resolution of all abnormalities after 20 days of therapy.

Fig. 4—Multifocal toxoplasma abscesses. Multiple deep and peripheral ring-enhancing lesions with and without edema.

CT scan several months before his autopsy diagnosis. Leukoencephalopathies were diagnosed in two patients. In one, CT scans showed widening of the frontal horns and bilateral low density of the adjacent white matter; these changes were more vividly displayed on MRI scans (Fig. 8). Neuropathologic evaluation at autopsy revealed a bifrontal leukoencephalitis characterized by demyelination and multinucleated giant cells. The second patient, in whom progressive multifocal leukoencephalopathy was diagnosed both by biopsy and at autopsy, had bilateral low-density areas near the external capsules without mass effect. One patient with herpes simplex type II encephalitis had bilateral low-density mass lesions with enhancement adjacent to the sylvian fissures; in the other patient with herpes simplex II and in the patient with mixed herpes simplex I and cytomegalovirus encephalitis, CT scans showed atrophy. Cerebral atrophy only was noted on the CT scans of the two patients with cryptococcal meningitis and the patient with coccidioidomycosis. The patient with *Candida albicans* infection had CT scans showing persistent, multiple, bilateral ring-enhancing lesions. The CT findings in

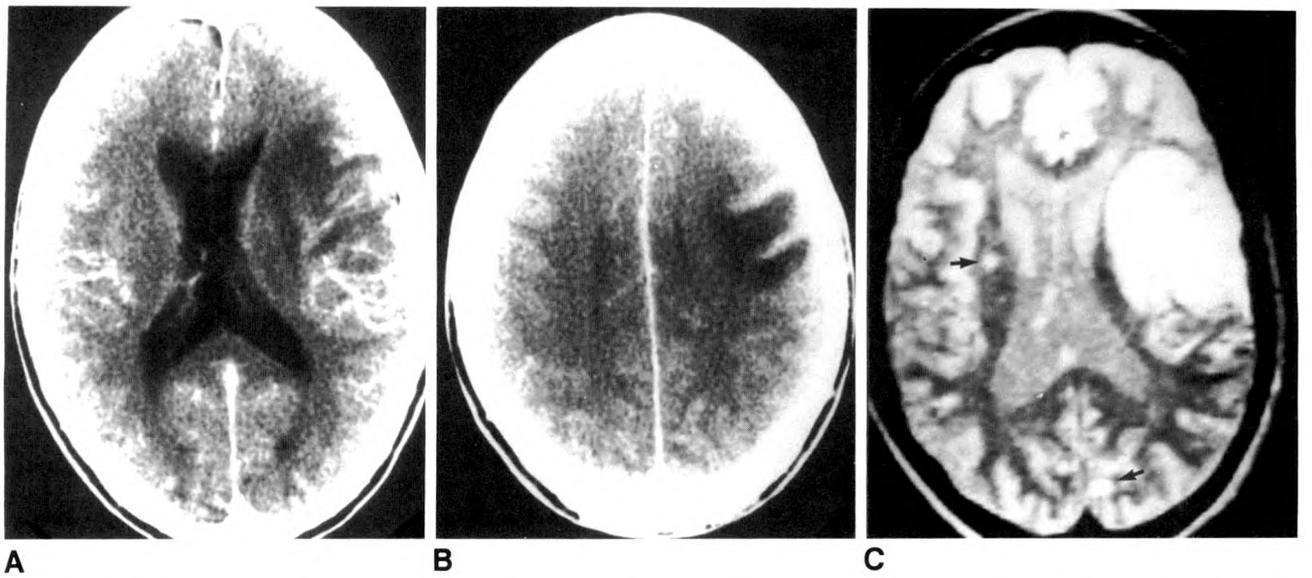


Fig. 5.—Atypical toxoplasmosis. **A** and **B**, CT scans showing left parietal edema with gyral enhancement and compression of left lateral ventricle. **C**, MRI scan obtained with spin-echo sequence (TR = 2000 msec, TE = 56 msec) on same day shows additional lesions in right corona radiata and in left occipital lobe (*arrows*).

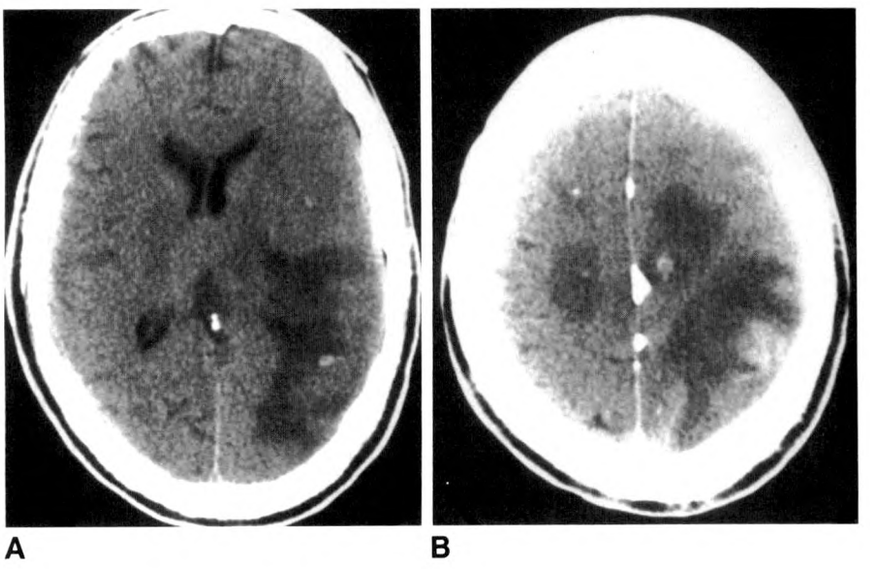


Fig. 6.—Hemorrhagic toxoplasmosis. **A** and **B**, Noncontrast scans showing bilateral low-density lesions containing focal areas of hemorrhage, which were confirmed at autopsy. Note mild left-to-right shift caused by mass effect of large left posteroparietal lesion.

the patient whose brain abscess was culture-negative consisted of bilateral ring-enhancing lesions in the vicinity of the basal ganglia and a solid lesion in the left parietal lobe; this scan was indistinguishable from those of patients with cerebral toxoplasmosis.

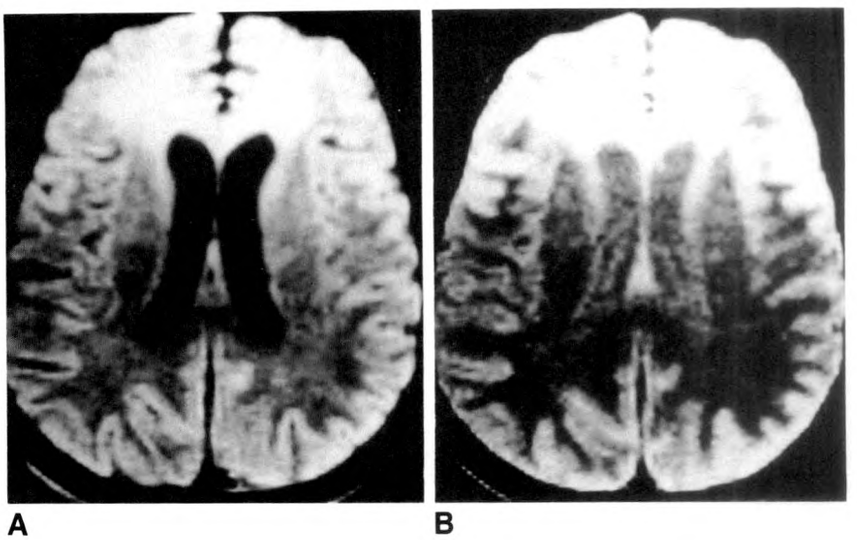
Histopathologic diagnoses were not available in 22 patients with focal lesions on CT. Five patients had compelling clinical evidence of cerebral toxoplasmosis. The remaining 17 patients had CT evidence of atrophy and small, usually nonenhancing, hypodense lesions distributed throughout the brain. None of these patients came to biopsy or postmortem examination; only one underwent serial CT scanning, which showed no significant change in the cerebral lesions over 3 months.

Discussion

The increasing number of AIDS patients and the high incidence of neurologic manifestations in this syndrome have led to a rapid increase in the frequency of neuroradiologic evaluation in patients with AIDS. Because these patients may have neurologic abnormalities seldom found in immunocompetent patients, and because the neuroradiologic findings are often confusing and nonspecific, it is particularly important to



Fig. 7.—Lymphoma mimicking toxoplasmosis. Enhanced scans show bilateral ring-enhancing lesions with surrounding edema that is indistinguishable from toxoplasma abscesses.



A B

Fig. 8.—Bifrontal leukoencephalitis. MRI shows widening of frontal horns and bilateral increases in signal intensity of adjacent white matter. **A**, T1-weighted scan; TR = 500 msec, TE = 28 msec. **B**, T2-weighted scan; TR = 2000 msec, TE = 56 msec.

correlate such findings with the natural history and histopathology of AIDS-related neurologic illnesses.

Of the 200 patients in this study, those who had initially normal CT scans constituted the largest group. Two of these 81 patients developed CT changes consistent with a diagnosis of toxoplasmosis; at autopsy, one additional patient was found to have primary CNS lymphoma and another had metastatic Kaposi's sarcoma. Thus, only four of 81 patients (5%) with initially normal CT scans later developed CT or histopathologic evidence of neurologic disease.

Patients with initial CT evidence of atrophy only (group 2) appeared to be at higher risk. Most of these patients were young, and there is little doubt that their atrophy was related to AIDS and not to normal aging. In all but three cases, the ventricular dilatation was proportional to the widening of the sulci and fissures. Recent studies have demonstrated a high incidence of primary CNS infection with human T-lymphotropic virus type III (HTLV-III), the virus thought to be causally related to AIDS [10]. As it has been suggested that such infection frequently may be the cause of encephalopathy in AIDS patients [11], it is possible that the cerebral atrophy seen in AIDS patients in whom additional cerebral abnormalities have not been identified may reflect infection with HTLV-III. Five of the 75 patients in this group subsequently developed cerebral toxoplasmosis that was evident on CT scans; seven other patients developed lesions that were found at autopsy, including cryptococcal meningitis in two, herpes simplex encephalitis in two, and toxoplasmosis, coccidioidomycosis, and primary CNS lymphoma in one each. Thus, of 75 patients in whom the initial CT scans showed evidence of atrophy only, 12 (16%) developed further neurologic abnormalities that were detected by repeat CT scanning or postmortem examination.

Once the presence of focal abnormalities on the CT scan was established, evaluation of further scans was complicated by variations in treatment administered by different physicians, by patient compliance, and by the duration of follow-up. Therefore, the presence of new lesions on subsequent CT scans probably does not reflect the sensitivity or the prognostic value of such studies in our patients.

Previous studies by ourselves and others [1, 3, 6] have indicated the high incidence of cerebral toxoplasmosis in patients with AIDS. In the present study, toxoplasmosis was the most common histopathologic diagnosis. Most patients with *T. gondii* infection appear to have characteristic CT findings, especially low-density mass lesions in the basal ganglia that enhance upon injection of contrast medium; these lesions are often multiple and bilateral and may develop rapidly. In two patients, follow-up CT scans demonstrated characteristic lesions 6 and 32 days, respectively, after normal CT scans had been obtained (Fig. 2).

The response of cerebral toxoplasmosis to pyrimethamine and sulfadiazine varied in degree and in latency. CT scans showed resolution of lesions as early as 20 days and as late as 6 months after the initiation of treatment (Fig. 3). Despite therapy, complete resolution was not the rule. Patients whose lesions did disappear with therapy usually had persistent CT evidence of atrophy. Double-dose contrast enhancement was not used in this study, however; it is possible that nonenhancing lesions or "completely resolved" lesions might have shown enhancement with such a technique [6]. Our experience also indicates that despite resolution of lesions on CT scans, cerebral toxoplasmosis will recur when treatment is discontinued. We have therefore recommended that once a diagnosis of toxoplasmosis has been established, lifelong antibiotic therapy should be administered [1].

Although it is tempting to suggest that AIDS patients with CT evidence of mass lesions be treated empirically for toxo-

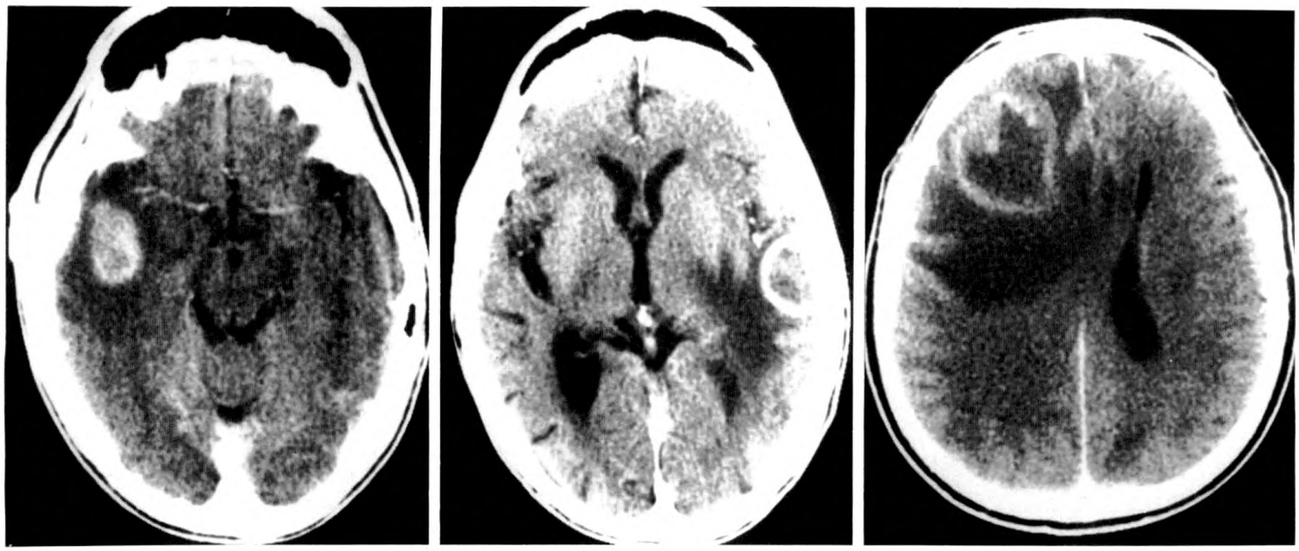


Fig. 9.—Atypical toxoplasmosis. **A**, Homogeneously enhancing right temporal lobe lesion with surrounding edema. **B**, Scan obtained 2 months later, during treatment for toxoplasmosis, shows a new left temporoparietal ring-enhancing lesion with surrounding edema. Original lesion in right temporal lobe has resolved.

Fig. 10.—Mixed toxoplasmosis and lymphoma. Large peripheral ring-enhancing right frontal lesion with surrounding edema and subfalcine herniation. This scan is indistinguishable from scans of patients with toxoplasmosis alone.

plasmosis, our experience indicates that this would be unwise. One patient, for example, whose CT scans showed lesions thought to be typical of cerebral toxoplasmosis was found to have primary CNS lymphoma. Another patient, while receiving empiric treatment for toxoplasmosis, developed new lesions after the initial focal abnormalities had resolved almost completely. This clinical picture suggests the emergence of another disease (Fig. 9). Five of six patients with multiple intracranial abnormalities had toxoplasmosis in addition to a second process; these processes were identified within the same lesion by needle biopsy in three patients and were in different sites in each of the other three. Therapy for toxoplasmosis alone would leave the second disease untreated. Therefore, biopsy appears to be necessary in all AIDS patients with CT evidence of mass lesions. If a patient has evidence of progression on subsequent CT scans, additional biopsies may be necessary to rule out the presence of multiple simultaneous intracranial diseases [12].

Lymphoma was the second most common pathologic finding in this series. Of the three patients with primary CNS lymphoma, one had a normal scan, one had atrophy only, and the third had bilateral ring-enhancing lesions that mimicked toxoplasmosis (Fig. 7). There were no differentiating features on CT to distinguish patients with toxoplasmosis from those with toxoplasmosis and lymphoma (Fig. 10). In contrast, progressive multifocal leukoencephalopathy can usually be distinguished from toxoplasmosis on CT scans by the absence of mass effect and enhancement and by the limitation of lesions to the white matter. These features were seen on the CT scans of the patient with progressive multifocal leukoencephalopathy and on the scans of the patient with bifrontal leukoencephalitis.

In several patients whose CT scans were normal, autopsy revealed CNS disease. There are several possible explanations for this apparent insensitivity of CT scanning. The first is a lengthy interval between CT scanning and postmortem diagnosis, which occurred in three of our cases. One patient with cryptococcal meningitis, whose initial CT scan showed only atrophy, developed a cryptococcoma that was discovered at autopsy 3 months later; two patients with normal CT scans were each found several months later to have a mass lesion (metastatic Kaposi's sarcoma and primary CNS lymphoma) that may well have been detected by follow-up CT scans. A second possible explanation is that toxoplasmosis, particularly in profoundly immunocompromised patients, frequently causes diffuse encephalitis without a secondary reaction. Thus, the brain is overwhelmed with *T. gondii*, but there is no abscess or focal lesion. In one patient, the presence of diffuse toxoplasma encephalitis without focal abscess formation was confirmed by autopsy 1 day after a normal CT scan had been obtained. A third possibility, which probably reflects an inherent limitation of this imaging technique, is that CT is insensitive despite the presence of local reaction. We have documented this with combined MRI and autopsy studies. Lesions missed by CT scans have ranged in size from a few millimeters to 2 cm or larger.

There is some indication that MRI may be more sensitive than CT in detecting intracranial abnormalities in patients with AIDS [1, 9]. All six MRI scans obtained in this series showed abnormalities that were not demonstrated by CT. In one patient with a normal CT scan, MRI showed multiple focal lesions; biopsy of these lesions led to the diagnosis of toxoplasmosis. Three of the patients who had MRI scans had CT evidence of atrophy only: in one, MRI demonstrated high

signal intensity throughout the white matter of both cerebral hemispheres, which was found at autopsy to represent leukoencephalopathy, and in the other two demonstrated focal lesions that have yet to be identified. One patient with toxoplasmosis had atypical findings on the CT scan; MRI revealed several lesions that were not evident on the CT scans (Fig. 5). Thus, it appears that MRI may be a valuable supplement to CT, especially when the CT scan shows evidence of atrophy only.

This study indicates that many AIDS patients with neurologic symptoms have normal CT scans and little risk of neurologic progression. In patients with CT evidence of diffuse cerebral atrophy, which in itself is nondiagnostic, there is a significant risk of neurologic and radiologic progression. Although *T. gondii* infection is the most frequent finding in patients with CT evidence of mass lesions, many diseases can mimic the CT appearance of toxoplasmosis, and AIDS patients often have multiple simultaneous intracranial abnormalities. Thus, it is unwise to assume that these lesions are caused by *T. gondii*, and biopsy is therefore recommended.

ACKNOWLEDGMENT

We thank Stephen Ordway for editorial assistance.

REFERENCES

1. Levy RM, Bredesen DE, Rosenblum ML. Neurological manifestations of the acquired immunodeficiency syndrome (AIDS): experience at UCSF and review of the literature. *J Neurosurg* **1985**;6:(2)475–495
2. Bredesen DE, Messing R. Neurological syndromes heralding the acquired immune deficiency syndrome. *Ann Neurol* **1983**; 14:141 (abstr)
3. Levy RM, Pons VG, Rosenblum ML. Central nervous system mass lesions in the acquired immunodeficiency syndrome (AIDS). *J Neurosurg* **1984**;61:9–16
4. Kelly WM, Brant-Zawadzki M. Acquired immunodeficiency syndrome: Neuroradiological findings. *Radiology* **1983**;149:485–491
5. Whelan MA, Kricheff II, Handler M, et al. Acquired immunodeficiency syndrome: cerebral computed tomographic manifestations. *Radiology* **1984**;149:477–484
6. Post MJD, Chan JC, Hensley GT, Hoffman TA, Moskowitz LB, Lippmann S. Toxoplasma encephalitis in Haitian adults with acquired immunodeficiency syndrome: a clinical-pathologic-CT correlation. *AJR* **1983**;140:861–868, *AJNR* **1983**;155–162
7. Bursztyn EM, Lee BCP, Bauman J. CT of acquired immunodeficiency syndrome. *AJNR* **1984**;5:711–714
8. Centers for Disease Control. Prevention of acquired immune deficiency syndrome (AIDS): report of interagency recommendations. *MMWR* **1982**;32:101–103
9. Levy RM, Bredesen DE, Moore S, Posin J, Mills C. Cranial MRI in the acquired immunodeficiency syndrome (AIDS): superiority to CT. *Soc Mag Res Med* **1985**;4:375 (abstr)
10. Gallo RC, Salahuddin SZ, Popovic M, et al. Frequent detection and isolation of cytopathic retroviruses (HTLV-III) from patients with AIDS and at risk for AIDS. *Science* **1984**;224:500–503
11. Shaw GM, Harper ME, Hahn BH, et al. HTLV-III infection in brains of children and adults with AIDS encephalopathy. *Science* **1985**;227:177–182
12. Levy RM, Bredesen DE, Davis RL, Rosenblum ML. Multiple simultaneous intracranial processes in the acquired immunodeficiency syndrome (AIDS). Abstract presented at the annual meeting of the Congress of Neurological Surgeons, Honolulu, October **1985**

Book Reviews

Nuclear Medicine in Clinical Oncology. Current Status and Future Aspects. Edited by Cuno Winkler, New York: Springer-Verlag, 402 pp., 1986. $90

The tumor symposium of the European Society of Nuclear Medicine, held in May 1985 in Bonn, Federal Republic of Germany, assembled international experts on diagnostic and therapeutic nuclear medicine procedures used in the evaluation and management of the cancer patient. Although much of the material presented is not new and is available, often in a more detailed and organized format in other sources, the published proceedings consolidate this information and introduce contributions to German investigators, much of which is not available in the United States. The book is divided into sections dealing with conventional nuclear medicine procedures, receptor imaging, immunoscintigraphy, and the latest advances in the high technology fields of positron emission tomography (PET) and MR imaging. The overviews provided at the beginning of each section vary in scope and quality, but in general they orient the reader to major developments and remaining problems in each field.

The quality of the individual presentations varies from excellent to poor and may be a result of the type of editing by each author before publication. Proceedings of such meetings must be published promptly to be current, but, unfortunately, this may affect the quality of the editing. Some papers are limited in scope and deal with preliminary research with data from too few patients to be useful for clinical conclusions. Many papers are not illustrated; the radionuclide images presented are small and have a high contrast; and the captions are not informative.

The sections dealing with MR are well written and accurately reflect the state of knowledge at the time of publication. The section on MR contrast agents is especially well written and informative.

The strong points of this book are its broad scope, the participation of leading clinicians and researchers from the United States and Europe, and up-to-date descriptions of new technologies. The lack of quality illustrations and poor editing by individual contributors limit its usefulness for radiologists and nuclear medicine physicians.

Manuel Cerqueira
VA Medical Center
Seattle, WA 98108

Magnetic Resonance Imaging: Principles and Applications. By David M. Kean and Michael A. Smith. Baltimore: Williams & Wilkins, 164 pp., 1986. $43.95

This concise text has been written for medical students, house officers, and clinicians who are seeking an introduction to MR imaging. The authors have met this goal admirably. The book is divided into 10 brief chapters that discuss the fundamentals of the NMR experiment, pulse sequences, and image production, as well as imaging of the head and neck, thorax, abdomen and pelvis, and the musculoskeletal system.

The greatest strength of this text lies in the second chapter, which focuses on the basic physical principles employed in MR imaging. Comprehension of this brief, eloquent explanation of NMR fundamentals requires only a modest knowledge of physics.

The section on pulse sequences is equally well written and includes clear diagrams. A nine-page discussion on image production, covering selective excitation, frequency, encoded spatial information, and two-dimensional Fourier transform, may offer more information than is required by a reader with only a passing interest in MR, but it is surely one of the most easily understood essays on these areas.

A significant area of weakness in this text is obvious in the clinical chapters, where the use of mainly low magnetic field images is an unfortunate shortcoming. The images of abnormalities within the brain are of acceptable quality, but those of the thorax, spinal canal, and extremities are not adequate for demonstrating optimal usage of MR. The images are presented on a black background, which does produce less glare than white pages. The index is appropriate for the text, as is the reference list.

I recommend this text for purchase by readers seeking an introduction to MR imaging. The first four chapters, carefully designed for the intended audience, are excellent. Although the images presented probably do not match in quality those produced at most imaging centers today, they are of value in indicating the spectrum of disease that can be diagnosed by MR.

Charles M. Citrin
Magnetic Imaging of Washington
5550 Friendship Boulevard
Chevy Chase, MD 20815

MR and CT of Occult Vascular Malformations of the Brain

Paul F. J. New[1]
Robert G. Ojemann[1]
Kenneth R. Davis[1]
Bruce R. Rosen[1]
Roberto Heros[1]
Raymond N. Kjellberg[1]
Raymond D. Adams[2]
E. P. Richardson[3]

The need for improved specificity in the diagnosis of "occult" vascular malformations led to the use of MR in suspected cases in order to determine MR's potential for improved diagnostic accuracy. Six patients with six lesions histologically diagnosed as vascular malformation after partial (1) or complete (5) microsurgical excision were studied by CT, MR, and selective magnification subtraction angiography. In all cases, the cerebral lesions were apparently solitary and were visible as focal lesions on both CT and MR. Since angiography failed to reveal the pathologic blood vessels of the lesions, and no arteriovenous shunting was evident, these lesions were termed vascular malformations occult to angiography (VMOTA). Angiography revealed a mass effect in only two cases. MR did not reveal additional vascular malformations missed by CT. In each case, MR, which was performed in an attempt to support the diagnosis suggested by CT, did in fact do so by revealing signal abnormalities indicative of nonacute hemorrhage within the lesion on T1- and T2-weighted pulse sequences. Although, as on CT, MR features of these lesions were found to be nonspecific, the MR criteria reinforced the probable diagnosis of VMOTA in an additional 30 cases that had shown similar nonspecific CT features. In this second group, excluded from this study, in which histologic verification was not obtained because of perceived hazards of surgery, the increased assurance regarding the diagnosis led to proton-beam therapy without histologic verification in 18 cases. It is concluded that MR can provide significant improvement in the accuracy of diagnosing VMOTA beyond that obtainable just by plain and contrast-enhanced CT.

Extensive experience with CT has led to the recognition of criteria for the diagnosis of vascular malformations occult to angiography (VMOTA) [1–8]. All varieties of vascular malformation have been identified in this group; arteriovenous malformations, cavernous malformations, venous malformations, and telangiectases [5, 8]. On plain CT, these lesions tend to present as hyperdense, or occasionally isodense, relatively small mass lesions, generally no more than 3 cm in diameter [8–11], often containing recognizable punctate or small dense foci indicative of areas of calcification. After intravenous contrast enhancement, relatively mild or moderate rather than marked enhancement is commonly seen. Occasionally, small regions of intense enhancement suggest the presence of contrast medium in small blood vessels. Although the CT features may be highly suggestive of the diagnosis, there is as a rule uncertainty in the differential diagnosis of these lesions from neoplasms, particularly low-grade astrocytomas and oligodendrogliomas. Granulomatous lesions may also show similar CT appearances and, rarely, avascular meningiomas may mimic VMOTAs. Because of the problems of accurate diagnosis, MR has been used at this center for approximately 2 years when this diagnosis has been suspected. This report documents our findings in six cases with surgical and histologic verification.

Subjects and Methods

Six patients for whom the diagnosis of a VMOTA was a major consideration were studied

This article appears in the September/October 1986 issue of *AJNR* and the November 1986 issue of *AJR*.

Received December 16, 1985; accepted after revision March 19, 1986.

Presented in part at the annual meeting of the American Society of Neuroradiology, San Diego, January 1986.

[1] Department of Radiology, Massachusetts General Hospital and Harvard Medical School, Boston, MA 02114. Address reprint requests to P. F. J. New, Dept. of Radiology, Section of Neuroradiology, Massachusetts General Hospital, Boston, MA 02114.

[2] Service of Neurology, Massachusetts General Hospital and Harvard Medical School, Boston, MA 02114.

[3] Department of Pathology (Charles S. Kubik Laboratory for Neuropathology), Massachusetts General Hospital and Harvard Medical School, Boston, MA 02114.

***AJR* 147:985–993, November 1986**
0361–803X/86/1475–0985
© American Roentgen Ray Society

TABLE 1: **Clinical, Surgical, and Histologic Features**

Case	Gender Age (yrs)	Site	Clinical	Surgery	Gross Appearance	Histology
1	M 26	L posterior temporal	3 mo. episodic headache, nausea and vomiting, difficulty reading	Excision	Encapsulated mass Old clot Gliosis	Vascular malformation
2	M 41	L pontocerebellar	1½ mo. episodic instability, dizziness, nausea, visual blurring	Excision	Tangle of vessels Gliosis, hematoma Cavity Thrombosed arteriovenous malformation	Arteriovenous malformation
3	M 27	Posterior pontomesencephalic	36 mo. episodic blurred vision, diplopia, headache, speech difficulty	Limited excision ventricular shunt	Encapsulated mass within old hemorrhage Thrombosed vascular malformation	Consistent with vascular malformation
4	M 40	L para-fourth ventricular	12 mo. episodic vertigo, nausea and vomiting, headache, diplopia, subarachnoid hemorrhage	Excision	Small mass Old hemorrhage Thrombosed arteriovenous malformation	Arteriovenous malformation
5	F 31	L frontal	8 mo. episodic minor seizures, recent generalized seizure	Excision	Encapsulated mass containing old hemorrhage Gliosis Vascular malformation	Arteriovenous malformation
6	F 40	L frontal	Many years of L frontal headache. 16 mo. earlier acute headache, nausea and vomiting, then obtundation, grand mal seizure	Excision	Localized mass Recent and old hemorrhage Gliosis Vascular malformation	Arteriovenous malformation

Note.—L = left.

by MR. CT was the initial imaging study in all cases and was performed using a variety of third- and fourth-configuration scanners, before and after intravenous contrast injection in all cases. Serial film selective catheter angiography, with magnification and subtraction, which in all cases failed to reveal either intrinsic abnormal vessels or vascular shunting, was performed either before or after MR. MR was performed using a superconductive whole-body system (Teslacon, Technicare Corp., Solon, OH) operating at 0.6 T (25.4 MHz). T1- and T2-weighted spin-echo (SE) pulse sequences and inversion recovery (IR) with spin-echo sequences were used. All patients had IR sequences with repetition times (TR) of 1500 or 1650 msec, inversion time (TI) of 400 or 450 msec, and echo time (TE) of 32 msec. Four acquisitions were averaged, except in one case, in which only a single acquisition was obtained. It is our usual practice to image the brain using the more T1-weighted IR sequence in preference to a short TR and TE SE sequence. One patient also had a less T1-weighted sequence, with TR 500 msec and TE 30 msec. One patient had in addition a mixed T1- T2-weighted SE sequence, TR 1500, TE 30. T2-weighted sequences were dual-echo SE 2000/60 and /120 msec, TR/TE, with four acquisitions, except for one patient who was examined with separate SE 1500/30 and 1500/60 sequences instead. The latter patient was examined with a single-section technique and 8-mm thick sections. The other patients all had multisection contiguous 7.5-mm slice technique. All patients were studied with axial sections. One patient had an additional IR sequence in the sagittal plane.

Data were acquired with 128-line resolution in the phase-encoded (Y) axis, interpolated to 256, and 256 lines in the frequency-encoded (X) axis, for a display matrix of 256 mm^2, giving pixel resolution of 2.0×1.0 mm.

Clinical Features

There were four men and two women, ranging in age from 26 to 41 years (mean, 34.1 years). In general, the predominant symptoms were similar to those described in earlier reports [3, 8]. Symptoms were typically episodic, over weeks, months, or years, and most frequently consisted of headache, with or without nausea and vomiting, seizures of various types, and focal neurologic deficits appropriate to the region involved (Table 1).

CT and MR

In each case, the pre- and postcontrast attenuation characteristics revealed by CT, and the signal intensities and their patterns on T1- and T2-weighted images, were analyzed and compared with those of normal anatomic structures shown in the same CT section and in the same MR image. T1 and T2 relaxation values were assessed qualitatively and were not measured or calculated.

Angiography

All angiograms were performed by selective catheterization, with magnification and subtraction. The examinations were all restudied retrospectively.

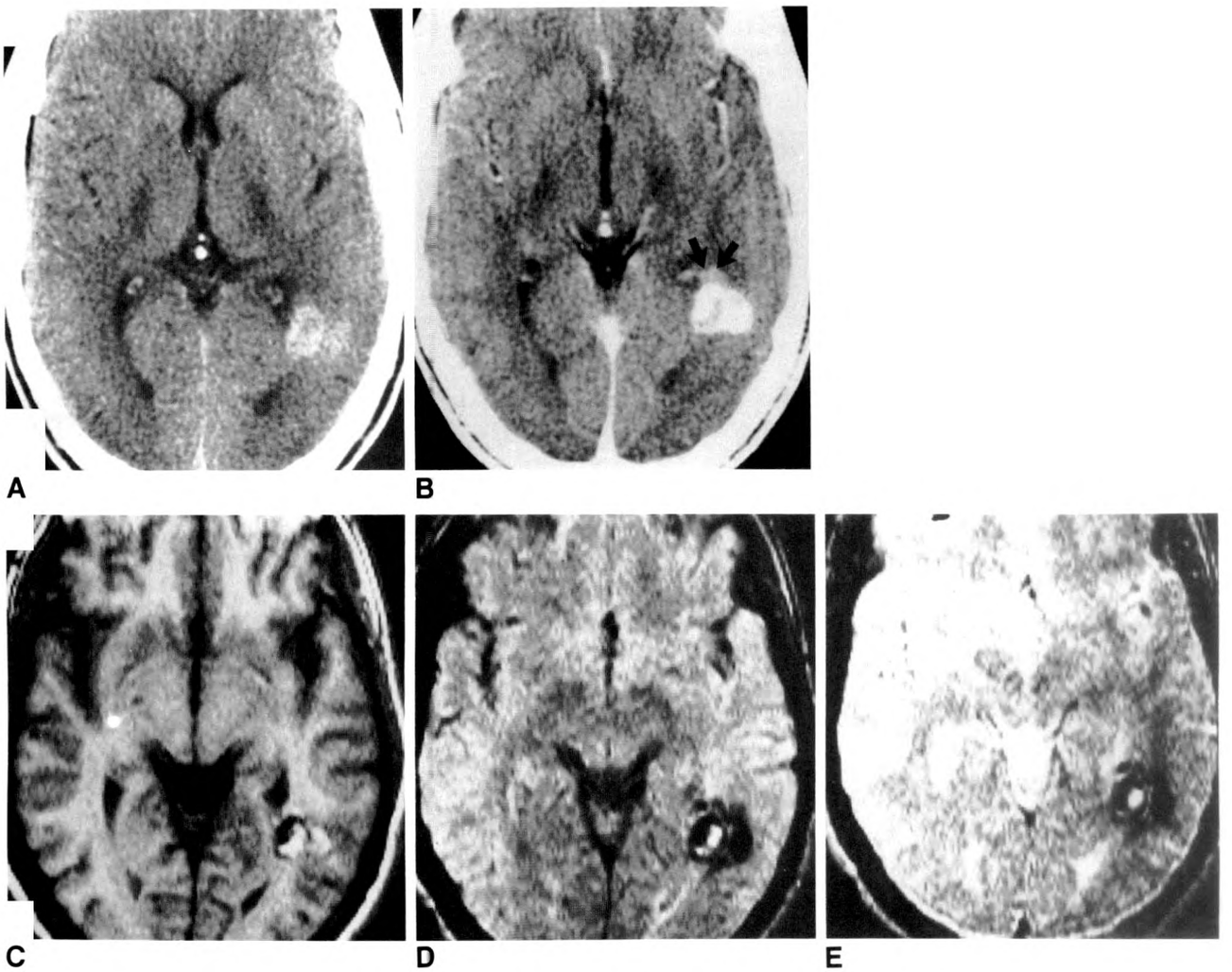


Fig. 1.—Case 1. **A**, Plain CT shows heterogeneous hyperdense lesion adjacent to trigone and occipital horn, probably but not definitely including punctate calcifications. **B**, After contrast, there is moderate heterogeneous enhancement of lesion, with appearance of small vessels anteriorly (*arrows*). Small vessels were apparent in lateral portion of lesion at time of acute hemorrhage 2½ months earlier (not shown). **C**, MR, 4 days later. IR 1650/450/32/4. Bright islands indicating short T1 are partly surrounded by areas of absent or near-absent signal. **D**, SE 2000/60/2 moderately T2-weighted sequence shows smaller bright islands of prolonged T2 within more extensive region of absent signal. **E**, Same sequence, but with TE 120. The bright foci are smaller than in **D**, but there is little change in appearance of surrounding area of signal void.

Results

Angiography

Each case satisfied the strict criteria for VMOTA in that no pathologic vessels or arteriovenous shunting were identified on careful retrospective study of the angiograms. There was no evidence of mass effect in four cases, and mass effect was identified in two cases.

CT

The lesions in all patients were 3 cm or less in diameter. All showed somewhat heterogeneous hyperdensity relative to brain on plain CT. In only two cases (cases 3 and 6) was definite granular calcification identified. In the lesions of three other cases (cases 1, 2, and 4), the heterogeneous hyperdensity raised suspicion of punctate calcifications, nonacute hemorrhage, dense soft tissues, or a combination of these. Case 5 had an isodense appearance, without mass effect on initial plain CT. Four months later, CT showed an irregular, thick ring with the density of relatively recent hemorrhage, and a lower mixed density centrally. The pattern suggested hemorrhage in a neoplasm, rather than a vascular malformation. In case 1, plain CT originally revealed a focal acute hemorrhage in the left temporal lobe, and intravenous contrast enhancement produced a slight increase in density at the periphery of the hematoma. Focal areas of this enhancement were consistent with small associated blood vessels. Two and a half months later, plain CT revealed a heterogeneous hyperdense lesion at the same site, and moderate, slightly heterogeneous enhancement occurred. There was again indication of small abnormal blood vessels in the region. In all



A



B



C



D

Fig. 2.—Case 2. **A**, Contrast CT shows moderate irregular enhancement of lesion, centered in left brachium pontis. In this and an adjacent section, enhancement of small vessels in and adjacent to lesion were seen (e.g., *arrow*). Noncontrast scan (not shown) revealed a heterogeneous, largely hyperdense lesion. **B**, MR, 2 days after CT, IR 1650/450/20/4, reveals largely homogeneous bright signal of short T1, consistent with nonacute hemorrhage. Areas of lesser signal centrally are consistent with hemorrhage and do not correspond to areas of enhancement suggestive of vessels on CT. **C**, SE 2000/60/4 moderately T2-weighted sequence 7.5 mm higher than section **B** shows large bright islands of increased T2, largely bounded by zone of absent signal and irregular areas of absent or reduced signal between the islands. With same SE sequence as at level in **B** (not shown), there was a narrow, almost completely circumferential, zone of absent signal around high signal. Posteriorly and laterally, a less intense signal around the lesion is indicative of edema. **D**, The same sequence, but with TE 120, more markedly T2-weighted. High-intensity islands and peripheral absent signal are much the same in distribution as in **C**. Perifocal edema is evident. Note that low signal regions between bright islands do not show appreciable increase in intensity (lack of second echo enhancement) and therefore are not suggestive of slowly flowing blood within vessels.

lesions, enhancement was mild or moderate in degree and heterogeneous in pattern. However, small rounded or arcuate foci of marked enhancement appeared in three cases (cases 1, 2, and 4), indicating the presence of small abnormal blood vessels (Figs. 1, 2, and 4; Table 2).

In summary, the findings on CT fitted well with the variety of appearances previously reported in VMOTA [1–8]. After angiography, VMOTA was the suspected diagnosis in all but cases 5 and 6, in which a hemorrhagic neoplasm (case 5) and a partially calcified glioma (case 6) were strongly suspected.

MR

Of the six cases, T1- weighted images revealed one or more foci of short T1, appearing as one or more bright "islands" in four cases (Figs. 1 and 2). Cases 4 and 6 showed only low signal (Figs. 3 and 4). In addition, areas of very low or absent signal on T1-weighted images were present peripherally and/or centrally in four cases and questionable in a fifth.

On T2-weighted images, one or more foci on long T2, appearing as one or more bright "islands," were seen in five cases. This was accompanied by very low or absent T2 signal (very short T2) in five cases, was arranged peripherally in four cases, and peripherally plus centrally in one case ("dark lakes"). In the remaining case (case 6), the entire area showed low to absent T2 signal (Fig. 4, Table 2).

Surgery

The lesion was excised partially in case 3 and completely in the remaining five cases, using microsurgical techniques. The gross appearance of the lesion at surgery was described as thrombosed arteriovenous malformation in cases 2 and 4 and as "vascular malformation" in the remaining cases.

All lesions appeared well encapsulated and showed gross evidence of old hemorrhage in cases 1–5 and of old and recent hemorrhage in case 6. Hemosiderin deposition was specifically commented upon in cases 5 and 6.

TABLE 2: **CT and MR Findings, and Time Intervals**

Case	CT		Interval to MR	MR			Interval to Surgery
	Plain	Enhanced		T1 Weighted	T2 Weighted	More T2 Weighted	
1	Acute hemorrhage 2½ mo. earlier; now hyperdense	Small vessels; moderate CE + small vessels	4 days	Confluent bright foci; adjacent signal void	Smaller bright islands within larger signal void	Same except smaller bright islands	4 weeks
2	Hyperdense	Mild to moderate CE + small vessels	2 days	Bright island; less intense area within	Bright islands; peripheral signal void	Same	2 days
3	Hyperdense; granular calcifications	Mild to moderate CE	21 weeks + multiple over 4½ yrs. postop. (unchanged)	Confluent bright islands, most within low or absent signal	Similar confluent bright islands; more obvious peripheral and central signal void	Similar	243 weeks after limited excision
4	Hyperdense, with some hypodensity	Mild CE + small vessels	9 days	Small focus of low signal (< gray matter)	Island of isointense signal within signal void	Lesion obscured by noise	3 days
5	Isodense 4 mo. earlier; now recent hemorrhage, peripheral denser than central	Moderate CE adjacent to recent hemorrhage	Same day	Large bright island; small central low signal focus	Bright island; narrow peripheral interrupted void	Not done	2 days
6	Hyperdense; granular calcifications	Mild CE	11 weeks	Low signal (< gray matter) only	Low signal and void	Larger signal void	5 weeks

Note.—CE = contrast enhancement.

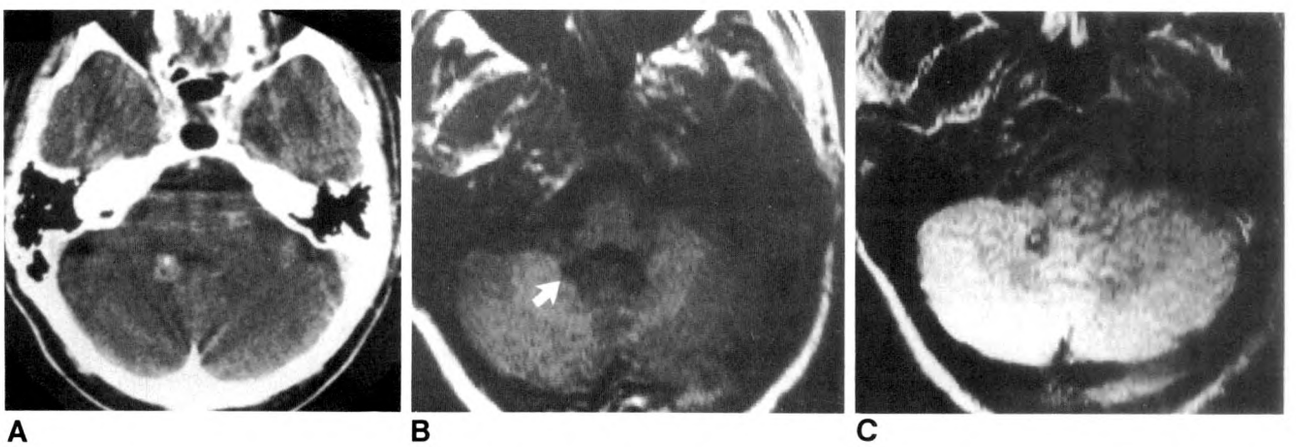


Fig. 3.—Case 4. **A**, Contrast-enhanced scan showing mild enhancement of this small, hyperdense lesion. One area of high density and a posterior arc of slightly increased density both suggest opacification of small blood vessels. Plain CT (not shown) showed mixed hyper- and hypodensity without definite calcification. The mass encroaches slightly upon the fourth ventricle. **B**, MR, 8 months later. IR 1500/450/4 T1-weighted section slightly below the level in **A**. There is small region of prolonged T1, similar to the T1 of gray matter, projecting into inferior portion of right cerebellar corpus medullaris from inferior vermis (*arrow*). No focus of short T1 is visible, presumably because hemorrhage was now many months old. **C**, SE 2000/60/2 moderately T2-weighted sequence at same level as **B.** A small area of approximately isointense signal is surrounded by zone of absent or near-absent signal. On same sequence with TE 120, no definite abnormality could be detected in this region, apparently because of the much higher noise level. (Note similarity to Fig. 5.)

Histology

Surgically excised material from each lesion was carefully reviewed. Because of the fragmentary character of the small tissue samples available, it was difficult to categorize with complete assurance the precise type of vascular malformation present in each case, although when viewed in light of the appearance at surgery, there was no doubt that these all represented vascular malformations. In various combinations, the following histologic features were observed: abnormally

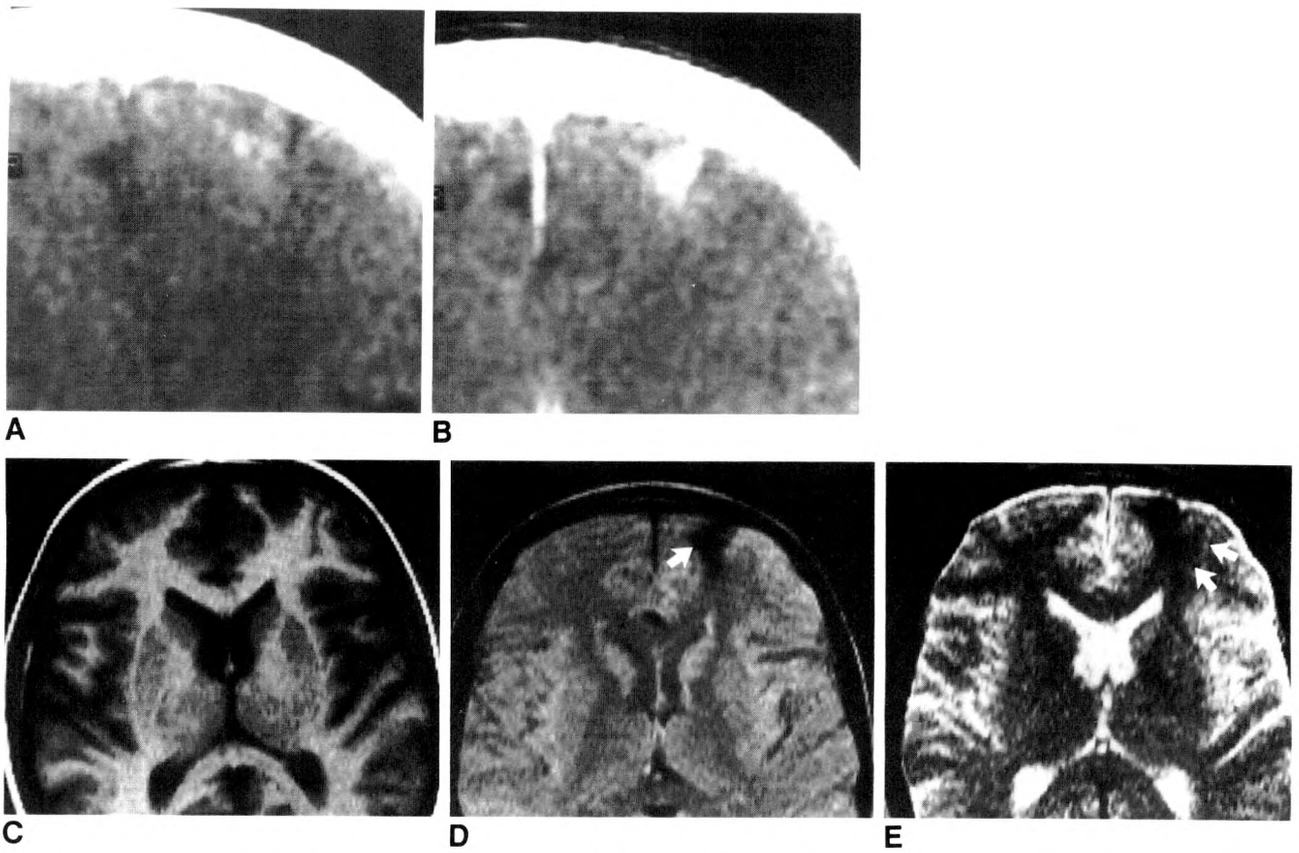


Fig. 4.—Case 6. **A**, Plain CT shows small hyperdense region in anterior left frontal lobe region, involving the cortex. Small granular calcifications are apparent. **B**, After intravenous contrast, area shows mild contrast enhancement surrounding calcifications. MR was performed 3 months after CT. **C**, IR 1500/450/4 sequence. A region of low signal, indicating T1 somewhat longer than gray matter, is shown extending from cortex into subcortical white matter. No mass effect is evident. **D**, SE 2000/60/2. The region of lesion (*arrow*) shows slightly heterogeneous pattern of absent to near-absent signal, indicating shortened T2, which is now confirmed by absent signal shown in **E** (*arrows*), obtained with a more strongly T2-weighted sequence, 2000/120/2. The lesion was excised 5 weeks later, when a little recent hemorrhage was identified in addition to much old clot and hemosiderin. It is probable that further hemorrhage occurred after MR.

formed blood vessels, many thrombosed or fibrosed; hyalinization of the walls of abnormal vessels; dystrophic calcifications; gliosis and hemosiderin deposition, frequently in high concentration; and evidence of old or recent and old hemorrhage (Table 1). Hemosiderin deposition was identified in tissue from all cases except case 1. Although the lesion was completely excised, only tiny fragments were available for microscopy. The final histologic diagnosis was arteriovenous malformation in one case, consistent with arteriovenous malformation in four cases, and vascular malformation of indeterminant type in one case (Table 1).

Discussion

Small vascular malformations became widely recognized after the report of Margolis et al. in 1951 [9], in which they called attention to small vascular malformations found on autopsy of six patients. Four of these were associated with fatal hemorrhage. Crawford and Russell [10] found that small vascular malformations were responsible for 20 of 461 cases of intracerebral hemorrhage. No abnormal vasculature was seen on angiography in two of the four patients who had this study. These authors introduced the term "cryptic" to describe these small malformations, because of their latent character both clinically and pathologically. Since that time, there have been many reports of arteriovenous malformations or other vascular malformations that were angiographically occult and responsible for spontaneous hemorrhage. Hashim et al. [8] recently reported three histologically proven VMOTAs. They were able to find only 47 reported cases of such histologically proven arteriovenous malformations not associated with clinically recognizable intracranial hemorrhage. The majority of these cases presented with seizures of various types and some with headaches. The lesions were generally detected by CT. Other vascular malformations with similar presentations have also been reported and include cavernous angiomas and venous angiomas [4, 5]. From previous reports, it is evident that VMOTAs are generally small, less than 2–3 cm in maximum size [8–11]. The true incidence is unknown, but their ratio to the classical malformations was 48:5, as detected in 48 autopsied cases by McCormick and Nofzinger [11]. They are usually said to give rise to signs and symptoms

when they hemorrhage, and hemorrhage may be massive. These lesions may present with neurologic symptoms without clinical evidence of intracranial hemorrhage. This was the case in each of our six cases, although the CT obtained at the time of a clinical exacerbation provided clear evidence of recent hemorrhage in two cases (cases 1 and 5). In the other four cases, CT did not reveal evidence of recent hemorrhage, owing either to failure to obtain CT at the appropriate time or to the presence of only a small seepage of recent hemorrhage, indistinguishable from the background hyperdensity of the VMOTA.

MR is steadily gaining acceptance as an important addition to the array of imaging techniques available for the investigation of neurologic disease, and it has been proposed as the diagnostic imaging method of choice for many forms of intracranial disease [12–15]. The capacity of MR to depict normal and abnormal vascular structures with high image contrast, without the need for intravascular contrast agents, has been demonstrated for normal vessels and a variety of vascular lesions [16–19]. A small number of cases has been reported in which intracranial vascular malformations have been identified by MR [20, 21]. A recent report of the comparative evaluation of CT and MR in 24 patients with 29 cerebral vascular malformations included 15 vascular malformations (in 11 patients) in which angiography revealed no pathologic circulation (VMOTAs) [20]. Histologic confirmation of the diagnosis was available in five of the 11 patients with VMOTAs. Ten of the 15 lesions could be seen equally well on CT and MR, three were more conspicuous on MR, and two were more conspicuous on CT. In the other six cases, the lesions were not safely accessible to biopsy or excision. Inherent hyperdensity was present on CT in 11 of the 15 lesions, and nonspecific enhancement, usually minimal, occurred in 13 lesions. Thirteen of 15 lesions were detected with MR, and the two that were missed were shown on CT only by virtue of fine punctate calcifications. Those that were shown by MR revealed relative signal void in three, hemorrhage in 12, and peripheral edema in seven. Evidence of slow flow (even-echo rephasing) could not be seen in any lesion. The regions of signal void were punctate or globular in all cases and were attributed to calcification rather than to high flow in vessels. However, the one illustrated case (Fig. 4) revealed a signal void much larger than the focus of calcification shown on CT and there were no corresponding opacified vessels. We suggest that the illustrated signal void in that case, and in our cases, is therefore most consistent with the selective effect of paramagnetic "clumps" (in this case hemosiderin deposits in macrophages) on spin-echo signal intensity. This manifests as a selective decrease in the apparent T2 of the region imaged, with lesser T1 effect. This phenomenon differs from that of the more commonly discussed interaction of uniformly distributed paramagnetic ions in solution (dipolar coupling), which affects T1 more strongly.

The effect we observe relates to the induction of local variations in the induced magnetic field (bulk susceptibility) by paramagnetic hemosiderin of the tissue under study. Paramagnetic materials, in addition to coupling directly to protons to increase relaxation rates, also have substantial fields induced when placed in a large external field; that is, they have large magnetic susceptibilities. This is due to the unpaired electron spins of the paramagnetic material, and the fields induced are much larger than those within normal, diamagnetic tissues. Clumps of paramagnetic substances, such as hemosiderin, would thus serve locally to distort the magnetic field "seen" by surrounding water protons. When water molecules diffuse through variations in magnetic field, their protons pick up phase changes that are not corrected for by the application of 180° refocusing pulses, since the field seen by a given proton is not constant with time. This results in a decrease in spin-echo signal intensity and would be observed as a decrease in the measured T2. This effect does not influence longitudinal relaxation, and hence a selective decrease in observed T2 is expected. This is in fact what was observed. The TE of 32 msec in the IR imaging introduces a T2 component, which can account for the absent signal regions on the T1-weighted images. Experience indicates that there is usually insufficient dense calcification in these lesions to produce sufficiently marked decrease in mobile proton density to explain signal void regions.

Kucharczyk et al. [20] conclude that at present CT detects VMOTAs more sensitively when faint calcification is the major evidence of their presence and MR is more accurate in evaluating associated hemorrhages, particularly when these have lost density with time or when they are located in the posterior fossa. Our experience conforms with these conclusions.

Lee et al. [21] included five cases of VMOTA, all in the posterior fossa. Two were verified by surgery. Hyperintense signal consistent with hemorrhage was shown on T1- and T2-weighted images in four cases. Multiple areas of decreased signal were shown within the hematomas in all these cases, and a curvilinear decreased signal was shown around the hematomas in three cases. In an additional case, a similar low signal was shown by the same pulsing techniques in a lesion having no evidence of hematoma. CT demonstrated increased attenuation in all five cases, with values consistent with calcification in only one case. They illustrate three cases of brainstem VMOTAs that have peripheral (three cases) and peripheral and central (two cases) very low signal intensity. This does not appear compatible with the presence of vascular signal voids, because the appearance and size of the signal-void regions do not correspond to the small size of vessels and the slow flow present in VMOTAs. In only one case was CT also illustrated, and this showed areas of calcific density that did not correspond to peripheral signal void on MR.

Studies in the first report cited above [20] were obtained at 0.35 T; those in the second report [21], at 0.5 T. The possibility of paramagnetic effects producing the low signal-to-signal void components of these lesions are not mentioned by either group. It has been stated that paramagnetic proton preferential T2 relaxation effects increase as the square of the magnetic field [22], and that certain paramagnetic effects are not likely to be shown by MR at lower field strengths (circa and below 0.5 T). It is possible that preferential T2 relaxation was not observed as regularly or prominently in



A B C

Fig. 5.—Multiple metastases of malignant melanoma, in which CT some time earlier had indicated neoplasm with probable hemorrhagic components. One of the multiple similar-appearing lesions in cerebellum and brainstem is illustrated here on paramedian sagittal sections. **A**, SE 500/30/4, mildly T1-weighted image, showing a low to absent signal in medial portion of cerebellar hemisphere. **B**, SE 2000/60/4, moderately T2-weighted sequence. There is a region of absent signal surrounding a small island that is isointense with cerebellar gray matter. **C**, SE 2000/120/4, strongly T2-weighted sequence, showing a small, intense focus of prolonged T2 within a region of low to absent signal. Note similarity to lesion shown in Figure 3.

the series reported by Kucharczyk et al. [20] or Lee et al. [21] for them to consider that this phenomenon was a plausible explanation for the low to absent signal regions associated with VMOTAs, rather than calcifications or vessels with high flow rates. Hemosiderin is a physiologically available paramagnetic relaxant, with a locally heterogeneous field varying slowly or not at all, and capable of producing locally heterogeneous magnetic susceptibility and local field gradients under the influence of a strongly applied magnetic field.

It is therefore our hypothesis that the regions of very low to absent signal described and illustrated in the above two reports [20, 21] and in our cases are due in fact to paramagnetic effects or magnetic susceptibility and not to vascular flow or to calcification. In our cases, the morphology of both the small vessels seen and the calcification, identified with certainty in only two cases, could not explain the patterns of signal void on MR.

Our results confirm the inability of CT to identify older parenchymal hemorrhages and add to a growing recognition that MR can reveal relatively characteristic and specific signal alterations (short T1, long T2) in nonacute hematomas [12, 22–27]. The short T1, believed to be due to the paramagnetic effect of methemoglobin, appearing after the first few days following hemorrhage and lasting for several months [28], represents an important advance over CT in imaging lesions consisting of or containing subacute and/or chronic hemorrhage. A feature corroborating hemorrhage, the appearance of absent or near-absent signal, presumed to be due to the magnetic susceptibility effect of hemosiderin, appears to be characteristic of lesions in which there has been considerable previous hemorrhage on one or more occasions. The presence of this signal pattern further helps characterize a hemorrhagic lesion in the type of case in which there is no clinical episode to suggest the occurrence of hemorrhage, such as in the present series of VMOTAs. This is presumably due to relatively slow seepage of small amounts of blood from relatively small vessels carrying slow flow under low pressure.

Although CT cannot always differentiate clusters of tiny calcifications from relatively dense soft tissues, slowly flowing blood, or blood clot, it can often distinguish small punctate or aggregated calcifications. Such small calcifications can generally not be identified by MR [29, 30]. With CT, the appearance of slight to moderate enhancement of these lesions is helpful in differential diagnosis, since low-grade gliomas, the principal differential consideration, generally do not show this type of enhancement. Nevertheless, since old hemorrhage cannot be identifed on CT, when angiography fails to reveal a pathologic circulation, it has been necessary in the past to undertake surgical confirmation by open operation or stereotactic biopsy, or to elect to perform serial CT scans over a protracted period.

Stereotactic biopsy is hazardous, since these occult lesions are prone to hemorrhage after this procedure with potentially fatal results [31]. Some deeply situated VMOTAs present at a ventricular surface (as in cases 2 and 4) and may be excisable by careful microsurgery [32], with low morbidity. However, many of these deep-seated lesions are not amenable to safe, open surgical exploration. Therefore, the unequivocal demonstration of significant previous hemorrhage or hemorrhages in these lesions by MR may provide greater assurance regarding the correct diagnosis, offering the opportunity of improved, particularly safer, patient management. In deeply seated lesions, not surgically accessible without undue hazard, the combination of typical findings on MR as well as by CT, may offer a better rationale for proton-beam therapy [33], without histologic confirmation. This approach was used in 18 of the initial 30 patients with clinical, CT, and MR features of VMOTA, in whom surgery of any type was judged to be unduly hazardous. Most of the lesions so treated involved the brainstem.

CT remains a necessary part of the evaluation of VMOTAs for the following reasons: follow-up CT a short time after an acute parenchymal hemorrhage will generally provide evidence that there is an underlying lesion (residual heterogeneous hyperdensity, with or without small calcifications, the opacification of very small intrinsic vascular channels in a

VMOTA, or evidence of an underlying neoplasm, particularly metastatic malignant melanoma or necrosing glioblastoma). These contributions to differential diagnosis are exemplified by our case 1 and by a case of hemorrhage into metastatic cerebellar melanoma (Fig. 5). In the latter case, the MR abnormalities of the individual lesions in themselves might not have provided the correct diagnosis. Low-grade gliomas may show small calcifications, but are unlikely to hemorrhage. Such a glioma may dedifferentiate, undergo necrosis, and thus become liable to hemorrhage. After hemorrhage, MR alone might not allow distinction from VMOTA, whereas CT can generally provide indication of underlying neoplasm by revealing a neoplastic pattern of contrast enhancement as the density of hemorrhage decreases. However, in case 5, both CT and MR suggested a hemorrhagic neoplasm.

We conclude from this study that CT and MR have complementary positions in the evaluation of suspected VMOTA.

Addendum

Since this report was completed, two further operated cases and one autopsied case (death from massive pontine hemorrhage from the VMOTA) showed CT and MR features similar to the six cases reported herein.

ACKNOWLEDGMENTS

We thank Paul Beaulieu, Bradley Field, and Maryann Kotowski for technological assistance, and Edith Bell for manuscript preparation.

REFERENCES

1. Kramer RA, Wing SD. Computed tomography of angiographically occult cerebral vascular malformations. *Radiology* **1977**;123:649–652
2. Bell BA, Kendall BE, Symon L. Angiographically occult arteriovenous malformations of the brain. *J Neurol Neurosurg Psychiatry* **1978**;41:1057–1064
3. Shuey HM Jr., Day AL, Quisling RG, Sypert GW. Angiographically cryptic cerebrovascular malformations. *Neurosurg* **1979**;5(4):476–479
4. Becker DH, Townsend JJ, Kramer RA, Newton TH. Occult cerebrovascular malformations. A series of 18 histologically verified cases with negative angiography. *Brain* **1979**;102:249–287
5. Cohen HCM, Tucker WS, Humphreys RP, Perrin RJ. Angiographically cryptic histologically verified cerebrovascular malformations. *Neurosurg* **1982**;10(6):704–714
6. Yeates A, Enzmann D. Cryptic vascular malformations involving the brainstem. *Radiology* **1983**;146:71–75
7. Mitnick JS, Pinto RS, Lin JP, Rose H, Lieberman A. CT of thrombosed arteriovenous malformations in children. *Radiology* **1984**;150:385–389
8. Hashim ASM, Asakura T, Koichi U, et al. Angiographically occult arteriovenous malformations. *Surg Neurol* **1985**;23:431–439
9. Margolis G, Odom GL, Woodhall B, et al. The role of small angiomatous malformations in the production of intracerebral hematomas. *J Neurosurg* **1951**;8:564–575
10. Crawford JV, Russell DS. Cryptic arteriovenous and venous hamartomas of the brain. *J Neurol Neurosurg Psychiatry* **1956**;19:1–11
11. McCormick WF, Nofzinger JD. "Cryptic" vascular malformations of the central nervous system. *J Neurosurg* **1966**;24:865–875
12. Bydder GM, Steiner RE, Young IR, et al. Clinical NMR imaging of the brain: 140 cases. *AJNR* **1982**;3:459–480, *AJR* **1982**;139:215–236
13. Brant-Zawadzki M, Davis PL, Crooks LE, et al. NMR demonstration of cerebral abnormalities: comparison with CT. *AJNR* **1983**;4:117–124, *AJR* **1983**;140:847–854
14. Bradley WG, Waluch V, Yadley RA, Wycoff RR. Comparison of CT and NMR in 400 patients with suspected disease of the brain and cervical spinal cord. *Radiology* **1984**;152:695–702
15. Lee BCP, Kneeland JB, Cahill PT, Deck MDF. MR recognition of supratentorial tumors. *AJNR* **1985**;6:871–878
16. Crooks LE, Mills CM, Davis PL, et al. Visualization of cerebral and vascular abnormalities by NMR imaging: the effects of imaging parameters on contrast. *Radiology* **1982**;144:843–852
17. Kaufman L, Crooks LE, Sheldon PE, et al. Evaluation of NMR imaging for detection and quantification of obstructions in vessels. *Invest Radiol* **1982**;17:554–560
18. Herfkens RJ, Higgins CB, Hricak H, et al. Nuclear magnetic resonance imaging of the cardiovascular system: normal and pathologic findings. *Radiology* **1983**;147:749–759
19. Bradley WG, Waluch V, Lai K, et al. The appearance of rapidly flowing blood on magnetic resonance images. *AJR* **1984**;143:1167–1174
20. Kucharczyk W, Lemme-Pleghos L, Uske A, Brant-Zawadzki M, Dooms G, Norman D. Intracranial vascular malformations: MR and CT imaging. *Radiology* **1985**;156:383–389
21. Lee BCP, Herzberg L, Zimmerman RD, Deck MDF. MR imaging of cerebral vascular malformations. *AJNR* **1985**;6:863–870
22. Gomori JM, Grossman RI, Goldberg HI, Zimmerman RA, Bilaniuk LT. Intracranial hematomas: imaging by high-field MR. *Radiology* **1985**;157:87–93
23. Sipponen JT, Sepponen RE, Sivula A. Nuclear magnetic resonance (NMR) imaging of intracerebral hemorrhage in the acute and resolving phases. *J Comput Assist Tomogr* **1983**;7:954–959
24. DeLaPaz RL, New PFJ, Buonanno FS, et al. NMR imaging of intracranial hemorrhage. *J Comput Assist Tomogr* **1984**;8:599–607
25. Bailes DR, Young IR, Thomas DJ, Straughan K, Bydder GM, Steiner RE. NMR imaging of the brain using spin-echo sequences. *Clin Radiol* **1982**;33:395–414
26. Brant-Zawadzki M, Davis PL, Crooks LE, et al. NMR demonstration of cerebral abnormalities: comparison with CT. *AJNR* **1983**;140:847–854
27. Pykett IL, Rosen BR, Buonanno FS, Brady TJ. Measurement of spin-lattice relaxation times in nuclear magnetic resonance imaging. *Phys Med Biol* **1983**;28:723–729
28. DiChiro G, Brooks RA, Girton ME, et al. Sequential MR studies of intracerebral hematomas in monkeys. *AJNR* **1986**;7:193–199
29. Holland BA, Kucharczyk W, Brant-Zawadzki M, Norman D, Haas DK, Harper PS. MR imaging of calcified intracranial lesions. *Radiology* **1985**;157:353–356
30. Oot RF, New PFJ, Rosen BR, Davis KR. The detection of intracranial calcifications by MR imaging. Presented at the 24th annual meeting of the American Society of Neuroradiology, San Diego, CA, January **1986**
31. Ahmadi J, Miller CA, Segall HD, Park S-H, Zee C-S, Becker RL. CT patterns in histopathologically complex cavernous hemangiomas. *AJNR* **1985**;6:389–393
32. Wilson CB, U HS, Domingue J. Microsurgical treatment of intracranial vascular malformations. *J Neurosurg* **1979**;51:446–454
33. Kjellberg RN, Hanamura T, Davis KR, Lyons SL, Adams RD. Bragg-Peak proton beam therapy for arteriovenous malformations of the brain. *N Engl J Med* **1983**;309:269–274

Book Reviews

Digital Subtraction Angiography: Practical Aspects. By Arina van Breda and Barry T. Katzen. New Jersey: Slack, Inc., 230 pp., 1986.

This well-written text, as the authors state, "presents a practical overview of the techniques involved in performing digital subtraction angiography (DSA) and optimizing image quality" and demonstrates its benefits in varied areas of vascular application. The text contains 14 chapters that cover the applications of DSA.

The first four chapters are technically oriented. The authors in a systematic fashion cover subjects such as design of an angiographic suite and selection of digital equipment. They then carefully describe angiographic techniques and thoroughly compare IV DSA and intra-arterial DSA (IA DSA). Management of complications is briefly described.

Chapters 4 through 10 describe the applications of DSA to different organ systems. In chapter 7, Alan G. Wasserman additionally describes the applications of computer software in the analysis of left ventricular ejection fraction and cardiac output. In all cases the practical aspects are well delineated and the clinical cases are relevant and well illustrated. The pitfalls of IV DSA and IA DSA are well discussed. The illustrations and legends are of good quality.

Chapter 11 relates to DSA and interventional radiology. The authors describe the uses of DSA in angioplasty, embolization, and drug infusion. This chapter is superbly illustrated. The authors describe methods of measurement of stenosis by computerized software and recommend standard angiography for measurement of vessel size before percutaneous transluminal angioplasty. It would have been helpful if the authors described the availability of higher resolution digital angiography systems as 1024 × 1024 and mentioned the applications of DSA to blood flow determinations. Chapter 12 describes uses of DSA in fistulograms and in the systemic veins. Chapter 13, contributed by Carol Mascioli, outlines the role of the special procedures technologist in digital vascular imaging. Chapter 14, contributed by Kay Lewis, describes nursing care of patients undergoing DSA. Both chapters are well written and concise, and are a perfect complement to descriptions of practical aspects of DSA.

In general, the text is well organized and beautifully illustrated. The clinical material is appropriate for the purposes of the book. The authors have achieved their goal and have provided a good understanding of the different applications of DSA. I recommend this book to general radiologists and cardiovascular radiologists interested in DSA.

Juan F. Lois
UCLA School of Medicine
Los Angeles, CA 90024

Echographie de la Prostate (Sonography of the Prostate). By Bruno Fornage. Paris: Vigot, 336 pp., 1985. hard cover

This nicely organized French-language book displays a well-balanced text with good attention to details. Supported by excellent illustrations, it provides a unique overview of sonography of the prostate.

The first chapter is about the anatomy of the prostate and is highlighted by pertinent anatomic drawings. The second chapter covers the technical aspects of variable instruments used in the evaluation of the prostate. The third chapter, which is abundant in illustrations, describes the normal sonographic appearance of the prostate and the male pelvis with emphasis on suprapubic and transrectal approach. The remaining chapters address pathologic conditions. Benign prostatic hypertrophy, carcinoma of the prostate, prostatitis and prostatic lithiasis are discussed with depth and clarity. The effects of prostatic disease on the urinary bladder and the upper urinary tracts, the postoperative states, and the role of sonography in the follow-up of the prostate after nonsurgical treatment are outlined as well. The sections on guided biopsy of the prostate and the dynamic evaluation of the bladder neck and the urethra have particularly elegant reproductions. Other diagnostic techniques used in the evaluation of the prostate are briefly discussed.

Echographie de la Prostate is the result of vast experience and outstanding work. Although its full advantage is restricted to those who can read French, the wealth of its illustrations should make it worthwhile for radiologists and urologists.

Joseph Fakhry
New York Medical College
Valhalla, NY 10595

Penetrating Vascular Injuries of the Face and Neck: Clinical and Angiographic Correlation

Charles M. North[1, 2]
Jamshid Ahmadi
Hervey D. Segall
Chi-Shing Zee

A retrospective review was made of 139 clinically stable patients who had sustained penetrating trauma to the face and neck. The study was done to learn more about the indications for angiography and the impact of angiography upon patient management. Some relationship between the physical examination and the angiographic findings was found. In the presence of any one of four physical signs or symptoms (absent pulse, bruit, hematoma, or alteration of neurologic status) there was a 30% incidence of vascular injury. However, it is unlikely that a clinically significant traumatic vascular lesion will be missed if angiography is not obtained when these clinical signs and symptoms are not present. In the group of 78 patients who presented with only a wound penetrating the platysma and no other findings or symptoms, just two had vascular injuries on angiograms; one of these lesions was minor and the other did not affect the patient's management. There was a substantially higher rate (50%) of vascular injury in patients with trauma cephalad to the angle of the mandible compared with 11% of patients who had neck trauma. Gunshot wounds were associated with vascular damage more frequently than were stab wounds.

Angiography is often performed in penetrating trauma to the head and neck to evaluate the possibility of vascular injury and to aid in planning appropriate management [1]. Nonetheless, the role of angiography in penetrating head and neck trauma has remained controversial. Some authors have advocated surgical exploration of all cases of penetrating wounds to the neck and face [2–4] while others have used angiography routinely in all cases in order to reduce the number of unnecessary surgical procedures [5, 6]. Angiography, however, is not completely without risk [7], and a more selective policy would be desirable. We retrospectively reviewed a consecutive series of 139 angiograms performed during an 18-month period and correlated the results of those studies with the clinical findings and outcome. The purpose of our study was to establish guidelines for performing angiography and to determine the impact of angiography upon patient management.

Subjects and Methods

We retrospectively reviewed the cases of 139 consecutive patients with neck and face trauma who underwent angiography of the brachiocephalic vessels from January 1, 1983, through June 30, 1984. The patients' ages ranged from 12 to 72 years with a mean age of 26 years. There were 135 male patients and 4 female patients. All the patients had been stabilized in the trauma admitting area prior to being referred for angiography. Therefore, our patient population excluded those so critically ill they required immediate exploration and those who succumbed to their trauma in the admitting area.

Angiograms were performed with percutaneous transfemoral technique. The filming sequence routinely included two exposures per second for 4 sec, followed by one exposure per second for 8 sec to facilitate visualization of the jugular veins. There were nine aortic arch studies and 130 selective angiograms. The latter included 84 left carotid, 55 right carotid, 26

This article appears in the September/October 1986 issue of *AJNR* and the November 1986 issue of *AJR*.

Received September 26, 1985; accepted after revision March 12, 1986.

[1] All authors: Department of Radiology, Section of Neuroradiology, University of Southern California School of Medicine, Los Angeles, CA 90033. Address reprint requests to J. Ahmadi, 1200 N. State St., Box 2, Los Angeles, CA 90033.

[2] Present address: Department of Radiology, Mercy Hospital, Bakersfield, CA 93301.

***AJR* 147:995–999, November 1986**
0361–803X/86/1475–0995
© American Roentgen Ray Society

left vertebral, 10 right vertebral, and 11 subclavian artery angiograms. Selective angiography was performed on the basis of location and path of the penetrating wound.

All angiograms were reviewed by staff neuroradiologists who had no knowledge of the details of the patients' clinical status. Two patients had minor complications of angiography; one had a transient diminution of the dorsalis pedis pulse, which resolved within 2 hr, and the other had a large hematoma at the puncture site. Observations made and data collected in 139 patients were tabulated according to the weapon used, the side and anatomic location involved, the symptomatology and physical findings resulting from the injury, the angiographic findings, and the management of the patient.

Results

Of the 139 patients, 62 sustained gunshot wounds and 77 sustained stab woulds. Fifty-five of the 77 patients sustaining stab wounds were injured on their left side, whereas gunshot wounds were evenly distributed between the left and right sides. Seventeen patients with gunshot wounds and six patients with stab wounds had positive angiographic findings. Trauma to the neck occurred in 119 patients, while 20 patients sustained facial trauma. Penetrating trauma above the angle of the jaw and to the face was associated with a higher frequency of abnormal angiographic findings (10 of 20 patients, or 50%) compared with neck trauma (13 of 119 patients, or 11%).

One hundred sixteen of the 139 patients had normal angiograms. Of the remaining 23 patients with abnormal angiograms, 12 sustained vascular injuries affecting or potentially affecting cerebral hemodynamics. This included entities such as arterial lacerations, narrowing and occlusions, arteriovenous fistulae, and a pseudoaneurysm (Fig. 1). Two patients had internal jugular vein lacerations. In these two patients compression of the internal jugular vein by hematoma was seen but the lacerations themselves were not apparent on the angiograms (Fig. 2). Seven patients had lesions affecting the external carotid circulation (four patients had branch occlusions of the external carotid that were clinically insignificant), one patient had a subclavian arteriovenous fistula associated with a large pseudoaneurysm (Fig. 3), and one patient had an injury to the thyrocervical trunk with fistulization into the jugular vein (Fig. 4).

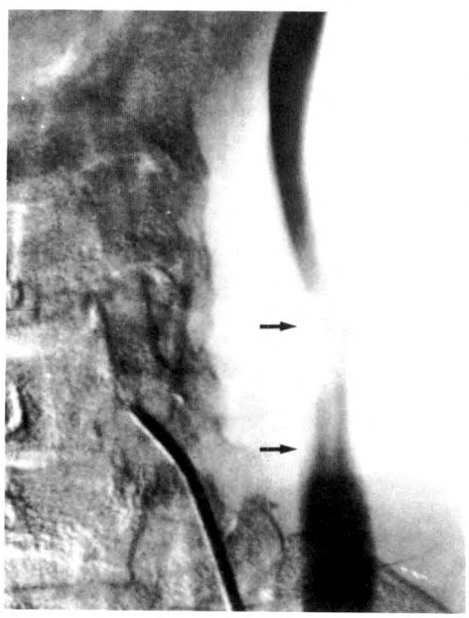
Clinical data on the 139 patients is correlated with angiographic findings in the following paragraphs. One group of patients had no signs or symptoms other than the wound itself. The remaining patients had various combinations of loss of consciousness or neurologic deficits, decreased or absent carotid pulses, bruits, or clinically detectable hematomas at the site of injury. It is important to note that some of the patients had more than one sign or symptom, and various clinical presentations overlapped.

Fifty-eight patients had clinically detectable hematomas at the site of injury. Among the 58 patients with hematoma, 44 presented with only the hematoma (Table 1). In the other 14 patients, the hematoma was associated with various combinations of other clinical findings, such as loss of consciousness, neurologic deficits, decreased or absent carotid pulses, or bruits (Table 2). In the total group of 58 patients with hematomas, 50 had a stable hematoma and eight had expanding hematomas. Of the 50 patients with stable hematomas, 16 had abnormal angiograms; of the eight patients with expanding hematomas, four had abnormal angiograms (Table 3).

Eighty-one patients had no hematoma at the site of injury (Table 4). Two of these patients presented with neurologic deficit (both had cranial nerve palsies and normal angiograms) and one patient presented with a bruit (this patient had a thyrocervical trunk—internal jugular vein fistula). The remain-



1

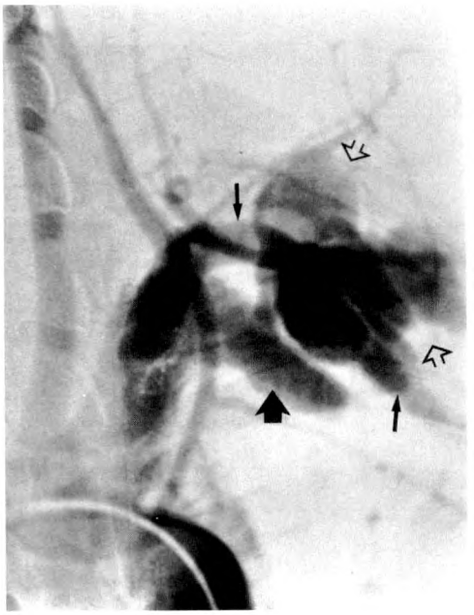


2

Fig. 1.—26-year-old man with expanding hematoma due to gunshot wound to right side of neck. Lateral projection of a common carotid angiogram shows pseudoaneurysm (*arrows*) of right internal carotid artery projecting anteriorly from its uppermost cervical portion. A Selverstone clamp was placed over the internal carotid artery followed by ligation 2 days later.

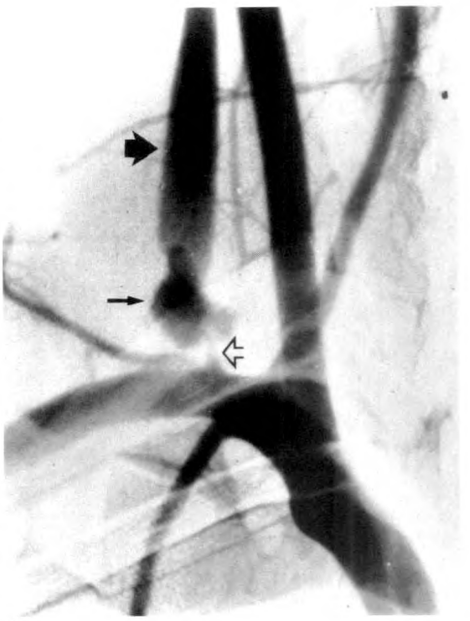
Fig. 2.—31-year-old man with large hematoma due to gunshot wound to neck. Anteroposterior projection of venous phase of angiogram shows compression of internal jugular vein by hematoma (*arrows*). Laceration of the vein was found and repaired at surgery.

Fig. 3.—22-year-old man with hematoma and bruit over lower portion of left side of neck due to gunshot wound. An arch aortogram obtained with a slightly oblique projection shows large pseudoaneurysm (*open arrows*) of left subclavian artery (*narrow arrows*) and fistulization into left subclavian vein (*wide arrow*). The pseudoaneurysm was resected and the subclavian artery and vein were repaired.



3

Fig. 4.—17-year-old man with a bruit at base of neck, but without a hematoma, caused by stab wound to right side of neck. An arch aortogram shows a pseudoaneurysm (*narrow arrow*) of thyrocervical artery (*open arrow*) and fistulization and reversal of direction of flow in the internal jugular vein (*wide arrow*). Thyrocervical artery was ligated and jugular vein repaired.



4

TABLE 1: **44 Patients with Only a Hematoma**

33 normal angiograms
28 observed
5 explored
2 retropharyngeal hematomas
1 perforated esophagus
2 negative explorations
11 patients with abnormal angiograms
3 observed
2 carotid or vertebral occlusions
1 carotid compression or spasm
6 explored
2 carotid compressions or spasm
1 pseudoaneurysm internal carotid artery (Fig. 1)
2 jugular vein lacerations (Fig. 2)
1 facial artery occlusion and submandibular gland laceration
2 embolized
2 pseudoaneurysms internal maxillary artery with arteriovenous fistulas

TABLE 2: **14 Patients with Hematomas Associated with Other Symptoms and Signs**

8 hematomas and loss of consciousness or neurologic deficits
4 normal angiograms
3 observed
1 observed (this patient had a facial hematoma; an associated ruptured globe was removed)
4 abnormal angiograms
1 observed
1 occlusion occipital artery
2 explored
1 extravasation internal maxillary artery
1 occlusion facial artery (open reduction, associated mandibular fracture)
1 embolized
1 carotid-cavernous fistula
1 hematoma with loss of consciousness and absent carotid pulse
1 abnormal angiogram
1 observed
1 occlusion carotid artery
2 hematomas with decreased or absent carotid pulse
2 abnormal angiograms
2 observed
1 occlusion carotid artery
1 intimal tear and laceration carotid artery
3 hematomas with bruit
1 normal angiogram
1 observed
2 abnormal angiograms
1 explored
1 pseudoaneurysm with subclavian arteriovenous fistula (Fig. 3)
1 embolized
1 carotid cavernous fistula

ing 78 patients had no signs or symptoms other than the wound itself. Of these 78, only two had abnormalities on angiograms while the remaining 76 had normal studies. Neither of the two patients with positive angiograms had clinical signs or symptoms of major significance; one, however, did have occlusion of a vertebral artery and the other patient had only an occlusion of an occipital artery.

Eleven patients had either loss of consciousness or neurologic deficits; nine of these patients had a hematoma (Table 2) and two did not (Table 4). In two patients with loss of consciousness, one had occlusion of the internal carotid and the other had a carotid cavernous fistula. In three patients, angiograms revealed injuries of external carotid artery branches. One of these had a peripheral facial nerve palsy, a mandibular fracture, and an occlusion of the facial artery; another patient had a peripheral facial nerve palsy associated with extravasation from the internal maxillary artery; and a third patient had an occipital artery occlusion (this patient had

TABLE 3: **Summary of Eight Patients with Expanding Hematomas**

Patient No.	Type of Wound/ Site of Trauma	Symptoms and Signs	Angiographic Results	Management
1	Gunshot/face	Expanding hematoma and bruit	Carotid-cavernous fistula	Embolized
2	Gunshot/face	Expanding hematoma	Pseudoaneurysm and arteriovenous fistula internal maxillary	Embolized
3	Gunshot/neck	Expanding hematoma	Pseudoaneurysm internal carotid artery	Selverstone clamp over internal carotid artery; ligated 2 days later
4	Gunshot/neck	Expanding hematoma	External compression or spasm carotid artery	Explored and hematoma evac.
5	Gunshot/neck	Expanding hematoma and RUE paraparesis and paresthesia	Normal	Observed
6	Stab/neck	Expanding retropharyngeal hematoma	Normal	Explored and hematoma evac.
7	Stab/neck	Expanding hematoma	Normal	Observed
8	Stab/neck	Expanding hematoma	Normal	Observed

TABLE 4: **81 Patients Without Hematomas**

3 patients with neurologic deficit or bruit
  2 with normal angiograms were observed
  1 with abnormal angiogram was explored
    1 thyrocervical—internal jugular vein fistula (Fig. 4)
78 patients with only wound itself
  76 had normal angiograms
    72 were observed
    4 were explored
      2 upper airway lacerations
      2 negative explorations
  2 had abnormal angiograms
    2 were observed
      1 left vertebral occlusion
      1 external carotid branch occlusion

loss of consciousness after cardiopulmonary arrest). In the remaining six patients, the angiograms were normal and the loss of consciousness or neurologic deficits were attributed to direct injuries to the nervous system.

Three patients had decreased or absent carotid pulses detected by physical examination. One of them had an intimal tear and laceration of the internal carotid artery while the other two had a total occlusion of the internal carotid artery.

Four patients had bruits on physical examination. One of these had a carotid-cavernous fistula, another had an arteriovenous fistula between the thyrocervical trunk and the internal jugular vein, and a third patient had a pseudoaneurysm of the subclavian artery with fistulization into the subclavian vein. The fourth patient with a bruit had a normal angiogram.

The 139 cases were managed as follows: (1) Twenty-three patients had abnormal angiograms. Of these, nine were observed, 10 underwent exploration (two of these 10 patients had internal jugular vein lacerations found at surgery with angiographic abnormalities noted only retrospectively), and four had intraarterial embolization. (2) Ten additional patients also had surgery despite normal angiography because they sustained injuries or were suspected of having other injuries to the face and upper respiratory or digestive tracts. Four of these had a negative exploration with no such injuries. (3) The other 106 patients had normal angiograms and conservative management.

Overall, 115 patients (83%) were just observed. Of the remaining 24 patients, only nine (6.5%) were explored or embolized as a result of what was found at angiography. The other 15 patients were operated on for nonvascular injuries.

Discussion

Since World War II, there has been a great deal of controversy over the management of penetrating injuries to the head and neck [2–6, 8–11]. In recent years, the concept of selective exploration seems to be replacing the earlier dictum of mandatory exploration of penetrating wounds [5, 6, 9–11]. In contrast to certain earlier opinions [4, 11], our work suggests some relationship between the clinical situation and the results of angiography. For example, in our series, there were 78 patients who presented with a wound penetrating the platysma but with no other clinical abnormalities. These patients had normal angiograms, except for two who had lesions that did not affect their management. Therefore, there appears to be a rational basis for using the clinical assessment as a guide when considering angiographic evaluation. In our series, 14% of patients with penetrating wounds underwent surgical exploration. Compared with earlier reports [2–6, 9–13], this is a significantly lower exploration rate. It should be kept in mind that our study included only stable patients who were referred for angiography; critically ill patients requiring immediate exploration were not part of the patient population described in this report.

It is interesting that stab wounds of the neck were associated with a relatively low incidence of significant vascular abnormalities at angiography; approximately 92% of these patients had a normal angiogram. Even with gunshot wounds to the neck, there was a 73% rate of negative angiographic studies.

In the group of 11 patients with loss of consciousness or neurologic findings, angiography revealed vascular injuries (significant with respect to the cerebral circulation) in only two patients. Direct injury to the nervous system accounted for the symptoms and findings in eight patients in this group, while one other patient had a cardiopulmonary arrest. However, in instances where neurologic abnormalities have a delayed onset after trauma (particularly when cranial CT fails to show intracranial lesions that can explain the patient's new findings), emergency cerebral angiography should be considered to search for a correctable vascular lesion.

Four of five patients with occlusions of the carotid and/or vertebral arteries had no evidence of cerebral ischemia because of collateral blood flow via the circle of Willis. These patients were managed conservatively.

The anatomic location of trauma to the neck has been divided into three zones [3, 4, 13]: zone I is the area below the level of the cricoid cartilage, zone II is between the cricoid and the angle of the mandible, and zone III is above the angle of the mandible. In this series there was a substantially higher rate of significant angiographic abnormalities in patients with trauma cephalad to the angle of the mandible. Fifty percent of angiograms were abnormal with injuries above the angle of the mandible compared with 11% below.

In view of the two cases of internal jugular vein lacerations where abnormalities were not initially detected at the time of angiography, subtraction films might be useful for the venous phase as well as the arterial phase to enable optimum diagnosis, even though most surgeons would not explore for an isolated venous laceration. The literature indicates that more venous than arterial injuries have been noted at exploration [2, 9, 11, 12]. In a series of 625 patients explored because of penetrating neck injuries, there was a 53% incidence of vascular injuries. Involvement of the venous system was noted in 61% of the vascular injuries [9]. It seems certain that many of these venous injuries are not detected on angiograms.

In our study, angiography had an impact on patient management. The exploration rate in this series was significantly lower than in earlier reports; a negative angiogram limited explorations in search of vascular traumatic lesions. Our experience also suggests that angiography is not necessary when there are no symptoms or signs other than the wound itself. One cannot be absolutely certain in such instances that a dissection or other vascular lesion is not present; however, the risk of missing a significant lesion with resultant serious harm to the patient is probably less than the potential risk of angiography itself. Although additional experience may further modify the use of angiography in such cases, we have shown that a clinically significant vascular lesion is unlikely under such circumstances.

REFERENCES

1. Davis JM, Zimmerman RA. Injury of the carotid and vertebral arteries. *Neuroradiology* **1983**;25:55–69
2. Markey JC, Hines JL, Nance FC. Penetrating neck wounds: a review of 218 cases. *Am Surg* **1975**;41:77–83
3. Saletta JD, Lowe RJ, Lim LT, Thornton J, Delk S, Moss GS. Penetrating trauma of the neck. *J Trauma* **1976**;16:579–587
4. Roon JA, Christensen N. Evaluation and treatment of penetrating cervical injuries. *J Trauma* **1979**;19:391–397
5. McCormick JM, Burch BH. Routine angiographic evaluation of neck and extremity injuries. *J Trauma* **1979**;19:384–387
6. Hiatt JR, Busuttil RW, Wilson SE. Impact of routine arteriography on management of penetrating neck injuries. *Vasc Surg* **1984**;1:860–866
7. Vitek JJ. Femoro-cerebral angiography: analysis of 2000 consecutive examinations; special emphasis on carotid artery catheterization in older patients. *AJR* **1973**;118:633–647
8. Giannotta SL, Ahmadi J. Vascular lesions with head injury. In: Wilkins RM, Rengachary SS, eds. *Neurosurgery*. New York: McGraw-Hill, **1985**:1678–1688
9. Sheely CH, Mattox KL, Reul GJ, Beall AC, DeBakey ME. Current concepts in the management of penetrating neck trauma. *J Trauma* **1975**;15:895–900
10. Elerding SC, Manari FD, Moore EE. Reappraisal of penetrating neck injury management. *J Trauma* **1930**;20:695–697
11. Rao PM, Bhatti MF, Gaudino J. Penetrating injuries of the neck: criteria for exploration. *J Trauma* **1983**;23:47–49
12. Massac EJR, Siram SM, Leffall LDJ. Penetrating neck wounds. *Am J Surg* **1983**;145:263–265
13. Monson DW, Saletta JD, Freeark RJ. Carotid-vertebral trauma. *J Trauma* **1969**;9:987–999

The reader's attention is directed to the Editorial on this article, which appears on the following pages.

Editorial

Angiography in Penetrating Neck Injuries

A paper by North and his colleagues in this issue [1] concerns emergency angiography in penetrating injuries of the neck and face. The information contained in that article should be carefully studied by radiologists who work in hospitals with large trauma services. Of particular interest are the 78 patients in whom emergency angiography was performed when there were no other physical or neurologic findings or symptoms, except for minor soft-tissue swelling at the wound-entry site. Seventy-six of those patients had normal angiography. In only one patient was there a significant finding—a vertebral artery occlusion—and in that case it did not affect the patient's treatment. The basic question is, therefore, whether angiography is justified under these circumstances, given the apparent low rate of positive findings and the inherent risks of carotid and vertebral arteriography.

Recommendations for routinely exploring all penetrating neck injuries that result from stab or gunshot wounds have been published in the surgical literature [2]. The object of these explorations was to directly visualize and repair, when necessary, those important structures that might have been damaged as a result of the injury. Contrary to this was the more conservative approach by Rao et al. [3]. Because these investigators believed that there would be a high probability of negative explorations if surgery were done in the absence of physical findings, they concluded that mandatory exploration was not required. In order to identify significant vascular injuries while avoiding unnecessary explorations, others have recommended routine angiography [4] so that patients requiring surgery for vascular injuries could be distinguished from patients who could simply be observed. This approach seemed sensible and in many trauma centers routine angiography became part of the standard protocol used in evaluating penetrating neck injuries.

Experience at our medical center with extremity injuries indicated that routine angiography was fruitful and directly affected patient management when there was a hematoma, active bleeding from the wound, absent pulses, a bruit/thrill, or neurologic findings [5]. When there were no significant findings, peripheral angiography was unrewarding. We believe that the same observations pertain to mid-neck injuries. After the receipt of North's paper, the chiefs of neuroradiology sections in eight hospitals that have large trauma services were contacted to see if North's and our experiences were shared by others. Specifically, the information sought was the procedure used when the surgeon ordered angiography for mid-neck injuries when there were no significant findings. These conversations indicated that although emergency angiography was done in such cases, the studies were uniformly negative. No one was able to recall a single positive case. It is of considerable interest that, as a result of North's data, surgeons at that hospital are now willing to carefully observe and monitor these patients rather than ordering routine angiography (H. Segall, personal communication).

Before confronting a surgeon in this potentially controversial area, the radiologist must be aware of how most surgeons view these injuries. It is commonplace to divide neck and face into three zones [6]: zone 1—below the cricoid cartilage; zone 2—between the cricoid cartilage and the mandible; zone 3—above the mandible. Because the clinical consequences of penetrating injuries to zone 1 (at or near the thoracic inlet) and zone 3 (high cervical area) may be occult and therefore difficult to monitor, angiography is usually advisable in these cases. When a proximity injury in those zones has caused a lacerated vessel, a pseudoaneurysm, or a fistula, intervention is usually required. Because zone 2 is more easily monitored, a strong stand for declining arteriography in the face of negative findings can be made for injuries in this area. While one could argue that after a gunshot wound to zone 2, a shock-wave effect could theoretically cause damage to the wall of a distant vessel and result in a subintimal tear, the possibility of that type of injury is extremely remote. Until data are presented to the contrary, the need to do emergency

This editorial appears in the September/October 1986 issue of the *AJNR* and the November 1986 issue of the *AJR*.

AJR 147:1000–1001, November 1986
0361–803X/86/1475–1000
© American Roentgen Ray Society

angiography in zone 2–penetrating injuries with no clinical findings is seriously questioned. Since all these patients are admitted to the hospital for observation, angiography could be performed if clinical signs develop.

To absolutely convince our surgical colleagues of the validity of this approach, a prospective multicenter study with the direct and active participation of each hospital's trauma service is desirable. A large amount of data, accumulated over a relatively short period of time, could then be evaluated. With this information, the interest of these traumatized patients will best be served and unnecessary angiography will be avoided.

REFERENCES

1. North CM, Ahmadi J, Segall HD, Zee CS. Penetrating vascular injuries of the face and neck: clinical and angiographic correlation. *AJNR* **1986**;7:855–859, *AJR* **1986**;147:995–999
2. Saleta JD, Lowe RJ, Lim LT, Thornton J, Delk S, Moss GS. Penetrating trauma of the neck. *J Trauma* **1976**;16:579–587
3. Rao PM, Bhatti FK, Gaudino J, et al. Penetrating injuries of the neck: criteria for exploration. *J Trauma* **1983**;23:47–49
4. McCormick TM, Burch BH. Routine angiographic evaluation of neck and extremity injuries. *J Trauma* **1979**;19:384–387
5. Gomez GA, Ratner L, Hernandez A, Russell E, Dove DB, Kreis DJ. Suspected vascular trauma of the extremities: the role of angiography in proximity injuries. *J Trauma* **1984**;24:660
6. Roon AJ, Christensen N. Evaluation and treatment of penetrating cervical injuries. *J Trauma* **1979**;19:391–397

Robert M. Quencer
University of Miami School of Medicine
Jackson Memorial Medical Center
Miami, FL 33136

UCSF Interventional Radiology Rounds

Interventional Radiologic Management of Sclerosing Cholangitis

Robert K. Kerlan, Jr.,[1,2] Jeanne M. LaBerge,[3] Henry I. Goldberg,[4] Anton C. Pogany,[5] and Ernest J. Ring[6]

This is a selection from the Interventional Radiology Rounds of the University of California, San Francisco. The discussion focuses on the radiologist's role in the management of patients with sclerosing cholangitis and includes clinical and radiologic descriptions of the disease and a discussion of the range of fluoroscopically guided catheter techniques.

Dr. LaBerge.—A 40-year-old man with a long history of ulcerative colitis, well controlled on Azulfidine, developed pruritis, jaundice, and a serum bilirubin of 15 mg/dl. Diagnostic ERCP was attempted but was unsuccessful. A percutaneous transhepatic cholangiogram was performed (Fig. 1). Dr. Pogany, would you comment on this study?

Dr. Pogany.—The cholangiogram shows good filling of both the right and left intrahepatic ducts. The right biliary radicles are unusually small and somewhat irregular in contour. Although the left duct is dilated centrally, its peripheral branches are attenuated and show contour irregularities. Localized areas of segmental narrowing are seen in the small intrahepatic branches. The extrahepatic duct is poorly filled. The lumen appears beaded with small saclike outpouchings. The most distal segment, barely visible on this radiograph, is very constricted. These cholangiographic findings are typical of primary sclerosing cholangitis.

Dr. LaBerge.—Because of persistent symptoms, the patient underwent surgery. An end-to-side choledochojejunostomy was constructed through which a T-tube was placed into the common bile duct. The patient did quite well after this procedure. His bilirubin dropped to 4.0 mg/dl, and the T-tube was removed.

Approximately 4 years later the jaundice recurred and the patient was readmitted to the hospital. An ERCP could not be performed, and a transhepatic cholangiogram was attempted. This procedure was very difficult. I understand that more than 50 passes were made in an attempt to opacify his biliary system. Dr. Ring, could you comment on the maximum number of passes that can be used to opacify the biliary tree during transhepatic cholangiography?

Dr. Ring.—In the 10 years or so since thin-needle cholangiography first became popular, vast experience has repeatedly demonstrated the safety of the method. Successive articles describing this procedure have progressively increased the recommended number of needle passes. It is my belief that because of the low risk involved, there is probably no limit to the number of passes that can be made. I do not use any fixed limit, but I terminate a procedure and declare it unsuccessful only because of increasing patient discomfort

Received April 28, 1986; accepted after revision June 13, 1986.

[1] Moderator.
[2] Scripps Memorial Hospital, Radiology Department, 9888 Genesee Ave., La Jolla, CA 92037.
[3] Tripler Army Medical Center, P. O. Box 890, Honolulu, HI 96818.
[4] University of California Medical School, Department of Radiology, Gastrointestinal/Body Computed Tomography Section, C-309, 501 Parnassus Ave., San Francisco, Ca 94143-0628.
[5] Alta Bates Medical Center, 2510 Webster St., Berkeley, CA 94705.
[6] University of California School of Medicine, Department of Radiology, Interventional Radiology Section, M-364, 501 Parnassus Ave., San Francisco, CA 94143-0628. Address reprint requests to E. J. Ring.

AJR 147:1002–1006, November 1986 0361–803X/86/1475–1002 © American Roentgen Ray Society

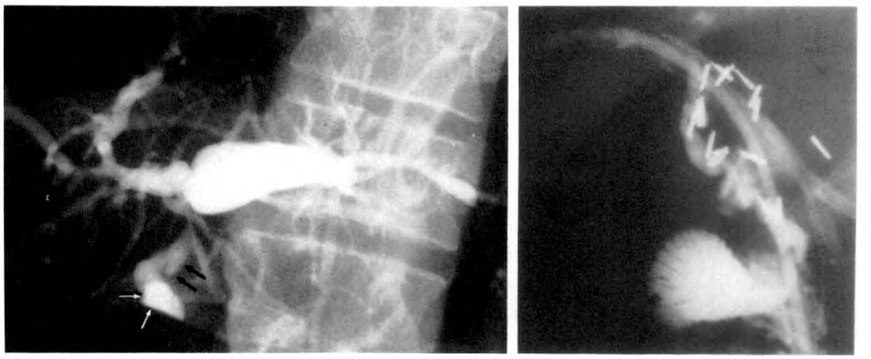


Fig. 1.—Percutaneous cholangiogram shows typical changes of primary sclerosing cholangitis. Peripheral intrahepatic ducts are narrowed and show contour irregularities. Extrahepatic duct is unusually tortuous with saclike outpouchings (*arrows*).

Fig. 2.—Injections of contrast medium through T-tube and U-tube show poor filling of intrahepatic ducts.

1 **2**

or, more commonly, because extravasated contrast medium from intraparenchymal injections completely obscures visibility.

Dr. Kerlan.—Have you ever had any problems with bleeding, abscesses, or infectious complications after performing a percutaneous cholangiogram?

Dr. Ring.—Complications of thin-needle cholangiography are infrequent. In a multiinstitutional review, Harbin et al. [1] reported a complication rate of only 3% out of 3596 procedures. Three types of risks are involved during the stages of thin-needle cholangiography. First are the chest complications that can occur if the needle traverses the costophrenic sulcus. Although this route of needle entry appears to be quite common, complications are uncommon. Second are the risks of the needle damaging the liver parenchyma, and these appear to be minimal when such a fine needle is used. The only bleeding complication I have seen after thin-needle cholangiography occurred when an uncooperative patient developed a liver laceration from thrashing about during the procedure. Finally, the most common complications of percutaneous cholangiography occur after a duct has been entered and contrast medium is injected. If an excessive amount of contrast medium is used, ductal pressure rises and sepsis may ensue. To reduce the risk of infectious complications, it is therefore extremely important to minimize the volume of contrast medium used and to employ gravity and positional changes for the portrayal of the ductal anatomy.

Dr. LaBerge.—Because of persistent symptoms and a rise in serum bilirubin from 4 to 12 mg/dl, the patient underwent a second operation. A U-tube was passed through a right hepatic duct across the choledochojejunostomy anastomosis to exit through the jejunal loop. A T-tube was also placed in the common duct. This procedure proved unsuccessful, and the patient became progressively more jaundiced. Injections of contrast material through the T-tube and U-tube showed that relatively few intrahepatic ducts were actually in continuity with the surgically placed tubes (Fig. 2).

The T-tube was then removed, and a catheter was manipulated through its tract to the origin of the right hepatic duct. Contrast medium injected through the catheter demonstrated that the right ductal system was isolated by a stricture proximal to the entrance of the U-tube (Fig. 3).

Dr. LaBerge.—Dr. Ring, could you comment on the methods you might use to ensure continued drainage of this ductal system?

Dr. Ring.—To maximize drainage of the right duct, I would prefer to dilate the stricture and then replace the existing T-tube with a long-stemmed T-tube through the strictured segment into the right duct. This technique was attempted; however, the anatomy was unfavorable, and the T-tube consistently buckled into the Roux-en-Y loop rather than advancing over the guidewire into the right hepatic duct.

An alternative procedure is percutaneous insertion of a transhepatic tube. I try to avoid this approach in patients with sclerosing cholangitis because the ducts are small and incapable of dilating and the drainage achieved is unpredictable. Tubes passed through long segments of strictured ducts in this disease can actually worsen the obstruction by impeding the inflow of bile from adjoining branches [2].

Dr. LaBerge.—Performing a transhepatic biliary drainage in a nondilated ductal system, as in this case, is obviously difficult. Dr. Kerlan, will you explain how the procedure was performed?

Dr. Kerlan.—Most transhepatic drainages are performed in patients with obstruction and dilated ducts. In these cases a 22-gauge needle is used to opacify the ducts, an appropriate puncture site is then selected, and a 5-French needle sheath is passed into the target duct. A torque-control guidewire is then passed through the sheath and directed across the obstruction to the duodenum [2].

For very small ducts we modify our approach considerably, because the small target is difficult to access and a large number of passes may be required. A 22-gauge needle is used both to puncture the small ducts and to begin the catheterization. Several systems have been developed that enable conversion of a 22-gauge needle puncture of a bile duct into a larger catheter guidewire system. Basically, all of these methods depend on unimpeded passage of a 0.018-in. (0.46-cm) guidewire well into the lumen of the duct. However, when the ducts are small, the tip of the guidewire will frequently push against the wall of the duct as it exits from the needle tip and cause the needle to recoil out of the duct. Furthermore, respiratory motion makes it difficult to keep the needle in a stable position within a narrowed duct. By revers-

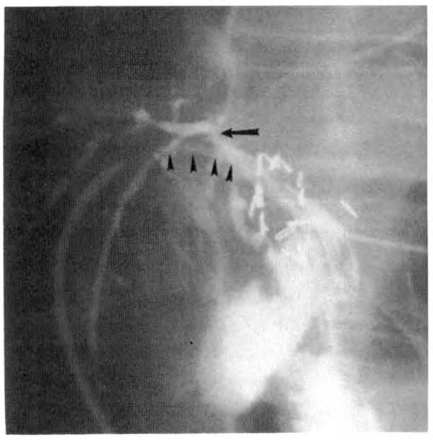


Fig. 3.—An angiographic catheter advanced through T-tube tract was manipulated through a stricture at origin of right hepatic duct (*arrow*). U-tube (*arrowheads*) enters duct below stricture.



Fig. 4.—After percutaneous biliary drainage through peripheral right hepatics, a new U-tube was inserted to drain right hepatic ducts.

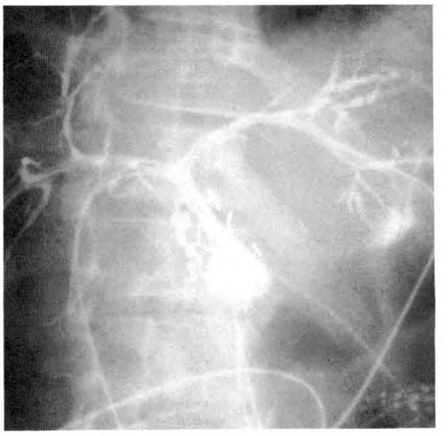


Fig. 5.—A second U-tube was percutaneously placed to drain left ducts.

ing the 0.018-in. guidewire and passing the stiff end through the duct into the liver parenchyma and beyond, enough stability is provided to insert a 3-French catheter over the guidewire. This catheter is comparable in diameter to an 0:038-in. (0.097 cm) guidewire and can be followed coaxially by a 5-French catheter. After the 5-French catheter has been introduced through the duct, it is slowly withdrawn while very small amounts of contrast medium are injected. When the tip of the catheter is in the lumen of the duct, an 0.038-in. torque-control guide can be inserted for precise manipulation through the ductal system.

With this particular patient, once the catheterization of the biliary tree was achieved, we decided to use this new access to create a U-tube. This can be done with little difficulty from a percutaneous approach whenever a portal of access already exists. In this case, the old T-tube tract served as the exit for the new U-tube. Once the sheath was through the stricture and in the extrahepatic biliary tree, a basket was manipulated through the T-tube tract and used to trap the transhepatic guidewire, which was then pulled out the T-tube tract, creating a U-configuration. A multi–side-hole silicone catheter was then passed over the guidewire to act as a new U-tube [Fig. 4].

Dr. LaBerge.—After this procedure, the patient's bilirubin decreased from 12 to 5 mg/dl. The procedure was then repeated on the left side, and a second new U-tube was inserted. Cholangiograms through the two new U-tubes demonstrated complete opacification of both the right and left ducts (Fig. 5). The patient did very well after the second procedure, and his bilirubin fell to 0.9 mg/dl. He has been followed for the past 11 months with interval cholangiograms and tube changes, and during this time his bilirubin has remained normal.

Dr. Kerlan.—Dr. Goldberg, you have extensive experience with the diagnosis and management of patients with sclerosing cholangitis. Would you review some of the important points about this problem?

Dr. Goldberg.—Sclerosing cholangitis is a difficult disease. It is a progressive process that ultimately leads to hepatic failure. The rate of progression varies with each patient, and the course of the disease in any individual is difficult to predict.

Clinically, 70% of patients with primary sclerosing cholangitis are men, and over 60% of these patients are less than 45 years old [3]. Seventy percent of patients have associated inflammatory bowel disease; chronic ulcerative colitis is by far the most common type.

The cause of this disease continues to be a mystery. Despite the clear association with inflammatory bowel disease, there does not appear to be a causal relationship. In fact, patients with chronic ulcerative colitis will occasionally develop primary sclerosing cholangitis years after total colectomies. Occasionally, patients will also have isolated cholangitis and subsequently develop symptoms related to inflammatory bowel disease.

A genetic predisposition has been suggested. In fact, sclerosing cholangitis and inflammatory bowel disease have been observed in siblings [4]. However, these correlations remain inconclusive. A relationship of the disease and HLA-B8 has also been detected [5]. Nevertheless, the diagnosis of sclerosing cholangitis can be difficult and involves biochemical, histologic, and cholangiographic criteria [6].

The histologic evaluation is often the most difficult. The process is characterized by a proliferation of connective tissue along the portal tracts associated with a mild infiltration of chronic inflammatory cells. Histologic changes typical of primary sclerosing cholangitis only occur early in the disease process. These changes include a fibrous-obliterative cholangitis in which solid cords of connective tissue replace ductal segments. However, in most patients, the disease process is more advanced by the time a liver biopsy is performed, and the histologic features are not specific.

Therefore, the cornerstone of establishing a diagnosis of sclerosing cholangitis is usually direct cholangiography. The optimal method to obtain a direct cholangiogram in this group of patients is through ERCP. This allows adequate visualization of the biliary system as well as the pancreatic duct. Although usually normal in patients with sclerosing cholangitis, the pancreatic duct can be involved in up to 8% of cases [7]. In addition, ERCP is often technically easier than percutaneous transhepatic cholangiography in these patients, who often have extremely attenuated ductal systems. When an ERCP cannot be performed for technical reasons, such as inability to cannulate the sphincter or the presence of choledochojejunostomy, percutaneous cholangiography remains a viable alternative.

The typical cholangiographic features include diffuse multifocal strictures involving both the intrahepatic and extrahepatic biliary system. In less than 30% of patients, only the intrahepatic ductal system is involved. Two cholangiographic features appear to be quite specific for sclerosing cholangitis: beading and diverticula formation. The beaded appearance is created by a series of short (1–10 mm) annular, bandlike strictures with intervening areas of dilatation [8–10]. Diverticula represent focal, eccentric 2–15 mm outpouchings of the ductal lumen, which are often, but not always, adjacent to areas of stricturing. Whether these are ulcers or diverticular outpouchings with a mucosal lining is not known.

The severity of sclerosing cholangitis can be categorized by the cholangiographic features into three types: mild, moderate, and severe [9]. The mild type is characterized by minor irregularities, as well as serrations and waviness in the mucosal surface. Moderate disease is indicated by the presence of multifocal bandlike strictures and diverticular outpouchings. In severe disease, large segments of the intrahepatic biliary system are replaced by fibrous tissue, giving rise to nonopacification or a "pruned tree" cholangiographic appearance.

Differential diagnoses of these cholangiographic patterns include secondary sclerosing cholangitis, primary biliary cirrhosis, and cholangiocarcinoma; ductal sclerosis has been induced by hepatic arterial infusion of 5-fluorouracil (FUDR) in patients with liver tumors [10].

Secondary sclerosing cholangitis must be suspected in any patient who has had biliary surgery other than a simple cholecystectomy. The cholangiographic pattern created by long-standing postsurgical strictures with recurrent pyogenic cholangitis can be nearly identical to the appearance of primary sclerosing cholangitis.

Primary biliary cirrhosis is generally easily differentiated by the fact that this disease never involves the extrahepatic biliary system. Furthermore, the ductal system, although narrowed, does not have areas of stricture and dilatation, nor is there irregularity of the duct contour. Since most patients with primary biliary cirrhosis will have antimitrochondrial antibodies present in their serum, clinical differentiation is usually not difficult.

The pattern of ductal sclerosis in patients who have been treated with hepatic artery therapy can be differentiated from primary sclerosing cholangitis because the ductal strictures in this entity are mainly localized to the common hepatic duct and proximal portion of the segmental ducts. The common bile duct and smaller peripheral ducts are typically not involved.

Cholangiocarcinoma may mimic primary sclerosing cholangitis. Rarely, a diffuse cholangiocarcinoma may be encountered that has cholangiographic features similar to primary sclerosing cholangitis [11]. However, the usual case of cholangiocarcinoma has a much more focal distribution with smooth dilation of the ductal system proximal to the site of obstruction. A more difficult problem is the possibility of cholangiocarcinoma developing in a patient with sclerosing cholangitis. An association between these diseases has been suggested [3]. Since patients with primary sclerosing cholangitis may develop cholangiocarcinoma, it may be impossible to determine when this event has occurred in the overall course of the disease. The presence of a complete obstruction of the extrahepatic bile duct should lead one to suspect neoplasm. Unfortunately, aspiration biopsy is of limited usefulness in diagnosing cholangiocarcinoma, which is frequently surrounded by a dense fibrous reaction. Likewise, transcatheter needle biopsy and brush cytology often fail to yield a diagnosis. In fact, pathologic differentiation between sclerosing cholangitis and cholangiocarcinoma can be difficult even with surgically resected specimens.

Dr. Kerlan.—Dr. Ring, would you elaborate upon the technical aspects of management in these difficult cases?

Dr. Ring.—My recommended management for patients with sclerosing cholangitis is a combined surgical–interventional radiologic approach. A surgical drainage procedure is performed and a conduit created so that subsequent interventions under fluoroscopic guidance can provide intermittent toilet of the biliary tree. Commonly, one or more tubes are introduced into the biliary tree as was done in this patient. More recently, a relatively simple access to the biliary tree has been used that avoids the annoyance of caring for permanent drainage tubes. With this approach a Roux-en-Y choledochojejunostomy is constructed at the time of surgery, and a segment of the Roux-en-Y loop is placed in an extraperitoneal location. In some medical centers this loop is connected to the skin as an open ostomy [12]. However, if the extraperitoneal segment is kept closed and marked with metal clips, it is relatively simple and safe to puncture the Roux-en-Y loop intermittently and introduce a catheter that can be manipulated into the biliary tree. In this way newly formed strictures can be dilated and stones removed. At the end of the procedure, the catheter is removed and the puncture site closes rapidly without concern about bile leakage or peritonitis [13].

In summary, the management of patients with sclerosing cholangitis remains frustrating. Ultimately, all patients with this disease will develop cirrhosis and liver failure. The methods of interventional radiology have been useful to delay the process and maintain bile flow as long as possible.

ACKNOWLEDGMENT

We thank Gala FitzGerald for editorial assistance.

REFERENCES

1. Harbin WP, Mueller PR, Ferrucci JT Jr. Transhepatic cholangiography: complications and use patterns of the fine-needle technique. A multi-institutional survey. *Radiology* **1980**;135:15–22
2. McLean GK, Ring EJ, Freiman DB. Therapeutic alternatives in the treatment of intrahepatic biliary obstruction. *Radiology* **1982**;145:289–295
3. La Russo NF, Weisner RH, Ludwig J, MacCarty RL. Primary sclerosing cholangitis. *N Engl J Med* **1984**;310:899–903
4. Quigley EMM, LaRusso NF, Ludwig J, MacSween RNM, Birnie GG, Watkinson G. Familial occurrence of primary sclerosing cholangitis and chronic ulcerative colitis. *Gastroenterology* **1983**;85:1160–1165
5. Chapman RW, Varghese Z, Gaul R, Kokinon N, Patel G, Sherlock S. Close association between HLA-B8 and primary sclerosing cholangitis (abstr). *Gut* **1981**;22:A871
6. Weisner RH, LaRusso NF. Clinicopathologic features of the syndrome of primary sclerosing cholangitis. *Gastroenterology* **1980**;79:200–206
7. MacCarty RL, La Russo NF, Weisner RH, Ludwig J. Primary sclerosing cholangitis: findings on cholangiography and pancreatography. *Radiology* **1983**;149:39–44
8. Krieger J, Seaman WB, Porter MR. The roentgenologic appearance of sclerosing cholangitis. *Radiology* **1970**;95:369–375
9. Chen LV, Goldberg HI. Sclerosing cholangitis: broad spectrum of radiologic features. *Gastrointest Radiol* **1984**;9:39–47
10. Shea WJ Jr, Demas BE, Goldberg HI, Hohn DC, Ferrell LO, Kerlan RK. Sclerosing cholangitis associated with hepatic arterial FUDR chemotherapy: radiologic-histologic correlation. *AJR* **1986**;146:717–722
11. Nichols DA, MacCarty RL, Gaffey TA. Cholangiographic evaluation of bile duct carcinoma. *AJR* **1983**;141:1291–1294
12. Barker EM, Winkler M. Permanent-access hepaticojejunostomy. *Br J Surg* **1984**;71:188–191
13. Russell E, Yrizarry JM, Huber JS, Nunez D Jr, Hutson DG, Schiff E. Percutaneous transjejunal biliary dilatation: alternate management of benign strictures. *Radiology* **1986**;159:209–214

Percutaneous Aspiration and Drainage of Pancreatic Pseudocysts

William E. Torres[1]
Michael B. Evert
Bruce R. Baumgartner
Michael E. Bernardino

Twenty-five patients with pancreatic pseudocysts had therapeutic intervention procedures that included diagnostic aspiration, short-term drainage (aspiration until completely drained), and long-term catheter drainage. Diagnostic aspirations were used to classify the pseudocysts as infected or noninfected. Short-term drainage was performed on six pseudocysts (two infected and four noninfected) with little success. One resolved and five recurred. Fifteen pseudocysts were treated by long-term catheter drainage. Eight of these (four infected and four noninfected) resolved after initial long-term drainage; two others resolved after additional drainage. The cure rate in these 15 patients was 67%. The other five patients were treated surgically after they had been stabilized but not cured by percutaneous drainage. Complications were few and uniformly minor except for one pneumothorax. Percutaneous aspiration should be used in the diagnosis of pancreatic fluid collections. In noninfected pseudocysts, drainage can be curative. In infected pseudocysts, percutaneous drainage is useful to stabilize the patient and can be either a cure or a temporizing measure until surgery can be performed.

Pancreatic pseudocysts reportedly occur in 2–18% of patients with pancreatic inflammatory disease [1, 2]. Although spontaneous resolution takes place in 8–20% of cases, it is rare in pseudocysts that have been present longer than 2 to 6 weeks [1, 3, 4]. Patients with pancreatic pseudocysts can develop severe complications, including pseudocyst rupture; abscess formation; and obstruction of adjacent bowel, bile ducts, or vessels. Percutaneous drainage of both infected and noninfected pseudocysts by means of CT and sonographic guidance has shown promising results [3, 5–8]. This report details our experience with percutaneous pseudocyst drainage and attempts to determine the usefulness of percutaneous aspiration and drainage in the treatment of complicated and uncomplicated pancreatic inflammatory disease.

Subjects and Methods

Fifteen men and 10 women with elevated serum amylase and symptoms of pancreatitis who had CT findings of pancreatic fluid collections were the basis for this study. The age range was 9 to 66 years (median 51, mean 47). Causes included acute and chronic alcoholic pancreatitis (nine), biliary pancreatitis (four), trauma (one), tumor (one), postoperative pancreatitis (two), and idiopathic pancreatitis (eight). After the extent of pancreatic inflammatory disease was determined by CT, guided diagnostic aspiration of the fluid collections was performed to determine whether the collections were infected. Fluid amylase level was determined for each aspirate. Gram stain and culture were obtained to exclude infection or to aid in the selection of appropriate antimicrobial therapy. The collections were then classified, on the basis of categories defined by Gerzof et al. [6], into infected and noninfected pseudocysts. No pancreatic phlegmons or pancreatic abscesses were included.

Four of the procedures were performed under sonographic guidance; the remaining 21 procedures were done with CT. Initial aspiration was performed by using 18- to 22-gauge needles, depending on the size and location of the fluid collection. Eighteen-gauge sheath

Received April 14, 1986; accepted after revision June 17, 1986.

[1] All authors: Department of Radiology, Emory University School of Medicine, 1364 Clifton Rd., N. E., Atlanta, GA 30322. Adddress reprint requests to W. E. Torres.

AJR 147:1007–1009, November 1986
0361–803X/86/1475–1007
© American Roentgen Ray Society

needles were preferred. Catheter drainage was initiated in all patients who had large, grossly purulent, or symptomatic fluid collections.

A variety of catheters were used: nine 12- or 14-French van-Sonnenberg sump catheters (without suction), thirteen 8.3-French all-purpose drainage catheters, and three miscellaneous-sized catheters. Two patients had two or more catheters inserted. The size of the catheter was chosen on the basis of the viscosity of the aspirate. Placement was determined by CT, sonography, and sinography.

Criteria for discontinuance of long-term catheter drainage were improvement in the patient's clinical status (e.g., afebrile), diminished or no catheter output, and collapse of the cavity as seen on CT or sonography. If clinical status worsened or if the evaluation of drainage showed evidence of residual collections or new collections were seen on CT, sonography, or sinography, additional catheters were inserted. Clamping catheters and rescanning after 1–2 days was another method used to decide when drainage should be terminated. If fluid reaccumulated, the catheter was left in place because this finding probably meant ductal communication; if no reaccumulation occurred, the catheter was withdrawn. In a third method, the catheter was exchanged for an end-hole catheter that was slowly withdrawn over several days.

Results

Diagnostic Aspiration

Fluid for diagnostic analysis was successfully obtained in all 25 patients. Five patients had no further radiographic or surgical intervention; they were managed medically, and their pseudocysts were followed by CT or sonography. These five pseudocysts resolved without additional therapy. Two additional patients had percutaneous drainage after cultures of their fluid aspirates were positive. The remaining 18 patients had therapeutic drainage at the time of the initial diagnostic aspiration because their pseudocysts were large and/or symptomatic or because the fluid aspirates were grossly purulent. Thus, 20 of the 25 patients had percutaneous drainage.

Short-Term Drainage

Six patients (two with infected pseudocysts, four with noninfected pseudocysts) had short-term drainage procedures. The pseudocyst contents were evacuated, but without placement of a long-term percutaneous indwelling catheter. After one-step drainage, one infected pseudocyst resolved without additional intervention; the remaining five pseudocysts recurred. One of these five was a noninfected pseudocyst that resolved after long-term percutaneous drainage by an indwelling catheter. In two of these five (one infected, one noninfected), repeat short-term drainage provided symptomatic relief from abdominal pain before surgery. The remaining two patients who had recurrence of their noninfected pseudocyst after a second attempt at short-term drainage were treated surgically.

Long-Term Percutaneous Drainage

Fifteen patients (nine with infected pseudocysts, six with noninfected pseudocysts) had long-term drainage after percutaneous placement of indwelling catheters. Long-term catheter placement ranged from 2 to 95 days (median 6, mean 17). The size of the catheter had no bearing on the eventual outcome. Two patients were managed as outpatients; one had an indwelling catheter for 12 weeks, and one had a percutaneously placed stent between the stomach and pancreatic pseudocyst left in place for 95 days. Eight pseudocysts (four infected, four noninfected) resolved after long-term drainage. One additional infected pseudocyst resolved after a second long-term percutaneous drainage. Another infected pseudocyst resolved after three attempts at percutaneous catheter drainage. Thus, 10 of the 15 pseudocysts resolved, resulting in a cure rate of 67%.

Five of the 15 patients were treated surgically after unsuccessful long-term catheter drainage. In two unstable patients catheter drainage was a temporizing measure that allowed time for clinical improvement before surgery. Three patients were treated surgically after long-term percutaneous treatment failed. Two of the three failures were attributed to fistulous communication between the pseudocyst and the main pancreatic duct that resulted in continuous drainage. The remaining failure was due to technical problems with catheter occlusion and inadequate drainage despite several attempts at repositioning and replacing the catheter.

A total of nine patients, therefore, ultimately required surgery. Four patients with infected pseudocysts had incision and drainage with debridement of the pancreatic bed; all did well postoperatively. Infected pseudocysts were differentiated from pancreatic phlegmons by the nature of the aspirated matter. An infected pseudocyst is a well-defined fluid mass that can be drained via a percutaneous catheter. A pancreatic phlegmon is an indurated inflammatory mass of pancreatic and adjacent tissue that cannot be drained. Of the five patients with noninfected pseudocysts, two had cystogastrostomy, one had a cystojejunostomy, and two had distal pancreatectomies and splenectomies. The three patients who had cystoenteric anastomosis all did well postoperatively without pseudocyst recurrence. One of the patients who had a distal pancreatectomy and splenectomy suffered a deteriorating course and died 7 weeks after the operation.

Complications

Three complications were the direct result of percutaneous drainage and were considered minor. One patient had a 20% pneumothorax, which resolved without intervention. A second patient, after a 12-week drainage, had *Candida albicans* infection of the tube tract, which had no effect on patient management. A third patient was thought to have a contaminated diagnostic aspirate, which resulted in a false-positive diagnosis. This patient was treated medically without radiologic or surgical intervention and did well.

Discussion

Management of the patient with a pancreatic pseudocyst is controversial. These patients can either be treated conservatively or with surgical (external or internal) or percuta-

neous drainage. The preferred nonemergent surgical management of noninfected pseudocysts is observation for approximately 6 weeks from the onset of symptoms while the fibrous membrane necessary for successful internal drainage develops around the pseudocyst. Decompression is then obtained via cystogastrostomy or cystojejunostomy. During this 6-week period spontaneous resolution is noted in 8–20% of cases. In the remaining group of patients, severe complications necessitating immediate surgery occur in 20% [1, 4]. Previously, acutely infected pseudocysts were managed by prompt external surgical drainage. However, percutaneous drainage is now being used with increasing frequency.

The high incidence of complications favors some type of early intervention, yet some uncomplicated pseudocysts resolve without intervention. Furthermore, surgical external drainage of the acute pseudocyst (less than 6-weeks duration) can result in a morbidity as high as 42%, with death after surgery in up to 19% of cases [9, 10]. Early external drainage, even though less desirable, has been advocated because of the severity of complications during the expectant period. Many believe that if a pseudocyst is present longer than 2 to 6 weeks, the chance of spontaneous resolution is poor and the likelihood of complication is great [4, 10]. The expectant period is not without problems, however; complications (rupture, ascites, hemorrhage, abscess formation, etc.) occur in 24% of the cases, with a resultant mortality of 6% [1].

When pancreatic pseudocysts are complicated by severe pain or biliary obstruction or infection, decompression should be performed immediately. Percutaneous aspiration and drainage usually can be performed at any time during the patient's course. In this series, as in others, the rate of radiologic complications is far less than those reported in the surgical literature [2, 3, 6, 10]. Our complication rate was extremely small, and the complications were minimal except for one pneumothorax. Furthermore, no infection developed in drained noninfected pseudocysts.

Infection cannot be predicted reliably by CT [11]. Diagnostic aspirations are performed on patients with pseudocysts who have abdominal pain or who have large fluid collections that may be infected. If the aspirate is grossly purulent or if the cultured aspirate is positive, long-term percutaneous drainage is undertaken. In large sterile collections, long-term catheter drainage is undertaken to minimize the risk of complications. Short-term drainage is not recommended because the benefit of this technique seems to be questionable. The resolution of one of six pseudocysts treated by short-term drainage is thought to be related to the natural history of the cyst rather than to the results of the drainage.

Five patients with noninfected pseudocysts had cyst aspiration and were treated medically until resolution. These patients were early ones in our series before strict criteria for drainage were developed.

Long-term drainage of pseudocysts was successful in 10 (67%) of 15 patients. This, plus the improved clinical status of the remaining five patients who eventually needed surgery, supports the belief that drainage should become the initial therapy for clinically symptomatic pseudocysts. For patients in whom drainage fails or in whom symptomatic pseudocysts persist after long-term drainage, surgery is recommended.

In summary, percutaneous aspiration should be used in the diagnosis of pancreatic fluid collections. In noninfected pseudocysts, drainage can be curative. In infected pseudocysts, percutaneous drainage is useful to stabilize the patient and can be either a cure or a temporizing measure until surgery can be performed. Complete evacuation of the pseudocyst without catheter drainage does not seem to be useful because most recur. In this series neither percutaneous drainage nor surgery yielded 100% cure, but combined radiologic and surgical techniques yielded optimum results with minimum morbidity.

REFERENCES

1. Colhoun E, Murphy JJ, MacErlean DP. Percutaneous drainage of pancreatic pseudocysts. *Br J Surg* **1984**;71:131–132
2. Julius AJ, Meijer S, Hoitsma HFW, Den Otter G. Surgical treatment of pseudocysts of the pancreas: guidelines for management. *Neth J Surg* **1984**;36(4):93–97
3. vanSonnenberg E, Wittich GR, Casola G, et al. Complicated pancreatic inflammatory disease: diagnostic and therapeutic role of interventional radiology. *Radiology* **1985**;155:335–340
4. Bradley EL, Clements JL, Gonazalez AC. The natural history of pancreatic pseudocysts: a unified concept of management. *Am J Surg* **1979**;137:135–141
5. Karlson KB, Martin EC, Fankuchen EI, et al. Percutaneous drainage of pancreatic pseudocysts and abscesses. *Radiology* **1982**;142:619–624
6. Gerzof SG, Johnson WC, Robbins AH, et al. Percutaneous drainage of infected pancreatic pseudocysts. *Arch Surg* **1984**;119:888–893
7. Barkin JS, Smith FR, Pereiras R, et al. Therapeutic percutaneous aspiration of pancreatic pseudocysts. *Dig Dis* **1981**;26:585–586
8. MacErlean DP, Bryan DJ, Murphy JJ. Pancreatic pseudocyst: management by ultrasonographically guided aspiration. *Gastrointest Radiol* **1980**;5:255–257
9. Kane MG, Krejs GJ. Pancreatic pseudocyst. *Adv Intern Med* **1984**;29:271–300
10. Shatney CH, Lillehei RC. The timing of surgical treatment of pancreatic pseudocysts. *Surg Gynecol Obstet* **1981**;151:809–812
11. Federle MP, Jeffrey RB, Crass RA, VanDalsem V. Computed tomography of pancreatic abscesses. *AJR* **1981**;136:879–882

Technical Note

Basket Extraction of Esophageal Foreign Bodies

Hubert A. Shaffer, Jr.,[1] Bennett A. Alford,[1,2] Eduard E. de Lange,[1] G. Andrew Meyer,[1] and Joan McIlhenny[1]

When a foreign body becomes lodged in the esophagus, appropriate management depends on the nature of the swallowed object [1]. Prompt endoscopic removal is recommended for a sharp-edged or pointed foreign body because of its potential for esophageal-wall penetration and perforation [2, 3]. Likewise, small disk batteries, such as those used in electronic watches and calculators, should be withdrawn without delay to prevent caustic erosion and perforation of the esophagus [4]. However, if the foreign body has smooth surfaces and is nontoxic, one may justify delaying extraction, because most blunt objects will pass spontaneously without incident [2, 5–7]. To hasten passage into the stomach, a number of noninvasive pharmacologic and mechanical measures have been advocated, such as glucagon to relieve lower esophageal sphincter spasm [1, 5, 8, 9], sublingual nitroglycerin to eliminate more widespread smooth muscle spasm [5], and carbon dioxide gas to distend the esophagus and push impacted food beyond fixed strictures [9, 10]. When noninvasive methods fail to dislodge a blunt object, extraction is required. Currently, most foreign bodies are removed with instruments passed through an endoscope or with a Foley catheter balloon inflated distal to the impaction and withdrawn under fluoroscopic control [11, 12].

We introduce a method for removing blunt foreign bodies from the esophagus using a Dormia-type wire basket under fluoroscopic guidance. The technique is a natural extension of the popular procedure developed by Burhenne [13] for removing residual bile duct stones through the T-tube tract. We have found the procedure particularly useful for removing soft food boluses and hard, spherical objects (such as fruit pits) that have become impacted above esophageal strictures.

Materials and Methods

Materials

A selection of biliary stone baskets (Medi-tech, Inc., Watertown, MA) measuring 15, 20, and 25 mm in diameter will permit extraction of esophageal foreign bodies in all patients, from infants to adults (Fig. 1). For each patient, a basket diameter is chosen to match the diameter of the esophagus so that there will be no space outside the basket into which the foreign body can escape during its removal. The 55-cm working length of these baskets is adequate to reach the distal esophagus, even in tall adults.

To introduce the basket into the esophagus, we prefer to use a 10-French feeding tube (Argyle, St. Louis, MO). It can be cut short enough to permit the basket to extend beyond its end and open fully. Because of the way the feeding tube is coiled in its sterile package, there are set curves approximately every 15 cm along its length. Cutting the tube at a selected point on one of these curves creates a custom-curved tip that can be torqued for directing a guidewire around lodged material and through eccentric strictures (Fig. 2). Gently heating the cut end of the tube will make it smooth. The other end snugly attaches to any Luer-Lok syringe with no need for an adapter. The tube has an opaque marker, making it easy to identify during fluoroscopy. The lumen is large enough to permit suctioning of tenacious secretions, which often accumulate above an impacted foreign body.

Other required equipment includes a tilting fluoroscopic table, topical anesthetic for the pharyngeal mucosa, an angiographic

Received April 14, 1986; accepted after revision June 9, 1986.
Presented at the annual meeting of the American Roentgen Ray Society, Washington, DC, April 1986.
[1] Department of Radiology, Box 170, University of Virginia Medical Center, Charlottesville, VA 22908. Address reprint requests to H. A. Shaffer.
[2] Present address: Department of Radiology, Children's Hospital, 1600 7th Ave., S., Birmingham, AL 35233.

 0361–803X/86/1475–1010 © American Roentgen Ray Society

Fig. 1.—Medi-tech biliary stone baskets ranging in diameter from 15–25 mm. Formed from four helical wires, these baskets work well for extraction of foreign bodies from the esophagus.

Fig. 2.—Argyle 10-French feeding tube used to introduce wire basket. On left, note that feeding tube, when removed from manufacturer's package, has set curves at intervals along its length. Tube may be cut to create any working length and custom-curved tip one desires (right). A Luer-Lok syringe is attached to proximal end of tube.

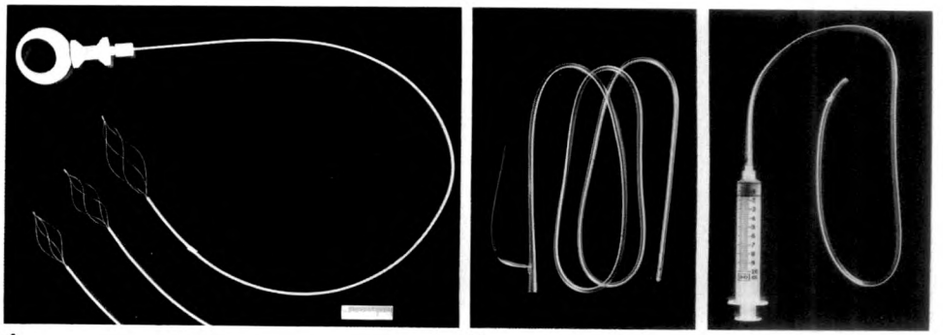
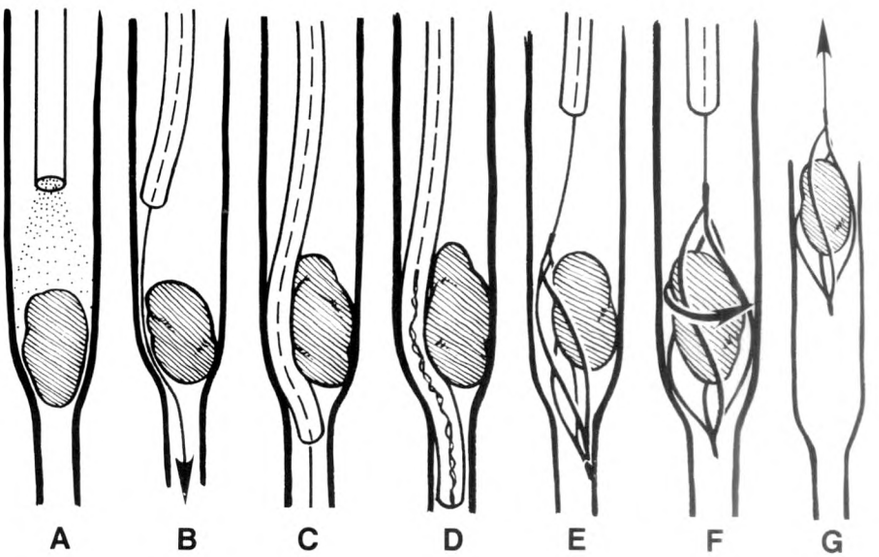


Fig. 3.—*A–G*, Diagram of steps in basket extraction technique. For details see text.



guidewire with a flexible "J" or straight tip, dilute barium sulfate, scissors, and two syringes (30–60 ml). Infants and young children must be secured in an immobilization device. A bite block or padded tongue depressor may be necessary to keep the teeth apart in a young child to allow free passage of the instruments. No sedation or general anesthesia is required.

Methods

A barium swallow should always be obtained first to evaluate the nature and location of the foreign body and to determine if a stricture is present. This knowledge allows one to select a basket of proper diameter and to custom-cut the length and the curve on the end of the feeding tube.

After the posterior oropharynx is sprayed with topical anesthetic, the modified feeding tube is passed through the mouth (*not the nose*) into the esophagus above the impaction. If the esophageal wall and foreign body are no longer outlined with barium, coating is reestablished by injecting a small amount of dilute barium through the tube (Fig. 3A). This is done with the head of the X-ray table elevated to reduce the chance of aspiration into the airway.

The guidewire is inserted into the feeding tube. By rotating the tube to deflect its tip to one side of the foreign body, the guidewire can be advanced carefully around the object under fluoroscopic control. The tip of the wire is passed well beyond the foreign body, often as far as the stomach (Fig. 3B). The feeding tube is then advanced over the guidewire well beyond the foreign body. This usually places the end of the tube within an underlying esophageal stricture (Fig. 3C).

The guidewire is removed from the feeding tube, and a basket of appropriate size is inserted. The basket is advanced inside the feeding tube until it is located beside the foreign body (Fig. 3D). The longitudinal midpoint of the basket must be positioned at or below the lower margin of the foreign body in order to capture the object when the basket is unsheathed. If the position of the basket must be adjusted, it should be advanced only within the protective cover of the feeding tube to avoid any risk of esophageal-wall penetration.

After the basket is properly positioned, the feeding tube is withdrawn to unsheath the basket. At first, the basket may not open fully because it is deformed by the adjacent foreign body and may be restricted by an underlying esophageal stricture (Fig. 3E). If the basket is withdrawn a short distance at this time, it will dislodge the foreign body upward from the stricture into the normal esophagus where the basket has room to expand fully. The foreign body is engaged in the basket by twirling the instrument until the object is enclosed within its wires (Fig. 3F).

The patient is turned onto his right side, and the X-ray table is turned to a head-down position to reduce the risk of aspiration during extraction. With the foreign body trapped and controlled within the basket, the feeding tube and basket are withdrawn together from the

esophagus through the mouth in one smooth, continuous motion (Fig. 3G). Transient resistance may be encountered as the mass passes the cricopharyngeus, but this is overcome by steady traction on the basket.

Results

Fluoroscopically guided basket extraction of 12 esophageal foreign bodies was accomplished in 11 patients. Patients ranged in age from 12 months to 71 years. Most (6/11) were infants and children. Impacted food was identified as the foreign material in 11 of 12 incidents. Poorly chewed meat was the cause in at least 10 of these. In addition to the 11 food impactions, one prune pit was extracted. In every case, there was an underlying abnormality of the esophageal wall that produced narrowing of the lumen and predisposed the patient to food impaction. Strictures developed at surgical anastomoses in five patients; two of these were complicated by a previous leak or perforation at the suture line. Stenoses in four patients were the result of gastroesophageal reflux: two peptic strictures, one Schatzki's ring, and one spastic muscular "A" ring. Single cases of stricture resulted from lye ingestion or iatrogenic laceration of a congenital web. Our first patient (Fig. 4) is a representative example of this series.

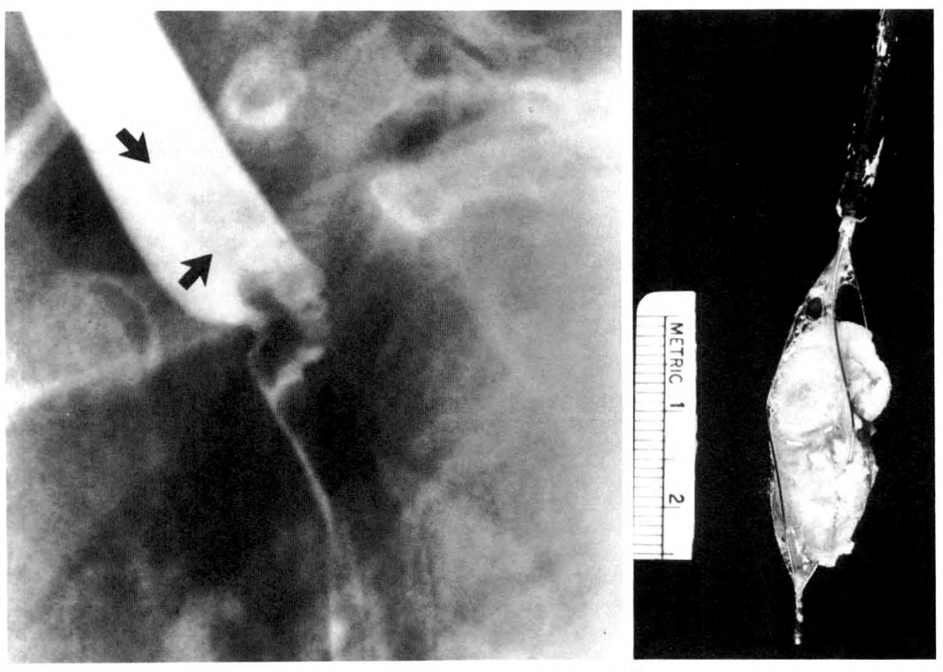
All patients were treated within 48 hr of their ingestion. In all but one, the foreign body was engaged and removed on the first pass of the basket. The lone exception was an infant with numerous impacted chunks of hot dog, which required three passes for complete removal. No complications were associated with the basket extractions. The basket showed no tendency to engage or snare mucosa in the esophagus as it occasionally does in the periampullary region during biliary stone removals.

Discussion

When noninvasive methods fail to dislodge a smooth, nontoxic foreign body, extraction is required. Currently, the methods usually considered are instrumentation through a rigid or flexible endoscope and the Foley catheter technique. In experienced hands, each of these techniques has a reported success rate of 90% or better and a complication rate of 1% or less [1, 7, 11, 14, 15]. Each method, however, has inherent disadvantages.

Since 1904, instrumentation through a rigid esophagoscope has been the standard procedure for removing esophageal foreign bodies [1]. The disadvantages of rigid endoscopy are that it requires general anesthesia, which increases the risk of the procedure, and frequently necessitates hospitalization, which makes it relatively expensive. In the past decade, fiberoptic flexible endoscopy has become a widely accepted alternative to rigid esophagoscopy. Although it can be performed as an outpatient procedure in most adults by using only sedation and topical anesthesia [1], children still require general anesthesia and hospitalization [16]. Another drawback is that a foreign body grasped by a snare or forceps cannot be withdrawn inside a fiberoptic scope for protection against escape and aspiration. Also, a large or fragmented foreign body that must be removed in pieces requires multiple insertions and withdrawals of the scope, adding to the discomfort and potential risk of the procedure [1, 17].

Regardless of whether a rigid or flexible scope is used, it is difficult or impossible to remove a smooth, hard, spherical object with a forceps or snare because there is nothing for the closing instrument to grasp. However, hard spheres (ball bearing, plastic bead, marble, and peach pit) have been removed endoscopically by using a Dormia basket [14, 16,



A B

Fig. 4.—10-year-old boy with esophageal lye stricture.

***A*, Barium swallow shows piece of pork chop (*arrows*) impacted above stricture.**

***B*, Photograph of extracted meat shows it still firmly contained in basket.**

18]. With this procedure, the basket must be inserted beyond the foreign body in order to capture it. Because the endoscopist cannot see around the impacted object, the tip of the advancing basket is not visually controlled. This blind insertion could lead to penetration of the esophageal wall, particularly when a stricture is present.

Another frequently used method is the Foley catheter technique. With this procedure, a Foley catheter balloon is inflated distal to the foreign body and is withdrawn together with the object under fluoroscopic guidance [1, 11, 19, 20]. This technique is easily performed, obviates hospitalization, and avoids the risks of general anesthesia and endoscopy [1, 7, 11, 20, 21]. The vast majority of the clinical experience has been with coins and other smooth, radiopaque objects, but nonopaque foreign bodies, including food impactions, have also been successfully removed [22]. Technical failures are most frequent when the foreign body is impacted in a stricture [11, 21]. Some consider the presence of esophageal stenosis to be a contraindication to Foley balloon inflation and extraction because of the potential for esophageal rupture [19, 22]. Concern has also been expressed about possible aspiration of the uncontrolled foreign body as it is dragged over the glottis [12, 15]. Although these are theoretical risks, we have found no reports of serious complications associated with the Foley catheter technique.

Although our series is relatively small, we have identified a number of advantages for fluoroscopically guided basket extraction of esophageal foreign bodies: (1) Being an outpatient procedure, it is relatively inexpensive. (2) There is no requirement for general anesthesia (or even sedation in most cases). (3) The method virtually eliminates the risk of esophageal perforation because the basket is advanced within a protective sheath, and the relationship between the basket tip and the esophageal wall beyond the foreign body can always be seen fluoroscopically. (4) Because an open basket is relatively flexible and under less tension than an inflated Foley balloon, the theoretical possibility of perforation should be even less. (5) Tracheal aspiration is very unlikely because the foreign material is trapped and controlled within the basket during withdrawal.

For removing coins and other discoid objects from the esophagus, we see no place for basket extraction. These flat, essentially two-dimensional objects would be very difficult to engage in the basket and secure against escape during withdrawal. However, we strongly advocate fluoroscopically guided basket extraction for removal of three-dimensional blunt foreign bodies, such as food boluses and hard spherical objects. We believe that this technique becomes the procedure of choice when there is an underlying esophageal stricture, a condition that makes other methods of extraction more difficult and dangerous.

Addendum

Since the acceptance date of this manuscript, the authors have performed successful basket extractions of retained food from four additional patients without complications. All had underlying esophageal strictures due to gastroesophageal reflux.

REFERENCES

1. Chaikhouni A, Kratz JM, Crawford FA. Foreign bodies of the esophagus. *Am Surg* **1985**;51:173–179
2. Vizcarrondo FJ, Brady PG, Nord HJ. Foreign bodies of the upper gastrointestinal tract. *Gastrointest Endosc* **1983**;29:208–210
3. Borden S IV. Removal of esophageal foreign bodies by balloon catheter. In: Athanasoulis CA, Pfister RC, Greene RE, Roberson GH, eds. *Interventional radiology*. Philadelphia: Saunders, **1982**:780–781
4. Jaffe RB, Corneli HM. Fluoroscopic removal of ingested alkaline batteries. *Radiology* **1984**;150:585–586
5. Spiro HM. *Clinical gastroenterology*, 3rd ed. New York: MacMillan, **1983**:99,120–121
6. Selivanov V, Sheldon GF, Cello JP, Crass RA. Management of foreign body ingestion. *Ann Surg* **1984**;199:187–191
7. Shaffer RD, Klug T. A comparative study of techniques for esophageal foreign body removal with special emphasis on meat bolus obstruction. *Wis Med J* **1981**;80:33–36
8. Trenkner SW, Maglinte DDT, Lehman GA, Chernish SM, Miller RE, Johnson CW. Esophageal food impaction: treatment with glucagon. *Radiology* **1983**;149:401–403
9. Friedland GW. The treatment of acute esophageal food impaction. *Radiology* **1983**;149:601–602
10. Rice BT, Spiegel PK, Dombrowski PJ. Acute esophageal food impaction treated by gas-forming agents. *Radiology* **1983**;146:299–301
11. Campbell JB, Quattromani FL, Foley LC. Foley catheter removal of blunt esophageal foreign bodies. Experience with 100 consecutive children. *Pediatr Radiol* **1983**;13:116–119
12. McGuirt WF. Use of Foley catheter for removal of esophageal foreign bodies. A survey. *Ann Otol Rhinol Laryngol* **1982**;91:599–601
13. Burhenne HJ. Garland lecture. Percutaneous extraction of retained biliary tract stones: 661 patients. *AJR* **1980**;134:889–898
14. Ricote GC, Torre LR, Perez De Ayala V, et al. Fiberendoscopic removal of foreign bodies of the upper part of the gastrointestinal tract. *Surg Gynecol Obstet* **1985**;160:499–504
15. Zonakis PM. Foley catheter technique (letter). *Arch Otolaryngol* **1984**;110:63
16. Bedogni G, Oselladore D, Ricci E, Rossoni R. *Operative endoscopy of the digestive tract. Text-atlas*. Padova, Italy: Piccin Medical Books, **1984**:1,2,8,19
17. Kozarek RA, Sanowski RA. Esophageal food impaction. Description of a new method for bolus removal. *Dig Dis Sci* **1980**;25:100–103
18. Schiratzki H. Removal of foreign bodies in the esophagus. An old device—a new procedure. *Arch Otolaryngol* **1976**;102:238–240
19. Kushner DC, Cleveland RH. Removal of esophageal foreign bodies in childhood. In: Ferrucci JT Jr, Wittenberg J, Mueller PR, Simeone JF, eds. *Interventional radiology of the abdomen*. Baltimore: Williams & Wilkins, **1984**:435–441
20. Campbell JB, Foley LC. A safe alternative to endoscopic removal of blunt esophageal foreign bodies. *Arch Otolaryngol* **1983**;109:323–325
21. O'Neill JA Jr, Holcomb GW Jr, Neblett WW. Management of tracheobronchial and esophageal foreign bodies in childhood. *J Pediatr Surg* **1983**;18:475–479
22. Nixon GW. Foley catheter method of esophageal foreign body removal: extension of applications. *AJR* **1979**;132:441–442

Technical Note

Effect of Suction on Biopsy Sample Size

Mark G. Hueftle[1] and John R. Haaga

In recent years many clinical reports of percutaneous procedures have appeared, but there are few data concerning the effects and duration of suction upon sizes of samples recovered. Out of 148 publications reviewed, only seven list methods of suction used [1–5]. Fifty-three authors made qualifying remarks, such as hard suction, continuous aspiration relative to duration, or maintenance of suction. In this same group, 27 advocated releasing suction and 15 supported maintaining suction.

Materials and Methods

A standard biopsy technique under controlled circumstances was used to evaluate the significance of (phase 1) effect of varying amounts of suction upon tissue recovery, and (phase 2) the impact of maintenance or release of suction.

The equipment used consisted of a 15-cm, 30°-bevel, 20-gauge needle (Universal Medical Instruments Corp., Ballston Spa, NY); a 12-cm, 60°-bevel, 18-guage Menghini needle (Becton-Dickinson, Rutherford, NJ); and a 50-ml Luer-Lok syringe (Becton-Dickinson, Rutherford, NJ). A Gram-atic balance (Mettler Instrument Corp., Hightstown, NJ, distributed by Fisher Scientific Co.), accurate to 0.1 ± 0.02 mg, was used.

Tissue used for the experiment was fresh, disease-free liver, both bovine and human. The liver specimen was placed on a table. By using a modified Menghini technique, a single pass was performed with the appropriate suction applied and a 3-cm incursion of the needle. The needle and syringe were weighed before and after the procedure. (The needle was wiped clean before weighing.) Size was the only difference between the two samples. The samples were taken from the same liver and from the same general area to avoid errors caused by density differences of the liver. A total of 290 biopsies were obtained (100 with 20-gauge needle and 190 with an 18-gauge needle).

Phase 1 was performed to assess the difference in sample size produced by variation of suction. The 20-gauge needle was evaluated with 5, 10, 20, and 30 ml and the 18-gauge needle with 0, 5, 10, 20, and 30 ml of negative pressure. For each set of data, five passes were made with each of the described amounts of suction. (The high and low values of each set were excluded from the average weight.) (Figs. 1 and 2). These data were compared with the expected theoretical data based on pressure change (Fig. 3).

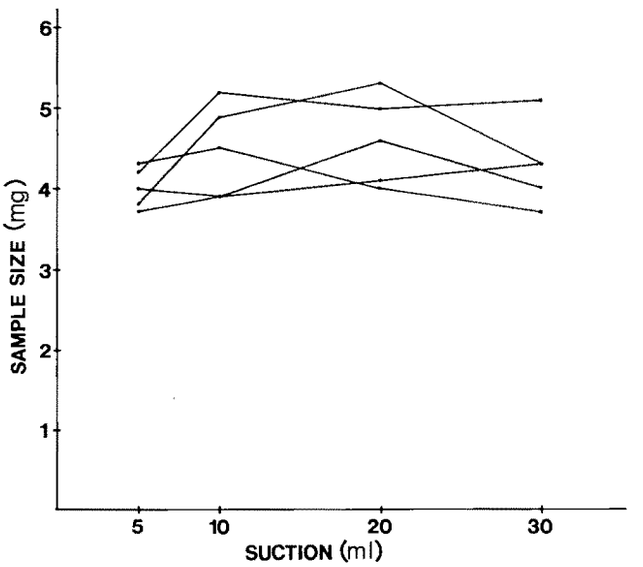


Fig. 1.—Sample size vs suction, 20-gauge needle. Each point = average of five samples.

Received April 28, 1986; accepted after revision June 17, 1986.
Both authors: Department of Radiology, University Hospitals of Cleveland, Cleveland, OH 44106. Address reprint requests to J. R. Haaga, Diagnostic Radiology, University Hospitals of Cleveland, 2074 Abington Rd., Cleveland, OH 44106.

 0361–803X/86/1475–1014 © American Roentgen Ray Society

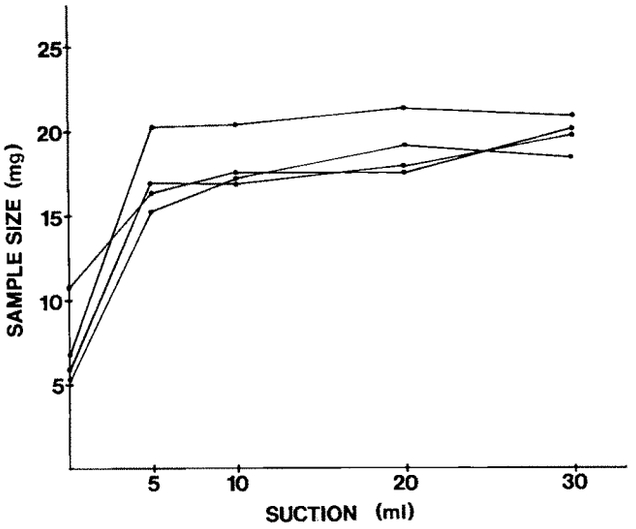


Fig. 2.— Sample size vs suction, 18-gauge needle. Each point = average of five samples.

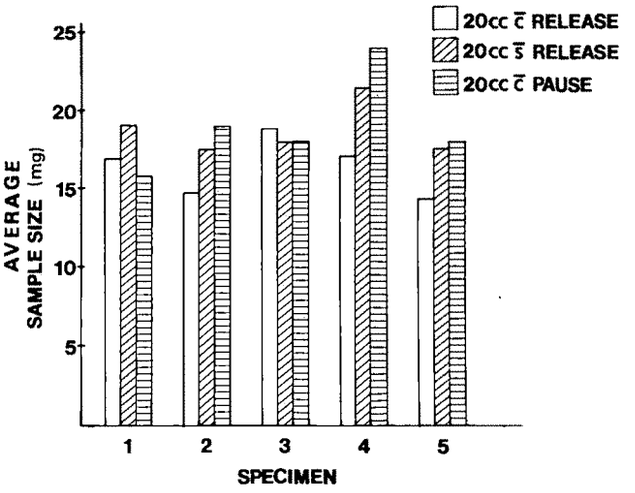


Fig. 4.—Variations in suction application. Specimens 1–4 = average of 5 samples (human), specimen 5 = average of 10 samples (bovine). c̄ = with, s̄ = without.

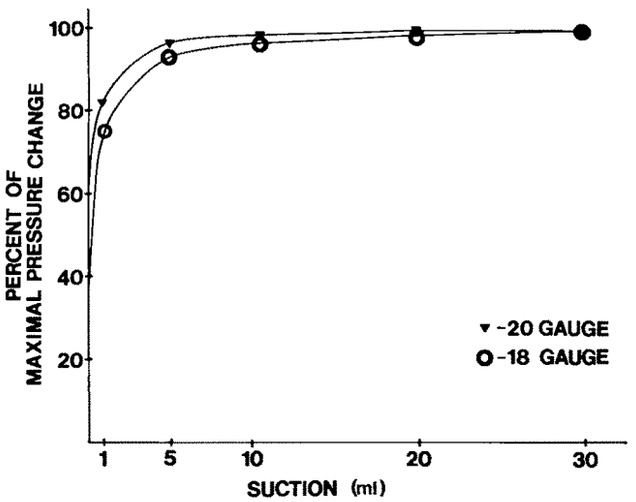


Fig. 3.—Theoretical pressure change as calculated by Poiseuille's law [6] for noncompressible fluids ($Q = \pi_8 \frac{pa^4}{1} n$. Q = volume of fluid through cylinder, P = pressure difference at ends of cylinder, a = radius of cylinder, l = length, n = viscosity of fluid) and Boyle's law [6] for ideal gasses ($P_1V_1 = P_2V_2$ at constant temperature, P_1 = initial pressure, V_1 = initial volume, P_2 = final pressure, V_2 = final volume.)

Phase 2 studied three variations with an 18-gauge needle: (1) 20 ml as in phase 1 but release of suction before withdrawal, (2) 20 ml of suction as in phase 1 with maintenance of suction, and (3) 20 ml as in phase 1 but with 1-sec pause at the peak depth of excursion (during needle removal the suction is maintained). Five passes were taken with each variation. Again the high and low values were excluded before getting the average. (This phase was repeated with beef liver with 10 passes taken.) These data illustrated in Fig. 4.

Results

The results of our study were consistent. We found no significant differences in sample sizes with variations of suction with a 20-gauge needle from 5–30 ml of suction. A plausible explanation is that with the 18-gauge needle, the sample size increases rapidly from 0 ml of suction and plateaus at 5–10 ml of suction. The curve maintains a similar shape with each sample (Fig. 2). The measured values showed good correlation with the calculated theoretical data (Fig. 3).

Using the same specimens as the data from Figure 2, we performed biopsies with the three variations in technique described above (Fig. 4). Because the results from the four human liver samples were variable, we repeated the study with fresh bovine liver. The results with the bovine samples showed a significant increase in sample size related to maintenance and increased duration of suction.

Discussion

In trying to improve yield of percutaneous biopsy procedures, suction is an important parameter to define. With the data about suction defined, the most satisfactory method of suction for many techniques can be further perfected. Knowing the optimal amount of suction, one can select the proper syringe size for the individual operator or for complex techniques like the "corkscrew" maneuver (large syringes are sometimes difficult to manipulate).

The data from our experiment on suction show that the recovery of tissue is dependent on suction but that the amount of suction required to obtain the maximum sample is somewhat low (Figs. 1 and 2). With the 20-gauge needle, the measured size of sample at 5 ml was 84% of the highest amount obtained and at 10 ml was 94% of the highest amount

obtained. This closely correlates with the theoretical pressure change (Fig. 3). The initial volume (V_1 of Boyle's law [6], Fig. 3) is the controlling factor, and these data are applicable to all needle sizes. The initial volume relates to the space within the bore of the needle (as well as the dead space in the syringe) and hence is larger with a bigger needle and smaller with a smaller needle. With a larger needle, the pressure change will be slightly more gradual with changes in suction and vice versa. With needles 18 gauge or smaller (e.g., 22 gauge), this difference in pressure change is not significant as long as 10 ml of suction are used.

The other information that we evaluated was the impact of duration of suction on sample size (i.e., releasing, sustaining, or maintaining suction during a biopsy procedure). Although with human samples the results were inconsistent, with the bovine livers we found almost a 20% larger sample size if suction was sustained during removal of the needle (Fig. 4). Maintaining suction for an additional second during maximum excursion of the needle showed a small percentage increase in sample size (Fig. 4).

These data appear to support the views of authors who claim that maintenance of suction obtains a larger sample [7, 8]. Previous concerns that aspiration of blood cells would confuse the cytopathologic interpretation are no longer valid [9–11]. New fixatives that lyse red cells and preserve cellular architecture are available (Nunez C, personal communication).

In conclusion, our in vitro study has shown that with different sizes of needles, one can use the amount of suction needed to maximize the sample recovered with aspiration biopsies. In our opinion, obtaining 90+% of the possible tissue is a reasonable goal and therefore we recommend the use of 10-ml suction for both the 20-gauge needle as well as the 18-gauge needle. These correlate with a theoretical pressure change of 98% and 96%, respectively. Although theoretically one could attempt to recover 99+% of the potential sample by using a larger amount of suction, our experimental data do not indicate that this will occur in the real biopsy setting.

REFERENCES

1. Clouse ME, Gregg JA, McDonald DG, Legg MA. Percutaneous fine needle aspiration biopsy of pancreatic carcinoma. *Gastrointest Radiol* **1977**;2:67–69
2. Cohen MM. Early diagnosis of pancreatic cancer using ultrasound and fine needle aspiration cytology. *Am Surg* **1979**; 45:715–717
3. Ihre TH, Pyk E, Raaschou-Nielsen T, Seligson U. Percutaneous fine-needle aspiration biopsy during endoscopic retrograde cholangiopancreatography. *Scand J Gastroenterol* **1978**;13:657–662
4. Ohto M, Karasawa E, Tsuchiya Y, et al. Ultrasonically guided percutaneous contrast medium injection and aspiration biopsy using a real-time puncture transducer. *Radiology* **1980**;136:171–176
5. Skolnick ML, Dekker A, Weinstein BJ. Ultrasound guided fine-needle aspiration biopsy of the liver: cytodiagnosis of hepatic cancer. *Acta Cytol (Baltimore)* **1979**;23(4):287–291
6. Sears FW, Zemansky MW. *University physics*, 3rd ed. Reading, MA: Addison-Wesley, **1963**
7. Dickey JE, Haaga JR, Schultz CL, Stellato TA, Hau T. Evaluation of CT guided percutaneous biopsies of the pancreas. Presented at the annual meeting of the American Roentgen Ray Society, Boston, MA, April **1985**
8. Menghini G. Two-operator needle biopsy of the liver. *Am J Dig Dis* **1959**;4:682–692
9. Hovdenak N, Lees WR, Pereira J, Beilby JOW, Cotton PB. Ultrasound-guided percutaneous fine-needle aspiration cytology in pancreatic cancer. *Br Med J* **1982**;285:1183–1185
10. Schwerk WB, Durr H-K, Schmitz-Moormann P. Ultrasound guided fine-needle biopsies in pancreatic and hepatic neoplasms. *Gastrointest Radiol* **1983**;8:219–225
11. Zornoza J. *Percutaneous needle biopsy*. Baltimore: Williams & Wilkins, **1981**

Technical Note

A Method for Retrieval of Retained Subcutaneous Catheter Fragments

Randy R. Sibbitt,[1,2] Julio C. Palmaz,[1] and Francisco Garcia[1]

Thoracentesis may be performed with a needle alone or with a catheter introduced through a needle. Occasionally the catheter may be cut off when it is inappropriately withdrawn against the cutting edge of the introducer needle [1, 2]. Such retained catheter fragments may extend from the pleural space to the subcutaneous muscle and fat layers of the chest wall. The plastic may act as a foreign body, inciting a sterile reaction, or serve as a focus for bacterial infection resulting in cellulitis or empyema [3]. Surgical removal can be difficult because the catheter fragment is soft, generally well below the skin and movable with respiration, making detection by palpation useless. We have treated two patients with retained thoracentesis catheter fragments and have developed and successfully used a percutaneous method for catheter fragment retrieval. The technique also has proven useful in retrieving the end of one biliary drainage catheter and one nephrostomy catheter, when the tubes were inadvertently cut or broken near the skin and well-timed deep inhalation by the patients pulled the catheter ends into the subcutaneous tissues of the puncture site.

Technique

The catheter fragment is generally radiopaque, allowing for easy localization [4]. Once the fragment is located, a tangential film obtained with fluoroscopic guidance helps to ascertain depth, and fluoroscopic observation of motion with respiration allows determination of pleural-space involvement. An 18- to 20-gauge needle is formed into a miniature hook by pressing the tip against a hard, sterile surface such as a surgical tray or bowl (Fig. 1). The small recurved hook at the tip permits unimpeded insertion of the needle. The skin over the catheter is infiltrated with local anesthetic, and a

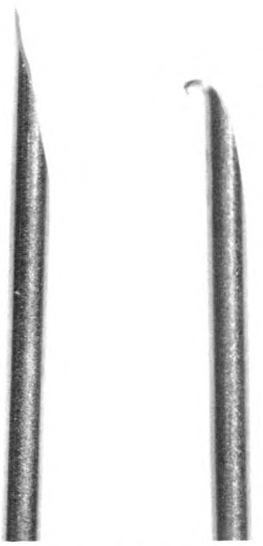


Fig. 1.—Small recurved hook at tip of 20-gauge needle formed through pressure against sterile metal surgical tray.



Fig. 2.—Case 1. Tangential view of catheter fragment hooked on needle tip (*arrow*) with removal by slow traction.

Received March 10, 1986; accepted after revision May 21, 1986.

[1] Department of Radiology, University of Texas Health Science Center at San Antonio, 7703 Floyd Curl Dr., San Antonio, TX 78284.

[2] Present address: Center for Noninvasive Diagnosis, University of New Mexico School of Medicine, Department of Radiology, Albuquerque, NM 87131. Address reprint requests to R. R. Sibbitt.

AJR **147:1017–1018, November 1986** 0361–803X/86/1475–1017 © American Roentgen Ray Society

small nick is made. The needle, oriented 90° to the most superficial portion of the catheter, is advanced past the catheter segment, rotated, and then pulled against it. The maneuver is repeated until the hook engages the catheter (Fig. 2). The fragment is then removed with gentle traction. If the catheter fragment remains bound by the surrounding tissue, a hemostat may be used to burrow along the needle to clear a path for removal. Multiple areas of partial catheter laceration were noted in our postthoracentesis patients, as occurred in one previous report [1]. Thus, an important part of the extraction is the slow traction on the retained fragment, since areas of weakening in the catheter wall are common. A constant smooth pulling motion avoids further breaks and ensures an easy, rapid retrieval. Postextraction chest fluoroscopy and radiographs confirm removal of all fragments and exclude pneumothorax.

Discussion

We successfully used this method in retrieving catheter fragments in two postthoracentesis patients and regaining purchase on the drainage catheters of two other patients. One percutaneous extraction was successful after a failed attempt at surgical removal. The patients tolerated the procedure well. After extraction, no chest-wall hematoma, hemothorax, pneumothorax, or infection occurred.

The best treatment for retained catheter fragments has not been established. If infection is present, the foreign body must be removed. The decision about whether to leave an uncomplicated catheter fragment in place should be based on a comparison of the damage that might be done by the removal process with the potential harm of a chronic foreign body. We have successfully used this nontraumatic method of catheter-fragment removal without complication and encourage its use as a simple solution to an unsettling iatrogenic problem.

REFERENCES

1. Sue D, Lam K. Retention of catheter fragment after thoracentesis. *Postgrad Med* **1982**;72:101–106
2. Richards V. Tube thoracostomy. *J Fam Prac* **1978**;6(3):629–635
3. Gilsanz V, Cleveland R. Pleural reaction to the thoracotomy tube. *Chest* **1978**;74:167–169
4. Gahhos F, Arons M. Soft-tissue foreign body removal: management and presentation of a new technique. *J Trauma* **1984**;24(4):340–341

Case Report

Small-Bowel Obstruction Due to an Intestinal Balloon: Treatment by Percutaneous Needle Puncture

Y. Sato,[1] E. Frey,[1] A. Foderaro,[2] and K. C. Pringle[3]

Intestinal obstruction is a rare but potentially serious complication of enteric alimentation, which sometimes necessitates laparotomy. We report a case of small-bowel obstruction caused by spontaneous inflation of the weight-bearing portion of a feeding catheter, which was successfully treated by percutaneous transabdominal puncture of the balloon.

Case Report

A 17-year-old woman with cerebral palsy underwent anterior fusion and Harrington rod placement for correction of scoliosis. Postoperatively the patient received enteric alimentation via a Keofeed (IVAC Corp., San Diego, CA) enteric tube (9.6 French, 109 cm) placed in the proximal jejunum. She suffered from intermittent feeding intolerance with increased gastric retention and bilious vomiting thereafter, which was treated conservatively. On the 45th postoperative day, she developed acute symptoms of abdominal distension and bilious vomiting. An attempt was made to exchange the feeding tube, which had been inserted 10 days before, but it could not be withdrawn. A supine abdominal film showed dilatation of the proximal small bowel and scattering of the metallic weights within the inflated weight-bearing portion of the catheter. The inflated portion measured 4.5 × 3 cm on the film.

Obstruction was confirmed by injection of water-soluble contrast material through the feeding tube (Fig. 1). A cross-table lateral film showed the inflated portion of the tube to be positioned just underneath the anterior abdominal wall without interposing intestinal loops. There were no clinical or laboratory signs or symptoms of peritonitis, so percutaneous transabdominal needle puncture of the balloon was performed under fluoroscopic guidance, by using a 22-gauge spinal needle.

On passage of the needle, the balloon deflated instantaneously with an audible popping sound. The catheter was retrieved without difficulty, and the patient's symptoms were relieved. Neither an immediate postprocedural abdominal film nor another taken on the following day showed pneumoperitoneum. Close inspection of the extracted catheter revealed a distended weight-bearing portion with greenish discoloration and an intact septum between the weight-bearing portion and the tube.

Discussion

Since the early description by Cantor in 1949 [1], intestinal obstruction caused by inadvertent inflation of the weight-bearing balloon of enteric alimentation catheters has been known to be a rare but potentially serious complication, which sometimes necessitates removal of the catheter by laparotomy. The complication has been reported both in single-lumen tubes, such as Cantor, Harris, or Kaslow tubes, and in double-lumen tubes with a balloon-vent cannula, such as Millar-Abbott or Dennis tubes [2, 3]. This complication should be considered in the differential diagnosis of intestinal obstruction in the patient undergoing long-term enteric feeding. Inflation of the balloon results from gas exchange occurring through the balloon wall in relation to the permeability of the balloon, the difference in pressure across the balloon wall, and the difference in composition of intestinal and balloon gases [1].

Received May 8, 1986; accepted after revision July 10, 1986.
[1] Department of Radiology, Division of Pediatric Radiology, University of Iowa Hospitals and Clinics, Iowa City, IA 52242. Address reprint requests to Y. Sato.
[2] Department of Radiology, University of Iowa Hospitals and Clinics, Iowa City, IA 52242.
[3] Department of Surgery, University of Iowa Hospitals and Clinics, Iowa City, IA 52242.

 0361–803X/86/1475–1019 © American Roentgen Ray Society



Fig. 1.—Water-soluble contrast material injected through feeding tube shows small-bowel obstruction proximal to inflated weight-bearing portion of the tube.

Nitrogen, carbon dioxide, and hydrogen sulfide are the intestinal gases most likely to diffuse into the balloon. To prevent this complication, using a thicker walled balloon constructed of a less permeable material and puncturing the balloon of a Cantor tube with a fine needle before intubation has been recommended [3].

The Keofeed tube has been on the market for about 5 years. The softness of the tube and compactness of the weight-bearing portion are suited to the size of the childhood intestinal tract. The weight-bearing portion, which is made of silicon rubber, is separated completely from the tube portion by a plastic wall of approximately 3 mm thickness. There is no vent hole or cannula attached.

The treatment for this complication must be individualized. Pulling and rupturing the bag often may be the easiest solution. A conservative attempt to deflate the balloon by decompressing the bowel, using a second tube, and reversing the diffusion effects on the balloon has been recommended [1]. Percutaneous transenteric fine-needle biopsy has been a safe and widely used procedure for such retroperitoneal abnormalities as pancreatic carcinoma and lymphadenopathies. Percutaneous needle puncture of a nondeflatable Foley balloon was performed safely [4]. If nonsurgical maneuvers fail, percutaneous transenteric needle puncture of an intestinal balloon should be considered before laparotomy in the patient who does not have symptoms of bowel necrosis.

REFERENCES

1. Cantor MO. *Intestinal intubation*. Springfield, IL: Thomas, **1949**:188–194, 243–263
2. Carlson DH, Slover WP. Radiographic detection of intestinal obstruction from a distended Kaslow tube. *J Can Assoc Radiol* **1971**;22:30–32
3. Fricke FJ, Niewodowski MA. Hazardous gaseous distention of intestinal balloons. *JAMA* **1976**;235:2611–2613
4. Higgins WL, Mace AH. Puncture of a nondeflatable Foley balloon using ultrasound guidance. *Radiology* **1984**;151:801

A Comparison of Techniques for Improved Visualization of the Arteries of the Distal Lower Extremity

Martin I. Cohen[1]
Robert L. Vogelzang

Intraarterial prostaglandin E_1, tolazoline, nitroglycerin, and tourniquet-induced reactive hyperemia were directly compared by paired analysis for their efficacy in improving visualization of distal lower extremity vessels during routine arteriography in 101 limbs (52 patients). Nitroglycerin and reactive hyperemia were equal in their effect and statistically superior to both tolazoline and prostaglandin E_1. Tolazoline was superior to prostaglandin E_1, which had little or no effect. Intraarterial nitroglycerin in a dose of 200 μg appears to be the method of choice for augmenting visualization of the distal arterial vascular system in lower-extremity arteriography.

Arterial circulation below the level of the midcalf frequently is neglected during lower-extremity arteriography. However, current trends in surgical revascularization of the lower extremity emphasize bypass grafts in the lower part of the leg and in the foot to increase outflow and thereby improve patency rates. Therefore, preoperative infomation on the status of the pedal arches is required because these vessels determine the success of distal grafts for the treatment of severe lower-extremity ischemia [1].

Reactive hyperemia and intraarterial administration of chemical vasodilators have been used for more than 20 years for improved visualization of the distal arteries of the lower extremity [2–6]. However, reported comparisons of reactive hyperemia and tolazoline used separate groups of patients rather than examining the efficacy of these techniques in the same patients [3]. Additionally, the relative efficacy of more recent techniques, including bolus injections of prostaglandin E_1 or nitroglycerin, has not been established.

For these reasons, we compared four different methods to improve small-vessel visualization of the distal leg and foot: tourniquet-induced reactive hyperemia and intraarterial injections of tolazoline, prostaglandin E_1, and nitroglycerin. Reactive hyperemia and tolazoline, reactive hyperemia and prostaglandin E_1, or tolazoline and prostaglandin E_1 were compared in three separate groups of patients with known atherosclerotic vascular disease. Reactive hyperemia and nitroglycerin were compared in a fourth group of patients after we became aware of the efficacy of intraarterial nitroglycerin in both angioplasty and routine arteriography.

Subjects and Methods

The subjects were patients with signs and symptoms of ischemia of the lower extremity, including claudication, rest pain, and ischemic ulceration. All had noninvasive arterial-flow studies before angiography, which was requested before surgery. Patients with serum creatinine levels greater than 2 mg/dl, serum uric acid levels greater than 8 mg/dl, or known multiple myeloma or diabetes were excluded from the study because of the increased potential for toxic effects associated with the additional contrast requirements of the protocol.

All patients were evaluated by the angiography service the night before angiography, and IV hydration was started then. Informed consent concerning the study was obtained from all

Received March 10, 1986; accepted after revision June 17, 1986.

[1] Both authors: Department of Diagnostic Radiology, Northwestern University Medical School and Northwestern Memorial Hospital, Chicago, IL 60611. Address reprint requests to R. L. Vogelzang, Department of Radiology/Olson Pav., Northwestern Memorial Hospital, Chicago, IL 60611.

AJR 147:1021–1024, November 1986
0361–803X/86/1475–1021
© American Roentgen Ray Society

patients. Arterial puncture was performed via the femoral approach in 50 patients and via the axillary approach in two.

To evaluate the abdominal aorta, a 5-French pigtail catheter was placed in the suprarenal aorta, and a single angiographic run with 40 ml of 76% diatrizoate (Renografin, Squibb, Princeton, NJ) was performed. The catheter was then withdrawn to the level of the aortic bifurcation, and a second angiographic run was done with 96 ml of 60% diatrizoate mixed with 100 mg of lidocaine and injected at 9 ml/sec. Radiographic exposures were obtained by using the four-shift capability of the Spectrum (Westville, NJ) programmable table to visualize the entire pelvis, lower extremity, and foot.

At this point, the first 36 patients were randomly assigned into three groups of techniques for visualization of the distal circulation. Each group was examined via two of three techniques (reactive hyperemia, tolazoline, and prostaglandin E_1). The groups comparing prostaglandin E_1 with reactive hyperemia and tolazoline with prostaglandin E_1 had 10 patients each. The group comparing reactive hyperemia with tolazoline had 16 patients. In all groups the sequence of performance of the two different techniques was randomized.

Reactive hyperemia was induced by placing inflatable tourniquets around both calves and rapidly inflating the tourniquets to 40 mm Hg above the systolic blood pressure. Rapid inflation prevents aching due to venous engorgement that results from slow or incomplete occlusion of the arterial inflow. After 5 min of inflation, the tourniquets were removed, and 60 sec later the angiographic run was performed with 45 ml of 60% diatrizoate mixed with 50 mg lidocaine. Radiographic exposures limited to the lower one-half of the calf and the foot were made every 3 sec after a delay of approximately 5 sec. A total of 12 films were obtained for each patient.

Intraarterial tolazoline was administered as a 50-mg dose diluted with saline to a volume of 10 ml. The angiographic run was begun 1 min after administration. The radiographic exposure sequence and contrast material were the same as those for reactive hyperemia.

Prostaglandin E_1, a vasodilator, was administered as an intraarterial bolus of 1 μg/kg. The bolus was followed by an immediate flush of 10 ml of saline before the angiographic run.

There was a 15-min interval between injections to allow the vasodilatory effects of the preceding technique to subside. The random determination of which agent to use first and the delay between injections was designed to eliminate the additive effects of the different methods.

In 16 additional patients, arterial opacification after reactive hyperemia was compared to opacification that occurred after intraarterial nitroglycerin. The technique for reactive hyperemia was as described previously. Nitroglycerin was administered as a 200-μg bolus (10 ml of a 20-μg/ml solution) and followed immediately by the angiographic sequence.

TABLE 1: **Comparison of Two Arteriographic Visualization Techniques in Each Lower Extremity**

Technique[a]	Grade A > B/Total	Grade A = B/Total	Grade B > A/Total
A vs B			
RH vs NG	9/32	12/32	11/32
RH vs TOL[b]	14/32	13/32	5/32
TOL vs PGE_1[b]	13/20	0/20	7/20
RH vs PGE_1[b, c]	15/17	0/17	2/17

[a] Numbers are for pooled data. RH = reactive hyperemia, NG = nitroglycerin, TOL = tolazoline, PGE_1 = prostaglandin E_1.
[b] Statistically significant via Wilcoxon signed-rank method (95% confidence level).
[c] Three unilateral lower-extremity amputees were included in this group.

Visualization of the vessels was graded according to the following schema: 0 = nonvisualization of the distal posterior tibial and anterior tibial arteries, 1 = clear visualization of these vessels, 2 = visualization of the proximal arteries of the foot, 3 = opacification of the pedal arch, and 4 = visualization of the arterial branches of the foot distal to the pedal arch.

Using four groups of patients allowed a direct comparison of two techniques in each individual limb. Data were statistically analyzed via the Wilcoxon signed-rank method, which is appropriate for paired subjective measurements.

The grade of arterial opacification was correlated with the extent of arterial-inflow disease for each individual technique. Arterial disease was evaluated at the aortoiliac, femoral-popliteal, and trifurcation levels, and note was made of severe atherosclerotic narrowing (greater than 75%). Finally, a subjective description of the level of discomfort caused by the techniques was obtained from each patient.

Results

The results of the two groups comparing reactive hyperemia or tolazoline vs prostaglandin E_1 (Table 1) indicated that prostaglandin E_1 was by far the inferior technique. In 30 of the 37 limbs examined after prostaglandin E_1 injection, there was no visualization of the arteries at the level of the ankle (grade 0).

Reactive hyperemia and tolazoline were compared in 32 limbs. In 14 limbs, reactive hyperemia resulted in visualization superior to that observed with tolazoline. In 13 limbs the results were equal, and in five tolazoline was superior to reactive hyperemia.

Reactive hyperemia was compared with nitroglycerin in 32 limbs. Nitroglycerin resulted in superior visualization in 11 limbs (Table 1). The results were equal in 12 limbs. In nine limbs reactive hyperemia was the superior technique.

Both reactive hyperemia and tolazoline were statistically superior to prostaglandin E_1 at the 95% confidence level. Reactive hyperemia was also statistically superior to tolazoline. There was no statistical difference between the efficacy of reactive hyperemia and nitroglycerin. There was no correlation between the extent of arterial-inflow disease and the grade of vascular opacification.

There was no difference in the severity of vascular disease or levels of occlusion in any of the patient groups. No patients had complete distal aortic occlusion.

An informal examination of the subjective responses to each technique indicated that tolazoline was the most uncomfortable. Reactive hyperemia caused minimal discomfort from the tourniquet application. Prostaglandin E_1 caused no discomfort, but one patient complained of nausea. No patients complained of discomfort with nitroglycerin administration.

Discussion

In clinical situations such as simple proximal (aortoiliac or femoral-popliteal) occlusive disease, routine unenhanced arteriography with a large contrast volume is sufficient to recognize tibial runoff and exclude occlusion. However, when popliteal and tibial disease is present and/or distal bypass

grafting is contemplated, detailed visualization of tibial vessels and the pedal arches is mandatory. In these circumstances or when tibial visualization is poor because of other factors, an additional angiographic run with enhancement techniques is required.

The purpose of this study was to determine which of the currently available techniques for improved visualization of the distal arteries of the lower extremity was most effective. Unlike previously reported series, a direct comparison of two randomly ordered techniques was made in each patient. The design of this series eliminated the inherent error that can occur when techniques are compared in small unmatched groups of patients.

Prostaglandin E_1 is a rapidly metabolized, potent vasodilator that has been shown to cause a 10-fold increase in arterial flow to the lower extremity when administered by a 10-min continuous-infusion technique [7]. However, because of recent reports of the efficacy and safety of bolus doses of up to 1.0 μg/kg for improved visualization of the mesenteric vasculature [8, 9] and of doses of 0.1 μg/kg for upper-extremity arteriography [10], we tested prostaglandin E_1 in lower-extremity arteriography. Our results indicate that high-dose bolus injection of prostaglandin E_1 is of no value in arteriography of the lower extremity. One possible explanation for the failure of prostaglandin E_1 may be related to the induction of increased flow through normal proximal vascular beds, producing a shunt phenomenon.

In addition to the apparent lack of efficacy, there are disadvantages to the use of prostaglandin E_1, including the need for refrigeration, the cost of $55 per ampule, and the requirement that any solution more than 24-hours old be discarded.

Tolazoline is an alpha-adrenergic blocker that has a direct histaminelike effect on vascular smooth muscle, which is thought to be the cause of the vasodilatation observed with intraarterial doses of 25–50 mg. Paradoxically, several authors have noted vasoconstriction of arteries during the first 30 sec after administration [11]. Therefore, the angiographic run should be delayed at least 30 sec after injection. Although tolazoline was not as effective as reactive hyperemia, it did improve arterial visualization. However, arrythmias, anginal pain, hypertension, and even myocardial infarction have been reported with doses of 25–50 mg administered directly into the vascular system. Therefore, tolazoline should not be administered to patients with known heart disease. Additionally, approximately one-third of the patients in our study reported a burning sensation after administration of the drug.

Our results indicate that reactive hyperemia is superior to prostaglandin E_1 and tolazoline for improved visualization of the distal vessels of the lower extremity. Additionally, there are no contraindications, and no systemic effects are seen.

One possible explanation for the superior results obtained with reactive hyperemia is that the occluding tourniquet produces uniform ischemia of the distal portion of the extremity, thereby inducing a diffuse increase in arterial perfusion when the tourniquet is removed. Shunting into proximal vascular beds does not occur. However, in 13% of our patients, the degree of visualization obtained with reactive hyperemia was graded as poor. This correlates well with the 10% frequency reported in the literature [5]. To our knowledge, no explanation for this phenomenon has been proposed. Another disadvantage is the need to maintain 5 min of tourniquet occlusion followed by a 1-min delay before the contrast infusion.

Nitroglycerin is a potent vasodilator that has been used intraarterially to prevent vascular spasm in patients undergoing angioplasty [12, 13]. It causes vasodilatation by activation of guanylate cyclase, leading to a local increase in cyclic-guanosine monophosphate [12, 13].

The second portion of this study was a direct comparison between reactive hyperemia and nitroglycerin in 32 limbs. Direct comparison between nitroglycerin and prostaglandin E_1 or tolazoline was not performed because we became aware of the benefits of nitroglycerin after we had begun the comparison between reactive hyperemia, prostaglandin E_1, and tolazoline. Because we observed clinically that nitroglycerin was an excellent agent for this purpose, we decided to compare directly the two best agents and eliminate the superfluous evaluation of prostaglandin E_1 and tolazoline. Although no statistical difference between reactive hyperemia and nitroglycerin was noted, we consider intraarterial nitroglycerin to be the preferred technique for improved visualization of the lower-extremity distal arteries because of ease of use, ready availability, and lack of side effects. We also now routinely use it as the vasodilating agent of choice in upper-extremity angiography and in the prevention of spasm during peripheral and renal angioplasty.

ACKNOWLEDGMENTS

Special thanks to Dorothy Woodward for typing and manuscript preparation and to Walter Bulawa for assistance with statistical analysis.

REFERENCES

1. O'Mara CS, Flinn WR, Neiman HL, Bergan JJ, Yao JST. Correlation of foot arterial anatomy with early tibial bypass patency. *Surgery* **1981**;89:743–752
2. Hishida Y. Peripheral arteriography using the reactive hyperemia. *Jpn Circ J* **1963**;27:349–358
3. Kahn PC, Callow AD. Selective vasodilatation as an aid to arteriography. *AJR* **1965**;94:213–220
4. Jacobs JB, Hanafee WN. The use of priscoline in peripheral arteriography. *Radiology* **1967**;88:957–960
5. Kahn PC, Boyer DN, Moran JM, Callow AD. Reactive hyperemia in lower extremity arteriography: an evaluation. *Radiology* **1968**;90:975–980
6. D'Souza V, Formanek A, Castaneda W, Knight L, Amplatz K. Peripheral angiography enhancement by long leg pneumatic boots. *Radiology* **1976**;120:209–212
7. Carlson LA, Ekelund LG, Oro L. Circulatory and respiratory effects of different doses of prostaglandin E-1 in man. *Acta Physiol Scand* **1969**;75:161–169
8. Cho JK, Chuang VP, Reuter SR. Prostaglandin E-1 as a phar-

macoangiographic agent for arterial portography. *Radiology* **1975**;116:207–209
9. Clark RA, Colley DP, Jacobson ED, Herman R, Tyler G, Stahl D. Superior mesenteric angiography and blood flow measurement following intra-arterial injection of prostaglandin E-1. *Radiology* **1980**;134:327–333
10. Levy JM, Joseph RB, Bodell LS, Nykarp DW, Hessel SJ. Prostaglandin E-1 in hand angiography. *AJR* **1983**;141:1043–1046
11. Friedman J, Zeit RM, Cope C, Bernhard VM. Optimal use of tolazoline in arteriography. *AJR* **1984**;142:817–820
12. Beinart C, Sos TA, Saddekni S, Weiner MA, Sniderman KW. Arterial spasm during renal angioplasty. *Radiology* **1983**;149:97–100
13. Kaltenbach M, Kober G, Scherer D. Transluminal coronary angioplasty and intracoronary thrombosis: transbrachial approach and prevention of thromboembolic complications. In: Kaltenbach M, Gruntzig A, Rentrop K, Bussman WD, eds. *Coronary heart disease IV*. New York: Springer, **1982**:23–40

Technical Note

Lower-Extremity Venography: Value of Femoral-Vein Compression

Tony P. Smith,[1] John F. Cardella, Michael D. Darcy, David W. Hunter, Wilfrido R. Castaneda-Zuniga, and Kurt Amplatz

Lower-extremity venography is usually performed with the patient positioned semiupright on a tilting table and with progressive lowering of the patient's head to visualize the more superior venous structures [1]. Because it is often necessary for the patient to remain recumbent, we have successfully used a technique of totally supine venography by using controlled femoral-vein compression with release just before pelvic filming. This technique yields excellent results with use of a minimal amount of contrast material.

Technique

If the study is to evaluate possible deep venous thrombosis, after cannulation of a dorsal pedal vein, tourniquets are placed above the ankle and below the knee. No tourniquets are used for evaluation of patients before in situ venous grafting [2]. The femoral artery is palpated, and hand compression is applied just medial to the artery in order to occlude venous flow. Depending on patient size, 40 to 90 ml of diatrizoate meglumine 60% are injected with an average total dose of 70 ml. Contrast material is injected either by power injection or by hand. With power injection, rates of 1–3 ml/sec are used. Images are then obtained, beginning distally, by using either serial filming or radiographic scanning with a slot device (Amplatz K, unpublished data). The tourniquets, if in place, are released, and the compression on the femoral vein is stopped 5 to 10 sec before the pelvic exposures are made. At least 150 ml of normal saline are flushed through the cannula before the examination is completed.

Results

Seventy-two lower-extremity venograms were performed on a total of 62 patients over a 6-month period. All examinations were done to evaluate possible deep venous thrombosis or for preoperative evaluation before in situ venous grafting. Vessels to the level of the bifurcation of the inferior vena cava were visualized (Fig. 1) in 70 of 72 cases. Six cases showed complete occlusion of the common femoral or iliac veins with well-delineated extensive collateral flow. The obstructions in these cases were subsequently documented by venography with more proximal injection of the contrast material.

Fifty-five venograms were performed to diagnose deep venous thrombosis: 18 were positive for thrombus, 37 were negative. Seventeen cases were performed for possible venous grafting; all adequately showed both the superficial and deep systems to the level of the lower inferior vena cava. A small amount of extravasation was noted at the puncture site in two cases, but follow-up examinations revealed no residual dermal injury. No adverse reactions were otherwise encountered.

Discussion

Many patients with suspected deep venous thrombosis are unstable and cannot be placed in a semiupright position for

Received January 13, 1986; accepted after revision June 11, 1986.

[1] All authors: Department of Radiology, University of Minnesota Hospitals and Clinics. Address reprint requests to K. Amplatz, University of Minnesota, Box 427, UMHC, 420 Delaware St., SE, Minneapolis, MN 55455.

AJR 147:1025–1026, November 1986 0361–803X/86/1475–1025 © American Roentgen Ray Society



Fig. 1.—Lower-limb venogram shows excellent filling of pelvic vessels after release of femoral vein compression.

venography to be done in the currently recommended manner. Often inflamed and painful legs are not easily elevated to assist in filling of the pelvic vessels. By use of the procedure recommended here, the patient remains supine and the leg is not disturbed.

Venography for possible venous in situ grafting was performed, when possible, immediately after arteriography. Performing the studies in this sequence enables accurate determination of the patient's candidacy for grafting and thus the need for venography. By using the technique described here, venography can be performed on the angiography table without moving the patient to a tilt apparatus. In addition, the patient need not be placed in a semierect position or undergo flexing of the hip after an arterial puncture.

Earlier studies [3] have shown that supine venography fills the pelvic vessels in a large percentage of the patients studied. However, at least 100 ml of contrast material are most often used. By using the compression technique, contrast material is trapped in the lower extremity and released to flow into the pelvic vessels at the critical time of filming, and less contrast material may be used. Excellent results were achieved with as little as 40 ml of contrast material, and no patient received more than 90 ml.

The rate of contrast injection is not critical because the femoral-vein compression prevents the flow of contrast material above the groin. The lack of discernible differences, despite a threefold difference in power-injection rates must be related to the trapping of contrast in the extremity. Equivalent filling was obtained with hand injection. Femoral compression allows the radiologist to control the outflow of contrast material, and thus film timing for calf and thigh vessels is not crucial.

The results presented here are comparable to current techniques using tilt tables and leg elevation to opacify pelvic vessels [4]. Although these techniques are adequate, we believe such maneuvers are unnecessary for good visualization of the pelvic venous system. Excellent lower-extremity venography can be obtained with the patient in the supine position, and the addition of femoral-vein compression with subsequent timely release aids further in pelvic vessel delineation with less contrast material.

REFERENCES

1. Rabinov K, Paulin S. Roentgen diagnosis of venous thrombosis in the leg. *Arch Surg* 1972;104:134–144
2. Hallin R. In situ saphenous vein bypass grafting. *Am J Surg* **1983**;145:626–629
3. Coel MN. Adequacy of lower limb venous opacification: comparison of supine and upright phlebography. *AJR* **1980**;134:163–165
4. Dure-Smith P, Tison JB. Ilio-femoral segment and inferior vena cava visualization using a non-catheter technique: an adjunct of leg phlebography. *Radiology* **1984**;153:251–252

MR Evaluation of the Portal Vein in Pediatric Liver Transplant Candidates

Deborah L. Day[1]
Janis G. Letourneau[1]
Bradford T. Allan[1]
Nancy L. Ascher[2]
Gunnar Lund[1]

Nine pediatric liver transplant candidates underwent preoperative MR evaluation of the portal vein and the inferior vena cava. Sonographic correlation was available in all patients and angiographic correlation was available in five. Pathologic correlation was obtained in seven cases either at liver transplantation or autopsy. MR demonstrated portal vein patency in three cases when it was not seen by angiography and confirmed portal vein patency in one patient when it was questionably identified on sonography. The portal vein was not seen on MR imaging in two cases when it was seen on sonography and angiography: in one case, it was small and to-and-fro flow was demonstrated angiographically; in the second case, the portal vein was occluded by tumor thrombus. Two vessels in two patients were misidentified by sonography and identified correctly by MR. These were an azygous continuation of the inferior vena cava and a large collateral vein in the portal region. Knowledge of the anatomy and documentation of vascular patency are essential in evaluation of patients before liver transplantation. In patients with complex anatomy or hemodynamics, it may be necessary to obtain this information from several imaging techniques (sonography, angiography, and MR).

Liver transplantation offers a prospect for survival for individuals afflicted with otherwise fatal liver diseases. Judicious selection of transplant recipients is essential since the demand for donor livers far exceeds the supply. Sonography, CT, angiography, and MR imaging are techniques that can define the vascular anatomy preoperatively [1–6] and, thus, can help determine which individuals have the greatest likelihood of survival after transplantation. Ten MR examinations, other radiologic studies, and pathologic data in nine liver-transplant candidates were studied.

Subjects and Methods

Ten MR scans were obtained in nine children before liver transplantation. The patients ranged in age from 4 to 46 months. Underlying conditions included extrahepatic biliary atresia (seven patients), hepatoblastoma (one patient), and cirrhosis secondary to α_1-antitrypsin deficiency (one patient).

A 1.0-T Siemens Magnetom (Iselin, NJ) superconducting MR system operating at 0.35 T was used. Slices (10 mm thick) were acquired with a 100% gap between sections. The gap was subsequently scanned and the images were interlaced for contiguous 1-cm images of the upper abdomen. Spin-echo (SE) sequences with TR 0.3 sec and TE 30 msec; TR 0.5 sec and TE 30 msec; and TR 1.5 sec and TE 35 and 70 msec were obtained in coronal, axial, and sagittal planes.

Real-time sonograms were obtained in all nine patients and angiography was performed in five patients before transplantation. Angiography included superior mesenteric and splenic arteriography in five patients, splenoportography in two patients, and wedge hepatic venography in two patients. Pathologic correlation was available in seven of the nine patients at surgery or autopsy. The interval between MR imaging and anatomic correlation ranged from 2 weeks to 4 months (mean, 1.3 months).

Received March 24, 1986; accepted after revision June 9, 1986.

Presented at the annual meeting of the American Roentgen Ray Society, Washington, DC, April 1986.

[1]Department of Diagnostic Radiology, University of Minnesota Hospital and Clinic, Box 292, Minneapolis, MN 55455. Address reprint requests to D. L. Day.

[2] Department of Surgery, University of Minnesota Hospital and Clinic, Minneapolis, MN 55455.

AJR 147:1027–1030, November 1986
0361–803X/86/1475–1027
© American Roentgen Ray Society

TABLE 1: **Clinical and Imaging Data on Liver Transplant Candidates**

Case No.	Age (months)	Gender	Diagnosis	Vessel	Vessel Size (mm)/Patency by:			
					MR Imaging	Sonography	Angiography	Pathologic Correlation
1	34	F	EHBA	PV	4	3–4	Not visualized	ND
				IVC	Patent	SIVC patent		
2	8	M	EHBA	PV	3	?3–4	ND	3
				IVC	Patent	Patent		
3	15	M	EHBA	PV	5	4–6	ND	4
				IVC	Patent	6–7		
4	9	M	EHBA	PV	3–4	2–4	Not seen	1–2
				IVC	Patent	Patent—?filling defect		Thrombosis
5	10	F	EHBA	PV	Not seen	4	3.3	3
				IVC	IIVC patent	Patent—compressed	10	
6	48	M	Hepatoblastoma	PV	Not seen	4	Thrombus	15
								Tumor thrombus
				IVC	Patent—displaced	Patent—compressed		
7	9	M	α_1-Antitrypsin deficiency	PV	5–6	5	ND	ND
				IVC	Patent	Patent		
8	34	M	EHBA	PV	5	3	ND	5
				IVC	IVC absent (large azygous)	Compressed		IVC absent
9	12	M	EHBA	PV	5	3–4	Not seen	8
				IVC	IIVC patent	IIVC patent		20

Note.—EHBA = extrahepatic biliary atresia; IVC = inferior vena cava; IIVC = infrahepatic IVC; ND = not done; PV = portal vein; SIVC = suprahepatic IVC.

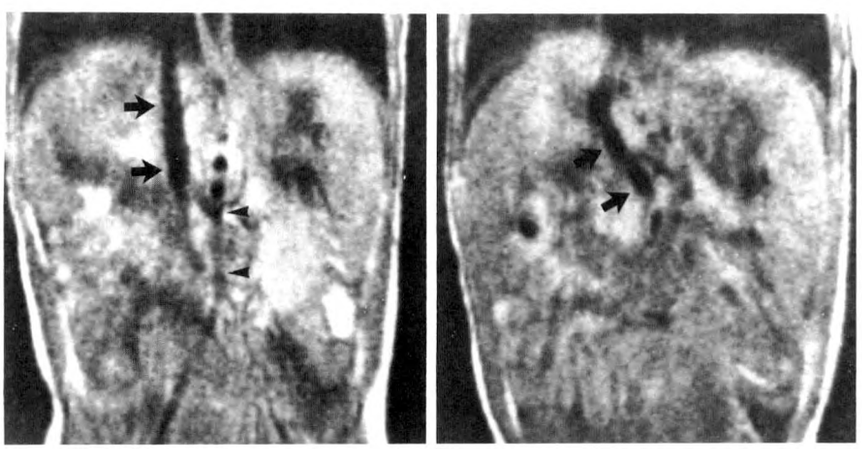


Fig. 1.—Case 7, 9-month-old boy with antitrypsin deficiency. Coronal MR images (SE 500/30).
***A*, Normal inferior vena cava (*arrows*), aorta (*arrowheads*), and aortic branches.**
***B*, Normal portal vein (*arrows*) imaged in more ventral plane.**

Results

The results of the various imaging studies are summarized in Table 1. Using MR, portal vein (PV) patency and size were best evaluated on T1-weighted SE sequences in the coronal plane (Figs. 1B and 2A), where it was imaged in seven of 10 examinations. The PV was also identified in eight of the nine patients sonographically and was tentatively seen in the ninth patient. The smallest PV imaged, 3 mm in diameter, was definitely seen on MR (Fig. 3) and questionably seen on sonography. One of the vessels identified as PV on sonography was actually a large venous collateral (case 6). In this same patient, the PV was not seen on MR (Fig. 4), and thrombus was seen within the PV on splenoportography. In three patients, the PV was identified on MR, but not identified on angiography because of hepatofugal flow in two patients and technical difficulties in the third. The PV was not seen on MR in two patients. In one patient (case 6), described above, the PV was filled with tumor thrombus. In the other (Fig. 5), splenoportography revealed a 3.3-mm-diameter PV with to-and-fro blood flow.

Surgical (four patients) or autopsy (three patients) correlation was available in seven of the nine transplant candidates. In the five patients in whom the PV was seen on MR and pathologic correlation was available, the PV was patent and similar to the size predicted by MR (Table 1). In one of the

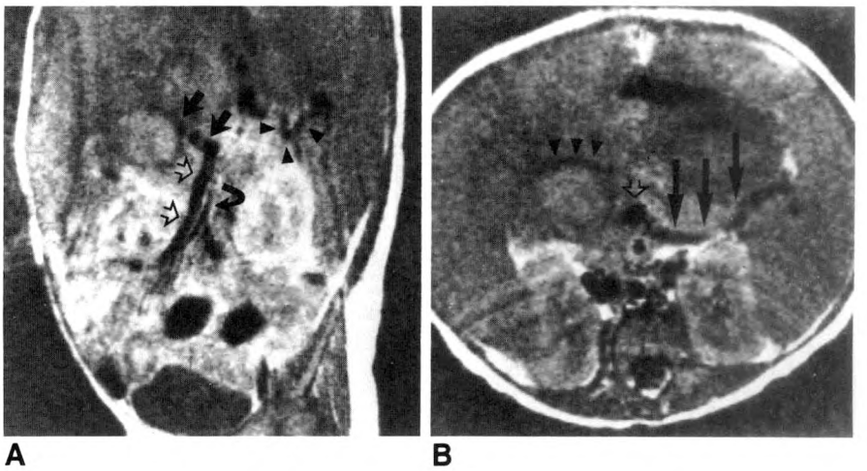


Fig. 2.—Case 1, 34-month-old girl with extrahepatic biliary atresia.

A, Coronal MR image (SE 500/30). Portions of splenic vein (*arrowheads*), inferior vena cava (*curved arrow*), and superior mesenteric vein (*open arrows*). Portal vein (*solid straight arrows*) is displaced superiorly by cystic dilatation of bile ducts in porta hepatis.

B, Transverse MR image (SE 300/35). Splenic vein (*solid arrows*) joining superior mesenteric vein (*open arrow*). Portion of portal vein (*arrowheads*) ventrally displaced in porta hepatis.



Fig. 3.—Case 2, 8-month-old boy with extrahepatic biliary atresia. Coronal MR image (SE 500/30). Tiny portal vein (*arrows*) in porta hepatis. Small portal vein contraindicates liver transplantation.

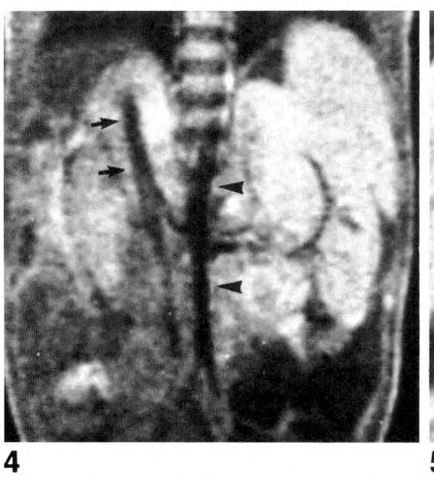


Fig. 4.—Case 6, 4-year-old boy who had undergone right hepatic lobectomy for hepatoblastoma. Coronal MR image (SE 500/30). Shift of intraheptaic inferior vena cava (*arrows*) to right. Aorta (*arrowheads*) is well demonstrated. Thrombus within portal vein and multiple venous collaterals were demonstrated on splenoportography.



Fig. 5.—Case 5, 10-month-old girl with extrahepatic biliary atresia. Coronal MR image (SE 500/30) of upper abdomen. Portal vein not seen and thought to be thrombosed. Multiple gastric and periportal venous collaterals (*arrows*) are seen. Note also ascites, inhomogeneous liver parenchyma (probably cirrhotic change), and relatively enlarged left hepatic lobe.

two patients in whom the PV was not seen on MR, it was about 3 mm in diameter at autopsy; as previously mentioned, it had to-and-fro flow on angiography. At transplantation, tumor thrombus filled the PV in the other patient in whom the PV was not seen on MR.

Portions of the inferior vena cava (IVC) were seen by MR in eight of the nine transplant candidates. In the ninth patient, no infrahepatic IVC was identified; rather, a large right paraspinal vessel was seen (Fig. 6) and identified as an azygous continuation of the IVC at surgery. This vessel was misidentified sonographically as the compressed infrahepatic IVC. In the other eight patients, sonography revealed patent, but sometimes compressed, IVCs.

The hepatic artery was seen in four of the nine patients who underwent MR imaging in the transverse plane. Multiple venous collaterals and/or enlarged azygous veins indicating portal hypertension were identified in eight of the nine patients (Fig. 6).

Discussion

Liver transplantation is becoming a routine transplantation procedure, offering the prospect of life for children and adults afflicted with otherwise fatal liver disease. Donor livers are in tremendous demand. Thus, it is essential to determine which

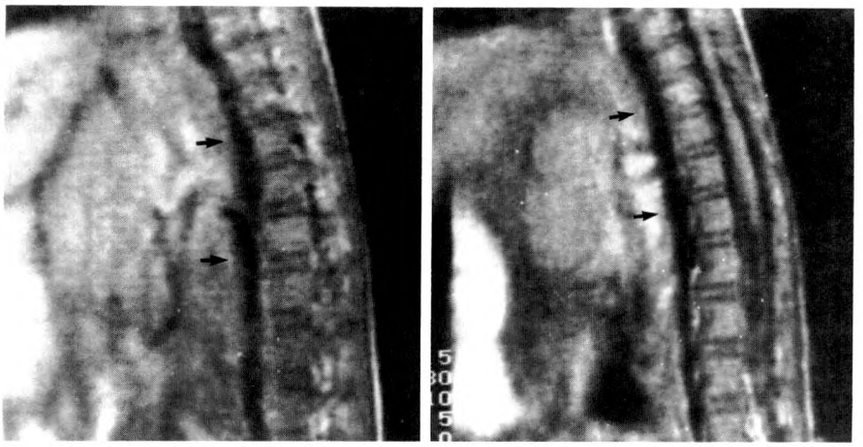


Fig. 6.—Case 8, 34-month-old boy with extrahepatic biliary atresia. Sagittal MR images (SE 500/30).

***A*, Right of midline. Large extrahepatic vessel (*arrows*) consistent with azygous continuation of inferior vena cava.**

***B*, Aorta (*arrows*) to left of midline.**

individuals cannot benefit from a liver transplant because of anomalous, thrombosed, absent, or small vessels. At our institution, surgeons require a PV diameter of at least 4 mm for the anastomosis to be technically feasible. Therefore, preoperative radiologic evaluation of the upper abdominal vascular anatomy is important.

Imaging techniques that aid in the evaluation of the vascular anatomy include sonography, CT, and angiography [1–3]. MR imaging provides an additional, often complementary, noninvasive means of evaluating blood vessels [4–6]. Direct multiplanar imaging is an inherent advantage of MR, as is the ability to scan the entire abdomen rather than portions of it. The latter is exemplified in case 8, a child with multiple congenital anomalies including extrahepatic biliary atresia and neonatal volvulus. Azygous continuation of the IVC was misidentified on real-time sonography as infrahepatic IVC but on MR imaging was shown to be extrahepatic. MR demonstrated the PV in three patients in whom it was not seen with angiography because of hepatofugal flow and/or technical problems (cases 1, 4, and 9).

Disadvantages of MR include the inability to image a vascular channel either when the flow is very slow (case 5) or when thrombus fills the vessel (case 6). The blood flow effects of MR are complex, but by using particular pulse sequences, MR has the potential to distinguish signal due to slow blood flow from true intraluminal thrombus [7].

Respiratory motion causes lack of sharpness and, thus, the exact vessel size cannot be determined by MR imaging. Despite the inherently increased examination time of 1.5–2 times associated with respiratory gating, it has the potential of removing gross motion artifacts and allowing better demonstration of small structures, such as the PV [8, 9]. MR can be tailored specifically for evaluation of vascular structures, thus eliminating unessential scans and image sequences and shortening the total time of the examination.

The primary screening procedure for evaluation of the hepatic transplant candidate is abdominal sonography [1]. Potential recipients often have distorted abdominal anatomy because of congenital anomalies, portal hypertension, tumor mass, and/or surgical change. In these difficult cases, when sonography is inconclusive in defining the vascular anatomy, MR and/or angiography are often useful. Because it is noninvasive, requires no contrast material, and uses no ionizing radiation, MR has the potential of replacing angiographic evaluation of the upper abdomen in transplant candidates.

REFERENCES

1. Ledesma-Medina J, Dominguez R, Bowen A, Young LW, Bron KM. Pediatric liver transplantation. Part 1. Standardization of preoperative diagnostic imaging. *Radiology* **1985**;157:335–338
2. Cardella JF, Castaneda-Zuniga WR, Hunter D, Young A, Amplatz K. Angiographic and interventional radiologic considerations in liver transplantation. *AJR* **1986**;146:143–153
3. Kane RA, Katz SG. The spectrum of sonographic findings in portal hypertension; a subject review and new observations. *Radiology* **1982**;142:453–458
4. Hricak H, Amparo E, Fisher MR, Crooks L, Higgins CB. Abdominal venous system: assessment using MR. *Radiology* **1985**; 156:415–422
5. Fisher MR, Wall SD, Hricak H, McCarthy S, Kerlan RK. Hepatic vascular anatomy on magnetic resonance imaging. *AJR* **1985**;144:739–746
6. Williams DM, Cho KJ, Aisen AM, Eckhauser FE. Portal hypertension evaluated by MR imaging. *Radiology* **1985**;157:703–706
7. Axel L. Blood flow effects in magnetic resonance imaging. *AJR* **1984**;143:1157–1166
8. Ahman RL, McNamara MT, Pallack M, Hricak H, Higgins CB. Magnetic resonance imaging with respiratory gating; techniques and advantages. *AJR* **1984**;143:1175–1182
9. Rung VM, Clanton JA, Partain CL, James AE Jr. Respiratory gating in magnetic resonance imaging at 0.5 tesla. *Radiology* **1984**;151:521–523

Pediatric Hypertrophic Gastropathy

Michael P. Marks[1]
Miguel V. Lanza[2]
Emily J. Kahlstrom[2]
Victor Mikity[1]
Susan Cadinha Marks[1]
Robert P. Kvalstad[1]

Four previously healthy children presented in a 6-week period with marked hypoproteinemia without liver disease, malnutrition, or significant proteinuria. They all had strikingly similar radiographic findings consisting of enlarged folds confined to the fundus and body of the stomach. Three of the children had prodromal symptoms suggesting a viral illness. Cytomegalovirus was cultured from the urine in all cases and from the gastric biopsy specimens in three patients. Two of these patients also showed intranuclear inclusions in their biopsy specimens compatible with cytomegalovirus. It is not certain if cytomegalovirus was the cause of the illness.

Menétrièr's disease in adults is an uncommon clinical entity marked by protein-losing enteropathy and hypertrophic gastropathy that has a predilection for the proximal portions of the stomach. In adults, this syndrome usually follows a chronic, unremitting course [1]. A similar but even more uncommon entity of protein-losing enteropathy and hypertrophic gastric rugae has been described in children. We are aware of 24 reported cases in children [2–10]. Radiographs show involvement of the proximal stomach and sparing of the antral region, as often happens in adult cases. The pediatric disease follows a more benign course, however, usually resolving spontaneously after weeks or months. The difference in the duration and course of symptoms suggests there may be a different pathogenesis. For this reason we prefer the term "pediatric hypertrophic gastropathy" to "Menétrièr's disease of childhood." Several causes have been invoked for the disease process in children. These include allergy [2] and infection, specifically with cytomegalovirus (CMV) [8–10].

We present a series of four children, three boys and one girl, who were admitted to the Pediatric Pavilion of Los Angeles County–USC Medical Center in a 6-week period during the fall of 1983. All had clinical evidence of a transient protein-losing enteropathy and radiographic evidence of enlarged gastric rugae. All four children had culture-proven evidence of concomitant CMV infection.

Subjects and Methods

The subjects were four children who presented between September 28 and November 10, 1983. All four children were admitted with hypoalbuminemia and suspected protein-losing enteropathy. A routine upper gastrointestinal tract (UGI) series was performed on each patient by using a barium sulfate suspension. All children subsequently underwent endoscopic evaluation. Peroral biopsies of 0.5–1.0 mm thickness were obtained from the fundal region during endoscopy and sent for CMV culture. Urine samples were also sent for CMV culture. All patients were seen in follow-up at 3–5 weeks. Serum albumin and total protein were measured at initial follow-up in three of the patients and at the 9-week follow-up in case 1.

Results

Pertinent history and admitting laboratory test results have been tabulated for

Received March 31, 1986; accepted after revision June 12, 1986.

[1] Department of Pediatric Radiology, University of Southern California, Los Angeles County–University of Southern California Medical Center, Los Angeles, CA 90033.

[2] Department of Pediatrics, Pediatric Pavilion, Los Angeles County–University of Southern California Medical Center, 1129 N. State St., Los Angeles, CA 90033. Address reprint requests to E. J. Kahlstrom.

AJR 147:1031–1034, October 1986
0361–803X/86/1475–1031
© American Roentgen Ray Society

the four cases (Table 1). The four children ranged in age from 22–48 months. Three of the four had a prodromal history suggesting an upper respiratory tract infection and/or gastrointestinal illness. Lower extremity and/or periorbital edema was noted in all the children between 3 and 5 days before admission. In addition to the laboratory values listed in Table 1, dipstick urinalysis on all patients was negative for protein. Their liver function tests were normal.

The upper gastrointestinal tract findings were identical for all; the series showed enlarged gastric folds in the fundus and body of the stomach, sparing the antrum (Fig. 1). The small-bowel mucosa was unremarkable and the transit time was normal. Endoscopy confirmed the presence of hypertrophic folds. Mucosal biopsies done at the time of endoscopy showed normal histology. Two of the patients (cases 1 and 3), however, had intranuclear inclusions compatible with CMV. CMV was cultured from the gastric biopsies of all patients except case 2. Gastric biopsy from case 4 was also positive for herpes simplex virus. CMV urine culture was positive in all cases.

The children were treated with diuretics and a high-protein diet. At the time of follow-up, all patients were asymptomatic, the edema had resolved, and serum albumin and total protein showed marked improvement or return to normal (Table 1).

Discussion

Clinically and radiologically, the four patients in this study are similar to prior case reports of transient protein-losing enteropathy and enlarged gastric rugae, which some authors have labeled Menétrièr's disease of childhood [2–7]. Our cases presented with hypoalbuminemia in the absence of discernible liver disease, proteinuria, or malnutrition. The hypoalbuminemia reversed in 3–5 weeks with symptomatic treatment. On upper gastrointestinal series, all the children had similar, distinctive radiographic changes consisting of enlarged rugae in the fundus and body of the stomach with relative antral sparing. These radiographic abnormalities were confirmed by endoscopy. Changes tended to be marked along the greater curvature of the stomach. Barium did not appear flocculated by excessive secretions and the stomach exhibited normal pliability. The small bowel mucosa and transit time were normal.

Previous reports of this entity in children show a similar pathologic picture to that of the adult Menétrièr's disease with hypertrophy of gastric glands, basilar cystic changes, and sometimes inflammatory cell infiltration [3–6]. In our patients, peroral gastric biopsies showed normal mucosa, but full-thickness surgical specimens were not obtained. Thickened hyperplastic mucosa exceeds the limits of the superficial specimen obtained by endoscopic biopsy [7, 11, 12]. The diagnosis of gastric mucosal hyperplasia is therefore only reliably made with a full-thickness surgical biopsy specimen.

Mild-to-moderate peripheral eosinophilia is frequently seen, found in about two-thirds of the reported cases [6]. Previous reports have postulated an allergic origin as the basis of peripheral eosinophilia and eosinophilic mucosal infiltrate [2]. Other reports have suggested a possible infectious cause and implicated CMV [8, 9]. Lachman et al. [8] presented a 7½-year-old boy whose biopsy of the gastric fundus showed cytomegalic inclusions. Leonidas et al. [9] also demonstrated intranuclear inclusions typical for CMV in a gastric biopsy and a diagnostic 16-fold rise in CMV complement-fixation titers in a 3½-year-old. Stillman et al. [10] reported two cases: a 5-year-old boy who had CMV cultured from urine, gastric aspirate, and gastric biopsy specimens, and a 3-year-old with a prodrome suggesting a viral illness from which CMV could not be isolated. Both of these patients had peripheral eosin-

TABLE 1: **Symptoms and Laboratory Test Results of Four Cases of Pediatric Hypertrophic Gastropathy**

Case	Age (mo.)	Gender	Prodromes	Admission Laboratory Results				Follow-up Laboratory Results	
				WBC Differential (1000/mm³)	Serum Albumin (mg/dl)	Total Protein (mg/dl)	IgG, IgA, IgM[a] (mg/dl)	Serum Albumin	Total Protein
1	22	F	2 wk history vomiting, diarrhea, productive cough	26.2: 48N, 5B, 45L, 2M[b]	1.6	3.0	398, 51, 100	4.4	6.7
2	26	M	none	15.0: 41N, 52L, 6M, 1E	1.8	3.1	213, 22, 45	3.9	6.5
3	45	M	2 wk history cough, rhinitis, fever	16.7: 57N, 25L, 18E	1.8	3.4	not obtained	2.8	4.5
4	48	M	5 day history vomiting, cough, rhinitis	16.8: 66N, 25L, 2B, 1M, 6E	2.4	4.0	161, 45, 32	4.3	6.4

[a] Normal values: IgG = 490–1390 mg/dl; IgA = 24–164 mg/dl; IgM = 36–200 mg/dl.
[b] N = neutrophil; B = band; L = lymphocyte; E = eosinophil; M = monocyte.

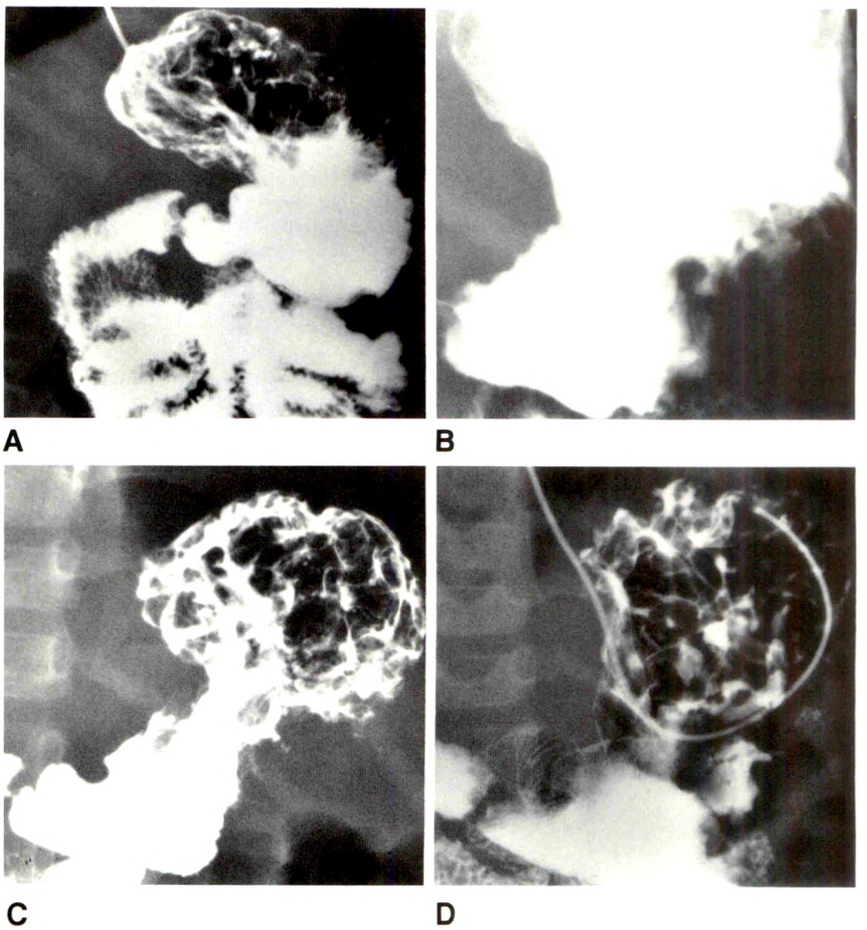


Fig. 1.—*A*, Case 1. Note rugal hypertrophy in fundus and body more marked along greater curvature.
***B*, Case 2. Enlarged folds shown in body along greater curvature.**
***C*, Case 3. Rugal hypertrophy seen in proximal portions of stomach with distal portions spared.**
***D*, Case 4. Enlarged folds again noted in fundus and body.**

ophilia, an eosinophilic mucosal infiltrate, and elevated serum IgE levels despite other serum immunoglobulins reduced below normal levels. Thus, an antibody-mediated allergic reaction may have occurred in both patients. Stillman et al. stated that the clinical presentation of one patient and the virologic data of the other suggested that a virus may have provoked an allergic reaction.

Three of the four children in our study had a prodromal history consistent with an acute viral illness beginning shortly before admission. In two of the cases CMV inclusions were seen in the gastric biopsy specimens. Three of the biopsy specimens were culture positive for CMV, and all four cases showed cytomegalic viruria. It is unclear whether the one negative biopsy culture was due to sampling error, fragility of the virus, or a true negative culture. Herpes virus was also cultured from the gastric biopsy specimen of one of the cases that was culture positive for CMV. Leukocytosis was seen in all of our cases, and two of our patients had a peripheral eosinophilia. Serum IgE levels were not obtained in our patients. It still remains unclear whether CMV or another viral agent is the cause of this syndrome or merely an opportunistic infection in tissues with altered immunologic resistance, which is suggested by a lowered level of immunoglobulins.

The incidence of urine excretion of CMV in our general pediatric population has not been determined, but it can be quite high in the preschool population. A recent study of children in a daycare center found active viral shedding in 59% of children from 1–5 years old by examination of urine or throat-swab specimens [13]. The frequency with which CMV can be detected in young children makes it hazardous to interpret our results as a cause-and-effect relationship. However, the presentation of four cases of a heretofore rarely reported entity presenting in a 6-week period at our institution suggests a possible infectious cause. Three of our patients had prodromes consistent with viral infections and all the patients showed evidence of concomitant CMV infection.

The presentation in children of hypoalbuminemia preceded by symptoms of a viral respiratory and/or gastrointestinal tract infection in the absence of nephrosis, liver disease, or malnutrition should suggest the diagnosis of pediatric hypertrophic gastropathy, which can be confirmed by an upper gastrointestinal series.

ACKNOWLEDGMENTS

The authors wish to thank Dr. B. Philip Citron, Clinical Professor of Pediatrics and Medicine, for gastroenterologic consultation and endoscopic procedures on all patients included in this series.

REFERENCES

1. Searcy RM, Malagelada JR. Menétrièr's disease and idiopathic hypertrophic gastropathy. *Ann Intern Med* **1984**;100:565–570
2. Burns B, Gay BB. Menétrièr's disease of the stomach in children. *AJR* **1968**;103:300–306
3. Kadlec G, Goodwin R, Fellows R, Andrews B. Menétrièr's disease in childhood. *South Med J* **1979**;72:33–36
4. Bloom RA, McQuaide JR. Benign hypertrophic gastropathy, Menétrièr's disease in childhood and adolescence. *Clin Pediatr (Phila)* **1980**;19:533–540
5. Kraut JR, Powell R, Hruby MA, Lloyd-Still JD. Menétrièr's disease in childhood: report of two cases and review of the literature. *J Pediatr Surg* **1981**;16:707–711
6. Chouraqui JP, Roy CC, Brochu P, Gregoire H, Morin CL, Weber AM. Menétrièr's disease in children: report of a patient and review of sixteen other cases. *Gastroenterology* **1981**;80:1042–1047
7. Knight JA, Matlak ME, Condon VR. Menétrièr's disease in children: report of a case and review of the pediatric literature. *Pediatr Pathol* **1983**;1:179–186
8. Lachman RS, Martin DJ, Vawter GF. Thick gastric folds in childhood. *AJR* **1971**;112:83–92
9. Leonidas JC, Beatty EC, Wenner HA. Menétrièr's disease and cytomegalovirus infection in childhood. *Am J Dis Child* **1973**;126:806–808
10. Stillman AE, Sieber O, Manthei U, Pinnas J. Transient protein-losing enteropathy and enlarged gastric rugae in childhood. *Am J Dis Child* **1981**;135:29–33
11. Stempien SJ, Dagradi AE, Reingold IM, et al. Hypertrophic hypersecretory gastropathy, analysis of 15 cases and a review of the pertinent literature. *Am J Dig Dis* **1964**;9:471–493
12. Case Records of the Massachusetts General Hospital (Case 41–1978). *N Engl J Med* **1978**;299:878–884
13. Pass RF, August AM, Dworsky M, Reynolds DW. Cytomegalovirus infection in a day-care center. *New Engl J Med* **1982**;307:477–479

Mesenchymal Hamartomas of the Liver in Childhood:
Sonographic and CT Findings



Philip Stanley[1,2]
Theodore R. Hall[1,2]
Morton M. Woolley[2,3]
Michael J. Diament[1,2]
Vicente Gilsanz[1,2]
John H. Miller[1,2]

Mesenchymal hamartomas of the liver usually present within the first 2 years of life. Abdominal enlargement and respiratory distress are the most common presenting features. Pathologically, the lesion is composed of large cysts separated by septations. Review of sonograms and CT scans in nine patients shows that a large, predominantly cystic mass with internal septae is characteristic of the tumor. Angiography shows peripheral hypervascularity with a septated avascular center. A confident preoperative diagnosis of mesenchymal hamartoma based on these features is possible.

Hepatic mesenchymal hamartoma is an uncommon benign lesion arising from the mesenchyme of the portal tract [1]. The hamartoma usually presents within the first 2 years of life, and abdominal swelling is usually the predominant clinical feature [1–4]. If fluid has rapidly accumulated within the mass, there may be respiratory distress as well [5, 6]. The tumor is often large [2] and usually cystic. It is usually located in the right lobe [2–4] but may be attached to the liver by a pedicle [1, 7, 8]. Because mesenchymal hamartomas are benign lesions with excellent prognosis, distinguishing them from other liver masses is important. We analyzed the appearance of the tumor in nine children with this disease.

Materials and Methods

During the past 10 years, eight patients with histologically proven hepatic mesenchymal hamartomas have been seen at Childrens Hospital of Los Angeles. In addition, one patient was referred for consultation after having been operated on elsewhere. The five girls and four boys ranged in age from 1 month to 4 years. Seven of the nine patients were asymptomatic children with an abdominal mass and without associated weight loss, fever, anorexia, or pain. Two patients had respiratory distress; in one of these patients this was relieved by placement of a catheter percutaneously into the largest cyst.

The first five patients had plain abdominal radiographs; IV urograms were performed in three. All nine patients had sonograms of the liver. Six patients had ^{99m}Tc sulfur colloid scintigraphy. In addition, one patient had a ^{99m}Tc-labeled RBC study. Arteriography was undertaken in six patients, and CT was performed in four. In all patients, the tumors were surgically removed and pathologic examination of the specimens was performed.

Results

Plain abdominal radiographs in five patients showed diffuse hepatic enlargement or a mass arising from the lower edge of the liver. No calcification was present. The three patients who had IV urograms demonstrated downward displacement of the right kidney and a septated cystic mass in the upper abdomen, which was seen in the total-body opacification stage of the examination.

Sonography was performed in nine patients. In eight, there was a mass with an

Received March 11, 1986; accepted after revision May 22, 1986.

[1] Department of Radiology, Childrens Hospital of Los Angeles, 4650 Sunset Blvd., Los Angeles, CA 90027. Address reprint requests to P. Stanley.

[2] University of Southern California School of Medicine, 2025 Zonal Ave., Los Angeles, CA 90033.

[3] Department of Surgery, Childrens Hospital of Los Angeles, 4650 Sunset Blvd., Los Angeles, CA 90027.

AJR 147:1035–1039, November 1986
0361–803X/86/1475–1035
© American Roentgen Ray Society

echo-free center and internal septations (Figs. 1A and 2A). No echogenic particulate material was present in the cysts, which varied in size, measuring up to 18 × 14 cm. In all eight patients, the findings on sonography suggested the diagnosis of a benign cystic tumor arising from or attached to the liver. There was compression of the adjacent liver, which was otherwise normal. The biliary system was normal. In the ninth patient, there was a well-defined homogeneous echogenic mass.

Three of the four patients with CT scans had similar appearances, with well-defined margins of the tumors. The mass had central diminished attenuation measuring 6 to 14 H with internal septations (Fig. 2B). Minimal or no enhancement of the mass or septae appeared after IV contrast injection (Figs. 1B and 2C). In a fourth patient, the study done before contrast injection showed a moderately well defined tumor of diminished attenuation with scattered areas of lower attenuation within the tumor (Fig. 3A). After IV contrast injection, patchy areas of enhancement appeared mixed with areas of low attenuation within the mass (Fig. 3B). No large cysts or septae were seen.

Scintigraphy with ^{99m}Tc sulfur colloid in six patients demonstrated solitary photopenic masses in five and two photopenic masses in the sixth patient. All masses appeared avascular on the initial scintiangiographic phase of the examinations, but a relatively vascular tumor rim was detected in the one patient who had a labeled-RBC study. Scintigraphy correctly showed that four of the tumors were intrahepatic and two were predominantly exophytic.

Angiography demonstrated major arterial variants in three of the patients. All six patients who had angiography showed vessel displacement around the mass with peripheral hypervascularity (Figs. 1C and 2D). The masses were all well-defined or moderately well defined; avascular centers were seen on the capillary phase in five patients (Figs. 1D and 2E). In the sixth patient, there was central hypervascularity intermingled with avascular areas.

All nine patients had surgical removal of the tumor. Two of the masses were predominantly exophytic, one having a broad pedicle. Seven of the patients had total or subtotal lobectomies, and two had trisegmentectomies. In one patient, macroscopic tumor was left behind on the undersurface of the right lobe of the liver; otherwise, the tumor was completely excised. Apart from postoperative adhesions, which required surgical lysis in one patient and a wound hematoma that spontaneously resolved in a second patient, there were no complications.

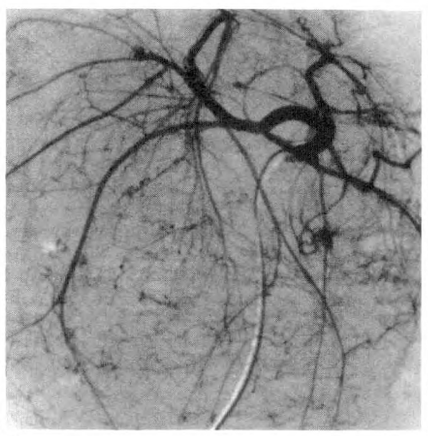
Pathologic examination of the gross specimens showed eight of the tumors to be cystic and one solid. The excised tumors weighed between 194 and 1037 g. One of the patients had a large single cyst; in the others there were multiple cysts separated by septae (Fig. 4). The fluid in the cysts was yellow or white and varied in consistency from clear to viscous. The cyst walls were thick and fibrous.



A



B



C



D

Fig. 1.—Case 7, 1-year-old boy with an abdominal mass.

***A*, Sonogram in longitudinal plane showing a sonolucent mass with internal septation.**

***B*, Postenhancement CT shows a large mass within right lobe of liver with central areas of diminished attenuation and septae.**

***C*, Selective celiac axis arteriogram in left anterior oblique position showing marked peripheral hypervascularity. Tumor involves whole right lobe of liver.**

***D*, Later phase of arteriogram showing multiple avascular areas with intervening septae within mass.**

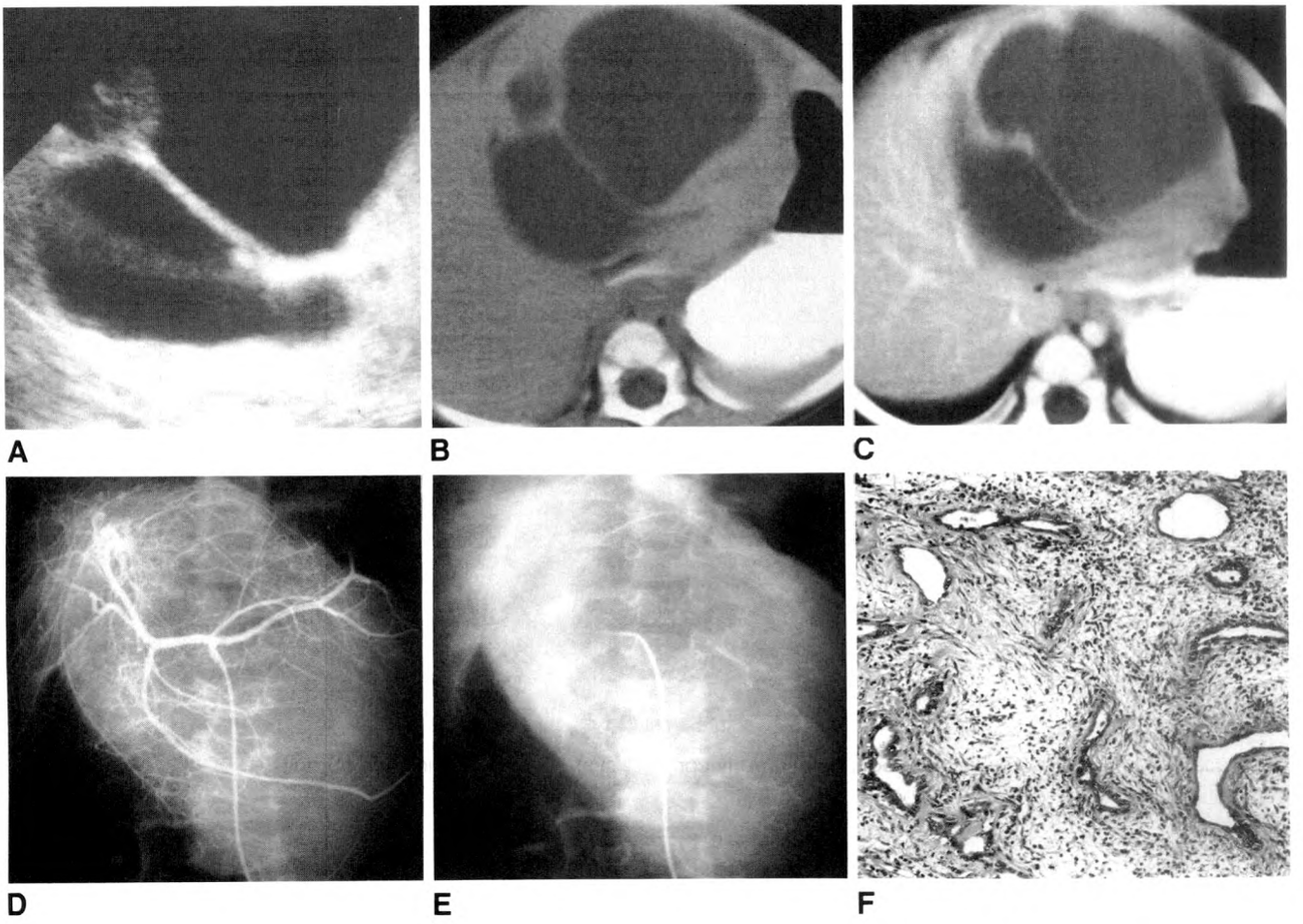


Fig. 2.—Case 8, 18-month-old boy with abdominal mass.

***A*, Sonogram in transverse plane showing multiple cystic areas within mass with intervening septae.**

***B*, Preenhancement CT shows a low-attenuation septated mass within left lobe of liver.**

***C*, Postenhancement CT at slightly more cranial level than Fig. *B*, showing faint enhancement of septation.**

***D*, Selective celiac axis arteriogram in anteroposterior projection shows vessels swept around periphery of mass with some increase in vascularity.**

***E*, Capillary phase of arteriogram showing central avascularity with clear plane of separation from adjacent liver.**

***F*, Photomicrograph showing mesenchymal hamartoma composed of dilated spaces lined by vascular endothelium and bile-duct epithelium surrounded by pale-staining connective tissue. (H and E ×100 original magnification) (Courtesy of Hart Isaacs, Jr.)**

The histology of all nine patients showed a consistent pattern of loose myxoid and fibrous stroma with entrapped bile ducts, small vessels, and islands of normal parenchyma. Some of the cysts were lined by various types of epithelium, including bile duct and vascular endothelium (Fig. 2F).

All nine children are alive and well between 6 months and 10 years later, with no evidence of tumor recurrence.

Discussion

In 1903, Maresch [9] described a lymphangioma of the liver in a 5-year-old girl with a 3-year history of abdominal swelling. Reports followed of cavernous lymphangiomatoid tumor, hamartomas, and solitary bile-cell fibroadenomas [1]. In his 1956 review, Edmondson [1] classified these tumors as mesenchymal hamartomas, using the term *hamartoma* first coined by Albrecht [10], implying a developmental anomaly rather than a true neoplasm. The mass arises from the indigenous mesoderm within the portal tracts.

Although mesenchymal hamartomas are most common before the age of 2 years [3], older children and young adults with the disease have been reported [11]. A slight male predilection has been noted [2, 3] but was not present in this series. The tumors usually grow slowly, and rapid increase in size [1, 3, 4] may signify accumulation of fluid within the cyst.

Most mesenchymal hamartomas are located within the right lobe of the liver [2–4]. The mass may blend with the adjacent liver [2], be encapsulated [2], or be attached to the liver by a pedicle [1, 7, 8]. Mesenchymal hamartomas are large tumors often weighing over 1000 g [2]. The cut surface shows a

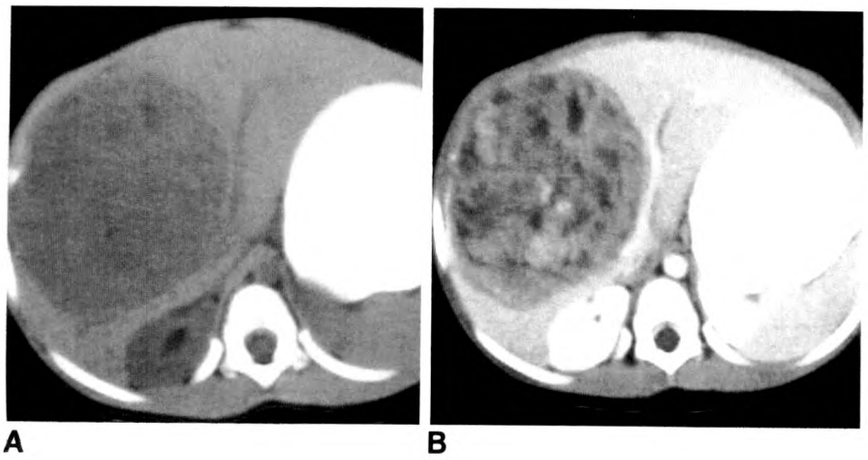


Fig. 3.—Case 6, 4-year-old boy with abdominal mass.

***A*, CT showing moderately well defined, 11-cm, slightly heterogeneous mass of diminished attenuation within right lobe of liver.**

***B*, Many areas of patchy enhancement and low attenuation within mass after IV contrast injection. There is displacement of left branch of portal vein by mass.**



Fig. 4.—Case 3, 14-month-old girl with abdominal mass. Bivalved specimen showing large central cyst with trabeculation of wall and several smaller cysts.

mixture of solid and cystic components; many tumors are predominantly cystic as seen in eight of our nine patients.

The microscopic features include cords of normal appearing hepatocytes lacking architectural landmarks and separated by zones of loose, poorly cellular mesenchyme. The porous nature of the mesenchyme permits accumulation of fluid [2]. The cysts consist primarily of dilated bile ducts or fluid accumulation in areas of degenerated mesenchyme.

Of the radiologic procedures performed, sonography was the most informative and should be the primary screening technique for this condition. CT supported the sonographic findings, confirming the extent of the mass and its relationship to adjacent structures. Arteriography was undertaken to demonstrate the arterial anatomy before extensive hepatic resection; it is unnecessary with a small or pedunculated tumor. Scintigraphy correctly demonstrated the site of the tumor but was nonspecific.

Previous reports of sonography in cystic mesenchymal hamartomas have described large cysts with internal septae or trabeculae [12–15]. The less common manifestation of smaller cysts with thickened septations [12, 15] was not represented sonographically in our eight patients, who showed large cysts with internal septation separate from a normal biliary tree. These findings appear to be specific for cystic mesenchymal hamartomas and not for other hepatic masses [16, 17]. Simple cysts are rare in children and do not have internal septae. Choledochal cysts are rarely septated and are associated with dilatation of the intra- or extrahepatic biliary system [18, 19]. Cysts of polycystic kidney disease are scattered throughout the liver and are associated with renal cysts. Abscesses usually show particulate matter within them, and the patients are often febrile.

On CT, mesenchymal hamartomas usually appear as well-defined masses with a central area of homogeneous low attenuation with internal septations [12, 15, 20]. Large cysts found in hamartomas and areas of extensive tumor necrosis seen in malignant hepatic neoplasms may have similar CT appearances. Therefore, if CT is performed first, it is important that sonography confirms that the areas of low attenuation within the hepatic mass represent cysts instead of tumor necrosis. There was a single hamartoma in our series that did not appear cystic on CT or sonography.

Scintigraphy correctly identifies the tumor. Because the hamartoma lacks Kupfer cells, there is no uptake of isotope-labeled sulfur colloid. A labeled RBC study was done in one of our patients and showed slight hypervascularity around the periphery of the tumor.

Although avascular and hypovascular tumors have been described [15, 21], angiography in our series showed that all tumors had various degrees of peripheral hypervascularity without contrast pooling or arteriovenous shunting. Well or moderately well defined tumor margins were present, and the cystic nature of the mass [22] was revealed in the capillary phase of the examination.

Mesenchymal hamartomas, large tumors that interfere with growth and respiration, should be surgically removed. Catheter drainage or marsupialization of the cyst may be needed before surgery [5]. In the past, postoperative deaths and other significant complications have been reported, but none

were present in our series. There has been no evidence of local recurrence or metastatic disease nor have these been reported [2, 3].

REFERENCES

1. Edmondson HA. Differential diagnosis of tumors and tumorlike lesions of liver in infancy and childhood. *Am J Dis Child* **1956**;91:168–186
2. Dehner LP. Hepatic tumors in the pediatric age group: a distinctive clinicopathologic spectrum. In: Rosenberg HS, Bolande RP, eds. *Perspectives in pediatric pathology*. Year Book Medical Publishing, **1978**;4:217–266
3. Stocker JT, Ishak KG. Mesenchymal hamartoma of the liver: report of 30 cases and review of the literature. *Pediatr Pathol* **1983**;1:245–267
4. Sutton CA, Eller JL. Mesenchymal hamartoma of the liver. *Cancer* **1968**;22:29–34
5. Srouji MN, Chatten J, Schulman WM, Ziegler MM, Koop CE. Mesenchymal hamartoma of the liver in infants. *Cancer* **1978**;42:2483–2489
6. Gilbert RF, Waugh DE, Clarke JS. Mesenchymal hamartoma of the liver. *South Med J* **1978**;71:530–532
7. Raffensperger JG, Gonzalez-Crussi F, Skeehan T. Mesenchymal hamartoma of the liver. *J Pediatr Surg* **1983**;18:585–587
8. Ito H, Kishikawa T, Toda T, Arai M, Muro H. Hepatic mesenchymal hamartoma of an infant. *J Pediatr Surg* **1984**;19:315–317
9. Maresch R. Ueber ein lymphangiom der liber. *Z Heilk Wiern Hepid* **1903**;24:30–40
10. Albrecht E. Ueber hamartome. *Verh Dtsch Ges Pathol* **1904**;7:153–157
11. Grases PJ, Matos-Villalobos M, Arcia-Romero F, Lecuna-Torres V. Mesenchymal hamartoma of the liver. *Gastroenterology* **1979**;76:1466–1469
12. Giyanani VL, Meyers PC, Wolfson JJ. Mesenchymal hamartoma of the liver: CT and ultrasonography. *J Comput Assist Tomogr* **1986**;10:51–54
13. Kaude JV, Felman AH, Hawkins IF. Ultrasonography in primary hepatic tumors in early childhood. *Pediatr Radiol* **1980**;9:77–83
14. Rosenbaum DM, Mindell HJ. Ultrasonographic findings in mesenchymal hamartoma of the liver. *Radiology* **1981**;138:425–427
15. Ros PR, Goodman ZD, Ishak KG, et al. Mesenchymal hamartoma of the liver: radiologic-pathologic correlation. *Radiology* **1986**; 158:619–624
16. Miller JH, Greenspan BS. Integrated imaging of hepatic tumors in childhood. Part I. Malignant lesions. *Radiology* **1985**;154:83–90
17. Miller JH, Greenspan BS. Integrated imaging of hepatic tumors in child. Part II. Benign lesions. *Radiology* **1985**;154:91–100
18. Han BK, Babcock DS, Gelfand MH. Choledochal cyst with bile duct dilatation. Sonography and ^{99m}Tc IDA cholescintigraphy. *AJR* **1981**;136:1075–1079
19. Kangerloo H, Sarti DA, Sample WF, Amundson G. Ultrasonic spectrum of choledochal cysts in children. *Pediatr Radiol* **1980**;9:15–18
20. Berger PE, Kuhn JP. Computed tomography of the hepatobiliary system in infancy and childhood. *Radiol Clin North Am* **1981**;19:431–444
21. Alpert S, Metcalf W, Vreede AA, Meng CH. Right hepatectomy for hamartoma in an eleven-month-old infant. *Ann Surg* **1967**;165:286–292
22. Wendth AJ, Shamoun J, Pantoja E, Luther P, Frede T. Cystic hamartoma of the liver in a pediatric patient. *Radiology* **1976**; 121:440

Book Review

The Radiologic Clinics of North America. Magnetic Resonance Imaging of Musculoskeletal System. Guest editor: Michael L. Richardson. Philadelphia: Saunders, June 1986;24(2), 335 pp. By subscription, 4 issues annually, $52

This timely edition of the *Radiologic Clinics of North America* includes contributions by a number of experts in the field of musculoskeletal imaging by MR, including Thomas H. Berquist, Harry K. Genant, Clyde A. Helms, Ray F. Kilcoyne, and Michael T. Modic. Appropriate space is delegated to each of the major areas in which MR imaging has either proven or potential applications to musculoskeletal disease. Two introductory chapters deal with practical considerations, including optimal pulse sequences, imaging pitfalls and artifacts, and normal variation. An overview of MR imaging as applied to articular disease is provided, along with site-specific chapters on the spine, menisci and ligaments of the knee, and temporomandibular joint. Separate discussions of disease processes including ischemic necrosis, bone-marrow disorders, trauma, neoplastic disease, and infection are also provided. The concluding chapter describes the proven and potential applications of MR spectroscopy to the study of the musculoskeletal system. The table of contents includes a brief synopsis of each article, and a comprehensive index to the entire volume is provided.

Although the volume as a whole is not quite current because of rapid advances in the field and expected publication delays, it constitutes an important and comprehensive overview of the subject that can be completely read in a reasonable period of time. In general, technical emphasis is placed on the application of multiple pulse sequences and surface coils; most of the images presented were obtained with relatively low–field-strength systems. The introductory chapter on optimizing pulse sequences suffers somewhat from brevity and assumes prior knowledge in basic physics of MR imaging. The discussion of artifacts, normal variants, and imaging pitfalls is well illustrated, although the text is extremely brief and the content is skewed toward axial sites. The overview chapter on joint disease includes equivalent consideration of disorders affecting subchondral bone, articular cartilage, tendons and ligaments, and synovium, and provides excellent correlative reference to conventional imaging methods. The discussion of temporomandibular-joint imaging is brief, but includes technical considerations as well as high-quality images. The chapter on osteonecrosis is excellent, and provides information concerning anatomy, cause, pathogenesis, and histology as well as MR imaging; the only limitation lies in its nearly exclusive consideration of the femoral head. The presentation on knee imaging appropriately considers the cruciate ligaments, capsular ligaments, and menisci, but the quality of the images (obtained at 0.15 Tesla) is not state-of-the-art. A comprehensive discussion of MR imaging applications in the spine is provided, although several of the illustrations in the article are inverted. The chapter on musculoskeletal infections suffers from images of inferior quality, but the text is comprehensive and well written. The discussion of neoplastic disease is brief but nicely illustrated and considers pulse-sequence optimization, histologic characterization, indications for MR imaging in staging, and paramagnetic contrast agents. The chapter on bone-marrow disorders is appropriate in length and content as well as beautifully illustrated, including correlative figures from histologic and conventional imaging studies. The presentation on musculoskeletal trauma is perhaps the most outstanding in the entire volume, from the standpoint of both comprehensiveness of content and quality of images. The concluding chapter on MR spectroscopy is appropriately superficial for the needs of the general radiologist, and includes a useful discussion of basic physics, a handy table summarizing the results of published human studies using the technique, and an extensive reference list.

In general, despite the limitations outlined above, this edition of the *Radiologic Clinics of North America* constitutes an important publication in the field of clinical MR imaging. Most previous attempts to summarize the proven and potential applications of this technology to musculoskeletal disorders have been in the form of single journal review articles, in which the text has been superficial and the number of images scanty because of space limitations. From the standpoint of information content, the volume compares favorably with the recently published textbook entitled *Magnetic Resonance of the Musculoskeletal System*, edited by Thomas H. Berquist (Raven Press, 1986), and many of the contributors are identical. While the latter currently sells for $38.50, an individual edition of the *Clinics* series can be obtained for approximately $15.00 from W. B. Saunders Company.

Despite the high probability that this book will be outdated in several years, and the fact that much of the technical information provided is scanner-specific as opposed to generally applicable, it is recommended highly to a broad range of radiologists. In both the academic and private settings, individuals with experience in neurologic and body MR imaging faced with an increasing volume of orthopedic and rheumatologic referrals will find the book extremely helpful. Other radiologists who are likely to benefit from its content include musculoskeletal specialists with no previous MR experience and residents or fellows in training. As many of the articles assume prior knowledge in basic physical principles of the technique, readers without such background may experience some difficulties. Nevertheless, the book would also be valuable to referring clinicians who deal with musculoskeletal disorders on a regular basis, as an overview of the diagnostic capabilities and limitations of MR imaging. Unquestionably, it is well worth its minimal cost, and constitutes yet another outstanding contribution from this series to the diagnostic imaging literature.

David J. Sartoris
UCSD Medical Center
San Diego, CA 92103

Case Report

Congenital Urethral Polyp

Pilar A. Caro,[1] Henrietta Kotlus Rosenberg,[1] and Howard McCrum Snyder III[2]

Congenital urethral polyps constitute a rare cause of bladder outlet obstruction in boys. These benign fibroepithelial structures originate from the verumontanum and appear on voiding cystourethrography as oval-shaped filling defects in the posterior urethra. In most reported cases, the diagnosis was established with voiding cystourethrography. Sonography, however, can provide specific information about the nature of the filling defect demonstrated on the voiding cystourethrogram [1].

Case Report

A healthy, 18-day-old white boy was seen in the Division of Urology at The Children's Hospital of Philadelphia for evaluation of an antenatal sonographic finding that suggested fetal hydroureter and hydronephrosis. Sonography demonstrated normal-size kidneys with minimal fullness of the left pelvocalyceal system and the distal right ureter. The renal texture was normal. Moderate thickening of the bladder wall was noted suggesting possible bladder outlet obstruction. An excretory urogram showed normal kidneys and minimal fullness of both lower ureters. A voiding cystourethrogram revealed minimal trabeculation of the bladder wall. The baby voided spontaneously and satisfactorily emptied the bladder without vesicoureteral reflux. A small, oval-shaped, radiolucent mass was noted at the level of the verumontanum in the posterior urethra (Fig. 1).

The initial diagnostic impression was that the mass was a harmartomatous polyp of the verumontanum. Because of the small size of the baby and the fact that the bladder was emptying well, resection was delayed.

Four months later, the kidneys appeared normal sonographically. Sonography, of the bladder showed a 7 × 7 × 9 mm polypoid mass at the bladder neck posteriorly (Fig. 2). The bladder wall was again slightly thickened. Cystoscopy revealed a pedunculated polyp of the posterior urethra. The stalk appeared to emanate from the top of the verumontanum, and the ejaculatory ducts seemed to be separate. A 10-French resectoscope with a Collings knife were used to incise the base of the stalk. The child tolerated this procedure well and was discharged the same day.

Pathologic studies showed a benign polyp covered by transitional epithelium with several von Brunn's nests. The child remained well. A follow-up voiding cystourethrogram done 3 months later showed a normal posterior urethra with no evidence of recurrent polyp.

Discussion

In 1982, only 50 cases of posterior urethral polyps had been reported in the literature [2]. The average age at the time of diagnosis was 8 years. Occasionally, the patient had a concomitant vesical calculus [3]. More recently, Downs [4] reported the use of sonography to demonstrate the lesion.

Polyps arising from the verumontanum in children are congenital in origin. They are solid, epithelialized, fibrous tumors that arise on or in the vicinity of the verumontanum and lie along the floor of the posterior urethra. These polyps have a tendency to protrude toward the bladder, causing intermittent obstruction. They may also obstruct the urethra if they are large enough. Obstructive symptoms occurred in 26 of 30 cases in a review of the literature [4]. In four cases, the sole complaint was hematuria. In general, symptoms are mild and

Received December 11, 1985; accepted after revision April 22, 1986.

[1] Department of Radiology, Division of Ultrasound, The Children's Hospital of Philadelphia, 34th St. and Civic Center Blvd., Philadelphia, PA 19104. Address reprint requests to P. A. Caro.

[2] Department of Surgery, Division of Urology, The Children's Hospital of Philadelphia, Philadelphia, PA 19104.

AJR 147:1041–1042, November 1986 0361–803X/86/1475–1041 © American Roentgen Ray Society



Fig. 1.—Voiding cystourethrogram demonstrates oval-shaped polypoid filling defect in posterior urethra (*arrow*).

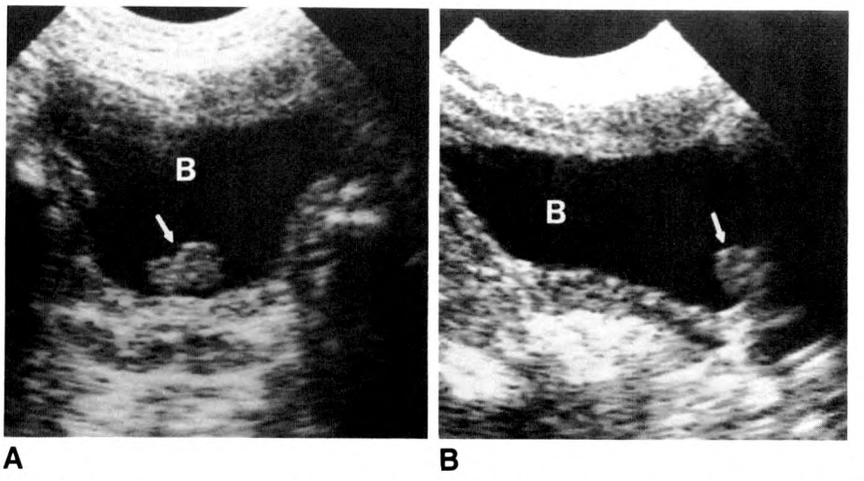


Fig. 2.—Transverse (*A*) and sagittal (*B*) bladder sonograms 4 months later show a solid polypoid mass (*arrow*) projecting from bladder neck into bladder lumen. B = bladder.

nonspecific. In the same review, 19 of the 30 cases were studied with urographic techniques. In 11 of the 19, dilatation of the upper urinary tract was documented. Reflux was demonstrated in three cases and diverticula in four. The voiding cystourethrogram demonstrated the polyp in 21 cases; seven were diagnosed endoscopically, and two were found at autopsy.

The presence and often the cause of upper and lower urinary tract obstruction in the neonate can be easily demonstrated by sonography. In the rare patient with a urethral polyp, sonography used in conjunction with voiding cystourethrography offers the added advantage of being able to differentiate the echogenic polypoid mass from a blood clot or stone.

ACKNOWLEDGMENT

We thank Janet Birkmann for secretarial assistance.

REFERENCES

1. de Filippi G, Derchi LE, Coppi M, Biggi E. Sonographic diagnosis of urethral polyp in a child. *Pediatr Radiol* **1983**;13:351–352
2. Kimche D, Lask D. Congenital polyp of the prostatic urethra. *J Urol* **1982**;127:134–135
3. Dalens B, Vanneuville G, Vincent L, Fabre J-L. Congenital polyp of the posterior urethra and vesical calculus in a boy. *J Urol* **1982**;128:1034–1035
4. Downs, RA. Congenital polyps of the prostatic urethra: a review of the literature and report of two cases. *Br J Urol* **1970**; 42:76–85

Sonographic Findings in Abdominal Pregnancy

John H. Stanley[1]
E. O. Horger III[2]
Charles J. Fagan[3]
Joseph G. Andriole[1]
Arthur C. Fleischer[4]

The sonograms of 20 proven cases of abdominal pregnancy were evaluated to determine the frequency of specific abnormalities associated with this condition. The most frequent and reliable finding was separation of the uterus from the fetus (90%). Extrauterine placenta (75%) and oligohydramnios (45%) were next in frequency. Other features such as fetal parts close to the maternal abdominal wall (25%), failure to visualize myometrium between the fetus or placenta and maternal bladder (15%), abnormal fetal lie (25%), poor visualization of the placenta (25%), and maternal bowel gas impeding fetal visualization (25%) were noted.

The early diagnosis of abdominal pregnancy is frequently difficult. Clinical findings are extremely variable, and the preoperative diagnosis is unsuspected in up to 60% of cases [1]. Frequent signs and symptoms include crampy abdominal pain, vaginal spotting or hemorrhage, nausea, vomiting, malaise, and painful fetal movement [1–4]. The most common physical findings are abdominal tenderness, an abnormal fetal position, and displacement of the cervix. The absence of uterine contractions during oxytocin challenge testing is highly suggestive of abdominal pregnancy [4]. Sonography is recommended as a rapid noninvasive method to aid in the diagnosis. Numerous single cases and studies of small series of patients that emphasize various diagnostic sonographic findings have been reported [5–17]. Despite this, the diagnosis remains difficult and is missed in one-fourth of reported cases. To aid in the sonographic diagnosis of this condition, sonograms of patients with abdominal pregnancies were acquired from several institutions and retrospectively reviewed to determine the prevalence and significance of reported sonographic findings.

Methods

A literature review [5–17] of the sonographic diagnosis of abdominal pregnancy suggested at least 12 sonographic criteria reported to occur in patients with this condition. To determine the relative frequency of these findings, 33 sonograms performed on 26 patients with abdominal pregnancy were accumulated from several institutions. Six patients were excluded because either a complete sonogram (transverse and longitudinal images) or surgical documentation was not available. The remaining 27 sonograms performed on 20 patients were retrospectively evaluated by three of the authors, and the sonographic findings and their frequency were compiled. Sonographic findings were considered positive only if all three examiners agreed to its presence.

Results

Twenty-seven sonograms of 20 patients with abdominal pregnancy were evaluated. The average maternal age was 29 years (range 19–42). Fifteen patients had only one sonogram obtained, three had two examinations, and two underwent

Received April 7, 1986; accepted after revision June 9, 1986.

[1] Department of Radiology, Medical University of South Carolina, 171 Ashley Ave., Charleston, SC 29425. Address reprint requests to J. H. Stanley.

[2] Department of Obstetrics and Gynecology, Department of Radiology, Medical University of South Carolina, 171 Ashley Ave., Charleston, SC 29425.

[3] Department of Radiology, The University of Texas Medical School, 301 University Blvd., Galveston, TX 77550.

[4] Department of Radiology, Department of Obstetrics and Gynecology, Vanderbilt University Medical Center, Nashville, TN 37232.

AJR 147:1043–1046, November 1986
0361–803X/86/1475–1043
© American Roentgen Ray Society

three examinations. Three patients had only real-time sonograms, 11 had only static gray-scale sonograms, and six had both static and real-time studies available for review. Fifty-five percent of the sonograms were performed during the last trimester of pregnancy, 25% in the first trimester, and 20% in the second trimester. The frequency of the sonographic findings seen in abdominal pregnancy are listed in Table 1. A prospective sonographic diagnosis of abdominal pregnancy was made in 14 (70%) of the 20 cases, suggested in one (5%), and missed in five (25%). The fetal mortality rate was 80% (16 of 20). Nine of 16 fetuses were dead at presentation. No maternal deaths occurred.

TABLE 1: **Sonographic Features in Abdominal Pregnancy**

	No. of Patients (%)
Uterus and fetus separate	18 (90)
Ectopic placenta	15 (75)
Oligohydramnios	9 (45)
Fetal parts in close proximity to maternal wall	5 (25)
Abnormal lie	5 (25)
Poor visualization of the placenta	5 (25)
Maternal bowel gas blocking visualization	5 (25)
Failure to visualize myometrium between fetus and maternal bladder	3 (15)
Failure to visualize myometrium between placenta and maternal bladder	3 (15)
Placenta previa appearance	2 (10)
Maternal peritoneal fluid	2 (10)

Note.—The total number of patients = 20.

Discussion

Abdominal pregnancy occurs uncommonly; the reported prevalence is between 1 in 3000 and 1 in 8000 deliveries [2, 3]. The condition most likely occurs secondary to rupture of a tubal pregnancy. Ovum fertilization outside the fallopian tube or uterine rupture with resultant abdominal implantation of a fertilized ovum are also possible explanations. Abdominal pregnancy is associated with maternal mortality rates from 6 to 18% [2, 3], perinatal mortality rates greater than 90%, and an increased incidence of congenital malformations [18]. Prompt diagnosis and management is needed to avert the associated complications. To aid in this difficult clinical and sonographic diagnosis, we have broadened and unified the data base by accumulating sonograms of proven cases of abdominal pregnancy from several institutions.

The most frequent and reliable sonographic finding was identification of an empty uterus separate from the fetus [6]. This was seen in 90% of the patients (Figs. 1A–C). In most cases the abdominal pregnancy was cephalad to the uterus, with downward displacement or compression of the uterus and bladder. To establish the diagnosis, clear identification of the empty uterus as a separate structure is important. This can be accomplished by giving close attention to the lower pelvis to ensure that there is continuity between normally appearing vaginal and endometrial echoes. Also, false-positive diagnoses must be avoided. Findings that mimic abdominal pregnancy include pregnancy in a bicornuate uterus (Fig. 2), pedunculated uterine fibroids associated with a gravid uterus, and even an early normal pregnancy in a sharply retroflexed or anteflexed uterus (Fig. 3).

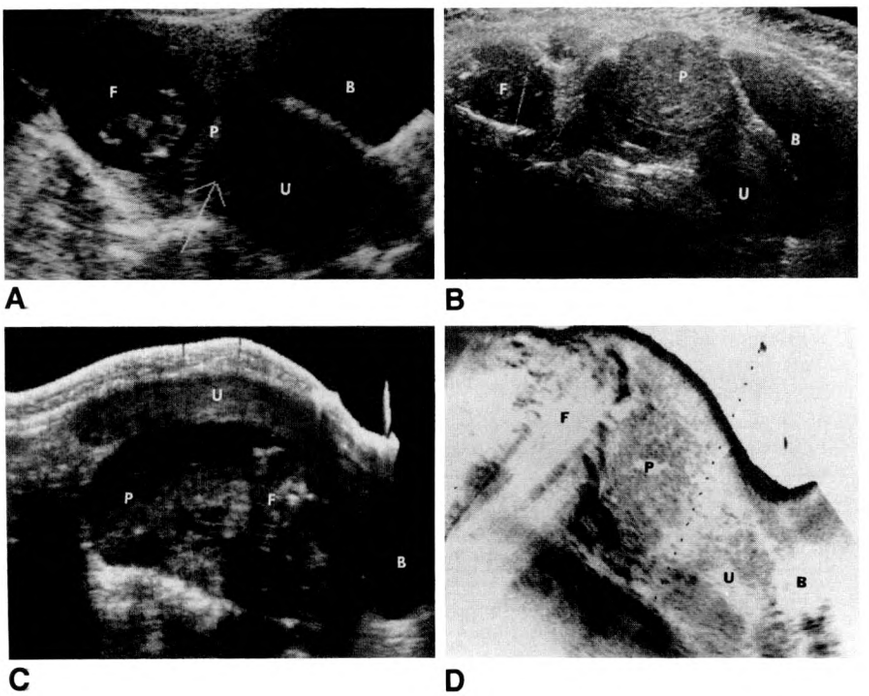


Fig. 1.—Sonograms at various stages of gestation showing several sonographic findings in abdominal pregnancy. (U = uterus, F = fetus, P = placenta, B = bladder).

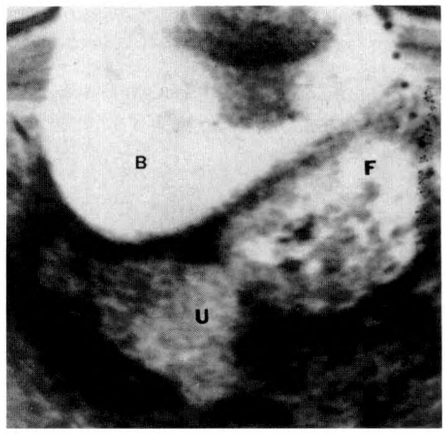
***A*, Longitudinal sonogram at 12-weeks gestation shows an abdominal pregnancy located on fundus of uterus, with a cleavage plane (*arrow*) between uterus and pregnancy.**

***B*, Longitudinal sonogram performed at 24-weeks gestation by using a water bath shows an extrauterine placenta implanted on uterine fundus. Fetal parts are located cephalad.**

***C*, Longitudinal sonogram shows a compressed elongated uterus anterior to placenta and fetus. This location of uterus occurred in only one patient; usually it was compressed inferiorly within lower pelvis.**

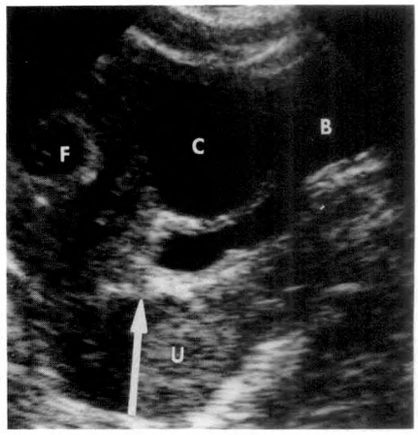
***D*, Longitudinal sonogram at term shows a pelvic mass produced by an enlarged uterus and placenta. Fetus is surrounded by loops of air-filled maternal bowel, resulting in poor fetal visualization. A viable abdominal pregnancy was found at laparotomy.**

Fig. 2.—Transverse sonogram shows a pregnancy in left side of a bicornuate uterus. Right side could be mistaken for "separate" uterus. (U = uterus, F = fetus, B = bladder.)



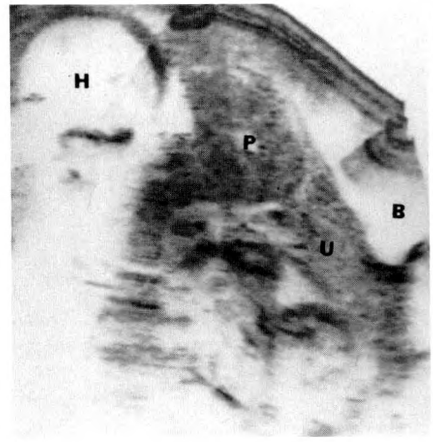
2

Fig. 3.—This sonogram was misinterpreted as representing an early abdominal pregnancy separate from uterus. On this longitudinal scan there is suggestion of a cleavage plane between uterus and fetus (*arrow*). At laparoscopy a normal anteflexed uterus was observed. Incidentally noted was a corpus leuteum cyst (C) inverting the dome of urinary bladder. (U = uterus, F = fetus, B = bladder.)



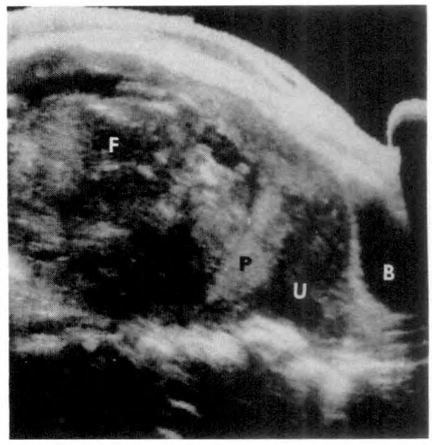
3

Fig. 4.—Longitudinal sonogram at approximately 32-weeks gestation shows fetal head (H) close to maternal abdominal wall. No identifiable myometrium is seen around fetal head, suggesting an abdominal pregnancy. At surgery, a viable abdominal pregnancy was found. (U = uterus, P = placenta, B = bladder.)



4

Fig. 5.—Longitudinal sonogram, thought to show a complete placenta previa, shows inferiorly displaced and compressed empty uterus that was wrongly called placenta. Extrauterine placenta about fetus is evident. At surgery an abdominal pregnancy was found. (U = uterus, F = fetus, P = placenta, B = bladder.)



5

The second most frequent finding was an extrauterine placenta which was seen in 75% of the patients (Fig. 1A). This occurred less frequently than identification of separation of the uterus and fetus because the placenta was poorly visualized or not seen in 25% of the examinations.

For the purpose of this study oligohydramnios was defined simply as the subjective determination of a reduced amount of amniotic fluid. This was present in 45% of the cases and is not specific for abdominal pregnancy. Fifty-five percent of the patients appeared to have a normal amount of amniotic fluid.

The remainder of the sonographic findings occurred in 25% or less of the patients and are less specific. Identification of fetal parts in close proximity to the maternal abdominal wall (25%) can be suggestive of abdominal pregnancy but is a subjective sonographic finding (Fig. 4). Failure to identify myometrium between the fetal head and maternal bladder (15%) or failure to visualize the myometrium between the placenta and maternal bladder (15%) should suggest the diagnosis of abdominal pregnancy (Fig. 1B). This finding may be difficult to appreciate because the myometrium can normally appear thin (5–10 mm). The presence of maternal bowel gas blocking visualization of the fetus (25%) (Fig. 1D) is not specific; this can occur in early pregnancy if the maternal urinary bladder fails to distend, with resultant displacement of maternal pelvic bowel loops. However, if such gas is identified in a properly performed examination, abdominal pregnancy should be considered. The presence of maternal peritoneal fluid (10%) is uncommon in normal pregnancy. It represented intraperitoneal bleeding on both occasions in our series and should be considered an ominous sonographic finding.

A final sonographic finding deserves comment, the appearance of a pseudo–"placenta previa" (10%). This occurred when the compressed empty uterus was displaced inferiorly into the pelvis by an ectopic placenta of similar echogenicity located on the fundus (Fig. 5). Pseudo–placenta previa was present in two patients and was followed over a 6-week period in both without suspicion of an abdominal pregnancy. This error could possibly have been avoided by closer atten-

tion to the differences in sonographic texture of the uterus and extrauterine placenta and by better identification of the lower uterine segment.

Some patients did not have both real-time and static examination; therefore a conclusion cannot be drawn as to which is superior for the diagnosis of abdominal pregnancy. We recommend both examinations in such complex cases because they can be complementary. Frequently, the lower pelvis can best be examined with the flexibility of the real-time transducer, whereas static serial echotomograms permit recognition of the overall total abdominal anatomy, which provides a better understanding of normal and abnormal relationships.

Although these studies were performed by experienced obstetric sonographers and sonologists, the diagnosis was missed in 25% of the cases. Retrospectively, the diagnosis can be made sonographically in 90% of the cases. The pregnancies would have been managed differently with earlier diagnosis. Thus, the sonographer and sonologist must maintain a high index of suspicion in the appropriate clinical situation, such as maternal pain or bleeding, to ensure the diagnosis of abdominal pregnancy is not missed.

ACKNOWLEDGMENTS

We thank Dallas Lovelace, Edward Shelley, Clifton Greer, Carol Mittelstaedt, Anita Kotheimer, and Issac Delke for providing case material for review and Juanita Landreth for preparing the manuscript.

REFERENCES

1. Rahman MS, Al-Suleiman SA, Rahman J, Al-Sibai MH. Advanced abdominal pregnancy: observations in 10 cases. *Obstet Gynecol* **1981**;59(3):366–372
2. Beacham WD, Hernquist WC, Beacham DW, et al. Abdominal pregnancy at Charity Hospital in New Orleans. *Am J Obstet Gynecol* **1962**;84:1257–1270
3. Strafford JC, Ragan WD. Abdominal pregnancy: review of current management. *Obstet Gynecol* **1977**;50(5):548–552
4. Delke I, Veridiano WP, Tawcer ML. Abdominal pregnancy: review of current management and addition of 10 cases. *Obstet Gynecol* **1982**;60:200–203
5. Ali V, Saldana LR, Balat IY, Katragadda R. Pitfalls in sonographic diagnosis of abdominal pregnancy. *South Med J* **1981**; 74(4):477–479
6. Allibone GW, Fagan CJ, Porter SC. The sonographic features of intraabdominal pregnancy. *J Clin Ultrasound* **1981**;9:383–387
7. Alexander MC, Horger EO. Early diagnosis of abdominal pregnancy by ultrasound. *J Clin Ultrasound* **1983**;11:45–48
8. Blackwelder T, Varner MW, Brown RC. Sonographic findings in advanced abdominal pregnancy. *AJR* **1981**;137:1259–1261
9. Garrett WJ, Crowe PH, Robinson DE. The interpretation of ultrasonic echograms in abdominal pregnancy. *Aust NZ J Obstet Gynaecol* **1969**;9:26–28
10. Graham D, Johnson RB, Sanders RC. Sonographic findings in abdominal pregnancy. *J Ultrasound Med* **1982**;1:71–74
11. Graham MF. First trimester abdominal pregnancy. *J Clin Ultrasound* **1977**;5(5):321–322
12. Hertz RH, Tritsch-Timor I, Sokol RJ, Zador I. Diagnostic studies and fetal assessment in advanced extrauterine pregnancy. *Obstet Gynecol* **1977**;50(1):62–65
13. Lee LL, McGahan JP. Combined use of ultrasound and computed tomography in evaluation of intraabdominal pregnancy and fetal demise. *J Comput Assist Tomogr* **1984**;8(4):770–771
14. Lorimer JD. Ultrasonography and advanced extrauterine pregnancy. *Br J Clin Pract* **1975**;29(12):349–358
15. Kurtz AB, Dubbins PA, Wapner RJ, Goldberg BB. Problem of abnormal fetal position. *JAMA* **1982**;247(23):3251–3252
16. Sauebrei E, Ants T, Effer SB, Fayle BWK. Intrauterine to intraabdominal pregnancy: ultrasound demonstrations. *AJR* **1979**; 133:132–134
17. Williams CH. Ultrasound evaluation of a near-term abdominal ectopic pregnancy. *J Clin Ultrasound* **1978**;6:264–266
18. Tan KL, Goon SM, Wee JH. The pediatric aspect of advanced abdominal pregnancy. *J Obstet Gynaecol Br Commonw* **1969**; 76:1021–1028

Fetal Omphalocele and Gastroschisis: A Review of 24 Cases

John H. Bair[1]
Paul D. Russ[1]
Dolores H. Pretorius[1]
David Manchester[2]
Michael L. Manco-Johnson[1]

Fetal omphalocele and gastroschisis are congenital defects of the abdominal wall that require prompt surgical management at the time of delivery. To evaluate the role of prenatal sonography in identifying factors that influence prognosis, 24 cases of abdominal-wall defect (16 omphalocele, eight gastroschisis) were reviewed. Sonograms were evaluated for location of umbilical cord insertion, contents of the ventral defect, presence or absence of a covering membrane, fetal ascites, bowel-wall thickening, and coexisting anomalies. Sonographic differentiation between omphalocele and gastroschisis was possible in 18 (75%) of 24 cases. Eighteen patients had congenital defects in addition to the abdominal-wall defect. Associated abnormalities were present in 14 (88%) of 16 fetuses with omphalocele and four (50%) of eight with gastroschisis. Overall survival rate was 50%, excluding six terminated pregnancies. Survival rate was 33% for neonates with omphalocele and 83% for those with gastroschisis. The better prognosis for neonates with gastroschisis appears to reflect the lower frequency of associated congenital anomalies.

Omphalocele and gastroschisis are congenital defects of the abdominal wall that occur in approximately 1 of 4000 and 1 of 12,000 pregnancies, respectively [1]. Before prenatal sonography, few ventral defects were anticipated before delivery. Sonography has made possible the prenatal diagnosis of both omphalocele and gastroschisis [2]. Sonographic criteria to distinguish omphalocele from gastroschisis include the site of umbilical cord insertion, the presence of a covering membrane, and the type of viscera protruding into the defect [2–5]. The overall survival rate for neonates born with an abdominal-wall defect has been reported to be 70–96% [6–10]. Patients with gastroschisis may have a better prognosis than those with omphalocele, because omphalocele is associated with a higher frequency of coexisting anomalies [7, 10, 11].

Twenty-four cases of congenital defects of the abdominal wall (16 omphaloceles, eight gastroschisis) detected in utero were reviewed retrospectively to evaluate the diagnostic potential of prenatal sonography. The accuracy of distinguishing omphalocele from gastroschisis and of identifying associated congenital abnormalities was assessed. The clinical course and outcome were reviewed to determine the impact of prenatal sonography, to evaluate the effect of coexisting malformations on survival rate, and to compare the survival rate to previously published results.

Materials and Methods

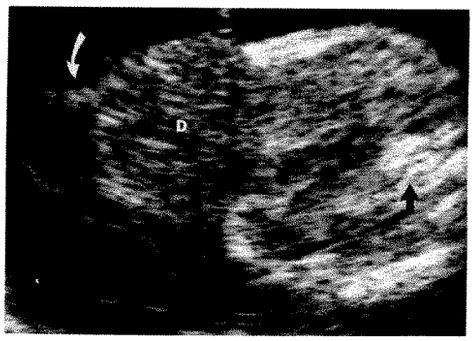
From 1977 to 1985, 24 fetuses with abdominal-wall defects were detected by prenatal sonography. Original sonograms were reviewed in 20 cases, and the sonographic reports were examined in all cases. The sonograms were obtained via a variety of commercially available static and real-time scanners with 3.5- and 5-MHz transducers. Medical records, autopsy reports, and/or clinical follow-up reports were available for all 24 cases. Data collected included maternal age, parity, and family history of abdominal-wall defects. Sonograms were

Received March 10, 1986; accepted after revision June 5, 1986.

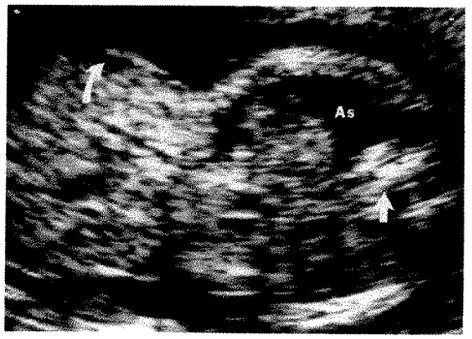
[1] Department of Radiology, University of Colorado Health Sciences Center, 4200 E. 9th Ave., Denver, CO 80262. Address reprint requests to D. H. Pretorius, Dept. of Radiology, UCSD Medical Center, 225 W. Dickinson St., San Diego, CA 92103.

[2] Department of Pediatrics, University of Colorado Health Sciences Center, 4200 E. 9th Ave., Denver, CO 80262.

AJR 147:1047–1051, November 1986
0361–803X/86/1475–1047
© American Roentgen Ray Society



1



2

Fig. 1.—Omphalocele. Transverse sonogram through abdomen of a 35-week-old fetus. Note spine (*black arrow*). Umbilical cord (*white arrow*) inserts onto abdominal-wall defect (D).

Fig. 2.—Omphalocele. Transverse sonogram through abdomen of a 25-week-old fetus. Spine (*straight arrow*). Ascites (As) is present in fetal abdomen and in abdominal-wall defect (*curved arrow*).

examined for volume of amniotic fluid, sizes of abdominal-wall defect and fetal abdomen, contents of the defect, presence of a covering membrane, location of cord insertion, fetal ascites, bowel-wall thickening, and presence of other fetal anomalies. In deciding which of the abdominal viscera were herniated into the abdominal-wall defect, liver was distinguished from bowel by its characteristic morphology and echo texture and by identification of the hepatic veins and adjacent gallbladder. A defect in the abdominal wall was classified as an omphalocele if a thin covering membrane of amnion and peritoneum was present or if the umbilical cord inserted onto the ventral defect; the diagnosis of gastroschisis was made if the umbilical cord inserted onto the fetal abdominal wall or if multiple images failed to demonstrate a covering membrane. Bowel-wall thickening was evaluated subjectively. Fetal and neonatal information evaluated included gestational age at diagnosis, gestational age at delivery, mode of delivery, birth weight, chromosomal analysis, and associated anomalies. Treatment techniques, complications, and outcome were reviewed.

Results

Maternal History

The average maternal age was 26 years (range, 18–35). Fifteen women were nulliparous; nine women were multiparous. None of the mothers had a personal history of an abdominal-wall defect or had had a previous gestation complicated by either an omphalocele or a gastroschisis.

Sonographic Findings

Sonograms or reports were reviewed for all patients. A diagnosis of an abdominal–wall defect was made when a mass composed of abdominal viscera protruding from the fetal abdomen was identified. The average gestational age as estimated by sonographic measurements at the time of diagnosis was 26 menstrual weeks (range, 17–36 weeks).

The volume of amniotic fluid evident on the sonogram was evaluated subjectively in 23 patients. In 16 the volume was normal. Five had polyhydramnios and two had oligohydramnios (one with premature rupture of membranes). All five pregnancies complicated by polyhydramnios were associated with fetuses who had omphaloceles. Of the two pregnancies complicated by oligohydramnios, one fetus had an omphalocele and one a gastroschisis.

The site of umbilical cord insertion could be determined in 12 cases (50%). Insertion onto the abdominal-wall defect could be seen in seven fetuses (Fig. 1). All seven of these defects were omphaloceles. Sonographically, cord insertion was considered to be lateral to the abdominal-wall defect in five cases. Four of these fetuses had gastroschises and one had an omphalocele. In 12 cases, the site of cord insertion was considered sonographically indeterminate.

A covering membrane could be identified in 11 fetuses, all of whom had an omphalocele. In six cases, sonographic images appeared to exclude a membrane. Five of these fetuses had a gastroschisis. One had an omphalocele with a covering membrane that was not sonographically apparent and did not have a ruptured membrane at autopsy. Seven sonograms were considered indeterminate for detecting the presence or absence of a covering membrane. Four of these fetuses had omphalocele, and three had gastroschises.

Seven ventral defects contained bowel only; six were gastroschises and one was an omphalocele. Four defects contained liver only; all four were omphaloceles. Eight abdominal-wall defects contained liver and bowel; seven were omphaloceles and one was a gastroschisis. Five additional defects containing liver and/or bowel were associated with ectopia cordis. Of the fetuses with ectopia cordis, four had omphalocele and one a gastroschisis. A total of 14 defects contained liver. Thirteen of these abdominal-wall defects were omphaloceles; only one was a gastroschisis.

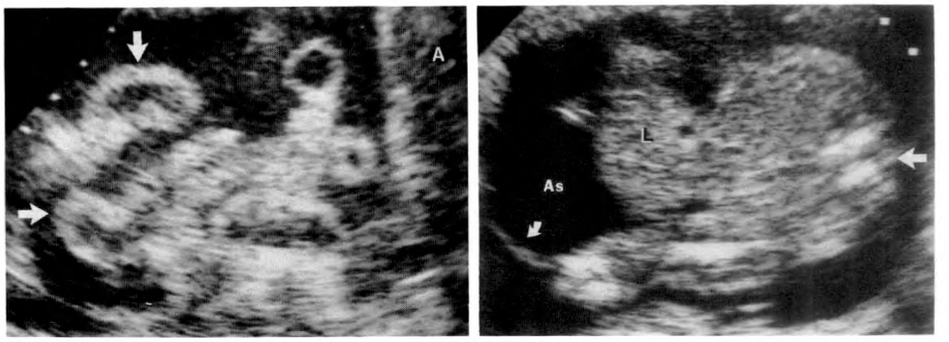
Ascites was detected in nine fetuses, all of whom had an omphalocele. Ascitic fluid was identified within either the fetal abdomen or the ventral defect (Fig. 2). Of these nine fetuses, six died, two survived, and one was terminated. Ascites was not demonstrated in any of the eight fetuses with gastroschisis.

Bowel-wall thickening was noted in four cases (Fig. 3). All four fetuses had gastroschisis. No fetus with an omphalocele had thickened bowel walls.

The average fetal abdominal circumference was 17 cm (range, 6.5–29). The average circumference of the abdominal-wall defect was 17 cm (range, 9.0–30). The circumference of the defect was greater than or equal to that of the fetal abdomen in 11 cases. Of these 11 fetuses, five (45%) were terminated, four (36%) died, and two (18%) survived. The circumference of the defect was less than the fetal abdominal

Fig. 3.—Gastroschisis. Transverse sonogram through abdomen of a 31-week-old fetus shows multiple bowel loops with thickened walls (*arrows*) floating anterior to fetal abdomen (A).

Fig. 4.—Omphalocele. Transverse sonogram through abdomen of a 22-week-old fetus. Note spine (*straight arrow*). Liver (L) protrudes into abdominal-wall defect. Ascites (As) outlines covering membrane (*curved arrow*) of omphalocele.



3 4

TABLE 1: **Associated Anomalies and Outcome of Omphalocele and Gastroschisis**

Case No.	AWD	Anomalies at Sonography	Anomalies at Birth	Outcome
1	Om	Amniotic bands, scoliosis	Amniotic bands, scoliosis, hypoplastic heart/lung, cloaca, Meckel's diverticulum	D
2	Om	Ectopia cordis, kyphosis	Ectopia cordis, skeletal anomalies, urethral agenesis, bladder exstrophy, imperforate anus	D
3	G	None	None	D
4	Om	None	Agenesis left kidney, patent urachus, cryptorchidism, Meckel's diverticulum	A
5	Om	None	Scoliosis, hypoplastic thorax, absent right hemidiaphragm, atrial septal defect	D
6	Om	Hypoplastic thorax	None	D
7	G	Hydronephrosis right kidney	None	A
8	Om	None	None	A
9	G	None	Ileal atresia, Meckel's diverticulum	A
10	G	None	Jejunal stenosis	A
11	Om	None	Bilateral inguinal hernias, undescended testis, patent foramen ovale	A
12	G	Amniotic bands, posterior encephalocele, hypoplastic thorax	Holoprosencephaly, encephalocele, absent right hemidiaphragm, atrial septal defect, hypoplastic thorax	T
13	Om	Ectopia cordis	Ectopia cordis	T
14	G	Ectopia cordis, scoliosis	Ectopia cordis, scoliosis	T
15	G	None	None	A
16	Om	Hypoplastic thorax	Amniotic bands, scoliosis, hypoplastic lungs	T
17	Om	Left diaphragmatic hernia	Left diaphragmatic hernia, undescended testis	D
18	Om	Hypoplastic thorax	Malrotation, Meckel's diverticulum	A
19	Om	Ectopia cordis, scoliosis	Ectopia cordis, scoliosis, left diaphragmatic hernia, short umbilical cord	T
20	Om	Abnormal cisterna magna	Cryptorchidism, craniofacial disporportion, club feet	D
21	G	None	None	A
22	Om	None	Extracranial occipital cyst	D
23	Om	Ectopia cordis, scoliosis, sacral cyst	Ectopia cordis, amniotic bands, sacral agenesis, sacral cyst, cloaca, bladder exstrophy, ileal atresia	T
24	Om	None	Hypoplastic lungs, atrial septal defect, patent ductus arteriosus, absent superior mesenteric artery, long-segment ileal atresia	D

Note.—AWD = abdominal wall defect, Om = omphalocele, G = gastroschisis. A = alive, D = dead, T = pregnancy terminated.

circumference in nine fetuses; five (56%) of these died and four (44%) survived. The relative circumference of the abdominal-wall defect compared with that of the fetal abdomen (i.e., larger or smaller) was not a useful predictor of fetal outcome for fetuses with either omphalocele or gastroschisis.

Associated congenital anomalies were detected at birth in 14 (88%) of 16 fetuses with an omphalocele and four (50%) of eight with a gastroschisis. Coexisting anomalies were suspected on the basis of sonography in 13 cases (Table 1). Nine of 18 fetuses were correctly identified as having coex-

isting anomalies on the basis of sonography; in four instances the suspected anomaly was not found to exist at birth (two cases of suspected hypoplastic thorax, one each of abnormal cisterna magna and unilateral hydronephrosis). In 11 fetuses no associated anomalies were detected by sonography, and none were found at birth in four of these. Seven fetuses without sonographically suspected anomalies were found to have additional abnormalities at birth, ranging from minor to life-threatening malformations (Table 1). However, only three of these fetuses had associated abnormalities that theoretically could have been detected by prenatal sonography.

On the basis of all available criteria, sonographic differentiation between omphalocele and gastroschisis was possible in 18 (75%) of 24 fetuses. A prenatal diagnosis of omphalocele was correct in 11 (100%) of 11 cases, whereas a diagnosis of gastroschisis was correct in 7 (70%) of 10 cases. Three fetuses with omphalocele were incorrectly diagnosed as having gastroschisis. Sonograms were considered indeterminate in three instances; one fetus had a gastroschisis and two had omphalocele.

Delivery

The gestational age at the time of delivery for the 18 pregnancies that were not terminated averaged 34 menstrual weeks (range, 22–40). There were 10 cesarean sections (nine live births and one stillbirth) and eight vaginal deliveries (six live births and two stillbirths). The presence of an abdominal-wall defect was mentioned specifically as a factor in electing cesarean section in four of 10 cases. The average birth weight for those pregnancies not terminated was 2186 g (range, 325–3920). The average weight for infants with omphalocele was 2151 g; for those with gastroschisis, 2253 g. Chromosomal analysis was performed for six neonates, all of whom had a normal karyotype.

Postnatal Course

Six of the 24 fetuses were terminated. Of the 18 nonterminated fetuses, 12 had omphalocele and six had gastroschisis. The overall survival rate of the nonterminated fetuses was 50% (9/18). Excluding terminated pregnancies, the survival rate of fetuses with omphalocele was 33% (4/12); for fetuses with gastroschisis the survival rate was 83% (5/6).

Of the 15 live born infants, 12 survived to undergo corrective surgery. A primary closure of the ventral defect was performed on two neonates with omphalocele and two with gastroschisis. A multistage closure by means of a Silastic (polymeric silicone) pouch was required in eight cases (five omphalocele, three gastroschisis). Three of the 12 neonates who underwent surgery subsequently died. All three were infants with omphalocele; one had been treated with primary closure, and two had required a multistage procedure. All survivors had corrective surgery but did not have severe coexisting congenital abnormalities (Table 1).

Discussion

An omphalocele is a midline defect in the anterior abdominal wall through which abdominal viscera herniate into the base of the umbilical cord. The protruding organs are covered by a thin membrane consisting of amnion, peritoneum, and Wharton's jelly; the umbilical cord inserts onto this membrane. Rarely, the covering membrane may rupture in utero and be sonographically inapparent. An omphalocele results from the failure of lateral body folds to migrate normally toward the midline, which produces a defect at the umbilical ring [12]. A high frequency of associated anomalies, including chromosomal abnormalities, ranging from 56 to 73% has been reported [7, 10, 11, 13].

Gastroschisis is a full-thickness paraumbilical defect in the abdominal wall, usually located to the right of the umbilical cord, through which abdominal viscera protrude; there is no covering membrane. The umbilical cord inserts normally onto the fetal abdomen. The pathogenesis of gastroschisis is controversial, but a recent theory suggests that it results from disruption of the right omphalomesenteric artery in early gestation [14]. The frequency of associated anomalies is much lower than with omphalocele, ranging from 8 to 21% [7, 10, 13].

The sonographic diagnosis of an abdominal-wall defect can be made when a mass containing viscera is seen to project from the anterior abdominal wall of the fetus. Sonographic differentiation of omphalocele from gastroschisis has been based on the site of cord insertion, the presence of a covering membrane, and the type of viscera protruding into the defect. In this study, the site of cord insertion was correctly identified in only 11 (46%) of 24 fetuses. A covering membrane was either detected or excluded correctly in 15 (63%) of 24 fetuses. Distinguishing omphalocele from gastroschisis by using all criteria was possible in 75% of cases.

Several authors [2, 5, 12] have reported that the presence of viscera other than bowel in an abdominal-wall defect is more likely with omphalocele than with gastroschisis. Redford et al. [2] stated that the liver is always in a normal location with gastroschisis. In our study, the liver protruded through the ventral defect in 14 fetuses, only one of whom had a gastroschisis. The presence of liver outside the fetal abdomen is strong evidence for an omphalocele. Ectopia cordis was present in five fetuses, four of whom had omphalocele. Ectopia cordis is frequently associated with omphalocele, and it results from abnormal formation of the cephalic body-fold as well as the lateral body-folds [5, 11, 12]. The presence of ectopia cordis suggests that an abdominal-wall defect is most likely an omphalocele.

Fetal ascites is a useful indicator of omphalocele. Ascites should be visualized only with omphalocele, because the membrane covering the ventral defect allows for the accumulation of ascitic fluid within the intact peritoneal cavity. With gastroschisis, the absence of a covering membrane allows any ascitic fluid generated within the peritoneal cavity to escape into the surrounding amniotic fluid. Theoretically, amniotic fluid could potentially accumulate in the abdomen of a fetus with gastroschisis, but this was not observed in any of the eight fetuses with gastroschisis. In this study, ascites was detected in nine fetuses with omphaloceles. In the usual case of omphalocele, ascites facilitated visualization of the covering membrane (Fig. 4). In one case, omphalocele could be diagnosed by the presence of ascitic fluid even though neither the

covering membrane nor the site of cord insertion could be demonstrated with certainty. The survival rate of fetuses with omphalocele complicated by ascites (two [25%] of eight nonterminated fetuses) was less than the survival rate of those with omphalocele and no ascites (two [50%] of four nonterminated fetuses).

With gastroschisis, bowel loops are often thickened and matted together. Bowel-wall thickening results from a chemical peritonitis caused by contact with fetal urine in the amniotic fluid [15]. Thickening of the bowel wall was noted in four fetuses during sonography, and all four had gastroschisis. In one of these, neither the site of cord insertion nor the presence or absence of a membrane could be determined with certainty; the diagnosis of gastroschisis was made on the basis of bowel-wall thickening. No fetus with an omphalocele had sonograms that showed thickened bowel walls. The presence of bowel-wall thickening did not adversely affect survival.

Stenotic or atretic bowel lesions were detected at surgery or autopsy in four neonates (three gastroschisis, one omphalocele). In retrospect, dilated loops of bowel were identifiable sonographically in two (50%) of these four. The bowel dilatation might have resulted from atretic or stenotic segments; however, four (80%) of five gastroschisis neonates who did not have atretic or stenotic bowel lesions also had sonographic evidence of dilated bowel. Bowel dilatation in fetuses with abdominal-wall defects is nonspecific, and the prenatal detection of bowel stenosis or atresia in these patients is problematic.

In this study, 18 (75%) of 24 fetuses had other anomalies in addition to their abdominal-wall defect. The severity of these associated malformations ranged from minor (e.g., cryptorchidism, inguinal hernia) to life threatening (e.g., long-segment intestinal atresia, absent hemidiaphragm, ectopia cordis). Associated deformities were either detected or correctly excluded in 13 (54%) of 24 fetuses. Several factors contributed to the difficulty in detecting associated malformations. First, five fetuses were examined before 1980 by means of less sophisticated equipment than that currently available. Second, some anomalies are difficult to evaluate sonographically (e.g., Meckel's diverticulum). In fact, of the 11 patients felt to have no additional anomalies on the basis of sonography, only three had defects that potentially could have been detected (unilateral renal agenesis, scoliosis, and hypoplastic lung). Third, associated congenital defects can be obscured or overlooked in the presence of a large extraabdominal mass. Once an abdominal-wall defect is identified, a detailed sonographic examination is required to detect associated malformations that could potentially affect outcome. Because a significant portion of these fetuses also have a cardiac abnormality (in our study, 9 [38%] of 24), a fetal echocardiogram should also be performed to detect cardiac anomalies whenever a sonogram shows a defect in the abdominal wall.

The overall survival of neonates in this series was 50% (nine of 18 nonterminated pregnancies). This rate is lower than the 70–96% survival rate reported [2–6]. Higher survival rates may reflect a greater proportion of patients with gastroschisis or preselection of patients who survive to undergo surgery. In this study, 33% of fetuses with omphalocele and 83% with gastroschisis survived. The better prognosis for gastroschisis appears to reflect the lower frequency of associated congenital anomalies. In addition, neonates who survived repair of omphalocele were those without severe coexisting malformations (Table 1). Although the absence of associated congenital anomalies did not guarantee a good outcome, most survivors in our study had either minor coexisting defects or no additional anomalies.

In conclusion, the survival rate of fetuses with an abdominal-wall defect is less than that reported for neonates with this condition. Sonography can be used to accurately diagnose abdominal-wall defects in utero and can distinguish between omphalocele and gastroschisis in most but not all cases. When an abdominal-wall defect is identified, a careful search, including a fetal echocardiogram, should be performed for associated anomalies.

REFERENCES

1. Baird PA, MacDonald EC. An epidemiologic study of congenital malformations of the anterior abdominal wall in more than half a million consecutive live births. *Am J Hum Genet* **1981**;33:470–478
2. Redford DHA, McNay MB, Whittle MJ. Gastroschisis and exomphalos: precise diagnosis by midpregnancy ultrasound. *Br J Obstet Gynaecol* **1985**;92:54–59
3. Grossman M, Fischermann EA, German J. Sonographic findings in gastroschisis. *J Clin Ultrasound* **1978**;6:175–176
4. Schaffer RM, Barone C, Friedman AP. The ultrasonographic spectrum of fetal omphalocele. *J Ultrasound Med* **1983**;2:219–222
5. Carpenter MW, Curci MR, Dibbins AW, Haddow JE. Perinatal management of ventral wall defects. *Obstet Gynecol* **1984**;64:646–651
6. Kirk EP, Wah RM. Obstetric management of the fetus with omphalocele or gastroschisis: a review and report of one hundred twelve cases. *Am J Obstet Gynecol* **1983**;146:512–518
7. Mabogunje OA, Mahour GH. Omphalocele and gastroschisis: trends in survival across two decades. *Am J Surg* **1984**;148:679–686
8. Schwartz MZ, Tyson KR, Milliorn K, Lobe TE. Staged reduction using a Silastic sac is the treatment of choice for large congenital abdominal wall defects. *J Pediatr Surg* **1983**;18:713–719
9. Schwaitzberg SD, Pokorny WJ, McGill CW, Harberg FJ. Gastroschisis and omphalocele. *Am J Surg* **1982**;144:650–654
10. Grossfeld JL, Dawes L, Weber TR. Congenital abdominal wall defects: current management and survival. *Surg Clin North Am* **1981**;61:1037–1049
11. Klein MD, Kosloske AM, Hertzler JH. Congenital defects of the abdominal wall: a review of the experience in New Mexico. *JAMA* **1981**;245:1643–1646
12. Klein MD, Hertzler JH. Congenital defects of the abdominal wall. *Surg Gynecol Obstet* **1981**;152:805–808
13. Colombani PM, Cunningham MD. Perinatal aspects of omphalocele and gastroschisis. *Am J Dis Child* **1977**;131:1386–1388
14. Hoyme HE, Jones MC, Jones KL. Gastroschisis: abdominal wall disruption secondary to early gestational interruption of the omphalomesenteric artery. *Semin Perinatol* **1983**;7:294–298
15. Kluck P, Tibboel D, van der Kamp AWM, Molenaar JC. The effect of fetal urine on the development of the bowel in gastroschisis. *J Pediatr Surg* **1983**;18:47–50

Technical Note

A Technique for Image Salvage in MR

Gunnar Lund[1] and Richard Morin

Two disadvantages of MR imaging are that data acquisition is a lengthy procedure, and image quality depends heavily on the patient's ability to remain immobile during the scan. Consequently, young children and uncooperative adults generally require some form of sedation.

If the child awakens during an imaging sequence, the ensuing motion will usually cause severe imaging artifacts. For safety reasons the patient will also have to be removed from the magnet. Often the acquisition sequence is aborted at this point, thus causing all information obtained before the patient's movement to be lost.

With most MR units, there are two methods of removing the patient. The technique that is most routinely used employs the table's electronic controls. Activating these controls during a measurement may completely abort the acquisition sequence. All information acquired up to that time is lost and no image is formed. The second option, available for emergency use, is a simple manual withdrawal of the patient table. Since the electronic controls are not activated, the system will continue the measurement, as if the patient were still within the magnet. After the measurement sequence is finished, images are reconstructed from patient data obtained before table withdrawal and from background electronic noise after withdrawal. We have found that images formed from such incomplete patient data sets can be useful in situations when patients have to be removed from the magnet because of motion. We report our procedure for implementing this "image salvage" technique, and illustrate its effect on image quality by describing a simple imaging experiment.

Materials and Methods

All patient images were obtained on a Siemens Magnetom (0.35 T). Images of the volunteer were obtained with the system operating at 1 T. Image acquisition was performed by using a two-dimensional Fourier transformation technique. When examining children under sedation, we monitor ECG and respiration. The patient is also observed via a TV camera. Awakening is usually preceded by an increase in heart rate. If movements are severe enough to require removal of the patient from the magnet, we manually withdraw the patient table without activating the table controls. This does not abort the measuring sequence. At the end of the measurement, images are reconstructed as usual by using standard system software.

Case Reports

We have used this technique in nine patients. Two of these patients are discussed below.

Patient 1

A 15-year-old girl was admitted for treatment of drug abuse. The patient was referred for MR to evaluate possible organic brain disease. Two multislice spin-echo sequences with a repetition time (TR) of 1.5 sec and echo-delay times (TE) of 35 and 70 msec were performed. With two acquisitions and a 256 × 256 acquisition matrix, each sequence lasts 12.9 min. Toward the end of the second sequence the patient removed herself from the head coil and crawled out of the magnet. The resulting images were of diagnostic quality, even though the patient was outside of the magnet for the last 2 min of the measurement (Fig. 1).

Received March 31, 1986; accepted after revision June 16, 1986.

[1] Both authors: Department of Radiology, University of Minnesota Hospitals, Box 292, 420 Delaware St. S.E., Minneapolis, MN 55455. Address reprint requests to G. Lund.

AJR 147:1052–1054, November 1986 0361–803X/86/1475–1052 © American Roentgen Ray Society

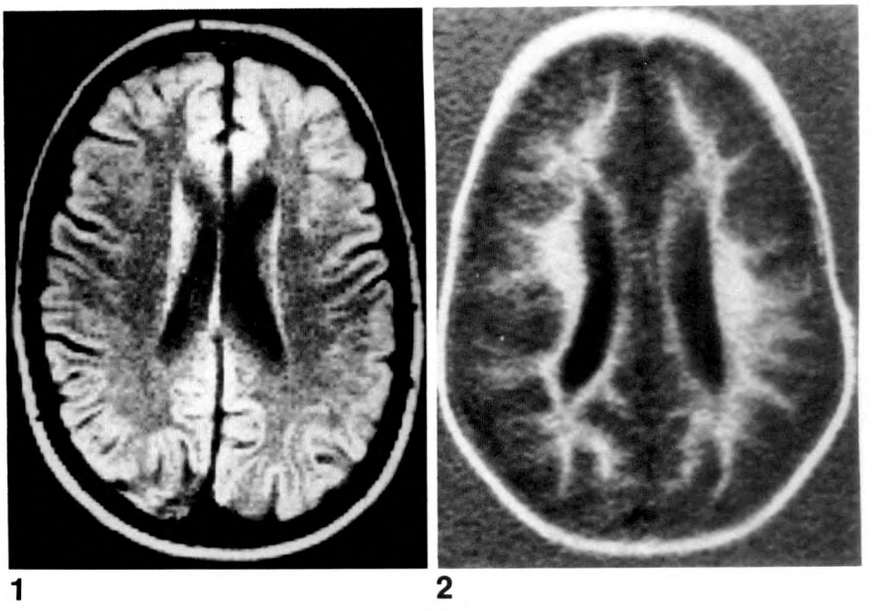


Fig. 1.—Axial spin-echo images reconstructed from incomplete patient data. SE 1.5/35. Patient was outside magnet for last 2 min of 12.9-min measurement.

Fig. 2.—Axial inversion recovery images reconstructed from incomplete patient data. Inversion recovery, 1.5/400/35 at two different slice positions. Patient was removed from magnet with 5 min of 12.9-min measurement remaining.

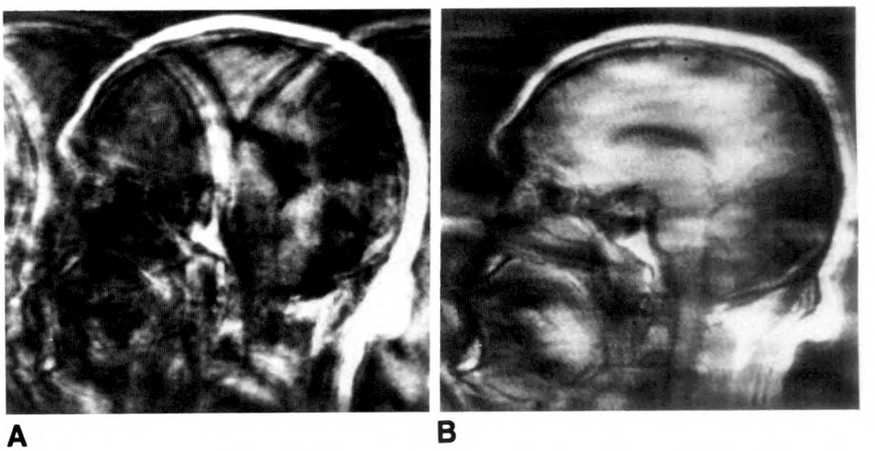


Fig. 3.—Sagittal spin-echo images of volunteer. Total measurement time 2 min, 47 sec; SE 0.5/17.

***A*, Movement (head nodding) during last 1 min of sequence.**

***B*, Same as *A*, but volunteer removed from magnet shortly after start of movement.**

Patient 2

A 15-month-old boy with developmental delay and suspected white-matter disease was referred for MR. The patient was sedated by using 80 mg/kg of chloral hydrate. Two spin-echo sequences with a TR of 1.5 sec and TE of 35 and 70 msec were performed. An inversion recovery sequence with TR 1.5 sec lasting 12.9 min was then started. The patient awoke with 5 min of the measurement left. Because of head and arm motion, the patient was removed from the magnet. The resulting images are shown in Figure 2. Despite some artifacts, the images allow evaluation of the extent of white matter development.

Imaging Experiment

To examine the influence of this technique on image quality and to see how the images were affected by withdrawal of the patient at different times during the measurement sequence, we carried out the following experiment. A normal adult volunteer was imaged using: (1) a sagittal multislice spin-echo sequence with TR 0.5 sec, TE 17 msec, 256 × 256 acquisition matrix, single acquisition (total time, 2 min 47 sec); (2) the identical sequence, but the volunteer was instructed to move (nodding motion) for the last 1 min of the measurement; (3) the identical sequence and motion, but the table was withdrawn shortly after the motion commenced; (4) the identical sequence with motion only during the last 30 sec; and (5) the same conditions as (4), but the table was withdrawn shortly after the motion started.

The image obtained with 1 min of motion (Fig. 3A) contains no useful information compared with a normal image. The image obtained after withdrawal of the table (Fig. 3B) is improved compared with Fig. 3A, but has phase distortions and decreased spatial resolution. The image obtained with

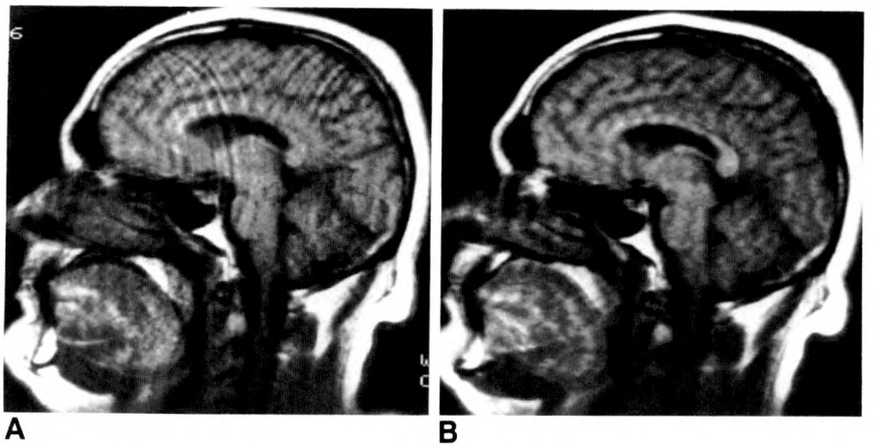


Fig. 4.—*A*, Movement during last 30 sec. *B*, Same as *A*, but with removal from magnet shortly after start of movement.

only 30 sec of movement (Fig. 4A) is less distorted than Fig. 3A, but is inferior to a regular image. The image obtained after withdrawal (Fig. 4B) is improved compared with Figs. 4A and 3B, but still shows residual phase distortions.

Discussion

Our experience with both patients and volunteers demonstrates that useful information is present even in images formed from limited patient data. In some situations these images may be valuable, compared with images obtained from a continuously moving patient.

Imaging techniques that use phase encoding and Fourier analysis for spatial localization and image formation are commonly employed in present-day MR scanners [1–3]. A complete set of raw data consisting of a number of different phase-encoding steps (equal to the matrix size) is required for the full Fourier-image reconstruction presently used. Interest in less than full Fourier imaging has been motivated mainly by the desire to shorten imaging time [4].

After the 90° radiofrequency pulse, the net magnetization evolves for a short time under the influence of a linear magnetic-field gradient along one axis. This phase-encoding gradient is subsequently turned off, and signal collection follows. The phase-encoding gradient results in the spins accumulating a phase angle dependent on their positions along the gradient. The strength of the gradient is varied for each subsequent measurement, and the number of measurements equals the required resolution along the direction of the phase-encoding gradient. In this way, a data set is collected with a sufficient number of lines to allow formation of an image.

Our system employs phase-encoding gradient steps such that the relative phase-encoding gradient varies (1) from -2π (N/2) to 2π (N/2 − 1), where N is the required gradient step. This means that the spin distribution will not be out of phase (zero phase angle) in the middle of the measuring sequence. The signal amplitude is largest when there is 0 phase angle, and the highest amplitude signal will therefore be collected at the middle of such a measurement. The beginning and end of a measurement sequence therefore contribute little to the overall signal but are required for high-spatial-frequency information resulting in edge sharpness. For the purposes of this discussion, ending the signal collection at any point beyond the middle of the sequence results in an image with overall good signal. However, as shown by our imaging experiment, there are increased noise, phase error, and loss of high-frequency information. These artifacts are less pronounced if more data are available for image reconstruction (Figs. 3 and 4). Provided the sequence proceeds beyond the point of 0 phase encoding there will be sufficient strength of signal. Some artifact results from the loss of higher frequency spatial resolution.

Alternative approaches, which may require software modifications, would allow either a choice of phase-encoding tables so that most of the signal could be collected at the start of the measurement rather than in the middle, or some form of less-than-full Fourier-image reconstruction in which the measurement could be stopped at any point with a "zero filling" of the missing data points and raw data filtering [4]. This would eliminate the electronic noise used to fill the missing data points in our technique and improve the signal-to-noise ratio in the image.

ACKNOWLEDGMENTS

We acknowledge the technical help of R. S. Wolla and J. Anton.

REFERENCES

1. Edelstein WA, Hutchinson JMS, Johnson G, Redpath T. Spin-warp NMR imaging and applications to human whole body imaging. *Phys Med Biol* **1980**;25:751–756
2. King KF, Moran PR. A unified description of NMR imaging, data-collection strategies, and reconstruction. *Med Phys* **1984**;11:1–14
3. Kumar A, Welti D, Ernst RR. NMR Fourier zeugmatography. *J Mag Resonance* **1975**;18:69–83
4. Margosian P. Faster MR imaging—imaging with half the data. Proc of the annual meeting of the Society of Magnetic Resonance in Medicine, London, August **1985**:1024–1025

The Scientific Literature in Diagnostic Radiology for American Readers: A Survey and Analysis of Journals, Papers, and Authors

Felix S. Chew[1]

The scientific literature in diagnostic radiology for American readers was surveyed by studying the recent growth of its journals, papers and authors. The number of journals has increased rapidly, following the growth in the production of papers. Of the 36 scientific diagnostic radiology journals available at a university medical center, 18 began publication in 1973 or later. The proliferation of new journals should moderate as the size of the American diagnostic radiology research community stabilizes and the newer journals publish a growing share of the papers. Citation analysis, a method of studying interrelationships between papers and journals, showed that citations from papers published in clinical journals to papers published in diagnostic radiology journals accounted for 6% of total citations made in those clinical journals. This observation indicates that research in diagnostic radiology has considerable relevance to research in clinical medicine. Although the number of papers from American diagnostic radiology researchers increased from 468 papers in two journals in 1960 to 2861 papers in 16 journals in 1984, the number of researchers increased more rapidly, resulting in a decline in aggregate productivity. At the same time, the average number of authors per paper increased from 2.15 in 1960 to 4.36 in 1985. The first authorship of a scientific paper appears to be the most suitable quantitative measure of research productivity. Study of a sample of 130 diagnostic radiology researchers showed that, on average, each researcher published 3.8 papers as first author in the 5 years from 1980 to 1984. The most prolific 15% of the authors published 52% of the papers.

As diagnostic radiology has grown and evolved, so has its scientific literature. Rapid advances made possible by technologic progress and a more sophisticated understanding of the human organism have generated an abundance of new information. This study examines the literature that conveys this infomation. The proliferation of new journals is studied first, and then the interrelationships between the literatures of diagnostic radiology and the clinical specialties are considered. The productivity and size of the American diagnostic radiology research community over 25 years are described. The trend towards multiple-author of papers is quantified and examined. A profile of contributors to diagnostic radiology journals and the distribution of their individual prolificacy is developed.

Materials and Methods

Journals

The number of diagnostic radiology journals readily available in the libraries of the State University of New York (SUNY) Health Science Center at Syracuse with format, content, and editorial policy appropriate for scientific papers was determined. The rate of proliferation of these journals was derived from their publication history. The criterion for ready availability was the ability to find actual issues of the journals. Selection factors for acquisition of particular journals were not examined; in general, the library system sought the largest collection of the most useful journals possible within its financial limitations.

The relationships between the scientific literature of diagnostic radiology and the biomedical

Received February 24, 1986; accepted after revision June 9, 1986.

[1] Department of Radiology, Health Science Center at Syracuse, State University of New York, 750 E. Adams St., Syracuse, NY 13210. Address reprint requests to F. S. Chew.

AJR 147:1055–1061, November 1986
0361–803X/86/1475–1055
© American Roentgen Ray Society

literature as a whole were studied by means of citation analysis [1]. Attention was focused on the use of nonradiologic research and knowledge in diagnostic radiology research and on the use of radiologic research and knowledge in nonradiologic research. A citation is the event that occurs when one paper (the cited paper) is used as a reference by another paper (the citing paper). A citation indicates that the cited paper, in at least one instance of the citing paper, has relevance to research subsequent to its publication, and implies a close link between the subjects of the two papers. If all of the citations made and received by all of the papers published in a particular journal are examined as a group, then the relationship of that journal to other journals can be described in terms of how frequently the other journals cite and are cited by the studied journal [1]. The *Journal Citation Reports* (*JCR*) of the *Science Citation Index* (*SCI*) [2] list data from which these relationships can be derived. Only those journals that were mentioned in the 1984 volumes of the *JCR* were included in the present study. Many journals, including most foreign ones, were excluded because data on their citations were unavailable. By using the method of Garfield [3], a core group of 10 diagnostic radiology journals was identified on the basis of the greatest number of citations received in 1984. The names of the 50 journals that cited these core journals most frequently and the names of the 50 journals that were cited by these core journals most frequently were obtained from data in the 1984 *JCR*.

Papers

Growth in the number of papers written by the American diagnostic radiology research community as a whole was studied in relation to the size of the research community during the 25 years from 1960 to 1984. The number of papers written by the American group was estimated by counting the number of papers published in journals that accepted predominantly original research contributions from Amerian academic departments of radiology. These journals were *American Journal of Roentgenology* (*AJR*), *Radiology*, *Journal of Nuclear Medicine*, *Investigative Radiology*, *Pediatric Radiology*, *Journal of Clinical Ultrasound* (*JCU*), *Journal of Computer Assisted Tomography*, *Clinical Nuclear Medicine*, *Gastrointestinal Radiology*, *Skeletal Radiology*, *Journal of Computed Tomography*, *Cardiovascular and Interventional Radiology*, *Urologic Radiology*, *Journal of Ultrasound in Medicine*, and *American Journal of Neuroradiology* (*AJNR*). Data were collected only about the number of papers, not about their length, quality, or subject material. Because none of these journals restricted itself to American contributions, this approach overestimated the number of papers from American researchers by counting papers from foreign radiologists as well as those from radiation oncologists and clinicians. The number of papers was underestimated by not counting papers published in other serials such as clinical journals or official journals of foreign radiologic societies. The number of full-time academic faculty in diagnostic radiology as reported by the American Medical Association in the annual medical education issues of *JAMA* was used as the number of American researchers in diagnostic radiology. The number of researchers in diagnostic radiology was overestimated by including academic radiation oncologists and underestimated by not counting researchers who were not full-time academic radiologists.

The growth of two diagnostic radiology journals, *AJR* and *Radiology*, was followed for the years 1950 to 1985. At 5-year intervals, the papers and authors in the July, August, and September issues were counted and multiplied by 4. The distribution of papers with more than one author was observed. No attempt was made to describe the time required for publication, the subject material, or the length or quality of the papers.

Authors

A sample of researchers in diagnostic radiology during a 5-year period was studied to observe the literary prolificacy of researchers individually. An arbitrary sample was obtained from the July 1982 issue of *AJR*, a large and eminent journal devoted exclusively to diagnostic radiology. Obtaining the sample in this way virtually excluded researchers in radiation oncology, physics, instrumentation, and related disciplines. The 130 authors of papers listed in the table of contents made up the sample; the authorship or coauthorship of a research paper in diagnostic radiology was considered strong presumptive evidence of significant research activity in that field. There were 34 first authors and 96 coauthors. Affiliation with a department of radiology or nuclear medicine was indicated by 106 of the researchers. Of the remaining 24 researchers, 13 were in surgery or related specialties, five were in medicine or related specialties, five were in pathology, and one was in basic science. By the end of the 5-year period being studied, 89 researchers were certified by the American Board of Radiology: three were certified in 1959 or earlier, 17 in 1960–1969, 18 in 1970–1974, 31 in 1975–1979, and 20 in 1980–1984 [4]. Those who were certified in 1980–1984 were presumed to be in training for a portion of the years studied. No attempt was made to establish whether each researcher was actively engaged in research for all of the 5 years studied.

For each researcher in the study sample, the number of papers published as first author in a journal of diagnostic radiology listed in the *Cumulated Index Medicus* [5] was counted for each year from 1980 to 1984. Papers coauthored by the researcher or published in other journals were not counted. A 5-year prolificacy profile was constructed by calculating the total number of publications for each researcher for the 5 years studied. The prolificacy of researchers in relation to the year of board certification was also studied.

Results

Journals

There were 36 scientific diagnostic radiology journals readily available in the libraries of SUNY Health Science Center at Syracuse in 1985. As shown in Table 1, nine journals began publication in the 62 years from 1896 through 1957. The number of journals in publication doubled to 18 only 14 years later in 1971 and doubled again to 36 only 13 years after that. Nearly all of these journals were published in North America and Europe, and in the English language.

Citation Analysis

Ten core journals of diagnostic radiology were identified as those that received the most citations in 1984 (Table 2). Six journals were general in scope; four were subspecialized: two in neuroradiology, one in nuclear medicine, and one in CT. As a group, they published 2641 papers in 1984 and made 42,029 citations, for an average of about 16 references per published paper. They were cited 48,385 times in 1984, which was 85% of the times the 35 diagnostic radiology journals covered in the 1984 *SCI* were cited. Other diagnostic radiology journals evidently received too few citations to reach the threshold for *SCI* coverage. Included among the 10 core journals were those with the longest publication histories, the greatest number of papers published per year, and the largest circulations.

TABLE 1: **Scientific Journals of Diagnostic Radiology Available at a University Medical Center**

Year of First Publication	Journal Title (Place of Publication)
1896	*British Journal of Radiology* (London)
1897	*RöFO: Fortschritte auf dem Gebiete der Röntgenstrahlen und der Nuklearmedizin* (Stuttgart)
1906	*AJR. American Journal of Roentgenology* (Baltimore)
1915	*Radiology* (Easton, PA)
1921	*Acta Radiologica: Diagnosis* (Stockholm)
1933	*Diagnostic Imaging in Clinical Medicine* (Basel)
1949	*Clinical Radiology* (Edinburgh)
1957	*Australasian Radiology* (Sydney)
1957	*Journal of Nuclear Medicine and Allied Sciences* (Torino)
1958	*Annales de Radiologie* (Paris)
1959	*Nuklearmedizin. Nuclear Medicine* (Stuttgart)
1960	*Journal of Nuclear Medicine* (New York)
1963	*Radiologic Clinics of North America* (Philadelphia)
1966	*Investigative Radiology* (Philadelphia)
1966	*Seminars in Roentgenology* (New York)
1970	*CRC Critical Reviews in Diagnostic Imaging* (Boca Raton, FL)
1970	*Neuroradiology* (Berlin)
1971	*Seminars in Nuclear Medicine* (New York)
1973	*JCU. Journal of Clinical Ultrasound* (Denver)
1973	*Journal of the Canadian Association of Radiologists* (Montreal)
1973	*Pediatric Radiology* (Berlin)
1976	*Clinical Nuclear Medicine* (Philadelphia)
1976	*European Journal of Nuclear Medicine* (Heidelberg)
1976	*Gastrointestinal Radiology* (Berlin)
1976	*Skeletal Radiology* (Berlin)
1977	*Computerized Radiology* (Elmsford, NY)
1977	*Journal of Computed Tomography* (New York)
1977	*Journal of Computer Assisted Tomography* (New York)
1978	*Cardiovascular and Interventional Radiology* (Berlin)
1979	*Urologic Radiology* (New York)
1980	*AJNR. American Journal of Neuroradiology* (Baltimore)
1980	*Seminars in Ultrasound, CT and MR* (New York)
1981	*Radiographics* (Easton, PA)
1982	*Journal of Ultrasound in Medicine* (Philadelphia)
1982	*Magnetic Resonance Imaging* (New York)
1984	*Seminars in Interventional Radiology* (New York)

TABLE 2: **1984 Core Journals of Diagnostic Radiology**

Journal	Papers Published in 1984	Citations in 1984	
		Received	Made
Radiology	647	17,792	9769
AJR	499	11,656	7527
J Nucl Med	193	5756	4346
Br J Radiol	205	3692	2934
J Comput Assist Tomogr	267	2875	3133
Invest Radiol	158	1588	3127
Clin Radiol	102	1370	1427
Neuroradiology	94	1345	1410
AJNR	163	1148	2858
RöFO	313	1163	5498

The 50 journals that cited the core diagnostic radiology journals most frequently in 1984 included the core journals and 18 other diagnostic radiology journals (Table 3). There were seven journals devoted to other aspects of radiology and 15 medical, surgical, or multidisciplinary clinical journals. These 50 journals cited the core journals 22,327 times, or 46% of all of the citations to the core journals in 1984. Citations to the core journals represented an average of 32% of total citations made in the 28 diagnostic radiology journals. Citations to the core were an average of 9% of total citations made in the journals devoted to other aspects of radiology. Citations to the core were an average of 6% of total citations made in the clinical journals.

The 50 journals cited most frequently in the bibliographies of papers published in the core diagnostic radiology journals in 1984 included the 10 core journals and seven other diagnostic radiology journals (Table 4). There were three journals devoted to other aspects of radiology, 15 medical and multidisciplinary clinical journals, 14 surgery journals, and one general science journal. These 50 journals were cited 24,099 times in the core journals, which made up 51% of all of the citations made by the core journals in 1984. For the 17 diagnostic radiology journals, citations in the core journals represented an average of 29% of their total citations received. For the three other radiology journals, citations in the core journals were an average of 8% of all citations received.

TABLE 3: **The 50 Journals That Cited the Core Diagnostic Radiology Journals Most Frequently in 1984**

1. *Radiology*	13. *Ann Radiol (Paris)*	25. *Med Phys*	38. *Int J Appl Radiat Isot*
2. *AJR*	14. *Clin Nucl Med*	26. *J Ultrasound Med*	39. *Strahlentherapie*
3. *RöFO*	15. *Neuroradiology*	27. *Surg Clin North Am*	40. *South Med J*
4. *Invest Radiol*	16. *Clin Radiol*	28. *J Urol*	41. *J Can Assoc Radiol*
5. *J Comput Assist Tomogr*	17. *Cancer*	29. *Acta Radiol [Diagn]* (Stockh)	42. *Phys Med Biol*
6. *J Nucl Med*	18. *J Comput Tomogr*	30. *Clin Gastroenterol*	43. *Am J Gastroenterol*
7. *AJNR*	19. *J Neurosurg*	31. *Skeletal Radiol*	44. *Mt Sinai J Med (NY)*
8. *Radiol Clin North Am*	20. *Radiologe*	32. *Clin Chest Med*	45. *Radiat Res*
9. *Br J Radiol*	21. *Eur J Nucl Med*	33. *Gastrointest Radiol*	46. *Proc Soc Photo Opt Instr*
10. *Int J Radiat Oncol Biol Phys*	22. *JCU*	34. *Nerosurgery*	47. *Diagn Imaging Clin Med*
11. *Semin Nucl Med*	23. *Med Clin North Am*	35. *Am J Cardiol*	48. *Comput Radiol*
12. *CRC Crit Rev Diagn Imging*	24. *Semin Roentgenol*	36. *Pediatr Radiol*	49. *Chest*
		37. *Surg Neurol*	50. *Clin Orthop*

Note.—Given in order of decreasing frequency of citation.

TABLE 4: **The 50 Journals That the Core Diagnostic Radiology Journals Cited Most Frequently in 1984**

1. *Radiology*	13. *Circulation*	25. *Surgery*	38. *Arch Neurol*
2. *AJR*	14. *J Urol*	26. *Acta Radiol [Diagn]* (Stockh)	39. *Pediatrics*
3. *J Nucl Med*	15. *JAMA*	27. *Am J Cardiol*	40. *Am J Med*
4. *J Comput Assist Tomogr*	16. *Lancet*	28. *Br Med J [Clin Res]*	41. *Urology*
5. *Br J Radiol*	17. *Arch Surg*	29. *Ann Intern Med*	42. *Am Rev Respir Dis*
6. *Cancer*	18. *Clin Radiol*	30. *Gastrointest Radiol*	43. *Clin Orthop*
7. *Invest Radiol*	19. *Am J Surg*	31. *J Pediatr*	44. *J Thorac Cardiovasc Surg*
8. *AJNR*	20. *Ann Surg*	32. *Br J Surg*	45. *Phys Med Biol*
9. *N Engl J Med*	21. *Radiol Clin North Am*	33. *Int J Radiat Oncol Biol Phys*	46. *Clin Nucl Med*
10. *RöFO*	22. *Gastroenterology*	34. *Neurology*	47. *Stroke*
11. *Neuroradiology*	23. *J Bone Joint Surg [Am]*	35. *Science*	48. *Surg Neurol*
12. *J Neurosurg*	24. *Surg Gynecol Obstet*	36. *JCU*	49. *Med Phys*
		37. *Semin Nucl Med*	50. *Semin Roentgenol*

Note.—Given in order of decreasing frequency of citation.

For the medical and multidisciplinary clinical journals, citations in the core journals were 1% of all citations received. For the surgery journals, citations in the core journals were 4% of all citations received.

For each individual core diagnostic radiology journal, the single journal that cited it most frequently was itself. The proportion of self-citedness ranged from 6 to 19% of all citations received. The journal most frequently cited by eight of the core journals was *Radiology*; such citations represented 11 to 18% of all citations made. The *British Journal of Radiology* and the *Journal of Nuclear Medicine* cited themselves most frequently and *Radiology* next most frequently.

Radiology and *AJR* received 64% and 63%, respectively, of their total citations from diagnostic radiology journals, and made 43% and 45%, respectively, of their total citations to diagnostic radiology journals. Of the total citations received by the *Journal of Nuclear Medicine*, 31% were in clinical nuclear radiology journals and 9% in other diagnostic radiology journals. Of the total citations made by the *Journal of Nuclear Medicine*, 23% were made to clinical nuclear radiology journals and 9% were made to other diagnostic radiology journals. Of the total citations received by *Neuroradiology* and *AJNR*, 43% and 67%, respectively, were from diagnostic radiology journals, and 35% and 13%, respectively, were from clinical neurology, neurosurgery, and psychiatry journals. Of the total citations made by *Neuroradiology* and *AJNR*, 46% and 40%, respectively, were made to diagnostic radiology journals, and 20% and 21%, respectively, were made to clinical neurology, neurosurgery, and psychiatry journals.

Papers

The numbers of papers from the American diagnostic radiology research community increased from 468 papers in two journals in 1960 to 2861 papers in 16 journals in 1984. At the same time, the number of researchers increased from 510 in 1960 [6] to 3457 in 1984 [7]. The increase in papers lagged behind the increase in researchers (Fig. 1), resulting in a decline in the average number of papers per researcher per year (Table 5). Since 1975, the producitivity has been returning towards the 1965 level.

The number of papers published yearly in *AJR* and *Radiology* combined increased from 368 in 1950 to 1148 in 1985 at a linear rate. The number of authors of papers increased from 664 in 1950 to 5000 in 1985 at an exponential rate. The ratio of authors to papers, or the mean number of authors per paper, increased from 1.80 in 1950 to 4.36 in 1985 (Table 6). A clear trend towards papers with more than one author was evident in the declining percentage of papers with one or two authors and the rising percentage of papers with five or more authors (Table 7). In 1950, 75% of the papers had one or two authors, and 2% had five or more. In 1985, 19% had one or two authors, and 42% had five or more.

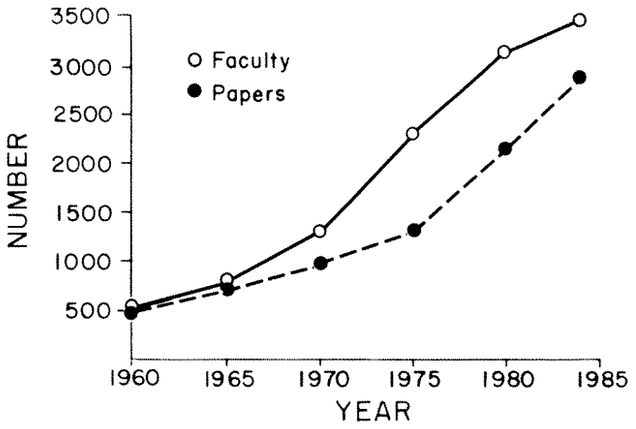


Fig. 1.—Increases in numbers of full-time American diagnostic radiology faculty and papers they publish.

TABLE 5: **Estimated Yearly Research Productivity of Full-Time American Academic Diagnostic Radiologists**

Year	Academic Radiologists	Papers	Papers per Radiologist
1960	510	468	0.92
1965	764	710	0.93
1970	1288	955	0.74
1975	2275	1294	0.57
1980	3113	2118	0.68
1984	3457	2861	0.83

TABLE 6: **Growth of *AJR* and *Radiology***

Year	Papers	Authors	Authors/Papers
1950	368	654	1.80
1955	392	788	2.01
1960	468	1008	2.15
1965	632	1440	2.28
1970	780	1944	2.49
1975	840	2620	3.12
1980	1068	3768	3.53
1985	1148	5000	4.36

Note.—Combined data.

Authors

Over the 5-year period studied, the 130 researchers in diagnostic radiology in the study sample published 492 papers in diagnostic radiology journals, an average total of 3.8 papers per researcher over 5 years. The distribution of prolificacy was such that the top 5% published 21% of the papers, the top 15% published 52%, and the top 50% published 94% (Table 8).

The three radiologists who were board certified before 1960 published six papers (1% of the total number of papers), the 17 certified in 1960–1969 published 53 (11%), the 18 certified in 1970–1974 published 110 (22%), the 31 certified in 1975–1979 published 187 (38%), and the 20 certified in 1980–1984 published 90 (18%). The 24 researchers without radiology or nuclear medicine affiliations published five papers (1%). The remaining 41 papers (8%) were written by the 17 researchers affiliated with departments of radiology or nuclear medicine who were not listed in the directory [4]. Of the 90 papers published by radiologists certified in 1980–1984, 23 were published in the years of or preceding board certification and were presumably written while the authors were in training. Thus, 5% of all papers were written by radiologists-in-training, and 86% were written by board-certified radiologists.

Examination of the number of papers published in relation to the number of years the first author was past board certification showed that those radiologists 1 to 5 years past board certification during the study period published 158 papers, those 6 to 10 years past board certification published 190, those 11 to 15 years past board certification published 49, and those 16 or more years past board certification published 24.

The number of papers published annually varied considerably from year to year for most individuals. Only 11% of the authors published at least one paper in each of the 5 years of the period studied; only 3% published at least two papers in each year. For most researchers in most years, no papers were published. The most prolific researcher published eight papers as first author in 1 year.

Discussion

Journals

The scientific literature of diagnostic radiology represents the accumulated knowledge and experience of 90 years of diagnostic medical imaging. It is a living and growing resource, a contemporaneous record that can be followed nearly a century into the past. The principal function of the scientific literature is to present new information, usually in the form of original scientific papers. Science grows exponentially. New data and ideas provide further opportunities for investigation, and successfully completed investigations result in papers. Publication of papers is an inherent feature of the scientific process, and consequently there is a continually growing need for suitable journals [8, 9]. Existing journals can increase their size, publish more frequently, divide into parts, and issue supplements. New journals are started when existing journals no longer fill the needs of growing numbers of contributors and more selective readers. In general, the newer journals are aimed at a specific audience and are narrower in scope, smaller, and issued less frequently than their established counterparts. The proliferation and growth of diagnostic radiology journals has followed the increase in the number of researchers in the specialty. The proliferation of new journals should moderate: the growth in the size of the diagnostic radiology research community has slowed, and existing journals can accommodate more papers than they now publish.

The sample of journals found during this survey represents only a fraction of the total world literature in diagnostic radiology. Libraries have limited space and money; conse-

TABLE 7: **Distribution of Authorship in *AJR* and *Radiology***

Year	Authors per Paper						
	1	2	3	4	5	6–7	8+
1950	52	23	20	3	2	0	0
1955	42	30	15	12	1	0	0
1960	41	26	17	11	3	2	0
1965	31	34	20	9	3	3	0
1970	22	34	27	11	5	2	0
1975	12	27	27	16	10	8	0
1980	15	16	24	20	13	10	3
1985	5	14	20	19	17	17	8

Note.—Combined data. Distribution given as percentages. Rows do not all add up to precisely 100% because of rounding.

TABLE 8: **Prolificacy of 130 Diagnostic Radiology Researchers Over 5 Years (1980–1984)**

Number of Researchers	Total Number of Papers Published As First Author	Percentile Rank
39	0	15
21	1	38
12	2	51
5	3	57
11	4	63
7	5	70
10	6	77
4	7	82
3	8	85
3	9	87
1	10	89
3	11	90
3	13	93
2	14	95
1	15	96
1	16	97
2	17	98
1	18	99
1	21	99.6

Note.—Percentages discussed in the text are not derivable directly from this table's data, because of differences due to rounding.

quently, they select for their patrons the largest and most carefully edited journals. Many foreign journals, particularly those not published in English and those with irregular publication schedules, would have relatively little interest for most American readers. The number of journals worldwide devoted to radiology is approximately 200 (Figley MM, personal communication).

Citation Analysis

Clinical diagnostic radiology is relevant to nearly every aspect of clinical medicine. Not unexpectedly, citation analysis demonstrates that diagnostic radiology research is relevant to clinical research. The scientific literature of diagnostic radiology is used in the research papers of other clinical specialties, and the literature of other clinical specialties is used in the research papers of diagnostic radiology. As a group, diagnostic radiology journals are cited by clinical journals proportionally more often than clinical journals are cited by diagnostic radiology journals.

The observed concentration of the citations to and from the diagnostic radiology literature among a relatively small number of journals is in keeping with bibliometric principles [10].

Papers

A research paper is not so much a parcel of truth and knowledge as it is a record of scientific work [11]. One way to measure scientific work is to count papers. The present study shows that although the number of papers written by the American diagnostic radiology research community increased steadily between 1960 and 1975, it lagged behind the growth in the size of the research community (Fig. 1). This has resulted in apparent decreases in unit productivity. Since 1975, the productivity has begun to return to the 1960 and 1965 levels. This lag may be due in part to the time required for new researchers to begin and complete research projects and shepherd them into publication. The most productive researchers are those who are 5 to 10 years beyond the completion of their training (as punctuated by board certification). This suggests that the aggregate productivity of the diagnostic radiology research community will approach the 1965 level, climb above it as a result of the demographic effect of a large cohort of researchers moving into their most productive years, and then decline as they pass their peak. Another relevant factor is that the modern scientific paper in diagnostic radiology has become much more carefully constructed, reviewed, and edited than in earlier years [12], so that the unit of measurement has been changing. This may be counterbalanced by the greater sophistication of modern researchers and more powerful research tools now available.

In diagnostic radiology, there are many more avenues for significant research than there are researchers. For example, the literature on CT is far from exhaustive in terms of the usual radiologic concerns: radiologic-anatomic-pathologic correlations; pitfalls in interpretation; technique and procedure; clinical indications; and usefulness and efficacy relative to alternative techniques. Nevertheless, many of the most prolific researchers have quit that research field to explore the same concerns in MR imaging. The amount of research that is accomplished is a function of the number of researchers, not a characteristic of diagnostic radiology.

Authors

A small proportion of highly prolific authors write most of the papers in diagnostic radiology. There are many more marginal and occasional researchers. This distribution of prolificacy is in agreement with the observation that, in general, the proportion of researchers in science with a particular number of publications over a unit of time decreases as the inverse square or cube of the number of publications [8–11]. This is related to the notion of cumulative advantage, in which the likelihood of publishing a paper is increased in relation to the number of previously published papers. Therefore, the most difficult step for a neophyte researcher is bringing the first paper to publication. The distribution of annual prolificacy and the small proportion of researchers publishing at least one paper each year as first author suggest that 1 year is too short an interval for assessing research performance in diagnostic radiology. Furthermore, the time required for publication, once a research project has been successfully completed and a manuscript submitted, typically ranges from 4 to 6 months [12]. If a manuscript is submitted to more than one journal before acceptance, the interval from first submission to publication is much longer. The decline in prolificacy of researchers who are more than 10 years beyond the completion of training may be related to changes in career orientation.

Multiple-Author Papers

The increasing complexity of diagnostic radiology may be, in part, responsible for the trend towards collaborative research and multiple-author papers. The complex case material most likely to form the basis for research is also most likely to involve many subspecialists whose cooperative research efforts will yield papers with many authors. Such a pattern can occur in teaching hospitals where there are many subspecialists and full-time academic faculty for whom there are considerable job-related incentives to publish and to publish frequently. An illusion of exceptional productivity may result if a researcher is a coauthor of several papers. The difficulties in trying to evaluate the productivity of a researcher whose portfolio bulges with dozens of papers of which the researcher is one of many authors is familiar enough to be the subject of humor [13]; the problem is real and likely to worsen. In 1985, coauthors outnumbered first authors by a factor greater than 3 (Table 6). This does not necessarily imply that a researcher who has made a substantive contribution to a project and the paper that reports it should not receive the credit of coauthorship or that such coauthorship is without value. However, a researcher's coauthorships represent a contribution to the literature as a whole primarily in the sense that the researcher's participation enhanced the prolificacy of the first author. The notion that more authors per paper produce better papers is untested. In evaluating the productivity of a researcher, there is a case for considering only the hard currency of first authorship. The number of first authors is limited by the number of papers, but the number of coauthors is limited only by the tolerance of the editor and the integrity of the authors themselves. This has permitted an exponential increase in authors with only a linear increase in papers.

ACKNOWLEDGMENTS

The editorial assistance of Annemarie Relyea-Chew is gratefully acknowledged. Data from the *Journal Citation Reports* of the *Science Citation Index* were used with permission of the publisher, the Institute for Scientific Information.

REFERENCES

1. Garfield E. *Citation indexing: its theory and application in science, technology, and humanities*. New York: Wiley, **1979**
2. Garfield E, ed. *SCI journal citation reports, science citation index 1984 annual*, vols. 15, 16. Philadelphia: ISI Press, **1985**
3. Garfield E. Journal citation studies. 45. Surgery journals: another operation in citation analysis. *Current Contents* **1985**;(21):3–18
4. American Board of Medical Specialties. *ABMS directory of certified radiologists*. Evanston, IL: ABMS, **1985**
5. National Library of Medicine. *Cumulated index medicus*. Bethesda, MD: U.S. Dept. of Health and Human Services, **1980–1984**
6. Wiggins WS, Laymaster GR, Taylor AN, Tipner A. Medical education in the United States and Canada. *JAMA* **1960**;174:1424–1476
7. American College of Radiology. *Manpower IV: a report of the ACR Committee on Manpower*. Chevy Chase, MD: Am. Coll. Radiol., **1985**
8. Price DJD. *Little science, big science*. New York: Columbia Univ. Press, **1963**
9. Price DJD. *Science since Babylon*. New Haven, CT: Yale Univ. Press, **1961**
10. Garfield E. Bradford's law and related statistical patterns. *Current Contents* **1980**;(19):5–12
11. Price DJD. The development and structure of the biomedical literature. In: Warren KS, ed. *Coping with the biomedical literature: a primer for the scientist and clinician*. New York: Praeger Scientific, **1981**:3–16
12. Figley MM. Publication in radiology: challenges to tradition. *Radiology* **1985**;157:633–636
13. Scheible W, Resnick D, Brahme F, Forrest J, Andre M. "Author inflation" or "CV creep." *AJR* **1985**;144:863

Memorial

Howard Alan Wexler, 1940–1986



Howard Alan Wexler died on January 31, 1986, having lost a valiant struggle against carcinoma of the colon.

Dr. Wexler was born September 9, 1940, in Mt. Kisco, N.Y. He was raised in Brooklyn and received his undergraduate education at Antioch College in Yellow Springs, OH, and at the University of Besancon in France. He graduated AOA from the University of Rochester School of Medicine in 1967. After an internal medicine internship in Boston City Hospital, he commenced residency training in radiology at the University of Miami/Jackson Memorial Medical Center, where he served in the capacity of Chief Resident during his final year of training, which was followed by fellowship training in pediatric radiology at the same institution.

On completion of his training, he joined the faculty of the University of Miami School of Medicine, where he served for 3 years as Assistant Professor of Radiology and Pediatrics.

Dr. Wexler was a brilliant, dynamic, enthusiastic, and energetic young academic radiologist who, in 3 short years, amassed a curriculum vitae that included 10 publications in peer-reviewed journals, a textbook on pediatric radiology, and 24 papers at local and national meetings; he also chaired two postgraduate seminars in pediatric radiology.

He left the University of Miami in 1977 to join Radiology Associates, P.A., in Fort Lauderdale, FL, where he brought to the private practice of radiology the same brilliance, dynamism, enthusiasm, and energy that had characterized his academic career.

Dr. Wexler was also a deeply religious man, totally dedicated to his family around whom his universe was centered. He shared with his family a devotion to animals, and his home was haven to many horses, dogs, and cats.

Dr. Wexler will be deeply missed by all his friends and colleagues, and our heartfelt sympathies go out to his beloved wife Pam, his devoted sons Nguyen and Seth, and his lovely daughter Muffy.

Catherine A. Poole
Gaston Mendez, Jr.
University of Miami School of Medicine
Miami, FL 33101

The Fibromatoses:
CT-Pathologic Correlation

Isaac R. Francis[1]
K. Dorovini-Zis[2]
Gary M. Glazer[1]
R. V. Lloyd[2]
Marco A. Amendola[1]
William Martel[1]

Although CT has been used in the evaluation of benign fibroblastic tumors (fibromatoses), data are lacking on radiologic-histopathologic correlation. In an attempt to explain the variable CT appearance of these lesions, a retrospective analysis was carried out of CT findings and histopathologic features in nine patients with fibromatoses. In three of four patients who had precontrast CT scans, the tumors were hyperdense relative to muscle, whereas in one patient the lesion was hypodense. The postenhancement appearance was variable. The pathologic specimens were analyzed and graded for (1) collagen content, (2) cellular content, (3) tumor necrosis, and (4) tumor vascularity. No consistent relationship could be established between the CT appearance of these lesions and their histologic appearance.

The fibromatoses constitute a group of benign fibroblastic soft-tissue tumors with a tendency for local invasion and recurrence. CT evaluation of these lesions provides fairly reliable information regarding anatomic relationships and tumor extent [1–7]. The CT findings have been recently reported [8, 9]; however, there is a lack of data correlating the varying CT features of these lesions with their histopathologic characteristics. The CT findings in nine patients (eight with extraabdominal and one with intraabdominal [mesenteric] lesions) were retrospectively analyzed and correlated with histopathologic data. These results form the basis of this report.

Materials and Methods

The CT findings in nine patients with fibromatoses in whom CT was performed between July 1980 and December 1985 were analyzed retrospectively. Eight of the nine patients were women and had extraabdominal lesions; the other was a man with Gardner's syndrome who had a large intraabdominal mesenteric lesion. In four of the patients, scans were obtained at the initial presentation of the lesions; in the other five patients, the scans were obtained to evaluate recurrent masses. The patients were 18–43 years old.

Seven patients were scanned on a GE 8800 or 9800 CT/T scanner. The other two were scanned on an EMI 5005 and a Technicare scanner, respectively. Contiguous 10- or 15-mm-thick sections were used in all cases. Noncontrast scans were obtained in two patients. In two other patients, both noncontrast and contrast-enhanced studies were performed, but in the other five patients, scans were acquired only after contrast enhancement. The contrast-enhanced scans were obtained after a bolus of 50–75 ml of meglumine iothalamate 60% (Conray 60) followed by rapid infusion of meglumine iothalamate 30% (Conray 30). From the CT images, the lesions were classified as hypodense, isodense, or hyperdense, with normal muscle as the standard for comparison. After surgical resection, the lesions were histopathologically analyzed and graded on the basis of their histology for (1) cellular content, (2) collagen content, (3) tumor necrosis, and (4) tumor vascularity by two of the authors independently, neither had prior knowledge of the radiologic findings. To avoid bias in analytic sampling and to obtain as true a representation of the entire lesion as possible, at least three areas of the specimen were histologically analyzed, and histologic features were graded on a 0–3 quantitative scale (0 = feature absent, 1 = feature present to small degree, 2 = feature present in moderate degree, 3 = feature prominent in specimen).

Received March 10, 1986; accepted after revision June 9, 1986.

[1] Department of Radiology, Box 30, University of Michigan Medical Center, Ann Arbor, MI 48109-030. Address reprint requests to I. R. Francis.

[2] Department of Pathology, University of Michigan Medical Center, Ann Arbor, MI 48109-030.

AJR **147:1063–1066, November 1986**
0361–803X/86/1475–1063
© American Roentgen Ray Society

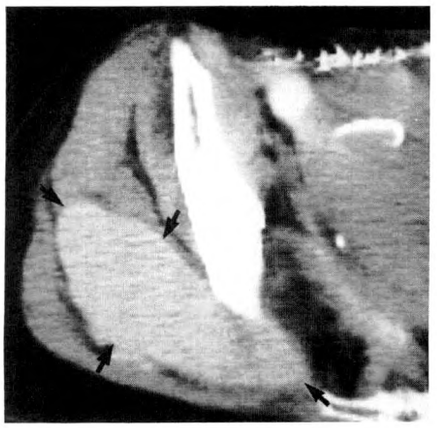
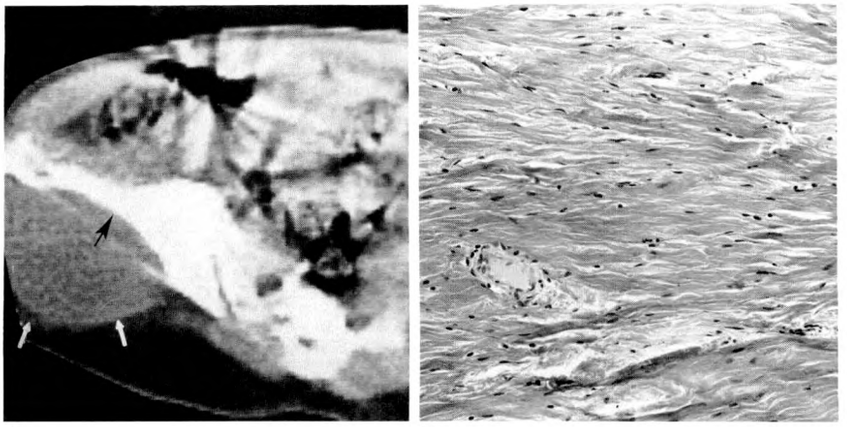
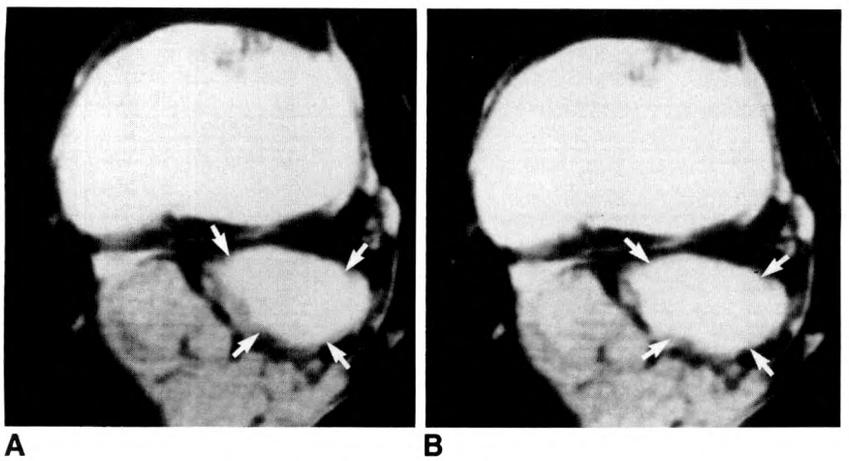


Fig. 1.—Unenhanced CT scan through pelvis. Oval hyperdense mass between gluteal muscles on right (*arrows*).



A B

Fig. 2.—*A*, Unenhanced CT scan through pelvis. Low-density mass involves right gluteal region (*white arrows*). Pressure erosion involves right ilium (*black arrow*).
B, Abundant dense collagen between slender fibroblasts characterizes this hypocellular lesion. (H and E ×188)



A B

Fig. 3.—*A*, Unenhanced CT scan through left distal femur. Hyperdense mass (*arrows*). *B*, After contrast infusion. Only minimal enhancement (*arrows*).

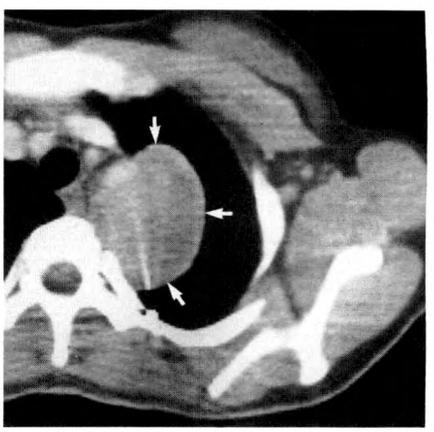


Fig. 4.—Large mass (*arrows*) that grew from cervical region into apex of left lung has mixed attenuation characteristics.

Results

Of the nine patients with fibromatoses, the eight women all had extraabdominal tumors and the one man had Gardner's syndrome with a large intraabdominal lesion. Ages of the patients were 18–43 years and the sizes of the lesions were 5–20 cm.

CT Findings

In three of four patients who had noncontrast scans, the lesions were hyperdense relative to skeletal muscle (Fig. 1), but in the last patient the lesion was hypodense (Fig. 2A). In the two patients imaged with both noncontrast and contrast-enhanced scans, the lesions showed only minimal contrast enhancement (Fig. 3). In four patients imaged only after contrast enhancement, two had lesions with mixed attenuation characteristics, containing both hyperdense and hypodense areas (Fig. 4), and the other three had uniformly hyperdense lesions (Fig. 5A).

Histopathologic Analysis

Microscopic examination showed all tumors to be composed of slender, elongated cells with wavy nuclei surrounded

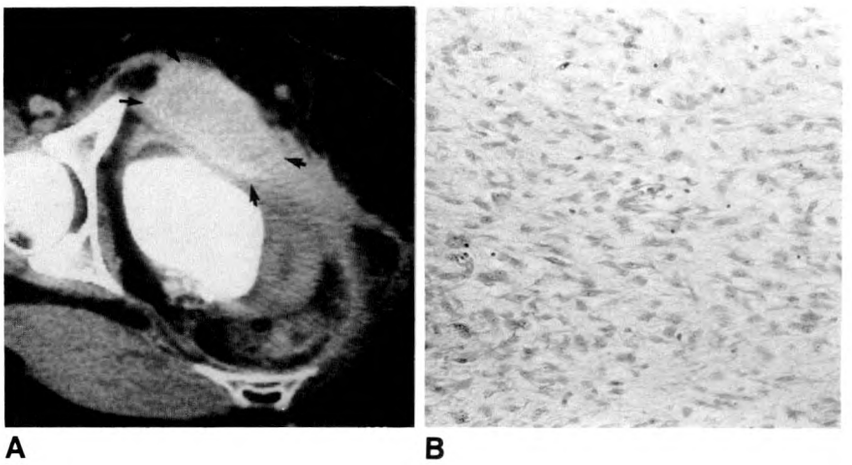


Fig. 5.—*A*, Postenhancement CT scan through pelvis of patient with prior hemipelvectomy for recurrent aggressive fibromatosis. Diffusely hyperdense lesion anterior to bladder (*arrows*).

***B*, Elongated fibroblasts with ovoid nuclei form interlacing bundles with small amounts of collagen separating individual cells in this moderately cellular lesion. (H and E ×188)**

by dense, collagenized matrix. The cellularity and the amount of collagen varied from lesion to lesion and within the same tumor. The tumors were either cellular with little collagen around the proliferating fibroblasts (Fig. 5B), moderately cellular, or hypocellular. The cells consisted of spindle-shaped fibroblasts widely separated by abundant collagenous stroma (Fig. 2B). Generally, the most cellular areas were present in the center of the lesion, whereas the periphery had less numerous fibroblasts and greater amounts of dense collagen. No significant variation in degree of vascularity was found, and no areas of tumor necrosis were seen in resected specimens from any of the nine patients.

Radiologic-Pathologic Correlation

Review of CT and histologic data showed no clear-cut correlation between the CT appearance of these tumors and their histologic features. Hence, tumors with identical histologic grades had varying CT appearances, and three tumors with the lowest collagen content had the highest attenuation values (Fig. 5A).

Discussion

The fibromatoses are a broad group of tumors characterized by benign fibrous tissue proliferation. Typically, their biologic behavior is intermediate between benign fibromas and fibrosarcomas [10, 11]. Fibromatoses often have an infiltrative growth pattern with a tendency toward local recurrence after surgical resection, but unlike fibrosarcomas, they do not metastasize. Histologically, the lesion consists of well-differentiated collagen and fibrous tissue, forming nonencapsulated, poorly circumscribed masses.

The CT appearance of fibromatoses in childhood was reported recently by Campbell et al. [8], and in all three cases, the lesions were hypodense on postcontrast scans. More recently, Hudson et al. [9] reported the CT and angiographic appearance of fibromatoses in 13 cases. They concluded that the tumors were usually better demonstrated after contrast infusion and that no relationship could be established between the vascularity of the tumors and their histologic features.

In our study, the tumors demonstrated varying appearances on CT and in this respect differed with the findings in the two studies cited above. In particular, three tumors were well demonstrated on precontrast scans and two showed only minimal enhancement after a bolus of iodinated IV contrast material. This latter observation was dissimilar to that reported by Hudson et al. [9].

Current concepts of CT tissue characterization suggest that fibrous tissue and collagen probably have high attenuation values, as was hypothesized by Kumar et al. [12] in their analysis of extracranial nerve sheath tumors. This view was not supported by our findings, as tumors with similar histologic grading had varying appearances and, conversely, three tumors with the highest attenuation values had the smallest amounts of collagen.

Although we found no significant correlation between the CT appearance of the fibromatoses and their histologic features, our study is limited in two aspects. First, the fibromatoses are a heterogeneous group of tumors with varying histologic features, and the character of the tissue within a lesion may vary. Second, in view of the small number of cases and the limited number of biopsy samples analyzed, actual histologic differences between these lesions may not have been detected. To fully understand the basis for the varying CT appearance of these tumors, further studies are required.

REFERENCES

1. Wilson JS, Korobkin M, Genant KH, Bovill EG. Computed tomography of musculoskeletal disorders. *AJR* **1978**;131:55–61
2. DeSantos LA, Goldstein HM, Murray JA, Wallace S. Computed tomography in the evaluation of musculoskeletal neoplasms. *Radiology* **1978**;128:89–94
3. Levine E, Lee KR, Neff JR, Maklad NF, Robinson RG, Preston

DF. Comparison of computed tomography and other imaging modalities in the evaluation of musculoskeletal tumors. *Radiology* **1979**;131:431–437
4. Heelan RT, Watson RL, Smith J. Computed tomography of lower extremity tumors. *AJR* **1979**;132:933–937
5. Hunter JC, Johnson WH, Genant KH. Computed tomography: evaluation of fatty tumors of the somatic soft tissues: clinical utility and radiologic pathological correlation. *Skeletal Radiol* **1979**;4:79–91
6. Egund N, Ekelund L, Sarko M, Persson B. CT of soft tissue tumors. *AJR* **1981**;137:725–729
7. Rosenthal DI. Computed tomography in bone and soft tissue neoplasm: application and pathological correlation. *CRC Crit Rev Diagn Imaging* **1982**;18:243–278
8. Campbell AN, Chan HSL, Daneman A, Martin DJ. Aggressive fibromatosis in childhood: computed tomographic findings in three patients. *J Assist Comput Tomogr* **1983**;7:109–113
9. Hudson TM, Vandergriend RA, Springfield DS, et al. Aggressive fibromatosis: evaluation by computed tomography and angiography. *Radiology* **1984**;150:495–501
10. Stout AP, Lattes R. Benign tumors of the soft tissue. In: Firminger HI, ed. *Atlas of tumor pathology*, 2d series, fasc. 1. Washington, DC: Armed Forces Institute of Pathology, **1967**
11. Allen PW. The fibromatosis: a clinical pathologic classification based on 140 cases. Parts I and II. *Am J Surg Pathol* **1977**;1(1):255–321
12. Kumar AJ, Kuhajda FP, Martinez CR, Fishman EK, Jezic DV, Siegelman SS. Computed tomography of extracranial nerve sheath tumors with pathological correlation. *J Comput Tomogr* **1983**;7:857–865

CT of Fibrous Tissues and Tumors with Sonographic Correlation

William A. Rubenstein[1]
George Gray[2]
Yong Ho Auh[1]
Christine L. Honig[2]
Bjorn Thorbjarnarson[3]
John J. Williams[3]
Allison B. Haimes[1]
Kenneth Zirinsky[1]
Elias Kazam[1]

Fibrous tissues and tumors may appear hyperdense relative to muscles and solid viscera on CT both before and after IV contrast injection. In addition, fibrous tissues generally have a homogeneously hypoechoic sonographic appearance. The diagnostic value of these criteria is illustrated in a group of 21 fibrous tissue abnormalities that includes retroperitoneal, mediastinal, and perigraft fibrosis, sclerosing pseudotumor of the orbit, generalized fibromatosis, desmoids, malignant fibrous histiocytoma, and normal tendons and ligaments. It is concluded that while hyperdensity on CT and echopenia on sonography are not pathognomonic of fibrous tissue, they occur with sufficient frequency that their presence raises the possibility of a fibrous lesion.

Several disorders are characterized by an abnormal proliferation of fibrous tissue in various parts of the body, including retroperitoneal, mediastinal, perianeurysmal, and perigraft fibrosis, sclerosing pseudotumor of the orbit, generalized fibromatosis, and desmoid tumors. The CT, sonographic, and conventional radiographic appearances of these disorders have been treated separately in many published reports [1–34]. We review our experience, accumulated over the past 9 years, studying fibrous tissues and tumors. We emphasize the CT and sonographic appearances that are common to many of these disorders and that are also shared by such normal fibrous tissues as fascia, tendons, and ligaments. The CT findings in tumefactive pancreatic retroperitoneal fibrosis and in idiopathic mediastinal fibrosis are illustrated. We also discuss perivascular inflammatory lesions and desmoplasia (fibrous tissue formation) induced by metastases, both of which may mimic primary fibrous disorders on CT and sonography.

Materials and Methods

The CT scans of 21 patients with surgically verified fibrous lesions were reviewed. These included seven cases of retroperitoneal fibrosis (Figs. 1A–C and 2A–B) associated with a fibrous pancreatic mass (Figs. 2A and B) and pleural fibrosis in one case and with mediastinal fibrosis in another (Fig. 3). Thus, among these seven patients, there were 10 fibrous lesions, eight of which were verified surgically. For the remaining two lesions, the mediastinal and pleural fibrosis was not directly confirmed at surgery, but was considered likely in view of the concurrent biopsy-proven retroperitoneal fibrosis and the 3–5 year follow-up obtained for both patients. In six of the patients with retroperitoneal fibrosis, there were plaquelike lesions along the aorta, vena cava, and iliac vessels (Figs. 1A–C and 2A–B). In one case with ulcerative colitis, not illustrated here, the fibrosis involved mainly the pancreatic head and body. Among the remaining 14 patients, there were 15 other fibrous lesions. These included one sclerosing pseudotumor of the orbit, two cases of perianeurysmal fibrosis, two cases of perigraft fibrosis (Fig. 4), one case of congenital generalized fibromatosis with two recurrent lesions (Fig. 5), three desmoid tumors (in the chest wall, abdominal wall [Fig. 6], and mesentery), one malignant fibrous histiocytoma (Fig. 7), one retroperitoneal fibrosarcoma, one ovarian fibroma, one case of pelvic fibrolipomatosis, and one fibrous mesothelioma of the pleura. The diagnosis for one of the fibromatosis lesions [Fig. 5] was not directly confirmed

Received December 13, 1985; accepted after revision June 23, 1986.

[1] Department of Radiology, The New York Hospital–Cornell Medical Center, 525 E. 68th St., New York, NY 10021. Address reprint requests to E. Kazam.

[2] Department of Pathology, The New York Hospital–Cornell Medical Center, New York, NY 10021.

[3] Department of Surgery, The New York Hospital–Cornell Medical Center, New York, NY 10021.

AJR 147:1067–1074, November 1986
0361–803X/86/1475–1067
© American Roentgen Ray Society

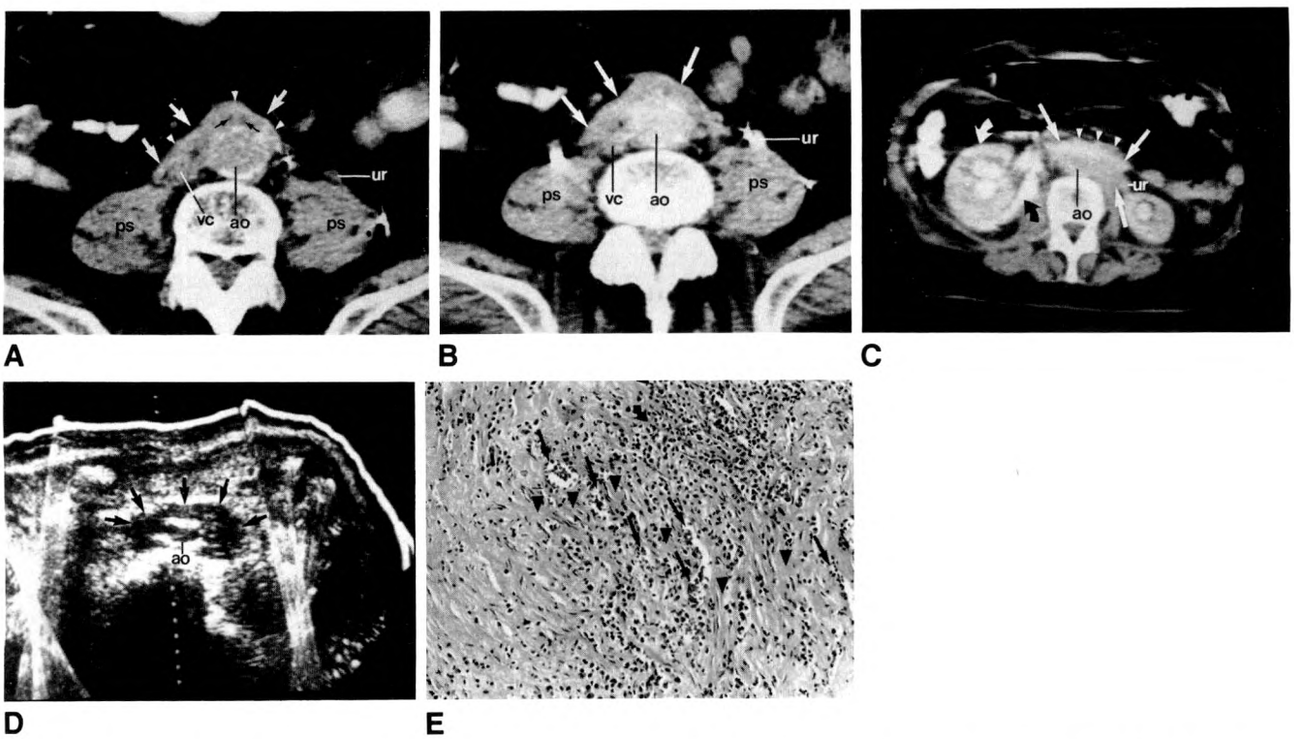


Fig. 1.—Retroperitoneal fibrosis.

A, CT before injection shows soft-tissue plaque (*large white arrows*) anterior to aorta (ao) and vena cava (vc). Peripheral, anterior portion (*arrowheads*) of plaque is denser than central portion (*small black arrows*) and hyperdense relative to caval lumen (vc) and psoas muscles (ps). ur = ureter.

B, Contrast-enhanced CT at approximate level of *A* obtained during an IV contrast drip of a 14 g/dl iodine solution. Soft-tissue plaque (*arrows*) has been enhanced by nearly 15% of its precontrast CT numbers, compared with a 68% enhancement of the aorta (ao) and a 1% enhancement of the psoas muscle (ps). Fibrotic plaque is now isodense with vena cava (vc). ur = ureter. Retroperitoneal fibrosis was confirmed at surgery.

C, Contrast-enhanced CT in another patient with proven retroperitoneal fibrosis. Scan was obtained 15 min after bolus injection of a solution containing 37 g of iodine. Anterior portion (*arrowheads*) of fibrotic plaque (*arrows*) has been enhanced more than aortic lumen (ao) and was also denser than aortic lumen on precontrast CT (not shown here). Extravasated contrast within a perinephric urinoma (*curved arrows*). ur = ureter.

D, Transverse sonogram at approximate level of *C*. Fibrotic tissue (*arrows*) is relatively hypoechoic. ao = aorta.

E, Microscopic section from lesion illustrated in *C* and *D*. Abundant capillaries (*arrows*) are interspersed with fibrous tissue (*arrowheads*). Chronic inflammatory cellular infiltrate (*curved arrows*).

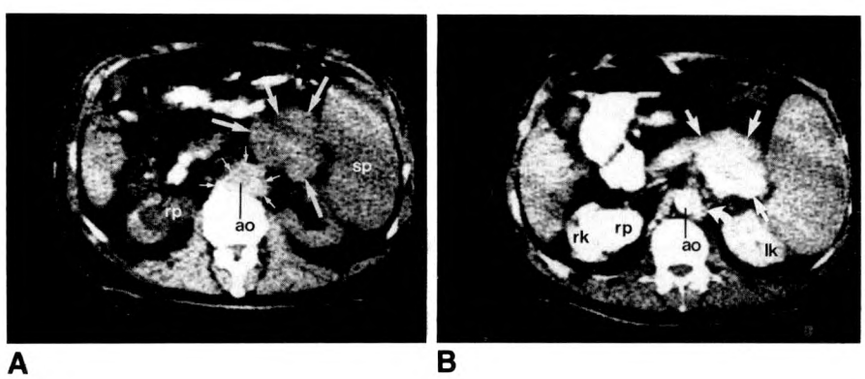


Fig. 2.—Tumefactive retroperitoneal fibrosis.

A, Precontrast CT shows mass (*large arrows*) in pancreatic tail that is isodense with enlarged spleen (sp). There is hyperdense tissue along the diaphragmatic crura (*small arrows*). ao = aorta. Right renal pelvis (rp) is dilated.

B, Contrast-enhanced CT at approximate level of *A*, obtained 10 min after a bolus of IV contrast media (37 g of iodine). Pancreatic tail mass (*straight arrows*) has been enhanced to nearly same degree as kidneys (rk, lk). Tissue along left diaphragmatic crus (*curved arrow*) also appears bright. ao = aorta; rp = right renal pelvis. Metastatic islet cell tumor of pancreas was diagnosed on CT, but retroperitoneal fibrosis involving pancreas and extending along aorta and iliac vessels was found at surgery. Mass was hypoechoic on sonography (not shown here), with a weak far wall, because of attenuation of sound beam. Three-year clinical follow-up excluded an underlying malignancy.

at surgery but appeared almost certain, as it occurred near a biopsy-proven fibroma in a patient with multiple postsurgical recurrences. In all, 25 fibrous lesions in 21 patients were studied.

We also reviewed nine surgically proven malignant lesions that were not primary fibrous tumors, yet resembled fibrous tissues on CT examination. These included four cases of lymphoma and five cases of desmoplastic metastases arising from primary malignancies in the breast, pancreas, and urothelium (Fig. 8). Four of these lesions were described as markedly desmoplastic at surgery.

Ten of the lesions were imaged with an 18-sec scanner (EMI), with

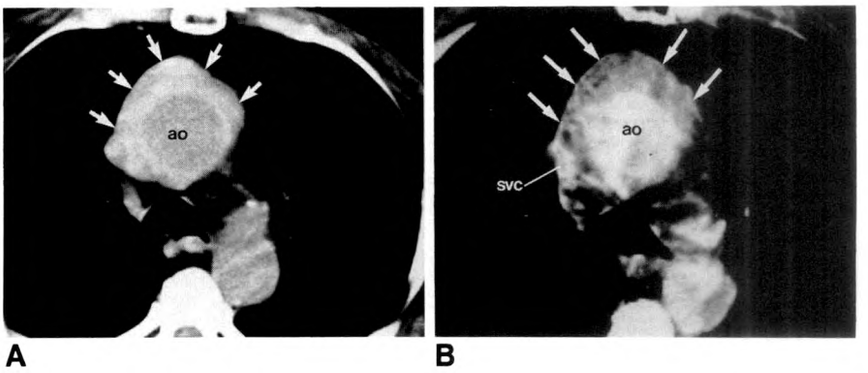


Fig. 3.—Mediastinal fibrosis.

***A*, Precontrast CT of same patient illustrated in 1*A* and 1*B*. Soft-tissue lesion (*arrows*) around distal ascending aorta (ao) has an average CT number of 56 H, compared with 46 H for the ascending aorta and 29 H for erector spinae muscles (not shown here).**

***B*, Contrast-enhanced CT at approximate level of *A* obained during drip infusion of a 14 g/dl iodine solution. Mediastinal lesion (*arrows*) has been enhanced by 41% of its precontrast CT number, compared with a 170% enhancement for the ascending aorta (ao). svc = superior vena cava.**

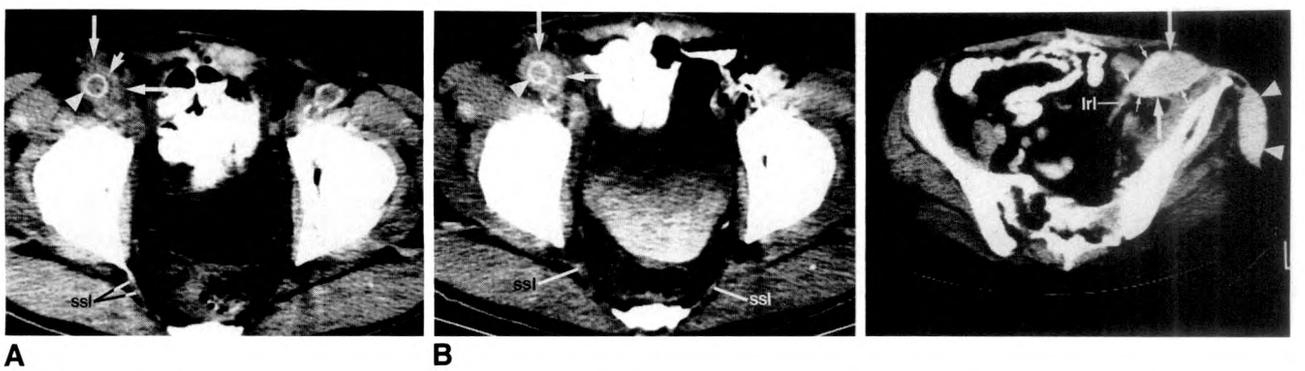


Fig. 4.—Perigraft fibrosis.

***A*, Precontrast CT. Soft-tissue plaque (*long arrows*) with hyperdense foci (*short arrow*) surrounds right aorticofemoral bypass graft (*arrowhead*). ssl = sacrospinous ligament.**

***B*, Contrast-enhanced CT at approximate level of *A* obtained during drip infusion of a 14 g/dl iodine solution. Plaque (*arrows*) surrounding graft (*arrowhead*) has been enhanced by more than 250% of its precontrast attenuation values. Peripherally, it contains foci that appear brighter than the graft lumen. Perigraft fibrosis was verified at surgery. ssl = sacrospinous ligament.**

Fig. 5.—Congenital generalized fibromatosis. Contrast-enhanced CT, obtained during drip infusion of a 14 g/dl iodine solution, shows intrapelvic (*large arrows*) and subcutaneous (*arrowheads*) hyperdense masses. Peripheral portion (*small arrows*) of intrapelvic mass is denser than more central portion. Left round ligament (lrl) is thickened and hyperdense. Pelvic lesion was proven to be a fibroma at surgery. Patient had multiple, recurring, and invasive fibromas of the lower extremities and pelvis.

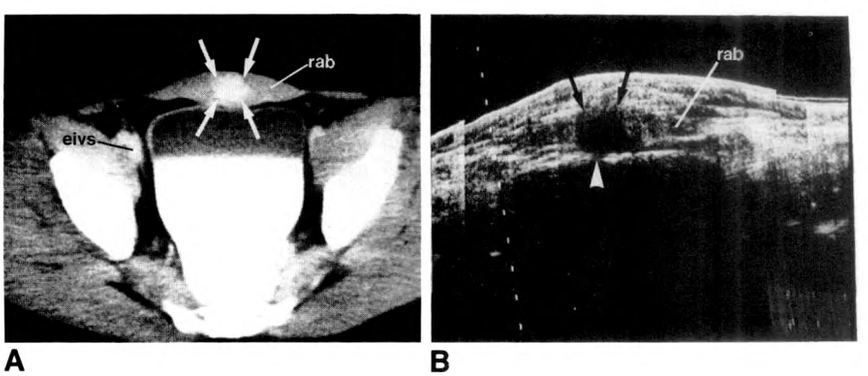


Fig. 6.—Abdominal wall desmoid.

***A*, Contrast-enhanced CT shows a midline mass (*arrows*), which occurred in a surgical scar after removal of a pelvic leiomyosarcoma. Mass enhanced markedly relative to its appearance on precontrast CT scan (not shown here) and appears nearly as bright as external iliac vessels (eivs). rab = rectus abdominis muscle.**

***B*, Transverse sonogram at level of *A*. Midline mass (*arrows*) is echo free but solid, with a poorly delineated far wall (*arrowhead*) due to attenuation of the sound beam. Fibrous tissue proliferation, rather than the clinically suspected recurrent leiomyosarcoma, was diagnosed on the basis of the CT and sonographic appearances. An abdominal wall desmoid was found at surgery. rab = rectus abdominis muscle.**

13-mm collimation. The remaining 15 lesions were evaluated with G. E. 8800 or 9800 equipment, with 10-mm collimation and scan times of 10 sec or 2–3 sec, respectively. Consecutive CT sections through the abdomen or chest were obtained in deep inspiration, with the patient supine, at intervals of 10–15 mm. Oral and IV contrast media were administered routinely, unless contraindicated. IV contrast material (meglumine diatrizoate) was administered either as a bolus injection containing 37 g of iodine, or as a drip infusion of 42 g of

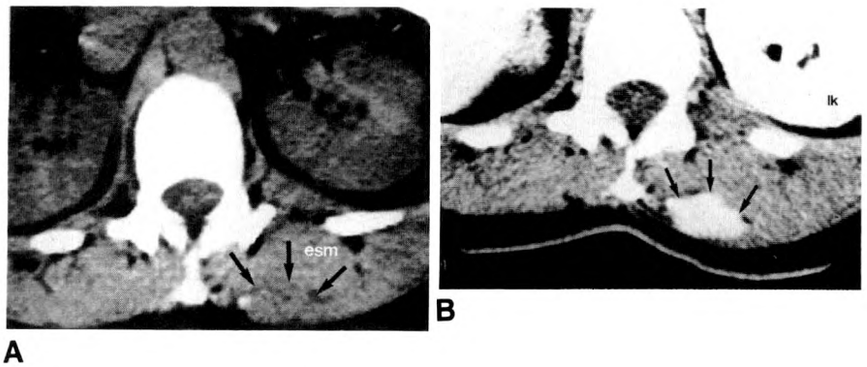


Fig. 7.—Malignant fibrous histiocytoma.

***A*, Precontrast CT shows a smoothly outlined, lobulated mass (*arrows*) that is slightly more radiolucent than the adjacent erector spinae muscles (esm).**

***B*, Contrast-enhanced CT at approximate level of *A*. Marked enhancement of mass (*arrows*), which is now nearly as radiodense as left kidney (lk). Mass was hypoechoic on sonography (not shown here), with a weak far wall due to attenuation of the sound beam. A desmoid was suspected at gross examination, but microscopy revealed a malignant fibrous histiocytoma.**

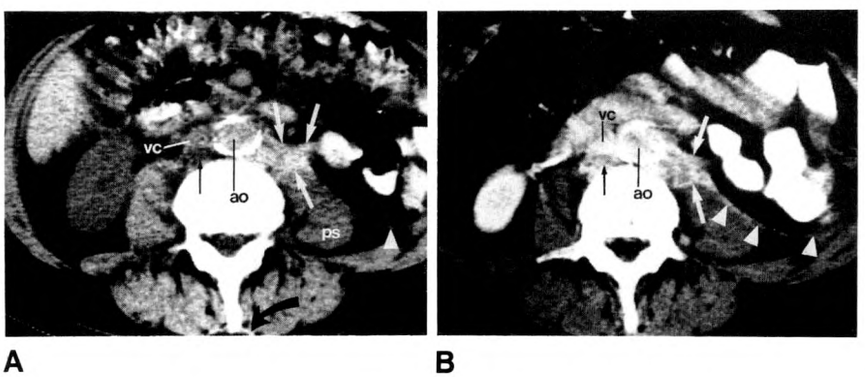


Fig. 8.—Malignant retroperitoneal fibrosis.

***A*, Precontrast CT shows an irregularly outlined hyperdense left paraaortic mass (*white arrows*). Posterior renal fascia (*arrowhead*) is thickened. A relatively lucent structure (*black straight arrow*) is visible behind vena cava (vc). ao = aorta; ps = psoas muscle. *Curved arrow* indicates thoracolumbar fascia.**

***B*, Contrast-enhanced CT at approximate level of *A*, obtained during drip infusion of a 14 g/dl iodine solution, shows a 67% increase in average CT number of left paraaortic mass (*white arrows*), most marked peripherally. This compares with an 84% enhancement for the aortic lumen (ao). Thickened left renal fascia (*arrowheads*) and retrocaval mass (*black arrow*) were also enhanced significantly. vc = vena cava. Gross and microscopic pathology demonstrated intense desmoplastic response to a recurrent transitional cell carcinoma of left kidney. Fibrous tissue had a rich network of capillaries.**

iodine, after a bolus of 15 g of iodine. Occasionally, rapid-sequence dynamic scans were performed after a bolus of 15 g of iodine. IV glucagon (1 ml) was administered for studies obtained with the 10-sec and 13-sec scanners.

Precontrast CT scans were available for 14 of the 25 primary fibrous lesions, and for three of the nine malignant tumors. Postcontrast CT scans were available for 24 of the 25 fibrous lesions and for all nine malignant tumors. On all CT scans, the attenuation of the lesions was compared with surrounding soft tissues by visual examination of the images, which were photographed at three different window widths and levels. Whenever possible, comparative CT numbers were also obtained.

Sonograms were available for 12 of the 25 fibrous lesions. The studies were performed initially with articulated-arm scanners connected to analog scan converters (Picker, G. E.), (Figs. 1D and 6B), and subsequently with real-time equipment (Diasonics). The highest frequency transducers that also allowed adequate penetration were used (2.5–10 MHz).

In addition, the CT appearances of some normally hyperdense fibrous tissues were assessed in a series of 50 consecutive scans, obtained with G. E. 8800 or 9800 equipment. These included the sacrospinous and sacrotuberous ligaments (Fig. 4), the thickened iliac fascia between the psoas and iliacus muscles (Fig. 9A), the hamstring tendons (Fig. 9B), and the thoracolumbar fascia (Fig. 8A). The 30 males and 20 females in this series ranged in age from 7 to 83 years. IV contrast media were administered in 45 of the 50 cases. Precontrast and postcontrast studies were available in one patient.

Finally, histologic slides from eight primary fibrous lesions and five malignancies were reviewed. These included four cases of retroperitoneal fibrosis (Fig. 1E), two cases of perianeurysmal fibrosis, one abdominal-wall desmoid, one congenital fibroma, two cases of lymphoma, two metastases from urothelial carcinoma, and one metastatic carcinoma of the pancreas.

Results

Primary Fibrous Lesions

On preconstrast CT scans, nine (64%) of the 14 lesions were either uniformly or focally denser, that is, hyperdense relative to adjacent soft tissues. These included five of seven with retroperitoneal fibrosis, one mediastinal fibrosis, one perigraft fibrosis, one orbital pseudotumor, and one of two desmoid tumors. Some lesions were diffusely hyperdense (Fig. 3A), while others appeared heterogeneous with dense foci that tended to occur peripherally (Figs. 1A and 4A). One fibrosarcoma appeared isodense with adjacent tissues on precontrast scans, while a malignant fibrous histiocytoma appeared slightly hypodense (Fig. 7A).

On postcontrast CT scans, 20 (83%) of 24 lesions were clearly hyperdense relative to adjacent soft tissues (Figs. 1C, 2B, 4B, 5, 6A, and 7B), or showed a marked enhancement when the postcontrast and precontrast CT scans were compared (Figs. 1B and 3B). These included six of eight with

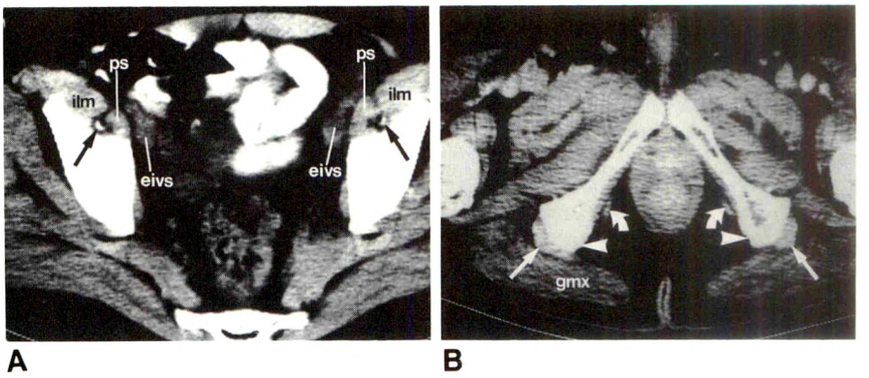


Fig. 9.—Hyperdense fascia and tendons.
***A*, Iliac fascia. Precontrast CT shows hyperdense structure (*arrows*) between psoas (ps) and iliacus (ilm) muscles that retains its relative hyperdensity on contrast-enhanced scans and represents thickened iliac fascia, not a blood vessel. eivs = external iliac vessels.**
***B*, Hamstring tendons. Tendons of biceps femoris, semitendinosus, and semimembranous muscles appear as confluent hyperdense structures (*straight arrows*) attached to ischial tuberosities (*arrowheads*). gmx = Gluteus maximus muscle. Pudendal canals (*curved arrows*), which contain pudendal vessels, are also hyperdense.**

retroperitoneal fibrosis, one mediastinal fibrosis, one pleural fibrosis, and four cases of perigraft or perianeurysmal fibrosis, one orbital pseudotumor, two congenital fibromas, two desmoid tumors, one malignant fibrous histiocytoma, one fibrosarcoma, and one fibrous mesothelioma of the pleura. The marked enhancement was observed even for masses that were not hyperdense on precontrast scans (Figs. 2A, 2B, 7A, and 7B). Lesions with peripheral foci of hyperdensity on precontrast scans tended to appear more homogeneously hyperdense on postcontrast studies (Figs. 1A, 1B, 4A, and 4B), although there was still some peripheral postcontrast hyperdensity (Fig. 5). One case of pelvic fibrolipomatosis and one ovarian fibroma appeared unenhanced on postcontrast scans. One desmoid tumor was not imaged with contrast-enhanced CT.

Review of the histologic slides from seven of the eight primary fibrous lesions showed abundant capillaries between the fibrocollagenous tissues. At times more blood vessels were seen than was suspected on initial examination. This vascularity was most marked for retroperitoneal and perigraft fibrosis (Fig. 1E), but was not thought to be characteristic of these entities only. Rather, the finding was considered to be typical of any fibrous or scar tissue in the acute or subacute stages of formation. The histologic slides from a pelvic congenital fibroma (Fig. 5) showed exuberant fibrous tissue without abundant vasculature.

The sonographic appearance of the fibrous lesions was consistent with their relatively homogeneous gross and microscopic appearances. In all, 11 (92%) of the 12 fibrous lesions were either echo free or hypoechoic on sonography (Figs. 1D and 6B). The single exception was a necrotic fibrosarcoma that had echogenicity comparable to renal cortex.

The diagnosis of a fibrotic process was suggested preoperatively in some cases on the basis of the CT and sonographic findings (Figs. 1, 3, 4, 6, 7). However, it was not possible to reliably differentiate benign from malignant fibrous lesions (compare Figs. 6 and 7). In one case of perigraft fibrosis, we were unable to distinguish the fibrotic plaque from an associated purulent exudate that also extended along the graft at surgery.

Malignancies with Desmoplastic Reaction

Among the nine malignancies that were not primary fibrous tumors, two of three (a breast metastasis and a urothelial metastasis) had a hyperdense precontrast CT appearance (Fig. 8A), while all nine appeared hyperdense on postcontrast scans (Fig. 8B). The masses in these cases tended to be focal and rounded, but were occasionally plaquelike (Fig. 8). Like the primary fibrous lesions, they were enhanced with contrast media, but not to the same extent as adjacent vessels (Figs. 8A and 8B). There was also a tendency for peripheral hyperdensity of some metastases (Fig. 8B). Four of the malignancies—a lymphoma, a pancreatic metastasis, and metastases from two urothelial tumors—were described as markedly desmoplastic and vascular at surgery. However, review of the biopsy specimens showed marked vascularity on microscopy in only one of four lesions.

Normal Fascia, Tendons, and Ligaments

Among the CT scans of 50 consecutive patients for which the appearance of some normal fibrous tissues were evaluated, the posterior portion of the thoracolumbar fascia near the midline was hyperdense in 49 (98%) (Fig. 8A), the iliac fascia between the psoas and iliacus muscles was hyperdense in 40 (80%) (Fig. 9A), the hamstring tendons were hyperdense in 43 (86%) (Fig. 9B), and the sacrospinous or sacrotuberous ligaments were hyperdense in 40 (80%) (Figs. 4A and 4B). The hyperdensity of these structures was a consistent finding on both precontrast and postcontrast scans, and therefore was not attributable solely to IV contrast enhancement. These same normal structures appeared hyperdense on the CT scans of the three cadavers that were studied.

Discussion

Most of the fibrous tissues in this study were hyperdense relative to adjacent soft tissues on CT and hypoechoic on sonography. Thus, on postcontrast CT, 83% of the histologically verified fibrous lesions appeared hyperdense or signifi-

cantly enhanced. On precontrast CT, 64% of the lesions were either uniformly or focally hyperdense. More than 90% of the lesions studied appeared hypoechoic sonographically. Clearly, these findings are not true of every primary fibrous lesion. Neither is CT hyperdensity universal for all normal fibrous tissues; it was observed in 80–98% of only portions of the fascia, tendons, and ligaments that we studied. Furthermore, some malignancies, especially those with associated desmoplasia, share the CT appearances of fibrous tissues. Nevertheless, these CT and/or sonographic findings occur often enough to be useful indicators for the presence of fibrous tissue. There were 18 primary fibrous lesions that were imaged with at least two of the following methods: precontrast CT, postcontrast CT, and sonography. Of these, 15 (83%) met at least two of the following criteria: hyperdense on precontrast CT, hyperdense on postcontrast CT, and echo free or hypoechoic on sonography.

The causes for the CT hyperdensity of the primary fibrous lesions in this study are not known. We propose two hypotheses to explain the CT appearance of most of these lesions.

Hypothesis A: The precontrast CT hyperdensity may reflect, in part, the high physical density of the collagen within these tissues. Attenuation is a function of both photoelectric and Compton interactions [35]. The photoelectric effect is related to the atomic number and is therefore increased for such elements as iodine, iron, and calcium. Compton scattering reflects the electron volume density, which is directly proportion to the physical density, that is, mass divided by volume [35]. Since no calcium was present in the pathologically proven fibrous lesions in this study, their elevated precontrast CT numbers may have been due to the relatively high physical density of collagen. Presumably, the variability in their precontrast CT numbers may reflect differences in collagen content.

Hypothesis B: The postcontrast CT hyperdensity of the fibrous lesions may be due in part to their abundant capillary network (Fig. 1E). This hypothesis is supported by our observation of a rich capillary network, on review of the histologic slides from seven of eight primary fibrous lesions. Contrast enhancement has been observed in retroperitoneal fibrosis during angiography [3, 36], although it is much easier to detect with CT scanning [1, 3]. Contrast enhancement has also been used in the CT differentiation of postoperative fibrous scars from recurrent intervertebral disk herniation [37–41]. Peripheral CT hyperdensity (Figs. 1B and 6A) has been reported previously in retroperitoneal fibrosis [3]. It may be due to differences in the maturation of the fibrous tissues within the lesion. Histochemical evidence has been presented for centrifugal spread of the fibrotic process in retroperitoneal fibrosis [42]. Thus, reduced postcontrast CT density in the center of the lesion may reflect the presence of mature fibrous tissue with a paucity of capillaries, whereas peripheral hyperdensity may be due to the more active, vascularized tissue at the advancing edge of the fibrosis [3].

Some fibrous lesions, such as ovarian fibromas and pleomorphic fibrosarcomas, contain fibroblasts on microscopic examination, but have relatively little collagen or few blood vessels within them [43]. According to hypotheses A and B above, these masses may not appear hyperdense on either precontrast or postcontrast CT scans. Indeed, neither the ovarian fibroma nor the necrotic fibrosarcoma appeared hyperdense on CT in our series. Clearly, however, these hypotheses do not explain the CT appearances of all the lesions in this study. In particular, relative abundance of collagen on histologic studies did not correlate consistently with hyperdensity on precontrast CT scans (Figs. 2A, 2B, 7A, and 7B). For example, the malignant fibrous histiocytoma was not hyperdense on the precontrast scan, despite its predominantly fibrotic internal structure (Fig. 7A). It was, however, enhanced markedly and uniformly with IV contrast media (Fig. 7B), mimicking a benign desmoid. A hyperdense CT appearance for malignant fibrous histioicytoma has not been described previously [44, 45].

Tumors that trigger a dense desmoplastic reaction, such as lymphomas and some metastatic carcinomas [3, 6, 46–54], may owe their CT hyperdensity to increased fibrous-tissue content (Figs. 8A and 8B). Differentiation of desmoplastic malignancies from primary fibrous lesions may therefore depend on morphology, rather than on CT attenuation alone [1, 6, 16, 17]. Tumors are usually more bulky and tend to displace adjacent vessels [5, 55] or invade bone. However, mass effect may also be seen with benign tumefactive retroperitoneal fibrosis [1] (Fig. 2) and in sclerosing pseudotumor of the orbit [56]. Definitive diagnosis, therefore, requires histologic examination and at times, subsequent clinical follow-up.

The CT hyperdensity of some of the normal fibrous tissues illustrated here may be due to their increased collagen content (Figs. 9A and 9B). Characteristically, collagen accounts for up to 30% of the wet weight of some tendons [57–59]. Internal vasculature is typically sparse within these tissues [60]. Since no histologic studies were made here, diffuse calcification in some of these tissues cannot be completely excluded. However, hyperdense fascia, ligaments, and tendons were observed on the CT scans of three children in our series, aged 7 to 9 years, where little or no calcification can be expected. Of interest, the fibrous tissue between the psoas and iliacus muscles was first thought to be a tendinous structure, but is well above the expected location of the psoas major tendon [60]. It corresponds in location to the iliac fascia, which is thickened at this level [60].

In conclusion, fibrous lesions should be added to the differential diagnostic list of masses that are hyperdense on postcontrast CT scans. This also includes vascular neoplastic and inflammatory masses, malignancies with desmoplastic reaction, acute hematomas, fluid collections with extravasated contrast media, and diffusely calcified masses. Extravasated contrast media, acute hematomas, and diffuse calcifications can be eliminated from the list, on the basis of their appearance on precontrast CT scans, sonography, and follow-up studies. With this approach, the possibility of a fibrotic process can be suggested strongly on the basis of the CT and sonographic findings. Histologic examination, however, is essential to distinguish benign from malignant fibrous lesions, and to diagnose an associated inflammatory process.

ACKNOWLEDGMENTS

The authors thank Fereshteh Kazam and Phyllis Fagan for manuscript preparation.

REFERENCES

1. Brun D, Laursen K, Sorensen IN, Lorentzen JE, Kristensen JK. CT in retroperitoneal fibrosis. *AJR* **1981**;137:535–538
2. Center S, Schwab R, Goldberg B. The value of ultrasonography as an aid in the treatment of idiopathic retroperitoneal fibrosis. *J Ultrasound Med* **1982**;1:87–89
3. Dalla-Palma I, Rocca-Rossetti S, Pozzi-Mucelli RS, Rizzatto G. Computed tomography in the diagnosis of retroperitoneal fibrosis. *Urol Radiol* **1981**;3:77–83
4. Fagan CJ, Amparo EG, Davis M. Retroperitoneal fibrosis. *Semin Ultrasound* **1982**;3:123–138
5. Fagan CJ, Larrieu AJ, Amparo EG. Retroperitoneal fibrosis: ultrasound and CT features. *AJR* **1979**;133:239–243
6. Feinstein RS, Gatewood OMB, Goldman SM, Copeland B, Walsh PC, Siegelman SS. Computerized tomography in the diagnosis of retroperitoneal fibrosis. J Urol. **1981**;126:255–259
7. Ardagh JW, Blake GB. Idiopathic retroperitoneal fibrosis. *NZ Med J* **1964**;63:362–366
8. Partington PF. Diffuse idiopathic fibrosis. *Am J Surg* **1961**;101:239–244
9. Morgan AD, Loughridge LW. Combined mediastinal and retroperitoneal fibrosis. *Lancet* **1966**;1:67–70
10. Weinstein JB, Aronberg DJ, Sagel SS. CT of fibrosing mediastinitis: findings and their utility. *AJR* **1983**;141:247–251
11. Tubbs OS. Superior vena caval obstruction due to chronic mediastinitis. *Thorax* **1946**;1:247–256
12. Inkley SR, Abbott GR. Unilateral pulmonary arteriosclerosis. *Arch Intern Med* **1961**;108:903–915
13. Cameron DG, Ing ST, Boyle M, Mathews WH. Idiopathic mediastinal and retroperitoneal fibrosis. *Can Med Assoc J* **1961**;85:227–232
14. Vint VC, Usselman JA, Warmath MA, Dilley RB. Aortic perianeurysmal fibrosis: CT density enhancement and ureteral obstruction. *AJR* **1980**;134:577–580
15. Megibow AJ, Ambos MA, Bosniak MA. Computed tomographic diagnosis of ureteral obstruction secondary to aneurysmal disease. *Urol Radiol* **1980**;1:211–215
16. Feldberg MAM, vanWaes PFGM, tenHaken GB. CT diagnosis of perianeurysmal fibrotic reactions in aortoiliac aneurysm. *J Comput Assist Tomogr* **1982**;6:465–471
17. Pahira JJ, Wein AJ, Barker CF, et al. Bilateral complete ureteral obstruction secondary to an abdominal aortic aneurysm with perianeurysmal fibrosis: diagnosis by computed tomography. *J Urol* **1979**;121:103–106
18. Henry LG, Doust B, Korns ME, Bernhard VM. Abdominal aortic aneurysm and retroperitoneal fibrosis. *Arch Surg* **1978**; 113:1456–1460
19. Reed GW, Stinely RW. Massive periaortic and periarterial fibrosis. *N Engl J Med* **1959**;261:320–323
20. Gyldensted C, Lester J, Fledelius H. Computed tomography of orbital lesions. A radiological study of 144 cases. *Neuroradiology* **1977**;13:141–150
21. Hilal SK, Trokel SL. Computerized tomography of the orbit using thin sections. *Semin Roentgenol* **1977**;12:137–147
22. Nugent RA, Rootman J, Robertson WD, et al. Acute orbital pseudotumors: classification and CT features. *AJR* **1981**; 137:957–962
23. Harr DL, Quencer RM, Abrams GW. Computed tomography and ultrasound in the evaluation of orbital infection and pseudotumor. *Radiology* **1982**;142:395–401
24. Wende S, Aulich A, Nover A, et al. Computed tomography of orbital lesions. *Neuroradiology* **1977**;13:123–124
25. Hurwitz BS, Citrin CM. Use of computerized axial tomography in evaluating therapy of orbital pseudotumor. *Ann Ophthalmol* **1979**;11:217–221
26. Enzmann D, Donaldson SS, Marshall WH, Kriss JR. Computed tomography in orbital pseudotumor (idiopathic orbital inflammation). *Radiology* **1976**;120:597–601
27. Edwards MK, Zauel DW, Gilmor RL, Muller J. Invasive orbital pseudotumor—CT demonstration of extension beyond the orbit. *Neuroradiology* **1982**;23:215–217
28. Hudson TM, Vandergriend RA, Springfield DS, et al. Aggressive fibromatosis: evaluation by computed tomography and angiography. *Radiology* **1984**;150:495–501
29. Allen PW. The fibromatoses: a clinicopathological classification based on 140 cases. *Am J Surg Pathol* **1977**;1:255–270, 305–321
30. Mackenzie DH. The fibromatoses: a clinicopathological concept. *Br J Med* **1972**;4:277–281
31. Hanson RD, Hunter TB, Haber K. Ultrasonographic appearance of anterior abdominal wall desmoid tumors. *J Ultrasound Med* **1983**;2:141–142
32. Miller EM, Newton TH. The angiographic features of extraabdominal desmoid tumors. *Radiology* **1979**;132:305–308
33. Totterman S, Reitamo JJ. Desmoid tumour: an angiographic study of five cases. *Br J Radiol* **1979**;52:936–941
34. Yeh H-C, Rabinowitz JG, Rosenblum M. Complementary role of CT and ultrasonography in the diagnosis of desmoid tumor of the abdominal wall. *Comput Radiol* **1982**;6:275–280
35. Phelps ME, Hoffman EJ, Ter-Pogossian MM. Attenuation coefficients of various body tissues, fluids, and lesions at photon energies of 18–136 keV. *Radiology* **1975**;117:573–583
36. Kees CJ. Angiographic staining and vascularity in a case of fibrous retroperitonitis. *Radiology* **1974**;113:329–330
37. Braun IF, Lin JP, Benjamin MV, Kricheff II. Computed tomography of the asymptomatic postsurgical lumbar spine: analysis of the physiological scar. *AJR* **1984**;142:140–152
38. Schubiger O, Valavanis A. CT differentiation between recurrent disc herniation and postoperative scar formation: the value of contrast enhancement. *Neuroradiology* **1982**;22:251–254
39. Teplick JG, Haskin ME. Computed tomography of the postoperative lumbar spine. *AJR* **1983**;141:865–884
40. Teplick JG, Haskin ME. CT of the postoperative lumbar spine. *Radiol Clin North Am* **1983**;21:395–420
41. Teplick JG, Haskin ME. Intravenous contrast enhanced CT of the postoperative lumbar spine: improved identification of recurrent disc herniation, scar, arachnoiditis, and diskitis. *AJR* **1984**;143:845–855
42. Catino D, Torack RM, Hagstrom JWC. Idiopathic retroperitoneal fibrosis: histochemical evidence for lateral spread of the process from the midline. *J Urol* **1967**;98:191–194
43. Robbins SL, Cotran RS, Kumar V. *Pathologic basis of disease*, 3rd ed. Philadelphia: Saunders, **1984**:269–270, 760–761, 1153, 1364–1365
44. Bernardino ME, Jing B-S, Thomas JL, Lindell MM, Zornoza J. The extremity soft tissue lesion: a comparative study of ultrasound, computed tomography, and xeroradiography. *Radiology* **1981**;139:53–59
45. Paling MR, Hyams DM. Computed tomography in malignant fibrous histiocytoma. *J Comput Assist Tomogr* **1982**;6:785–788

46. Lepor H, Walsh PC. Idiopathic retroperitoneal fibrosis. *J Urol* **1979**;122:1–6
47. Mieza M, Rotstein JM, Geffen A. CT demonstration of periureteral fibrosis of malignant etiology. *J Comput Assist Tomogr* **1982**;6:290–293
48. Usher SM, Brendler H, Ciavarra VA. Retroperitoneal fibrosis secondary to metastatic neoplasm. *Urology* **1977**;9:191–194
49. Webb AJ, Dawson-Edwards P. Malignant retroperitoneal fibrosis. *Br J Surg* **1967**;54:505–508
50. Kendall AR, Lakey WH. Sclerosing Hodgkin's disease vs. idiopathic retroperitoneal fibrosis. *J Urol* **1961**;86:217–221
51. Levine M, Schwartz S, Allen A, Narciso FV. Lymphosarcoma and periureteral fibrosis. *Radiology* **1964**;82:90–95
52. Nitz GL, Hewitt CB, Stratton RA, Kiser WS, Stewart BH. Retroperitoneal malignancy masquerading as benign retroperitoneal fibrosis. *J Urol* **1970**;103:46–49
53. Trever RW. Reticulum cell sarcoma producing retroperitoneal and periureteral fibrosis. *N Engl J Med* **1958**;258:268–270
54. Murray SM, Woo-Ming MO. Retroperitoneal fibrosis due to carcinoma of the ureter. *Br J Urol* **1966**;38:424–427
55. Degesys GE, Dunnick NR, Silverman PM, Cohan RH, Illescas FF, Castagno A. Retroperitoneal fibrosis: use of CT in distinguishing among possible causes. *AJR* **1986**;146:57–60
56. Blodi FC, Gass JDM. Inflammatory pseudotumor of the orbit. *Trans Am Acad Ophthalmol Otol* **1967**;71:303–323.
57. Hukins DWL. Biochemical properties of collagen. In: Weiss JB, Jayson MIV, eds. *Collagen in health and disease.* New York: Churchill Livingstone, 1982:49–72
58. Davison PF. Tendon. In: Weiss JB, Jayson MIV, eds. *Collagen in health and disease.* New York: Churchill Livingstone, **1982**:498–505
59. McGee JO'D. Liver. In: Weiss JB, Jayson MIV, eds. *Collagen in health and disease.* New York: Churchill Livingstone, **1982**:414–424
60. Williams PL, Warwick R, eds. *Gray's anatomy*, 36th ed. Philadelphia: Saunders, **1980**:474–475, 522–523, 542–543, 593

Computer Page

Some Applications for a Personal Computer Data-Base System in Radiology

F. Graham Sommer[1]

Applications for a personal-computer–based relational data-base system in an academic radiologist's office are described. These include archival and flexible retrieval of desired cases from clinical-case and teaching-file data bases and data-base management of a transparency-slide collection and radiology journal articles. All applications were implemented by using commercially available software that was specially adapted for each purpose. These data-base systems have been effective organizing tools over the past 4 years.

As the personal computer has become an increasingly ubiquitous feature of modern offices, including radiologists' offices, the question has arisen about the effective use of systems on a day-to-day basis. This report describes applications of a relational data-base management system that have been useful in organizing several aspects of the daily work of an academic radiologist over the past 4 years. Although specific hardware and software are described, such personalized applications can be implemented on virtually any microcomputer by means of a variety of commercially available data-base management software.

Applications include archival storage and retrieval of patient and teaching-file databases similar to those described for minicomputers [1, 2, 3] as well as archival storage and retrieval of transparency slides and journal articles. A microcomputer or personal computer that can be dedicated to the data-base requirements of a radiology office is more satisfactory than a minicomputer because computer-disk storage and computer access is unrestricted [4].

Two features of the system make the data-base management system practical: (1) a universal and simple case-coding system and (2) database programs or "command files" that present entry options for storage or retrieval in a structured, menu-driven format.

Methods

The data-base management functions were initially implemented on a variety of microcomputers by means of the dBASE II and dBASE III relational data-base management systems (Ashton-Tate Corp., Torrance, CA).

A common feature of the applications described is a system of case coding that represents radiographic findings with a three-letter code. The first letter represents the major anatomic area examined, the second represents the organ or subdivision involved, and the third represents the disease process involving that organ or subdivision. This simple coding system is used as a tool for storing and retrieving radiographic findings in the clinical-case and teaching-file data bases. Each patient record consists of a fixed record-length of 80 bytes divided into 22 fields. Each individual record contains 9 bytes entered as discrete fields, which are used to encode up to three radiographic findings per patient record. Patient data, including three-letter coding, are entered by a radiologic technologist with the aid of computer programs generated in the dBASE language (command files). The command file presents a series of menu-driven prompts that facilitate data entry. Although the command files themselves are

Received April 21, 1986; accepted after revision June 9, 1986.

[1] Department of Radiology, S-058, Stanford Medical Center, Stanford, CA 94305. Address reprint requests to F. G. Sommer.

AJR **147:1075–1077, November 1986**
0361–803X/86/1475–1075
© American Roentgen Ray Society

relatively lengthy, the general format is indicated in the three menus of Table 1. These three menus are used to ask for the major anatomic region, the organ or subdivision of one region, and the disease process. In addition to patient data, including the patient's name, medical record number, birth date, and scan date, a 38-character field is provided for a brief description of the indications for the scan and/or the patient's diagnosis.

Individual customized clinical data bases have been created for CT body, MR, and sonographic clinical cases and their corresponding teaching files. All may be searched on the basis of user-definable criteria, with the aid of command files. The organization of such searches is based on two primary strategies: either the three-letter codes for radiographic findings or the 38-character code for clinical indication or diagnosis. If the three-letter codes are used, the options are presented in a menu-driven fashion similar to that used for data entry. If the clinical indications or diagnoses are examined, a key word or portion of a desired word is entered and used as the basis for a search. Both types of search rely on the appropriate usage of "string" or character functions. Although the individual data bases contain data for only one type of examination, two or more data bases can be searched simultaneously to allow correlation among imaging techniques. When performing a search, the user is prompted to decide whether search output is to be directed to the terminal screen or to the printer. Although searches of teaching-file data bases, which are quite small, typically require only a few seconds, complete searches of patient data bases, such as the CT-body data base, which contains more than 13,000 entries, may take up to several minutes.

For all the data bases described, the information in any record can be altered retrospectively by an edit function. Primary data-base storage is on hard disk; backup storage of clinical and teaching-file data bases on floppy disks is performed automatically from command files.

Transparency slides of clinical cases, which may include several different types of radiographic examinations, are assigned case numbers. The case number is written on each slide, and each slide is also assigned a letter sequentially. The individual cases are filed physically in numeric order in a slide-storage case. The slides are then entered into a data base that uses the three-letter coding system; single-letter codes are also provided for the radiographic techniques represented. Table 2 is a sample menu from the command file prompting for type of examination. When the slide data base is searched, the opportunity is given to search for several subdivisions, disease processes, and types of radiographic examinations. For major radiology journals and subspecialty journals of interest, an article data base is maintained that again exploits the three-letter coding system and technique coding described. Entry and retrieval of article data are automated by command files.

Discussion

The described applications of personal-computer data base management in an academic radiology enviornment have been useful over the past 4 years and are offered as suggested applications for other radiologists. Although many details of the structure of the coding system and the manner in which searches are performed by the command files have been omitted, the principles behind the data base management applications are most important. Radiologists who desire to create applications such as those described undoubtedly will need customized software to conform to their specific requirements.

The patient data-base information, recorded in separate data bases according to the examination technique, has been particularly helpful. This data base has been used extensively for retrieval of case material for presentation at teaching conferences and seminars and for a variety of retrospective

TABLE 2: **Sample Menu for Type of Radiographic Examination**

Code	Technique
A	Angiogram
B	Barium study
C	CT scan
D	Diagram
H	Histologic/pathologic slide
I	IVP
M	MR image
T	Tomogram
U	Ultrasound (sonogram)
X	Plain X-ray
Z	Other

IVP = intravenous pyelogram (excretory urogram).

TABLE 1: **Sample Data-Base Menus for Three-Letter Coding of Radiographic Findings**

First Letter of Code: Anatomic Area	Second Letter of Code: Abdomen Subdivisions	Third Letter of Code: Type of Disease Process
A Abdomen	A Artery/Aorta	A Abscess/infection
C Chest	B Biliary ducts	C Congenital
E Extremity	D aDrenal	D Diffuse infiltration
N Neck	I Intestine	E Enlargement
O Obstetric	K Kidney	F Fluid (ascites, effusion)
P Pelvis	L Liver	G Good anatomy
S Scrotal	M Muscle	H Hematoma
	N lymph Nodes	L Lymphoma/leukemia
	P Pancreas	M Metastasis
	R Retroperitoneum	N Normal
	S Spleen	O Obstruction/stenosis
	T sTomach	S Stone/calcification
	U Unspecified (= all subdivisions)	T Tumor (primary)
	V Veins	Y cYst
	W Abdominal wall	

clinical studies. For both teaching-file and clinical data bases, the flexibility of search criteria (i.e., a wide variety of material may be searched either via case coding or text fields) maximizes the appropriate case material that can be retrieved.

Most data-base systems for radiology [1–4] have used the American College of Radiology (ACR) code [5] to encode numerically the major anatomic area and pathologic findings in a given examination. A simple letter code rather than a numeric code has several advantages in computer data-base management applications. The letter-coding system is simple and mnemonic and can be assimilated rather quickly; thus, after a short learning period, the user will know that "ALM" means "abdomen, liver metastases" and will not have to look up the code 761.339 in the ACR reference book to properly code this finding. Because a simple letter-coding system is so much easier to use, several findings per case can be entered, increasing the potential for recall of findings of interest on subsequent searches. Simple letter codes require less disk-storage space and are better suited for searches than the ACR coding language, at least when the dBASE relational data-base system is used. In my experience, the categories defined by the three-letter coding system are sufficiently narrow to allow for effective searches.

A perfect system for archival storage and retrieval of transparency slides or radiographic films is difficult to devise. If slides or films are filed solely on a physical basis, a choice must be made to file according to technique, part of the body examined, the disease identified, or a combination of these. Most cases that I photograph for slides include more than one imaging technique and often show several pathologic changes in different anatomic regions. Organization by means of a relational data base provides flexibility to search for slides or films on the basis of any of the aforementioned criteria and maximizes the possibility that the user will find exactly what is required in a search. The computer organization of the slide file as described has been useful for rapidly compiling lists of slides for specific conferences or lectures.

The use of a personal-computer data base for filing articles has advantages and disadvantages. The original reason for setting up this data base was the everyday problem of retrieving recent articles relevant to interesting or problematic clinical cases. If articles of interest are entered into a data base while the journals are being read, not much time is really expended in the data-entry process, and it is easy later to recall all relevant recent articles of interest. One disadvantage of such a procedure is that the journals must be read at the computer, generally in the office rather than at home.

The choice of microcomputer hardware and relational data-base software are probably of secondary importance. Many different personal computers and software packages are available to perform the functions described. The implementation of customized relational data-base routines, although somewhat time-consuming at first, can have great benefits in improving the organization of a radiologist's work life.

REFERENCES

1. Summers R, Axel L. A database for the management of clinical and technical information from MRI imaging. Presented at the annual congress of the American Association for Medical Systems and Informatics, San Francisco, August **1983**
2. Smith DR, Rowberg AA. Data-base management system on a CT scanner computer: application to teaching file and procedure records. *AJR* **1984**;142:1219–1223
3. Thompson WL, Murphy PH, Moore WH, Sonnemaker RE, Long SE, Burdine JA. Integration of database capabilities into a patient reporting system. *J Nucl Med* **1985**;26:770–774
4. Holshouser BA, Bradley WG Jr. Microcomputer patient database management system for MRI facility. *AJR* **1986**;146:871–874
5. American College of Radiology. *Index for roentgen diagnosis.* Chicago: Am Coll Radiol, **1975**

Opinion

Should Radiologists Perform Endoscopy?

Philip Shorvon[1] and Giles Stevenson

Fiberoptic endoscopy has revolutionized diagnostic investigation of the alimentary tract, yet radiologists have generally continued to use barium radiology despite a growing acceptance among clinicians of endoscopy as a primary diagnostic tool [1]. If trends continue, radiologists may no longer be called on to do imaging investigations of the alimentary tract. One alternative is for radiologists themselves to perform endoscopy, but before this can be recommended, a number of questions must be addressed.

To What Extent Should Endoscopy Replace Barium Radiology?

The answers to this question are complex and involve consideration of such factors as "accuracy," cost, safety, availability, and patient preference. These vary from one part of the alimentary tract to another. In the esophagus, barium studies are usually the only investigation needed for the diagnosis of gastroesophageal reflux and are superior to endoscopy for the diagnosis of motility disorders [2]. Many lesions will subsequently require biopsy, but endoscopy is an inappropriate first investigation [3].

In the investigation of dyspepsia, the situation is different. Early enthusiastic studies of endoscopic results revealed major inaccuracies in barium radiology but were biased toward endoscopy [4, 5]. Nevertheless, more recent and better-controlled studies rarely show barium radiology to be as accurate as endoscopy [6], although there may be little difference for significant lesions [7]. To those who perform both examinations, this difference is self-evident, especially for the elderly, the immobile, and those with previous gastric surgery. In the setting of acute upper gastrointestinal bleeding, a barium meal is contraindicated, because barium may preclude angiography and because radiologic identification of a lesion does not necessarily indicate the source of hemorrhage [8]. In addition, endoscopic findings of an adherent clot, a visible vessel, or Doppler-positive ulcer base are prognostic for further bleeding [9, 10], and some lesions are suitable for endoscopic therapy [11].

At present, expense precludes implementation of endoscopy for primary evaluation of dyspepsia in the United States. Because the diagnostic yields of barium meal and endoscopy are similar in cooperative patients [12], it is senseless for patients to pay $350 to $1400 for an endoscopy when they could pay $100 for a barium meal. However, these financial differences are actually outdated, because the skill required to produce good results on a barium-meal examination is greater than that needed to perform a good routine upper gastrointestinal endoscopy, and the actual costs per procedure are similar.

The danger of upper gastrointestinal endoscopy is probably overstressed. Published endoscopic complication rates indicate a morbidity rate of one in 500 cases and a mortality rate of one in 10,000 cases [13], but these figures are from the 1970s and ignore the fact that most problems arise in high-risk patients. These figures are almost certainly an overestimate today, when one considers increasing experience, the use of smaller caliber, more flexible instruments, and the tendency to use less sedation. Barium studies are undoubtedly still safer, although not completely hazard-free. However,

Received March 28, 1986; accepted after revision May 27, 1986.

[1] Both authors: Department of Radiology, McMaster University Medical Centre, 1200 Main St. W., Hamilton, Ontario L8N 3Z5, Canada. Address reprint requests to G. Stevenson.

the same factors that increase the risk of endoscopic complications also impair the quality of the barium-meal examination.

A final argument proposed against endoscopy is that it is an unpleasant procedure and that patients prefer a barium meal. However, there are few studies to determine if this is true [14]. In a study at our institution, two-thirds of patients had a preference for barium meal before undergoing either procedure. However, after having both procedures, 76% preferred endoscopy for any repeat examination (Frost RA, unpublished data).

In the colon, barium enema remains the optimal examination for routine investigation because it is substantially safer [15, 16] and less expensive. Although it can be as accurate as colonoscopy for the diagnosis of cancer [17], it is not always as accurate [18]. For polyp detection, even the double-contrast barium enema is about 10% less sensitive than colonoscopy [19–21], with most false-negative results occurring in examinations of the sigmoid [22]. However, colonoscopy fails to visualize the whole of the right colon in at least 10% of cases. Therefore, flexible sigmoidoscopy and barium enema are a powerful combination [23], potentially more accurate than colonoscopy or barium enema alone. Small polyps (less than 6 mm) still represent a problem, since even when technique is meticulous, barium enema will miss most small polyps. Half of them will be adenomatous with possible long-term, malignant potential. However, the chance of established malignancy in these tiny polyps is vanishingly small, and flexible sigmoidoscopy before barium enema would detect most of them. In inflammatory bowel disease colonoscopy is reserved for special indications [24], mainly to clarify radiologic appearances or obtain histologic material. The advent of the polyethylene-glycol–based oral purgation has so improved the accuracy of colonoscopy in patients with acute rectal bleeding that it is now probably the imaging investigation of choice.

ERCP is particularly suitable for radiologists to perform since the endoscope is used purely to facilitate a variety of diagnostic and therapeutic radiologic maneuvers. Therapeutic ERCP is increasing in popularity, versatility, and availability, and is probably safer than percutaneous procedures, as well as more comfortable for the patient. A variety of combined endoscopic/percutaneous techniques have been described [25–27]. The radiologist who is able to perform both techniques can more readily select the one that is most appropriate and change or combine the two as necessary.

Is It Appropriate for Radiologists to Perform Endoscopy?

It can be argued that endoscopy is not a radiologic procedure and therefore should not be performed by radiologists. This "purist" approach ignores the expansion of radiology beyond the narrow band of electromagnetic radiation into several new spheres of activity, such as sonography, thermography, nuclear medicine, and MR. Endoscopy is just another form of medical imaging, and there are compelling reasons to conclude that it is a suitable activity for radiologists. All physicians who perform endoscopy have found that directly viewing the mucosa considerably improves their ability to interpret barium radiographs.

Radiologists are in a unique position to influence the optimal use of barium radiology and endoscopy. A decade of endoscopy performed mainly by gastroenterologists has resulted in many patients still having inappropriate barium studies. If the cost of endoscopy can be reduced to that of barium studies, physicians will wish to obtain endoscopic examinations for some of their patients who currently have barium meals. Furthermore, many referring physicians may desire endoscopy by someone other than a gastroenterologist, because they do not wish to surrender clinical care of their patients, and some gastroenterologists do not accept the concept of endoscopy as a limited diagnostic encounter [28]. Radiologists are accustomed to acting as diagnosticians who do not take over the care of patients, and they already have the administrative framework with which to provide specific diagnostic services.

Closer cooperation between endoscopists and radiologists encourages a more integrated approach to gastrointestinal imaging, regardless of who actually performs the endoscopy [29]. Placing the endoscopy unit within the radiology department has many advantages, not the least of which is including the cost of endoscopy service in the radiology department budget. It also facilitates selection of the most appropriate procedure by the physicians actually performing the investigations. The fusion of endoscopic and radiologic services should facilitate research in areas that currently bridge the two specialties, such as endoscopic sonography [30], percutaneous gastrostomy [31, 32], and balloon dilatation of strictures [33–35].

Is It Feasible for Radiologists to Perform Endoscopy?

In some countries, gastrointestinal radiologists are already performing fiberoptic endoscopy. These are predominantly countries in which medical remuneration is not based on fee-for-service, and many gastroenterologists have been eager to train physicians from other specialties to provide endoscopic services.

In 1984, a number of radiologists who practice endoscopy in Great Britain formed a group that now has 35 members, and in January 1986 the British Institute of Radiology held its first conference devoted to endoscopy. Great advances have been made in gastrointestinal radiology and endoscopy in Japan, in part because so many physicians there practice both endoscopy and barium radiology. In Scandinavia, radiologists have been performing endoscopy for over a decade, and in Sweden they form an integral part of all endoscopic services [20].

For the last 2 years, surgical societies in North America have organized endoscopy workshops, as part of national efforts in Canada and the United States to promote the acceptance of endoscopy performed by surgeons. Individual surgeons have been frustrated in attempts to learn and practice endoscopy. The involvement of national surgical societies to establish endoscopy as a surgical residency training requirement was needed before substantial progress could be

made. Specific training in endoscopy for radiologists is now becoming available, but the involvement of substantial numbers of radiologists would probably similarly require the support of national radiologic societies.

American radiologists have lagged behind in the use of endoscopy because they have been reluctant to come into conflict with colleagues in gastroenterology, and also because CT and sonography have provided a challenge to compensate for the decline in numbers of barium studies. However, in other countries, such considerations have not prevented radiologists from successfully integrating endoscopy, along with the newer imaging techniques, into a broader concept of gastrointestinal radiology.

Radiologists will undoubtedly find it a struggle to set up endoscopic services in some situations, and ultimately each individual will decide whether the advantages outlined are worth the effort. Several difficulties may be encountered. (1) Adequate training may be difficult to obtain, since only a few centers in North America now offer teaching in endoscopy for radiologists. (2) Other specialists already performing endoscopy may object, and good professional relationships may suffer damage. Such considerations have not noticeably kept obstetricians, gynecologists, and cardiologists from setting up imaging facilities. (3) Clinicians may be reluctant to allow radiologists to assume the clinical responsibility implicit in performing endoscopy, although similar responsibilities are already commonplace for radiologists who do angiography and interventional techniques [36, 37]. (4) Difficulties may occur in obtaining referrals and therefore in establishing credibility as an endoscopist.

In summary, although barium radiology is still important, endoscopy has replaced it as the primary procedure in many clinical settings. Because of this, radiologists who wish to maintain a major interest in the diagnosis of alimentary-tract disease will find it difficult to do so without performing endoscopy. They will initially find it hard to establish endoscopy as part of their practice, but surgeons in the United States have demonstrated that such shifts in turf boundaries can be achieved without loss of good professional relationships. Radiologists abroad have already shown the feasibility of taking part in endoscopy and have been accepted in this role by their clinical colleagues. This involvement enhances radiologic practice and helps to achieve the goal of providing a flexible diagnostic service that offers patients the most appropriate tests with as few visits as possible.

REFERENCES

1. Dooley CP, Larson AW, Stace NH, et al. Double contrast barium meal and upper gastrointestinal endoscopy: a comparative study. *Ann Intern Med* **1984**;101:538–545
2. Ott DJ, Dodds WJ, Wu WC. Current status of radiology in evaluating gastroesophageal reflux disease. *J Clin Gastroenterol* **1982**;4:365–375
3. Edwards DAW. The problem of diagnosing reflux. In: Salmon PR, ed. *Gastrointestinal endoscopy: advances in diagnosis and therapy*, vol 1. London: Chapman and Hall, **1984**:142–153
4. Cotton PB. Fibreoptic endoscopy and the barium meal—results and implications. *Br Med J* **1973**;2:161–165
5. Tedesco FJ, Griffin JW, Crisp WL, et al. "Skinny upper gastrointestinal endoscopy"—the initial diagnostic tool. *J Clin Gastroenterol* **1980**;2:27–30
6. Cotton PB, Shorvon PJ. Analysis of endoscopy and radiography in the diagnosis, follow-up and treatment of peptic ulcer disease. *Clin Gastroenterol* **1984**;13:383–403
7. Gelfand DW, Ott DJ, Munitz HA, et al. Radiology and endoscopy: a radiologic viewpoint. *Ann Intern Med* **1984**;101:550–552
8. Silverstein FE, Gilbert DA, Tedesco FJ, et al. The national American Society of Gastrointestinal endoscopy (ASGE) survey on upper gastrointestinal bleeding. *Gastrointest Endosc* **1981**; 27:94–102
9. Foster DN, Miloszewski KJ, Losowski MS. Stigmata of recent hemorrhage in diagnosis and prognosis of upper gastrointestinal bleeding. *Br Med J* **1978**;2:1173–1177
10. Beckly DE, Casebow MP. Prediction of rebleeding from peptic ulcer: experience with an endoscopic Doppler device. *Gut* **1986**; 27:96–99
11. Swain CP, Salmon PR. Gastrointestinal bleeding—the upper gastrointestinal tract. *Scand J Gastroenterol* **1984**;19(Suppl 102):53–60
12. Laufer I, Mullens JE, Hamilton J. The diagnostic accuracy of barium studies of the stomach and duodenum—correlation with endoscopy. *Radiology* **1975**;115:569–573
13. Cotton PB, Williams CB. Upper gastrointestinal endoscopy—complications and precautions. In: *Practical gastrointestinal endoscopy*, 2nd ed. London: Blackwell, **1982**:44–46
14. Lichtenstein JL, Feinstein AR, Suzio KD. The effectiveness of panendoscopy on diagnostic and therapeutic decisions about chronic abdominal pain. *J Clin Gastroenterol* **1980**;2:31–36
15. Masel H, Masel JP, Casey KV. A survey of colon examination technique in Australia and New Zealand with a review of complications. *Australas Radiol* **1971**;15:140–147
16. Abrams JS. A second look at colonoscopy. *Arch Surg* **1982**;117:913–917
17. Kelvin FM, Gardiner R, Vas W, Stevenson GW. Colorectal carcinoma missed on double contrast barium enema study: a problem in perception. *AJR* **1981**;137:307–313
18. Gilbertsen VA, Williams SE, Schuman L, McHugh R. Colonoscopy in the detection of carcinoma of the intestine. *Surg Gynecol Obstet* **1979**;149:877–878
19. Waye JD, Braunfield S. Surveillance intervals after colonoscopic polypectomy. *Endoscopy* **1982**;14:79–81
20. Fork FT. Double contrast enema and colonoscopy in polyp detection. *Gut* **1981**;22:971–977
21. Williams CV, Macrae FA, Bartram CI. A prospective study of diagnostic methods in adenoma follow up. *Endoscopy* **1982**;14:74–78
22. Ott DJ, Gelfand DW, Wu WC, et al. Sensitivity of double contrast barium enema: emphasis on polyp detection. *AJR* **1980**; 135:327–330
23. Farrands PA, Vellacott KD, Amar SS, et al. Flexible fibreoptic sigmoidoscopy and double contrast barium enema examination in the identification of adenomas and carcinoma of the colon. *Dis Colon Rectum* **1983**;26:727–729
24. Teague RH, Waye JD. Inflammatory bowel disease. In: Hunt RH, Waye JD, eds. *Colonoscopy*—techniques, clinical practice and colour atlas. London: Chapman and Hall, **1981**:343–362
25. Passi RB, Rankin RN. The transhepatic approach to a failed endoscopic sphincterotomy. *Gastrointest Endosc* **1986**;32:221–225
26. Shorvon PJ, Cotton PB, Mason RR, et al. Percutaneous transhepatic assistance for duodenoscopic sphincterotomy. *Gut* **1985**;26:1373–1376

27. Kerlan RK, Pogansi AC, Ring EJ, et al. Biliary endoprosthesis: insertion using a combined peroral transhepatic method. *Radiology* **1984**;150:828–830
28. Spiro H. Endoscopy: a brief encounter. *J Clin Gastroenterol* **1980**;2:323–325
29. De Luca WA. The G.I. unit as a centralised interdepartmental hospital division. *J Clin Gastroenterol* **1980**;2:219–220
30. Cotton PB, Shorvon PJ, Lees WR. Endoscopic ultrasonography, a new look from within. *Br Med J* **1985**;290:1373
31. Ho CS, Gray RR, Goldfinger M, et al. Percutaneous gastrostomy for enteral feeding. *Radiology* **1985**;156:349–351
32. Gottfried EB, Plumser AB. Endoscopic gastrojejunostomy: a technique to establish small bowel feeding without laparotomy. *Gastrointest Endosc* **1984**;30:355–357
33. Dawson SL, Mueller PR, Ferrucci JT, et al. Severe esophageal strictures: indications for balloon catheter dilatation. *Radiology* **1984**;153:631–635
34. Graham DY, Smith JL. Balloon dilatation of benign and malignant esophageal strictures. *Gastrointest Endosc* **1985**;31:171–174
35. Kozarek RA. Hydrostatic balloon dilatation of gastrointestinal stenoses: a national survey. *Gastrointest Endosc* **1986**;32:15–19
36. Ring EJ, Kerlan RK. Inpatient management: a new role for interventional radiologists. *Radiology* **1985**;154:543
37. Evens RG. The radiologist as an attending physician: routine or special procedure? *Radiology* **1985**;154:545–546

The Society of Uroradiology: Abstracts from 1986 Meeting

Dedication

The Scientific Session of this meeting was dedicated to the memory of John Hodson, Professor Emeritus of Diagnostic Radiology at the Yale University School of Medicine who died on December 2, 1985, at the age of 69. I worked under him for 10 years, and many of you knew him for a longer time as a colleague and friend.

Although John was a member of many clubs and societies, the group that meant the most to him was the Society of Uroradiology. Many of us looked to him for advice and saw him as the prototypical model of what an academic uroradiologist should be. He consistently enlivened the society's scientific sessions with his knowledge and wit. It is appropriate that we dedicate this meeting to him because of his achievements in our field.

His career spanned many exciting changes in radiology. After receiving his medical degree in 1939 from London University followed by training in radiology, John served as a radiologist with the Royal Army Medical Corps in North Africa and Italy and had the distinction of being cited in dispatches in 1944 for his efforts. He had a number of subsequent appointments including Director of Radiology at University College Hospital in London, Chairman of Radiology at Memorial Hospital in Newfoundland, and Chief of Uroradiology at Yale.

By the time John had reached his 40s, he had achieved an international reputation primarily in his major field of interest, chest radiology. At this point in his career, when many would have rested on their laurels, he became interested in a number of unanswered problems regarding radiology of the urinary tract. You are all familiar with his uroradiology research, which occupied the rest of his life including his so-called retirement. He made observations that led to a clear definition of a number of radiologic patterns related to the kidney. He also devised a series of experiments that had a significant impact on pediatrics, pathology, and medicine, as well as radiology. His work taught us the pathophysiology of reflux nephropathy and showed us how to treat it and how to prevent it. Without a doubt, he was one of the outstanding researchers of our time.

John had many loves. He cared for his son, Ian, perhaps more than he cared for himself, and was justifiably proud of him. He loved people of all ages. Many of the fellows and residents coming through our department found a genuine friend in him. He treated them with dignity and offered them companionship and help. Finally, John loved the outdoors no matter what the weather. He listed his hobbies as "mountains, sailing, gardening, watercolor painting, and kidneys." Much of his free time was spent in the forest around his Connecticut home. He told his friends to come by on the weekend, but not to call before they came, because then he would have to go inside to answer the phone.

He did everything with an exactness that impressed all of us. His research was technically perfect. His watercolors were painstakingly plotted on a grid to reproduce the landscape with mapmaker's accuracy. His words were always carefully chosen. John was intimate with the classic languages. He coined the term "lobar nephronia" to reflect focal infection of the kidney, not just because he had once been a chest radiologist, but because he believed it was exactly the right phrase. When I tried to use the term "lobar testonia" to describe focal infection of a lobe of the testis, he became very upset. It turned out that he was not upset at my using a new term, but at my mixing the Greek word "lobe" with the Latin word "testis". It had to be "lobar orchonia," he explained to me, and so it was.

When Bob Hattery and I discussed the dedication of this session to John, the question of his name came up. For years, he had been C. John Hodson, but at the end of his life he was only John Hodson, and, in fact, he was adamant in refusing to have the initial "C" on papers. After talking to Bob, I looked up the name "Cecil," which is what the "C" stood for, and its derivation. It comes from the Latin adjective meaning "blind" or "dim-witted," which I think explains everything. Can you image John Hodson signing his name to reports 20 times a day, "dim-witted John Hodson"? He kept the "C" to humor those who had named him, but in the end he wanted his name exactly right.

There was another side to John, however. He could seem to be crusty, demanding, and difficult. In part, this was due to his background, for he grew up in staid pre–World-War-II Britain as an athlete, and he was a member of a generation of whom it might aptly be said that for them the war should

have never ended and they should never have grown too old to play rugby. In fact, John coached the Yale rugby team until he became ill. But more than his British background was responsible for John's behavior. It reflected his inability to tolerate inaccuracy and inexactness. He suffered fools poorly and he pursued the truth with a relentless honesty both in medicine and in life. This, at times, masked the real John Hodson.

The real John Hodson was an impressive man. The lesson he taught his residents, fellows, and colleagues was an important one: to look for "the blood behind the silver." Those were his own words, "the blood behind the silver," by which he meant that we should be concerned with the patient and not just the X-ray. He cared about the patient. His interest in "the blood behind the silver" and not a desire for academic success led him to his outstanding work.

He not only cared about the fellows, residents, and students he trained and befriended, he also cared about animals and plants. Once he made plans with some of the residents and fellows to cut down several dead trees at the periphery of his yard, which was adjacent to a forest. For days before the event, he plotted the exact way the trees should be cut down so that they would fall into the grassy yard instead of back into the forest. "Why not just let them fall into the forest?" his friends asked. He explained that he did not wish to damage the young trees in the forest.

He will be missed by his colleagues and friends, including the members of this society, who profited from his companionship, aid, and advice. The millions of young people whose renal disease is being correctly diagnosed and treated and whose lives are being changed because John Hodson cared about the "blood behind the silver" serve as his best memorial. And so we, the Society of Uroradiology, are using our Scientific Session to say good-bye to this scholar, to this physician, to this man who looked for the blood behind the silver. For him, the Romans had the most appropriate parting phrase, one that John would have understood, "Ave atque Vale," "Hail and Farewell".

Arthur T. Rosenfield
Yale University School of Medicine
New Haven, CT 06510

The Society of Uroradiology met in Scheveningen/The Hague, Holland, May 3 and 4, 1986. The following abstracts were presented at the meeting.

Contents

Advantages of nonionic contrast media for intravenous use. Fischer HW, Spataro R, Katzberg R, Morris T
The accuracy and reproducibility of a new contrast-clearance method for the determination of glomerular filtration rate. O'Reilly PH, Golman K
Glomerular filtration response to acute ureteral obstruction in the dog. Katzberg RW, Morris TW, DiMarco PL, Merguerian PA, Ventura JA, Linke CA, Fischer HW
Nonionic and ionic contrast material urography with mannitol. Lovett I, Benn R, Doust B, Benness GT
Patient attitudes about written informed consent for intravenous contrast-enhanced radiographic studies. Spring DB, Winfield AJ, Moss AA, Friedland G, Preger L, Eisenberg R
Results of PTA of renal arteries in patients with secondary singular kidneys, report of 20 cases. Lohr E, Kruger KG
Therapeutic segmental renal embolization. Chuang VP
Intercostal space nephrostomy for percutaneous stone removal. Picus D, Weyman PJ, Clayman RV, McClennan BL
Role of percutaneous procedures and ESWL in staghorn calculi. Pfister RC, Yoder IC, Papanicolaou N
Extracorporeal shock-wave lithotripsy: The radiologic experience after 1000 cases. Cochran ST, Barbaric ZL, Paranay G
Survey of complications of percutaneous stone extraction, dissolution or ultrasonic lithotripsy. Lang EK, McClennan B, Dunnick NR
Renal medullary calcification: Microradiographic studies of patterns and distribution. Olson SR, Clark RL, Cuttino JT
Changing patterns in the etiology of newborn hydronephrosis. Brown T, Mandell J, Lebowitz RL
Neonatal aortic thombrosis: Radionuclide and ultrasound diagnosis. Vailas G, Brouillette RT, Scott JP, Shkolnik MA, Conway JJ, Wiringa K
Imaging of paediatric renal tuberculosis. Cremin BJ
Vesicoureteral reflux in boys: a review of 196 cases. Sinai L, Ami TB, Hertz M, Boichis H
The incidence of vesicoureteral reflux in newborns with myelodysplasia. Fernbach SK, Conway JJ
Traumatic urethral fistulae in spinal cord injury patients: sonographic diagnosis. Perkash I, Friedland GW, Miller L
Results of tissue biopsy in renal transplant patients whose sonograms show collecting system thickening. Cunningham JJ
Acute hemorrhagic focal bacterial nephritis: findings on B-scan ultrasonography and computed tomography. Rigsby CM, Rosenfield AT, Glickman M, Hodson J
Comparison of computed and film-screen excretory urography: accuracy, certainty and costs. Hillman BJ, Fajardo L, Hunter TB, Claypool HR, Mockbee WB
Needle puncture of cystic renal masses: a survey of the membership of the Society of Uroradiology. Amis ES, Cronan JJ, Pfister RC
Spontaneous disappearance of hemorrhagic renal cysts: CT observations. Friedland GW
Accuracy and cost of examination sequences in renal mass evaluation. Fritzsche PJ, McDonald D, Holden B
Infiltrative growth in the kidney revisited: CT-sonographic-pathologic correlation. Hartman DS, Davidson AJ, Davis CJ, Goldman SM
Radiology of direct metastases to the ureter. Spataro RF, Totterman S, DeMarino G, Miller T, Rubens D, Katzberg RW
Uroepithelial metastases from hypernephroma. Mitty HA, Born R, Droller M
Intraarterial doxorubicin infusion treatment without and with temporary occlusion of the renal artery in rabbit renal VX-2 carcinoma. Gadeholt G, Gothlin JH
Magnetic resonance imaging in the detection and staging of carcinoma of the prostate. Spataro R. Thornbury JR, Cockett ATK, Disantagnese AP
Diagnostic and treatment impact of MR versus CT in staging of early carcinoma of the cervix. Thornbury JR, Rubens D, Weiss SL
Initial clinical experience with spectroscopic imaging by quadrature modulated echo time shifting. Friedenberg RM

Advantages of Nonionic Contrast Media for Intravenous Use: Fischer HW, Spataro R, Katzberg R, Morris T (Univ. of Rochester Medical Center, Rochester, NY 14642)

Evidence has now been obtained that compared to an ionic contrast medium, a nonionic medium liberates less histamine, inhibits acetylcholine-esterase less, and activates complement less, produces less bronchospasm, produces less depression of serum calcium ion and causes fewer EKG changes as well as producing less nausea and vomiting. When used in angiocardiography, pulmonary angiography and coronary arteriography, fewer hemodynamic disturbances and cardiac dysfunctions are produced. These new nonionics bind less to serum albumen (are more hydrophilic), alter the blood-brain barrier less and are of lowered neurotoxicity compared to the ionics. Independent of what single theory to explain adverse contrast media reactions one prefers, the radiologist is led to expect from this evidence that fewer adverse reactions - minor, intermediate, or severe, will result from the use of nonionics when used for intravenous urography and enhanced CT scanning. Preliminary evidence indicates this is so and there is preliminary evidence that patients who had a previous reaction to an ionic medium will be less likely to have a reaction to a nonionic one.

We have begun a study comparing the nonionics to the ionics in previous reactor patients and in patients with a true history of allergy and we are comparing the effects on systemic blood pressure and heart rate in intravenous administration.

The Accuracy and Reproducibility of a New Contrast-Clearance Method for the Determination of Glomerular Filtration Rate: O'Reilly PH, Golman K (Stepping Hill Hospital, Stockport, Manchester, UK; Malmo General Hospital, Univ. of Lund, Malmo, Sweden)

The results of an investigation into the accuracy and reproducibility of a new method for the determination of glomerular filtration rate are presented. The technique involves the determination of the clearance of iodinated contrast media from the plasma by an x-ray fluorescence method using purpose designed equipment. One hundred and eight patients were studied, 75 had simultaneous i.v. injection of 100 ml iohexol (Omnipaque^{R}) and 3.7MBq 51-Cr-EDTA. Venous samples were taken into heparinised syringes at hourly intervals for 4 hours. The plasma samples were divided into two for individual blind analysis of 51-Cr-EDTA and iohexol clearance. The procedure was repeated in 33 cases using half the dose of contrast. Twenty-four patients had simultaneous creatinine clearance measurement. The results showed excellent correlation between iodine and EDTA clearance using 100 ml contrast ($r=0.92$; $p=0.00001$) and 50 ml contrast ($r=0.88$; $p=0.00001$); creatinine clearance showed a weaker correlation with EDTA ($r=0.70$; $p=0.0009$). Reproducibility was good, variation between 60 studies over 6 weeks being 2ml/min - 10ml/min (mean 5.9ml/min). The technique is easy to perform , can be used as an adjunct to urography, CT and angiography and can be repeated for serial studies. The relative accuracy of present methods for determination of GFR will be discussed.

Glomerular Filtration Response to Acute Ureteral Obstruction in the Dog: Katzberg RW, Morris TW, DiMarco PL, Merguerian PA, Ventura JA, Linke CA, Fischer HW (Univ. of Rochester Medical Center, Rochester, NY 14642)

The glomerular filtration rate (GFR) has not been previously assessed in the whole kidney during complete ureteral obstruction. Timed urine collection clearance techniques are unsuitable for GFR measurements during ureteral obstruction since they require urine collections which would necessitate release of the obstruction. Our results show a 57% increase in renal blood flow (baseline: 203.8 ± 50.9 vs. 319 ± 69.4 ml/min at 105 minutes; $n = 7$) that was associated with monophasic decrease in filtration fraction to -70% at 120 minutes (0.26 ± 0.025 vs 0.08 ± 0.007) and an increase in ureteral pressure to 63.1 ± 6.1 mmHg at 120 minutes. A biphasic GFR response was noted with an initial small increase (baseline: 32.5 ± 7.5 vs. 36.3 ± 11.0 ml/min at 2 minutes) followed by a continual decline to -55% at 120 minutes (14.5 ± 2.6 ml/min). The techniques employed in this investigation provide a model to further explore whole kidney renal physiology with mechanical obstruction.

Nonionic and Ionic Contrast Material Urography with Mannitol: Lovett I, Benn R, Doust B, Benness GT (St. Vincents Hospital, Sydney, Australia)

While nephrogram quality mostly depends on blood contrast material (iodine) concentration and the renal blood flow, the pyelogram quality depends on urinary contrast material (iodine) concentration and diuresis.

This study was designed to compare the nephrogram and pyelogram (concentration and filling) quality with ionic contrast material and non-ionic contrast material with and without mannitol 25% (0.5ml/kg) diuresis.

A pilot study of 29 patients had randomized I.V. urography with contrast material doses of 300 mgI/kg. There was no prior fluid restriction. The I.V. injection was completed in 1 minute. Nephrogram films at 1, 2 and 5 minutes and pyelogram films at 2, 5, 10 and 20 minutes were compared with 2 selected studies (A and B). Better than A was graded excellent, between A and B was average and inferior to B was graded poor. The studies were graded by two radiologists who were blinded with regard to the contrast material chosen. Preinjection and post study urine samples were collected and urinary osmolality and urinary contrast material (iodine) concentration were measured.

Iopamidol, iopamidol and mannitol and urografin were administered in osmotic loads of 680 mO/kg, 1366 mO/kg and 1540 mO/kg respectively.

The results show that nephrogram quality was superior with iopamidol alone and that mannitol diuresis reduced the quality. Urografin was inferior to both. The pyelogram sequence showed iopamidol alone was superior to iopamidol with mannitol and urografin (equal). The preinjection urinary osmolality varied between 1117-210 mO/kg. The urinary iodine concentration was higher in the iopamidol group.

The study suggests that for equal iodine doses, urogram quality is improved when the osmotic load is reduced.

Patient Attitudes About Written Informed Consent for Intravenous Contrast-Enhanced Radiographic Studies: Spring DB, Winfield AJ, Moss AA, Friedland G, Preger L, Eisenberg R (Univ. of California, San Francisco, CA 94143)

In a multi-institutional study we surveyed over 1,000 patients having contrast-enhanced CT or urographic procedures concerning their feelings about reading written patient information describing some of the risks associated with radiographic contrast material. About 90% of patients said they preferred receiving information about risks. Ninety-one percent said their referring physician did not discuss any of the risks of the test with them.

Limitations in obtaining a truly informed consent were not uncommon and included true medical emergencies in 4% and limited understanding of risk disclosure information in 12% (comatose/semi-comatose (2.6%), aphasia (0.9%), dementia (1.5%), medication (0.7%), psychiatric problems (0.8%), inability to read (2.4%)). Two percent of patients were minors. Practical limitations of adequate risk disclosure are common but most patients desire and accept information about the risk of common minor and uncommon major adverse reactions.

Results of PTA of Renal Arteries in Patients with Secondary Singular Kidneys, Report of 20 Cases: Lohr E, Kruger KG (Univ. of Essen, FRG)

On the background of 280 patients treated by means of balloon dilatation because of stenosis of renal arteries, a follow-up study of 20 patients with singular kidneys is carried out. Four patients reached normal pressure ratios without any drug; in this group also creatinine reached normal values. In 7 cases the creatinine values did not change at all.

Complications: Out of 20 patients with 25 PTA's.

Dissection of the main artery with subtotal occlusion occured once;

Infarction of one lobar vessel without clinical manifestation (once).

General: Aneurysm due to puncture (1); fat embolism in the periphery.

Four of the group of 20 patients died owing to operation, not in immediate connection with the previous PTA.

The rate of complications is therefore remarkably higher than for the group with 2 kidneys where the whole rate of severe incidents ranges below 5%.

Therapeutic Segmental Renal Embolization: Chuang VP (Emory Univ. Hospital, Atlanta, GA 30322)

Segmental renal artery embolization (SRAE) can be utilized to treat lesions involving segmental renal artery in order to preserve residual renal parenchyma and to avoid nephrectomy. SRAE was performed in 20 patients for (1) post-trauma hemorrhage, (2) hypertension from segmental FMD, (3) congenital AVM, (4) solitary kidney with carcinoma, (5) pseudo-aneurysm following nephrostomy and PTA, and (6) post-biopsy AVF. The embolization materials included autogenous clot, gelfoam, Invalon, coil, ethanol, and barium sulfate. SRAE was successful in total or partial control of bleeding, hematuria, pain, or hypertension in these patients. No immediate complication developed from the embolization procedure. One patient had delayed hypertension requiring medication. One patient with solitary kidney required repeat embolizations for control of recurrent carcinoma over a four-year period. In summary, SRAE is a valuable method for the treatment of segmental renal disease prior to nephrectomy.

Intercostal Space Nephrostomy for Percutaneous Stone Removal: Picus D, Weyman PJ, Clayman RV, McClennan BL (Mallinckrodt Institute of Radiology, Washington Univ. School of Medicine, St. Louis, MO 63110)

Percutaneous removal of renal and ureteral calculi requires an accurately placed nephrostomy to provide the most direct access for stone manipulation. The standard nephrostomy, entering through a middle or lower pole calyx, does not provide optimal access for ureteral, upper pole renal, or large staghorn calculi. For treating these stones, we have found an intercostal, upper pole approach to be most efficacious.

We have used an intercostal approach to percutaneous stone removal in 50 of our last 122 patients. All calculi were successfully removed - 9 calyceal, 24 ureteral and 17 staghorns. In all cases, a chest x-ray was obtained immediately following the procedure. Complications included pneumothorax in 6 patients (12%) and hydro-urothorax in 2 patients. Four patients (18%) had chest tubes placed. These complications were felt to be due to air and/or fluid leaking through the wound when the working sheath was not in place.

The intercostal upper pole approach provides direct access to both upper pole and ureteral calculi, thus facilitating their removal. The straight tract permits the use of a rigid nephroscope for many of these stones, thereby allowing the use of larger grasping instruments, as well as ultrasonic lithotripsy. For staghorn calculi, the upper pole approach allows access to the ureter, as well as to the pelvic and lower pole portions of the stone. The intercostal approach to percutaneous stone removal greatly facilitates extraction of upper pole, ureteral, and staghorn calculi. Although the morbidity is slightly higher than the more traditional lower or middle pole approach, complications can generally be avoided by using a working sheath and placing a nephrostomy tube following the procedure.

Role of Percutaneous Procedures and ESWL in Staghorn Calculi: Pfister RC, Yoder IC, Papanicolaou N (Massachusetts General Hospital, Boston, MA 02114)

Large renal stones particularly the staghorn variety are difficult to treat. The residual calyceal stone fragment rate is significant when managed by percutaneous ultrasonic lithotripsy (PUL) and extraction only.

Prolonged ureteral obstruction is the usual outcome if staghorn calculi are only fragmented by the extracorporeal shock wave lithotriptor (ESWL) due to the excessive volume of granulated stone particles.

Currently in most cases, initial debulking of large stones by PUL is performed, followed by ESWL of the remaining retained calyceal stone fragments. Occasionally, in non-oxalate calculi, stone dissolution of post PUL and/or ESWL fragments is carried out through nephrostomy catheters. If a decompression percutaneous nephrostomy tube is needed for ESWL ureteral obstruction the usual 8-10 Fr catheters frequently become obstructed by stone debris; the larger continuous pyeloureteral catheter (24-8 Fr) is advantageous in this situation.

Extracorporeal Shock-Wave Lithotripsy: The Radiologic Experience After 1000 Cases: Cochran ST, Barbaric ZL, Paranay G (Univ. of California, Los Angeles, CA 90024)

Over 1000 extracorporeal shock-wave lithotripsy (ESWL) procedures have been performed at our institution. The impact this technology makes in a genitourinary radiology practice is quite significant.

Supine abdomen films and renal ultrasound studies are routine to follow the progress of stone discharge and monitor for obstruction. IVP, CT and MRI are used in a small percentage of cases following ESWL to monitor lucent stones and detect complications such as perinephric bleeding.

Percutaneous interventional procedures were needed in more than 10% of patients undergoing ESWL. These procedures were performed pre-ESWL to debulk large stones, or when the urologists were unable to dislodge a stone from the ureter or place a stent past the stone, or when the ureter was perforated during retrograde manipulation. These procedures were performed post-ESWL when the patient developed sepsis because of obstruction, or there was progressive dilatations and obstruction with poor passage of stone fragments, or pain was uncontrollable with narcotics.

Survey of Complications of Percutaneous Stone Extraction, Dissolution or Ultrasonic Lithotripsy: Lang EK, McClennan B, Dunnick NR (Louisiana State Univ. Medical Center, New Orleans, LA 70112)

An apparent rise in the incidence of complications attendant to percutaneous stone extraction and ultrasonic lithotripsy is investigated by means of a mail survey. Two hundred and eighty-six (286) questionaires have been mailed to North American institutions and/or urologists and radiologists; 72 to major foreign institutions and investigators. Returns (in progress) have been received and are tabulated. The complications reported are grouped into those attributable to "learning experience", variance of anatomy, attendant specific techniques, faulty techniques and underlying conditions.

Recommendations to avoid such complications will be based particularly on the findings in the groups "anatomical variance", "underlying conditions:, and "attributable to technique". Recommendations to modify or expand the preprocedural diagnostic workup to identify such variance as posterior locations of the colon and/or spleen will be formulated on basis of their statistical prevalence. Modifications of accepted techniques will be recommended if incriminated for a high incidence of complications. Similarly certain conditions predisposing to complications will be identified and modifications of management suggested.

Renal Medullary Calcification: Microradiographic Studies of Patterns and Distribution: Olson SR, Clark RL, Cuttino JT (Univ. of North Carolina School of Medicine, Chapel Hill, NC 27514)

Although microcalcifications frequently occur in the "normal" medulla, the progression of these mineral deposits to clinically apparent calculi has been difficult to document. Recently Bruwer suggested a new concept of stone formation, and his paper (Primary Renal Calculi: Anderson-Carr-Randall Progression? AJR 132:751, 1979) stimulated us to attempt to confirm his hypothesis.

Radiography of 144 grossly normal autopsy kidneys identified 84 containing parenchymal calcifications. A detailed study of involved areas using microradiographic and histologic techniques were performed.

Our results again document the striking frequency of medullary microcalcification. These deposits were usually present in the pertibular regions of the inner medulla and/or papilla. Less commonly, small stones were found in the suburothelial region of the calyceal fornix.

This study suggests that most primary calculi originate as mineralization in the papillary interstitium. Progressive conglomeration of the most superficial calcifications causes eventual erosion of the papillary surface resulting in calyceal access and the formation of "Randall's plaques". When a well anchored papillary nidus develops, continued calculus growth may occur if suitable environmental factors are present. We do not support Bruwer's hypothesis that papillary tip microcalcification migrates from the inner medulla.

Changing Patterns in the Etiology of Newborn Hydronephrosis: Brown T, Mandell J, Lebowitz RL (The Children's Hospital, Boston, MA 02115)

The detection of hydronephrosis in the fetus by ultrasonography has led to better understanding of hydronephrosis in the newborn infant.

During the thirty-year period, 1947-1977 (the pre-ultrasound era) 146 patients with significant neonatal hydronephrosis were seen. The majority were discovered because they had signs and/or symptoms - either an abdominal mass (an enlarged kidney or bladder) or urosepsis. The three most common conditions were obstruction of the ureteropelvic juntion (22%), posterior urethral valves (19%), and ectopic ureterocele (14%). During this period, 53 patients with multicystic dysplastic kidney were discovered (2 per year or 1 for every 3 patients with hydronephrosis).

During the six-year period, 1979-1985 (the ultrasound era) 141 patients with significant neonatal hydronephrosis have been seen. Seventy percent were discovered on fetal screening during maternal ultrasonography. (Maternal/fetal intervention was virtually never indicated.) Most babies were asymptomatic. The most common conditions were obstruction of the ureteropelvic junction (41%) and obstruction of the distal ureter (23%) (usually primary megaureter). Hydronephrosis associated with duplex anomalies accounted for 13% and posterior urethral valves 10% of the total. Seventeen patients with multicystic dysplastic kidney were seen (3 per year or 1 for every 8 patients with hydronephrosis).

This dramatic increase in the number of patients found to have neonatal hydronephrosis is primarily due to the widespread use of obstetrical ultrasonography and concomitant fetal screening. The previous pattern of etiologies represented the incidence of symptomatic lesions. The current pattern more accurately reflects the true incidence of congenital anomalies of the urinary tract.

Neonatal Aortic Thombrosis: Radionuclide and Ultrasound Diagnosis: Vallas G, Brouillette RT, Scott JP, Shkolnik MA, Conway JJ, Wiringa K (Children's Memorial Hospital, Chicago, IL 60614)

We reviewed 20 cases of aortic thrombosis associated with umbilical artery catheterization diagnosed by ultrasonography (16/20) or aortography (4/4) over a period of four years. Fourteen of 20 infants experienced severe perinatal asphyxia. Ultrasonography of the aorta provided information about the size, location and configuration of the thrombus and was useful in monitoring thrombus size response to therapy. Radionuclide renography-scintigraphy demonstrated abnormal renal function in all 11 patients studied. Six patients with minor thrombosis (hypertension as the only sign) improved without specific therapy. Nine infants had moderate thrombosis (multiple signs but normal urine output); all survived with a variety of therapies; two were not treated with anticoagulants or fibrinolytics; 3 improved with heparin alone and one had surgery without recurrence of the thrombus. Streptokinase resolved the thrombus in 2 of 3 infants with moderate thrombosis. All five babies with anuria from major thrombosis died. Hepatic infarction associated with aortic thrombosis was found in 3 of 3 autopsies. Asphyxiated infants with umbilical arterial catheters are at increased risk for aortic thrombosis. Because ultrasonography and radionuclide renography-scintigraphy provide anatomic and functional information respectively, both modalities should be used to study infants with this disease.

Imaging of Paediatric Renal Tuberculosis: Cremin BJ (Univ. of Cape Town, Cape Town, South Africa)

The diagnosis of renal tuberculosis in children is not common. The symptoms are benign and the original cortical lesion heals spontaneously so that radiological demonstration is delayed until there is spread to the medullary pyramids. The radiographs of 12 cases seen since 1960 were reviewed. The initial lesion was calyceal destruction but half the cases presented as autonephrectomy. In six of the cases the initial lesion was calyceal destruction with adjacent spread. In the other six, autonephrectomy had occurred to give relative non-visualization. Calcification in the kidneys was seen in two cases and in the abdominal glands in four cases. In two cases use was made of arteriography and CT.

Ultrasound has proved to be a most valuable initial examination. A child that presents with dysuria and haematuria should have ultrasound as a routine investigation after urine examination. A bladder that is contracted, has mucosal irregularities and gaping ureteric orifices must be strongly suspected. The change in the kidney will depend on the stage of the disease. The overall ultrasonic appearances may not be diagnostic but in the correct clinical setting they can be very specific. The ultrasound feature of two cases will be described.

Vesicoureteral Reflux in Boys: A Review of 196 Cases: Sinai L, Ami TB, Hertz M, Boichis H (Chaim Sheba Medical Center, Tel Hashomer, Israel)

Most reports on vesicoureteral reflux deal with girls who undergo micturating cystourethrography (MCU), because of urinary tract infection. We reviewed the charts of 196 boys (27%), with vesicoureteral reflux out of a total of 724 who underwent MCU between the years 1974-1984.

Urinary tract infection was the most frequent indication for the examination, present in 188 boys; 80 of them (42.5%) had reflux. Hypospadias was the second most common clinical setting. In these patients reflux was found in 17% of the cases, as was the case in other unrelated indications.

Seventy boys had a congenital anomaly of the kidney such as complete duplication (23), ectopia (10), and solitary kidney (12) had a high incidence of reflux.

Fourteen boys had posterior urethral valves, 9 of them with reflux. Our study shows that: 1) VUR is as common in boys as in girls with urinary tract infection, 2) that reflux is almost always primary and 3) that reflux is especially frequent in boys with renal anomalies.

The Incidence of Vesicoureteral Reflux in Newborns with Myelodysplasia: Fernbach SK, Conway JJ (Childrens Memorial Hospital, Chicago, IL 60614)

Functional and anatomic abnormalities of lower urinary tract are common in children with myelomeningocele (MM). When undetected or untreated, these functional problems are responsible for deteriorations of renal function. The radiologic standard for evaluating the lower urinary tract in the neonate has been radiologic voiding cystography (VCUG). To evaluate the role of cystography we reviewed 110 VCUG's and 16 radionuclide cystograms in neonates with MM.

The incidence of reflux detected by VCUG (26%) was similar to that detected by radionuclide cystography. Bladder capacity and the completeness of bladder emptying were measured by both techniques. The many anatomic abnormalities (trabecular, saccules, abnormal bladder contour) detected by VCUG were not surgically corrected. For these reasons and because of the significantly lower radiation exposure we now recommend that radioinuclide cystography be performed in neonates with MM.

Children without reflux might have a baseline excretory urography in infancy but, in general, may be followed with renal ultrasound. Children who reflux will need a baseline excretory urogram. After this, yearly radionuclide cystography should be done until reflux abates. The radionuclide renogram should be used in conjunction with clinical parameters to monitor renal function.

Traumatic Urethral Fistulae in Spinal Cord Injury Patients: Sonographic Diagnosis: Perkash I, Friedland GW, Miller L (Palo Alto V.A. Medical Center, Palo Alto, CA 94301)

False passages extending from the prostatic urethra in 10 spinal cord injury patients were examined via a sonographic voiding cystourethrogram (SVCU), a radiologic voiding cystourethrogram (RVCU), and urethroscopy. All patients were on intermittent catheterization, and all had difficulty with that procedure. Four had a posterior ledge at the bladder neck as previously described; 5 had a urethral stricture. False passages were seen at urethroscopy in 10 patients, on a SVCU in 9 patients, and on a RVCU in 2 patients. No patient had a retrograde urethrogram, since this examination is not routine in spinal cord injury patients. Despite the one miss, ultrasonography is an excellent modality for the detection of unsuspected false passages. The sagittal image enables the examiner to watch the progress of the catheter into false passages, and it can also detect false passages not seen on routine RVCU. The false passages were unroofed in all 10 patients, and all 10 were subsequently cured.

Results of Tissue Biopsy in Renal Transplant Patients Whose Sonograms Show Collecting System Thickening: Cunningham JJ (Ohio State Univ. Medical Center, Columbus, OH 43210)

Recent data has been presented which suggests that sonographic thickening of the collecting system in renal transplant patients is a reliable sign of rejection, particularly severe acute rejection. We reviewed the tissue biopsy results of a similar-sized series of transplant patients with sonographic evidence of thickening of the renal pelvis and calyces. Acute rejection was only one of several diseases found. Other patients had acute tubular necrosis, cyclosporine toxicity, hypertensive vasculopathy, ischemic necrosis, and a variety of other problems alone or in combination.

In our series, development of sonographic thickening (submucosal edema) of the collecting system is a non-specific finding and not a reliable indicator of rejection.

Acute Hemorrhagic Focal Bacterial Nephritis: Findings on B-Scan Ultrasonography and Computed Tomography: Rigsby CM, Rosenfield AT, Glickman M, Hodson J (Yale Univ. School of Medicine, New Haven, CT 06510)

Acute focal bacterial nephritis (AFBN) refers to focal parenchymal infection without liquefaction. The sonographic findings of a mass with an echogenicity equal to or less than normal renal parenchyma and the CT findings of a solid mass on precontrast scans with a nephrographic defect seen following contrast medium injection are well established. Five patients seen in the past year with AFBN presented a different imaging picture, explained by the occurrence of hemorrhagic AFBN. All patients had focal segments more echogenic than normal renal parenchyma. In four cases, precontrast computed tomography showed increased attenuation in the corresponding area and one of these four cases had evidence for low attenuation in the mass as well. The fifth case had a low attenuation segment compared to normal renal parenchyma. After administration of intravenous (IV) contrast medium, the typical findings of focally decreased enhancement were identified in all cases. In one patient, who also had delayed scans, the area of focally decreased enhancement on the initial scan was hyperdense on delayed scans confirming that the mass consisted of functioning renal parenchyma.

We conclude that the typical findings of focal hemorrhagic pyelonephritis are echogenic foci on ultrasound, high density on precontrast CT studies and an abnormal nephrogram without well defined margins on the post-contrast CT scans. The wedge-shaped area of decreased density on the noncontrast CT image in one patient and the mixture of high and low levels of density in patients who had echogenic foci in a similar area in the ultrasound study are also consistent with parenchymal hemorrhage at different stages.

Awareness of these findings on CT and ultrasound should lead to accurate diagnosis in almost all cases.

Comparison of Computed and Film-Screen Excretory Urography: Accuracy, Certainty and Costs: Hillman BJ, Fajardo L, Hunter TB, Claypool HR, Mockbee WB (Univ. of Arizona Health Sciences Center, Tucson, AZ 85724)

A recent radiologic innovation is the substitution of an electronic x-ray receptor for the conventional film-screen cassette. This bears the potential for increasing lesion conspicuity, and hence diagnostic facility, while reducing radiation and monetary costs. This presentation reports a prospective comparison of matched film-screen and digital excretory urogram exposures.

A statistically significant series of consecutive patients underwent excretory urography. Scout abdomen, scout renal tomogram, post-injection nephrotomogram, 10 minute ureteral compression and 15 minute compression release exposures were performed by film-screen and digital (Toshiba Computed Radiology - TCR) techniques on each patient following rapid bolus injection of contrast material. Digital exposures were performed at half the optimal film-screen radiographic technique. Three staff radiologists not involved in the performance of the examinations interpreted either the film screen or digital urograms, noting: the quality of the films; whether the study was normal or abnormal; if possible, a diagnosis; and their level of certainty. Diagnostic accuracy was evaluated by a review of the patients' records, or in the absence of a definitive diagnosis, a review of the complete case by a panel of radiologists. Analyses included diagnostic sensitivity, specificity, accuracy, receiver operator characteristic curves, and estimations of film and radiation costs. The results of these analyses and their implications will be the subject of the presentation.

Needle Puncture of Cystic Renal Masses: A Survey of the Membership of the Society of Uroradiology: Amis ES, Cronan JJ, Pfister RC (Naval Hospital, Bethesda, MD 20814)

The Society of Uroradiology was polled regarding cyst puncture. Sixty-four percent of the membership responded, relating experience with approximately 16,000 punctures of cystic renal masses. No respondent would currently puncture a lesion clearly defined as a simple cyst by nephrotomography and ultrasound. One hundred percent of the respondents accept CT as accurate in diagnosing simple cysts, while 92% accept sonography alone. Twenty percent are comfortable with diagnosing a simple cyst on nephrotomographic criteria alone, provided the criteria are rigidly met. Twenty-three percent, on finding clear fluid on puncture, discard the fluid without submitting it for further testing. If fluid is sent to the laboratory, virtually all respondents would order cytology, while less than a quarter would order culture, lipids, LDH, glucose, protein, or amylase. Four cases were reported where positive cytology or chemistry on clear fluid aspirated from a cystic mass was the only factor in diagnosing the lesion as malignant (0.025% of total lesions in this series). In none of these cases was CT reported as having been performed. Clear fluid (with or without positive cytology) has been reported in cystic renal malignancies. CT has been positive for tumor when performed in such cases. In view of the multiplicity of conflicting and overlapping findings in cases of cystic renal masses, to adhere to a specific algorithm in workup seems fraught with chances for error in diagnosis. CT should be the arbiter in establishing the final diagnosis of cystic lesions of the kidney. The character of fluid aspirated from cystic renal masses, while it may be suggestive of the nature of the lesion, cannot be considered conclusively diagnostic in that clear fluid with negative cytology has been associated with malignant renal lesions.

Spontaneous Disappearance of Hemorrhagic Renal Cysts: CT Observations: Friedland GW (Palo Alto VA Medical Center, Palo Alto, CA 94301)

We examined three patients with hematuria, in two of whom computed tomography suggested the presence of a single hemorrhagic cyst, and in the third acquired uremic cystic disease and one larger hemorrhagic cyst. Ultrasound demonstrated a complex mass in all three patients. Each was observed for 2-12 weeks; within that time CT revealed that the hemorrhagic cyst disappeared in all three patients leaving no scar in two patients, but some scarring in a third. Since there was no communication with the collecting system, we suspect that the cyst ruptured into the perirenal space after which the contents were absorbed. In patients with acquired uremic cystic disease, we suggest that this could be the mechanism by which they developed a perirenal hematoma, provided sufficient bleeding occurs after the rupture.

Accuracy and Cost of Examination Sequences in Renal Mass Evaluation: Fritzsche PJ, McDonald D, Holden B (Loma Linda Univ., Loma Linda, CA 92350)

A retrospective study was designed to look at the imaging sequences utilized at Loma Linda University Medical Center from 1978 to 1985 with particular emphasis on the cost and accuracy. Nearly 200 patients were selected on the basis of discharge diagnosis. Uroradiological examinations, including intravenous urography, ultrasound, CT and angiography were reviewed and the accuracy of each examination determined by correlation with the histology of the surgical or biopsy specimen. The accuracy of the examination was scored as 1) specific, 2) diagnostic but not specific; 3) not diagnostic. The number and cost of imaging procedures necessary to reach a specific correlation were calculated. The number of examinations performed in evaluation of the same mass beyond the specific diagnosis were considered excessive.

We found more examinations were used in evaluating malignant than benign lesions and excessive exams were particularly high when evaluating malignant lesions. The overall excess rate was approximately 15% reflecting an acquired reluctance to abandon examinations by both the radiologist and clinician even when specific diagnoses have been reached.

The cost of renal mass imaging evaluation can be reduced without sacrificing accuracy by utilizing out-patient facilities, less angiography and a systematic approach.

Infiltrative Growth in the Kidney Revisited: CT-Sonographic-Pathologic Correlation: Hartman DS, Davidson AJ, Davis CJ, Goldman SM (Armed Forces Institute of Pathology, Washington, D.C. 20306-6000)

Neoplastic and inflammatory diseases may infiltrate the kidney using nephrons, collecting ducts and blood vessels as the scaffolding for cellular proliferation. Initially, the renal margin and collecting system maintain a normal contour. With continued growth the calyces become attenuated and the renal contour is enlarged but the reniform shape is maintained. In 1977, Ambos et al described the urographic and angiographic findings of 4 cases of infiltrative growth within the renal parenchyma. Since this original description, little has been written concerning the CT and sonographic findings of this growth pattern. Twenty-three pathologically proven cases of infiltrative growth with CT and/or sonography were retrospectively correlated with their pathologic findings. On CT the infiltrating mass usually has an ill-defined interface with normal parenchyma but the reniform shape is maintained. In most cases, the mass encases the pelvocalyceal system and replaces the renal sinus fat. On sonographic examination the mass is ill-defined, has a heterogeneous echo pattern and is reniform. The renal sinus echos are frequently focally or diffusely absent. Pathologic processes which grow primarily by infiltrative growth include lymphoma, collecting system tumors, metastases, acute bacterial nephritis, mesoblastic nephroma and rarely renal cell carcinoma. CT and ultrasound are useful techniques in recognizing infiltrative growth within the kidney.

Radiology of Direct Metastases to the Ureter: Spataro RF, Totterman S, DeMarino G, Miller T, Rubens D, Katzberg RW (Univ. of Rochester, Rochester, NY 14642)

Metastases directly to the ureter are uncommon. Metastatic neoplasms generally involve the ureter by direct extension from adjacent organs or extension from lymph node metastases. In both of these cases,

ureteral obstruction may occur. Metastases directly to the ureter without evidence of surrounding mass or lymph node involvement is rare. Primary neoplasms which may metastasize directly to the ureter include: metastatic melanoma, breast, and lung carcinomas. In these cases, patients may present with ureteral obstruction or gross or microscopic hematuria. The radiology of metastatic neoplasm to the ureter will be described including the appearances on excretory urography and computed tomography. Examples of involvement of the ureter by metastatic melanoma, breast carcinoma and lung carcinoma will be presented. The use of retrograde, brush biopsy to differentiate metastatic intraluminal tumor as seen with metastatic melanoma and primary transitional cell carcinoma will be described.

Uroepithelial Metastases from Hypernephroma: Mitty HA, Born R, Droller M (Mount Sinai Medical Center, New York, NY 10029)

Post-mortem examination of patients succumbing to hypernephroma reveals ureteral metastases in 6.1% of cases that had renal vein tumor thrombus; 1.2% of cases without renal vein involvement also have ureteral metastases at post-mortum.

We have studied 6 patients with uroepithelial metastases from hypernephroma. The primary tumor was on the left in 5 of 6 cases. Four patients presented with hematuria after nephrectomy and proved to have recurrent tumor in the ipsilateral ureteral stump. Two patients had renal pelvic foci of hypernephroma that were not in continuity with the primary lesion. The original radiologic studies and/or surgical specimens revealed main renal vein involvement in 4 patients while the other 2 had microscopic venous involvement. Two patients with renal vein involvement also had lymphatic spread documented.

Since the number of patients reported with uroepithelial metastatic hypernephroma is small, routine nephroureterectomy has not been practiced. This operation should be considered in a patient with radiologic evidence of ipsilateral metastatic uroepithelial foci or if such involvement is found during nephrectomy.

Intraarterial Doxorubicin Infusion Treatment Without and With Temporary Occlusion of the Renal Artery in Rabbit Renal VX-2 Carcinoma: Gadeholt G, Gothlin JH (Bergen Univ., Bergen, Norway)

Doxorubicin was infused without and with temporary occlusion of the renal artery on three occasions in rabbits with VX-2 carcinoma percutaneously implanted into the left kidney. Control rabbits were treated three times with temporary occlusion and infusion of physiological saline. Temporary occlusion was obtained by advancing a catheter into wedge position.

In 22 rabbits renal- and capsular artery infusion was successful in 64 and 16 attempts, respectively, out of 66. Complication rate was low, with no vascular trauma seen after the first catheterization. At second and third catheterization altogether 6 vascular lesions were registered.

All rabbits were killed 64 days after tumorimplantation or before if they looked ill or were losing weight. Eight control- and 7 infusion occlusion rabbits sacrificed 32.5 and 56 days (median) after tumor implantation respectively, all had renal tumor and metastases. All 7 rabbits infused with doxorubicin were sacrificed after 64 days; 3 had renal tumor and metastases, 1 had renal tumor with local infiltration and 3 had no evidence of disease.

The rabbit kidney with implanted tumor is a suitable model for testing fractional schemes and doses for multiple intraarterial infusions of various antineoplastic drugs. Research continues to determine whether the results are consistent or may be attributed to technical or chance occurrence.

Magnetic Resonance Imaging in the Detection and Staging of Carcinoma of the Prostate: Spataro RF, Thornbury JR, Cockett ATK, Disantagnese AP (Univ. of Rochester Medical Center, Rochester, NY 14642)

Twelve patients with carcinoma of the prostate that had undergone magnetic resonance imaging (MRI) of the prostate gland had total prostatectomies. The prostatectomy specimens were serially sectioned and stained and a mapping of the location of the tumor was performed in conjunction with a uropathologist.

Correlation of the pathological specimens with the MR scans showed that magnetic resonance imaging was generally unable to detect the location of prostatic carcinoma within the prostate gland. Magnetic resonance signal intensity did not discriminate between prostatic carcinoma, benign prostatic hyperplasia and normal prostate.

Magnetic resonance imaging either understaged or overstaged the prostatic carcinoma in one-third of the cases. MRI was generally able to detect macroscopic extracapsular extension of prostatic carcinoma, invasion of the seminal vesicles and lymph node involvement when enlarged lymph nodes were present. However, MRI was unable to detect metastatic prostatic carcinoma in normal size lymph nodes or metastases to the seminal vesicles when they were microscopic in size.

This study showed that no tissue specific signal intensity was found in patients with prostatic carcinoma and there was poor pathological correlation between the suspected area of tumor involvement within the prostate gland and the sectioned pathological specimen after total prostatectomy. MRI was useful in the staging of prostate carcinoma but may not be significantly more sensitive than computed tomography in its ability to stage carcinoma of the prostate.

Diagnostic and Treatment Impact of MR Versus CT in Staging of Early Carcinoma of the Cervix: Thornbury JR, Rubens D, Weiss SL (Univ. of Rochester Medical Center, Rochester, NY 14642)

In April 1985 we began a comparison study of the usefulness of MR versus CT in the staging of early carcinoma of the cervix (IB to IIB). Data collected permits determination of sensitivity/specificity effect on treatment choice (surgery versus irradiation followed by surgery) and cost effectiveness.

A 1.5T superconducting magnet GE machine was used. MR examination included partial saturation (TR 600, TE 25) and T2 weighted, multislice spin echo (TR 2000 msec, TE 40 msec and 80 msec) pulse sequences. Both sagittal and axial formats were used. By April, 1986, 25 patients having uterine cancer had been examined. Five of these were early stage (IB to IIB) carcinoma of the cervix patients who then had surgical treatment permitting direct pathologic/imaging correlation.

Results indicate that pelvic examination under anesthesia (EUA) considerably underestimated the primary paracervical spread:

	Underest.	Overest.	Correct
EUA	2	1	2
MR	1	0	4

CT provided no helpful information about the configuration of the primary tumor and was very inaccurate in assessing paracervical spread. On T2 weighted MR images in all 5 patients, the primary squamous cell carcinoma tumor mass was well delineated by its high intensity signal. Thus, MR was more accurate in assessing the size, shape, and extent of the primary tumor than either EUA or CT. Most importantly, if MR findings had been considered in treatment decisions, 2 of 5 patients (40%) would have had radiation treatment prior to surgery; actually both patients had surgery alone.

Initial Clinical Experience with Spectroscopic Imaging by Quadrature Modulated Echo Time Shifting: Friedenberg RM (Univ. of California, Irvine, Orange, CA 92668)

Examples of normal and abnormal multiple organ scans including brain, extremities, and kidney will be shown utilizing a new proton spectroscopic imaging technique for resolving fat and water simultaneously. This new method is a variation of the echo encoded imaging technique which has high spatial resolution. The technique was initially tested with phantoms and then on normal brain and abdominal organs, and finally on appropriate lesions which benefit from fat and water shift. The author feels that this technique, when compared to the Dixon technique, reduces scan time, provides less motion and chemical shift artefact, and provides better spatial resolution.

Letters

Circumflex Retroesophageal Right Aortic Arch

The article by Shufford et al. [1], describing circumflex retroesophageal aortic arch points out the importance of differentiating this anomaly from a mediastinal tumor or thoracic aneurysm. Although this situation has been reported in previous studies, including my paper [2] in 1967, its importance is worth repeating because of its frequent occurrence. I have seen two to three chest films a year in patients with a right aortic arch, most of which are the more common variation with descent of the aorta on the right and which are frequently confused by the inexperienced radiologist with a right superior mediastinal mass. In these cases, the diverticulum so commonly present is mistaken for an aortic knob. The plain chest roentgenograms with or without barium will accurately characterize this variation without sophisticated imaging technique (Fig. 1). The characteristic posterior indentation on the esophagus or trachea will confirm the diagnosis. However, understanding the angiographic anatomy will help when interpreting CT and MR examinations in these patients.

I have evaluated eight aortograms in patients with circumflex right aortic arch, and I differ with Shufford et al. on two points. All but one of these patients were studied with biplane aortography, usually with a right posterior oblique projection as well. I disagree with their statement that it is impossible to determine on frontal aortography the anterior or posterior relationship of the circumflex arch to the esophagus. Nor do I think that simultaneous barium esophagography is important in demonstrating this anomaly. In all my cases, it was readily apparent on the anteroposterior aortogram that the arch passed to the right of the trachea and had a circumflex course. Admittedly, in these cases, the left-sided component was lower than the right arch (Fig. 2). Their one aortogram shows both the proximal and distal portions of the arch to be at the same level, but this variation does not occur in any form of a left aortic arch, and, therefore, it can only be right aortic arch. This may be a small point, but comparing frontal aortography with the frontal chest film is more convincing to the clinician of the nature of the mass. In addition to the frontal projection, a lateral or steep right posterior (left anterior) oblique projection is useful but generally not necessary in making the diagnosis.

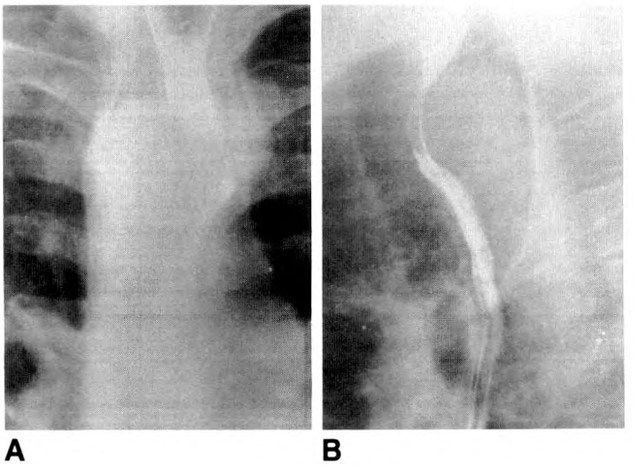


Fig. 1.—Posteroanterior (*A*) and lateral (*B*) chest films in patient with typical form of right aortic arch, aberrant left subclavian artery arising from a diverticulum, and right descending aorta. (Case 2 in [2]). Diverticulum compresses esophagus from the left and posteriorly and on posteroanterior film may be mistaken for left-sided aortic knob.

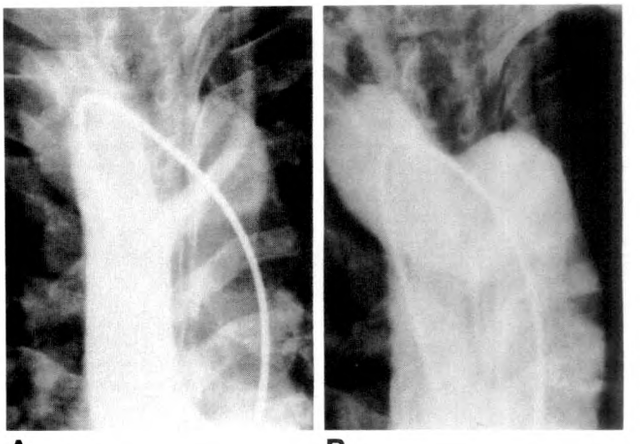


Fig. 2.—Frontal aortogram in patient studied because of chest film diagnosis of mediastinal mass. *A*, early phase; *B*, later phase. There is circumflex right aortic arch and aberrant left subclavian artery. Circumflex nature of right aortic arch is readily apparent in frontal aortogram, and the fact that it courses to left mediastinum to descend on the left indicates retroesophageal passage as the only possibility. (Courtesy of M. L. Daves, Denver, CO)

Also, this variation is not confined to patients with right aortic arch and an associated aberrant left subclavian artery, as Shufford et al. imply. In my eight cases, two had mirror-image branching (see published aortogram in [2]); four had aberrant left subclavian artery [Fig. 2]; and two had aberrant left innominate artery [3]. In the more common cases of right aortic arch with right descending thoracic aorta, 14 of 20 cases in which I have evaluated the aortograms had an aberrant left subclavian artery; the rest had mirror-image branching.

Julius H. Grollman, Jr.
Little Company of Mary Hospital
Torrance, CA 90509

REFERENCES

1. Shuford WH, Sybers RG, Gordon IR, Baron MG, Carson GC. Circumflex retroesophageal right aortic arch simulating mediastinal tumor or dissecting aneurysm. *AJR* **1986**;146:491–496
2. Grollman JH Jr, Harris CH, Hamilton LC. Congenital diverticula of the aortic arch. *N Engl J Med* **1967**;276:1178–1182
3. Grollman JH Jr, Bedynek JL, Henderson HS, Hall RJ. Right aortic arch with an aberrant retroesophageal innominate artery: angiographic diagnosis. *Radiology* **1968**;90:782–783

Reply

The case illustrated by Dr. Grollman is a different type of right arch from the ones we have reported. In his case the right and left components of the arch are at different levels. Essentially his case is a cervical right aortic arch. In our cases the right and left components of the arch are at the same level, and the curve of the aorta as it extends right to left is smooth and continuous.

The purpose of our paper was to point out that a circumflex right aortic arch can resemble a left aortic arch with mediastinal widening, simulating a mass. We agree with Dr. Grollman that a barium swallow is quite sufficient for its diagnosis.

However, if one does not suspect a circumflex right aortic arch and precedes with aortography, we wish to stress that the frontal aortogram may be misleading because the course of the aorta resembles a left arch (Fig. 2B, case 1, in our report). Dr. Grollman takes issue with our statement that it may be impossible to determine on the frontal aortogram whether the aorta is in front of or behind the esophagus. We know of no way to determine the anterior-posterior relationship of the arch to the esophagus on the frontal aortogram. It is the branching pattern of the arch vessels that establishes the diagnosis of right aortic arch. If one knows that a circumflex right aortic arch is present, then one knows that the aorta passes behind the esophagus.

In our reported cases of circumflex retroesophageal right aortic arch, the branching pattern of the arch vessels was that of an aberrant left subclavian artery. Our experience with right aortic arch and mirror-image branching has been quite different from Dr. Grollman's. We have not encountered any cases of right aortic arch with mirror-image branching with a retroesophageal aorta. In our experience with mirror-image right aortic arch, the descending aorta has always been on the right side.

Wade H. Shuford
Emory University School of Medicine
Atlanta, GA 30322

Significant Delayed Pneumothoraces

In the recent article [1] discussing the timing of chest films after transthoracic needle aspiration, the authors state that no "significant pneumothoraces" (defined as greater than 30% and requiring intervention) occurred more than 1 hr after the procedure. Perlmutt et al. conclude that a "chest radiograph obtained 1 hr after the procedure will detect 98% of pneumothoraces and identify all of those requiring intervention." In the last year at our institution, we have had two "significant pneumothoraces" detected approximately 9 hr and 2 days after subclavian line placement in which no pneumothorax was seen on 1-hr post-procedure films.

The placement of an introducer for subclavian line placement does require a larger-gauge needle (generally approximately 18 gauge); however, optimally it does not enter lung parenchyma. In the first case a radiograph taken approximately 1 hr after an uneventful left subclavian, triple-lumen catheter placement into the persistent left superior vena cava showed no pneumothorax. Approximately 10 hr later, the patient became short of breath and mildly hypotensive at which time a follow-up film showed almost complete collapse of the left lung and mild shift of the mediastinum consistent with a tension pneumothorax. The second case also had a normal chest radiograph after placement of a triple-lumen catheter. It was not until 2 days later when the patient complained of pleuritic chest pain after initiation of total parenteral nutrition through the subclavian catheter that a repeat film revealed an approximately 40% pneumothorax. Neither patient was on a ventilator during the time or had significant parenchymal disease.

These two cases certainly do not invalidate the excellent study by Perlmutt et al., but point out what everyone must expect: there will be a few exceptions to prove every rule.

Emily R. Fox
Wallace T. Miller
Hospital of the University of Pennsylvania
Philadelphia, PA 19104

REFERENCE

1. Perlmutt LM, Braun SD, Newman GE, Oke EJ, Dunnick NR. Timing of chest film follow-up after transthoracic needle aspiration. *AJR* **1986**;146:1049–1050

Reply

We appreciate the comments of Doctors Fox and Miller regarding the occurrence of delayed pneumothorax after a percutaneous thoracic procedure. Are they, however, comparing apples and oranges when relating a procedure that is performed blindly with a relatively large needle to one performed under fluoroscopic guidance with a small-caliber needle? As everyone has experienced, there are no absolutes in medicine, and we fully agree with their conclusion and so state in the last sentence of our paper.

Louis M. Perlmutt
Duke University Medical Center
Durham, NC 27710

Fluoroscopy of the Gastrointestinal Tract

Carlson, in his article [1] on the small bowel examination in Crohn's disease, emphasizes the importance of careful fluoroscopy and palpation for correct radiologic diagnosis. He also points out (correctly) that many radiology residents do not receive adequate training in fluoroscopy, and he makes a blunt statement that "most teachers are incapable of effectively and confidently performing diagnostic fluoroscopy" and that "some such teachers of high repute have said that the only usefulness of fluoroscopy was the proper positioning of the patient for films."

I concur with Carlson's opinion and with his remarks about the value of fluoroscopy. This opinion may be regarded as outrageous

by these teachers of "high repute" who have ignored the importance of fluoroscopy and have produced a generation of radiologists who lack the skills of fluoroscopy.

Peristaltic activity plays an important role in the diagnosis of gastrointestinal disease. It can be studied fluoroscopically, by recording on video tape (which does not require any additional radiation) or by cinefluorography. Motility and peristalsis cannot be appreciated on single radiographs, in particular when glucagon or some other antiperistaltic drug has been used, as recommended by most advocates of double contrast studies.

I wrote in 1967 [2], that "during fluoroscopy a static situation is built up to demonstrate normal or pathologic anatomy in a series of single films" and that "the films serve practically as documentation of the changes diagnosed at fluoroscopy, provided a good fluoroscopic technique is used."

In 1983, I noted [3] that the value of fluoroscopy should not be downgraded or even excluded from residents' training programs.

My teacher, Olle Olsson in Lund, Sweden, required that *all* diagnoses be made during fluoroscopy, even before the era of videofluoroscopy (televised image-intensifier fluoroscopy). The resident who performed fluoroscopy had to note the findings on the requisition form. The resident could see the *films* only if his/her fluoroscopic observations were incorrect, when he/she was either called to the film-viewing-and-interpretation area to discuss erroneous findings or told to go back and come up with a correct diagnosis. Of course, vigorous manual palpation was required for a correct fluoroscopic conclusion.

It is ironic that now, when the quality of modern image intensifiers permits the observation of lesions as small as 1 mm in the gastrointestinal tract, fluoroscopy has been neglected in many institutions. Radiologists who believe that fluoroscopy should be used only for positioning of the patient should be reminded that first the lesion must be observed during fluoroscopy. Even slight changes in positioning may decide if pathology can or cannot be demonstrated on films [4]. This is valid for both single and double contrast studies.

Some radiologists will disagree with Carlson about the non-value of small bowel enteroclysis and with his remarks and my opinion about the diagnostic importance of properly performed fluoroscopy. These radiologists really do not examine the patient but only read the films. In my experience, an examination performed under careful fluoroscopic control will provide the same, or even more, clinically important diagnostic information as a double contrast study (with possible exception for some very small colonic polyps) [3–5]. I believe that we should pay more attention to the training of residents in fluoroscopic skills, should not ignore the diagnostic value of fluoroscopy, and should not rely on radiographs obtained in standardized projections with either inadequate or no fluoroscopic control.

Also, valuable fluoroscopy of 1-min duration can be performed with approximately the same absorbed integral radiation dose to the patient that results from the exposure required for one 35 × 35 cm film [6].

Dr. Carlson is to be congratulated for his fine article.

Juri V. Kaude
University of Florida College of Medicine
Gainesville, FL 32610

REFERENCES

1. Carlson HC. Perspective: the small bowel examination in the diagnosis of Crohn's disease. *AJR* **1986**;147:63–65
2. Kaude J. Clinical studies on image intensifier fluorography and cinefluorography. *Acta Universitatis Lundensis* **1967**;II(18):3
3. Kaude JV. Fluoroscopically controlled examination of the upper gastrointestinal tract using low density barium. A review of 139 endoscopically proven lesions. *Europ J Radiol* **1983**;3:129–131
4. Kaude J. Hypotonic duodenography—too often performed but of too little value? A comparison with conventional spot films. *Gastrointest Radiol* **1978**;3:165–171
5. Kaude JV, Harty RF. Sensitivity of single contrast barium enema in regard to colorectal disease as diagnosed by colonoscopy. *Europ J Radiol* **1982**;2:290–292
6. Kaude J, Svahn G. Absorbed, gonad and integral doses to the patient and personnel for angiographic procedures. *Acta Radiol Diagn* **1974**;15:454–464

More on Fluoroscopy of the Gastrointestinal Tract

We agree with the statement by Dr. Carlson in his recent article on Crohn's disease that "detailed fluoroscopy and vigorous palpation should probably be revived." Careful, knowledgeable fluoroscopy *must* be revived.

The fluoroscopy-vs-films argument is the oldest controversy in radiology. Decades ago, however, knowledgeble radiologists concluded that optimal results are achieved by a combination of careful fluoroscopy and appropriate films. The atrophy of fluoroscopic skills referred to by Dr. Carlson is the result of at least three factors: (1) fewer gastrointestinal studies are being performed in many teaching hospitals, (2) many residents are taught fluoroscopy by teachers who were themselves never taught the full variety of fluoroscopic techniques, and (3) the past decade has witnessed an unfortunate deemphasis of single-contrast techniques and their requisite fluoroscopic skills.

We believe that the primary educational task in gastrointestinal radiology is that of teaching residents how to fluoroscope patients actively and accurately. If fluoroscopy is properly performed, teaching the interpretation of films becomes an easy matter, and the resulting examinations benefit from the enormous information obtained during fluoroscopy.

David W. Gelfand
David J. Ott
Bowman Gray School of Medicine
Winston-Salem, NC 27104

Screening Mammography

The agreement regarding recommendations for screening mammography is not as general as Dr. Hall suggests in his editorial [1] and certainly does not apply to women under 50 years of age. None of the screening studies cited have demonstrated a reduction in mortality to date for that age group. Possibly the most balanced statement is that of the American College of Physicians [2].

Another problem is the extremely variable natural history of breast cancer. Histologically similar, if not identical, cancers can behave in different ways in different patients [3]. Breast cancer is a disease of aging (10% of women will develop it during their lifetimes) with a rapid increase in prevalence until menopause (however, only 22% of breast cancers occur before age 50 and only 7% before age 40), suggesting that we are dealing with two diseases in which genetic elements have a greater role before age 50 and environmental factors, such as obesity and dietary fat, dominate thereafter [4].

Screening procedures should be sensitive, reasonably specific, safe, and inexpensive. As such, they will become widely available, which screening mammography is not today. Many of us do not know how effective or accurate we are with the procedure, and with few exceptions the examination is expensive. These and other factors suggest that the cost-effectiveness or affordability of compliance with the ACR/ACS guidelines is at least doubtful, especially for women under age 50 [5, 6]. Efforts to identify high-risk women (personal or

family history of breast cancer; previous biopsy, especially with proliferative breast disease with atypia [7]; a nipple discharge; a palpable mass) could improve this.

Another problem is the inability to respond effectively, even if clear benefits and cost-effectiveness are demonstrated because of the lack of competent personnel and adequate facilities to provide optimum screening mammography at low cost. The idea of using paramedics to sort positive from negative screening mammograms to reduce costs is intriguing. To my knowledge this has never been properly evaluated.

It is difficult to generalize about a procedure that is so emotionally charged and so dependent on the skills of the radiologist and technologist. We must evoke reproducible standards for quality assurance and determine our results and interpretative accuracy. The individual radiologist can do this with on-going careful pathologic correlations, as Dr. Hall as emphasized, but also by relatively simple data collection for accuracy determinations. A daily log to be completed at the time of interpretation of the mammograms should include: (1) the patient's name, age, and unit number; (2) nature and location of physical findings; (3) nature and location of mammographic findings, and an indication whether the findings are benign, malignant, or indeterminate. Arrangements should be made for clinical follow-up, especially pathologic information that includes the location, size, character, and cell type of all cancers and of any benign disease. With these data and correlations one can calculate sensitivity (false-negatives), specificity (false-positives), and determine true-positive biopsy rates and sizes, if not the stages of the cancers including the percentages of minimal, stage I, and other stages of cancers detected. The most difficult part is getting the system in place. As Dr. Hall suggests, overinterpretation based on fear of litigation is a disservice. A low false-negative rate at the expense of a high false-positive rate and the anxiety, additional tests, and unnecessary biopsies that this creates is unconscionable. A high true-positive biopsy rate when most of the cancers are over 2 cm in size is certainly no accomplishment.

Mammography is not an independent procedure [8]. Although mammography can detect breast cancer before it can be felt, to a lesser degree the opposite is also true. In our zeal to promote mammography we should not forget that it is a complementary procedure. It is part of the total evaluation of the patient, which includes clinical information, physical findings, and possibly laboratory data. The collaboration of clinician, surgeon, radiologist, pathologist, and oncologist has been one of the intellectually and professionally rewarding aspects of mammography. This on-going experience can materially improve confidence, competence, and accuracy with the procedure. It can also result in a sharing of responsibility in the management of the individual patient and can significantly reduce the likelihood of litigation.

Concerns, if not reservations, remain regarding the role of screening mammography, especially in women under age 50. The immediate challenge is to provide highest-quality images that are accurately interpreted at a reasonable cost [9, 10]. The latter may be the single greatest deterrent to the use of screening mammography today.

Robert McLelland
University of North Carolina at Chapel Hill
Chapel Hill, NC 27514

REFERENCES

1. Hall RM. Editorial. Screening mammography. *AJR* **1986**; 147:195–197
2. Mushlin AI. Health and Public Policy Committee, American College of Physicians. The use of diagnostic tests for screening and evaluating breast lesions. *Ann Int Med* **1985**;103:143–146
3. Fos MS. On the diagnosis and treatment of breast cancer. *JAMA* **1979**;241:489–494
4. Seidman H, Mushinski MH. Breast cancer: incidence, mortality, survival, and prognosis. In: Feig SA, McLelland R, eds. *Breast carcinoma: current diagnosis and treatment*. New York: ACR and Masson, **1983**:9–46
5. Bassett LW, Bunnell DH, Cerny JA, Gold RH. Screening mammography: a survey of 4200 referring physicians. *Radiology* **1985**;157:53
6. Survey of physicians' attitudes and practices in early cancer detection. *CA* **1985**;35:197–213
7. Dupont WD, Page DL. Risk factors for breast cancer in women with proliferative breast disease. *N Engl J Med* **1985**;312:146–151
8. Newsome JF, McLelland R. A word of caution concerning mammography. *JAMA* **1986**;255:528
9. McLelland R. Mammography 1984: Challenge to radiology. *AJR* **1984**;142:1–4
10. Editorial: Screening for breast cancer. *Lancet* **1985**:851–852

Reply

Dr. McLelland is correct in emphasizing that there is no general agreement as to the indications for screening mammography. The American Cancer Society, the American College of Radiology, the National Cancer Institute, the American College of Obstetrics and Gynecology, and the American Academy of Family Physicians all have similar policy statements recommending baseline mammograms at age 35 to 40, variable interval examinations until age 50, and annual mammography thereafter. The American Medical Association and the American College of Physicians have less specific and generally more restrictive recommendations, particularly for women under age 50 with no risk factors [1, 2]. Obviously, the opinions and practices of individual physicians are far more variable.

Controversy about screening mammography in women age 40 to 50 arises from the fact that, although there is a decrease in mortality from breast cancer in these individuals, the reduction has not achieved statistical significance [3–5]. Premenopausal breast carcinomas are relatively aggressive and yet screening mammograms in these women are generally recommended at only 2- to 3-year intervals. Annual screening of women 40–50 years old might result in the diagnosis of more early-stage carcinomas, with fewer advanced tumors being detected by palpation in the interval between mammograms. On the other hand, screening intervals of greater than 1 year may be as effective as annual examination in most postmenopausal women whose breast cancers appear to have slower doubling times. This is suggested by the report of Tabár et al. [5] who, in a randomized controlled trial, showed a 31% reduction in mortality in women over 50 who underwent screening mammograms every 2 to 3 years.

If these assumptions are confirmed, screening mammography might be performed more frequently than presently recommended in women 40–50 years old and less frequently in women over 50. The overall effect, a reduction in the total number of examinations and costs, is important. It is the cost-effectiveness of screening mammography that will determine its eventual use; its benefits are unquestioned.

My editorial concerned primarily the large number of breast biopsies and preoperative localization procedures resulting from false-positive mammographic interpretations. These indirect costs of screening mammography often relate to a lack of experience by the mammographer or to medicolegal considerations. The related issue of reducing the cost of individual screening mammograms has been recently addressed by Sickles et al. [6]. My suggestion was to have paramedical personnel screen and selectively read mammograms done in busy screening clinics. Obviously, this could substantially reduce costs and I have little doubt that it could be done without compromising the quality of interpretation. Documentation of the

effectiveness of such a program would be relatively easy and, indeed, receiver-operating-characteristic analyses for the interpretation of mammograms by radiologists and partially trained nonradiologic personnel have been published ([7], Lusted LB, personal communication). However, implementing such a program in the present medicolegal climate, and when many think that there is an oversupply or impending oversupply of radiologists, would be difficult.

Ferris M. Hall
Beth Israel Hospital
Boston, MA 02215

REFERENCES

1. Council on Scientific Affairs of the American Medical Association. Early detection of breast cancer. *JAMA* **1984**;252:3008–3011
2. Health and Public Policy Committee, American College of Physicians. The use of diagnostic tests for screening and evaluating breast cancer. *Ann Int Med* **1985**;103:143–146
3. Shapiro S, Venet W, Strax P, Venet L, Roeser R. Ten- to fourteen-year effect of screening on breast cancer mortality. *J Natl Cancer Inst* **1982**;69:349–355
4. Verbeek ALM, Hendriks JHCL, Holland R, Mravunac M, Sturmans F, Day NE. Reduction of breast cancer mortality through mass screening with modern mammography: first results of the Nijmegan project, 1975–1981. *Lancet* **1984**;1:1222–1224
5. Tabár L, Fagerberg CJG, Gad A, et al. Reduction in mortality from breast cancer after mass screening with mammography: randomized trial from the Breast Cancer Screening Working Group of the Swedish National Board of Health and Welfare. *Lancet* **1985**;1:829–832
6. Sickles EA, Weber WN, Galvin HB, Ominsky SH, Sollitto RA. Mammographic screening: how to operate successfully at low cost. *Radiology* **1986**;160:95–97
7. Lusted LB. Signal detection theory in the early diagnosis of cancer. In: Kessler II, ed. *Cancer control: contemporary views on screening, diagnosis and therapy*. Baltimore: Univ. Park Press, **1980**:105–118

IA-DSA and Rupture of Thoracic Aorta

In their recent article, Mirvis and coworkers [1] emphasize the use of intraarterial digital subtraction angiography (IA-DSA) in the diagnosis of presumed rupture of the thoracic aorta after blunt chest trauma. They believe it to be the method of choice because it is faster, less costly, and as accurate as conventional film-screen angiograms. But even in IA-DSA it is necessary to cross the damaged aorta and to pass a catheter through this portion of the vessel, manipulations that may lead to additional injuries to the vessel wall. Therefore, we replaced conventional aortography in this special subset of patients with IV-DSA and published our first promising results in 1983 [2]. Since then all patients with suspected traumatic laceration of the aortic arch have undergone only IV-DSA, except two cases in which questionable results of the IV studies necessitated an intraarterial study. According to the clinical follow-up of the patients, we missed no lacerations and all positive DSA findings were proven correct at surgery. Our policy is to do only an IV study, and to rarely perform an intraarterial study, if the IV-DSA is unrevealing. Obviously, the IV approach is faster and less costly than the IA-DSA, and, as an additional advantage, it carries virtually no risk and doesn't require a skilled angiographic team.

Mirvis and coworkers in their study used undiluted 76% meglumine diatrizoate for their IA-DSA studies in a quantity of up to 44 ml. According to our experience [3, 4] it is not necessary to use such high concentrations of contrast medium in intraarterial studies. The high contrast resolution of the current available DSA-units allows the use of diluted contrast-medium (1:1 up to 1:3 with isotone saline) in intraarterial studies without any reduction of the diagnostic information. There are two advantages to using diluted contrast medium. The first is a substantial reduction in the cost of contrast material, especially when nonionic compounds are used. The second is the reduction of the risk of nephrotoxic effects due to high doses of contrast medium and (in ionic compounds) the reduction of side effects that are due to the high osmolarity of the ionic contrast medium (i.e., heat sensations, pain, vasospasm). In virtually all intraarterial digital studies we use diluted contrast medium. According to our experiences, the use of diluted contrast medium results in a better diagnostic quality than the use of a reduced amount of undiluted contrast medium, probably because the higher injection volume of the former allows a more homogenous opacification of the vessel(s).

Klaus Rauber
Kliniken der Johann Wolfgang Goethe Universität
Frankfurt/Main, West Germany

REFERENCES

1. Mirvin SE, Pais SO, Gens DR. Thoracic aortic rupture: Advantages of intraarterial digital subtraction angiography. *AJR* **1986**;146:987–991
2. Rauber K, Kollath J. Die Diagnose der Aortenruptur durch digitale Subtraktionsangiographie (DSA). *Fortschr Rontgenstr* **1983**; 132:167–170
3. Rauber K, Starck, Sauer J, Kollath J, Riemann H. Kontrastmittelkonzentrationen zur intraarteriellen digitalen Subtraktionsangiographie der Extremitäten. *Fortschr Rontgenstr* **1986**; 143:526–529
4. Starck E, Rauber K, Knöner M, Sauer J, Kollath J. Digitale Subtraktionsangiographie in der Diagnostik von Nierenkarzinomen. *Digitale Bilddiagn* **1985**;5:89–95

Reply

Dr. Rauber first notes the possibility of further damaging an already injured aorta by passing a catheter through the injured region. Such damage is certainly a theoretical consideration. However, to our knowledge, not one report substantiates aggravation of traumatic injury to the aorta due to catheter manipulation, even though aortography has been the standard for establishing the diagnosis of traumatic aortic rupture for many years. This is not a valid reason to avoid aortography.

Dr. Rauber states that all patients admitted to his institution with suspected traumatic aortic rupture are examined by IV-DSA and that he has found this method to be accurate. We have had extensive experience with IV-DSA for both carotid and renal-artery imaging and have found that the contrast density, even using right atrial injections with a high volume of 76% meglumine diatrizoate, is so inadequate that images are not diagnostic. Dr. Rauber does not say how many patients he has studied in this fashion, but he does mention that in two cases questionable results necessitated additional arterial injections. This suggests that at least in some portion of his cases, the images were also inadequate by the IV approach.

We agree that if there were some major cost, safety, or time-saving advantage to using IV-DSA rather than the arterial route, this approach might be worth pursuing. However, in our hands, the introduction of a small intraarterial catheter takes no longer than the introduction of a catheter into the superior vena cava or right atrium, and the procedure is essentially without complication. Further, we believe that the so-called "invasiveness" and risk of introducing a 4- or 5-French catheter into the femoral artery is enormously exagger-

ated. On the other hand, the risk of introducing a catheter into the vena cava or right atrium is probably underestimated [1–3]. Therefore, we do not consider the IV route to be particularly advantageous in terms of time, safety, or cost. Also, in general it takes more, not less, contrast material to perform an IV rather than an intraarterial study, a further reason to prefer the arterial route.

As noted in our article, the ability to study quickly the great vessels in the head and neck without catheter exchange and, when necessary, to assess rapidly abdominal viscera for injury with or without selective injections is an additional advantage of IA-DSA over IV-DSA in assessing victims of multi-system trauma.

Finally, we will not take issue with Dr. Rauber's point that intraarterial studies of the thoracic aorta can be obtained by using more dilute contrast medium. This point was not addressed by our study and it may indeed be the case that less concentrated medium would have been adequate.

Stuart E. Mirivs
S. Osher Pais
University of Maryland Hospital
Baltimore, MD 21201

REFERENCES

1. Pinto RS, Manuell M, Kricheff II. Complications of digital intravenous angiography: experience in 2488 cervicocranial examinations. *AJNR* **1984**;5:553–557
2. Arbona GL, Verrill AD, Conrad WC, Paul DJ. Venous contrast extravasation during digital subtraction angiography. *Cardiovasc Intervent Radiol* **1985**;8(4):211–215
3. Aaron JO, Hesselink JR, Oot R, Jones RL, Davis KR, Taveras JM. Complications of intravenous DSA performed for carotid artery disease: A prospective study. *Radiology* **1984**; 153(3):675–678

Tracheal Dimensions in Childhood

As an anesthesiologist, I was interested in the recent publication by Griscom and Wohl [1]. The dimensions of the trachea are important to the anesthesiologist in the selection of appropriately sized tracheal tubes for children, and to the radiologist in the assessment of tracheal abnormalities. Previous studies reported in anesthetic and other literature have assessed tracheal size at postmortem [2], or by the use of endotracheal tubes or sounds [3–5]. The results of these studies have been plotted with those of the CT study (Fig. 1). By assuming a straight-line relationship between age and tracheal size, a line of best fit was drawn for the data; the values for slope and intercept are shown in Table 1. As can be seen from Figure 1, the data derived by sounding of the larynx and trachea deviate from that of the CT-derived tracheal diameter. Because the anesthesiologist is mainly interested in the narrowest point of the airway, these dimensions may represent laryngeal (subglottic) rather than tracheal size. The selection of a tracheal tube for a given patient is made by reference to formulae relating size to age. The correct size tube may be one size larger or smaller than this estimate. The two most used formulae ([age/4] + 4 or [age/4] + 4.5) refer to the size of tube in terms of internal diameter. This rather curious practice has arisen from the anesthesiologist's concern with airway resistance rather than external dimensions. The internal diameters for tubes selected in this way equate with the external diameters given by the formulae in Table 2.

Airway size is more closely related to height than age, but the latter is more convenient to use. Our purpose here is to suggest that a similar formula would be useful to the radiologist to compare between measured and predicted tracheal size or to assess the airway for intubation. Mostafa [5] has shown that 98% of the patients were successfully intubated with an endotracheal tube with internal diameter equivalent to (age/4) + 4. On the basis of these data it would seem appropriate to consider the trachea to be narrowed if its minimum transverse diameter is less than (0.33 × age) + 5.5 mm.

C. Nixon
University College Hospital
London, England

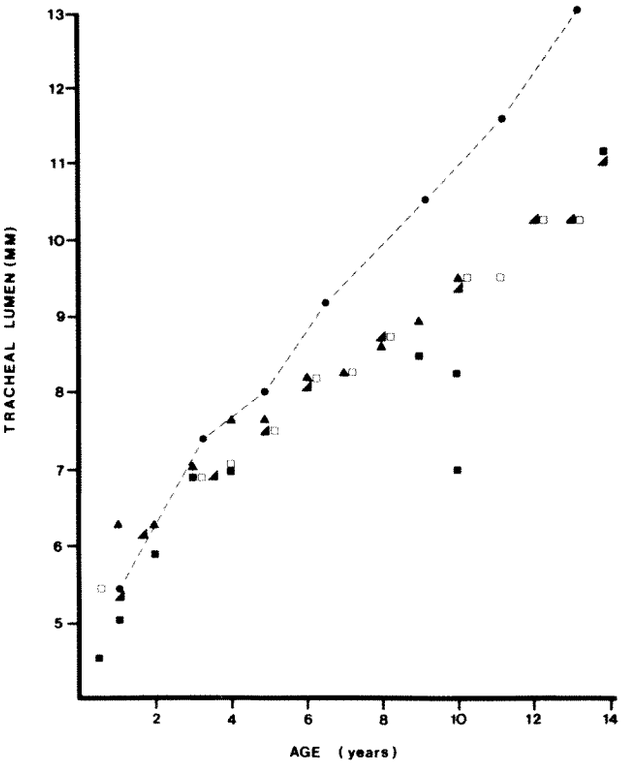


Fig. 1.—Tracheal diameter in children in relation to age as measured by CT, tracheal sounds, and at postmortem. Data are from references as follows: circle, [1]; equilateral triangle, [2]; closed square, [3]; isosceles triangle, [4]; open square, [5].

TABLE 1: **The Relation Between Tracheal Diameter and Age—Slope, Intercept, and Correlation Coefficient (r) for Lines of Best Fit**

Reference	No. of cases	Slope	Intercept	r
1	81	0.6	5.09	1.00
4	3956	0.44	5.29	0.95
2	24	0.48	4.02	0.94
3	452	0.41	5.39	0.99
5	2380	0.38	5.56	0.98

TABLE 2: **External Diameter of Portex Endotracheal Tubes Related to Formulae for Internal Diameter Based on Age**

Internal Diameter (mm)	External Diameter (mm)
(age/4) + 4.0	(0.33 × age) + 5.5
(age/4) + 4.5[7]	(0.35 × age) + 6.04

REFERENCES

1. Griscom NT, Wohl MEB. Dimensions of the growing trachea related to age and gender. *AJR* **1986**;146:233–237
2. Butz RO. Length and cross section growth patterns in the human trachea. *Pediatrics* **1968**;42:336–341
3. Keep PJ, Manford MLM. Endotracheal tube sizes for children. *Anaesthesia* **1974**;29:183–185
4. Slater HM, Sheridan CA, Ferguson RH. Endotracheal tube sizes for infants and children. *Anesthesiology* **1955**;16:950–952
5. Mostafa SM. Variations in subglottic size in children. *Proc R Soc Med* **1976**;69:793–795

Reply

We believe that the discrepancies, which occur only after about 5 years of age, between the tracheal diameters we found and those that Dr. Nixon cites, represent real differences. We relate those differences to the different conditions under which the measurements were made.

Most of our subjects less than 5 years old were examined asleep, and lung volumes were correspondingly low. At those ages there is reasonable agreement between our data and the sources Dr. Nixon cites; those diameters were also obtained at low lung volumes.

However, in older subjects, our measurements were obtained from children who were awake and alert. At and above the age of 6 the measurements were made at or near total lung capacity (full inspiration). The cited articles analyzed diameters by measuring slices of tracheas removed at autopsy, by passing laryngotracheal sounds in children prepared for surgery, or by retrieving from anesthesia records the endotracheal sizes actually used during surgery; in other words, the children were deeply sedated, under general anesthesia, or dead. Those lower measurements, therefore, must have been made somewhere near functional residual capacity or residual volume (i.e., deep in expiration). At low lung volumes one would anticipate smaller tracheal dimensions.

Also, the anteroposterior and transverse diameters we reported are the averages of many CT sections. There was only slight section-to-section variation in these diameters, but those sections often did not include the subglottic larynx. The measurements in three of the articles cited record only the *narrowest* point found below the vocal cords, and that was often in the subglottic larynx, not in the trachea proper.

We feel, therefore, that the diameters reported for middle and later childhood by Dr. Nixon's sources may well be correct for the circumstances in which they were measured: low lung volumes, measurements usually limited to the narrowest point found (often the subglottic larynx). However, we also feel that our data do indeed accurately represent children's tracheas under the circumstances of the study: awake and near full inspiration at age 6 and older, values averaged from many sections. Other workers, studying diameters [1, 2] and cross-sectional areas [3] in healthy subjects by different radiographic and CT systems, have reported results similar to those reached by our approach.

Thus, the discrepancies above age 5 emphasize the point that tracheal dimensions, as fluoroscopists have known for decades, vary with lung volumes and should be expected to be less when volumes are low.

N. Thorne Griscom
Mary Ellen B. Wohl
Children's Hospital
Boston, MA 02115

REFERENCES

1. Breatnach E, Abbott GC, Fraser RG. Dimensions of the normal human trachea. *AJR* **1984**;142:903–906
2. Osmanliev D, Bowley, Hunter DM, Pride NB. Relation between tracheal size and forced expiratory volume in one second in young men. *Am Rev Respir Dis* **1982**;126:179–182
3. Effmann EL, Fram EK, Vock P, Kirks DR. Tracheal cross-sectional area in children: CT determination. *Radiology* **1983**; 149:137–140

Papaverine as a Coronary Vasodilator

A recent article by Wilson and White [1] thoroughly and carefully documents the potential advantages of papaverine as a hyperemic stimulus in studies of coronary flow reserve. Although no serious adverse reactions were reported, and although we too have experienced no significant adverse responses with this approach other than QT prolongation on electrocardiography and rare, transient ventricular arrhythmias, several potentially important clinical observations have recently been made. Pilla et al. [2] have reported an incompatibility of Hexabrix (Mallinckrodt, St. Louis, MO), a new, low-osmolality contrast agent, with papaverine. Mixture of the two agents caused formation of a white, amorphous precipitate. Mixtures of papaverine with Conray 60% (Mallinckrodt, St. Louis, MO) and Amipaque (Winthrop-Breon, New York, NY) failed to show any interaction. Renografin-76 (Squibb, New Brunswick, NJ) produced a white suspension that disappeared after 1 to 2 min. The authors concluded that caution should be exercised when using papaverine and Hexabrix during angiography and that catheters should be flushed with saline between injections of these two agents.

In view of these findings, we tested Renografin-76 and two formulations of Omnipaque (iohexol 300 mgI/ml and 350 mgI/ml, Winthrop-Breon, New York, NY) with two lots of papaverine hydrochloride (Lilly, Indianapolis, IN) with pH = 6.8 and pH = 7.2. Contrast to papaverine ratios that were tested were 3:1, 2:1, 1:1, and 1:2. Immediate and 12-hr observations were made. With the pH = 6.8, papaverine and Renografin-76 caused a white suspension that was seen immediately and precipitation was noted in all dilutions within 15 min to 12 hr. With the pH = 7.2, no immediate suspension was observed in any dilution although all tubes contained precipitate at 12 hr. No immediate or late responses were noted with iohexol.

Although the practical, clinical implications of these observations are unknown, it is important for angiographers to recognize these interactions, particularly during coronary angiography if coronary flow reserve is to be assessed in larger numbers of patients with papaverine. The practice of flushing the papaverine dose with contrast medium should be discouraged. Some of the adverse clinical effects may be due to incompatibilities. We agree with the recommendations of Pilla et al. regarding the use of a saline flush between administration of Hexabrix and papaverine but would extend this recommendation even when Renografin-76 is used because of our observations when the more acidic preparation of papaverine was studied. Alternatively, agents such as iohexol might be preferable in order to minimize any risks when elective or experimental assessments of coronary flow reserve are undertaken.

G. B. John Mancini
Mark J. McGillem
University of Michigan Medical School
Ann Arbor, MI 48105

REFERENCES

1. Wilson RF, White CW. Intracoronary papaverine: an ideal coronary vasodilator for studies of the coronary circulation in con-

scious humans. *Circulation* **1986**;73:444–451
2. Pilla TJ, Beshany SE, Shields JB. Incompatibility of Hexabrix and papaverine. *AJR* **1986**;146:1300–1301

Reply

The discrepancy between our results and those of Dr. Mancini and his colleagues, when testing papaverine hydrochloride (HCl) (Lilly, Indianapolis, IN) with Renografin-76 (Squibb, New Brunswick, NJ), is apparently due to a pH difference in the papaverine HCl solutions. We have tested the pH of several vials of papaverine HCl (expiration date July 1, 1989) and have found them to vary from 3.6 to 3.7. The manufacturer states only that the pH of papaverine HCl has been adjusted to greater than 3. In view of these findings, iohexol (Winthrop-Breon, New York, NY) may be the preferred agent when papaverine HCl is used during an angiographic procedure. We will soon publish our results concerning the compatibility of other drugs used in angiography with contrast agents including the new low-osmolality agents.

Thomas J. Pilla
Shirley E. Beshany
John B. Shields
John R. Martin
St. Louis University Medical Center
St. Louis, MO 63104

Incompatibility of Hexabrix and Papaverine

In the June 1986 issue of the *AJR,* Pilla et al. [1] reported that ioxaglate-Hexabrix and papaverine precipitated upon contact. This chemical phenomenon was noticed previously by many users of Hexabrix in Europe when this contrast material was introduced (the first clinical trials in 1976; commercially available in 1979).

Since the manufacturer warned of this reaction with its recommendations for use, it is surprising that this reaction has only now been recognized in the American literature.

The use of papaverine as a vasodilator during angiographic examination is classic. We have performed hundreds of visceral angiographic investigations with papaverine and ioxaglate without incident.

Papaverine is used also in the radiologic investigation of impotence. Intracavernous injection of 60 mg of papaverine produces an intense arterial vasodilatation and an increased resistance of the venous outflow of the corpora cavernosa leading to an erection in normal potent man [2]. Pudendal arteriographies are now realized under local anesthesia with Hexabrix after intracavernous injection of papaverine. Intracavernous injection of papaverine is also used during cavernosographies without complications [3].

Our experience has shown that the use of these two components is safe if papaverine is not mixed directly with ioxaglate. When papaverine is injected alone and flushed with normal saline 30 sec before the injection of Hexabrix, no complications occur.

C. Delcour
Hospital Erasme
Universite Libre de Bruxelles
Route de Lennik 808 B-1070 Bruxelles
Belgium

REFERENCES

1. Pilla TJ, Beshany SE, Shields JB. Incompatibility of Hexabrix and papaverine. *AJR* **1986**;146:1300–1301
2. Virag R. Intracavernous injection of papaverine for erectile failure. *Lancet* **1982**;2:936
3. Delcour C, Wespes E, Vandenbosch G, Schulman CC, Struyven J. Radiologic and hemodynamics investigations of the venous system in impotence. *Radiology*, in press

Reply

The statement that the manufacturer recommends that Hexabrix not be mixed with any other substance is true. However, in the English recommendation provided by the manufacturer it states only that Hexabrix should not be mixed with any chemical substance in the same syringe. Our resident noted precipitation when papaverine HCl was injected through a catheter and then flushed with Hexabrix. This led to our study. Thus, the point of our article is that a saline flush is mandatory after injecting papaverine HCl before test-injecting with Hexabrix. Also, by diluting Hexabrix in 25 ml of normal saline, the possibility of any interaction between Hexabrix and papaverine HCl due to dead space within the catheter is further decreased. Hexabrix should never be used as a flush for any pharmacologic agent injected through a catheter before thorough flushing with a saline solution. We have contacted the manufacturer of Hexabrix and recommended that they revise their brochure supplied with the drug.

Also, you have failed to cite a reference to any article that describes this incompatibility, even though you state that it was observed several years ago in Europe by other clinical investigators. While we agree that papaverine HCl has been used for many years as a vasodilating agent in a variety of circumstances, none of the major textbooks in the English language, describing its administration, points out the possible adverse effects that may occur if contrast agents (i.e., Hexabrix) are used to flush papaverine HCl through a syringe [1, 2].

Thomas J. Pilla
Shirley E. Beshany
Michael K. Wolverson
Supranee Tantana
John R. Martin
St. Louis University Medical Center
St. Louis, MO 63104

REFERENCES

1. Bron KM. Arterial portography. In: Abrams HL, ed. *Angiography: vascular and interventional radiology.* Boston: Little, Brown, **1983**:1608
2. Gerlock AJ Jr, Mirfakhraee M. *Essentials of diagnostic and interventional angiographic techniques.* Philadelphia: Saunders, **1985**:246

Erratum

Sickles and Weber wrote a reply to a letter to the editor in the October 1986 issue of *AJR* (*AJR* 1986; 147:861–862); in publication of that reply, a typographic error was made. In the last paragraph of the reply, the first word in the fifth line should be "complex" instead of "complete." Therefore, the sentence should read, "For conventional mammography practices that mix *complex* cases with screening examinations, we strongly recommend our protocol of limiting grid use to women with thick or dense breasts." *AJR* regrets the error.

News

Physician's Imaging Courses 1986/87

The Dept. of Radiology, University of California, San Diego, Medical Center offers a 1- to 8-week program for physicians interested in updating their knowledge in diagnostic sonography—including carotid Doppler, or a combination of sonography-abdominal CT, and/or interventional radiology. Sonography and sonography–abdominal CT are offered weekly; abdominal CT alone is offered as an independent rotation. Interventional radiology is available any week throughout the year as arranged with Dr. Eric vanSonnenberg. Trainees may choose to concentrate on one specialty at a time or two or three together in the same session. Category 1 credit: 40 hr/week attendance. Information: Elizabeth Novak, Ultrasound Division, UCSD Medical Center, 225 Dickinson St., San Diego, CA 92103; (619) 543-6657; or to arrange participation in interventional radiology, call Dr. Eric vanSonnenberg (619) 543-6604.

Radiology and Early Colon Cancer Workshop

The Radiology Dept., Hospital of the University of Pennsylvania, will sponsor 3-hr workshops to acquaint radiologists and radiographers with screening programs for colorectal cancer and to provide data supporting the primary role of radiology. Dates and locations: Nov. 1, Montreal; Nov. 3, Milwaukee; Nov. 5, Seattle; Nov. 8, St. Louis; Dec. 11, Dallas; Dec. 13, New Orleans; Dec. 15, Birmingham; March 30, Denver. Category 1 credit: 3 hr (pending). Fee: $75: physicians; $35: technologists. Information: Janice L. Ford, Continuing Education Coordinator, Hospital of the University of Pennsylvania, 3400 Spruce St./G1, Philadelphia, PA 19104; (215) 662-4000.

Magnetic Resonance Imaging Seminar

The Continuing Education Committee of the Los Angeles Radiological Society announces a 2-day seminar in recent advances in MR imaging, Nov. 15–16, Century Plaza Hotel, Los Angeles, CA. Category 1 credit: 10 hr. Fee: $200: regular registrants; $175: LARS members; $125: residents (letter required); $125: technologists. Guest faculty: W. Bradley, B. Drayer, V. Haughter, A. Mancuso, R. Peshock, and J. Weinreb. Information: Attn. Diane L. Johnson, Los Angeles Radiological Society–MRI, P.O. Box 91215, Los Angeles, CA 90009-1215; (213) 642-0921.

Open Interim Meeting, RSNA

The Section on Radiology of the National Medical Association invites all interested radiologists and radiologic physicists to participate in its Open Interim Meeting during the meeting of the Radiological Society of North America in Chicago. The meeting begins 6 p.m. on Tuesday, Dec. 2 at the McCormick Center Hotel. Buffet served. Information: A. Oestreich, M.D., Radiology, Children's Hospital, Cincinnati, OH 45229; 513-559-4255.

Quantitative Thallium Myocardial Tomography

Emory University School of Medicine, Dept. of Radiology, announces a course designed for cardiologists, radiologists, and nuclear medicine physicians to familiarize them with basic principles and the clinical utility of quantitative thallium tomography, to be held at Emory University, Dec. 12–15. Information: Betty A. Allen, CME Program Coordinator, Emory University School of Medicine, Woodruff Health Sciences Center Administration Building, 1440 Clifton Road, N.E., Atlanta, GA 30322.

Nuclear Medicine Update: 1987

The Dept. of Radiology, Hospital of the University of Pennsylvania, announces a conference on nuclear medicine update for Jan. 19–22, 1987. Guest faculty: H. Berger, C. Gallagher, T. C. Hill, P. T. Makler, and A. Nunn. Category 1 credit: 20 hr (applied for). Fee: By Nov. 19, $395: physicians; $295: residents; $195: technologists. After Nov. 19: $445: physicians; $345: residents; $245: technologists. Information: Janice Ford, CME Coordinator, Dept. of Radiology, Hospital of the University of Pennsylvania, 3400 Spruce St., Philadelphia, PA 19104; (215) 662-6904 or (215) 662-6982.

Interventional Radiology and Didactic Imaging

The Dept. of Radiology, The Alexandria Hospital, announces a postgraduate course on interventional radiology and didactic imaging: Radiology 1987, Jan. 24–30, in St. Thomas, U.S. Virgin Islands. Faculty: E. M. Druy, B. Katzen, M. Reeder, E. J. Ring, A. R. Ross, and D. Schwarten. Category 1 credit: 24 hr (pending). Fee: $400. Information: Pam Donais, Dept. of Radiology, The Alexandria Hospital, 4320 Seminary Rd., Alexandria, VA 22304; (703) 379-3102.

Advanced Course in Diagnostic Imaging

The Academy of Medicine, Singapore, will hold an advanced course in diagnostic imaging in Singapore, Feb. 8–13, 1987. The course will emphasize MR and interventional radiology. Guest faculty: D. Allison, W. S. C. Hare, R. Herfkens, B. Katzen, J. K. T. Lee, F. Werhli, and B. Worthington. Information: Lenny Tan, Academy of Medicine, P.O. Box 694, Tiong Bahru Post Office, Singapore 911, Republic of Singapore.

Sun Valley Imaging

The Third Annual Sun Valley Imaging meeting will be held Feb. 14–21, 1987, in Sun Valley, ID. Reviews and discussions of the latest developments in sonography, CT, MR imaging, and interventional radiology will be included. Faculty: H. J. Burhenne, P. L. Cooperberg, G. Gamsu, G. R. Leopold, C. R. B. Merritt, A. A. Moss, W. Thompson. Category I credit: 20 hr. Fee: $425. Information: Sun Valley Imaging, 665–810 West Broadway, Vancouver, B.C., Canada. V5Z 4C9; (604) 875-4340.

EIGHTH ANNUAL INTERMOUNTAIN IMAGING CONFERENCE

The Intermountain Imaging Conference, sponsored by the Department of Radiology, the Medical College of Wisconsin, will be held Feb. 14–21, 1987, at Snowmass, CO. This 6-day program is designed to appeal to the physician interested in the application of digital imaging to clinical problems. Morning lecture and afternoon seminar sessions will explore the use of computer-based imaging systems in problem solving and their relationship to other conventional diagnostic techniques. The large number of simultaneous afternoon sessions will allow a wide variety of subject matter and a choice of programs. Guest faculty: P. O. Alderson, P. C. Freeny, P. Fritzsche, A. Hasso, R. P. Schwenker, E. vanSonnenberg, D. D. Stark, and F. W. Wehrli. Category I credit: 33 hr. Fee: $450. Information: Thomas L. Lawson, M.D., Dept. of Radiology, Milwaukee County Medical Complex, 8700 W. Wisconsin Ave., Milwaukee, WI 53226; (414) 257-6024 or (414) 257-7201.

Postgraduate Course in Diagnostic Imaging

Duke University, Dept. of Radiology, will present a 5-day postgraduate course in diagnostic imaging, Feb. 14–21, 1987, in Cancun, Mexico. It is designed to update participants in newer imaging techniques in diagnostic radiology, including MR, nuclear medicine, sonography, angiography, and general radiology. Category 1 credit: 22 hr. Fee: $450: physicians; $300: trainees. Information: Carl E. Ravin, M.D., Dept. of Radiology, Duke University Medical Center, P.O. Box 3808, Durham, NC 27710; (919) 681-2711, Ext. 226, 227.

University of Arizona Postgraduate Practical Radiology Course

The Dept. of Radiology at the University of Arizona will hold its annual postgraduate course *Practical Radiology*, Feb. 16–19, 1987, at Loews Ventana Canyon Resort, AZ. Category 1 credit: 17 hr. Information: Office of Medical Education, Arizona Health Sciences Center, Tucson, AZ 85716; (602) 626-6707.

Mammography: A Practical Approach

A course devoted to mammographic interpretation will be held in Aspen, CO, Feb. 16–20, 1987. Faculty: M. J. Homer. Category 1 credit: 14 hr. Fee: $450. Information: S. Hemley, M.D., Dept. of Radiology, 145 Westchester Ave., White Plains, NY 10601; (914) 682-0700 Ext. 318.

Sonomammography

The Division of Diagnostic Ultrasound, Thomas Jefferson University Hospital, will sponsor an intensive program emphasizing automative scanning with topics ranging from acoustic principles through advanced differential diagnosis of breast abnormalities, Feb. 16–20, 1987. Category 1 credit: for doctors: 19.5 hr/3 days; for technologists: 29 hr 5 days. Fee: $375: doctors; $525: technologists. Information: Thomas Jefferson University Hospital, Seventh Floor Main Building, 10th and Sansom Sts., Philadelphia, PA 19107; (215) 928-8533.

Radiologic-Pathologic Concepts in Diagnostic Radiology

The Ninth Annual Radiologic-Pathologic Concepts in Diagnostic Radiology will be presented by the Radiological Alumni of the AFIP at the Contemporary Resort Hotel in Walt Disney World, Lake Buena Vista, FL, Feb. 19–23, 1987. Lectures will emphasize pathologic correlation of diseases of the chest, abdomen, breast, and skeleton. Two sessions will be devoted to CT and MR of the chest and abdomen. Category 1 credit: 21 hr. Fee: $400: physicians; $300: residents/fellows. Information and registration: James C. Reed, M.D., Radiologic-Pathologic Concepts, Box 2065, New Bern, NC 28560.

Medical Imaging Conference in the High Sierras

The American College of Medical Imaging will hold a continuing medical education meeting, The eighth Annual Winter Conference in the High Sierras, Feb. 22–27, 1987, at Lake Tahoe, NV, at the Caesars Tahoe Hotel. Faculty: M. H. Gado, C. Kerber, T. P. Naidich, M. A. Weinstein. Program director: Allan M. Mannheim. Category 1 credit: 25 hr. Fee: $450; daily registration available at $125. Information: American College of Medical Imaging, 433 N. Camden Dr., #600, Beverly Hills, CA 90210.

Masters Diagnostic Radiology Conference

The University of Hawaii at Manoa will hold its sixth annual Masters Diagnostic Radiology Conference, Feb. 22–27, 1987, at the Royal Lahaina Resort and Hotel, Kaanaapali Beach, Maui, Hawaii. The program will include lectures and discussions in the fields of chest, skeletal and interventional radiology, CT, MR, sonography, and nuclear medicine. Faculty: T. G. Lee, L. R. Muroff, M. M. Reeder, P. Sheedy, and E. G. Theros. Workshops in fetal sonography, CT, and nuclear bone scanning will be presented. Program chairman: Maurice M. Reeder. Category 1 credit: 25 hr. Fee: $495: physicians; $350: residents and fellows. Information: M. M. Reeder, M.D., Dept. of Radiology, University of Hawaii School of Medicine, 1356 Lusitana St., Room 502, Honolulu, HI 96813; (808) 531-6471.

Practical Radiology 1987

The Dept. of Radiology, University of British Columbia, will sponsor a course for practicing radiologists at Whistler, a ski resort 75 miles from Vancouver, BC, Canada, March 1–6, 1987. Faculty: C. Putman, D. Resnick, C. Rohrmann, Jr., and faculty of the Dept. of Radiology, UBC. Category 1 credit: 21 hr. Fee: $325 US: physicians; $200 US: residents and fellows. Information: H. Joachim Burhenne, M.D., Dept. of Radiology, Vancouver, BC, Canada V5Z 1M9; (604) 875-4355.

Intermountain Imaging Conference–Extension

The Dept. of Radiology, Medical College of Wisconsin, will sponsor its second annual Intermountain Imaging Conference March 1–7, 1987, at Snowbird, UT. The 5-day program is designed for the physician interested in in-depth discussion of common problems in digital imaging. Topics have been selected because of their potential for differing opinions in imaging approach or difficulty in differential diagnosis. Faculty: L. R. Goodman, T. Lee, R. Vogelzang, and T. L. Lawson. Category 1 credit: 22 hr. Fee: $425. Information: Thomas L. Lawson, M.D., Dept. of Radiology, Milwaukee County Medical Complex, 8700 W. Wisconsin Ave., Milwaukee, WI 53226; (414) 257-6024 or (414) 257-7201.

Computed Body Tomography 1987–the Cutting Edge

The Johns Hopkins School of Medicine will hold a seminar on computed body tomography March 5–8, 1987, at Peabody-Orlando Hotel, Orlando, FL. The seminar will provide a comprehensive review of recent advances in CT of the chest and abdomen, including the spine, with some correlation with MR. Faculty: M. E. Bernardino, M. A. Bosniak, E. K. Fishman, B. W. Gayler, V. M. Haughton, B. Jones, D. Magid, J. C. Scatarige, M. J. Siegel, S. S. Siegelman, P. M. Som, E. A. Zerhouni. Category 1 credit: 22 hr. Fee: $350: physicians; $175: residents and technologists (letter needed). Program directors: Elliot K. Fishman and Stanley Siegelman. Information: Program Coordinator, Office of Continuing Education, Turner 22, 720 Rutland Ave., Baltimore, MD 21205; (301) 955-5880.

London Course in Whole-Body CT

The Royal College of Radiologists (with possible sponsorship by the American College of Radiologists) will hold a course at the Gleneagles Hotel, Auchterarder, Perthshire, Scotland, UK, March 15–19, 1987. The program will consist of lectures and small tutorial groups that will cover mainly body CT and also incorporate MR where appropriate. Faculty: M. Bernardino, J. Heiken, R. Levitt, J. Walsh, A. Dixon, S. Golding, I. K. Fry, B. Kendall, D. Nicholas, R. Reznek, and P. Peters. Course director: Janet E. Husband. Fee: 470 pounds sterling (includes food for duration of course). Information: Janice O'Donnell, Dept. of Radiology, Royal Marsden Hospital, Downs Road, Sutton, Surrey, UK SM2 5PT.

Ultrasound at Vail

The eighth annual Ultrasound at Vail Meeting will be held March 22–28, 1987, in Vail, CO. This meeting will include reviews and discussions of the latest developments in diagnostic ultrasound. Faculty: P. L. Cooperberg, E. A. Lyons, M. L. Manco-Johnson, B. A. Carroll, and F. A. Manning. Category I credit: 20 hr. Fee: $425. Information: Ultrasound at Vail, PO Box 6093, Cherry Creek Station, Denver Co 80206-0093; (604) 875-4340.

Diagnostic Angiography and Interventional Radiology

The Society of Cardiovascular & Interventional Radiology will hold its 1987 12th annual postgraduate course at the Hotel Intercontinental, San Diego, CA, March 23–26, 1987. Category 1 credit: 22 hr (submitted for approval). Fee: $395: physicians; $250: fellows, residents, nurses, and radiologic technologists. Information: for course and membership information: Society of Cardiovascular & Interventional Radiology, P.O. Box 44113, Pittsburgh, PA 15205; (412) 921-2636.

Intrauterine Diagnosis and Treatment: the New Frontier

The University of California, San Diego, School of Medicine announces a conference on intrauterine diagnosis and treatment on April 2–4, 1987, at Hotel Intercontinental, San Diego, CA. AMA/CMA credit: up to 19.5 hr; ACOG: pending; American Academy of Pediatrics: pending. Fee: to be announced. Information: Office of Continuing Medical Education, M-017, UC School of Medicine, La Jolla, CA 92093; (619) 534-3940 or (619) 452-3940.

The Asian-Oceanian Congress of Radiology

The 5th Asian-Oceanian Congress of Radiology will be held Sept. 21–25, 1987 at the Seoul Hilton International Hotel, Seoul, Korea. The official language will be English. The congress will sponsor scientific papers, scientific exhibitions, and technical exhibitions. Fee: Before Dec. 31, 1986—$250 US: physicians; $100 US: residents/trainees and accompanying persons. After Jan. 1, 1987—$300: physicians; $150: residents/trainees and accompanying persons. Information: Man Chung Han, M.D., Secretary General, The 5th Asian-Oceanian Congress of Radiology, Dept. of Diagnostic Radiology, Seoul National University Hospital, 28, Yunkun-dong, Chongro-ku, Seoul 110, Korea (K.P.O. Box 1880, Seoul 110, Korea). Telex: SNUH K25501; Telephone: 745-6826, 7601-2514.

American College of Radiology Announces 1986 Gold Medal Winners

Radiology's highest honor, the gold medal of the American College of Radiology, was awarded to Godfrey N. Hounsfield of Middlesex, England; Elias P. G. Theros of Winston-Salem, NC; Simon Kramer of Philadelphia, PA; and James H. Christie of Albuquerque, NM at the College's 63rd annual meeting in Baltimore, MD, Sept. 14–18, 1986.

Godfrey Hounsfield won the 1979 Nobel Prize for Medicine for his invention of the computerized axial tomography (CT) scanner. The CT scanner is considered the most significant imaging advancement in 50 years. Educated in England, Hounsfield has been honored worldwide for his innovative work.

Elias Theros served as registrar of the Registry of Radiological Pathology of the Armed Forces Institute of Pathology in Washington, DC, from 1966–1976. In addition to several academic appointments, Theros has published some 30 articles on diseases of the chest and skeletal system and has received numerous honors for his work.

Simon Kramer, a recognized leader in radiation oncology, initiated and organized the Patterns of Care Study of Radiation Therapy in the United States. This unique study has been the basis for an important quality assessment program for radiation oncologists. Kramer served as chairman of the Radiation Therapy and Nuclear Medicine department of the Thomas Jefferson Medical College in Philadelphia and led his department through a period of important growth.

James Christie, serving as professor of radiology and chief of the Division of Nuclear Medicine at the University of New Mexico in Albuquerque, has made significant contributions to the University's Nuclear Medicine Department and, as a teacher of radiology, has instructed students at every level. Christie has also contributed to the field of radiology through his work with professional radiologic societies.

Symposium Neuroradiologicum Fellowship Awards

The Fellowship Awards were established in Washington, DC, 1982, by the President, Giovanni Di Chiro, and the Vice President, Hillier L. Baker, Jr., of the XII Symposium Neuroradiologicum. The first awards were presented at the XIII Symposium in Stockholm for "the best original work by a radiologist relating to application of radiology and radiologic science to the study of the nervous system." Selected were the following: Isabelle Berry, Department of Radiology, University of Toulouse, Toulouse, France, and Department of Radiology, University of California, San Francisco; Robert R. Edelman, Department of Radiology, Massachusetts General Hospital, Boston; and Gerald V. O'Reilly, Department of Radiology, Beth Israel Hospital, Boston. Award winners received round-trip airfare to Stockholm, three days per diem, a cash prize, and a diploma.

The following were the winning manuscripts: I. Berry, M. Moseley, I. M. Germano, N. Ishige, M. C. Nishimura, H. M. Bartkowski, L. H.

Pitts, and L. M. Brant-Zawadzki. "Combined MRI and MRS in experimental regional injury of the brain: ischemia and impact trauma." R. R. Edelman, V. J. Wedeen, K. R. Davis, and T. J. Brady. "Multiphasic MRI: a new method for direct imaging and quantitation of pulsatile CSF flow." G. V. O'Reilly, M. D. Forrest, R. H. Clarke, and W. C. Schoene. "Intravascular laser coagulation of experimental aneurysms."

In addition to the award papers, the following two manuscripts were selected for honorable mention: T. Yamaguchi, H. Sasaki, T. Ogawa, K. Mineura, K. Uemura, I. Kanno, F. Shishido, M. Murakami, A. Inugami, and S. Higano. "Relationship between tissue nature and (18-F) fluorodeoxyglucose kinetics evaluated using dynamic positron emission tomography in human brain tumor." J. B. Rubin and D. R. Enzmann. "New concepts in magnetic resonance spine imaging: Exploiting CSF pulsation flow phenomenon." The senior authors of the two honorable-mention contributions were given a cash award and a diploma.

Presentations at NMA Meeting

The ninth Annual William E. Allen, Jr., Memorial Lecture of the Section on Radiology at the National Medical Association was delivered by Gatson J. Tarleton, Jr., of Nashville at the annual meeting of the NMA, in New York, July 23, 1986. The winner of the Resident/Fellow Paper Competition at the meeting was Catherine Brown of the University of California at Los Angeles.

Election Results

On May 4, 1986, at the annual meeting of the Society of Uroradiology held in The Hague, the following officers were elected: Robert R. Hattery, President; Robert L. Lebowitz, President Elect; Bruce L. McClennan, Secretary/Treasurer, and N. Reed Dunnick, Board of Directors.

Meeting and Course Review

For reader convenience, a summary of upcoming meetings and courses is provided. Detailed listings in the *AJR* issues are noted in parentheses.

UC San Francisco Courses; Diagnostic Radiology Seminars, Nov. 3–7, 1986, Maui Marriott Resort, Maui, Hawaii; Jan. 19–23, 1987, Camino Real, Ixtapa, Mexico; Feb. 1–6, 1987, The Gant, Aspen, CO; Feb. 22–27, 1987, Shadow Ridge, Park City, UT; **Diagnostic Imaging: 1987,** March 16–21, 1987, Waiohai, Kauai, HI (all Oct)
Weekend courses. Frontiers in Chest Diagnosis, Bone and Genitourinary Imaging, Nov. 3–7, Marbella, Spain (Feb)
Diagnostic Radiology Seminar, Nov. 3–7, Maui, HI (July)
University of Texas Continuing Medical Education, Sixth Semi-Annual Fundamentals of MRI, Nov. 5–8; **Radiation Safety Officer's Course,** Jan. 5–9, 1987, or May 18–22, 1987; **Radiotherapy Treatment Planning Anatomy,** Jan. 26–30, 1987; **Basic Radiologic Health,** Feb. 9–13, 1987; **Review of Radiation Calculations,** Feb. 16–18, 1987; **Advanced Radiologic Health,** May 11–15, 1987; all San Antonio, TX (all Sept)
Intervention Radiology for Practicing Physicians, Nov. 5–7, 1986, Charleston, SC (Sept)
Courses in Diagnostic Ultrasound, Nov. 7, Winston-Salem, NC (July)
Gastrointestinal Cancers, conference, Nov. 12–14, Houston (May)
Progress in Impotence: Diagnosis and Therapy, Nov. 13–15, 1986, San Diego (Oct)
Radiology Seminar, Gastrointestinal Diseases, Nov. 14–16, Scottsdale, AZ (Aug)
Brachytherapy of Choroidal Melanoma, Nov. 20–21, New York (Aug)
American Radiological Nurses Association Meeting, Nov. 29–Dec. 3, 1986, Chicago (Oct)
International Continuing Medical Education Series: Controversies in Medicine & Neurology, Dec. 2–9, 1986, Maui, HI; **Advances in Pediatric Clinical Care,** Dec. 24, 1986–Jan. 2, 1987, Cancun, Mexico; **Controversies in Medicine & Surgery,** Jan. 16–23, 1987, St. Moritz, Switzerland; **Clinical Update in Medicine & Surgery,** Feb. 10–17, 1987; Feb. 17–24, 1987, Maui, HI; **Topic to be announced,** March 14–21, 1987, Banff, Canada; **Topic to be announced,** May 20–26, 1987, Japan; **Topic to be announced,** May 20–26, 1987, Bermuda, **Topic to be announced,** June, 1987, Ireland; **Topic to be announced,** July 24–30, 1987, Pebble Beach, CA; **Topic to be announced,** Aug. 1987, Gstaad, Switzerland (all Oct)
MRI for Technologists, Dec. 5–6, Houston (June)
Indian Radiation Oncology Congress, Dec. 5–7, Bombay (April)
International Symposium on Breast Cancer, Jan. 1–4, 1987, New Delhi, India (Aug)
International Symposium on MR 1987, Jan. 29–Feb. 1, 1987, Garmisch-Partenkirchen, Bavaria (Aug)
Los Angeles Radiological Conference, Jan. 30–Feb. 1, 1987, Los Angeles (Oct)
Perspectives on Imaging Modalities, Feb. 2–6, 1987, Cancun, Mexico (Sept)
Palm Beach Magnetic Resonance Imaging Update, Feb. 8–11, 1987, West Palm Beach, FL (Oct)
Big Sky Radiology Conference, Feb. 8–13, 1987, Great Falls, MT (Oct)
Gastrointestinal Radiologists Meeting and Course, Feb. 8–13, 1987, Scottsdale, AZ (Aug)
Thoracic Imaging 1987, Feb. 16–19, Orlando, FL (May)
Diagnostic Radiology and Nuclear Medicine, Feb. 21–28, 1987, St. Thomas, U.S. Virgin Islands (Oct)
Radiation Research Society Meeting, Feb. 22–26, 1987, Atlanta, GA (July)
Advanced Perinatal Ultrasound Seminar, Feb. 26–28, 1987, Lake Buena Vista, FL (Aug)
Society for Magnetic Resonance Imaging, Feb. 28–March 4, 1987, San Antonio, TX (Oct)
Alexandria International Conference on Laryngeal Cancer, April 1–2, 1987, Alexandria, Egypt (Sept)
American Radium Society Meeting, April 6–10, 1987, London (Aug)
Annual Meeting, National Council on Radiation Protection and Measurements, April 8–9, 1987, Bethesda, MD (Sept)
Fleischner Society Annual Symposium, May 21–23, 1987, San Francisco, CA (July)
1987 Radiology Congress, Lisbon, May 31–June 6, 1987 (Aug)
American Board of Radiology Examinations, June 8–12, 1987; May 23–27, 1988 (Oct)
Euroson '87, June 14–18, 1987, Helsinki, Finland (Sept)
International Conference on Computer Assisted Radiology. July 1–4, 1987, West Berlin (Feb)
Sarcoidosis and Granulomatous Disorders, congress, Sept. 6–11, 1987, Milan (June)

AJR carries announcements of courses, symposia, and meetings of interest to its readers if received a minimum of 4 months before the event. There is no charge; receipt of items by the *AJR* Editorial Office is not acknowledged. Submit items for publication typed double spaced. Provide title, date, location, brief description, sponsor, course directors, fees, category I credit, and address and telephone number for additional information. Faculty from the host institution will not be listed. Guest faculty names will appear **only** if initials are provided. Mail news items to *AJR* Editorial Office, 2223 Avenida de la Playa, Suite 200, La Jolla, CA 92037.

Classified Advertising

Positions Available

DIAGNOSTIC RADIOLOGIST for small hospital and clinic practice San Francisco Bay Area. Write to J.J. Parker, M.D., Box 284, San Rafael, CA 94915. 11–12a

RADIOLOGICAL PHYSICISTS. The Dept. of Radiology at Thomas Jefferson University Hospital/Jefferson Medical College wishes to recruit two highly qualified radiologic physicists. The first position is for an MRI physicist to work with our GE 1.5T MRI system currently being installed. He/she will work closely with radiologists in our MRI division on applied and basic research. The second position is for a physicist with particular interests in image processing. The Dept. has a broad range of interests in digital radiography, DSA, PACS, and other methods of improving information content of radiologic images. Candidates for both positions should have strong academic records and current research interests. Hard money support is available for both positions. Contact David C. Levin, M.D., Chairman, Dept. of Radiology, Thomas Jefferson University Hospital, Philadelphia, PA 19107. 11–1a

MRI/ULTRASOUND RADIOLOGISTS. The Dept. of Radiology at Thomas Jefferson University Hospital/Jefferson Medical College is seeking two academically oriented radiologists to join its MRI and Ultrasound divisions. Both divisions are housed in modern, spacious facilities with state-of-the-art technology. A GE 1.5 T MRI unit is now being installed. Candidates will have the option of working in either of these divisions or both, according to their interests. The Dept. is currently under new leadership, and is expanding in both size and academic scope. Generous salaries and benefits are offered. Contact David C. Levin, M.D., Chairman, Dept. of Radiology, Thomas Jefferson University Hospital, Philadelphia, PA 19107. 11–1a

RADIOLOGIST, BOARD CERTIFIED/ELIGIBLE. Full- or part-time position available with two other radiologists in a hospital-based practice that includes diagnostic radiology, CT, ultrasound, angiography, nuclear medicine, and interventional procedures. Teaching hospital with residency programs. Please send CV and other inquiries to Douglas B. McGirr, M.D., Radiology Dept., San Joaquin General Hospital, P.O. Box 1020, Stockton, CA 95201. AA/EOE 11–12a

PERMANENT POSITION. Pediatric radiologist to cover high-risk nurseries at two hospitals approximately three miles apart. Approximately 15 high-risk beds at each hospital. Good pediatrician support. Anticipate growth of routine pediatric radiology as well. Large group, with full compensation package negotiable. Will give preference to person willing to do some plain film adult radiology. Write to C.M. Eiland, M.D., 1920 Huntington Rd., Birmingham, AL 35209. 11–12a

A 400-BED COMMUNITY HOSPITAL staffed by private practice group seeks a second neuroradiologist preferably with MR experience. Ongoing neuroradiologic service includes state-of-the-art CT, angiography with digital, and myelography. MR unit on order. Must be capable and willing to do general radiology also. Contact Ben R. Mayes, Jr., M.D., Radiology Dept., St. Luke's Hospital, 232 So. Woods Mill Rd., St. Louis, MO 63017, (314) 434-1500, ext. 4250. 11–1a

DIAGNOSTIC RADIOLOGIST. Need aggressive associate to perform all aspects of diagnostic radiology in well-equipped hospital with large outpatient component in South Texas. MR training a plus but not essential. Excellent salary and early partnership available. For confidential consideration please submit CV to Box H70, *AJR* (see address this section). 11xa

CHIEF, RADIOLOGY SERVICE. The academically affiliated Newington V.A. Medical Center invites applications of board-certified radiologists to fill this position. 190-bed medical center is a primary affiliate of the Univ. of Connecticut School of Medicine and has a University training program in radiology. Academic appointment commensurate with credentials. Excellent fringe benefits, no state tax, and malpractice coverage. Contact Chief of Staff, V.A. Medical Center, Newington, CT (203) 666-6951 X274. 11a

DIAGNOSTIC RADIOLOGIST with two years fellowship in interventional radiology to join 8-man hospital- and office-radiology group. Group involved in all diagnostic modalities including MRI. E.S.W.L. to be installed soon. Candidates must be skilled in interventional uroradiology and angioplasty. Must also be accomplished general radiologist. Position available on or before July 1, 1987 and leads to full partnership. Send CV to Paul R. Silk, M.D., Dept. of Medical Imaging, Albany Memorial Hospital, Albany, NY 12204. 11–12a

B/C - B/E DIAGNOSTIC RADIOLOGIST. Hospital and office practice. All modalities except MRI. Hands-on experience in real-time ultrasound desired. Excellent salary and benefits, commensurate with experience. Early partnership. Will consider locums. Send CV to Radiology, 5681 N. Fresno St., Fresno, CA 93710 (209) 439-2464. 11–12ap

RADIOLOGIST needed to serve as Chief of Radiology for modern progressive JCAH-accredited, 200-bed Medical/Surgical Center located at Central State Hospital, Milledgeville, GA. In addition to serving the 1,800 patients/residents of Central State Hospital, the center also serves other regional hospitals and state agencies under contract. Milledgeville is a beautiful middle Georgia college town of 15,000, only 2 hr from Atlanta, convenient to mountains and beaches, and immediately accessible to Lake Sinclair, which provides excellent recreational facilities. Annual salary range is $54,504–$74,934, beginning salary commensurate with qualifications. State service provides excellent fringe benefits, including free malpractice and administrative liability insurance, liberal sick and annual leave, 12 paid holidays annually, group term health and life insurance, continuing medical education program, tax-sheltered annuity, and retirement. Requirements are board-certification or board-eligibility in radiology and Georgia licensure. Contact Personnel Office, Central State Hospital, Milledgeville, GA 31062-9989 (912) 453-4094. Applications accepted continuously until suitable applicant located. EOE. 11a

THE DEPARTMENT OF RADIOLOGY, Medical College of Virginia, Richmond VA seeks qualified individuals for faculty positions in skeletal radiology, neuroradiology, and MRI. Must be ABR certified or eligible. Academic rank and salary commensurate with experience. Submit CV to William H. Brewer, M.D., Vice-Chairman, Dept. of Radiology, Medical College of Virginia, Box 470, Richmond, VA 23298. MCV is an equal opportunity, affirmative action employer. Women and minorities are encouraged to apply. 11–12a

PEDIATRIC RADIOLOGIST. Large hospital-based group seeks associate with recent pediatric radiology fellowship training. Busy private practice group needs second pediatric radiologist for coverage of small pediatric hospital. Practice would include 25% pediatric and 75% adult work. All modalities including MRI. Board certification mandatory. Opportunity for partnership in well-established western Washington practice. Reply Box H74, *AJR* (see address this section. 11–6a

NEW YORK CITY SUBURBAN PRACTICE seeks board-certified radiologist. Hands-on ultrasound skills essential. Solid imaging knowledge. Personality counts. High pay with early partnership for special individual. CV to Box 18, Meacham Station, Elmont, NY 11003. 10–11a

BOARD-CERTIFIED RADIOLOGIST–Six man radiology group seeks new associate with fellowship training in CT/ultrasound. The group provides complete radiologic services in fully-equipped 500 bed hospital with two G.E. 9800 CT scanners, and Acuson and Diasonics ultrasound. Private out-patient office also covered by the group. Send CV to Eric R. Rosenberg, M.D., Dept. of Radiology, New Hanover Memorial Hospital, Wilmington, NC 28403. 10–12ap

NEURORADIOLOGY/MRI. Private clinic seeks board certified radiologist with MRI experience to oversee and direct diagnostic center. Excellent salary and recreational activities. Reply: P.O. Box 292527, Davie, FL 33324. 6–11ap

CHIEF, BODY CT. The Dept. of Diagnostic Radiology of William Beaumont Hospital, a major tertiary care and academic institution in Michigan, is seeking a candidate to direct the division of body CT and participate in MR. Candidates must be board certified in diagnostic radiology and have significant academic achievements. Income is negotiable and competitive. Send CV to Jalil Farah, M.D., Director, Diagnostic Radiology, William Beaumont Hospital, 3601 West 13 Mile Road, Royal Oak, MI 48072. 10–12a

TWO YOUNG RADIOLOGISTS seek a third radiologist in expanding hospital-based practice near Canadian border in northern New York. All modalities available. Write P. Berman, HC 61 Box 454, Massena, NY 13662. 8–7a

BOARD CERTIFIED diagnostic radiologist. All diagnostic modalities except MR. MR installation planned in 1½ years. Busy in-patient and out-patient practice. Salary negotiable and early partnership available. Send CV to Box C23, AJR (see address this section). 6xa

BOARD CERTIFIED radiologist to do general diagnostic work, including CT, US, biopsies, mammography, and angio. Special training in angio desired. Excellent salary and full partnership 2nd yr. Busy hospital and office practice in suburban Washington, DC area. Send CV to Box F50, AJR (see address this section). 9-11a

GENERAL DIAGNOSTIC RADIOLOGIST, board certified to join hospital-based group. 200-bed hospital equipped with CT, US, nuclear medicine, special procedures, and interventional radiology. 20,000 exams/yr. Located in Alton, IL, 45 min. to downtown St. Louis. Competitive salary leading to early partnership. Contact Sumner Holtz, M.D., 232 So. Woodsmill Rd., Chesterfield, MO 63017 (314) 434-1500, ext. 4250. 9-11a

ISRAEL, DIAGNOSTIC RADIOLOGY. Opportunities for 3–4 week or longer working vacations in a number of Israeli medical centers, on a volunteer basis. Positions varied, arrangements flexible. For information contact: Jonathan H. Fish, M.D., 1844 San Miguel Dr., #302, Walnut Creek, CA 94596; (415) 947-0560. 8xa

Positions Desired

BOARD CERTIFIED RADIOLOGY GROUP with expertise in all modalities desires to relocate either to a moderate-size hospital or multi-speciality practice. All locations considered. Reply Box H72, *AJR* (see address this section). 11–12b

NEURORADIOLOGIST completing 2-yr-UCSD fellowship 6/87 (with 1.5T GE Signa experience throughout) seeks private practice position. P.O. Box 8107, La Jolla, CA 92038. 9-12b

BOARD-CERTIFIED RADIOLOGIST seeks part-time position in Philadelphia, South Jersey, Wilmington, Delaware area. Experienced in all imaging and invasive modalities except MRI. Reply Box G62, *AJR* (see address this section). 10–12b

PGY-3 RADIOLOGY RESIDENT seeking PGY-4 position beginning July 1987 at university-based program with MRI. Quality U.S. medical graduate. Dedicated, hard-working, easy-going. Reply Box G64, *AJR* (see address this section). 10–11bp

POST-DOCTORAL RESEARCH ASSOCIATE/ FELLOW in diagnostic radiology seeks position. Fully qualified, extensive experience in CT/US, installation to intervention. Over 10,000 CT/US cases, 500 CT/US intervention, biopsies, drainage. Adept also in angiography and general radiology. Write Box G66, *AJR* (see address this section) or call (914) 591-6234. 10–11b

BOARD-CERTIFIED DIAGNOSTIC RADIOLOGIST with interest in all areas of radiology seeks position beginning July 1987. Will have completed a formal postgraduate fellowship in CT/ultrasound/MRI. Have 1-yr extensive experience in angiography and interventional radiology procedures. Reply 251 Marengo Ave., Apt. 4F, Forest Park, IL 60130, (312) 366-0712. 10–12b

Fellowship and Residencies

FELLOW IN MRI - BUFFALO, NY. Available Jan. 1, 1987 a fellowship position is open in a 313-bed pediatric teaching hospital. Eight radiologists associated in practice; CT, nuclear medicine, 2 Acuson units, angiography, and Diasonics 0.5 Tesla Superconductive magnet in our department. Write to J.P. Kuhn, M.D., 219 Bryant St., Buffalo, NY 14222. 11–1a

Tutorials/Courses

CORTINA, ITALY—LONDON, ENGLAND. Winter Congress-Cortina, Jan 31–Feb 7, 1987: Winter Seminar-London, Feb 7–11, 1987. Attend one or both offering CME I accredited and presented by a renowned faculty. Topics in CT, US, MRI with correlation. Fees each meeting: to November 14, US$395, thereafter US$435 (combined fee US$450 and US$495, respectively). Contact Medical Seminars International, 21915 Roscoe Blvd., Ste. 222, Canoga Park, CA 91304 (818) 701-5143. 10–12d

NMR VISITING FELLOWSHIPS in Northern California. Intensive structured 1–6 week courses in clinical magnetic resonance with emphasis on CNS imaging. Integrated live instruction with 20 hr of dual projection slide presentations in week 1, extensive teaching file (600 cases), and updated videotape library. Certificate awarded on completion. References from prior fellows available. For further information contact: Murray A. Solomon, M.D., San Jose MRI Center, 361 S. Monroe St., San Jose, CA 95128. 6–11dp

ULTRASOUND AT SEA—Caribbean Cruise. Post RSNA CME 1 presented by Dr. Peter Cooperberg. Registration: $385 before Oct. 1; $425 thereafter. Info: Medical Seminars International, 21915 Roscoe Blvd., Ste. #222, Canoga Park, CA 91304, (818) 701-5143. 7–11d

Other

REALIZE THE VALUE of your practice. A group of successful and well-qualified radiologists is interested in acquiring established radiology practices. Hospital contracts, clinics, and private office settings are desired. Opportunity for radiologists considering retirement or reduction in practice activities to capitalize on the value of the practice they have built up during their careers. Alleviate the problems of professional recruitment or administrative pressures. Practices considered throughout the country. Flexible purchase options with opportunity for continuing relationship arrangements. Write Box C49, AJR, (see address this section). 6–5e

AJR Indexes

AJR CONSOLIDATED INDEXES available in limited quantities. Complete your journal collection. Order by index number. Indexes available, years covered and prices: 2, 1938–1942, $10; 3, 1943–1947, $22.50; 4, 1948–1952, $23.50; 5, 1953–1957, $25; 6, 1958–1962, $23.50; 7, 1963–1967, $30; 8, 1968–1972, $40; 9, 1973–1977, $34. Order from: Subscription Dept. Williams & Wilkins, 428 E. Preston, St. Baltimore, MD 21202; (301) 528-4000.

AJR Classified Advertising Information

Box Responses and Address for Ad Placement

Write Box _____, AJR, Suite 200, 2223 Avenida de la Playa, La Jolla, CA 92037; (619) 459-2229.

How to Place an Ad

AJR accepts classified advertising for Positions Available, Positions Desired, Fellowships and Residencies, and Tutorials/Courses. Ads are accepted by mail or telephone. Institutions should supply purchase orders.

Rates: $6.00/line with a $30 minimum charge. Box service is $10 additional for each month the ad appears. There are discounts for multiple insertions: 10% for 2–3 insertions; 20% for 4 or more. To estimate lines, count all words and divide by 5.5.

Billing: Ads may be prepaid or invoices will be sent after the ad appears.

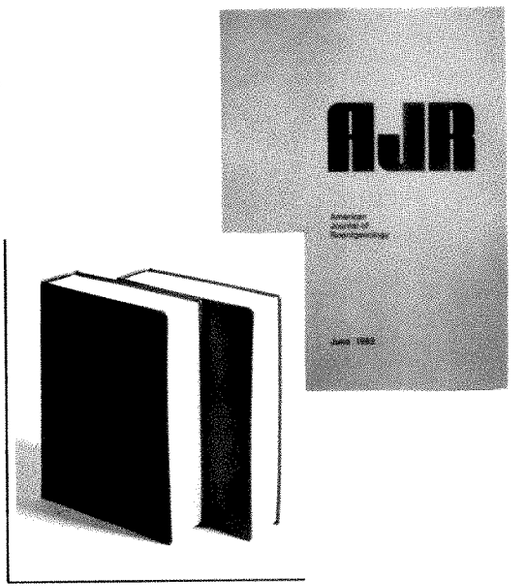
Deadlines. About 3 weeks before the issue mails. *AJR* issues mail in the middle of the month preceding the cover date (e.g., July mails June 17). For specific deadlines, write or telephone the AJR editorial office.

Estimating Ad Charges

Line charge: divide total words by 5.5 and multiply by $6.00	$
Multiple insertions? If so, multiply by number	×
Subtotal	$
Box response requested? If so, multiply number of months by $10.00	+
Subtotal	$
Discount applies to two or more insertions. Subtract 10% if ad appears 2–3 months, 20% if 4 months or more	−
Approximate advertising charge	$

AJR: American Journal of Roentgenology
Bound Volume Offer

A trouble-free way to keep your reference library up to date



As an **AJR** subscriber, you know how much useful information is packed into each issue. But you also probably know how frustrating and time-consuming it can be to try and locate one particular article from a back issue.

Find that back issue quickly and easily

Now you can get a year's worth of articles in bound volume form—a special offer available only to subscribers. So the information you need will be at your fingertips, handsomely preserved and ready for years of future reference.

You get the timely coverage only a journal can provide— penetrating discussions of the topics that interest you most, by the brightest names in your field—with all the durability and convenience of a hardcover edition. With a bound volume, you'll never again spend frustrating hours sifting through dog-eared back issues, only to discover that the article you need has been torn out. You'll have a year's worth of vital information all arranged and indexed in one sturdy source. And each carefully crafted volume will make a handsome addition to your permanent library.

Send in your paid order by October 31, 1986 and SAVE

Act now and receive the **1986 Bound Volumes** for only $55.00 for all prepaid orders, $2.00 off the regular price of $57.00. (Please add $10.00 to all orders outside the US.) Bound volumes are available for the current year only, and are in addition to the regular subscription price.

We'll help you keep your reference library up to date

Once a year, we'll send you a reminder so you can order the latest bound volumes. When you send in your paid order, a set will be reserved for you, to be sent as soon as available on 30-day approval. If you do not want the bound volumes for any reason, simply return them to us within 30 days for a courteous refund. It's that easy.

Williams & Wilkins
P.O. Box 23291 Baltimore, Maryland 21203
266 Fulham Road London SW10 9EL England

EASY ORDERING

Please send me the **AJR: American Journal of Roentgenology 1986 Bound Volumes** at $57.00 ($67.00 outside the US). I understand that I can save $2.00 by sending in my prepaid order (check or charge) by October 31, 1986. I also understand that this offer is in addition to my regular subscription, that it is available only to subscribers, and that I will have the option of ordering bound volumes for subsequent years as long as I remain a subscriber. I will receive my 1986 bound volumes in early 1987.

☐ Check enclosed ☐ Bill me
☐ VISA ☐ MasterCard ☐ American Express

Card # Exp. date

Signature/P.O.#

Please pay in US dollars. MD residents, please add 5% sales tax. Orders outside the US and Canada must be prepaid. Rates subject to change without notice. **All orders must be received by December 31, 1986.**

Name

Address

City/State/Zip

Date of order

ORDER FREE BY PHONE. Call 1-800-638-6423 from anywhere in the US except AK. MD residents, call 528-4105 collect.

Williams & Wilkins
P.O. Box 23291 Baltimore, Maryland 21203
266 Fulham Road London SW10 9EL England

Vital new references on 30-day FREE trial

EMERGENCY RADIOLOGY OF THE ACUTELY ILL OR INJURED CHILD
Second Edition

By **Leonard E. Swischuk, MD**

"Only Len Swischuk could produce a book quite like this....The reproductions, particularly of soft tissues, are superb....A true teacher, [Swischuk] stresses the basic facts, the simple, the obvious, the variations, and the pitfalls....This book should be in the library of even the smallest radiology department." — **J Can Assoc Radiol** (of the First Edition)

1986/622 pages/685 illustrations/#8049-0/$75.00

COMPUTED TOMOGRAPHY AND MAGNETIC RESONANCE IMAGING OF THE HEAD AND NECK
Second Edition

By **Anthony A. Mancuso, MD** and **William N. Hanafee, MD**
with a special contribution from ***John A. Kirchner, MD***

The leading guide to head and neck imaging now includes the first comprehensive discussion of otolaryngologic MRI, an extensively revised chapter on temporal bone, extraordinary images generated by state-of-the-art equipment, and more.

1985/504 pages/155 illustrations/#5476-7/$84.75

LYMPHATIC IMAGING
Lymphography, Computed Tomography and Scintigraphy
Second Edition

Edited by **Melvin E. Clouse, MD** and **Sidney Wallace, MD**

For assistance in selecting, performing and interpreting lymphatic images using state-of-the-art equipment and techniques, turn to the new *Second Edition* of the only book-length exploration of lymphatic evaluation.

1985/526 pages/252 illustrations/#1651-2/$87.50

COMPUTED TOMOGRAPHY IN TH EVALUATION OF TRAUMA
Second Edition

Edited by **Michael P. Federle, MD** and **Micha Brant-Zawadzki, MD**

In this new edition you'll find a thorough and up date discussion of the clinical indications for CT scanning in different types of trauma to virtually a areas of the body, keys to techniques of scanning a accurate interpretation, and comparisons of CT to radiographic procedures and laboratory tests.

1986/about 300 pages/about 370 illustrations/ #3102-3/about $58.95

CLINICAL ARTHROGRAPHY
Second Edition

By **Rolf-D. Arndt, MD, John W. Horns, MD,** a **Richard H. Gold, MD**
with a special contribution by ***Donald D. Blaschk DDS***

Including inflammatory diseases and other joint abnormalities, the *Second Edition* retains the emp on orthopedic disorders as it expands the basic pri ples of arthrography and adds new, recently publis concepts, such as double-contrast CT arthrography

1985/282 pages/147 illustrations/#0256-2/$62

Williams & Wilkins
428 E. Preston Street Baltimore, MD 21202

____ YES! Please rush my copy of _____

_____

_____

If not completely satisfied, I may return the books in 30 days at no further obligation. (US & Canada

PAYMENT OPTIONS
(Enclose payment or charge your order and Williams & Wilkins will pay all p and handling costs.)

☐ Check enclosed ☐ Bill me
☐ VISA ☐ MasterCard ☐ American Expres

card # ☐☐☐☐☐☐☐☐☐☐☐☐☐☐☐☐ exp. ☐☐

_____
signature/p.o. #

For fastest service...call 1-800-638-0672 toll free anywh the US except AK and HI; MD residents call 528-4221 col

Full Name _____

Address _____

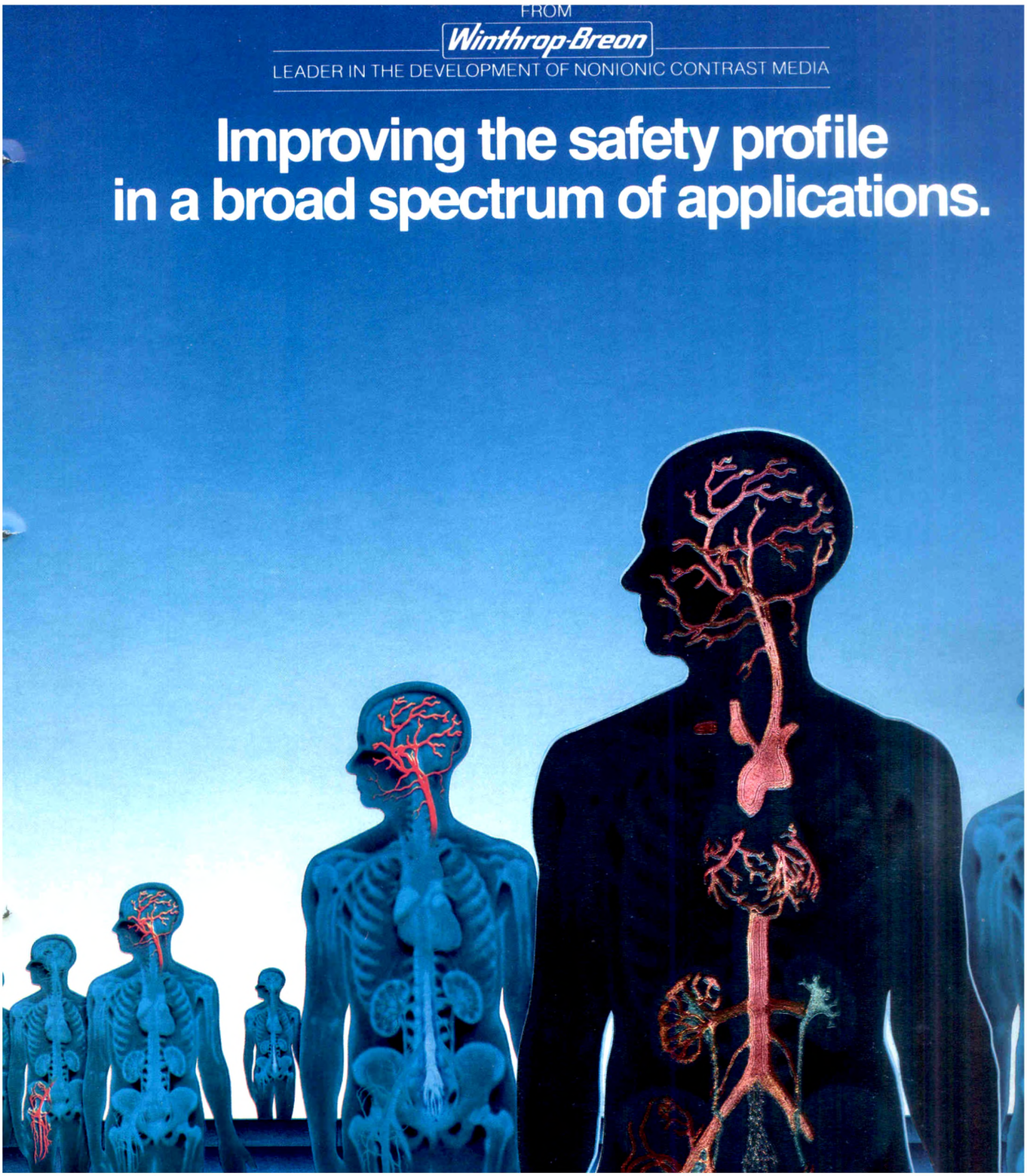
City _____ State _____ Zip _____

FROM

Winthrop-Breon

LEADER IN THE DEVELOPMENT OF NONIONIC CONTRAST MEDIA

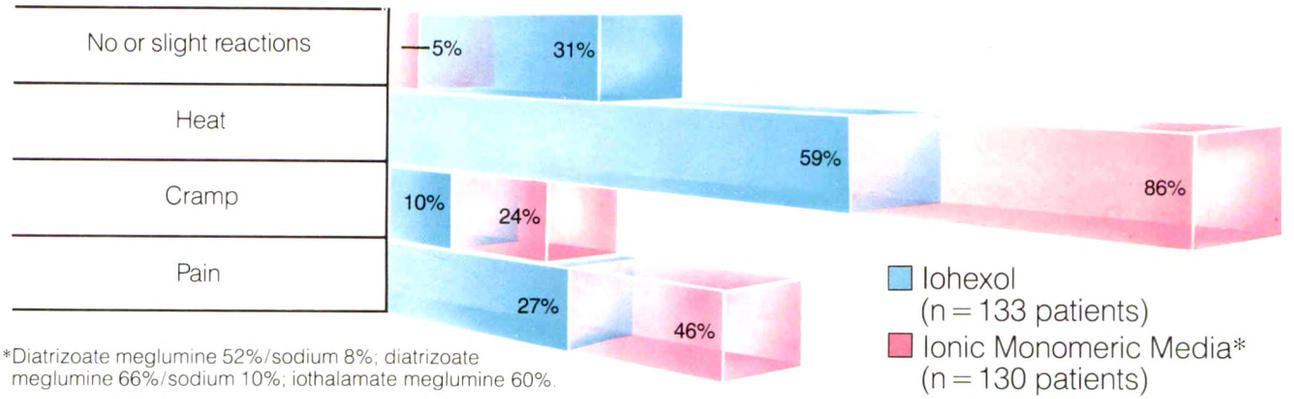
Improving the safety profile in a broad spectrum of applications.



Excellent vascular tolerance: low incidence of postphlebographic thrombosis.[1-3]

Significant improvement in comfort reduces patient motion[4,5]:
Less need for repeat examinations.

Subjective Sensations in Peripheral Arteriography



*Diatrizoate meglumine 52%/sodium 8%; diatrizoate meglumine 66%/sodium 10%; iothalamate meglumine 60%.

Improved hemodynamic profile over conventional ionic media.
Systolic and diastolic pressures are maintained near baseline levels.[6,7]

Improving the nephrotoxicity profile: Minimal effect on glomerular filtration rate, permeability, or albumin excretion.[8,9]

Not recommended for patients with anuria. Since adverse reactions can occur with nonionic media, similar preparations to those recommended for ionic media should be planned to handle severe or potentially fatal reactions.

Wider margin of safety even at higher iodine concentrations.[1-3]
Less potential for renal damage compared to conventional ionic media.
Minimal effect on creatinine levels and renal enzymes.[10]

Significant improvement in patient comfort in cerebral arteriography.

Significant improvement over conventional ionic contrast media:
Fewer and milder pain and warmth sensations.[11-15]
Excellent neurotoxicity profile.†

Excellent cardiovascular safety profile: Fewer injections accompanied by major changes in heart rate.[6,14,15]

For peripheral arteriography: Recommended concentrations—OMNIPAQUE 300 (300 mgI/mL) or OMNIPAQUE 350 (350 mgI/mL).
For cerebral arteriography: Recommended concentration—OMNIPAQUE 300 (300 mgI/mL).

Adapted from Wolf[4]; data on file, Winthrop-Breon Laboratories.[6]
†Comparable concentration and volume per injection.

Excellent diagnostic quality in intravenous digital subtraction angiography.

Greater patient comfort, better tolerance: Most subjective side effects are mild.[6,16-18]

Excellent diagnostic images: Significantly less image degradation secondary to swallowing, motion, coughing.[16]

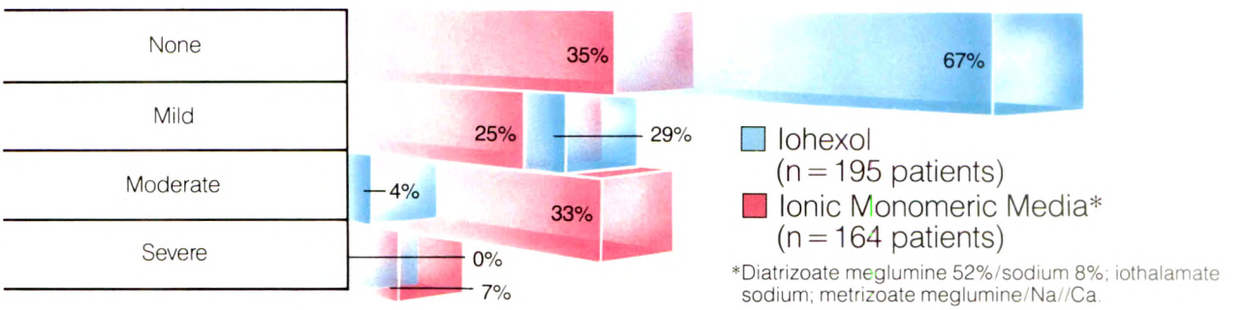
Good to excellent radiographic quality achieved in 94% of patients studied (n = 81).[6,16-18] 94% of carotid DSA studies conducted with no or only slight artifacts.[17]

Excellent patient tolerance in excretory urography.

Less nausea, vomiting, and heat sensation compared to conventional ionic contrast media.

In 96% of patients, discomfort was absent or mild.[6]

Discomfort in Urography



*Diatrizoate meglumine 52%/sodium 8%; iothalamate sodium; metrizoate meglumine/Na//Ca.

Data on file, Winthrop-Breon Laboratories.[6]

NONIONIC

OMNIPAQUE®

(IOHEXOL)

†See following pages for important product information concerning contraindications, warnings, adverse reactions, patient selection, and precautionary recommendations.

Improving the safety profile in a broad spectrum of applications.

Less chemotoxicity than ionic contrast media.[19]

Lower osmolality than conventional ionic media.[19]

Minimal effect on key physiologic parameters[19]**:** Well tolerated by most patients.

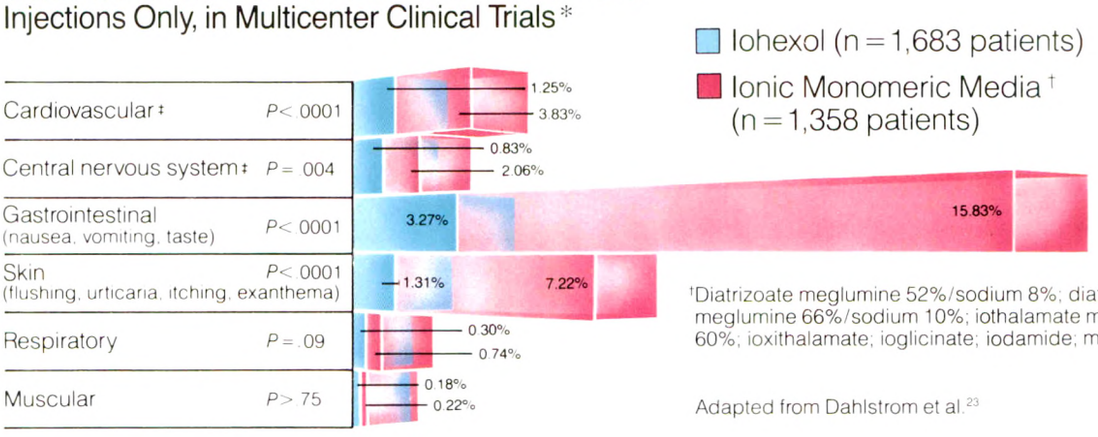
Less neurotoxic than conventional ionic media.

Few direct or indirect cardiovascular effects.[20,21]

Improved patient comfort: Fewer artifacts due to motion and swallowing.[16-18]

Less potential for allergic reactions.[22] Since adverse reactions can occur with nonionic media, similar preparations to those recommended for ionic media should be planned to handle severe or potentially fatal reactions.

Incidence of Adverse Reactions After Intravenous Injections Only, in Multicenter Clinical Trials *



†Diatrizoate meglumine 52%/sodium 8%; diatrizoate meglumine 66%/sodium 10%; iothalamate meglumine 60%; ioxithalamate; ioglicinate; iodamide; metrizoate.

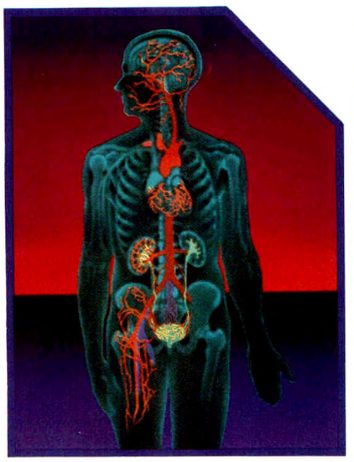
Adapted from Dahlstrom et al.[23]

Supplied in ready-to-use vials and bottles. No dilution or reconstitution necessary.

Product	Size (mL/unit)	Use
OMNIPAQUE® 180 (180 mgI/mL)	10 mL, 20 mL vials, Myelo-Kit™	Lumbar, Thoracic, and CT Myelography
OMNIPAQUE® 240 (240 mgI/mL)	10 mL, 100 mL vials, 200 mL bottle, Myelo-Kit	Lumbar and Thoracic Myelography, Peripheral Venography
OMNIPAQUE® 300 (300 mgI/mL)	10 mL, 30 mL, 50 mL, 100 mL vials	Urography, Cerebral Arteriography, Peripheral Arteriography, Peripheral Venography
OMNIPAQUE® 350 (350 mgI/mL)	50 mL, 100 mL vials, 200 mL bottle	Angiocardiography, Urography, Peripheral Arteriography, I.V. Digital Subtraction Angiography

*See following pages for important product information concerning contraindications, warnings, adverse reactions, patient selection, and precautionary recommendations.

‡In general, adverse reactions to the intravascular use of OMNIPAQUE have been mild and of short duration. The general incidence of these occurrences following total intravascular use is slightly higher, as shown in the product information on the last page.



OMNIPAQUE®
INJECTION (IOHEXOL)

180

240

300

350

PLEASE CONSULT FULL PRODUCT INFORMATION BEFORE USING.
A SUMMARY FOLLOWS:
OMNIPAQUE is a nonionic, water-soluble, radiographic contrast medium.
INDICATIONS AND USAGE: OMNIPAQUE is indicated in adults for angiocardiography (ventriculography, selective coronary arteriography); aortography, including studies of the aortic root, aortic arch, ascending aorta, abdominal aorta, and its branches; cerebral arteriography; digital subtraction angiography; peripheral angiography including arteriography and venography (phlebography); excretory urography; and lumbar and thoracic myelography, by conventional technique and in computerized tomography.

Administration of contrast media should be performed by qualified personnel familiar with the procedure and an appropriate technique should be utilized.
CONTRAINDICATIONS: OMNIPAQUE should not be administered to patients with a known hypersensitivity to iohexol.

Lumbar puncture ordinarily should not be performed in the presence of local or systemic infection where bacteremia is likely.

Intrathecal administration of corticosteroids with OMNIPAQUE is contraindicated.

Because of the possibility of overdosage, immediate repeat myelography in the event of technical failure is contraindicated (see DOSAGE AND ADMINISTRATION).
WARNINGS—General: OMNIPAQUE should be used with extreme care in patients with severe functional disturbances of the liver and kidneys, severe thyrotoxicosis, or myelomatosis. Diabetics with a serum creatinine level above 3 mg/dL should not be examined unless the possible benefits of the examination clearly outweigh the additional risk. OMNIPAQUE is not recommended for use in patients with anuria.

Radiopaque contrast agents are potentially hazardous in patients with multiple myeloma or other paraproteinemia, particularly in those with therapeutically resistant anuria. Although neither the contrast agent nor dehydration has separately proven to be the cause of anuria in myeloma, it has been speculated that the combination of both may be causative factors. The risk in myelomatous patients is not a contraindication; however, special precautions are necessary. Partial dehydration in the preparation of these patients prior to injection is not recommended since this may predispose the patient to precipitation of the myeloma protein in the renal tubules. No form of therapy, including dialysis, has been successful in reversing the effect. Myeloma, which occurs most commonly in persons over age 40, should be considered before instituting intravascular administration of contrast agents.

Ionic contrast media, when injected intravenously or intraarterially, may promote sickling in individuals who are homozygous for sickle cell disease.

Administration of radiopaque materials to patients known or suspected of having pheochromocytoma should be performed with extreme caution. If, in the opinion of the physician, the possible benefits of such procedures outweigh the considered risks, the procedures may be performed, however, the amount of radiopaque medium injected should be kept to an absolute minimum. The patient's blood pressure should be assessed throughout the procedure and measures for the treatment of hypertensive crisis should be readily available.

Reports of thyroid storm following the use of iodinated, ionic radiopaque contrast media in patients with hyperthyroidism or with autonomously functioning thyroid nodule suggest that this additional risk be evaluated in such patients before use of any contrast medium.

Urography should be performed with caution in patients with severely impaired renal function and patients with combined renal and hepatic disease.

Caution is advised in patients with a history of epilepsy, severe cardiovascular disease, chronic alcoholism, or multiple sclerosis.

Elderly patients may present a greater risk following myelography. The need for the procedure in these patients should be evaluated carefully. Special attention must be paid to dose and concentration of the medium, hydration, and technique used.

Patients who are receiving anticonvulsants should be maintained on this therapy. Should a seizure occur, intravenous diazepam or phenobarbital sodium is recommended. In patients with a history of seizure activity who are not on anticonvulsant therapy, premedication with barbiturates should be considered.

Prophylactic anticonvulsant treatment with barbiturates should be considered in patients with evidence of inadvertent intracranial entry of a large or concentrated bolus of the contrast medium since there may be an increased risk of seizure in such cases.

Drugs which lower the seizure threshold, especially phenothiazine derivatives, including those used for their antihistamine properties, should not be used with OMNIPAQUE. Others include MAO inhibitors, tricyclic antidepressants, CNS stimulants, and psychoactive drugs described as analeptics, major tranquilizers, or antipsychotic drugs. Such medication should be discontinued at least 48 hours before myelography, should not be used for the control of nausea and vomiting, and should not be resumed for at least 24 hours postprocedure.

Care is required in patient management to prevent inadvertent intracranial entry of a large dose or concentrated bolus of the medium. Also, effort should be directed to avoid rapid dispersion of the medium causing inadvertent rise to intracranial levels (eg, by active patient movement). Direct intracisternal or ventricular administration for standard radiography (not CT) is not recommended.

In most reported cases of major motor seizures with other nonionic myelographic media, one or more of the following factors were present. Therefore avoid:
- Deviations from recommended procedure or in myelographic management.
- Use in patients with a history of epilepsy.
- Overdosage.
- Intracranial entry of a bolus or premature diffusion of a high concentration of the medium.
- Medication with neuroleptic drugs or phenothiazine antinauseants.
- Failure to maintain elevation of the head during the procedure, on the stretcher, or in bed.
- Excessive and particularly active patient movement or straining.

If grossly bloody CSF is encountered, the possible benefits of a myelographic procedure should be considered in terms of the risk to the patient.

PRECAUTIONS—General: Diagnostic procedures which involve the use of radiopaque diagnostic agents should be carried out under the direction of personnel with the prerequisite training and with a thorough knowledge of the particular procedure to be performed. Appropriate facilities should be available for coping with any complication of the procedure, as well as for emergency treatment of severe reactions to the contrast agent itself. After parenteral administration of a radiopaque agent, competent personnel and emergency facilities should be available for at least 30 to 60 minutes since severe delayed reactions have occurred (see ADVERSE REACTIONS).

Preparatory dehydration is dangerous and may contribute to acute renal failure in patients with advanced vascular disease, diabetic patients, and in susceptible nondiabetic patients (often elderly with preexisting renal disease). Dehydration in these patients seems to be enhanced by the osmotic diuretic action of urographic agents. It is believed that overnight fluid restriction prior to excretory urography generally does not provide better visualization in normal patients. *Patients should be well hydrated prior to and following iohexol administration.*

In patients with severe renal insufficiency or failure, compensatory biliary excretion of the drug is anticipated to occur, with a slow clearance into the bile. Patients with hepatorenal insufficiency should not be examined unless the possibility of benefit clearly outweighs the additional risk.

Acute renal failure has been reported in diabetic patients with diabetic nephropathy and in susceptible nondiabetic patients (often elderly with preexisting renal disease) following excretory urography. Therefore, careful consideration of the potential risks should be given before performing this radiographic procedure in these patients.

Immediately following surgery, excretory urography should be used with caution in renal transplant recipients.

The possibility of a reaction, including serious, life-threatening, fatal, anaphylactoid, or cardiovascular reactions should always be considered (see ADVERSE REACTIONS). It is of utmost importance that a course of action be carefully planned in advance for immediate treatment of serious reactions, and that adequate and appropriate personnel be readily available in case a severe reaction should occur.

The possibility of an idiosyncratic reaction in susceptible patients should always be considered (see ADVERSE REACTIONS). The susceptible population includes patients with a previous reaction to contrast media, patients with a known sensitivity to iodine per se, and patients with a known clinical hypersensitivity: bronchial asthma, hay fever, and food allergies.

The occurrence of severe idiosyncratic reactions has prompted the use of several pretesting methods. However, pretesting cannot be relied upon to predict severe reactions and may itself be hazardous for the patient. It is suggested that a thorough medical history with emphasis on allergy and hypersensitivity, prior to the injection of any contrast media, may be more accurate than pretesting in predicting potential adverse reactions.

A positive history of allergies or hypersensitivity does not arbitrarily contraindicate the use of a contrast agent where a diagnostic procedure is thought essential, but caution should be exercised (see ADVERSE REACTIONS). Premedication with antihistamines or corticosteroids to avoid or minimize possible allergic reactions in such patients should be considered. Recent reports indicate that such pretreatment does not prevent serious life-threatening reactions, but may reduce both their incidence and severity.

Even though the osmolality of OMNIPAQUE is low compared to diatrizoate- or iothalamate-based ionic agents of comparable iodine concentration, the potential transitory increase in the circulatory osmotic load in patients with congestive heart failure requires caution during injection. These patients should be observed for several hours following the procedure to detect delayed hemodynamic disturbances.

General anesthesia may be indicated in the performance of some procedures in selected adult patients; however, a higher incidence of adverse reactions has been reported in these patients, and may be attributable to the inability of the patient to identify untoward symptoms, or to the hypotensive effect of anesthesia which can reduce cardiac output and increase the duration of exposure to the contrast agent.

Angiography should be avoided whenever possible in patients with homocystinuria, because of the risk of inducing thrombosis and embolism.

In angiographic procedures, the possibility of dislodging plaques or damaging or perforating the vessel wall should be borne in mind during the catheter manipulations and contrast medium injection. Test injections to ensure proper catheter placement are recommended.

Selective coronary arteriography should be performed only in those patients in whom the expected benefits outweigh the potential risk. The inherent risks of angiocardiography in patients with chronic pulmonary emphysema must be weighed against the necessity for performing this procedure.

Administration of contrast media should be performed by qualified personnel familiar with the procedure and appropriate patient management. Sterile technique must be used with any spinal puncture.

When OMNIPAQUE is to be injected using plastic disposable syringes, the contrast medium should be drawn into the syringe and used immediately.

If nondisposable equipment is used, scrupulous care should be taken to

prevent residual contamination with traces of cleansing agents.

Parenteral products should be inspected visually for particulate matter and discoloration prior to administration. If particulate matter or discoloration is present, do not use.

Repeat Procedures: If, in the clinical judgment of the physician, sequential or repeat subarachnoid examinations are required, a suitable interval of time between administrations should be observed to allow for normal clearance of the drug from the body.

Information for Patients: Patients receiving injectable radiopaque diagnostic agents should be instructed to:

1. Inform your physician if you are pregnant.
2. Inform your physician if you are diabetic or if you have multiple myeloma, pheochromocytoma, homozygous sickle cell disease or known thyroid disorder (see WARNINGS).
3. Inform your physician if you are allergic to any drugs, food, or if you had any reactions to previous injections of dyes used for x-ray procedures.
4. Inform your physician about any other medications you are currently taking, including nonprescription drugs, before you are administered this drug.

Drug/Laboratory Test Interaction: If iodine containing isotopes are to be administered for the diagnosis of thyroid disease, the iodine-binding capacity of thyroid tissue may be reduced for up to two weeks after contrast medium administration. Thyroid function tests which do not depend on iodine estimation, eg, T_3 resin uptake or direct thyroxin assays, are not affected.

Drug Interactions: Drugs which lower the seizure threshold—especially phenothiazine derivatives including those used for their antihistaminic or antinauseant properties—should not be used with OMNIPAQUE. Others include monoamine oxidase (MAO) inhibitors, tricyclic antidepressants, CNS stimulants, and psychoactive drugs described as analeptics, major tranquilizers, or antipsychotic drugs. Such medications should be discontinued at least 48 hours before myelography, should not be used for the control of nausea or vomiting during or after myelography, and should not be resumed for at least 24 hours postprocedure. In nonelective procedures in patients on these drugs, consider prophylactic use of anticonvulsants.

Carcinogenesis, Mutagenesis, Impairment of Fertility: No long-term animal studies have been performed to evaluate the potential of iohexol in these areas.

Pregnancy Category B: Reproduction studies have been performed in rats and rabbits with up to 100 times the recommended human dose. No evidence has been established of impaired fertility or harm to the fetus due to OMNIPAQUE; there are, however, no studies in pregnant women. Because animal reproduction studies are not always predictive of human response, this drug should be used during pregnancy only if clearly indicated.

Nursing Mothers: Caution should be exercised when OMNIPAQUE is administered to a nursing woman; it is not known to what extent iohexol is excreted in human milk.

Pediatric Use: Safety and effectiveness in children have not been established.

ADVERSE REACTIONS:

Intrathecal: Adverse reactions to the intrathecal use of OMNIPAQUE in general have been mild to moderate in degree, and of short duration. The incidence of these occurrences, based on clinical trials of 584 patients, is as follows:

Headaches: The most frequently occurring adverse reaction following myelography with OMNIPAQUE has been headache, with an incidence of less than 20%. Headache may be caused either as a direct effect of the contrast medium or by CSF leakage at the dural puncture site. However, in managing the patient, it is considered more important to minimize intracranial entry of contrast medium by postural management than to attempt to control possible CSF leakage.

Pain: Mild pain including backache, stiffness, and neuralgia occurred following injection with an incidence of about 8%.

Nausea and Vomiting: Nausea was reported, with an incidence of about 6%, and vomiting of about 3% (based on clinical trials of 584 patients—see PATIENT MANAGEMENT). Maintaining normal hydration is very important. The use of phenothiazine antinauseants is contraindicated. Reassuring the patient that the nausea will clear is usually all that is required.

Dizziness: Transient dizziness was reported in about 2% of the patients.

Other Reactions: Other reactions, occurring with an individual incidence of less than 0.1%, included feeling of heaviness, hypotension, hypertonia, sensation of heat, sweating, vertigo, and loss of appetite. All were transient and mild, with no clinical sequelae.

General Adverse Reactions to Contrast Media: Physicians should remain alert for the occurrence of adverse effects in addition to those discussed above, particularly those already reported in the literature for other nonionic, water-soluble myelographic contrast media. These have included but are not limited to aseptic and bacterial meningitis, and CNS and other neurologic disturbances.

Intravascular: Adverse reactions to the intravascular use of OMNIPAQUE have usually been of mild to moderate severity. However, serious, life-threatening and fatal reactions, mostly of cardiovascular origin, have been associated with the administration of iodine-containing contrast media, including OMNIPAQUE. The injection of contrast media is frequently associated with the sensation of warmth and pain, especially in peripheral angiography; pain and warmth are less frequent and less severe with OMNIPAQUE than with many ionic media, but lower osmolality media are similar in this respect. The incidence of these occurrences in clinical trials is as follows:

Cardiovascular System: Arrhythmias including PVCs and PACs (3%), angina/chest pain (2%), and hypotension (1%). Others including cardiac failure, asystole, bradycardia, tachycardia, and vasovagal reaction were reported with an individual incidence of less than 0.8%. In controlled clinical studies involving 900 patients, one fatality occurred. In widespread clinical use, the incidence of fatality is estimated at 0.0003%.

Nervous System: Pain (6%), photomas (3%), headache (2%), and metallic taste (0.8%). Others including anxiety, blurred vision, dizziness, fever, motor and speech dysfunction, convulsion, light-headedness, paresthesia, somnolence, vertigo, stiff neck, hemiparesis, and nystagmus were reported, with an individual incidence of less than 0.3%.

Respiratory System: Dyspnea, laryngitis, and throat irritation, with an individual incidence of 0.1%.

Gastrointestinal System: Nausea (2%) and vomiting (0.5%). Others including diarrhea, dyspepsia, and dry mouth were reported, with an individual incidence of 0.1%.

© 1986 WINTHROP-BREON LABORATORIES 41368/3737

OMNIPAQUE® (iohexol)

Skin and Appendages: Urticaria (0.3%) and purpura (0.1%).

Individual adverse reactions which occurred to a significantly greater extent for a specific procedure are listed under that indication.

General Adverse Reactions to Contrast Media: Physicians should remain alert for the occurrence of adverse effects in addition to those discussed above. The following reactions have been reported after administration of other intravascular iodinated contrast media. *Reactions due to technique:* hematomas and ecchymoses. *Hemodynamic reactions:* vein cramp and thrombophlebitis following intravenous injection. *Cardiovascular reactions:* rare cases of cardiac arrhythmias, reflex tachycardia, chest pain, cyanosis, hypertension, hypotension, peripheral vasodilatation, shock, and cardiac arrest. *Renal reactions:* occasionally, transient proteinuria, and rarely, oliguria or anuria. *Allergic reactions:* Asthmatic attacks, nasal and conjunctival symptoms, dermal reactions such as urticaria with or without pruritus, as well as pleomorphic rashes, sneezing and lacrimation and, rarely, anaphylactic reactions. Rare fatalities have occurred, due to this or unknown causes. *Signs and symptoms related to the respiratory system:* pulmonary or laryngeal edema, bronchospasm, dyspnea; *or to the nervous system:* restlessness, tremors, convulsions. *Other reactions:* flushing, pain, warmth, metallic taste, nausea, vomiting, anxiety, headache, confusion, pallor, weakness, sweating, localized areas of edema, especially facial cramps, neutropenia, and dizziness. Rarely, immediate or delayed rigors can occur, sometimes accompanied by hyperpyrexia. Infrequently, "iodism" (salivary gland swelling) from organic iodinated compounds appears two days after exposure and subsides by the sixth day.

CONSULT PACKAGE INSERT FOR A MORE DETAILED DISCUSSION OF ADVERSE REACTIONS to both intrathecal and intravascular use of OMNIPAQUE.

DOSAGE AND ADMINISTRATION: CONSULT FULL PACKAGE INSERT BEFORE USE. Details on dose, concentration, and administration are provided for each of the indicated procedures.

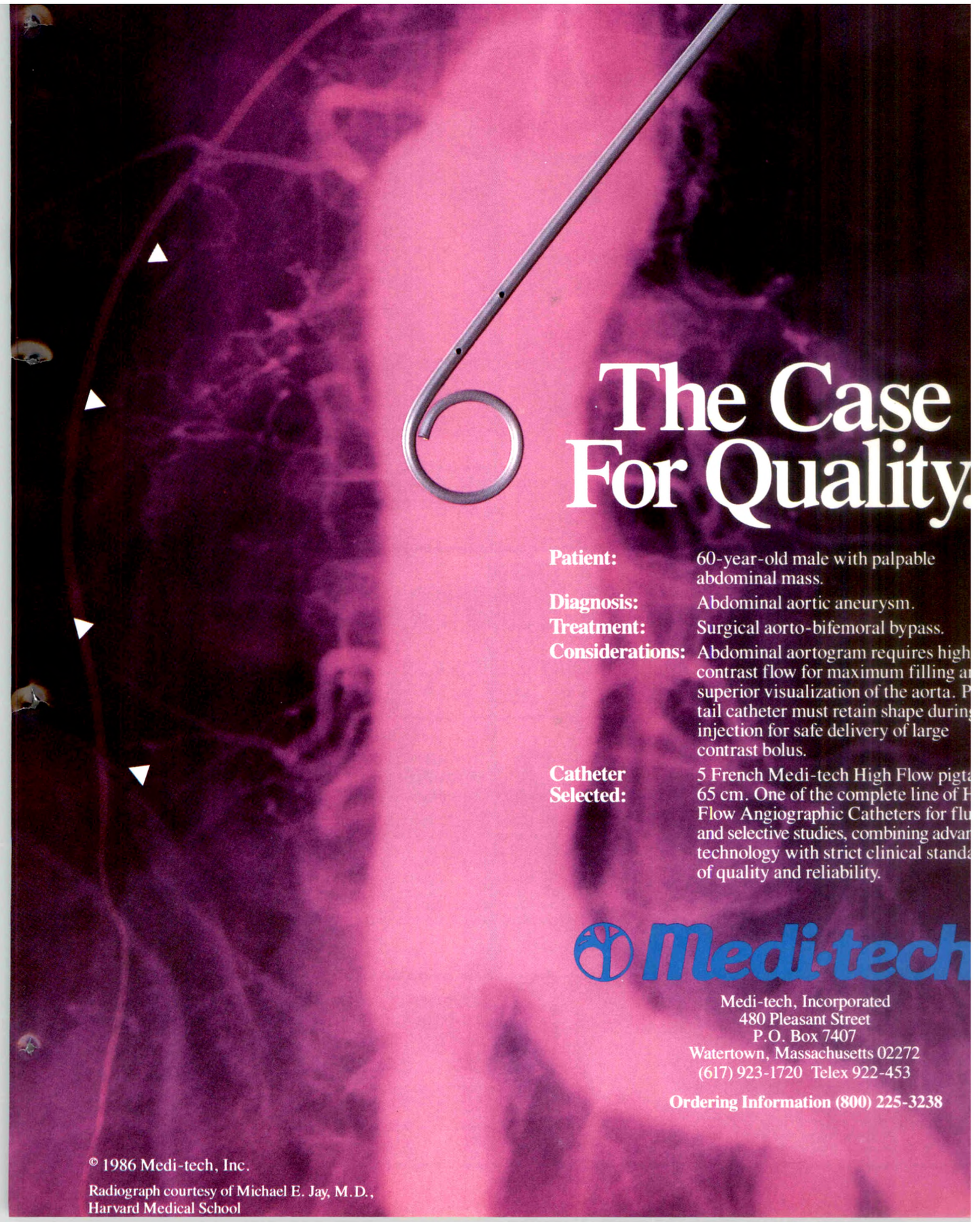
HOW SUPPLIED: OMNIPAQUE is available in the following packaging and concentrations, *requiring no dilutions or reconstitution:*

Vials of 10 mL, 180 mgI/mL, boxes of 10 (NDC 0024-1411-10)
Vials of 20 mL, 180 mgI/mL, boxes of 10 (NDC 0024-1411-20)
Vials of 10 mL, 240 mgI/mL, boxes of 10 (NDC 0024-1412-10)
Vials of 100 mL, 240 mgI/mL, boxes of 5 (NDC 0024-1412-15)
Bottles of 200 mL, 240 mgI/mL, boxes of 5 (NDC 0024-1412-25)
Vials of 10 mL, 300 mgI/mL, boxes of 10 (NDC 0024-1413-10)
Vials of 30 mL, 300 mgI/mL, boxes of 10 (NDC 0024-1413-30)
Vials of 50 mL, 300 mgI/mL, boxes of 10 (NDC 0024-1413-50)
Vials of 100 mL, 300 mgI/mL, boxes of 5 (NDC 0024-1413-15)
Vials of 50 mL, 350 mgI/mL, boxes of 10 (NDC 0024-1414-50)
Vials of 100 mL, 350 mgI/mL, boxes of 5 (NDC 0024-1414-15)
Bottles of 200 mL, 350 mgI/mL, boxes of 5 (NDC 0024-1414-25)
MYELO-KIT™ containing: One vial of 10 mL, 180 mgI/mL, and one sterile myelogram tray, boxes of 5 (NDC 0024-1411-05)
MYELO-KIT™ containing: One vial of 20 mL, 180 mgI/mL, and one sterile myelogram tray, boxes of 5 (NDC 0024-1411-51)
MYELO-KIT™ containing: One vial of 10 mL, 240 mgI/mL, and one sterile myelogram tray, boxes of 5 (NDC 0024-1412-05)

References: 1. Enge I: Phlebography: Survey and present state. *Acta Radiol* 1983; suppl 366, pp 50-53. **2.** Gjølberg T, Andrew E, Enge I: Iohexol in phlebography of the leg: A comparative investigation with meglumine metrizoate. *Acta Radiol* 1983; suppl 366, pp 65-69. **3.** Albrechtsson U, Fagher B, Lagerstedt C, et al: Double blind comparison between iohexol and metrizoate in phlebography of the lower limb. *Acta Radiol* 1983; suppl 366, pp 58-64. **4.** Wolf GL: Adult peripheral angiography: Results from four North American randomized clinical trials of ionic media versus iohexol. *Acta Radiol* 1983; suppl 366, pp 166-170. **5.** Gordon IJ, Skoblar RS, Chicatelli PD, et al: A comparison of iohexol and Conray-60 in peripheral angiography. *AJR* 1984; 142:563-565. **6.** Data on file, Winthrop-Breon Laboratories. **7.** Egsgaard H, Hørup A, Praestholm J: A controlled clinical trial of iohexol and diatrizoate in aortofemoral angiography. *Eur J Radiol* 1983; 3:14-17. **8.** Kolbenstvedt A: Iohexol in lower extremity, renal and visceral angiography: Survey and present state. *Acta Radiol* 1983; suppl 366, pp 153-157. **9.** Törnquist C, Holtås S: Renal angiography with iohexol and metrizoate. *Radiology* 1984; 150:331-334. **10.** Albrechtsson U, Hultberg B, Lárusdóttir H, et al: Nephrotoxicity of ionic and non-ionic contrast media in aorto-femoral angiography. *Acta Radiol* 1985; 5:615-618. **11.** Cronqvist S: Iohexol in cerebral angiography: Survey and present state. *Acta Radiol* 1983; suppl 366, pp 135-139. **12.** Ahlgren P: Iohexol compared to urografin meglumine in cerebral angiography: A randomized, double-blind cross-over study. *Neuroradiology* 1982; 23:195-198. **13.** Nakstad P, Sortland O, Aaserud O: Iohexol compared to meglumine-Ca-metrizoate in common carotid angiography: A randomized double-blind cross-over study in man. *Neuroradiology* 1983; 23:33-36. **14.** Kido DK, Morris TW, Ekholm S, et al: Comparison of iohexol and meglumine-Na diatrizoate in cerebral angiography. *Acta Radiol* 1983; suppl 366, pp 142-146. **15.** Amundsen P, Dugstad G, Presthus J, et al: Cerebral angiography with iohexol: A multicentre clinical trial. *Acta Radiol* 1982; 23:529-534. **16.** Cacayorin ED, Bernstein AD, Fruehan CT, et al: Intravenous digital subtraction angiography with iohexol. *AJNR* 4:329-332. **17.** Nakstad P: Digital subtraction angiography of the carotid arteries: A comparison of iohexol and metrizoate. *Acta Radiol* 1983; suppl 366, pp 89-93. **18.** Sackett JF, Bergsjordet B, Seeger JF, et al: Digital subtraction angiography: Comparison of meglumine-Na diatrizoate with iohexol. *Acta Radiol* 1983; suppl 366, pp 81-84. **19.** Dawson P: Some aspects of contrast medium toxicity. *Acta Radiol* 1983; suppl 366, pp 174-179. **20.** Bryan RN, Miller SL, Roehm JOF Jr, et al: Neuroangiography with iohexol. *AJNR* 1983; 4:344-346. **21.** Higgins CB, Mancini GBJ, Bloomquist JN, et al: Cardioangiography in man using iohexol and meglumine-Na diatrizoate: A comparison of hemodynamic and electrocardiographic effects. *Acta Radiol* 1983; suppl 366, pp 111-114. **22.** Holtås S: Iohexol in patients with previous adverse reactions to contrast media. *Invest Radiol* 1984; 19:563-565. **23.** Dahlstrom K, Shaw DD, Clauss W, et al: Summary of U.S. and European intravascular experience with iohexol based on the clinical program. *Invest Radiol* 1985; 20(suppl 1), pp 117-121.

Winthrop-Breon

Winthrop-Breon Laboratories
Division of Sterling Drug Inc.
New York, NY 10016



The Case For Quality.

Patient: 60-year-old male with palpable abdominal mass.

Diagnosis: Abdominal aortic aneurysm.

Treatment: Surgical aorto-bifemoral bypass.

Considerations: Abdominal aortogram requires high contrast flow for maximum filling a superior visualization of the aorta. P tail catheter must retain shape durin injection for safe delivery of large contrast bolus.

Catheter Selected: 5 French Medi-tech High Flow pigt 65 cm. One of the complete line of H Flow Angiographic Catheters for flu and selective studies, combining advan technology with strict clinical standa of quality and reliability.

Medi-tech

Medi-tech, Incorporated
480 Pleasant Street
P.O. Box 7407
Watertown, Massachusetts 02272
(617) 923-1720 Telex 922-453

Ordering Information (800) 225-3238

© 1986 Medi-tech, Inc.

Radiograph courtesy of Michael E. Jay, M.D., Harvard Medical School

Cut patien

Erbium x-ray filters reduce patie to 50% without loss of radiogra Operator doses are also significan

Erbium transmits only x rays that the radiographic image while absorl producing photons at the low and ends of the spectrum.

Erbium filters have demonstrated si reduction for a variety of technique

- Skull and abdominal examination
- Cerebral angiography
- Intravenous urography
- Pediatric fluoroscopy
- Ciné-radiography



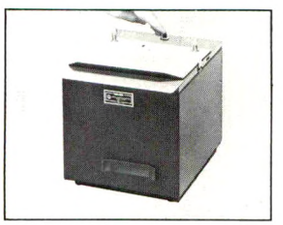
Two ste

Minimize X-ray exposu processor performanc

1. **The Tobias Model RF Wejex Sensitometer**

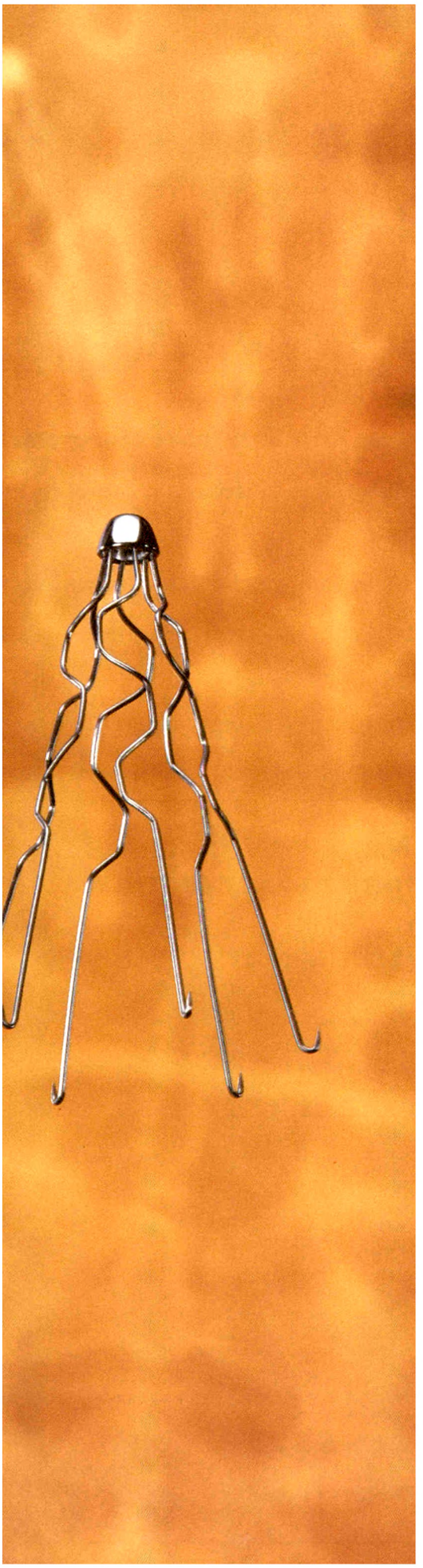
Produces a precise 11-step wedge on *your* X-ray film. Exposure made before processing eliminates latent fade problem.* Features: Precise sl exposure control. Variable lamp int Provisions for 2″×2″ ANSI blue, gr other filters, double sided exposure and 35mm test film alignment. And

*Lawrence, D.J.: **A Simple Method of Processor** Med. Rad. and Photog. 49, 2-6, 28, 1973 (Reprints on request)

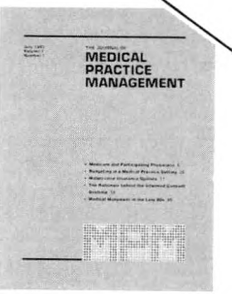


Weje Mode *Also* Weje Mode

For a demonstration, call your Tobias dealer.
Or write for our brochure. Ask about our 30 day f



Control the future of your practice



NEW!

The Journal of MEDICAL PRACTICE MANAGEMENT

Editor: **Marcel Frenkel, MD, MBA**

A new journal gives you the management skills you need to pull ahead

Right now you need information on some important topics that weren't covered in medical school. Topics that are having a profound impact on private practice and hospital-based physicians across the country.

Like competition from HMOs. Industrialization of medicine. The sheer number of physicians competing for your patients. Increasing costs.

You know the issues. What you need to know is the best way to face them so your practice will flourish in years to come.

And that's where **The Journal of Medical Practice Management** comes in.

Keep up with the issues that are changing your way of practice forever

The Journal of Medical Practice Management is a new quarterly publication that covers *your* concerns...issues affecting the way you practice now — and the way you'll practice in the future.

Four times a year, an expert editorial board headed by Dr. Marcel Frenkel brings you concise, readable coverage of today's issues and tomorrow's trends.

You'll find departments covering • office procedures and management • malpractice • marketing • manpower • computers • taxation • legal and legislative affairs • and health policy.

You'll also find pertinent features like the **Washington Report,** telling you what's up in the nation's capital and how it affects you...a **Letter from Abroad,** offering perspectives on how physicians are handling health care issues in other countries...and profiles of profit and not-for-profit health care delivery systems.

A multidisciplinary editorial board

Members of the editorial board for **The Journal of Medical Practice Management** have been carefully chosen for their knowledge of the management aspects of practicing medicine. These experts, many with experience in more than one field, give you the perspectives you need from medicine, law, management, government, and education.

You can control the future of your practice

The issues you can't afford to ignore are in **The Journal of Medical Practice Management.** It's a lot of information for a little money. And that's good business for you.

Reserve your charter subscription today!

Just return the attached coupon, or **call our FREE number,** 800-638-6423, from anywhere in the US except Alaska. In Maryland, call 528-4105 collect. **Quarterly**

Williams & Wilkins

428 East Preston Street
Baltimore, Maryland 21202

266 Fulham Road
London SW10 9EL England

YES, I want to control the future of my practice!

Please enter my subscription to **The Journal of Medical Practice Management** (quarterly)

☐ Individuals and Institutions $40

All subscribers: add $10 outside the U.S.

☐ Check enclosed ☐ Bill me
☐ MasterCard ☐ American Express ☐ VISA

Card # Exp. date

Signature

Name

Address

City/State/Zip

Maryland residents add 5% sales tax. Subscriptions outside the US must be prepaid. All subscriptions must be paid in US dollars. Rates valid through April 30, 1988.

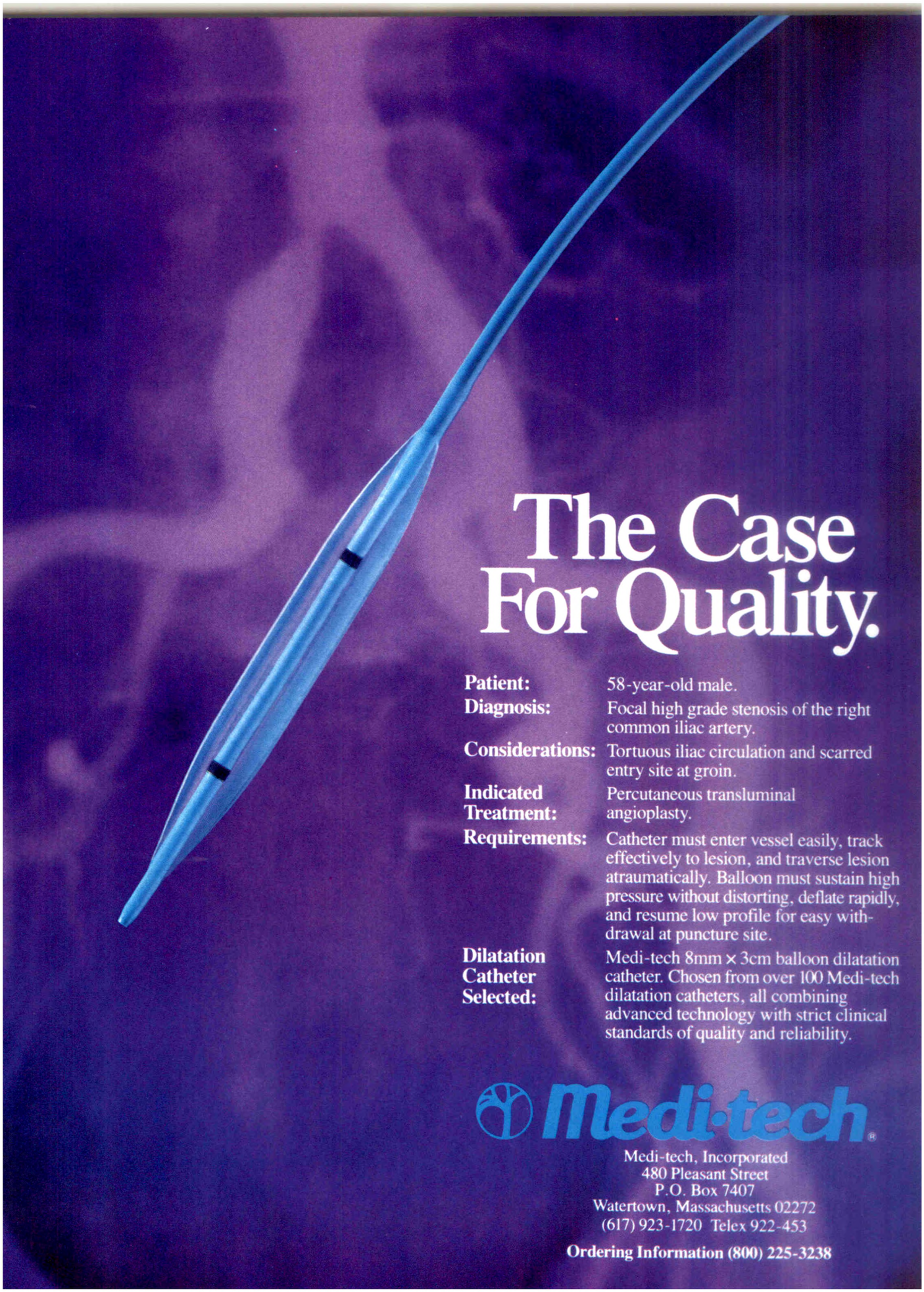
Please allow 8 weeks for delivery of your first issue, up to 16 weeks for surface delivery outside the US. Airmail rates available on request.

Williams & Wilkins

P.O. Box 23291
Baltimore, Maryland 21203

266 Fulham Road
London SW10 9EL England

MPMAD 95048 87



The Case For Quality.

Patient:	58-year-old male.
Diagnosis:	Focal high grade stenosis of the right common iliac artery.
Considerations:	Tortuous iliac circulation and scarred entry site at groin.
Indicated Treatment:	Percutaneous transluminal angioplasty.
Requirements:	Catheter must enter vessel easily, track effectively to lesion, and traverse lesion atraumatically. Balloon must sustain high pressure without distorting, deflate rapidly, and resume low profile for easy withdrawal at puncture site.
Dilatation Catheter Selected:	Medi-tech 8mm × 3cm balloon dilatation catheter. Chosen from over 100 Medi-tech dilatation catheters, all combining advanced technology with strict clinical standards of quality and reliability.

Medi-tech®

Medi-tech, Incorporated
480 Pleasant Street
P.O. Box 7407
Watertown, Massachusetts 02272
(617) 923-1720 Telex 922-453

Ordering Information (800) 225-3238

Radiology



St. Luke's\Roosevelt Hospital Center, a major teaching hospital affiliated with Columbia University, is seeking the following professionals:

General Diagnostic Radiologist

Opportunities exist for General diagnostic Radiologists, with expertise in *Urological* or *Skeletal Radiology.* Mammographic radiology experience a must. Fellowship or practice experience in addition to an interest in teaching, is highly desirable.

Radiologist

We are presently searching for a radiologist with board experienece in general radiology and with expertise in US/CT and mammography. Candidates should meet the requirements for faculty appointment.

Please send inquiries with CV indicating positions of interest to: Ronald C. Albow, M.D., Department of Radiology, St. Luke's\Roosevelt Hospital Center, Amsterdam Avenue & 114th Street, New York, N.Y. 10025.

In addition to a stimulating environment, St. Luke's\ Roosevelt Hospital Center, offers excellent remunerations. Equal Opportunity Employer M/F.

ST. LUKE'S\ROOSEVELT
Hospital Center

LONG BEACH VETERANS ADMINISTRATION MEDICAL CENTER
UNIVERSITY OF CALIFORNIA, IRVINE

The Long Beach Veterans Administration Medical Center and the University of California, Irvine are seeking a board certified radiologist for a staff position at the Long Beach Veterans Administration Medical Center. A position with an academic rank appropriate to experience is expected in the faculty of the Department of Radiological Sciences at the University of California, Irvine. The residency program is integrated between the two institutions, and teaching and research programs are closely coordinated.

Fellowship experience in neuro-radiology is necessary. Teaching experience and demonstrated interest in research are desirable. Salary is commensurate with experience.

The University of California, Irvine is an Equal Opportunity and Affirmative Action Employer. Interested candidates should forward their curriculum vitae and approximate date of availability to:

Richard M. Friedenberg, M.D.
Professor and Chairman
Department of Radiological Sciences
University of California, Irvine Medical Center
101 City Drive, South
Orange, CA 92668

LONG BEACH VETERANS ADMINISTRATION MEDICAL CENTER
UNIVERSITY OF CALIFORNIA, IRVINE

The Long Beach Veterans Administration Medical Center and the University of California, Irvine are seeking a board certified radiologist for a staff position at the Long Beach Veterans Administration Medical Center. A position with an academic rank appropriate to experience is expected in the faculty of the Department of Radiological Sciences at the University of California, Irvine.

The residency program is integrated between the two institutions, and teaching and research programs are closely coordinated. Specific training in ultrasound, body and head CT scanning and in neuro-radiology is necessary. Teaching experience and demonstrated interest in research are desirable. Salary is commensurate with experience.

The University of California, Irvine is an Equal Opportunity and Affirmative Action Employer. Interested candidates should forward their curriculum vitae and appropriate date of availability to:

Richard M. Friedenberg, M.D.
Professor and Chairman
Department of Radiological Sciences
University of California, Irvine Medical Center
101 City Drive, South
Orange, CA 92668

PULMONARY RADIOLOGIST

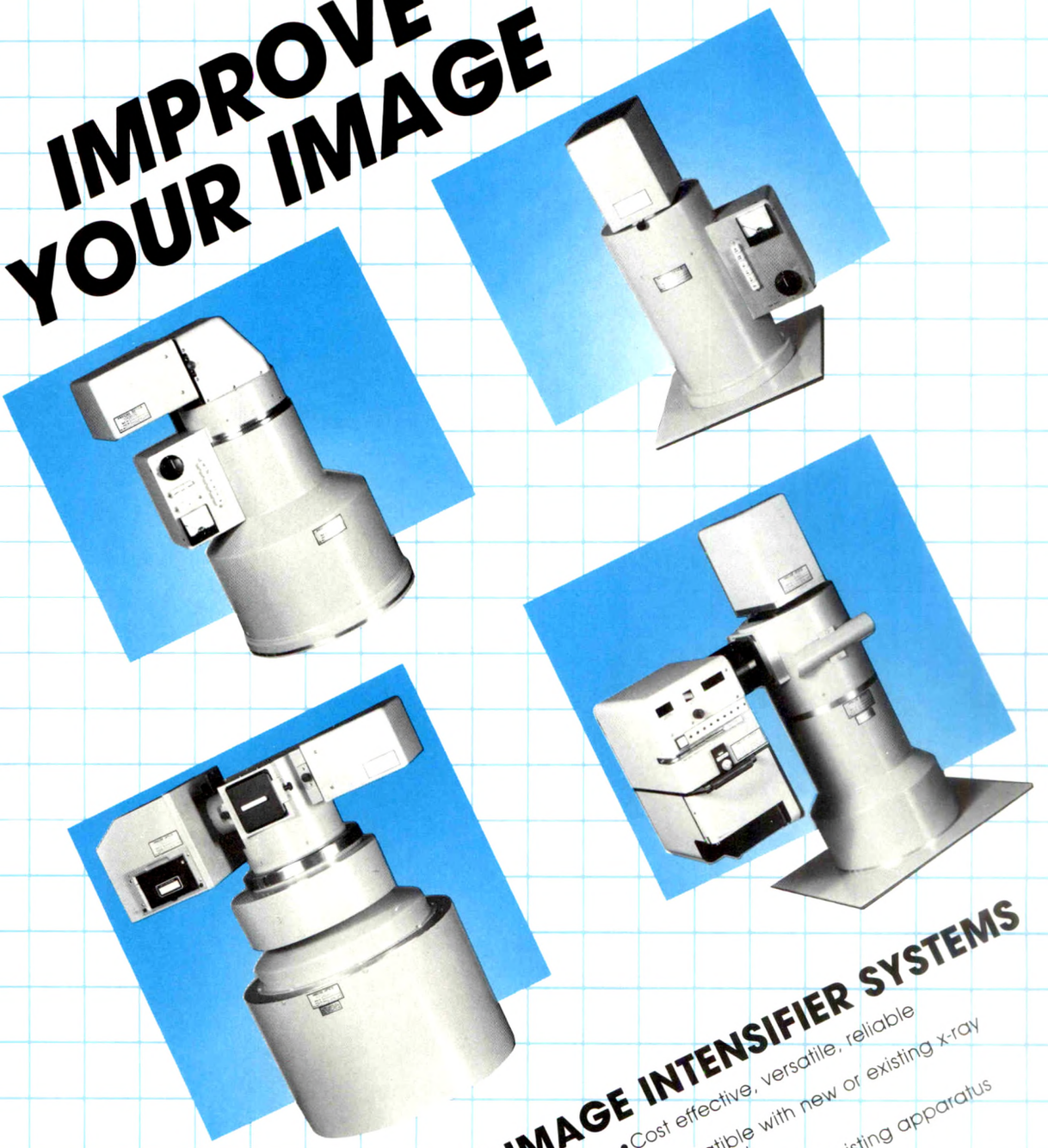
Temple University School of Medicine is seeking a Board certified Radiologist for faculty position, to direct the Section of Pulmonary Radiology. The candidate shall be proficient in all areas of pulmonary imaging, preferably with pulmonary radiology fellowship training, have demonstrated skills as a teacher and have an established reputation in research, preferably with grant funding. Applicant should send curriculum vitae and bibliography to **Francis J. Shea, MD, Director of Radiology,**

Temple University School of Medicine
Broad and Ontario Sts.
Phila., PA 19140.

TEMPLE UNIVERSITY

An Equal Opportunity, Affirmative Action Employer.

IMPROVE YOUR IMAGE

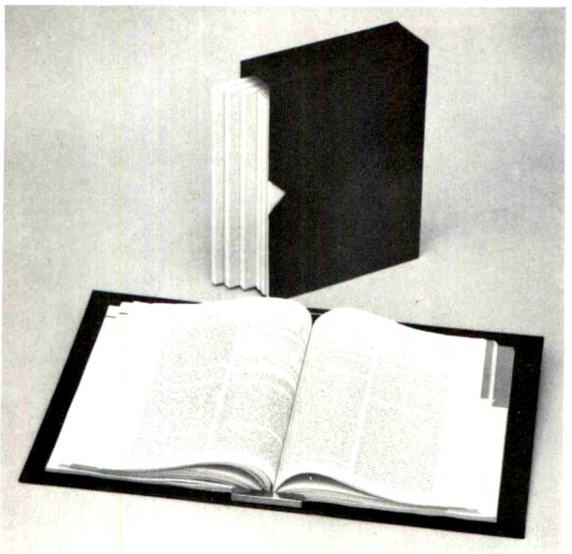


WITH PRECISE OPTICS IMAGE INTENSIFIER SYSTEMS

- The world's largest independent manufacturer of Image Intensifier Systems and components
- Over 30 years of experience in design and manufacture
- 6,9,12, and 16-Inch latest series image tubes for optimum performance
- 525/875/1023 line CCTV's, 6fps 100mm/105mm cameras
- Cost effective, versatile, reliable
- Compatible with new or existing x-ray equipment
- Extend the life of existing apparatus
- Worldwide dealer network

precise optics®
PHOTO MEDIC EQUIPMENT, INC.

239 South Fehr Way
Bay Shore, New York 11706
Tel.: 516 242-6600
TWX: 510-227-9837



Protect your copies of

AJNR: AMERICAN JOURNAL OF NEURORADIOLOGY

with Jesse Jones Binders or Files

Keep your journals clean, orderly, and readily accessible with Jesse Jones Binders or Files. One Binder or one box style File is all you need to accommodate a full year's worth of issues. Both Binders and Files are handsomely made with rich dark blue leatherette covers and gold leaf embossed lettering.

Jesse Jones Binders open flat for easy reading and reference and are economically priced at only $9.95 each; 3 for $27.95, or 6 for $52.95 postpaid. The rugged, compact box Files are only $7.95 each; 3 for $21.95, or 6 for $39.95. Add $1.00/unit postage and handling. (Outside the U.S. add $2.50/unit.)

For charge orders call toll free 1-800-972-5858. ($15.00 minimum).

Free gold transfer slips included for indexing volume and year.

Please allow four to five weeks for delivery.

TO: Jesse Jones Industries
499 E. Erie Avenue, DEPT. AJNR
Philadelphia, PA 19134

I enclose my check or money order for $_____
(PA residents add 6% sales tax)

Send me ____ ☐ Files ☐ Binders for my journals

Name

Address (will not ship to P.O. Box)

City/State/Zip

Satisfaction guaranteed.

INDEX TO ADVERTISEF

Acuson . . . . . A24, A25, A26, .

Adria Laboratories . . . . . .

Advanced Cardiovascular Systems . . . . . .

AGFA-Gevaert-Rex . . . . . A20, .

Bard Interventional Products . . . . . .

Eastman Kodak A5, A6, A7,

Elema Schonander, Inc. . . . . A14, .

E-Z-EM . . . . . Cover 2, .

General Electric . . . . . A10, A11, .

Medi-Tech . . . . . A45, A47, .

Nuclear Associates . . . . . .

Precise Optics/PME, Inc. . . . . .

Purdue Frederick . . . . . .

Pyne Corporation . . . . . Cove

Reactor Experiments . . . . . .

Shiley, Inc. . . . . A16, .

Siemens Corporation . . . . . A22, .

E. R. Squibb & Sons, Inc. . . . . A28, A29, .

S & S X-Ray . . . . . .

St. Luke's Roosevelt Hospital . . . . . .

Tecnomed . . . . . .

Temple University . . . . . .

Thompson CGR . . . . . A34, .

Tobias Associates . . . . . .

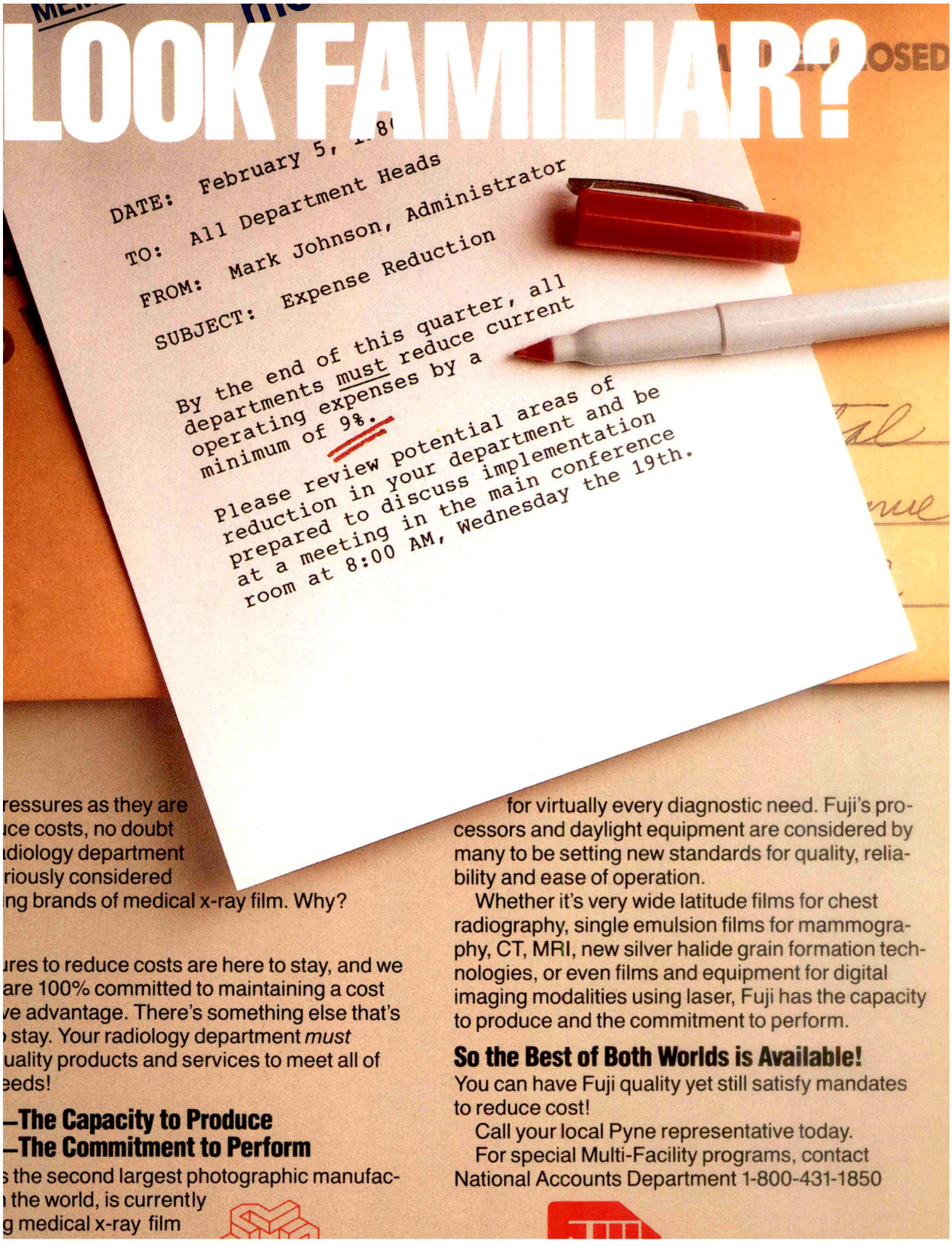
Toshiba Medical Systems . . . . . A18, .

University of California-Irvine . . . . . .

Winthrop Laboratories . . . A43, A44, A45, .
A47, .

Xerox Corporation . . . . . .

We try to present an accurate index. Occasionally this m.
be possible because of a last-minute change or an omis



ressures as they are
ıce costs, no doubt
ıdiology department
riously considered
ng brands of medical x-ray film. Why?

ures to reduce costs are here to stay, and we are 100% committed to maintaining a cost ve advantage. There's something else that's stay. Your radiology department *must* uality products and services to meet all of eeds!

—The Capacity to Produce
—The Commitment to Perform

s the second largest photographic manufac- the world, is currently g medical x-ray film for virtually every diagnostic need. Fuji's processors and daylight equipment are considered by many to be setting new standards for quality, reliability and ease of operation.

Whether it's very wide latitude films for chest radiography, single emulsion films for mammography, CT, MRI, new silver halide grain formation technologies, or even films and equipment for digital imaging modalities using laser, Fuji has the capacity to produce and the commitment to perform.

So the Best of Both Worlds is Available!

You can have Fuji quality yet still satisfy mandates to reduce cost!

Call your local Pyne representative today.

For special Multi-Facility programs, contact National Accounts Department 1-800-431-1850

Volume 147 American Journal of Roentgenology November 1986

SPECIAL ARTICLES

881 **Caldwell lecture. Armchair research and the practicing radiologist.** *Felson B*

891 **ARRS Executive Council Award paper. MR imaging of the lumbar spine: anatomic correlations and the effects of technical variations.** *Reicher MA, Gold RH, Halbach VV, Rauschning W, Wilson GH, Lufkin RB*

CARDIOPULMONARY RADIOLOGY

899 **Radiographic manifestations of bronchiolitis obliterans with organizing pneumonia vs usual interstitial pneumonia.** *Chandler PW, Shin MS, Friedman SE, Myers JL, Katzenstein A*

907 **CT of esophageal-pleural fistulae.** *Wechsler RJ*

911 **Postoperative recurrence of lung cancer: detection by whole-body gallium scintigraphy.** *Hatfield MK, MacMahon H, Ryan JW, et al.*

916 **Technical note. Cine-CT technique for evaluation of left ventricular function during supine exercise.** *Rees MR, MacMillan RM, Fender B, Clark DL*

GASTROINTESTINAL RADIOLOGY

919 **Pharyngeal Kaposi's sarcoma in patients with AIDS.** *Emery CD, Wall SD, Federle MP, Sooy CD*

923 **Pseudotumor of the quadrate lobe in hepatic sonography: a sign of generalized fatty infiltration.** *Sauerbrei EE, Lopez M*

929 **Benign pancreatic insulinoma: preoperative and intraoperative sonographic localization.** *Gorman B, Charboneau JW, James EM, et al.*

935 **Case report. Spontaneous rupture of a pancreatic pseudocyst into the portal venous system.** *Takayama T, Kato K, Sano H, Katada N, Takeichi M*

937 **Retractile mesenteritis involving the colon: barium enema, sonographic, and CT findings.** *Pérez-Fontán FJ, Soler R, Sanchez J, Iglesias P, Sanjurjo P, Ruiz J*

941 **Case report. CT diagnosis of primary small-bowel volvulus.** *Jaramillo D, Raval B*

SKELETAL RADIOLOGY

943 **Gaucher's disease type 1: assessment of bone involvement by CT and scintigraphy.** *Hermann G, Goldblatt J, Levy R, Goldsmith S, Desnick R, Grabowski G*

GENITOURINARY RADIOLOGY

949 **MR imaging of renal transplants.** *Baumgartner BR, Nelson RC, Ball TI, et al.*

954 **Commentary. Differential diagnosis of renal transplant rejection: is MR imaging the answer?** *Halasz NA*

957 **Excretory urography in patients with prostatism.** *Bundrick TJ, Katz PG*

960 **Commentary. Routine urography in men with prostatism.** *Talner LB*

NEURORADIOLOGY

963 **CT changes in dementing diseases: review.** *LeMay M*

977 **Neuroradiologic findings in AIDS: a review of 200 cases.** *Levy RM, Rosenbloom S, Perrett LV*

985 **MR and CT of occult vascular malformations of the brain.** *New PFJ, Ojemann RG, Davis KR, et al.*

995 **Penetrating vascular injuries of the face and neck: clinical and angiographic correlation.** *North CM, Ahmadi J, Segall HD, Zee C-S*

1000 **Editorial. Angiography in penetrating neck injuries.** *Quencer RM*

INTERVENTIONAL RADIOLOGY

1002 **UCSF interventional radiology rounds. Interventional radiologic management of sclerosing cholangitis.** *Kerlan RK Jr, LaBerge JM, Goldberg HI, Pogany AC, Ring EJ*

1007 **Percutaneous aspiration and drainage of pancreatic pseudocysts.** *Torres WE, Evert MB, Baumgartner BR, Bernardino ME*

1010 **Technical note. Basket extraction of esophageal foreign bodies.** *Shaffer HA Jr, Alford BA, de Lange EE, Meyer GA, McIlhenny J*

1014 **Technical note. Effect of suction on biopsy sample size.** *Hueftle MG, Haaga JR*

1017 **Technical note. A method for retrieval of retained subcutaneous catheter fragments.** *Sibbitt RR, Palmaz JC, Garcia F*

1019 **Case report. Small-bowel obstruction due to an intestinal balloon: treatment by percutaneous needle puncture.** *Sato Y, Frey E, Foderaro A, Pringle KC*

ANGIOGRAPHY

1021 **A comparison of techniques for improved visualization of the arteries of the distal lower extremity.** *Cohen MI, Vogelzang RL*

1025 **Technical note. Lower-extremity venography: value of femoral-vein compression.** *Smith TP, Cardella JF, Darcy MD, Hunter DW, Castaneda-Zuniga WR, Amplatz K*

PEDIATRIC RADIOLOGY

1027 **MR evaluation of the portal vein in pediatric liver transplant candidates.** *Day DL, Letourneau JG, Allan BT, Ascher NL, Lund G*

1031 **Pediatric hypertrophic gastropathy.** *Marks MP, Lanza MV, Kahlstrom EJ, Mikity V, Marks SC, Kvalstad RP*

1035 **Mesenchymal hamartomas of the liver in childhood: sonographic and CT findings.** *Stanley P, Hall TR, Woolley MM, Diament MJ, Gilsanz V, Miller JH*

1041 **Case report. Congenital urethral polyp.** *Caro PA, Rosenberg HK, Snyder HM III*

OBSTETRIC AND FETAL SONOGRAPHY

1043 **Sonographic findings in abdominal pregnancy.** *Stanley JH, Horger EO III, Fagan CJ, Andriole JG, Fleischer AC*

1047 **Fetal omphalocele and gastroschisis: a review of 24 cases.** *Bair JH, Russ PD, Pretorius DH, Manchester D, Manco-Johnson ML*

MR

1052 **Technical note. A technique for image salvage in MR.** *Lund G, Morin R*

RADIOLOGIC LITERATURE

1055 **The scientific literature in diagnostic radiology for American readers: a survey and analysis of journals, papers, and authors.** *Chew FS*

MISCELLANEOUS

1063 **The fibromatoses: CT-pathologic correlation.** *Francis IR, Dorovini-Zis K, Glazer GM, Lloyd RV, Amendola MA, Martel W*

1067 **CT of fibrous tissues and tumors with sonographic correlation.** *Rubenstein WA, Gray G, Auh YH, et al.*

COMPUTER PAGE

1075 **Some applications for a personal computer data-base system in radiology.** *Sommer FG*

OPINION

1078 **Should radiologists perform endoscopy?** *Shorvon P, Stevenson G*

OTHER CONTENT

910 **American Roentgen Ray Society Officers and Information**

928 **ARRS meeting information**

956 **Forthcoming articles**

1062 **Memorial**

1082 **Society of Uroradiology abstracts**

1089 **Letters**

1096 **Erratum**

1097 **News**

1101 **Classified ads**

Book reviews 962, 976, 984, 994, 1040

A2 **Guidelines for authors**

AJR

American
Journal of
Roentgenology





December 1986



Seri
side e

Pulling forward
of any of E-Z-EM
Adjust-A-Weight
garments has a
effect—it gradua
weight of the ga
shoulders to you
The amount tha
mines how the
spreading the lo
more comfortab

Our patented de
Velcro® brand fa
adjustment, and
of styles for radi
and operating ro
available in you
color, and trim.

To find out why
become the ind
for comfort, con
representative,
free at 800-645
call 516-333-82

E-Z-EM
More than ba
much more

Official Journal of the American Roentgen Ray Society

AJR

American Journal of Roentgenology
Diagnostic Imaging and Related Sciences

Editor-In-Chief Robert N. Berk, *San Diego, California*

Editor Emeritus Melvin M. Figley, *Seattle, Washington*

Associate Editors Alan J. Davidson, *Washington, District of Columbia*
Saskia von Waldenburg Hilton, *San Diego, California*
Juan M. Taveras, *Boston, Massachusetts*

Assistant Editors William L. Ashburn, *San Diego, California*
Charles C. Berry, *San Diego, California*
William G. Bradley Jr., *Pasadena, California*
Edward Buonocore, *Knoxville, Tennessee*
Peter L. Cooperberg, *Vancouver, British Columbia*
Peter Doubilet, *Boston, Massachusetts*
N. Reed Dunnick, *Durham, North Carolina*
Ronald G. Evens, *St. Louis, Missouri*
Henry I. Goldberg, *San Francisco, California*
William R. Hendee, *Chicago, Illinois*
John R. Hesselink, *San Diego, California*
Charles B. Higgins, *San Francisco, California*
Helen C. Redman, *Dallas, Texas*
Donald L. Resnick, *San Diego, California*
Stewart R. Reuter, *San Antonio, Texas*
Stuart S. Sagel, *St. Louis, Missouri*
Edward A. Sickles, *San Francisco, California*
Eric vanSonnenberg, *San Diego, California*

Editorial Staff: Gita S. Braude, *managing editor*; Elizabeth A. Whalen, *senior editor*; Linda Wood and Barbara Rose, *manuscript editors*; Nancy Rydbeck, *administrative assistant*; Sandra Wood, *administrative secretary*; Christina Sollazzo, *secretary*.

All business correspondence, including display (not classified) advertising, subscriptions, address changes, reprints, and permission requests should be addressed to Williams & Wilkins, 428 East Preston Street, Baltimore, MD 21202. Correspondence regarding editorial matters and classified advertising should be addressed to the editorial office, AJR, 2223 Avenida de la Playa, Suite 200, La Jolla, CA 92037. For manuscript submission, see Guidelines for Authors, next page. Undelivered or damaged copies replaced within 60 days of publication; 90 days for foreign subscribers. Allow 90 days for address changes.
AJR AMERICAN JOURNAL OF ROENTGENOLOGY (ISSN 0361 803X) is published monthly by American Roentgen Ray Society, 428 E. Preston Street, Baltimore, MD 21202. Annual dues include $50 for journal subscription. Second class postage paid at Baltimore, MD and at additional mailing offices. Postmaster send address changes (Form 3579) to Williams & Wilkins, 428 East Preston St., Baltimore, MD 21202. Subscription rates $90 ($120 foreign); institutions $100 ($130 foreign); in training $25; single copy $16 ($19). Japanese Yen price is available from our sole agent USACO Corporation, 13-12, Shimbashi 1-Chome, Minato-Ku, Tokyo 105, Japan, telephone 03-502-6471. Airmail rates furnished on request. Indexed by *Current Contents* and *Index Medicus*.
Copyright © 1986 by American Roentgen Ray Society.
0361-803X/86$2.00



AJR Guidelines for Authors

Address new and revised manuscripts, correspondence, and classified ads to:

AJR Editorial Office
2223 Avenida de la Playa, Suite 200
La Jolla, CA 92037
telephone: (619) 459-2229

Make inquiries regarding subscriptions, display advertising, reprints, or permission to republish *AJR* material to the publisher:

The Williams & Wilkins Co.
428 E. Preston St.
Baltimore, MD 21202
telephone: (301) 528-4133

Publication Policy

The *AJR* publishes original and timely contributions to the advancement of medical diagnosis and treatment with radiologic methods. Although content is predominantly clinical, laboratory investigations are accepted when their relevance to clinical practice is demonstrable. In prospective clinical investigations, authors should document that informed consent was obtained from patients. The material submitted **must** not have been previously published nor be currently submitted for publication elsewhere (prior publication of simple abstracts without illustrations or tables will not prejudice publication of the complete study). Papers dealing with **neuroradiology** should be addressed to: Editorial Office, American Journal of Neuroradiology, Dept. of Radiology, Massachusetts General Hospital, Boston, MA 02114; telephone: (617) 726–8342. At the discretion of the Editor of *AJR*, *AJNR* articles may be republished in *AJR*.

Decisions on manuscripts are based on peer review. Reviewers receive manuscripts without title pages to protect the identity of authors and to ensure an unbiased review; names of reviewers, in turn, are not revealed to the authors. Accepted manuscripts are subject to editing. Statements within an article, including changes made by the Editor or copy editor, are the responsibility of the author and not *AJR* or its publisher. Authors will receive the edited manuscript, galley proof, and proofs of illustrations usually 6–8 weeks after acceptance. If the corresponding author will not be available, arrangements should be made for a coauthor or colleague to read and return the proof.

Copyright Information

In accordance with *AJR* implementation of the U.S. Copyright Law, authors must release first and subsidiary rights to their manuscript at submission (unless the study was performed as part of their duties as an employee of a U.S. government agency). A dated letter with the signatures of all authors should state: "We, the authors, assign first and subsidiary rights to the American Roentgen Ray Society in the event that our manuscript [insert title] is published by *AJR*. We guarantee that this manuscript contains no matter libelous or otherwise unlawful or which invades individual privacy or which infringes any proprietary right. *AJR*, in turn, grants us the right of republication, subject only to crediting the original source of publication and receiving written permission from the publisher. We understand we will receive no royalty or other compensation from *AJR*. We guarantee that this article and illustrations have not been previously published elsewhere or, if previously published in part or in whole, that permission has been obtained for republication. Copies of these permissions are included and previously published text or illustrations have been identified in the manuscript." (Delete the last sentence if it does not apply.) The covering letter also should state that the manuscript has been seen and approved by all the authors.

Manuscript Form

AJR complies with the Uniform Requirements for Manuscripts Submitted to Biomedical Journals (*Ann Intern Med* 1979;90:95–99). Manuscripts must be ***typed double-space throughout***, including references, tables, and figure legends. Each table, the footnotes, and the figure legend section should begin on separate sheets; a separate title page should be provided. Send the original typescript, one copy, and two sets of illustrations (not photocopies). Authors' names should be on the title page **only** so that author anonymity can be maintained during the review process. Permission to reprint previously published material should accompany the manuscript.

Organization of Major Articles

Title Page

Titles should be brief yet precise, accurately conveying the content of the paper. Limit authors to those who made substantial contributions to the work. Include an address for *each* author, and ZIP or postal code; acknowledgment of grant or other financial support when appropriate; name of meeting, location, and date if the paper was presented; a running head (shortened title); and the name, address, and telephone number of the author to whom correspondence and requests for reprints should be addressed.

Abstract

A description of the purpose, methods, results, and conclusions of the study is required. The factual highlights of each section should be recapitulated.

Introduction

Clearly state the purpose of the investigation, including necessary background facts that indicate its current relevance.

Materials [or Subjects] and Methods

Describe the research plan, the materials or subjects, and the methods, in that order. Proof of disease and control of subjectivity in observations should be detailed. Metric measurements should be used throughout. Put measurements in the International System of Units (SI) in parentheses when appropriate; for example, 400 rad (4 Gy).

Results

Present results in logical sequence. If tables are used, do not duplicate tabular data but do describe important points and trends.

Case Reports

Individual cases can be described if there are only a few; one or more cases from a large series can be described individually as Representative Case Reports. Each report should concentrate on the radiologic information and its usefulness.

Discussion

Offer appropriate limitations about the research plan, materials or subjects, and methods to give perspective to their adequacy for the purpose of the study. Interpret the results to lend meaning and importance to the observations. Hypotheses and speculation based

on the results are encouraged. When results differ from those of previous investigations, an attempt should be made to explain the discrepancy. Conclude with a brief statement regarding clinical significance.

Acknowledgments

Acknowledge only persons who have made *substantive* contributions to the study. Mention grant support on the title page.

References

References should be offered to document major assertions of fact and any opposing evidence and concepts. Discretion in number is requested. References should be cited in the text by number (e.g., [3, 4]). The reference list should be arranged in the numeric order that references are cited in the text and ***typed double-spaced throughout***. References cited *first* or *only* in tables or figure legends should be numbered by the sequence in which the table or figure is first identified in the text. Data for each reference should be arranged according to the style adopted by the U.S. National Library of Medicine and used in *Index Medicus*. ***Accuracy of reference data is the responsibility of the author.*** Provide all authors' (or editors') names when fewer than seven; when seven or more, list the first three and add et al. Provide inclusive page numbers; if an article is only one page, please indicate. Abbreviations for titles of medical periodicals should conform to those published in *Index Medicus*. Articles that appear in both *AJR* and *AJNR* should be a single reference that cites both journals (example 3). Examples:

1. Kirks DR, Fram EK, Vock P, Effmann EL. Tracheal compression by mediastinal masses in children: CT evaluation. AJR 1983;141:647–651
2. Khansur T, Yam LT, Tavassoli M. Serum monitors of bone metastasis. In: Stoll BA, Parbhoo S, eds. Bone metastases: monitoring and treatment. New York: Raven, 1983:165–180
3. Sage MR. Review. Kinetics of water-soluble contrast media in the central nervous system. AJNR 1983;4:897–906, AJR 1983; 141:815–824

Unpublished data and personal communications should not be numbered references but should be put in parentheses in the text (e.g., Smith JD, personal communication).

Tables

Tables should be concise and organized to show trends, not merely compilations of raw data. (The Editor may request that tables of backup data too extensive to be published be deposited with the National Auxiliary Publications Service or made available by the author.) Include only data pertinent to the subject. Long itemized case histories are better presented in the text as case reports or summaries. Do not repeat in tabular form material presented in the text. Tables should have titles and headings, but no vertical or horizontal rules.

Illustrations

Figures should be submitted as 13 × 18 cm (5 × 7 inch) glossy, black-and-white prints, ***untrimmed and unmounted***. Labels and arrows must be of professional quality and removable. Number each figure to correspond with the figure legends and indicate the top. Avoid writing directly on the back of the print. Special permission for publication of facial photographs of patients or for previously published pictures is required. Line illustrations or graphs must be professionally drawn in black ink on white background; please send photographic prints (not photocopies), not originals, to avoid damage in handling. Color illustrations will be used at the discretion of the Editor; send color prints. Firm estimates of cost will be sent to the author(s) for approval before publication. Identical anatomic structures in color prints should be the same size to facilitate reproduction and reduce cost.

Legends

Figure legends should carry a title identifying the message of the illustration and the case number if individual cases are described in the text. Legends should be as brief as possible for the informed reader to understand the figure. Detailed clinical data should be avoided. Legends for previously published illustrations should cite the reference number of the source (e.g., Reprinted from [8]).

Organization of Case Reports

Concise case reports will be considered for publication if they present unusual experiences that are medically important and instructive. Clarity and brevity are essential. After preliminary screening by an editor to determine whether the requirement of medical significance has been met, qualifying papers will undergo the same peer review as major papers. To facilitate planning the order and layout of each issue, case reports are limited in length to two journal pages. The introduction should be one short paragraph that gives some general background of the disorder and the specific interest and message of the case presented. Only one case should be described in detail. The case report should concentrate on the radiologic information and its usefulness. The discussion should focus on the specific message of this report and the relevance of radiology in this instance. If the author has encountered other cases, they may be briefly mentioned, and possibly illustrated, but not described in detail. There should be no more than eight references. The figures should be limited to the minimum required to document the case findings, probably not more than four pictures, each a column wide (or the equivalent). Excess illustrations would require severely shortening the text. Figure legends should be as short as possible and should not repeat the text. There can be no tables and no acknowledgments. See previous sections for detailed instructions regarding references and illustrations.

Other Contributions

Technical Notes

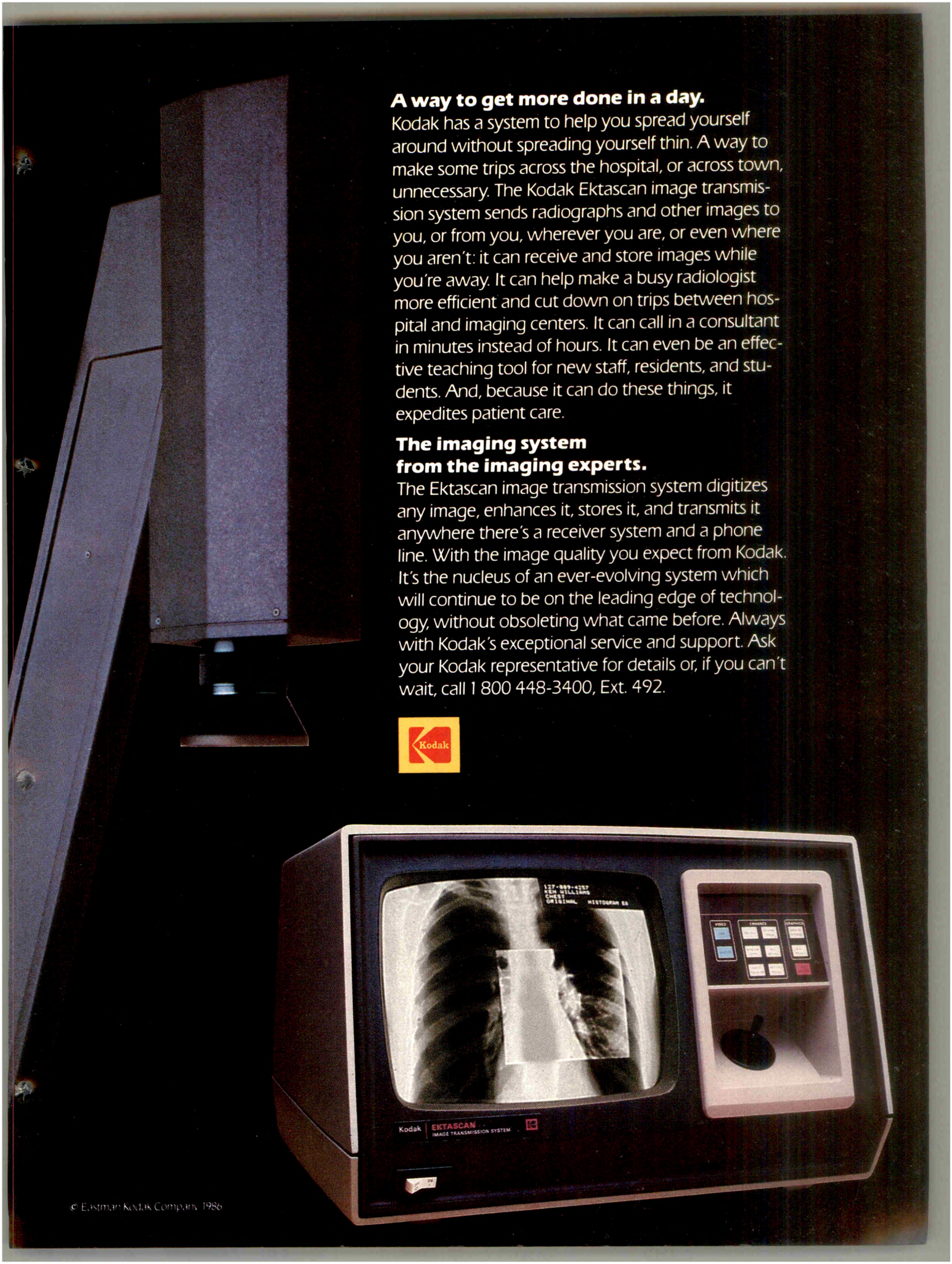
Brief descriptions of new techniques or significant modifications of older ones that are directly applicable to the clinical practice will be accepted if review is favorable. Technical notes do not carry abstracts or acknowledgments.

Letters to the Editor

Letters are subject to editing and condensation. Criticism of published articles should be objective and constructive. Letters also may discuss matters of general interest to radiologists.



Introducing a way to be everywhere at once. The new Kodak Ektascan image transmission system.



A way to get more done in a day.

Kodak has a system to help you spread yourself around without spreading yourself thin. A way to make some trips across the hospital, or across town, unnecessary. The Kodak Ektascan image transmission system sends radiographs and other images to you, or from you, wherever you are, or even where you aren't: it can receive and store images while you're away. It can help make a busy radiologist more efficient and cut down on trips between hospital and imaging centers. It can call in a consultant in minutes instead of hours. It can even be an effective teaching tool for new staff, residents, and students. And, because it can do these things, it expedites patient care.

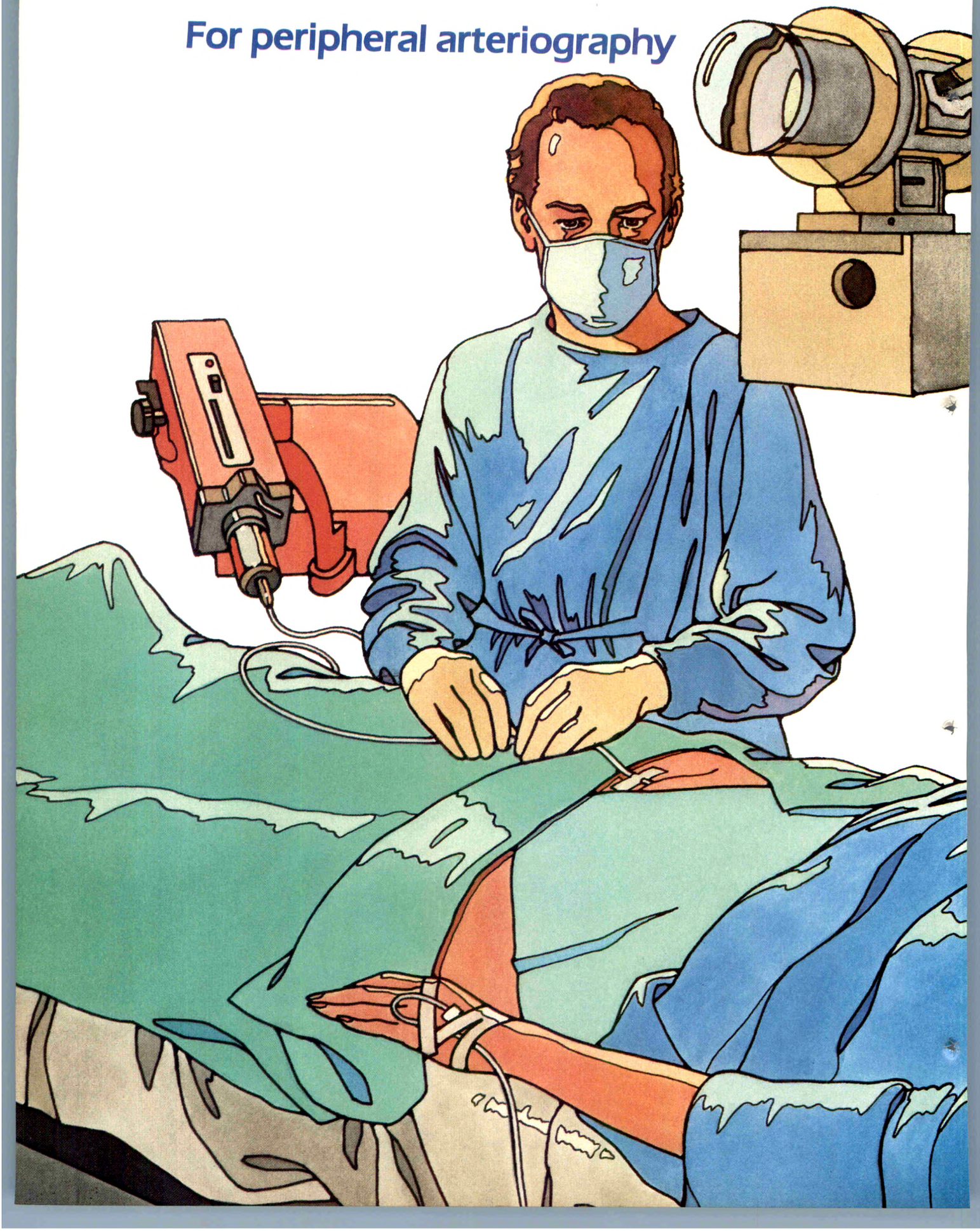
The imaging system from the imaging experts.

The Ektascan image transmission system digitizes any image, enhances it, stores it, and transmits it anywhere there's a receiver system and a phone line. With the image quality you expect from Kodak. It's the nucleus of an ever-evolving system which will continue to be on the leading edge of technology, without obsoleting what came before. Always with Kodak's exceptional service and support. Ask your Kodak representative for details or, if you can't wait, call 1 800 448-3400, Ext. 492.

Kodak

© Eastman Kodak Company, 1986

For peripheral arteriography



ISOVUE®-300
iopamidol injection 61%

Nonionic contrast media that causes less pain than a leading ionic agent.

With Isovue, patients found procedures less painful; physicians saw fewer signs of distress

Isovue-300 is low in osmolality—616 mOsm/kg water.

Using a visual analog scale, patients undergoing peripheral arteriography ranked their pain from "no pain" to "the worst pain I ever had." On a linear scale from zero to 12.4 cm, the mean pain rating for 99 patients given a total of 155 injections of Isovue-300 was 2.3 cm compared with 6.3 cm for 97 patients given a total of 144 injections of the ionic agent diatrizoate meglumine and diatrizoate sodium 52%/8%.

By observing signs of distress, such as movement and/or vocalization, physicians ranked patient distress as being absent, mild, moderate, or severe. When Isovue was compared with diatrizoate meglumine and diatrizoate sodium 52%/8%, the number of injections judged to cause severe distress was 2/299 (1%) compared with 23/293 (8%); moderate distress, 13/299 (4%) compared with 58/293 (20%); mild distress, 59/299 (20%) compared with 94/293 (32%); and no distress, 225/299 (75%) compared with 108/293 (37%), respectively.

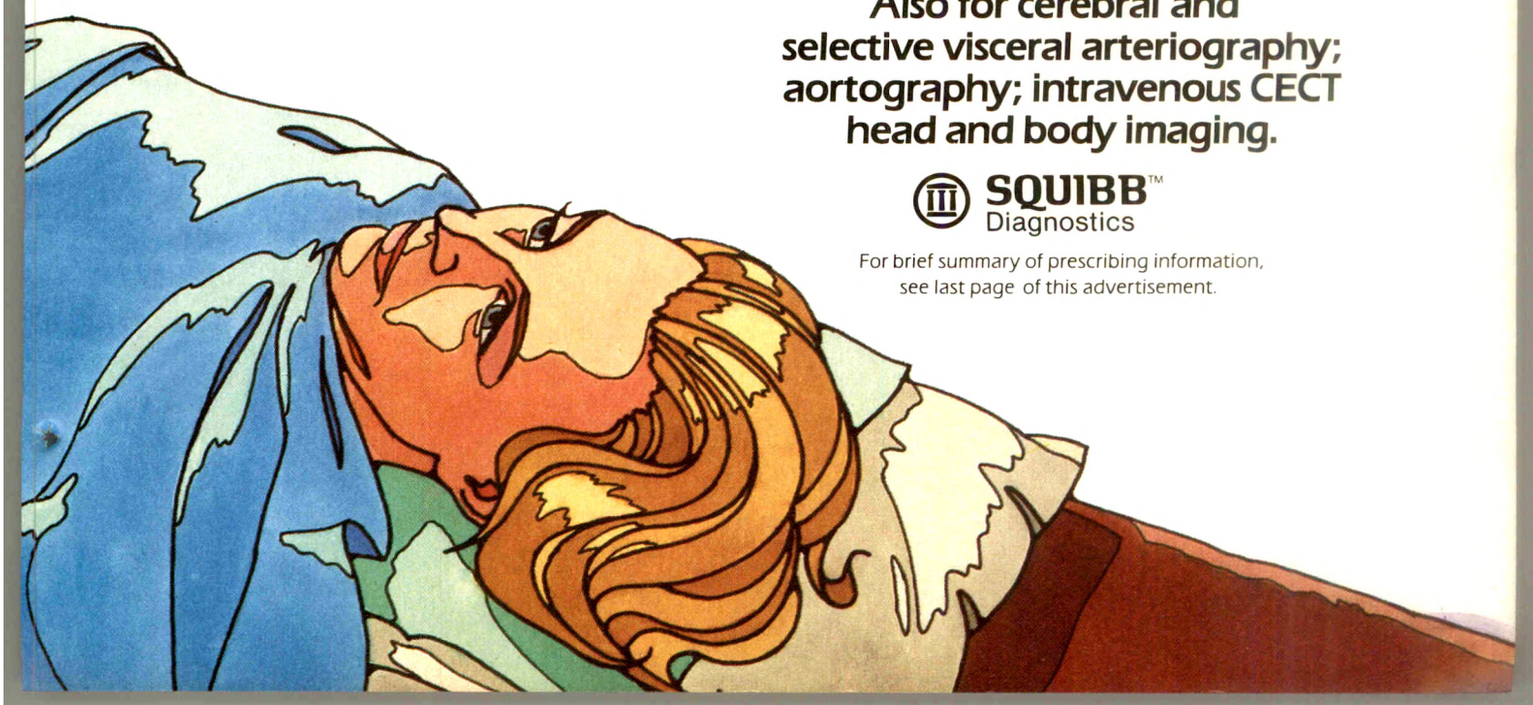
As with all injectable contrast agents, the possibility of severe reactions should be borne in mind. (See brief summary of prescribing information on the last pages of this advertisement for a discussion of CONTRAINDICATIONS, WARNINGS, PRECAUTIONS, and ADVERSE REACTIONS.)

ISOVUE®
iopamidol injection

Nonionic. Low in osmolality. Also for cerebral and selective visceral arteriography; aortography; intravenous CECT head and body imaging.

SQUIBB™
Diagnostics

For brief summary of prescribing information, see last page of this advertisement.



ISOVUE®-300
Iopamidol Injection 61%
ISOVUE®-370
Iopamidol Injection 76%

DESCRIPTION—ISOVUE (iopamidol injection) is a nonionic radiopaque contrast media for diagnostic use. The formulations are stable, aqueous, sterile, and nonpyrogenic solutions for intravascular administration. Each mL of ISOVUE-300 (iopamidol injection 61%) provides 612 mg iopamidol with 1 mg tromethamine and 0.39 mg edetate calcium disodium. The solution contains approximately 0.037 mg (0.002 mEq) sodium and 300 mg organically bound iodine per mL. Each mL of ISOVUE-370 (iopamidol injection 76%) provides 755 mg iopamidol with 1 mg tromethamine and 0.48 mg edetate calcium disodium. The solution contains approximately 0.046 mg (0.002 mEq) sodium and 370 mg organically bound iodine per mL. The pH has been adjusted to 6.5 to 7.5 with hydrochloric acid.

CONTRAINDICATIONS—None.

WARNINGS—Use caution in patients with severely impaired renal function, combined renal and hepatic disease, or anuria, particularly when larger doses are administered. Radiopaque diagnostic contrast agents are potentially hazardous in patients with multiple myeloma or other paraproteinemia, particularly in those with therapeutically resistant anuria. It has been speculated that the combination of the contrast agent and dehydration may be causative of anuria in myelomatous patients. This risk is not a contraindication; however, special precautions are required. Contrast media may promote sickling in individuals who are homozygous for sickle cell disease when injected intravenously or intraarterially. Administration to patients known or suspected of having pheochromocytoma should be performed with extreme caution. If the possible benefits outweigh the considered risks, the procedures may be performed; however, the amount of the medium injected should be kept to an absolute minimum. Assess blood pressure throughout the procedure and have measures for treatment of a hypertensive crisis available. Monitor such patients very closely. Use caution in patients with hyperthyroidism or with an autonomously functioning thyroid nodule because of risk of thyroid storm.

PRECAUTIONS: General—Diagnostic procedures should be carried out under the direction of personnel with the prerequisite training and a thorough knowledge of the particular procedure to be performed. Appropriate facilities should be available for coping with any complication of the procedure, or for emergency treatment of severe reaction to the agent itself. After parenteral administration, competent personnel and emergency facilities should be available for at least 30 to 60 minutes since severe delayed reactions may occur. Preparatory dehydration is dangerous and may contribute to acute renal failure in susceptible patients. *Patients should be well hydrated prior to and following administration.* Reactions to the medium, including serious, life-threatening, fatal, anaphylactoid or cardiovascular reactions, should always be considered (see ADVERSE REACTIONS in the product package insert). Patients at increased risk include those with a history of a previous reaction to a contrast medium, a known sensitivity to iodine per se, and a known clinical hypersensitivity (bronchial asthma, hay fever, and food allergies). Pretesting cannot be relied upon to predict severe reactions and may itself be hazardous for the patient. A thorough medical history with emphasis on allergy and hypersensitivity prior to the injection of any contrast medium may be more predictive and accurate than pretesting. Premedication with antihistamines or corticosteroids to avoid or minimize possible allergic reactions in such patients should be considered. General anesthesia may be indicated in some procedures in selected patients; however, a higher incidence of adverse reactions has been reported in anesthetized patients, which may be attributable to the inability of the patient to identify untoward symptoms, or to the hypotensive effect of anesthesia which can reduce cardiac output and increase the duration of exposure to the agent. Even though the osmolality is low compared to diatrizoate or iothalamate based ionic agents of comparable iodine concentration, the potential transitory increase in the circulatory osmotic load in patients with congestive heart failure requires caution during injection. Observe these patients for several hours following the procedure. In angiographic procedures, be aware of the possibility of dislodging plaques or damaging or perforating the vessel wall during catheter manipulations and contrast medium injection. Test injections to ensure proper catheter placement are suggested.

The inhibitory effects of nonionic contrast media on mechanisms of hemostasis have been shown, in vitro, to be less than ionic contrast media at comparable concentrations. For this reason, standard angiographic procedures should always be followed: angiographic catheters should be flushed frequently, and prolonged contact of blood with contrast in syringes and catheters should be avoided. Perform *selective coronary arteriography* only in those in whom the expected benefits outweigh the procedural risk. The inherent risks of *angiocardiography* in patients with chronic pulmonary emphysema must be weighed against the necessity for performing this procedure. *Angiography* should be avoided whenever possible in patients with homocystinuria, because of the risk of inducing thrombosis and embolism.

Drug Interactions—Renal toxicity has been reported in a few patients with liver dysfunction who were given oral cholecystographic agents followed by intravascular contrast agents. Administration of intravascular agents should therefore be postponed in any patient with a known or suspected hepatic or biliary disorder who has recently received a cholecystographic contrast agent. Other drugs should not be admixed with iopamidol.

Drug/Laboratory Test Interactions—PBI and radioactive iodine uptake studies will not accurately reflect thyroid function for up to 16 days following administration, however T3 resin uptake and total or free thyroxine (T4) assays are not affected. Any test which might be affected by contrast media should be performed prior to administration of the contrast media.

Carcinogenesis, Mutagenesis, Impairment of Fertility—In animal reproduction studies performed on rats, intravenously administered iopamidol did not induce adverse effects on fertility or general reproductive performance. In studies to determine mutagenic activity, iopamidol did not cause any increase in mutation rates.

Pregnancy Category B—No teratogenic effects attributable to iopamidol have been observed in teratology studies performed in animals. There are, however, no adequate and well controlled studies in pregnant women. It is not known whether iopamidol crosses the placental barrier or reaches fetal tissues. Because animal studies are not always predictive of human response, this drug should be used during pregnancy only if clearly needed. Radiologic procedures involve a certain risk related to the exposure of the fetus to ionizing radiation.

Labor and Delivery—It is not known whether use during labor or delivery has immediate or delayed adverse effects on the labor, the delivery or the newborn.

Nursing Mothers—It is not known whether iopamidol is excreted in human milk. Use caution when contrast media are administered to nursing women because of potential adverse reactions; consideration should be given to temporarily discontinuing nursing.

Pediatric Use—Safety and effectiveness in children have not been established.

ADVERSE REACTIONS—Usually mild to moderate, self-limited and transient. In angiocardiography (597 patients), the adverse reactions with an estimated incidence of one percent or higher are: hot flashes 3.4%; angina pectoris 3.0%; flushing 1.8%; bradycardia 1.3%; hypotension 1.0%; hives 1.0%. Intravascular injection is frequently associated with the sensation of warmth and pain, especially in peripheral arteriography; pain and warmth are less frequent and less severe with ISOVUE (iopamidol injection) than with diatrizoate meglumine and diatrizoate sodium injection. The following table of incidence of reactions is based on clinical studies with ISOVUE in about 1760 patients.

Adverse Reactions

	Estimated Overall Incidence	
System	>1%	≤1%
Cardiovascular	none	tachycardia hypotension hypertension myocardial ischemia circulatory collapse S-T segment depression bigeminy extrasystoles ventricular fibrillation angina pectoris bradycardia transient ischemic attack thrombophlebitis
Nervous	pain (2.2%) burning sensation (1.4%)	vasovagal reaction tingling in arms grimace faintness
Digestive	nausea (1.2%)	vomiting anorexia
Respiratory	none	throat constriction dyspnea pulmonary edema
Skin and Appendages	none	rash urticaria pruritus flushing
Body as a Whole	hot flashes (1.5%)	headache fever chills excessive sweating back spasm
Special Senses	none	taste alterations warmth in throat/arms/chest nasal congestion visual disturbances
Urogenital	none	urinary retention

Regardless of the agent employed, overall estimated incidence of serious adverse reactions is higher with *coronary arteriography* than with other procedures. Cardiac decompensation, serious arrhythmias, or myocardial ischemia or infarction may occur during *coronary arteriography and left ventriculography.* Following coronary and ventricular injections, certain electrocardiographic changes (increased QTc, increased R-R, T-wave amplitude) and certain hemodynamic changes (decreased systolic pressure) occurred less frequently with ISOVUE (iopamidol injection) than with diatrizoate meglumine and diatrizoate sodium injection; increased LVEDP occurred less frequently after ventricular iopamidol injections. In *aortography,* the risks of procedures also include injury to the aorta and neighboring organs, pleural puncture, renal damage including infarction and acute tubular necrosis with oliguria and anuria, accidental selective filling of the right renal artery during the translumbar procedure in the presence of preexisting renal disease, retroperitoneal hemorrhage from the translumbar approach, and spinal cord injury and pathology associated with the syndrome of transverse myelitis. Adverse effects reported in literature include arrhythmia, arterial spasms, hematuria, periorbital edema, involuntary leg movement, malaise, and triggering of deglutition; some of these may be procedural. Other reactions due to procedural hazards include hemorrhage or pseudoaneurysms at the puncture site, brachial plexus palsy following axillary artery injections, chest pain, myocardial infarction, and transient changes in hepatorenal chemistry tests; and rarely arterial thrombosis, displacement of arterial plaques, venous thrombosis, dissection of the coronary vessels and transient sinus arrest.

General Adverse Reactions To Contrast Media—Reactions known to occur with parenteral administration of iodinated ionic contrast agents (see the listing below) are possible with any nonionic agent. Life-threatening reactions and fatalities, mostly of cardiovascular origin, have occurred. Reported incidences of death from the administration of other iodinated contrast media range from 6.6 per 1 million (0.00066%) to 1 in 10,000 patients (0.01%). Foreign experience in approx. 2.4 million patients receiving iopamidol suggest a lower risk of mortality. Most deaths occur during injection or 5 to 10 minutes later, the main feature being cardiac arrest with cardiovascular disease as the main aggravating factor. Isolated reports of hypotensive collapse and shock (est. 0.005%) are found in the literature. Experience with iopamidol suggests there is much less discomfort (e.g., pain and/or warmth) with peripheral arteriography. Fewer changes are noted in ventricular function after ventriculography and coronary arteriography. The reported incidence of adverse reactions to contrast media in patients with a history of allergy is twice that for the general population; patients with a history of previous reactions to a contrast medium are three times more susceptible. Most reactions to intravascular contrast agents appear within 1-3 minutes after the start of injection, but delayed reactions may occur (see PRECAUTIONS, General). Adverse reactions reported with other intravascular contrast agents and theoretically possible with iopamidol include: *Cardiovascular:* vasodilation, cerebral hematomas, petechiae; *Nervous:* paresthesia, dizziness, convulsions, paralysis, coma; *Respiratory:* increased cough, asthma, laryngeal edema, pulmonary edema, bronchospasm, rhinitis; *Skin and Appendages:* injection site pain usually due to extravasation and/or erythematous swelling, skin necrosis; *Urogenital:* osmotic nephrosis of proximal tubular cells, renal failure, pain; *Special Senses:* bilateral ocular irritation; lacrimation; conjunctival chemosis, infection, and conjunctivitis; *Other:* neutropenia, thrombophlebitis, flushing, pallor, weakness, severe retching and choking, wheezing, cramps, tremors, and sneezing.

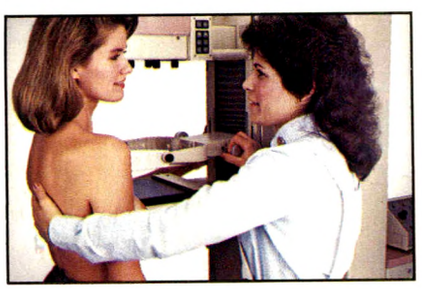
For full prescribing information consult package insert. (J3-652C)

Under license from Bracco Industria Chimica S.p.A. U.S. Patent #4,001,323

© 1986 E.R. Squibb & Sons, Inc., Princeton, NJ 646-503 Issued: Sept. 1986

The LORAD M-II™ Dedicated Mammography System...ideal for both Low Cost Screening and Sophisticated Diagnosis

✓	HIGH THRUPUT OF PATIENTS
✓	EASY, QUICK CASSETTE AND GRID CHANGES
✓	FAST ACCESS TO MAGNIFICATION AND BIOPSY MODES
✓	SUPERB RESOLUTION AND CONTRAST
✓	LOW DOSAGE



LOrad M-II meets the increasing demand for cost-effective mammographic screening systems. When operating in a screening mode, outstanding thruput results from LOrad M-II's compression and positioning controls, quick change cassette holders, continuously adjustable collimator, and automatic exposure. Easily mobile on large wheels, it plugs into any standard 115 volt power source, yet automatically delivers clean power at constant potential. And when a suspicious reading makes sophisticated diagnostic procedures advisable, LOrad's magnification and biopsy modes are easily attached.

Standard equipment includes:

Contact Film-screen Mode, with specially-designed breast compression devices and matching cassette holders.

Magnification Mode, including complete assembly which quickly attaches as a unit. It works with the new microfocus x-ray tube with rotating molybdenum target and alternative microfocal spot of .1 mm to give sharp, clearly-resolved magnified images. The special built-in LOrad 5-plate collimator with a light field indicator makes it easy to confine the beam precisely to the area of concern.

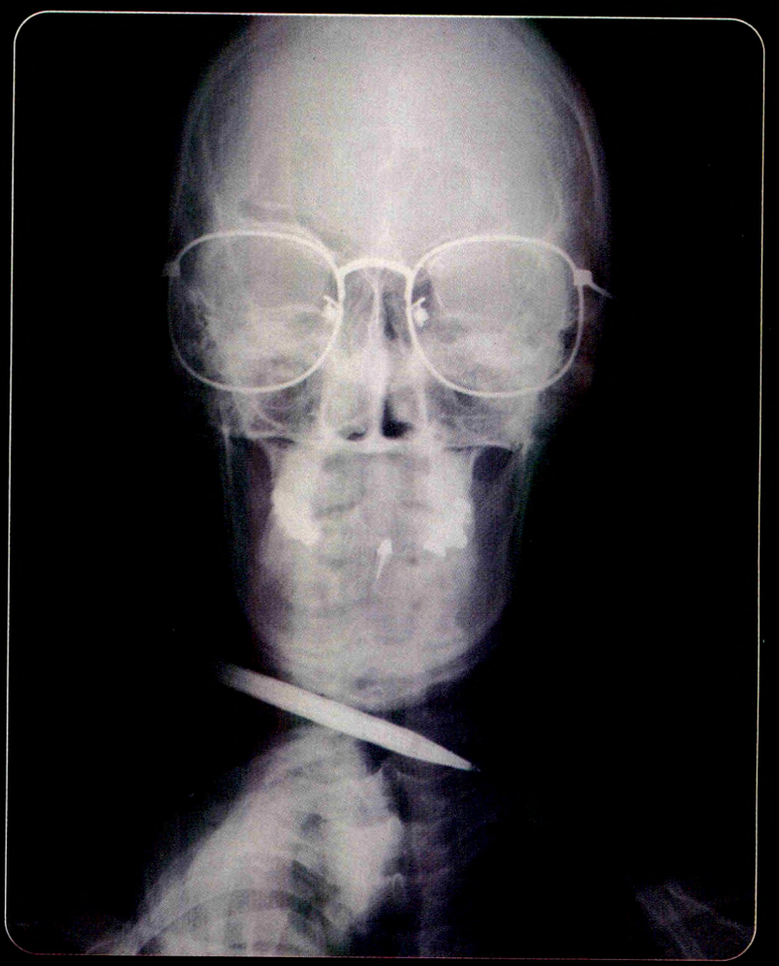
Biopsy localization mode. Its special compression device is perforated for a biopsy needle. The side-loading cassette allows the technologist to maintain positioning during film changes.

Grid Systems available.
The money-saving, time-saving new LOrad Permagrid™ has a stationary grid built into a specially engineered LOrad cassette holder. This slips easily onto the image receptor and accepts standard cassettes, and may be loaded and unloaded from either side. For those who prefer them, a Bucky moving grid or separate stationary grids are available.



LEASING PLANS AVAILABLE THROUGH YOUR DEALER. For his name, phone:

LOrad Medical Systems, Inc.
Eagle Road
Danbury, CT 06810
(203) 798-1127



YOU KNOW ALL ABOUT IMAGING NEGATIVES.



NOW, RAYTHEON OFFERS YOU SOME POSITIVES.

Take heart. Those imaging negatives you face every day may not be as overwhelming as they seem.

Dwindling budgets. Escalating costs. Runaway technology.

Problems, all. Negatives, all. Yet there is a way to cope. There is a way to convert those imaging negatives into positives.

Raytheon Medical Systems!

You demand quality imaging systems! Raytheon delivers. You demand prices that won't upset your budget! Raytheon delivers. And you demand excellent imaging results! Again, Raytheon delivers.

Because Raytheon Medical Systems believes that quality starts with fundamentals. And because we are part of a 7-billion-dollar multinational company, we offer the fundamentals that are important to you: strength, capability, support.

Raytheon Medical Systems can provide the knowledge, the resources, and the insight required to deliver the kind of imaging equipment you want.

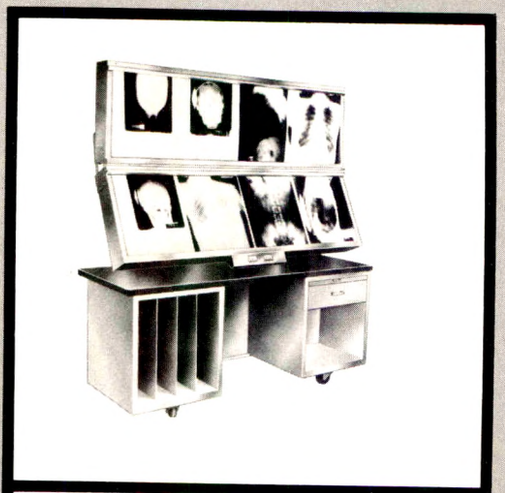
Raytheon Medical Systems. The one imaging company with the capabilities and the commitment that can change your negatives into positives.

Raytheon

MEDICAL SYSTEMS
2020 North Janice Avenue
Melrose Park, Illinois 60160
1-312-865-2600
1-800-323-2213

illumination

EXCELLENCE



Modular Mobile Illuminator

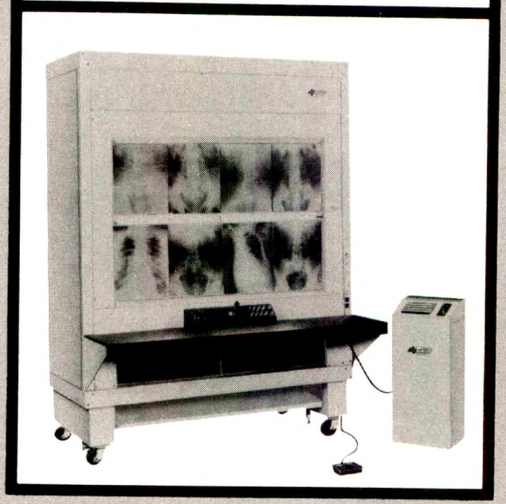
S&S X-Ray medical film reading illumination excellence has provided radiologists with unequalled quality and reliability for over 30 years.

The S&S commitment to quality and R&D has earned the reputation for excellence we enjoy, and has made S&S the world's largest manufacturer of Motorized Viewers.

Models' film capacity range from 48 14″x17″ radiographs to 400 (4 over 4).

Whether stationary or motorized, S&S viewers together with our complete line of x-ray accessories are designed and engineered to fit every need, every budget.

Catalog available upon request.



Model MV200A with optional MV 200C and MV200T

Engineered and produced by the world's leading manufacturer of X-Ray Accessories

S&S X-RAY PRODUCTS, INC.

87-93 Jay Street, Brooklyn, NY 11201
Telex: 219262 TLX UR
Tel: In NY State: (718) 852-6900
Toll Free: (800) 221-6634

Procedure trays to control costs ...new from E-Z-EM

The objective:
Respond to the demand for a set of disposable trays to help hospitals and private practices control biopsy costs on a per-procedure basis.

The result:
E-Z-EM's new PercuSet line of disposable biopsy trays creating a system of procedure trays—a system of trays which offers the doctor progressive degrees of procedure capability.

The PercuSet Skin Prep Tray includes every implement and agent needed to cleanse, aseptisize, and anesthetize the procedure area—for biopsy, or for any percutaneous procedure.

The PercuSet Basic Biopsy Tray includes all the elements of the Prep Tray, *plus* a needle stop, and a ruler/protractor, *and* the option of an E-Z-EM biopsy needle.

The PercuSet Expanded Biopsy Tray adds a specimen-handling section, for complete biopsy procedure capability, also with the option of an E-Z-EM biopsy needle.

PercuSet Biopsy Trays assure absolute sterility, minimize component handling, eliminate cross-contamination, and are laid out in a logical procedural sequence.

They provide effective cost control, and reduce inventory management of components.

For additional information and a color brochure that details the PercuSet System, contact your local representative, or call E-Z-EM toll-free at 800-645-3052. In New York call 516-333-8230.

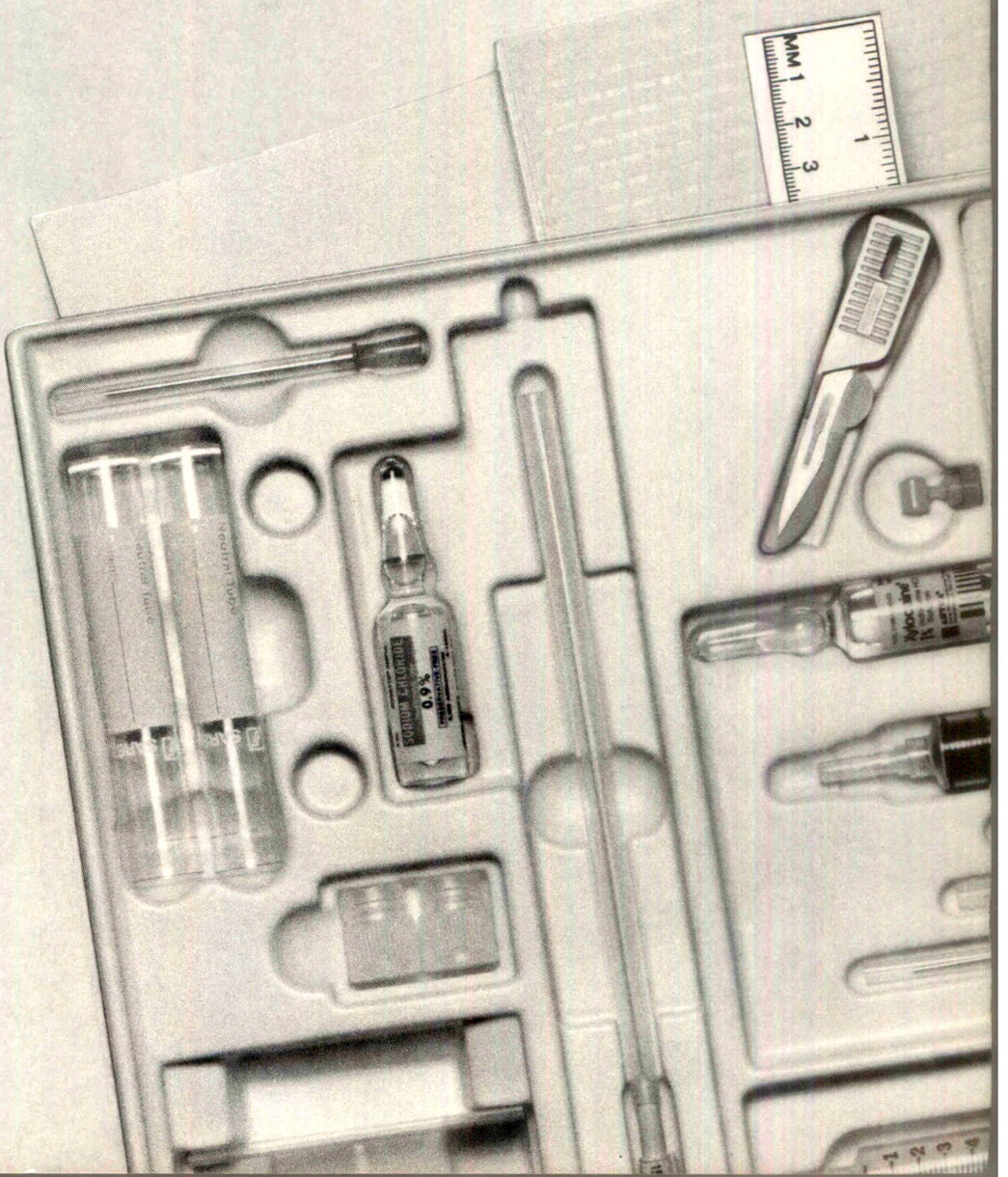
E-Z-EM

More than barium—
much more

E-Z-EM®
E-Z-EM, Inc.
7 Portland Avenue
Westbury, N.Y. 11590

© 1986 E-Z-EM, Inc.

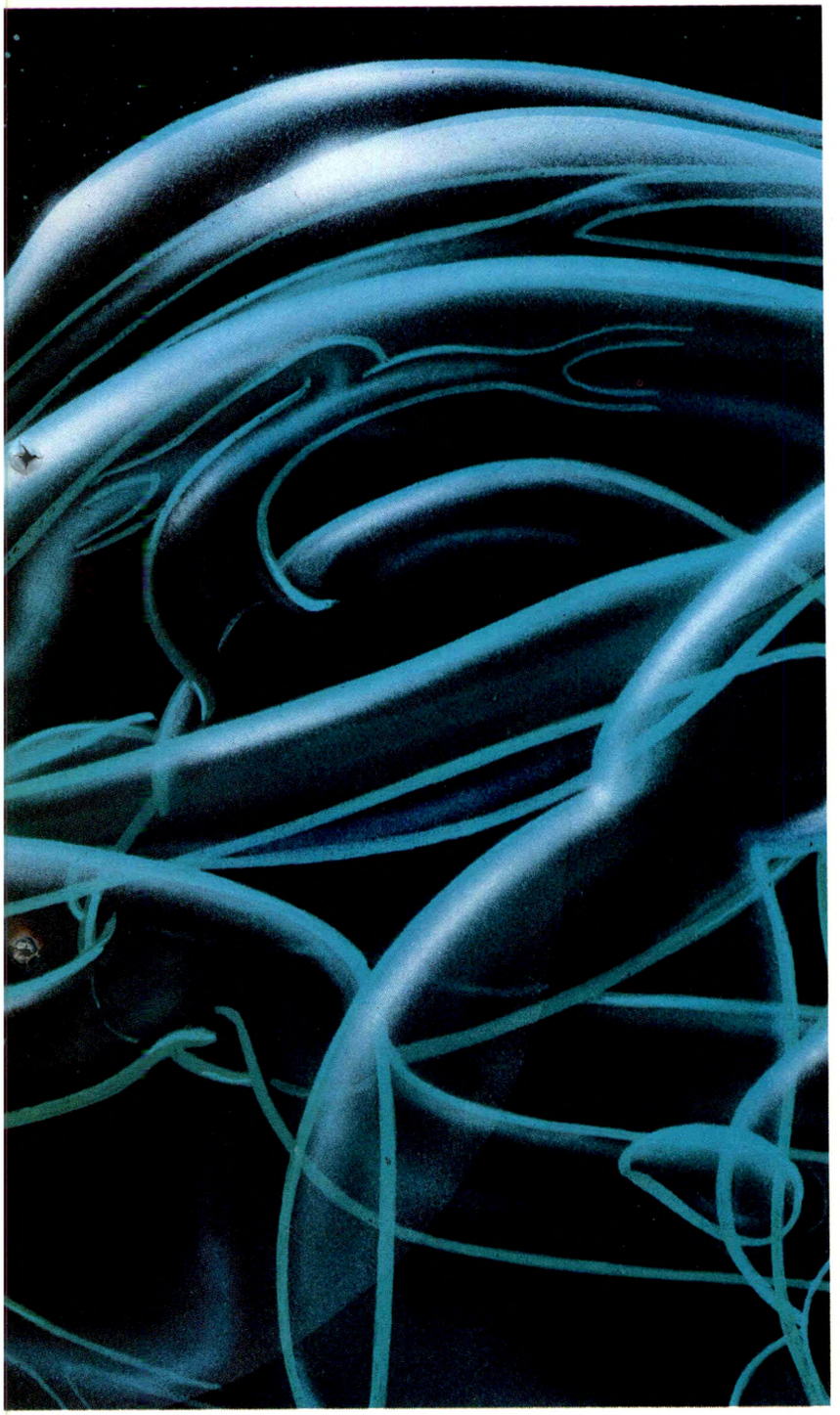
PercuSet™



Toshiba's TCT-900S...



one giant leap for CT!



CT beyond the fourth generation.

Toshiba's TCT-900S scanner is indisputably unique to the CT imaging industry. In fact, Toshiba's leading edge technology actually takes CT beyond the fourth generation into another dimension with these technological features found in no other comparable system:

1. Consistently superior image quality: just what you expect from Toshiba.
2. Nutate/Rotate geometry with continuous scan: thirty scans in thirty seconds.
3. True dynamic scan: no inter-scan delay.
4. Sub-second scanning: quality images in 0.6 seconds.

Let the competition tell you that CT technology can go no further. But you owe it to yourself to see just how far Toshiba can really go . . .

Call or write: Toshiba Medical Systems, 2441 Michelle Drive, Tustin, CA 92680. In California, call (714) 669-5419. Outside California, call toll-free (800) 421-1968. In Canada, call (416) 298-6100.

In Touch with Tomorrow

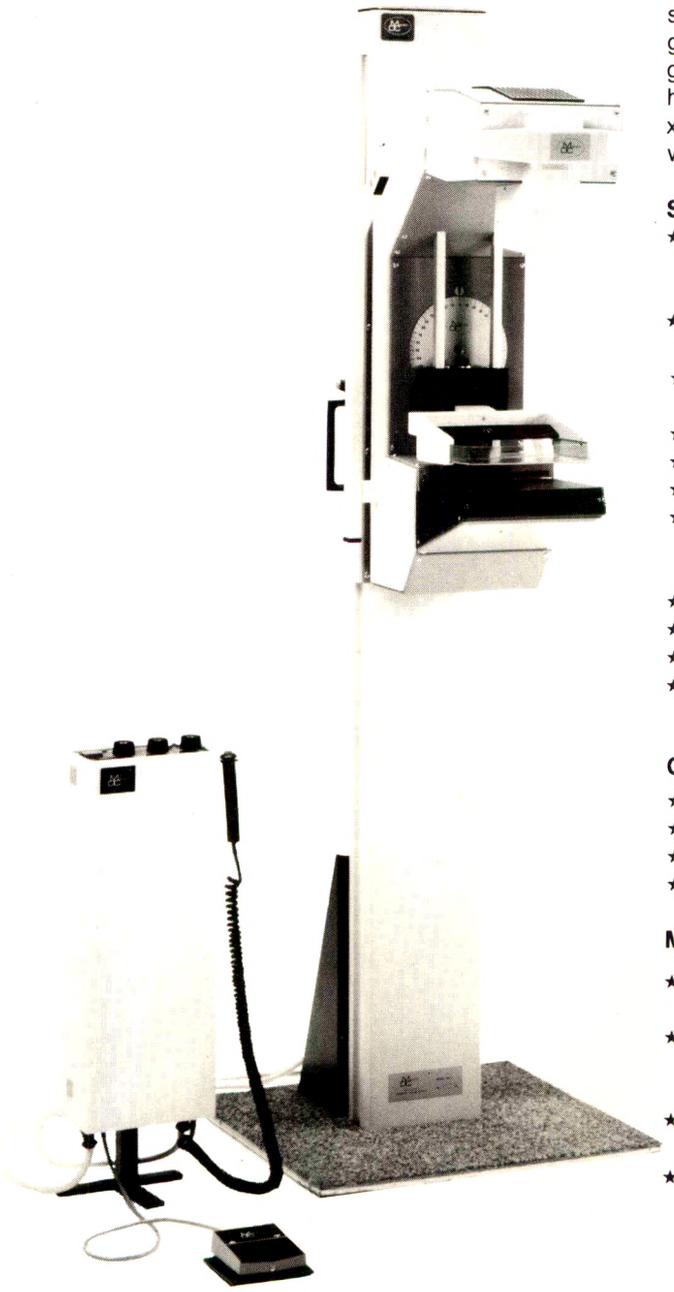
TOSHIBA

GLOBAL IMAGING SPECIALISTS

Tecnomed USA

Mamex DC

MAMMOGRAPHIC SYSTEM



Original MAMEX DC

In the beginning...
The original MAMEX DC

The Mamex DC is a complete mammographic system, consisting of a modern, efficient DC generator which virtually eliminates "ripple" and gives a higher resolution image with consistently higher subject contrast; a molybdenum anode x-ray tube; and a motorized compression system with floor remote control.

Standard features:

- ★ Compact DC generator with automatic exposure control.
  Exposures can be made once every 30 seconds.
- ★ Stand designed for x-ray examination of the breast.
- ★ Hardened glass screen protects technician during exposure.
- ★ Floor remote compression control.
- ★ Phototiming detector position selector.
- ★ Field light.
- ★ Breast compression plate;
  Biopsy compression plate;
  Spot cone compression plate.
- ★ 18x24cm Kodak Min-R cassette with screen.
- ★ Film identification markers.
- ★ Automatic line voltage compensation.
- ★ .6x.6 stationary anode molybdenum x-ray tube with beryllium window.

Options:

- ★ 200L 3.5:1 grid.
- ★ Carbon fiber cassette tunnel with grid pocket.
- ★ In-hospital wheel assembly (shown).
- ★ Van wheel assembly.

Mamex DC . . .

- ★ Five-year proven track record of performance and reliability;
- ★ Hundreds of satisfied physicians, clinics, and hospitals throughout the United States and internationally;
- ★ Full 12-month non-prorated warranty on the x-ray tube;
- ★ Average midbreast dosages, on a 2-film exam of a 6cm compressed breast, of .07R or less (as documented by the University of Michigan Breast Cancer Detection Center - Ingvar Andersson, M.D.)

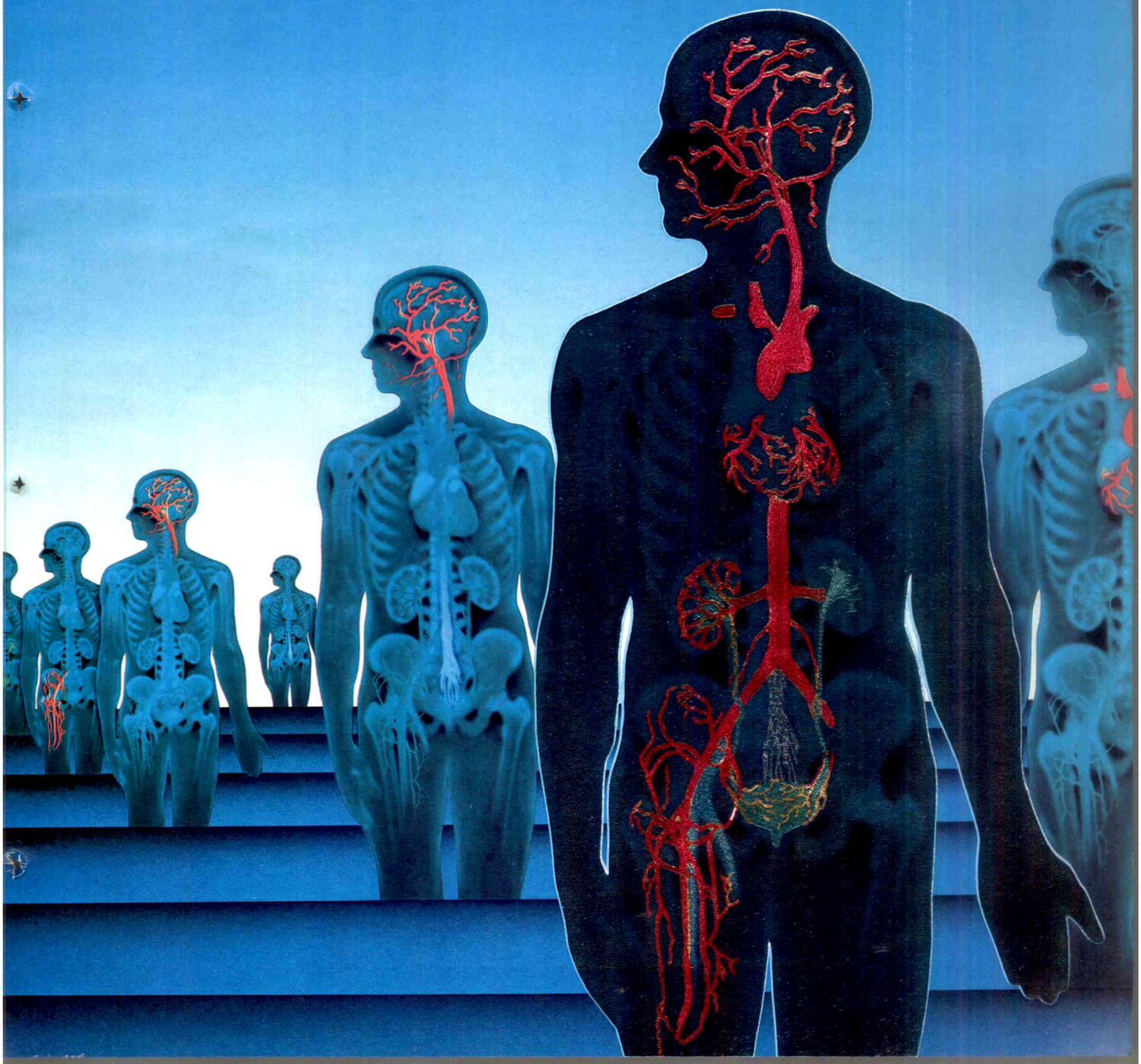
. . . offers your facility the very best in diagnostic equipment available in today's marketplace.

FROM

Winthrop-Breon

LEADER IN THE DEVELOPMENT OF NONIONIC CONTRAST MEDIA

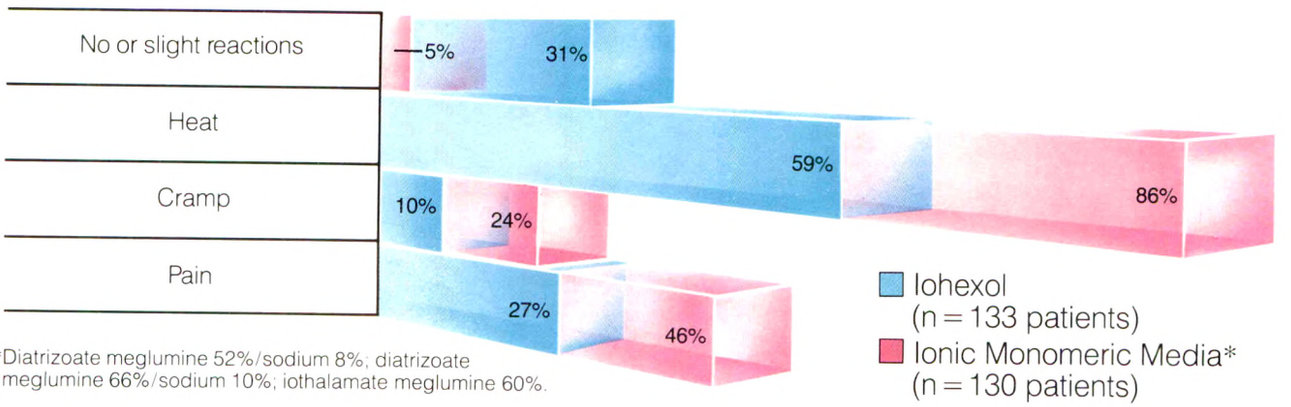
Improving the safety profile in a broad spectrum of applications.



Excellent vascular tolerance: low incidence of postphlebographic thrombosis.[1-3]

Significant improvement in comfort reduces patient motion[4,5]: Less need for repeat examinations.

Subjective Sensations in Peripheral Arteriography



*Diatrizoate meglumine 52%/sodium 8%; diatrizoate meglumine 66%/sodium 10%; iothalamate meglumine 60%.

Improved hemodynamic profile over conventional ionic media. Systolic and diastolic pressures are maintained near baseline levels.[6,7]

Improving the nephrotoxicity profile: Minimal effect on glomerular filtration rate, permeability, or albumin excretion.[8,9]

Not recommended for patients with anuria. Since adverse reactions can occur with nonionic media, similar preparations to those recommended for ionic media should be planned to handle severe or potentially fatal reactions.

Wider margin of safety even at higher iodine concentrations.[1-3] Less potential for renal damage compared to conventional ionic media. Minimal effect on creatinine levels and renal enzymes.[10]

Significant improvement in patient comfort in cerebral arteriography.

Significant improvement over conventional ionic contrast media: Fewer and milder pain and warmth sensations.[11-15] Excellent neurotoxicity profile.†

Excellent cardiovascular safety profile: Fewer injections accompanied by major changes in heart rate.[6,14,15]

For peripheral arteriography: Recommended concentrations—OMNIPAQUE 300 (300 mgI/mL) or OMNIPAQUE 350 (350 mgI/mL). For cerebral arteriography: Recommended concentration—OMNIPAQUE 300 (300 mgI/mL).

Adapted from Wolf[4]; data on file, Winthrop-Breon Laboratories.[6] Comparable concentration and volume per injection.

Excellent diagnostic quality in intravenous digital subtraction angiography.

Greater patient comfort, better tolerance: Most subjective side effects are mild.[6,16-18]

Excellent diagnostic images: Significantly less image degradation secondary to swallowing, motion, coughing.[16]

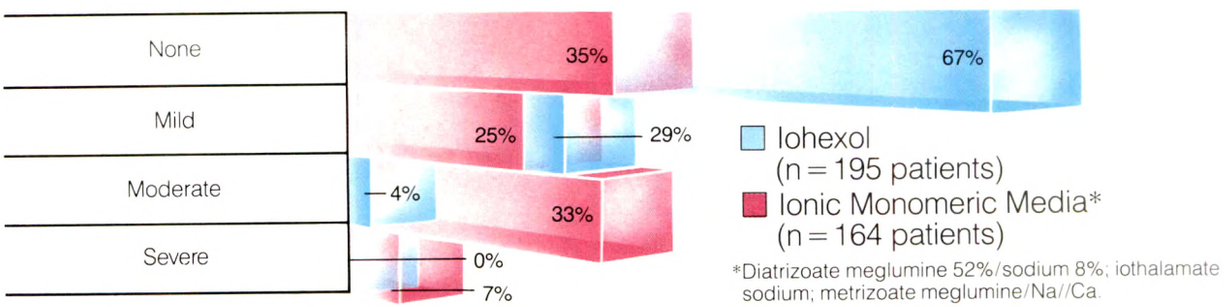
Good to excellent radiographic quality achieved in 94% of patients studied (n = 81).[6,16-18] 94% of carotid DSA studies conducted with no or only slight artifacts.[17]

Excellent patient tolerance in excretory urography.

Less nausea, vomiting, and heat sensation compared to conventional ionic contrast media.

In 96% of patients, discomfort was absent or mild.[6]

Discomfort in Urography



*Diatrizoate meglumine 52%/sodium 8%; iothalamate sodium; metrizoate meglumine/Na//Ca.

Data on file, Winthrop-Breon Laboratories.[6]

NONIONIC

OMNIPAQUE®

(IOHEXOL)

†See following pages for important product information concerning contraindications, warnings, adverse reactions, patient selection, and precautionary recommendations.

Improving the safety profile in a broad spectrum of applications.

Less chemotoxicity than ionic contrast media.[19]

Lower osmolality than conventional ionic media.[19]

Minimal effect on key physiologic parameters[19]**:** Well tolerated by most patients.

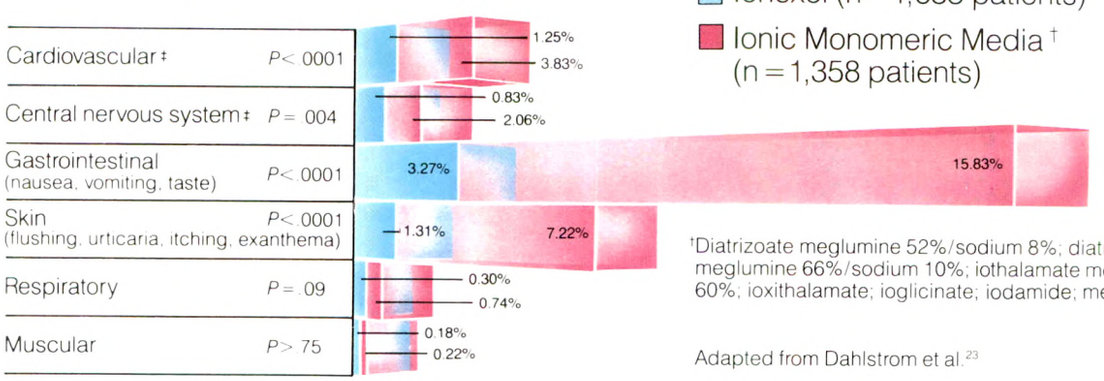
Less neurotoxic than conventional ionic media.

Few direct or indirect cardiovascular effects.[20,21]

Improved patient comfort: Fewer artifacts due to motion and swallowing.[16-18]

Less potential for allergic reactions.[22] Since adverse reactions can occur with nonionic media, similar preparations to those recommended for ionic media should be planned to handle severe or potentially fatal reactions.

Incidence of Adverse Reactions After Intravenous Injections Only, in Multicenter Clinical Trials*



†Diatrizoate meglumine 52%/sodium 8%; diatrizoate meglumine 66%/sodium 10%; iothalamate meglumine 60%; ioxithalamate; ioglicinate; iodamide; metrizoate.

Adapted from Dahlstrom et al.[23]

Supplied in ready-to-use vials and bottles. No dilution or reconstitution necessary.

Product	Size (mL/unit)	Use
OMNIPAQUE® 180 (180 mgI/mL)	10 mL, 20 mL vials, Myelo-Kit™	Lumbar, Thoracic, and CT Myelography
OMNIPAQUE® 240 (240 mgI/mL)	10 mL, 100 mL vials, 200 mL bottle, Myelo-Kit	Lumbar and Thoracic Myelography, Peripheral Venography
OMNIPAQUE® 300 (300 mgI/mL)	10 mL, 30 mL, 50 mL, 100 mL vials	Urography, Cerebral Arteriography, Peripheral Arteriography, Peripheral Venography
OMNIPAQUE® 350 (350 mgI/mL)	50 mL, 100 mL vials, 200 mL bottle	Angiocardiography, Urography, Peripheral Arteriography, I.V. Digital Subtraction Angiography

*See following pages for important product information concerning contraindications, warnings, adverse reactions, patient selection, and precautionary recommendations.

‡In general, adverse reactions to the intravascular use of OMNIPAQUE have been mild and of short duration. The general incidence of these occurrences following total intravascular use is slightly higher, as shown in the product information on the last page.



OMNIPAQUE®
INJECTION (IOHEXOL)

180

240

300

350

PLEASE CONSULT FULL PRODUCT INFORMATION BEFORE USING.
A SUMMARY FOLLOWS:
OMNIPAQUE is a nonionic, water-soluble, radiographic contrast medium.
INDICATIONS AND USAGE: OMNIPAQUE is indicated in adults for angiocardiography (ventriculography, selective coronary arteriography); aortography, including studies of the aortic root, aortic arch, ascending aorta, abdominal aorta, and its branches; cerebral arteriography; digital subtraction angiography; peripheral angiography including arteriography and venography (phlebography); excretory urography; and lumbar and thoracic myelography, by conventional technique and in computerized tomography.

Administration of contrast media should be performed by qualified personnel familiar with the procedure and an appropriate technique should be utilized.
CONTRAINDICATIONS: OMNIPAQUE should not be administered to patients with a known hypersensitivity to iohexol.

Lumbar puncture ordinarily should not be performed in the presence of local or systemic infection where bacteremia is likely.

Intrathecal administration of corticosteroids with OMNIPAQUE is contraindicated.

Because of the possibility of overdosage, immediate repeat myelography in the event of technical failure is contraindicated (see DOSAGE AND ADMINISTRATION).
WARNINGS—General: OMNIPAQUE should be used with extreme care in patients with severe functional disturbances of the liver and kidneys, severe thyrotoxicosis, or myelomatosis. Diabetics with a serum creatinine level above 3 mg/dL should not be examined unless the possible benefits of the examination clearly outweigh the additional risk. OMNIPAQUE is not recommended for use in patients with anuria.

Radiopaque contrast agents are potentially hazardous in patients with multiple myeloma or other paraproteinemia, particularly in those with therapeutically resistant anuria. Although neither the contrast agent nor dehydration has separately proven to be the cause of anuria in myeloma, it has been speculated that the combination of both may be causative factors. The risk in myelomatous patients is not a contraindication; however, special precautions are necessary. Partial dehydration in the preparation of these patients prior to injection is not recommended since this may predispose the patient to precipitation of the myeloma protein in the renal tubules. No form of therapy, including dialysis, has been successful in reversing the effect. Myeloma, which occurs most commonly in persons over age 40, should be considered before instituting intravascular administration of contrast agents.

Ionic contrast media, when injected intravenously or intraarterially, may promote sickling in individuals who are homozygous for sickle cell disease.

Administration of radiopaque materials to patients known or suspected of having pheochromocytoma should be performed with extreme caution. If, in the opinion of the physician, the possible benefits of such procedures outweigh the considered risks, the procedures may be performed; however, the amount of radiopaque medium injected should be kept to an absolute minimum. The patient's blood pressure should be assessed throughout the procedure and measures for the treatment of hypertensive crisis should be readily available.

Reports of thyroid storm following the use of iodinated, ionic radiopaque contrast media in patients with hyperthyroidism or with autonomously functioning thyroid nodule suggest that this additional risk be evaluated in such patients before use of any contrast medium.

Urography should be performed with caution in patients with severely impaired renal function and patients with combined renal and hepatic disease.

Caution is advised in patients with a history of epilepsy, severe cardiovascular disease, chronic alcoholism, or multiple sclerosis.

Elderly patients may present a greater risk following myelography. The need for the procedure in these patients should be evaluated carefully. Special attention must be paid to dose and concentration of the medium, hydration, and technique used.

Patients who are receiving anticonvulsants should be maintained on this therapy. Should a seizure occur, intravenous diazepam or phenobarbital sodium is recommended. In patients with a history of seizure activity who are not on anticonvulsant therapy, premedication with barbiturates should be considered.

Prophylactic anticonvulsant treatment with barbiturates should be considered in patients with evidence of inadvertent intracranial entry of a large or concentrated bolus of the contrast medium since there may be an increased risk of seizure in such cases.

Drugs which lower the seizure threshold, especially phenothiazine derivatives, including those used for their antihistamine properties, should not be used with OMNIPAQUE. Others include MAO inhibitors, tricyclic antidepressants, CNS stimulants, and psychoactive drugs described as analeptics, major tranquilizers, or antipsychotic drugs. Such medication should be discontinued at least 48 hours before myelography, should not be used for the control of nausea and vomiting, and should not be resumed for at least 24 hours postprocedure.

Care is required in patient management to prevent inadvertent intracranial entry of a large dose or concentrated bolus of the medium. Also, effort should be directed to avoid rapid dispersion of the medium causing inadvertent rise to intracranial levels (eg, by active patient movement). Direct intracisternal or ventricular administration for standard radiography (not CT) is not recommended.

In most reported cases of major motor seizures with other nonionic myelographic media, one or more of the following factors were present. Therefore avoid:
- Deviations from recommended procedure or in myelographic management.
- Use in patients with a history of epilepsy.
- Overdosage.
- Intracranial entry of a bolus or premature diffusion of a high concentration of the medium.
- Medication with neuroleptic drugs or phenothiazine antinauseants.
- Failure to maintain elevation of the head during the procedure, on the stretcher, or in bed.
- Excessive and particularly active patient movement or straining.

If grossly bloody CSF is encountered, the possible benefits of a myelographic procedure should be considered in terms of the risk to the patient.

PRECAUTIONS—General: Diagnostic procedures which involve the use of radiopaque diagnostic agents should be carried out under the direction of personnel with the prerequisite training and with a thorough knowledge of the particular procedure to be performed. Appropriate facilities should be available for coping with any complication of the procedure, as well as for emergency treatment of severe reactions to the contrast agent itself. After parenteral administration of a radiopaque agent, competent personnel and emergency facilities should be available for at least 30 to 60 minutes since severe delayed reactions have occurred (see ADVERSE REACTIONS).

Preparatory dehydration is dangerous and may contribute to acute renal failure in patients with advanced vascular disease, diabetic patients, and in susceptible nondiabetic patients (often elderly with preexisting renal disease). Dehydration in these patients seems to be enhanced by the osmotic diuretic action of urographic agents. It is believed that overnight fluid restriction prior to excretory urography generally does not provide better visualization in normal patients. *Patients should be well hydrated prior to and following iohexol administration.*

In patients with severe renal insufficiency or failure, compensatory biliary excretion of the drug is anticipated to occur, with a slow clearance into the bile. Patients with hepatorenal insufficiency should not be examined unless the possibility of benefit clearly outweighs the additional risk.

Acute renal failure has been reported in diabetic patients with diabetic nephropathy and in susceptible nondiabetic patients (often elderly with preexisting renal disease) following excretory urography. Therefore, careful consideration of the potential risks should be given before performing this radiographic procedure in these patients.

Immediately following surgery, excretory urography should be used with caution in renal transplant recipients.

The possibility of a reaction, including serious, life-threatening, fatal, anaphylactoid, or cardiovascular reactions should always be considered (see ADVERSE REACTIONS). It is of utmost importance that a course of action be carefully planned in advance for immediate treatment of serious reactions, and that adequate and appropriate personnel be readily available in case a severe reaction should occur.

The possibility of an idiosyncratic reaction in susceptible patients should always be considered (see ADVERSE REACTIONS). The susceptible population includes patients with a previous reaction to contrast media, patients with a known sensitivity to iodine per se, and patients with a known clinical hypersensitivity: bronchial asthma, hay fever, and food allergies.

The occurrence of severe idiosyncratic reactions has prompted the use of several pretesting methods. However, pretesting cannot be relied upon to predict severe reactions and may itself be hazardous for the patient. It is suggested that a thorough medical history with emphasis on allergy and hypersensitivity, prior to the injection of any contrast media, may be more accurate than pretesting in predicting potential adverse reactions.

A positive history of allergies or hypersensitivity does not arbitrarily contraindicate the use of a contrast agent where a diagnostic procedure is thought essential, but caution should be exercised (see ADVERSE REACTIONS). Premedication with antihistamines or corticosteroids to avoid or minimize possible allergic reactions in such patients should be considered. Recent reports indicate that such pretreatment does not prevent serious life-threatening reactions, but may reduce both their incidence and severity.

Even though the osmolality of OMNIPAQUE is low compared to diatrizoate- or iothalamate-based ionic agents of comparable iodine concentration, the potential transitory increase in the circulatory osmotic load in patients with congestive heart failure requires caution during injection. These patients should be observed for several hours following the procedure to detect delayed hemodynamic disturbances.

General anesthesia may be indicated in the performance of some procedures in selected adult patients; however, a higher incidence of adverse reactions has been reported in these patients, and may be attributable to the inability of the patient to identify untoward symptoms, or to the hypotensive effect of anesthesia which can reduce cardiac output and increase the duration of exposure to the contrast agent.

Angiography should be avoided whenever possible in patients with homocystinuria, because of the risk of inducing thrombosis and embolism.

In angiographic procedures, the possibility of dislodging plaques or damaging or perforating the vessel wall should be borne in mind during the catheter manipulations and contrast medium injection. Test injections to ensure proper catheter placement are recommended.

Selective coronary arteriography should be performed only in those patients in whom the expected benefits outweigh the potential risk. The inherent risks of angiocardiography in patients with chronic pulmonary emphysema must be weighed against the necessity for performing this procedure.

Administration of contrast media should be performed by qualified personnel familiar with the procedure and appropriate patient management. Sterile technique must be used with any spinal puncture.

When OMNIPAQUE is to be injected using plastic disposable syringes, the contrast medium should be drawn into the syringe and used immediately.

If nondisposable equipment is used, scrupulous care should be taken to

prevent residual contamination with traces of cleansing agents.

Parenteral products should be inspected visually for particulate matter and discoloration prior to administration. If particulate matter or discoloration is present, do not use.

Repeat Procedures: If, in the clinical judgment of the physician, sequential or repeat subarachnoid examinations are required, a suitable interval of time between administrations should be observed to allow for normal clearance of the drug from the body.

Information for Patients: Patients receiving injectable radiopaque diagnostic agents should be instructed to:

1. Inform your physician if you are pregnant.
2. Inform your physician if you are diabetic or if you have multiple myeloma, pheochromocytoma, homozygous sickle cell disease or known thyroid disorder (see WARNINGS).
3. Inform your physician if you are allergic to any drugs, food, or if you had any reactions to previous injections of dyes used for x-ray procedures.
4. Inform your physician about any other medications you are currently taking, including nonprescription drugs, before you are administered this drug.

Drug/Laboratory Test Interaction: If iodine containing isotopes are to be administered for the diagnosis of thyroid disease, the iodine-binding capacity of thyroid tissue may be reduced for up to two weeks after contrast medium administration. Thyroid function tests which do not depend on iodine estimation, eg, T_3 resin uptake or direct thyroxin assays, are not affected.

Drug Interactions: Drugs which lower the seizure threshold—especially phenothiazine derivatives including those used for their antihistaminic or antinauseant properties—should not be used with OMNIPAQUE. Others include monoamine oxidase (MAO) inhibitors, tricyclic antidepressants, CNS stimulants, and psychoactive drugs described as analeptics, major tranquilizers, or antipsychotic drugs. Such medications should be discontinued at least 48 hours before myelography, should not be used for the control of nausea or vomiting during or after myelography, and should not be resumed for at least 24 hours postprocedure. In nonelective procedures in patients on these drugs, consider prophylactic use of anticonvulsants.

Carcinogenesis, Mutagenesis, Impairment of Fertility: No long-term animal studies have been performed to evaluate the potential of iohexol in these areas.

Pregnancy Category B: Reproduction studies have been performed in rats and rabbits with up to 100 times the recommended human dose. No evidence has been established of impaired fertility or harm to the fetus due to OMNIPAQUE; there are, however, no studies in pregnant women. Because animal reproduction studies are not always predictive of human response, this drug should be used during pregnancy only if clearly indicated.

Nursing Mothers: Caution should be exercised when OMNIPAQUE is administered to a nursing woman; it is not known to what extent iohexol is excreted in human milk.

Pediatric Use: Safety and effectiveness in children have not been established.

ADVERSE REACTIONS:

Intrathecal: Adverse reactions to the intrathecal use of OMNIPAQUE in general have been mild to moderate in degree, and of short duration. The incidence of these occurrences, based on clinical trials of 584 patients, is as follows:

Headaches: The most frequently occurring adverse reaction following myelography with OMNIPAQUE has been headache, with an incidence of less than 20%. Headache may be caused either as a direct effect of the contrast medium or by CSF leakage at the dural puncture site. However, in managing the patient, it is considered more important to minimize intracranial entry of contrast medium by postural management than to attempt to control possible CSF leakage.

Pain: Mild pain including backache, stiffness, and neuralgia occurred following injection with an incidence of about 8%.

Nausea and Vomiting: Nausea was reported, with an incidence of about 6%, and vomiting of about 3% (based on clinical trials of 584 patients—see PATIENT MANAGEMENT). Maintaining normal hydration is very important. The use of phenothiazine antinauseants is contraindicated. Reassuring the patient that the nausea will clear is usually all that is required.

Dizziness: Transient dizziness was reported in about 2% of the patients.

Other Reactions: Other reactions, occurring with an individual incidence of less than 0.1%, included feeling of heaviness, hypotension, hypertonia, sensation of heat, sweating, vertigo, and loss of appetite. All were transient and mild, with no clinical sequelae.

General Adverse Reactions to Contrast Media: Physicians should remain alert for the occurrence of adverse effects in addition to those discussed above, particularly those already reported in the literature for other nonionic, water-soluble myelographic contrast media. These have included but are not limited to aseptic and bacterial meningitis, and CNS and other neurologic disturbances.

Intravascular: Adverse reactions to the intravascular use of OMNIPAQUE have usually been of mild to moderate severity. However, serious, life-threatening and fatal reactions, mostly of cardiovascular origin, have been associated with the administration of iodine-containing contrast media, including OMNIPAQUE. The injection of contrast media is frequently associated with the sensation of warmth and pain, especially in peripheral angiography; pain and warmth are less frequent and less severe with OMNIPAQUE than with many ionic media, but lower osmolality media are similar in this respect. The incidence of these occurrences in clinical trials is as follows:

Cardiovascular System: Arrhythmias including PVCs and PACs (3%), angina/chest pain (2%), and hypotension (1%). Others including cardiac failure, asystole, bradycardia, tachycardia, and vasovagal reaction were reported with an individual incidence of less than 0.8%. In controlled clinical studies involving 900 patients, one fatality occurred. In widespread clinical use, the incidence of fatality is estimated at 0.0003%.

Nervous System: Pain (6%), photomas (3%), headache (2%), and metallic taste (0.8%). Others including anxiety, blurred vision, dizziness, fever, motor and speech dysfunction, convulsion, light-headedness, paresthesia, somnolence, vertigo, stiff neck, hemiparesis, and nystagmus were reported, with an individual incidence of less than 0.3%.

Respiratory System: Dyspnea, laryngitis, and throat irritation, with an individual incidence of 0.1%.

Gastrointestinal System: Nausea (2%) and vomiting (0.5%). Others including diarrhea, dyspepsia, and dry mouth were reported, with an individual incidence of 0.1%.

© 1986 WINTHROP-BREON LABORATORIES 41368/3737

OMNIPAQUE® (iohexol)

Skin and Appendages: Urticaria (0.3%) and purpura (0.1%).

Individual adverse reactions which occurred to a significantly greater extent for a specific procedure are listed under that indication.

General Adverse Reactions to Contrast Media: Physicians should remain alert for the occurrence of adverse effects in addition to those discussed above. The following reactions have been reported after administration of other intravascular iodinated contrast media. *Reactions due to technique:* hematomas and ecchymoses. *Hemodynamic reactions:* vein cramp and thrombophlebitis following intravenous injection. *Cardiovascular reactions:* rare cases of cardiac arrhythmias, reflex tachycardia, chest pain, cyanosis, hypertension, hypotension, peripheral vasodilatation, shock, and cardiac arrest. *Renal reactions:* occasionally, transient proteinuria, and rarely, oliguria or anuria. *Allergic reactions:* Asthmatic attacks, nasal and conjunctival symptoms, dermal reactions such as urticaria with or without pruritus, as well as pleomorphic rashes, sneezing and lacrimation and, rarely, anaphylactic reactions. Rare fatalities have occurred, due to this or unknown causes. *Signs and symptoms related to the respiratory system:* pulmonary or laryngeal edema, bronchospasm, dyspnea; *or to the nervous system:* restlessness, tremors, convulsions. *Other reactions:* flushing, pain, warmth, metallic taste, nausea, vomiting, anxiety, headache, confusion, pallor, weakness, sweating, localized areas of edema, especially facial cramps, neutropenia, and dizziness. Rarely, immediate or delayed rigors can occur, sometimes accompanied by hyperpyrexia. Infrequently, "iodism" (salivary gland swelling) from organic iodinated compounds appears two days after exposure and subsides by the sixth day.

CONSULT PACKAGE INSERT FOR A MORE DETAILED DISCUSSION OF ADVERSE REACTIONS to both intrathecal and intravascular use of OMNIPAQUE.

DOSAGE AND ADMINISTRATION: CONSULT FULL PACKAGE INSERT BEFORE USE. Details on dose, concentration, and administration are provided for each of the indicated procedures.

HOW SUPPLIED: OMNIPAQUE is available in the following packaging and concentrations, *requiring no dilutions or reconstitution:*

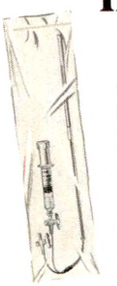
Vials of 10 mL, 180 mgI/mL, boxes of 10 (NDC 0024-1411-10)
Vials of 20 mL, 180 mgI/mL, boxes of 10 (NDC 0024-1411-20)
Vials of 10 mL, 240 mgI/mL, boxes of 10 (NDC 0024-1412-10)
Vials of 100 mL, 240 mgI/mL, boxes of 5 (NDC 0024-1412-15)
Bottles of 200 mL, 240 mgI/mL, boxes of 5 (NDC 0024-1412-25)
Vials of 10 mL, 300 mgI/mL, boxes of 10 (NDC 0024-1413-10)
Vials of 30 mL, 300 mgI/mL, boxes of 10 (NDC 0024-1413-30)
Vials of 50 mL, 300 mgI/mL, boxes of 10 (NDC 0024-1413-50)
Vials of 100 mL, 300 mgI/mL, boxes of 5 (NDC 0024-1413-15)
Vials of 50 mL, 350 mgI/mL, boxes of 10 (NDC 0024-1414-50)
Vials of 100 mL, 350 mgI/mL, boxes of 5 (NDC 0024-1414-15)
Bottles of 200 mL, 350 mgI/mL, boxes of 5 (NDC 0024-1414-25)
MYELO-KIT™ containing: One vial of 10 mL, 180 mgI/mL, and one sterile myelogram tray, boxes of 5 (NDC 0024-1411-05)
MYELO-KIT™ containing: One vial of 20 mL, 180 mgI/mL, and one sterile myelogram tray, boxes of 5 (NDC 0024-1411-51)
MYELO-KIT™ containing: One vial of 10 mL, 240 mgI/mL, and one sterile myelogram tray, boxes of 5 (NDC 0024-1412-05)

References: 1. Enge I: Phlebography: Survey and present state. *Acta Radiol* 1983; suppl 366, pp 50-53. **2.** Gjølberg T, Andrew E, Enge I: Iohexol in phlebography of the leg: A comparative investigation with meglumine metrizoate. *Acta Radiol* 1983; suppl 366, pp 65-69. **3.** Albrechtsson U, Fagher B, Lagerstedt C, et al: Double blind comparison between iohexol and metrizoate in phlebography of the lower limb. *Acta Radiol* 1983; suppl 366, pp 58-64. **4.** Wolf GL: Adult peripheral angiography: Results from four North American randomized clinical trials of ionic media versus iohexol. *Acta Radiol* 1983; suppl 366, pp 166-170. **5.** Gordon IJ, Skoblar RS, Chicatelli PD, et al: A comparison of iohexol and Conray-60 in peripheral angiography. *AJR* 1984; 142:563-565. **6.** Data on file, Winthrop-Breon Laboratories. **7.** Egsgaard H, Hørup A, Praestholm J: A controlled clinical trial of iohexol and diatrizoate in aortofemoral angiography. *Eur J Radiol* 1983; 3:14-17. **8.** Kolbenstvedt A: Iohexol in lower extremity, renal and visceral angiography: Survey and present state. *Acta Radiol* 1983; suppl 366, pp 153-157. **9.** Törnquist C, Holtås S: Renal angiography with iohexol and metrizoate. *Radiology* 1984; 150:331-334. **10.** Albrechtsson U, Hultberg B, Lárusdóttir H, et al: Nephrotoxicity of ionic and non-ionic contrast media in aorto-femoral angiography. *Acta Radiol* 1985; 5:615-618. **11.** Cronqvist S: Iohexol in cerebral angiography: Survey and present state. *Acta Radiol* 1983; suppl 366, pp 135-139. **12.** Åhlgren P: Iohexol compared to urografin meglumine in cerebral angiography: A randomized, double-blind cross-over study. *Neuroradiology* 1982; 23:195-198. **13.** Nakstad P, Sortland O, Aaserud O: Iohexol compared to meglumine-Ca-metrizoate in common carotid angiography: A randomized double-blind cross-over study in man. *Neuroradiology* 1983; 23:33-36. **14.** Kido DK, Morris TW, Ekholm S, et al: Comparison of iohexol and meglumine-Na diatrizoate in cerebral angiography. *Acta Radiol* 1983; suppl 366, pp 142-146. **15.** Amundsen P, Dugstad G, Presthus J, et al: Cerebral angiography with iohexol: A multicentre clinical trial. *Acta Radiol* 1982; 23:529-534. **16.** Cacayorin ED, Bernstein AD, Fruehan CT, et al: Intravenous digital subtraction angiography with iohexol. *AJNR* 4:329-332. **17.** Nakstad P: Digital subtraction angiography of the carotid arteries: A comparison of iohexol and metrizoate. *Acta Radiol* 1983; suppl 366, pp 89-93. **18.** Sackett JF, Bergsjordet B, Seeger JF, et al: Digital subtraction angiography: Comparison of meglumine-Na diatrizoate with iohexol. *Acta Radiol* 1983; suppl 366, pp 81-84. **19.** Dawson P: Some aspects of contrast medium toxicity. *Acta Radiol* 1983; suppl 366, pp 174-179. **20.** Bryan RN, Miller SL, Roehm JOF Jr, et al: Neuroangiography with iohexol. *AJNR* 1983; 4:344-346. **21.** Higgins CB, Mancini GBJ, Bloomquist JN, et al: Cardioangiography in man using iohexol and meglumine-Na diatrizoate: A comparison of hemodynamic and electrocardiographic effects. *Acta Radiol* 1983; suppl 366, pp 111-114. **22.** Holtås S: Iohexol in patients with previous adverse reactions to contrast media. *Invest Radiol* 1984; 19:563-565. **23.** Dahlstrom K, Shaw DD, Clauss W, et al: Summary of U.S. and European intravascular experience with iohexol based on the clinical program. *Invest Radiol* 1985; 20(suppl 1), pp 117-121.

Winthrop-Breon

Winthrop-Breon Laboratories
Division of Sterling Drug Inc
New York, NY 10016

The NEW Ackrad H/S Catheter Set for Hysterosalpingography

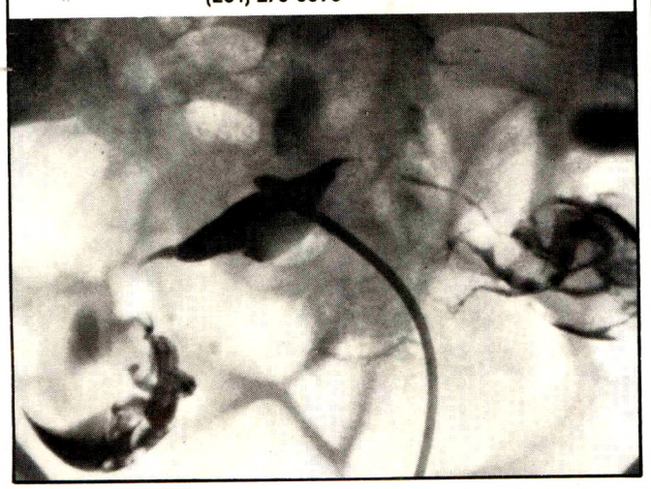


Now: Easier on the Patient . . .
Better for the Physician

The unique small sizes (5 and 7F) of the flexible balloon-bearing catheter provide previously unavailable freedom from trauma for the patient. A placement sheath and inflation syringe are included in the set for a rapid and efficient procedure.

Sample furnished on request.

ACKRAD LABORATORIES, Inc.
70 Jackson Drive, P.O. Box 1085, Cranford, NJ 07016
(201) 276-6390



FINALLY, WE'RE GIVING A KILLER DISEASE SOME OF ITS OWN MEDICINE.

A disease that once put an end to its victims, may soon be put to an end itself.

The disease, carnitine deficiency, destroys the body's ability to produce carnitine, a muscle-fueling substance. Until recently, carnitine deficiency meant certain disability. Often, it meant death.

In the past year, though, carnitine replacement therapy—developed with funding from the Muscular Dystrophy Association—has allowed fully half the patients treated to resume normal lives.

Carnitine replacement therapy is one of the most encouraging developments in MDA's fight against 40 neuromuscular diseases. And for one of those dread diseases, it could be the beginning of the end.

MDA

Muscular Dystrophy Association
Jerry Lewis, National Chairman

People Serving People.

Part of an International Fortune 500 Company with over $1 billion in sales, Konica Medical Corporation, has an important resource no other company can claim. Our people. Konica people. We've earned our reputation worldwide as quality imaging professionals. And serving you is what we do best, with a higher ratio of technical service and support personnel to customers than anyone else in the industry. We realize that having the best value in medical imaging products alone isn't enough in today's market. You also need the best value in service and support. That's why we're dedicated to supporting you in all phases of medical imaging. Promptly. Professionally. Comprehensively. We're Konica. We work harder for you.

Konica... The Image of Perfection, Since 1873.

KONICA

Konica Medical Corporation
411 Newark Pompton Turnpike, Wayne, NJ 07470 (201) 633-1500

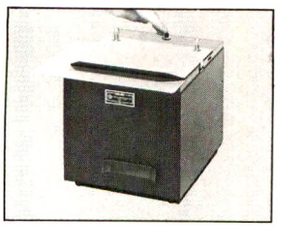
Two step film control

Minimize X-ray exposure. Optimize image quality. Stabilize film processor performance, film speed and contrast. Quickly. Easily.

1. **The Tobias Model RF Wejex Sensitometer**

Produces a precise 11-step wedge exposure on *your* X-ray film. Exposure made just before processing eliminates latent image fade problem.* Features: Precise shutter exposure control. Variable lamp intensity. Provisions for 2″×2″ ANSI blue, green or other filters, double sided exposures, 8″×10″ and 35mm test film alignment. And more.

*Lawrence, D.J.: **A Simple Method of Processor Control,** Med. Rad. and Photog. 49, 2-6, 28, 1973 (Reprints available on request)

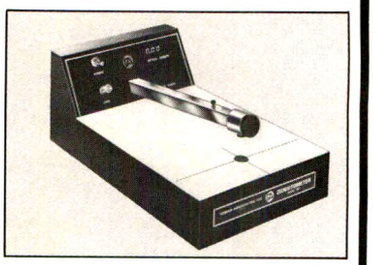


Wejex Universal Model RF
Also available: Wejex Standard Model R

For a demonstration, call your Tobias dealer.
Or write for our brochure. Ask about our 30 day free trial.

2. **The Tobias Model TBX Digital Densitometer**

Measures optical transmission density of the Wejex-exposed step wedge over a density range of 0 to 4.50. Accuracy ±0.02. Repeatability ±0.01. State-of-the-art electronics. Lighted digital display. 5 second warm up. Easily portable. Virtually no zero drift.



TOBIAS ASSOCIATES, INC.
50 Industrial Drive, P.O. Box 2699, Ivyland, PA 18974, (215) 322-1500

☐ Send literature on the Wejex Sensitometer and TBX Densitometer.

☐ Please send me a copy of D.J. Lawrence's "A Simple Method of Processor Control."

☐ Tell me more about your 30 day free trial policy.

Name _____
Title/Organization _____
_____
Address _____
City _____ State _____
Zip _____ Tel. _____

for prompt subscription service...

attach label here

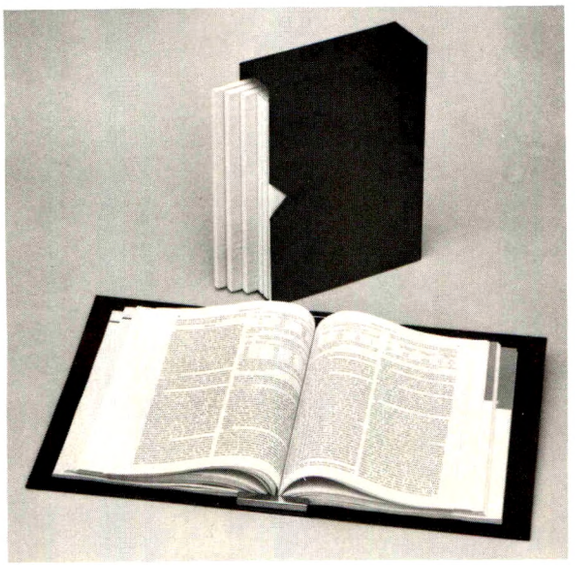
Please use this coupon and attach a *recent* label in the space provided when writing to us about:

- change of address
- renewal
- questions regarding your subscription

Please use the space below to indicate your *new* address.

Name of Journal _____
Name _____
Address _____
City/State/Zip _____

THE WILLIAMS & WILKINS COMPANY
428 East Preston Street/Baltimore, Maryland 21202



Protect your copies of

AJNR: AMERICAN JOURNAL OF NEURORADIOLOGY

with Jesse Jones Binders or Files

Keep your journals clean, orderly, and readily accessible with Jesse Jones Binders or Files. One Binder or one box style File is all you need to accommodate a full year's worth of issues. Both Binders and Files are handsomely made with rich dark blue leatherette covers and gold leaf embossed lettering.

Jesse Jones Binders open flat for easy reading and reference and are economically priced at only $9.95 each; 3 for $27.95, or 6 for $52.95 postpaid. The rugged, compact box Files are only $7.95 each; 3 for $21.95, or 6 for $39.95. Add $1.00/unit postage and handling. (Outside the U.S. add $2.50/unit.)

For charge orders call toll free 1-800-972-5858. ($15.00 minimum).

Free gold transfer slips included for indexing volume and year.

Please allow four to five weeks for delivery.

TO: Jesse Jones Industries
499 E. Erie Avenue, DEPT. AJNR
Philadelphia, PA 19134

I enclose my check or money order for $_____
(PA residents add 6% sales tax)

Send me ____ ☐ Files ☐ Binders for my journals

Name

Address (will not ship to P.O. Box)

City/State/Zip

Satisfaction guaranteed.

Nationwide Service and Support by Dedicated Professionals

Our imaging specialists and technical representatives are dedicated professionals. They stand behind every box of film. Through Radiology Support Programs and National Accounts Programs for Materials Management, they give you the right support for your specific imaging needs. And they'll keep you abreast of the latest developments and breakthroughs in medical imaging ...as well as administer our E.C.E. Approved Educational Programs, which provide excellent training for your staff personnel, radiology managers and technologists. From cost control and technique guidance to on-site computer generated reports for your information needs, helping you get the most out of your radiology departments is what we're all about. We're Konica. We work harder for you.

Konica... The Image of Perfection, Since 1873.

KONICA®

Konica Medical Corporation
411 Newark Pompton Turnpike, Wayne, NJ 07470 (201) 633-1500



USCI is Now Bard Interventional Products.

USCI, Products for Radiology, is now Bard Interventional Products. A new group with a strengthened commitment: innovative technologies for the interventional radiologist.

Many of the familiar and fundamental tools of interventional radiology were developed by USCI. New applications for these tools are being defined in the clinical arena, making interventional radiology one of the most dynamic, and demanding, fields in medicine.

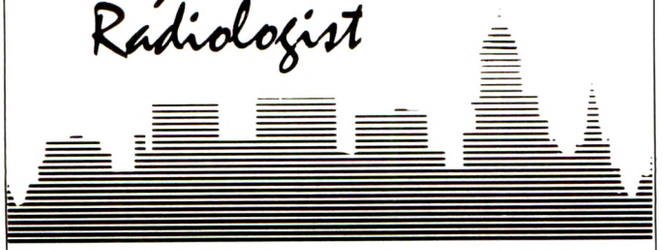
With Bard Interventional Products we are expanding our ability to work with you toward the development of new technologies based on our rigorous standards and applications-oriented know-how.

BARD
Interventional Products

The Bard Response to the Changes You've Made.

C.R. Bard Inc. 5 Federal Street P.O. Box 5069 Billerica, MA 01822
(617) 663-2244 • (800) 824-8724

Body MRI Radiologist



A Body MRI Radiologist with 2 or more years experience beyond fellowship being sought for St. Luke's\Roosevelt Hospital Center, a 1,315 bed voluntary facility university hospital of Columbia University College of Physicians and Surgeons. Strong interest in teaching and research as well as in patient care required.

Qualifications should meet requirements for Assistant or Associate Professor rank. Excellent remuneration. Please send inquiries with CV to:

Ronald C. Ablow, MD
Department of Radiology

ST. LUKE'S\ROOSEVELT
HospitalCenter

114th at Amsterdam Avenue
New York, NY 10025

Equal Opportunity Employer M/F



This publication is available in microform.

University Microfilms International reproduces this publication in microform: microfiche and 16mm or 35mm film. For information about this publication or any of the more than 13,000 titles we offer, complete and mail the coupon to: University Microfilms International, 300 N. Zeeb Road, Ann Arbor, MI 48106. Call us toll-free for an immediate response: 800-521-3044. Or call collect in Michigan, Alaska and Hawaii: 313-761-4700.

☐ Please send information about these titles:

_____

Name _____

Company/Institution _____

Address _____

City _____

State _____ Zip _____

Phone ( ) _____

University Microfilms International

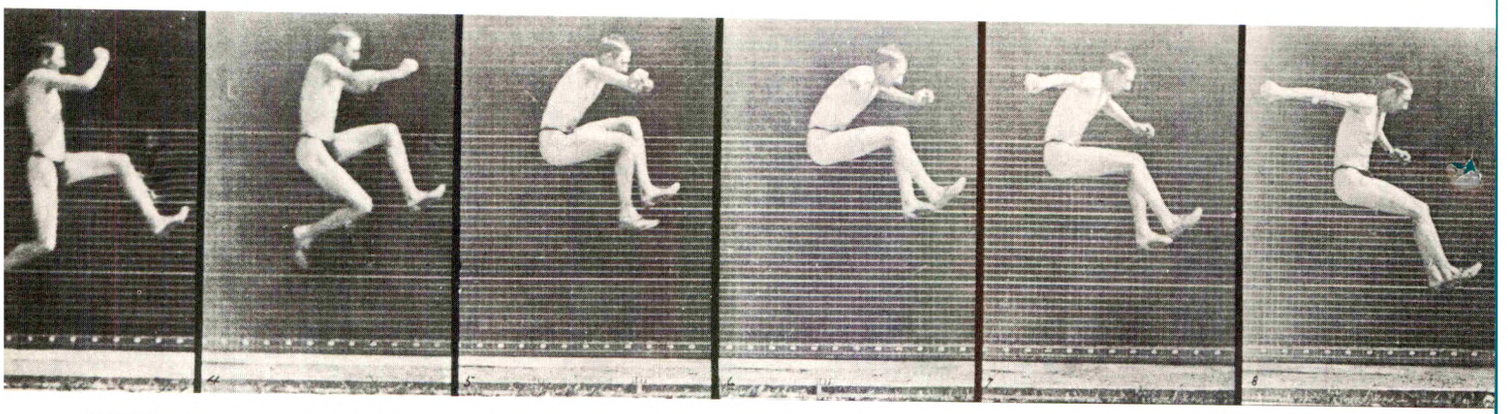
Technology & Products for State-Of-The-Art Imaging.

Since 1873, we've been a leader in advanced imaging research and technology. Today, we continue to meet your medical imaging needs by combining state-of-the-art computerized manufacturing with a strong commitment to research and development, and stringent quality control to create new, advanced medical imaging products. You can rely on us to provide sophisticated technologies in electronic imaging, automatic film processing, digital radiography systems, and the latest breakthrough in imaging film, New High Ortho Mono-Dispersed Grain Technology. At Konica we never stop working on new ideas for better imaging products. And we never will. We're Konica. We work harder for you.

Konica... The Image of Perfection, Since 1873.

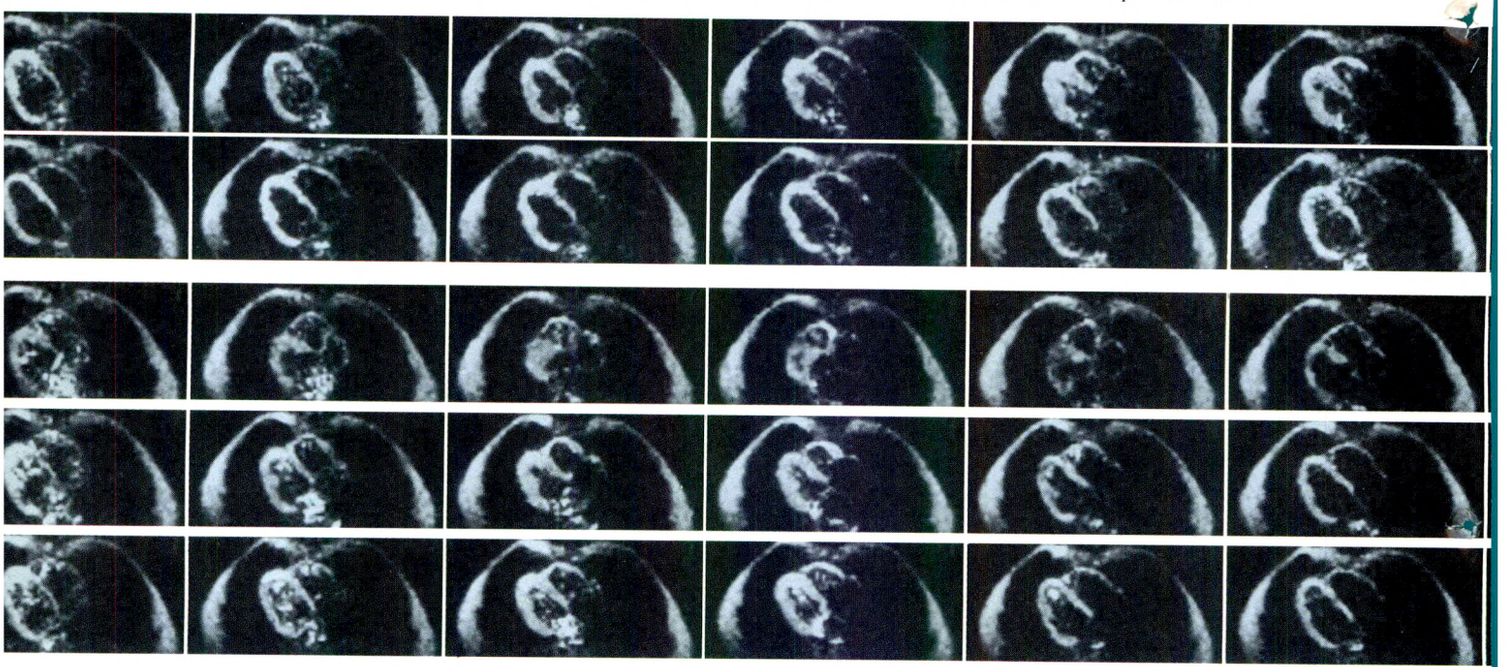
KONICA

Konica Medical Corporation
411 Newark Pompton Turnpike, Wayne, NJ 07470 (201) 633-1500

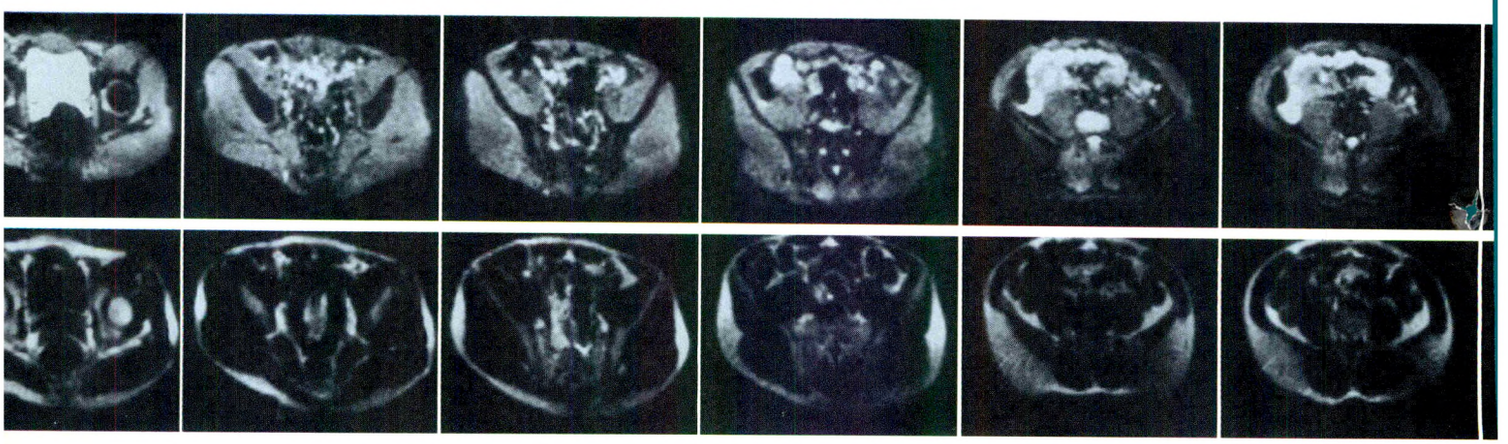


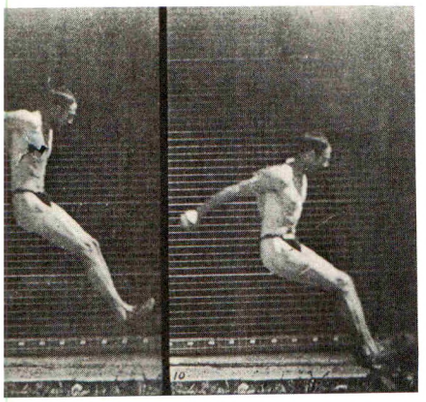
The Human Figure in Motion. "Man Performing Running Broad Jump," from Eadweard Muybridge's high-speed photographic sequence studies of the human figure in motion, first published in 1887.

The Human Heart in Motion. Top: Transaxial images from cardiac MR movie obtained through beating heart of adult human in single 16-sec. breath ho
Each instant image acquired in 1/25 second. Bottom: Single breath-hold cardiac MR movies. Three 6mm slices at sequential levels.

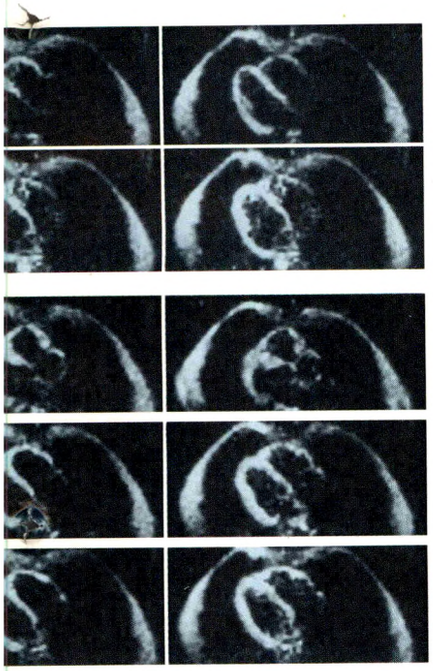


The Human Body Motion-Free. Motion artifact-free imaging of the body allows interactive definition of plane location and scan parameters.
Each 6mm slice obtained in 1/25 second. Top row: Water distribution. Bottom row: Fat distribution.



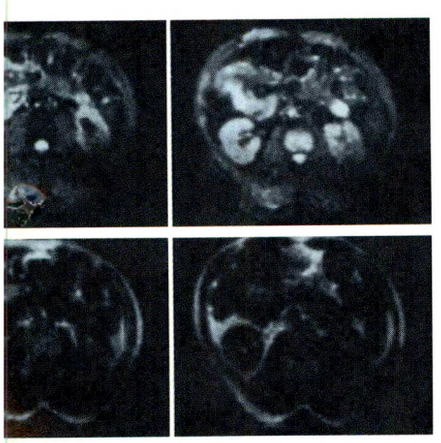


It's About Time.



Instant MR Images in 1/25 Second
Complete Cardiac Movies in One Breath Hold

Advanced NMR Systems' Instant Scan™ imaging mode produces motion artifact-free images in 1/25 second. An MR movie sequence may be obtained within one breath hold. This high speed technology significantly widens the diagnostic window in non-invasive cardiac studies and thoracic and abdominal imaging. It relegates the problem of motion artifact to history. And makes long image times a thing of the past. Patient throughput is optimized, making routine clinical use more cost-effective. If you are a clinical investigator, it's about time you looked into Advanced NMR Systems. If you are interested in a private screening of some of our short "takes," call us at (617) 938-6046 for further information.



Advanced NMR Systems, Inc.

30 Sonar Drive, Woburn, Massachusetts 01801 (617) 938-6046

Advanced NMR Systems, Inc.'s Magnetic Resonance Imaging unit is classified as an investigational device available for research applications only.

Magnetic Resonance Imaging. We're putting it in motion.
Catch our MR Movie Premiere at RSNA, Booth #5416.

You learn from your experience with

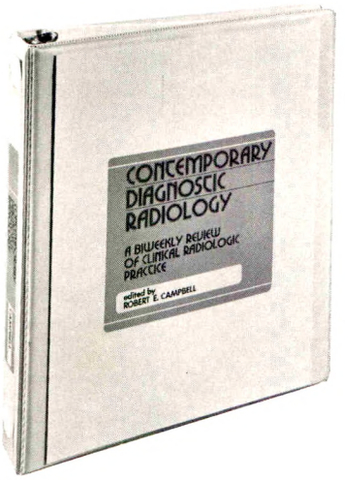
CONTEMPORARY DIAGNOSTIC RADIOLOGY

Editor: **Robert E. Campbell, M.D.**

A Biweekly Review of Clinical Radiologic Practice—26 issues a year!

One of your toughest jobs is keeping up with the many new developments that affect radiology. That's why you want **Contemporary Diagnostic Radiology**... an effective and convenient way to perfect your skills and maintain your professional status.

Contemporary Diagnostic Radiology is designed as a continuing education program that lets you work at your own pace. Every two weeks you'll receive an issue that covers a single topic or procedure in detail. Read the information and study the clearly reproduced radiographs—and then, if you choose, respond to a comprehensive examination in the strictest confidence. You set the pace.
Each biweekly lesson brings you pertinent review of the basics in bone radiology... gastrointestinal radiology... pediatric radiology... genitourinary radiology... MR imaging... and all of the topics you want to know more about.



Contemporary Diagnostic Radiology works *two ways*. You may choose to subscribe to the non-scoring version, receiving every issue as an important element of your professional reading. The scoring version, however, supplements your reading and computer-coded examinations with confidential result responses, making you eligible for Continuing Medical Education credits co-sponsored by the University of Pennsylvania School of Medicine.

"As an organization for continuing medical education, the University of Pennsylvania School of Medicine designates this continuing medical education activity as meeting the criteria for 1 credit hour per bi-weekly issue in Category I for Educational Materials for the Physician's Recognition Award of the American Medical Association provided it has been completed according to instructions."

You can begin this ongoing program **today**. **Contemporary Diagnostic Radiology** is a year-round program, so you can join at any time. To begin your lessons, just fill out the enclosed card and return it to us. Or call **FREE** 1-800-638-6423 (except from Alaska). In Maryland call **COLLECT** 528-4105. You'll find that **Contemporary Diagnostic Radiology** is the most efficient and inexpensive way to keep up with your dynamic field.

Williams & Wilkins

P.O. Box 23291
Baltimore, Maryland 21203

266 Fulham Road
London SW10 9EL England

clip & mail

CONTEMPORARY DIAGNOSTIC RADIOLOGY

☐ **Yes!** I want to keep pace in my field! Begin my 26-issue subscription:
☐ Send me the scoring version ($220)
☐ Send me the non-scoring version ($180)
☐ Send me the resident non-scoring version ($160)
(add $35 for optional air mail delivery outside the U.S.)
☐ new subscription
☐ renewal

name

address

city/state/zip

payment options
☐ payment enclosed ☐ bill me
☐ American Express ☐ MasterCard ☐ VISA

printed in USA

card # expiration date

signature/P.O. #

Maryland residents add 5% sales tax. Subscriptions outside the U.S. must be prepaid in U.S. dollars only. Rates subject to change without notice. Please allow 8 weeks for delivery of your first issue, up to 16 weeks for surface delivery outside the U.S. Optional airmail rates: add $35 per subscription.

Residents are eligible for the special in-training rate for up to three years. When requesting this rate, please include training status and institution.

Don't forget: you can order with a **FREE** phone call at 1-800-638-6423 (except from Alaska). In Maryland, call collect 528-4105.

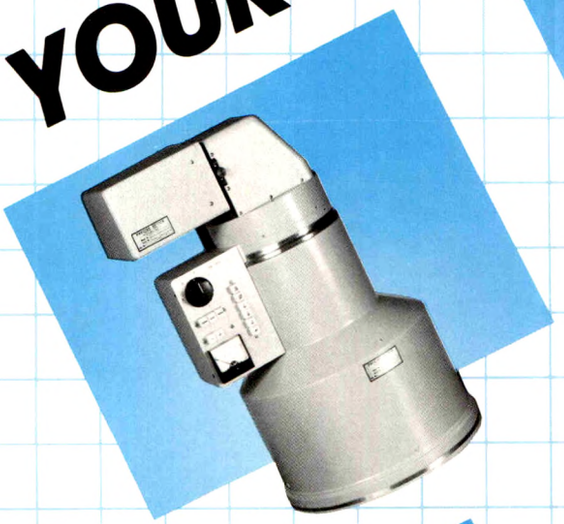
Williams & Wilkins

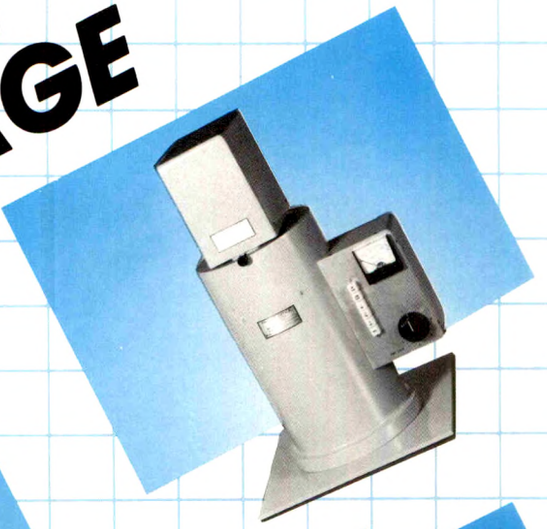
P.O. Box 23291
Baltimore, Maryland 21203

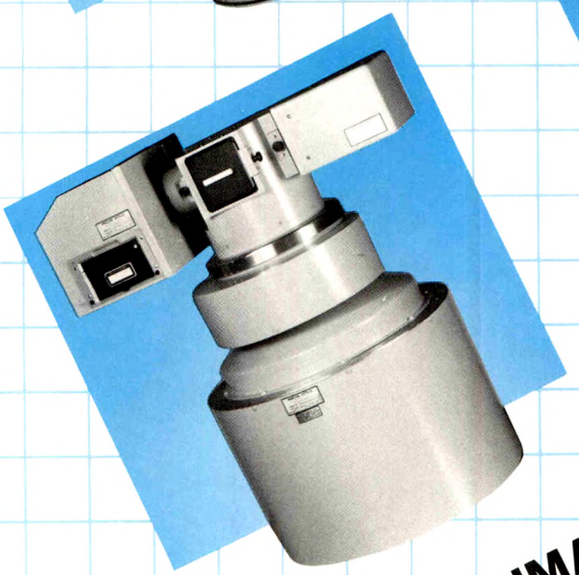
266 Fulham Road
London SW10 9EL England

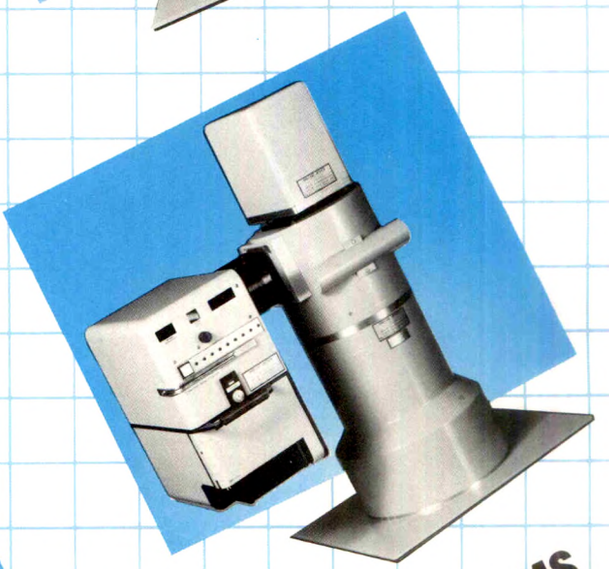
CDRAD 95191 87

IMPROVE YOUR IMAGE







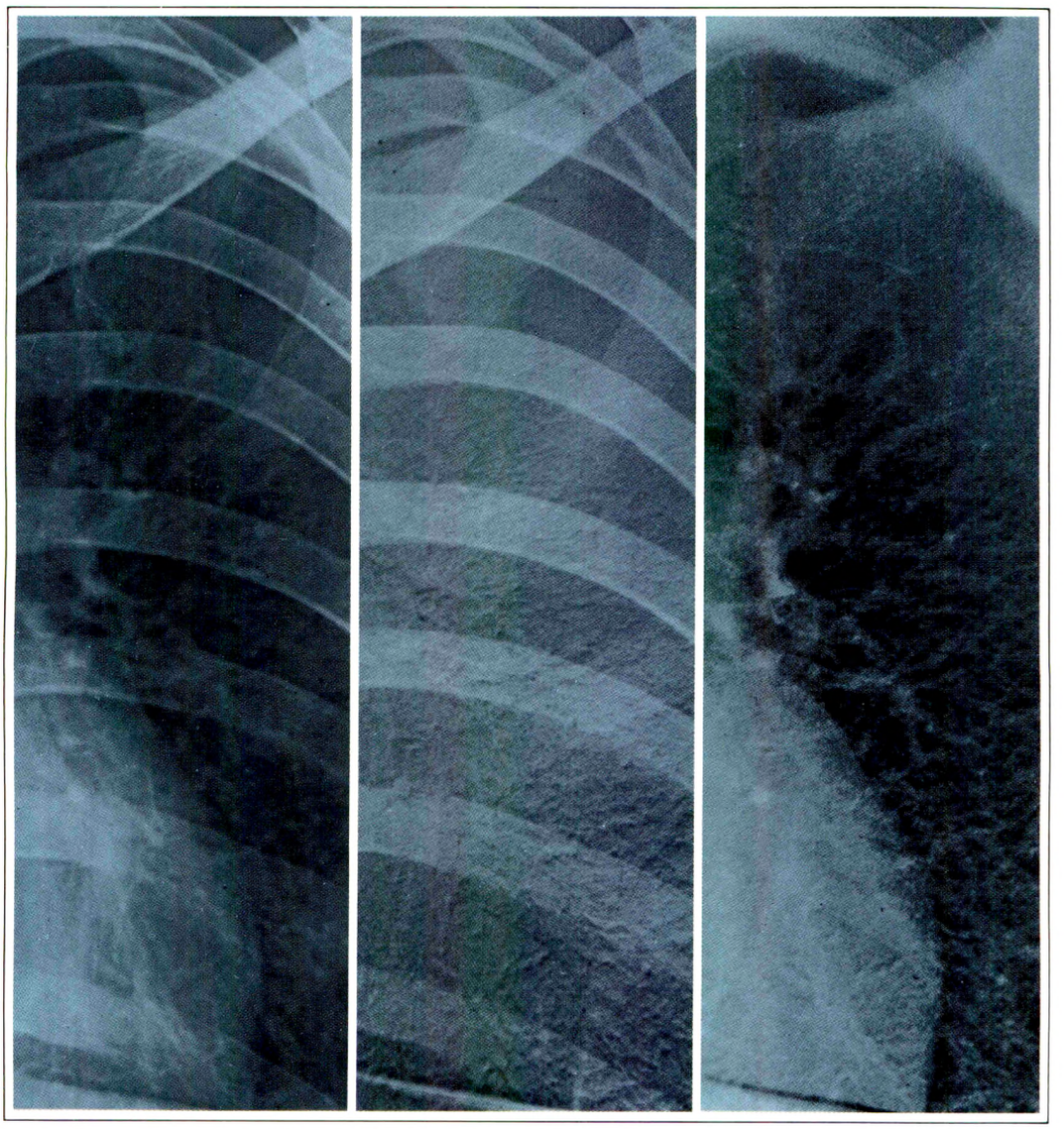


WITH PRECISE OPTICS IMAGE INTENSIFIER SYSTEMS

- The world's largest independent manufacturer of Image Intensifier Systems and components
- Over 30 years of experience in design and manufacture
- 6,9,12, and 16-Inch latest series image tubes for optimum performance
- 525/875/1023 line CCTV's, 6fps 100mm/105mm cameras
- Cost effective, versatile, reliable
- Compatible with new or existing x-ray equipment
- Extend the life of existing apparatus
- Worldwide dealer network

Precise® Optics
PHOTO MEDIC EQUIPMENT, INC.

239 South Fehr Way
Bay Shore, New York 11706
Tel.: 516 242-6600
TWX: 510-227-9837



A Philips computed radiograph acquired using stimulable phosphor technique. Left image: 60kV exposure (120kV not shown). Middle and right images: weighted, dual-energy subtractions.

"TRUTH FEARS NO TRIAL."

Thomas Fuller. M.D. 1732.

New projects in advanced development at Philips have brought the future of diagnostic imaging near enough to touch. Today, the Philips Computerized Radiography system produces radiographs of unequalled quality, requiring substantially fewer retakes and no change in conventional radiographic procedure. Tomorrow, this same system will be one major component of a digital image acquisition, storage and communications network that links physicians and radiology departments electronically. The day of high-speed access to a variety of patient images and information at remote locations is now at hand. Philips Medical Systems, Inc. Shelton, Connecticut 06484.

PHILIPS

PHILIPS

Efficient bowel evacuants for diagnostic procedures

Take one



Excellent visualization...fewer retakes

■ 95% efficacy proven with X-PREP® Liquid in 749 patients prepared for diagnostic procedures such as barium enemas and IVPs*

■ Effective for colonoscopy and sigmoidoscopy*

X-PREP® Liquid
2½ fl. oz. (74 ml) (standardized extract of senna fruit)

*Data on file, Medical Department, The Purdue Frederick Company.

Gray Pharmaceutical Co., Affiliate
The Purdue Frederick Company
Norwalk, CT 06856

X-PREP® Bowel Evacuant Kit-1
Contains two SENOKOT-S® Tablets (standardized senna concentrate and docusate sodium), one bottle of X-PREP Liquid 2½ fl. oz. (74 ml), one RECTOLAX® Suppository (bisacodyl 10 mg), plus easy-to-follow instructions.

X-PREP® Bowel Evacuant Kit-2
Contains one pack CITRALAX® Granules 1.06 oz. (effervescent citrate/sulfate of magnesia), one bottle of X-PREP Liquid 2½ fl. oz. (74 ml), one RECTOLAX Suppository, plus easy-to-follow instructions.



© 1984, Gray Pharmaceutical Co.

PFR-081/84

Leo J. Rigler Lecture

MR Imaging of the Liver

Joseph T. Ferrucci[1]

Recent technical and clinical advances in MR of the liver are reviewed with special reference to the role of MR as a primary screening technique for detection of space-occupying lesions, especially metastases. The major current problem in upper abdominal MR imaging is physiologic motions, and this appears to have been effectively solved by newly introduced pulse-sequence and timing-parameter strategies. Short-TR/TE spin-echo sequences with extensive signal averaging and heavy T1-weighting produce images with exceptional anatomic detail and liver-cancer contrast differences. With this sequence superior sensitivity for liver-cancer detection has been shown in quantitative signal-difference to noise comparisons with other pulse sequences and in clinical comparisons with CT. MR discovered 14% more individual metastases and 3% more patients with liver cancer than CT in a blinded comparative study of 142 patients undergoing both exams. MR also showed greater specificity (98%) than CT (91%) in distinguishing patients without liver metastases. Differentiation of hemangioma from metastases was possible with greater than 90% specificity by using heavily T2-weighted sequences. Use of a fast-scan, gradient-recalled echo technique can also produce good-quality, multislice, T1-weighted studies of the liver in 20 sec—a breath-hold. MR contrast agents (such as gadolinium-DTPA and reticuloendothelial-system–specific, superparamagnetic ferrite–iron-oxide particles) offer further promise for enhanced sensitivity for liver-cancer detection. When optimal pulse sequences are employed, MR can now be appropriate as a primary screening method for detecting liver neoplasms.

Despite several years of clinical experience with MR imaging, very few meaningful clinical applications for liver and upper abdominal disorders have appeared. The two factors limiting wide use of MR in the upper abdomen are (1) image artifacts due to various biological motions and (2) the lack of a suitable bowel contrast agent. Because of this delay and the critical importance of liver imaging to the general use of MR in the abdomen, considerable research is now focused on these two problems. Our efforts at Massachusetts General Hospital over the last 2–3 years have been directed mainly toward an in-depth study of MR in liver cancer. This review summarizes recent technical and clinical developments from the literature, as well as our laboratory and patient experience.

According to American Cancer Society statistics [1], nearly two million individuals annually are at risk of having liver metastases. Furthermore, with the introduction of aggressive extirpative surgical procedures, many patients now undergo extensive multisegmental hepatic resections in an attempt to cure demonstrated liver metastases, especially from colon primaries [2, 3]. Thus, in addition to merely detecting the existence of liver metastases in an all-or-none fashion, the more precise question of defining the extent of disease (i.e., the number and location of metastatic foci) becomes germane.

Currently, CT is the accepted gold standard for liver imaging, primarily because of its ability to show liver metastases with greater sensitivity and specificity than either sonography or radionuclide scanning [4]. Despite the apparent utility of MR in selected hepatic disorders such as hemochromatosis, portal hypertension, or

Received August 7, 1986; accepted after revision September 15, 1986.

This work was supported in part by Advanced Magnetics, Inc. (Cambridge, MA), Berlex Laboratories (Cedar Knolls, NJ), and Technicare Corp. (Solon, OH).

[1] Department of Radiology, Massachusetts General Hospital, Boston, MA 02114. Address reprint requests to J. T. Ferrucci.

***AJR* 147:1103–1116, December 1986**
0361–803X/86/1476–1103
© American Roentgen Ray Society

the Budd-Chiari syndrome, the practical question is whether MR can be effective as a primary screening technique for liver-cancer detection, especially metastasis.

The liver is indeed a fertile field for radiologic investigation because of its homogeneous parenchymal texture, dual blood supply, and varied physiologic and biochemical functions. A reflection of this complexity is the long and tortuous evolution that CT liver imaging has undergone with regard to the optimal use of iodinated contrast material. MR image formation is an order of magnitude more complicated than CT by virtue of the number of intrinsic and extrinsic factors independently influencing image contrast. These include native tissue characteristics such as proton spin density, T1 and T2 relaxation times, chemical shift, flow, diffusion, and magnetic susceptibility. Among the extrinsic factors are operator-selected instrument-pulse sequences, timing parameters, and paramagnetic MR contrast agents.

Despite its recognized potential, until recently published reports on the use of MR for detection of liver lesions have been infrequent and generally pessimistic [5, 6]. However, our current conviction is that with appropriate techniques, MR already possesses sufficient sensitivity and specificity (at least in our institution) to displace CT as the primary screening method for liver disease.

Strategies for Motion Reduction

The principal technical limitation on current acceptance of MR for imaging the liver and upper abdomen is image artifacts produced by physiologic movements, especially respiratory motions, cardiac and aortic pulsations, and intestinal peristalsis. The need for satisfactory solutions to these problems has been even further heightened by the unexpected and as yet unexplained tendency of high-field-strength systems to aggravate motion artifacts. Principal approaches to motion reduction have included (1) respiratory gating or respiratory software compensation; (2) fast imaging sequences; and (3) signal averaging.

Respirations cause two types of artifacts: (1) ghosting, usually ascribed to high signal from moving subcutaneous fat, which propagates periodically along the phase-encoding axis, and (2) imaging blurring. Direct respiratory gating has been generally abandoned as disappointing and impractical. Unlike cardiac gating, which is simplified by the availability of an electronic trigger (the ECG R wave), respiratory gating is much more difficult to implement because of the requirement for a mechanical hardware-linkage to convert chest-wall motion into an electrical signal. Furthermore, respiratory motion is neither periodic nor constant in amplitude, and thus only imperfect synchronization for data acquisition is possible. This is usually achieved only by rejecting data from unwanted portions of the respiratory cycle (i.e., data collection occurs only at end-expiration). Although this reduces motion artifacts, a significant time penalty is incurred in direct proportion to the fractional time of the respiratory cycle excluded [7, 8]. Not only does this result in an unacceptable 200% increase in imaging time, but also it fails to reduce other motion artifacts arising from cardiovascular pulsations and bowel peristalsis.

Respiratory-compensation software programs that seek to reduce the time penalty are being developed by several manufacturers. Bailes et al. (9], working with Picker International in England, described a method for data collection that uses preliminary monitoring of the breathing cycle to select the proper phase-encoding direction. The technique is termed respiratory-ordered phase encoding (ROPE), and a new version with multislice and multiaveraging (called COPE) is also under development. General Electric employs a similar software package (Exorcist). However, we believe the clinical role of these complex software compensation techniques is likely to be overshadowed by the rapidly accelerating evolution of fast scanning techniques.

The fast-scan approach involves extremely rapid data-acquisition sequences, often within a single breath-hold. A variety of different strategies are being examined by different manufacturers, including partial-saturation, gradient-recalled echo or FLASH (fast low-angle shot); echo-planar; driven-equilibrium; and half-Fourier scanning techniques.

The principles of partial-saturation fast imaging were recently described by Bydder and Young [10]. Haase et al. [11] have also recently detailed their FLASH technique. Partial-saturation, gradient-echo techniques differ from spin-echo sequences in the lack of a 180° refocusing pulse, tip angles less than 90°, and short repetition times (TR = 100–200 msec) and echo-delay times (TE = 8–30 msec). As a result, 11 slices (each 0.9 cm thick) can be obtained within 20 sec (i.e., within a single breath-hold). A complete multislice, T1-weighted survey of the liver, for example, can be obtained with images ready for viewing in 3–4 min. Although resultant images display somewhat less signal-to-noise ratio (SNR) than conventional spin-echo acquisitions and are more sensitive to vascular-flow artifacts, adequate T1-weighted images can usually be obtained. T2 images are presently of only marginal diagnostic quality. With total examination times potentially reduced fivefold compared with conventional studies, throughput advantages are obvious. As initially reported by Edelman et al. [12], we have now examined more than 90 patients with a variety of abdominal and liver disorders using the suspended-respiration, gradient-echo breath-hold technique. We consider that lesion conspicuity and anatomic detail are frequently of diagnostic quality even at this early stage. Undoubtedly, further improvements will ensue. Illustrative examples are shown in Figures 1 and 2.

The third major technique for reducing motion artifacts is signal averaging. Motion artifacts in MR images are not random; they occur when phase-encoding errors cause spatial misregistration of signal acquired from moving structures. Because of the periodicity of these effects, they are influenced by the ratio between pulse-sequence repetition time and respiratory cycle (i.e., they are coherent artifacts and can be reduced by averaging multiple data sets). Work in our department with a Technicare 0.6-T (Teslacon) system has permitted adaptation of short pulse-sequence timing parameters to allow averaging of a large number of data acquisitions without the need for gating or prolongation of imaging time. Stark et al. [13] have shown that use of multiple signal averages produces dramatic reductions in image noise and

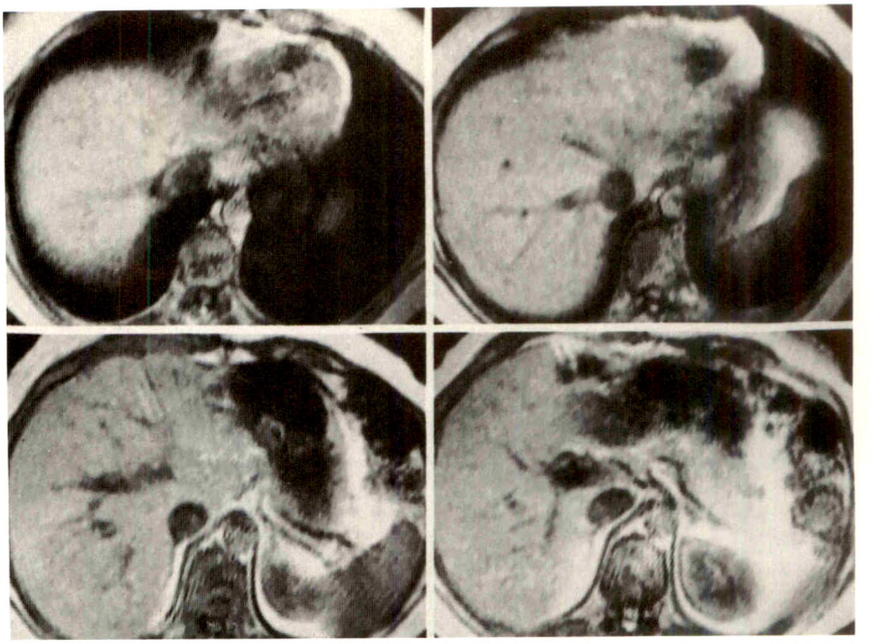


Fig. 1.—Gradient-recalled echo (partial-saturation) technique. Normal liver. T1-weighted sequence. Number of slices = 4 (contiguous), slice thickness = 1.2 cm, number of phase-encoding steps (Y lines) = 96, TR = 200 msec, TE = 11 msec, number of excitations = 1, total acquisition time = 20 sec. Images are slightly noisy, but there is adequate anatomic resolution of major intrahepatic vessels, diaphragmatic crura, and surface contours of liver, spleen, and kidney.

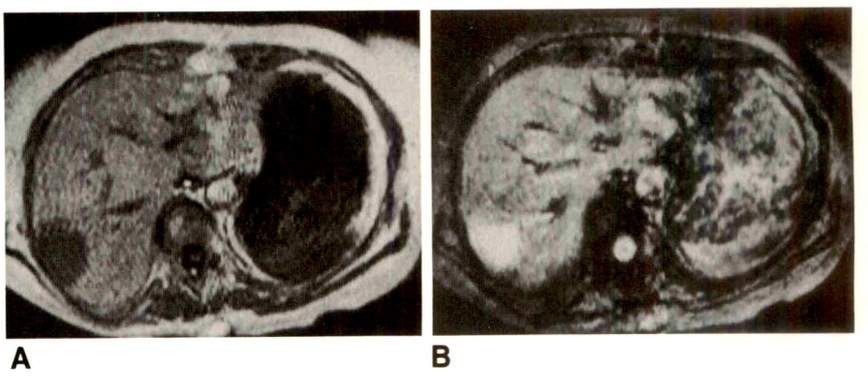


Fig. 2.—Gradient-recalled echo (partial-saturation) sequence of angiographically proven hepatic hemangioma.

***A*, T1-weighted image. Number of slices = 11, slice thickness = 1.2 cm, TR = 200 msec, TE = 11 msec, number of excitations = 1, acquisition time = 20 sec. Note well-seen typical long-T1 hemangioma. Some "corduroy" motion artifact is seen in right hepatic lobe and aortic ghosting in left hepatic lobe.**

***B*, T2-weighted image. Number of slices = 4, slice thickness = 1.5 cm, TR = 200 msec, TE = 30 msec, acquisition time = 20 sec. Note noise-degraded T2-weighted image. T2 contrast on gradient-recalled echo sequences is complicated combination of phase contrast and T2* differences. Nevertheless, the lesion is clearly visible.**

motion artifacts of all types, including cardiovascular pulsations. The result is strikingly improved anatomic resolution for imaging of the liver and upper abdomen (Fig. 3). Further explanation of the physical and theoretical principles of this technique and its application in clinical liver imaging with existing systems is a major focus of this review.

Short TR/TE, T1-Weighted, Spin-Echo Imaging

Extensive signal averaging to reduce biological motion artifacts requires availability of recently improved gradient and pulse-sequence software to expand the range of available timing parameters (TR, TE, and TI). The ability to reduce TR to 250–300 msec and TE to 14–20 msec creates synergistic effects that are beneficial to upper abdominal and liver imaging. First, the relationship between total-acquisition (scan) time, phase-encoding steps (Y lines), number of excitations (NEX), and TR is represented by the following equation [14]: Scan time = (Y lines) × (NEX) × (TR).

Shortening the TR allows more acquisitions to be obtained within a given imaging time. It is this additional data averaging that compensates for motion artifacts. Second, reduction in TE complements short TR by reducing signal loss due to dephasing of protons and thus preserving high SNR and anatomic resolution. Third, short TE reduces the contribution of T2-weighted contrast information, thereby preserving the overall T1-weighting. This is particularly noteworthy when compared with SE sequences formerly described as T1-weighted (i.e., SE 500/30). Fourth, shortened TE allows multislice capability according to the expression [15]: Number of sections = TR/(TE + constant). For example, 12 slices = 260 msec/(15 msec + 6 msec). The 6-msec "constant" is a pulse-sequence timing parameter related to gradient performance. This timing parameter varies widely among different imaging systems and may vary between pulse sequences on an individual system. This formula has considerable practical importance. More slices can be obtained with larger TR values or decreased TE values. For example, the entire liver span (a

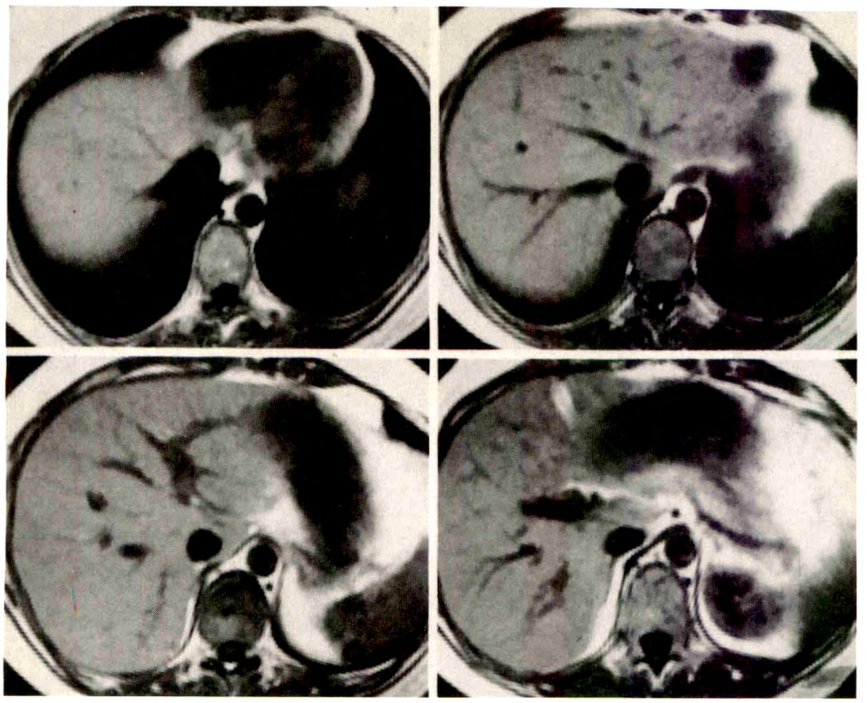


Fig. 3.—Short TR/TE (TR = 300 msec, TE = 14 msec), heavily T1-weighted spin-echo images. Normal liver. Same patient as in Fig. 1, four contiguous sections. TR = 300 msec, TE = 14 msec, number of excitations = 10, No. of slices = 13, acquisition time = 10.5 min. Signal averaging produces striking anatomic detail. No respiratory gating.

15–18 cm cranial-to-caudad distance) can be covered with a multislice technique that uses 1.5-cm slices.

This short-TR/TE, heavily T1-weighted, spin-echo technique (TR = 260–300 msec, TE = 14–20 msec), averaging 10–18 data acquisitions for a scan time of 10 min, has become our routine T1 sequence for screening for focal liver lesions. Indeed, inversion recovery sequences, the classic T1-weighted sequences, have essentially been abandoned in our department because of the well-known prolonged duration of scan time that is needed to complete the required number of slices.

Reduction in TE to less than 20 msec is the critical instrument parameter in this technique but to date has been available in only a few installed Technicare 0.6-T systems. The likelihood of similar software refinements for existing systems is presently unknown.

Image Contrast for Liver-Cancer Detection

Most solid tumors possess increased intracellular water and therefore show prolongation of T1 relaxation (spin-lattice) giving lesion blackening on T1-weighted images and prolongation of T2 relaxation (spin-spin) giving lesion brightening on T2-weighted images [16–18]. The prolonged relaxation times of neoplastic tissue set against the intrinsically short T1 and T2 values of normal liver parenchyma create good potential for striking tissue contrast on heavily T1-weighted images. Indeed, Moss et al. [19] showed a 40% prolongation in tumor T1 over normal liver but only a 26% prolongation of tumor T2 relaxation times. These data suggest the likelihood for greater exploitation of tissue-pair contrast differences by relying on T1-weighted information. The ability of short-TR/TE, spin-echo, T1-weighted imaging to benefit from this inherent tumor-liver contrast is illustrated in Figure 4.

Theoretical predictions from pulse-sequence performance considerations also suggest better contrast-to-noise ratios and therefore better cancer-liver discrimination from short-TR/TE spin-echo techniques [20, 21]. This advantage is confirmed by our clinical experience as well. For example, in a quantitative comparison of cancer-liver contrast-to-noise differences that we performed in 43 patients with liver metastases, Stark et al. [13] found short-TR/TE sequences (TR = 260 msec, TE = 18 msec) superior to 13 other standard and special pulse sequences (Table 1).

Many published reports on MR for liver tumors have been limited by system-selectable parameters restricted to the SE 500/30 pulse sequence for T1 information [19, 22–24]. This sequence in fact gives an offsetting balance of T1 and T2 contrast effects that often result in low ratios of image signal-difference to noise and poor lesion conspicuity (Fig. 5). In other reports on liver-cancer detection, T1 contrast was available mainly via inversion recovery, which inconveniently increased scan time and image noise [25]. As a result, most early published series emphasized the value of T2-weighted sequences for detection of liver metastases because of the high (bright tumor signal) contrast achieved [19, 22–24]. For clinical purposes we, nevertheless, advocate use of both T1- and T2-weighted sequences for liver imaging, because T2-weighted information provides confirmation of lesion detection and is particularly useful for tissue characterization and differential diagnosis of space-occupying lesions (discussed in a later section).

MR Detection of Liver Metastases: Comparison with CT

At present CT remains the accepted standard method for detection and staging of liver cancer, because recent careful series comparing MR with CT have shown no significant advantage to use of MR [24, 25]. Heiken et al. found no benefit of MR over CT in a study of 50 patients with hepatic metastases in which inversion recovery was used for T1 information and spin-echo sequences were used for T2 information. Therefore, CT was preferred as the screening test for hepatic metastases by virtue of its lower cost, better spatial resolution, and shorter imaging time. Glazer et al. [24] also found CT superior to MR in 27 patients with focal lesions, although their T1-weighted data were limited to an SE 500/30 sequence. Small lesions (<2 cm) were also much better shown with CT in this series. Demas et al. [22], however, gave an early indication of the sensitivity of MR by describing a group of eight patients in whom MR disclosed liver metastases when CT scans were negative. In two patients CT scans were of poor technical quality because of streak artifacts, and in the remaining six patients, CT scan quality was deemed acceptable.

The possibility that CT could be fallible in detecting liver metastases was recently highlighted in a meticulous study by Freeny et al. [26]. Despite use of state-of-the-art dynamic bolus-enhanced CT of the liver in staging colorectal carcinoma, 27% of liver metastases confirmed at surgery went undiscovered by CT. This surprisingly high false-negative CT result was considered more representative of the truth than earlier series (reporting 90–95% accuracy) in which "negative" CT scans were not accurately assessed by immediate exploratory surgery to determine the true miss rate.

On the basis of clinical results in more than 500 patients studied during the past 18 months, we find a clear advantage to heavily T1-weighted, short-TR/TE, spin-echo sequences in detection of liver metastases. More particularly, we performed a blinded retrospective comparison of CT and MR in 142

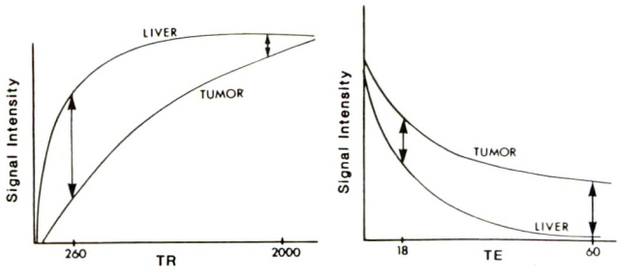


Fig. 4.—Origin of liver-tumor contrast enhancement obtained with short-TR/TE, heavily T1-weighted, spin-echo sequences. Inherently short T1 and T2 relaxation times of normal liver parenchyma compared with prolonged T1 and T2 values in malignant tumors is readily exploited by shortening both TR and TE.

***Left*, Short TR maximizes T1 contrast differences because shorter T1 time of normal liver allows quicker recovery of magnetization (i.e., signal intensity). Longer T1 of tumors does not allow recovery of signal intensity as promptly, resulting in darker signal from tumor. Much greater net tumor-liver contrast difference occurs at short TR than at long TR.**

***Right*, At very short TE values, differential signal loss between tumor and liver is minimal compared with the signal loss differences (i.e., tumor-liver contrast difference at long TEs). Thus, overall contribution of T2 contrast is minimized with short TEs, and overall image information is therefore heavily T1-weighted.**

TABLE 1: **Quantitative Pulse-Sequence Performance in Hepatic Metastases: Cancer-Liver Contrast-to-Noise Ratio**

Pulse Sequence	No. of Patients	C/N Magnitude	Rank Order of C/N Performance
SE 1500/30	7	1.9	14
SE 1500/60	7	3.5	12
SE 1500/90	6	5.5	9
SE 2000/30	27	2.4	13
SE 2000/60	33	4.7	10
SE 2000/90	27	7.5	5
SE 2000/120	5	7.7	4
SE 2000/180	4	4.2	11
IR 1500/450/30	33	6.2	8
IR 1500/450/18	35	7.9	3
IR 1500/280/18	30	7.2	6
SE 500/30	37	6.4	7
SE 260/30	32	8.1	2
SE 260/18	39	10.3	1

Note.—SE = spin echo; C/N = contrast to noise. Pulse sequence numbers are TR/TE or TR/TE/TI (all in msec). Data corrected to a standard 9-min scan time. The SE 260/18 (rank 1) pulse sequence yielded C/N ratios significantly greater than all other sequences. Modified with permission from Stark et al. [13].

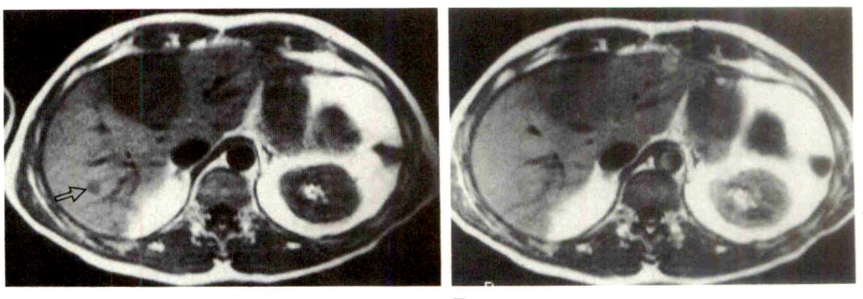


Fig. 5.—Advantage of heavily T1-weighted, short-TR/TE, spin-echo sequence (*A*) (TR = 260 msec, TE = 18 msec) compared with conventional, T1-weighted, spin-echo sequence (*B*) (TR = 500 msec, TE = 30 msec). Note sharper definition of hepatic vessels and large metastatic lesion in ventral portion of left hepatic lobe. Smaller lesion in posterior portion of right hepatic lobe (*arrow*) is seen only on short-TR/TE sequence.

patients to compare their relative sensitivity and specificity. The study group included 64 patients with known or suspected liver metastases, 31 with normal liver CT scans, 20 volunteers with normal MR images, and 27 patients with typical hepatic cysts or hemangiomas. MR imaging was performed on a 0.6-T Technicare (Teslacon) system by using inversion recovery, and both heavily T1-weighted and heavily T2-weighted spin-echo sequences. CT scans were obtained with a variety of techniques including noncontrast (14%), rapid drip-infusion (74%), and bolus techniques (12%), but no attempt was made to compare specific CT contrast techniques as separate variables.

In the first phase of a three-part analysis, separate MR and CT sequences were retrospectively reviewed in a blinded fashion by three radiologists. In the second, still-blinded phase of the study, all MR sequences for an indiviudal patient were combined and the entire examination read by each radiologist. Because there was no surgical proof available to confirm most individual metastatic lesions, we conducted a final third unblinded stage, in which the entire MR examination and the CT scans were read concurrently in a group review. An effort was made to obtain a final consensus on the image findings and clinical pathologic correlation from any available clinical details in the medical record.

The results of these studies are being reported in greater detail elsewhere. Preliminary analysis of data from the first 125 patients indicates a definite gain in accuracy with MR. MR had a sensitivity of 68% for detection of individual metastases, as opposed to a 54% sensitivity for CT. MR sensitivity for identifying individual patients who did or did not have liver cancer was 87%, as opposed to 84% for CT. Although the overall ability of MR to globally discriminate normal from tumor-bearing liver was not statistically better than CT, its 14% greater sensitivity for lesion detection was statistically significant. This increased sensitivity is clearly valuable for those patients in whom knowledge of the number and location

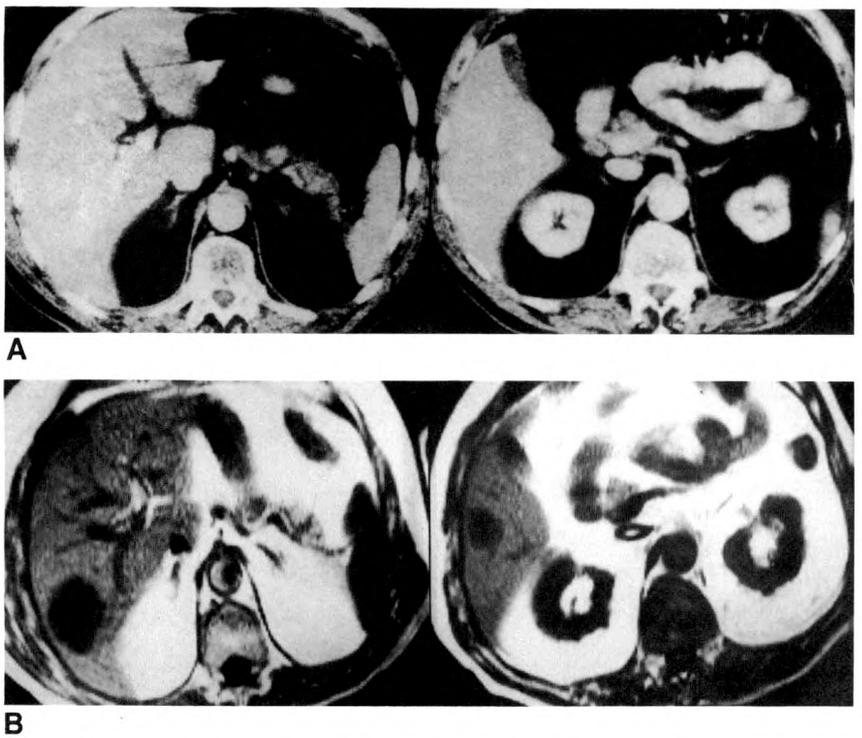


Fig. 6.—False-negative CT, and true-positive MR. Two separate metastatic lesions from colon primary are seen in inferior portion of right hepatic lobe.

***A*, Bolus-enhanced CT scan showing no abnormality on two adjacent sections.**

***B*, T1-weighted, short-TR/TE, spin-echo sequence, two comparable sections showing two typical long-T1 metastatic deposits.**

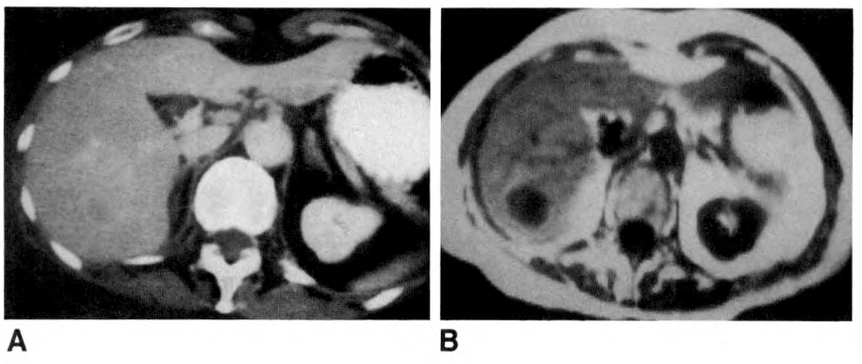


Fig. 7.—Negative/equivocal bolus CT scan with obvious positive MR for right hepatic lobe metastatic deposit. Breast primary.

***A*, CT scan was considered equivocal in right hepatic lobe for metastatic disease.**

***B*, Obvious 2–3 cm lesion in right hepatic lobe on short-TR/TE spin-echo sequence.**

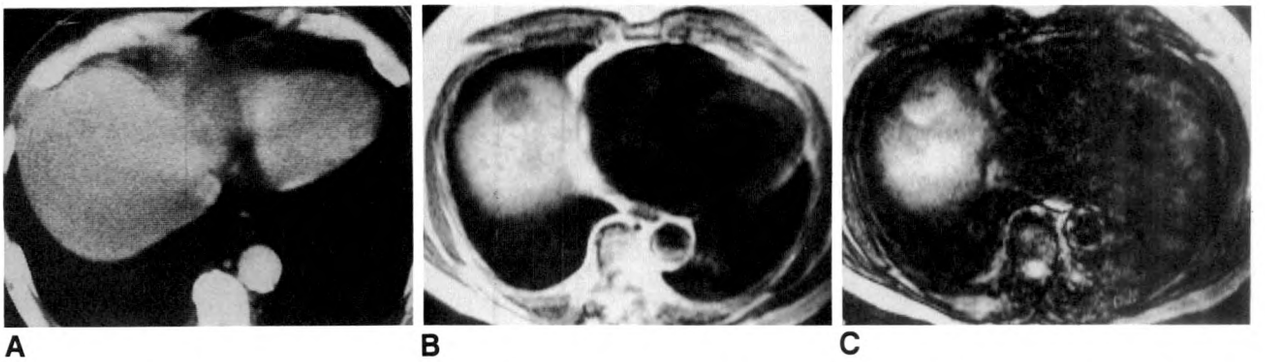


Fig. 8.—False-negative CT at dome of diaphragm. Colon primary.
***A*, Contrast-enhanced CT interpreted as negative.**
***B* and *C*, T1-weighted and T2-weighted (*C*) spin-echo sequences showing obvious lesion at anterior margin of liver. A second, less clearly defined lesion (partial volume) is apparent more medially and posteriorly.**

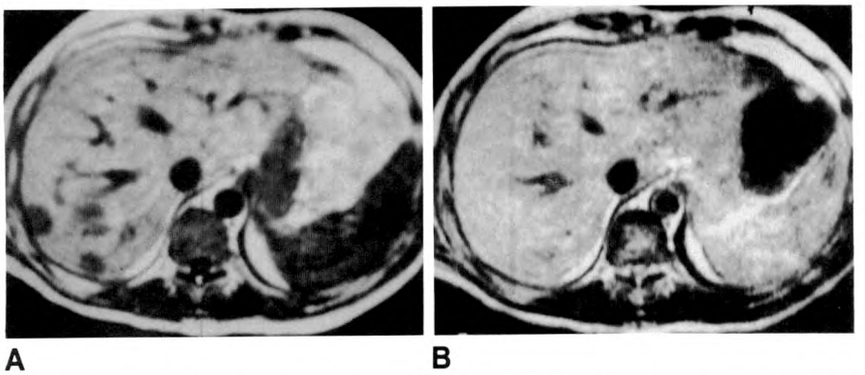


Fig. 9.—Variation in tumor signal intensity with pulse sequence may allow masking or obscuration of lesions especially on first-echo, T2-weighted, spin-echo sequences. Three 1–2 cm metastatic colon deposits in posterior portion of right hepatic lobe.
***A*, Short-TR/TE sequence (TR = 260 msec, TE = 18 msec) shows two clearly demarcated lesions at periphery of posterior right hepatic lobe with a third, more ventral, lesion less clearly seen.**
***B*, T2-weighted spin-echo sequence (TR = 2000 mec, TE = 60 msec) shows complete obscuration of all three lesions.**

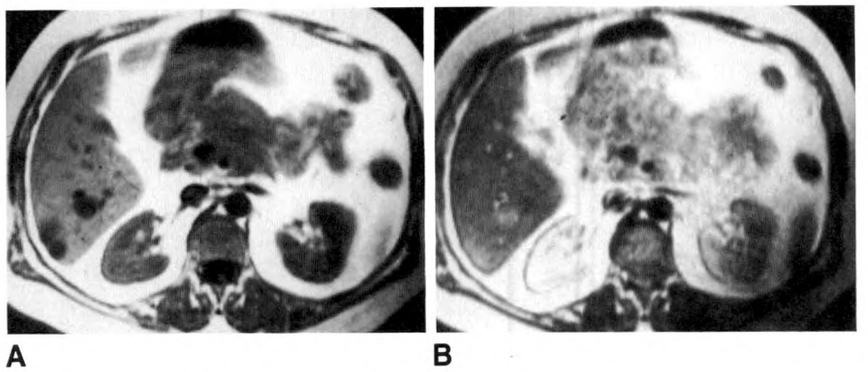


Fig. 10.—Another example of metastatic disease from pancreatic cancer obscured and blurred on first-echo, T2-weighted, spin-echo sequence. Cluster of three lesions from colon primary at tip of right hepatic lobe. Primary tumor can be seen in head of pancreas.
***A*, SE 260/18.**
***B*, SE 2000/60.**

of metastases could affect planned hepatic resections (i.e., colon metastases). MR was also less likely to give false positives, with a specificity of 98% vs 91% for CT. Also, for 10–12 patients with one or more metastatic lesions and negative or equivocal CT scans, MR showed conspicuous evidence of liver metastases [Figs. 6 and 7]. However, in only one patient were lesions seen on CT that were not visible on MR. MR was especially likely to reveal focal lesions in the dome of the liver, where CT detail was blurred because of cardiorespiratory motion (Fig. 8).

In a direct comparison of the sensitivity of individual pulse sequences for the presence of liver lesions, the short-TR/TE sequence proved superior to both first- and second-echo, T2-weighted, spin-echo sequences (69% vs 40% and 45%, respectively). As expected, tumor signal intensity varied greatly with pulse sequence. On the first echo (TE = 60 msec) of T2-weighted spin-echo sequences, the tumor often became isointense with normal liver (Figs. 9 and 10), or typical rounded-appearing lesions seen on heavily T1-weighted sequences acquired a blurred or geographic appearance and appeared larger in size. These changes are believed due to perifocal edema.

Cases in which numerous (>20) individual lesions were present were qualitatively graded, and the superior tissue contrast inherent in the MR signal was often evident on both heavily T1-weighted and heavily T2-weighted spin-echo sequences when compared with CT.

A potential criticism of our case material could be the

infrequent use of rapid, mechanically delivered, high-dose contrast injection combined with dynamic CT techniques (use did increase late in the study period). However, clinical practice across the nation does not uniformly use that technically demanding approach, and therefore our results more likely reflect the community standard. Moreover, perhaps the appropriate comparisons of MR and CT are yet to be made. For example, with the anticipated introduction of MR contrast agents for the liver such as gadolinium-DTPA, the validity of comparisons between enhanced-CT and unenhanced-MR techniques is questionable. If it is proper to compare unenhanced MR with dynamic bolus-enhanced CT, will it eventually be more proper to compare enhanced CT with gadolinium-DTPA–enhanced MR? As in the case of dynamic bolus CT, what percentage added yield in accuracy will justify the cost and risk of using contrast material in MR imaging?

MR Features of Liver Cancer

Morphologically, primary and metastatic liver cancers are generally indistinguishable from each other, although occasional suggestive MR imaging features are now being described. In the specific case of solid liver tumors, Moss et al. [19] were unable to record any specific T1 and T2 values among primary or metastatic tumors, among different primary tumor types, among similar tumor types in different patients, or among different regions of the same tumor nodule. These variations in T1 and T2 values were attributed to varying degrees of cellularity, hemorrhage, perfusion, and necrosis, as well as variations in normal tissue measurements. Overlapping morphologic patterns of contour sharpness, size, location, and local vascular displacement are also common.

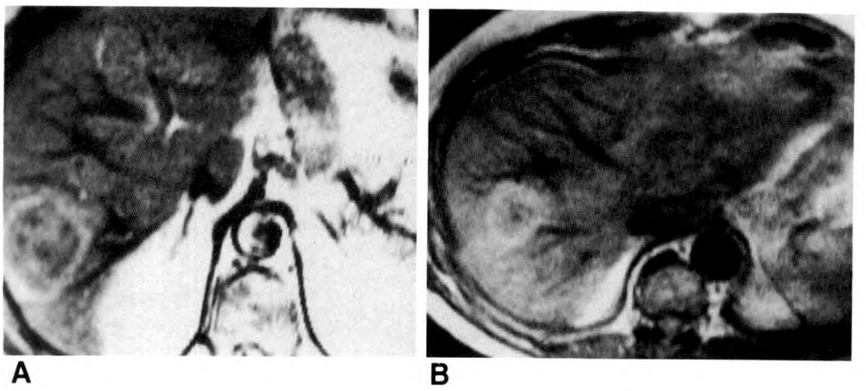
As in other organs, signal intensity of tumors in the liver varies with pulse sequence, becoming darker on T1-weighted and brighter on T2-weighted sequences and often isointense on balanced sequences. In our experience the most diagnostic finding in metastatic disease is a bright peripheral halo surrounding a low-density or isointense nodule on first- or second-echo delay T2-weighted sequences (Fig. 11). In our analysis of patients with proven metastatic liver cancer, this characteristic peripheral halo was present in approximately one-fourth of metastatic lesions, and was never observed in benign lesions such as cysts or hemangiomas. Although the exact cause of the halo is unknown, it is believed to reflect microscopic peritumoral edema. However, in primary hepatomas, a distinctive low-density peripheral rim may surround the tumor on T1-weighted images. In a study from Japan, Ebara et al. [27] found such a rim in 43% of cases and histologically confirmed its fibrous pseudocapsule origin. Occasional hepatomas also showed central steatosis within the tumor, giving short T1 values. In focal nodular hyperplasia, the characteristic stellate collagenous scar has also been observed by MR [28].

Other morphologic features of liver cancer are less common and less specific. With longer-echo-delay T2 sequences, solid tumors show gradual loss of hyperintensity and margin sharpness due to deteriorating SNR and the effects of respiratory motion. Tumors with central liquefaction necrosis or rich vascularization acquire characteristics of fluids and may show varying degrees of homogeneous persistence of bright signal on late-echo images. Such cases may mimic hemangiomas or cysts.

Differential Diagnosis: Tissue Characterization

Because as much as 10% of the adult population possesses either a benign hepatic hemangioma or simple liver cyst, MR screening for liver cancer will require at least some tissue specificity to be useful clinically. Because nearly all diseases cause prolongation of both T1 and T2 relaxation times in a nonspecific manner, ability to differentiate benign from malignant lesions has been limited. In particular, on T1-weighted screening sequences all space-occupying liver lesions (tumor, abscess, hemangioma, cyst) give a similar low-signal, dark appearance with few identifying features.

Cavernous hemangiomas present a particular problem in differential diagnosis from tumor because of their frequent incidental discovery as a solid focal lesion on routine sonography or CT. About 20% of hemangiomas lack the typical dense, hyperechoic, through-transmitting appearance on sonography. Even bolus-enhanced CT, the usual definitive noninvasive test, gives atypical results in 48% of cases if modern



A B

Fig. 11.—Typical bright signal peripheral halo surrounding metastatic colon carcinoma in right hepatic lobe. *A* and *B* are two different patients. This appearance occurred in approximately one-fourth of proven metastatic lesions and is best seen on first-echo (TE = 60 msec) or second-echo (TE = 120 msec) delay T2-weighted sequences. It is presumed to reflect perilesional inflammatory edema.

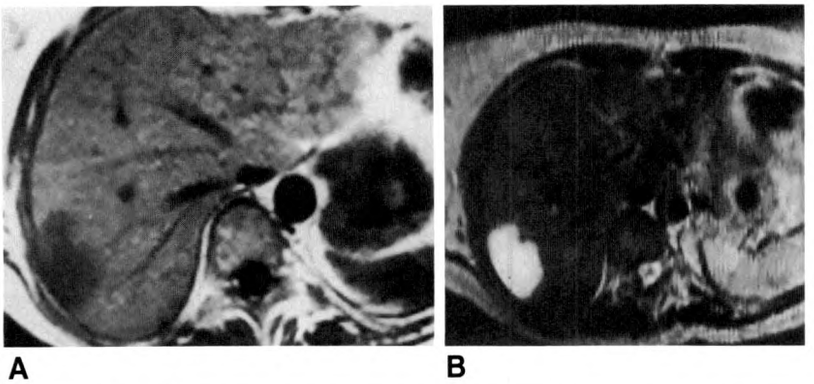


Fig. 12.—Hepatic hemangioma.
A, Short-TR/TE spin-echo sequence.
B, Heavily T2-weighted, second-echo, spin-echo image (TE = 120 msec). Single, intensely bright, homogeneous, long-T2 lesion. Characteristic appearance in periphery of right posterior hepatic lobe in subcapsular area.



Fig. 13.—Hepatic hemangioma. First-echo (*A*), second-echo (*B*), third-echo (*C*) delay spin-echo images (TE = 60, 120, 180 msec, repectively). Bright-signal hemangioma persists in homogeneous brightness despite increasing image noise. Metastatic lesions fill in and lose definition with longer echo delays.

strict criteria are applied [29]. Similarly, radionuclide blood-pool scanning is useful only in lesions exceeding 3 cm in diameter.

Recently, however, heavily T2-weighted spin-echo pulse sequences reflecting the presence of slowly flowing blood within the lesion have been found by several groups to give a highly reliable MR appearance [30–33]. Morphologically, hemangiomas most often appear as rounded, subcapsular, sharply marginated, homogeneously bright signal lesions on T2-weighted sequences (Fig. 12). Typically, and in contradistinction to solid cancers, the homogeneous, dense, bright signal and sharp margins persist on heavily T2-weighted delayed-echo images, whereas tumors fill in and become blurred (Fig. 13).

These features were accounted for by Itai et al. [30], who found prolongation of T2 relaxation times greater than 80 msec in 15 of 18 hemangiomas, while only one of 20 primary or secondary liver cancers under 3 cm showed similar prolongation. Stark et al. [31] also confirmed that hemangiomas have a quantitatively greater contrast-to-noise ratio than liver cancer ($p < .001$). Thus, greater sensitivity and specificity for diagnosis of hemangiomas over either contrast-enhanced CT or sonography can be achieved with heavy T2-weighting because of the extremely high lesion-liver contrast even with small (1–2 cm) lesions [30]. In our department, MR has replaced CT, radionuclide scans, and angiography as the study of choice for suspected hemangiomas.

In clinical practice, other differential diagnostic features of hemangioma may also be valuable. Small peripheral venous structures, tumors, and hemangiomas produce a similar round dark lesion on T1 images; on T2 images vessels remain black, and while both tumors and hemangiomas appear bright, tumor brightness fades whereas hemangioma brightness increases with longer echo delay. Simple benign hepatic cysts may give a similar bright-signal MR appearance on T2-weighted images, but these MR features are those of a typical benign lesion and the differentiation of an innocent cyst from a solid hemangioma can be readily made by sonography. However, in about 10% of cases of hemangioma, overlapping T1 and T2 values may create a diagnostic problem [34]. Necrotic or very vascular metastases may give a long T2, or fibrotic thrombosed hemangiomas may develop T2 shortening. Overall, however, with the use of a heavily T2-weighted sequence MR can detect and distinguish cavernous hemangioma from liver cancer with a sensitivity and specificity in excess of 90%. It can thus function well either as a screening procedure or tertiary problem-solving examination.

Other Pulse Sequences: The Fat-Liver Association

Fatty infiltration of the liver is commonly observed in association with advanced malignancy. At liver imaging, confusing diagnostic appearances may occur with geographic foci of

fat, tumor, or normal attenuation parenchyma. Similarly, MR is rather insensitive in detecting fatty infiltration. In experimental animals massive increases in triglyceride content produce only minimal increases in image signal intensity with conventional pulse sequences [35]. The normal liver contains only 5% fat by weight, but in cancer patients with associated fatty metamorphosis, the increased fat may be exploited by chemical-shift spectroscopic techniques that greatly enhance tumor-liver contrast.

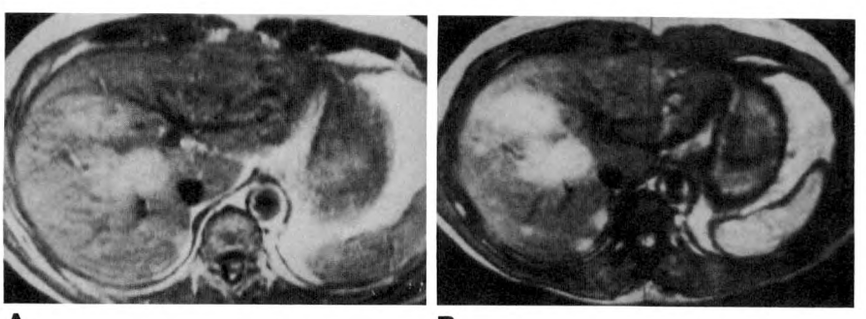
An innovative method for in vivo proton-spectroscopic chemical-shift imaging on commercial low-field systems was described by Dixon [36], who used a modification of the spin-echo sequence designed to display the difference in precession frequency between water and fat protons. Earlier work by Rosen et al. [37] had confirmed that chemical-shift imaging had a greater sensitivity than conventional MR imaging in detecting fatty liver, but the resulting images had poor spatial resolution. Dixon used a conventional clinical scanning system to produce high-quality images that were indivdually dependent on either the water or the fat content of the liver. Phase-contrast (opposed-phase) images were then generated by subtracting the water and fat magnetization. Increased hepatic fat signal subtracted from hepatic water protons gave a reduction in normal-liver signal intensity, and by using a T2-weighted spin-echo sequence tumors were easily distinguished as bright lesions against the black subtracted background of the fatty infiltrated liver (Fig. 14). High spatial resolution, contrast resolution, and convenient imaging speeds were preserved. Subsequent studies by Lee et al. [38] and Stark et al. [39] confirmed the superiority of opposed-phase images over conventional spin-echo techniques for detection of liver metastases. Stark et al. [39] found 72% of 40 patients with biopsy-proven metastatic liver cancer to show improved signal-difference to noise ratios over in-phase images with good preservation of anatomic detail. Signal intensity from malignant deposits showed no decline on opposed-phase images, presumably as a result of the lack of fatty accumulation within tumor tissue. The T2-weighted phase-contrast technique was thus suggested as a useful modification for T2-weighted imaging of suspected liver metastases [38]. However, we have not used this method routinely because of the high efficacy of our short TR/TE T1 and *multiecho T2 spin-echo* sequences.

In a different approach, suppression of the high-intensity signal from fat in the liver and in the entire upper abdomen was reported by Bydder and coworkers [40, 41] using a special inversion-recovery sequence with very short TI (inversion time). Termed STIR (short-inversion-time inversion recovery), this technique depends on the property that every tissue has a corresponding pair of TI and TR that will null out the signal for that tissue or any other tissue with a similar relaxation time. By using a sufficiently short TI TR sequence, the usual contrast relationships are reversed so that T1- and T2-dependent contrast after the 90° pulse is additive. For instance, on Bydder's 0.15-T system, an image obtained with an IR 1500/100/44 showed a liver tumor to appear brighter than normal liver parenchyma because the inversion time is shorter than the null point of the tumor. The normal liver parenchyma appears darker while the tumor appears brighter, giving the effect of a T2-weighted image. The STIR technique obtains similar results in imaging the CNS and upper abdomen where suppression of subcutaneous fat signal has the additional benefit of eliminating one of the major causes of respiratory ghosting, motion artifacts. A disadvantage of the STIR technique is that the images appear somewhat noisy; the method has not been widely used to date.

Hepatic MR Contrast Agents

The ability of exogenous pharmaceutical compounds to affect MR signal intensity by altering T1 and T2 relaxation values holds high promise for liver-cancer detection, and intense research is underway by many groups (including our own).

What is the rationale for developing MR contrast agents, given the apparent superiority of MR over CT in terms of contrast resolution for detection of focal liver metastases? Can the added cost and potential risk of toxicity be justified? Administration of a paramagnetic contrast agent that affects T1 and T2 values of normal diseased tissue pairs in predictable directions will allow preselection of a standardized, optimal set of instrument pulse sequences. In some instances the number of necessary pulse sequences could be reduced because of the highly predictable range of results expected. In other cases, because of the increased signal intensity generated by the contrast agent, repetition times and number of excitations could be reduced, thus also shortening overall scan time. The net result could be increased patient throughput and/or decreased examination costs. Increased contrast differences between normal and tumor tissue and patterns of tumor enhancement could also increase both the sensitivity



A B

Fig. 14.—Proton-spectroscopic chemical-shift imaging disclosing enhanced tumor-liver signal difference on phase-contrast (opposed-phase) image. Multiple right lobe deposits from carcinoid.

***A*, SE 2000/60 in phase image showing deposits as bright-signal areas in middle right hepatic lobe and along posterior right crural surface.**

***B*, SE 2000/60 opposed-phase chemical-shift image shows loss of liver signal due to hepatocyte fat, with resultant increases in visibility of metastatic lesions. Note especially two nodules along diaphragmatic crura.**

of disease detection and the specificity in tissue characterization. Both of the foregoing could increase the ability of MR to compete with CT as a primary screening method for the detection of metastatic liver cancer.

Contrast agents are most useful when selective accumulation occurs in only one of two tissues being compared [42]. In the case of a clinically applicable, liver-specific MR agent useful for cancer detection, requirements for a suitable compound would include (1) uptake by normal liver tissue, (2) exclusion by cancerous tissues, (3) magnetic activity sufficient to alter relaxation times of normal liver tissue without affecting adjacent tumor nodules, and (4) either low toxicity or a high margin of safety for the effective dose. Although an MR contrast agent that seeks a specific tumor is theoretically possible (e.g., monoclonal-antibody tagged), efforts to develop such tumor-selective agents for CT and sonography have met with little success. Similarly, exploitation of native physiologic mechanisms will probably be more fruitful with MR.

Three principal functions of the liver serve as possible routes for administration of a hepatic contrast agent: vascular flow, hepatobiliary excretion, and reticuloendothelial-system phagocytosis. Promising initial results have already been reported with all three mechanisms.

Gadolinium DTPA (Gd-DTPA) remains the best known paramagnetic substance currently available for human investigations [43–47]. As a result of proton-relaxation enhancement of nearby hydrogen nuclei, decreases in both T1 and T2 relaxation times occur, with T1 and T2 shortening predominating at lower and higher concentrations, respectively. The pharmacokinetic and biodistribution properties of Gd-DTPA are essentially analogous to that of conventional iodinated contrast agents used for CT [43, 44]. There is rapid plasma clearance and renal excretion by glomerular filtration. Both compounds are excluded by brain tissue with a physiologically intact blood-brain barrier and are selectively accumulated in abnormal tissues [45–47]. However, outside the CNS and in particular in the liver, GD-DTPA is distributed within the intravascular compartment initially and then diffuses in a nonspecific fashion throughout the interstitial extravascular tissue compartments, entirely analogous to the patterns of contrast enhancement seen with liver CT.

As a result of this nonspecific vascular distribution, early clinical trials of Gd-DTPA–enhanced liver MR for detection of liver metastases were disappointing [45]. In patients studied at the Hammersmith Hospital in London, a decrease in tumor-liver signal difference was frequently seen after an IV bolus infusion of 0.1 mmol/kg Gd-DTPA [45]. On postcontrast inversion-recovery scans, tumor nodules became isointense with surrounding liver and were obscured by extracellular, nonspecific distribution of the contrast agent, with "leakage" of the Gd-DTPA from the normal vascular space into the tumor. As with contrast-enhanced liver CT, equilibration into the interstitial compartment of the tumor resulted in a net loss in contrast.

In studies of Gd-DTPA imaging with a rat model of liver cancer from our laboratory, Saini et al. [48] emphasized the importance of immediate "dynamic" (1–2 min) postinjection scanning to maximize liver-tumor signal differences, just as with dynamic bolus CT. A short-TR/TE spin-echo sequence with 1–2 excitations showed threefold increase in tumor-liver signal-difference to noise ratio in the first minute after Gd-DTPA, with the two types of tissue returning to isointensity by 8 min (Fig. 15). The disappointing early Hammersmith results were postulated to reflect limitations imposed by the inversion-recovery-sequence timing parameters that resulted in images being obtained essentially in the equilibrium phase. Short-TR/TE, T1-weighted, spin-echo pulse sequences suitable for conventional MR liver imaging thus appear ideal for gadolinium-enhanced imaging of the liver as well. Indeed,

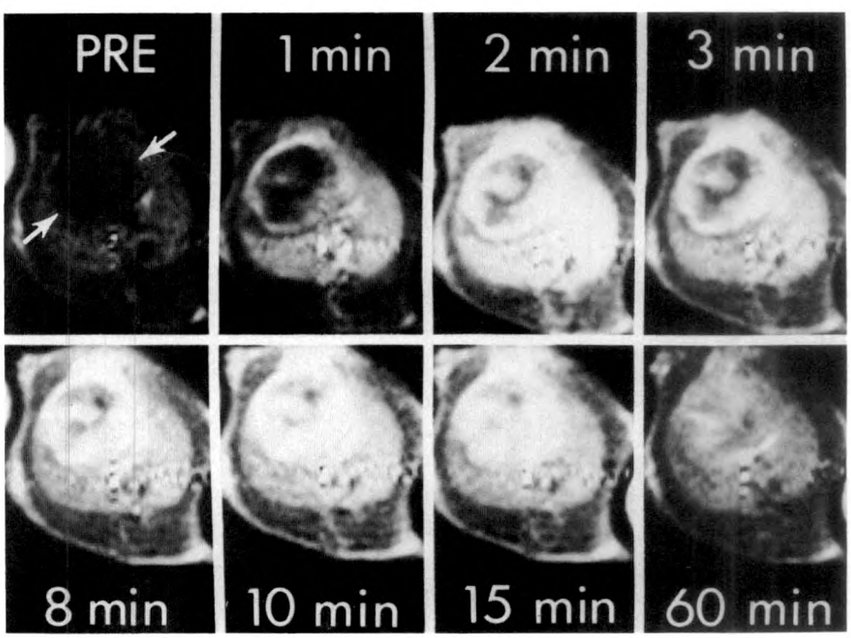


Fig. 15.—Rapid MR imaging of implanted adenocarcinoma in a rat liver after gadolinium-DTPA injection, SE 250/15/1 (0.6-min scan time). Pre-Gd-DTPA, tumor (*arrows*) has lower signal intensity than surrounding liver. Grainy image quality is due to poor signal-to-noise ratio. Post-Gd-DTPA images show an increase in signal intensity from normal liver. Early images (1, 2, and 3 min) show enhanced tumor-liver contrast, whereas later scans (8, 10 min) show reduction in tumor-liver contrast. At 10 and 15 min, tumor signal intensity actually exceeds that of liver. Sixty minutes after Gd-DTPA, some areas of tumor nodule once again show lower signal intensity than liver due to washout. (Reproduced with permission from Saini et al. [48]).

Wolf et al. [49] have also shown the speciifc advantages of gadolinium-enhanced liver imaging in animals with short-TE instrument parameters. T1-weighting, signal preservation due to less T2 decay, lower contrast dose, and shorter imaging time all follow. Ultimately it may therefore be possible to perform only gadolinium-enhanced scans without an initial unenhanced series, similar to commonly used CT techniques. Pilot studies on gadolinium imaging of human patients with liver metastases are now beginning in our department.

Among other possible liver MR contrast agents, a new class of compounds, superparamagnetic ferrite iron-oxide particles (Fe_2O_3), have attracted the attention of several groups (including our own) because of unique advantages related to their biodistribution, powerful relaxation mechanism, and low toxicity [50–53]. Prior medical uses of magnetic iron particles have included diagnostic immunoassay and magnetic separation techniques, magnetic labeling of cell surface-receptors and targeting of chemotherapeutic agents [50]. The ferrite-iron particles act by a unique superparamagnetic mechanism in which synergistic effects between molecules in a crystalline lattice create local field inhomogeneities when an external magnetic field is applied. Resulting powerful, selective T2 relaxation effects are 50 to 100 times more potent than the effects of Gd-DTPA on T1 relaxation rates as measured by the ED_{50} (effective dose 50 or dose required to reduce MR signal intensity by 50%) [54]. This indicates the potential for use of ferrite particles at low doses (Fig. 16). IV ferrite particles are rapidly sequestered from the blood stream by reticuloendothelial phagocytic functions of the liver, spleen, and bone marrow [50–53]. Because liver cancers contain no reticuloendothelial elements, exclusion of ferrite particles from cancer occurs. Wolf et al. [51] first used a VX2 rabbit carcinoma model to document that selective T2 relaxation effects occur in normal liver tissue relative to cancer tissues. Studies in our laboratory by Saini et al. [52] confirm striking differences in signal-difference to noise ratios of liver and tumor after μmole/kg doses of ferrite particles in rats with implanted mammary carcinomas. Imager pulse-sequence selection is simplified because of the predictable profound liver blackening and preservation of spatial resolution (Fig. 17). The effect resembles the ability of ferromagnetic iron proteins, ferritin, and hemosiderin to cause profound signal loss in iron-overloaded tissues (hemochromatosis). Hepatic iron overload is the experiment of nature that provided the basis for developing iron-oxide particles as MR contrast agents [55]. Crystalline ferrite particles can be fabricated at sizes less than 1 μm to avoid trapping in the pulmonary circulation. Coating with a variety of hydrophilic substances confers solubility for IV administration, and the potential for fashioning biodegradable particles further decreases risk of clinical toxicity.

Finally, both Gd-DTPA–enhanced and ferrite-enhanced liver MR may show special advantages in conjunction with fast imaging techniques, especially gradient-echo, partial-saturation sequences. The 10- to 20-sec acquisition times will allow dynamic-bolus phase imaging before the equilibration of Gd-DTPA into the interstitium that causes loss of tumor-liver signal difference. Hepatic flow and perfusion studies can also be envisioned [56]. In the case of ferrite, because the gradient-echo technique lacks a refocusing 180° pulse, its bulk magnetic susceptibility effects are increased, heightening sensitivity to the rapid proton dephasing of short T2 relaxation times [12]. This should further reduce the dose of ferrite required to cause the desired liver signal loss and proportionately increase the safety margin of this new agent.

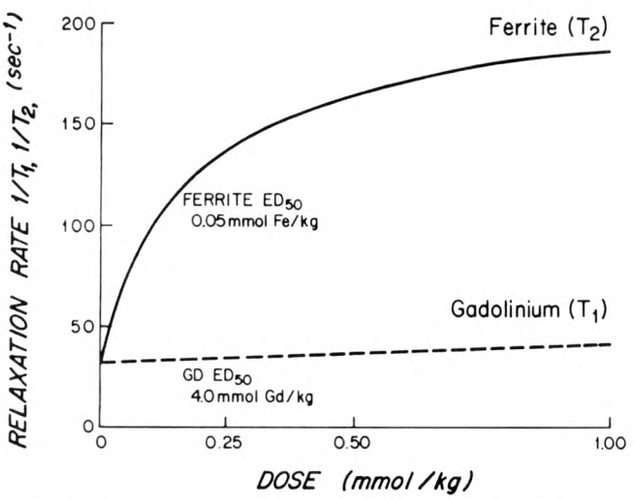


Fig. 16.—Comparison of ferrite vs Gd-DTPA liver relaxation. Gadolinium (T1 relaxation effect) shows a linear dose response with an ED_{50} of 4.0 mmol/kg of Gd. (ED_{50} = effective dose 50. This is the dose required to alter MR signal intensity by 50%.) The ability of ferrite to alter T2 relaxivity appears 80 times more powerful by virtue of an ED_{50} of 0.05 mmol Fe/kg. This nonlinear superparamagnetic effect on T2 relaxation will achieve the desired image signal blackening at minute dose levels.

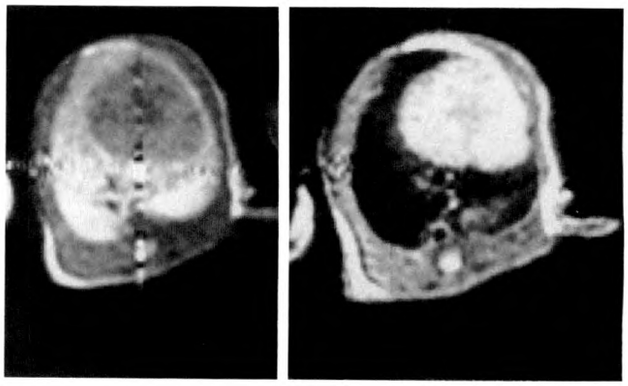


Fig. 17.—Ferrite-enhanced liver-tumor signal difference in a rat with implanted mammary adenocarcinoma.

***A*, Preferrite SE 250/15 image showing long-T1 tumor nodule darker than surrounding normal liver.**

***B*, After 1 mg IV ferrite-particle suspension. SE 500/30 showing striking signal blackening of normal liver with typical T2 brightening of tumor nodule. Specific reticuloendothelial system distribution of the ferrite with exclusion from tumor tissue is achieved.**

Conclusion

This review of clinical and laboratory directions in development of MR liver imaging illustrates the breadth and complexity of advances underway as well as the potential for future developments. Limitations of space have precluded consideration of the superior contributions of MR in major nonneoplastic conditions such as hepatic and portal venous disease and iron-overload states. Limited time is presently available on clinical MR systems for nonneurologic applications, but new system installations nationwide will probably create more opportunity for abdominal applications. Therefore, additional studies can be expected to extend present achievements. We, therefore, have reason to anticipate that MR will replace CT as the primary imaging method for detection of liver disease. Even if the accuracy of MR could only achieve parity with CT, the infrequent but well-understood serious risks of iodinated IV contrast material would result in the choice of MR [57]. The prospect that third-party payors might consider an either-or reimbursement choice between MR and CT, as injudicious as that might be, sharpens the issue further. In response, CT purists may insist that as a competing primary screening technique, MR should replace the clinical whole-abdomen–screening role of body CT completely if possible. To accomplish this, an effective gut contrast agent will be necessary to allow delineation of associated disease in the pancreas and retroperitoneum.

ACKNOWLEDGMENTS

The author acknowledges the contributions of his associates Jack Wittenberg, Thomas J. Brady, David D. Stark, Sanjay Saini, and Peter Hahn and the generous assistance of Diane McMahon and Lynda Bessette.

REFERENCES

1. *Cancer facts and figures*. New York: American Cancer Society, **1985**
2. Adson MA. Cannon lecture—hepatic metastases in perspective. *AJR* **1983**;140:695–700
3. Malt RA. Current concepts—surgery for hepatic neoplasms. *N Engl J Med* **1985**;313(25):1591–1596
4. Bernardino ME. The liver: anatomy and examination techniques. In: Taveras JM, Ferrucci JT, ed. *Radiology: diagnosis/imaging/intervention*, vol. IV. New York: Lippincott, **1986**
5. Doyle FH, Pennock JM, Banks LM, et al. Nuclear magnetic resonance imaging of the liver. *AJR* **1982**;138:193–200
6. Haaga JR. Magnetic resonance imaging of the liver. *Radiol Clin N Am* **1984**;22:879–890
7. Shultz CL, Alfidi RJ, Nelson AD, Kopiwoda SY, Clampitt ME. The effect of motion on two-dimensional Fourier transformation magnetic resonance images. *Radiology* **1984**;152:117–121
8. Ehman RL, McNamara MT, Pallack M, Hricak H, Higgins CB. Magnetic resonance imaging with respiratory gating: techniques and advantages. *AJR* **1984**;143:1175–1182
9. Bailes DR, Gilderdale DJ, Bydder GM, Collins AG, Firmin DN. Respiratory ordered phase encoding (ROPE): a method for reducing respiratory motion artifacts in MR imaging. *J Comput Assist Tomogr* **1985**;9(4):835–838
10. Bydder GM, Young IR. Clinical use of the partial saturation and saturation recovery sequences in MR imaging. *J Comput Assist Tomogr* **1985**;9(6):1020–1032
11. Haase A, Matthaei D, Hanicke W, Frahm J. Dynamic digital subtraction imaging using fast low-angle shot MR movie sequences. *Radiology* **1986**;160:537–541
12. Edelman RR, Hahn PF, Buxton R, Wittenberg J, Ferrucci JT, Brady TJ. Rapid magnetic resonance imaging with suspended respiration: initial clinical application in the abdomen. *Radiology* **1986**;161:125–132
13. Stark DD, Wittenberg J, Edelman RR, et al. Detection of hepatic metastases: analysis of pulse sequence performance in MR imaging. *Radiology* **1986**;159:365–370
14. Kneeland JB, Knowles RJR, Cahill PT. Magnetic resonance imaging systems: optimization in clinical use. *Radiology* **1984**;153:473–478
15. Kneeland JB, Knowles RJR, Cahill PT. Multisection multi-echo pulse magnetic resonance techniques: optimization in a clinical setting. *Radiology* **1985**;155:159–162
16. Davis PL, Kaufman L, Crooks LE, Miller TR. Detectability of hepatomas in rat livers by nuclear magnetic resonance imaging. *Invest Radiol* **1981**;16(5):354–358
17. Davis PL, Sheldon P, Kaufman L, et al. Nuclear magnetic resonance imaging of mammary adenocarcinoma in the rat. *Cancer* **1983**;51:433–439
18. Moon KL, Davis PL, Kaufman L, et al. Nuclear magnetic resonance imaging of a fibrosarcoma tumor implanted in the rat. *Radiology* **1983**;148:177–181
19. Moss AA, Goldberg HI, Stark DD, et al. Hepatic tumors: magnetic resonance and CT appearance. *Radiology* **1984**;150:141–147
20. Hendrick RE, Nelson TR, Hendee WR. Optimizing tissue contrast in magnetic resonance imaging. *Magnetic Resonance Imaging* **1984**;2:193–204
21. Wehrli FW, MacFall JR, Glover GH, Grigsby N. The dependence of nuclear magnetic resonance (NMR) image contrast on intrinsic and pulse sequence timing parameters. *Magnetic Resonance Imaging* **1984**;2:3–16
22. Demas BE, Hricak H, Goldberg HI, Margulis AR. Magnetic resonance imaging diagnosis of hepatic metastases in the presence of negative CT studies. *J Clin Gastroenterol* **1985**;7(6):553–560
23. Weinreb JC, Brateman L, Maravilla KR. Magnetic resonance imaging of hepatic lymphoma. *AJR* **1984**;143:1211–1214
24. Glazer GM, Aisen AM, Francis IR, Gross BH, Gyves JW, Ensminger WD. Evaluation of focal hepatic masses: a comparative study of MRI and CT. *Gastrointestinal Radiol* **1986**;11:263–268
25. Heiken JP, Lee JKT, Glazer HS, Ling D. Hepatic metastases studied with MR and CT. *Radiology* **1985**;156:423–427
26. Freeny PC, Marks WM, Ryan JA, Bolen JW. Colorectal carcinoma evaluation with CT: preoperative staging and detection of postoperative recurrence. *Radiology* **1986**;158:347–353
27. Ebara M, Ohto M, Watanabe Y, et al. Diagnosis of small hepatocellular carcinoma: correlation of MR imaging and tumor histologic studies. *Radiology* **1986**;159:371–377
28. Butch RJ, Stark DD, Malt RA. Magnetic resonance imaging of hepatic focal nodular hyperplasia. *J Comput Assist Tomogr* **1986**;10(5):874–877
29. Freeny PC, Marks WM. Patterns of contrast enhancement of benign and malignant hepatic neoplasms during bolus dynamic and delayed CT. *Radiology* **1986**;160:613–618
30. Itai Y, Ohtomo K, Furui S, Yamauchi T, Minami M, Yashiro N. Noninvasive diagnosis of small cavernous hemangioma of the liver: advantage of MRI. *AJR* **1985**;145:1195–1199
31. Stark DD, Felder RC, Wittenberg J, et al. Magnetic resonance

imaging of cavernous hemangioma of the liver: tissue-specific characterization. *AJR* **1985**;145:213–222
32. Glazer GM, Aisen AM, Francis IR, Gyves JW, Lande I, Adler DD. Hepatic cavernous hemangioma: magnetic resonance imaging. *Radiology* **1985**;155:417–420
33. Ohtomo K, Itai Y, Furui S, Yashiro N, Yoshikawa K, Iio M. Hepatic tumors: differentiation by transverse relaxation time (T2) of magnetic resonance imaging. *Radiology* **1985**;155:421–423
34. Takayasu K, Moriyama N, Shima Y, et al. Atypical radiographic findings in hepatic cavernous hemangioma: correlation with histologic features. *AJR* **1986**;146:1149–1153
35. Stark DD, Bass NM, Moss AA, et al. Nuclear magnetic resonance imaging of experimentally induced liver disease. *Radiology* **1983**;148:743–751
36. Dixon WT. Simple proton spectroscopic imaging. *Radiology* **1984**;153:189–194
37. Rosen BR, Carter EA, Pykett IL, Buchbinder BR, Brady TJ. Proton chemical shift imaging: an evaluation of its clinical potential using an in vivo fatty liver model. *Radiology* **1985**;154:469–472
38. Lee JKT, Heiken JP, Dixon WT. Detection of hepatic metastases by proton spectroscopic imaging. *Radiology* **1985**;156:429–433
39. Stark DD, Wittenberg J, Middleton MS, Ferrucci JT. Liver metastases: detection by phase-contrast MR imaging. *Radiology* **1986**;158:327–332
40. Bydder GM, Young IR. MR imaging: clinical use of the inversion recovery sequence. *J Comput Assist Tomogr* **1985**;9(4):659–675
41. Bydder GM, Steiner E, Blumgart LH, Khenia S, Young IR. MR imaging of the liver using short T1 inversion recovery sequences. *J Comput Assist Tomogr* **1985**;9(6):1084–1089
42. Brasch RC. Methods of contrast enhancement for NMR imaging and potential applications. *Radiology* **1983**;147:781–788
43. Weinmann HJ, Brasch RC, Press WR, Wesbey GE. Characteristics of gadolinium-DTPA complex: a potential NMR contrast agent. *AJR* **1984**;142:619–624
44. Brasch RC, Weinmann HJ, Wesbey GE. Contrast-enhanced NMR imaging: animal studies using gadolinium-DTPA complex. *AJR* **1984**;142:625–630
45. Carr DH, Brown J, Bydder GM, et al. Gadolinium-DTPA as a contrast agent in MRI: initial clinical experience in 20 patients. *AJR* **1984**;143:215–224
46. Carr DH. The use of proton relaxation enhancers in magnetic resonance imaging. *Magnetic Resonance Imaging* **1985**;3:17–25
47. Runge VM, Schoerner W, Niendorf HP, et al. Initial clinical evaluation of gadolinium-DTPA for contrast-enhanced magnetic resonance imaging. *Magnetic Resonance Imaging* **1985**;3:27–35
48. Saini S, Stark DD, Wittenberg J, Brady TJ, Ferrucci JT. Dynamic gadolinium-DTPA imaging of liver cancer: animal investigation. *AJR* **1986**;147:357–362
49. Wolf GL, Joseph PM, Goldstein EJ. Optimal pulsing sequences for MR contrast agents. *AJR* **1986**;147:367–371
50. Senyei AE, Widder KJ. Drug targeting: magnetically responsive albumin microspheres—a review. *Gynecol Oncol* **1981**;12:1–13
51. Wolf GL, Burnett KR, Goldstein EJ, Joseph PM. Contrast agents for magnetic resonance imaging. In: Kressel H, ed. *Magnetic resonance annual*, New York: Raven Press, **1985**:231–266
52. Saini S, Stark DD, Hahn PF, Wittenberg J, Brady TJ, Ferrucci JT. Ferrite particles: a superparamagnetic MR contrast agent for enhanced detection of liver cancer. *Radiology*, in press
53. Renshaw PF, Owen CS, McLaughlin AG, et al. Ferromagnetic contrast agents: a new approach. *Magnetic Resonance Med* **1986**;3:217–225
54. Wolf GL, Fobben ES. Tissue proton T1 and T2 response to gadolinium-DTPA injection in rabbits: a potential contrast agent for MR imaging. *Invest Radiol* **1984**;19:324–328
55. Stark DD, Moseley M, Bacon BR, et al. Magnetic resonance imaging and spectroscopy in hepatic iron overload. *Radiology* **1985**;154:137–142
56. Pettigrew RI, Avruch L, Dannels W, Coumans J, Bernardino ME. Fast-field-echo MR imaging with Gd-DTPA: physiologic evaluation of the kidney and liver. *Radiology* **1986**;160:561–563
57. Wolf GL. Opinion. Safer, more expensive iodinated contrast agents: how should we decide? *Radiology* **1986**;159:557–558

Cannon Lecture

The Impact of Radiology on Hepatology

Sheila Sherlock[1]
Robert Dick[2]

Because of remarkable advances in diagnostic imaging and the development of a variety of useful interventional techniques, radiology now plays a central role in the diagnosis and treatment of patients with hepatic disease. These include focal, vascular, and metabolic liver diseases, abnormalities of the biliary tract, and conditions associated with hepatic transplantation. Thus, optimal care of patients with liver disease now requires that there be close cooperation between the two specialties.

This lecture honors the memory of Walter B. Cannon (1880–1936), the distinguished Harvard physiologist who, as a medical student, realized the significance of X-ray in the study of the gastrointestinal tract. It was Cannon who made the first observations of gastrointestinal motility and, in particular, its relation to the emotions. Cannon could not have envisaged the developments of the next 40 years. In that interval the discipline of hepatology was born, and radiology progressed from its crude beginning to include sonography, CT, and MR imaging and the interventional procedures that they made possible [1, 2]. The lecture describes some important clinical situations in which the radiologist literally "takes over" from the hepatologist and shows how the two disciplines have developed in happy symbiosis.

Focal Lesions

Focal lesions can be divided into two classes: those that one wishes had never been seen and those that are clinically significant. Hemangiomas and simple cysts fall into the first category. They are diagnosed when a sonogram or CT is performed, often simply as a screening procedure when the clinician is driven, frequently by the patient, to make a diagnosis that would explain persistent, usually functional abdominal symptoms. Knowledge of the presence of the focal lesion can alarm the patient and confuse the physician. However, the imaging appearances are usually so characteristic that reassurance can be complete.

Hemangiomas are extremely common and are found in about 5% of autopsies. They may be single or multiple, small or large. They are usually asymptomatic and are occasionally painful as a result of intralesion hemorrhage. External rupture is virtually unknown. The contrast-enhanced CT scan is usually diagnostic, showing puddling of contrast material in venous channels followed by diffusion of contrast material from periphery to center with complete opacification in 30 to 60 min [3]. The hemangioma may be diagnosed by Technetium-99–labeled red-cell flow studies that show delayed filling of the lesion [4]. MR has been applied, since T2-weighted spin-echo imaging is the procedure of choice in distinguishing hemangiomas from liver cancers [5]. Sonography shows a well-defined area of increased echogenicity, and it and CT are so dependable in the diagnosis that the other techniques, including angiography, are rarely required.

Received March 27, 1986; accepted after revision July 7, 1986.

Presented in part at the annual meeting of the Association of Gastrointestinal Radiologists, Acapulco, Mexico, January 1986.

[1] Department of Surgery, Royal Free Hospital School of Medicine, Pond St., London NW3 2QG, England. Address reprint requests to S. Sherlock.

[2] Department of Radiology, Royal Free Hospital, London NW3 2QG, England.

AJR 147:1116–1122, December 1986
0361–803X/86/1476–1116
© American Roentgen Ray Society

Simple cysts show characteristic appearances on CT and sonography. Their diagnosis can be followed by complete reassurance of the patient. Liver failure never follows polycystic disease, however large the cysts are.

Hepatocellullar carcinoma is a scourge, particularly in areas where the carriage rate of hepatitis-B is high. The diagnosis is usually made late, after any possibility of surgical resection has passed. In areas such as Taipei, China, and Japan, diagnosis is being achieved by high-resolution, linear-array, real-time sonography [6–8]. Lesions as small as 1 cm can be detected. Hepatocellular cancers are usually hypoechoic, whereas small hemangiomas and some metastases are hyperechoic. Ideally, all hepatitis-B, surface-antigen–positive men more than 40 years old should have a sonogram and serum alpha-fetoprotein estimation every 6 months. The contrast-enhanced CT scan is of particular value and may show complications of the tumor, such as ascites or rupture.

Almost any lesion seen on imaging of the liver may safely be biopsied, with the exception of a large hemangioma. Direct (image-guided) liver biopsy gives a much higher percentage of positives than the nonguided percutaneous technique. The overall accuracy of diagnosis with the "blind" technique is 80%, but this can be raised to 95% if a directed form of liver biopsy is used [9]. In the last 4 years at the Royal Free Hospital, the number of liver biopsies performed by radiologists has markedly increased. A focal defect is recognized by sonography or CT, and, if coagulation and other conditions are satisfactory, a Trucut biopsy needle (Travenol, Deerfield, IL) is advanced into the lesion. The method of imaging for diagnosis has varied and includes scintigraphy, sonography (which has the advantage of not involving radiation and low cost), CT, and hepatic angiography [10]. In those with poor coagulation, a Gelfoam (Upjohn, Kalamazoo, MI) plug or steel coil may be injected through the outer cannula of the Trucut needle after the inner cutting needle, with its contained specimen, has been removed. At the Royal Free Hospital, this has been effective in preventing major bleeding after image-guided biopsies in those with coagulopathies. It is a quicker method than the transjugular route, which does not permit the biopsy needle to be directed toward a focal lesion.

Abscesses of the liver can be aspirated under direct guidance by sonography or CT (Fig. 1). This is the treatment of choice once hydatid disease has been excluded. The aspirated pus is cultured, and appropriate antibiotics are started. The aspiration can be repeated, or a catheter can be left in at the time of the first aspiration. Multiple abscesses are more difficult to treat, but sometimes percutaneous drainage of each is possible. Percutaneous sonographic or CT-guided catheter drainage has also been used for selected cases of amebic liver abscess [11]. Indications include uncertain diagnosis, imminent rupture, and a left-lobe or very large abscess.

Hepatic Vascular Lesions

Portal Vein

This should be demonstrated as soon as possible in any patient admitted with bleeding esophageal varices so as to determine whether the portal hypertension is due to portal vein block or cirrhosis (patients with portal vein block will have a better prognosis). The techniques, in order of invasiveness, are sonography, selective celiac angiography, percutaneous splenoportography, and transhepatic venography [1, 2]. Sonography has the advantage of simplicity but provides poor definition of the entire portal venous system. It is, however, very useful as an emergency screening procedure. Selective angiography has the advantage of relative safety and of showing the hepatic arterial anatomy and so diagnosing any coexistent hepatocellular carcinoma. Percutaneous splenoportography is still occasionally performed and gives the best definition of the extrahepatic portal anatomy. It is

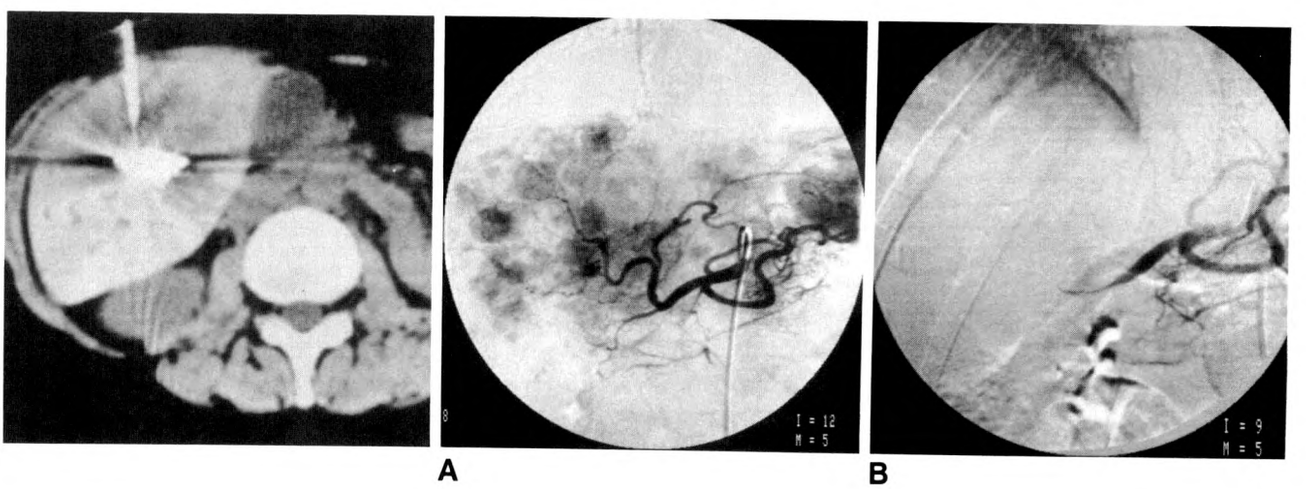


Fig. 1.—Patient with thalasemia and previous splenectomy and unexplained pyrexia. CT scan shows dense liver caused by iron overload and a liver abscess. Pus was aspirated and contrast material and antibiotic instilled into cavity.

Fig. 2.—Patient with resected primary carcinoid tumor of ileum and multiple symptomatic liver metastases.

***A*, Digital subtraction angiogram shows numerous vascular lesions.**

***B*, Repeat study after selective hepatic arterial embolization to ablate tumor function.**

especially useful when extrahepatic portal obstruction is suspected. Measurement of the intrasplenic pressure (portal blood pressure) is a bonus. Transhepatic portal venography gives the best definition of the portal vein and allows measurement of portal venous pressure, but is performed only when transhepatic variceal sclerosis is contemplated [12]. CT is useful in showing both subcutaneous and deep varices [13]. Percutaneous transhepatic angioplasty has been used to treat portal venous obstruction [14].

Hepatic Artery

Knowledge of anatomy is of value in diagnosing vascular anomalies and hepatic tumors and in planning surgery. The introduction of digital subtraction angiography has met with great approval from clinicians. This, along with the use of smaller-diameter catheters and smaller volumes of dilute nonionic contrast media, has enormously improved the safety of an angiogram, especially in the patient with poor liver function. Therapeutic embolization of the hepatic artery may be used for malignant tumors, particularly functioning endocrine ones (Fig. 2) [15]. Embolization for hepatocellular carcinoma is often complicated by nausea, pain, and fever. Abscess formation is rare. The tumor soon acquires a new arterial circulation via alternative vessels. Benign vascular masses such as adenomata and focal nodular hyperplasia may be embolized if causing symptoms.

Arteriovenous aneurysms after liver trauma, either from blunt abdominal injury or liver biopsy, may result in hemobilia. Embolization is the definitive treatment. Aneurysms, such as those caused by subacute bacterial endocarditis, may also be obliterated [16].

Some of the most bizarre changes in hepatic vasculature are found with hepatocellular carcinoma. Celiac angiography may show arteriovenous shunting, often with retrograde filling of the portal venous tree, perhaps associated with an abnormal circulation. The appearance is pathognomonic of primary liver cancer. Even without abnormal vessels, in a patient with cirrhosis and bleeding varices, demonstration by celiac angiography of a filling defect in the main portal vein suggests tumor invasion rather than clot (Fig. 3). Such a finding is of great practical value. Heroic efforts at resuscitation with massive blood transfusion, endoscopic sclerotherapy, and tamponade with the Sengstaken tube are clearly contraindicated. Invasion of the portal vein indicates that a terminal gastrointestinal hemorrhage is imminent.

Hepatic Vein

Hepatic venous obstruction (Budd-Chiari syndrome) is suspected when any patient develops sudden right upper quadrant pain with hepatomegaly and ascites. Selective celiac angiography, hepatic venography, and inferior venacavography with pressure measurements (taken in the inferior vena cava, hepatic vein, and right atrium) are essential to confirm the diagnosis and plan management. Bizarre and unexpected splanchnic vascular patterns may be revealed (Fig. 4). Most patients with Budd-Chiari syndrome due to a nonmalignant cause have an underlying disturbance in blood coagulation that may be a frank primary myeloproliferative disorder. The use of the in vitro erythroid colony formation test for myeloproliferative disorder suggests that this can exist without peripheral blood changes [17]. Polycythemia may sometimes be a consequence of hepatic vein occlusion. Finally, Budd-Chiari syndrome is increasingly recognized as being associated with collagen diseases, especially systemic lupus erythematosus, when accompanied by the circulating lupus anticoagulant [18, 19].

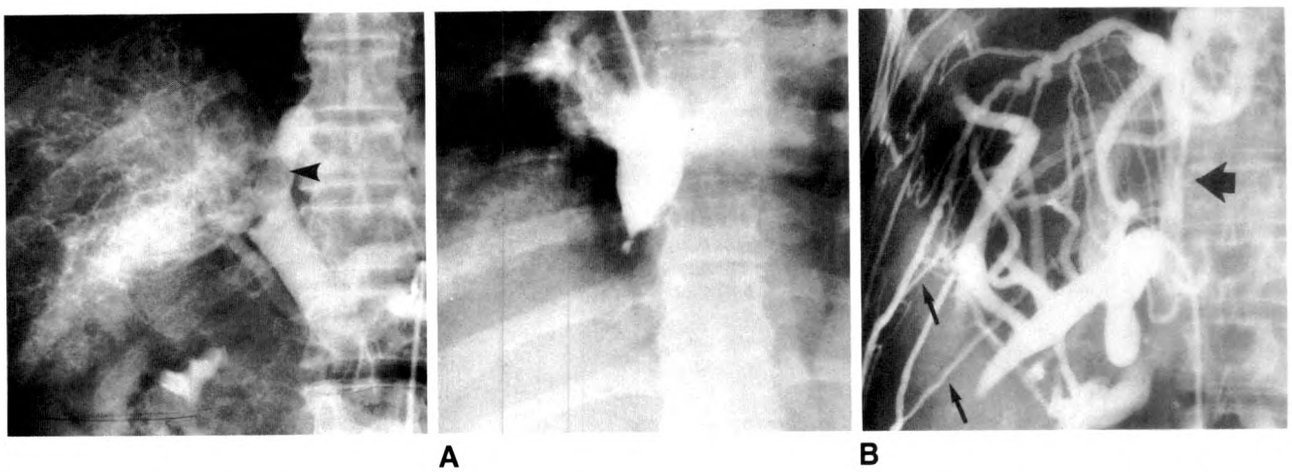


Fig. 3.—Celiac angiogram in patient with known cirrhosis, sudden deterioration in function, and rising alpha-fetoprotein level. Abnormal vessels in right lobe above hilum with massive and immediate arterioportal shunting. Appearances diagnostic of primary liver cancer. Defect in portal vein (*arrowhead*) represents tumor invasion rather than a clot.

Fig. 4.—Patient with systemic lupus erythematosus, circulating lupus anticoagulant, and Budd-Chiari syndrome.

***A*, Inferior venacavogram shows complete occlusion of suprahepatic portion of cava and major right and left hepatic veins.**

***B*, Selective injection of a dilated hepatic vein in lower right lobe of liver shows retrograde flow with diversion of blood to intercostal veins (*long arrows*) and hemiazygous system (*thick arrow*).**

Biliary Tract Diseases

Sonographic screening for the cause of jaundice has revolutionized management. It has reduced both diagnostic laparotomies and liver biopsies in cholestatic patients [10]. Radiologists have made a tremendous contribution through demonstration of the details of the biliary tree in the presence of obstructive jaundice.

The biliary radiopharmaceuticals have so improved that, for one of the newest, diethyliodo HIDA (Iodohida), preparation is easy and only 5% of the injected dose is excreted in the urine. Effective concentration in the bile duct is achieved in patients with "direct" reacting bilirubin levels exceeding 20 mg/dl. Cholescintigraphy may solve the diagnostic dilemma of neonatal jaundice. It can give conclusive evidence confirming the presence of biliary atresia (Fig. 5). It allows therapeutic plans to be formulated in the direction of either biliary enteric anastomosis (Kasai procedure) or later transplantation [20].

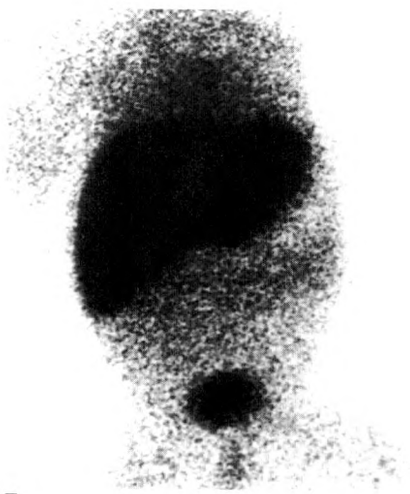
The advent of biliary imaging showed that the major intrahepatic bile ducts are abnormal in a large number of patients with ulcerative colitis. In an Oxford survey, 2% of 681 patients with ulcerative colitis had cholangiographic evidence of sclerosing cholangitis [21]. Most were asymptomatic and were suspected only because of a raised serum alkaline phosphatase level.

Sclerosing cholangitis has more than one cause. The "primary" type has a strong association with ulcerative colitis or, rarely, with Crohn's disease [22]. Sclerosing cholangitis may follow prolonged biliary inflammation secondary, for instance, to choledocholithiasis or chronic pancreatitis [23]. Typical sclerosing cholangitis may follow continuous hepatic infusion of fluorodeoxyuridine used to treat colorectal cancer [24–26]. The infusion may also cause cholecystitis [27]. Sclerosing cholangitis has followed the injection of substances such as formalin used to sterilize a hydatid cyst [28]. Histiocystosis X can also produce the picture of sclerosing cholangitis.

Endoscopic and percutaneous cholangiography provided new opportunities for access to the biliary tree without surgery and created the possibility for new therapy. Biliary obstruction can be relieved by the introduction of an endoprosthesis, either transhepatically [29] or endoscopically [30]. The percutaneous technique is probably more satisfactory for high biliary obstructions. The soft Carey-Coons' prosthesis (Radiologic, London, U.K.), made of percuflex, is easy to mold and remove, and the nonopaque pusher makes the radiopaque endoprosthesis easy to visualize [31]. If necessary, right and left hepatic ducts may be cannulated for the relief of high biliary obstruction caused by hilar carcinoma (Fig. 6). Percutaneously introduced prostheses avoid general anesthesia and surgery and cost less. In general, it is the older, poorer-risk patient who receives the nonsurgical prosthesis and the younger, fitter patient who has surgery. Hilar carcinomas are particularly suitable for prostheses as they are rarely resectable. Also, for large carcinomas of the head of the pancreas, a complicating gastric obstruction may be treated by peroral intubation under fluoroscopic control. With an ampullary carcinoma, if the patient is in suitable medical condition, the treatment should be surgery.

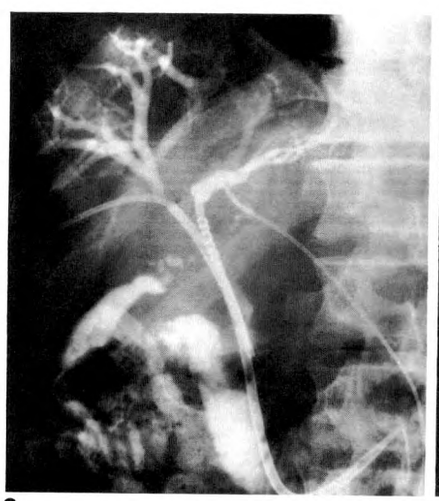
Aspiration cytology should be performed in all patients with noncalculous biliary obstruction when the diagnosis is uncertain. It may be performed under sonographic or CT control but sometimes gives inconclusive results, and a tissue diagnosis may not be possible.

Balloon dilatation of strictures in the extrahepatic bile ducts is possible whether by the transhepatic [32] or endoscopic



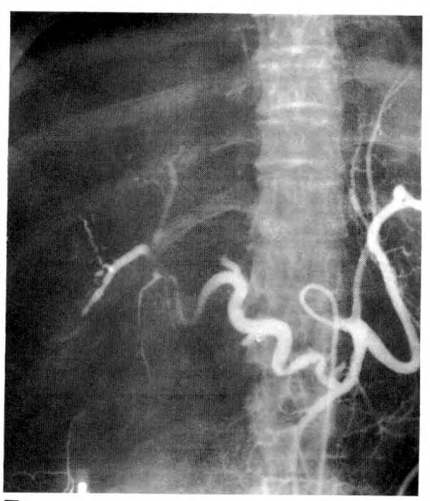
5

Fig. 5.—2-week-old infant with severe jaundice. Cholescintogram, using diethyliodo HIDA, shows radionuclide concentrated in liver, with some in urinary bladder. Biliary atresia was confirmed.



6

Fig. 6.—Cholangiocarcinoma at confluence of hepatic ducts (Klatskin tumor). An endoprosthesis has been passed percutaneously from right and left (Carey-Coons' on right, Burcharth prosthesis on left). Note external drainage catheters above stent for 24 hr for follow-up cholangiogram.



7

Fig. 7.—Deteriorating liver function 4 weeks after liver transplantation due to acute rejection. Celiac angiogram shows gross pruning of intrahepatic arterial tree. Filling did not improve later in series.

[33] route. Benign strictures of all types, including those that are secondary to surgery or sclerosing cholangitis, may be treated. Biliary-enteric anastomoses may be dilated. Dilatation may be used also as a preliminary step to the introduction of a transhepatic biliary endoprosthesis [34]. Skin stomas can be treated to provide access to biliary strictures via a small-bowel loop.

Metabolic Diseases

Imaging can help in the diagnosis and management of metabolic diseases and will play an even greater role in these areas when MR becomes more widely available.

Fatty Change

The sonographic appearances of fatty liver are of increased echogenicity [35]. Good correlation is shown between the CT density value of liver and the degree of histologic fat accumulation in liver cells, also between low Hounsfeld unit readings and raised gamma-GT enzyme levels in patients with a high alcohol consumption [36, 37]. MR may eventually be the most sensitive method of detecting hepatic fat [38]. Thus, diffuse fatty liver may be diagnosed in a number of situations without recourse to liver biopsy. These include acute fatty liver of pregnancy, diabetes, alcoholic liver disease, obesity, Reye's syndrome, and amiodarone therapy.

Focal fatty liver is a benign condition diagnosed by sonography or CT [39, 40]. Angular areas of increased echogenicity are usually peripherally placed. They may disappear only for new lesions to develop in other parts of the liver.

Iron and Copper

Hepatic density, determined by CT, is increased in iron overload. The CT scan shows relatively low-density, branching portal veins highlighted against the higher-density liver. Hepatic CT numbers normally vary between 35 and 65. A higher value accompanied by an increased serum ferritin level is diagnostic of increased iron stores [41]. If dual- (or tri-) energy CT is available, hepatic iron concentration may be measured. Unfortunately, this technique is not generally available. Liver copper usually has normal liver attenuation values on CT [42].

MR will offer greater possibilities [43]. Short TI values due to increased copper may be shown in Wilson's disease and primary biliary cirrhosis, and increased iron will be evident in hemochromatosis.

Hepatic Transplantation

The radiologist is a most important member of the hepatic transplantation team. Preoperatively, selective celiac and superior mesenteric angiography are necessary [44, 45]. The hepatic arterial tree must be visualized, and any anatomic abnormality, including aberrant origin of the hepatic artery and preduodenal portal vein, must be noted. The portal vein and inferior vena cava must be seen, since obstruction to either is usually a contraindication to transplantation. A selective right renal arteriogram is also performed, as failure to recognize the high position of a right kidney may result in unavoidable right nephrectomy at the time of liver transplantation. Demonstration of biliary ducts preoperatively is performed by cholangiography, usually endoscopic but percutaneous when endoscopic fails.

After transplantation, the radiologist's role varies at different stages [46]. Early complications (days 1–5) are largely technical and include hemorrhage and bile leaks. Biliary complications are particularly common and include malposition of T-tubes and later bile-duct obstruction caused by stricture. The arterial blood supply to the bile duct may have been disturbed, and this again leads to stricture formation. The most serious bile leak is due to necrosis of the complete donor bile duct secondary to hepatic artery thrombosis. In these patients a second transplant is required. CT imaging and HIDA, T-tube, or percutaneous biliary imaging are essential.

Sepsis (days 3–14) is related to biliary obstruction plus immunosuppression. Again, CT and sonography are needed to detect abscesses (which may be due to opportunistic organisms and fungi) and to institute drainage.

Rejection is seen in the third and fourth postoperative week. Angiography at this time may show arterial narrowing, slow flow, and poor intrahepatic arterial filling [44] (Fig. 7). Biliary strictures may be manifest many weeks or months after transplantation. Surgeons are keen for these to be treated nonoperatively, and some strictures respond to drainage, followed by dilatation and stenting.

REFERENCES

1. Sherlock S. *Diseases of the liver and biliary system*, 7th ed. Oxford: Blackwell Scientific, **1985**
2. Dooley JS, Dick R, Viamonte EM, Sherlock S, eds. *Imaging in hepatobiliary disease*. Oxford: Blackwell Scientific, in press
3. Johnson CM, Sheedy PF II, Stanson AW, Stephens DH, Hattery RR, Adson MA. Computed tomography and angiography of cavernous hemangioma of the liver. *Radiology* **1981**;138:115–121
4. Moinuddin M, Allison JR, Montgomery JH, Rockett JF, McMurray JM. Scintigraphic diagnosis of hepatic hemangioma: its role in the management of hepatic mass lesions. *AJR* **1985**;145:223–228
5. Stark DD, Felder RC, Wittenberg J, et al. Magnetic resonance imaging of cavernous hemangioma of the liver tissue-specific characterization. *AJR* **1985**;145:213–222
6. Sheu JC, Sung JL, Chen DS, et al. Ultrasonography of small hepatic tumours using high resolution linear-array real-time instruments. *Radiology* **1984**;150:797–802
7. Sheu JC, Sung JL, Chen DS, et al. Early detection of hepatocellular carcinoma by real-time ultrasonography. *Cancer* **1985**; 56:660–666
8. Shinagawa T, Ohoto M, Kimura K, et al. Diagnosis and clinical features of small hepatocellular carcinoma with emphasis on the utility of real-time ultrasonography; a study in 51 patients. *Gastroenterology* **1984**;86:495–502
9. Pagliaro L, Rinaldi F, Craxi A, et al. Percutaneous blind biopsy versus laparoscopy with guided biopsy in diagnosis of cirrhosis: a prospective randomized trial. *Dig Dis Sci* **1983**;28:39–43
10. Sherlock S, Dick R, Van Leeuwen DJ. Liver biopsy today. The

Royal Free Hospital experience. *J Hepatology* **1984**;1:75–85
11. vanSonnenberg E, Mueller PR, Schiffman HR, et al. Intrahepatic amebic abscesses: indications for and results of percutaneous catheter drainage. *Radiology* **1985**;156:631–635
12. Smith-Laing G, Camilo ME, Dick R, Sherlock S. Percutaneous transhepatic portography in the assessment of portal hypertension: clinical correlations and comparison of radiographic techniques. *Gastroenterology* **1980**;78:197–205
13. Balthazar EJ, Megbow A, Naidich D, LeFleur RS. Computed tomographic recognition of gastric varices. *AJR* **1984**;142:1121–1125
14. Uflacker R, Alves MA, Cantisani GG, Souza HP, Wagner J, Moraes LF. Treatment of portal vein obstruction by percutaneous transhepatic angioplasty. *Gastroenterology* **1985**;88:176–180
15. Allison DJ, Jordan H, Hennessey O. Therapeutic embolisation of the artery: a review of 75 procedures. *Lancet* **1985**;1:595–598
16. Kibbler CC, Cohten DL, Cruikshank JK, Kuswaha SS, Morgan MY, Dick R. Use of CAT scanning in the diagnosis and management of hepatic artery aneurysm. *Gut* **1985**;26:752–756
17. Valla D, Casadevall N, Lacombe C, et al. Primary myeloproliferative disorder and hepatic vein thrombosis: a prospective study of erythroid colony formation in vitro in 20 patients with Budd-Chiari syndrome. *Ann Intern Med* **1985**;102:329–334
18. Disney TF, Sullivan SN, Haddad RG, et al. Budd-Chiari syndrome with inferior vena cava obstruction associated with systemic lupus erythematosus. *J Clin Gastroent* **1984**;6:253–256
19. Pomeroy C, Knodell RG, Swain WR, Arneson P, Mahowald ML. Budd-Chiari syndrome in a patient with the lupus anticoagulant. *Gastroenterology* **1984**;86:158–161
20. Gartner JC Jr, Zitelli BJ, Malatack JJ, Shaw BW, Iwatsuki S, Starazite. Orthopotopic transplantation in children: two-year experience with 47 patients. *Pediatrics* **1984**;74:140–145
21. Shepherd HA, Selby WS, Chapman RWG, et al. Ulcerative colitis and persistent liver dysfunction. *Q J Med* **1983**;52:503–513
22. Chapman RWG, Arborgh VAM, Rhodes JM, et al. Primary sclerosing cholangitis: a review of its clinical features, cholangiography, and hepatic histology. *Gut* **1980**;21:870–877
23. Warwick F, Anderson RJL, Braganza JM. Sclerosing cholangitis like-changes in pancreatic disease. *Clin Radiol* **1985**;36:51–56
24. Kemeny MM, Battifora H, Blayney DW, et al. Sclerosing cholangitis after continuous hepatic artery infusion of FUDR. *Ann Surg* **1985**;202:176–181
25. Pien EH, Zepman RK, Venjamin SB, et al. Iatrogenic sclerosing cholangitis following hepatic arterial chemotherapy infusion. *Radiology* **1985**;156:329–330
26. Botet JF, Watson RC, Kemeny N, Daly JM, Yeh S. Cholangitis complicating intra-arterial chemotherapy in liver metastases. *Radiology* **1985**;156:335–337
27. Marymount JV, Dakhil SR, Travers H, Housholder DF. Chemical cholecystitis associated with hepatic arterial chemotherapy delivered by a permanently implanted pump. *Hum Pathol* **1985**; 16:986–990
28. Bories P, Mirouze D, Aubin JP, et al. Cholangite sclerosante apres traitement chirugical des kystes hydatiques due fie. Role probable de la formalisation des voies biliaires. *Gastroenterol Clin Biol* **1985**;9:113–116
29. Dooley JS, Dick R, George P, Kirk RM, Hobbs KEF, Sherlock S. Percutaneous transhepatic endoprosthesis for bile duct obstruction: complications and results. *Gastroenterology* **1984**;86:905–909
30. Huibregtse K, Tytgat GN. Palliative treatment of obstructive jaundice by transpapillary introduction of large bore bile duct endoprosthesis: experience in 45 patients. *Gut* **1982**;23:371–375
32. Gallacher DJ, Kadir S, Kaufman SL, et al. Non-operative management of benign post-operative biliary strictures. *Radiology* **1985**;156:625–629
33. Fonteh PG, Sivak MV Jr. Therapeutic endoscopic balloon dilatation of the extrahepatic biliary ducts. *Am J Gastroenterol* **1985**;80:575–580
34. Papnicolaou N, Dawson SL, Mueller PF, Ferrucci JT Jr. Insertion of a biliary endoprosthesis using a balloon dilatation catheter. *Gastrointest Radiol* **1985**;10:394–396
35. Scatarise JC, Scott WW, Donovan PJ, Siegelman SS, Sanders RC. Fatty infiltration of the liver: ultrasonographic and computed tomographic correlation. *J Ultrasound Med* **1984**;3:9–14
36. Bydder GM, Kreel L, Chapman RWG, Harry D, Sherlock S, Bassan L. Accuracy of computed tomography in diagnosis of iron overload liver. *Br Med J* **1980**;281:1042
37. Kawator F, Sakata K, Kunieda T, Sayi S, Doi H, Nozawa Y. Quantitative evaluation of fatty infiltration of the liver by computed tomography in rabbits. *AJR* **1984**;142:741–746
38. Lee JKT, Dixon WT, Ling D, Levitt RG, Murphy WA Jr. Fatty infiltration of the liver—demonstration by proton spectroscopic imaging: preliminary observations. *Radiology* **1984**;153:195–201
39. Clain JE, Stephens DH, Charboneau JW. Ultrasonography and computed tomography in focal fatty liver. *Gastroenterology* **1984**;87:948–952
40. Quinn SF, Gosink BB. Characteristic sonographic signs of hepatic fatty infiltration. *AJR* **1985**;145:753–755
41. Howard JM, Ghent CN, Carey LS, Flanagan PR, Valberg LS. Diagnostic efficacy of hepatic computed tomography in the detection of body iron overload. *Gastroenterology* **1983**;84:209–215
42. Smevik B, Rirland S, Nilsen T, Johansen O. Liver attenuation values at computed tomography related to liver copper content. *Scand J Gastroenterol* **1982**;17:883–893
43. Steiner RE. Magnetic resonance imaging: its impact on diagnostic radiology. *AJR* **1985**;145:883–893
44. Zajko AB, Bron KM, Starzlte, van Thiel DH, et al. Angiography of liver transplantation patients. *Radiology* **1985**;157:305–312
45. Ledesma-Medina A, Dominguez R, Bowen AD, Young LW, et al. Pediatric liver transplantation. Part L. Standardisation of preoperative diagnostic imaging. *Radiology* **1985**;157:335–344
46. Dominguez R, Young LW, Ledesma-Medina J, Cien Fuegos J, et al. Pediatric liver transplantation. Part II. Diagnostic imaging in post-operative management. *Radiology* **1985**;157:345–348

Aortic Dissection: A Statistical Analysis of the Usefulness of Plain Chest Radiographic Findings

Anand S. Jagannath[1]
Thomas A. Sos[1]
Stephen H. Lockhart[2]
Souheil Saddekni[3]
Kenneth W. Sniderman[4]

Findings on plain chest radiographs of patients with aortic dissection are variable and often overlap those of patients without dissection. To determine which findings were most useful in predicting aortic dissection, plain chest radiographs from 36 patients with aortographically proven aortic dissection and 36 patients from a control population were randomized and analyzed independently by five radiologists for the presence of various radiographic features associated with this condition. A widened aortic knob, widened descending aorta, and widened mediastinum showed the greatest interobserver agreement ($p < .001$) although the overall interobserver agreement was poor. The final conclusion of the radiologists was a better predictor of dissection than any of the individual radiographic features alone. Widening of the mediastinum ($p < .001$) and widening of the aortic knob ($p < .012$) were the only two radiographic features of significance in predicting dissection. In a stepwise multiple logistic regression model, the radiologists achieved an overall accuracy of 85%, a sensitivity of 81%, and a specificity of 89%. Although this illustrates the usefulness of plain chest radiographs in diagnosing aortic dissection, poor interobserver agreement dictates that further definitive investigation be undertaken.

Dissection of the aorta is a well-described entity in which blood dissects within the medial layer of the aorta [1–3]. Cardiovascular compromise produced by aortic dissection can be life threatening, but the initial signs and symptoms may be nonspecific and confusing [1, 2, 4, 5].

Findings on plain chest radiographs are variable and frequently overlap those of patients without dissection. To determine which findings were most useful in predicting the actual presence of dissection, we presented a group of radiologists with plain chest radiographs from a control group of patients with atherosclerosis and hypertension and from a group of patients in whom aortic dissection had been confirmed by aortography. The degree of agreement among the five radiologists' assessments of the presence or absence of various characteristics was calculated. In a statistical analysis, the average of the radiologists' subjective responses permitted calculation of the usefulness of the various features in predicting the presence of dissection. A mathematical model was used to calculate the overall diagnostic accuracy, specificity, and sensitivity of the different radiographic features and of the radiologists' conclusions.

Materials and Methods

The admission chest radiographs from 36 consecutive patients with aortographically proven dissection at The New York Hospital between 1965 and 1977 and a control group of 36 patients with hypertension and/or atherosclerotic cardiovascular disease were randomized, masked, and coded. Most were single frontal posteroanterior or portable anteroposterior views; a few were lateral projections or oblique views. A similar number of portable radiographs were included in both groups to avoid observer bias. The age range of the control group was 14 to 87 years (mean, 64); that of the group with dissection was 17 to 85 (mean,

Received February 4, 1986; accepted after revision June 27, 1986.

[1] Department of Radiology, The New York Hospital–Cornell Medical Center, 525 E. 68th St., New York, NY 10021. Address reprint requests to A. S. Jagannath, 435 E. 70th St., Apt. 25A, New York, NY 10021.

[2] Department of Biostatistics, Cornell University Medical College, Sloan Kettering Division, 1275 York Ave., New York, NY 10021.

[3] Department of Radiology, St. Luke's–Roosevelt Hospital Center, Amsterdam Ave. at 114th St., New York, NY 10025.

[4] Department of Radiology, Yale New Haven Hospital, 333 Cedar St., New Haven, CT 06510.

AJR 147:1123–1126, December 1986
0361–803X/86/1476–1123
© American Roentgen Ray Society

62). The number of men and women in the two groups was similar. Two-thirds of the group with known dissection had type B dissection. The entire set of radiographs was evaluated independently by five radiologists who were given a clinical history of "suspected aortic dissection" and asked to note the presence of specific findings and their degree of certainty. They could answer yes or no with a qualifier of definite, probable, or possible. The specific features to be assessed were blurring of the aortic knob, pleural effusion, tracheal shift, displacement of intimal calcification greater than 6 mm, localized lump on the aortic arch distal to the great vessels, and widening of the mediastinum, aortic knob, paraspinal shadow, and ascending and descending aorta. For each of the radiographs they were asked also to provide a final conclusion about the presence of dissection and to indicate the certainty of this conclusion.

The kappa statistic variant of Landis and Koch [6], the computed associated normal score (z), and p values were used to measure interobserver agreement in the experimental, control, and combined groups. If the agreement is perfect, kappa (κ) will be 1. Values below .40 represent poor agreement beyond that expected by chance, and values between .40 and .75 indicate fair to good agreement.

For each of the cases an average of the five radiologists' responses to each radiographic finding and their conclusions was calculated by assigning a value of 1 to 6 to the level of certainty that the radiologist expressed. For example, if definite yes is given a value of 6 and definite no a value of 1, then the average of four responses of definite yes and one response of definite no would be $(6 \times 4) + (1 \times 1) = 25/5 = 5$. By using this calculated average value for each of the radiographic findings as an independent variable and treating the known presence or absence of dissection as a dependent variable, a stepwise multiple logistic regression (SMLR) was performed to determine which of the radiographic findings was most significant in predicting aortic dissection. SMLR is a statistical technique used to analyze the ability of several factors to predict one of two outcomes (e.g., presence or absence of dissection). Only those factors that significantly add to the predictive value of the model are generated [7, 8]. By using an SMLR model, the predicted probability of dissection can be computed, and the sensitivity, specificity, and accuracy of the radiographic features and of the radiologists' final conclusions can be determined.

The software used for the analysis was RUNREGR, written by E. Krumblin (Department of Biostatistics, Memorial Sloan Kettering Cancer Center, New York). This program will run a dichotomous logistic regression with 14 covariates and up to 999 cases; it is similar to the program described in Lee [8].

The Spearman rank correlation coefficients were calculated to determine which radiographic features were associated with each other in predicting the presence of dissection. This correlation allows a test of significance of two continuous variables in which no assumption is made concerning normality of the variables.

Results

Table 1 shows the calculated kappa statistic for the control, experimental, and combined groups. Given six categories, overall agreement among the radiologists regarding the presence of the plain chest radiographic features of dissection was poor. Agreement was greatest in the findings of a wide aortic knob ($\kappa = .33$, $z = 18.3$, $p < .001$), wide descending aorta ($\kappa = .28$, $z = 15.6$, $p < .001$), and wide mediastinum ($\kappa = .28$, $z = 14$, $p < .001$).

The SMLR analysis showed that the final conclusion was a better predictor of dissection than any of the radiographic features alone ($p < .001$). Omitting the conclusion of the radiologists in the analysis showed that widening of the mediastinum ($p < .001$) and widening of the aortic knob ($p < .012$) were the two radiographic features of prognostic significance in recognizing aortic dissection.

The Spearman rank correlation coefficients of the association between the final conclusion and the various plain radiographic features ranged from .45 ($p < .001$) for displacement of intimal calcification to .86 ($p < .001$) for widening of the descending aorta. All the plain radiographic features also were correlated with presence of a wide mediastinum and widening of the aortic knob, with values ranging from .27 ($p < .02$) for displacement of intimal calcification to .86 ($p < .001$) for widening of the descending aorta. The SMLR model was used to compute the predicted probability of dissection. According to this model, those patients with a predicted probability of greater than .5 were considered to have aortic dissection and those with a value of less than .5 were predicted not to have dissection.

By using the plain chest radiographic features alone in the SMLR model, a specificity of 75%, a sensitivity of 81%, and an accuracy of 78% was achieved. Adding the conclusion of

TABLE 1: **Interobserver Agreement in the Control, Experimental, and Combined Groups for Plain Radiographic Features of Aortic Dissection and Radiologists' Final Conclusion**

Feature	With Dissection		Without Dissection		Combined	
	κ	z	κ	z	κ	z
Wide mediastinum	.22	7.1	.16	5.9	.28	14.0
Wide ascending aorta	.17	6.3	.27	10.0	.26	14.4
Wide descending aorta	.24	8.8	.24	8.6	.28	15.6
Wide aortic knob	.30	10.7	.20	6.9	.33	18.3
Blurred aortic knob	.20	6.7	.17	5.0	.23	10.5
Wide paraspinal shadow	.16	5.7	.30	8.8	.25	11.9
Pleural effusion	.22	8.5	.25	7.8	.27	13.5
Tracheal shift	.22	7.6	.15	4.7	.27	12.3
Calcification displacement	.12	3.5	.11	3.2	.13	5.4
Localized lump distal to vessels	.06	1.9	.05	1.3	.09	3.8
Conclusion	.14	5.4	.22	6.5	.24	13.3

Note.—Control = without dissection, experimental = with dissection, combined = control + experimental, κ = kappa statistic, z = associated normal score. All p values <.001 except for "localized lump" with ($p = .029$) and without ($p = .096$) dissection.

the radiologists raised the specificity of the model to 89%, the sensitivity to 81%, and the accuracy to 85%.

Discussion

The cause of spontaneous aortic dissection is not known. Approximately 70% of patients with aortic dissection have a history of systemic hypertension and left ventricular hypertrophy [1–4]. Our aim in this study was to analyze the usefulness of previously described plain chest radiographic findings of aortic dissection [9–12] by using a control population in whom an overlap of the findings might be expected. Objective measurements, although serving as a guideline in radiologic assessment, are often difficult to apply in an individual case because of the wide range of normal findings and a variety of technical considerations (e.g., supine views of poor inspiratory excursion). By quantifying the subjective evaluation of a group of radiologists, we wished to assess which of the features of plain chest radiographs would be most helpful in predicting aortic dissection. By using these data, specificity, sensitivity, and accuracy were calculated.

The kappa values in Table 1 suggest that agreement among the radiologists regarding the plain chest radiographic features of aortic dissection is not much greater than that expected at random. However, Table 2 shows that the level of agreement is related to the degree of certainty expressed by the radiologists. Agreement is fair to good at the definitive responses and low at the intermediate levels of certainty. None of the radiographic features had a high level of agreement within the intermediate levels. This suggests that there is little concordance among radiologists as to what constitutes possible and probable. The wide range of responses within the intermediate categories probably accounts for the overall low interobserver agreement. It may be inferred from this that the use of these ambiguous terms is not helpful in describing findings to other radiologists or clinicians and that it would be less confusing and more accurate to limit interpretation of radiographic findings to "yes," "no," or "I don't know." If only two responses had been allowed, agreement probably would be higher.

Logistic regression shows that the single best prognostic feature in predicting dissection was the final conclusion of the radiologists. Synthesis of all the radiographic features by the radiologists appears to be more important than the mere tabulation of the presence or absence of individual features. The generated accuracy, specificity, and sensitivity are simply another way of displaying the data generated by the regression model. Whenever possible, in this type of analysis, the regression equation should be checked (cross-validated) and coefficients reestimated on a data set different from that used for the initial variate selection [13]. The calculated accuracy, specificity, and sensitivity probably would be lower if a new set of similar patients was analyzed.

Using the averages of the five radiologists' responses may have resulted in a higher generated accuracy than would be found for the response of any single radiologist. However, our intention was to evaluate the usefulness of the radiographic features in predicting dissection, and, given the absence of absolute criteria, using an average of the radiologists' assessments is appropriate in the logistic regression.

The radiologists in our study were asked specifically to evaluate the findings related to suspected aortic dissection. To avoid further bias, they were not told the number of known cases. In practice, the radiologist may not even know that aortic dissection is suspected. The variety of radiographs in our study approached that of a clinical setting.

Although there is a correlation between the different radiographic features and the more predictive features of dissection, retrospective analysis of the radiographs showed that only one case showed clear displacement of calcification and only four cases showed evidence of pleural effusion. This suggests that these rarer findings are helpful, but their low frequency makes them less useful than other, more common findings.

CT has been helpful in the diagnosis of aortic dissection [14, 15] and has supplanted angiography at many centers. MR imaging also has been effective in diagnosing aortic dissection and may become the imaging technique of choice [16, 17]. Nevertheless, a plain chest radiograph is most often the preliminary radiographic examination useful in diagnosing aortic dissection. In an emergency clinical setting, CT and MR are rarely available immediately. In our study of suspected aortic dissection, widening of the mediastinum and aortic knob are the plain radiographic features of greatest predictive significance. However, in view of the overall low interobserver agreement, their absence must not deter further diagnostic evaluation.

ACKNOWLEDGMENTS

We thank Daniel Neistadt and David Olian for their assistance.

REFERENCES

1. Anagnostopulus CE, Prabhaker MJS, Kittle CF. Aortic dissections and dissecting aneurysms. *Am J Cardiol* **1972**;30:263–273

TABLE 2: **Spread of Interobserver Agreement and Level of Certainty of the Combined Group for Two Radiographic Features in Aortic Dissection**

Feature	κ						K
	Definite Absence	Probable Absence	Possible Absence	Possible Presence	Probable Presence	Definite Presence	
A	.51	.12	−.02	.06	.14	.59	.33
B	.52	.17	.05	.06	.04	.57	.28

Note.—Combined = control (without dissection) + experimental (with dissection). κ = kappa per level of certainty, K = kappa for total, A = widening of aortic knob, B = widening of descending aorta.

2. Hirst AEN, Johns VJ Jr, Kime SW Jr. Dissecting aneurysm of the aorta: a review of 505 cases. *Medicine* **1958**;37:217–279
3. Wilson KS, Hutchins GM. Aortic dissecting aneurysms: causative factors in 204 subjects. *Arch Pathol Lab Med* **1982**;106:175–180
4. Erb B, Tullis IF. Dissecting aneurysm of the aorta. *Circulation* **1960**;22:315–325
5. Lennard TWJ. Diagnosis not to be missed: dissecting aneurysms of the aorta. *Br J Hosp Med* **1981**;26:277–285
6. Fleiss JL. *Statistical methods for rates and proportions*, 2nd ed. New York: Wiley, **1981**
7. Halpern M, Blackwelder WC, Verter JI. Estimation of the multivariate logistic risk function: a comparison of the discriminant function and maximum likelihood approaches. *J Chronic Dis* **1971**;24:125–158
8. Lee DT. A computer program for linear logistic regression analysis. *Comput Programs Biomed* **1974**;4:80–92
9. Beachley MC, Ranniger K, Roth FJ. Roentgenographic evaluation of dissecting aneurysms of the aorta. *AJR* **1974**;121:617–625
10. Itzchak Y, Rosenthal T, Adar R, Rubenstein ZJ, Lieberman Y, Deutsch V. Dissecting aneurysm of thoracic aorta: reappraisal of radiologic diagnosis. *AJR* **1975**;125:559–570
11. Lodwick GW. Dissecting aneurysms of thoracic and abdominal aorta: report of six cases, discussion of roentgenologic findings and pathologic changes. *AJR* **1953**;69:907–925
12. Price JE, Gray RK, Grollman JH. Aortic wall thickness as an unreliable sign in the diagnosis of dissecting aneurysm of the thoracic aorta. *AJR* **1971**;113:710–712
13. Maindonald JH. *Statistical computation*. New York: Wiley, **1984**
14. Thorensen MK, San Dretto MA, Lawson TL, Foley WD, Smith DF, Berland LL. Dissecting aortic aneurysm: accuracy of computed tomographic diagnosis. *Radiology* **1983**;148:773–777
15. Oudkerk M, Overbosch E, Dee P. CT recognition of acute aortic dissection. *AJR* **1983**;141:671–676
16. Amparo EG, Higgins CB, Hricak H, Sollitto R. Aortic dissection: magnetic resonance imaging. *Radiology* **1985**;155:399–406
17. Geisinger MA, Risius B, O'Donnell JA, et al. Thoracic aortic dissection: magnetic resonance imaging. *Radiology* **1985**; 155:407–412

MR Imaging of the Central Pulmonary Arterial Tree in Conotruncal Malformation

Augustin G. Formanek[1]
Richard L. Witcofski
Vincent J. D'Souza
Kerry M. Link
Nolan Karstaedt

Successful MR imaging of the central pulmonary arterial tree was performed in four cases of conotruncal malformation and in one case of pulmonary arterial banding. Angiography performed near the time of MR imaging in three cases and 15 years earlier in two other cases did not visualize the central pulmonary arterial tree. Multiplanar imaging was necessary to fully visualize the anatomy of complex congenital defects of the pulmonary arterial tree; the choice of imaging plane varied depending on the portion of the pulmonary artery to be evaluated.

Two features in particular make MR useful for evaluating the anatomy of the cardiac chambers and great vessels: (1) lack of signal intensity from flowing blood (signal void), which provides excellent contrast between the lumen and the myocardium or vessel wall, and (2) simultaneous visualization of several or all cardiac components on multiple-plane tomographic images. The increasing number of reports on the application of gated MR in simple [1–3] and more complex [4–8] congenital cardiopathies confirm these advantages.

We report five cases of MR evaluation of the central pulmonary arterial tree, four in congenital cyanotic cardiac defects and one after palliative surgical interventions.

Materials and Methods

MR was performed to ascertain the anatomy of the pulmonary arteries in five patients, four with cardiac defects resulting in severe conotruncal malformation and one with subtotal occlusion of a major pulmonary artery branch secondary to pulmonary banding.

Images were obtained in the body coil of a Picker (Highland Heights, OH) Vista 1000 resistive 0.15-T imager with a proton-resonance frequency of 6.4 MHz. Cardiac gating was accomplished by a triggered data acquisition process in which the R wave initiated a view while the R-R time determined the pulse repeat time. A software-selectable time-delay parameter permitted imaging to begin at a prescribed point in the cardiac cycle.

Spin-echo scans were performed with an echo-delay time of 40 msec. Images were acquired with a multislice technique in which four adjacent 10-mm-thick sections were obtained with a time interval of 125 msec between slices (2, 4, 1, 3, slice order) and a 10-msec delay from the R wave of the ECG to the initiation of the pulse sequence. Each image used 128 views and four repetitions per view.

Case Reports

Case 1

The patient, a 38-year-old woman with tetralogy of Fallot, had undergone a left Blalock-Taussig shunt procedure at the age of 5 years. At recatheterization, the right ventricular infundibulum and main pulmonary trunk were absent. An angiogram in the shunt demonstrated a stenosis at the anastomosis and showed the left pulmonary artery only distal to the anastomosis. MR was performed to locate the proximal right pulmonary artery, if present (Fig. 1).

Received May 19, 1986; accepted after revision July 22, 1986.

[1] All authors: Department of Radiology, Bowman Gray School of Medicine of Wake Forest University, 300 S. Hawthorne Rd., Winston-Salem, NC 27103. Address reprint requests to A. G. Formanek.

AJR 147:1127–1131, December 1986
0361–803X/86/1476–1127
© American Roentgen Ray Society

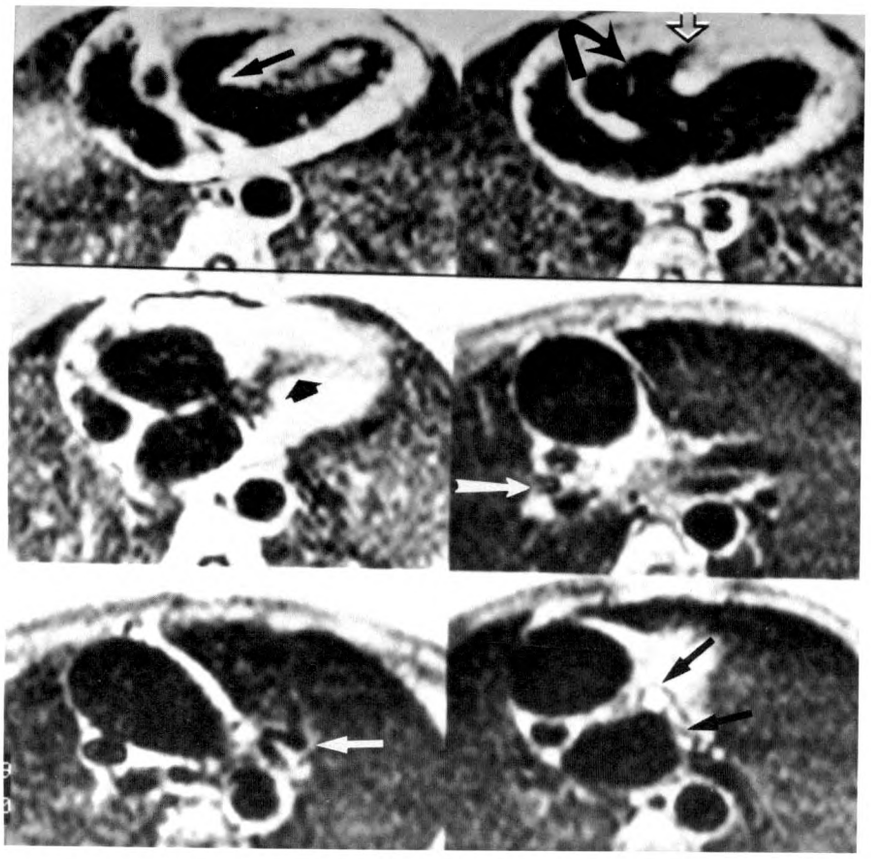


Fig. 1.—Patient 1. Transverse MR images in a patient with tetralogy of Fallot with infundibular and pulmonary artery atresia.

Top left, Subaortic ventricular septal defect (*arrow*).

Top right, Slice 1 cm more craniad shows large aortic root (*curved arrow*) overriding the defect and a small remnant of right ventricular outflow tract (*open arrow*).

More craniad (*middle left* and *middle right*), neither right ventricular outflow tract nor main pulmonary artery is seen.

Middle left, Small black arrow points to most superior aspect of left ventricle.

Middle right, Remnant of right pulmonary artery (*large white arrow*) is present posterior to superior vena cava.

Bottom left, At level of aortic arch, distal portion of Blalock-Taussig shunt connected to upper left pulmonary artery is seen (*white arrow*).

Bottom right, A large atrial branch of left circumflex coronary artery anastomosing with left lower lobar pulmonary artery is well demonstrated (*black arrows*).

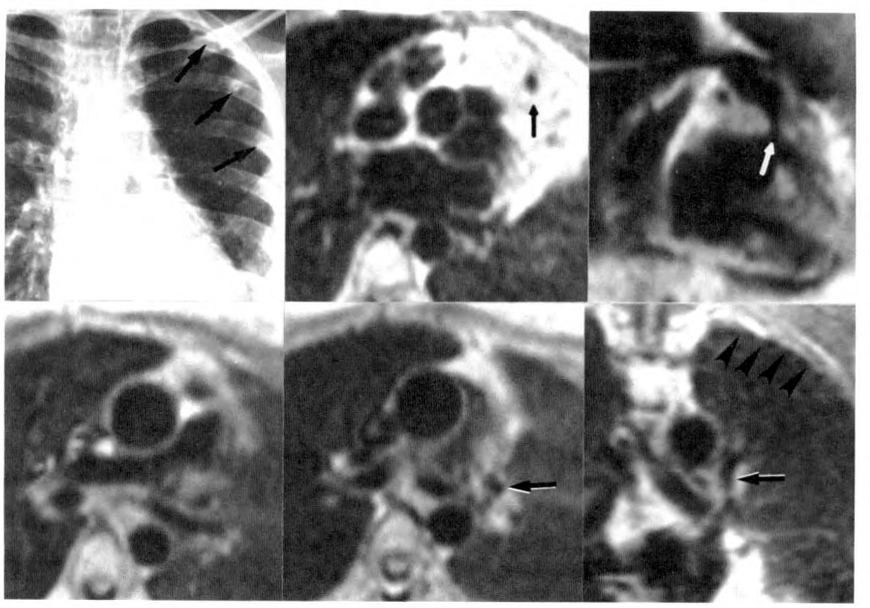


Fig. 2.—Patient 2. Tetralogy of Fallot with absent left pulmonary artery.

Top left, Close-up view of chest radiograph shows that left apical pleura is thickened and scalloped. Several small nodules in outermost left lung zones are present (*black arrows*).

MR images, *top middle* (transverse) and *top right* (coronal), depict well the extremely narrow infundibular channel (*arrows*) encircled by thick muscular ring.

In addition, on transverse MR scans, at height of pulmonary artery bifurcation (*bottom left* and *bottom middle*), main and right pulmonary trunks are seen, but from left pulmonary artery only a peripheral portion could be found (*arrow, bottom middle*).

Bottom right, Coronal slice shows only hilar part of left pulmonary artery (*arrow*) without its proximal segment. Multiple signal-free round structures (some marked by *arrowheads*) in apex and subcostal zones of left lung represent numerous transpleural collaterals to interrupted left pulmonary artery.

Case 2

The diagnosis of tetralogy of Fallot with severe infundibular stenosis was established by angiographic studies in a 24-year-old woman. The main and right pulmonary arteries were of adequate size, whereas the left pulmonary artery could not be seen. Because the chest radiograph (Fig. 2, upper left panel) showed a thickened and scalloped left apical pleura with several adjacent small nodular densities, interruption of the left pulmonary artery with transpleural collateral blood supply was considered as a possible explanation. For

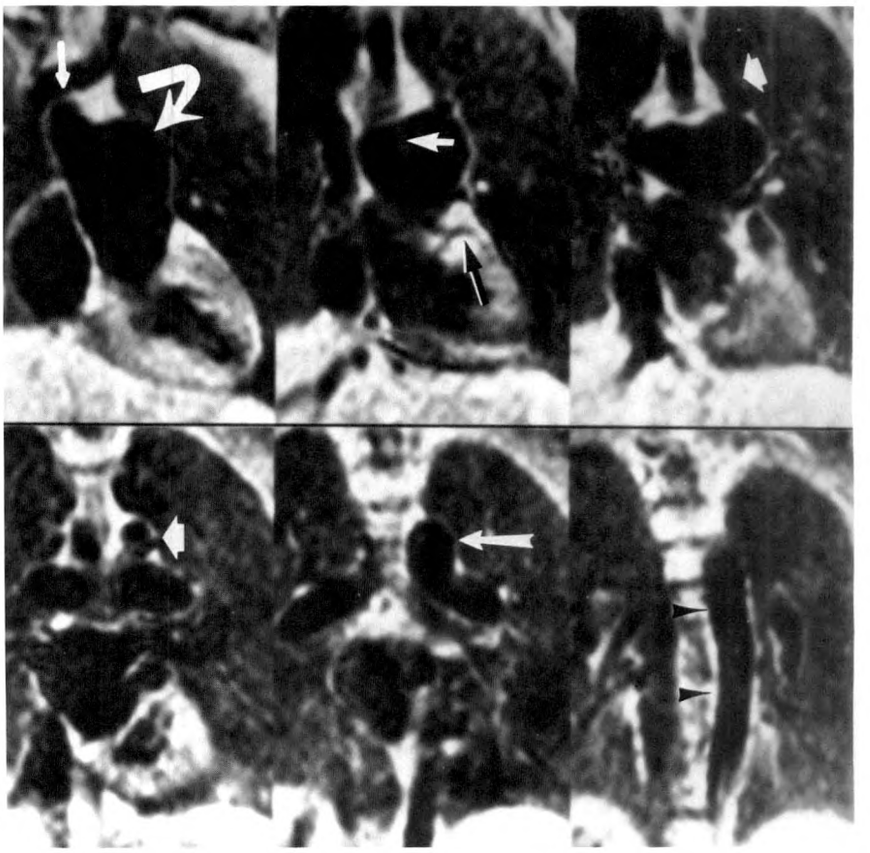


Fig. 3.—Patient 3. Coronal images in anteroposterior order in a patient with truncus arteriosus and interrupted aortic arch type B.

***Top left*, A large trunk divides into ascending aorta (*arrow*) and into vestigial pulmonary artery (*curved arrow*), but an aortic arch was not demonstrated.**

Separate close origin of two pulmonary artery branches at posterior aspect of pulmonary component is marked by a subtle septum superiorly (*white arrow, top middle*).

Identical shape and size of two central pulmonary arteries are well demonstrated (*top right* and *bottom left*. *Small arrows* mark left subclavian artery (*top right* and *bottom left*).

Large ductus arteriosus (*white arrow, bottom middle*) communicates with left pulmonary artery and descending aorta (*black arrowheads, bottom right*).

Left main coronary artery and its two branches reveal the good resolution of MR images (*black arrow, top middle*). Lack of a well-developed main pulmonary artery and close origin of two major pulmonary artery branches at posterior aspect of truncus allow its classification as an intermediate form between types 1 and 2.

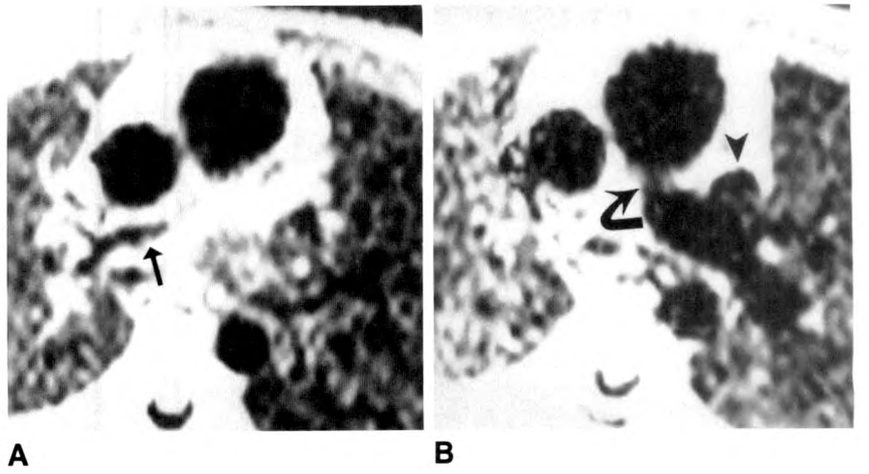


Fig. 4.—Patient 4. Transverse scans at level of great arteries in a patient with a complete form of persistent atrioventricular canal with banded pulmonary artery.

***A*, Small right pulmonary artery (*arrow*) measuring 4 mm in width is not in continuity with large main pulmonary artery.**

***B*, 0.7 cm more craniad, constriction of origin of left pulmonary artery by band (*curved arrow*) is well seen, but a proximal right pulmonary artery is missing. Persistent left superior vena cava is marked by *arrowhead*.**

more information, MR scans were obtained (see Fig. 2), and indeed, the absence of the proximal left pulmonary artery was verified.

Case 3

Persistent truncus arteriosus with interruption of the aortic arch (type B) distal to the left carotid artery was diagnosed in a cyanotic female infant at the age of 6 months. However, the anatomy of the truncal division and the pulmonary artery branching were not clear on the 16-mm cineangiogram. MR was performed at age 16, and an intermediate form between truncus type 1 and 2—the most common form [9]—was diagnosed in association with type B interruption of the aortic arch (Fig. 3).

Case 4

The main pulmonary artery was surgically banded for a left-to-right shunt in a 5-month-old boy with severe atrioventricular canal deformity. At the age of 7 years, during preoperative evaluation, the right

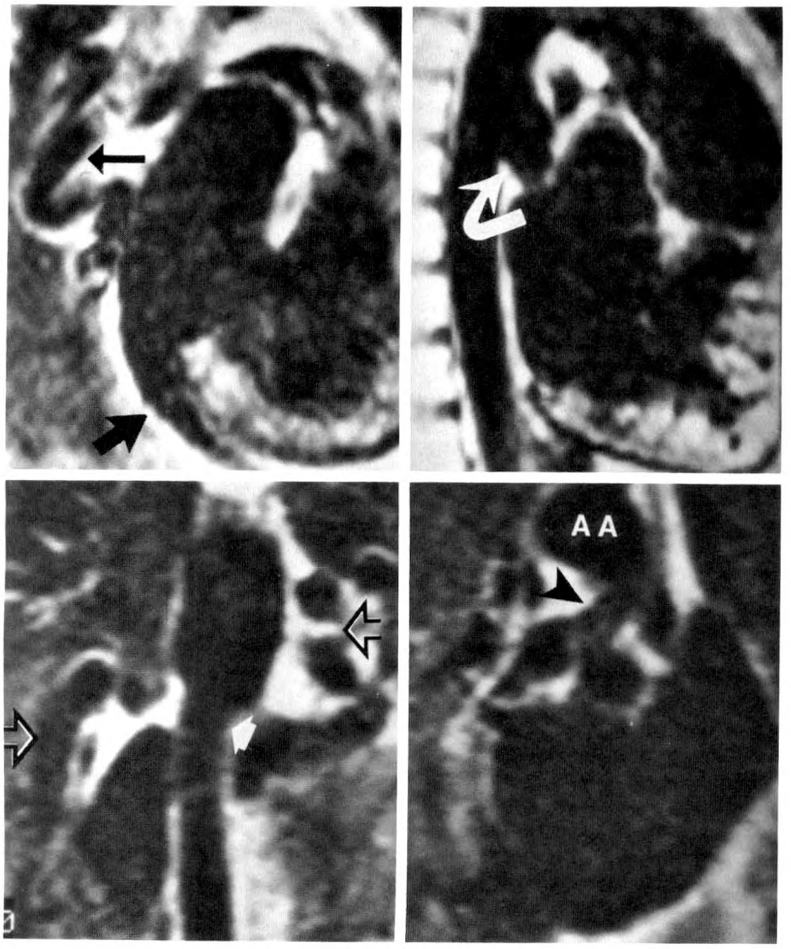


Fig. 5.—Patient 5. Two sagittal scans, in plane of left hilum (*top left*) and thoracic aorta (*top right*), respectively, show origin of a large systemic-pulmonary collateral vessel on anterior aspect of descending aorta (*curved arrow, top right*) and its left branch (*long arrow, top left*).

In *top left* panel, *thick black arrow* points to entrance of common hepatic vein into left portion of single atrium.

A posterior coronal slice (*bottom left*) shows sudden change in width of right-sided descending aorta (*closed arrow*) and large hilar pulmonary arteries (*open arrows*).

1.5 cm more anteriorly, bifurcating systemic-pulmonary collateral artery (*arrowhead, bottom right*) is seen.

Features of a single atrium and ventricle with one atrioventricular valve are well shown in *top left, top right,* and *bottom right* panels. AA = right aortic arch.

pulmonary artery could not be catheterized. After a pulmonary arteriogram showed only a wisp of contrast medium in the right pulmonary artery, an MR study was done to show the anatomy and size of the right pulmonary artery (Fig. 4), and only a 4-mm-wide distal right pulmonary artery was clearly seen.

Case 5

In a male infant, diagnosis of a single ventricle and probable pulmonary atresia was made. However, the central pulmonary arteries were not seen on the angiocardiograms. MR study when the patient was 16 years old led to the definitive diagnosis without the need for additional angiocardiograms (Fig. 5). A large vessel that originated from the ventral aspect of the proximal descending aorta bifurcated into moderately large right and left pulmonary arteries, indicating pulmonary artery atresia. Whether this vessel supplying the pulmonary artery branches is a ductus arteriosus or a large bronchial artery is not clear; thus it is appropriate to call this a systemic-pulmonary collateral [10]. The excellent blood flow to the pulmonary circulation may be inferred by the sudden decrease in the diameter of the aorta to approximately half its diameter immediately distal to the origin of the above-mentioned vessel. All other features of the complex anatomy were easily seen in the sagittal and coronal planes of MR study.

Discussion

In all of the patients described above, the pulmonary artery and its two major branches were profoundly distorted by faulty development or surgical intervention, and the anatomy of these great vessels was not satisfactorily demonstrated by angiocardiography. Signal void caused by the flowing blood results in excellent contrast and gives MR an advantage over angiocardiography in situations in which contrast medium cannot be delivered in an adequate amount.

For corrective surgery of congenital heart defects with conotruncal malformations, it is of paramount importance to know the exact anatomy of the aorta and central pulmonary arteries, and detailed angiographic studies immediately before surgery are warranted. MR imaging is indicated in patients with inconclusive angiographic findings.

In patient 1 with typical tetralogy of Fallot, atresia of the pulmonary artery apparently developed after a left-sided Blalock-Taussig procedure. The selective shuntogram did not opacify either the main or the right pulmonary arteries. MR images, however, clearly showed the absence of the right ventricular infundibulum and, from the right pulmonary artery only, showed the artery's peripheral minute branches to part before entering into the right hilum (Fig. 1, middle right panel). The small size of this artery indicates a long-standing decrease of blood flow; this finding together with that of the contrast shuntogram precluded surgical intervention.

In patient 2, the status of the left pulmonary artery not

visualized by the right ventriculogram could be evaluated either (1) by selective multivessel angiography (left subclavian artery branches, bronchial arteries) because of the posteroanterior chest film (Fig. 2, top left panel) indicating the presence of collaterals to peripheral pulmonary artery branches or (2) by MR scans. We chose MR imaging because of its noninvasiveness. Only a relatively small hilar portion (less than half of the diameter of the left bronchus) was seen (Fig. 2, bottom right panel). This MR information was sufficient to cause the surgeons to abandon their original intention to perform a graft from the main pulmonary artery to its left main branch. During the surgery for closure of the ventricular septal defect and the infundibular stenosis repair, absence of the entire proximal left pulmonary artery was confirmed.

In patient 4, the distally placed pulmonary artery band did not totally occlude the origin of the right pulmonary artery—the very faint blush during the pulmonary arteriogram (which showed no details) indicates minimal patency of the vessel. Therefore, the lack of signal-void in the proximal segment of the artery on MR images is compatible with subtotal occlusion. Even with 7-mm-thick slices, the spatial resolution of our MR images is insufficient to show tubular structures of very small caliber (the pulmonary artery with a likely diameter of less than 1 mm). A few centimeters distal, the 4-mm-wide right pulmonary artery, however, is well seen.

If small pulmonary artery branches are to be shown on MR scans, their course is important for selection of the proper imaging plane. The nearly horizontal course of the right pulmonary artery requires transverse (axial) images (patients 1 and 4). The hilar portion of the left pulmonary artery (and this most likely applies to the right pulmonary artery as well) is shown in detail on coronal scans (patient 2).

Patients 3 and 5 had their first angiographic examination in infancy, while the MR imaging was performed 15 years later. An initial MR study was chosen on the basis of the difficulties of obtaining a good angiocardiographic study in complex congenital heart defects in adults with increased pulmonary blood flow because of limitations in the total amount and volume of contrast medium used for a single angiographic study. In retrospect, in patient 5, selective angiogram of the systemic-pulmonary arterial collateral would likely have given adequate information about the anatomy of pulmonary blood supply. However, to obtain the anatomic details provided by MR (a single atrium and ventricle with one atrioventricular valve, trabeculation of the single ventricle classifying it as a primitive right ventricle, and drainage of the inferior vena cava) would require numerous, large-volume injections of contrast medium. MR provided, in addition to a detailed anatomy of the central pulmonary circulation (best seen on coronal and sagittal images), all the necessary information about the very complex anatomy of the heart.

In patient 3, the contrast medium probably would have obscured the subtle septum separating the orifices of the two pulmonary artery branches (Fig. 3, top middle), and the fast simultaneous clearance of contrast medium via four large channels (ascending aorta, ductus arteriosus, descending aorta, and two pulmonary arteries) might have interfered with a demonstration of the detailed anatomy. Imaging in coronal planes provides the most information in patients with persistent truncus arteriosus and interruption of the aortic arch. The spatial orientation of the two pulmonary arteries with the absence of the aortic arch is well seen, as well as the vascular complex of left pulmonary artery–ductus arteriosus–descending aorta. The patent ductus arteriosus, which continues with the descending aorta, is also visible on the sagittal slices. The coronal slices delineate the relationship of the left subclavian artery to the descending aorta (Fig. 3, top right and bottom left panels).

The potential of MR for diagnosis of the various congenital heart defects is not fully known. Published data and our experience suggest, however, that in complex cardiac defects and postsurgical complications, the information gained from MR images might not be obtainable by contrast-cine cardioangiograms. This applies particularly to imaging of the central pulmonary arterial tree, which may be inaccessible for selective catheterization in some cyanotic congenital malformations and postsurgical evaluations. These conclusions are similar to those reported in a recent publication of MR of the great arteries [11]. Although numerous angiograms might overcome these difficulties, the toxicity and the amount of contrast medium required are always limiting factors. MR imaging, therefore, is a valuable method for visualizing the central pulmonary arteries in severe congenital cyanotic heart diseases.

REFERENCES

1. Schiavone WA, O'Donnell JK. Congenital absence of the left portion of parietal pericardium demonstrated by nuclear magnetic resonance imaging. *Am J Cardiol* **1985**;55:1439–1440
2. Dinsmore RE, Wismer GL, Guyer D, et al. Magnetic resonance imaging of the interatrial septum and atrial septal defects. *AJR* **1985**;145:697–703
3. Stark DD, Higgins CB, Lanzer P, et al. Magnetic resonance imaging of the pericardium: normal and pathologic findings. *Radiology* **1984**;150:469–474
4. Fisher MR, Hricak H, Higgins CB. Magnetic resonance imaging of developmental venous anomalies. *AJR* **1985**;145:705–709
5. Jacobstein MD, Fletcher BD, Goldstein S, Riemenschneider TA. Magnetic resonance imaging in patients with hypoplastic right heart syndrome. *Am Heart J* **1985**;110:154–158
6. Higgins CB, Byrd BF II, McNamara MT, et al. Magnetic resonance imaging of the heart: a review of the experience in 172 subjects. *Radiology* **1985**;155:671–679
7. Jacobstein MD, Fletcher BD, Nelson AD, Clampitt M, Alfidi RJ, Riemenschneider TA. Magnetic resonance imaging: evaluation of palliative system–pulmonary artery shunts. *Circulation* **1984**;70:650–656
8. Fletcher BD, Jacobstein MD, Nelson AD, Riemenschneider TA, Alfidi RJ. Gated magnetic resonance imaging of congenital cardiac malformations. *Radiology* **1984**;150:137–140
9. Gedgaudas E, Moller JH, Castaneda-Zuniga WR, Amplatz K. Congenital heart disease: cyanosis and increased pulmonary arterial vascularity. In: *Cardiovascular radiology*, Philadelphia: Saunders, **1985**:113–125
10. Jefferson K, Rees S, Somerville J. Systemic arterial supply to the lungs in pulmonary atresia and its relation to pulmonary artery development. *Br Heart J* **1972**;34:418–427
11. Fletcher BD, Jacobstein MD. MRI of congenital abnormalities of the great arteries. *AJR* **1986**;146:941–948

Book Review

Practice of Coronary Angioplasty. By Thomas Ischinger. New York: Springer-Verlag, 325 pp., 1985. $79

Now that percutaneous transluminal coronary angioplasty (PTCA) has become an accepted procedure in over 350 centers in the United States, more than 100,000 coronary angioplasty procedures are performed annually. This text is not intended as a substitute for hands-on experience. Data document that success rates, complications, and procedural times are directly related to the experience of the operator. Few interventional procedures require greater technical skills than PTCA.

The volume, divided into 18 chapters, has several contributing authors, but the editor is the sole or participating author in 11 of these chapters. This is fortunate because his clarity and style are superb and his material is well organized.

Chapter four, "An Evaluation of the Coronary Arteriogram in Selection of Patients for Coronary Angioplasty," treats a topic that is well-established and frequently published, but which over the years has lost its excitement. The author, however, approaches the subject on the basis of the technical difficulties that the angiographer encounters during the procedure. He discusses the hazards of repeated manipulation, unnecessary forceful advancement, and trauma to the vessel intima; the inability to predict these technical problems by simple analysis of the arteriogram; the risks of iatrogenic side-branch occlusions; the protective role of coronary collaterals during the dilatation procedure; and the measurement of collateral functions, as well as other features, integrating the coronary artery anatomy with the clinical and technical decisions made at the time of the dilatation. Chapter six, "Cardiac Catheterization Laboratory for Coronary Angioplasty," equally well written, could serve as a model for laboratories planning a new installation. The author's recommend biplane fluoroscopic installation. Although most angiographers would agree with this, in Chapter 15, Hartzler claims that single-plane installations are quite adequate, even for the most complex of procedures. Differences of opinion by the experts is refreshing, which again reinforces the importance of "operator experience." Other superb chapters include a review of existing torque-control directional wires, balloons, varying profiles in the steerable systems, and guiding catheters. Only two of the multiple manufacturers involved in coronary artery PTCA equipment are discussed, which may be author preference or indicate a limited commercial market. Chapter 15, "Complex Coronary Angioplasty" by Hartzler, short, well-illustrated, and well-detailed, describes multiple vessel and lesion dilatations. He believes that multiple-lesion coronary angioplasty is now a realistic alternative to multiple-vessel bypass surgery in selected patients. Previously the procedure was limited to 5% to 10% of the patients undergoing coronary arteriography, but presently, in the author's experience, 50% of the patients undergoing arteriography may now be considered suitable candidates for a PTCA procedure.

Hollman and Ischinger, in their chapter, "The Problem of Restenosis," report that, although mortality, morbidity, abrupt occlusions, dissections, localized hematoma, and additional complications have all significantly improved, recurrent stenosis remains the most serious barrier to a wider application of the technique.

The chapter on saphenous vein-graft angioplasty could include a more detailed discussion of the pathology for the bypass graft. The technical success and long-term results of saphenous vein-graft angioplasty will vary depending on the presence of intimal hyperplasia, organized thrombus, or vein-graft atherosclerosis.

I recommend this book as "must reading" for all cardiologists who perform invasive procedures. Experienced physicians can compare these established techniques and results with their own, and beginners should commit the text to memory. I also consider the text "must reading" for radiologists involved in invasive interventional vascular procedures. Sophisticated wire and balloon technology developed for the coronary circulation is increasingly being applied by vascular radiologists in the peripheral and visceral circulation. Certainly the text should be a part of all departmental libraries.

Mark H. Wholey
Shadyside Hospital
Pittsburgh, PA 15232

MR Imaging of Pulmonary Emboli: An Experimental Study in Dogs

Mark G. Stein[1,2]
John V. Crues III[2]
William G. Bradley, Jr.[3]
Keith E. Kortman[3]
Terry A. Andrues[3]
Alan D. Waxman[2]
Robert W. Henderson[3]
Peter J. Julien[2]

Experimental pulmonary emboli, consisting of tantalum-labeled autologous blood clots and barium-labeled 3-mm plastic spheres that did not produce an MR signal, were introduced through the femoral vein into each of five dogs. The sensitivity of MR to detect autologous clots of known size was assessed, and the size of the clot on MR was compared with its actual size. Emboli were localized by using chest radiographs made in multiple projections. Cardiac-synchronized MR imaging was performed on a 0.35-T superconducting magnet and was followed by a ^{99m}Tc macroaggregated lung scan. All 12 blood clots larger than 3 mm, and three of 20 clots less than 3 mm in transverse diameter were correctly visualized with MR. Five of the 15 clots seen on MR were larger than 150% of the actual size. There were nine false-positive emboli on MR. Two of six plastic spheres resulted in an abnormal signal on MR. MR signal from pulmonary emboli results from the thrombus itself and probably also from slow blood flow proximal to the obstruction. MR may be of value in detecting pulmonary emboli; clinical trials to evaluate its usefulness should be carried out.

With its inherent contrast resolution between static and flowing blood, MR has the potential to image pulmonary emboli noninvasively [1–4]. Rapidly flowing blood and lung parenchyma produce almost no MR signal, whereas fresh clot should give a strong signal and good contrast with the surrounding lung. At least one experimental study and two case reports have demonstrated pulmonary emboli by MR [2–4], although not clot length or diameter [1].

The cause of the MR findings associated with pulmonary emboli has not been determined [5]. If the clot alone causes the signal in the region of the pulmonary embolus, the size of the clot detected on MR should be similar to that on radiographs. If the size on MR is larger, something other than the clot (e.g., slow flow) must be causing the signal. Similarly, if material that does not emit an MR signal is placed into the pulmonary arterial circulation and an abnormal signal is seen in that region, something in addition to the clot itself, such as slow flow or stagnant blood, must be causing the abnormal signal [5–10].

In this study, we assessed the sensitivity of MR to detect autologous clots of known size in the pulmonary circulation in dogs, and then we compared the size of the clot seen on MR to its actual size. We also imaged occluding plastic spheres (which produced no in vitro MR signal) in the pulmonary circulation to investigate further the cause of the signal produced by pulmonary emboli.

Methods

Five adult mongrel dogs weighing approximately 20 kg each were anesthetized with IV pentobarbitol (2 mg/kg) and morphine (1 mg/kg). Anesthesia was maintained with pentobarbitol as required. The heart rate of the dogs was maintained between 40 and 100 beats per min with IV propanolol (0.5 mg) or atropine (0.5 mg) as required.

Autologous blood clots labeled with radiopaque tantalum oxide and barium-labeled plastic spheres were embolized to the lungs from the femoral vein. Radiographs were obtained in

Received May 7, 1986; accepted after revision July 25, 1986.

[1] Present address: Department of Radiology, C-309, University of California San Francisco, San Francisco, CA 94143-0628. Address reprint requests to M. G. Stein.

[2] Department of Imaging, Cedars Sinai Medical Center, Los Angeles, CA 90048.

[3] Magnetic Resonance Imaging Laboratory, Huntington Medical Research Institutes, Pasadena, CA 91105.

AJR 147:1133–1137, December 1986
0361–803X/86/1476–1133
© American Roentgen Ray Society

different projections followed by MR and perfusion lung scans. The dogs were sacrificed with IV potassium chloride.

Autologous Blood Clots

Clots were made by mixing 2.7 ml of freshly drawn blood with 0.3 ml of aminocaproic acid (EACA 250 mg/ml) to stabilize the clots [2]. Approximately 0.1 ml of tantalum oxide was added to the mixture. The labeled blood was then allowed to clot in a 5-ml syringe (1 cm internal diameter), the tip of which had been cut off. The syringe was vigorously agitated until the blood clotted to ensure uniform distribution of tantalum oxide throughout the clot.

The in vitro MR signal intensity of the tantalum-labeled clots was found to be identical to unlabeled clots (made with 0.7 ml fresh blood and 0.3 ml EACA) with a repetition time (TR) of 1 sec and echo-delay time (TE) of 28 and 56 msec. The TR of 1 sec was chosen because it was the average TR of the cardiac-gated imaging (heart rate 40–100/min) used later for the in vivo studies.

Plastic Spheres

Two 3-mm plastic spheres labeled with radiopaque barium-impregnated wires were also injected into each of three dogs through the femoral vein. The labeled spheres gave no MR signal under identical procedures to those used for imaging the in vitro clots.

Animal Preparation

The femoral vein of each dog was then exposed, a venotomy was performed, and the clots were injected by inserting the 5-ml syringe directly into the vein. The distribution of the clots and spheres was directed by placing the lung to be embolized in a dependent position. Two clots were embolized to one lung in each of the first two dogs. In the next three dogs, two clots were placed in the right lung and two plastic spheres were placed in the left lung. After embolization, the femoral vein was ligated, and the dog was given 1 ml of EACA IV to maintain clot stability.

Radiographs

After embolization of the clots and spheres, chest radiographs were obtained in the anteroposterior, both oblique, and lateral projections. The film tube distance was 4 ft (3.7 m); the cassettes were placed immediately under the dog to decrease magnification.

MR

MR was performed with a Diasonics superconducting magnet system operating at 0.35 Tesla. ECG-synchronization was used for all studies. Axial spin-echo images, of 7-mm slice thickness with 3 mm between slices, were obtained from the lung apex to the lung base. Coronal imaging (7-mm slice thickness separated by 3 mm) from the spine to the sternum was also performed in three dogs. Two echoes were obtained in each sequence (TE) at 28 and 56 msec. TR was determined by the heart rate because of the use of ECG-gating, which varied between 1.5 and 0.5 sec for heart rates between 40 and 100 beats/min, gated to every heart beat.

Perfusion Lung Scans

Perfusion lung scans were performed on a large-field-of-view scintillation camera using 5 mCi (111 MBq) ^{99m}Tc macroaggregated albumin injected IV. Lung scan images were performed for 500,000 counts each in the left and right anterior and posterior oblique, anterior, posterior, and both lateral projections, for a total of eight views.

Interpretation

The MR studies were interpreted independently by two observers who did not know how many emboli were in each study. They circled the sites they interpreted as emboli. The MR findings were correlated with the radiographs and lung scans. The position of the clots and spheres in the axial and coronal projection was determined by correlating the various radiographic projections and fixing the position of each embolus in an axial view. Each radiograph was divided by transverse lines 1 cm apart, and axial projections were reconstructed with the embolus position. These projections were compared to the MR scan sections (also 1 cm apart). Some allowance was made for change in clot position because of the respiratory motion during the MR. The position of the clots was related to the dome of the diaphragm and to the hila of the lung. Both transverse and longitudinal measurements were obtained for all clots on both chest radiograph and MR images. For each abnormality noted on the MR, a corresponding embolus was looked for on the radiographs and vice versa. An embolus identified on MR that corresponded to an embolus on the radiographs was classified as a true positive. Abnormalities on MR that did not correspond to an embolus on the radiographs were classified as false positive. A false negative was an embolus on a radiograph not detected on MR.

The maximum length of the clots on MR was assessed by using a computer-generated measurement grid. An abnormality seen on MR was only considered larger than the clot seen on chest radiograph when the length was 50% greater than the X-ray size because of (1) the inherent decreased spatial resolution of MR, (2) difficulty in obtaining accurate measurements of less than 5 mm, and (3) the lack of standardization of the television display brightness. All these factors have some effect on the size seen on the video display.

The perfusion scans were used to determine whether sites of decreased perfusion corresponded to an embolus. Perfusion defects not corresponding to emboli and emboli without perfusion defects were also noted.

Results

After injection, each clot broke up into multiple smaller clots (Table 1, Fig. 1), probably because the tantalum oxide made them friable. All clots measured less than 1 cm in transverse diameter on radiographs. All the clots less than 3 mm in diameter were peripherally distributed. Half the clots >3 cm in diameter were in the midlung. No clots were centrally located. All the spheres were located centrally. The transverse

TABLE 1: **Numbers of Clots on Radiographs and MR (True Positives)**

Transverse Diameter of Clots on Radiographs (mm)	No. of Clots	
	On Radiographs (Tantalum-labeled)	On MR
3–8	12	12[a]
<3	20	3[b]

[a] Each observer failed to identify two clots. All clots were seen by at least one observer.
[b] Seventeen clots less than 3 mm in transverse diameter were not identified with MR.

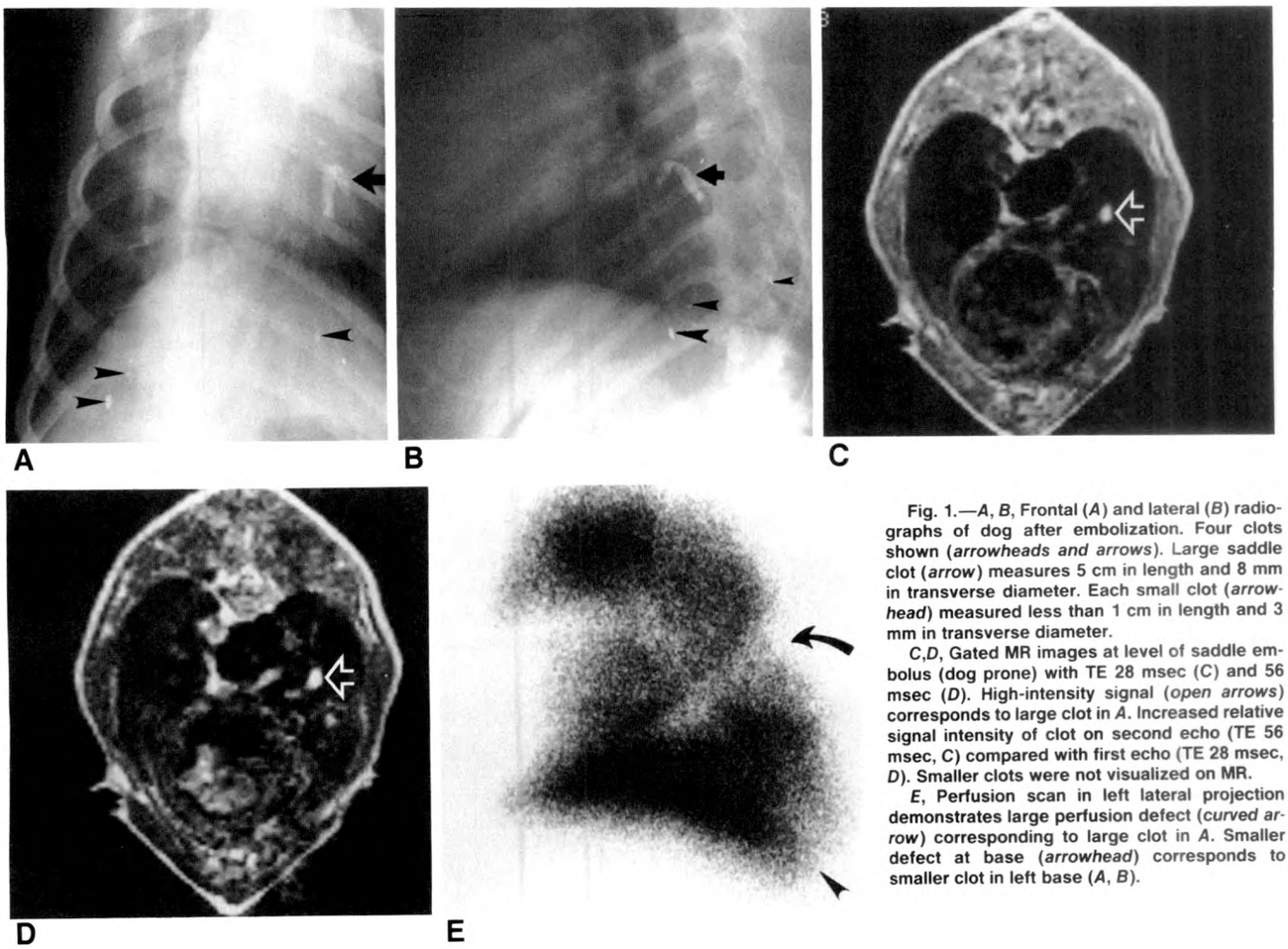


Fig. 1.—*A*, *B*, Frontal (*A*) and lateral (*B*) radiographs of dog after embolization. Four clots shown (*arrowheads and arrows*). Large saddle clot (*arrow*) measures 5 cm in length and 8 mm in transverse diameter. Each small clot (*arrowhead*) measured less than 1 cm in length and 3 mm in transverse diameter.

***C*,*D*, Gated MR images at level of saddle embolus (dog prone) with TE 28 msec (*C*) and 56 msec (*D*). High-intensity signal (*open arrows*) corresponds to large clot in *A*. Increased relative signal intensity of clot on second echo (TE 56 msec, *C*) compared with first echo (TE 28 msec, *D*). Smaller clots were not visualized on MR.**

***E*, Perfusion scan in left lateral projection demonstrates large perfusion defect (*curved arrow*) corresponding to large clot in *A*. Smaller defect at base (*arrowhead*) corresponds to smaller clot in left base (*A*, *B*).**

or smallest diameter of the clot (on radiographs) was used for evaluation of clot detection because it represented the diameter of the vessel in which the clot had stopped (presuming all clots to be occlusive). Perfusion defects were noted in all regions where clots were localized, suggesting that most were occlusive. One large segmental defect was seen that did not correspond to a labeled clot. All 12 clots that were 3 mm or more in transverse diameter were identified by at least one observer. Of these 12 clots, two were not identified by observer 1, and two separate clots were not identified by observer 2. The mean length of clots greater than 3 mm in transverse diameter was 17 mm (range 8–40 mm). Of the 20 clots that were less than 3 mm in transverse diameter, only three were identified. These had lengths of 4, 4, and 3 mm, respectively (mean, 3 mm). The length of clots not visualized ranged betwen 1 and 6 mm, with a mean of 3 mm. Coronal images showed only one clot not seen axially and missed many clots.

The maximum length of five of the 15 clots seen by MR was more than 150% of the largest measurement on radiographs. All these were less than 1.1 cm in largest radiographic measurement. No significant association was observed between increased MR measurement and increased relative signal intensity on the TE 56 msec second-echo images. The second-echo intensity was the same or increased compared to the first-echo intensity in 13 of 15 clots (87%) (Table 2, Fig. 2).

TABLE 2: **Relative Intensity of Clots on First-Echo and Second-Echo Images**

Size (mm)	No. Visualized	Second-Echo Intensity Compared to First-Echo (N)		
		Increased	Equal	Decreased
3–8	12	4	6	2
<3	3	2	1	0
Total	15	6	7	2

Two of the six 3-mm plastic spheres were associated with abnormal MR signal intensity. The second-echo intensity signal of each visualized ball was slightly greater than the first echo. In both cases, the length of abnormal signal was more than 6 mm in largest MR measurement and, therefore, unlikely to result from immediate local effects of balls, which were 3 mm in diameter.

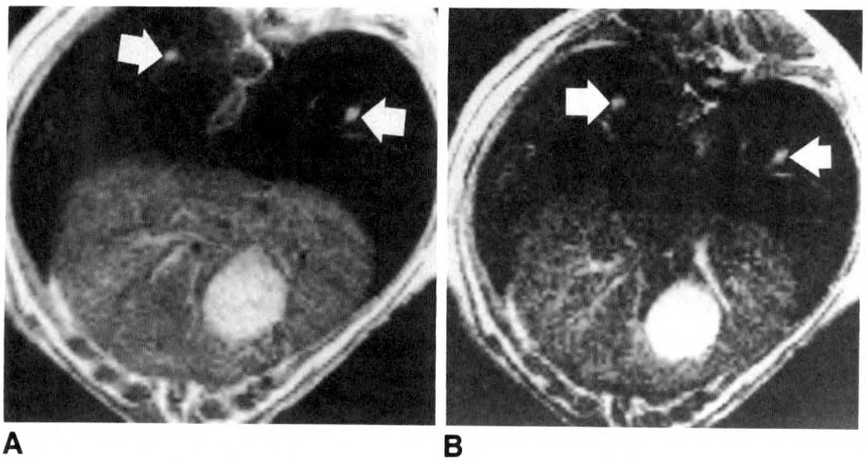


Fig. 2—*A,B*, Gated MR images of dog (prone) with TE 28 msec (*A*) and 56 msec (*B*) show large clot in each lower lobe (*arrows*). Slightly increased relative signal intensity seen on second echo.

Nine false-positive emboli were identified on the MR studies by the two observers (Table 3). False-positive 1, a high-intensity linear signal in the right hilum with no associated labeled clot, was interpreted as perihilar fat by interpreter 1 and an embolus by interpreter 2. However, a large perfusion scan defect, seen in the corresponding region on the lung scan, may have represented an unlabeled clot, possibly an in vivo embolus from the femoral vein stump. The remaining false-positive abnormalities could not be readily explained. No MR parenchymal abnormalities were seen on any scan distal to a labeled clot.

Discussion

The evaluation of pulmonary emboli by MR should be ideal because of the different MR properties of flowing blood, air-containing lung, and blood clot [5–9]. Fast, turbulent, or disturbed (pulsatile) flow of blood usually does not give an MR signal [8, 10]. Although gated MR studies usually have no signal in the pulmonary arteries during systole and early diastole [5, 6], some signal may be seen during late diastole as the rate of flow decreases to a speed at which the stimulated nuclei do not leave the planes of imaging during the relaxation phase (less than 10–15 cm/sec) [5]. Normal lung parenchyma (predominantly the air in the parenchyma) does not normally generate an observable MR signal.

Fresh blood clot, however, generates a strong signal on both T1- and T2-weighted imaging sequences [2]. Compared with the lack of surrounding signal (from flowing blood and lung), this strong signal provides good contrast on MR. In this study, clots larger than 3 mm in transverse diameter (longitudinal average, 17 mm) were routinely seen by at least one observer despite a 3-mm interslice distance. We believe that the interobserver difference may have resulted from inexperience, because the clots were easily seen in retrospect. Clots smaller than 3 mm were not routinely seen because (1) they tended to be more peripheral, and (2) the chance of such a small clot being predominantly in the interslice gap was increased. In the future, these problems may be reduced with respiratory gating, thinner sections, and contiguous spacing.

Further improvements in resolution may result from the use of a ECG-triggered permutation imaging sequence ("rotated gating") [10], in which the same slice is obtained during different phases of the cardiac cycle [5, 6], a process that

TABLE 3: **False-Positives: Radiographs Compared to Perfusion Defects on Lung Scan, Size of Defect on MR, and Intensity of Second Echo (TE 56 msec) Compared to First (TE 28 msec)**

False-Positive (No.)	Observer	Image No. in Gating Cycle[a]	Perfusion Defect	Intensity of Second Echo Compared to First	Length of Signal (cm)
1	1	1–5	Yes[b]	Increased	7
2	2	3, 4	No	Equal	2
3	1	2, 3	No	Equal	1.4
4	2	3, 4	No	Increased	1
5	2	1	No	Increased	1.2
6	2	1	No	Increased	1
7	2	5	No	Equal	2
8	2	1	No	Decreased	1
9	2	3, 4	No	Increased	1

Note.—No observers assessed the same area falsely positive.
[a] Image number in gating cycle indicates where in cardiac cycle signal occurred; 1 represents early systole and 5 late diastole.
[b] Possible unlabeled in vivo clot; see text.

helps to differentiate the signal of slowly flowing blood (e.g., late diastole) from clot.

In five of the 15 clots and two of the six plastic spheres, the MR signal was too large to be from the embolus alone. The signal was probably generated by abnormally slow-flowing or stagnant blood adjacent to the embolus [8, 9]. In one case of multiple small distal emboli in the same vessel, signal could be seen in the proximal segmental pulmonary artery. Perhaps the actual clots were enlarged because of in vivo clot proximal to the clot in an area of stasis. A rotated gating sequence [5], which may show some flow in this region, may help assess this ambiguity and exclude enlargement of the clot. Local parenchymal edema adjacent to the embolus is unlikely because the signal intensity was proximal to the clot, had a sharp, smooth margin, and was often tubular in configuration. The nine false-positive emboli (Table 3) were seen during all phases of the cardiac cycle and, therefore, could not all be explained solely as signal from slow flow. Other possible explanations include perihilar or peribronchial fat or bronchial mucous plugging [2]. The false positive associated with a large perfusion defect (number 1, Table 3) may have represented an in vivo thrombus.

Increased intensity on the second echo, which may occur from even-echo rephasing and signifies slow flow [9, 10], has been used to distinguish true-positive emboli with associated slow flow from a false-positive signal unassociated with flow abnormalities [2]. Blood clot will have an absolute second-echo intensity less than the first, while flowing blood may have an absolute increase in signal intensity on the second echo [10]. No differences in second-echo intensities were evident between the true and false positives in this study (Tables 2 and 3).

In a previous study [2], Gamsu et al. found fewer false-positive clots than our study. However, we had more clots and our observers were aware that the clots were small. Possibly they were overly alert to small defects. In this study, each observer identified 10/12 (83%) true positives as opposed to 63% for each observer in the Gamsu et al. study. The false negatives in that study may have been caused by the barium wire alone being visualized when a large amount of the adherent clot had broken off during the procedure. In our study, the clots themselves were labeled throughout with tantalum.

These autologous clots were all freshly formed within 3 hr of scanning. Red blood cells are trapped in acute clots, but not necessarily in in vivo subacute or chronic clots, where the red cells may have lysed, leaving only fibrin and tissue deficient in mobile protons. This process would result in the high signal intensities noted from the clots in this study, while older clots may not be as high in intensity [3]. Thus, MR of human pulmonary embolism clots may be dissimilar from the clots in this study.

We have not addressed the problem of differentiating pulmonary emboli from abnormal lung parenchyma, where the increased signal from the consolidated area as well as signal from slow-flowing blood may decrease contrast between clot and abnormal lung [5, 9]. Slow flow in pulmonary hypertension may also result in signal in patent vessels throughout the cardiac cycle, which may be mistaken for clot without a rotating gated imaging sequence [5]. Mucous plugs may also give a high-intensity MR signal indistinguishable from blood clot [2].

REFERENCES

1. Higgins CB. Cardiovascular imaging. In: James TL, Margulis AR, eds. *Biomedical magnetic resonance*. San Francisco: Radiology Research and Education Foundation, University of California, **1984**:135–142
2. Gamsu G, Hirji M, Moore E, Webb WR, Brito A. Experimental pulmonary emboli detected using magnetic resonance. *Radiology* **1984**;153:467–470
3. Moore EH, Gamsu G, Webb WR, Stulbarg MS. Pulmonary embolus: detection and follow-up using magnetic resonance. *Radiology* **1984**;153:471–472
4. Thickman D, Kressel HI, Axel L. Demonstration of pulmonary embolism by magnetic resonance imaging. *AJR* **1984**;142:921–922
5. von Schulthess GK, Fisher MR, Higgins CB. Pathologic blood flow in pulmonary vascular disease as shown by gated magnetic resonance imaging. *Ann Intern Med* **1985**;103:317–323
6. von Schulthess GK, Fisher MR, Crooks LE, Higgins CB. Gated MR imaging of the heart: intracardiac signals in patients and healthy subjects. *Radiology* **1985**;156:125–132
7. Wehrli FW, Shimakana A, Macfall JR, Axel L, Perman W. MR imaging of venous and arterial flow by a selective saturation-recovery spin echo (SSRSE) method. *J Comput Assist Tomogr* **1985**;19(3):537–545
8. Bradley WG, Waluch V, Ka-Siu Lai, Fernandez EJ, Spalter C. The appearance of rapidly flowing blood on magnetic resonance images. *AJR* **1984**;143:1167–1174
9. Waluch V, Bradley WG. NMR even echo rephasing in slow laminar flow. *J Comput Assist Tomogr* **1984**;8:594–598
10. von Schulthess GK, Higgins CB. Blood flow imaging with MR: spin phase phenomena. *Radiology* **1985**;157:687–695

Book Review

Cardiac Catheterization and Angiography, 3rd ed. Edited by William Grossman. Philadelphia: Lea & Febiger, 562 pp., 1986. $49.50

This third edition of a classic teaching textbook is designed to instruct physicians who are training to become cardiologists. The intent of this book is to provide practical, clear, and concise descriptions of major techniques currently being used in cardiac catheterization and angiography. I think that the authors have succeeded in these stated goals. The book is written by 23 authors including one radiologist, Sven Paulin.

The 33 chapters are grouped into seven separate parts. Part I deals with the general principles of cardiac catheterization and angiography, including a chapter by Robert Marco and Sven Paulin entitled "Angiography: Principles Underlying Proper Utilization of Radiologic and Cineangiographic Equipment." Part II deals with specific techniques of cardiac catheterization, including the direct brachial approach (which uses a single cutdown in the right antecubital fossa from which either a left or right heart catheterization can be performed) and the seldinger percutaneous femoral artery and vein techniques that are more familiar to radiologists. Part III deals with basic hemodynamic principles and part IV covers angiographic techniques, including coronary angiography, cardiac ventriculography, pulmonary angiography, and aortography. Part V discusses the methods used for evaluating cardiac function, such as dynamic and isometric exercise during cardiac catheterization. Part VI provides integrated hemodynamic and angiographic profiles of specific disorders such as valvular and coronary heart disease. The book concludes with part VII, which discusses specific advanced catheter techniques, including coronary angioplasty, percutaneous intraaortic balloon insertion, endomyocardial biopsy, pacemakers, and the potential role of lasers in the cardiac catheterization laboratory. An appendix of normal values relevant to cardiac catheterization and angiography are provided at the end of the book.

This well-written book provides a fairly succinct introduction to most of the important concepts in cardiac catheterization and angiography. Part IV provides good technical information on performing coronary angiography and ventriculography. The technical discussion of pulmonary angiography is somewhat brief, and I disagree with the position that the brachial approach should be used for pulmonary angiography in patients with suspected pulmonary embolism. Part VI presents good discussions of patients with a variety of disorders that should provide a radiologist with good insight into the total workup of a patient with serious heart disease. The chapters in this text that are devoted to hemodynamics and evaluation of cardiac function will be of little interest to most practicing radiologists, but these chapters do cover a lot of material in a clear and concise fashion.

The quality of the radiographic images throughout the text are good. My only complaint is that more images are not provided. The graphs and tables provided throughout the text are well done.

The book reads easily and since it is divided into separate parts, it is easy to focus on those items that are of most interest to the reader.

This book is too specialized for most practicing radiologists. It is a book that will be in most hospital libraries, and will be a valuable reference book to those radiology residents, fellows, and staff that are involved in the art and science of cardiac catheterization and angiography.

John D. Newell II
University of New Mexico Hospital
Albuquerque, NM 87131

New Cineradiographic Methods for Assessment of Bjork-Shiley Valve Integrity

Alan J. Cousin[1]
Benigno Soto

The Bjork-Shiley prosthesis has been used extensively for valvular replacement since 1969. Despite its widespread use, it is subject to complications that can be assessed with cineradiography. New methods are presented for assessment of incomplete closing and opening angles that occur with valvular malfunction. Alternative methods of cineradiographic measurement are compared with each other and with the new method. The new method is an appropriate alternative when the conventional double-profile method cannot be used and distributes the burden of performance and complexity between the technologist and radiologist. This new method is shown to be accurate to within 1°.

The Bjork-Shiley prosthesis has been used extensively for valvular replacement since its introduction in 1969 [1, 2]. Since that time it has undergone several revisions—one of which was to implant a tantalum foil loop in the outflow well of the disk. All disks manufactured after late 1975 have this radiopaque loop embedded in the pyrolytic carbon disk. More recently, the valve has been further modified with a convexoconcave design to reduce thrombus formation on the outflow side of the disk and to resolve other problems relating to the slow flow that occurs in the minor-outflow region of the valve [3].

Despite these revisions and its excellent hemodynamic attributes, the Bjork-Shiley valve is still not the ideal cardiac prosthesis. The most frequent complications are infected and noninfected paravalvular leakage, valvular dysfunction, and clot formation despite adequate anticoagulation [4–12]. Radiographic assessment of the Bjork-Shiley valve requires quantitation of base-ring movement as well as disk movement. Typically, this is easily accomplished with the valve in the aortic position by profiling simultaneously both base ring and disk, obtaining several cineradiographic frames, and then directly measuring the maximum opening angle. The normal value for maximum opening set at the time of manufacture is 60° but in vivo these values are often somewhat less than and occasionally more than 60° [13]. A new method for determining closing and opening angles is described and compared with other methods reported in the literature [13–16]. By appreciating the individual attributes of the several methods now available, one can easily choose the most appropriate method when confronted with a difficult valve measurement problem.

Received December 2, 1985; accepted after revision July 7, 1986.

[1] Both authors: Department of Radiology, Division of Cardiac Radiology, University of Alabama School of Medicine, Birmingham, AL 35233. Address reprint requests to A. J. Cousin, Department of Radiology, University Hospital, 619 S. 19th St., Birmingham, AL 35233.

AJR 147:1139–1144, December 1986
0361–803X/86/1476–1139
© American Roentgen Ray Society

Basis of the Proposed Methods

Computing the angle of valve opening involves finding the angle between two intersecting planes in space. In the special case when both planes can be projected in profile to the X-ray source, the angle can be measured directly and is not affected by the variations in distance between the X-ray source, valve, and detector.

The Bjork-Shiley valve prosthesis (boxed insert, Fig. 1) is radiographically imaged as a large-diameter circular shadow corresponding to the base ring and a thin,

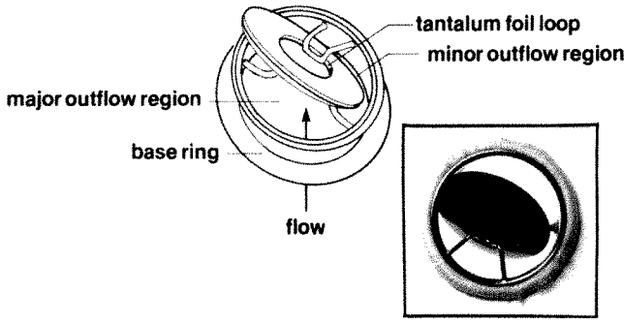


Fig. 1.—Schematic drawing and photograph (boxed insert) of Bjork-Shiley prosthesis.

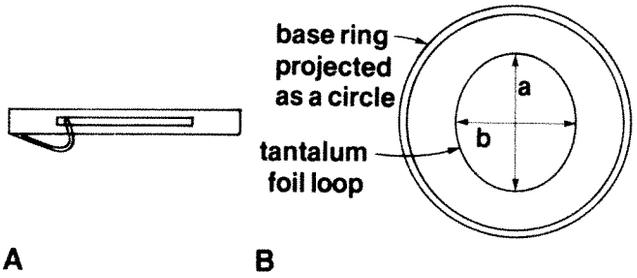


Fig. 2.—Closing angle assessment.

A, In many cases, base ring can be profiled and edge of tantalum foil loop through base ring can be viewed.

B, When disk reference cannot be clearly seen through base ring, an en face view can assess "circularity." See text (equation 1) for the calculation.

smaller-diameter circular shadow corresponding to the internal border of the valve disk that demarcates the impressed central portion from the raised, annular outer portion. The disk-ring shadow is produced as a consequence of the radiopaque tantalum foil loop embedded in the pyrolytic carbon disk material shown in the diagram in Figure 1. Consequently, any random projection will show the valve as two related rings that appear elliptical. Two special cases are (1) an en face projection in which the appropriate structure will appear as a perfect circle and (2) a profile (or tangent) projection in which the two rings appear as lines.

Closing Angle Assessment

Valve closure can become compromised mechanically by thrombus, usually on the low-flow side. For measurement of the closing angle, it is often possible to profile the base ring (refer to Fig. 2A) and to view the edge of the tantalum foil loop through the base ring [13].

When the disk reference cannot be clearly seen through the base ring, one can use an en face view to assess "circularity" as shown in Figure 2B. With an obstruction to closure, when the base ring is projected as a circle, the radiopaque portion of the disk will appear elliptical. With Bjork-Shiley valve in the mitral position and employing the same en face view during systole, the maximum and minimum diameters of the elliptical projection of the tantalum foil loop allow computation of the closing angle as:

$$\cos(\text{closing angle}) = \frac{b}{a} \qquad (1)$$

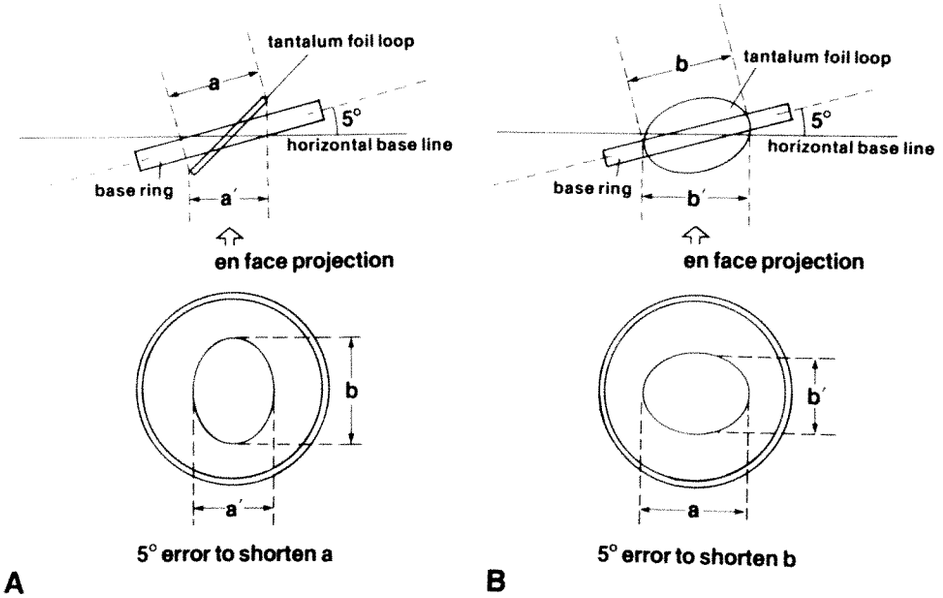


Fig. 3.—Errors in opening angle assessment by en face method.

A, Angulation from perfect en face projection shortens a to a′. Dimension b stays the same, but dimension a changes quickly, because cosine function is nearing its maximum slope and this value should be equal to actual error in degrees from true en face projection.

B, Angulation error is perpendicular to error in *A*. Dimension a stays the same, but b decreases by cosine of angle from perfect en face projection.

Bottom drawings, en face appearance of tantalum foil loop.

This method is identical to that of Godwin [13] that was used for the opening angle, but here it is applied to quantitate the closing angle. One could also obtain an en face projection of the disk, measure the "circularity" of the base ring, and obtain identical results.

Opening Angle Assessment

The simplest method to quantitate the opening angle is to obtain a simultaneous profile view of both base ring and disk. The maximum opening angle can be readily assessed either by direct measurement of the angle or by measurement of two sides of the triangle with the opening angle included between these two sides and use of a tangent loop-up table graph. This angle measurement is independent of the magnification caused by the variable distance between valve, X-ray source, and detector.

For cases when this double-profile view cannot be obtained, Venkataram et al. [14] have described a method that requires only a single projection but that uses numerous measurements of major and minor elliptoid axes and of one angle. The resulting equation is complex:

$$\text{Opening angle} = \beta = \cos^{-1} \frac{1}{a_1 a_2} \langle \cos \phi \{\sqrt{[a_1^2 - b_1^2][a_2^2 - b_2^2]}\} \pm b_1 b_2 \rangle \quad (2)$$

where ϕ is the angle between the major axes a_1 and a_2, and a_1, b_1, a_2, and b_2 are the major and minor axes of each ellipse, respectively.

A third method by Godwin [13] requires an en face projection of the base ring and only two measurements on a single view. Although this definitely has the advantage of simplicity, highly accurate en faceness is required. For example, if the base ring is not projected exactly en face the error can be significant. Potential error in this technique can be assessed by referring to Figure 3, in which two special cases are shown. With 5° as an illustrative error, the first case (Fig. 3A) results in the 5° error adding directly, while the second case (Fig. 3B) results in an error of approximately 0.2°. The general case would be an error of orientation intermediate between the above two, and consequently, the error should lie between 0.2° and 5°. These errors can, of course, be measured cineradiographically and then used to correct the calculated angle, but the method becomes complex. Although not mentioned by Godwin [13], this method also has the advantage that it can be used if only the disk can be projected en face; then analogous measurements can be made of the base ring to provide the opening angle measurement.

All three of the above methods—double profile, Venkataraman et al. [14] and Godwin [13]—share the advantage that only one cineradiographic view is required. However, with the exception of the first method in which a simultaneous profile of both base ring and disk can be obtained, each has its shortcomings as outlined. These limits must be considered in the context of the required accuracy and our desired sensitivity to changes in the opening angle related to disease. Also,

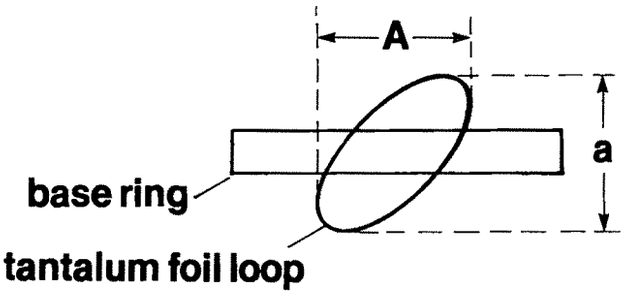


Fig. 4.—Required measurements from cineradiographic frame with base ring profiled.

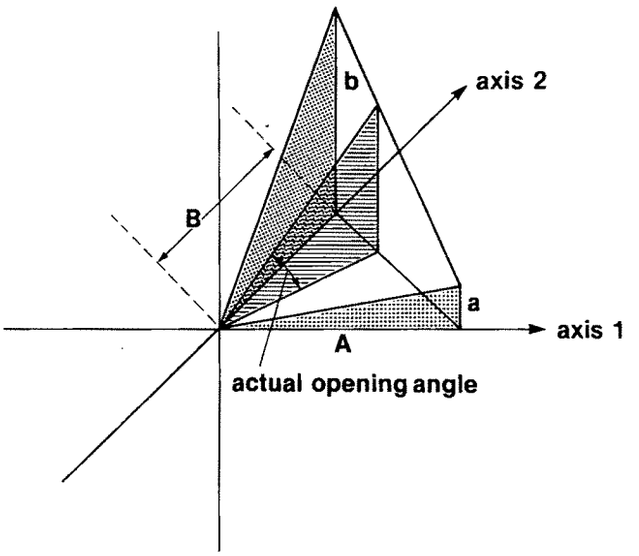


Fig. 5.—Three-dimensional line drawing that shows the measurements required for new method. Hatched triangle represents desired plane of measurement, which corresponds to orientation used in double-profile method whereby opening angle can be measured directly. Two dotted triangles correspond to two planes of measurement required for new method and are arranged ideally 90° apart.

the burden of measurement and complexity for the radiologist vs the skill required of the technologist in repeatably and reliably obtaining perfectly en face views must be evaluated.

We propose a new method employing *two* cineradiographic views to obtain the maximum opening angle. Specifically, if one obtains two different profile views of either the disk or the base ring, the resulting equation needed for calculating the opening angle is much simpler, and the technologist is only required to obtain profile views rather than en face views. Because this last requirement has a built-in control (i.e., the alignment of one edge of a circular structure with the other), results should be more repeatable and more accurate.

Geometrically, the problem is reduced to determining the angle between the planes of the two valve components given two views at known angles to each other. For the Bjork-

Shiley geometry, although the hinge point is not at the edge of the radiopaque disk, the valve can still be considered as two hinged planes without any change of reference points. If one constrains the cineradiographic view such that one of the two planes is tangent to the beam (i.e., in profile), the other will appear as an ellipse.

The two required measurements for each view are shown in Figure 4. This can be represented equivalently by a three-dimensional line drawing as shown in Figure 5. Geometric considerations from the two views (along axis 1 and axis 2) yield

$$\text{Opening angle} = \tan^{-1} \frac{a + b}{\sqrt{(B \sin c)^2 + (A \sin c)^2}} \quad (3)$$

where c is the angle between the two projections that is set by the technologist, and a, A, b, and B are the elevation and width of the disk in each view, respectively, and need to be measured on the appropriate cineradiographic frame as shown in Figure 4.

This equation can be further simplified if the two views can be obtained while maintaining the base ring in profile with an angle of 90° between the two views. The resulting opening angle can then be expressed as

$$\text{Opening angle} = \tan^{-1} \frac{a + b}{\sqrt{A^2 + B^2}} \quad (4)$$

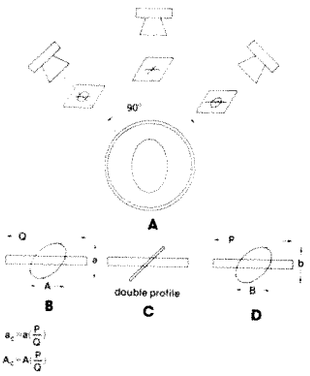


Fig. 6.—*A*, Overall schema of the new method and double-profile method with Bjork-Shiley valve held in maximum opening position.

***B*, *D*, Two views needed for new method. Only base ring is in profile; note two 90°-related views. Measurements from *B* and *D* allow calculation of opening angle by using a simple equation (see equation 4 in text). One should obtain 60° as opening angle after correcting for magnification. Magnification correction should be used for most accurate results.**

***C*, Resulting conventional double-profile image shows opening angle as 60°.**

Errors related to changes in magnification between the two views can be corrected by normalizing two of the four required measurements by the projected base-ring diameter ratio. Magnification correction should always be used for most accurate results.

Results

That the technique can be reduced to practice can be demonstrated in several ways. The overall schema of the new method and the double-profile method is shown in Figure 6A, with Figure 6C depicting the conventional double-profile image. The two views and required measurements are illustrated in Figures 6B and 6D. The series in Figure 7 shows use of the new method in an ex vivo environment that results in an accuracy of within 1° of the true value.

Sometimes the position of the tantalum loop that overlies the base ring will not be visible with a cineangiographic projector, but the location of the obscured portion can be readily estimated. Alternatively, for more accurate results, one can trace the visible portion of the tantalum loop and then, invoking symmetry arguments, flip over the paper image and align it with the projected image to obtain a continuous ellipse that is suitable for measurement. Our experience has been that only small errors (less than 1°) are introduced by estimating the position of the partially obscured loop.

Figure 8 illustrates the potential pitfalls of this method as applied to a valve located in the aortic position. In the case shown, insufficient craniocaudal tilt was applied to obtain the desired profile view. Also, the two views must be obtained 90° apart. The first error is apparent when the cineradiograph is viewed and is the source of the small difference in the angle computed by our method. The second error requires assurance from the technologist that the two views were orthogonal.

Discussion

The most straightforward method for obtaining the opening and closing angles of a Bjork-Shiley prosthesis is the double-profile method. This has the dual advantage of requiring only a single-profile view of the various valve components and a single geometric calculation or tangent table.

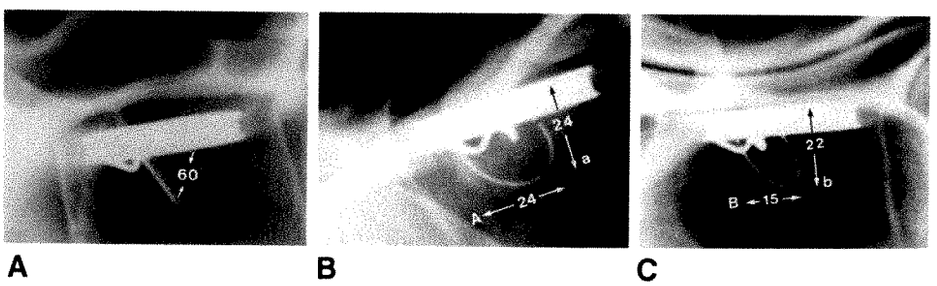


Fig. 7.—Ex vivo cineradiographic illustration of new method.

***A*, Double-profile view from which the opening angle of 60° can be directly measured.**

***B*, *C*, Two 90°-related views obtained with base ring in profile. Required measurements are noted, and putting these values into a simple equation (see equation 4 in text) yields a calculated opening angle of 58.4°. By using magnification correction as described in Fig. 6, one obtains opening angle of 59.1°—within 1° of the actual value.**

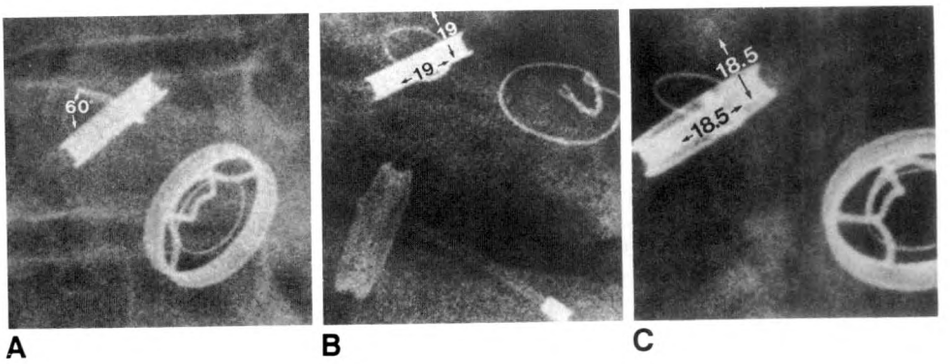


Fig. 8.—In vivo cineradiographic illustration of new method applied to a clinical case with valve in aortic position that shows potential pitfalls.

***A*, Double-profile view from which opening angle can be directly measured.**

***B*, *C*, Two views 90° apart with measurements yielding (after magnification correction) a computed opening angle of 55.4°. Geometric relationships partly compensate for varying magnification between the two views, and computed angle without magnification correction will differ only by 0.04° in this example. Base ring in *C* is not exactly in profile; insufficient craniocaudal tilt was applied to obtain desired profile view.**

TABLE 1: **Comparison of the Four Methods for Measurement of Opening Angle**

Method	Advantage	Disadvantage	Comments
Double profile	1. Only single view required 2. Technologist required to profile two structures 3. Direct measurement of the angle from one cineradiographic frame with essentially no calculations involved	Not always obtainable, particularly when the valve is in the mitral position and oriented cephalocaudad	Always use if this view is obtainable
Venkataraman et al. [14]	1. Only single view required 2. Wide range of orientation allowed	Complex calculations or table needed	Burden of expertise moved from the skill of technologist to a more complex cineradiographic calculation for the radiologist
Godwin [13]	1. Only single view required	Errors possible from inability to obtain a perfect en face view	Burden of expertise almost entirely on the technologist and accurate results critically dependent on the ability to obtain en face projections in real time
Cousin (this paper)	1. Simple calculation 2. Technologist required only to do profile views requiring straightforward alignment judgment	1. For best accuracy, correction for magnification needed 2. Two separate views required, ideally 90° apart	Burden distributed so that the technologist must obtain two views but the resulting calculations are considerably simplified

When this view cannot be obtained, three alternative approaches are now available. The method described by Venkataraman et al. [14] eases the technologist requirement to obtaining a single view depicting the elliptical projection of the base ring and foil loop. However, both the number of measurements and the complexity of the resulting equation increases for the radiologist. The method described by Godwin [13] shifts the burden to the technologist. The necessary calculations are quite straightforward, but the accuracy is critically dependent on the ability of the technologist to obtain an en face projection for cineradiographic analysis.

In the new method, the burden has been divided between radiologist and technologist. The technologist must obtain two views (i.e., one additional view), with either the base ring in profile in both views or the foil loop in profile in both views. Obtaining true single-profile views rather than en face views increases accuracy and repeatability. The advantages of the proposed technique are that (1) only four easily measured distances are required rather than four elliptoid related measurements plus an angle and (2) the resulting equation is considerably simplified. In addition the technologist does not need to obtain perfect en face views but only alignment in profile, which is easier to accomplish in practice and can be confirmed visually (see Fig. 8). The major disadvantage is that

two views are required. In our limited experience, we have encountered little difficulty in arranging these views to be obtained 90° to each other, thus greatly simplifying the resultant angle calculation. Of necessity the two views require twice as much radiation as other techniques and require the technologist to reliably obtain the two views 90° apart. Table 1 summarizes the advantages and disadvantages of all current techniques.

Our technique can be used for measurement of the angular relation between any two objects that have planar references, as can the other techniques. We specifically recommend this method for the case when the plane of the mitral prosthesis is oriented in a cephalocaudad direction and an effective profiling of both base ring and disk is impossible.

REFERENCES

1. Bjork VO. History of the Bjork-Shiley tilting valve. *Med Instrum* **1977**;11:80–81
2. Bjork VO. A new tilting disc valve prosthesis. *Scand J Thor Cardiovasc Surg* **1969**;3:1–10
3. Bjork VO. The improved Bjork-Shiley tilting disc valve prosthesis. *Scand J Thor Cardiovasc Surg* **1978**;12:81–84
4. Bjork VO, Henze A. Ten year's experience with a Bjork-Shiley tilting disc valve. *J Thorac Cardiovasc Surg* **1979**;78:331–342
5. Fernandez J, Samuel A, Yang SS, et al. Late thrombosis of the aortic Bjork-Shiley prosthesis. *Chest* **1976**;70:1–16
6. Yoganathan AP, Corcoran WH, Harrison EC, Curl JR. The Bjork-Shiley aortic prosthesis: flow characteristics, thrombus formation and tissue overgrowth. *Circulation* **1978**;58:70–76
7. Kazama S, Kim K, Sato K, et al. Malfunction of a Bjork-Shiley mitral valve prosthesis due to excessive platelet-fibrin deposition on its sewing cuff. *Jpn Heart J* **1980**;21:429–433
8. Karp RB, Cyrus RJ, Blackstone EH, Kirklin JW, Kouchoukos NT, Pacifico AD. The Bjork-Shiley valve intermediate term followup. *J Thorac Cardiovasc Surg* **1981**;81:602–614
9. Wright JO, Hiratzka LF, Brandt B III, Doty DB. Thrombosis of the Bjork-Shiley prosthesis: illustrative cases and review of the literature. *J Thorac Cardiovasc Surg* **1982**;84:138–144
10. Daenen W, Nevelsteen A, van Cauwelaert P, de Maesschalk E, Willems J, Stalpaert G. Nine year's experience with the Bjork-Shiley prosthetic valve: early and late results of 932 valve replacements. *Ann Thorac Surg* **1983**;35:651–663
11. Sabbagh AH. Clotted Bjork-Shiley mitral valve prostheses: early detection and surgical management. *Cardiovasc Res Cent Bull* **1983**;21:101–107
12. Martinell J, Salas J, de Vega NG, Moreno T, Fraile J, Rabago G. Thrombotic obstruction of the Bjork-Shiley aortic valve prosthesis. *Scand J Thor Cardiovasc Surg* **1979**;13:255–257
13. Godwin RJ. Cineradiographic assessment of Bjork-Shiley aortic and mitral prosthetic heart valves. *Clin Radiol* **1977**;28:355–360
14. Venkatamaran K, Beer RF, Mathews NP, et al. Thrombosis of Bjork-Shiley aortic valve prostheses. *Radiology* **1980**;137:43–47
15. de Leon AC Jr. How to recognize prosthetic valve dysfunction. *J Cardiovasc Med* **1984**;August:631–646
16. Verdel G, Heethaar RM, Jambroes G, van der Werf T. Assessment of the opening angle of implanted Bjork-Shiley prosthetic valves. *Circulation* **1983**;68:355–359

Rebound Thymic Hyperplasia After Treatment of Cushing's Syndrome

John L. Doppman[1]
Edward H. Oldfield[2]
George P. Chrousos[3]
Lynette Nieman[3]
Robert Udelsman[3]
Gordon B. Cutler[3]
D. Lynn Loriaux[3]

Rebound thymic hyperplasia has been described in children and young adults after recovery from stress. Similar thymic enlargement has been observed in patients after remission of Cushing's syndrome. In one patient successfully treated for ectopic adrenocorticotropic hormone (ACTH) syndrome by resection of a bronchial carcinoid with a hilar metastasis, the postoperative enlarging mediastinal mass suggested recurrent tumor. In another patient treated for an undetected ectopic ACTH source by a cortisol antagonist, the enlarging thymus could be confused with a thymic carcinoid. The typical thymic appearance on CT and the chronologic relation to declining cortisol levels should prevent such diagnostic errors.

Thymic enlargement after recovery from stress (e.g., burns [1], cardiac surgery [2], chemotherapy [3–7]) has been reported most often in children and adolescents. The mechanism is thymic depletion resulting from high plasma glucocorticoid concentrations [8], followed by rebound thymic hyperplasia when cortisol levels drop [9].

Cushing's syndrome occurs frequently in young adults and occasionally in adolescents. As residual thymic tissue may be demonstrated by CT in normal persons up to 40 years old [10–13], rebound enlargement might be anticipated in Cushing's patients when cortisol levels drop after resection of either an adrenal adenoma that produces cortisol or a pituitary adenoma that secretes adrenocorticotropic hormone (ACTH). When hypercortisolism results from ectopic ACTH production by a carcinoid tumor of the lung or mediastinum, the appearance of a mediastinal mass after surgery may incorrectly suggest recurrence. In addition, new glucocorticoid antagonists [14], such as RU 486, are being used to control the systemic manifestations of hypercortisolism in patients with ectopic ACTH syndrome when the occult source of ACTH cannot be found. An enlarging thymus associated with this therapy could be confused with a mediastinal carcinoid. Findling and Tyrrell [15] have recently reported the surgical removal of a "paradoxically enlarged but normal thymus" in a patient with ectopic ACTH syndrome.

We present three examples of rebound thymic hyperplasia. One patient had classic Cushing's disease responding to transsphenoidal resection of an ACTH-secreting pituitary microadenoma. The other two patients had ectopic ACTH syndrome, in one case resulting from a bronchial carcinoid (successfully resected), and in the second case resulting from an occult source of ACTH but responding to a glucocorticoid antagonist.

Case Reports

Case 1

A 15-year-old boy was referred with the diagnosis of hypercortisolism. High-dose dexamethasone suppression and elevated ACTH levels suggested classic Cushing's disease due

Received June 16, 1986; accepted after revision July 15, 1986.

[1] Diagnostic Radiology Department, The Clinical Center, National Institutes of Health, Building 10, Room 1C660, Bethesda, MD 20892. Address reprint requests to J. L. Doppman.
[2] National Institute of Neurological and Communicative Disorders and Stroke, Surgical Neurology Branch, National Institutes of Health, Bethesda, MD 20892.
[3] National Institute of Child Health and Human Development, Developmental Endocrinology Branch, National Institutes of Health, Bethesda, MD 20892.

AJR 147:1145–1147, December 1986
0361–803X/86/1476–1145
© American Roentgen Ray Society

to an ACTH-secreting pituitary adenoma. Thin-section enhanced coronal CT of the pituitary gland was negative, but petrosal sinus sampling diagnosed and lateralized an ACTH-producing microadenoma in the right lobe of the pituitary. The adenoma was successfully resected.

CT of the chest preoperatively had demonstrated a widened fat-filled anterior mediastinum containing a small thymic remnant (Fig. 1A). Three months after surgery, follow-up CT demonstrated a large anterior mediastinal mass (Fig. 1B). The patient has remained normocortisolemic for 2 years; no further follow-up of the CT findings has been performed.

Case 2

A 27-year-old woman with classic Cushing's features, hyperplastic adrenal glands, and elevated serum ACTH levels underwent transsphenoidal exploration of the pituitary gland. When no microadenoma was found, she was referred to National Institutes of Health for further diagnostic studies. The absence of elevated ACTH levels in either petrosal sinus before and after stimulation with corticotrophic releasing hormone established the diagnosis of ectopic ACTH syndrome.

A chest film was negative; pulmonary CT showed a small mass in the right lower lobe compatible with a bronchial carcinoid. The anterior mediastinum was widened by fatty infiltration and contained no detectable thymic remnant (Fig. 2A). At thoracotomy, a bronchial carcinoid tumor and a single right hilar node containing microscopic metastases were removed. Clinical features of Cushing's syndrome gradually receded and pituitary-adrenal function became normal.

Because of the metastatic hilar node, serial CT examinations of the chest were performed after the thoracotomy. Mediastinal lipomatosis regressed, but an anterior mediastinal mass appeared whose configuration resembled thymus. The follow-up studies 6 months later (Fig. 2B) have shown progressive thymic hyperplasia. All studies of pituitary adrenal function remain normal.

Case 3

A 35-year-old man presented with severe Cushing's syndrome and elevated peripheral ACTH levels. Petrosal sinus sampling revealed no ACTH gradients, confirming the clinical suspicion of ectopic ACTH production. A meticulous search, including CT of the chest and abdomen and wide-ranging venous sampling, failed to detect the ectopic ACTH source. Therapy with glucocorticoid antagonist RU 486 was started. The patient responded dramatically; all Cushing's

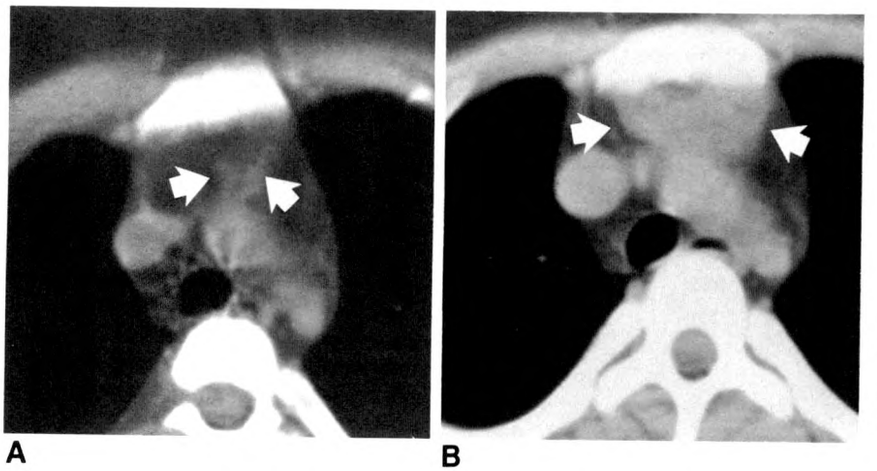


Fig. 1.—*A*, CT before surgery reveals widened fat-filled mediastinum with small residual thymic gland (*arrows*).
***B*, 3 months after successful pituitary surgery, mediastinal lipomatosis reduced but soft-tissue anterior mediastinal mass has enlarged (*arrows*).**

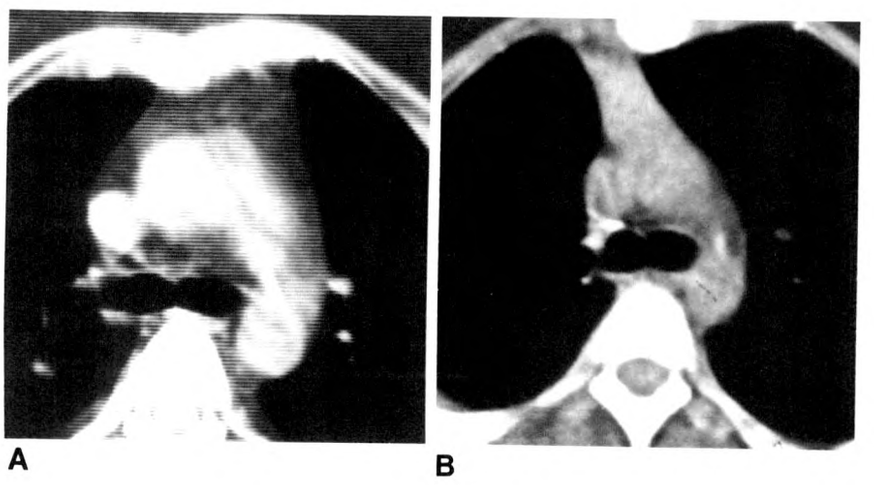


Fig. 2.—*A*, Before surgery, no thymic remnant seen in widened fat-filled mediastinum.
***B*, 6 months after surgery, regression of mediastinal lipomatosis and enlarged thymic mass.**

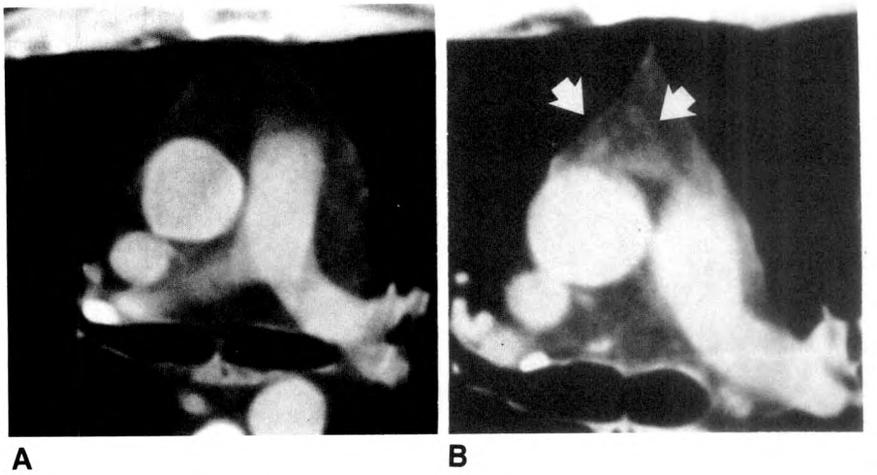


Fig. 3.—*A*, CT before glucocorticoid antagonist therapy.
***B*, CT 3 months after glucocorticoid antagonist therapy reveals reduction of mediastinal lipomatosis and appearance of thymus (*arrows*).**

features disappeared. Pulmonary CT before (Fig. 3A) and 3 months after (Fig. 3B) start of therapy revealed decrease of mediastinal fat and the appearance of a triangular soft-tissue density in the anterior mediastinum, compatible with thymic hyperplasia.

Discussion

Cortisol levels drop precipitously after resection of a cortisol-producing adrenal or an ACTH-producing pituitary adenoma. A period of relative adrenal insufficiency follows. Postoperative replacement steroid therapy is provided routinely, but the abrupt decline from elevated levels physiologically resembles the termination of stress associated with recovery from chemotherapy, burns, and so forth. Rebound hyperplasia of the thymus can be anticipated and poses no diagnostic problem unless the process is not recognized. Cohen et al. [3] performed two thoracotomies because of mediastinal widening after chemotherapy for childhood malignancies. Once they appreciated the phenomenon of thymic rebound after chemotherapy, they followed five subsequent patients conservatively. Thymic hyperplasia after chemotherapy for Hodgkin's disease has been reported [4–6]. Several authors accounted for the phenomenon as an immunologic response of T cells although all patients had received steroids as part of a chemotherapy protocol or for drug-induced pulmonary toxicity.

The size and configuration of a normal thymus on CT examination has been extensively described according to age categories [10–13]. Once one is familiar with the normal variation in the CT appearance of the thymus and aware that an abrupt decline in serum cortisol levels from any cause can lead to thymic hyperplasia, this phenomenon should be recognized and permit a conservative approach of follow-up examinations. Without serial studies, we cannot describe the chronological course of rebound thymic hyperplasia. In our cases and in those reported in the literature, thymic enlargement has been seen as early as 3–4 weeks after reduction of cortisol levels and has persisted for several months. In patient 2, thymic enlargement has persisted for 6 months. Regression is anticipated, but the time course is unknown. Serial CTs do not seem indicated in this benign physiologic phenomenon.

REFERENCES

1. Gelfand DW, Goldman AS, Law AJ. Thymic hyperplasia in children recovering from thermal burns. *J Trauma* **1972**;12:813–817
2. Rizk G, Cuteo L, Amplatz K. Rebound enlargement of the thymus after successful corrective surgery for transformation of the great vessels. *AJR* **1972**;116:528–530
3. Cohen M, Hill CA, Cangir A, Sullivan MP. Thymic rebound after treatment of childhood tumors. *AJR* **1980**;135:151–156
4. Shin MS, Kang-Jey H. Diffuse thymic hyperplasia following chemotherapy for nodular sclerosis Hodgkin's disease. *Cancer* **1983**;51:30–33
5. Grissom JR, Durant JR, Whitley RJ, Flint A. Thymic hyperplasia in a case of Hodgkin's disease. *Southern Med J* **1983**;76:1189–1192
6. Carmosina L, Di Benedetta A, Feffer S. Thymic hyperplasia following successful chemotherapy: a report of 2 cases and review of the literature. *Cancer* **1985**;56:1526–1528
7. Woodhead PJ. Thymic enlargement following chemotherapy. *Br J Radiol* **1984**;57:932–934
8. Caffey J, Di Liberti C. Acute atrophy of the thymus induced by adrenocorticosteroids: observed roentgenographically in living human infants. *AJR* **1969**;82:530–540
9. Caffey J, Sibley R. Results in overgrowth of the thymus after atrophy induced by oral administration of cortical steroids in human infants. *Pediatrics* **1960**;26:762–770
10. Heiberg E, Wolverson MK, Sundaram N, Nouri S. Normal thymus characteristics in subjects under 20. *AJR* **1982**;138:491–494
11. Baron RL, Lee JKT, Sagel SS, Peterson RR. Computed tomography of the normal thymus. *Radiology* **1982**;142:121–124
12. Moore AV, Korobkin M, Olanow W, et al. Age related changes in thymus gland: CT pathologic correlation. *AJR* **1983**;141:241–246
13. Francis JR, Glazer GM, Bookstein FL, Gross BH. The thymus: reexamination of age-related changes in size and shape. *AJR* **1985**;145:249–254
14. Nieman LK, Chrousos GP, Kellner C, et al. Successful treatment of Cushing's syndrome with the glucocorticoid antagonist RU 486. *J Clin Endocrinol Metab* **1985**;61:536–540
15. Findling JW, Tyrrell JP. Occult ectopic secretion of corticotropin. *Arch Intern Med* **1986**;146:929–933

Book Review

Atlas of Two-Dimensional Echocardiography in Congenital Cardiac Defects. By G. J. Van Mill, A. J. Moulaert, and E. Harrick. Dordrecht, The Netherlands: Martinus Nyhoff Publishers, 143 pp., 1985. $29.50, soft cover

Van Mill, Moulaert, and Harrick have put together in 14 chapters, along with still frames and illustrations, an atlas of a large number of congenital heart defects. An introductory section reviews the basic views used in their laboratory and offers clear explanations of diagrams used along with photographs of various sector images. The illustrations, which are clear and concise, are designed to illustrate not only the defect but the orientation of the transducer beam to the heart and chest.

The text describes various orientations and anatomy concisely and lends itself well to the illustration and photographs. The book is divided into sections on major congenital heart defects (e.g., ventricular septal defect, atrial septal defect). Descriptions in each group are excellent along with classifications of various abnormalities. The book progresses from the simple to the more complex lesions, ending with the criss-cross heart. The authors do not go into great depth with more complex anatomy but offer a basic approach and recognition that should be helpful to most technicians and clinicians. Several illustrations of contrast echocardiography are also offered along with clear illustrations of the images.

Criticisms of this book are few. One major problem is that the text and illustrations are often separated by several pages, which makes searching for specific explanation of technique or view somewhat tedious. Some of the photographs include catheters crossing some defects, which tends to be distracting. Most photographs are excellent. There will always be some difficulty in transferring that which one sees in a still image to that seen in real-time. It would be helpful if someone would produce a video atlas of congenital heart defects.

Overall, this book offers a very competent and straight-forward approach to the two-dimensional echocardiographic image. I recommend it to technicians and clinicians alike who are involved in the diagnosis of congenital heart disease in children.

James W. Wiggins, Jr.
University of Colorado Health Sciences Center
Denver, CO 80262

Baseline Screening Mammography: One vs Two Views per Breast

Edward A. Sickles[1]
William N. Weber
Helen B. Galvin
Steven H. Ominsky
Richard A. Sollitto

To compare the advantages of one-view vs two-view mammography screening, films were reviewed for 2500 consecutive asymptomatic women undergoing baseline mammography. To provide screening at low cost, examinations were limited to two radiographs per breast, one each in the craniocaudal and mediolateral oblique projections, with the understanding that those few patients with detected abnormalities would require additional mammograms, taken with an individually directed, problem-solving approach, at considerably higher cost. Two separate interpretations were made of each case, one using only the oblique projection images, the other using both oblique and craniocaudal views. Two-view interpretations not only identified more cancers than one-view readings (27 vs 25), they also required fewer additional mammograms to evaluate potential abnormalities (179 vs 642, 7% vs 26%). These advantages outweigh the additional radiation risk and added cost. Baseline screening mammography should be done with two views per breast.

Although still grossly underused, mammography screening is being done with increasing frequency. Also gaining in popularity is the concept of high-volume, streamlined screening at low cost [1–5]. Among the various methods suggested to reduce costs is the practice of imaging each breast with one rather than two standard projections [6–8]. This approach certainly will halve the cost of X-ray film, and it may also increase patient throughput and reduce interpretation time. In addition, despite the negligible difference in oncogenic risk [9, 10], mammography at half the radiation dose might well increase patient compliance [11, 12].

Among known mammography projections, it is generally recognized that the mediolateral oblique view, when properly performed, will image the greatest amount of breast tissue, especially the deepest part of the breast in the axillary tail region of the upper outer quadrant [6, 10, 13, 14]. For this reason, and also because of cost considerations, several large-scale mammography screening programs were begun that used only oblique views of each breast [6–8, 15].

However, the adequacy of this approach has been questioned by several authors, including some who are actively involved in one-view screening programs, primarily on the grounds that no single projection will identify all mammographically detectable cancers [14, 16–21]. Further objections have been raised because one-view screening may be more likely than two-view examination to result in requests for additional images to further characterize possible abnormalities [20–22]. The present study was designed to evaluate the differences between one- and two-view baseline screening examinations with respect to the frequency of call-back studies, the number of biopsies, and the cancers detected.

Subjects and Methods

The study population consisted of 2500 consecutive asymptomatic women undergoing mammography screening for the first time. The methods used in our screening program

Received June 30, 1986; accepted without revision July 29, 1986.

Presented in part at the annual meeting of the American Roentgen Ray Society, Washington, DC, April 1986.

[1] All authors: Department of Radiology, C-309, University of California School of Medicine, San Francisco, CA 94143. Address reprint requests to E. A. Sickles.

AJR 147:1149–1153, December 1986
0361–803X/86/1476–1149
© American Roentgen Ray Society

already have been reported in detail [4]; the emphasis is on producing excellent studies at low cost. Since the aim of screening is to detect unsuspected abnormalities rather than to characterize them fully, we streamline the imaging procedure to involve only two screen-film images of each breast, in mediolateral-oblique and craniocaudal projection. We also limit interpretation to two diagnoses, normal and abnormal, with the understanding that only a small percentage of examinations will be abnormal and therefore require additional imaging studies, at considerably higher cost. This overall approach provides high-quality mammography to a large number of asymptomatic women at less than one-third the price of an individually directed, problem-solving examination.

To investigate the full impact of screening with one rather than two standard views of each breast, a radiologist experienced in blinded image interpretation studies read each examination twice, first using only the oblique projection images, and then using both oblique and craniocaudal views. In this way it was possible to assess the differences in frequency of abnormal interpretation of one- and two-view-per-breast examinations and, therefore, the effects of single-view screening on the number of immediate call-backs for more complete mammography, the number of mammography-generated biopsies, and the number of mammography-detected cancers.

TABLE 1: **Results of Baseline Screening Mammography in 2500 Asymptomatic Women**

Results	Reading	
	One View per Breast	Two Views per Breast
Abnormal interpretations	642	179
Mammography-generated biopsies	76	83
Mammography-detected cancers	25	27

Results

Single-view baseline screening resulted in more than 3½ times the abnormal interpretations of two-view studies, with superimpositions accounting for the bulk of the abnormal cases (see Table 1). Most commonly, overlapping normal breast structures simulated masses on the oblique view, as illustrated in Figure 1. Less frequently, several isolated tiny calcific particles projected so close to one another on oblique view as to simulate a cluster of microcalcifications. In both of these circumstances, the additional perspective provided by a craniocaudal view was sufficient to eliminate any suspicion of malignancy, so that the standard two-view-per-breast examination was interpreted as normal. Another situation prompting abnormal interpretations on single-view examinations involved clustered calcifications in the skin that projected over fibroglandular tissues on the oblique view (Fig. 2). Demonstration of the true dermal location of the calcifications on a corresponding craniocaudal view permitted the two-view examination to be read as normal.

The additional information contained in craniocaudal projection images also generated some abnormal interpretations

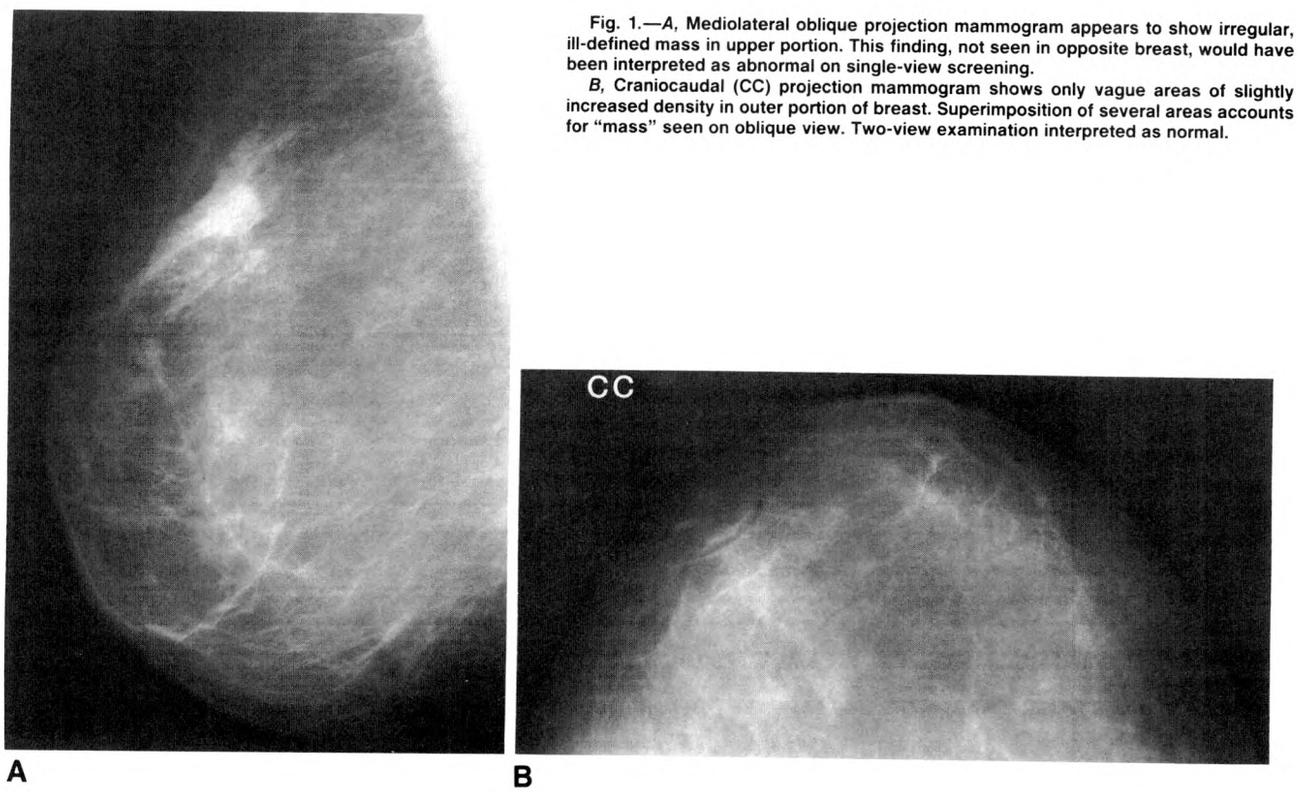


Fig. 1.—*A*, Mediolateral oblique projection mammogram appears to show irregular, ill-defined mass in upper portion. This finding, not seen in opposite breast, would have been interpreted as abnormal on single-view screening.

***B*, Craniocaudal (CC) projection mammogram shows only vague areas of slightly increased density in outer portion of breast. Superimposition of several areas accounts for "mass" seen on oblique view. Two-view examination interpreted as normal.**

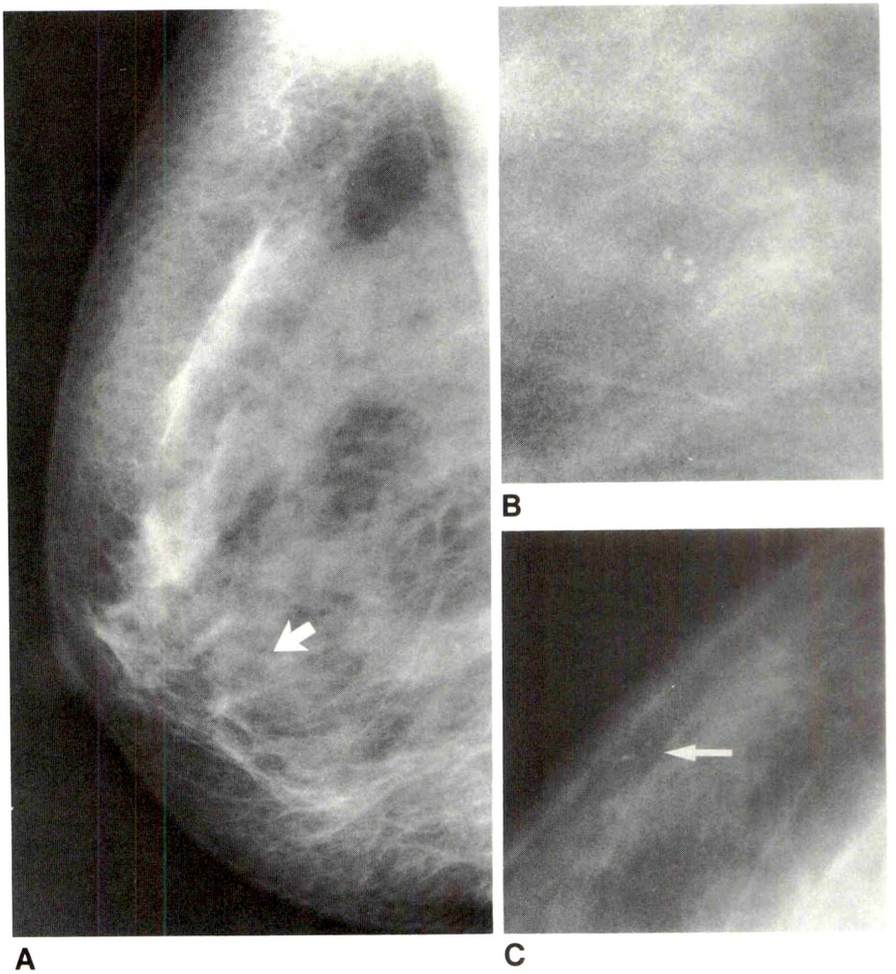


Fig. 2.—*A*, Mediolateral oblique projection mammogram shows cluster of tiny calcifications (*arrow*), apparently in retroareolar location. This finding also would have been interpreted as abnormal on single-view screening.

B, Photographic enlargement of area of interest shown in *A*.

C, Photographic enlargement of part of craniocaudal projection mammogram shows calcifications in superficial location (*arrow*) that establishes them as dermal deposits, a clearly benign mammographic finding. Two-view examination interpreted as normal.

that would not have been made based on single-oblique-view examinations alone. Occasionally an abnormality was seen only on craniocaudal view, either because it was located too far medially in the breast to be included on the oblique view, or because overlapping dense fibroglandular tissues obscured enough of the margins of a suspicious mass on the oblique projection image to prevent its detection. This resulted in seven biopsies that could be attributed solely to use of the craniocaudal view; two of these uncovered nonpalpable cancers (Table 1).

Discussion

It might be argued that, by halving the number of standard exposures with one-view screening, the proportionate reduction in radiation dose would encourage more patients and physicians to comply with mammography screening guidelines. However, viewed in the light of current low doses, the potential oncogenic risk of two-view examination is negligible [9, 10]. Therefore, patients who avoid mammography because of the ionizing radiation do so either because they lack knowledge of risks and benefits or because they fear radiation at any dose. Since neither of these obstacles would be overcome by further reducing a dose that already is very low, it is unlikely that single-view screening would meet with a substantially greater degree of compliance than current two-view examinations. For this reason, we have discounted considerations of radiation dose in assessing the relative merits of one- and two-view screening.

Our study reconfirms that two-view screening detects a slightly larger number of breast cancers than one-view examinations [14, 16–21]. No single mammographic projection portrays all of the tissues within the breast, so that the addition of a craniocaudal view to the mediolateral oblique view provides greater imaging coverage as well as a different perspective for observation. The resulting increase in lesion detection generates more biopsies and, thus, discovers more breast cancers. The price of several extra biopsies to detect a few additional cancers (seven biopsies for two cancers in our study) is one that traditionally has been accepted on the basis of both economic and social costs.

A large number of the abnormal interpretations from baseline mammography screening do not represent true lesions

detected [6, 8, 15, 22, 23]. Most management decisions, such as whether or not to biopsy, require more information than is provided by standard mammograms from either one- or two-view examinations, especially for the small and often subtle findings identified on screening. Only after more thorough characterization by additional imaging studies are some screening-detected abnormalities found to be clinically significant lesions. For this reason, single-view screening can result in many more abnormal interpretations, while two-view examinations actually generate more biopsies (Table 1).

The data collected in this study permit assessment of the relative dollar costs of one- and two-view mammography screening. Clearly, the operating expenses for one-view examinations are lower, by approximately $2.17 per patient, as summarized in Table 2. Not only are expendable supplies used up less rapidly, but there also is reduced wear and tear on fixed equipment, resulting in decreased costs for repairs and longer life in service. In addition, one-view examinations can be interpreted more rapidly than two-view studies because fewer films are read. Analysis of a consecutive series of 500 of our cases indicated a 40% reduction in interpretation time for one-view examinations. On the basis of our current $5 charge for reading two-view examinations, this could result in further savings of $2 per patient for one-view screening. One final consideration in assessing the cost savings of one-view examinations is the potential for increased patient throughput because fewer exposures are taken. However, most mammography screening programs manage patient flow efficiently by using two separate work stations, one for reception, the other for imaging. As a result, reduction in imaging time alone would not effectively increase throughput unless patient volume were high enough to justify twice as many work stations for reception as for imaging. Such an approach would require examining at least 80–100 patients per day, a volume that rarely is achieved in the United States. In summary, a realistic estimate of the total cost savings for one-view mammography screening amounts to approximately $4.17 per patient.

Weighed against these savings are the additional costs for follow-up imaging examinations generated by the increased number of abnormal interpretations resulting from one-view screening [20–23]. Our study clearly shows the magnitude of this problem, indicating that 19% more patients undergoing single-view (vs two-view) screening would require additional images to further characterize possible abnormalities. Assuming a charge of $100 for such additional problem-solving examinations, this would result in an average increase in cost of $19 per patient screened, more than four times the amount potentially saved by decreased operating expenses and interpretation fees. One-view mammography screening does not achieve substantial cost savings over two-view examinations, but rather proves to be more expensive.

The dollar costs calculated in our study apply primarily to low-cost screening programs patterned on the University of California San Francisco model [4]. However, geographic, economic, and political conditions in the United States vary sufficiently among communities to require different types of screening programs in many circumstances [2, 5]. As a result, the cost differentials between one- and two-view screening for such programs probably will not be the same as those reported here. However, our study shows that the cost excess for the additional call-back examinations generated by single-view screening is more than four times the concomitant cost saving resulting from decreased operating expenses and reduced interpretation fees. The sheer magnitude of this differential argues strongly that for any type of American screening program the overall cost of two-view examinations will be less than that of single-view screening. For this reason and because a few more early breast cancers will be detected, we recommend that baseline mammography screening be done by using two, not one, standard views per breast.

This recommendation applies only to the initial screening examination, and not to subsequent annual or biennial screenings. Many of the abnormal interpretations made on baseline examination will not be repeated on subsequent screenings [7, 24, 25], either because the abnormality will have been removed by biopsy or because the call-back examination generated by baseline screening will have shown the abnormality to be clinically insignificant. As a result, it may be appropriate to conduct follow-up screenings with single-view examinations, at least for women with fatty breasts [26, 27]. We plan to address this issue in a future study.

TABLE 2: **Estimated Savings in Operating Expenses for One-View (vs Two-View) Mammography Screening**

Operating Expense	Savings per Patient
X-ray film	$1.30
Screens	.01
Cassettes	.01
Film processor and chemicals	.12
Mammography unit	.73
Total	$2.17

Note.—Estimates of cost savings are based on actual experience whenever appropriate. Detailed explanation of these estimates will be provided by authors on request.

REFERENCES

1. Moskowitz M, Fox SH. Cost analysis of aggressive breast cancer screening. *Radiology* **1979**;130:253–256
2. Strax P. Mass screening for control of breast cancer. *Cancer* **1984**;53:665–670
3. McLelland R. Mammography 1984: challenge to radiology. *AJR* **1984**;143:1–4
4. Sickles EA, Weber WN, Galvin HB, Ominsky SH, Sollitto RA. Mammography screening: how to operate successfully at low cost. *Radiology* **1986**;160:95–97
5. Bird RE, McLelland R. How to initiate and operate a low-cost screening mammography center. *Radiology* **1986**, in press
6. Lundgren B, Jakobsson S. Single view mammography. A simple and efficient approach to breast cancer screening. *Cancer* **1976**;38:1124–1129
7. Lundgren B, Helleberg A. Single oblique-view mammography for periodic screening for breast cancer in women. *J Natl Cancer Inst* **1982**;68:351–355

8. Tabár L, Gad A, Åkerlund E, Holmberg L. Screening for breast cancer in Sweden. In: Feig SA, McLelland R, eds. *Breast carcinoma. Current diagnosis and treatment.* New York: Masson, **1983**:315–326
9. Feig SA. Radiation risk from mammography: is it clinically significant? *AJR* **1984**;143:469–475
10. National Council on Radiation Protection and Measurements. *Mammography—a user's guide.* Bethesda, MD: National Council on Radiation Protection and Measurements, **1986**:95–121
11. Buchanan JB, Jager RM. Single view negative mode xeromammography: an approach to reduce radiation exposure in breast cancer screening. *Radiology* **1977**;123:63–68
12. Bassett LW, Bunnell DH, Cerny JA, Gold RH. Screening mammography: referral practices of Los Angeles physicians. *AJR* **1986**;147:689–692
13. Lundgren B. The oblique view at mammography. *Br J Radiol* **1977**;50:626–628
14. Andersson I, Mühlow A, Pettersson H. Number of projections in mammography: influence on detection of breast disease. *AJR* **1978**;130:349–351
15. Tabár L, Gad A. Screening for breast cancer: the Swedish trial. *Radiology* **1981**;138:219–222
16. Libshitz HI, Fetouh S, Isley J, Lester RG. One-view mammographic screening. *Radiology* **1976**;120:719–722
17. Moskowitz M, Libshitz HI. Mammographic screening for breast cancer by lateral view only: is it practical? *J Can Assoc Radiol* **1977**;28:259–261
18. Pagani JJ, Bassett LW, Gold RH, et al. Efficacy of combined film-screen/xeromammography: preliminary report. *AJR* **1980**; 135:141–146
19. Bassett LW, Pagani JJ, Gold RH. Pitfalls in mammography. Demonstrating deep lesions. *Radiology* **1980**;136:641–645
20. Andersson I. Radiographic screening for breast carcinoma. III. Appearance of carcinoma and number of projections to be used at screening. *Acta Radiol [Diagn]* (Stockh) **1981**;22:407–420
21. Muir BB, Kirkpatrick AE, Roberts MM, Duffy SW. Oblique-view mammography: adequacy for screening. Work in progress. *Radiology* **1984**;151:39–41
22. Lundgren B, Jakobsson S. Screening for carcinoma of the breast with single-view mammography. *Medicamundi* **1976**;21:27–33
23. Andersson I, Andrén L, Hildell J, Linell F, Ljungqvist U, Pettersson H. Breast cancer screening with mammography. A population-based, randomized trial with mammography as the only screening mode. *Radiology* **1979**;132:273–276
24. Tabár L, Åkerlund E, Gad A. Five-year experience with single-view mammography randomized controlled screening in Sweden. In: Brünner S, Langfeldt B, Andersen PE, eds. *Early detection of breast cancer.* Berlin: Springer-Verlag, **1984**:105–113
25. Thomas BA, Price JL, Boulter PS, Gibbs NM. The first three years of the Guildford Breast Screening Project. In: Brünner S, Langfeldt B, Andersen PE, eds. *Early detection of breast cancer.* Berlin: Springer-Verlag, **1984**:195–199
26. Andersson I. Breast cancer screening in Malmö. In: Brünner S, Langfeldt B, Andersen PE, eds. *Early detection of breast cancer.* Berlin: Springer-Verlag, **1984**:114–116
27. Swedish National Board of Health and Welfare. *Recommendations for mammography screening procedures* [Swed]. Stockholm: Swedish National Board of Health and Welfare, in press

Forthcoming Articles

PULMONARY RADIOLOGY

Comparison of CT and fiberoptic bronchoscopy in the evaluation of bronchial disease. *Naidich DP, Lee J-J, Garay SM, McCauley DI, Aranda CP, Boyd AD*

CT of interstitial lung disease: a diagnostic approach. *Bergin CJ, Müller NL*

Occult pulmonary embolism: a common occurrence in deep venous thrombosis. *Dorfman GS, Cronan JJ, Tupper TB, Messersmith RN, Denny DF, Lee CH*

Kaposi's sarcoma of the lung in AIDS: a radiologic-pathologic analysis. *Sivit CJ, Schwartz AM, Rockoff SD*

Dystrophic calcification in carcinoma of the lung: demonstration by CT. *Stewart JG, MacMahon H, Vyborny CJ, Pollak ER*

Extension of ascites into the chest with hiatal hernia: visualization on CT. *Godwin JD, MacGregor JM*

CARDIAC RADIOLOGY

Measurement of canine left ventricular mass by using MR imaging. *Caputo GR, Tscholakoff D, Sechtem U, Higgins CB*

Primary angiosarcoma of the heart: CT characteristics. *Shin MS, Kirklin JK, Cain JB, Ho K-J*

BREAST RADIOLOGY

Mammographic detection of recurrent cancer in the irradiated breast. *Stomper PC, Recht A, Berenberg AL, Jochelson MS, Harris JR*

ENDOCRINE RADIOLOGY

Sonography in the follow-up of 100 patients with thyroid carcinoma. *Simeone JF, Daniels GH, Hall DA, et al.*

GENITOURINARY RADIOLOGY

MR imaging of the prostate gland: normal anatomy. *Hricak H, Dooms GC, McNeal JE, et al.*

Renal adenocarcinoma: CT staging of 100 tumors. *Johnson CD, Dunnick NR, Cohan RH, Illescas FF*

CT and sonography of advanced urinary tract tuberculosis. *Premkumar A, Lattimer J, Newhouse JH*

Diagnosis of subclinical varicocele in infertility. *Gonda RL Jr, Karo JJ, Forte RA, O'Donnell KT*

MUSCULOSKELETAL RADIOLOGY

MR imaging of the supraclavicular region: normal anatomy. *Kellman GM, Kneeland JB, Middleton WD, et al.*

MR imaging of the normal shoulder: anatomic correlation. *Seeger LL, Ruszkowski JT, Bassett LW, Kay SP, Kahmann RD, Ellman H*

The posterior vertebral body line: importance in the detection of burst fractures. *Daffner RH, Deeb ZL, Rothfus WE*

Spinal deformities and pseudofractures. *Boechat MI*

Prosthetic fit in below-knee amputation: evaluation with xeroradiography. *Irwin GAL, Friedman L, Shapiro D*

"Pseudobursae": a useful finding in patients with painful hip arthroplasty. *Berquist TH, Bender CE, Maus TP, Ward EM, Rand JA*

Dosimetric comparison of examination techniques in temporomandibular joint radiography, including CT and arthrography. *Christiansen EL, Moore RJ, Thompson JR, Hasso AN, Hinshaw DB Jr*

Scintigraphic diagnosis of sacral fractures. *Balseiro J, Brower AC, Ziessman HA*

GASTROINTESTINAL RADIOLOGY

Natural history of the obstructed rabbit appendix: observations with radiography, sonography, and CT. *Dachman AH, Nichols JB, Patrick DH, Lichtenstein JE*

CT evaluation of esophageal varices. *Balthazar EJ, Naidich DP, Megibow AJ, Lefleur RS*

CT diagnosis of occult incisional hernias. *Ghahremani GG, Jimenez MA, Rosenfeld M, Rochester D*

MR imaging of gallbladder carcinoma. *Rossmann MD, Friedman AC, Radecki PD, Caroline DF*

Radiolucency in the common bile duct simulating a gallstone. *Train JS, Novick A, Dan SJ, Efremidis S, Mitty HA*

Symptomatic congenital ectopic gastric mucosa in the upper esophagus. *Williams SM, May C, Krause DW, Harned RK*

Pneumoretroperitoneum secondary to hydrogen peroxide wound irrigations. *Swayne LC, Ginsberg HN, Ginsburg A*

FETAL AND OBSTETRIC RADIOLOGY

The significance of membrane thickness in the sonographic evaluation of twin gestations. *Hertzberg BS, Kurtz AB, Choi HY, et al.*

Severe polyhydramnios: incidence of anomalies. *Barkin SZ, Pretorius DH, Beckett MK, Manchester DK, Nelson TR, Manco-Johnson ML*

Sonographic spectrum of placental abruption. *Nyberg DA, Cyr DR, Mack LA, Wilson DA, Shuman WP*

Malignant gestational trophoblastic disease: CT findings. *Sanders C, Rubin E*

INTERVENTIONAL RADIOLOGY

Percutaneous balloon dilatation of ureteral strictures. *Johnson CD, Oke EJ, Dunnick NR, et al.*

Monooctanoin infusion and stone removal via the transparenchymal route: use in 17 patients. *Haskin PH, Teplick SK, Sammon JK, Gambescia RA, Zitomer N, Pavlides CA*

Percutaneous nephrostomy for endopyelotomy. *Lee WJ, Badlani GH, Smith AD*

PEDIATRIC RADIOLOGY

CT of children's feet: an immobilization technique. *Donaldson JS, Poznanski AK, Nieves A*

Normalized pediatric organ absorbed doses from CT examinations. *Fearon T, Vucich J*

NEURORADIOLOGY

The MR appearance of syringomyelia: new observations. *Sherman JL, Barkovich AJ, Citrin CM*

MR imaging of paragangliomas. *Olsen WL, Dillon WP, Kelly WM, Norman D, Brant-Zawadzki M, Newton TH*

Physiology of the CSF flow-void sign: modification by cardiac gating. *Citrin CM, Sherman JL, Gangarosa RE, Scanlon D*

Embolization of epistaxis and juvenile nasopharyngeal angiofibromas. *Davis KR*

MEDICOLEGAL RADIOLOGY

An overview of informed consent for radiologists. *Reuter SR*

Pictorial Essay

The Retroperitoneal Spaces Revisited

Wylie J. Dodds,[1] Reda M. A. Darweesh,[2] Thomas L. Lawson,[1] Edward T. Stewart,[1] W. Dennis Foley,[1] Soad M. A. Kishk,[1] and Michael Hollwarth[3]

Although progress has been made toward understanding retroperitoneal anatomy [1–5], it is still difficult to reconcile certain abdominal CT findings with prevailing concepts about the developmental and adult anatomy of the retroperitoneal spaces. Our aims here are to (1) review current concepts about the compartmental anatomy of the retroperitoneum, (2) present CT findings that are difficult to explain on the basis of current notions about the retroperitoneal spaces, and (3) propose a hypothesis that may help clarify the developmental and subsequent anatomic divisions of the retroperitoneum.

Background

Until recent years, despite detailed anatomic studies by Gerota [6], Tobin [7], and others [8–11], the boundaries and compartments of the retroperitoneum remained vague and controversial. During the past two decades, however, efforts spearheaded by the work of Meyers and Whalen [1–3] led to an enhanced understanding of retroperitoneal anatomy as well as the distribution and spread of retroperitoneal disease processes [12–16]. The prevalent current notion (Fig. 1) suggests that the retroperitoneum is divided into three compartments by the renal fasciae [1–5, 17–19].

The renal fasciae (Gerota's fasciae) develop as a discrete anterior layer (Zukerkandl's fascia) and posterior layer (Toldt's fascia) [6, 7]. These two layers are thought to fuse behind the ascending or descending colon, respectively, to form a single lateroconal fascia [1, 9] that blends in the flank with the peritoneal reflection that forms the paracolic gutter (Fig. 1B). The fused fasciae are thought to extend to the diaphragm (Fig. 1C). Lateral fusion of the renal fasciae forms an inverted hemicone of connective tissue that encompasses the kidney and adrenal gland. The lateroconal fascia is described as descending in the coronal plane to the level of the iliac fossa [1, 2, 9].

The following divisions have been suggested: (1) The anterior pararenal space lies between the posterior parietal peritoneum and the anterior renal fascia, and is bound laterally by the lateroconal fascia. This space contains alimentary structures (i.e., pancreas, duodenum, and retroperitoneal portions of the colon). (2) The perirenal space, enclosed by the anterior and posterior renal fascia, contains the kidney and adrenal gland. (3) The posterior pararenal space extends from the posterior renal fascia to the transversalis fascia and is continuous, external to the lateroconal fascia with the properitoneal fat stripe in the flank. This space does not contain any organs. (4) Above the kidney, the anterior pararenal space may extend cephalad to the bare area of the liver (Fig. 1C), while the posterior pararenal space projects higher on the diaphragm. (5) Below the free, caudal margin of the lateroconal fascia, the anterior and posterior pararenal spaces communicate with one another in the iliac fossa (Fig. 1C).

Analysis of CT Case Material

Certain findings from our clinical experience with 7000 abdominal CT examinations do not seem to fit current con-

Received April 4, 1986; accepted after revision July 21, 1986.

[1] Department of Radiology, Medical College of Wisconsin, Milwaukee County Medical Complex, 8700 W. Wisconsin Ave., Milwaukee, WI 53226. Address reprint requests to W. J. Dodds.

[2] Recipient of Peace Fellowship from Egypt.

[3] Department of Pediatric Surgery, University of Graz, Graz, Austria.

AJR 147:1155–1161, December 1986 0361–803X/86/1476–1155 © American Roentgen Ray Society

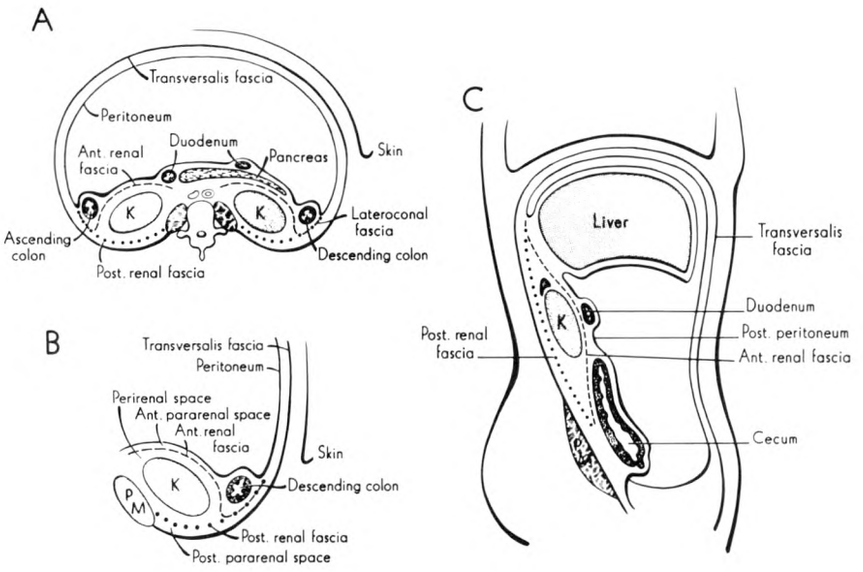
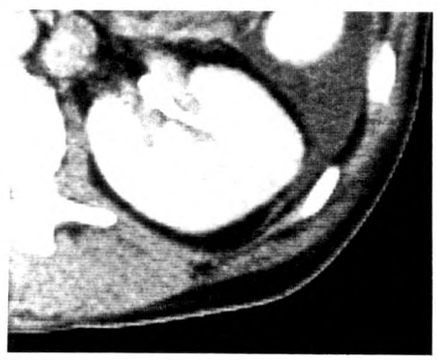


Fig. 1.—Schematic of retroperitoneal spaces based on current concept of retroperitoneal anatomy [1–5]. K = kidney; PM = psoas muscle. Anterior renal fascia (*dashed*) and posterior renal fascia (*dotted*) join to form lateroconel fascia (*dot-dashed*). These fasciae divided retroperitoneum into (1) anterior pararenal space that contains duodenum, pancreas, and right and left colon; (2) perirenal space that contains kidney and adrenal; and (3) posterior pararenal space that contains fat.

***A*, Axial section of pancreas.**

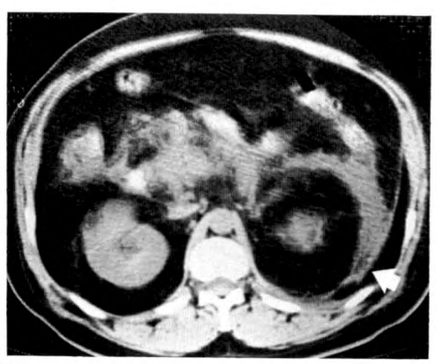
***B*, Axial section of left upper quadrant just caudal to pancreatic tail. Anterior pararenal space is subtended ventrally by posterior peritoneum and dorsolaterally by anterior renal fascia and lateroconal fascia. Posterior pararenal space is demarcated ventrally by posterior pararenal fascia and lateroconal fascia, and dorsolaterally by transversalis fascia.**

***C*, Parasagittal section through right kidney. Bare area of liver is in continuity with anterior pararenal space. Posterior pararenal space communicates with anterior pararenal space in iliac fossa, below perirenal space.**



2

Fig. 2.—Ascites level of left kidney has fork-tailed, or wishbone, configuration.



3

Fig. 3.—Peripancreatic fluid in patient with acute pancreatitis appears to be in "anterior pararenal space," but extends posterolateral to kidney (*arrow*) without involving fat-containing posterior pararenal space.

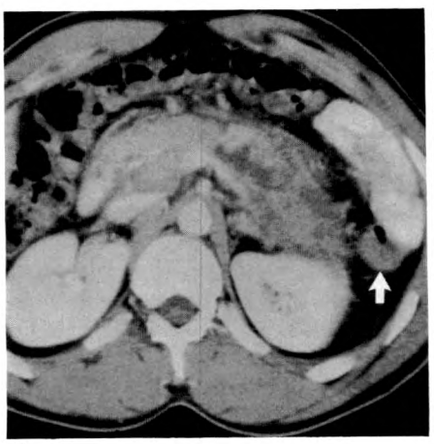
cepts about compartmental retroperitoneal anatomy, particularly as it applies to the "anterior pararenal space." For example, ascites commonly extends posterolaterally in the paracolic gutter to reach the meridian of the kidney or farther posteriorly. Ascitic fluid may extend dorsally in several patterns including a rounded, spikelike, or fork-tailed projection (Fig. 2). These patterns are difficult to explain by the conventional retroperitoneal anatomy shown in Figure 1B.

The spleen commonly extends posterolateral to the left kidney, while the liver does so occasionally on the right. These observations indicate that the lateral recess of the intraperitoneal cavity may extend posterior to the kidney. Additionally, other intraabdominal organs, such as the colonic flexures or small-bowel loops, may be located posterolateral to the kidney. These findings seem to differ substantially from the notion that a lateroconal renal fascia extends anterolateral to the kidney.

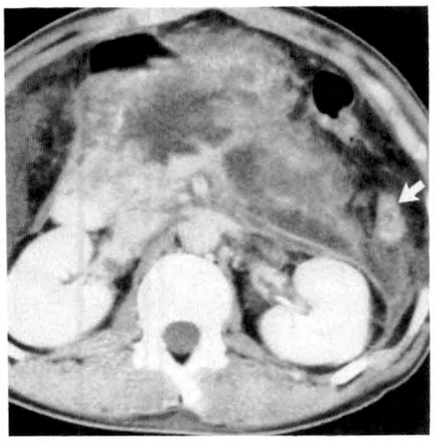
In some instances, fluid within the compartment called the "anterior pararenal space" does not conform to current concepts about the anatomic boundaries of the retroperitoneal spaces. For instance, extrapancreatic fluid in the left anterior pararenal space may appear to break into the posterior pararenal space and track behind the kidney while sparing the fat layer that is in the posterior pararenal space (Fig. 3). This pattern, which we observed in 10 patients with pancreatitis, is not explained adequately by the retroperitoneal anatomy depicted in Figure 1.

Peripancreatic fluid in the left anterior pararenal space tends to localize in the immediate vicinity of the pancreas without involving the retroperitoneal colon or extending below the level of the transverse mesocolon. Even large inflammatory fluid collections within the anterior pararenal space may spare the fat layer surrounding the retroperitoneal portion of colon (Fig. 4A).

In eight patients, a fluid collection in the "anterior pararenal space" extended caudally into the lower part of the iliac fossa, but did not show any communication with the fat plane of the posterior pararenal space (Fig. 5). Thus, these cases did not



A



B

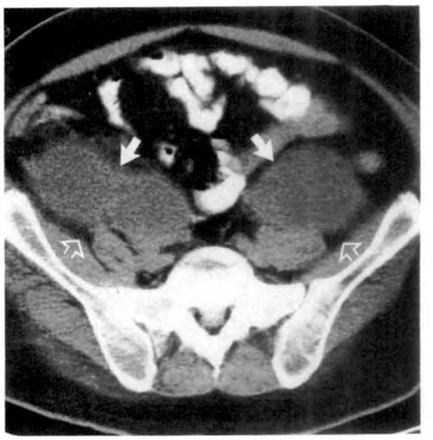


Fig. 4.—Peripancreatic fluid in two patients with pancreatitis.

***A*, Peripancreatic fluid in an anterior retroperitoneal space spares fat adjacent to retroperitoneal portion of descending colon (*arrow*). Ventral to retroperitoneal colon are contrast-filled loops of small bowel.**

***B*, Peripancreatic inflammatory fluid has dissected into the transverse mesocolon. Lateral extension of fluid obliterates fatty layer adjacent to posterior wall of retroperitoneal left colon (*arrow*). Ascites is seen on the right.**

Fig. 5.—Separation of an anterior retroperitoneal space from posterior pararenal space in left iliac fossa. In this patient with pancreatitis, fluid within anterior retroperitoneal spaces bilaterally (*white arrows*) does not affect fat layer in posterior pararenal spaces (*open arrows*).

exhibit any communication of the anterior and posterior pararenal space below an alleged free, caudal margin of the lateroconal fascia.

Proposed Explanation of CT Findings

To account for discrepancies between findings on abdominal CT and current concepts about retroperitoneal compartments, some workers have proposed variations in the posterior abdominal recess or lateroconal fascia [20–22]. We propose a different explanation based on embryologic principles.

Intermesenteric and Primary Retroperitoneal Domains

The gut and its derivatives develop within the intermesenteric domain, ventral to the domain of the primary retroperitoneum [23–27]. Thus, the gut, its derivatives, and their accompanying blood vessels serve as markers of the intermesenteric space, regardless of its embryologic migration, folding or fusion. In the embryo, and adult, the only potential communication between the intermesenteric and primitive retroperitoneal domains is normally at the root of the dorsal mesentery, where aortic and caval vessels supply structures in both domains. The twain intermesenteric and primary retroperitoneal domains can never meet, except at the mesenteric root. All abdominal structures, within both the intermesenteric and primary retroperitoneal domains, are really extraperitoneal. Structures termed "intraperitoneal," such as the stomach, liver, and transverse colon have a persistent dorsal or ventral mesentery but are actually intermesenteric rather than intraperitoneal.

Pancreaticoduodenal Space

Late in the first trimester of pregnancy, the bowel of the fetus rotates counterclockwise as it reenters the abdomen from the umbilical cord [26]. As the liver swings to the right and the stomach to the left (Fig. 6), the duodenum, pancreas, and their mesenteries lie parallel to the posterior abdominal wall (Fig. 7). The dorsal duodenal mesentery, or mesoduodenum, makes a hairpin turn so that part of the proximal mesoduodenum makes direct contact with the primary dorsal peritoneum. Later they fuse. The anterior part of the left mesoduodenum lies ventral to the duodenum and pancreas (Fig. 7B). The duodenum and pancreas lose their suspending mesentery and come to reside in a new, secondary retroperitoneal space, bound anteriorly by the left mesoduodenum and posteriorly by several layers of mesoduodenum that fuse with the primary dorsal peritoneum. The left leaf of mesoduodenum contributes centrally to the secondary posterior peritoneum of the adult. The pancreaticoduodenal space overlaps the lower half of the right kidney and most, or all, of the left kidney. It extends from a level just above the pancreatic body to a level slightly below the duodenum (Fig. 7C). A portion of mesoduodenum subtending the dorsal pancreas may fail to fuse completely with the primary dorsal peritoneum, thereby creating a retropancreatic recess [28]. Ascites in the retropancreatic recess can simulate a retroperitoneal-fluid collection (Fig. 8).

Colonic Retroperitoneal Space

The right and left colon rotate into the flanks (Fig. 9A) such that their dorsal mesentery, or mesocolon, lies parallel to the

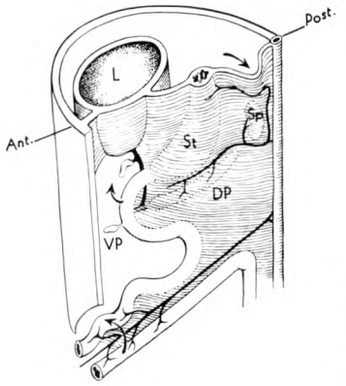


Fig. 6.—Upper abdomen in 8-week human embryo. Ant. = anterior; Post. = posterior. Liver (L) swings to the right while stomach (St) begins to rotate 90° counterclockwise, causing dorsal gastric mesentery, or mesogastrium, to buckle leftward (*dorsal curved arrow*) to form lesser sac. Dorsal pancreas (DP) is located in dorsal duodenal mesentery, or mesoduodenum. Ventral pancreas (VP) rotates counterclockwise behind duodenum as duodenum swings to the right (*ventral curved arrow*). Small and large bowels are seen herniated into the umbilicus. These structures are rotated 90° counterclockwise while within umbilicus and rotate another 180° as they return to abdomen. (Modified and reprinted with permission from Moore [26].)

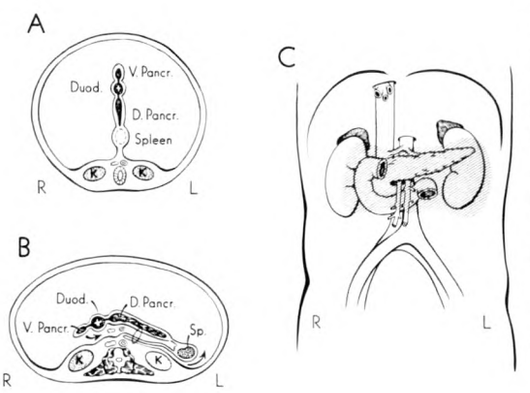


Fig. 7.—Pancreaticoduodenal space.

A, Axial section through second portion of duodenum in 6-week human embryo. Ventral-pancreas anlage within rudimentary ventral duodenal mesentery has lost its connection with anterior abdominal wall. Elongated dorsal pancreas located within mesoduodenum. At slightly cephalad level, spleen (*dashed line*) located within mesogastrum.

B, Axial view through dorsal pancreas in 10-week fetus represents a section several centimeters thick. Because of counterclockwise rotation of stomach and duodenum, mesogastrum and mesoduodenum swing to left so as to make hairpin turn at spleen. Dorsal half of the two leaves of mesogastrum and mesoduodenum lie flat against primary dorsal peritoneum. Dorsal pancreas is subtended ventrally by anterior, or left, leaf of mesogastrum and dorsally by right leaf, which has swung ventral to superior mesenteric vessels. Subsequently ventral pancreas rotates behind duodenum (*curved arrow*) to form pancreatic head. Later, three leaves of mesoduodenum and dorsal peritoneum, within the circle, fuse to form posterior boundary of pancreaticoduodenal space. Ventral portion of left leaf of mesoduodenum in front of pancreas becomes a secondary posterior peritoneum. A retropancreatic space persists when dorsal part of mesoduodenum fuses incompletely with posterior peritoneum.

C, Frontal view, adult upper abdomen. Area shaded by *diagonal lines* indicate coronal margins of pancreaticoduodenal space.

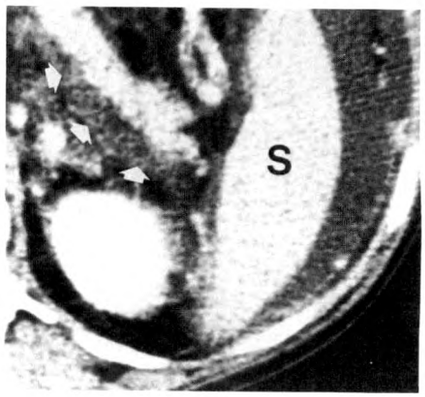


Fig. 8.—Retropancreatic peritoneal recess. Ascitic fluid (*arrows*) in persistent retropancreatic recess simulates retroperitoneal fluid collection. Intraabdominal ascites is seen around spleen (S).

posterior abdominal wall, overlying most of the duodenum [23, 26]. The right and left colon become fixed in position when the left leaf of their mesentery fuses (1) centrally to the mesentery covering the pancreaticoduodenal space and (2) laterally and inferiorly to the primary posterior parietal peritoneum (Fig. 10). According to Gerota [6], the mesocolon usually covers most or all of the left kidney and only the lower part of the right kidney. Fusion of the mesocolon extends bilaterally from about the second lumbar vertebrae to the iliac fossae (Fig. 9B). Caudally, the mesenteric fixation extends to the sigmoid on the left and generally to the cecal tip on the right. In about 10–20% of individuals the dorsal mesentery persists for the cecum and ascending colon. In this case, a secondary colonic retroperitoneal space does not form on the right (Fig. 11). By the processes described, the right and left colon usually come to reside in bilateral laminated spaces, sandwiched against the flattened pancreaticoduodenal space and primary retroperitoneum.

Most discrepancies between abdominal CT and the accepted retroperitoneal compartments relate to the "anterior pararenal space" and its relationship to the posterolateral peritoneal recess. The depth and configuration of the adult posterolateral peritoneal recess are influenced by the shape of the primary posterolateral recess, the amount of retroperitoneal fat, and the extent to which the mesocolon fuses laterally with the primary posterior peritoneum. In the embryo, the posterolateral peritoneal recesses extend posterior to the kidney. Thus, in adults, abdominal organs, bowel loops, and ascites commonly extend posterior to the kidney. In some patients, especially men, the ascending and descending colon have a ventral location because of retroperitoneal fat, whereas in others the lateral portions of colon are located posteriorly [29]. A major factor that determines the pattern of ascitic fluid in the paracolonic gutter is the lateral extent of mesocolonic fusion within the primitive peritoneal recess. Ascitic fluid in the paracolic gutter may assume a variable configuration (Fig. 12).

Primary Retroperitoneum

The domain of the primary embryonic retroperitoneum is confined ventrally by the primary posterior parietal peritoneum and posterolaterally by the transversalis fascia (Figs. 7A and 12A). The renal fasciae develop in the primitive mesenchyme

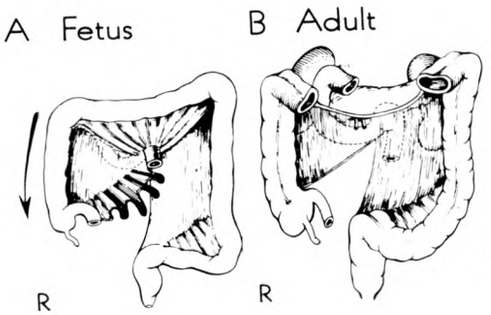


Fig. 9.—Colonic counterclockwise rotation and fixation. (Modified and reprinted with permission from Netter [23].)

A, Fetus of 18 weeks. During 270° counterclockwise rotation of colon (arrow), ascending colon lies flat along left posterior wall of abdomen while descending colon swings into right lower quadrant.

B, Adult configuration. Transverse colon and its free mesentery are cut away. Right leaf of ascending and descending colon, respectively, fuse with posterior abdominal wall to fix these colonic segments while left leaf of mesocolon contributes to adult posterior peritoneum. Normally, fixed portion of mesocolon covers lower third to one-half of right kidney and most or all of left kidney, and it extends into iliac fossae.

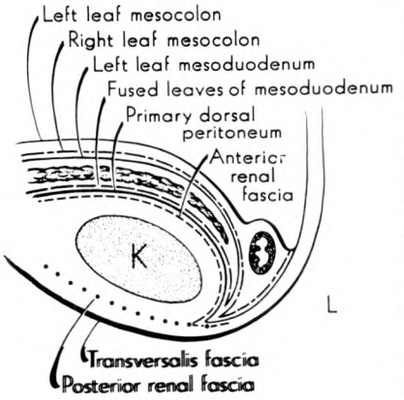


Fig. 10.—Adult retroperitoneal spaces at level of left kidney. Primary retroperitoneum is divided by anterior renal fascia (*dashed line*) and posterior renal fascia (*dotted line*) into a perirenal space and posterior pararenal space. Fusion of anterior renal fascia to primary dorsal peritoneum eliminates any anterior pararenal space. Ventral to primary retroperitoneum, a secondary retroperitoneum forms that consists of a pancreaticoduodenal space that is overlying a retroperitoneal colonic space. These secondary spaces are demarcated by folded, laminated leaves of mesentery that fuse with one another or primary dorsal peritoneum. K = kidney; L = left.



Fig. 11.—Failure of colonic fixation in a patient with abdominal carcinomatosis. Ascitic fluid clearly outlines a free mesentery (*arrow*) of right colon. Opacified blood vessels are seen within fat-filled mesentery of colon and small bowel, respectively. In this patient, a retroperitoneal colonic space does not exist on right side of abdomen because right colon is suspended by a free mesentery. A contrast-enhanced tumor implant is present on right ventral peritoneum.

as a prominent posterior layer and tenuous anterior layer [6, 7, 9]. The anterior renal fascia fuses with the primitive dorsal peritoneum [6, 7], thereby eliminating any potential anterior pararenal space. The posterior renal fascia attaches medially to the fascia that covers the psoas and quadratus muscles. Laterally, the posterior renal fascia joins the anterior renal fascia at a point near where they both fuse to the posterolateral peritoneum [7] or disappear into the properitoneal fat [6]. When present as such, the "lateroconal fascia," a term coined by Congdon and Edson [9], is always located dorsal to the primary posterior peritoneum. In the past, the lateral peritoneal reflection of the posterolateral peritoneal recess was often mistakenly called the lateroconal fascia. Superior to each kidney, the delicate anterior renal fascia does not extend above the level of the adrenal glands [9].

We suggest that the renal fasciae divide the true retroperitoneum into two compartments: (1) a perirenal space, subtended by the anterior and posterior renal fasciae, and (2) a posterior pararenal space bounded by the posterior renal fascia and transversalis fascia. The posterior pararenal space communicates with the properitoneal fat in the flank. Embryologically, no configuration of renal fasciae within the domain of the primary retroperitoneum exists that would define an "anterior renal space" containing gastrointestinal structures that originate within the intermesenteric domain.

Separation of Retroperitoneal Spaces

We propose that the adult retroperitoneum consists of two compartments, or domains: (1) the primary, primitive posterior retroperitoneum, which is located dorsal to the primary dorsal peritoneal membrane, contains exclusively structures of mesodermal origin, such as the kidney and adrenal glands; (2) a secondary retroperitoneum, which is located ventral to the primary posterior peritoneum, contains endodermal structures that develop in the intermesenteric space. Each major compartment contains two subcompartments (Fig. 10). The secondary retroperitoneum consists of the bilateral retroperitoneal colonic spaces that partially overlap the pancreaticoduodenal space. The primary retroperitoneum is divided by the renal fasciae into a perirenal space and posterior pararenal space. A parasagittal plane through the left kidney contains the following laminated membranes and spaces: (1) anterior, or left, leaf of mesocolon; (2) retroperitoneal colonic space; (3) posterior, or right, leaf of mesocolon that fuses with left leaf of mesoduodenum; (4) anterior, or left, leaf of mesoduodenum (secondary posterior peritoneum); (5) pancreaticoduodenal space; (6) several fused leaves of mesoduodenum that fuse with the primary posterior peritoneum; (7) primary posterior peritoneum; (8) anterior renal fascia that fuses with the primary posterior peritoneum; (9) perirenal space; (10) posterior pararenal space; and (11) transversalis fascia.

The notion of distinct pancreaticoduodenal and retroperitoneal colonic spaces is supported by findings at laparotomy and on CT examination. To mobilize the lateral colon, the surgeon makes an incision along a vertical white line, at the base of the paracolic gutter. This landmark, or line of Toldt, represents the fusion of the free mesenteric margin of the lateral colon with the primary dorsal peritoneum. The incision gains entry into the original intermesenteric space between the leaves of the dorsal colonic mesentery that contains

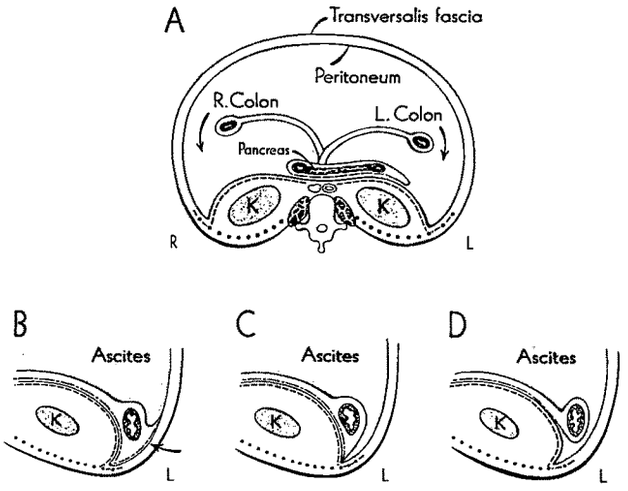


Fig. 12.—Schematic of retroperitoneal colonic space. K = kidney; R = right; L = left.

***A*, Axial section through pancreas of a 14-week human fetus. During colonic rotation (*arrows*), left and right colon swing toward flanks so that their dorsal mesentery, or mesocolon, lies flat against posterior abdominal wall. At this stage, mesentery of duodenum and pancreas have already fused with posterior peritoneum to form the pancreaticoduodenal space. Thus, bilateral retroperitoneal colonic spaces come to lie ventral to pancreaticoduodenal space, but extend more caudal.**

***B–D*, Different patterns that left colon and its dorsal mesentery assume in primary posterolateral peritoneal recess. Variable fusion occurs with primary posterior peritoneum. Sections are shown through lower pole of left kidney, just below caudal margin of pancreaticoduodenal space. Depending on depth of primary posterolateral peritoneal recess and extent of mesocolic fusion, ascites in the recess may have a configuration that is rounded (*B*), spiked (*C*), or forked (*D*). Right leaf of mesocolon (*long-short dashes*); anterior renal fascia (*short dashes*); posterior renal fascia (*dots*); lateroconal fascia (*dots and dashes*). Segment of membrane, designated by *arrow* in *B*, commonly labeled as lateroconal fascia is, in reality, peritoneum that forms lateral margin of primary posterolateral peritoneal recess along which right leaf of mesocolon may fuse. Lateroconal fascia either fuses with posterior peritoneum or disappears into subperitoneal fat [6].**

vessels to the lateral colon. These vessels are easily stripped away from the posterior abdominal wall to mobilize the lateral colon toward the midline. The duodenum and pancreas, however, remain enclosed within their own distinct space, demarcated ventrally by the posterior leaf of mesocolon that has fused with the anterior leaf of the mesoduodenum. To mobilize the pancreatic head and duodenal sweep, a Kocher maneuver is done by making a vertical incision through the membrane just lateral to the duodenum, and the pancreas along with its supplying vessels is lifted away from its retroperitoneal bed. Segregation of the pancreaticoduodenal and colonic subcompartments has also been shown by cadaver dissection [7].

Two observations from abdominal CT suggest that the pancreaticoduodenal space is generally separate from the bilateral retroperitoneal colonic spaces. First, extrapancreatic fluid generally does not extend appreciably caudad to the pancreas. If the pancreas were in the same space as the descending colon, however, frequent dissection of peripancreatic fluid into the left iliac fossa would be anticipated. Second, a sizable fluid collection in the retroperitoneal pancreaticoduodenal space often spares the fat plane around the retroperitoneal colon (Fig. 4A). A relatively common communication, however, between the pancreaticoduodenal and colonic retroperitoneal, spaces occurs along the root of the transverse mesocolon (Fig. 4B), which attaches along the inferior margin of the pancreas [30]. Such communication, however, involves disruption of the membrane that forms the ventral margin of the pancreaticoduodenal space (Fig. 13).

In some cases, inflammatory fluid within the pancreaticoduodenal space extends posteriorly and appears to communicate with the posterior pararenal space (e.g., Fig. 3). Dorsal fusion of mesoduodenum may extend sufficiently lateral to cover the medial wall of a deep posterolateral peritoneal recess that penetrates posterior to the kidney (Fig. 13A). In some patients, the mesenteric planes between the pancreaticoduodenal and retroperitoneal colonic space may be disrupted so that pancreatic fluid in the colonic space outlines the original primary posterior peritoneal recess that has been covered by mesocolon (Fig. 13B). In some cases, peripancreatic fluid gives the spurious appearance of having entered the posterior pararenal space (Fig. 3). In other cases, violation of fascial planes may occur with extension of inflammation into the posterior pararenal space and properitoneal fat in the flank.

Once fluid gains entry into the retroperitoneal colonic space (e.g., with pancreatitis), the fluid tends to dissect caudally because the colonic space extends into the iliac fossa. Fluid that reaches the iliac fossa, however, commonly remains separate from the posterior pararenal space, as shown in Figure 5. This finding challenges the concept that the anterior and posterior pararenal spaces are divided by a lateroconal fascia, but communicate in the iliac fossa. Fluid in both the colonic and posterior pararenal spaces indicates disruption of the primitive dorsal peritoneum.

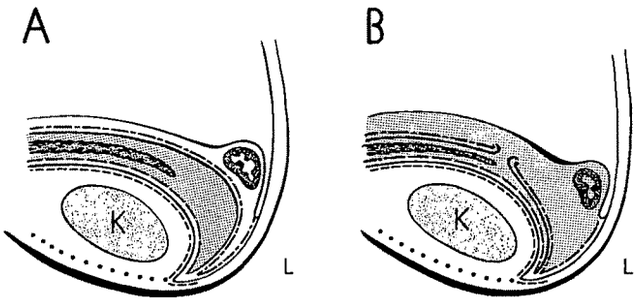


Fig. 13.—Schematic of posterior extension of peripancreatic fluid in the anterior, or secondary, retroperitoneal space. Fluid within anterior, or secondary, retroperitoneum extends posterior to kidney (K) without involving posterior pararenal space. L = left.

***A*, Fluid limited to pancreaticoduodenal space may extend posterior to the kidney. Uninvolved retroperitoneal colonic space and descending colon are displaced forward. Note that pericolonic rim of fat is preserved.**

***B*, Fluid within pancreaticoduodenal space has broken through into amesenteric colonic space. Descending colon is displaced forward, and its surrounding lucent-layer of fat is obliterated. In some instances, fluid from pancreaticoduodenal spaces reaches lateral portion of retroperitoneal colonic space by tracking along root of transverse mesocolon.**

Conclusions

We propose that (1) the kidneys and renal fasciae develop within the domain of the primary retroperitoneum, whereas all alimentary structures develop in the intermesenteric domain. (2) These two domains communicate only at the mesenteric root. (3) The anterior renal fascia and lateroconal fascia cannot demarcate a retroperitoneal space that contains alimentary-tract structures. (4) The secondary, or anterior, retroperitoneum is a laminated space, bounded by folded, fused leaves of mesentery, that contains distinct pancreaticoduodenal and colonic subcompartments. (5) The anterior and posterior pararenal spaces do not normally communicate caudally in the iliac fossa. We hope that our hypothesis helps resolve the apparent conflicts that exist between certain findings on abdominal CT and current notions about retroperitoneal compartmental anatomy. Like any hypothesis, however, our proposal must withstand critical scrutiny and testing before it merits general acceptance.

REFERENCES

1. Meyers MA, Whalen JP, Peele K, Berne AS. Radiologic features of extraperitoneal effusions: an anatomic approach. *Radiology* **1972**;104:249–257
2. Meyers MA. *Dynamic radiology of the abdomen: normal and pathologic anatomy*. New York: Springer-Verlag, **1976**
3. Whalen JP. *Radiology of the abdomen. Anatomic basis.* Philadelphia: Lea & Febiger, **1976**
4. Thornbury JR. Perirenal anatomy: normal and abnormal. *Radiol Clin North Am* **1979**;17:321–331
5. Love L, Meyers MA, Churchill RJ, Reynes CJ, Moncada R, Gibson D. Computed tomography of extraperitoneal spaces. *AJR* **1981**;136:781–789
6. Gerota D. Beitrage zur kenntnis des befestigungsapparates der niere. *Arch Anat Entwcklngsgech* **1895**;19:265–286
7. Tobin CE. The renal fascia and its relation to the transversalis fascia. *Anat Rec* **1944**;89:295–311
8. Mitchell GAG. The spread of retroperitoneal effusions arising in the renal regions. *Br Med J* **1939**;2:1134–1136
9. Congdon ED, Edson JN. The cone of renal fascia in the adult white male. *Anat Rec* **1941**;80:289–313
10. Daseler EH, Anson BJ. Anatomical relations of ectopic iliolumbar kidneys bilateral in adult, unilateral in fetus. *J Urol* **1943**;49:789–802
11. Mitchell GAG. The renal fascia. *Br J Surg* **1950**;37:257–266
12. Stevenson EO, Ozeran RS. Retroperitoneal space abscesses. *Surg Gynecol Obstet* **1969**;128:1202–1208
13. Meyers MA. Radiologic features of the spread and localization of extraperitoneal gas and their relationship to its souce: an anatomical approach. *Radiology* **1974**;111:17–26
14. Meyers MA. Uriniferous perirenal pseudocyst: new observations. *Radiology* **1975**;117:539–545
15. Barbaric Z. Renal fascia in urinary tract disease. *Radiology* **1976**;118:561–565
16. Parienty RA, Pradel J. Radiological evaluation of the peri- and para-renal spaces by computed tomography. *CRC Crit Rev Diagn Imaging* **1983**;20:1–26
17. Amin M, Blandford AT, Polk HC Jr. Renal fascia of Gerota. *Urology* **1976**;7:1–3
18. Reich NE, Haaga JR, Seidelmann FE, Havrilla TR, Alfidi RJ, Lipuma J. Computed tomography of the retroperitoneal fascia and compartments. *Comput Axial Tomogr* **1977**;1:205–212
19. Hunziker RJ. Pathologic effusions localized to the anterior pararenal space: an in vivo demonstration. *Gastrointest Radiol* **1978**;3:411–414
20. Hopper KD, Sherman JL. The variable fusion of the lateroconal fascia and its effect on the retroperitoneal colon. Presented at the annual meeting of the Radiological Society of North America, Washington, DC, November **1984**
21. Raptopoulos V, Kleinman PK, Marks S Jr, Snyder M, Silverman PM. Renal fascial pathways: posterior extension of pancreatic effusions within the anterior pararenal space. *Radiology* **1986**;158:367–374
22. Love L, Demon TC, Posniak H. CT of retrorenal fluid collections. *AJR* **1985**;145:87–91
23. Netter FH. *Lower digestive tract.* In: Oppenheimer, E., ed. *The Ciba collection of medical illustrations*, Part II of Vol. 3, *Digestive system.* New York: Ciba Publishers, **1962**
24. Goss CM, ed. *Anatomy of the human body*, 29th ed. Philadelphia: Lea & Febiger, **1973**
25. Patten BM, Carlson BM, ed. *Foundation of embryology*, 3rd ed. New York: McGraw-Hill, **1974**
26. Moore KL. *The developing human: clinically oriented embryology*, 3rd ed. Philadelphia: Saunders, **1982**
27. Dodds WJ, Foley WD, Lawson TL, Stewart ET, Taylor A. Anatomy and imaging of the lesser peritoneal sac. *AJR* **1985**;144:567–575
28. Rubenstein WA, Auh YH, Zirinsky K, Kneeland JB, Whalen JP, Kazam E. Posterior peritoneal recesses: assessment using CT. *Radiology* **1985**;156:461–468
29. Hadar H, Gadoth N. Positional relationships of the colon and kidney determined by perirenal fat. *AJR* **1984**;143:773–776
30. Jeffrey RB, Federle MP, Laing FC. Computed tomography of mesenteric involvement in fulminant pancreatitis. *Radiology* **1983**;147:185–188

The reader's attention is directed to the Commentary on this article, which appears on the following pages.

Commentary

Extraperitoneal Spaces

William A. Rubenstein[1] and Joseph P. Whalen

The preceding paper [1] presents several new and provocative concepts of the retroperitoneum which, if accurate, would require significant revision of our current understanding of the retroperitoneal space. Based on a review of embryology, the authors propose that the adult retroperitoneum consists of two distinct compartments: the primary posterior retroperitoneum, which contains the kidney and adrenal and is divided into perirenal and posterior pararenal spaces by the renal fascia; and the secondary or anterior retroperitoneum, which in turn is divided into two spaces that generally do not communicate—the pancreaticoduodenal space containing the duodenum and entire pancreas and the retroperitoneal colonic space containing the extraperitoneal ascending and descending colons.

Based on these concepts, two corollaries follow: First, our present understanding of an anterior pararenal space, being bordered posteriorly by anterior renal fascia, anteriorly by parietal peritoneum, and laterally by lateroconal fascia is erroneous. Fusion of the anterior renal fascia to the primary dorsal peritoneum eliminates the potential for any conventional anterior pararenal space. Instead, there is a secondary or anterior retroperitoneum that contains distinct pancreaticoduodenal and colonic subcompartments. Second, since there is no such entity as the anterior pararenal space, the conventional concept of an anterior pararenal space communicating with the posterior pararenal space in the iliac fossa is erroneous.

Using these concepts, the authors try to explain several findings on CT: (1) Peripancreatic fluid in the left upper quadrant tends to remain localized around the pancreas and spares the fat layer around the retroperitoneal descending colon (see Figs. 4A and 13A). According to the authors, this indicates that the pancreas and colon lie in two separate compartments. In some patients (presumably those with more severe pancreatitis, see Figs. 4B and 13B), "the mesenteric planes between the pancreaticoduodenal and retroperitoneal colonic space may be disrupted so that pancreatic fluid in the colonic space outlines the deep primary posterior peritoneal recess that has been covered by mesocolon." (2) Pancreatic fluid that reaches the retroperitoneal colonic space and dissects caudally into the iliac fossa commonly remains separate from posterior pararenal space fat (see Fig. 5). "This finding challenges the concept that the anterior and posterior pararenal spaces are divided cephalad by a lateroconal fascia, but communicate caudad in the iliac fossa."

With these hypotheses in mind, there are several discrepancies between the conclusions reached in this paper and currently accepted concepts of retroperitoneal anatomy. The authors' conclusions are based on correlating embryology with CT findings but are not supported by cadaver dissections or radiologic-anatomic studies that use injection of radiographic contrast media.

The authors conclude that no anterior parerenal space can exist since the anterior renal fascia fuses to the primary dorsal peritoneum. Yet anatomic studies by Southam [2], Tobin [3], Congdon and Edson [4], Whalen et al. [5], and Kazam and Whalen [6] have clearly shown the anterior renal fascia as a discrete structure, separate from the posterior parietal peritoneum. On sagittal anatomic sections, Southam [2] showed separate anterior renal fascia and posterior parietal peritoneum defining the anterior pararenal space, all of which extend from the diaphragm (superiorly) to below the iliac crest (inferiorly), and noted that while the anterior renal fascia may become contiguous with the posterior peritoneum [7–9], these two layers can be dissected from each other. Using serial sections of early embryos, 7–9 month fetuses, and

[1] Both authors: Department of Radiology, The New York Hospital-Cornell Medical Center, 525 E. 68 St., New York, NY 10021. Address reprint requests to W. A. Rubenstein.

AJR 147:1162–1164, December 1986 0361–803X/86/1476–1162 © American Roentgen Ray Society

adults, Tobin [3] exquisitely showed the anterior renal fascia and parietal peritoneum as separate structures. Similarly, by using transverse anatomic sections Congdon and Edson [4] and later Kazam and Whalen [6] showed that the anterior renal fascia and posterior parietal peritoneum are distinct structures, clearly separated from each other by the anterior pararenal space containing colon, pancreas, and/or fat. Meyers et al. [10], by using injection of iodinated contrast media into cadavers, clearly showed three distinct retroperitoneal spaces: anterior pararenal, posterior pararenal, and perirenal.

The authors conclude that the conventional anterior pararenal space and posterior pararenal space do not normally communicate caudally in the iliac fossa. Yet several previous investigators have shown that such communication commonly, if not always, exists. Using presacral retroperitoneal air insufflation, Whalen and coworkers [5, 11–13] showed free communication between the anterior and posterior pararenal spaces and the perirenal space. Meyers [14] showed that gas from perforated sigmoid diverticulitis originating below the cone of renal fascia can spread superiorly into both the anterior and posterior pararenal spaces. Similarly, gas from a perforated duodenum or pancreatic abscess within the anterior pararenal space can extend inferiorly below the cone of renal fascia and the limitation of the lateroconal fascia to gain access to the posterior pararenal space [15]. Using transverse and direct coronal CT scans, Feldberg [16] demonstrated anterior pararenal space fluid extending from the level of the left kidney and descending colon (superiorly) to the iliac fossa (inferiorly). On CT, fluid collections caused by pancreatitis [8, 17], perforations of the duodenum [18, 19] and rectum [2], and rupture of an internal iliac artery aneurysm [20] confirm the communication of the anterior and posterior pararenal spaces below the cone of renal fascia. Parienty and Pradel [8] demonstrated pancreatic phlegmons extending from the anterior pararenal space to the posterior pararenal space below the cone of renal fascia. Love et al. [17, 18] showed that at the level of the kidneys, fluid from pancreatitis or a duodenal leak occupied only the anterior pararenal space, but below the cone of renal fascia, occupied both the anterior and posterior pararenal spaces. Glazer et al. [19] showed that gas from duodenal rupture in the anterior pararenal space can escape below the apex of renal fascia and proceed up the flank into the peritoneal fat. Love et al. [21] demonstrated gas in all three retroperitoneal compartments resulting from rectal perforation. Similarly, hemorrhage from a ruptured internal iliac artery aneurysm may extend superiorly to involve both the anterior and posterior pararenal spaces around the kidney [20]. With respect to Figure 5, the observation that an inflammatory fluid collection (presumed to lie in the "anterior retroperitoneal space") does not communicate with the posterior pararenal space does not disprove the long-established concept that the anterior and posterior pararenal spaces communicate in the iliac fossa. Lack of communication in a given case could easily be due to loculation and/or presence of pyogenic membranes.

Anatomic dissections [2, 4, 5, 22, 23] have clearly shown that a structure corresponding to the lateroconal fascia exists and that the lateroconal fascia is distinct from parietal peritoneum. The authors' statement that the lateroconal fascia disappears into the properitoneal fat behind the primary dorsal peritoneum does not alter the established concept that the renal fascia divides the retroperitoneum into three distinct spaces: anterior pararenal, posterior pararenal, and perirenal. It has long been recognized that the fusion of the anterior and posterior renal fasciae, and hence the lateroconal fascia, is variable [2, 4, 22, 24]. Congdon and Edson [4] showed that in those occasional cases of no lateroconal fascia, the anterior and posterior renal fasciae simply fused directly with the lateral peritoneum, and Southam [2] showed that the lateroconal fascia could extend posterolateral to the peritoneum into the properitoneal fat. Fusion of the anterior and posterior renal fasciae to form the lateroconal fascia may be seen on plain radiographs [5, 25] and CT [16].

No new concepts are needed to explain the appearance of ascites in Figures 2, 11, and 12B–D. The extension of intraperitoneal fluid posterior to known extraperitoneal structures has previously been described and is due to posterior peritoneal recesses located at several areas within the abdomen [26]. Figures 2, 12B, and 12C demonstrate ascites in the inferior extension of the splenorenal recess and deep paracolic gutters. Figures 11 and 12D demonstrate the variable length of the mesocolon; in postmortem studies the ascending and descending colon may be on a mesentery in up to 26% and 36%, respectively [27, 28]. Similarly, the CT finding that the liver, spleen, and bowel may extend posterolateral to the kidney only indicates the variable site of fusion of the anterior and posterior renal fascia to form the lateroconal fascia [6, 17, 22, 24]. Furthermore, it has long been known that the posterior borders of the liver and spleen are outlined by extraperitoneal perivisceral fat [5, 25].

Current concepts of retroperitoneal anatomy explain the appearance of peripancreatic fluid in Figure 3. The observation that peripancreatic fluid in the left upper quadrant may extend posterolateral to the left kidney while sparing perinephric and/or posterior pararenal fat can be explained by any of three concepts: (1) The fluid may lie entirely within the anterior pararenal space, which extends posterolateral to the left kidney due to posterior fusion of the anterior and posterior renal fascia [17, 22, 24]; (2) fluid in the anterior pararenal space may dissect posterolateral to the left kidney within laminae of the posterior renal fascia [22]; (3) the fluid may actually be intraperitoneal within the inferior extension of the splenorenal recess [17, 26].

Although Dodds et al. [1] found that peripancreatic effusions related to pancreatitis tend to be localized around the pancreas (Fig. 4A), other investigators [16, 17, 29–34] have noted that peripancreatic fluid contiguous with the pancreas may also infiltrate pericolonic fat and involve the wall of the descending colon. In addition, we have been impressed with the aggressiveness of acute pancreatitis and by the ability of peripancreatic fluid collections to obliterate the fat planes around the colon as well as to dissect caudally into the iliac fossa. Before the introduction of CT, Meyers et al. [10] showed that anterior pararenal collections such as pancreatic pseudocysts resulted in localized changes in the descending colon.

It is somewhat difficult to reconcile the authors' conclusions with the work of previous investigators. It may be possible, however, to partially explain the discrepancies by several modifications of Figures 7B, 10, 12, and 13. Specifically, the proposed multilaminated fascial planes probably do not exist in the adult, but rather are resorbed after fusion of the dorsal mesentery with the primary posterior peritoneum in the fetus [23, 35–37]. The structure identified as anterior renal fascia

in the adult represents a single fascial plane composed of the fused embryological anterior renal fascia, primary dorsal peritoneum, and dorsal mesentery. This is the so-called "fusional fascia of Toldt" [2, 4, 16, 23], a term sometimes reserved for that part of the anterior renal fascia related to the colon. Congdon et al. [23] state explicitly that the adult anterior renal fascia, which lies posterior to the pancreas, is not trilaminar but rather a single fascial plane. The structure identified as posterior parietal peritoneum in the adult may represent the authors' "secondary posterior peritoneum"; that is, simply that portion of the parietal peritoneum derived from the reflected leaves of mesocolon. The proposed fascial plane that supposedly separates the pancreas and duodenum from colon is probably nonexistent. Williams and Warwick [35], Patten [36], Langman [37], and Congdon et al. [23] all indicate that significant portions of the mesoduodenum, mesocolon, and primary dorsal peritoneum are resorbed after fusion of these segments of dorsal mesentery with the primary dorsal peritoneum. Patten [36] states that the original peritoneal covering of the duodenum is completely resorbed, and the duodenum finally lies embedded in the dorsal body wall covered by a secondarily acquired peritoneal reflection of mesocolon.

In summary, there is overwhelming anatomic and radiographic evidence that the retroperitoneum is divided into three discrete and identifiable spaces by the renal fascia, and that these spaces communicate below the cone of renal fascia in the iliac fossa. Minor variations, such as occasional fusion of anterior renal fascia to posterior parietal peritoneum or absence of lateroconal fascia with direct fusion of anterior and posterior renal fascia to the lateral parietal peritoneum do not alter long-established concepts. The authors' CT observations may be explained by established anatomy.

REFERENCES

1. Dodds WJ, Darweesh RMA, Lawson TL, et al. The retroperitoneal spaces revisited. *AJR* **1986**;147:1155–1161
2. Southam AH. Fixation of the kidney. *Q J Med* **1923**;16:283–308
3. Tobin CE. The renal fascia and its relation to the transversalis fascia. *Anat Rec* **1944**;89:295–311
4. Congdon ED, Edson JN. The cone of renal fascia in the adult white male. *Anat Rec* **1941**;80:289–313
5. Whalen JP, Berne AS, Riemenschneider PA. The extraperitoneal perivisceral fat pad. I. Its role in the roentgenologic visualization of abdominal organs. *Radiology* **1969**;92:466–472
6. Kazam E, Whalen JP. Computed Tomography. In: Margulis AB, Burhenne HJ, eds. *Alimentary tract radiology*, 3rd ed. St. Louis: Mosby, **1983**:292–342
7. Parienty RA, Pradel J, Picard JD, Ducellier R, Lubrano JM, Smolarski N. Visibility and thickening of the renal fascia on computed tomograms. *Radiology* **1981**;139:119–124
8. Parienty RA, Pradel J. Radiological evaluation of the peri- and pararenal spaces by computed tomography. *CRC Crit Rev Diagn Imaging* **1983**;29:1–26
9. Mitchell GAG. The renal fascia. *Br J Surg* **1950**;37:257–266
10. Meyers MA, Whalen JP, Peelle K, Berne AS. Radiologic features of extraperitoneal effusions: an anatomic approach. *Radiology* **1972**;104:249–257
11. Whalen JP. *Radiology of the abdomen: anatomic basis.* Philadelphia: Lea & Febiger, **1976**:127
12. Whalen JP, Evans JA, Shanser J. Vector principle in the differential diagnosis of abdominal masses. I. The left upper quadrant. *AJR* **1971**;113:104–118
13. Whalen JP, Ziter FMH. Visualization of the renal fascia—a new sign in localization of abdominal masses. *Radiology* **1967**; 89:861–863
14. Meyers MA. Radiological features of the spread and localization of extraperitoneal gas and their relationship to its source: an anatomical approach. *Radiology* **1974**;111:17–26
15. Meyers MA. *Dynamic radiology of the abdomen: normal and pathological anatomy.* New York: Springer-Verlag, **1976**: 113–194
16. Feldberg MAM. *Computed tomography of the retroperitoneum. An anatomical and pathological atlas with emphasis on the fascial planes. Boston:* Martinns Nijhoff, **1983**
17. Love L, Demos TC, Posniak H. CT of retrorenal fluid collections. *AJR* **1985**;145:87–91
18. Love L, Meyers MA, Churchill RJ, Reynes CJ, Moncada R, Gibson D. Computed tomography of the extraperitoneal spaces. *AJR* **1981**;136:781–789
19. Glazer GM, Buy JN, Moss AA, Goldberg HI, Federle MP. CT detections of duodenal perforation. *AJR* **1981**;137:333–336
20. Samuelsson L, Albrechtsson U. Ruptured aneurysm of the internal iliac artery. *J Comput Assist Tomogr* **1982**;6:842–844
21. Love L, Reynes CJ, Churchill R, Moncada R. Third generation CT scanning in renal disease. *Radiol Clin North Am* **1979**;17: 77–90
22. Raptopoulos V, Kleinman PK, Marks S, Snyder M, Silverman PM. Renal fascial pathway: posterior extension of pancreatic effusions within the anterior pararenal space. *Radiology* **1986**;158:367–374
23. Congdon ED, Blumberg R, Henry W. Fasciae of fusion and elements of the fused enteric mesenteries in the human adult. *Am J Anat* **1942**;70:251–279
24. Sherman JL, Hopper KD, Greene AJ, Johns TT. The retrorenal colon on computed tomography. *J Comput Assist Tomogr* **1985**;9:339–341
25. Whalen JP, Berne AS. The extraperitoneal perivisceral fat pad. II. Roentgen interpretation of pathological alterations. *Radiology* **1969**;92:473–480
26. Rubenstein WA, Auh YH, Zirinsky K, Kneeland JB, Whalen JP, Kazam E. Posterior peritoneal recesses: assessment using CT. *Radiology* **1985**;156:461–469
27. Whalen JP, Riemenschneider PA. An analysis of the normal anatomic relationships of the colon as applied to roentgenographic observations. *AJR* **1967**;99:55–61
28. Whalen JP. Anatomy of the colon. Guide to intra-abdominal pathology. *AJR* **1975**;125:3–20
29. Siegelman SS, Copeland BE, Saba OP, Cameron JL, Sanders RC, Zerhouni EA. CT of fluid collections associated with pancreatitis. *AJR* **1980**;134:1121–1132
30. Donovan PJ, Sanders RC, Siegelman SS. Collections of fluid after pancreatitis: evaluation by computed tomography and ultrasonography. *Radiol Clin North Am* **1982**;20:653–665
31. Siegelman SS, Fishman EK. Computed tomography of pancreatitis. In: Siegelman SS, ed. *Computed tomography of the pancreas.* New York: Churchill Livingstone, **1983**:83–111
32. Strax R, Toombs BD, Rauschkolb EN. Correlation of barium enema and CT in acute pancreatitis. *AJR* **1981**;136:1219–1220
33. Federle MP, Goldberg HI. Computed tomography of the pancreas. In: Moss AA, Gamsu G, Genant HK, eds. *Computed tomography of the body.* Philadelphia: Saunders, **1983**:699–762
34. Mauro MA, Stanley RJ. Pancreas. In: Lee JKT, Sagel SS, Stanley RJ, eds. *Computed body tomography.* New York: Raven, **1983**:213–241
35. Williams PL, Warwick R, eds. *Gray's anatomy,* 35th ed. Philadelphia: Saunders, **1973**:173
36. Patten BM. *Human embryology,* 3rd ed. New York: McGraw-Hill, **1968**:421–422
37. Langman J. *Medical embryology,* 4th ed. Baltimore: Williams and Wilkins, **1981**:150–154

Esophageal Intramural Pseudodiverticulosis: A Reevaluation

Marc S. Levine[1]
David N. Moolten[2]
Hans Herlinger[1]
Igor Laufer[1]

Esophageal intramural pseudodiverticulosis is an unusual condition manifested by tiny flask-shaped outpouchings in the wall of the esophagus. The condition was diagnosed in 21 (0.15%) of 14,350 patients undergoing radiologic examinations of the esophagus at our hospitals. The pseudodiverticula were detected only by single-contrast technique in five of 18 patients (28%) who underwent both single- and double-contrast examinations. Thus, thin, low-density barium seems to enter these structures more readily than the high-density barium used for double-contrast esophagography. While most patients reported in the literature have diffuse or segmental pseudodiverticulosis associated with high esophageal strictures, the majority of our patients (11 [52%] of 21) had isolated involvement of the distal esophagus with 10 or fewer pseudodiverticula in the region of a peptic stricture. Other associated conditions included *Candida* esophagitis, herpes esophagitis, and squamous cell carcinoma of the esophagus. Our experience suggests that pseudodiverticulosis usually represents a sequela of reflux esophagitis, although the reason that so few patients with esophagitis develop this condition is unclear.

Esophageal intramural pseudodiverticulosis is an unusual condition manifested by multiple tiny, flask-shaped outpouchings in the wall of the esophagus and characteristic findings on esophagography [1–18]. Ninety percent of patients have associated strictures, most frequently in the upper third of the esophagus [16–18]. The disease may be either segmental or diffuse, but isolated involvement of the distal esophagus has been found in only 4% of all reported cases [17]. Recently, however, we observed several patients in whom these pseudodiverticula were confined to the distal esophagus in the region of a peptic stricture. The discrepancy between our observations and those reported in the literature led us to perform a retrospective review of patients seen at our hospitals to determine the prevalence of this condition, as well as the clinical and radiographic findings in these patients.

Materials and Methods

We examined log sheets of all esophagrams and upper gastrointestinal examinations performed at the Hospital of the University of Pennsylvania between 1980 and 1986. These records showed that pseudodiverticulosis was diagnosed radiographically in 16 patients during this period. Radiology log sheets from the Philadelphia Veterans Administration Hospital revealed five additional patients in 1985 and 1986. A total of approximately 14,350 esophagrams and upper gastrointestinal examinations were performed during those periods. Thus, pseudodiverticulosis was diagnosed in 0.15% of all patients undergoing radiologic examinations of the esophagus.

Eighteen of 21 patients with pseudodiverticulosis had biphasic examinations with upright double-contrast and prone single-contrast views of the esophagus. The double-contrast radiographs were obtained with a high-density barium suspension (E-Z-HD, E-Z-EM Co., Westbury NY), while the single-contrast radiographs were obtained with a thinner, low-density barium suspension (SOL-O-PAKE, E-Z-EM Co.). Of the remaining three patients, one had a single-contrast and two had double-contrast examinations. The radiographs were reviewed

Received July 7, 1986; accepted July 24, 1986.

[1] Department of Radiology, Hospital of the University of Pennsylvania, 3400 Spruce St., Philadelphia, PA 19104. Address reprint requests to M. S. Levine.

[2] University of Pennsylvania School of Medicine, Philadelphia, PA 19104.

AJR 147:1165–1170, December 1986
0361–803X/86/1476–1165
© American Roentgen Ray Society

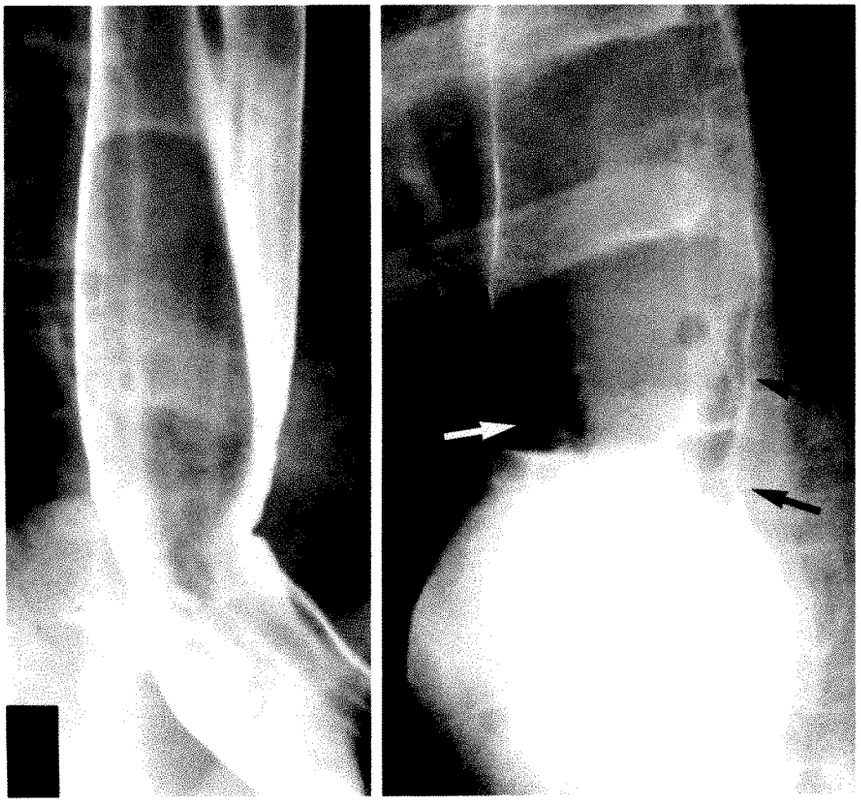


Fig. 1.—Biphasic esophagram with intramural pseudodiverticula only visualized by single-contrast technique.

***A*, Upright double-contrast view reveals minimal peptic scarring of distal esophagus without evidence of pseudodiverticulosis.**

***B*, However, prone single-contrast view with low-density barium shows several tiny pseudodiverticula (*arrows*) not seen, even in retrospect, on double-contrast view.**

retrospectively to determine the radiologic features of this condition, including the number, size, location, and appearance of the pseudodiverticula, as well as the presence or absence of strictures or other associated abnormalities in the esophagus. Medical records were also reviewed to determine the clinical and endoscopic findings in these patients.

Results

Clinical Findings

Fourteen patients were men and seven were women. The average age was 55 years (range, 22–74). Clinical data were available for 19 patients: 10 (53%) had reflux symptoms (i.e., heartburn, regurgitation), seven (37%) had dysphagia, two (11%) had odynophagia, one (5%) had upper gastrointestinal bleeding, and three (16%) had no esophageal complaints. The average duration of symptoms was 3.3 years, with a range of 3 months to 10 years. Associated esophageal diseases included *Candida* esophagitis (one patient), herpes esophagitis (one patient), esophageal varices (one patient), and squamous cell carcinoma of the esophagus (one patient). Five patients (26%) had a history of alcoholism, and two (11%) had AIDS.

Radiographic Findings

Pseudodiverticulosis was manifested radiographically by tiny flask-shaped outpouchings ranging from 1–4 mm in length and 1–2 mm in width (Figs. 1–6). The number of pseudodiverticula was 1–5 in eight patients (38%), 5–10 in eight patients (38%), 10–20 in one patient (5%), and 20 or greater in four patients (19%). In 18 patients (86%), the pseudodiverticula had a segmental distribution in the esophagus with involvement of the distal third in 12, middle third in five, and upper third in one patient. In the remaining three patients (14%), the pseudodiverticula were diffusely distributed throughout the thoracic esophagus. Branching of individual pseudodiverticula was observed in three patients, and intramural tracts with communication between adjacent pseudodiverticula in two (Fig. 3). When viewed in profile, some or all of the pseudodiverticula appeared not to communicate with the esophageal lumen in most cases (Figs. 2, 3, and 5).

The pseudodiverticula were visualized by single- and double-contrast technique in 13 (72%) of 18 patients who underwent biphasic examinations. In the remaining five patients (28%), pseudodiverticula were only visualized by single-contrast technique (Fig. 1B) and could not be recognized, even in retrospect, on the double-contrast portion of the examination (Fig. 1A).

Sixteen patients (76%) had associated strictures; 11 (69%) were located in the distal esophagus and five (31%) in the middle or upper esophagus. All 11 patients with distal strictures had a smooth or slightly irregular segment of esophageal narrowing extending several centimeters above the gastroesophageal junction with the typical appearance of a peptic stricture (Fig. 2). All 11 patients had associated hiatal hernias.

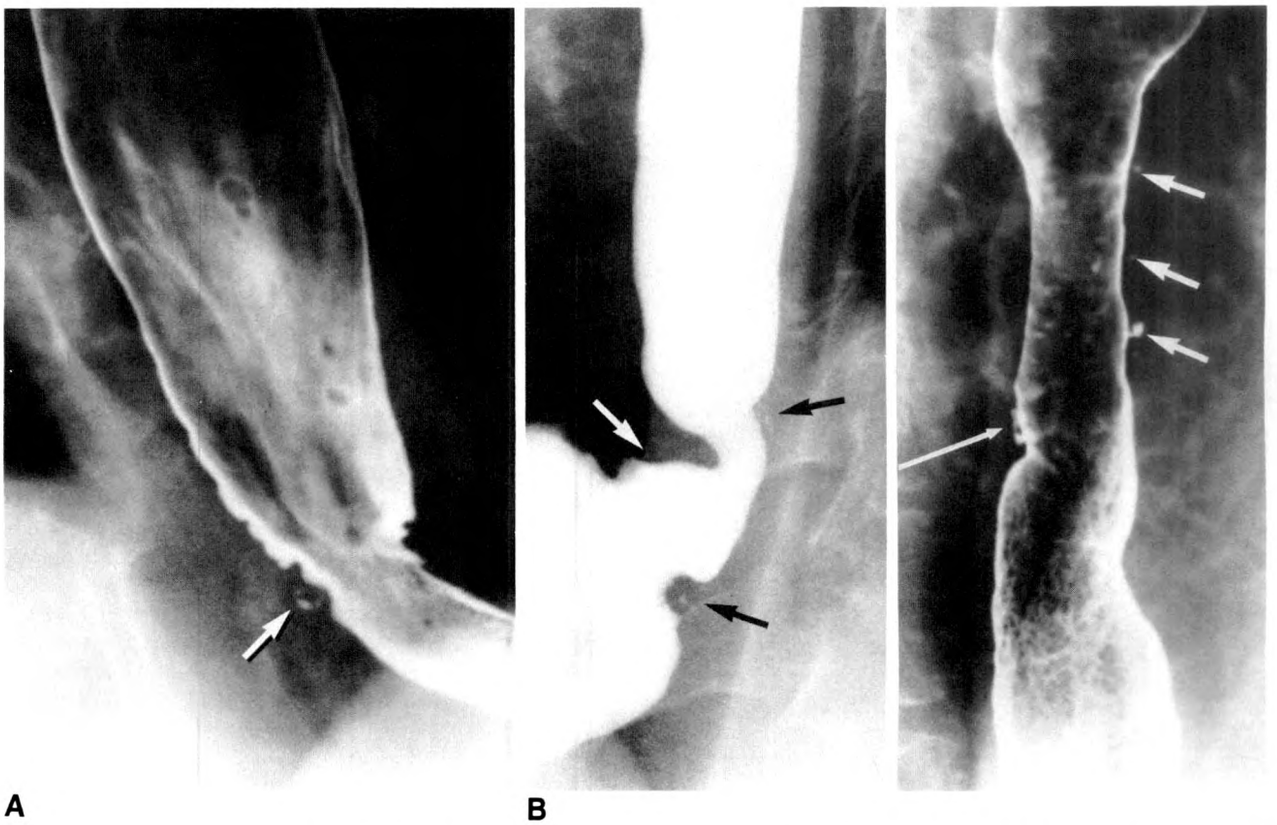


Fig. 2.—Double-contrast (*A*) and single-contrast (*B*) esophagrams in different patients showing peptic strictures with localized pseudodiverticulosis (*arrows*) in region of stricture. Most pseudodiverticula do not appear to communicate with esophageal lumen.

Fig. 3.—Midesophageal stricture with scattered pseudodiverticula (*short arrows*) in region of stricture. Communication between adjacent pseudodiverticula produces short intramural tract (*long arrow*). Reticular pattern of mucosa below stricture suggests presence of Barrett's esophagus, although endoscopic confirmation was not obtained in this case.

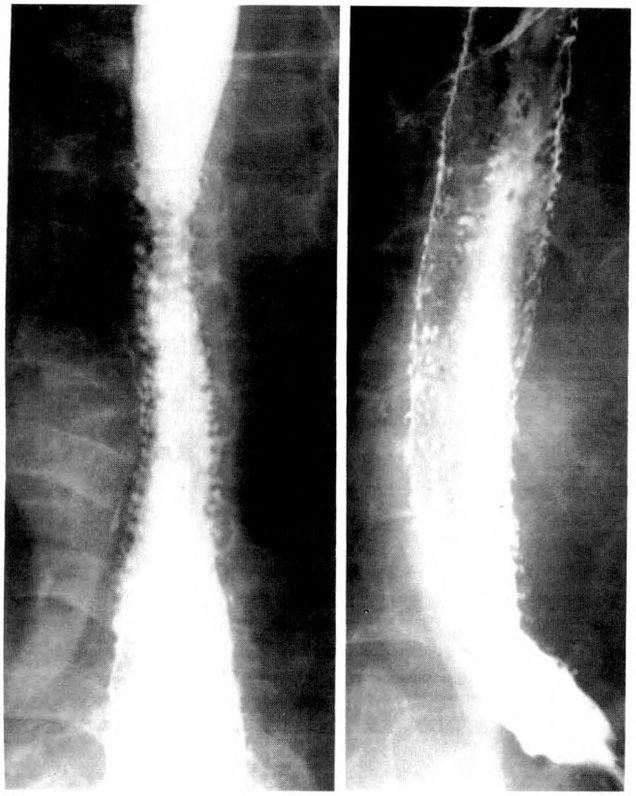
Two also had evidence of reflux esophagitis with superficial ulceration in the distal esophagus. In all patients with peptic strictures, the pseudodiverticula occurred at the level of the stricture, and in nine of those patients, there were five or fewer pseudodiverticula. Thus, the majority of patients with pseudodiverticulosis (i.e., 11 [52%] of 21) had isolated involvement of the distal esophagus with scattered pseudodiverticula in the region of a peptic stricture (Fig. 2).

Five patients had strictures in the middle (three cases) or upper (two cases) thoracic esophagus. Two patients with midesophageal strictures had associated hiatal hernias and gastroesophageal reflux with clinical evidence of reflux disease. Both patients were thought to have Barrett's esophagus (Fig. 3), although endoscopic confirmation was not obtained. In the remaining three patients, the cause of the stricture was unknown (Fig. 4). All five patients had smooth, concentric strictures ranging from 2–8 cm in length. The pseudodiverticula were confined to the level of the stricture in four cases (Fig. 3). The remaining patient had diffuse pseudodiverticulosis extending from a high stricture to the gastroesophageal junction (Fig. 4).

One patient with presumed *Candida* esophagitis (endoscopy was not performed) had extensive plaque formation throughout the esophagus with localized pseudodiverticula at the level of the aortic arch. Another patient with proven herpes esophagitis had discrete areas of superficial ulceration in the midesophagus with pseudodiverticula only in the diseased segment. Both patients with infectious esophagitis had AIDS. A third patient with irregular narrowing of the midesophagus due to squamous cell carcinoma had several pseudodiverticula at and just above the superior margin of the tumor (Fig. 5). Finally, two patients had an otherwise normal-appearing esophagus (Fig. 6). One had pseudodiverticula only in the distal esophagus and one had diffuse pseudodiverticulosis.

Endoscopic Findings

Only three (14%) of 21 patients had endoscopy. One patient had biopsy-proven squamous cell carcinoma of the midesophagus. The second had several shallow ulcers in the middle and distal esophagus with positive cytology for herpes



A B

Fig. 4.—High esophageal stricture with diffuse pseudodiverticulosis.
***A*, Single-contrast esophagram reveals smooth, tapered stricture of unknown cause in proximal thoracic esophagus; numerous pseudodiverticula in region of stricture.**
***B*, More distal radiograph shows widespread pseudodiverticulosis below stricture to gastroesophageal junction.**

esophagitis. The third had acute and chronic inflammation associated with a high esophageal stricture but no evidence of Barrett's esophagus or tumor. Intramural pseudodiverticula were not seen endoscopically in any case.

Discussion

Since its original description by Mendl in 1960 [1], nearly 100 cases of pseudodiverticulosis have been reported in the world literature [18]. Autopsy studies have shown that the pseudodiverticula represent dilated excretory ducts of deep mucous glands in the esophagus [9, 11, 19, 20]. In our study, pseudodiverticulosis was diagnosed in only 0.15% of all patients undergoing radiologic examinations of the esophagus. Nevertheless, esophagography is more sensitive than endoscopy in detecting these lesions because the orifices of the dilated excretory ducts are difficult to visualize endoscopically [17]. Furthermore, thin, low-density barium seems to enter these structures more readily than the high-density barium used for double-contrast esophagography. In our study, pseudodiverticula were detected only by single-contrast technique in 28% of patient who underwent both single- and double-contract examinations (Fig. 1). Thus, single-contrast esophagography is probably the best technique for diagnosing this condition.

Pseudodiverticulosis is classically thought to be manifested radiographically by innumerable, tiny (1–4 mm), flask-shaped outpouchings in longitudinal rows parallel to the long axis of the esophagus [7, 9, 11, 12, 16–18]. Because the necks of the pseudodiverticula are 1 mm or less in diameter, incomplete filling may erroneously suggest lack of communication with the esophageal lumen [16, 18]. Occasionally, bridging may occur between adjacent pseudodiverticula, producing discrete intramural tracts [2, 17]. According to the literature, about half the patients have diffuse disease and half have segmental disease [16–18], although it is rarely confined to the distal esophagus [17]. About 90% of reported patients have associated strictures, most frequently in the upper third of the esophagus [16–18]. In such cases, the pseudodiverticula often extend above and/or below the stricture [17].

In our study, however, almost 90% of patients had segmental disease, and two thirds of those patients had isolated involvement of the distal esophagus (Figs. 1 and 2). Furthermore, about 75% of patients had 10 or fewer pseudodiverticula. While most patients had associated strictures, 70% of those strictures were located in the distal esophagus and appeared radiographically as typical peptic strictures (Fig. 2). Thus, the majority of patients with pseudodiverticulosis had reflux disease with 10 or fewer pseudodiverticula in the region of a peptic stricture.

The explanation for this discrepancy between our findings and those reported previously is unclear. However, most publications on the subject are anecdotal, and it seems likely that the more spectacular cases have been reported rather than the more subtle ones with fewer pseudodiverticula. In any case, our experience suggests that pseudodiverticulosis is usually a localized disease in the distal esophagus associated with scarring from reflux esophagitis.

While pseudodiverticulosis is often associated with benign esophageal strictures, we encountered one case of irregular narrowing in the midesophagus due to squamous cell carcinoma in which several pseudodiverticula were detected at and just above the superior margin of the tumor (Fig. 5). Malignant degeneration may have occurred within a previ-esophageal strictures, we encountered one case of irregular narrowing in the midesophagus due to squamous cell carcinoma in which several pseudodiverticula were detected at and just above the superior margin of the tumor (Fig. 5). Malignant degeneration may have occurred within a previously benign stricture in this location. Whatever the explanation, this case indicates that strictures associated with pseudodiverticulosis are not always benign, and each case should be evaluated individually for radiologic signs of malignancy.

The cause of pseudodiverticulosis is uncertain. One infectious organism, *Candida albicans*, has been cultured from the esophagus in 34–48% of patients with pseudodiverticula [16–18]. In our study, however, only one patient had *Candida* esophagitis. A second patient had herpes esophagitis, a condition not previously associated with pseudodiverticulosis. We agree with other investigators that these organisms prob-

Fig. 5.—Double-contrast esophagram shows irregular narrowing of midesophagus from infiltrating squamous cell carcinoma. Scattered pseudodiverticula (*arrows*) at and just above superior margin of tumor.

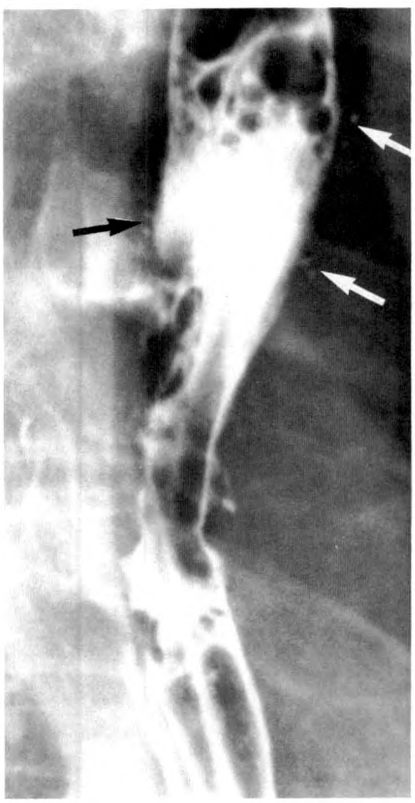
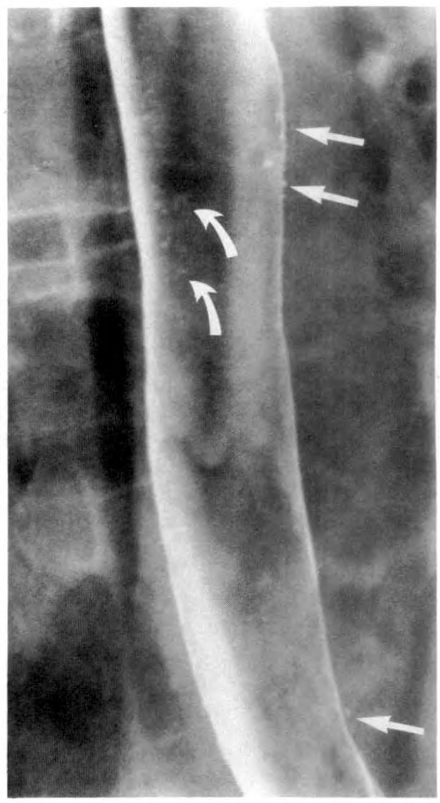


Fig. 6.—Double-contrast esophagram shows middle and distal pseudodiverticula in otherwise normal-appearing esophagus without evidence of stricture. Pseudodiverticula can be seen both in profile (*straight arrows*) and en face (*curved arrows*).



5 6

ably represent secondary esophageal invaders and are not important causal factors in the development of this condition [7–9, 13, 14, 20].

Others have postulated that ductal dilatation in pseudodiverticulosis results from plugging and obstruction of the ducts by thick, viscous mucus, inflammatory material, and/or desquamated epithelium [11, 19, 20]. Alternatively, the ducts may be extrinsically compressed by periductal inflammation and fibrosis that result from chronic esophagitis [15, 17, 18]. In various studies, 80–90% of patients with pseudodiverticulosis have endoscopic and/or histologic evidence of inflammatory changes in the esophagus [16, 18]. In our study, the majority of patients had evidence of reflux esophagitis. Thus, pseudodiverticulosis may be a sequela of chronic esophagitis, particularly reflux esophagitis, although the reasons that so few patients with esophagitis develop this condition are unclear.

Pseudodiverticulosis usually occurs in the elderly, with a slight male predominance [16–18]. Most patients present with intermittent or slowly progressive dysphagia due to the high prevalence of associated strictures [3, 5, 6, 8, 11–14, 16–18]. Treatment is therefore directed toward the underlying stricture because the pseudodiverticula themselves rarely cause problems. Mechanical dilatation of strictures produces a dramatic clinical response in almost all patients [12–14]. While the pseudodiverticula may persist or disappear after treatment, the fate of these structures has no relationship to the clinical course of the patient [16, 17].

In summary, pseudodiverticulosis has been diagnosed at our hospitals in only 0.15% of all patients undergoing radiologic examinations of the esophagus. Conventional single-contrast esophagography with a thin, low-density barium was the best technique for visualizing these structures. The majority of patients had isolated involvement of the distal esophagus with 10 or fewer pseudodiverticula associated with peptic strictures. We conclude that pseudodiverticulosis probably represents an uncommon sequela of chronic reflux esophagitis.

REFERENCES

1. Mendl K, McKay JM, Tanner CH. Intramural diverticulosis of the oesophagus and Rokitansky-Aschoff sinuses in the gallbladder. *Br J Radiol* **1960**;33:496–501
2. Hodes PJ, Atkins JP, Hodes BL. Esophageal intramural diverticulosis. *AJR* **1966**;96:411–413
3. Culver GJ, Chaudhari KR. Intramural esophageal diverticulosis. *AJR* **1967**;99:210–211
4. Troupin RH. Intramural esophageal diverticulosis and moniliasis. *AJR* **1968**;104:613–616
5. Zatzkin HR, Green S, La Vine JJ. Esophageal intramural diverticulosis. *Radiology* **1968**;90:1193–1194
6. Creely JJ, Trail ML. Intramural diverticulosis of the esophagus. *South Med J* **1970**;63:1257–1260
7. Sperling HV, D'Altorio RA. Intramural diverticulosis of the esophagus. *Am J Dig Dis* **1973**;18:978–982
8. Beauchamp JM, Nice CM, Belanger MA, Neitzchman HR. Esoph-

ageal intramural pseudodiverticulosis. *Radiology* **1974**;113 273–276
9. Boyd RM, Bogoch A, Greig JH, Trites EW. Esophageal intramural pseudodiverticulosis. *Radiology* **1974**;113:267–270
10. Lupovitch A, Tippins R. Esophageal intramural pseudodiverticulosis: a disease of adnexal glands. *Radiology* **1974**;113:271–272
11. Wightman AJA, Wright EA. Intramural esophageal diverticulosis: a correlation of radiological and pathological findings. *Br J Radiol* **1974**;47:496–498
12. Graham DY, Goyal RK, Sparkman J, Cagan ME, Pogonowska MJ. Diffuse intramural esophageal diverticulosis. *Gastroenterology* **1975**;68:781–785
13. Castillo S, Aburashed A, Kimmelman J, Alexander LC. Diffuse intramural esophageal pseudodiverticulosis. *Gastroenterology* **1977**;72:541–545
14. Shapiro MJ, Sloan WC. Intramural pseudodiverticulosis of the esophagus. *Ann Otol Rhinol Laryngol* **1977**;86:594–597
15. Muhletaler CA, Lams PM, Johnson AC. Occurrence of esophageal intramural pseudodiverticulosis in patients with pre-existing benign oesophageal stricture. *Br J Radiol* **1980**;53:299–303
16. Cho SR, Sanders MM, Turner MA, Liu CI, Kipreos BE. Esophageal intramural pseudodiverticulosis. *Gastrointest Radiol* **1981**;6:9–16
17. Bruhlmann WF, Zollikofer CL, Maranta E, et al. Intramural pseudodiverticulosis of the esophagus: report of seven cases and literature review. *Gastrointest Radiol* **1981**;6:199–208
18. Sabanathan S, Salama FD, Morgan WE. Oesophageal intramural pseudodiverticulosis. *Thorax* **1985**;40:849–857
19. Hammon JW, Rice RP, Postlethwait RW, Young WG. Esophageal intramural diverticulosis. *Ann Thorac Surg* **1974**;17:260–267
20. Umlas J, Sakhuja R. The pathology of esophageal intramural pseudodiverticulosis. *Am J Clin Pathol* **1976**;65:314–320

The Diagnosis of Acute Acalculous Cholecystitis: A Comparison of Sonography, Scintigraphy, and CT

Stuart E. Mirvis[1]
Julian R. Vainright[1]
Ava W. Nelson[1]
Gerald S. Johnston[1]
Robert Shorr[2]
Aurelio Rodriguez[3]
Nancy O. Whitley[1]

The clinical and laboratory diagnosis of acute acalculous cholecystitis is difficult, and the reliability of various diagnostic imaging techniques has not been established. The results of several imaging procedures performed over a 6-year period on 56 patients with clinically suspected acute acalculous cholecystitis were evaluated retrospectively. Sonography and CT were both highly sensitive (92% and 100%, respectively) and specific (96% and 100%, respectively). Hepatobiliary scintigraphy was compromised by frequent false-positives; the result was a specificity of only 38%. Percutaneous bile aspiration was insufficiently sensitive (33%) for diagnosis. Sonography was as sensitive as hepatobiliary scintigraphy and was more specific in establishing the diagnosis. Because sonography is relatively inexpensive and can be performed at the bedside, it should be regarded as a satisfactory screening procedure. However, CT is a good alternative in an easily transported patient when other intraabdominal disease is suspected.

Acute acalculous cholecystitis is an uncommon but potentially fatal complication of prolonged critical illness [1–4]. The condition most likely results from a gradual increase in bile viscosity, due to prolonged stasis, that leads to a functional obstruction of the cystic duct [1, 4]. Compromised perfusion of the metabolically active gallbladder mucosa may also be contributory [3]. Other factors such as prolonged hyperalimentation, prolonged suctioning by nasogastric tube, positive pressure ventilatory support, numerous transfusions, use of vasoactive amines, and use of morphine analgesia also have been implicated [1, 4].

Unfortunately, both clinical and laboratory tests lack sensitivity and specificity for arriving at a preoperative diagnosis [1–5]. Because patients with acute acalculous cholecystitis are typically victims of multisystem trauma or other severe illness, they represent a population for whom exploratory laparotomy should be avoided, if at all possible, as a means of diagnosing this condition. Although hepatobiliary scintigraphy and sonography have been valuable in the diagnosis of acute and chronic calculous cholecystitis, their usefulness and that of other techniques such as CT and percutaneous aspiration of bile have not been established in the diagnosis of acute acalculous cholecystitis [6–17].

To assess the value of imaging methods in the diagnosis of acute acalculous cholecystitis, we undertook a 6-year retrospective study of patients with clinically suspected acute acalculous cholecystitis in whom hepatobiliary scintigraphy, sonography, CT, or bile aspirations were performed.

Methods and Materials

Since 1980, 60 patients have been evaluated by diagnostic imaging methods for possible acute acalculous cholecystitis after trauma. Complete medical records and imaging study results were available in 56. All patients were admitted to the Shock Trauma Center of the University of Maryland Medical System/Hospital after major trauma. There were 37 men and

Received April 21, 1986; accepted after revision June 24, 1986.

[1] Department of Diagnostic Radiology, University of Maryland Medical System/Hospital, 22 S. Greene St., Baltimore, MD 21201. Address reprint requests to S. E. Mirvis.

[2] Department of Surgery, University of Southern California, Los Angeles, CA 90032.

[3] Maryland Institute for Emergency Medical Services System (MIEMSS), University of Maryland Medical System/Hospital, 22 S. Greene St., Baltimore, MD 21201.

AJR 147:1171–1175, December 1986
0361–803X/86/1476–1171
© American Roentgen Ray Society

19 women; the age range was 14 to 83 years, with a mean of 39. Most were injured in motor vehicle accidents (39); the remainder were involved in falls (four), crush injuries (three), diving accidents (two), ballistic injuries (two), or other accidents (10). Two patients were admitted for hyperbaric oxygen therapy for severe anaerobic soft-tissue infections. All studies were evaluated retrospectively without knowledge of results of other diagnostic procedures or final clinical outcome. No particular imaging sequence algorithm was followed as patients were cared for by a variety of different clinicians during the period of the study.

Hepatobiliary Scintigraphy

Hepatobiliary scintigraphy was performed on 45 patients injected intravenously with 5–10 mCi (185–370 MBq) of 99m-technetium–tagged paraisopropylacetanilidoiminodiacetic acid (PIPIDA, Diagnostic Isotopes, Bloomfield, NJ). Serial scintigrams were obtained at 5-min intervals. Static images were recorded at 2 hr and again at 4–6 hr if there was no visualization of the gallbladder. Static views were obtained from the anterior and right lateral projections. Imaging was performed by using a 37-tube Anger gamma camera. Studies were reviewed by two staff radiologists and were analyzed for hepatic uptake and excretion of tracer into the biliary system, time to visualization of activity in the small bowel, and time of visualization of the gallbladder if this occured within 6 hr. Studies demonstrating activity in the small bowel without visualization of the gallbladder within 6 hr were considered positive. Visualization of the gallbladder after 1 hr was considered to represent chronic cholecystitis. Cholecystokinin was administered to only one patient when the gallbladder had not been visualized 3 hr after injection of tracer.

Sonography

Sonographic examination of the gallbladder and right upper quadrant was performed in 40 patients by using real-time and/or articulating arm transducers. Imaging devices used included a Toshiba Sonolayer L (Model SAL-20A) (Toshiba America Inc., Tustin, CA), an ATL MK-100 Precision series (Advanced Technology Laboratories, Bellevue, WA), a Picker Echoview System 80-L (Picker International Inc., Northford, CT), and a Phillips Sono Diagnostic B (Phillips Ultrasound Inc., Santa Ana, CA). All images were obtained with either a 3- or 3.5-mHz transducer. When necessitated by the patient's clinical condition, portable studies were performed by using real-time equipment only. The studies generally were performed with the patients supine, although, when possible, patients also were examined in the right decubitus position. Erect images were seldom obtained due to the general severity of the illnesses. Sonographic studies were reviewed by two staff radiologists, and findings were divided into major and minor criteria as follows: Major criteria included a wall thickness of 4 mm or greater when the gallbladder was distended to at least 5 cm in the longitudinal dimension and there was no evidence of ascites or hypoalbuminemia (serum protein <3.2 mg/dl), the presence of pericholecystic fluid or subserosal edema, calculi, intramural gas, a sloughed mucosal membrane, or a complete lack of response to cholecystokinin. Minor criteria included the presence of echogenic bile (sludge), distension greater than 8 cm in the longitudinal or 5 cm in the transverse dimension, or a partial response (<50% decrease in longitudinal and transverse dimensions) after cholecystokinin injection. A study was considered positive if it included either a minimum of two major criteria or one major and two minor criteria. In five cases cholecystokinin (Kinevac, Squibb, Princeton, NJ) was administered at a dosage of 0.02 μg/kg, and the gallbladder was reexamined 15 min after the injection to assess for degree of contraction. Other evidence of disease detected in the right upper quadrant, such as an abscess, ascites, or biliary-tree dilatation, was also noted.

CT

As part of a general evaluation for possible sources of sepsis or evaluation of right upper quadrant pain, 15 patients had abdominal CT scans as part of their imaging workup, which included the liver and gallbladder. Studies were performed at 1-cm contiguous sections from the lung bases to the iliac crests or to the symphysis pubis if clinically warranted. When possible, both oral (2% diatrizoate sodium [Hypaque) and IV (50 ml bolus of diatrizoate meglumine/sodium [Angiovist 282]) contrast media were administered. Studies were conducted either on a General Electric 8800 or 9800, a CGR CT/T 10,000, or a Pfizer 0450. CT scans were reviewed by two staff radiologists for signs of gallbladder disease. Major criteria for the diagnosis of acute acalculous cholecystitis included wall thickening greater than 4 mm, pericholecystic fluid, or subserosal edema without ascites, intramural gas, or sloughed mucosa. Minor criteria included subjective distension or hyperdense bile. Other pathologic findings such as abscess, ascites, or pancreatic or hepatic lesions were also noted, as well as the status of the biliary system. No patient received cholecystokinin for the CT studies. A positive diagnosis was established by the presence of two major criteria or two minor and one major criteria.

Percutaneous Aspiration of Bile

Six patients underwent percutaneous aspiration of bile from the gallbladder guided by real-time sonography [5] or CT. Sonographic studies were performed by means of an ATL 100 portable sonographic unit with a biopsy transducer guide. All aspirations were performed by using a 20-gauge aspiration needle and an anterior transhepatic approach as described by McGahan and Walter [5]. Informed consent was obtained beforehand. On two occasions the bile was quite viscous, and a 19-gauge needle was required to obtain a sample. Bile samples were examined for bacteria and leukocytes and were cultured anaerobically and aerobically. No complications were encountered during or after these procedures. Four other patients had bile specimens obtained intraoperatively, which were cultured. These results are included with those from the percutaneously aspirated specimens.

Results

Hepatobiliary Scintigraphy

Hepatobiliary scintigraphy was performed on 46 patients with clinically suspected acute acalculous cholecystitis. In 19 (41%) the gallbladder was visualized within 1 hr after the injection and was considered normal. In all but one of these patients the clinical course suggested other causes for the patient's symptoms. However, one patient had normal findings on hepatobiliary scan but markedly abnormal findings on sonographic and CT studies. Persistent fever and right upper quadrant pain prompted cholecystectomy, which revealed acalculous cholecystitis.

In three patients gallbladder visualization was delayed (2–6 hr). In all cases subsequent clinical and sonographic correlation suggested chronic calculous cholecystitis. These patients were all managed without surgical intervention while recuperating from their acute traumatic injuries and had benign clinical courses.

Findings of hepatobiliary scintigrams were abnormal in 24 patients. In two the results were considered indeterminate for

the gallbladder because of poor hepatic function and failure to secrete sufficient tracer into the biliary system. Another patient had obstruction of the proximal hepatic duct and were thus indeterminate findings for the gallbladder but at surgery was shown to have both acute and chronic calculous cholecystitis. Eight patients with abnormal findings had acalculous (six), or calculous (two) acute cholecystitis established pathologically by the presence of acute inflammation, bacterial invasion, or necrosis of the gallbladder wall. One patient with acute acalculous cholecystitis received cholecystokinin, but visualization of the gallbladder still did not occur. However, there were 13 other patients with nonvisualization of the gallbladder in whom the clinical course (11), or surgical inspection alone (two) indicated a normal gallbladder. Considering all cases in which the gallbladder could be evaluated, 13 (54%) of 24 were false-positive, yielding a specificity of only 38% in the posttrauma population. Hepatobiliary scintigraphy was 95% sensitive in the diagnosis of posttraumatic acute cholecystitis.

Sonography

Sonographic studies were available from 40 patients. In 26 the study was considered negative by our established criteria (see Methods). Of this group two patients subsequently were shown at surgery to have either chronic calculous cholecystitis or both acute and chronic calculous cholecystitis. In the first patient sonography revealed only minimal wall thickening and echogenic bile without visualization of calculi. In the second the gallbladder was moderately distended with minimal echogenic bile but no definite calculi. Both studies were performed early in this series with less precise real-time equipment than is currently available.

In 14 patients sonographic findings were abnormal by our criteria. Seven had pathologically verified acute acalculous cholecystitis and five had acute and chronic calculous cholecystitis. One patient had an equivocal result: calculi and mild wall thickening (5 mm), but a partial response to cholecystokinin injection (longitudinal diameter decreased from 7.4 to 6.8 cm). This patient's symptoms and elevated bilirubin level resolved with conservative treatment. Three other patients injected with cholecystokinin failed to show any gallbladder contraction in 15 min and all had acute acalculous cholecystitis diagnosed pathologically. A single patient with abnormal sonographic findings improved clinically and thus was considered false-positive. Overall, sonography demonstrated a sensitivity of 92% for acute cholecystitis with or without calculi present and a specificity of 96% (Table 1).

CT

Results of CT were available for 15 patients. In five the study was positive by our criteria for acute acalculous cholecystitis, and all five cases were pathologically confirmed. Ten patients were considered to be negative for acute acalculous cholecystitis, and all 10 cases were confirmed by clinical course (eight) or surgical pathology (two). Thus, in this limited series CT was both 100% sensitive and 100% specific in the diagnosis of acute acalculous cholecystitis (Table 1).

TABLE 1: **Sonographic and CT Findings in Patients Evaluated for Acute Cholecystitis**

Findings	Sonography (N = 40)	CT (N = 15)
Minor criteria		
Distension[a]	17	5
Sludge	16	6
Partial response to CCK[b]	1	0
Major criteria		
Calculi	7	0
No response to CCK	4	0
Wall thickening ≥4 mm[c]	13	4
Pericholecystic fluid[d]	2	1
Subserosal edema (halo)	5	5
Positive (2 major or 1 major and 2 minor criteria)	14	5
Negative	26	10
True positive	13	5
True negative	24	10
Sensitivity (%)	92	100
Specificity (%)	96	100
Positive predictive value (%)	92	100
Negative predictive value (%)	92	100

[a] Longitudinal diameter >8 cm or transverse diameter >5 cm.
[b] <50% decrease in transverse or longitudinal axis. CCK = cholecystokinin.
[c] Serum protein >3.2 mg/dl.
[d] In absence of ascites.

Percutaneous Aspiration of Bile

Bile was aspirated percutaneously in six cases and obtained at surgery in four others. In two cases bacteria were obtained (*Citrobacter* and *Escherichia coli*), and both patients had pathologically verified acute acalculous cholecystitis. In four patients the aspirate was sterile and contained no leukocytes; these patients had normal clinical (three) or surgical (one) results. However, four other patients had sterile bile cultures and no organisms on Gram stains, as well as specimens without leukocytes, but had acute acalculous cholecystitis pathologically. Thus, although bile aspiration, either percutaneously or at surgery, was 100% specific, the method was only 33% sensitive in diagnosing acute gallbladder inflammation.

Discussion

The contribution of imaging studies to the diagnosis of acute cholecystitis in general is well established. Overall sensitivity and specificity for hepatobiliary scintigraphy in the diagnosis of acute cholecystitis are 95–100% and 81–100%, respectively, whereas the sensitivity and specificity of sonography is reported as 67–93% and 82–100%, respectively [8, 12–17]. These series in general represent a substantial majority of cases of acute calculous cholecystitis and reflect the preponderance of the calculous form in the general population [7]. However, the value of diagnostic imaging in establishing the diagnosis of acute *acalculous* cholecystitis is far less firmly established.

In 1983 Weissman et al. [11] described their experience with hepatobiliary scintigraphy and sonography in 15 patients with acute acalculous cholecystitis. They reported a 93% specificity and 93% accuracy for hepatobiliary scintigraphy

but found sonography to be far less reliable, with numerous false-positive and false-negative results. In 1984 Shuman et al. [7] evaluated hepatobiliary scintigraphy and sonography in 33 surgically proven cases of acute or chronic acalculous cholecystitis. They reported a sensitivity of only 67% for sonography and 68% for cholescintigraphy in establishing the diagnosis. They concluded that the imaging diagnosis of acalculous cholecystitis remains elusive.

Our results are at variance with these previous studies. Although we have found hepatobiliary scintigraphy to be highly sensitive (95%) with only a single false-negative result, many false-positive result led to low specificity (38%). The high frequency of false-positive results is not surprising because prolonged parenteral alimentation, prolonged fasting, severe nonbiliary intercurrent illness, and hepatocellular dysfunction are among the conditions known to produce false-positive results and are also commonly found in victims of major trauma [17–21].

By producing spasm of the sphincter of Oddi, morphine can increase pressure in the biliary system and direct flow of bile into the cystic duct [10]. In an effort to decrease false-positive cholescintigrams, Choy et al. [10] have suggested the use of IV morphine sulfate; however, they cautioned that morphine sulfate may produce false-negative results in cases of acalculous cholecystitis by overcoming a functional obstruction in the cystic duct. We did not assess the usefulness of morphine sulfate in this study.

Previous studies have suggested that injection of cholecystokinin to promote emptying of viscous bile from the gallbladder might decrease false-positive findings on scintograms. Davis et al. [22] evaluated cholecystokinin in the diagnosis of chronic acalculous cholecystitis and found it of little value in distinguishing symptomatic patients from volunteers. Proudfoot et al. [23] and Pickleman et al. [24], however, found the response to cholecystokinin useful in predicting symptomatic improvement after cholecystectomy. Experience with the use of cholecystokinin in the diagnosis of acute acalculous cholecystitis has been limited. Weissman et al. [25] specifically recommended injection of cholecystokinin in cases of possible acute acalculous cholecystitis. Choy et al. [10] raised the criticism that injection of cholecystokinin after nonvisualization of the gallbladder will necessitate reinjection of the radiopharmaceutical and unduly prolong the time of study. Although our experience with cholecystokinin is limited, the three patients with no sonographically demonstrable response were subsequently proven to have acute acalculous cholecystitis and the single patient with a partial response experienced clinical resolution.

One patient in our study had acute acalculous cholecystitis and normal findings on hepatobiliary scintigraphy. Shuman et al. [7] reported frequent false-negative results in their series of 33 patients, producing a low sensitivity of 68–76%. They suggested, as did Weissman et al. [25], that patency of the cystic duct can persist in acute acalculous cholecystitis despite inflammation of the gallbladder. The inclusion of nine cases of chronic acalculous cholecystitis in the Shuman study [7] may also have contributed to the frequency of false-negative results.

Sonography was useful in establishing the diagnosis of acute acalculous cholecystitis, with a sensitivity of 92% and a specificity of 96%. Although distension of the gallbladder and echogenic bile were frequent abnormalities shown in the posttrauma population, the detection of wall thickening, pericholecystic fluid, and subserosal edema were more indicative of acute cholecystitis. In 11 patients with acute cholecystitis examined by sonography, Marchal et al. [26] saw a sonolucent halo around the gallbladder, which was shown pathologically to represent subserosal edema and cellular infiltration. They believed that this sign was specific for acute cholecystitis. Five of our patients with this finding also had acute acalculous cholecystitis; the sign was never observed in any patient shown clinically or surgically to have a noninflamed gallbladder. Five of 12 patients with posttraumatic acute cholecystitis had calculi as shown by sonography and proven pathologically. This high percentage suggests that patients with calculi or chronic cholecystitis may be at increased risk for the development of acute inflammation after major trauma or similar prolonged critical illness.

CT was used to evaluate 15 patients with suspected acute acalculous cholecystitis and was 100% sensitive and specific in this limited series. The CT features of acute cholecystitis have been described previously [27–33]. Thickening or nodularity of the gallbladder wall, gallstones, poor definition of the gallbladder/liver interface, and pericholecystic fluid without ascites have been reported most frequently [27, 29, 31, 33]. The CT equivalent of the sonographic halo sign was present in all five patients with acute acalculous cholecystitis studied by CT. The rim of subserosal edema may mimic pericholecystic fluid, as recently reported by Goldstein et al. [34]. Although sonography and hepatobiliary scintigraphy have gained wide acceptance as initial screening studies for patients with symptoms suggestive of acute cholecystitis, the use of CT as an initial diagnostic procedure seems quite reasonable. In the typical case our posttrauma patients are referred for imaging evaluation if they have fever and sepsis of unknown source. They commonly also have associated liver enzyme abnormalities, often related to other aspects of their injury. The investigation of the abdomen by CT facilitates the search for occult abscesses and the evaluation of the biliary system. In many instances sonographic assessment of the abdomen is hindered by intestinal ileus or overlying bandages.

Recently, McGahan and Walter [5] reported their experience with percutaneous aspiration of bile in patients with suspected acute acalculous cholecystitis. They emphasized its value in suspected cases because of the potential for false-positive findings on cholescintigrams or false-negative findings on sonograms. They believe that aspiration of bile provides a method of excluding the gallbladder as a source of infection. However, four of our patients in whom bile aspiration was performed had pathologically verified acute acalculous cholecystitis despite the absence of bacteria or leukocytes in the bile specimen. Overall the technique was only 33% sensitive in determining patients with acute gallbladder inflammation. In describing the pathology of acute cholecystitis, Glenn [4] noted no significant difference in calculous vs acalculous disease. The number of leukocytes found in the gall-

bladder wall was variable; occasionally none were found. On the basis of this experience, we believe that the absence of leukocytes or bacteria in the bile should not exclude the diagnosis of acute calculous or acalculous cholecystitis.

In summary, our experience with 56 patients with clinically suspected acute acalculous cholecystitis has shown that sonography has sensitivity equivalent to and specificity superior to cholescintigraphy. CT was accurate in evaluating the gallbladder for suspected acute cholecystitis and should be regarded as a reasonable screening test, especially when other intraabdominal diseases are anticipated [4]. Finally, percutaneous aspiration of bile may be a valuable method for confirming the diagnosis of acute cholecystitis, but a sterile specimen without leukocytes cannot be used reliably to exclude the diagnosis.

REFERENCES

1. Dupriest RW, Khaveja SC, Cowley RA. Acute cholecystitis complicating trauma. *Ann Surg* **1979**;189:84–89
2. Eggermont AM, Lemeris JS, Jeakel J. Ultrasound guided percutaneous transhepatic cholecystostomy for acute acalculous cholecystitis. *Arch Surg* **1985**;1201:1354–1356
3. Long TN, Heimbach DM, Carrico CJ. Acalculous cholecystitis in critically ill patients. *Am J Surg* **1978**;136:31–46
4. Glenn F. Acute acalculous cholecystitis. *Ann Surg* **1979**; 189:458–465
5. McGahan JP, Walter JP. Diagnostic percutaneous aspiration of the gallbladder. *Radiology* **1985**;155:619–622
6. Harlin P, Jonsson PE, Karp W. Post-operative acute acalculous cholecystitis: an assessment of diagnostic procedures. *Gastrointest Radiol* **1980**;5:147–149
7. Shuman WP, Rogers JV, Rudd TG, Mack LA, Plumley T, Larson EB. Low sensitivity of sonography and cholescintigraphy in acalculous cholecystitis. *AJR* **1984**;132:531–534
8. Weissman HS, Frank M, Rosenblatt R, Goldman M, Freeman LM. Cholescintigraphy, ultrasound, and computerized tomography in the evaluation of biliary tract disorders. *Semin Nucl Med* **1979**;9:22–35
9. Matolo NM, Stadalnik RC, MaGahan JP. Comparison of ultrasound, computerized tomography, and radionuclide imaging in the diagnosis of acute and chronic cholecystitis. *Am J Surg* **1982**;144(6):676–681
10. Choy D, Shi EC, McLean RG, Hocshl R, Murray IPC, Ham JM. Cholescintigraphy in acute cholecystitis: use of intravenous morphine. *Radiology* **1984**;151:203–207
11. Weissman HS, Berkowitz D, Fox MS, et al. The role of technetium-99m iminodiacetic acid (IDA) cholescintigraphy in acute acalculous cholecystitis. *Radiology* **1983**;146:177–180
12. Zeman RK, Burrell MI, Cahou CF, Carida V. Diagnostic utility of cholescintigraphy and ultrasound in acute cholecystitis. *Am J Surg* **1981**;141:446–451
13. Worthen NJ, Uszher JM, Funamura JL. Cholecystitis: prospective evaluation of sonography and 99m Tc-HIDA cholescintigraphy. *AJR* **1981**;137:973–978
14. Cabellon S, Brown JM, Cavenaugh DG. Accuracy of the hepatobiliary scan in acute cholecystitis. *Am J Surg* **1984**;148:607–608
15. Suarez CA, Block F, Bernstein D, Serafin A, Rodman G, Zeppa R. The role of HIDA/PIPIDA scanning in diagnosing cystic duct obstruction. *Ann Surg* **1980**;191:392–396
16. Shuman WP, Mack LA, Rudd TG, Rogers JV, Gibbs P. Evaluation of acute upper quadrant pain: sonography and ^{99m}Tc-PIPIDA cholescintigraphy. *AJR* **1982**;139:61–64
17. Ralls PW, Colletti PM, Halls JM, Siemsen JK. Prospective evaluation of 99m Tc-IDA cholescintigraphy and grey-scale ultrasonography in the diagnosis of acute cholecystitis. *Radiology* **1982**;144:369–371
18. Womack NA, Bricker EM. Pathogenesis of cholecystitis. *Arch Surg* **1942**;44:658–660
19. Klingansmith WC III, Kuni CC. Radionuclide hepatobiliary imaging: non-visualization of the gallbladder secondary to prolonged fasting. *J Nucl Med* **1982**;23:1003–1005
20. Shuman WP, Gibbs P, Rudd TG, Mack LA. PIPIDA scintigraphy for cholecystitis: false positives in alcoholism and total parenteral nutrition. *AJR* **1982**;138:1–5
21. Kalff V, Froelich JW, Lloyd R, Thrall JH. Predictive value of an abnormal hepatobiliary scan in patients with severe intercurrent illness. *Radiology* **1983**;146:191–194
22. Davis GB, Berk RN, Scheible FW, et al. Cholecystokinin cholecystography, sonography, and scintigraphy: detection of chronic acalculous cholecystitis. *AJR* **1982**;139:1117–1121
23. Proudfoot R, Mattingly SS, Snodgrass S, Griffen WO. Cholecystokinin cholecystography: is it a useful test? *South Med J* **1985**;78(12):1443–1446
24. Pickleman J, Peiss RL, Henkin R, Salo B, Nagel P. The role of sincalide cholescintigraphy in the evaluation of patients with acalculous gallbladder disease. *Arch Surg* **1985**;120:693–697
25. Weissman HS, Frank MS, Bernstein LH, Freeman LM. Rapid and accurate diagnosis of acute cholecystitis with 99mTc-HIDA cholescintigraphy. *AJR* **1979**;132:523–528
26. Marchal GJF, Casaer M, Baeri AL, Goddeeris PG, Kerremans R, Fevery J. Gallbladder wall sonolucency in acute cholecystitis. *Radiology* **1979**;133:429–433
27. Kame RA, Costello P, Duszlak E. Computed tomography in acute cholecystitis: new observations. *AJR* **1983**;141:697–701
28. Jenkins M, Golding RH, Cooperberg PL. Sonography and computed tomography of hemorrhagic cholecystitis. *AJR* **1983**; 140:1197–1198
29. Nyman U, Rimer U, Zederfelt AB, et al. Intravenous computed tomographic cholangiography in acute cholangiography. *Acta Radiol [Diag]* **1984**;25:289–298
30. McMillin K. Computed tomography of emphysematous cholecystitis. *J Comput Assist Tomogr* **1985**;9(2):330–332
31. Terrier F, Becker CD, Stoller C, Triller JK. Computed tomography in complicated cholecystitis. *J Comput Assist Tomogr* **1984**; 8(1):58–62
32. Yiu-Chiu VS, Chiu LC, Wedel VJ. Acalculous hemorrhagic cholecystitis. *J Comput Assist Tomogr* **1980**;4(3):201–206
33. Toombs BD, Sandler CM, Conoley PM. Computed tomography of the non-visualizing gallbladder. *J Comput Assist Tomogr* **1981**;5(2):164–168
34. Goldstein RB, Wing VW, Laing FC, Jeffery RB. Computed tomography of thick-walled gallbladder mimicking pericholecystic fluid. *J Comput Assist Tomogr* **1986**;10(1):55–56

Book Review

Computed Tomography of the Gastrointestinal Tract Including the Peritoneal Cavity and Mesentery. Edited by Morton A. Meyers. New York: Springer-Verlag, 279 pp., 1986.

This book fulfills its purpose of providing a comprehensive, useful, up-to-date presentation of CT of the major disease states involving the gastrointestinal tract, mesentery, and peritoneal cavity. The book has contributions from major centers in the United States, Switzerland, The Netherlands, West Germany, and Japan. The 10 chapters include discussion of the value and limitations of CT for evaluation of tumors of the esophagus, stomach, and colon. Other topics are lymphoma and other nonepithelial tumors, inflammatory bowel disease, acute appendicitis, and lesions of the mesentery.

The chapter dealing with the peritoneum and the spread of disease in the subperitoneal space reflects the editor's expertise and numerous publications in this field, including the successful former book, *Dynamic Radiology of the Abdomen*.

The book is conveniently short (fewer than 300 pages), and the quality of the reproductions is excellent. The style of most of the discussions is authoritative, comprehensive, succinct, and practical. The chapter on carcinoma of the stomach, however, has an involved, lengthy, and at times confusing presentation of staging methods that is difficult to relate to the presentation of CT findings. For example, the staging method of Borrmann is cited in the text and illustrations but not specifically identified in the text. Also, the pertinent references are in the Japanese literature, which may not be readily available to American readers. Otherwise this chapter is an exhaustive summary of the extensive Japanese experience in the pathology, radiologic detection, and staging of gastric malignancies.

The chapter on subperitoneal spread of intraabdominal disease is an excellent exposition of a conceptual framework, devised by the authors, that provides the basis for ready analysis of many otherwise confusing appearances on complex CT images. This and the chapter on peritoneal fluid collections summarize the widely accepted concepts, largely developed by the editor and his coworkers, on which much of our present understanding of abdominal radiology is based.

Although the book provides an adequate summary of the current status of CT in gastrointestinal disease, it adds little to that covered by the several excellent current general texts on body CT imaging. It will probably be useful, however, to those with particular interest in gastrointestinal disease in providing a useful source of well-illustrated material in one place.

Michael K. Wolverson
St. Louis University Medical Center
St. Louis, MO 63104

Morphine-Augmented Cholescintigraphy in the Diagnosis of Acute Cholecystitis

E. Edmund Kim[1]
George Pjura[1]
Patricia Lowry[1]
Minh Nguyen[1]
Matthew Pollack[2]

Cholescintigraphy is a sensitive procedure for diagnosing or excluding acute cholecystitis. However, when rapid diagnosis is critical, the requirement for delayed images (4 hr or more after injection) to minimize the false-positive rate diminishes its utility. We prospectively evaluated 40 cholescintigraphic examinations that did not visualize the gallbladder 1 hr after injection of ^{99m}Tc diisopropyliminodiacetic acid. These examinations were then augmented by administration of IV morphine, followed by an additional 30 min of imaging. After the morphine, 18 of these examinations demonstrated visualization of the gallbladder; none subsequently required surgical exploration. Of the remaining 22, who demonstrated persistent nonvisualization of the gallbladder post-morphine, 11 were explored surgically and found to be abnormal. The 11 others were treated medically. Low-dose morphine administered when the gallbladder fails to visualize after 1 hr is a useful adjunct to conventional cholescintigraphy because it reduces the time required to obtain a diagnostic result and decreases the number of false-positive results.

Rapid diagnosis or exclusion of acute cholecystitis in the patient presenting with acute right-upper-quadrant pain is important to minimize morbidity and mortality. Most of these patients do not present with the typical additional findings of fever, leukocytosis, and a positive Murphy's sign [1]. Indeed, hepatocellular, renal, and bowel disease, as well as pancreatitis and peptic ulcer disease, are frequently difficult to distinguish on the basis of clinical findings alone. Documentation of cystic-duct obstruction, mechanical or functional, confirms the diagnosis of acute cholecystitis in most cases. Conversely, demonstrating patency of the cystic duct virtually excludes this diagnosis.

^{99m}Tc iminodiacetic acid (IDA) cholescintigraphy is the most sensitive method for assessing patency of the cystic duct [2]. Persistent nonvisualization of the gallbladder 4 hr after injection of a ^{99m}Tc IDA radiopharmaceutical, in the presence of prompt hepatic uptake and excretion into the intestine (i.e., within 1 hr), is consistent with cystic-duct obstruction. However, chronic cholecystitis, gallbladder carcinoma, pancreatitis, hepatocellular disease, severe illness, alcoholism, lack of adequate fasting, prolonged fasting, and physiologic gallbladder distension may also lead to nonvisualization of the gallbladder [3–6]. Recently, morphine injection has been reported effective in improving the specificity of cholescintigraphy for diagnosing acute cholecystitis from 83% to 100% of cases, without loss of sensitivity (96%) [7]. We prospectively assessed the value of morphine administration for reducing the time to diagnose acute cholecystitis.

Subjects and Methods

We prospectively evaluated 40 hepatobiliary scans that did not visualize the gallbladder at 1 hr after injection of ^{99m}Tc DISIDA and that were then augmented by the administration of IV morphine (0.04 mg/kg), followed by an additional 30 min of imaging. Imaging findings were correlated with sonographic and clinical findings in all 40 cases, and with pathologic studies

Received March 24, 1986; accepted after revision June 9, 1986.

[1] Department of Radiology, University of Texas Medical School, 6431 Fannin St., Houston, TX 77030. Address reprint requests to E. E. Kim.

[2] Department of Radiology, University of Pennsylvania, School of Medicine, Philadelphia, PA 19104.

AJR 147:1177–1179, December 1986
0361–803X/86/1476–1177
© American Roentgen Ray Society

in 11. All patients underwent radionuclide hepatobiliary imaging and real-time sonography performed within 48 hr of onset of acute illness and within 24 hr of each other. Twenty-five patients had fasted for more than 3 hr before the IV injection of 5 mCi (185 MBq) ^{99m}Tc DISIDA, while the remaining 15 had received IV hyperalimentation for at least 7 days. Sequential anterior static images with 500,000 counts per image were obtained with a large-field-of-view camera at 10- to 15-min intervals for a minimum of 50 min. Left anterior oblique and right lateral views were obtained as required at 50 min. If there was evidence of radioactivity in the duodenum but no filling of the gallbladder by 50 min, 0.04 mg/kg morphine sulfate diluted in 10 ml saline was given IV over a period of 3 min. Five-minute serial images were obtained for the next 30 min. Five of the patients with persistent nonvisualization of the gallbladder after the morphine injection were also imaged 4 hr after the radionuclide injection.

Results

Of 40 patients with nonvisualization of the gallbladder after 1 hr, 22 demonstrated persistent nonvisualization of the gallbladder even after the injection of morphine. Five of these were imaged again after 4 hr without a change in findings. Sonography of the 22 persistently nonvisualized gallbladders revealed gallstones in six, sludge in five, and acalculous cholecystitis (gallbladder-wall thickening, sludge, distension) in five. Of the remaining six, two showed contraction, one showed distension, and the other three were interpreted as normal. Eleven of the 22 were taken to surgery within 1–3 days after scintigraphy. Of these, pathology showed three with gallstones and two with acalculous cholecystitis to have acute cholecystitis. Another with acalculous cholecystitis had empyema of the gallbladder. Two with gallstones had chronic cholecystitis, and two with solitary common-bile-duct stones had a distended and a normal gallbladder, respectively. The remaining 11 were patients with massive trauma who were considered poor surgical risks and, therefore, treated medically. Eight of the 22 patients were on IV hyperalimentation; seven had alcoholic liver disease.

In the 18 cases with gallbladder visualization after morphine injection, sonography revealed nonobstructing gallstones in five, sludge in three, and normal findings in the remaining 10. Seven of these patients were receiving IV hyperalimentation; two were on tube feedings. Two had alcoholic liver disease, and one was postvagotomy. None had elevated serum amylase on admission. None required surgery, and all responded to conservative management.

Discussion

The scintigraphic diagnosis of acute cholecystitis is predicated on failure of the gallbladder to admit radionuclide within a specified interval of time, most commonly 1 hr. Weissmann et al. [8] report that with delayed imaging, up to 4 hr, the false-positive rate can be reduced from 9.9 to 0.6%. Zeman et al. [9] have even recommended 24-hr imaging in patients who have fasted longer than 1 day. Such delayed images are limited technically, however, by the progressive decline in activity within the biliary system that necessarily accompanies physiologic emptying and tracer decay. Furthermore, many clinicians with patients in acute distress are unwilling to accept such delays and turn instead to sonography in spite of its limited ability to diagnose acalculous cholecystitis and common duct stones [2, 8, 10]. Because hepatobiliary scintigraphy has demonstrated potential for greater specificity (93 vs 64%) and predictive value (77 vs 40%) [11], we were interested in exploring ways to increase its convenience by reducing the time to perform the study adequately.

The failure of radiopharmaceutical to enter an unobstructed gallbladder has been attributed to bile stasis within the gallbladder resulting either from a decrease in bile output from hepatocellular damage, or decrease in the release of endogenous cholecystokinin-pancreozymin from prolonged fasting [3]. In the latter case, the absence of repeated stimulation to contract and refill is postulated to leave the gallbladder sluggish and distended, unable to accept additional bile or radiopharmaceutical [9]. In chronic cholecystitis, thick, concentrated bile or sludge in a full gallbladder is thought to impede diffusion of the radiopharmaceutical [12]. Attempts to use cholecystokinin to promote emptying of the viscous bile have had little effect on the overall false-positive rate [3, 4, 7].

The administration of low-dose morphine approximately 40 min after injection of the hepatobiliary radiopharmaceutical produces improved specificity in the diagnosis of acute cholecystitis without loss of sensitivity. Morphine causes contraction of the spincter of Oddi [13]; as little as 2.5 mg IV has been reported to raise bile-duct pressure from 12.7 ± 1.2 to 20.0 ± 2.4 cm of saline within 5 min [14]. Presumably, if no obstruction exists, this increased pressure is sufficient to divert the flow of bile or radiopharmaceutical into a sluggish, distended, or sludge-filled gallbladder, thereby avoiding false-positive results. Surgical and gross pathologic studies of acute cholecystitis have demonstrated obliteration of the cystic duct with or without the presence of an impacted calculus [15]. Consequently, one would not anticipate an associated increase in false-negative results with morphine-augmented cholescintigraphy.

Our results support the findings of Choy et al. [7] on the utility of morphine-augmented cholescintigraphy. Furthermore, in more than 100 administrations of morphine, we have encountered no evidence of side effects and no false-negative results in cases of acalculous cholecystitis. Consequently, we consider this procedure safe and effective in the diagnosis of calculous and acalculous cholecystitis.

REFERENCES

1. Szlabick RE, Catto JA, Fink-Bennett D, Ventura V. Hepatobiliary scanning in the diagnosis of acute cholecystitis. *Arch Surg* **1980**;115:540–544
2. Weissmann HS, Rosenblatt R, Sugarman LA, Freeman LM. An update in radionuclide imaging in the diagnosis of cholecystitis. *JAMA* **1981**;246:1354–1357
3. Larsen MJ, Klingensmith WC III, Kuni CC. Radionuclide hepatobiliary imaging: non visualization of the gallbladder secondary to prolonged fasting. *J Nucl Med* **1982**;23:1003–1005
4. Shuman WP, Gibbs P, Rudd TG, Mack LA. PIPIDA scintigraphy for cholecystitis: false positives in alcoholism and total parenteral nutrition. *AJR* **1982**;138:1–5
5. Elund G, Kempi V, van der Linden W. Transient nonvisualization

of the gallbladder by Tc-99m HIDA cholescintigraphy in acute pancreatitis. *J Nucl Med* **1982**;23:1003–1005
6. Lecklitner ML, Rosen PR, Nusynowitz ML. Cholescintigraphy: gallbladder nonvisualization secondary to neoplasm. *J Nucl Med* **1981**;22:699–700
7. Choy D, Shi EC, McLean RG, Hoschl R, Murray IPC, Ham JM. Cholescintigraphy in acute cholecystitis: use of intravenous morphine. *Radiology* **1984**;151:203–207
8. Weissmann HS, Rosenblatt R, Freeman LM. An integrated imaging approach to disorders of the biliary tract. *Arch Clin Imaging* **1985**;1:57–64
9. Zeman RK, Segal HB, Caridre VJ. Tc-99m HIDA cholescintigraphy: the distended photon-deficient gallbladder. *J Nucl Med* **1981**;22:39–41
10. Weissmann HS, Berkowitz D, Fox MS, et al. The role of Tc-99m iminodiacetic acid (IDA) cholescintigraphy in acute acalculous cholecystitis. *Radiology* **1983**;146:177–180
11. Samuels BI, Freitas JE, Bree BL, Schwab RE, Heller ST. A comparison of radionuclide hepatobiliary imaging and real-time ultrasound for detection of acute cholecystitis. *Radiology* **1983**;147:207–210
12. Al-Sheikh W, Hourani M, Barkin JS, Clarke LP, Ashkar FS, Serafini AN. A sign of symptomatic chronic cholecystitis on biliary scintigraphy. *AJR* **1983**;140:283–285
13. Jaffe JH, Martin WR. Narcotic analgesics and antagonists. In: Goodman LS, Gilman A, eds. *The pharmacological basis of therapeutics*, 5th ed. New York: Macmillan, **1975**:253–254
14. Dedrick DF, Tanner WW, Bushkin FL. Common bile duct pressure during enflurane anesthesia. Effects of morphine and subsequent naloxone. *Arch Surg* **1980**;115:820–822
15. Glenn F: Acute acalculous cholecystitis. *Ann Surg* **1979**; 189:458–465

American Roentgen Ray Society:
Officers, Committees, and Meeting Information

Officers

President: Jerome F. Wiot
President- elect: Raymond A. Gagliardi
1st Vice-president: Lee F. Rogers
2nd Vice-president: Gerald D. Dodd
Secretary: Glen W. Hartman
Treasurer: Ronald G. Evens

Executive Council: E. Gedgaudas, J. F. Wiot, L. F. Rogers, R. A. Gagliardi, R. G. Evens, R. N. Berk, F. L. Angell, J. E. Madewell, M. P. Capp, G. W. Hartman, B. G. Brogdon, G. A. Kling, H. C. Carlson, A. K. Poznanski, A. E. James, Jr., J. A. Kirkpatrick, Jr., G. R. Leopold, G. D. Dodd, J. T. Ferrucci, Jr., R. H. Troupin, chairman

Committees 1986–1987

Editorial Policy: S. S. Sagel, W. J. Casarella, J. T. Ferrucci, Jr., N. C. Whitley, S. Hilton, A. J. Davidson, J. M. Taveras, R. N. Berk, M. P. Capp, chairman

Education and Research: C. E. Putman, A. R. Margulis, J. R. Thornbury, R. A. McLeod, J. T. Ferrucci, Jr., ex officio, B. G. Brogdon, chairman

Finance and Budget: B. P. Wood, L. R. James, J. A. Kirkpatrick, Jr., A. E. James, F. L. Angell, chairman

Instruction Courses: R. A. McLeod, associate chairman, J. T. Ferrucci, Jr., chairman

Program: J. Wiot, G. W. Hartman, J. A. Kirkpatrick, Jr., R. H. Troupin, M. P. Capp, J. E. Madewell, B. G. Brogdon, J. T. Ferrucci, Jr., G. A. Kling, G. G. Ghahremani, M. Viamonte, R. A. Gagliardi, chairman

Publications: W. J. Casarella, J. T. Ferrucci, Jr., S. S. Sagel, N. C. Whitley, M. P. Capp, chairman

Scientific Exhibits: S. G. Kirchner, A. V. Proto, S. M. Goldman, J. E. Madewell, chairman

Nominating: W. J. Casarella, H. C. Carlson, A. E. James, chairman.

Representatives to Other Organizations

American Board of Radiology: E. C. Klatte, R. W. McConnell, L. F. Rogers

American College of Radiology: J. L. Gwinn, G. A. Kling, G. W. Hartman, J. M. Dennis, E. J. Ferris, J. E. Madewell

American Medical Association House of Delegates: S. F. Ochsner, K. C. Krabbenhoft, alternate

American National Standards Institute: M. Haskin

National Council on Radiation Protection and Measurements: E. L. Saenger, H. L. Friedell

Meetings, Membership, Business Information

Annual Meetings: April 26–May 1, 1987, Fontainebleau-Hilton, Miami Beach; May 1–6, 1988, Westin Bonaventure, Los Angeles; May 7–13, 1989, Hilton, New Orleans.

Director Annual Meeting: George A. Kling, Harper Hospital, Detroit, MI 48201; (313) 494-8405.

ARRS Membership: Rosalind H. Troupin, Dept. of Radiology, Hospital of University of Pennsylvania, 3400 Spruce St., Philadelphia, PA 19104. The ARRS has two membership categories: active and in-training. For active membership, applicants must practice radiology in the U.S. or Canada. Each must have graduated in good standing from an approved medical school or hold an advanced degree in a physical, chemical, or biological science and be certified by the American Board of Radiology, the Royal College of Physicians and Surgeons of Canada, or otherwise adequately document training and credentials. A member-in-training must be in a radiology residency, a postresidency fellowship program, or a postgraduate student in an allied science. Status must be verified by the program director. For consideration during the 1987 ARRS meeting, completed applications must be received by Dr. Troupin no later than Feb. 1, 1987.

Business Office: Paul Fullagar, executive director, George J. O'Hop, controller, American Roentgen Ray Society, 1891 Preston White Dr., Reston, VA 22091; (703) 648-8900.

Case Reports

Anomalous Hepatic Duct Inserting into the Cystic Duct

Steven H. Reid,[1] Shao-Ru Cho,[1] Chung-I Shaw,[2] and Mary Ann Turner[1]

In a review of 2052 cases from nine studies, Berci and Hamlin [1] reported an average prevalence of anomalous biliary ducts of 12%. In their own experience, the most common biliary anomaly is an anomalous right hepatic duct emptying into the common hepatic or the cystic duct. Puente and Bannura [2] reported a prevalence of congenital abnormalities of the biliary tract of 18.5% and of anomalous hepatic ducts of 6.5% in a study of 3845 operative cholangiograms.

Three cases of an anomalous right hepatic duct (two cases of right aberrant hepatic duct and one case of right accessory hepatic duct) emptying into the cystic duct, identified by cholangiography, are presented. The first two cases were identified by intraoperative cholangiography, and the third was identified by preoperative ERCP. The importance of recognizing this anomaly before cholecystectomy is emphasized.

Case Reports

Case 1

An 82-year-old black woman was diagnosed with gallstones by sonography. An intraoperative cholangiogram showed clipping of the cystic duct just distal to its union with an accessory right hepatic duct (Fig. 1). Multiple stones were found in the distal common bile duct near the ampulla.

Case 2

A 21-year-old white woman presented with epigastric pain. Gallstones were demonstrated by sonography. An intraoperative cholangiogram demonstrated an aberrant right hepatic duct that emptied into the cystic duct (Fig. 2).

Case 3

A 65-year-old white man presented with upper abdominal pain and elevated serum amylase. The patient was admitted with a provisional diagnosis of acute pancreatitis. Subsequent sonography showed multiple gallstones. No common duct stones were identified by ERCP. However, an aberrant right hepatic duct that emptied into the midportion of the cystic duct was found (Fig. 3).

Discussion

Normally, the right and left hepatic ducts converge at the porta hepatis to form the common hepatic duct. The right hepatic duct has two major branches: a dorsocaudal (posterior) branch and a ventrocranial (anterior) branch [3]. Anomalous ducts can arise from either lobe of the liver, but those arising from the left lobe do not drain directly into the gallbladder or the cystic duct, and, therefore, are not susceptible to damage during cholecystectomy [3]. Anomalous right hepatic ducts are important to identify on the preoperative cholangiograms. Failure to do so may result in inadvertent ligation or severing of the anomalous duct. Ligation of an anomalous hepatic duct can result in significant segmental biliary obstructoin with resultant obstructive cholangitis [1]. This can progress to sepsis with hypotension [3]. A severed anomalous hepatic duct can result in biliary fistula formation and bile leakage [2, 3], which can progress to bile peritonitis [1].

An aberrant right hepatic duct (cases 2 and 3) drains into the common hepatic or cystic duct. This is an important abnormality, secondary to an inhibition of the primitive intes-

Received April 10, 1986; accepted after revision June 9, 1986.

[1] Department of Radiology, Medical College of Virginia/Virginia Commonwealth University, Richmond, VA 23298-0001. Address reprint requests to: S.-R. Cho, Dept. of Radiology, Box 615, MCV Station, Richmond, VA 23298-0001.

[2] Department of Radiology, McGuire Veterans Administration Medical Center, Richmond, VA 23249.

AJR 147:1181–1182, December 1986 0361–803X/86/1476–1181 © American Roentgen Ray Society

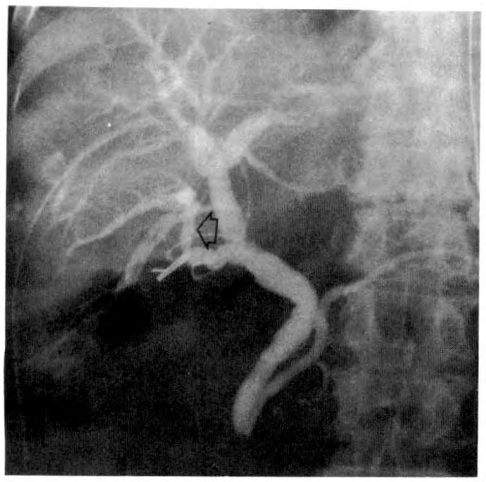


Fig. 1.—Intraoperative cholangiogram demonstrating accessory right hepatic duct (*arrowhead*) draining small area of liver and emptying into midportion of cystic duct. Note position of metallic clip across the cystic duct distal to its union with accessory right hepatic duct. Ligation of cystic duct at location of clip allows normal biliary drainage postoperatively. Note filling of pancreatic duct with small rounded filling defect at junction of common bile duct and pancreatic duct, which represents impacted stone.

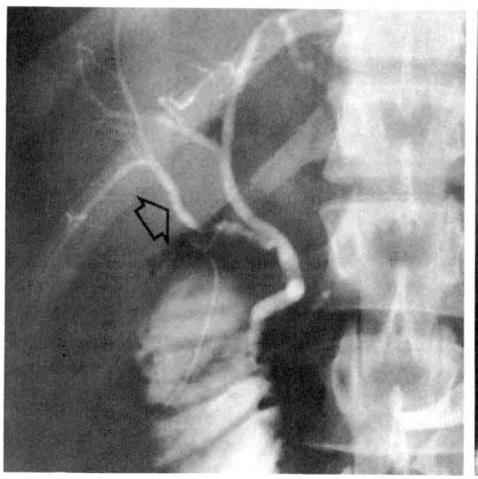


Fig. 2.—Intraoperative cholangiogram demonstrating aberrant right hepatic duct (*arrow*) draining large area of liver and emptying into midportion of cystic duct. Aberrant duct contains two major branches.

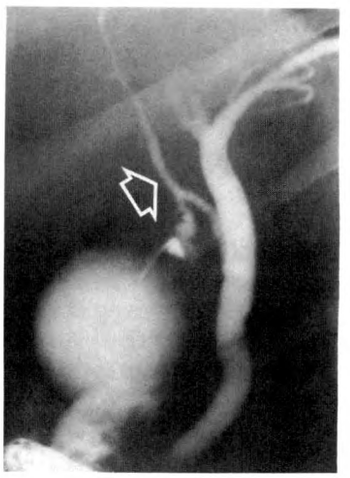


Fig. 3.—Preoperative endoscopic retrograde cholangiogram demonstrates aberrant right hepatic duct (*arrow*) emptying into midportion of cystic duct.

tinal bud [2]. A less frequent ductal anomaly is an accessory right hepatic duct (case 1), which also can empty into the common hepatic or cystic duct.

The occurrence of an anomalous right hepatic duct emptying into the cystic duct has been reported [1–6]. Puente and Bannura [2] reported that 177 (5%) cases in their study were aberrant hepatic ducts and 76 (2%) cases were accessory hepatic ducts, a total of 6.5% of anomalous biliary ducts. Berci and Hamlin [1] reviewed the literature and reported an average prevalence of anomalous biliary ducts of 12%. They also stated that an anomalous right hepatic duct emptying into the common hepatic or cystic duct was the most common biliary anomaly in their own experience. In 2 years, we have encountered three cases of an anomalous right hepatic duct emptying into the cystic duct. During that period, 112 ERCP and 155 intraoperative cholangiograms were performed in our institutions. In two of the three cases presented (cases 1 and 3), the anomalous right hepatic duct drained a small portion of the liver and emptied into the midportion of the cystic duct (Figs. 1 and 3). In the third case (case 2), the anomalous right hepatic duct consisted of two major branches, which drained a large portion of the liver. This duct also emptied into the midportion of the cystic duct (Fig. 2). When cholecystectomy is performed in patients with this anomaly, ligation of the cystic duct must be performed between the gallbladder and the junction of the anomalous right hepatic duct with the cystic duct. This will ensure normal drainage of the anomalous right hepatic duct into the common bile duct.

ACKNOWLEDGMENTS

The authors would like to thank Deborah Hogan and Rochelle Minter for their assistance in the preparation of this paper.

REFERENCES

1. Berci G, Hamlin JA. *Operative biliary radiology*. Baltimore: Williams & Wilkins, **1981**:110–116
2. Puente SG, Bannura GC. Radiological anatomy of the biliary tract: variations and congenital abnormalities. *World J Surg* **1983**;7:271–276
3. Rappoport AS, Diamond AB. Cholangiographic demonstration of postoperative bile leakage from aberrant biliary ducts. *Gastrointest Radiol* **1981**;6:273–276
4. Eisendrath AB. The clinical importance of anatomical anomalies in biliary surgery. *Boston Med Surg J* **1920**;182(23):573–578
5. Goor DA, Ebert PA. Anomalies of the biliary tree. *Arch Surg* **1972**;104:302–309
6. Schneiter R. Stepwise convergence of the bile ducts with implantation of the cystic duct on an ectopic right paramedial sectorial duct. *Gastroenterologia* **1967**;108:85–93

Technical Note

Value of Flow Technique for Double-Contrast Examination of the Stomach

Yoichi Kikuchi,[1] Marc S. Levine, Igor Laufer, and Hans Herlinger

In performing double-contrast upper-gastrointestinal examinations, we have found intentional manipulation of a thin barium pool extremely helpful for demonstrating lesions on the posterior gastric wall. Allowing a thin layer of barium to flow across the dependent surface of the stomach during the double-contrast examination has been referred to as "flow technique" by Engelholm of Brussels [1]. In our experience, flow technique has led to improved detection and characterization of subtle protruded or depressed lesions on the dependent wall of the stomach. As a result, we have incorporated this technique into our routine double-contrast examination. The advantages of this technique and a simple method for its performance are described.

Method

Double-contrast upper-gastrointestinal studies are routinely performed at our hospital, by using the technique previously described by Laufer [2, 3]. During the fluoroscopic examination, spot films of the stomach are obtained with the patient in supine, left posterior oblique (with respect to the table top), right posterior oblique, and right lateral positions. After the lateral view is obtained, "uphill" flow technique is performed by turning the patient onto his or her back and then slowly into a left posterior oblique position. This maneuver causes the barium pool to flow gradually from the antrum toward the body and fundus of the stomach. While the flow of barium is carefully monitored under fluoroscopy, 4-on-1 spot films of the upper and lower body and antrum of the stomach are obtained. These radiographs are deliberately taken while the posterior wall of the body and antrum are covered by a thin layer of barium to delineate shallow depressed or protruded lesions in this region (Fig. 1). Subsequently, "downhill" flow technique is performed by observing the stomach fluoroscopically as the patient is slowly turned to the right posterior oblique position. This maneuver causes the barium pool to flow from the fundus along the lesser curvature and posterior wall into the antrum, showing any lesions high on the lesser curvature of the stomach (Fig. 2). However, spot films of the region are only obtained when an abnormality is suspected fluoroscopically. The maneuvers required for uphill and downhill flow technique add one or two radiographs and about 30 sec of fluoroscopic time to the double-contrast examination.

Discussion

The double-contrast technique for an upper-gastrointestinal examination has been well described [2, 3]. Some authors favor a biphasic examination in which the double-contrast portion of the study is followed by single-contrast prone and upright compression views of the stomach and duodenum to better show anterior wall lesions [4, 5]. We routinely perform a biphasic upper-gastrointestinal examination at our hospital. However, we have also incorporated "flow technique" into our routine double-contrast study to better delineate lesions on the posterior wall and high on the lesser curvature.

In our experience, "uphill" flow technique can be used to facilitate detection of protruded or depressed lesions on the posterior gastric wall. Shallow protruded lesions such as varioliform erosions, polyps, and plaquelike carcinomas on the dependent surface may be recognized as radiolucent filling defects in the surrounding barium pool (Fig. 1B). In contrast, depressed lesions such as shallow ulcers or ulcerated carcinomas on the dependent surface may trap barium, producing a localized collection. In some cases, small, subtle, protruded or depressed lesions demonstrated by flow technique may not be visible on the initial double-contrast views (Fig. 1A).

"Downhill" flow technique is used primarily to demonstrate lesions high on the lesser curvature of the stomach. Subtle lesions in this region can be missed or misinterpreted on routine double-contrast radiographs (Fig. 2A). Because of the overlying rib cage, it is also difficult to obtain prone or upright compression views of this area. However, shallow ulcers or plaques, especially those extending from the lesser curvature onto the posterior wall, may be well delineated by this maneuver (Fig. 2B).

Received May 27, 1986; accepted after revision July 8, 1986.

[1] All authors: Department of Radiology, Hospital of the University of Pennsylvania, 3400 Spruce St., Philadelphia, PA 19104. Address reprint requests to M. S. Levine.

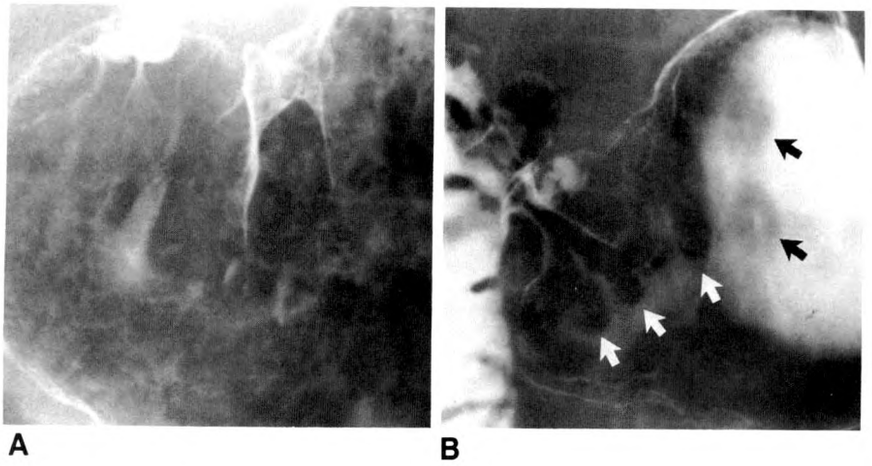


Fig. 1.—*A*, Double-contrast view of antrum shows irregular, nodular mucosa without discrete lesions.

***B*, Uphill-flow technique of antrum shows numerous varioliform erosions manifested by circular filling defects (*arrows*) in barium pool due to mound of edema surrounding central part of erosion. Even in retrospect, these lesions are barely discernible on earlier double-contrast view.**

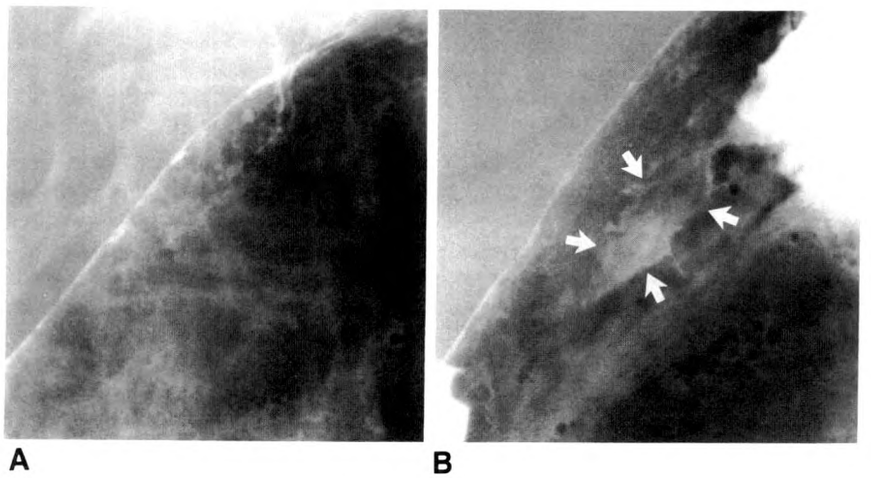


Fig. 2.—*A*, Radiograph of gastric body shows questionable area of mucosal irregularity high on lesser curvature, difficult to characterize on this initial double-contrast view.

***B*, Downhill-flow technique of same region has resulted in filling of shallow, irregular ulcer (*arrows*) on posterior wall near lesser curvature. Endoscopy confirmed presence of an ulcer high on lesser curvature.**

Flow technique is also useful for evaluating the nature and location of "ring shadows" in the stomach. A ring shadow may represent a variety of lesions, including a protruded or depressed lesion on the nondependent surface or a shallow depressed lesion on the dependent surface [6]. With flow technique, however, depressed lesions on the dependent surface should fill with barium, producing a discrete niche or collection. However, lesions on the nondependent surface should still be visible as ring shadows through the thin barium pool. In such cases, prone compression views should differentiate protruded from depressed lesions on the anterior gastric wall.

In difficult cases, flow technique can be adapted for evaluating anterior wall lesions in the stomach or lesions elsewhere in the gastrointestinal tract, particularly the colon, where it is possible to control and manipulate the barium pool. As a result, this technique may lead to improved detection of dependent-wall lesions throughout the gastrointestinal tract.

In summary, we believe that flow technique is a valuable adjunct to the routine double-contrast examination of the stomach, providing significant diagnostic information about lesions that are on the posterior wall and or high on the lesser curvature with only a small increase in examination time and radiation exposure.

REFERENCES

1. Engleholm L, Jeanmart L, DeToeuf J. Exploration gastro-duodenale et colique en double contraste. Belgium: European Press, **1978**
2. Laufer I. Upper gastrointestinal tract: technical aspects. *Double contrast gastrointestinal radiology*. Philadelphia: Saunders, **1979**:59–77
3. Laufer I. Double contrast examination of the stomach and duodenum. In: Marshak RH, Lindner AE, Maklansky D, eds. *Radiology of the stomach*. Philadelphia: Saunders, **1983**:1–27
4. Montagne JP, Moss AA, Margulis AR. Double-blind study of single and double contrast upper gastrointestinal examinations using endoscopy as a control. *AJR* **1978**;130:1041–1045
5. Margulis AR, Ominsky S. The biphasic examination of the upper gastrointestinal tract. In: Marshak RH, Lindner AE, Maklansky D, eds. *Radiology of the stomach*. Philadelphia: Saunders, **1983**:28–40
6. Kressel HY, Laufer I. Principles of double contrast diagnosis. In: Laufer I, ed. *Double contrast gastrointestinal radiology*. Philadelphia: Saunders, **1979**:11–58

UCSF Interventional Radiology Rounds

Angiographic Management of Upper Gastrointestinal Hemorrhage

Robert K. Kerlan, Jr.,[1,2] Anton C. Pogany,[1,3] Dana R. Burke,[1] and Ernest J. Ring[1]

This is a selection from the Interventional Radiology Rounds of the University of California, San Francisco. The discussion focuses on problems encountered with the diagnosis and management of upper gastrointestinal hemorrhage.

Dr. Burke.—A 53-year-old woman had a history of intermittent upper abdominal pain since childhood. At age 23 she was diagnosed as having chronic pancreatitis. The patient underwent numerous surgical procedures for recurrent abdominal pain, including a cholecystectomy in 1966, a gastrojejunostomy in 1968, and a pancreaticojejunostomy in 1971.

In 1978, at age 47, the patient developed jaundice. Transhepatic cholangiography revealed a high-grade stricture of the distal common bile duct. A choledochojejunostomy was performed; however, in 1980 the upper abdominal pain recurred. An upper gastrointestinal series disclosed ulceration at the gastrojejunal anastomosis, and a surgical revision of the gastrojejunostomy was performed. Unfortunately, the abdominal pain was not relieved, and 8 months later she underwent a total pancreatectomy and incidental splenectomy.

One year later the patient was readmitted to the hospital for abdominal pain. Upper gastrointestinal endoscopy revealed a deep ulceration at the gastrojejunal anastomosis. Despite intensive medical management, the pain persisted, and an erythematous area developed on her anterior abdominal wall. This area became fluctuant, and it was incised in the operating room. Purulent material was evacuated, and surgical drains were placed. One week later the drainage fluid became bilious, and an upper gastrointestinal series was performed (Fig. 1).

Dr. Kerlan.—Dr. Pogany, how would you interpret this study?

Dr. Pogany.—The gastric remnant is very irregular with thickened folds in its distal segment. A fistulous tract is originating from the lesser curvature and extending to the anterior abdominal wall.

Dr. Burke.—Five days later while walking on the ward, the patient collapsed and was found on the floor with copious amounts of blood pouring from her fistulous tract. She was unconscious, and her systolic blood pressure was 60 mm Hg. Diastolic blood pressure could not be determined.

Manual compression was applied to the drainage site, and IV fluids were administered. The bleeding stopped, and her blood pressure returned to the normal range. A nasogastric tube was put into place, and numerous blood clots were removed from the stomach.

Dr. Kerlan.—Dr. Pogany, from where do you think this bleeding was originating?

Dr. Pogany.—The bleeding was coming from a fistulous tract that communicated with the stomach, as confirmed by the presence of blood also found in the stomach. The two leading possibilities are hemorrhage from the fistulous tract itself or bleeding from the stomach that flowed out through

Received March 3, 1986; accepted after revision June 30, 1986.

[1] All authors: Department of Radiology, Interventional Radiology, Rm. M-361, University of California, San Francisco, 501 Parnassus Ave., San Francisco, CA 94143-0628. Address reprint requests to E. J. Ring.

[2] Present address: Radiology Department, Scripps Memorial Hospital, 9888 Genesee, San Diego, CA 92037.

[3] Present address: Alta Imaging Group, 2510 Webster St., Berkeley, CA 91703.

AJR 147:1185–1188, December 1986 0361–803X/86/1476–1185 © American Roentgen Ray Society

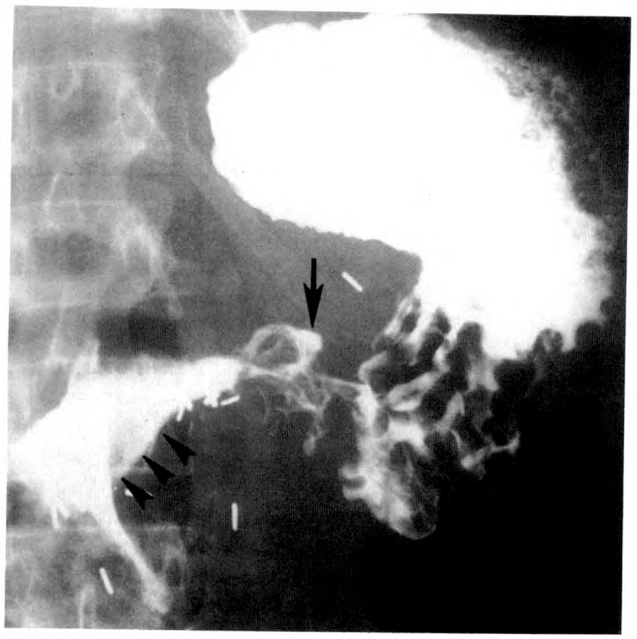


Fig. 1.—Frontal radiograph from upper gastrointestinal series shows an ulceration along the distal lower curve of gastric remnant (*arrow*). A sinus tract (*arrowheads*) extends from stomach to anterior abdominal wall. Gastrojejunal anastomosis is not shown.

the fistulous tract. The latter is the more reasonable possibility because hemorrhage from a well-formed fistulous tract extending to the anterior abdominal wall is quite unusual.

Dr. Kerlan.—Dr. Ring, what is your approach to treating patients with upper gastrointestinal hemorrhage?

Dr. Ring.—Upper gastrointestinal hemorrhage is an intriguing problem, and many techniques are available for diagnosis and treatment. From a clinical perspective, it is important to remember that bleeding will stop spontaneously in up to 75% of patients with supportive therapy and bed rest [1, 2]. However, it is clearly important to establish the source of bleeding in patients with significant gastrointestinal hemorrhage.

Recently, endoscopy has become the most efficient method for identifying the source of gastrointestinal hemorrhage. At our medical center all patients with significant upper gastrointestinal bleeding undergo endoscopy as the initial diagnostic test. With a diagnostic accuracy between 75% and 90% [3–5], endoscopy provides information regarding the cause as well as the site of bleeding.

Emergency arteriography has been relegated to a rather specific role in the diagnosis and management of gastrointestinal hemorrhage. Currently, we use arteriography for patients with bleeding unresponsive to conservative measures when (1) endoscopy and nuclear medicine imaging have failed to localize the bleeding site accurately, and the consulting surgeon desires more specific information; and (2) hemorrhage originates from a known area, but transcatheter infusion or embolization therapy is desired to control the bleeding.

Dr. Kerlan.—Dr. Ring, which patients are appropriate candidates for attempting control of upper gastrointestinal bleeding using transcatheter techniques?

Dr. Ring.—Transcatheter techniques have proven very effective for management of bleeding related to Mallory-Weiss tears, gastric ulcers, and gastritis [6–10]. In comparison, this form of therapy is relatively ineffective for bleeding duodenal ulcers [6, 11].

However, the clinical status of the patient must also be considered. With elderly patients, attempts at transcatheter control of hemorrhage may be indicated even if the bleeding is originating from an unfavorable site.

The patient we are discussing would appear to be a good candidate for angiographic therapy. The bleeding likely is originating from the stomach, and the numerous previous surgical procedures would make another operation in this area extremely difficult.

Dr. Kerlan.—Twenty-four hours later the patient experienced a second major episode of bleeding. Gastroscopy was performed, but the bleeding site could not be identified. She was brought to the angiography suite where a celiac and superior mesenteric arteriogram were performed (Fig. 2). Dr. Pogany, what is your interpretation of the study?

Dr. Pogany.—The anatomy of the celiac axis is very distorted, and the left gastric artery, right hepatic artery, and gastroduodenal artery are occluded. A relatively large vessel originates from the distal common hepatic artery and courses from right to left to supply the gastric remnant. No extravasation is demonstrated, but an aneurysm is present in the middle of this vessel.

Although the general appearance of the vessel suggests splenic artery, an oblique view confirms that this vessel is actually a right gastric artery that has enlarged to act as a source of collaterals because of occlusions involving the other branches supplying the stomach.

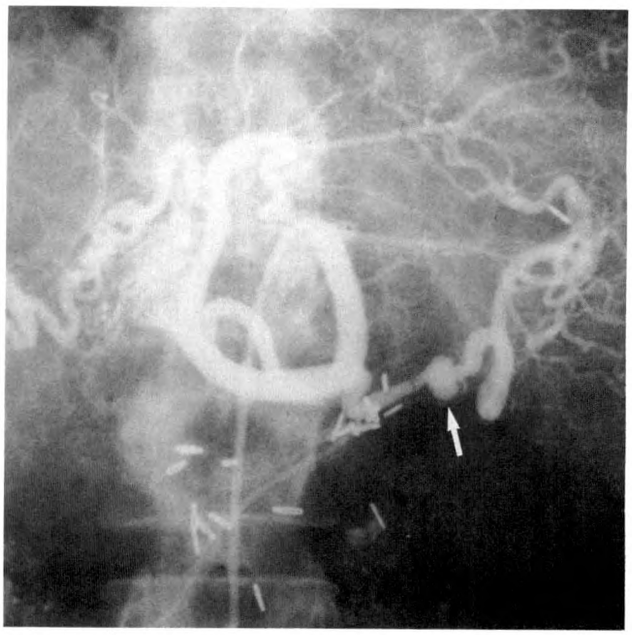


Fig. 2.—Midarterial phase of selective celiac injection shows splenic, left gastric, gastroduodenal, and right hepatic arterial occlusions. Aneurysm (*arrow*) is present in middle of right gastric artery.

Dr. Kerlan.—Do you always recommend beginning upper gastrointestinal bleeding studies with a celiac arteriogram?

Dr. Pogany.—A celiac arteriogram should be performed as the initial study in patients with upper gastrointestinal bleeding only when there is history of prior gastric surgery and the anatomy may be altered. However, in a patient with endoscopic evidence of gastric bleeding but without prior surgery, I begin with a selective left gastric injection, as more than 80% of gastric arterial hemorrhage is in the distribution of this vessel [12]. If the left gastric injection fails to reveal a bleeding site, I proceed to a celiac injection followed by selective splenic, hepatic, and superior mesenteric arteriograms, as necessary.

Dr. Kerlan.—What do you believe is the source of hemorrhage in this patient?

Dr. Pogany.—I do not detect any evidence of active extravasation at this time. However, on close inspection, a small ring of barium surrounds the aneurysm of the right gastric artery. When a radiograph from the previous upper gastrointestinal examination is compared to the arteriogram (Fig. 3), it is evident that the persistent barium is in the fistulous tract, contiguous with the ulcer, and that the aneurysm is located centrally within it. Therefore, I would assume that the ulcer has eroded into the right gastric artery causing a false aneurysm and that intermittent leakage from the aneurysm is the cause of the patient's recurrent hemorrhage.

Dr. Kerlan.—Dr. Ring, what are the therapeutic alternatives for this patient?

Dr. Ring.—Gastrointestinal hemorrhage can be controlled either through vasopressin infusion [13–15] or embolization [16–18]. Vasopressin appears to work well when superficial mucosal erosions are present; however, such infusion therapy would be unlikely to benefit this patient, whose bleeding originates from a large artery with an aneurysm that is probably mycotic.

Embolization is an alternative treatment, but in this patient the right gastric artery appears to be the sole arterial blood supply to the stomach. Although gastric infarction is a very rare complication of gastric embolization, this patient is undoubtedly at greater risk when compared with a patient who has conventional arterial anatomy. The degree of risk is difficult to estimate, but embolization in this case would appear to be somewhat analogous to embolization of a superior mesenteric or inferior mesenteric arterial branch. Although embolization of these vessels can be performed safely in some circumstances, some cases result in intestinal infarction.

Dr. Kerlan.—What embolic materials would you recommend?

Dr. Ring.—In most cases of embolization for gastrointestinal bleeding, Gelfoam (Upjohn, Kalamazoo, MI) cut into small pledgets is the material of choice. However, in this case, the bleeding originates from a relatively large artery. The ideal treatment would be to place occluding spring emboli or detachable balloons both proximal and distal to the aneurysm to avoid the necessity of occluding the smaller distal arteries and to decrease the possibility of gastric infarction.

Dr. Kerlan.—Dr. Burke, what approach was selected to treat this patient?

Dr. Burke.—We discussed the case with the referring surgeon, and, despite the possibility of gastric infarction, we were urged to attempt occlusion of the aneurysm.

Although the origin of the right gastric artery could be selectively catheterized, we could not advance the catheter a sufficient distance into the vessel to ensure safe delivery of an occluding spring embolus. However, as a result of catheter manipulation, a small intimal flap developed at the origin of the right gastric artery. The decision was made to attempt occluding the vessel by intentionally extending the dissection flap with a guidewire. This maneuver was successful (Fig. 4). The flap also extended proximally into the common hepatic artery.

After the procedure, the patient's blood pressure stabilized, and she experienced no further episodes of bleeding. Mild left upper quadrant discomfort developed but resolved spontaneously the next day. After 10 days of nasogastric suction, the fistula closed. She has subsequently done well, with no recurrence of abdominal pain during the 14-month follow-up period.

Comment

The role of angiography in the diagnosis and treatment of upper gastrointestinal bleeding has changed dramatically over

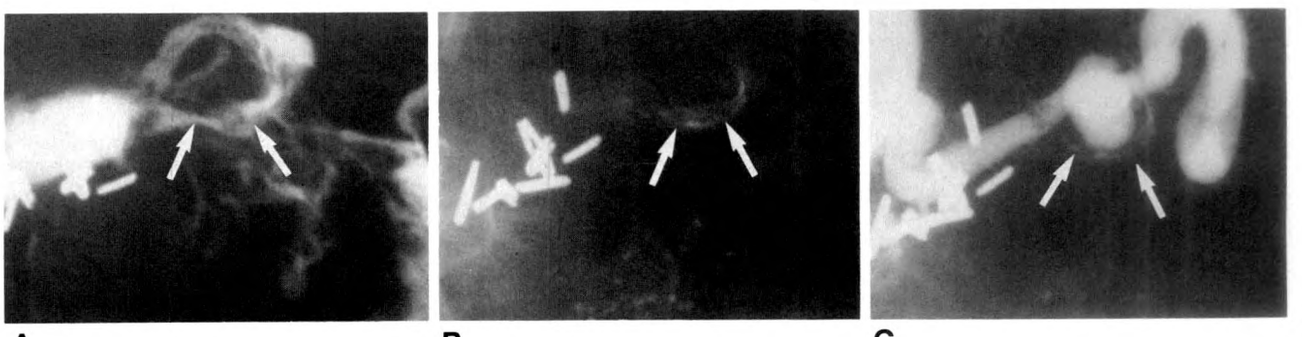


Fig. 3.—Close-up views of ulcer and ringlike barium collection (*arrows*).
***A*, Spot film from upper gastrointestinal series shows marginal ulcer.**
***B*, Preliminary film from angiogram shows residual barium in crater.**
***C*, Celiac artery injection shows pseudoaneurysm in center of ulcer crater.**

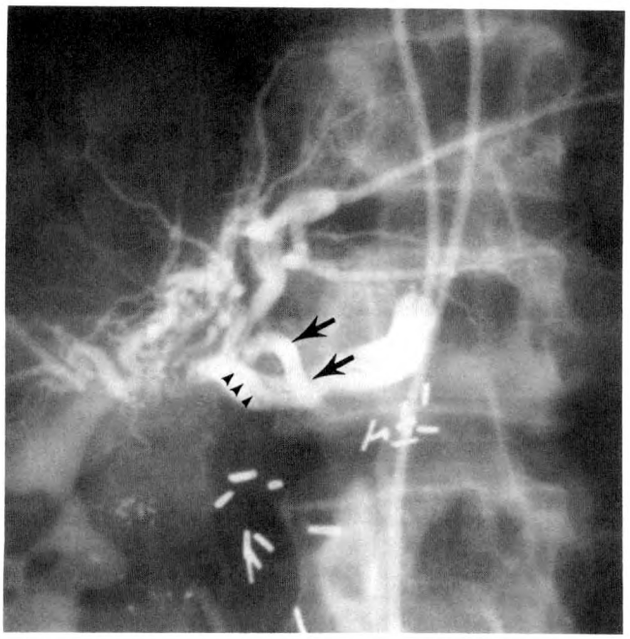


Fig. 4.—Midarterial phase of common hepatic arteriogram shows dissection flap (*arrowheads*) extending into proximal segment of right gastric artery (*arrows*), which is occluded and remains partially opacified by contrast material persisting from injection made during dissection maneuver. Note filling of peripheral hepatic arteries.

the past 5 years. The widespread application of flexible panendoscopy has reduced the number of angiograms performed for localization of bleeding sites. Moreover, the development of effective medication to block histamine-2 receptors has decreased the incidence of serious gastric hemorrhage. Nevertheless, in selected patients therapeutic angiography continues to be a valuable and effective form of management.

This case is unusual in two respects. First, the gastric arterial anatomy had been extensively modified by the previous surgical procedures. Second, the bleeding was originating from a large artery as opposed to smaller arterial and arteriolar sources, which are the common sources of gastric hemorrhage.

Ideally, occlusion of an artery of this size would entail deposition of the detachable balloon or coils both proximal and distal to the suspected site of hemorrhage. However, as with any interventional radiologic procedure, occasionally there are technical limitations to catheter manipulations that prevent attainment of the ideal goal. Fortunately, in this case, intentional dissection proved to be an effective alternative method for occluding the bleeding vessel.

ACKNOWLEDGMENT

We thank Gala FitzGerald for editorial assistance.

REFERENCES

1. Winans CS. Emergency upper gastrointestinal endoscopy: does haste make waste? *Am J Dig Dis* **1977**;22:536–540
2. Schrock TR. Does endoscopy affect the surgical approach to the patient with upper gastrointestinal bleeding? *Dig Dis Sci* **1981**;26:275–305
3. Steer ML, Silen W. Diagnostic procedures in gastrointestinal hemorrhage. *N Engl J Med* **1983**;309:646–650
4. Hoare AM. Comparative study between endoscopy and radiology in acute upper gastrointestinal hemorrhage. *Br J Med* **1975**;1:27–30
5. McGinn FP, Guyer PB, Wilken BJ, Steer HW. A prospective comparative trial between early endoscopy and radiology in acute upper gastrointestinal hemorrhage. *Gut* **1975**;16:707–713
6. Clark RA, Colley DP, Eggers FM. Acute gastrointestinal hemorrhage: efficacy of transcatheter control. *AJR* **1981**;136:1185–1189
7. Nusbaum M, Baum S, Blakemore WS. Clinical experience with diagnosis and management of gastrointestinal hemorrhage by selective mesenteric catheterization. *Am Surg* **1969**;170:506–514
8. Athanasoulis CA, Waltman AC, Novelline RA, Krudy AG, Sniderman KW. Angiography: its contribution to emergency management of G.I. bleeders. *Radiol Clin North Am* **1976**;14:265–280
9. Athanasoulis CA. Therapeutic applications of angiography. *N Engl J Med* **1980**;302:1117–1125
10. Fisher RG, Schwartz JT, Graham DY. Angiotherapy with Mallory-Weiss tear. *AJR* **1980**;134:679–684
11. Ring EJ, Oleaga JA, Freiman DB, Husted JW, Waltman AC, Baum S. Pitfalls in the angiographic management of hemorrhage: hemodynamic considerations. *AJR* **1977**;129:1007–1013
12. Kelemouridis V, Athanasoulis CA, Waltman AC. Gastric bleeding sites: an angiographic study. *Radiology* **1983**;149:643–648
13. Athanasoulis CA, Baum S, Waltman AC, Ring EJ, Imbembo A, Vandersalm TJ. Control of acute gastric mucosal hemorrhage with the intraarterial infusion of pituitary extract. *N Engl J Med* **1974**;290:597–603
14. Sherman LM, Shenoy SS, Cerra FB. Selective intraarterial vasopressin: clinical efficacy and complications. *Am J Surg* **1979**;189:298–302
15. Waltman AC, Greenfield AJ, Novelline RA, Athanasoulis CA. Pyloroduodenal bleeding and intraarterial vasopressin: clinical results. *AJR* **1979**;133:643–646
16. Gold RE, Grace DM. Gelfoam embolization of the left gastric artery for bleeding ulcers. *Radiology* **1975**;116:575–580
17. Goldman ML, Land WC, Bradley EL III, Anderson J. Transcatheter therapeutic embolization in management of massive upper gastrointestinal bleeding. *Radiology* **1976**;120:513–521
18. Katzen BT, Rossi P, Passarello R, Simonetti G. Transcatheter therapeutic arterial embolization. *Radiology* **1976**;120:523–531

Distal Ureteral Calculi:
Diagnosis by Transrectal Sonography

Robert M. Lerner[1]
Deborah Rubens

Eight patients were studied by both transrectal sonography and excretory urography for the presence of distal ureteral calculi. The sonographic diagnosis was correct in 5 of 5 true positives and 3 of 3 true negatives. Urography was correct in 4 of 5 true positives and 2 of 3 true negatives. None of the sonograms and two of the urograms were considered equivocal. Transrectal sonography appears to be a useful adjunct for the diagnosis of distal ureteral calculi when excretory urography is equivocal or contraindicated.

Excretory urography is accurate for diagnosing hydronephrosis and hydroureter and for demonstrating the level of distal ureteral obstruction, but occasionally it fails to establish the cause [1]. Small and/or radiolucent ureteral calculi may not appear on plain abdominal radiographs or urograms. Pelvic phleboliths and bowel contents may obscure the calculus. Obstruction by edema from recent passage of a calculus may be inferred from urograms, but unless the calculus is recovered the diagnosis is uncertain. If excretory urography does not identify the cause of distal ureteral obstruction, cystoscopy, antegrade or retrograde pyelography, or CT scans may be required for further evaluation.

A prospective study in eight patients with renal colic was undertaken to evaluate transrectal sonography for directly identifying distal ureteral calculi. These patients had a high probability of having distal ureteral calculi. In addition, a retrospective study in patients with a low probability was performed by reviewing 234 transrectal sonograms from patients under evaluation for prostate disease or rectal cancer.

Subjects and Methods

The transrectal ultrasound probe is a prototype manufactured by Toshiba Medical Systems (Tustin, CA). Designed for prostate and bladder examinations, it can operate with either a Toshiba SAL-20A or SAL-30 linear-array ultrasound analog unit. The probe is 2 cm in diameter and 15 cm in length; it has a 64-element, 3.5-MHz linear-array transducer focused at 3 cm. In use, the probe is covered by a latex condom filled with water to provide optimal acoustic coupling after rectal insertion. Informed consent was obtained. During the examination, the probe was rotated to view the rectal wall, the perirectal region, the inferior portion of the bladder, the prostate, and the seminal vesicles. All studies were performed by physicians, lasted approximately 5 min, and were done with the patient in the knee-elbow position. Patient tolerance of the examination was excellent. Only two out of 244 patients reported more discomfort than from a digital rectal examination. No complications were encountered.

The eight patients with renal colic (four men, four women, 34–85 years old) were examined with transrectal sonography for the presence of a lower ureteral calculus within 2 days after excretory urography. The urograms showed distal ureteral obstruction in all eight patients. In three, a definite calculus noted on urography was known at the time of transrectal sonography. The cause of the obstruction on the other five patients was unknown at the time of the sonogram. The final diagnosis of a distal ureteral calculus was documented by urography, cystoscopy, clinical follow-up, or surgery.

Received February 18, 1986; accepted after revision July 22, 1986.

[1] Both authors: Department of Radiology, Box 648, University of Rochester School of Medicine and Dentistry, Rochester, NY 14642. Address reprint requests to R. M. Lerner.

AJR 147:1189–1191, December 1986
0361–803X/86/1476–1189
© American Roentgen Ray Society

Criteria for diagnosis of distal ureteral calculi on transrectal sonography were (1) identification of a highly echogenic reflector with a distinct distal shadow located between the seminal vesicles and bladder in men (Fig. 1), or between the bladder and vagina or uterus in women (Fig. 2), and (2) a history of renal colic and/or a dilated ureter proximal to the shadowing reflector.

Results

Transrectal sonography showed distal ureteral calculi in five of the eight patients with renal colic. All five had the calculi confirmed, four by excretory urography and one by cystoscopy. The remaining three patients proved not to have calculi, two by urography and the clinical course, and the third by surgical exploration that confirmed the absence of a calculus. Only four calculi were detected by urography. These varied in size from 2 to 8 mm, as measured on the urogram, although they appeared larger on transrectal sonography (5–11 mm). The one radiolucent calculus measured 8 mm by transrectal sonography.

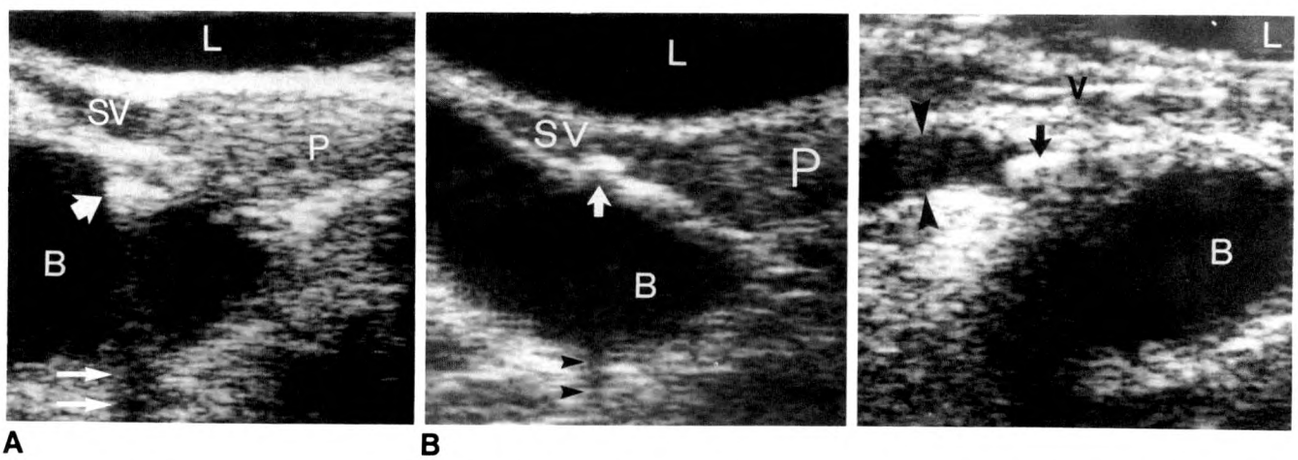
None of the transrectal sonograms were considered equivocal. The urographic diagnosis was correct in four of five patients with calculi and two of three without calculi. Two of the urograms showed evidence of distal ureteral obstruction but were equivocal for the presence of a calculus; one of these had a uric acid calculus at cystoscopy and the other had no calculus at surgery. The latter patient, who had a questionably positive urogram followed by a normal transrectal sonogram, might have passed a calculus during the interval between examinations, although the patient's pain had subsided 1 day before the urogram.

Although in three patients the diagnosis was known before transrectal sonography on the basis of urography, this knowledge is unlikely to have influenced the interpretation of the transrectal sonograms because the diagnostic criteria for calculi were readily apparent.

Review of the 234 transrectal sonograms performed primarily for prostate disease yielded only three patients with findings suspicious for distal ureteral calculi. These patients had echogenic reflectors with distal acoustic shadows adjacent to the seminal vesicles and bladder (criterion 1). Although none had recent symptoms of renal colic, and proof of distal ureteral calculi was lacking, two gave clinical histories consistent with earlier episodes of renal colic without recovery of a calculus, suggesting it was lodged in the distal ureter. In one patient, calcifications of the vas deferens (diagnosed by plain film) satisfied the reflector criterion but there was no history of renal colic or hydroureter (criterion 2). The remaining 231 patients showed no transrectal sonographic or clinical evidence of distal ureteral calculi.

Discussion

The diagnosis of distal ureteral calculi by using transabdominal sonography performed through a distended urinary bladder has recently been reported [2, 3]. Although 79% of calculi at the ureterovesical junction were detected by this technique, compared to 68% by excretory urography, only 25% of the calculi were observed directly by sonography [3]. The remaining 75% were inferred by the presence of moderate hydronephrosis and/or hydroureter on the symptomatic side. These criteria may not be adequate: Another report found that only 65% of patients with acute ureteral colic show hydronephrosis by sonography [4]. Thus, direct visualization of the obstructing calculus by transrectal sonography may provide a more reliable diagnosis than the presence of hydronephrosis or hydroureter.



A B

Fig. 1.—*A, B*, Transrectal sonograms in men, longitudinal projection with patients prone, heads to left. B = bladder; P = prostate; SV = seminal vesicles; L = fluid-filled condom containing transducer. Ureteral calculi present at the ureteral vesicle junction (*thick white arrow*). Note acoustic shadow caused by calculi (*long white arrows*) in *A*, *arrowheads* in *B*).

Fig. 2.—Transrectal sonogram in woman, same orientation as Fig. 1. V = vagina; B = bladder; L = fluid-filled condom containing transducer; *arrowheads* = ureter. Ureteral calculus (*arrow*) visible at ureteral vesicle junction. Radiolucent calculus was removed at cystoscopy.

Location of the distal ureter in men between the water-filled condom in the rectum and the urine-filled bladder, or between the uterus and urine-filled bladder in women, invariably provides an ideal sonic window for identification of distal ureteral calculi by transrectal sonography. Acoustic shadowing of distal ureteral calculi may be reliably detected because the shadow interrupts the bladder (Figs. 1 and 2). Shadow from a ureteral calculus imaged transabdominally may be difficult to perceive if the shadow is obscured by bowel gas. The bladder/urine interface, along with the excellent sonographic window provided by the fluid-filled condom surrounding the transrectal probe and the shorter soundpath (better lateral resolution), probably accounts for our high percentage of direct visualization (100%) of distal ureteral calculi by transrectal sonography, compared with approximately 25% reported by the transabdominal approach [3].

The calculi measured 0–3 mm larger on transrectal sonography than by urography. This discrepancy may be due to differences in orientation of the measured axis of the calculus, lateral beam-width uncertainty introduced by the sonographic transducer, or echogenic laminated material covering the radiopaque portion of the calculus.

In our experience, asymptomatic distal ureteral calculi are rare incidental findings on transrectal sonography. Calculi have been reported to lodge in the distal ureter without causing pain or obstruction [5] and without ureteral dilatation [2, 5]. Shadowing reflectors without continuity to dilated proximal ureters are equivocal for distal ureteral calculi in asymptomatic patients and may be due to phleboliths, calcified vas deferens, or nonobstructing calculi. In men, the vas deferens may occasionally appear as hypoechoic tubular structures (not associated with highly echogenic reflectors) adjacent to the seminal vesicles. The van deferens can be differentiated from a dilated ureter by their bilaterality and small size.

In this study, transrectal sonography shows promise for the diagnosis of distal ureteral calculi. Although the number of patients with calculi is small, the study suggests that transrectal sonography can accurately confirm the presence or absence of a calculus in the distal ureter. In addition to diagnosis, transrectal sonography may be valuable for monitoring passage of a calculus or as part of an interventional procedure. CT or cystoscopy may also document the presence of a calculus, but these procedures are more expensive or more invasive, respectively. Transrectal sonography should be considered an adjunct to urography in patients presenting with renal colic and distal ureteral obstruction of uncertain cause. In cases when urography should not be performed (i.e., pregnancy, contrast media allergy, lack of peripheral venous access), transrectal sonography is a sensitive examination for diagnosis of distal ureteral calculi and it complements abdominal sonography.

ACKNOWLEDGMENT

The authors gratefully acknowledge Beverly Pollet for her expert assistance in manuscript preparation.

REFERENCES

1. Thornbury JR, Parker TW. Ureteral calculi. *Semin Roentgenol* **1982**;17:133–138
2. Erwin BC, Carrol BA, Sommer FG. Renal colic: the role of ultrasound in initial evaluation. *Radiology* **1984**;152:147–150
3. Hill MC, Rich JI, Mardiat JG, Finder CA. Sonography vs excretory urography in acute flank pain. *AJR* **1985**;144:1235–1238
4. Laing FC, Jeffrey RB Jr, Wing VW. Ultrasound versus excretory urography in evaluating acute flank pain. *Radiology* **1985**; 154:613–615
5. Wolfman MG, Thornbury JR, Braunstein EM. Nonobstructing radioopaque ureteral calculi. *Urol Radiol* **1979**;1:97–104

American Roentgen Ray Society 87th Annual Meeting April 26–May 1, 1987, Miami Beach, FL Fontainebleau-Hilton Hotel

Registration and Hotel Reservations

Forms for advance registration and hotel reservations will be in the February and March 1987 issues of the *AJR*.

Refresher Course Program

A summary of the refresher courses will appear in the *AJR* in January along with advance registration forms. Early registration is an advantage in assuring preferred courses in this popular program. Dr. J. T. Ferruci, Jr. is program director.

Local Program

A program of sightseeing, shopping, and entertainment will be developed by the Local Arrangements Chairman. Information and advance registration forms will be in the January and February issues of the *AJR*.

President's Award Papers

The society offers several cash awards for the best scientific papers prepared by residents in radiology. The President's Award has a $1000 prize. There are two Executive Council awards of $500 each. All are presented at the annual meeting. Papers should be submitted by Jan. 31 for consideration in this competition. Send entries to:

B. G. Brogdon, M.D.
Dept. of Radiology
University of South Alabama Medical Center
2451 Fillingim Street
Mobile, AL 36617

ARRS Membership Requirements

The American Roentgen Ray Society (ARRS) has two membership categories: active and in-training. For active membership, applicants must practice radiology in the U.S. or Canada. Each must have graduated in good standing from an approved medical school or hold an advanced degree in physical, chemical, or biological science and be certified by the American Board of Radiology, the Royal College of Physicians and Surgeons of Canada, or otherwise adequately document training and credentials.

A member-in-training must be in a radiology residency or postresidency fellowship program or be a postgraduate student in an allied science. Status must be verified by the program director.

For consideration during the 1987 ARRS meeting, completed applications must be received no later than Feb. 1. Obtain forms and details from:

Rosalind H. Troupin, M.D.
Department of Radiology
Hospital of University of Pennsylvania
3400 Spruce St.
Philadelphia, PA 19104

Associated Society Meetings

Society for Pediatric Radiology and European Society of Pediatric Radiology

The inaugural conjoint International Pediatric Radiology '87 meeting will meet May 30–June 4, 1987 at the Westin Hotel, Toronto, Ontario, Canada. Deadline for receipt of abstracts is February 1, 1987. For details contact: Donald R. Kirks, M.D., Secretary, Society for Pediatric Radiology, c/o Dept. of Radiology, Childrens Hospital Medical Center, Elland and Bethesda Aves., Cincinnati, OH 45229, (513) 559-4880

Deadlines

President's Award papers: January 31
Membership applications February 1

Simultaneous Pancreatic-Renal Transplant Scintigraphy

Barry L. Shulkin[1]
Don C. Dafoe[2]
Richard L. Wahl[1]

^{99m}Tc-DTPA scintigraphy was evaluated in seven patients as a technique to assess perfusion of the transplanted pancreas and kidney. Such scans provide high-quality images of both organs in both the flow phase and later phases. The radionuclide is readily available and its brief effective half-life allows repeated evaluations at short intervals. ^{131}I-hippuran, the major radiopharmaceutical for renal transplant scintigraphy, does not allow visualization of the transplanted pancreas or evaluation of its blood supply. Although the blood glucose is a gross indicator of the function of the pancreatic allograft, pancreatic scintigraphy with ^{99m}Tc-DTPA in one case was capable of detecting graft dysfunction before elevation of the blood glucose occurred. While additional studies will be necessary to determine the predictive value of this test, ^{99m}Tc-DTPA is valuable for pancreatic-renal transplant evaluation.

Despite unfavorable results in the past, pancreatic transplantation continues to offer hope for physiologic control of blood glucose in diabetic patients. The immunosuppressive agent, cyclosporine, and improved surgical techniques have combined to provide a 40% 1-year pancreatic graft survival for those transplanted in 1983 and 1984 [1]. As pancreatic transplantation becomes more frequent, the availability of a noninvasive scintigraphic means of assessing function assumes increasing importance. Radionuclide scintigraphy of pancreatic transplants has been impaired by the lack of agents that specifically localize to exocrine pancreatic tissue. ^{75}Se-methionine may provide images of functioning pancreatic tissue but the low photon flux does not allow direct evaluation of blood flow [2]. ^{111}In-oxine platelets have been used to detect allograft rejection in people and dogs, but neither flow nor function can primarily be assessed by this method [3, 4].

Hahn et al. [5] recently reported the utility of ^{99m}Tc-DTPA in evaluating vascular compromise or rejection in pancreatic grafts of two patients. This paper describes the University of Michigan experience in which ^{99m}Tc-DTPA was used for simultaneous pancreatic-renal transplant scintigraphy and its value in monitoring graft function.

Methods and Case Illustrations

Seven patients with diabetes mellitus complicated by end-stage renal disease that required dialysis have received simultaneous cadaveric pancreatic-renal allografts at the University of Michigan. In five patients, both organs remain functional 10, 4, 4, 2, and ½ months after transplantation. Initial pancreatic-renal transplant scintigraphy was performed within 48 hr of surgery, with subsequent scans as clinically indicated. Flow to the organs was assessed by the bolus administration of 10–15 mCi (370–555 MBq) ^{99m}Tc-DTPA. Images were acquired every 2 sec for 60 sec, by using a large field-of-view gamma camera with a high-energy collimator interfaced with a computer. Serial 1-min images were then collected for 30 min. Upon completion of the ^{99m}Tc-DTPA acquisition, 0.25 mCi (9.25 MBq) ^{131}I-hippuran was injected. Serial 1-min images were acquired for 45 min. The following cases illustrate the scintigraphic findings in functioning and nonfunctioning transplants.

Received April 24, 1986; accepted after revision July 16, 1986

This work was supported in part by a grant from the Michigan Phoenix Foundation.

[1] Department of Internal Medicine, Division of Nuclear Medicine, B1G 412-0028, University of Michigan Hospitals, 1500 E. Medical Center Dr., Ann Arbor, MI 48109-0028. Address reprint requests to R. L. Wahl.

[2] Department of Surgery, University of Michigan Hospitals, 2926 Taubman, Box 0331, 1500 E. Medical Center Dr., Ann Arbor, MI 48109.

AJR 147:1193–1196, December 1986
0361–803X/86/1476–1193
© American Roentgen Ray Society

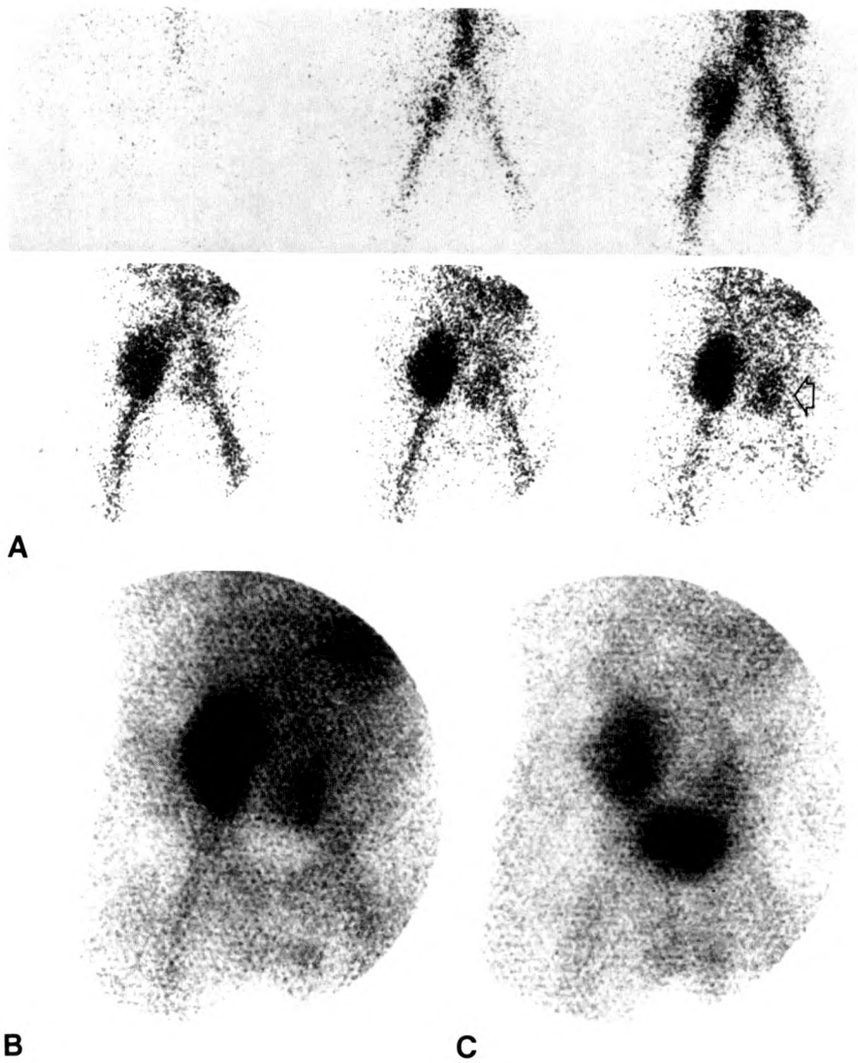


Fig. 1.—^{99m}Tc-DTPA scintigrams of patient 1.
***A*, Flow study (2 sec/frame)—excellent perfusion of both the pancreatic (*arrow*) and renal transplants.**
***B*, Image acquired 1 min after injection shows persistence of radioactivity in both organs.**
***C*, Image collected at 18 min shows decline in pancreatic radioactivity and appearance of bladder activity.**

Patient 1

A 33-year-old man with insulin-dependent diabetes mellitus, complicated by hypertension, retinopathy, neuropathy, and renal failure, began hemodialysis in 1981. He underwent splenectomy in 1982 as part of a pretransplantation protocol elsewhere. In June 1985, he received a cadaveric pancreatic-renal transplant, with the kidney placed in the right iliac fossa and the whole pancreas in the left. The pancreatic exocrine secretions were drained by using a periampullary "button" of donor duodenum into the urinary bladder. The grafts were tolerated well except for one episode of rejection that was treated successfully with large doses of glucocorticoids. Blood glucose rapidly became normal and the patient has not required supplemental insulin. Figure 1 shows the ^{99m}Tc-DTPA transplant scan obtained approximately 1 month postoperatively. Perfusion to the grafts (Fig. 1A) was excellent, and delayed images (Fig. 1B and 1C) showed substantial clearance of pancreatic activity over 20 min. However, ^{131}I-hippuran excretion study did not show visualization of the pancreas (Fig. 2). Nine months after transplantation, serum creatinine is 2.1 mg/dl and blood glucose 84 mg/dl.

Patient 2

A 38-year-old man with insulin-dependent diabetes mellitus for 20 years complicated by retinopathy, atherosclerotic heart disease, neuropathy, and renal failure was admitted for peritoneal dialysis. Early in his hospitalization, a donor pancreas-kidney became available. It was transplanted to the right iliac fossa, and the whole pancreas and donor spleen were transplanted to the left iliac fossa. The pancreatic exocrine secretions were drained through a C-loop of donor duodenum into the recipient's small bowel. Postoperatively, the patient suffered abdominal pain, swelling, and acidosis requiring large amounts of fluids, bicarbonate, and insulin.

A pancreatic-renal flow study was performed that evening (Fig. 3A). The functional renal transplant was evident in the right iliac fossa but no perfusion appeared in the area of the pancreas-spleen. Delayed images (Fig. 3B) showed a lack of radionuclide accumulation in the left iliac fossa extending superiorly into the abdomen. Because of the scintigraphic findings and clinical deterioration, the pancreatic-splenic grafts were removed. Histologic examination revealed edema and venous thrombosis from malpositioning of the graft portal vein. Renal function remains good, with serum creatinine stable at 2.1 mg/dl.

Patient 3

A 30-year-old man with insulin-dependent diabetes mellitus for 26 years, complicated by retinopathy, neuropathy, gastroparesis, and renal failure, underwent pancreatic-renal transplantation, with the kidney placed in the right and the pancreas in the left iliac fossa.

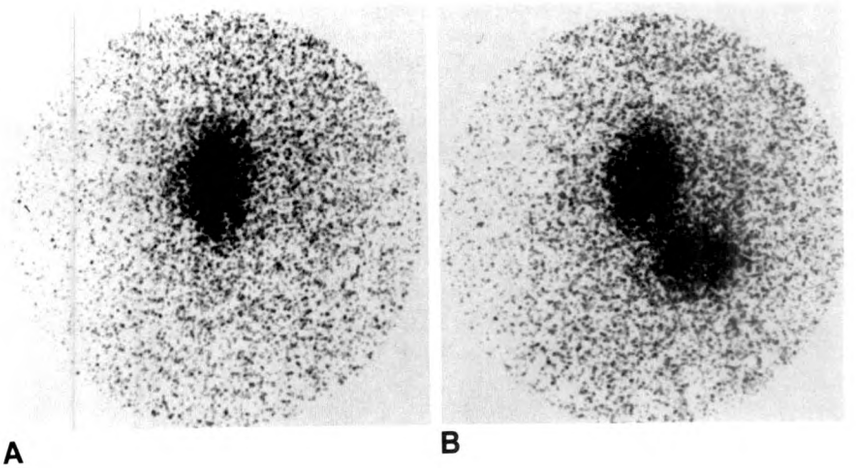


Fig. 2.—1-min images of patient 1 obtained at 3 min (*A*) and 10 min (*B*) after administration of 0.25 mCi (9.25 MBq) ^{131}I-hippuran, which is concentrated in kidney, not in pancreas, unlike ^{99m}Tc-DTPA. Ten-minute image shows bladder activity.

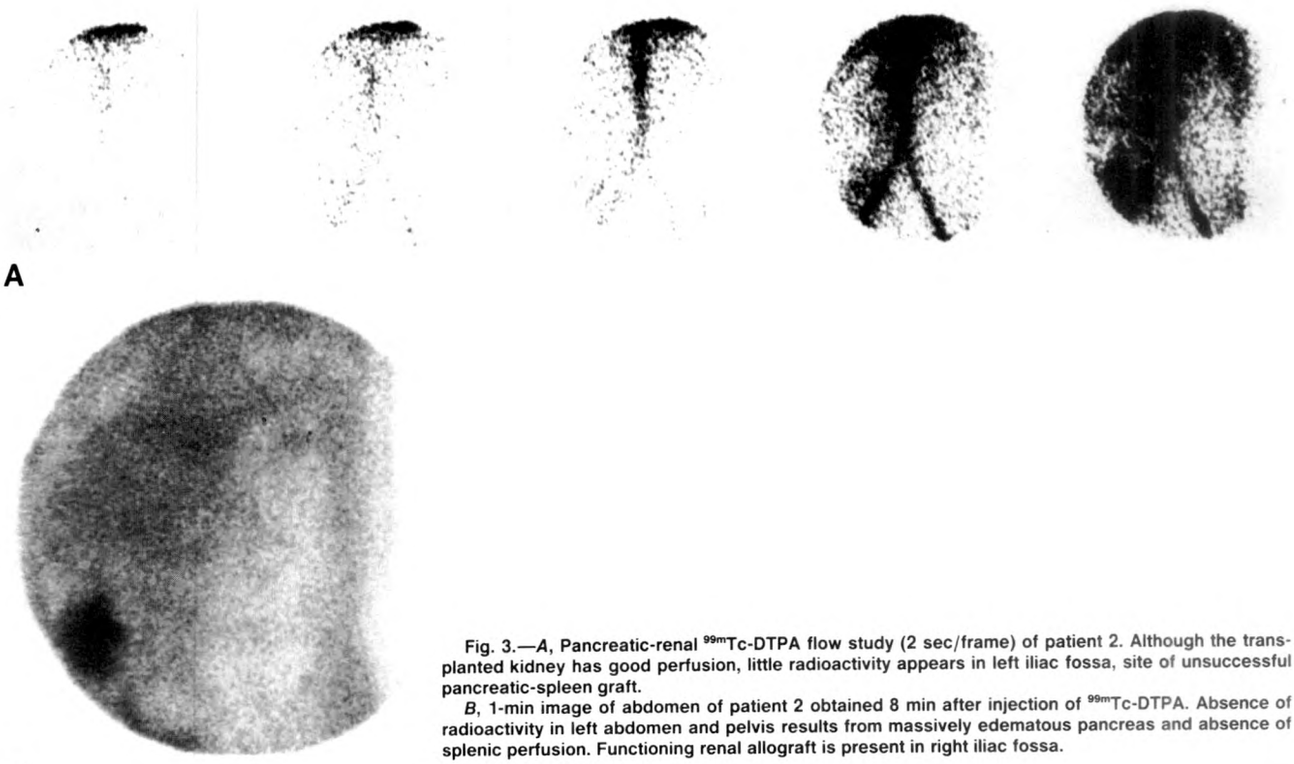


Fig. 3.—*A*, Pancreatic-renal ^{99m}Tc-DTPA flow study (2 sec/frame) of patient 2. Although the transplanted kidney has good perfusion, little radioactivity appears in left iliac fossa, site of unsuccessful pancreatic-spleen graft.

B, 1-min image of abdomen of patient 2 obtained 8 min after injection of ^{99m}Tc-DTPA. Absence of radioactivity in left abdomen and pelvis results from massively edematous pancreas and absence of splenic perfusion. Functioning renal allograft is present in right iliac fossa.

Pancreatic secretions were drained into the urinary bladder. Blood glucose fell promptly from 412 mg/dl preoperatively to 98 mg/dl within 6 hr of transplantation. Pancreatic-renal transplant scintigraphy was performed the following day and showed excellent visualization of the transplanted pancreas (Fig. 4). Serum creatinine declined to 1.3 mg/dl, and fasting blood glucose declined to 101 mg/dl. On the seventh postoperative day, the fasting blood glucose was 107 mg/dl, but the serum creatinine rose to 1.8 mg/dl. Repeat scintigraphy showed poor perfusion and visualization of the pancreas (Fig. 5). Renal biopsy showed moderate rejection. The patient was treated with high-dose steroids and antithymocyte globulin in addition to maintenance cyclosporine. Fasting blood glucose rose to 149 mg/dl and serum creatinine rose to 5.3 mg/dl on the 10th postoperative day. These values declined rapidly to 114 and 2.3, respectively, on the 14th postoperative day. The remainder of the hospital course was uncomplicated and the patient was discharged 21 days after surgery. Pancreatic-renal transplant scintigraphy was repeated on day 42, at which time the blood glucose was 101 mg/dl and the serum creatinine 1.8 mg/dl. Pancreatic perfusion and visualization (Fig. 6) were greatly improved.

Discussion

^{99m}Tc-DTPA can provide high-quality simultaneous pancreatic-renal transplant scintigraphy. Visualization of the pancreas is excellent early after administration, and most activity



Fig. 4.—Pancreatic-renal scan of patient 3, 1 min after injection of ^{99m}Tc-DTPA, 1 day after surgery. Excellent uptake by both organs (pancreas denoted by *arrow*). Renal transplant function as indicated by ^{131}I-hippuran excretion was good (not shown).

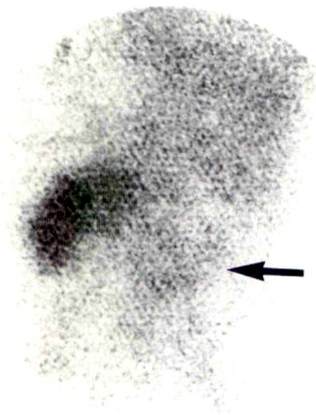


Fig. 5.—Pancreatic-renal ^{99m}Tc-DTPA study of patient 3 obtained 7 days after surgery. One-minute image shows poor accumulation of radiotracer by pancreatic transplant (*arrow*), interpreted as organ rejection. ^{131}I-hippuran excretion decreased compared with previous examination (not shown).

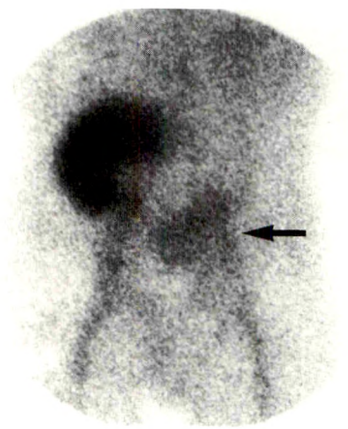


Fig. 6.—Pancreatic-renal ^{99m}Tc-DTPA study of patient 3, 6 weeks after transplantation. One-minute image shows much improvement in pancreatic visualization (*arrow*).

has cleared by 20 min after administration. The advantages of ^{99m}Tc-DTPA include its high photon-emission rate, allowing evaluation of blood flow, and low radiation dose. Its routine use in renal studies makes it readily available. The brief biologic half-life permits repeated evaluations in short intervals if necessary.

Toledo-Pereyra et al. [2] have previously suggested that pancreatic graft function is best assessed by the blood glucose level. Their studies, however, used ^{75}Se-methionine for scanning. As shown in case 3, scintigraphic abnormalities may precede functional impairment. Diminished perfusion of the pancreas was observed 2 days before elevation of the fasting blood glucose. Since pancreatic allograft rejection often accompanies renal allograft rejection [6], it seems likely that the decline in perfusion to the pancreas noted on the seventh postoperative day, along with the slight increase in blood glucose and serum creatinine, represented mild rejection. Blood glucose was relatively well preserved, presumably because of the B-cell reserve of the nondiabetic pancreas, which requires destruction of >90% of B-cells before insulin-dependent diabetes mellitus occurs [7]. Although glucocorticoids may impair carbohydrate metabolism, the decline in blood glucose after several days of glucocorticoid therapy supports a therapeutic rather than a causative role for these agents.

As cases 2 and 3 show, the course and function of the pancreatic graft may be quite unlike that of the transplanted kidney. Thus, a sensitive means of detecting early pancreatic graft dysfunction is important to allow specific interventions before irreversible damage occurs. Although visualization of the transplanted pancreas appears to represent nonspecific blood-pool activity of ^{99m}Tc-DTPA, the location of the graft in the pelvis is well suited to its scintigraphic detection, adjacent to the readily identified kidney and bladder. Additional studies will be needed to determine how commonly pancreatic scintigraphy can predict rejection before changes in the blood glucose and whether quantification of radioactivity will successfully predict rejection before clinical detection [8]. Further studies will also be necessary to determine whether this technique will allow differentiation of pancreatitis from rejection, or whether more specific probes of immunologic activity, such as radiolabeled antibodies reactive with cytotoxic lymphocytes, will be required [9]. At present, we believe ^{99m}Tc-DTPA is the scintigraphic agent of choice for combined pancreatic and renal transplants.

REFERENCES

1. Sutherland DER, Kendall DM. Pancreas transplantation—registry report and a commentary. *West J Med* **1985**;143:845–852
2. Toledo-Pereyra LH, Kristen KT, Mittal VK. Scintigraphy of pancreatic transplants. *AJR* **1982**;138:621–622
3. Jurewicz WA, Buckels JAC, Dykes JGA, et al. Indium-111 labeled platelets in monitoring pancreatic transplants in humans. *Transplant Proc* **1983**;16:720–723
4. Sollinger HW, Lieberman LM, Kamps D, Warner T, Cook K. Diagnosis of early pancreas allograft rejection with indium-111-oxine labeled platelets. *Transplant Proc* **1983**;16:785–788
5. Hahn D, Bull U, Land W. Pancreatic grafts. Nuclear perfusion imaging to detect vascular complications and rejection crises. *Horm Metab Res [Suppl]* **1983**;13:78–80
6. Severyn W, Olson L, Miller J, et al. Studies on the survival of simultaneous canine renal and segmental pancreatic allografts. *Transplantation* **1982**;33:606–612
7. Najarian JS, Sutherland DER, Baumgartner D, et al. Total or near total pancreatectomy and islet autotransplantation for treatment of chronic pancreatitis. *Ann Surg* **1980**;192:526–542
8. Perlman SB, Deierhoi MH, Wilson MA, Rowe B, Sollinger HW. Noninvasive evaluation of pancreatic allografts (abstr). *J Nucl Med* **1986**;27:909
9. Wahl RL, Parker CW. Monoclonal antibody radioimmunodetection of transplant rejection. *Transplantation* **1985**;40:451–454

Case Report

Uterine Duplication, Unilateral Imperforate Vagina, and Normal Kidneys

James Johnson[1] and Bruce J. Hillman

Developmental abnormalities of the uterus are common anomalies, usually resulting from abnormal fusion of the paired Müllerian ducts during organogenesis. The complex of complete Müllerian duplication with unilaterally imperforate vagina is rare: Only 92 cases have been reported [1–4]. In each case that had evaluation of the urinary system, renal agenesis was shown on the side of the imperforate vagina [2, 3]. This report presents the unusual complex of complete uterine duplication, unilateral imperforate vagina, and developmentally normal urinary tracts.

Case Report

A 21-year-old primigravida woman sought routine prenatal care at 13 weeks gestation. Pelvic examination revealed a large right-sided pelvic mass with displacement of the uterus to the left. A sonogram indicated the presence of a large cystic mass in the region of the right adnexa (Fig. 1). Limited excretory urography showed normal kidneys bilaterally except for mild right hydronephrosis and a gravid uterus, displaced out of the pelvis and to the left by a right lower quadrant mass (Fig. 2).

At surgery, a large cystic mass was found near the right vaginal apex, and 1100 ml of purulent, sanguinous fluid were drained. A second cervix was visible at the apex of the mass. The walls of the mass had the appearance of vaginal rugae. The diagnosis was hematocolpos and hematometra arising in a completely duplicated uterus (Fig. 3).

The patient's pregnancy continued without complications and she delivered a normal infant boy at 41 weeks gestation.

Discussion

Only 92 cases of the complex of uterus didelphys with unilateral imperforate vagina have been reported. All 67 cases in which the urinary tract was investigated showed renal agenesis on the side of the imperforate vagina [2, 3], as might be expected in view of the intimate developmental relationship shared by the genital and urinary systems.

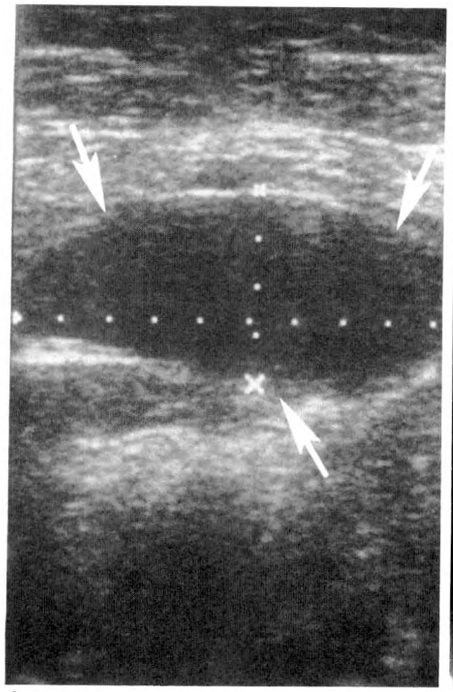
Some authors have postulated that the mesonephric ducts serve as a guide to the fusing of the paired Müllerian ducts [1, 5, 6]. Adopting this hypothesis, teratogenic insult affecting the mesonephric duct around 6 weeks after conception might well result in both abnormal Müllerian duct fusion—resulting in uterus didelphys and septate vagina—and aborted induction of the nephrogenic blastema by the mesonephric-duct-derived ureteric bud. Unilateral imperforate vagina in these cases may reflect unilateral failed invagination of the urogenital sinus that forms the distal third of the vagina, effectively resulting in a continuous separation from the vagina to the unresorbed septum derived of Müllerian origin (Fig. 3).

The classification scheme proposed by Magee et al. [7] classifies urogynecologic malformations by the embryologic stage of the abnormal development. Type I anomalies result from nondifferentiation of the nephrogenic ridge (before 4 weeks gestation) and result in unilateral or bilateral agenesis of the kidney and Müllerian structures. Type II anomalies occur during the fourth week of gestation, leading to an abnormal differentiation of the mesonephric duct and ureteral

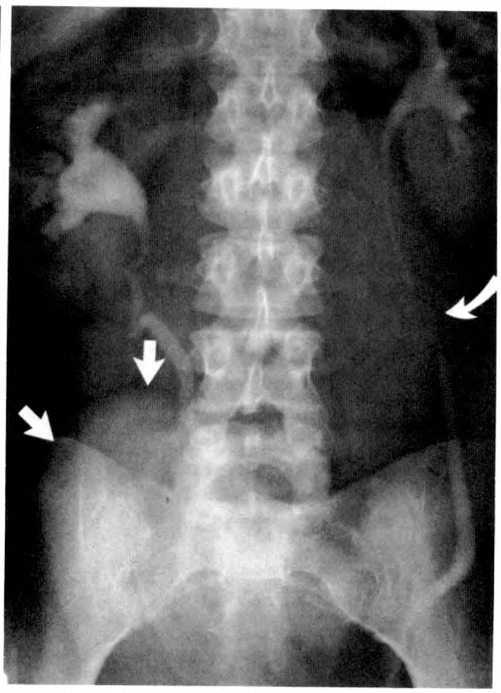
Received May 1, 1986; accepted after revision July 10, 1986.

[1] Both authors: Department of Radiology, University Medical Center, University of Arizona College of Medicine, Tucson, AZ 85734. Address reprint requests to B. J. Hillman.

AJR 147:1197–1198, December 1986 0361–803X/86/1476–1197 © American Roentgen Ray Society



1



2

Fig. 1.—Sonography shows oval cystic mass (*arrows*) 9.5 × 4.0 cm in right pelvis. Mass represents hematoculpos.

Fig. 2.—Excretory urography shows mild right pyelocalyceal blunting from extrinsic impingement by hematoculpos (*straight arrows*). Fetal parts faintly seen on the left (*curved arrow*).

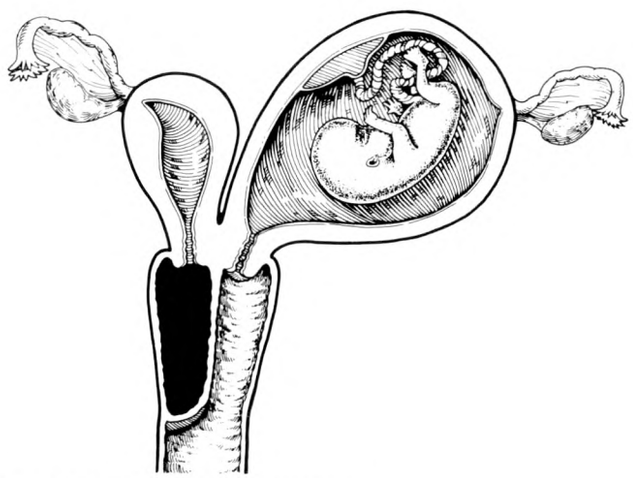


Fig. 3.—Diagram of genital tract anomalies.

bud. Patients with type II anomalies manifest incomplete fusion of the Müllerian structures and subsequent off-center contact with the urogenital sinus, leading to unilateral imperforate vagina. Type III anomalies involve nondifferentiation of the metanephric blastema from the nephrogenic cord at 4–6 weeks gestation, resulting in renal agenesis without genital maldevelopment because mesonephric and Müllerian duct development are unaffected.

This case represents a type II anomaly with respect to the genital tract but without developmental abnormality of the urinary tract. The reasons this patient showed no concomitant renal agenesis are unclear; possibly Müllerian developmental abnormalities of this type may arise de novo without antecedent mesonephric duct abnormalities.

The association between congenital urinary tract and genital anomalies is common in women. Thompson and Lynn [8] found genital anomalies in 37–44% of women with unilateral renal agenesis. Careful physical examination of the vagina and pelvis, as well as sonography of the uterus, are warranted in every young woman with unilateral renal agenesis. Conversely, the presence of genital abnormalities should precipitate imaging studies of the urinary tract.

REFERENCES

1. Beekhuis JR, Hage JC. The double uterus associated with an obstructed hemivagina and ipsilateral renal agenesis. *Eur J Obstet Gynecol Reprod Biol* **1983**;16:47–52
2. Rock JA, Jones HW. The double uterus associated with an obstructed hemivagina and ipsilateral renal agenesis. *Am J Obstet Gynecol* **1980**;138:339–342
3. Yoder IC, Pfister RC. Unilateral hematocolpos associated with agenesis of the kidney: report of two cases and review of the literature. *AJR* **1976**;127:303–308
4. Woolf RB, Allen WM. Concomitant malformations. The frequent, simultaneous occurrence of congenital malformations of the reproductive and urinary tracts. *Obstet Gynecol* **1953**;2:236–264
5. Goldstein, AI, Ackerman ES, Woodruff R, Poyas J. Vaginal and cervical communication with mesonephric duct remnants: relationship to unilateral renal agenesis. *Am J Obstet Gynecol* **1973**;116:101–105
6. Wiersma AF, Peterson LF, Justema EJ. Uterine anomalies associated with renal agenesis. *Obstet Gynecol* **1976**;47(6):654–657
7. Magee MC, Lucey DT, Fried FA. A new embryologic classification for uro-gynecologic malformations: the syndromes of mesonephric duct induced mullerian deformities. *J Urol* **1979**;121:265–267
8. Thompson DP, Lynn HB. Genital anomalies associated with solitary kidney. *Mayo Clin Proc* **1966**;41:538–548

Patterns of Liver Injury in Childhood: CT Analysis

H. Philip Stalker[1]
Robert A. Kaufman[1,2]
Richard Towbin[1,2]

Forty-eight consecutive cases of liver injury diagnosed by CT in hemodynamically stable children were analyzed retrospectively for anatomic location, type of injury, associated nonhepatic injuries, and complications. It was found that the right lobe was involved in 83% of all injuries, and that the posterior segment of the right lobe was injured most often. Right-sided injuries were usually superficial and simple, while left-sided injuries were more likely to be deep and complex. Significant complications were associated with deep, complex, perihilar injuries. Retroperitoneal blood collections were noted around the adrenal, in a distribution not previously described. Injuries of the hepatic dome were most characteristic and were often associated with injuries of the lung base, kidney, ribs, and pneumothorax.

Blunt abdominal trauma in childhood often results in solid-organ injury, commonly involving the spleen and liver. While the appearance of hepatic trauma on CT has been described in both children and adults, there has been no systematic evaluation of these injuries or of the likelihood of encountering a given type of injury. In a large series of children with the clinical and CT diagnosis of hepatic injury, we observed that hepatic injury occurs in predictable anatomic distributions, with commonly associated findings and complications.

Recently, in children with blunt abdominal trauma, nonoperative management of renal, splenic, and liver injuries [1–3] has become more commonplace. This is due in part to the accuracy and utility of CT for emergent evaluation of serious upper abdominal injury [4–6], coupled with selection of appropriate patients followed with careful serial clinical evaluations [1, 4]. Thus, recognition of common patterns of liver injury and predictors of possible complications should aid the successful management of blunt abdominal trauma in children.

Materials and Methods

Between August 1981 and September 1985, 216 consecutive hemodynamically stable children with blunt abdominal injury and clinical suspicion of solid-organ damage were evaluated by abdominal CT. Liver injury was diagnosed in 48. This subgroup was studied retrospectively to determine the distribution and type of hepatic injury, the presence and nature of associated injuries, the presence of intraabdominal bleeding, and complications of liver injury.

The mean age of all children in the study was 8 years (range, 1–16 years). Twenty-nine (60%) were boys and 19 (40%) were girls.

Injury Location

Injury location was described (1) by the hepatic segment(s) involved, (2) as deep or superficial, and (3) when appropriate, as perihilar or involving the liver dome. A *deep* lesion (Fig. 1) was defined as one that involved liver parenchyma in the region of the first two to three portal venous divisions, regardless of the volume of superficial liver tissue involved. In

Received June 2, 1986; accepted after revision July 11, 1986.

Presented at the annual meeting of the Society for Pediatric Radiology, Washington, DC, April 1986.

[1] Department of Radiology, University of Cincinnati College of Medicine, and Division of Radiology, Children's Hospital Medical Center, Elland and Bethesda Avenues, Cincinnati, OH 45229. Address reprint requests to R. A. Kaufman.

[2] Department of Pediatrics, University of Cincinnati College of Medicine, Cincinnati, OH 45229.

***AJR* 147:1199–1205, December 1986**
0361–803X/86/1476–1199
© American Roentgen Ray Society

most cases, it was a lesion closer to the hilus than to the peripheral hepatic surface. The remaining lesions were considered *superficial* (Fig. 2). *Perihilar* lesions (Fig. 3) were those that extended to the hilar hepatic surface. The *dome* (Fig. 4A) was considered the uppermost portion of the liver in contact with the diaphragm.

Imaging Appearance

Each injury was described as either simple or complex. All were of low attenuation on IV contrast-enhanced studies. *Simple* lesions (Fig. 2) were rounded (or linear) or well localized, or had short branches. *Complex* lesions (Fig. 5) were poorly localized and more disorganized, often with multiple long, branching segments.

Correlation with sonography and nuclear scintigraphy was not sought. The accuracy of CT relative to sonography and scintigraphy in the first 100 patients (including 19 liver injuries) has been reported [4]. Operative correlation was available in only two cases. Peritoneal lavage was not routinely performed.

All examinations were performed on a GE 8800 scanner, with oral–contrast-medium opacification of the upper gastrointestinal tract, IV contrast medium given as a bolus during scanning, and dynamic scanning with table incrementation. The details of the technique have been published [4].

Results

Age and Gender

No type of injury was more likely to occur in a given age group, and the ratio of boys to girls was approximately the same for each type of injury.

Distribution of Injuries

Table 1 summarizes the injuries by anatomic location. In 17 children (35%), multiple hepatic segments were injured, and four injuries (8%) involved more than one hepatic lobe. The right lobe of the liver was injured four times more often than the left and 20 times more often than the caudate lobe. Caudate injury occurred only with multilobar trauma. The posterior segment of the right lobe was the most vulnerable segment, injured in 65% of all patients.

Types of Injuries

Tables 2 and 3 analyze the injuries as simple vs complex and superficial vs deep. Although simple lesions were three times more common than complex ones in the right lobe, the two types occurred with nearly equal frequency in the left lobe. The frequencies of superficial and deep lesions in the right and left lobes were strikingly disparate, with right-sided injuries twice as likely to be superficial and left-sided injuries three times as likely to be deep.

There were 17 perihilar injuries, 35% of the total. Most deep injuries (17/22) were perihilar.

Associated Injuries

Right thoracic injuries.—Right-lung parenchymal abnormality, pleural fluid, pneumothorax, and rib fractures were frequently associated with hepatic injury. Some degree of consolidation in the right lung was detected by CT in nearly half (46%) of our patients. This was usually believed to represent contusion or atelectasis, although occasionally laceration was present. Ninety-five percent of the patients with

TABLE 1: **Anatomic Distribution of Injuries in 48 Children**

Site	No. of Patients (%)
Right lobe:	
Posterior segment	31 (65)
Dome	15 (31)
Anterior segment	10 (21)
Total[a]	40 (83)
Left lobe:	
Medial segment	7 (15)
Lateral segment	5 (10)
Total[a]	11 (23)
Caudate	2 (4)

[a] Numbers in columns add up to more than totals and totals do not add up to 48 because some children were injured in more than one site.

TABLE 2: **Characterization of Injuries in 48 Children: Simple vs Complex**

Type of Injury	No. of Patients (%)
Simple:	
Right lobe	30 (63)
Left lobe	6 (13)
Total[a]	35 (73)
Complex:	
Right lobe	10 (21)
Left lobe	5 (10)
Total[a]	13 (27)

[a] Some of the 48 children were injured in both the right and left lobes, which is the reason that numbers add up to more than totals.

TABLE 3: **Characterization of Injuries in 48 Children: Superficial vs Deep**

Type of Injury	No. of Patients (%)
Superficial:	
Right lobe	26 (54)
Left lobe	3 (6)
Total[a]	28 (58)
Deep:	
Right lobe	14 (29)
Left lobe	8 (17)
Total[a]	20 (42)

[a] Some of the 48 children were injured in both the right and left lobes, which is why numbers add up to more than totals.



Fig. 1.—Injury location: *deep*. Injury in anterior segment of right lobe involves parenchyma about proximal divisions of right portal vein. Type of injury: *simple*. Lesion is linear and moderately well defined, and only has short branches.



Fig. 2.—Injury location: *superficial*. Injury of posterior segment of right lobe involves more peripheral tissue. Type of injury: *simple* = focal.

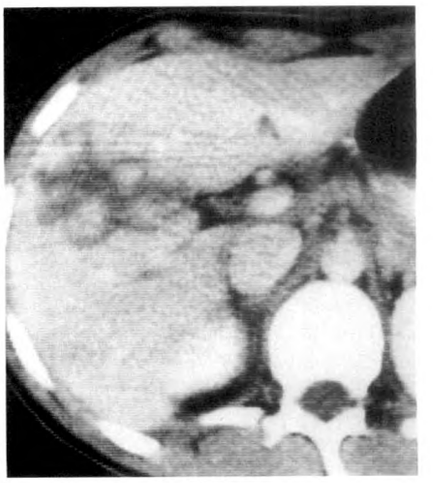
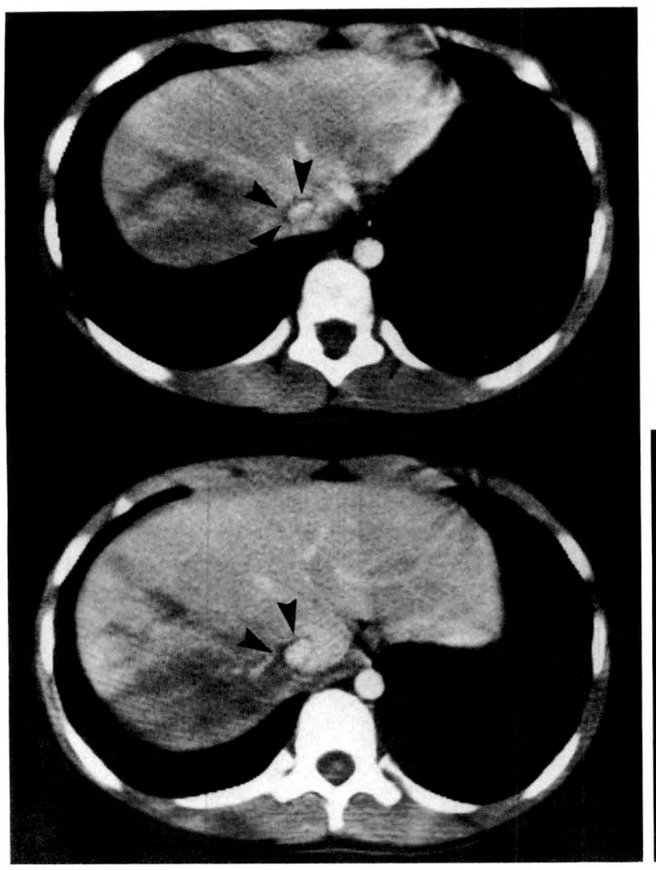
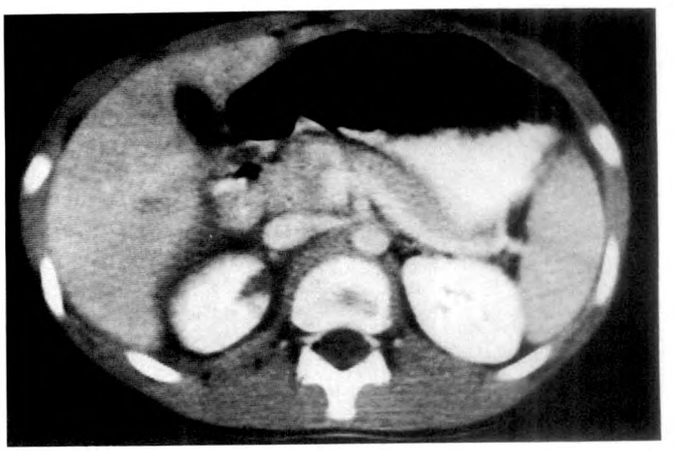


Fig. 3.—Injury location: *perihilar*, complex injury extending to hilar surface.



A



B

Fig. 4.—*A*, Injury location: *dome* injury involving most superior portion of liver in contact with hemidiaphragm. Type of injury: *complex*. Note also blood surrounding inferior vena cava producing "halo" sign (*arrowheads*).
B, Same patient. Associated contusion of ipsilateral kidney, with minor edema or hematoma in posterior pararenal space. (Reprinted from [7].)

right-lung abnormality had right-hepatic-lobe injury, and 68% had posterior-segment injury (Fig. 6). Two-thirds of all hepatic-dome injuries were associated with right-lung-base injury.

Nearly 23% (11/48) of all liver injuries were associated with right-sided pneumothoraces, and all right-sided pneumothoraces occurred in conjunction with right-hepatic-lobe injury. The largest percentage occurred with injury of the liver dome (45%). Conversely, one-third of hepatic-dome injuries were associated with right pneumothorax. Only 18% of the right pneumothoraces were associated with left-hepatic-lobe injury. Two children presented with left-sided pneumothoraces. Both had posterior-segment right-lobe trauma, and one also had a lateral-segment left-lobe injury, a right pneumothorax, and pneumomediastinum. Three other children with right-lobe injuries also had pneumomediastinum.

Rib fractures occurred in only seven patients (15%). All occurred in association with right-hepatic-lobe injury and were most likely to be seen in dome injury (33%). No right-sided rib fractures were associated with left-hepatic-lobe injury. Left-sided fractures were uncommon and were not tabulated.

Retroperitoneal injuries.—Right-renal, crus, paravertebral, and anterior-pararenal-space injuries were less common than thoracic injuries. All eight right-kidney injuries occurred in conjunction with right-hepatic-lobe trauma, and 75% of those were posterior-segment injuries. The liver injury most likely to be associated with renal trauma was the dome injury (27%) (Fig. 4).

Crus and paravertebral soft-tissue injuries were recognized as abnormal thickening and decreased attenuation, presumed to be swelling and/or hematoma. Three patients, all of whom had right-hepatic-lobe injury (two of three posterior segment), suffered injury of the right crus or paravertebral soft tissues.

Anterior-pararenal-space injuries involved the retroperitoneal duodenum and the pancreas. There were two such injuries, one pancreatic and one duodenal. Both occurred with left-hepatic-lobe injury, both involving the lateral segment, and one also involving the medial segment.



Fig. 5.—Type of injury: *complex*. Disorganized injury of right lobe is poorly localized. Injury location: *deep*. Injury extends into region of proximal portal venous divisions. Note also periadrenal space retroperitoneal blood (*arrows*).

Intraabdominal Blood Collections

Thirty-two of our 48 patients demonstrated intraabdominal blood collections. We described these collections as retroperitoneal, as intraperitoneal, or as perihepatic collections in hepatic fissures or in the subcapsular space.

Retroperitoneal collections.—Blood was seen surrounding the adrenal gland and/or the inferior vena cava (IVC) in 23 patients (48%). Periadrenal blood (Fig. 7), the more common of the two, occurred in 21 patients (44%) and either displaced or surrounded the adrenal. Collections encircling the IVC (Fig. 6B) have been described [4] and were noted in eight patients (17%). Twenty (95%) of 21 periadrenal collections and seven (88%) of eight IVC "halos" were seen in association with right-hepatic-lobe injury.

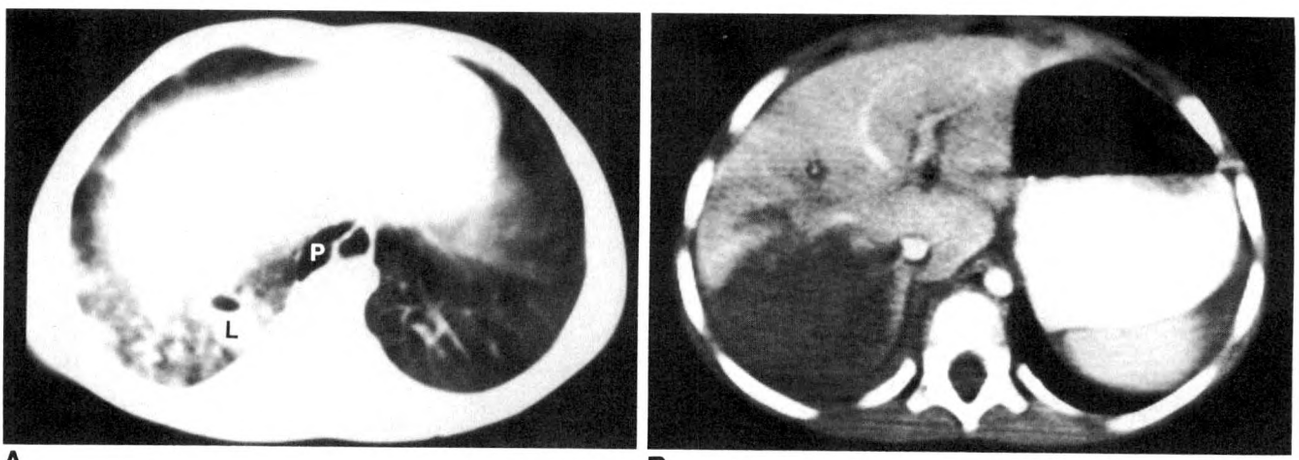


Fig. 6.—Right-lung-base injury is commonly associated with liver trauma. *A*, Contusion, laceration (L), and pneumomediastinum (P) in 4-year-old boy with, *B*, posterior-segment right-lobe injury. Note retroperitoneal blood and inferior vena cava "halo" sign.

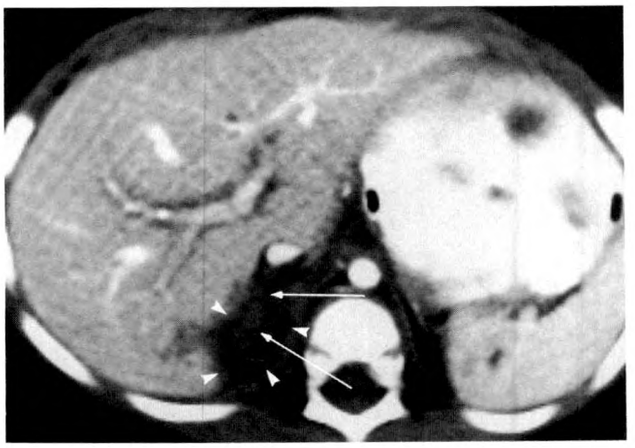


Fig. 7.—Periadrenal blood (*arrowheads*) lateral and medial to right adrenal gland (*arrows*) associated with posterior right-lobe-liver injury. Note also partial inferior vena cava "halo" and incidental splenic contusion.

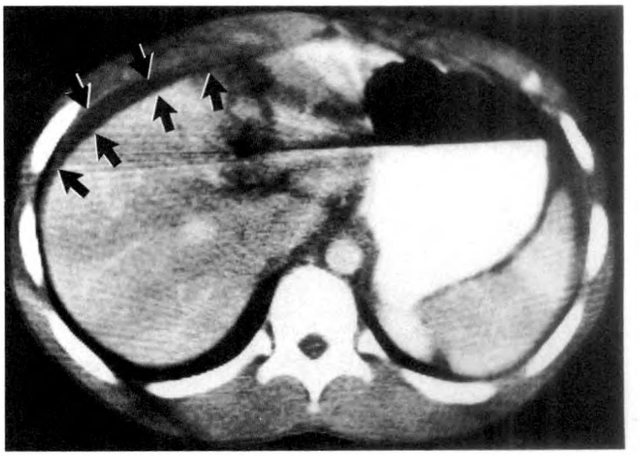
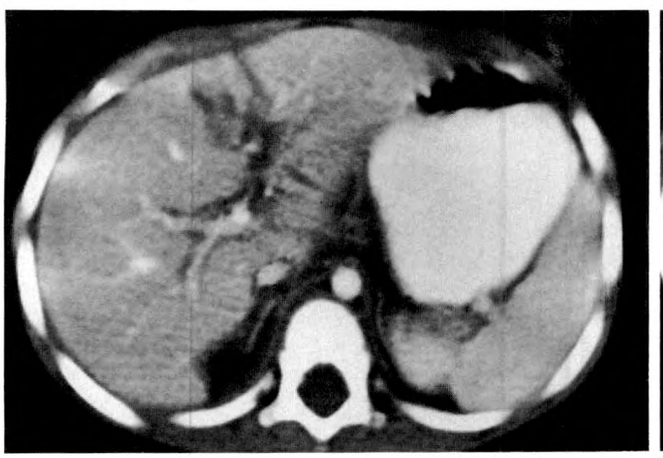
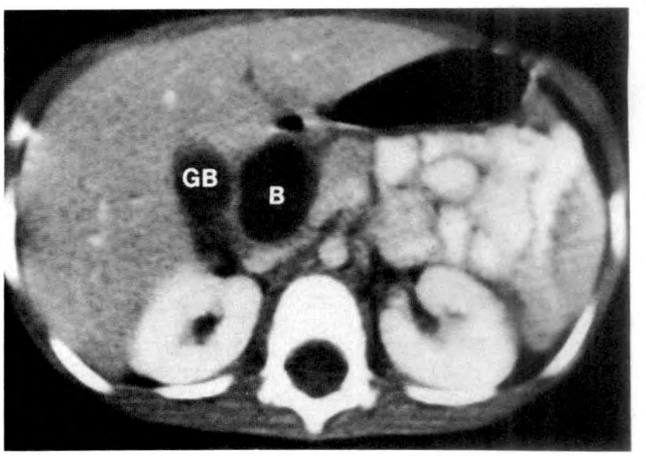


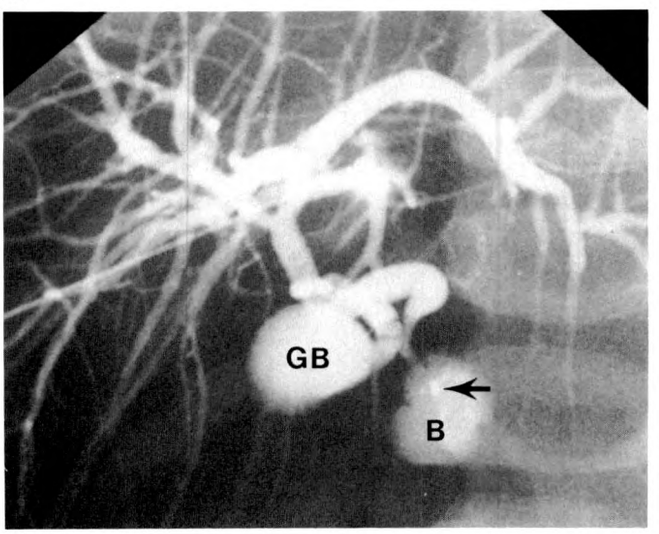
Fig. 8.—Subcapsular hematoma, associated with complex, deep medial-segment left-lobe injury, deforms anterolateral surface of liver (*arrows*). Note also free intraperitoneal blood lateral to spleen.



A



B



C

Fig. 9.—*A*, Complex medial-segment left-lobe injury in 3-year-old boy. Injury is deep and perihilar in location.

B, 3 weeks later. Biloma collection (B) caused by transection of common bile duct. GB = gallbladder.

C, Percutaneous transhepatic cholangiogram demonstrates site of injury (*arrow*).

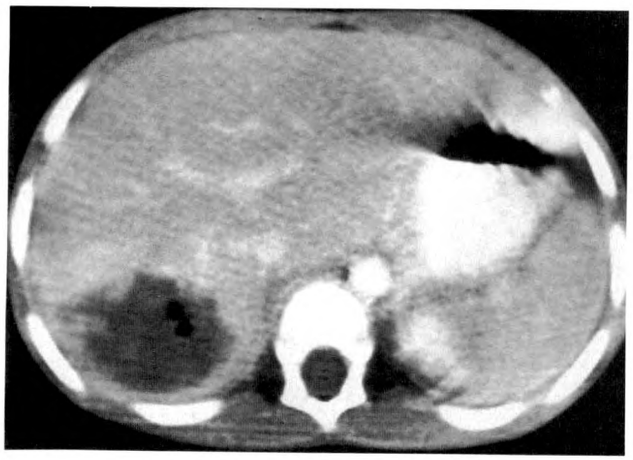


Fig. 10.—Infected hematoma? Gas formed in this superficial, simple right-lobe injury a few days after trauma. Cultures obtained by percutaneous aspiration were sterile, but patient had been treated with antibiotics.

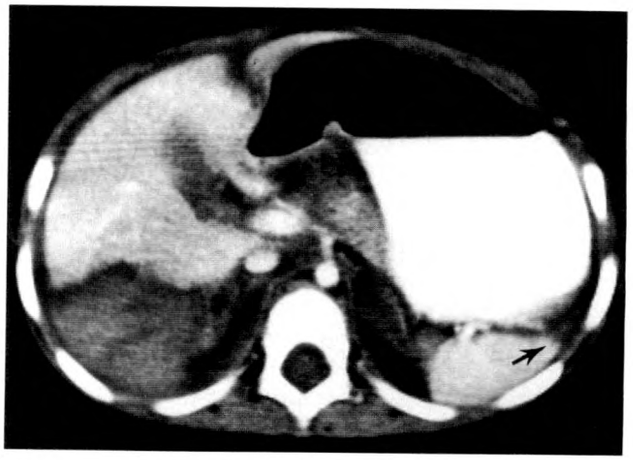


Fig. 11.—Right-lobe transection injury with devitalization, managed nonoperatively without complication. Note free intraperitoneal blood and small hematoma of spleen (*arrow*).

Intraperitoneal collections.—Sixteen patients (33%) demonstrated some intraperitoneal blood collection. Among these patients, 14 (88%) suffered injury of the right hepatic lobe and nearly all of these (13) were of the posterior segment.

Perihepatic collections.—Collections in the hepatic fissures and the subcapsular space were seen with parenchymal injury. Eight patients had subcapsular collections (Fig. 8), five demonstrated fluid distending the fissure for the ligamentum teres, and four had collections in the fissure for the gastrohepatic ligament.

Complications

Complications consisted of biloma (three patients), pancreatitis (two patients), delayed healing (one patient), and delayed hemobilia (one patient). Two patients required operative biloma drainage, and the third was done percutaneously. The pancreatitis and one biloma occurred with left-lobe injury (Fig. 9), while the other complications occurred with right-lobe injury. The bilomas, delayed healing, and delayed hemobilia all occurred with injuries that were complex and deep. The bilomas and the delayed hemobilia were also associated with perihilar injuries.

No cases were complicated by infection except possibly one. A 4-year-old boy with a superficial, simple, posterior-right-lobe injury became febrile 3 days after injury, and had leukocytosis and abdominal distension. A follow-up CT scan 7 days after injury showed gas in the liver hematoma (Fig. 10). Percutaneous aspiration demonstrated serosanguineous fluid containing leukocytes but no organisms on Gram stain or culture. The patient was placed on antibiotics; the fever defervesced and the leukocytosis resolved during the next 13 days. Unfortunately, when the patient was injured he had been taking antibiotics for an upper respiratory tract infection. Thus, we can only speculate about whether this case represents an infected hematoma or the phenomenon of gas liberated in a hepatic hematoma after injury [8].

Discussion

Categorization of hepatic injury by the anatomic segment(s) involved permits recognition of characteristic injury patterns. These are the right-lobe injury and the left-lobe injury. In our series, caudate injuries were never isolated and followed the pattern of the associated right- or left-lobe injury.

Most common is the right-hepatic-lobe injury, accounting for four of every five cases of liver trauma. The preponderance of these injuries has been noted in other series and has been attributed to the fact that the right lobe constitutes most of the volume of the liver [2]. We have extended these observations, finding that the posterior segment of the right lobe is involved in nearly two-thirds of all hepatic injuries. This may be because the posterior segment is surrounded by relatively "fixed" structures such as the ribs and spine, against which it may impact during blunt abdominal trauma. Fixation of the liver by the coronary ligaments in this region may locally enhance the effect of acceleration-deceleration injuries, as well. Right-lung-base injury, right renal injury, pneumothorax, right-sided rib fractures, and crus/paravertebral injuries were strongly associated with right-hepatic-lobe injury. The most characteristic of the right-sided injuries were those involving the hepatic "dome." Such injuries were associated with 70% of all rib fractures and approximately half of all pneumothoraces, right-lung parenchymal injuries, and right renal injuries.

Left hepatic lobe injury, while much less common, was uniquely associated with injuries of the pancreas and retroperitoneal duodenum. This occurred in only two patients, and in both there was lateral segment injury.

Previous investigators have described injury to the liver with terms such as hematoma or laceration. We chose to describe it as simple or complex, and found a marked tendency for right-lobe lesions to be simple and for left-lobe lesions to be complex. Similarly, right-lobe lesions tended to be superficial, while left-lobe lesions were more evenly divided between superficial and deep.

Consequently, the characteristic right-lobe injury was a simple, superficial lesion of the posterior segment, often with associated injury of the ipsilateral lung base and kidney, a right rib fracture, and a pneumothorax. Left-lobe injuries were more likely to be deep, complex lesions with associated anterior pararenal space injury. These two types of injuries are likely related to the vectors of force during trauma, compressing abdominal contents against the relatively fixed spine and ribs on impact. Although we did not systematically collect data on the circumstances surrounding these injuries, we informally observed that right-lobe injuries tended to occur in motor vehicle–pedestrian accidents in which children were struck from the side or from behind. Left-lobe injuries, however, tended to occur with forceful direct blows to the epigastrium.

Complications occurred infrequently in this group of predominantly nonoperatively managed patients. The most serious of these were a case of delayed healing and three bilomas. These complications arose from complex, deep injuries, and the bilomas from perihilar injuries. The complicated injuries were also more extensive than most, each covering a large volume of tissue and involving several hepatic segments. Although most complex, deep, extensive injuries were not associated with complications, it may be from this subgroup that complications are most likely to arise.

These four complications were all associated with some degree of intraperitoneal fluid collection. As has been suggested [9], this may indicate that hemoperitoneum increases the risk of complicated liver injury, although it should be stressed that children with complicated liver injury constituted a minority of the group with intraperitoneal collections.

We commonly noted retroperitoneal collections, particularly adjacent to the right adrenal. These were anteriorly or posteriorly displaced or surrounded the right adrenal. The adrenal lies within the perirenal space, above the inferior coronary ligament, behind the so-called "bare" area of the liver. In anatomic descriptions of adults, the anterior and posterior pararenal spaces extend superiorly until they merge with the diaphragm above the adrenal [10, 11]. Since these spaces are continuous at all levels, fluid introduced into a space should track through the length of that space. We observed paraadrenal collections in children that remained loculated and did not extend to the level of the kidneys. We conclude, therefore, either that the pararenal spaces do not necessarily extend to the adrenal level in children; that fluid collections may loculate within these spaces, analogous to the loculation of mediastinal air in newborn infants; or that there are other periadrenal retroperitoneal spaces in which fluid may collect.

A few injuries did not fit easily into our scheme for characterization. Of particular concern was one injury that transected and devitalized a superficial segment of the right lobe (Fig. 11). Although this child did well with nonoperative management, we suspect that the subgroup of transection injuries also may be at risk for complications.

ACKNOWLEDGMENTS

We thank Richard Isham for photography and Sherrie Henslee for manuscript preparation.

REFERENCES

1. Karp MP, Cooney DR, Berger PE, Kuhn JP, Jewett TC Jr. The role of computed tomography in the evaluation of blunt abdominal trauma in children. *J Pediatr Surg* **1981**;16:316–323
2. Moon KL Jr, Federle MP. Computed tomography in hepatic trauma. *AJR* **1983**;141:309–314
3. Meyer AA, Crass RA, Lim RC, Jeffrey RB Jr, Federle MP, Trunkey DD. Selective non-operative management of blunt liver injury using computed tomography. *Arch Surg* **1985**;120:550–554
4. Kaufman RA, Towbin R, Babcock DS, et al. Upper abdominal trauma in children: imaging evaluation. *AJR* **1984**;142:449–460
5. Berger PE, Kuhn JP. CT of blunt abdominal trauma in childhood. *AJR* **1981**;136:105–110
6. Federle MP, Goldberg HI, Kaiser JA, Moss AA, Jeffrey RB Jr, Mall JC. Evaluation of abdominal trauma by computed tomography. *Radiology* **1981**;138:637–644
7. Kaufman RA, Babcock DS. An approach to imaging the upper abdomen in the injured child. *Semin Roentgenol* **1984**;19:308–320
8. Panicek DM, Paquet DJ, Clark KG, Urrutia EJ, Brinsko RE. Hepatic parenchymal gas after blunt trauma. *Radiology* **1986**; 159:343–344
9. Federle MP, Jeffrey RB Jr. Hemoperitoneum studied by computed tomography. *Radiology* **1983**;148:187–192
10. Love L, Meyers MA, Churchill RJ, Reynes CJ, Moncada R, Gibson D. Computed tomography of extra-peritoneal spaces. *AJR* **1981**;136:781–789
11. Meyers MA. *Dynamic radiology of the abdomen. Normal and pathologic anatomy*, 2d ed. New York: Springer-Verlag, **1982**:105–186

Book Review

Digital Radiography; Selected Topics. Edited by James G. Kereiakes, Stephen R. Thomas, and Colin G. Orton. New York: Plenum, 194 pp., 1986.

The text has several contributors. The first chapter is an overview of the basic principles of digital radiography. In the remaining six chapters selected topics focusing primarily on digital subtraction angiography (DSA) are presented.

Image processors and processing techniques are discussed somewhat superficially in chapters 2 and 3. Chapter 4 is a very good review of noise analysis. The concept of noise in digital radiography is presented in a manner that can be understood by a reader without an extensive background in mathematics. However, as in the rest of the book, review of formulas and equations offers an interested reader the opportunity to study the subject in more depth. Chapter 5 describes quantitative aspects of digital X-ray imaging. The effect of physical degradation factors such as beam hardening, scatter, and veiling glare are well presented with techniques for reducing such factors. Also discussed is their effect on videodensitometer volume measurements. Applications of densitometric methods to stenosis and volume measurements are well described. However, blood flow applications of digital measurements are not included. Chapter 6 presents the applications of recursive filtering to DSA. The text concludes with a well presented chapter on energy selective radiography.

Although a multiauthor text, it can easily be read from cover to cover. It is well organized with minimal subject overlap. Tables and figures are adequate. Mathematical formulas are explicit but not too numerous. The print quality is good. The references at the end of each chapter are complete. The topics covered, especially noise analysis, provide an interesting presentation of the physical basis of digital radiography.

I recommend this book to radiologists, cardiologists, and physicists who are interested in a comprehensive exposure to the selected topics presented.

Juan F. Lois
UCLA School of Medicine
Los Angeles, CA 90024

Case Report

Prenatal Sonographic Diagnosis of Atrial Hemangioma

Richard E. Leithiser, Jr.,[1] Derek Fyfe,[2] Ellsworth Weatherby III,[3] Robert Sade,[4] A. Julian Garvin[5]

Primary cardiac tumors are rare in infants and children and most are benign rhabdomyomas, teratomas, and fibromas. They can be fatal if diagnosis and treatment are delayed [1]. In this paper, we report on a premature infant weighing 1280 g and having the prenatal sonographic diagnosis of a cardiac mass associated with a large pericardial effusion. Following further delineation after birth, a right atrial hemangioma was successfully resected.

Case Report

A 20-year-old, gravida 1 woman underwent prenatal sonography at a referring hospital to evaluate fetal age. The examination showed a single fetus consistent with the gestational age of 29 weeks. A lobulated pericardial mass arising from the right atrial wall and a large pericardial effusion were identified (Fig. 1). A small amount of ascites were also found, but there was no skin edema or polyhydramnios.

Labor began a few days later and the patient was transferred to Medical University of South Carolina. Emergency sonography suggested the presence of bilateral pleural effusions. Spontaneous vaginal delivery produced a boy of 30 weeks gestation weighing 1280 g. Apgar scores were 3 and 7 at 1 and 5 min, respectively. The neonate had cardiorespiratory distress soon after delivery, and chest tubes were placed bilaterally. The right tube drained 60 ml of serosanguineous fluid, and the left tube drained none. This fluid was initially presumed to be from the pleural space, but in retrospect was probably from the pericardial sac. The patient's hospital course was complicated by hyaline-membrane disease and increasing cardiomegaly. Postnatal cardiac sonography identified a right-sided anterior mediastinal mass contiguous with the right atrium and inseparable from the right coronary artery (Fig. 2). A large pericardial effusion had reaccumulated.

Surgery was done through a midline sternotomy with cardiopulmonary bypass and hypothermic circulatory arrest. A large intracavitary tumor mass replaced part of the right atrial wall and was contiguous with the right coronary artery and the tricuspid anulus (Fig. 3). The tumor mass was completely excised with the exception of a small portion adjacent to the right coronary artery. By preserving part of the atrial wall the defect could be closed by direct suture. After a complicated hospital course, the patient was discharged at age 2 months. The child is now 6 months old and well except for intermittent second-degree atrioventricular block.

On pathologic examination, the excised tumor was found to be lobulated with central areas of necrosis and dystrophic calcification. Microscopically, the tumor was composed of small, endothelium-lined capillary vessels that infiltrated the adjacent myocardial fibers. The final diagnosis was a hemangioma of the right atrial wall.

Discussion

Cardiac tumors are rare. The occurrence of cardiac tumors based on autopsy data that includes all ages is 1:5000 to 1:10,000. Such tumors are often metastatic and malignant in adults, whereas in children they are usually primary and benign [1, 2]. Until recently, the imaging of these tumors was limited to chest radiography and cineangiography, and diagnosis was often not made until autopsy. With the advent of two-dimensional echocardiography, however, cardiac tumors

Received May 5, 1986; accepted after revision July 24, 1986.
[1] Department of Radiology, Medical University of South Carolina, 171 Ashley Ave., Charleston, SC 29425. Address reprint requests to R. E. Leithiser.
[2] Department of Pediatric Cardiology, Medical University of South Carolina, 171 Ashley Ave., Charleston, SC 29425.
[3] Department of Radiology, Naval Hospital, Charleston, SC 29408.
[4] Department of Thoracic Surgery, Medical University of South Carolina, 171 Ashley Ave., Charleston, SC 29425.
[5] Department of Pathology, Medical University of South Carolina, 171 Ashley Ave., Charleston, SC 29425.

AJR 147:1207–1208, December 1986 0361–803X/86/1476–1207 © American Roentgen Ray Society

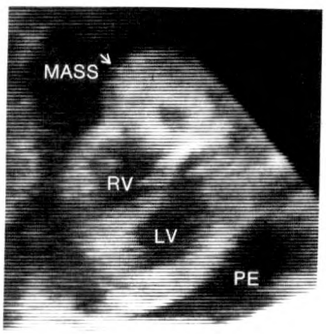


Fig. 1.—Prenatal, apical, four-chamber view shows tumor mass (*arrow*) occupying part of right atrium. Note anechoic area representing large pericardial effusions surrounding entire heart. (RV = right ventricle, LV = left ventricle, PE = pericardial effusion)

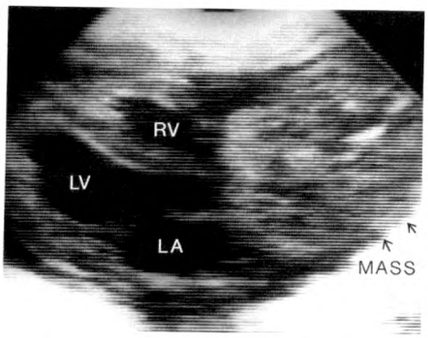


Fig. 2.—Postnatal echocardiogram performed in an angled, long-axis view shows large tumor mass (*arrows*) above right ventricle. Left atrium and left ventricle are identified. Note mixed echogenicity of tumor mass. (RV = right ventricle, LV = left ventricle, LA = left atrium)

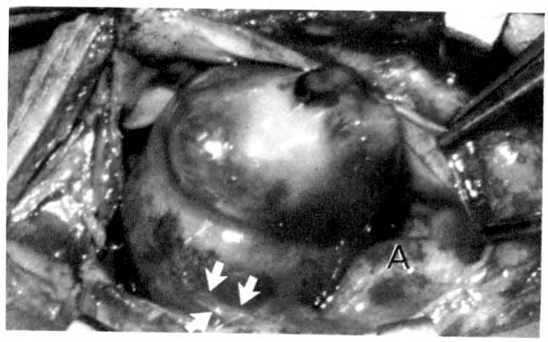


Fig. 3.—Operative photograph of large tumor mass arising from right atrial free wall, filling right side of the pericardial cavity. Forceps grasp free edge of incised pericardium. *Arrows*, atrial wall stretched over intracavitary portion of tumor. (A = ascending aorta)

are being recognized with increasing frequency and often prenatally [3–6). The common, primary cardiac tumors have specific fetal and neonatal echocardiographic features.

Hemangiomas are unusual; approximately 10 cases have been reported [1, 2, 3, 7]. Most are diagnosed in the neonatal period and they have a consistent echocardiographic appearance [3, 7]. The tumors are of mixed echogenicity because they consist of benign proliferations of endothelial cells in various stages of organization and thrombosis. Hemangiomas may arise from any site in the pericardium, myocardium, or ventricular cavity [2]. Most are seen as pericardial masses at the base of the heart adjacent to the right atrium, however, and frequently have an intracavitary component [3, 7]. The cardiac silhouette is often displaced into the left hemithorax by the mass, and a large pericardial effusion is usually present.

Rhabdomyomas, much more common than hemangiomas, make up about 60% of primary cardiac tumors in children [1, 6]. They originate in the atrial or ventricular myocardium and approximately half of them grow into a ventricular cavity. Echocardiographically, rhabdomyomas are uniform in echogenicity and can be recognized as nodular masses, often multiple, arising from the myocardial wall [5, 6]. Approximately half of all patients with cardiac rhabdomyomas have tuberous sclerosis. The cardiac lesions may remain asymptomatic and be discovered only incidentally during the evaluation of the patient for other stigmata of tuberous sclerosis [5, 6].

Teratomas constitute approximately 25% of pediatric cardiac tumors and have several typical features. The tumor masses are composed of all three germ layers and therefore can contain calcium, bone, or fat [2]. Echocardiographically, they are of mixed echogenicity related to their composition and frequently have posterior shadowing from bone or calcium within the mass, or focal increased echogenicity due to fat in the mass. Although intrapericardial, most are extracardiac and are attached to the root of the aorta or pulmonary artery by fine adventitial vessels. Almost all are associated with a large pericardial effusion [8].

Fibromas constitute approximately 12% of pediatric cardiac tumors [6]. The tumors are usually solitary, intramural masses, arising from the ventricular myocardium or septum. They may grow to be quite large and undergo central necrosis and calcification [2]. Echocardiographically, a fibroma is almost always a solitary mass in the ventricular myocardium or septum.

In this report, an accurate prenatal diagnosis of a cardiac tumor led to successful surgical resection in a very small premature infant. Fetal echocardiography is important in any patient with fetal hydrops because cardiac tumors may cause pericardial effusions, ascites, and edema. Careful attention to the location and the sonographic characteristics of cardiac masses is essential in attempting to distinguish among the varieties of cardiac tumors.

REFERENCES

1. Van der Hauwaert LG. Cardiac tumours in infancy and childhood. *Br Heart J* **1971**;33:125–132
2. McAllister HA Jr. Primary tumors of the heart and pericardium. *Pathol Ann* **1979**;14:325–355
3. Riggs T, Sholl JS, Ilbawi M, Gardner T. In utero diagnosis of pericardial tumor with successful surgical repair. *Pediatr Cardiol* **1984**;5:23–26
4. DeGeeter B, Kretz JG, Nisand I, Eisenmann B, Kieny M-Th, Kieny R. Intrapericardial teratoma in a newborn infant: use of fetal echocardiography. *Ann Thorac Surg* **1983**;35(6):664–666
5. Corno A, de Simone G, Catena G, Marcelletti C. Cardial rhabdomyoma: surgical treatment in the neonate. *J Thorac Cardiovasc Surg* **1984**;87:725–731
6. Dennis MA, Appareti K, Manco-Johnson ML, Clewell W, Wiggins J. The echocardiographic diagnosis of multiple fetal cardiac tumors. *J Ultrasound Med* **1985**;4:327–329
7. Ilbawi M, DeLeon S, Riggs T. Primary vascular tumors of the heart in infancy: report of a case with successful surgical management. *Chest* **1982**;81(4):511–512
8. Arciniegas E, Hakimi M, Farooki ZQ, Green EW. Intrapericardial teratoma in infancy. *J Thorac Cardiovasc Surg* **1980**;79:306–311

Subcortical Arteriosclerotic Encephalopathy: CT Spectrum and Pathologic Correlation

Preston R. Lotz[1, 2]
William E. Ballinger, Jr.[3]
Ronald G. Quisling[1]

Because of recent papers suggesting that subcortical arteriosclerotic encephalopathy (SAE) (Binswanger's disease) is more common than historically assumed, this investigation was initiated to assess the frequency of SAE, to gauge the reliability of CT in making this diagnosis, and to assess the strength of the correlation between SAE and arterial hypertension. Of 202 autopsied patients in a 17-month period, 82 had undergone antemortem CT. Of these, 20 had CT findings thought to represent varying degrees of the disease spectrum of SAE. Microscopy confirmed this diagnosis in 18 cases. The pattern of diminished attenuation in the white matter was periventricular in 16 patients (marked asymmetry in one) and limited to an isolated focus somewhat removed from the ependyma in two. Among the 16 with periventricular disease, the extent of the process by CT appeared mild in nine, moderate in five, and severe only in two. There were two false positive CT diagnoses of SAE. Among a control group of 10 patients with normal white matter by CT, seven had some microscopic evidence of SAE, although it was generally less severe than in those with positive CT scans. Subcortical arteriosclerotic encephalopathy is common and can be identified in its various forms by CT with a high degree of reliability.

Subcortical arteriosclerotic encephalopathy (SAE), or Binswanger's disease, is a sometimes dementing illness for which chronic arterial hypertension has been implicated as a major pathogenetic factor [1–6]. It had been considered to be rare, but recent reports suggest that it is fairly common [7–11]. Illustrations of CT images in this disorder have been restricted almost exclusively to severe cases [7, 9, 12–15]. The CT appearance of the advanced cases, specifically excessive periventricular radiolucency, is well known, but lesser degrees of involvement are less well appreciated.

The histologic abnormalities in SAE have been described in numerous small series and case reports, and include demyelination, axonal loss, and fibrous or "hyalinoid" thickening of the walls of small arteries in the deep cerebral white matter [2, 4, 5, 7, 12, 16–20]. The discovery of these typical findings in the postmortem examination of the brain of a patient with relatively modest periventricular lucency by CT in October 1982, prompted a prospective evaluation of autopsied patients whose CT scans suggested the presence of such changes to determine their frequency, the reliability of CT in detecting their presence, and the frequency of chronic arterial hypertension in affected patients.

Materials and Methods

During the 17 months from January 1983 through May 1984, the formalin-fixed brains of all autopsied patients whose antemortem cerebral CT studies showed abnormal radiolucent areas in the deep white matter thought likely to represent SAE were subjected to microscopic examination of suspicious areas. Those brains severely damaged by infarction or affected by cerebral edema of any cause between the antermortem scan and the patient's death were excluded.

This article appears in the September/October 1986 issue of *AJNR* and the December 1986 issue of *AJR*.

Received October 9, 1985; accepted after revision April 4, 1986.

Presented at the annual meeting of the American Society of Neuroradiology, Boston, June 1984.

[1] Department of Radiology, Veterans Administration Medical Center and Shands Teaching Hospital, University of Florida College of Medicine, Gainesville, FL 32602.

[2] Present address: Watson Clinic, P.O. Box 1429, Lakeland, FL 33802. Address reprint requests to P. R. Lotz.

[3] Department of Pathology, Veterans Administration Medical Center and Shands Teaching Hospital, University of Florida College of Medicine, Gainesville, FL 32602.

***AJR* 147:1209–1214, December 1986**
0361–803X/86/1476–1209
© American Roentgen Ray Society

The degree of white matter alteration by CT was graded subjectively by a neuroradiologist as mild, moderate, or severe, based on the extent of involvement rather than on the degree of radiolucency. The arteries of and near the circle of Willis were examined for atherosclerosis. Each brain was sectioned in a plane approximating that of the antemortem CT study. Specimens were taken from regions in the deep white matter identified as having abnormally low attenuation by CT. This included the white matter anterolateral to the frontal horns and posterolateral and superior to the trigones of the lateral ventricles in almost every case. Some overlying subcortical white matter, cerebral cortex, and ependyma were included in each specimen. Four sections were obtained from each specimen, one for each of four stains: hematoxylin and eosin (H and E), Masson trichrome (for collagen), Luxol Fast Blue with H and E (for myelin), and modified Seiver-Munger silver stain (for axons). The sections were examined for demyelination, axonal loss, and arterial/arteriolar wall thickening by a neuropathologist. The changes were graded as normal (−), mild (1+), moderate (2+), or severe (3+), based largely on the intensity of staining.

Ten brains from patients over 50 years old whose antemortem CT scans indicated no abnormal periventricular lucency to suggest the presence of SAE were subjected to the same sectioning and gross and microscopic examination in order to reveal the frequency of the disease changes of SAE in the presence of a normal CT scan. Bilateral sections from the same location already described adjacent to the frontal horns and trigones were obtained from each brain.

For both the abnormal and normal groups, the cardiac weight, thickness of the left ventricular wall, degree of coronary atherosclerosis, and evidence of myocardial infarction were recorded from the general autopsy data. Microscopic sections of the renal parenchyma in both patient groups were reviewed, and fibrous thickening of intrarenal small arteries and arterioles was graded on the same scale as were the cerebral vessels.

The charts of all patients were reviewed for evidence of chronic arterial hypertension, dementia, and factors that might have contributed to dementia or damage to the cerebral white matter. Any of the following could confirm the presence of chronic arterial hypertension: at least 3 recorded systolic pressures in excess of 150 mm Hg; at least 3 recorded diastolic pressures in excess of 90 mm Hg; left ventricular hypertrophy by postmortem examination (either simply recorded as such or recorded as a left ventricular mural thickness of at least 14 mm) in the absence of left ventricular outflow obstruction; or at least moderate arteriolarnephrosclerosis of the fibrous type typically caused by hypertension.

Results

The brains of 202 patients came to postmortem examination during the study period. Antemortem CT scans were available in 82 patients, 20 of which were deemed to have at least one area of diminished attenuation in the cerebral white matter suspicious for SAE. The CT scans were obtained within 1 month of death in 10 cases, between 1 and 6 months prior to death in four, between 6 and 12 months before death in four others, and from 12 to 26 months before death in two. The autopsy findings confirmed a diagnosis of SAE in 18 of the 20 suspected cases. These brains consistently showed the triad of demyelination, loss of axons, and fibrous thickening of the walls of small arteries in affected areas of the white matter, with the exception of one in which there was no demonstrable axonal loss in the specimens taken. The ages of these 18 individuals ranged from 56 to 93 years, with a mean age of 75 years. One case proved to have an occult focus of metastatic carcinoma (the lucency on CT presumably being edema). The last had demyelination and axonal loss with normal small arteries, but also had an aqueductal subependymoma that had caused an obstructive hydrocephalus.

Of the 18 patients with SAE, the demyelination was wholly periventricular in 15, limited to focus separated from the ependyma by apparently normal white matter in two, and a combination of these two patterns in one (Figs. 1–5). One of the 15 patients with a purely periventricular pattern had a striking asymmetry from side to side (Fig. 4).

The brains with normal white matter by CT exhibited generally far fewer changes, but seven did show some evidence of SAE. The ages of the CT-normal patients ranged from 54 to 89 years, with a mean age of 74 years. The microscopic findings in both groups (abnormal and normal white matter by CT) are given in Table 1. Loss of axons was less dramatic than the demyelination in both groups.

Arteriolar nephrosclerosis generally correlated with the degree of arteriolar sclerosis in the white matter (Table 2). The frequencies of systemic arterial hypertension, dementia, cerebral atherosclerosis, infarction in the brain, and myocardial infarcts in the two groups of patients is presented in Table 3. Among the abnormal group with periventricular demyelination, nine had involvement judged to be mild, five moderate, and two severe. There was no apparent correlation between the occurrence of dementia and the extent of the CT changes.

Discussion

The discovery of 18 cases of SAE among 82 autopsied patients with antemortem CT studies attests to its recently reported prevalence in the population over 50 years of age [7–11]. That more mild examples than moderate and severe cases combined should be encountered is in keeping with our day-to-day observations in cerebral imaging in a population of veterans.

The accuracy of CT in distinguishing SAE from other causes of low attentuation in the white matter was 90% (18 of 20) in this limited series. The false positive diagnosis of focal SAE in a patient with a nonenhancing metastasis is an error that we believe can be avoided in most cases by recognizing the typically more subcortical than subependymal location of the lucency and by subsequently using a higher dose of contrast agent and delayed CT imaging. Our other false positive case, a patient with a chronic aqueduct obstruction previously shunted, represents a rather rare circumstance, although we know of no way to distinguish the pattern of periventricular lucency in this case from that due to arteriolar sclerosis. Because of these factors and the experience gained during the 17-month period of study, we feel that our false positive rate in the diagnosis of SAE by CT is currently below 5%.

Based on the finding of at least minimal evidence of SAE in seven of our 10 cases with normal CT scans, it seems apparent that there exists a significant false negative diagnosis rate in cases at the mild end of the disease spectrum. It is therefore possible that cases appearing to be early or mild by CT are not so in terms of their clinical and pathologic evolution. MR holds promise for greater sensitivity than CT in detecting early cases of SAE [8, 11, 21].

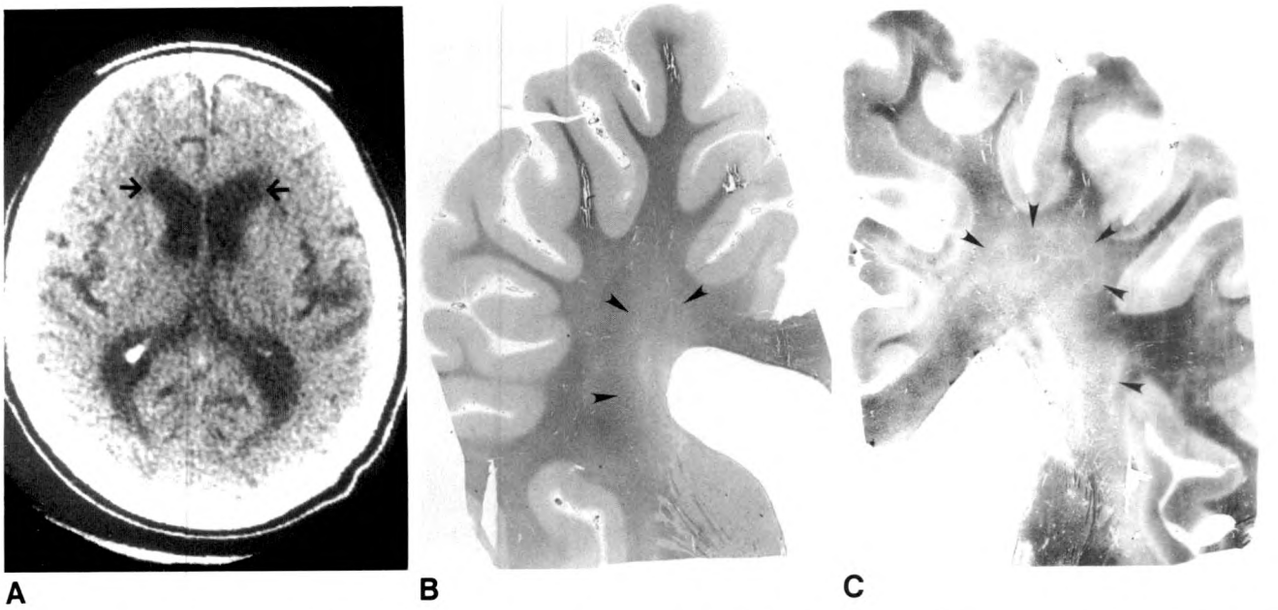


Fig. 1.—Mild periventricular form of subcortical arteriosclerotic encephalopathy. **A**, CT image showing abnormal lucencies (*arrows*) in white matter adjacent to frontal horns, small but quite apparent on left, barely detectable on right. **B** and **C**, Right and left quadrant sections, respectively, of brain (Luxol Fast Blue stain) showing areas of demyelination (*arrowheads*) somewhat larger than depicted by CT. Transitions to normal white matter are ill-defined.

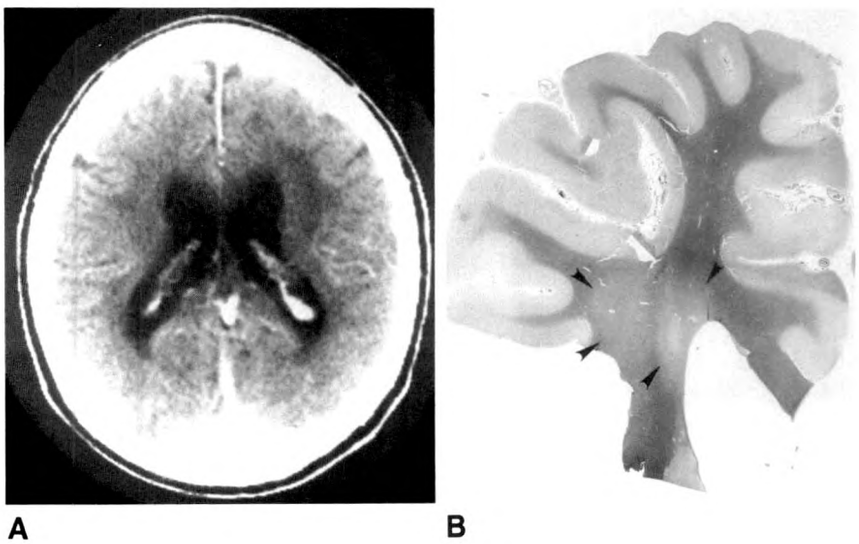


Fig. 2.—Moderate periventricular form of subcortical arteriosclerotic encephalopathy. **A**, CT section showing more extensive disease than in Figure 1A. **B**, Quadrant right frontal section (Luxol Fast Blue stain) showing greater degree and extent of demyelination (*arrowheads*) than in Figure 1B.

Discrete patches of low attenuation somewhat removed from the ventricular surface but not subcortical were identified in three of the 18 confirmed cases (Fig. 5). It seems entirely possible that such findings could be misconstrued as plaques of multiple sclerosis. This mistake appears even more likely with MR, given its greater likelihood of detecting such lesions on T2-weighted images. The radiologic distinction is likely to be a difficult one in many cases.

The periventricular lucency of SAE should not be mistaken for transependymal resorption of cerebrospinal fluid (TRCSF). We believe that the CT patterns of these two entities are sufficiently distinct to permit their separation by CT in nearly every instance. TRCSF produces zones of lucency that are centered somewhat anterior to the angles of the frontal horns and have a fairly sharp transition to the normal density of white matter along their outer margin (Fig. 6). The lucencies frequently extend through the full thickness of the corpus callosum. The frontal lucencies of SAE, on the other hand, usually are centered directly at the angles of the frontal horn, seldom extend into the genu of the corpus callosum (and do so less completely and with a lesser degree of radiolucency when they do), and have less sharply defined margins with adjacent, normal white matter (Figs. 1, 2, 3). Sparing of the medial subependymal regions along the trigones and occipital

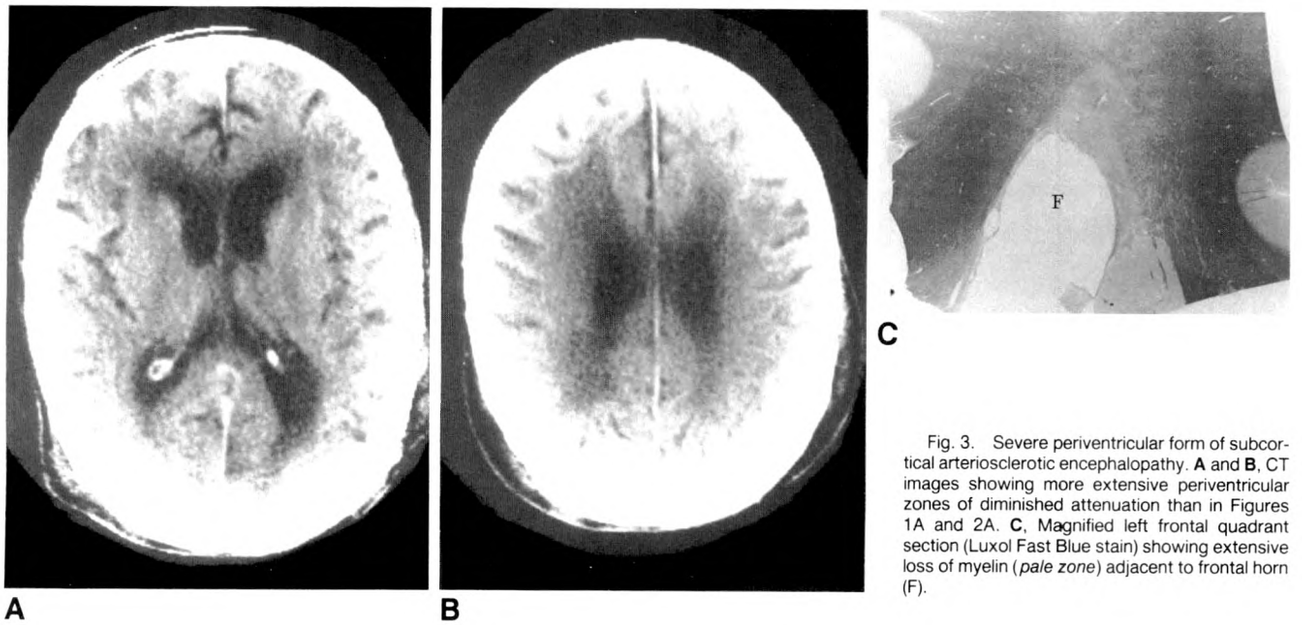


Fig. 3. Severe periventricular form of subcortical arteriosclerotic encephalopathy. **A** and **B**, CT images showing more extensive periventricular zones of diminished attenuation than in Figures 1A and 2A. **C**, Magnified left frontal quadrant section (Luxol Fast Blue stain) showing extensive loss of myelin (*pale zone*) adjacent to frontal horn (F).

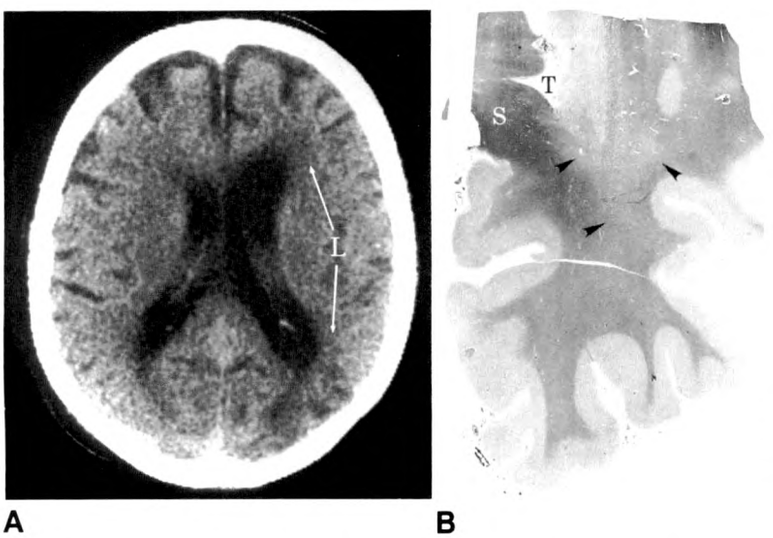


Fig. 4. Asymmetric periventricular form of subcortical arteriosclerotic encephalopathy. **A**, CT section showing moderate area of abnormal lucency (L) adjacent to left frontal horn and trigone with little or no involvement on right. **B**, Quadrant section (Luxol Fast Blue stain) including artefactually small left trigone (T) and splenium of corpus callosum (S) showing moderately extensive demyelination (*arrowheads*).

horns is a fairly consistent but not invariable finding with SAE, whereas TRCSF frequently produces sharply demarcated lucencies medial to the trigones and occipital horns. Given the prevalence of SAE, its coexistence in patients with various forms of hydrocephalus is to be expected. Decisions regarding the management of patients with hydrocephalus should not be based on the mistaken impression that transependymal migration of CSF is present when the zones of low attenuation seen at CT are really due to SAE. If there is doubt about the origin of periventricular lucencies, treatment decisions must be based wholly on clinical, laboratory, and other CT criteria.

In view of the loss of myelin and axons present with SAE, it seems reasonable to expect some degree of ventricular enlargement in affected individuals. Sporadic reports have indicated that this occurs [7, 13, 14, 17, 20, 22]. While the small number of patients in this series precluded a significant evaluation of this issue, we believe that many of these patients have enlarged ventricles, and this may explain some cases of so-called deep cerebral atrophy.

SAE, in its advanced form, can produce dementia and is called Binswanger's disease [1, 5–7, 9, 13, 14, 17, 22]. It has been considered uncommon [4, 23]. Recent papers have mentioned its clinically milder forms [7, 8, 11, 20, 21] and asymptomatic cases [11, 21]. Clinical evidence of dementia was noted in seven of our 16 cases with more than a solitary patch of SAE detected by CT (Table 3). Two of these seven had a postmortem tissue diagnosis of Alzheimer's disease, but three patients with mild SAE and two with moderate SAE had no other known explanations for their dementia. Interestingly, the two individuals with the most advanced SAE in this series had no record of an altered mental status. The presence of basal ganglionic and/or thalamic lacunae with SAE in nine of our 18 cases, and of small white-matter infarcts in seven, suggests a relationship between SAE and the lacunar

Fig. 5.—Patchy form of subcortical arteriosclerotic encephalopathy. CT image with patch of mild radiolucency (L) in left corona radiata and lacune (l) in subependymal region on right.



5

Fig. 6.—Transependymal resorption of subcortical arteriosclerotic encephalopathy. CT section in patient with hydrocephalus secondary to meningeal carcinomatosis showing lucent zones (*asterisks*) centered anterior to frontal horns with confluence in corpus callosum (*white arrow*) and extension of lucent zones medial to trigones and occipital horns (*black arrows*).



6

TABLE 1: **Microscopic Findings in Abnormal and Normal Groups**

	No. Patients by Pathologic Grade			
	–	1+	2+	3+
CT abnormal (n = 18)				
Arteriolarsclerosis	0	2	8	8
Demyelination	0	2	9	7
Loss of axons	1	9	8	0
CT normal (n = 10)				
Arteriolarsclerosis	3	4	2	1
Demyelination	3	7	0	0
Loss of axons	8	2	0	0

TABLE 2: **Correlation Between Cerebral and Renal Arteriolarsclerosis**

	No. of Patients			
	Grade of Arteriolarsclerosis in Cerebral White Matter			
Grade of arteriolar nephrosclerosis	0	1+	2+	3+
Abnormal group*				
0				
1+		1	3	
2+		1	1	5
3+			3	2
Normal group**				
0	1			
1+	1	3	1	1***
2+			1	
3+		1		

* Insufficient data on two patients; therefore, n = 16.
** Insufficient data on one patient; therefore, n = 9.
*** Very focal, limited extent, but severe.

TABLE 3: **Associated Findings in Abnormal and Normal Groups**

	CT Diagnosis	
	Abnormal (n = 18)	Normal (n = 10)
Hypertension	17	9
Dementia	7*	2*
Moderate or severe cerebral atherosclerosis**	9	3
Brain infarcts:***	16	1
Lacunar (basal ganglia and thalami)	9	1
White matter only	7	0
Cerebral cortical	10	0
Myocardial damage from coronary atherosclerosis	13	2

* Two had Alzheimer's disease.
** Based on autopsy findings.
*** Based on autopsy and CT findings.

state [14, 17, 22]. It is entirely possible that dementia heretofore attributed to the lacunar state really has been due to coexisting, undiagnosed SAE. Similarly, the occurrence of cortical infarcts in 10 of our patients strongly suggests a relationship between these lesions and SAE, thereby further stimulating the speculation that in some cases of multiinfarct dementia, the dementia is actually partly or wholly due to the coexisting SAE.

The relationship between systemic arterial hypertension and SAE is not clear. Hypertension might be the sole etiologic factor [3], a necessary but not the only causative agent [1, 2, 20, 22], or a contributing but nonrequisite element [14]. SAE has been said to occur in the absence of hypertension [7, 13, 24, 25]. Most patients in both of our groups were hypertensive (Table 3). Interestingly, the one patient in the normal CT group without any microscopic evidence of SAE was the only normotensive individual in that group. A large number of normal blood pressure recordings were available on this patient. It is unclear from these data whether SAE can occur in the absence of hypertension. That the arterial changes of SAE are due to exposure of vessel walls to intraarterial pressure over

time seems quite possible. That is, the greater the pressure and/or the life span of the individual, the more likely are these changes to be present. It follows that wholly normotensive persons would develop these changes if they lived long enough. This is of course speculative. By CT, several of our hypertensive patients with SAE only had normal blood pressure recordings in the months (or, at most, few years) preceding their deaths. It seems plausible that a reduced cardiac output may have contributed to the preterminal normotension. This phenomenon might explain the absence of hypertension in some reported cases of SAE. That other factors, including genetic ones, might contribute to the development of SAE is open to speculation, although Rothemunde and Frische [3] studied many factors and found a positive correlation with arterial hyalinosis only for long-standing arterial hypertension.

The ultimate pathogenetic factor very well may be ischemia. Although an ischemic origin is difficult to prove, it seems quite tenable in view of the severity of vascular changes in the territory of deep perforating arteries and the sparing of subcortical U-fibers, which are within the territory of supply of cortical branches [26].

It is highly uncertain whether the eight cases reported by Binswanger in 1894 [27] were all examples of the disease that has come to bear his name. Binswanger described a predominance of findings in the temporooccipital white matter, a distribution likewise mentioned by Farnell and Globus in 1932 [16]. These reports used autopsy data only. More recent literature, reporting the use of CT or MR to identify areas of involvement, illustrates the pattern seen in our patients, specifically that of predominant involvement near the frontal horns and superolateral to the trigones [7, 8, 14, 15].

SAE is being recognized increasingly by modern imaging methods. It is common, and can be diagnosed reliably, but much remains to be learned about its origin, especially regarding the role of arterial hypertension and about its importance as a cause of dementia and perhaps other disorders.

REFERENCES

1. Hughes W, Dodgson MCH, MacLennan DC. Chronic cerebral hypertensive disease. *Lancet* **1954**;2:770–774
2. Okeda R. Morphometrische Vergleichsuntersuchungen an Hirnarterien bei Binswangerscher Encephalopathie und Hochdruckencephalopathie. *Acta Neuropathol (Berl)* **1973**;26:23–43
3. Rothemunde E, Frische M. Klinisch-pathologische Studie zur Entstehung der intracerebralen Gefasshyalinose bein Hypertonie. *Arch Psychiat Nervenkr* **1973**;217:195–206
4. Burger PC, Burch JG, Kunze U. Subcortical arteriosclerotic encephalopathy (Binswanger's disease). A vascular etiology of dementia. *Stroke* **1976**;7:626–631
5. Janota I. Dementia, deep white matter damage and hypertension: "Binswanger's disease." *Psychol Med* **1981**;11:39–48
6. Tomonaga M, Hiroski Y, Tohgi H, Kameyama M. Clinicopathologic study of progressive subcortical vascular encephalopathy (Binswanger type) in the elderly. *J Am Geriatr Soc* **1982**;30:524–529
7. Goto K, Ishii N, Fukasawa H. Diffuse white matter disease in the geriatric population. A clinical neuropathological and CT study. *Radiology* **1981**;141:687–695
8. Bradley WG Jr, Waluch V, Brant-Zawadzki M, Yadley RA, Wycoff RR. Patchy, periventricular white matter lesions in the elderly: common observation during NMR imaging. *Noninvasive Med Imag* **1984**;1:35–41
9. Zeumer H, Hacke W, Hundgen R. Subkortikale arteriosklerotische Enzepahlopathie. Klinische, CT-morphologische, und elektrophysiologische Befunde. *Fortschr Neurol Psychiatr* **1981**; 49:223–231
10. Pullicino P, Eskin T, Ketonea L. Prevalence of Binswanger's disease. *Lancet* **1983**;1:939
11. Brant-Zawadzki M, Fein G, Van Dyke C, Kiernan R, Davenport L, de Groot J. MR imaging of the aging brain: patchy white matter lesions and dementia. *AJNR* **1985**;6:675–682
12. Rosenberg GA, Kornfeld M, Stovring J, Bicknell JM. Subcortical arteriosclerotic encephalopathy (Binswanger): computerized tomography. *Neurology (NY)* **1979**;29:1102–1106
13. Zeumer H, Schonsky B, Sturm KWQ. Predominant white matter involvement in subcortical arteriosclerotic encephalopathy. *J Comput Assist Tomogr* **1980**;4:14–19
14. Loizou LA, Kendall BE, Marshall J. Subcortical arteriosclerotic encephalopathy: a clinical and radiological investigation. *J Neurol Neurosurg Psychiatry* **1981**;44:294–304
15. Valentine AR, Moseley IF, Kendall BE. White matter abnormality in cerebral atrophy: clinicoradiological correlations. *J Neurol Neurosurg Psychiatry* **1980**;43:139–142
16. Farnell FJ, Globus JH. Chronic progressive vascular subcortical encephalopathy. *Arch Neurol Psychiatr (Chicago)* **1932**;27:593–604
17. Olszewski J. Subcortical arteriosclerotic encephalopathy. Review of the literature on the so-called Binswanger's disease and presentation of two cases. *World Neurol* **1962**;3:359–375
18. Jellinger K, Neumayer E. Progressive subcorticale vasculare Encephalopathie Binswanger. Eine klinisch-neuropathologische Studie. *Arch Psychiatr Z Ges Neurol* **1964**;205:523–554
19. Aronson SM, Perl DP. Clinical Neuropathological Conference. *Dis Nerv Syst* **1974**;35:286–291
20. DeReuck J, Crevits L, DeCoster W, Sieben G, vander Eecken H. Pathogenesis of Binswanger chronic progressive subcortical encephalopathy. *Neurology (NY)* **1980**;30:920–928
21. Erkinjuntti T, Sipponen JT, Iivanainen M, Ketonen L, Sulkava R, Sepponen RE. Cerebral NMR and CT imaging in dementia. *J Comput Assist Tomogr* **1984**;8:614–618
22. Caplan LR, Schoene WC. Clinical features of subcortical arteriosclerotic encephalopathy (Binswanger's disease). *Neurology (NY)* **1978**;28:1206–1215
23. Brust JCM. Dementia and cerebrovascular disease. In: Mayeax R, Rosen WG, eds. *The dementias*. New York: Raven Press, **1983**:131–147
24. Maeda S, Nakayama H, Isaka K. Aihara Y, Nemoto S. Familial unusual encephalopathy of Binswanger's type without hypertension. *Folia Psychiatr Neurol Jpn* **1976**;30:165–177
25. Tanaka M, Ikuta F, Oyake H. Report of a case of chronic progressive subcortical encephalopathy (Binswanger's disease) unassociated with hypertension. *Clin Neurol (Tokyo)* **1969**; 9:398–404
26. DeReuck J. The cortico-subcortical arterial angioarchitecture in the human brain. *Acta Neurol Belg* **1972**;72:323–329
27. Binswanger O. Die Abgrenzung der algemeinen progressiven paralyse. *Klin Wochenschr (Berl)* **1984**;31:1103–1105, 1137–1139, 1180–1186

Head Injury: Early Results of Comparing CT and High-Field MR

Robert A. Zimmerman[1]
Larissa T. Bilaniuk
David B. Hackney
Herbert I. Goldberg
Robert I. Grossman

The sensitivity and specificity of CT and high-field MR (1.5 T) were compared in an evaluation of 30 patients with head injuries (eight acute, 15 subacute, and seven chronic). By using T1- and T2-weighted images, it was possible to detect various stages of hemorrhages and their separation from edema. In the acute category, both CT and MR showed acute hemorrhagic lesions, but only MR demonstrated coexisting chronic hematomas or small hypothalamic or brainstem infarctions. MR was far superior to CT in the detection and characterization of subacute injuries, including shearing injuries, hemorrhagic and nonhemorrhagic contusions, and subdural hematomas. In chronic injury, atrophy was demonstrated by both techniques, but only MR showed parenchymal abnormalities and old hemorrhages. Its ease in monitoring patients and its greater speed make CT the procedure of choice for the evaluation of acute cases. CT also provides information that is useful in deciding between surgery and medical management. However, the more precise anatomic depiction of MR and its sensitivity to parenchymal abnormalities make MR the key to correct prognosis in patients with subacute or chronic injury.

In order for MR to replace or supplement CT in the evaluation of head injury, it will have to provide either new or better diagnostic information. MR at present requires significantly longer scan times than CT, and motion during these long scans can detract from image quality. Life-support and monitoring systems that perform well with CT function poorly with MR. The purpose of this study is to ascertain whether the information provided by high-field MR justifies the longer scan times and greater difficulty of patient management. To answer this question, we evaluated 30 head injury patients studied with 1.5-T MR and compared those findings with the CT findings when the trauma was acute, subacute, or chronic. The comparison was carried out for the three stages of trauma defined because of the now well-recognized changes in MR signal intensity of blood with time [1–4]. While the results in this series are preliminary, the data support the idea that MR contributes valuable information during the acute, subacute, and chronic stages after cerebral injury.

Materials and Methods

MR studies were performed on a 1.5-T GE Signa proton imaging system. T1-weighted images were obtained using a repetition time (TR) of 400 to 800 msec and an echo delay time (TE) of 20 to 25 msec. T2-weighted images used a TR of 2000–2500 msec and a TE of 30–80 msec. Two echoes were routinely obtained. Matrix size was 128 × 256, resulting in a pixel size of 1 mm × 0.5 mm. Slice thickness was either 3 or 5 mm. All images were done multislice using one average. Examination was initiated in the sagittal plane with subsequent T2 studies done in the axial and coronal planes. Coronal and/or axial T1-weighted images were also obtained, as indicated, primarily for evaluation of hematomas. A set of T1-weighted images took 2.5–3.3 min, while a set of T2-weighted images took 8.5–10.5 min.

CT studies were done on a GE 9800, GE 8800, or Philips 310 scanner. The CT studies

This article appears in the September/October 1986 issue of *AJNR* and the December 1986 issue of *AJR*.

Received February 5, 1986; accepted after revision May 1, 1986.

Presented at the annual meeting of the American Society of Neuroradiology, San Diego, January 1986.

[1] All authors: Department of Radiology, Hospital of the University of Pennsylvania, Philadelphia, PA 19104. Address reprint requests to R. A. Zimmerman.

***AJR* 147:1215–1222, December 1986**
0361–803X/86/1476–1215
© American Roentgen Ray Society

were done without contrast enhancement in the axial plane with slice thickness of 9–10 mm. MR studies, CT, clinical presentation, course, and outcome were reviewed.

Results

During a 1-year period, 1543 patients were examined for CNS diseases. Thirty patients with head injuries had 38 MR studies. There were 26 males and four females, ranging in age from 3 to 60 years; 60% were 29 years old or younger. Eight patients were initially examined acutely (within 72 hr of injury), 15 patients were examined subacutely (5 to 20 days after injury), and seven patients were examined chronically (1 month to 3 years after injury). Eight patients had follow-up examinations 1 to 3 months after the first study. All patients had CT scans without contrast enhancement.

Acute Head Injury

Seven of the eight patients had severe injuries and were stuporous to comatose at presentation (Table 1). Three patients underwent craniotomy after CT examination and before MR. All three had evacuation of acute subdural hematomas; one also underwent removal of an accompanying intracerebral hematoma and another removal of an epidural hematoma. Six of the eight patients showed evidence of hemorrhagic contusions, usually multiple, which appeared as areas of markedly decreased signal intensity on T2-weighted images owing to the presence of deoxyhemoglobin surrounded by a high signal intensity area caused by edema (Fig. 1). These areas appeared only as a region of moderate hypointensity on T1-weighted images (Fig. 1B). Edema and hemorrhage could not be separated on the T1-weighted images. In addition, four patients showed acute subdural hematomas, one with an additional chronic subdural hematoma, one with an intraventricular hemorrhage (Figs. 1D and 1E), one with a subarachnoid hemorrhage, and one with a posterior cerebral arterial territory infarct with hypothalamic and upper brainstem infarction (Fig. 2).

CT showed all the acute hemorrhagic contusions, the subdural hematomas, and the intraventricular bleed, but did not show a large isodense infratemporal-occipital chronic subdural hematoma in one patient or an infarction of the upper brainstem and hypothalamus in another (Fig. 2A).

TABLE 1: **Acute Head Injury**[a]

Finding[b]	CT	MR
Hemorrhagic contusions	6	6
Nonhemorrhagic contusion	0	1
Subarachnoid hemorrhage	1	1
Intraventricular hemorrhage	1	1
Acute subdural hematoma	4	4
Chronic subdural hematoma	0	1
Brainstem hypothalamic infarction	0	1
Posterocerebral infarction	1	1

[a] Eight patients were examined 1–3 days after injury.
[b] In some patients, there was more than one finding.

Subacute Injury

The patients in this stage fell into the moderate-to-severe head injury category and were confused, stuporous, or comatose. Four patients had surgery before MR, two for elevation of depressed fractures associated with underlying contusions, one for evacuation of an acute epidural hematoma, and one for evacuation of an acute intracerebral hematoma (Table 2). One patient had surgery after the MR examination for removal of a subacute (isodense on CT, high signal on T1- and T2-weighted images) subdural hematoma (Fig. 3). Subdural hematomas were found in five patients. Hemorrhagic contusions were found in 13 patients and nonhemorrhagic contusions in three patients. On T1-weighted images, contusional hemorrhages and related hematomas showed peripheral high-signal change early on, and more central high-signal change over time (Fig. 4) at sites of methemoglobin formation [3]. On T2-weighted images, signal change to high intensity was slightly delayed behind T1-weighted images, corresponding to a breakdown in the cell membrane surrounding methemoglobin. Intracellular methemoglobin has low signal intensity while extracellular methemoglobin has high signal intensity [3]. Shearing injuries were found in six patients. All the patients with shearing injury showed zones of high signal abnormality (T2-weighted image) in the cerebral white matter (corpus callosum = 4, basal ganglia = 1, corticomedullary juncture zones = 1) (Figs. 4C, 4D, and 5). Two patients with shearing injuries had focal hemorrhages at the site of injury. One patient had posterior cerebral artery territory infarction with involvement of the thalamus and hypothalamus. CT scans in these patients had not revealed the shearing injuries or subdural hematomas. Thirty-seven percent of the contusions seen on MR (including all nonhemorrhagic contusions) were not identified on CT.

Chronic Injuries

These patients had survived moderate-to-severe head injuries (Table 3). Two patients had had surgery, one for decompression of a frontal hemorrhagic contusion and one for removal of acute subdural and epidural hematomas. Five patients showed focal atrophy at a site consistent with old frontal or temporal contusions. Two patients showed generalized atrophy, one patient had evidence of diffuse gray- and white-matter damage, and another had evidence of multiple areas of old intracerebral hemorrhage (Fig. 6), including the brainstem. CT scans in these patients showed either focal or generalized loss of brain parenchyma.

Discussion

CT is the mainstay in the diagnostic armamentarium for evaluation of traumatic head injury. This is because of its rapid scan times and its ability to demonstrate, on the basis of density differences, the presence, location, and extent of intracerebral and extracerebral hemorrhage and hematomas, bony fractures, and compressed brain parenchyma, ventri-

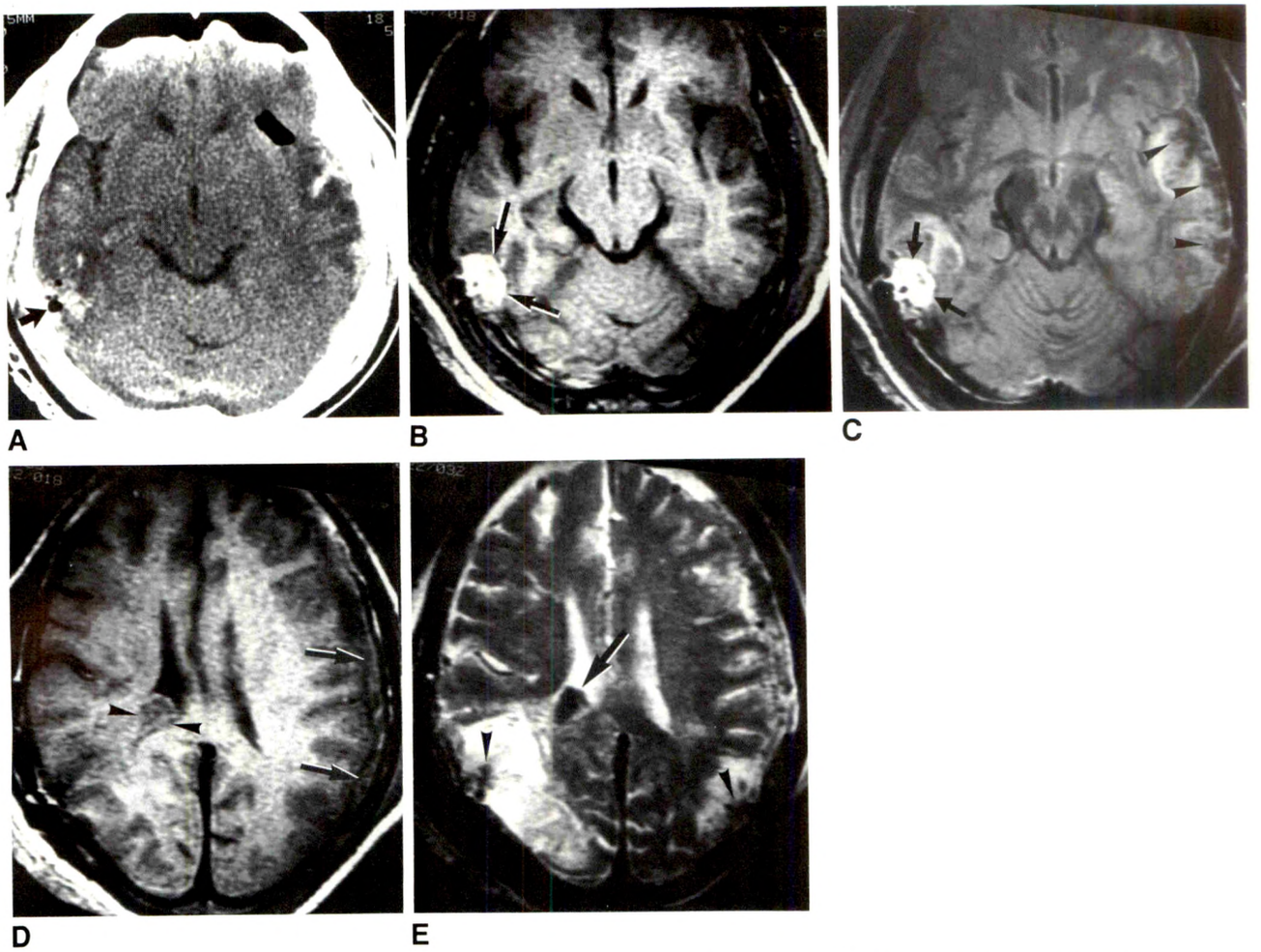
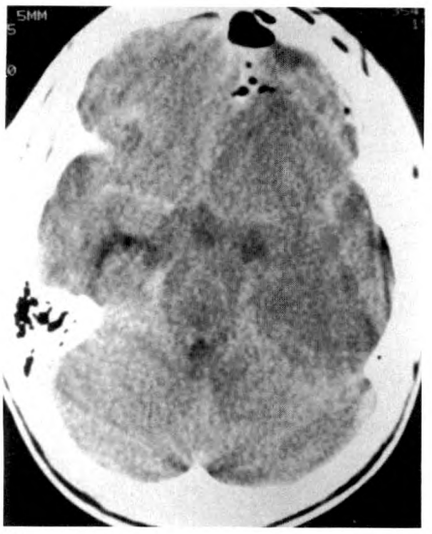


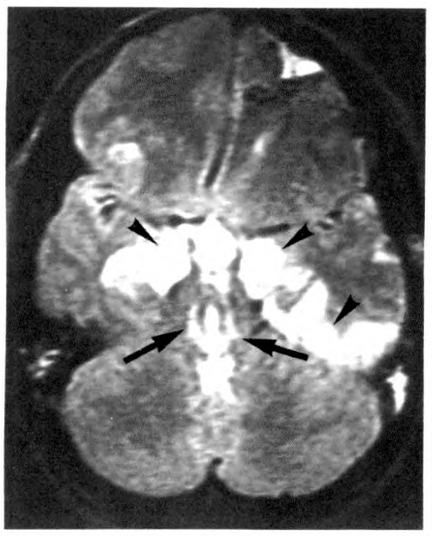
Fig. 1.—Acute brain injury in a 55-year-old man who was hit by a bus and rendered comatose. **A**, CT examination within 24 hr of injury, after evacuation of bilateral acute subdural hematomas, shows air over frontal lobes within subdural space, at craniotomy site (*arrow*), and at site of intratemporal hemorrhagic contusion. Left temporal lobe shows hemorrhagic contusion, edema, and residual subdural hematoma. **B,** Axial T1-weighted image (TR = 600 msec, TE = 25 msec). Examination performed approximately 1 hr after CT in **A** shows high intensity signal (methemoglobin) (*arrows*) at site of partially evacuated hemorrhagic contusion. Hemorrhagic contusion of surface of left temporal lobe is hypointense relative to nonhemorrhagic cortex. **C**, Axial T2-weighted image (done minutes after T1-weighted image) at same plane of section as in **B** (TR = 2500 msec, TE = 35 msec) shows high signal of extracellular methemoglobin (*arrows*) at same site as T-1 weighted image. Less intense high signal is present bilaterally in white matter underlying sites of hemorrhagic contusion secondary to edema. Marked hypointensity is seen from deoxyhemoglobin of hemorrhagically contused cortex (*arrowheads*) in left temporal lobe. **D**, Higher axial T1-weighted image (TR = 600 msec, TE = 25 msec) shows deoxyhemoglobin of intraventricular hematoma in right lateral ventricle as area of hypointensity relative to white matter, but more intense than CSF. Subdural hematoma on left is identifiable (*arrows*) as band of hypointensity distinguishable from more marked signal void of inner table of skull. **E**, Axial T2-weighted image (TR = 2500 msec, TE = 80 msec) shows high signal abnormalities of ischemia and edema involving both parietal occipital areas and underlying hypointense cortical areas of hemorrhagic contusion (*arrowheads*). Markedly hypointense clot (*arrow*) is present in right lateral ventricle, in part outlined by hyperintense CSF. Residual left acute subdural hematoma is seen as area of variable hypointensity. In this instance, areas of hyperintensity between acute subdural hematoma and inner table of skull are thought to represent serum extruded from clot retraction of subdural hematoma. Similar high intensity within subdural space is seen overlying upper portion of left and right frontal lobes. CSF within sulci is hyperintense.

cles, and subarachnoid space. The significance of CT findings is understood and their clinical importance recognized [5]. The limitations of CT are apparent in evaluation of the comatose patient and the patient with focal neurologic deficit whose CT examination appears normal [6, 7]. Superficial contusions of the cortex are frequently obscured on CT by volume averaging with contiguous bone. Small hypothalamic and brainstem infarcts are not resolved by CT, and shearing injuries of the cerebral white matter, unless hemorrhagic, usually are not identifiable [8]. Thus, there is a role for a new imaging technique that is both sensitive and reasonably specific in identifying those lesions that are poorly seen (or not seen at all) by CT. If MR can both identify and quantify these latter lesions while at the same time demonstrate the lesions already well shown by CT, then it has the potential to become the critical imaging technique in the evaluation of acute head injury.

Blood in acute intraparenchymal hematomas, in the state



A



B



C



D

Fig. 2.—Infarction of hypothalamus, midbrain, and vascular territory of posterior cerebral artery secondary to cerebral herniation caused by frontal intracerebral hematoma. Patient is a 23-year-old man who was involved in a motor vehicle accident and rendered comatose. First CT examination done within hours of injury revealed intracerebral hematoma. Surgical evacuation was undertaken, and CT and MR studies shown were performed 48 hr after trauma. **A**, CT scan shows air at operative site in left frontal lobe region, compression of chiasmatic cistern, and loss of ambiens cisterns. Subarachnoid hemorrhage is present in basilar cisterns. **B**, Axial T2-weighted image (TR = 2500 msec, TE = 35 msec) study done several hours after CT in **A** shows high signal intensity in midbrain (*arrows*) and medial temporal lobes (*arrowheads*) consistent with infarction. **C**, CT at a higher level shows area of hypodensity involving left occipital region, midline shift to right, and obliteration of atrial region of left lateral ventricle. Findings are consistent with infarction in distribution of left posterior cerebral artery. Subarachnoid hemorrhage is present in frontal interhemispheric fissure. **D**, Axial T2-weighted image (TR = 2500 msec, TE = 35 msec) shows area of high signal intensity in distribution of left posterior cerebral artery, consistent with infarction and midline shift to right.

TABLE 2: **Subacute Head Injury**[a]

Finding[b]	CT	MR
Hemorrhagic contusion	10	13
Nonhemorrhagic contusion	0	3
Shearing injury	0	6
Subdural hematoma	0	5
Posterocerebral infarction	1	1
Hypothalamic infarction	0	1

[a] Fifteen patients were examined 5–20 days after injury.
[b] In some patients, there was more than one finding.

of deoxyhemoglobin, examined at high field strength (1.5 T) appears as an area of slight hypointensity on T1-weighted images and as an area of marked hypointensity on T2-weighted images (Fig. 1) [3]. After oxidation to methemoglobin, the hematoma becomes high in signal intensity on T1-weighted images and eventually on T2-weighted images (Figs. 1, 3, 4, and 7B). This change occurs from the periphery centrally, and, in the nonoperated patient, was first seen 5 day after injury (Fig. 4B). At this stage, T2-weighted images still distinguish edema from hematoma because the intracellular methemoglobin remains low in signal intensity (Fig. 4C). However, as the cell membranes surrounding the methemoglobin lyse, the signal intensity changes, becoming higher [3]. In this case, a combination of T2- and T1-weighted images, done in the same plane, is needed in order to discriminate between edema and hematoma. Contusions and hematomas that are surgically exposed and that undergo oxidation at the time of craniotomy undergo rapid signal change, and high signal with both T1- and T2-weighted images may be seen on the immediate postoperative MR (Figs. 1B and

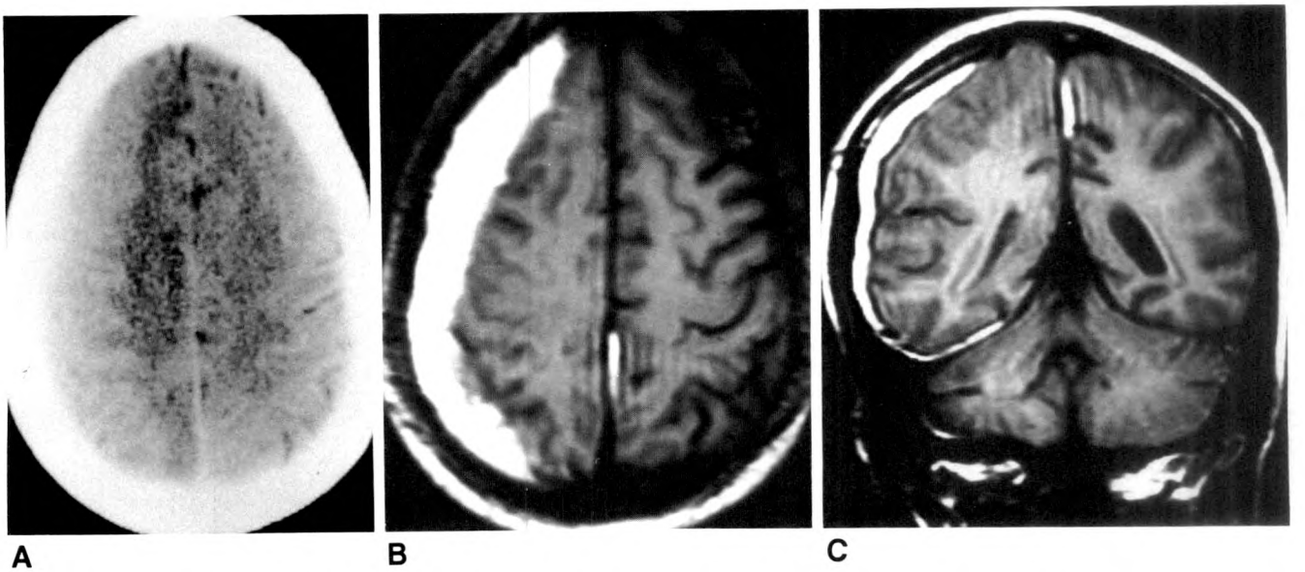
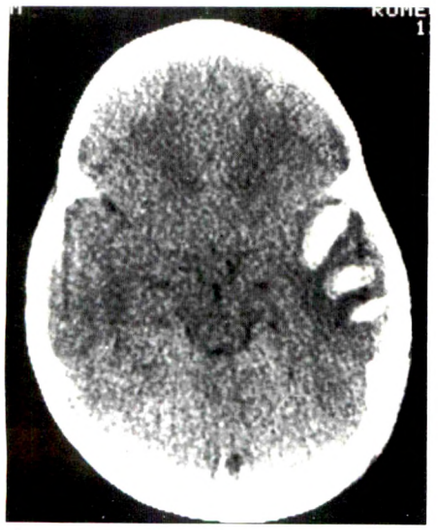


Fig. 3.—Subacute subdural hematoma in a 34-year-old man who was studied by CT and MR 12 days after a motor vehicle accident that resulted in an acute subdural hematoma, which was surgically removed. **A**, Axial CT was interpreted as showing no definite abnormality. In retrospect, cortical gray matter does not reach inner table of skull on right. **B**, Axial T1-weighted image (TR = 800 msec, TE = 20 msec) shows high signal intensity from a large subacute subdural hematoma that is displacing cortex medially. **C**, Coronal T1-weighted image (TR = 800 msec, TE = 20 msec) shows subdural hematoma to cover lateral convexity, extending infratemporal with a small interhemispheric component. Atrium of right lateral ventricle is smaller than left.

1C). With breakdown of the hematoma, macrophagic activity results in removal of blood products. The hemosiderin in these products produce a marked hypointensity on T2-weighted images on the periphery of the hematoma (Fig. 6) [3].

In this series, the eight patients with acute head injury all had initial CT examinations and the MR was done after any emergency surgical procedure or medical therapy that was indicated. At the time the MR study was done, its success was equal to that of CT in identifying the hemorrhagic contusions and focal hematomas within the brain, ventricles, and subdural space. Only one patient was examined who had evidence of significant subarachnoid hemorrhage, and in this instance, both the CT (day 1) and MR examination (day 3) were positive. This series does not represent sufficient experience to permit us to draw conclusions regarding the ability of MR to demonstrate subarachnoid hemorrhage.

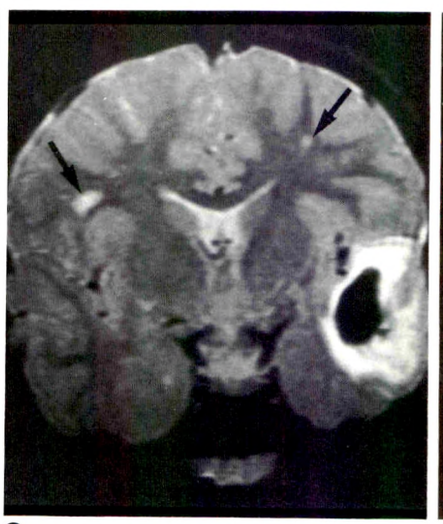
In the acute patients, the multiplanar MR examination, using coronal and sagittal planes in addition to the axial, gave much better localization and assessment of the extent of contusions and hematomas. The acute cortical hemorrhagic contusion is identified not only because of the hypointensity of the blood, but also because of the hyperintensity on the T2-weighted image of the surrounding edema and the interspersed necrotic brain tissue. In the acute injury patient, a difference in signal intensity between the normal and edematous cortex from the hypointense calvarium serves to identify the extracerebral hematoma. On the T2-weighted image, the hypointensity of the acute subdural hematoma may appear similar to the signal void of the nonmobile protons in the inner table of the calvarium. In this instance, the T1-weighted image is apt to show a higher signal intensity from the acute subdural hematoma than from the cortical bone, identifying the presence and location of the extracerebral hematoma [Fig. 1D]. However, the extrusion of serum from the acute subdural hematoma (because of clot retraction) can produce a thin rim of high-intensity signal (T2-weighted image) on the inner and/or outer margins of the subdural hematoma (Fig. 1E) that also helps to identify the extracerebral hematoma. With CT, in the smaller acute subdural hematomas, there may be relatively little contrast between the hematoma and the calvarium. With MR, using both T1- and T2-weighted images, we have found better contrast overall between brain, hematoma, and calvarium. Although we did not examine an acute epidural hematoma in this series, we would expect on the T2-weighted image that the hypointensity of the deoxyhemoglobin in the acute epidural hematoma would not be easily separable from the lack of signal in both the displaced dura and in the calvarium, and that the MR diagnosis would depend more on the T1-weighted image difference in signal intensity between dura, clot, and calvarium as well as on the configuration of the extracerebral hematoma. Air, regardless of its location, produces a signal void, and, as such, may not be separable from the hypointensity of the deoxyhemoglobin on T2-weighted images. However, on T1-weighted images, the signal intensity of air is less than that of deoxyhemoglobin, thus allowing separation. The signal void associated with rapidly flowing blood in surface arteries will not be easily separated from the hypointensity of an acute subdural hematoma on T2-weighted images. Once the signal intensity of the hematoma has become higher, the displaced vessels are easily



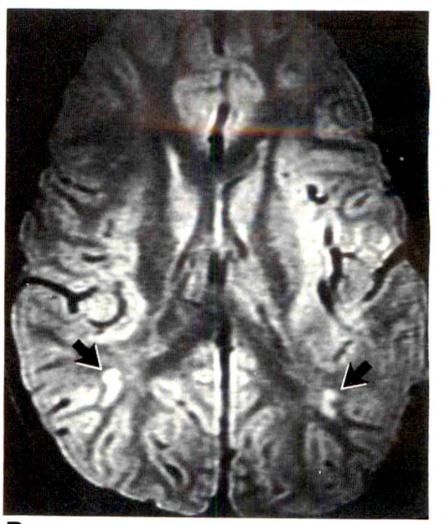
A



B



C



D

Fig. 4.—Subacute examination of intratemporal hematomas and shearing injury in a 5-year-old boy who was thrown from a motor vehicle during a high-speed collision. CT examination on day of injury; MR study 5 days after injury. **A**, Axial CT shows three intratemporal hematomas surrounded by some edema. No other abnormalities were identified on either this CT examination or on follow-up examinations. **B**, Sagittal T1-weighted image (TR = 800 msec, TE = 20 msec) shows peripheral high signal intensity of methemoglobin at site of one intracerebral hematoma within temporal lobe. Temporal lobe is enlarged. **C**, Coronal T2-weighted image (TR = 2000 msec, TE = 40 msec) shows marked hypointensity centrally within temporal intracerebral hematoma. Peripheral high signal intensity corresponds to edema. Intracellular methemoglobin on periphery is not of high signal intensity. Note two scattered areas of high signal intensity near corticomedullary junctures (*arrows*) secondary to shearing injury. **D**, Axial T2-weighted image (TR = 2000 msec, TE = 40 msec). Same bilateral parietal high signal areas at corticomedullary junctures (*arrows*) are seen.

identified by their signal void.

With the conversion of deoxyhemoglobin to methemoglobin, the signal intensity becomes high on T1-weighted images [1]. This high signal intensity on T1-weighted images provides very precise gyral localization of hemorrhagic contusions and graphically shows the location and extent of the extracerebral hematomas (Fig. 3). Again, relative to CT, the multiplanar capabilities of MR make a more precise anatomic depiction possible.

However impressive the subacute demonstration of focal hemorrhages and hematomas may be, it is the demonstration of nonhemorrhagic parenchymal changes that is the real province of MR. These are areas of edema that occur at sites of brain injury as a result of shearing injuries and necrosis, nonhemorrhagic contusions, and infarction (Figs. 2 and 5). In this series, the majority of patients showing the nonhemorrhagic consequences of trauma fell into the head injury group that was studied subacutely. One of the eight acute head injury patients also demonstrated such findings—infarction of the upper brainstem and hypothalamus—not seen on CT (Fig. 2A). MR demonstration of infarctive changes and non-

TABLE 3: **Chronic Head Injury**[a]

Finding[b]	CT	MR
Shearing injury	0	1
Focal contusional encephalomalacia	5	5
General atrophy	2	2
Gray-white matter damage	1	1
Old intracerebral hemorrhage	0	1

[a] Seven patients were examined 1 month to 3 years after injury.
[b] In some patients, there was more than one finding.

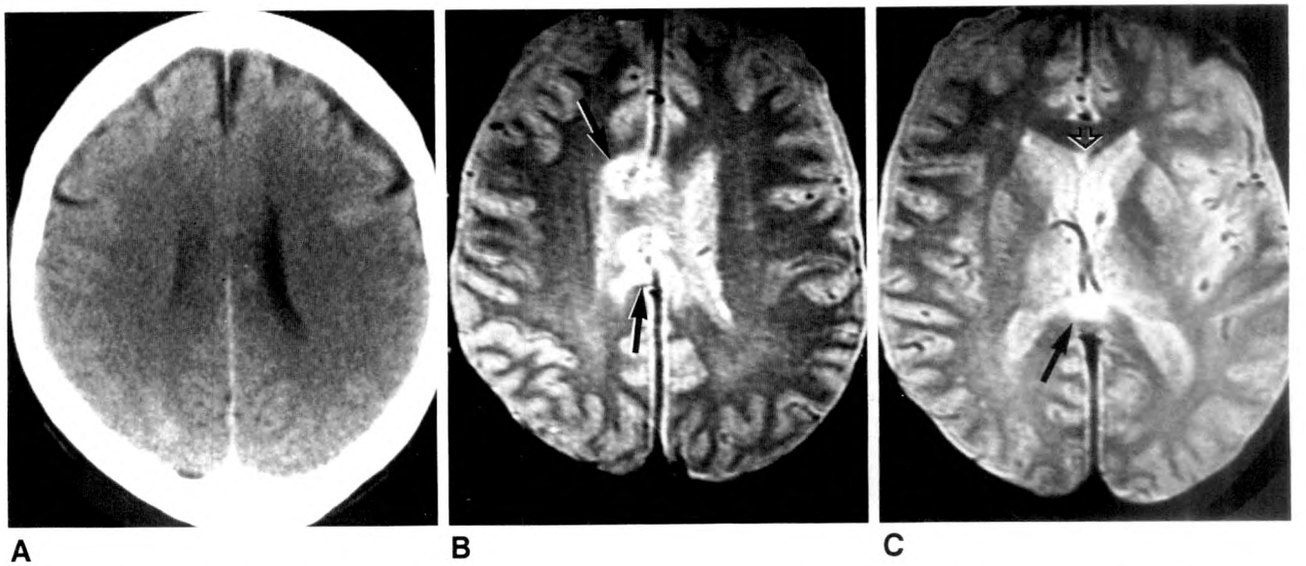


Fig. 5.—Shearing injury corpus callosum in a 60-year-old woman rendered comatose by a motor vehicle accident. **A**, CT scan on day of accident shows no apparent abnormality at level of corpus callosum. **B**, Axial T2-weighted image (TR = 2500 msec, TE = 40 msec), 6 days after accident, shows high signal abnormality involving corpus callosum (*arrows*). **C**, Lower axial section T2-weighted image (TR = 2500 msec, TE = 40 msec) shows high signal abnormality in splenium of corpus callosum (*arrow*) and in septum pellucidum (*open arrowhead*).

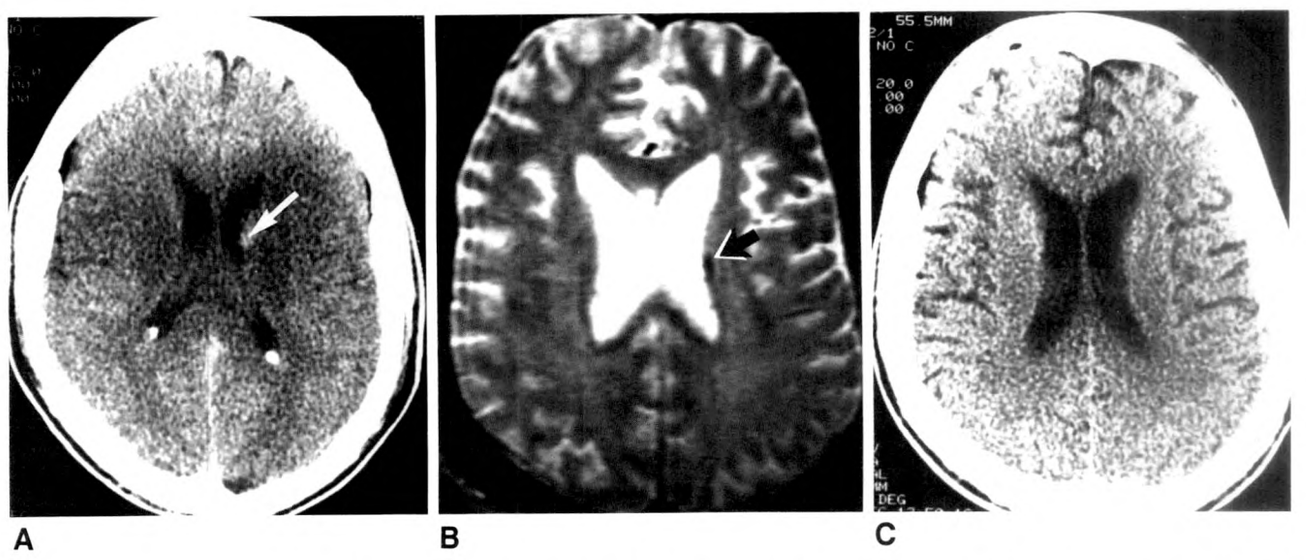


Fig. 6.—Hemosiderin deposition at site of old injury. Patient is a 38-year old man who suffered shearing injury with hemorrhages in brainstem and white matter of centrum semiovale after a motor vehicle accident. CT examination at time of injury, and at 6 months; MR examination at 6 months. **A**, Axial CT section shows hemorrhage (*arrow*) in white matter contiguous to body of left lateral ventricle. **B**, Axial T2-weighted image (TR = 2000 msec, TE = 80 msec) shows area of marked signal hypointensity at site of hemosiderin deposition from previous hemorrhage (*arrow*). **C**, CT done at same time as MR shows enlargement of lateral ventricles, sylvian fissures, and sulci and no abnormality in region of old hemorrhage.

hemorrhagic shearing injuries are findings of prognostic significance [7, 8] since these lesions are either fatal or result in poor recovery.

Subacutely, on CT the high density of the hematoma fades [9]. On MR, the hyperintensity on T1- and T2-weighted images remains [2–4, 10, 11]. Thus, in one patient with an acute subdural hematoma, a subacute subdural hematoma in an infratemporal occipital location was found on MR. This had not been seen on CT. A second isodense subacute subdural hematoma was missed on CT but showed clearly on MR (Fig. 3).

In the chronic phase after injury, focal or generalized atrophic changes are well seen with both CT and MR. Multiplanar MR displays the exact gyral or lobar involvement of



Fig. 7.—Hemorrhagic contusion of temporal lobes. Patient is a 30-year-old man who presented in a coma after being knocked off a bike by a car. CT and MR examinations 17 days after injury. **A**, CT shows bilateral temporal lobe mass effect consisting of edema within white matter and more superficial irregular areas of minimal hypodensity. Findings are consistent with bilateral temporal lobe hemorrhagic contusions. **B**, Sagittal T1-weighted image shows high signal from methemoglobin at site of hemorrhagically contused right middle and inferior temporal gyri.

the atrophic process better than CT, when focal. In this series the atrophic process was often the result of prior contusion. This anatomic information is invaluable in correlating the structural image with the functional abnormalities determined by psychological testing [12].

In the eight patients who had follow-up examinations, the additional benefits of MR were the demonstration of transverse sinus thrombosis in one, putaminal and uncal high-signal abnormalities in another, and progressive generalized atrophy in another, with abnormal high-signal changes in the white matter after a shearing injury.

Conclusions

Although the number of patients studied in each category is limited, certain preliminary conclusions appear to be warranted. The nonhemorrhagic consequences of trauma are much better displayed by MR than CT. Infarction, shearing injuries, and nonhemorrhagic contusions should be identifiable not only subacutely but acutely, and because they are significant consequences of trauma that are not well shown by CT, they should stimulate further efforts toward refinement of monitoring and life-support equipment for MR use with acute head injuries. CT remains the first diagnostic step in treating the emergency patient who needs a rapid examination to determine whether surgical evacuation of a hematoma or medical management is indicated. MR has the capacity to demonstrate the cause of unexplained coma and focal neurologic deficits as well as to provide more routine diagnostic information. Subacutely, MR has an edge over CT in that it can demonstrate with graphic and precise localization extra- and intracerebral hematomas, even when these are isodense on CT. In the chronic patient, while both CT and MR demonstrate local and generalized parenchymal loss, MR gives the type of anatomic information that is needed to make sense of the patient's functional state [12]. In addition, old nonhemorrhagic and hemorrhagic areas can be demonstrated.

REFERENCES

1. Bradley WG, Schmidt PG. Effect of methemoglobin formation on the MR appearance of subarachnoid hemorrhage. *Radiology* **1984**;156:99–103
2. Zimmerman RA, Bilaniuk LT, Grossman RI, et al. Resistive NMR of intracranial hematomas. *Neuroradiology* **1985**;27:16–20
3. Gomori JM, Grossman HI, Goldberg HI, Zimmerman RA, Bilaniuk LT. High field magnetic resonance imaging of intracranial hematomas. *Radiology* **1985**;157:87–93
4. Zimmerman RA, Bilaniuk LT. MRI evaluation of subacute head injury. In: *Proc Meeting European Society of Neuroradiology*. Amsterdam, Holland: Elsevier, in press
5. Zimmerman RA, Bilaniuk LT. Radiology of craniocerebral trauma. In: Rosenberg, RN, Heinz R, eds., *The clinical neurosciences*, New York: Churchill & Livingston, **1984**:483–524
6. Zimmerman RA, Bllaniuk LT, Dolinskas C, Gennarelli T, Bruce D, Uzzell B. Computed tomography of acute intracerebral hemorrhagic contusion. *J Comput Tomogr* **1977**;1:271–280
7. Zimmerman RA, Bilaniuk LT, Gennarelli T. Computed tomography of shearing injuries of the cerebral white matter. *Radiology* **1978**;127:393–396
8. Zimmerman RA. Supratentorial trauma. In: Taveras J, Ferrucci J, eds., *Radiology: diagnosis/imaging/intervention*. Philadelphia: J.B. Lippincott, **1986**:1–18
9. Dolinskas CA, Zimmerman RA, Bllaniuk LT, Gennarelli T. Computed tomography of post-traumatic extracerebral hematomas: comparison to pathophysiology and responses to therapy. *J Trauma* **1979**;19:163–169
10. Han JS, Kaufman B, Alfidi RJ, et al. Head trauma evaluated by magnetic resonance and computed tomography: a comparison. *Radiology* **1984**;150:71–77
11. Sipponen JT, Sepponen RE, Sivulo A. A chronic subdural hematoma: demonstration by magnetic resonance. *Radiology* **1984**;15:79–85
12. Uzzell BP, Zimmerman RA, Dolinskas CA, Obrist WD. Lateralized psychological impairment associated with CT lesions in head injured patients. *Cortex* **1979**;XV:391–401

Gd-DTPA in Clinical MR of the Brain: 1. Intraaxial Lesions

Michael Brant-Zawadzki[1]
Isabelle Berry[1, 2]
Luci Osaki[1]
Robert Brasch[1]
Judith Murovic[3]
David Norman[1]

Over 35 intraaxial lesions in 15 patients suspected of having intracranial tumors were studied with MR before and after injection of Gadolinium-DTPA (Gd-DTPA). Diseases included primary and metastatic brain tumors, plaques of multiple sclerosis, occult arteriovenous malformations, lymphoma, toxoplasmosis, and pituitary adenoma. The precontrast T2-weighted sequence (SE 2000/30, 60) was found to be most sensitive in detecting intraaxial lesions, showing 17 lesions that were not seen on the post-Gd-DTPA T1-weighted sequence (SE 500/30). In one case of multiple sclerosis, several lesions seen on the pre-Gd-DTPA study on T2-weighted images faded after injection of Gd-DTPA (due to T2 shortening). In two patients with large metastatic foci, other small metastatic lesions were seen better after Gd-DTPA on both T1- and T2-weighted sequences. Four other patients with only one focal-enhancing lesion and one patient with multifocal lesions on T1-weighted images actually had a much larger single glioma depicted on pre-Gd-DTPA T2-weighted images. In a patient with AIDS, a ring-enhancing lesion thought to be an abscess proved to be lymphoma. The cryptic arteriovenous malformations enhanced but showed more characteristic findings, such as hemorrhage, on pre-Gd-DTPA studies. Our experience suggests that Gd-DTPA may not improve sensitivity of MR in the detection of intraaxial lesions. However, functional aspects of brain disease, such as the presence of perfusion of a lesion and active breach of the blood-brain barrier, are depicted well with Gd-DTPA and are vital for proper diagnosis in many instances.

Early limitations of MR included relatively long study times, suboptimal characterization of disease and its chronicity, perceived inability to separate tumor from edema, and, on occasion, suboptimal sensitivity. CT had similar problems in its early stages, with suboptimal sensitivity being the most unacceptable problem but the one most easily remedied through the use of preexisting iodinated contrast agents. The impact of such contrast agents on CT provided a historical precedent for the development of paramagnetic contrast agents. Gadolinium-DTPA (Gd-DTPA) was the first such substance to be tested for human use in European trials, with the brain and spinal cord as early targets [1–3]. Enthusiasm for this agent's utility is evident in these early trials. The first American clinical trials of Gd-DTPA have been completed and the initial results of tolerance, toxicity, and efficacy from the phase II multicenter trial have been reported [4]. This and the following article (5] elucidate the clinical experience with Gd-DTPA from a referral center for neurologic disease where MR had been used routinely by neuroradiologists for 4 years prior to the introduction of this agent.

Subjects and Methods

Thirty patients at the University of California, San Francisco (UCSF), were enrolled in a multicenter clinical trial of Gd-DTPA under the guidelines of the Food and Drug Administration, the Human Research Committee at UCSF, and the commercial developer of the product (Berlex Laboratories, New Jersey). Fully informed consent was obtained from every patient.

This article appears in the September/October 1986 issue of *AJNR* and the December 1986 issue of *AJR*.

Received December 20, 1985; accepted after revision April 2, 1986.

Presented at the American Society of Neuroradiology, San Diego, CA, January 1986.

This work was supported in part by Berlex Laboratories, New Jersey.

[1] Department of Radiology, University of California, San Franscisco, CA 94143. Address reprint requests to M. Brant-Zawadzki, Dept. of Radiology C309, UCSF School of Medicine, San Francisco, CA 94143.

[2] Department of Neuroradiology, Hôpital Purpan, Toulouse, France.

[3] Department of Neurosurgery, University of California, San Francisco, CA 94143.

***AJR* 147:1223–1230, December 1986**
0361–803X/86/1476–1223
© American Roentgen Ray Society

TABLE 1: **Clinical Data in 13 Patients with Definitive Diagnosis**

Age	Gender	Clinical Symptoms	Histology
Primary Brain Tumors			
55	M	Progressive difficulty in verbal fluency	Anaplastic astrocytoma
53	M	Grand mal seizures	Multicentric anaplastic astrocytoma
42	M	Grand mal and focal seizures	Anaplastic astrocytoma
34	M	Grand mal seizures	Anaplastic astrocytoma
56	M	History of astrocytoma treated by radiation; homonymous hemianopsia	Radionecrosis residual astrocytoma
32	M	Petit mal seizures	Anaplastic astrocytoma
Secondary Brain Tumors			
59	F	Sensory seizures	Adenocarcinoma metastasis
62	M	Left arm weakness and dysarthria	Adenosarcoma metastasis
53	F	History of breast carcinoma; left hemiparesis	Breast carcinoma* metastasis
Miscellaneous Lesions			
43	M	Altered mental status; AIDS	Lymphoma and toxoplasmosis
37	M	History of seminoma; multifocal neurologic signs	Multiple sclerosis*
53	F	Visual flashes; hearing loss	Cryptic arteriovenous malformation
31	M	Incidental discovery; head trauma	Pituitary adenoma

* Denotes clinical diagnosis only.

The enrollment requirements included strong suspicion of intracranial tumor (based either on CT studies or clinical criteria) in adult patients. Women of child-bearing age were excluded. Following a battery of baseline laboratory studies [4], MR was performed before and after the intravenous administration of Gd-DTPA (0.1 mmol/kg), at 0.35 T with dual spin-echo (TE 30, 60 msec) sequences using TR of 2000 msec (sequence A) and 500 msec (sequence B). The order of sequences was A/B, B/A/B/A/B, with Gd-DTPA delivered after the first A/B pair. The image matrix was 256 × 256, or 128 × 128 when the patient's condition necessitated a more rapid study. The imaging time for an A/B pair at a matrix of 128 was 13 min; at a matrix of 256, it was 26 min. Slices were contiguous and 5 or 10 mm in thickness, depending on the anatomic region of interest. Quantitative measurements of tissue intensity were carried out before and after administration of Gd-DTPA by circumscribing a region of interest with an interactive cursor. This procedure allowed calculation of T1 and T2 relaxation values in normal and pathologic foci. The quantitative aspects of the intraaxial lesions considered here are reported elsewhere as part of an overall study [6].

Visual evaluation of the degree of enhancement in the intraaxial lesions considered here was scored on a 0–2 scale by two of the authors (MBZ, IB), with 0 = no enhancement, 1 = equivocal enhancement, 2 = definite enhancement. The same scoring scale was used to judge the ability of MR before and after the injection of Gd-DTPA to separate tumor from edema, identify focal cyst or necrosis, and provide a site for biopsy, if applicable. Finally, an overall judgment was made regarding the effects of Gd-DTPA on the general diagnostic efficacy of MR. The effect was judged positive if this agent improved sensitivity or made the lesion easier to see, or if it helped characterize the disease process. For all these judgments, *both* A and B sequences before Gd-DTPA administration were used and compared with both sequences after the agent was given.

Results

Fifteen of the 30 patients enrolled in the study had over 35 intraaxial lesions. The patient tolerance and toxicity data relative to Gd-DTPA administration is the subject of the multicenter report [4] and will not be considered here. The variety of diseases encountered are listed in Table 1. Histologic proof of the diagnosis was available in 11 of the 15 patients. In two others with multifocal lesions, the diagnosis was based on the imaging studies and on definitive clinical criteria (multiple sclerosis, metastases). Two patients with a focal MR abnormality are being followed with no firm diagnosis to date. Therefore, 13 patients with an established diagnosis form the basis of this study. Five of the patients were on steroid therapy when undergoing the imaging study. No correlation between enhancement or lack thereof and such therapy was noted in this small group of patients (only one patient on steroids had a nonenhancing lesion). Overall, almost half (17) of all the lesions detected with MR showed

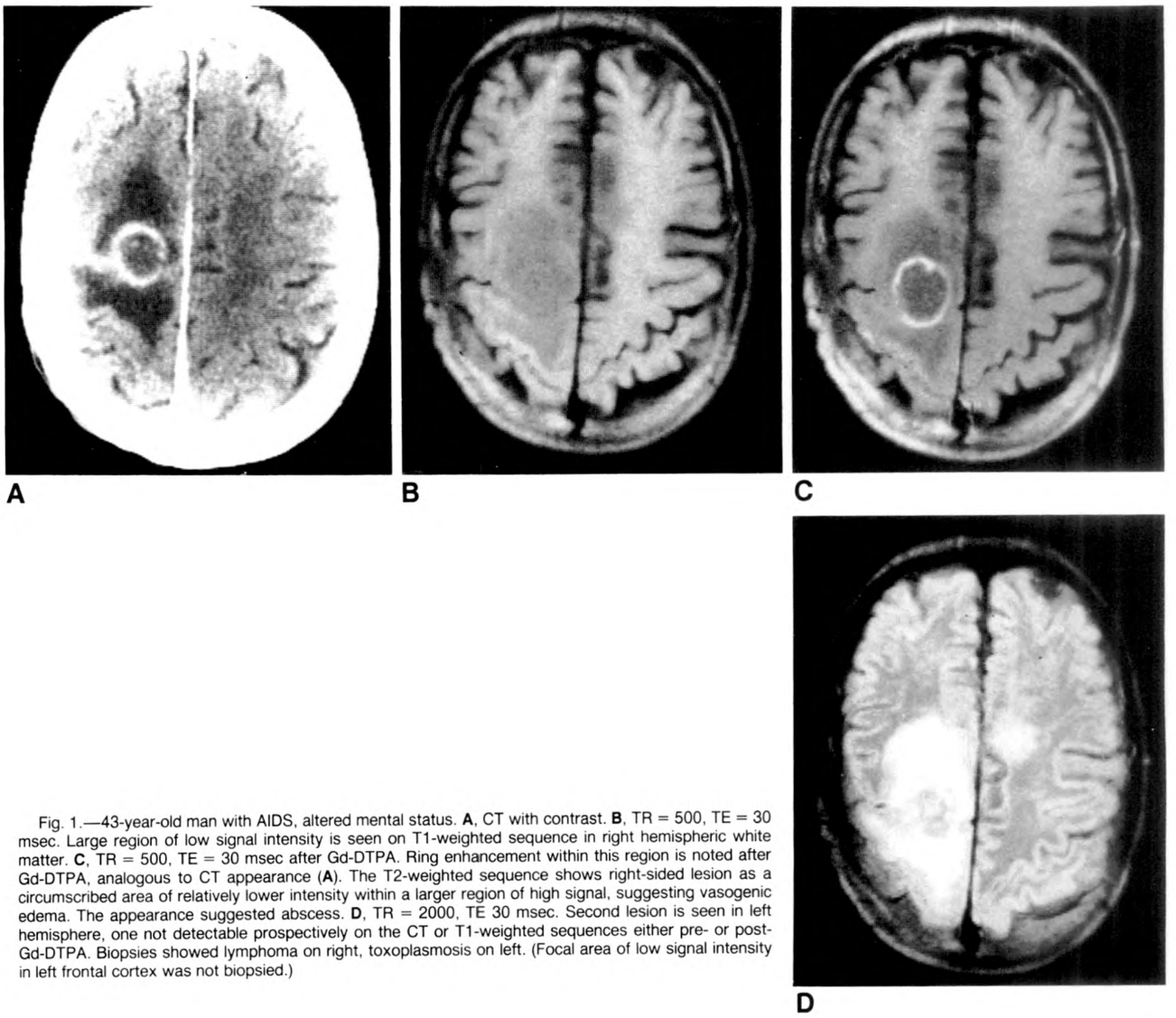


Fig. 1.—43-year-old man with AIDS, altered mental status. **A**, CT with contrast. **B**, TR = 500, TE = 30 msec. Large region of low signal intensity is seen on T1-weighted sequence in right hemispheric white matter. **C**, TR = 500, TE = 30 msec after Gd-DTPA. Ring enhancement within this region is noted after Gd-DTPA, analogous to CT appearance (**A**). The T2-weighted sequence shows right-sided lesion as a circumscribed area of relatively lower intensity within a larger region of high signal, suggesting vasogenic edema. The appearance suggested abscess. **D**, TR = 2000, TE 30 msec. Second lesion is seen in left hemisphere, one not detectable prospectively on the CT or T1-weighted sequences either pre- or post-Gd-DTPA. Biopsies showed lymphoma on right, toxoplasmosis on left. (Focal area of low signal intensity in left frontal cortex was not biopsied.)

no definite enhancement with Gd-DTPA. However, 10 of these were demyelinating plaques in a single patient with multiple sclerosis. The agent's effects on overall diagnostic capability was judged as positive in two of 15 patients and negative in two others.

Detection of Enhancement

Prior to Gd-DTPA injection, the T2-weighted sequence (sequence A) was the most sensitive in detecting focal lesions within the brain, showing 17 such lesions that were not seen (score 0 or 1) on the post-Gd-DTPA, T1-weighted sequence (sequence B). The lesions missed on post-Gd-DTPA sequence B included the majority of the plaques in the patient with multiple sclerosis (only 10 of which were counted for the purpose of this study), the lesions of toxoplasmosis and primary cerebral lymphoma (Fig. 1) in the patient with AIDS, two foci of astrocytoma in a patient with multicentric astrocytoma, one large infiltrating temporal astrocytoma in which only a punctate focus enhanced with Gd-DTPA on sequence B, a large parietal astrocytoma involving the thalamus (Fig. 2), the major component of a diffusely infiltrating astrocytoma in which a subfrontal and posterior parietal focus of enhancement was seen, and a frontal astrocytoma in which a punctate hemorrhagic focus was noted. In a minority of these cases, minimal (equivocal) increase in signal intensity (score 1) was faintly visible on the post-Gd-DTPA sequence B when the pre-Gd-DTPA sequence was available for side-by-side comparison.

The optimal sensitivity of the T2-weighted sequence A was maintained after injection of Gd-DTPA with two notable exceptions. Several of the multiple sclerosis plaques seen on the pre-Gd-DTPA T2-weighted sequence A disappeared on

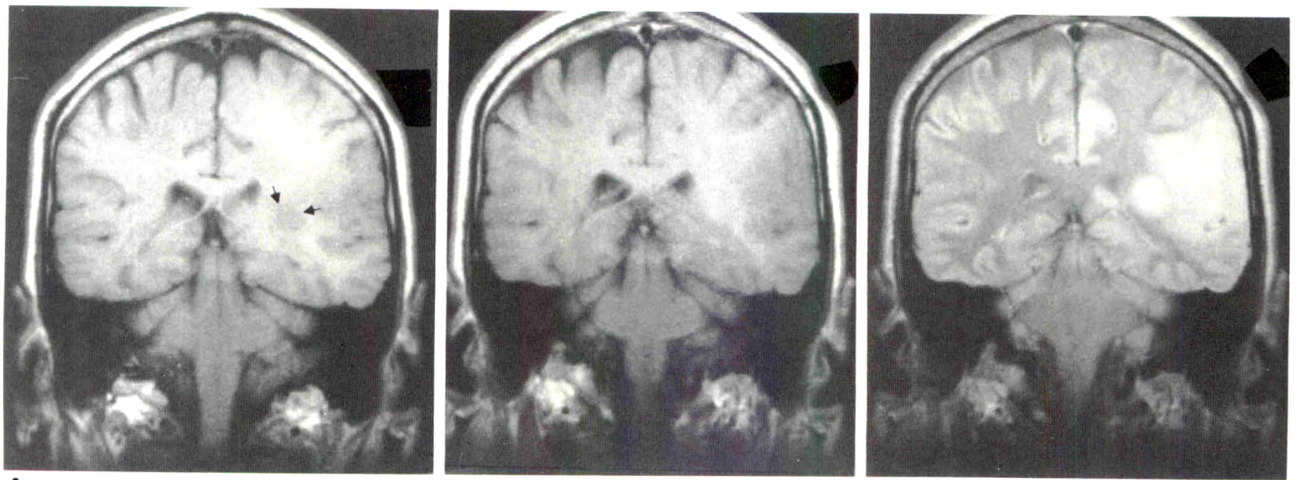


Fig. 2.—55-year-old man with progressive difficulty in verbal fluency; astrocytoma. **A**, TR = 500, TE = 30 msec. Small region of lower intensity (*arrows*) and subtle cortical mass effect is seen on T1-weighted sequence prior to Gd-DTPA. **B**, TR = 500, TE = 30 msec after Gd-DTPA. Administration of Gd-DTPA yields no obvious enhancement of the lesion. **C**, TR = 2000, TE = 30 msec. T2-weighted sequence shows circumscribed area of high signal intensity with even brighter nidus in its deep portion corresponding to low-intensity focus seen in **A**.

that sequence after injection of Gd-DTPA (Fig. 3) because of shortening of T2 relaxation values [6]. The intensity of one, focal, hyperintense site within an astrocytoma faded on the T2-weighted sequence A post-Gd-DTPA when compared with that pre-Gd-DTPA sequence.

Gd-DTPA did improve the sensitivity of both A and B sequences in two of the three patients with metastatic disease (adenosarcoma, adenocarcinoma). Both patients exhibited a single enhancing lesion on CT. The pre-Gd-DTPA MR (sequences A and B) showed a single lesion in one patient and two lesions in the other patient. In both patients, an additional punctate focus of enhancement post-Gd-DTPA was noted on sequences B and A (Fig. 4).

Of the remaining cases, Gd-DTPA-enhanced lesions on T1-weighted sequence B were also detected pre-Gd-DTPA in a patient with multiple breast metastases, in an AIDS patient with cerebral lymphoma (whose toxoplasmosis lesions did not enhance—see Fig. 1), in a patient with multifocal familial occult arteriovenous malformations (Fig. 5), and in a patient with a large pituitary tumor. In all cases that had enhancement, the phenomenon was detectable on the first T1-weighted sequence after injection; however, several multiple sclerosis plaques and two punctate metastatic foci showed more conspicuous enhancement after a 20-min delay.

Characterization

In four of the patients (two with metastases, one with lymphoma, and one with treated astrocytoma), CT showed definite segmentation of the lesion into an enhancing component surrounded by low density—an appearance strongly suggestive of tumor surrounded by edema. In all four cases, the combination of sequence A and B pre-Gd-DTPA also indicated such segmentation. In some cases, the very low intensity focus on T1-weighted sequence B corresponded to the enhancing central component on CT, while T2-weighted sequence A showed the extensive surrounding high intensity consistent with edema (Fig. 4). Post-Gd-DTPA sequence B showed enhancement corresponding to that of CT in these cases. In others, the T2-weighted sequence A showed diffuse high signal intensity, suggesting edema in a vasogenic pattern, circumscribing a garland-shaped low-intensity center (Fig. 1).

Cystic or necrotic components in these intraaxial lesions were identifiable by low-intensity foci on T1-weighted sequence B, and Gd-DTPA offered little to their characterization other than the delayed increase in intensity of the central nidus of such lesions when compared with their periphery.

Hemorrhagic foci within tumors and the occult arteriovenous malformations could be identifed only on the pre-Gd-DTPA pair of sequences based on the high signal intensity of such foci on both A and B sequences. After Gd-DTPA, distinguishing the hemorrhagic focus from an enhancing one was not possible (Fig. 5).

The pattern of enhancement offered little advantage over the morphologic pattern of the lesion before Gd-DTPA. For example, prior to biopsy, the lymphoma lesion in the AIDS patient was thought more likely to represent an abscess based on the ring-enhancing pattern with both CT and MR sequence B. Enhancement in a homogenous or garland-shaped manner was seen in primary as well as metastatic lesions. Thus, in any individual case, these patterns were not predictive of the disease. Although multifocal enhancement with Gd-DTPA did significantly alter the diagnostic differential in two patients with metastatic foci, such multifocal enhancement post-Gd-DTPA would have negatively altered the differ-

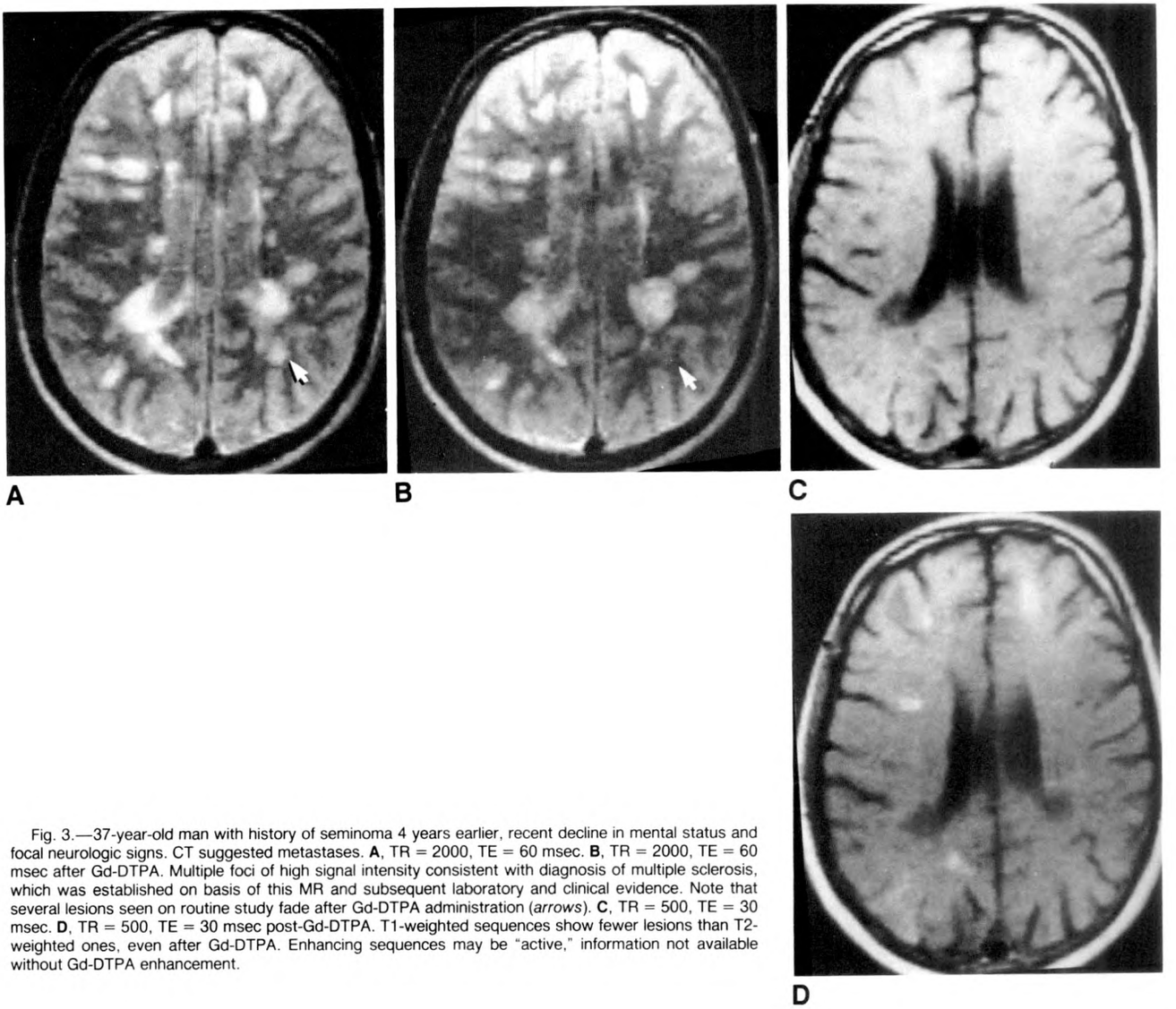


Fig. 3.—37-year-old man with history of seminoma 4 years earlier, recent decline in mental status and focal neurologic signs. CT suggested metastases. **A**, TR = 2000, TE = 60 msec. **B**, TR = 2000, TE = 60 msec after Gd-DTPA. Multiple foci of high signal intensity consistent with diagnosis of multiple sclerosis, which was established on basis of this MR and subsequent laboratory and clinical evidence. Note that several lesions seen on routine study fade after Gd-DTPA administration (*arrows*). **C**, TR = 500, TE = 30 msec. **D**, TR = 500, TE = 30 msec post-Gd-DTPA. T1-weighted sequences show fewer lesions than T2-weighted ones, even after Gd-DTPA. Enhancing sequences may be "active," information not available without Gd-DTPA enhancement.

ential considerations in three patients with primary astrocytomas were it not for the picture of nonenhancing contiguous infiltration seen with the T2-weighted sequence A.

Discussion

The superiority of T2-weighted sequences in the detection of intraaxial brain disease when compared with Gd-DTPA-enhanced T1-weighted sequences as documented by the limited experience reported here is easily understood in light of the pathophysiology of brain disorders. Contrast agents for CT, as well as Gd-DTPA, are large molecules that require both intact perfusion and gross active disruption of the blood–brain barrier (BBB) for their accumulation within the diseased tissues. However, only minimal BBB breakdown may be needed for water to leak out into abnormal tissue. Such water accumulation may predate the more severe BBB disruption needed for leakage of larger proteins across this barrier [7]. Water is an inherent contrast-enhancing substance for T2-weighted images. Indeed, increased water may be seen in diseased tissues (such as demyelinated plaques) even when no active BBB breakdown is present. MR's superior sensitivity to increased tissue water compared with contrast-enhanced CT is well documented and accounts for its diagnostic advantage (8]. Given the pathophysiology of BBB breakdown, then, it is implausible that Gd-DTPA would accumulate in a site that did not also contain abnormal amounts of water. Such sites routinely yield a high signal on T2-weighted sequences. The two "missed" metastatic lesions prior to Gd-DTPA in this series run counter to the above analysis. However, they were both punctate and subject to partial volume

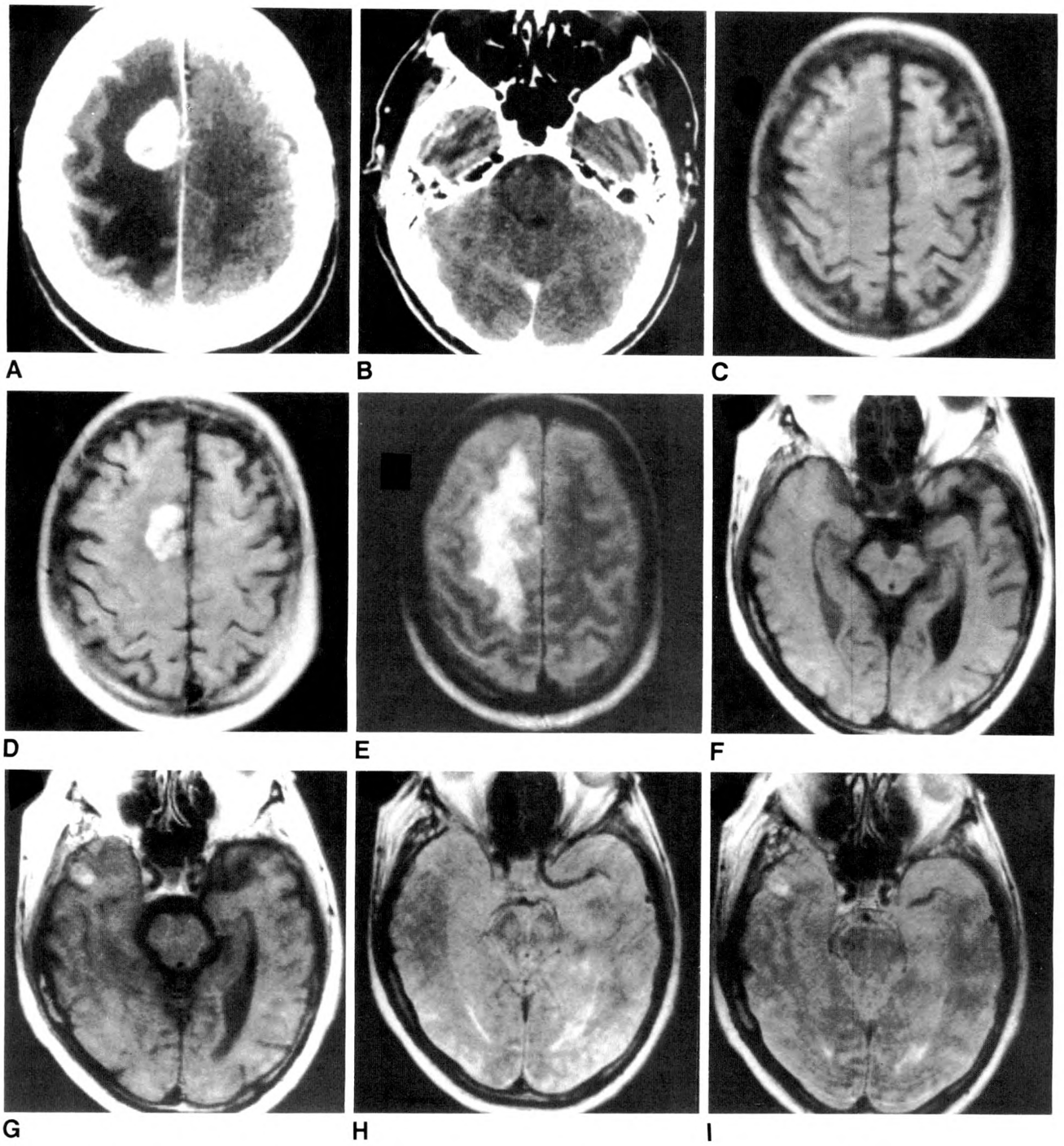


Fig. 4.—62-year-old man with left arm weakness and dysarthria progressing over 3 weeks. **A**, CT shows enhancing lesion in right hemispheric white matter, surrounded by low density. **B**, CT section of temporal lobes degraded by streak artifact. **C**, TR = 500, TE = 30 msec. **D**, TR = 500, TE = 30 msec after Gd-DTPA. Lesion enhances. **E**, TR = 2000, TE = 60 msec. Localization of lesion and differentiation from surrounding edema are possible on pre-Gd-DTPA sequences (**C**, **E**). Primary tumor was suspected. **F**, TR = 500, TE = 30 msec. **G**, TR = 500, TE = 30 msec after Gd-DTPA. **H**, TR 2000, TE = 60 msec. **I**, TR 2000, TE = 60 msec after Gd-DTPA. Temporal focus seen after Gd-DTPA (**G**, **I**) is not visible on CT (**B**) or on sequences before Gd-DTPA (**F**, **H**). Note slight differences of slice orientation, indicating patient motion between pre- and post-Gd-DTPA sequences. On biopsy of large lesion, adenosarcoma was found.

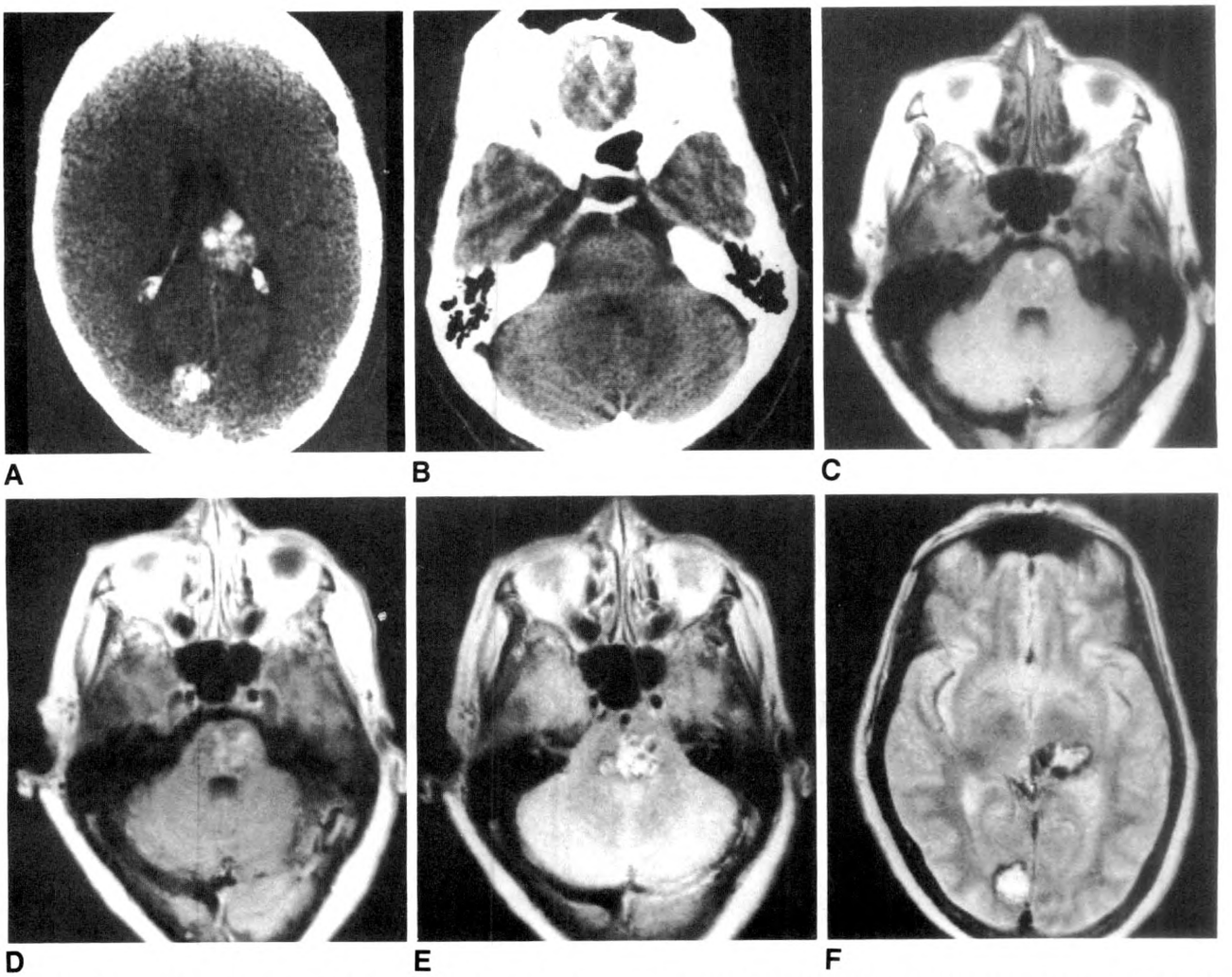


Fig. 5.—53-year-old woman with visual flashes, hearing loss. **A**, **B**, CT shows two partially calcified lesions; one in left thalamus, one in right occipital cortex. Brainstem appears normal. Angiography was negative. **C**, TR = 500, TE = 30 msec. MR shows third lesion in brainstem, missed with CT. High-intensity foci on T1- and T2-weighted sequences suggested subacute bleeding in lesion. Lack of brainstem signs or symptoms suggested occult arteriovenous malformations; biopsy of occipital lesion confirmed this. **D**, TR = 500, TE = 30 msec post-Gd-DTPA. Enhanced MR cannot distinguish foci of enhancement from foci of hemorrhage. **E**, TR = 2000, TE = 60 msec. **F**, TR = 2000, TE = 60 msec. T2-weighted sequences pre-Gd-DTPA show all three lesions with regions of signal void suggesting calcification, although hemosiderin deposition accounting for signal void cannot be excluded.

effects in patients who moved slightly between the pre- and postcontrast sequences. Our results are affected, of course, by the pulse sequences used and by the selected population. The inclusion of 10 demyelinating plaques in one patient heavily weighted the nonenhancing lesions. Also, the relatively large number of primary brain tumors in our material should be noted.

A major difference between the use of contrast agents in CT and their use in MR is documented. In CT, the greater the concentration of iodine in the abnormal tissue, the greater its enhancement. In MR, too much Gd-DTPA may produce an unwanted effect of decreasing the T2 relaxation time, which causes signal decay, as opposed to the typical signal enhancement based on more rapid T1 relaxation produced by appropriate amounts of the agent (Fig. 3).

Given the observed results, the expectation that Gd-DTPA might speed up the MR procedure obviating T2-weighted sequences will not be realized. Another early expectation—based on an analogy with CT—that contrast would significantly improve sensitivity, is also not entirely fulfilled. However, as in the case of two of our patients with metastatic disease, punctate foci of BBB breakdown may be more conspicuous after Gd-DTPA. It should be noted that slice thickness of 10 mm and the slight motion of the patients between the pre- and post-Gd-DTPA sequences detracted from a truly rigorous analysis of the comparison. It does conform to the CT analogy, however, in that early generation CT scanners with less than optimal image quality were those that especially benefited from a contrast agent.

The role of Gd-DTPA in helping to characterize disease was limited. When enhancement was seen, however, definite evidence of perfusion into and BBB breakdown around the

lesion was obtained. Such information is analogous to that obtained with contrast-enhanced CT. Both techniques can mask the presence of underlying hemorrhage if contrast-only studies are performed. The separation of tumor and edema is inaccurate on CT or MR even when a focal-enhancing lesion surrounded by low density is seen. All that is shown is the site of greatest BBB disruption, not tumor margins. Another observation dispels the misconception that contrast enhancement correlates with tumor margins (or the degree of malignancy). A number of tumors (both in this series and elsewhere) either did not enhance at all or exhibited only select foci of enhancement within a much larger tumor mass, despite their malignancy.

In view of this limited early experience, it is perhaps premature to discuss the eventual rational use of Gd-DTPA in MR of the brain. Certain preliminary points can be made, however. It is an open question whether Gd-DTPA will be used as liberally as iodinated agents are in CT for initial screening studies. The optimal sensitivity of T2-weighted sequences will ensure their routine use unless new, more sensitive sequences are developed. Nevertheless, when the information that Gd-DTPA can provide is needed, its use will significantly aid the characterization of disease on MR images. The major role for Gd-DTPA will likely be the identification of active BBB disruption, especially in patients who are known to have underlying CNS disease. Thus, once the screening T2-weighted sequence shows abnormalities, a T1-weighted sequence with Gd-DTPA may well be obtained to characterize the activity of the process. For example, in the population over the age of 65, a high incidence of abnormal high-signal foci on T2-weighted sequences is known to exist. The use of Gd-DTPA may be routine in this age group when MR is ordered to look for metastases, recent infarction, or some other process that disrupts the BBB. Such active processes should enhance on T1-weighted sequences, differentiating them from the underlying chronic high-signal foci on T2-weighted sequences. Of course, if hemorrhage (e.g., hypertensive stroke) is in the differential diagnosis, both a pre- and post-Gd-DTPA T1-weighted sequence may be needed. Gd-DTPA may be used when searching for pituitary microadenomas. The lack of a BBB in the pituitary will allow enhancement of its extracellular space and show the hypercellular or cystic microadenoma as a nonenhancing focus. In patients with previously diagnosed infection or tumor who are undergoing therapy, Gd-DTPA will be useful during follow-up in evaluating response to therapy, identifying new foci within surrounding edema, or separating such foci from demyelination due to radiation therapy.

REFERENCES

1. Felix R, Schorner W, Laniado M, et al. Brain tumors: MR imaging with Gadolinium-DTPA. *Radiology* **1985**;156:681–688
2. Graif M, Bydder GM, Steiner RE, Niendorf P, Thomas D, Young I. Contrast-enhanced MR imaging of malignant brain tumors. *AJNR* **1985**;6:855–862
3. Bydder GM, Niendorf P, Young I. Enhancement of cervical intraspinal tumors with intravenous Gd-DTPA. Abstract no. 49. Presented at the 71st annual meeting of the Radiological Society of North America, Chicago, November **1985**
4. Bradley W, Brant-Zawadzki M, Knop R, et al. Gd-DTPA in MR imaging of malignant brain tumors. Abstract no. 321. Presented at the 71st annual meeting of the Radiological Society of North America, Chicago, November **1985**
5. Berry I, Brant-Zawadzki M, Osaki L, Brasch B, Murovic J, Newton T. Gd-DTPA in clinical MR of the brain. 2: Extraaxial lesions and normal structures. *AJNR* **1986**;7:789–793
6. Berry I, Brant-Zawadzki M, Brasch R, et al. T1 and T2 values in enhancing (Gd-DTPA) vs nonenhancing brain lesions on MR imaging. Abstract. Presented at the 71st annual meeting of the Radiological Society of North America, Chicago, November **1985**
7. Bell BA, Symon L, Branston N. CBF and time thresholds for the formation of ischemic cerebral edema and effect of reperfusion in baboons. *J Neurosurg* **1985**;62:31–42
8. Brant-Zawadzki M, Norman D, Newton T, et al. Magnetic resonance of the brain: the optimal screening technique. *Radiology* **1984**;152:71–77

Gd-DTPA in Clinical MR of the Brain: 2. Extraaxial Lesions and Normal Structures

Isabelle Berry[1, 2]
Michael Brant-Zawadzki[1]
Luci Osaki[1]
Robert Brasch[1]
Judith Murovic[3]
Thomas H. Newton[1]

Fifteen patients with suspected extraaxial tumors were evaluated with MR before and after intravenous injection of Gadolinium-DTPA (Gd-DTPA). Meningiomas (7), neurinomas (4), chordomas (2), a previously irradiated dural metastasis, and a giant aneurysm were studied. All the lesions except the dural metastasis enhanced. In two patients with asymptomatic meningiomas, the use of Gd-DTPA with MR allowed definitive diagnosis of the lesions when the routine MR did not. Gd-DTPA also provided improved definition of intracranial tumor margins, produced differential enhancement of dura and nasopharyngeal mucosa from tumor, and caused enhancement of the choroid plexus, some venous structures, the pituitary gland, and its stalk. The enhancement of the pituitary suggests a role for Gd-DTPA in the diagnosis of microadenomas. Routine T2-weighted images without Gd-DTPA were useful in differentiating neurinomas from meningiomas. Judicious use of Gd-DTPA should improve the ability of MR to detect extraaxial lesions, delineate their extent, and characterize their perfusion.

Extraaxial lesions offer a different challenge for MR than do intraaxial ones. Their location on the periphery of the brain—and therefore the edges of an axial section—makes them less conspicuous and subject to partial volume averaging with CSF. These lesions may be calcified (e.g., meningioma) or they may possess tissue with signal characteristics similar to normal brain (e.g., neurinoma). Both factors can contribute to making their MR signal similar to normal brain parenchyma. Indeed, problems with the identification of extraaxial lesions on routine MR have been encountered [1–3]. Unlike the brain, however, these extraaxial lesions lack a blood-brain barrier (BBB). Therefore, most of them should be ideal candidates for enhancement with a paramagnetic contrast agent such as Gd-DTPA [4]. The evaluation of this agent for this purpose is the topic of our study. Because such tumors often abut the normal brain, meninges, and even the nasopharynx, the enhancement characteristics of these structures are also briefly considered.

Subjects and Methods

A total of 15 patients form the basis of this study. Their lesions consisted of meningioma (7), neurinoma (4), chordoma (2), dural metastasis from prostate primary (1), and giant cavernous aneurysm (1). All the solid tumors were verified histologically; the aneurysm by angiography.

The patient selection criteria, MR sequences, and dose of Gd-DTPA delivered were the same as those described in the preceding article [5]. The same sequential acquisition of long (2000 msec) and short (500 msec) TR sequences was performed. It is notable that five of the seven patients with meningioma were specifically referred for the MR study by their clinicians because of the difficulty in delineating the lesion with CT based on location (e.g., foramen magnum).

Regions of interest were defined within the lesions, and the intensity values obtained were used for quantitative analysis of relaxation effects, the topic of a previous report [6]. Visible enhancement of the lesions was scored on a 0–2 basis by experienced observers (IB, MBZ):

This article appears in the September/October 1986 issue of *AJNR* and the December 1986 issue of *AJR*.

Received December 20, 1985; accepted after revision April 2, 1986.

Presented at the American Society of Neuroradiology, San Diego, CA, January 1986.

This work was supported in part by Berlex Laboratories, New Jersey.

[1] Department of Radiology, University of California, San Francisco, CA 94143. Address reprint requests to M. Brant-Zawadzki, Dept. of Radiology C309, UCSF School of Medicine, San Francisco, CA 94143.

[2] Department of Neuroradiology, Hôpital Purpan, Toulouse, France.

[3] Department of Neurosurgery, University of California, San Francisco, CA 94143.

***AJR* 147:1231–1235, December 1986**
0361–803X/86/1476–1231
© American Roentgen Ray Society

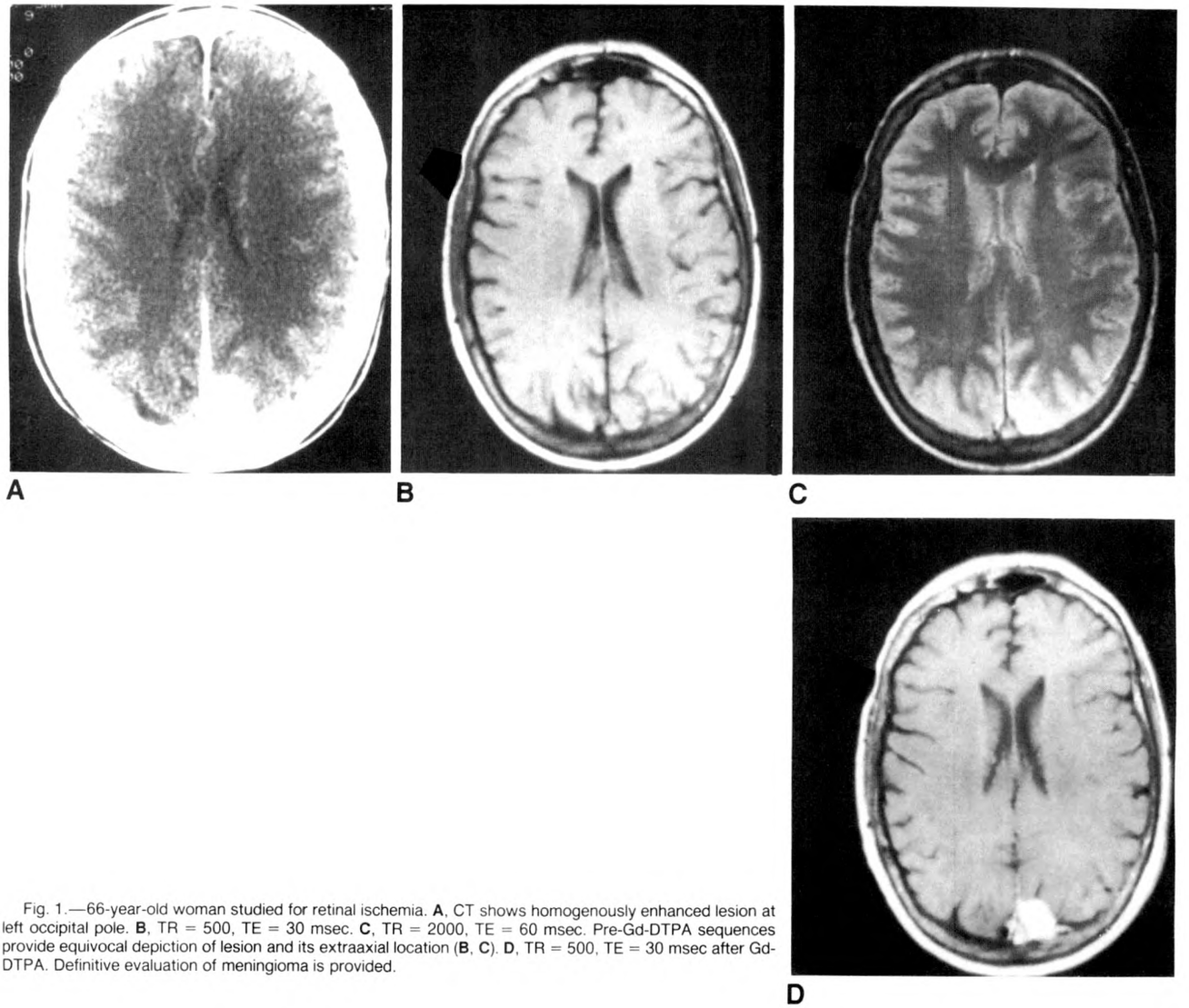


Fig. 1.—66-year-old woman studied for retinal ischemia. **A**, CT shows homogenously enhanced lesion at left occipital pole. **B**, TR = 500, TE = 30 msec. **C**, TR = 2000, TE = 60 msec. Pre-Gd-DTPA sequences provide equivocal depiction of lesion and its extraaxial location (**B**, **C**). **D**, TR = 500, TE = 30 msec after Gd-DTPA. Definitive evaluation of meningioma is provided.

0 = no enhancement, 1 = equivocal enhancement (detected only if the pre-Gd-DTPA image was available for side-by-side comparison), and 2 = definite enhancement. Normal structures that were included in the analysis included large arteries, veins, dura, gray and white matter, pituitary stalk and gland, choroid plexus, and nasopharyngeal mucosa.

Results

Enhancement with Gd-DTPA was noticeable in all but one of these lesions and was best seen on the initial short TR (T1-weighted) sequence obtained after Gd-DTPA. The one exception was a nonenhancing dural metastasis in a patient who had undergone whole cranium radiation (3000 rad) for bone involvement by metastases from prostate carcinoma.

Enhancement with Gd-DTPA improved the conspicuousness of all the meningiomas and, in two patients, allowed the definitive diagnosis to be made (Fig. 1). In both patients, the lesions were asymptomatic and discovered incidentially on CT done for other reasons. The routine MR images before contrast did not provide reliable identification of the lesion in one patient, and were not definitive of an extraaxial lesion in the other. Following Gd-DTPA, the homogenous enhancement of the lesions, their extraaxial location, and broad dural base were easily seen.

Unlike CT, MR allowed enhancement of the meningiomas, while arteries coursing through the lesions or adjacent to them did not enhance. Therefore, MR provided better anatomic information for the surgeon (Fig. 2). The normal dura enhanced and washed out quickly, but meningiomas retained their enhancement longer. This allowed differentiation of a small meningioma of the planum sphenoidal from the surrounding dura in a patient with visual loss (Fig. 3). Finally, after Gd-DTPA, the margins of several of the meningiomas

(corresponding to the capsule seen at surgery) exhibited a hyperintense appearance when compared with the body of the tumor.

All the neurinomas were easy to identify as high-intensity foci on the routine T2-weighted images before Gd-DTPA. In all cases their enhancement with the agent contributed little to the diagnosis. In the cases of chordoma, their high intensity on T2-weighted images before Gd-DTPA and their prominent early enhancement made differentiation of their margins from adjacent nasopharyngeal mucosa difficult. The mucosa faded on subsequent images, however, while the chordoma's enhanced intensity persisted (Fig. 4). Also of interest was the

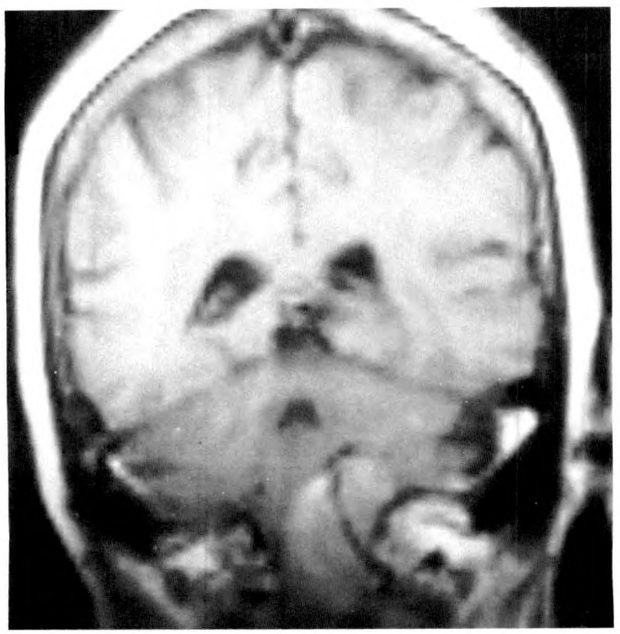
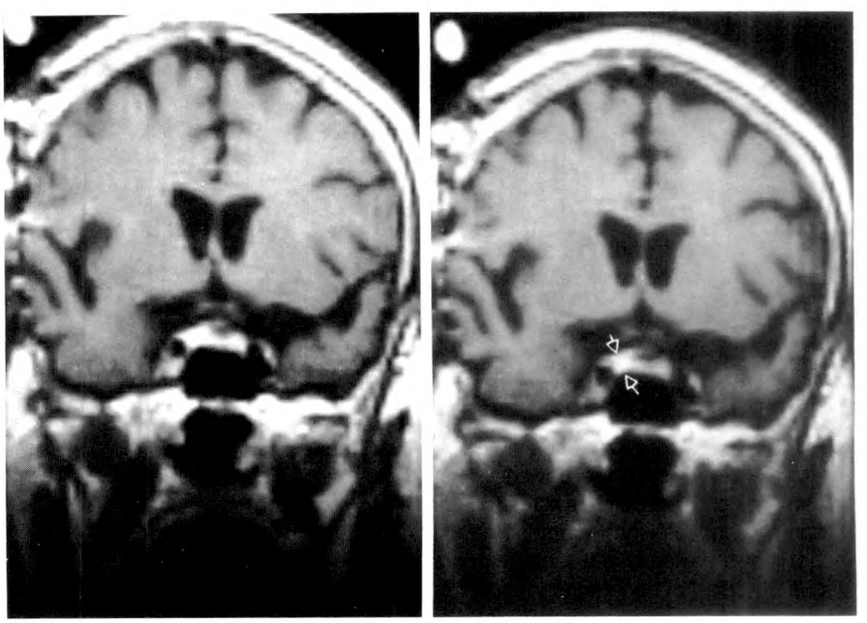


Fig. 2.—67-year-old woman with meningioma of foramen magnum. MR image (TR = 500, TE = 30 msec) after Gd-DTPA shows enhancing lesion, with vertebral artery within it seen because of signal void from rapid flow.



Fig. 4.—20-year-old man with chordoma of clivus. MR (TR = 500, TE = 30 msec) immediately after Gd-DTPA delineates tumor within nasopharynx. Note lesser intensity of intracranial component. Pituitary gland and basilar venous plexus enhance markedly on this early sequence, as does nasopharyngeal mucosa.



A B

Fig. 3.—70-year-old woman with visual loss in right eye due to meningioma of planum sphenoidal. **A**, **B**, TR = 500, TE = 30 msec. Sequences obtained 5 and 45 min after Gd-DTPA. Small meningioma (*arrows*) retains contrast agent longer than dura of cavernous sinus.

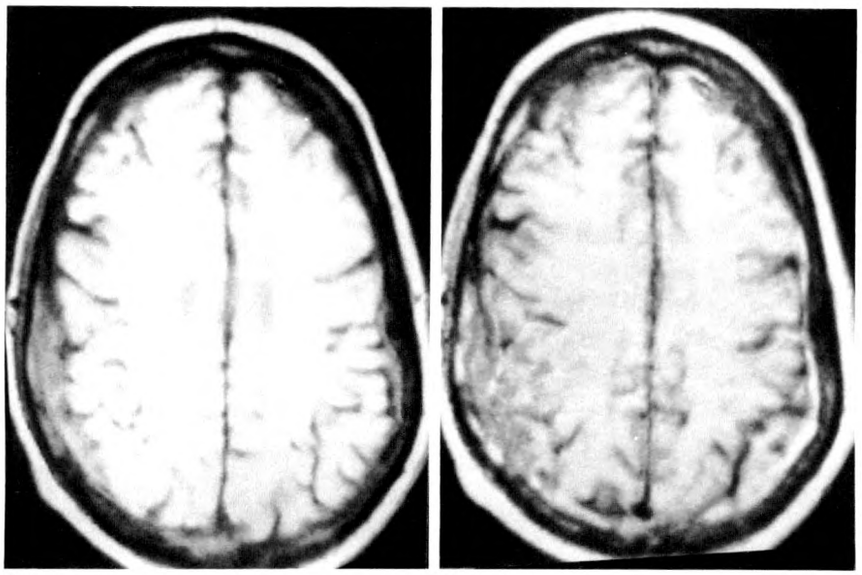


Fig. 5.—58-year-old man previously treated (3000 rad) for metastases to cranial vault from prostatic carcinoma. **A**, TR = 500, TE = 30 msec. **B**, TR = 500, TE = 30 msec after Gd-DTPA. Extraaxial mass is seen in high, right parietal convexity with no definite enhancement of mass itself; note dural and leptomeningeal enhancement.

one chordoma's intracranial component that was less enhanced than its extracranial portion.

The lack of definite enhancement of the dural metastasis (Fig. 5). was probably due to the patient's previous radiation therapy, which may have affected the vascularity of the dura. The lesion was hyperdense on CT before iodinated contrast, showed no obvious enhancement after contrast, and appeared relatively low in intensity on pre-Gd-DTPA MR sequences. A densely fibrotic, thickened region of dura infiltrated with prostatic carcinoma was found at autopsy 1 month later.

Finally, MR helped define a partially thrombosed, giant, cavernous aneurysm (Fig. 6), thought possibly to represent a parasellar meningioma on CT. Gd-DTPA added no diagnostic information, but did enhance slow component of flow in the lumen as well as the thrombus (presumably due to recanalized channels with slow flow). The slowed flow could be defined on the basis of second-echo rephasing [7] prior to Gd-DTPA on the T2-weighted images.

Of interest was the lack of visible enhancement of the gray or white matter, although the pituitary stalk and gland showed a prominent increase in signal after Gd-DTPA. Slowly flowing blood in veins and dural sinuses exhibited varying degrees of enhancement, as did the choroid plexus; all these structures enhanced early and washed out on the subsequent sequences.

Discussion

The difficulties encountered in identifying meningiomas with MR relate to several factors: small size, plaquelike configuration, and relatively isointense characteristics on routine sequences. These may all contribute to the nondiagnostic appearance of these lesions. On the other hand, their usually typical vascularity and lack of a BBB make meningiomas ideal lesions for enhancement with Gd-DTPA. The role of Gd-DTPA in this context needs some clarification. Most meningiomas that produce symptoms or signs of mass effect on adjacent brain will readily be recognized on routine MR images because of the anatomic distortion produced, if not by altered signal characteristics. However, when characteristic symptoms of visual loss, cavernous sinus involvement, or lower cranial nerve dysfunction suggest a planum sphenoidal, parasellar, or foramen magnum lesion, Gd-DTPA should be used routinely. Appropriate timing of the study may be necessary to separate small lesions from adjacent dura.

Neurinomas did not require Gd-DTPA for definitive evaluation in our series. However, no solely intracanalicular lesion was included. Whether Gd-DTPA will aid the identification of such small tumors remains to be seen. The similar degree of enhancement of meningiomas and neurinomas with Gd-DTPA abolishes their distinctly different intensity features on pre-Gd-DTPA T2-weighted sequences. Neurinomas routinely showed high intensity on such sequences, whereas meningiomas do so rarely in our experience, and none of the ones in this series exhibited such intensity. Finally, the limited experience described suggests other important aspects of Gd-DTPA. The potential value of Gd-DTPA in differentiating nasopharyngeal neoplasms is suggested by the rapid enhancement and washout of normal tissue in this region and the temporally differential enhancement of the chordoma invading it.

The enhancement of the normal pituitary suggests a role for Gd-DTPA similar to that of iodinated agents with CT in diagnosing microadenomas. The lack of enhancement of normal gray matter and normal arterial structures is a relative, albeit minor, shortcoming. Further experience with Gd-DTPA is needed before its complementary role to routine MR can be fully defined.

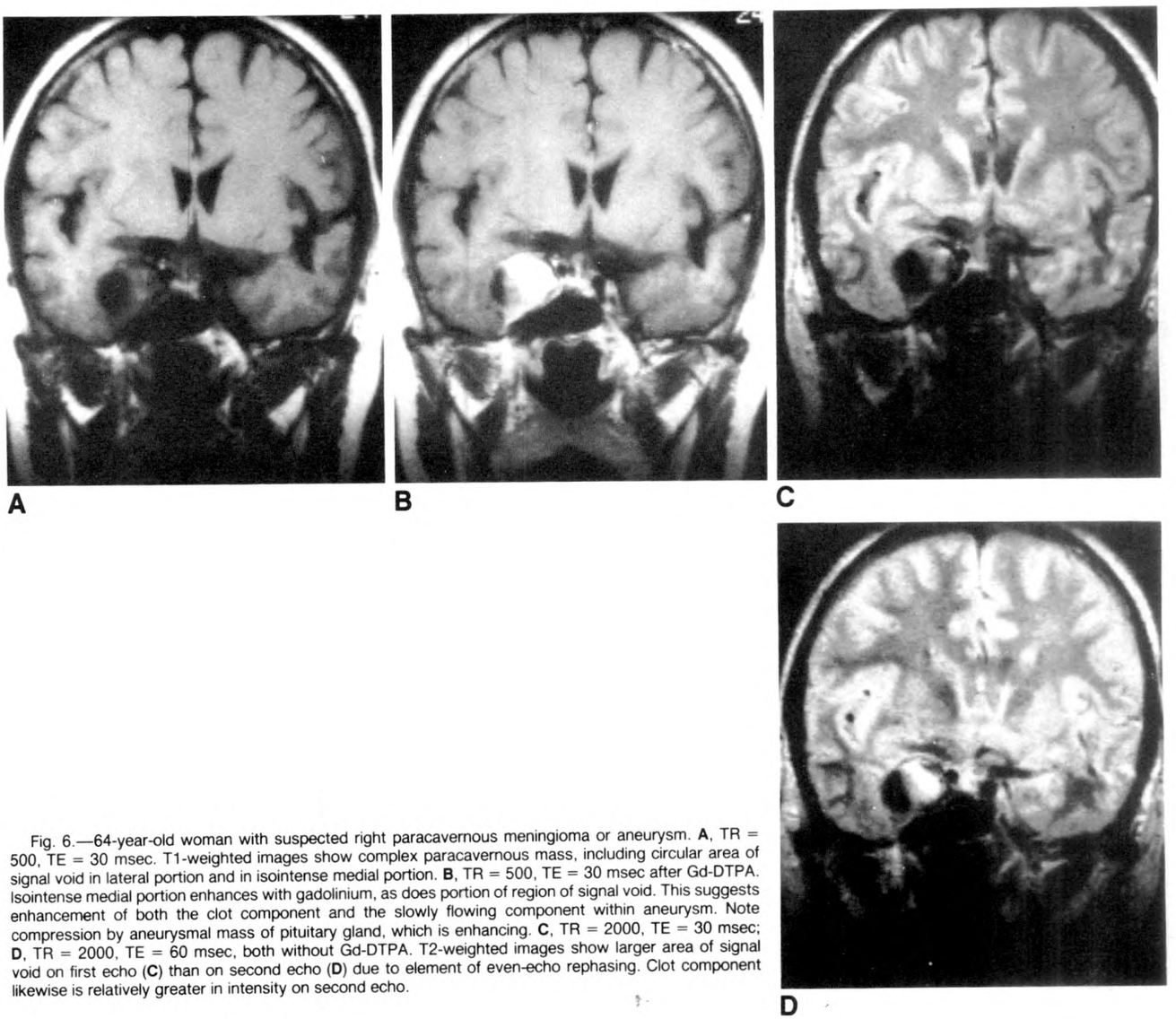


Fig. 6.—64-year-old woman with suspected right paracavernous meningioma or aneurysm. **A**, TR = 500, TE = 30 msec. T1-weighted images show complex paracavernous mass, including circular area of signal void in lateral portion and in isointense medial portion. **B**, TR = 500, TE = 30 msec after Gd-DTPA. Isointense medial portion enhances with gadolinium, as does portion of region of signal void. This suggests enhancement of both the clot component and the slowly flowing component within aneurysm. Note compression by aneurysmal mass of pituitary gland, which is enhancing. **C**, TR = 2000, TE = 30 msec; **D**, TR = 2000, TE = 60 msec, both without Gd-DTPA. T2-weighted images show larger area of signal void on first echo (**C**) than on second echo (**D**) due to element of even-echo rephasing. Clot component likewise is relatively greater in intensity on second echo.

REFERENCES

1. Zimmerman RD, Fleming CA, Saint-Louis L, Lee B, Manning J, Deck M. Magnetic resonance imaging of meningiomas. *AJNR* **1985**;6:149–157
2. New P, Bachow T, Wismer G, Rosen B, Brady T. MR imaging of the acoustic nerves and small acoustic neuromas at 0.6 T. *AJNR* **1985**;6:165–170
3. Mikhael M, Ciric I, Wolff A. Differentiation of cerebellopontine angle neuromas and meningiomas with MR imaging. *J Comput Assist Tomogr* **1985**;9:852–856
4. Bydder G, Kingsley P, Brown J, Niendorf H, Young I. MR imaging of meningiomas including studies with and without Gadolinium-DTPA. *J Comput Assist Tomogr* **1985**;9:690–697
5. Brant-Zawadzki M, Berry I, Osaki L, Brasch R, Murovic J, Norman D. Gd-DTPA in clinical MR of the brain. 1: Intraaxial lesions. *AJNR* **1986**;7:781–788
6. Berry I, Brant-Zawadzki M, Osaki L, et al. T1 and T2 values in enhancing (Gd-DTPA) vs nonenhancing brain lesions on MR imaging. Abstract. Presented at the 71st annual meeting of the Radiological Society of North America, Chicago, November **1985**
7. Waluch V, Bradley W. NMR even echo rephasing in slow laminar flow. *J Comput Assist Tomogr* **1984**;8:594–598

Book Reviews

Atoms, Radiation, and Radiation Protection. By James E. Turner. New York: Pergamon Press, 324 pp., 1986. Soft cover

This textbook is a collection of material that has been used in teaching over many years. The first three chapters, "Atomic Physics," "Atomic Structure," and "The Nucleus," will be of general interest to radiologists. The material is presented in a lucid and interesting manner. The remaining material is essentially a textbook of physics and radiation protection, at a level for students in physics. The presentation of problems with their solutions in this text will be helpful to students.

This book might also serve as a reference for radiation safety officers and as a source for the preparation of courses for nonphysicists.

The chapters on biologic effects are the weakest, as one would expect in a physics test. This is particularly true in the sections dealing with clinical response. However, physicists, nuclear engineers, and environmental health scientists with a good mathematics background will find this a useful book.

Reynold F. Brown
University of California, San Francisco
San Francisco, CA 94143

Diagnostic Patient Studies in Surgery. By Bernard Sigel. Philadelphia: Lea & Febiger, 450 pp., 1986. $60

This is a well-illustrated text primarily written to assist surgeons in the diagnostic workup of patients. The author believes that errors that may occur in the diagnostic workup are often related to the choice of tests to perform and the reasons for the choices. Since half of this book is devoted to imaging and half to endoscopy, function studies, and MR it should also benefit radiologists who would like to participate in the complete workup of surgical patients. Part 1 covers imaging and provides a comprehensive overview of all imaging techniques with particular reference to surgical problems. Although the individual chapters are written by specialists in their field, there does not appear to be any overlap between the chapters. Some of the individual chapters, such as CT, are excellent introductions for those new to the field. Part 2, on endoscopy, function studies, and MR, offers radiologists an updated review of the other half of the surgical workup. The chapters on gastrointestinal endoscopy are excellent and important for radiologists. Both radiologists and surgeons can benefit from this book.

Leonard Goldberg
Toronto, Ontario M6R 2M2
Canada

Percutaneous Drainage of Subphrenic Abscess: A Review of 62 Patients

Peter R. Mueller[1]
Joseph F. Simeone
Rodney J. Butch
Sanjay Saini
Susan A. Stafford
Luis Gaston Vici
Carlos Soto-Rivera
Joseph T. Ferrucci, Jr.

Sixty-two patients who presented with subphrenic abscesses had the abscesses drained percutaneously. Diagnosis of a subphrenic collection was usually made with sonography. Initial percutaneous drainage was accomplished with a combination of sonography and fluoroscopic guidance. More recently (in the last 31 cases) most drainages were done with sonographic guidance alone. Successful catheter drainage was achieved in 85% with a complication rate of 4.8%. Failure of catheter drainage (defined as any patient who was not cured by percutaneous drainage alone) occurred in patients with multiple collections or in whom the primary cause of the abscess necessitated surgery, for example, perforated ulcer, acute cholecystitis. Considerations for successful drainage include understanding the anatomy of the subphrenic space, recognizing the importance of a correct access route (avoidance of the pleura and lung), and the long time necessary for adequate drainage (longer than 10 days in 60%). An angled subcostal approach to the subphrenic space was used in 56 (90%) of 62 cases. No complications occurred in this group. The one pneumothorax that occurred in the remaining six cases was a direct result of using an intercostal approach through the parietal pleura into a subphrenic collection. We conclude that percutaneous drainage is a safe and effective method of treatment of subphrenic abscesses.

When a percutaneous drainage of an intraabdominal abscess is performed, the origin of the abscess, its relationship to adjacent anatomic spaces, the type of content, and the presence of fistulas are the main factors that determine the outcome. These points are also important in the results achieved with percutaneous drainage of bilomas [1, 2], lymphoceles [3], enteric fistulas [4], amebic abscesses [5], pancreatic abscesses [6], pyogenic intrahepatic abscesses [7], and psoas abscesses [8]. However, despite the common occurrence of subphrenic abscesses in posttraumatic and postoperative patients [9, 10], the specific factors that relate to the results of percutaneous drainage have not been stressed [11–15].

We report a series of 62 subphrenic abscesses treated by percutaneous drainage with a success rate of approximately 85% and a complication rate of 1.6%. Analysis of the cases shows that important factors in the outcome concern the anatomic location, the determination of the correct access route (avoidance of the pleura and the lung), and the duration of catheter drainage (generally longer than 10 days).

Materials and Methods

Sixty-two cases of subphrenic abscesses were percutaneously drained under radiologic guidance during 5 years between January 1981 and December 1985. Twenty of these cases were included in an earlier report [14]. In 52 of the patients, collections were postoperative complications after biliary (38) or gastrointestinal (14) surgery. In the other 10 patients, the cause was diffuse ascites with subphrenic loculations (three patients), gallbladder perforation (two), perforated ulcer (one), perforated adenocarcinoma of the colon (one), Crohn's disease (one), and uncertain cause (two). Forty of the collections were located in the right subphrenic space and 16 in the left. Six patients had bilateral collections.

Received May 20, 1986; accepted after revision July 24, 1986.

[1] All authors: Department of Radiology, Massachusetts General Hospital and Harvard Medical School, Boston, MA 02114. Address reprint requests to P. R. Mueller.

AJR 147:1237–1240, December 1986
0361–803X/86/1476–1237
© American Roentgen Ray Society

Detection and aspiration of an abscess and insertion of a catheter for therapeutic drainage were usually made by using sonography, CT, and/or fluoroscopy (Table 1).

Technique

Fifty-six (90%) of the 62 catheters were inserted via an anterior or lateral subcostal access route (Fig. 1). Needle aspiration and subsequent catheter placement were purposely not done via a direct intercostal approach to avoid puncturing the pleura or lung (Figs. 2 and 3). Attempts were made to ensure that the initial insertion of a diagnostic needle and/or catheter were positioned below the seventh rib anteriorly or 10th rib laterally. After initial identification of the subphrenic abscess, a 20-gauge needle angled in a caudad to cephalad direction was directed toward the potential space between the liver/spleen and the lateral abdominal wall (Fig. 1). After confirmation of the presence of purulent material and the location of needle, the drainage catheter was placed by either the Seldinger or the trocar method. With either method, a guidewire was usually used to enter the potential space medial to the lateral abdominal wall. Even when trocar placement was used, a guidewire was placed through the cannula after insertion for use as a "protected" guide [16]. Abscess drainage catheters of 9- to 14-French size were used. Catheter care and follow-up was done in the standard manner [11–14].

TABLE 1: **Guidance Technique Used for Catheter Placement**

Stage: Study	No. of Cases (%) (n = 62)	
	First 31 Cases	Last 31 Cases
Diagnosis:		
Sonography	24 (77)	21 (68)
CT	4 (13)	9 (29)
Fluoroscopy	3 (10)	1 (3)
Treatment:		
Sonography	3 (10)	20 (65)
CT	1 (3)	4 (13)
Fluoroscopy	4 (13)	1 (3)
Combined[a]	23 (74)	6 (19)

[a] Sonography and fluoroscopy; CT and fluoroscopy.

Results

Successful catheter drainage (defined as no surgical intervention required) was achieved in 43 of 62 patients. In nine patients the cavity was completely drained, but surgery was performed for other reasons. This included failure of the referring physician to believe that percutaneous drainage would be successful (four patients) and curative surgery for the underlying process that caused the abscess (five patients). The latter included biliary/small-bowel fistula (two), perforated cholecystitis (one), perforated duodenal ulcer (one), and perforated adenocarcinoma of the colon (one). One patient died of unrelated causes and was not considered in the overall results. Thus, an overall success rate of 85% (52 of 61) was achieved.

Nine patients were considered failures of percutaneous treatment. Seven of these had multiple abscesses in the subphrenic space and other noncontiguous locations. They required surgical exploration and drainage for complete cure. Two other patients who had unsuccessful drainages had perforation of the gallbladder from acute cholecystitis (one) and diffuse peritonitis from Crohn's disease (one).

Catheter drainage required for cure of the subphrenic abscesses was generally longer than necessary for abscesses in other locations [11–13]. Twenty cases required catheter drainage for less than 7 days and 32 required drainage for 10 days or longer. In the latter group, 24 (75%) of the 32 had a catheter in place for at least 21 days. Eleven patients there had a low-flow fistulous communication with the biliary tree or small bowel or an enteric biliary anastomosis (Fig. 3).

Complications of the drainage procedure were uncommon (4.8%): Two patients developed septicemia (defined as hypotension with positive blood cultures) after catheter insertion. Both of these patients were treated successfully with antibiotics and fluid therapy. One patient developed pleural contamination and resulting empyema from inadvertent entrance of the catheter into the pleural space.

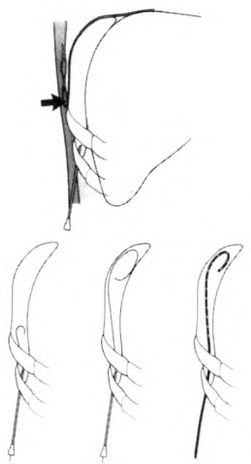


Fig. 1.—Diagram of subcostal approach to subphrenic space.

***Top,* After confirmation of subphrenic collection by sonography or CT, needle is placed subcostally below pleura reflection (*arrow*). Needle is directed laterally and cephalad to inferior extent of subphrenic collection.**

***Bottom,* Course and position of drainage catheter placed via anterolateral subcostal approach. Note that guidewire prevents perforation through diaphragm.**

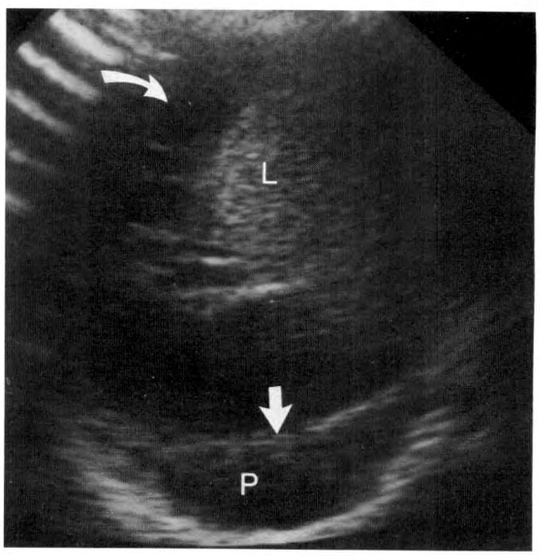


Fig. 2.—Example of ability of sonography to delineate anatomic relationships of subphrenic space. Transverse sonogram demonstrates excellent visualization of location and extent of subphrenic collection (*curved arrow*). Note good delineation of relationship between diaphragm (*straight arrow*), pleural effusion (P), and liver (L).

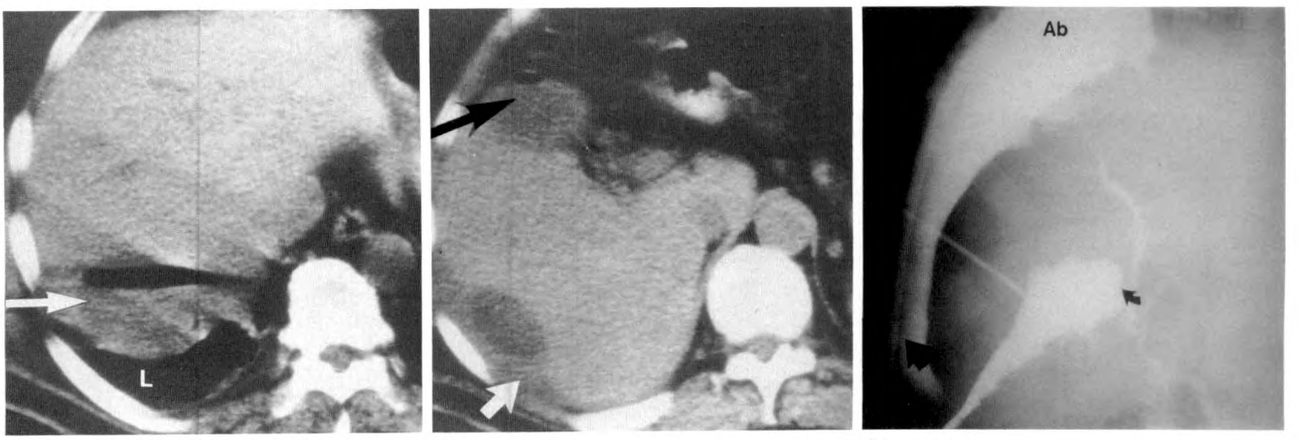


Fig. 3.—Example of lateral subcostal approach to avoid puncturing lung in high subphrenic abscess in a 52-year-old man 2 weeks after cholecystectomy, who had fever and right shoulder pain.

***A*, CT scan demonstrates air-fluid level in most cephalad portion of subphrenic space. Note that direct approach (*arrow*) would result in transgression of lung (L).**

***B*, Scan 3 cm inferior depicts caudal extent of collection (*short arrow*). Aspiration of abscess and insertion of drainage catheter were performed in this portion of collection. Second collection is in gallbladder bed (*black arrow*).**

***C*, Frontal radiograph showing contrast material in subphrenic cavity 2 days after insertion of catheters into subphrenic spaces and gallbladder bed. Actual entrance to abscess is subcostal (*straight arrow*), well below inferior extent of pleura. Ab refers to that portion of abscess seen on CT scan (*A*). Injection of catheter in gallbladder bed demonstrates communication with biliary system (*curved arrow*) and explains cause of subphrenic abscess. Catheter in gallbladder bed stopped draining after 5 days and was removed 2 days later. Subphrenic catheter remained in place for 3 weeks.**

Discussion

In the postsurgical and/or posttraumatic patient, subphrenic abscesses are most commonly diagnosed by sonography and CT. In their classic treatise describing surgical experience with 3372 patients, Ochsner and Graves [9] stressed that drainage should be performed via an extraperitoneal and extrapleural approach. Early radiologically guided procedures were performed according to this surgical dictum and also employed an extrapleural and/or extraperitoneal approach to the subphrenic space [11–13, 17]. Percutaneous drainage was performed via a posterior angled approach through the back with the patient positioned prone. More recently, others [10] have stressed that a transperitoneal approach can be performed safely if pleural contamination is avoided. This makes drainage through the retroperitoneum unnecessary.

The subphrenic collections in this series were detected by sonography, CT, and fluoroscopy (Table 1). Initially, sonography was used most often for diagnosis, but was combined with fluoroscopy for catheter placement. Fluoroscopy was helpful in determining the exact location of the pleura and led to an understanding of the anatomy of the subphrenic space. More recently (last 31 cases), sonography has been used not only for diagnosis but also for monitoring catheter placement. During the same time, the use of CT for diagnosis has increased from 13 to 29%, and for guiding the actual catheter insertion from 3 to 13%.

We have successfully used a lateral or anterior subcostal transperitoneal insertion in over 90% of cases. Placement of the catheter so that it enters below the seventh rib anteriorly or 10th rib laterally assures avoidance of contamination of the pleural space (Figs. 1 and 2). The catheter can then be angled in a caudad to cephalad manner until the collection is encountered. Most often in subphrenic collections, the lateral aspect of the liver/spleen is separated from the intercostal muscles and the abdominal wall, and a catheter can be easily directed into the collection.

The most important technical consideration is avoiding contamination of the pleura and lung. Several series have described infrequent but serious complications associated with puncture of the pleura during percutaneous biliary drainage [18, 19] (Fig. 4). However, in patients with a subphrenic collection, the inferior extent of the pleural reflection may be obliterated because of an inflammatory reaction from the adjacent subphrenic abscess. Consequently, transgression through this space may be safe. Ten percent of the cases in our series were drained through an intercostal approach. However, it is difficult to decide prospectively which patients will tolerate an intercostal approach so that complications may be avoided. In most cases, a low subcostal approach is safe, easy, and practical. But in patients in whom a subcostal angulation is not possible, an intercostal puncture provides a viable, though more risky, alternative.

The duration of catheter drainage in 32 (62%) of 52 patients in our series was somewhat longer than the 5–7 days that has been suggested in previous reports [11–13]. One-third of the abscess cavities in our patient group communicated with small bowel or the biliary tree and required several weeks of continuous drainage until the fistula closed. In the other two-thirds, a longer time of drainage was required when compared with intrahepatic abscesses [7]. Other explanations for the greater duration of drainage must be considered. For example, after the contents of an intrahepatic liver abscess have been removed, normal hepatic parenchyma surrounding the collection collapses and granulates around the catheter quite readily. Well-vascularized normal hepatic parenchyma will accelerate the healing process. Subphrenic collections,

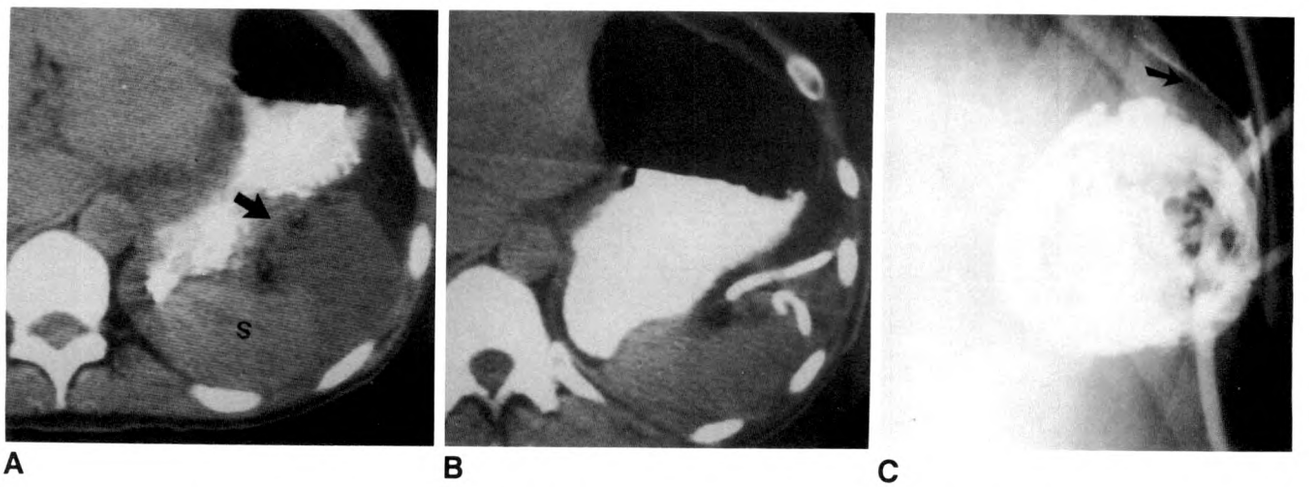


Fig. 4.—Postoperative patient 10 days after extensive pancreatic surgery wih fever and subphrenic collection.

***A*, Transverse CT scan demonstrates small collection (*arrow*) in left subphrenic space bordered posteriorly and inferiorly by spleen (S), thus precluding standard subcostal approach.**

***B*, CT scan showing position of catheter that was placed under CT guidance by using direct intercostal approach into subphrenic collection.**

***C*, Catheter injection 10 days after insertion. Small amount of contrast material extending into pleural space (*arrow*). Catheter eventually became dislodged, and patient developed tension pneumothorax that was relieved by placement of catheter under fluoroscopic guidance.**

however, occupy "potential" intraperitoneal spaces that may not heal as readily as vascularized spaces. Therefore, prolonged, sustained catheter drainage of infected material is required for total evacuation of the infected material. Although there may be improvement in the patient's condition because the purulent material has been removed, continuous drainage may be required for several weeks. As in all cases of abscess drainage, catheter removal should be determined by the quantity and duration of drainage.

Failure of percutaneous drainage to completely cure subphrenic abscesses is predictable and depends on the presence of multiple noncontiguous collections or the cause of the collection. Patients in our series with perforated ulcers and/or gallbladder disease had their subphrenic collections completely drained but still required surgery for the primary problem.

REFERENCES

1. Mueller PR, Ferrucci JT Jr, Simeone JF, et al. Detection and drainage of bilomas: special considerations. *AJR* **1983**;140:715–720
2. Vujic I, Brock JB. Biloma: aspiration for diagnosis and treatment. *Gastrointest Radiol* **1982**;7:251–254
3. White EM, Mueller PR, Ferrucci JT Jr, et al. Percutaneous drainage of postoperative abdominal and pelvic lymphoceles. *AJR* **1985**;145:1065–1069
4. Kerlan R, Jeffrey RB Jr, Pogany AC, Ring EJ. Abdominal abscess with low output fistula: successful percutaneous drainage. *Radiology* **1985**;155:73–75
5. vanSonnenberg E, Mueller PR, Schiffman HR, et al. Intrahepatic amebic abscesses: indications for and results of percutaneous catheter drainage. *Radiology* **1985**;156:631–635
6. vanSonnenberg E, Wittich GR, Casola G, et al. Complicated pancreatic inflammatory disease: diagnostic and therapeutic role of interventional radiology. *Radiology* **1985**;155:335–340
7. Kuligowska E, Conners SK, Shapiro JN. Liver abscess: sonography in diagnosis and treatment. *AJR* **1982**;138:253–256
8. Mueller PR, Ferrucci JT Jr, Wittenberg J, Simeone JF, Butch RJ. Iliopsoas abscess: treatment by CT-guided percutaneous catheter drainage. *AJR* **1984**;142:359–362
9. Ochsner A, Graves A. Subphrenic abscess. *Ann Surg* **1933**;98:961–987
10. Serrano A, Dahl EP, Rubin RH, Ferrucci JT Jr, Mueller PR, Malt RA. Eclectic drainage of subphrenic abscesses. *Arch Surg* **1984**;119:942–945
11. Gerzof SG, Robbins AH, Johnson WC, Birkett DH, Nabseth HD. Percutaneous catheter drainage of abdominal abscesses. *N Engl J Med* **1981**;305:653–657
12. Haaga JR, Alfidi RJ, Harrill AT, et al. CT detection and aspiration of abdominal abscesses. *AJR* **1977**;128:465–477
13. vanSonnenberg E, Ferrucci JT Jr, Mueller PR, Wittenberg J, Simeone JF. Percutaneous drainage of abscesses and fluid collections: technique, results and applications. *Radiology* **1982**;142:1–10
14. vanSonnenberg E, Mueller PR, Ferrucci JT Jr. Percutaneous drainage of 250 abdominal abscesses and fluid collections. Part I. Results, failures, and complications. *Radiology* **1984**; 151:337–341
15. Mueller PR, vanSonnenberg E, Ferrucci JT Jr. Percutaneous drainage of 250 abdominal abscesses and fluid collections. Part II. Current procedural concepts. *Radiology* **1984**;151:343–347
16. vanSonnenberg E, Polansky AD, Wittich GR, et al. Guide wire protection for trocar puncture of fluid collections. *AJR* **1985**;145:831–832
17. vanSonnenberg E, Wittenberg J, Ferrucci JT Jr, Mueller PR, Simeone JF. Triangulation method for percutaneous needle guidance: the angled approach to upper abdominal masses. *AJR* **1981**;137:757–761
18. Neff CC, Mueller PR, Ferrucci JT Jr, et al. Serious complications following transgression of the pleural space in drainage procedures. *Radiology* **1984**;152:335–341
19. Nichols DM, Golding RH, Cooperberg PL, et al. The safe intercostal approach? Pleural complications in abdominal radiology. *AJR* **1984**;142:1013–1018

Portable Real-Time Sonographic and Needle Guidance Systems for Aspiration and Drainage

John P. McGahan[1]
Mark W. Anderson
John P. Walter

One hundred and two aspiration or drainage procedures were reviewed to determine the value of portable sonographic and real-time needle guidance systems. While the majority of thoracenteses or abdominal paracenteses were performed without the aid of real-time guidance, these systems were instrumental in the development of new procedures such as percutaneous cholecystostomy and in the drainage of small fluid collections in critical areas. Portable sonographic guidance was used in 32 cases, mostly for thoracentesis or abdominal paracentesis, but it had its greatest value in guiding drainage procedures at the bedside in critically ill patients. These portable drainage procedures included four cholecystostomies, one nephrostomy, drainage of two abdominal abscesses, and two empyema drainages. Complications included one case of an enterocutaneous fistula and one case of hemoptysis after thoracentesis. The failure rate was less than 7%. The use of portable real-time sonographic and needle-guidance systems has a direct impact on improving patient care.

Sonography has previously been described as a method to aid in the guidance of aspiration and drainage procedures [1, 2]. These procedures were usually performed in the radiology department by use of the sonographic probe to mark the site, depth, and angle, but with the probe removed for needle insertion. Recent technologic advances in sonographic instrumentation have allowed sonographic equipment to be transported throughout the hospital [3]. In addition, most manufacturers have introduced needle-guidance systems that allow for direct needle visualization with real-time sonography [3, 4]. We analyzed the impact and the utility of portable real-time sonography and the use of newer guidance systems in 102 aspiration and/or drainage procedures performed under sonographic guidance over the last year.

Materials and Methods

From the last 4000 exams performed in our department, the charts and sonograms from 102 patients in whom aspiration or drainage procedures were performed under sonographic guidance were retrospectively reviewed. Amniocenteses performed within our department were not included in this series. Data were analyzed as to the site of aspiration, failures, complications, type of guidance systems, type of procedure, and the physical location of the sonographic unit at the time of drainage, that is, at bedside or in the radiology department.

Sonographic guidance of aspiration or drainage was accomplished by using one of two methods. The "conventional" method consisted of marking the site of aspiration on the skin and removing the probe at the time of needle insertion. For instance, in performance of thoracentesis, the sonographic probe was used to mark the site and depth of fluid. A 22-gauge injection needle connected to a 12-ml syringe was passed into the suspected fluid collection and needle suction was applied. If this was unsuccessful, a similar technique was used with a 20-gauge injection needle or a 20-gauge spinal needle. Abdominal paracentesis was performed in a similar manner.

Real-time needle guidance was performed with an ATL (Advanced Technology Laboratories, Bothell, WA) MK600 real-time biopsy guidance system using a roughened Teflon-coated

Received February 3, 1986; accepted after revision June 30, 1986.

[1] All authors: Department of Radiology, Division of Diagnostic Radiology, University of California, Davis, Medical Center, Sacramento, CA 95817. Address reprint requests to J. P. McGahan, Dept. of Radiology, 4301 X St., Room 109R, Sacramento, CA 95817.

AJR 147:1241–1246, December 1986
0361–803X/86/1476–1241
© American Roentgen Ray Society

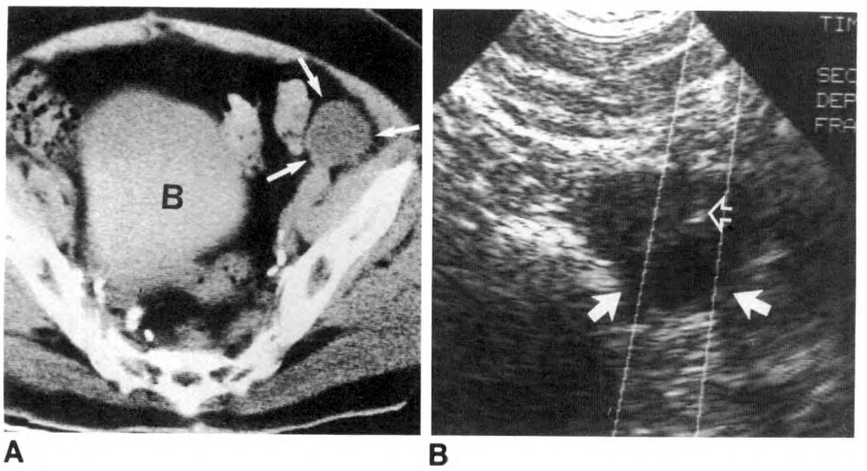


Fig. 1.—Aspiration of lymphocyst.
A, CT scan of pelvis showing well-circumscribed lymphocyst (*arrows*) anterior to left ilium. B = bladder.
B, Under sonographic control, a 22-gauge roughened needle (*open arrow*) was placed into lymphocyst (*arrows*) for complete aspiration.

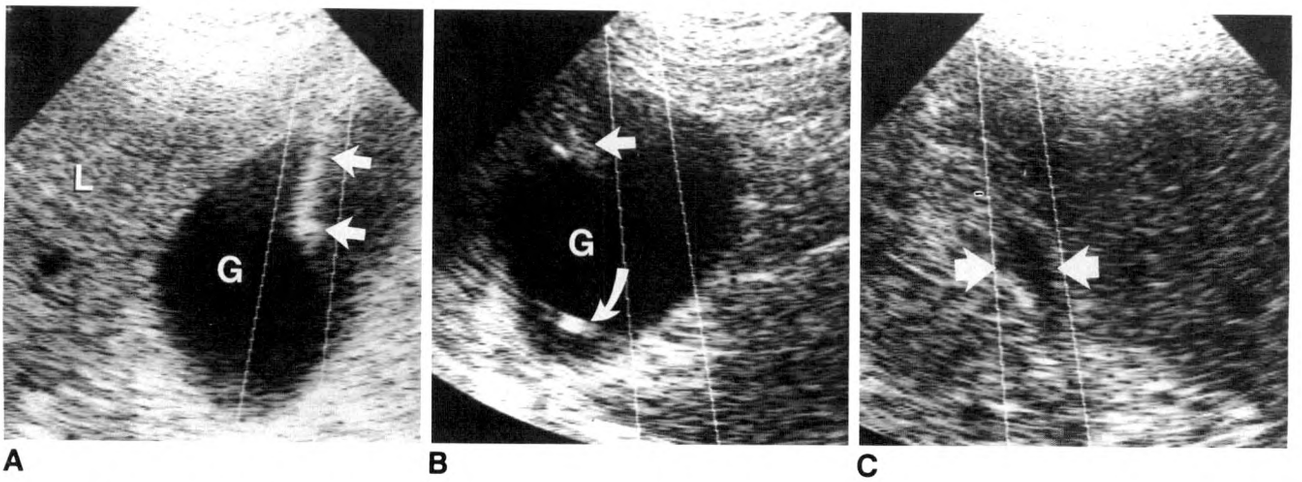


Fig. 2.—Percutaneous cholecystostomy.
A, Roughened Teflon-coated 22-gauge needle placed into gallbladder under sonographic guidance (*arrows*). G = gallbladder; L = liver.
B, Catheter placed through gallbladder wall under sonographic control (*arrow*) showing a portion of catheter coiled within gallbladder lumen (*curved arrow*). G = gallbladder.
C, Gallbladder markedly decreased in size after percutaneous drainage (*arrows*).

needle (Cook, Bloomington, IN). In this technique, a sterile glove was placed over the sonographic probe, the biopsy guide was attached to the transducer, and the needle was inserted into the target area under real-time visualization (Figs. 1–3).

Drainage was performed by either the conventional technique or real-time sonography using a variety of catheters. When a drainage procedure was performed, an initial fluid aspirate was usually obtained after passage of a 20- or 22-gauge needle under one of the two techniques outlined previously. A drainage catheter was then inserted under either sonographic or fluoroscopic control after passage of an 18-gauge sheath needle [2]. Alternatively, when a trocar method of catheter insertion was performed, the catheter was usually passed using real-time sonographic guidance. When the trocar was sufficiently larger than the opening of the biopsy guide, the sonographic transducer was placed to the side of the catheter, which allowed for trocar visualization under real-time control [5] (Fig. 4).

Results

Results are tabulated in Table 1. In general, the most frequently performed procedures were thoracentesis or thoracic fluid drainage. Suspected pleural fluid collections were aspirated by the "conventional" technique. Abdominal paracentesis was usually performed in a similar manner.

In general, the biopsy guidance system was most helpful in aspiration and drainage procedures involving the gallbladder, kidney, or other portions of the abdomen and pelvis. The real-time system was used in 36 cases. Real-time guidance was especially useful in aspiration of small fluid collections that were once considered too small or located in too critical an area for attempted "conventional" aspiration (Figs. 1 and 3). Real-time guidance was also used in most percutaneous

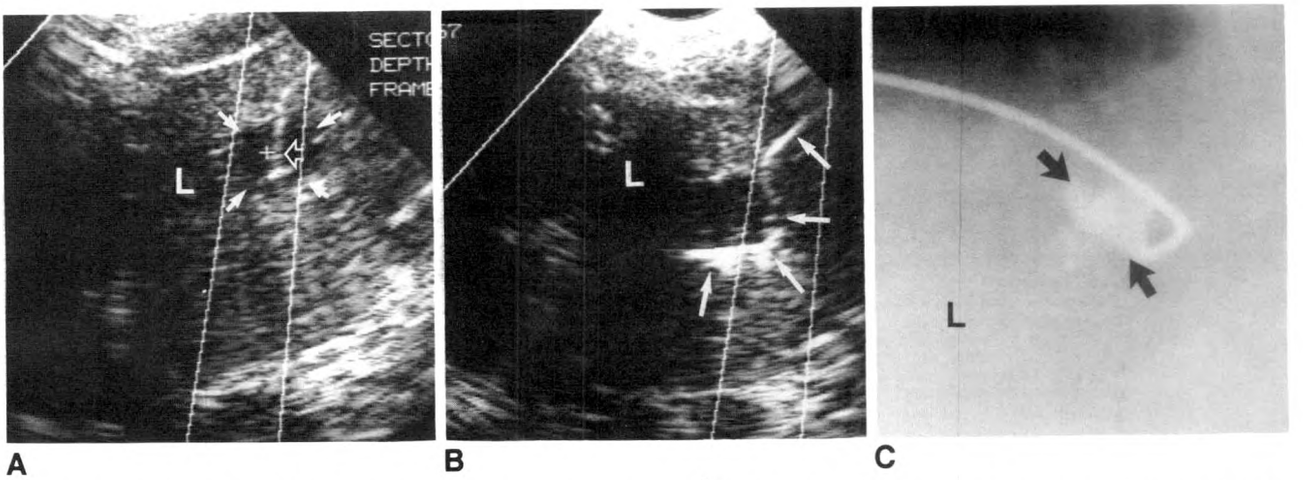


Fig. 3.—Drainage of infected biloma on a 1-year-old child with a liver transplant.

A, Sonogram shows a well-circumscribed fluid collection (1 cm in diameter) in left lobe (*arrows*). A roughened Teflon-coated needle (*open arrow*) is placed into infected biloma. L = liver.

B, Sonogram shows a 0.018-in. (0.05-cm) guidewire (*arrows*) passing through the 22-gauge needle and coiling within the fluid collection. L = liver.

C, Using a modified Seldinger technique, a 5-French catheter was placed under fluoroscopic control. Injection of contrast material outlines biloma cavity (*arrows*). L = liver.

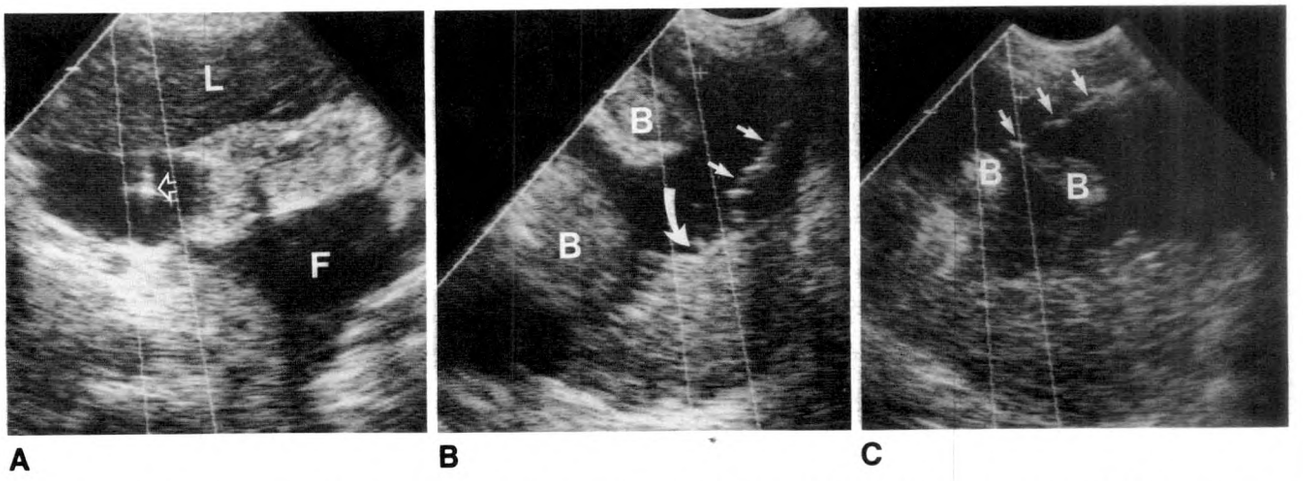


Fig. 4.—Portable sonography-guided percutaneous aspiration and drainage.

A, Transverse scan demonstrating a 22-gauge needle being passed into a fluid collection (*open arrow*) lying posterior to left lobe of liver (L). This and a second aspirated fluid collection (F) were loculated, noninfected ascites.

B, Transverse scan of left flank shows a 12-French catheter (*arrows*) in a third fluid collection that had a layer of fluid and debris (*curved arrow*) and was an abdominal abscess. B = bowel.

C, A second catheter (*arrows*) was placed anterior and cephalad to first catheter under sonographic guidance with catheter tip lying adjacent to a loop of bowel (B). Neither catheter was placed through the needle guidance system; instead the sonographic probe was held adjacent to the catheter as it was being placed. An enterocutaneous fistula developed in this patient 1 week after drainage.

drainage procedures, including nephrostomies, cholecystostomies, or abscess drainage (Figs. 2 and 4) (Table 1).

Sonographic aspiration or drainage was performed at the patient's bedside in 32 of the cases, most commonly for thoracentesis or abdominal paracentesis. Nine drainage procedures were performed at the patient's bedside including four portable cholecystostomies, two empyema drainages, one nephrostomy, and two abscess drainages (Fig. 5).

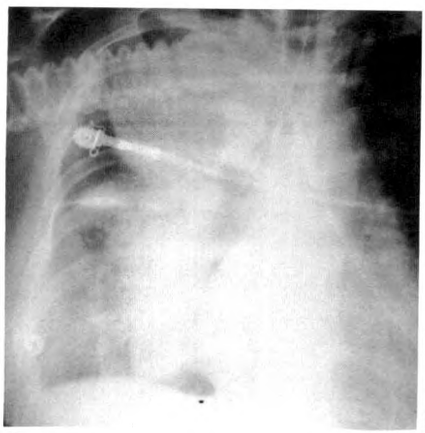
There were two complications in the 102 procedures. In one case, an enterocutaneous fistula occurred after abdominal abscess drainage (Fig. 4). This was probably secondary to inadvertent puncture of the small bowel. Also, one episode of hemoptysis lasted 2 to 3 hr after thoracentesis. This occurred in conjunction with a fluoroscopy-guided biopsy of a pulmonary nodule performed at the same sitting.

Failures at different sites are listed in Table 2. We listed

TABLE 1: **Aspiration Drainage Procedures**

Location[a]	Total	Guide[b]	No Guide[c]	Drainage[d]	Portable[e]
Gallbladder	8	8	0	4	8
Ascites/abdomen	27	9	18	9	11
Thorax	28	0	28	2	10
Renal/retroperitoneal	14	9	5	5	1
Pelvis	13	5	8	1	1
Subcutaneous	2	0	2	0	0
Liver	8	3	5	2	1
Pancreas	2	2	0	1	0
Total	102	36	66	24	32

[a] Anatomic location of aspiration or drainage procedure.
[b] Number of procedures in which guidance system was used.
[c] Number of procedures in which no guidance system was used.
[d] Number of drainage procedures.
[e] Number of procedures performed portably.



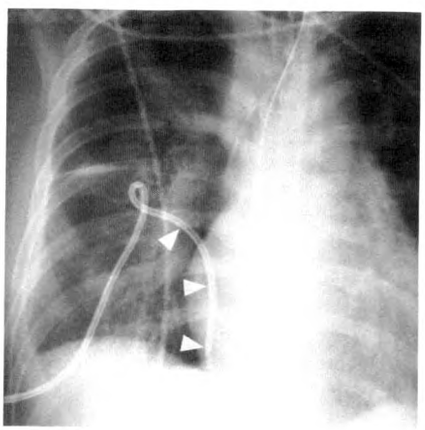
A



B



C



D

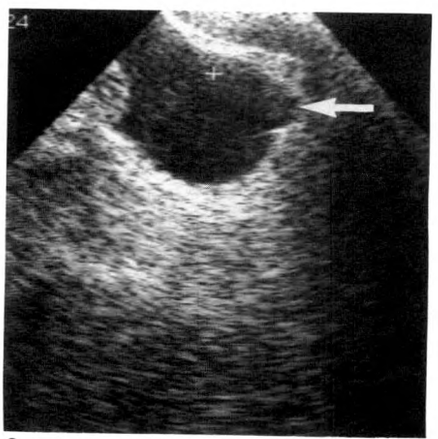
Fig. 5.—Portable empyema drainage.

***A*, Portable chest radiograph of a 28-year-old woman with multiple trauma who was suspected of having a right-sided empyema.**

***B*, Because patient was septic and too ill to be moved, real-time guidance was used to aspirate a large fluid collection (*curved arrow*), revealing purulent material.**

***C*, Following a "positive" aspirate, a 12-French catheter was placed (*curved arrow*) through posterolateral approach by trocar method.**

***D*, Chest radiograph 1 week later documented catheter position (*arrowheads*) and almost complete resolution of patient's empyema.**



6

Fig. 6.—Failed abdominal paracentesis. Longitudinal scan showing abdominal fluid (*arrow*). Site of aspiration had been marked on the skin for the primary physician and procedure was done after patient was moved back to his bed on the ward. Aspiration was unsuccessful.

seven of 102 cases as failures, which gave us an overall failure rate of 7%. Specific analysis shows failure of fluid aspiration in the abdomen in three cases; the first was a probable hematoma, the second was failure of aspiration of the pancreatic duct, and the last failure of aspiration was by the ward team after abdominal fluid was marked in the radiology department and the patient returned to the ward (Fig. 6). Parenthetically, this is the only case in which a nonradiologist attempted aspiration in this series. The pancreatic duct aspiration was performed with direct sonographic guidance and was unsuccessful because of the deflection of the needle tip in the densely calcified pancreas. Failure to

TABLE 2: **Failures of Aspiration or Drainage by Anatomic Site**

Location	Failure	Reason	Guidance System
Liver	No fluid	Probable hematoma	No
Ascites	No fluid	Aspirated by ward team	No
Pancreatic duct	No fluid	Densely calcified pancreas	Yes
Pleural fluid	No fluid	Pleural thickening	No
Pleural fluid	No fluid	Pleural thickening	No
Pleural fluid	No fluid	Aspirated blood	No
Kidney	Tube reposition	Poor tube visualization	Yes

obtain fluid occurred three times in the thorax, two of which were probably secondary to an attempt to aspirate pleural thickening rather than fluid and one in which the procedure was stopped after 3 ml of blood was aspirated. No further aspiration was performed in either of the three failed abdominal or the three failed thoracic cases.

Four problems occurred with drainage procedures, including one cathether that clotted, two failed drainages, and one catheter that had to be repositioned. Only the latter of these cases can be attributed to failure of the guidance system. This was a patient in whom percutaneous nephrostomy was performed under direct sonographic guidance at the bedside. Two days later when the patient could be moved, the tip of the tube was found to be located just within the renal calyx and had to be repositioned under fluoroscopic control.

Discussion

Percutaneous aspiration and biopsy techniques have assumed importance with the development of newer imaging methods such as CT and sonography. Sonography was initially shown to be useful in guiding the aspiration of large fluid collections [1]. The site of aspiration or drainage was marked on the skin after sonographic imaging, the probe removed, and the needle placed without direct sonographic visualization [2]. Only limited initial reports demonstrated the ability of sonography in a direct needle visualization [5]. An important recent technological advance has been the development of a variety of sonographic needle-guidance systems that allow for real-time visualization of the needle as it is passed into a fluid collection [3, 4, 6]. This study was performed to evaluate the effect of these portable sonographic guidance systems on the performance of aspiration and drainage procedures.

Needle aspiration or drainage was performed after removal of the sonographic transducer in approximately two-thirds of our cases. This technique was most commonly used for thoracentesis and thoracic fluid drainage. While there have been advocates of needle-guidance systems for biopsy of pleural-based masses [7], we have found that thoracentesis is best performed without a biopsy attachment. With our current biopsy guidance system, it is difficult to image the target without hitting the overlying rib with the needle. In fact, using the "conventional" technique, we have had only three failures and one complication of attempted thoracentesis in the 28 cases (89% success). The most common reason for requested sonographic guidance of thoracentesis was a failed attempt by the patient's primary physician. Therefore, we believe that the high success rate and negligible morbidity of the "conventional" sonographic method of thoracentesis is a marked improvement over the attempted "blind" aspiration of thoracic fluid by the primary physician. Sonographic guidance of thoracic fluid drainage had a high success rate (25 of 28 cases) with low morbidity (1 of 28 cases) and was well tolerated by the patients.

Sonographic biopsy attachments were most helpful in guidance of aspiration of small fluid collections within the abdomen or pelvis (Figs. 1 and 3). We used direct sonographic needle guidance whenever we thought that needle visualization would increase the retrieval rate or avoid potential complications. In fluid collections that are small, inaccessible, or adjacent to vital structures such as vessels or bowel, we feel more comfortable using direct needle visualization under real-time guidance rather than using the "conventional" technique.

Drainage procedures are readily performed under sonographic guidance and account for one-fourth of our cases. Drainages were performed by using the modified Seldinger technique for the nephrostomies and three of the abscess drainages. After initial needle placement under sonography, fluoroscopic guidance was used [8]. A standard or modified trocar method was always used to perform percutaneous cholecystostomies—in six of the nine abdominal abscess drainages and in the two empyema drainages (Figs. 2, 4, and 5). The percutaneous cholecystostomies were always performed at the patients' bedside with the final catheter position documented with sonography or a portable abscessogram [4] (Fig. 2). Percutaneous procedures not previously performed in our hospital, such as percutaneous cholecystostomies, are now routinely performed exclusively under direct sonographic guidance.

One-third of the 102 aspiration and drainage procedures were performed at the bedside of the critically ill patient. In addition to the cholecystostomies, two abdominal abscess drainages, two empyema drainages, and one nephrostomy were performed in the intensive-care units (Figs. 4 and 5). While portable diagnostic aspiration and drainage may be inconvenient for the radiologist, often these patients are so ill that they cannot be moved to either the radiology department or the operating room for drainage [3, 4]. This may have the most significant impact in terms of direct patient care since obtaining even a negative aspiration at the patient's bedside

may alleviate the need for exploratory surgery. Alternatively, a positive aspirate and accompanying drainage is often lifesaving and previously could not be performed without such technologic advances as portable real-time guidance systems. If major cardiovascular complications occur in these patients, they are better handled in the intensive-care unit than in the radiology department [3, 9].

One shortcoming of portable sonographic drainage of intraabdominal abscesses is the unreliability in visualization of bowel lying between the skin surface and the fluid collection. This may result in inadvertent bowel perforation, and therefore a CT guidance is suggested in drainage of intraabdominal abscesses whenever possible (Fig. 4).

Failures in this series are few. Failure of aspiration of a suspected fluid collection was the most commonly encountered problem. While we list seven of the 102 cases (7%) as failures, the exact number of failures is probably less. The incidence of false-negative tests cannot be reliably ascertained in the cases in which fluid was not obtained. A specific comment should be made concerning the one case in which the site of suspected ascitic fluid was marked and the patient was transported to the ward team for aspiration. Although this method was used once in our series of 102 cases, we advise against it. This method presents numerous problems because the exact angle and depth for aspirate cannot be duplicated once the patient is moved; the abdominal fluid and bowel shift as the patient changes position; and finally, the question of liability concerning the radiologist's role and any complications encountered by the ward team can be raised (Fig. 6).

Failure of complete drainage secondary to faulty sonographic guidance occurred in only one case. This was a portable percutaneous nephrostomy that was successfully performed but in which good catheter position could not be documented until the patient was moved to fluoroscopy 2 days later. From this experience we would advise against portable percutaneous nephrostomy-tube placement unless the patient cannot be moved and there is concomitant massive dilatation of the renal collecting structures as visualized with sonography.

We have found that a roughened Teflon-coated needle can be detected more readily than a nonroughened needle [10] (Figs. 1 and 2). Although these roughened needles are more visible, suboptimal needle visualization can occur, for example, with needle deflection. If the needle is deflected out of the path of the image, then rocking the transducer into the path of the needle or removing the needle from the biopsy guide and placing the transducer to the side of the needle may be helpful [5]. Visualization of the needle may be improved by gently jiggling it or by moving the inner stylet up and down [10].

In summary, the sonographic method of removing the transducer before needle insertion was useful in aspirating large abdominal fluid collections or in performing thoracentesis. This method of sonography-guided thoracentesis or abdominal paracentesis was a marked improvement over "blind" aspirate by the ward team. Real-time sonographic needle-guidance systems were most helpful in aspiration of fluid collections that were small, inaccessible, or adjacent to vital structures such as vessels or bowel. Portable real-time sonographic guidance had its greatest impact, in terms of direct patient care, in guiding lifesaving percutaneous drainage procedures at the bedside of critically ill patients.

ACKNOWLEDGMENTS

Special thanks to Karen Anderson for typing the manuscript and to Joen Traeger, Mercedes Valandon, Cheri Robertson, and Sandra Maleski for technical assistance.

REFERENCES

1. Als O. Puncture of intraabdominal fluid collections. In: Holm HH, Kristensen JK, eds. *Ultrasonically guided puncture technique*. Philadelphia: Saunders, **1980**:83–86
2. Gronvall S, Gammelgaard J, Haubek A, Holm HH. Drainage of abdominal abscesses guided by sonography. *AJR* **1982**; 138:527–529
3. McGahan JP. Aspiration drainage procedures in the intensive care unit: percutaneous sonographic guidance. *Radiology* **1985**; 154:531–532
4. McGahan JP, Walter JP. Diagnostic percutaneous aspiration of the gallbladder. *Radiology* **1985**;155:619–622
5. Cooperberg PL, Carpenter CW. Real-time ultrasound as an aid in intrauterine transfusion. *Radiology* **1978**;127:535–537
6. Buonocore E, Skipper GJ. Steerable real-time sonographically guided needle biopsy. *AJR* **1981**;136:387–392
7. Izumi S, Tamaki S, Natori H, et al. Ultrasonically guided aspiration needle biopsy in disease of the chest. *Am Rev Respir Dis* **1982**;125:460–464
8. Zegel HG, Pollack HM, Banner MP, et al. Percutaneous nephrostomy: comparison of sonographic and fluoroscopic guidance. *AJR* **1981**;137:925–927
9. vanSonnenberg E, Wing VW, Pollard JW, Casola G. Life-threatening vagal reactions associated with percutaneous cholecystostomy. *Radiology* **1984**;151:377–380
10. McGahan JP. Laboratory assessment of ultrasonic needle and catheter visualization. *J Ultrasound Med* **1986**;5:373–377

Inferior Vena Caval Stent Filter

M. J. Wallace[1]
K. Ogawa[2]
K. Wright[2]
C. H. Carrasco[2]
William Richli[2]
C. Charnsangavej[2]

New inferior vena caval filters for percutaneous placement were made by attaching filter wires similar to those in the bird's nest inferior vena caval filter onto expandable metallic stents. These stents formed a base on which to anchor the filter to the wall of the inferior vena cava. The stent filter can be introduced through a 12- to 13-French catheter sheath system. The system was successfully tested in 13 dogs.

For the past 20 years, interruption of the inferior vena cava has been employed for the management of pulmonary thromboembolism [1–5]. Various filters are available for placement into the inferior vena cava to trap clots from the veins of the pelvis and lower extremities [2, 6–9]. Although these filters effectively prevent pulmonary embolism, the techniques of installation are difficult and cumbersome, the mechanism of fixation precarious, the site of deposition critical, and the filters themselves may result in occlusion of the inferior vena cava [10–13].

Recently, Gianturco et al. [8] formulated and Roehm et al. [12] clinically tested a filter based on a tangle of four wires, known as the bird's nest filter. Gianturco also designed an expandable metallic stent that is relatively nonthrombogenic, can be introduced percutaneously into the inferior vena cava, and is fixed in place by local dilatation of the vessel [14, 15]. In an attempt to simplify both the device and the method of placement, a variety of inferior vena cava filters incorporating the advantages of Gianturco's two innovations are presented.

Materials and Methods

For these experiments, expansile stents were constructed of round stainless-steel wire (0.018 in. [0.05 cm] in diameter) in a zigzag configuration of five to seven bends. The length of the stents was arbitrarily set at 2.5 cm with an expanded diameter of 4 cm. Single or multiple stents were incorporated into the designs of the filter.

Five different types of filter designs were used (Fig. 1). Type 1 was used in one dog; type 2 in four dogs; type 3 (six bends) in three dogs; type 3 (seven bends) in two dogs; type 4 in two dogs; and type 5 in one dog.

Experimental Studies

Thirteen adult mongrel dogs (15–27 kg) were anesthetized with an IV injection of 30 mg/kg sodium pentobarbital (Nembutal, Abbott, North Chicago, IL). The femoral vein was surgically isolated. An incision was made in the vessel and a 13-French sheath containing a 12-French Teflon catheter with a tapered tip was inserted. Under fluoroscopic guidance, the assembly was advanced into the inferior vena cava just beyond the area of interest and the Teflon catheter was removed. The stent with the attached filter within a 12-French Teflon cartridge was introduced into the 13-French sheath. The filter was advanced through the sheath with an introducer or pusher, actually a flat-ended, 12-French polyethylene catheter or cable. When the stent reached the end of the sheath, the introducer was held in place as the sheath was withdrawn. While a portion of the stent was still within the sheath, the entire

Received March 17, 1986; accepted after revision June 16, 1986

This work was supported in part by the John S. Dunn Research Foundation and the George A. Cook Memorial Fund.

[1] John S. Dunn Summer Student Grant Program, The University of Texas M. D. Anderson Hospital and Tumor Institute at Houston, 6723 Bertner Ave., Houston, TX 77030.

[2] Division of Diagnostic Imaging, Department of Diagnostic Radiology, The University of Texas M. D. Anderson Hospital and Tumor Institute at Houston, 6723 Bertner Ave., Houston, TX 77030. Address reprint requests to C. Charnsangavej.

***AJR* 147:1247–1250, December 1986**
0361–803X/86/1476–1250
© American Roentgen Ray Society

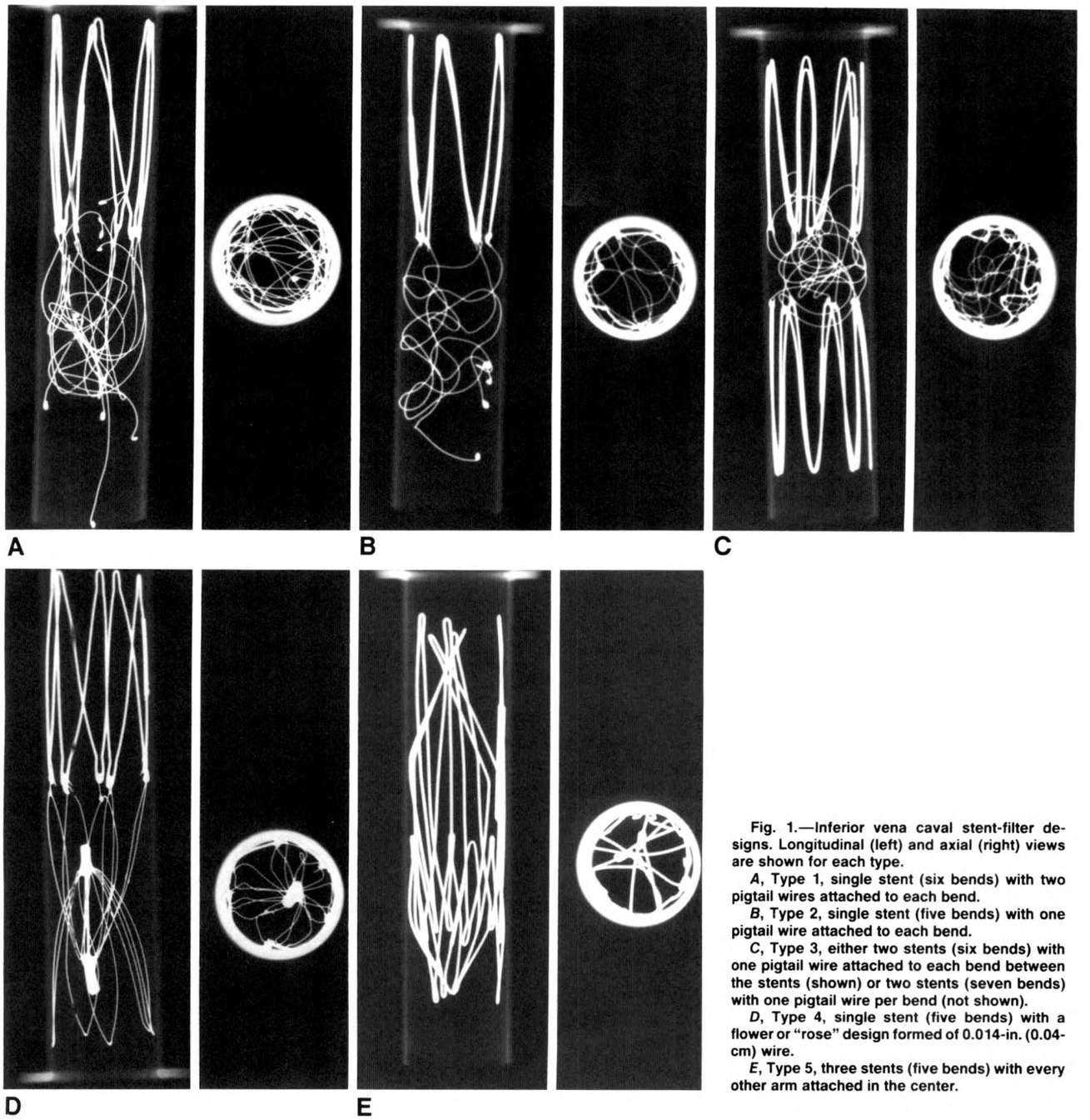


Fig. 1.—Inferior vena caval stent-filter designs. Longitudinal (left) and axial (right) views are shown for each type.

***A*, Type 1, single stent (six bends) with two pigtail wires attached to each bend.**

***B*, Type 2, single stent (five bends) with one pigtail wire attached to each bend.**

***C*, Type 3, either two stents (six bends) with one pigtail wire attached to each bend between the stents (shown) or two stents (seven bends) with one pigtail wire per bend (not shown).**

***D*, Type 4, single stent (five bends) with a flower or "rose" design formed of 0.014-in. (0.04-cm) wire.**

***E*, Type 5, three stents (five bends) with every other arm attached in the center.**

mechanism could be moved within the vena cava. Once released, realignment of the device was difficult if not impossible. The expanded stent impinged on the wall of the vessel; the purpose of the overdistension was to fix the stent in position.

When two stents were employed with intervening attached wires, before its release the wire mesh was crowded together by an upward movement of the second stent to almost abut against the first stent before its release. Inferior venacavography was performed immediately, 1 week after placement, and then at monthly intervals for up to 5 months.

The parameters investigated included (1) migration, (2) flow defects created by the filter, (3) inferior vena caval and renal vein patency, and (4) the ability to trap clots. Barium-impregnated blood clot and Gelfoam particles (3 mm × 3 mm × 3 mm) or long segments (3 mm × 3 mm × 30 mm) were injected into a saphenous vein. Radiographs of the dog's abdomen and the lungs were taken to determine the ability of the device to trap the radiopaque clots.

The animals were killed at the end of the study (6–20 weeks) by exsanguination under deep sodium pentobarbital anesthesia, and a complete necropsy was performed.

Results

The placement of the filters was executed without difficulty. The stents were positioned below the renal veins in three animals and purposefully bridging the veins in 10. In one animal, the lower of the two stents of type 3 was in the common iliac vein. No edema of the extremity due to venous occlusion or vessel perforation was encountered. The animals showed no evidence of distress that could be attributed to the stents. It was difficult to bunch up the pigtail wires in the vena cava without causing a change in stent position. By 4 weeks one pigtail wire broke in two animals with no obvious consequences.

Patency.—Inferior venacavography revealed that the stent filter often increased the diameter of the cava, but a stenosis occurred just below the stent in one animal with type 2, one with type 3 above the lower of the two stents, and one with type 4 at the upper stent. The inferior vena cava and the renal veins remained patent even when the stent bridged the renal veins.

Flow defects.—There were flow defects seen at cavography, but at necropsy these were found to be related to the position of the filter rather than thrombi.

Migration.—The expansion of the stent distending the inferior vena cava maintained the stent filter in position in 12 of the 13 animals. The migration of 1.5 cm occurred in only one animal within the first week after placement. Because of this, 12 stents with three barbs on each were introduced into the vessels of three additional animals. Each barb was made of a 1-cm segment of wire with a distal portion (2 mm) bent at a right angle and projecting beyond the margin of the stent. The barbs were attached at equidistance from the upper bends of the stent. The stents with barbs remained in place during 3 months of observation with no complications.

Clot entrapment.—The stent filters, especially those with pigtail wires (types 1, 2, and 3), trapped both small and large thrombi (Fig. 2). Types 4 and 5 were successful only in impeding the passage of the larger clots.

Postmortem.—Cellular proliferation occurred around all the stent filters where the wires came in contact with the vessel wall, and cellular deposits were seen on all solder points. Within 4 weeks after placement, the stent filters were almost completely covered with intima while by 12 weeks all were encased. Even after 20 weeks no cell growth was noted on the wire segments that bridged the renal veins. No erosion of the vascular wall was noted.

Microscopically, the stent-filter wires were located deep within the vessel wall and were encased by an extension of the intima. Immediately surrounding the wires were multiple layers of endothelium covered by a layer of fibrous connective tissue of similar thickness. A single layer of endothelium lined the vascular lumen.



Fig. 2.—Inferior vena caval stent-filter function. Large and small particles of blood clot, Gelfoam, and barium were effectively trapped within stent filter (type 2).

Discussion

Pulmonary embolism is still a significant cause of death in patients after surgical procedures, congestive heart failure, pulmonary disease, and carcinomatosis. Interruption of the inferior vena cava is recommended when anticoagulation or fibrinolytic therapy fails or is contraindicated. Interruption by surgical ligation or plication may be associated with mortality rates ranging from 0 to 39% and may not sufficiently prevent subsequent embolism [1, 3, 5]. Several mechanical devices have been designed to trap the large clot that arises from the veins of the pelvis and lower extremities.

Of the surgically placed filters, most of the clinical experience has been with the Mobin-Uddin filter [2, 7, 11]. This filter has an umbrella configuration with the tips of the spokes penetrating the caval wall for anchoring. The silastic webbing is heparin impregnated and has 18 3-mm holes. The placement requires a surgical cutdown. The Kimray-Greenfield filter, another frequently used device, has hooks to provide fixation to the caval wall without complete penetration [6, 10]. It permits filling of 70% of the cone with blood clots with a decrease in the cross-sectional diameter of 50%. This filter was originally placed through the catheter by a surgical cutdown technique, but recently it was modified and was placed percutaneously through a 24-French catheter [13].

The patency rate of surgically placed IV devices is 27% for the Mobin-Uddin and 95% for the Kimray-Greenfield [11]. Both the Mobin-Uddin and the Kimray-Greenfield filters have a pulmonary embolism recurrence rate of 2–3%. There is also an increase in the prevalence of lower-extremity edema with the Mobin-Uddin of 75% as compared with 38% with the Kimray-Greenfield.

A percutaneous approach to the placement of an inferior vena cava filter has captured the imagination of both the radiologist and the clinician. Tadavarthy et al. [13] modified the technique of placement of the Kimray-Greenfield filter to a percutaneous approach using a 24-French catheter. Lund et al. [16] modified the Kimray-Greenfield filter so that it can be placed through a 10-French catheter and can be retrieved from the opposite direction. Simon et al. [9] employed Nitinol (an expensive alloy of nickel and aluminum) to construct a filter, and Cragg et al. [17] used Nitinol forming a helical cone

for a filter. This Nitinol wire can be placed through an 8-French catheter.

Gianturco et al. [8] designed a filter by using 0.152-mm-thick stainless-steel wire forming a mesh, attached to four wire prongs that were used to anchor the wire mesh to the wall of the vena cava. This filter, also called a bird's nest filter, is currently undergoing clinical evaluation by Roehm et al. [12]. Gunther et al. [18] made a filter consisting of a pliable basket, similar to a Dormia basket, and anchoring legs made of stainless-steel wire. The filter can be placed through a 10-French Teflon catheter and can also be retrieved with a snare or forceps.

The stent filter described here compares well with the other percutaneously placed filters. The wire mesh used for trapping the blood clot is similar to the bird's nest filter. The fixation mechanism is different; this filter is fixed to the vessel wall by the expandable metallic stent, but the bird's nest filter is attached by the wire prongs. As a result, the introduction of this stent filter is simpler than that of the bird's nest filter. A 13-French sheath is required for the installation of the stent filter rather than the 10-French sheath needed for the bird's nest filter. Migration of the stent filter can be prevented by overdistension and by lateral barbs. Another advantage of the stent filter is its expandability, which may prevent the stenosis observed with other types of filters. The type 2 stent filter was the preferred design because of the simplicity of its construction and because of its ability to trap clots.

The ease of placement and the expansile nature of the metallic stent in combination with the ability of the bird's nest filter to trap blood clots should provide an effective filter for the management of pulmonary embolism.

ACKNOWLEDGMENTS

The authors wish to acknowledge the assistance and guidance of Raquel Collins and Irene Szwarc, the photography of Gene Szwarc and Charles Buegeler, and secretarial support of Erlinda S. Alabastro.

REFERENCES

1. Amador E, Li TK, Crane C. Ligation of inferior vena cava for thromboembolism. Clinical and autopsy correlation in 119 cases. *JAMA* **1968**;206:1758–1760
2. Mobin-Uddin K, McLean R, Jude JR. A new catheter technique of interruption of inferior vena cava for prevention of pulmonary embolism. *Am Surg* **1969**;35:889–894
3. Piccone VAJ, Vidal E, Yarnos M, Glass P, LeVeen HH. The later results of caval ligation. *Surgery* **1970**;68:980–998
4. Blumberg RL, Gelfand ML. Long-term follow-up of vena cava clips and umbrellas. *Am J Surg* **1977**;134:205–208
5. Bernstein EF. The role of operative inferior vena caval interruption in the management of venous thromboembolism. *World J Surg* **1978**;2:61–71
6. Greenfield LJ, McCurdy JR, Brown PP, Elkins RC. A new intracaval filter permitting continued flow and resolution of emboli. *Surgery* **1973**;73:599–606
7. Mobin-Uddin K, Callard GM, Bolooki H, Robinson R, Michie D, Jude JR. Transvenous caval interruption with umbrella filter. *N Engl J Med* **1972**;286:55–58
8. Gianturco C, Anderson JH, Wallace S. A new vena cava filter: experimental animal evaluation. *Radiology* **1980**;137:835–837
9. Simon M, Kaplow R, Salzman E, Freiman D. A vena cava filter using thermal shaped memory alloy. *Radiology* **1977**;125:89–94
10. Greenfield LJ, Peyton R, Crute S, Barnes R. Greenfield vena cava filter experience. *Arch Surg* **1981**;116:1451–1456
11. Cimochowski GE, Evans RH, Zarins CK, Luch T, DeMeester TR. Greenfield filter versus Mobin-Uddin umbrella: the continuing quest for the ideal method of vena caval interruption. *J Thorac Cardiovasc Surg* **1980**;79:358–365
12. Roehm JOF, Gianturco C, Barth BH, Wright KC. Percutaneous transcatheter filter for the inferior vena cava. *Radiology* **1984**;150:255–257
13. Tadavarthy SM, Castaneda-Zuniga W, Salomonowitz E, et al. Kimray-Greenfield vena cava filters: percutaneous introduction. *Radiology* **1984**;151:525–526
14. Wright KC, Wallace S, Charnsangavej C, Carrasco CH, Gianturco C. Percutaneous endovascular stents: an experimental evaluation. *Radiology* **1985**;156:69–72
15. Charnsangavej C, Wallace S, Wright KC, Carrasco CH, Gianturco C. Endovascular stent for use in aortic dissection: an in vitro experiment. *Radiology* **1985**;157:323–324
16. Lund G, Rysavy J, Hunter DW, Castaneda-Zuniga WR, Amplatz K. Retrievable vena caval filter percutaneously introduced. *Radiology* **1985**;155:831
17. Cragg A, Lund G, Salomonowitz E, et al. A new percutaneous vena cava filter. *AJR* **1983**;141:601–604
18. Gunther RW, Schild H, Fries A, Storkel S. Vena caval filter to prevent pulmonary embolism: experimental study. *Radiology* **1985**;156:315–320

Expandable Intrahepatic Portacaval Shunt Stents in Dogs with Chronic Portal Hypertension

Julio C. Palmaz[1]
Francisco Garcia[1]
Randy R. Sibbitt[1]
Fermin O. Tio[2]
David T. Kopp[1]
Wayne Schwesinger[3]
Jack L. Lancaster[1]
Peter Chang[1]

A canine experimental model was used to investigate the feasibility of using balloon-expandable portacaval shunts in humans with chronic portal hypertension. Intrahepatic portacaval shunts were created in nine dogs with stable portal hypertension previously induced by intraportal injections of polyvinyl alcohol (Ivalon). Embolic material was injected periodically through a subcutaneous port that allowed repeated access to the portal system. Shunts were placed 14 weeks after the last embolization. A shunt patency rate of 100% was observed up to 48 weeks. Low portacaval pressure gradient and high shunt flow accounted for the good results.

In a previous report [1] we described a method of creating intrahepatic portacaval shunts in experimental animals. The technique, modified from that of Rosch et al. [2], involved placement of a balloon-expandable metal stent within a liver-tissue track previously formed by a transjugular needle puncture. Unlike previously described intrahepatic shunts [2–7], ours directly connected the inferior vena cava with the portal bifurcation in a side-to-side fashion. Most of our reported shunts remained patent for as long as they were under study; nevertheless, more than half required recanalization of the lumen by balloon angioplasty after early thrombosis. Although these initial failures were associated with technical errors that resulted in obstruction of shunt flow, the lack of sustained portal hypertension and high flow in the shunt must have contributed substantially to the occlusions.

To evaluate the performance of balloon-expandable portacaval shunts with sustained elevation of the portal pressure, we injected several doses of polyvinyl alcohol (Ivalon) into the portal circulation of large, adult dogs before placing percutaneous transjugular portacaval shunts. The objective of this study was to investigate further the feasibility of human application of the technique by studying the short- and long-term performance of intrahepatic shunt stents in experimentally created chronic portal hypertension.

Materials and Methods

Induction of Experimental Chronic Portal Hypertension

Nine dogs had injection ports placed subcutaneously as vascular access to the portal system for repeated particle embolization (Fig. 1). The ports (Norfolk Medical Products, Inc., Skokie, IL) consisted of a diaphragm placed subcutaneously in the right abdominal flank and connected to a silicone rubber 7-French tube that was introduced into the superior mesenteric vein through a mesenteric vein branch. An 18-gauge Huberd deflected-point needle (Norfolk) was used to gain access to the subcutaneous diaphragm, measure pressures, inject contrast material, and create embolisms in the portal system. Barium-impregnated Ivalon powder (Unipoint Industries, High Point, NC) with a particle size of 250–400 μm was suspended in saline and injected at a dosage of 0.5 g/week for a maximum of four doses. Embolization was avoided if the preembolization portal pressure was 20 cm of saline or higher. Before each embolization, a portogram was obtained by injecting 76% contrast material through the

Received May 5, 1986; accepted after revision July 8, 1986.

Presented at the annual meeting of the American Roentgen Ray Society, Washington, DC, April 1986.

This work was supported by the University of Texas Health Center, Grant No. 2S07-RR05654-17.

[1] Department of Radiology, University of Texas Health Science Center at San Antonio, 7703 Floyd Curl Dr., San Antonio, TX 78284-7800. Address reprint requests to J. C. Palmaz.

[2] Department of Pathology, University of Texas Health Science Center at San Antonio, 7703 Floyd Curl Dr., San Antonio, TX 78284-7800.

[3] Department of Surgery, University of Texas Health Science Center at San Antonio, 7703 Floyd Curl Dr., San Antonio, TX 78284-7800.

***AJR* 147:1251–1254, December 1986**
0361–803X/86/1476–1251
© American Roentgen Ray Society

port (Fig. 2). Four weeks after initial placement, the port was removed through a small skin incision. Biochemical liver profiles were assessed by SMA-12 (SMA = sequential multichannel autoanalyzer) analysis every week during the embolization period and every other week thereafter. A percutaneous liver biopsy was performed with a 14.5 gauge Tru-Cut needle (Travenol, Inc., Deerfield, IL) immediately before shunt placement.

Placement of Percutaneous Portacaval Shunt

Each dog was given general gaseous anesthesia, and a valved 12-French introducer sheath (Cook, Inc., Bloomington, IN) was placed percutaneously in the right jugular vein while the animal was lying on its left side. A 12-French Teflon dilator mounted on an 8-French Teflon catheter was advanced in the inferior vena cava to the level of the hepatic veins. The inner catheter was removed, and an 18-gauge cannula with a diamond-tipped mandril [1] was introduced. The needle tip was oriented toward the portal vein bifurcation by using (as a "road map") a previously obtained portogram of the dog in an identical position. After the needle penetrated the portal vein, which was perceived as a sudden give to the operator's hand, the trocar was removed, and portal blood was aspirated. A guidewire 260 cm long and 0.09 cm (0.035-in.) in diameter was advanced into the superior mesenteric vein. After the needle was removed, the 8-French Teflon dilator and 12-French sheath were advanced across the needle track with a rotary motion. The dilators were then exchanged for an 8 mm × 4 cm balloon angioplasty catheter, and the balloon was expanded for 3 min after the injection of 1500 units of heparin into the portal vein. The site where the balloon was indented before full expansion was used as a landmark to position the stent.

A 30 × 3.7 mm stainless steel stent was mounted snugly over a 10 mm × 4 cm high-pressure angioplasty balloon catheter. Unlike the stent used in our previous series, the new one was a single piece, a stainless steel tube with parallel staggered slots etched in the wall. On inflation each slot became a diamond-shaped space. The wall thickness of the stent was 0.15 mm (0.006 in.); therefore, the diameter of the collapsed stent-balloon assembly was only slightly wider than the folded balloon and was easily introduced through the sheath's valve. After adequate positioning of the stent, the balloon was inflated and immediately deflated, leaving the expanded stent in place. After balloon withdrawal, pressure measurements in the portal vein, inferior vena cava, and right atrium and a portogram were obtained.

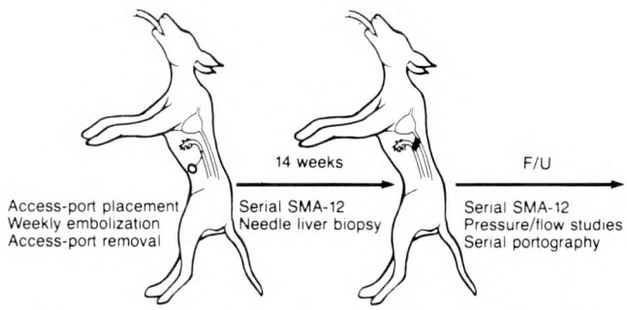


Fig. 1.—Experimental design. SMA = sequential multichannel autoanalyzer; F/U = follow-up.

Postshunt Evaluation

Percutaneous transjugular portograms, serial SMA-12 analysis, and pressure measurements were obtained after shunt placement. Portograms and pressure studies were performed at 1, 3, 6, and 12 weeks after shunt placement and were repeated every 12 weeks thereafter. Occlusive and opening portal pressures were recorded only once by means of a rubber occlusive balloon in the shunt lumen 3 to 6 weeks after shunt placement.

The fraction of portal flow shunted to the systemic circulation was established by injecting ^{99m}Tc-labeled human albumin microspheres into the portal vein and inferior vena cava circulations and then comparing the corresponding radioactivity in a region of interest (ROI)

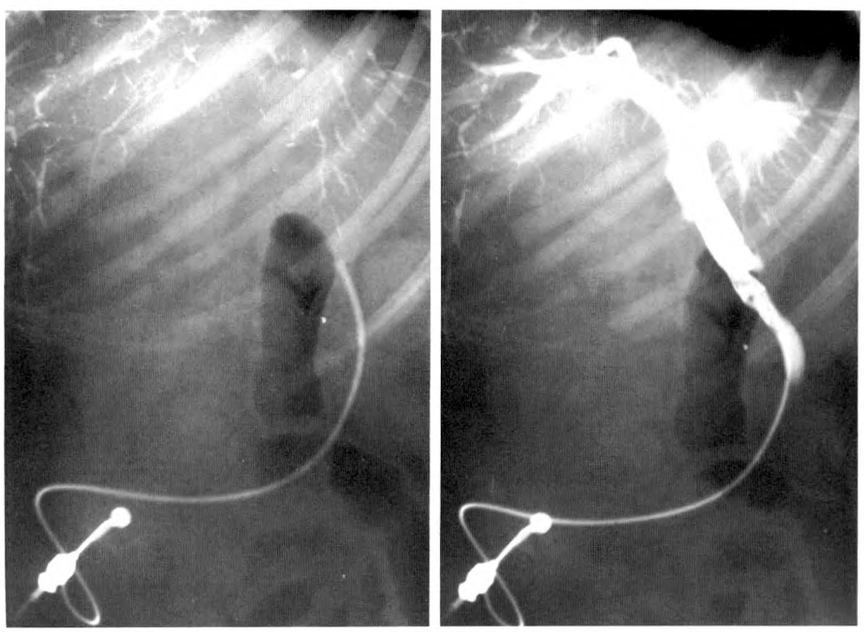


Fig. 2.—*A*, After last embolization portal radicles are extensively filled with opaque embolic material.

***B*, Contrast injection through percutaneous needle shows patency of portal system.**

in the upper lungs. Counts within the ROI were assumed to be proportional to the amount of radioactivity injected directly into the inferior vena cava (A_{ivc}) or indirectly through the portal shunt (A_{ps}). Attempts were made to inject for each dog similar amounts of radioactive material into the inferior vena cava and into the portal vein. Average radioactivity was 1.1 mCi (40.7 MBq) per injection (range, 0.63–2.3 mCi [23.3–85.1 MBq]). It was assumed that the distribution in the lungs was the same for material entering the vena cava directly or indirectly, that the small number of microspheres per dose (20,000) would not alter pulmonary flow distribution, and that mixing of the labeled microspheres with blood was adequately accomplished by giving injections through side-hole catheters. Given these assumptions, the following relationship applies:

$$ROIcts_{ivc}/ROIcts_{pv} = A_{ivc}/A_{ps} = A_{ivc}/(A_{pv} \times f)$$

where $ROIcts_{ivc}$ and $ROIcts_{pv}$ represent the net counts within the lung ROI for the inferior vena cava and portal vein injections, respectively. The fraction (f) of flow from the portal vein to the inferior vena cava is given then by

$$f = (ROIcts_{pv}/A_{pv})/(ROIcts_{ivc}/A_{ivc})$$

This implies that the fraction of flow to the lungs via the portacaval shunt is equal to the ratio of the observed net counts over the lung ROI, with the observed count weighted for the amount of radioactivity injected. The possibility of passage of microspheres through spontaneous portosystemic collaterals was ruled out by observing the absence of such collateral flow in a portogram performed before the microspheres were injected. The catheter position was identical in both studies.

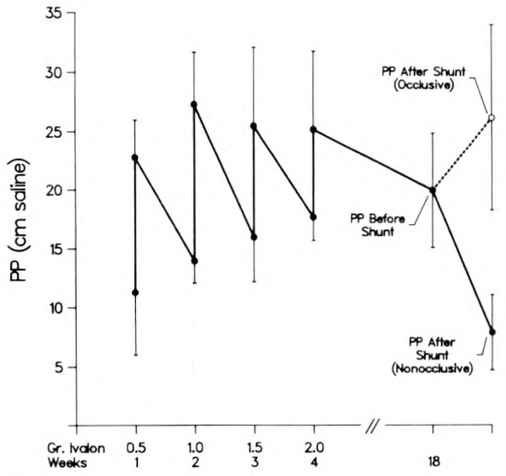
Results

Eight animals completed the embolization schedule and had a percutaneous transjugular shunt. One dog had thrombosis of the portal vein at the time of portacaval shunt placement. Before shunt placement, one dog received two embolizations of Ivalon and two received three because the portal pressure was higher than 20 cm of saline at the time of embolization. The rest of the dogs received four embolizations (2 g of embolic material). The portal pressure rose immediately after each embolization and dropped before the next one (Fig. 3). The mean postembolization pressure peak reached maximal values after the second embolization and was lower in the last two. The mean portal pressure of 11 ± 5.3 cm of saline before embolization steadily increased and reached the highest value of 20 ± 4.9 cm of saline ($p < .02$) before shunt placement. Serial measurements of serum transaminases (SGOT, SGPT) and lactic dehydrogenase showed an expected transient elevation immediately after placement of the subcutaneous port and then a decline to normal levels. After shunt placement there was a transient second elevation of the enzymes that leveled off, but at higher levels than those found before the shunt was placed. Serum bilirubin also showed this bimodal elevation. Serum albumin was lowered substantially after placement of the shunt, probably reflecting the lower protein concentration of the postshunt diet. The results of percutaneous liver biopsy showed that most of the portal areas were normal, with occasional mild periportal fibrosis and proliferation of the bile ducts. Ivalon filled up portal veins as small as 0.045 mm in diameter. The portal veins that remained patent appeared distended and were surrounded by prominent perivenous capillaries. The hepatic sinusoids were distended. No liver-cell necrosis or cirrhosis was present.

All shunts remained open, as shown by contrast examinations, for a maximum follow-up of 48 weeks, and none of them had early thrombosis. The mean lumen of the shunt as measured on the last portogram was 79 ± 12% of the radiopaque graft diameter. Contrast injections in the portal system showed that most of the flow was directed to the shunt, with little or no flow into the portal radicles (Fig. 4). Portograms taken late in the study often showed reversed flow in the portal branches. The mean portal pressure of 26 ± 7.9 cm of saline after inflation of an occlusive rubber balloon in the shunt lumen dropped to 8 ± 3.1 cm of saline after balloon deflation (Fig. 3). The pressure gradients across the shunt remained remarkably stable throughout the postshunt follow-up studies, averaging 2.4 ± 1.9 cm of saline. The estimated fraction of portal flow shunted to the inferior vena cava by ^{99m}Tc-labeled microspheres was 95 ± 11% (range, 76–110%). The percentage in excess of 100% was assumed to be within the margin of error of the method.

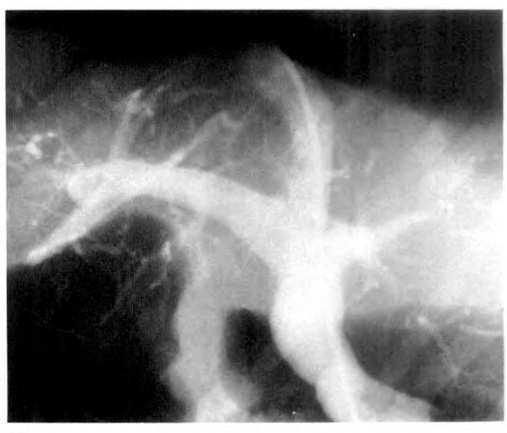
Discussion

Creation of stable chronic portal hypertension in dogs by repeated injections of Ivalon was first described by Buergener et al. [8]. This model is well suited to the study of percuta-



3

Fig. 3.—Portal pressure (PP) fluctuations during embolizations and after shunt placement. Each dot represents mean value ± 1 standard deviation (bars). (For clarity, standard deviation values overlapping vertical lines between dots are not indicated.)



4

Fig. 4.—Contrast injection into portal vein through a transjugular catheter introduced across shunt.

neous portosystemic shunts because there is no hepatocellular damage; therefore, the animals remain healthy and in a good nutritional state if they are adequately supported. The portal obstruction is presinusoidal, but the portal vein bifurcation and the major portal branches remain open, allowing the creation of an intrahepatic shunt with the inferior vena cava. We modified the method of Buergener's group by temporarily placing an injection access-port in the portal system and by simplifying the embolization schedule. The benefit of having rapid access to the portal system through an injection port for embolization, pressure measurement, and contrast injection offset the extra cost and time involved in placing and removing the device. With successive embolizations of Ivalon, the portal flow slows, and the possibility of portal thrombosis induced by the presence of the port catheter increases. Therefore, the port must be removed as soon as a total of 2 g of Ivalon have been injected or the portal pressure has been 20 cm of saline or higher for 2 consecutive weeks. With this method, only one animal developed portal thrombosis. The radiopacity provided by the barium mixed with the Ivalon was quite useful because it indicated the degree of filling of the portal radicles, the symmetry of distribution throughout the lobes, and the progressive loss of volume of the liver (Fig. 2A).

Examination of the liver biopsies done before shunt placement showed no significant abnormalities. Periportal fibrosis was seen only occasionally. The lack of histologic abnormalities correlated with the essentially normal liver chemistry profiles before shunt placement. After shunting, the abnormal serum enzyme levels reflected parenchymal liver atrophy caused by the effect of portal flow diversion and high resistance in the hepatic portal circulation.

The mean postembolization elevation of portal pressure was maximal after the second embolization and lower after the following ones. This could have been caused by the development of portosystemic collaterals that dampened the pressure rise of additional embolizations. Those collaterals probably atrophied or decreased in diameter a few weeks after shunt placement as indicated by the high occlusive pressures. Postshunt atrophy of the collaterals caused a "tighter" portal system and, therefore, high occlusive pressures. The portal pressure before each embolization increased steadily, indicating that collateral circulation, just as in human portal hypertension, is insufficient to effectively decompress the portal system. The radiopacity of the metal stent made the follow-up catheterizations simple. The regular, cylindrical lumen permitted measurement of occlusive pressure by means of an occlusive rubber balloon. Although the physiologic value of the test should be further evaluated, the portal pressure measured beyond an occlusive balloon indicated the perfusion pressure of the liver and the degree of atrophy of the portosystemic collaterals.

In contrast to our earlier experience, in which half the shunts thrombosed during the first week [1], all shunts remained open at the latest follow-up study of 48 weeks without the need for recanalization. The shunt lumen averaged 79% of the metal stent diameter as compared with 69% in our first series [1]. The pressure gradient across the shunt was 2.37 cm of saline as compared with 4.9 cm of saline. These findings indicate the beneficial effects of the high shunt flow caused by the portal hypertension. This observation is confirmed by the measurements of shunted portal flow fraction via labeled microsphere, which indicated an almost complete portal flow diversion. The use of a new stent with lower profile and a "learning-curve" effect in the performance of the shunt procedure may have contributed to the improved results. Probably, high shunt flow is necessary to protect against thrombosis before the endothelization of the inner surface of the shunt develops.

Direct intrahepatic portacaval shunting may be hazardous in humans because of the risk of hemorrhage caused by the violation of the peritoneal space. Extensive anatomic studies must be completed before such an approach is considered. Until such time, adequate results may be attained by placing stents between proximal hepatic and portal veins, a modification of the method used by Colapinto et al. [6].

ACKNOWLEDGMENTS

We acknowledge the contributions of Genaro Leija and Cono Farias.

REFERENCES

1. Palmaz JC, Sibbitt RR, Reuter SR, Garcia F, Tio FO. Expandable intrahepatic portocaval shunt stents: early experience in the dog. *AJR* **1985**;145:821–825
2. Rosch J, Hanafee WN, Snow H. Transjugular portal venography and radiological portocaval shunt: an experimental study. *Radiology* **1969**;92:1112–1114
3. Koch G, Rigler B, Tentzeris M, Schuy S, Sakulin M, Schmidt-Kloiber H. Der intrahepatische porto-cavale Shunt. *Langenbecks Arch Chir* **1973**;333:237–244
4. Reich M, Olumide F, Jorgensen E, Eisenman B. Experimental cryoprobe production of intrahepatic portocaval shunt. *J Surg Res* **1977**;23:14–18
5. Buergener FA, Gutierrez OH. Nonsurgical production of intrahepatic portosystemic shunts in portal hypertension with the double lumen balloon catheter. *ROFO* **1979**;130:686–688
6. Colapinto RF, Stronell RD, Gildiner M, et al. Formation of intrahepatic portosystemic shunts using a balloon dilatation catheter: preliminary clinical experience. *Can Med Assoc J* **1982**;126:267–268
7. Buergener FA, Gutierrez OH. Produktion einer intrahepatischen portokavalen Fistel im Hund mit Leberzirrhose und Pfortaderhonchdruck. *ROFO* **1984**;141:327–332
8. Buergener FA, Gutierrez OH, Logsdon GA. Angiographic, hemodynamic and histologic evaluation of portal hypertension and periportal fibrosis induced in the dog by intraportal polyvinyl alcohol injections. *Radiology* **1982**;143:379–395

MR Imaging of the Thyroid

Charles B. Higgins[1]
Michael T. McNamara[1]
Madeleine R. Fisher[1]
Orlo H. Clark[2]

The thyroid gland was evaluated with MR imaging in six normal subjects and 32 patients with thyroid disease. The purpose was to evaluate signal characteristics of normal and diseased thyroid tissue; determine the contrast between normal and diseased tissue on T1- and T2-weighted images; compare relaxation times of normal thyroid, adenomas, and carcinoma; and assess the capability of MR for showing the extent of large thyroid masses. Adenomas and carcinomas were frequently isointense with normal thyroid tissue on T1-weighted images but had markedly higher intensity on T2-weighted images. The mean T1 (1202 ± 717 msec) and T2 (118 ± 48 msec) relaxation times of adenomas were markedly longer than the T1 (721 ± 97 msec) and T2 (59 ± 10 msec) times of normal thyroid tissue. Likewise, the T1 and T2 values of carcinomas were markedly prolonged compared with normal thyroid but the values overlapped with those of the adenomas. Sagittal and coronal images effectively depicted the extent of large goiters, adenomas, and carcinomas and indicated extension below the cervicothoracic junction. The marked prolongation of relaxation times associated with thyroid disease causes excellent contrast of lesions with normal thyroid and surrounding structures. The large field of view possible with coronal and sagittal images is useful for assessing extensive thyroid masses. These attributes indicate the potential clinical utility of MR for evaluating thyroid disease.

Because the neck is only minimally subjected to the degrading influence of cardiac and respiratory motion, adequate evaluation of the thyroid by using MR imaging is possible even with the relatively long image-acquisition times currently being used for clinical imaging. In this regard MR has been effective for defining the normal anatomy [1, 2] and tumors [3] of the larynx. However, no reports have yet appeared evaluating the specific use of MR for evaluation of thyroid disease.

The purposes of our current study were to (1) determine the signal characteristics of the normal and diseased thyroid; (2) evaluate the contrast between thyroid and adjacent tissues (muscle and fat) and the contrast between normal thyroid and various thyroid masses on T1- and T2-weighted images; (3) define the magnetic relaxation times of normal thyroid, adenomas, and carcinoma; and (4) assess the capability of MR imaging for defining the extent of large thyroid masses.

Subjects and Methods

Patient Population

Six normal subjects (aged 24–38 years) and 32 patients with thyroid disease (aged 29–79 years) underwent MR studies. The types of thyroid abnormalities were adenoma (eight patients), goiter (five patients), primary carcinoma (three patients), recurrent carcinoma (nine patients), suspected but not confirmed recurrent carcinoma (three patients), cyst (two patients), thyroiditis (one patient), and postthyroidectomy (one patient). Patients referred for MR to evaluate thyroid disease between May 1983 and October 1985 were included in this study. A few patients studied in late 1983 are not included in this study because these MR studies could not be obtained for analysis.

Received April 8, 1986; accepted after revision July 7, 1986.

[1] Department of Radiology, Box 0628, University of California San Francisco Medical Center, San Francisco, CA 94143. Address reprint requests to C. B. Higgins.

[2] Department of Surgery, University of California San Francisco Medical Center, San Francisco, CA 94143.

***AJR* 147:1255–1261, December 1986**
0361–803X/86/1476–1255
© American Roentgen Ray Society

Imager and Imaging Protocol

MR spin-echo imaging was done with a 0.35-T cryogenic imaging system that has been described [4]. Multislice images were obtained with repetition time (TR) values varying from 0.5 to 2.0 sec and echo times (TEs) of 28 or 30 msec (first echo) and 56 or 60 msec (second echo). In nearly all patients two sets of transverse images were obtained: a single-echo TR 0.5-sec sequence (10 sections imaged) and a dual-echo TR 2.0-sec sequence (20 sections imaged). Standard slice thickness (z axis) was 10 mm with no gap between slices. In studies performed before February 1985, slice thickness was 7 mm with 3-mm gap between slices. In a few patients, thin slices (5 mm) were also obtained. In patients with large neck masses or with suspected substernal extension of thyroid masses or goiters, a set of coronal images was also obtained. Coronal images were obtained with dual-echo multislice sequences by using a TR of either 1.5 or 2.0 sec.

The standard resolution mode was used, which has a 256 × 256 image matrix and an in-plane spatial resolution of 1.8 mm. The number of excitations per line was two for TR 2.0-sec sequences and four for TR 0.5-sec sequences. The imaging time for TR 0.5 sequence was 8.3 min and for TR 2.0 sequence was 17 min. An elliptical RF coil was used with a y axis of 30 cm and an x axis of 58 cm.

Verification of Thyroid Abnormalities

Twenty-seven of 30 abnormalities were established from operative findings along with gross and microscopic pathologic examination. In two other patients, needle aspirates at sites of possible recurrence of thyroid carcinoma were negative. In two patients with multinodular goiter, neither surgery nor a needle biopsy was done. In one patient with possible recurrence of thyroid carcinoma, a reoperation has not yet been performed.

Image Analysis

The images were analyzed retrospectively by two reviewers to determine the morphologic appearance and visible signal characteristics of the normal and diseased thyroids on the T1- and T2- weighted images. This consisted of a judgment regarding asymmetry or enlargement of the thyroid; abnormal increase or decrease in signal of regions of the thyroid; invasion or displacement of adjacent tissues, airways, or blood vessels by tumors; or recurrence of thyroid carcinomas.

The quantitative analysis involved the determination of the percentage contrast for normal thyroid tissue relative to adjacent fat and muscle on T1- and T2-weighted images with regions of interest placed over normal (average 15 pixels) and diseased (average 17 pixels) thyroid tissue. This was calculated by the following formula, % Contrast = (Ix − I thyroid)/(Ix + I thyroid/2), where I = image intensity and x = muscle or fat.

The percentage of contrast between thyroid masses and normal thyroid tissue was also calculated on both T1- and T2-weighted images. This was calculated by the formula, % Contrast = (I mass − I thyroid)/(I mass + I thyroid/2).

The T1 and T2 relaxation times were determined for normal thyroid (six), adenomas (eight), and carcinomas (four) by using the double spin-echo formula [5]. These values were not obtained for all adenomas and carcinomas, because in some instances either data were not available (deletion of a necessary pulse sequence) or regions of interest were considered too small to provide reasonable measurements.

Qualitative observations on MR images were correlated with operative and histologic findings. Both qualitative and quantitative analysis of the images were done in most instances with knowledge of these findings. Indeed, the gross and microscopic pathologies were used to guide the site for placement of regions of interest. Because this was a retrospective study, no attempt was made to define the diagnostic accuracy of MR in regard to other imaging techniques in these patients.

Results

Normal Subjects

The normal thyroid gland had medium intensity on the T1-weighted (TR 0.5, TE 30) images; signal intensity was much lower than surrounding fat and slightly to moderately higher than that of overlying strap muscles (Fig. 1). On the T2-weighted (TR 2.0, TE 60) images, the intensity of the thyroid showed a relative increase compared with the T1-weighted images; signal intensity was distinctly greater than that of the overlying strap muscles. The intensity of the thyroid was always homogeneous on T1-weighted images and usually homogeneous on T2-weighted images (Fig. 1). However, two volunteers had nonhomogeneous intensity on T2-weighted

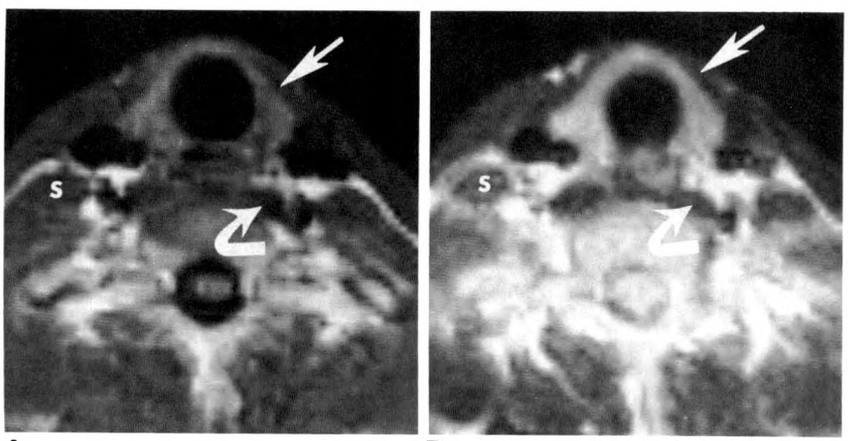


Fig. 1.—T1- (*A*) and T2- (*B*) weighted images of thyroid in normal subject. Transverse images at same anatomic level through middle of gland. Strap muscles (*straight arrows*), longus colli muscle (*curved arrows*), anterior scalene muscle (s).

images; small regions of high intensity were evenly and diffusely distributed throughout both lobes.

Quantitation of contrast between thyroid and adjacent tissues and measurement of relaxation times were consistent with the above qualitative observations. The percentage of contrast between thyroid and fat on T1- and T2-weighted images was 75.6 ± 12.7% and 58.5 ± 14.3%, respectively. The contrast between thyroid and muscle on T1- and T2-weighted images was 23.8 ± 6.5% and 65.3 ± 15.4%, respectively. The T1 and T2 relaxation times of thyroid tissue were 571.6 ± 30.7 and 49.6 ± 8.6 msec, respectively.

Goiter

Goiters showed low to medium intensity on the T1-weighted images (Fig. 2). The intensity was similar or only slightly increased compared with the normal thyroid. On the T2-weighted images, all five goiters were heterogeneous and contained multiple regions of high signal intensity (Figs. 2 and 3). Three of the five goiters were composed of substernal portions; the coronal images displayed penetration through the cervicothoracic junction and the extent of the mediastinal mass (Fig. 3).

Four of the five goiters contained focal adenomatous changes at pathologic examination. These regions had higher signal intensity than the remainder of the thyroid on the T2-weighted images in all four patients (Fig. 2B). Relaxation times could be measured in three of these patients; the T1 values of these adenomatous foci ranged from 815 to 990 msec among these patients, while the T2 values ranged 59 to 158 msec, respectively. Both values were higher than the remainder of the thyroid in these patients and in the range observed for true adenomas in patients without goiters. For determinations of percentage contrast and relaxation times, the values for these regions of focal adenomatous hyperplasia (four patients) were grouped with the values for solitary adenomas.

Adenoma

The eight benign adenomas were grouped together regardless of histologic type because of the limited number of subjects. Visual inspection of the T1-weighted images showed asymmetry of the lobe at the site of the adenoma. Intensity of the adenoma was more than 10% higher than that of normal thyroid on T1-weighted images for five of the eight patients in whom such measurements were possible. However, increased intensity of the adenoma was visually discernible in only one subject (Fig. 4). The other seven adenomas were nearly isointense (six patients) or slightly hypointense (one patient) with the normal thyroid tissue (Fig. 5). On the T2-weighted images all the adenomas had markedly higher intensity than the normal thyroid tissue (Figs. 4 and 5).

Coronal images displayed the full extent of the adenoma. They provided a clear depiction of the relationship of the mass to the cervicothoracic junction and of its effect on the airway (Fig. 5).

The percentage of contrast between adenoma and normal thyroid could be calculated for T1- and T2-weighted images in seven and eight patients, respectively. The mean percentage contrast was 11.9 ± 8.4% for the T1-weighted images and 51.9 ± 14.9% for T2-weighted images. The T1 and T2 relaxation times for the adenomas were 1202.8 ± 517.8 and 118.1 ± 48.8 msec, respectively. In each subject, the T1 and T2 times were greater for the adenoma when compared with normal thyroid tissue. However, within the group of patients, T2 values overlapped for normal and adenomatous regions in three instances, but T1 values overlapped in one instance.

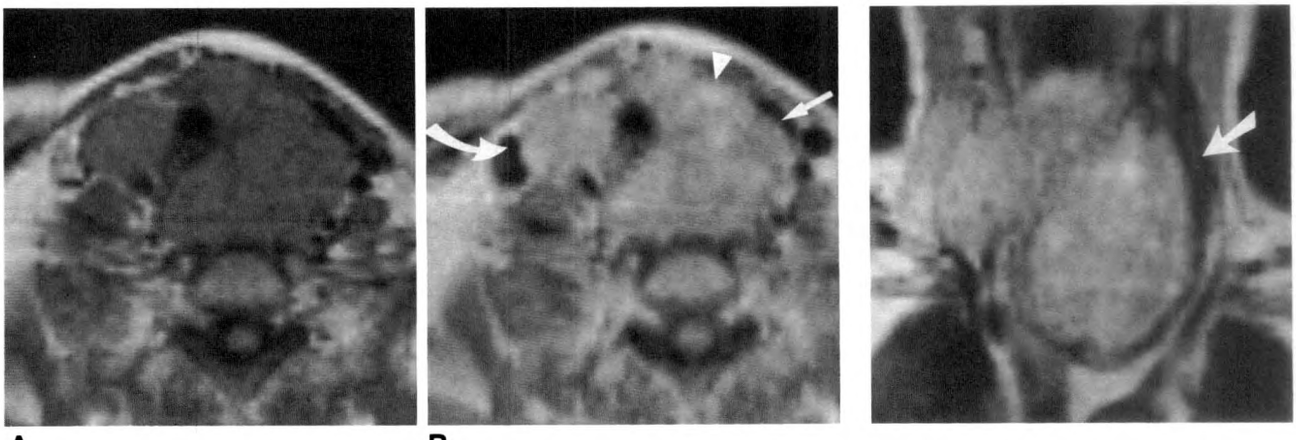


Fig. 2.—T1- (*A*) and T2- (*B*) weighted images in patient with multinodular goiter. Goiter has low, homogeneous intensity on T1-weighted image and high, heterogeneous intensity on T2-weighted image. Some regions of adenomatous hyperplasia (*arrowhead*) have higher intensity than remainder of goiter. Note compression of left jugular vein (*straight arrow*) and displacement of right jugular vein (*curved arrow*). Goiter extends behind and anteriorly displaces trachea.

Fig. 3.—Coronal image reveals substernal extension of multinodular goiter. Note lateral displacement of left neurovascular bundle (*arrow*).

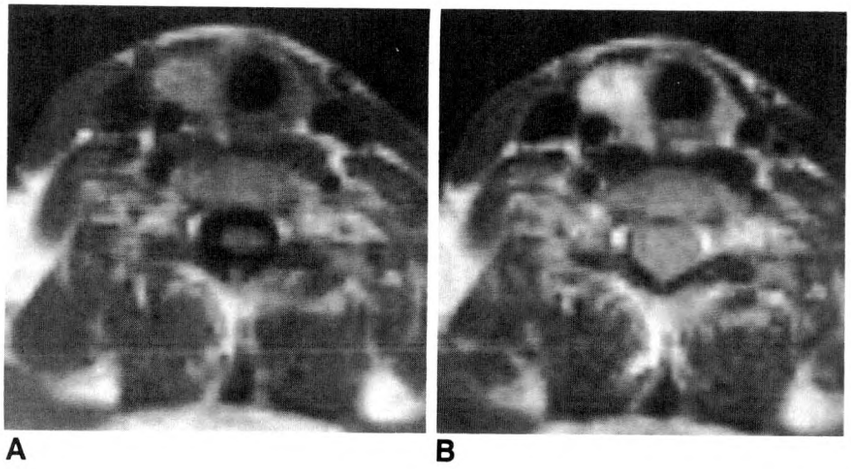


Fig. 4.—T1- (*A*) and T2- (*B*) weighted images of patient with single nonfunctioning nodule. Adenoma has high intensity on both images.

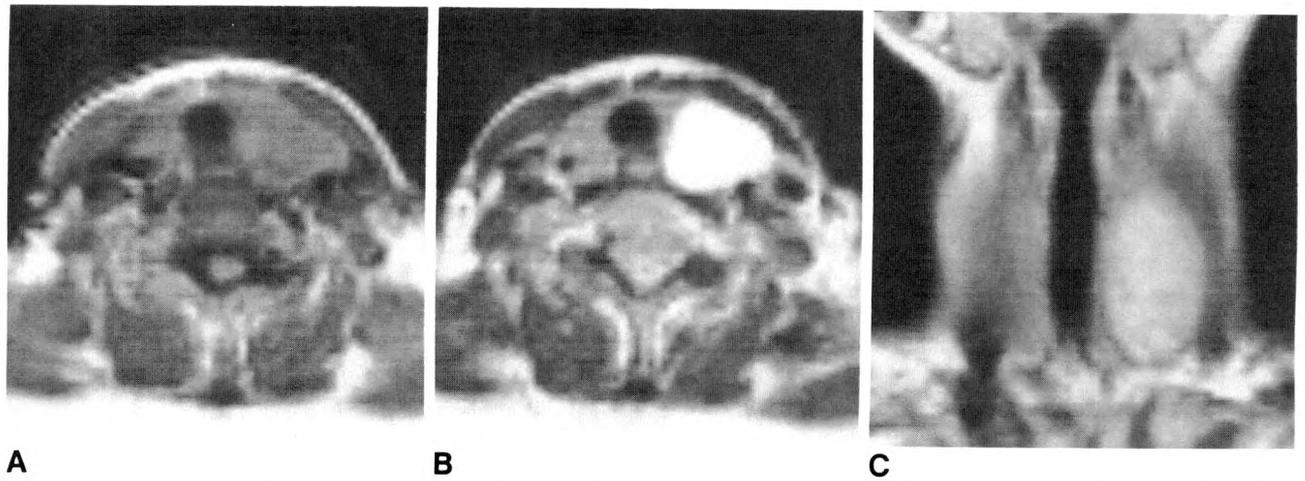


Fig. 5.—Transverse T1- (*A*) and T2- (*B*) weighted and coronal (*C*) images show large adenoma of left lobe of thyroid. It is isointense on T1-weighted image and markedly increases in intensity on most T2-weighted image. Coronal image displays full extent of large adenoma.

Carcinoma

T1-weighted images were available in seven and T2-weighted images in all 12 patients with thyroid carcinoma. The tumors were recurrent in nine of the 12 patients. In three patients, comparison with normal thyroid tissue could be made. The intensity of the carcinoma was less than normal thyroid (Fig. 6) in two patients and greater than normal thyroid in the one patient (Fig. 7) on the T1-weighted images. The carcinoma was also essentially homogeneous on these images. However, most of the mass had higher intensity than normal thyroid in all patients on T2-weighted images. Both primary and recurrent carcinoma showed heterogeneous intensity on T2-weighted images in all but one patient.

The MR images demonstrated well the displacement and impingement on the neurovascular bundles (Figs. 6 and 8), displacement and invasion of the larynx and trachea (Fig. 6), and invasion of surrounding muscles (Fig. 8). The coronal and sagittal images provided a composite view of the extent of the mass and invasion into the mediastinum (Figs. 6 and 8). The MR images showed extensive invasion of the neck and mediastinum in the two patients with anaplastic carcinoma and in another patient with recurrent papillary carcinoma (Figs. 6 and 8).

In the three patients with carcinomas, the percentage of contrast between carcinoma and normal thyroid ranged from 3.6 to 11% on T1-weighted images and from 40.5 to 75.9% on T2-weighted images. The T1 and T2 relaxation times were 1244.7 ± 440.3 and 94.3 ± 10.5 msec, respectively.

MR showed small to extensive local recurrences in five patients and recurrence to local lymph nodes in three subjects (Fig. 9). Recurrence in mediastinal lymph nodes was demonstrated in three patients. These were demonstrated with optimal contrast on T1-weighted images, where nodes had low signal intensity compared with surrounding fat.

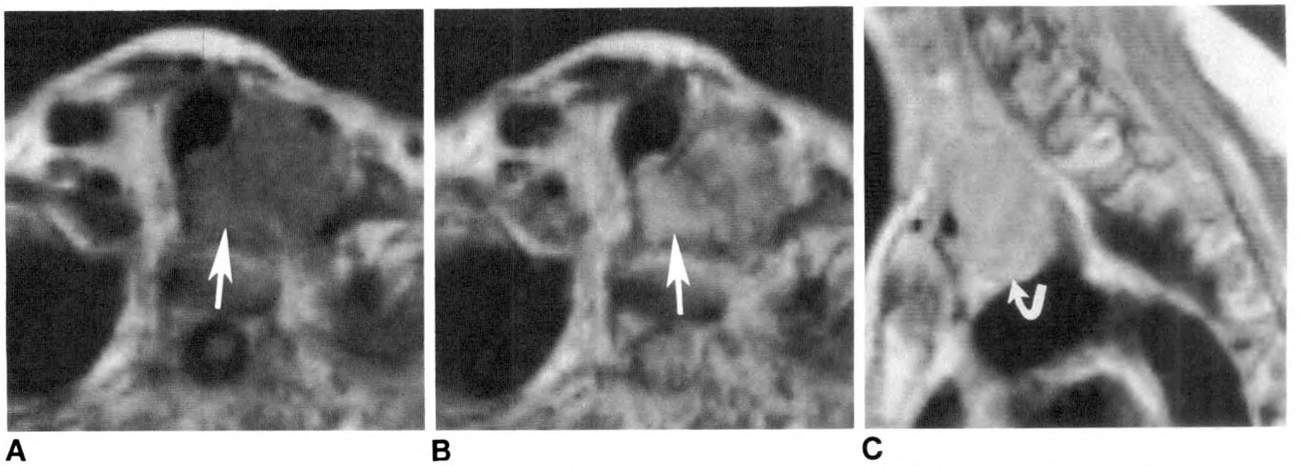


Fig. 6.—Recurrent thyroid carcinoma. Transverse T1- (*A*) and T2- (*B*) weighted and parasagittal (*C*) images. Carcinoma has low intensity on T1-weighted image and heterogeneous higher intensity on T2-weighted image. Tumor extends into trachea and longus colli muscles (*straight arrows*). Full extent of invasive carcinoma is displayed by parasagittal image; tumor extends deeply into mediastinum to level of aortic arch (*curved arrow*).

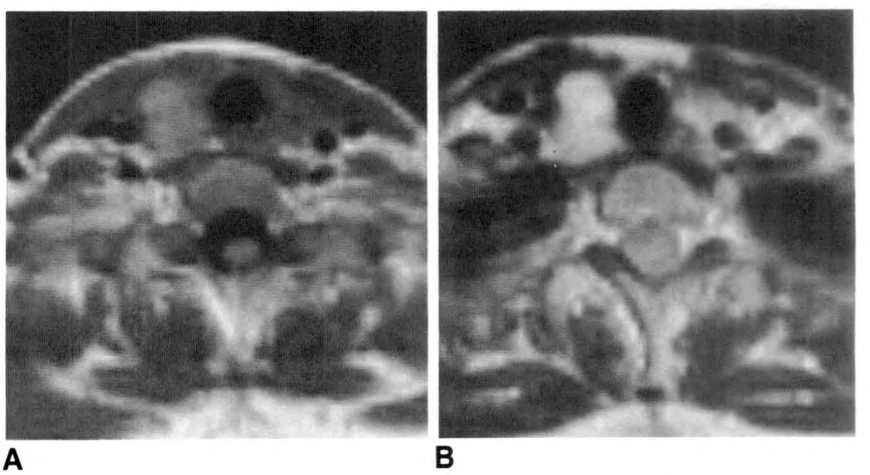


Fig. 7.—T1- (*A*) and T2- (*B*) weighted images of follicular carcinoma. Tumor has higher intensity than normal thyroid on both images.

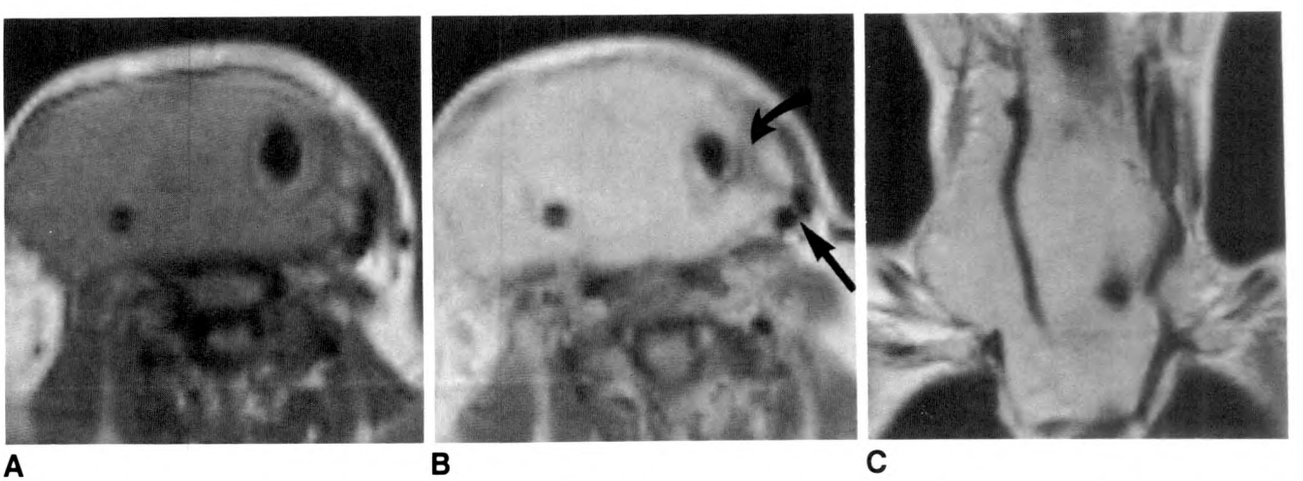
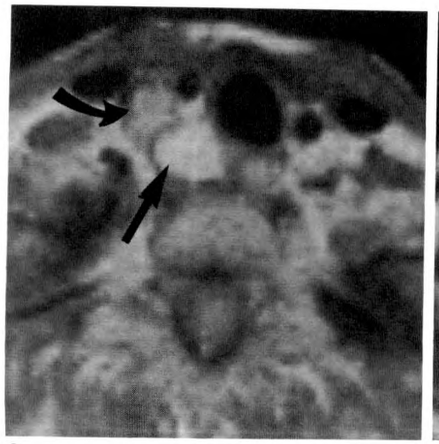
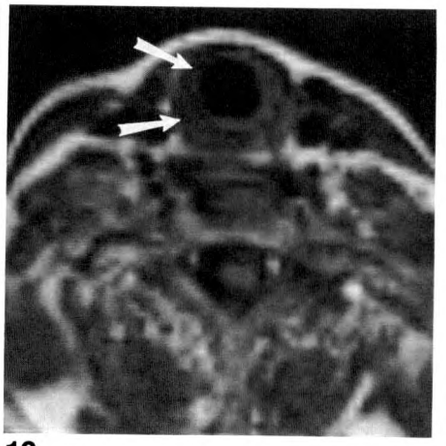


Fig. 8.—Anaplastic invasive carcinoma. Transverse T1- (*A*) and T2- (*B*) weighted and coronal (*C*) images. Tumor has low intensity on T1- weighted image, where its interface with fat is distinct. It has high intensity on T2-weighted image and can be distinguished from small region of residual normal thyroid (*curved arrow*). Trachea and left neurovascular bundle (*straight arrow*) are displaced laterally by tumor. Right jugular is occluded. Coronal image shows extension of mass deeply into mediastinum.



9



10

Fig. 9.—Transverse image shows recurrent thyroid tumor (*straight arrow*) and overlying metastatic lymph node (*curved arrow*). Trachea and esophagus are displaced leftward.

Fig. 10.—Transverse image shows rim of low-intensity tissue (*arrows*) surrounding trachea in area of resected thyroid bed. This rim of fibrous tissue is normal postthyroidectomy appearance.

Miscellaneous Abnormalities

A thyroid cyst (blue dome) had increased intensity relative to normal thyroid on both T1- and T2-weighted images. In a patient with granulomatous thyroiditis, the thyroid gland was enlarged with the right lobe enlarged asymmetrically. Compared with the values of the normal thyroid glands, both T1 (1046 msec) and T2 (61 msec) times were prolonged.

Postoperative Changes

Twelve patients were studied to detect or determine the extent of possible local or nodal recurrence of thyroid carcinomas. Recurrence in the neck was demonstrated in nine patients. Recurrence was confirmed by surgery in seven patients, but no recurrence was found in one patient in whom MR suggested recurrence anterior to the jugular veins bilaterally. The remaining patient has not had another operation. In two patients, extensive local recurrences were demonstrated (Fig. 8). Recurrences were demonstrated in cervical (Fig. 9) and mediastinal lymph nodes. In all subjects who had thyroidectomy, a rim of low-intensity tissue surrounded the trachea (Fig. 10). This tissue showed a relative decrease in signal intensity compared with muscle on T2-weighted images and presumably represented fibrosis in the thyroid bed.

Discussion

Our study indicates that, on MR, the thyroid gland has a signal intensity distinct from other tissues in the neck when both T1- and T2-weighted images are used. The maximum contrast between adenoma and carcinoma compared with normal thyroid tissue was observed on T2-weighted images, which reflected a more than twofold higher mean T2 time for tumors compared with normal thyroid. Since the average T2 for the adenomas was greater than 90 msec, it is likely that the contrast would be greater with even more T2 weighting, achieved by prolonging the TE to 90 msec. The T1-weighted images are also useful for evaluating thyroid masses, because they provide clear definition of the interface between infiltrating tumors and surrounding fat and the best contrast between lymph nodes and the fat [5].

Some thyroid nodules show high signal intensity on T1- as well as on T2-weighted images. This can be expected when there has been hemorrhage into a cyst or adenoma or in the presence of colloid degeneration in an adenoma. Highly proteinaceous fluids have a relatively short T1 [6].

The average T2 relaxation time of adenoma is longer than that observed for other tumors [7]. Only 11 and 7% of primary hepatic tumors had T2 values greater than 90 and 100 msec, respectively [7]. In our current study, the mean T2 value for adenomas exceeded 100 msec and for carcinomas exceeded 90 msec. Five of nine thyroid carcinomas had T2 values greater than 100 msec. However, the range of T2 values for adenomas was very wide. Both T1 and T2 values had some overlap between benign adenomas and carcinomas. Thus, with current techniques for estimating relaxation times, specific tissue characterization for thyroid mass does not seem possible.

MR imaging and other techniques are used to detect recurrence of carcinoma after thyroidectomy. Recurrent tumor in the resected thyroid bed or along the course of the jugular vein must be distinguished from postoperative fibrosis. Fibrous tissue has a short T2 relaxation time [8], which should reduce signal intensity on T2-weighted images. In our current study, a rim of tissue with low signal intensity was observed in the thyroid bed after thyroidectomy. This characteristic of fibrous tissue differs considerably from the qualities of tumor, which typically has a long T2 relaxation time [7, 8]. However, in one instance, a substantial amount of soft tissue beneath the sternocleidomastoid muscle after neck dissection had a medium-intensity signal on T2-weighted images and was misinterpreted as probable recurrent tumor. This experience suggests that differentiation of recurrent tumor and postoperative fibrosis may not always be possible based upon tissue appearance on T2-weighted images.

Radionuclide imaging has traditionally been the primary procedure used in the assessment of thyroid abnormalities; it defines the function of thyroid tissue and shows if palpable

nodules are composed of functioning thyroid tissue [9]. It also defines the presence of residual or recurrent functioning thyroid tissue after thyroidectomy for carcinoma. Compared with other techniques, it has the limitation of low spatial resolution.

Sonography defines thyroid masses and is especially accurate for determining the solid or cystic nature of thyroid nodules [10, 11]. Sonography is limited in defining substernal extension and retrotracheal components of thyroid masses.

The role of MR in thyroid imaging is probably similar to that of CT [12–14]. Both techniques are useful for defining the extent of large tumors, especially in depicting substernal extension and components located behind the airways. Likewise, these techniques are useful in determining the infiltration of masses into surrounding tissues. MR has some potential advantages over CT for the assessment of invasive carcinomas of the thyroid. The direct coronal images available with MR provide a large field of view and demonstrate the neck, cervicothoracic junction, and superior mediastinum on one or two images. This enables composite visualization of the full extent of large thyroid malignancies and substernal goiters. The excellent contrast between tumor and normal muscle on MR is useful for assessing muscle invasion; abnormalities involving the muscles cause an alteration in the signal intensity of the muscle [15].

At this stage in the evaluation of MR for the diagnosis of thyroid disease, it seems to have a role in two areas: (1) to assess the extent and invasiveness of large thyroid carcinomas and the extent of substernal goiters, and (2) to detect and define the extent of recurrent thyroid carcinoma.

REFERENCES

1. Stark DD, Moss AA, Gamsu G, Clark OH, Gooding GAW, Webb WR. Magnetic resonance imaging of the neck. *Radiology* **1984**;150:455–461
2. Lufkin RB, Hanafee WN. Application of surface coils to MR anatomy of the larynx. *AJR* **1985**;145:483–489
3. Lufkin RB, Hanafee WN, Wortham D, Hoover L. Larynx and hypopharynx: MR imaging with surface coils. *Radiology* **1986**;158:747–754
4. Crooks LE, Arakawa M, Hoenninger J, et al. Nuclear magnetic resonance whole body imager operating at 3.5 kgauss. *Radiology* **1982**;143:169–174
5. Dooms GC, Hricak H, Crooks LE, Higgins CB. Magnetic resonance imaging of the lymph nodes: comparison with CT. *Radiology* **1984**;153:719–728
6. Fullerton GD, Potter JL, Dornbluth NC. NMR relaxation of protons in tissues and other macromolecular water solutions. *Magnetic Resonance Imaging* **1982**;1:209–228
7. Schmidt HC, Tscholakoff D, Hricak H, Higgins CB. MR image contrast and relaxation times of solid tumors in the chest, abdomen and pelvis. *J Comput Assist Tomogr* **1985**;9:738–748
8. Herfkens R, Davis PL, Crooks LE, et al. Nuclear magnetic resonance of the abnormal live rat and correlation with tissue characteristics. *Radiology* **1981**;141:211–218
9. Pinsky S, Ryo VY. Thyroid imaging: a current status report. In: Freeman LM, Weissman HS, eds. *Nuclear medicine annual 1981*, New York: Raven, **1981**:157–193
10. Simeone JF, Daniels GH, Mueller PR, et al. High resolution real time sonography of the thyroid. *Radiology* **1982**;145:431–435
11. Schieble W, Leopold GR, Woo VL, Gosink BB. High resolution real time sonography of thyroid nodules. *Radiology* **1979**;133:413–417
12. Bashist B, Ellis K, Gold RP. Computed tomography of intrathoracic goiter. *AJR* **1983**;140:455–460
13. Reede DC, Bergeron RT, McCauley DI. CT of the thyroid and of other thoracic inlet disorders. *J Otolaryngol* **1982**;11:349–357
14. Silverman PM, Newman GE, Korobkin M, Workman JB, Moore AV, Coleman RE. Computed tomography in the evaluation of thyroid disease. *AJR* **1984**;142:897–902
15. Murphy WA, Totly WG, Carroll JE. MRI of normal and pathologic skeletal muscle. *AJR* **1986**;146:565–574

Book Review

Diagnostic Nuclear Medicine. By Henry N. Wagner, Jr., Julia W. Buchanan, and Danilo Espinola-Vassallo. Chicago, Year Book Medical, 430 pp, 1986.

The 18 chapters of this book cover such topics as the brain, heart, lung, thyroid, bone, liver, spleen, gastrointestinal tract, gallbladder, kidney, testes, lymph nodes, subphrenic space, iliopsoas space, peripheral vascular system, salivary glands, adrenal glands, blood platelets, and surgical shunts. In addition, most topics are broken down into common disease states, such as depression and Alzheimer's disease for the brain. There is an appendix of commonly used radiopharmaceuticals at the end of the book.

The organization of the book is good and the quality of illustrations varies from good to excellent. The text is easy to read with only a few typographical errors. Some discrepancy between the forward and the preface of the book exists; this is not a comprehensive coverage of the field of nuclear medicine and is geared more to the general practitioner, radiology resident, the nuclear medicine resident, and the medical student rather than the full-fledged practitioner of the specialty of nuclear medicine. It does, however, represent a good didactic approach to the teaching and application of the specialty of nuclear medicine in the evaluation of the patient.

The references are generally up to date. Although I cannot agree with all the legends and points covered in the discussion, this book presents a particular philosophy and subjectivity of its authors. The textbook does not have a thorough review of the literature nor a comprehensive review of the subject material.

The undue emphasis on the use of positron emission tomography (PET) in the brain section relfects the subjectivity of the authors, since this is a major area of research from their institution. The coverage of PET for the heart, for example, is not presented, which places out of perspective the availability and prevalence of PET for brain imaging as a routine study in most major hospitals.

The American College of Radiology periodically produces a nuclear radiology syllabus. Although their syllabus does not cover all the topics in such a systematic manner as this textbook does, it does present an excellent didactic approach that is more comprehensive and thought-provoking than the *Diagnostic Nuclear Medicine* textbook. It is also less subjective.

The textbook under review presents the opportunity to review quickly the various disease states in a somewhat simplified manner in which the specialty of nuclear medicine could benefit the patient. It is, however, not a textbook on nuclear medicine, nor does it thoroughly evaluate other diagnostic techniques for a particular patient problem. This is a weakness of the book, since other techniques, such as sonography, MR, and CT, are important in the evaluation of the patient and in many instances the question is: which is the most cost effective or the most efficacious test in the workup of the patient?

Robert C. Stadalnik
UC Davis Medical Center
Sacramento, CA 95817

Comparison of the Contrast-Enhancing Properties of Albumin-(Gd-DTPA) and Gd-DTPA at 2.0 T: An Experimental Study in Rats

Udo Schmiedl[1]
Marc D. Ogan[1]
Mike E. Moseley[2]
Robert C. Brasch[1]

Albumin-(gadolinium-diethylenetriaminepentaacetic acid), albumin-(Gd-DTPA), a macromolecular MR contrast agent designed for intravascular distribution, was compared with gadolinium-diethylenetriaminepentaacetic acid (Gd-DTPA), an extracellular fluid agent, for imaging characteristics in normal rats at 2.0 T. Albumin-(Gd-DTPA) produced larger-intensity increases in myocardium (125%), liver (114%), and brain (21%), at a dose of 0.062 mmol Gd/kg than did Gd-DTPA at a dose of 0.2 mmol/kg. The duration and pattern of enhancement differed between the two compounds; the enhancement with albumin-(Gd-DTPA) persisted at relatively constant levels from 2 min to 1 hr. The Gd-DTPA tissue enhancement peaked at 2 min and had virtually disappeared at 60 min. Gd-DTPA better enhanced subcutaneous tissues, presumably because of capillary permeability and enhancement of the abundant extracellular fluid space. When albumin-(Gd-DTPA) is used, the strong persistent enhancement of the microvascular compartment is well demonstrated on subtracted images and supports potential application of albumin-(Gd-DTPA) for blood-volume and perfusion-dependent contrast enhancement of myocardium, liver, and brain.

IV administration of gadolinium-diethylenetriaminepentaacetic acid (Gd-DTPA), as shown in experimental animals [1–4] and more recently in clinical trials [5], can dramatically change the MR imaging appearance of specific tissues. Like classic iodinated contrast agents (e.g., diatrizoate) used in conventional radiography, Gd-DTPA distributes after IV administration within the extracellular fluid compartment (ECF), does not penetrate the blood-brain barrier, and is rapidly eliminated by the kidney [2, 4, 6–9]. This particular distribution allows for application of Gd-DTPA as a contrast medium for urographic imaging, for demonstration of abnormal capillary permeability associated with inflammation and tumors [2, 5], and for evaluation of blood-brain barrier integrity [5–7].

Gd-DTPA, however, has certain limitations for use in contrast enhancement of perfusion or blood-volume abnormalities. Experimental data indicate that 5 min after IV injection, 80% of the administered Gd-DTPA dose has disappeared from the intravascular space [8]. About 50% of this compound is cleared from the capillaries into the interstitial space on the first pass (Weinmann H-J, personal communication). This rapid distribution of Gd-DTPA into the ECF does not permit a selective enhancement of the intravascular space, which is desired for assessment of blood volume or tissue perfusion. A contrast agent retained in the vascular space could, in theory, provide direct, specific information on blood volume and tissue perfusion.

Human serum albumin has been paramagnetically labeled by covalently binding an average of 16 Gd-DTPA chelates to each molecule of albumin [10]. This product had an exceptionally high T1 relaxivity (R1) (relaxation rate per millimolar agent) of R1 = 313 mM^{-1} sec^{-1} relative to protein concentration when measured at 10.7 MHz. For comparison, the R1 value of Gd-DTPA is 4.9 mM^{-1} sec^{-1} [4]. Thus the molar relaxivity of each Gd-DTPA chelate was increased approximately threefold

Received May 7, 1986; accepted after revision July 22, 1986.

This work was supported in part by grant R01-AM31937 from the National Institute of Arthritis, Diabetes, Digestive and Kidney Diseases and by Schering A.G., Berlin.

U. Schmiedl is on leave from the Medizinisches Strahleninstitut, Universitaet Tuebingen, Roentgenweg 11, 7400 Tuebingen, West Germany. He is the recipient of a fellowship from the Deutsche Forschungsgemeinschaft, Bonn, West Germany.

[1]Department of Radiology, C309, Contrast Media Laboratory, University of California School of Medicine, San Francisco, CA 94143-0628. Address reprint requests to R. C. Brasch.

[2]Department of Radiology, Magnetic Resonance Spectroscopy Laboratory, University of California School of Medicine, San Francisco, CA 94143-0628.

AJR **147:1263–1270, December 1986**
0361–803X/86/1476–1263
© American Roentgen Ray Society

by binding it to albumin [10]. Both biodistribution and preliminary in vivo imaging studies have shown that albumin-(Gd-DTPA) remains largely confined to the vascular space for up to 90 min after IV injection in rats [11].

The goal of our present study was to compare the in vivo contrast-enhancing properties of albumin-(Gd-DTPA) and Gd-DTPA in normal rodent tissues including the heart, liver, and brain by using short pulse sequence settings at 2.0 T. It was postulated that the enhancement after IV injection of albumin-(Gd-DTPA), compared with Gd-DTPA, would produce equal or larger tissue-intensity gains for a longer time interval, and that the pattern of enhancement would differ from that of Gd-DTPA.

Materials and Methods

Contrast Media

Human serum albumin was labeled with Gd-DTPA and characterized as previously described [10, 11]. The albumin-(Gd-DTPA) used for the present study had an average of 31 Gd ions per albumin molecule and had a T1 relaxivity of R1 = 350 mM^{-1} sec^{-1} at 2.0 T. The T1 and T2 relaxivities, measured at 0.25 T, were R1 = 424 mM^{-1} sec^{-1} and R2 = 569 mM^{-1} sec^{-1}. An aqueous solution of native bovine serum albumin, obtained in crystalline form (Sigma Chemical, St. Louis) was used in control experiments. Both native bovine serum albumin and albumin-(Gd-DTPA) were administered by IV injection of 160 mg/kg (0.0024 mmol protein/kg). The dimeglumine salt of Gd-DTPA (Schering A.G., Berlin) was administered intravenously at a dose of 0.2 mmol/kg.

Imager Pulse Sequences and Image Subtraction Technique

All imaging experiments were performed with a General Electric CSI-II 2.0-T (85.6-MHz proton-resonant frequency) chemical-shift-imaging spectrometer (GE Medical Systems, Fremont, CA). The proton imaging sequence used throughout this study was that of a standard spin-warp 2DFT sequence that employed a single 2-mm slice thickness with four phase-cycled signal acquisitions. The raw data matrix size was 128 phase-encoding cycles by 512 complex data points (quadrature detection mode) transposed to 512 × 512 image-output pixels (256 level gray scale) over a 150 × 150 mm field of view (FOV). Only repetition time (TR) and echo time (TE) values were varied; all other parameters (FOV, gain, image processing) were held constant. A specially designed 53-mm outer-diameter (130-mm-long) imaging coil of the low-pass birdcage resonator design [12] was employed with a balanced-matched tuning network [13] for all images. This design allowed for near-complete coil filling with excellent sensitivity and B1 homogeneity over the imaged volume.

Postcontrast-minus-precontrast image subtraction was performed by signal subtraction of the original, precontrast 128 × 512 raw data matrices from the postcontrast matrices followed by the standard image processing technique used for all images.

Selection of Pulse Sequence and Dose

Test-tube phantoms were prepared by addition of 0.0, 1.8, 3.7, 5.6, 7.5, 9.5, 11.5, 13.6, 15.7, 17.8, and 20.0 mg of albumin-(Gd-DTPA) to samples of 4.5 ml of human plasma. These dilutions correspond to an increase in total plasma albumin concentration of 0%, 1%, 2%, 3%, 4%, 5%, 6%, 7%, 8%, 9%, and 10% (albumin-[Gd-DTPA]/total albumin).

Transverse spin-echo (SE) images of the tubes were obtained by using pulse sequences of SE 220/14, SE 220/28, SE 300/14, SE 300/28, SE 460/14, and SE 460/28, where the first number designates the TR (msec) and the second number designates the TE (msec). A test tube filled with commercial corn oil was used as an intensity standard. Signal intensities for the images of the test tubes were determined by region-of-interest (ROI) measurements (minimum 60 pixels/ROI) over the center of each tube.

The influence of various pulse-sequence settings was further investigated in two rats. After intraperitoneal injection of sodium pentobarbital (Sodium Pentobarbital Injection C, Anthony Products, Arcadia, CA) (40–50 mg/kg), the 200-g female Spraque-Daweley rats were separately positioned supine in the coil. Coronal SE images that had TR and TE times of SE 220/14, SE 220/28, SE 300/14, SE 300/28, SE 460/14, and SE 460/28, respectively, were obtained at the level of the left ventricle, and the images were qualitatively evaluated for chamber and major vessel resolution.

Comparison of Albumin-(Gd-DTPA) and Gd-DTPA

Animals were prepared for imaging by intraperitoneal injection of 40–50 mg/kg sodium pentobarbital. A 23-gauge scalp-vein catheter was placed into the tail vein of each 200-g female Spraque-Daweley rat. Each of the 12 rats was imaged separately, lying supine in the coil, with the head elevated 1 cm. Precontrast single-slice SE images of the animals were obtained in the coronal plane at the level of the left ventricle, brain, and liver. Single-slice SE images (SE 300/14) were chosen (see Results) for the comparison of albumin-(Gd-DTPA) and Gd-DTPA. Five rats received 160 mg/kg (0.0024 mmol protein/kg) of albumin-(Gd-DTPA), five rats received 0.2 mmol/kg of Gd-DTPA, and two rats received 160 mg/kg of native bovine serum albumin. Images were acquired before and at 2, 20, and 60 min after injection of albumin-Gd-DTPA ($n = 5$), Gd-DTPA ($n = 5$), or native serum albumin ($n = 2$).

In addition, the degree of contrast enhancement and the distribution properties of albumin-(Gd-DTPA) for various anatomic structures were studied. Without changing the position of the rat, images of the head, thorax, and upper abdomen were obtained in the coronal plane at 12 different levels, from the spine to the anterior chest wall. Each contiguous slice had a thickness of 2 mm. The first image was obtained 60 min after injection of 160 mg/kg of albumin-(Gd-DTPA) while the last image, due to acquisition and data-processing time, was completed 180 min after injection.

Intensity Measurements

The image gray scale using the CSI-II 2.0 T imager was automatically adjusted to the highest image intensity. Thus, signal intensity values obtained for the plasma phantom model with various pulse-sequence settings were not directly comparable. In comparison of ROI intensity data for various pulse-repetition times, the intensity data of the plasma phantoms were normalized by means of the ratio of intensities for the oil phantom, which was measured at the different TRs.

Signal-intensity values were determined for all pre- and postcontrast images of rats by ROI measurements over the parenchyma of the left lobe of the liver, the left ventricular wall, the left hemisphere of the brain, and the corn-oil phantom. The ROIs incuded a minimum of 20 pixels and were held constant while the pre- and postcontrast signal intensity of each organ was measured. The intensity values were normalized for each image with the equation, relative intensity = intensity of sample/intensity of standard.

The intensity values were presented as mean ± 1 SD on an

arbitrary linear scale. Differences between pre- and postcontrast signal intensities were assessed, as appropriate, for significance by means of the paired t test. Scores of $p < .01$ were considered significant.

Results

Selection of Pulse Sequence and Dose

Intensity data from the doped plasma solutions demonstrated the effects of different concentrations of albumin-(Gd-DTPA) and of pulse-sequence settings on the image intensity (Fig. 1). Long TR and short TE values produced high absolute signal intensity for all solutions. This behavior is consistent with the SE intensity equation [14].

In comparing the effect of the concentrations of albumin-(Gd-DTPA) at TRs of 220, 300, and 460 msec on the signal intensity, the maximum intensities were observed, respectively, at 5%, 3.5%, and 2.5% concentrations of paramagnetic albumin relative to total plasma albumin (TE = 14 msec). With the same TR values and a TE of 28 msec, the optimal concentrations were found to be at 4%, 3%, and 2% (Fig. 1). Thus, the longer TR interval (460 msec) could be used advantageously to yield comparatively high signal intensities with small doses (2.5% or 2%) of paramagnetic agent.

Yet another factor in the selection of pulse settings for in vivo studies was anatomic resolution. For resolution of the beating rodent heart, the TR value of 300 msec in combination with a TE value of 14 msec produced the sharpest delineation of the cardiac chambers.

While a long TR interval of 460 msec produced a high signal intensity with a low dose of paramagnetic agent, contrast differences with and without paramagnetic agents are better emphasized with a shorter TR time [1, 2, 15] that would favor the use of a TR of 220 msec. As a compromise, the SE 300/14 parameters and a 160 mg/kg albumin-(Gd-DTPA) dose [16, 17] were selected for subsequent in vivo imaging.

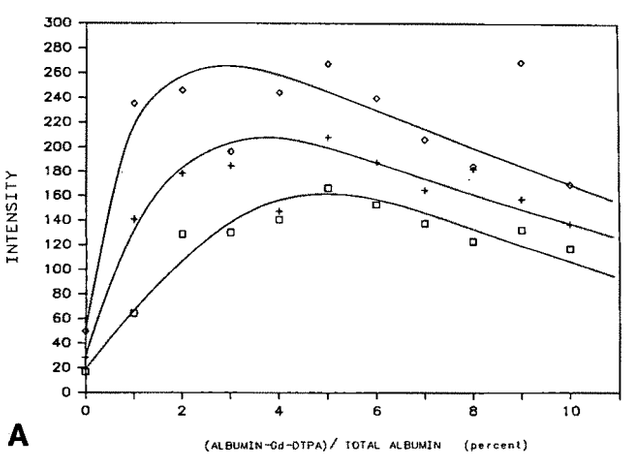
Comparison of Albumin-(Gd-DTPA) and Gd-DTPA Enhancement

All images obtained in this series of 12 rats provided excellent anatomic resolution of the brain, liver, and heart using an SE 300/14 sequence (Figs. 2–4). No signal was observed from flowing blood in the major vessels and cardiac chambers before administration of contrast media (Figs. 2 and 4). Without ECG gating, the images allowed for delineation of the left and right ventricular walls and the interventricular septum before and after injection of albumin-(Gd-DTPA) ($n = 5$), of Gd-DTPA ($n = 5$), or of unlabeled albumin ($n = 2$) (Figs. 2–6).

Enhancement of the liver parenchyma, the myocardium, the brain, and several large venous structures was observed 2, 20, and 60 min after injection of 160 mg/kg of albumin-(Gd-DTPA) (Fig. 2). Signal enhancement of slowly flowing blood was observed in the atrial appendices, veins of the liver, upper extremities, and mediastinum. This enhancement persisted qualitatively unchanged for 60 min after injection (Fig. 2). In two animals that were reimaged 72 hr after injection of albumin-(Gd-DTPA) ($n = 2$), the signal of previously enhanced tissues had returned to baseline levels of intensity.

Quantitative analysis of the signal intensity data obtained from five animals that received albumin-(Gd-DTPA) showed that, by 2 min postinjection, the liver parenchyma was enhanced by 114%, the myocardium by 125%, and the brain by 21% relative to respective precontrast values (Fig. 7). The signal intensity of these tissues remained unchanged for 60 min. The increases in tissue signal intensities measured at 2, 20, and 60 min after administration of albumin-(Gd-DTPA) were significant ($p < .01$) in each case, but time-dependent variations in intensities for each tissue were not significant. Administration of unlabeled albumin ($n = 2$) did not alter the image intensities.

Images of one rat studied at 12 different coronal planes with 2-mm contiguous slices after administration of 160 mg/



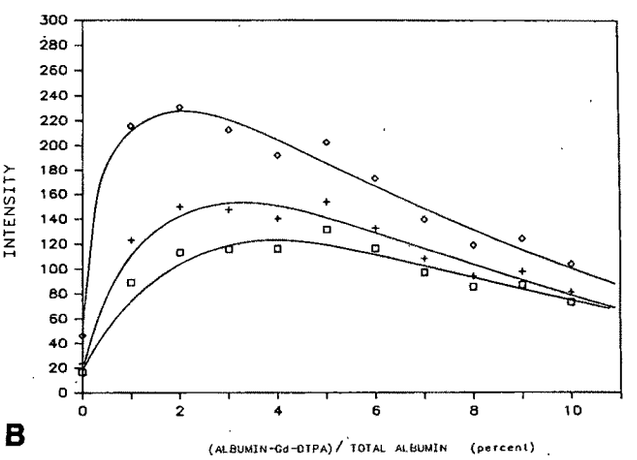


Fig. 1.—Signal intensities of test tubes containing concentrations of 0–10% albumin-(Gd-DTPA) in plasma as measured on spin-echo images acquired with three repetition times: 220 (□), 300 (+), and 460 (◇) msec; and two echo times: 14 (*A*) and 28 (*B*) msec.

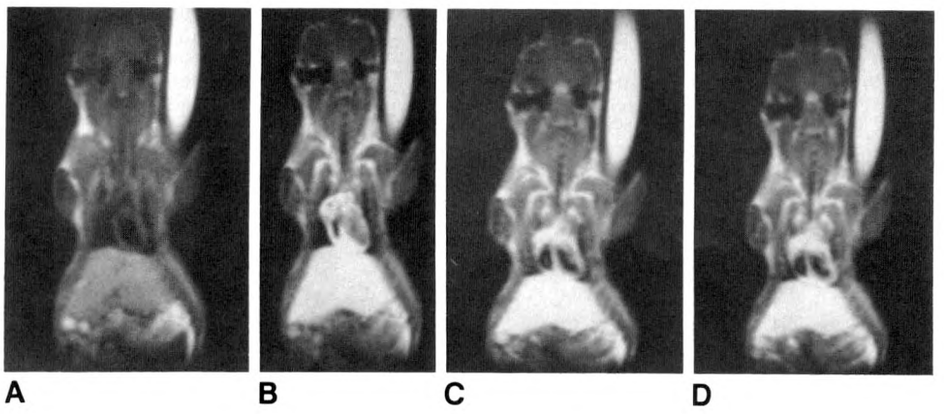


Fig. 2.—Coronal spin-echo images (SE 300/14) of rat before (*A*) and 2 min (*B*), 20 min (*C*), and 60 min (*D*) after IV injection 160 mg/kg albumin-(Gd-DTPA). Test tube containing commercial corn oil is attached to rat. Time-consistent signal enhancement is seen of myocardium, liver, and slow-flowing blood in several vascular structures including brachiocephalic veins.

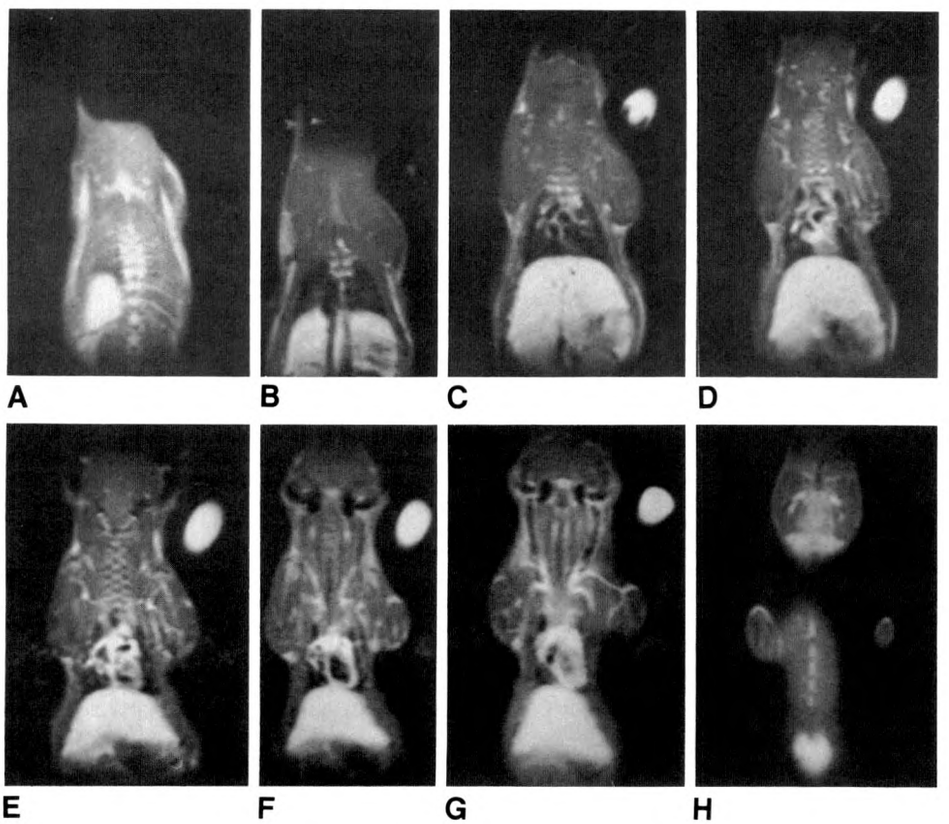


Fig. 3.—From a series of 12 contiguous coronal spin-echo images (SE 300/14), selected slices are included from level of posterior mediastinum (*A*) up to anterior chest wall (*H*). Rat had supine position in coil with head elevated by 1 cm. First image (*A*) was acquired 60 min after IV injection of 160 mg/kg albumin-(Gd-DTPA). Last image (*H*) was acquired 3 hr after injection of contrast medium. Note enhancement of liver (*A–H*), myocardium (*E–G*), and bone marrow (*A* and *H*). Contrast between flowing blood in inferior vena cava and descending aorta is best seen on *B*. Enhancement of slow-flowing blood in pituitary (*G*) and choroid plexus (*H*) and brachiocephalic veins (*F* and *G*) can be appreciated.

kg albumin-(Gd-DTPA) showed a more complete pattern of enhancement, including all walls of the cardiac chambers (Figs. 3E–3G). The two strongly enhanced areas at the base of the heart probably represented relatively stagnant blood in the atrial appendices (Fig. 3F). Blood flowing centrally in the internal jugular veins showed no enhancement, while a slight enhancement caused by laminar flow was noted close to the walls of both of these veins (Fig. 3G). The rapidly flowing blood in the hepatic and supradiaphragmatical portions of the inferior vena cava, cardiac ventricles, and abdominal aorta did not show enhancement (Fig. 3B). No signal enhancement was seen in the blood in the ascending and descending aorta or in the main pulmonary artery (Figs. 3B–3E).

The blood in the liver veins appeared brighter than the surrounding liver parenchyma (Fig. 3B). The spleen was seen as a small triangular area of high signal intensity in the left midabdomen (Fig. 3C). In the brain, after administration of albumin-(Gd-DTPA), several vascular structures were en-

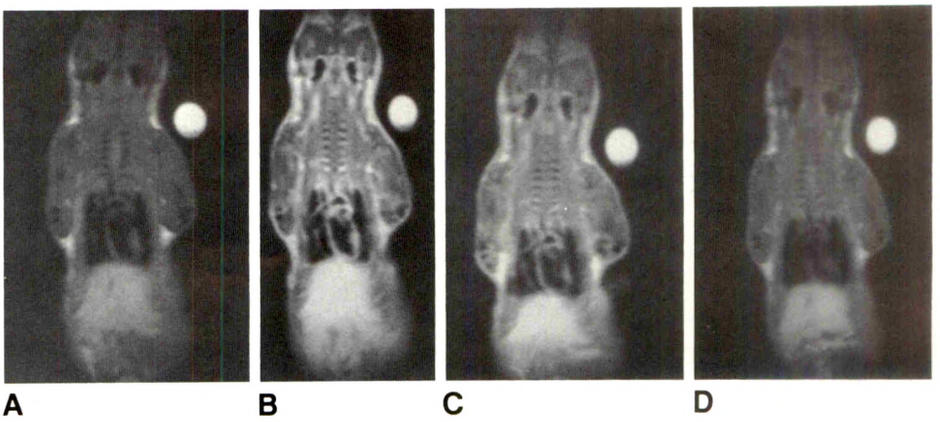


Fig. 4.—Series of coronal spin-echo images (SE 300/14) of a rat before (*A*) and 2 min (*B*), 20 min (*C*), and 60 min (*D*) after IV injection of 0.2 mmol/kg Gd-DTPA. Myocardium, liver, and subcutaneous tissue appear enhanced (*B*).

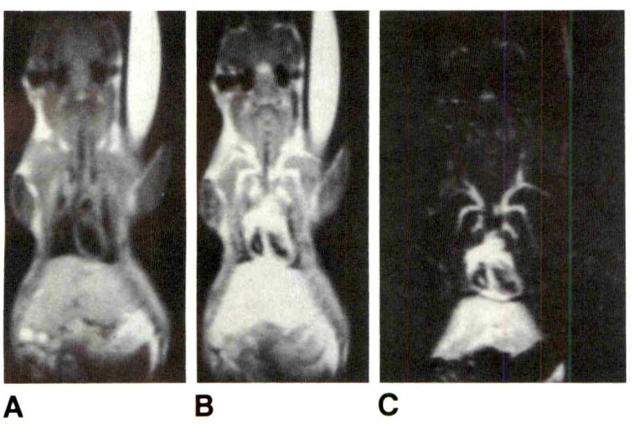


Fig. 5.—Distribution of albumin-(Gd-DTPA) 60 min after injection. Precontrast image (*A*), image acquired 60 min after injection of 160 mg/kg albumin-(Gd-DTPA) (*B*) (both *A* and *B* spin-echo 300/14), and subtracted image (*C*) are shown.

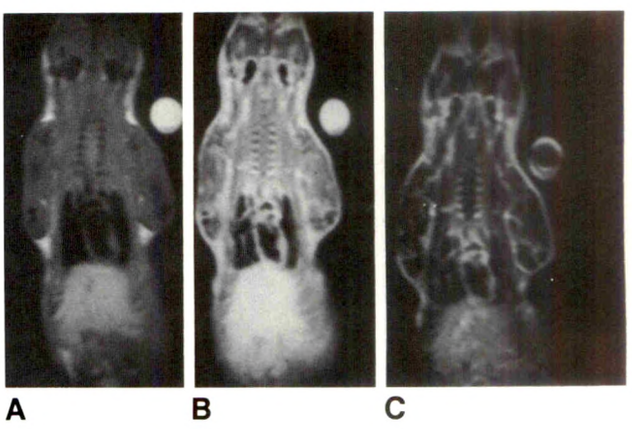


Fig. 6.—Distribution of Gd-DTPA 2 min after injection. Coronal precontrast (*A*), 2 min postcontrast (*B*) (both spin-echo 300/14), and subtracted (*C*) images are shown.

hanced including the pituitary and the choroid plexus (Figs. 3F–3H).

The macromolecular contrast medium appeared to accumulate in the bone marrow producing in-signal enhancement of the vertebral bodies, pedicles, ribs, and sternum, compatible with the large blood volume of the bone marrow (Figs. 3A, 3B, and 3H).

Because of the image-acquisition and data-processing times for each single-slice image, the images shown in this series were acquired between 1 hr (Fig. 3A) and 3 hr (Fig. 3H) after IV injection of albumin-(Gd-DTPA). Contrast enhancement was still appreciable at 3 hr after administration of the contrast medium.

At 2 min after administration of 0.2 mmol/kg of Gd-DTPA, enhancement was observed of the myocardium, liver parenchyma, and subcutaneous tissues (Fig. 4). Blood in the hepatic veins and the choroid plexus also showed signal enhancement (Fig. 4). Signal enhancement of these tissues was already considerably decreased by 20 min and had returned to baseline 60 min after injection (Fig. 4).

Quantitative analysis of the intensity data obtained in five rats at 2 min after injection of Gd-DTPA showed that the signal intensity of the myocardium was increased by 80% ($p < .01$) (Fig. 8). The intensity of the liver parenchyma increased by 60% at 2 min postinjection relative to the precontrast value (Fig. 8). Liver enhancement was significant at a score of $p < .05$ but not at $p < .01$. The signal intensity for heart and liver showed a substantial progressive decline over 60 min. At 20 and 60 min after injection of Gd-DTPA, no significant change in signal intensity relative to the precontrast values could be recorded. The intensity changes in the brain were not significant at any point.

The subtracted images clearly showed the different biodistribution of albumin-(Gd-DTPA) and Gd-DTPA (Figs. 5 and 6). The myocardium, liver parenchyma, and spleen, as well as the blood in the liver veins, the brachiocephalic veins, and

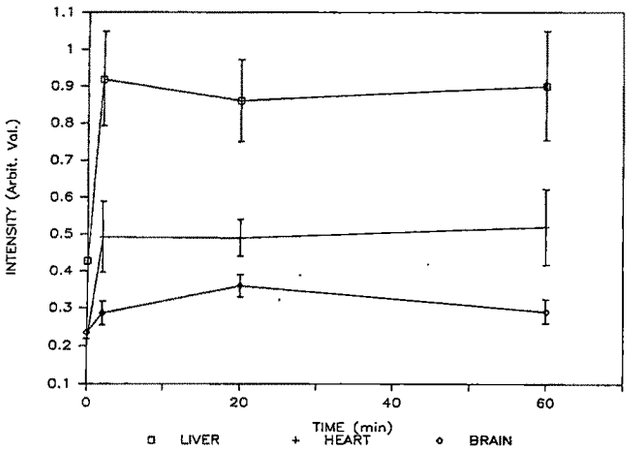


Fig. 7.—Time-dependent signal-intensity changes (mean values ± 1 SD, $n = 5$) of brain, heart, and liver before and 2 min, 20 min, and 60 min after IV injection of 160 mg/kg albumin-(Gd-DTPA). All changes were significant ($p < .01$).

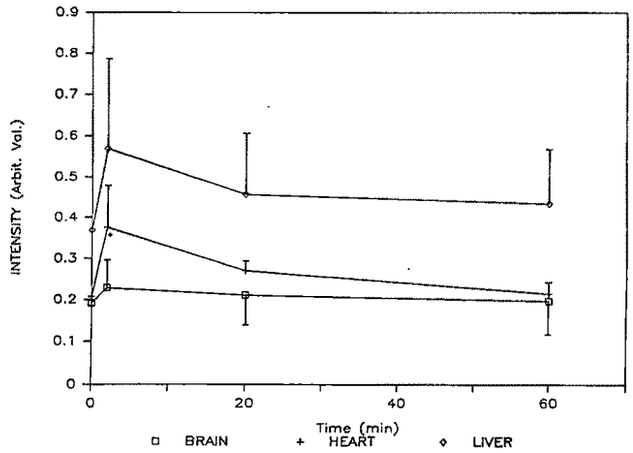


Fig. 8.—Signal-intensity changes (mean values ± 1 SD, $n = 5$) of brain, heart, and liver before and 2 min, 20 min, and 60 min after IV injection of 0.2 mmol/kg Gd-DTPA. Significant ($p < .01$) changes are indicated by plus sign.

the vascular plexus in the pituitary fossa, showed observable signal enhancement on the 60-min postcontrast minus precontrast image after injection of albumin-(Gd-DTPA) (Fig. 5).

The 2-min-postcontrast minus precontrast subtracted image after administration of Gd-DTPA showed enhancement of the myocardium, liver parenchyma, marrow, and subcutaneous tissue (Fig. 6). Enhancement in the blood of the liver veins could also be appreciated. The postcontrast-minus-precontrast image obtained 60 min after injection did not reveal any remaining contrast-enhancing effect of Gd-DTPA.

Discussion

The results of this comparative imaging study of Gd-DTPA (0.2 mmol/kg) and albumin-(Gd-DTPA) (0.062 mmol Gd/kg) demonstrated that both contrast media produced easily observed enhancement of highly vascular tissues, including the myocardium and liver. Important differences were (1) the macromolecular albumin-(Gd-DTPA) induced greater intensity changes and that these changes persisted for 60 min as compared with the gradual loss of enhancement with Gd-DTPA; (2) only albumin-(Gd-DTPA) produced significant enhancement of the brain; (3) the patterns of distribution varied, as expected for an intravascular agent, albumin-(Gd-DTPA), and Gd-DTPA, that equilibrates with the interstitial extravascular space; (4) with Gd-DTPA, there was a clear enhancement of subcutaneous tissues that was not observed with albumin-(Gd-DTPA); (5) albumin-(Gd-DTPA) induced significant enhancement of the bone marrow and of the blood in mediastinal veins and atrial appendices; this enhancement of the normal blood pool demonstrated by albumin-(Gd-DTPA) may prove useful for diagnosing abnormalities of tissue blood volume or perfusion.

Gd-DTPA has been studied extensively as an MR contrast agent in laboratory experimentation and in clinical trials [1–8]. This small molecule (590 daltons) distributes throughout the interstitial space after IV administration, allowing for enhancement of inflammatory lesions [2] and tumors [5–7] with abnormal capillary permeabilities and expanded interstitial spaces. An estimated 50% of Gd-DTPA is cleared from the vascular space into the extravascular compartment on the initial pass through the capillaries (Weinmann H-J, personal communication). Ex vivo studies of canine myocardial ischemia using Gd-DTPA have shown a dynamic distribution and enhancement pattern with this compound [15, 18]. Initially the contrast agent enhances normal myocardium with no effect on ischemic and infarcted regions, but after 5 min the relative enhancement reverses [18]. This dynamic pattern presents a disadvantage for the application of Gd-DTPA for the assessment of perfusion; the accumulation of this agent depends not only on perfusion but also on capillary permeability and the size of the interstitial space. A paramagnetic agent largely confined to the vascular space might be used advantageously for direct assessment of tissue perfusion.

The image subtraction technique was particularly useful to highlight the in vivo differences in distribution between Gd-DTPA and albumin-(Gd-DTPA). Postcontrast-minus-precontrast subtracted images only displayed the enhanced tissues. Elimination of background signal may prove useful for detection of small, enhancing lesions, for defining the vascular anatomy, and for detection of small differences in enhancement. With the subtraction technique, a substantial signal enhancement of highly vascularized tissues and of slow-flowing blood in small-to-medium–sized veins was seen clearly on images up to 60 min after injection (Fig. 5). The myocardium and liver parenchyma are highly vascular tissues with average measured blood volumes in the rat of 262 μl/g

and 270 μl/g, respectively [19]. The blood volume of brain tissue, 33 μl/g, is considerably lower [19]. These differences in organ blood volumes explain, apart from the inherent T1 and T2 values of the tissues, the strong signal enhancement in myocardium and liver and the considerably lesser enhancement in the brain with albumin-(Gd-DTPA) and the absent cerebral effect with Gd-DTPA.

Albumin-(Gd-DTPA) is a relatively new contrast agent for MR imaging, and its pharmacologic properties are not yet fully defined. This conjugate is synthesized by reaction of the cyclic anhydride of DTPA with albumin and subsequent addition of an excess of Gd^{+3} ions before purification by extensive dialysis [10]. The DTPA groups are covalently linked to the amine moieties of albumin, and the Gd^{+3} ion is chelated in the DTPA ligand.

Our present imaging results with albumin-(Gd-DTPA) confirm previous in vitro biodistribution studies conducted in rats over a 90-min observation period [11]. These earlier data indicate relative constant accumulation levels in the blood, heart, lung, liver, kidney, and brain, listed in order of decreasing concentrations [11]. In our present in vivo study, tissue enhancement was greatest for the heart, followed by the liver and brain. No loss of contrast enhancement was observed over 60 min. The degree of tissue enhancement was excellent, exceeding that observed with Gd-DTPA. Lung and renal enhancement could not be adequately evaluated on the coronal images used in this study for assessment of brain, heart, and liver.

In our study, ECG gating was not used (not available with our imaging system); but in a previous study [11], with the same dose of albumin-(Gd-DTPA) at 0.35-T in gated SE images, we observed a 32% myocardial enhancement, persisting up to 23 min after injection. This degree of enhancement points out the importance of pulse-sequence settings on the effectiveness of contrast media. The gated cardiac images, acquired with a TE of 28 msec, had an effective TR greater than 500 msec, and thus, were not as T1-weighted as the pulse sequence used advantageously in the present study (SE 300/14). The contrast enhancement was apparently stifled by using the longer TR and TE times. It is postulated that at short TRs, the water protons interacting with the paramagnetic contrast agent will relax fast enough to provide signal intensity, whereas tissue water unaffected by contrast agent will quickly become saturated and will fail to contribute to the signal intensity. The overall image intensity will diminish; however, signal intensity caused by contrast-mediated relaxation, and thus contrast enhancement, will provide a large percentage of image intensity.

High field strength had apparently little influence on contrast enhancement. High field strengths are known to generally attenuate proton relaxation effectiveness of paramagnetic contrast media [20, 21]. Also, the R1 relaxivities of albumin-(Gd-DTPA) were shown to be 350 mM^{-1} sec^{-1} at 2.0 T and 424 mM^{-1} sec^{-1} at 0.25 T. Yet the anticipated loss of enhancing effectiveness at higher fields was negated by the use of heavily T1-weighted pulse sequences. The observed enhancement from albumin-(Gd-DTPA) and Gd-DTPA might be even more dramatic at lower field strengths, if we assume constant pulse-sequence settings.

No adverse reactions to 160 mg/kg albumin-(Gd-DTPA) were observed in six rats, but complete toxicologic assays are not yet available. For reference, albumin used as a plasma expander in man can be administered intravenously in doses exceeding 1 g/kg, a sixfold higher dose than used in this study. The possible immunologic consequences of using a modified protein must be examined before clinical testing. Also lacking are studies of metabolism and elimination of labeled albumin. Rather, the goal of this study was to demonstrate the effectiveness and to suggest potential applications of paramagnetic macromolecular contrast media; the optimal compound of this class must yet be determined before clinical studies can be started.

The potential applications of albumin-(Gd-DTPA), a prototype intravascular, macromolecular contrast-enhancing agent, might include the demonstration and gradation of ischemia in myocardial, hepatic, and cerebral tissues. The assessment of blood volume and perfusion may also be possible for tumors, inflammatory lesions, and organs not investigated in this study. The combination of albumin-(Gd-DTPA) and recently available fast image-acquisition sequences may provide useful information about the initial distribution phase of this intravascular agent. The addition of functional information about tissue perfusion and blood volume might expand the diagnostic value of MR imaging.

REFERENCES

1. Brasch RC. Work in progress. Methods of contrast enhancement for NMR imaging and potential applications. *Radiology* **1983**;147:781–788
2. Brasch RC, Weinmann H-J, Wesbey GE. Contrast-enhanced MR imaging: animal studies using gadolinium-DTPA complex. *AJR* **1984**;142:625–630
3. Runge VM, Clanton JA, Herzer WA, et al. Intravascular contrast agents suitable for magnetic resonance imaging. *Radiology* **1984**;153:171–176
4. Weinmann H-J, Brasch RC, Press W-R, Wesbey GE. Characteristics of gadolinium-DTPA complex: a potential NMR contrast agent. *AJR* **1984**;142:619–624
5. Carr DH, Brown J, Bydder GM, et al. Gadolinium-DTPA as a contrast agent in MRI: initial clinical experience in 20 patients. *AJR* **1984**;143:215–224
6. Carr DH, Brown J, Bydder GM, et al. Clinical use of intravenous gadolinium-DTPA as a contrast agent in NMR imaging of cerebral tumors. *Lancet* **1984**;1:484–486
7. Felix R, Schoerner W, Laniado M, et al. Brain tumors: MR imaging with gadolinium-DTPA. *Radiology* **1985**;156:681–688
8. Strich G, Hagan PL, Gerber KH, Slutsky RA. Tissue distribution and magnetic resonance spin lattice relaxation effects of gadolinium-DTPA. *Radiology* **1985**;154:723–726
9. Kormano M, Dean PB. Extravascular contrast material: the major component of contrast enhancement. *Radiology* **1976**;121:379–382
10. Ogan MD, Grodd W, Paajanen H, et al. Approaches to the chemical synthesis of macromolecular MR imaging contrast media for perfusion-dependent enhancement. *Radiology* **1985**; 157(P):100

11. Grodd W, Ogan MD, Sosnovsky G, et al. Perfusion contrast agents for MR imaging: evaluation of two paramagnetically labeled albumins. *Radiology* **1985**;157(P):100
12. Hayes CE, Edelstein WA, Schenk JF, Mueller OM, Eash M. An efficient, highly homogeneous radiofrequency coil for whole body NMR imaging at 1.5 T. *J Magnetic Resonance* **1985**;63:622–628
13. Murphy-Boesch J, Koretsky AP. An in vivo NMR probe circuit for improved sensitivity. *J Magnetic Resonance* **1983**;54:526–532
14. Wehrli FW, MacFall JR, Newton TH. Parameters determining the appearance of NMR images. In: Newton TH, Potts DG, eds. *Advanced imaging techniques*. San Anselmo, CA: Clavadel, **1983**:81–117
15. McNamara MT, Higgins CB, Ehman RL, Revel D, Sievers R, Brasch RC. Acute myocardial ischemia: magnetic resonance contrast enhancement with gadolinium-DTPA. *Radiology* **1984**;153:157–163
16. Kozoma CK, Weisbroth SH, Stratman SL, Conejeros M. Normal biological values for Long-Evans rats. *Lab Anim Sci* **1969**;19:746–755
17. Yale CE, Torhorst JB. Critical bleeding and plasma volumes of adult germ-free rats. *Lab Anim Sci* **1972**;22:497–502
18. Wesbey GE, Higgins CB, McNamara MT, et al. Effect of gadolinium-DTPA on the magnetic relaxation times of normal and infarcted myocardium. *Radiology* **1984**;153:165–169
19. Altmann PL, Dittmar DS. Volume of blood in tissue: vertebrates. In: *Respiration and circulation*. Bethesda, MD: Federation of the American Society for Experimental Biology, **1979**;148:383–387
20. Koenig SH, Baglin C, Brown RD III. Magnetic field dependence of solvent proton relaxation induced by Gd^{3+} and Mn^{2+} complexes. *Magnetic Resonance Med* **184**;1:496–501
21. Koenig SH, Brown RD III. Relaxation of solvent protons by paramagnetic ions and its dependence on magnetic field and chemical environment: implications for NMR imaging. *Magnetic Resonance Med* **1984**;1:478–495

MR Artifacts: A Review

Errol M. Bellon[1-3]
E. Mark Haacke[1, 4]
Paul E. Coleman[3]
Damon C. Sacco[1, 2]
David A. Steiger[1, 2]
Raymond E. Gangarosa[3]

The process of creating MR images frequently gives rise to artifacts in the final display. Many artifacts may be corrected or ameliorated through an understanding of their cause. This requires familiarity with scanner design; theory of operation; and image acquisition, generation, and display. Some artifacts are obvious, totally degrading the image; others are regional, leaving much of the scan undisturbed. In some cases, the degradation is permanent; in others, the data can be reprocessed or manipulated to yield artifact-free images. Some artifacts are overt and easily identified. Others, such as those caused by phase-shift or gradient-strength effects, are subtle and require careful observation for detection.

The acceptance of MR imaging in clinical practice has brought with it a requirement for recognition and understanding of the various artifacts that may occur during each step of the scanning process, from data acquisition through image display. As is the case with each of the other radiologic techniques, numerous artifacts are associated with MR scanning [1–5]. With an understanding of their cause, many may be corrected, minimized, or avoided, either at the source before data acquisition or at the reconstruction stage after data acquisition. Although artifacts are capable of causing severe image degradation, many more subtle effects exist that can also lead to misinterpretation of the image. Our main concern here is to draw attention to both the subtle and obvious changes in contrast that may lead to misdiagnosis.

Artifacts are a problem in MR imaging because the complexity of the imaging sequences introduces the opportunity for multiple sources of systematic error. Physical constraints, such as the presence of field inhomogeneity, and hardware limitations contribute further problems. Also, numerous sources of spurious noise (both sequence- and system-related) can cause image degradation.

The various artifacts may conveniently be considered under the following headings: sequence, reconstruction algorithm, field, and noise. Each category can in turn be subdivided into system- and patient-related artifacts. Many of the artifacts demonstrated here were deliberately generated for illustrative purposes. They in no way represent the image quality to be expected from a properly functioning, well-calibrated scanner.

Technique and Methods

Two-dimensional Fourier transform (2DFT) imaging is now the standard method for acquiring data in MR imaging [6]. The most common technique is the spin-echo sequence (Fig. 1) used to refocus static field inhomogeneities. This sequence requires the application of a 90° RF pulse to rotate the magnetization into the plane transverse to the static magnetic field. A gradient is often applied in one direction during the RF to select a slice of interest. At an echo time (TE) of TE/2 later, a 180° refocusing RF pulse is applied so that at a time TE

Received February 14, 1986; accepted after revision June 27, 1986.

The work on which this report is based was carried out at the Clinical Science Center, NMR Division, Picker International, Highland Heights, OH (Surya Mohapatra, Director).

[1]Department of Radiology, Case Western Reserve University, Cleveland, OH 44106.

[2]Department of Radiology, Cuyahoga County Hospital, 3395 Scranton Rd., Cleveland, OH 44109. Address reprint requests to E. M. Bellon.

[3] Clinical Science Center, Picker International, Highland Heights, OH 44143.

[4]Department of Physics, Case Western Reserve University, Cleveland, OH 44106.

***AJR* 147:1271–1281, December 1986**
0361–803X/86/1476–1271
© American Roentgen Ray Society

after the initial excitation the magnetization refocuses or echoes even in the presence of field inhomogeneities. The data are then sampled centered about this time.

In order to extract two-dimensional information, the spins are spatially encoded in one direction by phase encoding and in the other by frequency encoding. This is accomplished in the latter case by applying a dephasing gradient between the 90° and 180° pulses and then a rephasing or read gradient centered about TE so that the spins still echo at TE. In the former case, the phase encoding can take place before or after the 180° RF pulse but must be changed each time the sequence is rerun. Each such collection of data is referred to as a view, with all views collectively representing a complete scan. The time between each view is the repetition time (TR).

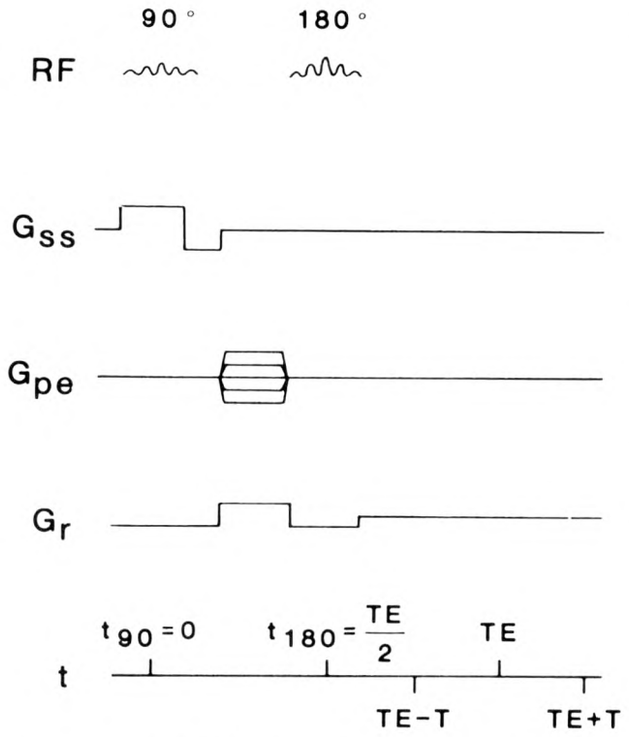


Fig. 1.—Standard 2DFT sequence structure showing radiofrequency and gradient timing and profiles. Timing (t) is counted from center of 90° pulse, with echo occurring at t = TE. Sampling runs from TE − T to TE + T being of duration $T_s = 2T$. G_{ss} = section select gradient; G_{pe} = phase encoding gradient; G_r = read gradient.

The number of sample points and the number of views determine the amount of spatial information or resolution for that scan. The field of view (FOV) is also determined by the appropriate choice of sampling time and gradient strength. Smaller FOVs are normally achieved by increasing the gradient strength. Finally, the data are sampled and a two-dimensional discrete inverse Fourier transform performed to produce an image. Most images presented in this article are based on spin-echo sequences with the parameters: sampling time, 80 μsec; read gradient, 1 mT/m; FOV, 30 cm (head), 45 cm (body); sampling points, 256; and views, 256. Where deviations from this parameter set occur, the values of the modified parameters will be stated.

Sequence Artifacts

System-Related

Inherent in all MR techniques is the assumption that the RF pulses are ideal. For example, in a spin-echo multislice experiment, it is assumed that slices have square profiles and the RF field distribution is uniform throughout the plane. Deviations from ideal pulses can cause various artifacts: broad slice profiles or perfect thick slices produce partial-volume effects (Fig. 2A), and profiles with multiple lobes produce scan sections that contain contributions from out-of-slice material (Fig. 2B). In the former case, a small tumor could be lost in a thick slice if surrounded by high-intensity tissue. (However, even going to a thin slice may not allow identification of the tumor if contrast-to-noise is now too low.) The latter is caused by 180° pulses acting as 90° pulses



A



B

Fig. 2.—Partial-volume effect.

A, Coronal section through cervical spine at nominal 10-mm section thickness contains information from outside ideal slice. Note transverse contributions (*arrows*) from intervertebral disks anterior to plane of section, projecting faintly over cord (TR 700, TE 40).

B, Out-of-slice contribution in region of liver, with single acquisition. Vertical line with alternating intensity colloquially referred to as the "zipper" artifact.

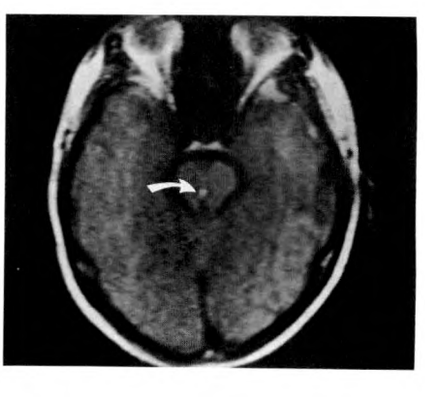


Fig. 3.—Central point artifact. When direct current level of each view in scan is not constant, line artifact occurs in phase-encoded direction. When all views have same direct current offset, line reduces to a point artifact (*arrow*). Image is a transverse pilot brain scan with 128 phase-encoding steps (views) and TR 200, TE 40.

outside the slice and is overcome by appropriately phase-alternating one of the pulses and combining the data from two acquisitions. This twofold excitation removes the artifact. When clinical requirements necessitate a short scan time and only a single acquisition is used, the resulting artifact is a line (or lines) through the image along (parallel to) the frequency-encoded axis. With ideal RF pulses, high-quality, artifact-free images are routinely obtained, even with one acquisition.

A similar artifact occurs if the direct current (DC) level of each phase-encoding step (view) in the scan is not constant. This leads to a line along the phase-encoded axis. If all views have the same DC offset, the artifact reduces to a central point (Fig. 3). This point actually gets spread over several pixels because of the finite number of data points used. It may be particularly troublesome if located over a clinically significant region. For example, when the artifact falls over the midbrain or pons, it needs to be distinguished from a small infarct. The solution again involves appropriate RF phase cycling and data subtraction.

Image quality is also sensitive to the read-gradient level. The read gradient and the size of the FOV together determine the sampling rate and hence the frequency content per pixel in the image. Normally, the read gradient is set high to minimize field inhomogeneity effects. However, if the ratio of total sampling time (T_o) to the T_2 value is on the order of unity, image contrast and resolution will change. Such may be the case with body scanning where this effect may be pronounced, especially with low read gradients (Fig. 4). This edge enhancement due to finite T_2 values should not be confused with the Gibbs phenomenon caused by data truncation (see discussion of patient-related noise artifacts).

A practical problem also associated with the gradients is the correct setting of the FOV. If the FOV selected is too small, the image will wrap back into itself (aliasing). Nevertheless, if the overlap does not obscure the region of interest, the image is still usable (Fig. 5). A FOV that produces aliasing may be a deliberate choice to obtain a higher-resolution image in a central region of interest. This aliasing may be avoided even with the incorrect setting in the frequency-encoded direction if the analog filter bandwidth is reduced accordingly. This is not possible in the phase-encoded direction because of the discrete steps used.

Patient-Related

Since the patient has electric and magnetic properties (such as conductivity, permitivity, and permeability) different from free space, it is not possible to have uniform distribution of

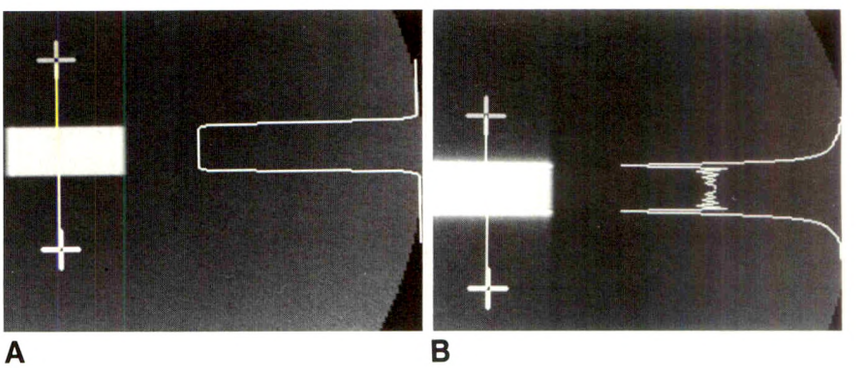


Fig. 4.—Read gradient and size of field of view together determine sampling rate and thus frequency content per pixel. Image contrast and resolution are affected by setting of read gradient, especially low read-gradient levels.

***A*, Simulated image of rectangular box with R = $T_o/2T_2$ = 0.03.**

***B*, As in *A*, but with R = 1.28. Note edge enhancement and increase in systematic noise in central region. There is also loss of resolution at edges due to increased dispersive nature of signal.**

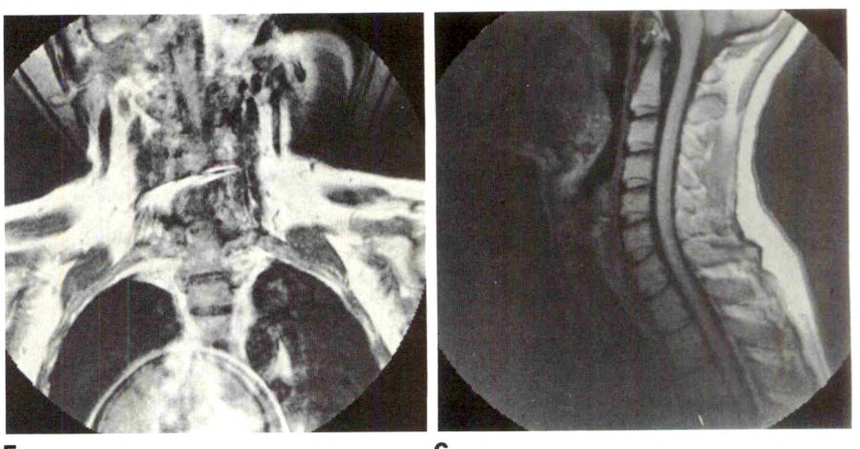


Fig. 5.—Aliasing—image appears wrapped around into itself. Picture elements that correctly belong at top of field are projected along bottom, and vice versa. Vertical phase-encoding was used for this scan; when horizontal phase-encoding is used, artifact occurs along left and right margins instead. Artifact occurs because field of view selected is too small for particular body region being imaged. Note that although artifact is usually present peripherally, central regions of image are unaffected and quite usable.

Fig. 6.—Surface-coil hot spot. Response of the particular coil employed here varies as function of position, so tissues close to coil are imaged much more intensely than those farther away. In this case, subcutaneous fat near coil is much more intense than farther away from coil. Note also lack of resolution in anterior neck structures. The problem is due to nonuniform reception of signal throughout scan slice.

an RF pulse throughout the scan slice [7]. This leads to an RF penetration problem where a tissue of uniform composition exhibits a change in intensity depending on its location in the image plane. Similar, but less complicated, effects occur when using surface coils [8] where their response varies as a function of position, thus producing intense regions close to the coil with significant falloff in tissue farther away from the coil (Fig. 6).

The signal from flowing blood can be significantly affected by the sequence parameters [9]. For example, flowing blood can appear hyper- or hypointense depending on the rate and direction of flow, whether the sequence used was single- or multislice, and whether broad-band or selective pulses were used. A knowledge of vascular anatomy is essential for the differentiation of low-intensity areas on T1-weighted images, so as to permit distinction of vascular structures from neoplasm or other abnormality. Flowing blood can also produce an artificially enhanced signal [10, 11], so that before pathologic conditions can be diagnosed, the possibility of artifactually enhanced areas caused by flowing blood should be excluded.

Reconstruction Algorithm Artifacts

System-Related

The mainstay of current sequence design and reconstruction algorithms is 2DFT imaging. The types of artifact associated with this method are different from those associated with other techniques (such as projection reconstruction, echo planar [12], and Hybrid [13, 14]). In this article, only 2DFT-related techniques will be considered.

The peak signal changes drastically as a function of sequence and object being imaged, so that the signal is attenuated to make the peak signal compatible with the computational range of the computer. If the signal does not lie within the required limits, data clipping occurs (the large numbers become smaller numbers lying in the available integer range) and information is destroyed and is not recoverable. In this case, the image is often rendered useless (Fig. 7), even though only a small central portion of the data is corrupted (see also Fig. 9).

Another example is hardware failure during the experiment, with only one data channel surviving. The image will appear as if it has been reflected about both the phase-encoded axis and the frequency-encoded axis [1] (Fig. 8). However, in those regions where no overlap occurs, the information is still accurate and diagnostically useful.

Patient-Related

The data-clipping artifact can also occur if there is patient movement during the period the signal attenuator is being set. For example, with respiratory motion, a bowel loop may move in and out of the plane of interest. Since bowel tissue has characteristics different from other tissues, including those in the plane of interest, setting the attenuator when a bowel loop is in the plane will produce an incorrect attenuator setting with respect to the desired plane. This may lead to data clipping for that plane if the attenuator setting is not determined for a sufficient length of time.

Flow and motion within the subject also lead to image degradation and changes in contrast. This is manifest by a

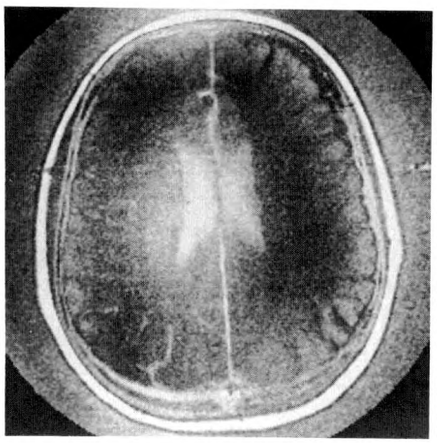


Fig. 7.—Data clipping. If peak signal does not lie within computational range of computer and software used in image reconstruction, severe arithmetic errors occur, and incorrect pixel values are assigned. Image has significant low spatial frequency distortion giving it a "ghostlike," unreal quality with loss of contrast and resolution.

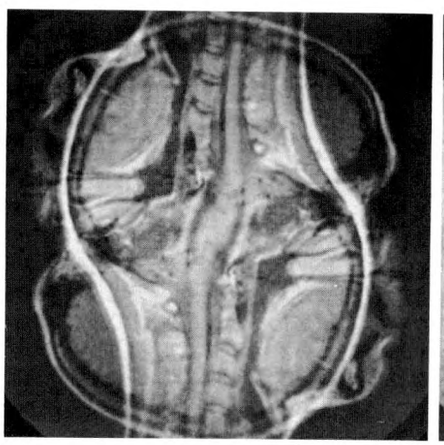


Fig. 8.—Failure of one data channel, an example of hardware failure. Image resembles that caused by aliasing (Fig. 5), but is reflected about both phase-encoded and frequency-encoded axes. There are small regions where no overlap occurs and image is still usable (TR 600, TE 40).

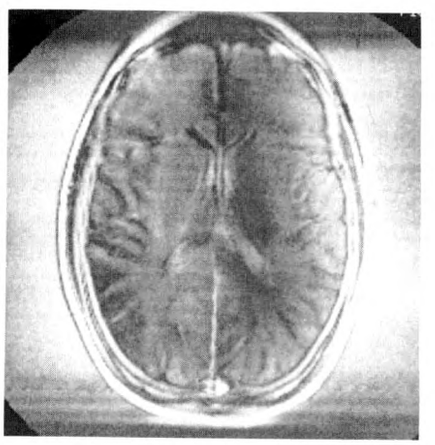


Fig. 9.—Motion during central view acquisition. Normal volunteer was instructed to turn the head to the side once only during a few central scan views (near view 128) and then resume original scan position. The scan had 256 phase-encoding steps (views). The image is totally degraded, shows altered contrast, and a "ghostlike" quality similar to data clipping (compare with Fig. 7). Movement early (near view 5) or late (near view 250) does not degrade image.

loss in resolution for motion and by phase-encoded noise through the affected region for both motion and flow. The simple 2DFT algorithm is not equipped to handle the phase errors associated with motion; however, an appropriate reconstruction technique may be able to do so [15]. The induced phase-encoded noise aspect of this problem and methods of alleviating the problem are addressed under Noise Artifacts. The use of phase-ordering techniques [14, 16] during data acquisition eliminates the noise in the phase-encoded direction, leaving only the resolution loss due to gross body-part motion itself. Scaling techniques [15, 17] operating on the raw data may then be used to further improve the resolution.

An image with loss of resolution only may also occur if the patient moves during the critical period when the central views (region of zero or low phase-encoding) are being acquired. Either a single deep inspiration or turning of the head is sufficient to produce severe image degradation (Fig. 9).

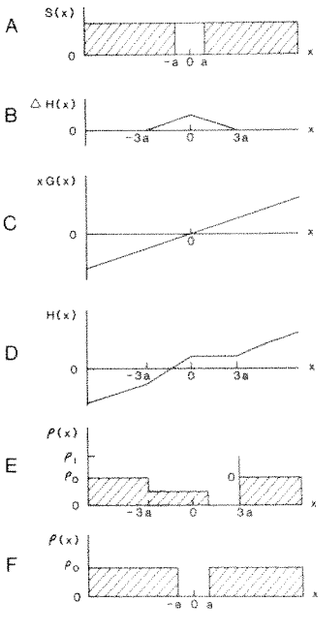


Fig. 10.—Geometric (field) distortion in frequency-encoded direction: effect of field inhomogeneity. Artifactual expansion or contraction, as well as intensity change and altered contrast and resolution, result from macroscopic imperfections in magnetic field, especially due to magnetic substances.

***A*, Cross section of hypothetical object. Cross-hatched area denotes normal tissue, and unmarked area contains material with significantly different susceptibility of length 2a.**

***B*, Hypothetical field inhomogeneity (true field profile has been simplified for purpose of illustration).**

***C*, Field due to applied gradient.**

***D*, Total field.**

***E*, Image intensity as function of position. Here $\rho_1 = \rho_0[1 + (\alpha/3\Delta\chi)]$, where $\Delta\chi$ is pixel size.**

***F*, Ideal image intensity.**

Field Artifacts

System-Related

The relationship between the read-gradient level and the FOV, which together determine the sampling rate and hence the frequency content per pixel in the image, was discussed under Sequence Artifacts. Particularly in the case of body scanning, and in situations where low read gradients are used, field inhomogeneity effects may result in altered image contrast and resolution.

Geometric distortion only occurs along the frequency-encoded axis and arises because macroscopic imperfections of the magnetic field lead to nonparallel flux lines that, when mapped onto an orthogonal (square) grid, cause deformation of the image. These imperfections may be caused by large static field inhomogeneities or by field changes resulting from the presence of a magnetic substance in an otherwise constant field. The induced field deviations produce artifactual expansion or contraction of the image, accompanied by changes in image intensity and resolution. For demonstration purposes (Fig. 10), let the substance induce a field change (G') linear to the center of the modified region and of opposite slope and equal magnitude beyond the center, as shown in Figure 10B. Taking the magnitude to be the same as that of the read gradient (G), one can easily see that in the region of the increased field gradient (Fig. 10D), the object appears stretched, decreasing the image intensity while simultaneously increasing resolution (Fig. 10E). Conversely, where the field is now constant, the object gets mapped to a point. Since this information has been collapsed to a point, the image intensity is increased and all resolution is lost. While ferromagnetic objects cause the field deformations discussed above, diamagnetic objects cause much smaller changes and the stretching and compressing are reversed with respect to the frequency direction.

The ratio G'/G determines the degree of stretching and compression. This can be expressed equivalently by the ratio $\gamma\Delta H/\Delta f$, where ΔH is the field inhomogeneity across a pixel and Δf ($= \gamma G\Delta\chi$) is the frequency per pixel. Since the size of the read gradient controls the amount of distortion, allowable changes in TE or TR will not affect the distortion. Unfortunately, although an increase in the read gradient will reduce the distortion, it will also decrease the signal to noise (S:N) ratio. This can be understood since, as the bandwidth increases by a factor of A, the incoherent (white) noise increases by a factor of $\sqrt{A}$. In some cases, suffering the slight distortions may well be worth the extra S:N margin.

The effect of the field distortions may be central or peripheral, symmetric or asymmetric, and the distortion produced may be pincushion- or barrel-type. While the clinical impact of the artifact is that linearity of the image is lost, resolution may actually be degraded or enhanced. As an example, vertebral bodies may appear smaller or larger at the periphery of the field than at the center (Fig. 11).

Patient-Related

As discussed above, ferromagnetic objects produce artifacts because their higher magnetic susceptibility relative to tissue produces localized field changes. This results in image distortion and associated contrast changes [18–20]. The direction of the misregistration is determined by the direction of the read gradient used for the particular MR experiment. As described earlier, the characteristic appearance on the image is a low-intensity region or void adjacent to or surrounded by regions of high signal intensity (Fig. 12). Very often bizarre, nonanatomic, elongated distortions are seen (Fig. 13). Depending on the quantity, shape, and susceptibility of the metal present, there may be so much distortion as to make the image anatomically unrecognizable.

While metals are classified as ferromagnetic and diamagnetic, the mechanism of image distortion is the same in both cases, differing only in magnitude and direction. A ferromag-



Fig. 11.—Field distortion—loss of linearity. Vertebral bodies appear disproportionately smaller at top and bottom of image than at center. Image is not linear. This may occur along one of or both x and y axes. Note that resolution may in fact be enhanced or degraded. (Aliasing artifact partially obscures upper portion of field.)



A B

Fig. 12.—Typical ferromagnetic artifact. Low-intensity central region in *A* is partly surrounded by a high-intensity border along same direction as read gradient. This requires distinction from true pathologic abnormality, such as scalp fibroma in *B*, which exhibits low-intensity central region, but lacks peripheral zone of intensity.

netic surgical clip will produce a larger void area than an equivalently sized nonferromagnetic clip. Substances not thought to contain ferromagnetic materials, such as dental crowns, in fact frequently are not made of precious metals and may contain significant quantities of nickel, cobalt, or chromium, in which case they do produce severe artifacts. Dental amalgam contains silver, tin, and mercury (occasionally tin substitutes for the silver) and does not produce artifacts. Ferromagnetic material is present in wire surgical sutures, protheses of all kinds, zippers, safety pins, support wiring in wigs, corset stays, non–precious-metal jewelry, and mascara (Steiger DA, unpublished data).

Although the chemical-shift dispersion of hydrogen in tissues is invaluable for spectroscopic investigations, chemical shift becomes a problem in evaluating images [21–23], especially those produced at very high fields where the ratio R_{CS} of chemical shift (CS) in frequency (Δf_{CS}) to bandwidth per pixel (Δf) is large. This ratio could, in turn, be reduced by increasing the read gradient but at the expense of S:N ratio. The effect is due to the fact that protons in water resonate at a different frequency than those in lipids. The chemical shift separation of fat and water protons is about 3.35 ppm [24], which corresponds to $\Delta f_{CS} = 71.4$ Hz at 0.5 T.

For values of R_{CS} less than unity, regions containing both water and fat will be unaffected for an ideal spin-echo sequence. If the timing of the 180° pulse is incorrect, the fat will gain a relative phase with respect to the water, and the intensity of the signal will change even though no shift in position occurs [25]. With or without these relative changes in phase, the two-component nature of the signal causes T1 and T2 to be inaccurately determined because of the now multiexponential nature of the signal. With new techniques that account for field inhomogeneities in the separation of water and fat [26], the separated components of T1 and T2 can be accurately found.

When R_{CS} is greater than unity, the fat is shifted by one or more pixels from its actual position with respect to the water. This may be a problem when a predominantly fat-containing area is shifted far enough to overlap a region of interest. This effect is significant in the orbit, where it may degrade what would otherwise be a high-resolution scan. It is also significant in the spine, where the superior and inferior margins of the vertebral bodies may show reduced or increased intensity, and in the kidneys (Fig. 14). Clinically, the shift is unimportant for brain imaging since the lipid (myelin) signal intensity from brain is negligible relative to that from water.

Similar intensity changes and distortions can occur from in vivo local field inhomogeneities because of tissue magnetic properties. These inhomogeneities are caused by changes in susceptibility between tissues (or air) in the body (for example, near the paranasal sinuses). These, as well as other field distortions, also cause local phase changes. For techniques that need phase information, such as water/fat separation, these phase changes can wreak havoc with the images. Techniques that account for such effects are then required [27].

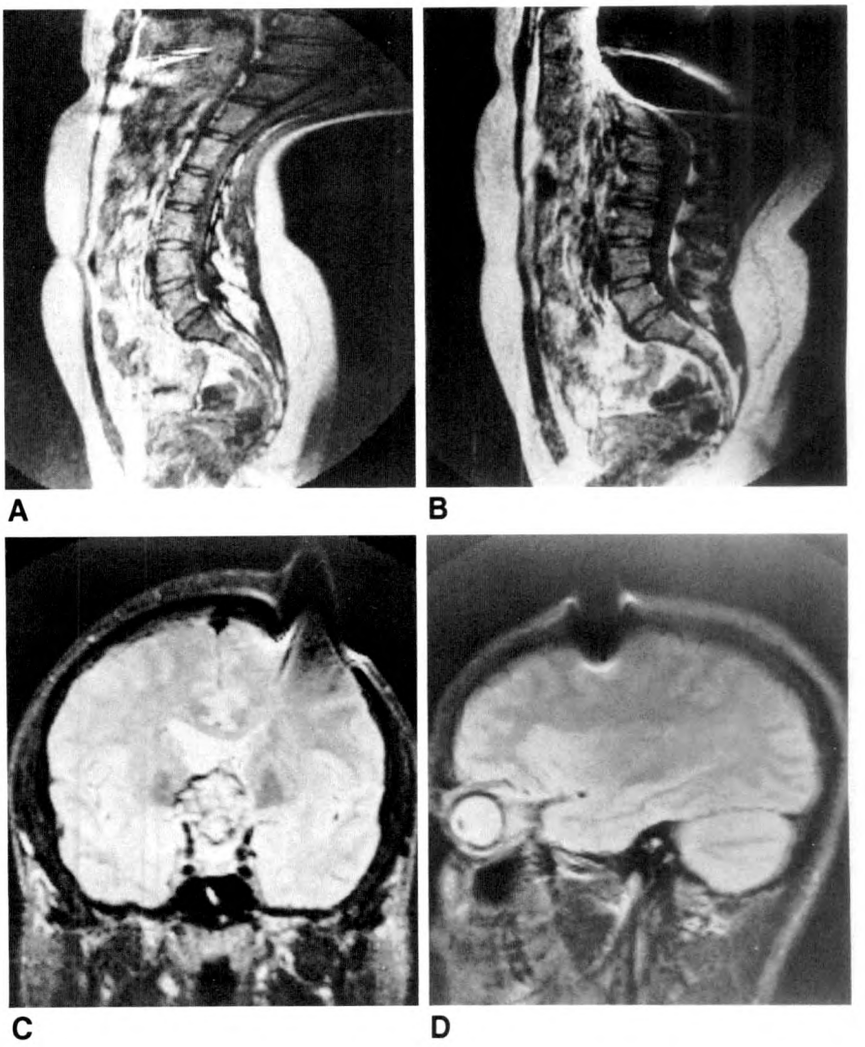


Fig. 13.—Bizarre ferromagnetic effects may occur, usually related to quantity, shape, and susceptibility of metal present. Note area of intensity extending well beyond anatomic boundaries of subject, in frequency-encoded direction.

A and *B*, Artifact caused by metal fasteners of a seven-hook bra. Note distortion is to left in *A* and to right in *B*. This is due to alternate-slice orientation of frequency-encoding gradient (see Fig. 10).

C and *D*, Artifact due to shunt-tube reservoir. Note localized tearing and stretching of image (TR 2000, TE 40).

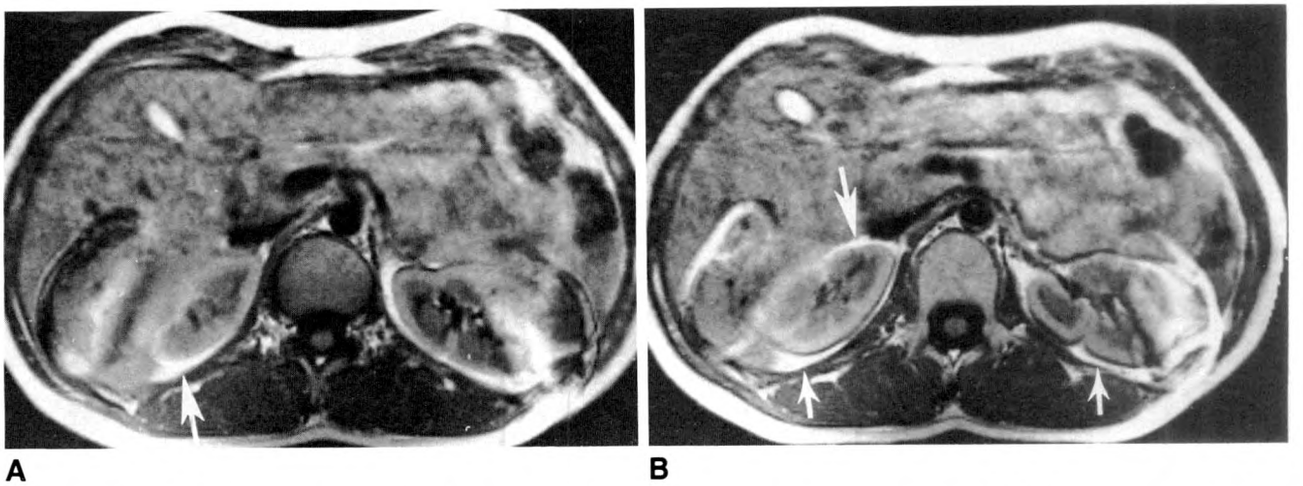


Fig. 14.—Chemical-shift artifact. *A* and *B*, Kidneys show area of intensity (*long arrows*) along inferior margin in *A* and superior edge in *B*. Also, in *B*, inferior margin has changed from intense to dark line (*short arrows*). Intensity change is caused by differential shift of protons in fat vs those in water, and occurs in frequency-encoded direction. In *A*, frequency-encoded direction is vertically upward, while in *B*, it is vertically downward. Changing direction of gradient is a useful method of confirming that changes observed are artifactual in nature. (TR 700, TE 40.)

Noise Artifacts

System-Related

Noise may be considered as any information in the signal that does not contribute to characterization of the biologic sample being imaged. Sources of white noise include random thermal variation in the sample and electronic noise from scanner hardware. Extraneous broadcast RF energy acts as another source of noise that affects a specific frequency. While scanner design optimization involves tradeoffs that maximize the S:N ratio, even under ideal circumstances the signal is generally only one or two orders of magnitude greater than the noise level.

Thermal (incoherent) noise produces diffuse increase in image mottle. The effects of thermal noise are diminished in surface-coil applications, where signal detection falls off rapidly as a function of depth, and the coil effectively does not see the thermal noise from more distant tissues [28].

Radiofrequency interference is due to detection of extraneous broadcast energy by the receiver coils of the scanner. Since the operating frequency of the scanner is directly related to magnet field strength, the frequency is essentially fixed around a narrow range (for example, 21.3 MHz for 0.5 T, or 64.0 MHz for 1.5 T), and any extraneous broadcast energy near this frequency may be detected. These sources include fluorescent lights (starter and ballast) and electric motors (especially direct current). Television and radio transmissions are also a problem, since 21.3 MHz is within the frequency assigned to amateur radio operators (21.0–21.5 MHz); 64.0 MHz falls within the frequency assigned to channel 3 (60–66 MHz); and 85.0 MHz lies within the FM radio band. Base-to-base and mobile communications are in the range 5–50 MHz. Similarly, 60 Hz noise in the electric power supply can also affect the image. The artifact produced is usually a linear band across the image (Fig. 15), apparent where the noise overwhelms the tissue signal. It is perpendicualr to the frequency-encoded direction, and its position is related to the difference in frequency between the center frequency of the scanner and the extraneous signal. This determines the distance to which the artifact is displaced from the center frequency (and thus from the center of the image).

Patient-Related

Systematic sources of noise are induced by nonideal circumstances in the scan. These include errors in establishing the correct phase relationship at each position due to nonlinear gradients, field inhomogeneities, motion, or flow. In particular, patient motion of any type degrades image quality because it produces data-phase errors. Phase information is used by the reconstruction algorithm in the process of voxel to pixel mapping. Motion-induced phase errors result in blurring, "ghosting," or mottled bands propagated in the phase-encoded direction. Even when the patient is externally quiescent, biologic activity associated with cardiac, respiratory, blood flow, and peristaltic motion continues. While the artifact produced by these activities may appear in the region of interest, it should not be considered as random white noise. It is in fact misregistered tissue information that cannot be properly positioned by current reconstruction algorithms. Future sequence and software developments [14, 15] will most likely correct phase errors so that physiologic motion will have a less detrimental effect on image quality.

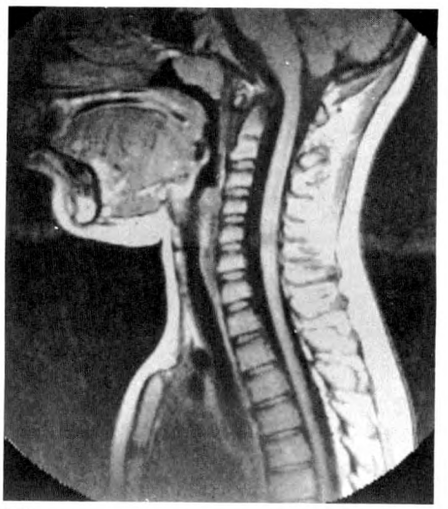
For obvious reasons, motion produces a loss of resolution when it is significant with respect to the TR, as occurs, for example, when the patient turns, fidgets, or repositions a limb. This type of motion unsharpness is also seen with physiologic activities—the pancreas moves 2.0 cm on average in the craniocaudad direction during tidal respiration [29]. The magnitude of this excursion dwarfs the dimensions of the voxels commonly used in imaging and thus completely destroys the image. However, motion also induces phase

Fig. 15.—Radiofrequency artifact. Extraneous RF energy sources near scanner operational frequency produce linear band across image, perpendicular to frequency-encoded direction. Its exact position is determined by difference between center frequency of scanner and extraneous signal. (TR 600, TE 40.)



15

Fig. 16.—Swallowing artifact has produced horizontal band of noise along phase-encoded direction. Where it passes over vertebral body and spinal cord, there are local intensity and contrast changes, rendering these portions of scan suspect. If desired, artifact may be overcome by changing phase-encoded gradient to vertical direction, so that noise is propagated off regions of interest.



16

changes to which 2DFT is extremely sensitive (see later discussion). These phase changes lead to noise throughout the affected region along the phase-encoded direction.

Artifacts due to body-part motion, such as flow, blinking, swallowing, or chewing, are a form of coherent noise. Although often not important locally, they may affect a critical region of the image by producing a band of noise propagated across the field in the phase-encoded direction. This will cause areas of increased or diminished intensity in the region of interest, creating doubt as to the presence of abnormality and hence rendering the scan useless for diagnosis (Fig. 16). Flow artifacts from the internal carotid artery, carotid siphon, or jugular bulb are frequently encountered in scans of the head. They are much more evident in surface-coil applications because of the improved S:N ratio [7]. Depending on the image plane, the artifact may be redirected to noncritical areas of the image through proper selection of the phase-encoded direction. Phase-encoded flow artifacts may be seen in arteries, veins [10, 11], or any other fluid system, including the CSF [30, 31].

Chewing and talking produce mandibular, lingual, and laryngeal musculature motion that result in obvious image degradation, both locally and over the neck and cervical spine. Another problem occurs in imaging patients with oropharyngeal or laryngeal tumors, as well as lesions of the tongue and oropharynx, where secretions and saliva require frequent clearing and swallowing. This is also important with certain neurologic disorders involving the brainstem and lower cranial nerves.

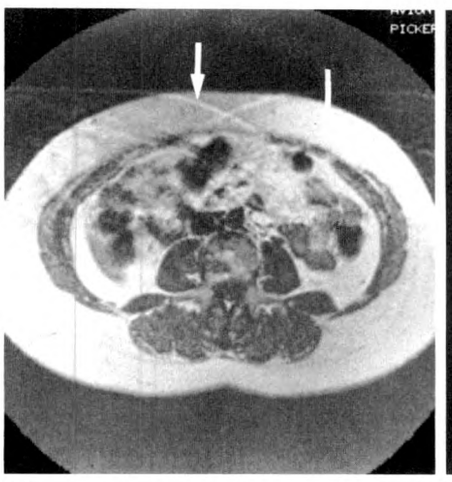
Peristalsis may be a major source of artifact when the upper abdomen and pelvis are imaged (Fig. 17), especially with the longer scan sequences. Significant reduction is possible through use of glucagon to eliminate gastrointestinal tract peristalsis. Since the sensitive region of surface coils is limited, they can be positioned so as to receive signal from nonmoving tissue only [28, 32, 33], thus minimizing the noise.

Respiratory motion produces a form of coherent noise distributed across the image as a periodic artifact [14, 34]. In the head, the major contribution is from eye movement, while in the body the major contribution is from high-intensity areas in the subcutaneous and retroperitoneal fat. Throughout the body the pulsatile component of blood flow may also produce artifacts. These artifacts are produced in the phase-encoded direction, regardless of the direction of the motion causing them. The ghost images are partial copies of the original static structure, with interference effects producing areas of reinforcement or cancellation. In the case of respiratory artifacts, the ghost images become more widely separated with increasing respiratory rate or prolonged TR; increased respiratory amplitude produces only increased blurring of both the original and ghost images, but no positional change [8, 14, 28, 34, 35]. Multiple acquisitions can remove the worst of these artifacts if the product of the number of averages and TR is approximately equal to the respiratory period [14, 36].

The Gibbs phenomenon causes a ringing in the image (Fig. 18) due to data truncation [37]. This can resemble the periodic ghosting in the vicinity of edges as in the case of motion artifact.

Cardiac and respiratory motion produce sufficient pixel misregistration and phase shift to totally degrade the image, unless some form of gating or specialized data-collection method is used. Gating is a technique that essentially removes both motion problems (loss of resolution and phase-encoded noise). Although respiratory gating may extend scan times by factors of 2 to 4, significant image improvement results (Fig. 19). Methods using phase reordering to destroy the periodicity of the respiratory motion, such as centrally ordered phase encoding (COPE) and respiratory ordered phase encoding (ROPE) [14, 16, 17], remove only the phase-encoded smearing, without increasing the scan time. Figure 20 demonstrates the improvement achieved with COPE for dealing with respiratory motion. Without phase-encoded reordering, the noise

Fig. 17.—Peristalsis and respiratory artifacts. Wide band of artifact extends horizontally across anterior half of abdomen in phase-encoded direction. Blurring is caused by peristalsis, while curvilinear replication of subcutaneous fat (*arrows*) is caused by respiration.



17

Fig. 18.—Ringing artifact due to data truncation. Note periodic nature of ringing. This should not be confused with motion artifact.



18

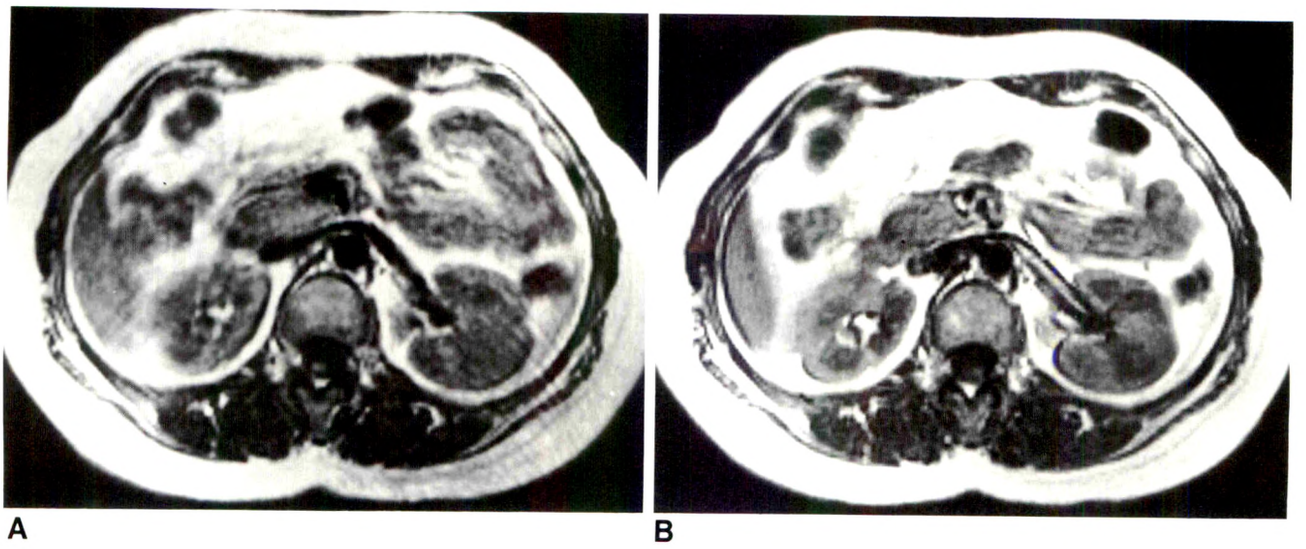


Fig. 19.—Respiratory gating. Transverse section through abdomen at level of head of pancreas and kidneys. Multislice scan (six slices), TR 500, TE 40.
A, Without gating, 4-min scan.
B, With gating, 10-min scan.

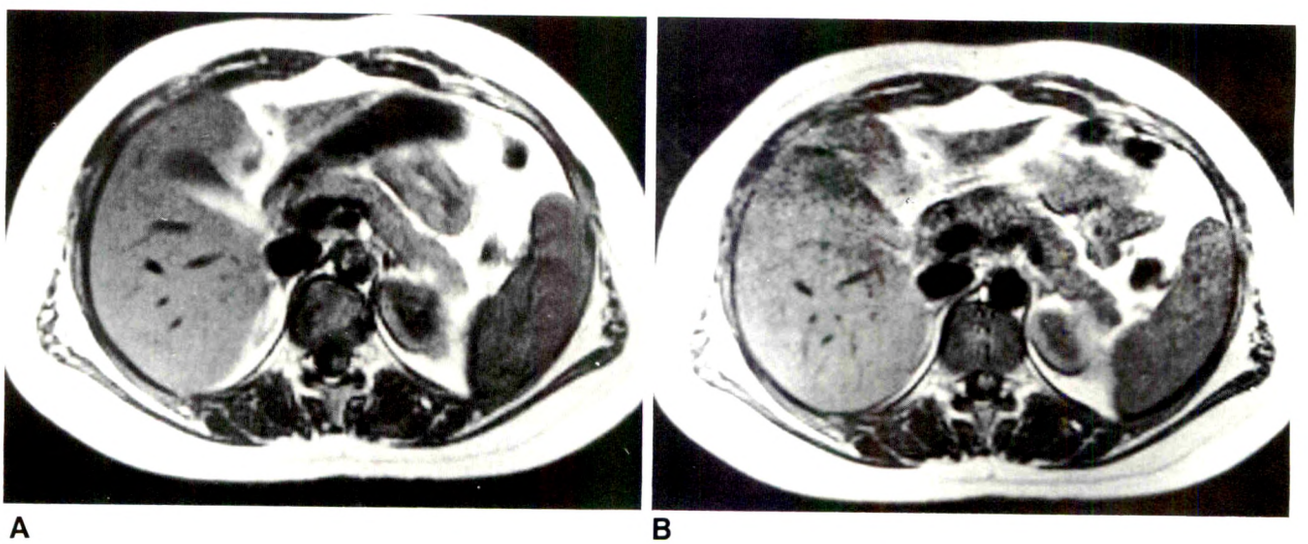


Fig. 20.—Respiratory artifact—improvement with COPE.
A, With respiratory gating, 10-min scan, TR 500, TE 40.
B, Monitoring motion and collecting data with appropriate values of phase-encoded gradient according to COPE technique. Some small background noise artifact remains because actual movement itself has not been accounted for. Scan time was only 4 min.

can also be reduced and redistributed by using the Hybrid fast-scan technique. In principle, both COPE and Hybrid could be combined to yield high-quality, short-time body images.

ACKNOWLEDGMENTS

We thank Michael A. Profeta, Eileen Strauss, Douglas Jarvis, and Jan Harrison for technical assistance; Laura Lewis for secretarial support; Michael Pettit and David Sabol for their photographic skills, and John Patrick, Leonard Weiss, and Ernest Wiesen for their contributions of time and information.

REFERENCES

1. Haacke EM, Clayton JR, Lampman DA, Linga NR. Artifacts in two-dimensional Fourier transform imaging (abstr). Program of the annual meeting of the Society of Magnetic Resonance in Medicine, New York, August **1984**:288–289
2. Yamanashi WS, Wheatley KK, Lester PD, Anderson DW. Technical artifacts in magnetic resonance imaging. *Physiol Chem Phys Med NMR* **1984**;16:237–250
3. Pusey E, Brown RKJ, Lufkin R, Solomon M, Hanafee W. Artifacts

in MR imaging: mechanisms and clinical significance (abstr). *Radiology* **1985**;157(P):296
4. Hastrup W, Porter BA, Olson DO, et al. Classification and investigation of artifacts in MR imaging (abstr). *Radiology* **1985**;157(P):397
5. Kulkarni MV, Patton JA, Wolfe O, et al. Techniques, pitfalls, and artifacts in MR imaging (abstr). *Radiology* **1985**;157(P):398
6. Haacke EM, Bellon EM. Artifacts produced by Fourier transform inversion techniques in magnetic resonance imaging. In: Stark DD, Bradley WG, eds. *Magnetic resonance imaging*. St. Louis: Mosby, in press
7. Glover GH, Hayes CE, Pelc NJ, et al. Comparison of linear and circular polarization for magnetic resonance imaging. *J Magnetic Resonance* **1985**;64:255–270
8. Ehman RL. MR imaging with surface coils. *Radiology* **1985**;157:549–550
9. Moran PR, Moran RA, Karstaedt N. Verification and evaluation of internal flow and motion. True magnetic resonance imaging by the phase gradient modulation method. *Radiology* **1985**; 154:433–441
10. Bradley WG, Waluch V, Lai K-S, Fernandez EJ, Spalter C. The appearance of rapidly flowing blood on magnetic resonance images. *AJR* **1984**;143:1167–1174
11. Bradley WG, Waluch V. Blood flow: magnetic resonance imaging. *Radiology* **1985**;154:443–450
12. Mansfield P, Pykett IL. Biological and medical imaging by NMR. *J Magnetic Resonance* **1978**;29:355–373
13. Haacke EM, Bearden FH, Clayton JR, Linga NR. Reduction of MR imaging time by the Hybrid fast-scan technique. *Radiology* **1986**;158:521–529
14. Haacke EM, Patrick JL. Reducing motion artifacts in two-dimensional Fourier transform imaging. *Magnetic resonance imaging* **1986**;4:359–376
15. Haacke EM. Application of a generalized transform to image reconstruction in MRI (abstr). Program of the annual meeting of the Society of Magnetic Resonance in Medicine, London, August **1985**:975–976
16. Bailes DR, Gilderdale DJ, Bydder GM, Collins AG, Firmin DN. Respiratory ordered phase encoding (ROPE): a method for reducing respiratory motion artefacts in MR imaging. *J Comput Assist Tomogr* **1985**;9:835–838
17. Haacke EM, Patrick JL, Bond CK, Blakely DM. Correction for motion artifacts based on a linear expansion model (abstr). Program of the annual meeting of the Society of Magnetic Resonance in Medicine, London, August **1985**:977
18. Finn EJ, Di Chiro G, Brooks RA, Sato S. Ferromagnetic materials in patients: detection before MR imaging. *Radiology* **1985**; 156:139–141
19. New PFJ, Rosen BR, Brady TJ, et al. Potential hazards and artifacts of ferromagnetic and nonferromagnetic surgical and dental materials and devices in nuclear magnetic resonance imaging. *Radiology* **1985**;147:139–148
20. Laakman RW, Kaufman B, Han JS, et al. MR imaging in patients with metallic implants. *Radiology* **1985**;157:711–714
21. Soila KP, Viamonte M, Starewicz PM. Chemical shift misregistration effect in magnetic resonance imaging. *Radiololgy* **1984**;153:819–820
22. Hricak H, Williams RD, Moon KL, et al. Nuclear magnetic resonance imaging of the kidney: renal masses. *Radiology* **1983**;147:765–772
23. Babcock EE, Brateman L, Weinreb JC, Horner SD, Nunnally RL. Edge artifacts in MR images: chemical shift effect. *J Comput Assist Tomogr* **1985**;9:252–257
24. Maudsley AA, Hilal SK. Field inhomogeneity correction and data processing for spectroscopic imaging. *Magnetic Resonance Med* **1985**;2:218–233
25. Dixon WT. Simple proton spectroscopic imaging. *Radiology* **1984**;153:189–194
26. Patrick JL, Haacke EM, Hahn JE. Evaluation of T1 and T2 from water and fat separated images (abstr). *Radiology* **1985**; 157(P):220
27. Patrick JL, Haacke EM, Hahn JE. Water/fat separation and chemical shift artifact corrections using a single scan (abstr). Program of the annual meeting of the Society of Magnetic Resonance in Medicine, London, August **1985**:174–175
28. White EM, Edelman RR, Stark DD, et al. Surface coil MR imaging of abdominal viscera. Part II. The adrenal glands. *Radiology* **1985**;157:431–436
29. Suramo I, Paivansalo M, Myllyla V. Cranio-caudal movements of the liver, pancreas and kidneys in respiration. *Acta Radiol [Diagn]* (Stockh) **1984**;25:129–131
30. Bradley WG, Kortman KE, Burgoyne B. The variable MR intensity of ventricular CSF: effect of flow (abstr). Program of the annual meeting of the Society of Magnetic Resonance in Medicine, London, August **1985**:319–320
31. Sherman JL, Citrin CM. Magnetic resonance demonstration of normal CSF flow. *AJNR* **1986**;7:3–6
32. Edelmann RR, McFarland E, Stark DD, et al. Surface coil MR imaging of abdominal viscera. Part I. Theory, technique, and initial results. *Radiology* **1985**;157:425–430
33. Simeone JF, Edelman RR, Stark DD, et al. Surface coil MR imaging of abdominal viscera. Part III. The pancreas. *Radiology* **1985**;157:437–441
34. Wood ML, Henkelman RM. MR imaging artifacts from periodic motion. *Med Phys* **1985**;12:143–151
35. Schultz CL, Alfidi RJ, Nelson AD, Kopiwoda SY, Clampitt ME. The effect of motion on two-dimensional Fourier transformation magnetic resonance images. *Radiology* **1984**;152:117–121
36. Haacke EM, Lenz GW, Nelson AD. Pseudo-gating: elimination of periodic motion artifacts in magnetic resonance imaging without gating. *Magnetic Resonance Med*, in press
37. Wood ML, Henkelman RM. Truncation artifacts in magnetic resonance imaging. *Magnetic Resonance Med* **1985**;2:517–526

American Roentgen Ray Society
Resident Award Papers, 1987

The ARRS announces competition for the 1987 President's Award and two Executive Council's Awards for the best papers concerning the clinical application of the radiological sciences.

Awards

The winner of the President's Award will receive a certificate and a $1000 prize. The winners of the two Executive Council Awards will each be given a certificate and a prize of $500. The winners will be announced March 1, 1987.

Regulations

Papers written and submitted by residents in radiology are eligible. The resident must be the sole or senior author and be responsible for all or most of the project.

Submitted manuscripts must not exceed 5000 words and have no more than 15 illustrations. Four copies of the manuscript and the illustrations are required.

Winning papers will be presented at the annual meeting of the American Roentgen Ray Society, Fountainbleau Hilton Hotel, Miami Beach, FL, April 26–May 1, 1987.

Winning papers will be submitted for early publication in the *American Journal of Roentgenology*. All other manuscripts will be returned to the authors.

Deadline for submissions is January 31, 1987. Send papers to

Byron G. Brogdon, M.D.
Department of Radiology
University of South Alabama Medical Center
2451 Fillingim Street
Mobile, AL 30617

Boundary Artifact Due to Truncation Errors in MR Imaging

Robert B. Lufkin[1]
Elizabeth Pusey[1]
David D. Stark[2]
Richard Brown[1]
Bernard Leikind[3]
William N. Hanafee[1]

A boundary artifact in MR images due to truncation of the infinite Fourier series necessary to encode tissue discontinuities was investigated by using doped water phantoms and normal volunteers. All images were obtained on 0.3-T permanent and 0.6-T superconducting MR imagers with varying phase and frequency sampling rates. The artifact appeared in both the phase and frequency encoding direction as parallel lines or ringing adjacent to borders or tissue discontinuities. This was unlike motion artifacts, which occur predominately in the phase direction, and chemical shift misregistration errors, which are most pronounced in the frequency direction. Increasing the sampling frequency from 128 to 512 resulted in higher frequency ringing and more rapid drop-off in amplitude. Low-pass digital filtering also decreased the ringing at the expense of fine detail. The truncation of the infinite Fourier series necessary to encode edges to the 128–512 terms used for most MR imaging produces the artifact. It is important to recognize this common artifact and not mistake it for patient motion or disease.

The two-dimensional Fourier transformation (2DFT) technique used for image reconstruction on most MR imagers is associated with several artifacts that must be recognized and differentiated from normal anatomy and disease [1–3]. Motion is a familiar problem that produces blurring and ghost images, or image harmonics, along the phase-encoding direction [4, 5]. Chemical shift is another source of artifacts in MR imaging that causes misregistration of fat/water interfaces along the frequency direction [6–9]. A third type of artifact similar in appearance to motion occurs at boundaries or tissue discontinuities but is unrelated to movement and is found in both the phase and frequency directions. In this study, we investigate the effect of this third phenomenon on MR images.

Methods

All images were obtained on a 0.3-T permanent magnet (Fonar B-3000, Melville, NY) or 0.6-T superconducting magnet (Technicare Teslacon, Solon, OH) whole-body MR imager. Spin-echo pulse sequences were used for all studies. The MR images acquired and reconstructed with the 2DFT technique, currently used by most manufacturers, produced planar images in which one dimension, or direction, was encoded with phase and the other with frequency of the MR signal. The phase direction was encoded by applying variable-magnetic-field gradient pulses for a fixed duration. The number of phase-encoding gradient levels determined the sampling frequency for the phase direction of the image. The sampling frequency of the frequency direction was determined by how finely the analog signal was digitized into its amplitude values when the frequency read-out magnetic field gradient was turned on. A 2DFT was then applied to this phase and frequency data to produce the image.

A uniform phantom consisting of a 9-cm lucite cube filled with 5 mM NiCl (T1 = 463 msec at 0.3 T) was imaged with various spin-echo pulse sequences. Symmetric data sampling frequencies in both the phase and frequency directions were varied from 128 to 512 levels. Images were reconstructed both with and without low-pass digital filters to remove high spatial frequency information. The filters were standard gaussian circular digital filters with a

Received April 8, 1986; accepted after revision July 10, 1986.

This work was supported in part by Public Health Service grant 1K08 CA 00979-01, awarded by the National Cancer Institute, U. S. Department of Health and Human Services.

[1] Department of Radiological Sciences, UCLA School of Medicine, UCLA Medical Center, Los Angeles, CA 90024. Address reprint requests to R. B. Lufkin.

[2] Department of Radiology, Massachusetts General Hospital, Boston, MA 02114.

[3] Department of Physics, UCLA School of Medicine, Los Angeles, CA 90024.

AJR 147:1283–1287, December 1986
0361–803X/86/1476-1283
© American Roentgen Ray Society

variable-taper function applied before the Fourier transformation [10]. For all studies, intensity values were plotted across the phantoms.

Normal volunteers were studied with these specialized data-collection pulse sequences as well as with standard pulse sequences. The standard sequences had asymmetric data sampling frequencies of 128–384 in the phase direction and 256–512 in the frequency direction. The standard asymmetric sequences were designed to minimize the data-sampling frequencies in the time-consuming phase-direction acquisition.

Results

In the phantom study obtained with 128 × 128 data sampling, alternating parallel bands of high and low signal were present along abrupt transitions from the high-signal NiCl solution to the low-signal lucite (Fig. 1). As the data-sampling frequencies were increased from 128 to 256 to 512, the spatial frequency of the ringing increased. The amplitude decay rate of the ringing also increased, until at the 512 level, the ringing was almost lost in background image noise. For data-sampling frequencies of 128, 256, and 512, the spatial frequency of the ringing was 2, 4, and 8 per cm, respectively. The ringing could be removed by the addition of a low-pass filter (Fig. 2). The loss of high spatial frequencies because of the filter resulted in a smoothed image with no visible ringing.

In normal volunteers, the symmetric 256 × 256 data-sampling acquisition resulted in symmetric ringing at tissue discontinuities such as the inner table of the skull or sclera (Fig. 3A). Low-pass filtering with the same acquisition technique removed the artifact at the expense of high spatial frequency information (Fig. 3B).

With standard pulse sequences and asymmetric data-sampling frequencies, the artifact occurred with a different frequency in each direction, depending on the sampling fre-

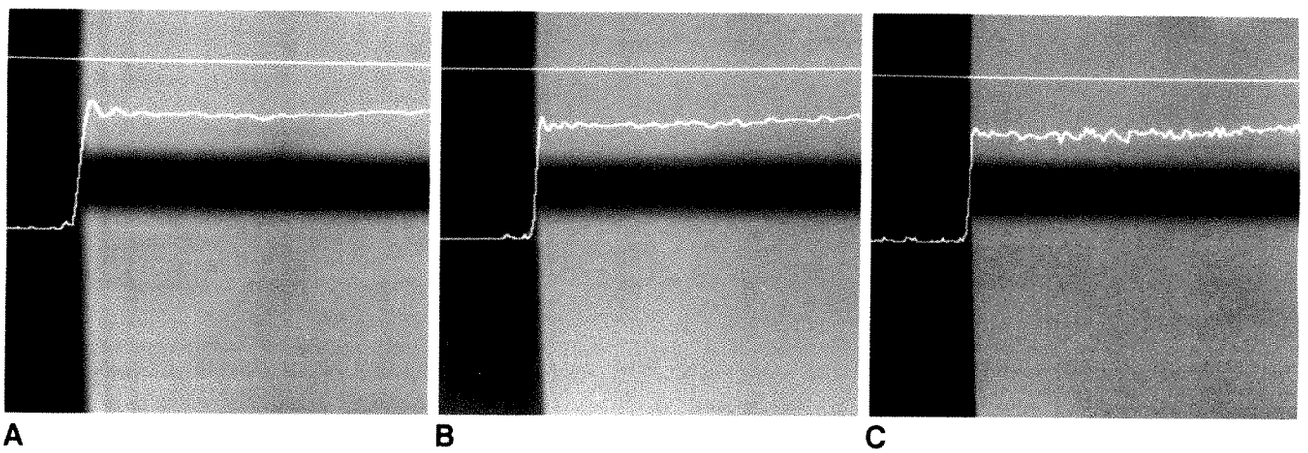


Fig. 1.—2.5-mM NiCl phantom imaged with symmetric data acquisition (phase = frequency sampling frequencies) shows effect on truncation artifact. Signal intensity across line is plotted on graph.

***A*, 128 × 128 levels. Pronounced ringing present.**
***B*, 256 × 256 levels. Artifact diminished**
***C*, 512 × 512. Ringing now almost lost in background noise.**

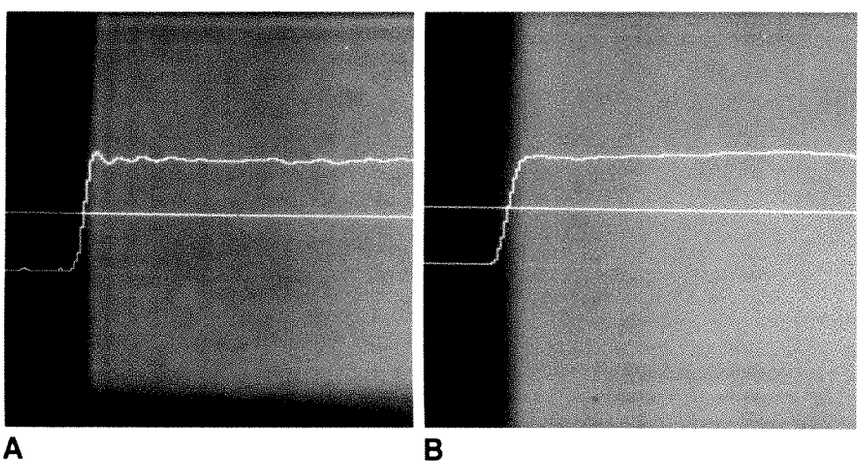


Fig. 2.—The effect of low-pass filters is shown on the phantom scanned with 256 × 256 level acquisition.

***A*, Ringing present at boundary from truncation errors.**

***B*, Low-pass filter removes ringing artifact but also diminishes image sharpness.**

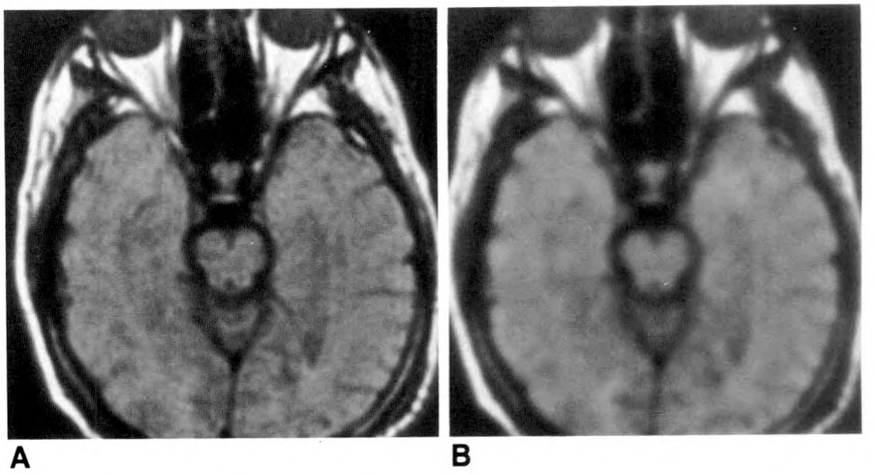


Fig. 3.—Normal volunteer scanned with and without filters. Symmetric data acquisition (256 × 256) used.

***A*, Without filters, pronounced truncation artifacts present along inner table of skull because of abrupt tissue transition.**

***B*, Addition of filters results in elimination of the ringing artifact at expense of overall image sharpness.**

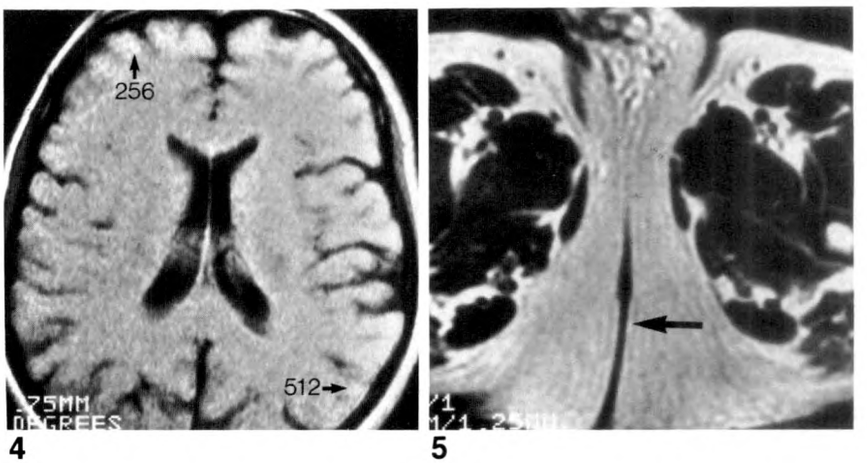


Fig. 4.—Standard asymmetric data acquisition of normal volunteer. 256 levels are acquired along phase direction and frequency is sampled at 512. Truncation ringing more prominent along interfaces in phase direction (256→) than in frequency direction (512→).

Fig. 5—Body coil image of normal volunteer (SE/2000/84) with marked ringing (*arrow*) at fat/muscle interfaces in soft tissues of pelvis.

quency, and was most pronounced in the phase direction because of generally lower sampling frequencies in this dimension (Fig. 4). The artifact appeared in images independent of pulse-sequence parameters (TR, TE) or coils used (body, head, surface coils) (Figs. 5 and 6). The ringing artifact was also decreased by increasing the data-sampling frequency in the phase direction (Fig. 7).

Discussion

2DFT techniques transform the MR signal to spatial-intensity image data with frequency and phase information encoding each direction or axis in the plane of the scan. Complex shapes are specified by a series of sine and cosine waves of various frequencies, phase, and amplitude. Some shapes are more difficult to encode than others. The most difficult shapes to represent with a Fourier series of terms are wave forms with instantaneous transitions, tissue discontinuities, or edges [2, 3]. This situation occurs often in the human body, for example, at the junction of the low-signal inner table of the skull with the adjacent brain, or at the high-signal subcutaneous fat adjacent to low-signal air. For the most accurate representation of an instantaneous transition with a series of terms for Fourier analysis, an infinite number of frequency-phase terms are necessary. Because an infinite number is not possible in real life, the ideal infinite Fourier series must be truncated to a more manageable number of components for patient studies. (The truncation of an infinite series is a familiar concept. We routinely approximate ⅓ as 0.33333, although, strictly speaking, the decimal approximation is an infinite series of 3s.) The truncation of the Fourier series in MR imaging results in errors or approximations in reconstructing the appearance of the original object. The Fourier transformation of the real truncated data equals the Fourier transformation of the real infinite data convolved with a sinc function ([sin x]/x). As fewer data terms are used, these errors become more pronounced because of the decreased frequency of ringing and diminished decay rate of ringing amplitude. In images or the spatial-frequency domain, the oscillations, or ringing, appear as parallel bands of high and low signal adjacent to tissue discontinuities, or edges.

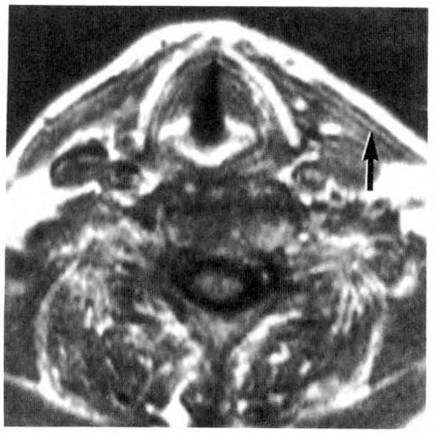
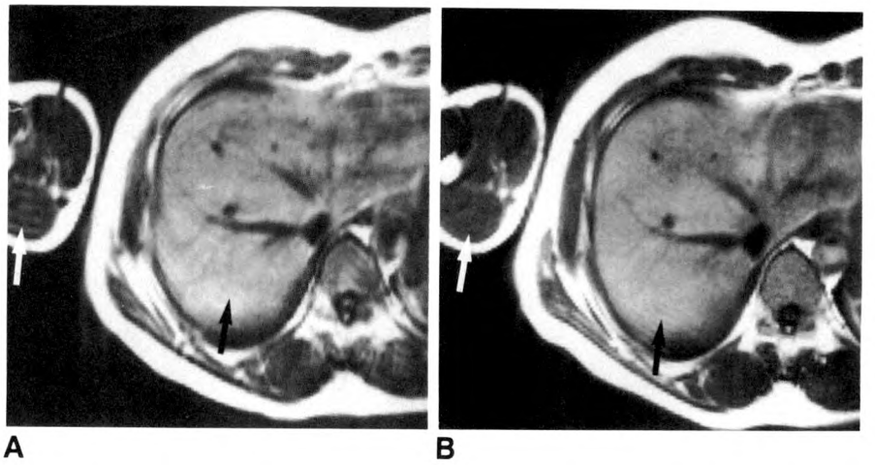


Fig. 6.—Surface-coil image of larynx (SE/500/28) with truncation artifacts (*arrow*) along phase direction (256 levels) at fat/muscle and thyroid-cartilage/vocal-cord interfaces.



A B

Fig. 7.—Axial images of liver (SE/260/15) in normal volunteer. Short TR and TE diminish motion artifact but truncation errors persist (*arrows*).
A, Acquisition with 128-phase levels results in prominent ringing along phase direction.
B, Increasing phase acquisition to 192 levels decreases effect of artifact.

TABLE 1: **Characteristics of Edge Artifacts**

Characteristic	Type of Artifact		
	Truncation	Motion	Chemical Shift
Axes involved	Phase & frequency	Phase only	Frequency only
Periodicity	Constant for axis	Variable	Single offset
Amplitude	Uniform decay	Variable	Single offset
Dependent on	Sampling rates	TR, TE, velocity,signal averaging, periodicity	Fat/water interfaces, Larmor frequency
Mechanism	Fourier series truncation	Interference phenomenon	Spatial encoding, error due to frequency variations in chemical species

Even if it were possible to include an infinite number of terms in the Fourier series to eliminate the ringing due to truncation, one small artifact at tissue discontinuities would still persist. Known as Gibb's phenomenon, this artifact is a small signal overshoot at the boundary that equals 8.95% of the discontinuity amplitude [2, 3].

Another artifact of 2DFT imaging similar in appearance to truncation errors is the artifact due to motion [4, 5]. Position change during the various phase-encoding levels of image acquisition results in inconsistent image reconstruction along the phase direction, regardless of whether the motion is in the phase or frequency direction. Errors in phase location result in "ghost images," or image harmonics produced at periodic intervals along the phase direction. Image harmonics are also most pronounced at edges or tissue discontinuities. Unlike truncation artifacts, they depend on TR and TE and are most pronounced in the phase direction. Truncation artifacts also show strictly periodic decay of ringing, while motion artifacts show irregular periodicity depending on the periodicity of the motion and irregular amplitude and spacing depending on the number of signals averaged (Table I). Finally, motion artifacts are not necessarily close to the original edge, as truncation errors are.

A third edge artifact is due to chemical shift [6–9]. The slightly different Larmor frequency of differing chemical species, such as fat and water in proton imaging, produces spatial errors in image reconstruction. The artifact appears as dark and light bands along the fat/water interfaces offset along the frequency direction. The fat/water shift (50 Hz at 0.3 T) is enhanced at higher magnetic-field strengths and shallower magnetic-field gradients used for imaging. Unlike truncation artifacts, chemical shift produces a single offset rather than periodic ringing (Table I).

In addition to degrading the image, truncation artifacts can obscure normal anatomy and be mistaken for disease. Several strategies can decrease the effect of truncation artifacts on

an image. If more phase and frequency terms are added during data collection, the ringing will have a higher frequency, decay more rapidly, and be generally less noticeable (Figs. 1 and 7). Unfortunately, because the sampling frequency in the phase direction, or the number of phase levels acquired, determines the overall scan time, increasing it may result in unrealistic patient examination times. Most manufacturers already implement asymmetric data-sampling rates with 128–256 phase levels and 256–1024 levels obtained in the non–time-dependent frequency direction. Thus, the artifact is usually most noticeable because of the lower data sampling rates in the phase direction.

When the structures being imaged have many edges that occur in one direction, the effects of truncation can be decreased if the patient is positioned so that the edges lie along the frequency direction, which usually has the higher sampling frequency. Adding a low-pass filter to the data may remove high spatial frequency information from the signal data, which will eliminate most of the ringing due to truncation effects but will also remove a great deal of the image sharpness (Figs. 2 and 3). The ringing can also be reduced by modification of the phases of the complex data samples [11], by applying a quartic phase shift in succession to each column of image data. Although more data processing is required to perform this modification, the technique results in less blurring than in simple low-pass filtering.

In this paper, we describe a ringing edge artifact in MR imaging due to truncation of the infinite Fourier series necessary to encode tissue discontinuities or edges. Unlike edge artifacts due to motion or chemical shift, truncation artifacts occur in both the phase and frequency direction and depend on data-sampling frequency. It is important to recognize this common artifact of 2DFT MR techniques and to not mistake it for disease.

ACKNOWLEDGMENTS

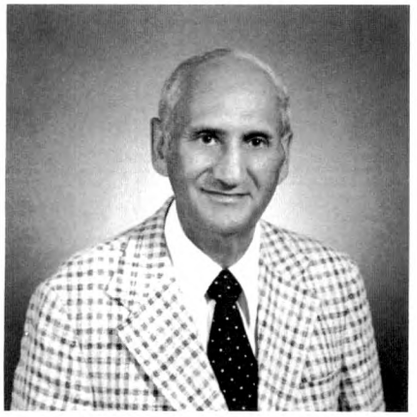
We would like to thank David Smith and the late Theo Andrikos of Fonar Corporation for their helpful comments regarding 2DFT imaging techniques.

REFERENCES

1. Kumar A, Welti D, Ernst J. NMR Fourier zeumatography. *J Magnetic Resonance* **1975**;18:69–83
2. Bracewell RN. *The Fourier transformation and its applications.* New York: McGraw-Hill, **1978**
3. Ramirez R. *The FFT: fundamentals and concepts.* Beaverton, OR: Tektronix, Inc., **1977**
4. Runge VM, Clanton JA, Partain CL, James AE. Respiratory gating in magnetic resonance imaging at 0.5 Tesla. *Radiology* **1984**;151:521–523
5. Schultz CL, Alfidi RJ, Nelson AD, Kopiwoda SY, Clampitt ME. The effect of motion on two-dimensional Fourier transformation magnetic resonance images. *Radiology* **1984**;152:117–122
6. Babcock EE, Brateman L, Weinreb JC, Horner SD, Nunnally RL. Edge artifacts in MR images: chemical shift effect. *J Comput Asst Tomogr* **1985**;9(2):252–257
7. Soila KP, Viamonte M, Starewicz PM. Chemical shift misregistration effect in magnetic resonance imaging. *Radiology* **1984**; 153:8819–8820
8. Weinreb JC, Brateman L, Babcock EE, Maravilla KR, Cohen JM, Horner SD. Chemical shift artifact in clinical magnetic resonance images at 0.35 T. *AJR* **1985**;145:183–185
9. Dixon WT. Simple proton spectroscopic imaging. *Radiology* **1984**;153:189–194
10. Oppenheim AV, Schafer RW. *Digital signal processing.* Englewood Cliffs, NJ: Prentice-Hall, **1975**:239–250
11. Wood ML, Henkelman RM. Truncation artifacts in magnetic resonance imaging. *J Magnetic Resonance Med* **1985**;2:517–526

Memorial

Raymond M. Abrams, 1917–1986



Raymond M. Abrams died on June 3, 1986, at the age of 69, and we who worked with him are deprived of his warmth and wisdom, his zeal, and his probing mind. For more than a decade, Ray wrestled with and overcame ill health until his magnificent heart finally gave out.

Wrestling was not new to Ray; he was an intercollegiate champion at Michigan and came away from Ann Arbor with a varsity letter and a baccalaureate. Chemistry next claimed his attention and led to an M.S. degree from the University of Richmond. Medicine called him to St. Louis University where he obtained his M.D. in 1943. When military obligations were over, Ray found himself in another wrestling match, this time between Internal Medicine and Radiology. Fortunately, Radiology won. After residency at the New York Post Graduate Medical School, he spent the next 27 years at the NYU medical center attaining full professorial status in 1968. This rank was earned and deserved, not only for his publications, including pioneering work in angiography, but more so for the stimulation he provided to students, residents, and junior staff. From NYU, Ray came to St. Mary's Hospital in Waterbury, CT. Under his skillful guidance, an outstanding department evolved. On retirement in 1981, Ray gave his time to Yale, unencumbered by administrative restraints. His curiosity was insatiable, driving him to improve on what we had, to create what did not exist. The end interrupted joyful exploration of refinements in lithotripsy and imaging with monoclonal antibodies.

While Ray's own heart failed him, he failed no one. Many of us who were fortunate enough to know him became infused with his enthusiasm and zest. At his memorial services, his son, Paul, noted that his father gave "the last full measure of devotion" to those whose paths crossed his and who needed his help. He constantly offered his assistance to friends, colleagues, and patients, both those who were close to him and those he had recently met. He took on their problems as his own. His selfless approach to life included not just counsel and encouragement to others, but active time-consuming efforts on their behalf. Although he was at Yale a short time, his impact on the department was enormous for he taught us how to live and behave as well as how to interpret films. A lecture will be given in his honor this year at the Yale Radiology Grand Rounds.

His friends will miss hours of conversation and fiercely fought tennis matches whether won or lost.

He leaves behind his wife, Lennie, sons, Paul, Alan, and Richard, and his adored grandson, Jake. They are, of course, his greatest contributions but more, he has touched us all.

Solomon S. Schwartz
Arthur T. Rosenfield
New Haven, CT 06511

Technical Note

A New Device for Exercise MR Imaging

Saul Schaefer,[1] Ronald M. Peshock,[1] Robert W. Parkey,[2] and James T. Willerson[1]

Although dynamic exercise is an effective method for inducing myocardial ischemia in patients with coronary artery disease [1], the limited sensitivity and specificity of the standard exercise test have stimulated efforts to use imaging techniques to improve its diagnostic accuracy [2, 3]. MR provides excellent anatomic detail of the heart that can detect regional wall-motion abnormalities [4], changes in ejection fraction [5], and, possibly, perfusion defects [6]. The abilities to perform graded dynamic exercise in an MR system and accurately measure these variables could improve the usefulness of exercise to detect ischemic heart disease. With this goal in mind, we have designed and built an exercise device to be used in an MR system.

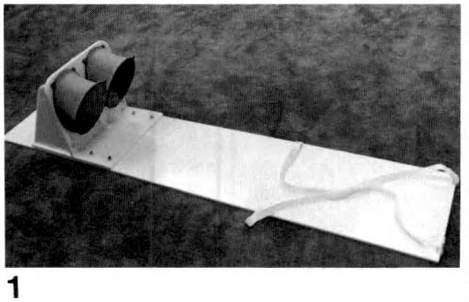
Design goals for this device were that (1) it should operate within the MR system without requiring equipment modification, (2) it should allow graded dynamic exercise with the patient in the normal supine position, and (3) MR data acquisition should be obtained while the patient exercises. Imaging interference by ferromagnetic materials, as well as the physical limitations of the scanner bore, eliminated conventional exercise devices from consideration.

Technique

Our device (Fig. 1) consists of a high-strength polypropylene frame on which two air-bellows pressure pumps with 16 cm of travel are mounted. The pump assembly is adjustable over a 30-cm range to accommodate patients at different heights. The output lines of the pumps have orifices that allow variable resistance to movement and enable calibration of the work required to depress the pump fully. The exercise device fits into the patient table (Fig. 2) of the Diasonics MT/S system without any table modification. The patient is positioned supine so that he or she is able to compress the pumps using both

Fig. 1.—Exercise device constructed of high-strength polypropylene with pump adjustable longitudinally to accommodate varying patient heights.

Fig. 2.—Patient lies supine so that both upper- and lower-leg muscles are used in exercise. Position is maintained by diagonal shoulder straps, and exercise is performed in magnet bore.



1



2

Received May 30, 1986; accepted after revision July 2, 1986.
This work was supported totally by Ischemic Heart SCOR Grant, National Institutes of Health grant HL-17669, and the Moss Heart Fund, Dallax, TX.
[1] Department of Internal Medicine (Cardiology), The University of Texas Health Center at Dallas, 5323 Harry Hines Blvd., Dallas, TX 75235. Address reprint requests to S. Schaefer.
[2] Department of Radiology (Nuclear Medicine), The University of Texas Health Center at Dallas, 5323 Harry Hines Blvd., Dallas, TX 75235.

AJR **147:1289–1290, December 1986** 0361–803X/86/1476–1289 © American Roentgen Ray Society

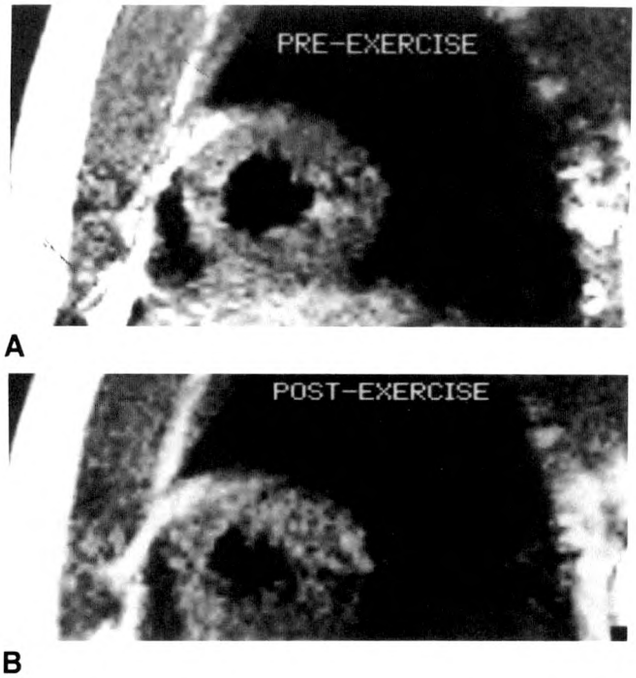


Fig. 3.—Short-axis scans in normal volunteer before exercise (*A*) and after (*B*). Increased wall thickness and smaller cavity dimensions occur at same time in cardiac cycle.

upper- and lower-leg muscles; diagonal shoulder and body straps maintain position during exercise. After we obtain baseline views of the left ventricle, the patient can exercise to either time or heart-rate limits. Continuous ECG monitoring (Diasonics ECG cardiac gating control system and monitor) allows the physician to detect arrhythmias and follow the heart-rate response to exercise. Blood pressure is obtained at appropriate intervals by using a modified Sunbeam model 7620 digital sphygmomanometer. The patient's pumping rate on the device can be regulated by using an electronic metronome, thus allowing staging of the exercise protocol. At the end of exercise, another scan is performed without repositioning or retuning. This is diagnostically relevant because segmental left ventricular wall-motion abnormalities sometimes persist for several minutes after the end of exercise, and some current techniques, such as exercise echocardiography, rely on the persistence of these wall-motion abnormalities to detect ischemic heart disease noninvasively.

The images obtainable with exercise MR are illustrated in Fig. 3, which shows the pre- and postexercise scan obtained in a true short-axis plane in a normal volunteer. This person exercised to a target heart rate, and image acquisition began immediately at the end of exercise. A 256 × 128 pixel, 2-acquisition, single spin-echo routine was used to obtain images in approximately 4 min.

Discussion

Images suitable for analysis of ejection-fraction and wall-motion abnormalities require acquisition of the same cardiac slice both at the end of systole and diastole. Current imaging routines require significantly longer than 4 min for this process. However, technical developments in the near future should appreciably shorten this time requirement and improve the diagnostic yield of exercise MR. These developments include (1) rapid, small-flip-angle, short-TR routines that take less time and provide blood-flow and velocity information in addition to wall-motion data; (2) paramagnetic contrast agents to define perfusion defects; and (3) advanced computerized processing to quantify accurately the image information. These developments may also allow imaging during exercise, which is difficult now because of image degradation from patient motion.

Interpretation of ECG ST-segment and T-wave changes is impaired in the presence of magnetic fields of 0.3 T or greater. T-wave abnormalities, previously noted [7], are thought to be caused by the induced electromagnetic force associated with high-velocity blood flow perpendicular to the static magnetic field. Although no arrhythmias or heart rate changes have been induced, the diagnostic usefulness of the ECG in this setting is diminished.

In summary, we have developed an exercise device that can be used to perform graded exercise in a commercial MR system. Images obtained before and after exercise can be analyzed for changes reflecting myocardial ischemia. With further development of image acquisition and processing routines, this device should provide useful information for the noninvasive diagnosis of cardiovascular disease.

REFERENCES

1. Ellestead MH, Allen W, Wan MCK, Kemp GL. Maximal treadmill stress testing for cardiovascular evaluation. *Circulation* **1969**; 39:517–522
2. Bailey IK, Griffith LSC, Rouleou J, Strauss HW, Pitt W. Thallium-201 myocardial perfusion imaging at rest and during exercise. Comparative sensitivity to electrocardiography in coronary artery disease. *Circulation* **1979**;55:79–87
3. Corbett JR, Nicod PH, Huxley RL, Lewis SE, Rude RE, Willerson JT. Left ventricular functional alterations at rest and during submaximal exercise in patients with recent myocardial infarction. *Am J Med* **1983**;74:577–591
4. Rokey R, Malloy CR, Keller AM, et al. Regional systolic wall thickening assessed with magnetic resonance imaging (abstr). *Circulation* **1985**;72:III-23
5. Stratemeier EJ, Thompson R, Brady TJ, et al. Ejection fraction determination by MR imaging: comparison with left ventricular angiography. *Radiology* **1986**;158:775–777
6. McNamara MF, Higgins CB, Ehman RL, Revel D, Sievers R, Brasch RC. Acute myocardial ischemia: magnetic resonance contrast enhancement with gadolinium-DTPA. *Radiology* **1984**; 153:157–163
7. Budinger TF, Cullander C. Biophysical phenomena and health hazards of in vivo magnetic resonance. In: Margolis AR, ed. *Clinical magnetic resonance imaging.* San Francisco: Radiology Research and Education Foundation, **1983**:303–320

Malpractice and Radiologists, Update 1986:
An 11.5-Year Perspective

Leonard Berlin[1]

All medical malpractice lawsuits filed in Cook County, IL, from January 1, 1980, through June 30, 1986, were reviewed and compared with similar data for the period of January 1, 1975, through December 30, 1979. A total of 11,203 suits were filed during the 11.5-year period; of these, 1391 (12%) were radiology related. The latter were categorized into six groups. The largest was missed radiologic diagnoses, which accounted for 40% of the total. The remaining groups included complications, 19%; failure to order, 17%; radiation therapy, 11%; slip and fall, 5%; and miscellaneous, 8%. Over the 1975–1986 period, the rise in the number of suits alleging radiologic misses outpaced all other groups. Although the most common type of miss continues to involve fractures, the frequency of missed carcinomas has grown at a disproportionately faster rate. Misses specifically involving CT, nuclear medicine, and sonography also are becoming more prevalent. Radiographic misses continue to occur at an average rate of 30%, with little hope of improvement. Methods to combat the rising number of malpractice suits are discussed. It is concluded that although programs to educate radiologists on risk management should continue, the ultimate solution may be a more enlightened public attitude as to what actually constitutes malpractice, and institution of tort reform measures by federal and state legislatures.

It has now been 6 years since the *American Journal of Roentgenology* published a special report that listed and categorized all radiology-related malpractice lawsuits filed during the period from 1975 to 1980 in a large metropolitan region [1]. This article is a continuing survey of similar lawsuits and focuses on the questions of how many and for what reasons radiologists are sued for medical malpractice. Its purpose is to uncover the changing patterns that have occurred in the nature of allegations made in radiologic suits and to discuss how radiologists can more effectively reduce the causes of these suits.

Materials and Methods

The geographic region of Cook County, IL, includes the city of Chicago and many of its suburbs. The population is about 6 million. Its approximate medical composition includes 9000 physicians (520 of whom are radiologists), 94 hospitals, and 31,000 beds.

Malpractice suits in Cook County are filed in the Law Division of the Circuit Court in Chicago. *The Cook County Jury Verdict Reporter* is a private monthly service that lists every lawsuit filed, names all plaintiffs and defendants, and provides a brief summary of the allegations. Material for this report was gathered from every issue of the *Verdict Reporter* published between January 1, 1980, and June 30, 1986. All medical malpractice suits were categorized on the basis of the defendants and the complaints. Those suits that named a radiologist or involved a radiologic procedure were analyzed, and this material was then compared with similar data from the 1975 through 1979 period. Thus, an 11.5-year span is covered.

Published descriptions of these lawsuits contain preliminary allegations only. During the legal process, charges are often modified, deleted, or added, and the names and number of defendants are frequently changed. No study of these changes is included in this report.

Received June 5, 1986; accepted after revision July 25, 1986.

[1] Department of Radiology, Skokie Valley Hospital, Skokie, IL, and University of Illinois College of Medicine, Chicago, IL. Address reprint requests to L. Berlin, Skokie Valley Hospital, 9600 Gross Point Rd., Skokie, IL 60076.

***AJR* 147:1291–1298, December 1986**
0361–803X/86/1476–1291
© American Roentgen Ray Society

TABLE 1: **Annual Totals of Radiology-Related Malpractice Lawsuits in Cook County, IL, 1975–1986**

Year	Total Radiology-Related Suits	Slip and Fall	Radiation Therapy	Failure to Order	Complications	Misses	Misc.
1980	140	9	22	20	30	47	12
1981	114	7	12	15	22	48	10
1982	127	9	10	23	27	52	6
1983	138	2	4	12	28	81	11
1984	168	8	8	43	32	69	8
1985	222	8	12	28	51	93	30
1986[a]	17	0	1	6	3	7	0
Subtotal[b]	926	43 (5)	69 (7)	147 (16)	193 (21)	397 (43)	77 (8)
1975	129	10	39	18	13	37	12
1976	82	4	18	19	9	27	5
1977	66	6	5	14	11	24	6
1978	70	2	6	18	10	29	5
1979	118	10	13	26	20	42	7
Subtotal[b]	465	32 (7)	81 (17)	95 (20)	63 (14)	159 (34)	35 (8)
11.5-year total[b]	1391	75 (5)	150 (11)	242 (17)	256 (19)	556 (40)	112 (8)

[a] First 6 months only.
[b] Numbers in parentheses are percentages.

Lawsuits have three possible outcomes: They are won by the plaintiff, won by the defendant, or settled. It is beyond the scope of this paper to research the final disposition of these suits, although a study that does so is now in progress.

No article can possibly list every grievance made by patients against physicians; many disputes are settled before legal action, thus escaping public record. I have deliberately focused on patient grievances rather than on actual injuries sustained. Although the latter are most important in determining final compensation, the specific allegations of wrongdoing are most useful to groups evaluating risk-management procedures.

TABLE 2: **Slip-and-Fall Cases, 1980–1986**

Injury	Number
Fell from wheelchair or cart in or near X-ray department	13
Fell from stool or table in X-ray department	15
Struck by X-ray equipment	9
Body injured by X-ray technician or radiologist	4
Sexually assaulted by X-ray technician	2
Total	43

Note.—Data for 1986 are for first 6 months only.

Results and Observations

During the 78-month period from 1980 to 1986, 8136 medical malpractice lawsuits were filed against hospitals and physicians. This number does not include suits naming only dentists, podiatrists, or chiropractors. Of the total, 926 suits involved radiologists or radiologic procedures.

Suits involving radiology may be divided into several categories for convenient discussion: (1) Cases that do not challenge professional conduct. These include injuries resulting from slips or falls within, or in transit to, radiology departments, from being struck by X-ray equipment, or from manipulation by the radiologist or technologist. Such cases, termed "slip-and-fall" suits by attorneys, are covered by professional liability insurance. (2) Suits that allege injury from radiation therapy. (3) Litigation termed "failure to order." Defendants in these suits usually are not radiologists, but other physicians sued for failing to order a specific radiologic procedure. From an economic point of view, this type of suit assumes great importance. (4) Cases that allege misinterpretation of radiographs or radiologic procedures. Most name the radiologist as the defendant, but in some cases a hospital alone is named. (5) Suits that allege complications from radiologic procedures. (6) Miscellaneous cases. In 70% of these, radiologists were sued without apparent cause along with several other defendants.

Table 1 summarizes the annual totals of various lawsuit categories both in the current 6.5-year period and in the 1975–1979 period [1].

Slip-and-Fall Cases

A total of 43 cases were reported (Table 2); 37 of these arose from injuries sustained as a result of falling in or near the X-ray department or of being inadvertently struck by various types of X-ray equipment. In four cases, patients alleged injury caused by rough handling by the X-ray technologist or the radiologist. In two, sexual assault by the X-ray technician was claimed.

Slip-and-fall cases accounted for about 5% of all radiology-related suits. As can be seen in Table 1, this figure is rather consistent throughout the 11.5-year span.

TABLE 3: **Suits Alleging Injury from Radiation Therapy, 1980–1986**

Suit	Number
Thyroid carcinoma from childhood irradiation at Michael Reese Hospital	22
Late carcinoma from other childhood irradiation	6
Miscellaneous tissue damage from improper X-ray therapy	35
Unnecessary therapy due to mistaken diagnosis	3
Failure to administer X-ray therapy	3
Total	69

Note.—Data for 1986 are for first 6 months only.

Injury from Radiation Therapy

Sixty-nine cases claimed injury from radiation therapy (Table 3). Of these, 22 were related to alleged development of thyroid carcinoma due to previous childhood irradiation at Michael Reese Hospital in Chicago. As pointed out in the previous report [1], after Michael Reese undertook a massive program recalling for thyroid evaluation patients who previously had been irradiated, a large number of lawsuits were filed. Forty-six were filed in the 1976 through 1979 period. In the current period, the number fell to 22, half of which were filed in 1980. Six additional cases alleged carcinoma due to previous childhood irradiation involving non–Michael Reese radiologists.

Three suits alleged unnecessary therapy because of mistaken diagnoses, and three suits alleged failure to administer any radiation therapy at all. There remained only 35 cases over the 6-year period that actually claimed tissue damage from radiation therapy. This small figure represents less than 4% of all radiology-related malpractice suits and should have little impact on the overall practice of radiology.

Failure to Order Radiologic Procedures

Most defendants in these suits (Table 4) were nonradiology physicians. Although more than one-third of these cases were related to bone injuries, many other radiologic procedures also were included. Noteworthy are five cases in which patients who later developed lung carcinomas or metastatic lesions sued for failure to receive chest radiography in a timely fashion and six in which women who later developed breast carcinomas sued their physicians for failure to order mammograms. Ten suits specifically mentioned failure to order a CT scan, eight mentioned sonograms, and seven mentioned nuclear medicine scans.

These figures indicate that attorneys have developed a greater knowledge of radiology. They also explain a major cause of "defensive" medicine: Clinicians order many tests in an effort to avoid lawsuits. The conflict between the need to practice defensive medicine and the pressure to comply with cost-containment measures instituted by Medicare's diagnosis-related groupings, various insurance companies, preferred-provider organizations, and health-maintenance organizations is obvious.

TABLE 4: **Suits Alleging Failure to Order a Radiologic Procedure, 1980–1986**

Procedure	Number
Radiographs for	
Fractures and dislocations	54
Bone malignancies	2
Mandibular and teeth lesions	4
Miscellaneous bone conditions and osteomyelitis	7
Spine abnormalities	3
Skull abnormalities	2
Loose bodies in elbow	1
Chest carcinoma or metastases	5
Miscellaneous chest conditions, chest tube placement	3
Gastrointestinal carcinomas and ulcers	3
Foreign bodies	10
Neck before intubation	1
Kidney biopsy	1
Mammograms for breast cancer	6
Angiograms	9
Myelograms	4
Operating room cholangiogram	2
Pelvimetry	1
CT scans of	
Head, for tumor, trauma, and anomalies	7
Abdomen and spine	3
Sonograms for	
Fetal abnormalities	6
Ectopic pregnancy	1
Kidney carcinoma	1
Nuclear medicine scans for	
Lung emboli	2
Heart	2
Bone	1
Testicles for torsion	1
Spleen for trauma	1
Ventriculogram	1
Unspecified	3
Total	147

Note.—Data for 1986 are for first 6 months only.

Radiologic Misses

The largest single category of radiology-related lawsuits is still the missed diagnosis, which can arise from either failing to "see" a significant finding on a radiograph or attaching the wrong significance to a finding that is readily seen. Not noticing a fracture or pulmonary nodule are examples of the former; incorrectly labeling a breast density as "fibrocystic disease" rather than "suspicious for carcinoma," the latter. Whereas in the 1975 through 1979 period, misses accounted for 34% of the lawsuits, in the 1980–1986 period, misses rose to 43%. A comparison of the 397 alleged misses in 1980–1986 (Table 5) with the previous data [1] shows a dramatic increase in radiologists' liability in cases involving carcinomas, CT scans, radionuclide examinations, and sonographic studies.

Not unexpectedly, misses centering on fractures and dislocations of bones remained the most frequent, rising in number from 102 in the first 5-year period to 153 in the current 6-year period. However, misses of various carcinomas increased strikingly from a previous 29 to a current 92. Suits

TABLE 5: **Suits Alleging Radiologic Misses, 1980–1986**

Radiologic Miss	Number
Fractures, dislocations, and separations	153
Delayed union or nonunion of fractures	10
Lung malignancies: carcinoma, lymphoma, metastases	47
Bone tumors	12
Breast carcinomas (mammography)	15
Gastrointestinal carcinomas: upper and lower tract, pancreas	9
Carcinoma, type not specified	9
Brain tumors, on radiograph and/or CT	7
Miscellaneous bone conditions: osteomyelitis, degenerative changes, aseptic necrosis	17
Miscellaneous chest conditions: heart, asthma, silicosis	4
Miscellaneous gastrointestinal conditions: gallbladder disease, ulcer, obstruction	14
Head trauma: hematomas, vascular lesions	4
Head CT, miscellaneous misdiagnoses	9
Abdominal and spine CT, miscellaneous	5
Angiographic and venous thromboses	5
Aneurysms: aortic, renal	4
Throat and neck abnormalities	4
Foreign bodies	9
Myelogram	7
Arthrogram, shoulder	1
Scoliosis of spine	2
Bent hip prosthesis	1
Fetal death and position, on plain radiograph	3
Urinary tract, miscellaneous	3
Nuclear medicine scans: bone, heart, thyroid	3
Hysterosalpingogram: tubal patency	1
Sonography: fetal age, position, anomalies	15
Sonography, ectopic pregnancy	5
Sonography, miscellaneous abnormalities	3
Unspecified	16
Total	397

Note.—Data for 1986 are for first 6 months only.

TABLE 6: **Suits Alleging Complications from Radiologic Procedures, 1980–1986**

Procedure or Complication	Number
Angiography	69
Colon perforation from barium enema (air contrast specified in four)	14
Bartum enema, miscellaneous (obstruction)	2
Excretory urography	13
Venogram	13
CT injection	7
Myelogram	24
Arthrogram	2
Pregnancy aborted because of diagnostic X-ray	24
^{131}I, diagnostic, causing fetal anomaly	1
Fetal anomaly from gallbladder and small-bladder examination	1
Male infertility from multiple X-rays	1
Vas deferens injection	2
Nonspecific injury from too much X-ray	1
Bronchogram	1
Injury from bowel preparation for gastrointestinal series	1
Retrograde pyelogram	3
Endourological procedures	2
Informed consent for stone removal	1
Embolization procedure	1
Aspiration during upper gastrointestinal series	1
Digital subtraction angiography	1
ERCP	2
Discogram	2
Morphine before CT	1
Gallium scan	1
Bone scan	1
Percutaneous transhepatic cholangiogram	1
Total	193

Note.—Data for 1986 are for first 6 months only.

alleging missed lung malignancies rose from 16 to 47, those claiming missed breast carcinomas jumped from four to 15, and those involving missed gastrointestinal carcinomas tripled from three to nine. Missed CT, nuclear medicine, and sonographic examinations were specifically mentioned in 40 cases in the current period, compared with only two cases in the 1975–1979 listing.

Complications of Radiologic Procedures

Table 6 lists 193 suits that alleged complications from radiologic procedures, accounting in the current period for 21% of all radiology-related suits. Leading the list are 69 complications from angiography. There were 14 colon perforations secondary to barium enemas, of which four specified air-contrast examinations. Twenty-six complications resulted from excretory urograms and venograms and another seven from CT injection. Myelograms accounted for 24 cases. Again reflecting the increasing sophistication of plaintiffs' attorneys, suits arising from complications from specific examinations such as digital subtraction angiography, ERCP, and endourologic procedures were filed also. Two cases of complications were from nuclear medicine diagnostic examinations: one from a gallium study and one from a technetium scan of bone.

Twenty-four cases alleged abortions that had occurred either spontaneously or on the order of a physician, and one additional case alleged fetal anomalies. All of these were supposedly the result of diagnostic X-ray procedures. Also, one case alleged male infertility caused by diagnostic X-ray procedures.

Miscellaneous Suits

Table 7 lists 77 miscellaneous suits; 57 of these named a radiologist along with several other defendants in cases that apparently were not directly related to radiology. In 10 cases it was alleged that the radiologist failed to communicate results of a study to either the patient or the patient's physician. In one case the radiologist was sued for failing to follow up proper treatment of a patient in whom a diagnosis of lung tuberculosis was made. One rather unusual case concerned a patient who alleged humiliation because her mammogram, which had shown a breast carcinoma, was displayed in a Xerox Corp. exhibit.

TABLE 7: **Miscellaneous Malpractice Suits, 1980–1986**

Description of Suit	Number
Failure to communicate results to patient or referring physician	10
Several defendants, including radiologist (in some cases apparently not related to radiologic procedures)	57
Failure to follow up pulmonary tuberculosis	1
Unnecessary myelogram	1
Foot radiograph improperly developed	1
Wrong hand X-rayed	1
Breast biopsy not done after suggested by findings on mammogram	1
Nonspecific allegation	1
Poor hip pinning due to equipment failure	2
Failure to interpret radiographs in timely fashion	1
Mammogram showing breast carcinoma given to Xerox Corp., causing humiliation	1
Total	77

Note.—Data for 1986 are for first 6 months only.

TABLE 8: **Relationship Between Radiology-Related Lawsuits and All Malpractice Suits in Cook County, IL, 1975–1986**

Year	Total Number of Malpractice Suits	Number of Radiology-Related Suits	Percentage
1980	858	140	16
1981	906	114	13
1982	1103	127	12
1983	1312	138	11
1984	1393	168	12
1985	2364	222	9
1986[a]	200	17	9
Subtotal	8136	926	11
1975	847	129	15
1976	507	82	16
1977	443	66	15
1978	515	70	14
1979	755	118	16
Subtotal	3067	465	15
11.5-year total	11,203	1391	12

[a] First 6 months only.

Relation between Radiology-Related Lawsuits and All Malpractice Suits in Cook County

The overall percentage of radiology-related lawsuits has not only stabilized but has actually dropped somewhat. As can be seen in Table 8, radiology-related lawsuits accounted for 11% of all malpractice suits filed between 1980 and 1986, slightly less than in the 1975–1979 period, when they accounted for 15%. However, a look at the numbers of suits tells a different story. As can be seen in Table 8 and Figure 1, the total number of malpractice suits filed in Cook County in the 1980–1986 period is more than double the number filed in 1976–1979. This is in keeping with a national trend of a burgeoning growth of medical malpractice litigation.

The large number of suits filed in 1985 may reflect passage of a malpractice-reform bill by the Illinois State Legislature. This bill placed certain requirements on plaintiffs before the filing of a lawsuit, limited financial compensation to the injured patient, and lowered lawyers' contingency fees. The effective date of this legislation was August 15, 1985. As a result, an onslaught of suits was filed just before that date. Whereas in all of 1985 a total of 2364 suits was filed, 2298 of them were filed before August 15. In the period from August 16 to December 31, 1985, a total of only 66 malpractice suits was filed, of which just 12 were related to radiology.

This "postlegislative depression" in malpractice lawsuit filings has continued well into 1986. During the first 6 months of 1986, the total number of malpractice suits filed was only 200; of these just 17 were radiology-related. This is in considerable contrast to the 1045 malpractice suits filed, of which 96 were radiology-related, during the corresponding 6-month period in 1985. Clearly, the impact of tort reform legislation in Cook County has been felt, although it may be short-lived. Most plaintiffs' attorneys had accelerated the preparation of lawsuits that normally would have been filed in late 1985 and early 1986 to meet the deadline of August 15, 1985. In this way they escaped the new restrictions imposed by the legislative reforms. A study of the 11-year trend (Figs. 1 and 2) suggests that malpractice filings are likely to resume their upward climb.

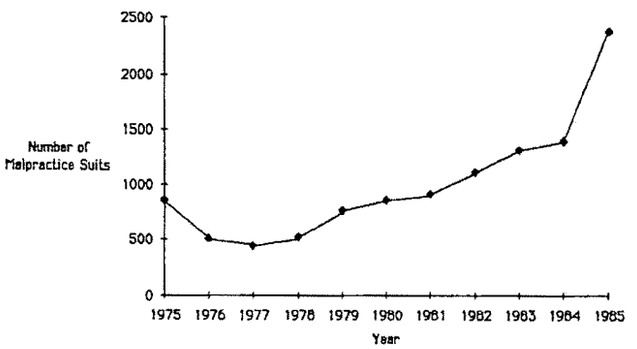


Fig. 1.—Number of malpractice suits in Cook County, IL, 1975–1985.

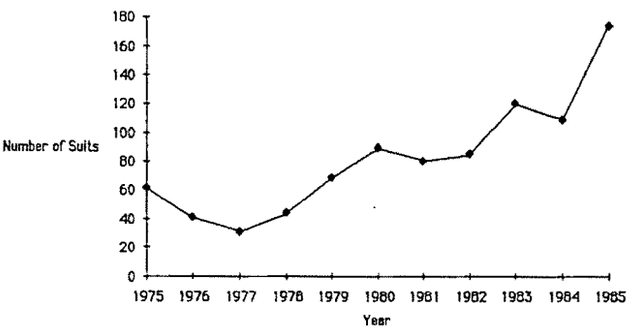


Fig. 2.—Number of lawsuits directly involving radiologists (misses, complications, and miscellaneous) in Cook County, IL, 1975–1985.

Discussion and Perspective

Lawsuits alleging misses and complications of radiologic procedures, plus the miscellaneous group, have the most direct bearing on the everyday practice of radiology. Together, they number 667 in the current 6-year reporting period, representing 72% of all radiology-related suits and 8% of all medical malpractice lawsuits. When we include similar cases from 1975–1979, these three groups of suits accounted for 66% of all radiology-related litigation in the 11.5-year period and slightly more than 8% of all medical malpractice lawsuits. Although the actual number of these suits has dramatically increased during the 11-year period, as shown in Fig. 2, when measured as a percentage the increase has been only moderate. Furthermore, the overall ratio of radiology-related to total medical malpractice suits has even decreased slightly (Table 8).

These percentages unfortunately are of little comfort to the practicing radiologist. As seen in Table 1 and in Figs. 1 and 2, the actual number of total medical malpractice suits and the actual number of suits alleging radiologic misses, complications, and miscellaneous injuries have soared in the past 5 years. This spectacular rise has far-reaching effects on all radiologists.

Radiologic Misses: Can We Avoid Them?

Closer scrutiny of the data reveals that radiologic misses constitute an even greater threat of involving the diagnostic radiologist in a malpractice lawsuit than previously imagined. In the 11.5-year reporting period, there were 556 suits alleging a missed diagnosis, representing 40% of the 1391 radiology-related suits. If we exclude those suits related to issues usually not under the direct professional control of the diagnostic radiologist (i.e., the slip-and-fall, radiation therapy, and failure-to-order cases) and the 57 cases in which the radiologist was sued along with several other defendants in matters not directly related to radiology, the figure of 1391 is reduced to 867. This number more realistically reflects the number of cases wherein the professional conduct of the radiologist is called into question and is the one against which the 556 misses should be measured. Thus, we see that radiologic misses really account for 64%, not 40%, of lawsuits filed against the practicing diagnostic radiologist. A decrease in the number of misses could alleviate the burden of malpractice litigation. However, this is not an easy task.

The published data [2–6] that document the number of significant errors committed by well-trained, competent radiologists is astonishing. Table 9 summarizes these studies. From the pioneering work of Garland [2] in 1949, who found a nearly 20% error rate and a 50% disagreement rate among radiologists, through the classic work of Yerushalmy [4] 1969, who showed a 30% error rate, to the most recently published studies of Lehr et al. [6] in 1976, who showed an overall error rate of 33% in radiographic interpretations, it can be seen that radiologic misses continue to occur in a surprisingly consistent and predictable manner. What Garland [2] said about error rates is as accurate and meaningful in 1986 as it was in 1949: "The first reaction of every new observer is, 'This does not happen to me.' To these, we suggest, 'Try it systematically,' That this (high error rate) should happen to amateurs is accepted, but that it should happen to experts is now for the first time thoroughly proved statistically."

TABLE 9: **Accuracy of Radiologic Examinations**

Area of Study	Error Rate (%)	Reference
Chest radiographs	20	Garland 1949 [2]
Chest radiographs	30	Garland 1959 [3]
Chest radiographs	30	Yerushalmy 1969 [4]
Chest radiographs	41	Herman et al. 1975 [5]
Various studies	33	Lehr et al. 1976 [6]

Can error rates be lowered? Logic suggests that as radiologists gain experience, their error rates will become lower. The facts, however, dispute this. In an exhaustive study of error rates in 2000 cases, Lehr et al. [6] found that experience had little to do with accuracy. The error rate among staff radiologists was 30%; among third- and fourth-year residents, 33%; and among second-year residents, 31%.

Logic also suggests that lengthening the time spent interpreting a radiograph will increase accuracy, but Lehr et al. [6] found just the opposite. In their study, erroneous readings averaged 147 sec, the correct ones 113 sec.

Logic further suggests that double reading is an effective and practical method of reducing error rates, but the evidence is mixed. Stitik and Tockman [7] did indeed find that the miss rate decreased from 31% to 18% by double reading, Yerushalmy et al. [8] found it decreased from 32% to 21%, and Guiss and Kuensler [9] showed a decrease from 34% to 25%. At the same time, each of these studies showed that two readers reading the same radiograph disagreed with each other an average of 58% of the time. Hessel et al. [10] found that double reading reduced errors by 37% and increased correct interpretations by 18%. But they also showed that double reading added 19% to the cost of procedures (because of additional time and manpower spent on arbitration of the two different opinions) and that it increased the false-positive diagnoses by 100%. Thus, as a practical or efficient means of reducing error rates among radiologists who practice in a hospital or a private office, double reading is, at best, of dubious value.

The improvement in error rate achieved by repeated reading by the same radiologist also has been called into question. Yerushalmy [4] found that radiologists disagree with their own reading of the same radiographs, made at different times, 21% of the time.

It is logical to assume that accuracy in the clinical setting is improved if the radiologist compares radiographs with previous similar studies and radiologic reports, if a complete patient history accompanies the radiologic request form, and if there is consultation with the referring physician. I know of no data in the literature that specifically support or contradict these assumptions, but Smith [11], in his book on errors in

diagnostic radiology, raised caveats about them. He described in detail how clinical history and laboratory results occasionally may lead the radiologist to draw incorrect conclusions or to overlook pertinent radiographic findings. He also showed how a review of a previous similar radiograph and its accompanying radiologist's report can sometimes cause the radiologist to repeat an error made by a predecessor or to commit a new error.

In view of the published data on radiologic errors, it is doubtful that radiologic misses will ever be significantly lowered, as long as human beings continue to interpret radiographs. However, some basic common sense guidelines can help the radiologist minimize errors. These include (1) acquiring and maintaining an adequate level of knowledge before interpreting specific radiographs, (2) not attempting to interpret radiologic studies in areas in which the radiologist does not feel competent, (3) spending enough time to properly give a complete interpretation, (4) making comparisons with previous radiologic studies and reports, (5) having adequate clinical information, (6) making sure the radiographs are of good quality, and (7) discussing the radiographic findings with the referring physician whenever possible. Following these guidelines cannot ensure elimination of or even a decrease in errors, but not following them most likely will result in an increase.

Malpractice and Risk Management

Many causes of radiologic malpractice litigation other than the missed diagnosis can be minimized if not eliminated. Measures to ensure proper handling and transportation of patients, especially when they are confined to wheelchairs or carts; safe operation and accurate calibration of all radiologic equipment; efficient filing, storage, and retrieval of radiographs and radiologic reports; and effective timely transmission of X-ray reports to referring physicians can be developed and implemented by the radiologist in conjunction with technical and administrative personnel. Special procedure techniques, including the content of explanations and informed consents given to patients, can be reviewed in hopes of reducing complications and misunderstandings. Guidelines about the performance of radiologic procedures in the potentially pregnant patient can be formulated.

Ongoing efforts to educate radiologists on the subject of risk management must be expanded. The American College of Radiology, through its malpractice awareness task force and its publication of the booklet, *Medical Radiation: A Guide to Good Practice*, is participating in this effort. The Radiological Society of North America, by scheduling a course on risk management in radiology at its annual scientific assembly, is also aiding in this educational process. State radiologic organizations, state medical societies, and many hospitals are also devoting much attention to risk-management procedures, which are geared to reducing the causes of malpractice litigation. Such continuing efforts are a high-priority challenge.

Whether good risk-management programs will substantially reduce radiologic malpractice litigation remains to be determined. Already established programs have thus far done little to stem the rising number of malpractice suits. Although the radiologic profession must continue to do its part in reducing the causes of malpractice, the ultimate solution may lie elsewhere. The question of whether every radiologic miss constitutes malpractice is a complex one that has been discussed before [12, 13]. Perhaps the public, through the court system and both federal and state legislatures, must restate the definition of medical malpractice and must realize that ordinary radiologic errors and complications resulting from special procedures should not be construed as malpractice. Perhaps the public must also devise a system of reasonable compensation to injured parties that will not overburden the hospital and medical establishments.

Although it is beyond the scope of this paper to discuss monetary awards arising from these suits, others have done so [13, 14]. Radiologists should keep these accelerating verdict and settlement dollar awards in mind when determining their need for appropriate professional liability coverage. Increasing coverage unfortunately leads to higher insurance premiums, but the malpractice problem extends beyond the actual costs—it touches on the availability of coverage. In some states, Illinois for example, insurance carriers are beginning to deny insurance to physicians who have an unfavorable claims history. Increasing numbers of malpractice suits unavoidably will be accompanied by increasing numbers of radiologists with poor claims histories; this ultimately will have an adverse impact on both the cost and the availability of professional liability insurance.

As can be seen by the precipitous drop in the number of malpractice suits filed in Cook County after August 15, 1985, reform tort legislation holds considerable promise in ultimately alleviating the malpractice quagmire. Eventually, a combination of actions from the legislature, enlightened public attitudes toward malpractice, efforts to minimize misses and complications, and more effective communications with patients may help to curtail permanently the spiraling number of malpractice suits.

Conclusions

Malpractice litigation in Cook County, IL, permeates every aspect of medical practice. Although the percentage of suits involving radiologists seems to have leveled off, if not decreased, the absolute number of radiology-related suits continues to rise. Perhaps as a result of greater sophistication among plaintiffs' attorneys, the types of radiologic procedures called into legal question have been expanded to include CT, sonography, and nuclear medicine examinations. MR imaging cannot be far behind.

Radiologic professional organizations must continue efforts to educate their members on risk management, on ways of reducing litigation exposure, and on how to better defend oneself when sued. Simultaneously, federal and state tort reform legislation seems to be moving slowly forward. In the

meantime, the threat and the reality of malpractice litigation influences virtually every facet of the radiologist's practice. As this report demonstrates, that threat and reality are not likely to diminish soon.

REFERENCES

1. Berlin L. Malpractice and radiologists. *AJR* **1980**;135:587–591
2. Garland LH. On the scientific evaluation of diagnostic procedures. *Radiology* **1949**;52:309–328
3. Garland LH. Studies on the accuracy of diagnostic procedures. *AJR* **1959**;82:25–38
4. Yerushalmy J. The statistical assessment of the variability in observer perception and description of roentgenographic pulmonary shadows. *Radiol Clin North Am* **1969**;7:381–392
5. Herman PG, Gerson DE, Hessel SG, et al. Disagreements in chest roentgen interpretation. *Chest* **1975**;68:278–282
6. Lehr JL, Lodwick GS, Farrell C, Braaten MO, Virtama P, Kolvisto EL. Direct measurement of the effect of film miniaturization on diagnostic accuracy. *Radiology* **1976**;118:257–263
7. Stitik FP, Tockman MS. Radiographic screening in the early detection of lung cancer. *Radiol Clin North Am* **1978**;16:347–366
8. Yerushalmy J, Harkness JT, Cope JH, Kennedy BR. The role of dual reading in mass radiography. *Am Rev Tuberc* **1950**;61:443–464
9. Guiss LW, Kuensler P. A retrospective view of survey photofluorograms of persons with lung cancer. *Cancer* **1960**;13:91–95
10. Hessel SJ, Herman PG, Swensson RG. Improving performance by multiple interpretation of chest radiographs: effectiveness and cost. *Radiology* **1978**;127:589–594
11. Smith MJ. *Error and variation in diagnostic radiology*. Springfield, IL: Thomas, **1967**:23, 24, 41, 42, 75–77
12. Berlin L. Does the "missed" radiographic diagnosis constitute malpractice? *Radiology* **1977**;123:523–527
13. Berlin L. Is a radiologic "miss" malpractice? An ominous example. *AJR* **1983**;140:1031–1034
14. Spring DB, Tennenhouse DJ. Radiology malpractice lawsuits: California jury verdicts. *Radiology* **1986**;159:811–814

MR Imaging and CT of Extrahepatic Cavernous Hemangiomas

Errol Levine[1]
Louis H. Wetzel[1]
James R. Neff[2]

Ten extrahepatic cavernous hemangiomas in seven patients were evaluated by MR and CT. MR was done with a 1.0-T superconducting magnet and spin-echo imaging. The lesions occurred in the musculoskeletal system, parotid gland, and spleen. MR and CT features of hemangiomas were compared, and MR findings in hemangiomas were also compared with those in eight musculoskeletal tumors of nonvascular origin. MR detected 10 hemangiomas, while nine were shown by CT. Also, MR was more accurate than CT in three patients in determining the true extent of hemangiomas. At a pulse-repetition interval of 2000 msec and an echo delay time of 90 msec, all hemangiomas were markedly hyperintense compared with skeletal muscle. Quantitatively, at this pulse sequence, intensity ratios of hemangiomas to skeletal muscle were all seven or greater (mean = 9.89), while the ratios for other tumors were usually less than seven (mean = 5.14). These means differed significantly ($p < .001$). Small cavernous hemangiomas were homogeneous, well-defined round or oval lesions, while large hemangiomas consisted of dilated, tortuous vascular channels. Other tumors, however, were usually heterogeneous owing to hemorrhage and necrosis and had irregular margins. MR may, therefore, be useful for distinguishing cavernous hemangiomas from other soft-tissue tumors, particularly sarcomas.

Cavernous hemangiomas occur commonly in the liver where CT often suggests the correct diagnosis [1, 2]. Recent studies indicate that MR imaging also often permits tissue-specific characterization of liver cavernous hemangiomas [3, 4]. They are usually markedly hyperintense compared with normal liver on MR scans obtained using long pulse-repetition intervals (TRs) and long echo-delay times (TEs) [3, 4]. Cavernous hemangiomas occur in many anatomic sites other than the liver [5], but there is little information about their CT and MR features [6–8]. The present study was done retrospectively to establish the utility of MR in evaluating extrahepatic cavernous hemangiomas and to compare it with CT.

Materials and Methods

During a 6-month period, 10 cavernous hemangiomas occurring in seven patients were studied by MR and CT. CT was the first study in all patients and preceded MR by intervals of 1–26 days. The MR and CT findings were evaluated retrospectively and compared with surgical and pathologic findings. Both studies were interpreted together for each patient with emphasis on determining the ability of MR and CT to establish the diagnosis and to determine the extent of the lesion. We also attempted to determine whether MR could differentiate cavernous hemangiomas from other tumors by evaluating MR features of eight histologically confirmed musculoskeletal tumors of nonvascular origin. They included two malignant fibrous histiocytomas, three neurofibrosarcomas, a chest-wall lymphoma, and soft-tissue components of an osteosarcoma and a chondrosarcoma.

The patients with hemangiomas consisted of six men and one woman aged 12–53 years (mean, 27 years). Most complained of soft-tissue masses. One patient had neurologic symptoms due to extradural extension of a vertebral hemangioma. Lesion locations included the thigh muscles (two), ankle (three in one patient), foot (one), parotid gland (one), fifth

Received June 27, 1986; accepted after revision July 30, 1986.

Presented at the annual meeting of the Society of Computed Body Tomography, Hilton Head, SC, March 1986.

[1] Department of Diagnostic Radiology, 2-169 Bell Memorial Hospital, University of Kansas College of Health Sciences and Hospital, Rainbow Blvd. at 39th St., Kansas City, KS 66103. Address reprint requests to E. Levine.

[2] Department of Surgery, Division of Orthopedic Surgery, University of Kansas College of Health Sciences and Hospital, Kansas City, KS 66103.

AJR **147:1299–1304, December 1986**
0361–803X/86/1476–1299
© American Roentgen Ray Society

thoracic vertebra (one), and abdominal wall (one). The last was associated with a splenic lesion. Six lesions were resected. Surgical biopsies of three lesions were done. All diagnoses were confirmed histologically except for the splenic lesion. This was diagnosed from CT findings of peripheral contrast enhancement and delayed "filling-in" of the lesion [1, 2]. Three lesions were considered histologically to be mixed capillary-cavernous hemangiomas, although the cavernous element always predominated.

All patients had CT scans. Dynamic CT scanning after bolus injections of urographic contrast material was done in three cases. In others, CT was done during rapid IV infusions of 150 ml of 60% meglumine iothalamate. Contiguous sections of 5 to 10 mm were obtained. MR was done in all patients by using a superconducting magnet (Siemens) operated at 1.0 T and multisection spin-echo (SE) imaging. Two pulse sequences were always used, one with a TR of 500 msec and a TE of 30 msec and another with a TR of 2000 msec and TEs of 30 and 90 msec. Two data acquisitions were always averaged for each image. Contiguous sections of 5 or 10 mm were obtained by interleaving. Axial images were always obtained and were supplemented by sagittal or coronal images.

MR intensity measurements of eight of 10 hemangiomas, other tumors, and adjacent skeletal muscle and fat were obtained by using an electronic cursor to define regions of interest. Intensity and other measurements were not obtained for either the splenic lesion or an 8-mm ankle hemangioma in which partial-volume averaging precluded accurate measurements. When possible, all intensity measurements were made with the same x coordinate (i.e., same y axis) to minimize the effects of artifacts. Intensity ratios of cavernous hemangiomas and other tumors to muscle and fat were calculated for all pulse sequences. T1 and T2 relaxation times were measured for eight hemangiomas and all other tumors by using commercially available scanner software. MR images were evaluated for flow-related effects such as flow enhancement and high-velocity signal loss. The mean intensity ratios (Table 1) and mean T1 and T2 relaxation times for hemangiomas and other tumors were compared by using the two-sample t test.

Results

Six hemangiomas were 2 cm or smaller (mean size, 1.6 cm; range, 0.8–2 cm in maximum dimension), while four measured 5.3, 6.2, 8.3, and 15.6 cm, respectively, in the long axes.

CT identified nine of 10 hemangiomas. An ankle lesion measuring 8 mm was not detected. Three cavernous hemangiomas contained phleboliths that were shown by CT but not by MR (Fig. 1). On CT, all hemangiomas showed variable degrees of contrast enhancement. Of five lesions measuring 2 cm or less, two showed diffuse enhancement similar in degree to that in adjacent large blood vessels (Fig. 2), while three showed denser peripheral enhancement (Fig. 3). Two of four large hemangiomas exhibited enhancing tubular vascular structures (Fig. 4), while two showed no definite vessels (Fig. 1). One of the latter, a vertebral hemangioma, was suspected on CT from prominent vertical trabeculae seen in cross section in the vertebral body with a nonspecific extradural mass. On CT, the smaller hemangiomas were round or oval and had smooth, well-defined contours (Figs. 2 and 3). The larger lesions had poorly defined interfaces with adjacent tissues and irregular contours in three patients (Figs. 1 and 4).

Hemangiomas showed consistent MR appearances at various SE pulse sequences. Visually, they were slightly or somewhat more intense than skeletal muscle on SE images obtained at TR = 500 msec, TE = 30 msec (Fig. 3). Hemangiomas were usually considerably more intense than muscle on SE 2000/30 images (Fig. 1), but were markedly hyperintense compared with muscle on SE 2000/90 images (Figs. 1–4). Hemangiomas were usually significantly less intense than fat on SE 500/30 images (Fig. 3) and were slightly less intense than fat on SE 2000/30 images (Fig. 1). The lesions were somewhat more intense than fat on SE 2000/90 images (Figs. 1–4). Consequently, the best contrast between hemangiomas and surrounding tissues was obtained at the TR = 2000 msec, TE = 90 msec pulse sequence. Other tumors showed similar findings but were usually not as hyperintense compared with muscle and fat on SE 2000/90 images.

Of the various means calculated, only the mean lesion/muscle ratios obtained at TR = 2000, TE = 90 msec differed significantly for hemangiomas and other tumors ($p < .001$) (Table 1). The intensity ratios of hemangiomas to skeletal muscle were all seven or greater, while the ratios for other tumors were less than seven, except for a neurofibrosarcoma, which had a ratio of nine. The mean T1 relaxation time for hemangiomas was 1725 msec (SD, 558; range, 983–2745 msec), while the mean T1 value for other tumors was 1273 msec (SD, 415; range, 743–2151 msec). The mean T2 relaxation time for hemangiomas was 128 msec (SD, 40; range, 89–212 msec), while the mean T2 value for other tumors was 99 msec (SD, 34; range, 73–157 msec). These means did not differ significantly ($p > .05$, two-sample t test).

The smaller hemangiomas were homogeneous in appearance at all pulse sequences, were round or oval in shape, and had smooth, well-defined contours (Figs. 2 and 3). The larger

TABLE 1: **Mean MR Intensity Ratios of Cavernous Hemangiomas and Other Tumors to Muscle and Fat at Different Pulse Sequences**

Pulse Sequences	Cavernous Hemangiomas ($n = 8$)				Other Tumors ($n = 8$)			
	Lesion/Muscle		Lesion/Fat		Lesion/Muscle		Lesion/Fat	
	Mean (SD)	Range	Mean (SD)	Range	Mean (SD)	Range	Mean (SD)	Range
TR 500/TE 30 msec	1.55 (0.01)	1.4–1.6	0.39 (0.01)	0.2–0.5	1.31 (0.57)	0.8–2.6	0.33 (0.01)	0.2–0.5
TR 2000/TE 30 msec	1.99 (0.37)	1.6–2.6	0.86 (0.19)	0.5–1.2	1.79 (0.31)	1.4–2.4	0.64 (0.18)	0.3–0.9
TR 2000/TE 90 msec	9.89[a] (2.08)	7.0–12.9	2.21 (1.16)	1.2–4.8	5.14[a] (1.81)	3.6–9.0	1.41 (0.42)	0.8–1.8

Note.—TR = repetition time; TE = echo time.
[a] p value for difference between means <.001, two-sample t test.

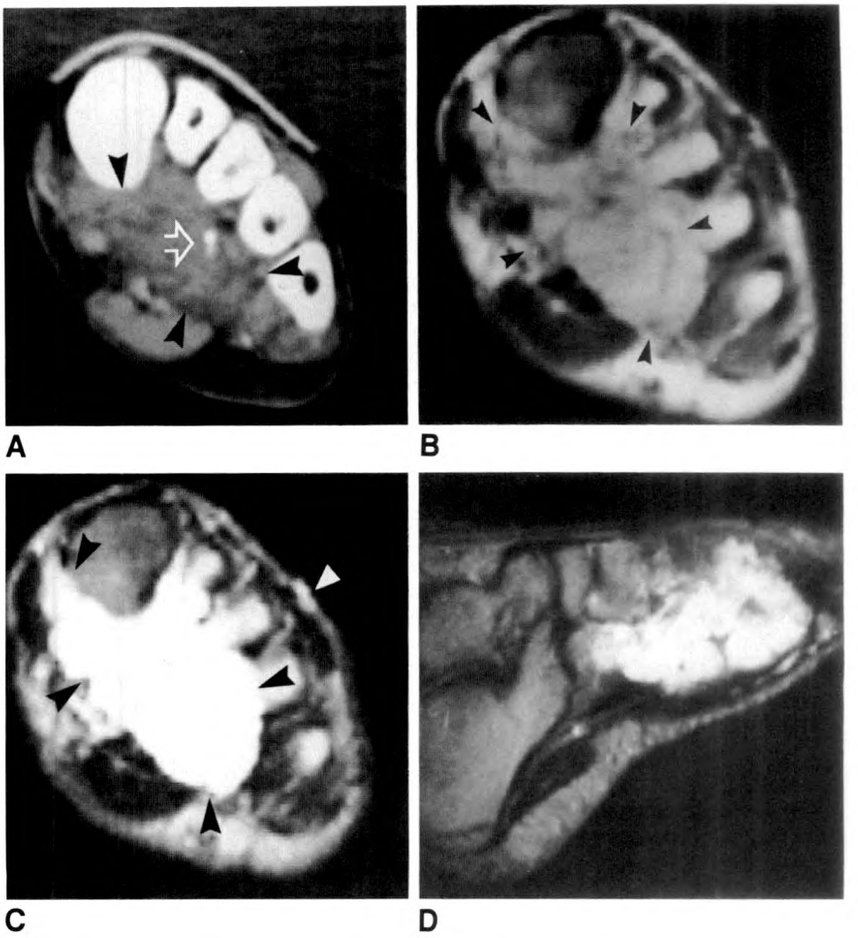


Fig. 1.—Cavernous hemangioma of foot.

A, CT shows deep mass (*arrowheads*) between metatarsals and plantar muscles. Demarcation between tumor and muscle is not clearly defined. Note calcified phleboliths (*arrow*).

B, MR (TR 2000/TE 30) reveals that hemangioma (*arrowheads*) is significantly more intense than muscle, but only slightly less intense than fat.

C, MR (TR 2000/TE 90) exhibits markedly hyperintense appearance of hemangioma (*black arrowheads*). Lesion is more intense than both fat and muscle and has high signal intensity similar to superficial veins (*white arrowhead*). True extent of hemangioma is well displayed because of high contrast.

D, Extent of hemangioma is well demonstrated on sagittal MR image (TR 2000/TE 90). Hemangioma is composed of large tortuous vascular structures separated by low-intensity fibrous connective tissue stroma.

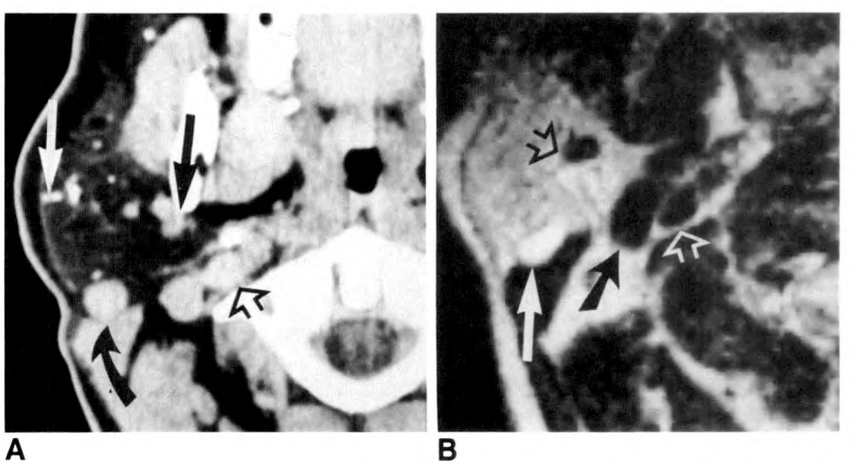


Fig. 2.—Cavernous hemangioma of right parotid gland.

A, Contrast-enhanced CT shows well-defined, homogeneously enhancing lesion (*curved arrow*) with smooth contour located posteriorly in parotid gland anterior to sternocleidomastoid muscle. Note contrast material in parotid duct (*white arrow*) from sialogram. Internal jugular vein (*open arrow*), junction of maxillary and superficial temporal veins (*straight black arrow*).

B, MR (TR 2000/TE 90) exhibits well-defined, markedly hyperintense, homogeneous parotid nodule (*solid white arrow*). Junction of superficial temporal and maxillary veins (*open black arrow*), posterior belly of digastric muscle (*solid black arrow*), internal jugular vein (*open white arrow*).

lesions were composed of dilated, tortuous vascular structures separated by low-intensity linear structures and had somewhat irregular margins (Figs. 1 and 4). Of eight other tumors, only two were homogeneous at all pulse sequences. The rest displayed heterogeneous internal architectures caused by areas of hemorrhage and necrosis, and all had poorly defined, irregular margins.

The intensities of hemangiomas could be compared with those of adjacent veins in six patients. In four, hemangiomas and adjacent peripheral veins showed similar high signal

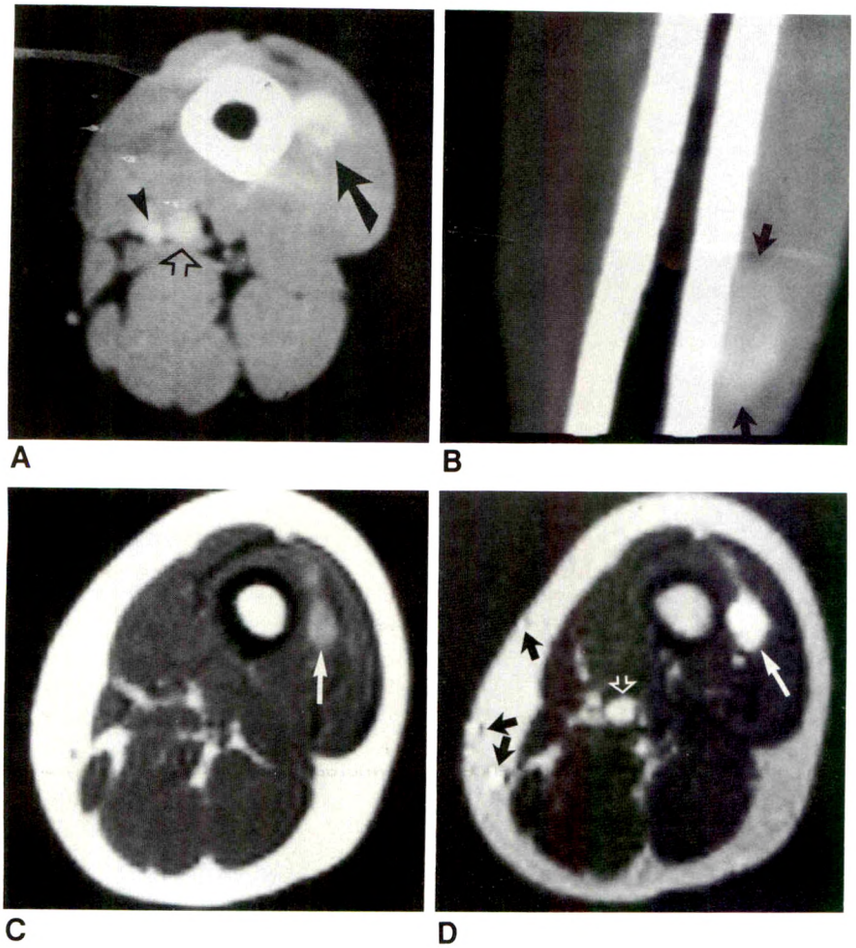


Fig. 3.—Intramuscular cavernous hemangioma of thigh.

A, Contrast-enhanced CT shows juxtafemoral lesion (*solid arrow*) in left vastus lateralis and vastus intermedius muscles. Lesion demonstrates degree of enhancement similar to popliteal artery (*arrowhead*) and vein (*open arrow*).

B, Coronal reconstructed CT image displays denser peripheral enhancement in hemangioma (*arrows*).

C, MR (TR 500/TE 30) shows that hemangioma (*arrow*) is more intense than surrounding muscle.

D, MR (TR 2000/TE 90) reveals that hemangioma (*solid arrow*) is hyperintense compared with muscle and fat and has a signal intensity similar to that in popliteal vein (*open arrow*) and subcutaneous saphenous veins (*black arrows*).

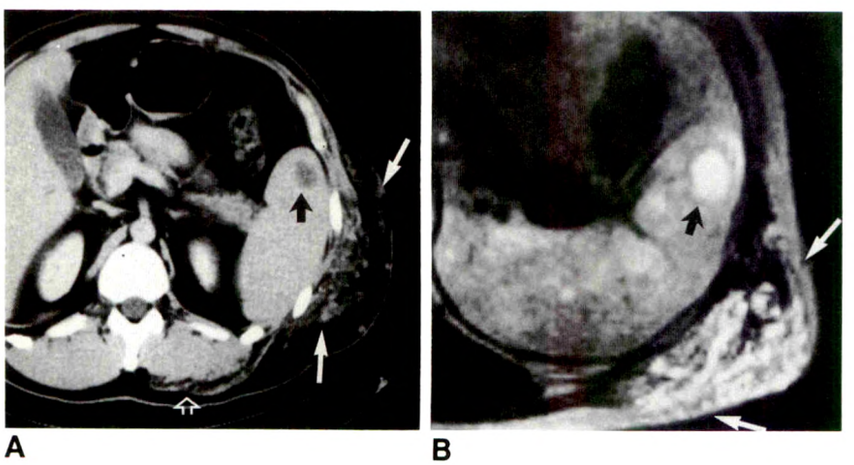


Fig. 4.—Cavernous hemangioma of abdominal wall and spleen.

A, Contrast-enhanced CT scan shows dilated tortuous vascular channels (*white arrows*) in subcutaneous tissues of left lateral abdominal wall. Lesion extends deeply to involve muscles and posteriorly to involve left erector spinae muscle (*open arrow*). Focal splenic lesion (*black arrow*) shows peripheral contrast enhancement.

B, MR (TR = 2000/TE = 90) shows hyperintense appearance of dilated vascular channels separated by low-intensity connective tissue stroma (*white arrows*). Muscular extension is well shown. Splenic lesion (*black arrow*) also exhibits hyperintense appearance.

intensities at the TR = 2000 msec, TE = 90 msec pulse sequence (Figs. 1 and 3). In two patients (with parotid and abdominal wall lesions), adjacent large veins such as the internal jugular vein (Fig. 2) and inferior vena cava showed no signal. Five peripheral tumors in the comparison group showed lower intensities than adjacent veins at the TR = 2000 msec, TE = 90 msec pulse sequence.

CT and MR gave similar information about the extent of hemangiomas in seven of 10 lesions (Figs. 2 and 3). In three large lesions, MR gave a better indication than CT of the

extent of hemangiomas and their relationships to adjacent structures. This resulted from greater contrast between hemangiomas and adjacent structures such as muscles on MR (Figs. 1 and 4) and from the ability of MR to provide direct sagittal and coronal images (Fig. 1).

Discussion

Cavernous hemangiomas are found most often in the liver, where they occur with reported frequencies of 0.4–7.3% in autopsy series [9]. They also occur commonly in skeletal muscle, where they vary from small to extensive lesions [10–12]. Deep intramuscular cavernous hemangiomas are difficult to diagnose clinically and may be confused with soft-tissue sarcomas [11, 12]. Hemangiomas occur less commonly in bone [5], salivary glands [13], and spleen [14].

Diagnosis of cavernous hemangiomas is important, since the lesions are always benign [12]. Consequently, surgical resection is often reserved for only large, symptomatic liver and musculoskeletal lesions [3, 12]. If resection is required, precise preoperative determination of lesion extent is necessary because, despite their benign nature, soft-tissue cavernous hemangiomas frequently extend insidiously across the normal tissue barriers to tumor growth [12]. Incomplete resection is almost invariably followed by recurrence [12]. Sometimes, preoperative radiologic studies may indicate that a lesion is so extensive that definitive surgery would be markedly disabling and therefore unwarranted [12].

Conventional radiographs may help in the diagnosis of hemangiomas by showing phleboliths [12]. However, phleboliths occurred in only 30% of lesions in our series. Also, conventional radiography does not show the size or extent of hemangiomas. Arteriography often shows that peripheral hemangiomas are composed of tortuous dilated vessles [6, 15], but differentiation between hemangiomas and malignant soft-tissue tumors is not always possible [15]. Moreover, angiography does not usually show the relationship of lesions to adjacent structures well enough to allow accurate surgical planning [6, 12]. Accordingly, the role of angiography is limited to identification of major feeding vessels for planning surgical or embolic therapy [6].

CT and MR are useful in evaluating cavernous hemangiomas [1, 2, 6]. In our present study, MR was slightly more sensitive than CT in detecting hemangiomas. Small hemangiomas may be suspected on CT if they show peripheral (Fig. 3) or diffuse (Fig. 2) contrast enhancement similar to that of adjacent blood vessels. Larger lesions may be diagnosed from the presence of phleboliths (Fig. 1), which are not shown by MR, and the presence after contrast enhancement of punctate or curvilinear structures that have attenuation values similar to nearby vessels (Fig. 4) [6]. However, unless IV bolus contrast injections and dynamic scanning are used, hemangiomas may not be distinguishable from other soft-tissue tumors on CT [6].

On MR, hemangiomas appear markedly hyperintense compared with skeletal muscle on images obtained at long TR and TE intervals (Figs. 1–4). Small lesions are homogeneous in appearance and have smooth, well-defined contours (Figs. 2 and 3). Larger lesions exhibit dilated vascular channels separated by low-intensity linear structures probably representing loose fibrous connective tissue stroma (Figs. 1 and 4) [16]. They do not usually show heterogeneity of the internal architecture or markedly irregular margins seen in malignant soft-tissue tumors. However, cavernous hemangiomas may manifest a spectrum of histopathologic changes including hemorrhage, thrombosis, extensive hyalinization, and hemosiderin and mineral deposits [17, 18]. These histologic changes may affect CT [17, 18] and MR appearances by causing heterogeneity. Consequently, confusion between hemangiomas and malignant tumors sometimes occurs on both CT and MR [3, 4, 17, 18].

Quantification of T1 and T2 relaxation rates is not useful in characterizing hemangiomas. However, the intensity ratio of hemangioma to skeletal muscle at the TR = 2000 msec, TE = 90 msec pulse sequence is useful in diagnosis. In our system operated at 1.0 T, hemangiomas always had ratios of seven or greater. Only one other tumor had a ratio greater than seven, but this lesion was also heterogeneous in appearance and had an irregular margin. Accordingly, both morphologic and quantitative features may help in distinguishing hemangiomas from other soft-tissue tumors.

MR also helps distinguish cavernous hemangiomas from arteriovenous malformations [19]. Rapid flow in the enlarged vessels of these lesions causes high-velocity signal loss at all pulse sequences [19], whereas hemangiomas typically show increased signal intensity on T2-weighted images. We did not study any malignant tumors of vascular origin such as hemangiopericytomas or hemangioendotheliomas. To our knowledge, their MR features have not been described. However, on CT, malignant soft-tissue hemangiopericytomas differ from cavernous hemangiomas in that they usually consist of large, lobular masses with areas of cystic degeneration and hemorrhage [20]. Hemangioendotheliomas affect bones more often than soft tissues and generally have obvious malignant features on conventional radiography [12]. It is therefore unlikely that these rare tumors will be confused with hemangiomas on MR.

Both MR and CT are useful in determining the true extent of hemangiomas. However, MR was more accurate than CT in this respect in three patients in our study because of the greater contrast between lesions and adjacent structures on T2-weighted images and the ability of MR to provide direct sagittal and coronal images. MR provides excellent delineation of the relationships of hemangiomas to specific muscle groups, fascial planes, and blood vessels and therefore facilitates planning of curative surgery.

It is likely that the marked hyperintensity of cavernous hemangiomas compared with muscle at the TR = 2000 msec, TE = 90 msec pulse sequence is related to slow blood flow known to occur in these lesions [16]. The similar intensities of peripheral hemangiomas and adjacent small veins at this pulse sequence in some of our patients supports this hypothesis (Figs. 1 and 3) [21]. Hemangiomas in locations such as the parotid gland and abdominal wall showed much higher signal intensities than did the internal jugular vein (Fig. 2) and inferior vena cava, which had signal voids probably because of high-velocity blood flow [21].

In summary, cavernous hemangiomas often manifest distinctive findings on MR and CT that permit their differentiation from other soft-tissue lesions such as sarcomas. This is important prognostically and therapeutically since cavernous hemangiomas are always benign. However, since atypical liver hemangiomas may be confused with malignant lesions on MR [3, 4] and CT [17], it is likely that similar difficulties sometimes will be encountered with extrahepatic hemangiomas. It is also possible, that as with a neurofibrosarcoma in our series, sarcomas sometimes may have features found in hemangiomas. Our series is small and our results require validation by studies of larger series of patients with hemangiomas and sarcomas.

REFERENCES

1. Freeny PC, Vimont TR, Barnett DC. Cavernous hemangioma of the liver: ultrasonography, arteriography and computed tomography. *Radiology* **1979**;132:143–148
2. Johnson CM, Sheedy PF, Stanson AW, Stephens DH, Hattery RR, Adson MA. Computed tomography and angiography of cavernous hemangiomas of the liver. *Radiology* **1981**;138:115–121
3. Glazer GM, Aisen AM, Francis IR, Gyves JW, Lande I, Adler DD. Hepatic cavernous hemangioma: magnetic resonance imaging. *Radiology* **1985**;155:417–420
4. Stark DD, Felder RC, Wittenberg J, et al. Magnetic resonance imaging of cavernous hemangioma of the liver: tissue-specific characterization. *AJR* **1985**;145:213–222
5. Watson WL, McCarthy WD. Blood and lymph vessel tumors. Report of 1056 cases. *Surg Gynecol Obstet* **1940**;71:569–588
6. Rauch RF, Silverman PM, Korobkin M, et al. Computed tomography of benign angiomatous lesions of the extremities. *J Comput Assist Tomogr* **1984**;8:1143–1146
7. Moon KL, Genant HK, Helms CA, Chafetz NI, Crooks LE, Kaufman L. Musculoskeletal applications of nuclear magnetic resonance. *Radiology* **1983**;147:161–171
8. Augustyn GT, Scott JA, Olson E, Gilmor RL, Edwards MK. Cerebral venous angiomas: MR imaging. *Radiology* **1985**; 156:391–395
9. Ishak KG, Rabin L. Benign tumors of the liver. *Med Clin North Am* **1975**;59:995–1013
10. Allen PW, Enzinger FM. Hemangioma of skeletal muscle: an analysis of 89 cases. *Cancer* **1972**;29:8–22
11. Fergusson ILC. Hemangiomata of skeletal muscle. *Br J Surg* **1972**;59:634–637
12. Enneking WF. *Musculoskeletal tumor surgery*, vol 2. New York: Churchill Livingstone, **1983**:1175–1223
13. Nussbaum M, Tan S, Som ML. Hemangiomas of the salivary glands. *Laryngoscope* **1976**;86:1015–1019
14. Moss CN, Van Dyke JA, Koehler RE, Smedberg CT. Multiple cavernous hemangiomas of the spleen: CT findings. *J Comput Assist Tomogr* **1986**;10:338–340
15. Levin DC, Gordon DH, McSweeney J. Arteriography of peripheral hemangiomas. *Radiology* **1976**;121:625–630
16. Olmsted WW, Stocker JT. Cavernous hemangioma of the liver. *Radiology* **1975**;117:59–62
17. Takayasu K, Moriyama N, Shima Y, et al. Atypical radiographic findings in hepatic cavernous hemangioma: correlation with histologic features. *AJR* **1986**;146:1149–1153
18. Ahmadi J, Miller CA, Segall HD, Park SH, Zee CS, Becker RL. CT patterns in histopathologically complex cavernous hemangiomas. *AJNR* **1985**;6:389–393
19. Cohen JM, Weinreb JC, Redman HC. Arteriovenous malformations of the extremities: MR imaging. *Radiology* **1986**;158:475–479
20. Alpern MB, Thorsen MK, Kellman GM, Pojunas K, Lawson TL. CT appearance of hemangiopericytoma. *J Comput Assist Tomogr* **1986**;10:264–267
21. Bradley WG, Waluch V, Lai KS, Fernandez EJ, Spalter C. The appearance of rapidly flowing blood on magnetic resonance images. *AJR* **1984**;143:1167–1174

Case Report

Multiple Granular Cell Tumors of the Skin and Gastrointestinal Tract

D. Randall Radin,[1] Richard Zelner,[2] Marilyn J. Ray,[1] Hartley Cohen,[2] and James M. Halls[1]

Granular cell tumors are uncommon lesions of probable Schwann cell origin [1]. In the past they were called granular cell myoblastoma because of suspected muscle origin [2]. Almost always benign, granular cell tumors are found in patients of all ages, from 4 months to 79 years, with approximately equal frequency in both sexes [2–4]; there appears to be a relatively greater prevalence in blacks than in whites [3]. Although almost any organ may be involved, 70–80% of granular cell tumors appear as small asymptomatic masses in the skin, subcutaneous tissue, or mouth (particularly on the tongue) [2, 3]. Only 5–7% of these lesions are detected in the gastrointestinal tract [3]. Seven to 16% of affected patients have two or more tumors, usually in a single organ but occasionally involving several organs [2, 3, 5]. We wish to report an unusual patient with granular cell tumors of the skin, esophagus, stomach, colon, and perianal region who had gastrointestinal hemorrhage.

Case Report

A 51-year-old black woman complained of epigastric pain, nausea, vomiting, and melena. Firm, mobile cutaneous nodules 1 cm in diameter were palpated on her left anterior chest wall and left wrist. She reported that she had undergone excision of several similar nodules and had been told that they were benign. After transfusion with two units of packed RBCs to raise her hematocrit to 27%, upper endoscopy was performed. A small extramucosal mass was detected in the distal esophagus, and a 4-cm mass with a deep central ulceration was seen on the greater curvature of the body of the stomach. Biopsy specimens of the gastric lesion showed acute and chronic inflammatory changes. Both lesions were seen on findings of an upper gastrointestinal series (Figs. 1A and 1B). The patient underwent subtotal gastrectomy and gastrojejunostomy. A 3-cm mass in the transverse colon was discovered incidentally during surgery, and segmental resection with primary anastomosis was performed. Pathologic examination revealed that both lesions were granular cell tumors. The gastric mass was located in the submucosa; the colonic mass arose in the muscularis. Subsequent CT showed two cutaneous nodules in the vulva and the perianal region that had escaped detection on initial physical examination (Fig. 1C). In addition, an intraluminal polypoid mass 2–3 cm in diameter was noted in the ascending colon. This was confirmed by barium enema (Fig. 1D). The mucosa overlying this pedunculated mass was intact at colonoscopy. The polyp was removed with an electrosurgical snare but, unfortunately, was lost before histologic examination.

Discussion

Granular cell tumors occur as intramural lesions throughout the gastrointestinal tract. In 1981, Johnston and Helwig [4] reported 74 cases and reviewed an additional 66 cases in the world literature. These tumors were distributed as follows: esophagus, 30%; stomach, 19%; small bowel, 2%; appendix, 3%; colon, 23%; and perianal region, 23%. Twelve percent of their patients had several granular cell tumors occurring either in the same area of the bowel or in other organs, most commonly the skin.

Coutinho et al. [6] reviewed 117 cases of granular cell

Received May 14, 1986; accepted after revision July 1, 1986.

[1] Department of Radiology, University of Southern California School of Medicine, Los Angeles County–USC Medical Center, 1200 N. State St., Los Angeles, CA 90033. Address reprint requests to D. R. Radin.

[2] Department of Medicine, Gastroenterology Section, University of Southern California School of Medicine, Los Angeles, CA 90033.

AJR 147:1305–1307 0361–803X/86/1476–1305 © American Roentgen Ray Society

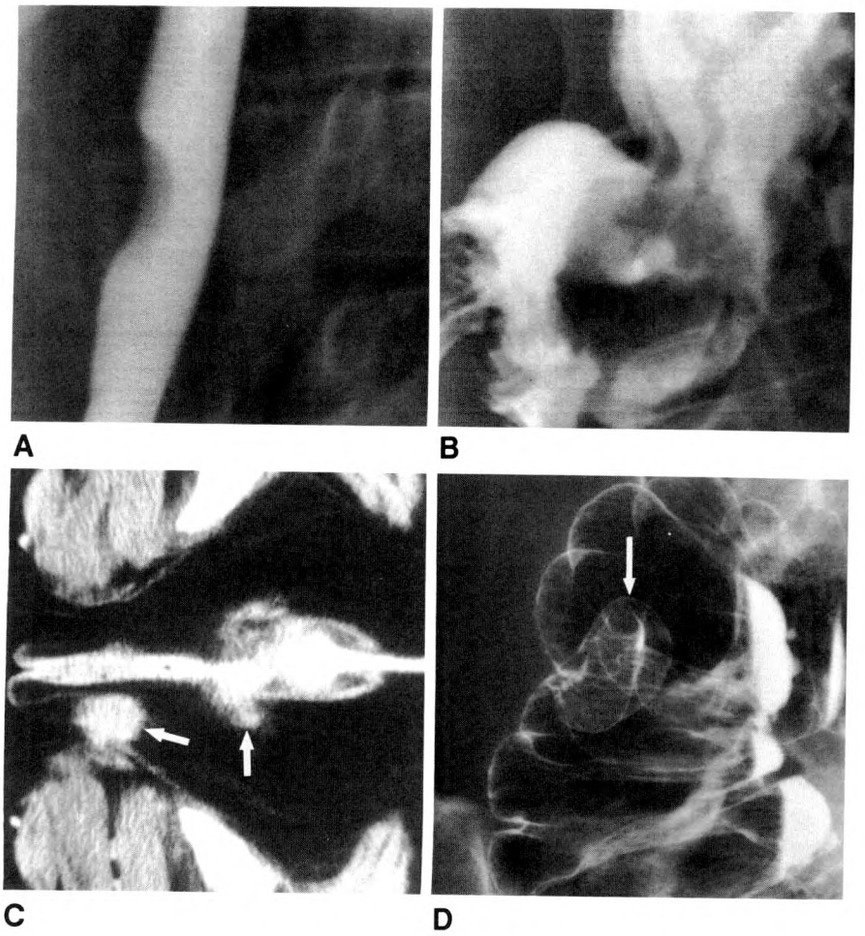


Fig. 1.—*A*, Spot film of distal esophagus. Small extramucosal mass on anterolateral wall.
***B*, Spot film of body of stomach. Large polypoid filling defect with central ulceration.**
***C*, CT scan of perineum. Two small soft-tissue nodules (*arrows*) in right labium majus and perianal region.**
***D*, Spot film of hepatic flexure. Polypoid mass (*arrow*) arising from posterolateral wall.**

tumor of the esophagus reported in the world literature through December 1984 and added two cases of their own. Age of the patients was 19 to 72 years, with an average in the early 40s. Men outnumbered women by almost 2 to 1, and a relatively high prevalence was found in blacks. Symptoms were present in approximately 50% of patients and occurred more frequently with larger lesions. Dysphagia was the most common symptom, followed by upper abdominal pain and thoracic pain. Sixty-three percent of the tumors were located in the lower esophagus, 19% in the middle, and 18% in the upper. Most were less than 2 cm in diameter; only four were larger than 4 cm. Malignant changes were described in four cases (3%). The nonspecific radiographic appearance of a small extramucosal esophageal mass, as seen in our patient, was typical.

We are aware of literature reports of 36 patients with granular cell tumors of the stomach [1, 4, 7–9]. The age distribution of these patients was almost identical to that of patients with esophageal involvement. However, there was a reversal of the sex ratio, with a 2:1 female preponderance among patients with gastric lesions. At least half of the patients were black. The gastric tumor was an incidental finding in one-third of the patients. Symptomatic patients were clinically suspected of having peptic ulcer disease, as was our patient. Epigastric pain occurred in 75%, vomiting in 25%, and gastrointestinal bleeding in 20%. The tumors occurred more commonly on the lesser curvature. As with esophageal lesions, about 80% of gastric granular cell tumors were less than 2 cm in diameter, with only a few greater than 4 cm. No malignant granular cell tumor of the stomach has been reported. These tumors appeared radiographically as intramural gastric masses, occasionally with ulceration of the overlying mucosa. Two or more gastric lesions were present in 15–20% of the patients reported. Eleven percent of patients had granular cell tumors elsewhere in the gastrointestinal tract, and 17% had extraintestinal lesions, usually cutaneous or subcutaneous.

Johnston and Helwig [4] reported on 20 patients with granular cell tumors of the colon and reviewed an additional 12 cases from the literature. These patients averaged 47 years of age (range, 17–79) and were evenly divided by gender. A disproportionately large number were black. Although a few patients had rectal bleeding or discomfort attributable to the granular cell tumor, most of the lesions were discovered incidentally on rectal examination or barium enema. The cecum and rectosigmoid were the most frequent

sites. Twenty percent had several colonic lesions, and 6% had a concurrent gastric granular cell tumor. All of the colonic tumors were small benign submucosal masses. The right colonic lesion in our patient was radiographically indistinguishable from an adenomatous polyp. However, its submucosal location was evident at colonoscopy.

Although uncommon, granular cell tumor should be included in the differential diagnosis of an intramural mass in the gastrointestinal tract. Major surgical resection is probably unnecessary when a small asymptomatic submucosal tumor is detected in the esophagus, stomach, or colon of a patient with a history of histologically proven granular cell tumor of the skin or gastrointestinal tract.

REFERENCES

1. Seo IS, Azzarelli B, Warner TF, Goheen MP, Senteney GE. Multiple visceral and cutaneous granular cell tumors. *Cancer* **1984**;53:2104–2110
2. Strong EW, McDivitt RW, Brasfield RD. Granular cell myoblastoma. *Cancer* **1970**;25:415–422
3. Lack EE, Worsham GF, Callihan MD, et al. Granular cell tumor: a clinicopathologic study of 110 patients. *J Surg Oncol* **1980**;13:301–316
4. Johnston J, Helwig EB. Granular cell tumors of gastrointestinal tract and perianal region: a study of 74 cases. *Dig Dis Sci* **1981**;26:807–816
5. Rubesin S, Herlinger H, Sigal H. Granular cell tumors of the esophagus. *Gastrointest Radiol* **1985**;10:11–15
6. Coutinho DS, Soga J, Yoshikawa T, et al. Granular cell tumors of the esophagus: a report of two cases and review of the literature. *Am J Gastroenterol* **1985**;80:758–762
7. Abdelwahab IF, Klein MJ. Granular cell tumor of the stomach: a case report and review of the literature. *Am J Gastroenterol* **1983**;78:71–76
8. Fried KS, Arden JL, Gouge TH, Balthazar EJ. Multifocal granular cell tumors of the gastrointestinal tract. *Am J Gastroenterol* **1984**;79:751–755
9. Chen KTK. Multifocal benign granular cell tumor of the stomach. *J Clin Gastroenterol* **1981**;3[Suppl 1]:65–67

Tailgut Cyst: Diagnosis With CT and Sonography

Alan R. Johnson[1,2]
Pablo R. Ros[2,3]
Brent M. Hjermstad[4]

Tailgut cyst is a rare congenital lesion that presents as a presacral mass, found in infancy or persisting undetected into adulthood, and characterized by multiple cysts lined with a gastrointestinal type of epithelium. In a retrospective review of five patients whose ages ranged from 1 month to 42 years—three cases with CT and two with sonograms—tailgut cyst appeared as a complex mass on both procedures, representing its composition of multiple small cysts filled with keratinous material and other debris. Other CT and sonographic features include well-defined borders, and, in one case, presentation as a mass lateral to the midline. CT also shows preservation of adjacent fat planes. Tailgut cyst should be included in the differential diagnosis of a retrorectal mass at any age.

Tailgut cyst, or retrorectal cystic hamartoma, is a rare congenital lesion that typically occurs between the rectum and the sacrum. It is thought to arise from a vestige of the embryonic hindgut and is characterized by multiple cysts lined by a variety of intestinal types of epithelium, most often a columnar epithelium [1]. Squamous and transitional epithelia are also common.

Tailgut cyst has been described in the surgical and pathologic literature [2, 3], but only its appearance on barium enema examination has been noted in the radiologic literature [1]. We describe the radiographic findings in five patients with this abnormality (four with CT and/or sonography, one with barium enema alone), and correlate the radiographic and pathologic abnormalities.

Materials and Methods

The clinical history, imaging studies, and pathology specimens of five patients with tailgut cyst (on file at the Radiologic Pathology Registry of the Armed Forces Institute of Pathology) were retrospectively reviewed. Four patients were imaged with CT or sonography: two had only pelvic CT, one had only a pelvic sonogram, and one had both studies. One patient, an infant, had only a barium enema. The CT scans were performed with both oral and IV contrast and with 10-mm slice thickness.

Results

The four patients evaluated by CT or sonography averaged 32 years old (range, 17–42 years). The fifth patient, a 1-month-old infant evaluated only by barium enema, is included to emphasize that this abnormality can be found in children. Of the adult patients, three were women and one was a man. Two patients presented with an asymptomatic retrorectal mass incidentally found at physical exam, and the other two presented with rectal fullness or pain, accompanied by change in bowel habits. Barium enema showed an extrinsic retrorectal mass in each case.

In all three cases imaged by CT, a well-defined homogeneous retrorectal mass appeared. Adjacent fat planes were preserved, and the mass smoothly indented the rectum. No sacral destruction or defect was seen. In two cases, the mass lay

Received June 9, 1986; accepted after revision July 25, 1986.

The opinions or assertions contained herein are those of the authors and should not be construed as being official or as necessarily reflecting the views of the Department of the Navy, Army or Air Force or of the Department of Defense.

[1] Imaging Section, Department of Radiology, Naval Medical Center, National Capital Region, Bethesda, MD 20814.

[2] Department of Radiology, Uniformed Services University of Health Sciences, Bethesda, MD 20814.

[3] Section of Gastrointestinal Radiology, Department of Radiologic Pathology, Armed Forces Institute of Pathology, Washington, DC 20360-6000. Address reprint requests to P. R. Ros.

[4] Department of Gastrointestinal Pathology, Armed Forces Institute of Pathology, Washington, DC 20306.

AJR 147:1309–1311, December 1986
0361–803X/86/1476-1309
© American Roentgen Ray Society

in the midline, and in the third case the mass lay to the right of the midline, displacing the rectum to the left. In one case, the mass exhibited a density similar to that seen in an adjacent ovarian cyst, and had an attenuation value of 22 H (Fig. 1). A second case also had a density near that of water, although an attenuation value was not calculated. In a third case, the mass had a density similar to that of adjacent solid pelvic organs and an attenuation of 39 H (Fig. 2).

By sonography, one case showed a round retrorectal mass with a well-defined back wall but with low-level internal echoes and no obvious increase through transmission of sound. The second case had low-level internal echoes and minimal increase through transmission of sound, but no well-defined back wall (Fig. 3).

In each case the appearance of a discrete well-defined mass with no evidence of invasion of contiguous structures was confirmed at surgery. The gross pathologic evaluation showed each mass to be composed of many small cysts containing keratinous or mucoid debris. In the case in which CT showed a homogeneous mass with a density near that of water, a single dominant cyst was found with the other smaller cysts identified only by microscopic examination of the wall. In all cases, microscopic examination showed the typical gastrointestinal epithelia that establishes the diagnosis of tailgut cyst. An inflammatory infiltrate was noted in the cyst wall in two cases.

Discussion

Tailgut cyst is a rare congenital lesion thought to arise from vestiges of the embryonic hindgut and found in the presacral (retrorectal) space. Microscopically, it contains a variety of epithelia but always some elements of intestinal epithelium. Squamous, simple, and stratified columnar cells (mucus-secreting, ciliated, and goblet types) and transitional and cuboidal cells may be encountered, often in combination. The lining is usually flattened and does not have a complex structure with villi and crypts, as seen in normal bowel. An incomplete muscle layer is often associated with the cyst wall [2, 3].

Grossly, tailgut cyst is a multiloculated cystic mass, usually adherent to sacrum or rectum. If uninfected, it is usually thin walled with a glistening lining and is filled with a mucoid material. Infection or inflammation may cause fibrosis of the cyst wall and breakdown of the cyst lining. Such changes are seen in about half of all cases. The entire mass usually measures several cm in diameter [2].

Early in development, the embryo possesses a true tail and the primitive hindgut extends into this tail caudal to the point of subsequent formation of the anus. The caudal extension is called the postanal gut or tailgut (Fig. 4). The tail and tailgut normally involute by the eighth week of embryonic development. If tailgut remnants persist, they may give rise to a tailgut cyst [3, 5].

Tailgut cyst is more common in women and usually presents in middle age, but it can be detected at any age, including infancy. The lesion is usually detected as an asymptomatic mass during physical examination or at childbirth. Tailgut cyst may also come to medical attention when it becomes infected, at which time it may be misdiagnosed as a pilonidal cyst or anorectal fistula. A common history is that of recurring retrorectal abscesses or repeated surgical procedures for anal fistulae [3]. Several cases of malignant degeneration have been documented in the literature; however, this is a rare complication [2, 4].

CT examination shows a discrete well-marginated retrorectal mass with CT numbers varying from water to soft-tissue density (Figs. 1 and 2). The small cysts within the center of the tailgut cyst and the keratinous or inflammatory debris may account for the solid appearance seen in some cases and the Hounsfield numbers in the soft-tissue range. The presence of

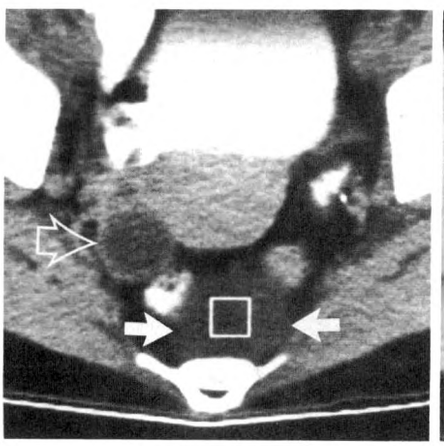


Fig. 1.—Well-defined hypodense pelvic mass (*white arrows*) suggestive of cyst. Incidentally noted right ovarian cyst (*open arrow*).

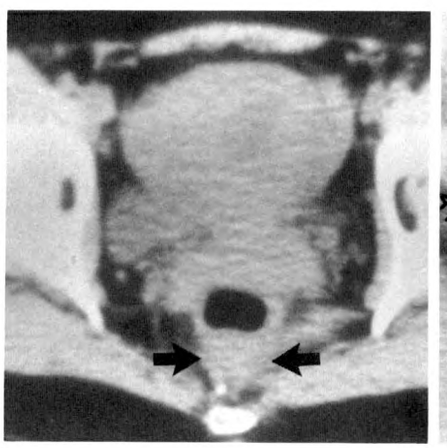


Fig. 2.—Homogeneous retrorectal mass (*arrows*). Density of mass similar to that of solid pelvic organs such as uterus.

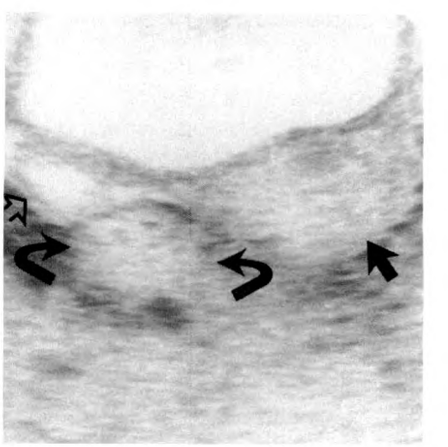


Fig. 3.—Transverse pelvic sonogram. Complex retrorectal mass with minimal through transmission (*curved arrows*). Uterus (*straight arrow*). Right adnexa (*open arrow*).

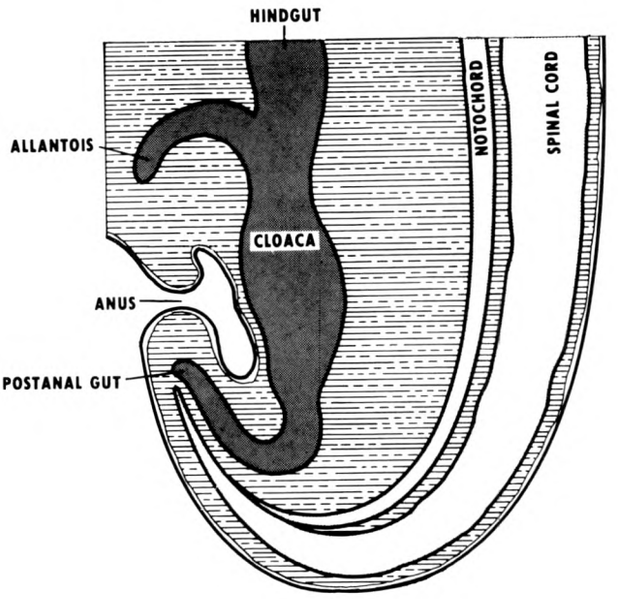


Fig. 4.—Cross-section diagram of 6.5-mm human embryo. Postanal gut is most caudal part of hindgut, distal to future anus. (Modified from Whittaker and Pemberton [4].)

a dominant cyst and little debris may cause a more cystic appearance, with attenuation similar to water. No calcification is detected within the mass, and none was seen microscopically in our series. The rectum is displaced by the mass, and the adjacent wall of the rectum may be indented. There is no evidence of invasion or destruction of adjacent structures, and the adjacent fat planes are intact. If there is concurrent infection or malignant degeneration, CT may show loss of discrete margins and involvement of contiguous structures. Sonography shows a complex mass not characteristic of a simple cyst. Low-level internal echoes were demonstrated in both of our studies with sonography (Fig. 3). A well-defined back wall and increased through transmission were not consistently demonstrated. The internal echoes of the tailgut cyst appear to result from the multicystic nature of the mass and the presence of keratinous material or inflammatory debris within the lumen. These features could also account for increased absorption of ultrasound within the cyst, thereby decreasing through transmission and causing the back wall to appear less distinct. Water enema may help to show the retrorectal location of tailgut cyst on sonogram.

Other diagnoses that should be considered are teratoma, epidermal cyst, rectal duplication, anal gland cyst, neuroblastoma, anterior meningocele, and chordoma. Meningocele and chordoma show evidence of sacral defect or invasion. Rectal duplication is often anterior to the rectum. Teratoma, chordoma, neuroblastoma, or mucinous adenocarcinoma may show calcification on CT. Teratoma may have a fatty component. Epidermal or anal gland cyst commonly has an associated cutaneous defect.

REFERENCES

1. Campbell W, Wolff M. Retrorectal cysts of developmental origin. *Am J Radiol* **1973**;117:307–313
2. Hjermstad B. Case for diagnosis. *Milit Med* **1985**;150:218–220
3. Mills T, Walker A, Stallings R, Allen M. Retrorectal cystic hamartoma. *Arch Pathol Lab Med* **1984**;108:737–740
4. Whittaker ID, Pemberton J. Tumors ventral to the sacrum. *Ann Surg* **1983**;107:96–106
5. Marco V, Autonell J, Farre J, Fernandez-Layos M, Doncel F. Retrorectal cyst hamartomas. *Am J Surg Pathol* **1982**;6:707–714

Technical Note

Double Images in Plain Film Radiography: A Motion Artifact

David Marinelli[1] and Wallace T. Miller

Movement of a patient during X-ray exposure causes blurring of the resulting image. How motion can lead to two or more discrete images is perhaps less apparent. We describe how a radiograph of an oscillating structure can cause an apparent double image. Failure to appreciate the origin of this artifact can lead to the erroneous conclusion that a double exposure has occurred, resulting in unnecessary reexamination.

Figure 1 is a detail of a lateral chest radiograph obtained with a phototimed exposure limited to 0.8 sec. The clip on the aorta marks the proximal anastomosis of a bypass graft. The tip of the pacemaker wire is in the right ventricle, and the aortic valve frame is in the root of the aorta. All three metal objects have indistinct margins due to motion. In addition, each object has produced two discrete images in the radiograph. Our hypothesis is that these objects are oscillating because of cardiac motion, that they are momentarily stationary at both extremes of their excursion, and that the exposure is long enough to show them at both extremes. In a patient with a heart rate greater than 70 cycles/min, the average cycle lasts less than 0.86 sec. An exposure time of this magnitude would not be unusual when patient is large or when portable equipment is used.

To test our hypothesis, we constructed a simple pendulum from an angiographic wire, using a hemostat as a weight. We adjusted the length to yield 70 cycles/min and obtained a radiograph with a 0.8-sec exposure time. No attempt was made to initiate the exposure during a particular phase of the pendulum's swing. A detail of the radiograph is shown in Figure 2. Two discrete images of the wire and weight can be seen, with a blurred density in between.

The motion of the pendulum can be represented by a sine wave in a time-displacement curve, as in Figure 3. When the pendulum passes through the midpoint of its swing, the velocity is maximum. At the extremes of excursion (represented by points A and B in Fig. 3), the velocity is 0. A radiograph of an oscillating object will always give an image of the object at both extremes of excursion if the exposure time is greater than or equal to one cycle time. If the exposure is between ½ and 1 cycle time, the image will always include one of the stationary points and will sometimes include both stationary points, depending on the initiation of exposure. For example, an exposure from t_1 to t_2 in Figure 3 will include both extremes of excursion, even though t_2 minus t_1 is less than the time necessary for a complete cycle.

It follows from this discussion that a double image is more likely to be formed when exposure times are longer. We have observed the double-image artifact more often on portable and lateral radiographs and on radiographs of large patients. Radiographs obtained with shorter exposure times are more likely to show a single blurred image.

Once the double-image artifact is recognized, it can easily be differentiated from a double exposure caused by equipment malfunction, and repeat examinations can be avoided.



Fig. 1.—Detail of lateral chest radiograph shows double images of a vascular clip, a pacemaker wire, and a prosthetic aortic valve.

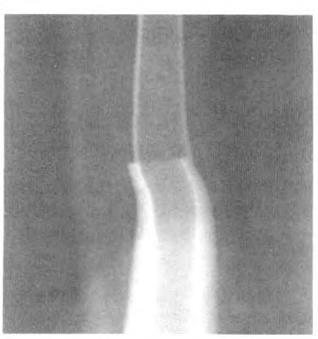


Fig. 2.—Detail of a radiograph of a pendulum in motion shows discrete images at extremes of excursion.

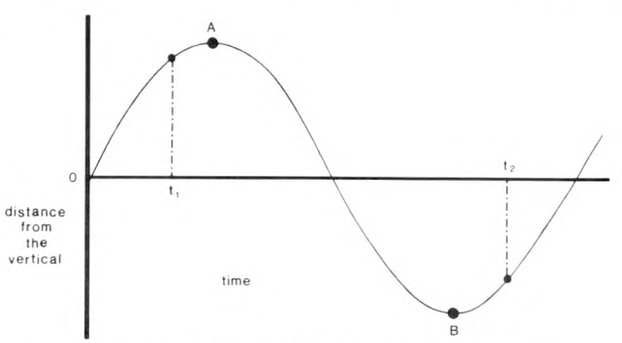


Fig. 3.—Time-displacement curve of a pendulum in motion.

Received April 28, 1986; accepted after revision June 30, 1986.

[1] Both authors: Department of Radiology, Hospital of the University of Pennsylvania, 3400 Spruce St., Philadelphia, PA 19104. Address reprint requests to W. T. Miller.

Communicating the Significance of Radiologic Test Results:
The Likelihood Ratio

William C. Black[1]
Peter Armstrong

The likelihood ratio is a useful but simple concept that helps the radiologist communicate to the clinician the significance of radiologic findings. It is defined as the ratio of the probabilities of a particular test result among patients with and without disease. Readily derivable from sensitivity and specificity, the likelihood ratio represents the degree to which a test result is positive or negative and serves as a proportionality constant that relates the pre- and posttest odds of disease in a linear manner. The linearity of the relationship permits the impact of a test result to be easily understood and allows for the integration of additional test results. The concept of likelihood ratio is explained in straightforward algebraic terms, and its practical application to clinical radiology is demonstrated by using several specific medical examples.

Although radiologists traditionally have been schooled in the recognition of pathognomonic findings, in the day-to-day practice of radiology few findings have enough predictive power to diagnose or exclude disease with certainty. Most radiologic tests can produce a diverse spectrum of results that vary greatly in their degree of positivity or negativity. When the radiologic findings are not pathognomonic or unequivocally normal, the radiologist often has difficulty communicating the significance of the test result, because the predictive value of such results depends not only on the characteristics of the test but also on the pretest probability of disease. Frequently, therefore, the radiologist's report contains terms such as "consistent with" or "cannot exclude," leaving the clinician relatively unenlightened as to the posttest probability of the disease in question. However, by using the concept of likelihood ratio (LR), a ratio of the probabilities of a given test result among patients who do and do not have the disease, the radiologist can precisely describe the degree of test positivity or negativity and the impact of the test result on the disease probability. Because the likelihood ratio and the pretest probability are independent, they can be combined to yield the posttest probability whenever the clinical information becomes available.

The concept of likelihood ratio has previously been applied to ECG stress testing [1], a reporting method for pathologists [2], the interpretation of the ventilation/perfusion (V/Q) scan in the diagnosis of pulmonary embolism (PE) [3, 4], and determination of the diagnostic usefulness of excretory urography [5]. Despite these publications, we believe that the concept of LR is not widely understood and should be applied more extensively in the clinical practice of radiology, especially considering the growing impact of radiologic imaging on patient management. Therefore, we review the concepts of likelihood ratio and odds and show how LR relates pre- and posttest odds of disease in a simple linear fashion according to Bayes' theorem. Using specific medical examples, we then demonstrate the application of LR to clinical radiology.

Likelihood Ratio

The likelihood ratio is the probability of a particular test result given disease

Received May 22, 1986; accepted after revision July 31, 1986.

[1] Both authors: Department of Radiology, University of Virginia Medical Center, Charlottesville, VA 22908. Address reprint requests to W. C. Black, Department of Radiology, Box 170, University of Virginia Medical Center, Charlottesville, VA 22908.

AJR 147:1313–1318, December 1986
0361–803X/86/1476–1313
© American Roentgen Ray Society

divided by the probability of the same test result given no disease. For a dichotomous test result, LR can be derived from the sensitivity (S, the probability of a positive result given disease) and specificity (Sp, the probability of a negative result given no disease) of the test. For a positive test result,

$$LR = \frac{S}{1 - Sp} \quad (1)$$

and for a negative test result,

$$LR = \frac{1 - S}{Sp} \quad (2)$$

The LR varies in value from 0 to infinity, depending on the degree of positivity or negativity of the test result. A test result that is strongly positive has an LR much greater than 1.0, one that is strongly negative has an LR close to 0, and one that is intermediate has an LR close to 1.0. Table 1 lists likelihood ratios derived from reported sensitivities and specificities of some commonly performed radiologic tests [6–11].

Most radiologic tests have several possible test results for which the terms positive and negative do not properly apply. Instead, each of these particular results can be described in terms of its LR, which can be determined by dividing the conditional probabilities of the particular test result with and without disease [12, 13]. (Note: These conditional probabilities are not the same as sensitivity [the probability of a test result being at least as positive as a particular one given the disease] and one minus specificity [the probability of a test result being at least as positive as a particular one given no disease].) Alternatively, if these conditional probabilities are not available, the LR of each particular test result can be derived from the sensitivities and specificities defined by the criteria that bound the test result. Whereas the LRs of the most positive and negative test results can be calculated from equations 1 and 2, respectively, the LR of an intermediate test result, bounded by criteria a and b, can be determined as follows:

$$LR = \frac{S_a - S_b}{Sp_b - Sp_a} \quad (3)$$

where S_a, S_b, Sp_a, and Sp_b are the sensitivities and specificities defined by the criteria a and b (see the appendix).

For example, in the evaluation of lung cancer patients for possible mediastinal lymph-node metastasis, chest CT may reveal mediastinal lymph nodes of various sizes. Likelihood ratios for neoplastic involvement can be determined according to short-axis lymph-node diameters [14] (Table 2).

The conditional probability of a lymph node measuring between 15 and 20 mm in diameter in a patient with mediastinal involvement divided by the conditional probability of a lymph node measuring between 15 and 20 mm in a patient without mediastinal involvement is 3.3. In a similar fashion, likelihood ratios for different size mediastinal lymph nodes can be determined. Notice that the LR can be calculated for each range of diameters between upper and lower cutoff points, while the terms sensitivity and specificity impose a "positivity" criterion placing all diameters into only one of two broad categories. (Actually, the test results in Table 1 are

TABLE 2: **Likelihood Ratios of Mediastinal Lymph Nodes in Lung Cancer Patients**

Short-Axis Diameter (mm)	Likelihood Ratios[a]
0–9	0.16
10–14	0.23
15–19	3.3
20–29	13.3
30–infinity	Infinity

[a] Derived from sensitivities and specificities plotted on receiver-operating characteristics curve by Glazer et al. [14]: diameter greater than or equal to 10 mm, sensitivity 0.95, specificity 0.30; diameter greater than or equal to 15 mm, sensitivity 0.80, specificity 0.94; diameter greater than or equal to 20 mm, sensitivity 0.70, specificity 0.97; diameter greater than or equal to 30 mm, sensitivity 0.30, specificity 1.0.

TABLE 1: **Likelihood Ratios of Commonly Performed Radiologic Tests**

Radiologic Test	Disease	Sensitivity	Specificity	Likelihood Ratio[a]	
				Positive Result	Negative Result
RBC ^{99m}Tc liver scintigram	Hemangioma [6]	0.90	1.00	Infinity	0.10
Renal sonogram	Gross hydronephrosis [7]	0.98	0.97	32.7	0.02
Abdominal CT scan	Splenic injury [8]	0.95	0.96	23.8	0.05
Abdominal sonogram	Acute cholecystitis [9]	0.86	0.90	8.6	0.16
Mammogram	Occult breast cancer [10]	0.92	0.25	1.2	0.32
Chest radiograph	Hilar metastasis [11] (known lung cancer)	0.53	0.85	3.5	0.55
Chest radiograph	Mediastinal metastasis [11] (known lung cancer)	0.05	1.00	Infinity	0.95

[a] Derived from the reported sensitivities and specificities. See text.

not dichotomous, but conditional probability data pertaining to all the possible results are not available.)

Odds

Odds and probabilities can be easily converted. The odds favoring the occurrence of an event are defined as the probability of an event (P) divided by the probability of that event not occurring (1 − P).

$$\text{Odds} = \frac{P}{1 - P} \quad (4)$$

For example, if the probability of lung cancer in a particular patient is 0.90, then the odds favoring the diagnosis is 0.90 divided by 0.10, or 9:1. Similarly, the odds against the diagnosis of lung cancer is 1:9.

Bayes' Theorem

Bayes' theorem relates the posttest probability of disease (P′) to the pretest probability (P), sensitivity (S), and specificity (Sp) of the test [15]. For a positive test result,

$$P' = \frac{P \times S}{P \times S + (1 - P) \times (1 - Sp)} \quad (5)$$

and for a negative test result,

$$P' = \frac{P \times (1 - S)}{P \times (1 - S) + (1 - P) \times Sp} \quad (6)$$

This familiar form of Bayes' theorem can be reduced to a simple linear equation when LR is substituted for sensitivity and specificity, and probabilities are converted to odds.

$$\text{Posttest odds} = \text{pretest odds} \times \text{LR} \quad (7)$$

This multiplicative form of Bayes' theorem allows both the radiologist and clinician to easily understand the impact of a test result on disease probability. It is simpler to multiply pretest odds times LR than to calculate Equations 5 and 6. For example, consider a patient with lung cancer who has pretest odds of mediastinal involvement of 1:3. If a chest CT shows a mediastinal lymph node measuring between 15 and 20 mm, then the posttest odds of mediastinal involvement is 1:3 × 3.3 (Table 2), or 1.1:1. With roughly even odds of mediastinal involvement, preoperative mediastinoscopy would be advised.

Furthermore, the linearity provides for the easy integration of other test results. For two conditionally independent tests,

$$\text{Posttest odds} = \text{pretest odds} \times LR_1 \times LR_2 \quad (8)$$

where LR_1 and LR_2 are the likelihood ratios of the two test results.

In fact, for any number (n) of conditionally independent tests, posttest odds can be determined as a linear function of the pretest odds and the LRs of the test performed [12]:

$$\text{Posttest odds} = \text{pretest odds} \times LR_1 \times LR_2 \times \ldots \times LR_n \quad (9)$$

Clinical Applications

The following examples illustrate the usefulness of the LR in evaluating the significance of radiologic findings with (1) a negative test result, (2) a positive test result, (3) test results with various degrees of positivity, and (4) several test results. For simplicity, only one disease entity is considered in each example. When several tests are used, the results are assumed to be independent.

Negative Test Result

Clinical problem.—Patient A, a 50-year-old man with a 50-pack-year history of cigarette smoking, comes to his internist with an asymptomatic, 1.5-cm pulmonary nodule that was not present on a chest radiograph taken 2 years earlier. On the basis of the clinical features and chest radiograph, the internist estimates the probability of lung cancer before percutaneous needle biopsy to be 0.90 (pretest odds of 9:1). Patient B has a similar-appearing lung nodule but is 30 years old, has never smoked, and has no previous radiographs to determine the growth rate of the nodule. The clinician estimates the probability of lung cancer in patient B to be 0.02 (pretest odds of 1:49). If a percutaneous needle biopsy were to be performed, what would be the significance of a negative result in these two patients?

According to the criteria that a percutaneous needle biopsy is considered positive if the results show carcinoma and negative if they show otherwise, the sensitivity and specificity are 0.87 and 0.98, respectively [16].

Calculations.—For LR of negative percutaneous needle biopsy,

$$LR(-) = \frac{1.0 - 0.87}{0.98} = 0.13$$

For patient A (pretest odds = 9:1),

$$\text{Posttest odds} = 0.13 \times 9{:}1 = 1.17{:}1$$

(Posttest probability = 0.54)

For patient B (pretest odds = 1:49),

$$\text{Posttest odds} = 0.13 \times 1{:}49 = 1{:}377$$

(Posttest probability = 0.003)

Comment.—The posttest odds are easily assessed by multiplying the pretest odds and LR(−). Despite the negative findings on percutaneous needle biopsy, the odds of cancer in patient A remain greater than 1:1 (1.17:1) because of the high pretest odds. However, in patient B the negative findings virtually exclude carcinoma by reducing the odds to 1:377.

Positive Test Result

Clinical problem.—Patient A has had a partial colectomy for Dukes' C adenocarcinoma and is being evaluated for occult liver metastasis with abdominal CT. Patient B, also undergoing CT, has had a sigmoid polypectomy for a pedunculated adenomatous polyp with carcinoma in situ confined to the head. The probability of liver metastasis in patient A is about 0.29 (pretest odds = 1:2.4) [17]. The probability of metastasis in patient B is very low, less than 0.01 (pretest odds less than 1:99) [18]. The CT scan in both patients reveals a solitary low-density defect 2 cm in diameter in the right lobe of the liver. What are the odds that the CT findings represent a liver metastasis in these two patients?

The sensitivity and specificity of CT in the evaluation of liver metastasis has been reported as 0.90 and 0.87, respectively [19].

Calculations.—For LR of positive findings on CT,

$$LR(+) = \frac{0.90}{1.0 - 0.87} = 6.9$$

For patient A (pretest odds = 1:2.4),

Posttest odds = 6.9 × 1:2.4 = 2.9:1

(Posttest probability = 0.74)

For patient B (pretest odds = 1:99),

Posttest odds = 6.9 × 1:99 = 1:14

(Posttest probability = 0.065)

Comment.—The finding of a low-density defect on the abdominal CT scan is more likely to represent a liver metastasis than anything else in patient A (2.9:1). However, the same finding in patient B is more likely to be a false-positive result than an actual liver metastasis (less than 1:14).

Degrees of Test Positivity

The LR is especially useful in expressing the degree of positivity or negativity of a test result. Communicating the significance of a lung ventilation/perfusion (V/Q) scan pattern in the diagnosis of pulmonary embolism is a good example of this particular application.

Clinical problem.—A 30-year-old woman comes to the emergency room with an estimated 0.33 probability of having pulmonary embolus (PE) (pretest odds = 1:2). If a lung V/Q scan were to be performed, what would be the significance of the various possible scan patterns?

In a recent paper [20], conditional probabilities were determined for four mutually exclusive categories of possible V/Q scan results. Pattern 4 was defined as a segmental or larger perfusion defect with normal chest radiograph; pattern 3, subsegmental defect with normal chest radiograph; pattern 2, any perfusion defect with a corresponding chest radiograph abnormality; and pattern 1, normal V/Q scan. Conditional probabilities were reported as follows: P(pattern 4 | PE+) = 0.80, P(pattern 4 | PE−) = 0.14; P(pattern 3 | PE+) = 0.16, P(pattern 3 | PE−) = 0.18; P(pattern 2 | PE+) = 0.04, P(pattern 2 | PE−) = 0.10; P(pattern 1 | PE+) = 0, P(pattern 1 | PE−) = 0.58. The likelihood ratios of the various V/Q scan patterns can be calculated directly from the conditional probabilities.

Calculations.—LRs of V/Q scan patterns are

$$\text{Pattern 4: } LR_4 = \frac{0.80}{0.14} = 5.7$$

$$\text{Pattern 3: } LR_3 = \frac{0.16}{0.18} = 0.89$$

$$\text{Pattern 2: } LR_2 = \frac{0.04}{0.10} = 0.40$$

$$\text{Pattern 1: } LR_1 = \frac{0}{0.58} = 0$$

Therefore, posttest odds of pulmonary embolism are

Pattern 4: Posttest odds = 5.7 × 1:2 = 2.8:1

(Posttest probability = 0.74)

Pattern 3: Posttest odds = 0.89 × 1:2 = 1:2.2

(Posttest probability = 0.31)

Pattern 2: Posttest = 0.40 × 1:2 = 1:5

(Posttest probability = 0.16)

Pattern 1: Posttest = 0 × 1:2 = 0

(Posttest probability = 0)

Comments.—With a normal (pattern 1) V/Q scan, the posttest odds of PE are close to zero. Pattern 2 decreases the odds of PE by a factor of 0.40. If pattern 4 is obtained, the posttest odds of PE are high (2.8:1) because of the relatively high LR (5.7) of the V/Q scan result. However, because the LR of pattern 3 is close to unity (0.89), this test result has very little impact on the odds of PE. In other words, this test result does not change the odds of PE from the original clinical estimate. The radiologist could simply describe the V/Q scan as having an LR of near unity, thus highlighting the importance of the clinical information. If it were revealed subsequently that the patient was at high risk for PE (because of taking oral contraceptives and smoking), then the posttest odds could be recalculated on the basis of a new, higher, pretest odds estimate of PE. Similarly, if the patient were reclassified as low risk, then the pre- and posttest odds could be sufficiently lowered to spare the patient additional workup for PE.

Several Test Results

Clinical Problem.—A 50-year-old woman who had a cholecystectomy for cholelithiasis 2 years ago comes to the emergency room. Her chief complaint is acute pain in the right upper quadrant. The working diagnosis to be excluded is recurrent gallstones causing obstruction of the common bile duct (probability = 0.50, pretest odds = 1:1). Sonography is performed first. If the sonographer sees a normal-sized common bile duct and no gallstones in the biliary tree, is choledocholithiasis causing acute bile-duct obstruction completely

ruled out? What if a subsequent hepatobiliary scintiscan shows delayed excretion into the biliary tree or bowel?

According to the criterion that a common bile duct greater than 6 mm is obstructed, the sensitivity and specificity of sonography are approximately 0.55 and 0.90, respectively [21]. If delayed excretion into the biliary tree or intestines is considered the criterion for positivity for the hepatobiliary scintigram, then the sensitivity and specificity of the scintigram are 0.80 and 0.95, respectively [22].

Calculations.—For negative findings on sonography (S−),

$$LR_{S-} = \frac{1.0 - 0.55}{0.90} = 0.50$$

For positive findings on hepatobiliary scintiscan (HBS+),

$$LR_{HBS+} = \frac{0.80}{1.0 - 0.95} = 16.0$$

The *posttest odds of obstruction* for negative findings on sonography are

$$\text{Posttest odds} = 0.50 \times 1{:}1 = 1{:}2$$

$$(\text{Posttest probability} = 0.33)$$

and for negative findings on sonography and positive findings on hepatobiliary scintiscan,

$$\text{Posttest odds} = 0.50 \times 16.0 \times 1{:}1 = 8{:}1$$

$$(\text{Posttest probability} = 0.89)$$

With such a low sensitivity, a negative finding on sonography would only halve the odds of acute biliary obstruction, $LR_{S-} = 0.50$. Although less likely, acute biliary obstruction would not be decisively excluded. If sonography were to be followed by a hepatobiliary scintigram that showed delayed excretion into the biliary tree or intestines, then the odds favoring acute biliary obstruction would be high (8:1) because of the high LR of 16.0 of the positive scintigram. Confusion over which examination should be believed would be eliminated—the positive scintigram would greatly outweigh the negative sonogram.

Discussion

The application of the likelihood ratio to the interpretation of diagnostic tests is not new. Rifkin and Hood [1] assigned LR values to different degrees of ST depression on the ECG exercise stress test according to how these results increased the risk of coronary artery disease. For example, ST depression in the range of 1.0–1.49 mm had a likelihood ratio of 2.35, whereas depression in the range of 2.0–2.49 mm was associated with a much higher likelihood ratio of 21.33. These authors used the nonlinear form of Bayes' theorem to calculate the posterior probability of coronary artery disease rather than the more convenient multiplicative form described in this paper. Similarly, McNeil [3] assigned likelihood ratios to different ventilation-perfusion patterns in the diagnosis of pulmonary embolism. Schwartz et al. [2] proposed a change in the reporting method for pathologists that would permit better integration of clinical data and pathologic findings than the conventional intuitive method does. Using their approach, the pathologist would estimate the relative likelihoods of observed biopsy findings in patients with each disease considered in the differential diagnosis of the clinician. These estimates, independently determined by the pathologist, would be multiplied by the clinician's estimates of the relative likelihood of each disease calculated before the biopsy to yield products that could be normalized into posttest probabilities. Because the analysis was applied to a differential diagnosis of diseases rather than to simply the presence or absence of one disease, the calculations of the posttest probabilities were more complicated than those in our examples.

It is the role of the radiologist to communicate effectively to clinicians the significance of radiologic findings. It is not enough just to describe the findings and to assume that the clinician knows their significance. A radiologist who reports the probability of disease based on a radiologic test result, however, must know not only the sensitivity and specificity of the test result but also the likelihood of disease before the test. For various reasons, the radiologist is frequently unable to accurately estimate the pretest probability. Indeed, this estimate often changes as the diagnostic workup proceeds. The radiologist can, however, report the intrinsic significance of the radiologic findings as a likelihood ratio, a term that incorporates sensitivity and specificity in a way that allows easy integration with the pretest probability of the disease in question.

Because LR is independent of pretest probability, the radiology report is valid over a large range of pretest probability values. In the past, when diagnostic testing was used primarily to confirm disease, the pretest probabilities often were high. Today, the pretest probability is frequently very small because advances in medical treatment, increasing availability of diagnostic tests, and threat of litigation all lower the physician's threshold for diagnostic testing. Abnormal test results, sometimes incidental, are therefore often found in patients with low pretest probability. The use of LR also allows recalculation of the posttest odds, as discussed in our example of suspected pulmonary embolism, if the clinician's perception of pretest probability changes. Furthermore, use of the likelihood ratio in the multiplicative form of Bayes' theorem allows for the integration of additional, sometimes conflicting, test results. Any number of likelihood ratios can be integrated by simple multiplication to yield a single likelihood ratio for the combination of test results, provided that the test results are independent [12].

Unfortunately, the subject of test independence is complex. However, tests that rely on similar methods of detection generate results that are generally more dependent on one another than tests that operate on different principles. For example, detection of a mass in the middle of a lung by either a plain chest radiograph or CT scan is dependent on the same principles of size and density, so the results of these two tests are interdependent, and sequential application of Bayes' theorem does not apply. Although independence of test results cannot necessarily be logically deduced, statistical methods are available to determine independence.

The likelihood ratio has other limitations. A major one is

that its practical application is limited by the same restrictions that govern the use of sensitivity and specificity. The disease must be regarded as either present or absent, and only one disease process can be considered at a time. The LR can be applied to differential diagnosis as demonstrated by Schwartz et al. [2], but the analysis becomes complicated and requires the input of conditional probabilities for which objective data are not always available.

Conclusion

The likelihood ratio is a simple concept that can help the radiologist communicate to the clinician the significance of a test result. Using the concept, the radiologist can precisely describe the degree of positivity or negativity of a test result in a quantitative form readily derived from sensitivity and specificity. Because the likelihood ratio can be used to relate pre- and posttest odds of disease linearly, it makes understanding a test result easy and allows for the integration of several, sometimes conflicting, test results.

ACKNOWLEDGMENTS

We thank Shirley Yowell and Sherry Deane for secretarial assistance.

REFERENCES

1. Rifkin RD, Hood WB Jr. Bayesian analysis of electrocardiographic exercise stress testing. *N Engl J Med* **1977**;297:681–686
2. Schwartz WB, Wolfe JH, Pauker SG. Pathology and probabilities: a new approach to interpreting and reporting biopsies. *N Engl J Med* **1981**;305:917–923
3. McNeil BJ. Ventilation-perfusion studies and the diagnosis of pulmonary embolism: concise communication. *J Nucl Med* **1980**;2:319–323
4. Blinder RA, Coleman RE. Evaluation of pulmonary embolism. *Radiol Clin North Am* **1985**;23:391–405
5. Thornbury JR, Fryback DG, Edwards W. Likelihood ratios as a measure of the diagnostic usefulness of excretory urogram information. *Radiology* **1975**;114:561–565
6. Rabinowitz SA, McKusick KA, Strauss HW. ^{99m}Tc red blood cell scintigraphy in evaluating focal liver lesions. *AJR* **1984**; 143:63–68
7. Ellenbogen PH, Scheible FW, Talner LB, et al. Sensitivity of gray scale ultrasound in detecting urinary tract obstruction. *AJR* **1978**;130:731–733
8. Jeffrey RB, Laing FC, Federle MP, et al. Computed tomography of splenic trauma. *Radiology* **1981**;141:729–732
9. Ralls PW, Colletti PM, Halls JM, et al. Prospective evaluation of ^{99m}Tc-IDA cholecystitis. *Radiology* **1982**;144:369–377
10. Stomper PL. Breast carcinoma: initial staging. In: McNeil BJ, Abrams HL, eds. *Brigham and Women's Hospital handbook of diagnostic imaging.* Boston: Little, Brown, **1986**:250–251
11. Osborne DR, Korobkin M, Ravin CE, et al. Comparison of plain radiography, conventional tomography, and computed tomography in detecting intrathoracic lymph node metastases from lung carcinoma. *Radiology* **1982**;142:157–161
12. Sackett DL. Interpretation of diagnostic data. 5. How to do it with simple math. *Can Med Assoc J* **1983**;129:947–954
13. Weinstein MC, Fineberg HV. *Clinical decision analysis.* Philadelphia: Saunders, **1980**:103–104
14. Glazer GM, Orringer MB, Gross BH, Quint LE. The mediastinum in non-small cell lung cancer: CT-surgical correlation. *AJR* **1984**;142:1101–1105
15. Phillips WC, Scott JA, Blasczcynski GI. How sensitive is "sensitivity"; how specific is "specificity"? *AJR* **1983**;140:1265–1270
16. Calhoun P, Feldman PS, Armstrong P, et al. The clinical outcome of needle aspirations of the lung when cancer is not diagnosed. *Ann Thorac Surg* **1986**;41:592–596
17. Finlay JG, Meek DR, Gray HW, Duncan JG, McArdle CS. Incidence and detection of occult hepatic metastases in colorectal carcinoma. *Br Med J* **1982**;284:803–805
18. Christie JP. Malignant colon polyps: cure by colonoscopy or colectomy? *Am J Gastroenterol* **1984**;79:543–547
19. Drum DE. Hepatic metastases in nonlymphomatous tumors. In: McNeil, BJ, Abrams HL, eds. *Brigham and Women's Hospital handbook of diagnostic imaging.* Boston: Little, Brown, **1986**:239–243
20. Vea HW, Sirotta PS, Nelp WB. Ventilation-perfusion scanning for pulmonary embolism: refinement of predictive value through Bayesian analysis. *AJR* **1985**;145:967–972
21. Zeman RK, Lee C, Jaffe MH, Burrell MI. Hepatobiliary scintigraphy and sonography in early biliary obstruction. *Radiology* **1984**;153:793–798
22. Kaplun L, Weissmann HS, Rosenblatt RR, Freeman LM. The early diagnosis of common bile duct obstruction using cholescintigraphy. *JAMA* **1985**;254:2431–2434

Appendix

Calculating Likelihood Ratios for Intermediate Test Results

Let a and b be two different criteria for test positivity that divide the set of possible test results R into three mutually exclusive subsets, R_1, R_2, and R_3, where $R_1 < a \leq R_2 < b \leq R_3$, and $P(R) = P(R_1) + P(R_2) + P(R_3) = 1.0$. The likelihood ratio for result R_2 [$LR(R_2)$] can be defined as follows:

$$LR(R_2) = \frac{P(a \leq R < b \mid D+)}{P(a \leq R < b \mid D-)} \quad \text{(A1)}$$

$$\begin{aligned} P(a \leq R < b \mid D+) &= P(R \geq a \mid D+) - P(R \geq b \mid D+) \\ &= S_a - S_b \end{aligned} \quad \text{(A2)}$$

where S_a equals the sensitivity of the test using criterion a and S_b equals the sensitivity of the test using criterion b.

$$\begin{aligned} P(a \leq R < b \mid D-) &= P(R \geq a \mid D-) - P(R \geq b \mid D-) \\ &= [1 - P(R < a \mid D-)] \\ &\quad - [1 - P(R < b \mid D-)] \\ &= P(R < b \mid D-) - P(R < a \mid D-) \\ &= Sp_b - Sp_a \end{aligned} \quad \text{(A3)}$$

where Sp_a equals specificity of the test using criterion a, and Sp_b equals the specificity of the test using criterion b. Substituting equations A2 and A3 into equation A1 yields

$$LR(R_2) = \frac{S_a - S_b}{Sp_b - Sp_a}. \quad \text{(A4)}$$

Computer Page

Microcomputer-Based Graphics for Radiology

George A. Taylor[1]

Personal computers, an increasingly familiar sight in radiology departments, are being used for a variety of tasks, including data management, word processing, scheduling, and quality control [1, 2]. Despite the proliferation of these machines and accompanying software, the potential of using personal computers to generate high-quality graphics for use as teaching tools, illustrations, or slide presentations has not been explored. This paper gives several examples of how anatomic drawings and charts may be created or modified by using a personal computer as a desktop typesetting tool.

Materials and Methods

My department currently has a MacIntosh 512-K personal computer (Apple Corp., Cupertino, CA) that it uses for word processing, data management, and graphics preparation for some of the staff radiologists. In addition to the basic graphics and word processing programs supplied by Apple (MacPaint and MacWrite), other commercial software applications were used in the preparation of this manuscript (see Results). A dot matrix printer (Imagewriter) was used to generate hard copies. The images shown were created in 20 min or less.

Results

Anatomic Drawings

Several ways of creating or manipulating images are available. Original drawings require little artistic talent and may be created by using a combination of circles, ovals, and straight lines provided by software (MacPaint) or drawn freehand by using a desktop cursor controller (mouse). Detailed or fine artwork is possible by means of a magnified pixel map of the image (Fig. 1). Shading or background patterns can be selected from a group of preset options available from a "palette" menu on the screen. Titles or labels may be added as finishing touches by using a variety of typefaces (fonts) and type sizes accessible from a pulldown menu. Commercially produced anatomic drawings (MacAnatomy, MacMedic Publications, Inc., Houston, TX) are also available for immediate use or for modification by the user by means of the aforementioned techniques (Fig. 2).

The second method of creating drawings involves the use of a digitizer. Several different types, which vary in price and sophistication, are available commercially. The apparatus described here (Thunderscan, Thunderware, Inc., Orinda, CA) consists of a relatively inexpensive ($175) optical density reader that converts reflected light intensities from analog to digital form and displays them on the computer monitor. The original artwork is placed on the printer roller, and the digitizer is mounted on the printer head (after removal of the ribbon cartridge). The digitizer then reads the image line by line and creates an electronic pixel map of the original. With Thunderscan, anatomic drawings of excellent quality that are available in printed form [3] may be copied and manipulated according to the needs of the user. Once the image is stored in memory, the whole image or parts of it may be recopied and modified (Fig. 3). Finally, different techniques can be combined to produce a particular effect or drawing.

Charts and Typesetting

Complex data relationships often can be more easily understood when presented in graphic form. Many data-base,

Received May 12, 1986; accepted after revision June 27, 1986.

[1] Departments of Radiology and Child Health and Development, The Children's Hospital National Medical Center and The George Washington University School of Health Sciences, Washington, DC. Address reprint requests to G. A. Taylor, the Children's Hospital National Medical Center, 111 Michigan Ave. NW, Washington, DC 20010.

AJR 147:1319–1321, December 1986 0361–803X/86/1476–1319 © American Roentgen Ray Society

statistical, and charting programs are available that offer graphic capabilities for data display. However, few allow complete customization of the graph. This may be accomplished by copying the chart from its original data base or statistical application to a graphics program that permits the creation of composite graphs, use of different fonts, and accurate centering of text on the page (Fig. 4).

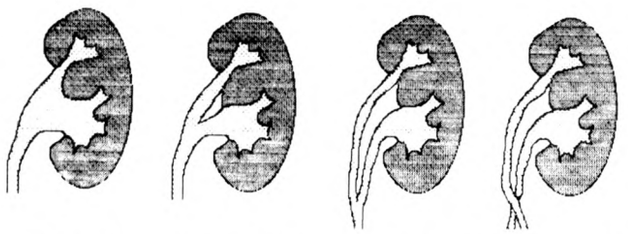


Fig. 1.—Example of original drawing made by using computer-generated curved lines, background patterns, and freehand drawing with a desktop cursor controller.

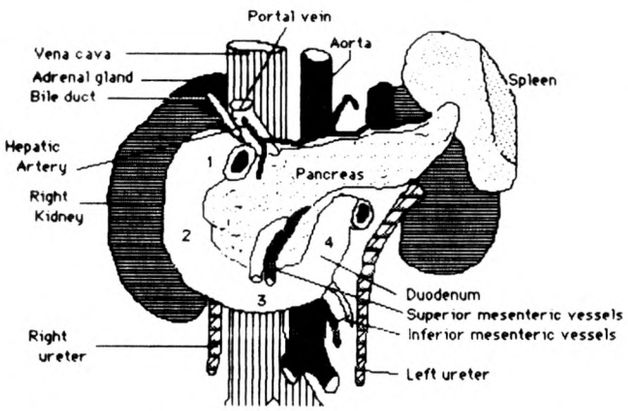


Fig. 2.—Example of anatomic drawings available commercially in diskette form. (Reprinted with permission from MacMedic Publications, 1985.)

Discussion

Personal computer–based graphics can be used in a variety of applications as shown. This capability could be useful to smaller radiology departments or to those with limited access to medical illustrators for preparation of manuscripts, lectures, or teaching conferences. The main advantage of computer-generated graphics is the ability to create rapidly customized, high-quality images and text that can be modified easily, and stored for future use. Computerized drawings made by means of this system have been well accepted and have been used in recent publications [4, 5] and national presentations [6]. Several other graphics and image-manipulation software packages are available for the MacIntosh that permit more complex tasks such as rotation, distortion, magnification, and overlaying of images. Detailed description of these applications is beyond the scope of this paper and can be found in most popular personal computer publications such as *MacWorld* and *Byte*.

The current configuration of the IBM (International Business Machines, Boca Raton, FL) personal computer will produce bar and line graphs and pie charts in color but will not produce more complex images such as anatomic drawings. However, MacIntosh and IBM personal computers can be linked through network communications software that enables both machines to share text and numeric data files. Thus, raw numeric data can be sent from the IBM personal computer to the MacIntosh and converted into graph or chart form, which in turn could be further modified by using the more powerful graphics applications available for the MacIntosh.

A limitation of the system presented is the relatively low resolution of most dot matrix printers, which may cause an image to look unacceptably coarse. This can be overcome by making a relatively large original drawing on the computer.

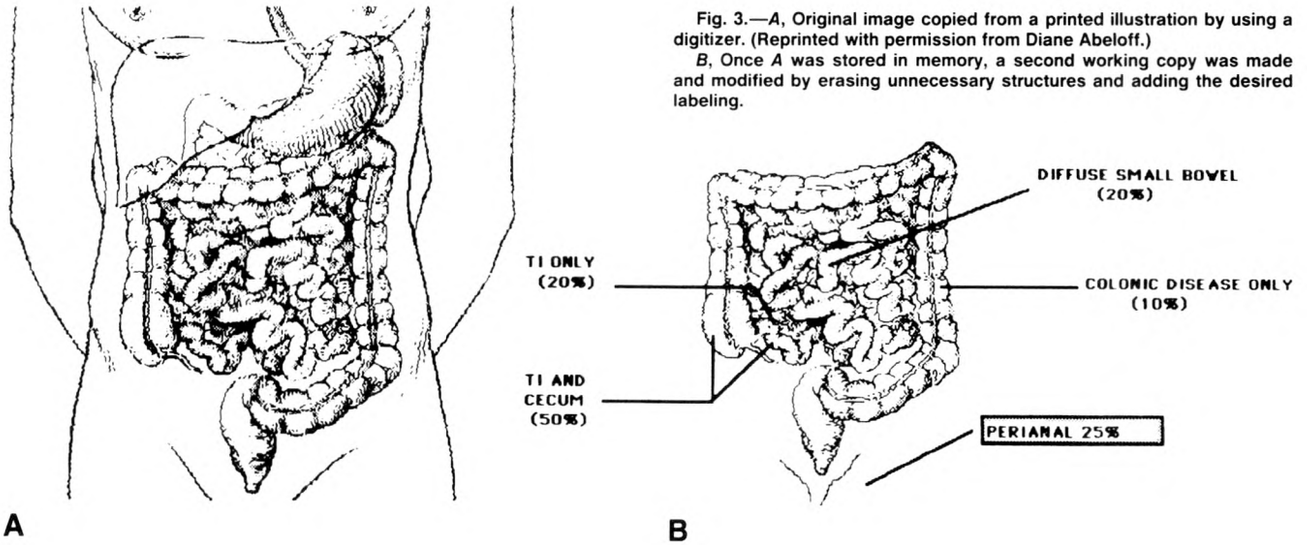


Fig. 3.—*A*, Original image copied from a printed illustration by using a digitizer. (Reprinted with permission from Diane Abeloff.)
B, Once *A* was stored in memory, a second working copy was made and modified by erasing unnecessary structures and adding the desired labeling.

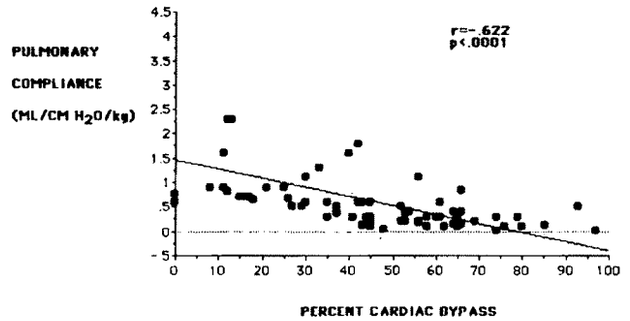


Fig. 4.—A simple regression line between two variables generated by a statistical data-base program and copied to a graphics program. Labels were customized to the author's needs.

Photographic minification then can smooth many of the minor irregularities present on the printout. Use of a laser printer can make a significant difference in resolution attained (300 dots/in. compared with 80 dots/in. for standard dot matrix printer). However, the prohibitive cost of laser printers ($3000–6000) make them impractical for all but large departments.

The total cost for this system, including software, was $2500. Although purchase of a personal computer for the sole purpose of producing graphics is not cost-effective, the utilization of its graphics potential in addition to already established data-management and word-processing capabilities can be both time saving and cost-effective.

REFERENCES

1. Holshouser BA, Bradley WG. Microcomputer patient database management system for an MRI facility. *AJR* **1986**;146:871–874
2. Barnhard HJ, Lane GB. The computerized diagnostic radiology department: update 1982. *Radiology* **1982**;145:551–558
3. Abeloff D. *Medical art graphics for use.* Baltimore: Williams & Wilkins, **1985**
4. Nancarrow PA, Edwards DK. Kinked catheters: radiographic appearance of functionally significant bends. *AJR* **1986**;146: 789–792
5. Taylor GA, Kirkpatrick JA. Periosteal reactions in children. *Contemp Diagn Radiol* **1985**;8:1–5
6. Fitz CR. *Pediatric brain tumors.* Presented at the annual Advanced Neuroradiology Seminar of the University of South Florida College of Medicine, Orlando, FL, October **1985**

Opinion

Technological Volatility and the Aging Radiologist

Alan J. Davidson[1]

Experience gives birth to expertise, perspective, and judgment. These qualities, in turn, may be expected to attract the young to the fount of their elders for guidance and wisdom. That, at least, is the usual expectation of the aging professional. But is radiology the exception? Has the technological volatility of recent years deprived the graying radiologist of the 1980s of this reward? Probably yes, and in more ways than one.

In just 13 years' time, three new technologies—sonography, CT, and MR—and their modifications have wrought fundamental changes in the nature of radiologic science and practice. Table 1 highlights the milestones of this period.

Landmark developments have been made at such a rapid pace that before one technique could become established another had come into use. The focus has been and continues to be on the new: new physical principles to learn; new technological skills to acquire; a new technique to exploit clinically; and, moving out, an entire new generation of gifted young radiologists who are already much closer to the cutting edge of these techniques than most of their elders can ever hope to be. How many have these changes affected and in what way? Has the white water of this turbulent stream eroded the foundation stones on which our discipline rests?

Demographic data available from the American Medical Association [1] and the American College of Radiology [2] provide estimates of the number of current American radiologists and the year they first entered practice. Relating this information to the year the various new procedures were added to training programs makes it possible to estimate the percentage of current American radiologists who were not trained in new techniques as part of their primary residency education (Table 2).

It is difficult to gauge precisely all of the ramifications of rapid technological change. Certainly many—perhaps most—radiologists have kept abreast of these developments, as surely they must. Our ample educational resources—heavily attended refresher courses and national meetings, fine journals, and vigorous book publishing enterprises—support this trend. Clearly, though, the focus of radiologic education as well as everyday radiologic practice has shifted away from the fundamentals of yesteryear. Technological tours de force now dominate our teaching institutions as well as the average radiologic department in American hospitals. Not unrelated, these landmark events have coincided with the beginning of a fundamental restructuring of the social and economic context in which medicine is practiced. Faced with the threat of technological obsolescence and the turmoil of our changing health-care system, the temptation must be great for many of today's radiologists to retire early. Indeed, reducing the number of practitioners would in one sense help the widely acknowledged impending oversupply of radiologists.

TABLE 1: **Milestones in the Development of Radiologic Technology, 1978–1984**

Sonography
1973—Bistable
1978—Gray scale
1980—Real time
CT
1973—Head
1975—Body
1978—High resolution, fast scan
MR
1984—Investigational device

Received May 2, 1986; accepted after revision July 22, 1986.

[1] Department of Radiologic Pathology, Armed Forces Institute of Pathology, Washington, DC 20306-6000.

 0361–803X/86/1476–1322 © American Roentgen Ray Society

TABLE 2: **Estimates of Percentage of Radiologists Without Primary Training in Sonography, CT, and MR**

New Technology	Threshold[a] Year	Percentage of Current United States Radiologists Without Primary Training
Sonography		
Bistable	1976	62
Gray scale	1981	83
CT		
Head/body	1978	71
MR	1986	>99

[a] Threshold year is based on the assumption that the average training program in the United States introduced a new technology into its curriculum within 2 years of its initial commercial availability and that a training period of at least 1 year ensued before a resident first entered practice fully trained in a new technique.

If this be so, the implications could be serious. Valuable as the new technologies are, they do have their negative aspects. They produce redundant information because they overlap. They carry the potential for fiscal and clinical excesses as well as the potential for fiscal and clinical efficiency. And in many respects, they have divided and compartmentalized the discipline of radiology and thereby laid the groundwork for possible disintegration. Not surprisingly, and quite naturally, the advances and the fragmentation are most notable in academic health centers, which provide the formative environment for new generations of radiologists. And beyond radiology itself, primary care, wellness, clinical efficiency, and fiscal conservatism are emerging as the imperatives of a new health-care philosophy. The fact of the matter is that radiologists will soon be held in higher esteem for doing less, rather than more, to solve a clinical problem.

Radiologists must increasingly assume the critical and subtle role of guiding and counseling their clinical colleagues in the application of the total radiologic discipline to a patient's welfare. It is in this very area that younger radiologists are least prepared, by virtue of both the nature of technique-oriented contemporary training programs and a simple lack of experience. Judgment, perspective, and clinical understanding are the requisite values for the maturation of technically skilled young radiologists and for the preservation of the integrity and credibility of our discipline. Now, more than ever, the experienced radiologist is needed to contribute these qualities and to help steady the course into the future.

REFERENCES

1. *Physician characteristics and distribution in the United States.* Chicago: American Medical Association, **1984**
2. *Manpower IV. A report of the ACR committee on manpower.* Chicago: American College of Radiology, **1985**

Perspective

The American Board of Radiology to Consider *Added Qualifications*

Lee F. Rogers[1]

Subspecialization is thought by some to be the inevitable consequence of increasing medical knowledge that has led to the significant advances in modern medicine. Others view it as alarming evidence of the fragmentation of medicine and contrary to the best interests of patient care. Despite this difference of opinion, increasing numbers of physicians seek fellowship training and become subspecialized. Nearly half of all recent graduates of diagnostic radiology residency-training programs have gone on to take 1 or more additional years of training. Few decry the presence of such programs or belittle the advantages of such training. Indeed, the skill and competence of those so trained is readily acknowledged and eagerly employed. Nevertheless, few prospects in diagnostic radiology are more controversial than the formal recognition of subspecialization.

Opponents of subspecialty recognition state that it would lead to fragmentation of the specialty, dilute the value of the general board certificate, create issues of turf among radiologists, and disenfranchise the generalist. Some claim subspecialization would subject the generalist to greater risk for malpractice claims, although a recent review revealed no case of malpractice brought for lack of subspecialty expertise or training. It is said that more radiologists would be required, which would increase the cost of care. It is also said that the general radiologists would be subjected to exploitation by clinician specialists regarding interpretation of certain examinations. For instance, were recognition of subspecialty expertise to be granted in neuroradiology, the neurologist might claim that there were two classes of radiologists, recognized neuroradiologist and general radiologist. In the absence of a certified neuroradiologist, the neurologists might argue they have more knowledge of neurologic disease than the general radiologist, and are therefore more qualified to interpret and perform neurologic imaging procedures than the general radiologist.

These arguments are countered by proponents of certification who maintain that subspecialty certification has improved and advanced internal medicine, pediatrics, and pathology, and that the subspecialty-trained radiologist is more knowledgeable and thus more aware of the imaging needs of their clinical counterparts. Proponents believe subspecialty recognition would be valuable in issues of turf between the radiologists and clinicians. Such expertise in radiology would defuse the movement by clinicians to perform their own imaging studies. Cardiologists have already captured cardiac angiography and are making inroads in nuclear cardiology. Internal medicine specialists are poised to control MR spectroscopy. There is an ongoing dispute with obstetricians over the performance of obstetric sonography and most outpatient orthopedic radiology is now performed in orthopedists' offices. Some claim that subspecialization already exists in radiology, informally by those who limit their practice to some degree, particularly in academic centers and large group practices, and formally by recognition of special competence in nuclear medicine and by the long-standing division into diagnostic and therapeutic radiology. Certainly most scientific articles in radiologic journals and presentations at national radiologic meetings and symposia are the work of subspe-

Disclaimer: Although Dr. Lee F. Rogers is a Trustee of the American Board of Radiology, the views expressed are his own and do not in any way represent either the positions of the American Board of Radiology or viewpoints of other Trustees in this matter (Editor).

[1] Department of Radiology, Northwestern University Medical School, 710 N. Fairbanks, Chicago, IL 60611. Address reprint requests to Lee F. Rogers.

AJR 147:1324–1326, December 1986 0361–803X/86/1476–1324 © American Roentgen Ray Society

cialists. Furthermore, certain subspecialty areas in radiology meet the requirements outlined by the American Board of Medical Specialists (ABMS) and are deserving of recognition.

Another specter has been raised: Suppose radiology decided not to offer subspecialty recognition of any type in any area. Would other primary boards argue that general radiologists are inadequately trained to meet their imaging requirements and that they must establish certification in imaging within their own specialties to meet their special needs (e.g., cardiology, in cardiac imaging; neurology, in neurologic imaging; obstetrics and gynecology in obstetric and gynecologic imaging; and emergency medicine in emergency medicine imaging)?

The pressure for credentialing of subspecialties exists in many specialties. During the 1940s, subspecialty certification was issued in only seven areas, by 1970 this had doubled, and by 1980 quadrupled to a total of 28. The 23 primary boards now issue 34 different subspecialty certificates, among them 11 in internal medicine, nine in pathology, eight in pediatrics, and four in obstetrics and gynecology. In the years between 1975 and 1984, the primary boards certified 164,289 general specialists and, surprisingly, 30,418 subspecialists: roughly one subspecialist for every five specialists.

The ABMS, the governing body of the 23 primary medical specialty boards, has long been concerned with the effects of subspecialization, particularly its impact on both the cost and accessibility of medical care. A policy statement issued by the ABMS [1] declares, "There is no requirement nor necessity for a diplomat in a recognized specialty to hold special certification in a subspecialty of that field in order to be considered qualified to include aspects of that subspecialty within a specialty practice. Under no circumstances should a diplomat be considered unqualified to practice within an area of subspecialty solely because of lack of subspecialty certification . . . Such special certification . . . has not been created to justify a differential fee schedule or to confer other professional advantages over other diplomats not so certified." One of the principal problems is the perception that many who have received fellowship training are either reluctant or refuse to practice in the primary field in areas beyond their subspecialty interests.

Until recently the ABMS allowed only two types of certification, first, general certification, conferred on diplomats meeting the requirements of a primary board (e.g., pediatrics); and second, special qualifications limited to a specified portion of the primary field (e.g., nephrology in pediatrics). Upon successful completion of an examination in the first type, the physician is awarded a general certificate: certified in pediatrics. In the second, the certificate covers only the subspecialty: certified in pediatric nephrology. Because subspecialty certification could be acquired without the requirement of full training and credentials in the primary specialty, serious questions were raised. The ABMS recognized that subspecialty certification granted without prior certification in the general field of the specialty is conducive to the limitation of practice to that specific field.

In light of these concerns and after considerable deliberation, the ABMS announced, in its annual report of 1985, a third type of certification, termed *Added Qualifications*, as a means of correcting this problem. *Added Qualifications* constitutes a modification of an approved general certificate to reflect (1) additional training of at least 1 year beyond that required for the primary board and (2) satisfactory completion of an additional examination. The certificate would reflect this difference: certified in pediatrics with *Added Qualifications* in pediatric nephrology. The training program must be associated with an accredited residency and, of importance to radiology, incorporate a specific identifiable body of knowledge that may include, but not be limited to, isolated technical skills. The distinction between subspecialty certification and added qualifications is more than semantic. An individual granted *Added Qualifications* must first be certified by the parent board and thereby qualified in the general specialty.

Added Qualifications cannot be established simply by action of a primary board. Before a primary board may establish any new type of certification, it is required to obtain prior approval of two-thirds of the member boards of the ABMS. Such a proposal must be announced to all member organizations at least 1 year before the proposal is submitted for a vote. Extensive documentation is required, including evidence of the professional and scientific status of this special field as acknowledged by the existence of a group of physicians concentrating their practice in this field, the number and geographic distribution of such physicians, their annual rate of increase, the existence of national societies dedicated to this field, number and location of medical-school and hospital departments devoted to the field, number and names of institutions providing training programs, number of positions available, number of trainees completing training programs annually, and the duration and curriculum of existing programs. In addition, a written statement indicating concurrence or specific grounds for objection is required from each primary board having expressed interest in certifying in the same field. A minimum of 4 or 5 years would be required to assemble the documents and receive approval from the ABMS before any examination could be initiated and the first certificates with *Added Qualifications* could be granted.

Fellowships are now treated differently from residencies. The credentialing of residency training, which is a two-prong process, includes accreditation of residency-training programs by the Residency Review Committee and certification of graduates of such programs by the appropriate specialty board. It might seem logical to assume that a similar process would be required for fellowship training. However, to date, most subspecialty certification has been accomplished without review of training programs. Despite the American Board of Internal Medicine's long history of subspecialty certification, fellowship-training program review has been under consideration only in the past year.

Approximately 40 to 60% of recent graduates of diagnostic radiology residency-training programs have taken 1 or more additional years of fellowship training. Most programs are educational, but others, regrettably, are exploitative or at best marginal. At present there is no way of evaluating the body of knowledge taught, the skills learned, or the quality of the experience offered, except by the reputation of the institution

and the preceptor under whom the training is received. We therefore allow claims of competence without knowing the nature of the training experience or confirming competence by passage of an examination.

Some radiologists believe that programmatic review and accreditation is warranted to assure both the profession and the public that programs meet minimum standards. Programmatic accreditation is also viewed as an intermediate and less divisive step in subspecialty recognition than the granting of certificates to the graduates of such programs.

Over the past several years, various subspecialists within orthopedics have sought subspecialty certification from the American Board of Orthopedic Surgery, which is similar to our experience with neuroradiology and pediatric radiology. To prevent fragmentation and maintain unity, orthopedists have sought and obtained approval from the Accreditation Council of Graduate Medical Education (ACGME) for the Orthopedic Residency Review Committee to review and approve fellowship training programs without requiring subspecialty certification by the American Board of Orthopedic Surgery. This required an agreed-upon definition of subspecialties within orthopedic surgery. This would pose a problem in diagnostic radiology. While it is possible to define certain subspecialties (e.g., nuclear radiology, pediatric radiology, and neuroradiology), others are not so easily defined (e.g., abdominal imaging, angiography and interventional imaging, and the various combinations of CT, sonography, and MR).

Because of concerns regarding quality of training, the Society of Pediatric Radiology is considering a request of the Radiology Residency Review Committee (RRC) to review fellowship-training programs in pediatric radiology. The American Society of Neuroradiology is considering a similar request of the RRC and has engaged in discussions with representatives of the American Board of Radiology (ABR) to encourage the establishment of *Added Qualifications in Neuroradiology*. The Society of Pediatric Radiology does not intend to petition the ABR for certification with *Added Qualifications* in Pediatric Radiology at this time.

Recognizing the profound implications for radiology and in light of the establishment of the new type of certification by the ABMS, the ABR, at its January 1986 meeting, approved a motion to inform all national radiologic organizations of its intent to carefully consider the question of *Added Qualifications* at its January 1987 meeting. Comment has been solicited and welcomed from all organizations and interested individuals. It was to be a major topic at this year's Summit meeting and was discussed in an open forum at the annual meeting of the Radiological Society of North America.

The actions, if any, of the ABR cannot be predicted. It is important to recognize that the ABR intends only to consider these issues: there is no mandate to decide or take final action at that time.

Should the ABR offer *Added Qualifications* or encourage the Residency Review Committee to establish a mechanism for the accreditation of fellowship programs? Should it do both? Or should it maintain the status quo? Are fellowships analogous to residencies? Since we require the credentialing of residency-training programs, why don't we do the same with fellowships? The issues are not simply parochial interests of subspecialists, such as pediatric radiologists and neuroradiologists, but of the more encompassing concerns, "What should be the shape of radiology in the future? What is best for the people we serve? How do we prosper? And more to the point, how do we best survive? What is best for all of radiology?" This is the context in which the question of *Added Qualifications* will be considered.

REFERENCE

1. American Board of Medical Specialties. Certification. In: *Annual report and reference handbook, 1985*. Evanston, IL: ABMS, **1985**:78–81

Perspective

Localized Tissue MR Spectroscopy

Alexander R. Margulis[1] and Thomas L. James[2]

Proton MR imaging has in a very short time become a clinically useful and, for some disease conditions, an indispensable diagnostic technique. It owes its advantages over other clinically useful diagnostic tests to the numerous physical parameters within the imaged tissue that determine the quality of the MR signal. These parameters (proton density, T1, T2, diffusion constants, chemical shift, bulk proton motion, and magnetic susceptibility) permit selection of appropriate pulse sequences, thereby emphasizing the distinction between types of tissue as well as between normal and abnormal tissues. Such differentiation is further enhanced by the ability of MR to provide images directly in multiple planes. The speed and spatial resolution of MR imaging are continually being improved, providing images that now display findings unobtainable even a short time ago. Yet these advancements, while providing improvements in sensitivity of detection of abnormalities in many areas, have failed to meet the expectations of marked improvement in specificity.

Tumors and chronic inflammatory disease are often indistinguishable from each other on MR images. In most cases, the capability to detect an abnormality has failed to be matched by a capability to give information about the nature of the abnormality. Use of paramagnetic contrast media has improved the method's sensitivity only in detecting disease.

MR spectroscopy in vivo has started to provide valuable data about numerous metabolic processes. ^{31}P spectra have been studied most commonly, but valuable in vivo information has also been obtained from ^{13}C, ^{19}F, ^{23}Na, and H spectra. Compared with MR imaging, MR spectroscopy requires higher magnetic field strength, and much better magnetic field uniformity is needed in order to obtain good separation between peaks in the spectrum and to reduce noise. Until recently, however, high–field-strength magnets had very small bores, which limited in vivo studies to small animals and upper limbs of humans. With advancing magnet technology, spurred on by increasing clinical demand for imaging, 1.5- and 2.0-T, 1-m bore magnets are becoming fairly common, and 4.7-T, 33-cm bore magnets, which can produce spectra from tissue of experimental animals as well as images, are now being introduced into research laboratories.

While spectra obtained by means of the higher field instruments are generally superior to those from 2-T imaging spectrometers, the spectra obtained from the lower field imaging spectrometers are definitely of high quality [1–6]. These spectra are usually tissue specific, and the techniques for localizing the MR spectroscopic signal are rapidly improving. Localizing the site of origin of the spectra is extremely important. Much effort is going into the solution of this problem, and recent successful methods have already been described for use in humans [1–6].

Present work in many laboratories is most encouraging in attempting to impart to the high sensitivity of MR imaging the greater specificity of localized tissue MR spectroscopy. Spectroscopic studies, primarily with animals, have already shown an ability to elucidate interesting facets of normal physiology [7–9] and pathophysiology [8–11]. For example, abnormal metabolic features of myocardial and cerebral infarcts have been examined, as have tumor growth and response to radiotherapeutic and chemotherapeutic intervention. The use of various substances as tracers in normal and abnormal animals opens a whole range of metabolic tracer MR spectroscopic studies.

With the addition of spectroscopic consoles to 1.5-T, clinical, 1-m-bore imaging machines, studies on human subjects are being undertaken. MR spectroscopy will not have the same spatial resolution as MR imaging. MR imaging can

[1] Department of Radiology, C-309, University of California School of Medicine, San Francisco, CA 94143-0628. Address reprint requests to A. R. Margulis.
[2] Department of Pharmaceutical Chemistry, School of Pharmacy, University of California, San Francisco, CA 94143-0628.

AJR 147:1327–1328, December 1986 0361–803X/86/1476–1327 © American Roentgen Ray Society

produce useful images with a voxel size of 1 mm^3 or less, but MR spectroscopy requires a voxel size of at least 1 cm^3 to produce diagnostic spectra.

MR spectroscopy promises to become a clinical reality as research in animals progresses. The strategy is (1) to localize and differentiate various atomic nuclei within specific tissue in the animal model, usually on high-field magnets (4.7 T or higher), then (2) to transfer the techniques to MR imager-spectrometers having 1-m bores with 1.5 or 2.0 T. MR images can then be used to identify in animals and humans the locus of interest for spectroscopic in vivo studies of normal and abnormal tissue and of metabolic processes. Clinical work will proceed on the basis of the experience obtained.

A few areas of MR spectroscopic research appear especially promising for clinical application. MR spectroscopic diagnosis of myopathy has been demonstrated [8, 9]. MR spectroscopy has shown potential [10] to aid in follow-up assessment of response of tumors to therapy and in choice of appropriate treatment. On the basis of kidney studies in rats, pigs, dogs, and humans [12], MR spectroscopy also appears to be predictive of renal transplant viability and may prove useful in monitoring the state of the transplanted kidneys. MR spectroscopic detection of testis dysfunction also appears to have potential on the basis of recent animal work [13]. The noninvasive monitoring of metabolic processes in selected areas of the human body is technically demanding; but recent developments have shown the feasibility of such noninvasive monitoring by MR spectroscopy. Many groups of investigators are currently developing and examining the clinical applications of this elegant approach.

REFERENCES

1. Styles P, Scott CA, Radda GK. A method for localizing high-resolution NMR spectra from human subjects. *Magnetic Resonance Med* **1985**;2:402–409
2. Bottomley PA. Noninvasive study of high-energy phosphate metabolism in human heart by depth-resolved ^{31}P NMR spectroscopy. *Science* **1985**;229:769–772
3. Bottomley PA, Smith LS, Leue WM, Charles C. Slice-interleaved depth-resolved surface-coil spectroscopy (SLIT DRESS) for rapid ^{31}P NMR in vivo. *J Magnetic Resonance* **1985**;64:347–351
4. Chance B, Clark BJ, Nioka S, et al. Phosphorus nuclear magnetic resonance spectroscopy in vivo. *Circulation* **1985**;72(Suppl IV): 103–110
5. Grist TM, Jesmanowicz A, Froncisz W, Hyde JS. 1.5T in vivo ^{31}P NMR spectroscopy of the human liver using a sectorial resonator. *Magnetic Resonance Med* **1986**;3:135–139
6. Ordidge RJ, Connelly A, Lohman JAB. Image-selected in vivo spectroscopy (ISIS). A new technique for spatially selective NMR spectroscopy. *J Magnetic Resonance* **1986**;66:283–294
7. Stromski ME, Arias-Mendoza F, Alger JR, Shulman RG. Hepatic gluconeogenesis from alanine: ^{13}C nuclear magnetic resonance methodology for in vivo studies. *Magnetic Resonance Med* **1986**;3:24–32
8. Chance B. Studies of exercise performance, vascular disease, and genetic disease. In: James TL, Margulis AR, eds. *Biomedical magnetic resonance.* San Francisco: Radiology Research and Education Foundation, **1984**:187–199
9. Radda GK, Shulman RG. Nuclear magnetic resonance of in vivo metabolism: from normal to pathophysiology. In: James TL, Margulis AR, eds. *Biomedical magnetic resonance.* San Francisco: Radiology Research and Education Foundation, **1984**:201–207
10. Litt L, Gonzalez-Mendez R, Severinghaus JW, et al. Cerebral intracellular changes during supercarbia: an in vivo ^{31}P nuclear magnetic resonance study in rats. *J Cereb Blood Flow Metab* **1985**;5:537–544
11. Evanochko WT, Ng TC, Glickson JD. Application of in vivo NMR spectroscopy to cancer. *Magnetic Resonance Med* **1984**;1:508–534
12. Bretan PN Jr, Vigneron DB, James TL, et al. Assessment of renal viability by phosphorus-31 magnetic resonance spectroscopy. *J Urol* **1986**;135:866–871
13. Bretan PN Jr, Hricak H, Vigneron DB, et al. Assessment of testicular metabolic integrity of phosphorus-31 magnetic resonance spectroscopy. *Radiology*, in press

Letters

Densitometric Screening for Osteoporosis: A Radiologist's Perspective

Two recent articles in the internal medicine literature have sharply criticized the potential role of noninvasive densitometric techniques in screening for osteoporosis [1, 2]. Using an epidemiologic approach, Cummings and Black [1] have concluded that screening is warranted because of the serious consequences of hip fracture, but that it may not be justified to identify individuals at risk for vertebral and distal radial fractures, which have relatively minor clinical sequelae. They also contend that screening is indicated only if the results would influence the decision regarding long-term preventive therapy. In addition, emphasis is placed on the imprecision of existing densitometric technology and on the limited predictive value for fracture afforded by these methods at sites other than the spine.

In a discussion of similar concepts, Ott [2] concluded that advertisements recommending osteoporosis screening for women between the ages of 45 and 70 years are misleading. She also alluded to the great financial profit that can be made by performing densitometric studies on a large number of patients.

While these criticisms have merit, both articles failed to consider several important aspects of the osteoporosis problem. Densitometric screening of women has significant merit even if its only consequence is an increasing awareness of the disease on the part of the general public. The tragic fact that most American women are calcium-deficient and/or have lifestyle habits that are detrimental to skeletal integrity indicates that our health-care system has not placed sufficient emphasis on preventive medicine, particularly for younger women. Current evidence indicates that osteoporosis is a disease that should be attacked in adolescence, with strategies including educational programs in schools aimed at encouraging optimal dietary and exercise regimens. Nevertheless, the ability of a woman at any age to have a simple, noninvasive, and safe test that can tell her the status of her bones as compared with age-matched peers can, in our experience, contribute greatly to the adoption of an appropriate lifestyle.

Another important concept not addressed by the articles under discussion involves the therapeutic approach to osteoporosis. Cummings and Black hint that the risk-benefit ratio for low-dose estrogen replacement may be low enough to warrant its indiscriminate use in all perimenopausal women, which would obviate densitometric screening. However, they fail to indicate that other potential therapeutic options are currently being explored at many research institutions, including our own. It is entirely possible that fluoride, calcitonin, vitamin D, and other yet-to-be discovered agents, alone or in combination, may be viable alternatives to estrogen replacement in certain individuals. Both articles argue that newer densitometric techniques with improved clinical reproducibility and/or the capability for measuring bone quality and geometric structure must be developed before osteoporosis screening can be justified, but the authors fail to recognize that the optimal means for treating the disease is also not currently available. The ability to successfully monitor the disease and its response to specific therapeutic regimens has been demonstrated in a large number of studies [3–6], despite the fact that the long-term precision of existing densitometric measurements may not be perfect.

It is our belief that Cummings and Black have inappropriately deemphasized the potential impact that a fracture of the spine or distal radius may have on the patient. Both are associated with pain and disability, albeit transient [7, 8], and no patient would choose the "dowager's hump" deformity (resulting from multiple vertebral fractures) if it could be avoided by early detection and treatment of the underlying disease. Thus, although screening for increased risk of fracture at these sites may not be justified from an epidemiologic standpoint, it most certainly is from a personal perspective. The authors may be interested to know that our institution was able to purchase its single- and dual-photon absorptiometers through the generosity of a 92-year-old woman with severe osteoporosis, whose lifestyle had been limited by disabling deformities.

Finally, both articles are critical of the cost and potential profit motive involved in noninvasive densitometric techniques. As pointed out by Cummings and Black, the number of clinics offering bone-mass determinations (chiefly by single-photon absorptiometry of the distal radius, which is less reliably predictive of mineral status at axial sites of osteoporotic fracture than direct measurement) is projected to increase from approximately 25 in 1984 to over 500 by the end of this year. Unfortunately, the inevitable has indeed happened in a capitalistic nation; money is being made from osteoporosis by a variety of businesses, including private entrepreneurs. Calcium supplement tablets, dairy council advertisements, calcium in breakfast cereals and soft drinks, antacids marketed for the skeleton as opposed to the stomach, and such densitometric clinics are a reflection of this tragic fact. As radiologists and nuclear medicine physicians, it is our duty to maintain the costs of bone-density measurements as low as possible. Medicine should never be a business, and it is our conviction that every woman has a right to know truthfully the risk of fracture at important sites. The criticisms of our internal medicine colleagues need not be justified. Our advocation of densitometric

screening for osteoporosis should stem from one or more of the concepts outlined above rather than a profit motive.

David J. Sartoris
UCSD Medical Center
San Diego, CA 92103
Donald Resnick
Veterans Admininstration Medical Center
San Diego, CA 92161

REFERENCES

1. Cummings SR, Black D. Should perimenopausal women be screened for osteoporosis? *Ann Intern Med* **1986**;104:817–823
2. Ott S. Should women get screening bone mass measurements? *Ann Intern Med* (Editorial) **1986**;104:874–876
3. Recker RR, Saville PD, Heaney RP. Effects of estrogens and calcium carbonate on bone loss in postmenopausal women. *Ann Intern Med* **1977**;87:649–655
4. Genant HK, Cann CE, Ettinger B, Gordan GS. Quantitative computed tomography of vertebral spongiosa: a sensitive method for detecting early bone loss after oophorectomy. *Ann Intern Med* **1982**;97:699–705
5. Chesney RW, Rose PG, Mazess RB. Persistence of diminished bone mineral content following renal transplantation in childhood. *Pediatrics* **1984**;73:459–466
6. Ruegsegger P, Dambacher MA, Ruegsegger E, Fischer JA, Anliker M. Bone loss of premenopausal and postmenopausal women. *J Bone Joint Surg (Am)* **1984**;66:1015–1023
7. Frost HM. Clinical management of the symptomatic osteoporotic patient. *Orthop Clin North Am* **1981**;12:671–681
8. Garraway WM, Stauffer RN, Kurland LT, O'Fallon WM. Limb fractures in a defined population. II. Orthopedic treatment and utilization of health care. *Mayo Clin Proc* **1979**;54:708–713

Dynamic Upper Airway Narrowing in Patients with Obstructive Sleep Apnea

In a recent study Ell et al. [1] employed cine CT scans to show the dynamic upper airway narrowing in four patients with obstructive sleep apnea. The authors concluded that cine CT is a rapid, simple, and noninvasive method for screening patients with suspected sleep apnea, and is by far more sensitive than other diagnostic-imaging methods of the upper airways.

We wish to point out several problems that may compromise the use of this technique as a screening test in patients with obstructive sleep apnea. First, the cine CT data were acquired during one respiratory cycle; despite the authors' assertion that this is a dynamic technique, they presented no data describing the variation in upper airway cross-sectional area with lung volume. Single measurement of pharyngeal cross-sectional area at functional residual capacity may not be sufficient to differentiate normal subjects from patients with obstructive sleep apnea, since nonapneic snorers also have reduced cross-sectional area at functional residual capacity. However, the amount of reduction in cross-sectional area between functional residual capacity and residual volume (i.e., lung volume dependence of pharyngeal area [2, 3]) permits differentiation among the three groups: nonapneic snorers, nonapneic nonsnorers, and patients with obstructive sleep apnea. These subtle differences in dynamic pharyngeal cross-sectional area further emphasize the necessity for selecting a proper control group when reporting pharyngeal cross-sectional area.

Second, the cine CT technique appears to be incapable of providing another important characteristic that differentiates patients with sleep apnea from nonapneic controls–namely pharyngeal compliance, which is increased in these patients [4, 5], even in the presence of normal cross-sectional area at functional residual capacity. Thus, it is surprising that the authors found no change in extrathoracic upper airway cross-sectional area with the Mueller maneuver.

The third point concerns the fact that all four patients studied by Ell et al. had gross anatomic abnormalities of their upper airways during breathing. Most patients with obstructive sleep apnea have no obvious anatomic deformities of their upper airways and from the data presented by the authors it is not clear whether the sensitivity and reproducibility of the cine CT technique would permit detection of subtle changes in pharyngeal geometry in such cases.

Age and gender are also known to influence pharyngeal area [6, 7] and its lung volume dependence; therefore these factors should also be considered when reporting pharyngeal cross-sectional areas.

Our comments are not intended to criticize the authors' effort to develop an objective and dynamic method of imaging upper airways. Rather, they are intended to reemphasize the difficulties with studying upper airway geometry under dynamic conditions and the need for further appropriately designed studies to validate the usefulness of new techniques. Presently, the cine CT technique has some obvious drawbacks: it exposes the subject to considerable radiation; it does not permit a truly dynamic (i.e., breath-by-breath) imaging of the upper airways; and it requires considerable financial resources. We wish, therefore, to point out a new method [8] that is currently being explored in our laboratory. It employs sound waves to infer the cross-sectional area of the upper airways at least up to and perhaps a few centimeters past the carina. This method is noninvasive, simple, reproducible, inexpensive, and permits the measurements of upper airway cross-sectional area in the supine position as frequently as 5 times/sec. So far, this technique has been applied to only a few human studies, but it appears to have a considerable potential as a dynamic imaging technique for the upper airways, particularly in patients with suspected obstructive sleep apnea.

I. Rubinstein
N. Zamel
V. Hoffstein
Toronto General, Mt. Sinai, and St. Michael's Hospitals
University of Toronto
Toronto, Ontario, Canada MSB 1W8

REFERENCES

1. Ell SR, Jolles H, Galvin JR. Cine CT demonstration of nonfixed upper airway obstruction. *AJR* **1986**;146:669–677
2. Hoffstein V, Zamel N, Phillipson EA. Lung volume dependence of pharyngeal cross-sectional area in patients with obstructive sleep apnea. *Am Rev Respir Dis* **1984**;130:175–178
3. Hoffstein V, Bradley D, Brown I, Zamel N, Martinez D, Grossman RF. Pharynx in snorers, non-snorers, and patients with obstructive sleep apnea. *Am Rev Respir Dis* **1986**;133:A148
4. Brown IG, Bradley TD, Phillipson EA, Zamel N, Hoffstein V. Pharyngeal compliance in snoring subjects with and without obstructive sleep apnea. *Am Rev Respir Dis* **1985**;132:211–215
5. Issa FG, Sullivan CE. Upper airway closing pressures in obstructive sleep apnea. *J Appl Physiol* **1984**;57:520–527
6. White DP, Lombard RM, Cadieux RJ, Zwillich CW. Pharyngeal resistance in normal humans: influence of gender, age, and obesity. *J Appl Physiol* **1985**;58:365–371
7. Hoffstein V, Brown IG, Zamel N. Pharyngeal cross-sectional area in normal men and women. *Am Rev Respir Dis* **1986**;133:A306
8. Hoffstein V, Zamel N. Tracheal stenosis measured by acoustic reflection technique. *Am Rev Respir Dis* **1984**;130:355–357

Reply

The letter from Dr. Hoffstein and associates raises several questions that merit response. The complexities of upper airway caliber in various physiologic situations have been well documented. That does not exclude the possibility that obstructive sleep apnea patients will differ from normal subjects when imaged in a way hitherto impossible. We stressed in our article that the work presented represented early experience with a new technique and was not highly structured and tightly controlled scientific research. We would anticipate considerable refinement both in technique and diagnostic criteria as experience accumulates. Stanford et al. [1] have continued this study, refining the diagnostic criteria and finding a greater variation among normal subjects, as one would expect, but still with excellent results in diagnosing obstructive sleep apnea. Despite the complexities of this condition, cine CT has so far remained reliable in diagnosis.

The query regarding the lack of significant airway change during Mueller maneuver and lack of definite measurement of compliance is justified. The results we obtained are correct, but the Mueller maneuver was modified. We instructed patients and controls to exert only the effort necessary to take a normal breath. We were aware of the Griscom paper and thought that a gentler Mueller maneuver might reveal airways susceptible to collapse at mild negative pressures. We regret that this was not made clear in the text. At the same time, however, we believed that this modified maneuver might be an indirect indicator of pharyngeal compliance, as borne out by our results.

The radiation dose *is* low relative to other imaging techniques. The acoustic reflection technique recommended by Dr. Hoffstein is *not* an imaging technique, but a system of inferring cross-sectional areas. While the patients we studied had gross abnormalities, as we pointed out, they were obvious, indeed detectible radiographically, only on cine CT (except for one). Thus, at least in terms of radiographic techniques we were justified in claiming a high sensitivity. Which tests will ultimately prove optimal in diagnosing obstructive sleep apnea remain to be determined.

The Imatron C-100 Cine CT scanner is expensive. Since this is a very quick exam, it need not be prohibitively expensive. It seems unlikely that anyone would purchase a Cine CT unit solely to study airways, and since most hospitals have CT scanners (the Imatron also can do routine studies), the financial question is of dubious relevance.

The criticism of our claims relative to this technique relates to at least three areas. We do feel the cine CT technique is the most sensitive noninvasive *imaging* technique available. Conventional CT and fluoroscopy have disadvantages we have discussed. Again, acoustic reflection is *not* an imaging technique. Second, cine CT does have dynamic capability. Acoustic reflection can sample airway area 5 times/sec but cine CT can do so 16 times/sec. The technique we used samples over a longer time, but that was our choice, not a limitation of the scanner. We stated that 5 sec of scanning were always sufficient to image one respiratory cycle. That does not, however, mean that that is all we ever studied. Perusal of our illustrations would show that most of our subjects breathed twice. Third, questions of reproducibility and control group choice were raised. We are unsure of the importance of the first point. If a patient shows an abnormality we consider indicative of obstructive sleep apnea, are we to reexamine him several times (more radiation) to determine if that abnormality is always present? The control group was problematic. We described it and recognized variations in upper airway size and compliance with age and other factors. Nonetheless, we used criteria of abnormality that were extreme, so that we purposefully rendered our test *less* sensitive than if we had simply taken as abnormal that not seen in our control group. Obviously, further refinement is needed (and indeed has come) in this area.

Overall, we do not feel inclined to retract anything we said. The fact that a phenomenon is complex does not necessarily mean that it cannot be diagnosed or strongly suspected from a simple test. The appropriate and expedient means to diagnose obstructive sleep apnea remain unclear. We did not make such a claim for cine CT. We regret that the language of our paper lent itself to such misinterpretation. Any lack of clarity is a fault.

S. R. Ell
H. Jolles
J. R. Galvin
University of Chicago
Chicago, IL 60637

REFERENCE

1. Stanford W, Rooholamini M, Galvin J, Dicken S, Crockett D, Ell S. Cine CT in the evaluation of sleep apnea. Presented at annual meeting of Society of Thoracic Radiology. Newport Beach, CA, February **1986**

CT Evaluation of Soft-Tissue Hemorrhage

In the June 1986 issue of *AJR*, Illescas et al. [1] described the CT evaluation of soft-tissue hemorrhage, suggesting a specific "sign" of contiguity of the high-density soft-tissue mass with the inguinal vessels.

The authors stated that "surgery is performed if there is evidence of continued bleeding." They point out that the size of the hematoma can be precisely measured. Presumably then, serial CT studies would be required, with enlarging dimensions suggesting continual hemorrhage in these cases in which clinical evidence for continued extravasation is often absent.

Reversal of anticoagulation or surgical intervention are steps that should be taken only when there is definitive evidence for continued extravasation. Changes in dimension(s) of a soft-tissue hematoma may erroneously suggest continued extravasation when only a change in configuration is manifest because of partial resorption or influx of extravascular fluid.

I have used a simple, essentially noninvasive and potentially portable scintigraphic technique for assessing "activity" of hemorrhage into soft-tissue spaces [2]. Several techniques are now commercially available for labeling autologous RBC with ^{99m}Tc. The technique involves the administration of IV ^{99m}Tc-labeled RBC with subsequent imaging over the area of interest in multiple planar views or tomographic planes (single-photon emission CT, or SPECT is now widely available).

Dynamic imaging with computer acquisition will frequently demonstrate active bleeding within minutes of ^{99m}Tc-RBC administration. When initial imaging for 30 to 90 min is negative, repeat scintigraphy is performed at 4 to 6 hr, providing an accurate method of documenting continued slow or intermittent extravasation in that changes in both physical dimensions as well as decay-corrected count density can be quantitated. Occasionally, delayed imaging up to 24 hr may be necessary to confirm continued bleeding.

High-risk patients can be given an injection at the conclusion of angiography. Iliac vessels are readily identified on both planar and SPECT-imaging studies of ^{99m}Tc-labeled RBC distribution. The ^{99m}Tc-labeled RBC technique might be performed in conjunction with the postangiographic CT study to confirm active bleeding if the specificity for the "sign" reported by Illescas et al. is validated in larger series.

Stephen R. Bunker
Children's Hospital of San Francisco
San Francisco, CA 94118

REFERENCES

1. Illescas FF, Baker ME, McCann R, Cohan RH, Silverman PM, Dunnick NR. CT evaluation of retroperitoneal hemorrhage associated with femoral arteriography. *AJR* **1986**;146:1289–1292
2. Bunker SR, Kolina JS, Kaplan KA, McAuley RJ, Lull RJ. Scintigraphic detection of occult hemorrhage using RBCs labeled in vitro with technetium Tc 99m sodium pertechnetate. *Arch Intern Med* **1983**;143:1027–1028

Reply

We appreciate the opportunity to respond to the comments of Dr. Bunker. We agree that soft-tissue hemorrhage and confirmation of continued bleeding may be difficult to assess and has significant clinical implications. In the proper clinical setting when retroperitoneal hemorrhage is suspected, the role of CT is to confirm the presence of hemorrhage, determine its size, location, and extent within the retroperitoneal compartments, and when possible, identify the cause of hemorrhage. CT is the best imaging technique to assess these parameters, although it cannot assess the "activity" of hemorrhage as does scintigraphy.

A single CT examination cannot be used to determine the persistence of bleeding. However, in our experience, clinical and laboratory parameters are usually present when there is continued hemorrhage, and imaging techniques only serve to confirm this clinical suspicion. Of the three patients taken to surgery in our series, the preoperative clinical evaluation regarding persistence of bleeding was correct in all three. In the patient described by Dr. Bunker, clinical parameters indicated the presence of ongoing bleeding, which was subsequently confirmed by scintigraphy.

After confirmation of the presence of a hematoma by CT, the described scintigraphic technique may be used to confirm active bleeding when clinical evidence of such is equivocal. How often this occurs requires further study, and until then this scintigraphic technique in conjunction with CT may be helpful in selected difficult cases.

Fernando F. Illescas
McGill University
Montreal, Quebec
Canada H3G 1A4

Avascular Necrosis of the Hip

In the July 1986 issue of *AJR*, Mitchell et al. [1] reported a comparison of MR, CT, and scintigraphy as imaging techniques for the diagnosis of avascular necrosis (AVN) of the hip. Their results confirm the earlier conclusions of Easton et al. [2], as well as their own preliminary reports [3, 4].

It should be noted, however, that current radionuclide (RN) bone scanning techniques are no longer limited to planar and pinhole-imaging routines. Recent preliminary data suggest that the increased contrast resolution of single-photon emission CT (SPECT) provides improved sensitivity over standard RN techniques applied to the hip [5]. In addition, SPECT images can be formatted into transaxial, coronal, and parasagittal planes, which allow for more precise comparisons with both CT and MR.

Our own initial experience in cases studied prospectively by both MR and SPECT has shown virtually 100% correlation in both early and late AVN, as well as in normal hips. In the cost-conscious environment of current health care, the economics of the various imaging techniques must also be considered. Since SPECT remains the least expensive of the three (San Francisco Bay Area total charges for MR is $800, CT $420, and SPECT $340), initial screening for AVN with this technique may be preferable, with MR evaluation reserved for evaluation of the extent of disease when SPECT is positive or for those cases when strong clinical evidence for hip disease exists despite negative screening with SPECT. It would seem that larger prospective series comparing MR and SPECT will be required before definitive conclusions about the proper diagnostic algorithm can be made.

Stephen R. Bunker
Hirsch Handmaker
Children's Hospital of San Francisco
San Francisco, CA 94118

REFERENCES

1. Mitchell MD, Kundel HL, Steinberg ME, Kressel HY, Alavi A, Axel L. Avascular necrosis of the hip: comparison of MR, CT, and scintigraphy. *AJR* **1986**;147:67–71
2. Easton E, Zuger J, Salmon R, Floyd M. Superiority of magnetic resonance imaging in the detection of avascular necrosis of the femoral head. Presented at the annual meeting of the Society of Magnetic Resonance in Medicine, New York, August **1984**
3. Thickman D, Axel L, Kressel HY, et al. MR imaging of avascular necrosis of the femoral head. *Radiology* **1984**;153(P):137
4. Kundel HL, Mitchell M, Steinberg ME, Kressel HY, Alavi A. Comparison of MR, CT, and RN imaging of avascular necrosis of the hip using ROC curves. *Radiology* **1984**;153(P):137
5. Collier BD, Carrera GF, Johnson RP, et al. Detection of femoral head avascular necrosis in adults by SPECT. *J Nucl Med* **1985**;26:979–987

Reply

We thank Doctors Bunker and Handmaker for bringing this new technique to our attention. We hope they will pursue their evaluation of SPECT and publish quantitative data on its efficacy and a comparison of it with MR.

Meanwhile, a recent presentation to the American Orthopedic Association gave preliminary evidence that MR is more sensitive than SPECT in the diagnosis of early AVN [1]. It should be remembered that SPECT is in its clinical infancy. Cost-benefit analysis will be appropriate only when the efficacy of SPECT is ascertained.

Matthew D. Mitchell
Harold L. Kundel
Marvin E. Steinberg
Herbert Y. Kressel
Abass Alavi
Leon Axel
University of Pennsylvania Medical School
Philadelphia, PA 19104

REFERENCE

1. Levine M, Roth AI, Stulberg BN, Pflanze W, Feiglin DHI, Wilde AH. The identification of preradiographic disease in non-traumatic osteonecrosis of the femoral head: a prospective protocol. Presented at the annual meeting of the American Orthopedics Association, Hot Springs, VA, June **1986**

The Mammography Report

The editorial by Dr. Homer, "The Mammography Report", published in the March 1984 issue of the *AJR* [1] is in such conflict with my belief, which is that such reports should reflect only the radiologist's diagnostic opinion rather than any management recommendations, that I wish to respond.

Dr. Homer states, "The clinician is interested in only three things:

(1) Is there an abnormal or suspicious area on the mammogram? (2) If so, must a biopsy be done immediately? (3) If not, what follow-up is needed"? I suggest that many clinicians are only interested in the first of these questions. I believe that surgeons should be given the same consideration that Dr. Homer would give to a clinician treating pneumonia who, according to Dr. Homer, "usually is aware of the appropriate type of follow-up required."

Do not all situations demand complete knowledge of the clinical setting for optimal decision making, a circumstance usually not available to the radiologist? I believe that all decisions must be made on clinical grounds, which by definition include history, physical examination, laboratory and imaging tests, and even social and economic considerations.

I submit that Dr. Homer is dealing with an unusual segment of the medical community that needs so much guidance. When a radiologist and a clinician need to confer, much can be done by direct or telephone communication without creating a medical-legal problem as a result of unsolicited radiologic recommendations.

Robert T. Schorr
San Diego, CA 92120

REFERENCE

1. Homer MJ. The mammography report. *AJR* **1984**;142:643–644

Reply

I believe that the X-ray requisition is not an order form but rather is a request for a radiographic consultation. I have elaborated upon this premise elsewhere [1]. Management recommendations are an appropriate component of a consultation. If Dr. Schorr disagrees with this premise, as his remarks indicate, then he is not taking full advantage of the expertise of his colleagues in radiology. He may only be interested in whether there is an abnormality or suspicious area on the mammogram, but I hope his is a minority opinion among surgeons. My clinical colleagues realize that the knowledgeable radiologist can often provide help in the best management of their patients. Work-up and management of an area of five microcalcifications, an asymmetric density, or a sharply marginated mass are different, and excisional biopsy is not the only option. If Dr. Schorr expects mammographic reports to read either normal or abnormal, then he does not understand the complexities of the examination.

I have no basis upon which I can judge Dr. Schorr's acumen, but I would be curious to know how his surgical training has prepared him to manage nonpalpable breast abnormalities. What is the surgical standard for follow-up of the nonpalpable sharply marginated 6-mm breast mass? What is the traditional surgical teaching regarding the reliability of differentiating benign from malignant microcalcifications? What do the textbooks of breast surgery say about the management of the nonpalpable asymmetric density? I suspect that his surgical training was similar to others and these problems did not exist, because until recently mammography was never performed routinely on asymptomatic women. If Dr. Schorr has been basing management of his patients on anecdotal experience, then he has bypassed valuable input from the radiologist, who should be well versed in the current mammographic literature.

While it is true that social and economic situations may weigh into management decisions, I remain steadfast in stating that there is absolutely no clinical correlation for the nonpalpable mammographic abnormality in the healthy asymptomatic woman. The responsibility of the radiologist in this situation should be quite obvious since he alone has raised the possibility of a breast abnormality, and it seems quite logical to me that input from the radiologist should be sought in determining management recommendations for radiographic abnormalities.

I am fortunate to be part of a dedicated team of physicians who devote much of their time to the diagnosis and treatment of women with all forms of breast disease. I do not function in a vacuum, and the structure of my report fulfills the needs of my referring clinicians in helping them to determine the most appropriate course of action for radiographic findings they cannot palpate.

I am a firm believer in constant communication between the referring clinician and the radiology consultant. However, in my experience, especially when a patient is mismanaged, the substance of the telephone conversation is often difficult to recall at a later date. The mammography report is the only documentation that the radiologist has regarding his consultation. I truly hope that Dr. Schorr will recognize the indispensable help that he can receive from radiologists experienced in mammographic interpretation. If a clinician never seeks advice from his consultant, then I cannot imagine how he can provide optimal and cost-effective care to his patients.

Marc J. Homer
Tufts–New England Medical Center
Boston, MA 02111

REFERENCE

1. Homer MJ. A radiologist's point of view. *JAMA* **1981**;246:2581–2582

What Really Happens in Imaging Centers: Issues of Finance and Control

No subject in the radiologic community stirs up more emotional conflict than the legal, ethical, and financial issues in the development of free-standing outpatient-imaging centers. In a recent issue of this journal, Baum, Zeman, and Eliott debated the ethical nature of imaging-center capitalization, in particular nonradiologist, referring-physician investorship [1, 2]. Some thoughts and experiences of imaging-center radiologists are in order.

The economic resource most commonly available to the radiologist for acquiring high-technology devices (the hospital) is no longer as willing or able to go along with massive expenditures, especially considering the present prospective payment reimbursement schemes (put into place by Medicare). The introduction of MR into clinical practice has exacerbated this problem. The need for capital and the demand for service has produced a new type of venture, which is a pooling of resources from radiologists, nonradiologist referring physicians, venture capitalists, and/or a hospital. Clearly, some, but not all, of the impetus for developing outpatient imaging centers is the profit motive.

Some people assume that the monetary participation of nonradiologist referring physicians in the imaging-center capital pool is unethical and undesirable because such arrangements constitute an economic incentive to refer their own patients to the imaging center, with potential for abuse, and because control of imaging services shifts from the radiologist to the referring physician. A well-constructed and realistic prospectus of a typical imaging center partnership usually describes a return on investment that is insignificant in relationship to a referring physician's total earned income. The minimal tax advantages (e.g., depreciation) may make the physician a slightly more willing investor and reduce some financial risk. However, this benefit is not related to the direct and ongoing referral of patients. The physicians who invested in our center are responsible for a small fraction of the total business that is performed. For this reason, it is hard to sell limited partnership interests in imaging centers to skeptical physicians when the focus is on finances alone.

Physician investorship is a result of several factors. Many physicians are unhappy with the efficiency, level of service, and cost structure of imaging that is provided in the hospital. They see many

hospitals as being monolithic, manipulative, and cumbersomely slow in the ability to respond to their practice needs. The opportunity to invest in a radiology center provides them with a fairly quick and direct way of procuring services without being involved in the politics and encumbrances of hospital administration. Physician investment in radiology may be a greater demonstration of frustration with respect to the hospital and the changing economic forces of medicine than it is a function of personal greed. Our experience would support the statements of Zeman and Elliott that referring physicians are more interested in providing high-quality, prompt and cost-efficient care for their patients than in the minimal return that they might receive from sending those patients to an imaging center in which they are invested. Undoubtedly, some physicians will attempt to exploit the imaging-center concept for excessive personal gain. The practices and investment opportunities created by this minority can be easily spotted and avoided by legitimate practitioners when armed with the appropriate facts about imaging-center operation.

Venture capitalists are becoming more involved in the financing of outpatient radiology centers. However, the involvement of a corporation in the imaging-center "joint venture" may be welcomed by all parties. The referring physician–investment group, the radiologist, and hospital (if investors) may seek to reduce their financial liability with additional capital. The physician and hospital groups may also want help with the problems of outpatient-imaging administration. Often, the independent corporate entity will function as "facilitator" of this complex venture in which the parties have had a history of conflict, turmoil, and/or nonperformance in previous business arrangements.

In his article, Baum stated that the hospital (corporately owned or not) should be the major financial partner in radiology imaging centers since they are "committed to high levels of care" and have produced relationships that have worked in the past. However, none of us is convinced of this altruistic assessment. The hospital is also a corporate business that has its own problem with the diverse environment that it administers. Outpatient radiology centers are large and complex businesses that demand greater administrative specialization and attention. In the background, the Federal Government, large and impersonal conglomerates, insurance companies, and HMOs loom as our financial partners.

We believe, unequivocally, that the quality of care and level of radiologic practice in an outpatient imaging center is controlled by the radiologists. In a limited-partnership structure, by definition, the investor has no say in the operation of the center nor any voice in its management. Other organizational arrangements may be different. However, radiologists would do well not to enter into those kinds of structures. The investing physician exerts no more control than the noninvesting physician. His (her) demands on a radiology practice are similar to those in a hospital setting. The independent corporate business partner is prohibited by law from interfering in the practice of medicine (California Statute). The possible pressures that could be brought to bear on the radiologist to streamline practice procedures and become more efficient are really no different from those that are instituted currently in the hospital environment. Corporate investor and management companies realize that the success of the center is largely dependent on the creation of strong relationships between referring doctors and radiologists, which in a competitive environment means supporting a quality practice. Conflict in matters of business or professional practice between radiologists and corporate partners is detrimental to this goal and everyone works to diminish or resolve it. Adequate safeguards are usually provided against encroachment on medical practices. However, it is the radiologist's responsibility to demand and get control of those portions of practice in which no other individual or group should meddle.

Perhaps the controversy among radiologists surrounding issues in outpatient imaging is really borne out of fear. Many radiologists (by virtue of their exclusive hospital contract and unofficial territorial boundaries) are unaccustomed to and afraid of the potential for competition that the establishment of outpatient investor-owned imaging centers implies, especially if they are uninitiated and insecure about independent practice in a rapidly changing environment. Imaging centers do not threaten traditional radiologic practice. HMOs, insurance companies, and government agencies do. It is early enough in the imaging-center phenomenon to establish rules that are fair and efficient. Radiologists must grasp this opportunity to mold the rules and create an environment that is to our liking. Clearly this means forging bold new relationships and new business strategies in the provision of radiologic care.

Keith R. Burnett
Joel B. Levine
Long Beach Medical Imaging Clinic
Long Beach, CA 90804

REFERENCES

1. Baum S. Physician investment in free-standing imaging centers: in opposition. *AJR* **1986**;147:412–413
2. Zeman RK, Elliott LP. In defense. *AJR* **1986**;147:414–416

Free-Standing Imaging Centers

This letter is to provide support for the argument by Baum against nonradiologic physician investment in imaging centers [1]. Although data are scarce, there has been at least one substantial investigation of the influence of ownership on the frequency of use of diagnostic radiologic studies [2]. The survey by Childs and Hunter of 7300 patients found that nonradiologists with a financial interest in providing their own radiologic services obtained studies twice as frequently as physicians referring patients to radiologists. The data supported a conclusion that physicians having an economic interest in radiologic equipment are encouraged to obtain more radiologic studies on their patients than physicians without a similar economic interest.

In our locality, a large health maintenance organization found that, in randomly referring patients to specialists in the community, one particular group owning a CT scanner incurred far greater costs. On further analysis, it was appreciated that they obtained more than nine times as many CT scans as similar specialists who did not own a CT scanner. There is no question in my mind that economic interest in an imaging center encourages physicians to order more studies that are either unnecessary or marginally indicated. I know of no study showing that physicians with such an interest order fewer studies.

Diagnostic imaging is one of the fastest growing components of medical costs and is under increasing regulatory pressure from providers. Hospital-based radiologists in particular are being subjected to these efforts in the form of DRGs, regulated fee schedules, and limited approval of equipment installations. In view of this, radiologists should point out to all parties that much of the increase in cost of diagnostic imaging procedures is taking place in a setting of self-referral. The most obvious solution to this problem would be the refusal of providers to pay for examinations that are self-referred. Unless steps are taken by radiologists to encourage the elimination of self-referral, cost-containment efforts in diagnostic testing will in large measure continue to be directed at radiologists, particularly hospital-based radiologists, who are the individuals least involved in these abuses.

David W. Gelfand
Bowman Gray School of Medicine
Winston-Salem, NC 27103

REFERENCES

1. Baum S. Physician investment in free-standing imaging centers. In opposition. *AJR* **1986**;147:412–413
2. Childs AW, Hunter ED. Non-medical factors influencing use of diagnostic x-ray by physicians. *Med Care* **1972**;10:323–335

Reply

It is naive for advocates of free-standing medical imaging centers to believe that venture capital or corporate business entities are not concerned about maximizing profits. By definition, a commercial venture is concerned about making money whether it involves the operation of a hot dog stand or an imaging center.

Burnett and Levine's argument that "free-standing outpatient imaging centers save money in this environment of cost containment" is simply not true. As Gelfand points out, physician self-referral has always resulted in marked increase in use of radiologic procedures when compared with physicians without a similar economic interest.

The fact that free-standing outpatient-imaging centers stir so many emotions and ethical questions is an indication that most of us realize that these entities represent an intrusion of business and commercialism into the practice of radiology. The corporate mentality that goes directly to the bottom line threatens the moral and ethical foundation of our profession.

As radiologists, we have traditionally been rewarded with professional fees for the rendering of a professional consultation. We have not benefited financially because we have invested in the facility. It has been customary practice to have referring physicians send us patients because they value our professional opinion. The unsavory practice of having a referring physician own a financial piece of an imaging center raises many ethical issues and any argument that tries to justify "innocent" self-referral is simply rationalization. This type of self-referral has been judged unethical by our professional organizations as well as by state legislation that prohibits physicians from referring patients to any facility in which the referring physician has a financial interest.

The proliferation of outpatient imaging centers poses many other problems as well. What accommodations have been made in these business ventures for the care of the indigent? In our region of the country the only patients studied at these imaging centers are those having either insurance coverage or the ability to pay directly out of pocket. If this trend continues, there will almost certainly be an erosion of the hospital-based departments of Radiology as the percentage of indigent care increases and the so-called "financial cream" is skimmed from the top by the imaging center.

A great deal of the so-called inefficiency of hospital-based radiology practice is due to housestaff training. Where would these efficient physician businessmen receive their radiologic training? Certainly not in a free-standing imaging center. In my opinion, the removal of high-technology facilities from hospital practice will spell disaster for the future training of radiologists. We have an obligation to leave our successors a profession that is at least as exciting as the one we have inherited. If there are problems in the way hospital practices relate to patients' needs, let us try to improve our mode of practice and procedures and not try to take down the entire house.

Stanley Baum
University of Pennsylvania
Philadelphia, PA 19104

More on Free-Standing Imaging Centers

In their defense of free-standing imaging centers, Zeman and Elliott delude themselves if they really believe that referring physicians invest in such enterprises not for financial gain, but rather because "unfair charges, lack of available services, and inaccurate or slow reporting of findings" occur in already existing hospitals or office radiologic facilities. I have never seen a prospectus for such a venture that lists these reasons to entice doctor-investors. What is emphasized in a prospectus is the potential for a high "return on investment." These enterprises are indeed profit-driven; goals such as preferred treatment and better service for patients, if present at all, are secondary.

As one who has been involved in a free-standing CT facility owned exclusively by radiologists [1] and a free-standing MR facility owned partly by nonradiologic physicians [2], I can state that there is one, and only one, purpose in enlisting the participation of physician-owners: the hope that a referring physician, because of a financial interest in an imaging center in which a return on investment varies directly with the volume of business conducted in that center, will refer patients to the center who ordinarily would be referred elsewhere.

Radiologists who are contemplating formation of a free-standing imaging center owned by nonradiologic physicians should consider the following three potential drawbacks before proceeding. (1) Periodic financial reports of the operation, which contain the income of the radiologist, must be distributed to every owner. As radiologists in private practice know, some of our nonradiologic physician colleagues are envious of the radiologist even when they don't know his exact income. Knowledge of the exact income could well magnify those feelings. Some situations could create conflicts among the doctors. If the enterprise runs at a loss, the physician-owners will lose money, while the radiologist will be collecting his professional fees. If the business operates at a break-even level, the investor makes nothing, but the radiologist still earns his fees. If the center runs well in the black, the physician-investor will earn a small or moderate return on his investment, but the professional fees of the radiologist would probably rise markedly. Any of these scenarios could cause antagonism toward the radiologist by the physician-investors and adversely affect referrals. (2) Physicians who are not investors may be alienated. Referring physicians who choose not to be investors in the center might be competitors of physicians who are investors. This spirit of competition, along with perhaps local medical politics, could lead noninvestor physicians to boycott the imaging center to prevent their competitors from making a profit from their patients. The radiologist would then be an innocent victim, in the middle of such a dispute. The noninvesting physicians could become so angry with the radiologist because he set up such a venture that they would extend the boycott to the radiologist's hospital practice as well. (3) A physician-investor might take the position that since he's an owner, the technologists and the radiologist work for him. This could lead, at the least, to interference with the radiologist's ability to manage the facility; at worst, it could create considerable unpleasantness by placing the radiologist in a subservient position relative to his investor-doctor-owners.

As to moral and ethical considerations, I equate a radiologist's participation in a free-standing imaging center with his carrying a radar detector in his automobile. Both are theoretically immoral and unethical—the former because the purpose is to entice the referring physician to refer patients on the basis of financial reward rather than quality of the radiologic facility, the latter because the purpose is to entice the driver of the auto to speed when he knows there is no law enforcement officer in the vicinity. Notwithstanding the potential for abuse, most of us might indulge in the use of radar detectors because we feel they are practical and not immoral or unethical to the degree that strains our consciences. In the same vein, I believe that if radiologists think that they must organize or participate in a free-standing imaging center partially owned by physician-investors, as a defensive measure and in order to maintain their own professional

viability and financial position by "locking in" their referring physicians before they are attracted to another venture by some other entrepreneur, then they should by all means go ahead and do it. At the same time, however, let us not delude ourselves into believing that such business endeavors are altruistic, highly moral, or without downside risks; for they, like radar detectors, are not.

Leonard Berlin
Skokie Valley Hospital
Skokie, IL 60076; and
University of Illinois College of Medicine,
Chicago, IL 60637

REFERENCES

1. Berlin L. Our health planners are fiddling while I'm burning. *Med Economics* **1980**;57:85–87
2. Berlin L. I'm betting my bundle on NMR. *Med Economics* **1984**;61:108–115

Free-Standing Imaging Centers

This letter is a response to Zeman and Elliott's editorial "In Defense" [1] that appeared in the August 1986 issue of the *AJR*. Most of the joint ventures that have proliferated throughout the country have put the radiologists at a percentage arrangement rather than fee for service. As venture income drops, tax laws change, or equipment is replaced, these percentage arrangements will be altered or new, more compliant radiologists will be hired.

Although most imaging centers do comply with federal law that requires rules for purchase of shares without regard to percentage of patients referred, their selection of investors excludes those who would not refer large numbers of patients to the centers. This provides an unhealthy climate for excessive referral.

The editorial also states that doctors in office practice will not perform their own radiographic procedures if they belong to an imaging center but will instead refer patients to their imaging center. This in fact does not happen because the doctors are not giving up a large source of income by charging the total component in their office for write-off and some income in the clinic.

The only justification for a free-standing out-patient center that I can agree with from practical experience is when a local hospital does not have technical capability, prompt service, or competent radiologists to adequately service their patients. Nonradiologic physicians are becoming entrepreneurs at the expense of the radiologists and their patients. Radiologists should not be a part of this charade.

J. Stolzenberg
Miami Heart Institute
Miami Beach, FL 33140-2999

REFERENCE

1. Zeman, RK, Elliott LP. In defense. *AJR* **1986**;147:414–416

Replies

First, in regard to the letter by Stolzenberg, our opinions are based on our own experiences and those of our fellow radiologists who actually participate in imaging centers. The actual contractual relationship between general partners and radiologists are negotiated up front, as they are in many hospital-based practices. As in a hospital setting, if a contract that is favorable to the radiologist exists, there is always vulnerability. The administration may seek to alter the relationship or hire a new radiologist, just as Stolzenberg suggests may happen in an imaging center.

On the basis of our own experience, after a little less than 1 year of operation, most of our referrals have come from physicians in the Washington suburban area who have no financial interest in our center. This obviously suggests that clinical needs and appropriate referrals are financially driving the center. Stolzenberg is partially correct when he says that nonradiologic physicians will not give up practicing radiology in their offices because of imaging centers. We know of a precipitous drop in the number of fluoroscopic procedures and urograms being performed by clinicians, but bone and chest films are still performed and interpreted by many nonradiologists in this community.

Second, Berlin raises several hypothetical considerations to which we would like to respond. Our dealings with physicians in our imaging center have been extremely positive. We have many noninvestor referrers who do not hesitate to volunteer that our superior service is the reason that we get referrals.

Jealousy over income levels of radiologists, animosity between investor and noninvestor referrers, and the physician-investor as the radiologist's boss are admittedly potential problems. These problems, however, are ones that radiologists must deal with in varying degrees in many forms of practice. Secrecy about one's income is dying fast in radiology. In university hospitals, the hospital administration and medical school have easy access to that information. In many hospital-based practices, billing of radiology professional fees is based on a centralized hospital computer that undergoes numerous checks and audits. Practice-plan income may easily be determined by the many committees involved in managing the hospital's fiscal affairs. Frankly, the new generation of radiologists feels that only those with unethically high incomes have something to hide. Following a well-established precedent in the legal profession, a minority of radiology groups take advantage of their junior, nonvested members. Perhaps some disclosure is not all that bad.

We have not experienced alienation of physicians in our community who are not investors. To the contrary, they have been very supportive. In theory, however, Berlin makes a valid point. To amplify this further, most of the negative reaction that has arisen to our imaging center has been a result of the omnipresent town vs gown dilemma. Our department, like most university departments, has often been viewed as a hibernating bear. Academic departments traditionally have their activities greatly restricted by their parent university. They must shoulder the responsibility for a greater amount of charity than their surburban counterparts. They are vulnerable to suburban practices draining off their patients because urban hospitals are inaccessible and inconvenient. Even their former residents establish practices next door. Academic radiologists are finding many exciting practice opportunities in suburban areas. As this trend spreads to other specialties, our nonuniversity colleagues in and outside of radiology are becoming increasingly nervous about competition from academic physicians, which is the greatest reason for animosity that we have experienced.

The issue of "Who's working for Whom?" is always a concern for the radiologist. We are in a profession that provides a service not only to patients but also to referring physicians. The nature of our profession, whether or not we work in an imaging center, requires immediate response to requests from referring physicians. A radiologist's own integrity and the hands-off corporate structure inherent to the limited-partnership relationship allows a clear distinction as to who works for whom.

We agree with Berlin that every radiologist must analyze his local situation and search his own soul for guidance. Imaging centers are a double-edged sword, but radiology cannot close its eyes and hope that they will go away.

Robert K. Zeman
Larry P. Elliott
Georgetown University Hospital
Washington, DC 20007

Recognition of Manuscript Reviewers, Abstractors, and Book Reviewers for 1986

The editors and the editorial staff wish to express their heartfelt appreciation to the following colleagues, who as reviewers have spent many hours in 1986 helping to select only the most authentic, original, and useful articles for publication in the *AJR*, and to those responsible for abstracts and book reviews.

Each manuscript received by the Journal is anonymously forwarded to two knowledgeable reviewers for their opinions concerning the worthiness of the paper for publication and/or their suggestions for improvement. The reviewers do this without compensation and with no recognition, except for this acknowledgment. The Journal receives 1200 manuscripts annually, of which only 50% of major papers and 15% of case reports are accepted for publication. Authors are nearly always required to revise accepted papers, often more than once, in accordance with the reviewer's (and the editor's) recommendations.

Book reviewers have been equally generous with their time, evaluating for the readers the burgeoning number of textbooks published each year. Finally, those who write or select abstracts of other literature for publication in the Journal help readers stay au courant in a rapidly evolving specialty.

In the aggregate, these many contributors have added immeasurably to the value, scientific merit, and interest of the Journal. The quality of the Journal is in their hands. We are grateful for the erudite and conscientious manner in which they discharge these imposing responsibilities.

Robert N. Berk
Editor-in-Chief

F. P. Agha
A. M. Aisen
N. P. Alazraki
P. O. Alderson
N. K. Allan
J. R. Amberg
E. S. Amis, Jr.
J. H. Anderson
M. Andre
J. H. Arndt
D. Aronberg
H. L. Atkins
J. H. M. Austin
L. Axel
J. W. Baer
N. A. Baily
D. H. Baker
S. R. Baker
D. M. Balfe
E. J. Balthazar
M. P. Banner
M. G. Baron
K. H. Barth
R. J. Bartrum, Jr.
L. W. Bassett
S. Baum
J. W. Beabout
J. A. Becker
C. B. Begg
T. C. Beneventano
W. E. Berdon
P. Berger
M. E. Bernardino
M. A. Bettmann
M. K. Bilbao
A. Bjorkengren
M. D. Blaufox
J. D. Blumhagen
S. P. Bohrer
J. J. Bookstein
G. P. Borkowski

J. D. Bowie
L. M. Boxt
T. J. Brady
D. G. Bragg
F. J. Brahme
M. N. Brant-Zawadzki
R. C. Brasch
L. Brateman
E. M. Braunstein
R. L. Bree
W. H. Brewer
A. C. Brower
J. J. Brown
L. R. Brown
R. C. Brown
R. F. Brown
P. J. Bryan
R. E. Buenger
H. J. Burhenne
H. Burko
A. J. Buschi
W. H. Bush, Jr.
R. J. Butch
P. W. Callen
W. L. Campbell
M. P. Capp
D. H. Carlson
H. Carlson
E. Carlsson
B. A. Carroll
W. J. Casarella
P. N. Cascade
G. Casola
W. R. Castaneda-Zuniga
R. A. Castellino
M. Cerqueira
A. Chait
C. H. J. Chang
J. W. Charboneau
J. R. Charters
N. E. Chase

C. H. Chesnut III
K. J. Cho
V. P. Chuang
R. J. Churchill
C. M. Citrin
R. A. Clark
J. L. Clements, Jr.
W. P. Cockshott
A. M. Cohen
M. D. Cohen
C. Cole-Beuglet
R. S. Colvin
W. G. Connor
C. Cope
P. Costello
L. E. Crooks
A. B. Crummy
D. A. Cubberley
J. J. Cunningham
R. H. Daffner
M. K. Dalinka
D. B. Darling
F. L. Datz
G. B. Davis
J. B. Dealy, Jr.
D. J. Delany
T. C. Demos
A. A. De Smet
W. C. Diner
R. E. Dinsmore
G. D. Dodd
W. J. Dodds
M. W. Donner
J. L. Doppman
J. P. Dorst
E. M. Druy
G. L. Dubuque
J. S. Dunbar
S. J. Dwyer III
M. R. Eckstein
J. Edeiken

D. Edwards
E. L. Effman
J. C. Ehrhardt
R. L. Eisenberg
J. I. Eisenman
G. Y. El-Khoury
K. Ellis
R. A. Ellwood
B. L. Engelstad
J. Fakhry
J. Farman
M. P. Federle
S. A. Feig
D. Feiglin
S. B. Feinberg
F. Feldman
S. K. Fernbach
E. J. Ferris
J. T. Ferrucci, Jr.
M. M. Figley
E. J. Finck
D. W. Fitting
A. C. Fleischer
W. D. Foley
J. B. Foreman
J. Forrest
D. M. Forrester
L. A. Forstrom
E. A. Franken, Jr.
P. C. Freeny
R. H. Freiberger
I. M. Freundlich
D. G. Frey
A. M. Fried
R. M. Friedenberg
G. W. Friedland
A. Friedman
A. C. Friedman
P. J. Friedman
P. Fritzsche
D. G. Fryback

G. D. Fullerton
G. Gamsu
R. Gardiner
B. B. Gay, Jr.
M. A. Geisinger
D. W. Gelfand
S. C. Geller
M. I. Gelman
H. Genant
A. J. Gerlock, Jr.
S. G. Gerzof
L. Gilula
S. N. Glick
M. Glickman
J. D. Godwin
T. C. Goergen
R. E. Gold
R. H. Gold
R. P. Gold
B. B. Goldberg
L. Goldberg
M. E. Goldberg
L. E. Goldberger
A. B. Goldman
H. S. Goldman
M. L. Goldman
H. M. Goldstein
A. S. Gomes
C. A. Gooding
L. R. Goodman
D. A. Goodwin
R. M. Gore
B. B. Gosink
A. F. Govoni
C. B. Graham
H. F. Gramm
J. E. Gray
E. V. Grayson
C. E. Green
R. Greene
R. A. Greenes

A. Greenfield
G. Greenway
N. T. Griscom
J. H. Grollman, Jr.
D. F. Guthaner
J. R. Haaga
K. Haber
F. Hall
J. O. Haller
J. M. Halls
W. Hanafee
R. K. Harned
D. P. Harrington
G. B. C. Harris
J. H. Harris, Jr.
R. D. Harris
D. Hartman
G. W. Hartman
D. Harwood-Nash
M. E. Haskin
R. R. Hattery
I. F. Hawkins, Jr.
M. Healy
C. A. Helms
R. Herfkens
H. Herlinger
B. J. Hillman
J. Hilton
W. S. Hinshaw
P. B. Hoffer
R. A. Holmes
C. S. Houston
H. Hricak
H. K. Huang
K. F. Hubner
T. B. Hunter
D. E. Hutchinson
T. J. Imray
G. A. L. Irwin
K. L. Jackson
H. G. Jacobson

C. C. Jaffe
R. B. Jaffe
E. Janon
M. L. Janower
P. F. Jaques
B. Jeffrey
P. S. Jensen
M. Jochelson
G. C. Johnson
M. A. Johnson
I. S. Johnsrude
B. Jones
R. G. Jost
G. W. Kabalka
S. Kadir
A. R. Kagan
K. Kandarpa
H. Kangarloo
P. A. Kaplan
D. Karasick
N. Karstaedt
R. W. Katzberg
B. T. Katzen
D. Katzman
R. A. Kaufman
S. L. Kaufman
C. Kay
J. J. Kaye
E. Kazam
T. E. Keats
N. N. Keep
F. S. Keller
M. J. Kelley
F. M. Kelvin
P. Kidd
R. Kidd
T. S. Kilcheski
R. F. Kilcoyne
P. T. Kirchner
J. A. Kirkpatrick, Jr.
D. R. Kirks

E. C. Klatte
R. M. Klein
J. B. Kneeland
P. R. Koehler
D. B. Kopans
M. Korobkin
K. L. Krabbenhoft
H. Y. Kressel
A. G. Krudy
R. A. Kubicka
M. V. Kulkarni
H. L. Kundel
A. B. Kurtz
D. C. Kushner
F. C. Laing
M. J. Landay
E. K. Lang
E. C. Lasser
I. Laufer
P. C. Lauterbur
T. L. Lawson
E. A. Lebowitz
R. L. Lebowitz
J. K. T. Lee
T. G. Lee
J. L. Lehr
J. C. Leonidas
J. R. LePage
R. M. Lerner
A. J. LeRoy
D. C. Levin
E. Levine
R. G. Levitt
E. Lewis
D. K. Li
J. E. Lichtenstein
A. Lieber
D. P. Link
M. J. Lipton
J. P. LiPuma
G. S. Lodwick
W. Logan
W. K. Logan
J. F. Lois
J. W. Loop
L. Love
R. B. Lufkin

C. J. Lundell
E. A. Lyons
R. L. MacCarty
W. J. MacIntyre
L. A. Mack
H. MacMahon
D. T. Maglinte
N. F. Maklad
D. Maklansky
M. L. Manco-Johnson
F. A. Mann
C. Marcus
S. I. Marglin
C. Markivee
W. Martel
E. C. Martin
J. E. Martin
J. F. Martin
L. O. Martinez
T. A. S. Matalon
R. Mattrey
A. H. Maurer
G. R. May
R. B. Mazess
J. G. McAfee
W. H. McAlister
R. W. McCallum
M. J. McCarthy
B. L. McClennan
J. McCort
J. P. McGahan
G. K. McLean
R. A. McLeod
T. C. McLoud
T. F. Meaney
H. E. Meema
A. J. Megibow
G. L. Melson
L. Menuch
C. R. B. Merritt
C. E. Metz
M. A. Meyers
R. S. Mezrich
M. S. Middleton
V. G. Millan
F. J. Miller
R. H. Miller III

S. W. Miller
W. T. Miller
H. J. Mindell
C. A. Mistretta
C. A. Mittlelstaedt
H. A. Mitty
M. T. Modic
R. Moncada
W. E. Moore
R. L. Morin
T. W. Morris
R. D. Moseley, Jr.
R. P. Moser, Jr.
M. Moskowitz
P. S. Moskowitz
A. A. Moss
P. R. Mueller
J. R. Muhm
L. R. Muroff
W. A. Murphy
R. C. Murry
H. L. Neiman
W. B. Nelp
J. A. Nelson
T. R. Nelson
A. A. Nemcek
A. H. Newberg
J. D. Newell II
J. H. Newhouse
H. Newmark III
A. Norman
R. L. Nunnally
M. J. O'Brien
M. K. O'Connor
L. Olson
D. J. Ott
T. W. Oviit
M. B. Ozonoff
J. C. Palmaz
A. M. Pantone
B. R. Parker
R. G. Parker
C. L. Partain
S. K. Patel
J. A. Patton
W. Pavlicek
H. Pavlov

A. S. Pearlman
W. Peck
J. P. Petasnick
R. C. Pfister
H. M. Pollack
A. K. Poznanski
S. C. Prasad
D. H. Pretorius
L. A. Prewitt, Jr.
D. C. Price
A. V. Proto
S. Quinn
J. G. Rabinowitz
P. A. Randall
V. Raptopoulos
B. J. Reilly
C. S. Resnick
C. J. Reynes
J. Reynolds
T. Richards
M. D. Rifkin
J. Riley
E. J. Ring
B. Robbins
A. E. Robinson
R. G. Robinson
S. D. Rockoff
J. O. F. Roehm, Jr.
L. F. Rogers
C. A. Rohrmann
F. D. Rollo
P. R. Ros
R. J. Rosen
D. M. Rosenbaum
A. Rosenfield
H. Rosenkrantz
D. Rosenthal
L. Rosenthall
R. P. Rossi
A. Rowberg
V. A. Rowley
J. M. Rubin
C. M. Rumack
V. M. Runge
A. H. Russell
F. F. Ruzicka, Jr.

K. Ryan
N. L. Sadowsky
D. J. Sahn
L. J. Saidman
R. C. Sanders
M. P. Sandler
E. N. Sargent
S. K. Sargent
D. J. Sartoris
M. Sarwar
E. Sauerbrei
S. C. Schatzki
M. S. Schechter
W. Scheible
H. R. Schelbert
H. Schiffman
M. H. Schreiber
P. S. Schulman
S. S. Schwartz
W. B. Seaman
J. I. Sebes
A. M. Segal
J. H. Shapiro
D. R. Shearer
P. F. Sheedy II
W. H. Shehadi
W. P. Shuman
A. Siegal
B. A. Siegel
H. A. Siegel
M. E. Siegel
M. J. Siegel
E. B. Silberstein
T. M. Silver
P. M. Silverman
J. F. Simeone
A. L. Simon
E. B. Singleton
M. L. Skolnick
J. Skucas
J. G. Smirniotopoulos
C. Smith
E. H. Smith
H. J. Smith
J. Smith
K. W. Sniderman

T. A. Sos
B. Soto
R. L. Soulen
R. P. Spencer
D. Spigos
H. Spindola-Franco
B. A. Spirt
D. B. Spring
R. C. Stadalnik
P. Stanley
R. J. Stanley
T. W. Staple
D. D. Stark
G. M. Stevens
R. K. Stevens
G. Stevenson
E. Stewart
D. A. Stringer
J. R. Sty
M. Sundaram
L. Swischuk
L. Talner
J. P. Tampas
J. M. Taveras
G. A. Taylor
K. Taylor
C. D. Teates
R. Teele
C. J. Tegtmeyer
S. K. Teplick
F. D. Thomas
W. M. Thompson
J. R. Thornbury
J. Tisnado
I. L. D. Tonkin
T. A. Tristan
R. H. Troupin
D. A. Turner
J. A. Usselman
R. L. Van Heertum
M. Viamonte, Jr.
C. W. Vick III
M. R. Violante
V. A. Vix
S. D. Wall
S. Wallace

W. J. Walls
J. W. Walsh
J. F. Walter
A. C. Waltman
V. Waluch
Y. Wang
J. F. Ward
W. R. Webb
F. W. Wehrli
J. C. Weinreb
B. N. Weissman
H. S. Weissman
J. L. Westcott
L. Wexler
P. J. Weyman
J. P. Whalen
R. I. White, Jr.
N. O. Whitley
M. H. Wholey
S. N. Wiener
W. A. Wilcox
R. H. Wilkinson
S. M. Williams
B. R. J. Williamson
S. Wilson
V. W. Wing
F. Winsberg
P. F. Winter
G. G. Winzelberg
J. F. Wiot
R. L. Witcofski
H. R. Withers
D. M. Witten
J. Wittenberg
G. L. Wolf
J. N. Wolfe
A. H. Wolson
M. K. Wolverson
I. C. Yoder
L. W. Young
H. Y. Yune
R. A. Zamenhof
R. K. Zeman
E. A. Zerhouni
J. Zornoza
C. J. Zylak

News

1987 Diagnostic Ultrasound Training Courses

Thomas Jefferson University will schedule weekly courses in diagnostic radiology covering abdomen, obstetrics and gynecology, noninvasive vascular diagnosis, neonatal brain, sonomammography, and echocardiography. Program director: Barry B. Goldberg. Information: Education coordinator, Division of Diagnostic Ultrasound, Thomas Jefferson University, 7th Floor, Main Building, Philadelphia, PA 19107; (215) 928-8533.

Uroradiology Course

The Armed Forces Institute of Pathology, the American Registry of Pathology, and the American College of Radiology will sponsor a uroradiology course on Jan. 19–20, 1987, at the Holiday Inn of Bethesda, Bethesda, MD 20814. The purpose of this course is to teach basic genitourinary radiology to urologists and urology residents. Faculty: E. S. Amis, Jr., A. J. Davidson, M. S. Debbas, S. M. Goldman, and D. S. Hartman. Course director: David S. Hartman. Category 1 credit: 15 hr. Fee: $200: nonfederal physicians; active duty military and other full-time federal salaried physicians with authorized approval are exempt from the fee. Information: Uroradiology Course, Armed Forces Institute of Pathology, Washington, DC 20306; (202) 576-2934.

Palm Beach Magnetic Resonance Imaging Update

Boston University Medical Center and JFK Memorial Hospital, Lake Worth, FL, announce an MR imaging course, Feb. 8–11, 1987, at the Hyatt Palm Beaches, West Palm Beach, FL. Course directors: Allan M. Green and Neil Steinmetz. Category 1 credit: 18 hr. Fee: $385: physicians; $285: residents and technologists. Information: Dept. of CME, Boston University School of Medicine, 80 E. Concord St., Boston, MA 02118; (617) 638-4605.

The Pacific Radiological Institute Courses

The Pacific Radiological Institute was founded to bring together diagnostic radiologists from both sides of the Pacific for the exchange of ideas and talents. Twelve weekly courses (Feb.–April 1987) will be offered, with guest faculties. Category 1 credit: 35 hr/week, or 140 hr for 4-week program. Fee: $475: physicians; $325: residents and fellows; $1750/month: physicians; $1200/month: residents and fellows. Information: Pacific Radiological Institute, 104 Poipu Dr., Honolulu, HI 96825.

Vail Winter Imaging Seminar III

Western Pennsylvania Hospital will sponsor their Vail Winter Imaging Seminar III, Feb. 21–28, 1987, at The Marriott's Mark Resort in Vail, CO. Current applications of diagnostic sonography, body CT, MR, nuclear medicine, and interventional radiology will be presented. Faculty: R. Bree, S. Hissong, N. Joseph, G. Kellman, E. Mendelson, P. Mueller, H. Neiman, E. Russell, S. Sagel, J. H. Thrall, G. L. Wolf. Category 1 credit: 23 hr. Fee: $425: physicians; $325: residents, fellows, sonographers. Information: Joanne Bondarenka, Vail Winter Imaging Seminar III, The Western Pennsylvania Hospital, 4800 Friendship Ave., Pittsburgh, PA 15224; (412) 578-17800.

Winter Imaging at Stowe VT

NYU Medical Center will hold its First Annual Winter Imaging course, March 2–6, 1987, at Topnotch Inn and Conference Center, Stowe, VT. This 5-day course will cover the use of new imaging techniques in a wide variety of clinical practice situations. CT, MR, sonography, digital radiology, information systems, and interventional radiology will be highlighted and appropriate imaging strategies in useful day-to-day practice will be developed. Category 1 credit: 25 hr. Fee: $425. Information: NYU Medical Center Postgraduate Medical School, 550 First Ave., New York, NY 10016; (212) 340-5295.

Diagnostic Imaging and Interventional Radiology

The University of Utah Medical Center, Dept. of Radiology, will hold a diagnostic imaging and interventional radiology course at Park City, UT, March 8–13, 1987. Visiting faculty: D. Stark and T. McNamara. Category 1 credit: 22 hr. Fee: $395. Information: Judy Gallegos, Dept. of Radiology, School of Medicine, 1A71 Medical Center, Salt Lake City, UT 84132; (801) 581-7553.

Positron Emission Tomography and the Chemistry of Mental Illness

The Johns Hopkins Medical Institutions will offer a course on positron emission tomography and the chemistry of mental illness, on March 12–13 at the Johns Hopkins Medical Institutions, Baltimore, MD. The basic principles and techniques of positron emission tomography will be covered together with research and clinical results. The program is designed to meet the needs and interests of psychiatrists, psychologists, basic and clinical neuroscientists, neurologists, nuclear medicine physician, neuroradiologists, and others interested in the

brain and its relation to the mind. Course director: Henry N. Wagner; course codirector: Julia W. Buchanan. Category 1 credit: 15 hr. Fee: $275: physicians; $175: residents and fellows. Information: Pamela E. Macedonia, program coordinator, Turner 22, 729 Rutland Ave., Baltimore, MD 21205; (301) 955-8582.

Diagnostic Radiology Conference on Imaging Modalities in Chest and Abdomen

Loyola University of Chicago Medical Center will sponsor its 8th midwinter diagnostic radiology conference on imaging techniques in the chest and abdomen, including MR, CT, and sonography, March 16–20, 1987, at the Royal Lahaina Resort, Maui, HI. Category 1 credit: 20 hr. Information: Dr. Linda Gunzburger, Assoc. Dean of Educational Research and Development, Continuing Medical Education, and the Learning Resource Center, Loyola University Stritch School of Medicine, 2160 S. 1st Ave. Maywood, IL 60153; (312) 531-3237.

Federation of Western Societies of Neurological Science Meeting

The 24th annual meeting of the Federation of Western Societies of Neurological Science will be held March 30–April 1, 1987, at Hotel del Coronado, Coronado, CA. Interdisciplinary concerns of neurologists, neurosurgeons, neuroradiologists, and neuropsychiatrists will be discussed. Category 1 credit: 19 hr. Program chairman: Patrick D. Lyden, Dept. of Neurosciences, UCSD Medical Center H815-A, 225 W. Dickinson St., San Diego, CA 92103; (619) 294-6737.

Society of Computed Tomography Meeting/Course

The 10th annual course of the Society of Computed Body Tomography will be held March 30–April 3, 1987, at the Hotel Inter-Continental in San Diego, CA. The faculty will present 22 hr of formal lectures, four 1-hr workshops, and a new 2-hr "CT Club." The focus will be on anatomy, techniques, indications, advantages, and pitfalls of CT. MR will also be covered. The course will be aimed at the needs of the practicing radiologist. Fee: $475: physicians; $375: residents and fellows. Category I credit: 28.5 hr. Information: Society of Computed Body Tomography, % Matrix Meetings, Inc., Barbara McLeod, Meeting Manager, P.O. Box 1103, Rochester, MN 55903; (507) 288-5620.

Radiation Therapy Clinical Research Seminar

The Radiation Therapy Division, University of Florida, Division of Continuing Medical Education, University of Florida, and the American Cancer Society, Florida Division, Inc., will sponsor the 17th annual radiation therapy clinical research seminar April 23–25, 1987, at University Centre Hotel, Gainsville, FL. The seminar will include a 3-day cancer conference with 1 day of case presentations and 2 days of clinical research papers. Category 1 credit: 18 hr. Fee: $200: radiation therapists; no fee for residents. Information: Timonthy A. Brant, M.D., 1987 Seminar Coordinator, Radiation Therapy Div., Box J-385, J. Hillis Miller Health Center, Gainesville, FL 32610; (904) 395-0316.

George Simon Award—The Fleischner Society

Established to honor the memory of George Simon, the George Simon Memorial Fellowship Award is presented annually by the Fleischner Society for the best original work relating to radiologic or other imaging of the respiratory system. The winning author will receive a cash prize and an all-expense paid trip to the Fleischner Society Meeting and Course to present the award paper. In 1987, the Society will meet in San Francisco, CA, May 17–23. The award paper may be the result of work done by several investigators, but the senior author should be the applicant and responsible for most of the work. Papers previously published or submitted for publication are not eligible. Applicants should not be more than 40 years old. Manuscripts must be in the form of a complete scientific paper, no longer than 25 typed, double-spaced pages, and must be submitted in triplicate. Submissions should be sent to: Richard H. Greenspan, M.D., Dept. of Diagnostic Radiology, Yale University School of Medicine, 333 Cedar St., New Haven, CT 06510. Deadline by which papers must be received is March 1, 1987.

Society of Nuclear Medicine Annual Meeting

The 34th annual meeting of the Society of Nuclear Medicine will be held June 2–5, 1987, at the Toronto Convention Center, Toronto, Ontario, Canada. Deadline for submission for abstracts: Scientific papers—Jan. 8, 1987; Scientific exhibits—Jan. 22, 1987; Works-in-progress—April 9, 1987. Fee: $120; members; $125: nonmembers. Information: Society of Nuclear Medicine, Education & Meetings Dept., 136 Madison Ave., New York, NY 10016; (212) 889-0717.

Correction—The American Board of Radiology Examinations

The dates published in the Sept.–Nov. *AJR* issues for the American Board of Radiology examinations were incorrect. Written examinations will be held Oct. 8–9, 1987; Oct. 6–7, 1988; and Oct. 5–6, 1989. Oral examinations will be held at the Executive West Hotel in Louisville, KY, on June 8–12, 1987; May 23–27, 1988; and June 5–9, 1989. The ABR will accept applications for admission to the examinations after April 1, but not later than September 30, of the year *before* the examination is to be taken. For application forms and further information: Office of the Secretary, The American Board of Radiology, 300 Park, Ste. 440, Birmingham, MI 48009.

AJR carries announcements of courses, symposia, and meetings of interest to its readers if received a minimum of 5 months before the event. There is no charge; receipt of items by the *AJR* Editorial Office is not acknowledged. Submit items for publication typed double spaced. Provide title, date, location, brief description, sponsor, course directors, fees, category I credit, and address and telephone number for additional information. Faculty from the host institution will not be listed. Guest faculty names will appear **only** if initials are provided. Mail news items to *AJR* Editorial Office, 2223 Avenida de la Playa, Suite 200, La Jolla, CA 92037.

Classified Advertising

Positions Available

NEURORADIOLOGIST. Applications are being sought for an academically oriented neuroradiologist for a 612-bed teaching hospital. Position to start July 1987. Candidate should be board certified preferably with 2 yr of neuroradiology fellowship. Training in MR, CT, angiography, and myelography necessary. Individual will be the second neuroradiologist in an active, aggressive section. Private practice. Send current CV to Harvey L. Neiman, M.D., Chairman, Dept. of Radiology, The Western Pennsylvania Hospital, 4800 Friendship Ave., Pittsburgh, PA 15224. 12–2a

NUCLEAR MEDICINE PHYSICIAN. Opportunity at the Assistant Professor level in major Northeast University Department. Successful candidate must be certified in radiology or internal medicine and board certified/eligible in nuclear medicine. Excellent clinical and research opportunity. Send CV to Arnold M. Strashun, M.D., Div. of Nuclear Medicine, Dept. of Radiology, State University of New York, Health Science Center at Brooklyn, 450 Clarkson Ave., Box 1210, Brooklyn, NY 11203. EO/AA Employer. 12a

CHIEF OF RADIOLOGY HARBORVIEW MEDICAL CENTER. The University of Washington School of Medicine, Seattle, WA, invites nominations and applications for the position of Chief of Radiology at the Harborview Medical Center, a University of Washington teaching hospital. We seek an experienced physician/administrator with strong commitment to academic radiology, patient care, and teaching. The candidate must be board certified by the American Board of Radiology and meet the academic requirements for Professor or Associate Professor at the University of Washington School of Medicine. The individual chosen as Chief of Radiology will be responsible for all professional radiologic and nuclear medicine services and must have the vision, vigor, and will to build an academic radiology program commensurate with the mission of the Harborview Medical Center. The University of Washington School of Medicine is an equal opportunity employer. Please send CV to Charles A. Rohrmann, Jr., M.D., Professor of Radiology, Chairman HMC Radiology Search Committee, University of Washington, SB-05, Seattle, WA 98195. 12a

DIAGNOSTIC RADIOLOGY FACULTY MEMBER. The McGill University Dept. of Diagnostic Radiology is seeking an additional faculty member. The successful candidate will have responsibilities in research, teaching, and clinical work. He/she will lead the division of gastrointestinal radiology and will be part of the abdominal imaging team. He/she will be responsible for a research project on digital imaging of the gastrointestinal tract. He/she will be based primarily in one of the major teaching hospitals of the University, where approximately 120,000 cases are performed each year and state-of-the-art equipment is available in conventional diagnostic imaging, as well as ultrasound and CT. In accordance with Canadian immigration requirements, priority will be given to Canadian citizens or landed immigrants. Applicants should send their CV and three letters of reference to Dr. Patrice M. Bret, Radiologist-in-Chief, Dept. of Diagnostic Radiology, Montreal General Hospital, 1650 Cedar Ave., Montreal, Quebec H3G 1A4, Canada; (514) 934-8003. 12a

ISRAEL, DIAGNOSTIC RADIOLOGY. Opportunities for 3–4 week or longer working vacations in a number of Israeli medical centers, on a volunteer basis. Positions varied, arrangements flexible. For information contact: Jonathan H. Fish, M.D., 1844 San Miguel Dr., #302, Walnut Creek, CA 94596; (415) 947-0560. 8xa

RADIOLOGY INSTRUCTOR to assist candidate in preparation for Oral Radiology Boards. Candidate needs practice in formally discussing cases and answering board-type questions. Would like to meet on a weekly basis beginning early 1987. Fee negotiable. Please call (215) 342-4110 or (615) 359-7092 eves. 12–2a

UNIVERSITY HOSPITALS OF CLEVELAND is seeking a board-certified radiologist for an assistant professor position in nuclear medicine. Position entails work in both conventional nuclear medicine and in the PET facility. Teaching experience and demonstrated interest in research are desirable. Salary commensurate with experience. University Hospitals of Cleveland is a 900-bed hospital associated with Case Western Reserve University. Interested candidates should forward CV and approximate date of availability to Floro Miraldi, M.D., Director, Division of Nuclear Radiology, University Hospitals of Cleveland, 2074 Abington Rd., Cleveland, OH 44106. AA/EOE. 12–1a

PEDIATRIC NEURORADIOLOGIST. The Dept. of Radiology at Childrens Hospital of Los Angeles and the University of Southern California is seeking a pediatric neuroradiologist with strong commitment in teaching, patient care, and research. Applicants should be board certified and must qualify for licensure in California. Faculty rank would be predicated upon the qualifications. Interested applicants should send CV and names and addresses of three references to John L. Gwinn, M.D., Radiologist-in-Chief, Childrens Hospital of Los Angeles, P.O. Box 54700, Los Angeles, CA 90054. Qualified individuals from minority groups and women are encouraged to apply. 12a

RADIOLOGICAL PHYSICISTS. The Dept. of Radiology at Thomas Jefferson University Hospital/Jefferson Medical College wishes to recruit two highly qualified radiologic physicists. The first position is for an MRI physicist to work with our GE 1.5T MRI system currently being installed. He/she will work closely with radiologists in our MRI division on applied and basic research. The second position is for a physicist with particular interests in image processing. The Dept. has a broad range of interests in digital radiography, DSA, PACS, and other methods of improving information content of radiologic images. Candidates for both positions should have strong academic records and current research interests. Hard money support is available for both positions. Contact David C. Levin, M.D., Chairman, Dept. of Radiology, Thomas Jefferson University Hospital, Philadelphia, PA 19107. 11–1a

MRI/ULTRASOUND RADIOLOGISTS. The Dept. of Radiology at Thomas Jefferson University Hospital/Jefferson Medical College is seeking two academically oriented radiologists to join its MRI and Ultrasound divisions. Both divisions are housed in modern, spacious facilities with state-of-the-art technology. A GE 1.5 T MRI unit is now being installed. Candidates will have the option of working in either of these divisions or both, according to their interests. The Dept. is currently under new leadership, and is expanding in both size and academic scope. Generous salaries and benefits are offered. Contact David C. Levin, M.D., Chairman, Dept. of Radiology, Thomas Jefferson University Hospital, Philadelphia, PA 19107. 11–1a

DIAGNOSTIC RADIOLOGIST. Need aggressive associate to perform all aspects of diagnostic radiology in well-equipped hospital with large outpatient component in South Texas. MR training a plus but not essential. Excellent salary and early partnership available. For confidential consideration please submit CV to Box H70, *AJR* (see address this section). 11xa

RADIOLOGIST, BOARD CERTIFIED/ELIGIBLE. Full- or part-time position available with two other radiologists in a hospital-based practice that includes diagnostic radiology, CT, ultrasound, angiography, nuclear medicine, and interventional procedures. Teaching hospital with residency programs. Please send CV and other inquiries to Douglas B. McGirr, M.D., Radiology Dept., San Joaquin General Hospital, P.O. Box 1020, Stockton, CA 95201. AA/EOE 11–12a

DIAGNOSTIC RADIOLOGIST for small hospital and clinic practice San Francisco Bay Area. Write to J.J. Parker, M.D., Box 284, San Rafael, CA 94915. 11–12a

PERMANENT POSITION. Pediatric radiologist to cover high-risk nurseries at two hospitals approximately three miles apart. Approximately 15 high-risk beds at each hospital. Good pediatrician support. Anticipate growth of routine pediatric radiology as well. Large group, with full compensation package negotiable. Will give preference to person willing to do some plain film adult radiology. Write to C.M. Eiland, M.D., 1920 Huntington Rd., Birmingham, AL 35209. 11–12a

A 400-BED COMMUNITY HOSPITAL staffed by private practice group seeks a second neuroradiologist preferably with MR experience. Ongoing neuroradiologic service includes state-of-the-art CT, angiography with digital, and myelography. MR unit on order. Must be capable and willing to do general radiology also. Contact Ben R. Mayes, Jr., M.D., Radiology Dept., St. Luke's Hospital, 232 So. Woods Mill Rd., St. Louis, MO 63017, (314) 434-1500, ext. 4250. 11–1a

DIAGNOSTIC RADIOLOGIST with two years fellowship in interventional radiology to join 8-man hospital- and office-radiology group. Group involved in all diagnostic modalities including MRI. E.S.W.L. to be installed soon. Candidates must be skilled in interventional uroradiology and angioplasty. Must also be accomplished general radiologist. Position available on or before July 1, 1987 and leads to full partnership. Send CV to Paul R. Silk, M.D., Dept. of Medical Imaging, Albany Memorial Hospital, Albany, NY 12204. 11–12a

THE DEPARTMENT OF RADIOLOGY, Medical College of Virginia, Richmond VA seeks qualified individuals for faculty positions in skeletal radiology, neuroradiology, and MRI. Must be ABR certified or eligible. Academic rank and salary commensurate with experience. Submit CV to Search Committee, Dept. of Radiology, Medical College of Virginia, Box 470, Richmond, VA 23298. MCV is an equal opportunity, affirmative action employer. Women and minorities are encouraged to apply. 11–12a

PEDIATRIC RADIOLOGIST. Large hospital-based group seeks associate with recent pediatric radiology fellowship training. Busy private practice group needs second pediatric radiologist for coverage of small pediatric hospital. Practice would include 25% pediatric and 75% adult work. All modalities including MRI. Board certification mandatory. Opportunity for partnership in well-established western Washington practice. Reply Box H74, *AJR* (see address this section. 11–6a

TWO YOUNG RADIOLOGISTS seek a third radiologist in expanding hospital-based practice near Canadian border in northern New York. All modalities available. Write P. Berman, HC 61 Box 454, Massena, NY 13662. 8–7a

BOARD CERTIFIED diagnostic radiologist. All diagnostic modalities except MR. MR installation planned in 1½ years. Busy in-patient and out-patient practice. Salary negotiable and early partnership available. Send CV to Box C23, AJR (see address this section). 6xa

BOARD-CERTIFIED DIAGNOSTIC RADIOLOGIST to join multispecialty private corporation, with a well-equipped X-ray area, dedicated mammography, nuclear medicine, high-resolution real-time ultrasound, and whole-body CT scanner. Send CV and reply to Raymond Kuntz, Administrator, Johnson Clinic, P.D., P.O. Box 315, Rugby, ND 58368. 12–1a

BOARD-CERTIFIED RADIOLOGIST–Six man radiology group seeks new associate with fellowship training in CT/ultrasound. The group provides complete radiologic services in fully-equipped 500 bed hospital with two G.E. 9800 CT scanners, and Acuson and Diasonics ultrasound. Private out-patient office also covered by the group. Send CV to Eric R. Rosenberg, M.D., Dept. of Radiology, New Hanover Memorial Hospital, Wilmington, NC 28403. 10–12ap

CHIEF, BODY CT. The Dept. of Diagnostic Radiology of William Beaumont Hospital, a major tertiary care and academic institution in Michigan, is seeking a candidate to direct the division of body CT and participate in MR. Candidates must be board certified in diagnostic radiology and have significant academic achievements. Income is negotiable and competitive. Send CV to Jalil Farah, M.D., Director, Diagnostic Radiology, William Beaumont Hospital, 3601 West 13 Mile Road, Royal Oak, MI 48072. 10–12a

B/C - B/E DIAGNOSTIC RADIOLOGIST. Hospital and office practice. All modalities except MRI. Hands-on experience in real-time ultrasound desired. Excellent salary and benefits, commensurate with experience. Early partnership. Will consider locums. Send CV to Radiology, 5681 N. Fresno St., Fresno, CA 93710 (209) 439-2464. 11–12ap

Positions Desired

PGY-2 OR PGY-3 DIAGNOSTIC RADIOLOGY POSITION sought by resident with 16 months' training at midwest university program. Currently involved in MR and contrast research. Affable and committed. Available January 1987. Reply Box I90, *AJR* (see address this section). 12–1b

BOARD-CERTIFIED RADIOLOGIST seeks position in general radiology including CT, ultrasound, nuclear medicine, neuroradiology, GI, mammography, angiography, and interventional radiology. Three years' experience modernizing a busy community hospital and expanding private office. I would like to enhance and expand practice, leading to partnership. Send reply to Box I91, *AJR* (see address this section). 12b

BOARD CERTIFIED RADIOLOGY GROUP with expertise in all modalities desires to relocate either to a moderate-size hospital or multispecialty practice. All locations considered. Reply Box H72, *AJR* (see address this section). 11–12b

BOARD-CERTIFIED RADIOLOGIST seeks part-time position in Philadelphia, South Jersey, Wilmington, Delaware area. Experienced in all imaging and invasive modalities except MRI. Reply Box G62, *AJR* (see address this section). 10–12b

NEURORADIOLOGIST completing 2-yr-UCSD fellowship 6/87 (with 1.5T GE Signa experience throughout) seeks private practice position. P.O. Box 8107, La Jolla, CA 92038. 9-12b

Fellowship and Residencies

RESIDENCY POSITION. Fourth-year radiology residency position available at a university teaching hospital in the Midwest. Emphasis can be placed on special procedures if desired. Send

CARDIOVASCULAR INTERVENTIONAL RADIOLOGY FELLOWSHIP. Opening for fellowship program beginning July 1, 1987. Also, now accepting applications for candidates for July 1, 1988. One-year program at 454-bed teaching hospital with departmental affiliation to the University of Pittsburgh. Busy dept. covering all aspects of cardiovascular and neurovascular imaging, as well as, vascular and nonvascular interventional techniques. Ideally suited for candidates wishing to pursue cardiovascular interventional radiology in private practice. Inquiries to Mark H. Wholey, M.D., Director, Dept. of Radiological Sciences and Diagnostic Imaging, Shadyside Hospital, 5230 Centre Ave., Pittsburgh, PA 15232; (412) 622-2083. 12c

FELLOW IN MRI - BUFFALO, NY. Available Jan. 1, 1987 a fellowship position is open in a 313-bed pediatric teaching hospital. Eight radiologists associated in practice; CT, nuclear medicine, 2 Acuson units, angiography, and Diasonics 0.5 Tesla Superconductive magnet in our department. Write to J.P. Kuhn, M.D., 219 Bryant St., Buffalo, NY 14222. 11–1a

Tutorials/Courses

CORTINA, ITALY—LONDON, ENGLAND. Winter Congress-Cortina, Jan 31–Feb 7, 1987: Winter Seminar-London, Feb 7–11, 1987. Attend one or both offering CME I accredited and presented by a renowned faculty. Topics in CT, US, MRI with correlation. Fees each meeting: to November 14, US$395, thereafter US$435 (combined fee US$450 and US$495, respectively). Contact Medical Seminars International, 21915 Roscoe Blvd., Ste. 222, Canoga Park, CA 91304 (818) 701-5143. 10–12d

Other

RADIOLOGY OFFICE FOR LEASE, SALE, OR JOINT VENTURE. Rapidly growing area, S.E. Florida Coast Hospital and three-medical building complex. 30 physicians. Send reply to Box I88, *AJR* (see address this section). 12d

REALIZE THE VALUE of your practice. A group of successful and well-qualified radiologists is interested in acquiring established radiology practices. Hospital contracts, clinics, and private office settings are desired. Opportunity for radiologists considering retirement or reduction in practice activities to capitalize on the value of the practice they have built up during their careers. Alleviate the problems of professional recruitment or administrative pressures. Practices considered throughout the country. Flexible purchase options with opportunity for continuing relationship arrangements. Write Box C49, *AJR* (see address this section). 6–5e

AJR Classified Advertising Information

Box Responses and Address for Ad Placement

Write Box _____, AJR, Suite 200, 2223 Avenida de la Playa, La Jolla, CA 92037; (619) 459-2229.

How to Place an Ad

AJR accepts classified advertising for Positions Available, Positions Desired, Fellowships and Residencies, and Tutorials/Courses. Ads are accepted by mail or telephone. Institutions should supply purchase orders.

Rates: $6.00/line with a $30 minimum charge. Box service is $10 additional for each month the ad appears. There are discounts for multiple insertions: 10% for 2–3 insertions; 20% for 4 or more. To estimate lines, count all words and divide by 5.5.

Billing: Ads may be prepaid or invoices will be sent after the ad appears.

Deadlines. About 3 weeks before the issue mails. *AJR* issues mail in the middle of the month preceding the cover date (e.g., July mails June 17). For specific deadlines, write or telephone the AJR editorial office.

Estimating Ad Charges

Line charge: divide total words by 5.5 and multiply by $6.00	$
Multiple insertions? If so, multiply by number	×
Subtotal	$
Box response requested? If so, multiply number of months by $10.00	+
Subtotal	$
Discount applies to two or more insertions. Subtract 10% if ad appears 2–3 months, 20% if 4 months or more	−
Approximate advertising charge	$

Combined Author Index Volumes 146–147

Authors of *AJR* articles are also included in the 5-year cumulative index published in *Radiology*.

A

Abbas S, **146:**819
Abrams DI, **146:**7
Abramson S, **146:**239
Adams RD, **147:**985
Adler DD, **147:**843
Adler LP, **146:**459
Adler YT, **146:**415
Agha FP, **146:**25, **146:**527, **147:**216
Ahmadi J, **146:**257, **147:**995
Aiach M, **146:**157
Aisen AM, **146:**749, **146:**1179, **147:**33, **147:**843
Ajani J, **147:**149
Alavi A, **147:**67, **147:**1332
Alavi SM, **147:**552
Alazraki N, **146:**621, **146:**1100
Alazraki NP, **146:**87
Alford BA, **147:**1010
Al-Kawi MZ, **147:**767
Allan BT, **147:**1027
Al-Mefty O, **147:**767
Alspaugh JP, **146:**881
Altman DF, **146:**1
Altman DH, **146:**1261
Altman NR, **146:**1261
Alzate GD, **147:**822
Amberg JR, **147:**257
Amendola MA, **146:**1179, **147:**1063
Amodio J, **146:**239
Amorosa JK, **146:**649, **146:**1047
Amplatz K, **146:**143, **146:**849, **147:**161, **147:**836, **147:**1025
Amsler LC, **146:**44
Anderson GH Jr, **146:**67
Anderson MW, **147:**1241
Andre M, **147:**545
Andrew ER, **146:**1314
Andrews WL, **147:**801
Andriole JG, **147:**1043
Andrues TA, **147:**1133
Angel C-Y, **146:**853
Anschuetz SL, **146:**1165
Antony AC, **147:**846
Applbaum YN, **146:**61
Applebaum DM, **147:**177
Araki T, **146:**729
Argila C, **146:**605
Armstrong E, **147:**785
Armstrong P, **147:**1313
Aronberg DJ, **147:**17
Aronchick JM, **147:**227
Ascher NL, **147:**1027
Ashburn WL, **146:**1010
Athey PA, **147:**725
Atkins HL, **146:**1100
Atkinson GO Jr, **146:**113
Atlas SW, **146:**277, **147:**575
Aufderheide AC, **146:**93
Auh YH, **147:**1067
Auster M, **146:**1025
Austin J, **146:**883
Awwad EE, **146:**359
Axel L, **146:**1215, **147:**67, **147:**1332

B

Babcock DS, **146:**609
Bagg MNJ, **147:**185
Bain J, **146:**349
Bair JH, **147:**1047
Bakal CW, **146:**169, **146:**590, **147:**438
Baker ME, **146:**845, **146:**1289
Baker MK, **147:**846
Baker SR, **147:**637
Balachandran S, **147:**173
Ball MR, **147:**119
Ball TI, **147:**806, **147:**949
Ball WS Jr, **147:**791
Ballinger WE Jr, **147:**1209
Balthazar EJ, **147:**696, **147:**705
Ban N, **146:**735
Banner MP, **147:**94
Barakos JA, **146:**1161
Barbier PA, **147:**519
Barloon TJ, **146:**323
Barnes PD, **147:**339
Barnes RW, **147:**173
Baron MG, **146:**491
Bartholomot B, **146:**263
Bashir R, **147:**767
Bassett L, **146:**409
Bassett LW, **147:**689
Baum S, **147:**412, **147:**1335
Baumgartner BR, **147:**949, **147:**1007
Baumstark AE, **146:**424
Becker CD, **147:**519
Becker GJ, **147:**685
Bedrossian J, **146:**853
Beggs I, **147:**860
Bell G, **147:**757
Bell RM, **147:**613
Bellinger MF, **146:**615
Bellon EM, **147:**1271
Belt TG, **146:**955
Benenati JF, **147:**685
Beneventano TC, **146:**519
Ben-Menachem Y, **146:**422, **146:**809
Beranbaum ER, **147:**705
Berdon W, **146:**239
Beres J, **147:**613
Berger T, **146:**373
Bergin CJ, **146:**477
Berk RN, **146:**171, **146:**879, **146:**1311
Berland LL, **146:**155, **146:**421
Berlin L, **147:**1291, **147:**1335
Berman HL, **146:**169, **146:**590, **147:**632
Bernardino ME, **147:**9, **147:**949, **147:**1007
Bernstein LH, **146:**519
Berquist TH, **146:**93
Berry I, **147:**1223, **147:**1231
Besarab A, **146:**267
Beschorner WE, **146:**691
Beshany SE, **146:**1300, **147:**1096
Bester L, **147:**185
Bettmann MA, **147:**621
Bianchini M, **146:**523
Biberstein M, **146:**823
Bieber FR, **147:**598
Bieberstein MP, **146:**1099
Bielecki D, **147:**545
Bielecki DK, **147:**83
Bierre A, **147:**598
Bilaniuk LT, **147:**1215
Bisker J, **146:**716
Bjorkengren A, **147:**66
Bjorkengren AG, **147:**739
Black WC, **147:**1313
Blackbourne B, **146:**895
Blickman JG, **146:**245
Blinder RA, **147:**497
Bloem JL, **147:**79
Bloom RA, **146:**549
Bluemm RG, **147:**79
Blumhagen JD, **146:**249, **146:**1268
Bluth EI, **146:**1061
Bober-Sorcinelli KE, **146:**1298
Bohrer SP, **146:**216, **147:**216
Bonamo J, **146:**361
Bonneville JF, **146:**263
Bookstein FL, **147:**469
Borns PF, **147:**317
Boswell WD Jr, **146:**741
Bottles K, **146:**7
Boumphrey F, **147:**757
Bourke E, **147:**949
Bowen A'D, **146:**137
Bowie JD, **146:**337
Boxt LM, **146:**831
Boyd CM, **147:**173
Boyer RS, **146:**83
Bozymski EM, **147:**57
Bradley WG Jr, **146:**871, **146:**1307, **147:**1133
Brady TJ, **146:**75, **146:**309, **146:**1286, **147:**357, **147:**553
Bragg DG, **147:**696
Brandt LJ, **146:**519
Brannen GE, **147:**89
Brant-Zawadzki M, **146:**649, **146:**1223, **147:**331, **147:**1223, **147:**1231
Brasch R, **147:**1223, **147:**1231
Brasch RC, **147:**1263
Brateman L, **146:**971
Braun IF, **147:**587
Braun SD, **146:**881, **146:**1049, **147:**39
Braunstein EM, **146:**749
Bressler EL, **147:**646
Bret PM, **147:**513
Breton G, **146:**53, **147:**505
Brewer WH, **146:**533
Brewster DC, **146:**711
Bried J, **146:**839
Brill PW, **146:**471
Brisset J-M, **146:**853
Brock R, **146:**869
Brody BA, **146:**1067
Brody WR, **146:**248
Brogdon BG, **147:**848
Bron KM, **146:**137, **147:**657
Brown LK, **146:**577
Brown LR, **147:**191
Brown R, **147:**1283
Brown RF, **147:**1236
Brunberg JA, **147:**293
Bruner JM, **147:**111, **147:**747
Bryan PJ, **146:**543, **147:**291
Buckspan MB, **146:**349
Buckwalter KA, **147:**33
Buda AJ, **147:**33
Bundrick TJ, **147:**957
Bunker SR, **147:**1331, **147:**1332
Bunnell DH, **147:**689
Burger P, **147:**103
Burk DL Jr, **147:**293
Burke DR, **146:**383, **147:**1185
Burks DD, **146:**1187
Burnett KR, **147:**1333
Burrows PE, **146:**211
Bush WH, **147:**89, **147:**962
Butch RJ, **146:**1155, **147:**1237
Butler HE, **146:**543

C

Caballero P, **147:**859
Cabrera OA, **146:**327, **146:**581
Cacayorin ED, **146:**1246
Cadavid G, **147:**725

Cady B, **147:**665
Calvanese J, **147:**854
Cameron JL, **147:**271
Campatelli A, **146:**523
Campbell JB, **146:**577
Cann C, **147:**21
Capitanio MA, **146:**227
Caputo G, **146:**925
Cardella JF, **146:**143, **146:**849, **147:**1025
Carey PH, **147:**822
Carithers RL, **146:**533
Carlson DH, **146:**238, **147:**398
Carlson HC, **147:**63
Caro PA, **147:**1041
Caroline DF, **146:**351, **146:**1167
Carrasco CH, **146:**375, **146:**591, **147:**149, **147:**155, **147:**1247
Carroll JE, **146:**565
Carson GC, **146:**491
Casarella WJ, **146:**881
Cascade PN, **147:**78
Casola G, **146:**327, **146:**581, **147:**513
Cass OW, **146:**93
Castagno A, **146:**57
Castaneda-Zuniga W, **147:**836
Castaneda-Zuniga WR, **146:**143, **146:**849, **147:**161, **147:**1025
Castell DO, **147:**693
Cattin F, **146:**263
Cerny JA, **147:**689
Cerqueira M, **147:**984
Chandler PW, **147:**899
Chang P, **147:**1251
Chang R, **146:**1025
Chan-Yeung M, **146:**477
Charboneau JW, **147:**929
Charlebois N, **146:**369
Charnsangavej C, **147:**149, **147:**155, **147:**1247
Chase B, **147:**665
Chen JTT, **146:**757, **147:**674
Chen YM, **146:**875, **146:**993, **146:**1317, **147:**261, **147:**693, **147:**697
Chernin MM, **147:**257
Chew FS, **147:**1055
Chia KB, **147:**145
Chick BE, **146:**1100
Chin JK, **146:**1273
Cho S-R, **147:**1181
Choplin RH, **146:**665
Chrousos GP, **147:**1145
Chuang VP, **146:**839, **146:**881
Churchill RJ, **146:**601
Citrin CM, **147:**984
Clark DL, **147:**916
Clark JW, **146:**51
Clark OH, **147:**1255
Clarke NMP, **147:**317
Clayman RV, **147:**393
Clere P, **146:**263
Cleveland RH, **146:**1273
Clouse M, **147:**665
Clouse ME, **146:**163, **146:**1141
Coblentz C, **147:**477
Cohan RH, **146:**57, **146:**1289
Cohen AM, **146:**543
Cohen H, **147:**1305
Cohen JM, **146:**597, **146:**679, **147:**785
Cohen LM, **147:**141
Cohen MD, **146:**639, **146:**955, **146:**1293
Cohen MI, **147:**1021
Cohen RA, **146:**97
Colapinto RF, **146:**859
Coleman PE, **147:**1271
Colletti PM, **146:**741
Compton CC, **147:**721
Compton T, **146:**1192, **146:**1204
Condon VR, **146:**83
Connor TP, **146:**767
Conrad MR, **146:**645
Constantin A, **146:**53
Conti J, **146:**1178
Coombs RRH, **147:**167
Coons HG, **147:**822
Cooper HS, **146:**1011
Cooper R, **146:**471
Cooperberg PL, **146:**174, **146:**345, **147:**509
Cope C, **146:**160, **147:**383
Cory DA, **146:**955, **146:**1293
Cosman E, **146:**163
Costello P, **146:**163, **146:**1005
Coupal JJ, **146:**333
Cousin AJ, **147:**1139
Craig EV, **146:**561, **147:**647
Cramer BC, **147:**133, **147:**801
Cramer FM, **147:**155
Crass JR, **146:**413, **146:**561, **147:**647
Cromwell LD, **147:**627
Cronan JJ, **146:**425, **146:**1317
Crooks LE, **146:**931
Crues JV III, **147:**1133
Crummy AB, **147:**338
Cubberley DA, **146:**327, **146:**577
Cuenin E, **146:**263
Cummings T, **147:**729
Curnes JT, **147:**119
Currarino G, **146:**757
Curtis HW, **147:**742
Cutler GB, **147:**1145

D

Dachman AH, **147:**537
Daffner RH, **146:**80, **146:**119, **146:**353, **147:**562
Dafoe DC, **147:**1193
Dake MD, **147:**583
Dalal PS, **146:**1246
Daley C, **147:**29
Dalinka M, **146:**1215
Dan SJ, **147:**51
Daneman A, **146:**763
Daniels DL, **146:**1235
Darcy MD, **147:**161, **147:**836, **147:**1025
Darling RC, **146:**711
Darweesh RMA, **147:**1155
Darwin R, **147:**103
Dash N, **146:**119, **146:**353
Datz FL, **146:**621, **147:**809, **147:**813
Daves ML, **147:**209
Davidson AJ, **147:**1322
Davis KR, **147:**353, **147:**985
Davis PC, **147:**587
Davis RL, **147:**331
Davis S, **146:**465
Davison NE, **146:**341
Day DL, **146:**395, **147:**1027
De Armond SJ, **147:**331
de Geer G, **147:**21
de Jong TEAM, **146:**421
de Lange EE, **147:**1010
de Roos A, **147:**79
De Verbizier G, **146:**1316
De Vuyst P, **146:**73
Deck MDF, **146:**443
Dedrick CG, **146:**1129
Deeb ZL, **146:**119, **146:**353
Degesys GE, **146:**57
DeLand FH, **146:**333, **147:**181
Delaney V, **147:**949
Delcour C, **147:**1096
D'Elia F, **146:**523
Dellagiovampaola C, **146:**523
Demas B, **146:**163
Demas BE, **146:**717
DeMeester TR, **147:**911
Demos TC, **146:**45, **146:**601
Denny DF, **146:**863
Denny DF Jr, **146:**425, **146:**1317
Derauf BJ, **146:**849
Dershaw DD, **146:**127, **147:**491
Derugin N, **146:**925
Desnick RJ, **147:**943
Dev P, **147:**545
Dhumeaux D, **147:**635
Diakoumakis EE, **147:**593
Diament MJ, **147:**1035
Diamond AB, **146:**61
Diamond NG, **147:**834
Diáz FJ, **147:**859
Diaz RD, **147:**125
DiCandio G, **146:**523
Dick R, **147:**1117
Dickerson N, **147:**191
Didier D, **146:**919
Dietrich RB, **146:**251
Dillon EC, **146:**507
Dillon ML, **146:**497
Dillon WP, **147:**583
Dilworth LR, **147:**33
Dinkel E, **146:**775
Dinsmore RE, **146:**309, **146:**1286
DiPietro MA, **146:**1067
DiSantis DJ, **147:**850
Dittrich M, **146:**775
Docken WP, **147:**742
Dodds WJ, **146:**21, **147:**1155
Doherty P, **147:**721
Domstad PA, **146:**333, **147:**181
Donaldson JS, **146:**781
Donohue HJ, **146:**1038
Doppman JL, **147:**493, **147:**1145
Dorfman GS, **146:**425, **146:**1317
Dorne HL, **146:**175
Dorovini-Zis K, **147:**1063
D'Orsi CJ, **147:**721
Dorwart RH, **147:**583
Doubilet PM, **147:**598
Doumanian HO, **146:**1101
Drayer B, **147:**103
Dritschilo A, **147:**275
Drolshagen LF, **146:**1187
Drouineau J, **146:**1316
D'Souza VJ, **147:**1127
duCret RP, **146:**341
Duke RA, **146:**575
Dumont A, **147:**505
Dumortier P, **146:**73
Dunnick NR, **146:**57, **146:**1049, **146:**1289, **147:**39, **147:**832
Dwyer AJ, **147:**493
Dyer RB, **146:**665

E

Ebara M, **147:**531
Edeiken-Monroe B, **146:**803
Edelman RR, **146:**1286
Edwards DK, **146:**789
Edwards M, **146:**1223
Edwards MK, **147:**571
Eenmaa J, **146:**14
Eisenberg D, **147:**279
Eisenman JI, **146:**86, **147:**562
Eismont FJ, **147:**125
Ekholm SE, **146:**1057
Eli SR, **147:**1331
Ell SR, **146:**669
Elliott J, **147:**822
Elliott LP, **147:**414
Emery CD, **147:**919
Enzmann DR, **146:**1239
Epstein DM, **147:**227
Eraklis A, **146:**787
Erickson DL, **146:**849
Erickson J, **146:**1057
Eshghi M, **147:**283
Evens RG, **147:**166, **147:**856
Evert MB, **147:**1007

F

Fagan CJ, **147:**1043
Fakhry J, **147:**728, **147:**994
Farber LR, **146:**1298
Farlow MR, **147:**571
Farr G, **146:**1061
Farrell FW Jr, **146:**476
Feczko PJ, **146:**697, **147:**646
Federle MP, **146:**7, **146:**685, **146:**1161, **147:**406, **147:**919
Feigin DS, **146:**295, **147:**439
Fein AB, **146:**337
Feinberg SB, **146:**561, **147:**647
Fellmeth BD, **146:**619
Fellows KE, **146:**785, **146:**787
Felson B, **147:**881
Fender B, **147:**916
Ferguson M, **147:**911
Fernandes BJ, **146:**349
Fernbach SK, **146:**415
Ferrell LD, **146:**717
Ferris EJ, **146:**845, **147:**173
Ferrucci JT, **147:**1103
Ferrucci JT Jr, **146:**711, **146:**1141, **146:**1155, **147:**357, **147:**1237
Fields WS, **146:**809
Fierer J, **147:**83
Fiessinger J-N, **146:**157
Fifer M, **146:**1286
Figley MM, **147:**16
Filly RA, **146:**1099, **147:**411
Finck EJ, **146:**422
Firooznia H, **146:**361
Fischi M, **146:**1229
Fisher DR, **146:**634, **146:**1087
Fisher MR, **147:**1255
Fisher RG, **146:**422
Fishman EK, **146:**291, **146:**691, **146:**997, **146:**1167, **147:**271
Fitzer PM, **147:**439
Flannigan B, **147:**363, **147:**379
Fleischer AC, **146:**619, **146:**1187, **147:**1043
Fleming CA, **146:**443
Fletcher BD, **146:**941
Fletcher JW, **146:**819
Flisak ME, **146:**45
Flores A, **146:**787
Foderaro A, **147:**1019
Foley WD, **147:**613, **147:**1155
Fong KW, **146:**767
Foreman M, **146:**1061
Forman JM, **146:**155
Formanek AG, **147:**1127
Fornage BD, **147:**567
Fortner A, **146:**621
Foster WL, **146:**537
Foster WL Jr, **146:**703
Fox ER, **147:**1090
Fox JL, **147:**767
Frager DH, **146:**519
Frager J, **146:**519
Francis IR, **146:**285, **146:**1179, **147:**469, **147:**1063
Francis RS, **146:**649
Frank J, **147:**493
Frank JL, **146:**217
Franken EA, **146:**323
Fraser RG, **146:**883
Freedom RM, **146:**211
Freeman MP, **146:**533
Freeny PC, **147:**627, **147:**711
Frey E, **147:**1019
Frey GD, **146:**476, **147:**720

Fried AM, **146:**497
Friedman AC, **146:**351, **146:**997, **146:**1167
Friedman AK, **147:**776
Friedman EL, **146:**745
Friedman PJ, **147:**17
Friedman SE, **147:**899
Fugate JH, **146:**1273
Furui S, **146:**723
Furukawa H, **146:**513
Fyfe D, **147:**1207

G

Gagliardi RA, **146:**80, **146:**716, **147:**422
Gagnadoux MF, **146:**593
Gale ME, **146:**981
Galiber AK, **147:**929
Galloway SJ, **147:**753
Galvin HB, **147:**1149
Galvin JR, **146:**669, **147:**1331
Gamsu G, **147:**21
Gangarosa RE, **147:**1271
Ganti SR, **146:**451
Ganz P, **146:**831
Garcia F, **147:**1017, **147:**1251
Gardiner GA Jr, **146:**831, **147:**621
Garel L, **146:**593
Gariépy G, **147:**505
Garnick MB, **146:**745
Garvin AJ, **146:**113, **147:**1207
Gaux J-C, **146:**157, **146:**853
Gay BB Jr, **146:**113
Gebhardt MC, **147:**553
Gedgaudas E, **146:**93
Gefter WB, **146:**1215, **147:**227
Geisinger KR, **146:**665
Gelfand DW, **146:**424, **146:**875, **146:**993, **146:**1317, **147:**261, **147:**693, **147:**697, **147:**1091, **147:**1334
Gelford GJ, **147:**38
Geller M, **147:**266
Gens DR, **146:**987
Gerlock AJ Jr, **147:**776
Gersten K, **146:**843
Ghaed N, **146:**1038
Gibbons R, **146:**537, **146:**703
Gibbons RP, **147:**89
Gibbs JF, **146:**577
Gibson RN, **146:**1099, **147:**404
Gilsanz V, **146:**781, **147:**1035
Gilula LA, 1204, **146:**645, **146:**1192
Ginalski J-M, **146:**647
Ginsberg F, **146:**459
Gisvold JJ, **147:**191
Glass RBJ, **146:**644
Glazer GM, **146:**285, **146:**1179, **147:**469, **147:**843, **147:**1063
Glazer HS, **146:**403, **147:**17, **147:**188
Glenn W, **147:**199
Glick SN, **146:**648
Glickman MG, **146:**1173, **146:**1298
Glickstein M, **147:**227
Glowalla M, **146:**1184
Gluck WL, **146:**39
Godwin JD, **147:**674
Goergen TG, **147:**766
Goiney RC, **146:**553
Gold RH, **147:**689
Gold RH, **147:**891
Goldberg BB, **146:**1011
Goldberg H, **146:**163
Goldberg HI, **146:**1, **146:**717, **146:**940, **147:**1002, **147:**1215
Goldberg L, **147:**372, **147:**1236
Goldberg R, **147:**721
Goldblatt J, **147:**943
Goldfinger M, **146:**349
Goldsmith SJ, **147:**943
Goldstein EJ, **147:**367
Golimbu C, **146:**361
Golomb HM, **147:**911
Gomes AS, **146:**835, **146:**1031
Gonzalez CF, **146:**267
Goodman J, **146:**49
Goodman PC, **147:**29
Goodman ZD, **146:**997
Goormastic M, **147:**757
Gordon IJ, **146:**491
Gordon P, **146:**1005
Gordon RB, **147:**705
Gorman B, **147:**929
Goto H, **147:**525
Govoni AF, **147:**864
Grabowski GA, **147:**943
Graeb DA, **146:**103
Graef JW, **146:**245
Gramm HF, **146:**39
Graney DO, **146:**553
Grant CS, **147:**929
Grant EG, **147:**275
Gray G, **147:**1067
Gray JE, **146:**93
Graziano SL, **146:**1246
Green BA, **147:**125
Greenspan B, **146:**843
Greenstein S, **147:**271
Greenwood LH, **146:**863
Grillo HC, **146:**1129
Griscom NT, **146:**233, **147:**1095
Grizzard JD, **147:**301
Grollman JH Jr, **147:**1089
Gross BH, **146:**285
Gross GW, **146:**615
Gross RC, **147:**389
Grossman HB, **146:**1179
Grossman RI, **147:**1215
Grufferman S, **146:**337
Grumbach K, **146:**997
Guilbert M, **146:**593
Guillaumin ES, **146:**685
Guinet C, **147:**635
Gurney JW, **147:**641
Guter M, **146:**294

H

Haacke EM, **147:**1271
Haaga JR, **146:**543, **147:**1014
Hackney DB, **147:**1215
Hadlock FP, **146:**422
Haghighi P, **147:**83, **147:**739
Hahn PF, **146:**1141
Haimes AB, **147:**1067
Halasz NA, **146:**327, **147:**954
Halbach VV, **147:**891
Hale JD, **146:**931
Hall A, **146:**1239
Hall FM, **146:**424, **146:**425, **146:**648, **147:**195, **147:**646, **147:**742, **147:**860, **147:**1092
Hall TR, **147:**1035
Hall-Craggs MA, **147:**399
Halls JM, **146:**321, **146:**741, **147:**1305
Halpert RD, **146:**697, **147:**646
Halvorsen RA, **146:**537, **146:**703
Hampson LG, **147:**513
Han BK, **146:**609
Han SY, **147:**268
Hanafee W, **147:**199, **147:**363, **147:**379
Hanafee WN, **146:**409, **147:**1283
Handmaker H, **147:**1332
Harcke HT, **147:**317
Hardy DC, **147:**557
Harnsberger R, **146:**518
Harrington DP, **146:**831, **147:**621
Harris AB, **146:**14, **147:**627
Harris J, **146:**883
Harris JH Jr, **146:**803
Harris RD, **146:**986, **147:**524
Harter KW, **147:**275
Hartz WH, **146:**383
Hasegawa H, **147:**525
Hashim SW, **146:**863
Haskin PH, **147:**164
Hatfield MK, **147:**911
Haughton VM, **146:**1235
Hayman LA, **146:**415
Healy M, **146:**1282
Healy ME, **147:**544
Heavey LR, **146:**285
Heller VL, **147:**598
Hendee WR, **147:**490
Henderson AR, **147:**839
Henderson RG, **147:**167
Henderson RW, **147:**1133
Henry RE, **146:**1302
Hensley GT, **146:**1229
Herba MJ, **147:**513
Herfkens R, **147:**103
Herfkens RJ, **147:**497
Herlinger H, **146:**35, **146:**1318, **147:**1165, **147:**1183
Herman SD, **146:**351
Herman TE, **146:**1273
Hermann G, **147:**943
Heros R, **147:**985
Hertz D, **147:**363
Herzenberg JE, **146:**644
Hewes RC, **146:**1025, **146:**1219
Heystraten FM, **146:**303
Higgins CB, **146:**315, **146:**907, **146:**919, **146:**925, **146:**931, **147:**239, **147:**245, **147:**253, **147:**1255
Hightower DR, **146:**1161, **147:**406
Hilal SK, **146:**451
Hill MC, **146:**1277
Hillman AL, **146:**963
Hillman BJ, **147:**1197
Hilpert PL, **146:**1167
Hilton SvW, **147:**479
Hinke ML, **146:**627, **146:**631, **146:**634, **146:**637, **146:**1074, **146:**1080, **146:**1087, **146:**1094
Hirohashi S, **146:**1149
Hirohasi S, **147:**525
Hirooka N, **147:**531
Hirsch J, **146:**1019
Hjermstad BM, **147:**1309
Ho K-J, **146:**155, **147:**268
Hoddick W, **146:**163
Hodgman CH, **146:**639
Hodson J, **146:**1173
Hoffman JC Jr, **147:**587
Hoffman PC, **147:**911
Hoffstein V, **147:**1330
Hofmann AF, **146:**865
Hogan WJ, **146:**21
Hohn DC, **146:**717
Holden RW, **147:**685
Hollwarth M, **147:**1155
Holmburg CE, **147:**737
Holshouser BA, **146:**871
Holt RW, **147:**275
Homer MJ, **147:**1333
Honickman S, **146:**605
Honig CL, **147:**1067
Hopper J, **146:**465
Horger EO III, **147:**1043
Horwitz TA, **147:**185
Houston LW, **146:**637, **146:**1094
Hricak H, **146:**1115
Huber JS, **146:**587
Hudon G, **146:**369
Hueftle MG, **147:**1014
Hulnick D, **147:**705
Hunter D, **146:**143
Hunter DW, **147:**161, **147:**836, **147:**1025
Hunter TB, **146:**248, **147:**504
Hurwitz L, **147:**279
Hussain S, **146:**1316
Hutton L, **147:**839
Hydovitz JD, **147:**819

I

Iglesias P, **147:**937
Illescas FF, **146:**57, **146:**1289, **147:**1332
Imai Y, **147:**701
Inoue K, **146:**1101
Irwin GAL, **147:**530
Ishigour S, **146:**513
Itai Y, **146:**723, **146:**729
Itzchak Y, **146:**549

J

Jack CR Jr, **146:**271
Jackson H, **146:**883
Jackson J, **146:**421
Jackson KL, **147:**32
Jackson VP, **146:**341
Jacobstein MD, **146:**941
Jacoby CG, **146:**174
Jaffe RB, **146:**83, **147:**863
Jagannath AS, **147:**1123
James AE Jr, **146:**1187
James EM, **147:**929
James TL, **147:**1327
Jaques P, **146:**1041
Jaques PF, **147:**57
Jaramillo D, **147:**72, **147:**610, **147:**941
Jardin M, **147:**457
Jeffrey RB Jr, **146:**7, **146:**1161, **147:**406, **147:**828
Jenkins R, **147:**665
Jequier S, **147:**133
Jiang J-H, **147:**861
Jinkins JR, **147:**767
Jochelson MS, **146:**745
Johnson AR, **147:**1309
Johnson CM III, **147:**782
Johnson GA, **147:**103
Johnson GC, **147:**409
Johnson J, **147:**1197
Johnson N, **146:**1098
Johnston GS, **147:**1171
Johnston WK, **146:**859
Johnstone GF, **147:**293
Jolles H, **146:**669, **147:**1331
Jones B, **146:**691, **147:**271
Jones D, **146:**67
Joseph PM, **147:**367
Julien PJ, **147:**1133

K

Kadar N, **146:**1098
Kadir S, **146:**1025
Kagan AR, **146:**64, **146:**251, **146:**1184
Kahlstrom EJ, **147:**1031
Kahrilas PJ, **146:**21
Kanagasuntheram R, **147:**145
Kanal E, **147:**293
Kandarpa K, **146:**787, **146:**831, **147:**621
Kane R, **146:**163, **147:**665
Kangarloo H, **146:**251
Kanter SA, **146:**484
Kanzer M, **146:**1246
Karellas A, **147:**729
Karl EM, **146:**1187
Karlik S, **147:**839
Karlinsky JB, **146:**981

Karstaedt N, 147:1127
Kass EG, 147:593
Kassabian JP, 147:28
Katada N, 147:935
Kato K, 147:935
Katz J, 147:665
Katz ME, 147:322
Katz PG, 147:957
Katz RL, 147:155
Katz SG, 146:169, 146:590, 147:627
Katzenstein A-L, 147:899
Kaude JV, 147:1090
Kaufman L, 146:931
Kaufman RA, 146:97, 147:1199
Kaufman SL, 146:1025
Kaul S, 146:75
Kawamoto EH, 146:665
Kay CJ, 146:940
Kay D, 146:1061
Kaye A, 146:465
Kazam E, 147:1067
Keats TE, 147:782
Keen R, 147:199
Keep NN, 146:1276
Keller FS, 147:268, 147:289
Kelvin FM, 146:39, 146:537
Kenney PJ, 146:67, 147:289
Kent SG, 146:1277
Keramati B, 147:501
Kerber CW, 147:627
Kerlan RK, 146:717
Kerlan RK Jr, 146:882, 147:1002, 147:1185
Keshavarzian A, 147:167
Ketelbant P, 146:73
Khan RK, 146:882
Khettry U, 147:665
Khoo FY, 147:145
Kido DK, 146:1057
Kier R, 147:497
Kikuchi Y, 147:1183
Kilcoyne RF, 146:232
Kim EE, 147:610, 147:1177
Kim KS, 146:277, 147:575
Kimura K, 147:531
Kinard RE, 147:848
King HA, 146:1268
King PS, 146:345
Kingma LM, 146:303
Kinnison ML, 146:1025
Kintanar C, 147:801
Kipper S, 146:1099
Kirkaldy-Willis WH, 146:882
Kirklin JW, 146:155
Kirks DR, 146:757
Kishi K, 147:525
Kishk SM, 146:21
Kishk SMA, 147:1155
Kjellberg RN, 147:985
Klein JL, 146:823
Klein RM, 147:38
Kleinman PK, 146:895
Kling TF, 146:749
Knol E, 146:793
Koehler RE, 147:268, 147:289
Koerner FC, 146:133
Kogan FJ, 147:257
Kokubo T, 146:723, 146:729
Koltun W, 147:621
Konrad J, 146:373
Koonce TW, 146:646
Kopans DB, 146:133
Kopecky KK, 147:846
Kopiwoda SY, 146:543
Kopp DT, 147:1251
Kornstein MJ, 147:227
Kortman KE, 147:1133
Kramer SS, 146:691
Krasna IH, 146:1047
Kraus R, 146:609
Krauss AN, 146:471
Krausz T, 147:167
Kressel HY, 146:1167, 146:1215, 147:67, 147:1332
Kriesmer P, 146:1257
Krohn KA, 146:690
Kucharczyk W, 146:1223
Kuhn G, 146:73
Kuligowska E, 146:1283
Kulkarni MV, 147:373
Kumakura K, 147:701
Kumpe DA, 147:159
Kundel HL, 147:67, 147:1332
Kunin M, 146:882
Kunz LL, 147:627
Kursunoglu S, 147:545
Kurtz AB, 146:1011
Kushner DC, 146:1273
Kvalstad RP, 147:1031
Kwan ESK, 146:1239

L

LaBerge JM, 147:1002
Laberge JM, 146:882
Lacquet LK, 146:303
Lacy J, 146:1298
Lafortune M, 146:53, 147:505
Laing FC, 146:7, 146:1099, 146:1161
Lake AM, 146:691
Lamki N, 147:725
Lampmann LEH, 146:421
Lancaster JL, 147:1251
Lande IM, 146:1277
Lanza MV, 147:1031
Lapin SA, 146:741
Lapointe JS, 146:103
Lapointe R, 147:505
Larsen JW, 146:1277
Laster DW, 147:119
Latchaw R, 147:777
Laufer I, 146:31, 146:507, 147:1165, 147:1183
Lavain J, 146:465
Lavender JP, 147:167
Lawdahl RB, 147:744
Lawson TL, 147:1155
Lebensart PD, 146:549
Lebowitz RL, 147:313
Lee AA, 146:581
Lee BCP, 146:443
Lee EL, 147:61
Lee HH, 146:25
Lee JKT, 146:403, 147:732
Lee K, 147:372
Lee MS, 147:317
Lee WJ, 147:97, 147:283, 147:830
Lee WS, 147:145
Lee Y-Y, 147:111, 147:747
Lees WR, 147:399
Leight GS, 147:497
Leikind B, 147:1283
Leithiser RE Jr, 146:227, 147:1207
Lemak NA, 146:809
LeMay M, 147:963
Lemme-Plaghos L, 146:1223
Leonard JC, 147:596
Leopold GR, 147:479
Lerner RM, 147:1189
Lester PD, 147:339
Letourneau JG, 147:1027
Levin DC, 146:604, 147:1, 147:621
Levine E, 147:1299
Levine JB, 147:1333
Levine MS, 146:31, 146:507, 147:1165, 147:1183
Levinsohn EM, 146:67, 146:1246
Levy DW, 146:997
Levy LM, 147:283
Levy RM, 147:977
Levy RN, 147:943
Lewall DB, 146:391
Lewis BD, 147:598
Lewis GP, 147:89
Li C-Y, 147:181
Liberthson RR, 146:309
Libshitz HI, 147:747
Libson E, 146:549
Lichtenstein JE, 147:537
Liddell HT, 146:1187
Lieber A, 146:333, 147:44
Lieberman RP, 146:595, 147:439
Lindfors KK, 146:133, 147:797
Ling D, 146:403
Link KM, 147:1127
Lipchik EO, 147:613
LiPuma JP, 146:543
Little AG, 147:911
Liu G-C, 146:845
Liu P, 146:309, 146:763
Lloyd RV, 147:1063
Lock JE, 146:785
Lock MM, 146:64
Lockhart SH, 147:1123
Lois JF, 146:835, 146:1031, 147:994, 147:1148, 147:1206
Lokich JJ, 146:39
Longmaid HE III, 146:1005
Lopez M, 147:923
Lorenzo RL, 146:113
Loriaux DL, 147:1145
Lotz PR, 147:1209
Lough J, 147:513
Lowe R, 146:341
Lowry P, 147:1177
Lufkin RB, 146:409, 147:199, 147:363, 147:379, 147:891, 147:1283
Lund G, 147:836, 147:1027, 147:1052
Lundell CJ, 146:422
Lupetin AR, 146:119, 146:353
Lyons JW, 146:581

M

MacEwen GD, 147:317
Machan L, 147:509
Mack LA, 146:1019
MacMahon H, 147:911
MacMillan RM, 147:916
Macpherson RI, 146:227
Madigan SM, 146:345
Magill HL, 147:325
Magilner AD, 147:329
Mahan J, 146:395
Mail JT, 147:685
Makuuchi M, 146:1149, 147:525
Malik S, 147:491
Mallett E, 147:97
Mamourian AC, 146:485
Manaster BJ, 146:87, 146:1100, 147:563
Manchester D, 147:1047
Mancini GBJ, 147:33, 147:1095
Manco-Johnson ML, 147:1047
Mankovich NJ, 146:835
Marcus CS, 147:728
Mareschal JL, 146:593
Margulis AR, 146:1, 147:1327
Marincek B, 147:519
Marinelli D, 147:1312
Mark AS, 146:685
Markarian B, 146:67, 146:1246
Markivee CR, 146:819, 146:830, 147:144
Marks MP, 147:1031
Marks SC, 146:895, 147:1031
Marks WM, 147:711
Marshall J, 146:309
Martel W, 146:749, 147:1063
Martin B, 147:291
Martin DS, 146:774
Martin JR, 147:1096
Martin KW, 147:670
Martin L, 147:477
Martin LG, 146:881, 147:9
Martin RL, 147:834
Maruyama Y, 147:181
Marx M, 147:1
Masaryk T, 147:757
Mathieu D, 147:635
Mattrey RF, 146:327
Maurer AH, 147:530
Mauro M, 146:1041
Mauro MA, 147:57
Mawad M, 146:451
Mayer JH, 146:1101
McAfee JG, 146:67
McAlister WH, 146:1140, 147:322
McCallum RW, 147:544
McCann R, 146:1289
McCarthy KA, 146:133
McClennan BL, 147:188, 147:393
McCorkell SJ, 146:391
McCoy RD, 146:1031
McCrea ES, 147:501
McDermott W, 147:665
McDougal WS, 146:1187
McDougall IR, 147:601
McGahan JP, 147:797, 147:1241
McGillem MJ, 147:1095
McGuire W, 146:1293
McIlhenny J, 147:1010
McKenna S, 146:955
McLean GK, 146:383
McLelland R, 147:1091
McLoud TC, 146:309, 146:1129
McMillin KI, 146:749
McNamara MT, 146:315, 147:1255
Megibow AJ, 147:705
Melada GA, 147:819
Melson GL, 146:555
Melvin IG, 146:497
Mendez G, 146:587
Mendez G Jr, 147:1062
Meranze SG, 146:383
Merritt CRB, 146:1061
Merten DF, 147:87
Métreau J-M, 147:635
Mettler D, 147:519
Meyer GA, 147:1010
Meyer JE, 146:133
Meyerovitz MF, 146:831, 147:621
Meyers TP, 147:834
Meziane MA, 146:1167
Middaugh D, 147:338
Middleton WD, 146:555
Mikity V, 147:1031
Milde MW, 147:613
Miller CL, 147:45
Miller CM, 147:51
Miller DA, 147:155
Miller DL, 146:949, 146:1317, 147:438
Miller GA Jr, 146:326
Miller JH, 146:781, 147:1035
Miller SW, 146:309, 146:1286
Miller W, 147:227
Miller WT, 147:1090, 147:1312
Mills NL, 146:1061
Mills SE, 146:665
Minagi H, 147:29
Minami M, 146:723, 146:729
Minitz HA, 146:1317
Minkoff J, 146:361
Mirivs SE, 147:1093
Mirvis SE, 146:987, 147:501, 147:1171
Mishkin FS, 147:815

Mitchell DG, **146:**1167, **146:**1215
Mitchell MD, **147:**67, **147:**1332
Mitchell SE, **146:**387, **146:**1025
Mitty HA, **147:**51
Miyake T, **146:**735
Modic MT, **147:**757
Moes CAF, **146:**211
Moinuddin M, **147:**607
Momoshima S, **147:**701
Montalvo BM, **146:**815, **147:**125
Montana MA, **147:**516
Moody DM, **147:**119
Moolten DN, **147:**1165
Moore EH, **146:**1123
Moore S, **146:**163
Moore WE, **146:**678
Mootz A, **146:**679
Morgan TR, **147:**257
Moriarty AT, **147:**846
Morin R, **147:**1052
Moriyama N, **146:**1149, **147:**525
Moriyasu F, **146:**735
Morrison G, **146:**1261
Morse SS, **146:**863, **147:**391
Mosca F, **146:**523
Moseley ME, **147:**1263
Moser R, **147:**111
Moskowitz GW, **147:**283
Moskowitz LB, **146:**1229
Moss A, **146:**163
Moss CN, **147:**744
Mueller PR, **146:**711, **146:**869, **146:**1155, **147:**1237
Muller N, **146:**1123
Müller NL, **146:**477, **147:**509
Mulopulos GP, **146:**51, **147:**291
Munitz A, **146:**875
Munitz HA, **146:**993, **147:**261
Murakami ME, **146:**51
Muramatsu Y, **146:**1149, **147:**525
Murari PJ, **147:**537
Murovic J, **147:**1223, **147:**1231
Murphy FB, **147:**9
Murphy K, **146:**87, **146:**1100
Murphy WA, **146:**555, **146:**565
Murray DR, **146:**839
Murray RR, **146:**1025
Myers JL, **147:**899
Myers PA, **146:**97

N

Naidich DP, **147:**705
Naidich T, **146:**1246
Nakamura T, **146:**735
Nancarrow PA, **146:**785, **146:**789
Neblett WW, **146:**619
Needell GS, **146:**1047
Needleman L, **146:**1011
Neff JR, **147:**1299
Nelson AD, **146:**543
Nelson AW, **147:**1171
Nelson RC, **147:**949
Nemcek AA Jr, **146:**1324
Nemcek AA Sr, **147:**737
Neoptolemus J, **146:**865
New PFJ, **147:**985
Newbold RG, **147:**87
Newell JD, **146:**248
Newell JD II, **147:**1138
Newman GE, **146:**1049, **147:**39
Newmark H III, **146:**484, **146:**1276
Newton TH, **146:**1223, **147:**331, **147:**1231
Ng HW, **147:**145
Nguyen DL, **147:**596
Nguyen M, **147:**1177
Nieman L, **147:**1145
Nishida O, **146:**735
Nixon C, **147:**1094
Nixon GW, **146:**83
Norman D, **146:**1223, **147:**331, **147:**1223
North CM, **146:**257, **147:**995
Nosher JL, **146:**1047
Notman DNH, **146:**93
Nozick J, **146:**605
Nugent RA, **146:**103
Nunez D Jr, **146:**587
Nyberg D, **146:**1019
Nyberg DA, **146:**7, **146:**1099

O

Ocon E, **147:**859
Oestreich AE, **146:**609, **147:**863, **147:**864
Ogan MD, **147:**1263
Ogawa K, **147:**1247
O'Gorman AM, **147:**133
Ohto M, **147:**531
Ohtomo K, **146:**723, **146:**729
Ojemann RG, **147:**985
Okada RD, **146:**309
Okawara S-H, **146:**1057
Okazaki N, **147:**525
Oke EJ, **146:**1049, **147:**832
Okuda K, **147:**531
Oldfield EH, **147:**1145
Olmsted WW, **147:**537
Oloff J, **146:**1192, 1204
Oloff LM, **146:**1192, 1204
Olsen R, **147:**363
Olson LK, **146:**1140, **147:**479
Olutola PS, **147:**839
Ominsky S, **146:**1
Ominsky SH, **147:**1149
Onik G, **146:**163, **147:**665
Op den Orth JO, **146:**1017, **147:**281
Orringer MB, **146:**285, **147:**469
Orrison WW, **147:**848
Ortendahl DA, **146:**931
Orth S, **146:**775
Osaki L, **147:**1223, **147:**1231
Osborn AG, **146:**518
Oster ZH, **146:**1100
Ott DJ, **146:**424, **146:**875, **146:**993, **146:**1317, **147:**261, **147:**693, **147:**697, **147:**1091

P

Pae WE, **146:**485
Page AC, **146:**81
Page DL, **147:**487
Pais SO, **146:**987, **147:**1093
Palayew MJ, **146:**175
Palmaz JC, **147:**1017, **147:**1251
Papanicolaou N, **146:**711
Papin PJ, **146:**835
Parer JT, **147:**411
Pariente D, **146:**593
Parkey RW, **147:**1289
Pasto ME, **146:**1011
Pate D, **147:**545
Patel R, **147:**815
Patriquin H, **146:**1253
Patten RM, **146:**1019
Patton JA, **147:**373
Patwardhan NA, **147:**721
Pearl GS, **147:**587
Pearlman AS, **146:**44
Penkrot RJ, **146:**137
Pennes DR, **146:**1100
Penning L, **146:**793
Pérez-Fontán FJ, **147:**937
Perkins CL, **146:**1
Perlman JM, **147:**322
Perlmutt LM, **146:**1049, **147:**39, **147:**832, **147:**1090
Pernes J-M, **146:**157
Perrett LV, **147:**977
Peshock RM, **147:**1289
Peters ME, **146:**627, **146:**1080
Peterson HdeC, **146:**471
Pettersson H, **146:**1314
Pevsner P, **146:**1038
Peylan-Ramu N, **146:**549
Peyster RG, **146:**459
Phillips WA, **146:**749
Picus D, **147:**393
Pietra GG, **147:**227
Piggott B, **146:**1041
Pilla TJ, **146:**1300, **147:**1096
Pillari G, **146:**843
Pjura G, **147:**1177
Pochaczevsky R, **147:**97
Pogany AC, **146:**882, **147:**1002, **147:**1185
Point S, **147:**657
Pojunas KW, **146:**1235
Pollack H, **146:**67
Pollack HM, **147:**94
Pollack M, **147:**1177
Poole CA, **146:**217, **147:**1062
Pope TL, **146:**665
Portha C, **146:**263
Poskitt K, **146:**174
Posmituck G, **146:**1051
Posniak HV, **146:**601
Post MJD, **146:**1229, **147:**125
Postma MP, **147:**287
Preger L, **146:**30
Pretorius DH, **147:**552, **147:**1047
Price RR, **147:**373
Prince JR, **147:**339
Princenthal RA, **146:**581, **146:**865
Pring DJ, **147:**167
Pringle KC, **147:**1019
Pryor DB, **146:**337
Pusey E, **147:**1283
Pyatt RS, **146:**997

Q

Qin D, **147:**543
Quencer RM, **146:**815, **147:**125, **147:**1000
Quinn J, **147:**199
Quinn MF, **146:**422
Quinn SF, **146:**581
Quint LE, **147:**469
Quisling RG, **147:**1209

R

Rabinowitz JG, **146:**49
Radecki PD, **146:**351, **146:**997, **146:**1167
Radin DR, **146:**321, **146:**741, **147:**1305
Rafii M, **146:**361
Rahmani MR, **146:**767
Ralls PW, **146:**741
Randall PA, **146:**30, **147:**184
Ranfranz MK, **147:**191
Rao BK, **146:**631, **146:**1074
Rao V, **146:**1215
Rappoport AS, **146:**61
Raptopoulos V, **147:**721, **147:**729
Ratcliff G, **147:**777
Rauber K, **147:**1093
Rauch RF II, **146:**337
Rauschning W, **147:**891
Raval B, **146:**421, **147:**941
Ray MJ, **146:**321, **147:**1305
Raygor DJ, **147:**191
Raynaud A, **146:**853
Read RC, **147:**173
Reading CC, **147:**929
Redman HC, **146:**415, **146:**597
Reed LD, **146:**819
Reed M, **146:**1038
Rees C, **146:**341
Rees MR, **147:**916
Reese DF, **146:**271
Regenbogen V, **147:**575
Regenbogen VS, **146:**277
Reicher M, **146:**409
Reicher MA, **147:**363, **147:**891
Reid SH, **147:**1181
Reid WD, **147:**801
Reifsteck JR, **146:**845
Reinig JW, **146:**949, **147:**493
Reinus WR, **146:**555, **146:**645, **147:**203
Remy J, **147:**457
Remy P, **146:**853
Resnick D, **147:**83, **147:**545, **147:**739
Resnick MI, **146:**543
Resnik CS, **147:**301
Reyes PF, **146:**267
Rhodes M, **147:**199
Rholl KS, **147:**732
Rice RP, **146:**537
Rich M, **147:**830
Richards T, **147:**144
Richardson EP, **147:**985
Richie JP, **146:**745
Richli W, **146:**591, **147:**149, **147:**1247
Richmand D, **146:**605
Richter JE, **147:**693
Riederer S, **147:**103
Riemenschneider PA, **146:**172
Rifkin MD, **146:**1011
Rigsby CM, **146:**1173
Rindsberg S, **146:**997
Ring EJ, **146:**882, **147:**1002, **147:**1185
Rivett AG, **147:**167
Roberts L, **146:**537, **146:**703
Roberts SR, **146:**20
Robertson WD, **146:**103
Robins AG, **146:**981
Robitaille P, **146:**1253
Robledo AG, **147:**859
Rockett J, **147:**607
Rockoff SD, **147:**141
Rocmans P, **146:**73
Rodgers B, **146:**605
Rodgers JE, **147:**275
Rodriguez A, **147:**1171
Rogers LF, **146:**277, **147:**575, **147:**1324
Rohrmann CA, **147:**516
Romero R, **146:**1098
Roncato M, **146:**157
Roos MS, **146:**931
Root L, **146:**1219
Ros PR, **146:**997, **147:**537, **147:**1309
Rosas G, **146:**217
Rose SC, **147:**159
Rose TH, **146:**767
Rosen BR, **146:**1286, **147:**985
Rosen E, **146:**843
Rosenbaum DM, **146:**249, **146:**1268
Rosenberg HK, **146:**109, **147:**1041
Rosenbloom S, **147:**977
Rosenbusch G, **146:**303
Rosenfield AT, **146:**1173, **147:**1082
Rosenthal DI, **147:**553
Rothberg R, **146:**349
Roy S III, **147:**325
Rubens D, **147:**1189
Rubenstein WA, **147:**1067, **147:**1162
Rubesin SE, **146:**35, **146:**1318
Rubinsky B, **147:**665
Rubinstein I, **147:**1330
Ruchti C, **147:**519

Ruiz J, 147:937
Rumack C, 146:415
Russ PD, 147:1047
Russell AH, 146:970
Russell E, 146:587
Rustgi SN, 147:275
Ryan JW, 147:911

S

Sacco DC, 147:1271
Saddekni S, 147:1123
Sade R, 147:1207
Safrit H, 146:1041
Sagel SS, 147:17, 147:26, 147:670
Saini S, 146:309, 146:1155, 147:357, 147:1237
Saint-Georges G, 146:369
Saint-Louis LA, 146:443
Sakai M, 146:735
Sakai Y, 146:513
Sakimura IT, 147:177
Salazar JE, 146:575
Salzman L, 146:1283
Samaan NA, 147:149
Sammon JK, 147:164
Sampliner RE, 147:257
Sanchez FW, 146:839
Sanchez J, 147:937
Sandler MP, 146:619
Sandler S, 147:777
Sane P, 146:451
Sanjurjo P, 147:937
Sano H, 147:935
Santos GW, 146:691
Saral R, 146:691
Sargent SK, 146:690
Sartoris D, 147:83
Sartoris DJ, 146:1030, 146:1046, 146:1268, 147:545, 147:739, 147:1040, 147:1329
Sarwar M, 147:570
Satin R, 146:175
Sato T, 146:513
Sato Y, 147:1019
Sauerbrei EE, 147:923
Saul SH, 146:507
Saunders DR, 146:294
Sauser DD, 146:1219
Sauvegrain J, 146:593
Savit RM, 146:644
Sax SL, 147:725
Scanlan KA, 146:631, 146:1074
Scatarige JC, 146:291
Schaefer S, 147:1289
Schapiro RL, 146:119, 146:353
Scheible FW, 146:327
Scheinman JI, 146:395
Scheithauer BW, 146:271
Schernberg FL, 147:567
Schier D, 146:1051
Schiff RG, 147:283
Schlater M, 146:1061
Schlesinger AE, 146:1133
Schmiedl U, 147:1263
Schorr RT, 147:1332
Schulte-Wissermann H, 146:775
Schwartz AM, 147:141
Schwartz AN, 146:553
Schwartz E, 146:549
Schwartz JS, 146:963
Schwartz MM, 146:51
Schwartz SS, 147:1288
Schwarz W, 146:605
Schwesinger W, 147:1251
Scott JA, 147:553
Scott WW Jr, 146:387, 146:423
Sebrechts C, 146:823
Sechtem U, 146:925, 147:239, 147:245
Sechtem UP, 147:140
Sefczek RJ, 146:119, 146:353
Segal MC, 146:137
Segal SR, 146:109
Segall GM, 147:601
Segall HD, 146:257, 147:995
Seibert JJ, 146:255
Seife B, 147:593
Sekine Y, 147:701
Seltzer SE, 146:1005
Selwyn AP, 146:831
Semine A, 146:1283
Service FJ, 147:929
Shaffer HA Jr, 147:1010
Shah HR, 147:173
Shane OC III, 146:93
Shapiro MD, 147:753
Shapiro R, 147:753
Sharpless T, 147:379
Shaw C-I, 147:1181
Shaw CM, 147:627
Shea WJ Jr, 146:717
Sheldon JJ, 147:125
Shepard JO, 146:1129
Sherlock S, 147:1117
Sherman P, 146:763
Sherry CS, 147:834
Shields JB, 146:1300, 147:1096
Shih W-J, 147:181
Shih WJ, 146:333
Shima Y, 146:1149, 147:525
Shin MS, 146:155, 146:421, 147:899
Shires GT III, 147:9
Shorr R, 147:1171
Short BL, 146:1257
Shorvon P, 147:1078
Shuford WH, 146:491, 147:1090
Shulkin BL, 147:1193
Shuman WP, 146:175
Sibbitt RR, 147:1017, 147:1251
Siber FJ, 146:774
Sickles EA, 146:661, 146:1137, 147:861, 147:1149
Siegel BA, 147:670, 147:784
Siegel ME, 147:177, 147:372
Siegelman SS, 146:291, 146:691, 146:997, 147:271
Silber JH, 146:459
Silva W, 147:729
Silver AJ, 146:451
Silverman PM, 146:57, 146:1289, 147:497
Silverstein GS, 146:423
Simeone JF, 146:711, 146:1155, 147:347, 147:1237
Simmons BP, 147:301
Simon JH, 146:1057
Simon M, 146:883
Simpson A, 146:605
Sinning L, 147:317
Sistrom CL, 147:782
Sivit CJ, 146:1277
Skidmore MB, 146:767
Skolkin MD, 146:839
Skolnick ML, 146:137
Sleder PR, 146:595, 147:439
Sleight G, 146:64
Sloan K, 146:1061
Smith AD, 147:283
Smith DF, 147:613
Smith EH, 147:721, 147:729
Smith HJ, 147:61
Smith JA, 146:955, 146:1293
Smith R, 147:287
Smith S, 147:363
Smith SD, 146:409
Smith T, 147:785
Smith TP, 147:161, 147:836, 147:1025
Sniderman KW, 146:863, 147:1123
Snyder HM III, 147:1041
Snyder LL, 146:646
Soler R, 147:937
Sollitto R, 146:1, 146:1123
Sollitto RA, 147:1149
Solomon MA, 146:1192, 146:1204
Sommer FG, 147:1075
Sooy CD, 147:919
Sörensen R, 146:373
Sos TA, 146:604, 147:1123
Soto B, 147:1139
Soto-Rivera C, 147:1237
Spencer R, 147:791
Spencer RP, 146:1010
Spirt BA, 147:976
Spizarny DL, 146:1129
Sprayregen S, 147:438
Spritzer CE, 146:1215
St. Amour TE, 147:188
Staab EV, 147:57
Stadalnik RC, 147:1262
Stafford SA, 147:553, 147:1237
Stalker HP, 147:1199
Stanley JH, 147:1043
Stanley P, 147:1035
Stapleton FB, 147:325
Stark DD, 146:1141, 146:1155, 147:357, 147:411, 147:1283
Stark P, 147:72
Starzl TE, 146:137, 147:657
Stauffer AE, 146:711
Steckel RJ, 146:64, 146:251, 146:1184
Steele G, 147:665
Steiger DA, 147:1271
Stein BM, 146:451
Stein EJ, 146:383
Stein HD, 147:637
Stein MG, 147:1133
Steinberg EP, 147:453
Steinberg HV, 147:9
Steinberg M, 146:1215
Steinberg ME, 147:67, 147:1332
Steiner E, 146:1057
Stevens JC, 147:571
Stevenson G, 147:1078
Stewart CA, 147:177
Stewart ET, 146:21, 147:1155
Stewart J, 146:1061
Stewart WA, 146:1246
Stolar C, 146:239
Stoll S, 146:349
Stolzenberg J, 147:1336
Stomper PC, 146:745
Stratemeir EJ, 146:309
Strauss EB, 146:863, 147:391
Strauss S, 146:549
Streeten DHP, 146:1246
Strife JL, 147:791
Stringer DA, 146:15, 146:763
Stronell RD, 146:859
Sugino Y, 147:701
Sullivan L, 146:174
Sullivan M, 146:1061
Sumida M, 147:531
Sumpio BE, 147:391
Sundaram M, 146:359, 147:238
Sussman SK, 147:39, 147:832
Sutton D, 147:216
Swantkowski TM, 147:57
Swee RG, 147:191
Swensen HE, 147:293
Sybers RG, 146:491
Sze G, 147:331
Szwarc IA, 146:591

T

Tack ED, 147:322
Takayama T, 147:935
Takayasu K, 146:1149, 147:525
Takeichi M, 147:935
Talner LB, 147:960
Tanenbaum LB, 146:577
Tantana S, 147:1096
Tarr R, 147:501
Tash RR, 147:266
Tashjian J, 146:93
Taus RH, 146:831
Taveras JM, 147:353
Taylor A Jr, 146:621
Taylor GA, 146:647, 146:1257, 147:1319
Taylor KJW, 146:533
Tchang SPK, 146:882
Teele RL, 146:1067
Tegtmeyer CJ, 147:504
Telander RL, 147:929
Teo AT, 147:145
Teplick SK, 147:164
Tepper JE, 146:1155
Thieme GA, 146:619
Thompson BW, 147:173
Thompson R, 146:309
Thompson WM, 146:537, 146:703
Thorbjarnarson B, 147:1067
Thornburg AJ, 146:615
Thorne DA, 147:809
Thorsen MK, 146:1235
Tihansky DP, 147:627
Tio FO, 147:1251
Tirman RM, 146:646
Tocino IM, 146:487
Torres WE, 147:1007
Totty WG, 146:555, 146:565, 146:645, 147:203
Towbin R, 147:791, 147:863, 147:1199
Towbin RB, 146:97
Train JS, 147:51
Trapnell D, 146:883
Traughber P, 146:1100
Traughber PD, 146:87
Trenkner SW, 146:647
Tress BM, 146:465
Trey C, 146:1141
Tscholakoff D, 146:925, 147:239, 147:245
Tucker GF Jr, 146:1133
Turner DA, 146:51
Turner MA, 147:1181
Tutschka P, 146:691
Tuttle R, 147:477

U

Uchino H, 146:735
Udelsman R, 147:1145
Unger EC, 146:403
Unger JM, 146:627, 146:1080
Uske A, 146:1223
Utz JA, 147:497

V

Vainright JR, 147:1171
Valk PE, 146:931
Vallee C, 146:53
Van Allen M, 146:1019
Van Dyke JA, 147:744
van Heerden JA, 147:929
van Heesch HAJM, 146:421
Van Lom K, 147:83
van Meerten ELvP, 147:79
Van Tassel P, 147:111, 147:747
van Woerden HH, 146:793
Vanden Brink J, 146:419
Vandiviere HM, 146:497
vanSonnenberg E, 146:327, 146:577, 146:581, 146:865, 146:1099
Vargas B, 147:313

Vasile N, **147:**635
Vassiliadis A, **147:**545
Vedal S, **146:**477
Verstandig A, **146:**31
Viamont T, **146:**1019
Vici LG, **147:**1237
Vick CW, **146:**533
Villarica J, **147:**389
Vitoux J-F, **146:**157
Vlahakes GJ, **146:**1286
Vogelzang RL, **146:**381, **146:**1165, **147:**1021
Vogler JB III, **147:**557
Volkman DJ, **146:**949
Votruba J, **146:**409

W

Wagner LK, **146:**803
Wahl RL, **147:**1193
Wall RT, **147:**438
Wall SD, **146:**1, **146:**7, **147:**919
Wallace MJ, **147:**1247
Wallace S, **146:**375, **146:**591, **147:**149, **147:**155
Walter JP, **147:**797, **147:**1241
Waltman AC, **146:**711
Wang Y, **147:**205
Watanabe A, **146:**487
Waxman AD, **147:**1133
Weatherby E III, **147:**1207
Webb WR, **146:**1123, **147:**21
Weber ER, **146:**646
Weber WN, **146:**1137, **147:**861, **147:**1149
Wechsler RJ, **147:**45, **147:**907
Wedeen VJ, **146:**1286
Weetman R, **146:**955
Weil R III, **147:**159
Weinberg B, **147:**593
Weingarten M, **147:**266
Weinreb JC, **146:**597, **146:**679, **147:**785
Weiss MH, **146:**257
Wells T Jr, **146:**163
Wetzel LH, **147:**1299
Weyman PJ, **147:**393
Whalen JP, **147:**1162
Wheeler PS, **146:**387, **146:**418
White RH, **147:**557
White RI Jr, **146:**1025
Whitley NO, **147:**1171
Whittemore A, **147:**621
Wholey MH, **147:**1132
Widder DJ, **147:**347, **147:**353
Wiener MD, **147:**87
Wiggins JW Jr, **147:**1148, **147:**1206
Wigton RS, **147:**641
Wilcox WA, **146:**518, **147:**44
Wilkinson RH, **146:**245
Willerson JT, **147:**1289
Williams AL, **146:**1235
Williams DL, **146:**532
Williams JJ, **147:**1067
Williams TD, **146:**497
Williamson MR, **146:**255, **147:**173, **147:**216
Williamson SL, **146:**255
Williford ME, **146:**537
Wills JS, **147:**826
Willson SA, **147:**479
Willson SW, **146:**865
Wilmink JT, **146:**793
Wilson D, **146:**1019
Wilson GH, **147:**891
Winchester P, **146:**471
Winer-Muram HT, **146:**575
Winfield AC, **147:**487
Wing VW, **146:**7, **146:**1099, **146:**1161, **147:**406
Winkler ML, **147:**253
Winter J, **147:**363
Winter PF, **147:**408
Winzelberg GG, **147:**819
Wiot JF, **146:**181, **147:**417
Wismer GL, **146:**75, **146:**309
Witcofski RL, **147:**119, **147:**1127
Withers CE, **146:**1282
Wittenberg J, **146:**711, **146:**1155, **147:**357
Wittich GR, **146:**327, **146:**577, **146:**581, **146:**865
Witzel MA, **146:**15
Witztum KF, **146:**823
Wohl MEB, **146:**233, **147:**1095
Wolf EL, **146:**519
Wolf GL, **147:**293, **147:**367
Wolf R, **147:**363
Wolfe SA, **146:**1261
Wolverson MK, **147:**1096, **147:**1176
Wood BP, **146:**20, **146:**227, **146:**639, **146:**1098
Woodring JH, **146:**497
Woods DM, **146:**375
Woolley MM, **147:**1035
Wootton P, **146:**24, **146:**678
Wozney P, **147:**657
Wright K, **147:**1247
Wright KC, **146:**375
Wu WC, **146:**875, **146:**993, **147:**261, **147:**693, **147:**697
Wulff K, **146:**645
Wyly JB, **147:**806, **147:**949

Y

Yagan R, **147:**858
Yaghmai I, **147:**301
Yakes WF, **146:**1038
Yamada T, **146:**1149, **147:**525
Yamanashi WS, **147:**339
Yamasaki S, **146:**1149, **147:**525
Yamauchi T, **146:**723, **146:**729
Yankaskas B, **146:**1041
Yashiro N, **146:**723, **146:**729
Yeager AM, **146:**691
Yeh H-C, **146:**49
Yernault J-C, **146:**73
Yolken RH, **146:**691
Young A, **146:**143
Young JWR, **147:**501
Yousem DM, **146:**291
Yrizarry JM, **146:**587
Yu AC, **147:**279

Z

Zaatari GS, **146:**113
Zajko AB, **146:**137, **147:**657
Zalewska MK, **146:**267
Zamel N, **147:**1330
Zee C-S, **147:**995
Zee CS, **146:**257
Zeit R, **147:**383
Zelner R, **147:**1305
Zeman RK, **147:**414, **147:**1336
Zimmerman RA, **147:**1215
Zimmerman RD, **146:**443
Zirinski K, **147:**1067
Zito J, **146:**843
Zorba J, **146:**1051
Zornes SL, **147:**268
Zvi ZB, **147:**593

Combined Subject Index Volumes 146–147

AJR articles are also included in the 5-year cumulative index published in *Radiology*.

Index Key: a = abstract, b = book review, e = editorial, l = letter, m = memorial, p = pictorial essay

Subjects in this index are catalogued by body part where possible. Disease entities unique to a body part are listed by that part; other more general diseases have separate listing by name. Technical procedures are also listed by part, as appropriate. Because of general interest, subjects dealing with computed tomography, magnetic resonance imaging, ultrasound, radionuclide imaging, and pediatric radiology are listed under those headings as well as under appropriate body part and/or disease.

A

Abdomen
appendicitis, CT findings, **147:**705
pain, plain film evaluation, **147:**501
percutaneous abscess, digital-scout-radiograph-assisted drainage, **147:**406
subphrenic abscess, percutaneous drainage, **147:**1237
Abrams, Raymond M. (m), **147:**1288
Abscess, *see* specific organ; region
Achalasia, nongastrointestinal malignancies and (a), **147:**442
Achilles tendon
computed tomography (a), **146:**1104
tendinopathies, sonography of (a), **146:**429
Acoustic neuroma, diagnosis (a), **147:**218
Acquired immune deficiency syndrome
abdominal CT in, **146:**7
cytomegalic inclusion virus encephalitis with, CT, **146:**1229
gastrointestinal tract, multifocal abnormalities of, **146:**1
Kaposi's sarcoma with, **147:**919
neurological manifestations of (a), **146:**1106
neuroradiologic findings in, **147:**977
pneumonia, spontaneous pneumothorax with, **147:**29
Adenoid cystic carcinoma, trachea, CT, **146:**1129
Adenoma, *see* specific organ
Adrenal disease, functional, anomalous kidneys with, radiology, **147:**289
Adrenal gland
Cushing syndrome, CT, **146:**1235
intermediate masses, MRI, **147:**493
Aerodigestive tract, multiple primary epidermoid carcinoma (a), **146:**1320
Air bronchogram, sonographic demonstration, **147:**593
Airway
obstruction, nonfixed, cine CT, **146:**669
upper, dynamic narrowing, obstructive sleep apnea and (l), **147:**1330
Albumin, Tc-99m macroaggregated, evaluation of peritoneovenous shunt patency, **147:**177
Alzheimer's type dementia, CT, **147:**963
American Roentgen Ray Society, **147:**1192
awards for distinguished service to radiology, B147:420
case of day: 1986, **146:**626, **146:**1073
invitation to membership, B147:430
1986 meeting, Washington, DC, **146:**181, **146:**340, **146:**618, **146:**740
new members, **147:**428
officers, committees, and meeting information, **147:**1180
presidential address, **147:**417
scientific exhibits, 1986 meeting, B147:426
1986 scientific program, **146:**183
secretary's report, 1986 meeting, **147:**422
section on instructions: courses and symposium, **146:**189
Amyl nitrite test, radiologic, pseudoachalasia distinguished from idiopathic achalasia, **146:**21
Anatomy, sectional human (b), **146:**940
Anderson-Carr progression, sonographic demonstration, **146:**1253
Anechoic crescent, abdominal aortic aneurysm, **146:**345
Aneurysm
see also specific artery; Aorta; Heart
abdominal aortic
anechoic crescent in, **146:**345
CT evaluation of, **146:**711
presentation as a pulmonary mass, **146:**155
chronic posttraumatic, thoracic aorta, **146:**303
coagulation of, direct percutaneous thrombin injection, **147:**383
dissecting, circumflex retroesophageal right aortic arch simulation of, **146:**491
hepatic artery, sonography in diagnosis, **147:**725
natural history of (a), **146:**653
Angiography
see also specific organ; artery; vein
Budd-Chiari syndrome, **147:**9
coronary, power injector, **146:**831
gastrointestinal hemorrhage, **146:**1031
interventional considerations, liver transplantation, **146:**143
liver transplantation, vascular complications after, **147:**657
occlusion balloons, removal of bile duct stones, **146:**383
penetrating vascular injuries, face and neck, **147:**995, (e)**147:**1000
portal vein thrombosis, liver cirrhosis (a), **146:**427
primary central nervous system lymphoma, **146:**271
saphenous vein bypass, **147:**51
small hepatocellular carcinoma, **147:**525, **147:**531
Takayasu's arteritis, **146:**949
thoracic aortic aneurysms, **146:**309
transluminal angioplasty, aortic narrowing (a), **146:**178
trauma, arterial occlusion due to pneumatic antishock garment, **147:**391
upper gastrointestinal hemorrhage, **147:**1185
Angiography, digital subtraction
crossed-leg technique, **146:**843
intraarterial
cerebral ischemia (a), **146:**430
thoracic aortic rupture, **146:**987
IV and intraarterial hybrid, **147:**613
pediatric (a), **146:**1323
rapid-sequence, intracranial circulation, **146:**1239
surgically implantable pump-catheter systems, **146:**839
thoracic aorta rupture (l), **147:**1093
transbrachial approach, **146:**649
Angioma, *see* specific organ
Angiomyolipoma, renal, abdominal case of day, **146:**1078
Angiopathic dementia, CT, **147:**963
Angioplasty
brachiocephalic, washout technique for, **146:**849
femoral artery, superficial, **146:**1025
iliac artery rupture related to, treatment without surgery, **147:**389
percutaneous transluminal
aortic rupture and, **146:**373
balloon catheter for (l), **146:**1101
lower abdominal aorta, **146:**369
renal transplant arterial stenosis, **146:**853
superficial femoral artery, antegrade puncture, **147:**632
thrombectomy and, thrombosed synthetic hemodialysis access fistulas, **147:**161
transluminal, complete iliac obstructions, **146:**859
venous, treatment of superior vena cava syndrome, **147:**834
Ankle, CT scanning, **146:**1192, **146:**1204
Aorta
abdominal
aneurysm, anechoic crescent in, **146:**345

aneurysm presenting as pulmonary mass, **146:**155
percutaneous transluminal angioplasty, **146:**369
ascending, laceration (l), **146:**422
calcified ascending, after radiation therapy, **147:**477
coarctation
mediastinal collateral arteries, **146:**757
pulsed Doppler findings (a), **147:**217
dissection
detection of intimal flap, unenhanced CT images, **146:**601
MRI of, **146:**1286
plain chest radiographic findings, **147:**1123
narrowing, transluminal angioplasty of (a), **146:**178
regurgitation, evaluation with Doppler echocardiography (a), **147:**863
rupture
retroperitoneum (l), **146:**421
transluminal angioplasty and, **146:**373
thoracic, rupture, intraarterial digital subtraction angiography, **146:**987
thoracic aneurysm
clinical and radiographic findings, **146:**303
MRI, **146:**309
thrombosis, umbilical artery catheterization, **146:**619
Aortic arch
circumflex retroesophageal right, simulating mediastinal tumor or dissecting aneurysm, **146:**491
regurgitant fraction, Doppler echocardiographic measurement (a), **147:**217
retroesophageal right, circumflex (l), **147:**1089
Aortic stenosis, calcific, echocardiographic (a), **146:**650
Aortitis, clinical, pathologic and radiologic aspects (b), **146:**1276
Aortography, *see* Angiography; Aorta
Aortoiliac compression, neonatal, distended bladder, sonography, **146:**1273
Aortoiliac disease, assessment, hemodynamic measures (a), **146:**1322
Appendectomy, nonsurgical drainage of abscesses and, **146:**587
Appendicitis, CT findings, **147:**705
Appendix, coiled spring sign of the cecum, acute appendicitis, **146:**45
Arachnoid cyst
intradural, neuroradiology case of day, **146:**1095
sacrum, MRI, **146:**359
Areae gastricae, delineation of, barium suspension viscosity and, **146:**35
Arterial calcification, idiopathic, sonographic recognition, **146:**249
Arterial disease, lower extremity, young adults (a), **146:**1322
Arteriography, femoral, retroperitoneal hemorrhage, CT evaluation, **146:**1289
Arteriography, lower extremity, improved visualization, **147:**1021
Arterioportal shunt, CT features of, hepatocellular carcinoma, **146:**723
Arterior venous fistula, iatrogenic, percutaneous management (a), **146:**885
Arteriovenous malformation
see also organ; region
brain, natural history of (a), **146:**1107
ileal, coil embolization, **146:**787
intraosseous, embolization of, **146:**785
natural history of (a), **146:**653
symptomatic, serial embolizations of, **146:**1038
Artery
see also specific artery; organ; region
ischemia, lower limbs, **146:**157
Arthritis, rheumatoid, juvenile, changes in cervical spine (a), **147:**443
Arthrography
see also specific joint
apophyseal joint (a), **146:**652
aspiration and, negative bone scans after, experimental studies, **146:**87
CT, capsular structures of shoulder, **146:**361
digital, wrist, **147:**563
distal humerus, infants (a), **147:**649
knee locking and unlocking, **146:**575
midcarpal wrist (l), **146:**645
shoulder, after rotator cuff repair (a), **147:**219
temporomandibular joint (a), **146:**1104
torn rotator cuff (l), **147:**646
Aspirin, serpiginous gastric erosions caused by, **146:**31
Asterisk sign, ischemic necrosis, femoral head (a), **146:**652
Atelectasis
round (a), **146:**176
subpulmonic pleural effusions and, CT value in, **146:**685
Atheromatous placques, laser effects on (a), **146:**1106
Atlantoaxial instability, Down syndrome, **146:**1269
Atrium, *see* Heart
Avascular necrosis, *see* Bone

B

Bacterial meningitis, recurrent, CT (a), **146:**1108
Baltaxe, Harold A. (m), 146:604
Barium sulfate
double-contrast, hemoccult screening and, **146:**697
multifocal abnormalities in gastrointestinal tract, acquired immune deficiency syndrome, **146:**7
single- vs double-contrast, colonic polyps, **146:**993
suspension viscosity, delineation of areae gastricae and, **146:**35
suspension viscosity (l), **146:**1317
Barium sulfate, retractile mesenteritis, colon, **147:**937
Barrett's esophagus
radiologic diagnosis (a), **147:**441
radiologic studies, **147:**257
Behcet syndrome, gastrointestinal system involvement, children (a), **147:**218
Biceps tendon, ultrasound (a), **147:**648
Biello, Daniel R. (m), 147:784
Bile acid, malabsorption (a), **146:**428
Bile duct
cholangitis
sclerosing, interventional radiology, **147:**1002
sclerosing, hepatic arterial FUDR chemotherapy, **146:**717
dilatation
after laparotomy, **147:**729
immunodeficiency and, children (a), **146:**432
obstruction, floating gallstones, without added contrast material, **146:**49
removal of stones, angiographic occlusion balloons, **146:**383
stones, optimal cholangiographic technique, **146:**537
varices (a), **146:**1321
Biliary drainage
complications of, malignant pleural effusion, **146:**1165
pain control after (l), **147:**438
percutaneous
diffuse Caroli's disease, **147:**159
obstructive jaundice and (a), **147:**444
Biliary endoprosthesis, insertion via T-tube tract, **147:**164
Biliary sludge, nature of (a), **147:**441
Biliary tract
endoprosthesis blockage, **147:**404
percutaneous drainage, pain control after, **146:**595
Biliary tumors, fine-needle aspiration biopsy in, **147:**399
Binswanger's disease, *see* Subcortical arteriosclerotic encephalopathy
Biopsy
see also specific organ
CT-guided, body stereotaxis, **146:**163
endoscopic, MRI and, Egyptian mummies, **146:**93
fine needle aspiration, **147:**155, pancreatic and biliary tumors, **147:**399
puncture, new needle for, **147:**543
sample size, suction effects, **147:**1014
Bjork-Shiley valve, integrity, cineradiographic methods for assessment, **147:**1139
Bladder
calculi, scrotal cystocele with, **147:**287
carcinoma, MRI-CT-surgical correlation, **146:**1179
distended, neonatal aortoiliac compression caused by, **146:**1273
MRI value in review, **147:**732
tumors, ultrasound diagnosis (a), **147:**443
Blastomycosis, adult respiratory distress syndrome and, chest case of day, **146:**1085
Blood, MRI appearance of, **146:**1293
Blood flow, MRI spin-echo, **146:**931
Blood pool, radionuclide venography, **146:**1051
Bone
see also specific bone
avascular necrosis
hip, **147:**67
hip (l), **147:**1332
density, spinal and hip fractures (a), **146:**1104
Gaucher's disease type 1, CT and scintigraphy, **147:**943
metastases, radiologic contributions to management, **147:**305
negative scans, after aspiration (l), **146:**1100
neoplasm, renal tumors of childhood that metastasize to, clear cell sarcoma, **146:**64
percutaneous trephine biopsy, thoracic spine (a), **146:**1103
stress fracture, MRI, **147:**553
tumors
computer tomography (a), **147:**443
diagnosis (b), **146:**1046
primary and soft tissue, MRI and CT, **146:**749
radiology in (a), **146:**1104
Bone, radionuclide imaging
hepatic metastases from colonic carcinoma, ^{99m}TC-HMDP in, **146:**333
negative scans after aspiration or arthrography, experimental studies, **146:**87
Bone marrow
malignant infiltration, MRI detection of, **146:**353
transplantation
esophageal infections after (a), **146:**427
gastrointestinal inflammation after, CT, **146:**691
intestinal and hepatic complications of (a), **147:**440
Book reviews
aortitis: clinical, pathologic and radiologic aspects, **146:**1276
atlas for maxillofacial pantomographic interpretation, **146:**1324
atlas of normal fetal ultrasonographic anatomy, **147:**552
atlas of two-dimensional echocardiography in congenital cardiac defects, **147:**1148
atoms, radiation, and radiation protection, **147:**1236
bockus gastroenterology, **146:**294
cardiac catheterization and angiography, **147:**1138
cardiac imaging and image processing, **147:**140
cervico-occipital joint (RX, CT), **147:**525
clinical computed tomography illustrated procedural guide, **147:**524

clinical diagnostic ultrasound, **147:**976
clinical radiology of the spine and spinal cord, **147:**776
computed tomography and magnetic resonance imaging of the head and neck, **146:**518
computed tomography of the gastrointestinal tract including the peritoneal cavity and mesentery, **147:**1176
computed tomography of trauma, **147:**562
computer assisted radiology. Computergestützte radiologie, **146:**484
consultation in diagnostic imaging. medical consultation series, **146:**986
cranial computed tomography: a comprehensive text, **147:**544
diagnostic cardiology, **146:**44
diagnostic imaging in clinical medicine, **146:**216
diagnostic imaging in hemophilia: musculoskeletal and other hemorrhagic complications, **146:**80
diagnostic imaging in ophthalmology, **146:**1282, **147:**562
diagnostic imaging of the acutely injured patient, **147:**766
diagnostic nuclear medicine, **147:**1262
diagnostic patient studies in surgery, **147:**1236
differential diagnosis of soft tissue and bone tumors, **146:**1046
digital cardiac imaging, **146:**484
digital radiography; selected topics, **147:**1148, **147:**1206
digital subtraction angiography, **147:**994
double contrast examination of the colon: principles and practice, **147:**38
echographie de la prostate, **147:**994
essentials of radiology physics, **146:**518
functional mapping of the brain in vascular disorders, **147:**570
guide pratique d'echographie scrotale, **147:**728
guide to prosthetic cardiac valves, **147:**338
handbook of physics for radiologists and radiographers, **146:**678
handbook of radioactivity measurements procedures, **146:**532
hand-held and automated breast ultrasound, **147:**44
imaging of orthopedic trauma and surgery, **147:**238
information processing in medical imaging, **146:**476
joints and vertebral connections clinical radiology, **146:**1268
learning to heal—the development of American medical education, **147:**166
lung cancer, **146:**774
lymphatic imaging: lymphography, computed tomography and scintigraphy, **147:**776
magnetic resonance imaging: principles and applications, **147:**984
metabolism of the human brain studied with positron emission tomography, **146:**690
musculoskeletal magnetic resonance imaging, **147:**544
myelofibrosis, **146:**30
noninvasive diagnostic techniques in vascular disease, **146:**30
nuclear medicine annual 1985, **146:**294
nuclear medicine in clinical oncology, **147:**984
nuclear pharmacy, **147:**728
oncologic imaging, **146:**1140
pediatric magnetic resonance imaging, **146:**1140
pediatric ultrasonography, **146:**1282
pocket atlas of normal ultrasound anatomy, **146:**690
practice enhancement, **146:**716
practice of coronary angioplasty, **147:**1132, **147:**184
proceedings of the Eighth Conference on Computer Applications in Radiology, **146:**248
progress in medical radiation physics, **146:**24
progress in radiopharmacology 1985, **147:**44
radiation oncology: a handbook for residents and the allied health professions, **146:**970
radiodiagnosis of the skull, **146:**476
radioisotope studies in cardiology, **146:**1010
radiolabeled cellular blood elements, **147:**525
radiological physicists, **146:**678
radiologic clinics of North America: symposium on digital radiography, **146:**86
radiologic diagnosis of renal transplant complications, **147:**962
radiology of adverse reactions to drugs and toxic hazards, **147:**696
radiology of liver circulation, **147:**504
radiology of lymphomas, **147:**696
radiology of the hand. a diagnostic synopsis of many general diseases, **147:**66
radiology of the spine, tumors, **147:**552
radiology of the spine tumors, **146:**1030
radiology review cards, **147:**367
radiology today, **146:**940
radionuclide imaging techniques, **147:**367
recent developments in digital imaging, **146:**248
roentgen signs in diagnostic imaging, **146:**238, **147:**398
sectional human anatomy, **146:**940
self assessment in radiology and imaging 2. gastrointestinal radiology, **146:**1276
self assessment in radiology 1. ear, nose and throat, **146:**1276
sensitivity and specificity of common scintigraphic procedures, **146:**716
single photon emission computed tomography, **147:**720
some issues important in developing basic radiation protection recommendations. National Council on Radiation Protection and Measurements Proceedings No. 6, **147:**32
Stafne's oral radiographic diagnosis, **147:**338
the fundamentals of x-ray and radium physics, **147:**144
the radiologic clinics of North America. symposium on advances in cardiac imaging, **147:**78
the radiologic clinics of North America, **147:**408, **147:**504, **147:**1040
the selection and performance of radiologic equipment, **147:**144
thyroid and parathyroid imaging, **146:**1010
ultrasound physics and instrumentation, **147:**490
World Health Organization basic radiological system. Manual of radiographic interpretation for general practitioners, **146:**80
x-ray imaging equipment, **146:**232
x-rays: health effects of common exams, **146:**774

Bowel, *see* Colon; Intestine

Brain
abscesses, indium-111 leukocyte scans (a), **146:**885
aging and (a), **146:**1107
anterior frontal horns, MRI, **147:**331
arteriovenous malformation (a), **146:**1107
chemotherapy
supraophthalmic carotid infusion (a), **146:**653
Gd-DTPA, clinical MRI, **147:**1223, **147:**1231
glucose utilization, aging and (a), **146:**430
minimal asymmetry of, CT brain scans, **147:**753
occult vascular formations, MRI and CT, **147:**985
positron emission tomography (b), **146:**690
torcular Herophili, sonographic appearance of, **146:**109
torulosis, CT (a), **146:**652

Brain, CT, organized intracerebral hematoma, acute hemorrhage and, **147:**111

Brain, MRI
iron in, **147:**103
radiation injury, **147:**119

Brain, ultrasound
compressed and asymmetric lateral ventricles, neonate, **146:**471
craniocervical junction, neonate, **147:**133
periventricular stereotaxis (a), **146:**178
torcular Herophili, **146:**109

Brain tumor, surrounding oedematous tissue and, measurements (a), **146:**430

Breast
carcinoma
calcifications, mammograms (a), **147:**864
diaphanography in (a), **146:**431
internal mammary lymphoscintigraphy (a), **146:**431
disease
male, mammography, **146:**127
MRI in diagnosis, **146:**119
images, high-contrast mammography with a moving grid, **146:**1137
lesions
diagnostic tests for (a), **146:**1323
mammography and transillumination light scanning comparison, **147:**191
neoplasm
metastasis to intramammary lymph nodes, **146:**133
nonpalpable, mammographic features of, **146:**661

Bronchiolitis obliterans, with organizing pneumonia, vs. usual interstitial pneumonia, **147:**899

Bronchopulmonary dysplasia, changing picture, persistent pulmonary abnormalities (a), **147:**649

Bronchopulmonary foregut, congenital malformations, **146:**227

Bronchovascular anatomy, segmental, lower lobes, **147:**457

Bronchus, solid mediastinal cyst, mineralogic analysis, **146:**73

Bucrylate-pantopaque mixture, histologic analysis of, **147:**627

Budd-Chiari syndrome, *see* Liver

Bupivacaine, pain control, after percutaneous biliary drainage, **146:**595

C

Calcaneus, fractures, CT (l), **146:**644

Calcification
see also specific organ; region
arterial, idiopathic, sonographic recognition, **146:**249
dystrophic, umbilical artery, children (a), **146:**654
intracranial, chronic lead exposure, CT findings, **146:**267
midline cerebral, cause of (a), **146:**1108

Canal stenosis, lumbar herniated disk disease and, coil MR, CT, and myelography, **147:**757

Cancer, *see* specific organ; region

Carcinoid syndrome, palliation, hepatic artery embolization, **149:**149

Cardiology, diagnostic (b), **146:**44

Cardiovascular shunt, cardiovascular lesions, MRI estimation of pulmonary vascular resistance, **146:**919

Caroli's disease, diffuse, percutaneous biliary drainage, **147:**159

Carotid artery, plaque, sonographic characterization of, **146:**1061

Carotid body, bifurcation, incremental dynamic CT, **146:**465

Carotid placque, asymptomatic (a), **146:**1322

Carpal bones, incomplete coalition, **147:**301

Carpal tunnel syndrome, idiopathic, plate thermography in (a), **146:**1106

Carpus, *see* Wrist

Case of day
abdominal, **146:**631, **146:**1074
chest, **146:**627, **146:**1080
musculoskeletal, **146:**634, **146:**1087
neuroradiological, **146:**634, **146:**1094

Catheter
arterial, determination of entry site (l), **147:**438

ultrasound-guided, microbubbles as contrast agent for, **147:**347
Catheterization
see also organ; blood vessel
arterial
complications arising from, neonates (a), **146:**655
entry site determination (l), **146:**175, **146:**1101
Cope-style drainage catheter, **146:**169
Cope-style loop retention, replacing broken suture in, **146:**590
impending perforation, superior vena cava, radiographic recognition of, **146:**487
intractable pericatheter leakage, Hollister disk and bag system for, **146:**869
kinked, radiographic appearance, **146:**789
nonsurgical drainage, appendiceal abscesses, **146:**587
percutaneous drainage, transrectal pelvic abscess, sonographic guidance, **146:**1047
percutaneous transluminal angioplasty (l), **146:**1101
pump-catheter systems, surgically implantable, **146:**839
retrograde ureteral, via the ileal conduit, **146:**61
transhepatic biliary drainage, complications of, **146:**1165
umbilical artery, evaluation of neonatal aortic thrombosis, **146:**619
Catheterization, retained subcutaneous fragments, method for retrieval, **147:**1017
Cat scratch disease, CNS involvement (a), **147:**649
Caudal regression syndrome, abdominal case of day, **146:**1074
Cavernous sinus
clinical syndrome, CT diagnosis (a), **146:**885
invasion by pituitary adenoma, CT and MRI signs, **146:**257
Cavum septi pellucidi, hemorrhage and cyst development in (a), **146:**888
Cecum, *see* Colon
Central nervous system
cat scratch disease and (a), **147:**649
primary lymphoma
CT and pathologic correlation, **147:**747
radiographic findings, **146:**271
ventricular fluid from, coxsackievirus group B antibodies from (a), **146:**179
Cerebral artery, *see* Brain; specific artery
Cerebral hypoperfusion, focal, dysphasia or attention deficit disorder, children (a), **146:**655
Cerebral ischemia, intraarterial digital angiography (a), **146:**430
Cerebral palsy
see also body part
athetoid-dystonic, cervical spondylotic radiculomyelopathy in (a), **146:**178
spastic, hip changes in, **146:**1219
Cerebral vein, *see* Brain
Cerebrospinal fluid, rhinorrhea, metrizamide CT cisternography (a), **146:**885
Chemical shift, imaging, **146:**971
Chemonucleolysis, septic complications of (a), **146:**1107
Chemotherapy
see also specific drug; organ
advanced seminoma, CT evaluation of, **146:**745
hepatic arterial FUDR, sclerosing cholangitis associated with, **146:**717
intraarterial, short-term flow occlusion in, **146:**375
residual masses after, testicular carcinoma, **146:**1184
Chest, *see* Thorax
Chest phantom, CT nodule densitometry, **147:**21
Cholangiocarcinoma
choledochal cyst, preoperative diagnosis, **147:**516
complication of choledochoenteric anastomoses, **147:**513
Cholangiography
optimal technique, bile duct stones, **146:**537
percutaneous, obstructive jaundice and (a), **147:**444
Cholangiohepatitis, oriental, diagnostic imaging and management, **146:**327
Cholangitis, *see* Bile duct
Cholecystitis, *see* Gallbladder
Cholecystography
cholecystokinetic (a), **146:**651
oral, gallbladder function (a), **146:**651
Cholecystostomy, percutaneous, gallstone dissolution, methyl-tert-butyl ether, **146:**865
Choledochal cyst, cholangiocarcinoma in, preoperative diagnosis, **147:**516
Choledochoenteric anastomoses, cholangiocarcinoma as a complication of, **147:**513
Choledocholithiasis, ultrasound detection of (a), **147:**441
Cholescintigraphy
functional obstruction of sphincter of Oddi (a), **147:**442
morphine-augmented, acute cholecystitis, **147:**1177
Cholestasis, total parenteral nutrition (a), **146:**1102
Chondroblastoma, review (a), **146:**652
Chondroma
see also specific organ
cricoid cartilage, neuroradiology case of day, **146:**1096
Chron's disease, recurrence after surgery (a), **146:**177
Cilia syndrome, chest film in (a), **147:**863
Cineradiography, assessment, Bjork-Shiley valve integrity, **147:**1139
Cirrhosis
regenerating nodules in, sonography, **146:**533
splenorenal shunts, postoperative assessment with MRI, **146:**597
Colitis, *see* Colon
Colles' fracture, trabecular osteopenia in (a), **147:**443
Colon
adenoma, familial polyposis coli and, **147:**61
coiled spring sign of the cecum, acute appendicitis, **146:**45
colorectal carcinoma
floxuridine therapy, small-bowel toxicity due to, **146:**39
hepatic metastases from, **146:**333
simulation of, ischemia and (a), **146:**176
diminutive polyps, radiographic detection (e), **146:**875
diverticulitis, CT findings, **147:**271
megacolon, idiopathic, radiologic definition (a), **146:**651
microcolon, premature infant, **146:**239
polyps, single-contrast vs double-contrast barium enema, **146:**993
retractile mesenteritis involving, **147:**268, barium, sonography, and computed tomography, **147:**937
small bowel, obstruction, intestinal balloon and, **147:**1019
small-bowel volvulus, CT diagnosis, **147:**941
volvulus (a), **146:**1321
Colorectal cancer
adenomas, prognostic factors (a), **146:**427
Dukes' C class of (a), **146:**1321
multiple, comparison in ulcerative colitis, familial polyposis coli, and *de novo* cancer (a), **146:**1320
preoperative imaging (a), **146:**1320
Column of Bertin, hypertrophied, sonography of, **146:**53
Computed tomography
see also specific type; organ
Achilles tendon (a), **146:**1104
advanced seminoma, chemotherapy treatment and, **146:**745
AIDS, cytomegalic inclusion virus encephalitis with, **146:**1229
angio- (a), **146:**433
body stereotaxis, **146:**163
body worksheet, **147:**848
calcaneal fractures (l), **146:**644
diagnostic procedures, cost-effectiveness vs. accuracy (l), **146:**174
experimental design, need for precision in (l), **146:**174
fibromatoses, **147:**1063
fibrous tissues, **147:**1067
following diphenylhydantoin intoxication (a), **146:**179
foot and ankle, **146:**1192
inferior lumbar hernia, **147:**744
Kimray-Greenfield filter complications, **147:**45
metrizamide, traumatic dural tear (a), **146:**654
metrizamide myelography and (a), **146:**1108
pediatric, retinoblastoma (a), **146:**179
pheochromocytoma, **146:**741
primary bone and soft-tissue tumors, **146:**749
quantitative, vertebral body compressive fractures (a), **146:**1104
retroperitoneal hemorrhage, femoral arteriography and, **146:**1289
sagittal, temporomandibular joint (a), **146:**179
soft tissue hemorrhage (l), **147:**1331
subcortical arteriosclerotic encephalopathy, **147:**1209
three-dimensional reformation, children, **146:**1261
Computed tomography, abdomen
acquired immune deficiency syndrome, **146:**7
acute acalculous cholecystitis, **147:**1171
aortic aneurysms, **146:**711
appendicitis, **147:**705
compartmental anatomy of retroperitoneum (p), **147:**1155
extraperitoneal spaces, **147:**1162
gastric diverticulum, simulating adrenal mass, **146:**553
gastrointestinal inflammation, after bone marrow transplantation, **146:**691
intraabdominal abscesses, percutaneous drainage, **146:**1041
ovarian cancer, liver metastasis and (a), **147:**444
periappendiceal abscess, **146:**1161
peritoneal and mesenteric, malignancies (a), **147:**864
renal angiomyolipoma, **146:**1078
residual masses after chemotherapy, testicular carcinoma, **146:**1184
subpulmonic pleural effusions, atelectasis and, **146:**685
tailgut cyst, **147:**1309
Computed tomography, adrenal, malignant and benign masses (l), **146:**1316
Computed tomography, bladder, MRI-surgical correlations, staging of carcinoma, **146:**1179
Computed tomography, bone, Gaucher's disease type 1, **147:**943
Computed tomography, brain
dementing diseases, **147:**963
minimal asymmetry in, **147:**753
Computed tomography, chest
benign schwannomas, **147:**141
nodule densitometry, chest phantom for, **147:**21
silicosis, **146:**477
Computed tomography, cine, nonfixed upper airway obstruction, **146:**669
Computed tomography, colon, retractile mesenteritis, **147:**937
Computed tomography, cranium
abused child with head injury, **146:**97
brain and cervical spine diseases, MRI comparison (a), **146:**653

cavernous sinus, clinical syndrome and diagnosis (a), **146:**885
cerebral bleeding, central traumatic (a), **146:**1108
cerebral torulosis (a), **146:**652
chronic lead exposure, intracranial calcification in, **146:**267
evaluation of radiation therapy, **147:**587
exophthalmos, excessive fat and, **146:**459
glioma, chronic seizure disorder caused by (a), **146:**886
head injury, **147:**1215
MRI and, head and neck (b), **146:**518
neurosarcoidosis, steroids and, **146:**819
NMR and, dementia (a), **146:**178
opsomyoclonus, **146:**781
primary CNS lymphoma, **146:**271
severe diffuse injury (a), **146:**654
Computed tomography, esophagus
esophageal-pleural fistula, **147:**907
sclerotherapy, **147:**57
Computed tomography, eye, intraocular foreign bodies (a), **146:**1107
Computed tomography, heart, aortic dissection, detection of intimal flap of, **146:**601
Computed tomography, hip, avascular necrosis, **147:**67
Computed tomography, hypopharynx, carcinoma (a), **146:**430
Computed tomography, intestine, small bowel diverticulitis, **147:**271
Computed tomography, kidney
hemorrhagic focal bacterial nephritis, **146:**1173
retroperitoneal fibrosis, **146:**57
Computed tomography, liver
Budd-Chiari syndrome, **147:**9
children, **147:**785
dynamic bolus, hemangioma, **147:**711
extrahepatic cavernous hemangiomas, **147:**1299
hepatocellular carcinoma, **146:**1005
arterioportal shunts in, **146:**723
in vivo volume determination (a), **146:**177
masses, **146:**729
mesenchymal hamartomas, **147:**1035
multiple bile-duct hamartomas, simulating malignant disease, **147:**279
patterns of injury, **147:**1199
transplants, impaired lymphatic drainage, **147:**519
Computed tomography, lung
lower lobes, segmental bronchovascular anatomy, **147:**457
non-small-cell bronchogenic carcinoma, preoperative staging, **146:**285
pulmonary infiltrates, mosaic oligemia simulating, **147:**670
Computed tomography, lymph nodes
calcified mediastinal, new ATS classification (p), **147:**17
mediastinal, detection and sizing, autopsy and, **147:**469
Computed tomography, mediastinum, solid bronchogenic cyst, mineralogic analysis, **146:**73
Computed tomography, musculoskeletal system, three-dimensional imaging; **147:**545
Computed tomography, neck
calcific tendinitis, longus coli, **147:**742
incremental dynamic, carotid bifurcation, **146:**465
MRI and, head and neck (b), **146:**518
Computed tomography, pancreas
mass occupying lesions (a), **146:**428
prediction of pancreatitis (a), **146:**1321
Computed tomography, pelvis, septic hip, psoas abscess mimicking of (a), **146:**1105
Computed tomography, pineal, region tumors, **146:**451
Computed tomography, pituitary
adenoma, cavernous sinus invasion by, **146:**257
Cushing syndrome, **146:**1235
posterior, **146:**263
Computed tomography, prostate, carcinoma detection, **146:**351
Computed tomography, rapid-acquisition, left ventricular function, supine exercise, **147:**916
Computed tomography, rectum
carcinoma, pre- and postoperative staging, **146:**703
staging cancer, **146:**1155
Computed tomography, shoulder
capsular structures, CT arthrography of, **146:**361
intra-articular penetration of a screw (a), **146:**1105
Computed tomography, small bowel, volvulus, **147:**941
Computed tomography, spine
cervical spine and brain diseases, MRI comparison, **146:**653
cystic necrosis, compressive cervical myelopathy, **147:**767
degenerative disorders, myelographic data, **146:**793
disk-space hypersensitivity (a), **146:**429
extraarachnoid metrizamide instillation, **147:**583
intravenous contrast enhancement, intraspinal tumors, **146:**103
lumbar herniated disk disease, canal stenosis and, **147:**757
malignant diseases (a), **146:**431
pathomorphology of stenosis (a), **146:**1109
primary central nervous system lymphoma, **147:**747
Computed tomography, spleen, hepatosplenic neoplasia, thorotrast-induced, **146:**997
Computed tomography, sternum, abnormalities (p), **147:**72
Computed tomography, testis, malignancy, **146:**291
Computed tomography, thigh, nutritional assessment, pediatrics (a), **147:**650
Computed tomography, trachea
adenoid cystic carcinoma, **146:**1129
growing, age and gender in, **146:**233
Computer, radiology and (b), **146:**484
Computer, reference management and, **147:**641
Computer page
database management, MRI facility, **146:**871
microcomputer-based graphics, **147:**1319
personal, low-volume imaging department, **146:**1302
personal computer data-base system, radiology, **147:**1075
scheduling for radiologists, **147:**203
Computer tomography, bone and soft tissue tumors, thoracic wall (a), **147:**443
Congenital abnormality, *see* organ; part
Congestion index, portal vein, **146:**735
Contrast medium
see also specific medium
floating gallstones without added contrast material, bile, **146:**49
hexabrix and papaverine, incompatibility of, **146:**1300
high- and low-osmolality, intravenous, comparison, **147:**185
intravenous contrast enhancement, CT evaluation of intraspinal tumors, **146:**103
microbubbles, catheter manipulation, **147:**347
MRI, optimal pulsing sequences for, **147:**367
parenteral radiographic, acute thrombocytopenia induced by, **146:**1298
transient reaction to, pancreatic mumps, **147:**188
Cope introducer, modified, **147:**828
Coronary artery, bypass graft anastomoses, evaluation with epicardial echocardiography (a), **147:**863
Coxsackievirus group B antibodies, ventricular fluids, infants with severe anatomic defects in central nervous system (a), **146:**179
Cranial vault, giant cell reparative granuloma, pediatric (a), **146:**655
Creutzfeldt-Jakob disease, CT, **147:**963
Cricoid cartillage, elliptical, congenital subglottic stenosis, **146:**1133
Crohn disease
postsurgical recurrence, sonographic detection of, **146:**523
real-time ultrasound in, **146:**1102
small bowel examination, **147:**63
Cryosurgery, hepatic, ultrasound monitoring of, **147:**665
Cushing's syndrome, hyperplasia after treatment, **147:**1145
Cyst
nonparasitic splenic, radiologic-pathologic correlation, **147:**537
see also specific organ or part
Cystic duct, anomalous hepatic duct inserting into, **147:**1181
Cystography, *see* Bladder; other organs

D

Dementia
see also Brain
cerebral NMR and CT imaging in (a), **146:**178
diseases causes, CT changes in, **147:**963
Densitometric screening, osteoporosis (l), **147:**1329
Diabetes, lumbar myelography complications in, **146:**1057
Dialysis, pediatric complications, CT peritoneography, **147:**325
Diaphanography, breast carcinoma (a), **146:**431
Diarrhea, post-irradiation, pathogenesis of (a), **146:**650
Diffuse idiopathic skeletal hyperostosis, quadriplegia in, after minor trauma (l), **147:**858
Digital subtraction angiography, *see* Angiography
Diphenylhydantoin, intoxication, CT findings following (a), **146:**179
Diskitis, computed tomography (a), **146:**429
Diverticulitis, *see* Colon
Diverticulum, *see* specific organ
Dopamine receptors, images, PET (a), **146:**886
Doppler, *see* Ultrasound
Dosimetry, multipoint real-time thermal, clinical microwave hyperthermia system with (a), **147:**219
Double-contrast barium enema, *see* Barium sulfate
Down syndrome, atlantooccipital instability in, **146:**1269
Drainage procedures, *see* specific organ
Drug uptake, experimental enhancement, short-term flow occlusion, **146:**375
Duodenum
bulb, hypertrophied fold (l), **146:**647
ulcer, radiologic search (l), **146:**424
Dural arteriovenous malformations, intracranial hemorrhage and (a), **146:**431

E

Echinococcal cysts, rupture of, **146:**391
Echocardiography
see also Heart; Ultrasound
amyloid heart disease (a), **147:**217
calcific aortic stenosis (a), **146:**650
Doppler
evaluation of aortic regurgitation (a), **147:**863
Kawasaki disease (a), **147:**218
epicardial, coronary artery bypass graft anastomoses evaluation (a), **147:**863
mitral regurgitation (a), **146:**650
updated Doppler measurement, regurgitant fraction, aortic arch (a), **147:**217
Editorials
angiography in penetrating neck injuries, **147:**1000

changing of the guard, **146:**171
classification of non-Hodgkin's lymphoma, **147:**205
device identification: deficient marking systems, **146:**418
impact of maternity on radiologists, **146:**415
language of certainty, **147:**209
new assistant editors, **146:**1311
physician investment in free-standing imaging centers: in opposition, **147:**412
physician investment in free-standing imaging centers: in defense, **147:**414
presence of parents with children during imaging procedures, **146:**639
radiographic detection of polyps of the colon, **146:**875
radiology manpower: where are we?, **146:**172
screening mammography, **147:**195
the dense mammogram, **147:**487
the diffusion of MRI in the United States: What is fact and what is speculation, **147:**856
what radiologists say about PACS, **146:**419
Effusion, *see* specific region
Ejection-fraction determination, right anterior oblique view, gated cardiac MRI, **147:**33
Elbow, radial head—capitellum view, trauma, **146:**81
Embolization
hepatic artery, carcinoid syndrome, **147:**149
ileal arteriovenous malformation, **146:**787
intraosseous arteriovenous malformation, **146:**787
male infertility and, **147:**97
Encephalitis
see also Brain
cytomegalic inclusion virus, AIDS and, CT, **146:**1229
Endoprosthesis, biliary, blockage, **147:**404
Endoscopy
see also specific organ
lower esophageal mucosal ring, **147:**261
pneumatic balloon dilatation, achalasia, esophagus, **146:**25
radiologist performance of, **147:**1078
Endourology, current trends (a), **146:**429
Enteroclysis
plasma electrolyte status after, **146:**323
radiologic examination, small intestine, **147:**63
Enterocyst, formation, neonatal necrotizing enterocolitis, **147:**806
Epidermoid carcinoma, multiple primary, aerodigestive tract (a), **146:**1320
Epilepsy, temporal lobe, NMR in (a), **146:**653
Epinephrine, pain control, percutaneous biliary drainage, **146:**595
Esophagitis, reflux, radiographic examination (a), **147:**441
Esophagography
double-contrast, alternative technique, **147:**266
intramural pseudodiverticulosis, **147:**1165
Esophagus
atresia, hypertrophic pyloric stenosis and, **147:**329
early cancer, **146:**507
endoscopic pneumatic balloon dilatation, achalasia, **146:**25
fistula, CT, **147:**907
foreign bodies, basket extraction of, **147:**1010
function tests (a), **146:**428
idiopathic achalasia, pseudoachalasia distinguished from, radiologic amyl nitrite test, **146:**21
infections, after marrow transplantation (a), **146:**427
intramural pseudodiverticulosis, **147:**1165
laser treatment for obstructing carcinoma, radiographic appearance after, **146:**519
lower mucosal ring, radiographic and endoscopic sensitivity, **147:**261
motor function, muscular dystrophy and (a), **147:**442
nutcracker, radiologic and manometric correlation in, **147:**693
pseudoachalasia, idiopathic achalasia distinguished from, radiologic amyl nitrite test, **146:**21
strictures, balloon dilatation (a), **146:**427
uncomplicated sclerotherapy, CT after, **147:**57
varices, splenorenal shunt surgery for, MRI postoperative assessment of, **146:**597
Ethanol, renal ablation, fatal outcome in end-stage kidneys, **146:**593
Ewing sarcoma, *see* Bone
Exophthalmos, *see* Eye
Extracorporeal shock wave lithotripsy, percutaneous stone procedures, **147:**89, **147:**94
Eye
exophthalmos, excessive fat effects CT, **146:**459
intraocular foreign bodies, CT localization of (a), **146:**1107

F

Facet joint injection, low back pain (a), **147:**219
Familial amyloid polyneuropathy, echocardiographic assessment (a), **147:**217
Familial polyposis coli, uncomplicated adenomas in, **147:**61
Felty's syndrome, radiocolloid scintigraphy, **147:**181
Femopropopliteal grafts, occluded, thrombolysis of, **147:**621
Femoral artery
guided direct antegrade puncture, **147:**632
superficial angioplasty, **146:**1025
Femoral vein, compression, lower-extremity venography, **147:**1025
Femur
head, avascular necrosis (a), **146:**1104
ischemic necrosis, asterisk sign and (a), **146:**652
transient ischaemia, bone scintimetry for (a), **146:**1104
Fibromatoses, CT-pathologic correlation, **147:**1063
Fibromuscular dysplasia, renal, reversible, **147:**737
Fibrosis, *see* specific organ; region
Fibrous tissue, tumors and, CT and sonographic correlation, **147:**1067
Fleischner Society, glossary, **146:**883
Floxuridine
hepatic arterial chemotherapy, sclerosing cholangitis associated with, **146:**717
therapy, small-bowel toxicity due to, **146:**39
Fluoroscopy, gastrointestinal tract (l), **147:**1090, **147:**1091
Focal lytic lesion, acetabular loosening, total hip prosthesis (l), **146:**423
Foley catheter, simulating nasopharyngeal mass, neuroradiology case of day, **146:**1095
Fontanelle, *see* Skull
Foot, CT scanning, **146:**1192, **146:**1204
Fracture
see also specific bone
burst, spine, radiography, **147:**575
stress
MRI, **147:**553
second metatarsal, Lisfranc's joint (a), **147:**219
trampoline, proximal tibia in children, **146:**83
FUDR, *see* Floxuridine

G

Gadolinium-DTPA, MRI, liver cancer, **147:**357
Gallbladder
carcinoma, anomalous pancreaticobiliary ductal union and, **147:**442
cholecystitis
acute, cholescintigraphy, morphine augmented, **147:**1177
acute acalculous, indium-111-labeled leukocyte imaging, **147:**813
acute acalculous, sonography, scintigraphy, and CT, **147:**1171
acute, hepatobiliary imaging and real-time ultrasound (a), **146:**1319
chronic acalculous disease, multimaging evaluation, **147:**721
floating gallstones in bile, without added contrast material, **146:**49
function, oral cholecystography, **146:**651
gallstones, sonographic screening for, **146:**337
wall, V-shaped artifact, **147:**505
Gallstone
dissolution with methyl-tert-butyl ether, percutaneous cholecystostomy, **146:**865
symptomatic and asymptomatic (a), **146:**1319
Ganglion, *see* organ; part
Gastric antrum, hypertrophied fold (l), **146:**647
Gastric carcinoma, gastroplasty stoma dilatation and, application of percutaneous gastrostomy, **147:**826
Gastric cardia, diverticulum simulating adrenal mass, CT, **146:**553
Gastric emptying
measurement, real-time ultrasonography (a), **147:**442
renal failure and (a), **146:**428
Gastritis, erosive, aspirin and other nonsteroidal antiinflammatory drugs, **146:**31
Gastroenterology, bockus (b), **146:**294
Gastroenterostomy, percutaneous, **146:**577, **146:**581
Gastrointestinal stenoses, hydrostatic balloon dilation (a), **147:**440
Gastrointestinal tract
biphasic enteroclysis (a), **146:**176
examination, hypotonia, ear acupuncture and (l), **147:**862
fluoroscopy (l), **147:**1090, **147:**1091
granular cell tumors, **147:**1305
hemorrhage, angiographic treatment of, **146:**1031
inflammation, after bone marrow transplantation, CT, **146:**691
intussusception, adults, **146:**527
linear erosions, radiologic findings, **147:**701
malformations, fetal, antenatal sonographic diagnosis (a), **146:**432
multifocal abnormalities, acquired immune deficiency syndrome, **146:**1
perforations, mechanically ventilated neonates (a), **146:**432
ulcer, radiographic efficacy in, **147:**697
upper
hemorrhage, angiography, **147:**1185
management (a), **147:**440
Gastroschisis
omphalocele and
fetal, B147:1047
fetal, sonographic diagnosis, **147:**797
Gastrostomy
percutaneous, **146:**577, **146:**581
gastric carcinoma and gastroplasty stoma dilatation, **147:**826
jejunal feeding, **147:**822
percutaneous endoscopic (a), **146:**1323
Gaucher's disease type 1, bone involvement, CT and scintigraphy, **147:**943
Genitalia, *see* specific organ
Genitourinary tract, interventional radiology, children, **147:**791
Gestational sac, HCG levels and, sonography (l), **146:**1098
Glioma
see also Brain
prediction of survival, positron emission tomography (a), **146:**653
seizure disorder caused by, CT (a), **146:**886

Glioma, optic nerve, posterior visual pathway involvement (a), **147:**864
Glomus tumor, intraosseous, review, **147:**739
Granular-cell tumor, skin and GI tract, **147:**1305
Granuloma
see also specific organ
eosinophilic, chest case of day, **146:**1080
plasma cell, lung, chest case of day, **146:**1080
Granulomatosis, *see* specific organ
Graves disease, *see* Thyroid gland
Great arteries, congenital abnormalities, MRI, **146:**941
Gruentzig, Andreas Roland (m), **146:**118
Guide wire
see also Catheterization
exchange problems (l), **146:**881

H

Harrington instrumentation, thoracolumbar spine (a), **146:**652
Harrison, R. Stewart (m), **147:**28
Head
injury
abused child, cranial CT in, **146:**97
CT and highfield MR, **147:**1215
Heart
see also Aortic valve; Mitral valve
atrial hemangioma, prenatal sonographic diagnosis, **147:**1207
atrial septal defect, noninvasive pulsed Doppler echocardiographic detection (a), **146:**176
digital imaging (b), **146:**484
function, MR overview, **146:**907
ischemic, coronary thrombolytic therapy, **147:**1
radioisotope studies (b), **146:**1010
selective angiography, power injector, **146:**831
Heart, computed tomography, rapid-acquisition, left ventricular function during supine exercise, **147:**916
Heart, magnetic resonance imaging
measurement of normal left dimensions, **146:**75
myocardial infarction, **146:**925
strangulated hernia, pneumothorax and, **146:**321
Heart, ultrasound
noninvasive evaluation, aortic regurgitant fraction, Doppler echocardiography (a), **146:**1319
thoracic aortic aneurysms, **146:**309
Hemangioma
see also organ; region
atrial, prenatal sonographic diagnosis, **147:**1207
hepatic, dynamic bolus CT, **147:**711
hepatic cavernous, atypical radiographic findings in, **146:**1149
Hematoma
see also organ; region
extracranial, MRI, **146:**403
Hematopoiesis, extramedullary, acute lymphocytic leukemia, **147:**846
Hemoccult tests,
cost comparison (l), **147:**646
role of radiology in, **146:**697
Hemodialysis, thrombosed synthetic, access fistulas, **147:**161
Hemoglobinuria, paroxysmal nocturnal, magnetic resonance imaging, kidney, **146:**51
Hemolymphangiomatosis, musculoskeletal case of day, **146:**1087
Hemorrhagic infarction, delayed, pediatric (a), **146:**888
Henoch-Schonlein purpura, ileal stricture and (a), **147:**443
Hepatic artery
aneurysms, sonography in diagnosis, **147:**725
embolization, palliation of carcinoid syndrome, **147:**149
thrombosis, after liver transplantation, **146:**137
Hepatic duct, anomalous, inserting into cystic duct, **147:**1181
Hepatocellular carcinoma
see also Liver
arterioportal shunts in, CT features of, **146:**723
primary extrahepatic mass, CT, **146:**1005
scintigraphy in diagnosis (a), **146:**884
small, angiography of, **147:**525, **147:**531
Hepatology, radiology impact on, **147:**1117
Hepatosplenic neoplasia, thorotrast-induced, CT identification, **146:**997
Hernia, inferior lumbar, CT, **147:**744
Herophili, torcular, sonographic appearance of, **146:**109
Hexabrix, incompatibility with papaverine, **146:**1300, (l)**147:**1096
Hip
avascular necrosis (l), **147:**1332
changes, spastic cerebral palsy, **146:**1219
normal and ischemic, joint fluid, MRI, **146:**1215
ossification, infant, sonographic and radiographic correlation, **147:**317
prosthesis, acetabular loosening, focal lytic lesions with (l), **146:**423
Histocytosis X, healing rates in bones, children (a), **146:**655
Hodgkin's lymphoma, thallium-201 parathyroid scan, mediastinum, **147:**819
Hodson, John (m), **146:**1154
Huntington's chorea, CT, **147:**963
Hyatid cyst, splenic (l), **147:**859
Hydatid disease, rupture of echinococcal cysts, **146:**391
Hydrocephalic dementia, CT, **147:**963
Hydrocephalus, idiopathic external, benign familial macrocephaly relations (a), **147:**863
Hyperimmunoglobulinemia E syndrome, pulmonary imaging (a), **147:**864
Hyperoxaluria, primary, radiologic aspects of, **146:**395
Hypertension
see also specific type
chronic portal, expandable intrahepatic portacaval shunt stents, **147:**1251
flank mass and, **146:**67
portal, porto-caval anastomosis in, children (a), **146:**654
Hypertrophic gastropathy, pediatric, **147:**1031
Hypertrophic pyloric stenosis, esophageal atresia and, **147:**329
Hypopharynx, *see* Pharynx
Hypotonia, GI examination, ear acupuncture for (l), **147:**862
Hysterosalpingography, low-osmolality contrast medium in (a), **146:**428

I

Ileal conduit, retrograde ureteral catheterization via, **146:**61
Ileum
obstruction, transluminal angioplasty, **146:**859
stricture, Henoch-Schonlein purpura and (a), **147:**443
Iliac artery, angioplasty-related rupture, treatment without surgery, **147:**389
Imaging
see also Radiography; Computed Tomography; Ultrasound
cerebral perfusion, iodine 123-labeled amines (a), **146:**886
chemical shift, **146:**971
children, presence of parents during (e), **146:**639
diagnostic
clinical medicine (b), **146:**216
consultation in (b), **146:**986
roentgen signs of (b), **146:**238
digital (b), **146:**248
information processing (b), **146:**476
kidney mass (a), **146:**429
oncologic (b), **146:**1140
renal failure (a), **146:**651
Imaging centers
finance and control (l), **147:**1333
free-standing, physician investment in (e), **147:**412
free-standing (l), **147:**1334, **147:**1335, **147:**1336
Imaging equipment, x-ray (b), **146:**232
Imaging processing, digital, cardiac (b), **146:**484
Imaging techniques, tarsal coalitions (a), **146:**885
Implanted devices, markers for, **146:**387
Indium-111
leukocyte scan
acute acalculous cholecystitis, **147:**813
brain abscesses (a), **146:**885
chronicity of infection and, **147:**809
early myocarditis in Kawasaki disease, **146:**255
febrile renal transplant patients, **146:**823
uptake by tumors, **146:**621
white blood cells, lung uptake of, **147:**601
Indium-granulocyte scanning, painful prosthetic joint, **147:**167
Infertility, male, thermography, spermatic venography, and embolization in, **147:**97
Insulinoma, benign pancreatic, sonography, **147:**929
Intestinal hypomotility, bile-duct dilatation, after laparotomy, **147:**729
Intestine
complications of bone marrow transplant (a), **147:**440
small bowel diverticulitis, CT findings, **147:**271
small bowel examination, Crohn's disease, **147:**63
small-bowel toxicity, floxuridine therapy and, **146:**39
Intracranial circulation, quantitative analysis, rapid-sequence DSA, **146:**1239
Intracranial hemorrhage, NMR imaging of (a), **146:**1106
Intravascular mass, non-Wilms', childhood (l), **146:**1098
Intravascular retrieval, percutaneous, foreign body, **146:**863
Intussusception
see also specific organ
adults, **146:**527
Iohexol, metrizamide comparison, cognitive and affective changes after, **147:**777
Ischemia
arterial, lower limbs, **146:**157
simulation of colonic carcinoma by (a), **146:**176
Islet-cell tumors, small, localization (a), **146:**884

J

Jaundice
obstructive
percutaneous cholangiography and biliary drainage in (a), **147:**444
sonographic parallel channel sign in (l), **146:**645
Jejunal feeding, percutaneous gastrostomy and, **147:**822, **147:**826
Jejunostomy, percutaneous, **146:**577, **146:**581
Jejunum
enteroclysis, plasma electrolyte status after, **146:**323
percutaneous bioplasty (a), **146:**1102
Job syndrome, gallium-67 imaging, **147:**610
Joint
see also specific joint
aspiration or arthrography, negative bone scans after, experimental study, **146:**87
hip, fluid, vacuum phenomenon and (a), **147:**218
knee, locking and unlocking, arthrography, **146:**575
prosthetic, pain, indium-granulocyte scanning in, **147:**167
temporomandibular, sagittal computed tomography (a), **146:**179

K

Kaposi's sarcoma, AIDS and, **147:**919
Kawasaki disease

early myocarditis in, indium-111 leukocyte scanning localization, **146:**255
tricuspid regurgitation, Doppler detection (a), **147:**218
Kidney
anomalous, functional renal disease in, radiology, **147:**289
calculi
extracorporeal shock wave lithotripsy, **147:**89, **147:**94
removal, intercostal-space nephrostomy for, **147:**393
candidiasis, neonatal, sonographic diagnosis, **147:**801
clear cell sarcoma, tumor of childhood that metastasizes to bone, **146:**64
cyst, hemorrhagic, MRI, **146:**1167
failure
acute rhabdomyolysis with, technetium-99m pyrophosphate imaging in, **147:**815
current imaging (a), **146:**651
gastric emptying in (a), **146:**428
mass, current imaging (a), **146:**429
normal growth, myelodysplasia, **146:**615
percutaneous nephrostolithotomy, **147:**283
polycystic disease, MRI, **146:**1167
simultaneous pancreatic transplant, scintigraphy, **147:**1193
staghorn, large pelvic stones and (a), **146:**652
transplant
febrile patients, indium-111 leukocyte scanning, **146:**823
MRI, **147:**949
rejection, MRI, **147:**954
Wilms' tumor, MRI, **146:**955
Kidney, angioplasty, transplant arterial stenosis, **146:**853
Kidney, magnetic resonance imaging, paroxysmal nocturnal hemoglobinuria, **146:**51
Kidney, ultrasound
American Burkitt lymphoma, **146:**549
calcium deposition, children, **146:**1253
cystic disease, fetal, **146:**767
Kimray-Greenfield filter
complications, CT evaluation of, **147:**45
percutaneous femoral introduction (l), **146:**424
percutaneous placement (l), **146:**1317
Klatskin tumor, sonographic diagnosis of, **147:**509
Klippel-Trenaunay-Weber syndrome, cutaneous and visceral hemangiomata, sonography, **147:**598
Knee
locking and unlocking, arthrographic demonstration, **146:**575
1.5-T surface-coil MRI, **147:**293

L

Laparotomy, bile-duct dilatation after, **147:**729
Laser therapy, obstructing carcinoma, esophagus and stomach, radiographic appearance after, **146:**519
Lead poisoning
intracranial calcification in, CT findings, **146:**267
radiologic diagnosis of, **146:**245
Leriche syndrome, angiography, CT, and sonography (a), **146:**1106
Leukemia, lymphocytic, extramedullary hematopoeisis in, **147:**846
Leukocyte scan
indium-111, myocarditis (l), **147:**216
indium-111-labeled, chronicity of infection and, **147:**809
tumor uptake of indium-111, **146:**621
Leukocytes, indium-111-labeled, detection of prosthetic vascular graft infections, **147:**173
Leydig-cell tumor, ultrasound in (a), **146:**177
Limb-body wall complex, in utero sonographic diagnosis, **146:**1019
Lisfranc's joint, stress fractures of second metatarsal (a), **147:**219
Liver
Budd-Chiari syndrome
MRI, **146:**1141
review, **147:**9
cancer, gadolinium-DTPA, MRI, **147:**357
cirrhosis
portal vein thrombosis in (a), **146:**427
ruptured hepatocellular carcinoma complicating (a), **146:**178
complications of bone marrow transplant (a), **147:**440
disease, radiology impact on, **147:**1117
extrahepatic cavernous hemangiomas, CT and MRI, **147:**1299
hemangioma, dynamic bolus CT, **147:**711
hepatic cavernous hemangioma, atypical radiographic findings in, **146:**1149
ischemic necrosis, fetal liver calcification and, **147:**596
malignant disease, multiple bile-duct hamartoma simulation of, CT and sonography for, **147:**279
mesenchymal hamartomas, sonographic and CT findings, **147:**1035
metastases
colonic carcinoma, ^{99m}TC-HMDP in, **146:**333
interstitial radiation therapy for, **147:**275
preoperative imaging (a), **146:**1320
MRI, **147:**1103
patterns of childhood injury, computed tomography, **147:**1199
pediatric, CT and MRI, **147:**785
quadrate lobe, pseudotumor in, sonography, **147:**923
subcapsular metastasis, ovarian cancer and (a), **147:**444
transplantation
angiographic and radiologic interventional considerations, **146:**143
hepatic artery thrombosis after, **146:**137
impaired lymphatic drainage in, CT, **147:**519
MRI evaluation of portal vein, **147:**1027
vascular complications after, **147:**657
volume determination, sonography and CT (a), **146:**177
Liver, computed tomography, masses, **146:**729
Liver, ultrasound
diffuse benign disease, **146:**1011
diffuse parenchymal disease (a), **146:**177
monitoring of cryosurgery, **147:**665
regenerating nodules, cirrhosis, **146:**533
Longus coli, calcific tendinitis of, CT, **147:**742
Lumbar herniated disk disease, canal stenosis and, coil MR, CT, and myelography, **147:**757
Lung
air bronchogram, sonography, **147:**593
amiodarone toxicity, gallium scintigraphy, **147:**607
cancer
postoperative recurrence, whole-body gallium scintigraphy, **147:**911
radiotherapy (b), **146:**774
horseshoe, **146:**211, **146:**217
indium-111 oxine-labeled white blood cell uptake, **147:**601
lower lobes, segmental bronchovascular anatomy, CT, **147:**457
metastases, radiologic contributions to management, **147:**473
nonlymphomatous lymphoid disorders, **147:**227
non-small-cell bronchogenic carcinoma, CT in preoperative staging, **146:**285
parenchyma, CT, mosaic oligemia, **147:**670
persistent abnormalities, bronchopulmonary dysplasia (a), **147:**649
plasma cell granuloma, case of day, **146:**1080
pulmonary emboli, MRI, **147:**1133
tuberculosis, radiographic features, **146:**497
Lung, radiography, carcinoid, atypical, **146:**665
Lymphadenopathy, sinus histiocytosis with (a), **146:**179
Lymphangioma
intra-abdominal cystic, mesenteric cysts and (a), **146:**1319
vertebral, lymphographic documentation of (a), **146:**177
Lymphangiomyomatosis, pulmonary, chest case of day, **146:**1083
Lymph node
see also Lymphoma
calicfied mediastinal, CT demonstration (p), **147:**17
impaired drainage, liver transplants and, CT, **147:**519
intramammary, breast cancer metastasis to, **146:**133
mediastinal, CT and autopsy, **147:**469
Lymphography, vertebral lymphangioma (a), **146:**177
Lymphoid disorders, nonlymphomatous, lung, **147:**227
Lymphoma
American Burkitt, renal sonography in, **146:**549
early gastric, radiologic manifestations of, **146:**513
Hodgkin's, thallium-201 parathyroid scan of mediastinum in, **147:**819
non-Hodgkin
bone, musculoskeletal case of day, **146:**1088
central nervous system involvement (a), **146:**887
classification (e), **147:**205
primary central nervous system, CT and pathologic correlation, **147:**747
Lymphoscintigraphy, internal mammary, breast carcinoma (a), **146:**431

M

Magnetic resonance imaging
abnormal pericardium, **147:**245
albumin-(Gd-DTPA) and Gd-DTPA comparison, **147:**1263
arachnoid cysts, sacrum, **146:**359
artifacts, **147:**1271, **147:**1283, **147:**797
blood and blood products, **146:**1293
Budd-Chiari syndrome, **146:**1141
cardiac gated, perivalvular infectious pseudoaneurysms, **147:**253
chemical shift, **146:**971
comparing costs and efficacy, commentary, **146:**1307
comparison with CT, brain and cervical spine diseases (a), **146:**653
contrast agents, optimal pulsing sequences, **147:**367
contrast imaging (a), **146:**433
CT and
cerebral, dementia (a), **146:**178
head and neck (b), **146:**518
diffusion in U.S. (e), **147:**856
diffusion of, **146:**963
endoscopic biopsy and, Egyptian mummies, **146:**93
exercise, new device, **147:**1289
facility, computer patient database management, **146:**871
gated cardiac, right anterior oblique position, **147:**33
intervertebral disk (a), **146:**429
localized tissue spectroscopy, **147:**1327
multiple sclerosis, **147:**571
neuroblastoma, **146:**251
neurosarcoidosis, steroids and, **146:**819
nonorthogonal, multiple-angle, variable-interval, **147:**363
normal pericardium, **147:**239
optimally oriented, measurement of normal left heart dimensions, **146:**75
orthopaedic surgery (a), **146:**884

pediatric (b), **146:**1140
periventricular hyperintensity, **146:**443
primary bone and soft-tissue tumors, **146:**749
simulator, instruction in pulse-sequence selection, **147:**199
skeletal muscle, **146:**565
solenoid surface coils in, **146:**409
spectroscopy (a), **146:**1107
spin-echo, blood flow and, **146:**931
status in 1986, 453
stroke syndromes (a), **146:**431
surface coil (a), **146:**178
technique for image salvage, **147:**1052
temporal lobe epilepsy (a), **146:**653
two-dimensional Fourier transformation technique, truncation errors, **147:**1283
vascular malformations, **146:**1223
Magnetic resonance imaging, abdomen
puerperal ovarian-vein, **147:**291
sickle cell anemia, **147:**843
Wilms' tumor, **146:**955
Magnetic resonance imaging, adrenal, indeterminate masses, **147:**493
Magnetic resonance imaging, arteries
congenital abnormalities, **146:**941
Takayasu's arteritis, angiography and, **146:**949
Magnetic resonance imaging, bladder
CT-surgical correlation, staging of carcinoma, **146:**1179
prostate and, value in review of, **147:**732
Magnetic resonance imaging, bone
malignant infiltration, **146:**353
stress fracture, **147:**553
Magnetic resonance imaging, brain
foci of signal, anterior frontal horns, **147:**331
iron, **147:**103
occult vascular formations, **147:**985
radiation injury, **147:**119
Magnetic resonance imaging, breast, diagnosis of disease, **146:**119
Magnetic resonance imaging, cranium
CT comparison, head injury, **147:**1215
extracranial hematoma, **146:**403
Gd-DTPA, brain, **147:**1223, **147:**1231
intracranial hemorrhage (a), **146:**1106
pediatric abnormalities (a), **146:**886
Magnetic resonance imaging, heart
central pulmonary arterial tree, conotruncal malformation, **147:**1127
dissection of the aorta, **146:**1286
myocardial infarction, **146:**315
overview, **146:**907
reperfused myocardial infarct, dog, **146:**925
thoracic aortic aneurysms, **146:**309
Magnetic resonance imaging, hip, avascular necrosis, **147:**67
Magnetic resonance imaging, joint, fluid, normal and ischemic hip, **146:**1215
Magnetic resonance imaging, kidney
paroxysmal nocturnal hemoglobinuria, **146:**51
polycystic disease, renal cysts in, **146:**1167
transplantation, **147:**949, rejection in, **147:**954
Magnetic resonance imaging, knee, 1.5-T surface-coil, **147:**293
Magnetic resonance imaging, liver
Budd-Chiari syndrome, **147:**9
children, **147:**785
dynamic spin-echo, gadolinium-DTPA, **147:**357
extrahepatic cavernous hemangiomas, **147:**1299
hepatic venous drainage, inferior vena cava obstruction, **147:**635
splenorenal shunts, **146:**597
technical and clinical advances, **147:**1103
transplant, MRI evaluation of portal vein, **147:**1027
Magnetic resonance imaging, lung
pulmonary airspace disease, **146:**1123
pulmonary emboli, **147:**1133
pulmonary vascular resistance, congenital cardiovascular shunt lesions, **146:**919
Magnetic resonance imaging, neck, normal and diseased thyroid, **147:**1255
Magnetic resonance imaging, parathyroid gland, tumors, surface coils, **147:**497
Magnetic resonance imaging, pelvis
female, **146:**1115
pelvimetry, **147:**409
Magnetic resonance imaging, pituitary, adenoma, cavernous sinus invasion by, **146:**257
Magnetic resonance imaging, prostate
bladder and, value in review of, **147:**732
carcinoma detection, **146:**351, **146:**543
Magnetic resonance imaging, rectum, staging cancer, **146:**1155
Magnetic resonance imaging, spine
chronic injury, **147:**125
dysraphism, infants and children, **147:**339
lesions of posterior fossa and upper cervical cord, childhood (a), **146:**179
lumbar, anatomic correlations and technical variations, **147:**891
lumbar herniated disk disease, canal stenosis and, **147:**757
surface coils in, **147:**373, dynamic range compression, **147:**379
tuberculous spondylitis, **147:**79
Magnetic resonance imaging, thorax, venous obstruction, **146:**679
malignant and benign masses, CT discriminators of (l), **146:**1316
Malpractice, radiologists and, **147:**1291
Mammography
breast cancer
metastasis, intramammary lymph nodes, **146:**133
nonpalpable, **146:**661
calcification in, significance in breast carcinoma (a), **147:**864
density of tissue (e), **147:**487
grids, stationary and moving, **147:**491
grids and (l), **147:**860
high-contrast, moving grid, **146:**1137
male breast disease, **146:**127
report (l), **147:**1332
screening, **147:**689, baseline, **147:**1149
screening (e), **147:**195
screening (l), **147:**1091
therapy (l), **146:**1100
transillumination light scanning comparison, breast lesions, **147:**191
Maternity, impact on radiologists (e), **146:**415
Maxial-orbital fractures, medial, CT (a), **146:**1108
Maxillofacial pantomography, interpretation (b), **146:**1324
Mediastinal collateral arteries, coarctation of the aorta, **146:**757
Mediastinum
mass, pericardial effusion presenting as (a), **146:**1102
solid bronchogenic cyst, mineralogic analysis, **146:**73
transesophageal sonography (a), **146:**1102
tumor, circumflex retroesophageal right aortic arch simulation of, **146:**491
venous obstruction, MRI, **146:**679
Medtronic hall valve prosthesis, radiographic appearance, **146:**485
Megacalyces, congenital, primary megaureter and, **147:**313
Megacolon, *see* Colon
Megaureter, primary, congenital megacalyces and, **147:**313
Memorials
Abrams, Raymond M., 1917–1986, **147:**1288
Baltaxe, Harold A., 1931–1985, **146:**604
Biello, Daniel R., 1947–1986, **147:**784
Bird, Gustavus C., Jr., 1910–1984, **146:**1326
Dotter, Charles Theodore, 1920–1985, **146:**1321
Gruentzig, Andreas Roland, 1939–1985, **146:**118
Harrison, R. Stewart, 1906–1986, **147:**28
Judkins, Melvin P., 1922–1985, **146:**1324
Miller, George Andrew, Sr., 1920–1985, **146:**326
Ricketts, Howard James, 1932–1986, **147:**16
Wexler, Howard Alan, 1940–1986, **147:**1062
Meniscus, *see* Knee
Mesenteritis, retractile, colon, **147:**937
Mesentery
cysts
intra-abdominal cystic lymphangiomas and (a), **146:**1319
retroperitoneal cysts and (a), **146:**1320
Metaphyseal lesion, abused infants, radiologic characteristics, **146:**895
Methyl-tert-butyl ether, gallstone dissolution with, percutaneous cholecystostomy, **146:**865
Metoclopramide, pancreatic sonography and, **146:**341
Metrizamide
CT cisternography, cerebrospinal fluid rhinorrhea (a), **146:**885
lumbar myelography
aseptic meningitis secondary to, infant (a), **146:**655
complications in diabetics, **146:**1057
myelography
cervical (a), **146:**1109
CT scanning and (a), **146:**1108
Metrizamide, iohexol comparison, cognitive and affective changes after, **147:**777
Microbubbles, contrast agent, catheter manipulation, **147:**347
Microcolon, *see* Colon
Miller, George Andrew, Sr. (m), 146:326
Mitral valve, regurgitation, echocardiography (a), **146:**650
Mosaic oligemia, simulation of pulmonary infiltrates, CT, **147:**670
MRI in, **146:**443
Mucopolysaccharidosis, narrow trachea in (a), **146:**180
Multiimaging evaluation, chronic acalculous gallbladder disease, **147:**721
Multiple sclerosis
see also Brain
MRI and clinical correlation, **147:**571
Muscle, skeletal, MRI imaging, **146:**565
Muscular dystrophy, esophageal motor function in (a), **147:**442
Musculoskeletal system
case of day, **146:**634, **146:**1090
three-dimensional imaging, **147:**545
Myelodysplasia, normal kidney growth and, children, **146:**615
Myelofibrosis (b), **146:**30
Myelography
cervical, metrizamide (a), **146:**1109
cognitive and affective changes after, metrizamide and iohexol, **147:**777
CT scanning and, metrizamide (a), **146:**1108
cystic necrosis, compressive cervical myelopathy, **147:**767
lumbar
metrizamide, aseptic meningitis secondary to, infant (a), **146:**655
metrizamide, complications in diabetics, **146:**1057
outpatient (a), **146:**885
lumbar herniated disk disease, canal stenosis and, **147:**757
Myelomeningocele, progressive spasticity and scoliosis in (a), **146:**653
Myelopathy, compressive cervical, CT-myelography, **147:**767
Myocarditis
indium-111 leukocyte scanning (l), **147:**216
Kawasaki disease in, indium-111 leukocyte scanning localization in, **146:**255
Myocardium, *see* Heart

Myositis ossificans, musculoskeletal case of day, **146:**1090

N

Nasal cavity, pseudotumor, anatomic basis of, **147:**782
Nasopharyngeal mass, Foley catheter simulation of, neuroradiology case of day, **146:**1095
Nasopharyngography, normal (p), **147:**145
Neck
carotid bifurcation, incremental dynamic CT, **146:**465
masses, ultrasound, children, **146:**609
penetrating vascular injuries, angiography, **147:**995, (e)**147:**1000
Necrotizing enterocolitis, neonatal, enterocyst formation as a complication of, **147:**806
Needle guidance system, aspiration and drainage, **147:**1241
Neoplasm, *see* specific organ; region
Nephritis, hemorrhagic focal bacterial, Gray-scale sonography and CT findings, **146:**1173
Nephrostolithotomy
kidney changes after, **147:**283
percutaneous (a), **146:**887
Nephrostomy
intercostal-space, percutaneous stone removal and, **147:**393
percutaneous catheter, indwelling ureteral stent placement and, **147:**832
percutaneous (l), **146:**882
Neuroblastoma
cystic, infants, **146:**113
egg-shell calcifications, children (a), **146:**432
magnetic resonance imaging, **146:**251
opsomyoclonus, CT scanning in, **146:**781
primary (a), **146:**1108
Neuroradiology
AIDS, **147:**977
case of day, **146:**637
Neurosarcoidosis, steroids and, CT and MRI, **146:**819
Neurosonography
intraoperative, time requirement for, **146:**815
microbubbles as contrast agent for, catheter manipulation, **147:**347
Nonsteroidal antiinflammatory drugs, serpiginous gastric erosions caused by, **146:**31
Nuclear magnetic resonance imaging, *see* Magnetic resonance imaging
Nuclear medicine
annual 1985 (b), **146:**294
Budd-Chiari syndrome, **147:**9
Nucleus polposus, herniated, spontaneous regression (l), **146:**882

O

Occlusion, short-term, drug uptake and, **146:**375
Oligohydramnios, 16 and 30 weeks gestation, sonographic evaluation, **146:**1277
Omphalocele
gastroschisis and
fetal, **147:**1047
fetal, sonographic diagnosis, **147:**797
Oncology
diagnostic, clear cell sarcoma of the kidney, **146:**64
radiation (b), **146:**970
Ophthalmology, diagnostic imaging (b), **146:**1282
Opsomyoclonus, CT scanning in, **146:**781
Optic nerve, meningiomas (a), **146:**430
Orthopedic surgery, MRI (a), **146:**884
Osteoblastoma, spine (a), **147:**648
Osteoid-osteoma, spine (a), **147:**648
Osteoma
see also Bone
osteoid, musculoskeletal case of day, **146:**1092
Osteomyelitis, multifocal, chronic recurrent, **147:**87
Osteoporosis, densitometric screening for (l), **147:**1329
Osteosarcoma
see also Bone
parosteal, radiolucencies (a), **146:**884
Ovary, cancer, subcapsular liver metastasis in (a), **147:**444

P

PACS, what radiologists say (e), **146:**418
Pancreas
benign insulinoma, sonography, **147:**929
calcifications, pancreatic insufficiency and (a), **147:**441
fat depositions, sonography and, **146:**1017
lipomatosis, Schwachman-Diamond syndrome (a), **146:**433
mass occupying lesions, CT diagnosis (a), **146:**428
pancreatitis
abscesses in, CT (a), **146:**1321
diagnosis of (a), **146:**177
pseudocyst
percutaneous aspiration and drainage, **147:**1007
spontaneous rupture into portal venous system, **147:**935
simultaneous renal transplant, scintigraphy, **147:**1193
tumors, fine-needle aspiration biopsy in, **147:**399
Pancreas, ultrasound, metoclopramide and, **146:**341
Pancreatic mumps, reaction to contrast media, **147:**188
Pancreaticobiliary ductal union, gallbladder carcinoma and, **147:**442
Pancreatic pseudomass, second portion of duodenum, water-aided sonography and, **147:**281
Pancreatitis, *see* Pancreas
Pancreatography, retrograde dorsal (a), **147:**441
Papaverine
coronary vasodilator (l), **147:**1095
incompatibility with hexabrix, **146:**1300
incompatibility with hexabrix (l), **147:**1096
Parathyroid gland
imaging (b), **146:**1010
tumors, MRI with surface coils, **147:**497
Pediatric radiology
aortoiliac compression, distended bladder, **146:**1273
arterial catheters, complications of (a), **146:**655
aseptic meningitis, secondary to metrizamide lumbar myelography, infant (a), **146:**655
Bechet syndrome, involving gastrointestinal tract (a), **147:**218
bile duct dilation, immunodeficiency and (a), **146:**432
bronchopulmonary foregut malformations, **146:**227
cerebral abnormalities (a), **146:**886
chronic recurrent multifocal osteomyelitis, **147:**87
cilia syndrome, chest film in (a), **147:**863
cranial radiation, CT evaluation of, **147:**587
craniocervical junction, ultrasound, **147:**133
delayed hemorrhagic infarction (a), **146:**888
digital subtraction angiography (a), **146:**1323
end-stage kidneys, fatal outcome after renal ablation, **146:**593
facial port-wine stains, Sturge-Weber syndrome and (a), **146:**432
fetal anomalies, oligohydramnios between 16 and 30 weeks gestation, **146:**1277
focal cerebral hypoperfusion, dysphasia or attention deficit disorder (a), **146:**655
gastrointestinal malformations, antenatal sonographic diagnosis of (a), **146:**432
giant cell reparative granuloma, cranial vault (a), **146:**655
hemorrhage and cyst development, cavum septi pellucidi (a), **146:**888
hip joint fluid, vacuum phenomenon and (a), **147:**218
histiocytosis X, healing rates in bone (a), **146:**655
horseshoe lung, **146:**211, **146:**217
humerus, distal end, arthrography of fractures (a), **147:**649
Hurler's syndrome (a), **146:**433
hydrocephalus, idiopathic external (a), **147:**863
hyperimmunoglobulinemia E syndrome (a), **147:**864
hypertrophic gastropathy, **147:**1031
hypertrophic pyloric stenosis, sonography (a), **147:**649
ileal stricture, complication of Henoch-Schonlein purpura (a), **147:**443
indium-111 leukocyte scanning, early myocarditis in Kawasaki disease, **146:**255
infantile infectious sacroiliitis (a), **146:**888
interventional genitourinary, **147:**791
ischemic hepatic necrosis, fetal, **147:**596
Kawasaki disease, Doppler detection of (a), **147:**218
liver, MRI and CT, **147:**785
liver injury, CT, **147:**1199
liver transplant, MRI evaluation of portal vein, **147:**1027
malignancies, peritoneal and mesenteric involvement, CT (a), **147:**864
mechanical ventilation, gastrointestinal perforation in (a), **146:**432
mesenchymal hamartomas, liver, **147:**1035
metaphyseal lesion, abused infants, **146:**895
microcolon of prematurity, **146:**239
MRI in neuroblastoma, **146:**251
neck masses, sonography, **146:**609
neonatal chest, extracorporeal membrane oxygenation, **146:**1257
neuroblastoma, egg-shell calcifications (a), **146:**432
normal renal growth, myelodysplasia and, **146:**615
omphalocele and gastroschisis, fetal, **147:**797
opaque chest, bronchial foreign body (a), **147:**649
optic nerve glioma, posterior visual pathway involvement (a), **147:**864
pancreatic lipomatosis, Schwachman-Diamond syndrome (a), **146:**433
percutaneous endoscopic gastrostomies (a), **146:**1323
percutaneous nephrostolithotomy (a), **146:**887
persistent pulmonary abnormalities, bronchopulmonary dysplasia (a), **147:**649
portal hypertension, porto-caval anastomosis in (a), **146:**654
preoral pneumocolon, **146:**763
presence of parents during imaging procedures (e), **146:**639
pseudoomphalocele, **146:**1283, **147:**797
radial growth plate, stress-related widening of (a), **147:**863
renal calcium deposition, ultrasound, **146:**1253
renal candidiasis, neonatal, **147:**801
renal cystic disease, fetal, **146:**767
respiratory syncytial virus infection (a), **147:**218
rib osteomyelitis (a), **146:**654
septic shock, group B streptococcal sepsis and periventricular leukomalacia (a), **146:**432
soft tissue calcification, vitamin E injection and (a), **147:**443
sonographic study, cerebral ventricles, neonate, **146:**471
subdural hemorrhage, in utero (a), **146:**887
thigh, computed axial tomographic scanning (a), **147:**650
three-dimensional CT reformation, **146:**1261
tracheal dimensions, **146:**233
tracheal dimensions (l), **147:**1094
tracheobronchitis, necrotizing (a), **147:**443

traumatic uteropelvic disruption (a), **147:**218
ultrasound, idiopathic arterial calcification, **146:**249
umbilical artery, dystrophic calcification in (a), **146:**654
urinary tract, contrast sonography (a), **147:**649
Pelvimetry, MRI, **147:**409
Percutaneous puncture, serial embolization, extremity arteriovenous malformation, **146:**1038
Percutaneous transluminal angioplasty, *see* Angioplasty
Periappendiceal abscess, CT in management of, **146:**1161
Pericardium
abnormal, MRI, **147:**245
normal, MRI, **147:**239
Peritoneography, CT, pediatric dialysis complications, **147:**325
Peritoneovenous shunt, evaluation of patency, intraperitoneal Tc-99m macroaggregated albumin, **147:**177
Perivalvular abscesses, MRI, **147:**253
Perivalvular infectious pseudoaneurysms, MRI, **147:**253
Periventricular hyperintensity, MRI in, **146:**443
Periventricular leukomalacia, sonography, **146:**1067
Petit's hernia, CT, **147:**744
Pharynx, hypopharynx tumors, CT (a), **146:**430
Pheochromocytoma, unenhanced CT, **146:**741
Phlebitis, portal, abdominal case of day, **146:**1077
Phlegmons, CT in management of, **146:**1161
Physics, radiological (b), **146:**678
Pick's disease, CT, **147:**963
Pineal gland
germinal-cell tumor, **146:**1246
tumors, CT of, **146:**451
Pituitary gland
adenoma, cavernous sinus invasion by, CT and MRI signs of, **146:**257
Cushing syndrome, CT, **146:**1235
posterior, CT demonstration of, **146:**263
Pituitary tumors, CT (a), **146:**886
Plasma cell disease, review (a), **146:**429
Pleural effusion, malignant, complication of biliary drainage, **146:**1165
Pneumatic antishock garment, apparent arterial occlusion and, traumatic angiography, **147:**391
Pneumocolon, preoral, children, **146:**763
Pneumocystis carinii, pneumonia, spontaneous pneumothorax with, AIDS patients, **147:**29
Pneumonia
organizing, bronchiolitis obliterans with, **147:**899
Pneumocystis carinii, spontaneous pneumothorax with, AIDS patients, **147:**29
Pneumosinus dilatans, orbital (a), **146:**430
Pneumothorax
colopleural fistula, strangulated diaphragmatic hernia with, **146:**321
significant delayed (l), **147:**1090
spontaneous, with pneumonia, AIDS patients, **147:**29
Polycystic kidney disease, *see* Kidney
Polyvinyl alcohol foam, embolization, radiopaque suspension, **146:**591
Portacaval shunt, expandable intrahepatic, chronic portal hypertension, **147:**1251
Portal venous system
congestion index, **146:**735
rupture of pseudocyst, pancreatic, **147:**935
sonographic and pulsed-Doppler evaluation (a), **147:**864
Portography, digital indirect, **147:**39
Positron emission tomography
brain (b), **146:**690
dopamine receptor images (a), **146:**886
glioma patients (a), **146:**653
Posttraumatic dementia, CT, **147:**963
Pregnancy
abdominal, sonographic findings, **147:**1043
fluoroscopy and (e), **146:**415
Proptosis, CT volumetric analysis, **146:**459
Prostate
cancer, MRI, **146:**543
carcinoma, MRI/CT-guided biopsy, **146:**351
lesions, transrectal sonography, **146:**1187
MRI value in review, **147:**732
Prostatism
excretory urography in, **147:**957
routine urography in, **147:**960
Pseudarthrosis, diagnosis, posterior spinal fusion for scoliosis (a), **146:**1103
Pseudocyst
pancreatic
benign rupture into portal venous system, **147:**935
percutaneous aspiration and drainage, **147:**1007
Pseudoomphalocele, fetal sonography, **146:**1283, **147:**797
Pseudotumor
nasal cavity, radiography, **147:**782
quadrate lobe, liver, sonography, **147:**923
Psoas abscess, CT diagnosis (a), **146:**1105
Pulmonary airspace disease, MRI, **146:**1123
Pulmonary alveolar proteinosis, bronchopulmonary lavage in, chest radiography, **146:**981
Pulmonary artery, central, MRI, conotruncal malformation, **147:**1127
Pulmonary disease, talc and, **146:**295
Pulmonary embolism
perfusion impairment, radiographic assessment (a), **147:**440
short-term prophylaxis, retrievable vena cava filter, **147:**836
Pulmonary function tests, CT correlation with, silicosis, **146:**477
Pulmonary nodule, solitary, CT, **147:**21, **147:**26
Pulse-sequence selection, instruction for, MRI simulator, **147:**199
Pyelography, emergency intravenous (a), **146:**1322
Pylethrombosis, protean manifestations of (a), **146:**1321

Q

Quadriplegia, diffuse idiopathic skeletal hyperostosis, after minor trauma (l), **147:**858

R

Radial growth plate, stress-related widening, adolescents (a), **147:**863
Radiation injury, brain, MRI, **147:**119
Radiation physics, medical, progress in (b), **146:**24
Radiation therapy
calcified ascending aorta after, **147:**477
cranial, CT evaluation of effects, **147:**587
interstitial, hepatic metastases, **147:**275
Radioactivity, measurements procedures (b), **146:**532
Radiodiagnosis, skull (b), **146:**476
Radiography
see also specific organ
interpretation for general practitioners (b), **146:**80
x-rays, health effects (b), **146:**774
Radiography, digital, symposium on (b), **146:**86
Radiography, imaging, oriental cholangiohepatitis, **146:**327
Radiography, injurious effects, contrast medium, acute thrombocytopenia, **146:**1298
Radiography, technique
assessment of perfusion impairment, pulmonary embolism (a), **147:**440
atypical carcinoid, lung, **146:**665
bladder calculi, scrotal cystocele with, **147:**287
bronchiolitis obliterans, with organizing pneumonia, **147:**899
catheter perforation, superior vena cava, **146:**487
cervical spine, hyperextension dislocation, **146:**803
chest
aortic dissection, **147:**1123
CT and pulmonary function test correlation, silicosis, **146:**477
extracorporeal membrane oxygenation, neonatal, **146:**1257
colonic polyps, single-contrast vs double-contrast barium enema in, **146:**993
computer-generated examinations, **146:**413
congenital megacalyces, primary megaureter and, **147:**313
contrast agents, comparison of, **147:**185
conventional and computed tomography, spiral fractures of tibia (a), **147:**219
cystic neuroblastoma, **146:**113
digital-scout, drainage of percutaneous abscess, **147:**406
diminutive polyps, colon (e), **146:**875
double-contrast, esophageal mucosa (a), **146:**651
early esophageal cancer, **146:**507
elbow trauma, radial head—capitellum view, **146:**81
esophagus and stomach, laser treatment for obstructing carcinoma, **146:**519
functional adrenal disease, anomalous kidneys and, **147:**289
hemophilia, diagnostic imaging (b), **146:**80
hepatic cavernous hemangioma, **146:**1149
hip changes, spastic cerebral palsy, **146:**1219
hip ossification, infant, **147:**317
horseshoe lung, **146:**211
incomplete carpal coalition, **147:**301
kinked catheters, **146:**789
lower esophageal mucosal ring, **147:**261
Medtronic hall valve prosthesis, **146:**485
multiphasic, reflux esophagitis (a), **147:**441
plain film evaluation
abdominal pain, **147:**501
double images, **147:**1312
primary central nervous system lymphoma, **146:**271
pseudotumor, nasal cavity, **147:**782
pulmonary alveolar proteinosis, **146:**981
pulmonary tuberculosis, **146:**497
radial head—capitellum view, elbow trauma, **146:**81
single-contrast and multiphasic, gastric ulcer, **147:**697
solenoid surface coils, MRI, **146:**409
spine
burst fractures of, **147:**575
infection, intraosseous and intradiscal gas and, **147:**83
strangulated diaphragmatic hernia, pneumothorax and, **146:**321
thoracic venous anatomy (p), **147:**674
transhiatal esophagectomy, gastric interposition following (a), **146:**651
Radioisotope studies, cardiology (b), **146:**1010
Radiologic-pathologic correlation conference, flank mass and hypertension, **146:**67
Radiologist, practicing, armchair research and, Caldwell Lecture, **147:**881
Radiology
AIDS, **147:**977
amyl nitrite test, pseudoachalasia distinguished from idiopathic achalasia, **146:**21
Barrett's esophagus, **147:**257
cancer management and, **147:**473
computer applications in (b), **146:**248
congenital bronchopulmonary foregut malformations, **146:**227
consultation, acute care surgical ward, **147:**637
device identification (e), **146:**418
diagnosis and management of bone tumors (a), **146:**1104

diagnostic, scientific literature in, **147:**1055
double-contrast technique, stomach, **147:**1183
duodenal ulcer detection (l), **146:**424
early American, **147:**850
early gastric lymphoma, **146:**513
hepatic artery thrombosis, after liver transplantation, **146:**137
horseshoe lung, **146:**217
hyperoxaluria, **146:**395
idiopathic megacolon (a), **146:**651
impact on hepatology, **147:**1117
interventional
biliary, removal of bile duct stones, **146:**383
Cope introduction set, **146:**381
liver transplantation, **146:**143
interventional management, sclerosing cholangitis, **147:**1002
lead poisoning, **146:**245
linear gastric erosions, **147:**701
microcomputer-based graphics for, **147:**1319
night (l), **146:**1100
pediatric: *see* Pediatric radiology
personal computer data-base system in, **147:**1075
physics, essentials of (b), **146:**518
physics (b), **146:**678
respiratory syncytial virus infection, children (a), **147:**218
saphenous vein bypass graft, **146:**605
self assessment
ear, nose, and throat (b), **146:**1276
gastrointestinal (b), **146:**1276
small-bowel toxicity, floxuridine therapy, **146:**39
subspecialty, **147:**1324
techological volatility, aging radiologist and, **147:**1322
terminology (l), **146:**425
test results, significance of, **147:**1313
today (b), **146:**940
X-ray imaging equipment (b), **146:**232
Radiology, clinical, joints and vertebral connections (b), **146:**1268
Radiology, operations
computer-assisted (b), **146:**484
computer-assisted scheduling, **147:**203
hemoccult screening, **146:**697
manpower: where are we? (e), **146:**172
spine tumors (b), **146:**1030
Radiology, pediatric, *see* Pediatric radiology
Radiology, training, residents, computer-generated examinations, **146:**413
Radiolucencies, parosteal osteosarcoma (a), **146:**884
Radionuclide imaging, *see* Scintigraphy
Radiopaque suspension, polyvinyl alcohol foam for embolization, **146:**591
Radiotherapy, lung cancer (b), **146:**774
Rectosigmoid carcinoma, CT staging of, **146:**703
Rectum
cancer, MR and CT staging of, **146:**1155
rectosigmoid carcinoma, CT staging of, **146:**703
Renal artery, fibromuscular dysplasia, reversible, **147:**737
Renografin-60, urography, **147:**839
Respiratory distress syndrome, adult, chest case of day, **146:**1085
Respiratory syncytial virus infection, radiology in children (a), **147:**218
Retinoblastoma, computed tomography (a), **146:**179
Retractile mesenteritis, colon, **147:**268
Retroperitoneal cysts, mesenteric cysts and (a), **146:**1320
Retroperitoneum
anatomy (p), **147:**1155
aortic rupture into (l), **146:**421
extraperitoneal spaces, **147:**1162
fibrosis, CT in distinguishing cause of, **146:**57
hemorrhage, femoral arteriography and, CT, **146:**1289
mass with intradural extension, magnetic resonance imaging, **146:**251
Retrorectal cystic hamartoma, *see* Tailgut cyst
Rhabdomyolysis, nontraumatic, acute renal failure with, technetium-99m pyrophosphate imaging in, **147:**815
Ricketts, Howard James (m), 147:16
Rotator cuff
disorders (a), **146:**1105
impingement, **147:**557
operative repair, sonographic and arthrographic assessment (l), **147:**646
sonography of, **146:**555, **146:**561
torn, arthrography after operative repair (a), **147:**219
ultrasound (a), **147:**648

S

Sacroilitis, infantile infectious (a), **146:**888
Sacrum
arachnoid cysts, MRI, **146:**359
foraminal lines (l), **146:**648
upper, transverse fracture (a), **146:**1103
Saphenous vein
bypass
angiography of, **147:**51
radiologic aspects, **146:**605
Schilder's disease, myelinoclastic diffuse sclerosis (a), **146:**1108
Schwachman-Diamond syndrome, pancreatic lipomatosis and (a), **146:**433
Schwannomas, benign, CT inhomogeneities, **147:**141
Scimitar syndrome, horseshoe lung and, **146:**211
Scintigraphy
acute acalculous cholecystitis, **147:**1171
gallium, amiodarone lung toxicity, **147:**607
Gaucher's disease type 1, **147:**943
hepatocellular carcinoma (a), **146:**884
hip, avascular necrosis, **147:**67
procedures (b), **146:**716
radiocolloid, Felty's syndrome, **147:**181
simultaneous pancreatic-renal transplant, **147:**1193
whole-body gallium, lung cancer, postoperative recurrence, **147:**911
Scintimetry, bone (a), **146:**1104
Scoliosis
see also Spine
idiopathic, isotope scanning with Tc-99m MDP (a), **146:**1103
posterior spinal fusion for, diagnosis of pseudarthrosis (a), **146:**1103
Scrotal cystocele, bladder calculi and, **147:**287
Seminoma
see also body part
advanced, chemotherapy treatment, CT evaluation, **146:**745
Septic shock, group B streptococcal sepsis, periventricular leukomalacia and (a), **146:**432
Shoulder, rotator cuff diseases (a), **146:**884
Shoulder impingement syndrome, radiographic findings, **147:**557
Sickle cell anemia, MRI, spleen, **147:**843
Sigmoid diverticular disease, neoplasms and (a), **146:**1320
Silicosis, CT, correlation with plain films and pulmonary function tests, **146:**47
Skin, granular cell tumors, **147:**1305
Skull
radiodiagnosis (b), **146:**476
solitary eosinophilic granuloma (a), **146:**654
Sleep apnea, obstructive, dynamic upper airway narrowing (l), **147:**1330
Small bowel, *see* Intestine, Jejunum, Ileum
Society for Pediatric Radiology
abstracts from 1986 meeting, **147:**865
1986 scientific program, Washington, DC, **146:**642
Society of Magnetic Resonance in Medicine, meeting in London, commentary, **146:**1314
Society of Uroradiology, abstracts from 1986 meeting, **147:**1082
Soft tissue
calcification, vitamin E injection and (a), **147:**443
hemorrhage, CT evaluation (l), **147:**1331
tumors
aspiration cytology in (a), **146:**1105
computer tomography (a), **147:**443
diagnosis (b), **146:**1046
MRI and CT evaluation of, **146:**749
Solenoid surface coils, MRI, **146:**409
Sonography, *see* Ultrasound
Spectroscopy
MR, localized tissue, **147:**1327
NMR (a), **146:**1107
Speech, velopharyngeal insufficiency, videofluoroscopy of, **146:**15
Spermatic cord, tension (a), **146:**1103
Sphincter of Oddi, functional obstruction, cholescintigraphic detection (a), **147:**442
Sphincterotomy, antegrade transcholecystic (a), **147:**442
Spine
burst fractures, radiography, **147:**575
cervical, changes in juvenile rheumatoid arthritis (a), **147:**443
cystic necrosis, compressive cervical myelopathy, **147:**767
degenerative disorders, CT myelographic data, **146:**793
dysraphism, infants and children, MRI, **147:**339
extraarachnoid metrizamide instillation, CT, **147:**583
hyperextension dislocation, radiographic features, **146:**803
infection, intraosseous and intradiscal gas, **147:**83
injuries, spondylosis and, **146:**277
lumbar
MRI, **147:**891
stenosis (a), **146:**1322
osteoid-osteoma, osteoblastoma and (a), **147:**648
pathomorphology of stenosis, CT (a), **146:**1109
radiology of tumors (b), **146:**1030
stenosis (a), **146:**887
thoracolumbar, Harrington instrumentation of (a), **146:**652
Spine, computed tomography, intraspinal tumors, intravenous contrast enhancement, **146:**103
Spine, magnetic resonance imaging
chronic injury, **147:**125
lesions of posterior fossa and upper cervical cord (a), **146:**179
Spine, ultrasound, focal stenosis, disc disease and (a), **147:**443
Spleen
hyatid cyst (l), **147:**859
nonparasitic cysts, radiologic-pathologic correlation, **147:**537
Splenorenal shunt, postoperative assessment with MRI, **146:**597
Spondylarthrography, apophyseal joint arthrography (a), **146:**652
Spondylosis, cervical spinal cord injuries and, **146:**277
Steinberg, Samuel S. (m), 146:1178
Stent introducer, universal, **147:**830
Sternum, computed tomography (p), **147:**72
Steroids, neurosarcoidosis responding to, CT findings, **146:**819
Stomach
double-contrast examination, flow technique for, **147:**1183
laser treatment for obstructing carcinoma, radiographic appearance after, **146:**519
Stroke syndromes, MRI in (a), **146:**431

Sturge-Weber syndrome, facial port-wine stains and, pediatric radiology (a), **146:**432
Subcortical arteriosclerotic encephalopathy, CT spectrum, **147:**1209
Subdural hemorrhage, in utero (a), **146:**887
Subglottic stenosis, congenital, elliptical cricoid cartilage, **146:**1133
Subphrenic abscess, percutaneous drainage, **147:**1237
Suprasellar epidermoid, neuroradiology case of day, **146:**1094
Suture anchor, visceral drainage, **146:**160

T

Tailgut cyst, CT and sonography, **147:**1309
Takayasu's arteritis, vascular imaging, MRI, **146:**949
Talc
inhalation or intravenous administration, manifestations in chest, **146:**295
manifestations in the chest (l), **147:**439
Tarsal coalitions, imaging techniques (a), **146:**885
Technetium-99m pyrophosphate imaging, acute renal failure, nontraumatic rhabdomyolysis, **147:**815
Temporal lobe, epilepsy, NMR in (a), **146:**653
Tendinitis, calcific, longus coli, CT, **147:**742
Testis
carcinoma, residual masses after successful chemotherapy, **146:**1184
embryonal carcinoma, non-Wilms' intravascular mass, childhood (l), **146:**1098
impalpable neoplasm, sonography, **146:**349
malignancy, low-attenuation thoracic metastases, **146:**291
Thermography
liquid crystal, thyroid (a), **147:**444
male infertility and, **147:**97
plate, carpal tunnel syndrome (a), **146:**1106
Thoracic aorta, rupture, digital subtraction angiography (l), **147:**1093
Thoracic inlet, venous obstruction, MRI, **146:**679
Thoracic outlet syndrome, athletes, **146:**809
Thoracic venous anatomy, chest radiography (p), **147:**674
Thorax
case of day, **146:**627, **146:**1080
extracorporeal membrane oxygenation, neonatal chest, radiographic appearance of, **146:**1257
opaque, bronchial foreign body, children (a), **147:**649
percutaneous trephine bone biopsy (a), **146:**1103
pulmonary alveolar proteinosis, **146:**981
rib osteomyelitis, radiologic and ultrasonic findings, children (a), **146:**654
talc manifestations in chest, **146:**295
timing of film follow-up, after transthoracic needle aspiration, **146:**1049
Thorotrast, hepatosplenic neoplasia, CT, **146:**997
Thrombectomy, angioplasty and, thrombosed synthetic hemodialysis access fistulas, **147:**161
Thrombin, direct percutaneous injection, coagulation of aneurysms and, **147:**383
Thrombocytopenia, acute, parenteral radiographic contrast medium, **146:**1298
Thrombolysis, occluded femoropopliteal grafts, **147:**621
Thrombolytic therapy, state of the art, **147:**1
Thrombosis
acute coronary, state of the art, **147:**1
deep venous, effect of anatomic variations, **146:**845
hepatic artery, after liver transplantation, **146:**137
puerperal ovarian-vein, MRI, **147:**291
Thymus, hyperplasia, after Cushing's syndrome, **147:**1145
Thyroid gland
imaging (b), **146:**1010
liquid crystal thermography (a), **147:**444
MRI, **147:**1255
Tibia, proximal metaphysis, trampoline fracture in children, **146:**83
Tongue, infiltrations, sonographical-clinical-surgical correlation (a), **147:**444
Trabecular osteopenia, Colles' fracture (a), **147:**443
Trachea
CT, adenoid cystic carcinoma, **146:**1129
dimensions, childhood (l), **147:**1094
growing, age and gender in, computed tomography, **146:**233
narrow, mucopolysaccharidoses (a), **146:**180
Tracheobronchitis, necrotizing (a), **147:**444
Transillumination light scanning, mammography comparison, breast lesion detection, **147:**191
Transplant
liver
angiographic and interventional radiologic considerations in, **146:**143
hepatic artery thrombosis after, **146:**137
vascular complications after, **147:**657
renal
MRI, **147:**949
rejection, MRI, **147:**954
Transthoracic needle aspiration, pulmonary lesions, **146:**1049
T-tube tract, insertion of biliary endoprosthesis, **147:**164
Tuberculosis, pulmonary, radiographic features, **146:**497
Tuberculous spondylitis, MRI of, **147:**79

U

Ultrasound
see also specific organ; region
CT correlation, fibrous tissues and tumors, **147:**1067
diffuse parenchymal liver disease (a), **146:**177
endoscopic (a), **146:**427
fetal
limb-body wall complex, **146:**1019
oligohydramnios, 16 and 30 weeks gestation, **146:**1277
pseudoomphalocele, **146:**1283
Gray-scale, hemorrhagic focal bacterial nephritis, **146:**1173
hypertrophic pyloric stenosis, children (a), **147:**649
idiopathic arterial calcification, infancy, **146:**249
Klippel-Trenaunay-Weber syndrome, **147:**598
normal anatomy (b), **146:**690
obstructive jaundice (l), **146:**645
pediatric (b), **146:**1282
physics and instrumentation (b), **147:**490
real-time
acute cholecystitis (a), **146:**1319
aspiration and drainage, **147:**1241
tendinopathies, Achilles tendon, athletes (a), **146:**429
tongue infiltrations (a), **147:**444
torcular herophili, **146:**109
transesophageal mediastinal (a), **146:**1102
urinary tract, children (a), **147:**649
Ultrasound, abdomen
abdominal pregnancy, **147:**1043
acute acalculous cholecystitis, **147:**1171
aortic aneurysm, anechoic crescent in, **146:**345
bile-duct dilatation, after laparotomy, **147:**729
gallbladder wall, V-shaped artifact, **147:**505
portal venous system (a), **147:**864
real-time, Crohn's disease (a), **146:**1102
tailgut cyst, **147:**1309
water-aided, pancreatic pseudomass, **147:**281
Ultrasound, bladder
diagnosis of tumors (a), **147:**443
neonatal aortoiliac compression, **146:**1273
Ultrasound, brain
compressed and asymmetric lateral ventricles, neonates, **146:**471
craniocervical junction, neonate, **147:**133
periventricular stereotaxis (a), **146:**178
Ultrasound, breast, real-time, **147:**479
Ultrasound, carotid artery, hemorrhage detection, carotid plaque, **146:**1061
Ultrasound, colon, retractile mesenteritis, **147:**937
Ultrasound, cranium, peritrigonal echogenic blush on, **146:**1067
Ultrasound, extremities, distal, foreign bodies in, **147:**567
Ultrasound, gallbladder, gallstones, chest pain and normal coronary arteries, **146:**337
Ultrasound, genitourinary system, Leydig-cell tumors (a), **146:**177
Ultrasound, heart
atrial hemangioma, prenatal diagnosis, **147:**1207
laser Doppler velocimetry relations, simplified Bernoulli relations and (a), **147:**216
noninvasive pulsed Doppler echocardiographic detection, atrial septal defect (a), **146:**176
thoracic aortic aneurysms, **146:**309
ventricular shunt patency, **147:**353
Ultrasound, hip, ossification, infant, **147:**317
Ultrasound, intestines
Crohn disease, postsurgical recurrence of, **146:**523
real-time, measurement of gastric emptying (a), **147:**442
Ultrasound, kidney
American Burkitt lymphoma, **146:**549
calcium deposition, children, **146:**1253
choledocholithiasis (a), **147:**441
cystic disease, fetal, **146:**767
hypertrophied column of Bertin, **146:**53
urinary tract infection, differentiation of upper and lower, **146:**775
Ultrasound, liver
artery aneurysms, **147:**725
Budd-Chiari syndrome, **147:**9
cryosurgery, monitoring of, **147:**665
diffuse benign disease, **146:**1011
in vivo volume determination (a), **146:**177
Klatskin tumor, **147:**509
mesenchymal hamartomas, **147:**1035
metastases, interstitial radiation therapy, **147:**275
multiple bile-duct hamartomas, simulating malignant disease, **147:**279
quadrate lobe, pseudotumor in, **147:**923
regenerating nodules, cirrhosis, **146:**533
Ultrasound, lung, air bronchogram, **147:**593
Ultrasound, neck, masses, children, **146:**609
Ultrasound, pancreas
benign insulinoma, **147:**929
fat deposition in, **146:**1017
metoclopramide enhancement, **146:**341
Ultrasound, pediatric
omphalocele and gastroschisis, **147:**797
renal candidiasis, neonatal, **147:**801
Ultrasound, pelvis, hip disease, children (a), **146:**1105
Ultrasound, rectum, transrectal pelvic abscess drainage, **146:**1047
Ultrasound, shoulder
rotator cuff, **146:**555, **146:**561
rotator cuff and biceps tendon (a), **147:**648
torn rotator cuff (l), **147:**646
Ultrasound, spine
focal stenosis, disc disease and (a), **147:**443
intraoperative, spinal (a), **146:**887
Ultrasound, testicular, impalpable neoplasm, **146:**349
Ultrasound, transrectal
distal ureteral calculi, **147:**1189
prostatic lesions, **146:**1187
Ultrasound, umbilical, pseudoaneurysm, **147:**322
Umbilical artery
dystrophic calcification in, children (a), **146:**654

pseudoaneurysms, sonography, **147:**322
Urachus, carcinoma, abdominal case of day, **146:**1075
Uremia, terminal, ethanol renal ablation and, **146:**593
Ureter
distal, calculi, transrectal sonography, **147:**1189
polyps, congenital, **147:**1041
retrograde catheterization, via the ileal conduit, **146:**61
vesicoureteral reflux, excretory urography (l), **146:**647
Ureteral stent
antegrade insertion, universal introducer, **147:**830
placement, shearing percutaneous nephrostomy catheter during, **147:**832
Ureteropelvic disruption, children (a), **147:**218
Ureteropelvic junction, obstruction, abdominal pain (a), **146:**1103
Urinary tract
contrast sonography (a), **147:**649
upper and lower infection, sonography in differentiation of, **146:**775
Urography
excretory
distal ureteral calculi, **147:**1189
patients with prostatism, **147:**957
vesicoureteral reflux (l), **146:**647
renografin-60 for, **147:**839
routine, men with prostatism, **147:**960
Urokinase-lys-plasminogen, intraarterial infusion therapy, complications in arterial ischemia of lower limbs, **146:**157
Uterus, developmental abnormalities, **147:**1197

V

Vacuum phenomenon
hip joint fluid (a), **147:**218
intervertebral disk, **147:**83
Vagina, unilateral imperforate, uterine duplication and normal kidneys, **147:**1197
Vascular disease, noninvasive diagnostic techniques (b), **146:**30
Vascular grafts, infections, indium-111-labeled leukocyte detection of, **147:**173
Vascular malformations, angiographically occult, MRI imaging of, **146:**1223
Vasopressin, infusion, gastrointestinal hemorrhage, **146:**1031
Velocimetry, laser Doppler, ultrasound relations, heart (a), **147:**216
Velopharyngeal insufficiency, videofluoroscopy, **146:**15
Vena cava
hepatic venous drainage in, MRI, **147:**635
impending catheter perforation, radiographic recognition, **146:**487
inferior stent filter, **147:**1247
retrievable filter, pulmonary embolism, short-term prophylaxis of, **147:**836
superior
obstruction, digital subtraction venography, 685
obstruction, treatment by venous angioplasty, **147:**834
Venography
see also Angiography; specific vein; organ; region
lower-extremity, femoral vein compression and, **147:**1025
positive contrast, deep venous thrombosis of lower extremity, **146:**845
radionuclide, blood pool, **146:**1051
spermatic, male infertility and, **147:**97
Venography, digital subtraction, central venous obstruction and, **147:**685
Ventricular shunt, patency, assessment by sonography, **147:**353
Vesicoureteral reflux, *see* Ureter
Videofluoroscopy, velopharyngeal insufficiency, **146:**15
Viscera, hollow, suture anchor for drainage, **146:**160

W

Wexler, Howard Alan (m), **147:**1062
Wilms' tumor, *see* Kidney
Wrist
digital arthrography, **147:**563
midcarpal, arthrography (l), **146:**645

X

Xeroangiography, technique and application (a), **147:**864
X-rays, *see* Radiography

U.S. Postal Service

STATEMENT OF OWNERSHIP, MANAGEMENT AND CIRCULATION

Required by 39 U.S.C. 3685)

1A. TITLE OF PUBLICATION	1B. PUBLICATION NO.	2. DATE OF FILING
AJR - AMERICAN JOURNAL OF ROENTGENOLOGY	0 3 6 1 8 0 3 x	Oct. 1, 1986
3. FREQUENCY OF ISSUE	3A. NO. OF ISSUES PUBLISHED ANNUALLY	3B. ANNUAL SUBSCRIPTION PRICE
Monthly	12	$90.00

4. COMPLETE MAILING ADDRESS OF KNOWN OFFICE OF PUBLICATION *(Street, City, County, State and ZIP+4 Code) (Not printer)*

428 East Preston Street, Baltimore, Maryland 21202

5. COMPLETE MAILING ADDRESS OF THE HEADQUARTERS OF GENERAL BUSINESS OFFICES OF THE PUBLISHER *(Not printer)*

428 East Preston Street, Baltimore, Maryland 21202

6. FULL NAMES AND COMPLETE MAILING ADDRESS OF PUBLISHER, EDITOR, AND MANAGING EDITOR *(This item MUST NOT be blank)*

PUBLISHER *(Name and Complete Mailing Address)*

Williams & Wilkins, 428 E. Preston St., Baltimore, MD 21202

EDITOR *(Name and Complete Mailing Address)*

Robert N. Berk, M.D., Editor, 2223 Avenida de La Playa, Suite 200, La Jolla, CA 92037

MANAGING EDITOR *(Name and Complete Mailing Address)*

7. OWNER *(If owned by a corporation, its name and address must be stated and also immediately thereunder the names and addresses of stockholders owning or holding 1 percent or more of total amount of stock. If not owned by a corporation, the names and addresses of the individual owners must be given. If owned by a partnership or other unincorporated firm, its name and address, as well as that of each individual must be given. If the publication is published by a nonprofit organization, its name and address must be stated.) (Item must be completed.)*

FULL NAME	COMPLETE MAILING ADDRESS
American Roentgen Ray Society	1891 Preston White Drive Reston, VA 22091

8. KNOWN BONDHOLDERS, MORTGAGEES, AND OTHER SECURITY HOLDERS OWNING OR HOLDING 1 PERCENT OR MORE OF TOTAL AMOUNT OF BONDS, MORTGAGES OR OTHER SECURITIES *(If there are none, so state)*

FULL NAME	COMPLETE MAILING ADDRESS
NONE	

9. FOR COMPLETION BY NONPROFIT ORGANIZATIONS AUTHORIZED TO MAIL AT SPECIAL RATES *(Section 423.12 DMM only)*
The purpose, function, and nonprofit status of this organization and the exempt status for Federal income tax purposes *(Check one)*

[X] (1) HAS NOT CHANGED DURING PRECEDING 12 MONTHS
[ ] (2) HAS CHANGED DURING PRECEDING 12 MONTHS *(If changed, publisher must submit explanation of change with this statement.)*

10. EXTENT AND NATURE OF CIRCULATION *(See instructions on reverse side)*	AVERAGE NO. COPIES EACH ISSUE DURING PRECEDING 12 MONTHS	ACTUAL NO. COPIES OF SINGLE ISSUE PUBLISHED NEAREST TO FILING DATE
A. TOTAL NO. COPIES *(Net Press Run)*	22900	21406
B. PAID AND/OR REQUESTED CIRCULATION 1. Sales through dealers and carriers, street vendors and counter sales	See line 11 645	621
2. Mail Subscription *(Paid and/or requested)*	18400	18525
C. TOTAL PAID AND/OR REQUESTED CIRCULATION *(Sum of 10B1 and 10B2)*	19045	19146
D. FREE DISTRIBUTION BY MAIL, CARRIER OR OTHER MEANS SAMPLES, COMPLIMENTARY, AND OTHER FREE COPIES	250	260
E. TOTAL DISTRIBUTION *(Sum of C and D)*	19295	19406
F. COPIES NOT DISTRIBUTED 1. Office use, left over, unaccounted, spoiled after printing	3605	2000
2. Return from News Agents	NONE	NONE
G. TOTAL *(Sum of E, F1 and 2--should equal net press run shown in A)*	22900	21406

11. I certify that the statements made by me above are correct and complete

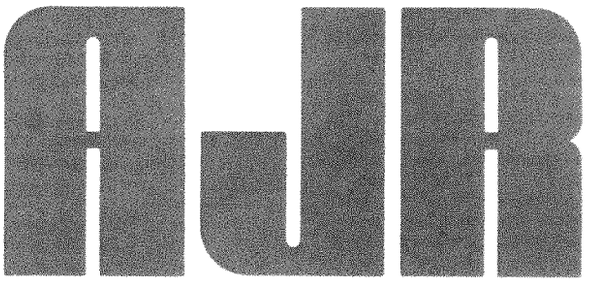
SIGNATURE AND TITLE OF EDITOR, PUBLISHER, BUSINESS MANAGER, OR OWNER
Publisher Alan J. Willis

Paid Subs. mailed Via Canada Post

PS Form 3526, Dec. 1985 *(See instruction on reverse)*

Volume 147

Official Journal of the American Roentgen Ray Society



American Journal of Roentgenology
Diagnostic Imaging and Related Sciences

Editor-In-Chief Robert N. Berk, *San Diego, California*

Editor Emeritus Melvin M. Figley, *Seattle, Washington*

Associate Editors Alan J. Davidson, *Washington, District of Columbia*
Saskia von Waldenburg Hilton, *San Diego, California*
Juan M. Taveras, *Boston, Massachusetts*

Assistant Editors William L. Ashburn, *San Diego, California*
Charles C. Berry, *San Diego, California*
William G. Bradley Jr., *Pasadena, California*
Edward Buonocore, *Knoxville, Tennessee*
Peter L. Cooperberg, *Vancouver, British Columbia*
Peter Doubilet, *Boston, Massachusetts*
N. Reed Dunnick, *Durham, North Carolina*
Ronald G. Evens, *St. Louis, Missouri*
Henry I. Goldberg, *San Francisco, California*
William R. Hendee, *Chicago, Illinois*
John R. Hesselink, *San Diego, California*
Charles B. Higgins, *San Francisco, California*
Helen C. Redman, *Dallas, Texas*
Donald L. Resnick, *San Diego, California*
Stewart R. Reuter, *San Antonio, Texas*
Stuart S. Sagel, *St. Louis, Missouri*
Edward A. Sickles, *San Francisco, California*
Eric vanSonnenberg, *San Diego, California*

Editorial Staff: Gita S. Braude, *managing editor*; Elizabeth A. Whalen, *senior editor*; Linda Wood and Barbara Rose, *manuscript editors*; Nancy Rydbeck, *administrative assistant*; Sandra Wood, *administrative secretary*; Christina Sollazzo, *secretary*.

All business correspondence, including display (not classified) advertising, subscriptions, address changes, reprints, and permission requests should be addressed to Williams & Wilkins, 428 East Preston Street, Baltimore, MD 21202. Correspondence regarding editorial matters and classified advertising should be addressed to the editorial office, AJR, 2223 Avenida de la Playa, Suite 200, La Jolla, CA 92037. For manuscript submission, see Guidelines for Authors, next page. Undelivered or damaged copies replaced within 60 days of publication; 90 days for foreign subscribers. Allow 90 days for address changes.

AJR AMERICAN JOURNAL OF ROENTGENOLOGY (ISSN 0361 803X) is published monthly by American Roentgen Ray Society, 428 E. Preston Street, Baltimore, MD 21202. Annual dues include $50 for journal subscription. Second class postage paid at Baltimore, MD and at additional mailing offices. Postmaster send address changes (Form 3579) to Williams & Wilkins, 428 East Preston St., Baltimore, MD 21202. Subscription rates $90 ($120 foreign); institutions $100 ($130 foreign); in training $25; single copy $16 ($19). Japanese Yen price is available from our sole agent USACO Corporation, 13-12, Shimbashi 1-Chome, Minato-Ku, Tokyo 105, Japan, telephone 03-502-6471. Airmail rates furnished on request. Indexed by *Current Contents* and *Index Medicus*.

Copyright © 1986 by American Roentgen Ray Society.

0361-803X/86$2.00

American Roentgen Ray Society:
Officers, Committees, and Meeting Information

Officers

President: Jerome F. Wiot
President- elect: Raymond A. Gagliardi
1st Vice-president: Lee F. Rogers
2nd Vice-president: Gerald D. Dodd
Secretary: Glen W. Hartman
Treasurer: Ronald G. Evens

Executive Council: E. Gedgaudas, J. F. Wiot, L. F. Rogers, R. A. Gagliardi, R. G. Evens, R. N. Berk, F. L. Angell, J. E. Madewell, M. P. Capp, G. W. Hartman, B. G. Brogdon, G. A. Kling, H. C. Carlson, A. K. Poznanski, A. E. James, Jr., J. A. Kirkpatrick, Jr., G. R. Leopold, G. D. Dodd, J. T. Ferrucci, Jr., R. H. Troupin, chairman

Committees 1986–1987

Editorial Policy: S. S. Sagel, W. J. Casarella, J. T. Ferrucci, Jr., N. C. Whitley, S. Hilton, A. J. Davidson, J. M. Taveras, R. N. Berk, M. P. Capp, chairman

Education and Research: C. E. Putman, A. R. Margulis, J. R. Thornbury, R. A. McLeod, J. T. Ferrucci, Jr., ex officio, B. G. Brogdon, chairman

Finance and Budget: B. P. Wood, L. R. James, J. A. Kirkpatrick, Jr., A. E. James, F. L. Angell, chairman

Instruction Courses: R. A. McLeod, associate chairman, J. T. Ferrucci, Jr., chairman

Program: J. Wiot, G. W. Hartman, J. A. Kirkpatrick, Jr., R. H. Troupin, M. P. Capp, J. E. Madewell, B. G. Brogdon, J. T. Ferrucci, Jr., G. A. Kling, G. G. Ghahremani, M. Viamonte, R. A. Gagliardi, chairman

Publications: W. J. Casarella, J. T. Ferrucci, Jr., S. S. Sagel, N. C. Whitley, M. P. Capp, chairman

Scientific Exhibits: S. G. Kirchner, A. V. Proto, S. M. Goldman, J. E. Madewell, chairman

Nominating: W. J. Casarella, H. C. Carlson, A. E. James, chairman.

Representatives to Other Organizations

American Board of Radiology: E. C. Klatte, R. W. McConnell, L. F. Rogers

American College of Radiology: J. L. Gwinn, G. A. Kling, G. W. Hartman, J. M. Dennis, E. J. Ferris, J. E. Madewell

American Medical Association House of Delegates: S. F. Ochsner, K. C. Krabbenhoft, alternate

American National Standards Institute: M. Haskin

National Council on Radiation Protection and Measurements: E. L. Saenger, H. L. Friedell

Meetings, Membership, Business Information

Annual Meetings: April 26–May 1, 1987, Fontainebleau-Hilton, Miami Beach; May 1–6, 1988, Westin Bonaventure, Los Angeles; May 7–13, 1989, Hilton, New Orleans.

Director Annual Meeting: George A. Kling, Harper Hospital, Detroit, MI 48201; (313) 494-8405.

ARRS Membership: Rosalind H. Troupin, Dept. of Radiology, Hospital of University of Pennsylvania, 3400 Spruce St., Philadelphia, PA 19104. The ARRS has two membership categories: active and in-training. For active membership, applicants must practice radiology in the U.S. or Canada. Each must have graduated in good standing from an approved medical school or hold an advanced degree in a physical, chemical, or biological science and be certified by the American Board of Radiology, the Royal College of Physicians and Surgeons of Canada, or otherwise adequately document training and credentials. A member-in-training must be in a radiology residency, a postresidency fellowship program, or a postgraduate student in an allied science. Status must be verified by the program director. For consideration during the 1987 ARRS meeting, completed applications must be received by Dr. Troupin no later than Feb. 1, 1987.

Business Office: Paul Fullagar, executive director, George J. O'Hop, controller, American Roentgen Ray Society, 1891 Preston White Dr., Reston, VA 22091; (703) 648-8900.

July 1986

SPECIAL ARTICLES

1 **Coronary thrombolytic therapy: state of the art.** *Marx M, Levin DC*
9 **The Budd-Chiari syndrome: a review.** *Murphy FB, Steinberg HV, Shires GT III, Martin LG, Bernardino ME*

THORACIC RADIOLOGY

17 **Pictorial essay. CT demonstration of calcified mediastinal lymph nodes: a guide to the new ATS classification.** *Glazer HS, Aronberg DJ, Sagel SS, Friedman PJ*
21 **Evaluation of a chest phantom for CT nodule densitometry.** *de Geer G, Gamsu G, Cann C, Webb WR*
26 **Commentary. The solitary pulmonary nodule: role of CT.** *Sagel SS*
29 **Spontaneous pneumothorax in AIDS patients with *Pneumocystis carinii* pneumonia.** *Goodman PC, Daley C, Minagi H*

CARDIOVASCULAR RADIOLOGY

33 **Gated cardiac MRI: ejection fraction determination using right anterior oblique view.** *Buckwalter KA, Aisen AM, Dilworth LR, Mancini GBJ, Buda AJ*
39 **Digital indirect portography.** *Sussman SK, Braun SD, Perlmutt LM, Newman GE, Dunnick NR*
45 **CT evaluation of Kimray-Greenfield filter complications.** *Miller CL, Wechsler RJ*
51 **Angiography in the in situ saphenous vein bypass.** *Dan SJ, Train JS, Mitty HA, Miller CM*

GASTROINTESTINAL RADIOLOGY

57 **CT after uncomplicated esophageal sclerotherapy.** *Mauro MA, Jaques PF, Swantkowski TM, Staab EV, Bozymski EM*
61 **Umbilicated adenomas in familial polyposis coli: radiologic and histologic correlation (case report).** *Smith HJ, Lee EL*
63 **Perspective: the small bowel examination in the diagnosis of Crohn's disease.** *Carlson HC*

SKELETAL RADIOLOGY

67 **Avascular necrosis of the hip: comparison of MR, CT, and scintigraphy.** *Mitchell MD, Kundel HL, Steinberg ME, Kressel HY, Alavi A, Axel L*
72 **Pictorial essay. CT of the sternum.** *Stark P, Jaramillo D*
79 **MRI of tuberculous spondylitis.** *de Roos A, van Persijn van Meerten EL, Bloem JL, Bluemm RG*
83 **Intraosseous and intradiscal gas in association with spinal infection: report of three cases.** *Bielecki DK, Sartoris D, Resnick D, Van Lom K, Fierer J, Haghighi P*
87 **Chronic recurrent multifocal osteomyelitis (case report).** *Wiener MD, Newbold RG, Merten DF*

GENITOURINARY RADIOLOGY

89 **Impact of extracorporeal shock wave lithotripsy on percutaneous stone procedures.** *Bush WH, Gibbons RP, Lewis GP, Brannen GE*
94 **Commentary. Extracorporeal shock wave lithotripsy and the radiologist.** *Pollack HM, Banner MP*
97 **Management of male infertility: roles of contact thermography, spermatic venography, and embolization.** *Pochaczevsky R, Lee WJ, Mallett E*

NEURORADIOLOGY

103 **MRI of brain iron.** *Drayer B, Burger P, Darwin R, Riederer S, Herfkens R, Johnson GA*
111 **Organized intracerebral hematoma with acute hemorrhage: CT patterns and pathologic correlations.** *Lee Y-Y, Moser R, Brunner JM, Van Tassel P*
119 **MRI of radiation injury to the brain.** *Curnes JT, Laster DW, Ball MR, Moody DM, Witcofski RL*
125 **MRI of the chronically injured cervical spinal cord.** *Quencer RM, Sheldon JJ, Post MJD, Diaz RD, Montalvo BM, Green BA, Eismont FJ*
133 **Sonography of the neonatal craniocervical junction.** *Cramer BC, Joguier S, O'Gorman AM*
141 **Benign schwannomas: pathologic basis for CT inhomogeneities.** *Cohen LM, Schwartz AM, Rockoff SD*
145 **Pictorial essay. The normal nasopharyngogram.** *Khoo FY, Kanagasuntheram R, Chia KB, Lee WS, Teo AT, Ng HW*

INTERVENTIONAL RADIOLOGY

149 **The carcinoid syndrome: palliation by hepatic artery embolization.** *Carrasco CH, Charnsangavej C, Ajani J, Samaan NA, Richli W, Wallace S*
155 **Fine needle aspiration biopsy: the role of immediate cytologic assessment.** *Miller DA, Carrasco CH, Katz RL, Cramer FM, Wallace S, Charnsangavej C*
159 **Percutaneous biliary drainage in diffuse Caroli's disease (case report).** *Rose SC, Kumpe DA, Weil R III*
161 **Thrombosed synthetic hemodialysis access fistulas: the success of combined thrombectomy and angioplasty (technical note).** *Smith TP, Hunter DW, Darcy MD, Castaneda-Zuniga WR, Amplatz K*
164 **Insertion of a large-caliber biliary endoprosthesis via the T-tube tract (technical note).** *Sammon JK, Teplick SK, Haskin PH*

NUCLEAR MEDICINE

167 **Indium-granulocyte scanning in the painful prosthetic joint.** *Pring DJ, Henderson RG, Keshavarzian A, Rivett AG, Krausz T, Coombs RRH, Lavender JP*
173 **111 In-labeled leukocytes in the detection of prosthetic vascular graft infections.** *Williamson MR, Boyd CM, Read RC, Thompson BW, Barnes RW, Shah HR, Balachandran S, Ferris EJ*
177 **Evaluation of peritoneovenous shunt patency by intraperitoneal Tc-99m macroaggregate albumin: clinical experience.** *Stewart CA, Sakimura IT, Applebaum DM, Siegel ME*
181 **Radiocolloid scintigraphy in Felty's syndrome.** *Shih W-J, Domstad PA, Li C-Y, DeLand FH, Maruyama Y*

CONTRAST MEDIA

185 **Comparison of patient responses to high- and low-osmolality contrast agents injected intravenously.** *Bagg MNJ, Horwitz TA, Bester L*
188 **Pancreatic mumps: a transient reaction to IV contrast media (case report).** *St Amour TE, McClennan BL, Glazer HS*

BREAST RADIOLOGY

191 **Comparison of mammography and transillumination light scanning in the detection of breast lesions.** *Gisvold JJ, Brown LR, Swee RG, Raygor DJ, Dickerson N, Ranfranz MK*
195 **Editorial. Screening mammography.** *Hall FM*

MRI

199 **MRI simulator for instruction in pulse-sequence selection.** *Lufkin RB, Keen R, Rhodes M, Quinn J, Glenn W, Hanafee W*

COMPUTER PAGE

203 **Computer-assisted scheduling of radiologists.** *Reinus WR, Totty WG*

OTHER CONTENT

205 **Editorials. Classification of non-Hodgkin's lymphoma.** *Wang Y;* **Language of certainty.** *Daves ML*
211 **ARRS 1987 meeting summary, calls for papers and exhibits**
216 **Letters**
217 **Abstracts**
220 **News**
223 **Classified ads**
Book reviews 32, 38, 44, 66, 78, 140, 144, 166, 184
Memorials 16, 28
A2 **Guidelines for authors**
A8 **ARRS information**

August 1986

CHEST RADIOLOGY

227 **Nonlymphomatous lymphoid disorders of the lung.** *Glickstein M, Kornstein MJ, Pietra GG, et al*
239 **MRI of the normal pericardium.** *Sechtem U, Tscholakoff D, Higgins CB*
245 **MRI of the abnormal pericardium.** *Sechtem U, Tscholakoff D, Higgins CB*
253 **MRI of perivalvular infectious pseudoaneurysms.** *Winkler ML, Higgins CB*

ABDOMINAL RADIOLOGY

257 **Efficacy of radiologic studies in the detection of Barrett's esophagus.** *Chernin MM, Amberg JR, Kogan FJ, Morgan TR, Sampliner RE*
261 **Radiographic and endoscopic sensitivity in detecting lower esophageal mucosal ring.** *Ott DJ, Chen YM, Wu WC, Gelfand DW, Munitz HA*
266 **An alternative technique for double-contrast esophagography (technical note).** *Tash RR, Weingarten M, Geller M*
268 **Retractile mesenteritis involving the colon: pathologic and radiologic correlation (case report).** *Han SY, Koehler RE, Keller FS, Ho K-J, Zornes SL*
271 **Small-bowel diverticulitis: CT findings.** *Greenstein S, Jones B, Fishman EK, Cameron JL, Siegelman SS*
275 **Interstitial radiation therapy for hepatic metastases: sonographic guidance for applicator placement.** *Dritschilo A, Grant EG, Harter KW, Holt RW, Rustgi SN, Rodgers JE*
279 **CT and sonography of multiple bile duct hamartomas simulating malignant liver disease (case report).** *Eisenberg D, Hurwitz L, Yu AC*
281 **Pancreatic pseudomass caused by the second portion of the duodenum: a pitfall during water-aided sonography (technical note).** *Op den Orth JO*

GENITOURINARY RADIOLOGY

283 **Morphologic and functional changes of the kidney after percutaneous nephrosto-lithotomy.** *Schiff RG, Lee WJ, Eshghi M, Moskowitz GW, Levy LM, Smith AD*
287 **Scrotal cystocele with bladder calculi (case report).** *Postma MP, Smith R*
289 **Functional adrenal disease: radiologic evaluation in a patient with anomalous kidneys (case report).** *Kenney PJ, Keller FS, Koehler RE*
291 **MRI of puerperal ovarian vein thrombosis (case report).** *Martin B, Mulopulos GP, Bryan PJ*

SKELETAL RADIOLOGY

293 **1.5-T surface-coil MRI of the knee.** *Burk DL Jr., Kanal E, Brunberg JA, Johnstone GF, Swensen HE, Wolf GL*
301 **Incomplete carpal coalition.** *Resnick CS, Grizzard JD, Simmons BP, Yaghmai I*
305 **Radiologic contributions to cancer management. Bone metastases.** *Kagan AR, Bassett LW, Steckel RJ, Gold RH*

PEDIATRIC RADIOLOGY

313 **The coexistence of congenital megacalyces and primary megaureter.** *Vargas B, Lebowitz RL*
317 **Ossification center of the infant hip: sonographic and radiographic correlation.** *Harcke HT, Lee MS, Sinning L, Clarke NMP, Borns PF, MacEwen GD*
322 **Neonatal umbilical artery pseudoaneurysm: sonographic evaluation (case report).** *Katz ME, Perlman JM, Tack ED, McAlister WH*
325 **CT peritoneography in evaluation of pediatric dialysis complications.** *Magill HL, Roy S III, Stapleton FB*
329 **Esophageal atresia and hypertrophic pyloric stenosis: sequential coexistence of disease (case report).** *Magilner AD*

NEURORADIOLOGY

331 **Foci of MRI signal (pseudo lesions) anterior to the frontal horns: histologic correlations of a normal**
339 **MRI in infants and children with spinal dysraphism.** *Barnes PD, Lester PD, Yamanashi WS, Prince JR*
347 **Microbubbles as a contrast agent for neurosonography and ultrasound-guided catheter manipulation: in vitro studies.** *Widder DJ, Simeone JF*
353 **Assessment of ventricular shunt patency by sonography: a new noninvasive test.** *Widder DJ, Davis KR, Taveras JM*

MAGNETIC RESONANCE

357 **Dynamic spin-echo MRI of liver cancer using gadolinium-DTPA: animal investigation.** *Saini S, Stark DD, Brady TJ, Wittenberg J, Ferrucci JT Jr*
363 **Multiple-angle variable-interval nonorthogonal MRI.** *Reicher MA, Lufkin RB, Smith S, et al.*
367 **Optimal pulsing sequences for MR contrast agents.** *Wolf GL, Joseph PM, Goldstein EJ*
373 **Technical considerations for the use of surface coils in MRI.** *Kulkarni MV, Patton JA, Price RR*
379 **Dynamic-range compression in surface-coil MRI.** *Lufkin RB, Sharpless T, Flannigan B, Hanafee W*

VASCULAR RADIOLOGY

383 **Coagulation of aneurysms by direct percutaneous thrombin injection.** *Cope C, Zeit R*
389 **Treatment of angioplasty-related iliac artery rupture without bypass surgery (case report).** *Villarica J, Gross RC*
391 **Apparent arterial occlusion due to pneumatic antishock garment: pitfall in trauma angiography (case report).** *Morse SS, Strauss EB, Sumpio BE*

INTERVENTIONAL RADIOLOGY

393 **Intercostal-space nephrostomy for percutaneous stone removal.** *Picus D, Weyman PJ, Clayman RV, McClennan BL*
399 **Fine needle aspiration biopsy: pancreatic and biliary tumors.** *Hall-Craggs MA, Lees WR*
404 **Biliary endoprosthesis blockage: clearance using a 22-gauge needle (technical note).** *Gibson RN*
406 **Digital-scout-radiograph–assisted percutaneous abscess drainage (technical note).** *Wing VW, Jeffrey RB, Hightower DR, Federle MP*

COMMENTARY

409 **Pelvimetry revisited.** *Johnson GC*
411 **Response.** *Filly RA, Parer JT, Stark DD*

EDITORIALS

412 **Physician investment in free-standing imaging centers. In opposition.** *Baum S.* **In defense.** *Zeman RK, Elliott LP*

ARRS NEWS

417 **ARRS presidential address. Radiology, it's not the same!** *Wiot JF*
420 **1986 ARRS awards for distinguished service to radiology.** *Wiot JF*
422 **ARRS secretary's report.** *Gagliardi R*
426 **ARRS award-winning scientific exhibits, 1986**
428 **ARRS new members**
430 **ARRS membership invitation and application**
433 **ARRS 1987 meeting summary and call for papers and exhibits**

OTHER CONTENT

388 **Forthcoming articles**
438 **Letters**
440 **Abstracts**
445 **News**
450 **Classified ads**
Book reviews 238, 270, 338, 372, 398, 408, 411
446 **Editorial office address change**

September 1986

SPECIAL ARTICLE

453 **The status of MRI in 1986: rates of adoption in the United States and worldwide.** *Steinberg EP*

THORACIC RADIOLOGY

457 **Segmental bronchovascular anatomy of the lower lobes: CT analysis.** *Jardin M, Remy J*

469 **Mediastinal lymph node detection and sizing at CT and autopsy.** *Quint LE, Glazer GM, Orringer MB, Francis IR, Bookstein FL*

473 **Radiologic contributions to cancer management. Lung metastases.** *Kagan AR, Steckel RJ*

477 **Case report. Calcified ascending aorta after radiation therapy.** *Coblentz C, Martin L, Tuttle R*

BREAST RADIOLOGY

479 **Real-time breast sonography: application in 300 consecutive patients.** *Hilton SvW, Leopold GR, Olson LK, Willson SA*

487 **Editorial. The dense mammogram.** *Page DL, Winfield AC*

491 **Stationary and moving mammography grids: comparative radiation dose.** *Dershaw DD, Malik S*

ENDOCRINE RADIOLOGY

493 **MRI of indeterminate adrenal masses.** *Reinig JW, Doppman JL, Dwyer AJ, Frank J*

497 **MRI with surface coils for parathyroid tumors: preliminary investigation.** *Kier R, Herfkens RJ, Blinder RA, Leight GS, Utz JA, Silverman PM*

ABDOMINAL RADIOLOGY

501 **Plain film evaluation of patients with abdominal pain: are three radiographs necessary?** *Mirvis SE, Young JWR, Keramati B, McCrea ES, Tarr R*

505 **The V-shaped artifact of the gallbladder wall: a sonographic sign of chronic disease.** *Lafortune M, Gariépy G, Dumont A, Breton G, Lapointe R*

509 **Sonographic diagnosis of Klatskin tumors.** *Machan L, Müller NL, Cooperberg PL*

513 **Cholangiocarcinoma as a late complication of choledochoenteric anastomoses.** *Herba MJ, Casola G, Bret PM, Lough J, Hampson LG*

516 **Case report. Cholangiocarcinoma in the choledochal cyst: preoperative diagnosis.** *Montana MA, Rohrmann CA*

519 **CT appearance of impaired lymphatic drainage in liver transplants.** *Marincek B, Barbier PA, Becker CD, Mettler D, Ruchti C*

525 **Angiography of small hepatocellular carcinomas: analysis of 105 resected tumors.** *Takayasu K, Shima Y, Muramatsu Y, et al.*

531 **Accuracy of angiography in the diagnosis of small hepatocellular carcinoma.** *Sumida M, Ohto M, Ebara M, Kimura K, Okuda K, Hirooka N*

537 **Nonparasitic splenic cysts: a report of 52 cases with radiologic-pathologic correlation.** *Dachman AH, Ros PR, Murari PJ, Olmsted WW, Lichtenstein JE*

543 **Technical note. A new needle for puncture biopsy.** *Qin D*

MUSCULOSKELETAL RADIOLOGY

545 **Perspective. Three-dimensional imaging of the musculoskeletal system.** *Pate D, Resnick D, Andre M, et al.*

553 **Case report. MRI in stress fracture.** *Stafford SA, Rosenthal DI, Gebhardt MC, Brady TJ, Scott JA*

557 **The shoulder impingement syndrome: prevalence of radiographic findings and correlation with response to therapy.** *Hardy DC, Vogler JB III, White RH*

563 **Digital wrist arthrography: precision in determining the site of radiocarpal-midcarpal communication.** *Manaster BJ*

567 **Sonographic diagnosis of foreign bodies of the distal extremities.** *Fornage BD, Schernberg FL*

NEURORADIOLOGY

571 **Multiple sclerosis: MRI and clinical correlation.** *Edwards MK, Farlow MR, Stevens JC*

575 **The radiographic characterization of burst fractures of the spine.** *Atlas SW, Regenbogen V, Rogers LF, Kim KS*

583 **CT of extraarachnoid metrizamide instillation.** *Dake MD, Dillon WP, Dorwart RH*

587 **CT evaluation of effects of cranial radiation therapy in children.** *Davis PC, Hoffman JC Jr, Pearl GS, Braun IF*

FETAL AND PEDIATRIC RADIOLOGY

593 **The air bronchogram: sonographic demonstration.** *Weinberg B, Diakoumakis EE, Kass EG, Seife B, Zvi ZB*

596 **Case report. Ischemic hepatic necrosis: a cause of fetal liver calcification.** *Nguyen DL, Leonard JC*

598 **Case report. Cutaneous and visceral hemangiomata in the Klippel-Trenaunay-Weber syndrome: antenatal sonographic detection.** *Lewis BD, Doubilet PM, Heller VL, Bierre A, Bieber FR*

NUCLEAR MEDICINE

601 **Diagnostic value of lung uptake of indium-III oxine-labeled white blood cells.** *Segall GM, McDougall IR*

607 **Gallium scintigraphy in the detection of amiodarone lung toxicity.** *Moinuddin M, Rockett J*

610 **Case report. Demonstration of a cold abscess by gallium-67 imaging in a patient with Job syndrome.** *Jaramillo D, Kim EE*

VASCULAR RADIOLOGY

613 **IV and intraarterial hybrid DSA: clinical evaluation.** *Foley WD, Beres J, Smith DF, Bell RM, Milde MW, Lipchik EO*

621 **Thrombolysis of occluded femoropopliteal grafts.** *Gardiner GA Jr, Koltun W, Kandarpa K, et al.*

627 **Histologic analysis of tissue response to bucrylate-pantopaque mixture.** *Cromwell LD, Freeny PC, Kerber CW, Kunz LL, Harris AB, Shaw CM*

632 **Technical note. Guided direct antegrade puncture of the superficial femoral artery.** *Berman HL, Katz SG, Tihansky DP*

635 **Case report. Unusual hepatic venous drainage in inferior vena cava obstruction: demonstration by MRI.** *Guinet C, Mathieu D, Métreau J-M, Dhumeaux D, Vasile N*

RADIOLOGY PRACTICE

637 **Radiology consultation: its application to an acute care surgical ward.** *Baker SR, Stein HD*

COMPUTER PAGE

641 **Computerized reference management: searching the literature.** *Gurney JW, Wigton RS*

OTHER CONTENT

456 **ARRS Meeting, 1987**
503 **Erratum**
518 **Forthcoming articles**
529 **Call for papers**
646 **Letters**
648 **Abstracts**
651 **News**
654 **Classified ads**
Book reviews 490, 504, 524, 530, 544, 552, 562, 570
A2 **Guidelines for authors**
A22 **American Roentgen Ray Society information**

October 1986

SPECIAL ARTICLE

657 **Vascular complications after liver transplantation: a 5-year experience.** *Wozney P, Zajko AB, Bron KM, Point S, Starzl TE*

ROSCOE E. MILLER AWARD, SOCIETY OF GASTROINTESTINAL RADIOLOGY

665 **Monitoring hepatic cryosurgery with sonography.** *Onik G, Kane R, Steele G, et al.*

PULMONARY RADIOLOGY

670 **Case report. Mosaic oligemia simulating pulmonary infiltrates on CT.** *Martin KW, Sagel SS, Siegel BA*

674 **Pictorial essay. Thoracic venous anatomy.** *Godwin JD, Chen JTT*

685 **Digital subtraction venography in central venous obstruction.** *Benenati JF, Becker GJ, Mail JT, Holden RW*

BREAST RADIOLOGY

689 **Screening mammography: referral practices of Los Angeles physicians.** *Bassett LW, Bunnell DH, Cerny JA, Gold RH*

GASTROINTESTINAL RADIOLOGY

693 **Radiologic and manometric correlation in "nutcracker esophagus."** *Ott DJ, Richter JE, Wu WC, Chen YM, Gelfand DW, Castell DO*

697 **Radiographic efficacy in gastric ulcer: comparison of single-contrast and multiphasic examinations.** *Ott DJ, Chen YM, Gelfand DW, Wu WC*

701 **Radiologic findings of linear gastric erosions.** *Momoshima S, Imai Y, Sugino Y, Sekine Y, Kumakura K*

705 **CT of appendicitis.** *Balthazar EJ, Megibow AJ, Hulnick D, Gordon RB, Naidich DP, Beranbaum ER*

711 **Hepatic hemangioma: dynamic bolus CT.** *Freeny PC, Marks WM*

721 **Chronic acalculous gallbladder disease: multiimaging evaluation with clinical-pathologic correlation.** *Raptopoulos V, Compton CC, Doherty P, et al.*

725 **Sonography in the diagnosis of hepatic artery aneurysms.** *Athey PA, Sax SL, Lamki N, Cadavid G*

729 **Bile-duct dilatation after laparotomy: a potential effect of intestinal hypomotility.** *Raptopoulos V, Smith EH, Cummings T, Silva W, Karellas A*

GENITOURINARY RADIOLOGY

732 **Review article. MRI of the bladder and prostate.** *Lee JKT, Rholl KS*

737 **Case report. Reversible renal fibromuscular dysplasia.** *Nemcek AA Sr, Holmburg CE*

MUSCULOSKELETAL RADIOLOGY

739 **Case report. Intraosseous glomus tumor: report of a case and review of the literature.** *Bjorkengren AG, Resnick D, Haghighi P, Sartoris DJ*

742 **Case report. Calcific tendinitis of the longus coli: diagnosis by CT.** *Hall FM, Docken WP, Curtis HW*

744 **Case report. Inferior lumbar (Petit's) hernia.** *Lawdahl RB, Moss CN, Van Dyke JA*

NEURORADIOLOGY

747 **Primary central nervous system lymphoma: CT and pathologic correlation.** *Lee Y-Y, Bruner JM, Van Tassel P, Libshitz HI*

753 **Minimal asymmetry of the brain: a normal variant.** *Shapiro R, Galloway SJ, Shapiro MD*

757 **Lumbar herniated disk disease and canal stenosis: prospective evaluation by surface coil MR, CT, and myelography.** *Modic MT, Masaryk T, Boumphrey F, Goormastic M, Bell G*

767 **Cystic necrosis of the spinal cord in compressive cervical myelopathy: demonstration by iopamidol CT-myelography.** *Jinkins JR, Bashir R, Al-Mefty O, Al-Kawi MZ, Fox JL*

777 **Cognitive and affective changes after myelography: a comparison of metrizamide and iohexol.** *Ratcliff G, Sandler S, Latchaw R*

782 **Technical note. The anatomic basis of the pseudotumor of the nasal cavity.** *Sistrom CL, Keats TE, Johnson CM III*

PEDIATRIC RADIOLOGY

785 **Imaging the pediatric liver: MRI and CT.** *Weinreb JC, Cohen JM, Armstrong E, Smith T*

791 **Interventional genitourinary radiology in children: a review of 61 procedures.** *Ball WS Jr, Towbin R, Strife JL, Spencer R*

797 **Fetal omphalocele and gastroschisis: pitfalls in sonographic diagnosis.** *Lindfors KK, McGahan JP, Walter JP*

801 **Neonatal renal candidiasis: sonographic diagnosis.** *Kintanar C, Cramer BC, Reid WD, Andrews WL*

806 **Case report. Enterocyst formation: a late complication of neonatal necrotizing enterocolitis.** *Ball TI, Wyly JB*

NUCLEAR MEDICINE

809 **Effect of chronicity of infection on the sensitivity of the In-III labeled leukocyte scan.** *Datz FL, Thorne DA*

813 **Case report. Utility of In-III labeled leukocyte imaging in acute acalculous cholecystitis.** *Datz FL*

815 **Technetium-99m pyrophosphate imaging in acute renal failure associated with nontraumatic rhabdomyolysis.** *Patel R, Mishkin FS*

819 **Case report. False-positive thallium-201 parathyroid scan of the mediastinum in Hodgkin's lymphoma.** *Winzelberg GG, Melada GA, Hydovitz JD*

INTERVENTIONAL RADIOLOGY

822 **Technical note. Percutaneous gastrostomy for jejunal feeding: a new technique.** *Alzate GD, Coons HG, Elliott J, Carey PH*

826 **Case report. Percutaneous gastrostomy: applications in gastric carcinoma and gastroplasty stoma dilatation.** *Wills JS*

828 **Technical note. A modified Cope introducer set for rapid insertion of a safety wire.** *Jeffrey RB Jr*

830 **Technical note. The universal stent introducer: a simplified approach to antegrade ureteral stent insertion.** *Lee WJ, Rich M*

832 **Case report. Shearing of percutaneous nephrostomy catheter during indwelling ureteral stent placement.** *Sussman SK, Oke EJ, Perlmutt LM, Dunnick NR*

834 **Case report. Successful treatment of superior vena cava syndrome by venous angioplasty.** *Sherry CS, Diamond NG, Meyers TP, Martin RL*

836 **Case report. Short-term prophylaxis of pulmonary embolism by using a retrievable vena cava filter.** *Darcy MD, Smith TP, Hunter DW, Castaneda-Zuniga W, Lund G, Amplatz K*

MISCELLANEOUS

839 **Renografin-60 for urography: effect on serum, electrolytes and proteins in adults.** *Olutola PS, Hutton L, Karlik S, Henderson AR*

843 **MRI of the spleen: normal appearance and findings in sickle-cell anemia.** *Adler DD, Glazer GM, Aisen AM*

846 **Case report. Extramedullary hematopoeisis in acute lymphocytic leukemia masquerading as hepatic, renal, and splenic microabscesses.** *Kopecky KK, Moriarty AT, Antony AC, Baker MK*

848 **Technical note. The value of a worksheet in reporting body-CT examinations.** *Kinard RE, Orrison WW, Brogdon BG*

HISTORY OF RADIOLOGY

850 **Early American radiology: the pioneer years.** *DiSantis DJ*

COMMENTARY

854 **Should we X-ray Halloween candy?** *Calvanese J*

EDITORIAL

856 **The diffusion of MRI in the United States: what is fact and what is speculation.** *Evens RG*

OTHER CONTENT

664 **ARRS 1987 meeting**
704 **Forthcoming articles**
784 **Memorial**
858 **Letters**
863 **Abstracts**
865 **Society for Pediatric Radiology Abstracts**
874 **News**
877 **Classified ads**
Book reviews 696, 720, 728, 766, 776
A2 **Guidelines for authors**
A20 **American Roentgen Ray Society information**

November 1986

SPECIAL ARTICLES

881 **Caldwell lecture. Armchair research and the practicing radiologist.** *Felson B*

891 **ARRS Executive Council Award paper. MR imaging of the lumbar spine: anatomic correlations and the effects of technical variations.** *Reicher MA, Gold RH, Halbach VV, Rauschning W, Wilson GH, Lufkin RB*

CARDIOPULMONARY RADIOLOGY

899 **Radiographic manifestations of bronchiolitis obliterans with organizing pneumonia vs usual interstitial pneumonia.** *Chandler PW, Shin MS, Friedman SE, Myers JL, Katzenstein A*

907 **CT of esophageal-pleural fistulae.** *Wechsler RJ*

911 **Postoperative recurrence of lung cancer: detection by whole-body gallium scintigraphy.** *Hatfield MK, MacMahon H, Ryan JW, et al.*

916 **Technical note. Cine-CT technique for evaluation of left ventricular function during supine exercise.** *Rees MR, MacMillan RM, Fender B, Clark DL*

GASTROINTESTINAL RADIOLOGY

919 **Pharyngeal Kaposi's sarcoma in patients with AIDS.** *Emery CD, Wall SD, Federle MP, Sooy CD*

923 **Pseudotumor of the quadrate lobe in hepatic sonography: a sign of generalized fatty infiltration.** *Sauerbrei EE, Lopez M*

929 **Benign pancreatic insulinoma: preoperative and intraoperative sonographic localization.** *Gorman B, Charboneau JW, James EM, et al.*

935 **Case report. Spontaneous rupture of a pancreatic pseudocyst into the portal venous system.** *Takayama T, Kato K, Sano H, Katada N, Takeichi M*

937 **Retractile mesenteritis involving the colon: barium enema, sonographic, and CT findings.** *Pérez-Fontán FJ, Soler R, Sanchez J, Iglesias P, Sanjurjo P, Ruiz J*

941 **Case report. CT diagnosis of primary small-bowel volvulus.** *Jaramillo D, Raval B*

SKELETAL RADIOLOGY

943 **Gaucher's disease type 1: assessment of bone involvement by CT and scintigraphy.** *Hermann G, Goldblatt J, Levy R, Goldsmith S, Desnick R, Grabowski G*

GENITOURINARY RADIOLOGY

949 **MR imaging of renal transplants.** *Baumgartner BR, Nelson RC, Ball TI, et al.*

954 **Commentary. Differential diagnosis of renal transplant rejection: is MR imaging the answer?** *Halasz NA*

957 **Excretory urography in patients with prostatism.** *Bundrick TJ, Katz PG*

960 **Commentary. Routine urography in men with prostatism.** *Talner LB*

NEURORADIOLOGY

963 **CT changes in dementing diseases: review.** *LeMay M*

977 **Neuroradiologic findings in AIDS: a review of 200 cases.** *Levy RM, Rosenbloom S, Perrett LV*

985 **MR and CT of occult vascular malformations of the brain.** *New PFJ, Ojemann RG, Davis KR, et al.*

995 **Penetrating vascular injuries of the face and neck: clinical and angiographic correlation.** *North CM, Ahmadi J, Segall HD, Zee C-S*

1000 **Editorial. Angiography in penetrating neck injuries.** *Quencer RM*

INTERVENTIONAL RADIOLOGY

1002 **UCSF interventional radiology rounds. Interventional radiologic management of sclerosing cholangitis.** *Kerlan RK Jr, LaBerge JM, Goldberg HI, Pogany AC, Ring EJ*

1007 **Percutaneous aspiration and drainage of pancreatic pseudocysts.** *Torres WE, Evert MB, Baumgartner BR, Bernardino ME*

1010 **Technical note. Basket extraction of esophageal foreign bodies.** *Shaffer HA Jr, Alford BA, de Lange EE, Meyer GA, McIlhenny J*

1014 **Technical note. Effect of suction on biopsy sample size.** *Hueftle MG, Haaga JR*

1017 **Technical note. A method for retrieval of retained subcutaneous catheter fragments.** *Sibbitt RR, Palmaz JC, Garcia F*

1019 **Case report. Small-bowel obstruction due to an intestinal balloon: treatment by percutaneous needle puncture.** *Sato Y, Frey E, Foderaro A, Pringle KC*

ANGIOGRAPHY

1021 **A comparison of techniques for improved visualization of the arteries of the distal lower extremity.** *Cohen MI, Vogelzang RL*

1025 **Technical note. Lower-extremity venography: value of femoral-vein compression.** *Smith TP, Cardella JF, Darcy MD, Hunter DW, Castaneda-Zuniga WR, Amplatz K*

PEDIATRIC RADIOLOGY

1027 **MR evaluation of the portal vein in pediatric liver transplant candidates.** *Day DL, Letourneau JG, Allan BT, Ascher NL, Lund G*

1031 **Pediatric hypertrophic gastropathy.** *Marks MP, Lanza MV, Kahlstrom EJ, Mikity V, Marks SC, Kvalstad RP*

1035 **Mesenchymal hamartomas of the liver in childhood: sonographic and CT findings.** *Stanley P, Hall TR, Woolley MM, Diament MJ, Gilsanz V, Miller JH*

1041 **Case report. Congenital urethral polyp.** *Caro PA, Rosenberg HK, Snyder HM III*

OBSTETRIC AND FETAL SONOGRAPHY

1043 **Sonographic findings in abdominal pregnancy.** *Stanley JH, Horger EO III, Fagan CJ, Andriole JG, Fleischer AC*

1047 **Fetal omphalocele and gastroschisis: a review of 24 cases.** *Bair JH, Russ PD, Pretorius DH, Manchester D, Manco-Johnson ML*

MR

1052 **Technical note. A technique for image salvage in MR.** *Lund G, Morin R*

RADIOLOGIC LITERATURE

1055 **The scientific literature in diagnostic radiology for American readers: a survey and analysis of journals, papers, and authors.** *Chew FS*

MISCELLANEOUS

1063 **The fibromatoses: CT-pathologic correlation.** *Francis IR, Dorovini-Zis K, Glazer GM, Lloyd RV, Amendola MA, Martel W*

1067 **CT of fibrous tissues and tumors with sonographic correlation.** *Rubenstein WA, Gray G, Auh YH, et al.*

COMPUTER PAGE

1075 **Some applications for a personal computer data-base system in radiology.** *Sommer FG*

OPINION

1078 **Should radiologists perform endoscopy?** *Shorvon P, Stevenson G*

OTHER CONTENT

910 **American Roentgen Ray Society Officers and Information**

928 **ARRS meeting information**

956 **Forthcoming articles**

1062 **Memorial**

1082 **Society of Uroradiology abstracts**

1089 **Letters**

1096 **Erratum**

1097 **News**

1101 **Classified ads**

Book reviews 962, 976, 984, 994, 1040

A2 **Guidelines for authors**

December 1986

SPECIAL ARTICLES

1103 **Leo J. Rigler lecture. MR imaging of the liver.** *Ferrucci JT*

1117 **Cannon lecture. The impact of radiology on hepatology.** *Sherlock S, Dick R*

CARDIOVASCULAR RADIOLOGY

1123 **Aortic dissection: a statistical analysis of the usefulness of plain chest radiographic findings.** *Jagannath AS, Sos TA, Lockhart SH, Saddekni S, Sniderman KW*

1127 **MR imaging of the central pulmonary arterial tree in conotruncal malformation.** *Formanek AG, Witcofski RL, D'Souza VJ, Link KM, Karstaedt N*

1133 **MR imaging of pulmonary emboli: an experimental study in dogs.** *Stein MG, Crues JV III, Bradley WG Jr, et al.*

1139 **New cineradiographic methods for assessment of Bjork-Shiley valve integrity.** *Cousin AJ, Soto B*

CHEST

1145 **Rebound thymic hyperplasia after treatment of Cushing's syndrome.** *Doppman JL, Oldfield EH, Chrousos GP, et al.*

BREAST RADIOLOGY

1149 **Baseline screening mammography: one vs two views per breast.** *Sickles EA, Weber WN, Galvin HB, Ominsky SH, Sollitto RA*

GASTROINTESTINAL RADIOLOGY

1155 **Pictorial essay. The retroperitoneal spaces revisited.** *Dodds WJ, Darweesh RMA, Lawson TL, et al.*

1162 **Commentary. Extraperitoneal spaces.** *Rubenstein WA, Whalen JP*

1165 **Esophageal intramural pseudodiverticulosis: a reevaluation.** *Levine MS, Moolten DN, Herlinger H, Laufer I*

1171 **The diagnosis of acute acalculous cholecystitis: a comparison of sonography, scintigraphy, and CT.** *Mirvis SE, Vainright JR, Nelson AW, et al.*

1177 **Morphine-augmented cholescintigraphy in the diagnosis of acute cholecystitis.** *Kim EE, Pjura G, Lowry P, Nguyen M, Pollack M*

1181 **Case report. Anomalous hepatic duct inserting into the cystic duct.** *Reid SH, Cho S-R, Shaw C-I, Turner MA*

1183 **Technical note. Value of flow technique for double-contrast examination of the stomach.** *Kikuchi Y, Levine MS, Laufer I, Herlinger H*

1185 **UCSF Interventional radiology rounds. Angiographic management of upper gastrointestinal hemorrhage.** *Kerlan RK Jr, Pogany AC, Burke DR, Ring EJ*

GENITOURINARY RADIOLOGY

1189 **Distal ureteral calculi: diagnosis by transrectal sonography.** *Lerner RM, Rubens D*

1193 **Simultaneous pancreatic-renal transplant scintigraphy.** *Shulkin BL, Dafoe DC, Wahl RL*

1197 **Case report. Uterine duplication, unilateral imperforate vagina, and normal kidneys.** *Johnson J, Hillman BJ*

PEDIATRIC AND FETAL RADIOLOGY

1199 **Patterns of liver injury in childhood: CT analysis.** *Stalker HP, Kaufman RA, Towbin R*

1207 **Case report. Prenatal sonographic diagnosis of atrial hemangioma.** *Leithiser RE Jr, Fyfe D, Weatherby E III, Sade R, Garvin AJ*

NEURORADIOLOGY

1209 **Subcortical arteriosclerotic encephalopathy: CT spectrum and pathologic correlation.** *Lotz PR, Ballinger WE Jr, Quisling RG*

1215 **Head injury: early results of comparing CT and high-field MR.** *Zimmerman RA, Bilaniuk LT, Hackney DB, Goldberg HI, Grossman RI*

1223 **Gd-DTPA in clinical MR of the brain: 1. Intraaxial lesions.** *Brant-Zawadzki M, Berry I, Osaki L, Brasch R, Murovic J, Norman D*

1231 **Gd-DTPA in clinical MR of the brain: 2. Extraaxial lesions and normal structures.** *Berry I, Brant-Zawadzki M, Osaki L, Brasch R, Murovic J, Newton TH*

INTERVENTIONAL RADIOLOGY

1237 **Percutaneous drainage of subphrenic abscess: a review of 62 patients.** *Mueller PR, Simeone JF, Butch RJ, et al.*

1241 **Portable real-time sonography and needle guidance systems for aspiration and drainage.** *McGahan JP, Anderson MW, Walter JP*

1247 **Inferior vena caval stent filter.** *Wallace MJ, Ogawa K, Wright K, Carrasco CH, Richli W, Charnsangavej C*

1251 **Expandable intrahepatic portacaval shunt stents in dogs with chronic portal hypertension.** *Palmaz JC, Garcia F, Sibbitt RR, et al.*

MR

1255 **MR imaging of the thyroid.** *Higgins CB, McNamara MT, Fisher MR, Clark OH*

1263 **Comparison of the contrast-enhancing properties of albumin-(Gd-DTPA) and Gd-DTPA at 2.0 T: an experimental study in rats.** *Schmiedl U, Ogan MD, Moseley ME, Brasch RC*

1271 **MR artifacts: a review.** *Bellon EM, Haacke EM, Coleman PE, Sacco DC, Steiger DA, Gangarosa RE*

1283 **Boundary artifact due to truncation errors in MR imaging.** *Lufkin RB, Pusey E, Stark DD, Brown R, Leikind B, Hanafee WN*

1289 **Technical note. A new device for exercise MR imaging.** *Schaefer S, Peshock RM, Parkey RW, Willerson JT*

MEDICOLEGAL RADIOLOGY

1291 **Malpractice and radiologists, update 1986: an 11.5 year perspective.** *Berlin L*

MISCELLANEOUS

1299 **MR imaging and CT of extrahepatic cavernous hemangiomas.** *Levine E, Wetzel LH, Neff JR*

1305 **Case report. Multiple granular cell tumors of the skin and gastrointestinal tract.** *Radin DR, Zelner R, Ray MJ, Cohen H, Halls JM*

1309 **Tailgut cyst: diagnosis with CT and sonography.** *Johnson AR, Ros PR, Hjermstad BM*

1312 **Technical note. Double images in plain film radiography: a motion artifact.** *Marinelli D, Miller WT*

1313 **Communicating the significance of radiologic test results: the likelihood ratio.** *Black WC, Armstrong P*

COMPUTER PAGE

1319 **Microcomputer-based graphics.** *Taylor GA*

OPINION

1322 **Technological volatility and the aging radiologist.** *Davidson AJ*

PERSPECTIVES

1324 **The American Board of Radiology to consider *Added Qualifications*.** *Rogers LF*

1327 **Localized tissue MR spectroscopy.** *Margulis AR, James TL*

OTHER CONTENT

1154 **Forthcoming articles**

1180 **American Roentgen Ray Society information**

1192 **ARRS meeting information**

1282 **Deadlines for submission of residents' award papers**

1329 **Letters**

1337 **Recognition of manuscript reviewers, abstractors, and book reviewers for 1986**

1339 **News**

1341 **Classified ads**

1343 **Index, volume 147**

Book reviews 1132, 1138, 1148, 1176, 1206, 1236,1262

Memorial 1288

i **Masthead and contents, volume 147**

A2 **Guidelines for authors**

Vital new references on 30-day FREE trial

EMERGENCY RADIOLOGY OF THE ACUTELY ILL OR INJURED CHILD
Second Edition

By **Leonard E. Swischuk, MD**

"Only Len Swischuk could produce a book quite like this....The reproductions, particularly of soft tissues, are superb....A true teacher, [Swischuk] stresses the basic facts, the simple, the obvious, the variations, and the pitfalls....This book should be in the library of even the smallest radiology department." — **J Can Assoc Radiol** (of the First Edition)

1986/622 pages/685 illustrations/#8049-0/$75.00

COMPUTED TOMOGRAPHY AND MAGNETIC RESONANCE IMAGING OF THE HEAD AND NECK
Second Edition

By **Anthony A. Mancuso, MD** and **William N. Hanafee, MD**
with a special contribution from ***John A. Kirchner, MD***

The leading guide to head and neck imaging now includes the first comprehensive discussion of otolaryngologic MRI, an extensively revised chapter on temporal bone, extraordinary images generated by state-of-the-art equipment, and more.

1985/504 pages/155 illustrations/#5476-7/$84.75

LYMPHATIC IMAGING
Lymphography, Computed Tomography and Scintigraphy
Second Edition

Edited by **Melvin E. Clouse, MD** and **Sidney Wallace, MD**

For assistance in selecting, performing and interpreting lymphatic images using state-of-the-art equipment and techniques, turn to the new *Second Edition* of the only book-length exploration of lymphatic evaluation.

1985/[illegible] pages/[illegible] illustrations/#1851-2/$87.50

COMPUTED TOMOGRAPHY IN THE EVALUATION OF TRAUMA
Second Edition

Edited by **Michael P. Federle, MD** and **Michael Brant-Zawadzki, MD**

In this new edition you'll find a thorough and up-to-date discussion of the clinical indications for CT scanning in different types of trauma to virtually all areas of the body, keys to techniques of scanning and to accurate interpretation, and comparisons of CT to other radiographic procedures and laboratory tests.

1986/about 300 pages/about 370 illustrations/#3102-3/about $58.95

CLINICAL ARTHROGRAPHY
Second Edition

By **Rolf-D. Arndt, MD, John W. Horns, MD,** and **Richard H. Gold, MD**
with a special contribution by ***Donald D. Blaschke, DDS***

Including inflammatory diseases and other joint abnormalities, the *Second Edition* retains the emphasis on orthopedic disorders as it expands the basic principles of arthrography and adds new, recently published concepts, such as double-contrast CT arthrography.

1985/282 pages/147 illustrations/#0256-2/$62.50

Williams & Wilkins
428 E. Preston Street Baltimore, MD 21202

___ YES! Please rush my copy of _____

If not completely satisfied, I may return the books within 30 days at no further obligation. (US & Canada only).

PAYMENT OPTIONS
(Enclose payment or charge your order and Williams & Wilkins will pay all postage and handling costs.)

☐ Check enclosed ☐ Bill me
☐ VISA ☐ MasterCard ☐ American Express

card # ☐☐☐☐☐☐☐☐☐☐☐☐☐☐☐☐ exp. ☐☐-☐☐

_____
signature/p.o. #

For fastest service...call 1-800-638-0672 toll free anywhere in the US except AK and HI; MD residents call 528-4221 collect.

Full Name _____

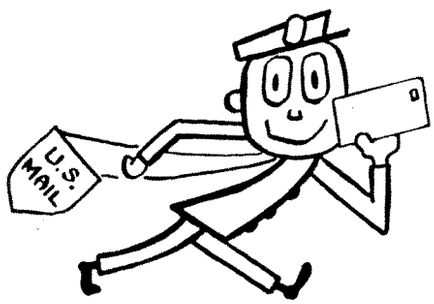
Address _____

City _____ State _____ Zip _____

Help us to serve you better.....

If your mailing label does not contain your zip code, note it on the label and return it to us for correction.

Remember, your Zip Code provides faster, more direct delivery of your journals. Use it on all correspondence, too.



INDEX TO ADVERTISERS

Ackrad Laboratories, Inc. A23

Advanced NMR A28, A29

Bard Interventional Products A26

Eastman Kodak A4, A5

E-Z-EM Company ..... Cover 2, A13

Konica Medical Corporation ... A23, A25, A27

Lorad Medical Systems, Inc. A9

Philips Medical Systems, Inc. A32, A33

Precise Optics/PME, Inc. A31

Purdue Frederick Company A34

Pyne Corporation ..... Cover 3

Raytheon Medical Systems A10, A11

Squibb A6, A7, A8

S & S X-Ray A12

St. Luke's Roosevelt Hospital A27

Tecnomed USA A16

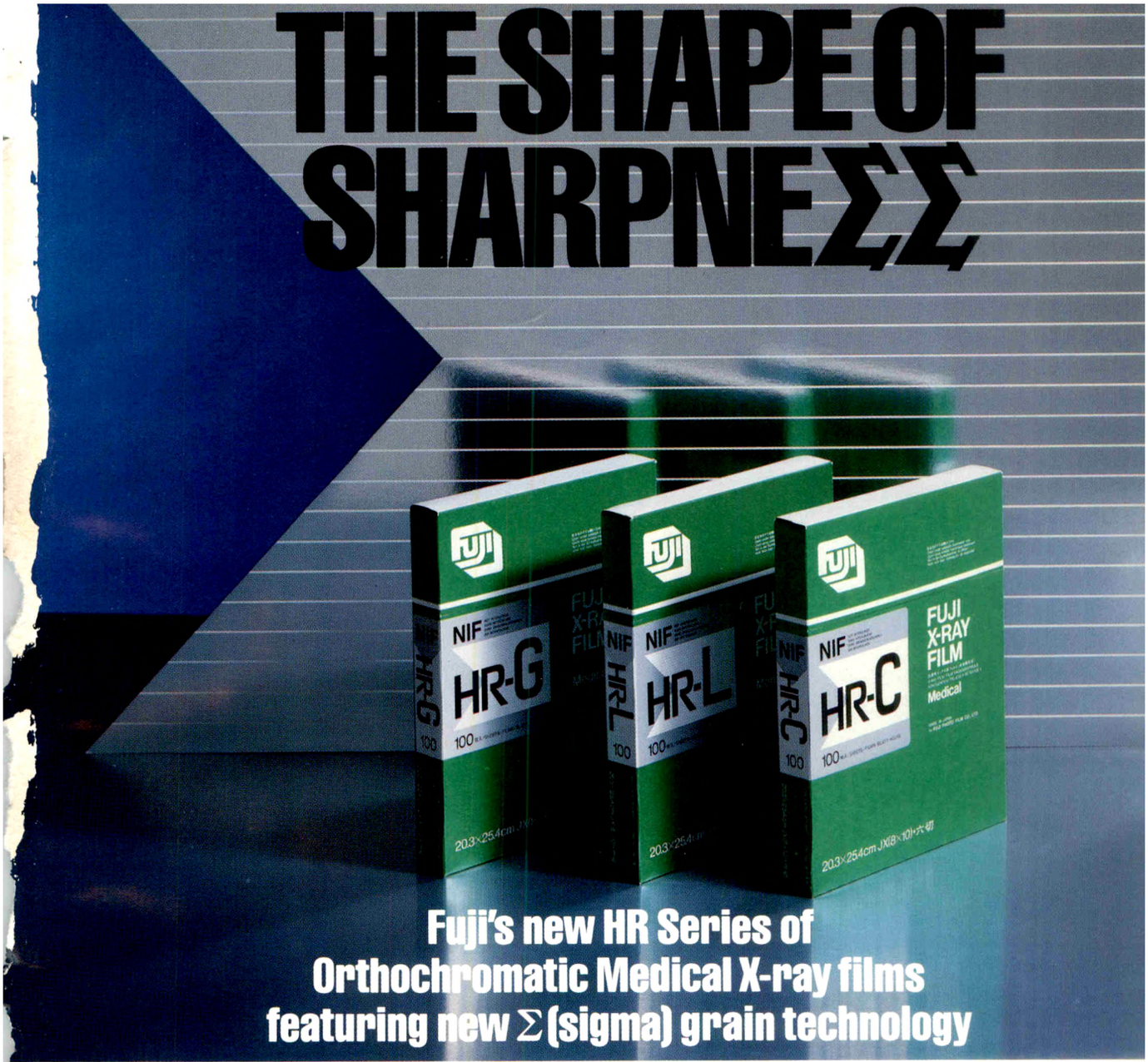
Tobias Associates A24

Toshiba Medical Systems A14, A15

Winthrop Laboratories .. A17, A18, A19, A20, A21, A22

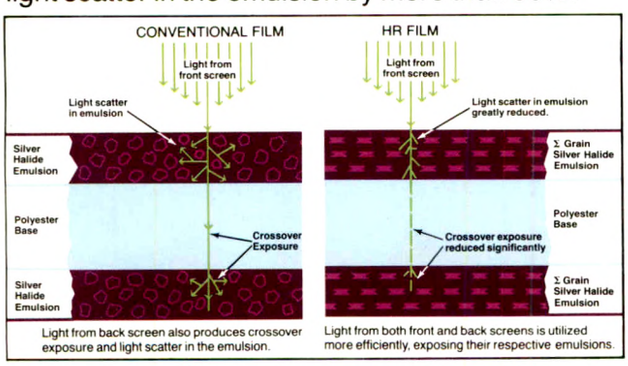
We try to present an accurate index. Occasionally this may not be possible because of a last-minute change or an omission.

THE SHAPE OF SHARPNEΣΣ



Fuji's new HR Series of Orthochromatic Medical X-ray films featuring new Σ (sigma) grain technology

Through the use of new silver halide formation technology and higher optimized amounts of spectral sensitizing dye, Fuji's new Sigma Grain Technology can reduce cross-over exposure and light scatter in the emulsion by more than 50%!



The very small (one micron mean diameter) Σ grains are systematically arranged in the toward the intensifying screen for maximum light absorption. The result is increased resolution and extremely fine grain with no loss of film speed.

Prove it to yourself

Simply put, the Fuji HR series of medical x-ray films provide the highest resolution images obtain able today. Call your Pyne representative today toll free 1-800-431-1850.

THE REASON FOR CHANGE

PYNE CORPORATION

Volume 147 **American Journal of Roentgenology** December 1986

SPECIAL ARTICLES

1103 **Leo J. Rigler lecture. MR imaging of the liver.** *Ferrucci JT*

1117 **Cannon lecture. The impact of radiology on hepatology.** *Sherlock S, Dick R*

CARDIOVASCULAR RADIOLOGY

1123 **Aortic dissection: a statistical analysis of the usefulness of plain chest radiographic findings.** *Jagannath AS, Sos TA, Lockhart SH, Saddekni S, Sniderman KW*

1127 **MR imaging of the central pulmonary arterial tree in conotruncal malformation.** *Formanek AG, Witcofski RL, D'Souza VJ, Link KM, Karstaedt N*

1133 **MR imaging of pulmonary emboli: an experimental study in dogs.** *Stein MG, Crues JV III, Bradley WG Jr, et al.*

1139 **New cineradiographic methods for assessment of Bjork-Shiley valve integrity.** *Cousin AJ, Soto B*

CHEST

1145 **Rebound thymic hyperplasia after treatment of Cushing's syndrome.** *Doppman JL, Oldfield EH, Chrousos GP, et al.*

BREAST RADIOLOGY

1149 **Baseline screening mammography: one vs two views per breast.** *Sickles EA, Weber WN, Galvin HB, Ominsky SH, Sollitto RA*

GASTROINTESTINAL RADIOLOGY

1155 **Pictorial essay. The retroperitoneal spaces revisited.** *Dodds WJ, Darweesh RMA, Lawson TL, et al.*

1162 **Commentary. Extraperitoneal spaces.** *Rubenstein WA, Whalen JP*

1165 **Esophageal intramural pseudodiverticulosis: a reevaluation.** *Levine MS, Moolten DN, Herlinger H, Laufer I*

1171 **The diagnosis of acute acalculous cholecystitis: a comparison of sonography, scintigraphy, and CT.** *Mirvis SE, Vainright JR, Nelson AW, et al.*

1177 **Morphine-augmented cholescintigraphy in the diagnosis of acute cholecystitis.** *Kim EE, Pjura G, Lowry P, Nguyen M, Pollack M*

1181 **Case report. Anomalous hepatic duct inserting into the cystic duct.** *Reid SH, Cho S-R, Shaw C-I, Turner MA*

1183 **Technical note. Value of flow technique for double-contrast examination of the stomach.** *Kikuchi Y, Levine MS, Laufer I, Herlinger H*

1185 **UCSF Interventional radiology rounds. Angiographic management of upper gastrointestinal hemorrhage.** *Kerlan RK Jr, Pogany AC, Burke DR, Ring EJ*

GENITOURINARY RADIOLOGY

1189 **Distal ureteral calculi: diagnosis by transrectal sonography.** *Lerner RM, Rubens D*

1193 **Simultaneous pancreatic-renal transplant scintigraphy.** *Shulkin BL, Dafoe DC, Wahl RL*

1197 **Case report. Uterine duplication, unilateral imperforate vagina, and normal kidneys.** *Johnson J, Hillman BJ*

PEDIATRIC AND FETAL RADIOLOGY

1199 **Patterns of liver injury in childhood: CT analysis.** *Stalker HP, Kaufman RA, Towbin R*

1207 **Case report. Prenatal sonographic diagnosis of atrial hemangioma.** *Leithiser RE Jr, Fyfe D, Weatherby E III, Sade R, Garvin AJ*

NEURORADIOLOGY

1209 **Subcortical arteriosclerotic encephalopathy: CT spectrum and pathologic correlation.** *Lotz PR, Ballinger WE Jr, Quisling RG*

1215 **Head injury: early results of comparing CT and high-field MR.** *Zimmerman RA, Bilaniuk LT, Hackney DB, Goldberg HI, Grossman RI*

1223 **Gd-DTPA in clinical MR of the brain: 1. Intraaxial lesions.** *Brant-Zawadzki M, Berry I, Osaki L, Brasch R, Murovic J, Norman D*

1231 **Gd-DTPA in clinical MR of the brain: 2. Extraaxial lesions and normal structures.** *Berry I, Brant-Zawadzki M, Osaki L, Brasch R, Murovic J, Newton TH*

INTERVENTIONAL RADIOLOGY

1237 **Percutaneous drainage of subphrenic abscess: a review of 62 patients.** *Mueller PR, Simeone JF, Butch RJ, et al.*

1241 **Portable real-time sonography and needle guidance systems for aspiration and drainage.** *McGahan JP, Anderson MW, Walter JP*

1247 **Inferior vena caval stent filter.** *Wallace MJ, Ogawa K, Wright K, Carrasco CH, Richli W, Charnsangavej C*

1251 **Expandable intrahepatic portacaval shunt stents in dogs with chronic portal hypertension.** *Palmaz JC, Garcia F, Sibbitt RR, et al.*

MR

1255 **MR imaging of the thyroid.** *Higgins CB, McNamara MT, Fisher MR, Clark OH*

1263 **Comparison of the contrast-enhancing properties of albumin-(Gd-DTPA) and Gd-DTPA at 2.0 T: an experimental study in rats.** *Schmiedl U, Ogan MD, Moseley ME, Brasch RC*

1271 **MR artifacts: a review.** *Bellon EM, Haacke EM, Coleman PE, Sacco DC, Steiger DA, Gangarosa RE*

1283 **Boundary artifact due to truncation errors in MR imaging.** *Lufkin RB, Pusey E, Stark DD, Brown R, Leikind B, Hanafee WN*

1289 **Technical note. A new device for exercise MR imaging.** *Schaefer S, Peshock RM, Parkey RW, Willerson JT*

MEDICOLEGAL RADIOLOGY

1291 **Malpractice and radiologists, update 1986: an 11.5 year perspective.** *Berlin L*

MISCELLANEOUS

1299 **MR imaging and CT of extrahepatic cavernous hemangiomas.** *Levine E, Wetzel LH, Neff JR*

1305 **Case report. Multiple granular cell tumors of the skin and gastrointestinal tract.** *Radin DR, Zelner R, Ray MJ, Cohen H, Halls JM*

1309 **Tailgut cyst: diagnosis with CT and sonography.** *Johnson AR, Ros PR, Hjermstad BM*

1312 **Technical note. Double images in plain film radiography: a motion artifact.** *Marinelli D, Miller WT*

1313 **Communicating the significance of radiologic test results: the likelihood ratio.** *Black WC, Armstrong P*

COMPUTER PAGE

1319 **Microcomputer-based graphics.** *Taylor GA*

OPINION

1322 **Technological volatility and the aging radiologist.** *Davidson AJ*

PERSPECTIVES

1324 **The American Board of Radiology to consider *Added Qualifications*.** *Rogers LF*

1327 **Localized tissue MR spectroscopy.** *Margulis AR, James TL*

OTHER CONTENT

1154 **Forthcoming articles**

1180 **American Roentgen Ray Society information**

1192 **ARRS meeting information**

1282 **Deadlines for submission of residents' award papers**

1329 **Letters**

1337 **Recognition of manuscript reviewers, abstractors, and book reviewers for 1986**

1339 **News**

1341 **Classified ads**

1343 **Index, volume 147**

Book reviews 1132, 1138, 1148, 1176, 1206, 1236, 1262

Memorial 1288

i **Masthead and contents, volume 147**

A2 **Guidelines for authors**

1987 ARRS Meeting: April 26–May 1, Miami Beach, FL